Proceedings

Strategic Alliance Acceleration in Natural Resources Utilisation and Hazard Mitigation for National Resilience

JCB 2021

JOINT CONVENTION BANDUNG

23 - 25 November 2021

JOINT CONVENTION BANDUNG 2021
PROCEEDINGS

November 23rd - November 25th 2021

Theme

"Strategic Alliance Acceleration in Natural Resources Utilisation and Hazard Mitigation for National Resilience"

Bandung
November 23rd - December 25th 2021, Indonesia

Published By

Himpunan Ahli Geofisika Indonesia (HAGI)
The Indonesian Association of Geophysicists

Ikatan Ahli Geologi Indonesia (IAGI)
Indonesian Association of Geologists

Ikatan Ahli Fasilitas Produksi Minyak dan Gas Bumi Indonesia (IAFMI)
The Indonesia Association of Oil and Gas Production Facilities Professionals

Ikatan Ahli Teknik Perminyakan Indonesia (IATMI)
The Indonesian Association of Petroleum Engineer

Secretariat
Jl. Ciledug Raya Kav.109, Cipulir, Kebayoran Lama,
Jakarta Selatan 12230, Indonesia
Phone: +62 (021) 739 4422 ext.1914

PROCEEDINGS OF
JOINT CONVENTION BANDUNG 2021

November 23rd - November 25th 2021, Bandung, Indonesia

Himpunan Ahli Geofisika Indonesia (HAGI)
Ikatan Ahli Geologi Indonesia (IAGI)
Ikatan Ahli Fasilitas Produksi Minyak dan Gas Bumi Indonesia (IAFMI)
Ikatan Ahli Teknik Perminyakan Indonesia (IATMI)

EDITOR

Advisor	Mohammad Syaiful (Universitas Pakuan)
Chief Editor	Muhammad Azka Yusuf (BAUER Pratama Indonesia)
Proceedings Editor	Wildan Tri Koesmawardani (Universitas Trisakti) Andi St Waiyah Andisa (Rimau Group)
Technical Program Committee	Julianta Parlindungan Panjaitan (Medco EP International) Argya Hastubrata Basundara (Geoservices Indonesia) Aji Rahmat Ginanjar (Pertamina EP) Muhammad Ridha (ESRI Indonesia) Bella Dina Safitri (Seleraya Merangin Dua) Widiastuti Nur farida (Pertamina Hulu Rokan) Josia Timothy Simanjuntak (IAFMI) Ricki Daniel Marbun (HAGI) Indra Luthfiana (Petrochina) Ivan Ibrahim (Rajamandala Indonesia) Tsara Kamilah (Universiti Teknologi PETRONAS) Ekkal Diyanto (HAGI) Arnold S. Layuk (IAFMI) Farhan Febrianto (IAFMI) Albertus Angga (IAGI)
Technical Secretariat	Ramoth Pambudi (IATMI)

Publisher	Ikatan Ahli Teknik Perminyakan Indonesia (IATMI)
Publisher Address	Jl. Ciledug Raya Kav.109, Cipulir, Kebayoran Lama, Jakarta Selatan 12230, Indonesia
Email	pusat@iatmi.or.id
Website	www.iatmi.or.id

PROCEEDINGS OF
JOINT CONVENTION BANDUNG 2021
November 23rd - November 25th 2021, Bandung, Indonesia

Himpunan Ahli Geofisika Indonesia (HAGI)
Ikatan Ahli Geologi Indonesia (IAGI)
Ikatan Ahli Fasilitas Produksi Minyak dan Gas Bumi Indonesia (IAFMI)
Ikatan Ahli Teknik Perminyakan Indonesia (IATMI)

REVIEWER

Imam Setiaji Ronoatmojo	**Trisakti University**
Urwatul Wusqa	**University of Indonesia**
Misbahudin	**Pertamina University**
David Ontosari	**Pertamina Hulu Rokan**
Yuniarti Ulfa	**Institut Teknologi Bandung**
I Gde Budi Indrawan	**Gadjah Mada University**
Yuniar Zhafira Abdillah	**Institut Teknologi Bandung**
Sukiato Khurniawan	**University of Indonesia**
Rosmalia Dita Nugraheni	**Trisakti University**
Budi R Permana	**ConocoPhillips**
Paramitha Tedja Trisnaning	**Institut Teknologi Nasional Yogyakarta**
Epo Prasetya Kusumah	**Pertamina University**
Haryo Edi Wibowo	**Gadjah Mada University**
Erlangga Septama	**PT.Pertamina (Persero)**
Irwan Susilo	**PT. Geospasia Wahana Jaya**
Herning Dyah Kusuma Wijayanti	**Keong Energy Indonesia Ltd.**
Dwandari Ralanarko	**PERTAMINA EP**
Merza Media Adesyofi	**Schlumberger**
Ricki Marbun	**Schlumberger**
Marsha Sakira	**Schlumberger**
Febrian Arie Wibowo	**Schlumberger**
Dedi Juandi	**Schlumberger**
Sonny Ari Wiyoga	**Schlumberger**
Hafiz Hamdalah	**UPN "Veteran" Yogyakarta**
Adi Widyantoro	**PERTAMINA EP**
Rinaldi Sudarwoto	**Schlumberger**
Sriyanta Hadi	**PETRONAS**
Yunita Dyah	**Harbour Energy**
Silvya	**Institut Teknologi Bandung**

PROCEEDINGS OF
JOINT CONVENTION BANDUNG 2021
November 23rd - November 25th 2021, Bandung, Indonesia

Himpunan Ahli Geofisika Indonesia (HAGI)
Ikatan Ahli Geologi Indonesia (IAGI)
Ikatan Ahli Fasilitas Produksi Minyak dan Gas Bumi Indonesia (IAFMI)
Ikatan Ahli Teknik Perminyakan Indonesia (IATMI)

REVIEWER

Radya Senoputra	**North Oil Company Qatar**
Alfian	**Independent Petroleum Engineer Specialist**
Andry Halim	**PT. Pertamina (Persero)**
Dodi Miyondri	**SKK Migas**
Erwinsyah Putra	**PT Pertamina Hulu Energi**
Imam M Purnama	**Canadian Emirates Western Engineering Co LLC**
Mujibul Anam	**PETRONAS**
Dr. Silviana	**Diponegoro University**
Dr. Fauzan Amir	**SKK Migas**
Farida	**SKK Migas**
Tigor Hutabarat	**PT. Blue Ocean Services**
John Hotman R Purba	**INPEX Corporation**
Marly Resdi	**SKK Migas**
Trian Asmoro	**JOB.Pertamina-Medco E & P Tomori Sulawesi**
Edwin Badrusomad	**Medco E&P Indonesia**
Fara Umainah	**SKK Migas**
Dr. Ir. Bambang Widyanto	**Institut Teknologi Bandung**
PD Suprijadi	**BP Berau Ltd.**
Budi Prasodjo	**PT Duta Marine**
Andi Palkar	**BP Berau Ltd.**
Desi A. Mahdi	**IAFMI**
Ilham Budi	**SKK Migas**

PROCEEDINGS OF
JOINT CONVENTION BANDUNG 2021

November 23rd - November 25th 2021, Bandung, Indonesia

Himpunan Ahli Geofisika Indonesia (HAGI)
Ikatan Ahli Geologi Indonesia (IAGI)
Ikatan Ahli Fasilitas Produksi Minyak dan Gas Bumi Indonesia (IAFMI)
Ikatan Ahli Teknik Perminyakan Indonesia (IATMI)

COMMITTEE

Advisor	John Hisar Simamora (Pertamina EP)
	Taufik Aditiyawarman (Pertamina EP)
	M Burhannuddin Nur (Trisakti)
	Muharram Jaya Parungseng (Pertamina EP)
Steering Committee	Hadi Ismoyo (Petrogas Group)
	G. Daru Dewanto (SKK Migas)
	Desi Mahdi (IAFMI)
	Iryanto Rompo (J-Resources)
	M. Syaiful (Universitas Pakuan)
	Rosalyn Wullandhary (Harita Group)
Organizing Committee	
Chairman	**Ari Iskandar (SKK Migas)**
Co-chairman	Surya (Pertamina Hulu Energi)
Sponsorship	**Novie (Schlumberger)**
	Yulia, Irfan Anshory (Pertamina EP)
	Laila Dzaikra Habsari (IAGI)
	Dwi Grevani Hayuti (DNP)
Treasury	**Astri Kania (Pertamina EP)**
	Aurora Juniarti (Trisakti)
	Iwan Gunawan (RPE)
Secretariat	**Syamsul Irham (Trisakti)**
	Muhammad Addiansyah (IAGI)
	Ngurah Beni Setiawan (Schlumberger)
	Sofyanudin (IATMI)
Pre-event JCB 2021	
Chairman	**Areiyando (Independent)**
Short Course/Workshop	**Yarris Ibdian Cakra Putra (PHI)**
	Desi A. Mahdi (IAFMI)
	Fraga Luzmi Fahmi (IAGI)
Geo-photo Contest	**Dwandari Ralanarko (Pertamina EP)**
Fieldtrip	**Kuntadi (Pertamina Hulu Energi)**
Golf Tournament	**Gilang Ary (Independent)**

PROCEEDINGS OF
JOINT CONVENTION BANDUNG 2021

November 23rd - November 25th 2021, Bandung, Indonesia

Himpunan Ahli Geofisika Indonesia (HAGI)
Ikatan Ahli Geologi Indonesia (IAGI)
Ikatan Ahli Fasilitas Produksi Minyak dan Gas Bumi Indonesia (IAFMI)
Ikatan Ahli Teknik Perminyakan Indonesia (IATMI)

COMMITTEE

Technical Program

Chair Person	**Julianta Parlindungan Panjaitan (Medco EP International)**
Paper Reviewer	**Erlangga Septama (IAGI)**
Oral Presentation Session	**Argya Hastubrata Basundara (Geoservices)** Widiastuti Nur Farida (Pertamina Hulu Rokan) Josia Timothy Simanjuntak (SKK Migas) Indra luthfiana (Petrochina)
Poster Presentation Session	**Aji Rahmat Ginanjar (Pertamina EP)** Arnold Layuk (Pertamina EP) Farhan Febrianto (IAFMI) Trian Hendroasmoro (Medco EP) Bella Dina Safitri (Seleraya Merangin Dua) Albertus Angga (IAGI) M. Ridha (ESRI Indonesia)
Proceedings	**Muhammad Azka Yusuf (BAUER Pratama Indonesia)** Wildan Tri Koesmawardani (Universitas Trisakti) Andi St Waiyah Andisa (Rimau Group)
Student Competition	**Prillia Aufa (IAGI)** Yury Prastika Januari (IAGI)
Session Chair & Judge	**Rizqi Syawal (IAGI)** Ivan Ibrahim (IAGI) Noezran (IAFMI)

PROCEEDINGS OF
JOINT CONVENTION BANDUNG 2021

November 23rd - November 25th 2021, Bandung, Indonesia

Himpunan Ahli Geofisika Indonesia (HAGI)
Ikatan Ahli Geologi Indonesia (IAGI)
Ikatan Ahli Fasilitas Produksi Minyak dan Gas Bumi Indonesia (IAFMI)
Ikatan Ahli Teknik Perminyakan Indonesia (IATMI)

COMMITTEE

Non-technical Program

Chair Person	**Nuli Rakhmad Widodo (SKK Migas)**
Co-chair Person	Hermansyah Nasroen (Pertamina EP) Jenary Kaban (SKK Migas)
Exhibition	**Reizky Azhar (RFD)** M. Kurnia Oktavianto (HAGI) Nur Qosim Ghozali (Pertamina Hulu Rokan)
Registration	**Sheila Kusuma Putri (HAGI)** Eksi (ENI) Gievany (IATMI) Fhirdha Rizqi (IAGI) Fraga Luzmi Fahmi (IAGI) Chintya Meidina Azwar (Institut Teknologi Bandung)
Courtesy Relation	**Bina (IATMI)** Erry Prihandry (SAKA) Bagus Guspudin (Pertamina EP Cepu) Ledi Priscilia Anjani (SAKA) Reza Riezqi Ramadhan (ANTAM)
Venue Facility	**Shanti (Pertamina EP Regional 2)** Putu Ayu Saraswati (HAGI) Ira Bangun (Pertamina EP)
IT Support (Online & Offline)	**Ahmad Aksin (Elnusa)** Ricki Daniel Marbun (Schlumberger) Oza Reisman (IATMI)

PROCEEDINGS OF
JOINT CONVENTION BANDUNG 2021

November 23rd - November 25th 2021, Bandung, Indonesia

Himpunan Ahli Geofisika Indonesia (HAGI)
Ikatan Ahli Geologi Indonesia (IAGI)
Ikatan Ahli Fasilitas Produksi Minyak dan Gas Bumi Indonesia (IAFMI)
Ikatan Ahli Teknik Perminyakan Indonesia (IATMI)

COMMITTEE

Non-technical Program

Logistic	**Mahtubah (IATMI)** Syifa (IAFMI) Yulita (IAFMI)
Media & Publication	**Nurcholis (IAGI)** Muhajir (HAGI) Inge Sondaryani (IATMI) Yunita (IAFMI)
Event Documentation	**Novie Hernawati (Independent)**
Transportation & Acommodation	**Luthfi Naufal (Huaneng Nova Energy)** Fakhrur Razi (SKK Migas)
Student Volunteer	**Afifah Nurul Maulina (HAGI)** Danya (Independent) Aji Ekananda (J-Ressources) Firman Herdiansyah (Trisakti)

FOREWORDS

Welcome to the HAGI-IAGI-IAFMI-IATMI 2021 JCB !

This has been a tough year for the Oil Industry. It started previous year with a pandemic, business is slowing down in general, unemployment and high inflation rate becomes a nightmare for almost every country who has been struggling to overcome the economic crisis. The good news is Crude Oil price hopefully will average around $60+ per barrel in 2021. This represents a rebound from the 2020 yearly average of $41 per barrel, but it is still lower than pre-Covid levels.

This year, the 4th Joint Convex 2021 is held with the theme of "Strategic Alliance Acceleration in Natural Resources Utilisation and Hazard Mitigation for National Resilience". The theme couldn't be more accurate in delivering all the issues and opportunities we need to address. As Indonesia's population and economy continue to grow, the demand for energy -in which oil and gas play a significant role- will also continue to grow.

In the current global oil and gas environment, both countries and investors are in strong competition. Countries must compete globally to win foreign investment as the current global opportunities exceed the total available capital, specifically in the energy sector. And the investors still see strong competition to secure the best of these resources. Both must make a choice as it is a long-term commitment that is made and the success of a project is a joint responsibility that depends on know-how, technology and experience from the operating company and stable environment, efficient regulations, and equitable fiscal terms from country.

In this Joint Convex meeting we will have panel discussions on how Strategic Alliance can accelerate the process of increasing Resources-to-Production ratios, special talks related to latest issues in the global market, and technical presentations on the future landscape of the oil and gas industry in Indonesia.

We invite you to joint this great event as sponsor, 400+ papers/posters will be presented covering multi-disciplinary topic geology, geophysics, petroleum engineering, and production facility, 1000+ professionals will attend the seminar and exhibitions, including the top management from all KKKS who has working area throughout Indonesia. And not to forget the prestigious 5-star venue in the beautiful city of Bandung will ensure your company brand exposure in the industry.

Look forward to seeing you in the 2021 Joint Convex!

Ir. Ari Iskandar, S.T. – JCB 2021 Chairman

PROCEEDINGS OF

JOINT CONVENTION BANDUNG 2021

November 23rd - November 25th 2021, Bandung, Indonesia

Himpunan Ahli Geofisika Indonesia (HAGI)
Ikatan Ahli Geologi Indonesia (IAGI)
Ikatan Ahli Fasilitas Produksi Minyak dan Gas Bumi Indonesia (IAFMI)
Ikatan Ahli Teknik Perminyakan Indonesia (IATMI)

FOREWORDS

It is with the greatest pleasure that I Welcome you all to Bandung to take part in the Joint Convention HAGI-IAGI-IAFMI-IATMI witch will be held on 23-25 November 2021. The theme of joint confrence is "***Strategic Alliance Acceleration in Natural Resources Utilization and Hazard Mitigation for National Resilience***" give opportunity to share our knowledge and enhance our network/collaboration among us from different aspect including academician, researcher and industry practitioner in the geosciences, petroleum and surface facilities fields.

During this joint conference, a series scientific presentation have been organized on a diverse range of topic. Recent issue about oil & gas exploration, renewable energy, unconventional energy and major disaster, remind us of that multi-disciplinary study and collaboration is very Important.

On behalf of the committee and members of HAGI, we invite you to participate as delegated, presenters, exhibitor and sponsors. I wiss all the participants a pleasant time in the Joint Convention HAGI-IAGI-IAFMI-IATMI 2021 in Bandung and look forward for your participant.

Muharram Jaya Panguriseng – President of HAGI

PROCEEDINGS OF
JOINT CONVENTION BANDUNG 2021

November 23rd - November 25th 2021, Bandung, Indonesia

Himpunan Ahli Geofisika Indonesia (HAGI)
Ikatan Ahli Geologi Indonesia (IAGI)
Ikatan Ahli Fasilitas Produksi Minyak dan Gas Bumi Indonesia (IAFMI)
Ikatan Ahli Teknik Perminyakan Indonesia (IATMI)

FOREWORDS

Dear Earth Friends,

We all know that Indonesia lies in a complex and dynamic geological setting. This condition has implications for the large variety of potential Earth resources and disasters in Indonesia. From the perspective of Earth resources, Indonesia's geological position is very advantageous because there are many types of economic commodities that can be used as a means for the welfare of the Indonesian people. But on the other hand, Indonesia's geological position also causes various types of potential Earth disasters that can threaten the safety of the Indonesian people. Based on these conditions, IAGI – HAGI – IATMI - IAFMI took the initiative to hold the Joint Convention Bandung (JCB) 2021 as a joint routine event with the theme "Strategic Alliance Acceleration in Natural Resources Utilization and Hazard Mitigation for National Resilience" on 23-25 November 2021.

The theme was chosen as IAGI - HAGI - IATMI - IAFMI's concern and response to Indonesia's geological conditions and their derivative impacts. Moreover, Indonesia has often been hit by a number of disasters in recent times, while at the same time development programs and the welfare of the Indonesian people must be carried out simultaneously.

IAGI - HAGI - IATMI - IAFMI believes that there is a need to accelerate strategic alliances to synergize national to local policies based on technical recommendations in responding to various Earth dynamics that occur in Indonesia. JCB 2021 is designed to be a momentum to catalyze the strategic cross-sectoral alliance process through a series of events that have been designed by the committee.

In the end, IAGI - HAGI - IATMI - IAFMI as the joint committee of JCB 2021 hopes that all Earth enthusiast and Earth pentahelixes can be actively involved, so that joint works and recommendations can be produced as a contribution of JCB 2021 in realizing national resilience which can be started from natural resources utilization and hazard mitigation.

M. Burhannudinnur – Chairman of IAGI

FOREWORDS

Greetings from The Indonesian Association of Oil and Gas Production Facilities Professional (IAFMI) as we invite you to participate in Joint Convention Bandung 2021 (JCB 2021), hosted by the four Indonesian Professionals Associations namely: The Indonesian Association of Geophysicists (HAGI), The Indonesian Association of Geologists (IAGI), The Indonesia Association of Oil and Gas Production Facilities Professionals (IAFMI) and The Indonesian Association of Petroleum Engineer (IATMI).

As a regular bi-yearly event, the Joint Convention is one of the biggest convention of Geo-Science and Production Facilities held in Indonesia. The convention brings together the stakeholders from energy business in Indonesia including Government Agencies, Top Management, Legislators, Experts and Professionals that are intimately involved in the industry to discuss matters pertinent to strategic, regulatory, technical and commercials side of the business. The theme of this year Convention is "Strategic Alliance Acceleration in Natural Resource Utilisation and Hazard Mitigation for National Resilience".

The last event of Joint Convention was done in Yogyakarta in 2019, prior to the global pandemic which has changed the way we conduct our meetings and convention. This year, as the situation progresses towards better outcome, we hope to bring you a slightly different format of Convention which will combine both virtual and face-to-face convention and exhibition. We believe that this Hybrid approach is a better solution for the current situation, and with proper planning this can be a new and engaging experience for the speakers, exhibitors and participants.

On behalf of the committee and members of IAFMI, we welcome and encourage your participation to support this event through choices of sponsorship packages or items described in this proposal. Your participation means a great deal for us to push forward the agenda for strategic alliance in Indonesia Energy Industry.

Together let us create this JCB 2021 to be a successful and fruitful event.

Ir. Taufik Aditiyawarman, M.M, PMP – Chairman of IAFMI

PROCEEDINGS OF
JOINT CONVENTION BANDUNG 2021

November 23rd - November 25th 2021, Bandung, Indonesia

Himpunan Ahli Geofisika Indonesia (HAGI)
Ikatan Ahli Geologi Indonesia (IAGI)
Ikatan Ahli Fasilitas Produksi Minyak dan Gas Bumi Indonesia (IAFMI)
Ikatan Ahli Teknik Perminyakan Indonesia (IATMI)

FOREWORDS

One behalf of the Indonesian Petroleum Engineers Association (IATMI), we are pleased to invite your organization to participate in the 2021 Joint Convention Bandung. This event will benefit oil and gas and mining industries in general, as well professionals and academicians. An ambitious goal is declared, a production target of 1 Million BOPD oil and 12 BSCFD gas, which indeed, is a challenging objective. However, we believe this target can be reach with support from all stakeholders in oil and gas industry such as Government, Contractor PSC (K3S) including Pertamina SHU, Technology Provider, Local Government, and as well all the professional in oil and gas industry, in the whole level from top to the bottom of organization.

"Strategic Alliance Acceleration in Natural Resources Utilisation and Hazard Mitigation For National Resillience", will give us strong message to achieve the target by speeding up the strategic alliance to increase production, especially on marginal, idle field, discovery undeveloped, IOR, Minyak Non Conventional and EOR. It is important to note that the investor commitment rely on GOI's willingness to give the incentive and sweetening, to increase IRR of the project.

Without willingness GoI to change oil and gas investment climate investment to attract more capital from outside, it is very difficult to hit the ambitious production target above. Currently, the global oil and gas industry is race one to another to give sweet incentive, there for strategic decision should be taken and in-place as soon as possible. In reality investors share the burden and scarifying from the beginning , first well exploration until oil and gas on-stream. It vary from 5 years to even 15 years from discovery. Last but not least, Maximizing the undeveloped reserves and resources through digitalization data (big data) and reservoir management with IoT is urgently needed and would expedite additional reserves.

In Joint Convention Bandung 2021, we hope all the stakeholder meet and discuss professionally, to solve the technical and non technical issue and find best solution to it. Thank you in advance for your participation and on behalf of the committee, we look forward to your attendance and support.

John Hisar Simamora – Chairman of IATMI

CONTENTS

Prefaces ..... **VII**

Topic 1 **PROFESSIONAL ORAL PRESENTATION** **1**
Big Data Analysis, Machine Learning, Data Sciences, AI

Topic 2 **PROFESSIONAL ORAL PRESENTATION** **31**
Business Development

Topic 3 **PROFESSIONAL ORAL PRESENTATION** **37**
Codes and Standard for Oil and Gas Facilities

Topic 4 **PROFESSIONAL ORAL PRESENTATION** **40**
Digital Oil Field

Topic 5 **PROFESSIONAL ORAL PRESENTATION** **45**
Drilling, Completion and Well Intervention

Topic 6 **PROFESSIONAL ORAL PRESENTATION** **61**
Environmental and Hazard Mitigation

Topic 7 **PROFESSIONAL ORAL PRESENTATION** **95**
Formation Evaluation

Topic 8 **PROFESSIONAL ORAL PRESENTATION** **100**
G&G Methods, Technology and Application

Topic 9 **PROFESSIONAL ORAL PRESENTATION** **131**
Geodynamics, Seismology, Petrology, Volcanology, and Metamorphic

Topic 10 **PROFESSIONAL ORAL PRESENTATION** **137**
Geomechanics

Topic 11 **PROFESSIONAL ORAL PRESENTATION** **140**
Geophysics, Hydrology & Oceanography

Topic 12 **PROFESSIONAL ORAL PRESENTATION** **168**
Geosciences and Technology Educational Trend and Concept

Topic 13 **PROFESSIONAL ORAL PRESENTATION** **176**
Geotourism

CONTENTS

Topic 14 **PROFESSIONAL ORAL PRESENTATION** **195**
Health Safety Environment

Topic 15 **PROFESSIONAL ORAL PRESENTATION** **199**
Infrastructure & Engineering Geology

Topic 16 **PROFESSIONAL ORAL PRESENTATION** **214**
IOR/EOR

Topic 17 **PROFESSIONAL ORAL PRESENTATION** **245**
Marginal Field Development

Topic 18 **PROFESSIONAL ORAL PRESENTATION** **249**
Marine Geology, Marine Geophysics, Marine Exploration, Marine Geology Hazard & Environmental

Topic 19 **PROFESSIONAL ORAL PRESENTATION** **251**
Mature Field Rejuvenation

Topic 20 **PROFESSIONAL ORAL PRESENTATION** **286**
Meteorology and Climatology

Topic 21 **PROFESSIONAL ORAL PRESENTATION** **292**
Mineral & Coal, Mining, Geothermal and REE

Topic 22 **PROFESSIONAL ORAL PRESENTATION** **311**
Mining Geophysics

Topic 23 **PROFESSIONAL ORAL PRESENTATION** **316**
Naturally Fracture Reservoir

Topic 24 **PROFESSIONAL ORAL PRESENTATION** **333**
Operational Safety

Topic 25 **PROFESSIONAL ORAL PRESENTATION** **343**
Operations and Integrity Management

Topic 26 **PROFESSIONAL ORAL PRESENTATION** **358**
Petroleum Geoscience

CONTENTS

Topic 27 **PROFESSIONAL ORAL PRESENTATION** **437**
Predictive Maintenance

Topic 28 **PROFESSIONAL ORAL PRESENTATION** **444**
Production Optimization

Topic 29 **PROFESSIONAL ORAL PRESENTATION** **454**
Production Technology

Topic 30 **PROFESSIONAL ORAL PRESENTATION** **479**
Project Cost Optimization

Topic 31 **PROFESSIONAL ORAL PRESENTATION** **498**
Reservoir and Production Management

Topic 32 **PROFESSIONAL ORAL PRESENTATION** **516**
Reservoir Characterization

Topic 33 **PROFESSIONAL ORAL PRESENTATION** **559**
Reservoir Engineering, Simulation, and Modelling

Topic 34 **PROFESSIONAL ORAL PRESENTATION** **641**
Sedimentology and Stratigraphy

Topic 35 **PROFESSIONAL ORAL PRESENTATION** **650**
Structural Geology

Topic 36 **PROFESSIONAL ORAL PRESENTATION** **656**
Unconventional and Renewable Energy

CONTENTS

Topic 1 **STUDENT ORAL PRESENTATION** **673**
Big Data Analysis, Machine Learning, Data Sciences, AI

Topic 2 **STUDENT ORAL PRESENTATION** **683**
Codes and Standard for Oil and Gas Facilities

Topic 3 **STUDENT ORAL PRESENTATION** **690**
Contract Risk Management

Topic 4 **STUDENT ORAL PRESENTATION** **696**
Environmental and Hazard Mitigation

Topic 5 **STUDENT ORAL PRESENTATION** **744**
G&G Methods, Technology, and Application

Topic 6 **STUDENT ORAL PRESENTATION** **765**
Geodynamics, Seismology, Petrology, Volcanology, and Metamorphic

Topic 7 **STUDENT ORAL PRESENTATION** **790**
Geomechanics

Topic 8 **STUDENT ORAL PRESENTATION** **800**
Geophysics, Hydrology & Oceanography

Topic 9 **STUDENT ORAL PRESENTATION** **867**
Geosciences and Technology Educational Trend and Concept

Topic 10 **STUDENT ORAL PRESENTATION** **873**
Geotourism

Topic 11 **PSTUDENT ORAL PRESENTATION** **898**
GIS Application for Energy Security and Mitigation

Topic 12 **STUDENT ORAL PRESENTATION** **941**
IOR/EOR

Topic 13 **STUDENT ORAL PRESENTATION** **978**
Mineral & Coal, Mining, Geothermal and REE

CONTENTS

Topic 14 **STUDENT ORAL PRESENTATION** **1042**
Petroleum Geoscience

Topic 15 **STUDENT ORAL PRESENTATION** **1053**
Production Technology

Topic 16 **STUDENT ORAL PRESENTATION** **1059**
Reservoir Characterization

Topic 17 **STUDENT ORAL PRESENTATION** **1076**
Reservoir Engineering, Simulation, and Modelling

Topic 18 **STUDENT ORAL PRESENTATION** **1091**
Sedimentology and Stratigraphy

Topic 19 **STUDENT ORAL PRESENTATION** **1129**
Structural Geology

Topic 20 **STUDENT ORAL PRESENTATION** **1151**
Unconventional and Renewable Energy

PROCEEDINGS
JOINT CONVENTION BANDUNG (JCB)2021
November 23rd – 25th 2021

A Comprehensive Review on Machine Learning Application to Solve Operational Challenges in Indonesia's Brownfield Upstream Surface Facility

Muhammad Riandhy[1,2], M. Rizqi Al Asy'ari[1,3,4], Muhammad Faza Adiyat[1,5], Vincentius Adven Brilian[1,6], Alief Thandi Yufadio[1,7]

[1]Enerka Bhumi Pratama, Kawasan Komersial Cilandak Gudang 410, Jakarta Selatan 12560, Indonesia
[2]Pertamina Hulu Rokan, Jakarta Pusat 12560, Indonesia
[3]Geoenergi Solusi Indonesia (GEOENERGIS), Cibis Nine Building 11th Floor, Jakarta Selatan 12560, Indonesia;
[4]UPN "Veteran" Yogyakarta, Yogyakarta 55283, Indonesia
[5]Universitas Pertamina, Jakarta 12220, Indonesia
[6]Universitas Gadjah Mada, Yogyakarta 55281, Indonesia
[7]Universitas Islam Riau, Pekanbaru 28284, Indonesia

Abstract
Operating brownfield upstream surface facilities has become more and more complicated and challenging nowadays. As a result of these challenges, the oil & gas industry has suffered loss of production that may affect the expected profit from production. Some notable operational challenges faced by upstream facilities are theft, aging equipment, and corroded pipeline, disruption in power lines, and challenging oil and gas characteristics that may lead to scaling and congealing problems in pipelines. To overcome this problem using conventional methods will result in exhaustive resources, hence will need new approaches and methods to effectively solve these problems using efficient resources. Machine learning methods provide excellent alternative solutions to solving the challenges. This research aims to provide comprehensive insights regarding the successful implementation of machine learning methods that has solved some of the most challenging operational issues in brownfield's surface facilities as well as explore potential application of machine learning methods to solve other challenging operational issues. To make the scope more focus, the use cases discussed in this paper only originated from Indonesia. This paper summarizes the machine learning methods that have been successfully implemented in surface facilities in Indonesia and summarizes the opportunities to adopt machine learning methods that have been implemented abroad to solve similar operational challenges in Indonesia. The authors strongly believe that this research will be useful for energy practitioners involved in the upstream oil and gas industry, specifically in the surface facilities engineering team. Moreover, this research can be a reference for production & surface facilities engineering teams who are looking for ideas to implement machine learning technology to improve their operational safety, reliability and cost-effectiveness. As the result, the transition to digital oilfield or oil and gas 4.0 in Indonesia will be smoother since many of the important stakeholders (oil and gas companies, government bodies, education providers) will understand more about machine learning technology and its potential application for solving the most challenging surface facility issues. Implementation of digital oilfield will be a key enabler to achieve Indonesia's ambition to produce 1 MMBOPD by 2030 safely, reliably and cost-effectively.

Introduction

Oil & Gas Surface Facility Overview

The role of a surface production facility is to separate the well into three components - typical "phases" (oil, gas and water) - and to process or distribute these phases into marketable products. Gas is flashed from the liquids and 'free water' from the oil is extracted in mechanical instruments called 'separators.' (K. Arnold,et.al, 2008)

As shown on Figure 1, after the well fluid reaches the surface, the fluid is flowed to the block station (BS) through flow pipes to separate water, oil, and natural gas. Apart from being directly used for industrial gas, gas lift injection or pressure maintenance can also be used, while crude oil is generally stored in the oil collection center before being sent to a refinery or terminal for shipment.

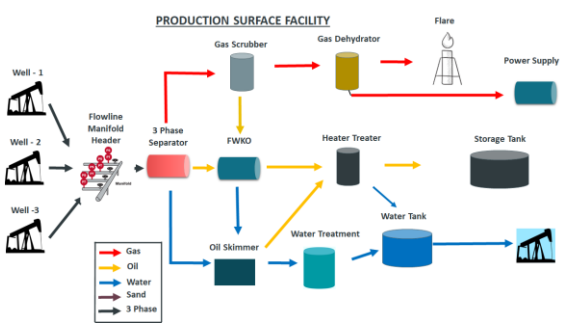

Figure 1: Simplified Design of Oil Production Surface Facility

Data Science and Machine Learning Overview

Data science is the evolution of statistics capable of producing vast volumes of data, which integrates methods from computer science into the statistics toolbox. The capacity to work with huge data and experience with machine learning, computers, and development methods distinguishes data scientists from statisticians (Cielen et al., 2016).

Figure 2: Data Science Process (Modified from Cielen et al., 2016)

PROCEEDINGS
JOINT CONVENTION BANDUNG (JCB)2021
November 23rd – 25th 2021

In data science and Big data, you will find different types of data, and each of them tends to require different tools and techniques. The main categories of data are:

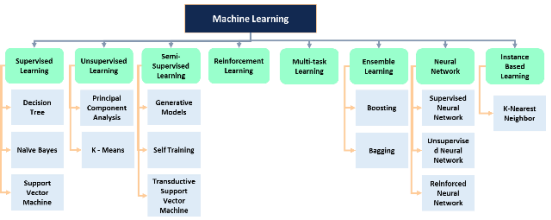

Figure 3: Type of machine learning (Modified from Dey, 2016)

1. Supervised Learning
Supervised machine learning algorithms are ones that require external assistance to operate. The input dataset is separated into two sections: train and test. The train dataset contains an output variable that requires prediction or classification. All algorithms extract patterns from the training set and apply them to the test set in order to make predictions or classify objects (Kotsiantis et al., 2007). Decision Tree, Naive Bayes, and Support Vector Machine are three of the most well-known supervised machine learning algorithms.

2. Unsupervised Learning
Unsupervised learning methods extract a limited number of features from the data. When new data is introduced, the system makes use of previously learnt features to determine the data's class. It is mostly used for feature reduction and grouping (Dey, 2016). K-Means Clustering and also Principal Component Analysis are two examples of methods for dimensionality reduction and clustering techniques.

3. Semi-supervised Learning
Semi-supervised learning algorithms are a type of machine learning technique that combine the advantages of supervised and unsupervised learning. It may be advantageous in fields like machine learning and data mining where unlabeled data is already present and obtaining labeled data is a time-consuming procedure (Zhu, et al., 2009). There are numerous classifications of semi-supervised learning, for example, Generative Models, Self-Training, and Transductive SVM.

4. Reinforcement Learning
Reinforcement learning is a sort of learning in which decisions are made about which actions to take in order to maximize the likelihood of a good outcome. Until a circumstance is presented to the student, the learner has no idea what actions to take. The learner's actions may have an effect on future situations and their actions. Reinforcement is based entirely on two criteria: trial and error searching and delayed outcome (Sutton, 1992).

5. Multitask Learning
Multitasking has the simple purpose of assisting other learners in performing better. When multitask learning algorithms are applied to a task, the algorithm retains the technique by which it solved the problem or arrived at the desired result. The algorithms then apply these processes to other similar problems or tasks. This assistance from one algorithm to another is also called / entitled to as inductive transfer. If learners share their experiences with one another, they can learn concurrently rather than individually, which results in a considerably faster learning process (Caruana, 1997).

6. Ensemble Learning
When multiple individual learners are merged to produce a single learner, this is referred to as ensemble learning. Individual learners may take the form of Naive Bayes, decision trees, or neural networks. Since the 1990s, ensemble learning has been a popular issue. It has been discovered that a group of learners is nearly always superior to an individual student at performing a particular task (Opitz et al., 1999). Boosting and Bagging are two common Ensemble Learning strategies.

7. Neural Network Learning
The neural network (or artificial neural network, or ANN) is a biological term derived from the concept of neurons. In the brain, a neuron is a cell-like structure. Dendrites, nucleus, soma, and axon are the four components. A neural network, on the other hand, behaves similarly. It operates on a three-tiered system. The input layer accepts data (much like dendrites). The input is processed by the hidden layer (like soma and axon). Finally, the output layer transmits the calculated output (along the lines of dendritic terminals) (Sharma et al., 2012). Artificial neural networks are classified into three types: supervised, unsupervised, and reinforced (Hiregoudar et al., 2014).

8. Instance-Based Learning
Instance-based learning algorithms are classified as lazy learning algorithms. (Mitchell, 1997), as they postpone induction or generalization until classification is performed. While lazy-learning algorithms (such as decision trees, neural networks, and Bayes nets) require less computation time during the training phase, they demand more computation time during the classification phase. The closest neighbor algorithm is one of the simplest and straightforward instance-based learning techniques (Kotsiantis et al., 2007).

Data and Method
The aims of this study is to give comprehensive insight regarding the application of machine learning that including preventive action and reaction regarding the operational challenges in brownfield's surface facility. The authors strongly believe that this research can be useful especially for energy practitioners that involved in upstream of oil and gas industry, specifically in surface facilities engineers team. This paper will give a review and summary about the machine learning application and will be an integrated effort in order to tackle operational challenges in brownfield's surface facilities. As the result future engineer can more understanding and make a proactive action to optimize oil and gas production. Integrated effort in this discussion is refers to all of related teams, especially for surface facilities and production engineer teams, to solve, mitigate, and fasting decision-maker of future problem in surface facility.

In order to achieve the objectives of this research, the authors of this study make a comprehensive overview to analyze actual problem in oil and gas field that related to the production problem followed by the example of the machine learning application to solve that objective.

The methodology that used in this study are literature review, and group discussion. In order to achieve the study objectives, this study is answering based on explored several questions as follows:

1. What kind of brownfield's surface facilities operational challenges that common to occur during production operation?
2. How the machine learning can help to overcome those challenges?
3. What kind of application that can be applied to solve brownfield's surface facilities operational challenges.
4. What kind of machine learning application to solve the current challenges in Indonesia?

Furthermore, the authors strongly believe this study can eventually become one of the important steps of accelerating the oilfield digitalization program and creating a guideline for implementing this method to prevent and overcome operational challenges in future production operations

Result and Discussion

Operational Challenges in Brownfield's Surface Facilities

1. Theft

Due to inaccessible facilities and compact operations leading to effective security surveillance, offshore assets appear to be insulated from these constant thefts. However, this is not the case for land assets, which generally have a large asset footprint, caused by traditional development concepts, considered simple and low-cost. These traditional concepts result in wells drilled from multiple locations with multiple pipelines spanning many communities, and make effective surveillance nearly impossible. Attackers usually target mobile assets like wellhead fixtures, Christmas trees, and oil production lines in low-activity areas. Inactive oil production lines / wells are good candidates for minimal risk. This behavior increases operating costs and in most cases will cause environmental contamination because the thief did not bother to clean up the mess they are making (Obi et al., 2021).

2. Pipeline Leakage

During continuous production processes over-time, oil and gas production pipelines may eventually fail because of corrosion, weld defects, third-party injury, and different reasons. This would lead to pipeline leakage accidents. Many experts have concluded that the failure modes of the gas pipeline are largely corrosion, both internal and external corrosion. Oil and gas pipeline leakage is one amongst the common kinds of accidents and is additionally one amongst the most causes of significant losses. The leakage accident not solely affects the routine operation of the pipeline, but additionally harms the environment and safety for surrounding humans (Lu et al., 2020).

3. Congealing

All crude oils become more viscous as they cool, but only oils freeze and precipitate paraffin, causing problems in the production of. These oils contain a lot of wax. When dealing with these high wax oils, three different problems may be encountered before the oil reaches the refinery. The first problem is sedimentation and paraffin accumulation in the well, whether in the oil string, or in the working surface and sand pores. The second problem is the accumulation of paraffin and the solidification of oil in the transportation pipeline. The third problem is paraffin precipitation and tank bottom formation (Reistle, 2017).

4. Vegetation Risk on Surface Facility/Powerline

The emerging vegetation around the surface facility and powerlines could hinder the field's operation. One of the most frequent causes of electrically induced fires is high impedance faults caused by contact with vegetation. Not to mention the major production outage from power loss. Therefore, routine surveillance is required to maintain intervals between surface facility & powerline and the growing vegetation.

5. Scaling

Oilfield scale deposits usually contain inorganic deposits and also some organic deposits (hydrate, wax, asphaltene) or corrosion, and commonly could be found in many places, such as valves, pipe walls, wells, and pumps. Scale deposition is the formation of crystalline deposits of mineral compounds in water. When the mineral concentration exceeds its saturation limit, scale manifests itself as mineral descending precipitation. This may be due to changes in certain physical properties of the fluid (usually water), such as pressure, temperature, and pH. The biggest threat to carbonate precipitation is water. When the total dissolved solids content is low, the solubility of the carbonate is low and precipitation will occur. (Rostron, 2018).

6. Corrosion

Corrosion is the damaging attack of a material by reaction with its environment and a natural potential hazard related to oil and gas facilities. Nearly every aqueous condition can support the occurrence of corrosion that happens beneath varied complex conditions in oil and gas production, processing, and pipeline systems. Crude oil and natural gas will carry varied high-impurity substances which are inherently corrosive. Within the case of oil and gas wells and pipelines, such extremely corrosive media are dioxide (CO2), hydrogen sulphide (H2S), and free water. The pipelines and also the element fittings of the lines would bear material degradations with the variable conditions of the well due to changes in fluid compositions, spoilage of wells over the amount, and changes in operating conditions of the pressures and temperatures. This material degradation ends up in the loss of mechanical properties like strength, ductility, and impact strength, subsequently loss of materials, reduction in thickness, and occasionally final failure (Popoola et al., 2013).

7. Aging Equipment

In recent years, there has been a growing interest in oil and gas equipment health prediction that identifies aging effects. The aging of a technical system may be a degradation process caused by a variety of different factors like strain, stresses, fatigue, and environmental factors. Several vital and advanced machines like gas turbines, pumps and compressors in oil and gas production facilities will finally face the top of their designed operational lifespan. The increases in demand are too little to warrant whole new installations. Understanding the residual lifetime of a technical system ensures that it is operated up to or perhaps longer than its designed operational life (Hui et al., 2014).

8. Gas Oil Separation

In brownfields, water cut of the production fluid is higher than in newly developed fields. Additionally, with breakthrough from water flood and expanded gas lift circulation, the produced fluid water cut and gas-oil ratio is ever changing. In many cases, the separator fluid loading exceeds the vessel's initial design capacity. As a result, many

companies discover that their separator is no longer sufficient to meet the required oil and water effluent requirements, or even that their gas has a high liquid carry-over. (Choi, 2010).

Machine Learning in Oil & Gas Industry

Machine learning (ML), nowadays become the most important technologies to be deployed, because this can create significant potential for innovations (WIPO, 2019). Concept of machine learning is already triggered and rooted to substantial changes and lead digital transformation in all aspect of current job and company. According to (Iansiti M, 2020) that rather than focusing on traditional, also human-centered business processes, companies across a wide range of industries are generating value through AI and machine learning applications.

Oil and gas industry is become one of industrial that categorized of latecomers to digitalization (Kohli R, 2011 and Kane G, 2015) and now the oil and gas industry become proactive for AI and machine learning applications since several years ago (BCG, 2019). This suitable with the main strategy is to enhance value by leveraging advanced technologies toward the oil and gas industrial revolution 4.0 concept (Lu H, 2019). Machine learning application can boost the decision-making and process to tackle surface facility operational challenges.

Machine Learning Application Regarding Brownfield Upstream Surface Facility Challenges

1. Process to Enhance Non-Metallic Pipe Deployments

This project aims to find recommended optimal non-metallic pipe technology, generate automatic work coverage for optimal field results, and predict business planning requirements for various fields at different operating conditions.

When applied to the design of surface non-metallic piping, the application of Artificial Intelligence in the design process of surface pipeline systems is particularly beneficial. This is because there are many different kinds of non-metallics, with each varied applications depending on pressures, ODs, temperatures, H2S levels, and a variety of other factors. As a result, the design of non-metallic surface applications makes it an excellent possibility to apply artificial intelligence in this activity. In the industry, significant improvements can be gained by combining the use of artificial intelligence with the application of non-metallic technologies.

This process was developed for several types of non-metal pipe technology, both rigid and flexible types, such as Reinforced Thermoplastic Pipe (RTP), both carbon fibre and steel-reinforced, Thermoplastic Composite Pipe (TCP), Reinforced Thermosetting Resin (RTR)) and Internal Layers using data. Historical as well as Classification Algorithms (Decision Tree) workflows for different data sets. The Decision Tree makes use of the minimum and maximum permissible operating conditions for all different technology types in different diameters, combinations, and operating conditions against technical and statistical parameters to predict the optimal type of each non-metallic pipe technology for a given field, in any given area of time (Alrabeh & Abuzaid, 2020).

2. Decision Support System for Optimizing GOSP Operation

This project aims to develop a generic integrated framework for optimizing oil recovery by optimizing the gas-oil-separation-plant (GOSP) parameters. To mimic an oil train, a model comprises of multi-stage separators, stabilization units, and a stock tank in this project. Among the various parameters, only controllable parameters such as pressure and temperature were considered optimization parameters to achieve the maximum oil recovery. The relationship based on the input fluid composition, gas and liquid rate and process parameters was established using AI techniques. The Low-Pressure Production Tap pressure was found to affect the oil recovery from the individual separation stage significantly.

The results of application machine learning in this activity can offer process optimization and Operation Decision Support System (ODSS) as stated in Figure 4.

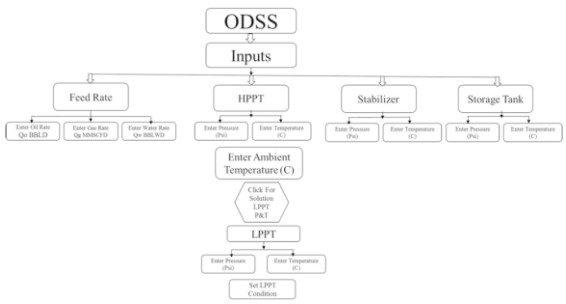

Figure 4: Conceptual model of Operation Decision Support System (ODSS) (Al-Dossary et al., 2020)

The optimum pressure was predicted with high accuracy using an artificial neural network (ANN). The pressure and temperature effect can be predicted using an AI model that takes the fluid composition as inputs. With all data provided before, Decision Support System can be created and deployed (Al-Dossary et al., 2020).

3. CO_2 Corrosion Prediction

This project aims to predict CO_2 corrosion in fluid transmission pipelines. CO_2 corrosion is a significant issue in the production and transportation of petroleum products. Most oil/gas fields are characterized by low porosity and low permeability with high CO_2 content. CO_2 corrosion in oil pipes is a complex process affected by various parameters, such as temperature, CO_2 partial pressure and pH, that can impact the service life of the integrated tubing and casing for oil and gas production. The computational fluid dynamics (CFD) model was then utilized to forecast the corrosion rate by computing the electrochemical reactions occurring at the metal surfaces. The corrosion rate is then used as the target variable, using seven parameters as input features: flow velocity, pH value, CO2 concentration, inner pipe diameter, pipe bend angle, radius, and temperature. To predict CO2 corrosion in aqueous pipelines with varied pipe bending angles, this project uses Light Gradient Boosting Machine (LightGBM) and Multiple Layer Perceptron Neural Network (MLPNN) models. For the prediction of CO2 corrosion in pipelines with bends, CFD simulation-based MLPNN and LightGBM algorithms have been developed. The cross plots show that the test data samples are well predicted with an R^2 of 0.9985 for LightGBM and 0.9931 for MLPNN. The 10-fold cross-validation results demonstrate that both methods are stable and generalizable. Data science ML model provides an effective alternative to the CFD modeling procedure if large amount of CFD results can be obtained efficiently using the

under-utilized software license and computer capacity during off-peak hours (Yang et al., 2020).

4. Detecting & Treating Flowline Emulsions in Oil Well
This project aims to detect emulsions in flowlines. Artificial Intelligence (AI) is then employed to identify and understand factors related to emulsion and optimization treatment programs. Once the wells are treated and the method is confirmed to prove emulsion existence, a focused approach is carried out to understand it further. Wells are categorized based on their production response to standard demulsifier bull heading. The project's first step is to classify the data using the Pearson correlation coefficient (R) based on pressure and temperature, then use Random Forest to improve the prediction (Esbai et al., 2020).

5. Pipeline Remote Surveillance
This project aims to increase the frequency and effectiveness of pipeline surveillance for the anomaly (3rd party damage, vegetation, unsafe pipe condition) early detection, reduce illegal tapping impact on the environment, LPO and pipeline integrity. The process uses a drone with a beyond range visual line of sight (BVLOS) and night flight mode to watch the pipeline. Combined with the AI object detection, based on deep learning, it will detect five main objects: cars, motorcycles, people, cargo trucks, and oil trucks. It also will divide the detected objects into segmentation areas like houses, roads, and pipelines. If suspicious object is detected near the pipeline, the system will have a warning or reminder system that the officer will receive SMS through their mobile phones (Renyut et al., 2020).

6. Illegal Tapping Risk Modeling
This project aims to increase the frequency and effectiveness of pipeline surveillance for the anomaly (3rd party damage, vegetation, unsafe pipe condition) early detection, reduce illegal tapping impact on the environment, LPO and pipeline integrity. The process will rank the risk based on the incidents historical data, existing ArcGIS data (map, aerial photo), google street data, field verification data, and pipeline data. It is processed with Case-based Reasoning (CBR) Correlation Analytics using the tree-based algorithm (Random Forest, Extreme Gradient Boosting, and Light Gradient Boosting). The higher risk will be prioritized for surveillance (Herlianto et al., 2020).

7. Congeal Integrated Prediction and Prevention Tool
This project aims to predict and prevent wax deposition on the flowline. Pipelines were congealed, causing production loss and pipe rupture and leakage. Many factors may aggravate oil congealing, such as ageing pipeline, long length of the pipeline, lack of external insulation, soil interaction, low fluid velocity, other deposits and rainfall intensity. The process will use the weather data flow assurance, and oil characteristics to predict the pressure on the flowline. The prediction is then produced using the tree-based algorithm (Random Forest, Extreme Gradient Boosting, and Light Gradient Boosting). When the system tells there will be high pressure, the team can inject PPD to prevent the wax deposition (Iyengar et al., 2020).

The authors also summarizing current application about the machine learning application regarding brownfield upstream surface facility challenges that already summarized in Table 1.

Machine Learning Potential to Solve Current Problem in Indonesia

1. Automatic High Level Alarm Set Point Determination
This solution aims to make an alarm for the high point on the oil tank. Oil spillover from tanks has a high risk to the facility, such as the impact on the environment (and even further extent, company image), interruption of production, and risk to personnel. API RP 2350 provided guidance to avoid risk due to spillover. It will calculate the set point for high levels in tanks. However, the formula needs the volumetric flow rate data from the incoming wells. The volumetric flow rate data is not usually available since the volumetric flow rate from the surface facility is usually measured at the outgoing production header after metering. Moreover, the optimal alarm level calculation that is calculated manually needs a lengthy amount of time. So, by using time series-based machine learning to predict the volumetric flow from the well, the alarm set point can be calculated instant and accurate. The parameter for the prediction will be the production data, and the result can also be displayed through mobile apps or web clients in the control room.

2. Sand Producing Prediction
This solution aims to predict and prevent sand on the surface facility. Predicting sanding rate, particularly for gas fields, has historically been complicated, owing to the sporadic nature of sand formation, weak quantification of fundamental physics, and a lack of representative laboratory testing and reliable field calibration. With machine learning, especially the tree-based algorithm (Random Forest, Extreme Gradient Boosting, and Light Gradient Boosting), it is possible to make prediction easier. The algorithm's parameters will be the subsurface data, sand producing historical data, and problem in the surface facility due to sand. The result can help the entire team make a proper maintenance schedule and avoid failure of the surface facility.

3. H_2S Prediction
This solution aims to predict and prevent H2S contamination on the surface facility. High H2S concentrations in produced gas are a serious problem because of the environmental impact, the impossibility to transmit acid gas to the distribution network, and asset deterioration. The algorithm's parameters will be the subsurface data, H_2S historical data, and problem in the surface facility due to H_2S, then it processed using tree-based algorithm machine learning (Random Forest, Extreme Gradient Boosting, and Light Gradient Boosting). The result can be expressed into preventive warnings and a monitoring system. Ultimately, this solution ensures the constant flow of the gas into the distribution network, avoids or mitigate halts in production, and guarantees asset integrity.

4. Pipeline Theft Detection System
This solution aims to prevent theft throughout the pipeline. The general process of theft in the pipeline, which make a hole to spill the oil off the pipeline, can lead to many problems such as corrosion, mechanical failure, and even environmental issue. The solution will combine the sensor data and surveillance data. The sensor data will be made from the pressure gauge and flowrate data to predict and detect the anomaly in the data that can indicate pipeline leaks. On the other side, drone with a beyond range visual line of sight (BVLOS) and night flight mode can monitor the pipeline. The drone will be able to recognize and detect several objects such as people, pipelines, and vehicles. All

the data above are then processed using deep learning to determine the theft activities. The product result will be a notification to security officers through their mobile phones and alarm monitoring system.

5. Thunderstorm Effect on Power Generation

Since Indonesia is a tropical country, the thunderstorm risk is always available, especially during the rainy season. Lightning discharges contain tremendous amounts of electrical energy. The impact of a direct strike is immediately evident since it typically results in damaged structures, scarred trees, and physical harm or death. Transient over-voltages, or short-duration, high-voltage spikes, are a secondary lightning strike effects Electrical equipment and electronics inside power plants can suffer as catastrophic, albeit less visually visible, damage as a result of these events. Damage to the electrical system means there will be a problem with a surface facility such as compressor, booster, and heater that can lead to a bigger problem. The method of this solution will make a prediction model (neural network algorithm or deep learning) based on weather data, incidents historical data, existing ArcGIS data (map, aerial photo, HCA), google street data, field verification data, and pipeline data. The result will be a notification system to the personnel whenever the bad condition is predicted to come.

The authors also summarizing current application about the machine learning application regarding brownfield upstream surface facility challenges that already summarized in Table 2.

Conclusions

In conclusion, several problems related to brownfield surface facilities can happen, such as theft, pipeline leakage, congealing, vegetation risk, scaling, corrosion, ageing equipment, and gas oil separation. In order to help solve them, machine learning can make the job faster and easier to execute. There are some examples of machine learning applications in order to help surface facilities problems. This study also delivers some potential ideas regarding machine learning applications in brownfield surface facilities in Indonesia.

PROCEEDINGS
JOINT CONVENTION BANDUNG (JCB)|2021
November 23rd – 25th 2021

References

Al-Dossary, B., Al-Naser, M., Al-Dogail, A., Gajbhiye, R., Al-Qathmi, A., Mahmoud, M., 2020, Decision Support System for Optimizing GOSP Operation. International Petroleum Technology Conference 13-15 January 2020. Dhahran, Saudi Arabia. IPTC-20021-Abstract

Alrabeh, M., Abuzaid, A., ,2020, New Artificial Intelligence and Big Data Analytics Process to Enhance Non-Metallic Pipe Deployments in Digital Oil Fields Using Workflows for Disparate Data Sets. Abu Dhabi International Petroleum Exhibition & Conference, 9 – 12 November 2020. SPE-202926-MS.

BCG., 2019, Going digital is hard for oil and gas companies —but the payoff is worth it 2019. https://www.bcg.com/ru-ru/publications/2019/digital-value-oil-gas.aspx.

BCG., 2019, Big oil, big data, big value 2019. https://www.bcg.com/publications/2019/big-oil-data-value.aspx.

Dey, A., 2016, Machine Learning Algorithms: A Review. *(IJCSIT) International Journal of Computer Science and Information Technologies. Vol. 7 (3)* (pp. 1174-1179). Tamil Nadu: AIRCC Publishing Corporation.

Esbai, R., Al Rumaidh, A., Sharaf, S., 2020, Detecting and Treating Flowline Emulsions in Oil Wells Using Surface Temperature, Pressure, and the Application of Artificial Intelligence. International Petroleum Technology Conference 13-15 January 2020. Dhahran, Saudi Arabia. IPTC-20231-M

Herlianto, P. A., Aji, A. Z. S., Negara, A. S., Handjoyo, T., Nugroho J., Hermawan, Y., 2020, Digital Quick Wins – Illegal Tapping Risk Modeling (AI Approach) for Duri Dumai, Minas Duri, Kotabatak Pipeline Segments. Digital Innovation and Acceleration Newsletter.

Hiregoudar, S. B. Manjunath, K. Patil, K. S., 2014, A Survey: Research Summary on Neural Networks. International Journal of Research in Engineering and Technology, ISSN: 2319 1163, Volume 03, Special Issue 03, pages 385-389.

Hui, K. H., Hee, L. M., & Leong, M. S., 2014, Equipment aging, aging detection, and aging management: A review. *Applied Mechanics and Materials*, *575*, 935–938. https://doi.org/10.4028/www.scientific.net/AMM. 575.935

Iansiti M, Lakhani KR., 2020, Competing in the age of AI. Harvard Bus Rev 2020 (January–February). [Online]. Available: https://hbr.org/2020/01/competing-in-the-age-of-ai .

Iyengar, M., Arora, V., Syukirman., Wilantara, D., Han, J., Ahba, H., 2020, Expansion of Congeal Integrated Prediction and Prevention Tool (IPPT) Kotabatak Shipping Line Wax Deposition Mitigation Tool Development. Digital Innovation and Acceleration Newsletter

Kane G. C, Palmer D, Phillips A, Kiron D, Buckley N., 2015, Strategy, not technology, drives digital transformation. MIT Sloan Manag Rev 2015.

Kohli, R. and Johnson, S., 2011, Digital transformation in latecomer" vol. 10, no. 4, pp. 141–156.

Kotsiantis, S.B., Zaharakis, I.D. & Pintelas, P.E., 2007, Machine learning: a review of classification and combining techniques. *Artif Intell Rev* 26, 159–190.

Koroteev, D. and Tekic, Z., 2021, Artificial Intelligence in Oil and Gas Upstream: Trends, Challenges, and Scenarios for The Future, Energy and AI 3 100041.

Lu H, Guo L, Azimi M, Huang K., 2019 Oil and gas 4.0 era: a systematic review and outlook. Comput Ind 2019;111(June): 68–90. doi: 10.1016/j.compind.2019.06.007.

Lu, H., Iseley, T., Behbahani, S., & Fu, L., 2020, Leakage detection techniques for oil and gas pipelines: State-of-the-art. *Tunnelling and Underground Space Technology*, *98* https://doi.org/10.1016/j.tust.2019.103249

Mitchell, T. 1997, Machine learning. McGraw Hill.

Opitz, D., Maclin, R., 1999. Popular Ensemble Methods: An Empirical Study. Journal of Artificial Intelligence Research, 11, Pages 169-198.

Popoola, L. T., Grema, A. S., Latinwo, G. K., Gutti, B., & Balogun, A. S., 2013, Corrosion problems during oil and gas production and its mitigation. *International Journal of Industrial Chemistry*, *4*(1), 1–15. https://doi.org/10.1186/2228-5547-4-35

Renyut, B., Palahniuk, M., Zulkarnaini, Aji, A., Simanungkalit, S., Brahmantyo, A., Permadi, R., Hermawan, Y., Susanto, I., Nugroho, J., Wibawa, R., Arianto, T., Paean, D., Murdiyono., Sadikin, A., Isa, M. A. N., Supriyatno, E., Kamal, F., Ozma, R., 2020, Drone Beyond Visual Line of Sight (BVLOS) with Artificial Intelligence (AI) for Pipeline Remote Surveillance. Digital Innovation and Acceleration Newsletter.

Rostron, P., 2018, Critical Review of Pipeline Scale Measurement Technologies. *Indian Journal of Science and Technology*, *11*(17), 1–18. https://doi.org/10.17485/ijst/2018/v11i17/121459

Sharma, V. Rai, S. Dev, A., 2012, A Comprehensive Study of Artificial Neural Networks, International Journal of Advanced Research in Computer Science and Software Engineering, ISSN 2277128X, Volume 2, Issue 10.

Stewart, M., Arnold, K., 2008, Surface Production Operations Design of Oil Handling Systems and Facilities Third Edition, Elsevier: United States

Sutton, R. S., 1992. Introduction: The Challenge of Reinforcement Learning. Machine Learning, 8, Page 225-227, Kluwer Academic Publishers, Boston.

WIPO., 2019, WIPO technology trends 2019, Geneva, Switzerland: Artificial Intelligence.

Yang, H., Lu, L., Tsai, K., 2020, Machine Learning Based Predictive Models for CO2 Corrosion in Pipelines with Various Bending Angles. SPE Annual Technical Conference & Exhibition 26 - 29 October 2020. SPE-201275-MS.

Zhu, X., & Goldberg, A. B., 2009. Introduction to Semi-Supervised Learning. Synthesis Lectures on Artificial Intelligence and Machine Learning, 3(1), 1–130.

PROCEEDINGS
JOINT CONVENTION BANDUNG (JCB)2021
November 23rd – 25th 2021

Appendix

Table 1: Current Application About the Machine Learning Application Regarding Brownfield Upstream Surface Facility Challenges

No	Author	Main Focus	Description	Algorithm / ML Method
1	Majed Alrabeh and Abdulrahman Abuzaid	Process to Enhance Non-Metallic Pipe Deployments	To find recommended optimal non-metallic pipe technology, generate automatic work coverage for optimal field results, and predict business planning requirements for various fields at different operating conditions.	Decision Tree
2	Badr Al-Dossary, et al.	Decision Support System for Optimizing GOSP Operation	To develop a generic integrated framework for optimizing oil recovery by optimizing the gas-oil-separation-plant (GOSP) parameters.	Artificial Neural Network
3	Huihui Yang, et al.	CO_2 Corrosion Prediction	To predict CO_2 corrosion in aqueous pipelines with different pipe bending angles.	Light Gradient Boosting Machine (LightGBM) and Multiple Layer Perceptron Neural Network (MLPNN)
4	Rami Esbai, et al.	Detecting & Treating Flowline Emulsions in Oil Well	To detect emulsions in flowlines, identify and understand factors related to emulsion, and optimisation treatment programs.	Random Forest
5	Budianto Renyut, et al.	Pipeline Remote Surveillance	To increase the frequency and effectiveness of pipeline surveillance for the anomaly (3rd party damage, vegetation, unsafe pipe condition) early detection, reduce illegal tapping impact on the environment, LPO and pipeline integrity.	Deep Learning
6	Pramudyana Agus Herlianto, et al.	Illegal Tapping Risk Modeling	Make a risk model based on the incident's historical data, existing SMO ArcGIS data (map, aerial photo, HCA), google street data, field verification data, and pipeline data.	Tree-based algorithm (Random Forest, Extreme Gradient Boosting, and Light Gradient Boosting)
7	Madhu Iyengar, et al.	Congeal Integrated Prediction and Prevention Tool	To predict and prevent wax deposition on the flowline. The process will use the weather data flow assurance and oil characteristics to predict the pressure on the flowline.	Tree-based algorithm (Random Forest, Extreme Gradient Boosting, and Light Gradient Boosting)

PROCEEDINGS
JOINT CONVENTION BANDUNG (JCB)2021
November 23rd – 25th 2021

Table 2: Machine Learning Potential to Solve Current Problem in Indonesia

No	Main Idea	Description	Algorithm / ML Method
1	Automatic High-level Alarm Set Point Determination	A high alarm point on the oil tank based on API RP 2350 with the predicted volumetric flow makes it automatic and easier to calculate.	Time Series Forecasting
2	Sand Producing Prediction	Predict and prevent sand on the surface facility based on subsurface data and historical problem data. The result can help the entire team make a proper maintenance schedule and avoid failure of the surface facility.	Tree-based algorithm (Random Forest, Extreme Gradient Boosting, and Light Gradient Boosting)
3	H_2S Prediction	Predict and prevent H_2S contamination on the surface facility based on subsurface data, historical problem data. Preventive warning and monitoring systems can improve safety for the entire operation.	Tree-based algorithm (Random Forest, Extreme Gradient Boosting, and Light Gradient Boosting)
4	Pipeline Theft Detection System	Prevent theft throughout the pipeline. Combine the sensor data and surveillance data from drone and make a decision and notification when it detects an anomaly.	Deep Learning
5	Thunderstorm Effect On Power Generation	Prediction of thunderstorm effect on the powerline based on weather, historical data, mapping data, and pipeline data, and make a notification system to personnel to be more aware of the upcoming event.	Neural Network or Deep Learning

PROCEEDINGS
JOINT CONVENTION BANDUNG (JCB)2021
November 23rd – 25th 2021

Turning Cameras into Eyes – Success Stories and Lessons Learned From Leveraging Computer Vision to Improve Safety and Reliability in Facility Operations

Muhammad Riandhy Anindika Y[1], Muhammad Rismananda Pratama[1], Ari Sukma Negara[1], Ramdhan Ari Wibawa[1], Ade Anggi Naluriawan Santoso[1]
[1]PT. Pertamina Hulu Rokan, Duri 28784 Indonesia

Abstract
Indonesia upstream sector operates more than 5,000 km of power lines, more than 30,000 km pipelines and more than 100 gathering stations consisted of more than 1000 equipment. All those assets shall be monitored and inspected regularly to ensure its mechanical integrity and security, a component of safe and reliable operations. Given its vast coverage area, the current method of manual inspection and monitoring is not very effective since it took considerably long period of time to complete and can only cover a limited area for each inspection activity session. As a result, the inspection and monitoring program was sub-optimal to detect potential threat to operations, such as theft, illegal tapping, and vegetation risk, earlier.

The advances in digital technology, particularly computer vision, cloud computing and artificial intelligence, enable every device with a camera and internet connection to become additional "eyes" that monitor, inspect and analyze everything in sight. This opens the opportunity to leverage the existing camera equipment such as CCTV in the facilities as well as Unmanned Aerial Vehicle (UAV) drone that have the capability to monitor a larger area for inspection and surveillance. Hence, we could automate the inspection and surveillance activities and even improve its effectiveness and efficiency compared with the manual method.

In this paper, we will discuss the successful implementation of computer vision and artificial intelligence technology in facility operations that has improved the effectiveness of the surveillance program at lower cost. There will be 3 success stories presented, namely CCTV object detection to prevent theft in the facility, drone object detection to prevent theft and illegal tapping in pipeline and drone aerial mapping and object detection to identify vegetation risk and insulator failure in power line. We will also discuss other potential opportunities of computer vision and artificial intelligence that will improve the effectiveness and efficiency of other types of visual inspection programs currently conducted manually, such as corrosion detection, oil spill detection, defect detection during remote Factory Acceptance Test, safety compliance on site monitoring and many more.

Introduction
Based on SKK Migas data[1], Indonesia currently has more than 1000 oil and gas fields consisted of more than 30,000 wells scattered among 94 operating areas with a total operating area of 750,000 km^2. The fields produced a total 706.7 MBOPD of oil that flows in more than 20,300 km of pipeline and processed by more than 100 gathering stations. To power the whole operations, more than 3000 km of power line consisted of more than 20,000 power poles are laid out across the operating area.

Such massive operations has its inherent operational hazards and threats. Some of those hazards and threats posed major consequences to the operations, such as:

a. Theft
b. Illegal tapping
c. Natural disruptions
d. Public exposure to oil spill or leakage
e. Weathering that leads to corrosion in equipment

As a countermeasure, multiple surveillance equipment and programs are put in place as safeguards to the hazards to lower the risks of operation. The critical facilities are monitored by CCTVs, with a total of more than 100 CCTVs in place. There are even Unmanned Aerial Vehicles (UAV) or drones implemented for added surveillance and monitoring to cover the vast operating areas. However, the effectiveness of the surveillance equipment and programs are still highly dependent on the performance of the human personnel in charge for monitoring. A slip of performance will be costly. Therefore, there is an opportunity to leverage digital technology to improve the effectiveness of these programs and improve the safety and reliability of the upstream operations, especially in the surface facility operations.

The technology in discussion is best known as computer vision. Computer vision is a field of artificial intelligence that enable computers and systems to derive meaningful information from digital images, videos and other visual inputs and take actions or make recommendations based on that information. Simply put, if artificial intelligence enables computers to think, computer vision raised the bar higher by enabling computers to see, observe and understand. With many visual inputs available to be used and exploited (CCTVs, drone cameras, cellphone cameras), the potential applications for computer vision to improve the safety and reliability of the surface facilities operations are limitless. In this paper, we will discuss 3 successful application of computer vision in surface facility operations that has been proven to improve operational safety and reliability despite the major threats inherently embedded into the surface facility operations.

Data and Method
Computer vision technology deployed in surface facility operations to enhance the capability of the surveillance visual devices to detect objects are developed based on two major machine learning algorithms class, namely:

- Supervised classification learning
- Deep learning

Let's discuss the basics of each method one by one.

Supervised learning methods or algorithms include learning algorithms that take in data samples (known as training data) and associated outputs (known as labels or responses) with each data sample during the model training process. The main objective is to learn a mapping or association between input data samples x and their corresponding outputs y based on multiple training data instances. This learned knowledge

PROCEEDINGS
JOINT CONVENTION BANDUNG (JCB)2021
November 23rd – 25th 2021

can then be used in the future to predict an output y′ for any new input data sample x′ which was previously unknown or unseen during the model training process. These methods are termed as supervised because the model learns on data samples where the desired output responses/labels are already known beforehand in the training phase.

Supervised learning basically tries to model the relationship between the inputs and their corresponding outputs from the training data so that we would be able to predict output responses for new data inputs based on the knowledge it gained earlier with regard to relationships and mappings between the inputs and their target outputs. This is precisely why supervised learning methods are extensively used in predictive analytics where the main objective is to predict some response for some input data that's typically fed into a trained supervised machine learning model. Supervised learning methods are categorized into two major classes based on the type of Machine Learning tasks they aim to solve:

- Classification
- Regression

The classification based tasks are a sub-field under supervised Machine Learning, where the key objective is to predict output labels or responses that are categorical in nature for input data based on what the model has learned in the training phase. Output labels here are also known as classes or class labels are these are categorical in nature meaning they are unordered and discrete values. Thus, each output response belongs to a specific discrete class or category.

One successful application of supervised classification learning algorithm for computer vision in surface facility operation is automatic analysis of CCTV stream to detect people in restricted/limited area and sending alert to security on duty. The algorithm used for the application is called support vector machine (SVM). As opposed to many of the machine learning algorithms where the objective function is to minimize a cost function, the objective in SVM is to maximize the cost function or margin between support vectors through a separating hyperplane[3].

A simple SVM is illustrated in Figure 1 where a separating hyperplane (solid black line) is drawn to separate blue instances from the green ones. This hyperplane is drawn in a manner to maximize the margin from both sides. Please note that the widest possible stretch must be drawn to separate the green and blue instances. The closest blue and green instances to the separating hyperplane are referred to as support vectors and this is why this algorithm is called support vector machine. The distance between the dashed lines near the blue and green instances to the separating hyperplane (solid black line) is called the "margin." As previously mentioned, the idea is to maximize the margin from both sides.

This illustration in Figure 1 is for a two-dimensional space and hyperplane will be n-1 for n-dimensional space. For instance, for a two-dimensional space (two features), the hyperplane will be one dimension, which is just a line. For a three dimensional space (three input features), the hyperplane becomes a two dimensional plane. For a four-dimensional space (four features), the hyperplane would have three dimensions. This figure illustrates the simplest form of classification problem for linearly separable cases.

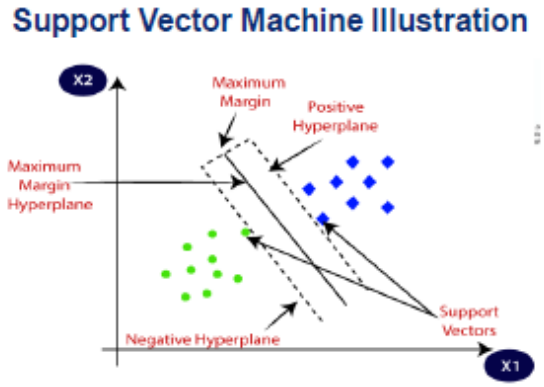

Figure 1 Support Vector Machine Illustration

The support vectors we want to separate using SVM algorithm are the class we want the SVM to learn and classify based on the set of features we feed into the algorithm. For the CCTV analysis, the features of a person that the computer vision will detect is taken from each of the image frame that made up the CCTV video stream. To deal with image data, the core principles to remember is that any image can be represented as a matrix of numeric pixel values. Therefore we could apply matrix-based feature descriptor algorithm such as Histogram of Oriented Gradient (HoG) into the each of the image frame that made up the CCTV video stream to extract the features of the object or class we want to classify. The HoG works by counting occurrences of gradient orientation in the localized portion of the image and iterates for the whole image. For each of the regions of the image it generates histograms using the magnitude and orientations of the gradient. Using this histogram, the features of the image (for example the curves, the head, etc) can be extracted for classification[4]. Figure 2 provides a simple illustration for HoG to extract the features of a person in a photo image.

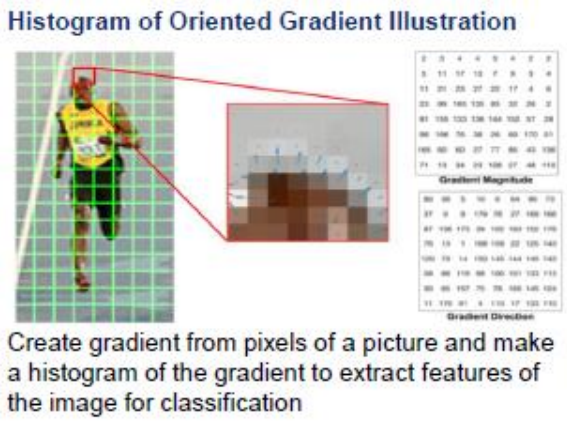

Figure 2 Histogram of Oriented Gradient

Another algorithm that can be used for object detection is deep learning. Deep learning can be considered as an extension of Artificial Neural Networks (ANNs). Neural networks were first introduced as a method of learning by Frank Rosenblatt in 1958, although the learning model called perceptron was different from modern day neural networks, we can still regard the perceptron as the first artificial neural network[3].

Artificial neural networks loosely work on the principle of learning a distributed distribution of data. The underlying

PROCEEDINGS
JOINT CONVENTION BANDUNG (JCB)2021
November 23rd – 25th 2021

assumption is that the generated data is a result of nonlinear combination of a set of latent factors and if we are able to learn this distributed representation then we can make accurate predictions about a new set of unknown data. The simplest neural network will have an input layer, a hidden layer (a result of applying a nonlinear transformation to the input data), and an output layer. The parameters of the ANN model are the weights of each connection that exist in the network and sometimes a bias parameter. This simple neural network is represented as shown in Figure 3.

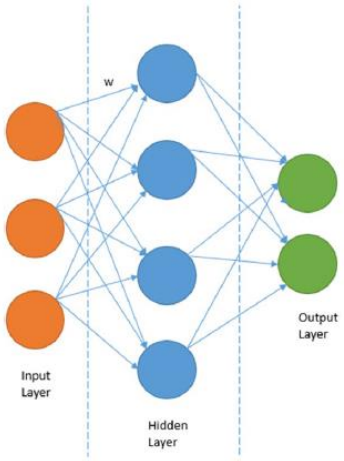

Figure 3 Simple ANN Illustration

This network is having an input vector of size 3, a hidden layer of size 4, and a binary output layer. The process of learning an ANN will involve the following steps.

1. Define the structure or architecture of the network we want to use. This is critical as if we choose a very extensive network containing a lot of neurons/units (each circle in Figure 3 can be labeled as neuron or a unit) then we can overfit our training data and our model won't generalize well.
2. Choose the nonlinear transformation to be applied to each connection. This transformation controls the activeness of each neuron in the network.
3. Decide on a loss function we will use for the output layer. This is applicable in the case when we have a supervised learning problem, i.e. we have an output label associated with each of the input data points.
4. Learning the parameters of the neural network , i.e. determine the values of each connection weight. Each arrow in Figure 3 carries a connection weight. We will learn these weights by optimizing our loss function using some optimization algorithm and a method called backpropagation.

There are three major differences that deep neural networks have as compared to normal neural networks.

1. Number of Layers
   Normal neural networks are shallow, which means that they will have at max one or two hidden layers. Whereas the major difference in deep neural networks is that they have a lot more hidden layers. And this number is usually very large. For example, the Google brain project used a neural network that had millions of neurons.
2. Diverse Architectures
   There are a wide variety of deep neural network architectures available ranging from Deep Neural Network (DNNs), Convolutional Neural Network (CNNs), Recurrent Neural Network (RNNs), and Long Short Term Memory (LSTMs). This is significantly more diverse than the traditional ANN architecture.
3. Computation Power
   The larger the network and the more layers it has, the more complex the network becomes and training it takes a lot of time and resources. Deep neural networks work best on GPU based architectures and take far less time to train than on traditional CPUs, although recent improvements have vastly decreased training times.

The deep learning algorithm used in computer vision application in surface facility operation is based on CNN. Convolutional Neural Networks (CNNs) are similar to the general artificial neural networks illustrated in Figure 3. The additional explicit assumption of input being an image (tensor) is what makes CNNs optimized and different than the usual neural networks. This explicit assumption is what allows us to design deep CNNs while keeping the number of trainable parameters in check (in comparison to general neural networks). The following are the key concepts of CNN:

- Convolutional Layer: This is the key differentiating component of a CNN as compared to other neural networks. Convolutional layer or conv layer is a set of learnable filters. These filters help capture spatial features. These are usually small (along the width and height) but cover the full depth (color range) of the image. During the forward pass, we slide the filter across the width and the height of the image while computing the dot product between the filter attributes and the input at any position. The output is a two-dimensional activation map from each filter, which are then stacked to get the final output.
- Pooling Layer: These are basically down-sampling layers used to reduce spatial size and number of parameters. These layers also help in controlling overfitting. Pooling layers are inserted in between conv layers. Pooling layers can perform down sampling using functions such as max, average, L2-norm, and so on.
- Fully Connected Layer: Also known as FC layer. These are similar to fully connected layers in general neural networks. These have full connections to all neurons in the previous layer. This layer helps perform the tasks of classification.
- Parameter Sharing: The unique thing about CNNs apart from the conv layer is parameter sharing. Conv layers use same set of weights across the filters thus reducing the overall number of parameters required.

A typical CNN architecture with all the components is depicted in Figure 4, which is a LeNet CNN model (Source: deeplearning.net).

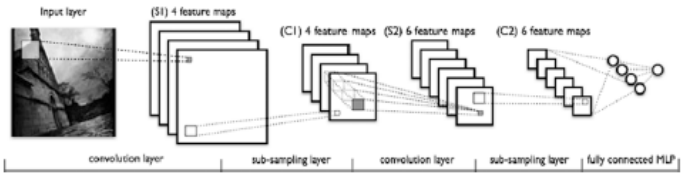

Figure 4 LeNet CNN Architecture

PROCEEDINGS
JOINT CONVENTION BANDUNG (JCB)2021
November 23rd – 25th 2021

Convolutional Neural Networks are prime examples of the potential and power of neural networks to learn detailed feature representations and patterns from images and perform complex tasks, ranging from object recognition to image classification and many more. CNNs have gone through tremendous research and advancements have led to more complex and power architectures, like VGG-16, VGG-19, Inception V3, and many more interesting models. For the application we discuss the deep learning architecture used for object detection is called You Only Look Once version 4 (Yolov4).

Deep learning is used to detect and segment objects in pipeline and power line that has the potential to pose threat to operations. Among the objects detected are suspicious people in the pipeline, suspicious tanker truck, suspicious house, vegetation near power line and broken insulator in power pole. These objects have the potential to disrupt operations by causing loss of production due to illegal tapping and power outage. Therefore early detection of these objects through application of deep learning computer vision algorithm on the video surveillance taken by drones, CCTVs and cameras will improve operational safety and reliability.

Result and Discussion

The result of the computer vision application will be discussed per case:

1. **Computer vision to detect suspicious people in the facility from CCTV stream**

   The CCTV that has been enhanced with computer vision algorithm that used HoG and SVM combination was able to detect suspicious people and send alert through messaging app to security team to take action. Figure 5 provides a snapshot of the implementation result.

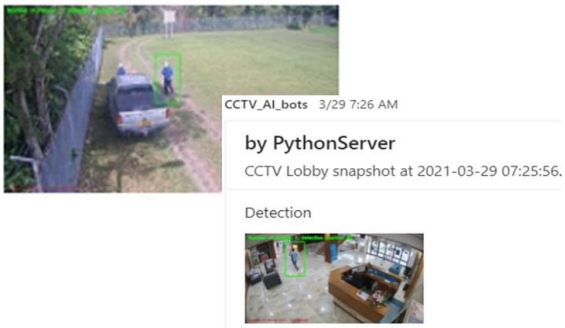

Figure 5 Result of CCTV object detection

2. **Computer vision to detect suspicious people, tanker and house near pipeline from drone surveillance video**

   The drone that has been enhanced with computer vision algorithm based on deep learning was able to detect suspicious activities near the pipeline and send alert to Security team to take action through SMS. Figure 6 provides a snapshot of the implementation result.

Figure 6 Drone with computer vision result in pipeline

3. **Computer vision to detect broken insulator in power line from drone surveillance video**

   The drone that has been enhanced with computer vision algorithm based on deep learning was able to detect broken insulator and differentiate it from the good insulator with high accuracy (> 90%). Figure 7 provides a snapshot of the implementation result.

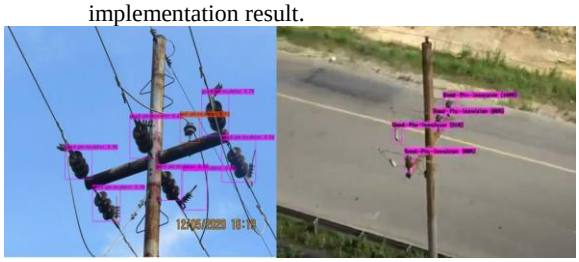

Figure 7 Drone with computer vision result in power line

4. **Computer vision to detect vegetation risk in power line from drone surveillance video**

   The drone that has been enhanced with computer vision algorithm based on deep learning was able to detect vegetation with high accuracy (> 90%) and send the location to visualization dashboard to alert Operations and Maintenance team to take action. Figure 8 provides a snapshot of the implementation result

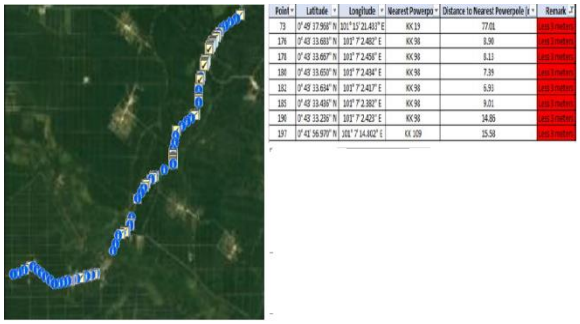

Figure 8 Drone with computer vision result in power line

The total cost saving from the 4 application to date is almost USD 100,000. This is significantly larger than the cost to produce the solution which is roughly 20 – 30% of the cost savings. The large savings was possible since the solution was made in house by the Company's own engineer. This avoids the high cost of using a third party vendor to develop the full solution.

Using similar method as the successful implementation cases, computer vision can also be used for other applications in surface facility, namely:

- Product defect detection during Remote FAT
- Physical distancing detection
- Virtual fencing
- Unsafe behavior detection (mask & PPE usage)
- Oil spill detection
- Corrosion detection in pipeline/powerline

The generalized computer vision workflow in Figure 9 can be adopted for any future application in surface facility.

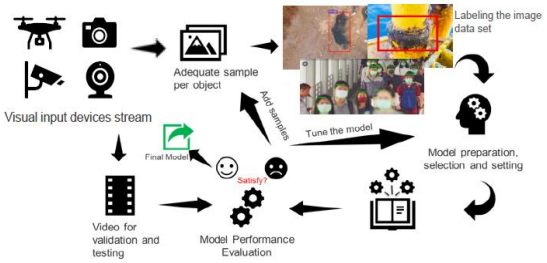

Figure 9 Generalized Computer Vision Workflow

Conclusions and Lessons Learned

- Application of computer vision algorithm to existing visual input devices has been proven to dramatically improved the effectiveness and efficiency of inspection and surveillance program
- Combination of domain expertise from functional team with AI/DS capability of IT has been proven to deliver innovative solutions for challenging operational issues (i.e., inspection in difficult location, theft detection, oil spill detection vegetation mapping, etc.)
- Indonesian resource has the capability to develop a highly accurate, cost effective computer vision solution using the latest open source technology that rivals the high cost solutions developed by developed countries.
- The availability, quality and accessibility of training data for specific application (i.e., insulator failure data) is important to ensure high accuracy computer vision model. To solve this challenge, it is advised to collect as much data as possible to be used for training data and store it in easily accessible data storage (e.g. cloud). The data source can be from previous inspections and trial runs with visual input devices of choice (drone camera, CCTV, cellphone camera, etc)
- Performing computer vision work needs high specification processing power hence needs a full upgrade from the standard PC. Therefore need to invest in high specification PC/laptop if computer vision application is considered to be applied in your facility.
- For special circumstances like night flight, there is special drone camera available for night vision. However, the challenge came from government regulation for night flights which require additional permit. Therefore, it is important to fulfill all the permit required for the full application.

References

1. https://www.skkmigas.go.id/infografis/fakta-umum-industri-hulu-migas
2. Belyadi, H., and A. Haghighat, 2021, Machine Learning Guide for Oil and Gas Using Python
3. Sarkar, D., R. Bali, and T. Sharma, 2018, Practical Machine Learning with Python
4. Tyagi, M., 2021, https://towardsdatascience.com/hog-histogram-of-oriented-gradients-67ecd887675f

PROCEEDINGS
JOINT CONVENTION BANDUNG (JCB)2021
November 23rd – 25th 2021

Wax Deposition Rate Predictive Model for Two Phase Flow Using Supervised Machine Learning

Jalest Septiano, [1]; Amega Yasutra, [1]; Sylvia Dewi Rahmawati[1]
[1]Institut Teknologi Bandung

Abstract
Wax deposit is one of the major problems experienced in the process of oil production and transportation from sub-surface to surface. There have been many models that define wax deposition in pipe streams for single-phase and multiphase flows. Nevertheless, large amounts of data are required to perform modeling using existing thermodynamic models such as carbon number data obtained from HGTC. In this paper, a supervised machine learning model, namely an artificial neural network (ANN), random forest, and support vector machine (SVM) will be implemented to determine the wax deposition rate in a two-phase water in oil flow using unified model approach. Two types of input are implemented in order to simulate influence of feature selection used in training and testing machine learning which are input A consists of water volume fraction (fw), shear stress (τ_w), effective viscosity (μe), wax concentration gradient (dC/dT), and temperature gradient (dT/dR) and input B consists of water volume fraction (fw), shear stress (τ_w), effective viscosity (μe), wax concentration gradient (dC/dT), temperature gradient (dT/dR), shear stripping variable (SV) dan diffusion variable (DV) . The random forest with Ntree = 500 known to be the best machine learning method compared to others. Based on accuracy parameter it achieves input A R^2 for training, testing and total data are 0.999, 0.992, 0.9975 and input B R^2 for training, testing and total data are 0.999, 0.993, 0.9977.
Keywords: wax deposit, machine learning, wax deposition rate, two-phase water in oil flow.

Introduction

Wax deposit is one of the problems in the process of production and transportation of oil and gas. Wax molecules will precipitate from the oil when the oil temperature is below the wax appearance temperature (WAT) (Arya et al., 2014; Onwuegbuchulem, 2015; Obaseki & Elijah, 2020). The difference in temperature between the temperature in the bulk oil and around the inner wall causes a difference in the concentration of wax dissolved in the oil. Molecular diffusion can occur due to differences in concentration. This is the most reliable mechanism that causes wax to accumulate on the pipe walls (Burger et al., 1981; Azevedo & Teixeira, 2003; Sousa et al., 2019). The presence of wax deposits in the pipe walls and reservoirs can cause the pipe walls to become smaller, reduce oil production capacity, increase handling costs, increase production downtime, reduce production efficiency and cause pipe damage when the pressure due to wax deposits is greater than the maximum yield strength of the pipe. (Adewusi, 1997; Zuo et al., 2001; Wu et al., 2002; Dalirsefat and Feyzi 2007; KhaksarManshad et al., 2012).

Massive research has been done in modeling the mechanism of deposition of wax on the pipe wall. There are 2 existing models that can be used, namely the RRR model and the Matzain model. The RRR model is used in a multiphase model by considering 2 mechanisms, namely molecular diffusion and shear dispersion. In the matzain model, 3 mechanisms are considered, namely molecular dispersion and shear dispersion as a mechanism for wax formation and shear stripping as a wax grinding mechanism (Giachetta et al., 2018). The two models above are 2 of 3 models available in commercial software. The use of the above model requires many and complex inputs such as oil and wax composition data, oil and wax physical properties data, and pipe specification data.

Huang (2008) developed a unified model using flow loop test data from 9 types of crude oil. The concept of effective wax precipitation (EWP) and effective deposition ratio (EDR) to calculate the wax deposition rate formed at a certain temperature. This model considers 4 parameters that affect wax deposition on the pipe wall, namely shear stress (τw), viscosity (μe), wax concentration gradient (dC/dT) and temperature gradient near the pipe wall (dT/dR).

$$W = f\{\tau w, \mu e, dC/dT, dT/dR) \quad (1)$$

The wax deposition rate here shows how dangerous the condition of wax deposits that form on the pipe wall is (Huang, 2008). Shear stress and viscosity are variables that show the shear stripping mechanism and the wax concentration gradient and the temperature gradient near the pipe wall indicate the molecular diffusion mechanism.

Despite the convenience offered by this unified model, the exclusion of the water fraction in the parameters that affect the deposition of wax in the pipe wall makes this model not universally applicable. In the field, oil production along with water is a certainty that must be faced, especially when production has been carried out for a long period of time (Zheng, 2019). It has been known previously that the presence of water in waxy crude oil will reduce the formation of wax deposits. This is because the diffusion rate will be smaller when there is water dispersed in waxy crude oil compared to single phase waxy crude oil (Fan et al., 2015). Although water will increase the temperature of the flowing fluid because water has a greater heat capacity than oil, the diffusion rate effect of the wax concentration gradient will be more dominant (Couto et al., 2008; Bruno et al., 2008). The effect of water will be clearly seen in the initial wax deposition occured which is further away from the inlet due to a gentler decrease in temperature compared to single phase waxy crude oil flow (Zheng, 2019).

The development of computational technology increases the development of wax deposition rate prediction models using machine learning algorithms. Qiyu & Ma (2008) predict wax deposition rate using BP Neural network of 26 unified model data and it showed R^2 of training and testing data set 0.97 and 0.95. Wei et al (2010) proposed a seven hidden neurons back-propagation neural network to estimate wax deposition rate for single phase flow. The estimated result indicated that the error is less than 2%. Kamari et al (2014) proposed LSSVM with coupled simulated annealing as optimization strategy to predict wax deposition for single phase flow in 10 different data. This

method has R^2 in training and testing data with a value of 0.999. In this paper, two phase water in oil flow wax deposition will be modeled using a unified model approach (Huang, 2008). By considering shear stress, effective oil viscosity, wax concentration gradient, near wall temperature gradient and water volume fraction as input and wax deposition rate as the target supervised machine learning model is created. Supervised machine learning is known to have the ability in self-learning, self-adaptability and successive non-linear fitting. Several supervised machine learning algorithms such as artificial neural network, support vector machine, and random forest will be used to determine the best model to predict wax deposition rate. The best machine learning algorithm will be used as the next wax deposition rate prediction model.

Data and Method

Selection of good input parameters is very necessary for the development of machine learning in making accurate predictions. The use of 75 data from Kamari (2014), Fan et al (2015), and Xie (2016) is selected. On that data wax deposition rate based on laboratory experiment only available until fw = 0.3. In addition to variate the data, a wax deposition model based on the commercial software hypothetical case was created with the existing wax components. The carbon distribution components of the gas chromatography results based on the Sample Case are shown in Figure 1 While the wax precipitation curve in Figure 2 wax precipitation curve can be obtained from the results of differential scanning calorimetry (DSC) or other heat testing experiment. From that figure, it is also known that the wax appearance temperature is 63.83 °C. Multiflash results from the known carbon number distribution are then prepared as input in commercial software.

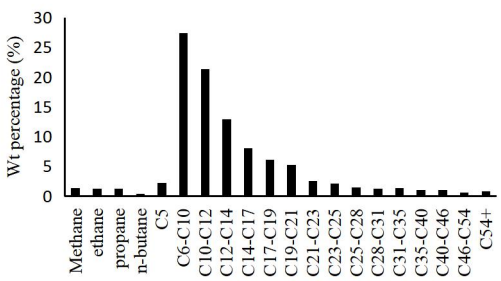

Figure1: Carbon Number Distribution of Crude Oil A (Sample Case, 2017)

Before conducting the simulation, it is necessary to know the basic assumptions used in this study are:

1. Wax only diffuses through the oil molecules
2. Condition of water in oil flow on horizontal pipe
3. Pipe roughness is considered as smooth pipe
4. Fw in deposit is the same as fw in liquid flow.

PVT data and wax data is then used in the simulation. A horizontal pipe with a length of 8.2 km is made by discretization per 40 m. This follows a sample case from commercial software simulation. The data pipeline is presented as follows:

1. OD : 0.17 m
2. ID : 0.166 m
3. Material : steel
4. ρ_{pipe} : 7850 kg/m3
5. k_{Pipe} : 50 W/mK
6. Cp_{Pipe} : 485 J/KgC
7. T_{in} : 70 °C
8. T_{out} : 20 °C
9. Tamb : 5 °C
10. Pout : 20 bar
11. Q : 1891 m3/d

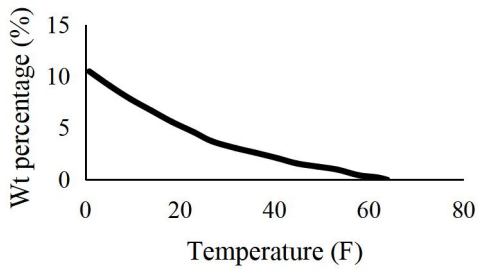

Figure 2:Wax Precipitation Curve of Crude Oil A (Sample Case, 2017)

The above simulation was carried out until the 3rd day to determine the amount of wax deposition rate. As the purposeof this paper is to build a wax deposition model for water in oil flow, the sensitivity to water cut is carried out from 0.1 to 0.9. Water inversion viscosity will be set at water volume fraction 0.9. In addition to the water cut, other parameters that were carried out by sensitivity analysis were liquid flow rate (Q), inlet temperature (T_{in}). Table 1 below shows the sensitivity of these variables.

No	Fw (-)	Q (m^3/d)	T_{in}(°C)
1	0-0.9	1891	60, 70, 80
2	0-0.9	2500	60, 70, 80
3	0-0.9	5000	60, 70, 80

Table 1: Simulation Sensitivitas Analysis

The image below shows the simulation results of several scenarios used. Figure 3 shows the effect of fw on the same Q and Tin values. It can be seen that the greater the value of fw, the lower the wax deposition rate and the first wax appearance is further away from the starting point of the inlet (Fan et al., 2015; Zheng, 2019). A sharp decline occurs at the beginning of the increase in the value of fw but tends to decrease when the value of fw is above 0.8.

Figure 4 shows the wax deposition rate curve at different Q values for the same Tin and fw values. It can be seen that the greater the value of Q, the lower the value of the wax deposition rate because Q is directly proportional to the shear stress at the wall which becomes the greater the shear stripping or negative effect on the development of wax deposition. Nevertheless, a larger Q value also causes a slower heat reduction so that the dT/dR value will be even greater especially at the near outlet. dT/dR here shows that it has a greater effect than shear stress at the wall (Xie, 2016). Figure 5 shows the wax deposition rate curve at the same Q and fw and different Tin values. From this curve, it can be seen that the larger the value of the Tin the farther first wax appearance from the inlet and the value of the wax deposition rate will tend to decrease. This is because the value of dT/dR and dC/dT will be smaller when the Tin

value is getting smaller, especially in the section approaching the outlet.

After performing sensitivity with several cases selected variables such as water volume fraction (fw), shear stress at wall (τw), effective oil viscosity (μe), wax concentration gradient (dC/dT), temperature gradient near wall (dT/dR) and the wax deposition rate (W) which will be used as input for machine learning. The value of the water volume fraction and the effective viscosity of the oil can be directly obtained from the simulation results. Values for τw and dT/dR can be calculated based on the output data from simulation. τw is calculated using the Newtonian fluid flow equation assumption for the correlation of turbulent Darcy/Fanning fraction factor with Reynolds number (Wang & Huang, 2014; Li et al., 2019).

$$\tau_w = 4.94\ x\ 10^{-3} RE^{0.75} \frac{8V}{ID} \mu e \quad (2)$$

For laminar flow,

$$\tau_w = \frac{8V}{ID} \mu e \quad (3)$$

Meanwhile dT/dR can be calculated using the equations given in the commercial software manual (Gianchetta et al., 2018; Montero, 2020).

$$dT/dR = \left(\frac{(Tb-Tws)}{kmix} hhin\right) /1000 \quad (4)$$

Lastly, the dC/dT value can be calculated based on the equation of the line formed in Figure 2.

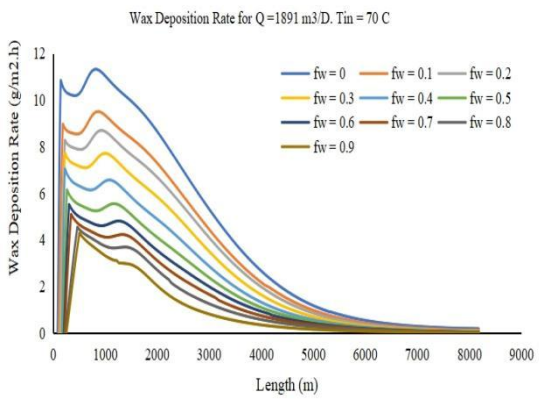

Figure 3:Wax Deposition Rate on Different Water Fraction

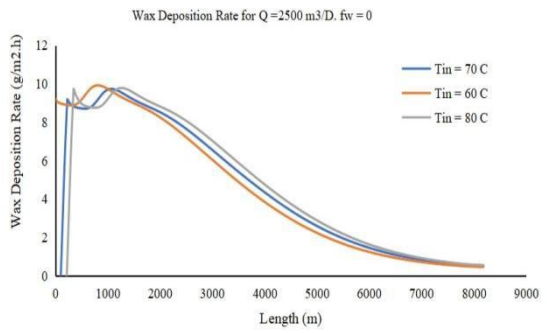

Figure 4:Wax Deposition Rate on Different Rate

Based on the simulation results, there are a total of 13995 total input data which will be the final data in making machine learning. The distribution of data for each variable such as the minimum, maximum, standard deviation, and average values is shown in Table 2 below. Results obtained quite diverse, especially in the value of W which has the smallest range of 0.023 – 18.7 g/m2h.

In knowing the relationship between each variable, the correlation coefficient is made as shown in Figure 6. It is known that the wax concentration gradient (dC/dT) temperature gradient near the wall have a positive effect on the wax deposition rate. Meanwhile, 3 other variables such as water volume fraction (fw), shear stress (τ_w) and effective oil viscosity (μe) have a negative effect on wax deposition rate. The relationship between water volume fraction and wax concentration gradient shows an inverse relationship. This indicates that the diffusion rate will be smaller when the water volume fraction is getting bigger (Fan, 2015; Zheng, 2019). While the water volume fraction has a directly proportional relationship with the viscosity and shear stress. This is because the greater the water volume fraction, the greater the viscosity of the emulsion and the greater the shear stress on the pipe wall. This input data will be divided randomly into 80% as training data and 20% as testing data.

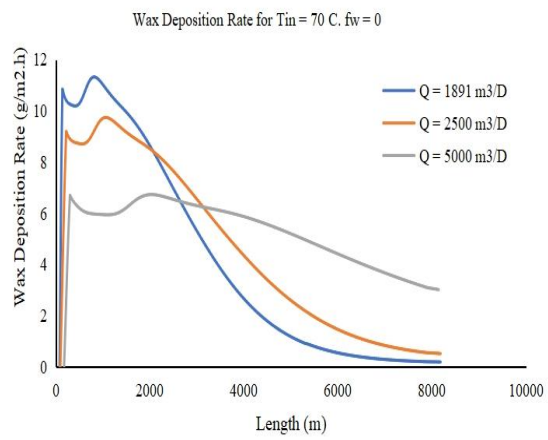

Figure 5: Wax Deposition Rate on Different Tin

	fw (-)	τw (Pa)	μe (mPa.s)	dC/dT (10-3/oC)	dT/dR (oC/mm)	W (g/m2.h)
Amount	13995	13995	13995	13995	13995	13995
Max	0.9	87.9	780.5	5.073	29.54	18.7
Min	0	1	1.11	0.00007	0.011	0.023
SDV	0.29	16.01	182.84	0.65	4.10	2.16
Ave	0.44	13.65	84.26	0.41	3.31	2.60

Table 2: Input Data Distribution

eature Engineering Method

In producing robust machine learning, it is necessary to determine the input parameters that have the best relationship to the output or target being sought. The closer the value of correlation coefficient to 1 or -1, the better the relationship between the input and the output. As previously stated regarding the correlation coefficient, the ariables dC/dT and dT/dR have the highest relationship. Meanwhile, viscosity and shear stress have smaller correlation values. To increase the correlation value, feature engineering is carried out on the data. Because the

shear stress and viscosity variables are known to have an inverse relationship, they are divided into 1/τw and 1/μe. Meanwhile, the variables dC/dT and dT/dR are multiplied by the normal log so that they become ln (dC/dT) and ln (dT/dR). With this new data, it can be seen that there is an increase in the correlation value between the input and the target W as shown in Figure 7.

Previously, the relationship between μe and W was only -0.28, after feature selection the correlation relationship between 1/μe and W was increased to 0.613. Meanwhile, ln (dC/dT) and ln (dT/dR) also showed an increase in correlation, from 0.76 and 0.64 to 0.85 and 0.69. Nevertheless, this is not indicated by 1/τw. the value of the relationship between 1/τw and W becomes 0.16 which previously was -0.17. Therefore, 2 additional features were introduced, namely shear stripping variable and diffusion variable. In the shear stripping variable, the new variables from the 2 basic variables are carried out mathematical operations as follows.

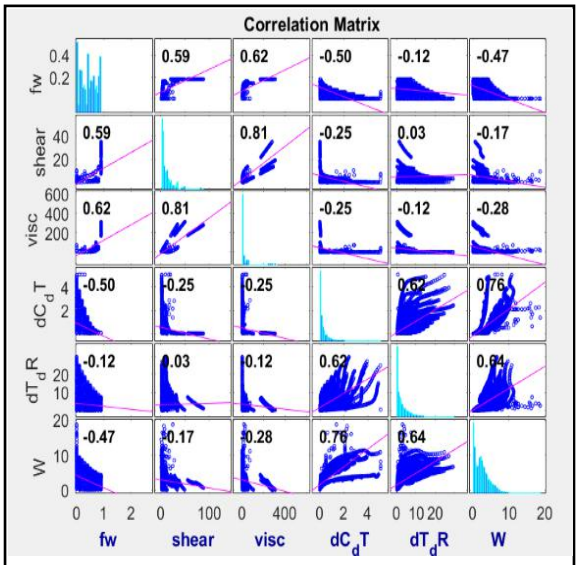

Figure 6: Correlation Matrix of Base Data

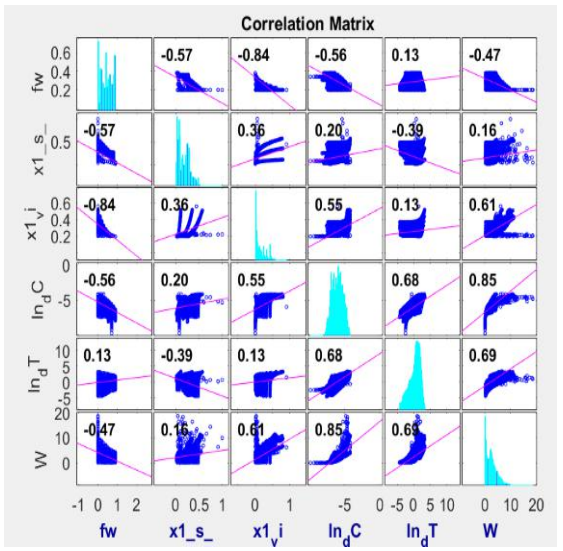

Figure 7: Correlation Matrix after Feature Engineering A

•

$$SV = \frac{1}{\tau_w \times \mu e} \quad (5)$$

While the diffusion variable is formulated as follows.

$$DV = \ln (dC/dT \times dT/dR) \quad (6)$$

These two additional features are then included in the correlation coefficient analysis. It was found that these two variables had a fairly good correlation value to the target, namely the shear stripping variable and the diffusion variable respectively 0.46 and 0.83. The relationship between these two variables with other parameters can also be seen in Figure 8.

The results of these feature engineering strategy will be used in a supervised machine learning development strategy. Both will be compared in terms of the ability to predict train data and test data that have been generated previously. Table 3 shows 2 types of strategies used in making machine learning models based on the results of feature engineering that has been carried out.

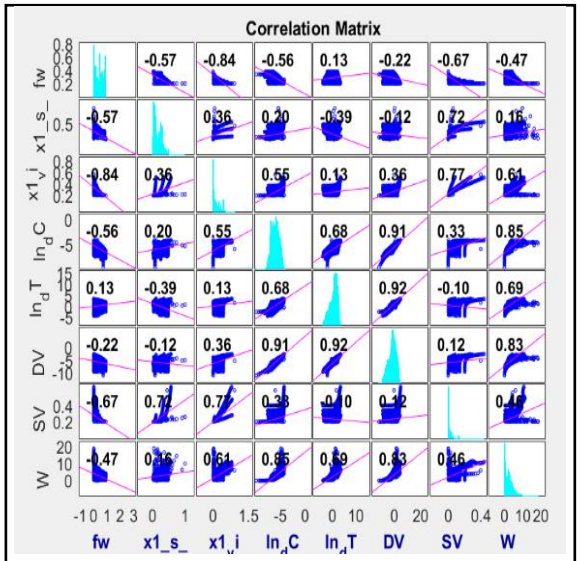

Figure 8: Correlation Matrix after Feature Engineering B

Scenario	Input Machine Learning							
A	fw	1/τw	1/μe	ln(dC/dT)	ln(dT/dR)	W		
B	fw	1/τw	1/μe	ln(dC/dT)	ln(dT/dR)	DV	SV	W

Table 3: Featured Used on Machine Learning

Data Preprocessing

The data that will be used as machine learning input will be normalized into a simpler form that is -1 to 1. Min – max normalization of machine learning input data is done using the following equation.

$$norm = \frac{x_{act} - x_{min}}{x_{max} - x_{min}} (norm_{max} - norm_{min}) + norm_{min} \quad (7)$$

Machine Learning Development

Making machine learning in predicting regression of existing data is done using 3 machine learning algorithms, namely artificial neural network, random forest and support vector machine. Artificial neural network systems

are made up of processing units called neurons. The ANN training process is used to achieve a balance between memorization and generalization abilities. Thus, the results of the ANN that have been created can be perfectly reused for other new data inputs whose quantities are still within the range of the previous training process (Agustin & Prahasto, 2012).

The first thing to do is to prepare a training sample consisting of inputs and ideal outputs. In this case the inputs are shown in Table 3. When the results of the calculation of the output match the ideal output, the training is stopped. This process can be repeated automatically with self-adaptation of the weight and activation value until the ideal output is obtained (Wei, 2010).

Back propagation artificial neural network (BP-ANN) is used in this paper. In this algorithm, each unit that is in the input layer is associated with the hidden layer and continues to be interconnected with the output layer. This network can consist of 1 hidden layer or many (multilayer network). When this network is given input as training data, then the pattern goes to the hidden layer units to be forwarded to the units in the output layer. Then the output layer units will respond as the target/output of the neural network. When the output does not match the expected target, the output will be returned backward to the hidden layer and input layer and the output will be recalculated (Agustin & Prahasto, 2012). This condition will continue to repeat until the error value between the target and the output is minimal.

Network created using Levenberg-marquardt training function and gradient descent adaptive learning. The use of Levenberg-Marquardt training function because it has a good fitting ability on the training set and also has the fastest training network (Huang, 2008). The amount of learning rate used is 0.01 with the activation function used, namely the tansig function for the input, hidden layer, and output layer. The number of hidden layers and hidden neurons becomes the sensitivity parameter. Table 4 below shows the sensitivity of BP-ANN.

Random forest is a supervised machine learning development of an iterative decision tree so as to produce a better level of accuracy. Because random forest is an ensemble method from CART, random forest also has no assumptions or is good for use in nonparametric cases (Mulyahati, 2020). This method is used to build a decision tree consisting of root nodes, internal nodes, and leaf nodes by taking attributes and data randomly according to the applicable provisions (Siburian & Mulyana, 2018). The root node variable which is also the separator variable is a determinant in making the splitting tree which can be done by using the MSE value, Gini ratio, and entropy/information ratio. After getting the separator attribute with the lowest MSE/gini ratio value, it will proceed to the next branch. This continues until the stopping criteria are met, namely the minimum leaf node is met (Mulyahati, 2020).

The final prediction results can be calculated by combining or aggregating the prediction results of each decision tree which can be shown in the following equation.

$$Y_i = \frac{1}{Ntree}\sum_{n-1}^{Ntree} Y_n \quad (8)$$

No	Hidden Layer	Hidden Neuron 1	Hidden Neuron 2
1	1	5	
2	1	7	
3	1	9	
4	1	10	
5	1	15	
6	1	20	
7	1	25	
8	1	30	
9	1	35	
10	1	40	
11	1	42	
12	1	44	
13	1	46	
14	1	48	
15	1	50	
16	1	52	
17	1	54	
18	1	56	
19	1	58	
20	1	60	
21	2	5	5
22	2	7	7
23	2	9	9
24	2	10	10
25	2	15	15
26	2	20	20
27	2	25	25
28	2	30	30
29	2	35	35
30	2	40	40
31	2	42	42
32	2	44	44
33	2	46	46
34	2	48	48
35	2	50	50
36	2	52	52
37	2	54	54
38	2	56	56
39	2	58	58
40	2	60	60

Table 4: BP-ANN Model Scenario

Random forest was created using Orange data mining software by varying the Ntree value. Based on Breiman (2001) the Ntree value of 50 has resulted in a satisfactory predictive value. Meanwhile, according to Sutton (2004) the value of Ntree > 100 will produce a low level of error. Therefore, the Ntree values of 50, 100, 200, 300, 400, 500, 600, 700, 800, 900, 1000, are used to produce variations in accuracy.

The third machine learning is support vector machine. Support vector machine basically uses the basic principle of linear classifier. By using kernel functions such as gaussian or polynomial, classification and prediction can be used in non-linear cases. In a space with high dimensions, a hyperplane (hyperplane) that can maximize the distance (margin) between data classes. Hyperplane in SVM can be defined as follows (Santosa, 2007; Octaviani et al, 2014):

$$f(x) = w^T x + b \quad (9)$$

Where w is the linear regression slope, x is the input vector of the model, b is the intercept linear regression and T is the transpose matrix (Kamari et al., 2014). While the function of the gaussian kernel is defined as follows (Kamari et al., 2014).

$$K(x_i, x_j) = \exp\left(-\frac{[|x_i - x_j|]^2}{2\sigma}\right) \quad (10)$$

Trial and error of cost and regression loss epsilon (σ) has been done to acquire best SVM prediction. Figure 9 shows

the scheme used in making machine learning using Orange data mining.

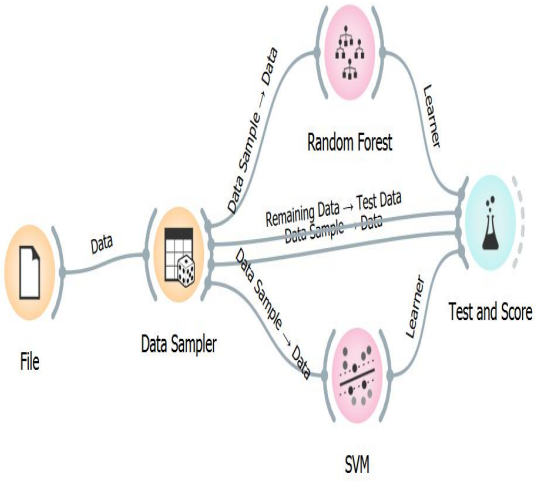

Figure 9: Model Establishment of Machine Learning at Orange Data Mining

These three machine learning models will be compared based on the MAE, MSE, RMSE, and R2 error parameters using the following equation.

$$\mathrm{MAE} = \frac{1}{n}\sum_{j=1}^{n}\left|W_{pred} - W_{act}\right| \quad (11)$$

$$\mathrm{MSE} = \frac{1}{n}\sum_{j=1}^{n}\left(W_{pred} - W_{act}\right)^2 \quad (12)$$

$$\mathrm{RMSE} = \sqrt{\frac{1}{n}\sum_{j=1}^{n}\left(W_{pred} - W_{act}\right)^2} \quad (13)$$

$$R^2 = 1 - \frac{\sum_{j=1}^{n}\left(W_{(i)act} - W_{(i)pred}\right)^2}{\sum_{j=1}^{n}\left(W_{(i)pred} - \mathrm{average}W_{(i)pred}\right)^2} \quad (14)$$

Result and Discussion

In the experiment using BP-ANN using input scenario A, it was found that the BP-ANN scenario no. 38 where using 2 hidden layers with each hidden layer is 56 has the best error and accuracy. The scheme of BP-ANN is showed on Figure 10.

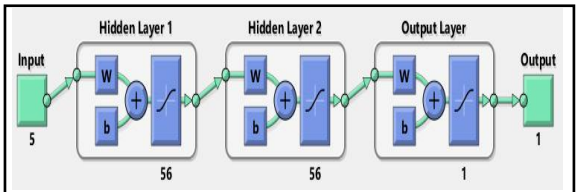

Figure 10: Best BP ANN Scheme

The error and accuracy values for training, testing and total data using input scenario A are shown in Table 5. Using this model on input scenario B achieve error and accuracy better than input scenario A. The error and accuracy values for training, testing and total data are shown in Table 6. It was also found that the more hidden layers used the better adjustable parameters to define the nonlinear relationship between input parameters and output parameters. This has a positive impact on the network that is made, it will be better at storing memory about the predictions made. So that a more precise solution will be obtained when making predictions using other data (Wei, 2010). Nonetheless, the training time will be longer when hidden layer increase. In this best parameter ANN, it takes 143.3 seconds of training time for input scenario A and 156.2 seconds for input scenario B. The addition of additional feature variables seems to only affect the training time not significantly.

	MSE	RMSE	MAE	R
Total	0.022	0.147	0.052	0.995
Training	0.0074	0.087	0.019	0.998
Testing	0.033	0.182	0.04	0.992

Table 5: Input A Scenario Accuracy and Error using Best BP-ANN

	MSE	RMSE	MAE	R
Total	0.014	0.117	0.043	0.997
Training	0.00684	0.083	0.018	0.998
Testing	0.031	0.175	0.04	0.992

Table 6: Input B Scenario Accuracy and Error using Best BP-ANN

The result of feature selection that has been done previously also shows that the presence of additional features as input for scenario B will result in a better level of predictability than input for scenario A. The increase in total data R^2 from 0.995 to 0.997 indicates that the SV and DV parameters have a positive effect on machine learning's ability to recognize target. Figure 11 describe predicted and actual wax deposition rate using input scenario B.

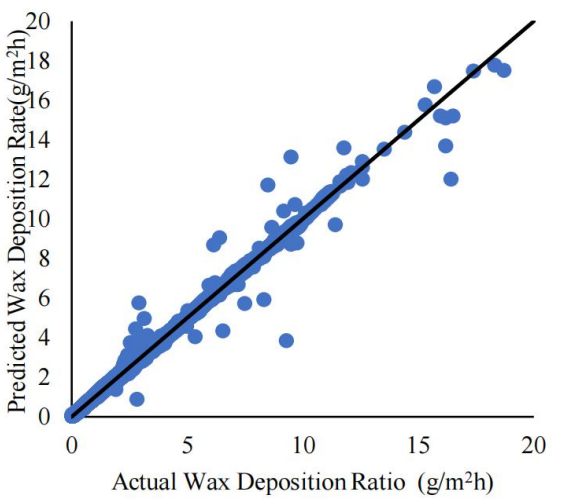

Figure 11: Input B Scenario Comparison Between Predicted and Actual Wax Deposition Rate for Best BP-ANN

Sensitivity of the Ntree value will be carried out when modelling using a random forest. The value of growth control on leaf nodes and individual trees is not limited. Based on the experimental results, it was found that Ntree = 500 produced the best error and accuracy values compared to the others with a fairly fast training time of

21.06 seconds. The results of the accuracy and error of the random forest model Ntree = 500 can be seen in Table 7. The use of input B scenarios at the same Ntree = 500 also shows an increase in the accuracy and error obtained. It can be seen in Table 8.

	MSE	RMSE	MAE	R
Total	0.012	0.109	0.022	0.9775
Training	0.006	0.081	0.017	0.999
Testing	0.033	0.182	0.04	0.992

Table 7: Input A Scenario Accuracy and Error using Best Random Forest

	MSE	RMSE	MAE	R
Total	0.011	0.104	0.022	0.9777
Training	0.006	0.083	0.017	0.999
Testing	0.029	0.173	0.04	0.993

Table 8: Input B Scenario Accuracy and Error using Best Random Forest

The addition of additional features in the use of random forest also increases the required training time to 22.14 seconds. This condition is similar to the experiment using the best parameter BP-ANN. Increasing the Ntree above 500 did not improve the accuracy and error parameter values obtained. The addition of Ntree will only increase the training time so that it will take longer to perform calculations. Here figure 13 described actual vs predicted wax deposition rates for input scenario B using random forest.

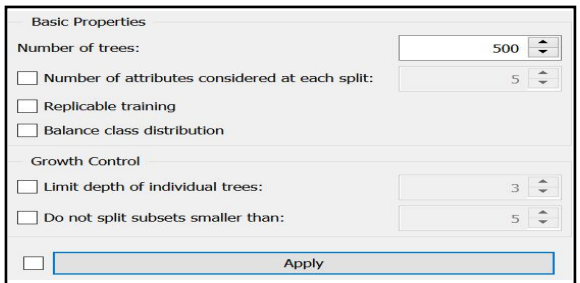

Figure 12: Random Forest Widget on Orange Data Mining

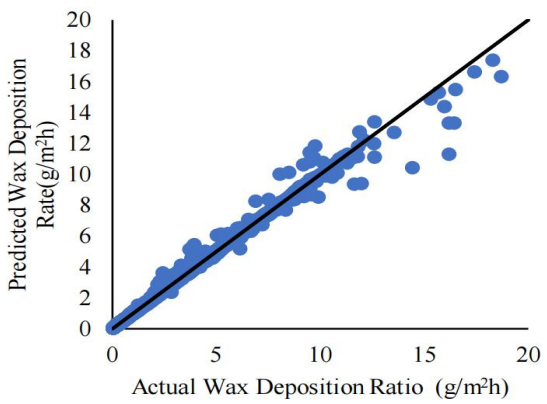

Figure 13: Input B Scenario Comparison Between Predicted and Actual Wax Deposition Rate for Best Random Forest

The last machine learning is SVM. In making the best SVM model the cost value and regression loss epsilon (σ) values are varied. It was found that in the input scenario A, the best error and accuracy values were in the combination of cost and regression loss epsilon (σ) of 2.05 and 0.1, respectively. The error and accuracy values for training, testing and total can be seen in Table 9. Meanwhile in the input scenario B, the use of cost and regression loss epsilon (σ) of 2.05 and 0.1, respectively, produces better error and accuracy values than the input scenario A. This can be seen in Table 10.

	MSE	RMSE	MAE	R
Total	0.25	0.5	0.369	0.948
Training	0.252	0.5	0.37	0.946
Testing	0.246	0.496	0.365	0.945

Table 9: Input A Scenario Accuracy and Error using Best SVM

	MSE	RMSE	MAE	R
Total	0.25	0.5	0.361	0.949
Training	0.253	0.5	0.363	0.946
Testing	0.239	0.489	0.355	0.946

Table 10: Input B Scenario Accuracy and Error using Best SVM

When the cost value is fixed, an increase in epsilon regression loss will reduce prediction accuracy. Meanwhile, at a fixed epsilon regression loss value, an increase in cost value will increase the predictive ability of the data and then it will decrease that predictive ability. In this case the use of cost 2.05 is the optimum value. The use of the SVM algorithm also requires the fastest training time compared to other machine learning used in this paper. Input scenario A training time is needed for 0.485 seconds and for input scenario B it takes as much as 0.611 seconds. This can also be observed in the use of BP-ANN and random forest. The addition of parameter SV and DV also increases the predictive ability for SVM model. Figure 14 showed actual vs predicted wax deposition rates for the input scenario B using SVM.

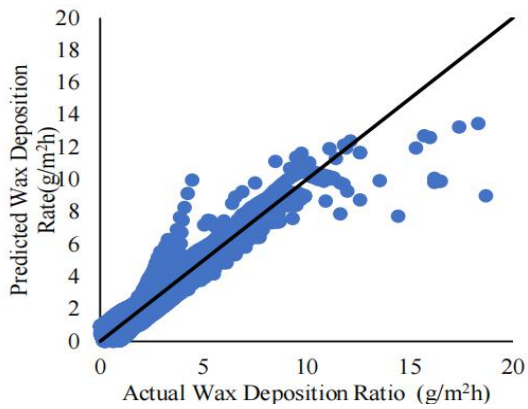

Figure 14: Input B Scenario Comparison Between Predicted and Actual Wax Deposition Rate for Best Random Forest

Regardless type of machine learning used, it was found that the use of random forest produces the best error and accuracy values in the use of input scenario A and input scenario B. In addition, the use of input scenario B which defines additional parameters or features increases the predictive ability. As for each machine learning, slightly increase of accuracy observed from random forest which has total data R2 = 0.9975 to R2 = 0.9977, BP-ANN which has total data R2 = 0.995 to R2 = 0.997 and SVM which has total data R2 = 0.948 to R2 = 0.949. Addition another feature which has a better correlation with target can be one of strategy in order to increase predictability of machine learning.

Application of Best Machine Learning

Based on the results that have been shown previously, a random forest algorithm was chosen with the best predictive accuracy value. To prove the ability of the random forest algorithm that has been made previously in making predictions, in this section predictions will be made in several cases. The case used in this prediction is still the same as that described in the Data and Method section.

Figure 15 shows the results of predictions and calculations using dynamic multiphase flow at a flow rate of 1891 m3/D, an inlet temperature of 70 °C, and variations of water fraction 0, 0.2, 0.4, 0.6, and 0.8 (case 1). The results of the predictions using the random forest used show a similar pattern to the results of calculations using dynamic multiphase flow for each case. The mean absolute percentage error (MAPE) obtained also shows a value of 0.73% to 1.32%. Another case is shown in Figure 16 where the water fraction is 0 and the inlet temperature is 70°C (case 2). The good predictive ability of random forest can also be seen in this case. MAPE values ranging from 0.34 % - 1.1 %. This indicates that the predictive ability of the random forest algorithm is quite good when compared to using a dynamic multiphase flow simulator.

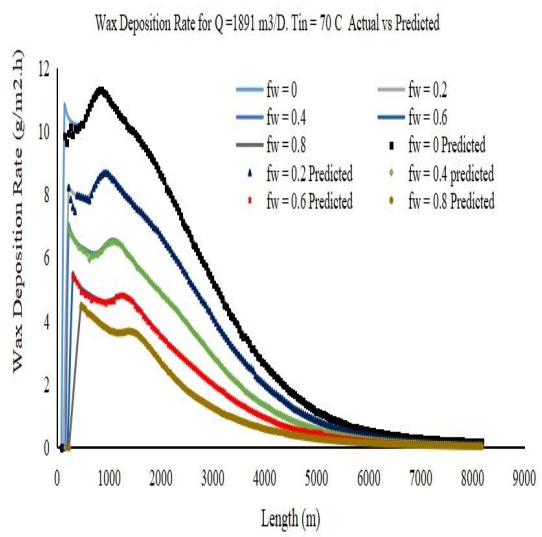

Figure 15: Comparisons of Wax Deposition Ratio Between Dynamic Multiphase Flow and Best Machine Learning (Case 1)

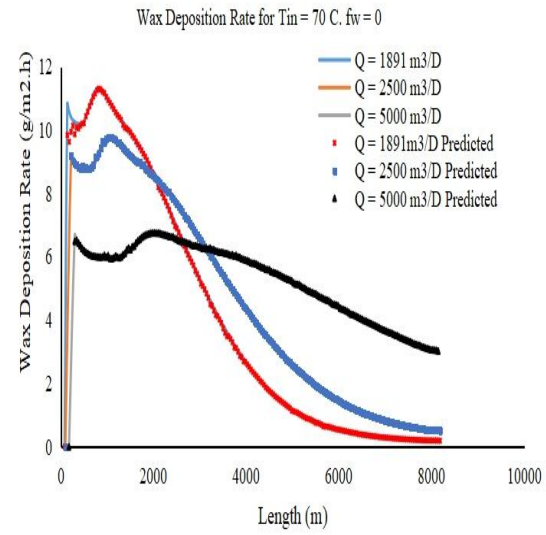

Figure 16: Comparisons of Wax Deposition Ratio Between Dynamic Multiphase Flow and Best Machine Learning (Case 2)

Case	fw	Q	Tin	MAPE (%)
1	0	1891	70	1.10
	0.2	1891	70	0.73
	0.4	1891	70	0.82
	0.6	1891	70	1.32
	0.8	1891	70	0.98
2	0	1891	70	1.10
	0	2500	70	0.43
	0	5000	70	0.34

Table 11: MAPE of Predicted Wax Deposition Rate

Conclusions

Prediction of wax deposition is very important in oil and gas transportation and production operations. The conditions of oil production followed by water will affect how the wax is formed. In this paper, 3 machine learning algorithms (BP-ANN, random forest, and SVM) were developed to calculate the wax deposition rate in streams with different fw. Two types of input after feature engineering is used. Based on the data obtained from the results of simulations using commercial software, it is known that the use of machine learning algorithms in the form of random forests with Ntree = 500 produces the best predictive ability based on the error values obtained for both types of input scenarios. It has R2 for training, testing and total data are 0.999, 0.992, 0.9975, respectively. The strategy to include additional features is also known to improve predictability for best parameter random forests even on slightly values. Using the same parameter of best random forest achieves R2 for training, testing and total data are 0.999, 0.993, 0.9977, respectively. Beside that prediction using random forest while compare to the result from dynamic multiphase flow showed good prediction. It can be seen on the value of MAPE obtained is under 10%. Establishment of machine learning for next study can be made by varying input of simulation and apply another feature which has better correlation with target so it can

have wider range of data that can be predict and also increase accuracy of predicted data.

Nomeclature:

μe	: Effective viscosity of oil, cP
ρ_{fluid}	: Fluid density, kg/m^3
τ_w	: Liquid shear stress at wall, Pa
Cp_{Pipe}	: Heat capacity of pipe, J/KgC
dC/dT	: Wax concentration gradient, 10^{-3}/°C
dT/dR	: Temperature gradient near wall, °C/mm
fw	: volume fraction of water, (-)
hhin	: Inner wall heat transfer coefficient, W/m2-C
ID	: Pipe inside diameter, m
k_{mix}	: Conductivity of fluid, W/m°C
k_{Pipe}	: Pipe conductivity, W/mK
OD	: Pipe outside diameter, m
P_{out}	: Outlet Pressure, bar
Q	: Liquid flow Rate, m^3/D
RE	: Reynold Number, (-)
T_{amb}	: Ambient temperature, °C
T_b	: Bulk temperature, °C
T_{in}	: Inlet temperature, °C
T_{out}	: Outlet temperature, °C
T_{ws}	: Wall surface temperature, °C
V	: Liquid flow velocity, (m/s)
W	: Wax deposition rate, g/m^{2}h
W_{act}	: Actual wax deposition rate, g/m^{2}h
W_{pred}	: Predicted wax deposition rate, g/m^{2}h

References

Adewusi, V. A., 1997, Fuel, **76**, 1079–1083.
Agustin, M., and Prahasto, T., 2012, Sistem Informasi Bisnis, **2**, 89 – 97.
Arya, H.P., Khalik, M.S., Andhy, A.E., Azuraien, B.J., and Lukeman, I., 2014, J. Appl. Mech. Mater, **625**, 196-200. Azevedo, L. F. A., and Teixeira, A. M., 2003, Petroleum
Science and Technology, **21**, 393-408
Breiman, L., 2001, Machine Learning, **45**, 5-32
Bruno, A., Sarica, C., Chen, H., Volk, M., 2008, SPE 114474.
Burger, E. D., Perkins, T. K., and Striegler, J. H., 1981, Journal of Petroleum Technology, **33**, 1075-1086.
Couto, G. H., Chen, E., Dellecase, E., Sarica, C., and Volk,M., 2008, SPE Production & Operations, **23**, 49 – 55.
Dalirsefat, R., and Feyzi, F., 2007, *Fuel*, **86**, 1402–1408. Fan, K., Huang, Q., Li, S., and Yu, W., 2015, Journal of Dispersion Science and Technology, **38,** 8 - 18.
Giacchetta, G., Marchetti, B., Leporini, M., Terenzi, A., Dall'Acqua, D., Capece, L., Grifoni, R. C., 2017, Petroleum, **5**, 206-213.
Huang, Q., Li, Y., Zhang, J., 2008, *Acta. Petrolei. Sinica. (in Chinese)*, **29**, 459-462.
Kamari, A., Mohammadi, A, H., Bahadori, A., & Zendehboudi, S., 2014, Petroleum Science and Technology, **32**, 2837-2844.
Khaksar Manshad, A., Ashoori, S., Khaksar Manshad, M., and Omidvar, P., 2012, Petroleum Science and Technology, **30**, 1369–1378.
Li, R., Huang, Q., Huo F., Fan, K., Li, W., Zhang, D., 2019, Journal of Petroleum of Science and Engineering, **181**, 1- 44.
Mulyahati, I. L.,2020, B.S. thesis, Universitas Islam Indonesia.
Montero, F., 2020, M.S. thesis, Aalborg University.
Obaseki, M., and Elijah, P. T., 2020, Journal of King Saud University, **33**, 437-445.
Octaviani, P. A., Wilandari, Y., and Ispriyanti, D., 2014, Gaussian, 3, 811 – 820.
Onwuegbuchulem, C., 2015, M.S. thesis, Federal universityof Owerri.
Qiyu, H., and Ma, J., 2008, International Pipeline Conference, IPC-64225.
Santosa, B., 2007, Graha Ilmu.
Siburian, V. W., and Mulyana, I. E., 2018, Annual ResearchSeminar, **4**, 144-147.
Sutton, C. D., 2004, Handbook of Statistics, 24, 303-329. Sousa, A. M., Matos, H. A., and Guerreiro, L., 2019,
Petroleum, 6, 215-225.
Wang, W., and Huang, Q., 2014, Journal of Energy Institute, 87, 196 – 207.
Wei, Y., Wu, M., and Ling, Z., 2010, Sixth International Conference on Natural Computation.
Wu, C. H., Wang, K. S., Shuler, P. J., Tang, Y., Creek, J. L., Carlson, R. M., and Cheung, S., 2002, AIChE J. 48, 2107–2110.
Xie, Y., and Xing, Y., 2016, Petroleum, 3, 237-241.
Zheng, S., 2017, Ph.D. Dissertation, University of Michigan Zuo,
J. Y., Zhang, D. D., and Ng, Heng-Joo., 2001. Chemical engineering science, 56, 6941–6947

PROCEEDINGS
JOINT CONVENTION BANDUNG (JCB) 2021
November 23rd – 25th 2021

Lateral Heterogeneity Analysis using Multiwell ZVSP Unsupervised Machine Learning Classification

Fahdi Maula
SIS SCHLUMBERGER, Qatar

Abstract

In 3D and 2D surface seismic interpretation, seismic waveform shapes and attributes can define facies and reservoir parameters laterally with more details than traditional amplitude mapping. I adapted this method on 1D zero offset VSP (ZVSP) data, giving a unique perspective of lateral heterogeneity analysis using VSP seismic waveform shapes and attributes. The downgoing wavefield of VSP measures seismic wave variation in the vertical direction. When there are enough VSPs covering an area, we can combine them to get an insight into both vertical and lateral variations.

I used a machine learning unsupervised classification algorithm based on K-means and self-organizing maps (SOM) to group the waveforms based on their shape similarity and attributes (frequency spectrum). The algorithm produced a cluster map, a probability map, and a typical wavelet for each cluster. These were then used to analyze the vertical and lateral heterogeneity from well to well based on VSP waveform attributes. The example data used were an open dataset, the Poseidon 3D data from the NW Shelf, Australia (Browse Basin), provided by GEOscience Australia. There were six wells available with VSP datasets.

This method can be useful to integrate additional attributes from VSP into broader 3D subsurface interpretations. For precautions, the VSP measurement or data preconditioning must be done consistently before classification. Such method may work well for vertical well ZVSP where we only observed variation because of the vertical seismic ray path.

With this work, the application of VSP data has been extended from the conventional single well-to-well basis. This study shows the value of integrating VSP characterization from multiple wells and multiple measurements to discern both vertical and lateral heterogeneity in an area.

Keywords: VSP Machine Learning, Waveform Classification

Introduction

Seismic waveform shapes and attributes carry information about facies and reservoir parameters. In 2D and 3D surface seismic data, this attribute mapping analysis provides lateral details about the reservoir to balance traditional structural mapping analysis. The waveform shapes interpretation method normally integrated into the seismic waveform's classifications. Andersen and Boyd (2004) depicted a two type classification methods; unsupervised and supervised classifications used to describe and display the seismic reflection character. They reported that this method can identify character differences among thousands of data points.

In the present study, the seismic waveforms classification was adapted on 1D zero-offset VSP (ZVSP) data which provides a unique perspective on lateral heterogeneity analysis based on VSP seismic waveform shapes and attributes. Traditionally, Vertical Seismic Profiles (VSP) is employed to provide seismic traces of the well for correlation with surface seismic. With VSP having vertical wavefield propagation, it carries vertical high-resolution information. In addition, the waveshape would be useful to extract valuable information on the wavefield propagations. This data could be extracted in the form of direct measurement of attenuation (Q), geometric divergence, or amplitude analysis for the correlation of acoustic impedance inversion (Campbell, et. al, 2005).

When there are enough VSPs covering an area, they can be combined to get an insight into both vertical and lateral variations. In this paper, we used the unsupervised machine learning classification to describe and show seismic characters found in VSPs waveforms. In particular, the waveform shapes and attributes of the VSPs downgoing waveforms.

Data and Method

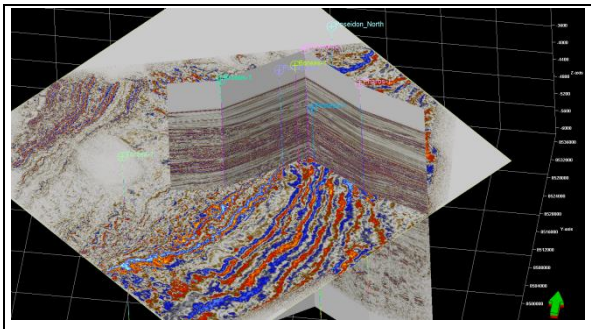

Figure 1: Wells location and example of 3D seismic time slice and random line. Data provided by GEOScience Australia.

The example data used were an open dataset, the Poseidon 3D data from the NW Shelf, Australia (Browse Basin), provided by GEOscience Australia. There were six wells available with VSP datasets. The Browse Basin covers an area of approximately 140,000 km^2 and lies entirely offshore, north of Broome. The Browse Basin, which forms part of the Westralian Superbasin, is a northeast-trending depocenter containing up to 15 km of Paleozoic to Cenozoic sediments (Government of Western Australia, Dept of Mines and Petroleum, 2014).

Ideally, the waveforms classification only deals with the variation due to geology. However, the challenge of working with multiple VSP datasets from multiple Wells is the difference in the acquisition system (different tools, different gun systems, etc.). This is the case that was observed with Browse VSP data. The table below summarized the variation in the acquisition system,

PROCEEDINGS
JOINT CONVENTION BANDUNG (JCB)2021
November 23rd – 25th 2021

Table 1: List of available wells and the downhole tools

Well Name	Years	Downhole Tools
Kronos-1	2010	VSI
Pharos-1	2014	VSI
Poseidon-1	2009	VSI
Posideon-2	2010	VSI & QAST
Proteus-1ST2	2014	VSI
Torosa-1	2006	VSI

Data preconditioning was applied only for geometric correction and waveforms normalization. The downgoing wavefield was extracted using a median velocity filter. It was noticed that this preconditioning did not solve the issue with the variation in acquisition. However, the waveforms classification algorithm will be tested if it also picked up any variation due to acquisitions.

The unsupervised classification was used to provide insights about waveforms variation without prior information. The employed algorithms were K-means and Self-Organizing Map (SOM). The process consists of two stages, the learning phase, and classification. Within the first stage, the typical waveform for every class was defined. In the second stage, the program calculated the similarity or probability value which is a measure for the resemblance with the master waveforms for every seismic waveform. The highest probability range is defining the class category for the waveform under examination.

During the classification, two waveform segments will be placed in the same class if their waveforms have a similarity, it can be calculated from the distance between the waveforms, the distance can therefore be taken for example as the square difference between two waveforms.

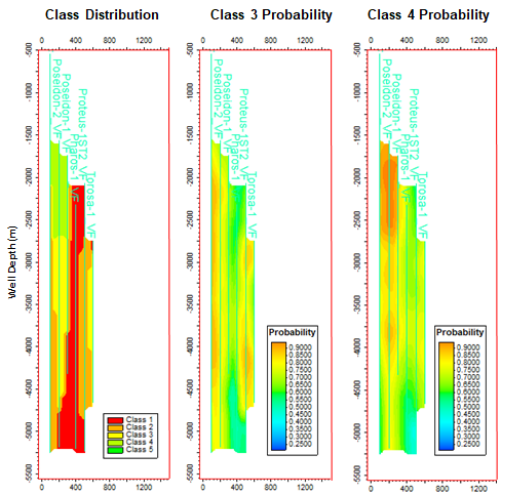

Figure 2: Left panel shows waveforms class distribution (K-Means) in all wells. Middle and Right panel shows an example of the Probability Map for Waveforms Class 3 and Waveforms Class 4.

The parameter used to compute similarity was mainly based on the downgoing waveforms shapes. Sensitivity analysis using various windows and methods was also tested in the exercises to compute similarity. It was concluded to compute the similarity distance using a combination of correlation coefficient and square difference. And the waveforms were limited to a 50 ms window in the analysis.

The workflow output classification map, the probability map for each wavelet class, and the typical wavelet for each class were used to analyze the vertical and lateral heterogeneity from well to well based on VSP waveform attributes.

Result and Discussion

Both K-means and SOM algorithms were utilized for the classifications. The results showed that K-means was more sensitive in classifying the waveforms. It was suggested that SOM was maybe too sensitive to the noise present in the dataset. These two methods require a number of clusters to be classified (K number in K-means). In this paper, a number of clusters were derived based on the interpretation of lithology distribution observed in the well logs. Parameter testing was conducted to assess the sensitivity of the cluster's distributions; we used 5 classes for distribution. The results are displayed in Figure 2 left panel. The class distribution map was defined based on the probability of each class. For instance, Class 3 and Class 4 probability map was displayed in the same figure (middle panel and right panel).

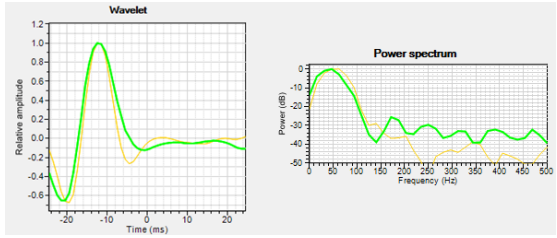

Figure 3: Typical downgoing wavelet for Class 3 (Dark Yellow) and Class 4 (Green)

Since the classification distance is based on waveforms shape and spectrum, it was predictable to see a strong correlation of classes' distribution with depth. The start of certain classes observed to be different from well to well, that may correlate with the geological structure or other subsurface properties.

The classification workflow can be used to identify similar downgoing characters in multiple wells. Hence, it can be used to map out the lateral character heterogeneity seen by downgoing VSP waveforms. For example, Class 3 and Class 4 were showing distinctive changes in waveforms within shallower depths. Such change in waveforms is identified in the estimated typical waveforms for each cluster displayed in Figure 3. This character was also showing between Poseidon-1 and Poseidon-2, and slightly similar for farther well such as Torosa-1.

Another way to analyze the classification results was to compare them with the surface seismic. The classification results can be plotted as discrete log in each well. The example in Figure 4 shows cross-section through Kronos-1, Poseidon-2, and Proteus-1ST2. Similar classification results were observed at time intervals between 2000 to 3000 ms, between Kronos-1 and Proteus-1ST2, whilst Poseidon-2 that showed some difference. Such outcomes require further analysis by integrating the geological interpretation and VSP waveforms attribute.

PROCEEDINGS
JOINT CONVENTION BANDUNG (JCB) 2021
November 23rd – 25th 2021

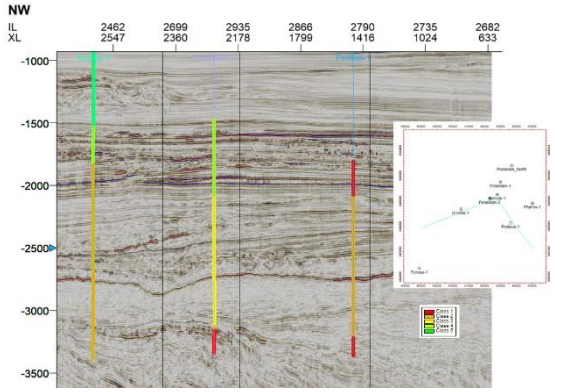

Figure 4: Random line crossing Kronos-1, Poseidon-2, and Proteus-1ST2. Showing comparison of classifications results with seismic.

Conclusions

This study showed the value of integrating VSP characterization from multiple wells using machine learning to discern an area's vertical and lateral heterogeneity. With more data being acquired, the conventional VSP analysis can be expanded from a single well-to-well basis into a more integrated multi-well interpretation for an oilfield. While machine learning can be very influential, its use relies upon the formulation of the right questions to ask from the data. Specifically for subsurface data analysis, information from geology knowledge should consistently be included as a priori information.

References

Andersen, A., and J. Boyd, 2004, CSEG Recorder, **29**, Issue No. 03.

Campbell, A., Fryer, A., Wakeman, S., 2005, The Leading Edge, **24**, 694-697.

Government of Western Australia, Dept. of Mines and Petroleum, (2014), Western Australia's Petroluem and Geothermal Explorer's Guide

Acknowledgements

The author would like to thank SIS SCHLUMBERGER, Qatar for the support and all the reviewers for the helpful suggestions for the writing of this extended abstract.

PROCEEDINGS
JOINT CONVENTION BANDUNG (JCB) 2021
November 23rd – 25th 2021

Principal Component Analysis (PCA) in ichnology

Ery Arifullah,[1)]
[1]Department of Geology, Universitas Muhammadiyah Kalimantan Timur
email: earifullah27@gmail.com

Abstract

I observed the ichnofabric variable on 600 ichnofabric units in the Samarinda area of Kutai Basin. Five ichnofabric variables are bioturbation index (BI), biodiversity (ID), number of behaviors (NB), penetration depth (PD), and burrow diameter (DM) that perform as a semi-quantitative form. It must process the data with principal component analysis (PCA) to extract useful information from the data. Results of the PCA are the new principal components (PC), the loading of the ichnofabric variables in the PC-1 and PC-2, and the scattered pattern of the ichnofabric unit scores in PC-1 PC-2 axes. PC-1 has a "strong" positive correlation with ID and NB, a "moderate" positive correlation with BI, and a "weak" positive correlation with PD and DM. In contrast, the PC-2 correlates positively with BI, PD, and DM and correlates negatively with ID and NB. The PC-2 correlates moderately with PD and DM and correlates weakly with BI, ID, and NB. The dispersion pattern of the ichnofabric unit scores on PC-1 and PC-2 axes shown no simple pattern. PC-1 and PC-2 are interpreted as ichnodisparity and space utilization, respectively. The results of the PCA might be the unique indicators for a Miocene brackish depositional system in the study area. The application of PCA in this study has helped to know that the sediment source comes from land and the sea (tides and waves).

Introduction

In ichnofabric studies, I need semi-quantitative data to study deposition systems (Arifullah et al. 2021). Analysis of significant components (PCA) has been widely applied. I applied it in ichnology (e.g., Arifullah et al. 2017, 2018, 2019; Arifullah, 2019), paleoecology (Van der Zwan and Jorrisen, 1991), hydrogeology (Liu et al. 2003).

An enormous amount of data with over two-variable needs data processing, making it easier for further data analysis. This is because not all data variables are needed. Usually, several variables are discarded and maintain others. This way is subjective. The aim is to allow the data set to reveal the weight of its relevant variable. For this reason, I use principal component analysis (PCA). With PCA, the semi-quantitative ichnofabric variable (Arifullah, 2019; Arifullah et al. 2021) can be reduced to two components that group the ichnofabric variable.

Data and Method

The basis data for PCA were the observed 600 ichnofabric units in the Serravallian-Tortonian sequence of Kutai Basin, East Kalimantan, Indonesia (Figure 1). Each ichnofabric unit had five ichnofabric variables, i.e., bioturbation index (BI), ichnodiversity (ID), number of behavior (NB), penetration depth (PD), and burrow diameter (DM) in numerical form (see in Arifullah, 2019).

I assumed the five ichnofabric variables as the five axes in the Cartesian coordinate system. The problem was how to draw those axes and how to visualize the point of ichnofabric unit do. Were those variables critical? If only some parts were necessary, several variables must be maintained, and others must be discarded. However, it was

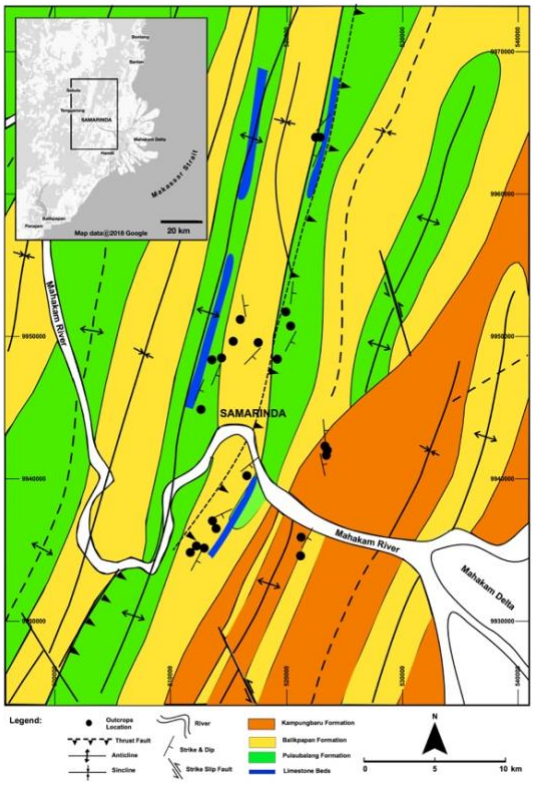

Figure 1. Geological map of Samarinda Area, Indonesia (modified after Supriatna et al. 1995). Reprinted with permission from the Geological Agency, Ministry of Energy and Mineral Resources of Indonesia.

a subjective approach. The aim approach was to allow the data to reveal its variable weights. PCA permits me to keep the original data and simplify them into 2 or 3 dimensions without reducing the original structure significantly. That 2 or 3 dimensions were the new coordinate axes that called principal components (PC). In addition, PAST-4 was the free software that helps with PCA.

Since BI, ID, NB, PD, and DM are in different units, I standardized them (Arifullah et al. 2017, Arifullah, 2019). There are two ways for standardization. First, by statistics formula and the second by transforming the continuous value (i.e., PD and DM) to discrete one (see Table 2 and 3 in Arifullah et al. 2021). I created a Pareto histogram that ranks the PCs with the highest% cumulative frequency to the lowest one. The x-axis represents the principal component (PC) comprising PC-1, PC-2, PC-3, PC-4, PC-5. There are two y-axes on the axis that describe the PC's eigenvalue and cumulative frequency percentage. The

PROCEEDINGS
JOINT CONVENTION BANDUNG (JCB)2021
November 23rd – 25th 2021

purpose of having an axis showing the cumulative frequency presentation of PCs is to determine a 60% cutoff with precision to determine a representative PC as directed by Jollife (2002).

I choose the principal component based on a 60% to 90% cutoff of cumulative variance (Jollife, 2002), and the principal components should have a minimum eigenvalue of 1 (Kaiser, 1960). The first principal component is PC-1, the second principal component is PC-1, the third principal component is PC-3, etc. The eigenvalue of PC-1 > PC-2 > PC-3 > PC-n and so on. If the eigenvalue is the value that shows how the power of PC to spreading of data, then PC-1 is more powerful than PC-2, and PC-2 is more potent than PC-3, and so on.

The new PC had ichnofabric variables with a different weight of contribution that was shown by coefficient correlation value. If coefficient correlation index > 0,75, 0,75 to 0,5 and 0,5 to 0,3, then represent "strong", "medium" and "weak" correlation respectively to PC (see Liu et al. 2003).

Result

Principal components

If the cumulative frequency curve cuts the 60% cutoff line from the y-axis, then only PC-1 and PC-2 are qualified to represent all existing PCs (Figure 2). The cumulative frequency is 62.40%, while the remaining 37.6% is the cumulative frequency of PC-3, PC-4, and PC-5. Likewise, if based on the eigenvalues, PC-1 and PC-2 are 2 of 5 PCs with an eigenvalue of over 1, i.e., 1.87 and 1.25. Thus, PC-1 and PC-2 are priorities to be discussed further in this paper.

PCA helps me learn and understand the interrelationship between five ichnofabric variables (i.e., BI, ID, NB, PD, and DM). The interrelationship between BI, ID, NB, PD, and DM variables to the PC-1 and PC-2 can be from the different correlation coefficients (Figure 3). Based on the strength of the correlation, PC-1 has a "strong" correlation with ID and NB, a "moderate" correlation with BI, and a "weak" correlation with PD and DM. In contrast, PC-2 correlates positively with BI, PD, and DM and negatively correlates with ID and NB. Based on the strength of the correlation, PC-2 correlated "moderately" with PD and DM and "weak" with BI, ID, and NB. Thus PC-1 represents the BI, ID, and

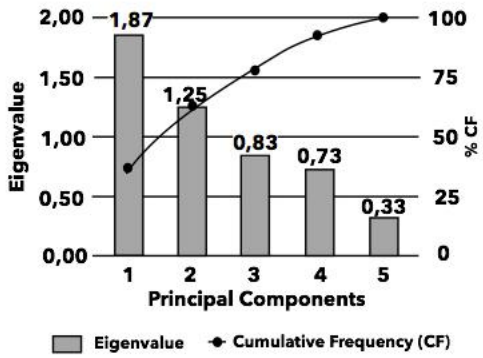

Figure 2. Pareto histogram of PCs. Each PC shows its eigenvalue and cumulative frequency (Arifullah, 2019).

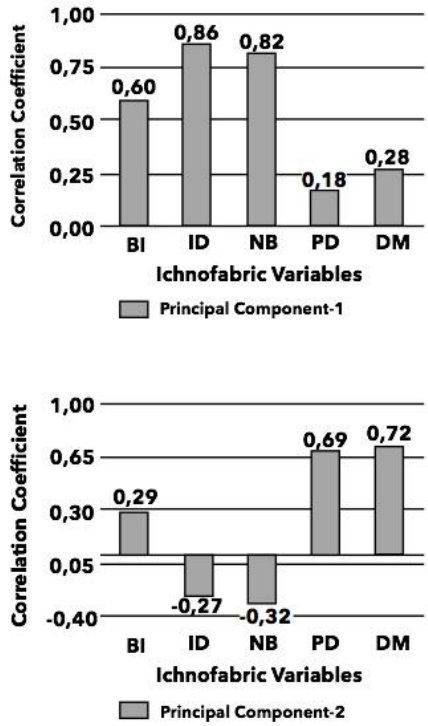

Figure 3. The relationship between ichnofabric variables (BI, ID, NB, PD, and DM) with PC-1 and PC-2 (Arifullah, 2019).

NB, and PC-2 represents PD and DM. The next task is to find out what variables PC-1 and PC-2 are.

Ichnofabric units score and scattered diagram

As already mentioned, each of the ichnofabric units has the values of the ichnofabric variable (i.e., BI, ID, NB, PD, and DM). Each of the ichnofabric variables has a different load in each PC-1 and PC-2. Thus, each ichnofabric unit has a value on PC-1 and PC-2, referred to as a score. Since I studied 600 ichnofabric units, there are 600 x 2 PC = 1200 scores, as exemplified in Table 1. The scatter diagram shows the relationship between PC-1 and PC-2 measured in the same ichnofabric units (Figure 4). The dots in the scatter diagram represent ichnofabric units. Figure 4 displays a scatter diagram, and the type of relation between PC-1 and PC-2 implies a no linear relation (r = 0,000).

Table 1. Examples of tabulations showing PC-1 and PC-2 scores in each ichnofabric unit (Arifullah, 2019).

N	Ichnofabric unit	PC-1 score	PC-2 score
1	01-Op-07	0,28	1,32
2	01-Ch-03	1,34	0,66
3	01-Pa-03	0,47	0,41
4	01-Ch-04	-1,14	1,03
5	01-Op-08	-1,43	-0,36
….	….	…	…
600	16-Sk-05	-1,62	-1,28

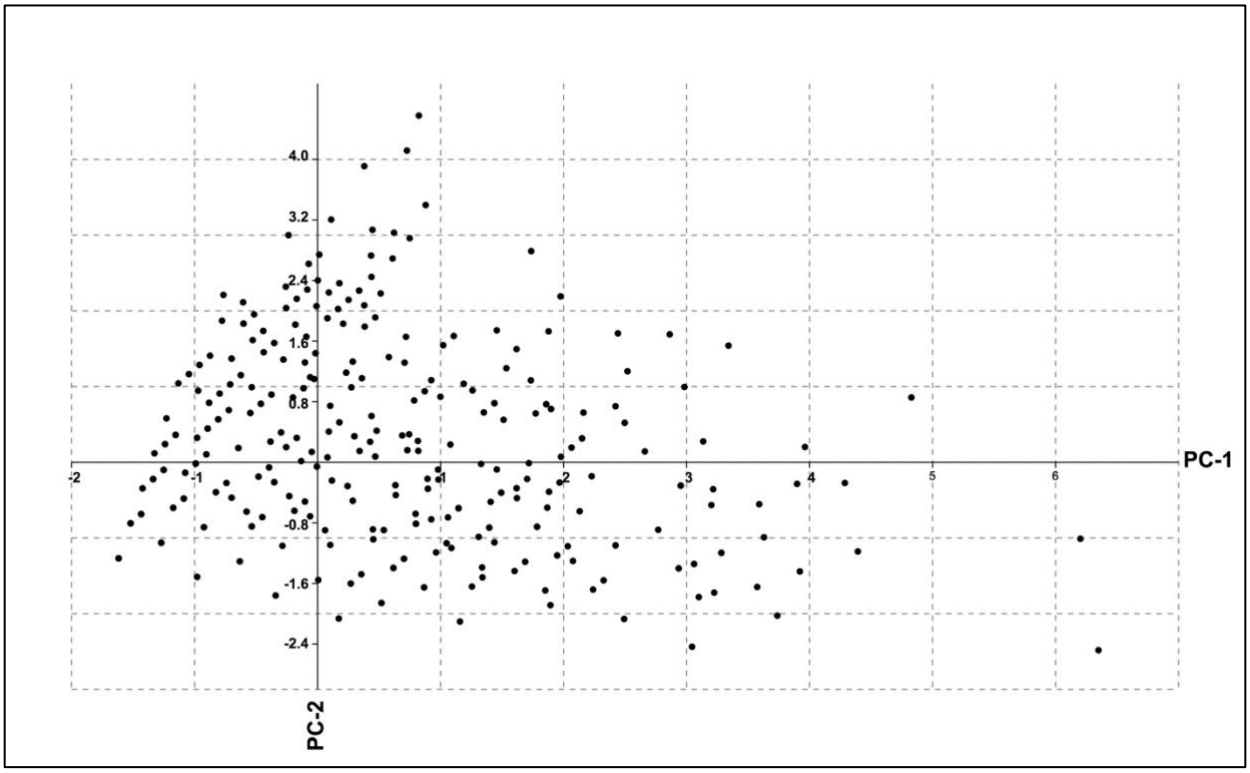

Figure 4. The scatter diagram shows the relationship between PC-1 and PC-2 measured in the same ichnofabric units. The dots in the diagram represents ichnofabric units (Arifullah, 2019). Type of relation between PC-1 and PC-2 implies a no linear relation (r = 0,000).

Discussion

The strength of PCA

PCA allows us to study and understand the depositional system, helping the geologist see in two PC that otherwise would have to be seen in over five variables (i.e., BI, ID, NB, PD, and DM) to be studied. I can consider PCA the best technique to approach any semi-quantitative data. PCA is a handy tool for dealing with some problems with fluvial-marine transition depositional systems.

In that system, I respect the environmental variables which regulate the ichnofabric variable. In reality, complicated interrelationships happen in this depositional system, including positive and negative feedback loops. However, PCA makes it simpler to understand. The five ichnofabric variables (i.e., BI, ID, NB, PD, and DM) are reduced become two components (i.e., PC-1 and PC-2).

Paleoecology

BI, ID, and NB suggest innovation, mobility, and fauna behavior (Arifullah, 2019) which Buatois and Mángano (2013) called ichnodisparity. Thus, PC-1 represents ichnodisparity (Arifullah, 2019). PD and DM show a positive correlation with the larger size of the fauna, followed by increasing the penetration depth (Arifullah, 2019). Referring to Levinton (1977) and Reise (1979), then PC-2 is a component of space utilization. If referring to Fig.3, then the PC-1 axis is ichnodisparity and PC-2 is space utilization.

Since the food resources are a common factor considered in the ecological analysis (Bambach, 1983), then the ichnodisparity reflects the factor food supply. A particular mechanism supplies food to the ecosystem. Since the interaction of fluvial and marine processes in the basin (Bachtiar, 2003; Arifullah, 2005; Arifullah, 2019), the food supply is from land and marine (Van Der Zwaan and Jorissen, 1991; Brencley and Harper, 1998). Food is supplied as seston, bound to sediment grains (Brenchley and Harper, 1998).

The component of space utilization reflects paleosalinity and paleotemperature fluctuation in the depositional system. There is an interaction between the fluvial processes and the origin of the sea in the Kutai Basin. The fluctuating salinity and temperature are general conditions in a brackish environment (Dalrymple and Choi, 2007; Buatois and Mangano, 2011).

Depositional processes

The question is the meaning of the scatter diagram, and the type of relation implies a nonlinear relationship. There is no relationship between ichnodisparity and space utilization or no linear relationship between food supply and palosalinity-paleotemperature fluctuation. Thus, food supply and paleosalinity-paleotemperature fluctuation can be directly proportional or inversely proportional. If the food supply from land increases, there will be a decrease in paleosalinity and paleotemperature fluctuation.

On the one hand, if the food supply of land origin increases, there will be an increase in paleosalinity and

paleotemperature fluctuation. Thus, the food supply can cause an increase and decrease in paleosalinity-paleotemperature fluctuation. I interpreted if food supply as a fluvial input function, then it is natural that fluvial inputs increase, then there will be a decrease in paleosalinity-paleotemperature fluctuation. However, what happened was precisely an uncommon thing. So, I interpret that food supply comes from land and the sea (tides and waves).

The existence of both inputs shows the fluvial process, and the process of sea origin modifies each other's deposition system in Serravallian-Tortonian intervals. The interaction of fluvial processes and ocean origin forms a delta or estuary or both at once. What is interesting here is that ichnofossil can determine the proportion of fluvial processes and processes of ocean origin (tides and waves).

Conclusions

Results derived from PCA present an actual picture of paleoecology and depositional processes of the Serravallian-Tortonian fluvial-marine transition zone with no data manipulation. PCA may help me to interpret the paleoecology and depositional processes easily.

References

Arifullah, E., 2005, M.S, thesis, Institut Teknologi Bandung.
Arifullah, E., 2019, Ph.D., dissertation, Institut Teknologi Bandung.
Arifullah, E., Zaim, Y., Aswan., Djuhaeni, 2017, Proceeding of Joint Convention Malang.
Arifullah, E., Zaim, Y., Aswan., Djuhaeni, 2021, Journal of Mathematical and Fundamental Sciences **53**, 285-304.
Bachtiar, A., 2004, Ph.D., dissertation, Institut Teknologi Bandung.
Bambach, R., 1983, Topics in Geobiology, 719-746.
Brencley, P.J., and Harper, D.A.T., 1998, Chapman & Hall.
Jollife, I., 2002, Springer, 2nd edition.
Kaiser, H.F., 1960, Educ. Psychol. Meas **20**, 141-151.
Liu, C.W., Lin, K.H., Kuo, Y.M., 2003, The Science of the Total Environment **313**, 77-89.
Reise, K., 1979, Helgolander wiss. Meeresunters **32**, 55-72.
Supriatna, S., Sukardi, and Rustandi, E., 1995, Peta Geologi Lembar Samarinda, Puslitbang Geologi.
Van der Zwaan, G.J., and Jorissen, F.J., 1991, Geological Society Spec. Publ. **58**, 65-82.

PROCEEDINGS
JOINT CONVENTION BANDUNG (JCB)2021
November 23rd – 25th 2021

UNDERSTANDING LAND ACQUISITION AND LOCAL COMMUNITY ISSUES IN INDONESIA GEOTHERMAL EXPLORATION PROJECT

Amrullah Farad Sunaryo[1], Dorman Purba[1] Nabila Azarine Zahraf[1] Erica Prasetyo[1], and Mochamad Risyad Rizkyafdhal[1]

[1]Enerka Bhumi Pratama, Cibis Nine Building 11th Floor, Jakarta Selatan 12560, Indonesia;

ABSTRACT

Indonesia is in the process of increasing geothermal energy utilization in its energy mix. The identified challenges considered by many lies in the exploration phase since most of geothermal prospect in Indonesia has not yet been explored properly. Obviously, in doing exploration activities, any geothermal developers will have to deal with land acquisition and local community issues.

Several potential issues in the land acquisition process are lack of understanding of regulations, failure to determine fair prices, local community resistance, lack of communication skill from both sides, technical incompetence, and environmental impacts. Failure to address these issues will potentially bring failure in getting the required land, which consequently leads to failure in completing the exploration project.

This study aims to discuss in detail several potential problems that might occur in land acquisition activities that are most likely correlated with local community rejection, based on literature review and interview with practitioners who has experiences in land acquisition. This research aims to provide a simple guidance yet useful for geothermal developers to mitigate problems in the land acquisition process. Additionally, this paper also summarizes some aspects related with land requirements, regulations, standards, and case studies, which relevant to geothermal exploration project in Indonesia.

Keywords: *Geothermal, land acquisition, community, exploration, drilling, rejection, livelihood, Indonesi*

1. INTRODUCTION

1.1. Current Development of Geothermal Energy in Indonesia

No	Field	Unit	Total Capacity	Reservoir	Technology
1	Sibayak	Monoblok 2 MW. Unit-2–3, 2 × 5 MW	12 MW	Water dominated	Single-flash
2	Ulubelu	Unit-1–3; 3 × 55 MW	165 MW	Water dominated	Single-flash
3	Salak	Unit-1–3, 3 × 60 MW. Unit 4–6 3 × 65.6 MW	377 MW	Water dominated	Single-flash
4	Wayang Windu	Unit-1: 110 MW Unit 2: 117 MW	227 MW	Water dominated	Single-flash
5	Patuha	Unit 1: 55 MW	55 MW	Water dominated	Single-flash
6	Kamojang	Unit-1: 30 MW Unit 2–3: 2 × 55 MW Unit 4: 60 MW Unit 5: 35 MW	235 MW	Vapor dominated	Dry steam plant
7	Darajat	Unit-1: 55 MW Unit-2: 94 MW Unit 3: 121	270 MW	Vapor dominated	Dry steam plant
8	Dieng	1 × 60 MW	60 MW	Water dominated	Single-flash
9	Lahendong	Unit 1–6: 6 × 20 MW	120 MW	Water dominated	Single-flash
10	Ulumbu	Unit 1–4: 4 × 2.5 MW	10 MW	Water dominated	Single-flash
11	Mataloko	2.5 MW	2.5 MW	Water dominated	Single-flash
Total			1533.5 MW		

Fig. 1. Geothermal Powerplant in Indonesia (N.A. Pambudi, 2017)

Indonesia is a country that has enormous geothermal potential. Indonesia has geothermal energy potential of more than 23.9 Gigawatts (GW) (EBTKE, 2019). This abundance of geothermal resources can help meet the increasing demand and increase the electrification rate. Based on data from the Direktorat Panas Bumi, currently Indonesia has utilized 8.9% or 2,130.6 MW, the utilization of geothermal energy in Indonesia can be considered quite small in terms of the amount of potential it has. Therefore, it is known that the government is targeting an increase in geothermal utilization to 7,241.5 MW or 16.8% in 2025.

If we compared Indonesia's geothermal development with other countries, it is indeed still classified as low. But there are several fields we could find in Indonesia that were successful to install geothermal powerplant as shown in the table below.

There are a lot of issues that make geothermal development is challenging such as government policy, regulation, incentive infrastructure, and predominantly when doing the processes land acquisition. Land plays an important role as a financial asset. The process of land acquisition takes place gradually, which land has the potential to be developed. Even when the process of land acquisition itself goes well, there are still an issue from local community. The purpose of this preliminary study is to discuss in detail several potential problems that might occur in land acquisition activities

1.2. Research Objective and Method

1.2.1 Research Objective

This study aims to discuss in detail several potential problems that might occur in land acquisition activities that are most likely correlated with local community rejection, based on literature review and interview with practitioners who has experiences in land acquisition. This paper also are completed by land requirements, regulations, standards, and it hopefully could be a simple guidance for geothermal developers to mitigate problems in the land acquisition process.

In order to ripen the main questions, this research started by offering question below:

1. What is the land acquisition for?
2. What is the effect on geothermal exploration from regulations that governing land acquisition?
3. How much land is required for infrastructure specifications?
4. How long the land is needed for the geothermal development project?
5. What procedure are needed before buying land?
6. What are the challenges of geothermal land acquisition? How to prevent that?

1.2.2 Research Method

In order to know how several aspects relate to the land acquisition process for a geothermal project in Indonesia and it could be made up as a guidance, the authors conducted a literature review of various sources regarding laws and regulation of geothermal land acquisition, technical aspects that must be concerned, the procedure of land acquisition and challenges that will meet them on geothermal project land acquisition in Indonesia. In addition, we also interviewed practitioners who already had been through the land acquisition process to get the point of view from them based on real experience.

2. RESULTS AND DISCUSSION

2.1 Laws and Regulation

Regulations that greatly affect the process of geothermal land acquisition in Indonesia in terms of exploration are Presidential Regulation Number 71 of 2012 and Government Regulation Number 7 of 2017. Meanwhile, from the investment side, it is influenced by the IFC (International Finance Cooperation) Performance Standard-5.

2.1.1. Presidential Decree No. 71 of 2012

Referring to Presidential Decree No. 71 of 2012, the land acquisition process related to the public interest must be led by a governor where the governor will form a team consisting of the mayor, provincial level task force, agencies requiring land, and other supporting agencies (Dewi et al., 2013).

2.1.2. Republic of Indonesia Law No. 5 of 1990

The prospect of geothermal that is located in conservation areas and protected forests and requires test drilling to make the exploration process limited to land use acquisition. Because there is Law no. 5 of 1990, especially in articles 1, 2, and 3 which emphasize aspects of ecosystem balance.

2.1.3. Government Regulations No. 7 of 2017

In Government Regulation No. 7 of 2017, land acquisition needs to be stated in IPB (Geothermal Exploitation Permit) which consists of commitments and must be approved by the Director General and IPB holders. Exploration commitments that must be fulfilled are in the form of financial guarantees to drill exploration wells.

2.1.4. IFC Performance Standard-5

One of the main investments in the energy sector in Indonesia is funding from the World Bank, where the agency enforces a fairly strict IFC-5 Standard of Work. This standard is the reference for most energy sector loan operators. The essence of this regulation states that displacement of affected people must be strictly avoided. However, if there is something that has a major and significant impact on the wider community, the company can provide compensation in the form of physical compensation including providing cash compensation for affected people including plants and buildings, providing resettlement places and housing, facilitating the relocation process, and livelihood restoration program.

Government Regulation No. 7 of 2017 can be a way out for cases of land use in protected forest areas, because the agency entitled to issue IPB is the Ministry of Energy and Mineral Resources, which must coexist with the Ministry of Environment and Forestry. Therefore, technical design is very important to reduce the impact of changes in forest ecosystems.

2.2 Technical Aspects

Acquisition of land is carried out to do geothermal exploitation activities. For determining whether an area has geothermal prospects, exploration is implemented to determine the presence of hot water or steam in the reservoir. The exploration activity itself is divided into several parts, namely preliminary exploration, further exploration, and exploration drilling (Syahda et al, 2019). The objectives of the preliminary exploration activities are to determine the areas that become geothermal fields that show manifestations on the surface, as well as obtain a geological description of the area. After conducting preliminary exploration, further or detailed exploration, which collects data through field surveys. To sort out the land that will be used for geothermal exploration, data is required using a field survey. The survey consists of geological, geophysical, hydrological, and geochemical surveys (Juanda, 2020). The survey was conducted to identify that an area is likely to contain geothermal sources and has economic value to develop. After that, exploration drilling activities were carried out which proved that there was a presence of geothermal heat below the surface.

Towards conduct drilling, several infrastructures are needed to support geothermal exploration activities.

2.2.1 Access Road

Road access is one of the important things for geothermal exploration. This road access will facilitate the implementation of exploration activities starting from the delivery of tools, equipment, and materials to the area until eventually facilitating mobilization during drilling. Land acquisition at the start of a project is usually based on gaining access from a road built by the government to the desired area where exploration will take place, which is commonly referred to as a drilling site or well pad (Purba D.P.,et.al, 2020).

Geothermal systems are frequently found in volcanic environments, where the terrain is steep and access is difficult. which implies that for usable access roads to be made, massive earth has to be excavated (Miyora, 2015). To open a new road, the construction of this road will destroy forest areas, vegetation, and traffic activities for the general public. The width of land to be used for the construction of this road generally ranges from 8 to 15 meters which will include road and streamline access (Purba D.P.,et.al, 2020).

2.2.2 Well pad

Well pad is a very necessary infrastructure for drilling. This is because the well pad is a well facility which is the main asset in carrying out geothermal development projects. Well

pad contains the basement which is where the hole is drilled. A well pad might have a recirculation pool which is used to fill water from the holes drilled and will be reused for drilling.

According to industry estimates, the average size of a multi-well pad for the drilling and fracturing phase of operations is 0.014 km; 006 km² is the estimated average after the required partial reclamation (SGEIS 2011, chapter 5). The area of the well depends on what type of well will be drilled. Geothermal well types are classified into 3 types based on the size or diameter of the well bore, specifically big hole, standard hole, and slim hole. Slim and standard hole well have a size in width and length each one 40 meters and 50 meters; 70 meters and 120 meters

A well pad is a relatively flat work area within the geothermal field (surface location) that is used for drilling a well or wells and producing from the well once it is completed (TEEIC, 2015). The well location is at least 100 meters from housing, roads, and public construction (BSN,2002). The existence of a gap between the well location and community facilities will mitigate the negative impact of drilling on the community

2.2.3 Base camp, Warehouse, and Site office

Base camp, warehouse, and site office this place was built in the early stages of the project. Base camp it is no less important for geothermal project development. This place is a place to live and rest for workers. All drilling materials, such as casing, liner, wellhead, cementing material, and drilling fluid material, are stored in a warehouse. A site office, on the other hand, is a working space established near the project site (Purba D.P.,et.al, 2020)

This area usually has an area of 42.000. But depending on the number of rigs operating and also the more rigs built, the larger the building area. This place is located not far from the main well drilling area to facilitate project work.

2.2.4 Staging area

Drilling necessitates the use of bulky hardware as well as consumables. This area is used to store various materials used in the construction of well pads and drilling structures. The staging area is usually chosen in the flat area between the well pad and the basecamp, closer to the well pad than to the basecamp. The staging area typically requires much less land than the basecamp and well pad area, which can range from 1.000 to 5.000 (Purba D.P.,et.al,2020).

2.2.5 Period of time the land is used

The development of geothermal projects necessitates a lengthy period of time therefore, the land is used for an extended period of time. According to Permen ESDM No.36 tahun 2017, geothermal exploration activities can take a long time. The time is divided into two parts: preliminary survey and exploration along with pre-feasibility. This activity requires a long duration with a span of approximately 7 years. Then the land is used for exploitation and utilization of geothermal which takes more than 30 years.

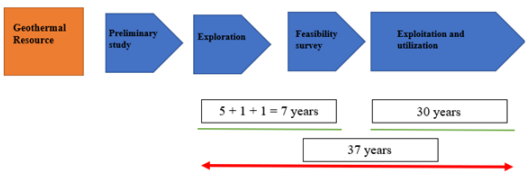

Fig. 2. Indonesia Geothermal Development Period

2.3 Land Acquisition Procedure

It is necessary to know the landowner's status before buying the land for the project. There are two types of land status, they are land state and non-land state. Each of the lands has several procedures that must be done.

2.3.1 State Land

If the land available is state land, there are several processes that should be follow.

2.3.1.1 Valuation Process

After surveying suitable land for the project, it is important to know the land prices in the area. To know the land prices in an area, do a land prices valuation can be a solution. A land prices valuation is conducted to achieve a reference for determining the nominal value. Land prices can be affected by the existing crops and land statuses. It is possible to use consulting services to research prices for the land.

2.3.1.2 Negotiation Process

After getting a land price from the valuation process, The Land Acquisition Team will negotiate with the landowner by giving a benchmark price. The negotiation will be successful if the landowner and the negotiator have a deal on the final price.

2.3.1.3 Ownership Process

To accomplish a successful transaction, the negotiator team need proper legal documentation. There is identification of the legal status of land to acquired that divided into two, forestry area and non-forestry area, and based on (OTP Geothermal, 2013), the documentation needed are:

Forestry Area:

1. Proof of Heritage and Inheritance
2. Surat Pernyataan Penguasaan Fisik Bidang Tanah
3. Signature of adjacent owner
4. Kartu Tanda Penduduk (KTP)

Non-Foresty Area

1. Proof of Heritage and Inheritance
2. Surat Keterangan Tanah signed by the Village Head and subdistrict Head
3. Signature of adjacent owner
4. Kartu Tanda Penduduk (KTP)

2.3.1.4 Purchase and Financial Transaction Process

The process to have legal ownership for forest area and non-forestry would be different but the transaction method will be decided at the discretion of the landowner (OTP Geothermal, 2015). To finalize the transaction process will need a few documents required. The forestry area needs Surat Pelepasan Penguasaan Hak and the non-forestry area needs Berita Acara of Transaction and Surat Pelepasan Hak Ganti Rugi. In the forestry area, the document required the detail of the provision of the peace settlement and should be conducted by a notary. While in a non-forest area will involve a certified notary to legalize the area and payment of compensation will follow en-suite. After this step is done, the payment can be made with several steps: cash-call and transfer by finance, witness allowance (approved documents on rates are available) and photographs of each transaction (OTP Geothermal, 2015).

2.3.2 Non-State Land

If the only suitable land available is non-state lands, there are several steps that should be follow in each agreement.

2.3.2.1 Voluntary Land-Use Agreement
This agreement happens when the local landowner willing to give the land for the project team but in consideration the project team will give the community member the benefit of the project.

2.3.2.1 Land-Purchase through Negotiated Agreement
This agreement happens when the local landowner willing to sell part of their land and the land may be purchased through negotiated agreement following the Land Act.

2.3.2.2 Third-Party Verification
This agreement happens when both voluntary land-use agreements and negotiated purchase agreements will be verified by a third-party Non-Government Organization (NGO) (Asian Development Bank, 2015).

2.4 Challenges in Geothermal Land Acquisition

2.4.1 Based on Literature Review

Based on the literature review, this research categorizes some aspects that can be the main challenges for the land acquisition.

2.4.1.1 Technical

As an engineer, this aspect must be considered before designing land necessity. Land boundaries are often lost/damaged, documentation has not been handled properly, and some lands that do not have official certificate documents are some of the technical challenges that should not be ignored (Pertamina report, 2018). If they had to, they would have caused the potential for reduced land assets, the potential for land misuse, the potential for conflict with the surrounding environment, difficulty to inventory and consolidate company land. Therefore, the developers can use a tool like Pertamina had which is in the form of a GIS (Geographic Information System) based on land acquisition application that records all land data from the procurement process, measurement, payment, and the issuance of land acquisition certificates into a centralized system using the PGE LAND application.

2.4.1.2 Internal (Community) Problem

Internal problem is the most frequent aspect that happens in almost every land acquisition process. Local people generally do not know buying and selling mechanism and lack understanding of the geothermal project (Ginting et al, 2017). These problems can lead to delay the project because the developer must spare extra time and even money to socialize them.

Besides that, land in several regions in Indonesia is not owned by one person but owned communally by one the whole village (Purba et al, 2021). This means that all decisions related to the land must be discussed together and take a long time, especially if one of the community members disagrees. It might take a long time, so the developer has to wait or find another land if it is reasonable.

2.4.1.3 Refusal of Inhabitant

From the previous point, it only happens when people do not know about the geothermal project at all. However, this aspect is one of the resistances that internal residences already know a little bit about a geothermal project but not in detail. They do not meet adequate information from trustworthy sources so they are afraid of being deceived by the company (Purbat et al, 2021). Another example is they are worried that the drilling activity would cause a Lapindo-like even though they have been explained a technical aspect from the developer. These effects might make them unwilling to sell their land, and it causes a delay for the geothermal project (Purbat et al, 2021). Thus, the ultimate task of a facilitator is not to explain the geothermal project in technical terms but to serve as a bridge in any disputes that occur between the people. Moreover, developing direct-use facilities to bring economic impact to local communities while serving as geothermal education media. This campaign is suggested to be conducted in the very early phase of the exploration project to increase local community awareness of the geothermal exploration project before the project itself commenced.

Apart from that, some people do not allow the geothermal project because they think geothermal development can destruct a historical value in the hot spring area (Ginting et al, 2017). Since the developer has to respect everyone's faith, it must pay attention to be careful, maintain and build the value of local community wisdom.

2.4.1.4 Social Environment

Developing geothermal energy does not mean it has not social environment issue. As an engineer, you also have to look forward to this aspect. Before you negotiate a land, you have to think about the condition of land where you want to construct. If you do not notice appropriately, it will cause erosion or even a landslide (Supremenergy, 2017). Hence, mitigation is needed to limit impacts on air, water, agricultural land, and wildlife habitats. In addition, developers have to consider the needs of the local community, such as road improvements, public health, and other facilities like schooling and housing (Supremenergy, 2017).

2.4.2 Based on Practitioners Interview

Referred to the interview section, there are some factors that can be the main challenges for land acquisition. They will be discussed by each practitioner. This section provides info that is not available in the literature review.

2.4.2.1 Dorman Purba

Dorman currently works as an energy consultant in the world bank. He has been active in geothermal projects since 2014, particularly between 2014 and 2017 which he succeeded in two land acquisition projects in North Sumatra and East Nusa Tenggara. Based on his experience, there are some obstacles in the land acquisition process.

1. Technical

There was a case when the landowner whose land in the center of the project. He did not want to sell it, so it could fail the entire project. It could be done after a long time of negotiation until it could meet at a fair price.

2. Price

When we want to acquire the land of the geothermal project, we normally need not only a village, so we have to negotiate

with more than one village. Because every village does not have the same price for a meter of land, the developer has to make a smart plan for the transaction scheme. If it had not been made, the price would have experienced a drastic increase, and it will cause an imbalance in the project balance sheet.

3. Local Community

There were some land owners who lived there, but he had not property rights or place where they live. There were also some landowners when they were in negotiating, and their family members were not there. Moreover, there was customary land where it was not clear who owned it. These aspects will hamper the transaction process. There is no way to solve that unless you want to wait in an unspecified time or you find another location.

4. Government

Land acquisition surely involves the local government coordinating with stakeholders. There was a case when government delivers a different perception as the developer had told about, so it needed extra time to socialize again with the local residences. In the future, the developer has to ensure the understanding of the project is well delivered enough to the government.

5. The Incitement of Other Parties

This is the aspect that the developer does not underestimate because it can happen at every stage of the project. It happens when there are some people in the village whose land which it is not sold while the neighbor's land is sold to the developer, so they become envious. It can be dangerous because they will incite others to do not sell the land, which can hamper another land acquisition process. This problem can be solved through negotiation at a fair price.

There are some tips from Mr. Dorman for geothermal land acquisition in the future, such as training and development of land acquisition for people involved in geothermal projects, land mapping in Indonesia could be improved, and permit access should not be complicated and increase quantity of geothermal practitioner.

2.4.2.2 Vicky Chandra

Vicky is a geologist at PT. Geo Dipa Energy who has been participating in geothermal projects for nine years. He has completely finished a geothermal land acquisition project from 2015 to 2017 in East Nusa Tenggara. Regarding his past experience, he classifies the land acquisition process's resistances into some elements.

1. Technical

As an engineer, you have to be able to design a geothermal land regardless of size. In fact, the land that you finally acquired is not always as you planned before, so you have to be competent in it. Besides that, do not forget to pay attention to other aspects related to technical, such as the environment. In some case, there was a case when drains are blocked by the project, and even worse, causes a landslide. Therefore, you have to master your competencies, not only one field.

2. Price

The land that the developer usually acquired the land where it is plantation land, so lots of plants are growing there. Normally, it has a problem with the pricing. It is very difficult to determine the correct calculation method, so it needs a consultant to help us. However, the landowner sometimes does not agree with the price, and they want a higher price. To solve this problem needs an advanced strategy, and it usually surveys from surroundings.
Besides that, sometimes there is an obstacle in corporate bureaucracy. When the developer has dealt with the landowner, the corporate needs a long time to transfer the money. It should be made easier.

3. The Incitement of Other Parties

As mentioned before, it does not take it easy for the whole project. In this case, what differentiates it from Mr. Dorman is the influence from local NGOs who does not get a project from the developer. It must need dealing a negotiation to overcome this.

There are some tips from Mr. Vicky for geothermal land acquisition in the future such as companies must welcome in society, make an advanced masterplan and great strategy for negotiation, flexibility in internal corporate, enhance a negotiation skill for people who involve in a geothermal project, competent skill for engineering, and can predict the future of the project..

3. CONCLUSION

1. This land acquisition is intended to carry out geothermal development projects. Will be used as the main infrastructure for developing a geothermal exploration project. The land was used for a span of approximately 37 years.
2. Regulations in Indonesia require that an exploration project be financially secure in order to obtain an IPB, where in order to obtain financing, the exploration must comply with the regulation that all affected communities are guaranteed their rights. Throughout the land acquisition, the company will also be supervised by a provincial-level task force.
3. It is important to know the landowner’s status and prepare several documents needed before buying the land. For state land and non-state land have different steps that must be remembered.
4. Regarding both literature review and practitioners interview, several aspects such as technical, refusal of inhabitant, social environment and government are the main obstacles that will hamper the land acquisition process. Hence, the developers should be appropriately flexible in terms of technical aspects and the communication with the local community. Moreover, the government must have the same vision and command in the land acquisition process, simplify the access to permit for the bureaucracy and must develop tools such as the national center of land information system.

4. PATH FORWARD

1. The government, both national and local, must have the same vision and command in the land acquisition process so that there is no misinterpretation during actions in the field. Then, the government simplify the access to permit for the bureaucracy. Then, the government must develop a tool such as the national center of land information system. Actually, Pertamina has made it, and it could be developed further. The system contains spatial (graphical) and non-spatial (physical land information, legal data, financial data, administrative data, environmental visuals), which are managed in digital form. It is built with the purpose of monitoring land availability financially, such as safeguarding the system of

company land assets and non-financially such as eases the status of land acquisition progress, avoids fraud in the land acquisition process, the data consolidation process can be done in real-time. Moreover, the government must increase practitioners in the geothermal sector because the ratio of the number of projects and practitioners involved is very disproportionate.

2. A developer company must make strategic plans as much as possible and must be flexible, and provide spare time. In fact, this land acquisition process takes unpredictable times and many unwanted events occur. The company should also conduct land acquisition training and development for people involved in geothermal projects so that people at least know how to do it.

5. ACKNOWLEDGEMENT

The authors would like to express their deepest gratitude towards PT. Enerka Bhumi Pratama for their support for providing the facilities and the data. Comfortable gratitude for the practitioners that supporting the information of geothermal land acquisition challenges based on their real experience in this research.

REFERENCES

Asian Development Bank. (2015). Building Resilience to Climate Change in PNG: Voluntary Land Use/Negotiated Settlement Framework.

Dewi, A.N.R.P., Chatim, L., Lukito, L., et. al. (2013). What Are the Benefits and Challenges: Land Acquisition Process Based on Presidential Regulation No. 71 Year 2012 Versus IFC Performance Standard 5. *The 37th Indonesian Petroleum Association Proceedings.* Jakarta.

Ginting, Febrianti. "Studi Sosial Potensi Energi Panas Bumi Di Kabupaten Bantul." Publikauma: Jurnal Administrasi Publik Universitas Medan Area 5.1 (2017): 13-17.

Hunt T.M.(2012). Geothermal Resources, Environmental Aspects of. In: Meyers R.A. (eds) Encyclopedia of Sustainability Science and Technology. Springer, New York.

Intenational Council on Mining & Metals. (2015). Land acquisition and resettlement: Lessons learned. Intenational Council on Mining & Metals. London.

International Finance Corporation. (2012). Performance Standard 5: Land Acquisition and Involuntary Resettlement. *In book: IFC Performance Standards on Environmental and Social Sustainability*. World Bank Group. Washington D.C.

Ongau M.T. (2015). Introduction To Geothermal Drilling. Short Course X on Exploration for Geothermal Resources, organized by UNU-GTP, GDC and KenGen, at Lake Bogoria and Lake Naivasha, Kenya.

OTP Geothermal. (2013). Land Acquisition Processes.

Pambudi, Nugroho. (2017). Geothermal power generation in Indonesia, a country within the ring of fire: Current status, future development and policy. http://dx.doi.org/10.1016/j.rser.2017.06.096

Peraturan Pemerintah Republik Indonesia Nomor 7 Tahun 2017 *Panas Bumi untuk Pemanfaatan Tidak Langsung*. 21 Februari 2017. Lembaran Negara Republik Indonesia Tahun 2017 Nomor 30. Jakarta

Peraturan Pemerintah ESDM No. 36 Tahun 2017 tentang Tata Cara Penugasan Survei Pendahuluan Dan Penugasan Survei Pendahuluan Dan Eksplorasi Panas Bumi. 18 Mei 2017. Lembaran Negara Republik Indonesia Tahun 2017 Nomor 36. Jakarta

Peraturan Presiden Nomor 71 Tahun 2012 *Penyelenggaraan Pengadaan Tanah Bagi Pembangunan Untuk Kepentingan Umum*. 8 Agustus 2012. Lembaran Negara Republik Indonesia Tahun 2012 Nomor 156. Jakarta

Pertamina Geothermal Energy.: PGE Land One Map One Solution. Geomatics & ICT, (2021).

Purba, D., Adityatama, D.W., Soedarsa. (2021). A Study on Competency Assessment of the Geothermal Exploration Project Manager in Indonesia. *World Geothermal Congress.* Reykjavik.

Purba D.P.,et.al. (2021). Drilling Infrastructure Construction Challenges in Geothermal Exploration Project in Eastern Indonesia. *World Geothermal Congress.* Reykjavik

Purba D.P.,et.al. (2019). Review on Geothermal Direct Use Application as an Alternative Approach in Community Engagement at Early Exploration Phase in Indonesia. *Workshop on Geothermal Reservoir Engineering Stanford University. Stanford*, California.

Supremeenergy. Rencana Kegiatan Pengusahaan Panas Bumi untuk PLTP Rantau Dedap 250 MW. (2017)

Undang-undang Republik Indonesia Nomor 5 Tahun 1990 *Konservasi Sumber Daya Alam Hayati dan Ekosistemnya*. 10 Agustus 1990. Lembaran Negara Tahun 1990 Nomor 49. Jakarta

Yousefi H., et.al. (2007). Environmental Aspects of Geothermal Energy Development in Iran. Conference: The 5th International Workshop on Earth Sciences and Technology. Fukuoka, Japan.

PROCEEDINGS
JOINT CONVENTION BANDUNG (JCB) 2021
November 23rd – 25th 2021

What's New in API 610 12th Edition?

Suharto

PT Duraquipt Cemerlang

Abstract
A centrifugal pump standard, API 610 12th edition was just published in January 2021. This is still quite fresh and it will take time for the API 610 pumps manufacturers and end users to adapt to this new API 610 standard.

There are few International Standards for pumps which are used in Oil & Gas Industry. But, API 610 is the most popular pump standard and used widely all over the world, especially in the Oil & Gas Industry.

This paper is trying to discuss several things that are new in API 610 12th edition when compared to previous API 610 11th edition, including:

1. BB1 pumps. In the previous API 610, there is only 1 type of BB1 pump. But, now it is divided into 2 types, namely BB1-A: Foot Mounted and BB1-B: Near-centerline Mounted.
2. Hierarchy of Requirements. The hierarchy of the documents shall be stated by the purchaser.
3. Equipment Reliability. If requested by the purchaser, only field-proven pumps, as defined by the purchaser are accepted.
4. Parallel operation. Pumps with a discharge size greater than 3 inches that are operated in parallel, there is an additional requirement that in the preferred operating range (POR), the head different shall be within 3% of each pump.
5. Head rise to shut off (HRTSO). It is noted that pumps with head curve that continues to rise towards the shut off (stable curve) are preferred for all applications. However, this is not possible for all types of pumps.
6. Couplings. In API 610 11th edition, the coupling should be balanced with grade G6.3, but in 12th edition, the balancing grade is not stated, but it should be specified by the purchaser.
7. Shaft guards. In addition to the coupling guard installed between the driver and the pump, a shaft guard shall also be installed between the bearing housing and the mechanical seal.
8. Baseplates. The baseplate for the OH2 pump shall have nothing (auxiliaries or seal flush plan) mounted beside or above the coupling or bearing housing.
9. Performance test. The distance of each test point in the allowable operating range (AOR) should not be more than 35% of the rated flow. Hence, the test point is increased from 6 to 9 points.
10. Material Classes. Bronze, Ni-Resist and cast iron materials are no longer used for either the casing or impeller. Minimum material for casing and impeller is carbon steel.
11. Special-purpose Centrifugal Pumps. A special-purpose centrifugal pump is a pump that meets one or more of the following criteria:
a. Operating in a severe, critical application;
b. A prototype;
c. High energy levels.

Introduction
API 610 Pump Standard 12th edition was just published in January 2021. This is still quite fresh and it will take time for API 610 pumps manufacturers and users to adapt to the new API 610 standard.

In addition to the API 610 Pump standard (Centrifugal Pump) there are several other pump standards that are used in the Oil and Gas industry, namely API 674 (Reciprocating Pumps), API 675 (Controlled volume/Metering/Dosing pumps), API 676 (Rotary pumps), API 685 (Sealless Centrifugal Pumps) and ANSI/ASME B73.1 (Centrifugal Pump).

API 610 Pump Standard is the most popular pump standard in the oil and gas industry. API 610 Pump Standard was first published in 1954. Table 1 shows the years of publication of the API 610 standard from 1st edition to the last edition, which is 12th edition.

Table 1: Publishing History of API 610

Edition	Year of publication	Title	Number of pages	Years between editions
1	1954	API Specifications for Pumps for General Refinery Services	20	
1	Jan-55	Supplementary 1 Mechanical Seals	1	
1	Jan-55	Supplementary 2 Vertical Pumps	3	
2	Jan-57	Centrifugal Pumps for General Refinery Service	22	2
3	Jan-60	Centrifugal Pumps for General Refinery Service	26	3
4	Jul-65	Centrifugal Pumps for General Refinery Service	26	5
5	Mar-71	Centrifugal Pumps for General Refinery Service	35	6
6	Jan-81	Centrifugal Pumps for General Refinery Service	62	10
7	Feb-89	Centrifugal Pumps for General Refinery Service	139	8
8	Aug-95	Centrifugal Pumps for Petroleum, Heavy Duty Chemical, and Gas Industry Services	193	6
9	Dec-02	Centrifugal Pumps for Petroleum, Petrochemical and Natural Gas Industries	192	7
10	Oct-04	Centrifugal Pumps for Petroleum, Petrochemical and Natural Gas Industries	184	2
11	Sep-10	Centrifugal Pumps for Petroleum, Petrochemical and Natural Gas Industries	205	6
12	Jan-21	Centrifugal Pumps for Petroleum, Petrochemical and Natural Gas Industries	223	11

Compared to other pump standards, the API 610 standard is the most popular pump standard and the most frequently updated.

Data and Method
Most of data in this paper are taken from API 610 12th and 11th edition. Method used in this paper is comparative, i.e. comparing API 610 12th edition with the previous API 610 11th edition.

Result and Discussion
In API 610 12th edition there are several things that are new when compared to API 610 11th edition, including the following. To make it easier to check in API 610 12th edition, the API 610 paragraph is provided in parentheses.

PROCEEDINGS
JOINT CONVENTION BANDUNG (JCB) 2021
November 23rd – 25th 2021

1. BB1 Pumps (4.2.2.8)
BB1 pump type, which previously only has 1 type, is now divided into 2 types, namely BB1-A: Foot Mounted and BB1-B: Near-centerline Mounted. See figure 1a & 1b respectively. BB1-A pumps may be used for service temperature below 150 ^{O}C.

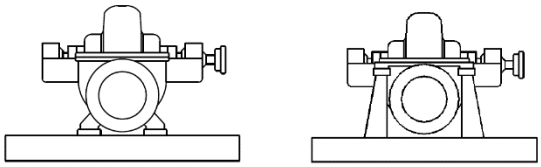

Figure 1a. BB1-A: Foot Mounted

Figure 1b. BB1-B: Near-centerline Mounted

2. Hierarchy of Requirements (5.3.3)
In API 610 12th edition there is an addition that the hierarchy of documents shall be specified by purchaser. This is certainly very useful to avoid any conflicts that may occur between one document and another. So it is clear that the document with the highest hierarchy shall be used as a reference. In case of conflict between the standard and the inquiry, the inquiry shall govern. At the time of the order, the purchase order shall govern.

3. Equipment Reliability (6.1.1)
In API 610 11th edition, pumps shall be designed and manufactured for a minimum of 20 years of service life (excluding normal wear of parts specified in Table 20 of API 610 11th edition) and a minimum of 3 years of uninterrupted operation. Whereas In API 610 12th edition, if requested by the purchaser, only field-proven pumps, as determined by the purchaser, are acceptable.

Purchaser can use their engineering judgment in determining what equipment is field-proven. API 691 can be used as a reference.

If specified, the vendor shall provide documentation to demonstrate that all proposed equipment qualifies as field proven.

If the equipment is not available, vendors shall submit an explanation of how their proposed equipment can be considered field-proven. A possible explanation is that all the components that make up the assembly machine meet field-proven definitions.

4. Parallel operation (6.1.13)
Pumps with a discharge nozzle size greater than 3 inches that are operated in parallel, there is an additional requirement that in the preferred operating range (POR), the head values must be within 3% of each pump. This means that the head difference of each pump which is operated in parallel cannot be more than 3%.

5. Head rise to shut off (HRTSO) (6.1.15)
It is noted that pumps with a head curve that continues to rise towards the shut off (stable curve) are preferred for all applications. However, this is not possible for all types of pumps. The shape of the head curve is dependent on several factors specific to the hydraulic design of the pump.

6. Couplings (7.2.2.g)
In API 610 11th edition, if specified, the couplings shall be balanced according to ISO 1940-1 grade G6.3, but in 12th edition major coupling components (hubs and spacer/flex element) shall be balanced in accordance with ISO 21940-11, but the balance grade is determined by the purchaser.

Balancing grade G6.3 is good enough for the coupling. So far so good, no problem.

7. Shaft guards (7.3.3)
In addition to coupling guard between driver and driven equipment (pump), a shaft guard shall also be installed between bearing housing and mechanical seal.

The shaft guard shall sufficiently vented to prevent the accumulation of seal emissions, liquid, or vapor and allow visual inspection of the seal without removal of guard;

8. Baseplates (7.4.6)
Baseplates for OH2 pumps shall have nothing (auxiliaries or seal flush plan) mounted beside or above the coupling or bearing housing. If the auxiliaries or seal flush plan shall be mounted on the baseplate, the increased length standard baseplate shall be used and the auxiliaries and/or seal flush plan shall be mounted adjacent to the suction nozzle. See figure 2.

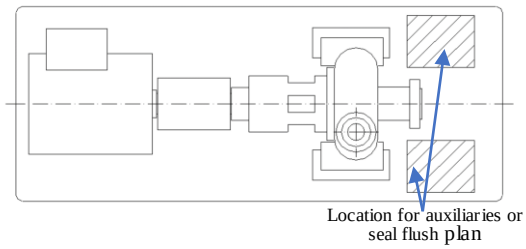

Figure 2. Baseplate for OH2 Pumps

This is intended that the auxiliary systems will not block access when maintain the pump, motor, and coupling.

Table 2. Dimensions of Standard Baseplates

Dimensions in millimetres (inches)

Baseplate number	Number of holes per side	l_1 +13 (0,5)	l_2 −25 (1,0)	l_3 −3 (0,12)	l_4 +3 (0,12)	l_5 +3 (0,12)
0.5	These baseplate numbers are deleted in API 610 12th edition					
1						
1.5						
2						
2.5	3	915 (36,0)	1 535 (60,5)	615 (24,25)	615 (24,25)	840 (33,0)
3	3	915 (36,0)	1 840 (72,5)	770 (30,25)	770 (30,25)	840 (33,0)
3.5	4	915 (36,0)	2 145 (84,5)	920 (36,25)	615 (24,16)	840 (330)
4	4	915 (36,0)	2 450 (96,5)	1 075 (42,25)	715 (28,16)	840 (33,0)
5	3	1 065 (42,0)	1 840 (72,5)	770 (30,25)	770 (30,25)	990 (39,0)
5.5	4	1 065 (42,0)	2 145 (84,5)	920 (36,25)	615 (24,16)	990 (39,0)
6	4	1 065 (42,0)	2 450 (96,5)	1 075 (42,25)	715 (28,16)	990 (39,0)
6.5	5	1 065 (42,0)	2 755 (108,5)	1 225 (48,25)	615 (24,12)	990 (39,0)
7	4	1 245 (49,0)	2 145 (84,5)	920 (36,25)	615 (24,16)	1 170 (46,0)
7.5	4	1 245 (49,0)	2 450 (96,5)	1 075 (42,25)	715 (28,16)	1 170 (46,0)
8	5	1 245 (49,0)	2 755 (108,5)	1 225 (48,25)	615 (24,12)	1 170 (46,0)
9	4	1 395 (55,0)	2 145 (84,5)	920 (36,25)	615 (24,16)	1 320 (52,0)
9.5	4	1 395 (55,0)	2 450 (96,5)	1 075 (42,25)	715 (28,16)	1 320 (52,0)
10	5	1 395 (55,0)	2 755 (108,5)	1 225 (48,25)	615 (24,12)	1 320 (52,0)
11	4	1 550 (61,0)	2 145 (84,5)	920 (36,25)	615 (24,16)	1 475 (58,0)
11.5	4	1 550 (61,0)	2 450 (96,5)	1 075 (42,25)	715 (28,16)	1 475 (58,0)
12	5	1 550 (61,0)	2 755 (108,5)	1 225 (48,25)	615 (24,12)	1 475 (58,0)

PROCEEDINGS
JOINT CONVENTION BANDUNG (JCB) 2021
November 23rd – 25th 2021

Baseplate size in API 610 12th edition starts with the baseplate size number 2.5 – 12, while in the previous edition the size starts from the number 0.5 – 12. See Table 2.

9. Performance test (8.3.3.4.1)
The distance of each test point in the allowable operating range (AOR) shall be no more than 35% of the rated flow. The number of test points is 9. See figure 3.

Table 3 shows the differences in its test points between API 610 11th and 12th editions.

Table 3: Comparison of test points of API 610 11th edition vs 12th edition.

11th Edition	12th Edition
1. Shutoff;	1. Shutoff;
2. Minimum continuous stable flow;	2. Minimum continuous stable flow;
	3. Halfway between minimum continuous stable flow and minimum preferred operating flow;
	4. Minimum preferred operating flow;
	5. Halfway between minimum preferred operating flow and rated flow;
3. Between 95 % and 99 % of rated flow;	6. Between 95 % and 99 % of rated flow;
4. Between rated flow and 105 % of rated flow;	7. Between rated flow and 105 % of rated flow;
5. Approximately BEP flow (if rated flow is not within 5 % of BEP flow);	
6. End of allowable operating region.	8. End of preferred operating region;
	9. End of allowable operating region if different from the end of the preferred operating region.

For pumps with low capacity, below 50 gpm (11 m^3/hr), test points no. 3 and 5 are not required.

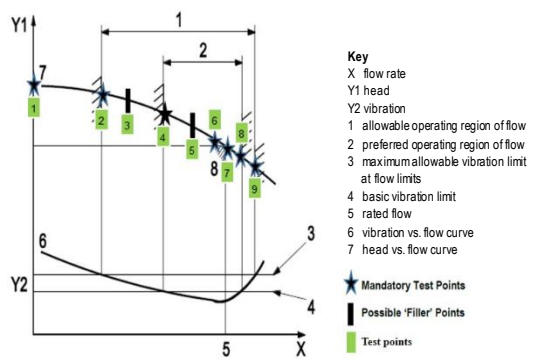

Figure 3. Test points

10. Material Classes (Table H.1)
In API 610 12th edition, bronze, Ni-Resist and cast iron materials are no longer used for either casing or impeller. Minimum material for casing and impeller is now carbon steel. So the material class starts from S-4. Material classes I-1, I-2, S-1 and S3 are removed from the API 610 12th edition.

For the last few years back, the requirement of cast iron material for API 610 pump is very seldom. Cast iron is fragile and not suitable for high pressure. Moreover, it is difficult to repair when welding is required.

11. Special-purpose Centrifugal Pumps (Annex O)
A special-purpose centrifugal pump is a pump that meets one or more of the following criteria:

a. Operating in a severe, critical application;
b. A prototype – a design that is sufficiently different from existing designs to warrant, in either the manufacturer's or the purchaser's opinion, the extent of engineering analysis and manufacturing process specified in Annex O of API 610 12th edition;
c. High energy levels.

High energy is a term that has been used by some in the oil and gas industry to define if a design requires more attention to engineering and manufacturing than is required by API 610. High energy has many definitions (shaft power, power per stage, head per stage, pressure rise per stage, value of first stage impeller inlet peripheral velocity), none of which are sufficiently encompassing to qualify as a single definition.

Conclusions
This paper has highlighted some significant new requirement in API 610 12th edition. Both pumps manufacturers and end users shall adapt their pumps design and requirement to this new API 610 12th edition.

There is no change in bare pump design like: maximum allowable working pressure (MAWP), corrosion allowance, bearing life, shaft deflection, etc. The significant change occurred in pump requirement like: pump reliability, parallel operation, head rise to shut off, performance test, material classes & special purpose pumps, and also pump accessories like: coupling, shaft guard & baseplate.

References
ANSI/API Standard 610, 2021, Centrifugal Pumps for Petroleum, Petrochemical and Natural Gas Industries, 12th Edition.
ANSI/API Standard 610, 2010, Centrifugal Pumps for Petroleum, Petrochemical and Natural Gas Industries, 11th Edition.
Suharto, 2016, POMPA SENTRIFUGAL Panduan Lengkap: Standarisasi, Teori, Pemilihan, Pembelian, Pengoperasian, *Maintenance* dan *Troubleshooting.*

PROCEEDINGS
JOINT CONVENTION BANDUNG (JCB) 2021
November 23rd – 25th 2021

Development of an Integrated Operation Center (IOC): Streamlining Upstream Oil and Gas Production Monitoring in Indonesia

*(M. Fauzan Amir, Alfandra I, Amalia KD, Vitrisia K, Widi K.P, M. Ridlo Rosyid, Bong Anthony, Yogi A, Panca D. N, Mildo N, Bambang P, Ngatijan)**
**) SKK Migas*

Abstract
As appointed to represent Indonesia government for managing the entire business and operational aspects of upstream oil and gas in Indonesia, Special Task Force For Upstream Oil and Gas Business Republic of Indonesia or known as SKK Migas have established a vision to integrate operation monitoring of all oil and gas blocks in Indonesia, by means of an Integrated Operation Center (IOC) that transform the previous conventional approach in to an unified online monitoring system. It has been motivated by digital transformation trend in oil and gas industry which bring a new wave of opportunities in order to raise effectivity and efficiency in terms of monitoring and supervision.

Motivated by the fact that the old vision of the integration that never come true—due to the complicated proposed solutions at that time, therefore, a simpler method is required. Supported by the better infrastructure condition and more developed web-based technology, finally the system has been successfully built. By combining in time and real-time connections based on web-based application, the IOC is able to provide more than 2500 derived monitoring dashboards covering oil and gas production operation and plant information management system (PIMS) in Indonesia. The system is used to monitor the daily production data of around 670,000 barrels oil per day and close to 7,000 millions standard cubic feet per day gas and, from the whole PSC companies in Indonesia, where 80% of them are in real time monitoring.

The dashboards are available in two platforms, i.e. desktop and mobile application which gives flexibility in terms of connection and access as long as internet connection available. During the pandemic COVID-19 which restricts inspection activities going to the fields, the system is proven effective in monitoring point of view, without losing the essence of direct supervision over the operational assets which usually locates on the stranded and limited areas.

In conclusion, the contribution of the presented work is the digital transformation in oil and gas sector in Indonesia, which successfully creates collaborative working environment in managing the oil and gas production operation. It changes the interaction approach between the regulator and PSC operators in terms of process monitoring as well as underlying the foundation of the data management toward the preliminary development of data analytics as path forward of the oil gas operation management in Indonesia

Introduction

Since 2019, SKK Migas has launched an upstream oil and gas transformation program that carries a big vision to return to oil production of 1 million barrels of oil per day and gas production of 12,000 MMSCFD. This vision is realistically achievable if there are giant discoveries that are supported by improvements in upstream oil and gas governance. Furthermore, the transformation pillars underlying the process improvement are translated into programs like organizational and human resource management towards a center of excellence, simplification of permit process through a one door service policy, acceleration of commercial potential and last but not least digitalization programs.

The digitalization in oil and gas sector is actually not new, as in fact that has been developed for quite a long time, in accordance with the characteristics of the oil and gas industry that requires high technology. The digital application has obviously played an important role in the upstream industry, including in Indonesia, generally placing the technology development at the forefront compared to other industrial sectors. However, in the integrated management point of view in Indonesia, the digitalization just plays the partial role, where the production sharing contracts were formerly managed in individual systems, without the support of an integrated system which supposes to help process monitoring more effective and efficient.

The old ideas to build such system have been actually discussed formerly, but they were too complicated and hard to be implemented considering high costs, large resources and long project time duration. In addition to that, the information technology infrastructures between BPMigas/SKK Migas and PSC operators at that time was not pretty good and still in early development phase of integration, so that raising the complexity of the implementation.

The unavailability of the integrated system leaves some concern of the operation supervision of oil and gas production facilities, as follows [1]:

1. Limited available information
   The availability of operation information was generally limited, usually manual or offline and unidirectional (without comparison). With other words, the human dependency plays important role in providing the data or information, not based on a system-driven
2. Monitoring system
   The unavailability of a real-time monitoring system made it difficult in terms of the immediate need of monitoring PSC operational disruptions or in some cases for which requires direct approval or close monitoring of the regulatory body
3. Transparency and data openness
   Due to the absence of the online monitoring system, the data submitted by PSC operators is sometimes not transparent, un-comparable and relying only on the one-way information
4. Effectiveness of supervision
   Monitoring of operational activities requiring hands-on supervision is sometimes ineffective because the personnel mobilization for the field visit requires time and administrative processes, while the availability of information is needed right away

PROCEEDINGS
JOINT CONVENTION BANDUNG (JCB) 2021
November 23rd – 25th 2021

The development of Integrated Operation Center in SKK Migas is therefore intended to overcome the problems mentioned above. It is motivated by efforts to carry out the transformation pillar for the upstream oil and gas operation which improves the good governance of oil and gas industry in Indonesia.

This paper presents the contribution of the development of integrated operation center (IOC) in SKK Migas in the context of oil and gas production operation. Introduced system in first section by some issues of the unavailability of the integrated and the justification of the IOC development, the next one describes the data and method used in building the integrated operation system. The emphasis is placed on the technology selection, step-by-step approaches of the engineering implementation and proposed system architecture as well. The next section explains the dashboard design and examples of the real time monitoring system and its associated results, while the last one presents the conclusion of the presented work and the way forward for next development.

Building System of Production IOC

The use of digital technology in the oil and gas world has grown rapidly. Driven by a high level of competition in creating added value for companies [2,3], innovation in the digital sector is exponentially growing in various fields leading to the development of data integration, modern visualization processes as well as increasingly sophisticated analytical data management systems.

Many international oil and gas companies have succeeded in developing data integration centers and analytics systems to integrate the operating systems of oil and gas production facilities that are scattered everywhere. As shown in Figure 1, an oil and gas company in UAE (ADNOC), for example, has developed an Integrated Operation Center (IOC) which unites its subsidiaries from upstream to downstream. The modern management of the oil and gas industry not only provides efficiency values in terms of monitoring oil and gas production operations, but also provides a positive reputation in terms of modernizing oil and gas management, thus indirectly becoming an effective marketing strategy.

Figure 1. ADNOC – Panorama [4]

Driven by the success of the companies, SKK Migas has benchmarked several typical companies and invited some PSC operators to share their experiences and to formulate the idea to realize the development of the IOC. Brain storming, discussions and exploring some options were conducted to determine the best option which is appropriate to the limited budget and the time given. By empowering internal resources in designing the system supported by the local technology provider, the IOC was finally launched and inaugurated by the Minister of Energy and Mineral Resources Republic of Indonesia by the end of 2019, as shown in Figure 2.

Figure 2. The IOC Soft Launching in SKK Migas

Basically, the Integrated Operation Center (IOC) of SKK Migas consists of some dashboard modules, namely production, drilling, project, maintenance and HSE, which combine in time and real time data. Here, in this paper, the concentration is only focused on the development of the production module due to the large scope of operation, which covers:

1. The daily production dashboard of all PSC operators in Indonesia
2. Plant Information Management System (abbr. PIMS) enabling the live monitoring of production operation of in Indonesia

The both items above adequately provides a representative picture of the production operation conditions of the upstream oil and gas in Indonesia. The users are given by various national data and displays of oil and gas production, lifting, stock, gas balance, gas utilization and reconciliation including thousands of the derived sub-dashboards, which are useful for monitoring operation condition all at once evaluating the operation performance.

Having the system like the IOC obviously offers some advantages. First, the production data including the derived one can be stored permanently. The data can be easily accessed, traceable, kept safely, instead of using the conventional storage devices like hard disks that prone to damage. Second, the data can be displayed systematically, integrated in structured visualizations, so that providing the transparent data, open, in an attractive modern design. Third, the information is quickly available to meet the demand. Live access featured in the plant information management system provides even the instant information on what's going on in the plant in real time. By doing so, the interaction approach in terms of monitoring is changing significantly which is creating new values in supervision and monitoring of upstream oil and gas operation in Indonesia.

Using the same reference by [1], there are some criterion used to build the production modules. First, the financial aspect, where it is expected to be as low as possible without sacrificing quality. The second one is the project duration, which is challenged that must be completed in

relatively short time. Third, the data can be transmitted in online in a combination of daily data and real time one with a configuration of 1 minute or less of the refreshment time. Fourth, the system must be designed securely and protected, so that minimizing the cyber threat risk. Fifth, the system should have good reliability in terms of connection, so that it is operable for a long time. The last one is flexibility. The system should be accessible anytime and anywhere, without limited by time and location.

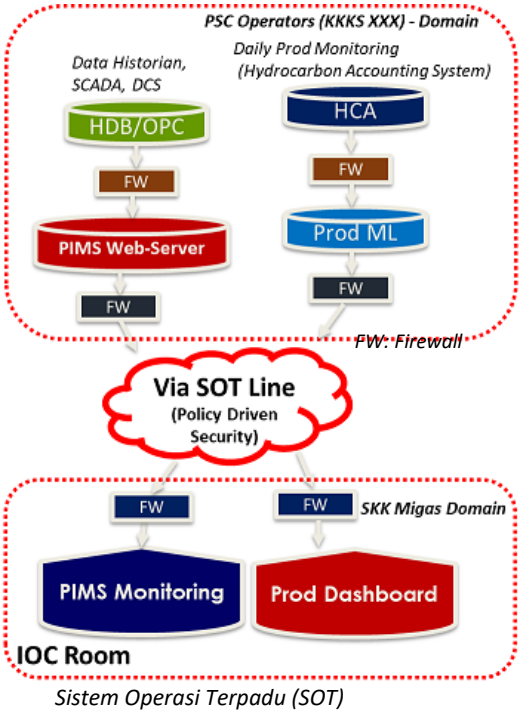

Figure 3. The Simplified System Architecture

The simplified system architecture is shown in Figure 3. The real time data from SCADA systems or automation systems is consolidated in the historian database or connected through the open platform communication or well knows as OPC. The data is then sent to the PIMS server for further translation to the SKK Migas network via the SOT line. Through a layered security system, the PIMS application can be accessed safely at SKK Migas. On the other side, the daily data like production, lifting and stock sourced from hydrocarbon accounting system of the associated PSC is translated into a prod ML format and sent to the SOT server in SKK Migas. The SOT data is afterward visualized into production dashboards including their derivatives.

In general, the production dashboards contain main production information as follows:

- Management dashboard that informs the production and lifting key performance indicators
- Oil and gas production including the details of daily & historical production data, activity contribution, well performance and data reconciliation
- Oil and gas lifting including oil stock and operational reconciliation data
- Gas balance composing gas lifting, fuel, flare, impurities and discrepancy
- Gas utilization displaying gas buyers, associated industry classification and comparison contract versus actual sales
- Plant Information Management System (PIMS) providing real time plant data from well summary to custody points

The next section describes in more details the displays available on the IOC, including the associated features.

Production Dashboards

This module basically represents the national scope of the production monitoring reflected by 15 main production displays with more than 2500 sub-dashboards of the operational data across all PSC operators including oil and gas production, oil and gas lifting, oil and condensate stocks, gas balance and gas utilization.

Desktop Dashboards
Once the application is launched, the viewers are brought to the front page which provides general information about oil and gas operation. As seen in Figure 4, the today oil and gas production, the oil and gas lifting, the national oil stock, the drilling progress information and the planned maintenance monitoring are the presented data based on the last report status updated regularly by associated functions in SKK Migas.

Figure 4. The IOC landing page

Moving on the next menu, the user is presented the drop down features that can select the desired dashboard, for example, operation management as pictured in Figure 5. This page is intended to the management level to see the helicopter view of the major parameters in operation, among others production operation, drilling operation, project management, maintenance and operation support.

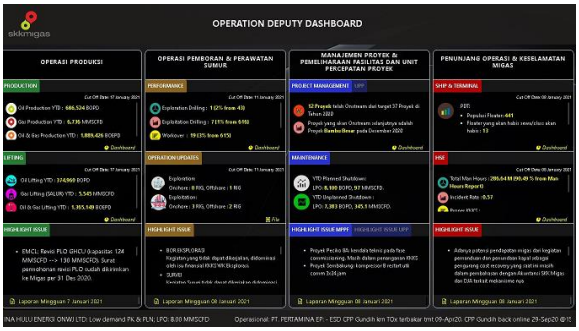

Figure 5. Operation Management Dashboard

The main production page as available on the Figure 6 shows the data of today oil and gas production rate,

monthly average, yearly average, top oil and gas producers, and historical data all at once the production notes appointed to the production curve and running text updated regularly.

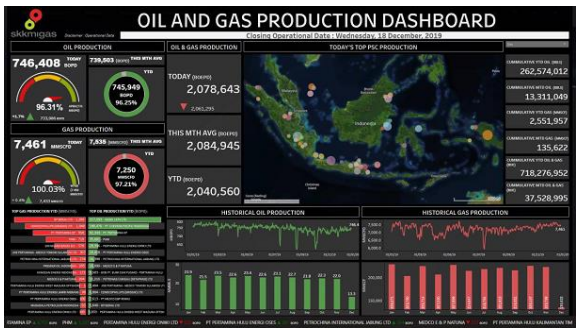

Figure 6. The oil and gas production page

Like the production page, the lifting dashboard is designed similarly as presented in Figure 6. The lifting operation displays shows the oil and gas lifting data from today, monthly, yearly average and the lifting distribution of the all PSC operators. Furthermore, the associated data can be filtered in national or PSC operator category including its accumulation as well as top lifting PSC operators today in Indonesia. The oil stock complementing the lifting reports is then available from the major terminals in Indonesia. Then, the LPG lifting volume is also presented in the same display including monthly and its related yearly average.

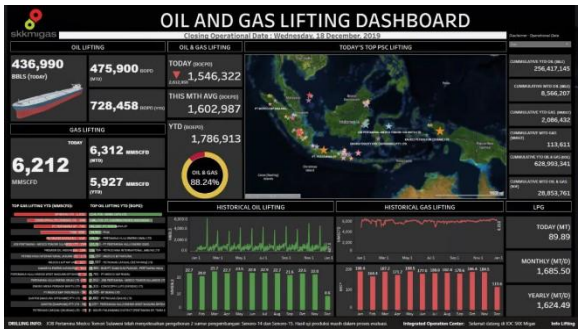

Figure 7. The oil and gas lifting page

In addition to that, there are also available on the advanced dashboard analysis related to the performance of oil and gas wells, the production contribution from drilling, work overs and well services activities, the top 10 rankings of oil and gas development wells, to the comparison of the number of on stream wells with respect to the monthly plan. The gas balance user interface describing the flare data, gas consumption, impurities, discrepancy and gas lifting are also available on the other window equipped by the filter to select national or individual data of PSC operator, as desired. We also develop a gas utilization dashboard, displaying a helicopter view of the gas distribution to the all buyers as well as related industries in Indonesia. Once can see the data of the main gas buyers including the daily contract quantity (DCQ) compared to the actual sale volume to see the gas lifting performance.

PIMS Dashboards

Completing the in-time data, the IOC also provides real-time features via PIMS application. The PIMS dashboards are designed to represent the live actual data of the PSC operators, from the well heads to the metering systems that constructs the surface production facilities. Usually, there are some requirement of process visualization, which present the oil and gas production operation in terms of simplified process diagrams, namely:

1. Well summary
2. Production rate
3. Major/critical equipment (corresponding to
4. production impact)
5. Gas flaring system
6. Fuel gas system
7. Power generation system
8. Metering system (custody)
9. Air pressure system
10. Oil inventory system

The samples of the PIMS dashboards are shown in Figure 8, which basically meets the main points above. Currently, the number of the PSC operators which are connected to the IOC PIMS covering around 80% of the oil and gas production all over Indonesia. So far, it is sufficient to describe the dynamics of major operations in the PSC fields, as the main objective of the real time monitoring.

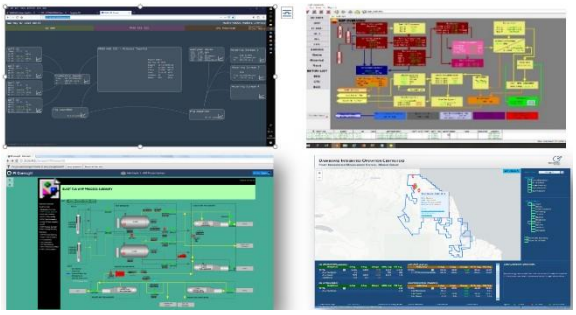

Figure 8. The examples of the PIMS application

All the critical equipment corresponding to the production impact is included in the PIMS. Thus, the process disruption occurring on the plants is easily known and checked without waiting the PSC operator response which usually take time. The users can easily monitor the shutdown execution and ensuring the process startup is on time as planned. If something happened, the historical data for the analysis purpose can be called easily. One can set the initial time and the interval duration, and then the historical trending is immediately available as expected. By these features, the users are helped, to improve the data evaluation quickly and overcome the slow response issue of the PSC operators, whenever the data anomaly is detected.

IOC Mobile Version

Besides being available in the desktop format, the IOC is made in a mobile version as well. As shown in Figure 9 above, the users can see the production operation data in the mobile version, following the technology trend recently. This application facilitates the data monitoring easier, quicker and more flexible in the context of the data access and transfer without necessarily opening the desktop application whenever requiring some data access instantly. The user can adequately check the data from the mobile dashboards, or screen-shoot and send it to the other user by means of the trending medias like whatsup, telegram or others.

PROCEEDINGS
JOINT CONVENTION BANDUNG (JCB) 2021
November 23rd – 25th 2021

Figure 9. The IOC Mobile Version

Conclusions

This paper presents an innovation of the development of an integrated operation center (IOC) to streamline the production operation in upstream oil and gas industry in Indonesia. The old vision finally comes true, so helping SKK Migas as an appointed government body to supervise and monitor the whole upstream production operation in Indonesia easily using the digital technology.

The development of new features in the IOC is still ongoing. By equipping early warning systems and automatic reporting, the process monitoring is expected easier and quicker so that resulting in the more effective approach in terms of supervision. Moreover, we also currently plan to develop a new approach in forecasting the oil production data for oil lifting management based on an analytical tool like machine learning or other advanced method. The result is expected to be more accurate and consistent so that further calculation such as based on the data become more precise to achieve the optimum oil lifting management.

References

[1] M.F. Amir, Yogi A, Rossupanji P, Bambang P, Ngatijan, “Proceedings IPA”, September 2021
[2] Alexander Clark, Henrik W. Larsen, Jan-Erik Nordtvedt, Bart T. Stafford, Kevin Stewart, Bård-Henning Tvedt, Ådne Tveit, ,” SPE Annual Technical Conference and Exhibition, 30 September - 2 October, Calgary, Alberta, Canada
[3] Claudio L, Osvaldo L. Gonçalves Quelhas, Gilson Brito Alves L, Rodrigo N. F. Value and approach in the oil industry” 2015
[4] https://www.smartindustry.com/articles/2019/adnoc-pioneering-oil-and-gas-4-0/

Acknowledgements

The authors gratefully acknowledge the support of SKK Migas, PSC operators, and other parties (who, unfortunately, could not be mentioned one by one) in finishing the projects and creation of this paper.

PROCEEDINGS
JOINT CONVENTION BANDUNG (JCB)|2021
November 23rd – 25th 2021

Application of Managed Pressure Drilling Successfully Navigating Narrow Drilling Window Enabling Opportunity for Offshore Depleted Reservoir

Insan Faza[1], Ali[1], Fikri Irawan[1], Andry Prasthio[1]
[1]Weatherford

ABSTRACT

Extending field productivity within the reservoir which is currently facing natural decrease from virgin pressure is common challenge in mature field development. The depleted reservoir changes formation properties such as pore pressure and fracture pressure when the drilling window becomes narrower promotes further challenges.

As the reservoir pressure window becomes narrow, implementation of conventional drilling technique may induce common drilling problems, such as loss circulation, kick, differential sticking and so on. An alternative method known as Managed Pressure Drilling (MPD) which actively controls the annular hydraulic pressure while drilling, making connections, and tripping operation was implemented in this operation.

At the beginning of the 8.5in. section, extensive drilling window of 6.33ppg observed based on the subsurface information and preliminary study. The challenges appear when the well had just been drilled in less than for 2,300ft where the drilling window significantly reduced to 0.93ppg as a result of pore pressure ramp up. Meanwhile, fracture pressure point decreases at the same section which result in narrow drilling window of the 8.5in hole. At this condition, the utilization of conventional drilling methods promotes high risk of inviting undesirable conditions such as loss and kick. Without MPD implementation, it is considered impossible to reach target depth successfully.

Weatherford MPD system computes precise ECD model based on real-time drilling parameters and downhole condition. Surface Back Pressure is exerted during pipe connection to keep the well overbalance until target depth achieved.

This paper describes MPD utilization as unconventional method to overcome drilling hazard related to pressure depletion and extend technical limits for prolonged and developed field. The publication is expected to unlock further advancement in Indonesia developed field with similar approach by other operators.

Keywords: Narrow pressure window, managed pressure drilling, equivalent circulating density.

INTRODUCTION

Drilling a new well is a crucial step toward boosting oil and gas recovery. However, for some depleted fields, drilling of new wells is difficult due to constrained operational drilling window. This is due to the field's production history and is especially linked to formation pressure depletion.

The difference between the highest pore pressure gradient and the lowest fracture gradient determines the operational drilling window of each section. The operational drilling window has a different value at each depth of the wellbore.

All producing oil and gas fields will experience pressure depletion issues. This factor will determine the economic conclusion of that area. The use of conventional drilling techniques in places where these difficulties exist promotes higher risk of causing kicks and losses. It is necessary to drill a well by maintaining the bottom pressure within the pressure drilling window. Managed Pressure Drilling (MPD) is the fit-to-purpose drilling method to complete this objective. By utilizing MPD technique, the bottom hole pressure is consistently and accurately adjusted to remain above the pore pressure and below the fracture pressure during drilling and connection.

MANAGED PRESSURE DRILLING

MPD is a drilling method used to accurately regulate annular pressure in order to prevent influx entering the wellbore. MPD equipment develop a closed-loop drilling system to manage the annular pressure profile by exerting Surface Back Pressure (SBP) to easily manage the bottom hole pressure while drilling, pipe connection, or even running completion string *(Agustinus, 2016).*

Distinctive to conventional drilling, the determination of bottom hole pressure using MPD includes one additional factor as explained in the equations below.

PROCEEDINGS
JOINT CONVENTION BANDUNG (JCB)2021
November 23rd – 25th 2021

$$BHP_{static} = HP + SBP$$

$$BHP_{dynamic} = HP + AFP + SBP$$

BHP_{static} = Bottom Hole Pressure while no circulation

$BHP_{dynamic}$ = Bottom Hole Pressure while circulation

HP = Hydrostatic Pressure Mud

AFP = Annular Friction Pressure

SBP = Surface Back Pressure

MPD EQUIPMENT

Rotating Control Device

Rotating Control Device (RCD) is an equipment which is installed above the annular BOP or riser, depending on the type of BOP set on the well. While drilling, RCD will seal the annulus surrounding the drill pipe to produce a closed and pressured annulus system. The primary function of the RCD is to enable closed-loop system through a dual sealing element installed inside the RCD Bearing. RCD installed in this project is RCD Marine Series to align with its offshore shallow water operation. The RCD Bearing can be installed directly into RCD housing without any man riding operation on the BOP area. The RCD is completed with three primary outlet with two side outlet sized 7-1/16in. for return line and emergency fill up line as well as one outlet sized 2-1/16in. for injection, trip tank line and bleed off line.

MPD Automatic Choke Manifold

MPD manipulates the bottom hole pressure by applying additional pressure at the surface, which is referred as SBP. The SBP is generated when the flow through the MPD manifold is restricted by a surface choke. The MPD Automatic Choke manifold system is capable to change the proportion of choke opening based on the desired SBP set point. When the requisite SBP is higher, the choke will be closed until the required SBP is reached. When the requisite SBP is lower, choke system will perform the opposite action. The MPD Manifold is completed with two chokes sized 3in. that can be utilized separately or simultaneously depending on the operation necessities.

MPD Automatic Choke Manifold enables to detect loss and kick within seconds, making it a reliable tool to mitigate loss and kick to be handled promptly and minimize catastrophic well control related issue. MPD Automatic Choke manifold system is completed with Coriolis Flow Meter for flow detection capability. It can measure accurate flow out rate, mud density and returned temperature. All of these data then combined with drilling parameters from WITS and installed surface sensors to be analyzed by the MPD control system in real time to deliver annulus pressure management during drilling operation.

MPD OPERATION

Preliminary MPD simulation was completed in advance prior to drilling commencement. This study was used to simulate actual MPD condition in order to obtain the optimum mud weight design and SBP range. Drilling parameters such as RPM, WOB, ROP, mud rheology and well trajectory were simulated in order to acquire the optimized ECD. According to the MPD simulation, 13.66ppg mud and 150 psi SBP would be applied at a depth in 8.5in. section where the estimated depleted pressure regime.

According to the geological data modeling, extensive drilling window of 6.33ppg was expected at the beginning of the 8.5in. section. The difficulty arises when the drilling operation reached 2,300ft below the last casing shoe where the drilling window drastically reduced into 0.93ppg due to the pore pressure ramp up and decrease of fracture pressure gradient in the same hole section as illustrate in Figure 5. Depleted formation occurs in the same section because production operations have proceeded in that location for many years, resulting in pore pressure and fracture pressure drop at certain layer. The combination of these two factors results in an extremely narrow pressure window. To successfully drill this well, ECD needs to be controlled precisely within the drilling window by utilizing MPD technique.

MPD equipment such as RCD, MPD Automatic Choke manifold system, and accessories were pre-installed before the 8.5in. section. Then fingerprinting and familiarization were performed to personnel involved, such as essential rig contractor team, mud engineer, wireline crew, and drilling supervisors, on how MPD works were performed. The system SBP resulted by flowing at drilling rate to MPD Automatic Choke manifold system with choke at fully open was measured to be 33psi.

Existing mud weight set in the wellbore at 10.83ppg. At the beginning of 8.5in. section, drilling commenced conventionally without exerting SBP while circulation or pipe connection because of extensive drilling window. MPD system were activated in EKD mode to detect unwanted kick or loss to minimize aftermath impact.

The mud weight was then increased periodically prior to the estimated depth of depleted zone. At this depth the mud weight used was 13.66ppg. It was decided to proceed drilling the sequential depth without additional SBP while drilling as the ECD generated shall be overbalance and exceed the safety margin. However, during pipe connection, the MPD Automatic choke system applied 150 psi SBP in the annulus to maintain ESD above the pore pressure and allowing drilling to continue safely and effectively until the TD was reached.

The objective of the CBHP technique is to prevent and control hydrocarbon migration to surface by using the mud density as near as possible to the pore pressure. In some cases, the mud density is designed in slightly underbalanced condition; in other cases, it is designed at balanced condition. The mud design will be adapted with the drilling window profile and will be limited by formation strength, fracture leak-off point, and equipment specification *(Dharma D.S., 2016).*

During drilling, the ECD was observed from MPD real-time bottom hole pressure model (generated by MPD software platform) in conjunction with the PWD sensor readings installed in the BHA. Both of these technology controlled independently. The ECD was monitored during dynamic and static condition i.e. pump off. During no circulation, the annulus friction pressure would disappear and MPD system anticipated this condition with the exertion of SBP.

The basic principle of having a back-pressure pump diverted across an MPD choke at surface is that the pressure loss created at the choke is directly transmitted to the annulus, since there is full column of fluid at all times. Hence even though the flow from the back-pressure pump does not pass downhole, but through the surface line on the rig, the pressure in the annulus is still able to be manipulated as required *(Zein, J., 2016)*. The MPD Automatic Choke system will adjust the choke opening to build pressure along the surface line, which will be delivered to the bottom hole pressure through the annulus.

MPD connection proceeds according to the illustration in Figure 3. The ECD value was maintained at 13.95ppg during static conditions. The flow from drill string gradually decreased at the same time the back-pressure pump is increased gradually to compensate friction pressure lost. Simultaneously, MPD Choke will adjust the choke opening until the required SBP is achieved according to the pressure schedule. When the mud pump is completely shut off and the desired SBP has been reached, the drill pipe connection can be initiated.

Reverse procedure is in place after the connection, prior to continue drilling. The flow from drill string will be gradually increased while the back-pressure pump rate decreases at the same time. Drilling to be resumed safely while the MPD system monitors the parameters until the target depth is achieved.

Conclusions

Hydrocarbon extraction from the reservoir that have been producing for years result in pore pressure depletion. In this particular field, the decline lead to reduction in pore pressure and fracture pressure of certain layer. While at the non-producing layer, both of these pressures remain constant. This event ultimately caused the narrow pressure window existence within one drilling section which will lead to kick and loss drilling hazard. The used of MPD technique allows drilling operation to overcome this challenges by maintaining bottom hole pressure within the pressure window. MPD is proven to be successful in drilling wells with narrow drilling window until the target depth is safely achieved.

Acknowledgements

The authors would like to express their appreciation to Weatherford management for their permission to publish these results and all valuable contributors of Indonesia MPD team.

References

Zein, J., Irawan, F., Hidayat A.M., et al. “Case Study-Constant Bottom Hole Pressure of Managed Pressure Drilling Utilization to Maintain Wellbore Instability in East Java Drilling Operation, Indonesia”, Presented in Asia Pacific Oil & Gas Conference and Exhibition (APOGCE) 2016 in Perth, Australia, 25-27 Oct 2016. SPE-182212-MS.

Agustinus, K., Zein, J., Irawan, F. et al. “Managed Pressure Drilling Application to Deploy Lower Completion Safely and Efficiently in Static-Underbalanced Well”, Presented at Offshore Technology Conference Asia held in Kuala Lumpur, Malaysia, 22–25 March 2016. OTC-26713-MS.

Dharma D.S., Hidayat. A.M., Irawan F., “Enhance ECD Management using Sub-Based Uninterrupted Circulating System Application”, Presented in Abu Dhabi International Petroleum Exhibition and Conference held in Abu Dhabi, UAE, 7–10 November 2016. SPE-183132-MS.

Figure 1: RCD Installed on BOP

Figure 2: MPD Automatic Choke Manifold

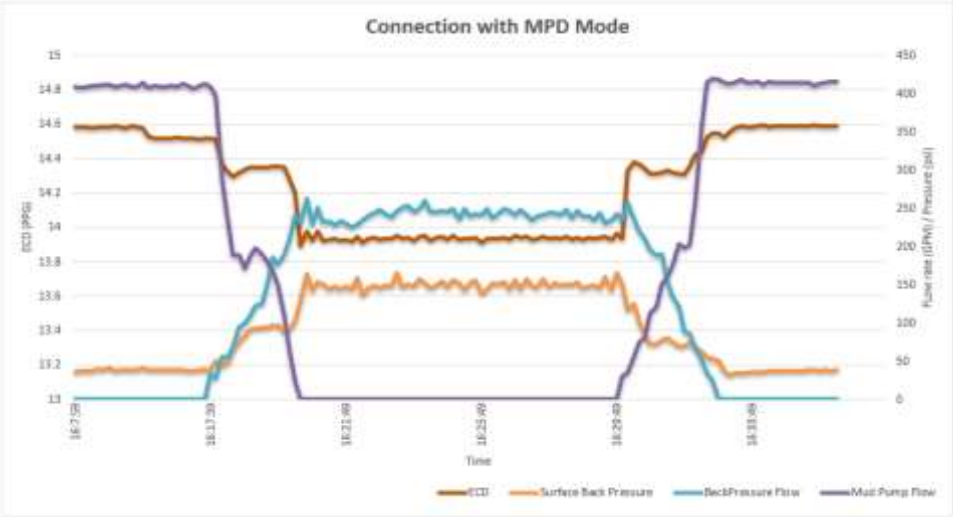

Figure 3: Ramp Pump Schedule during Connection with MPD Mode.

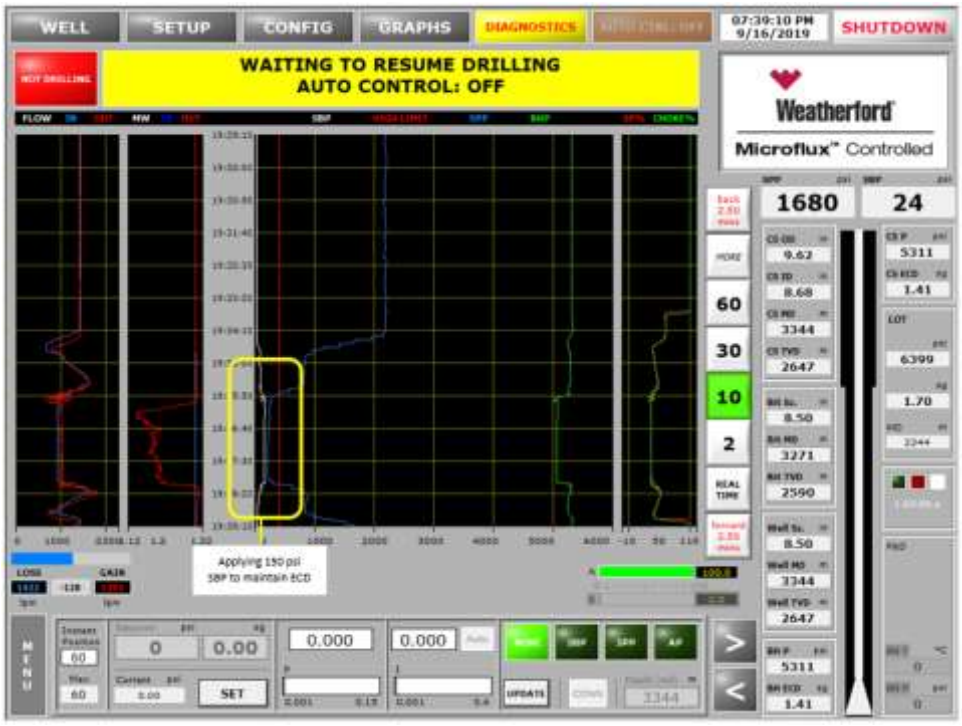

Figure 4: Applying SBP during Connection to maintain ECD.

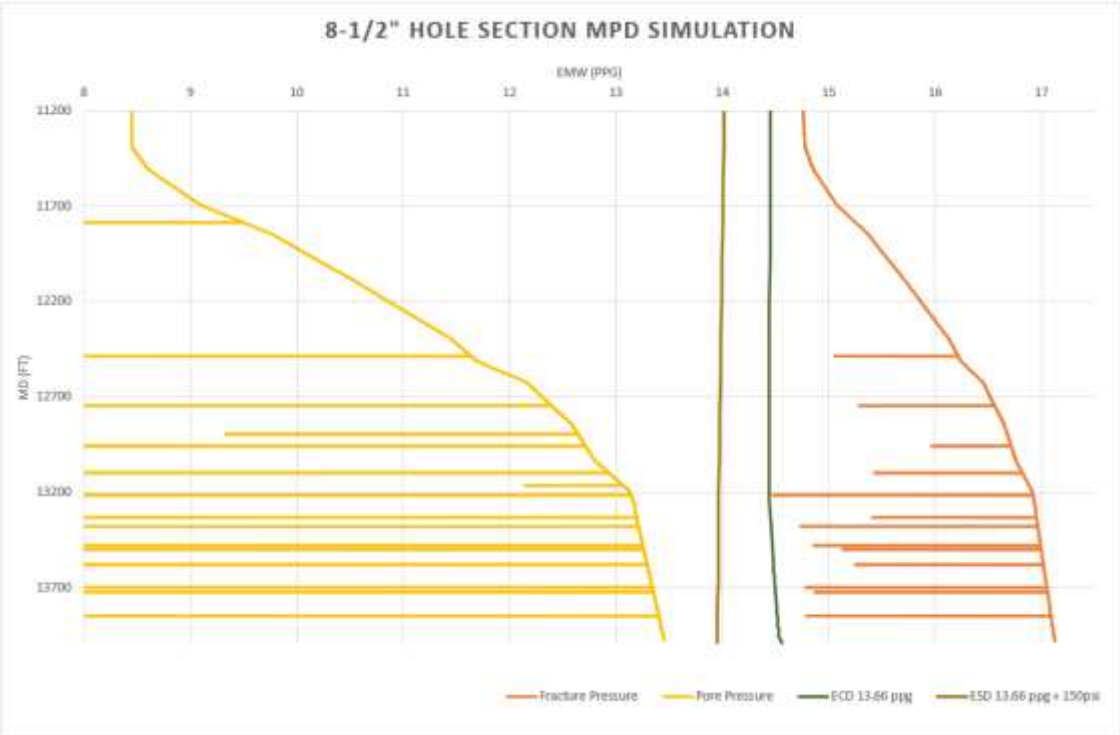

Figure 5: Drilling window of 8.5in. hole section.

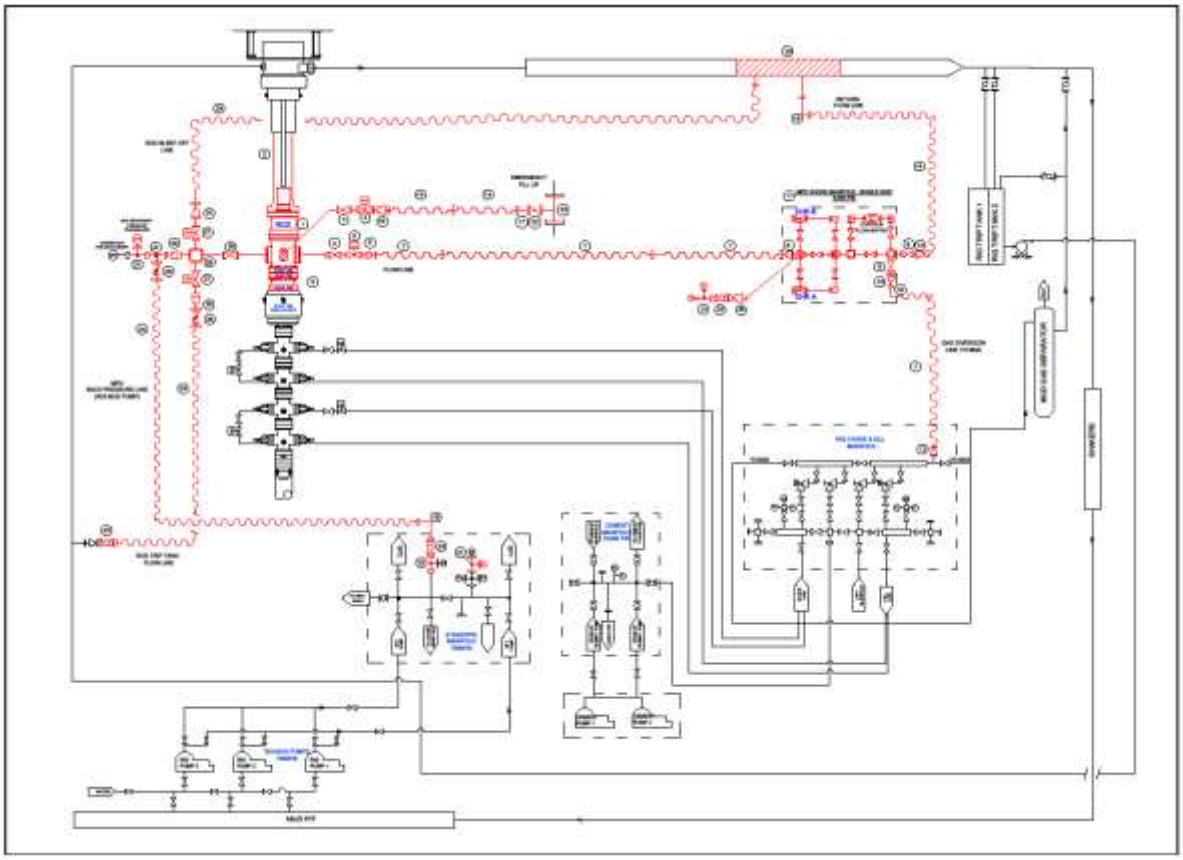

Figure 6: Piping and Instrumentation Diagram.

PROCEEDINGS
JOINT CONVENTION BANDUNG (JCB)2021
November 23rd – 25th 2021

EVALUATION OF LOSS CIRCULATION TREATMENT IN WELL Z-5, Z-10, Z-12 AND Z-13 AT L FIELD

Muhammad Zulka

Abstract

Loss circulation is a problem of partial or complete loss of the drilling fluid into the formation, causing fluid circulation becomes impaired. This final assignment will discuss about the loss of circulation in field L. There are 4 development wells in field L, which is Z-5, Z-10, Z-12, and Z-13. Some loss circulations in some depths are caused by natural factors. Some depths during loss circulation being evaluated are in Cisubuh and Parigi formations with limestone rock and claystone rock lithology, which have a large pore size in the drilling mud to enter and loss into the formation.

Treatment loss circulation in this field is blocking with loss circulation material with various compositions. However, some depths after the LCM blockage has not been successfully handled, so the cementing plug process is performed to overcome the loss circulation. The treatment that carried out in the loss zones have been successfully stopped the loss circulation, so that the drilling process can be continued to reach the desired final depth of the well.

Keywords: Loss Circulation, Natural Fracture, Treatment, Lithology, Loss Circulation Material, Cementing Plug

Introduction

Field L is part of the Northwest Java Basin which was formed due to the rifting phase in the Eocene period and is also the edge of the Sundaland continent. The Northwest Java Basin consists of 4 depocenters, namely the North, Central, South Arjuna sub-basins, and the Jatibarang sub-basins. The depocenter is filled predominantly by Tertiary sediment deposits with a thickness of more than 5500 meters.

Field L is located in the Talang Akar and Baturaja formations. The Talang Akar Formation contains quartz sandstone, shale, coal and there is a small amount of limestone which is located alternately. Meanwhile, the Baturaja formation contains carbonate rocks and is used as a significant seismic marker for the L field. For the depositional environment, this formation comes from a deltaic environment and there are also fluvial deposits.

Based on the Tertiary stratigraphy region, there are 6 formations in the Northwest Java Basin, namely Banuwati/Jatibarang, Talang Akar, Baturaja, Main-Massive, PreParigi-Parigi, and Cisubuh. For the Talang Akar, Baturaja, Main-Massive, and Parigi formations, they act as effective traps for hydrocarbon accumulation.

Loss circulation is most or all of the drilling fluid into the formation so that the fluid circulation is not perfect. In general, the loss of circulation occurs because the hydrostatic pressure of the mud is greater than the formation pressure so that the mud enters the formation.

In this study, we will discuss how the circulation loss occurs, as well as take effective countermeasures so that drilling can be resumed. Well Z in L is a development well located in the west of the Java Sea, close to the Thousand Islands. These wells will penetrate the Cisubuh, Parigi, Baturaja, Talang Root, Jatibarang and Basement formations. In wells Z-5 and Z-10 there is a loss circulation on the 17-1/2" route, while in wells Z-12 and Z-13 there is a loss circulation on the 12-1/4" route with the types of loss namely total loss and partial loss so that Circulation loss is handled by lowering pump pressure, reducing material loss circulation, and cementing plugs.

Loss circulation is the loss of a number of drilling fluids that enter the formation, caused by the presence of open spaces in the formation that exceed the diameter of the mud particles or caused by the borehole pressure is too high that exceeds the formation fracturing pressure.

Open space formations which are natural conditions are usually found in permeable sand formations with coarse grains and are not well consolidated. Caves or open cavities are found in compact formations, while natural fractures can be found in every rock layer. This type of fractured rock is often found in geothermal areas.

Sometimes the loss of circulation is also caused by the drilling operation itself. This is caused by the borehole pressure that is too high due to the pressure of the mud column in the borehole and the addition of pressure from the mechanical pressure that occurs during the drilling operation, thus exceeding the fracture pressure. Loss of circulation is a serious and expensive problem to treat. This problem occurs in the drilling area, depth, rock type and geological age of the rock.

Loss circulation can be caused by the type of formation, namely because of the type of porosity and large permeability and the presence of caves and formation fractures.

PROCEEDINGS
JOINT CONVENTION BANDUNG (JCB)|2021
November 23rd – 25th 2021

In terms of formation, mud loss can occur in Coarsely permeable formations (formations with permeable coarse grains), Cavernous formations (open caves), fissures, fractures, faults.

The occurrence of lost mud circulation can be classified according to the amount or volume of mud lost into 3 types, namely Seepage losses, Partial losses and Total losses.

Seepage is when the mud is lost in relatively small amounts, ranging from 1-10 bbl/hour, it can occur in every type of formation consisting of porous sand and gravel, natural fractures and in formations with fractures (limestone) and induced fracture (fracturing is not natural).

Partial is the occurrence of mud that is only partially lost and there is still mud flowing to the surface. The mud that has the potential to be lost to the formation will range from 10-500 bbl/hour. Generally it can occur in formations consisting of porous sand and gravel, and occasionally occurs in rocks containing fractures (natural fractures and fractures induced).

Complete is the total loss of mud or no return of mud to the surface. There will be a decrease in hydrostatic pressure, which can cause a well kick.

This problem has the potential to occur in formations that contain caves as well as very large fractures and formations with subnormal pressure.
Loss circulation can cause several problems and losses, for example: Loss of mud, danger of pipe jamming, formation damage, lost time, not getting cuttings for sample logs, subsidence of mud surface can cause blowout in the next formation.

To avoid problems that arise due to loss circulation, it must be prevented or overcome when it occurs. Some methods that can be used to overcome circulation loss are:

- Reducing Pump Pressure
- Reducing Sludge Weight
- Increases Viscosity and Gel Strength
- Reducing Borehole Surge Pressure
- Loss Circulating Material (LCM)
    - Fibrous Material
    - Material Flakes
    - Granular Material
- Cement
- Blind Drilling

Data and Method

The purpose of this research is to evaluate whether the cause of loss circulation is caused by natural factors or caused by mechanical factors such as hydrostatic pressure, the value of Equivalent Circulating Density, Bottom Hole Circulating Pressure, and Pressure Surge. Thus, from this analysis, it is possible to determine what methods are appropriate to overcome problems in loss circulation in the L field.

Leak Off Test is performed to determine the pressure at which the formation begins to fracture. The goal is to determine the maximum surface pressure and maximum mud weight.

The calculation of equivalent circulating density and bottom hole circulating pressure is carried out to determine whether ECD and BHCP pass the formation fracture pressure or not.

Calculation of pressure surge is carried out to determine whether this surge pressure exceeds the fracture pressure or does not exceed the fracture pressure. Here is the result of the calculation.

Result and Discussion

Loss circulation problems in this field occur in wells Z-5, Z-10, Z-12 and Z-13 and are found in various formations in the field. Loss circulation in this field can be caused by various obstacles, some of which occur due to the type of formation that has coarse-grained rocks and can also occur due to pressure factors. The rock lithology in these wells is dominated by limestone so that there are natural fractures and has a low formation pressure gradient. It is important to evaluate the physical properties of the drilling mud and the use of loss circulation material used in drilling this well. In the wells in field L there is a loss of circulation and the types of losses are partial loss and total loss, and the amount is different. In Table 4.1 the following is a table of data on the number of losses, types of losses and formations contained in Field L:

Table 4.1
Loss Circulation on Field L

Well	Traject	Depth	Formation	loss	MW
	inch	Ft TVD		bph	ppg
Z-5	17-1/2	928	Cisubuh	400	9
Z-5	17-1/2	1104	Cisubuh	Total	9
Z-10	17-1/2	409	Cisubuh	200	9
Z-10	17-1/2	800	Cisubuh	300	9,2
Z-12	12-1/4	1998	Parigi	60	9,2
Z-12	12-1/4	2325	Parigi	60	9,3
Z-13	12-1/4	2531,5	Parigi	Total	9,3
Z-13	12-1/4	2614,4	Parigi	79	9,2

PROCEEDINGS
JOINT CONVENTION BANDUNG (JCB)2021
November 23rd – 25th 2021

Loss circulation will hinder the drilling operation so that an analysis is carried out to determine the cause of the lost circulation. Therefore, the calculations carried out are the calculation of Hydro-static Pressure (Ph), Formation Pressure (Pf), Formation Fracture Pressure (Pfr), Equivalent Circulating Density (ECD), Bottom Hole Circulating Pressure (BHCP), and Pressure Surge (Psurge). Calculation of formation fracture pressure using equation (3.16).

Meanwhile, to calculate the hydrostatic pressure of the mud at the time of loss using equation (3.14), and to calculate the formation pressure can use equation (3.13).

Table 4.2 below shows the results of the calculation of formation fracture pressure, hydrostatic pressure and formation pressure in Field L:

Table 4.2
Result Pressure in Field L

Well	**Depth**	**Pfr**	**ρmax**	**Phyd when loss**	**Pf**
	Ft TVD	**psia**	**ppg**	**psia**	**psia**
Z-5	928	532,30	11,03	434,3	334,46
Z-5	1104	614,67	10,71	516,67	370,01
Z-10	409	241,41	11,35	191,41	157,62
Z-10	800	582,72	14,01	382,72	474,08
Z-12	1998	1160,84	11,17	955,84	742,26
Z-12	2325	1329,37	11	1124,37	831,55
Z-13	2531,5	1446,23	10,99	1224,23	903,60
Z-13	2614,4	1472,73	10,83	1250,73	901,89

The bottom hole assembly used in the 928 ft TVD depth is 17-1/2" BHA. The calculations carried out are the calculation of the velocity of the mud flow in the annulus using equation (3-8) and the critical flow velocity in the annulus with equation (3-9), as well as calculating the pressure loss with equation (3-10).

In Table 4.3 below are the results of the calculation of flow velocity and critical velocity at a depth of 928 ft TVD in well Z-5:

Table 4.3
Annual Velocity and Critical Velocity on 928 ft TVD

BHA	Va	Vc	Ploss
	ft/min	ft/min	psia
Sperry Lobe	114,70	384,17	0,27
Float Sub	101,14	366,25	0,01
NMDC	101,14	370,29	0,05
LWD	103,95	370,29	0,14
Power Pulse	103,95	361,50	0,19
NMDC	98	366,25	0,18
UBHO Sub	101,14	364,99	0,02
Over Sub	100,28	348,87	0,02
HWDP	90,66	348,87	0,86
Drilling Jar	92,80	352,84	0,16
Drill Pipe	87,11	341,54	4,26

So that the value of the velocity of the mud flow in the annulus, the critical velocity and the value of the pressure loss are obtained. So the total pressure loss at a depth of 928 ft TVD is 6.17 psia. The bottom hole assembly used at a depth of 409 ft TVD is BHA 17-1/2".

In Table 4.4 the following are the results of the calculation of flow velocity and critical velocity at a depth of 409 ft TVD in well Z-10:

Tabel 4.4
Annual Velocity and Critical Velocity on 409 ft TVD

BHA	Va	Vc	Ploss
	ft/min	ft/min	psia
Drilling Motor	52	326,29	0,06
Stabilizer	65,74	401,90	0,04
NMDC	65,74	401,90	0,12
LWD	66,86	405,57	0,11
Power Pulse	66,86	405,57	0,15
NMDC	65,74	401,90	0,13
UBHO Sub	65,74	401,90	0,01
X-Over Sub	65,74	401,90	0,02
HWDP	56,62	365,98	0,58
Drilling Jar	60,32	382,29	0,13
Drill Pipe	56,62	365,98	2,21

So, the total pressure loss at 409 ft TVD is 3.54 psia. The bottom hole assembly used in the 1998 ft TVD depth is 12-1/4" BHA.

In Table 4.5 the following are the results of the calculation of flow velocity and critical velocity at a depth of 1998 ft TVD in well Z-12:

Table 4.5
Annual Velocity and Critical Velocity on 1998 ft TVD

BHA	Va	Vc	Ploss
	ft/min	ft/min	psia
Drilling Motor	384	592,15	2,95
MWD Sub	268,90	536,37	0,12
MWD Ontrack	268,90	536,37	0,83
MWD Modular	268,90	536,37	0,27
MWD BCPM	268,90	536,37	0,51
MWD Top	268,90	536,37	0,12
NMDC	256,21	528,79	1,03
X-Over Sub	268,90	536,37	0,16

HWDP	184,04	474,35	8,46
X-Over Sub	214,50	500,42	0,08
Drilling Jar	204,52	492,55	0,74
X-Over Sub	214,50	500,42	0,09
Drill Pipe	184,04	474,35	7,85

So the total pressure loss at 1998 ft TVD is 23.20 psia. The bottom hole assembly used at a depth of 2531.5 ft TVD is BHA 12-1/4".

In Table 4.6 the following is the result of calculating the flow velocity and critical velocity at a depth of 2531.5 ft TVD in well Z-13:

Table 4.6
Annual Velocity amd Critical Velocity on 2531,5 ft TVD

BHA	Va	Vc	Ploss
	ft/min	ft/min	Psia
Drilling Motor	405,33	580,73	2,71
MWD Sub	283,84	500,21	0,10
MWD Ontrack	283,84	500,21	0,70
MWD Modular	283,84	500,21	0,23
MWD BCPM	283,84	500,21	0,43
MWD Top	283,84	500,21	0,10
NMDC	270,44	489,58	0,84
X-Over Sub	283,84	500,21	0,14
HWDP	194,26	415,56	6,29
X-Over Sub	226,42	450,49	0,06
Drilling Jar	215,88	439,85	0,59
X-Over Sub	226,42	450,49	0,07
Drill Pipe	194,26	415,56	5,91

So the total pressure loss at a depth of 1998 ft TVD is 18.17 psia.

Equivalent Circulating Density (ECD) and Bottom Hole Circulating Pressure (BHCP) which exceed the formation fracture pressure will cause the formation to fracture and cause drilling fluid to enter the formation. After calculating the total pressure loss that occurs in each drilling series in the lost circulation zone, the ECD value can be calculated using equation (3-11) and also the BHCP value (3-12).
In Table 4.7 the following are the results of the ECD and BHCP calculations for wells Z-5, Z-10, Z-12, and Z-13:

Table 4.7
ECD and BHCP in Field L

Well	Traject	Depth	ECD	BHCP
	inch	Ft TVD	ppg	Psia
Z-5	17-1/2	928	9,13	440,47
Z-5	17-1/2	1104	9,08	521,24
Z-10	17-1/2	409	9,17	194,96
Z-10	17-1/2	800	9,30	386,90
Z-12	12-1/4	1998	9,42	979,04
Z-12	12-1/4	2325	9,50	1148,05
Z-13	12-1/4	2531,5	9,44	1242,41
Z-13	12-1/4	2614,4	9,33	1268,90

Pressure Surge is the pressure that occurs when inserting the drill string into the drill hole. The nature of the mud and the procedure for inserting the tool must be controlled and observed so that the pressure surge is not too high. A pressure surge that is too high can cause the formation to fracture and drilling mud into the formation, this can also be one of the causes of loss circulation. Calculation of the pressure surge in the Z-5 well is done by determining the fluid velocity with the equation (3-7), the flow velocity (Va), determining the maxi-mum pipe velocity (Vm) with the equation (3-21), and determining the pressure loss (Ps) with equation (3-22). The pressure surge value can be calculated using the equation (3.23).

In Table 4.8 the following are the results of the calculation of the pressure surge in Field L:

Table 4.8
Pressure Surge in Field L

Well	Depth	N	k	Ploss Total	Psurge
	Ft TVD			psia	psia
Z-5	928	0,41	4,22	7,27	441,57
Z-5	1104	0,41	4,22	5,38	522,05
Z-10	409	0,51	3,10	4,36	195,77
Z-10	800	0,51	3,10	5,14	387,86
Z-12	1998	0,38	6,44	27,07	982,91
Z-12	2325	0,38	6,44	27,63	1152,00
Z-13	2531,5	0,52	2,64	22,47	1246,70
Z-13	2614,4	0,52	2,64	22,47	1273,20

In the Z-5 well at a depth of 928 ft TVD and 1104 ft TVD loss circulation occurs, therefore, countermeasures are carried out so that the loss does not occur again.

When making holes 17 - 1/2" at a depth of 928 ft TVD found a dynamic loss of 400 bpd. Handling is done by stopping the pump and observing a static loss of 120 bpd. Then mixing 50 bbls stop loss, pump again with 20 bbls Hi-Vis + 50 bbls stop loss + 10 bbls Hi-Vis. When the stop loss is immersed for 1 hour the well is observed to be static, then the bit is removed until the shoe is 30" Conductor pipe at a depth of 380 ft MD, and the pump pressure is raised again to 1000 gpm so that dynamic loss does not occur again.

While continuing to make holes 17 - 1/2" at a depth of 1104 ft TVD, there was a total loss of circulation. The initial treatment was to lower the pump pressure from 900 gpm to 300 gpm. After observing the loss to 395 bpd. The next treatment is by pumping the LCM (20 ppb Fibroseal M + 20 ppb CaCO3 M), then increasing the pump pressure to 1000 gpm so that dynamic loss does not occur again.

In the Z-10 well at a depth of 409 ft TVD and 800 ft TVD loss circulation occurs, therefore, countermeasures are carried out so that the loss does not occur again. At a depth of 409 ft TVD, a dynamic loss of 200 bpd was found. The treatment was carried out by pumping 50 bbls LCM (20 ppb CaCO3 M + Fibroseal M) 3 times and performing Cement Plug 3 times. The first cement plug was carried out by pumping 10 bbls of seawater and 110 bbls of cement slurry. The second cement plug is carried out by pumping 10 bbls of seawater and 140 bbls of cement slurry. The third cement plug is carried out by pumping 172 bbls of cement slurry, so that the lost circulation can be overcome and the hole making can be resumed. At a depth of 800 ft TVD a dynamic loss of 300 bpd occurs. Handling is done by lowering the pump pressure to 400 gpm, but the loss of circulation only decreases slightly to 270 bph. Then re-spot LCM (20 ppb CaCO3 M + 30 ppb Fibroseal M and perform a cementing plug with a composition of 10 bbls sea water +170 bbls cement slurry so that lost circulation can be overcome.

In the Z-12 well at a depth of 1998 ft TVD and 2325 ft TVD loss circulation occurred, therefore countermeasures were carried out to prevent the loss from occurring again. When making a 12-1/4 hole from a depth of 2440 ft to 2827 ft MD/2048 ft TVD with a pump pressure of 850/900 gpm, a dynamic loss at a depth of 1998 ft was found at 60 bpd. The handling is done by reducing the flow rate from 930 gpm to 900 gpm, after observing that there is no static loss. And when reducing the flow rate again to 850 gpm the dynamic loss was successfully overcome so that the hole making could be resumed. The depth that experienced the next loss of circulation was a depth of 2325 ft TVD. At this depth there is a dynamic loss of 60 bpd, by pumping the LCM and reducing the pump pressure to 850 gpm, the loss of circulation has been overcome.

In the Z-13 well at a depth of 2531.5 ft TVD and 2614.4 ft TVD loss circulation occurs, therefore countermeasures are carried out so that the loss does not occur again. At a depth of 3667 ft MD / 2531.5 ft TVD total dynamic loss was found, so a cement plug was performed by pumping 5 bbls DW spacer and test lines up to 1000 psi. The circulation is stopped slowly until the pump pressure becomes 200 gpm and the pump rate is raised again to 800 gpm so that the loss can be overcome. Dynamic loss was initially 93 bpd at 3632 ft depth and increased to 120 bpd at 3667 ft MD. By lowering the pump pressure, the loss of circulation at this depth can be overcome. The next depth that experienced loss of circulation was 2614.4 ft TVD, found a dynamic loss of 79 bpd so a cement plug was performed by pumping 5 bbls DW spacer and test lines up to 1000 psi. The next step is to lower the pump pressure to 850 gpm so that the dynamic loss at this depth can be overcome.

Conclusions

Some of the conclusions obtained from the results of this research that have been carried out are as follows:

1. Based on the depth analyzed in field L, the types of losses that occur are partial loss and total loss. By lowering the pump pressure, pumping out lost circulation material (Fibroseal and CaCO3), and performing a cementing plug so that the lost circulation at any depth in the L field was successfully overcome.
2. Based on the leak off test (LOT) data conducted on the Z-5 well, the formation will fracture at 10.91 ppg. While the LOT carried out on the Z-10, Z-12, and Z-13 formations will fracture at 16.91 ppg, 11.49 ppg, 11.07 ppg. The leak off test data is used as an evaluation limit of the ECD and BHCP values.
3. The addition of mud density called equivalent circulating density in the Z-5 well at a depth of 928 ft TVD is 9.13 ppg and at a depth of 1104 ft TVD is 9.08 ppg. Meanwhile in the Z-10 well at a depth of 409 ft, which is 9.17 ppg and at a depth of 800 ft, TVD is 9.30 ppg. So it can be interpreted that the ECD value in the Z-5 well and the Z-10 well does not exceed the maximum mud density value limit.
4. The formation fracturing pressure found in the Z-12 well at a depth of 1998 ft is 1160.84 psia and at a depth of 2325 ft is 1329.37 psia. Meanwhile, the value of the formation fracture pressure in the Z-13 well at a depth of 2531.5 ft is 1446.23 psia and at a depth of 2614.4 ft is 1472.73 psia.
5. In the Z-12 well, the pressure caused by the addition of mud density (BHCP) at a depth of 1998 ft is 979.04 psia and at a depth of 2325 ft the BHCP value is 1148.05 psia. Meanwhile, in the Z-13 well, the BHCP value at a depth of 2531.5 ft is 1242.41 psia and at a depth of 2614.4 ft the BHCP value is 1268.90 psia. This indicates that the BHCP value for each depth does not exceed the fracture pressure of the existing formation.
6. In wells Z-5 and wells Z-10 circulation is lost due not to mechanical factors but due to the type of formation. The type of formation is the Cisubuh Formation with its rock lithology, namely clay-stone which has large pores and is interconnected, causing loss of circulation.
7. Based on the results of calculations that have been carried out on wells Z-12 and wells Z-

13, that the loss of circulation is not due to the weight of the mud, pumping pressure and even pressure surges, but is caused by the formation, namely the Parigi formation with limestone rock lithology. has a large and interconnected porosity that can cause drilling fluids to be lost into the formation.

References

1. AADE, "Review of Loss Circulation Materials and Treatments with an Updated Classification", Guston, Texas, 2014.
2. "Daily Mud Report", PT PHE ONWJ. Jakarta, 2014.
3. "Daily Operational Report", PT PHE ONWJ. Jakarta, 2014.
4. Lapeyrouse, Norton J. "Formulas and Calculations for Drilling Production and Workover", Gulf Publishing Company, Houston, Texas, 1982.
5. Rubiandini, Rudi, "Teknik Operasi Pemboran", Departemen Teknik Perminyakan, ITB, Bandung, 2012.
6. Rubiandini, Rudi, "Teknik Pemboran Lanjut", Departemen Teknik Perminyakan, ITB, Bandung, 2012.

PROCEEDINGS
JOINT CONVENTION BANDUNG (JCB)2021
November 23rd – 25th 2021

Reactivation of Gas Well With Lower Master Valve Problem Using Hottapping Method

Reza Alfajri[1], Sakti Parsaulian Siregar[1]
Pertamina[1]

Abstract
Lower master valve is the most crucial part of a christmas tree in a producing well. This valve is directly connected to the well, which means it has direct contact with pressured fluid from reservoir. Therefore, excellent condition for lower master valve is a must.

M-03 is a gas well in M structure Pertamina that had failure in its lower master valve. This well was forced to stop producing due to problem in lower master valve. The disk in the lower master valve was stuck in closed position so that the well couldn't produce. The problem escalated once the valve's condition deteriorated. It started leaking gas that made a hazard to the surroundings. For safety reason, an action needed to be taken, however there was no path to kill the well. An alternative solution was needed to solve the problem.

In order to stop gas leak and recover production, hottapping method to make a hole in the lower master valve's disk was performed. First scaffolding is needed for safety during operation. For this, hoist rotary table was used. Another master valve was added to be the new lower master valve, ignoring the broken original lower master valve. Hottapping assembly was installed above this valve, the rest of the christmas tree was taken down. The drill inside hottapping assembly was moved by air compressor. Once the operation finished, a path for production in the stuck disk was made, christmas tree was reinstalled with one added master valve, flow line was modified, and well was producing again safely (no more gas leak). This solution regained production from well M-03 of 1.5 MMSCFD gas as well as stopping HSSE hazard (gas leak) from the well.

Having this method as a solution provide safety nets if the same problem ever happened at other wells in Pertamina. HSSE problem is something that could not be taken lightly in oil and gas industry. This project served that purpose as well as put the well back into production, which ultimately affected company's sales revenue.

Introduction
The loss of well integrity can result in major accidents and presents a severe risk to the environment (Raj 2014). No matter how old a well is, well integrity still needs to be maintained. M Structure in Pertamina was a gas structure with 30 MMSCFD gas and 350 bopd condensate production. This structure had 17 wells with 13 producing wells. Well M-03 is one of those 13 producing wells in M Structure. This well was shut in for quite a long time with last production of 3 MMSCFD and 20 bbls/day condensate. This well had a broken lower master valve that could not be opened. Beside of suspended production due to this problem, safety aspect needed to be considered. With average tubing pressure of 970 psi, this well needed to be put back on production to prevent any outside disturbance that can put safety at risk. Figure 1 shows the condition of suspended well M-03.

Figure 1 Well M-03 Condition

Well integrity is "the qualification that testifies to the well's sound capability to perform its function to contain and control the flow of fluids within the predetermined barriers throughout its designed life" (Sultan 2009). Since lower master valve in well M-03 could not perform its function, it means that M-03 had well integrity problem. Therefore well intervention was needed.

Data and Method
The condition of Well M-03 was active reservoir with perforated interval and complete production string. Estimated tubing string from this well was quite high (> 900) psi. There were two options that could be taken to solve this problem: kill or reactivate the well. In order to perform either options, connection from surface to reservoir was needed. Killing the well straight away could not be performed because no pathway from string due to stuck disk in the lower master valve. Killing from the well's annulus was also negative due to the presence of packer in the production string. Therefore, creating pathway safely through the stuck disk in existing lower master valve was chosen as solution.

The next consideration was either to kill or reactivate the well. Killing the well would mean giving disturbance to an active natural flow reservoir, something that should be avoided without emergency reasons. Bearing that in mind, after creating pathway in the problematic lower master valve, a new x-mas tree would be installed to safely reactivate the well.

The stuck disk in the lower master valve would be drilled to create a hole with sufficient size that considered inside diameter of the valve (3-1/8"). In order to perform this job safey, job safety analysis was laid out and some mitigations would be taken as precautions:

- With a quite high average tubing pressure of 970 psi and an active gas reservoir below, drilling the disk

PROCEEDINGS
JOINT CONVENTION BANDUNG (JCB) 2021
November 23rd – 25th 2021

should be performed with proper equipments that can handle high pressure and a good condition. Based on the requirements, drilling machine D-904 that can handle up to 2,200 psi at 100^0 F was selected. The pressure capacity that was alsmost twice the average tubing pressure in M Structrure was selected to accommodate the actual range of tubing pressure in M Structure, which was 900 – 1500 psi. Traveling bar of the machine was 28" in length, with a twist drill was 8.5" long and 1" diameter.

- Before performing the job, an isolation valve was installed above the stuck master valve so that when the job was finished, travelling bar of the drilling machine could be safely extracted, the well could be temporarily shut in to release remaining pressure and gas above the isolation valve, and the rest of new x-mas tree could safely be installed.
- The job would be performed at height more than 2 meters, so scaffolding was needed. The scaffolding should be firm and stable enough to perform the job. Furthermore, clearance from the stuck valve to the surface of the scaffolding must be enough to accommodate drilling machine. The scaffolding should also be not too high so that the drilling machine could be operated safely and comfortably on the scaffolding. Rig/hoist rotary table met all of these requirements and would be used as the scaffolding during the job.
- Since the strength of valve disk material should be strong enough to handle up to 1500 psi pressure, drilling job should be taken quite some time and could not be performed solely on human strength. An air compressor would be utilized as a prime mover for the drilling machine.
- Fluid inside the drilling machine and master valve was needed for cooling and lubrication. Lubricant would be used as the fluid.
- All the equipments that would be directly in contact to pressure from the reservoir should passed pressure test on maximum estimated pressure when drilling job finished.
- All the safety documents should be provided and discussed before executing the job, and revisited in pre job safety meeting on site.

In summary, job procedure of drilling the stuck disk valve were as follow:

- Clean and dry the stuck disk valve.
- Nipple up isolation valve on top of the stuck valve.
- Setting scaffolding (rotary/hoist table) surrounding Well M-03 wellhead
- Prepare drilling machine, connect twist drill to the machine.
- Nipple up drilling machine on top of the isolation valve.
- Pressure test drilling machine and isolation valve.
- Connect air compressor and execute the job.
- When the drilling finished, extract travelling bar back into the drilling machine, close isolation valve, bleed off pressure from needle valve on the drilling machine.
- Nipple up new x-mas tree (isolation valve as new lower master valve).
- Connect line to Emergency Shut Down Valve (ESDV), put the well back on production.

Figure 2 shows the description of D-904 drilling machine. As shown in Figure 2, since the stuck master valve was a flange type master valve, threaded valve adapter was not used. Also instead of hole saw, twisted drill was utilized. Figure 3 to 11 show job execution along with the explanation.

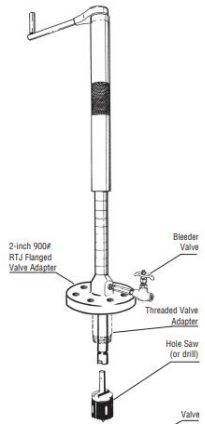

Figure 2 D-904 TD Williamson Drilling Machine

Figure 3 Stuck disk of the problematic lower master valve

Before the job, the above part of the master valve was cleaned and dried so that no debris on the soon to be drilled valve's disk.

Figure 4 Installation of Isolation Valve on Top of the Stuck Valve

PROCEEDINGS
JOINT CONVENTION BANDUNG (JCB)2021
November 23rd – 25th 2021

Figure 5 Setting Scaffolding (Rotary Table)

Figure 6 Setting D-904 Drilling Machine, Complete with Twist Drill

Figure 7 Installing Drilling Machine on Top of the Isolation Valve

Figure 8 Pressure Test Drilling Machine and Isolation Valve

Figure 9 Execution of Drilling the Stuck Disk

Figure 10 Well M-03 was Back on Production after Drilling the Stuck Valve

After the well was put back into production, well test and monitoring was performed to evaluate the newly back on production Well M-03.

Result and Discussion

Well test and monitoring was performed after Well M-03 was back on production. Figure 11 shows production performance before and after the job.

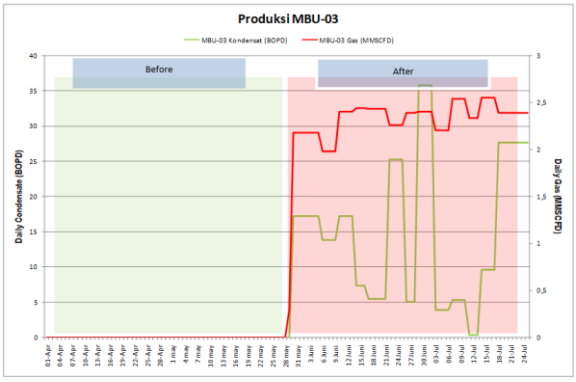

Figure 11 Well M-03 Production Performance Before and After the Job

It can be seen that average production of Well M-03 was 2.34 MMSCFD and 14.91 bopd.

Gas handling in Gas Compressing Station in M structure has maximum allowable gas temperature to be allowed entry, which was 130^0 F. Average temperature of Well M-03 was 120^0 F, hence the restriction did not apply for its gas.

PROCEEDINGS
JOINT CONVENTION BANDUNG (JCB)2021
November 23rd – 25th 2021

Therefore, putting Well M-03 successfully added the whole structure gas production from 29.98 to 31.34 MMSCFD. Figure 12 shows M Structure gas production before and after putting Well M-03 back on production.

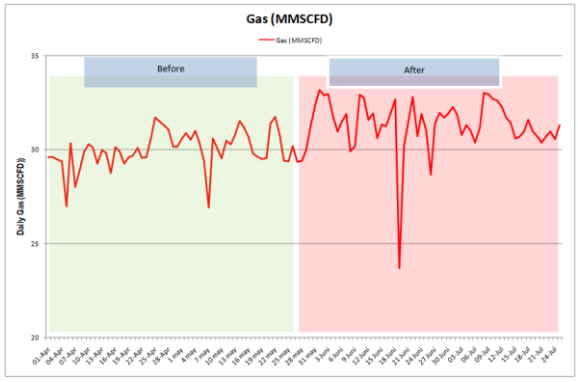

Figure 12 M Structure Production Performance Before and After Reactivating of Well M-03

Figure 11 and 12 show that this project was successfully carried out safely. Aside from economical aspect of added gas production, safety aspect in term of well integrity was also successfully regained. Furthermore no disturbance to the active gas reservoir, so this method was also a success in reservoir management aspect.

Conclusions

Reactivation of Well M-03 by performing drilling stuck disk of lower master valve was a success in economics, safety, and also technical aspect in oil and gas industry. It would be wise to prevent the same thing from happening in the future by performing good housekeeping and equipment maintenance for each producing well. However, if the same were unavoidable, this method would be the solution.

References

Raj, M., 2014, Well Integrity - Christmas Tree Acceptable Leakage Rate and Sustained Casing Pressure, Symposium Series, **159**, 1–13.

Sultan, A. A., 2009, Well Integrity Management Systems; Achievements versus Expectations, presented at the International Petroleum Technology Conference, Doha, Qatar.

Acknowledgements (Optional)

Our gratitude to all of our comrades in Pertamina and all parties involved for the collaboration effort to make this project successful.

PROCEEDINGS
JOINT CONVENTION BANDUNG (JCB) 2021
November 23rd – 25th 2021

Efforts to Reduce Sulfur CPP Gundih Operational Costs With Changes in Environmental Permits From Handling Sulfur in B3 Waste To Non B3 Waste Through Sulfur Characteristic Test PT. Pertamina EP Field Cepu

Ardi, Hadi Akmalunas, Adha Bayu Wijaya, A. Zainal Abidin, Adiguna Candrawisesa Heriwijaya, Astika Titistiti, Bayu Laksono Putro

Abstract
PT. Pertamina EP Field Cepu owns a gas field along with gas purification facilities in the form of the Gundih Central Processing Plant (CPP) which is the backbone with a gas production figure of 70 MMSCFD, gas sales figure of 50 MMSCFD, condensate of 500 BCPD and sulfur pellets of 8-12 tons/ day. Currently, sulfur handling costs are relatively large, reaching 25 billion/year. CPP Gundih sulfur is produced with the aim of reducing H2S levels in the process, with limitation if burned it will become SO2 with maximum value of 2600 mg/Nm3 accordance *Kep/MenLH/129/2003*. The process of reducing / managing H2S at CPP Gundih is by converting H2S into Elemental Sulfur (S8) using bacteria in the Biological Sulfur Recovery Unit (BSRU).

The specification of sulfur purity level reaches 97% which can be categorized as a selling value product. The current condition is that the management of sulfur is constrained by issues of licensing and corporate taxation so it does not generate revenue or reduce production costs for the company. Based on the applicable Gundih environmental permit, namely the Environmental Permit for East Java Gas Development Activities in the Kedungtuban, Randublatung and Kedunglusi – Gundih Areas, on page. 24 no. 8 and the above conditions, the sulfur management at CPP Gundih is managed as waste B3 resulting in the cost of handling the sulfur being expensive, which is Rp. 5 Million/Ton or Rp. 25 Billion/Year.

The most efficient way to reduce the cost of sulfur handling, is change the environmental permit regarding the handling of sulfur which was originally B3 waste by law into non-B3 waste. Changes in the sulfur environmental permit regarding non-B3 waste management of sulfur reduces the cost of handling sulfur to Rp. 1.3 Million/Ton or Rp. 6.5 billion/year so that it has a cost saving impact of Rp. 3.7 Million/Ton or Rp. 18.7 billion/year and the potential for the utilization of sulfur into derivative materials that are more valuable, such as asphalt and paving.

Introduction

The H2S gas content in the Gundih field of 5200 ppm must be reduced to a maximum of 6 ppm as required by the gas sales PJBG. The process of decreasing the H2S content is through absorption on the H2S Absorber which uses the caustic NaOH solvent. Then the H2S is converted into elemental sulfur (S8) using thiobacilus microbes in the bioreactor at BSRU. The elemental sulfur is then concentrated and formed into sulfur pellets in the Melter Sulfur Pelleting & Packaging (MSPP) unit. The content should not be released into the open air nor should it only be burned in a Thermal Oxidizer (TOx) with a maximum SO2 content limit of 2600 Mg/NM.

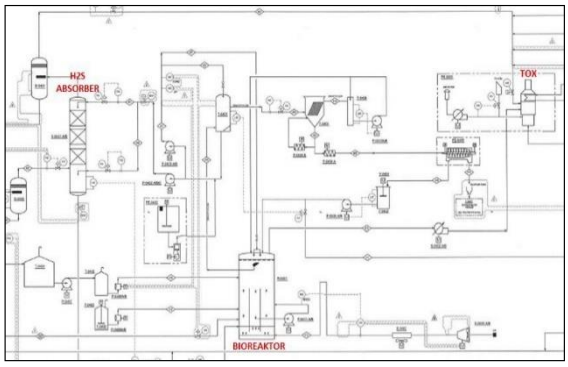

Figure 1: PFD BSRU, showing the position of the unit that plays a role in the absorption of H2S and converts H2S into Elemental Sulfur.

In accordance with the applicable environmental permit, namely Kep/MenLH/129/2003 concerning Environmental Permits for East Java Gas Development Activities in the Kedungtuban, Randublatung and Kedunglusi – Gundih Areas, on p. 24 no. 8, where sulfur management can be carried out as follows:

1. Sale / commercialization of CPP Gundih sulfur.
2. Cooperation with third parties who already have a permit from the Ministry of Environment / relevant agencies starting from storage in containers, temporary shelter, transportation to processing.

KEPUTUSAN MENTERI LINGKUNGAN HIDUP REPUBLIK INDONESIA
NOMOR 437 TAHUN 2013
TENTANG
IZIN LINGKUNGAN KEGIATAN PENGEMBANGAN GAS JAWA BAGIAN TIMUR
LAPANGAN KEDUNGTUBAN, RANDUBLATUNG
DAN KEDUNGLUSI-AREA GUNDIH
OLEH PT. PERTAMINA EP-PROYEK PENGEMBANGAN GAS
JAWA BAGIAN TIMUR (PPGJ)

					se pengolahannya.				
8.	Limbah padat sulfur dari Kegiatan Operasional CPP	Pemurnian kualitas air permukaan	a. PP No. 18 Jo No. 85 Tahun 1999 b. PP No. 82/2001 untuk Baku Mutu Air Kelas III	Memenuhi persyaratan pemurnian kualitasnya permukaan	Dijual atau hasil sama dengan pihak ketiga yang telah memiliki ijin KEMENTERIAN LINGKUNGAN HIDUP / instansi terkait mulai dari penyimpanan dalam kontainer, penampungan sementara, transportasi sampai ke pengolahannya.	Kompleks CPP	Selama kegiatan operasional CPP	PT. Pertamina EP-PPGJ	Pemerintah Kabupaten Blora	a. Instansi Pengelola Lingkungan Hidup Kabupaten Blora b. Bapedal Provinsi Jawa Tengah c. Dirjen Migas, Kementerian ESDM d. Kementerian Lingkungan Hidup
9.	Operasional CPP	Meningkatnya	Adanya tersimpanan	Memenuhi persyaratan					

Figure 2: Kep/MenLH/129/2003

Sulfur management by third parties uses Government Regulation no. 18 Jo No. 85 of 1999 concerning Management of Hazardous and Toxic Waste and Government Regulation no. 82 of 2001 concerning Water Quality Management and Water Pollution Control.

Alternative sale / commercialization of CPP Gundih sulfur ref. Minutes of Meeting (MoM) Discussion Meeting on the Status of Sulfur Gundih on June 4 2018, point no. 2, there is currently no decision on the form of cooperation in the sale and purchase of sulfur so that a follow-up meeting will be held which is coordinated with the OGM (Oil & Gas Monetization) function involving SKK Migas, the Ministry of Energy and Mineral Resources and the Ministry of Environment and Forestry.

PROCEEDINGS
JOINT CONVENTION BANDUNG (JCB) 2021
November 23rd – 25th 2021

Ref. Minutes of Meeting (MoM) Discussion of the Sulfur Sale and Purchase Agreement on 17 May 2017 between PT. Pertamina EP and SKK Migas, with the following information:

1. Background on the Value Added Tax on Goods and Services and Sales Tax on Luxury Goods ("VAT Law") related to the Sulfur Sale and Purchase Agreement (PJBS).
2. PEP conveys about the potential imposition of VAT on sulfur and CO2, as a by-product of hydrocarbons, which can result in the determination of the status of a Taxable Entrepreneur (PKP) to PEP with all the consequences.
3. SKK Migas conveyed about the approach that has been taken in handling sulfur in other KKKS Working Areas that categorize sulfur as waste (not a by-product) needs further study.
4. Follow-up actions include the following: PEP will conduct a study on sulfur as waste; SKK Migas will facilitate meetings with other KKKS for the purpose of studying sulfur handlers.

Measurement Condition

Instrument: EDX-8000 Atmosphere: Air Collimator: 10(mm)

Analyte	TG kV	uA	FI	Acq.(keV)	Anal.(keV)	Time(sec)	DT(%)
Al-U	Rh 50	69-Auto	----	0 - 40	0.00-40.00	Live- 100	30
C-Sc	Rh 15	342-Auto	----	0 - 20	0.00- 4.40	Live- 100	30

Quantitative Result

Analyte	Result	[3-sigma]	Proc.-Calc.	Line	Int.(cps/uA)
S	97.866 %	[0.140]	Quan-FP	S Ka	131.4569
Al	1.458 %	[0.094]	Quan-FP	AlKa	0.1480
Si	0.223 %	[0.027]	Quan-FP	SiKa	0.0783
P	0.151 %	[0.018]	Quan-FP	P Ka	0.1231
Cs	0.143 %	[0.021]	Quan-FP	CsLa	0.1174
K	0.141 %	[0.020]	Quan-FP	K Ka	0.3362
Cu	0.018 %	[0.001]	Quan-FP	CuKa	1.6400

Figure 3: Results of Analysis of Sulfur Purity by Study Center Gajah Mada University Energy.

Identitas	Penetapan	Hasil	Satuan	Metoda
275/20 – 2020002685 Padatan (**Sulfur #1**)	Sulfur	99.15	% wt	XRF
276/20 – 2020002686 Padatan (**Sulfur #2**)	Sulfur	99.12	% wt	XRF
277/20 – 2020002687 Padatan (**Sulfur #3**)	Sulfur	98.76	% wt	XRF

Figure 4: Report of Sulfur Content Laboratory Test Results by LEMIGAS.

Alternative sulfur management through cooperation with a third party that already has a permit by the relevant ministry is the chosen alternative which has a cost of up to Rp. 5 Million / Ton or Rp. 25 Billion / Year. The current condition of the sulfur pellets have sulfur purity levels of 97.866% - 99.78% which can be categorized as a selling value product.

Data and Method

With the spirit of cost saving in handling sulfur CPP Gundih, efforts are made to revise the environmental permit which originally used the B3 waste legislation to become Non B3 waste. The use of the approach method is as follows:

1. Test the characteristics of B3 waste by using the Toxicity Characteristic Leaching Procedure (TCLP) parameter.

LABORATORY TEST RESULT

JOB NUMBER: ENV-2190244 — Date : February 20, 2019
Customer : PT. PERTAMINA ASSET 4 CEPU FIELD — Attention: -

Customer Sample ID. : **Sulfur Sludge**
Location Coodinate : -
Date Sampled : 29/01/2019
Time Sampled : 11:55
Sample Matrix : Sludge

Laboratory Sample ID. : 2190244-3
Date Received : 30/01/2019
Time Received : 08:00
Interval Analysis : 30Jan - 11Feb

NO.	TEST DESCRIPTION	RESULT	REGULATORY LIMIT* TCLP - A	TCLP - B	UNIT	METHOD
	ANORGANIC PARAMETERS					
1	Antimony, Sb	0.144	6	1	mg/L	EPA 1311:1992,EI 36.098 (AAS)
2	Arsenic, As	0.02	3	0.5	mg/L	EPA 1311:1992,EI 36.098 (AAS)
3	Barium, Ba*	2.68	210	35	mg/L	EPA SW 846 6010
4	Berilium, Be*	< 0.02	4	0.5	mg/L	EPA 1311:1992,EI 36.098 (AAS)
5	Boron, B*	0.64	150	25	mg/L	EPA SW 846 6010
6	Cadmium, Cd	0.08	0.9	0.15	mg/L	EPA 1311:1992,SNI 6989.16:2009
7	Hexavalent Chromium, Cr^{6+}	0.07	15	3	mg/L	EPA 1311:1992,SNI 6989.71:2009
8	Copper, Cu	< 0.05	60	10	mg/L	EPA 1311:1992,SNI 6989.6:2009
9	Lead, Pb	0.08	3	0.5	mg/L	EPA 1311:1992,SNI 6989.8:2009
10	Mercury, Hg	< 0.00002	0.3	0.05	mg/L	EPA 1311:1992,EI 36.098 (AAS)
11	Molybdenum, Mo*	< 0.002	21	3.5	mg/L	EPA SW 846 7480
12	Nickel, Ni	0.14	21	3.5	mg/L	EPA 1311:1992,SNI 6989.18:2009
13	Selenium, Se	< 0.00007	3	0.5	mg/L	EPA 1311:1992,EI 36.098 (AAS)
14	Silver, Ag*	< 0.007	40	5	mg/L	EPA SW 846 6010
15	Tributyltin Oxide*	< 0.001	0.4	0.05	mg/L	Gas Chromatography-MS
16	Zinc, Zn	0.28	300	50	mg/L	EPA 1311:1992,SNI 6989.7:2009
	ANION					
17	Chloride, Cl	2	75000	12500	mg/L	EPA 1311:1992,SNI 6989.19:2009
18	Cyanide, CN	0.13	21	3.5	mg/L	EPA 1311:1992,EI 36.138 (AAS)
19	Fluorides, F-	< 0.05	450	75	mg/L	EPA 1311:1992,SNI 6989.29:2005
20	Iodide, I^-	< 0.01	40	5	mg/L	Spectrophotometric
21	Nitrate, NO_3^-	0.04	15000	2500	mg/L	EPA 1311:1992,SNI 6989.79:2011
22	Nitrite, NO_2^-	< 0.002	900	150	mg/L	EPA 1311:1992,SNI 06-6989.9:2004
	ORGANIC					
23	Benzene	< 0.2	3	0.5	mg/L	EI 36.093 (Gas Chromatography-FID)
24	Benzo pirene*	< 0.00019	0.004	0.0005	mg/L	Gas Chromatography-MS
25	Carbon tetrachloride*	< 0.0028	1.2	0.2	mg/L	EPA SW 846 8240
26	Chlorobenzene*	< 0.006	120	15	mg/L	EPA SW 846 8240
27	Chloroform*	< 0.0016	24	3	mg/L	EPA SW 846 8240
28	2-Chloro Phenol*	< 0.01	120	5	mg/L	Gas Chromatography-MS
29	Total Cresol*	< 0.001	800	100	mg/L	EPA SW 846 8270
30	2-Ethylheksil Ftalat*	< 0.004	2.4	0.4	mg/L	Gas Chromatography-MS
31	1,2-Dichlorobenzene*	< 0.004	300	50	mg/L	Gas Chromatography-MS
32	1,4-Dichlorobenzene*	< 0.0003	90	15	mg/L	EPA SW 846 8270
33	1,2-Dichloroethane*	< 0.00003	15	2.5	mg/L	EPA SW 846 8240
34	1,1-Dichloroethylene*	< 0.00012	12	3	mg/L	EPA SW 846 8240
35	1,2-Dichloroethylene*	< 0.00012	15	2.5	mg/L	Gas Chromatography-MS
36	Dichlorometane (metilen chlorida)*	< 0.002	6	1	mg/L	Gas Chromatography-MS
37	2,4-Dichlorofenol*	< 0.0057	80	10	mg/L	Gas Chromatography-MS
38	2,4-Dinitrotoluene*	< 0.0057	0.52	0.065	mg/L	EPA SW 846 8270
39	Etilbenzene*	< 0.002	90	15	mg/L	Gas Chromatography-MS
40	Ethylene diamine tetra acetic acid (EDTA)*	< 0.004	180	30	mg/L	Gas Chromatography-MS
41	Formaldehide*	< 0.006	200	25		Gas Chromatography-MS
42	Hexachlorobutadiene*	< 0.00011	0.18	0.03	mg/L	EPA SW 846 8270
43	Methyl ethyl ketone	< 0.01	800	100	mg/L	EPA SW 846 8240
44	Nitrobenzene*	< 0.01	8	1	mg/L	EPA SW 846 8270
45	Fenol (total, non-terhalogenasi)	< 0.05	56	7	mg/L	Gas Chromatography-MS
46	Stirene*	0.2	6	1	mg/L	Gas Chromatography-MS
47	1,1,1,2-Tetrachloroethane*	< 0.002	40	4	mg/L	Gas Chromatography-MS
48	1,1,2,2-Tetrachloroethane*	< 0.002	5.2	0.65	mg/L	Gas Chromatography-MS
49	Tetrachloroethylene (PCE)*	< 0.002	20	2.5	mg/L	EPA SW 846 8240
50	Toluene	< 0.7	210	35	mg/L	EI 36.093 (Gas Chromatography-FID)
51	Trichlorobenzene (total)*	0.012	12	1.5	mg/L	Gas Chromatography-MS
52	1,1,1-Trichloroethane*	< 0.002	120	15	mg/L	Gas Chromatography-MS
53	1,1,2-Trichloroethane*	< 0.002	4.8	0.6	mg/L	Gas Chromatography-MS
54	Trichloroethylene (TCE)*	< 0.002	2	0.25	mg/L	EPA SW 846 8240
55	2,4,5-Trichlorophenol*	< 0.01	1600	200	mg/L	EPA SW 846 8270
56	2,4,6-Trichlorophenol*	< 0.01	8	1	mg/L	EPA SW 846 8270
57	Vinyl chloride*	< 0.00018	0.12	0.015	mg/L	EPA SW 846 8240
58	Xylene total*	< 0.6	150	25	mg/L	Gas Chromatography-MS
	PESTICIDE					
59	Aldrin + Dieldrin*	< 0.000012	0.009	0.0015	mg/L	EPA SW 846 8080
60	DDT + DDD + DDE*	< 0.001	0.3	0.05	mg/L	Gas Chromatography-MS
61	2,4-D (2,4-Dichloro phenoxyacetic acid)*	< 0.0012	9	1.5	mg/L	EPA SW 846 8150
62	Chlordane*	< 0.000014	0.06	0.01	mg/L	EPA SW 846 8080
63	Heptachlor + Heptachlor epoxide*	< 0.000083	0.12	0.015	mg/L	EPA SW 846 8080
64	Lindane*	< 0.000004	0.6	0.1	mg/L	EPA SW 846 8080
65	Methoxychlor*	< 0.00096	6	1	mg/L	EPA SW 846 8080
66	Pentachlorophenol*	< 0.05	2.7	0.45	mg/L	EPA SW 846 8270
	ADDITIONAL PARAMETERS					
67	Endrin*	< 0.000006	0.12	0.02	mg/L	EPA SW 846 8080
68	Hexachlorobenzene*	< 0.0019	0.8	0.13	mg/L	EPA SW 846 8270
69	Hexachloroethane*	< 0.01	18	3	mg/L	EPA SW 846 8270
70	Pyridine*	< 0.01	30	5	mg/L	EPA SW 846 8270
71	Toxaphene*	< 0.0024	3	0.5	mg/L	EPA SW 846 8080
72	2,4,5-TP (Silvex)*	< 0.01	6	1	mg/L	EPA SW 846 8150

Figure 5: The results of the Sulfur TCLP analysis on 20 February 2019 which resulted in Gundih CPP sulfur being in the Non B3 category

2. Study on the sulfur status of CPP Gundih, the conclusion of the study is CPP Gundih sulfur can be categorized as a by-product of CPP Gundih (not as waste) so it can be equated as a raw material for the H2SO4 industry at PT Petrokimia Gresik.

Figure 6: Photos of Sulfur Pellets in the report on the Sulfur Quality Study from the Bio Desulfurization Process.

3. Comparative study with similar facilities. The study was conducted at CPP Donggi – Matindok which has a similar process as CPP Gundih, namely Bio Desulfurization, where the environmental permit there states that the sulfur produced can be managed as Non B3.

PROCEEDINGS
JOINT CONVENTION BANDUNG (JCB) 2021
November 23rd – 25th 2021

Result and Discussion

The revision of the environmental permit of CPP Gundih has been issued, namely *KepMen KLHK No. SK. 710/Menlhk/Setjen/PLA.4/9/2019* concerning Amendment to the Decree of the Minister of the Environment Number 437 of 2013 concerning Environmental Permits for East Java Gas Development Activities in the Kedungtuban, Randublatung and Kedunglusi – Gundih Areas by PT. Pertamina EP - East Java Gas Development Project (PPGJ).

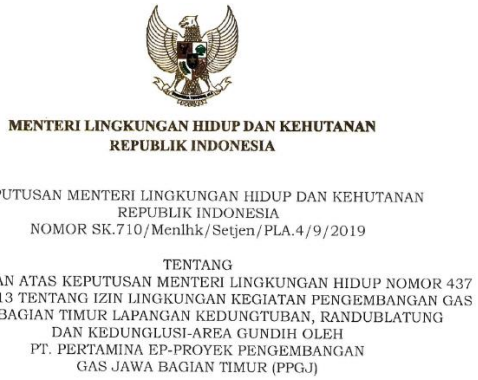

MENTERI LINGKUNGAN HIDUP DAN KEHUTANAN
REPUBLIK INDONESIA

KEPUTUSAN MENTERI LINGKUNGAN HIDUP DAN KEHUTANAN
REPUBLIK INDONESIA
NOMOR SK.710/Menlhk/Setjen/PLA.4/9/2019

TENTANG
PERUBAHAN ATAS KEPUTUSAN MENTERI LINGKUNGAN HIDUP NOMOR 437
TAHUN 2013 TENTANG IZIN LINGKUNGAN KEGIATAN PENGEMBANGAN GAS
JAWA BAGIAN TIMUR LAPANGAN KEDUNGTUBAN, RANDUBLATUNG
DAN KEDUNGLUSI-AREA GUNDIH OLEH
PT. PERTAMINA EP-PROYEK PENGEMBANGAN
GAS JAWA BAGIAN TIMUR (PPGJ)

Figure 7: KepMen KLHK No. SK. 710/Menlhk/Setjen/PLA.4/9/2019.

Conclusions

From the above conditions, the following conclusions can be drawn:

1. Sulfur CPP Gundih reaches sulfur purity levels of 97.866% - 99.78% which can be categorized as a selling value product.
2. Sulfur CPP Gundih cannot be managed using the commercialization method due to taxation issues, so sulfur management is managed by a third party with the relevant official permit.
3. Revision of the environmental permit for handling sulfur CPP Gundih changed the management of sulfur which originally used PP No. 18/1999 on Hazardous Waste Management to become PP No. 19/2010 concerning Liquid Waste Quality Standards for Oil and Gas Activities and the Earth.
4. The cost of handling sulfur which was originally managed using the B3 waste legislation is ± Rp. 5 Million/Ton or Rp. 25 Billion/Year then if using the Non-B3 waste legislation is Rp. 1.3 Million/Ton or Rp 6.5 Billion/Year. Therefore, sulfur handling costs can be reduced by Rp. 18.7 Billion/Year.

References

KepMen No.710/Menlhk/Setjen/PLA.4/9/2019.
Kep/MenLH/129/2003.
PP No. 19/2010 concerning Liquid Waste Quality Standards for Oil and Gas Activities and the Earth.
PP No. 18/1999 concerning Hazardous Waste Management.
PP No. 82/2001 concerning Water Quality Management and Water Pollution Control.
Laboratory TCLP Result of Sulfur Pellet, 2019, PT. Envilab
Master Data of Engineering Process CPP Gundih.
Dr. Ir.P. Sumardi , SU, 2018, IPM, Study of sulfur quality from the cpp bio desulfurization process – Gundih Pertamina EP Asset 4 Cepu Field, Center for Energy Studies (PSE) – UGM.
Report of Sulfur Content Laboratory Test Results by LEMIGAS, 19 May 2020.

Acknowledgements

We dedicate this thank you to the Operation Production Team and the HSSE Team of PT Pertamina EP Asset 4 Field Cepu and all related parties who have helped and been involved in making this proceedings, which the authors cannot mention one by one.

PROCEEDINGS
JOINT CONVENTION BANDUNG (JCB) 2021
November 23rd – 25th 2021

Earthquake and Tsunami Hazards Identification of Bali Cultural Center Development Area in Klungkung Regency Bali

Iman Fatchurochman[1)], Dwi Hartanto[2)], Sigit Pramono[1)], Rudy Darsono[2)], Tomy Gunawan[2)], Fajri. Syukur Rahmatullah[1)], Adityo Mursitantyo[2)], Kautsar Nafi[2)], Aditya Setyo Rahman[1)]
[1)]Meteorology Climatology and Geophysics Agency - Center, Jakarta
[2)]Meteorology Climatology and Geophysics Agency - Regional Center III, Denpasar

Abstract
The Government of Bali has plans to build a monumental masterpiece project of the Bali Cultural Center (PKB) to preserve and promote Balinese culture, art, and tourism located in the ex-excavation area - C, Gunaksa Area, Klungkung Regency, Bali. A study of potential earthquake and tsunami hazards in the PKB area is needed to provide recommendations for project design and disaster management plans. Potential earthquake hazards are identified by analyzing the history of earthquakes in Bali and modeling the peak ground acceleration (ShakeMap) for three significant earthquake scenarios. Seismic microzonation mapping was carried out using Multichannel Analysis of Surface Waves (MASW) at 31 locations and Spatial Auto-Correlation (SPAC) at 3 locations to identify average shear wave velocity to a depth of 30 meters (Vs30), ground site class, and engineering bedrock depth. Meanwhile, tsunami potential is determined by modeling tsunami wave propagation and inundation based on two earthquake-tsunami scenarios in the south of Bali. The ShakeMap modeling reveals that the PKB area has the potential of earthquake intensity up to severe category (VIII MMI). The analysis of microtremor data shows that the value of Vs30 is varied from SC class (very dense soil / soft rock) to SE (soft soil). The results of SPAC estimate the depth of the engineering bedrock is progressively deeper from the higher measurement area to the lower region (coastal area), which is from 71.4 meters to 108.8 meters. The tsunami modeling results indicate that the site is prone to tsunamis; the height reaches up to 4 meters with an inundation of up to 1500 meters.

Keywords: earthquake, microzonation, tsunami

Introduction

The Bali Cultural Center (PKB) is a monumental masterpiece project aiming to preserve and promote Balinese culture, art, and tourism. The construction is located in the ex-excavation area C, Klungkung Regency, which includes Klungkung and Dawan sub-districts, often referred to as the Gunaksa area. The project will be developed on an area of 320 hectares at the coordinates of 8°32’41.35” - 8°34’30.94” S and 115°24’54.92” - 115°26’6.99” E (Figure 1).

As the PKB area is located in a highly seismic active area (Eurasia - Indo-Australia Plate Megathrust (south), Flores Back Arc Thrust (north), and Lombok Strait Fault (east)), the area is very prone to earthquake disaster. Moreover, as the project will be developed in Tukad Unda Estuary to the open sea of the Indian Ocean, a tsunami will be a significant threat to the development area. Therefore, a study of the ground shaking, microzonation, and tsunami hazards are needed to provide recommendations to project design and disaster management strategy of the PKB development plans. The aim is to diminish the negative impacts of hazards, e.g., infrastructure damage and fatalities.

This study highlights the potential seismic hazard, which comprises of 1) ShakeMap modeling to illustrate earthquake ground-shaking model, 2) microzonation to identify average shear wave velocity to a depth of 30 meters (Vs30), ground site class, and engineering bedrock depth, 3) tsunami hazards modeling to forecast potential tsunami flow depth and inundation.

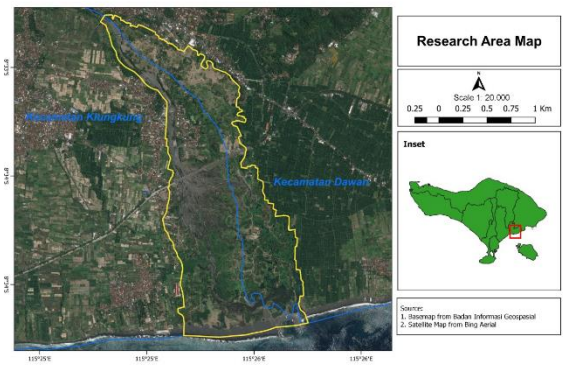

Figure 1. The Study Site of the Bali Cultural Center.

Data and Method

Earthquake ShakeMaps. In this study, the ShakeMaps were modeled using the ShakeMap software developed by the United States Geological Survey (USGS) [1]. The calculation of the post-earthquake MMI (Modified Mercalli Intensity) intensity scale is based on ground motion modeling using earthquake parameters such as magnitude, location, depth, and mechanism of the earthquake source.

The ground-shaking value is correlated with the earthquake intensity parameter (MMI scale), which means the higher the PGA (Peak Ground Acceleration) and PGV (Peak Ground Velocity) values compensate the higher MMI intensity value as given by equations (1) and (2). MMA is the MMI value derived from the PGA value, while MMV is derived from the PGV value [2].

$$MMI = 0.46MMA + 0.52MMV \quad (1)$$

$$MMI = (MMA + MMV) / 2 \quad (2)$$

Microzonation

Earthquake ground shaking level on the surface is not only affected by earthquake magnitude and hypocenter distance but also by local soil characteristics as a medium for the propagation of earthquake waves from the bedrock to the ground surface [3]. The variations and changes of surficial soil structure are obtained and presented into a micro-scale spatial distribution on the microzonation map. The aim is to estimate the amplification factor of the ground shaking due to strong earthquakes. In this study, the microzonation

PROCEEDINGS
JOINT CONVENTION BANDUNG (JCB) 2021
November 23rd – 25th 2021

method was carried out using Multichannel Analysis of Surface Waves (MASW) and Spatial Auto-Correlation (SPAC) with the distribution of measurement points are shown in Figure 2.

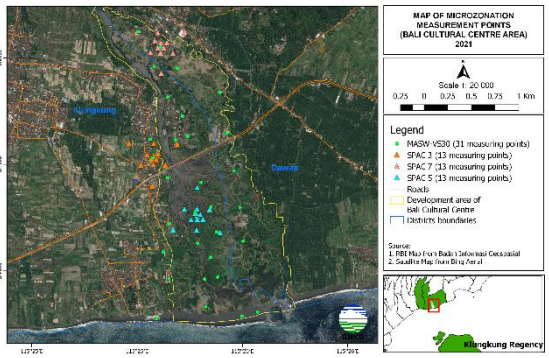

Figure 2. Measurement Points of Microzonastion in the PKB area.

Multichannel Analysis of Surface Waves (MASW). MASW method is a seismic method to measure the average velocity of shear waves to a depth of 30m (Vs30). Vs30 is an indicator to describe the stiffness and strength of the soil. The principle of the MASW is based on the Rayleigh surface wave theory generated from the interaction of the shear wave with the soil surface [3]. As the average Vs30 value is obtained, the site class is determined using the SNI 1726-2012 criteria [4].

Spatial Auto-Correlation (SPAC).
SPAC is a microtremor array survey method based on Rayleigh surface wave propagation theory. The method uses a passive source with varying frequencies. As a result, the wave's penetration can reach a deeper depth and predict the engineering bedrock depth, generally at a depth of more than 30 meters. In the SPAC method, microtremor wave is recorded using sensor configuration (array). This study uses an isotropic/ triangular shape, then the wave's phase velocity forms dispersion curves from all directions [3].

Tsunami Modeling. The modeling process is divided into three steps:

1) Determination of tsunami-genic earthquake
The scenario is applied as the initial model and the basis in seafloor shifting modeling. In this study, the determination of earthquake scenarios is carried out through a literature review of research conducted by Pusat Studi Gempa Nasional (PuSGeN) 2017 [5]. Two strong earthquake scenarios located in the south of Bali, due to the activity of megathrust Indo-Australia and Eurasia Plate, have been selected for tsunami modeling, i.e., Sumba Megathrust segment (M 8.5) and East Java Megathrust segment (M 8.7).

2) Tsunami wave propagation modeling
In this study, the tsunami modeling has resulted from the application of ComMIT (Community Model Interface for Tsunami) developed by the NOAA Center for Tsunami Research (NCTR). The application uses a numerical model, namely MOST (Method of Splitting Tsunami). The MOST numerical model simulates three stages of tsunami evolution, which comprises earthquake, trans-oceanic wave propagation, and tsunami inundation [6]. The initial study of the tsunami model using 1 arc-minutes ETOPO1 bathymetry data while topographic data (derived from the 90m CGIAR SRTM digital elevation model available in the ComMIT application) do not represent the actual geographical condition of the Gunaksa Area. Therefore, additional input of geographical data is required, namely 1 arc-second SRTM data provided by USGS (http://earthexplorer.usgs.gov/) and 30 arc-second GEBCO bathymetry data (https://www.gebco.net/).

3) Tsunami inundation map
Tsunami wave inundation modeling, using the ComMIT application (https://nctr.pmel.noaa.gov/ComMIT/), creates inundation data illustrating the height and distance of tsunami waves that hit the mainland. Then, the data is processed using the Q-GIS application (https://qgis.org/en/site/), which is based on a geographic information system.

Result and Discussion

ShakeMap Scenario
The ground-shaking level analysis of the study site used three earthquake scenarios according to PuSGeN 2017, i.e., Megathrust Zone M 9.0 (south), Lombok Strait Fault M 7.6 (east), and Flores Back Arc Thrust M 7.4 (north). The ShakeMap scenarios are shown in Figure 3 to Figure 8.

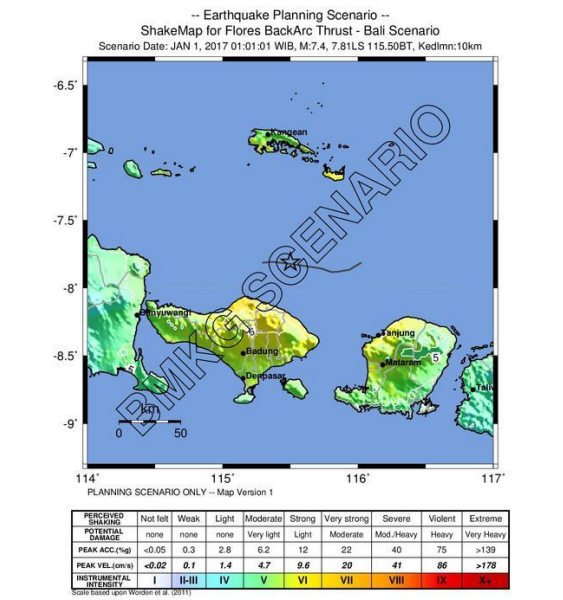

Figure 3. ShakeMap for the Flores Back Arc Thrust Scenario in Bali Region.

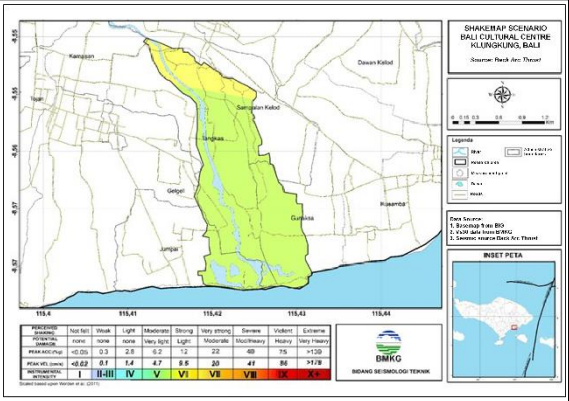

Figure 4. ShakeMap for the Flores Back Arc Thrust Scenario in the PKB Area.

PROCEEDINGS
JOINT CONVENTION BANDUNG (JCB) 2021
November 23rd – 25th 2021

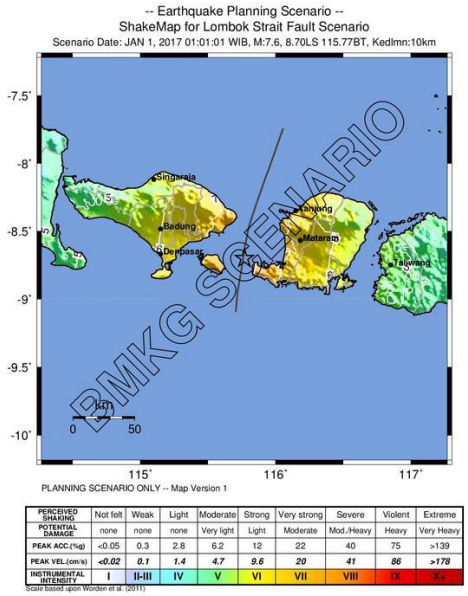

Figure 5. ShakeMap for the Lombok Strait Fault Scenario in Bali Region.

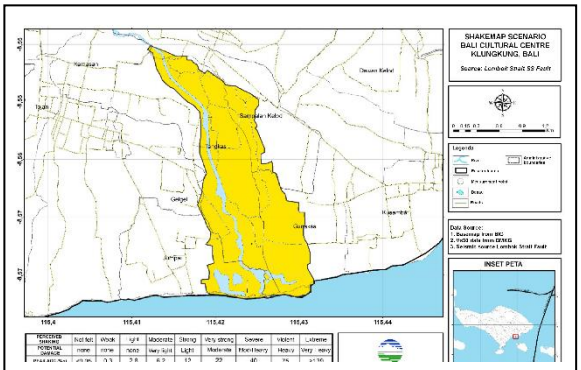

Figure 6. ShakeMap for the Lombok Strait Fault Scenario in the PKB Area

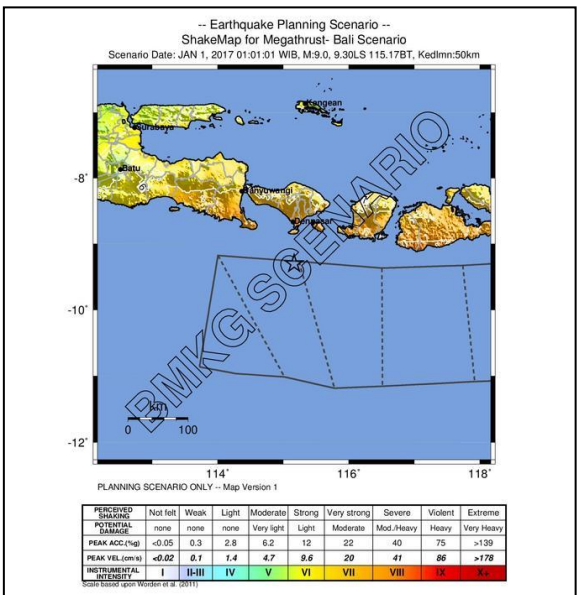

Figure 7. ShakeMap for the Megathrust - Bali Scenario in Bali Region.

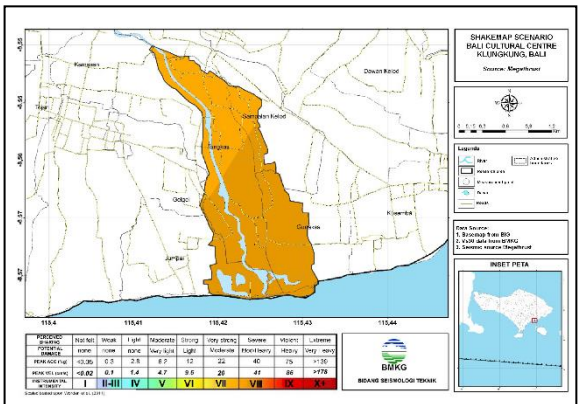

Figure 8. ShakeMap for the Megathrust - Bali Scenario in the Study Site.

The results of the ShakeMap scenario indicate that the maximum level of ground shaking which potentially occurs in the study site is varied from V to VIII MMI (Figure 3 to Figure 8). Earthquakes located in East Java Megathrust are predicted to cause the most severe damage with the maximum intensity of VIII MMI, which means *"Damage slight in specially designed structures; considerable damage in ordinary substantial buildings with partial collapse. Damage great in poorly built structures. Fall of chimneys, factory stacks, columns, monuments, walls. Heavy furniture overturned"*. The earthquake parameters and intensity prediction from the ShakeMap modeling are shown in Table 1.

Table 1. The Parameter of Earthquake Scenario

Earthquake Parameter					
M	**Latitude**	**Longitude**	**Depth (km)**	**MMI**	**Note**
7.4	-7.81°	115.50°	10	V	Florest Back Arc Thrust
7.6	-8.70°	115.77°	10	VII	Lombok Strait Strike-slip North
9.0	-9.30°	115.17°	50	VIII	Megathrust East Java

Microzonation
Multichannel Analysis of Surface Waves (MASW)

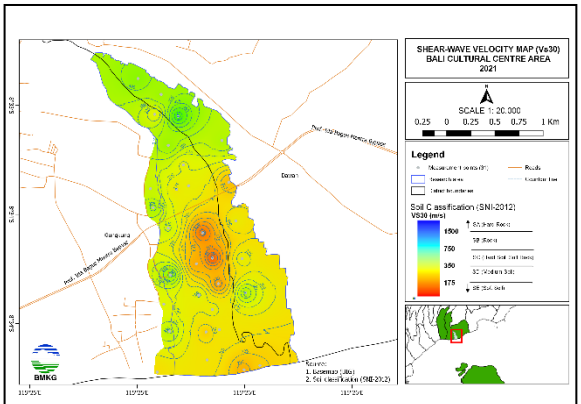

Figure 9. Vs30 Contour Map of the PKB Area.

The analysis of 31 measurement points showed that the Vs30 value at the study site varied from 97.38 m/s (SE class – soft soil) to 487.62 m/s (SC class – hard soil or soft rock). Vs30 contour map (Figure 9) indicates that the northern part

PROCEEDINGS
JOINT CONVENTION BANDUNG (JCB) 2021
November 23rd – 25th 2021

of the project site has relatively hard soil (SC class), while the middle area (the south of the Ida Bagus Mantra Highway Bridge) is dominated by soft soil (SE class). The other areas are classified as medium soil (SD class) as the most dominant site class in the study area.

Spatial Auto-Correlation (SPAC).
The estimated engineering bedrock is obtained by analyzing the S-wave velocity and depth profile, which is shown in the profiles of Figure 10.a, 10.b, and 10.c.

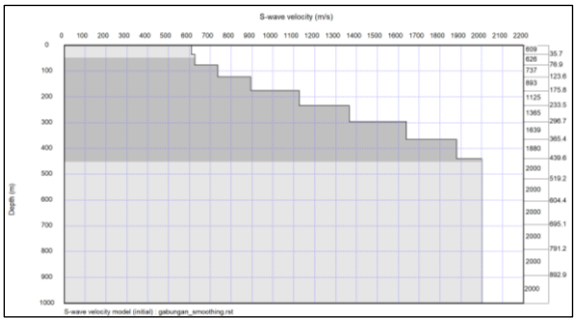

Figure 10.a. The profile of S velocity and depth at SPAC3.

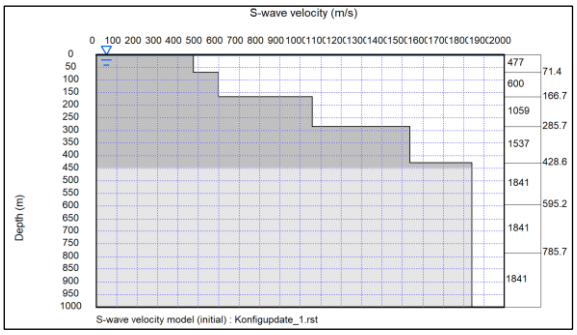

Figure 10.a. The profile of S velocity and depth at SPAC5.

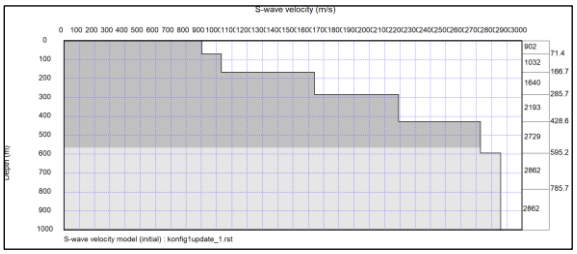

Figure 10.a. The profile of S velocity and depth at SPAC7.

The results of SPAC analysis show that the estimated engineering bedrock depth is varied from 71.4 meters to 108.8 meters. The depth is increasingly deeper from the higher measurement area to the lower direction (coastal area). The Vs value and estimated bedrock depth are shown in Table 2.

Table 2. Average Vs30 Value and Estimated Bedrock Depth based on SPAC Analysis.

Measuring Point	Avg. Vs30 Value	Estimated Bedrock Depth
SPAC-7	903 m/s	71.4 m
SPAC-3	760 m/s	83,8 m
SPAC-5	477 m/s	108.8 m

Tsunami Modeling
The Sumba Megathrust Earthquake M 8.5
Based on the tsunami modeling due to the M8.5 Sumba Megathrust earthquake (Figure 11), the PKB development site is included in the tsunami-affected area. The result shows that the flow depth is estimated at 6.8 m in the west of the site's coastal area while at the PKB site reaches 4 m.

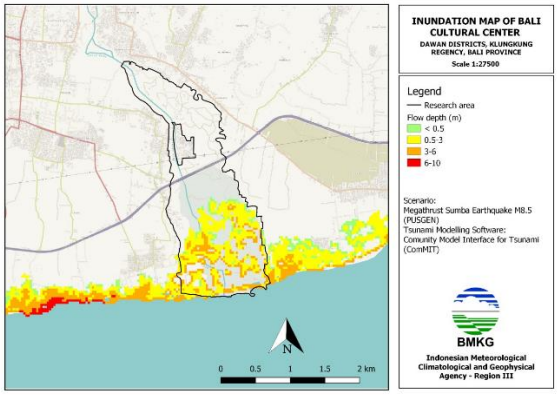

Figure 11. Inundation map due to the Sumba Megathrust earthquake M8.5.

The profiles of the recorded tsunami waves of the eight scenarios can be observed by installing artificial tide gauges at four points along the coast of the PKB location and its surroundings (Figure 12). The tsunami modeling's synthetic tide gauge (mareogram) recording shows that the tsunami wave height when it reaches the shoreline of the PKB location can reach 3-6 meters (Figure 13).

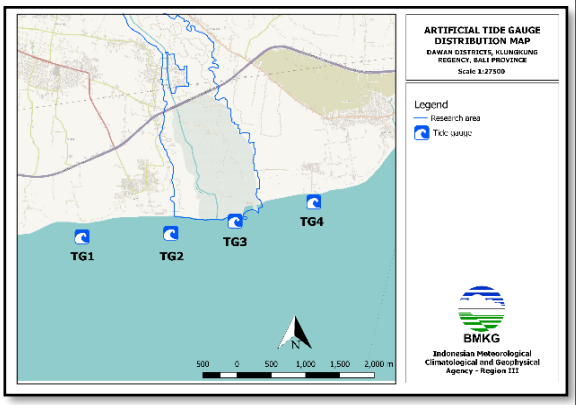

Figure 12. Artificial tide gauge distribution map.

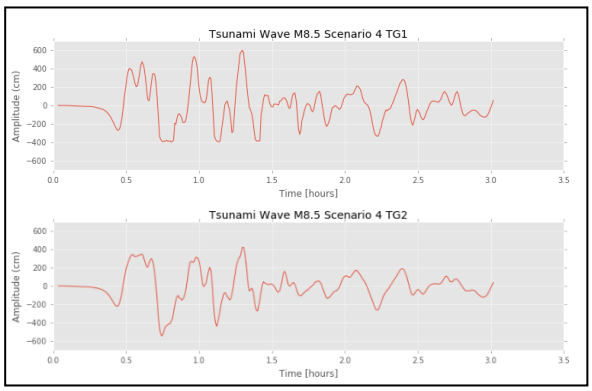

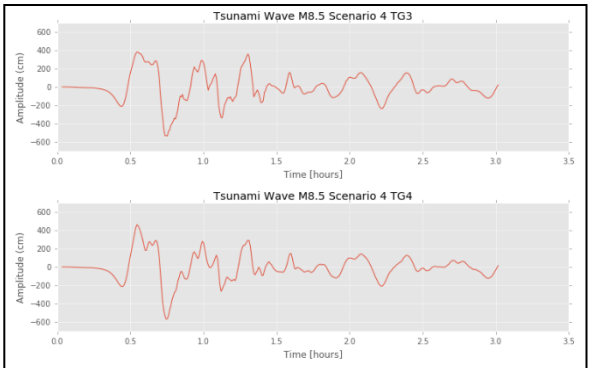

Figure 13. Artificial tsunami wave records at the coastline based on the Sumba Megathrust earthquake M8.5 scenario.

The East Java Megathrust Earthquake M8.7

Similar to the Sumba Megathrust M 8.5 earthquake, the tsunami modeling also shows that the PKB area is included in the tsunami-affected area due to the East Java Megathrust earthquake. In comparison, the tsunami impact from the Megathrust East Java M8.7 earthquake was slightly lower than the tsunami impact from the Megathrust Sumba M 8.5 earthquake (Figure 14). The tsunami inundation from the ground surface (flow depth) can reach 6.2 meters on the west coast of the area. In the development area, the flow depth can reach 3.7 meters. Similar to the previous scenario, the results of recorded artificial tide gauges at four points along the coast indicate that the height of the tsunami when it reaches the shoreline is between 3-6 meters (Figure 15).

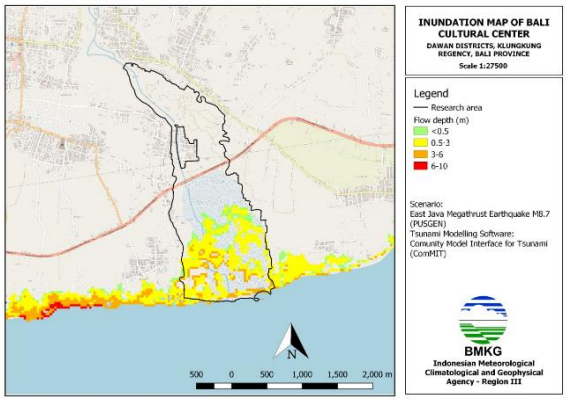

Figure 14. Inundation map due to the East Java Megathrust Earthquake M8.7.

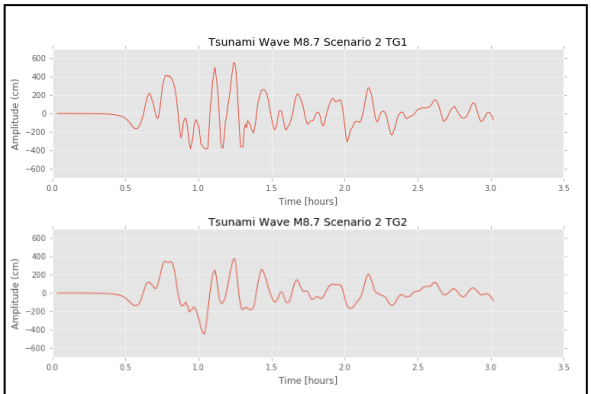

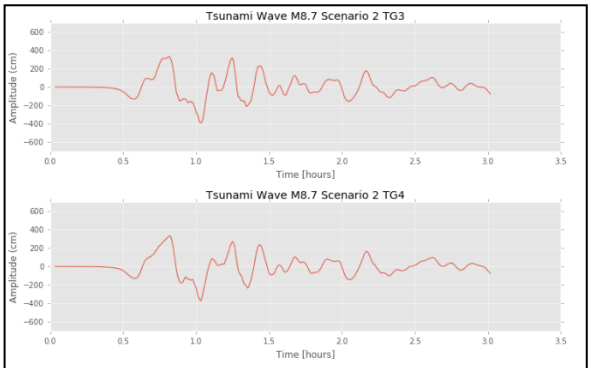

Figure 15. Artificial tsunami wave records at the coastline based on the East Java Megathrust earthquake M 8.7 scenario.

Combined Tsunami Modeling Scenario

The worst scenario of tsunami modeling is obtained by combining two tsunami models due to the Sumba Megathrust M 8.5 and East Java Megathrust M 8.7 earthquakes (Figure 16). The flow depth reaches 6.8 m on the west coast of the project location. For PKB locations, the flow depth is up to 4 meters. The tsunami inundation distance at the PKB area reaches a farther extent (up to 1500 meters) than its surroundings, which only range from 300 to 700 meters from the coastline (Figure 17). It is in accordance with the tsunami probabilistic analysis on the coast of Bali, with a 10% chance of a tsunami with a height of higher than 0.5 meters [7].

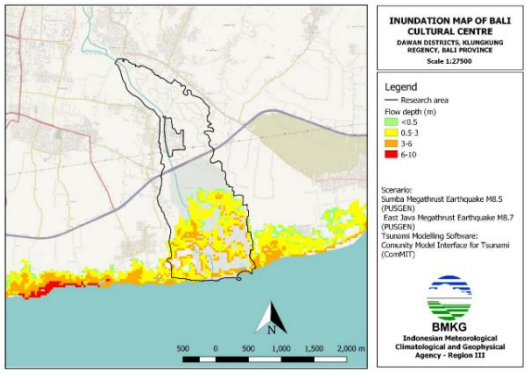

Figure 16. Composite inundation map due to the Sumba Megathrust earthquake M 8.5 and East Java Megathrust earthquake M 8.7

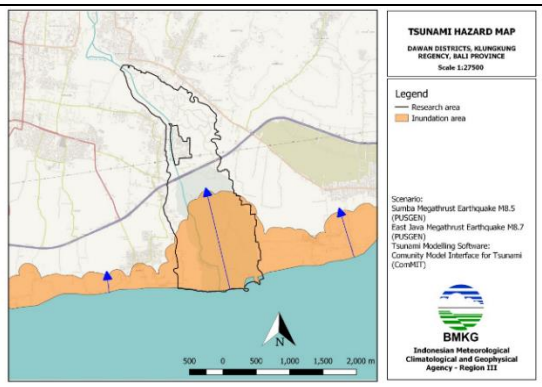

Figure 17. Tsunami hazard map of Bali Cultural Centre area. Blue arrow from the left to the right 300 meters, 1500 meters, and 700 meters.

PROCEEDINGS
JOINT CONVENTION BANDUNG (JCB) 2021
November 23rd – 25th 2021

Conclusions and Recommendations

1. The maximum intensity level of ground shaking in the PKB area is up to VIII MMI due to an activity of the East Java Megathrust segment.
2. Based on the MASW analysis, the PKB area is dominated by medium soil (SD class), while the middle and northern area has soft soil class (SE class) and hard soil/ soft rock class (SD class), respectively.
3. The results of SPAC analysis estimate that the depth of engineering bedrock in the PKB area is increasingly deeper from the higher measurement area (71.4 m) to the lower/ coastal area (108.8 m).
4. The tsunami flow depth in the PKB area is forecasted up to 4 meters, with a tsunami height on the shoreline is from 3 to 6 meters. As the project site is located in the estuary area, a tsunami inundation potentially reaches a farther extent (up to 1500 meters) than the surrounding area (300-700 meters).
5. We recommend that the building construction plan should adjust the level of ground-shaking threat in the area. Critical buildings that impact operational systems and humans should be built on hard soil areas. If the buildings have to be constructed on soft soil, it is necessary to design a more robust building and adjust the threat level due to the potential for seismic wave amplification. Meanwhile, buildings on medium and hard soil should also adjust the threat level, referring to the building code and technical instructions for constructing earthquake-resistant buildings.
6. As the PKB area is located in a tsunami-prone area, it is recommended to provide tsunami evacuation maps and assembly points (for tsunami shelter is higher than 4 meters while open space is farther than 1500 meters from the shoreline).

References:

[1] Wald, D.J., Worden, B.C., Quitoriano, V., and Pankow, K.L, 2006, ShakeMap Manual, Reston: USGS.
[2] Worden, Charles & Gerstenberger, M. & Rhoades, D. & Wald, D., 2012, The Bulletin of the Seismological Society of America. 102. 204-221.
[3] Seismologi Teknik BMKG, 2021, Laporan Mikrozonasi, BMKG.
[4] BSN, 2012, SNI 1726:2012, 17-18.
[5] PuSGeN, 2017, Puslitbang Kementrian PUPR.
[6] Synolakis, C.E., E.N. Bernard, V.V. Titov, U. Kânoğlu, and F.I. González, 2007, NOAA Tech. Memo. OAR PMEL-135, NOAA/Pacific Marine Environmental Laboratory, Seattle, WA, 55.
[7] N. Horspool, I. Pranantyo, J. Griffin, H. Latief, D. H. Natawidjaja, W. Kongko, A. Cipta, B. Bustaman, S. D. Anugrah, and H. K. Thio, 2014, Nat. Hazards Earth Syst. Sci., 14, 3105–3122, 2014.

PROCEEDINGS
JOINT CONVENTION BANDUNG (JCB) 2021
November 23rd – 25th 2021

PRELIMINARY CONCEPT AS EARLY STEP DEVELOPMENT OF GMPE BACK ARC THRUST-WEST NUSATENGGARA, INDONESIA

I Gusti Ketut Satria Bunaga[1], Sigit Pramono[2], Rian Mahendra Taruna[1], Danis Istiqomah[1], Ardhianto Septiadhi[1], Bambang Setiyo Prayitno[1], Dadang Permana[1]
[1]Indonesian Agency for Meteorological, Climatological and Geophysics, Mataram 83124, Indonesia
[2]Indonesian Agency for Meteorological, Climatological and Geophysics, Jakarta 10620, Indonesia

Abstract

The 2018 Lombok Earthquake has caused major destruction in the Lombok area, it caused of building design code to be upgraded related to actual the threat level of impact earthquake motion, especially struck from the Back-arc thrust source in the northern part of Lombok and Sumbawa Region. However, the others earthquake source was not involved in this research. The main target is to propose an early technical design of the Ground Motion Model to estimate PGA value predictive related to the seismicity intensity in Lombok and Sumbawa and to reveal concept design in step preparation. It has involved the design of distribution accelerometer sensors, selected catalog, site parameter, and deployed 2 the accelerometer sensors as temporary monitoring, 8 accelerometer existing sensors in Lombok Island and 6 accelerometer sensors in Sumbawa Island. Those GMPE will be developed using geometric means from the X and Y-axis components. The results show the technical design of instruments distribution and parameters which are collected to be involved in the processing. Then it would be continued to develop the empirical formula as represented for back-arc thrust Lombok-west Nusa Tenggara.

Keywords: Ground Motion Prediction Equation (GMPE), PGA, Seismic Intensity

Introduction

West Nusa Tenggara is one of Indonesia's regions that has frequently experience significant earthquakes and tsunami. There are six seismic sources that geologically affects West Nusa Tenggara Region (Figure 1); namely the subduction, Flores Back-arc Thrust, Lombok Strait Strike-Slip Fault, Sumbawa Strait Strike Fault, Teluk Panas Fault, and Sape Strike-Slip (Irsyam *et al.* 2017).

Five significant earthquakes on 29 July 2018 (M 6.4), on 5 August 2018 (M 7.0), on 9 August 2018 (M 6.2), on 19 August (M 6.3 & M 6.9) occurred in the northern part of West Nusa Tenggara. Numerous studies were committed to the investigation had a strong impact on civil infrastructure and caused severe loss of life and properties (Irsyam *et al.* 2017). Moreover, based on the BNPB report that the earthquakes caused 7.1 trillion Indonesian Rupiah economic losses and 71,740 damaged houses. According to the hypocenter relocation and focal mechanism, the earthquakes were caused by Back-arc Thrust activity (Supendi *et al.* 2020). This condition represents that West Nusa Tenggara has a high level of seismic hazard, particularly the north part seismic source (Back-arc Thrust mechanism). For that reason, the establishment of a ground motion model is very suitable for characterizing it.

The present effort that BMKG expanded the accelerograph station, totally of 669 sites. In addition to this strong-motion instrument, the recordings are needed to use in a ground motion prediction equation (GMPE). This model expresses the predicted ground motion with a fairly long period. Because of suitable for future use, BMKG is going to establish GMPE of Indonesia, particularly for Back-arc Thrust in West Nusa Tenggara (Figure 2). In this study, we are motivated to make the preliminary concept an early step in the development of the GMPE Back-arc Thrust conditioned northern part of Lombok and Sumbawa region. This result allows us to know the technical design of instrument distribution and parameters which are collected to be involved in the processing, particularly the empirical formula in the Back-arc Thrust region as it is modeled in the development of GMPE in the future.

Data and Method

This research is carried out based on the grand design of developing GMPE Indonesia (Figure2). In other words, this development captures the expected future ground motion in the area of interest. There are 11 locations that are BMKG's major issues (Figure 3). In 2021, we set the Back-arc Thrust source mechanism as the first project.

We used data from BMKG's accelerometer sensors for our technical design. We specify the recordings of

as many as eight existing sensors in Lombok Island and six sensors in Sumbawa Island. Two accelerometer sensors as temporary monitoring are added due to the lack of available recording in the northern and the center of Lombok Island (Figure). Moreover, the determination of temporary monitoring considered the distribution with the tight network, ideal location, and source power (Figure 4). We performed 119 selected earthquakes for the period extending from July 2016 to August 2021 (Figure 1). The Indonesian Tsunami Early Warning System (InaTEWS) data catalog is used reported by BMKG. The procedures are described here begin with restricting the recordings at distances < 300 km with the earthquake source within The Flores Back-arc Thrust region.

The Peak Ground Acceleration (PGA) data were successfully obtained based on the shakemap repository of the BMKG catalog (https://shakemap.bmkg.go.id/). To determine the value of temporary sensors, we conducted peak and valleys analysis using obspy software (Beyreuther *et al*. 2010). Figure 5 and figure 6 illustrate the example of accelerograms of temporary monitors.

The time-averaged shear-wave velocity in the upper 30m of the site (Vs30) value needed for this early concept is assigned using between measured Vs30 and bedrock engineering depth estimation (BMKG-UI report). Figure 7 shows the domination of soft soil and stiff soil in the Lombok region and the 33 sites that the locations of in situ geophysical measurement obtained by Multichannel Analysis of Surface Wave (MASW) method. Based on Pramono *et al* (2020), the local characteristics site of Lombok Area was variated, it's consequently the GMPE would have represented more actual condition in Lombok area if when the implementation of GMPE using the actual strong motion data from Lombok region.

Result and Discussion

The early concept results are shown as the graphic that cumulative numbers of recordings and event since 2016 (Figure 8). There are three categories in the database; 243 recordings from 119 events (existed accelerograph), 19 recordings from 20 events (temporary accelerograph at Central Lombok), and 2 recordings from 20 events (temporary accelerograph at North Lombok).

This database is well-populated for the 300 km distance range, from magnitude between 2 and 7 with all of the events are shallow depth (5-38 km). The location of events occurred in the Back-arc Thrust area and we assumed it related to the region and depth shallower hypocenter. As mentioned before, the database will be upgraded by some supporting parameters.

Lesson learned of Lombok earrhquake 2018 recommended the needs of PGA calculated value with local characteristic data support. To be realized and implemented BMKG's program, in 2021 BMKG develop of GMPE with the back arc thrust seismic source.

BMKG has committed to implement earthquake hazard assessments to reach the high-quality calculation. However, it would be related to the existing model of GMPE in Indonesia. The seriously efforts have to be prepared and should be planned in the short and long BMKG national priority project. The development of GMPE already started in Indonesia in a few years ago. Megawati and Pan (2009) had developed with the earthquake source of the western part of Sumatera, Prakoso and Sukanta (2015) has developed for the southern part of Java Island and the last just published of ground motion model for low to intermediate magnitude with the shallow crustal background for Central Sulawesi (Pramono *et al*, 2020).

Conclusions

GMPE is one of the important elements of seismic hazard. We described the preliminary concept used to develop a GMPE for the Back-arc Thrust region in West Nusa Tenggara. This study will likely be used for future references of engineering applications.

References

Irsyam, M., 2017, Peta sumber dan bahaya gempa Indonesia tahun 2017 (in Indonesian).
Supendi, P., *et al* 2020, Geophysical Journal International, 221, 1845-1855.
Beyreuther, M., 2010, Seismological Research Letters, 81, 3.
Pramono, S., *et al* 2020, International Journal of Technology, 11, 743-753.
Pramono, S., *et al* 2020, International Journal of GEOMATE, 19, 61-68.
Megawati, K., Pan, T.C., 2009, Bulletin of Seismological Society of America, 99, 566-584
Prakoso, W.A., Sukanta, I.N., 2015, Jurnal Teknologi, 77:11, 83-90.

Acknowledgements (Optional)

We would like to thank for the Indonesian Agency for Meteorological, Climatological and Geophysics for supporting and facilitating this research.

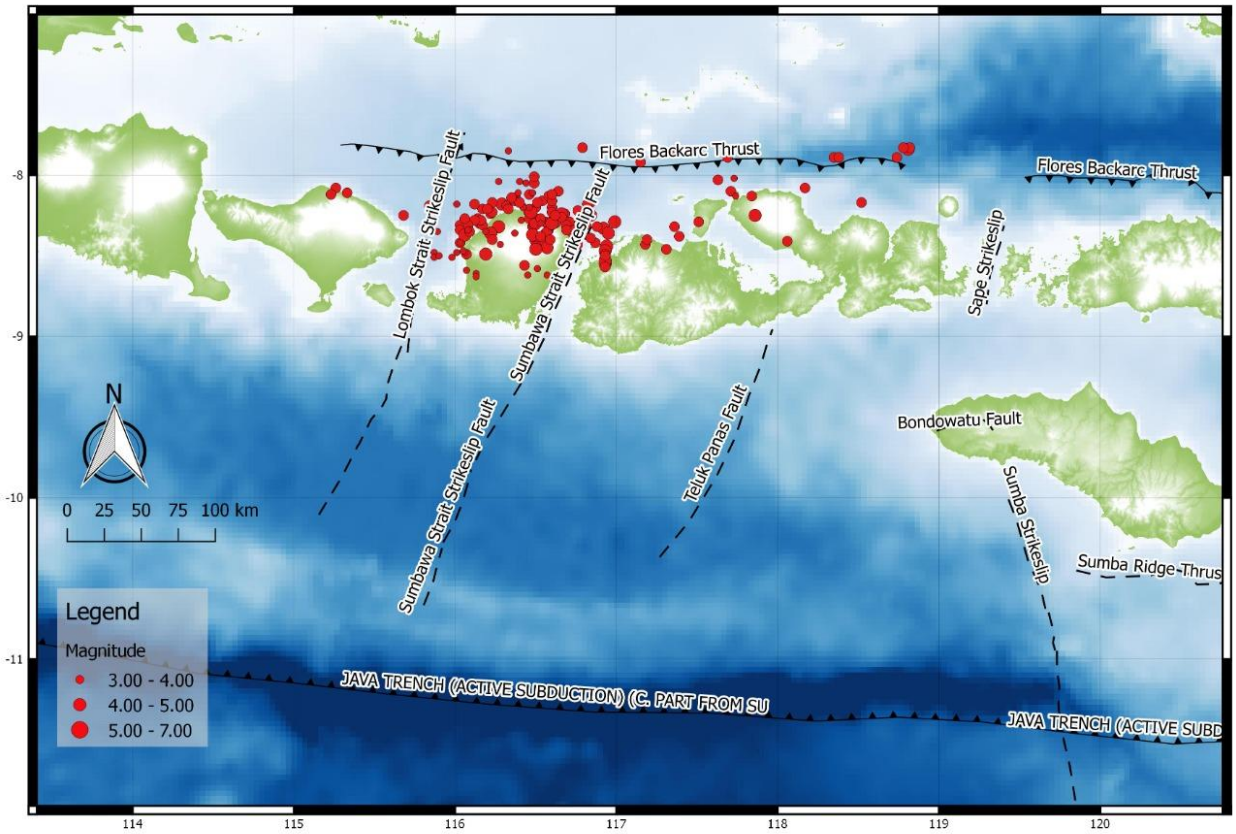

Figure 1: Tectonic setting of West Nusa Tenggara including the subduction, Flores Back-arc Thrust, Lombok Strait Strike-Slip Fault, Sumbawa Strait Strike Fault, Teluk Panas Fault, and Sape Strike-Slip. Red dots mark the earthquakes that were used in our study.

PROCEEDINGS
JOINT CONVENTION BANDUNG (JCB) 2021
November 23rd – 25th 2021

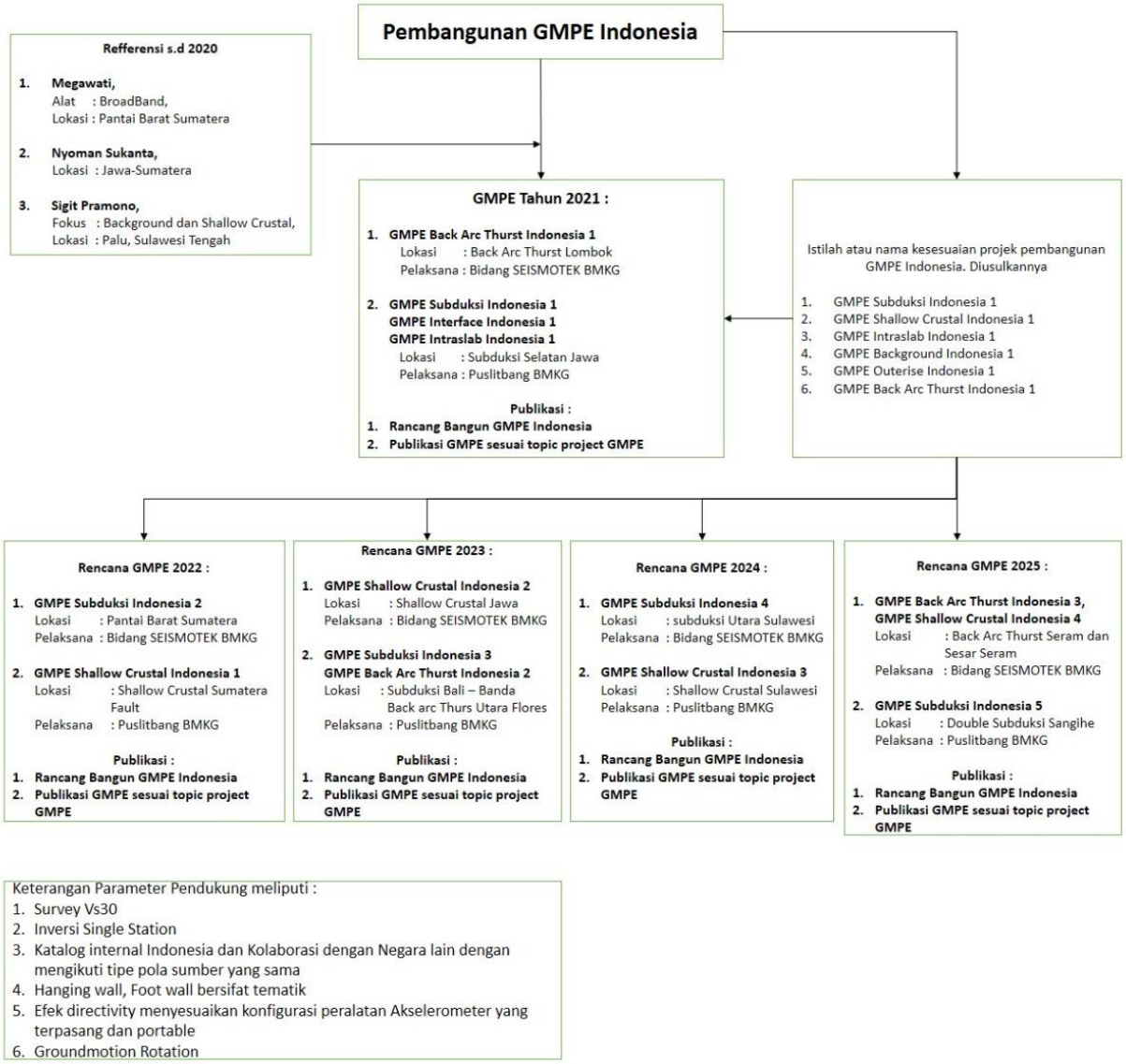

Figure 2: The GMPE Grand Design of Indonesia between 2021 and 2025.

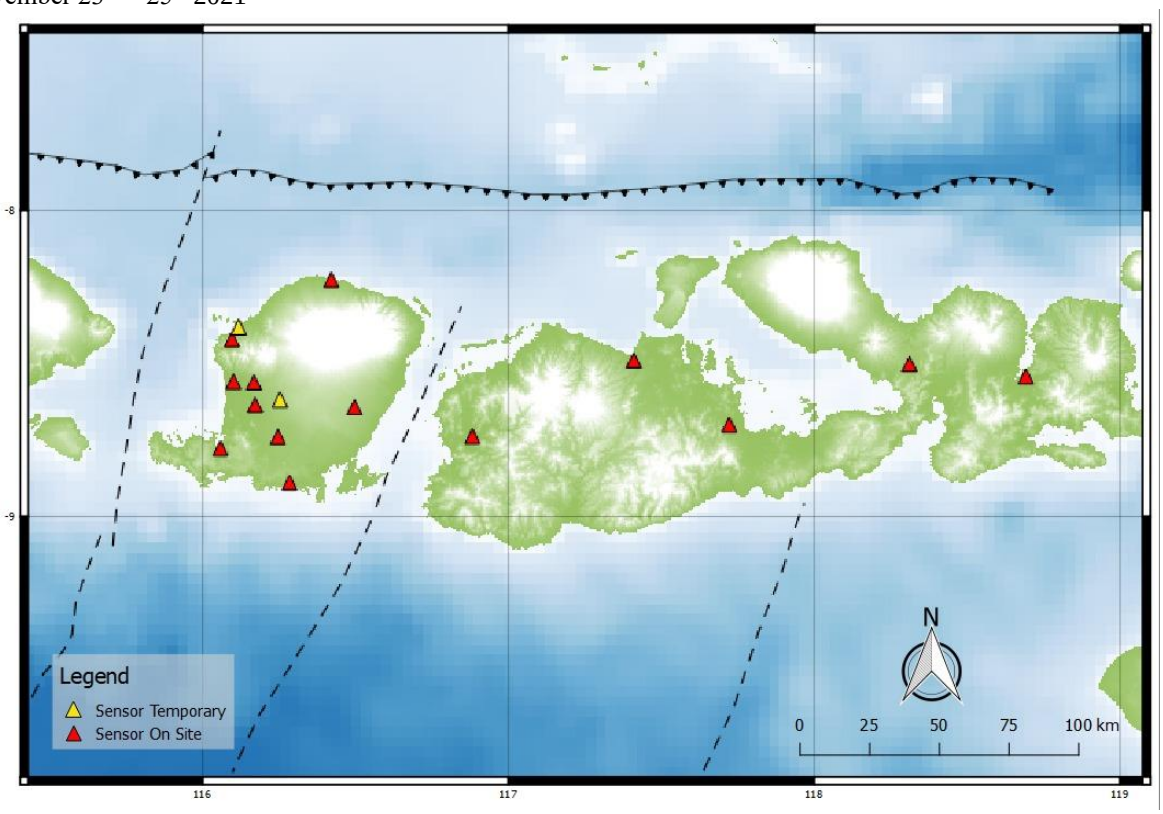

Figure 3: Spatial distribution of accelerograph sites in West Nusa Tenggara region.

Figure 4: Location observation and coordination with stakeholders for temporary accelerograph installation.

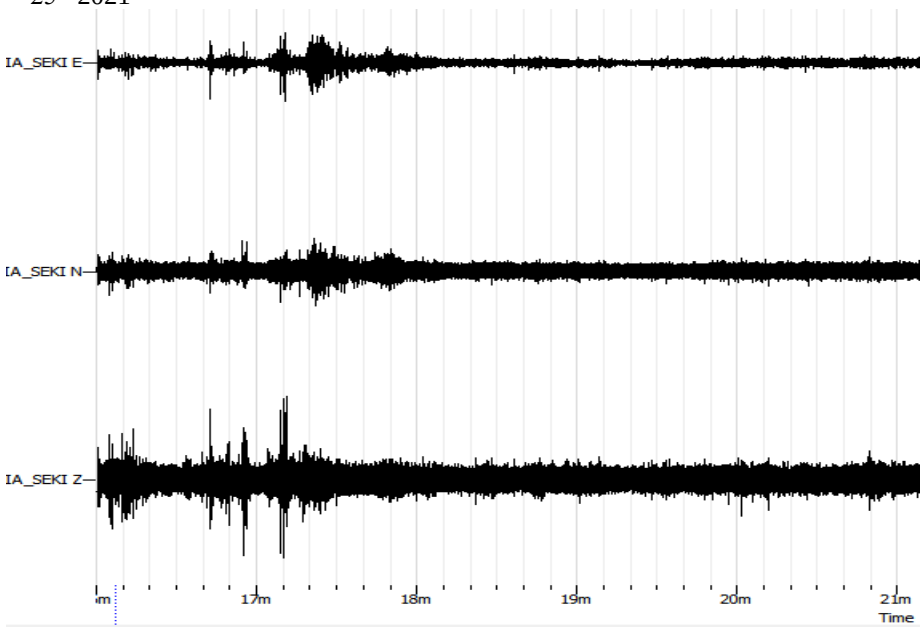

Figure 5: Recording at North Lombok site from an event on 22 Juny 2021 (M 3.6), three component.

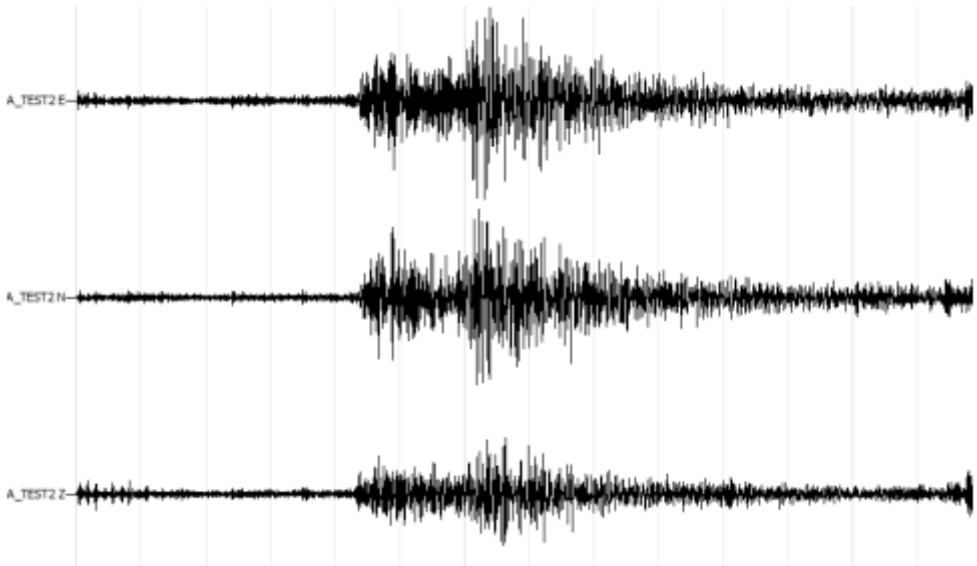

Figure 6: Recording at Central Lombok (Pringgarata) site from an event on 12 August 2021 (M 3.7), three component.

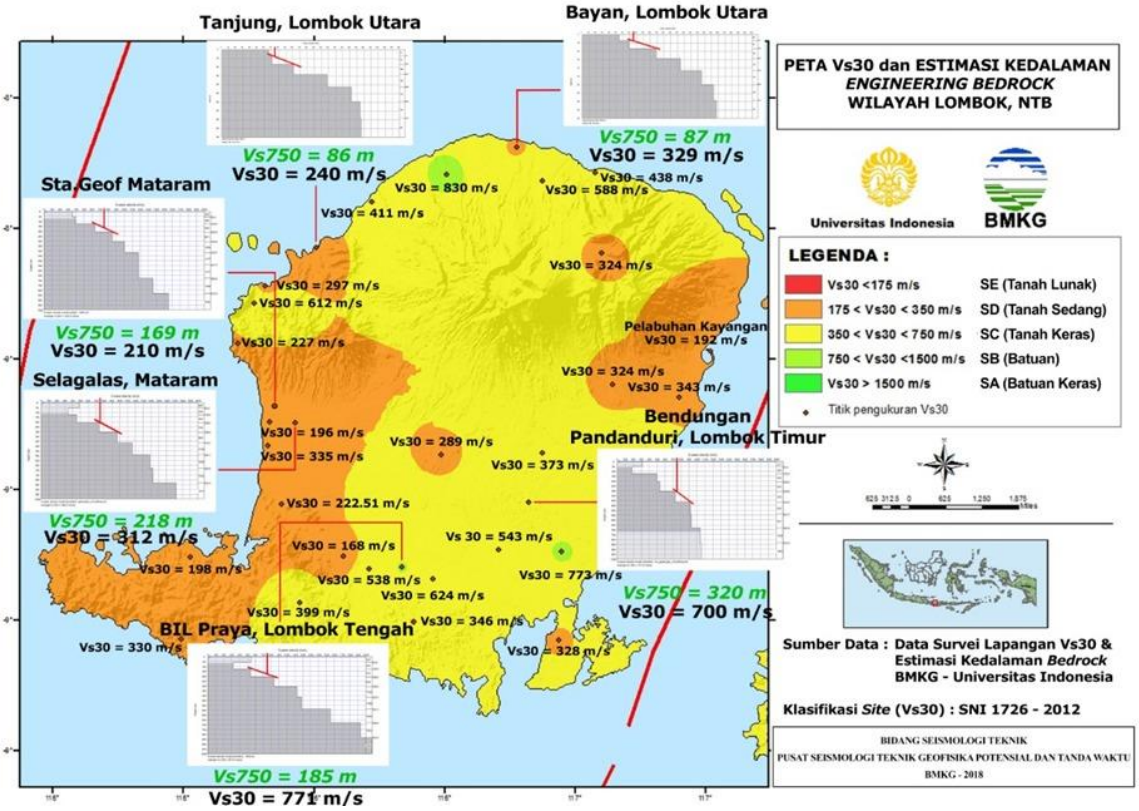

Figure 7: Vs 30 map based on in situ geophysical measurements with MASW method.

Figure 8: Cumulative numbers from 3 category monitorings between 2016-2021 (yellow and green bars for recordings and events, respectively).

PROCEEDINGS
JOINT CONVENTION BANDUNG (JCB) 2021
November 23rd – 25th 2021

V_{s30} Analysis in Daerah Istimewa Yogyakarta Using Simulated Annealing HVSR Inversion

Sandy Tri Gustono[1], Yoga Dharma Persada[2] and Fajri SyukurRahmatullah[2]

1. *Geophysics Department, School of Meteorology, Climatology and Geophysics*
2. *Meteorological Climatological and Geophysical Agency Indonesia*

Abstract

The 2006 Bantul Earthquake caused massive damage and casualties, so it needs action as mitigation to prevent any possibilities of a similar earthquake in Yogyakarta region, for instance, a survey of types and characteristics of sites there. Microtremor is one of the most effective and easily handled surveys of site conditions. Microtremor data processed by Horizontal to Vertical Spectral Ratio (HVSR) method as input for the inversion process. The simulated annealing method is used for inversion calculation. This method is chosen because it is more relevant to the true condition based on the probability function. The result is a shear wave velocity model which can be converted to v_{s30} value. That value has a correlation with site characteristics and type. Shear wave velocity shows different types at some point that differ from each other as prove that stratigraphy and lithology were heterogeneous. v_{s30} of the Yogyakarta region has a value from 179 to 524 m/s. The northern region is classified as hard soil correlated with a higher v_{s30} value. Meanwhile, the eastern part showed the opposite value and to be classified as soft soil type. There is a correlation between site classification and v_{s30} value mapping with damages from the Bantul earthquake 2006.

Introduction

Indonesia is one of the countries which had a high number of disasters. One of them is an earthquake. The earthquake happened on the border of a subduction area or land fault. The 2006 Yogyakarta earthquake is categorized as the significant earthquake that had been occurred in Indonesia with many casualties and damages. Around 70 thousand houses were totally broken and there were medium to slightly damaged houses.

Earthquakes can't be predicted. But there is a solution to minimize the damage that could happen when an earthquake occurs. It can be from building collapse or from ground shaking. So, it is important to know what soil types are from an area, in this case, is Daerah Istimewa Yogyakarta region. Supartoyo (2016) defined the biggest factor which determined how destructive the 2006 earthquake was local site condition.

There are many methods to determine local site conditions. One example was based on the v_{s30} value. This value is obtained from mean shear wave velocity until 30-meter depth. This value could justify surface condition based on the assumption that until 30-meter depth all the soil responses are the same (Martin, 2004).

Based on the geological structure, the Yogyakarta region is majority composed of sedimentation of Merapi mountain (Sukandarrumidi, 1995). This sedimentation is divided into young sedimentation and old one. Young sedimentation from Merapi mountain consists of tuff sand (Trisnaning, 2015). It is loose and has low hardness. Soehaimi (2016) said that soil type from young sedimentation of Merapi mountain might be categorized as soft soil. This condition could generate big destruction from earthquakes. The old sedimentation has the same composer as young sedimentation, but andesite and basalt rock also could be found on that. There are also other formations of rock in Yogyakarta, for example, Semilir formation and Nglanggran formation. Geological conditions from the area of interest can be seen in Figure 1.

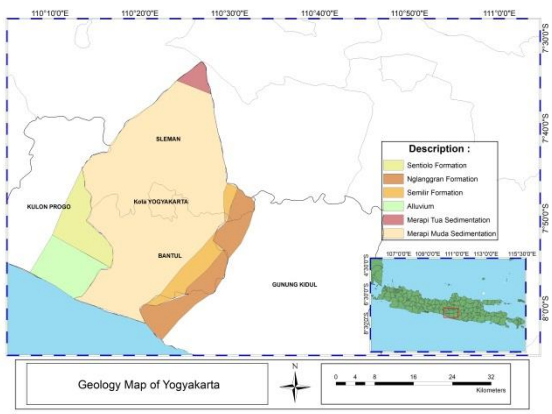

Figure 1: Geology map of Daerah Istimewa Yogyakarta (Sukandarrumidi, 1995).

The v_{s30} or mean shear wave velocity until 30 meters depth value is determined by using the inversion process. The inversion was a fitting data process from observed data with model data. The algorithm which used in this study is simulated annealing algorithm. The simulated annealing algorithm is one of nonlinear inversion that is based on the analogy of thermodynamics process (Grandis, 2009).

Data and Method

The microtremor data is used for this research collected from the Meteorological, Climatological, and Geophysical Agency of Indonesia (BMKG) using broadband accelerometer in 2014 around Daerah Istimewa Yogyakarta. The study area is located between $8^0 30'$ to $7^0 20'$ South and $109^0 40'$ to $111^0 0'$ East. There are 51 points location of the microtremor measurement and can be seen in Figure 2. The initial model for the inversion process was collected using the MASW (Multichannel Analysis of Surface Wave) method.

PROCEEDINGS
JOINT CONVENTION BANDUNG (JCB) 2021
November 23rd – 25th 2021

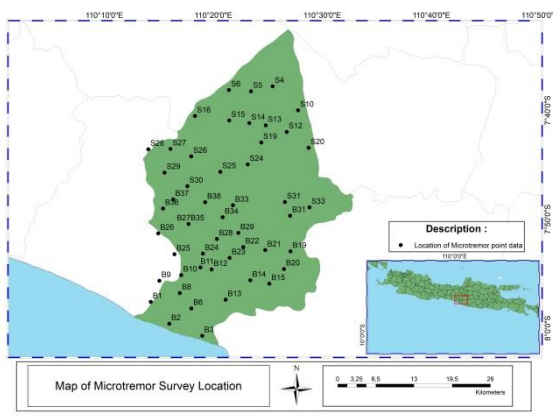

Figure 2: Location of microtremor data.

Microtremor data used as input for HVSR (Horizontal to Vertical Spectral ratio) process. This method is used to identify soil characteristic determined from amplification of sediment layer in the top of bedrock (Nakamura, 2008). Mathematical formulation of HVSR process (Almendros, et al., 2004) mentioned in Equation 1, could be defined as a ratio from the horizontal component of observed microtremor data with their vertical component. Calculation of observed HVSR curve helped by Geopsy software which developed by SESAME (Site Effects Assessment using Ambient Excitations) European research project.

Theoretically, there are assumptions in HVSR. Piña-Flores et al (2016) mentioned that H/V or HVSR curve consists of all body and surface waves, so that assumption is named as diffuse field assumption. The H/V curve is also proportional with the ratio from diffuse field energy based on their direction. It is written in Equation 2 as the ratio from the imaginer part of the green function (Sánchez-Sesma et al., 2011). So, this assumption is used to make a theoretical curve that will be compared with the observed curve in the inversion process.

After calculations of the observed HVSR curve and theoretical HVSR curve are done, the next step is the inversion process, in which both curves have compared each other. There are iterations processes which all calculations will be repeated until we found minimum misfit. Misfit, also known as error, is the difference between the observation curve and the theoretical one. The inversion process was done by using HVInv software (Sánchez-Sesma et al., 2011; Piña-Flores et al, 2016).

The initial model to make the first theoretical curve was collected from MASW data. MASW data are based on the ground roll principle. From the inversion of the dispersion curve by using the least square method (Park, 1997), we got the initial velocity of the P and S waves. All inversion process from MASW data are calculated using SeisImager software tool. Meanwhile, the initial density data were obtained from a geological map from Sukandarrumidi (1995).

Change of model (also called as a neighbor model) from inversion process are calculated with perturbation model using simulated annealing algorithm based on Yamanaka (2005). The next generated model was made reflected from some of the thresholds. Where if the difference between the misfit of the generated model and the misfit from the past model had a negative value, the neighbor model is used as the next initial model. If the difference was a positive value, last the initial model was kept as the initial model. Another threshold used is the probability function as seen in Equation 8.

The output from inversion process is the velocity model of S wave and P wave at each point. Therefore, to get the v_{s30} value, each of v_s models is processed by Equation 9. After we got the v_{s30} value, the last step was an interpolation. All the v_{s30} data was interpolated into the v_{s30} map.

Calculation of HVSR curve from observed data using:

$$HVSR(\mathrm{f}) = \frac{\sqrt{A_{east}(f)^2 + A_{north}(f)^2}}{A_{vertical\,(f)}} \qquad (1)$$

Where A_{east} is amplitude from east-west component and A_{north} is amplitude in north-south direction. Meanwhile $A_{vertical}$ is amplitude from up-down direction.

Calculation of HVSR theoretical curve using:

$$\frac{H}{V}(x,\omega) = \sqrt{\frac{Im[G_{11}(x,x;\omega)] + Im[G_{22}(x,x;\omega)]}{Im[G_{33}(x,x;\omega)]}} \qquad (2)$$

$G_{ij}(X_A, X_B; \omega)$ are expressed as green tensor from X_B point and X_A point.

The inversion process is based on:

$$E = \sum_{i=1}^{n} \frac{(HV_{obs}(\omega_i) - HV_{theo}(\omega_i))^2}{\sigma_{HV}(\omega_i)^2} \qquad (3)$$

Misfit or E are calculated from observed curve with theoretical curve. HV_{obs} is amplitude observed curve at each frequency, on the other side, HV_{theo} is from theoretical curve. Standard deviation written as σ_{HV}.

Perturbation model is calculated using:

$$m_1{}^i = m_0{}^i + y_i\left(m_{max}{}^i - m_{min}{}^i\right) \qquad (4)$$

m_{max} and m_{min} are upper and lower limit from model changes, define by researcher. Initial model is m_0 and neighbor model is m_1. Parameter which control change of value in model is y_i.

$$y_i = sgn(u_i - 0{,}5)T_k\left[(1 + {}^1/_{T_k})^{[2u_i - 1]} - 1\right] \qquad (5)$$

This calculation using random number which distributed randomly from 0 to 1, in Equation 5 expressed as u_i. T_k is cooling schedule shown in Equation 6.

$$T_k = T_0 \exp(-ck^a) \qquad (6)$$

a and c are constants. Meanwhile T_0 is initial temperature, also define by researcher. Number of iterations expressed as k.

Misfit is the difference of neighbor model with initial model, written as

$$\Delta E = E(m_1) - E(m_0) \qquad (7)$$

Misfit or error from neighbor model is $E(m_1)$ and misfit from initial model is $E(m_0)$.

Probability function to determine whether the model is accepted or not is calculated using:

$$P = \exp\left({}^{-\Delta E}/_{T}\right) \qquad (8)$$

Probabilty function or P are exponential function with T is temperature corresponded to number iteration.

PROCEEDINGS
JOINT CONVENTION BANDUNG (JCB) 2021
November 23rd – 25th 2021

The v_{s30} is calculated using:

$$v_{s30} = \sum h_i \Big/ \sum_{i=1}^{N} \left(h_i / v_i \right) \qquad (9)$$

h_i is thickness of layer and v_i is shear wave velocity in corresponded layer

Flowchart of this research is shown below in Figure 3.

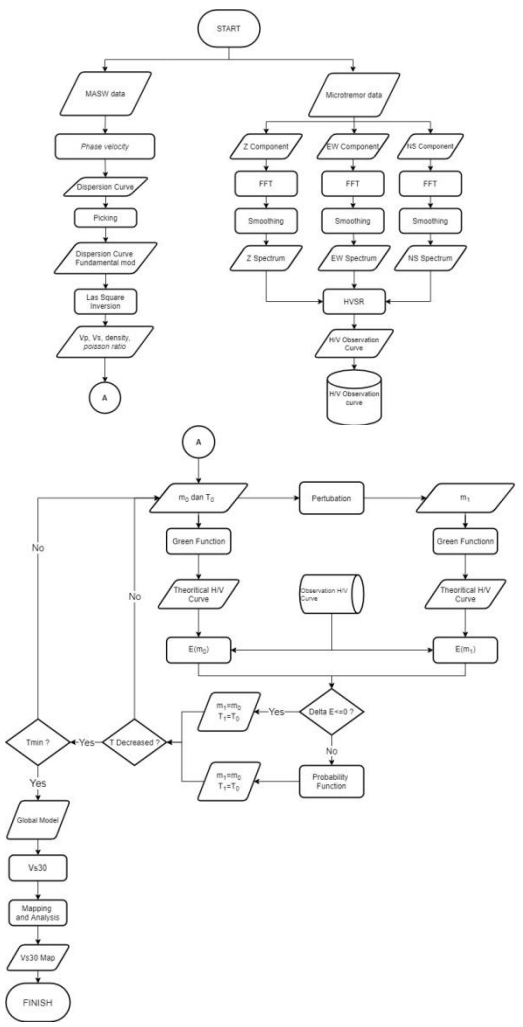

Figure 3: Flowchart of the research.

Result and Discussion

1-D Shear Wave Velocity each Points

The south side of the study area has a low value of v_s until 30 meters depth. It shows the sediment thickness of the layer around each point is thick. There are some points that have low velocity layer in the south side, for example, B1 and B8. For B8 value of v_s relatively higher than others, but the thickness of low velocity layer was found bigger than others too. It is shown that the south side of the study area has a value of v_s from around 175 until 750 m/s, which a higher value could be found in B8.

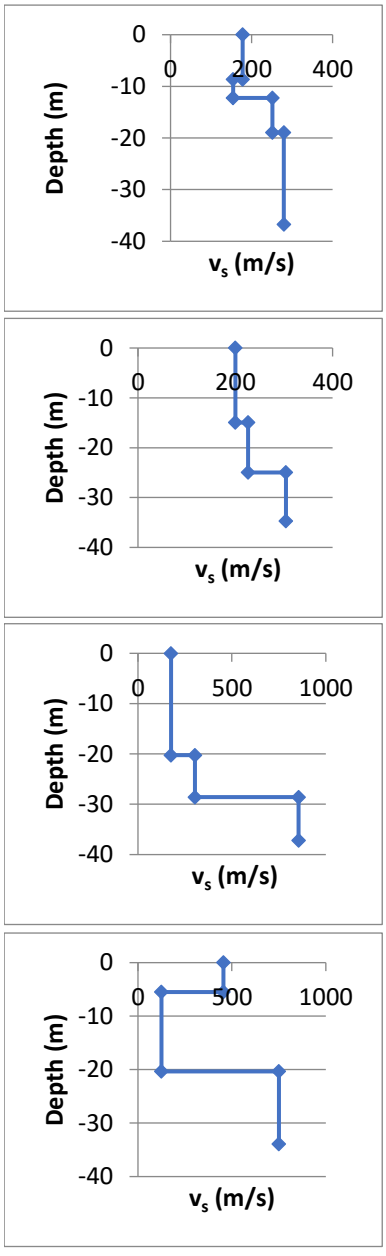

Figure 4: 1-D v_s model from some example points in south side area, a) B1, b) B2, c) B6 and d) B8.

Based on the research of Naing et al (2009) in Figure 6a, there are some correlations of 1-D v_s model. The result of SASW method used by Naing et al shows some similarities. The result in the Sanden area from Naing et al (2009) shows the same range value with B1 and B2. There is low velocity layer from 5 to 8 meters depth which is also found in B1. Meanwhile, B6 and B8 are slightly different where both have higher values than the result of the Sanden area. That result shows B1 and B2 are relatively homogeneous and same geological structure with Sanden area result and show that all the southside area is heterogeneous.

The middle side of the study area relatively has higher shear wave velocity than the south side. It means, on the

middle side, the soil characteristic is denser than on the south side. Since the sedimentation process in lower topography areas has high sedimentation deposits, this 1-D result can show that. As we know the south area is a lower topography area, so the sedimentation deposit is thicker than in the middle area.

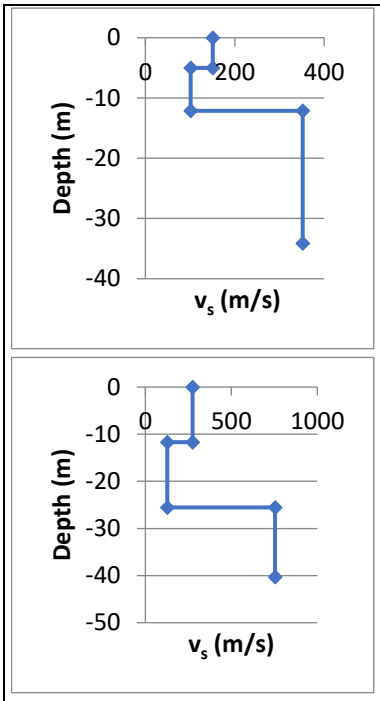

Figure 5: 1-D v_s model from some example points in south side area, a) B28 and b) B34.

B28 and B34 as examples, show the same pattern of 1-D v_s model. Where two of them have low velocity layer. The B34 low velocity layer is thicker than B28.

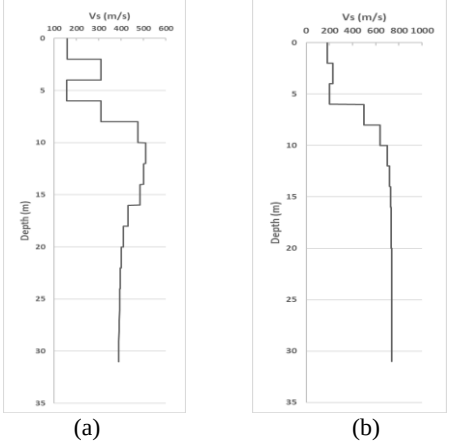

Figure 6: 1-D v_s model from Naing et al (2009), a) Sanden and b) Bantul.

This result also shows sedimentation phenomena. The Low velocity layer could be formed when the layer is sediment. By some process, it is cover with some materials which will be weathered later. B34 has low thick sediment layer, as could see in Figure 5b. Topography of B34 is higher topography area than B28 make B34 have a low sediment layer. Also, because geology in middle to the north side of Yogyakarta is old Merapi sedimentation formation which is denser than young Merapi sedimentation formation.

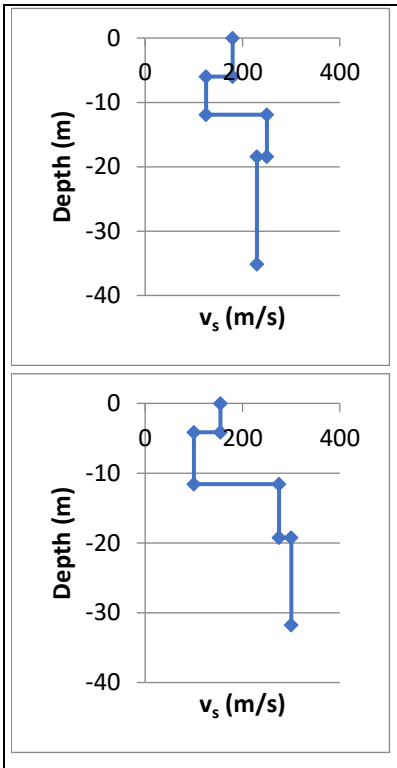

Figure 7: 1-D v_s model from some example points in west and east side area, a) B9 and b) B13.

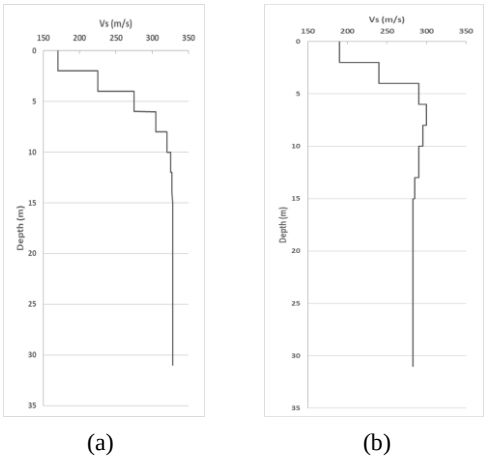

Figure 8: 1-D v_s model from Naing et al (2009), a) west Yogyakarta and b) east Yogyakarta.

Similarities were also found with the result from Naing et al (2009) as shown in Figure 6b. The result in Bantul area was correlated with the middle area Yogyakarta. From Naing et al (2009), the v_s value is from 200 to 750 m/s, which is quite similar to B28 and B34. B28 has a lower value because the location of B28 is in lower topography.

The west area of Yogyakarta has a thick sediment layer. Based on B9 v_s model, low values of v_s around 150 to 250 m/s are found until 30 meters depth. This result shows until

30 meters depth are still sediment layer. Sunardi et al (2017) also described that west area of Yogyakarta has 20-30 meters of sedimentation layer.

Like the west area, the east area of Yogyakarta also has a thick sediment layer. For example, B13 v_s model where is on the east of Yogyakarta. 1-D v_s model from B13 shows until 30 meters depth range values of shear wave velocity are relatively low. v_s has value from 150 to 300 m/s up to 30 meters depth.

The result from the west and east area are also correlated to Naing et al (2009) result. From Naing et al 2009, values of v_s are similar. Until 30 meters depth, either west or east area have low shear wave velocity value. It means both the west and east area have thick sediment layers.

Unlikely other sides, the north side of Yogyakarta have high v_s values based on their 1-D model result. For example, S27 and S6 points. S27 has a low sediment layer around 7 meters thick. Meanwhile, S6 is composed of high velocity layer.

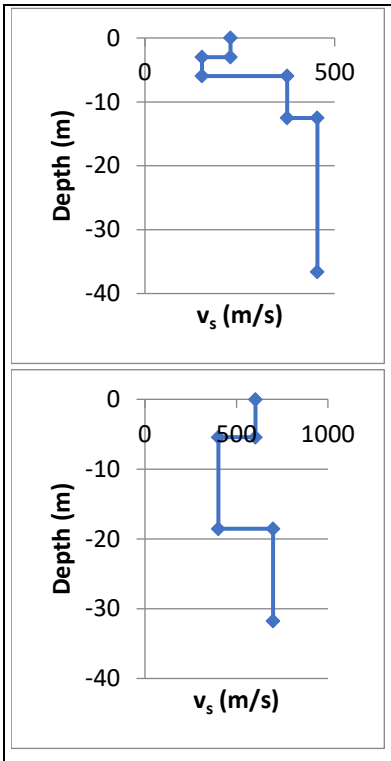

Figure 9: 1-D v_s model from two sample points in north side area, a) S27 and b) S6.

Location of S6 where higher in topography shows topography effect in sedimentation process. Almost all of datasets on the north side are in high topography. Make all of them have high v_s value. The other reason is the geological structure on the north side which consist of rock include andesite and basalt rock.

Based on the analysis of the 1-D v_s model, there is an advantage of using simulated annealing inversion. The advantage by using this algorithm is the low velocity layer could be found.

V_{s30} map

All 1-D v_s models from each data point were interpolated into 1 map. The result shows that almost the east side of the study area has low v_{s30} values. This low v_{s30} value shows that characteristics from the east side are soft soil. This type of soil is dangerous to earthquake ground shaking, which could make an amplification effect. The result also correlated with impact data from earthquake 2006 in Figure 12, where the most significant impact is on the east side.

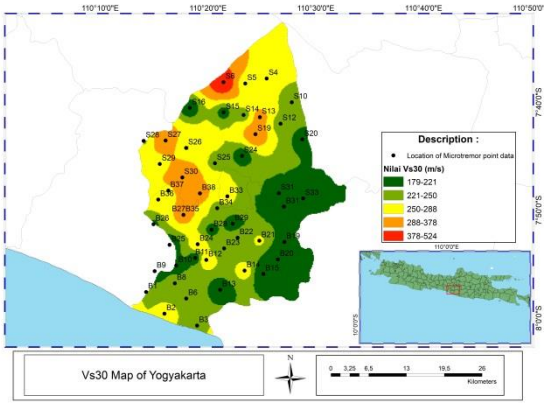

Figure 10: v_{s30} map. The green to red color scale indicates areas with low to high values, respectively.

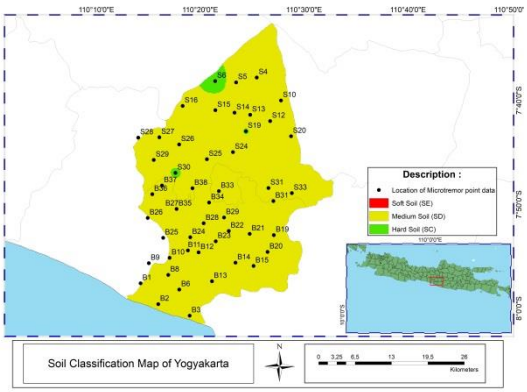

Figure 11: Soil classification map. The green color scale indicates the hard soil whereas the yellow is medium soil.

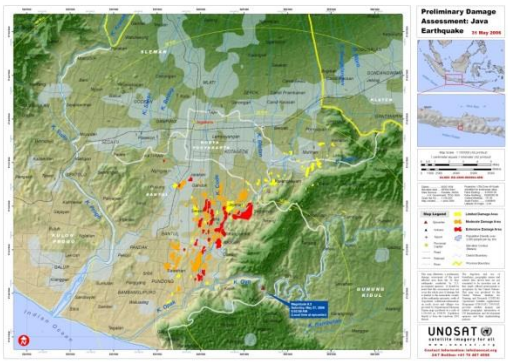

Figure 12: Areas damaged by the Bantul 2006 earthquake. The red color scale indicates heavily damaged and the yellow is slightly damaged.

The south side areas also have low v_{s30} values. It might be because the south side is in the lower topography area. The lower topography areas are the place where all the transport of sediment process ended. Therefore, it makes sediment deposits are thicker in the south side.

West to North side area have high v_{s30} values. This result could determine that the west to north sides have denser soil. The north side is also an area that has highest v_{s30} value. The area which has the highest value v_{s30} might be categorized as hard soil. The north side of Yogyakarta is

low v_{s30} value area. This could be concluded that the soil condition is very heterogeneous. Based on the impact map of the 2006 earthquake, easily we can see that some of the areas which far away from the source are also damaged by the earthquake. Low v_{s30} area might answer it. The area damaged by earthquake should be soft soil, so easily generate amplification effect.

Site class categorization can be seen in Figure 11. Almost all of them are categorized as medium soil with some hard soil. Also, there is one dataset categorized as soft soil in B20. Soft soil is dangerous for earthquakes. So, it is important to do a more specific survey in that dataset. That category of soil type is based on Badan Standardisasi Nasional (2012).

The v_{s30} map on this research then is compared to the research from Muzli et al (2016) in the same area. There are similarity patterns and range values. Based on Muzli et al (2016), the east side and south side are the areas that have low v_{s30} values. The same result is showed in the north area, where high v_{s30} are found there.

Misfit and probabilty function

Almost all of the misfits from each data set are relatively minimal. Most misfit is under 600. This misfit value is a collective error from each amplitude between observed data with theoretical data. It could be concluded that the result from inversion is good related to their misfit and secondary data from geological structure or past research.

As mentioned before, the probability function decides the model is accepted with the real condition or not. Lower misfit has a higher chance one model could be accepted with real conditions (Beaty et al, 2002). At some point, it does not always the same. Sometimes higher misfit shows real soil condition. So, it is important to validate the result with geological data or past research.

Misfit is also controlled by temperature from inversion process. The change of temperature is related to the thermodynamics principle. The lower temperature could be reached by a substance is proportional to the energy that is released. Energy in this case is a misfit. So, if inversion process could reach minimum temperature in the same way misfit will be minimum too.

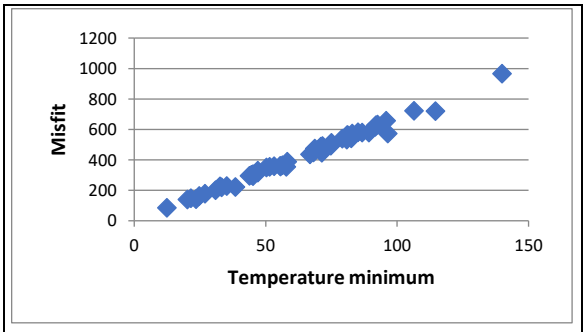

Figure 13: Correlation between misfit and temperature.

Conclusions

From the result, we can conclude this research as follow:

1. Either 1-D v_s model or v_{s30} map show the values that can be concluded as most areas of Yogyakarta are medium soil. Some of the hard soil and soft soil type can be found too. It is important to underline the fact that medium to soft soil types are dangerous for earthquakes, it can be seen from the impact of the 2006 earthquake.
2. Simulated annealing can make reliable v_s model, which can be seen from some low velocity layers are found. This algorithm can be an alternative method which more reliable and effective to find a proper model for site class and soil characteristic investigation.

References

Almendros, J., Luzon, F. And Posadas, A., 2004, Pure and Applied Geophysics, **161**, 1579-1596.
Badan Standardisasi Nasional, 2012, **1726**, BSN.
Beaty et al, 2002, Geophysical Journal International, **151**, 622-631.
Grandis, H., 2009, Himpunan Ahli Geofisika, Vol -, Ed -.
Martin, A.J. and Diehl, G.J., 2004, 13th World Conference on Earthquake Engineering.
Muzli et al, 2016, Jurnal Meteorologi dan Geofisika, **1**, **17**, 25-32.
Naing et al, 2009, Journal SE Asian Applied Geophysics, **2**, **1,** 60-77.
Nakamura, Y., 2008, The 12th WCEE.
Park, C.B., Miller, R.D. and Xia, J., 1997, Kansas Geological Survey.
Piña-Flores et al, 2016, Geophysical Journal International, **1**, **208**, 577-588.
Sánchez-Sesma et al, 2011, Geophysical Journal International, **186**, 221-225.
Soehaimi, A., Marjiyono and Setia, N.R, 2016, Geomagz, **2**, **6**, 30-33.
Sukandarrumidi, R.W. and Rosidi, H.M.D., 1995, Pusat Penelitian dan Pengembangan Geologi, **2**.
Sunardi et al, 2017, Jurnal Riset Geofisika, **2**, **1**, 47-53.
Supartoyo, Abdurahman, O. and Kurnia, A., 2016, Geomagz, **2**, **6**, 18-23.
Trisnaning, P.T., 2015, Proceeding seminar nasional kebumian ke-8.
Yamanaka, H., 2005, Tokyo Institute of Technology.

Acknowledgements

Thank you to all the institutions who support this research. Especially for the Meteorological, Climatological, and Geophysical Agency of Indonesia (BMKG) by supporting the data of this research, and also State College of Meteorology, Climatology, and Geophysics (STMKG).

PROCEEDINGS
JOINT CONVENTION BANDUNG (JCB) 2021
November 23rd – 25th 2021

Internet of Things Application used Arduino Based Fuzzy Logic Method for Flood Disaster Mitigation on Krukut River, Jakarta Selatan Indonesia

Adi Gunawan[1]

Geopangea Reasearch Group [1]

History recorded DKI Jakarta area flooded in 1619 when the Dutch East Indies government. The flood was caused by the geology aspect and morphometry of the thirteen river flows that crossed the DKI Jakarta area so that it became access for surface water flow (direct runoff) sourced from rainfall. Height of rainfall with an average of 208-256 mm that it can not accumulate standing water of 135x6 M^3 (one hundred thirty five million cubic) in the city.

The thirteen streams, there is the Krukut river watershed which has a morphometry of 37 km long, 98 km2 wide and the lowest elevation of 117 meters which has an impact on flood disasters in DKI Jakarta, changes in morphology, spatial planning, narrowing and silting of watersheds (DAS).) the Krukut river caused a two-meter flood residential areas in South Jakarta without any predictions and warnings, causing material losses. Referring to these problems, people needs fast and accurate data for alert system during a disaster so that disaster necessary actions can be organized quickly, accurately, and thoroughly by government agencies. Information and communication technologies have a majorrole in helping the process of collecting data accurately and fast. Therefore utilization of IOT (Internet of Things) technology by arduino device using the fuzzy logic method to determine the percentage of flooding that will occur. Installation of three main sensors in the form of 1). Ultrasonic 40 Khz : High water level 2). Tipping bucket: Application of local rainfall 3). Flow water meter : water velocity. The sensor will give a report flood alert status to microchip.

Data processing on the Arduino Microchip will calculate and send warnings of rainfall, alert status, and flooding potential through the android application and automatically display the data on the mobile phone dashboard in real time. the use of microcontroller technology in areas that often experience floods will make it easier to carry out disaster mitigation to reduce material losses and reduce the number of fatalities.

Keywords : *Flood, Disaster,* Arduino, Fuzzy logic, *Warning Alert*

Background

Floods disaster cannot be separated from the lives of people living in the DKI Jakarta area and its surroundings capital. Some areas are hit by floods every year, so that it can cause huge losses for the government and people. Naturally, flooding in DKI Jakarta is a natural and man-made factor, which geological conditions affect that process. With advances in technology such as Internet of Things (IOT), able to help the people. Develop of a alert security system to announcements a sign if there is a change in the condition of changes in the character of the river such as water level, speed of water discharge and local rainfall conditions.

Geology Regional

Study area is dominated by quaternary deposits with tertiary bedrock, bounded on western is Tangerang High and on eastern is Rengasdengklok high Figure 1. Sedimentary basin are thickening towards to the east and thinning between Pamanukan-Jatibarang. The southern region is bounded by the Mount Gede-Gunung Salak quarter volcano. Quaternary deposits are volcanic alluvium fan units, coastal alluvium units, and rivers, those lithology unit are interfingering. Thickness of the sediment deposit is estimated 65 meters (in the present Ciputat area) to 300 meters (in the present Jakarta Kota area). Whith lithology dominan are clay (claystone), marl (marl) and reefal limestone layer that was deposited on Pliocene. Quaternary deposits are located unconformably above tertiary sedimentary bedrock (Martodjodjo 1984). Quaternary deposits are formed by Plio-Plistocene (1–2 million years ago) to recent, with lithofacies is volcanic fan deposits resulting volcanic eruptions southern of Jakarta. During this period there was a process of erosion, developed of river channels, coastal plain, and shallow marine sedimentation. This stage resulted in quarterly deposits in depocenter of Jakarta are Volcanic fan alluvium, river channel, and coastal deposits that have an interfingering correlation. That provenan sediment Volcanic Fan Alluvium from Mount Gede and Mount Salak. Deposition area from the Bogor area which spreads to North Jakarta. which has a elongated coastal plain morphology directional west to east bounded with java sea, with altitude 0–16 m above sea level and slope 0–1%. Lithology dominant is clay to coarse sand. These geological conditions have the potential for flooded areas in DKI Jakarta.

Morfometry & Hidrology

Jakarta has a flood abundant morphology. The flood plain is an area formed by the sedimentation process during a rainy and flood. Generaly flood plains are located around meandering rivers or confluence of a tributary with the main river such as ; Ciliwung River and Krukut River. With the existence of thirteen rivers that cross the city of Jakarta, that impact in many scattered floodplains Figure 2 .

Thirteen rivers that cross the city of Jakarta, the Ciliwung River is the river with the largest contribution to the potential for flooding in the DKI Jakarta area. According to NEDECO (1973), Ciliwung Watershed (DAS) is about 347 km2, the widest compared to the other. Length of the Ciliwung River flow upstream position in the Mounth Gede and Mounth Pangrango area (Bogor) to its downstream area in the Pluit

(North Jakarta) area is 117 km, the longest compared to other river flows, Budi Harsoyo (2012).

Furthermore Krukut River also contributes significantly to the potential for flooding in the south Jakarta area. The Krukut watershed has an area of about 98 km2 with a main river flow length of 37 km, the highest elevation is 7 and the lowest is 117 meters.Tabel.1. The Krukut River flows through many villages, densely populated settlements and slums. The flow of this river also has direct access to the heart of Jakarta, where the location of the Central Government is located, so if the average rainfall is above >150mm/day until 208-256 mm/day, the river overflows and floods South Jakarta in a relatively long time so that it has an impact on economic, social and other activities. government centered in the city of Jakarta Figure 3. This study introduces the findings of a flood disaster mitigation monitoring system in real time to control readings of rainfall, water flow velocity and water level installed in low river morphometry with IoT technology without requiring human interaction or from human to computer devices. avoid loss of life and material loss.

Methodology

Morphological, geology map data and interpretation flood risk maps as determination to the identification worst locations. Then Ultrasonic sensors, rainfall gouge sensor and water flowmeter working to sending a reading signal on watershed based on the program and then waiting for the signal to be received back by the reed switch, the data from the signal is processed using software and will send a buzzer that converts electricity into sound and displays a signal dashboard using a modem Figure 3. On each citizen's smartphone to find out the water level. The installation position of the tool is determined based on the character data and river morphometric conditions. those tool provides government solutions in providing solutions in handling flood disasters.

IoT Devices

Equipment built on this tool consists of several components including hardware and software Figure 4:

1. Microcontroller is a compressed micro computer manufactured to control the functions of embedded systems in machines, robots, and a number of other gadgets. A microcontroller is comprises components like - memory, peripherals and most importantly a processor

2. The Arduino is an open-source electronics platform based on easy-to-use hardware and software used to build electronics this projects. All Arduino boards have one thing in common which is a microcontroller

3. Buzzer Piezoelectric Piezoelectric sounders are sound components which generate sound suitable for use as input signals (including multi-tone, melody and so forth) without built-in oscillation circuits. This characteristic allows them to be used in a wide range of applications, using respon logic if 0 than on, and buzzer will noise.

4. A tipping bucket rain gauge is one of the most traditional tools used for weather station applications. These rain gauges include a rain-collecting funnel, two carefully calibrated “buckets” mounted on a fulcrum, and an electronic switch. Rain is channeled through the funnel to the one of the tiny buckets, or catchments. The catchment area of these buckets is usually only a few hundred centimeters squared. Once it fills, it becomes overbalanced and tips down, emptying itself into the outer shell of the gauge as the other bucket is raised to position for the next reading.

5. *Reed switch* The Reed contact switch is a lamina (normally open) which closes in the presence of a magnetic field, The logic output of the Reed Switch module produces a logic 0, when a magnet is attached to the Reed Switch, the logic output of the Reed Switch module changes to logic 1. This condition is used to detect rainfall conditions. Rain conditions are known to be 3, namely drizzling rain, moderate rain and heavy rain. Rain conditions can be distinguished by detecting how long the time lag between the first active reed switch to the second active reed switch.

6. Modulator Demodulator (MODEM GSM). The modulator is the part that converts the information signal into a carrier signal and is ready to be sent, while the demodulator is the part that separates the information signal (which contains data or messages) from the received carrier signal so that the information can be received properly.

Fuzzy Logic

Fuzzy logic developed boolean logic by Lotfi Zadeh in 1965, it presenting the idea of degrees in verifying a condition, that it allows a condition to be in a state other than true or false such as slow, rather fast, fast and very fast. Fuzzy logic has abilities such as reasoning in the human brain where a set can represent two linguistic variables at once based on the degree value. Case study in the Krukut river, the Fuzzy logic method is conditioned if the water level high on 150 Cm and the rainfall conditions are > 60 ml/min, it will give a gradual signal for Alert 1, Standby 2 and Alert 3, with the reference formula in Figure 5.

Installation Device for Reduce Flood Risk

The installation GPS (Global Position System) UTM point 6°18'30.8"S 106°48'07.3"E, the device uses the survey results of the flood maps, interpreted river characterizatio such as water flowmeter, water level, and a map flood distribution, then the tool system will work by reading the water level using an ultrasonic sensor and processed by a microcontroller on the river watershed Figure 6. Device will work based on water level conditions : standby 3 or standby 2 or standby 1. and the sensor will display of rainfall conditions with status of rain or moderate rain or heavy rain with the IoT mechanism are:

1. If water status condition standby three (3) is Normal and rain fall is drizzle. Devices will send data and dashboard information will showing risk flood potential 10-30%.

2. If water status condition standby two (2) is beware and rain fall is moderate to heavey. Devices will send data and dashboard information will showing risk flood potential 30-70%.

3. If water status condition standby one (1) is alert and rain fall is heavy-very heavy. Devices will send data and dashboard information will showing risk flood potential 70-90%.

Device will sending data and processed by the microcontroller with standby condition 1, the buzzer will sound to notify the surrounding community then send data and display the dashboard in real time. In the future, the tool will be combined with turning on the pump engine to siphon flood to flowing into the absorption green area.

Resume

Results of research and discussion, it is concluded such as :

1. Geomorphology of DKI Jakarta is a flood plain with the dominant lithology of the constituent being claystone which is impermeable to water.

2. The Krukut watershed has an area 98 km2 with a main river flow length of 37 km, the highest elevation is 7 and the lowest is 117 meters, with an average rainfall above >150 mm/min resulting in runoff in the lowlands.

3. This study introduces the findings of a flood disaster mitigation monitoring system in real time to control rainfall readings, water flow rates and water levels installed in low river morphometry with IoT technology

4. The design of an automatic flood detection monitoring tool that is connected to the Mobile Dashboard display has been successfully created and can be used.

References

Nedeco. 1973. Masterplan for Drainage and Flood Control of Jakarta, Jakarta Indonesia. Kementerian Pekerjaan Umum, Direktorat Jenderal Sumberdaya Air.

A. A. K. Ramadhan, E. Kurniawan & A. Sugiana, 2019. Perancangan Sistem Peringatan Dini Banjir Berbasis Mikrokontroller dan Short Message Service (SMS). Universitas Telkom bandung.

Harsoyo, 2013. Mengulas Penyebab Banjir Di Wilayah Dki Jakarta Dari Sudut Pandang Geologi, Geomorfologi Dan Morfometri. Jurnal Sains & Teknologi Modifikasi Cuaca, Vol 14, No.1, Juni 2013 Hal.: 37 – 43

Indriasari1, 2014 Analisis dan Perancangan Sistem Pengumpulan Data Bencana Alam. Program Studi Teknik Informatika, Universitas Atma Jaya Yogyakarta

Wicaksono, 2019 Rancang Bangun Alat Pendeteksi Banjir Menggunakan Arduino Dengan Metode Fuzzy Logic Jurnal Teknologi Elektro, Universitas Mercu Buana ISSN: 2086 - 9479

Muh. Ahyar, Muh. Fajri Raharjo, Ibrahim Abduh and Hafsah Nirwana, 2018 A Novel Prototype Of Flood Early Warning System Using Analytical Hierarchy Process (Ahp) Based Internet Of Things (Iot), ICIC International 2018 ISSN 2185-2766

M. Ridwan, S. Widiyantoro, M. Irsyam, Afnimar and H. Yamanaka, 28 July 2016 Development of an engineering bedrock map beneath Jakarta based on microtremor array measurements, Geological Society, London, Special Publications, 441, 153-165,

Tabel.1 Discharge Data Calculation Results with Area – Speed Method (continued)

Lokasi	Luas [m²]	Vm [m/s]	MA [m]	Q [m³/s]
Kali Krukut-Benhil	22.00	0.78	1.20	17.16
	35.00	0.92	1.70	32.20
	55.00	1.15	2.20	63.25
	78.00	1.23	2.70	95.94

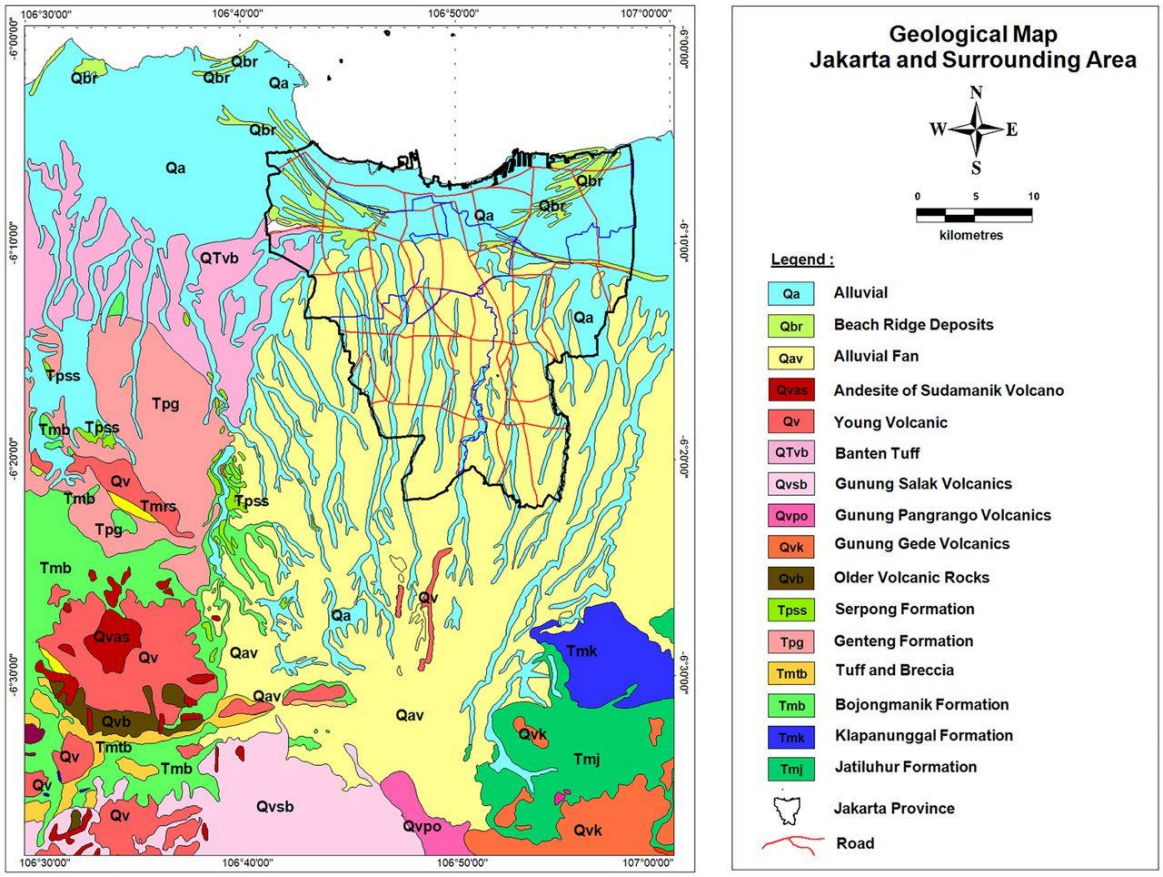

Figure.1 Geology Map of DKI Jakarta (modified from Turkandi et al. 1992; Effendi et al. 1998)

PROCEEDINGS
JOINT CONVENTION BANDUNG (JCB) 2021
November 23rd – 25th 2021

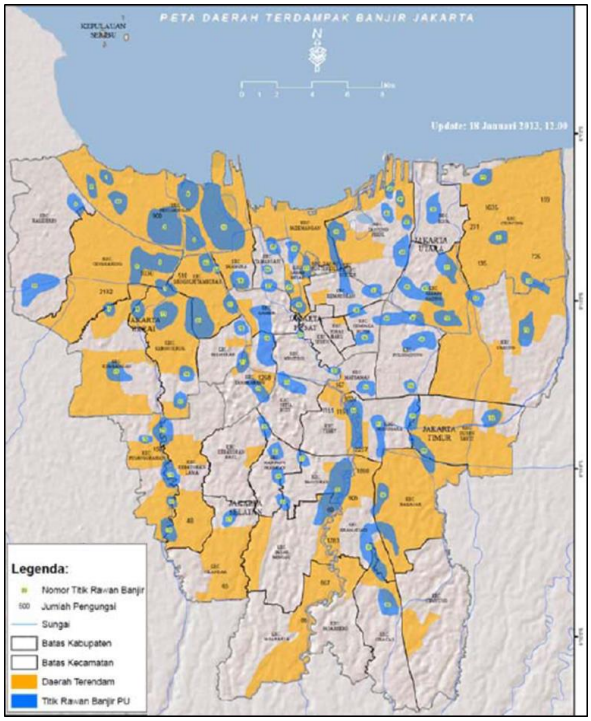

Figure.2 Flood Plain Jakarta Maps (BNPB)

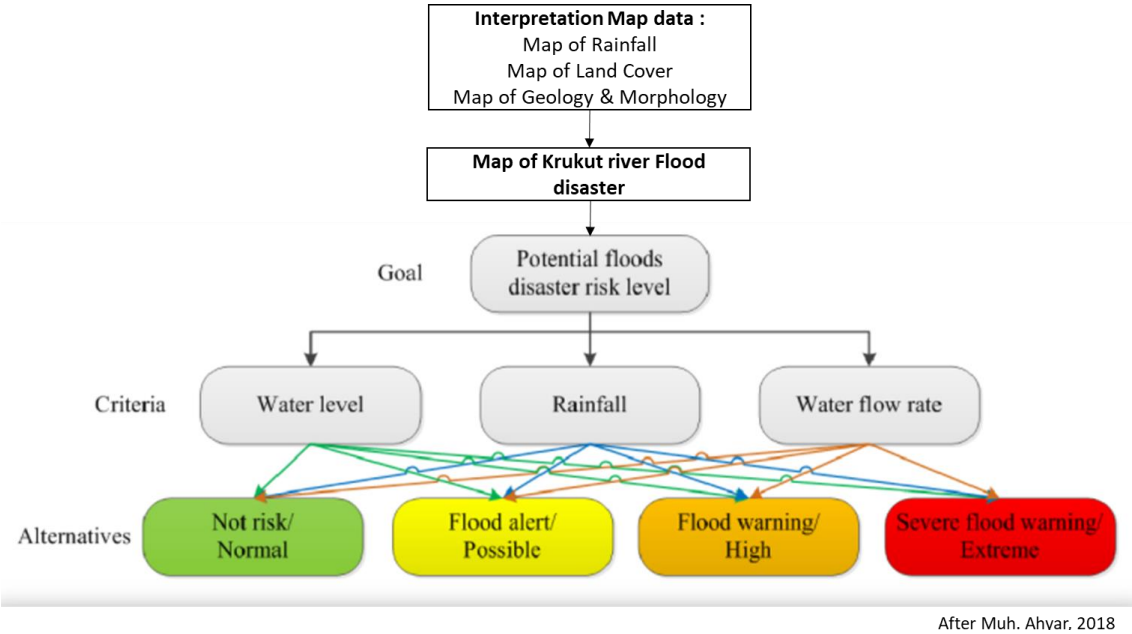

Figure.3 Data & Methodology

PROCEEDINGS
JOINT CONVENTION BANDUNG (JCB) 2021
November 23rd – 25th 2021

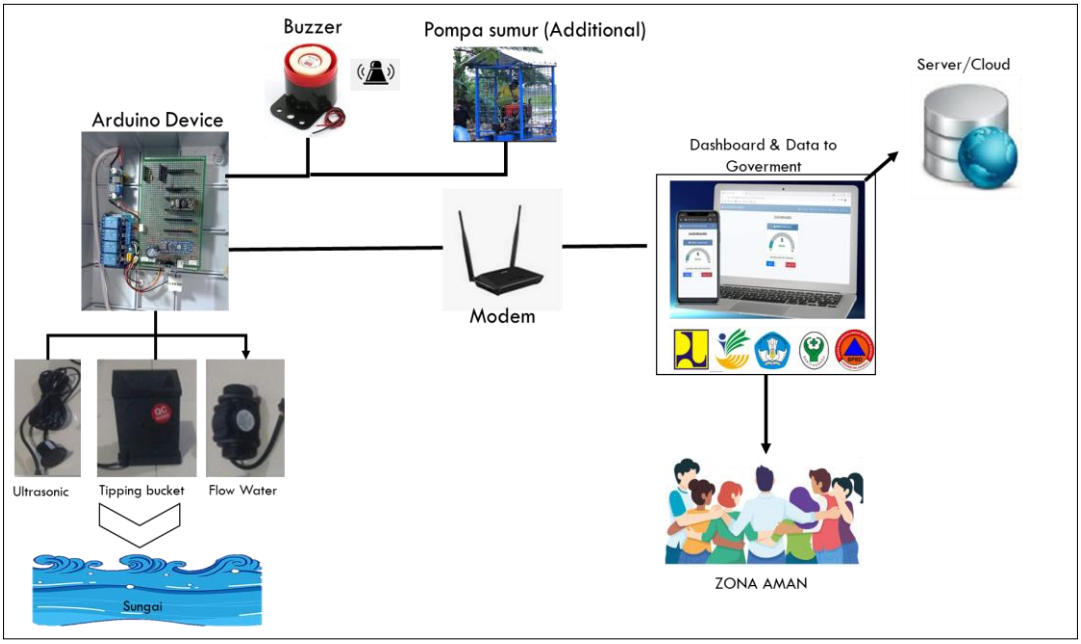

Figure.4 Alert System use IOT method

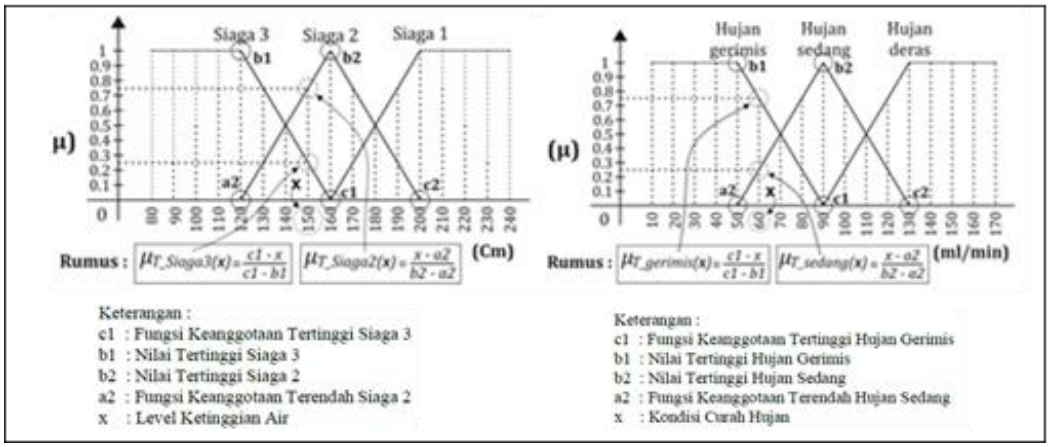

Figure.5 Fuzzy logic Formula using water level 150 Cm and rainfall 60 ml/minutes

Figure.5 (A) Krukut River and Device Installation (B) Flood plain condition house in Jakarta Selatan

PROCEEDINGS
JOINT CONVENTION BANDUNG (JCB) 2021
November 23rd – 25th 2021

Lesson Learned from Banjarpanji LUSI Mud Extrusion, Sidoarjo, East Java, Indonesia

Prihadi SUMINTADIREJA*, Bambang ISTADI**

*Applied Geology Research Division, Faculty Earth Science and Technology, Institut Teknologi Bandung, Jl. Ganesha 10, Bandung 40132, Indonesia, email: prihadi@gl.itb.ac.id
**Independent Consulting Geologist, Jakarta, Indonesia, email: Bambang.istadi@yahoo.com

Abstract

The objective of this paper is to revisit 15 years after the occurrences of mud eruption and source of ejected materials of LUSI area. On May 29, 2006, near the Banjarpanji-1 well marked the beginning of the ongoing mud flows covering the surrounding area, which still continues up to now. Several cited references demonstrate possible triggering mechanism for mud eruption. Speculative drilling theories and strong earthquake were amongst the hotly debated triggering mechanism.

The early research of several field works such as aerial photography, gravity, resistivity, and micro-earthquake monitoring resulted in a better understanding of the geology of the area. Subsequent investigations using sophisticated remote sensing using satellite aperture radar combine with GPS continues monitoring were deployed. Early mud eruption suggested the Late Pliocene over-pressured shale sequence as a major source of the mud, composed of 45% clay mineral (smectite, illite, kaolinite and chlorite), 45% quartz and 10 % others. Vitrinite reflectance data (Ro 0.64%) and paleontological correlations suggested the majority of mud source is from 4000-6000 ft depth. Log analyses of Banjarpanji-1 well, such as GR, Density and Sonic log, exhibit an anomaly within rock strata and indicated an under-compacted environment. More recently, a much deeper muds and rocks were indicated with gas sources related to a magmatic intrusion.

Although the occurrence of mud volcanoes in East Java is prevalent, but LUSI is a different case, and has been identified as a hybrid system, it is a sedimentary system with magmatic association, and hence has been described as a sediment hosted hydrothermal system (SHHS). More recent findings were the rare earth elements within Lusi mud, thought to have been found in quantities to be determined if can be economically extracted from the mud accumulations.

Keywords: LUSI (Lumpur Sidoarjo), over pressured shale, rare earth elements

Introduction

The LUSI mud volcano has been widely studied, written and discussed by many experts since 2007 and particularly more thoroughly and published in 2009 special edition of the journal of Marine and Petroleum Geology. The papers are wide ranging, from geology, geophysics, geochemistry, drilling engineering and other special approaches.

This paper's aim is to mainly discuss the early stages of research designed to describe and understand the mud volcano phenomena and how to best deal with the problem of mud eruption. Quick and prompt yet proper actions were needed in selecting several methods of geological, geophysical and geochemical to gain data to identify specific subsurface conditions, which were causing and affecting the mud eruption. Most of these early-stage surveys and study results were discussed in Sumintadireja et.al. 2007, Istadi et,al. 2009. One of the more significant findings are the subsurface mud volume calculated based on gravity data and seismic data of about 910,000,000 - 1,400,000,000 m3. The assumption average mud eruption rate of 100,000 m3 per day, therefore, the eruption was predicted would last for another 25-38 years (PT. LAPI ITB, 2006, unpublished). This prediction changed the course of action on how to manage the eruption in a long term. The mud eruption is a unique phenomenon which has attracted many scientists worldwide.

Method

The early field surveys were designed to identify shallow and deep information of mud eruption, the adjacent and surrounding areas. In the first weeks of the mud eruption the priority was to estimate the daily mud flow rate, and to cope with the problems, the

PROCEEDINGS
JOINT CONVENTION BANDUNG (JCB) 2021
November 23rd – 25th 2021

simplified workflow is shown in Figure 1. An aero-modelling remote sensing using simple plane equipped with GPS and fly 300 meters above ground were applied. During those days in 2006 there were no drones like nowadays. Subsequently, combined with ground check measurement of mud depths using simplified bamboo metering. Therefore, the volume in the surface is calculated from the multiplying the area covered the mud with the mud depths at multiple points, divided with number of days of flow activities. An estimated flow of 50,000 m3 per day was derived and reported to the authorities after 2 weeks of field surveys . Field geological observations (Figure 2) approach was carried out in order to find the watukosek fault plane which was predicted have a major role as mud eruption channel(s). This dynamic geological condition caused difficulties to stop the mud flow using directional drilling, in other words the success of drilling activities was hard to attain. Trenching and shallow drilling are also carried out to find data which were correlated with fault reactivation.

Data

The faults are shown in Figures 3 and 4. Since the aim of the study was also to investigate soil condition shallow drilling data methods were used to calibrate the resistivity data measurements. Based on gravity spatial temporal measurements within 1 month interval period, the mud movements were clearly identified (PT. LAPI ITB 2006, Istadi et.al 2009). During the early stages continues geodetic monitoring surveys were also carried out by Abidin H.Z. et.al., 2008. In order to find the most possible location of mud, mud analysis such as X-ray diffraction is the appropriate tool. The result illustrates mud framework. Mud is composed by 45% clay mineral (smectite, illite, kaolinite and chlorite), 45% quartz and 10 % others. This composition demonstrates non carbonate environment for the source of mud. Moreover, vitrinite reflectance data (Ro 0.64%) suggest source of mud equivalent to depth 4000-6000 ft. To sum up, mud was originated from non carbonate or clastic sequence of the Late Pliocene shale sequence. An under compacted zone exists within Plio-Pleistocene strata. Sonic logs (DTC) of Banjarpanji-1 well exhibit an anomaly within rock strata. This zone is located between 2800 and 6200 ft depth and it is dominated by thick shale layer. Within this zone the velocity is not increasing with depth as the normal shale compaction. The velocity becomes slower with depth especially at depth ranges from 2800 ft down to 6200 ft. Comparison between GR log and density log demonstrate interesting features. The drawing straight line on the assumed shale base line, there are two separated layer that have low GR with low density. These two layers (4400-4800 ft, 5400-5800 feet) are still shale layer as a represented by cutting sample. The possible explanation why those two shale strata have lower GR and lower density is as follow. Due to the faulting, the thick shale strata were crushed and forced as fault zone. Moreover, the undercompacted zone is segmented into three overpressure zones, the interval between 3652-4400 ft (OP-1 interval), 4800-5400 ft (OP-2 interval) and 5800-6200 ft (OP-3 interval). Only two intervals, OP-1 and OP-2, have maximum water saturation as indicated by resistivity of these zones. Resistivity of un-invaded zone is as high as resistivity of water (0.32 ohm). Two separated fault zones also exist within under compacted zone. They are 4400-4800 ft and 5500-5800 ft interval. Between OP-1 and OP-2 are separated by fault zone that consist of cataclastic material. This fault zone is characterized by lower GR, lower density, and slower compressional velocity compared to adjacent strata. The first fault zone has the highest water saturation compared to other zones and it is acting as conduit and escape route for mud and water from over pressured zone.

Discussion

The latest study 10 years of Lusi eruption: Lessons learned from multidisciplinary studies (LUSI LAB), have been published in Marine and Petroleum Geology, 90, 2018 which contains publications of many serious follow up research to supplement the early field surveys carried out by LAPI ITB. More recent studies describing the mechanism of reactivation watukosek fault during Plio Pleistocene period, based on integrated approach by Andrea Moscariello et.al., 2018, the summary of the results confirmed a large deformation zone complex referred as the Watukosek fault system has previously been identified. The early deformation phase causing the development of basement segmentation in the E-W orientation developed. The N40ºE orientation of Watukosek fault system as tensional lineament, possibly during Middle Eocene. The present-day N40oE oriented sinistral strike slip Watukosek At depth, the Watukosek fault system is linked to a complex of synthetic and antithetic fault segments forming large triangular fault zones, deeply rooted in pre-Oligocene successions.

Recent Studies, the rare earth elements contained in mud sample has already been scrutinized by Didi Supriadi et.al, 2017, this important information needs to be followed up with a possible resources calculation for commercial purposes. The fault plane information and geological map of old mud volcano previously identified could have same potential to be explored. Nowadays, the rare earth elements study is one of the main priority data inventories done by Geological Agency.

Conclusions

Field observation is important in the explanation and analysis of the active fault reactivation. The

observation. However, should be supplemented by various geophysical measurement methods as well logging information from borehole. When combined, it is thought to be the best techniques in extracting information to revealing both shallow and deeper subsurface geological conditions. However, the already new available data and analysis makes the understanding about LUSI mud extrusion clearer.

References

PT. LAPI-ITB, 2006, Geohazard Surveillance of Banjarpanji Mud Extrusion Areas, Sidoarjo, East Java. Unpublished Report for PT. Lapindo Brantas Inc

PT. LAPI-ITB, 2006, Integrated Geological, Geophysical, and Geochemical Study of Mud Extrusion and Its Controlling Factors in Banjarpanji Area. Unpublished Report for PT. Lapindo Brantas Inc.

Sumintadireja P, Indro P. B. Istadi, A.B.Darmoyo, 2007, Geology and geophysics study in revealing subsurface condition of Banjarpanji mud extrusion, Sidoarjo, East Java, Indonesia, IUGG XXIV, Perugia, Italy.

Abidin, H.Z., M.A Kusuma, H Andreas, M.Gamal and P.Sumintadireja, 2008, GPS-Ba sed Monitoring of Surface Displacements in the Mud Volcano Area, Sidoarjo, East Java. In Observing Our Changing Earth, International Association of Geodesy (IAG) Symposia,.

A. Mazzini, H. Svensen, G.G. Akhmanov, G. Aloisi, S. Planke a.d, A. Malthe-Sørenssen, B. Istadi, 2007, Triggering and dynamic evolution of the LUSI mud volcano, Indonesia, Earth and Planetary Science Letters 261, pp.375–388.

B. Istadi, G Pramono, P Sumintadireja, S Alam, 2009, Modeling Study of Growth and Potential Geohazard for LUSI Mud Volcano East Java Indonesia, Marine and Petroleum Geology xxx 1-16.

Andrea Moscariello, Damien Do Couto, Fiammetta Mondino, Jacqueline Booth, Matteo Lupi, Adriano Mazzini, 2018, Genesis and evolution of the Watukosek fault system in the Lusi area (East Java), Marine and Petroleum Geology 90 pp. 125-132.

Didi Supriadi Agustawijaya, Karyadi Karyadi, Baiq Dewi Krisnayanti, and Sutanto Sutanto, 2017, Rare earth element contents of the Lusi mud: An attempt to identify the environmental origin of thehot mudflow in East Java – Indonesia, De Gruyter Open Geosci. 9. pp. 689–706

PROCEEDINGS
JOINT CONVENTION BANDUNG (JCB) 2021
November 23rd – 25th 2021

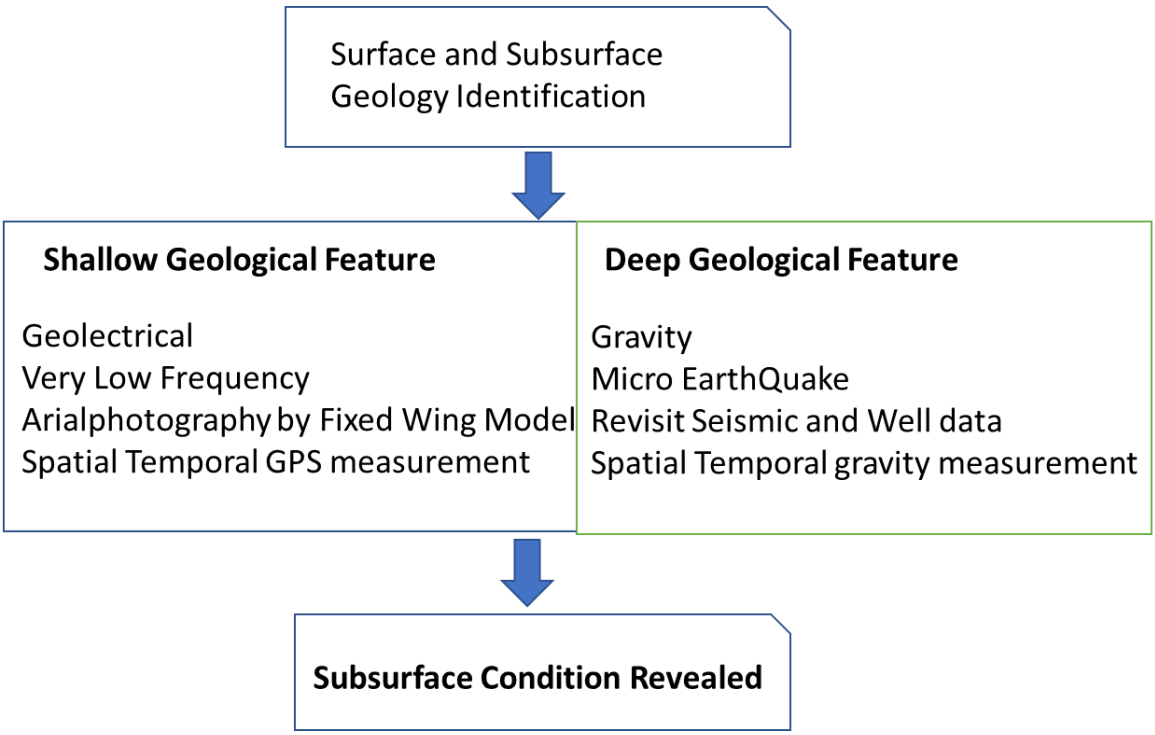

Figure 1: Simplified Flow Chart

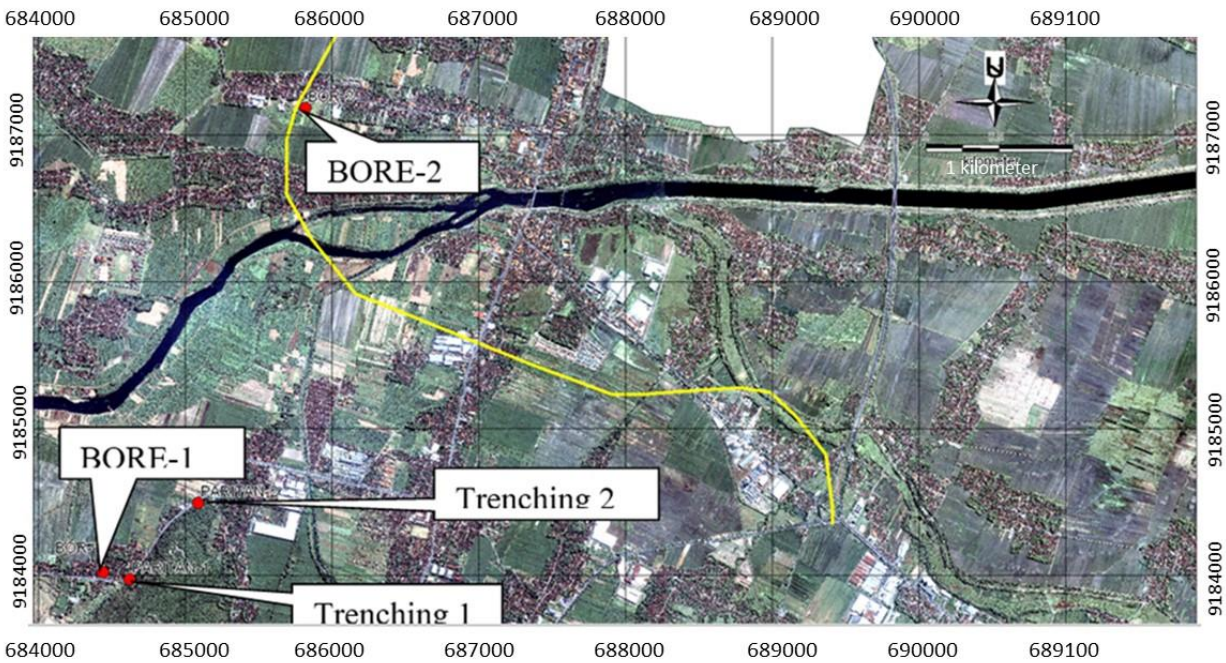

Figure 2: Observation of shallow drilling and trenching (2x3x5 meter size)

frame.

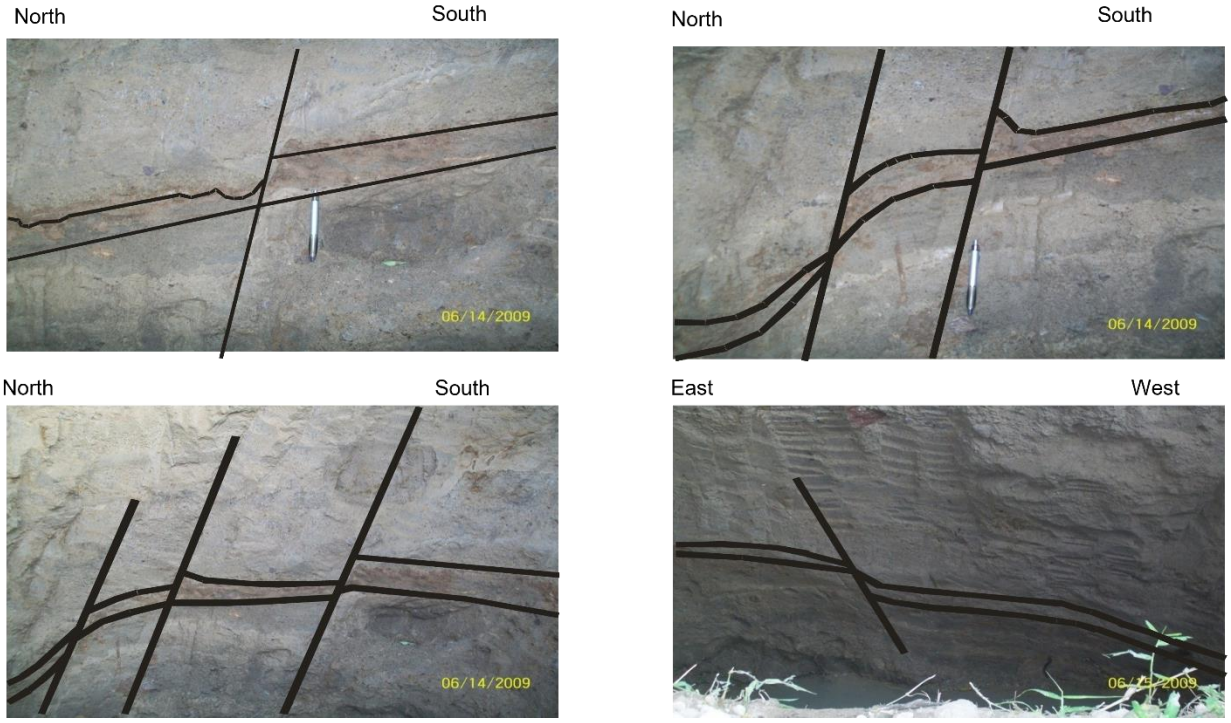

Figure 3: Trenching Location 1, Showing layer offset with West East plane

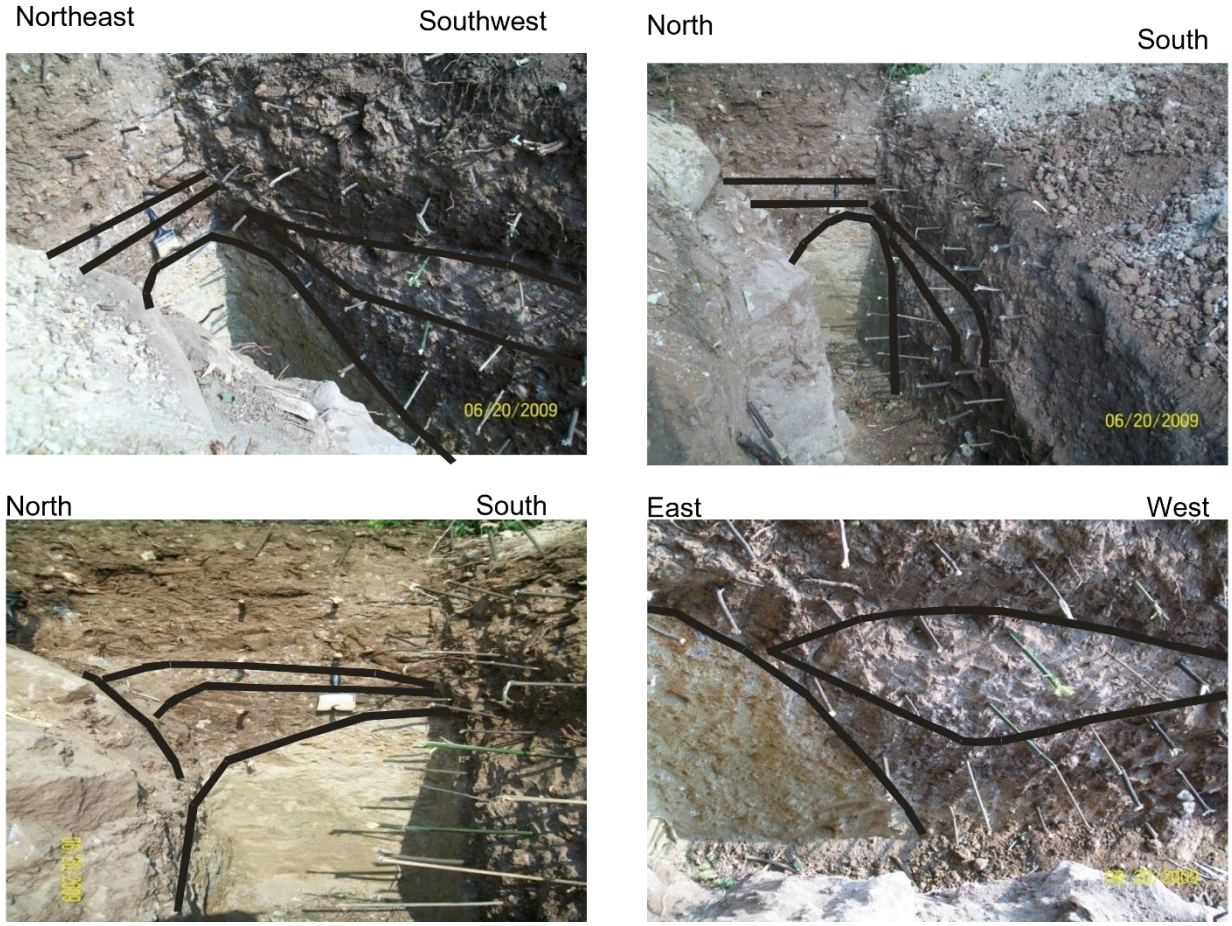

Figure 4: Trenching Location 2, Showing layer offset with West East plane

PROCEEDINGS
JOINT CONVENTION BANDUNG (JCB)2021
November 23rd – 25th 2021

Identification and Characterization of Low Resistivity Pay Zone, Case Study "L" Field

Muhammad Ilham Barustan[1], Dirsya Felizarda Corbafo Siki[1], Elrey Fernando Butarbutar[2], Pambudi Suseno[2],
[1]PT Geosain Delta Andalan
[2]PT Pertamina Hulu Rokan Regional 1 Zona 4

Abstract

In general, sandstone reservoir containing hydrocarbons has high resistivity values based on the response of well log measurement. This is because hydrocarbons are unable or difficult to conduct electric current (resistive). However, in some cases, rocks with low resistivity value have the potential to become hydrocarbon reservoirs.

On the other side, the decrease of production makes the company need new approach to increase oil production. One of the alternative methods is to reevaluate the well log data in suspended well, especially in low resistivity pay zone. Low resistivity pay zone is a unique reservoir that usually identified as water bearing zone, but in fact has hydrocarbon potential. Test production on several wells in L Field shows the presence of hydrocarbon with resistivity value less than 10 ohmm (2 – 5 ohmm). By focusing on the low resistivity pay zone, the company can also reduce the production costs by opening new layers on existing wells instead of drilling new wells.

This paper focuses on identifying the main causes of low resistivity pay zone in L' Field, South Sumatera Basin. By using openhole log, core data, petrography analysis, and cutting data, it can be concluded that the main cause of low resistivity pay zone in this area are the presence of illite & kaolinite as clay minerals, sand shale lamination, silty-fine sand grain size and conductive minerals.

Keywords: *Air Benakat Formation, Low resistivity pay zone, Low resistivity reservoir, Shalysand*

Introduction

The low resistivity reservoir was initially considered unattractive because in general reservoir which contain hydrocarbon would have high resistivity. However, in some cases, rocks with low resistivity have the potential to become hydrocarbon reservoir.

L field is mature oil field operated by Pertamina that located in Prabumulih, South Sumatra Basin with more than 250 wells. The main reservoir target is from Talang Akar and Baturaja formation which deposited in Fluvial Deltaic to Shallow Marine environment. However, decrease in production and the downtum of oil price made the company must find the alternative ways to increase hydrocarbon production, one of the best strategy is to reevaluate well logging data in suspended well especially in low resistivity pay zone which initially considered as water bearing zone.

In 2019, the journey began, it started with collecting & digitizing well log data at the shallow interval because most of the well in L Field only have digital log (las) in main reservoir. After reevaluating the openhole log, core and cutting data, several layers of prospect zone were defined. These layers were tested with various result, some have unsatisfied result but others have promising opportunity.

Data and Method

The integrated analysis of openhole log, core and cutting data were performed in order to have better understanding of low resistivity pay zone. From openhole data, Gamma ray log show sand shale lamination, with resistivity value of oil bearing zone is about 2-2.4 ohmm which shows at well L-82 and L-215. On the other side, the resistivity of Gas bearing zone around 3 – 4.3 ohmm at well L-170 & LC-13.

Core data acquisition and analysis were carried out from Air Benakat Formation in well L-306. The cored interval consists of silty-shale and sandy-shale which can be divided into a lower interval of parallel laminated, sideritic silty shale (interval 666.00-687.10 m), and upper interval of faintly laminated silty and sandy shale (interval 660.00-666.00 m). The depositional environment is interpreted to be low energy, outer shelf to offshore and the upper shale may represent a slightly shallower environment than the lower shale.

Petrography data shows that rocks are containing common silt to sand grains with mean grain sizes are 0.03 to 0.2 mm. Grains are angular to subrounded, locally concentrated and appear as burrow structure and as laminae form. Grains is dominant with Quartz with rock fragment (chert, granitic and volcanic type), K-feldspar, plagioclase, and accessories minerals such as glaucony, muscovite, phosphatic material and chlorite.

Clay matrix is locally disrupted with bioturbation, and partially also replaced by microcrystalline siderite. But at several intervals, has strongly been replaced by microcrystalline siderite, and rock is called sideritized silty/sandy claystone. Secondary minerals area occurring as grain replacement and locally preserved

in primary pore and identified as siderite, kaolinite, calcite and pyrite. Illite and chlorite replace unstable grain and also recrystallized clay matrix. Calcite and pyrite is encountered filling chamber of foraminifera.

SEM image shows quartz (Qz) surrounded with clay matrix and the matrix is partially recrystallized to illite and kaolinite and replaced by siderite (Sid). Pyrite (Py) disperses in the matrix and locally is seen concentrated. Chamber of foraminifera filled by kaolinite, pyrite and clays, but sometimes by filled by cements and creates primary intraparticle pore. SEM image observations shows the abundance of clay matrix that would reduce reservoir porosity and permeability. The presence has disrupted the smooth fluid flows.

XRD result of L-306 showed that mineralogy are controlled by clay mineral (49%-62%), followed with quartz (26%-34%). Common siderite is recorded in several depth (2%-20%). The presence of high quartz is synchronized with thin sectioned observations that the rocks are containing common silt to sand grains.

Result and Discussion

Based on integration of openhole log, core and cutting data, the main causes of low resistivity pay zone are clay minerals, sand shale lamination, grain size and conductive minerals.

Clay minerals are classified into two, namely allogenic and authigenic clay. Allogenic clay is detrital clay, which comes from an area and is then transported from its source to another place with certain media. Authigenic clay is a clay mineral formed insitu during burial and affected of chemical reactions between rock fluids (pore water) and minerals (lithic fragments, feldspar, volcanic glass, and ferromagnesian minerals). Authigenic clay minerals in sandstones are generally divided into three, namely:

1. Discrete Particle or pore filling, clay structure formed from migrating clay flakes to fill voids between rocks. The clay flakes do not follow the shape of the rock grain surface but will form their straightness according to the direction of migration. This structure is usually formed in kaolinite clay minerals.
2. Pore-lining or grain coating, clay minerals are formed on the surface of the rock grains to cover the rock grains (coating). The clay minerals that make up the structure are chlorite, illite, smectite.
3. Pore bridging clay, formed when the clay-covered granules have touched each other to form new clumps, Clay minerals that make up the pore bridging clay structure are illite, smectite, and mixed illite-smectite.

Clay minerals can reduce resistivity readings because they contain bound water that is retained in the clay minerals. It is affected by the amount of these compensating ions constitutes the Cation Exchange Capacity which is commonly referred to asthe CEC (meq/ 100 g dry rock) or Qv (meq/ cm total pore volume). CEC is related to the specific surface area of a clay mineral. It has its lowest value in kaolinite and its highest values in montmorillonite. The larger the surface area it will hold very significant bound water.

Based on XRD data, it can be showed that illite and kaolinite are the dominant clay, where Illite has a high surface area. In authigenic clay which is distributed as pore-lining and pore bridging clay, it will hold very significant bound water in the clay which is spread out in hydrocarbon reservoirs. So that the reading of the hydrocarbon fluid is disturbed by the clay bound water.

Sand shale lamination is one of the factors that affect the reading of the resistivity log. Core and cutting data shows that the formation has sand shale lamination with thickness around 0.5 to 1 cm, meanwhile, the vertical resolution of the conventional log is about 5 to 80 cm. Thomas-Stieber Crossplot also shows that the distribution of clay minerals is Laminated (20-80%). This might affect the reading of the resistivity log because the lamination is too thin to be resolved. The reading of resistivity might appear low because the shale content of the lamination has higher conductivity (low resistivity) than the layer with hydrocarbon content, thus could bypass the potential zone.

Identification of grain size distribution on the target layer using petrographic data represented by the L-306 well. Petrographic analysis shows a silt-sandstone lithology with mean grain sizes are 0.03 to 0.2 mm. Grains are angular to subrounded, the finer the grain size of the rock, the higher the water saturation in the rock which cannot be replaced by hydrocarbons (Swirr). Reservoir with fine-very fine grain size would lead to high irreducible water saturation (Swirr). This would reduce the value of resistivity log although there might be hydrocarbon in its pores.

Each mineral has different conductivity properties. Conductive minerals are minerals that are good at conducting electricity when an electric current is applied. These minerals can reduce the resistivity log reading, so it will read low even though the rock contains hydrocarbons. Conductive minerals usually contain Ferrum (Fe) or Magnesium (Mg) element (ferromagnesian minerals such as Pyrite (FeS2) and Siderite (FeCO3).

Petrography and SEM analysis from Well L-306 showed the presence of these two minerals. SEM image detailed shows that that siderite replace partially clay matrix, where the clay matrix is locally dissolved resulting secondary pore (SP) and pyrite disperse within it.

Conclusions

The main causes of low resistivity pay zone On L Field are:

- Clay minerals composed by Illite & Kaolinite which hold very significant bound water in the clay that can disturb the reading of hydrocarbon content in the reservoir.
- Very thin sand shale lamination that can affect the reading of the resistivity log because of bad resolution. It can also make the resistivity of reservoir with hydrocarbon content appear lower because the shale content of the lamination has high conductivity (thus low resistivity).
- The grain size of silt-sandstone would lead to high irreducible water saturation (Swirr), because the finer the grain size of the rock, the higher the water saturation in the rock which cannot be replaced by hydrocarbons (Swirr). Therefore, reservoir with fine-very fine grain size would reduce the value of resistivity log although there might be hydrocarbon in its pores.
- Conductive minerals with composition of pyrite and siderite. These two minerals has good conductivity properties thus can reduce the resistivity log reading even though the rock might contains hydrocarbons.

References

Worthington, P. F., 1997, Society of Petroleum Engineers, **SPE 38035**, 157-171

Chu, W., and Welch, P. M., 2008, Society of Petroleum Engineers, **SPE 114478**

Hamada, G.M. & Al Awad, M.N.J, 2001, ”Log Evaluation of Low Resistivity Sandstone Reservoirs, Society of Petroleum Engineers 70040.

Kantorowicz, J. 1984, “The Nature, Origin, and Distribution of Authigenic Clay Minerals From Middle Jurassic Ravenscar and Brent Group Sandstones”, Clay Minerals, page 359-375.

Sarkisyan, S.G. 1972, “Origin of Authigenic Clay Minerals and Their Significance in Petroleum Geology”. Amsterdam. Sedimentary Geology-Elsevier Publishing Company, Page 1-22.

Neasham, W.J. 1977, " The Morphology of Dispersed Clay in Sandstone Reservoirs and Its Effect on Sandstone Shaliness, Pore Space, and Fluid Properties", Society of Petroleum Engineers

PROCEEDINGS
JOINT CONVENTION BANDUNG (JCB)2021
November 23rd – 25th 2021

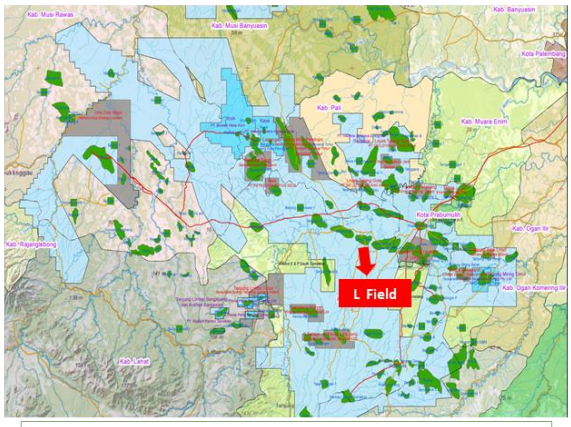

Location of L Field in South Sumatera Basin

Well	Zone	Average Resistivity	Test Data
L-170	3rd Layer	3.1 Ohmm	Gas 1.2 MMSCFD, no water
L-82	1st Layer	2.4 Ohmm	Oil rate 160 BOPD, wc 3%
LC-13	6th Layer	4.5 Ohmm	Gas 2.4 MMSCFD, no water
L-215	1st Layer	2 ohmm	Oil Rate 64 BOPD, wc 75%
L-195	6th Layer	1.5 ohmm	Swab WC 100% Cumm 310.5 bbls

Test Result of Low Resistivity Reservoir in L Field

Figure 1. Location of L Field and test data of low resistivity pay zone

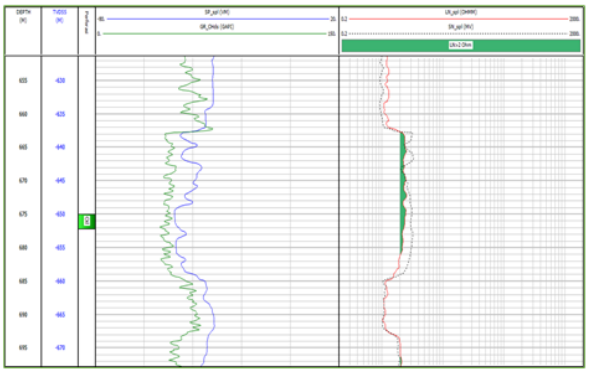

L-82 Typelog (Oil Bearing Zone)

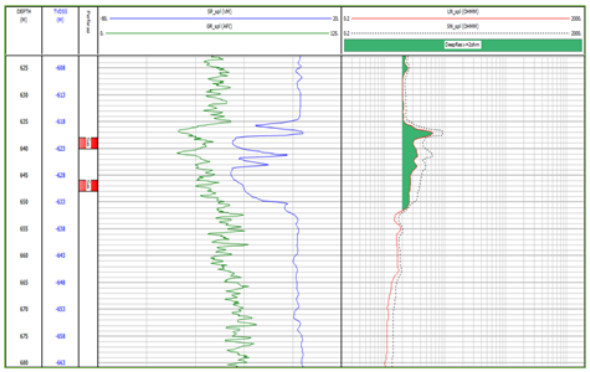

L-170 Typelog (Gas Bearing Zone)

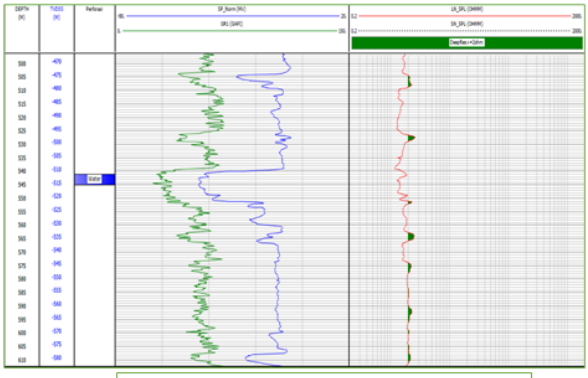

L-195 Typelog (Water Bearing Zone)

Figure 2. Typical typelog of low resistivity pay zone at L field, in well L-82 with average resistivity about 2.4 ohmm resulted oil after perforated, whereas in well L-170 resulted gas with average resistivity of 3.1 ohmm and in L-195 with average resistivity about 1.5 ohmm resulted water.

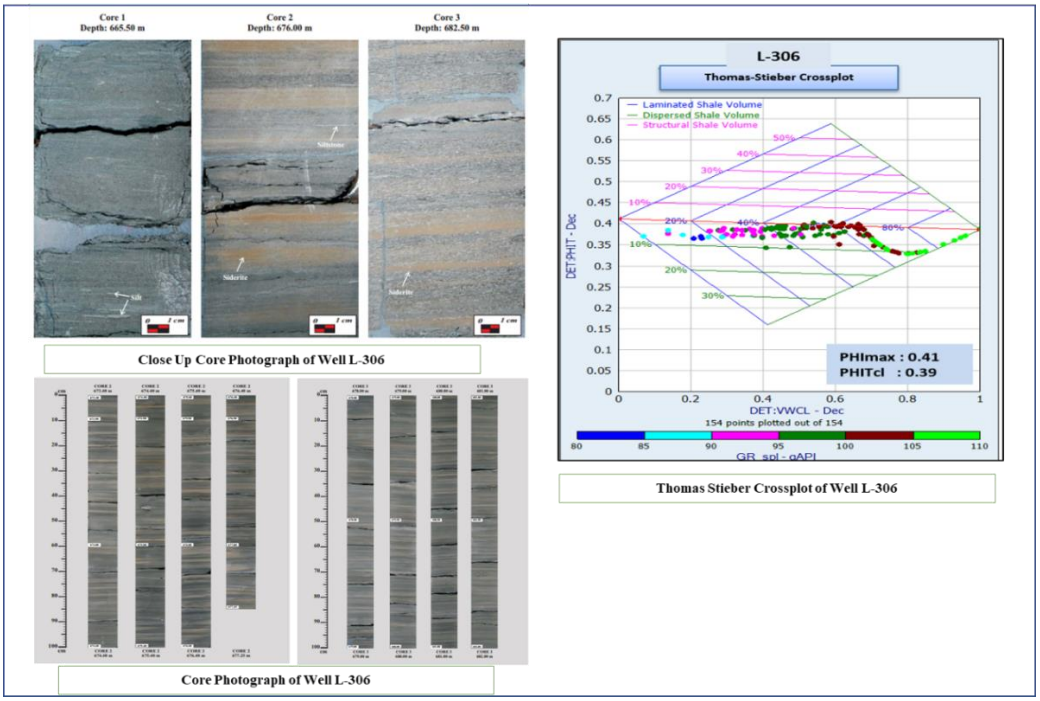

Figure 3. Core Photographs show parallel lamination, with the presence of Siderite as conductive minerals. Thomas Stieber crossplot also show the dominance of laminated shale volume.

No	Depth *meter*	Clay Minerals %				Carbonate Minerals %			Other Mineral %								Total %		
		Smectite	Illite	Kaolinite	Chlorite	Calcite	Dolomite	Siderite	Quartz	K-Feldspar	Plagioclase	Pyroxene	Pyrite	Hematite	Halite	Gypsum	Clay	Carbonate	Other
1	666.55	-	33	12	8	tr	-	10	31	3	3	-	tr	-	-	-	53	10	37
2	667.40	-	30	11	8	tr	-	20	26	2	3	-	tr	-	-	-	49	20	31
3	667.92	-	34	14	9	tr	-	6	31	3	3	-	tr	-	-	-	57	6	37
4	669.50	-	31	12	9	tr	-	6	34	3	5	-	tr	-	-	-	52	6	42
5	670.00	-	35	14	10	tr	-	2	32	3	4	-	tr	-	-	-	59	2	39
6	670.77	-	34	13	9	tr	-	2	33	4	5	-	tr	-	-	-	56	2	42
7	671.25	-	32	12	8	tr	-	7	34	3	4	-	-	-	-	1	52	7	41
8	675.4	-	34	13	9	tr	-	7	31	3	3	-	-	-	-	1	56	7	37
9	683.80	-	37	15	10	tr	-	4	28	3	3	-	-	-	-	-	62	4	34

XRD Data of Well L-306

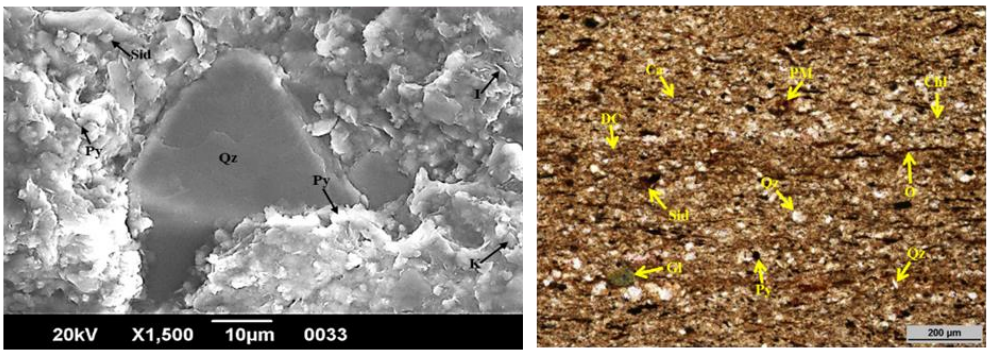

SEM Analysis of well L-306

Petrography Analysis of Well L-306

Figure 4. Based on XRD Data, the clay minerals are dominated by Illite and kaolinite whereas from SEM & Petrography Analysis show the presence of Siderite, Pyrite and Glauconite.

PROCEEDINGS
JOINT CONVENTION BANDUNG (JCB) 2021
November 23rd – 25th 2021

3D Seismic Acquisition and Processing in South Sumatra Basin: Challenging to Improve the Better Basement

Riky Hendrawan B Pandito[1], Dody Apriadi[1], M Fery Mustofa[1], Arya Nugraha[1], Rocky Yudistira[1], Haryo Dwi[1] , Ahmad Zazeli Fuadi[2]*
[1]Pertamina Hulu Rokan/PHE Jambi Merang
[2]PHE Subholding Upstream
**Corresponding author's email: riky.pandito@pertamina.com*

Abstract

In 2019, PHE Jambi Merang acquired 3D seismic processing with area coverage 387 km2. The purpose of this activity is to pursue the naturally fractured basement in the South Sumatra Basin. However, several rock formations above it, such as the Talang Akar Formation, also as secondary target. Some of the challenges in this acquisition can be divided into technical issue and social aspects. From a technical point of view, the presence of the Kasai Formation with the characteristics of pumice, conglomerate, and tuffaceous sandstone is quite an obstacle as a damper that signal of seismic penetrates through this layer. On the social aspect, it becomes a challenge because the work has to pass through productive Acacia plantations and several residential areas. The data used as a comparison is 2D seismic which was acquired in 2002. The latest acquisition increase frequency bandwidth in 8 Hz until 90 Hz with better signal to noise ratio. Good reflection not only in the deepest target (basement ~ 2000 ms) but also in the shallow target (~ 600 ms). To improve the quality of data acquisition, several processing methods were carried out, such as 5D interpolation and OVT on PSTM and tomography on PSDM. From those methods, technically the frequency content and fold coverage have increased quite significantly imaging (from 63 – 221 – 500 %).

Keywords: Abstract, Template, up to 5 words arranged in alphabetical order.

Introduction

The South Sumatra Basin is located along the NW-SE direction and is bordered by the Barisan Mountains in the west, Bangka-Biliton Island in the east, Tigapuluh Mountains in the north and Tinggian Lampung in the south (Fig. 1). The South Sumatra Basin is one of the most extensive basins, up to 85,670 km2, in which it is divided into several sub-sections, such as the Jambi sub-basin and the Palembang sub-basin. The tectonic phase that works in the Jambi sub-basin is relatively the same as the tectonic pattern of the South Sumatra Basin, which is much influenced by the convergent pattern transform that forms a pull apart basin of late createaceous to early tertiary age. In simple terms, there are three tectonic phases that occur in the South Sumatra Basin, namely the compression phase in the late Jurassic to early Createaceous. The next phase is extension as a result of changes in the direction of subduction and its speed that occurs in the late cretaceous to early tertiary. The last phase is the compression phase that has occurred in the middle miocene to date. The increase in subduction activity causes reactivation of old faults, thus forming an inversion structure. At the same time, it also forms a NNW-SSE trend. The results of this tectonic activity are indirectly reflected in the stratigraphic pattern of the Jambi Basin. The stratigraphy of this basin can be divided into two parts, which reflect the tectonic strain of TAF, Pendopo Fm, Baturaja and Gumai. Meanwhile, those that reflect the compression and regression regime of the marine environment can be seen in the Air Benakat and Muara Enim Formations.

Jambi Merang Working Area is currently managed by a subsidiary of Pertamina Hulu Energi. Covering an area of 1,080 km2, located in the northern part of the South Sumatra Basin, Indonesia, approximately 40 km to the southeast of the city of Jambi. Currently, the block produces up to 84.75 MMSFD of gas and 4,346 BCPD. Jambi Merang working area block is divided into two parts, the southern and northern parts. In the southern part, many fields are produced from stratigraphic traps in the Baturaja Formation Carbonate. Meanwhile in the north, it will pursue potential naturally fractured basement, structural trap and stratigraphic trap.The last seismic data acquired in the area was 2D data taken in 2002.

In 2019, PHE Jambi Merang carried out seismic acquisition activities in the northern block to pursue the potential of hydrocarbons in the area..

Data and Methods

To pursue deep targets as well as shallow targets with optimal resolution, it is necessary to design specific acquisition parameters. It is aims to kwowing the direction of the fault, subsurface structure and basement fracture in detail. The difference in target

depth variation is one of the considerations in determining the design of 3D seismic parameters. In addition, the faults that exist below the surface are also a separate consideration in designing this seismic. The last design used is the direction of the receiver line (RL) so that it cuts perpendicular to the existing fault, so that the RL azimuth design with the direction of N 114o E, with a distance of 300 m for each path. While the direction of shooting was decided to be in the direction of N 240 E with each shooting being 400 m. To obtain data with a high density, a receiver interval of 25 m is made and the shot point distance is every 50 m.

Bin Size calculation is obtained using the following mathematical approach:

$$Bin\ Size = \frac{V}{4\ F\ Sin\ \alpha}$$

By knowing the maximum dip in the area, frequency and average velocity, the optimal bin size is 12.5 m x 12.5 meters. Meanwhile, the direction of the trajectory is about N 1140 E, with the SP perpendicular to about N 240 E. Using active channels more than 4000, with orthogonal symmetry shooting mode, the maximum fold coverage is 63%. This figure is 2 times larger than the existing 2D data.

In this study, to improve the resolution and quality of seismic data, processing was carried out from the PSTM to PSDM stages (figure 3 and 4). The data received and processed from the field are in the form of raw gathers, observer reports, supporting files and others. Data from field processing found that there are some noise problems such as direct wave, multiple and diffraction. From these two methods, the target of this processing is to get 3D Wide Azimuth Anisotrophy Pre Stack Time Migration Volume which preserves amplitude which is commonly called beam migration.

At the PSTM stage, one that can be highlighted is 5D interpolation and regulation as well as OVT Partitioning. This stage is carried out before the pre stack migration. This process is an interpolation of traces on 5 domains simultaneously. These five domains can be grouped inline, Xline, Offset, Azimuth and Frequency/Time. Another grouping is the Source Receiver on X and Y and Frequency/Time. The idea of this method is to create a tighter acquisition model to fill in the blank data due to the geometry itself. From the two interpolation models, the first method is used interpolation based on inline, crossline, etc.

For OVT Partioning, it is done after 5D interpolation. This method basically divides the OVT (Offset Vector Tile) class on each vector of the receiver component and SP on each CDP (illustration in Figure 7). The result of this OVT theoretically increases the fold coverage from 63 to 221.
At the PSDM stage, of the 3 available wells, but only 1 well is carried out for the next process. This is because the well is located in 3D Seismic.

Initial velocity model building is one of the stages carried out in PSDM. This stage is carried out by comparing the speed conversion in the study area using contrained velocity inversion (CVI) and DIX with test intervals of 1, 3 and 5 km. Smoothing is done to reduce the effect of the speed anomaly locally.

Basement Velocity Model
This process is the final process that is carried out after the speed model in the main body (shallow layer to top basement) is correct. Furthermore, basement velocity analysis/scanning is carried out to obtain the most optimal velocity model estimate. This modeling provides an estimate of velocity in the top basement of 4800 m/s graded down.

360 degree Modeling
This method is an advance method of Common Reflection Angle Migration which is a migration method with multi arrival ray tracing. This method uses up going ray tracing to generate seismic information called the local angle domain (LAD). This information controls all ray tracing pairs at each point of occurrence and keeps the phase preserved. This method allows to produce 2 types of 3D angle gather, namely directional and reflection. Direction gather allows specular and diffraction imaging in isotropic 3D geological models. This information can be helpful in structural imaging and interpretation, especially in areas with faults and small fractures.

Post Migration
In addition to the residual velocity analysis, azimuthal residual velocity analysis was also carried out. The presence of vertical fractures in rocks can be modeled as orthorhombic anisotropy. This analysis provides several outputs including fast, slow and azimuth vslow speeds.

Result and Discussion

The results of this acquisition and processing provide a better basement image than the previous seismic data. This can be seen from the comparison of PSTM and PSDM data. In PSDM, the suspected fracture lines clearly cut off seismic signals, especially in the event after the top basement.

To strengthen the hypothesis of fracture, seismic attribute analysis was carried out using Symmetry I3D. The major faults are well characterized, and the fractures are mapped predominantly in a northeasterly direction.

Another strengthening analysis is the vfast slicing in the basement area. It can be seen that the basement area has a slowdown in its velocity data. This is one of the characteristics that the area has an anisotropy homogeneous distribution.

The analysis and model above is only based on seismic and other data. The existence of a fracture must be proven by drilling exploration wells.

References

Badley, M.E., 1985. Practical seismic interpretation.

Ginger, D. and Fielding, K., 2005. The petroleum systems and future potential of the South Sumatra Basin.

Liu, E. and Martinez, A., 2014. Seismic fracture characterization (Vol. 575). EAGE.

Tsvankin, I. and Grechka, V., 2011. Seismology of azimuthally anisotropic media and seismic fracture characterization. Society of Exploration Geophysicists.

Yilmaz, Ö., 2001. Seismic data analysis: Processing, inversion, and interpretation of seismic data. Society of exploration geophysicists.

Acknowledgements (Optional)

Thank you for all management Pertamina Hulu Rokan and Pertamina Hulu Energy support to our study. Also thanks to Teguh Suroso – Pertamina for full support.

PROCEEDINGS
JOINT CONVENTION BANDUNG (JCB) 2021
November 23rd – 25th 2021

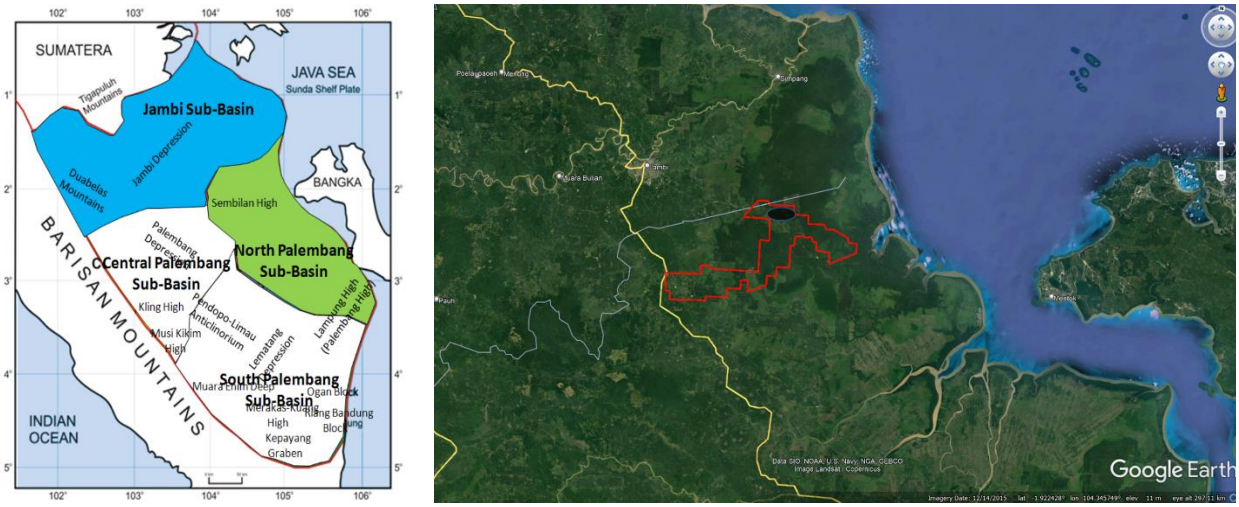

Figure 1. Elemental Structure of the South Sumatra Basin. Bounded by several morphologies such as Bukit Barisan, Bangka Island and the Tigapuluh Mountains (Ginger and Fielding, 2005). Focus study is marked with a black elipse (right).

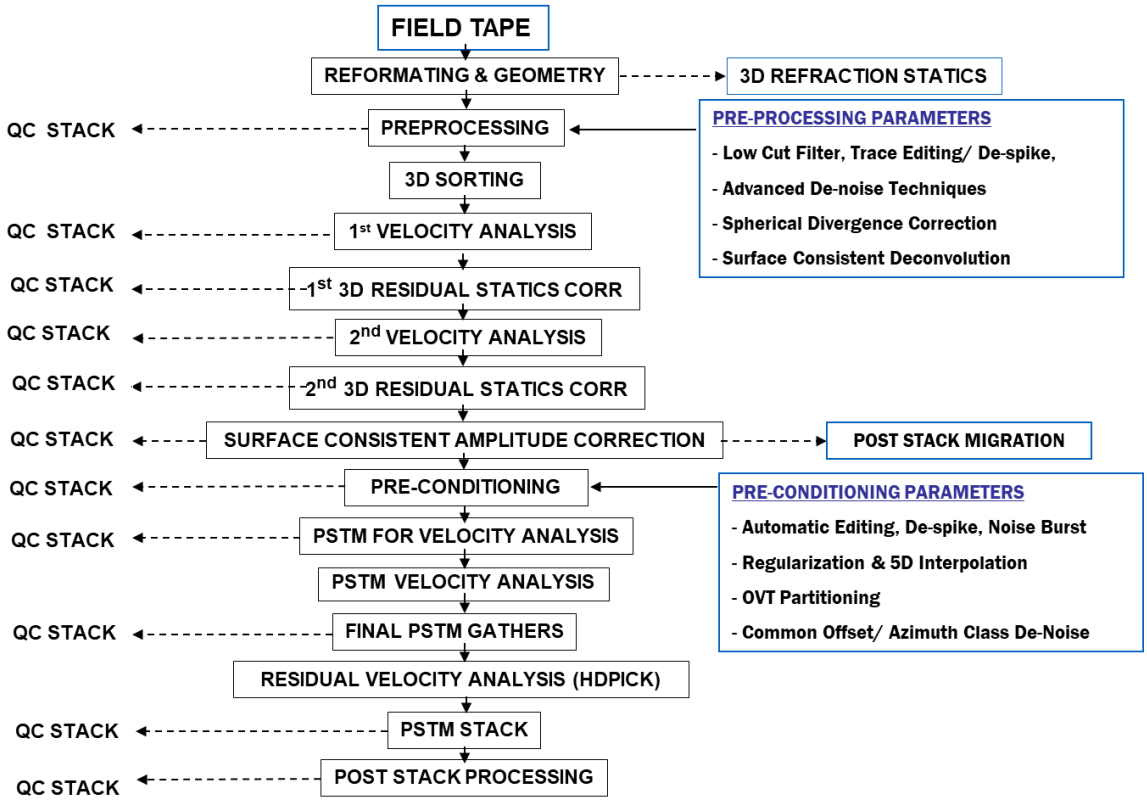

Figure 2. PSTM Workflow

PROCEEDINGS
JOINT CONVENTION BANDUNG (JCB) 2021
November 23rd – 25th 2021

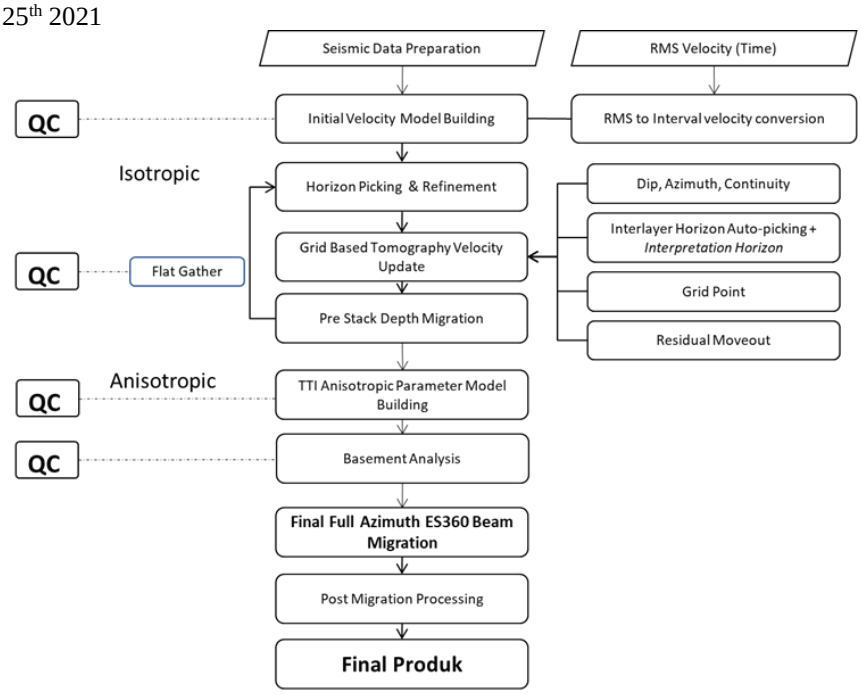

Figure 3. PSDM Workflow

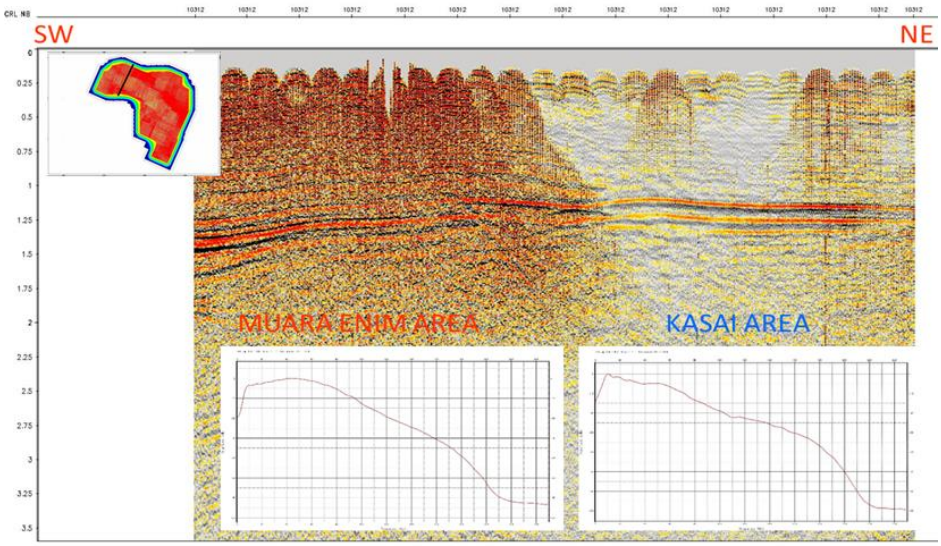

Figure 4. Obstacle in the Kasai Formation. This formation is composed of tuffaceous sandstone, claystone and thin coal causing the seismic signal quality to decrease when compared to other areas.

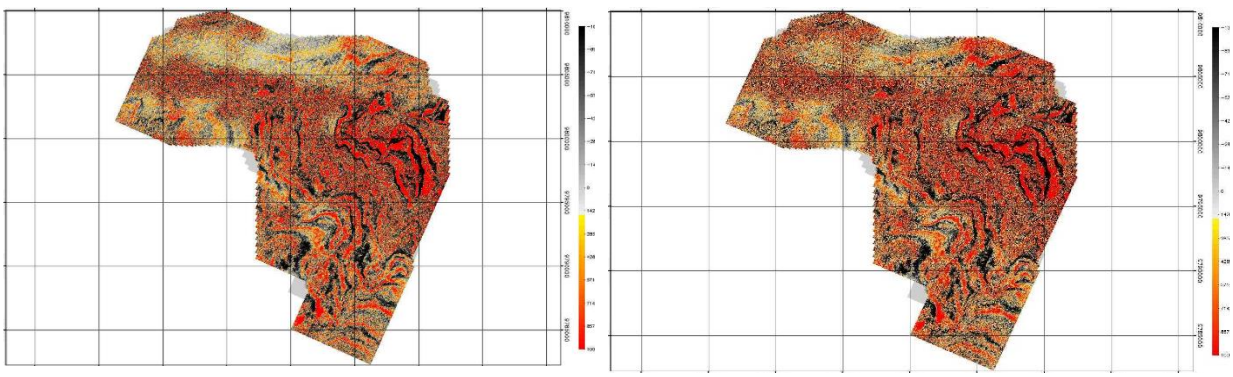

Figure 5. Time slice in shallow section before scale (left) and after scale (right)

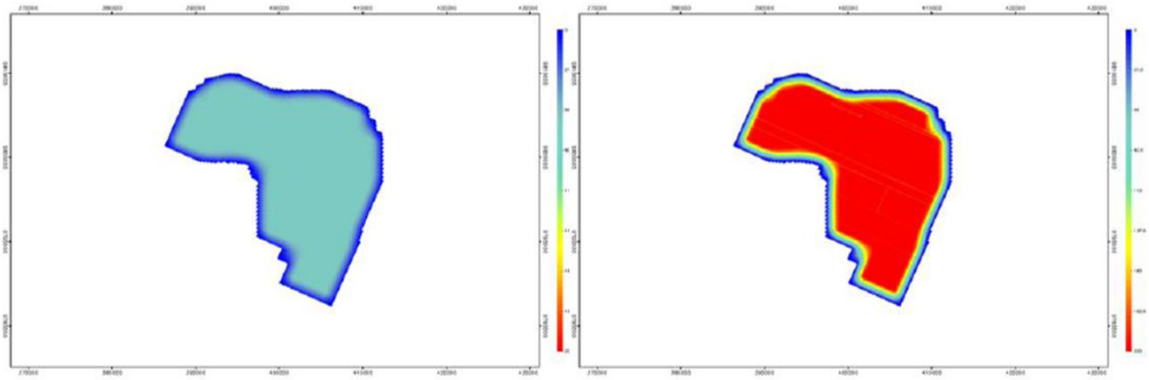

Figure 6. Fold map before 5D interpolation 63 (left) and after interpolation 221 (right)

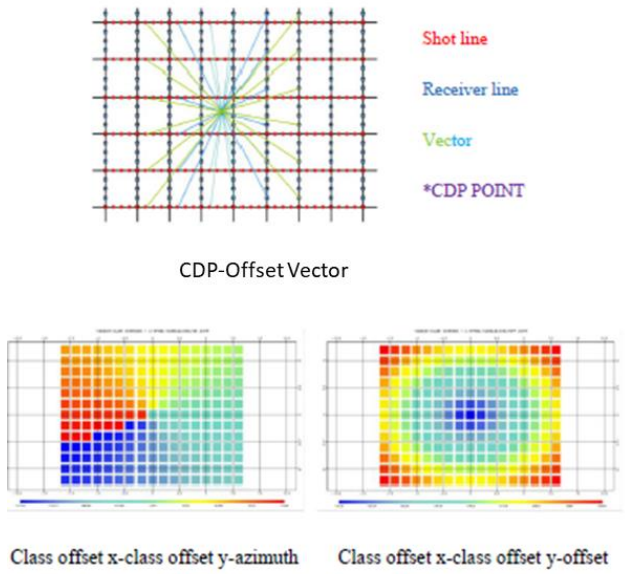

Figure 7. OVT Azimuth and Offset

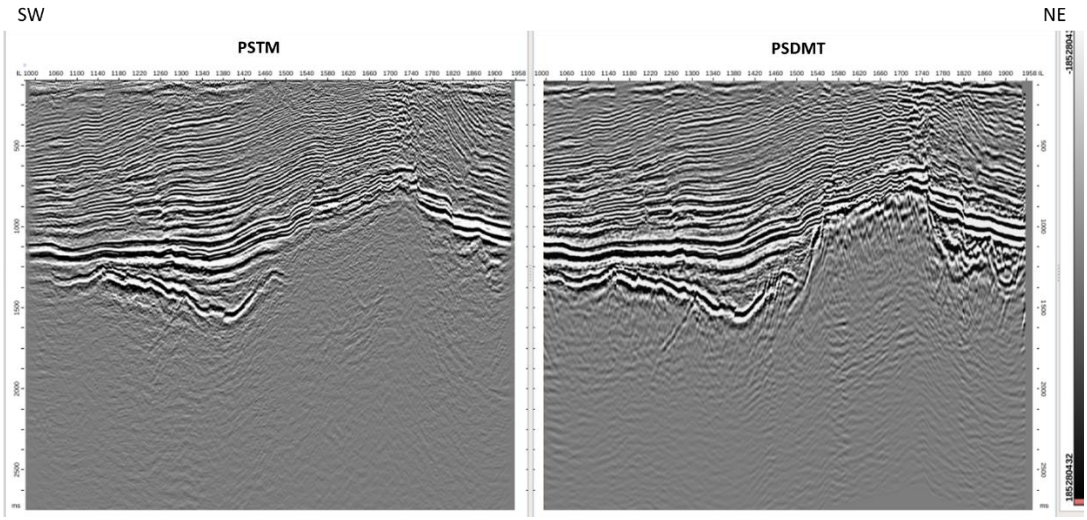

Figure 8. PSTM and PSDM Section SW to NE. PSDM (right) imaging fracture better than PSTM

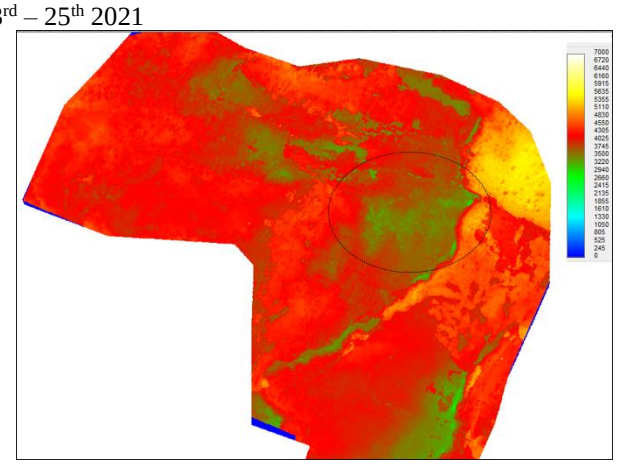

Figure 9. Vfast in basement area (circle) showing the anomaly, velocity slower than other. Assuming the product is homogeneous anisotrophy.

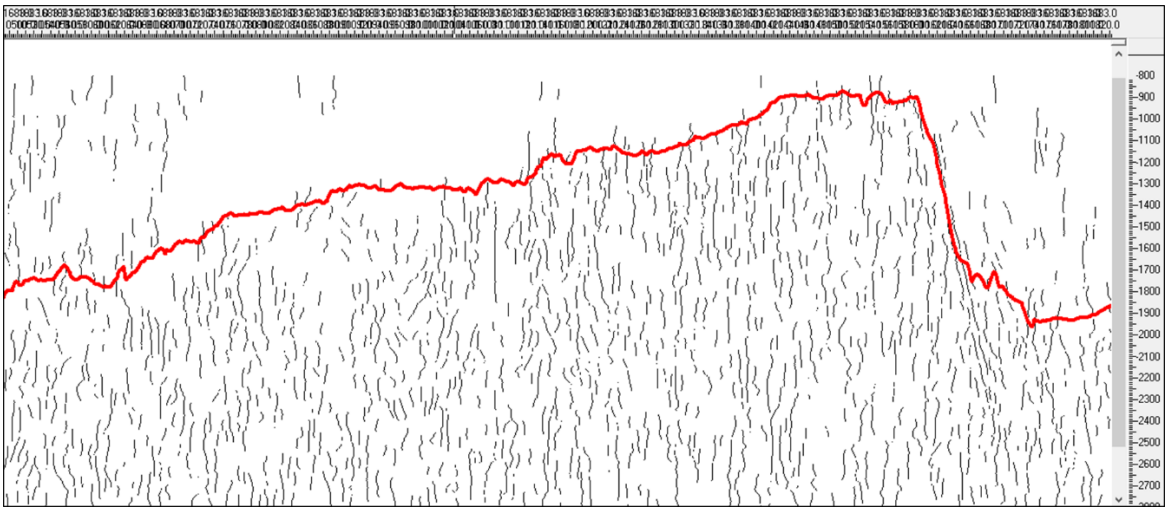

Figure 10. Seismic fault attribute cross section showing fracture formation under top basement (red horizon)

PROCEEDINGS
JOINT CONVENTION BANDUNG (JCB)|2021
November 23rd – 25th 2021

AVO Analysis Success Story: Carbonate Build-Up Step Out Well Prospect Case Study

Mualimin (1), Ibnu Suhartanto (1), Nanang Yulianto (1), Suryana (2), Farid Hosni (2)
(1) Pertamina Hulu Energi, (2) Pertamina EP

Abstract

The BBS-STO prospect is a proposed step out well which identified based on the appearance of seismic reflector and interpreted as an isolated carbonate build-up that forms a 4-way dip closure. This prospect is a proven petroleum system that located in the Kepuh Sub Basin, a part of the North West Java Basin. BBS-STO is approximate 3 km North of the Bambu Besar (BBS) Field which is an existing hydrocarbon producing Field. BBS-STO build-up position is more up dip than the carbonate build-up BBS. The challenge in this prospect is whether there are hydrocarbons trapped in this the isolated carbonate build up.

AVO analysis is used as a DHI method: Near & Far Angle Stack analysis and derivatives between Normal Incident and Gradient known as "Fluid Index". The analysis was carried out on both of the top carbonate build-up of the BBS-STO and existing BBS to confirm the AVO response. Near & Far Angle Stack analysis of the existing BBS shows that the amplitude changes to be more negative at the Far than the Near Angle Stack, the same response is also shown by the BBS-STO. The Fluid Index is derived from the cross plot between Intercept and Gradient, then the background trend line is determined from it, this background trend line interpreted as a shale and wet sand line. The data that move away from the trend line indicated the presence of hydrocarbons.

These methods have proven identified the presence of hydrocarbon, indicated by the data during drilling: limestone cutting with gas reading C1-nC5 with Total – Background Gas ratio more than 25 and 5% oil show. It is also confirmed from the downhole fluid analysis data which shows the presence of oil. Furthermore, this carbonate build-up was perforated and succeeded in obtaining oil with Qoi: 1569.48 bopd/0% WC.

Keywords: AVO, carbonate build-up, Fluid Index, Intercept-Gradient, Near & Far Angle Stack.

Introduction

Bambu Besar structure is an oil and gas field that located in the Kepuh Sub basin, a part of North West Java basin. Main reservoir, BBS structure is a build-up carbonate, Upper Cibulakan formation (Figure 1)

3D PSTM seismic data interpretation result for BBS area shows some feature appearance of “build-up carbonate” bodies surrounded the existing body. The chosen carbonate body for step-out well candidate (BBS-STO) is located +/- 3 km Northern existing BBS in the up-dip position (Figure 2 & 3). In the perspective of petroleum system component, the only challenge of this prospect is whether there is trapped hydrocarbon inside the 4-way dip closure.

Hydrocarbon occurrence detected by AVO method and due to no well in the build-up carbonate BBS-STO, Direct Hydrocarbon Indicator method conducted based on pre-stacked data (gather). BBS-STO analysis result qualitatively validated based on the existing BBS to confirm hydrocarbon occurrence in the area of interest, BBS-STO well proposal.

Data and Method

Fluid identification in this study is narrowly based on seismic particularly CDP gather since there is no well in the target area. Analysis of AVO result data validation for BBS-STO prospect conducted qualitatively for BBS existing.

Data Preparation

The main objective of preparation stage to enhance the CDP gather by removing noise, frequency filtering and NMP correction optimization. Random and coherent noise eliminated to increase the quality of CDP gather by applying high-resolution sparse radon transform algorithm as stated by Trad et al (2003). Filter of frequency domain applied to eliminate noise particularly high frequency also to balance the frequency of near offset with the far offset.

The most important step for CDP gather analysis is optimization of NMO correction to match the event in the near offset with the event in the far offset. The applied method is offset cross-correlation to get the highest correlation and optimum time shift hence the inter offset represents identical event (Culunay et. Al., 2007)

The final step of data preparation process is converting the CDP gather in the offset domain to angle domain in the form of angle stack in alignment with all formula of AVO analysis and all derivatives.

Atribut AVO

Once CDP gather clean, this data used for the next process, to produce AVO attribute as Intercept and Gradient by using Shuey's formula that derived from two terms formula based on less than 35-degree angle in the CDP gather as consideration (Shuey, 1985).

After Intercept and Gradient volume produced, cross-plot analysis conducted in the target depth interval continued with background-trend-line definition. Castagna et al. (1997 and 1998) mentioned that trend-line-background could be interpreted as shale line and wet sand as function of Vp/Vs. Data points that located offset the trend line represents hydrocarbon appearance or lithology.

Fluid Index

Distance measurement of data points to the background trend using distance formula with intercept input, gradient and the trend itself as input by which defined as Fluid Index, with the following formula:

Fluid Index = f (intercept, gradient, trend line)

There are positive and negative results from Fluid Index calculation, the negative value shows that the data point located below trend line. These negative values are important and closely related to reservoir top in several AVO classes (I, II, III and IV) as described by Castagna et al. (1997) whilst is the reservoir base that located across.

Result and Discussion

Figure 4 shows the angle stack in existing structure area whilst Figure 5 is the angle stack in step-out structure area, both shows AVO anomaly in the carbonate top

Figure 7 shows Fluid Index section derived from AVO attribute. Both Fluid Indexes, in the existing BBS top carbonate and BBS step-out are negative and is consistent with the result from oil and gas-cap well. Negative values spreads in the step-out area as shown in Figure 8.

Both methods have successfully identified hydrocarbon appearance and confirmed with the actual data of limestone drilling cutting gas reading with 2679.42 unit of total gas C1-nC5 and 80-100 unit of background gas and 5% of oil show. Hydrocarbon appearance in the build-up carbonate also confirmed from downhole fluid analysis data that shows oil appearance. The build-up carbonate layer proven by production of 1569.48 bopd/ 0% WC oil after perforation.

Conclusions

AVO qualitative partial stack analysis method and attribute calculation (Fluid Index) that derived from intercept-Gradient has proven the appearance of oil hydrocarbon in step-out well (BBS-STO)

References

Castagna, J.P., Swan, H.W., 1997. Principles of AVO crossplotting. Lead. Edge 16, 337–344.

Castagna, J.P., Swan, H.W., and Foster, D.J., 1998, Framework for AVO gradient and intercept interpretation: Geophysics, 63, 948-956.

Gulunay, N., M. Magesan, and, H. Roende (2007b) Gather Flattening, The Leading Edge, December 2007 issue

Pertamina EP., 2019. Internal Report.

Shuey, R.T., 1985, A simplification of the Zoeppritz equations: Geophysics, 50, 609-614.

Trad, D., Ulrych, T., and Sacchi M., 2003, Latest views of the sparse Radon transform: Geophysics, 68, 386–399.

Acknowledgements (Optional)

Appreciation and thanks the author gave to Pertamina Upstream Management for permission granted for this publication. Team Revisit G&G Exploitation PEP Head Office for the support.

PROCEEDINGS
JOINT CONVENTION BANDUNG (JCB)2021
November 23rd – 25th 2021

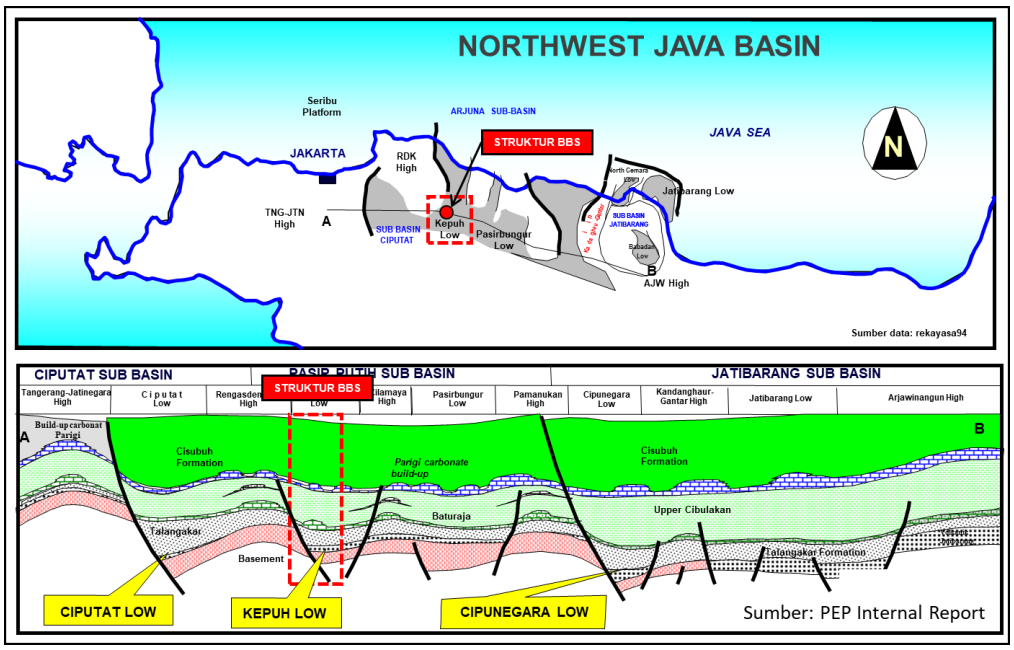

Figure 1: Regional geology. The BBS Step Out (BBS-STO) is located in a proven petroleum system in the Kepuh Sub Basin, a part of the North West Java Basin.

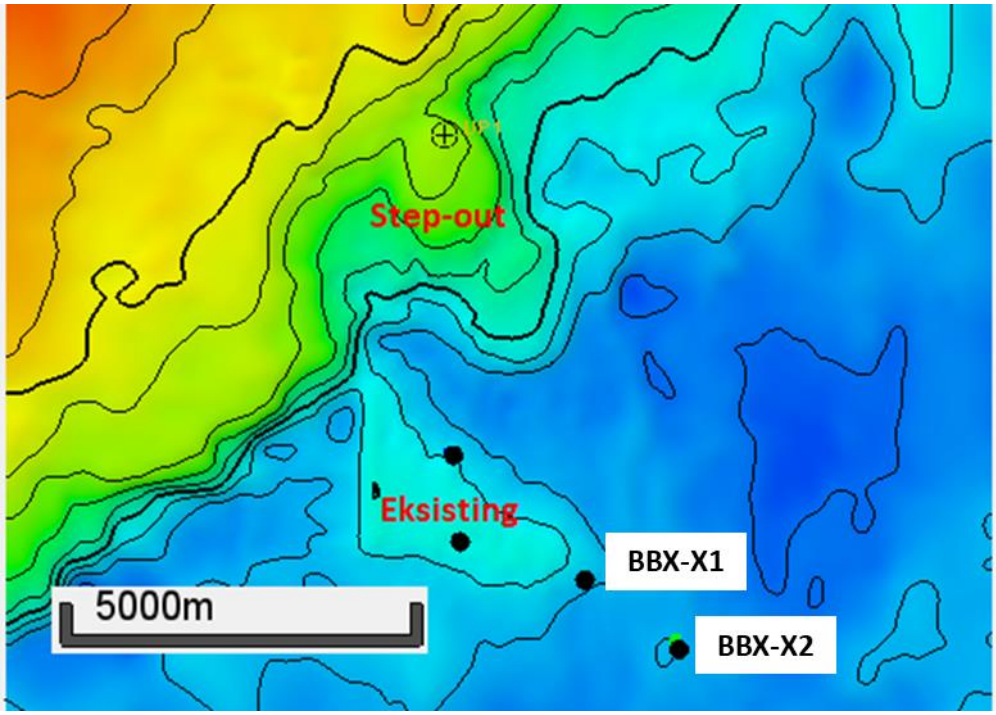

Figure 2: Location of existing Bambu Besar Field and Bambu Besar Step Out (BBS-STO), BBS-STO is approximate 3 km North of the Bambu Besar (BBS).

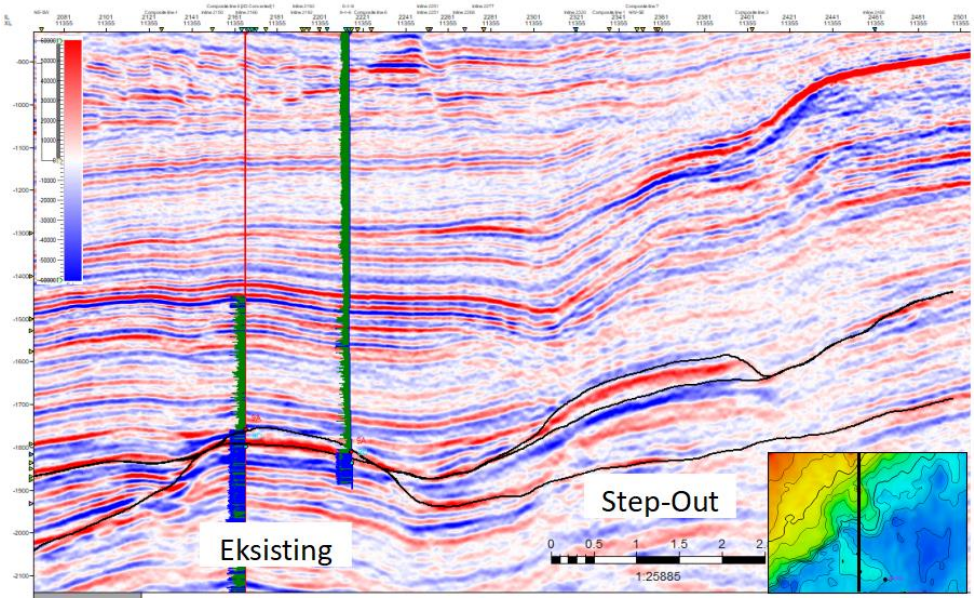

Figure 3: Seismic appearance of PSTM data showing BBS-STO prospect intepreted as "carbonate build-up" same as existing producing BBS Field.

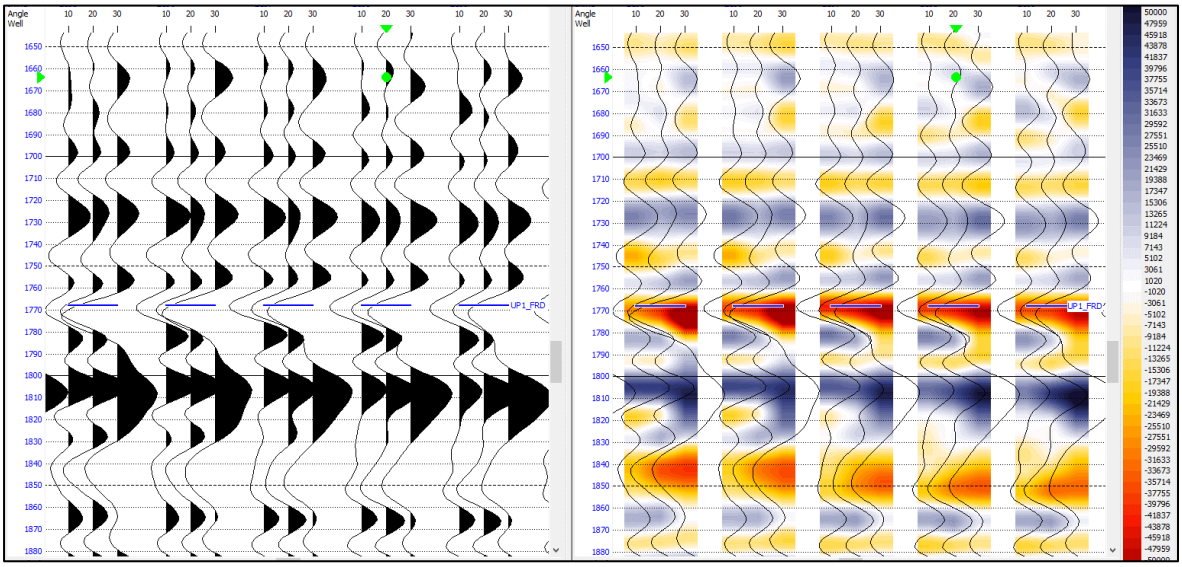

Figure 4: Agle stack at existing BBS Field showing variation amplitude versus angle/offset.

PROCEEDINGS
JOINT CONVENTION BANDUNG (JCB)2021
November 23rd – 25th 2021

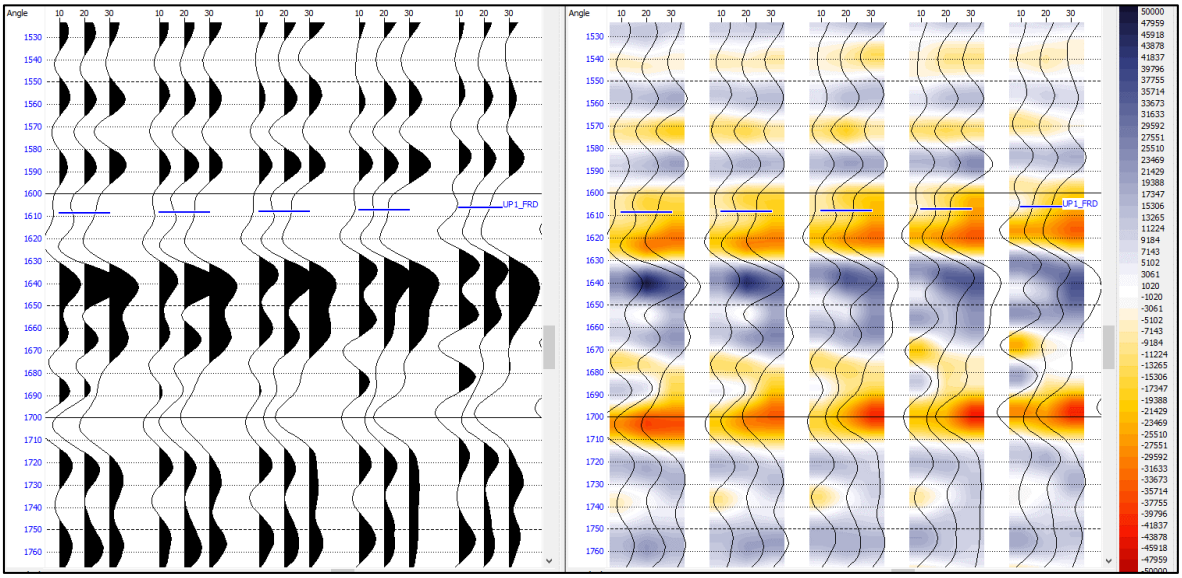

Figure 5: Agle stack at BBS-STO prospect showing variation amplitude versus angle/offset.

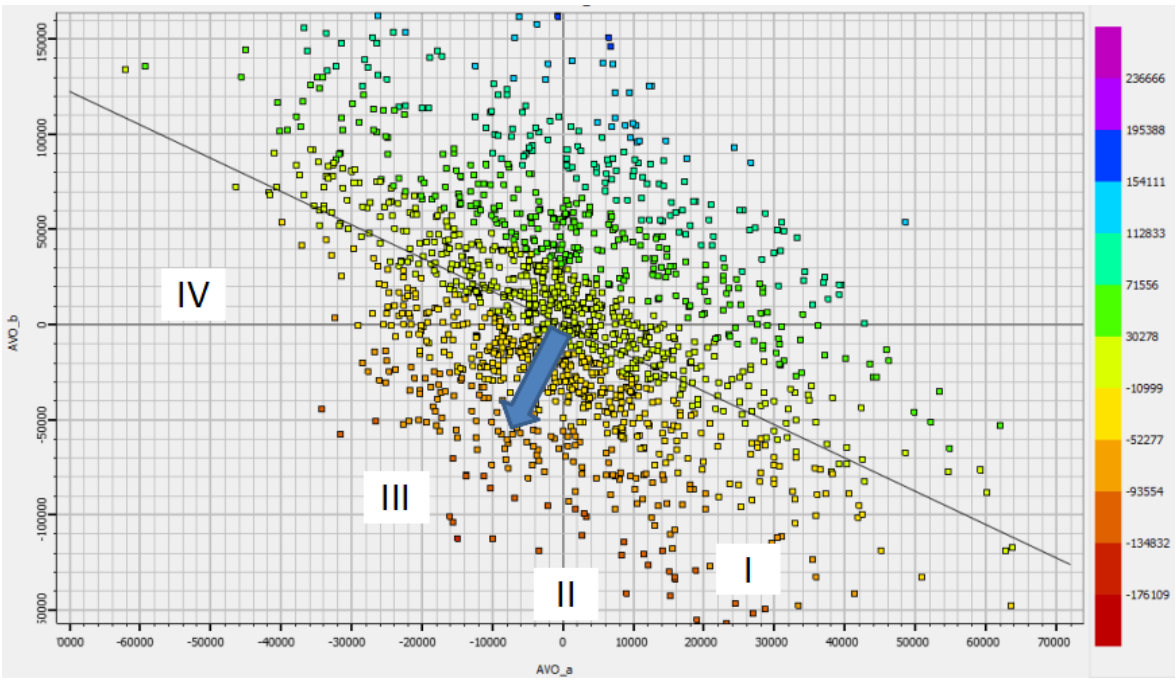

Figure 6: Crossplot Intercept (horizontal) and Gradient (vertical), black line as background trend line. Colour data is distance between data to trendline.

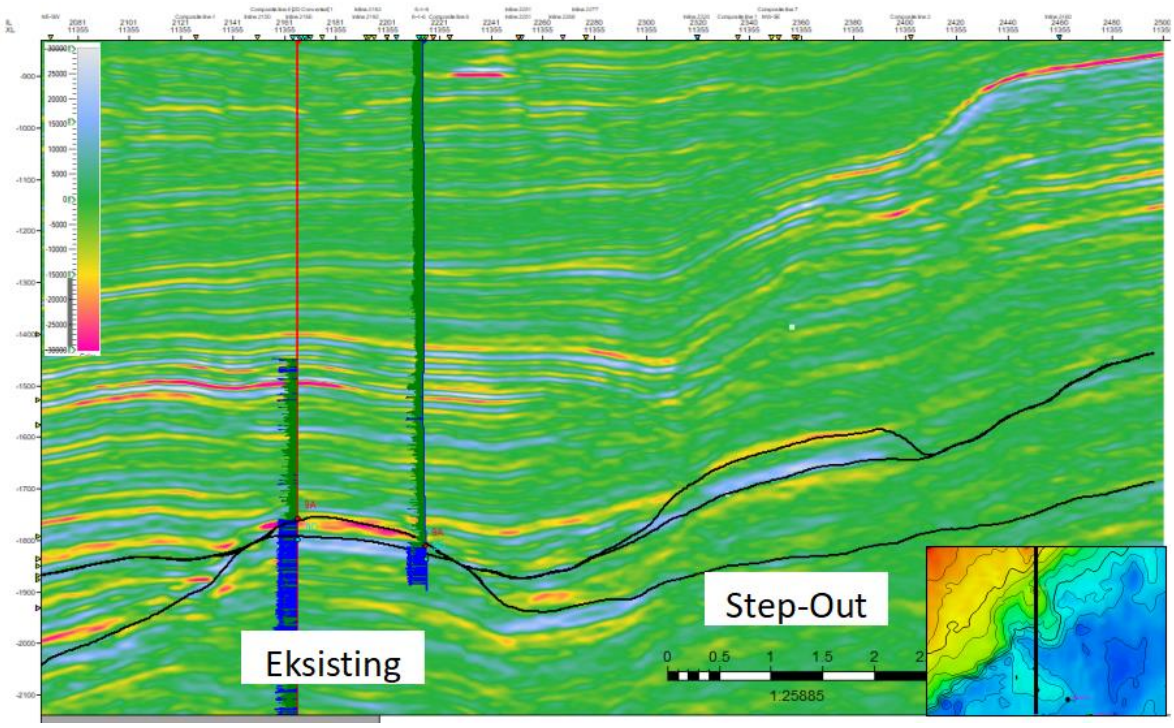

Figure 7: "Fluid Index" section, both of BBS existing Field and BBS-STO has negative value.

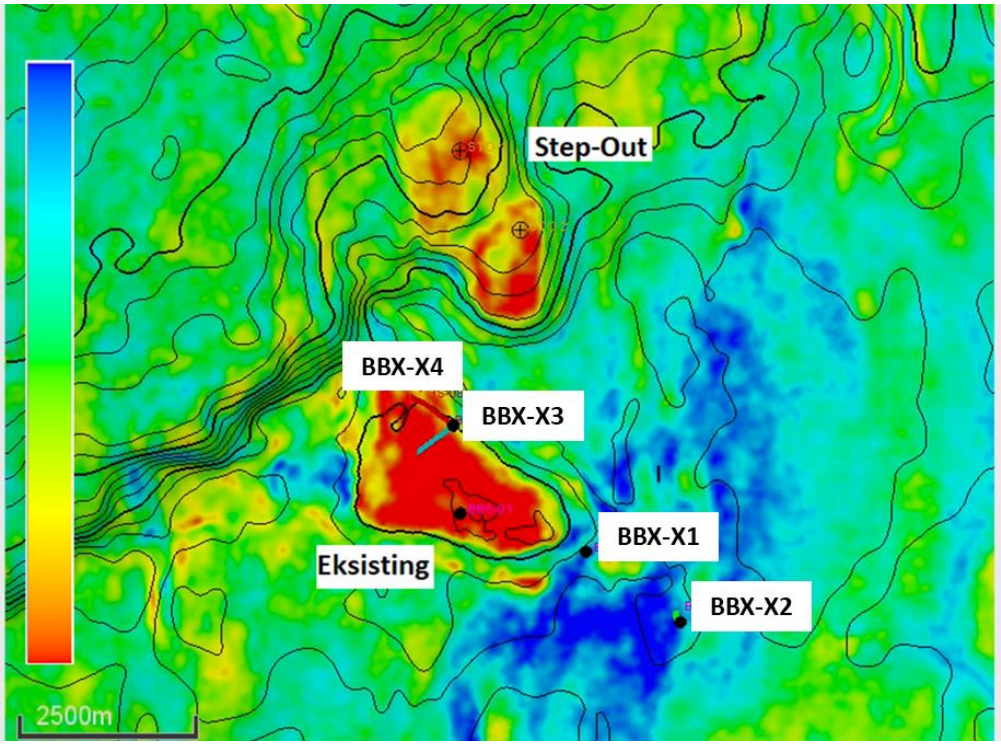

Figure 8: "Fluid Index" map, both of carbonate build-up BBS existing Field and BBS-STO has negative value.

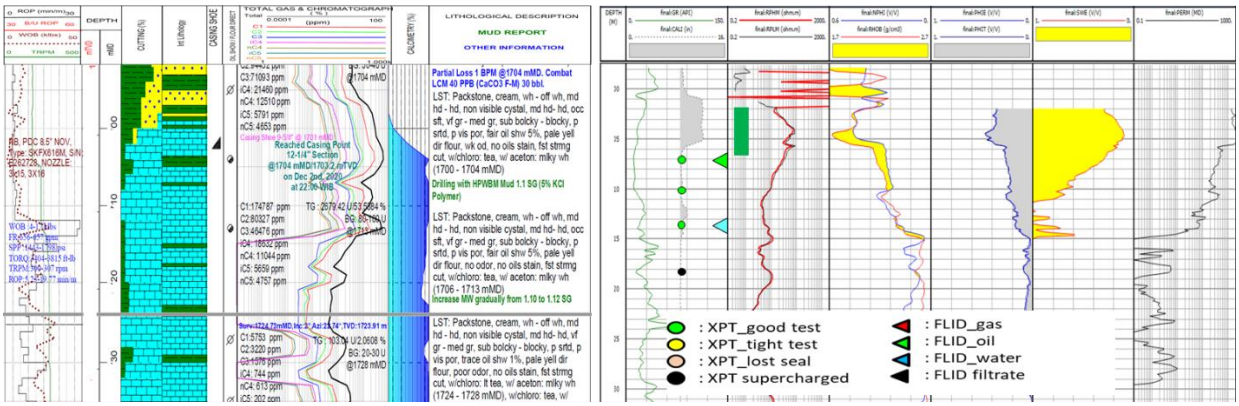

Figure 9: Mudlog data of BBS-STO, cutting data consist of limestone with C1-nC5 gas reading, Total Gas 2679.42 unit, Background gas 80-100 Unit and 5% oil show (left). Right: Open hole log overlaid by downhole fluid analysis point which proving oil (green triangle), green bar is perforation interval which producing oil with initial rate Qoi: 1569.48 bopd/0% WC.

.

PROCEEDINGS
JOINT CONVENTION BANDUNG (JCB) 2021
November 23rd – 25th 2021

Quantifying Pore Scale Heterogeneity of Carbonate Reservoir using Digital Rock Approach

Pongga Wardaya[1], Richie Pratama[1], Erlanga Septama[1], Rusalida Raguwanti[1], Vida Irine[1]
[1]Upstream Research and Technology Innovation, PERTAMINA

Abstract

Digital rock physics technology shifts the laboratory routines into the computer simulation domain to obtain rock physical properties e.g permeability, bulk and shear modulus, formation factor, thermal conductivity, NMR properties, and their transport properties. Many studies have shown that there is profound agreement between digital rock petrophysical properties calculation to those from manual laboratory measurement. However, this conclusion is not too valid for heterogeneous sample like carbonate rock, where results from both laboratory and digital rock physics simulation may differ significantly. To comprehend this observation, quantifying the heterogeneity is the key aspect to describe the relevancy of the digital rock physics result when being compared to the laboratory measurement. This study aims at investigating the micro scale pore heterogeneity of the x-ray micro-CT scanned rock of the carbonate reservoir.

Keywords: Abstract, Template, up to 5 words arranged in alphabetical order.

Introduction

In reservoir characterization and evaluation, core analysis has a very significant meaning for giving a profound understanding of the petrophysical properties of the reservoir rock. Basically, the routine involves the several measurements of the perophysical properties including permeability, porosity, wettability, formation factor, spectral gamma, multi-phase flow, etc. All these laboratory measurements are undertaken at the rock sample or core plug taken from the reservoir during the "expensive" drilling program. However, the intensive laboratory experiments and multi-treatments to the core samples can damage the internal or whole structure of them. After experience the varying high pressures and saturated by various fluids there must be changes in the rock structure such as the pore addition or reduction by the closing or opening of microcracks, matrix dissolution, pore shape changes, and pore connectivity changes. Unfortunately, these changes may result in different experiment reading as compared when the original structure is preserved. For example, the pore shape is highly controlling the formation factor and the pore connectivity is controlling the permeability of the rock. When the core sample experiences this damage, a big question is, "Is it still representative for the further analysis?"

Fortunately, nowadays technology of non destructive testing brings the great promise on the new perspective on core analysis. By using the X-ray CT-scan technology adopted from the medical application, the core analysis can be now undertaken digitally, in the computer instead of laboratory, and without damaging any pieces of the core sample. As the imaging takes place in 3D, the real geometry and pore structure can be extracted for giving the more accurate interpretation that the conventional petrographic analysis cannot. More interestingly, once the digital core imaged, it becomes eternally documented. In addition, not only sample friendly, digital core analysis also provides the infinitely repeatable analysis that cannot be done in the laboratory.

Digital core analysis (originally named digital rock physics) is a relatively a new study in the area of geosciences that applies the combination of the recent advances of multi scientific and engineering approacesh to address the issues related to the rock problems. The workflow consists of three main parts: 1) digital imaging, 2) data processing, and 3) physical process simulation (Dvorkin et al., 2011). The imaging part makes use the physical phenomena of the X-ray absorption or attenuation by the material placed in the X-Ray computed tomography instrument. This technique allows the measurement of the x-ray absorption at the millimeter to centimeter scale sample and produces the number of 2D slices to be reconstructed for building the 3D volume of the rock sample. The recording yields the grayscale images whose brightness is proportional to the CT-number of the material (Mees et al., 2003).

The processing part mainly lies on the segmentation process to differentiate between the solid phases and pore spaces. The original X-ray recording basically provides the distinct brightness between the two phases due to the different X-ray energy absorption. The segmentation process aims at creating the binary images whose pores generally treated as the region of interest and hence valued 1 while the solid matrix is terminated. Image segmentation is basically an active research area in image processing disciplines that giving the numerous techniques to segment the interested object from its background. The method comprises automated and manual segmentation. The former utilizes the use of supervised and unsupervised classification using the K-mean clustering, backpropagation neural network,

PROCEEDINGS
JOINT CONVENTION BANDUNG (JCB) 2021
November 23rd – 25th 2021

radial basis function neural network, or self organizing maps. The further discussion of these techniques can be found in Richa et a.l, (2006) and Wardaya et al., (2013a). On the other hand manual segmentation mainly employs the tresholding method that can be done in single band or multi-band of images (Richa et al, 2006; Andra et al., (2013a).

The third part involves the fundamental theory of physical process brought into the computer simulation. This part is also adopted from the very active research development in the area of computational physics. For many years, computer simulation gives the significant role by bridging the gap between theoretical and experimental physics. While the laboratory work deals with the real phenomena, the computer simulation deals with the solving of the physical-mathematical formulation digitized by using numerical techniques. Physical processes simulated into computer in the last digital rock physics development comprises the transport phenomena (single or multi phase of fluid flow and electrical flow) for calculating the absolute permeability and effective formation factor (Keehm, 2003; Richa, 2010; Andra et al, 2013b; Kameda, 2004; Sain, 2010), elastodynamic problem (wave propagation) for calculating the effective elastic moduli (Garbozci, 1998; Arns et al, 2002; Dvorkin et al, 2011; Saenger et al, 2011; Arns et al, 2007; Saenger et al, 2006; Andra et al, 2013b), and magnetic phenomena for investigating the NMR response (Talabi, 2008) of the digital rocks. These physical phenomena are simulated on the digital cores by using the various numerical methods in which each has the unique advantages or disadvantages. The most important issue about the digital rock physics is to find the best computational method to provide the closest result to the real laboratory measurement.

This paper presents the result of porosity heterogeneity in the carbonate using X-Ray micro-CT scanned rock sample. The aims of the evaluation is to obtain the spatial heterogeneity of the pore spaces.

Data and Method

X-ray computed tomography of carbonate sample taken from the benchmark dataset of Andra et al, (2013) are used in this study. The sample was taken at different imaging resolution and recorded as RAW grayscale data with size of 1024x1024x1024voxel. We processed the data by implementing the image processing routine to segment between pore and solid part of the rock. Otsu's segmentation technique was used to create the binary image that can be further quantified. The heterogeneity assessment was performed by analyzing the porosity of various size sub samples cut at different position. The representative elementary volume (REV) was then determined to obtain the scale dependent porosity heterogeneity.

The workflow of the method is presented in the figure 1 below

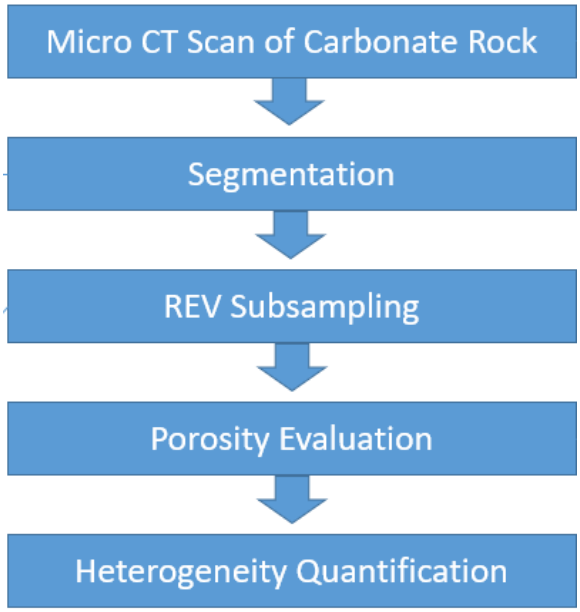

Figure 1. Workflow of the proposed method.

Micro CT Scan Data

Figure 2 depicts the 3D reconstruction result of the X-Ray micro-CT scan imaging. In contrary, figure 3 shows the depth slice of the figure 3. In this figure, it is noted that the darker regions corresponding to the pore spaces can be discriminated easily from the surrounding matrix shown as lighter regions. The carbonate matrix is seen composed of different constituents indicated by various level of brightness present. Brighter regions correspond to the higher density matrix component and vice versa. Some fossils are seen in various size within the matrix.

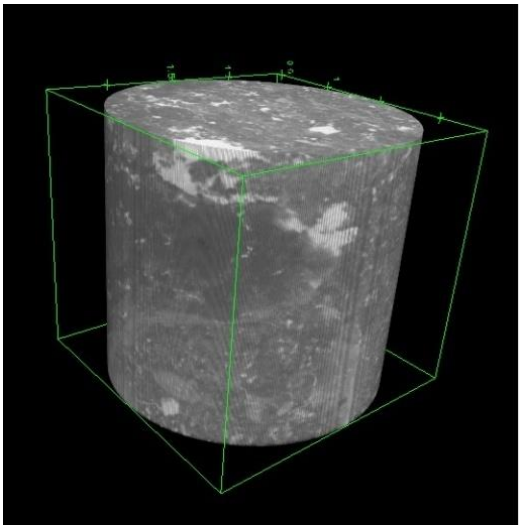

Figure 2. 3D reconstruction of the carbonate micro CT scan data

PROCEEDINGS
JOINT CONVENTION BANDUNG (JCB) 2021
November 23rd – 25th 2021

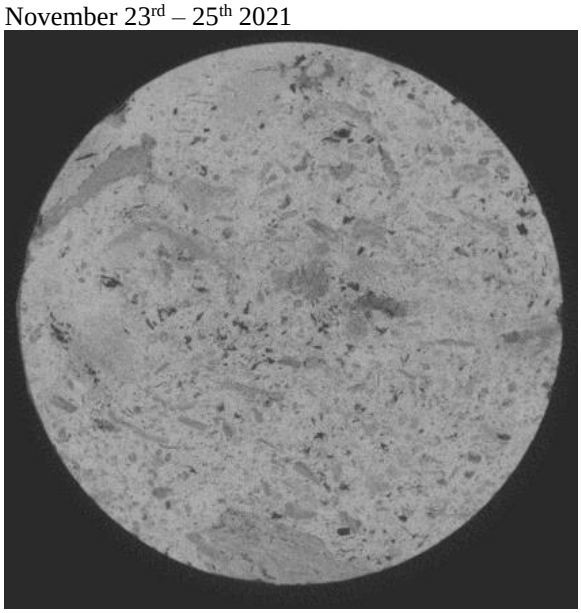

Figure 3. the depth slice of the figure 2.

Sample selection and Image Segmentation

The corresponding 3D sample in figure 2 is cylindrical and comprises loo large volumes for the digital rock analysis. Since digital rock analysis routine requires a clear distinction between the matrix and pore spaces, the zoom in version is needed. Thus, a smaller sample having a shape of cube is selected from the cylindrical image. The selection should consider the region of interest, i.e. specific pore or fracture if any. This procedures also ensure that the computation time will be more efficient yet captures the variations present in the rock sample.

The selected cube is then passed to the image segmentation part. The segmentation procedure follows method introduced by Wardaya et al, (2013) by using Neural Network assisted segmentation. The method has been reported providing faster yet accurate segmentation as compared to more manual method such as watershed or Otsu segmentation. The segmentation transform the greyscale image into binary image where pixel corresponding to the pore spaces will be addressed by 1, while the matrix as 0. The total number of pixel valued 1 divided by the total pixel in the image is the value of the porosity. Figure 4 shows the segmentation result.

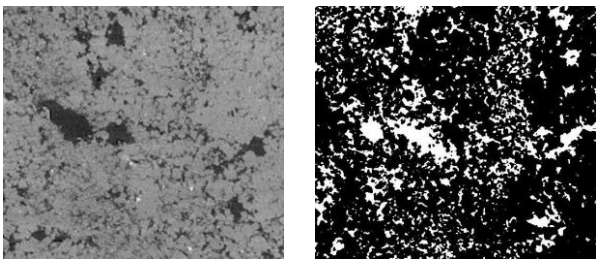

Figure 4. left: original image. Right: segmented image

Subsampling procedure

Spatial heterogeneity is defined as the variation of porosity value sampled at different location of the sample. For heterogeneous rocks, the variation of the porosity at different sampling points might be prominent as compared to that of homogeneous rock samples. Even at pore scale, in this case, at 1024^3 voxel, porosity value at this size might significantly differ to the same sample analyzed at half of its size, 512^3 voxel. Therefore, analyzing the porosity at various cube sizes can provide a reliable measure at which the size of the sub sample yields the same value of porosity of the whole sample. This is the concept of representative elementary volume (REV).

In this step, we selected various sizes of subsamples ranging from 100^3, 200^3, 300^3, 400^3, 500^3, and 600^3 voxel. In the sampling, overlapping is allowed so long it is not more than half of the overlapped section. Consequently, the smallest subsamples have the most number while the biggest subsamples at 600^3 has the least.

The subsampling procedure is illustrated in the figure 5 below

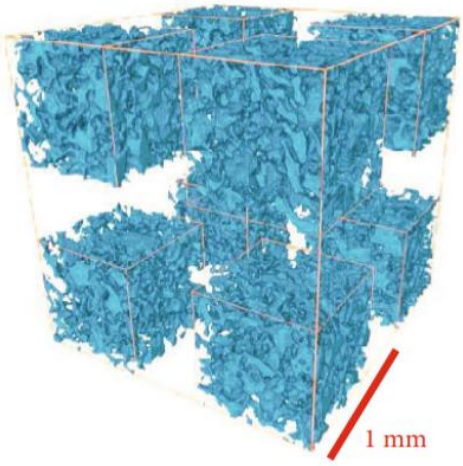

Figure 5. Subsampling procedure.

Porosity Heterogeneity

Porosity is calculated automatically by the method described in the segmentation section. The neural network algorithm performed the calculation automatically using the training basis given in the 2D slice of the data. Once training was given, the algorithm run the segmentation slice by slice from the bottom to the topmost part of the data.

The porosity value of each subsample is plotted against the sample size, presented as subsample volume. Figure 6 depicts the porosity against sub sample size.

PROCEEDINGS
JOINT CONVENTION BANDUNG (JCB) 2021
November 23rd – 25th 2021

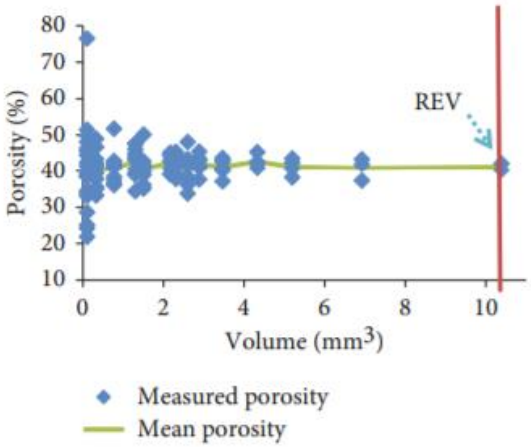

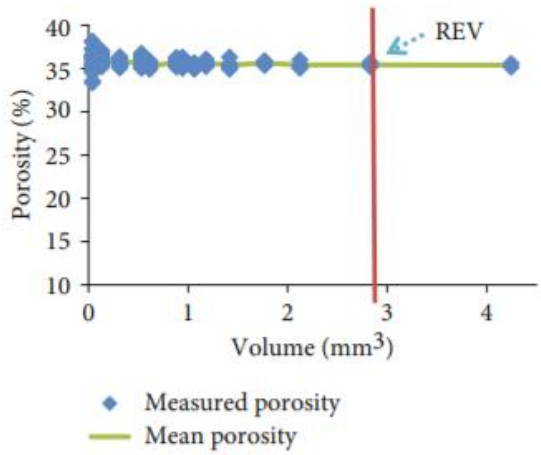

Figure 6. Porosity versus sample volume.

From figure 6 above, we can see that the mean porosity of the sample is 40%. This value confirms the porosity run at the whole sample at 1024^3 voxel size. Smallest samples of 100^3 corresponding to 0.3^3 mm^3 yield the highest variation in the measured porosity value. This happened since majority of pore spaces has size larger than 0.3mm. Subsample at 0.3^3 mm^3 sometimes covered half of the individual pores paces, whole individual pore spaces, parts of few neighboring pore spaces, and even very little part of the pore spaces.

However, as the size of the subsample gets larger, the variability in the porosity is smaller, and is close the mean porosity value. It is observed that the REV for this sample is at $10.3mm^3$ where the porosity value at this sample exactly matches the mean porosity value.

This finding implies a relatively larger heterogeneity in the sample. The scale dependent heterogeneity is represented by the REV where larger REV implies a larger heterogeneity. The smallest subsamples selected at various location within the larger cube capture the spatial distribution of the pore spaces. Larger variability of porosity measured at this size indicates the spatial heterogeneity of the sample.

As the benchmark, we analyzed the relatively homogeneous sample, a Berea sandstone whose porosity against subsample volume plot is given in the figure 7. It is evident that the scale dependent heterogeneity in the sandstone sample is smaller than in carbonate as indicated by the smaller REV value at $2.8mm^3$. In addition, the spatial heterogeneity is also smaller, indicated by smaller variation in the porosity value measured at the smallest subsamples. In contrary to the carbonate sample, their porosity is very close to the mean value already.

Conclusion

Carbonate sample evaluated in this study shows significantly high heterogeneity. Both scale dependent and spatial heterogeneity can be observed through plot of porosity versus subsample size. REV can be used as the indicator of scale dependent heterogeneity. As compared to sandstone sample, carbonate is more heterogeneous.

Acknowledgement

The authors thank to PERTAMINA for giving permission to publish this work.

References

Andra, H., et al. 2013a. Digital rock physics benchmarks-part 1: imaging and segmentation. Computer and Geosciences 50, 25-32

Andra et al., 2013b. Digital rock physics benchmark-part 2: Computing effective properties. Computer and Geosciences, 50, 33-43.

Arns, C.H., Knackstedt, M.A., Pinczewski, W.V., Garboczi, E.J., 2002. Computation of linear elastic properties from microtomographic images: methodology and agreement between theory and experiment. Geophysics 67 (5), P1395–P1405.

Dvorkin, J, Derzhi, N., Diaz, E., Fang, Q., 2011. Relevance of computational rock physics. Geophysics 76, E141–E153.

Wardaya, P.D., Khairy, H, and Sum, C.W., 2013a. Integrating Neural network and image processing for estimating porosity from thin section images. 6th IPTC, Beijing.

PROCEEDINGS
JOINT CONVENTION BANDUNG (JCB) 2021
November 23rd – 25th 2021

Exploration of Hidden Geothermal System by Utilizing Micro Seismic Method

Gilang Wiranda[1], Bambang Mujihardi[2], Hary Koestono[3], Taufiq[4], Satryo Budiraharjo[5]
[12345]PT Pertamina Research & Technology Innovation

Abstract
Not all geothermal resources have surface manifestations as identifier. Therefore, subsurface exploration activities are needed to identify the existence of hidden geothermal systems. To get information in the form of geothermal reservoirs and heat rock sources, comprehensive mapping is needed so that the right information can be used as a determination of injection and production well points. One commonly used method is the micro-seismic method. The micro-seismic method is a method already used to map subsurface conditions in geothermal areas, generally by using Pressure (P) and Shear (S) wave delay time calculations to map velocity. Data are processed in the form of analysis of seismic energy decay that propagates in rocks. The analysis provides valuable information in the form of Q which is a quality factor for rocks in seismic term. In this study, passive seismic data processing was carried out in the Hululais geothermal area taken in 2019. Through the cooperation of Pertamina Research & Technology Innovation (RTI) and Universitas Pertamina, passive seismic data processing is carried out using seismic attenuation techniques. Through the processing of data from 156 mobile stations obtained, 85 seismic events were identified, but only 28 seismic events entered the research area. Attenuation processing results provide anomalies of Q values relatively consistent with rock velocity, where high Q conditions are generally found in the High V zone. Attenuation tomography also showed a positive correlation between low-speed anomalies and low attenuation anomalies. This can be attributed to the presence of rocks that are integrated by high temperature fluids that are thought to be reservoirs in geothermal fields. Tomography attenuation methods can map the subsurface conditions of geothermal areas well.

Introduction
Indonesia history of geothermal exploration looking back to 19th century when German volcanologist study and mapping number of manifestations on java region. Progressing into 20th century, efforts for mapping the potential of national geothermal resources began in 1970 for high temperature system (Hochstein & Sudarman, 2008). The journey of geothermal reconnaissance and surveys since the 1960s show that more than 200 geothermal prospects with significant active surface manifestations occur throughout Indonesia. Most of the resource mapped are geothermal systems with visible surface manifestation and relatively identifiable geological features marking them (Heiken et al., 1993).

Not all geothermal area shows clear visible surface manifestation such as fumaroles, hot springs, and minerals. Hidden geothermal are hydrothermal systems that lack surface thermal features, it is also known as blind geothermal system. Conventional geothermal resource and hidden geothermal system share many features in common such as a permeable reservoir that allows for circulation of hydrothermal fluids at depth (Dobson, 2016). Some efforts in Indonesia of identifying the features of hidden geothermal have been done using 3D gravity method to map the concealed underground heat sources (Martakusumah et al., 2015).

Geophysical exploration provides subsurface imaging that identifies subsurface structure and hidden geothermal system. Common geophysical method used in geothermal project are magnetic, gravity, magneto telluric (MT), and micro earthquake (micro seismic). A proper geophysical data acquisition helps the conceptual model of geothermal system (Harthill, 1973). One of the geophysical methods used is Micro Seismic Tomography, using natural earthquake or subsurface disturbance as sources that usually in a low-frequency form. Exploration could be done by measuring the hypocenter, travel time, rock velocity, and even the waveform itself. Originally, the method of mapping the hypocenter of every isolated small earthquake produces a map that predicts earth crustal structure such as subduction, large basin, or heat source rocks. In geothermal, the micro earthquake resulted from interaction of rock, fluid, and reservoir provides information of zonal porosity and permeability from the assumption of probability of seismic activity at subsurface faults. The advance of computational technology gives the researcher more possibilities to utilize the earth natural source of seismic waves using velocity tomography that calculates the ray path from the source to the signal receiver.

This research aims to analyzes attenuation phenomenon of seismic waves that propagate in a medium using Q-Tomography. The attenuation parameter obtained from the method will be useful to estimate potential geothermal reservoirs, especially in hidden system where no visible manifestation occurs on the surface.

Data and Method

In 2019, the ambient noise tomography survey was done by Pertamina Upstream Research & Technological Innovation (URTI) with Universitas Gadjah Mada (UGM) and obtained good insight about the study area. The passive seismic data considered to be useful for exploration research and studies. The data consisted of 152 data of moving seismogram measurement. Each of the data consisted of 3 to 4 days of passive seismic recording on an array that covers the Hululais area. In 2020, the same data is processed with Q Tomography method with partnership of Universitas Pertamina. The data originally purposed for ambient noise tomography, which the recording duration is not very ideal for micro seismic research because of the shorter duration. Nevertheless, we look to utilize the available data to give an insight of what this method could produce with those limitations. The attenuation parameter

PROCEEDINGS
JOINT CONVENTION BANDUNG (JCB) 2021
November 23rd – 25th 2021

of rock could be obtained by calculation of energy reduction of seismic wave received by the recorder.

Table 1 The Characteristic of Q Vp, Vp/Vs and other Geophysical Properties

Characteristic of *Q*, *Vp*, *Vp*/*Vs* and other geophysical properties	Lab or Field Research	Reference
Qp decreases rapidly with increasing temperature	Lab	Sato *et al.* (1989)
Low *Qp* correlated with the increase in the melting volume correlating and high temperature	Lab	Mavko (1980)
Qp decreases with the increase of fluid content	Field	Haberland & Rietbrock (2001)
Sedimentary basin and magmatic in Central Java (*Qp* < 100; low *Vp*; high electrical conductivity)	Field	Bohm *et al.* (2013)
Ventura Basin California (low *Qp* < 100)	Field	Hauksson & Shearer (2006)
Low *Vp* and high *Vp*/*Vs* is related to high fluid saturation	Field	Julian *et al.* (1996) Husen *et al.* (2004) Haberland *et al.* (2009)
Low *Q*, low *Vp* and low *Vs* beneath Mt Guntur complex	Field	Priyono *et al.* (2011)
Gas-filled volume beneath the Yellowstone caldera (low *Vp* and low *Vp*/*Vs*)	Field	Husen *et al.* (2004)

From the research done by Sato,1989 (Sato et al., 1989), it was observed that a dry spinel lherzolite in high pressure and temperature condition have a decrease in Quality Factor (Qp), which meant that acoustic wave energy adsorption in the material increased with the temperature. Fluid content in rock formations also has a decrease in Qp value. The results are given from the research on local earthquake traveltime tomography analysis. Using both natural earthquake and explosive source, subsurface velocity and attenuation are obtained and analyzes. It is found that the area that likely to have a partial melting and also fluid-saturated sediment have a relatively lower Qp. (Haberland et al., 2009)Research in Mt. Guntur by Priyono (2011) shown that the decrease of Vp/Vs value correlates with the low Q anomaly in that area. The decrease of the value interpreted as a weak zone of volcanic materials, probably caused by high temperature and fluid-saturated rock beneath the surface. (Priyono et al., 2011)

Inversion for Tomography Attenuation is obtained by determining the attenuation parameter *t**, which correlates with the earthquake signal amplitude spectrum.

$$A(f) = 2\pi f \Omega 0 \frac{f_c^2}{(f_c^2 + f^2)} \exp[-\pi f (t^*)]$$

The equation above shown that t* causing amplitude spectrum attenuation. Other parameter affects it is spectra level (Ω0) and corner frequency (*f*c). The Three parameters of those estimated by spectra fitting shown in Figure 1 & 2. (Scherbaum, 1990) Waveforms around the P-wave arrival time are chosen then a Fourier Transform is applied to obtain the spectrum. Based on the spectrum data, a spectra fitting is done to obtain the three parameters (Ω0, *f*c, & *t**). Inversion of 3D Q Attenuation then obtained by 3D velocity inversion, using the number of t* from some earthquake source and 3D velocity structure from velocity tomography. Q attenuation structure then obtained from t* inversion along the ray path, which fulfil the equation of:

$$t^* = \int_{Ray\ path} \frac{1}{[Q(s) \cdot V(s)]} ds + t * station$$

Results and Discussion

A rock velocity value defines a speed of wave propagating through rock body. Variations of seismic wave velocity usually affected by the rock material properties. A less compacted rock often giving a lower velocity result while a more dense and compact rock giving a higher velocity result. There are other parameters affecting velocity in rock in geophysical aspect such as fluid content, elasticity, etc. but in this research, we focus on the correlation with attenuation parameter (Q) in the following sections.

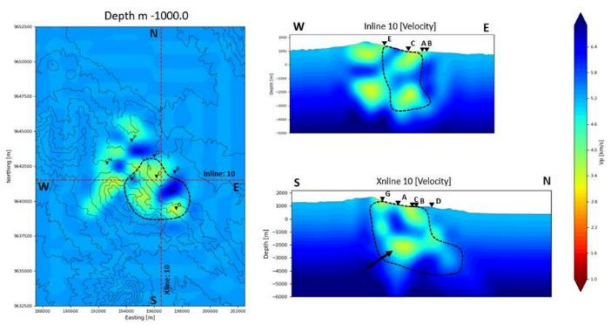

Figure 1: Velocity Section of Inline and Crossline 10, and Horizontal Slice of -1000msl Depth

PROCEEDINGS
JOINT CONVENTION BANDUNG (JCB) 2021
November 23rd – 25th 2021

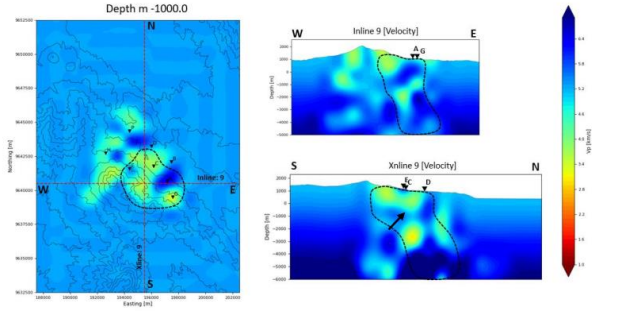

Figure 2: Velocity Section of Inline and Crossline 9, and Horizontal Slice of -1000msl Depth

The Vp obtained from 6 iterations of the inversion, with damping and smoothing parameters from trade-off results and optimized regularization. It is shown in Figure 5 that in the depth of -1000msl, the bright zone that indicates lower velocity appear below well E, C, A, and G. The bright zone also appears on the boundary of well D and B. The Vp value in inline and crossline 10, low-velocity anomaly that appears in the 1000-0 MSL and -2500msl showed indications of geothermal system components such as reservoir zone saturated by geothermal fluid. The area shown is still in the dash line boundary, so it is considered a good resolution.

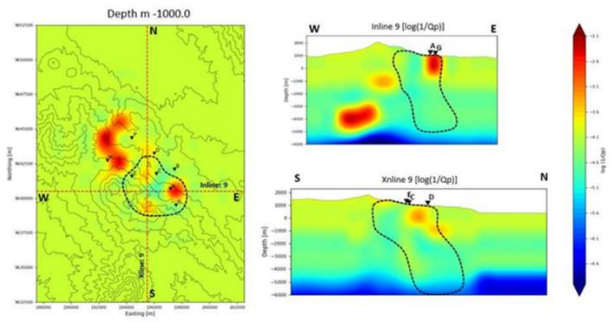

Figure 3: Attenuation (1/logQp) section of Inline and Crossline 9, and a horizontal slice of -1000msl depth.

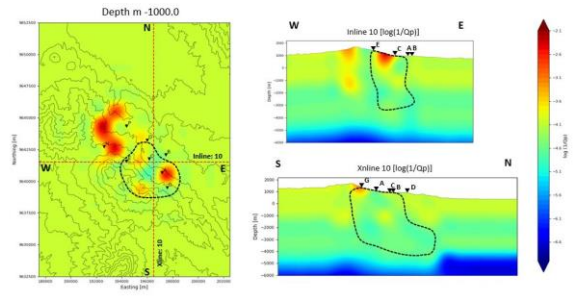

Figure 4: Attenuation (1/logQp) section of Inline and Crossline 9, and a horizontal slice of -1000msl depth.

From the attenuation factor in Figure 7 and Figure, zones with high and low attenuation are shown. In line 9, it is seen between E and C well, the depth of 0 to 1000m appears to be a low-velocity anomaly. It is estimated to be a response from rock saturated by hot fluid that is a geothermal reservoir of Hululais. Using the formula from (Jackson et al., 1992), a temperature estimation from the Q factor is obtained. The estimated reservoir temperature of the Hululais geothermal area shown in the temperature estimation is around 220°C.

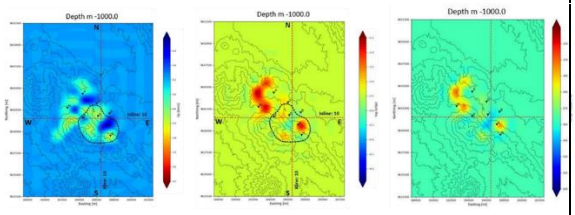

Figure 5: Comparison between 3 extracted parameters from the data processed with Vp (left), Qp (middle), and temperature (right)

The three parameters of Vp, Q, and T estimation are compared and analyzed. From Figure 5, it is shown that around Well A, it has a high attenuation (1/logQp) and high-velocity section (Vp). The section results on C well shown an opposite value between velocity and attenuation, with relatively medium-high attenuation and medium-low velocity. The temperature estimation value in this map shown a relatively consistent with the attenuation value because of the few variables affects the equation. There are also many interesting features in the northwest zone of the map, showing a highly attenuative anomaly stretching from well P to well N.

Conclusions

With the method of microseismic tomography such the example of Hululais Geothermal Area, the extracted parameter of primary velocity (Vp) and P-wave quality factor (Qp) is obtained. Using the Q-Tomography technique paired with velocity tomography, a good understanding of the subsurface area in the geothermal area could be done. The method of using available passive seismic data proven to be valuable. Using short period passive seismic data of three to four days, we could see an acceptable tomography that differentiate between high or low attenuation zone which information could help identify geothermal reservoir. A better result will be expected with a longer recording period of Micro seismic data that produce more ray paths in the process. From the extracted parameter, we observed that in Hululais Area attenuated zone below, well A and G are anomalous, which have an opposite value between P-attenuation and P-velocity. The rest of the observed area showed a consistent result of low-velocity section with high attenuation that consistent with many references that a reservoir filled with geothermal fluid may presents certain spots in subsurface. This method could help in identify hidden geothermal system on a prospected geothermal area.

References

Dobson, P. F. (2016). A Review of Exploration Methods for Discovering Hidden Geothermal Systems. *GRC Transactions*, *40*. https://www.eia.gov/electricity/data/eia860/;

Haberland, C., Rietbrock, A., Lange, D., Bataille, K., & Dahm, T. (2009). Structure of the seismogenic zone of the southcentral Chilean margin revealed by local earthquake traveltime tomography. *Journal of Geophysical Research: Solid Earth*, *114*(B1). https://doi.org/10.1029/2008JB005802

Heiken, G. H., Ander, M. E., Shankland, T. J., Vesnaver, A., Lin, R., Zhao, L. F., Xie, X. B., He, J. K., Tian, X., Yao, Z. X., Hochstein, M. P., & Sudarman, S. (1993). Geothermal resources of Sumatra. *Earth and Planetary Science Letters*, *64*(26), 181–200. https://doi.org/10.1016/j.jappgeo.2019.04.004

Hochstein, M. P., & Sudarman, S. (2008). History of geothermal exploration in Indonesia from 1970 to 2000. *Geothermics*, *37*(3), 220–266. https://doi.org/10.1016/j.geothermics.2008.01.001

Jackson, I., Paterson, M. S., & Fitz Gerald, J. D. (1992). Seismic wave dispersion and attenuation in Åheim dunite: an experimental study. *Geophysical Journal International*, *108*(2), 517–534. https://doi.org/10.1111/j.1365-246X.1992.tb04633.x

Martakusumah, R., Suryantini, W. S., Pratama, A. B., & Haans, A. (2015). Gravity Analysis for Hidden Geothermal System in Cipanas , Tasikmalaya Regency , West Java. *World Geothermal Congress 2015*, *April*, 19–25.

Priyono, A., Suantika, G., Widiyantoro, S., Priadi, B., & Surono. (2011). Three-dimensional P- and S-wave velocity structures of Mt. Guntur, West Java, Indonesia, from seismic tomography. *International Journal of Tomography and Statistics*, *16*(W11), 1–11.

Sato, H., Sacks, I. S., Murase, T., Muncill, G., & Fukuyama, H. (1989). melting temperature relation in peridotite at high pressure and temperature: Attenuation mechanism and implications for the mechanical properties of the upper mantle. *Journal of Geophysical Research: Solid Earth*, *94*(B8), 10647–10661. https://doi.org/10.1029/JB094iB08p10647

Acknowledgements (Optional)
The authors want to thank Pertamina for the funding source of the q-tomography research and team of Universitas Pertamina for the research partnership that has been done in 2020. The data and the project backing this paper is part of the Corporate and University continuous partnership in research programs.

PROCEEDINGS
JOINT CONVENTION BANDUNG (JCB)2021
November 23rd – 25th 2021

Wellbore Stability on Shale Gas Reservoir with 1D Geomechanical Model, Keluarga Field, Central Sumatra Basin

Santika Satya Widita, Benyamin Sapiie**
**) Geological Engineering, Institut Teknologi Bandung*

Abstract

Shale gas is categorized as an unconventional hydrocarbon. Shale gas does not require hydrocarbon trap components, cap rocks, migration pathways, or reservoir rocks and only requires source rock. The source rock in the "Keluarga" Field, Central Sumatra Basin, is dominated by lacustrine deposits from the Brown Shale Formation, Pematang Group, which accumulated in syn-depositional extensional graben with a north-south and northwest-southeast trend. However, the production of shale gas is different from conventional hydrocarbons. It needs hydraulic fracture through horizontal drilling to enhance permeability.
The geomechanical model analysis is needed in shale gas production to determine the in-situ stress conditions below the surface and understand the wellbore stability. To understand the in-situ stress conditions, one-dimensional geomechanical model analysis from the well data needs to be analyzed. R-3 well is used in the analysis of one-dimensional geomechanical models.

The analysis includes calculating vertical stress, pore pressure, rock elastic properties such as Young's modulus and Poisson's ratio, rock strength such as Unconfined Compressive Strength (UCS) and friction angle, horizontal stress orientation, and magnitude wellbore stability analysis. The result of the one-dimensional geomechanical modeling shows that the pore pressure condition of the "Keluarga" Field reservoir is under pressure while the shale layer is close to the hydrostatic value of 0.43 psi/ft or 8.33 ppg and validated with formation pressure test data. The vertical stress shows an average gradient of 1.01 psi/ft. The values of Young's modulus, Poisson Ratio, Unconfined Compressive Strength (UCS), and friction angle are validated with Triaxial Compressive Strength test data. The horizontal stress analysis showed that the "Keluarga" Field's stress regime is normal to a strike-slip fault. Meanwhile, wellbore stability analysis indicated that the borehole was stable and able to withstand mud weight up to 13.10 ppg on the shale interval, Brown Shale Formation.

Keywords: shale gas, geomechanical model, in-situ stress, wellbore stability.

Introduction

"Keluarga" Field is one of Rokan's Product Sharing Contract (PSC) fields located 72 km southwest of Dumai city, Central Sumatra Province, Indonesia (Figure 1). The main targets of the "Keluarga" field are oil and gas hydrocarbons that have accumulated in the Sihapas Group fluvial sandstone reservoir of the early Miocene age in a half-graben structure.

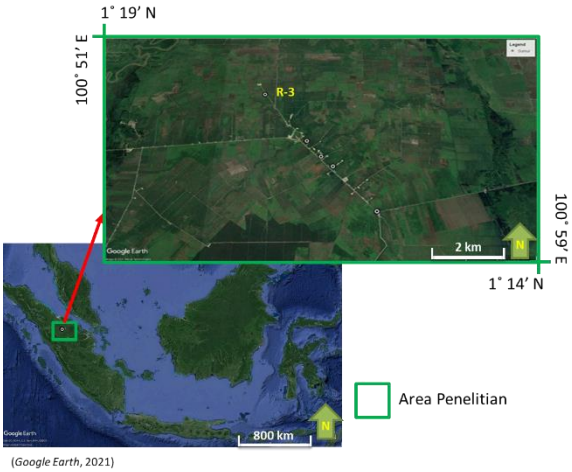

Figure 1. "Keluarga" Field marked with a box. (Google Earth, 2021).

The tectonic regime of the Central Sumatra Basin distinguished between Pre-Tertiary, Middle Eocene, and Middle Miocene ages. The Pre-rift basement of the Pre-Tertiary age is a series of accretionary terranes intruded by granite and shows a structural trend in the northwest – southeast (NW – SE) direction. During the Middle Eocene, a collision between the Indian sub-continent and the South Asian plate boundary resulted in a relatively deep extensional graben formation in a north – south direction, while a shallow half-graben formed along with the northwest – southeast (NW – SE) trend. The succession of the Pematang Group consisting of fluvial and lacustrine deposits in the form of the Brown Shale Formation accumulated in several grabens. The deep lacustrine shale sediment deposits are deposits in rich organic material and oil-prone. Some shallow graben coal facies are deposited with the potential for gas, condensate, and light oil. In the inversion and partial erosion period, the graben filled with transgression clastic sediment deposits from the Sihapas group. The Sihapas Group deposition was formed due to a transgressive cycle starting from Late Miocene fluvial sandstones from the Menggala Formation to transgressive marine shale deposits from the Telisa Formation (Figure 2).

PROCEEDINGS
JOINT CONVENTION BANDUNG (JCB)2021
November 23rd – 25th 2021

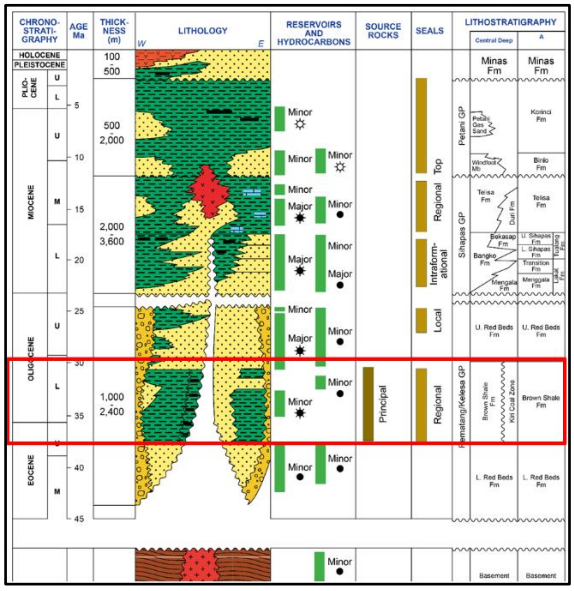

Figure 2. Stratigraphic column of the Central Sumatra Basin (IHS, 2015).

During the Middle Miocene, the northward movement of the Indo-Australian plate relative to the Southeast Asian plate formed a compression force that resulted in a shift of the dextral plate (right lateral) with a northwest – southeast (NW – SE) trend. It formed the Great Sumatra Fault Zone which where the uplift of the Bukit Barisan took place. The deposition of sandstone deposits that occurred in the Middle Miocene age resulted from Bukit Barisan's erosion and regressively deposited in the Petani Group. Compression forces in the Central Sumatra Basin occur to date and affect the in-situ stresses below the surface (Figure 3).

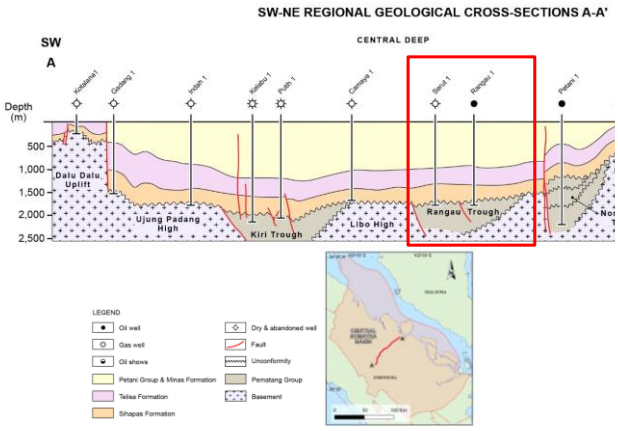

Figure 3. Cross-section area of the Central Sumatra Basin, the cross-section marked with a red box (Petroconsulants, 1990).

In-situ stress accumulates in rock formations before experiencing external disturbances such as the drilling process. The in-situ stress component consists of one component directed vertically and two components directed horizontally. The magnitude and orientation of the subsurface in-situ stresses could be estimated by one-dimensional geomechanical models of the well and three-dimensionally from seismic and well data. The in-situ stress is also known as far-field stress, while the stress around the borehole is called near-field stress because the stress is affected by drilling conditions. This study will discuss how the stress conditions work in the near-field or one dimension from the well data.

Data and Method

The challenge faced in geomechanics work is the availability of data. Geomechanical modeling requires the integration of data from various sources to get good results. Coates & Denoo (1981) provide guidelines for what data are needed to build a geomechanical model. The data used in this study consisted of primary and secondary data. Primary data is well data in the form of wireline logs consisting of gamma ray logs, bulk density logs, resistivity logs, compressional slowness logs, image logs, and calipers logs. In contrast, the secondary data are drilling reports, formation pressure test data, Triaxial Compressive Strength test data, and literature studies. This study focuses on R-3 well, which the availability of the data listed in (Table 1).

Table 1. Data availability of R-3 well (Available data in green and not available data in red)

Data	Well R-3
Well data	
Sonic DT compressional slowness	
Sonic DTSM shear slowness	
Density	
Gamma Ray	
Resistivity	
Petrophysical interpretation (VCL, PHIE, PHIT)	
Caliper logs	
Trajectory / deviation for offset and plan well	
Equivalent circulating Density log / ECD log	
Formation pressure point (MDT / DST / RFT)	
Image Logs - FMI, UBI, OBMI, AND etc.,	
LOT / XLOT, and or DataFRAC, and or FIT and or step rate tests – Pressure vs time (pdf and LAS)	
Rock mechanics laboratory core test results	
Drilling Data	
Mud log / Master Log / Litholog	
Geological final report / Final Well Report	
Mud log type data (TGAS, MWTI.,etc)	
Daily drilling reports and/or End of wells reports	
Stratigraphic column/formation top	
Geological Data	
Structural Map	

The R-3 well data will be used as a representative well for validation because the data is complete and reaches the Brown Shale Formation. R-3 also has Triaxial Compressive Strength test data and drilling reports. R-3 was drilled for the first time in May 1969 and reached TD (Total Depth) at a depth of 8520ft after three months of drilling in July 1969. The only recorded drilling events in the R-3 were pipe pinching and fishing. Another drilling incident was the increase in mud weight at a depth of 7200ft due to a very high gas cut in the drilling mud, so that the mud weight had to increase from 10.16 ppg to 11.90 – 13.10 ppg. The drilling conditions would be later used in the analysis of the stability of the borehole, especially for the safe weight window of drilling mud.

Methodology

The importance of geomechanical models are to explain how the conditions of stress, pressure, and

PROCEEDINGS
JOINT CONVENTION BANDUNG (JCB) 2021
November 23rd – 25th 2021

rock strength are relate with depth which refer to the stratigraphic column (Brata, 2018). Parameters in the continuous profile will be generated from the one-dimensional geomechanical model. That parameters are rock elastic properties including Young's Modulus and Poisson's Ratio; rock strength parameters in the form of Unconfined Compressive Strength (UCS), tensile strength and angle of internal friction; and stress model in the form of vertical stress, magnitude, and orientation of minimum and maximum horizontal stress, and pore pressure (Figure 4). If the geomechanical model has formed, an analysis of the in-situ stress could carry out to predict the mud weight for safer drilling.

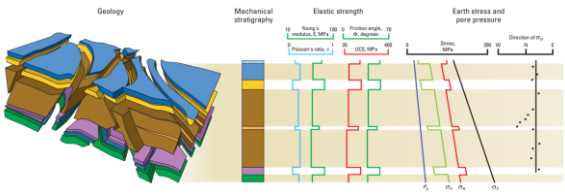

Figure 4. Stages of processing a one-dimensional geomechanical model (Ali, 2013).

The first workflow to do is data adjustment. Each well was reviewed, especially the triple combo log data (gamma-ray, resistivity, and density) and compressional sonic logs (compressional slowness). All wells do not have shear slowness, so the synthetic logs must be processed using the Castagna equation (Castagna et al., 1985) with the input parameters of the compressional sonic log. Bulk density log data in all wells were not acquired from the surface but only at the formation target, such as in R-3 well. Which was only from 5200ft to 8520ft, so the density log had to be extrapolated using a linear equation so that the density value was known from the surface to the total depth (Fig. 5). In addition, caving was recognized in the R-3 borehole or also known as badhole conditions. These conditions affect the density log reading, which is very sensitive to borehole conditions. Density log conditioning was done by correcting the badhole interval based on the density value approximated from the compressional slowness log using the Gardner method. After examining all the wireline log data, it was continued with the analysis of vertical stress and pore pressure.

Vertical Stress and Pore Pressure

The vertical stress was processed by integrating the formation density. In general, formation density can be obtained from wireline logs or density of sample core, but the density used is log bulk density for this study. The equation for vertical stress is indicated by the parameters (ρ_b) bulk density, (Z) vertical depth, and (g) gravity in equation (1) below:

$$\sigma(z) = \int_0^z \rho_b(z).g.dz \qquad (1)$$

The results of the vertical stress are shown in (Figure 5) and have a gradient value of 1.05 psi/ft

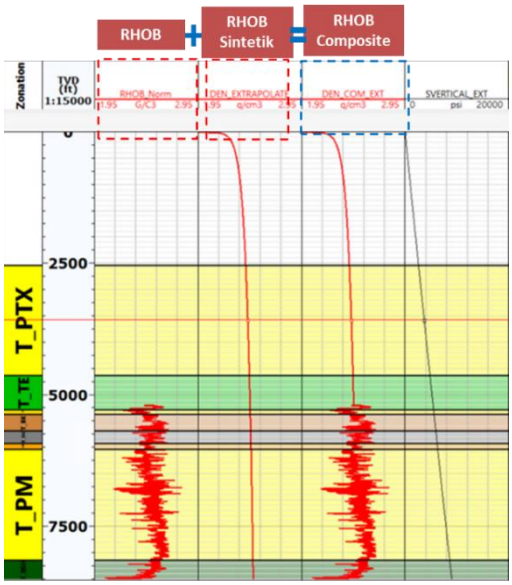

Figure 5. Extrapolation of density logs and plots of vertical stress (overburden) results.

Pore pressure is an essential component in geomechanical models because it is needed in the calculation of horizontal stress, borehole stability analysis, and other geomechanical applications. Pore pressure can be estimated from the sonic log and resistivity log data by several methods such as the Eaton method, Bowers method, the Equivalent Depth method, and others, which calculations are only valid for shale lithology. R-14 well is a key well for pore pressure analysis because R-14 well has formation pressure test data in the form of Repeat Formation Test (RFT) (Figure 6).

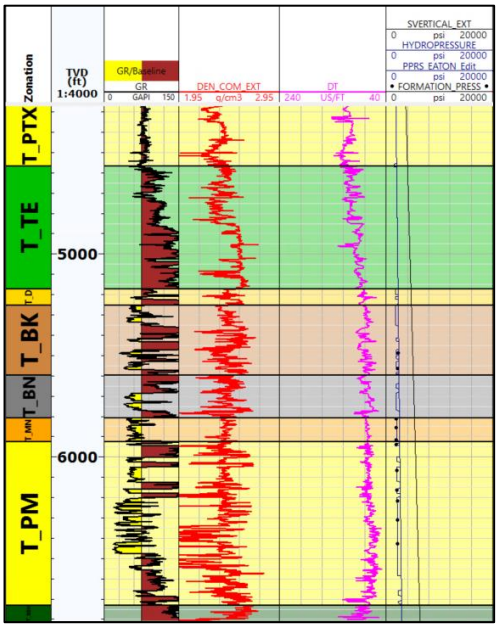

Figure 6. R-14 well as validation for pore pressure gradient treatment.

PROCEEDINGS
JOINT CONVENTION BANDUNG (JCB)2021
November 23rd – 25th 2021

Furthermore, the value of the formation pressure test is plotted with the depth value to obtain a linear equation (Figure 7) which will be used to determine the pore pressure gradient in the R-3 well.

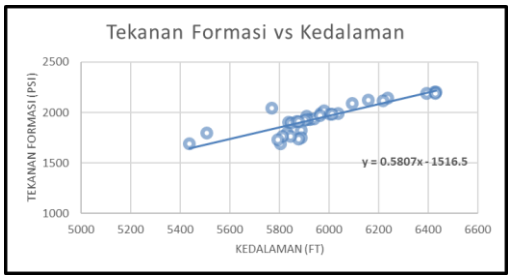

Figure 7. Plot of formation pressure and depth test from R-14 well.

Pore pressure calculation using sonic log with Eaton method was calibrated with formation pressure test data. The pore pressure conditions in the shale lithology are close to the hydrostatic pressure of 0.43 psi/ft or 8.33 ppg. Meanwhile, the pore pressure conditions in the Upper Red Bed Formation, Menggala Formation, and Bangko Formation reservoirs are under pressure because they have been produced for years. (Figure 8).

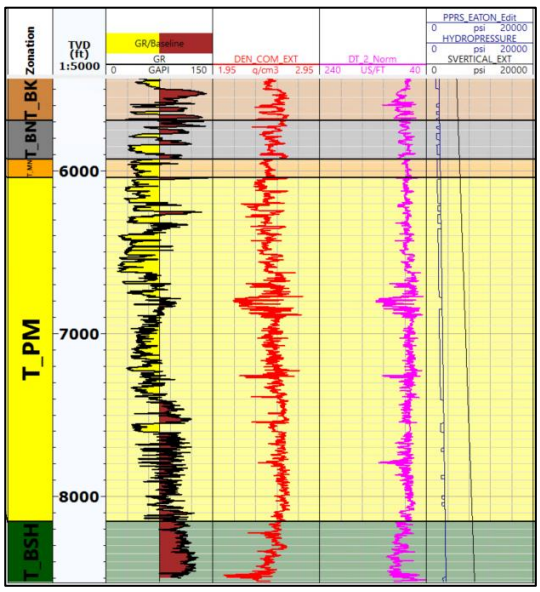

Figure 8. Results of pore pressure analysis in R-3 well.

Rock Elastic Properties

The elastic properties of rocks reflect the stress and strain properties of rocks which are highly dependent on the rock type. In this study, the rock material is assumed to be an isotropic elastic material and its value is represented by the parameters of Young's Modulus and Poisson's Ratio. Rock elastic properties were divided into two types, namely static and dynamic. Static properties are usually obtained from direct measurements such as stress–strain curves from laboratory compression tests. Dynamic properties can be calculated from the log compressional slowness (Δt_c), log shear slowness (Δt_s), and log bulk density (ρ_b). The dynamic elastic properties, namely dynamic shear modulus G_{dyn}, dynamic bulk modulus K_{dyn}, dynamic Young's Modulus E_{dyn}, and dynamic Poisson's Ratio v_{dyn}, are calculated using the Horsud (2001) equation as follows:

$$G_{dyn} = (13474.45)\frac{\rho_b}{(\Delta t_s)^2} \quad (2)$$

$$K_{dyn} = (13474.45)\rho_b\left[\frac{1}{(\Delta t_c)^2}\right] - \frac{4}{3}G_{dyn} \quad (3)$$

$$E_{dyn} = \frac{9\times G_{dyn}\times K_{dyn}}{G_{dyn}+3\times K_{dyn}} \quad (4)$$

$$v_{dyn} = \frac{\frac{1}{2}(\Delta t_s/\Delta t_c)^2-1}{(\Delta t_s/\Delta t_c)^2-1} \quad (5)$$

Furthermore, the value of the dynamic elastic property is used to calculate the static elastic property. The static modulus differs from the dynamic modulus due to the magnitude of the strain. Sonic logs use acoustic waves to calculate deceleration. Acoustic measurements require energy waves that are small enough and are reversible so that the recorded rock elastic values describe the actual adaptable conditions in the rock. Static modulus measurement by core rock test requires large strains during loading, and some are irreversible. The modulus measurement is not entirely elastic, but irreversible deformation occurs due to frictional forces (TerraTek, 1998). So that the value of the static modulus will be smaller than the value of the dynamic modulus. While the value of the static strain is inversely proportional to the dynamic strain, which is a larger value (Plumb, 2000).

Calculation of the static Young's Modulus using the Lacy equation (1997) below:

$$E_{st} = 0.018E_{dyn}^2 + 0.422E_{dyn} \quad (6)$$

The equation is generated from the core rock test of sandstone, shale, limestone and dolomite. Lacy's equation is a fairly good and can be applied to a wide range of lithologies. As for the static Poisson Ratio, shown by the equation below:

$$v_{st} = v_{dyn} * PR\ multiplier \quad (7)$$

Basically, dynamic and static Poisson Ratios are assumed to be the same. Still, there is a multiplier or *PR multiplier* to validate the Poisson Ratio value with rock test data. The ratio between static and dynamic Young's modulus depends on porosity, confining pressure, loading, and other factors, making dynamic Young's modulus two to three times greater than static. Calibration with Triaxial Compressive Strength test has been carried out on well R-3. The static Young's modulus and static Poisson's ratio from core rock test data in the Upper Red Bed Formation are 4.48 Mpsi and 0.15, while the Brown Shale Formation is 2.65 Mpsi and 0.24 (Figure 9).

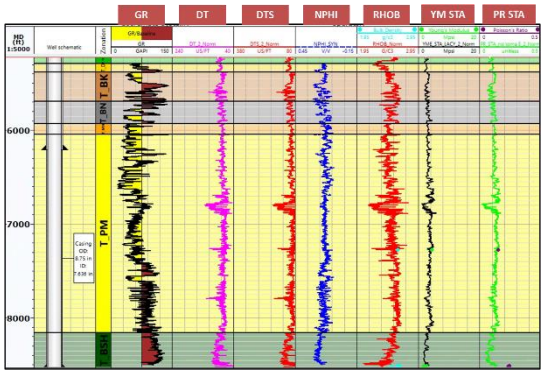

Figure 9. The results of the analysis of the elastic properties of rocks in accordance with the compressive test data of rocks.

Rock Strength Properties

Rock strength is the rock's ability to withstand in-situ stress conditions around the borehole. Rock strength properties include Unconfined Compressive Strength (UCS), tensile strength, and rock friction angle. The UCS parameter is a parameter that is widely used because it can determine the damage to the borehole during drilling, obtained from the Triaxial Compressive Strength test on the core rock. These values will be used as validation points for the continuous profile. The calculation of UCS on a constant profile is carried out using the McNally equation (McNally, 1990), as follows:

$$UCS = 1200\exp^{-0.036*\Delta t_c} \quad (8)$$

The UCS continuous profile was validated with Triaxial Compressive Strength test data on R-3 well. Core rock was tested in an unsaturated or unconfined state and samples were taken from the Upper Red Bed Formation sandstone at a depth of 7277 ft at 13200 psi and Brown Shale Formation at depth of 8513 ft at 10021 psi. The parameters in the calculation of UCS in R-3 well will also be used for other wells. Tensile strength is used to determine the tensile failure in boreholes caused by stress release. Tensile strength is assumed to be 0.1 of UCS. The value of 0.1 is a facies and zone factor based on Griffith Elastic-brittle theory which gives a ratio between compressive strength and tensile strength of 8 ~ 12.

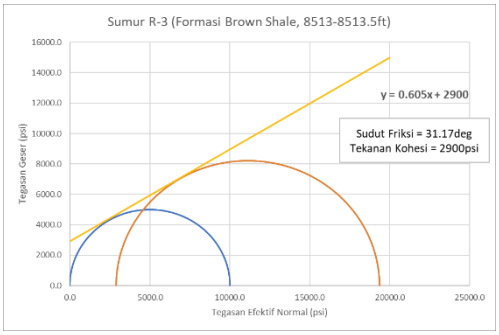

Figure 10. Mohr-Coulomb diagram as validation of rock friction angle.

Furthermore, the rock friction angle is determined from the log compressional slowness. It is based on the increase in rock strength values along with increasing compaction. So that rock strength parameters can be approached by measuring wire rope logs such as porosity, density, and compressional slowness logs (Lal, 1999). The validation of the friction angle is obtained from the Mohr-Coulomb diagram based on the shear stress and normal effective stress from the Triaxial Compressive Strength test. Based on the graph, the friction angle value is 31.17 degrees, and the cohesive pressure is 2900 psi, according to the empirical friction angle calculation in the FANG_DT log (Figure 10). The result of rock strength analysis could be seen in the Figure 11.

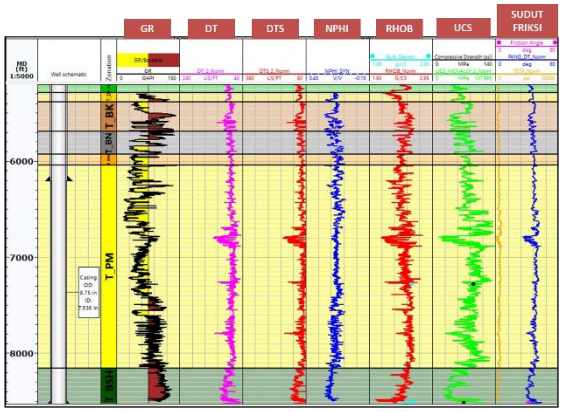

Figure 11. Results of rock strength analysis in accordance with rock compressive test data.

Horizontal Stress

Horizontal stress is caused by tectonic events that occur on earth. Horizontal stress cannot be measured directly but can be approximated by stress and strain measurements such as the Leak-Off Test (LOT), Formation Integrity Test (FIT), or from drilling events such as breakouts and drilling-induced tensile fractures.

The poroelastic model by Blanton and Olson (1999) explains that it can determine the maximum and minimum horizontal stress magnitudes through the parameters of static Young's modulus and static Poisson Ratio. The model also adds tectonic strain parameters and geothermal effects into the calculation to accommodate anisotropic horizontal stress conditions. The poroelastic model is shown in the following equation:

$$\sigma_h = \frac{v}{1-v}\sigma_V + \frac{1-2v}{1-v}\alpha P_p + \frac{E}{1-v^2}\varepsilon_x + \frac{vE}{1-v^2}\varepsilon_y \quad (9)$$

$$\sigma_H = \frac{v}{1-v}\sigma_V + \frac{1-2v}{1-v}\alpha P_p + \frac{E}{1-v^2}\varepsilon_y + \frac{vE}{1-v^2}\varepsilon_x \quad (10)$$

The results of maximum and minimum horizontal stress cannot be validated with pressure test data because data is unavailable, so validation is carried out based on borehole conditions observed by caliper logs and bit size logs. Meanwhile, the tectonic regime in

PROCEEDINGS
JOINT CONVENTION BANDUNG (JCB)2021
November 23rd – 25th 2021

the study area shows a normal fault regime as indicated by the value of the vertical stress being greater than the two horizontal stresses. The maximum horizontal stress direction is parallel to the direction of Sumatran subduction, which is N35^{0}E (NE – SW) (Figure 12).

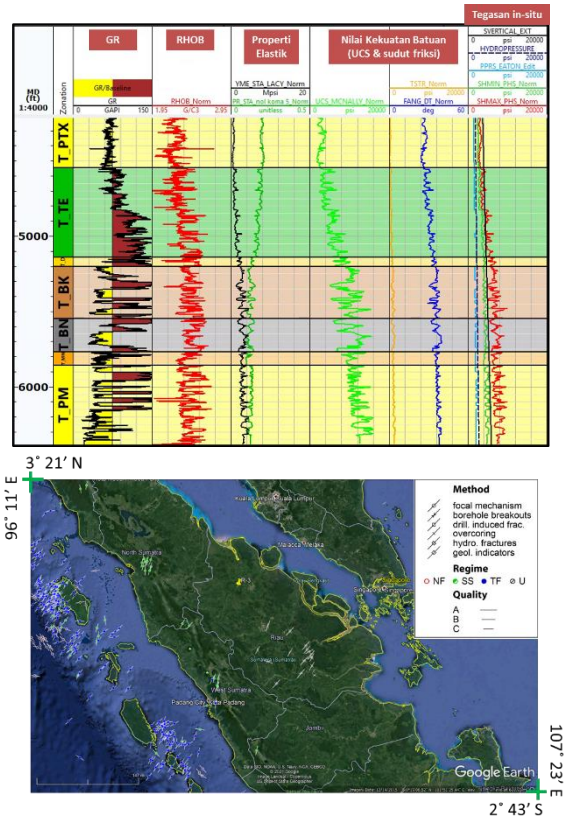

Figure 12. Results of horizontal stress analysis (upper image = magnitude of horizontal stress, lower image = orientation of horizontal stress).

One-dimensional geomechanical models can be analyzed through borehole stability analysis. Pore pressure, vertical stress, elastic property, rock strength, horizontal stress magnitude, and drilling mud weight are the key parameters for conducting borehole stability analysis. The analysis results can be validated using drilling events such as breakouts, drilling-induced tensile fractures, and losses, which can be observed from drawing logs, calipers logs, or drilling reports. R-3 well does not have an image log, so validation is only performed against the caliper log.

Analysis of borehole stability uses the Mohr-Coulomb method as failure criteria to determine shear failure and tensile failure. Mohr-Coulomb uses input data in the form of Uniaxial Compressive Strength (UCS) and rock friction angle to determine the failure envelope. The results of the borehole stability analysis illustrate that when there is an increase in the weight of the mud at a depth of 7340 ft, the borehole is still stable. This was validated based on drilling reports that did not record any drilling events such as breakouts, drilling-induced tensile fractures, kicks or losses.

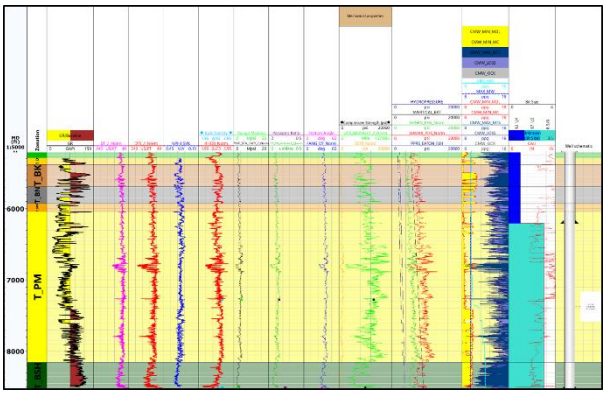

Figure 13. Results of borehole stability analysis in R-3 well shown in column 12.

Result and Discussion

The pore pressure at the reservoir interval in well R-3 shows the results of under pressure. It is known from the test data of formation pressure in the reservoir interval. Meanwhile, at the shale interval, the pore pressure is close to the hydrostatic pressure, which is 0.43 psi/ft or 8.33 ppg. The elastic properties of Young's modulus and Poisson's static ratio, as well as rock strength, have been validated with Triaxial Compressive Strength test data. Meanwhile, the results of the maximum and minimum horizontal stresses analysis using the poroelastic method showed a normal to strike-slip fault regime and an orientation of N35^{0}E. The results of the borehole stability analysis show that the borehole is in a stable condition. The borehole stability analysis showed no drilling events such as breakouts, drilling-induced tensile fracture, and losses. Although there was an increase in mud weight at a depth of 7340 ft from 10.4 ppg to 11.2 ppg, the borehole was stable, and the formation pressure was still able to withstand the pressure from the drilling mud (Figure 13).

Discussion

Based on the analysis carried out on the drilling report, especially in the R-3 well, shows that there are several intervals that are analyzed as bad holes. This makes the density log reading not very accurate and causes caving, especially in sandstone reservoirs. Some of the depth intervals experiencing bad holes are at a depth of 5769 – 5795ft, 5838 – 5901ft, 5938 – 6040ft, 6282 – 6322ft, 6384 – 7280ft so that the depth interval is improved by reducing the density value of the log compressional slowness through the Gardner equation.

Table 2. Triaxial Compressive Strength test results on R-3 well.

Triaxial Compressive Test Result (R-3)							
Sample Number	Depth	Test Temperature	Confining Pressure	Bulk Density	Compressive Strength	Young's Modulus	Poisson's Ratio
Unit	ft	degF	(psi)	g/cm3	psi	Mpsi	
1V	7277	70	100	2.62	13300	4.48	0.15
10V	8511.1	70	2900	2.64	24570	2.65	0.24
11V	8513	70	0	2.51	10021	1.72	0.24
12V	8513.5	300	2900	2.61	19360	2.46	0.23

The value of the rock elastic parameter Young's modulus indicates the change in length of a material which is the rock to a given strain. In other words, Young's modulus calculates the tensile stiffness of the rock. A high value of Young's modulus indicates inelastic or stiff rock, while a low value of Young's modulus indicates an elastic rock. Based on Howard and Fast (1970) and Fjaer et al. (2008) the value of Young's static modulus in shale is around 0.1 – 1.0 Mpsi, sandstone is about 2 – 10 Mpsi, and limestone is around 8 – 12 Mpsi. The Young's modulus analysis (Figure 9) shows that the static Young's modulus derived from the compressional slowness log has a value range of 2-4 Mpsi and has been validated with Triaxial Compressive Strength test data (Table 2). It also shows that the shale in the Brown Shale Formation shows a fairly high Young's modulus value of 2.46 Mpsi, which indicates the rock is stiff. Stiff shale layers are best for hydraulic fracturing because they will make it easier for the fracture to propagate.

Poisson's ratio elastic parameter value shows the material change when given a strain or the ratio between transverse strain and axial strain. The value of the Poisson ratio is in the range of 0 – 0.5 and is unitless. Elastic materials such as rubber have a Poisson ratio close to 0.5, while solid materials are around 0.2 – 0.3. Gercek (2007) describes the Poisson ratio in rock (Figure 14), which shows that shale is in the range 0.05 – 0.32, sandstone is in the range 0.05 – 0.4, and limestone is in the range 0.1 – 0.32. the Poisson ratio analysis (Figure 9) shows that the static Poisson ratio derived from the compressional slowness log has a value range of 0 – 0.2 and has been validated with Triaxial Compressive Strength test data (Table 2). The Brown Shale Formation shows a low Poisson ratio, so it is very good for hydraulic fracturing.

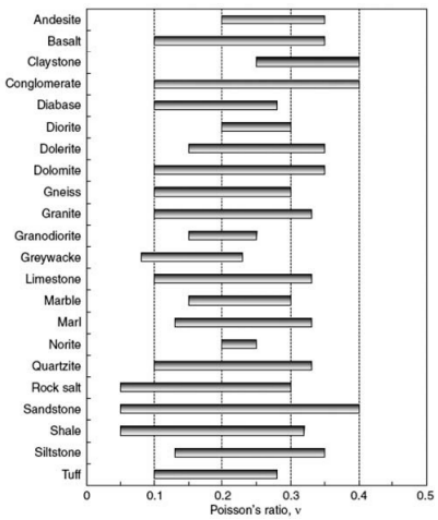

Figure 14. Poisson's range of rock values (Gercek, 2007).

Unconfined Compressive Strength (UCS) rock strength values and rock friction angles show the rock's ability when the compression forces applied. The higher the UCS value, the greater the rock's ability to withstand the given compression force. Based on Zoback (2007), the UCS value in shale lithology has a value range of 70 – 120 Mpa (Figure 15). In comparison, the friction angle shows the angle of shear strength given to the rock. The friction angle also shows how the relationship between particles (particle interlocking) or rock matrix. The greater value of the friction angle, so the greater interlocking between the rock matrix and the more compact the rock. The friction angle in sedimentary rocks varies in the range of 25 to 30 degrees (Jang, 2018). From the analysis results, carried out, the UCS value and friction angle have an average of 76 Mpa and 36 degrees (Figure 10). Especially in the Brown Shale Formation, the range of UCS values was quite low, which means that the rock will be easier to do hydraulic fracturing.

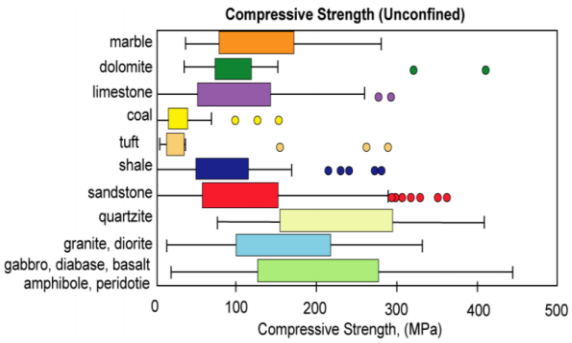

Figure 15. Range of UCS values in rocks (Zoback, 2007)

The analysis of the horizontal stress value was validated based on the caliper value and the occurrence of drilling because the R-3 well did not have image log data. In addition, borehole stability analysis can only be validated through mud weight values and drilling reports.

Conclusions

Based on the analysis of vertical stress, pore pressure, rock elastic properties, rock strength, and horizontal stress has been validated with Repeat Formation Tester formation pressure test data, Triaxial Compressive Strength test data, and drilling reports, the analysis of the stability of the R-3 well borehole can be concluded in stable condition and able to withstand mud weight up to 13.10 ppg at shale interval, Brown Shale Formation. This research can be continued as a reference in making three-dimensional geomechanical models to determine the lateral distribution of in situ stresses. So that it is useful in determining the best area and direction of hydraulic fracturing in horizontal wells, as well as increasing hydrocarbon production in Indonesia.

References

Blanton T. L., & Olson J. E., 1999, Stress Magnitudes from Logs – Effects of Tectonic Strains and Temperature; SPE 54653.

Brata, R., Mahardi, M. Y., Anis, A. S. L., Bahesti, F., 2018, Geomechanics Wellbore Stability Analysis in Successful Drilling of a Challenging HPHT Exploration Well in North Sumatra, Forty-Second Annual Convention & Exhibition, Indonesian Petroleum Association.

Castagna, J.P., Batzle, M.L., Eastwood, R.L., 1985, "Relationship Between Compressional-Wave and Shear Wave Velocities in Clastic Silicate Rocks", Geophysics, VOL. 50, NO.4, p.571-581.

Coates G. R., & Denoo S. A., 1981, Mechanical Properties Program Using Borehole Analysis and Mohr's Circle; 22nd SPWLA Ann. Logging Symp.; Mexico City, June 1981.

Eaton B., 1975, The Equation for Geopressure Prediction from Well Logs; SPE 5544.

Fjaer, E.; Horsrud, H.P., Raaen, A.M., Risnes, R., 2008, Petroleum Related Rock Mechanics; Elsevier B. V.: Amsterdam, The Netherlands

Gercek H., 2007, Int. J. Rock Mech. Min. Sci., 44, 1–13

Horsrud, P., 2001, Estimating Mechanical Properties of Shale from Empirical Correlations; SPE 56017

Howard, G.C.; Fast, C.R. Hydraulic Fracturing. dalam Doherty Memorial Fund of AIME, Society of Petroleum Engineers of AIME; Henry L.: New York, NY, USA, 1970; Monograph Volume 2 of SPE.

IHS Markit, 2015, Central Sumatra Basin: Basin Summary Report. Unpublished.

Jang, HS., Zhang, QZ., Kang, SS. et al., 2018, Determination of the Basic Friction Angle of Rock Surfaces by Tilt Tests. Rock Mech Rock Eng 51, 989–1004

Lacy L.L., 1997, Dynamic Rock Mechanics Testing for Optimized Fracture Designs; SPE 38716, presented at the 1997 SPE Annual Technical Conference and Exhibition held in San Antonio, Texas, 5-8 October 1996.

Lal, M. (1999). Shale Stability: Drilling Fluid Interaction and Shale Strength. SPE Asia Pacific Oil and Gas Conference and Exhibition. doi:10.2118/54356-ms

McNally, G.H., 1990, The prediction of geotechnical rock properties from sonic and neutron log; Exploration Geophysics, 21, 65–71.

Petroconsultants, 1990. Central Sumatra Basin. Southeast Asia Basin Opportunities, Petroconsultants Non-Exclusive Report, 14. Page(s) 73

Plumb R, Edwards S., Pidcock G., & Lee, D., 2000, The Mechanical Earth Model Concept and its Application to High-Risk Well Construction Projects; SPE 59128.

TerraTek Inc., 1998, The Difference Between Static and Dynamic Mechanical Properties; TerraTek Standard Publications, June 1998.

Zoback, M. D. (2007) Reservoir Geomechanics, Reservoir Geomechanics. doi: 10.1017/CBO9780511586477.

Reference from website:

Central Sumatra Maps as study area, accessed from https://earth.google.com at 20 June 2021.

Acknowledgments

The author would like to thank SKK Migas and Schlumberger for providing access to the data and software used in this research. The researcher also thanks to the supervisor, Prof. Benjamin Sapiie PhD. and external supervisors Mr. Sunjaya Eka Saputra, Mas Aryo Radityo, Mr. I Ngurah Beni Setiawan, and Mas Bayu Wisnubroto for their suggestions and input on this research.

PROCEEDINGS
JOINT CONVENTION BANDUNG (JCB) 2021
November 23rd – 25th 2021

Pre-1963 Mount Agung Eruption History And Magma Evolution Based On Petrological, Mineralogical, And Geochemical Analysis

Aulia Syafitri[1], I G.B. Eddy Sucipta[2], Adzkia Noerma Arifa[1], Asep Saepuloh[2], Sri Widiyantoro[3,4]
[1]Laboratory of SEM-EDS UPP Chevron – Bandung Institute of Technology, Indonesia
[2]Petrology, Volcanology, and Geochemistry Research Group, Geological Engineering, Faculty of Earth Science and Technology – Bandung Institute of Technology, Indonesia
[3]Global Geophysics Research Group, Faculty of Mining and Petroleum Engineering – Bandung Institute of Technology, Indonesia
[4]Faculty of Engineering, Maranatha Christian University, Bandung, Indonesia.

Abstract
Mount Agung is an active stratovolcano located on Bali island. The eruption of Mount Agung in 1963 was the largest eruption after Mount Krakatoa in 1883 and became one of the most important eruptions of the 20th century. The prior eruption history of Mount Agung has yet to be known in detail. This study aims to determine the history of the pre-1963 volcanic activity of Mount Agung. Based on the results of published data statistical analysis and our petrological and/or mineralogical data, we found that the pre-1963 eruption of Mount Agung was influenced by three cogenetic magmas and can be divided into 4 eruption periods, i.e. pre-3200 ± 60 BP, 3200 ± 60 – 1870 ± 40 BP, 1870 ± 40 – 1040 ± 50 BP, and post-1040 ± 50 BP. Mount Agung's historical activity was marked by the start of the basaltic magma injection in the pre-3200 ± 60 BP period and reached its peak in the 3200 ± 60 – 1870 ± 40 BP period. Both periods produced dominant basalt to basaltic andesite lava units (SiO_2 51 – 56%) and at the end of the 3200 ± 60 – 1870 ± 40 BP period was marked by the formation of Bukit Pawon parasitic cone. In the period of 1870 ± 40 – 1040 ± 50 BP, in addition to the emergence of basalt to andesite lava units, many pyroclastic flow units were formed. During this period, magma continued to differentiate, as indicated by the increase of SiO_2 (51 – 58%), which was controlled by crystal fractionation. During this period, a slight injection of basaltic magma also occurred which causes magma mixing with the previously differentiated magma. At the beginning of the post-1040 ± 50 BP period, there was a slight injection of basaltic magma. Then, magma undergoes intensive differentiation, which is in line with the increase of SiO_2 (53 – 63%), in the form of crystal fractionation and slight crustal contamination, so it was capable to produce pyroclastic fall, pyroclastics flow, and lava units.

Keywords: Agung volcano, eruption periods, magmatic differentiation.

Introduction

Only 69 out of 120 volcanoes in Indonesia are monitored by the Center of Volcanology and Geological Hazard Mitigation (PVMBG). Besides the highest number of volcanoes, the number of victims due to volcanic disasters is also ranked first in the world (Ministry of Energy and Mineral Resources, 2020). It shows that studies on volcanoes in Indonesia and their disaster mitigation are still far from optimal. According to Fontjin et al. (2015), one of the critical information needed in volcanic hazard assessment is detailed historical records of volcanic activity.

Mount Agung is an active stratovolcano located in Karangasem Regency, eastern Bali Province. The eruption of Mount Agung in 1963 was the largest eruption with the highest magnitude in Indonesia, after Mount Krakatoa in 1883, and became one of the most pre-dominant events in the 20th century due to its influence on the global climate (Self and Rampino, 2012). This eruption released lahars, pyroclastic flows, lava, and volcanic earthquakes, which caused more than 2000 deaths (Zen and Hadikusumo, 1964 in Geiger et al., 2018; Tanguy et al., 1998 in Self and Rampino, 2012).

Previous research on Mount Agung mainly focused on the 1963 eruption (Self and Rampino, 2012). However, the volcanic activity before is not well recorded. Information is based only on Balinese historical records, which mention eruptions in the 16th to 18th centuries, precisely in 1843, 1821, 1808, and 1711 (Fontijn et al., 2015). Therefore, this research conduct to study the historical activity of Mount Agung, especially prior to 1963.

Mount Agung has one main crater at 3014 meters above sea level. In addition, Mount Agung also has a parasitic cone, Bukit Pawon, on the southeast slope with an altitude of 800 meters above sea level. The pre-1963 volcanic deposits consist of 12-lava units, 5-flow pyroclastic units, and 2-fall pyroclastic units (Nasution et al., 2004). Based on the volcano-stratigraphy, Mount Agung produced dominant lava units in the older period. Pyroclastic flow units began to appear in 1870 ± 40 BP, and pyroclastic fall units began to form in 1040 ± 40 BP.

Data and Method

Well-preserved lava samples were taken from 18 outcrop locations around Mount Agung (Fig. 1). Microscopic observations using a polarizing microscope were conducted on all lava samples to discover the mineral contained. Mineral chemistry analysis was carried out on 6-selected samples using Scanning Electron Microscopy-Energy Dispersive X-Ray Spectrometry (SEM-EDS) JEOL JSM-IT-300 of SEM-EDS Laboratory of Chevron-Bandung Insitute of Technology, Indonesia. This test aimed to identify the major and minor element's content (such as Ti, Al, Fe, Mn, Mg, Ca, Na, K, P, Cr, Ni) of the phenocrysts in the sample.

As support, bulk geochemical analysis is obtained using published data research from Fontjin et al. (2015) (48 samples) and Dempsey (2013) (18 samples). Those data, taken from volcanic rocks, consists of the major elements (SiO_2, Al_2O_3, Fe_2O_3, FeO, MnO, MgO, CaO, Na_2O, K_2O, TiO_2, P_2O_5) and trace elements (Rb, Sr, Y, Nb, Zr, Cr, Ni, Cu, Zn, Ga, Ba, Pb, Th, U, La, Ce, Nd, Sm).

PROCEEDINGS
JOINT CONVENTION BANDUNG (JCB) 2021
November 23rd – 25th 2021

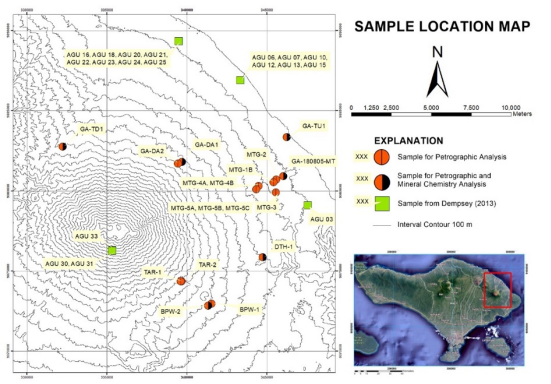

Fig. 1: Sampling location of this study. Dempsey (2013) sample location is included.

For better understanding, data and stratigraphic correlation were needed to find the connection between all of the existing samples used in this research. The correlation is based on: (1) the same absolute age in Nasution et al. (2004) and Fontjin et al. (2015) (Table. 1); (2) SiO_2 vs. K_2O diagram, which shows the existence of 3 cogenetic magma-differentiation (Fig. 2). With those basics, the authors divided the pre-1963 Mount Agung's volcanic activity into 4-periods, namely the post-1040 ± 50 BP, 1870 ± 40 BP – 1040 ± 50 BP, 3200 ± 60 BP – 1870 ± 40 BP, and the pre-3200 ± 60 BP period.

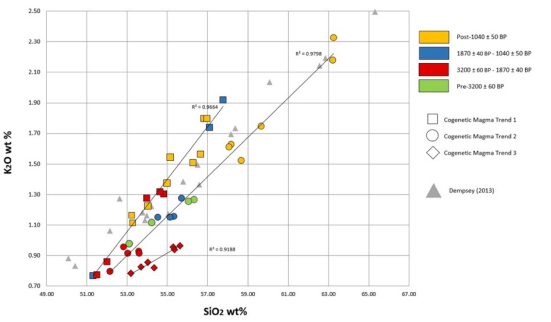

Fig. 2: SiO_2 against K_2O diagram. The data used is from Fontjin et al. (2015). Dempsey's (2013) data is used as a comparison.

Result

Petrography and Mineral Composition

Based on microscopic observations of 18 lava samples, all eruption periods produced pyroxene-andesite rocks (name using Williams et al. (1982) classification), which have a porphyritic texture. The phenocrysts contained are dominated by plagioclase, followed by pyroxene, opaque minerals, and olivine.

Plagioclase is the predominant phenocryst present in all samples. It is found as subhedral crystals that showed varying microtextures. Coarse sieve is abundant followed by glomerocryst, fine sieve, fine-oscillatory zoning, and resorption surface. Based on the An composition taken from mineral chemistry analysis, in pre-3200 ± 60 BP period, plagioclase contains a long-range of $An_{38–89}$. The core tends to be more calcic than the rim. In 3200 ± 60 – 1870 ± 40 BP BP period, the An content decreased to $An_{67–83}$. Both core and rim have a wide range of An. In 1870 ± 40 – 1040 ± 50 BP, the An composition generally decreased again to $An_{43–88}$. In the post-1040 ± 50 BP period, plagioclase minerals have $An_{38–86}$, with the same distribution pattern as the first period. The core is more calcic than the rim. Based on the scanline test, in each eruption period, plagioclase has a decreasing percent mass of Ca from the core to the rim (Fig. 3A).

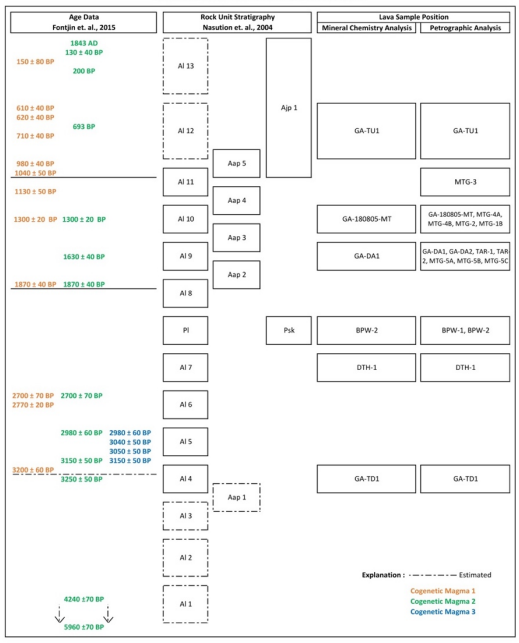

Table 1: Data and stratigraphic correlation table of age data (Fontjin et al., 2015), rock units (Nasution et al., 2004), and sample positions representing the rock units.

Pyroxene minerals as phenocrysts are present in subhedral–anhedral forms. Locally, pyroxenes are found as cumulocryst along with plagioclase, olivine, and opaque minerals. There are two types of pyroxene observed in each sample, orthopyroxene and clinopyroxene. Orthopyroxene has enstatite composition, while clinopyroxene has augite composition (classify using Morimoto et al., 1988). Based on mineral chemistry analysis, In pre-3200 ± 60 BP period, enstatite has $Mg\#_{61–77}$, whereas augite has $Mg\#_{73–78}$. In the following period, the Mg# content in enstatite generally increased to $Mg\#_{65-76}$, but augite's Mg# decreased to $Mg\#_{71–76}$. In 1870 ± 40 – 1040 ± 50 BP period, the Mg# composition in enstatite and augite generally decrease, to $Mg\#_{65–75}$ and $Mg_{\#72–77}$ in order. In post-1040 ± 50 BP period, the Mg# content in enstatite and augite tend to increase, to $Mg\#_{67–72}$ and $Mg\#_{67–81}$. Based on the scanline test, enstatite and augite from each eruption period, in general, have an increasing percent mass of Mg from the core to the rim (Fig. 3B and 3C).

Generally, olivine minerals found in pre-1963 eruption samples are present as microphenocrysts with subhedral–anhedral forms. Olivine dominantly has a reaction rim composed of pigeonite or enstatite (classify using Morimoto et al., 1988). Based on mineral chemistry analysis, olivine in pre-3200 ± 60 BP period contains $Fo_{62–78}$ with more Mg-rich core than the rim. In 3200 ± 60 – 1870 ± 40 BP, the Fo content tends to decrease, become $Fo_{60–71}$, but both core and rim have a wide range of Fo. In 1870 ± 40 – 1040 ± 50 BP period, the Fo content slightly decreased to $Fo_{59–71}$. Then, in

PROCEEDINGS
JOINT CONVENTION BANDUNG (JCB) 2021
November 23rd – 25th 2021

post-1040 ± 50 BP, the Fo composition increase to $Fo_{66–76}$. The core is also more Mg-rich than the rim. Based on the scanline tests on individual minerals, olivine from each period has decreasing percent mass of Mg from core to the rim (Fig. 3D), which can be caused by the presence of reaction rim.

Opaque minerals are present as phenocrysts with anhedral shapes. Locally, it is found as a cumulocryst along with plagioclase, pyroxene, and olivine. Based on the mineral chemistry test, the opaque mineral from all eruption periods has a magnetite composition (classify using Buddington dan Lindsley., 1964 in Souza et al., 2020).

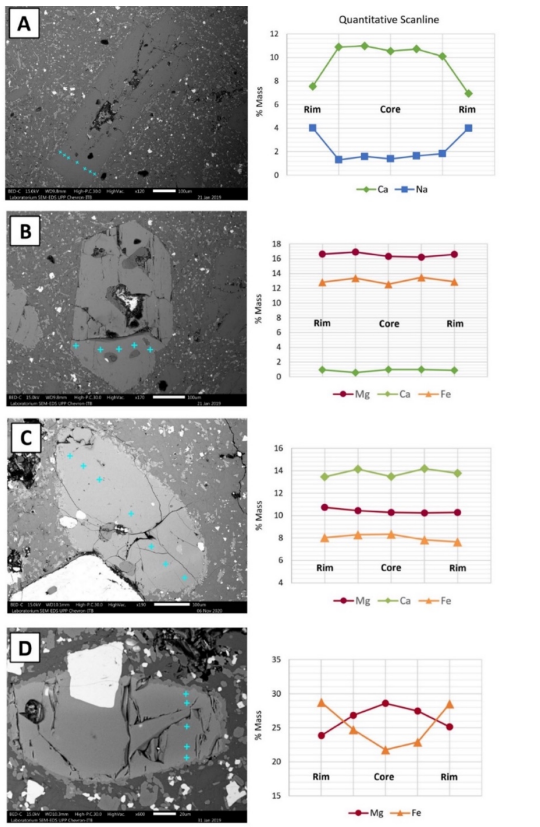

Fig. 3: Selected electron images of minerals from SEM-EDS mineral chemistry analysis and its quantitative scanline result. Blue + : approximate analyzed points. (A) Plagioclase of Sample GA-TD1 (pre-3200 ± 60 BP period). (B) Enstatite of Sample GA-TD1 (pre-3200 ± 60 BP period). (C) Augite of Sample DTH-1 (3200 ± 60 – 1870 ± 40 BP period). (D) Olivine with reaction rim of Sample GA-TU1 (post-1040 ± 50 BP).

Geochemical Analysis

Bulk geochemical analysis was carried out using primary data from published journals by Fontjin et al. (2015). As a comparison, Dempsey's (2013) data was also used in this study, especially to see the data clusters distribution suitability. The first analysis is the normative mineral that expressed their molecular proportion (Kelsey, 1965). This paper used the CIPW calculation excel sheet program written by Hollocher (2004). Based on Table 2, all samples from each period are characterized by the presence of quartz and hypersthene that shows saturated to highly saturated silica magma.

Eruption Period	Pre-3200 ± 60 BP	3200 ± 60 BP - 1870 ± 40 BP	1870 ± 40 BP - 1040 ± 50 BP	Post-1040 ± 50 BP
Deposit Type	Scoria, Pyroclastic Flow	Scoria, Ash Fall	Scoria, Ash Fall, Pyroclastic Flow	Pyroclastic Dlow, Pumice, Scoria, Ash Fall
Normative Mineral (wt%)				
Quartz	2.92 - 6.34	1.35 - 6.92	0.39 - 8.26	2.76 - 15.57
Plagioclase	59.99 - 67.66	56.61 - 72.14	55.35 - 68.3	55.1 - 59.82
Orthoclase	5.73 - 7.45	4.61 - 7.68	4.55 - 11.46	6.68 - 10.7
Corundum	0	0 - 0.64	0	0
Diopside	1.22 - 6.66	0 - 8.36	3.13 - 6.43	0.52 - 8.49
Hypersthene	13.85 - 21.34	13.53 - 24.61	13.66 - 25.49	10.48 - 19.56
Ilmenite	1.44 - 2.07	1.42 - 2.22	1.58 - 2.03	1.12 - 1.73
Magnetite	1.09 - 1.59	1.07 - 1.83	1.15 - 1.59	0.87 - 1.48
Apatite	0.53 - 0.65	0.35 - 0.65	0.37 - 0.65	0.53 - 0.63
Zircon	0.01	0.01	0.01 - 0.03	0.01 - 0.03

Table 2: Percentage of normative minerals present in each period of the pre-1963 eruption of Mount Agung. The data used are geochemistry data from Fontjin et al. (2015).

Using plotted data on the diagram of total alkali (Na_2O + K_2O) against SiO_2 in Le Bas et al. (1986) diagram (Fig. 4), the eruption products from each period are as follows: (1) The pre-3200 ± 60 BP period consist of basaltic andesite rocks with SiO_2 53 – 56 wt%; (2) 3200 ± 60 – 1870 ± 40 BP consists of basalt to andesite basaltic rocks with SiO_2 51 – 56 wt%; (3) 1870 ± 40 – 1040 ± 50 BP consists of basalt to andesite rocks with SiO_2 53 – 58 wt%; (4) The post-1040 ± 50 BP period consists of basaltic andesite to dacite rocks with SiO_2 53 – 63% wt%.

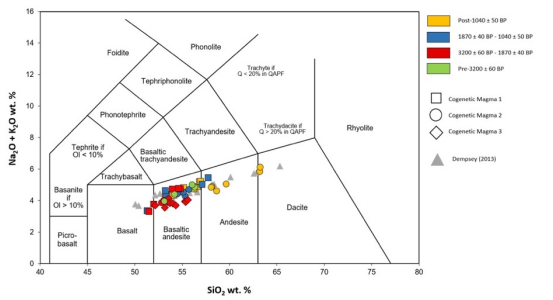

Fig. 4: The results of data plotting from Fontjin et al. (2015) on the Na_2O + K_2O vs. SiO_2 diagram (Le Bas et al., 1986). Dempsey's (2013) data is used as a comparison.

Magma series or magma affinity can interpret the volcano-tectonic setting (Wilson, 1989). data plot result to Peccerillo and Taylor (1976) diagram (Fig. 5) shows that all samples are from the calc-alkaline magma series. According to Wilson (1989), it is a feature of convergent plate boundaries (subduction).

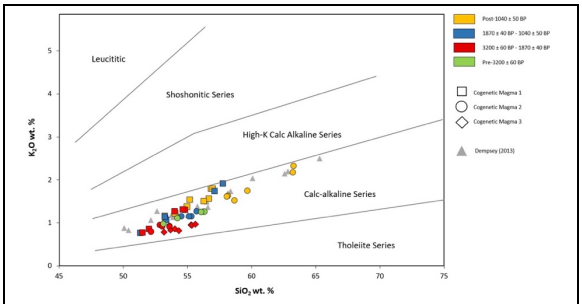

Fig. 5: The results of data plotting of Fontjin et al. (2015) on the K_2O vs. SiO_2 diagram (Peccerillo and Taylor, 1976). Dempsey's (2013) data is used as a comparison.

Harker diagrams show the change of major elements to SiO_2 that provide magmatic activity interpretation (Harker, 1909 in Winter, 2014). Crystal fractionation is characterized by a curved pattern due to the depletion of certain compatible elements from the magma solution that depends on the mineral phase undergoing crystallization (Novak and

Bacon, 1986). Harker Diagram of TiO_2, MgO, Fe_2O_3, and CaO (Fig. 6) shows the occurrence of this process. The older period (pre-1040 ± 50 BP) indicates the fractionation of magnetite, olivine, and/or pyroxene. Next, the CaO diagram exhibits the plagioclase fractionation, which predominantly happened in the younger period (post-1040 ± 50 BP) instead. The differences in the minerals that undergoing fractionation is also supported by Dempsey's (2013) research, which stated that there are two fractionation vectors during the magma differentiation process. The cause can be identified from plagioclase minerals (Parman et al., 2011; Dempsey, 2013).

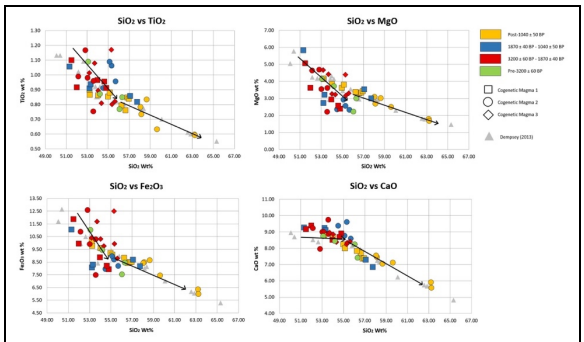

Fig. 6: Selected Harker Diagram. The data plotted is from Fontjin et al. (2015) and Dempsey (2013) that is used as a comparison.

Fig. 7 shows data distribution against the two trendlines of plagioclase fractionation from Parman et al. (2011). It can be seen that all pre-1040 ± 50 BP periods, in general, followed the curved line indicating that the plagioclase fractionation was restrained. In contrast, the post-1040 ± 50 BP period, in general, followed the other line that show the occurrence of plagioclase fractionation. These differences correspond to Dempsey (2013) and Geiger et al. (2018), which said that Mount Agung is possibly controlled by the presence of a high pressure-deep magma reservoir that can withstand plagioclase fractionation and also a shallow magma reservoir with lower pressure.

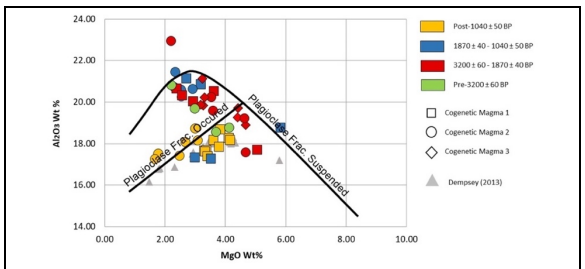

Fig. 7: Diagram of MgO against Al_2O_3 with two trendlines of plagioclase fractionation (Parman et al., 2011; Dempsey, 2013). The data used is from Fontjin et al. (2015) with Dempsey (2013) as a comparison.

Discovering the tectonic setting can be done by plotting trace elements that have been normalized with the primitive mantle onto a spider diagram (Sun and McDonough, 1989). From Fig. 8, it can be seen that the Rb, Ba, Th, and K (LILE) and La – Sm (LREE) contents are enriched, while Eu - Lu (HREE) experienced depletion. In addition, the Nb content also shows a negative anomaly. It can be inferred that Mount Agung comes from a volcanic associated with a convergent plate boundary (subduction) (Wilson, 1989; Dirk, 2008).

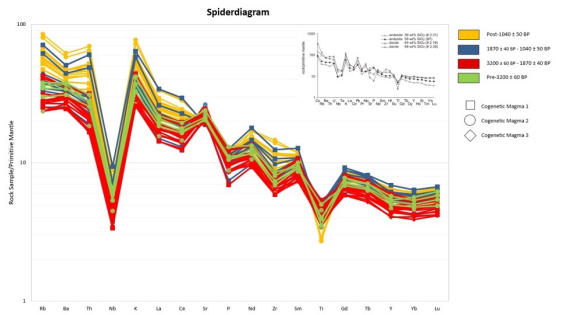

Fig. 8: Spider diagram of the pre-1963 product of Mount Agung. The data comes from Fontjin et al. (2015) that was normalized against the primitive mantle (Sun and Mcdonough, 1989). The diagram of Mount Batur eruption products (Reubi and Nicholls, 2005) was used as a comparison.

The types of subduction, island arc or active continental margin, can be distinguished using the ratio of Zr to Zr/Y from Pearce (1983). Based on Fig. 9A, Mount Agung originates from the subduction of oceanic crust beneath continental crust. Next, the La/Sm to Th/Nb diagram can specify the differentiation type influenced by its tectonic setting (Plank, 2005 in Barresi et al., 2015). Fig. 9B shows that in the older period (pre-1040 ± 50 BP), the magma differentiation process is subduction-related enrichment. Whereas in the younger period (post-1040 ± 50 BP), there may be a slight influence from the presence of crustal contamination.

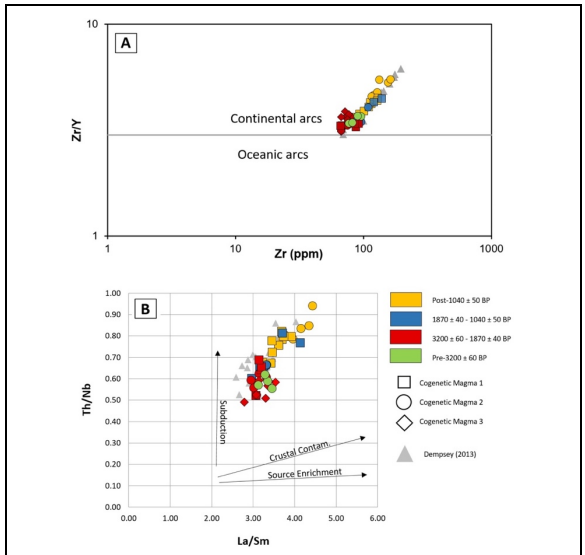

Fig. 9: (A) Diagram of Zr vs. Zr/Y which distinguishes between oceanic arc and continental arc (Pearce, 1983). (B) La/Sm vs. Th/Nb diagram with several differentiation vectors (Plank, 2005 in Barresi et al., 2015). The rock geochemistry data is from Fontjin et al., (2015). Dempsey's (2013) data is used as a comparison.

Discussion

Thus, the pre-1963 Mount Agung's magma evolution can be discussed comprehensively from the geochemical analysis. It was later strengthened by the petrographic and mineral chemical analysis.

Magma source interpretation of Mount Agung can be acquired by looking at the Fo content in olivine phenocrysts (Rogkala et al., 2019). Magma originating directly from the

mantle source has fosterite content more than Fo_{88} (Wilson, 1989; Arai,1994). The Fo in olivine from the pre-1963 eruption ranged from $Fo_{60–78}$. It proves that the primitive magma of Mount Agung originates from the partial melting process instead. The SiO_2 content of the primitive magma of Mount Agung can be interpreted from K_2O against SiO_2 diagram (Fig. 2), assuming that the K_2O content is not affected by the crystal fractionation process and can represent the actual content of the magma. Based on the diagram, three trendlines come from one point at lower SiO_2. Therefore, it indicates that the three cogenetic magmas may originate from the same source. By extending the trendline, the primitive magma has a SiO_2 content of ~50 wt%.

Magma evolution started at the pre-3200 ± 60 BP period, which produced basaltic andesite with 53 – 56 wt% SiO_2. From the beginning to the end of this period, SiO_2 content in the rock sample continued to decrease. That indicates a basaltic magma injection. In the 3200 ± 60 – 1870 ± 40 BP period, Mount Agung released eruption products of basalt to basaltic andesite with SiO_2 51 – 56 wt%. The increasing hypersthene as the normative minerals shows that the level of magma saturation had decreased. This era also produced low SiO_2 samples. Based on this evidence, the 3200 ± 60 – 1870 ± 40 BP period may become the peak of the basaltic magma injection, which had begun at the previous period. Then, towards the end of the period, the SiO_2 content in the rock samples increased, indicating that magma underwent a differentiation process in the form of olivine-pyroxene-magnetite fractionation based on previous analysis. At the beginning of 1870 ± 40 – 1040 ± 50 BP, Mount Agung released eruptive products with the lowest SiO_2 value. It was expected that magma injection may have occurred at the beginning of the period and may cause magma mixing with previously differentiated magma. In general, this period's eruption produced basalt to andesite composition with a dominant SiO_2 value at 53 – 58 wt%. The percentage of normative quartz increased, which suggests magma saturation level rose. Based on these marks, magma continued to differentiate. In the beginning post-1040 ± 50 BP period, compared to late 1870 ± 40 – 1040 ± 50 BP, there was a decrease in SiO_2 and K_2O value. It indicates that this period started with magma injection first. Then gradually, Mount Agung's eruption produced basaltic to dacite andesite rocks with a long interval of SiO_2, 53 – 63 wt%. The normative quartz became more abundant, while the hypersthene was less. It interprets that magma experienced intensive differentiation during this period. Based on the geochemical analysis, this differentiation is influenced by plagioclase fractionation and a slight presence of crustal contamination based on the geochemical analysis.

The petrographic analysis supports this evolution. The predominant minerals found are plagioclase, therefore there are many typical plagioclase textures. It can imply the processes that happened during magma evolution (Renjith, 2014). Table 3 shows the presence of plagioclase microtextures in each period. The most abundant textures are coarse sieve that suggested magma dominantly undergoes a decompression process. It developed simultaneously with the differentiation process that occurred. The differentiation will cause the magma to become saturated with SiO_2 that in line with the percentage of shallow-tail and broken crystal textures developing in each period. Judging from the fine sieve and resorption surface, they imply that basaltic magma injection appeared in each period. In 3200 ± 60 – 1870 ± 40 BP, the abundance of those textures rose compared to the pre-3200 ± 60 BP. It means that magma injection in this period was more intensive. The peak of magma injection occurred at 3200 ± 60 – 1870 ± 40 BP was shown by the coarse sieve microtextures, which present was highest during this period. The increase of fine sieve and resorption surface in 1870 ± 40 – 1040 ± 50 BP can be affected by the injection of more basaltic magma, which caused magma mixing with previously differentiated magma. Thus, the dissolution process in plagioclase increases. In the post-1040 ± 50 BP period, fine sieve and resorption surface percentage decreased compared to the previous period. It proves that magma injection was not taking place intensively.

Eruption Period	Pre-3200 ± 60 BP	3200 ± 60 BP - 1870 ± 40 BP	1870 ± 40 BP - 1040 ± 50 BP	Post-1040 ± 50 BP
Plagioclase Microtexture (%)				
Coarse Sieve	31	29 – 43	14 – 35	27
Glomerocryst	24	10 – 17	7 – 13	31
Fine Sieve	5	0 – 12	0 – 26	6
Resorption Surface	2	3 – 5	0 – 8	-
Fine Oscillatory Zoning	8	4 – 10	5 – 13	6
Rounded Zone	4	0 – 3	0 – 6	-
Synneusis	2	0 – 3	0 – 5	2
Shallow Tail	-	0 – 6	0 – 9	-
Broken Crystal	24	24 – 33	25 – 40	28

Table 3: The plagioclase microtextures percentage of the samples representing each eruption period of Mount Agung.

The interpretation of mineral chemistry was carried out based on the development of %mol fosterite (Fo) in olivine (Fig. 10A), %mol of anorthite (An) in plagioclase (Fig. 14B), %mol Mg# in orthopyroxene (Fig. 10C) and in clinopyroxene (Fig. 10D).

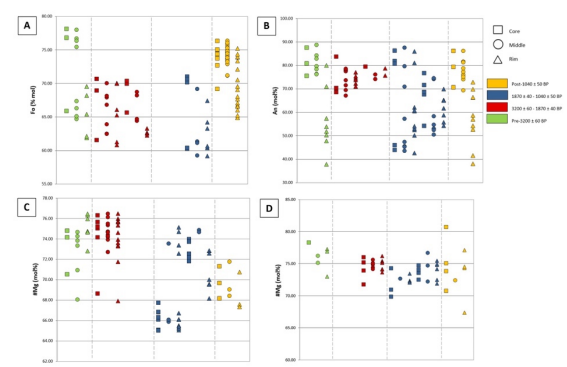

Fig. 10: The development of Fo composition in olivine (A), An composition in plagioclase (B), Mg# composition in orthopyroxene (C), and Mg# composition in clinopyroxene phenocrysts (D) in each period.

Those figures show that Mount Agung's magma was dominantly undergo a differentiation process. In the pre-3200 ± 60 BP period, minerals with high Fo, Mg#, and An contents were produced. Magma injection occurrence during this period was recorded in orthopyroxene and clinopyroxene, which had an increasing %mass of Mg from the core to the rim. In 3200 ± 60 – 1870 ± 40 BP, the peak of magma injection occurred. This period sequentially produced Agung Lava Units 5 to 8 (Al 5 – 8), Pawon Lava Units (Pl), and Pawon Scorias (Psk) (Nasution et al., 2004). The peak of magma injection is hypothesized to occur during the formation of the Agung Lava Units 5 to 6 (Al 5 – 6). Then, the differentiation process took place and formed the Agung Lava Unit 7 (Al 7), Pawon Lava Unit (Pl), Skoria Pawon (Psk), and Agung Lava Unit 8 (Al 8). This can be seen from the Fo, Mg#, and An content, which decreased in

the samples of DTH-1 (Al 7) and BPW 2 (Pl). The peak of magma injection during the formation of Agung Lava Units 5 to 6 (Al 5 – 6) is also supported by the increase of Mg# in orthopyroxene minerals (Fig. 10C). Based on the two-phase incongruent melting, if olivine has excess silica, which in this case is olivine in the Agung Lava Units 5 and 6 (Al 5 – 6), enstatite minerals will be formed in the following unit, the Agung Lava Unit 7 (Al 7). This is proven by the dominant presence of enstatite in the DTH-1 (Al 7). Then in the period 1870 ± 40 – 1040 ± 50 BP, the %mol of Fo, An, and Mg# tended to decrease. This shows that magma continued to undergo a differentiation process. The presence of more basaltic magma injection during this period was recorded in enstatite and augite with the increasing %mass Mg# from the core to the rim. In the post-1040 ± 50 BP, in general, Fo, Mg#, and An increased compared to the previous period. This period is represented by Sample GA-TU1, Agung Lava Unit 12 (Al 12), which was formed at the beginning of the period. Based on the previous geochemical interpretation, at the beginning of the period, there was an injection of basaltic magma. This is what causes a rise in the content of Fo, Mg#, and An in minerals. Then, the differentiation process takes place again. This can be seen from the scanline results of plagioclase and olivine minerals which show decreasing An and Fo content.

Conclusions

Based on the discussion above, the history of pre-1963 Mount Agung activity in summary is as follows. The volcanic activity of Mount Agung was caused by partial melting due to the subduction of the convergent plate boundaries (active continental margin) between the Indo-Australian and the Eurasian Plate during the Quaternary Period, which formed magma with calc-alkali affinity. Mount Agung's primitive magma probably contains ~50 wt% SiO_2. As it rose to the surface, the primitive magma underwent differentiation and divided into three cogenetic magmas. The magmatic activity of Mount Agung begins in the pre-3200 ± 60 BP period. The eruption of this period resulted dominant lava units. In this period, the injection of basaltic magma began to occur and reached its peak in the 3200 ± 60 – 1870 ± 40 BP. Then, magma went through a differentiation process, olivine-pyroxene-magnetite fractionation. This period also produced dominant lava units. At the end of it, there was an eruption at the Bukit Pawon parasitic cone. In the next period, 1870 ± 40 – 1040 ± 50 BP, in addition to producing lava units, Mount Agung eruption formed quite a lot of pyroclastic flow units. It symbolizes that magma continues to differentiate. At the beginning of the period, basaltic magma injection took place, caused magma mixing with previously differentiated magma. The magma then underwent re-differentiation, controlled by the olivine-pyroxene-magnetite fractionation. At the start of the post-1040 ± 60 BP, there was a little magma injection. After that, there was an intensive differentiation process, in the form of plagioclase fractionation and probably slight influence from crustal contamination. Thus, Mount Agung could produce thick pyroclastic fall units, followed by pyroclastic flow and lava units.

References

Arai, S., 1994, Chemical Geology, **113**, 191 – 204.
Barresi, T., J.L. Nelson, J. Dostal, and R. Friedman, 2015, Can. J. Earth Sci, **52**, 466–494.
Dempsey, S. R., 2013, Durham thesis, Durham University.
Dirk, M. H. J., 2008, Pusat Survei Geologi Jurnal Geologi Indonesia, **3**, 23-35.
Fontijn, K., F. Costa, I. Sutawidjaja, C. G. Newhall, and J. S. Harrin, 2015, Bull Volcanol, **77**, 59.
Geiger, H., V. R. Troll, E. M. Jolis, F. M. Deegan, C. Harris, D. R. Hilton, and C. Freda, 2018, scientific reports, **8**, 10547.
Hollocher, K., 2004, Geology Department, Union College.
Kelsey, C. H., 1965, Mineral. Mag., **34**, 276-282
Le Bas, M. J., R. W. Le Maitre, A. L. Streckeisen, and B. Zanettin, 1986, Journal of Petrology, **27**, 745-50.
Ministry of Energy and Mineral Resources, 2020, magma.esdm.go.id.
Morimoto, N., J. Fabries, A. K. Fergusson, I. D. Guizbourg, M. Ross, F. A Seifert, J. Zussman, K. Aoki, and G. Gottardi, 1988, Am. Mineral, 173.
Nasution, A., N. Haerani, D. Mulyadi, and M. Hendrasto,, 2004, Direktorat Vulkanologi dan Mitigasi Bencana Geologi.
Novak, S. W. and C. R. Bacon, 1986, *Geological Survey Professional Paper 1383*.
Parman, S. W., T. L. Grove, K. A. Kelley, and T. Plank, 2011, *Journal of Petrology*, **52**, 2, 257-278.
Peccerrillo, R., and S. R. Taylor, 1976, Contribution to Mineralogy and Petrololgy, **58**, 63-81.
Pearce, J. A., 1983, Continental Basalt and Mantle Xenolith, 230-249.
Renjith, M. L., 2014, Geoscience Frontiers, **5**, 113-126
Reubi, O. I., and A. Nicholls, 2005, Journal of Petrology, **46**, 7.
Rogkala, A., P. Petrounias, B. Tsikouras, P. P. Giannakopoulou, and K. Hatzipanagiotou, 2019, *Minerals,* **9**, 120.
Self, S., and M. R. Rampino, 2012, Bull Volcanol, **74**, pp. 1521-1536.
Souza, I. M. B. A, I. P Guimarães, S. B. Barreto, G. L. Santos, J. F. A. Neto, 2020, Brazilian Journal of Geology.
Sun, S.S., and W. F. McDonough, 1989, Geological Society of London, **42**, 313- 345.
Williams, H., F. J. Turner, and C. M. Gilbert, 1982, W. H. Freeman and Company, San Francisco.
Wilson, M., 1989, Springer, Netherland.
Winter, J. D., 2014, Pearson New International Edition. Pearson Educational Limited, United States.

PROCEEDINGS
JOINT CONVENTION BANDUNG (JCB) 2021
November 23rd – 25th 2021

Software Development using Machine Learning to Predict PPFG and 3D Geomechanics

Pipit Irfani Amorokhman[1], Allen Haryanto Lukmana[2], Pertamina Research Technology Innovation[1] UPN Veteran Yogyakarta[2]

Abstract

Pressure prediction plays a fundamental role to design mud weight and well trajectory for wellbore stability and prevents stuck pipe. Some manual calculations are only able to calculate on certain condition such as clean-shale formation and under-compaction mechanism formation. Unfortunately, real formation can be very heterogenic. A method to produce independent formation type shall be developed solve the issue. Therefore, software using machine learning (ML) were developed to generate scrupulous pressure prediction.

Logging data (e.g., Density, Sonic, Gamma Ray) and drilling parameter (e.g., ROP, RPM, WOB) from 2 wells (MLC-01, TTA-01) were used as machine learning input. In this research, 3 methods which are Artificial Neural Network (ANN) Feedforward type, Random Forest (RF), and Support Vector Machine (SVM) were applied.

The result exhibits (1) ANN showed the least Root Square Mean Error (RSME) of 0.11401 in comparison to the other 3 methods, Determination Coefficient (R^2) 0.9789. Thus, ANN will be used for the rest of the analysis. (2) 4 data (Density, Sonic, Gamma Ray, Depth) together achieve the most precise with actual condition with RSME 0.0714 and R^2 0.9826. (3) After plotting the result in one graph, pore pressure prediction from ANN method is closer to actual pore pressure rather than manual calculation result.

It is to conclude that this software gives a promising result to predict Pore Pressure, Fracture Gradient, and Shear Failure Gradient. The comparative analysis results show that ANN Feedforward type has the feature estimation by its shorter time prediction and high accuracy (a coefficient of determination of 0.99 and RSME 0.08 – 0.23. The overpressure prediction, XRD and Geomechanics can be analysis in one integrated software.

Introduction

Basic geomechanical components are include pore pressure (PP), unconfined compression strength (UCS), Overburden or Vertical stress (Sv), Minimum horizontal stress (Shmin), and maximum horizontal stress (SHmax). These component gained from core measurement. However, core measurement cannot performed in the whole interval regarding of core limitation. Prediction calculation can be alternative, but it require many data and only specific condition to use the method

Pore pressure at depth is equivalent to hydraulic potential measurement respect of earth surface. Assumed to be uniform in small volume of interconnected pores. Therefore, pore pressure can be variated refer to geological events. Overpressure occurs as several factors such as Disequilibrium compaction, tectonic compaction, hydrocarbon column height, Aqua-thermal compaction, mineral diagenesis, and hydrocarbon maturation.

.

Artificial Intelligence (AI) and Machine Learning (ML) grown its popularity among various industry. Its supported by development of technology in computer service makes big data acquisition is more easier than before. However, energy sector is still left behind.

In this paper we rise a case study using data from 2 exploration wells located in North Sumatera. Depth of well reached to 9000 ft, TTA-01 and MLC-01. Overpressure occurred for both of wells during drilling activity. Team developing a software using AI and ML to predict PP from existing log and drilling data. The result of AI prediction will be compared to manual calculations and recorded data.

Data and Method

Geological and Stratigraphical Setting

The fold system is dominated by the WNW-ESE trending anticlinoria. Generally forming an en-echelon pattern explanation:

- Wrench movement along the NW-SE basement faults (related to the Paleogene graben system) (Harding,1988) .
-Draping over uplifted blocks due to compressive regime of the subduction (Moulds, 1989).

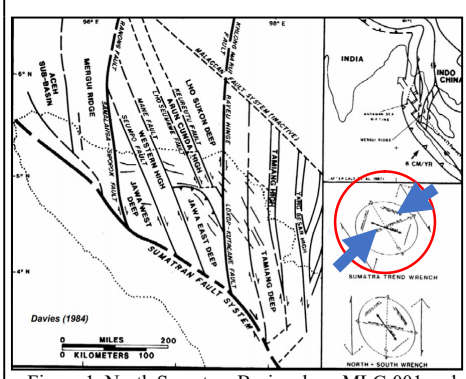

Figure 1. North Sumatera Basin where MLC-001 and TTA-001 Location

The Present Stress was dominantly from Plio-Pleistocene Stress. Well MLC-1 dan TTA-1 are under U-S pattern with stress direction NE-SW (N 020 E – N 060 E) & (N 200 E – N 240 E).

Log and Drilling Data

Data from well TTA-01 will be input as learning data, consist of RHOB, DTCO, GR, ECD, RPM, WOB, ROP,

PROCEEDINGS
JOINT CONVENTION BANDUNG (JCB) 2021
November 23rd – 25th 2021

and recorded pore pressure. The final model will be used to predict pore pressure for well MLC-001

DEPTH	ECD	RPM	WOB	ROP	PorePressure
xx5.724	10.912	20.133	2.778	132.929	9.753
xx5.877	10.912	20.134	2.778	132.935	9.754
xx6.029	10.912	20.135	2.777	132.942	9.755
xx6.182	10.912	20.137	2.777	132.949	9.756
xx6.334	10.912	20.138	2.779	132.956	9.757
xx6.486	10.912	20.139	2.782	132.962	9.758
xx6.639	10.912	20.14	2.783	132.969	9.759
xx6.791	10.912	20.142	2.783	132.976	9.76
xx6.944	10.912	20.143	2.787	132.983	9.761

Figure 2. Drilling Parameter of Welll TTA-01

Method:

Artificial Neural Network (ANN)

ANN is a method which inspired by "neuron" system in human brain. It is using connectivity between "neuron" to find the right model. The target can be iterations limit or maximum error value determine by researchers.

$$y = ax + by + cz + \ldots\ldots\ldots + mn$$

$a, b, c, \ldots, m$ is input variable

$x, y, z, \ldots, n$ is training weight

Analysis Steps:

Preprocessing

The data cleaning process required raw data preprocessing. Then it will be divided into 2 types of data input, training and testing.

- Data 1: in this process, all of data output (Pore Pressure) smaller than 0 (negative) will be deleted.
- Data 2: in this process, all of data output (Pore Pressure) smaller than 0 (negative) will be convert 0.

Testing

Machine Learning Method

Testing process will determine the most suitable machine learning methods and final validation will use 10-fold cross. The method with result R^2 closest to 1, RSME closest to 0, and optimum training time.

Metode	*Best* RMSE	*Best* R^2	10-*fold* RMSE	10-*fold* R
ANN	0.11401	0.9789	0.1240	0.9644
RF	0.36512	0.9213	0.841	0.918
SVM	0.4771	0.946	0.5112	0.933

Table 1. Accuracy of Machine Learning Methods

Based on table 1, ANN show the best result with the lowest RMSE 0.11401 and R^2 0.9644. ANN will be use as ML method in this research.

Result and Discussion

Learning Rate

Learning Rate	Best RMSE (nilai LR)	Best R^2 (nilai LR)
0.1 – 0.5	3.274 (0.1)	0.847 (0.1)
0.05 – 0.1	1.172 (0.05)	0.912 (0.05)
0.01 – 0.05	0.1121 (0.01)	0.978 (0.01)
0.0005 – 0.01	0.110 (0.00025)	0.979 (0.00025)

Table 2. Determination of Optimum Learning Rate

We need to find the correct learning rate for well TTA-001. Normally, the smaller learning rate the smaller error rate will gain but the longer convergent time needed. So the optimum value should be obtained by trial and error.

Learning rate 0.01 shown as optimum value as RSME had reached 0.1121 and R^2 0.978. Researcher tried to decrease learning rate to 0.00025 as RSME and R^2 improved insignificantly yet had increased learning time significantly.

Error Threshold

Error threshold is limit of training process time. If error threshold reached its value, then the training will stop. If value of error threshold is too large the training will stop faster causing the optimal condition has not been achieved (error percentage may still high). However, if error threshold value is too small then training will last longer, and most likely stop because the maximum iteration has been reached before error threshold value is reached. In this paper, there were 4 error threshold values tested with result below.

Error Threshold	RMSE	R^2
0.001	0.4016	0.9013
0.0005	0.1104	0.9781
0.00025	0.1121	0.9671
0.0001	N/A	N/A

Table 3. Determination of Error Threshold

Error threshold 0.0001 cannot be reach because training process stopped first (500.000 iterations). Error threshold value 0.0005 result RSME 0.1104 and R^2 0.9781. However, error threshold value 0.00025 give insignificant improved result but it took a longer training process time.

Data Combination

The quantity of neuron in hidden layer determine complexity of ANN. The greater amount of neuron, the more complex and time consuming the process will be. There will be 4 data combinations as the input training parameters with minimum 3 input variable. The result is combinations of depth, DTCO, GR, and RHOB got the lowest RMSE with R^2 closest to 1.

PROCEEDINGS
JOINT CONVENTION BANDUNG (JCB) 2021
November 23rd – 25th 2021

Kombinasi Variabel	RMSE	R^2
DEPTH + DTCO + GR	0.3124	0.8901
DEPTH + DTCO + RHOB	0.1123	0.9223
DEPTH + GR + RHOB	0.412	0.901
DTCO + GR + RHOB	0.1819	0.9633
DEPTH + DTCO + GR + RHOB	0.0714	0.9826

Table 4. Determination of Optimal Data Combinations

Comparison Between Machine Learning Result vs Calculation Result

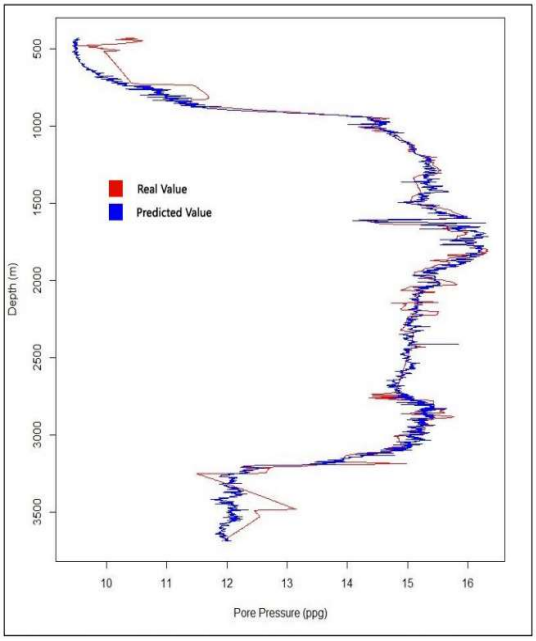

Figure 3. Comparison Between Manual Calculation and Predicted Pressure by Machine Learning

The picture shows that machine learning is having the same capacity to predict pore pressure as manual calculation. The input data used in this calculation is wireline log data.

Conclusions

1. Artificial Neural Network (ANN) is the most suitable machine learning method with R^2 0.9789, RSME 0.11401, 10-Fold RSME 0.1240, 10-Fold R^2 0.9644.
2. In this case study using learning rate 0.01, error threshold 0.1 as the optimum training variable.
3. Machine learning are able to predict pressure with a more efficient and faster result compared to manual calculation.

References

Moulds, P.J 1989, Ann. Conv. Indonesia Petroleum Association (IPA), **18**, 217-245.
Wilcox, R.E., T.P. Harding & D.R. Seeley 1973. American Assoc. Petrol. Geol. (AAPG) Bull. 57, 74-96.

PROCEEDINGS
JOINT CONVENTION BANDUNG (JCB) 2021
November 23rd – 25th 2021

Seawater Intrusion Zone in the Karst Baruga Area, Bantimurung-Bulusaraung

Muhammad Altin Massinai[1], Muhammad Fawzy Ismullah Massinai[1], Muh. Farid Wajedy[1], Virman[2]*
[1]Geophysics Department, Hasanuddin University, Makassar, Indonesia
[2]Physics Education Department, Cendrawasih University, Jayapura, Indonesia
[*]altin@science.unhas.ac.id

Abstract
The Bantimurung – Bulusaraung karst area is residential, especially in the Baruga – Maros area. In this area in the valley of Mount Bulusaraung, people find it difficult to get clean water, especially groundwater. This is due to the mixing of groundwater with brine. However, the community benefits from the entry of seawater in the karst pores to meet the brine needs of the community's ponds. This study aims to determine the effect of daily sea level on freshwater and brine interfaces and identify the depth of the seawater intrusion zone based on the results of a 2-D inversion resistivity section in the Baruga Bantimurung-Bulusaraung karst area. The method used in this study is the Wenner-Schlumberger configuration resistivity geoelectric method and uses the Ghyben-Herzberg formula. The results of interpretation and analysis show that tidal events influence the depth of the fresh and brine interface. If the seawater experiences a tide, the fresh water and brine interface depth will be small, and vice versa. If the seawater recedes, the depth of the fresh water and brine interface will be high. Moreover, seawater intrusion occurs in dolomite rock with good porosity and permeability with a resistivity value of 4.68 Ωm – 12.8 Ωm, which has a depth varying from ± 2.5 meters – 20 meters.

Introduction
Groundwater is a natural renewable resource that is limited and plays an essential role in meeting clean water needs. As time goes by, groundwater uses as a medium for daily needs both in the industrial sector. Moreover, household needs will increase (Massinai et al., 2020). Groundwater extraction that is carried out continuously by ignoring environmental aspects will cause groundwater production to exceed the productivity of the aquifer itself (Prusty & Farooq, 2020).

The main problem faced in nearshore areas is seawater intrusion into the aquifer, affecting groundwater quality (Prusty & Farooq, 2020). Seawater intrusion is a stage where seawater enters the aquifer to replace groundwater. Freshwater is located above brine because of the density difference between freshwater and brine. Brine has a higher density than freshwater because brine has more mineral content than freshwater (Flower et al., 2017).

In addition to the negative impacts caused by seawater intrusion in an area, seawater intrusion also positively impacts human life. Communities in the Karst area of Baruga, Bantimurung - Bulusaraung, take advantage of seawater intrusion to meet the water needs of their ponds, which are always in short supply of brine.

One of the appropriate methods to detect seawater intrusion zones is the Electrical Resistivity Tomography (ERT) method. The electrical Resistivity Tomography (ERT) method is a geophysical method used to study rock resistivity. The basic principle of the resistivity method is to inject electricity into the earth and measure the earth's response through the value of the resulting potential difference. The potential difference value obtained will be inverted to obtain the resistivity value, and a 2D cross-section can be made to provide information about changes in resistivity values both vertically and horizontally (Alamry et al., 2017).

Previous research on seawater intrusion was conducted by Kazakis et al. (2016). The result achieved is the intrusion of seawater aquifers in coastal areas consisting of clay, sand, gravel, and sandstone using the Electrical Resistivity Tomography (ERT) method. The resistivity value in brine aquifers consisting of sand and gravel material ranges from 0.1-15 m, while clay has a resistivity of 1-10 m (Kazakis et al., 2016). The purpose of this study was to determine the effect of daily sea level on fresh and brine interfaces and to identify the depth of the seawater intrusion zone based on the results of a 2-D inversion resistivity section.

Research Methodology
This research is located in the Karst area of Baruga, Bantimurung-Bulusaraung. The following map shows the location of the field measurements.

PROCEEDINGS
JOINT CONVENTION BANDUNG (JCB) 2021
November 23rd – 25th 2021

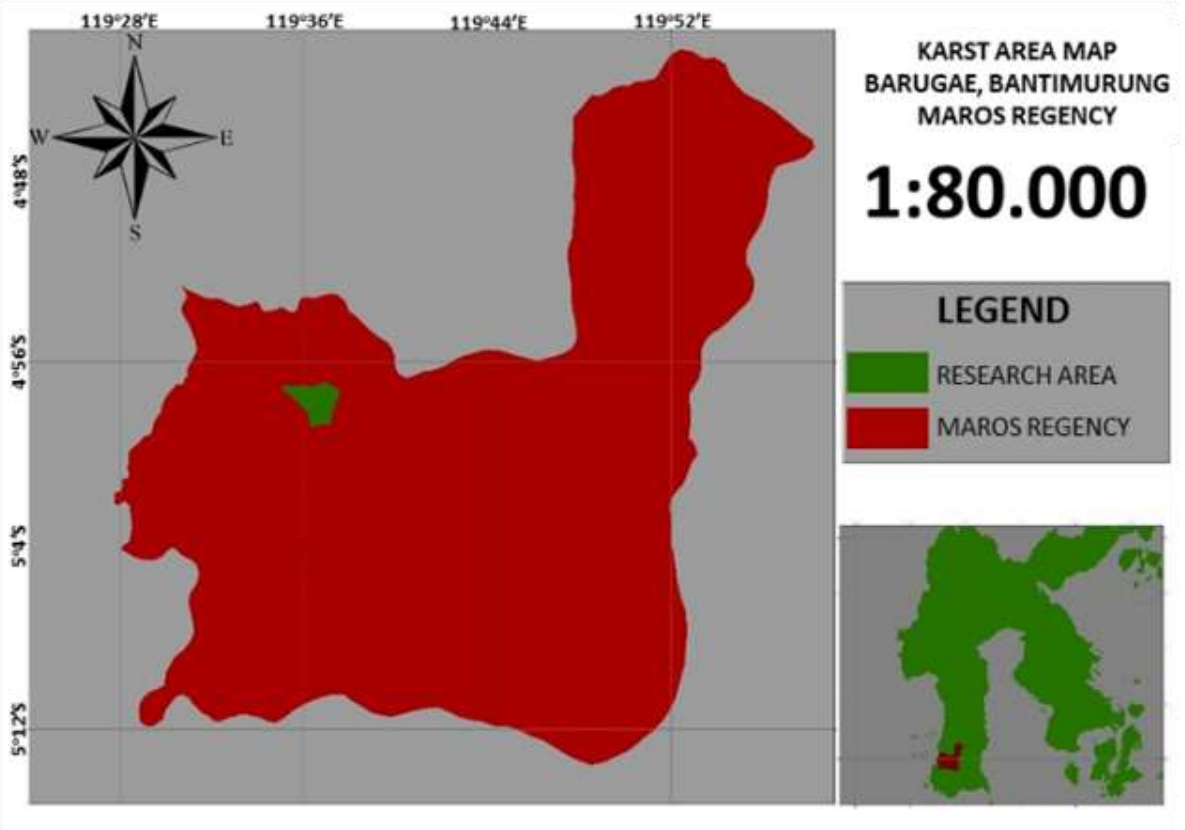

Figure 1: Research Location Map

Geoelectric data retrieval in the field was carried out with two-line length 300 m using the Wenner-Schlumberger configuration. Geoelectric data processing in this study was carried out using the RES2DINV application.

Tidal data processing was carried out using Microsoft Excel and the Ghyben-Herzberg formula (Masciopinto & Liso, 2016). This formula is used to get the value of the interface depth of fresh water and brine.

Result and Discussion

Freshwater and Brine Interface Depth

Tides are a phenomenon of periodic sea-level rise and fall that occurs in all parts of the earth due to tidal generating forces, mainly from the sun and moon (Tan et al., 2021). This tidal phenomenon is known to generate ocean currents known as tidal currents (Owen, 2020). The tide chart for the Maros area can be seen in Figure 2 below.

Tidal charts are very influential on seawater intrusion in the kart area. Tides can enter through the limestone pores in this area.

The Ghyben-Herzberg calculation in this study was carried out to determine the interface of fresh water and brine, which assists in interpreting geoelectrical data. The graph of Ghyben-Herzberg calculation processing can be seen in Figure 3 below.

Figure 3 shows the fluctuation of fresh water and brine at the study site every hour. The Y-axis represents the interface depth (m), while the X-axis represents the time (hours).

The results of calculating the freshwater and brine interface depth using The Ghyben-Herzberg equation (Figure 3) show that the fresh and brine interface depth is strongly influenced by daily tidal events (Figure 2). This can be seen from the graph of the fresh and brine interface depth with the tide graph. If the seawater is high, then the freshwater and brine interface will be below, and vice versa; if the seawater recedes, the freshwater and brine interface depth will be profound. At the research location, it was found that the average depth of the fresh and brine interface was 9 meters from MSL (Mean Sea Level).

Geoelectrical Resistivity

In this study, the method used is the geoelectric resistivity method of the Wenner-Schlumberger configuration consisting of two paths, each of which is 300 meters long. The first line runs from North to South, and the second line runs from West to East (Figure 4). The data processing is carried out using the inversion method, which aims to obtain the model parameter values from the field data, in this case, the resistivity value.

Geoelectric resistivity data processing in this study was carried out using the inversion method. The inversion method is one of the methods by modifying the field data to get the desired model parameter value in this case, is the resistivity value (Ansari et al., 2021).

Line 1
The first line stretches from North to South with a line length of 300 meters. The number of electrodes is 60 with a distance between electrodes of 5 meters and has a

penetration depth of 50 meters. The results obtained can be seen in Figure 5.

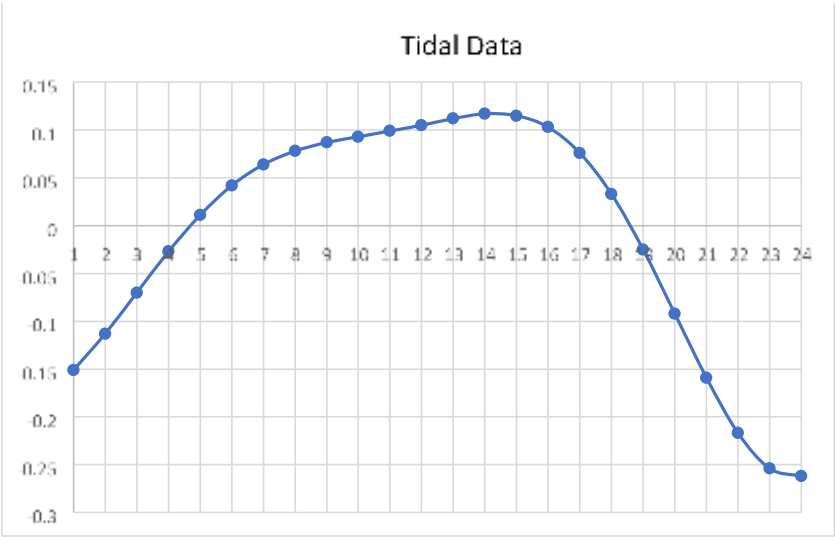

Figure 2: Tidal Data Graph

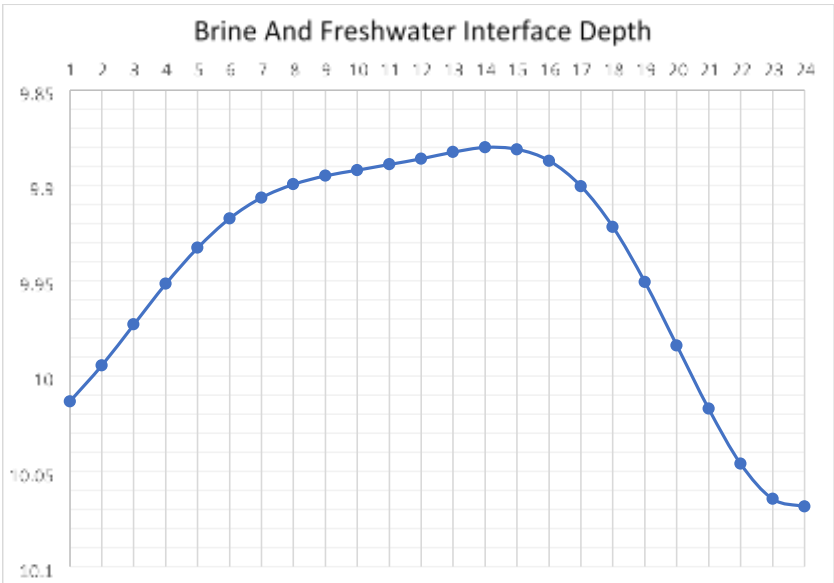

Figure 3: Graphics of Freshwater and Brine Interface

Figure 4: Line Measurement Map from Google Earth

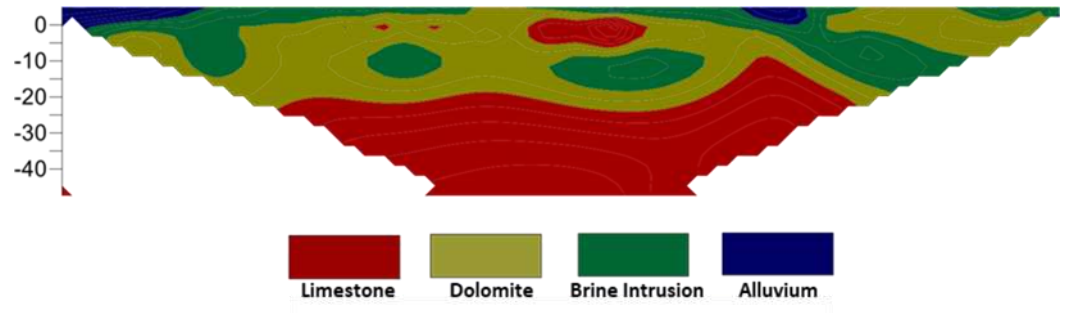

Figure 5: Cross Section Resistivity of Line 1

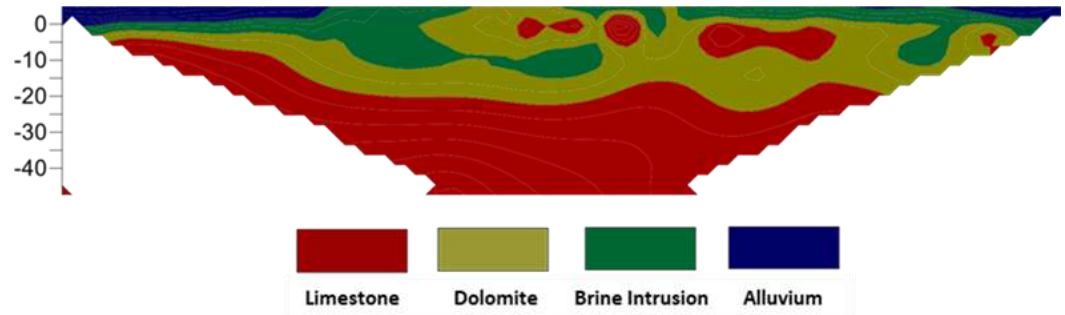

Figure 6: Cross Section Resistivity of Line 2

Based on the resistivity cross-section of Figure 5, it can be indicated that there are three layers contained in the research location. The first layer is alluvial deposits with resistivity values ranging from 1.37 Ωm – 3.10 Ωm, represented by dark blue. The second layer consists of dolomite-type carbonate rock with a resistivity value of 4.68 Ωm – 10.6 Ωm, which is depicted in green to yellow. In comparison, the third layer consists of massive limestone with a resistivity value of 16.0 Ωm – 24.1 Ωm (red color). The seawater intrusion is indicated to be in the second layer composed of dolomite represented in green.

Line 2

On the second line, the direction of the stretch leads to the West-East, which has a line length of 300 meters. The number of electrodes used is the same as the first line, which is 60 pieces that have a distance between the electrodes of 5 meters with a penetration depth of 50 meters. With the inversion results contained in Figure 6.

The results of the cross-sectional resistivity of line 2 (Figure 6) are indicated to consist of alluvium in the first layer with a resistivity value of 1.34 Ωm – 3.31 Ωm with a thickness of ± 1 meter – 7 meters which are depicted in blue. The resistivity value of 5.19 Ωm – 12.8 Ωm is indicated to consist of dolomite with a thickness of ± 5 meters – 20 meters (green to yellow). In the cross-sectional image, the red resistivity is composed of limestone with a resistivity value of 20 Ωm – 31.4 Ωm, with a thickness of ± 20 meters – 40 meters. Seawater intrusion is indicated to occur in layers composed of dolomite (green color). Dolomite is a type of carbonate rock with good porosity and permeability to store and pass fluids. At the research location, seawater intrusion occurs due to the entry of seawater into the river network around the research location, which then seeps through dolomite rock which can store and pass fluids.

Conclusions

1. The depth of the fresh and brine interface is affected by tidal events. If the seawater experiences a tide, the fresh water and brine interface depth will be small, and vice versa. If the seawater recedes, the depth of the fresh water and brine interface will be high.
2. Seawater intrusion occurs in dolomite rock with good porosity and permeability with a resistivity value of 4.68 Ωm – 12.8 Ωm which varies in depth from ± 2.5 meters – 20 meters.

References

Alamry, A. S., M. van der Meijde, M. Noomen, E. A. Addink, R. van Benthem, and S. M. de Jong, 2017, CATENA, **157**, 388–396. https://doi.org/https://doi.org/10.1016/j.catena.2017.06.001

Ansari, S., R. Norooz, A. Zeynolabedin, H. Foadi, and R. Ghiassi, 2021, Journal of Applied Geophysics, **104391**. https://doi.org/https://doi.org/10.1016/j.jappgeo.2021.104391

Flower, H., M. Rains, D. Lewis, J.-Z. Zhang, and R. Price, 2017, Estuarine, Coastal and Shelf Science, **184**, 166–176. https://doi.org/https://doi.org/10.1016/j.ecss.2016.11.013

Kazakis, N., A. Pavlou, G. Vargemezis, K. S. Voudouris, G. Soulios, F. Pliakas, and G. Tsokas, 2016, Science of The Total Environment, **543**, 373–387. https://doi.org/https://doi.org/10.1016/j.scitotenv.2015.11.041

Masciopinto, C., and I. S. Liso, 2016, Science of The Total Environment, **569–570**, 672–680. https://doi.org/https://doi.org/10.1016/j.scitotenv.2016.06.183

Massinai, M. A., E. Syamsuddin, Paharuddin, M. F. I. Massinai, M. A. Madda, 2020, Journal of Advance Research in Dynamical and Control Systems, **12(5)**, 550–561. https://doi.org/10.5373/JARDCS/V12I5/20201974

Owen, A., 2020, Tidal Current Energy: Origins and Challenges. In T. M. B. T.-F. E. (Third E. Letcher (Ed.), Future Energy (Third Edit, pp. 357–374). Elsevier.

https://doi.org/https://doi.org/10.1016/B978-0-08-102886-5.00017-7

Prusty, P., and S. H. Farooq, 2020, HydroResearch, **3**, 61–74. https://doi.org/https://doi.org/10.1016/j.hydres.2020.06.001

Tan, H., O. Francis, G. Wu, G. Yang, J. Wang, X. Zhang, J. Huang., and C. Shen, 2021, Geodesy and Geodynamics. https://doi.org/https://doi.org/10.1016/j.geog.2021.08.001

PROCEEDINGS
JOINT CONVENTION BANDUNG (JCB) 2021
November 23rd – 25th 2021

Interbed Multiple Attenuation

Ladaya A. Rakhmawati[1], Awali Priyono[1], Nurudin Mahmud[2], Hudzaifah[3]
[1]Geophysical Engineering, Faculty of Mining and Petroleum Engineering, Bandung Institute of Technology
[2] PT. Pertamina Hulu Indonesia
[3]PT. Pertamina Hulu Energi – ONWJ

Abstract

The appearance of multiples in marine seismic data provides pseudo layer effects that should not exist. The existing method such as predictive filter, f-k filter, and radon transform can reduce most multiples. However, interbed multiples are challenging to be reduced with usual methods. Interbed multiples occur at the subsurface due to impedance contrast between layers. In this research, we perform seismic data processing to reduce interbed multiples in 2D marine seismic data at ONWJ Basin, Indonesia. We apply the data-driven method. The concept is to define all multiple events as convolutions of primary events, then perform auto-convolution to predict the interbed multiples and subtract them adaptively from the seismic data. The result shows that the interbed multiple elimination method could reduce the interbed multiples contamination optimally. However, the result is obtained after performing more than one iteration using the same procedure involving all suspected interfaces as interbed multiples generators.

Keywords: Attenuation, Interbed multiples, Subsurface.

Introduction

Multiples need to be attenuated from the data in the processing steps. The existence of multiples can give ambiguous effects while interpreting the marine seismic data. Multiples are events that have at least one downward reflection at the surface or the subsurface. Most multiples can be reduced using an existing de-multiple method, e.g., Radon Transform, F-K filter, or predictive filter. However, this does not apply to interbed multiples. Interbed multiples have at least one downward reflection at the subsurface. Zaske (2000) and Verschuur (2013) stated that interbed multiples occur because the low-velocity layer is interbedded between the high-velocity layers. Interbed multiples are more difficult to distinguish than surface multiples. They have higher move-out velocity and are slightly close to primaries. Interbed multiples also have a similar frequency with primaries. These characteristics cause interbed multiples to be challenging to remove using predictive filter or Radon Transform method (Griffiths, 2011).

Some previous researches showed that interbed multiples appearances could lead to misinterpretation. El Emam (2005) and Griffiths (2011) showed that interbed multiples affected the structure accuracy and stratigraphy mapping. Interbed multiples can also cause seismic records on actual data not to correlate with synthetic records (Gan et al., 2018). These researches show that interbed multiples yield subsurface interpretation uncertainty.

Based on Verschuur et al. (1997) and Jiawen (2013), Interbed multiples can be removed by applying a method with prediction and subtraction concepts. In this research, we are implementing this concept into ONWJ Basin seismic dataset. The result shows that interbed multiples contamination on the data disappeared, confirmed in the shot gather domain display. However, we obtain the optimal result after applying more than one iteration processing on the same dataset.

Data and Method

Interbed multiple elimination method (IME) is a modification of an existing method that aims at surface-related multiples. The method is the Surface Related Multiple Elimination method (SRME). Thus, the IME method has a similar implementation concept to the SRME method.

A. Interbed Multiple Prediction

Surface multiple prediction can be written as,

$$M_0(x_r, x_s, f) = -\int_{x_k} X_0(x_r, x_k, f) P(x_r, x_k, f) dx_k$$

Or

$$M_0(x_r, x_s, f) = -\sum X_0(x_r, x_k, f) P(x_r, x_k, f)$$

Where x_s and x_s is source and receiver location respectively, x_k is the position of the reflection. The minus sign shows that the reflection waves are opposite to the surface. In matrix form become,

$$\mathbf{M}_0 = -\mathbf{X}_0\mathbf{P}$$

Based on Verschuur and Berkhout (1997), the reflected plane from the interbed multiples needs to be moved to the depth of the interface while the source and receiver remain on the surface (Figure 1). Therefore, the location of some components of the seismic data need~~s~~ to be changed. Then, the prediction multiples for interbed multiples become~~s~~,

PROCEEDINGS
JOINT CONVENTION BANDUNG (JCB) 2021
November 23rd – 25th 2021

$$M_n^{(i)}(x_r, z_0, x_s, z_0, f) = \sum_{x_k} \bar{P}_n^{(i-1)}(x_r, z_0, x_s, z_n, f)\bar{P}_{n-1}(x_k, z_n, x_s, z_0, f)$$

In matrix form,

$$\mathbf{M}_n^{(i)}(z_0, z_0) = \overline{\mathbf{P}}_n^{(i-1)}(z_0, z_n)\overline{\mathbf{P}}_{n-1}(z_n, z_0)$$

Where M_n show the multiples prediction for n at z_n, $\overline{\mathbf{P}}_{n-1}(z_n, z_0)$ describe all the reflected events that have been removed above z_n . $\overline{\mathbf{P}}_n(z_0, z_n)$ represent the primary events with the receiver at the surface and the source at the depth z_n, (z_n, z_0), or (z_0, z_n) is the receiver and source depth respectively. In the multiples prediction results, the source signature causes the amplitude of the predicted results to become inconsistent compared to the initial seismic data, so adaptive reduction is needed as an additional step for this process (Jiawen, 2013).

B. Adaptive Subtraction

In the multiple prediction process, there are amplitude and arrival times that are not perfectly predictable. These conditions happen due to auto-convolution. Adaptive subtraction works by dividing the data into several windows that have an estimated matching filter. Then, the windows are converted into a time or space domain, and the new matching filter is calculated.

Adaptive subtraction on surface multiples case can be written as,

$$P_0^{(i)}(x_r, x_s, f) = P(x_r, x_s, f) - A(f)M_0^{(i)}(x_r, x_s, f)$$

Whereas on interbed multiples case becomes,

$$P_n^{(i)}(x_r, z_0, x_s, z_0, f = P_{n-1}(x_r, z_0, x_s, z_n, f) - A(f)M_n^i(x_r, z_n, x_s, z_0, f)$$

In matrix form,

$$\mathbf{P}_n^{(i)} = \mathbf{P}_{n-1}(z_0, z_0) - A_n(f)\mathbf{M}_n^{(i)}(z_0, z_0)$$

$A_n(f)$ describes the matching operator between multiples predicted result and the original multiple. So, this adaptive reduction process produces an amplitude that matches the original data. Levinson's recursion aids the overall adaptive subtraction process.

Based on this theory, the process of eliminating interbed multiples can be carried out in four stages, they are:

- Define~~s~~ the suspected interface that generates interbed multiples and then move~~s~~ the position of x_k to that interface.
- Apply the displacement to the shot record and temporarily remove the reflection above the selected reflector.
- Predict interbed multiples.
- Adaptively subtract the interbed multiples prediction~~s~~ with original data.

Before processing the data, several conditions need to be met, there are:

- The data must be clean from noise such as direct waves, reverberation, or multiples other than interbed multiple.
- The layer above the generator indication's layer should be temporarily muted.
- It should have precise 2D geometry, with no near offset gaps and no lost shot or receiver recording data.
- Perform offset regularization to fill in unrecorded traces.

We used marine 2D seismic data from the Basin Offshore Northwest Java (ONWJ). The streamer is 4000 m long, with the number of channels 640 m, the group interval is 6.25 m, and the shooting point interval is 25 m. The displayed data have undergone the missing near offset reconstruction process. Based on Dragoset (2010) and Jiawen (2013), in order to predict the multiples correctly, the essential preprocessing step is to extend the offsets to zero offsets. Any missing trace will act as a noise source and generate artifacts. However, the preconditioning gathers results that cannot be shown due to proprietary issues.

The 2D marine seismic data in the stack section can be seen in Figure 2. In Figure 2, there are seven interfaces (borders between layers). Where A is the boundary between the sea and the water-bottom and interface G is the layer boundary between the basement and the layer above it. The reflectors below the basement are suspected as interbed multiples. Interbed multiples existent on that area are verified by velocity semblance panel. Interbed multiples have higher velocity than surface multiples. Surface multiples generator is water-bottom; therefore, surface multiples have the same energy as water-bottom. Meanwhile, a source layer resurrects interbed multiples at a depth. Thus, the energy is also equivalent. So that the white circles on the velocity semblance panel (Figure. 2b) are confirmed as interbed multiples and green arrows also indicate the interbed multiple.

Result and Discussion

The interbed multiples attenuation process is carried out after preconditioning the data. Before predicting the interbed multiples, it is necessary to determine the new surface, which creates them. The chosen horizon is determined by strong amplitude horizon existence on stack section, caused by contrast of acoustic impedance due to velocity change and by analyzing the energy of the velocity semblance panel.

PROCEEDINGS
JOINT CONVENTION BANDUNG (JCB) 2021
November 23rd – 25th 2021

The new surface is the realization of x_k. In this research, we used interface F as the new surface. The layers above F should be muted so the data above them do not get into the processing steps. The interbed multiple elimination method works in the shot gather domain; therefore, the prediction multiples and subtraction process is all in shot gather. As a result, after predict interbed multiples and subtract them on all datasets, the interbed multiples that initially appeared at 3 s – 4 s have already decreased, but not thoroughly. So that the interbed multiples still give an ambiguous effect on the real data.

The interbed multiple elimination method (IME) procedures need to be repeated. Repetition of the process is done by applying the results of the previous procedure as an input and using other surfaces (other interfaces), which are also considered to have a relationship with interbed multiples occurrences. In this second elimination procedure, interface E becomes the new surface. Then, in the same way as before, multiples estimations are obtained, then adaptively subtracted, resulting in a significant change (Figure 3). In this picture, the interbed multiples look well attenuated.

Interface D also needs to be involved in processing using this IME method because it relates to interbed multiples existence. However, Figure 3 showed that the interbed multiples have been eliminated and no longer interfere with seismic data. The velocity semblance panel also reinforces this result in Figure 3b. It shows that the energy of interbed multiples are reduced. Thus, the elimination process involving interface D is not required. In addition, important to note is the existence of an adaptive reduction procedure. When subtraction is applied, it is feared that not only multiples will be eliminated, but also the primary data. This result proves that the IME method can attenuate the interbed multiples.

Conclusions

This research concludes that the interbed multiple elimination (IME) method could optimally attenuate the interbed multiples. Although, there was a need for alignment during the data processing process. However, we also need to repeat processes according to the interface relations with interbed multiple. Aside from that, not all interbed multiple related interfaces should be removed. It depends on the previous processing IME result. If we force to use all related interfaces, we should concern about losing the primary data.

References

Berkhout, A.J. and Verschuur, D.J, 1997, Geophysics, **62**, 1586-1595.

Dragoset, B., Verschuur, E., Moore, I., and Bisley, R, 2010, Geophysics, **75**, 75A245-75A261.

El-Emam, A., Moore, I., and Shabrawi, A, 2005, 75th Annual International Meeting SEG Extended Abstracts, 448-451.

Gan, L., Xiao, F., Dai, X., Yang, H., Xu, Y., Ran, Q., Wei, C., Xie, Z., Zhang, X., Liu, W., Zhang, M., Song, J., dan Li, Y, 2018, Petrol. Explor. Develop., **45**, 1023-1035.

Griffiths, M., Hembd, J., and Prigent, H, 2011, The Leading Edge, **30**, 906-912.

Song, J., Verschuur, E., and Chen, X, 2013, Journal of Applied Geophysics, **95**, 66-76.

Verschuur, D.J, 2013, EAGE Publications bv, Houten, Dutch.

Verschuur, D.J. and Berkhout A.J., 1997, Geophysics, **62**, 1596-1611.

Zaske, J., 2000, Ph.D. dissertation, Karlsruhe University.

Acknowledgements

The authors thank PT. Pertamina Hulu Energi – Offshore North West Java (PHE-ONWJ) for permission to publish this work.

PROCEEDINGS
JOINT CONVENTION BANDUNG (JCB) 2021
November 23rd – 25th 2021

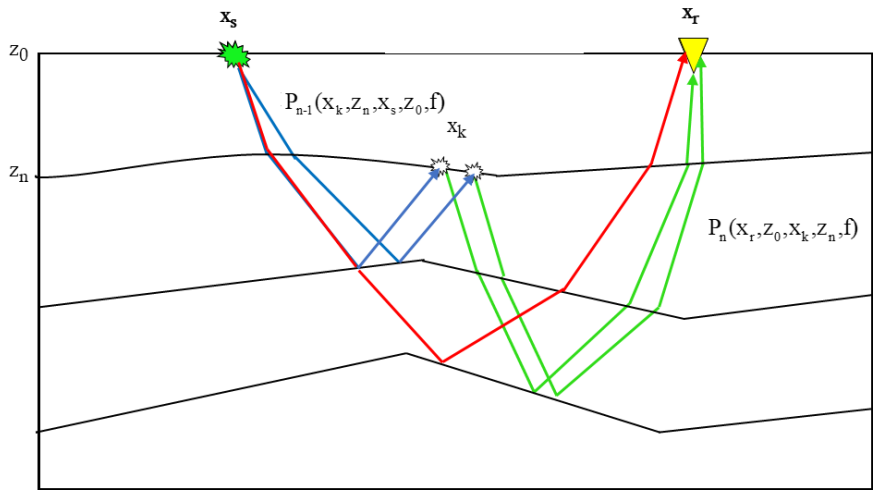

Figure 1: Multiples prediction construction. The red ray-path is an ideal ray-path illustration when firing a signal to x_s. The non-ideal event illustrated by the blue ray-path, show the signal that fired by x_s being received at x_k because it bounces first at a location, then forwarded until receive at x_r (green ray-path). These non-ideal events illustrate multiples (blue and green ray-paths). In surface multiples case, x_k is located in the surface (z_0) . Meanwhile, in interbed multiples case, x_k is located in the subsurface (z_n) (Verschuur, 2013).

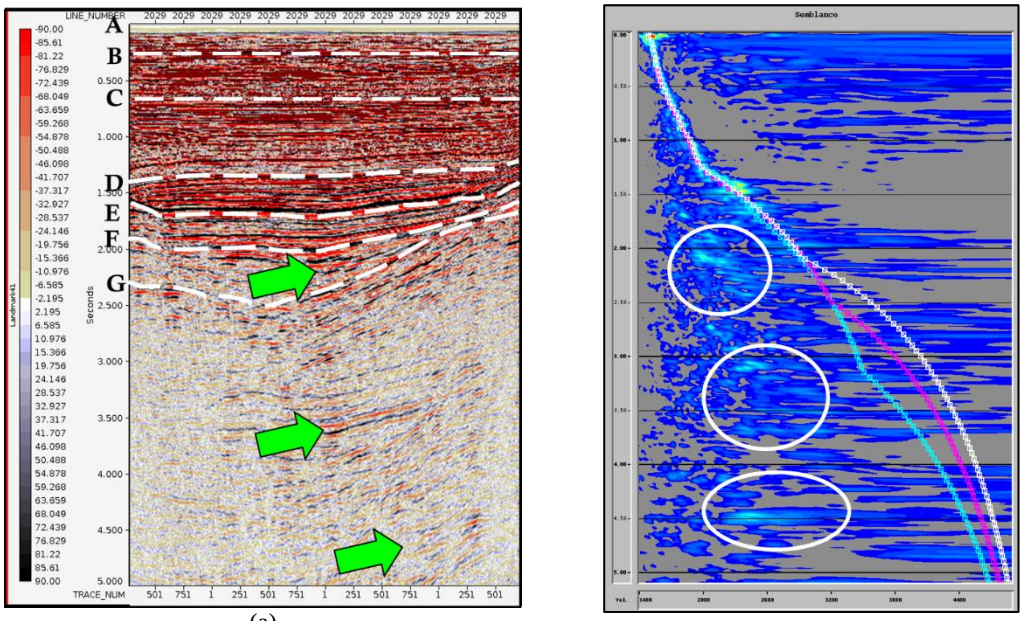

(a) (b)

Figure 2: (a) Stack section from seismic data. (b) Velocity semblance panel corresponding to (a). Green arrows and white circles indicate interbed multiples.

PROCEEDINGS
JOINT CONVENTION BANDUNG (JCB) 2021
November 23rd – 25th 2021

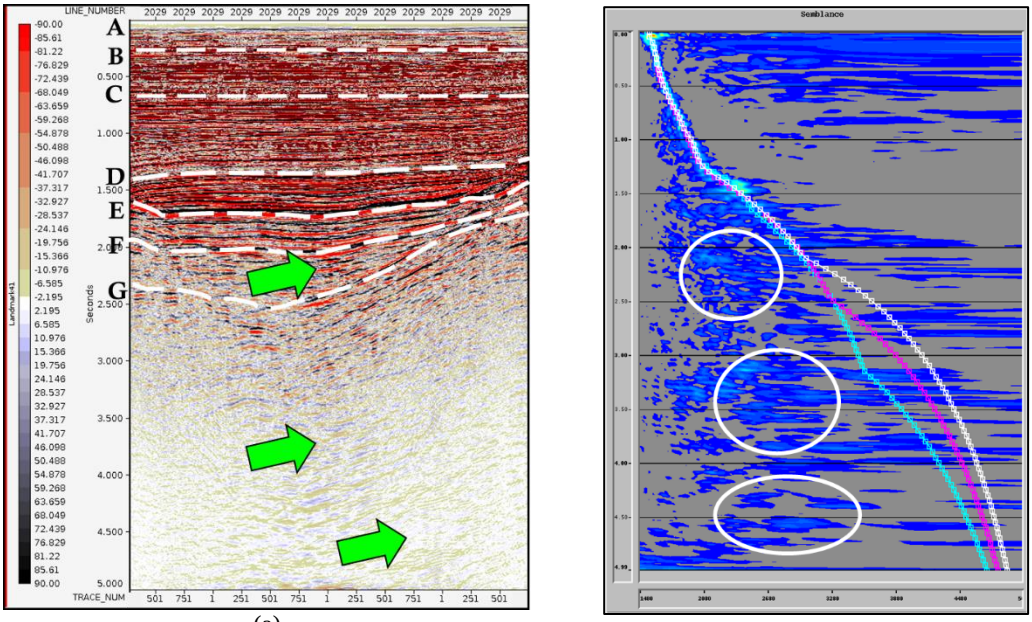

(a) (b)

Figure 3: (a) Stack section after processing. (b) Velocity semblance panel corresponding to (a). Green arrows and white circles indicate interbed multiples.

PROCEEDINGS
JOINT CONVENTION BANDUNG (JCB) 2021
November 23rd – 25th 2021

Characteristics of Oceanographic Conditions in Skipjack Tuna (Katsuwonus Pelamis) Catching Areas in Indonesian Waters

Audia Azizah Azani
Bitung Maritime Meteorological Station, Indonesian Agency of Meteorology Climatology and Geophysics

Abstract
This paper aims to determine the oceanographic characteristics of the skipjack tuna catching area (Katsuwonus pelamis), especially in Indonesian waters, based on several studies that have been carried out. Oceanographic elements that are generally studied in these studies include sea surface temperature (SST), chlorophyll-a, salinity, and sea current. Most of the researches were conducted used satellite imagery to obtain the required data. Based on these studies, the optimum skipjack tuna catch was found in conditions of warm SST (around 27,0-31,5°C) and chlorophyll-a concentration of 0.10-0.35 mg/m^3. The range of optimum SST and chlorophyll-a for catching skipjack tuna in eastern Indonesian waters is wider than in western Indonesian waters. The peak of fish catch is different in each water, depending on the characteristics of the water and the climate condition of the water. However, in general, the areas with the best catch are around the coast, while the best season for catching skipjack tuna is generally in the dry season. It is necessary to further investigate the dynamics of oceanographic conditions in the long term to see whether climate change or climate variability affects determining the optimum skipjack tuna catch area.
Keywords: *skipjack tuna, sea surface temperature, chlorophyll-a, salinity, sea current*

Introduction

Skipjack tuna (Katsuwonus pelamis) is a fast-swimming pelagic fish that lives in open waters and flocks when searching for food (Zulkhasyni, 2015). This fish is found in almost all Indonesian waters. The distribution of skipjack tuna in Indonesian waters includes the Indian Ocean (Waters of western Sumatra, southern Java, Bali, and Nusa Tenggara), eastern Indonesian waters (Sulawesi Sea, Maluku Sea, Banda Sea, Flores Sea, Makassar Strait), and the Pacific Ocean (Northern waters) (Anjarsari, 2018). According to the Food and Agriculture Organization (FAO) in 2009, skipjack tuna is commercially important, ranked among the first 10 species that have contributed highly to global catches in previous years (Mugo et al, 2010).

Generally, fishing areas are not fixed because they are always changing and moving following the movement of environmental conditions. The distribution of skipjack tuna is also influenced by oceanographic conditions. They are what usually determine the fertility of the waters. Fertile waters have high nutrient content, such as orthophosphate, nitrite, and other nutrients (Fajar et al, 2020). Another factor that affects the production of skipjack catches is the presence of small pelagic fish that are used as bait in the process of the pole and line catching (Fajrianti et al, 2016).

Some waters such as Bone Bay and Maluku Sea are potential areas for catching skipjack tuna. However, the catch of fishermen per trip and the total catch per year are still low due to the uncertain location and timing of catching (Fajrianti et al, 2016). For these reasons, information on fishing grounds is needed for more efficient catching in terms of fuel consumption, energy, and operating time (Simbolon, 2010). This paper summarizes several studies on the oceanographic conditions of skipjack tuna catching areas in some waters in Indonesia so that the oceanographic characteristics of skipjack tuna catching areas, in general, are known.

Data and Method

In determining the oceanographic parameters used in research, the most common way is to use remote sensing. Remote sensing can be used to determine the fishing position and data information from the distribution of oceanographic parameters in the fishing area. Oceanographic data such as sea surface temperature, chlorophyll-a, and salinity were taken from the Aqua/Terra MODIS satellite available at https://oceancolor.gsfc.nasa.gov/. This data is usually processed spatially with geographic information system applications.

The oceanographic data obtained were then compared with data on fish catches obtained from the mental maps of local fishermen (Huda et al, 2019) and Fish Landing Site (Zulkhasyni, 2015). This primary data can also be obtained by directly following skipjack tuna fishing activities carried out by fishermen using the pole and line method (Sarianto, 2018; Fajar et al, 2020) or purse seine method (Simbolon, 2010; Pratiwi, 2018; Pamungkas et al, 2020).

Result and Discussion

Sea surface temperature (SST)

Sea surface temperature is very influential on fish life such as fish growth, activity, mobility of movement, migration, distribution, abundance, schooling, maturation, spawning fecundity, incubation and hatching periods of eggs, and survival of fish larvae (Fajarianti et al, 2016). Its fluctuations, as well as geographic changes, are important factors in stimulating and determining the concentration of schools of fish (Fajar et al, 2020; Pratiwi, 2018; Simbolon, 2010). The spatial distribution of skipjack tuna catching activity shows a seasonal pattern related to environmental conditions where the temperature is the main variable that can be used to predict skipjack tuna habitat (Mugo et al, 2010). Furthermore, SST images can be used to monitor the dynamics of oceanographic phenomena such as thermal fronts and upwelling locations where this location is usually a flocking place for fish (Zainudin et al, 2015).

According to Gunarso (in Fajar et al, 2020), the ideal water temperature for skipjack tuna is between 26°C-32°C. Several studies were conducted to prove this statement (as shown in Table 1). In Bone Bay, the optimum SST for skipjack tuna is in the range of 29.0°C – 31.5°C. Especially for January to June, it is in the range of 29.75°C and 30.25°C. Meanwhile, in the south of West Java, the

Table 1. Optimal SST results of skipjack tuna catch from several studies

Author, Year	Research Area	Research Time	Optimal SST Result (°C)
Zainuddin and Farhum, 2010	Bone Bay	April – July 2009	29,5 – 31,5
Fajrianti et al, 2016	Bone Bay	2011 - 2014	29,5 – 30,0
Zainuddin et al, 2015	Bone Bay – Flores Sea	January – June 2014	29,75 – 30,25
Rahman et al, 2020	Southern of West Java Waters	2014 - 2016	28,0 – 28,3
Anjarsari, 2018	Bone Bay	June – September 2016	29,0 – 31,0
Ismunandar, 2018	Bone Bay	April – September 2017	28,5 – 29,3
Sarianto, 2018	Bacan and Obi, Southern Halmahera	May – June 2018	29,7
Tangke et al, 2019	Ternate Water	June – November 2018	27,0 – 30,9
Pamungkas et al, 2020	Maluku Sea	December 2018 – March 2019	28,0 – 29,0
Safruddin et al, 2020	Western of Makassar Strait, Southern of Flores Sea, and Eastern of Bone Bay	January – August 2019	29,0 – 29,5
Fajar et al, 2020	Bacan Island, Southern Halmahera	March – May 2019	30,1 – 31,0

optimum condition where skipjack is caught between SST of 28°C – 28.3°C. Around Maluku Island, such as in Ternate waters and around Southern Halmahera, the optimum SST is 27.0°C – 31.0°C. These results show that the waters in eastern Indonesia have a wide range of SST to catch the fish in optimal results, while waters around western Indonesia have a narrow SST range. However, there should be more comprehensive researches to confirm this result.

Not only from the number of catches, but some also stated that SST affected the size of the fish caught where large fish (≥36.4 cm) is dominantly caught at a temperature range of 28°C – 28.99°C and small fish (≤31.4 cm) is dominantly caught at a temperature of 30°C - 30.99°C (Pamungkas et al, 2020). This is in line with Simbolon (2010) which states that large skipjack tuna is caught at varying SST, while small skipjack tuna is caught at warmer temperatures. It is because large fish is generally influenced by a better metabolic system so that it can adapt to various water temperature ranges.

Although several studies have stated that there is a strong relationship between SST and skipjack catch, some results are showing that SST does not affect it. According to Sarianto (2018), SST does not affect spatially because all fishing areas have a homogeneous SST distribution and are in the optimum SST range for skipjack tuna catch. Simbolon (2010) observed that SST did not affect the number of skipjack tuna catch in Pelabuhanratu Bay during August – October 2007, but it only affects the size of the fish caught.

Based on the researches that have been done, Indonesian waters are very possible for skipjack tuna catching areas because they have a homogeneous and warm SST. Skipjack tuna is more likely to be in a relatively warm temperature range. Skipjack tuna is not abundant at low temperatures because low sea surface temperatures can reduce the rate of photosynthesis so that skipjack tuna food tends to be lacking at these low temperatures (Rahman et al, 2019).

Chlorophyll-a

Chlorophyll-a is closely related to primary productivity as indicated by a large amount of phytoplankton biomass which is the first food chain for small fish which will then become food for larger fish including pelagic fish such as skipjack tuna (Fajar et al, 2020). The number of plankton evaluated based on the content of chlorophyll-a depends on seasonal changes. In addition, variations in chlorophyll-a are caused by differences in the intensity of sunlight and the concentration of nutrients contained in the waters (Fajarianti et al, 2016). Nutrients have a low concentration and fluctuate at sea level. Their concentration will increase with increasing depth and will reach a maximum concentration around the water area (Safruddin et al, 2020). The presence of chlorophyll-a at sea level is also influenced by other oceanographic physical parameters such as salinity and Total Suspended Solid (TSS) (Huda et al, 2019).

Chlorophyll-a is one indicator of the front area that can provide the path of the tuna migration area (Polovina et al, 2001). In the sea, the concentration of chlorophyll-a is higher in coastal and coastal waters, and lower in offshore waters (Fajrianti et al, 2016). The high distribution of chlorophyll-a concentrations in coastal and coastal waters is due to the presence of a large supply of nutrients through run-off from the mainland, while the low concentration of chlorophyll-a in offshore waters is due to the absence of direct nutrient supply from land (Presetiahadi, 1994). The content of chlorophyll-a affected the composition of the number of fish caught (Sarianto, 2018).

Based on the researches that have been done (Table 2), the optimum chlorophyll-a in southern Java is 0.2 – 0.25 mg/m^3. Around Maluku Island, the optimum is 0.18 – 0.35 mg/m^3. Meanwhile, in Bone Bay, skipjack tuna was mostly caught in the range of 0.15 – 0.35 mg/m^3. This result is quite similar to SST, where the range of optimum chlorophyll-a in eastern Indonesia waters is wider than in western Indonesia. At any rate, skipjack tuna is generally concentrated in the chlorophyll-a range of 0.2 – 0.3 mg/m^3, which is assumed as the range where the front zone is located.

Other Oceanographic Factors

Salinity is a parameter that affects potential fishing areas. It states the level of dissolved salts in water that causes

PROCEEDINGS
JOINT CONVENTION BANDUNG (JCB) 2021
November 23rd – 25th 2021

Table 2. Optimal chlorophyll-a results of skipjack tuna catch from several studies

Author, Year	Research Area	Research Time	Optimal Chlorophyll-a Result (mg/m^3)
Zainuddin and Farhum, 2010	Bone Bay	April – July 2009	0,15 – 0,35
Fajrianti et al, 2016	Bone Bay	2011 - 2014	0,22 – 0,25
Zainuddin et al, 2015	Bone Bay – Flores Sea	January – June 2014	0,125 – 0,213
Rahman et al, 2020	Southern of West Java Waters	2014 - 2016	0,20 – 0,25
Anjarsari, 2018	Bone Bay	June – September 2016	0,20 – 0,30
Ismunandar, 2018	Bone Bay	April – September 2017	0,20 – 0,34
Tangke et al, 2019	Ternate Water	June – November 2018	0,20 – 0,35
Safruddin et al, 2020	Western of Makassar Strait, Southern of Flores Sea, and Eastern of Bone Bay	January – August 2019	0,10 – 0,15
Fajar et al, 2020	Bacan Island, South Halmahera	March – May 2019	0,18 – 0,27

osmotic pressure between the organism's body and seawater. The higher the salt level, the more it will reduce the presence of phytoplankton (Huda et al, 2019; Tangke et al, 2020).

According to Sandi (in Pratiwi, 2018), skipjack tuna tends to be in the waters with salinity levels of 33-35 ppt. In Pratiwi's research (2018), the most influential parameter on catches in Bone Bay is salinity. In the Maluku Sea, the highest average catch is in the salinity range of 31 – 31.9 ppt, while the lowest is within a salinity of 34 – 35 ppt. The relationship between salinity and length of fish is not strong, but there is a pattern that small fish is more dominantly caught at high salinity (Pamungkas et al, 2020).

Another factor that affects the presence of skipjack tuna is sea current. Indonesian waters are generally influenced by monsoon winds so that the current pattern formed is determined by the ongoing season. The waters closest to the waters studied also affect the characteristics of the waters, such as the Southern Waters of West Java which are influenced by water masses from the Indian Ocean and the Sunda Strait, or the Makassar Strait which is influenced by the Pacific Ocean. This water mass movement affects the migration pattern of high migratory species such as Katsuwonus pelamis (Safruddin et al, 2020).

Skipjack tuna generally tends to be in waters with weak sea currents (Simbolon and Girsang, 2009). The meeting of two water masses is a barrier to fish migration because of the fast movement of water and big waves. Therefore, the front area is a suitable area for the distribution of tuna species (Sarianto, 2018).

Catching Area Analysis

Fishing areas are always changing according to environmental factors and oceanographic dynamics of the waters because fish will choose habitats that are more suitable for feeding, housing, reproduction, and migration (Wailerunny et al, 2014; Rahman et al 2019). The further away from the coast, the lower the potential skipjack tuna catching zone. This is related to the nutrients that act as a food supply for phytoplankton originating from sedimentation material flowing by the river that does not allow it to move to the high seas (Huda et al, 2019). In the Banda Sea, there is a change in skipjack tuna fishing areas according to seasonal changes with a fairly large distribution of fishing in coastal areas near the island (Wailerunny et al, 2014). However, this result is different from the waters of Western of Makassar Strait, Southern of the Flores Sea, and Eastern of Bone Bay where skipjack fish tends to occupy space in the offshore area (Safruddin et al, 2020).

The productivity level of skipjack tuna catch itself is influenced by the climate which also affects the levels of chlorophyll-a, TSS, and salinity in the waters. For instance, the highest production of skipjack tuna in the Southern Makassar Strait occurs in the dry months (June, July, August) with a total of 15.3 tons in line with the upwelling

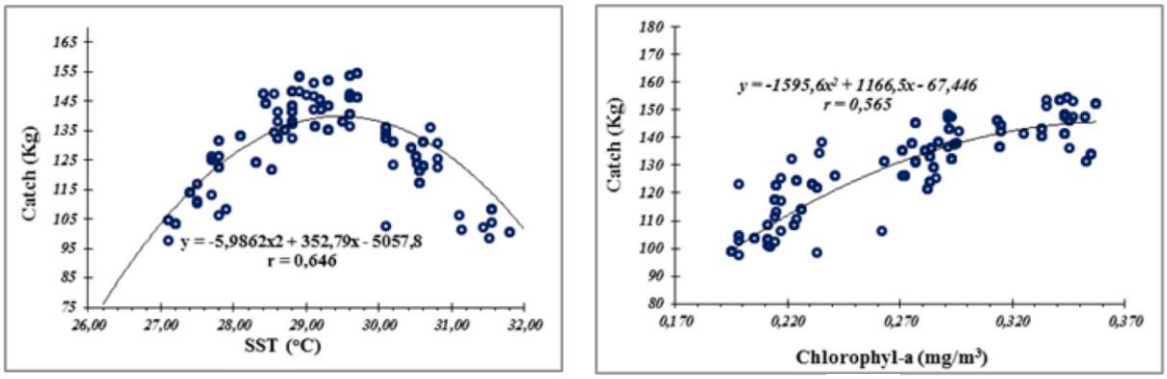

[a] [b]

Figure 1. The relationship between oceanographic conditions (SST [a] and chlorophyll-a [b]) and tuna catch (Tangke et al, 2020)

phenomenon, while the lowest production occurs in the wet months, especially in January, February, and March (Huda et al, 2019). The same results were observed in the Southern Waters of West Java, where the maximum catch was in the dry season of 2015 and the lowest catch was in the wet season of 2016. It is because the high waves occurred during the wet season so that the intensity of fishing was also less (Rahman et al, 2019).

There is a specific relationship between the dynamics of the distribution of sea surface temperature and chlorophyll-a with the presence of skipjack tuna as shown in Figure 1 (Tangke et al, 2020; Safruddin et al, 2020). SST and chlorophyll-a are significant predictors that affect the distribution pattern and abundance of skipjack tuna. It is shown by the characteristics of the catchment area in Bone Bay when the temperature was highest and chlorophyll-a increased in May (Zainuddin et al, 2015). Skipjack tuna will be concentrated when the front develops characterized by optimum temperature and chlorophyll-a conditions. Fishing activities that are not in the optimum temperature range or chlorophyll-a result in the non-optimal catch (Zainuddin and Farhum, 2010).

Several studies have proven the effect of SST and chlorophyll-a on skipjack tuna catch areas. However, Simbolon and Limbong (2012) suggested that SST and chlorophyll-a may not have a direct effect on the formation of fishing grounds. For this reason, it is necessary to obtain more oceanographic information so that the skipjack tuna catching area can be ascertained. By combining the oceanographic parameters such as SST, chlorophyll-a, salinity, and sea currents, the accuracy of fishing grounds identification can be improved. Besides that, oceanographic conditions are closely related to climatic conditions. It is needed to study the dynamics of oceanographic conditions in the long term to see whether climate change or climate variability affects the determination of the optimum skipjack tuna catching area in Indonesia.

Conclusions

Several attempts to determine skipjack tuna fishing areas in Indonesian waters have been carried out by utilizing oceanographic parameters such as sea surface temperature, chlorophyll-a, salinity, and sea current. In general, the optimum yield of skipjack tuna is in waters with warm temperatures in the range of 27,0-31,5°C and chlorophyll-a in the range of 0.10-0.35 mg/m^3. The range of optimum SST and chlorophyll-a for catching skipjack tuna in eastern Indonesian waters is wider than in western Indonesian waters. The areas with the best catch are around the coast, while the best season for catching skipjack tuna is generally in the dry season. However, this condition also depends on the nature of the waters and the climate in the catching area. Further study is needed on the dynamics of oceanographic conditions in the long term to see whether climate change or climate variability affects determining the optimum skipjack tuna catching area.

References

Anjarsari, L., 2018, Minithesis, Universitas Hasanuddin.
Fajar, P., Kadir, I. A., & Wahiddin, N., 2020, Hemyscyllium, 1, 93-113.
Fajrianti, D., Mallawa, A., & Musbir, M., 2016, Jurnal IPTEKS Pemanfaatan Sumberdaya Perikanan, 3, 469-483.
Huda, D. N., Nurhuda, A., & Lubis, M. Y., 2019, Prosiding Seminar Nasional Penginderaan Jauh, 6, 409-417.
Ismunandar, I., 2018, Minithesis, Universitas Hasanuddin.
Mugo, R., Saitoh, S. I., Nihira, A., & Kuroyama, T., 2010, Fisheries Oceanography, 19, 382-396.
Pamungkas, P. A., Kusdinar, A., & Halim, S., 2020, Jurnal Penyuluhan Perikanan dan Kelautan, 14, 13-26.
Polovina, J. J., Howell, E., Kobayashi, D. R., & Seki, M. P., 2001, Progress in Oceanography, 49, 469-483.
Presetiahadi, K., 1994, Minithesis. Institut Pertanian Bogor.
Pratiwi, D., 2018, Minithesis, Universitas Hasanuddin.
Rahman, M. A., Syamsudin, M. L., & Agung, M. U. K, 2019, Jurnal Perikanan Kelautan, 10, 92-102.
Safruddin, Hidayat, R., & Zainuddin, M., 2020, Journal of Fisheries and Marine Science, 3, 1-10.
Sarianto, D., 2018, SEMAH Jurnal Pengelolaan Sumberdaya Perairan, 2.
Simbolon, D., 2010, Jurnal Mangrove dan Pesisir, 10, 42-49.
Simbolon, D., & Girsang, H. S., 2009, Jurnal Penelitian Perikanan Indonesia, 15, 297-305.
Simbolon, D., & Limbong, M., 2012, Journal of Coastal Development, 15, 225-233.
Tangke, U., Silooy, F. D., & Saing, Z., 2020, Journal of Physics: Conference Series, 1517, 012039.
Wailerunny, W., Wiyono E. S., Wisudo, S. H., Purbayanto, A., & Nurani, T. W., 2014, Jurnal Teknologi Perikanan dan Kelautan, 5, 41-54.
Zainuddin, M., & Farhum, A., 2017, Jurnal Penelitian Perikanan Indonesia, 16, 115-123.
Zainuddin, M., Safruddin, S., Nelwan, A., Selamat, M. B., Hidayat, S., & Sudirman, S., 2015, Jurnal IPTEKS Pemanfaatan Sumberdaya Perikanan, 2, 228-237.
Zulkhasyni, Z., 2015, Jurnal Agroqua: Media Informasi Agronomi dan Budidaya Perairan, 13, 68-73.

PROCEEDINGS
JOINT CONVENTION BANDUNG (JCB) 2021
November 23rd – 25th 2021

PENYELIDIKAN AIR TANAH DAERAH KARST DI KABUPATEN WONOGIRI BAGIAN SELATAN, PROVINSI JAWA TENGAH

Wiyono, Acep Ruchimat, Erika Purwaningsih
Pusat Air Tanah dan Geologi Tata Lingkungan, Badan Geologi
Jl. Diponegoro No.57 Bandung 40122.

Abstract

Groundwater investigation activities in the southern part of Wonogiri Regency have been successfully carried out. Most of locations in this area are dominated by karst morphology and geologically consists of the Wonosari – Punung Formation (Tmwl) which is composed of limestone, marl limestone to tuffaceous, conglomerate limestone, sandstone, tuff and siltstone. Based on the hydrogeological map, the aquifer system of this area is form of flow through fissures, fractures and solution channels. The research methodology includes hydrogeological and geophysical methods was conducted. Hydrogeological investigations consisted of observing the physical and chemical properties of water, while geophysical investigations used a 2-dimensional (2-D) resistivity method, using 48 channels and 20 meters electrode spacing with Wenner-Schlumberger configuration. The results of the hydrogeological study show that there is no significant difference between the physical and chemical properties of water obtained from dug wells, drilled wells, springs and ponds. The results of the analysis on the water samples were found to be freshwater with a Ca – Mg – HCO3 facies with a relatively high secondary alkalinity. Groundwater flow patterns in general are N 130° – 150° E. Water isotope analysis shows the groundwater recharge area is at an elevation of > 300 m above sea level and the groundwater discharge area is at an altitude of < 300 m above sea level. The results of the analysis and interpretation of the geoelectrical section showed that the subsurface conditions at each location were dominated by limestone with different lithological characteristics. The results of the interpretation of the geoelectrical section can be distinguished from the condition of rocks containing groundwater (specific resistance value 12.7 – 134.6 Ωm) and empty/dry rocks (134.6 – 437.6 Ωm). In some cross sections also found the presence of voids with specific resistivity values >437.5 Ωm which are not visible on the ground surface.

Keywords: *geophysics, hydrogeology, karst, resistivty, Wonogiri*

Pendahuluan

Bagian selatan Kabupaten Wonogiri merupakan daerah perbukitan Karst yang menjadi bagian dari perbukitan karst Gunung Sewu. Kawasan karst ini membentang di tiga provinsi, yaitu dari Gunung Kidul – DI. Yogyakarta hingga ke Pacitan – Jawa Timur. Daerah Karst adalah salah satu bentang alam geologi yang tergolong unik dengan bentukan bukit-bukit batu gamping yang tandus. Tak jarang keberadaan morfologi karst ini mengakibatkan masyarakat di daerah ini mengalami kesulitan air bersih sebagai akibat dari proses pembentukan dan pola pelarutan batu gamping yang mengakibatkan kondisi permukaan daerah karst menjadi kering. Jika dilihat dari proses pembentukan karst, yang diawali dengan munculnya rongga sebagai akibat proses pelarutan maka sebenarnya daerah karst ini memiliki potensi air tanah yang cukup bila kondisi bawah permukaannya mampu terpetakan dengan baik, khususnya memetakan pola aliran serta rangkaian rongga di bawah tanah, baik rongga yang terisi air maupun rongga yang kosong. Untuk itu perlu adanya penyelidikan air tanah yang komprehensif untuk mengetahui kondisi bawah permukaan daerah karst, sehingga dapat diketahui penyebaran dan potensi air tanah di daerah ini. Dengan begitu masyarakat di sekitar daerah ini dapat memanfaatkan air tanah yang ada di daerah karst secara optimal sehingga pada akhirnya dapat memenuhi kebutuhan masyarakat dalam penyediaan air bersih.

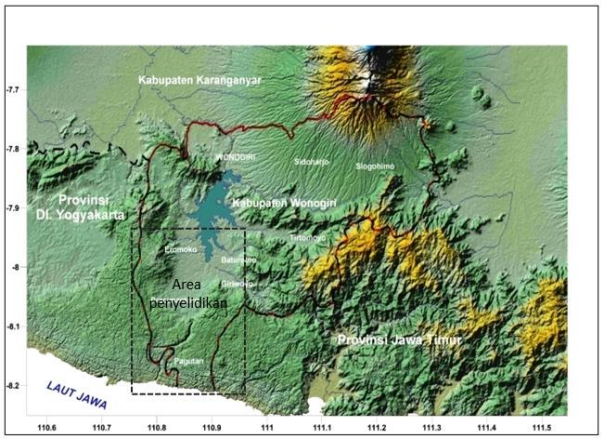

Gambar 1: Peta lokasi penyelidikan

Lokasi Penyelidikan

Lokasi penyelidikan secara administratif menempati wilayah di bagian selatan Kabupaten Wonogiri,

PROCEEDINGS
JOINT CONVENTION BANDUNG (JCB) 2021
November 23rd – 25th 2021

Provinsi Jawa Tengah (Gambar 1) yang merupakan bagian dari bentang alam karst Gunung Sewu. Lokasi ini terbentang mulai dari 110º45'35" sampai dengan 110º59'55" BT dan 7º55'38" sampai dengan 8º13'54" LS.

Morfologi Daerah

Berdasarkan bentuk bentang alam yang ada di wilayah Kabupaten Wonogiri maka secara morfologi daerah ini dapat dikelompokkan menjadi 4 satuan, yaitu: Satuan Morfologi Dataran, Satuan Morfologi Perbukitan Sedimen, Satuan Morfologi Pegunungan Vulkanik, dan Satuan Morfologi Karst. Variasi ketinggian (elevasi) daerah ini adalah antara 0 hingga 1.600 meter di atas muka laut (m.aml). Daerah penelitian sebagian besar berada pada daerah dengan Morfologi karst.

Kondisi Geologi

Wilayah Kabupaten Wonogori dibentuk oleh berbagai jenis batuan yang tersusun dalam beberapa formasi batuan (Gambar 4). Mengacu pada peta geologi skala 1:100.000, Lembar Surakarta – Giritontro (Surono, B. Toha, dan I. Sudarno, PPPG, 1992), Lembar Ponorogo (Sampurno dan H. Samodra, PPPG, 1997), dan Lembar Pacitan (H. Samodra, S. Gafoer dan S. Tjokrosapoetro, PPPG, 1992) daerah penyelidikan pada bagian utara terdapat Formasi Baruretno (Qb) yang tersusun atas lempung hitam, lumpur, lanau dan pasir. Satuan batuan ini berumur Plistosen.

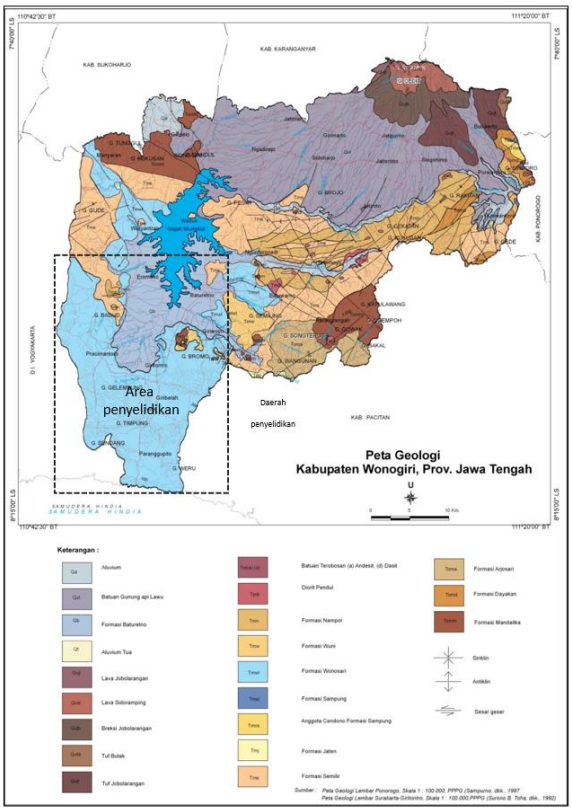

Gambar 2: Peta geologi daerah penyelidikan

Satuan ini dijumpai di sekitar Sungai Bengawan Solo dan daerah dataran sekitar Waduk Gajah Mungkur sedangkan di bagian selatan daerah penyelidikan terhampar Formasi Wonosari – Punung (Tmwl), tersusun atas batugamping, batugamping napalan hingga tufan, batugamping konglomeratan, batupasir, tuf dan batulanau. Satuan batuan ini berumur Miosen Tengah hingga Pliosen dan diendapkan pada lingkungan laut dangkal (*neritik*). Satuan batuan ini tersebar secara luas di daerah penyelidikan bagian selatan.

Hidrogeologi

Mengacu pada Peta Hidrogeologi Lembar Yogyakarta (Gambar 3) dengan Skala 1 : 250.000 (A. Djaeni, 1982), daerah ini terbagi berdasarkan kelompok keterdapatan air tanah dan produktivitasnya. Wilayah penyelidikan termasuk pada daerah akuifer dengan aliran melalui celahan, rekahan dan saluran.

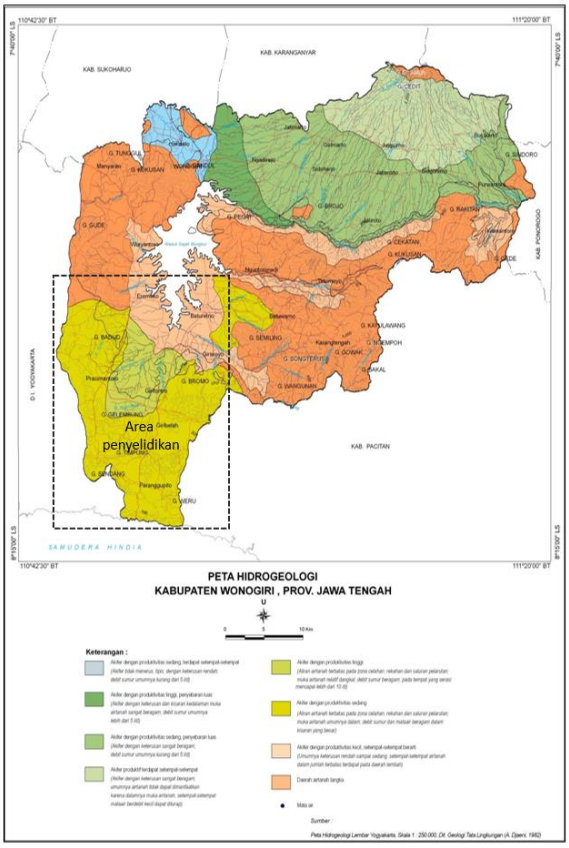

Gambar 3: Peta hidrogeologi daerah penyelidikan

Wilayah ini terdapat di bagian selatan atau di sekitar daerah batuan gamping yang terbagi lagi dalam kelompok:

• Akuifer dengan produktivitas tinggi: umumnya aliran air tanah terbatas pada zona celahan, rekahan dan saluran pelarutan dengan muka air tanah yang relatif dangkal dengan debit sumur yang beragam.

• Akuifer dengan produktivitas sedang: aliran air tanah umumnya terbatas pada zona celahan, rekahan

dan saluran pelarutan dengan muka air tanah yang dalam.

Metodologi Penyelidikan

Metode yang dilakukan dalam penyelidikan ini adalah melakukan pengamatan di lapangan dengan mengukur dan mengamati kondisi morfologi, geologi dan hidrogeologi. Pengamatan hidrogeologi meliputi pengamatan sifat fisika dan kimia air tanah. Pengamatan aspek kimia dilakukan dengan mengukur sifat kimia baik yang dilakukan di lapangan maupun di laboratorium untuk mendukung kajian sistem aliran air tanahnya. Pengujian percontoh air di lakukan di laboratorium kimia air Pusat Air Tanah dan Geologi Tata Lingkungan dan laboratorium isotop BATAN untuk mendapatkan data yang diperlukan dalam kegiatan pemantauan.

Metode geofisika yang digunakan adalah metode geolistrik (*resistivity*) dua dimensi (2-D) di lokasi-lokasi yang dianggap mewakili kondisi daerah penelitian. Metode ini dianggap cocok untuk menentukan sebaran litologi, struktur karst di daerah ini serta kondisi bawah permukaan yang ada di daerah Kabupaten Wonogiri. Pengambilan data dilakukan menggunakan alat resistivity 48 channel dengan spasi elektroda 20 meter dan konfigurasi Wenner-Schlumberger (Loke, 2000).

Prinsip metode geolistrik adalah mengalirkan arus listrik DC (*Dirrect Current*) ke dalam tanah. Injeksi arus listrik ini menggunakan 2 buah elektroda arus A dan B yang ditancapkan ke dalam tanah dengan jarak tertentu. Semakin panjang jarak elektroda AB akan menyebabkan aliran arus listrik bisa menembus lapisan batuan lebih dalam. Dengan adanya aliran arus listrik tersebut maka akan menimbulkan tegangan listrik di dalam tanah (Telford, dkk, 1996). Tegangan listrik yang terjadi di permukaan tanah diukur dengan menggunakan alat penerima (*receiver*) yang terhubung melalui dua buah elektroda tegangan M dan N yang jaraknya lebih pendek dari pada jarak elektroda AB. Bila posisi jarak elektroda AB diubah menjadi lebih besar maka tegangan listrik yang terjadi pada elektroda MN ikut berubah sesuai dengan informasi jenis batuan yang ikut terinjeksi pada kedalaman yang lebih besar. Nilai resistivitas dirumuskan oleh:

$$\rho_a = K\frac{\nabla V}{I}$$

Dimana : ρ_a = Resistivitas semu (Ohm-m), K = Faktor Geometri, V = Beda potesial listrik (Volt) dan I= arus yang diinjeksikan ke bawah permukaan (Ampere)

Hasil dan Analisis

Hasil pengamatan hidrogeologi dan geofisika baik yang berasal dari data langsung di lapangan maupun data sekunder (dari berbagai instansi terkait) diolah, dievaluasi dan dianalisis dengan pendekatan hidrogeologi untuk melakukan hipotesa genesa sistem aliran air tanah di wilayah penyelidikan. Hasil kajian ini diharapkan dapat memberikan kontribusi dalam mengetahui sistem aliran air tanah, konfigurasi akuifer dan keterdapatan air tanah.

Pengambilan sampel air di lapangan dilakukan pada lokasi yang berbeda-beda sebanyak 44 lokasi sampel yang tersebar di daerah penyelidikan. Distribusi pengambilan sampel air sebagian besar dilakukan pada sumur gali sebanyak 15 lokasi, sumur bor 11 lokasi, mata air 17 lokasi, dan telaga 1 lokasi. Adapun lokasi pengukuran dan pengambilan sampel air tanah terdapat pada Gambar 4.

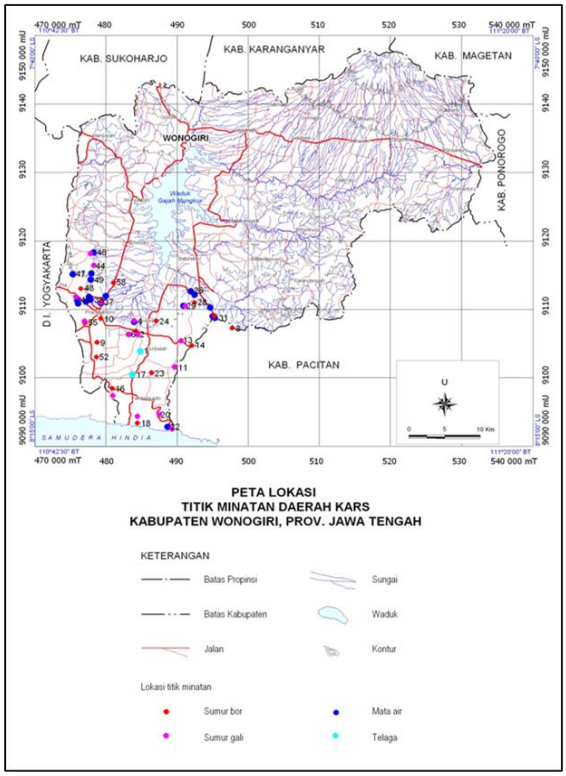

Gambar 4: sebaran pengukuran titik minatan hidrogeologi

Hidrogeologi

Sifat Fisika dan Kimia Air Tanah

Sifat fisika air tanah diukur secara langsung pada saat pengamatan di lapangan. Kemudian contoh air tanah pada lokasi tertentu diambil untuk dilakukan analisis di laboratorium.

• Temperatur Air Tanah

Berdasarkan hasil pengukuran langsung di lapangan menunjukkan bahwa suhu air tanah pada lapisan akuifer tidak tertekan (*unconfined aquifer*) berkisar antara 26.5 ºC hingga 30.7 ºC rata – rata 28,36 ºC. Hasil pengukuran pada sumur bor dengan kedalaman 75 hingga 170 m di bawah muka tanah (m.bmt) menunjukkan suhu sekitar 27.9 hingga 37.6 ºC dan rata–rata 30,7 ºC. Hasil pengukuran pada mata air menunjukkan suhu sekitar 26.7 hingga 33.5 ºC dan rata–rata 29,02 ºC. Hasil pengukuran pada air telaga

menunjukkan suhu sekitar 27.7 hingga 28.7 °C dan rata–rata 28,2 °C

• Daya hantar listrik

Berdasarkan hasil pengukuran di lapangan menunjukkan bahwa daya hantar listrik pada sumur gali berkisar antara 520 uS/cm hingga 716 uS/cm rata – rata 628 uS/cm. Hasil pengukuran pada sumur bor dengan kedalaman 75 hingga 170 mbmt menunjukkan nilai daya hantar listrik antara 357 uS/cm hingga 700 uS/cm dan rata–rata 543 uS/cm. Hasil pengukuran pada mata air menunjukkan nilai daya hantar listrik sekitar 272 uS/cm hingga 639 uS/cm dan rata–rata 539 uS/cm. Hasil pengukuran pada air telaga menunjukkan nilai daya hantar listrik berkisar antara 511 uS/cm hingga 557 uS/cm dan rata–rata 534 uS/cm.

• Derajat keasaman (pH)

Berdasarkan pengukuran langsung di lapangan nilai pH untuk air tanah pada sumur gali berkisar antara 6,82 hingga 7,94 dengan rata–rata 7,47 sedangkan untuk air tanah pada sumur bor menunjukkan nilai pH 7,05 hingga 8,0 dengan rata – rata 7,52. Nilai pH pada mata air berkisar antara 7,13 hingga 8,04 dengan rata – rata 7,65 sedangkan pada telaga nilai pH yang didapat adalah berkisar antara 6,72 hingga 7,87 dengan rata – rata sebesar 7,29.

• Kandungan ion terlarut

Hasil analisis hidrokimia ion utama untuk contoh air tanah yang diambil dari sumur gali, sumur bor dan mata air di daerah penyelidikan menunjukkan nilai yang relatif sama. Kation utama yang melimpah adalah ion kalsium (Ca2+). Nilai rata–rata untuk sumur gali 86,81 mg/l, sumur bor 87 mg/l,dan mata air 95,12 mg/l. Anion utama yang melimpah adalah ion klorida (Cl-) dengan rata–rata untuk sumur gali 41,4 mg/l, sumur bor 22,7 mg/l, mata air 21,7 mg/l dan ion bikarbonat (HCO3-), rata–rata untuk sumur gali 318,7 mg/l, sumur bor 320,9 mg/l, mata air 346,92 mg/l.

• Kesadahan

Hasil analisis nilai kesadahan di laboratorium menunjukkan bahwa pada air yang diambil dari sumur gali, sumur bor, mata air dan telaga mempunyai kisaran nilai antara 121,7 hingga 362,9 mg/l CaCO3 dengan nilai rata–rata 273,67 mg/l CaCO3. Berdasarkan klasifikasi menurut Todd (1980), kondisi air tanah di daerah penyelidikan, baik yang berupa air tanah dari sumur gali, air dari sumur bor, mata air, maupun air telaga pada umumnya sifatnya sadah - sangat sadah.

Analisis Kualitas Air Tanah

Analisis Diagram Piper

Berdasarkan hasil analisis diagram piper terlihat bahwa contoh air yang berasal dari sumur gali, sumur bor, mata air dan telaga mempunya fasies yang relatif sama yaitu fasies Ca – Mg – HCO3. Air tanah pada fasies ini mempunyai sifat tawar. Alkalinitas sekunder pada fasies ini relatif tinggi dengan ditandai dengan kandungan ion Ca2+ dan ion bikarbonat (HCO3) yang dominan. Pada proses ini terjadi reaksi dengan batugamping murni (Gambar 5).

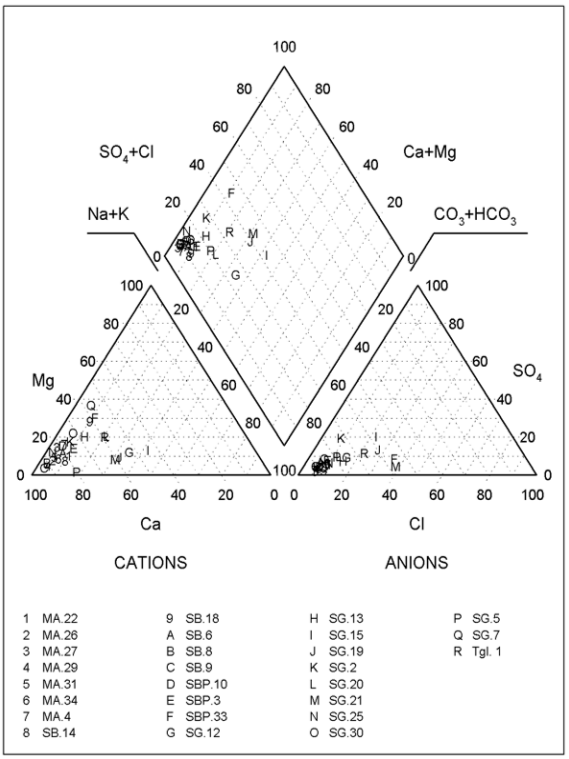

Gambar 5: Diagram Piper contoh air di daerah penyelidikan

Analisis Isotop Air tanah

Data isotop yang digunakan dalam penyelidikan di daerah ini adalah isotop deuterium (δ2H) dan isotop oksigen-18 (δ18O). Hasil laboratorium terhadap isotop ini menunjukkan bahwa air yang berasal dari sumur bor dan mata air secara umum masih berada dekat dengan garis meteorik lokal (Gambar 6).

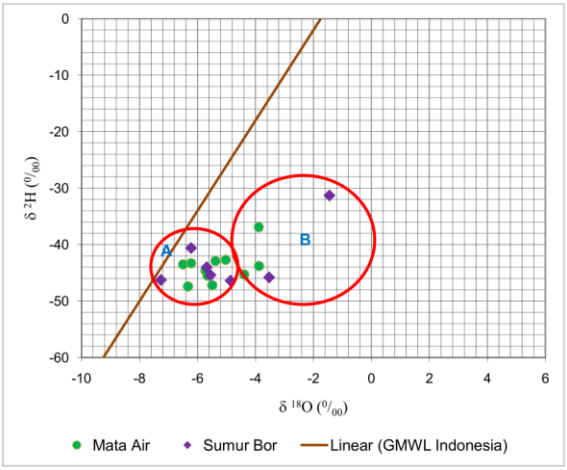

Gambar 6: Grafik hasil pengeplotan δ^2H dan $\delta^{18}O$ di daerah karst Wonogiri

PROCEEDINGS
JOINT CONVENTION BANDUNG (JCB) 2021
November 23rd – 25th 2021

Hal ini memperlihatkan bahwa air tersebut masih terkait dengan siklus hidrologi atau dipengaruhi oleh suatu proses pengimbuhan (Domenico dan Schwartz, 1990) dan dapat dikelompokkan menjadi 2 kelompok yaitu contoh air tanah yang diambil dari daerah imbuhan (A) dan daerah lepasan (B). Berdasarkan hasil pengeplotan antara elevasi dan nilai isotop O-18 dan hasil pengeplotan antara elevasi dan debit dapat digambarkan bahwa daerah imbuhan berada pada elevasi sekitar > 300 mdpl dan daerah lepasan berada pada ketinggian < 300 mdpl.

Distribusi Mata Air

Wonogiri bagian selatan yang mempunyai litologi berupa batugamping, terdapat sekitar 32 mata air karst dan 102 luweng atau gua berair. Keterdapatan mata air dapat dijumpai terutama pada daerah baratlaut Kabupaten Wonogiri yaitu di daerah Pracimantoro. Keterdapatan mataair tersebut sebagian besar dikontrol oleh kontak dengan batuan yang bersifat kedap air seperti napal maupun batulempung (*contact free draining spring*). Luweng atau gua berair merupakan bagian atau interface dari sistem sungai bawah tanah. Daerah dengan keterdapatan luweng atau gua berair tersebut merupakan daerah yang sangat potensial akan sumberdaya airnya. Keterdapatan luweng atau gua berair secara luas terdapat pada bagian selatan mulai dari Kecamatan Paranggupito hingga berbatasan langsung dengan Samudera Hindia, dan secara setempat berada pada bagian baratlaut dan timurlaut area penyelidikan.

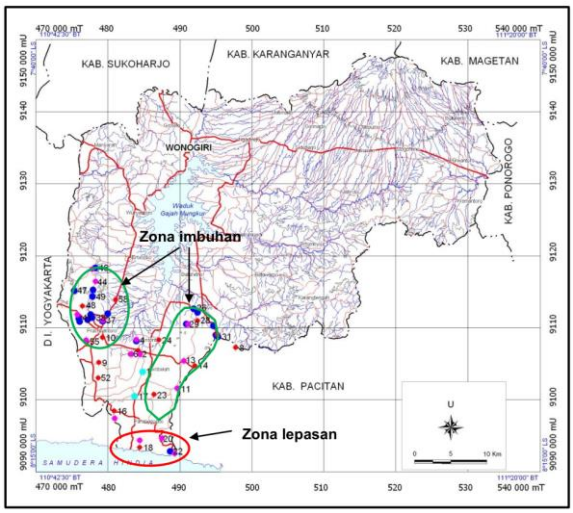

Gambar 7: Area zona imbuhan dan lepasan air tanah di daerah karst Wonogiri

Hidrogeofisika

Pengambilan data geolistrik 2 dimensi (2-D) pada daerah karst di Kabupaten Wonogiri berhasil mendapatkan total 20 penampang geolistrik dengan sebaran dapat dilihat pada Gambar 8. Masing-masing penampang mempunyai bentangan 940 m dengan spasi elektroda 20 m. Pada beberapa penampang geolistrik terdapat fenomena yang cukup menarik pada penyelidikan ini.

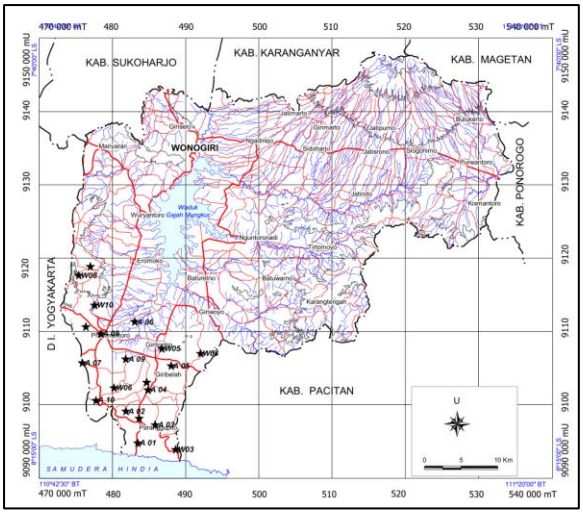

Gambar 8: Sebaran lokasi pengambilan data geolistrik 2D

- **Penampang tahanan jenis W02 (Desa Johonut, Kecamatan Paranggupito)**

Pada penampang tahanan jenis W02 terlihat sebaran batuan di bawah permukaan terdiri dua lapisan, yaitu: Lapisan pertama merupakan lapisan akuifer, berupa lapisan dengan tahanan jenis 19.5 - 134.65 Ohm-meter yang diinterpretasikan sebagai lapisan batugamping pasiran, batugamping berongga/ rekah. Lapisan tersebut memiliki ketebalan 25 - 66 meter (kedalaman 0 – 66 meter). Selain itu pada jarak X = 25 – 175 meter terdapat lapisan non akuifer dengan tahanan jenis < 19.5 Oh-meter yang diinterpretasikan sebagai lempung, napal. Lapisan tersebut memiliki ketebalan 33 meter.

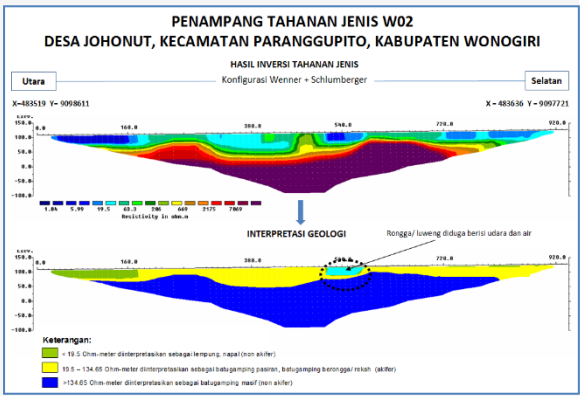

Gambar 9: Penampang tahanan jenis W02 di daerah Desa Johonut, Kecamatan Paranggupito

Selain itu pada lapisan ini terdapat juga lapisan dengan pola bentuk tahanan jenis menyerupai bentuk geometri ellips hingga agak segi empat. Lapisan tersebut memiliki tahanan jenis < 19 Ohm-meter yang diinterpretasikan rongga/ luweng berisi udara dan air. Rongga/ luweng tersebut terletak pada jarak X = 510 - 575 meter dengan ketebalan 58.34 meter (kedalaman 8.33 - 66.67 meter),Lapisan kedua merupakan lapisan

non akuifer, berupa lapisan dengan tahanan jenis 134.65 Ohm-meter yang diinterpretasikan sebagai lapisan batugamping masif. Lapisan tersebut muncul mulai dari kedalaman 25 meter).

- **Penampang tahanan jenis W04 (Desa Girikikis, Kecamatan Giritontro)**

Dari penampang tahanan jenis W04 terlihat sebaran batuan di bawah permukaan terdiri dua lapisan, yaitu: Lapisan pertama adalah lapisan non akuifer, berupa lapisan dengan tahanan jenis 134.65 - 437.65 Ohm-meter yang diinterpretasikan sebagai batugamping masif. Lapisan tersebut memiliki ketebalan 68 - 90 meter (Kedalaman 0 - 91 meter). Selain itu pada lapisan ini terdapat lapisan dengan pola bentuk tahanan jenis menyerupai bentuk geometri ellips hingga agak segi empat. Lapisan tersebut memiliki tahanan jenis 12.745 - 134.65 Ohm-meter yang diinterpretasikan sebagai rongga/ luweng yang berisi udara dan air yang ditunjukkan oleh warna biru muda. Rongga/ luweng tersebut terletak pada jarak X = 140 – 180 meter dengan ketebalan 22 meter (kedalaman 34 - 57 meter), Selain itu juga pada lapisan ini terdapat lapisan dengan pola bentuk tahanan jenis menyerupai bentuk geometri ellips hingga agak segi empat. Lapisan tersebut memiliki tahanan jenis > 437.65 Ohm-meter yang diinterpretasikan sebagai rongga/ luweng yang berisi udara yang ditunjukkan oleh warna biru muda. Rongga/ luweng tersebut terletak pada jarak X = 330 - 390 meter dengan ketebalan 45 meter (kedalaman 22 - 67 meter, Lapisan kedua adalah lapisan akuifer, berupa lapisan dengan tahanan jenis 12.745 - 134.65 Ohm-meter yang diinterpretasikan sebagai batugamping pasiran, batugamping berongga/ rekah. Lapisan tersebut memiliki ketebalan 17 - 140 meter (Kedalaman 0 - 140 meter).

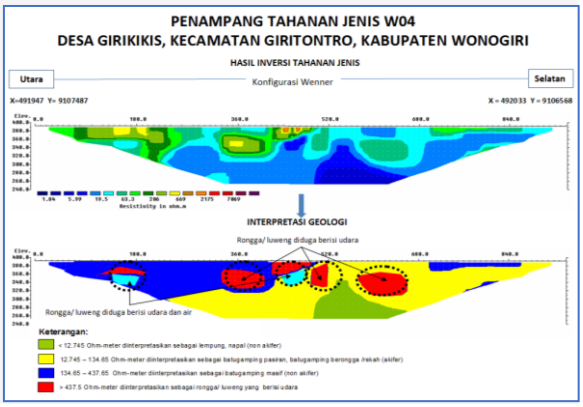

Gambar 10: Penampang tahanan jenis W04 di daerah Desa Girikikis, Kecamatan Giritontro

Selain itu pada lapisan ini terdapat lapisan dengan pola bentuk tahanan jenis menyerupai bentuk geometri ellips hingga agak segi empat. Lapisan tersebut memiliki tahanan jenis > 1422 Ohm-meter yang diinterpretasikan sebagai rongga/ luweng yang berisi udara yang ditunjukkan oleh warna merah. Rongga/ luweng tersebut terletak pada jarak X = 490 – 520 meter dengan ketebalan 45 meter (kedalaman 17 - 62 meter), X = 580 - 660 meter dengan ketebalan 57 meter (kedalaman 28 – 85 meter). Terdapat juga lapisan yang memiliki tahanan jenis 19.5 – 206 Ohm-meter yang diinterpretasikan sebagai rongga/ luweng yang berisi udara dan air yang ditunjukan oleh warna biru muda. Rongga/ luweng berisi udara dan air tersebut terletak pada jarak X = 440 – 480 meter dengan ketebalan 28 meter (kedalaman 28 – 57 meter. Selain itu juga terdapat bongkah dengan tahanan jenis < 12.745. Bongka tersebut ditafsirkan sebagai bongkah lempung, napal. Lapisan tersebut terdapat pada X = 490 – 650 meter dan mulai muncul pada kedalaman 45 meter.

- **Penampang tahanan jenis A03 (Desa Gendayakan, Kecamatan Paranggupito)**

Pada penampang tahanan jenis A03 terlihat penyebaran batuan di bawah permukaan terdiri satu lapisan, yaitu: Lapisan non akuifer, berupa lapisan dengan tahanan jenis 206 - 1422 Ohm-meter yang diinterpretasikan sebagai batugamping masif. Selain itu pada lapisan ini terdapat lapisan dengan pola bentuk tahanan jenis menyerupai bentuk geometri ellips hingga agak segi empat. Lapisan tersebut memiliki tahanan jenis > 1422 Ohm-meter yang diinterpretasikan sebagai rongga/ luweng yang berisi udara yang ditunjukkan oleh warna merah.

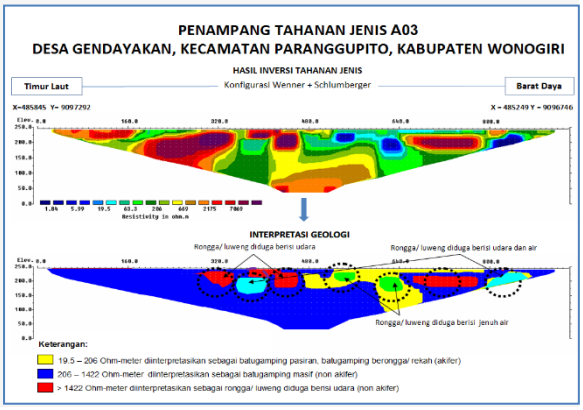

Gambar 11: Penampang tahanan jenis A03 di daerah Desa Gendayaan, Kecamatan Paranggupito

Rongga/ luweng tersebut terletak pada jarak X = 290 – 340 meter dengan ketebalan 58.34 meter (kedalaman 8.33 – 66.67 meter), X = 420 – 460 meter dengan ketebalan 50.01 meter (kedalaman 16.66 – 66.67 meter) dan X = 655 - 760 meter dengan ketebalan 33.35 meter (kedalaman 33.32 - 66.67 meter). Terdapat juga lapisan yang memiliki tahanan jenis 19.5 - 206 Ohm-meter yang diinterpretasikan sebagai rongga/ luweng yang berisi udara dan air yang ditunjukan oleh warna biru muda.

Rongga/ luweng berisi udara dan air tersebut terletak pada jarak X = 350 - 400 meter dengan ketebalan 58.31 meter (kedalaman 33.32 – 91.63 meter) dan X = 790 - 860 meter dengan ketebalan 41.65 meter (kedalaman 16.66 - 58.31 meter). Terdapat juga

lapisan yang memiliki tahanan jenis 19.5 – 206 Ohm-meter yang diinterpretasikan sebagai rongga/ luweng yang berisi jenuh air yang ditunjukan ole warna hijau. Rongga/ luweng berisi udara dan air tersebut terletak pada jarak X = 350 – 400 meter dengan ketebalan 24.99 meter (kedalaman 16.66 – 41.65 meter) dan X = 790 – 860 meter dengan ketebalan 49.98 meter (kedalaman 33.32 – 83.3 meter)

Kesimpulan

Hasil dari penyelidikan daerah karst di Kab. Wonogiri bagian selatan, berupa pengambilan data hidrogeologi dan geofisika memberikan beberapa hasil yang dapat disimpulkan sebagai berikut:

- Berdasarkan hasil pengukuran sifat fisika dan kimia air tanah yaitu nilai temperatur/suhu, sifat daya hantar listrik (EC), derajat keasaman (pH), zat padat terlarut dan kesadahan, baik dari contoh sumur gali, sumur bor, maupun mata air dan telaga diketahui bahwa tidak ada perbedaan yang mencolok terhadap sifat fisika dan kimia air tersebut dan air yang dianalisis tersebut adalah termasuk air tanah tawar.
- Jenis fasies air daerah karst di Kabupaten Wonogiri adalah fasies Ca – Mg – HCO3, dengan alkalinitas sekunder pada fasies ini relatif tinggi yang ditandai dengan kandungan ion Ca2+ dan ion bikarbonat (HCO3) yang dominan.
- Berdasarkan analisis isotop air tanah daerah karst di Kabupaten Wonogiri diketahui bahwa daerah imbuhan berada pada elevasi sekitar > 300 mdpl dan daerah lepasan berada pada ketinggian < 300 mdpl.
- Hasil analisis dan interpretasi penampang geolistrik didapatkan bahwa pada masing-masing lokasi memiliki karakteristik litologi yang berbeda-beda. Namun demikian, metode ini mampu menunjukan kondisi batuan yang mengandung air dan yang kering/kosong Pada beberapa penampang juga muncul fitur khas karst yang ada dibawah permukaaan berupa rongga/luweng yang tidak terlihat di permukaan tanah.

Daftar Pustaka

Djaeni A., 1982, Peta Hidrogeologi Indonesia Skala 1 : 250.000 Lembar Yogyakarta, Direktorat Geologi Tata Lingkungan, Bandung.

Domenico, P. A., dan Schwartz, F.W., 1990, Physical and Chemical Hydrogeology, John Wiley & Sons, New York.

Loke M. H. , 2000, Tutorial : 2-D and 3-D electrical imaging surveys. www.geoelectrical.com

Samodra H., S. Gafoer, dan S. Tjokrosapoetro, 1992, Peta Geologi skala 1:100.000 Lembar Pacitan, Pusat Penelitian dan Pengembangan Geologi, Bandung.

Sampurno,H. Samodra, 1997, Peta Geologi skala 1:100.000 Lembar Ponorogo, Pusat Penelitian dan Pengembangan Geologi, Bandung.

Schwartz, F. W., dan Zhang, H., 2003, Fundamentals of Groundwater, John Wiley & Sons, New York.

Surono, B. Toha, dan I. Sudarno, 1992, Peta Geologi skala 1:100.000 Lembar Surakarta – Giritontro, Pusat Penelitian dan Pengembangan Geologi, Bandung.

Telford, W.M., Geldart L.P dan Sheriff R.E., 1996, Applied Geophysics. Second edition, Cambridge.

Todd, D. K., 1980, Groundwater Hydrology, 2nd ed., John Wiley and Sons, New York.

Wartono R., Sukandarrumidi, Rosidi, 1995, Peta Geologi Skala 1:100.000 Lembar Yogyakarta, Jawa, Pusat Penelitian dan Pengembangan Geologi, Bandung.Castagna, J. P., 1993, The Leading Edge, **12**, 172–179.

PROCEEDINGS
JOINT CONVENTION BANDUNG (JCB) 2021
November 23rd – 25th 2021

KAJIAN KONDISI BAWAH PERMUKAAN DI AREA MUSEUM KARST INDONESIA MENGGUNAKAN METODE ELECTRICAL RESISTIVITY TOMOGRAPHY (ERT) DAN GROUND PENETRATING RADAR (GPR)

Wiyono, Acep Ruchimat
Pusat Air Tanah dan Geologi Tata Lingkungan, Badan Geologi
Jl. Diponegoro No.57 Bandung 40122.

Abstract

Flash flood events that occurred in most parts of southern Java on November 28, 2017 caused problems in structure of the Indonesian Karst Museum (MKI) building. In several locations there were cracks at buildings appeared, decreasing some part of the floors, and also cracks on the walls of the museum. These conditions are feared to have an effect on the stability structure of the museum building. To ensure the condition of the MKI structure building caused by flash flood and also to delineate the subsurface structure and possibility of cavities under and surrounding the museum building, the geophysical subsurface study was carried out in the area of the Indonesian Karst Museum. In this study, two geophysical methods were used. First method was used an Electrical Resistivity Tomography (ERT) method and second method used Ground Penetrating Radar (GPR). The ERT method at this area was used IRIS Syscal-Pro instrument with 36 electrodes and 3 m spacing every electrode. With this configuration, the total length of the cable stretch is 105 m. The electrode configuration (array type) used is the Dipole-dipole configuration. While the GPR instrument used is the IDS – instrument. Data acquisition for these methods were point mode measurement with 30 cm spacing between single measurements. The results of the analysis show that the structural condition of the main building of the Indonesian Karst Museum in general is still good, this can be seen from the subsurface conditions in the interior of the museum which is illustrated in the results of GPR data processing, there are no fracture anomalies or underground cavities. The condition of the building structure in front of the museum (hallway) seems to need to be repaired and must be fine a solution because it is indicated that there is seepage (leakage) in some parts which is likely to get bigger if left unchecked. Around the museum there found indications of the existence of cavities in limestone, this condition needs to be verified and further researched on its effect with the existence of the Indonesian Karst Museum building.

Keywords: *GPR, Indonesian Karst Museum, Resistivity, Wonogiri*

Pendahuluan

Karst merupakan bentuk bentang alam yang berkembang pada batugambing/karbonat dan juga pada batuan dolomit. Karst dibentuk dan dipengaruhi proses pelarutan batuan tersebut oleh air. Proses pembentukan karst disebut sebagai proses karstifikasi (Rahmadi, dkk, 2014). Karst Gunung Sewu merupakan kawasan karst terluas di Pulau Jawa (Prakarsa dan Ahmadin, 2017) dan sudah mendapat pengakuan sebagai warisan dunia (*World Heritage Site*) dan juga telah menjadi salah satu bagian dari jaringan geopark dunia (*Global Geopark Network*) dari UNESCO (Hasibuan dalam Hartawan, dkk, 2020).

Museum Karst Indonesia (MKI) merupan satu-satunya museum karst yang ada di Indonesia. Museum ini dibangun di area karst gunung sewu yang ada di Kabupaten Wonogiri, Jawa Tengah. Peristiwa bencana alam berupa banjir bandang yang terjadi pada beberapa wilayah di Jawa bagian selatan pada tanggal 28 November 2018 telah mengakibatkan adalah permasalahan pada bangunan Museum Karst Indonesia. Pada beberapa lokasi bangunan muncul adanya retakan, penurunan lantai di beberapa lokasi, serta adanya dinding bangunan museum yang mengalami pergeseran. Hal ini dikawatirkan akan berpengaruh kepada kestabilan struktur bangunan gedung MKI. Untuk memastikan kondisi struktur bangunan dan mendeliniasi kemungkinan adanya rongga di bawah tanah dan sekitar bangunan MKI, maka dilakukan kegiatan kajian kondisi bawah permukaan di area Museum Karst Indonesia.

Gambar 1: Lokasi penyelidikan di sekitar area Museum Karst Indonesia

Lokasi Penyelidikan

Lokasi kegiatan adalah di area sekitar bangunan Museum Karst Indonesia yang berada di Desa

PROCEEDINGS
JOINT CONVENTION BANDUNG (JCB) 2021
November 23rd – 25th 2021

Gebangharjo, Kecamatan Pracimantoro, Kabuparen Wonogiri, Provinsi Jawa Tengah. Pengambilan data dilakukan pada lokasi dimana terdapat adanya retakan di lantai bangunan maupun area di sekitar gedung museum yang mempunyai indikasi terdapat rongga ataupun luweng di bawah tanah (Gambar 1).

Kondisi Morfologi dan Geologi

Museum Karst Indonesia secara umum berada pada satuan morfologi perbukitan karst. Bukit-bukit berupa kerucut karst beserta lembahnya sebagian besar meliputi daerah di sekitar museum karst. Morfologi ini pada umumnya menunjukkan daerah yang mengalami proses pelarutan yang aktif sehingga kehadiran goa-goa, ponor *(luweng)*, dan lubang pelarutan sering dijumpai. Posisi bangunan MKI ini sangat tidak menguntungkan karena berada pada bagian lembah yang apabila ditelusuri merupakan ujung dari daerah aliran sungai tipe dendritik.

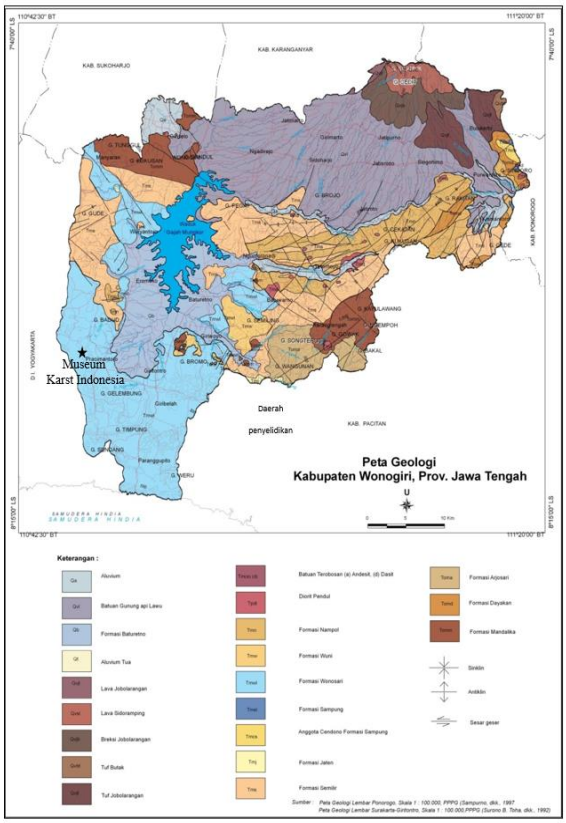

Gambar 2: Peta geologi daerah penyelidikan, lokasi MKI berada dibagian bawah kiri peta (simbol bintang).

Geologi permukaan daerah Kabupaten Wonogiri bagian selatan, didominasi oleh batuan gamping berbentuk karst. Disebelah utara lokasi pengukuran, terdapat formasi Baturetno yang terdiri dari lumpur hitam, lempung, lanau, pasir (Qb). Formasi ini menurut Surono, dkk (1992) berada di atas formasi Wuni yang terdiri dari Aglomerate bersisipan batupasir tufan dan batupasir kasar. Lokasi MKI sendiri berada pada formasi Wonosari yang terdiri dari batugamping, batugamping napalan-tufan, batugamping konglomerat, batupasir tufan dan batulanau (Gambar 2).

Metodologi Penyelidikan

Pengambilan data geofisika yang digunakan dalam kegiatan ini berupa data geofisika bawah permukaan menggunakan 2 buah metode geofisika yaitu metode Electrical Resistivity Thomography (ERT) atau sering disebut dengan metode tahanan jenis 2-D serta metode Ground Penetrating Radar (GPR) atau sering juga disebut dengan georadar.

Kedua metode diharapkan mampu melihat kemungkinan adanya struktur anomali di bawah permukaan khususnya di area sekitar gedung MKI yang mengalami beberapa retakan dan penurunan lantai bangunan. Instrumen resistivity yang digunakan adalah IRIS Syscal-Pro. Elektroda yang digunakan berjumlah 36 buah dengan spasi antar elektroda adalah 3 m sehingga total panjang bentangan kabel adalah 105 m. Konfigurasi elektroda (*array type*) yang digunakan dan adalah konfigurasi Dipole-dipole. Sedangkan instrument GPR yang digunakan adalah IDS-instrument menggunakan metode pengukuran *point mode* dengan spasi antar pengukuran 30 cm.

Metode ERT

Prinsip metode geolistrik adalah mengalirkan arus listrik DC (*Dirrect Current*) ke dalam tanah. Injeksi arus listrik ini menggunakan 2 buah elektroda arus A dan B yang ditancapkan ke dalam tanah dengan jarak tertentu. Semakin panjang jarak elektroda AB akan menyebabkan aliran arus listrik bisa menembus lapisan batuan lebih dalam. Dengan adanya aliran arus listrik tersebut maka akan menimbulkan tegangan listrik di dalam tanah (Telford, dkk, 1996). Tegangan listrik yang terjadi di permukaan tanah diukur dengan menggunakan alat penerima (*receiver*) yang terhubung melalui dua buah elektroda tegangan M dan N yang jaraknya lebih pendek dari pada jarak elektroda AB. Bila posisi jarak elektroda AB diubah menjadi lebih besar maka tegangan listrik yang terjadi pada elektroda MN ikut berubah sesuai dengan informasi jenis batuan yang ikut terinjeksi pada kedalaman yang lebih besar. Nilai resistivitas dirumuskan oleh:

$$\rho_a = K\frac{\nabla V}{I}$$

Dimana : ρ_a = resistivitas semu (Ohm-m), K = Faktor Geometri, V = Beda potesial listrik (Volt) dan I= arus yang diinjeksikan ke bawah permukaan (Ampere)

Metode GPR

Suatu sistem georadar terdiri dari sebuah pembangkit sinyal, antenna transmisi dan sebuah penerima yang berfungsi untuk merekam keluaran yang dihasilkan. Sistem radar menyebabkan antenna tranmisi menghasilkan serangkaian gelombang radio yang akan ditransmisikan melewati medium dan apabila

terjadi perbedaan permitivitas ataupun konduktivitas maka sinyal tersebut akan direfleksikan kembali dan diterima oleh antenna penerima *(receiver)* dalam orde nano detik (ns) (Gambar 3). Sistem peralatan georadar secara konsep sangat sederhana. Inti dari sistem tersebut adalah timing unit yang mengontrol pembangkitan sinyal radar dan kemudian mendeteksi sinyal yang diterima sebagai fungsi waktu.

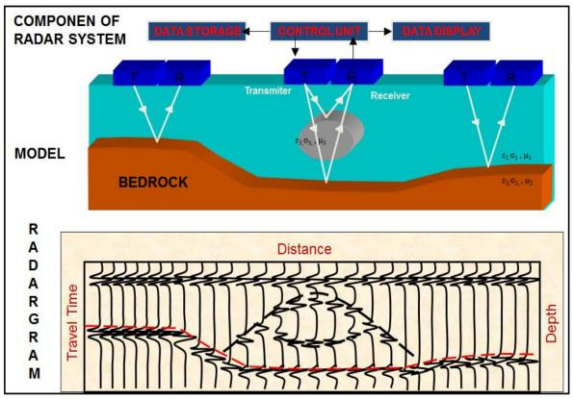

Gambar 3: Skema proses pengambilan data GPR, gelombang elektromagnetik dipancarkan oleh transmiter ke bawah permukaan bumi, kemudian sinyal tersebut akan direfleksikan, terefraksikan maupun diteruskan oleh lapisan di bawahnya, kemudian sinyal yang keatas akan diterima oleh receiver.

Sinyal yang direfleksikan diperkuat, ditrans-formasikan ke dalam jangkauan frekuensi audio, direkam, diproses dan ditampilkan. Pendeteksian GPR selanjutnya adalah merupakan masalah penginderaan dan pengukuran respon target menggunakan suatu sinyal masukan (*input signal*) yang telah diketahui dan melakukan analisis sinyal keluaran (*output signal*) yang diobservasi. Dari tampilan rekaman, gambaran bawah permukaan dapat diidentifikasi.

Pengambilan Data

Pengambilan data Electrical Resistivity Tomography (ERT) dilaksanakan di sekitar bangunan MKI menggunakan instrument IRIS Syscal pro dengan menggunakan total 36 channel elektroda. Pengukuran ERT di area MKI dilakukan sebanyak 3 line (MKI-1, MKI-2, MKI-3) yang keseluruhannya berada di sekitar gedung utama museum. Line MKI-1 berada di samping kiri bangunan museum dan berarah Utara – Selatan, Line MKI-2 berada di depan bangunan museum berarah Barat – Timur, dan MKI-3, berada di samping kiri museum dengan arah bentangan Barat – Timur (Gambar 4).

Pengambilan data Ground Penetrating Radar (GPR) dilaksanakan di beberapa lokasi gedung utama museum yaitu di bagian dalam lantai 1 (dekat maket gua) dan di area halaman bagian depan museum (selasar gedung). Total jumlah penampang GPR adalah 7 line, dengan penampang bagian depan (utara) berjumlah 3 penampang dan di bagian dalam gedung (selatan) adalah 4 penampang (line).

Gambar 4: Pengambilan data ERT dan GPR di area MKI. Pengukuran ERT dilakukan sebanyak 3 penampang, sedangkan data GPR diambil 7 buah penampang.

Hasil dan Analisis

Pengolahan data ERT menghasilkan sebaran nilai resistivity batuan di bawah permukaan yang dapat diinterpretasi menjadi sebaran endapan batuan bawah permukaan, baik sebaran secara vertikal maupun lateral. Berikut adalah hasil pengolahan dan interpretasi data ERT yang telah dilakukan di area sekitar museum karst.

- **Penampang ERT line MKI-1**

Hasil pengolahan data ERT line MKI-1 menunjukkan adanya perubahan nilai resistivity yang kontras di bawah permukaan yang diinterpretasi sebagai bentuk perubahan perlapisan batuan (Gambar 5). Pada bagian atas penampang terlihat nilai resistivity rendah, yang diduga merupakan endapan terarosa, sedangkan nilai resistivity tinggi merupakan bongkah batuan gamping.

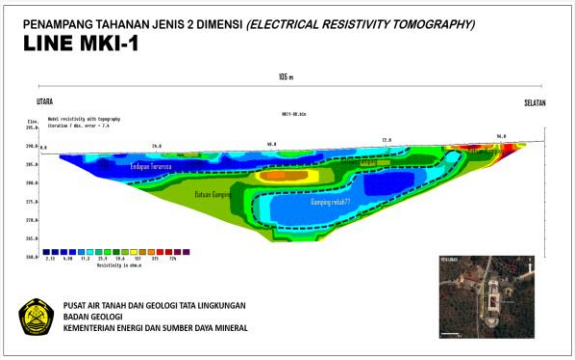

Gambar 5: Hasil pengolahan data ERT penampang MKI-1

Dari penampang MKI-1 terlihat pola perlapisan mengikuti topografi yaitu dipping kearah utara. Posisi endapan terarosa berdasarkan penampang ini adalah mencapai 9 m dari permukaan tanah. Pada bagian bawah terlihat nilai resistivitas menunjukkan peningkatan yang diinterpretasi sebagai batuan gamping, dengan pola lapisan yang miring kearah utara. Pada bagian kiri penampang terlihat batuan gamping mengalami penebalan. Pada kedalaman 10 hingga 25 m dari permukaan tanah, pada bagian tengah penampang terlihat adanya anomali berupa nilai resistivity yang rendah. Kondisi ini diinterpretasi

sebagai lapisan batuan gamping rekah yang kemungkinan terisi oleh fluida sehingga menghasilkan nilai resistivitas yang kecil. Ketebalan lapisan ini sekitar 10 m dan berada pada kedalaman 12 m di titik tengah penampang.

➢ **Penampang ERT line MKI-2**

Hasil pengolahan data menunjukkan kondisi bawah permukaan penampang ERT line MKI-2 (Gambar 6). Posisi penampang ini berada di depan museum karst (sebelah utara) gedung utama museum. Dari hasil pengolahan data didapatkan nilai resistivitas tinggi pada hampir seluruh bagian penampang. Hal ini diinterpretasi sebagai lapisan batuan gamping yang tersebar cukup signifikan. Pada bagian kiri penampang (arah barat) dijumpai nilai resistivitas rendah yang diinterpretasi sebagai endapan terarosa. Pada sebelah kanan penampang bagian bawah, dijumpai anomali berupa nilai resistivity rendah yang diinterpretasi sebagai batuan gamping rekah atau gamping berongga. Dari penampang, terlihat indikasi rongga ini berada pada kedalaman 5 – 10 m dari permukaan tanah dan kemungkinan rekahan atau rongga ini berisi fluida sehingga menghasilkan nilai resistivity yang relatif rendah.

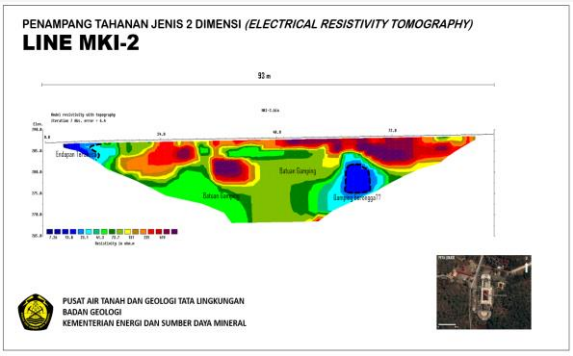

Gambar 6: Hasil pengolahan data ERT penampang MKI-2

➢ **Penampang ERT line MKI-3**

Hasil pengolahan data ERT line MKI-3 (Gambar 7) menunjukkan kondisi bawah permukaan berupa nilai resistivitas batuan yang relatif besar pada bagian tengah dan kanan penampang. Kondisi ini diinterpretasi sebagai batuan gamping yang relative kompak, terutama pada bagian atas penampang. Pada ujung kiri dan kanan penampang terlihat nilai resistivitas yang rendah, kondisi ini diduga merupakan lapisan endapan terarosa yang juga terlihat pada penampang MKI-2. Pada bagian kiri bawah hingga tengah penampang, terdapat pola memanjang dengan nilai resistivitas yang relative kecil dan diapit nilai resistivitas besar. Anomali ini terlihat seperti pola chanel atau aliran dari kiri ke kanan. Dari indikasi tersebut lapisan ini diinterpretasi sebagai lapisan gamping rekah, yang membentuk pola aliran. Kemungkinan lapisan ini yang mengadung fluida sehingga nilai resistivitas terlihat turun. Pada bagian tengah bawah penampang, nilai resistivitas terlihat rendah yang mengindikasikan adanya batuan gamping yang berongga.

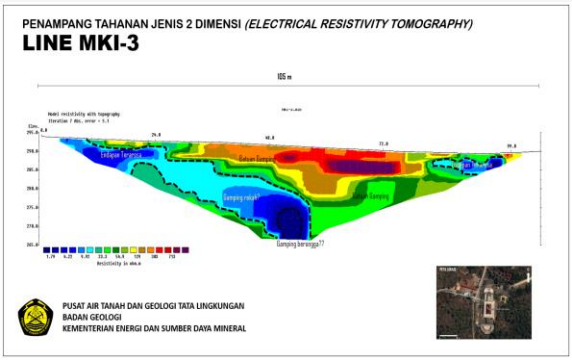

Gambar 7: Hasil pengolahan data ERT penampang MKI-3

Hasil pengolahan data Ground Penetrating Radar (GPR)

Pengolahan data GPR di area MKI menghasilkan gambaran amplitudo dan kecepatan gelombang elektromagnetik di bawah permukaan tanah. Hasil metode ini kemudian dapat diinterpretasikan menjadi struktur bawah permukaan baik secara vertikal maupun lateral. Beberapa penampang GPR yang menarik dapat dijelaskan sebagai berikut.

➢ **Penampang GPR : Line GR-1**

Hasil pengolahan data GPR pada line GR-1 menunjukkan bahwa kondisi bawah permukaan pada penampang ini relatif tidak terganggu. Tidak terdapat anomali struktur yang mengindikasikan adanya rekahan. Pada bagian atas, dari bentuk amplitude gelombangnya, dapat diinterpretasi berupa endapan terarosa yang kurang padat bersama dengan tanah urugan. Lapisan dibawahnya juga berupa endapan terarosa, namun relative lebih padat, ini terlihat dari kecepatan gelombang elektromagnetik yang sedikit naik. Lapisan ini berada hingga kedalaman 18 m. Pada lapisan terakhir dijumpai terarosa yang sudah cukup padat, atau bisa juga berupa endapan batuan gamping (Gambar 8).

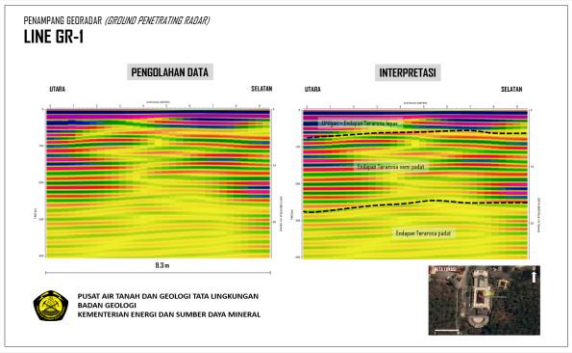

Gambar 8: Hasil pengolahan data GPR penampang GR-1

➢ **Penampang GPR : Line GR-5**

Pengolahan data GPR line GR-5 yang berada di sisi kiri bangunan museum menunjukkan kondisi bawah permukaan berupa endapan terarosa lepas dan urugan

pada kedalaman hingga 5 m (Gambar 9). Hal ini diindikasikan dari pola amplitudo gelombang serta kecepatan gelombang yang rendah.

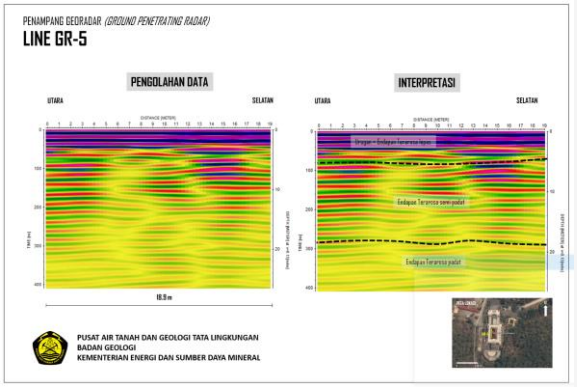

Gambar 9: Hasil pengolahan data GPR penampang GR-5

Di bawah lapisan terarosa lepas dan urugan, terlihat kecepatan gelombang elektromagnetik sedikit naik, dengan pola amplitude yang berubah. Kondisi ini diinterpretasi sebagai endapan terarosa juga, namun kemungkinan sudah semi padat. Terlihat pola lapisan ini berada hingga kedalaman 19 m. Kondisi di bawahnya terlihat kecepatan gelombang semakin naik dengan amplitudo yang semakin kecil, diinterpretasi sebagai endapan terarosa padat atau kemungkinan batuan gamping hingga kedalaman 26 m dari permukaan tanah. Pada penampang ini tidak ditemukan adanya anomali struktur yang tidak menerus dan pola difraksi yang dapat diindikasikan sebagai pola rekahan atau rongga.

- **Penampang GPR : GRS-1**

Hasil pengolahan data menunjukkan nilai kecepatan gelombang elektromagnetik terlihat membesar dari atas ke bawah (Gambar 10). Pada bagian atas, dari permukaan hingga kedalaman 10 m terdapat struktur menerus yang diduga merupakan urugan dan endapan alluvium berupa terarosa. Pada bagian atas, kiri dan kanan penampang terlihat adanya anomali berupa struktur vertikal yang diduga merupakan bentuk rekahan akibat adanya aliran air yang masuk dari atas ke bagian bawah (lingkaran merah).

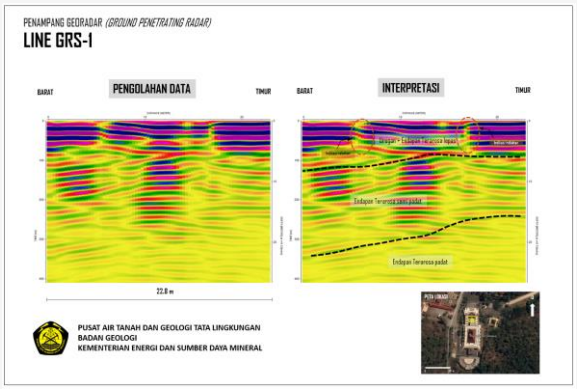

Gambar 10: Hasil pengolahan data GPR penampang GRS-1

Dari penampang GRS-1 juga terlihat adanya kemiringan lapisan / dipping, yang terlihat kearah barat (kiri penampang). Demikian juga dengan kondisi lapisan di bawahnya yang berupa endapan terarosa semi padat, terlihat mengalami kemiringan kearah yang sama. Endapan ini terlihat berada hingga kedalaman 24 m dari permukaan tanah. Pada lapisan terakhir, diduga masih berupa endapan terarosa namun sudah padat ataupun batuan gamping.

- **Penampang GPR : GRS-3**

Hasil pengolahan data GPR Line GRS-3 menunjukkan kondisi bawah permukaan hingga kedalaman 26 m. Pada bagian atas penampang terlihat struktur mendatar yang diinterpretasi sebagai urugan dan endapan terarosa yang belum padu (lepas).

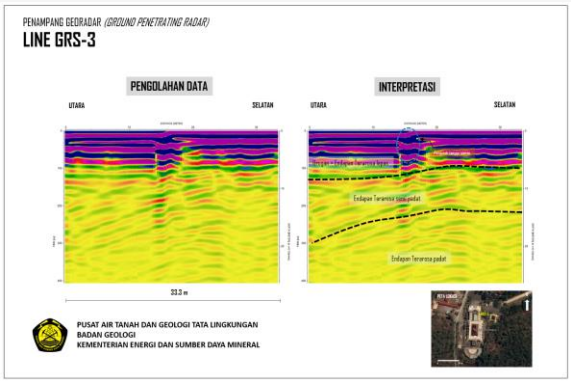

Gambar 11: Hasil pengolahan data GPR penampang GRS-3

Pada bagian tengah lapisan terdapat anomali, berupa displacement yang setelah dilakukan pengecekan, ternyata merupakan anomali yang berasal dari tangga lantai yang berundak, bukan struktur bawah permukaan. Pada bagian di bawahnya diduga terdapat endapan terarosa semi padat, hingga kedalaman 20 m dari permukaan tanah. Lapisan terakhir di duga berupa endapan terarosa padat ataupun batuan gamping. Pola perlapisan pada line ini terlihat sedikit mengalami *dipping* kearah utara (depan bangunan).

Kesimpulan

Hasil dari penyelidikan daerah karst di Kab. Wonogiri berupa pengambilan data hidrogeologi dan geofisika memberikan beberapa hasil yang dapat disimpulkan sebagai berikut:

- Kondisi struktur bangunan utama museum karst secara umum masih baik, hal ini terlihat dari kondisi bawah permukaan di bagian dalam museum yang tergambar pada hasil pengolahan data GPR tidak dijumpai adanya anomali rekahan atau rongga di bawah tanah.
- Kondisi bangunan bagian depan museum (selasar) terlihat perlu diperbaiki dan dicari solusi karena diindikasikan terdapat rembesan (*leakage*) pada

beberapa bagian yang kemungkinan akan semakin membesar jika dibiarkan.

- Kondisi disekitar museum dijumpai terdapat indikasi keberadaan rongga pada batuan gamping yaitu terlihat pada line MKI-2 dan line MKI-3. Kondisi ini perlu diverikasi kebenarannya dan diteliti lebih lanjut pengaruhnya terhadap kestabilan bangunan Museum Karst Indonesia.

Daftar Pustaka

Hartawan, B.S., Erwandha, R, Irsyadi, M.B, Hidayat, M.R.A., and Sholih, D., 2020, Characteristics of Sewu Mountain Karst as Geopark Area, Journal of Global Environmental Science, 1 (1), 7-12.

Loke M.H. , 2001, Tutorial : 2-D and 3-D electrical imaging surveys. www.geoelectrical.com.

Prakarsa, T .B .P. and K. Ahmadin.,2017, Diversitas Arthropoda Gua di kawasan Karst Gunung Sewu, Studi Gua-Gua di Kabupaten Wonogiri, The Journal of Tropical Biology, 1(2), pp.31-36.

Rahmadi, C, Sigit Wiantoro, Hari Nugroho, 2018, Sejarah Alam Gunung Sewu, Lembaga Ilmu Pengetahuan Indonesia, Jakarta

Samodra H., S. Gafoer, dan S. Tjokrosapoetro, 1992, Peta Geologi skala 1:100.000 Lembar Pacitan, Pusat Penelitian dan Pengembangan Geologi, Bandung.

Surono, J.B. , Toha, B. dan Sudarno, I., 1992, Peta geologi lembar Surakarta dan Giritontro, Pusat Penelitian dan Pengembangan Geologi, Bandung.

Wartono, R., Sukandarrumidi, Rosidi, H.M.D, 1995, Peta geologi lembar Yogyakarta, Pusat Penelitian dan Pengembangan Geologi, Bandung.

PROCEEDINGS
JOINT CONVENTION BANDUNG (JCB)|2021
November 23rd – 25th 2021

Virtual Vlog Field Trip": The New Methodology and Delivery of the Field-Based Course for the Undergraduate Geoscience Students using VGEMS

Widodo Nugroho[1], Rizki Nanda[1], Berli Sahala Simorangkir[1], Faris Fardan Nugroho[1], Faisal Adhitama[1], Saptono Budi Samodra, S.T., M.Sc[2], Salahuddin Husein, Ph.D[2]

(1) PT. Geodwipa Teknika Nusantara (GTN),
(2) Geological Engineering Department, Faculty of Engineering, Universitas Gadjah Mada (UGM)

Abstract

COVID-19 pandemic forces undergraduate geoscience education to transform their field-based courses to remote learning with virtual outcrops from outdated and incomplete documentation as an alternative. The Geological Engineering Department, Universitas Gadjah Mada (UGM), requested GTN deliver Regional Geology Excursion (RGE), one of their field-based courses, online. GTN proposed a new concept of field-based course through the Virtual Vlog Field Trip Methodology with VGEMS (Virtual E-learning Geodwipa Management System), a web-based Learning Management System developed by and proprietary of GTN.

This new field-based course methodology and delivery is a complete blended learning package that comprises three major stages. Firstly, Data Collection by visiting and capturing every component of the outcrops and taping a comprehensive geological explanation video of that area in front of the camera. Secondly, Data Processing by editing and improving all the recorded videos and images to become integrated, intuitive, and engaging online RGE delivery. Thirdly, Delivery by VGEMS as the platform to do all online learning activities and access the processed videos, course modules, tests, evaluation sheets, and other related documents with tiered access, including the roles and security to ensure the students could get optimum benefits. Virtual Vlog Field Trip methodology using VGEMS encourages the students to self-learn and exercise as if they were experiencing in the real offline RGE. At the same time, the committee enables the evaluation of the students as well. The final goal of this new methodology is to deliver field-based courses for undergraduate geoscience students effectively and safely during the COVID-19 pandemic. The students always keep up to date and do not lose their basic field mapping skills and regional geology knowledge. Geological Engineering Department of UGM has collaborated with GTN to deliver an online RGE course to undergraduate geoscience students. In 2021, RGE in UGM were delivered using the above methodology and technology.

Keywords: geological field trip, learning management system, virtual field trip, virtual vlog field trip, VGEMS

Introduction

One of the main reasons for organizing a geological field-based course or field trip is to sharpen geological mapping skills utilizing all geological senses. It provides real experiences and opportunities to interact with the outcrops physically. The field-based course helps to understand alive to what the students have learned in the classroom or textbook.

Recently, the COVID-19 pandemic forced undergraduate geoscience education to postpone or cancel their scheduled field-based courses. In specific locations, many of them are no more able to visit the outcrops physically due to strict regulations of covid-19 safety protocol. The increasing number of daily cases covid-19 and the high potential risk of being affected have made many of them switch the delivery method of field-based courses.

The challenges that grow along with organizing field-based courses have become a serious concern. Field-based courses should not be ignored or removed from the geosciences curriculum. Many educational institutions believe that the best substitution to experience authentic field trips is a virtual field trip. Virtual field trips in essence try to capture the real world environment of a specific location or region through a collection of data, photographs, cartography and other technologies such as GIS, without the cost of physically being there (Carmichael & Tscholl, 2011). It is a technology-based experience that allows participants to take field journeys without leaving the classroom.

The aim of virtual field trip has not been to replace field trips but rather to introduce students to various aspects and develop some of the basic skills needed and to prepare students for going into the field or as follow up exercises after a real field trip (Gilmour, 1997). But generally, virtual field trips use outdated and incomplete documentation of outcrops as an alternative. In many cases, virtual field trips only use presentation slides with simple photos or videos taken from a few months or a few years ago. There is no further live interaction that the participants can do to the outcrops.

Sriarunrasme, et.al (2015) stated that the integration of teaching and learning are then better adjusted to the difference inability of students, by utilizing information communication technology as a tool to convey the knowledge, and as a mean of communication between teachers and students. Students can learn without time and place limitation; it opens up the opportunity to learn leading to educational equality. With enriched modern technology platforms, students can exchange knowledge communicate across the board rapidly. Students have opportunity in thinking, deciding in learning context, priority knowledge, controlling the learning channels, and presenting their projects. Cassady and Mullen (2006) stated that the virtual field trip is a good alternative for the educational program, which can pass over the difficulties. The teachers and students can experience the virtual field trip any time any way, enriched by modern information and communication technologies. It reduces down many limitations in organizing a real trip, on the contrary, increases the equal opportunity to those students who do not have a chance. Cassady and Mullen (2006) also suggested that the virtual field trip cannot replace real field trip or a real site visit. But the virtual field trip can result in higher learning level, skills and experience than the real field trip. The integrated technology in virtual filed trip is another complement element to fulfill the in-class teaching and to reduce the limitation of activity outside classroom. The teachers will help in stimulating the capability of learners in seeking information by themselves. This is an alternative in leisure-education development and well-suited with the learners'ability and quality; which well supports the educational policy and contributes to leverage the national education quality in the future (Sriarunrasme, et.al. 2015)

This paper presents a new methodology to this challenge called Virtual "Vlog" Field Trip (VVFT). The "Vlog" is the recorded explanation videos about the outcrops and then delivered on Virtual Geodwipa E-learning Management System (VGEMS), a web-based Learning Management System. VGEMS enables students to watch repeatedly at their pace. Together, these features make active learning in virtual field trips possible and practical from anywhere. The following describes a complete workflow from data collecting, data processing, and delivery on VGEMS.

Data and Method

Virtual "vlog" geological field trip

Virtual "vlog" geological field trip is a new field trip method with camera tapping in front of the outcrops. The instructor's explanation was recorded and taken using a video camera.

VGEMS (Virtual Geodwipa E-learning Management System)

VGEMS is an all-in-one Learning Management System (LMS) for organizational & corporate learning, training, meeting, onboarding, assessment, and remote working.

Online Regional Geology Excursion (RGE)

Online Regional Geology Excursion (RGE) is a virtual geological field trip for 3rd-year students in Universitas Gadjah Mada (UGM). In 2021, RGE took field trip zone in South Serayu Mountain & North Serayu Mountain with 6 stopsites (Table 1). Online RGE consists of 6-9 persons as field trip instructors and 5-6 crews.

1. Data Collecting

The team conducted fact-finding and field observation before camera tapping. The crews recorded the outcrops using DSLR cameras and a drone by visiting and capturing every component of the outcrops and taping a comprehensive geological explanation video of that area in front of the camera (Figur 1, 2, 3, &4).

2. Data Processing

The data processor edits and improving all the recorded videos and images to become integrated, intuitive, and engaging online RGE delivery, using the Video Editor and Graphics Editor Softwares (Figure 5).

3. Delivery by VGEMS

The platform to do all online learning activities and access the processed videos, course modules, tests, evaluation sheets, and other related documents with tiered access, including the roles and security, ensures the students could get optimum benefits (Figure 6 & 7).

Result and Discussion

Based on the results of using the Virtual "vlog" Field Trip method for Regional Geological Excursion activities, field trip participants could get natural field vibration and knowledge "like" in the field wherever they accessed the video. During a normal Field Trip, taking pictures through various angles (such as close up, wide-angle, drone view, detailed view, etc.) can provide comprehensive outcrop observations and show geomorphological conditions and geological structures. Megascopic observation of rock samples will also help participants to understand the texture and structure of rocks.

In addition, the existence of the VGEMS platform greatly assists the delivery process of the videos because of the automatic attendance feature, participant progress records, learning modules, and exams.

Conclusions

The Virtual Vlog Geological Field Trip method using VGEMS is a comprehensive alternative way for

improving field trip participants' understanding and feeling working experience in the field during the Covid-19 Pandemic. Further development of this method and platform is needed, especially for 3D Field Outcrop experience, gamification, Sample photos, and assessment of effectiveness of virtual field trip.

Acknowledgements

We would like to say our gratitude for Geological Engineering Department Universitas Gadjah Mada as our partner for delivering this method to the curriculum.

References

Carmichael, P., & Tscholl, M. (2011). *Cases, simulacra and semantic web technologies*. Journal of Computer Assisted Learning

Gilmour, I. (1997). Skiddaw virtual field trip. A study of thermal metamorphism. Retrieved from http://earth2.open.ac.uk/Skiddaw/Text/Skiddaw.html

Jerrell C. Cassady & Laurie J. Mullen (2006) *Reconceptualizing electronic field trips: a Deweyian perspective*, Learning, Media and Technology, 31:2, 149-161

Sriarunrasmee, J., Praweenya Suwannatthacho, P. & Dechakupt, P. (2015). *Virtual Field Trips with Inquiry learning and Critical Thinking Process: A Learning Model to Enhance Students' Science Learning Outcomes.* In 7th World Conference on Educational Sciences (WCES-2015). Athens Convention Center, Athens, Greece.

No	Stopsite	Location
1	Micro Hydro Power Plant, Merden	Jeblogan, Merden Village, Kebumen, Central Java
2	Hydroelectric Power Plant, Wadas Lintang	Sigudeg, Sendangdalem Village, Kebumen, Central Java
3	Kemutuk River (Kalitelu)	Kalitelu, Panerusan Village, Wonosobo, Central Java
4	Quarry Paweden	Kalianus, Paweden Village, Banjarnegara, Central Java
5	Merdada Lake	Pauan, Karangtengah Village, Banjarnegara, Central Java
6	Liyangan Site	Liyangan, Purbosari Village, Temanggung, Central Java

Table 1: Stopsites of Online Regional Geology Excursion (RGE) UGM in 2021

Figure 1: Data Collecting by video tapping in front of the outcrop

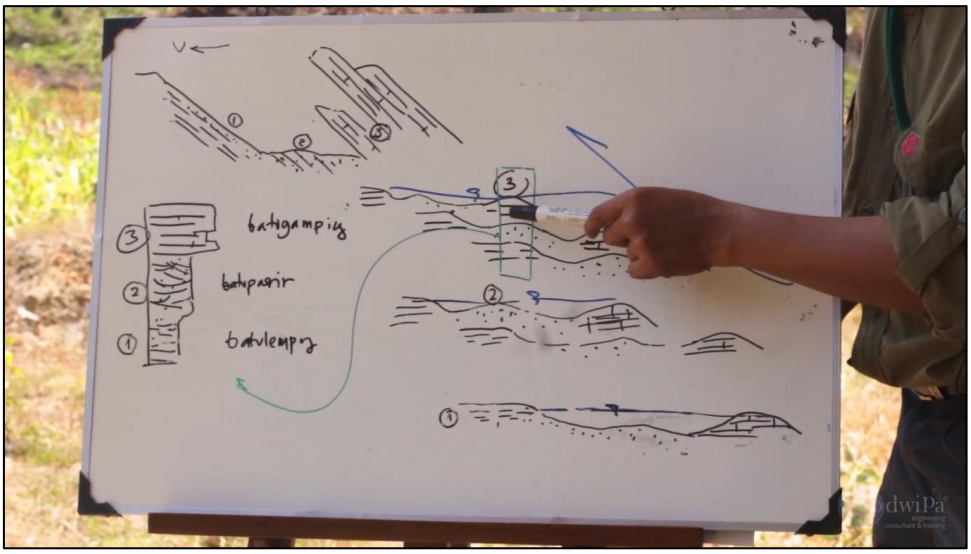

Figure 2: Explanation of the field trip leader for enhance the understanding of participants

Figure 3: Detailed view of the vein structures founded in the igneous rock

Figure 4: The drone view represent the scale of the outcrop compared with the man size

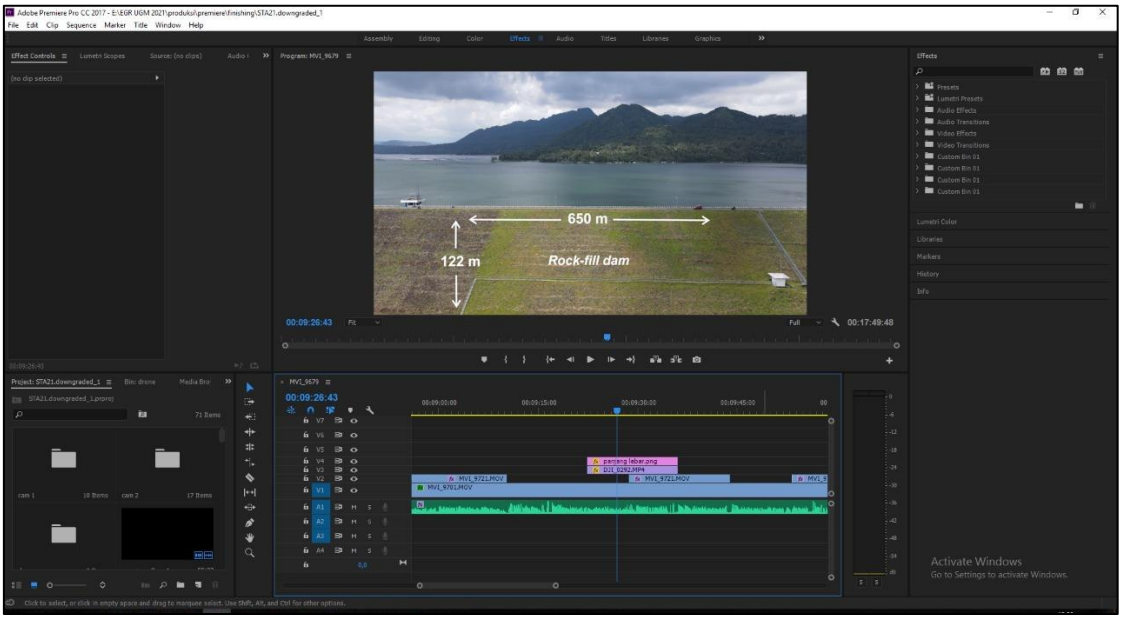

Figure 5: The video editing using the Video Editor and Graphics Editor Softwares.
Some figures added in this video used for increasing the understanding of the participants

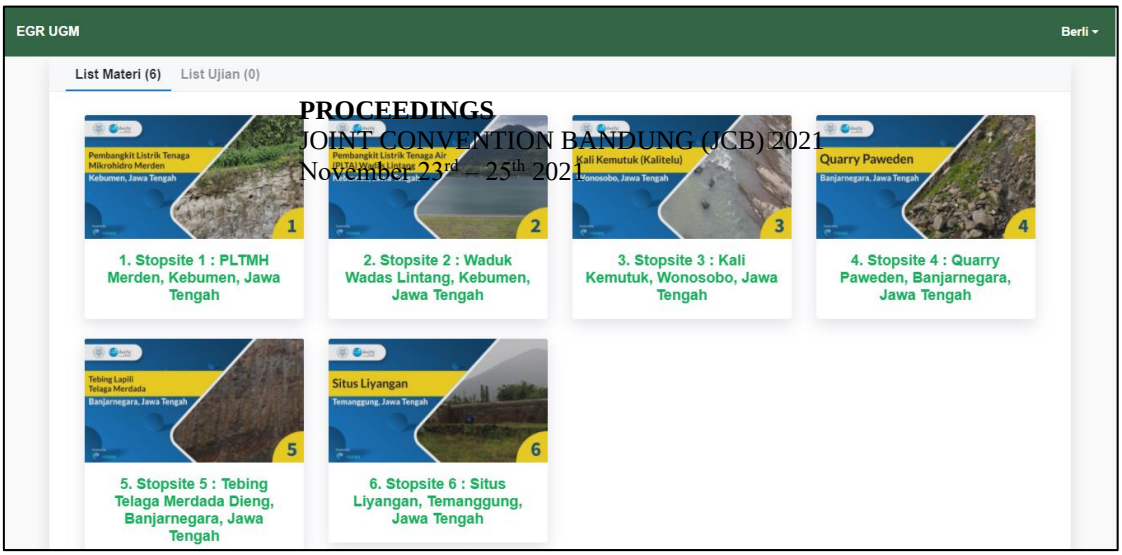

PROCEEDINGS
JOINT CONVENTION BANDUNG (JCB)2021
November 23rd – 25th 2021

Figure 6: Delivery method using Virtual Geodwipa E-learning Management System (VGEMS)

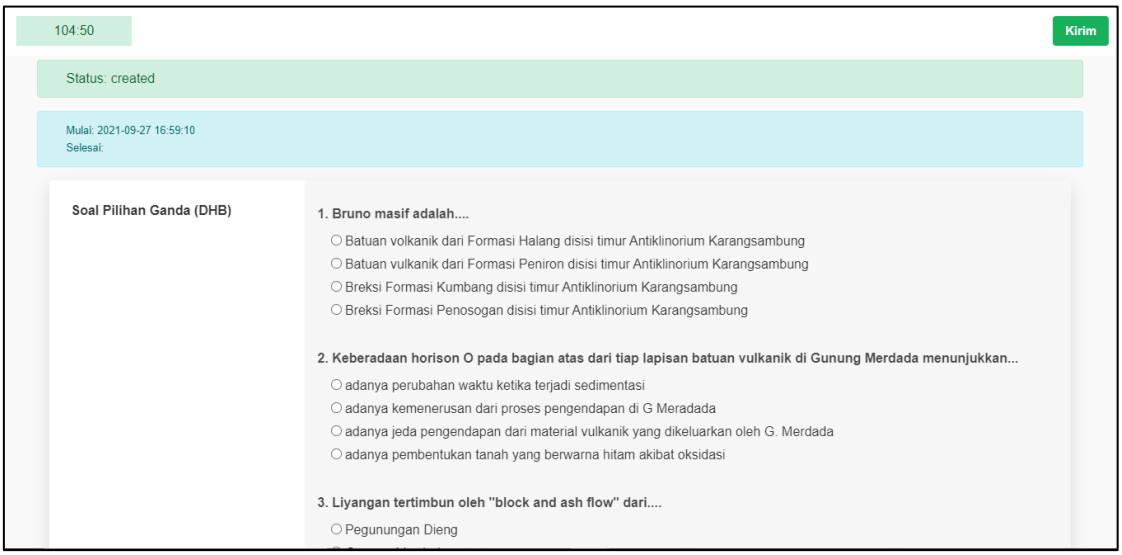

Figure 7: Tests of each videos are delivered and completed
in Virtual Geodwipa E-learning Management System (VGEMS)

PROCEEDINGS
JOINT CONVENTION BANDUNG (JCB)2021
November 23rd – 25th 2021

New Era Geological Map of Indonesia

Sony Malik Kartanegara, Muhammad Kamal Ramdhani, Muhammad Yusuf Abdul Madjid,
Muhammad Edo Marshal Nurshal, Nailul Marom
GEAR ID.

Abstract

Database is one of the most important things for geoscientist nowadays. One of the basic information that geoscientist must know or have is regional geology map. Several institutions have already created, compiled and published the geological map of Indonesia but still in picture, pdf or shp format.

GEAR-ID tried to transform the old format of geological map to an easy access, open and browse all around Indonesia with high resolution. By compiling all Indonesia geological map (regional scale) to one application. Not only seeing the geological map, GEAR-ID designed to be database for outcrop, geological information and also media sharing for all Indonesian geoscientists.

All the database will be open access and everyone can use it for any purposed: applied geoscience, engineering and academic.

Keywords: Database, Geological Map, Application.

Introduction

Geological Map data is one of the most important data that all geologist must have. Several institutions have already created, compiled and published the geological map of Indonesia but still in picture, pdf or shp format. In thus digital area people demand to access the data faster and simpler.

Based on explanation above, GEAR-ID (a mobile apps) tried to transform the old format of geological map to an easy access, open and browse all around Indonesia with high resolution. By compiling all Indonesia geological map (regional scale) to one application. Thus, everyone can access the geological information anywhere, anytime.

The apps is designed also as outcrop, geological information and also media sharing for all Indonesian geoscientists. The database will be open access and everyone can use it for any purposed: applied geoscience, engineering and academic.

Data and Method

The process of building the apps is start from compiling all geological map from OneMap by Ministry of Energy & mineral resources and several geological map from Geological Engineering Institute Technology Bandung. All of the maps then digitize using GIS software to create .shp data. Each polygon of formation contained description including name of formation, lithology and references.

After all of map in .shp data completed, we start building the application using android platform and mapbox. Then upload all geological map and information to application.

Result

The name of the application that we build is GEAR ID. The apps can display all of the geological information that uploaded, geological map, geological structure, lithology, and reference (Figure 1).

Figure 1: Geological Map of Indonesia from GEAR ID Apps

GEAR ID is also designed as outcrop and geological information sharing. GEAR ID provide page for you can sharing outcrop and its geological information

such as coordinate, lithology, description and interpretation. The location of the outcrop will be automated show on the geological maps.

More user upload and share the outcrop and geological information, richer the database, so the geological map will be updates and more accurate. Not only the geological map, the database can use for any purposed: applied geoscience, engineering and academic

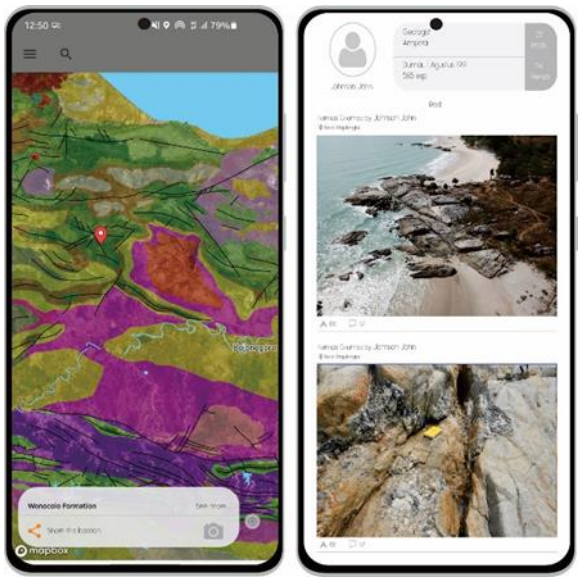

Figure 2: outcrop sharing view from GEAR ID

Conclusions

GEAR ID is built to help all Indonesian geoscientist can access geological map, outcrop and geological information all around Indonesia, without border only using smartphone.

PROCEEDINGS
JOINT CONVENTION BANDUNG (JCB)2021
November 23rd – 25th 2021

Preliminary Geological Heritage Assessment in Poso Tectonic Lake, Potential Geotourism Destination of Indonesia

Fhirdha Rizqi [1], Reza Permadi [2]
[1]Tim Ekspedisi Poso
[2]Ikatan Ahli Geologi Indonesia .

Abstract

This paper presents a preliminary assessment of geological diversity in Poso Tectonic Lake that can assist in sustainable planning and management and provide protection for national geological heritage sites. The landscape of Poso tectonic lake is characterized by structural and karst landforms. The method used in this research is an inventory of geological diversity with field data collection and self-assessment using the Geological Survey Center Classification, Geological Agency, Ministry of Energy and Mineral Resources (2017), whose assessment is based on four aspects, namely aspects of scientific value, educational value, tourism value, and potential degradation value. Each scoring point has a value converted to a percentage that is summarized to classify the geological heritage as high, medium, or low value. Based on field inventories and independent assessments, the Poso Tectonic Lake area has 20 geological diversity. 19 geological diversity have a moderate classification value, some of which are of Saluopa waterfall; Padamarari; Bancea to Petirodongi, and one site has a high classification value namely Pamona cave. These results can help provide a geological diversity protection status to become a geological heritage and the development of geotourism destination management.

Keywords: Lake; Tectonic; Heritage; Diversity

Introduction

Several locations around Poso Tectonic Lake, Central Sulawesi Province, are already well-known as general tourism locations, such as Pada Marari, Saluopa waterfalls, beaches, valleys and others. These locations are geologically based, meaning that these locations are the formation of natural geological processes that have the potential for geotourism.

The information regarding the processes of formation according to geological science is very much needed as educational material, nature and environmental conservation so that awareness will arise to maintain the heritage (conservation) and will create sustainable tourism development based on local wisdom. The results of this survey are the first step to manage geotourism development opportunities and also as a data preparation step for the conservation of the geological heritage site and the development of geotourism potential in Poso Tectonic Lake.

The purpose of this study is to determine the potential of a geological diversity as an initial initiation to become a geological heritage site, so that the wealth of geotourism objects is becomes part of the economic development of the community, can open development in the area starting from roads, social facilities, and others. This study aimed to determine the general geological conditions of the geological diversity and to understand the potential of the geological heritage around Poso Tectonic Lake. The survey activity locations for geological diversity in Poso Regency are located in 5 sub-districts, namely North Pamona Subdistrict, Pamona Pusalemba, West Pamona, South Pamona and Southeast Pamona, Poso Regency, Central Sulawesi Province. Geographically, the activity location is between 120° 10' 00"- 120° 50' 30 "and 1° 37' 10" - 1° 59' 00" South Latitude

Regional Geological Condition

Sulawesi Island is located at the convergence of the Eurasian, Indo-Australian and Philippine tectonic plates. Its tectonic evolution is not only influenced by the process of convergence with a complex history of subduction, extension, ophiolite obduction and continental collision (Katili 1978; Hamilton 1979; Silver et al. 1983a, b; Hall 1996, 2002; Parkinson 1998; Calvert & Hall 2003; van Leeuwen & Muhardjo 2005). The island consists of four elongated 'arms', widely associated with lithotectonic units (Sukamto 1975; Hamilton 1979). The northern arm consists of a Neogene island arc underlain by oceanic crust, with small fragments of continental crust (Taylor & van Leeuwen 1980; Elburg et al. 2003; van Leeuwen et al. 2007).

Regional Stratigraphy of the research area starting from the oldest formed:

- **Pompangeo Complex (MTmp)**

  It consists of a complex of bedrock, including schist, graphite, slate, genes, serpentinite, quartzite, limestone, and local breccia. The schist consists of mica schist; hyacinth mica schist;

sericite schist; muscovite schist; chlorite-seritic schist; green schist; glaucophan schist; pumpelite schist and yakut-amphibolite schist. Genes consist of albt-muscovite genes, quartz-biotite genes and epidote-muscovite-plagioclase genes. The age of the unit is thought to be older than the Cretaceous. Its thickness is thought to be thousands of meters.

- **Metamorphoic Limestone (MTmm)**

Consisting of lithology in the form of marble and leafed limestone, the color is light gray to greenish-gray, brown to brownish red. This unit is thought to originate from deep-sea Pelagos sediments, while its age is probably older than limestone.

- **Poso Formation (Tppl)**

It consists of lithology in the form of limestone, tuffaceous sandstone, and conglomerate. Foraminifera fossil content indicates Pliocene age, while the depositional environment is the shallow sea. The thickness of the formation reaches 800 m.

- **Puna Formation (Tpps)**

The lithology consists of conglomerate, sandstone, silt, shale, calcareous claystone, and limestone. The conglomerate comprises leafed limestone, schist, genes, and milk quartz, with carbonate cement, solid and hard. The sandstone is greenish-brown to blackish, dense, hard, well layered (30-200 cm). The silt is gray to blackish gray, slightly hard, well layered (10-30 cm). Shale gray, slightly hard and dense, well layered; Limestone clay is brownish yellow to gray, less dense. Limestone is generally in the form of coral limestone. Foraminifera fossils in calcareous clay show Pliocene age, while the depositional environment is shallow. The thickness of the formation is about 800 m. This formation overlaps with the Pompangeo formation.

- **Lake Sediment (Ql)**

It consists of clay, silt, sand, and gravel, showing a horizontal layer, a few meters to tens of meters thick (T.O. Simandjuntak, Surono, and J.B. Supandjono, 1997).

- **Coastal Deposits (Qal)**

Consists of sand, clay, mud, gravel and gravel (T.O. Simandjuntak, Surono, and J.B. Supandjono, 1997).

Regional Tectonics

Physiographically, the Poso Lake area is part of the Poso Basin from the Kuku Village area to the north of Boe Village which extends towards the south. This zone has a Basin morphology; hills and lakes are controlled by the active Poso fault structure. The type of lithology that forms the morphology of this zone consists of sedimentary and metamorphic rocks and alluvial deposits. The morphology of this zone is also influenced by geological structures that develop, such as faults. The spread of the Metamorphic Belt in the Poso area and its surroundings is included in the Central Sulawesi Metamorphic Belt. It consists of metamorphic bedrock dominated by schist, serpentinite, metamorphic limestone, and muscovite minerals older than Cretaceous with an estimated thickness of thousands of meters.

Data and Method

Data collection or inventory is carried out and identifies each location that can become a geological heritage site that will be taken to represent the geological condition of the area in the research area and summarized into geological diversity data. The report writing stage is carried out before collecting data for research methods and the basic theory that underlies the research. Followed by writing the contents and conclusions of the research. At this stage, an analysis of the geological data that has been obtained and the self-assessment based on the criteria according to the Center for the Geological Survey (2017) of the locations that will be designated as geological heritage site for geotourism around Poso Tectonic Lake

Result and Discussion

Lake Poso is a part of the Poso Basin, the type of lithology that forms the morphology of this zone consists of sedimentary and metamorphic rocks and alluvial deposits. The morphology of this zone is also influenced by geological structures that develop, such as faults. In the Poso Lake area, there are twenty geological diversity that can become geological heritage sites and are spread over several areas. Sites explained the geological diversity as evidence of history of geological activity and forms due to geological processes. Briefly, the location and name of the site can be seen in Figure 1 and Table 1.

Based on the results of the assessment, the lowest value contribution is from the scientific aspect, this is due to the lack of scientific publications on geology in Poso Tectonic Lake. In addition, the development of access and other supporting facilities must be improved. So that within the framework of developing as geological heritage sites from geological diversity it must be equipped with facilities and infrastructure to support it, both from the aspect of amenities and educational elements in the form of preparing information panels and

interpretations of geological, culture and biological aspects as well as the interrelationships of these three aspects, and their conservation for protection from the degradation of damaged both by nature and by the actions of irresponsible visitors.

Twenty geological diversity are starting from the west to east of the research area as a primary initiation and forwarded to potential geological heritage sites, which are summarized and sorted based on the top value from the classification of the Geological Survey Center (2017).

Conclusions

Based on the results of the analysis using the Geological Survey Center method (2017) geological diversity in the Poso Lake area still need further development. From these methods there are several points that must be addressed, namely:

1. Expand scientific publications, especially in the field of geology, both at national and international levels
2. Expand geological education materials in geosites and information centers
3. Increasing local products and tourism facilities to support economic value
4. Prepare amenity and supporting infrastructure to preserve the object, safety and comfort of visitors.

The geological diversity in Poso Lake area can't be separated from the existing geological diversity. The geological heritage that is superior and has the potential to become a world-class geological heritage is seen from its unique geological feature and geological history, including metamorphic rocks, limestones, quaternary and marine deposits as well as geological structures related to the Poso fault. For geological heritage, the national scale is dominated by geomorphological sites with beaches, waterfalls and caves and hills. For national-scale heritage in this area, it emphasizes the natural beauty and uniqueness of the existing rocks, besides that the geotourism activities that have been developed in the Poso Lake area are the main attraction.

References

Aubert M et al. 2014 Pleistocene cave art from Sulawesi, Indonesia. Nature 514, 223– 227. (doi:10. 1038/nature13422)

Bemmelen, Van. 1949. The Geology of Indonesia and Adjacent Archipelagoes. Government Printing Office. Den Haag. Vol I, IA and IB, 732p.

Frantz LAF et al. 2018 Data from: Synchronous diversification of Sulawesi's iconic artiodactyls driven by recent geological events. Dryad Digital Repository. (https://doi.org/10.5061/dryad.dv322)

Moss SJ, Wilson MEJ. 1998 Biogeographic implications from the Tertiary palaeogeographic evolution of Sulawesi and Borneo. In Biogeography and geological evolution of SE Asia (eds R Hall, JD Holloway), pp. 133 – 163. Leiden, The Netherlands: Backhuys Publishers.

Nugraha, A. M. S. & Hall, Robert., 2016. Late Cenozoic Paleogeography of Sulawesi, Indonesia. Journal Elsevier.

Nugraha, A. M. S. & Hall, Robert., dkk. Nugraha, A. M. S. & Hall, Robert., 2018. An Outline of Sedimentology, Stratigraphy, and Provenance of Poso Depression and its Implication to the Late Cenozoic Evolution of Central Sulawesi, Indonesia. Poster FOSI-IAS-SEPM.

Pusat Survei Geologi. 2017. Petunjuk Teknis Asesmen Sumberdaya Warisan Geologi. Badan Geologi Pusat Survei Geologi. 2017. Standar Teknis Inventarisasi Keragaman Geologi dan Identifikasi Warisan Geologi. Badan Geologi

Russell, J. M. dkk. 2016. The Towuti Drilling Project: paleoenvironments, biological evolution, and geomicrobiology of a tropical Pacific lake, Towuti Lake, South Sulawesi. 2016. Scientifis Driling Journal (Open Access). Simandjuntak, T. O.,

Rusmana, E., Surono., Supandjono, J. B., 1991. Geologi Lembar Malili, skala 1:250.000. Pusat Penelitian dan Pengembangan Geologi, Bandung. Simandjuntak, T. O.,

Surono., Supandjono, J. B., 1997. Geologi Lembar Poso, skala 1:250.000. Pusat Penelitian dan Pengembangan Geologi, Bandung.

Sompotan, A. F., 2012. Struktur Geologi Sulawesi. Perpustakaan Sains Kebumian Institut Teknologi Bandung, Bandung

.

Acknowledgements

We gratefully thank the Poso Expedition Team for financial support.

PROCEEDINGS
JOINT CONVENTION BANDUNG (JCB)2021
November 23rd – 25th 2021

Table 1: Geological heritage Self-assesment

	LOCATION / GEOHERITAGE SITE											
Assessment criteria	Blue & Green Schist	Petiro Dongi	Wawondoda 1	Wawondoda 2	Goa Tangkadao	Goa Latea	Situs Ue Datu	Situs Ua Tangkaboba	Goa Pamona	Situs Posunga Bangke	Situs Posunga Kodi	Kompleks Goa Torau
Scientific Value	101.25	60	50	46.25	42.5	46.25	42.5	46.25	66.25	50	46.25	62.5
Education Value	66.25	62.5	51.25	48.75	51.25	48.75	50	48.75	83.75	51.25	48.75	71.25
Tourism Value	55	57.5	61.25	60	58.75	71.25	77.5	67.5	77.5	61.25	61.25	57.5
Degradation Risk Value	42.5	73.75	57.5	55	58.75	43.75	68.75	65	88.75	60	60	77.5
Total	265	253.75	220	210	211.25	210	238.75	227.5	316.25	222.5	216.25	268.75
Evaluation	Moderate	Moderate	Moderate	Moderate	Moderate	Moderate	Moderate	Moderate	High	Moderate	Moderate	Moderate

	LOCATION / GEOHERITAGE SITE							
Assessment criteria	Air Terjun Saluopa	Pantai Siuri	Pada Marari	Bancea	Situs Makilo	Bukit Lamusa	Situs Kandela	Watu Pangasa
Scientific Value	78.75	80	87.5	91.25	81.25	58.75	77.5	56.25
Education Value	75	86.25	70	70	75	66.25	80.25	66.25
Tourism Value	77.5	67.5	61.25	60	67.5	58.75	71.25	71.25
Degradation Risk Value	50	42.5	61.25	56.25	47.5	38.75	40	61.25
Total	281.25	276.25	280	277.5	271.25	222.5	269	255
Evaluation	Moderate	Moderate	Moderate	Moderate	Moderate	Moderate	Moderate	Moderate

CODE & SITES	CATEGORY	LOCATION	COORDINATE	PHOTO	DESCRIPTION
SWG-01 Green Schist & Blue Schist	Lithology	Village: Kuku District: Pamona Utara Regency: Poso		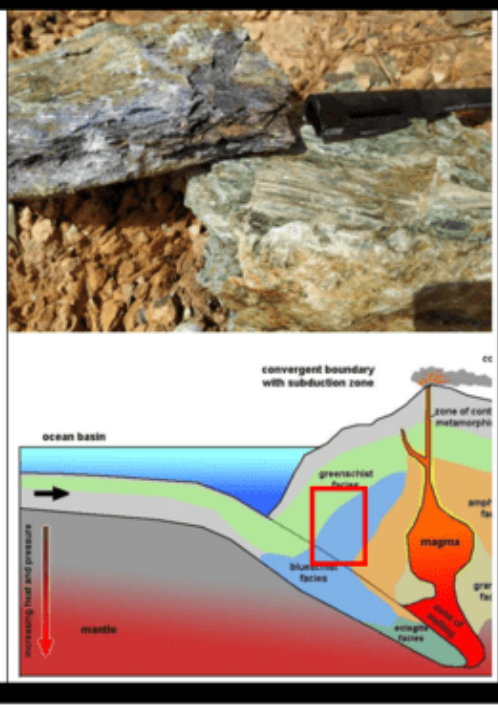	Blueschist and Greenschist are included in the Pompangeo Complex. The Pompangeo is an older formation than the Cretaceous. Generally this lithology is below the surface (bedrock), but exposed on the surface. Greenschist is a facies formed at low temperature with medium pressure. Blueschist is a facies formed at low temperature and high pressure This outcrop was found around Jalan Kuku - Panjoka

Figure 1: Matrix of Green Schist & Blue Schist Geoheritage Site

PROCEEDINGS
JOINT CONVENTION BANDUNG (JCB)2021
November 23rd – 25th 2021

SWG-02 Petirodongi	Lithology and Structural Geologu	Village : Petirodongi District: Pamona Utara Regency: Poso	120,65825 - 1,73016667	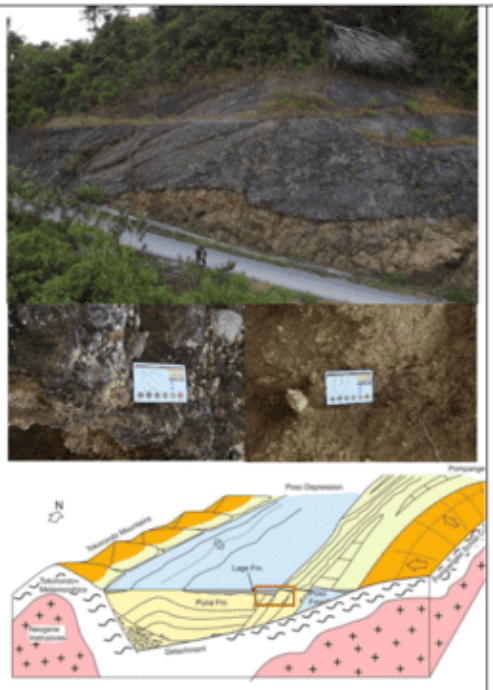	Is a rock outcrop consisting of the Puna Formation (Tpps) and the Lage Formation (Tppl) Puna Formation (Tpps) It consists of lithology in the form of ultramafic rocks of Pliocene age, while the depositional environment is shallow sea. The thickness of the formation is about 800 m. This formation overlaps with the Pompangeo formation. The Lage Formation is a formation rich in metamorphic products This outcrop was formed due to normal faults that cut sedimentary rocks in the Neogene Poso Valley.

Figure 2: Matrix of Petirodongi Geoheritage Site

SWG-03 Wawondoda 1	Geo-Archaeology	Village: Sawidago District: Pamona Utara Regency: Poso	120.7303 -1.9781		The Wawondoda 1 site is composed of Malih limestone lithology from the Pompangeo Complex (MTmp) which is older than the Cretaceous. There are archaeological features found at this location including: Human skulls and skeletons, wooden coffins, pottery.

Figure 3: Matrix of Wawondoda-1 Geoheritage Site

SWG-04 Wawondoda 2	Geo-Archaeology	Village: Sawidago District: Pamona Utara Regency: Poso	120.7294 -1.8911		The Wawondoda 2 site is composed of Malih limestone lithology from the Pompangeo Complex (MTmp) which is older than the Cretaceous. There are archaeological features found at this location including: human skeletons, wooden coffins, pottery

Figure 4: Matrix of Wawondoda-2 Geoheritage Site

SWG-05 Tangkadao Cave	Geo-Archaeology	Village: Dulumai District: Pamona Utara Regency: Poso	120.6645 -1.9184		The Tangkadao 1 Cave site is composed of Malih limestone lithology from the Pompangeo Complex (MTmp) which is older than the Cretaceous. There are archaeological features found at this location including: Human skulls and skeletons, wooden coffins, pottery.

Figure 5: Matrix of Wawondoda 2 Geoheritage Site

SWG-06 Latea Cave	Geo-Archaeology	Village: Tentena District: Pamona Utara Regency: Poso	120.8955 -1.86		The Latea Cave site is composed of limestone lithology from the Poso Formation (Tppl) aged Pliocene There are archaeological features found at this location including: Human skulls and skeletons, wooden tombs, bronze bracelets, silver bracelets, ceramics, pens, mirrors, pottery

Figure 6: Matrix of Latea Cave Geoheritage Site

SWG-07 Situs Ue Datu	Geo-Archaeology	Village: Tentena District: Pamona Utara Regency: Poso	120.640831 -1.757949		The Ue Datu site is composed of Sand Deposits from Pliocene to Holocene Lake (Ql) deposits which show horizontal layers and their thickness ranges from several meters to tens of meters. There are archaeological features found in this location including: The spring is sacred to the local population

Figure 7 : Matrix of Ue Datu Geoheritage Site

SWG-08 Situs Ua Tangkaboba	Geo-Archaeology	Village: Tentena Distrcit: Pamona Utara Regency: Poso	120.8658333 -1.9247222		The Latea Cave site is composed of limestone lithology from the Poso Formation (Tppl) aged Pliocene There are archaeological features found at this location including: Human skulls and skeletons, wooden coffins, pottery fragments, ceramic fragments

Figure 8 : Matrix of Ua Tangkaboba Geoheritage Site

SWG-09 Pamona Cave	Geo-Archaeology	Village: Pamona District: Pamona Pusalemba Regency: Poso	120,638381 -1,763859	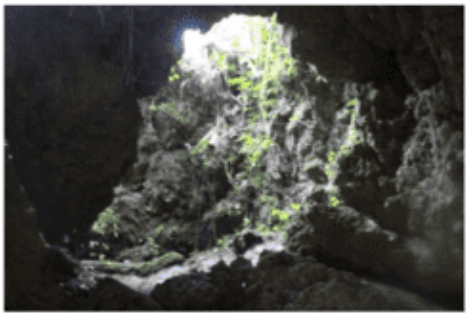	Composed of limestone lithology from the Poso Formation (Tppl) of Pliocene age. There are 2 visible feature processes, including exogenous processes, namely degradation where the clastic limestone that forms Pamona Cave undergoes chemical weathering by water that is absorbed and dissolves the minerals in the rock and the agradation process where minerals dissolved by water form minerals that make them stalactites. and stalagmites Human skeleton, remains of wooden coffin

Figure 9 : Matrix of Pamona Cave Geoheritage Site

SWG-10 Situs Posunga Bangke	Geo-Archaeology	Village : Pamona District: Pamona Utara Regency: Poso	120.52111111 -1.766944444		The Posunga Bangke site is composed of limestone lithology from the Poso Formation (Tppl) of Pliocene age There are archaeological features found at this location including: pottery fragments, terraced punden, stone foundation pillars of traditional houses

Figure 10 : Matrix of Posunga Bangke Geoheritage Site

SWG-11 Situs Posunga Kodi	Geo-Archaeology	Village: Pamona Distrcit: Pamona Utara Regency: Poso	120.640666 -1.7569166		The Posunga Kodi site is composed of limestone lithology from the Poso Formation (Tppl) of Pliocene age There are archaeological features found at this location including: Human skulls and skeletons, wooden coffins, intact earthenware jars, offerings, iron trays

Figure 11 : Matrix of Posunga Kodi Geoheritage Site

SWG-12 Torau Cave Complex	Geo-Archaeology	Village : Leboni District : Pamona Pusalemba Regency : Poso	120,5191361 - 1,78610556	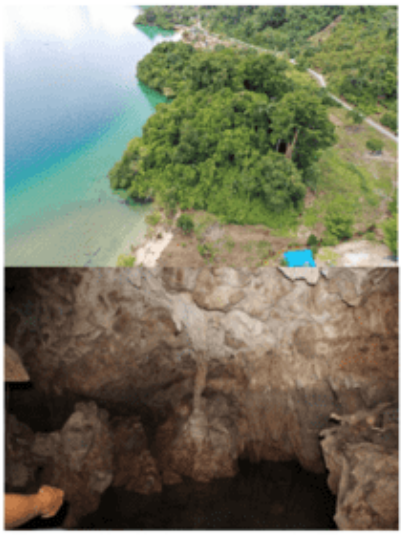	Included in the Endokarst Phenomenon is a cave composed of limestone lithology from the Poso Formation Limestone (Tppl) members of Pliocene age. It is called a complex because there are several caves with chambers and overdrafts with a depth of ±45m. There are 2 feature processes that can be seen, including exogenous processes, namely degradation where the clastic limestone that forms Torau Cave undergoes chemical weathering by water that is absorbed and dissolves the minerals in the rock and the agradation process in which minerals dissolved by water form minerals that make them stalactites. and stalagmites Then in it there are archaeological features in the form of a human skeleton skull.

Figure 12 : Matrix of Torau Complex Cave Geoheritage Site

SWG-13 Saluopa Waterfall	Structural Geology	Village : Pamona Distrcit : Pamona Pusalemba Regency : Poso	120,5415833 - 1,736075		It is a waterfall formed by the western Poso fault. Composed of tuffaceous limestone lithology from the Poso Formation (Tppl) of Pliocene age. Formed due to tectonic activity, this waterfall has 12 waterfall steps.

Figure 13 : Matrix of Saluopa Waterfall Geoheritage Site

SWG-014 Siuri Beach	Morphology	Village : Pamona District : Pamona Pusalemba Regency : Poso	120,5184167 - 1,80116944		The stretch of beach on the shore of the lake with white sand dominated by quartz sand and into the Pleistocene – Holocene Lake Deposit (Ql).

Figure 14 : Matrix of Siuri Beach Geoheritage Site

SWG-015 Pada Marari	Geomorphology	Village : Pamona District: Pamona Pusalemba Regency: Poso	120,5540278 - 1,93541667		It is a complex hill of metamorphic rock with the lithology of the bedrock including schist and quartzite. Enter the Pompangeo Complex (MTmp) which is older than the Kapur.

Figure 15 : Matrix of Pada Marari Geoheritage Site

SWG-16 Bancea	Geo-Archaeology	Village: Bancea Distrcit: Pamona Utara Regency: Poso	120.3219444 -2.1986111		This Bancea site is composed of limestone lithology from the Pompangeo Complex (MTmp) which is older than the Cretaceous. There are archaeological features found at this location including: Human skeleton, wooden coffin

Figure 16 : Matrix of Bancea Geoheritage Site

SWG-17 Makilo Cave	Geo-Archaeology	Village : Makilo Distrcit: Pamona Selatan Regency: Poso	120,62575 -- 2,06222222		The Makilo site is composed of Malih limestone lithology from the Pompangeo Complex (MTmp) which is older than the Cretaceous. There are archaeological features found at this location including: Human skulls and skeletons, wooden coffins, iron tombs, pottery, ceramic plates, wooden barrels, baskets

Figure 17 : Matrix of Makilo Cave Geoheritage Site

SWG-18 Lamusa Hills	Geo-Archaeology	Village : Korobono District: Pamona Tenggara Regency: Poso	120.7391555 -2.05247222		The Lemusa Hill site is composed of Malih limestone lithology from the Pompangeo Complex (MTmp) which is older than the Cretaceous. There are archaeological features found at this location including: Collection of kitchen waste shells (kjokkenmondinger)

Figure 18 : Matrix of Lamusa Hills Geoheritage Site

SWG-19 Kandela Site	Geo-Archaeology	Kelurahan : Tindoli Kecamatan : Pamona Tenggara Kabupaten : Poso	120,6614444 - -1,761		Situs Kandela ini tersusun atas litologi batugamping malih dari **Kompleks Pompangeo (MTmp)** berumur lebih tua dari Kapur. Terdapat fitur arkeologi yang ditemukan di lokasi ini diantaranya : Tengkorak dan kerangka manusia, peti kubur kayu, fragmen keramik Eropa, manik-manik, fragmen gerabah.

Figure 19 : Matrix of Kandela Geoheritage Site

SWG-20 Watu Pangasa	Lithology	Village : Sangele District: Pamona Utara Regency: Poso	120,6380 -1,7728		It is a limestone outcrop on the shores of Lake Poso with limestone lithology belonging to the Pliocene Clastic Limestone Member of the Poso Formation (Tppl).

Figure 20 : Matrix of Watu Pangasa Geoheritage Site

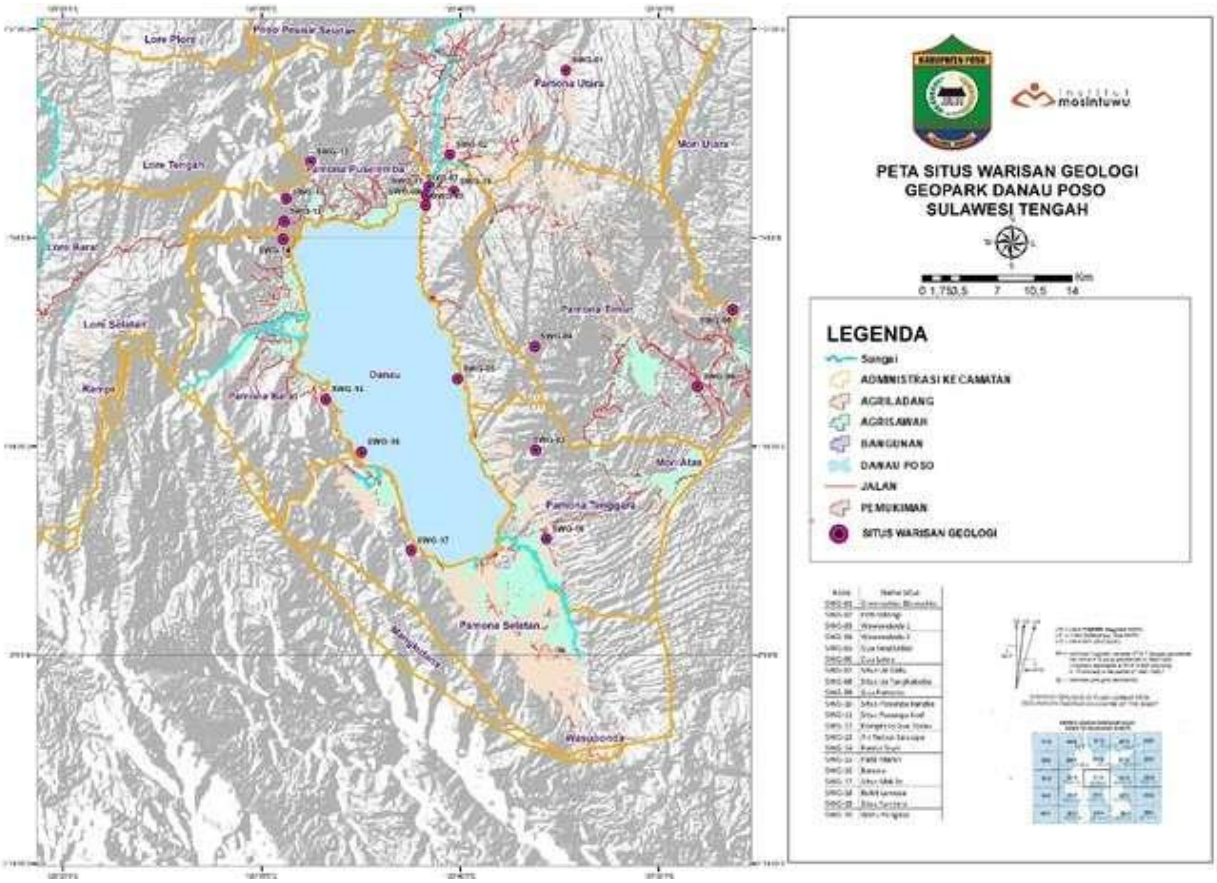

Figure 21: Geological diversity map of Poso Tectonic Lake

PROCEEDINGS
JOINT CONVENTION BANDUNG (JCB)2021
November 23rd – 25th 2021

Tourism Geology Contribution for Tourism Development in the Mandalika Special Economic Zone, Lombok Island, Indonesia

Yudi Satria Purnama (Environment Tourism and Social Development Centre - ETSDC, Bandung)

Abstract
An area in the eastern part of the Lombok island -Mandalika Special Economic Zone (SEZ)- is being developed by government to accelerate economic growth through tourism sector. The author interest to explore geology of Mandalika SEZ and use it to be tourist attraction and its activities.

This desk study uses tourism geology perspective, not geotourism view. In context of tourist interest, tourism geology embraces many tourist interest types. In other hand, geotourism focus on geoscientific interest. The outcome of this study is many potential tourist interests able to be accommodated by Mandalika SEZ geology. They are geoscientific, sightseeing, curative and physical outdoor activity interests, i.e. aerosport, rock climbing, off road motorcycle riding, cliff diving, swimming and thriathlon. Those attractions and activities status are range from proven, probable to possible.

This study concerns activity risk, environmental impact and risk relate to natural hazard. Activity risks are typically low to high risks in physical outdoor activity (depend on activity types), and low to no risks for geoscientific, sightseeing and speleotherapy activities. Environmental impact of physical outdoor activities is low to high impacts, while low to no impact for geoscientific, sightseeing and speleotherapy. Risk related to natural hazard in study area is earthquake, prone to tsunami flood, and vulnerable to ground motion in medium degree.

The study results have consequences for various tourism markets, concern for safety and awareness of environmental impacts. Geotourism, health tourism, sport tourism and adventure tourism are tourism market types relate to interest types recommended. In addition, field investigation is important in possible activity status to ensure whether or not the activity could be performed and to ensure safety, and also to reduce / eliminate risk particularly on moderate to high activity risks. Furthermore, each activity which has environmental impact should be further evaluated whether it is accepted by local community or government.

A. Introduction

Lombok Island is a well-known Indonesia tourist destination. An area in the eastern part of the island is being developed by government to be a special economic zone. It is called the Mandalika Special Economic Zone (SEZ; Figure.1). The Mandalika SEZ has been being developing to be a world class destination and to accelerate economic growth of surrounding area through tourism sector. In addition, within the area there is Mandalika International Street Circuit ready to be used for international MotoGP championship which able to accommodate about 195 thousand visitors. Thus, the market demand for tourist attraction and activity most likely will be very large.

Figure 1. Study Area of Mandalika SEZ (yellow) and surrounding area.

The author explores geology of the area to be used for tourist attraction. Uniquely, this study uses tourism geology perspective, not geotourism view. Tourism geology differs with geotourism. Geotourism is tourism concept rely on geological feature and man-made work related to geology while tourism geology is geological concept applied to tourism (Purnama, 2020 in Purnama, 2020). Tourism geology is similar with other applied geology, e.g. engineering geology or petroleum geology.

One of many differences between geotourism and tourism geology is geotourism focus on geoscientific tourist interest, while tourism geology acknowledges many tourist interests as long as relate to geological feature (Table 1; Purnama, 2020 in Purnama, 2020). As consequence, tourism geology embraces many tourist interests such as scenic beauty, physical outdoor activity, curative and art-related stone and minerals interests. Thus, this paper purpose is to expose geological interpretation of study area for various tourist attractions and its activities.

Table 1. Difference of Geotourism and Tourism Geology (Purnama, 2020 in Purnama, 2020)

Aspect	Geotourism	Tourism Geology
Purpose	To support geological conservation, to be sustainable tourism, to improve visitor experience and to encourage local economic growth.	To support tourism by deliver proper geological knowledge to make the tourism-related professional able to solve tourism problem linked to the geological feature
Variable Type	Mostly non-geological variables	Mostly geological variables
Knowledge Type Generated	Non-geological knowledge since social variables plays critical roles.	Geological knowledge
Outcome	Tourism products connected to geology	Geologic publication or report
User Type	end-user (tourist) and also nextuser (tourism-related professional)	next-user (tourism-related professional and other practitioner)
Tourist Interest Type	Geologic interest	All tourist interest that connected to geological feature
Tourism Market Target	Geotourism, Ecotourism (?)	All tourism market applied to geological feature

PROCEEDINGS
JOINT CONVENTION BANDUNG (JCB)2021
November 23rd – 25th 2021

B. Method

There are six stages of this desk study. Sequentially, it is composed of collecting data, mapping attraction zone (use work of Purnama et al, 2020 in Purnama, 2020), defining attraction and activity types, defining status of attraction and activity (include risk), defining environmental impact of each activity, and identify natural process as hazard. Data and information were derived from internet source, scientific publication, and personal experience.

Interpretation of attraction and activity need to be categorized into three level of status, that is proven, probable and possible (Purnama et al, 2020 in Purnama, 2020). Those three levels are not considered whether or not the destination is developed. The statuses are described below.

- Proven: the attraction and activity confirm exist. It might be confirmed by tourist reports from various media types, research, mentioned in a document because of its attractiveness, the place where an attraction-related event was held, fieldtrip stop sites or personal experience.
- Probable: the attraction and activity are probable because it has similar geological character to the proven attraction where the position is relatively near. However, there is no tourist report found or there is a report, but no geographical points reported, e.g. points on the Google Maps. Investigation might be needed to ensure whether the activity able to be performed but low urgency.
- Possible: the attraction is identified from an analysis on data and/or information. There is no visitation recorded. Investigation is highly needed to ensure whether the activity able to be performed and also relate to safety issue (high urgency).

Those statuses have consequence to new tourist attraction, new tourism product, and new target tourism market.

Particularly in safety context, potential risk of each activity should be estimated. The risk is as follow.

- High risk when fatality is potentially high.
- Moderate risk when physical injury is likely high.
- Low risk when physical injury is potentially low.
- No risk when no physical injury will be potentially occurred. The risk that arises during reaching the location is another case.

The consequence of those risk levels is the need of engineering or field investigation to eliminate or reduce the risk.

Regarding to environmental impact because of activity, there are four levels as follows.

- High impact when the feature is extremely hard to restore to earlier condition or to be restored.
- Moderate impact when the feature is possible to restore, with high effort and costly.
- Low impact when the feature is easily to restore, with low effort.
- No impact when nothing significantly changes on environment.

Those impacts at least need to be considered by government or local people whether it is accepted or not.

C. Geomorphology

Study area is characterized by hilly area in the northern side with steeper slope and coastline in the south. Land cover mostly plantation, bush, and grassland. Flat area near coastline is urban area.

Purnama et al (2020 in Purnama, 2020) described Landform Zone Map for Geological-related Attraction of the Lombok island (Figure 2). There are four landscapes with eleven landforms, as shown below.

- Volcanic Landscape:
  - Rinjani Upper Cone (A1)
  - Rinjani Lower Cone (A2)
  - Punikan Volcanic Cone (A3)
  - Pusuk-Nangi Volcanic Cone (A4).
- Coastal Landscape:
  - Pengulung-Kuta Rocky Coast (B1)
  - Malimbu Rocky Coast (B2)
  - Rinjani Sandy Coast (B3)
- Faulted Hill Landscape:
  - Pengulung Undulated (C1)
  - Kuta Undulated (C2)
- Karst Landscape:
  - Ekas Carbonate (D1)
  - Pengulung Isolated Carbonate (D2)

Based on their work, study area falls to three of eleven landform units. They are Pengulung-Kuta Rocky Coast (coastal landscape), Kuta Undulated (faulted hill landscape) and Pengulung Isolated Carbonate (Karst Landscape).

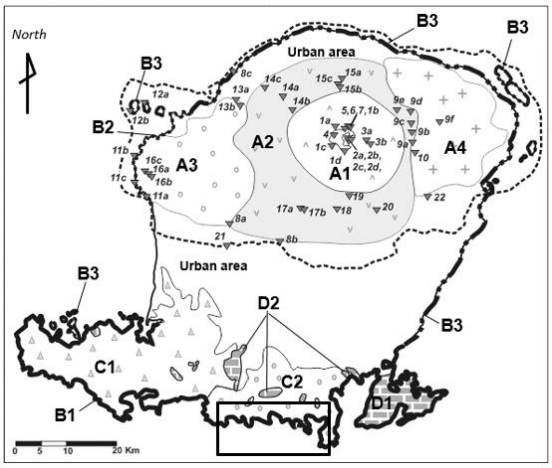

Figure 2. Landform Zone Map for Geological-related Attraction (Purnama et al, 2020 in Purnama, 2020) with four landscape (A, B, C, D) and eleven landform units (A1, B2, C3, and so on). Area with dashed line is Rinjani-Lombok Geopark Area where small triangles are geological sites. Study area (box area) is composed of Pengulung Isolated Carbonate (D2), Pengulung-Kuta Rocky Coast (B1), and Kuta Undulated (C2).

C.1. Pengulung-Kuta Rocky Coast (Coastal Landscape)

This landform is one of the tourism icons of Lombok. This rocky coast is situated in the southern coast, to the south of Pengulung Undulated Area (C1) and Kuta Undulated Area (C2). Coast character is curvature shoreline, various seabed slope from shore to deep water, pocket beach, and erosional feature (e.g. sea stack or sea cliff). Various sand type is reported, such as pink beach sand in the southeastern coast, white beach sand in the gili's and southern coast, while few beaches have round sand from biota. Rock type is breccia, lava, tuff of Pengulung Formation and quartz sandstone and claystone of Kawangan Formation (Mangga et al, 1994). Both formations have Oligocene to Early Miocene age.

Calcarenite of Ekas Formation (Late Miocene age) in southeastern coast. This coast is prone to tsunami flood.

C.2. Kuta Undulated (Faulted Hill Landscape)
The southern part is the location of this landform unit. The character is hilly area, slope typically up to 45º, elevation range 5 meter to less than 300 meter. Rock type is breccia, lava, tuff of Pengulung Formation and quartz sandstone and claystone of Kawangan Formation (Mangga et al, 1994). Those formations have Oligocene to Early Miocene age. This area has medium degree of ground motion vulnerability zone (Pusat Vulkanologi dan Mitigasi Bencana Geologi, 2009) while earthquake prone character in this area falls to high hazard zone (Suartika & Turjono, 2009).

C.3. Pengulung Isolated Carbonate (Karst Landscape)
This unit is in southwestern area of the island. It is typically by isolated carbonate located in Pengulung undulated area and Kuta undulated area, slope typically 10º - 30º, elevation range 5 meter – 400 meter. Rock type is Carbonate of Ekas Formation (Late Miocene age, Mangga et al, 1994)). Domination of medium degree of ground motion vulnerability zone is character this isolated carbonate (Pusat Vulkanologi dan Mitigasi Bencana Geologi, 2009). Earthquake character in this area is moderate hazard zone (Suartika & Turjono, 2009).

D. Tourist Interest and Activity
The study outcome shows there are various geological-related attractions which relate to various tourist interests. Those attractions able to fulfill four tourist interests: geoscientific, scenic beauty, curative, and physical outdoor activities. Below is description of each attraction type including potential risk and environmental impact of each activity.

D.1. Geoscientific Interest
Geological feature of geoscientific attraction is composed of unique sand beach, Oligo-Miocene outcrops, landform (e.g. erosional features) and landscape. Those features are generally located in coastal area (Pengulung-Kuta Rocky Coast).

Activity itself is learning geological information of the features which range to proven to probable (for new site). Potential risk of this activity is low. However, rock or sand collecting is possible where it causes to low environmental impact. This interest is strongly related to geotourism market.

D.2. Scenic Beauty Interest
This activity is the most tourist activity in Kuta Undulated Area. The feature is the landform and landscape seen. Appreciate or observe the landform or landscape is the activity conducted. The points to see those features is mostly located in promontory with low vegetation as landcover, e.g. Bukit Merese. Other locations are many but probably underexplored due to accessibility. This activity has no potential risk, no environmental impact, and status activity is proven to probable.

D.3. Curative Interest (Speleotherapy)
A cave (Gua Bangkang Prabu) found in Pengulung Isolated Carbonate landform and already become a well-known destination. While no other cave reported surround the area, it is expected many other cave entrances have not reported or underexplored. Such cave possibly able to be utilized for speleotherapy.

Speleotherapy means a therapy activity carried out in the cave for a certain time to heal respiratory disease, e,g. asthma. The attraction of cave environment for this therapy is cave microclimate which at least free from pollutant, dust, and pollen. Activity type during therapy session basically refer to breathing exercise in cave environment. The activity may vary from just lying down to light exercise. This therapy can be repeated several times in months, depending on medical advice. Such activity has no potential risk and no environmental impact.

Status activity is possible. It means the site need to be investigated whether or not suitable for speleotherapy and also for safety reason. This interest is strongly related to medical or health tourism market.

D.4. Physical Outdoor Activity Interest
This interest varies and require particular landform for each activity. For instance, flat to steep slope combined with mud on off road route are suitable for motorcycle riding on off road track, cliff diving potential to be performed on erosional feature landform which face to the standing body of water, while swimming needs our knowledge of safety nearshore.

The physical outdoor activity type in this study is aerosport, rock climbing, off road motorcycle riding, cliff diving, swimming, and triathlon. Those outdoor activity interests are strongly related to sport or adventure tourism markets.

D.4.1. Physical Outdoor Activity: Aerosport
Some take off sites of aerosport are proven on hill slope facing to the ocean, such as Seger beach and Torok Aik Beleq. Such area is typically on Kuta Undulated Landform which utilize deflected wind when wind strikes obstacle (hill, mountain ridge or cliff). It is also called ridge lift or slope lift. Similar site characters are also probable on several locations. There is no environmental impact of take off activity. Potential risk of this activity is moderate. Status activity is proven to probable (for new site).

D.4.2. Physical Outdoor Activity: Rock Climbing
Rock climbing activity require vertical cliff to overhang on hard rock. Such features in study area are mostly situated on erosional features on Pengulung-Kuta Rocky Coast landform. For instance, some spot candidates in Pengulung-Kuta Rocky Coast landform are Gili Penyu Tunak and Batu Payung Loteng. Most likely this activity is categorized as possible since it is lack of documentation. Difficulty rating of this activity is unknown. Environmental impact of this activity is high where potential some tools put on the wall will create damage on it. Potential risk activity probably moderate to high.

D.4.3. Physical Outdoor Activity: Off road Motorcycle Riding
Kuta Undulated landform has slope range from 20º – 45º. Those slope range challenging for off road motorbike trails. Difficulty rating will vary from moderate to hard which follows the steepness of the slope. Moreover, surrounding scenery such as hilly areas with plantation, bush, grassland, and coastal areas as backdrop add the attraction value for land crossing. Riding status in this area is probable to

possible since it is lack of documentation. Environmental Impact of this activity is most likely low to moderate (soil erosion). Potential risk activity is low to moderate.

D.4.4. Physical Outdoor Activity: Cliff Diving
Perhaps, this activity is little bit extreme for some people. However, some spots in Pengulung-Kuta Rocky Coast landform are possible to be performed this activity. A spot candidate as example in Pengulung-Kuta Rocky Coast landform is Gili Penyu Tunak. Such spots character is vertical cliff and the height probably maximum 10 meter for untrained people.

World High Diving Federation considers water depths of 13 to 15 meters adequate for dives from 20 meters or less (as quoted by Kolich, 2009). Hence, if someone jump from cliff maximum 10 meter, then the water depth should be minimum 6.5 to 7.5 meters. In addition, the water should be clear to know seabed surface.

Status activity is possible which require field investigation. There is no environmental impact of this activity. Potential risk of this activity is most likely moderate.

D.4.5. Physical Outdoor Activity: Swimming
Playing on the nearshore of Pengulung-Kuta Rocky Coast landform is one of the most tourist activity does. Whether it is swimming, surfing or other activities in the water, safety is a requirement. Mostly, accident in nearshore is due to rip current. Thus, it requires our knowledge on safety nearshore.

The bay in study area has two coast slope types, flat – drop off type and ramp – drop off type (Figure 3). Particularly on promontory, coast slope type is drop off type. Flat - drop off type is characterized by shallow water depth in flat zone. During low tide, deepest part is about a waist height. Water depth is deeper abruptly in the drop off zone.

Rip current is less likely occurred in the flat zone which make this coast type to be the safest nearshore. Hence, swimming or other activity in the flat zone almost has no risk.

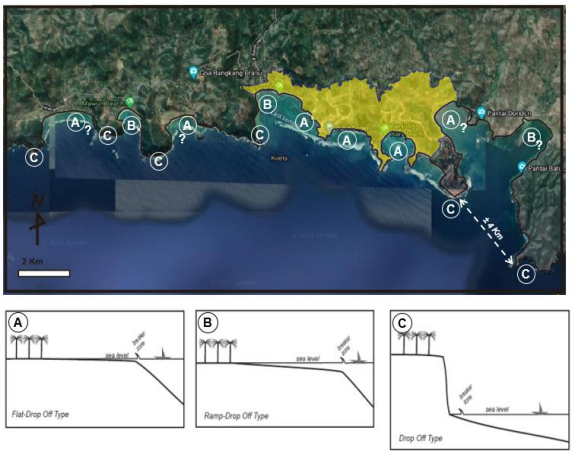

Figure 3. Coast slope type in study area: flat – drop off type (A), ramp – drop off type (B), and drop off type (C) particularly on promontory.

The slope of ramp - drop off type is probably up to 11º in the ramp zone. However, in the drop off zone, the slope is steeper and water column is deeper abruptly. Rip current often occurred in ramp zone. Consequently, swimming in the zone is moderate to high risks, e.g. caught by rip current and drowning. However, surfing in this coast is one of the best things to do. Whatever the activity in the nearshore, it is interpreted this activity has no environmental impact.

Drop off type is typical in promontory where the vertical cliff facing to the ocean. On this coast type, cliff diving activity possible to be performed if water depth deep enough and the water is clear.

D.4.6. Physical Outdoor Activity: Triathlon
It is interest to propose triathlon (swim-bike-run) in study area because there is nearshore, where distance of the promontory reach 4 Km in SE coast (Figure 3). Land route for biking and running may use main road in the southern area. Scenic beauty of Kuta Undulated and Pengulung-Kuta Rocky Coast landforms is also the advantage points for international event of sport tourism.

Potential environmental impact is interpreted low (soil erosion). Potential risk of this activity is moderate (injury). Status activity is possible.

E. Risk related to Natural Hazard
There are several geological characters in study area relate to safety should be considered for tourism. It is earthquake, ground motion vulnerability, and tsunami. Study area has high hazard zone means area potentially affected by earthquake with intensity scale of VII MMI, potentially to have earthquake features (Suartika & Turjono, 2009).

Study area also has medium degree zone for Ground Motion Vulnerability Zone (Pusat Vulkanologi dan Mitigasi Bencana Geologi, 2009). It is the area of ground motion occurred at the edge of river valley, cliff, road cut or when a slope disturbed and might triggered by heavy rain.

Flat area -particularly near bay zone- is prone to tsunami flood. Fortunately, the bay is bounded by hill in promontory. It can be used as natural evacuation area. Such area should be prepared with properly sign, board, ladder, shelter, etc. Such preparation can be used for tourism branding, such as 'the safest beach ever'.

F. Conclusion
Study area has various geological attraction potential with various attraction statuses, risk, and environmental impact (Table 2). The attraction is composed of geoscientific (proven - probable), sightseeing (proven - probable), curative (possible) and physical outdoor activity (proven – possible, depend on the type). In addition, potential risk related natural hazard such as earthquake, tsunami flood and vulnerable to ground motion in medium degree particularly on the edge of river valley, cliff, and road cut.

There is consequence of this study outcome. Firstly, there is various types of tourism markets might be influenced that is geotourism, medical or health tourism, sport tourism and adventure tourism. Those are tourism market types relate to interest types recommended.

PROCEEDINGS
JOINT CONVENTION BANDUNG (JCB)2021
November 23rd – 25th 2021

Table 2. Tourist Interest Type, Activity Status, Risk and Environmental Impact and Landform Type for each activity.

Tourist Interest Type	Activity	Proven	Probable	Possible	Risk of Activity	Environ-mental Impact	Land-form
Geoscientific	Geological activity	X	X		Low	Low	A
Scenic Beauty	Sightseeing	X	X		-	-	B (mostly)
Curative	Speleotherapy			X	-	-	C
Physical Outdoor Activity	Aerosport	X	X		Moderate	-	B
	Rock Climbing			X	Moderate to High	High	A
	Off road Motorcycle Riding		X	X	Low to Moderate	Low to Moderate	B (mostly)
	Cliff Diving			X	Moderate	-	A
	Swimming	X	X		Moerate to High	-	A
	Triathlon			X	Moderate	Low	A & B

Note
A: Pengulung-Kuta Rocky Coast
B: Kuta Undulated
C: Pengulung Isolated Carbonate

Secondly, field investigation urgency for two reasons. The first is on the site which has possible activity status, investigation is needed to ensure whether or not the activity can be performed and to ensure safety. The second is on activity risk which has particularly moderate to high risk, field investigation is needed to reduce / eliminate the risks.

Thirdly is the need of awareness on environmental impacts will be affected by each recommended tourist activity. Any activities recommended in this paper should be further evaluated whether or not the impact is accepted by local community or government.

Reference Cited

Kolich, H., (2009), How Cliff Diving Works, 5 October 2009, HowStuffWorks.com, https://adventure.howstuffworks.com/outdoor-activities/water-sports/cliff-diving.htm, visited 12 September 2021.

Mangga, S. A., Atmawinata, S., Hermanto, B., Setyogroho, B. & Amin, T.C. (1994) Geological Map of the Lombok Sheet, West Nusatenggara, Scale 1:250,000. Geological Research and Development Centre, Bandung, Indonesia.

Purnama, Y.S., (2020), Chapter 2: Reshaping Geology and Tourism Relation,p.13 – 85, in Purnama, Y.S., (2020), You Say Geotourism, I Say Tourism Geology!, Elmarkazi, 454 pp.

Purnama, Y.S., Lumanauw, N., & Rachmat, H., (2020), Chapter 10: Highlights of t he Geological-related Attractions and Turism Development off Rinjani – Lombok Geopark and Lombok Island.,p.374 – 407, in Purnama, Y.S., (2020), You Say Geotourism, I Say Tourism Geology!, Elmarkazi, 454 pp.

Pusat Vulkanologi dan Mitigasi Bencana Geologi, (2009) Peta Zona Kerentanan Gerakan Tanah Provinsi Nusa Tenggara Barat, Pusat Vulkanologi dan Mitigasi Bencana Geologi, Bandung.

Suartika, K.P. & Turjono, G., (2009) Earthquake Hazard Prone Map of Lombok Island West Nusa Tenggara, Scale 1:250,000. Pusat Vulkanologi dan Mitigasi Bencana Geologi, Bandung.

PROCEEDINGS
JOINT CONVENTION BANDUNG (JCB) 2021
November 23rd – 25th 2021

Harnessing the Operational Learning Method to Uncover Process Improvement Opportunities that Improves Process Safety and Operation Efficiency

Muhammad Riandhy Anindika Y[1], Muhammad Rismananda Pratama[1], Marthin Winner Adhyaksa Simanjuntak[1]
[1]PT. Pertamina Hulu Rokan, Duri 28784 Indonesia

Abstract
Learning is an important part of continuous improvement culture. Effective learning investigates and studies the root causes and contributing factors of a successful event or a failure event and uncover improvement opportunities to make the process safer and more efficient. One proven method for learning to improve the system holistically is operational learning. Operational learning leverages open and honest communication to learn how the work was done by the people who did the work. By having open and honest communication, it seeks to understand the context behind the actions taken by the worker and the associated human performance factors related to the work, an important aspect the root cause that traditional root cause analysis was unable to capture. Through its holistic approach that studies both the human and system aspect of the process, operational learning delivered tremendous improvement in overall process safety as well as operational efficiency. A sample of its power will be discussed in this paper taking the case of power outage response learning team as case study. The operational learning method inherently leverage friendly conversation to obtain all related contributing factors which aligned with Indonesian people's chatty culture. This advantage contributes significantly to the success of this method implementation in one of the KKKS.

In Q2 2020, an abrupt major power outage happened and caused loss of containment at multiple GS facility due to slow outage response. Operational learning method was used to identify the cause of slow response and learn how to improve response time for power outage. The learning session involved many key Operations personnel that were present during the event. During the session, the Operations personnel communicated openly about the key contributing factors. They also proposed alternative opportunities that will improve the response time to power outage that will prevent the occurrence of the loss of containment event in the future. The team successfully identified 6 major themes of issues to be improved.

One of the key improvement theme derived from the learnings that has been proven to reduce response time and increase operational efficiency is the development of fit-for-purpose online reference that provides the front-liners with the most updated condition of the power distribution network and informed its impacts to the power supply to the field. The Live One Line Diagram enabled Operations to make prompt decision to respond the changes in the power distribution network thus minimizing its impact to the plant and field operations. The presence of live one line diagram reduces the response time to power outage by 1 hour, which translated to around USD 5,000 savings per power outage.

Introduction

There are 4 pillars of Process Safety Management based on CCPS Risk Based Process Safety (Figure – 1), where one of the pillar is focused on learning from experience. Under the learning from experience pillar, there are 4 elements, namely incident investigation, measurement and metrics, auditing, management review and continuous improvement.

Learning from experience pillars involves monitoring, and acting on, internal and external sources of information. Despite a company's best efforts, operations do not always proceed as planned, so organizations must be ready to turn their mistakes – and those of others – into opportunities to improve process safety efforts. The most cost effective ways to learn from experience are to:
(1) Apply best practices to make the most effective use of available resources.
(2) Correct deficiencies exposed by internal incidents and near misses.
(3) Apply lessons learned from other organizations.

In addition to recognizing these opportunities to better manage risk, companies must also develop a culture and infrastructure that helps them remember the lessons and apply them in the future. Metrics can be used to provide timely feedback on the workings of Risk Based Process Safety management systems, and management review, a periodic honest self-evaluation, helps sustain existing performance and drive improvement in areas deemed important by management.

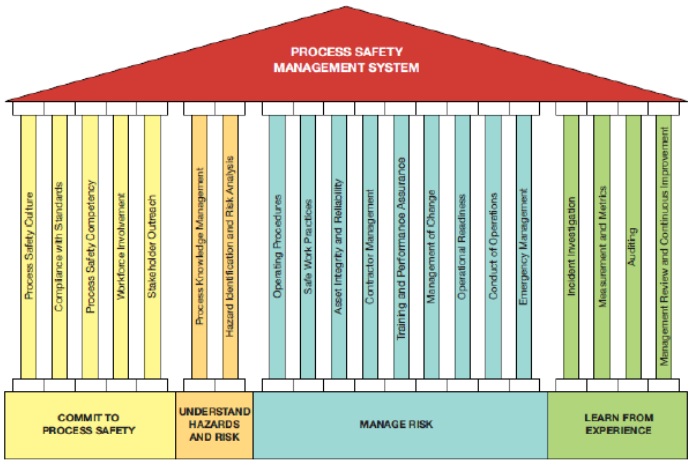

Figure 1 Risk Based Process Safety

Learning is an important part of continuous improvement culture. Effective learning investigates and studies the root causes and contributing factors of a successful event or a failure event and uncover improvement opportunities to make the process safer and more efficient. There are many tools that could be used for learning. Among them are root cause analysis and operational learning.

Root cause analysis (RCA) is defined as a formalized and systematic approach to determine the underlying reasons for an event. The underlying reasons, or best known as root causes, are the system level causes that can be reasonably

PROCEEDINGS
JOINT CONVENTION BANDUNG (JCB) 2021
November 23rd – 25th 2021

identified and that we have control to fix. If the root causes are eliminated or fixed, then the event will be prevented from recurrence. Figure 2 illustrate the RCA process using one of the most widely known method, the why tree method.

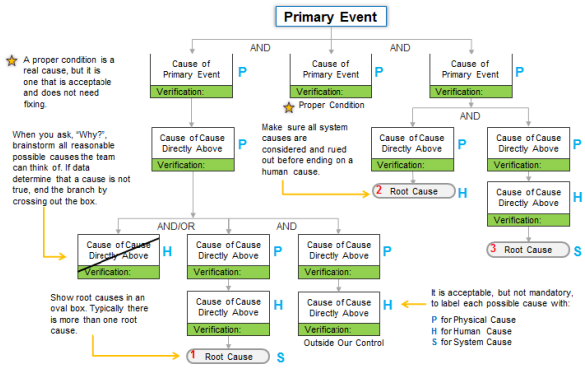

Figure 2 RCA process illustrated.

Operational learning is a method of evaluating an event though learning of work "as done" by the front line. Figure 2 illustrate the difference between the works as done vs the work as planned and the gaps that we aim to learn using operational learning method. Learning team method leverages open and honest communication to learn how the work was done by the people who did the work. By having open and honest communication, it seeks to understand the context behind the actions taken by the worker and the associated human performance factors related to the work, an important aspect that the root cause that traditional root cause analysis was unable to capture. Through its holistic approach that studies both the human and system aspect of the process, operational learning delivered tremendous improvement in overall process safety as well as operational efficiency. The method inherent intensive use of friendly conversation is aligned with Indonesian people's chatty culture which contributes significantly to the success of this method implementation in one of the KKKS in Indonesia, which will be discussed in this paper as case study.

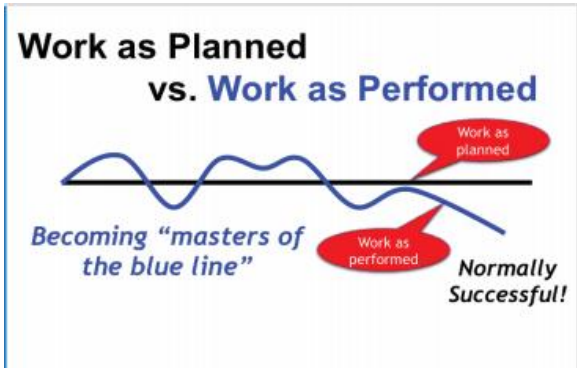

Figure 3 Operational learning illustrated

The key difference between Operational Learning and traditional why tree RCA method is in the structure of the investigation. While why tree method is structured since the beginning, operational learning is abstract in the beginning. However, through its abstraction, it can uncover the root causes and significant contributing factors that cannot be uncovered through the traditional RCA method which made it a powerful alternative to the traditional RCA method for incident investigation.

Data and Method

Operational learning bring people closest to the work together, to create a shared understanding of how a particular work activity actually gets done. This unique approach to learning provides an environment of open communication and makes it easier for others to understand the complexity involved in different types of work. When we provide the time and space for operational knowledge to be shared, we can discover and learn many things (e.g., potential vulnerabilities, how our systems' goals may conflict with one another) that can help to strengthen our safeguards.

Oftentimes, work is handed off between the owner's personnel and one or more contractor companies. When workers discuss their views, they discover they have different perspectives. During discussions, participants build off of each other's viewpoints and gain a better understanding of how to improve the work activity and do it more safely. They can identify gaps in the way people assume work is done (work as planned).

A key premise of an operational learning is that the people doing the work are best positioned to ensure safeguards are sufficient and in place. Oftentimes discussions result in improved methods to get work done. Through the operational learning process the group:

- Discovers how the system, process and people interact to get work done.
- Identifies gaps and weak signals that exist in the system or process that could result in an event.
- Identifies safeguards that can be improved or added to create capacity to fail safely.

One of the most impactful ways of learning is to recognize system gaps before they result in an event. In other words, when work is completed without incident, it does not necessarily mean that work processes and procedures were completed perfectly, rather in successful work, the combination of circumstances simply did not result in a negative outcome. By intentionally listening to the worker, we can identify weaknesses in our system that, under different conditions, may result in a negative outcome. Discussions with these workers allow us to take proactive action to reduce or eliminate that gap.

Ideally, the operational learning process can be completed in four hours or less. However, the four hours should be split into two sessions. Provide a one-hour break or overnight period between sessions to allow participants to consider discussions from the first session.

Figure 4 illustrate the operational learning process and its sessions. There are 5 steps in conduction operational learning:

1. Prepare
    a. Define the scope – not too broad, not too narrow
    b. Pull the right people together
2. Session 1 – learn
    a. Takes around 60–90 minutes
    b. Learn and discover how work gets done vs. how it should be done
    c. Discuss conditions around the work
3. Soak

a. Ideally soak time is overnight, but it can be over an extended lunchtime between session 1 and 2
b. New insights may emerge that can be shared in session 2

4. Session 2 – brainstorm & prioritize
   a. Identify the error traps and evaluate the safeguards
   b. Agree on what to improve first
   c. Capture ideas that are within the team's control to try
5. Take action
   a. Document and share the learning team results with leadership
   b. Implement the approved solutions and confirm they are working as intended
   c. Share lessons learned with others

Figure 4 Operational learning process

As a case study to see how the method is implemented, we will discuss the abrupt major power outage that happened at one of the KKKS operational area and caused loss of containment at multiple gathering station facilities due to slow outage response in Q2 2020. Operational learning method was used to identify the cause of slow response and learn how to improve response time for power outage. The learning session involved many key Operations personnel that were present during the event, who knew the event to the little details.

During the session, the Operations personnel communicated openly about the event chronology, how was their state of psychology and health during the event, the situation they were in, the challenges that they faced in responding to the event and other concerns. All of those concerns, opinions and statements were properly documented by the facilitators as basis for finding the root causes and the key contributing factors of the event. After all of the concerns were properly noted, the team moved to identification of root causes based on the notes in the documentation. The team successfully grouped the issues that was jotted down in the notes and identified 6 major themes of issues to be improved. The team brainstormed alternative opportunities that could be proposed to improve the response time to power outage which will prevent the occurrence of the loss of containment event in the future.

If the investigation is carried out using the traditional RCA method, only root causes that directly related to event will be uncovered. All other root causes, especially related to human performance will not be uncovered. Therefore, there will be possibilities that in the future the human performance root cause will cause similar incident to occur.

Result and Discussion

One of the key improvement theme derived from the learnings that has been proven to reduce response time and increase operational efficiency is the development of fit-for-purpose online reference that provides the front-liners with the most updated condition of the power distribution network and informed its impacts to the power supply to the field. The reference, called The Live One Line Diagram, enabled Operations to make prompt decision to respond the changes in the power distribution network thus minimizing its impact to the plant and field operations. The presence of live one line diagram reduces the response time to power outage by 1.3 hour from 2.71 hours/outage to 1.4 hours per outage, which translated to around USD 5,000 savings per power outage. Within the first 2 months of its commencement the Live One Line Diagram has delivered a total benefit of USD 744,410 from loss of production avoidance due to shorter response time to power outage.

The identification of such high value improvements was enabled by the inherent nature of openness in the method itself, which allows the team involved in the learning to see the process as it is without the bias of what the process should have been. The team openly communicated that the lack of accurate reference in responding to the event was the main cause of the slow response. Therefore it was the most prioritized area to be improved, which was confirmed to deliver the highest improvement value to operations.

Conclusions

- Operational learning was able to deliver more tremendous improvement in overall process safety as well as operational efficiency compared to traditional root cause analysis due to its inherent openness in learning how the work was done by the people who did the work and its focus on human performance.
- Operational learning method inherently exploits intensive use of friendly conversation which is aligned with Indonesian people's chatty culture. This contributes significantly to the success of this method implementation in Indonesia.

References

1. Sullivan, Mark, Sahika Korkmaz, Matt Korfist, Tanya Lughermo, Errol Munro, 2018, Operational Learning Pocket Guide

PROCEEDINGS
JOINT CONVENTION BANDUNG (JCB) 2021
November 23rd – 25th 2021

Effect of Structural Density on Peridotite Rock Quality, East Kolaka, Southeast Sulawesi

Bambang Hambar Eko Prasetyo – Independent Researcher

Abstract

Construction works has facing a rapid expansion by means development any infrastructure facilities to enhance national economics. Infrastructure developing that being main work is national road, higway road, bridge, dam, building nor another public facilities. Infrastructure work needs various supporting material of construction, ones is a rocks. The aim of this research to know how geological structure influenced rock quality of peridotite which is include as ultramafic rock that affordable for construction material. Approach method that applied is fault fracture density (FFD) using SRTM 1 arc-second remote sensing by hill, valley and river lineament. Rock quality testing consist of compressive strength, bulk specific gravity and soundness test. Laboratory testing of rock sample based on SNI 2825-2008, SNI 03-2437-1991 and SNI 3407-2008. Lineament from SRTM remote sensing obtained density value of structure at location A B and C successive 5,11 km/km² ; 2,77 km/km² ; and 6,64 km/km². Result from compressive strength testing obtained a successive value 1.091,76 kg/cm² ; 1.562,13 kg/cm² ; and 556,67 kg/cm². Bulk specific gravity testing in a successive value 3,263 ; 3,336 ; and 2,907. And soundness test is 1,07% ; 0,89% ; and 1,94%. Correlation between lineament structure from FFD method explain that location B have a low density. Its impact to good rate of rock quality just than another location with high rate of strength and bulk specific gravity and low rate of soundness value. Inspite of that, in a general three rock location is affordable in usage all of that as a supporting material for construction due to appropriate with construction technical specification.

Keyword: *structure, FFD, UCS, Soundness, Quality*

Introduction

In recent years, work in the construction sector has experienced a significant increase. This demands to maximize the potential of natural resources that exist in each region. The southeastern arm of Sulawesi has abundant peridotite rock manifestations. These rocks are black-green ultramafic igneous rocks located in the limestone-aged ultramafic (Ku) complex formation. In East Kolaka district, there are several places where the mountains appear composed of peridotite rocks, where the distribution is not continuous. Observations and data taken are based on three mountainous locations, namely locations A, B and C which can be seen in the following (**Figure 1**).

In terms of engineering, there are several aspects that need to be considered from peridotite rocks to be used as construction materials. These aspects include compressive strength, specific gravity, soundness, and so on depending on the technical specifications of each field of construction work.

In terms of geology, the main aspect that will greatly affect the engineering value of rocks is the presence of rock structures on a micro scale and morphological lineament on a macro scale. Therefore, it is reviewed qualitatively on the morphological lineament to determine the density of the structure in the peridotite rock mountains.

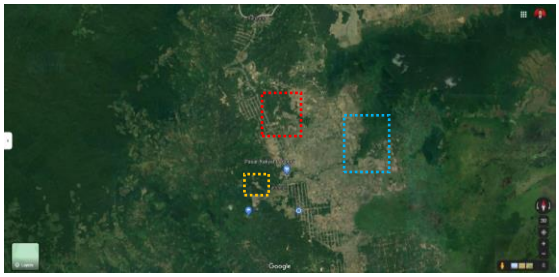

Figure 1: Location Map of Peridotite Manifestation

Data and Method

In this study using two main methods, namely geology and geomechanics.

- Geology section, the method used is morphological lineament using SRTM 1-Arc second satellite imagery to then draw the lineaments morphology.
- Geomechanics section, sample testing in the laboratory uses standard reference testing procedures from SNI 03-2437-1991 (Methods to determine the parameters of the physical properties of rock samples), SNI 3407-2008 (Method of testing the conservation of aggregate properties by immersion using sodium sulfate solution or magnesium sulfate), SNI 2825-2008 (Uniaxial rock compressive strength test method).

After the morphological lineament analysis and rock engineering tests are carried out, the final results of the analysis can be obtained.

Result and Discussion

Lineament Morphology

Analysis of the 1-Arc second SRTM satellite image aims to obtain a linearization of morphology. Liniation can indicate the existence of a structural pattern, the presence of a structure and the level of density.

Based on the results of the analysis, it can be seen that the structural patterns that work at each location have different directions. Locations A and B have the same direction, which is northwest-southeast. Location C is relatively north-south (**Figure 2**).

PROCEEDINGS
JOINT CONVENTION BANDUNG (JCB) 2021
November 23rd – 25th 2021

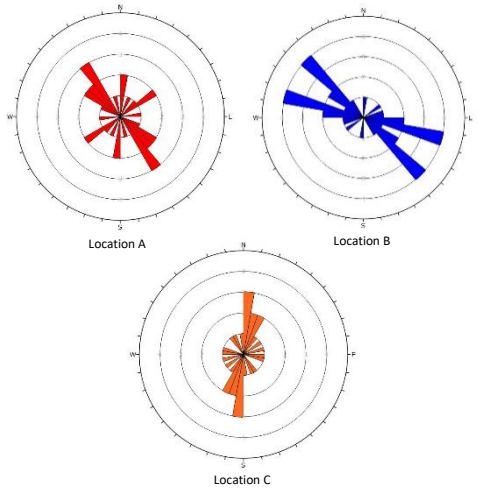

Figure 2 : Lineament Pattern of Peridotite Mountains

If the rock mass is assessed based on the rock mass rating (*RMR*), the rock mass values will be 69 (*good rock mass*), 71 (*good rock mass*) and 51 (*fair rock mass*). Rock mass values can characterize rock mechanical parameters empirically. Rocks in the good category have a cohesion value of 0.3-0.4 MPa and an internal friction angle of 35-45°, while the fair category has a cohesion value of 0.2-0.3 MPa and an internal friction angle of 25-35° (**Tabel 1**).

Tabel 1 : Rock mass rating in peridotite quarry

ROCK MASS RATING (Bieniawski, 1979)					
Nama Lokasi : Quarry A			Nama Batuan : Peridotite		
NO	**PARAMETERS**	**UNIT**	**VALUE**	**DESCRIPTION**	**RATING**
1	Strength of Intact Rock	Mpa	100 - 250	Very Strong	12
2	Rock Quality Designation	%	75 - 90	Good	17
3	Spacing of Discontinuity	m	0,6 - 2 m	Wide	15
4	Condition of Discontinuity				
	a. Discontinuity Length	m	3 - 10 m	Moderate	2
	b. Separation / Aperture	mm	> 5 mm	> 5 mm	0
	c. Roughness of Discontinuity Surface	-	Slightly Rough	Slightly Rough	3
	d. Infillings / Gouge	mm	Hard Filling > 5 mm	Hard Filling > 5 mm	2
	e. Weathering Discontinuity Surface		Moderately Weathered	Moderately Weathered	3
5	Groundwater Condition	L/min	0	Completely Dry	15
	TOTAL RMR RATING =				**69,00**

ROCK MASS RATING (Bieniawski, 1979)					
Nama Proyek : Quarry B			Nama Batuan : Peridotite		
NO	**PARAMETERS**	**UNIT**	**VALUE**	**DESCRIPTION**	**RATING**
1	Strength of Intact Rock	Mpa	100 - 250	Very Strong	12
2	Rock Quality Designation	%	75 - 90	Good	17
3	Spacing of Discontinuity	m	0,6 - 2 m	Wide	15
4	Condition of Discontinuity				
	a. Discontinuity Length	m	3 - 10 m	Moderate	2
	b. Separation / Aperture	mm	> 5 mm	> 5 mm	0
	c. Roughness of Discontinuity Surface	-	Slightly Rough	Slightly Rough	3
	d. Infillings / Gouge	mm	Hard Filling > 5 mm	Hard Filling > 5 mm	2
	e. Weathering Discontinuity Surface	-	Slighty Weathered	Slighty Weathered	5
5	Groundwater Condition	L/min	0	Completely Dry	15
	TOTAL RMR RATING =				**71,00**

ROCK MASS RATING (Bieniawski, 1979)					
Nama Proyek : Quarry C			Nama Batuan : Peridotite		
NO	**PARAMETERS**	**UNIT**	**VALUE**	**DESCRIPTION**	**RATING**
1	Strength of Intact Rock	Mpa	50 - 100	Strong	7
2	Rock Quality Designation	%	50 - 75	Fair	13
3	Spacing of Discontinuity	m	0,2 - 0,6 m	Moderate	10
4	Condition of Discontinuity				
	a. Discontinuity Length	m	3 - 10 m	Moderate	2
	b. Separation / Aperture	mm	> 5 mm	> 5 mm	0
	c. Roughness of Discontinuity Surface	-	Smooth	Smooth	1
	d. Infillings / Gouge	mm	Soft Filling > 5 mm	Soft Filling > 5 mm	0
	e. Weathering Discontinuity Surface	-	Moderately Weathered	Moderately Weathered	3
5	Groundwater Condition	L/min	0	Completely Dry	15
	TOTAL RMR RATING =				**51,00**

Then the density analysis of the structure was carried out at the three locations resulting in different density values. At location "A" the density value of the structure 5,11 km/km², location "B" has the value 2,77 km/km² and location "C" has the value 6,64 km/km² (**Figure 3**).

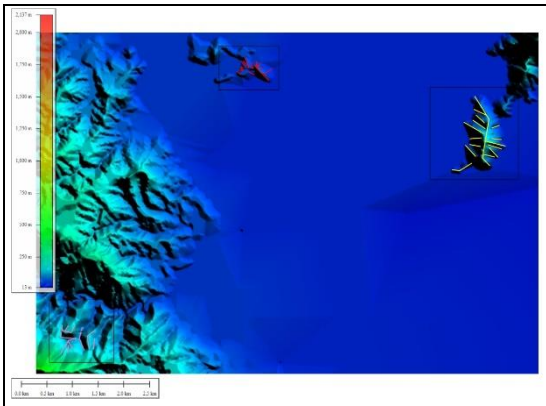

Figure 3 : Lineament Morphology Using SRTM 1-Arc Second

Geomechanics Testing

Geomechanical testing in the laboratory was taken from rock samples from quarry locations A, B and C. The rock samples were used to determine rock engineering parameters, including compressive strength, specific gravity and soundness as shown in the table below (**Tabel 2**).

Tabel 2 : Summary of peridotite rock engineering test

No	Engineering Parameters	Location		
		A	B	C
1	Uniaxial Compressive Strength (kg/cm²)	1.091,76	1.562,13	556,67
2	Spesific Gravity	3,263	3,336	2,907
3	Soundness (%)	1,07	0,89	1,94

Based on the table above, it can be seen that from the three observation locations, location "B" is the area with the highest average sample with a higher compressive strength value of 470,37 kg/cm2 compared to location "A" and 1,005.46 kg/cm2 compared to location "C". Specific gravity value location "B" is 0.073 greater than location "A" and 0.429 greater than location "C". The percentage of soundness value at location "B" is 0.18 less than location "A" and 1.05 less than location "C". So that, the technical parameter values can be sorted from the highest to the lowest value based on location, namely locations B, A and C.

Rock Quality Relationship

All geological and geomechanical data are connected or correlated to obtain the quality of the peridotite rock mass at each of the observation sites. The structural density which has the lowest value is the best because the rock does not have intense cracking. The lowest density is at location "B" with a result of 2.77 km/km².

The high compressive strength of rock and specific gravity will provide additional resistance and strength to concrete, embankments, and counterweights. The highest value is at location "B" with a compressive strength of 1562.13 kg/cm² and a specific gravity of 3.336. While the lower soundness will provide good resistance to the chemical effects of

climate change. Location "B" has the lowest soundness value, which is 0.89%.

So it can be assumed that location "B" has the best potential to be used as construction material. However, locations "A" and "C" can also be used in construction work considering their relatively high parameters.

Conclusions

Based on the observations and data analysis that has been done, it can be concluded that:

a. The structural density obtained from lineament morphology shows that location B has the lowest structural density, while location C has the highest structural density.

b. The rock engineering parameter at location B is the best because it has high compressive strength and specific gravity values and low soundness.

c. In general, peridotite rocks at all locations are good enough to be used in civil construction buildings, it is necessary to adjust the technical specifications of each work.

References

Bieniawski, Z.T .1989. Engineering Rock Mass Classification. John Wiley & Sons : Canada

Rocksciences. 2019 . Dips 7.0 Graphical and Statistical Analysis of Orientation Data. Rocksciences

Singh, Bhawani., and Goel. R.K, 2011, Engineering Rock Mass Classification. Butterworth-Heinemann : Toronto

SNI 03-2437-1991. Metode Pengujian Laboratorium untuk Menentukan parameter Sifat Fisika Pada Contoh Batu.

SNI 3407-2008. Cara Uji Sifat Kekekalan Agregat Dengan Cara Perendaman Menggunakan Larutan Natrium Sulfat atau Magnesium Sulfat.

SNI 2825-2008. Cara Uji Kuat Tekan Batu Uniaksial.

Trip, Gerald .2004. Fault/Fracture Density and Mineralization: a Contouring Method for Targeting in Gold Exploration. Journal of Structural Geology : Australia

PROCEEDINGS
JOINT CONVENTION BANDUNG (JCB) 2021
November 23rd – 25th 2021

Application of Decision-Making Model Based on Slope Stability Limit Equilibrium Analysis to Determine Safest and Most Beneficial Method in Open Pit Waste Dumping

Rieza Rachmat Putra[1], Guruh Charismaputra[2], Rama Surya Purnama[3]

[1]Thiess Indonesia, [2]Meares Soputan Mining, [3]Arutmin Indonesia

Abstract

Fast-paced and demanding-safe-factor are two inseparable components in open pit mining activity. All limitation related to design execution must be mapped properly to resulting measured controllable method in order to construct waste disposal from pit removal materials. This paper will focus on bridging the precursor analysis for geotechnically safest waste dump stage plan with unit availability to removing geotechnical hazard during construction using bulldozer D8 and D10 class of heavy equipment. Limit Equilibrium Method (LEM) used to identify the global minimum safety factor that has framed into decision tree model.

Decision tree model (DTM) was built with two basic criterion of waste dump design: slope height on 5 and 10 meters, slope angle on 25, 30, 37, 40 degrees as designated primary and secondary input. Process of DTM will presumed causing two types of failure: cracking on tip-head (TH) and cracking on designated distance (DD) of dumping point. All of the DTM will resulting degree of consequences each unit of bulldozer with respecting to construction and repairing the volume of failure cost.

Results of DTM shows the threshold of safest and conventional way of dumping process is using 5 meters height and 25 to 30 degrees of slope angle both in tip-head and designated distance. Any condition necessary to implement above the threshold must not exceed 10 meters height and 25 degrees of slope angle as resulted will causing unstable condition on tip-head and crowded surface for D10 and not applicable for D8 class.

This engineering processes give us a detail of safety factor and unit availability matrix to solve a limitation of design execution at open pit mining area. Given matrix also can provide preliminary assessment for any given design planned at working area which can be useful to develop new standard of geotechnical risk management in the future.

Keywords: decision-making, risk management, slope stability.

Introduction

The purpose of mining activity is to achieve safest operation with avoid the landslide hazard. Mining outline must consider geotechnical hazard during plan and execution. Working area is currently has limitation about design provided which also not considering about detailed geotechnical assessment and need to be bridged.

Regarding to geotechnical hazard in dumping activity, we focus to identify the safest and effective way of dumping process in waste dump with optimization of dozer availability.

The dumping activity itself are considered as high-risk activity due to its construction are beyond design criteria. Thus, it shall managed with putting additional control such as predicted crown-failure location.

Controlled crown-failure location supposed to be eliminated by dozing activity, started from outer arc of the crown and smoothed it to the toe of disposal.

Data and Method

The study will be conducted by using Decision Tree Model (DTM), which consists of framework for dealing with difficult decision-making processes in order to lead decision makers to make better decisions.

Basically, DTM can provide structured way of think about decision and required structure. The purpose of DTM is to help a decision maker to think systematically about complex problems and improve the quality of resulting decision. DTM will consists of two basic criterion of waste dump design: slope height on 5 and 10 meters, slope angle on 25, 30, 37, 40 degrees as designated primary and secondary input as shown in figure 1.

Field observation shows that dumping activities will causing two types of failure: cracking on tip-head (TH) and cracking on 15 meters as designated distance (DD) of dumping point and then to be inputted into geotechnical modelling. DTM will processing the consequences degree of two class of bulldozer (D8

and D10) with respecting to construction and repairment of failure cost.

Result and Discussion

General iteration resume

Tip head stability reach minimum safety threshold if only use 20 30 degree with 5 meters of slope height, critical condition in 33 40 degree with 5 meters of slope height. All of slope design within 10 meters height will causing tip head instability.

Designated distance stability reaches minimum safety threshold if only use 25 degree with 10 meters of slope height, critical condition in 30 degree with 10 meters of slope height All of slope design within 5 meters height will produce safe designated distance stability.

Bulldozer D8 Utilization

All of 5 meters design produce no repairing allocation. As per geotechnical models only shows tip head instability. Dozer D8 will only run for smoothing on crest no longer than 0.8 – 1.0 hour of work.

All of 10 meters design will require minimum construction hours allocation. As per geotechnical models shows only 25 degree of slope angle will not causing excessive work for dozer D8. Greater than 25 degree will causing required excessive repairing hours (6-8 hours) as shown in figure 3.

Bulldozer D10 Utilization

All of 5 meters design produce no repairing allocation. As per geotechnical models only shows tip head instability Dozer D10 will only running for smoothing on crest no longer than 0.5 hours work.

All of 10 meters design will require minimum construction hours allocation. As per geotechnical models shows only 25 degree of slope angle will not causing excessive work for dozer D 10 (only A) Greater than 25 degree will causing required excessive repairing hours (2-4 hours) as shown in figure 4.

Conclusions

As shown in table. 2 Geotechnical model iteration shows conservatives way of sequences in dumping activity is to create 5 meters of disposal height with 25 30 degrees of slope angle (available for D10 and D8).

With 5 meters height and 37-40 degrees design, only D10 are executable smoothing in tip head failure.

With 10 meters height design, will causing instability tip head area. Allocation of D10 still causing crowded condition at disposal, need to relocate the dumping point at the lower level to accommodate the volume.

References

Arifani, Widjojo, Risk based decision making in highway slope geometry design, MATEC Web of Conferences 270, 02001 (2019) ConCERN 2 2018.

J. Rupke, M. Huisman, H.M. Kruse, Stability of Man Made Slopes, Eng. Geol., 91, 16 24, (2007)

K. K. Phoon, F. Kulhawy , M.D. Grigoriu , Reliability Based Design of Foundation for Transmission Line Structure (Cornell University, Geotechnical Engineering. Ithaca, New York: Electric Power Research Institue. 1995)

K. K. Phoon, J. V. Retief, Reliability of Geotechnical Structure in ISO2394 (CRC Press, 2016) 5.

K. K. Phoon, Reliability Based Design in Geotechnical Engineering (Taylor & Francis, 2008).

PROCEEDINGS
JOINT CONVENTION BANDUNG (JCB) 2021
November 23rd – 25th 2021

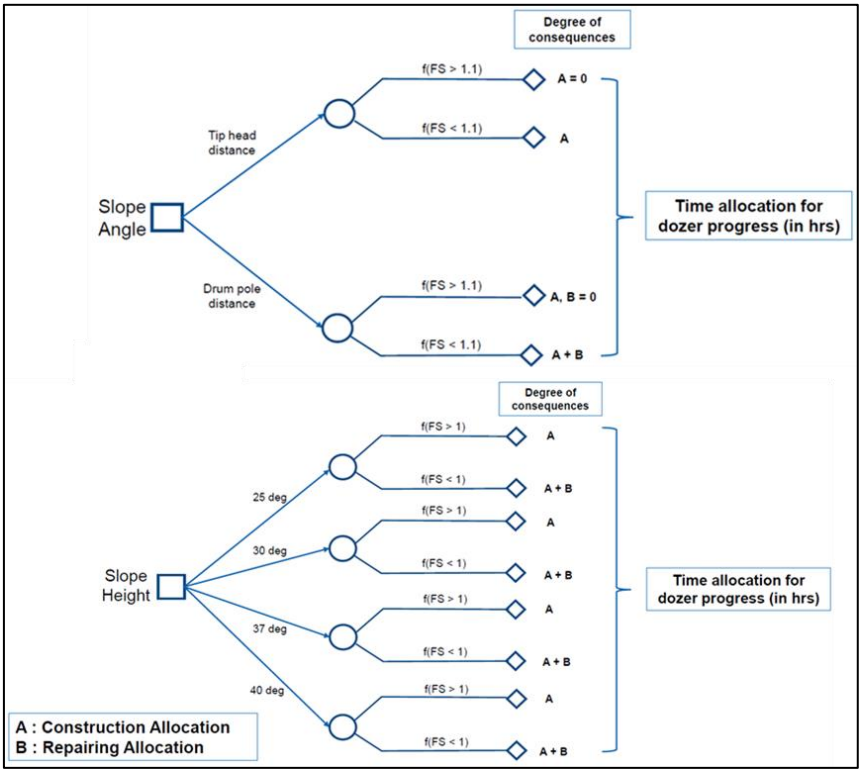

Figure 1: Decision Tree Model (DTM) framework for disposal design study

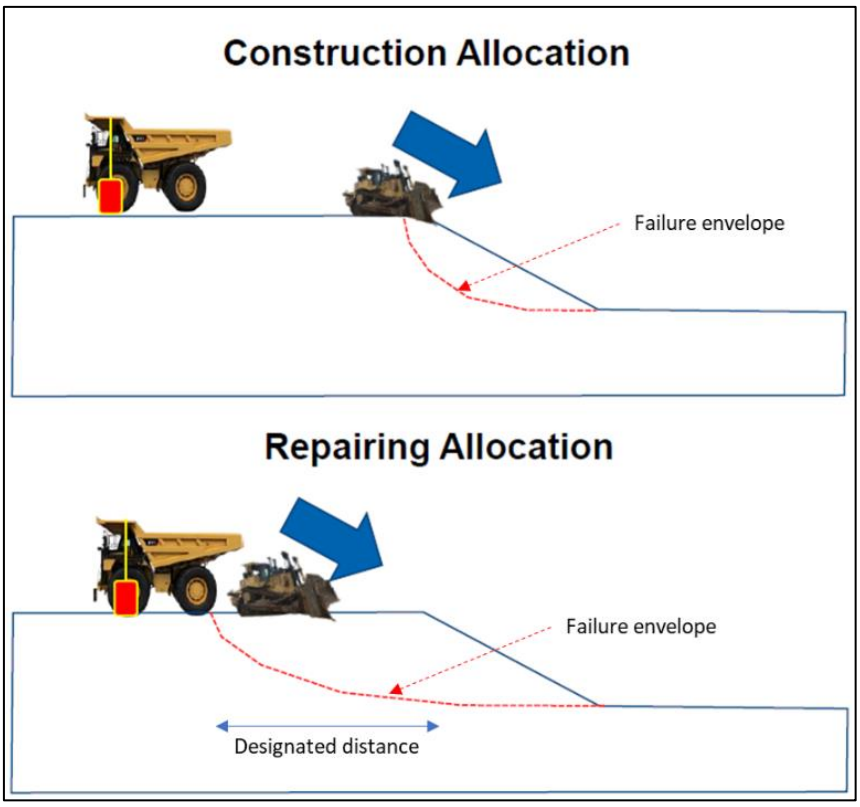

Figure 2: Illustration of dozer activity in predicted failure area which classify as construction and repairing allocation

PROCEEDINGS
JOINT CONVENTION BANDUNG (JCB) 2021
November 23rd – 25th 2021

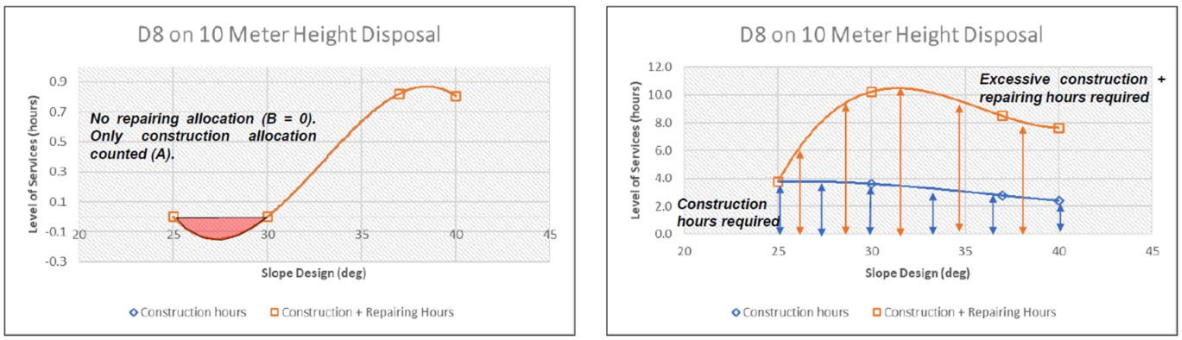

Figure 3: Left: D8 class bulldozer level of service in 5 meters height disposal. Right: D8 class bulldozer level of service in 10 meters height disposal

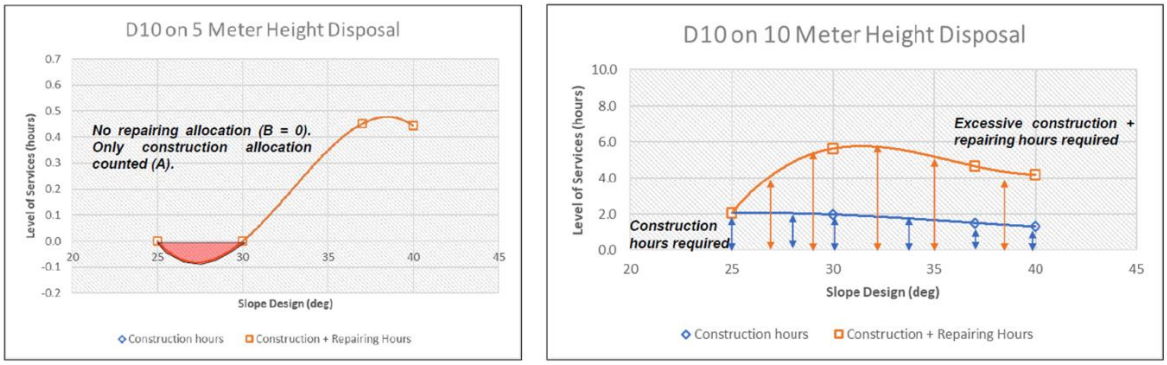

Figure 4: Left: D10 class bulldozer level of service in 5 meters height disposal. Right: D10 class bulldozer level of service in 10 meters height disposal

PROCEEDINGS
JOINT CONVENTION BANDUNG (JCB) 2021
November 23rd – 25th 2021

Table 1. Resume of iteration

Slope Height (m)	Slope Angle (deg)	Safety Factor		Failure Section Volume (BCM)		Level of Services at crest disposal (hrs) - D10			Level of Services at crest disposal (hrs) - D8		
		Tiphead (Global Minimum)	Designated Distance	Tiphead	Drum Pole Distance	Construction (A)	Repairing (B)	Construction + Repairing (A+B)	Construction (A)	Repairing (B)	Construction + Repairing (A+B)
5	25	1.301	1.613	749.56	1,638.55	0.0	0.0	0.0	0.0	0.0	0.0
	30	1.172	1.529	565.54	1,501.63	0.0	0.0	0.0	0.0	0.0	0.0
	37	1.044	1.4	451.08	1,279.25	0.5	0.0	0.5	0.8	0.0	0.8
	40	1.002	1.391	443.36	1,334.04	0.4	0.0	0.4	0.7	0.0	0.7
10	25	0.99	1.174	2,054.18	3,385.18	2.1	0.0	2.1	3.4	0.0	3.4
	30	0.938	1.002	1,987.47	3,640.64	2.0	3.6	5.6	3.3	6.1	9.4
	37	0.82	0.973	1,528.36	3,142.61	1.5	3.1	4.7	2.5	5.2	7.8
	40	0.787	0.931	1,319.19	2,883.12	1.3	2.9	4.2	2.2	4.8	7.0

Dozer D10 pdty	1,000	BCM/hrs
Dozer D8 pdty	600	BCM/hrs

Table 2. Disposal risk matrix of study area

Disposal Risk Based Matrix			Safety Factor		Level of Services	
			Tiphead (Global Minimum)	Drum Pole Distance	D10	D8
Slope height (m) and slope (deg)	5	25	Stable	Stable	Executable	Executable
		30	Stable	Stable	Executable	Executable
		37	Critical	Stable	Executable	Crowded
		40	Critical	Stable	Executable	Crowded
	10	25	Unstable	Stable	Crowded	Not_applicable
		30	Unstable	Critical	Crowded	Not_applicable
		37	Unstable	Unstable	Crowded	Not_applicable
		40	Unstable	Unstable	Crowded	Not_applicable

PROCEEDINGS
JOINT CONVENTION BANDUNG (JCB) 2021
November 23rd – 25th 2021

Optimization of Highwall Pit Y – East Asam Area based on Geotechnical Mapping Data

Zohar Mustari[1], Teten Risyana[1]
1. PT. Arutmin Indonesia

Abstract

East Asam area is a part of Asamasam Mine located in Jorong District, Tanah Laut Regency, South Kalimantan. Pit Y is an open pit mine in East Asam which still has economic reserves and has not been mined optimally. The lack of geotechnical drilling data in the East Asam is one of the obstacles in conducting slope stability analysis in this area. Last data from geotechnical drilling was carried out in 2014 with total 5 drillholes, where all of them located on the west side of the Pit Y.

Geotechnical mapping is a method to collect rock properties data from outcrops. Other than that, the aims of geotechnical mapping are to describe the slope stratigraphy and identify weak plane (joint, bedding, fault) and their orientation also weak layer such as carbonaceous mudstone. To cover all lithology of Pit Y, geotechnical mapping was carried out in several parts, including Lowwall, Highwall, West Sidewall, and East Sidewall. Result from this mapping consists of : type of lithology, lithology thickness, strength, and discontinuities information (persistence, roughness, filling, aperture, weathering, etc).

Preliminary analysis based on geotechnical drillhole samples in 2014 shows that the Highwall Pit Y can be construct with maximum overall slope 30° and maximum overall height 110 m. With the additional data from geotechnical mapping, design Highwall Pit Y can be optimized to be stepper. This optimization design can also reduce the stripping ratio (SR), so this will affect to efficiency of mining costs.

Keywords: highwall, optimization, overall slope, safety factor

Introduction

Asam Asam Mine is one of the open pit mining which owned by PT. Arutmin Indonesia. Asam Asam Mine, situated at Jorong, Tanah Laut Regency approximately 121 km south east of Banjarmasin **(Figure 1)**.

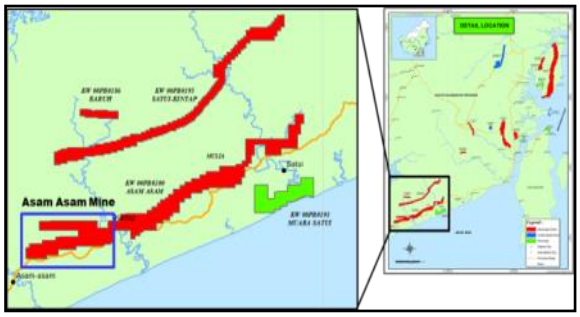

Figure 1. Asam Asam Mine location

East Asam is one of mining area at the Asam Asam Mine. There are 2 mining areas in the East Asam, namely Pit Y and Pit Z. The Pit Z area has been mined out since 2018 and became an inpit dump. Meanwhile, the Pit Y is still became an active pit until the end of 2020.

Mining activity in Pit Y is planned to be reactivated soon so it need optimal and efficient mine planning. One of them is by designing mine slope as steep as possible to minimize the overburden volume so it can reduce stripping ratio and mining costs. The constraint in designing mine slope in the East Asam area is the lack of geotechnical data. There are only 5 geotechnical drillholes. All of them located on the west side of Pit Y and Pit Z. This causes a lack of confidence to use material properties data from drillholes to design the mine slope, especially in the Middle and East part of Pit Y.

One of the methods to obtain material properties data apart from drillhole is by conducting geotechnical mapping. This project aims to get the optimal slope angle that may be construct at Highwall Pit Y based on geotechnical mapping data so it meets the safety criteria based on the FoS value which have determined.

Figure 2. Drone view of Pit Y East Asam

PROCEEDINGS
JOINT CONVENTION BANDUNG (JCB) 2021
November 23rd – 25th 2021

Regional Geology of Asam Asam Mine

Asam Asam Mine is located in Tanah Laut Regency, South Kalimantan. Regionally, Asam-Asam Mine is included in Banjarmasin Sheet (N. Sikumbang & R. Heryanto. 1994). Asam-Asam Mine located in the intersection of two tertiary basins, Asam-Asam Basin located in the South and Juntai Basin in the North. Both basins was formed during Paleocene then reactivated in Tertiary period.

Sedimentary rocks in Asam-Asam Mine are part of the Warukin Formation (Tmw) which is dominated by coarse-fine grained quartz sandstones, conglomerate, claystone with siltstone laminated, and sub-bituminous coal which deposited in Miocene.

Coal deposits in Asam Asam Mine are included in the Warukin Formation which has a relatively southwest-northeast direction with a relative slope of 25 ° - 45 ° towards the Southeast.

Data and Method

a. Material Properties Data

Material properties data were obtained from laboratory tests of rock core samples. These core samples were obtained from geotechnical drilling which carried out in Asam Asam Mine. These core samples then prepared and tested in geotechnical laboratory, including Direct Shear (DS) and Physical Properties (PP) tests.

Table 1. Material properties of Pit Y based on geotechnical drilling

From	To	Thickness (m)	Lithology	Cohesion (KPa)		Internal Friction Angle (...°)		Density (kN/m3)
				Peak	Residual	Peak	Residual	
47.70	92.81	45.11	Claystone	132	72	24.12	15.21	19.10
92.81	97.30	4.49	Sandstone	165	91	33.51	17.54	18.90
97.30	156.57	59.27	Claystone	129	69	25.07	14.61	20.70
156.57	188.21	31.64	Sandstone	117	71	29.70	19.71	21.70
188.21	201.35	13.14	Claystone	129	69	25.07	14.61	20.70
201.35	211.19	9.84	Sandstone	117	71	29.70	19.71	21.70
211.19	216.35	5.16	Claystone	129	69	25.07	14.61	20.70
216.35	224.97	8.62	Sandstone	117	71	29.70	19.71	21.70
224.97	244.43	19.46	Claystone	129	69	25.07	14.61	20.70
244.43	253.40	8.97	Coal BU1	153	54	49.92	38.07	13.40

b. Geotechnical Mapping

Geotechnical mapping is a procedure to determine the quality of rock mass (Norokallio, 2015). Geotechnical mapping can be performed by two procedures :

1. Scanline mapping
   Geotechnical mapping procedure by measuring and documenting the characteristics of all areas of discontinuity that intersect the measurement line / sampling line (Read & Stacey, 2009)
2. Window mapping
   Geotechnical mapping procedure by collecting all discontinuity field data in a certain area (Read & Stacey, 2009)

In order to identify the quality of rock mass, it is necessary to classify the rock mass. To classify rock mass there are several parameters that can be indicators of rock mass quality, including:

- Uniaxial Compressive Strength (UCS)
  The maximum stress given to material sample before the sample breaks
- Rock Quality Designation (RQD)
  The percentage between total core recovery with ≥10 cm length with the total core length in one drilling run (Deere, 1989). The equation to get the RQD value is :

$$RQD = \frac{\text{total core recovery with} \geq 10\text{ cm}}{\text{total core length}} \times 100\%$$

- Joint spacing
  Distance between joints at core in one drilling run (Palmstrom, 2001). The equation to get the joint spacing value is :

$$\text{Joint spacing} = \frac{\text{Drilling run length}}{\text{Joint frequency in one drilling run}}$$

- Joint condition;
  Discontinuity plane conditions which include : joint length, joint width, joint surface roughness, type of joint filling material, and weathering level.
- Groundwater condition
  A measure that states the presence of water in the discontinuity plane

There are several methods to classifying rock mass :

a. Rock Mass Rating (RMR) Method
   RMR method introduced by Bieniawski (1989). With the RMR method, weighting is refers to 5 parameters rock mass quality include UCS, RQD, joint spacing, joint conditions, and groundwater conditions. After weighting the five parameters, then the weights are added to get the total value of the five weights. The RMR weighting is shown in the Figure 3.
b. Geological Strength Index (GSI) Method
   GSI method only considers two parameters of rock mass quality indicators (weight of joint conditions and RQD) to calculate it.

A. CLASSIFICATION PARAMETERS AND THEIR RATINGS									
Parameter			Range of values						
1	Strength of intact rock material	Point-load strength index	>10 MPa	4 - 10 MPa	2 - 4 MPa	1 - 2 MPa	For this low range - uniaxial compressive test is preferred		
		Uniaxial comp. strength	>250 MPa	100 - 250 MPa	50 - 100 MPa	25 - 50 MPa	5 - 25 MPa	1 - 5 MPa	< 1 MPa
	Rating		15	12	7	4	2	1	0
2	Drill core Quality RQD		90% - 100%	75% - 90%	50% - 75%	25% - 50%	< 25%		
	Rating		20	17	13	8	3		
3	Spacing of		> 2 m	0.6 - 2. m	200 - 600 mm	60 - 200 mm	< 60 mm		
	Rating		20	15	10	8	5		
4	Condition of discontinuities (See E)		Very rough surfaces Not continuous No separation Unweathered wall rock	Slightly rough surfaces Separation < 1 mm Slightly weathered walls	Slightly rough surfaces Separation < 1 mm Highly weathered walls	Slickensided surfaces or Gouge < 5 mm thick or Separation 1-5 mm Continuous	Soft gouge >5 mm thick or Separation > 5 mm Continuous		
	Rating		30	25	20	10	0		
5	Groundwater	Inflow per 10 m tunnel length (lm)	None	< 10	10 - 25	25 - 125	> 125		
		(Joint water press)/ (Major principal σ)	0	< 0.1	0.1, - 0.2	0.2 - 0.5	> 0.5		
		General conditions	Completely dry	Damp	Wet	Dripping	Flowing		
	Rating		15	10	7	4	0		

Figure 3. RMR classification parameters and ratings (Bienawski, 1989)

Geotechnical mapping was carried out in 4 areas which covering from Lowwall to Highwall Pit Y. The mapping procedure uses scanline mapping by stretching a rope on outcrop that will be described.

Some of the parameters that will be described include :

- Lithology
- Top & Bottom Lithology
- Discontinuity information :

PROCEEDINGS
JOINT CONVENTION BANDUNG (JCB) 2021
November 23rd – 25th 2021

- Persistence

Persistence in discontinuities can be measured but the opportunity to make these measurements is limited to outcrop scale so persistence cannot be measured from rock core (Price et al., 2008).

- Roughness

Surface area of discontinuity can have a certain level of roughness. The level of surface roughness of discontinuity plane can be observed from surface waveform.

- Infill

Some defect can be filled with certain materials. This filling material can be claystone, shale, gouge, quartz, and calcite.

- Aperture

Aperture is the width of defect in discontinuity plane, either open or filled with material. The fracture shear strength will be high if fracture gap or joint is very tight.

- Weathering

Degree of weathering in discontinuity plane can be observed through the color of material in discontinuity plane. The more a material decomposes and changes in color, the more clearly it indicates that material is getting weathered.

E. GUIDELINES FOR CLASSIFICATION OF DISCONTINUITY conditions					
Discontinuity length (persistence) Rating	< 1 m 6	1 - 3 m 4	3 - 10 m 2	10 - 20 m 1	> 20 m 0
Separation (aperture) Rating	None 6	< 0.1 mm 5	0.1 - 1.0 mm 4	1 - 5 mm 1	> 5 mm 0
Roughness Rating	Very rough 6	Rough 5	Slightly rough 3	Smooth 1	Slickensided 0
Infilling (gouge) Rating	None 6	Hard filling < 5 mm 4	Hard filling > 5 mm 2	Soft filling < 5 mm 2	Soft filling > 5 mm 0
Weathering Ratings	Unweathered 6	Slightly weathered 5	Moderately weathered 3	Highly weathered 1	Decomposed 0

Figure 4. Guidelines for discontinuity classification (Bienawski, 1989)

Figure 5. Scanline mapping area 1

Figure 6. Scanline mapping area 2

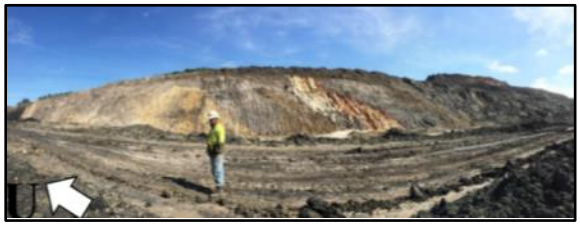

Figure 7. Scanline mapping area 3

Figure 8. Scanline mapping area 4

Hoek-Brown & Mohr-Coulomb Failure Criterion

The Hoek-Brown failure criterion is an empirical method whose function is to describe non-linear relationships in isotropic rock materials by comparing the rock strength values when confining stress is also added. The basic difference between Hoek-Brown and Mohr-Coulomb is the typical of collapse curve, in Mohr-Coulomb it is linear, whereas in Hoek-Brown the failure criterion is non-linear. Laboratory test that usually uses Mohr-Coulomb is Direct Shear with output parameters are *Internal Friction Angle (ϕ)* and *Cohesion (C)*. Meanwhile, laboratory tests that use Hoek-Brown collapse criteria are UCS and Triaxial.

Hoek-Brown assumes that failure at rock material is caused by major stress at $\sigma 1$ and minor stress at $\sigma 3$, while for Mohr-Coulomb is dominated by minor stress at $\sigma 3$.

Limit Equilibrium Analysis Method

Limit equilibrium types of analysis to assess stability have been used in geotechnical engineering for decades. The concepts have been widely applied to the stability analysis of earth slopes. The idea of discretizing a potential sliding mass into vertical slices was introduced early in the 20th century.

Slope stability analysis carried out in sections A – A', B – B', and C – C', using limit equilibrium method by Slope/W software. Slope/W formulation is based on principles of limiting equilibrium.

Factor of Safety (FoS) recommended for Pit Y East Asam area is FoS ≥ 1.250. Assumption used in this analysis are :

- Geological model : *Astim_Jun19*
- Pitshell using design *1911_Redgn_SR4_R* with highest elevation at RL50 and lowest elevation at RLM80
- Analysis method using Mohr-Coulomb (based on Direct Shear data from geotechnical drilling

sample) and Hoek-Brown (based on geotechnical mapping data and UCS value)

- No surcharge loads
- Maximum groundwater level assumed at ¾ slope height and saturated at ½ slope height
- Failure mechanism at Highwall area is circular failure

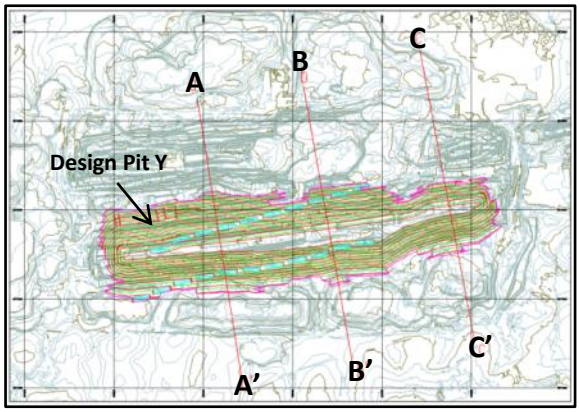

Figure 9. Section line view at Pit Y

Result and Discussion

a. Rock Mass Calculation at Pit Y

- **Area 1**

Scanline mapping was carried out with 165.99 m length. Rock masss classification based on geotechnical mapping result at Area 1 can see in table below.

Table 2. Rock mass classification at Area 1

Interval		Lithology	UCS	Discontinuities Information					Discontinuities Spacing	RQD	Groundwater	RMR	GSI
From (m)	To (m)			Persistance	Roughness	Infill	Aperture	Weathering					
0.00	13.80	CO	1	4	3	6	1	5	15	20	15	70	65
13.80	14.30	CY	1	2	3	6	5	5	15	20	15	72	67
14.30	18.23	CO	1	4	3	6	1	5	15	20	15	70	65
18.23	20.64	ST	1	4	3	6	5	5	10	20	15	69	64
20.64	23.14	CY	1	4	3	6	5	5	10	20	15	69	64
23.14	27.21	ST	1	4	3	6	5	5	10	20	15	69	64
27.21	31.01	SS	1	2	3	6	5	5	20	20	15	77	72
31.01	35.41	ST	1	4	3	6	5	5	10	20	15	69	64
35.41	35.68	CO	1	4	3	6	1	5	10	20	15	65	60
35.68	37.24	ST	1	2	3	6	5	5	15	20	15	72	67
37.24	37.55	CM	1	2	3	6	5	5	10	20	15	67	62
37.55	38.22	CY	1	2	3	6	5	5	15	20	15	72	67
38.22	38.39	CM	1	2	3	6	5	5	8	20	15	65	60
38.39	39.39	CY	1	2	3	6	5	5	15	20	15	72	67
39.39	40.69	SS	1	2	3	6	5	5	15	20	15	72	67
40.69	41.45	CM	1	2	3	6	5	5	15	20	15	72	67
41.45	41.56	CO	2	6	3	6	1	5	8	17	15	63	58
41.56	44.16	CY	1	4	3	6	5	5	10	20	15	69	64
44.16	44.96	CY	1	2	3	6	5	5	10	20	15	67	62
44.96	49.16	CO	2	4	3	6	1	5	8	17	15	61	56
49.16	54.10	CY	1	2	3	6	5	5	20	20	15	77	72
54.10	57.70	ST	1	2	3	6	5	5	20	20	15	77	72
57.70	63.30	SS	1	2	3	6	5	5	20	20	15	77	72
63.30	72.20	CO	2	4	3	6	1	5	15	20	15	71	66
72.20	72.97	SS	1	2	3	6	5	5	10	20	15	67	62
72.97	73.17	CO	1	4	3	6	1	5	8	17	15	60	55
73.17	73.61	SS	1	2	3	6	5	5	10	20	15	67	62
73.61	103.33	CY	1	2	3	6	5	5	20	20	15	77	72
103.33	105.60	SS	1	2	3	6	5	5	20	20	15	77	72
105.60	107.35	CY	1	2	3	6	5	5	15	20	15	72	67
107.35	108.70	SS	1	2	3	6	5	5	15	20	15	72	67
108.70	124.57	CY	1	2	3	6	5	5	20	20	15	77	72
124.57	127.07	ST	1	2	3	6	5	5	20	20	15	77	72
127.07	133.60	SS	1	2	3	6	5	5	20	20	15	77	72
133.60	165.99	CY	1	2	3	6	5	5	20	20	15	77	72

- **Area 2**

Scanline mapping was carried out with 106.39 m length. Rock masss classification based on geotechnical mapping result at Area 2 can see in table below.

Table 3. Rock mass classification at Area 2

Interval		Lithology	UCS	Discontinuities Information					Discontinuities Spacing	RQD	Groundwater	RMR	GSI
From (m)	To (m)			Persistance	Roughness	Infill	Aperture	Weathering					
0.00	**3.55**	**ST**	**1**	**4**	**3**	**6**	**5**	**5**	**20**	**20**	**15**	**79**	**74**
3.55	3.75	CM	1	2	3	6	5	5	10	20	15	67	62
3.75	8.90	ST	1	2	3	6	5	5	20	20	15	77	72
8.90	9.50	CM	1	2	3	6	5	5	15	20	15	72	67
9.50	14.00	ST	1	2	3	6	5	5	20	20	15	77	72
14.00	14.40	CM	1	2	3	6	5	5	10	20	15	67	62
14.40	16.50	ST	1	2	3	6	5	5	8	20	15	65	60
16.50	16.75	CM	1	2	3	6	5	5	10	20	15	67	62
16.75	20.50	SS	1	2	3	6	5	5	20	20	15	77	72
20.50	23.50	ST	1	2	3	6	5	5	20	20	15	77	72
23.50	23.70	CY	1	2	3	6	5	5	10	20	15	67	62
23.70	24.12	CO	2	4	3	6	1	5	8	17	15	61	56
24.12	28.33	CY	1	2	3	6	5	5	20	20	15	77	72
28.33	33.38	CO	2	4	3	6	1	5	8	17	15	61	56
33.38	37.46	CY	1	2	3	6	5	5	20	20	15	77	72
37.46	38.39	CO	2	4	3	6	1	5	8	17	15	61	56
38.39	58.62	ST	1	2	3	6	5	5	20	20	15	77	72
58.62	62.70	SS	1	2	3	6	5	5	20	20	15	77	72
62.70	64.50	ST	1	2	3	6	5	5	20	20	15	77	72
64.50	64.60	CM	1	2	3	6	5	5	8	20	15	65	60
64.60	65.77	ST	1	2	3	6	5	5	20	20	15	77	72
65.77	66.09	CO	2	4	3	6	1	5	8	17	15	61	56
66.09	67.89	ST	1	2	3	6	5	5	15	20	15	72	67
67.89	106.39	CY	1	2	3	6	5	5	20	20	15	77	72

- **Area 3**

Scanline mapping was carried out with 92.09 m length. Rock masss classification based on geotechnical mapping result at Area 3 can see in table below.

Table 4. Rock mass classification at Area 3

Interval		Lithology	UCS	Discontinuities Information					Discontinuities Spacing	RQD	Groundwater	RMR	GSI
From (m)	To (m)			Persistance	Roughness	Infill	Aperture	Weathering					
0.00	10.50	CO	1	4	3	6	1	5	10	17	15	62	57
10.50	15.70	CY	1	4	3	6	1	5	20	20	15	75	70
15.70	22.94	SS	1	2	3	6	5	5	20	20	15	77	72
22.94	59.02	CY	1	4	3	6	1	5	20	20	15	75	70
59.02	71.15	ST	1	2	3	6	5	5	20	20	15	77	72
71.15	88.79	SS	1	2	3	6	5	5	20	20	15	77	72
88.79	92.09	CY	1	2	3	6	5	5	20	20	15	77	72

- **Area 4**

Scanline mapping was carried out with 85.8 m length. Rock masss classification based on geotechnical mapping result at Area 4 can see in table below.

Table 5. Rock mass classification at Area 4

Interval		Lithology	UCS	Discontinuities Information					Discontinuities Spacing	RQD	Groundwater	RMR	GSI
From (m)	To (m)			Persistance	Roughness	Infill	Aperture	Weathering					
0.00	2.34	SO											
2.34	50.40	CY	1	2	3	6	5	5	20	20	15	77	72
50.40	64.55	SS	2	2	3	6	1	5	20	20	15	73	68
64.55	80.20	CY	1	2	3	6	5	5	20	20	15	77	72
80.20	82.30	ST	1	2	3	6	5	5	20	20	15	77	72
82.30	85.80	SS	2	2	3	6	5	5	20	20	15	78	73

b. Slope Stability Analysis Design Highwall Pit Y

- Section A – A'

Slope analysis at Highwall Pit Y section A – A' based on material properties from geotechnical drilling data shows FoS 1.371, which means Highwall in safe condition. While slope analysis based on geotechnical mapping data shows FoS 1.422, which means Highwall also in safe condition. Highwall section A – A' have 90 m height with overall slope 27°.

Based on FoS value for both analysis result, it shows that Highwall still can be optimized to reduce FoS until approaches the recommended value.

Optimization is performed by redesign the Highwall slope steeper than the original design.

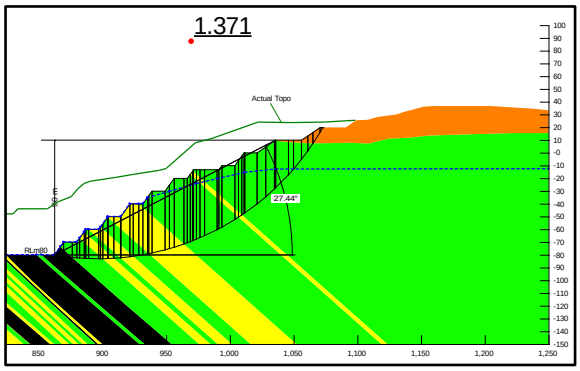

Figure 10. Slope analysis design Highwall Pit Y section A-A' based on drillhole data

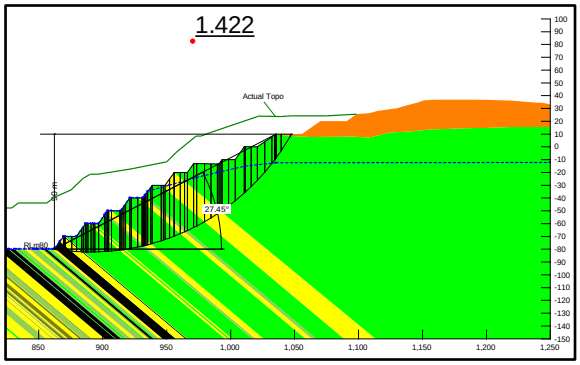

Figure 11. Slope analysis design Highwall Pit Y section A-A' based on geotechnical mapping data

- Section B – B'

Slope analysis at Highwall Pit Y section B – B' based on material properties from geotechnical drilling data shows FoS 1.306, which means Highwall in safe condition. While slope analysis based on geotechnical mapping data shows FoS 1.398 which means Highwall also in safe condition. Highwall section A – A' have 90 m height with overall slope 28°.

Based on FoS value for both analysis result, it shows that Highwall still can be optimized to reduce FoS until approaches the recommended value. Optimization is performed by redesign the Highwall slope steeper than the original design.

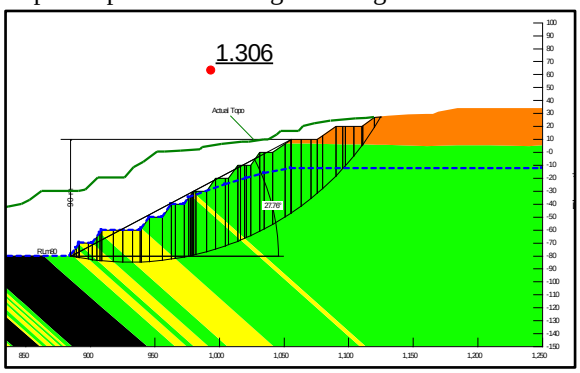

Figure 12. Slope analysis design Highwall Pit Y section B-B' based on drillhole data

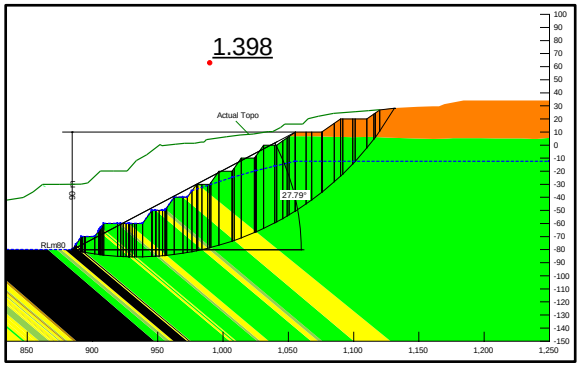

Figure 13. Slope analysis design Highwall Pit Y section B-B' based on geotechnical mapping data

- Section C – C'

Slope analysis at Highwall Pit Y section C – C' based on material properties from geotechnical drilling data shows FoS 1.256, which means Highwall in safe condition. Based on FoS value, it shows that Highwall has reached the optimal slope design indicated by FoS value which already approaching the recommended value. It means, Highwall at section C-C' based on drillhole data no need to optimize again.

While slope analysis based on geotechnical mapping data shows FoS 1.412, which means Highwall also in safe condition. Highwall section C – C' have 90 m height with overall slope 31°. Based on FoS value, it shows that Highwall still can be optimized to reduce FoS until approaches the recommended value. Optimization is performed by redesign the Highwall slope steeper than the original design.

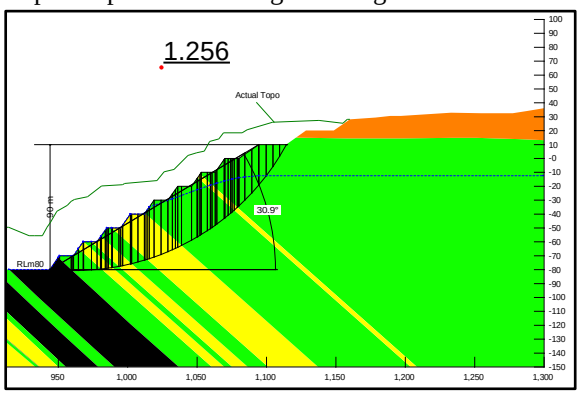

Figure 14. Slope analysis design Highwall Pit Y section C-C' based on drillhole data

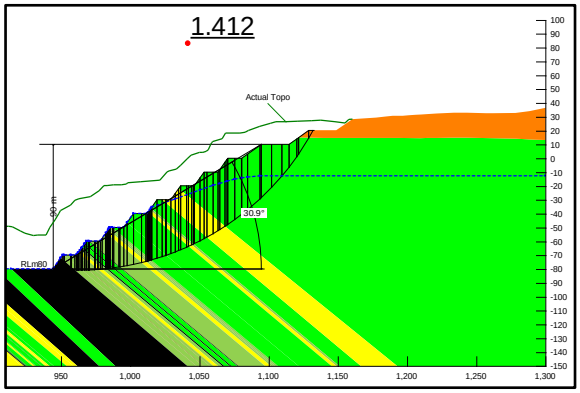

Figure 15. Slope analysis design Highwall Pit Y section C-C' based on geotechnical mapping data

c. Slope Stability Analysis Design Optimization Highwall Pit Y

- Section A – A'

Slope analysis at optimization design Highwall Pit Y section A – A' based on material properties from geotechnical drilling data shows FoS 1.257, which means Highwall in safe condition. Slope optimization is performed by reduce bench width at RL0 – RLm70 from 10 to 8 m. Highwall section A – A' have 90 m height with overall slope 31°.

While slope analysis based on geotechnical mapping data shows FoS 1.251, which means Highwall also in safe condition. Slope optimization is performed by reduce bench width at RL0 – RLm70 from 10 to 5 m. Highwall section A – A' have 90 m height with overall slope 33°.

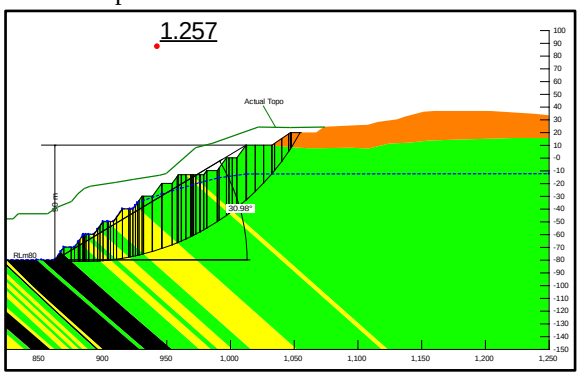

Figure 16. Slope analysis design optimization Highwall Pit Y section A-A' based on drillhole data

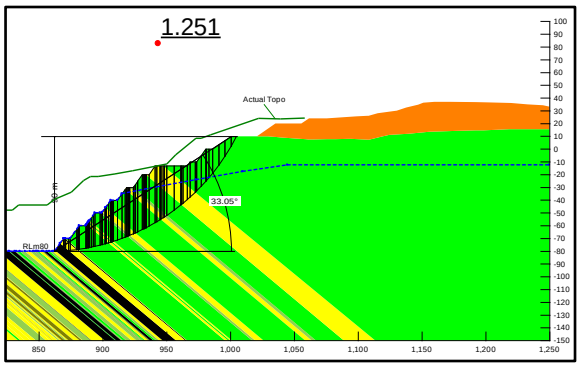

Figure 17. Slope analysis design optimization Highwall Pit Y section A-A' based on geotechnical mapping data

- Section B – B'

Slope analysis for optimization design Highwall Pit Y section B – B' based on material properties from geotechnical drilling data shows FoS 1.251, which means Highwall in safe condition. Slope optimization is performed by reduce bench width at RL0 – RLm70 from 10 to 8 m. Highwall section B – B' have 90 m height with overall slope 31°.

While slope analysis based on geotechnical mapping data shows FoS 1.252, which means Highwall also in safe condition. Slope optimization is performed by reduce bench width at RL0 – RLm70 from 10 to 5 m. Highwall section A – A' have 90 m height with overall slope 34°.

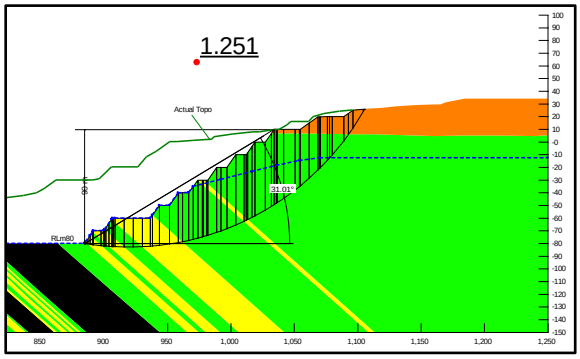

Figure 18. Slope analysis design optimization Highwall Pit Y section B-B' based on drillhole data

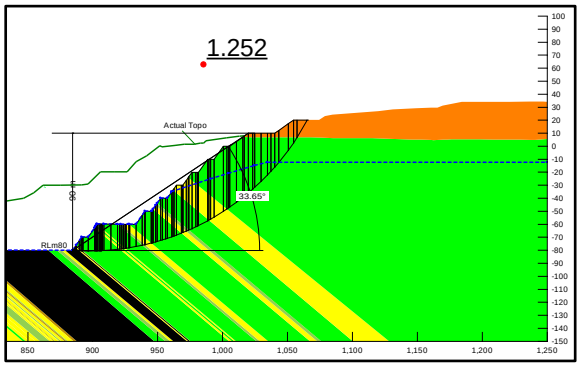

Figure 19. Slope analysis design optimization Highwall Pit Y section B-B' based on geotechnical mapping data

- Section C – C'

Slope analysis for optimization design Highwall Pit Y section C – C' based on geotechnical mapping data shows FoS 1.252, which means Highwall in safe condition. Slope optimization is performed by reduce bench width at RL0 – RLm70 from 10 to 7 m. Highwall section C – C' have 90 m height with overall slope 36°.

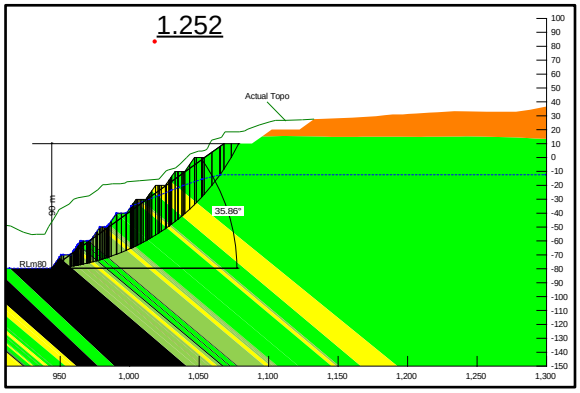

Figure 20. Slope analysis design optimization Highwall Pit Y section C-C' based on geotechnical mapping data

d. Comparison Between Previous Study and Re-Analysis with Geotechnical Mapping Data

Based on the data above, analysis in previous studies can tried to re-analysis again using the latest data from geotechnical mapping.

In the previous study Highwall Pit Y can be construct with overall slope 30° and overall height 110 m. After re-analysis using the update data from geotechnical mapping, for 110 m Highwall height can be construct with overall slope 32°.

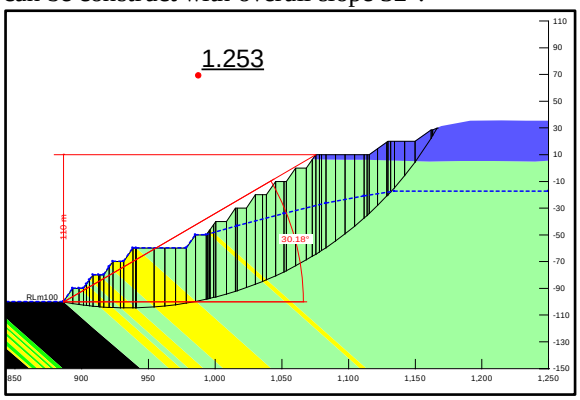

Figure 21. Slope analysis Highwall Pit Y in previous study

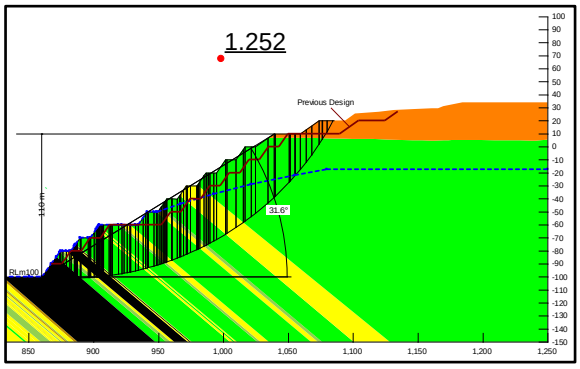

Figure 21. Re-analysis previous design Highwall Pit Y with latest data from geotechnical mapping

Table 6. Summary of analysis result for design Highwall Pit Y - East Asam Area

Section	Highwall					FoS	
	Single Slope			Overall Slope		Data Drilling	Data Mapping
	Height (m)	Slope (…°)	Width (m)	Height (m)	Slope (…°)		
A – A'	10	45	10	90	27	1.371	1.422
B – B'	10	45	10	90	28	1.306	1.398
C – C'	10	45	10	90	31	1.256	1.412

Table 7. Summary of analysis result for optimization design Highwall Pit Y based on drillholes data

Section	Highwall					FoS
	Single Slope			Overall Slope		
	Height (m)	Slope (…°)	Width (m)	Height (m)	Slope (…°)	
A – A'	10	55	8	90	31	1.257
B – B'	10	55	8	90	31	1.251

Table 8. Summary of analysis result for optimization design Highwall Pit Y based on geotechnical mapping data

Section	Highwall					FoS
	Single Slope			Overall Slope		
	Height (m)	Slope (…°)	Width (m)	Height (m)	Slope (…°)	
A – A'	10	55	5	90	33	1.251
B – B'	10	55	5	90	34	1.252
C – C'	10	55	7	90	36	1.252

Conclusions

1. Based on slope stability analysis results using geotechnical drilling data in Pit Y East Asam area, it shows that the Pit Y design can be optimized up to 31° for a slope height of 90 m (3-4° steeper than original design).
2. Meanwhile, slope stability analysis results based on geotechnical mapping data show that the Pit Y design can still be optimized up to 36° for a slope height of 90 m (5-6° steeper than original design).
3. Comparison between analysis on previous study and re-analysis with geotechnical mapping data shows that Highwall Pit Y can be optimized 2° stepper compared than previous design
4. This project shows that geotechnical mapping data can be very useful for analyze mine slopes stability and can be used to increase confidence level of determine rocks strength at mine slopes.

References

Bieniawski, Z.T; 1989; Engineering Rock Mass Classifications

Hoek, E. & Brown, ET; 2018; The Hoek-Brown failure criterion and GSI - 2018 edition; Journal of Rock Mechanics and Geotechnical Engineering (2018)

Norokallio, J; 2015; Geological and Geotechnical Mapping Procedures in Use in the Onkalo

Price, D. G; 2008; Engineering Geology : Principles and Practice; Springer

Read, J. & Stacey, P; 2009; Guidelines for Open Pit Slope Design

Sikumbang, N. & Heryanto, R; 1994; Regional Geology of Banjarmasin, Southern Kalimantan

Acknowledgements

Authors would like to thanks PT. Arutmin Indonesia ECMP Management for allowed us to publish this paper and to Geotcechnical Section team for all support during this project.

PROCEEDINGS
JOINT CONVENTION BANDUNG (JCB) 2021
November 23rd – 25th 2021

Improving EOR Selection Efficiency with Novel EOR Screening Software: Applied Machine Learning

Fransiskus Ondihon S (1), Sumadi Paryoto (1), Victor Sitompul (1), Denie Winata (1), Tino Diharja (1), Gunawan Sutadiwiria (1), Muhammad Alfian (1)
(1) Pertamina Upstream Research Technology & Innovation

Abstract

With the decreasing rate of production, the application of Enhanced Oil Recovery (EOR) technology is one solution to increase the recovery of oil production from reservoirs. EOR is a method to increase production by influencing the interaction between fluids and reservoir rocks. Before an EOR method is implemented, it is necessary to conduct EOR screening so that the EOR method is most suitable for field conditions and the increase in oil production is achieved optimally. Conventionally, EOR screening methods are done manually matching field parameters with criteria sourced from Taber et al (1997) and from Al-Adasani et al (2010). This method has several drawbacks including taking a long time, high subjectivity, and qualitative. As a result, screening results using this method have poor accuracy, low effectiveness, and have high uncertainty. In this study, we proposed quantitative methods for EOR screening based on automation systems in software built with Machine Learning algorithms. This screening method is based on a static and probabilistic evaluation of the most suitable combination of 8 parameters of oil and reservoir characteristics and tested on 5 different fields based on Taber et al (1997) and Al-Adasani & Bai (2010) criteria. Based on the test results, the order of conformity rating of EOR method is obtained along with the evaluation of the score. Furthermore, a comparative analysis is conducted with the results of EOR screening manually and with the results of screening using other commercial software. The results of this study show that the proposed method can produce better output because the process is efficient in terms of computational time, more reliable results, and quantitative. This method is expected to be one of the solutions for the acceleration of the EOR program in support of the target of increasing national oil production.

Keywords: Enhanced Oil Recovery, Machine Learning, Screening Technology, Software

Introduction

Hydrocarbon fields after a long-time production is going to natural decline due to the reduced energy to remove fluids from the well. The reduced propulsion force is usually overcome by installing a pump or gas lift in a natural well. However, over time, artificial lift well will gradually find it difficult to flow due to the limited drainage area. To increase the field drainage area and driving force, there are developed a few techniques that are called Enhanced Oil Recovery (EOR) or now better known as Improved Oil Recovery (IOR). But how to determine the appropriate EOR method (EOR Screening) for existing oil fields?

EOR screening is a technique to choose the right EOR method that can be used in a particular reservoir. This screening process is strongly influenced by the method of assessing the level of compatibility between the reservoir properties and the EOR method. There have been many studies and publications that discuss methods to perform statistical EOR Screening or with an artificial intelligence approach. EOR screening was initially carried out using a statistical approach but over time several other approaches have been taken such as cluster and composite methods, artificial intelligence (AI) methods and machine learning (ML) methods. Taber et al (1983) developed a technical guidance to determine the EOR method by collecting data from successful EOR projects worldwide and dividing them into two parts, there are oil properties and reservoir characteristics. The result of this study is that Taber et al. presented the technical selection criteria in the form of tables and graphs accompanied by the basis of the lifting mechanism and the limitations of each method. Al-Adasani et al (2010) updated the screening criteria for the selection of the EOR method by adding the latest EOR project data. This study adds data from the results of the EOR survey from 1998 to 2010 into the screening criteria that have been made by Taber (1997). In addition to updating the screening criteria, this study also investigates the distribution of EOR projects with reservoir properties. There is still a lot of literature that has discussed how to determine the EOR method that is suitable for a field. However, there are several gaps including: i) most of them are still manual, ii) high subjectivity, and iii) one method/technology is limited to one field or only one type of EOR method. This paper tries to fill the gap by using PertaEOR software. PertaEOR is an EOR software made by Pertamina Upstream Research & Technology Innovation (URTI) which can perform EOR screening based on machine learning and automated statistical algorithms. It is hoped that the screening results will be better, more accurate, and quantitative so the EOR methods can be compared.

Data and Method

PertaEOR was tested on 5 fields in Indonesia. The five fields are named after fields A, B, C, D, and E. The naming is to maintain data confidentiality. Field A operates in South Sumatra, Field B&E in East Java, and Fields C&D in Jambi.

Oil & Reservoir Properties

Oil and reservoir characteristics include 9 parameters including: Oil gravity, viscosity, porosity, oil saturation, formation type, permeability, net thickness, depth, and temperature. Data from 5 different real fields have been provided as in table 1.

EOR Screening

It is a process of selecting a suitable EOR method based on oil and reservoir data in a field. There are 3 types of ways / techniques are carried out including:

Manual Screening

Manual screening carried out by using guidelines from Al-Adasani & Bai (2010) and Taber et al (1997) in table 2. Oil & reservoir properties data of a field will be matched with data from tables 2 and 3. Al-Adasani & Bai (2010) and Taber et al (1997) grouped oil & reservoir properties into an EOR Method based on success stories of field implementations that have been carried out previously around the world.

Determination of the EOR method using reference data Taber et al. (1997) seen from the suitability of the oil properties and reservoir characteristics in the field, it includes 9 (nine) parameters as follows:

a. Oil API Gravity
b. Oil viscosity
c. Oil Composition
d. Reservoir oil saturation
e. Reservoir formation type
f. Reservoir net thickness
g. Average permeability
h. Reservoir depth
i. Reservoir temperature

Match level is depicted in cell colors, which are green (if the value is within the range and supports the related EOR method), yellow (if the value is slightly out of range and there is still a chance for the related EOR method), and red (if the value is outside the range).

Determination of the EOR method using reference data Al-Adasani & Bai (2010) saw the suitability of the oil properties data and reservoir characteristics in the field covering 9 (nine) parameters as follows:

a. Oil API Gravity
b. Oil viscosity
c. Oil Composition
d. Reservoir porosity
e. Reservoir oil saturation
f. Reservoir formation type
g. Average permeability
h. Reservoir depth
i. Reservoir temperature

Same with Taber et al. (1997) the match level is depicted in green (if the value is within the range and supports the related EOR method), yellow (if the value is slightly out of range and there is still a chance for the related EOR method), and red (if the value is slightly out of range.

PertaEOR

It is PERTAMINA's software that has an EOR screening module. Using machine learning with scoring and weighting based on statistical and technical algorithms. Statistical algorithms are algorithms with purely statistical data considerations. While the engineering algorithm includes engineering sense. In addition, there is also a penalty algorithm if the input data is too far from the range of criteria data that is suitable for an EOR method. The combination of all these algorithms will be used to determine the suitability rating of the input field data.

The determination of the EOR method using PertaEOR Software was based on the match of 9 (nine) oil properties and reservoir characteristics of the field to the database which included the reference of Taber et al. (1997), Al-Adasani & Bai (2010) and Oil & Gas Journal (2020). For a target reservoir, the EOR method that has the highest probability value will be selected and ranked as the best EOR method for the target reservoir. The nine parameters analyzed are as follows:

a. Oil API Gravity
b. Oil viscosity
c. Oil Composition
d. Reservoir porosity
e. Reservoir oil saturation
f. Reservoir formation type
g. Average permeability
h. Reservoir depth
i. Reservoir temperature

Other EOR Screening Software

As a reference for commercial software, EORGui from Petroleum Solutions is used. The determination of the EOR method using the EORGui Screening Software is based on the suitability of the oil properties and reservoir characteristics data in the field covering 9 (nine) parameters as follows:

a. Oil API Gravity
b. Oil viscosity
c. Oil Composition
d. Reservoir oil saturation

e. Reservoir formation type
f. Reservoir net thickness
g. Average permeability
h. Reservoir depth
i. Reservoir temperature

These 3 (three) methods are used to do the screening process on 5 (five) different fields. There are two carbonate reservoirs and three sandstone reservoirs with different oil properties. So, the differences between these screening methods/technologies are known.

Result and Discussion

Screening using PertaEOR resulting list of EOR methods. The suitability of 9 oil and reservoir parameters is represented by a match probability score as shown in Figure 1. The match probability score of an EOR method regarding to oil and reservoir data is calculated using an equation involving the multiplication of the probability number per parameter with a weighting factor value. Figure 2 is a ranking of the EOR methods starting from the most suitable to the least suitable in the D fields.

Manual EOR Screening using Al-Adasani & Bai (2010) and Taber et al. (1997) results can be seen in table 3. The suitable EOR method is sorted by the total number of parameters whose values are in the range and the number of parameters whose values are slightly out of the range. All parameters assume equal and there is no penalty score if the input data are too far from the database.

Screening using EORGui software gives results as shown in Figure 2. The results are a spider chart and table of suitability from each parameter with certain EOR methods. The level of compatibility of EOR methods is indicated by dark green, green, and red colors for each parameter. They are sorted according to the match percent value. The correlation between the green, bright green, and red colors is still unknown to the percent match value that appears in spider chat.

In terms of results, it was found that the order of screening between PertaEOR and the literature (manual screening) was quite consistent. Although in the manual screening several EOR methods are included in one group due to the difficulty of sorting if they have the same number of green columns. This does not happen in PertaEOR, because the value has been calculated based on the algorithm that has been compiled. The results of the screening using EORGui also show conformity with PertaEOR, but some EOR methods are not found in EORGui such as miscible gas injection. In fact, if we look at the example in the E field, miscible gas injection ranks first in both manual screening and PertaEOR.

PertaEOR screening results in accordance with study work or implementation in the 5 fields. Field B located in East Java is a carbonate field and understudy of CO2 EOR study align with PertaEOR suggests (figure 1 match probability). Likewise, the A, C, D, & E fields are currently under Chemical EOR study and those are align with the results of PertaEOR screening.

PertaEOR has a complete feature which can accept single-value and distributed value data input. The result is fair since every parameter has a weighting factor based on the database. And if the data is too far from range, the match probability score will be reduced by the penalty algorithm**.**

Conclusions

The results of this study indicate that the technical and statistical algorithm, also penalty algorithm in PertaEOR can produce better output because the process is efficient in terms of computational time compared to manual screening, the results are more reliable because it was objective, quantitative, fair with addition of weighting value and penalty score, and cover almost all types of EOR methods. This method is expected to be one of the solutions to accelerate the EOR program in supporting the target to increase national oil production.

References

Al-Adasani, A., Bai, B., 2010. Recent developments and updated screening criteria of enhanced oil recovery techniques. In: International Oil and Gas Conference and Exhibition in China.Baker, D. W., and N. L. Carter, 1972, American Geophysical Union Geophysical Monographs **16**, 157–166.

Taber, J.J., 1983. Technical screening guides for the enhanced recovery of oil. In: SPE Annual Technical Conference and Exhibition.

Taber, J.J., Martin, F.D., Seright, R.S., Aug. 1997a. EOR screening criteria revisited – Part 1: introduction to screening criteria and enhanced recovery field projects. SPE Reservoir Eng. 12 (03), 189–198.

Oil & Gas Journal (2020)

Acknowledgements

Authors would like to say thank you to Pertamina Upstream Research Technology & Innovation (URTI) and PT LAPI ITB for the support and assistance.

PROCEEDINGS
JOINT CONVENTION BANDUNG (JCB) 2021
November 23rd – 25th 2021

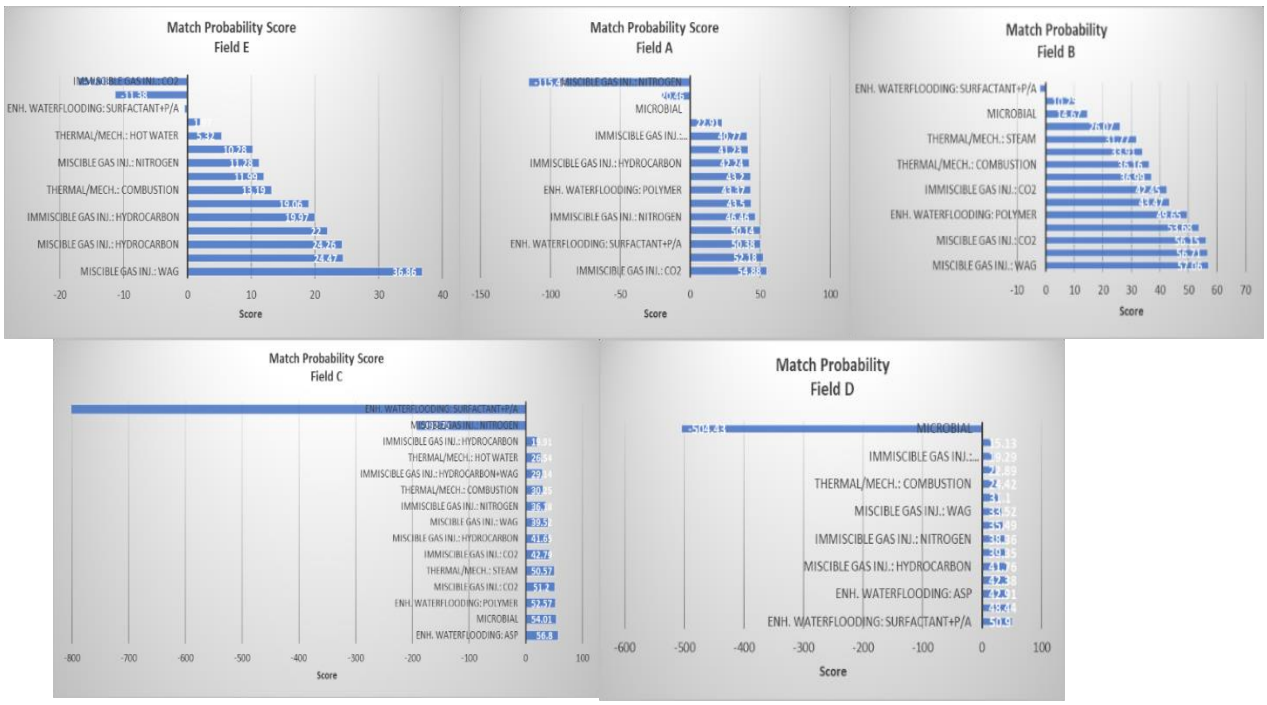

Figure 1: Match Probability Score for each field (A to E) using PertaEOR

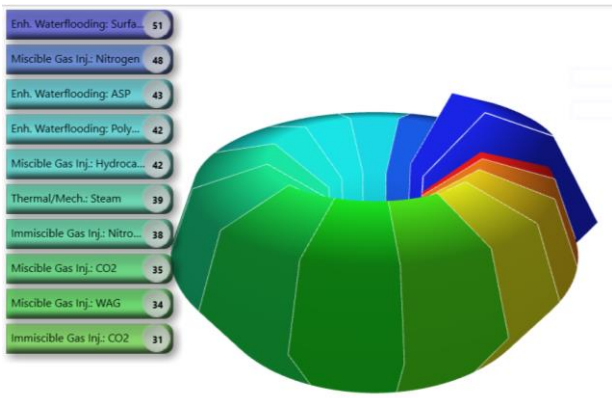

Figure 2: PertaEOR Screening Result on D field

Field Id	Oil Properties			Reservoir Characteristics					
	Gravity (deg API)	Viscosity (cp)	Composition	Oil Saturation (% PV)	Formation Type	Net Thickness (ft)	Average Permeability (md)	Depth (ft)	Temperature (deg F)
A	26.56	5.25	C5-C12	40	Sandstone	26.67	99	3938.92	198
B	40.6	1.42	NC	48.6	Carbonate	114.02	117	5815	235
C	46	0.52	High % C5-C11	48	Sandstone	261.31514	225	2798.5564	141
D	47	0.51	High % C5-C12	59.1	Sandstone	41.33	16.54	2795.28	149
E	32.1-33.3 mean=32.4	0.51-1.13 mean=0.66	High % C5-C12	70-85 mean = 75	Carbonate	947	10-1000 mean=100	4035-4982 mean=4500	263-267 mean: 265

Table 1: Oil and Reservoir Data

Figure 3: Other Software Screening Result on E field

No.	EOR Method	Oil Properties		Reservoir Characteristics						
		Gravity (°API)	Viscosity (cp)	Porosity (%)	Oil Saturation (% PV)	Formation Type	Permeability (md)	Net Thickness (ft)	Depth (ft)	Temperature (°F)
Miscible Gas Injection										
1	CO2	28[22]-45 Avg. 37	35-0 Avg. 2.1	3-37 Avg. 14.8	15-89 Avg. 46	Sandstone or Carbonate	1.5-4500 Avg. 201.1	[Wide Range]	1500°-13365 Avg. 6171.2	82-250 Avg. 136.3
2	Hydrocarbon	23-57 Avg. 38.3	18000-0.04 Avg. 286.1	4.25-45 Avg. 14.5	30-98 Avg. 71	Sandstone or Carbonate	0.1-5000 Avg. 726.2	[Thin unless dipping]	4040[4000]-15900 Avg. 8343.6	85-329 Avg. 202.2
3	WAG	33-39 Avg. 35.6	0.3-0 Avg. 0.6	11-24 Avg. 18.3		Sandstone	130-1000 Avg. 1043.3	NC	7545-8887 Avg. 8216.8	194-253 Avg. 229.4
4	Nitrogen	38[35]-54 Avg. 47.6	0.2-0 Avg. 0.07	7.5-14 Avg. 11.2	0.76[0.4]-0.8 Avg. 0.78	Sandstone or Carbonate	0.2-35 Avg. 15.0	[Thin unless dipping]	10000[6000]-18500 Avg. 14633.3	190-325 Avg. 266.6
Immiscible Gas Injection										
5	Nitrogen	16-54 Avg. 34.6	18000-0 Avg. 2256.8	11-28 Avg. 19.46	47-98.5 Avg. 71	Sandstone	3-2800 Avg. 1041.7		1700-18500 Avg. 7914.2	82-325 Avg. 173.1
6	CO2	11-35 Avg. 22.6	592-0.6 Avg. 65.5	17-32 Avg. 26.3	42-78 Avg. 56	Sandstone or Carbonate	30-1000 Avg. 217		1150-8500 Avg. 3385	82-198 Avg. 124
7	Hydrocarbon	22-48 Avg. 35	4-0.25 Avg. 2.1	5-22 Avg. 13.5	75-83 Avg. 79	Sandstone	40-1000 Avg. 520		6000-7000 Avg. 6500	170-180 Avg. 175
8	Hydrocarbon + WAG	9.3-41 Avg. 31	16000 - 0.17 Avg. 3948.2	18-31.9 Avg. 25.09	Avg. 88	Sandstone or Carbonate	100-6600 Avg. 2392		2650 -9199 Avg. 7218.71	131-267 Avg. 198.7
(Enhanced) Waterflooding										
9	Polymer	13-42.5 Avg. 26.5	4000°-0.4 Avg. 123.2	10.4-33 Avg. 22.5	34-82 Avg. 64	Sandstone	1.8°-5500 Avg. 834.1	[NC]	700-9460 Avg. 4221.9	74-237.2 Avg. 167
10	Alkaline Surfactant Polymer (ASP)	23[20]-34[35] Avg. 32.6	6500°-11 Avg. 875.8	26-32 Avg. 26.6	68[35]-74.8 Avg. 73.7	Sandstone	596[10]-1520	[NC]	2723-3900[9000] Avg. 2984.5	118 [80]-158[200] Avg. 121.6
11	Surfactant + P/A	22-39 Avg. 31	15.6-3 Avg. 9.3	16-16.8 Avg. 16.4	43.5-53 Avg. 48	Sandstone	50-60 Avg. 55	[NC]	625-5300 Avg. 2941.6	122-155 Avg. 138.5
Thermal/Mechanical										
12	Combustion	10-38 Avg. 23.6	2770-1.44 Avg. 504.8	14-35 Avg. 23.3	50-94 Avg. 67	Sandstone or Carbonate [Preferably Carbonate]	10-15000 Avg. 1981.5	[>10]	400-11300 Avg. 5569.6	64.4-230 Avg. 175.5
13	Steam	8-30 Avg. 14.5	5E6-3° Avg. 3297.3	12-65 Avg. 32.2	35-90 Avg. 66	Sandstone	1°-15000 Avg. 2605.7	[>20]	200-9000 Avg. 1643.6	10-350 Avg. 105.8
14	Hot Water	12 -25 Avg. 18.6	8000-170 Avg. 2002	25-37 Avg. 31.2	15-85 Avg. 58.5	Sandstone	900-6000 Avg. 3346	-	500-2950 Avg. 1942	75-135 Avg. 98.5
Microbial										
16	Microbial	12-33 Avg. 26.6	8900-1.7 Avg. 2977.5	12-26 Avg. 19	55-65 Avg. 60	Sandstone	180-200 Avg. 190	-	1572-3464 Avg. 2445.3	86-90 Avg. 88
The following reported EOR reservoir characteristics have extreme values that impact the respective average and range in Table 1.										

Table 2: Manual Screening using Al-Adasani&Bai (2010) on C field

		Oil Properties			Reservoir Characteristics					
Detail Table in Ref. 16	EOR Method	Gravity (deg API)	Viscosity (cp)	Composition	Oil Saturation (% PV)	Formation Type	Net Thickness (ft)	Average Permeability (md)	Depth (ft)	Temperature (deg F)
Gas Injection Methods (Miscible)										
1	Nitrogen and flue gas	>35↑ avg: 48↑	<0.4 ↓ avg: 0.2↓	High percent of C_1 to C_7	>40↑ avg:75↑	Sandstone or carbonate	Thin unless dipping	NC	>6,000	NC
2	Hydrocarbon	>23↑ avg:41↑	<3↓ avg:0.5↓	High percent of C_2 to C_7	>30↑ avg:80↑	Sandstone or carbonate	Thin unless dipping	NC	>4,000	NC
3	CO_2	>22↑ avg:36F ↑	<10↓ avg:1.5↓	High percent of C_5 to C_{12}	>20↑ avg:55↑	Sandstone or carbonate	Wide range	NC	>2,500[a]	NC
4	Immiscible gases	>12	<600	NC	>35↑ avg:70↑	NC	NC if dipping and/or good vertical permeability	NC	>1,800	NC
(Enhanced) Waterflooding										
5	Micellar/ Polymer, ASP, and Alkaline Flooding	>20↑ avg:35↑	<35↓ avg:13↓	Light, intermediate, some organic acids for alkaline floods	>35↑ avg:53↑	Sandstone preferred	NC	>10↑ avg:450↑	<9,000↓ avg:3,250	<200↓ avg:80
6	Polymer Flooding	>15	<150, >10	NC	>50↑ avg:80↑	Sandstone preferred	NC	>10↑ avg:800↑ [b]	<9,000	<200↓ avg: 140
Thermal/Mechanical										
7	Combustion	>10↑ avg:16→?	<5,000↓ avg: 1,200↓	Some asphaltic components	>50↑ avg:72↑	High-porosity sand/ sandstone	>10	>50 [c]	<11,500↓ avg:3,500	>100↑ avg: 135
8	Steam	>8 to 13.5→?	<200,000↓ avg: 4,700↓	NC	>40↑ avg:66↑	High-porosity sand/ sandstone	>20	>200↑ avg:2,540↑ [d]	<4,500↓ avg:1,500	NC
NC=not critical.										
NC=not										

Table 2: Manual Screening Result using Taber et al. (1997) on C field

Rank\Field	A	B	C	D	E
Taber et al. (1997)					
1	Combustion	Combustion	Misc CO2 /Steam injection	Misc CO2 inj/Polymer	Misc CO2 inj
2	ASP Flooding	Misc. CO2 Injection	ASP Flooding	ASP Inj	Combustion
3	Polymer flooding/Miscible CO2 Injection	ASP Flooding	Combustion	Steam	Imsc Gas Injection
4	Immiscible Gas/ Steam Injection	Steam/Imsc. Gas/Misc HC	Polymer Flooding	Combustion	Misc HC inj/Polymer Flooding/ ASP Flooding
5	Miscible HC Injection	Polymer	Imsc. Gas Injection	Imm Gas	Steam Injection
6	N2 & Flue Gas	N2 & Flue gas	Misc HC injection	Mis HC Inj	Misc N2 Injection
7			Misc N2 Injection	Misc N2	
Aladasani & Bai (2010)					
1	Misc CO2/Steam	Misc CO2 /HC	Misc Co2/Imm N2	Imm N2	Misc CO2/HC
2	Polymer/Combustion	Imm N2/HC-WAG/Polymer	Misc HC/Polymer/Steam	Misc CO2/HC	Imm N2
3	Misc HC/Imm N2	Imm CO2/Combustion/Steam	Imsc CO2/Imsc HC-WAG/ASP	Combustion/Steam	Imm Co2
4	Imm Co2/ASP	Misc N2	Ims HC/Surfactant/Hot Water	Polymer	Imm HC-WAG/Combustion
5	Imm HC-WAG/Surfactant	Imm HC	Misc WAG/Misc N2/	Imm Co2/ ASP/HC-WAG	Steam
6	Imm HC/Microbial	WAG	Microbial	Misc N2/Imm HC/ Microbial	Polymer
7	Misc WAG/Mic N2	ASP/Surfactant/Hot Water		Misc WAG/Surfactan/ Hot Water	Misc N2
8	Hot Water	Microbial			Immiscible Co2 Injection
9					ASP/Surfactan/WAG/Hot Water

Table 3: Manual Screening Result using Taber et al. (1997) and Al-Adasani & Bai (2010)

PROCEEDINGS
JOINT CONVENTION BANDUNG (JCB) 2021
November 23rd – 25th 2021

Investigation of Performance of Electromagnetic Heating with Nano-Ferro Fluid and NaCl Solution for Recovery Heavy Oil Deposits

Bely Juliantoro, Fairuz Athallah, Erdila Indriani, Bambang Yudho Suranta
Oil and Gas Production Engineering, PEM Akamigas, Indonesia

Abstract

In providing a solution for lifting up the viscous oil which is immensely concerned in a mature field, thermal recovery is commonly applied to recover the oil with API gravities approximately 20 by using the steam injection and in situ combustions. It had been the way out to lower enough the viscosity so that the oil would flow toward more effortless than the viscous one for the recent times. Applying electromagnetic microwave to heat up the reservoir can overcome the depth limitation which is often found in conventional thermal recovery methods. This method uses the nano-ferro fluid as a stimulant that conveniently radiates heat in a reservoir. It is important to analyze the brine formation in affecting the optimization of the thermal period while the nano-ferro fluid being directly introduced to formation fluid. Therefore, NaCl solution becomes variable which was used to represent brine formation in investigating the heating time of saturated artificial cores. Meanwhile, the optimal concentration of nano-ferro had been recognized. The microwave was also varied in the sequence of power, 378 Watt, 468 Watt, 657 Watt, 792 Watt, and 900 Watt. For example, applying 50,000 ppm, 100,000 ppm, and 350,000 ppm in performing an investigation that would give a significant performance while thermal process. When 657 Watt was set to heat up the compartment contained an artificial core, the temperature could reach up to 90 °C in 110 seconds, 82 seconds, and 54 seconds consecutively from low to high NaCl solution. In that way, the sensitivity of this variable was proved that NaCl solution greatly affects the temperature increment in times. Furthermore, this research can be a considerable study in finding out the behavior of formation fluid which contributes to optimizing nano-ferro fluid thermal recovery.

Keywords: Electromagnetic Microwave, Heavy Oil, NaCl Solution, Nano-Ferro Fluid, Thermal Enhanced Oil Recovery.

Introduction

Petroleum liquids are classified as either light, medium or heavy oil based on their API gravity, a type of inverse specific gravity commonly used in the oil and gas industry, referenced to water properties at standard conditions of 60 °F and atmospheric pressure. Heavy oil is defined as liquid petroleum of less than 20 °API gravity or more than 200 cp viscosity at reservoir conditions. Heavy oil and bitumen resources account for approximately 70% of the remaining oil discovered to date in the world (Nizamidin, 2016). Further, in contrast to conventional crude oils, heavy crude oils are darker in color and may even be black. In addition to high viscosity and high specific gravity, heavy oils typically have low hydrogen-to-carbon ratios, high contents of asphalting, high carbon residues, sulfur, nitrogen, and heavy-metal content, as well as higher acid numbers (Alabdulmohsen, 2015; Carrizales, 2010; Green & Willhite, 1998; Nizamidin, 2016; Sahni et al., 2000; Silset, 2008). While heavy oil is abundant, it also presents significant economic and technological challenges. High viscosity is a major concern for the recovery from heavy-oil reservoirs. However, as the world energy demands grow, major conventional oil discoveries are rare (and difficult to find) and the costs of discovering and producing conventional oil go up, the economics of heavy oil will steadily improve.

If the heavy oil/bitumen reservoirs are shallow, surface mining is used. Otherwise, introducing heat to the formation has proven to be an effective way of lowering the oil viscosity by raising the temperature in the host formation. Thermal recovery involves well-known processes such as steam injection (cyclic steam stimulation or huff and puff, steam drive, and steam-assisted gravity drainage), in situ combustions, and a more recent technique that consists of heating the reservoir with electrical energy. Thermal recovery methods have the common objective of accelerating the hydrocarbon recovery process (Carrizales, 2010). Steam injection is the most effective method for improving heavy oil production. However, there are certain situations where it may not work very well (Sahni et al., 2000).

Generally, for steam stimulation and steam drive techniques, where heat loss occurs along the wellbore, the maximum depth of the well is 3,000 ft. While for in-situ combustion the maximum depth of the well is 11,500 ft due to the difficulty of maintaining air injection pressure to stay above the reservoir pressure due to the decrease of pressure along the wellbore. Another obstacle to forward in-situ combustion technique is the availability of sufficient crude oil in the reservoir to maintain the combustion front (Green & Willhite, 1998).

PROCEEDINGS
JOINT CONVENTION BANDUNG (JCB)|2021
November 23rd – 25th 2021

Electromagnetic Heating (EM) can be considered as an alternative recovery technique from heavy oil reservoirs that are not attractive to steam because of steam flooding many limitations. EM heating does not require a heat transporting fluid such as steam or a hot fluid injection process. EM heating can apply to situations where generating and injecting steam may be environmentally unacceptable, a single well can be used to introduce energy to the formation through a power source as well as to recover produced fluids. Production may occur during or immediately after EM heating if the formation pressure is large enough. With EM, the higher heat efficiency is achieved for thin pay-zones, where the use of steam is not economically feasible because of excessive heat loss through the overburden.

Electromagnetic (EM) heating is a process where high-frequency electrical energy is transformed into heat energy by dielectric losses when an electromagnetic wave is radiated from antennas into oil-bearing formations.

By EM heating, energy is propagated by electromagnetic waves from antennas that are impeded and absorbed by the polar molecules (water) and other reservoir materials, providing resistance to the flow. As a result, the intensity of the propagating wave is reduced and the energy is converted to heat, and then transferred by conduction to the oil and reservoir rock increasing the formation temperature. Figure 1 shows a schematic view of the EM heating process for co-current flow. The antenna is placed at the center of an injector well in front of the reservoir confined by the adjacent layers. EM energy flows into the formation and is transformed into heat with the subsequent increase of fluid flowing toward the producing well located at the opposite end of the system. Two wells are used for this EM heating process (Carrizales, 2010).

Electrical heating of a formation can occurs in three ways, depending on the frequency of the electrical current namely; low-frequency Electric Resistive Heating (ERH), high-frequency microwave heating and inductive heating.

The radiation with frequencies within a range of 300 MHz to 300 GHz and corresponding wavelengths from 1 to 0.001 m are referred to as microwaves (MW). The analysis of high-frequency heating is described by Maxwell's equations with material properties represented by permittivity (ε), magnetic permeability (μ), and electrical conductivity (σ).

At high frequencies, dielectric heating dominates and heat is generated through the absorption of electromagnetic energy by the polar molecules (connate water) in the formation.

The amount of energy absorbed will depend on the electrical properties of the formation, which are a function of its composition and water saturation as well as on the operating frequency. The magnitude of the change in temperature of the formation will depend on the energy absorbed.

For linear and homogeneous conducting medium, plane radiation propagating in the +x direction will be absorbed according to the following relationship (Santoso et al., 2016):

$$\frac{d\phi\,(x)}{dx} = -\alpha\,\phi\,(x) \qquad (1)$$

Where,
$\phi\,(x)$ = power density, Watt/cm^3
x = position coordinate, cm
α = power absorption coefficient, 1/cm

The power absorption coefficient (α) depends on the properties of the absorbing medium in the following manner:

$$\alpha = 0.02 \qquad (2)$$

And

$$\alpha_0^2 = \frac{\omega^2 \underline{\mu}\,\varepsilon}{2}\left\{\left(1 + \left[\frac{\sigma}{\omega\,\varepsilon}\right]^2\right)^{\frac{3}{2}} - 1\right\} \qquad (3)$$

Where,
α_0 = electric field absorption coefficient, 1/cm
σ = conductivity, mho/meter
$\underline{\mu}$ = permeability, H/meter
ε = permittivity, F/meter
ω = angular frequency, ($2\pi \times$ frequency)

As the porous media absorbs electromagnetic energy, the increase in temperature can be calculated from the following simple equation:

$$\frac{dT}{dt} = \frac{\sigma E^2}{\rho c_p} \qquad (4)$$

Where,
c_p = specific heat at constant pressure
E = electric field intensity, Volt/meter
ρ = mass density, Kg/m^3

Varied materials have varying specific heat capacities. Or rather, different amounts of energy are needed to heat different materials. When salt is dissolved in water, it changes several properties, one of which is the specific heat capacity. The experiment showed that as the concentration of salt increased, the specific capacity of the solution decreased (Qu, 2016).

Recent studies have been conducted for heavy oil recovery that coupled Microwave Heating with Nano Ferro Fluid (Indriani et al., 2017). In their study, the primary objective was to investigate the effects of nano ferrous concentrations on the temperature changes of the sand pack due to microwave heating. To reflect the real reservoir microwave heating in laboratory experiments, they used sand pack consists of sand, heavy oil (22 °API), brine or nano ferrous (Fe_2O_3) fluid and emulsifier (oil-based, 3%).

Therefore, the study intends to investigate the effects of the added salinity concentration of the brine on the temperature changes (rise) of the formation (and pack) and hence the viscosity of heavy oil. Combining solvent injection and EM heating might further reduce the energy intensity of the process. The merits of using a solvent in EM heating include diluting heavy oil and thereby increasing its mobility, serving as a heat carrier by reinforcing heat convection in porous media and facilitating gravity drainage by forming a vapor chamber (Hu et al., 2016).

Data and Method

This study will employ the same sand pack compositions used in (Indriani et al., 2017) experimental work.

Artificial cores are made by mixing the sand and resin with approximately 5% of the total mass. The artificial core will then be weighed in its dry weight. Furthermore, porosity measurements would be taken. The artificial core will then be saturated with heavy oil.

The nanoparticles that will be used is nano-ferrous (hematite, α-Fe_2O_3). The nano-ferro fluids of 14 ppm concentration are made up by mixing nano-ferro powder with brine (density of 1.024 gr/ml) using both handshaking and sonicator for not less than 20 minutes.

The heating process will be conducted by using a microwave heating technique. It includes the assembly of microwave circuits, magnetron, waveguide, sand pack, and thermometer for experimental measurement. There are 4 thermometers that are separated 2 cm each other vertically and are inserted into the middle of the sand pack to measure the change of temperature. Then the heating of the sand pack will be conducted by varying the power input and salinity concentration of the brine.

In both cases, the changes in temperature of sand pack and heavy oil viscosity (measured by viscometer) will be recorded at every 20 seconds from 25 °C until any point of measurement reaches the heating temperature of 90 °C to avoid water evaporation and oil flows through the slits between thermometer and the glass container, both happen at temperature of 100 °C.

Result and Discussion

The results of the experiment with the salinity concentration of the brine varied show that it could lead to the optimum heating temperature as well. The experiment conditions are made up of 50,000 ppm salinity concentration. Furthermore, by using 900 watt power of electromagnetic heating, the temperature of the sand pack performing increases up to 90 °C in 40 seconds. On the other way, the temperature increment had already occurred using 14 ppm of nano-ferro fluid in an identic condition which is influenced by 900 watt power of electromagnetic heating. Furthermore, it needs 100 seconds to reach 90 °C with 14 ppm of nano-ferro fluid in the same conditions even it was at point 1 which is the nearest one to the heat source. It is shown that the 10 ppm of nano-ferro fluid provides the temperature target more than 100 seconds as well. It could notice that high salinity brine has considerable influence as a heating stimulant to the sand pack according to the thermal heating time to reach 90 °C.

At the lowest point, the heating process could not reach to 90 °C due to the lowest power was used that leads to reduce the performance of heating distribution in which 50,000 ppm of brine applied.

Besides using 50,000 ppm salinity of the brine, the experiment also used 100,000 ppm and 350,000 ppm salinity of the brine. The results indicate that the high salinity of the brine can significantly affect the performance of the increasing temperature of the sand pack. In other words, performing heat in using a huge salinity can reduce the time needed for the heating process. Moreover, the heating process under higher salinity has a great influence to obtain the high temperature as well.

As indicated, a gradually decreasing power used also provides an effect on the performance of the heating process. The lower the power used, the longer the temperature increment takes due to the frequency radiated regarding the applied power. The thermal produced by the low power needs more time to heat up in certain conditions in which using either nano-ferro fluid or high salinity brine as a stimulant. As indicated below, the usage of higher salinity brine apparently has less time needed to heat up which is compared to the high concentration of nano-ferro fluid as a stimulant.

Furthermore, the study could bring to indicating the condition of the minimum cost as using for heating stimulant according to the time taken in which heating process. Obviously, the figure 5 shows that the usage of NaCl solution has less heating time which can minimize the heating cost up to 60% compared to exposing nano-ferro fluid. In most cases, to provide the high concentration salinity fluid could be said reasonably affordable in which conducting to brine formation.

Conclusions

In accordance with the data obtained during the experiment, it obviously indicates that NaCl solution has a significant influence to enhance the radiating thermal process for reducing the viscosity of heavy oil of the sand pack. Accordingly, it is pointed out that the thermal process using a high concentration of nano-ferro fluid as a stimulant requires more time to heat up the sand pack containing heavy oil to the temperature set up which is compared to the usage of high NaCl solution.

In other words, applying the NaCl solution as a heating stimulant can reduce the heating cost regarding less time taken in power consumption to heat up the sand pack. Approximately it would be minimized up to 60% compared to the introduction of nano-ferro fluid. By way of this case, the salinity can be a considerable parameter to compensate for the high concentration of nano-ferro fluid as a thermal stimulant fluid which can optimize the time needed in lowering a huge viscosity of heavy oil.

References

Alabdulmohsen, Z., 2015, Thesis, Missouri University of Science and Technology.

Carrizales, M. A., 2010, Thesis, The University of Texas at Austin.

Green, D. W., & Willhite, G. P., 1998, Enhanced Oil Recovery, In SPE Textbook Series (Second Edi, Vol. 6), Society of Petroleum Engineers.

Hu, L., Li, H. A., Babadagli, T., & Ahmadloo, M., 2016, SPE Canada Heavy Oil Technical Conference.

Indriani, E., Anugerah, Rachmat, S., & Munir, A., 2017, Progress in Electromagnetics Research Symposium - Fall (PIERS - FALL), 2608–2611.

Nizamidin, N., 2016, Thesis, The University of Texas at Austin.

Qu, L., 2016, Thesis, Queensland Academies Science Mathemathics & Technology Campus.

Sahni, A., Kumar, M., & Knapp, R. B., 2000, SPE/AAPG Western Regional Meeting, 257–266.

Santoso, R. K., Rachmat, S., Resha, A. H., Putra, W. D. K., Hartowo, H., & Setiawati, O., 2016, SPE Asia Pacific Oil & Gas Conference and Exhibition.

Silset, A., 2008, Thesis, Norwegian University of Science and Technology.

Acknowledgements

The authors wish to thank all kind support and contributions provided by Polytechnic of Energy and Mineral “Akamigas” Cepu

PROCEEDINGS
JOINT CONVENTION BANDUNG (JCB) 2021
November 23rd – 25th 2021

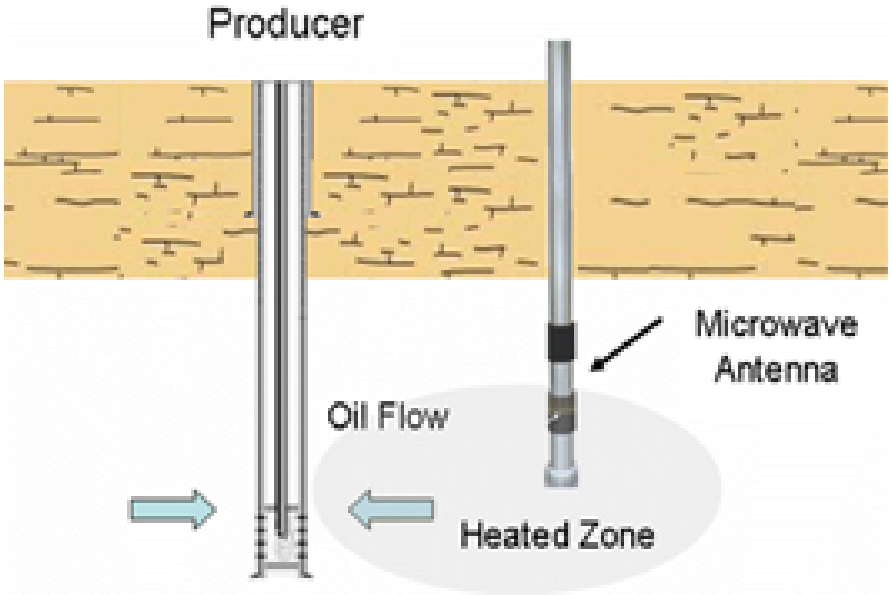

Figure 1: Schematic view of EM heating process for co-current flow (Carrizales, 2010)

The main source of heat generation in this study is microwave heating, it comprises of the microwave circuit, waveguide, and magnetron. The other tools used during the heating process of heavy oil in a laboratory are such as thermometers, containers, beakers, sonicators (agitator), viscometer, stopwatch, and cooling fans.

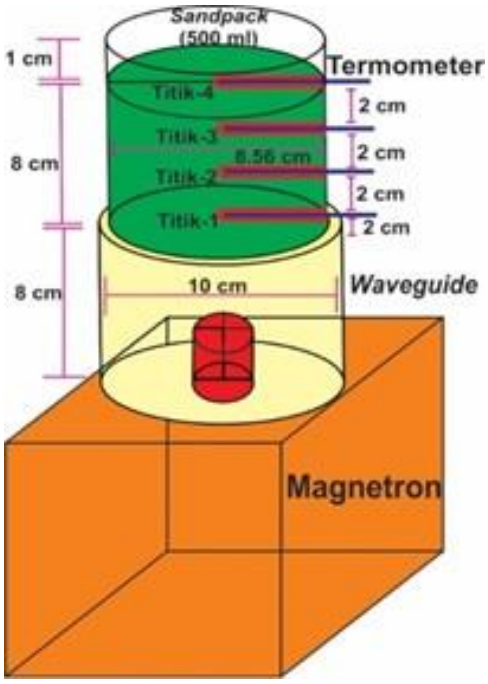

Figure 2: Microwave heating configuration (Indriani et al., 2017)

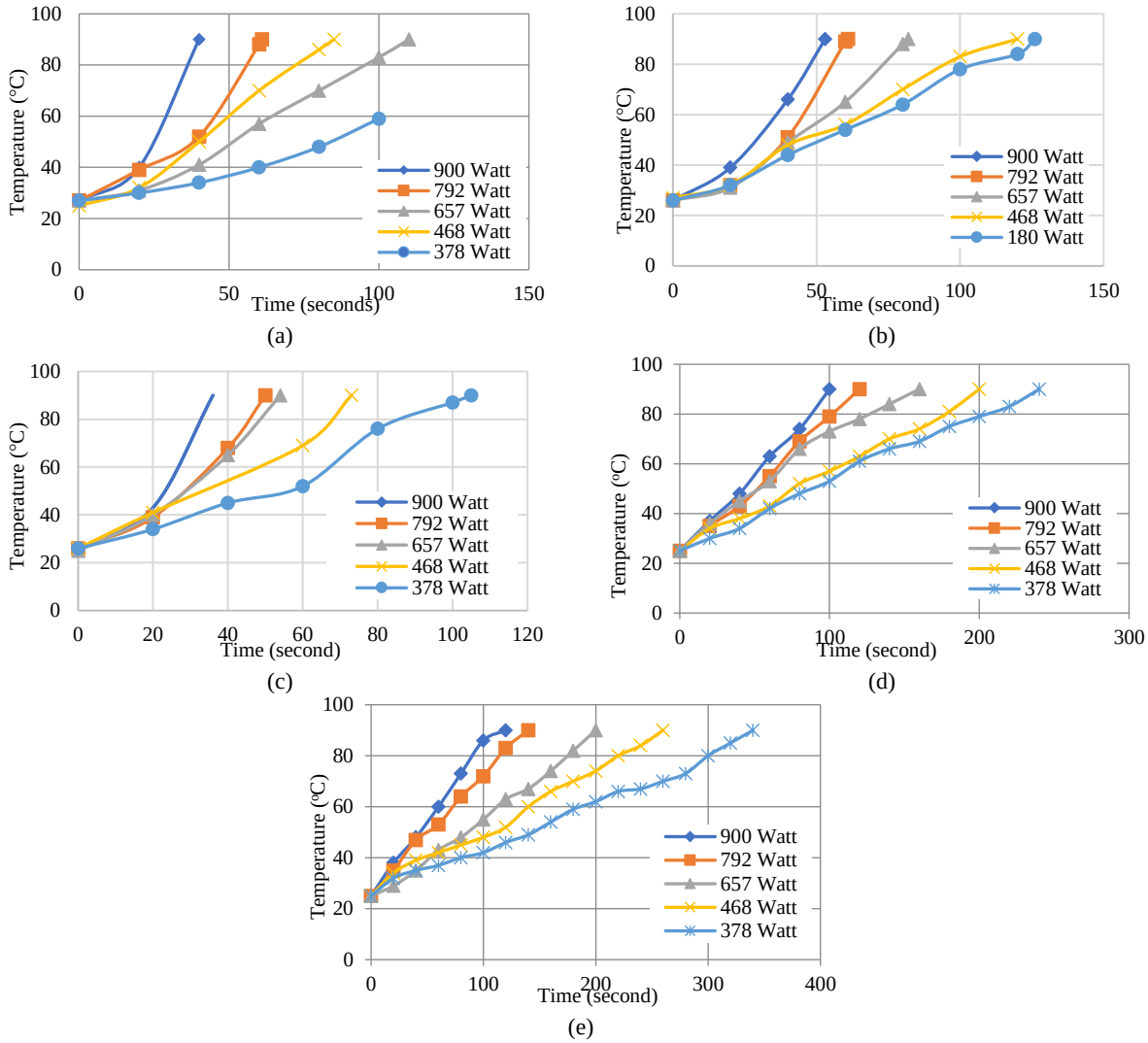

Figure 3: T (°C) vs time (second) using power varied with (a) 50,000 ppm; (b) 100,000 ppm; (c) 350,000 ppm salinity concentration of the brine, (d) 14 ppm; (e) 10 ppm of nano ferro fluid

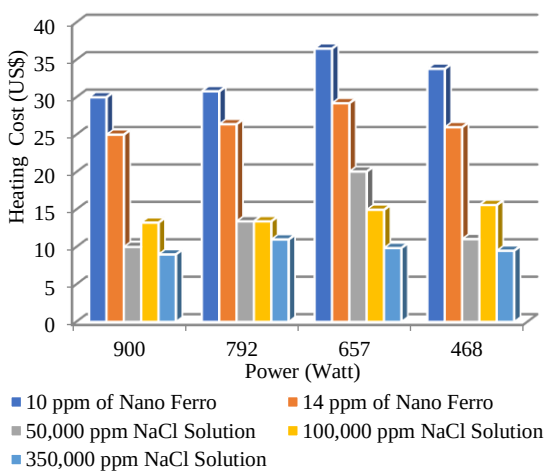

Figure 4: Comparison of heating cost within nano ferro fluid and solution of NaCl

PROCEEDINGS
JOINT CONVENTION BANDUNG (JCB)|2021
November 23rd – 25th 2021

Investigation of Polymer Flood Performance in Light Oil Reservoir: Laboratory Case Study

Dadan DSM Saputra[1], Bayu D Prasetiyo[1], Hestuti Eni[1], Yudha Taufantri[1], Ghifahri Damara[1], Yusuf D Rendragraha[1]
[1]R&D Centre for Oil and Gas Technology "LEMIGAS"

Abstract

The use of polymer solutions in the application of chemical EOR injection technology has a role in increasing oil recovery effort by improving oil mobility in porous media. The addition of the polymer solution is expected to increase the viscosity value of the displacement fluid so that it can form a "piston-like" effect with the aim of increasing the volumetric sweep efficiency of the light oil reservoir.

The polymer used in this study was HPAM with using 3 concentrations, namely 500 ppm, 1000 ppm, and 1500 ppm conducted at temperature of 70 °C. The rheology test of the polymer included concentration vs temperature, and shear rate vs viscosity. Thermal stability testing of polymer for 7, 14, 30, 60, and 90 days at 70 °C was done to determine the stability of the polymer solution. Filtration testing was conducted with the criteria of FR <1.2. The static adsorption test has been done with the standard limit of adsorption value <400 µg / gr. Polymer injectivity test using 3 variations of injection rates and coreflooding test were conducted to determine the reduction of Sor in reservoirs due to polymer displacement.

From the polymer testing stage, it was found that HPAM polymers at 3 concentrations were compatible with the injection. This is indicated with the clear solution for 3 concentrations at room temperature and at 70 °C. The rheology test results showed that the polymer solution with 3 concentrations was decreased in viscosity with the addition of the shear rate value. In the thermal stability test, the viscosity value of the HPAM with 500 ppm was relatively constant. The value of the FR for HPAM 500 ppm is 1.1, HPAM 1000 ppm is 1.07 and HPAM is 1500 ppm is 1.03. The results of the static adsorption test showed the lowest HPAM value of 500 ppm was 156 µg/gr. In the injectivity test results, the resistance residual factor (RRF) values at injection rates of 0.3, 0.6, and 1 cc/min were 0.8, 1.04, and 1.12. With the RRF value close to 1, indicating that after injection of 500 ppm of HPAM tended to not experience plugging. Polymer flooding shows the oil recovery factor (RF) of water injection is 39% OOIP, and RF after polymer injection with 0.35 PV with flush water is 13.5% OOIP or 22% Sor.

By knowing the behavior of HPAM polymer with various concentration to be used for chemical EOR injection, it could provide advantages for future implementation in the light oil reservoir in Indonesia.

Keywords: filtration, injectivity, light oil, polymer flooding, rheology.

Introduction

The use of polymer solutions in the application of chemical EOR injection technology have a role in increasing oil recovery effort by improving oil mobility in porous media. The addition of the polymer solution is expected to increase the viscosity value of the displacement fluid so that it can form a "piston like" effect with the aim of increasing volumetric sweep efficiency of the light oil reservoir. (Sheng, 2010; Seright et al, 2008; Shah and Schechter, 1977)

The polymer screening and performance testing must be done before pilot scale implementation in the oil fields. The partially hydrolyzed polyacrylamide (HPAM) polymer were used in this study. There are several tests which have to be passed to make sure the HPAM polymer performance in reservoir condition meet the criteria which will improve the oil recovery of the mature fields. Several test which must be done were screening tests or rheology evaluation such as compatibility tests, viscosity vs. shear rate tests, thermal stability tests, filtration tests, and static adsorption tests. The injectivity tests and coreflooding test were also carried out to know the performance of the polymer injection into the native and/or synthetic core.

The purpose of this study is to investigate the performance of the HPAM polymer injection in increasing oil recovery in light oil reservoir.

Research Methodology

This research study begins to understand the rheological properties of the polymeric material and providing more insight about the adequacy of polymer HPAM from its behavior through porous media (reservoirs). HPAM concentration that were tested were at 500, 1000 and 1500 ppm. The material of HPAM was mixed in a brine water that has a

designated salinity of roughly 2800 ppm (see **Table 1** for brine water composition). The experiment consists of several tests, started by testing compatibility, shear test, filtration, adsorption, thermal degradation, injectivity, and coreflooding (Poettman and Hause, 1978; Lemigas, 2008). All the tests were carried out at 70°C as the light oil reservoir temperature.

- **Compatibility test**
  The solubility of HPAM with various concentrations were visually observed at both room and 70 °C temperature to investigate the phase solution, color changing, and precipitation.
- **Shear test**
  All the rheological experiments were performed on Brookfield DVIII with UL adaptor. For each test (viscosity vs concentration and viscosity vs shear rate), the polymer solutions were prepared with varying concentrations. Concentrations ranged from 500 ppm to 1500 ppm of polymeric material in brine. The viscosity vs concentration of HPAM was measured using shear rate 7 rpm and the viscosity vs shear rate was measured using shear rate from 50 rpm to 250 rpm.
- **Filtration test**
  A filtration test was conducted to evaluate the polymer solution has free of aggregates which could lead to formation plugging. The measurement of filter test is pumped through 3 µm membrane with a differential pressure of 2 bars.
- **Adsorption test**
  The polymer solutions were prepared to conduct static adsorption test according to Recommended Practice (RP 63).
- **Thermal degradation test**
  Tests were performed during 3 months at 70 °C temperature under anaerobic conditions in sealed glass ampoules.
- **Injectivity test**
  HPAM injectivity test was run at concentration 500 ppm, temperature of 70 °C, and slow injection rates of 0.3 cc/min, 0.6 cc/min, and 1 cc/min.
- **Coreflooding test**
  During the flooding experiment, the injection rate of the displacing fluids was controlled at 0.3 cc/min with polymer injection 0.35 PV.

Result and Discussion

Polymer flooding is intentionally conducted to reduce relative permeability of water in the reservoir, therefore can improve the production of oil, as well as to enlarge the swept volume of the reservoir. Recent popular material of polymer that assured to accommodate in oil fields is HPAM. HPAM has most often been used to achieve a more favorable mobility ratio and improve macroscopic sweep in chemical EOR by increasing viscosity of the water. When dissolved in fluid, the polymer solutions have a viscosity that depends on many aspects: concentration, molecular weight, temperature, and salinity (Lemigas, 2008). In this study, the investigation of polymer flood has been performed using light crude oil. The characteristic of light crude oil has been shown in **Table 2**. Based on the result, the °API of crude oil was approaching 28 and this has to do with designing the compatible of HPAM type. Besides, the water analysis demonstrates roughly 2800 ppm salinity brine.

The compatibility of the polymer solution was first conducted at both room and 70 °C temperature. This presents in **Figure 1**, with the good result of the clear phase solution, the color of the solution was not changing, and no precipitation, which is essential to obtain distinctly sufficient chemicals.

The rheological properties of the HPAM polymer solution were evaluated by measuring the apparent viscosity vs concentration and viscosity vs shear rate. This experiment is one of the most prominent screening of an injected chasing fluid during the chemical flooding process. **Figure 2** demonstrates variation shear rate from 50 rpm to 250 rpm was conducted on the viscosity of 3 concentrations polymer at 70 °C temperature. This result presents HPAM is generally classified as a non-Newtonian fluid, because the viscosity changes when shear rate was applied. Thus, the type of fluid rheology is pseudo-plastic fluid. In this desired condition, pseudo-plastic fluid was known as shear thinning, in which viscosity decreases as shear rate increases.
The experiment result of viscosity vs concentration was demonstrated the viscosity increasing steadily with increasing polymer concentration at 70 °C temperature. This behavior greatly contributes to the shear thickening of the HPAM solution for when the polymer flows at a high shear rate in porous media.

The filtration test was performed to determine the polymer can flow through the rock pores and evaluating the effect of debris. **Figure 3** informs a volume plot graph against time of the polymer with 3 concentrations. Each of concentration solution was ensured that polymer hydration had been achieved. The value of the FR for HPAM 500 ppm is 1.1, HPAM 1000 ppm is 1.07, and HPAM 1500 ppm is 1.03. This result rapidly indicates HPAM are acceptable as it has no tendency to plug porous media in the reservoir because the requirement of the filtration ratio (FR) value was below 1.2.

The thermal degradation test was conducted during 3 months at 70 °C temperature to investigate the remaining viscosity of HPAM. The result is presented in **Figure 4**. The viscosity of 500 ppm maintains a constant value in the last 30 days, and the

rest after 3 months of aging period, it decreases slowly from 10 cP to 7 cP with a viscosity retention percentage of 30%. Comparatively, the remaining viscosity of the two concentrations left was demonstrated at 1000 ppm and 1500 ppm with increasing the number viscosity due to the changing of the colloidal system solution, likely through hydrolysis reaction. Thus, more effective preparations should be developed to improve their thermal degradation.

To understand the performance of the polymer to the rocks, injectivity and coreflooding tests were carried out. The characteristic of the rocks that were used is sandstone native core plugs with permeability range of 1500 to 2500 mD and average porosity of 0.26.

The injectivity tests were carried out using step-up rate of 0.3, 0.6 and 1 cc/min for every concentration of polymer solution. The results of the polymer injectivity can be seen in **Figure 5**. From the test results, the polymer has Residual Resistance Factor (RRF) value near to 1 (one) which means that the permeability of the core plugs after polymer injection were not changing as much and also indicates plugging did not happen after polymer injection.

From coreflooding test result, recovery factor (RF) after waterflood is at 7.2 cc or 38.7 % (OOIP) and Sor after waterflood is at 11.4 cc (61.3% OOIP). With injecting 0.35 PV polymer, recovery of oil is at 2.4 cc or 13% OOIP. This result shows that by injecting polymer after waterflood, additional oil recovery can be gained about 13.5% OOIP or about 22% ROIP **(**see **Figure 6).**

Conclusion

The test results for all of the parameters are already meet the criteria for polymer screening as chemical EOR. Based on the polymer screening test and polymer performance test that have been done, polymer concentration of 1000 ppm is suitable for polymer injection with rule of thumb polymer viscosity should be four times higher than oil viscosity (6.988 cSt) which gives about 26 cP and from coreflood result which gives about 22% ROIP. From these results, this polymer has potential to be implemented on the pilot scale on light oil reservoir.

References

Lemigas, 2008, Prosedur Analisis Surfaktan dan Polimer untuk EOR, Lemigas, Jakarta.

Poettman, Fred. H., Hause, R., 1978, SPE 7068. 5th Symposium on Improved Methods for Oil Recovery of the Society of Petroleum Engineers of AIME.

Seright, et al., 2008, SPE 115142. SPE Annual Technical Conference & Exhibition.

Shah, D.O., Schechter, R.S., 1977, Improved Oil Recovery by Surfactant and Polymer Flooding.

Sheng, J.J., 2010., Burlington, Massachusetts: Gulf Professional Publishing/ Elsevier.

Acknowledgements

Thank you to the Exploitation Department in R&D Center for Oil and Gas Technology “LEMIGAS” for the technical and non-technical supports for this research.

Table 1 Brine water composition

	Unit	Result
ANION		
Chloride	mg/L	709.06
Bicarbonate	mg/L	1037.31
Sulfate	mg/L	0.07
Carbonate	mg/L	120.02
Hydroxide	mg/L	0.00
KATION		
Sodium	mg/L	891.1
Calcium	mg/L	20.04
Magnesium	mg/L	15.19
Iron	mg/L	0.00
Barium	mg/L	0.00
Total Dissolve Solid	mg/L	2792.81
pH		8.71

Table 2 Characteristic of light crude oil

Determination	**Unit**	**Result**	**Method**
Density at 15◦C	g/cm3	0.8792	ASTM D. 5002
◦API Gravity	-	27.5588	ASTM D. 5002
Kin. Viscosity at 70◦C	cSt	6.9884	ASTM D. 445
Pour Point	◦C	45	ASTM S. 5853
Asphaltene	%wt	0.374	IP. 143
Total Acid Number	mg KOH/g	0.0156	ASTM D. 664
Saturated	%wt	52.20	Column Chromatography
Aromatic	%wt	16.04	Column Chromatography

PROCEEDINGS
JOINT CONVENTION BANDUNG (JCB)2021
November 23rd – 25th 2021

Figure 1
Compatibility polymer solution at room temperature (a) and 70 °C (b)

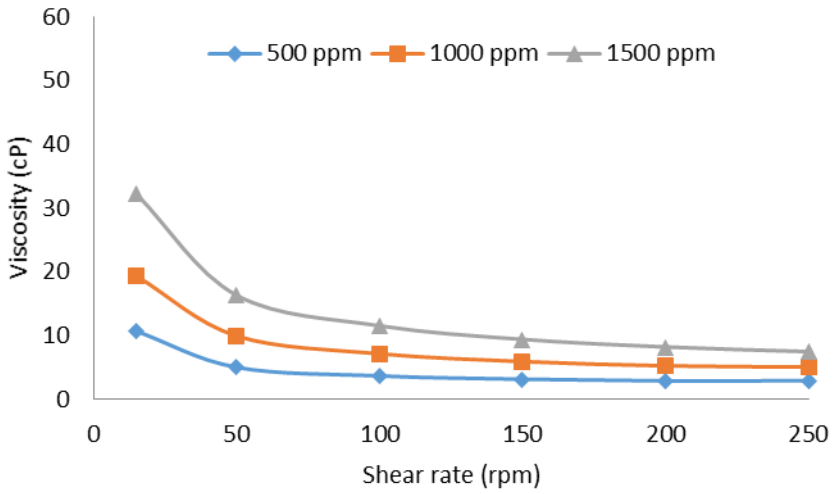

Figure 2
Effect of polymer on shear rate test results

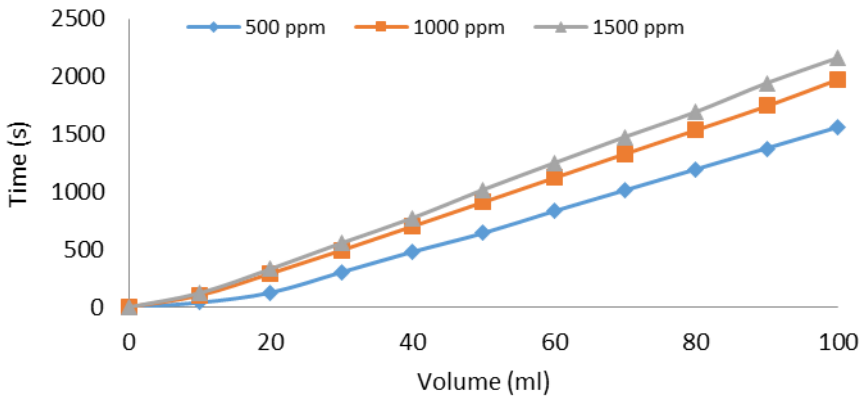

Figure 3
Filter test using 3 µm membrane results

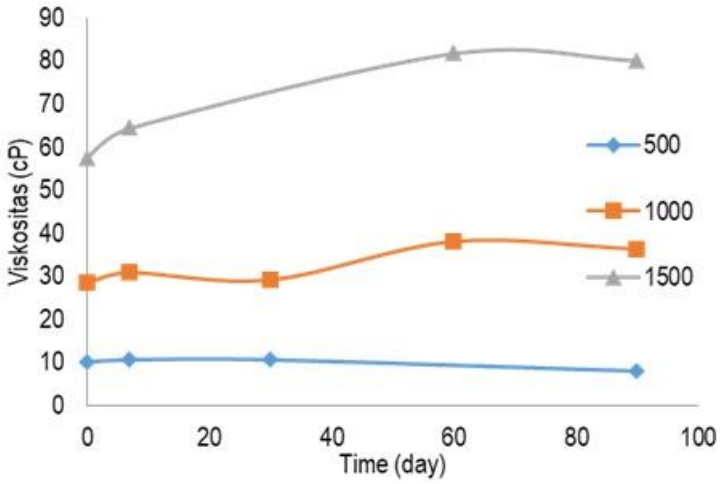

Figure 4
Thermal degradation test results

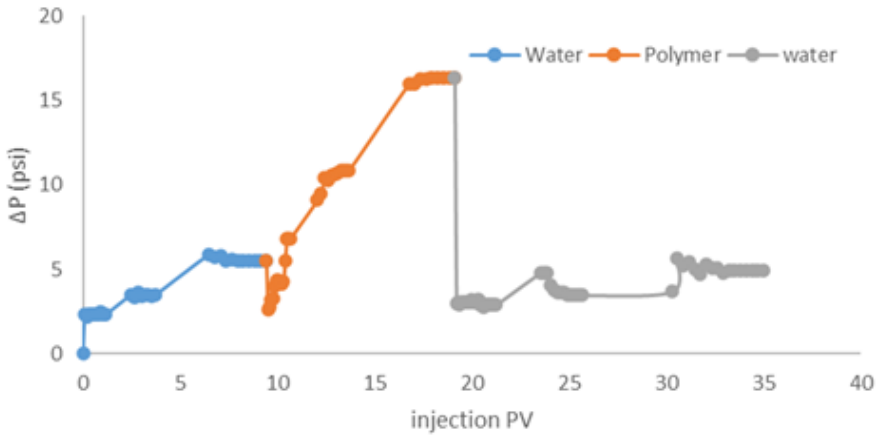

Figure 5
Injectivity test results

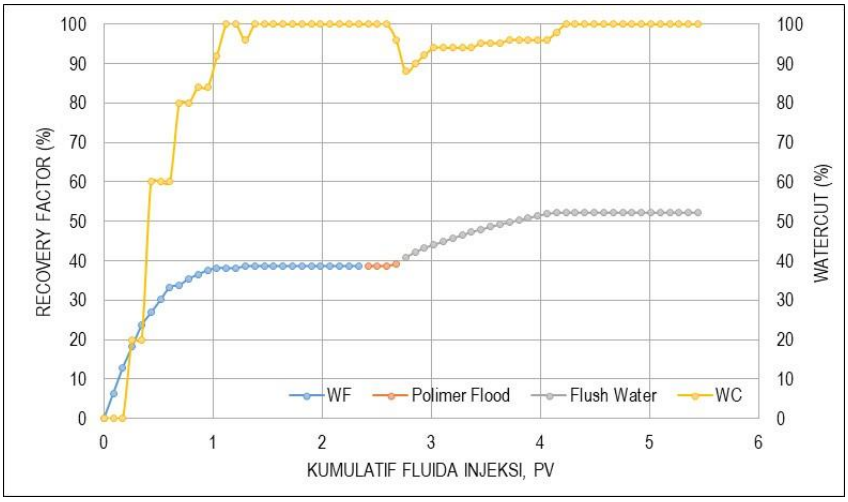

Figure 6
Coreflooding test results

PROCEEDINGS
JOINT CONVENTION BANDUNG (JCB)2021
November 23rd – 25th 2021

Analytics-Driven Method for Injectivity Analysis in Tight and Heterogeneous Waterflooded Reservoir

Richard Arnold, PT Medco E&P Indonesia

Abstract
Waterflood is one of the most reliable methods to enhance oil recovery. Among many factors governing waterflood performance, injectors' injectivity is considered as the key factor. Throughout the life of a waterflooded reservoir, injectivity impairment occurs which can have a negative impact on pressure maintenance and sweep efficiency provided by the waterflood, which both have a direct impact on production. This study aims to establish an integrated, analytics-driven method that will be leveraged to analyze injectors' performance in a tight and heterogeneous reservoir and monitor the evolution of their injectivity over time. An injectivity diagnostic methodology was developed by incorporating daily injection data and integrating various analytical techniques including instantaneous injectivity index, Hearn plot, Hall plot, derivative Hall plot, and falloff test and analysis. The resulting analytics performed well in assessing the performance of all injectors in the studied reservoir and identifying which injectors were experiencing formation damage and need stimulation. Instantaneous injectivity index quantifies the injectivity of each well. Hearn plot presents the change of the reciprocal injectivity index throughout the injection period. Hall plot provides qualitative indicators of formation damage and stimulation in each injector. Derivative Hall plot was able to capture subtle changes in injectivity that cannot be detected by conventional Hall plot, making it a powerful tool for real-time injectivity monitoring. Falloff analysis provides well and reservoir characterization in a particular injector, proving the low permeability and fractured characteristics in the injector. Each technique has its advantages and limitations and the best practice was implemented by combining all the techniques to obtain a clearer and bigger picture of the performance of all injectors. This paper describes the integrated data analysis for injectivity analysis in a tight and heterogeneous reservoir. The workflow presented is practically applicable and highly recommended for monitoring and evaluating injectors' performance in any reservoir, including the most complex ones.

Introduction

Field Overview

The reservoir of interest in this study is the TK reservoir, which is currently operated by PT. Medco E&P Indonesia. This reservoir is located onshore Sumatra, approximately 70 km northwest of Palembang City. TK is a saturated, low permeability, shaly, and heterogeneous sandstone reservoir. The key properties of this reservoir is summarized in Table 1. Due to the relatively low reservoir permeability, all TK wells are hydraulically fractured to enable production. The production started in 2002. After fast production build up in the early stage of the production life, the reservoir pressure dropped significantly.

Considering the weak pressure support provided by the solution-gas drive, water injection was then established in 2009 as a means of pressure maintenance. The required injectors are put in place by conducting convert-to-injector (CTI) jobs to convert producers that were inactive or had low oil reserve to be water injection wells. This strategy is beneficial, not only because it is significantly more economical than drilling new injectors, but also because the conversion process will maintain the existing fractures thereby allowing the injectors to have high injectivity.

Table 1. TK reservoir properties summary

Parameters	Value
Lithology	Sandstone
Depth (ft-TVD)	2,000 – 3,000
Initial Pressure (psia)	1,230
Current Pressure (psia)	500 – 1,230
Initial Temperature (°F)	175
Porosity (%)	10 – 20
Permeability (mD)	5 – 50
Average Net Pay (ft)	29
Initial Water Saturation (%)	40 – 65
Drive Mechanism	Solution-gas Drive
Production Commencement	Year 2002
Production Commencement	Year 2009

Since the beginning of its operation, water injection has been the main energy source supporting TK. Therefore, the performance of the water injection will strongly influence the production performance, and hence, the ultimate recovery factor of the reservoir. Among many factors affecting the performance of water injection, it is considered that injectors' injectivity plays the key role (Palsson, 2003). It is thus very important to monitor, diagnose, and thoroughly evaluate the injectivity of all injectors on the field; necessary actions to maintain or to improve the injectivity can then be formulated based on the evaluation. This study aims to analyze the performance of the water injection wells in the TK field and evaluate the evolution of their injectivity over time.

Data and Method

Five analytical techniques, incorporating injection flowrate and pressure data, were leveraged to evaluate the evolution of injectivity of the water injectors in TK reservoir: (i) instantaneous injectivity index, (ii) Hearn plot or reciprocal injectivity index plot, (iii) Hall plot, (iv) derivative Hall plot, and (v) falloff test and analysis.

Instantaneous Injectivity Index

The instantaneous injectivity index (II) combines all of the factors affecting the injection performance, which include effective permeability to water (k_w), effective injection zone thickness (h), water viscosity (μ_w), reservoir radius (r_e), wellbore radius (r_w), and skin factor (s). In oilfield units, assuming that the injection establishes a radial flow regime, the injectivity index can be calculated using Eq. 1.

$$II = \frac{k_w h}{141.2\ \mu_w B_w \left(\ln\left(\frac{r_e}{r_w}\right) + s\right)} = \frac{i_w}{P_{bhi} - \bar{P}_r} \qquad \text{Eq. 1}$$

The advantage of this method is that the injectivity can be directly expressed quantitatively without the need of further interpretations. Also, the injection rate and the wellhead injection pressure are normally available in timely basis. The main disadvantage of this method is that fluctuations in the measured rates and injection pressure, which normally occur during injection either due to inaccurate measurement or because of transient effects caused by reservoir or operational changes, will also result in fluctuating injectivity index. This fluctuations can sometimes be so significant such that the real instantaneous injectivity index value cannot be identified. Other drawbacks of this technique are the uncertainty in both the reservoir pressure and the bottomhole injection pressure predictions. Obtaining the actual reservoir pressure requires shutting in well(s) which is not always desirable. Bottomhole injection pressure can be predicted by calculating the friction loss across the tubing as well as the hydrostatic pressure, as expressed by Eq. 2-4.

$$P_{bhi} = P_{whi} - h_f + P_{hyd} \qquad \text{Eq. 2}$$

$$h_f = 2.083\ x\ \left(\frac{100}{C}\right)^{1.85}\ x\ \left(\frac{\left[\frac{i_w}{34.3}\right]^{1.85}}{ID^{4.8655}}\right) \qquad \text{Eq. 3}$$

$$P_{hyd} = fluid\ gradient \text{ x } midperf\ depth \qquad \text{Eq. 4}$$

Hearn Plot

Hearn plot (Hearn, 1983) is also called reciprocal injectivity index plot. This method presents the reciprocal of the injectivity index plotted against cumulative water injection volume. In cases where the injection rate and/or injection pressure fluctuates significantly due to operational or subsurface reasons, which will result in fluctuating injectivity, this plot is often more applicable as it is less sensitive to fluctuations.

Hall Plot

Hall plot (Hall, 1963) is arguably the most popular method for injectivity monitoring and analysis. This technique incorporates the following data to generate the plot:

- Average monthly bottomhole injection pressures obtained either from direct measurement with downhole pressure gauges or predicted from wellhead injection pressures using flow correlations
- Average reservoir pressure in the injection zone
- Water injection rates and/or volumes (daily or monthly)
- Injection elapsed time

This method assumes that the steady-state water injection has been achieved and can be described by Darcy's equation as shown in Eq. 5.

$$i_w = \frac{0.00708\ k_w\ h\ (P_{bhi} - \bar{P}_r)}{\mu_w B_w \left[\ln\left(\frac{r_e}{r_w}\right) - 0.75 + s\right]} \qquad \text{Eq. 5}$$

The plot is generated by plotting the cumulative pressure-time product ($i.e. \int_0^t (P_{bhi} - \bar{P}_r) dt$) against the cumulative volume of water injected ($i.e. \int_0^t i_w\ dt$). Hall plot provides a visual indication of the injection behavior where a change in injectivity, which is primarily caused by the change in skin factor, appears as a change in the slope of this plot as mathematically expressed by Eq. 6.

$$slope = \frac{141.2 \mu_w B_w \left[\ln\left(\frac{r_e}{r_w}\right) - 0.75 + s\right]}{k_w\ h} \qquad \text{Eq. 6}$$

This cumulative summing reduces fluctuations in the injectivity index which makes this tool more useful compared to injectivity index plot and Hearn plot.

Derivative Hall Plot

The advantage of the Hall plot, *i.e.* not susceptible to fluctuations, in many cases becomes the major drawback of this technique. It should be noticed that the changes in the slope of Hall Plot usually occurs gradually as it involves cumulative summation. A slight or sudden change of injectivity can easily be masked making it difficult for engineers to notice it. Due to this limitation, Hall plot is incapable of performing real-time monitoring and diagnostics.

To overcome this, Izgec and Kabir (2009) developed an extension to the Hall plot which involves plotting the derivative (DHI) of the Hall integral (HI) on the same axis. This will visually signify the injectivity changes thereby improving its diagnostic capability to capture small and sudden injectivity changes and making it applicable for real-time observation.

The derivative of the Hall integral can be calculated using Eq. 7:

$$DHI = \frac{d(HI)}{d(\ln(W_{inj}))} \approx \frac{(HI)_{t+1} - (HI)_t}{\left[\ln(W_{inj})_{t+1} - \ln(W_{inj})_t\right]} \qquad \text{Eq. 7}$$

Plotting the HI and DHI on the same Cartesian scale would reveal the following behaviors:

- If both plots trace the same path, then neither wellbore stimulation (e.g., fracturing or acidizing) nor formation damage (e.g., plugging or scaling) occurs
- If DHI plot falls below HI plot, then wellbore stimulation is indicated
- If DHI falls above HI plot, then wellbore plugging is indicated

Falloff Test

A falloff test is actually the pressure build-up version for injectors. It is a pressure transient test that is done by injecting water into the reservoir for a certain period of time and then shutting in the injector while measuring the pressure falloff. As this test requires the injector under investigation to be shut-in, this test is not routinely done in many operations.

This test provides useful information regarding the injector and the reservoir including the average reservoir pressure, effective permeability-thickness product, skin factor, and

fracture characteristics (e.g., conductivity, dimensionless conductivity, and half-length). From this analysis, reservoir permeability can be determined by incorporating injection zone thickness obtained from log analysis or production/injection logging analysis.

Result and Discussion

Instantaneous Injectivity Index

Instantaneous injectivity index plots are generated for all the injectors. Injectivity index plot of one of the injector is shown in Figure 1.

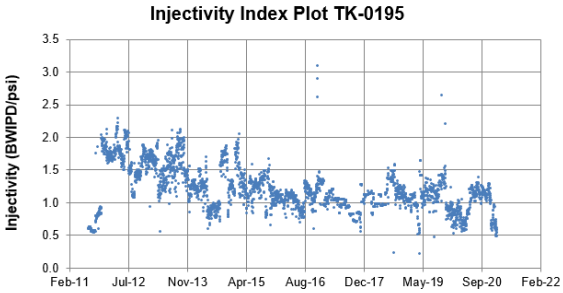

Figure 1: Injectivity index plot of injector TK-0195

As can be seen from Figure 1, there was a continuous decline of injectivity from approximately 2.0 BWIPD/psi in 2011 to about 1.0 BWIPD/psi in end of 2013. Since then, the average injectivity tends to be stabilized though the instantaneous injectivity keeps fluctuating. The latest trend of injectivity profile however shows a sharp injectivity impairment. This observation was important as an input for further investigation before the best remedial action to improve the injectivity can be formulated and conducted.

Hearn Plot

Hearn plots were also constructed for all injectors along with the injectivity index plot. This technique plots the reciprocal injectivity index against the cumulative water injection volume to measure the injection performance of the injector for every available data point. It has the same weakness as the instantaneous injectivity index plot although it is slightly less reactive to fluctuations in injection rate and pressure. Hearn plot of TK-0195 is presented in Figure 2.

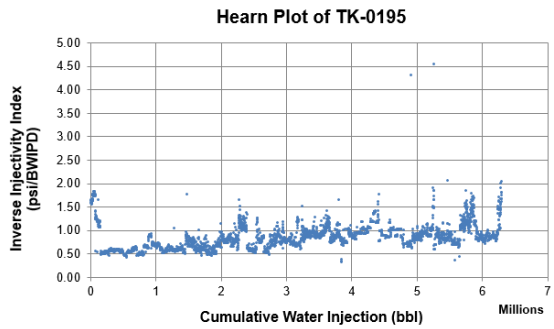

Figure 2: Hearn plot of injector TK-0195

As can be inferred from Figure 2, in average, there was a continuous increase of inverse injectivity index in the early operation of this injector. After the injection volume of 3 MMbbls was reached, the average reciprocal injectivity was relatively constant although instantaneously it keeps fluctuating. The latest reciprocal injectivity trend however shows a significant increase which indicates wellbore plugging that needs further study and action.

Hall Plot

As a best practice, Hall plots were generated for all injectors as illustrated in Figure 3. Based on the Hall plots, some injectors maintained their initial injectivity even after years of injection operation, while several others showed injectivity impairment. The main cause of injectivity decline was the accumulation of oil and suspended solids carried by the injection water. The other sources of injectivity impairment were sand and proppant build-ups covering the perforation or the choked fracture caused by the loss of proppant bed conductivity at sandface as the proppant were pushed by the injection water towards the reservoir.

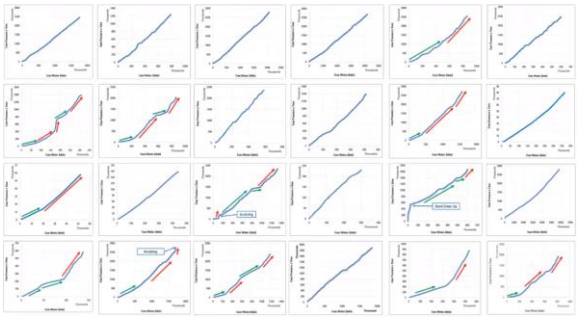

Figure 3: Hall plots of several TK injectors (Arnold & Asrul, 2020)

Using this analytical tool, injection performance of each injector can be monitored and analyzed. For comparative analysis, all Hall plots were plotted on a same graph, and based on the slope of each plot, each injector was then categorized into one of the two groups, as shown in Figure 4. The two groups are separated by the unit-slope line. Steep slope of the Hall plot or slope higher than unity indicates low injectivity or high resistance to flow, which can be caused by low reservoir permeability, formation damage, or local over-pressurization that minimizes the injection driving force. On the other hand, gentle Hall slope or slope lower than unity suggests high injectivity or low resistance to flow, which can be due to high reservoir permeability, connection with high permeability layer, or low reservoir pressure which maximizes the injection driving force.

Based on the comparative Hall plots, it was found that most of the injectors exhibited high resistance to injection. There was one injector that outperformed other injectors, both in terms of injectivity and injection sustainability. There are several possible reasons for this, including waterflood-induced fracturing that improved and sustained the injectivity, connection to high permeability streaks or to other zone, or wellbore leakage. Comprehensive investigation including reservoir, geomechanics, and wellbore integrity studies is required to identify the root cause of this anomaly.

PROCEEDINGS
JOINT CONVENTION BANDUNG (JCB)2021
November 23rd – 25th 2021

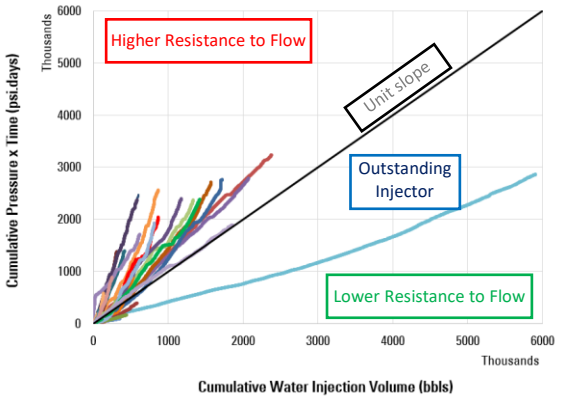

Figure 4: Comparative analysis with Hall plot (Arnold & Asrul, 2020)

Derivative Hall Plot

Derivative Hall plots were constructed for all injectors along with the construction of Hall plots. Hall plot and derivative Hall plot of TK-0195 is depicted in Figure 5.

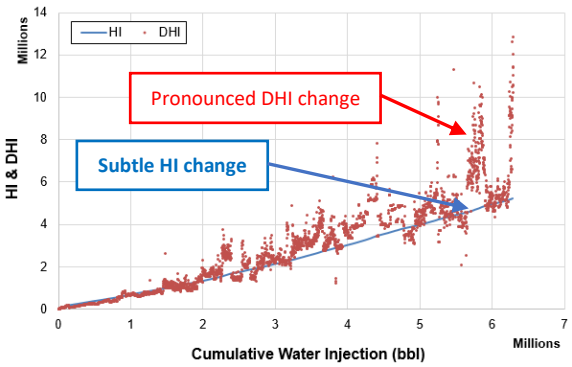

Figure 5: Hall plot and derivative Hall plot of TK-0195

As evidenced in Figure 5, the changes in slope of the Hall plot was subtle, making it difficult to identify the injectivity change. However, the derivative nature of the DHI plot is able to magnify these changes, making it easy to detect whether the injector experienced well stimulation or wellbore plugging.

In addition, the instantaneous injectivity, Hall plot, and derivative plot can be combined on the same graph to create a more comprehensive injectivity monitoring tool (Onwuchekwa, 2019) as demonstrated in Figure 6.

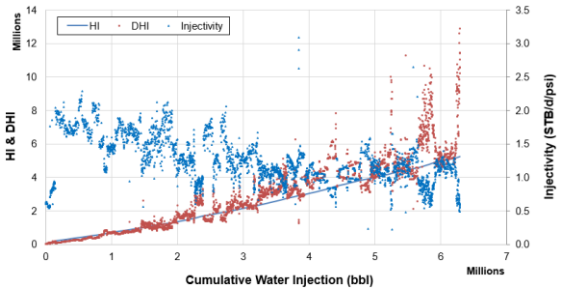

Figure 6: Combination of injectivity plot, Hall plot, and derivative Hall plot of TK-0195

Falloff Test

Due to the requirement of shutting in the injector of interest, falloff test was rarely executed. This test is only performed when there is a strong need of reservoir or well data, for example reservoir pressure to validate the reservoir simulation, fracture conductivity to validate the fracture simulation results following hydraulic fracturing execution, or permeability-thickness product to greatly enhance the quality of the injection analysis.

The latest falloff test conducted in TK field was performed in TK-0257. The log-log plot result of this test is shown in Figure 7. This analysis highlighted three important things, which are:

- Very high reservoir pressure exceeding the original reservoir pressure, which can be caused by continuous water injection within the reservoir zone that has low continuity to the far field area resulting in localized pressurization
- Low reservoir permeability of 7 mD, which confirmed the tight characteristic of TK reservoir
- Fracture half-length of about 300 ft, which validated the fracture analysis.

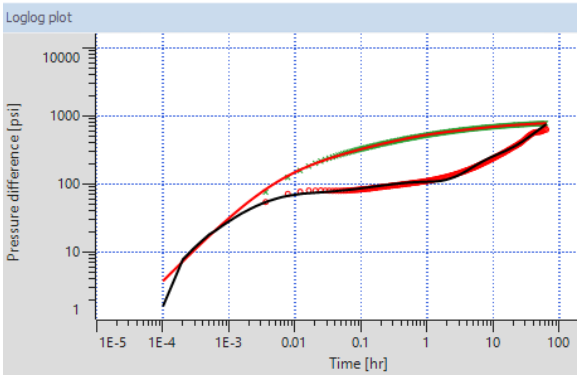

Figure 7: Log-log plot of falloff analysis in TK-0257

Conclusions

In this study, an integrated injectivity analysis methodology was developed by incorporating daily injection data and various analytical techniques including instantaneous injectivity index, Hearn plot, Hall plot, derivative Hall plot, and falloff test and analysis. Each technique has its advantages and drawbacks and the best practice was leveraged by combining all the techniques to obtain a clearer and bigger picture of the performance of all injectors in TK reservoir. The resulting analytical methodology performed well in assessing the injectivity of all injectors and identifying which injectors were experiencing formation damage and in need of wellbore stimulation. This method is very useful as it provides more accurate well performance assessment and faster opportunities identifier to improve injectors' performance.

Nomenclature:

B_w = water formation volume factor (RB/STB)
h_f = pressure drop due to friction (psia)
ID = tubing internal diameter (inch)
k_w = effective permeability to water, mD
h = effective injection zone thickness, ft
II = injectivity index (BWIPD/psi)
i_w = water injection rate (BWIPD)

PROCEEDINGS
JOINT CONVENTION BANDUNG (JCB) 2021
November 23rd – 25th 2021

μ_w = water viscosity, cp
P_{bhi} = bottomhole injection pressure (psia)
P_h = hydrostatic pressure (psia)
$\bar{P}_r$ = average reservoir pressure (psia)
P_{whi} = wellhead injection pressure (psia)
r_e = reservoir radius, ft
r_w = wellbore radius, ft
s = skin factor

References

Palsson, B., Davies, D. R., Todd, A. C., and J. M. Somerville. "A Holistic Review of the Water Injection Process." Paper presented at the SPE European Formation Damage Conference, The Hague, Netherlands, May 2003.

Hearn, C. L. (1983): "Method Analyzes Injection Well Pressure and Rate Data," Oil and Gas Journal (No 81) (April.1983) 117–120.

Hall, H. N. (1963): "How To Analyze Waterflood Injection Well Performance," World Oil 128-30.

Izgec, Bulent, and C. Shah Kabir. "Real-Time Performance Analysis of Water-Injection Wells." SPE Res Eval & Eng 12 (2009): 116–123.

Arnold, R. and Asrul, F. 2020. Waterflood Surveillance Best Practice in a Tight, Heterogeneous, Water-Sensitive, and Massively Fractured Reservoir. Paper IATMI20-87. Presented at IATMI Simposium 2020, 24 – 25 October 2020

Rothkopf, B., Fredrickson, S., & Hermann, J. (2003, January 1). Case Study: Merging Modern Reservoir Characterization with Traditional Reservoir Engineering. Society of Petroleum Engineers.

Onwuchekwa, Vincente, Usman, Musa, Wantong, Paterne, Biu, Victor, and Jed Oukmal. "Injectivity Monitoring & Evolution for Water Injectors in a Deepwater Turbidite Field." Paper presented at the SPE Nigeria Annual International Conference and Exhibition, Lagos, Nigeria, August 2019.

Acknowledgements

The author expresses sincere thanks to team members of PT Medco E&P Indonesia Resource Development Area-1, Saras N.H, Febrian A., Geraldus Y. S. R. S., Dian U., and Elsa F. S., for their priceless contributions in developing the reservoir presented in this paper. Special thanks to Medco management for allowing the publication of this paper.

PROCEEDINGS
JOINT CONVENTION BANDUNG (JCB) 2021
November 23rd – 25th 2021

Challenges of MEOR Implementation in Indonesia

Sumadi Paryoto, Victor Sitompul, Denie Tirta Winata, Tino Diharja, Muhammad Alfian, Fransiskus Ondihon Sitompul, Gunawan Sutadiwiria
Upstream Research & Technology Innovation – PT. Pertamina (Persero)

Abstract

The target of oil production Indonesia in 2030 has been set at 1 million bopd. Opportunities and challenges to achieve these production figures are certainly not easy. One of these efforts is the application of EOR methods.

Microbial Enhance Oil Recovery (MEOR) technology is one of the EOR methods by utilizing microbes that will degrade types of oil to make it easier to flow as well as a producer of bio surfactants that can reduce surface tension or internal force tension (IFT). Before implementing MEOR, screening is carried out which includes reservoir parameters, selection the type of microbes to be used and proper nutrition. All over the world this technology has been tried in 17 countries with positive results in 10 countries.

Several fields in Indonesia have been tested for MEOR implementation, including Cepu, Ledok, Bentayan and Mangunjaya. MEOR implementation is carried out with the Huff and Puff system of nutrient injection and microbial injection in production wells. The problem in implementing MEOR is the selection of appropriate nutrients and microbes, besides that when implementing the huff and puff system it takes a relatively long time for soaking. To maintain the production of huff and puff wells, it is necessary to repeat the injection work.

The factors that support this success are reservoir screening, nutrient selection and injection technique. The results of laboratory tests in 3 fields showed that MEOR resulted increasing Recovery Factor (RF) more than 10% and from the implementation of huff and puff in 4 fields, it showed a decrease in water content and a gradually increasing production after soaking.

Keywords: MEOR, Microbe, Nutrient.

Introduction

The target of oil production Indonesia in 2030 has been set at 1 million bopd. Opportunities and challenges to achieve these production figures are certainly not easy. One of these efforts is the application of EOR methods.

Microbial Enhance Oil Recovery (MEOR) technology is one of the EOR methods by utilizing microbes. Increasing production from the MEOR application occurred as a result of a decreasing in oil viscosity, an increasing in API gravity, and a decreasing in pour point *(Harry Budiharjo et al (4)*). MEOR applications in Indonesia have implemented in several fields, including Prabumulih (1992), Klamono and Kawengan (1993), Ledok (1999), Chevron Pacific Indonesia (CPI, 2001), Bentayan (2017) and Mangunjaya (2017). From several fields that have been carried out by MEOR in Indonesia, production increases ranging from 8-66%. The increasing production occurs after some time from the moment of injection.

This paper aims to provide an overview of MEOR cases in Indonesia, MEOR requirements, types of microbes for MEOR, optimal conditions for microbial development in reservoirs, nutrient injection and several fields that potential for MEOR candidates. The writing is based on a literature study of several papers on MEOR and some data from the fields.

MEOR Technology

MEOR is one of the EOR technologies aimed to increasing oil recovery by injecting nutrients and microbes into the reservoir. In the presence of nutrients, microbes in the reservoir will thrive. In addition to degrading hydrocarbons into lighter oils, microbial metabolism also produces gases, acids, biomass and polymers. Gas produced by microbes, it could be rising up reservoir pressure and decrease oil

viscosity by dissolving it. Acid could dissolve carbonate. Biopolymer could increases water viscosity in water flooding activity.

An increase lots of microbes could also cause plugging in the oil zone and acid can cause corrosion in equipment.

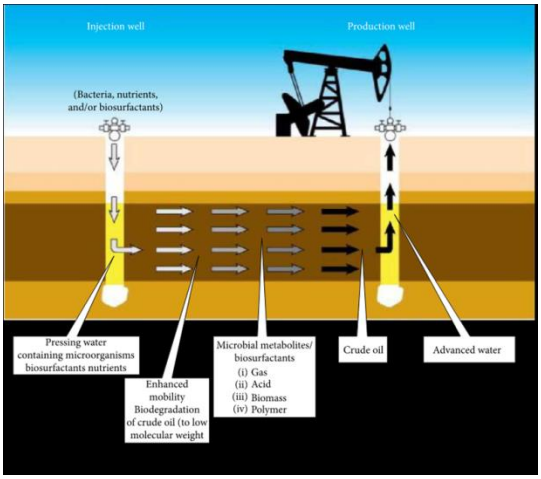

Figure 1 – MEOR Process in Reservoir. *Haicheng She et al. (3)*

Based on the use of MEOR, the process is divided into several there are including microbial flooding recovery (MFR), cycle microbial recovery (CMR), microbial selective plugging recovery (MSPR), and others. According to the strain, it is divided into 2, namely Indigenous and Exogenous. Indigenous microbes come from reservoirs. Exogenous microbes are selected and come from outside the reservoir. Currently, the most developed microbes are indigenous microbes because they are more adaptive and avoid the use of microbes from outside.

Based on the growth that needed oxygen or not, it could be divided into aerobic bacteria, facultative bacteria, and anaerobic bacteria. Based on their effect on oil production, there are microbes in the reservoir that are good for oil production and some are not. To detect microbes, complex high-tech biotechnology equipment is used, such as terminal restriction fragment length polymorphism (T-RFLP), gene bank, denaturing gradient gel electrophoresis (DGGE) and most probable number (MPN).

The MEOR process mechanism is:

1. Oil Degradation by Microorganisms
2. Biosurfactants in Microbial Metabolism
3. Emulsification
4. Altering Reservoir Physical Properties
5. Microscopic Mechanism

Planning in Conducting MEOR

The microbial flooding system includes activating material composition, slug injection, nutrient concentration, nutrient sizing and slug injection. The increase in recovery occurred after the growth period.

Referring to laboratory research and field tests in China, there are 8 main parameters for reservoir screening and evaluation for microbial flooding as follows (CNPC MEOR Screening criteria):

Table 1 – CNPC MEOR Parameters. *Haicheng She et al. (3)*

Parameter	Value Range	Optimum
Formation temperature (°C)	20-80	30-60
Crude viscosity (mPa·s)	10-500	30-150
Permeability (mD)	≥50	≥ 150
Porosity (%)	12-25	17-25
Brine salinity (g/L)	≥300	≥100
Wax content (%)	≥4	≥7
Water cut (%)	40-95	60-85
Total bacterial concentration in produced fluid (number/mL)	≥100	≥1000

Considering the results of that research, the parameters for the Shengli Oil Field test are as follows:

Table 2 – Shengli Oil Field MEOR Parameters. *Haicheng She et al. (3)*

Formation temperature(°C)	Permeability (mD)	Formation brine (pH)	Formation brine salinity (mg/L)	Dead oil viscosity at 50°C
≤80	≥50	6~8	≤150000	≤3000

Microbial flooding recovery field test in China showed an increase in oil recovery at 4.95% with 0.1 PV slug.

There are several types of microbes and their applications in MEOR as follows:

Table 3 – Types of Microbes and MEOR Applications (*McInerney MJ et al., 2002*), (*Harry Budiharjo et al (4)*)

Microbial Product	Example Microbes	Application in MEOR
Bio-mass	Biomass Bacillus, Leuconostoc, Xanthomonas	Selective plugging and wettability alteration
Surfactant	Acinetobacter, Arthrobacter, Bacillus, Pseudomonas	Emulsification and de-emulsification through reduction of IFT
Polymer	Bacillus, Brevibacterium, Leuconostoc, Xanthomonas	Injectivity profile and viscosity modification, selective plugging
Solvent	Clostridium, Zymomonas, Klebsiella	Rock dissolution for better permeability, oil viscosity reduction
Acids	Clostridium, Enterobacter, Mixed acidogens	Permeability increase, emulsification
Gasses	Clostridium, Enterobacter Methanobacterium	Increased pressure, oil swelling, IFT and viscosity reduction

Based on the pressure, the maximum pressure for live microbes is 7000 – 8000 psi, above that it will have a negative impact on microbial growth. Based on temperature, there are 3 types of microbes, namely Psychrophiles (<25°C), Mesophiles (25-45°C) and Thermopiles (45-60°C).

MEOR Implementation Worldwide

There are 17 countries that have implemented the MEOR besides Indonesia. This implementation is intended to overcome production problems, namely: formation damage; low oil relative permeability; trapped oil due to capillary forces; poor sweep efficiency channeling; unfavorable mobility ratio; low sweep efficiency; water or gas coning. Positive implementation results were found in 10 countries and negative results were found in 6 countries and 1 country for which there was no report *(I Lazar et al. (5)).*

MEOR in Indonesia.

MEOR has been tested and researched in Indonesia since 1992 at Pertamina EP in Prabumulih Field. There are several fields that have been tested by MEOR, including Prabumulih, Cepu (not specifically named), Ledok, Kawengan, Klamono, Bentayan, Mangunjaya and PT Chevron Pacific Indonesia in Balam South, Bangko and Minas Fields. There are at least 7 SPE papers that discuss MEOR technology in Indonesia. In this paper, we will discuss the implementation of MEOR in Cepu, Ledok, Bentayan and Mangunjaya.

MEOR in Cepu

MEOR has been implemented in 10 wells. Microbial selection is based on reservoir permeability, pressure and temperature. Clostridium sp. and Bacillus sp was chosen because it can grow in conditions of temperatures up to 230°F (110°C) and pressures up to 7000 psi. The lowest permeability in the 10 wells is 7 – 38 mD, while for the other 9 wells the permeability is categorized according to *Kalish et. Al, 1964* is a medium category that has a pore size of 4.5 – 5 μm. The width of the Clostridium sp. and Bacillus sp is 0.1 - 0.3 μm so it can be transported and grow in rock pores. Success analysis is in 2 ways, the first is the analysis from oil sample and the second is the analysis from production data before and after MEOR.

Table 4 – Pore size category and permeability range according to *Kalish et. Al, 1964 (Harry Budiharjo et al (4)*) as follows:

Type of Permeability	Permeability Range (mD)	Pore Size (μm)
High	278 - 400	5,5 – 6,0
Medium	130 -162	4,5 - 5
Low	17,7 - 48,3	3,5 - 4

Table 5 – MEOR Screening by *Ahmed Eltayeb et al., 2013 (Harry Budiharjo et al (4))* as follows:

Factor	Limit	Optimum	Comment
Pressure (Psi)	Not Critical	-	Extremely high pressure are troublesome to non adapted bacteria
Temperature (^{o}C)	<80	30 – 50	Depend on the microbe
Viscosity (CP)	>20	-	The upper limiting value wasn't reported
API Gravity (^{o})	>15	30 – 40	Heavier crude information wasn't sufficient
pH	5 – 9	6 – 8	Main Factor
Salinity (ppm)	<10% NaCl<150000	-	-
Lithology	Not Critical	Carbonate	-
Depth (ft)	<7800	-	Depend on the corresponding temperature
Porosity (%)	>10	>10	Not limiting
Permeability (mD)	>50	>150	-
Oil Saturation (%)	-	>25	Successful trials with a low saturation was reported

PROCEEDINGS
JOINT CONVENTION BANDUNG (JCB)2021
November 23rd – 25th 2021

In the analysis of oil and brine used 4 parameters, there are oil viscosity, API gravity, pour point and stability index (SI). The results of the analysis showed that there was a decrease in oil viscosity by 13% - 31.3% in 6 wells and a decrease in viscosity of less than 10% in 4 wells. There is an increase in API gravity of 1.5%-9.3% in 5 wells and an increase of 0.5%-0.9% in 5 wells. There was a pour point decrease of 3%-21% in 9 wells. SI analysis shows an increase in 10 wells, it shows that it could be make scale in production facilities which can reduce production.

In the analysis of production after 21 days MEOR shows an increasing production. The largest increasing production was 66% and the smallest increase in production was 8%. There are 2 wells that experienced a decrease in production indicating failure which was probably caused by the large stability index. The results of the SI analysis show an increase.

The comparison graph before and after MEOR is as follows *(Harry Budiharjo et al (4))*:

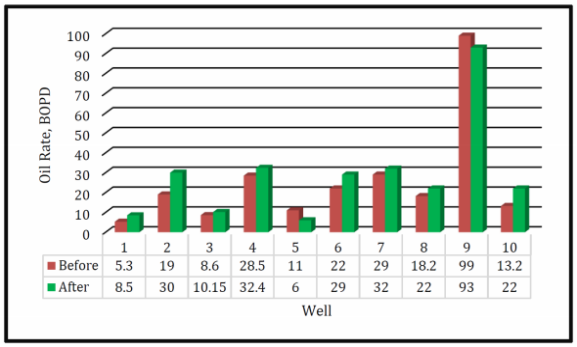

Figure 3 – The comparison graph before and after MEOR

MEOR in Ledok

In Ledok, huff and puff MEOR is implemented in the LDK-132 well. Prior to the field test, a lab test was conducted with the fluid taken from the well head and native core from the LDK-P1 well for comparison with the standard core (Classach) from Scotland. Core of LDK-P1 with a permeability of 140 mD. The microbes used were indigenous from LDK-132 enriched with Bacillus licheniformis and M4+. The results of the lab test test can increase the gain by 12.58%, reduce the permeability by 52.11%.

Table 6 – Coreflood Test Result with MEOR. *A. Yusuf et al (1)*

No.	Core Sample	Pore Vol. (cc)	Initial Water Saturation (cc)	Initial Water Saturation %PV	Initial Oil Saturation (cc)	Initial Oil Saturation %PV	Oil Production Water Injection (cc)	Oil Production Water Injection %OOIP	Type Of Microbes	Shut In (days)	Oil Production Microbes Inject. (cc)	Oil Production Microbes Inject. %OOIP	Oil Rec. Factor (%)
1	LDK-P1	23.20	7.15	30.80	16.05	69.20	8.10	50.10	LDK-132 + BC	21	1.00	6.23	12.58
2	CLASSACH	13.73	4.03	29.33	9.70	70.67	5.93	61.13	LDK-132 + BL	16	0.80	8.25	21.22

Field test was conducted on July 8, 1999, there was an increasing production of 8.18 bopd on June 15, 1999. Investment of 3000 USD with income above cost of 926.4 USD for 4 weeks.

MEOR in Bentayan

Lab tests were carried out in wells BN-38 and BN-81. Screening based on a combination of Aladasani and Bryant methods. During the lab test, the number of bacteria during the incubation period was observed every 7 days using the Total Plate Count (TPC) method on Nutrient Agar (NA) media for aerobic facultative bacteria and Reinforced Clostridial Medium (RCM) for anaerobic bacteria. Optimum nutrient composition consists of molasses, nitrogen salt of the type $(NH4)_2PO4$ and NPK type phosphate salt for well BN-38. In contrast to BN-81, especially in the concentration of molasses. The composition after treatment was observed with GC/MS clearly to be a lighter composition. Heptane plus degraded more than 30%. Decreased viscosity to 43.68% in BN-38 and 47.83% in BN-81. The imbibition experiment showed RF 56% and optimum soaking for 7 days in BN-81.

PROCEEDINGS
JOINT CONVENTION BANDUNG (JCB)2021
November 23rd – 25th 2021

Table 7 – Screening Method by Aladasani and Bryant . *(D. I. Astuti et al (2))* as follows:

Parameter	Reference	
	Aladasani (2012)	Bryant (1991)
API	12.0 – 33.0	>15
Viscosity (CP)	1.7 – 8900	-
Porosity (%)	12.0 – 28.0	-
Oil Saturation (%CP)	55 – 65	>25
Formation Type	Sandstone	-
Permeability (mD)	60 – 200	>50
Depth (ft)	1572 – 3464	<8000
Temperature (oF)	86 - 90	<170

Flow chart of the imbibition test for Well BN-81 is as follows:

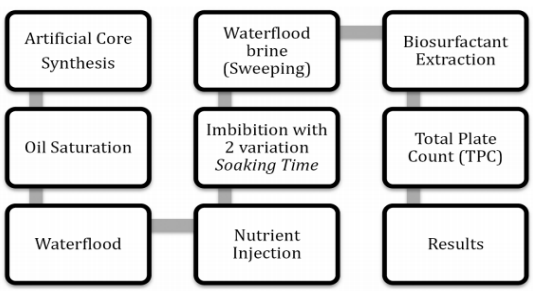

Figure 4 – Imbibition Flow Chart Analysis. *D. I. Astuti et al (2)*

The most optimum nutrient composition consisted of 7.16% w/v molasses, 0.3% w/v $(NH4)_2PO4$ and 0.26% w/v NPK.

In the pilot test with a gradually nutrient injection program of 500 bbls nutrient followed by 100 bbls post flush then a second nutrient injection of 1500 bbls nutrient followed by 100 bbls of post flush. After injection, soaking is done for 14 days. Then 2000 bbls post flush injection was performed and soaked again for 7 days. After 3 months of observation the production of aerobic microbial abundance increased by 1000-fold and anaerobes increased 10-fold. This abundance changes the physical and chemical conditions of oil and reduces oil viscosity by 24 percent and IFT by 47 percent. In both wells the water cut reduces from 99% to 92% and increases oil production by 1395 bbls. Economic calculations show Pay Out Time (POT) for 4 months and a production gain of 1750 bbls.

MEOR in Mangunjaya

Applied with the Huff and Puff method in the MJ-122 and MJ-125 wells. Reservoir parameter screening based on Aladasani and Bryant method. Screening on 5 wells, namely MJ-122, MJ-74, MJ-125, MJ-116, MJ-42. From that five wells, based on laboratory tests, the best results were MJ-122 and MJ-125. Monitoring was carried out for 6 months consisting of microbial population, composition analysis of oil production samples and production performance. Bacterial growth all of them was in the range of 2x103 CFU/mL – 5 x106 for 176 days in MJ-122 and more than 500x106 CFU/mL in MJ 125 for 122 days. After 3 months monitoring the biodegradation reached 34%. Field test results showed MJ-122 water content decreased at low production. MJ-125 experienced an increase in oil production by 20% with a decrease in water content at low and high production rates.

Huff and Puff field test MEOR process flow is as follows:

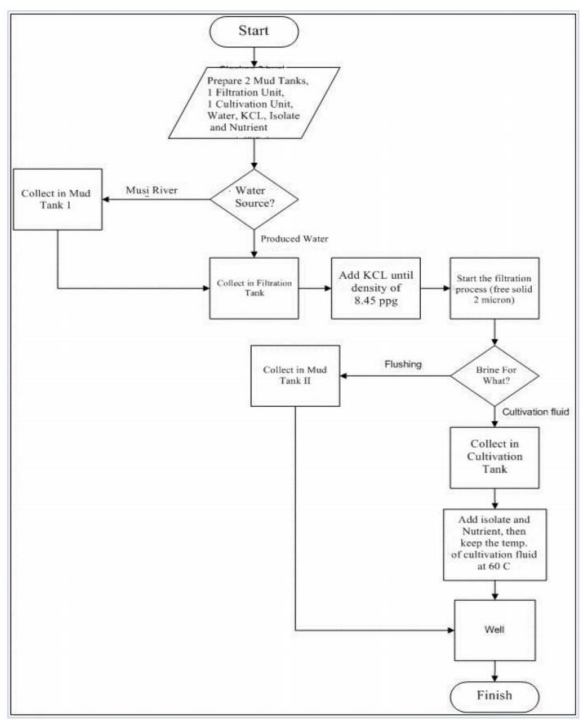

Figure 5 – Process Flow MEOR Injection. *T. Ariadji et al (9)*

PROCEEDINGS
JOINT CONVENTION BANDUNG (JCB)2021
November 23rd – 25th 2021

Table 8 – The flow of fluid requirements (*T. Ariadji et al (9)*):

50 bbls	200 bbls	50 bbls	Soaking	200 bbls	200 bbls	Soaking	600 bbls	Soaking
Pre-flush (brine)	Inject MEOR (100 formation + 98 brine + 2 bbls oil)	Post Flush (brine)	7 days	Inject MEOR (100 formation + 98 brine + 2 bbls oil)	Post Flush after jobs (brine)	3 days	Post Flush after soaking 3 days (brine)	1 day

Discussion

Based on several references in the application of MEOR as mentioned above, it indicates that need a reservoir screening consisting of fluid, rock and reservoir conditions. Prior to implementation in the field, several tests were carried out in the laboratory consisting of testing the nutritional composition, microbial growth and coreflood. Usually it will be selected if the coreflood results show an increaseing gain of more than 10%. After testing in the laboratory is completed and getting the best nutritional formula, then proceed with implementation in the field. In Indonesia, the implementation in the field that has been done using huff and puff.

From several examples of implementation above, it is found that the implementation in Cepu resulted in an increase production by 8%-66%. The number of wells implemented is also at most 10 wells, while in Mangunjaya and Bentayan there are 2 production wells and Ledok 1 production well. MEOR implementation can also reduce water content, so that if gross production is also reduced, the nett production obtained is not so visible. The parameters of these success criteria must refer to good engineering practice based on the ability of the wells tested before MEOR is carried out. The effect of MEOR on the huff and puff system is usually up to 3 months after injection and soaking In order to maintain production, the huff and puff must be repeated.

Based on MEOR screening by Aladasani, Bryant, Ahmed Eltayeb and CNPC with parameters API Gravity and Temperature there are several oil fields in Indonesia may suitable to MEOR implementation.

Table 9 – The structure of oil fields in Indonesia that are suitable as initial MEOR candidates there are:

Oil Fields	^{o}API Oil at max 33°	T Reservoir (^{o}F) at max 170°F
Kenali Asam	18 - 21	115 - 138
Setiti	24 - 27	125 - 135
Ketaling Timur	20 - 31	119 - 149
Tempino	20 - 23	100 - 115
Bentayan	20	155
Mangunjaya	22 - 28	122
Ibul Tenggara	30 - 35	250 - 260
Dewa	16 - 35	250 - 260
Abab	22 - 30	220 - 230
Raja	22 - 34	250 - 260
Benakat Barat	19 - 35	130 - 180
Jirak	23 - 36	130 - 180
Talang Akar	30 - 35	130 - 180
Sopa	30 - 40	280 - 300
Ogan	25	168 - 200
Talang jimar	28	170 - 212
Tanjung Miring Barat	29	150 - 210
Tanjung Miring Timur	27	180 - 200
Kawengan	31 - 36	130 - 145
Ledok	26 - 42	130 - 145
Warukin	25 - 33	104 - 140
Klamono	19	140 - 158
Linda	18	167 - 183

Conclusion

1. MEOR has been implemented in several oil fields in Indonesia including Cepu, Ledok, Bentayan and Mangunjaya
2. The implementation in several fields was carried out by Huff and Puff and some managed to get a fairly good increase in production.
3. The length of time for the operation of MEOR huff and puff injection and soaking is relatively long, so it is necessary to select candidate wells through field screening and laboratory testing with many candidates and test variations.
4. Success criteria parameters should be determined prior to MEOR implementation based on good engineering practice and well production testing should be carried out to obtain optimum production figures before MEOR is carried out.
5. Based on the screening criteria, there are still many potential MEOR candidates in several fields in Indonesia.

Acknowledgement

Thank you to VP URTI Mrs. Merry Marteighianty who has given the opportunity to write this paper. Thank you are also to Mrs. Belladona Troxylon who has provided some suggestion and input in technical writing. And also thank you conveyed to all friends at URTI for their support and assistance during writing this paper.

References

1. A. Yusuf, Sri Kadarwati, Nurkamelia, LEMIGAS, and Sumaryana, PERTAMINA, "Field Test of the Indigenous Microbes for Oil Recovery, Ledok Field, Central Java", Society of Petroleum Engineers, SPE 57309.
2. D.I. Astuti, T. Ariadji, P. Aditiawati, I. A. Purwasena, G. P. Persada, A. A. Ananggadipa, U. R. Dewi, D. D. Khendarsyah, and R. Rizki, Bandung Institute of Technology; M. H. Abqory and R. N. Ardianto, PT Pertamina EP, "A Comprehensive Preparation Study for Microbial Nutrient Injection of Microbial Enhanched Oil Recovery : Reservoir Screening and Laboratory Analysis – Case Study Bentayan Field", Society of Petroleum Engineers, SPE-186249-MS.
3. Haicheng She, School of Civil Engineering and Architecture, Xi'an University of Technology, Xi'an, 710048 Shaanxi, China; Debin Kong, Yiqiang Li, State Key Laboratory of Petroleum Resources and Prospecting, China University of Petroleum-Beijing, Beijing 102249, China; Zaiqiang Hu, School of Civil Engineering and Architecture, Xi'an University of Technology, Xi'an, 710048 Shaanxi, China; Hu Guo, School of Petroleum Engineering and Environment Engineering, Yan'an University, Yan'an, 716000 Shaanxi, China, "Recent Advance of Microbial Enhanced Oil Recovery(MEOR) in China", Hindawi, Geofluids Volume 2019, Article ID 1871392.
4. Harry Budiharjo, Nur Suhascaryo, Handika Agung Nugroho, and Benny Ariandy Saputra, Universitas Pembangunan Nasional Veteran Yogyakarta, "Optimizing Oil Recovery through Microbial Injection to Support the Increasing Demand for Oil in Indonesia", Society of Petroleum Engineers, SPE-186214-MS.
5. I. Lazar , I. G. Petrisor & T. F. Yen (2007), "Microbial Enhanced Oil Recovery (MEOR)", Petroleum Science and Technology, 25:11, 1353-1366, DOI: 10.1080/ 10916460701287714.
6. Lewis R Brown, Mississippi State University, Biological Sciences, "Microbial enhanced oil recovery (MEOR)", Science Direct, Elsevier.
7. Saikrishna Maudgalya, SPE, Anadarko Petroleum Corp., and Roy M. Knapp, SPE, and Michael J. McInerney, SPE, U. of Oklahoma, Norman, "Microbial Enhanced-Oil-Recovery Technologies: A Review of the Past, Present, and Future", Society of Petroleum Engineers, SPE 106978.
8. Steven L. Bryant, The University of Texas at Austin, and Thomas P. Lockhart, SPE, Enitecnologie, "Reservoir Engineering Analysis of Microbial Enhanced Oil Recovery", Society of Petroleum Engineers Inc, SPE 63229.
9. T. Ariadji, D. I. Astuti, P. Aditiawati, I. A. Purwasena, G. P. Persada, M. R. Soeparmono, N. H. Amirudin, A. A. Ananggadipa, and S. Y. Sasongko, Bandung Institute of Technology; M. H. Abqory and R. N. Ardianto, Pertamina EP; E. Subiantoro and G. H. Aditya, EMP Malacca Strait, "Microbial Huff and Puff Project at Mangunjaya Field Wells: The First in Indonesia Towards Successful MEOR Implementation", Society of Petroleum Engineers, SPE-186361-MS.
10. T. Ariadji, D. I. Astuti, N. Priharto, A. A. Ananggadipa, G. P. Persada, and E. Subiantoro, Bandung Institute of Technology; P. E. Erwanto and M. H. Abqory, PT Pertamina EP, "Field Implementation of Nutrient Huff and Puff in Bentayan Field, South Sumatera: Towards a Low-Cost EOR", Society of Petroleum Engineers, SPE-196536-MS.

Appendix

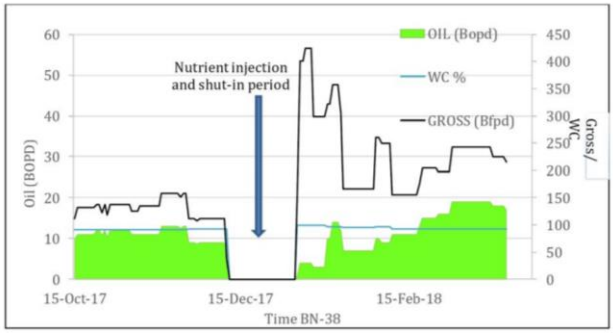

Figure 6 – MEOR Production Performance at well BN-38. *T. Ariadji et al (12)*

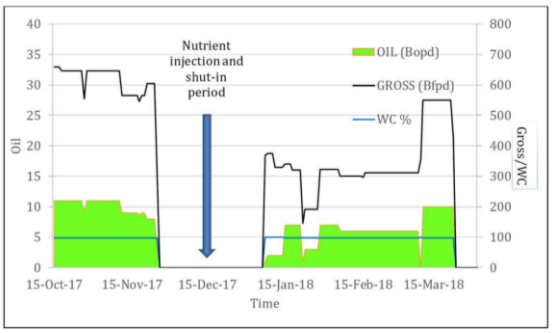

Figure 7 – MEOR Production Performance at well BN-81. *T. Ariadji et al (12)*

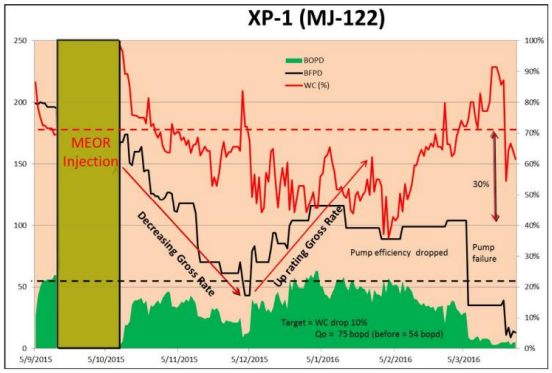

Figure 8 – MEOR production performance at well MJ-122. *T. Ariadji et al (11)*

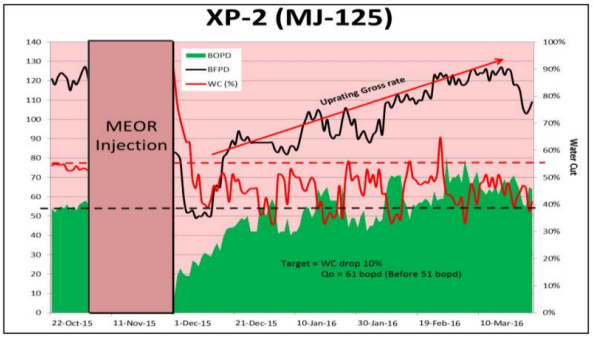

Figure 9 – MEOR Production Performance at well MJ-125. *T. Ariadji et al (11)*

PROCEEDINGS
JOINT CONVENTION BANDUNG (JCB) 2021
November 23rd – 25th 2021

How to Deal with Producing Very Mature Field: case L Field Pertamina

Reza Alfajri[1], Tantowi Tandean[1], Herbert Sipahutar[1]
Pertamina[1]

Abstract
As national oil and gas company that was founded 63 years ago, Pertamina deals with quite a lot of mature fields. L Field was first explored in 1925, which precede Pertamina. This field produces with wells that are mostly on more than 90% water cut. Dealing with this very mature filed is quite tricky. Selective work plan needs to be performed to achieve optimum results.

Three general approaches that are performed for L Field for the last three years are: decreasing water cut, balancing produced water and injection water, searching for remaining oil prospects. In order to decrease water cut, reversed coning treatment package was performed. The package consists of perforation cleaning using high pressure flush, paraffin solvent and relative permeability modifier stimulation, and reversed coning tool. Balancing injection and produced water was achieved by performing acidizing or solvent stimulation to injector wells to remove perforation plugging. RST log was utilized to search for remaining oil in a well.

Well M-36 was treated with reversed coning treatment package in 2019. This treatment was performed under performance based contract. Having performance based stipulation to handle mature field economically makes sense since production is not going to be really big. Powerwave tools was used to mechanically clean perforation. This tool increase fluid pressure that flows through its nozzles. Paraffin solvent stimulation then entered the picture to dissolve oil's paraffin content. Relative permeability modifier was then pumped to block water movement in the reservoir. Last, mechanical reversed coning tool was installed to attempt breaking existing water coning shaped. After treatment, well M-36 produced oil more than twice its pretreatment production from 5 to 12 bbls/day. Injector stimulation was performed for seven wells, which had drops in injection rate. Out of these seven wells, 63% success ratio was achieved. This treatment successfully maintain L-Field Production. RST log was performed on well L-071. From RST, remaining oil from potential layers in this well was found and perforated. Its oil production was the highest in L field in the last 5 years with 80 bopd with water cut as low as 30%.

These three general approaches are proven to be quite effective in producing very mature field such as this L Field. When water handling was done right, any excess from injection rate compared to produced water can be used to perform production optimization. While waiting for discoveries on new prospects in a mature field the approaches in this paper can be used as a template work plans.

Introduction
L Field was first explored in 1925 by Standard Oil of New Jersey (America) and Nederlanse Koloniale Petroleum Maatschapij (Netherland). The first oil producing well L-003 found in 1936. In 1941 Sago structure was developed with S-010 well initial rate 850 BOPD. L Field reached its peak production 30.000 BOPD in 1958 with average water cut around 30%. Pertamina operated L Field from 1983 and now its producing 1600 BOPD from 109 producing wells with 98.8% water cut and injecting around 150,000 BLPD produced water through 57 injector wells. L Field has reached a mature stage with 52% recovery factor. L field has sufficient wells drilled to adequately drain the productive reservoirs, no new wells are considered necessary to be drilled, as 1986 study suggested. One way to increase oil production is gross up optimization which causes the increment of water production.

With this condition, L Field facing some major problems:
- High water cut
- Water management
- Low remaining reserves

For the last three years several efforts performed to decrease water cut, balancing produced water and injection water, and look for remaining oil prospects. This paper will explain it further.

Data and Method
A. Reverse Coning Package Method
As we know reverse coning method often used to prevent water coning or thin hydrocarbon layer. In this case, we combined several techniques and performed it as one job sequence. This job sequence consists of:
1. Powerwave tools
Water was injected through powerwave tools that have a nozzle on the tip. This tool increase fluid pressure that flows through its nozzle, creating jetting effect to mechanically clean the perforated zone. The powerwave technology is based on internal differential pressure forcing the flow to oscillate from nozzle exit to the other, these burst of fluid create pulsating pressure waves within wellbore and formation fluid that break up and removing near wellbore damage. Figure 1 shows description of this tool.

Figure 1 Powerwave tool

PROCEEDINGS
JOINT CONVENTION BANDUNG (JCB) 2021
November 23rd – 25th 2021

2. Paraffin Solvent
   L Field has paraffinic oil with API gravity 34 and pour point 108ºF. Therefore, paraffin solvent stimulation can be utilized to chemically clean the wellbore. It dissolves oil's paraffin content and deposition near wellbore. Relative permeability modifier was then pumped to block water movement in the reservoir.
3. Reverse Coning Tool
   Mechanical reversed coning tool was installed to attempt breaking existing water coning shaped. Figure 2 shows how water coning in the reservoir is broken by installing reverse coning tool. This tool is shown in Figure 3. Reverse Coning Tool developed to extract oil in watery region by reversing the water through the bottom of the device and allowing oil flow from reservoir into the well that is shown in the following figure. With this approach, the oil recovery can be raised

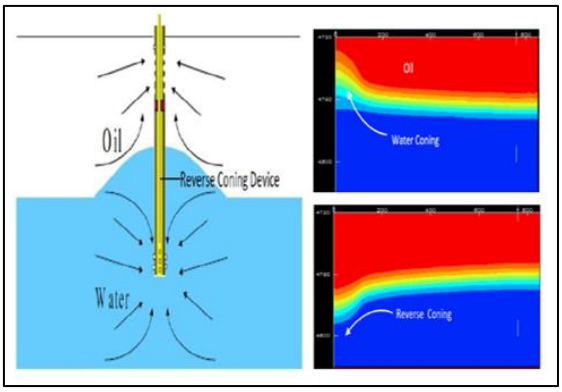

Figure 2 Reverse Coning Concept

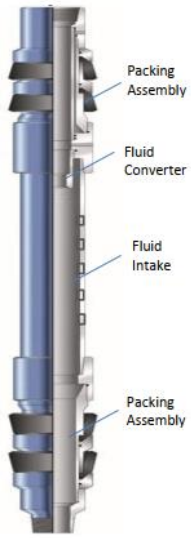

Figure 3 Reverse Coning Tool

B. Injection Well Stimulation
   With 150,000 bbls of production water, L field only had 57 injector wells. Overtime, injection wells capacity started to decline due to blockage of the perforation caused by paraffin wax and scale deposition. Optimization on injector wells must be performed, while looking for new injection well candidates. Therefore, anti-paraffin agent was injected to dissolves paraffin wax, followed by acid stimulation to dissolve scale accumulation. Figure 4 and Table 1 show the form of paraffinic oil in L field and results of paraffin solvent solubility test of the oil.

Figure 4 Crude Oil from L-Field

m_{oil}	10.9018	gr
m_{screen}	2.9721	gr
m_{final}	2.987	gr
$m_{insoluble}$	0.0149	gr
$m_{soluble}$	10.8869	gr
% solubility	**99.86%**	

Table 1 L Field Crude Oil Solubility Test Result with Paraffinic Solvent

C. C/O log
   C/O log is a logging tool that measures the carbon-oxygen content of a formation and its contained fluids. The C/O ratio proved to be reliable indicator of hydrocarbons in sandstone formations, independent of formation water salinity and, in most instances, independent of turbidity.

   In addition to the C/O log, a continuous log similar to an ordinary neutron log can be run. Also, by selective timing within the tool, gamma ray responses indicative of silicon and calcium can be recorded to aid in interpreting the C/O log in areas of unknown lithology or mixed lithology. In a practical sense, this tool has the capability to obtain information on the hydrocarbon content and porosity of a formation, as well as to differentiate sandstone from carbonates and clean sands from limy sands. Figure 4 shows C/O example of C/O log interpretation.

PROCEEDINGS
JOINT CONVENTION BANDUNG (JCB) 2021
November 23rd – 25th 2021

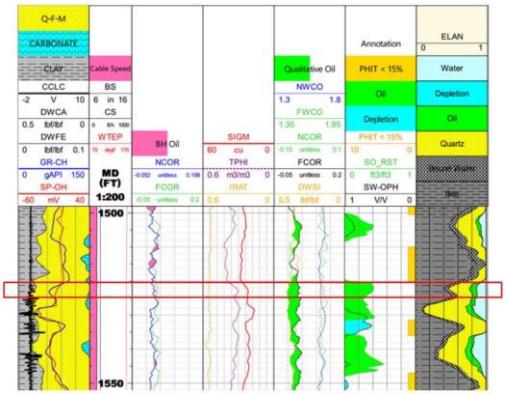

Figure 5 C/O log interpretation Example

Result and Discussion

A. Reverse Coning Package Method

M-036 well met the criteria to be applied with reverse coning package method. Its water cut rapidly increase from 94.2% to 98.8% after artificial lift optimization. Figure 6 shows this well's Chan Plot that indicated a bottom-water coning. The reverse coning package aimed to decrease water cut so that water management for this well could be easier to handle.

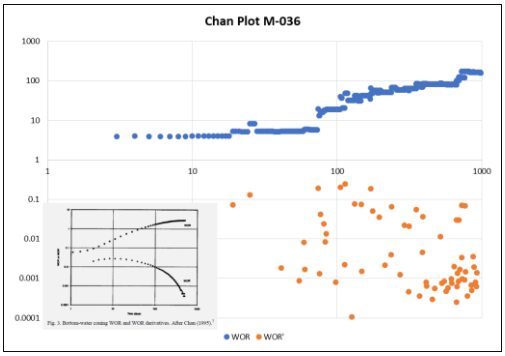

Figure 6 Chan Plot of M-036 well

M-036 was producing 5 BOPD before treatment. After Reverse Coning stimulation job in January 2020, M-036 produced averagely 12 BOPD, although no significant decrease in water cut (99.6% to 98.2%) and still producing at 6 BOPD and 99.5% water cut at the end of 2020 (Figure 7). It seems that its water cut went back to the pre-treatment condition after almost a year. It can be concluded that the treatment is effectively decrease M-036 water cut, with 1 year lifetime. Next tasks to carry are to evaluate the effectiveness of powerwave tool, paraffin stimulation, and reverse coning tool separately and the optimum period to repeat treatment process in a well.

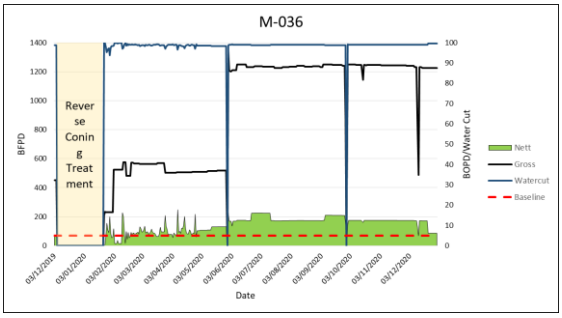

Figure 7 M-036 Production Performance

B. Injection Well Stimulation

Acid and Anti-paraffin stimulation was performed to 8 injection wells, which had drops in injection rate. The method is as follow:

a) **Pre-job injectivity rate test** with brine to identify the stimulation operating rate and pressure
b) **Inject anti-paraffin chemical** and soak for two hours.
c) **Inject acid chemical** to dissolve scale deposition near wellbore and soak for two hours.
d) **Post job injectivity rate test** to compare before-after performance.

Some wells immediately performed better while stimulation, yet a few showed improvement after soaking the chemical. Overall, 5 out of 8 injection wells showed improvement in injection rate (63% success ratio). Figure 8 to 11 show one of the successful injection well stimulation case in Well N-082 L Field.

Rate (BPM)	Pressure (psi)
0.5	290
0.75	350
1	405
1.25	445
1.5	460
1.75	490
2	505
2.25	510
2.5	515

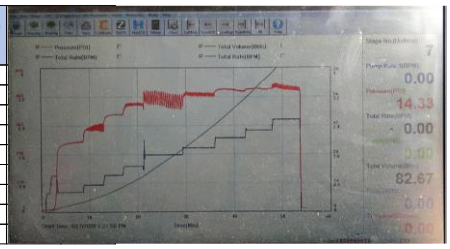

Figure 8 Anti-parafin injection of N-082 well, L Field

Rate (BPM)	Pressure (psi)
1	270
2	400
2	190
2	320

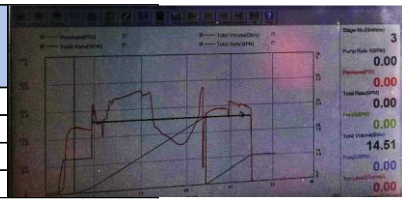

Figure 9 Anti-parafin injection of N-082 well, L Field

The graph showed pressure decline while injection of anti-parafin, indicating that chemicals reacted well and clean the wellbore.

Rate (BPM)	Pressure (psi)
0.5	15
1	120
1.75	320
2	360
2.5	420
2.75	450
3	460
3.5	500

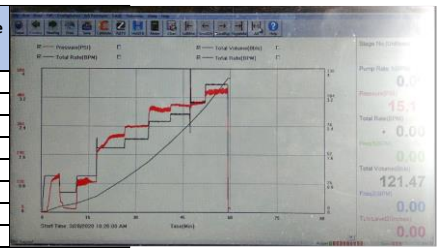

Figure 10 Post-job injectivity rate test of N-082 well, L Field

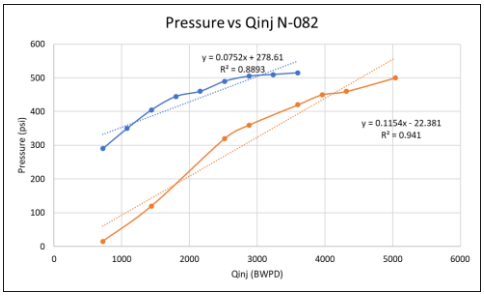

Figure 11 Pre-job and Post-job injectivity rate comparison

PROCEEDINGS
JOINT CONVENTION BANDUNG (JCB) 2021
November 23rd – 25th 2021

This shows that the injectivity rate was better after stimulation. With the same injection pressure, it could be injected with more volume after stimulation.

Injection well stimulation successfully increased injection capacity in L Field and ease the water management. Resulting space for surface facilities and artificial lift optimization.

C. C/O log

A C/O log was done on suspended well L-071 to seek hidden potential hydrocarbon resources. Figure 12 shows C/O log from Well L-071.

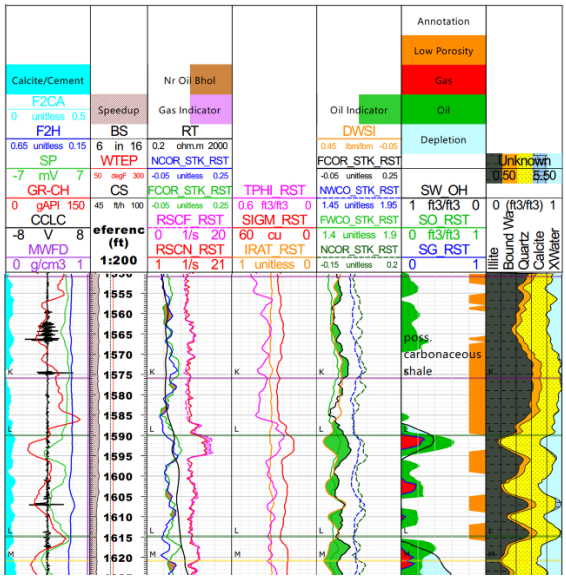

Figure 12 C/O log of L-071 well

The C/O log interpretation found an interesting zone on L layer (1590 – 1594 ftMD).

Production performance of this Well L-071 after performing well intervention based on the C/O log result is shown in Figure 13.

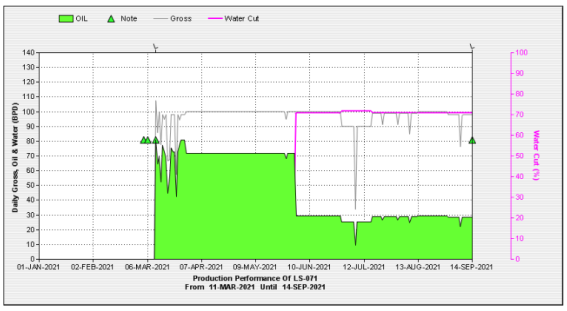

Figure 13 L-071 Production Performance

L layer of L-071 was opened with initial production = 108 BFPD, 81 BOPD, and 25% water cut. It was a huge achievement for L field and unlocked new opportunities on L layer near L-071 well to be developed.

Conclusions

These three general approaches are proven to be quite effective in producing very mature field such as L Field. When water handling was done right, any excess from injection rate compared to produced water can be used to perform production optimization. While waiting for discoveries on new prospects in a mature field the approaches in this paper can be used as a template work plans

References

Jockel, D. et.all. 2014. "Fluid Oscillation Tool Restores Gas Delivery Rate from Storage Wells". SPE- 91390-MS

Willemse, Emanuel J.M. et.all. 2015. "Optimizing Stimulation Treatments in Straddled Completions". SPE-93071-MS

Wichmann, P.A. dan Hopkinson, E.C.1976. "The Carbon/Oxygen Log Measurement". SPWLA

Harthy, A. et.all. 2004. "Screen and Near-Wellbore Cleaning and Stimulation Tools Evaluation: Recent Experience in Well Operation". SPE-89653-MS

Acknowledgements (Optional)

We would like to thank our comrades in Pertamina and others that were involved in supporting this work.

PROCEEDINGS
JOINT CONVENTION BANDUNG (JCB)2021
November 23rd – 25th 2021

Basin geometry and deep-water deposition,Tertiary Bampo-Bruksah Petroleum System, offshore North Sumatra Basin

Chris Sim, Jens Beenfeldt, Eric Mueller, PGS.

Abstract
The North Sumatra Basin, Indonesia, is a prolific back-arc basin with a proven Tertiary petroleum system evidenced by onshore and offshore oil and gas discoveries. Multisensor 3D seismic data covering the underexplored deep water offshore northern North Sumatra-Mergui Basin provides detailed insights into the syn- and post-rift depositional system and the relationship to the underlying pre-rift sequence of the area. Direct Hydrocarbon Indicators (DHI) in pre-rift fault blocks and amplitude anomalies in the post-rift section, suggests the potential extension of the prolific petroleum system proven across the Central Trough-Malacca Platform.

Data quality allows a detailed evaluation of pre-rift basin structure and its imprint on subsequent syn- and post rift deposition. A number of flat spots are present towards the top of the syn-rift section, either associated with large anticlines or more limited in tilted fault blocks.

Structural movement is reflected in post-rift thickness changes and the location of mass transport complexes that have shed off local highs. Subtle basin morphology and temporal shifting of depocenters are recorded in sediment thickness distribution. Ponding of thick mass transport complexes in front of post-rift basin inflection points is suggested based on the location of stacked amplitude anomalies. Slope and basin floor settings can be derived from horizon attribute maps representing laterally continuous reflectors. However, single high amplitude events with lateral phase change and amplitude shut-offs in overlying sections may be evidence for reservoir potential in more distal locations. Basin modelling suggests the eastern part of the study area is at present mature for hydrocarbon generation from Oligocene marine source rocks when extrapolating the high thermal gradient reported in wells. Deeper source rocks, potentially located in the pre-rift section could also provide charge in the western part of the study area. The combination of direct hydrocarbon indications, seismic stratigraphic interpretation and thermal modelling results attest to the extension of the North Sumatra Basin petroleum system into the offshore deep water area and suggest significant petroleum potential in the clastic syn- and post-rift sections of the basin.

Introduction
The North Sumatra Basin (NSB), Indonesia, is a prolific back-arc basin which hosts a proven Tertiary petroleum system evidenced by a number of onshore and offshore oil and gas discoveries. Only a limited number of wells have been

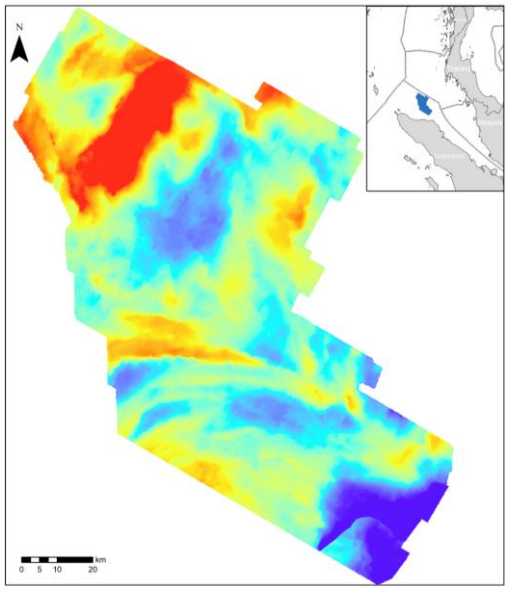

Figure 1: Total sediment twt isochron (red: thin, blue: thick). Inset location map, blue polygon designates 3D multisensor data cover.

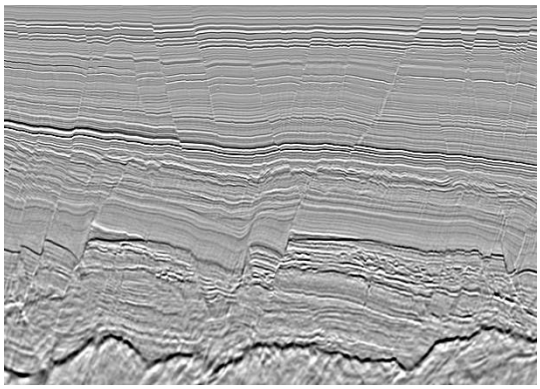

Fig. 2: Prominent flat spots in the Bruksah Formation.

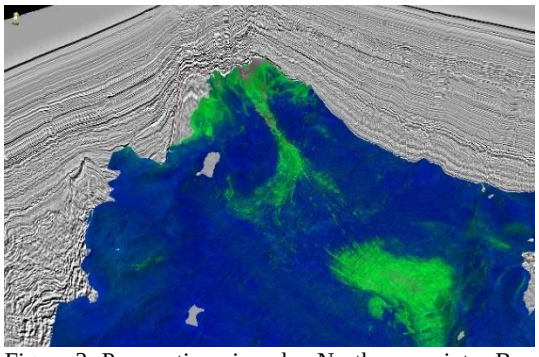

Figure 3: Perspective view due North on an intra Bampo deep water channel-fan system shed off a basement high.

drilled in the offshore deep water northern North Sumatra-Mergui Basin and 2D and 3D seismic data cover of the

area is sparse (https://geoportal.esdm.go.id/migas/). Newly acquired 3D multisensor seismic data provide new insights into the syn- and post-rift depositional system of this underexplored area. Direct Hydrocarbon Indicators (DHI) in pre-rift fault blocks, overburden gas clouds and various amplitude anomalies in the syn-rift section, suggests the potential extension of the prolific petroleum system proven onshore and locally offshore into the deep-water area of the NSB.

Data

9276 km2 PGS multi-client multisensor seismic data were acquired in 2018 (Figure 1) with a NW-SE shooting direction in 60-1500m water depth. A 10 streamers setup with 8025m streamer length and 112.5 m separation acquired 10s record length at 2 ms sampling rate. Processing steps included e.g. 3D surface related multiple elimination, full waveform inversion (FWI) and Kirchhoff prestack depth migration (KPSDM).

Result and Discussion

Published data suggests a segmentation of the offshore NSB into N-S arranged highs and intervening sub-basins (Doust and Noble, 2008). However, the new data show the presence of local irregular and E-W arranged highs, which control the deposition of overlying sections (Figure 1) and distribution of syn-rift reservoir sediment facies. There is little suggestion for a significant extension of the Peutu carbonate play into the distal offshore parts of the NSB covered by the multisensor survey. However, a number of flat spots in tilted fault blocks and anticlinal structures located within the Bruksah Formation are apparent and attest to a working petroleum system (Figure 2). The flat spots comprise sizable areas and structure apex consideration suggest significant hydrocarbon column heights. The continental character of this section (Meckel, 2013) is expressed in the internal seismic configuration, high impedance contrast and channel features (Figure 2) which changes laterally away from basement structural features to more parallel and subtle impedance contrast seismic facies in basinal settings.

Local depocenters appear to host late syn-rift deep-water clastics and turbidites described also from areas close to the Sumatra coast of the NSB (Meckel, 2013). Figure 3 shows an RMS amplitude map extracted from an intra-Bampo Formation horizon. Seismic morphology interpretation suggests deep water sands shed from a local basement high along a slope valley pouring out onto the paleo-basin floor. Further outboard seismic attributes indicate detached or ponded sands which are trapped along the flank of a local inversion structure.

Extensive gas chimneys, often associated with the above mentioned local highs, but also found above local inversion structures, attest to a prolific petroleum system present in the area. The gas chimneys charge traps in the shallow Miocene Keutapang section, where presumably gas filled stacked sands appear as bright low impedance seismic events. High density normal fault systems controlled by underlying structure and substrate provide obvious migration pathways. In cases the faults terminate close to the surface providing evidence for recent tectonic activity.

Although local kitchen potential in the segmented area is evident, Petroleum systems modelling of the area suggests hydrocarbon generation can only occur from the Bampo Formation and older syn-rift sections, even considering high heat flow as suggested from thermal gradients reported in the wells drilled in the area. The Bampo shales suggested as one potential source rock horizon with dispersed gas-prone organic matter in the NSB (Doust and Noble, 2013) may not be mature enough to explain the location of gas chimneys. These gas chimneys may indicate the presence of oil-prone lacustrine sources rocks occurring within the underlying Bruksah Formation (Machette-Downes et al., 1994).

Conclusions

New 3D multisensor seismic data provide unprecedented detail of the structure, geometry and depositional patterns of the syn- and post-rift sections in the underexplored offshore deep water NSB. Numerous conventional, combined and stratigraphic traps can be identified. Seismic direct hydrocarbon indications are frequent in the area and presence and locations suggest viable petroleum systems which potentially give rise to sizable petroleum accumulations as indicated by prominent flat spots.

References

Doust, H., and R.A. Noble, 2008, Marine Petroleum Geology **25**, 103-129.

Matchette-Downes, C.J., A.E. Fallick, E., Karmajaya, and S. Rowland, 1994, Geological Society Special Publication **77**, 139-148

Meckel, L.D., 2012, AAPG Search and Discovery #10464

Meckel, L.D., 2013, Berita Sedimentologi **27**, 15-17

Acknowledgements

The authors thank PGS for permission to publish and internal reviewers for their suggestions.

PROCEEDINGS
JOINT CONVENTION BANDUNG (JCB)|2021
November 23rd – 25th 2021

Rejuvenating an Overlooked Formation by Unlocking by-Passed Hydrocarbon in Belanak Mature Field of West Natuna Basin

Ayub Budi Hartono (1), Agung Ertanto (1), Haniva Navilova (1), Bintang Putra Melanes (1), Tejo Sukotrihadiyono (1), Mudji Prajitno (1)
1) Medco E&P

Abstract

Arang Formation is one of the sandstone reservoirs in the Belanak Field, which was previously overlooked and has already been stated as depleted gas reservoir with latest production rate of 4.3 MMSCFD, after being produced since 2005. A detailed study, which integrates dynamic production data analysis, stratigraphic concept, and seismic attribute, then was carried out to pursue the opportunity of finding hydrocarbon potential and rejuvenating the production from this formation.

There are two main parts of the study: first is the evaluation of unconnected gas in place volume which combining volumetric in place evaluation from a seismic attribute assisted well-to-well correlation update and dynamic production data evaluation from both static and flowing material balance while also rates the transient analysis. Several hydrocarbon saturation logs were performed in some wells to confirm this by-passed or unproduced zone. The second part is creating development plan of the potential zones that were found as very challenging, not only due to distribution of the reservoir zone, but also because of limited available data of reservoir permeability. The inflow performance prediction was created using a porosity-permeability averaging model which is calibrated with the production performance data and then combined with skin model which refers to analog field data statistic. The gas deliverability forecast then performed by integrating material balance, well flow performance, and production system model.

This study has identified 11 new potential zones which will be developed through three scenarios of direct add perforation programs, cement packer well service program, and re-completion program using Hydraulic Workover Unit (HWU) technology. Two initial programs were proven and successful by using 20% choke opening due to sand screen limitation which able to increase gas production from this formation by 8 (eight) fold. Other programs are in progress for execution and predicted to further double up the gas production by early of 2022.

This paper will describe a full reservoir description and development plan that will rejuvenate the production of Arang Formation.

Keywords: Mature Field, Unlocking by-Passed, Reservoir Description, Integrated GGR Study, Development Plan

Introduction

Belanak field is a mature field located approximately 100 km north of Matak island base and 150 km east of the Belida Field with water depth is 300' with 20 year production history (Figure 1). The primary targets for the Belanak field are oil and gas bearing sands of the Arang, Gabus Massive and Gabus Zone-3. The Belanak Arang formation is the uppermost formation in Belanak field. Some wells were completed to produce Arang formation start from the beginning, while most other wells were initially completed at the deeper zone of Gabus Massive or Gabus Zone-3.

The Belanak Arang formation is divided into eight different reservoirs, named A1 to A8 from lower to the upper section respectively. Most of them are considered as gas bearing reservoir A2, A3, A4, A5, A6, A7 and A8 zones (Figure-2 &-3). These zones are not laterally extensive and are isolated from each other. Most of its gas in place is contained in four major sandstone reservoir : the Arang-2 reservoir (A2 zone), Arang-3 reservoir (A3 zone), Arang-4 reservoir (A4 zone), Arang-5 reservoir (A5 zone).

The Belanak Arang formation was deposited in deltaic-fluvial environment which has various types of facies, e.g. main fluvial channel, point bar, crevasses splays, levee, oxbow lake and other flood plain deposits. It was offered many opportunities and challenges of hidden hydrocarbon potential waiting to be identified. The reservoirs are categorized as dry gas reservoirs with depletion drive mechanism supported by weak aquifer influx.

The Arang sands are very fine to fine grained, occasionally medium grained. They are moderately well sorted, poorly consolidated, friable and non-calcareous. Porosity derived from petrophysical analysis indicates these sands have good inter-granular porosity, ranging between 14% and 27% with an average of 22%.

PROCEEDINGS
JOINT CONVENTION BANDUNG (JCB)|2021
November 23rd – 25th 2021

Belanak Arang has been producing since July 2005, reached peak production of 86 MMSCFD in mid of 2008 , from three (3) wells. The last development in Belanak Arang was in 2013 from 2 infill drilling of B-22 well and A-29 well. In 2020, the production has declined sharply to 4.3 MMSCFD after being produced for 15 year with cumulative production of almost 59% of the Initial in Place number.

Successful of cement packer technology, and changing sand control type from frac-pack to inserted screen at adjencent field, lead to lower development cost, thus open more opportunity to develop previously marginal field targets.

A detailed study, which integrates dynamic production data analysis, stratigraphic concept, and seismic attribute, then was carried out to find more hydrocarbon potential. The incremental gas production is targeted to fulfill the increasing gas demand.

Data and Method

Geophysic Data

Seismic interpretation is based on a portion of the 780 sq.km. Natuna Sea Area Block 'B' 3D Seismic survey which was acquired in 1997. PSTM Seismic reprocessing was then carried out in 2005 to increase S/N ratio of legacy seismic data. Prior to the reprocessing of seismic data, series of geophysical works took place. Figure-2 show seismic section in Belanak field.

Geology Data

The Arang sands have been penetrated by most wells in the Belanak field. All wells have electric logs, good composite log data and mud log data including gas chromatography. The nature of isolated reservoirs in Arang formation bring the big challenge in reservoir mapping and well to well correlation.

Petrophysic Data

Belanak Arang has limited data of rock properties. The core is not available and only log data were used for petrophysical evaluation.

Reservoir & Production Data

The reservoir engineering dataset consist of production and pressure history data taken from RFT's / MDT and static gradient surveys (SGS). 70 pressure data points from MDT/RFT were taken from 7 wells at 8 different reservoirs. Unfortunately, there is no DST and PVT data available, while pressure transient data only available from pressure build test of two reservoirs (A2 zone and A3 zone) during their initial production.

Production data is available from daily allocation based on regular test from each wells. The wellhead and surface pressure also available from real time surveillance tools. Five (5) wells (A-17, A-18ST1, A-29, B-13 and B-22) have been produced from Arang formation.

This paper presents a analysis method in rejuvenating the production of Arang Formation by integrating geological understandings, comprehensive reservoir engineering analysis results and technical measures.

The first methodology is the evaluation of unconnected gas in place volume.

The method used in this study involves well correlation, well-seismic tie, seismic interpretation and mapping, depositional environment and integration of pressure and production data with geological and geophysical interpretations.

Unconnected reservoirs ares identified by integrating static evaluation of volumetric in place from geological model and dynamic evaluation from reservoir pressure and production performance. The geological model was improved by using seismic attribute analysis to guide the facies and properties distribution and also provide indication of lateral connectivity in the reservoir. Figure 4 shows the workflow of geological modelling in this study.

Reservoir engineering data was used to assist integrating static evaluation of volumetric in place. Reservoir pressure data are predicted based on trendline pressure gradient from MDT/RFT data. Most of good pressure test data show gas gradient of about 0.06 psi/ft and water gradient about 0.433 psi/ft, which indicates the reservoir to be normally pressured (Figure 5). Pressure interpretation result was also used to define gas water contact (GWC).

Synthetic PVT model was created to support dynamic data evaluation. The fluid properties refer to analog of PVT laboratory data from adjacent field which has the similar gas composition and was taken from the Arang formation (Figure 6).

PVT synthetic Belanak Arang was generated from PVT laboratorium data at SW Bawal field by using PVTp simulation. The fluid properties of SW Bawal field was used in the PVTp simulation and matching PVT laboratorium data. It's showed as red line colour (Figure 7). By changing input data in PVTp simulation with Belanak Arang data, the sintesis PVT Belanak Arang could be generated, shown as yellow dot.

The dynamic data evaluation was performed to identify reservoir volume that are connected to current producing wells. The evaluation consist of material balance or p/z plot, flowing material balance, and rate transient analysis. Saturation log data acquisition and evaluation were also added once the unconnected

reservoir was identified as the instrument for final confirmation.
The detail workflow of unconnected reservoir evaluation is shown in Figure 8.

The second methodology is Development Plan.
The keys to reservoir development planning are reservoir performance prediction, reservoir accessibility from existing wells, gas deliverability plan, and project economics.

Reservoir production performance is strongly related to inflow performance relationship evaluation which is a function of reservoir permeability in the well candidate. The analytical method by matching production data to the model is carried out to determine the permeability which will be used as input into the model. Matching on wells producing from single zones shows that the permeability resulting from petrophysic calculations using the Timur equation with the geometric averaging method requires a Skin value that is smaller than zero (Figure 9). So that the single zone well can be matched with arithmetic average. From the results of the interpretation of Pressure Build Up (PBU) in Block B wells which are completed using FracPack, the skin range is between 20 – 30. As for wells that produce from multi zones, production test data can be matched using permeability from the Timur equation with the geometric averaging method and the skin value in accordance with the PBU interpretation results (Figure 10). In addition to the arithmetic and geometric averaging method, Permeability and Skin values figures from the interpretation of Rate Transient Analysis (RTA) are also used for model calibration of which the results show that the values producedfrom the model are close to the production test data.

The type of screen that will be used in the Belanak Arang wells completion is Insert Screen (Through Tubing) and will be installed above the top interval. From the results of the C-02 well production test in the North Belut field which also uses the Insert Screen, it shows that the skin is around +7. For all programs (direct add perforation cement packer well service program, and re-completion program using Hydraulic Workover Unit (HWU)), Skin= +10 is used as input data.

The inflow performance prediction was created using a porosity-permeability averaging model which is calibrated with the production performance data and then combined with skin model which refers to analog field data statistic.

Final production and gas deliverability forecast was performed by using integrated production system model that incorporate reservoir material balance, well production performance, and surface system models. The detail workflow of development plan is shown in Figure 8.

In addition, Arang formation is the shallowest hydrocarbon bearing in Belanak field. Evaluation of Top Of Cement (TOC) in Annulus-B is critical to develop the development strategy Arang since mostly old type wells completion have not been cementing on Arang zones. Therefore, the existing wellbores can be utilized to evaluate and further develop Arang formation (Figure 11).

Based on the evaluation of completion existing wells and the selection of candidate wells that can access the potential reservoir zones, the completion strategy plan can be divided into three (3) catagories as following:

1. Direct perforation program
   If the reservoir zones in Arang formation are well insulated with cement and the presence of available packers above the zone, it requires the direct perforation program.
2. Cement Packer Well Services Program
   If the reservoir zones in Arang formation are well insulated with cement and the presence of available packers under these zones, it requires the work of installing the packer above the interest zone.
3. Re-completion using Hydraulic Workover Unit (HWU)
   If the reservoir zones in Arang formation are not isolated by cement, the annulus cementing work is required. It's needed Hydraulic Workover Unit to pull out tubing and re-install, cementing job and bridge plug installation if needed.

When the potential zones can be accessed by one of the appropriate completion strategy programs, the program implementation will consider the economic of the project. When the project is economically viable and secure internal and external approval, the project will be executed.

Result and Discussion

Revealing unconnected area in A2 reservoir zone

A-18ST1 is the first well producing in Belanak Arang from A2 zone. This well reached peak production of 15 MMSCFD in March 2008. Well testing & Pressure Build up (PBU) was conducted on the well in early production.

This well has good performance production with slight decline. In end of 2020, this well had loaded up problem after 12 years production with the last production was about 0.58 MMSCFD in December 2013. The current recovery factor of this well is 67%. This well was completed with single target zone and has good flowing tubing head pressure (FTHP) trend data. It's showed in dynamic production data analysis. The Flowing Material Balance (FMB) analysis shows good trendline of P/z vs. cumulative production and

confirms boundary dominated reservoir by PI trend (Figure 12). Flowing Material Balance plot using flowing pressure and cumulative production data showed the connected reservoir volume is 3% lower than the calculated volume in place.

Rate Transient Analysis (RTA) have been conducted in A18ST1 well A2 zone. The interpretation of production data & pressure data is showed good matching actual data with Agrawal-Gardner type curve and Blasingame type curve (Figure 13). These type curves matching results are showed the connected reservoir volume is 3% lower than the calculated volume in place.

Static material balance evaluation (P/Z vs Cumulative Production) was also conducted in A-18ST1. The well has six (6) reservoir pressure data, consits of one (1) data taken in the starting production (PBU data) and the others from Static Gradient Survey (SGS). The first three (3) data show straight line, the others data show indication of water support from aquifer (Figure-14). It was confirmed that this well has increasing water production in late life production naturally before this well was shut in due to water load up.

P/z plot between cumulative production and static bottom-hole pressure data showed the connected reservoir volume is 4% lower than the calculated volume in place.

All the dynamic data evaluation resulted in lower connected volume compared to the calculated volumetric in place in WHPA area which indicated that there is unconnected area of A2 reservoir zone that is not depleted yet by A-18ST1 well production (Figure 15).

It's also important to analyze production reservoir vertically. It's needed to confirm of the fluid system in terms of gas and liquid in sand reservoir by saturation log tool. The objective of saturation log at A-07 well is confirm the potential undrain are in A2 zone. The saturation log result showed the zone is still saturated with gas (Figure 16), although A2 zone (NE) is lower than A2 zone (Middle and SW) structurally. It also confirmed that A2 zone in the NE has separate channel reservoir with A2 zone in the SW part (Figure 15).

Revealing unconnected area in A3 reservoir zone

B-13 well is the third well producing in Belanak Arang. This well was produced commingle from A2 & A3 zones. This well reached peak production of 35 MMSCFD in June 2008. This well has good performance in term of gas production, but sharply declining after experiencing water breakthrough in early 2013. In mid of 2014, this well was have loaded up problem after 6 years production. The last production was intermittent at about 2.38 MMSCFD in end of July 2015. The water production was suspected coming from A2 zone. It was confirmed at A-18ST1 that the well has water problem, however, B-13 A2 zone has stronger water support with water production up to 2200 BWPD. B-13 A3 zone has low water production that confirmed by B-22 well.

B-22 is the fifth well producing in Belanak Arang. This well has good production performance with slight decline. The current recovery factor of this well is 60%. This well was completed on single target zone and has good flowing tubing head pressure (FTHP) trend data. It's showed in dynamic production data analysis. The Flowing Material Balance (FMB) analysis shows good trendline of P/z vs. cumulative production and confirms boundary dominated reservoir by PI trend (Figure 17). Flowing Material Balance plot using flowing pressure and cumulative production data showed the connected reservoir volume from this well is 1% lower than the calculated volume in place.

Rate Transient Analysis (RTA) was conducted in B22 well A3 sand. The interpretation of production data & pressure data is showed good matching actual data with Agrawal-Gardner type curve and Blasingame type curve (Figure 18). These type curves matching results are showed the connected reservoir volume is 1% lower than the calculated volume in place.

The static material balance evaluation (P/Z vs Cumulative Production) was also conducted in B-22 well. The well has three (3) reservoir pressure data, consits of one (1) data was taken in the starting production (PBU data) and the others from Static Gradient Survey (SGS). All pressure data shows straight line (Figure 19).

P/z plot between cumulative production and static bottom-hole pressure data showed the connected reservoir volume is 2% lower than the calculated volume in place.

Based on well by well correlation at A3 zone, it shows separated zones in Arang 3 consist of Arang 3 (lower) and A3A zone (upper) (Figure 20).

It's also important to analyze production reservoir vertically. It's needed to confirm of the fluid system in terms of gas and liquid in sand reservoir by saturation log tool. The objective of saturation log in B-14 well is to confirm the potential undrained area in A3 zone. The saturation log result showed good potential high gas saturation (Figure 21). It also confirmed that A3A zone (upper) has a channel reservoir separated from A3 (lower) loop and also to confirm this by-passed or unproduced zone

PROCEEDINGS
JOINT CONVENTION BANDUNG (JCB)2021
November 23rd – 25th 2021

(Figure 20). The A3 zone (lower) shows shifting of tphi vs phi which indicate the zone has been depleted.

The following is the OGIP comparison beetwen connected volume with volumetric calculation in produced reservoirs.

Table-1. Summary of OGIP comparison

Wells	Reservoir	OGIP Static P/Z of Volumetric Calc	OGIP FMB P/Z of Volumetric Calc
A-17	A4+A5	4%	
A-18ST1	A2	4%	3%
A-29	A7+A8	2%	
B-13	A2+A3	1%	
B-22	A3	2%	1%

Table-1 is shows a good correlation between connected volumes and the OGIP volumetric calculation for the depleted zone. This result increases the confidence level of the OGIP calculation using volumetric method for the virgin zones that will be the targets of the further development programs.

This study result increases gas in place about 21% of original in place as shown in Figure 22.

Unconnected gas in place volume in other reservoirs zones

The study has done Geomodeling as a geological workflow in Arang formation. One by one deltaic type reservoir has been identified that be assisted well-to-well correlation update to getting better understanding of reservoir distribution laterally such as the finding of A4A zone (Figure 23).

Finally, this study has identified 11 new potential zones, consist of A2A zone, A2 zone (North East loop), A 4A zone , A4C zone , A5A zone , A6A zone, A6B zone, A6 zone, A8A zone, A9 zone and A10 zone as shown in the following cross-section schematic (Figure 24).

Development Plan

Belanak Arang which has been producing since 2005 still has unopened zones in the existing wells both dedicated to Arang and other zones (Zone-3, Lower Gabus/SB90 and Gabus Massive). The newly drilled wells with remaining gas potential in Arang formation have cement in annulus B. Therefore, recompletion is not required to access the zones. However, the old existing wells require further evaluation whether the interest zones are isolated by cement.

The study has identified unconnected new potential zones, it requires development plan to optimize recoverable reserves. The development strategy has been completed with selected five (5) zones that can be accessed by six (6) wells thru one (1) direct perforation program, two (2) cement packer well services program and three (3) wells HWU workover program. The six (6) programs were consist of five (5) cominggle production and one (1) progam with single production. All programs candidat have fullfilled project economical internally and government approval has been secured through Work Program & Budget in 2020 & 2021. The following is the schedule execution programs :

Tabel-2: Schedule Programs

Wells/Programs	Target Reservoir Zones	2020						2021												2022
		Jul	Aug	Sept	Oct	Nov	Dec	Jan	Feb	Mar	Apr	May	Jun	Jul	Aug	Sept	Oct	Nov	Dec	Jan
A-02ST2 (Direct Perfo)	A2A, A4A																			
B-13 (CP)	A6A, A6																			
A-07 (HWU)	A2																			
A-01ST1 (HWU)	A4A, A6A																			
A-26 (CP)	A4A, A4C																			
B-05 (HWU)	A4A, A5A																			

The first batch was direct perforation of A2A and A4A zones in A02ST2 well. The well successfully produced gas with initial rate higher than expectation. The well production was choked at 20% opening to avoid sand production from the reservoir. The second batch was B-13 Cement Packer program to produce gas from A4A zone &A6 zone. Prior to the Cement Packer program, B-13 well is an idle well and shut in due to water load up. Additional gas from A-02ST2 well and B-13 well increased Belanak Arang production to 40 MMSCFD. Other workover programs using HWU in the next three (3) wells are in progress for execution and expected to increase gas production from Belanak Arang to 70 MMscfd in early of 2022 (Figure 25).

Conclusions

- Detailed integrated static & dynamic data analysis and saturation log can be used for assessment and identification of unconnected reservoir zones; two (2) zones reservoir have been confirmed consist of A2 zone (NE loop) and A3A zone.
- For depleted zones, connected volumes derived from dynamic data shows good agreement with OGIP calculated using volumetric. This result increases the confidence level of the OGIP calculation using volumetric method for the virgin zones that will be the targets of the futher development program. An integrated geomodelling study has identified 11 new potential zones with increases gas in place about 21% of Original In Place which will be developed through three scenarios of direct add perforation programs, Cement Packer well service program, and re-completion program using Hydraulic Workover Unit (HWU) technology. Two initial programs (A-02ST2 and B-13) were successfully increased Belanak Arang production to 40 MMSCFD.

PROCEEDINGS
JOINT CONVENTION BANDUNG (JCB)2021
November 23rd – 25th 2021

References

ConocoPhillips Indonesia., 2003, Plan of Development Block B Integrated Gas Project, South Natuna Sea Block B PSC, p. 18-30.

Medco E&P, 2017, Plan of Future Development Belanak Field, South Natuna Sea Block B PSC, p.11.

Matter, L., Anderson, D. "Dynamic Material Balance (Oil or Gas in place without shut in-s)".Proceeding The Petroleum Society's 6th Canadian International Petroleum Conference (56th Annual Technical Meeting), Calgary, Alberta, Canada, june 2005.

Mattar, L., and R. McNeil. "The Flowing Gas Material Balance," Journal of Canadian Petroleum Technology. 37.2 (1998).

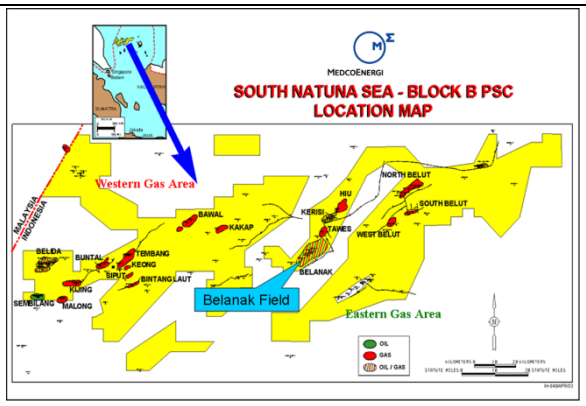

Figure 1: Belanak field location

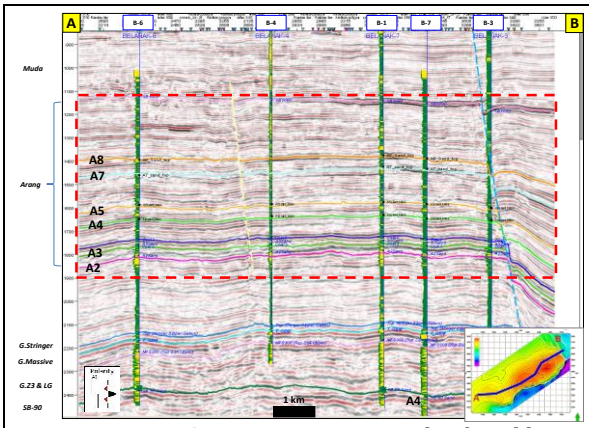

Figure 2: Seismic cross section Belanak Field

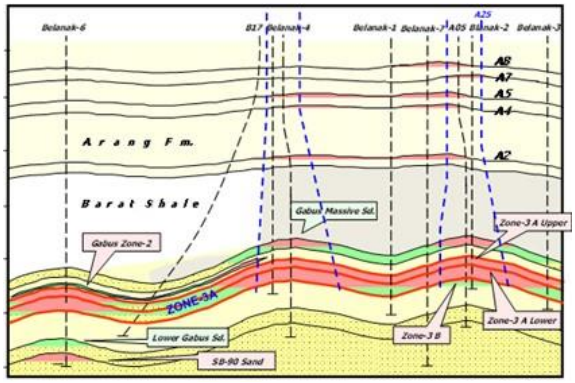

Figure 3: Belanak field schematic X-section

Acknowledgements

The Authors would like to thank to Medco E&P, Dirjen Migas and SKK Migas for their permission to publish this paper. Special thanks to Mr. Redo Dwandy Waworuntu for his consultancy during this study.

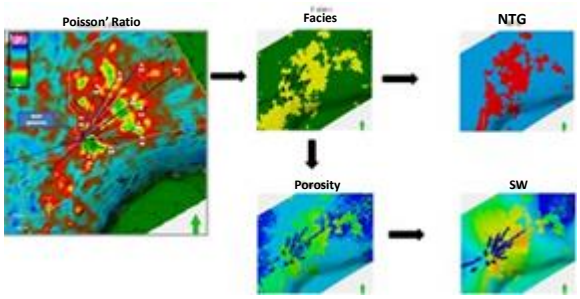

Figure 4: Geomodeling work

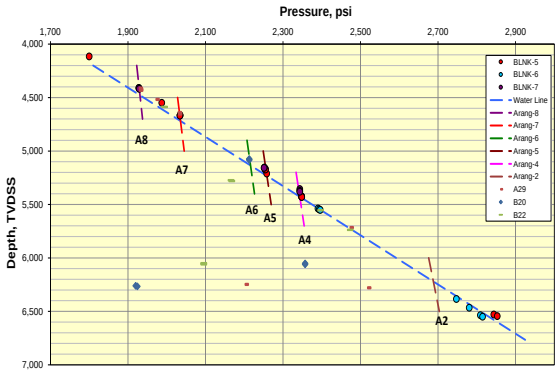

Figure 5: Reservoir pressure trendline at Belanak Arang

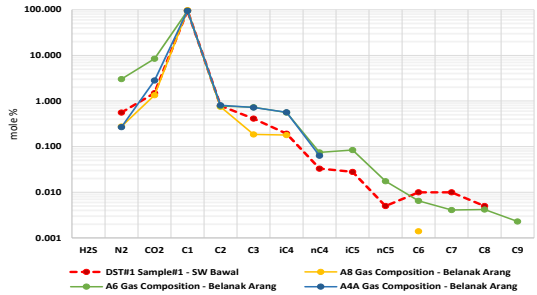

Figure 6: Gas composition Belanak Arang and SW Bawal

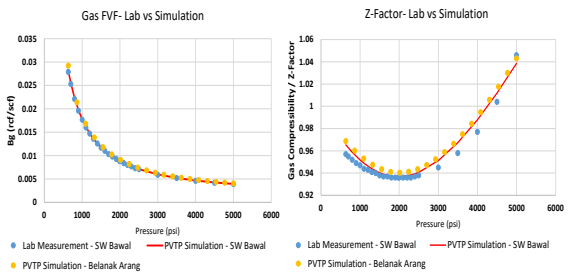

Figure 7: PVT synthetic Belanak Arang

PROCEEDINGS
JOINT CONVENTION BANDUNG (JCB)2021
November 23rd – 25th 2021

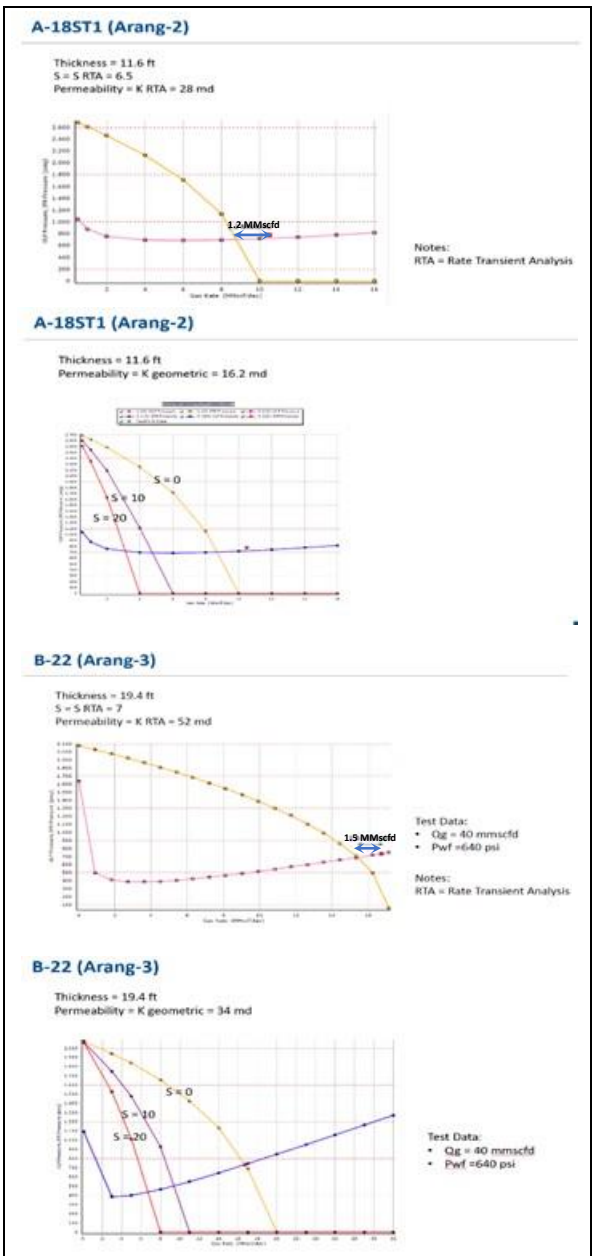

Figure 9: The process of matching production data with models for wells that have a single zone

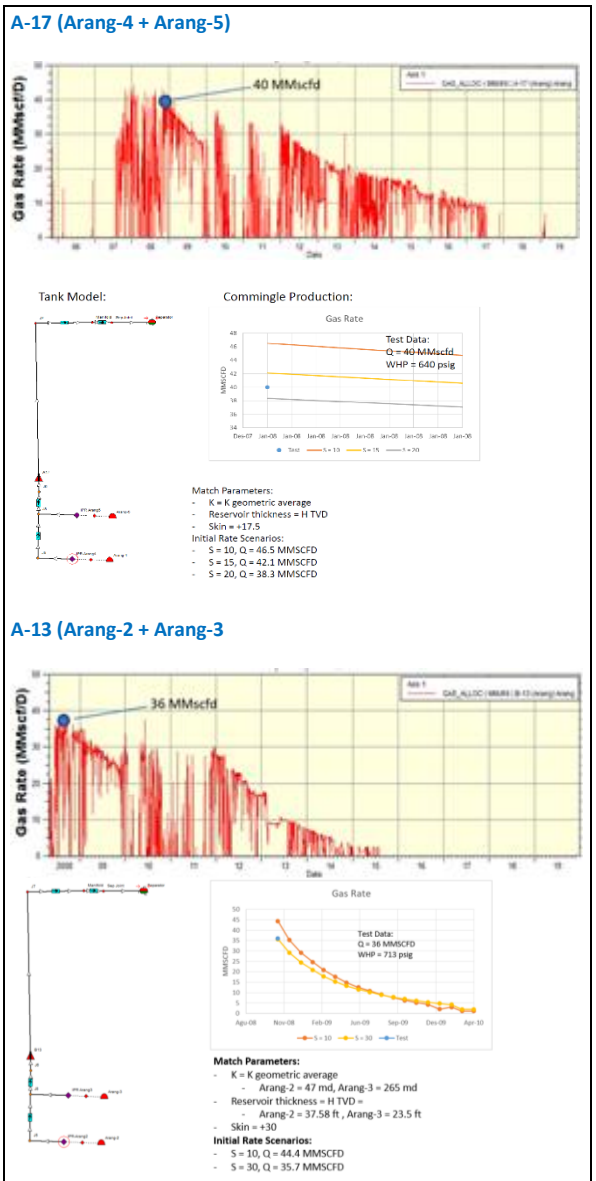

Figure 10: The process of matching production data with models for wells that have a comingle zone

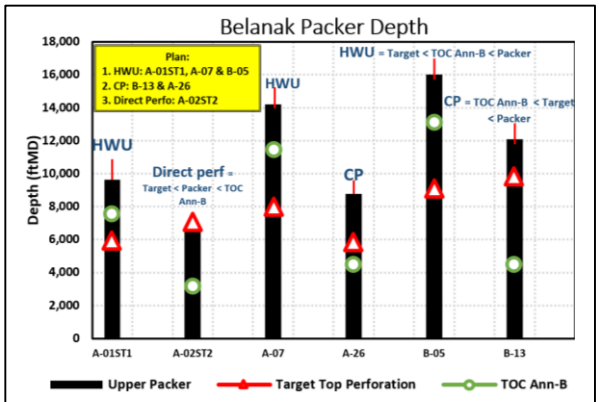

Figure 11: The completion strategy programs

PROCEEDINGS
JOINT CONVENTION BANDUNG (JCB)2021
November 23rd – 25th 2021

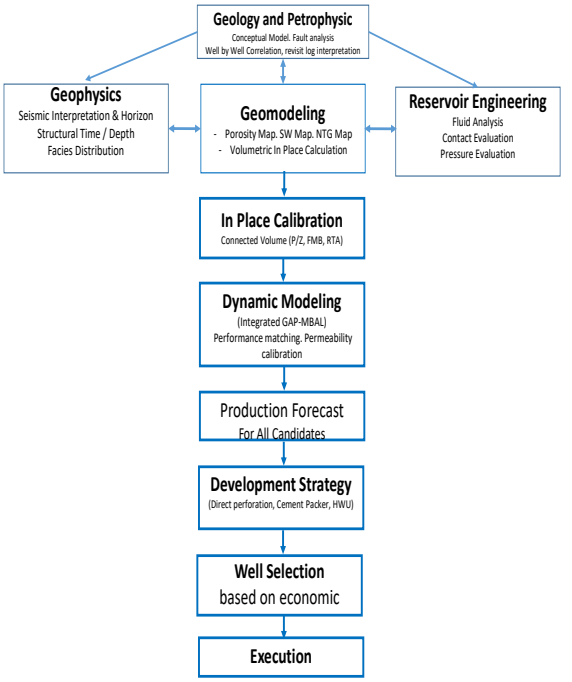

Figure 8: Flow chart workflow of unconnected reservoir evaluation and development plan

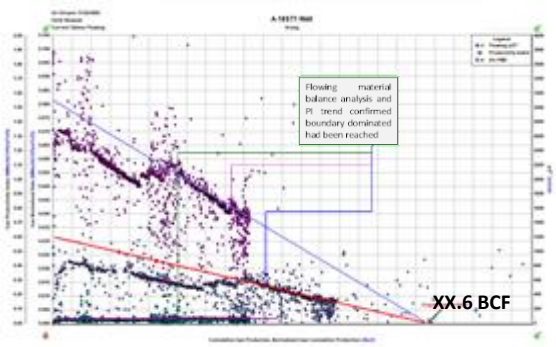

Figure 12: Flowing Material Balance at A18ST1 well

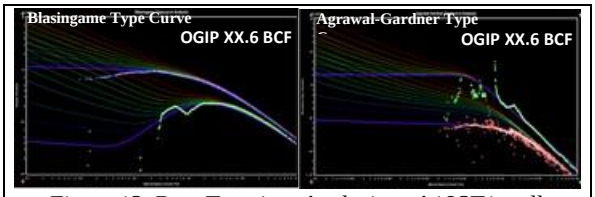

Figure 13: Rate Transient Analysis at A18ST1 well

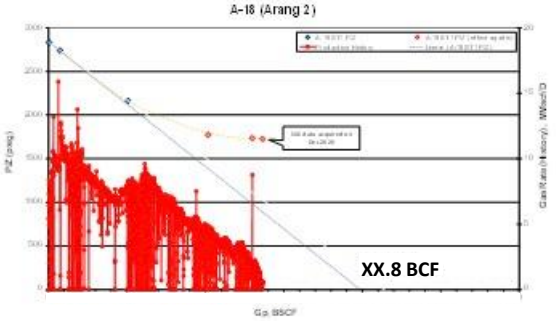

Figure 14: P/Z vs Cummulative production at A-18ST1

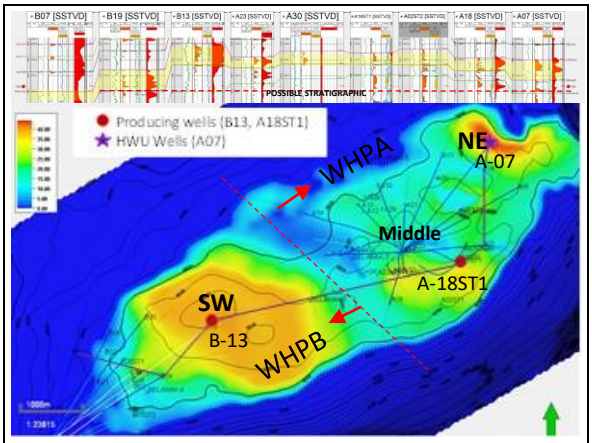

Figure 15: Structure Map & Net Pay A2 sand

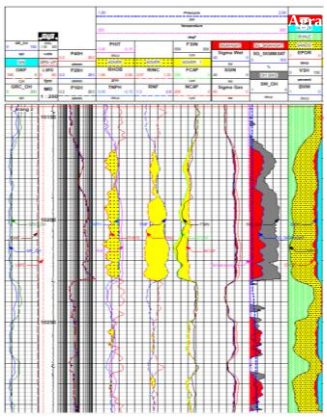

The Calculated remaining gas saturation is about 30%

Strong indication of gas from qualitative curves (FCAP-NCAP)

Figure 16: Saturation log result at A-07 well

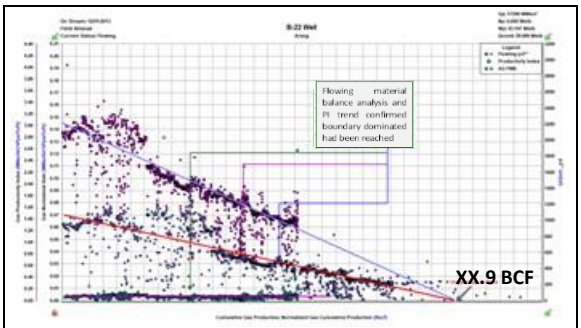

Figure 17: Flowing Material Balance at B22 well

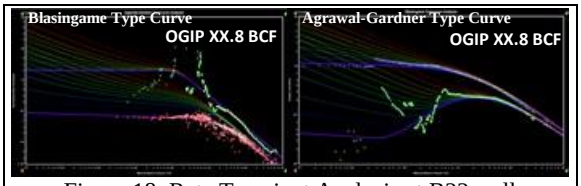

Figure 18: Rate Transient Analysis at B22 well

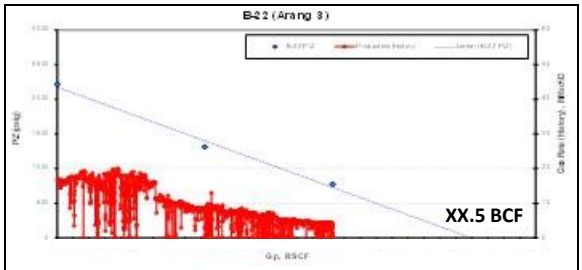

Figure 19: P/Z vs Cumulative production at B-22

PROCEEDINGS
JOINT CONVENTION BANDUNG (JCB)2021
November 23rd – 25th 2021

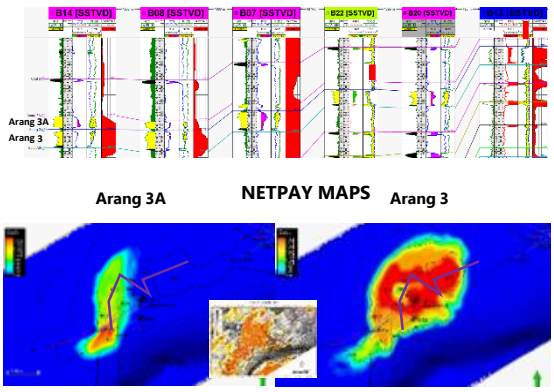

Figure 20. Wells cross section, Poisson's ratio map and net pay map A3 & A3A sand

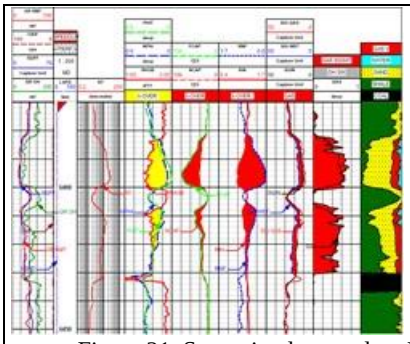

Based on tphi vs phi, there is no shifts in the upper part sand

Large X-over of NCAP FCAP suggesting virgin zone in the upper part sand

40-70% of gas saturation observed

Figure 21: Saturation log result at B-14 well

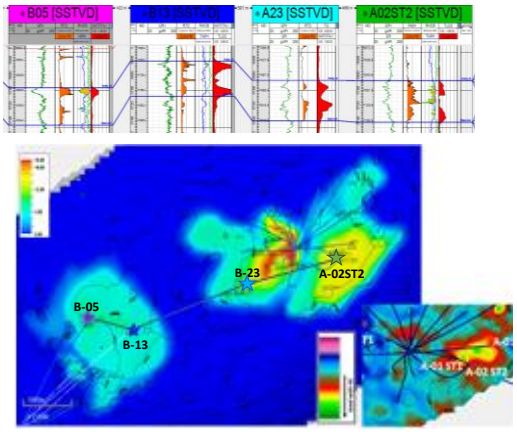

Figure 23: Wells cross section, Poisson's ratio map and net pay map A4A sand (new potential zone)

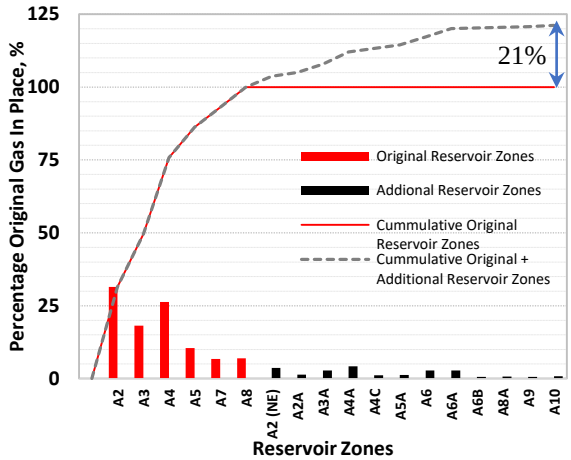

Figure 22: The percentage each reservoir zones to Original Gas In Place

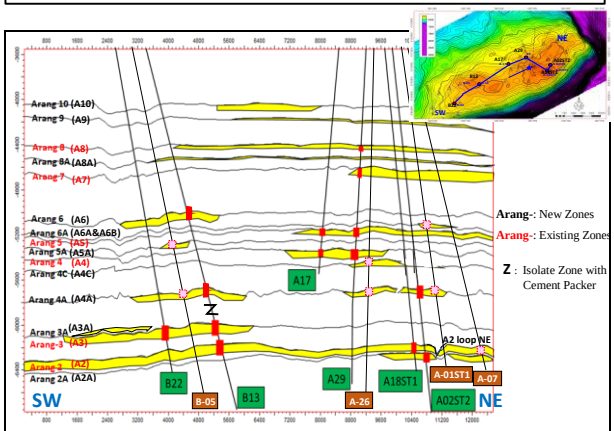

Figure 24: Schematic cross section of new potential zones

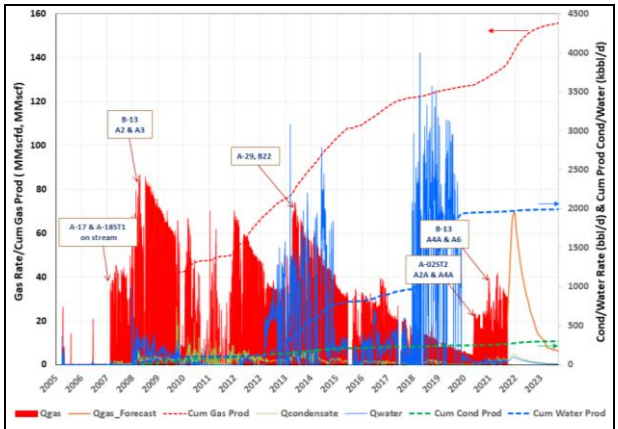

Figure 25: Production profile Belanak Arang

PROCEEDINGS
JOINT CONVENTION BANDUNG (JCB)2021
November 23rd – 25th 2021

Mature Gas Field as New Challenge for New Operator at Block B Aceh by Generating Surface Production Facility Interventions for Optimization (Increasing Gas Sales and Fuel Efficiency)

Helmi[1], Edy Kurniawan[1], and M. Akbarul Syah Alam[1].

[1] *Badan Pengelola Migas Aceh (BPMA)*

Abstract

Mature gas field optimization shall begin with main production problems identification, for Block B operation, the main problem is the production facility equipment need to be modified by intervention through surface production facility to adapt the current operating conditions. Excessive fuel own use has more challenging for new operator in Block B.

First and foremost, generating surface production facility intervention programs that directly contribute to reduce fuel own use should be put on priority.

There are two projects where located in Point B (Ex-Arun LNG) processing area that will be executed to reducing fuel own use and increasing sales gas. Firstly, replace existing TEG Dehydration and Regeneration Package suitable with current operating condition, and secondly replacement for Booster Compressor.

The new TEG Dehydration and Regeneration package will reduce fuel gas consumption in amount of 5 MMSCFD. This project will contribute the revenue for new operator to increase the amount of sales gas. While the Booster Compressor will reduce fuel consumption in amount of 4 MMSCFD. Therefore, the amount of total fuel own use that could be reduced is ± 9 MMSCFD. This portion is divided between PGE and PHE NSO based on throughput feed gas.

In the next stage, several surface facility interventions will be selected to additionally offer utilized innovations in various units, such as power generation system and gas compressor in APO field and other ageing facility.

Introduction

Arun field is well-known for its remarkable hydrocarbon resource in Indonesia. Discovered in 1971, the field has supported Liquefied Natural Gas (LNG) sales to Asian market (Pathak, 2004). The Arun field has been producing since 1977. Currently more than 99% of expected ultimate gas recovery has been produced. Surface facilities were designed for a peak capacity of 3,500 MMSCFD with multiple well clusters and production trains. (Avida, 2013).

First gas was produced in July 1977, and the first condensate was exported in October 1977 and the first LNG tanker was loaded in October 1978 (Pathak, 2004).

Since 17 May 2021, this field has been operated by PT Pema Global Energi (PGE) as a new operator (Production Sharing Contractor) to Aceh Upstream Oil and Gas Management Agency (hereinafter called "BPMA"). Previously, the field had been operated by PHE-NSB.

The production field area consists of Arun, South Lhok Sukon A (SLS-A) and South Lhok Sukon D (SLS-D), (Luthfi, 2019). Gas production from the fields will be transported via 42-inch pipeline 32 km to Point B treating unit ex.PT Arun NGL and PHE-NSO Onshore for blending and further process with gas from PHE-NSO and from Triangle Pase Indonesia.

This study describes intervention surface production facilities to reduce fuel own use consumption. The effective implementation of the concept to reduce cost and fuel own use shall be analyze comprehensively. In the next stage, several surface facility interventions will be selected to additionally offer utilized innovations in various units, such as power generation system and gas compressor in Aceh Production Operation (APO) field and other ageing facility. The issue of ageing facilities leading to an increased risk of loss of containment and other failures due to plant and equipment deterioration. The significance of deterioration and damage relates to the potential effect on the equipment's availability and reliability. Ageing facilities which are no longer considered fully fit for purpose due to obsolescence in its integrity or functional performance (P Horrock, 2010). The traditional approaches to reduce the cost production and fuel consumption is to change the existing surface production facility which appropriate with the current operating condition.

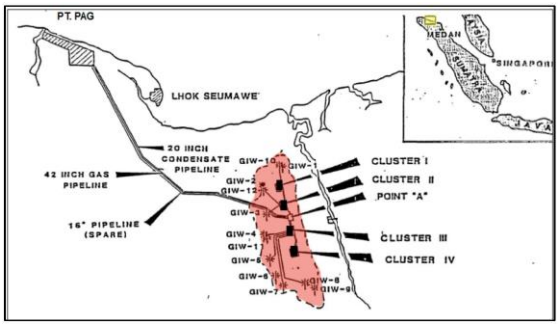

Figure 1: Arun Field Map (Suhendro, 2017)

Data and Method

Currently, the production from PGE (APO) approximately is 50 MMSFD and 1000 barrels of stabilized condensate per day.

The APO field information as shown in Table. 1

Table 1. APO Field Information

Field Information	Arun	SLS-A	SLS-D
Discovery	1971	1972	1991
No. of Wells	141	14	16
No. Active Wells	43	2	8
IGIP (Bscf)	14,112	306	696
Gp (Bscf)	13,267	286	616
Rem. Reserve (BCF)	56	1	3
Gas Prod. (MMscf/d)	36.62	2.18	6.19
RF (%)	94	94	89

The Arun field consist of Cluster I, II, III and IV and each cluster consisted of production wells and other surface facilities. Gas from SLS-A, SLS-D delivered to Cluster IV as well as gas from Cluster I, II and III. In cluster IV, stream gas undergoes a three-phase separation and then refrigerated dehydration unit. Dry gas and separated condensate are then delivered to metering station in Point A by Booster compressor K-4920 (located in Cluster-IV) before transfer to the Point B (Avida, 2013).

Feed gas from the PGE (APO field) still contains impurities. Feed gas from PGE and PHE NSO (outlet SRU unit) will be commingled shared facilities booster gas compressor (KGT-2601), the feed gas will require further purification and processing to remove impurities and condensate stabilization before delivered to the buyer. Gas purification and processing in this step causes a large consumption of fuel for its own use (FOU).

The operation scheme at Point B using Facility Sharing Agreement (FSA) and the FSA is operated by PHE-NSO. In addition, there are cost for utilities service that provided by PT. PAG in this area. The utilities services are intended for two main area, namely Sulfur Recovery Unit (dedicated for PHE-NSO) and the other Gas Treating and Condensate Treating Unit (share between PGE and PHE NSO). For Gas Treating unit, the allocation of cost sharing will be based on ratio of the volume of feed gas rate. And for condensate treating unit, the allocation cost will be based on the ratio of the rate of volume of the condensate.

Table 2. Gas Composition From APO

No.	Component	Composition Mol Fraction
1	N2	0.0045
2	CH4	0.6845
3	H2S	0.000
4	CO2	0.2156
5	C2H6	0.0514
6	C3H8	0.0203
7	iC4H10	0.0051
8	nC4H10	0.0063
9	iC5H12	0.0033
10	nC5H12	0.0021
11	C6H14+	0.0069
TOTAL		1.0000

After purified, gas is then delivered to buyer according to gas nomination. This gas is also used for operational needs at Point B. On the other hand, to support operating gas purification and processing, both parties need additional items including services and consumable such as manpower, chemical & catalyst, lubricant, and other supporting utilities. Different strategies were created by previous operator (ExxonMobil) to maintain profitability of mature field. Arun Cluster Project Consolidation Project (ACCP) were started in 2004 to centralize gas dehydration and booster compression facilities into one cluster. The benefit from this project is reduced active assets by 60%, reducing operating expense by $350K annually, and saving fuel gas consumption by 9 MMSCFD by deactivated 2-unit gas turbine booster compressor. The ACCP was followed by the Liquid Handling Project (LHP) to consolidate liquid separation and transfer facilities from four clusters into two. Deactivation of two condensate pumps enabled until 20% reduction of power consumption. In addition to the condensate pumps, the LHP also eliminated several other types of equipment, including condensate-water separators, produced water treatment tanks, and produced water transfer pumps (Avida, 2013).

Cost Sharing, Feed Gas and Gas Supply

The treated gas that is flowed from the shared facility to all buyers is a commingled gas sale of the parties. Sales gas each party is measured based on feed gas after deduction with fuel consumption.

Gas for fuel is taken from treated gas from shared facilities, the fuel gas is used for power plants, steam generators, gas turbine for booster compressor and NSO facilities. Measurement of fuel consumption is carried out at the measuring point of each equipment.

Fuel consumption for NSO treating unit will be borne by NSO, and the fuel consumption used for PGE treating unit (APO field) is also fully borne by PGE.

Gas from the parties entering the sharing facilities is measured at the Gas Transition Point in volume units (MMSCFD) using the following measuring tools:

PGE gas is measured flow meter FQI-56001/2 which is a as flow meter PGE. Gas from NSO is measured as the difference from the combined gas measured by flow meter FQI-2602A that located down stream of booster compressor unit-26.

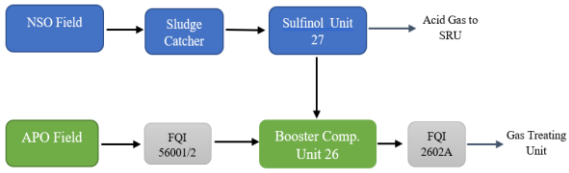

Figure 2: Commingle of Feed Gas

Gas for fuel is taken from the gas that has entered the shared facility, which will be used as fuel for booster compressor (Unit-26). The fuel consumption for booster compressor will be charged to each party (PGE and NSO) proportionally based on the feed gas volume of each party. Fuel consumption for power plants and steam generators is charged on a prorated basis based on the use of electricity and use of steam by each party. Feed gas volume from each party is measured by flow meter. The recording of the feed gas volume measurement is carried out on daily at 00:00 - 24:00. Analysis of gas composition to determine the GHV value is carried out on a weekly basis.

The volume of gas sales to each buyer is commingle gas sales by PGE and NSO, measured by the flow meter as shown in Table 3.

Table 3. Custody Meter Supply Gas

Tag Number	Services	Remark
FQI-6751	Total Treated Gas	
FQI-1905	Gas to Arbel	KIM and Jargas Lhoksukon
M-401/402	PT Pupuk Iskandar Muda	
M-403/404	PT Kertas Kraft Aceh (KKA)	PLN-KKA
CM	Jargas Aceh Utara	
CM	Jargas Lhokseumawe	

The recording of the sales gas volume measurement is carried out on daily at 00:00 - 24:00. Analysis of gas composition to obtain the GHV value will be carried out periodically in accordance with the agreement with each buyer. Recording and reading of gas usage in the system is carry out on each daily, weekly, and monthly.

Sales gas for each party's is calculated prorated based on the comparison of each party's feed gas after deducting for fuel consumption (PGE and NSO) as described below.

Sales Gas PGE.

$$Total\ gas\ sales\ x \frac{Feed\ Gas\ PGE - Fuel\ PGE}{(Feed\ Gas\ NSO - Fuel\ NSO) + (Feed\ Gas\ PGE - Fuel\ PGE)}$$

Sales Gas NSO.

$$Total\ gas\ sales\ x \frac{Feed\ Gas\ NSO - Fuel\ NSO}{(Feed\ Gas\ NSO - Fuel\ NSO) + (Feed\ Gas\ PGE - Fuel\ PGE)}$$

The calculation of fuel own use is carried out in energy units. The measurement of the volume of gas fuel own use and heating value at the measuring point is described in Table 4 below.

Table 4. Measuring Point of Fuel Own Use

No.	Equipment	Meter	Remark
1	Condensate Stripper	FI-2760	Dedicated NSO
2	SRU Plant	FI-6702	Dedicated NSO
3	HRSG	FI-9239	Share base on using of steam
4	Power Generation	FI-9001	Share base on electricity consumption after deduction with load of PAG.
5	KGT-2601	FI-5731	Sahre base on feed gas volume
6	KGT-4501	FI-4562	Share base on feed gas volume

In many mature gas fields, the production and fuel own use is a big issue. For APO field, optimal use of existing surface facilities or by intervention of surface equipment including install the new facilities to adapt with current condition is the key to reducing production costs and increase economic value.

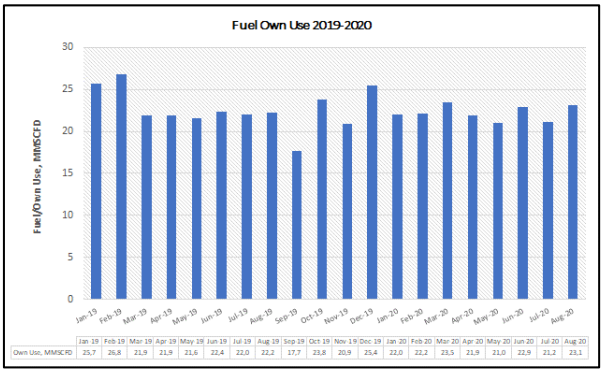

Figure 3. Fuel Own Use 2019-2020

Result and Discussion

The Arun and SLS A/D fields are mature fields with the oil and gas depletion rate reaching by 94%. The carbonate reservoir drain rate is generally below 80%. The rate of decline in natural production from year to year reaches 20%. Apart from that, along with decline of gas production and excessive fuel own use in Block B cause on production life becomes shorter and at certain times, all the production will be used for fuel gas only.

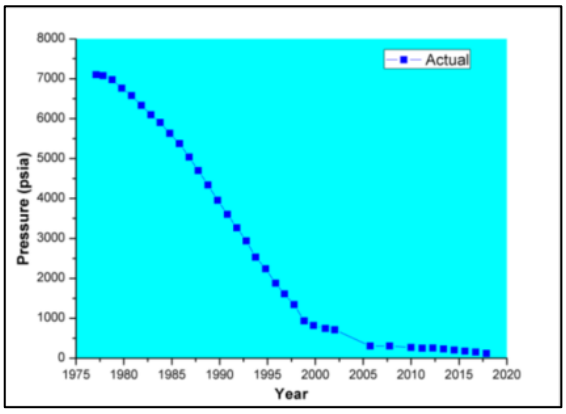

Figure 4. Arun Field Reservoir Pressure (Luthfi, 2019)

With the existing operating conditions, economic value of the Arun field will be negative in 2022/2023. To prevent this event, PGE as new operator should define the objective to be achieved, including prioritization and identify effectiveness of production cost.

Average production of gas from APO field is 48 MMSCFD (August 2021), and total fuel consumption at APO field is 8.25 MMSCFD. In this field, the biggest consumption is for booster compressor KGT-4920 that consume 3.7 MMSCFD. After deduction with fuel own use in APO field, feed gas be delivered to Point B in amount of 41 MMSCFD. At point B, feed gas form APO field will commingle with gas from NSO (outlet of unit 27), with the amount 21 MMSCFD and from TPI is 1.42 MMSCFD only. The total feed gas commingled at Point B is 63 MMSCFD.

From the amount of feed gas, 20,24 MMSCFD is used for fuel own use, and this is heavily influencing the commercialization of sales gas from WK-B. The biggest fuel own use in Point B is treating unit that consume 10 MMSCFD and following by power generator consume 7.5 MMSCFD. The amount of impurities gas is 18,44 MMSCFD. Finally, total amount sales gas is 21.3 MMSCFD with 15.05 MMSCFD for PGE portion, 5,25 MMSCFD for NSO and 0.99 for TPI. (This data base on PGE daily report August 2021).

First and foremost, generating surface production facility intervention programs that directly contribute to reduce fuel own use (efficiency) should be put on priority. In this scenario, there are two projects that located at Point B processing area that will be executed to reducing fuel own use and increasing sales gas.

TEG Dehydration & Regeneration Package

First project is to optimize the system in Unit 45 (liquefaction system) with deactivated the Scrubbing & Refrigeration System and deactivated Fuel Gas Compressor Unit and replace the existing Gas Dehydration Unit (Molecular-Sieve Drier) with a new TEG dehydration unit that suitable with current condition. The existing refrigeration system consume fuel gas 5.7 MMSCFD meanwhile fuel gas compressor unit requires power of 4.2MW or equivalent to 1.3 MMSCFD of fuel gas.

The new TEG Dehydration package will be installed with a capacity of 60 MMSCFD. This equipment is required to replace the existing unit. This scenario will contribute gas treating unit becomes more efficient. TEG Dehydration package easier to operate and requires less fuel gas consumption compared to existing (Mole-Strainer Dehydration System).

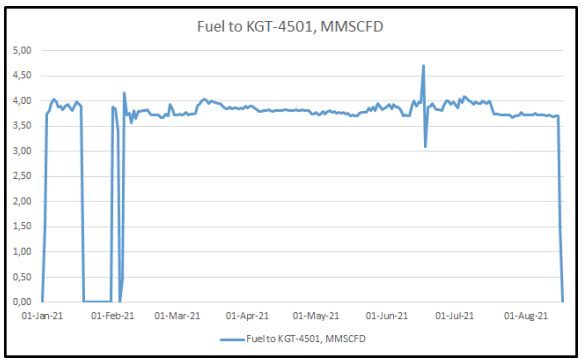

Figure 5. Fuel Consumption KGT-4501

From this optimization, it is expected that there will be a fuel savings by installing this TEG Dehydration unit can reach ± 5 MMSCFD. The saving of this gas fuel can be additional sales gas and revenue for both parties.

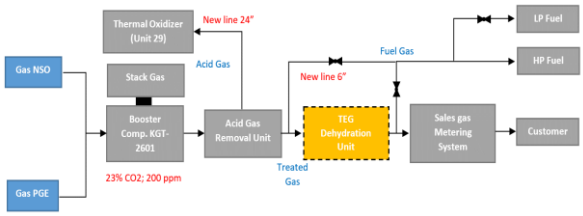

Figure 6. Modified TEG Dehydration Unit

Replacement Booster Compressor K-2601

Second project is replacing the existing Booster Compressor (Unit-26) which has a design capacity of 450 MMSCFD with a new booster compressor unit that adjusts to the total feed in amount of 60 MMSCFD.

Unit 26 is a booster compressor (K/KGT-2601) which aims to increase feed gas pressure for the treating unit and dehydration unit. The feed gas comes from PGE gas and NSO gas. Existing K-2601 is a centrifugal compressor that has two stages of compression with a gas turbine driven.

The current condition of feed gas to K-2601 is 60 MMSCFD. The inlet pressure is 265 psig and outlet pressure is 738 psig. To compress this amount of untreated gas, K-2601 requires treated gas fuel of 6.3 MMSCFD which the amount of fuel is not much different from the design fuel requirement.

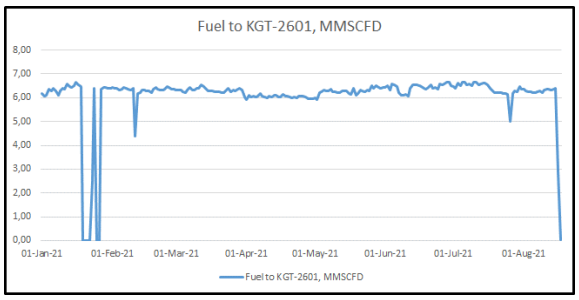

Figure 7. Fuel Consumption KGT-2601

By reducing fuel gas consumption at the booster compressor unit by replacing the booster compressor with a smaller capacity, adjusts to the current amount of gas feed. Decrease in fuel gas consumption can be used as additional gas sales to increase gas revenue. The new booster compressor will be selected with fuel gas consumption maximum 2 to 3 MMSCFD, therefore will be a fuel saving from this unit can reach 4 MMSCFD and this fuel saving can be additional sales gas.

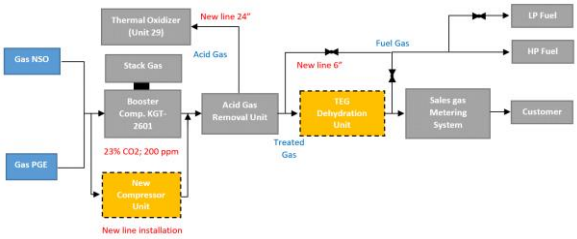

Figure 8. Modified New Booster Compressor Unit

Raise in economically viable awareness of current operation mode have led to increased fuel efficiency at point B processing and treating unit for almost 9 MMSCFD. This fuel saving provides economic advantage for PGE and NSO. This portion is divided between PGE and PHE NSO based on throughput feed gas.

A Sustainable Efficiency Effort of Each Parties

In the next option, several surface facility interventions will be selected to additionally offer utilized innovations in various units, such as power generation system, gas compressor and gas purification and treating unit in APO field.

This scenario will focus on APO Field only. Existing surface production will be changed or modified. This program optimizing production facilities by reducing the fuel own use.

Average production of raw gas at SLS is 8-9 MMSCFD, meanwhile average sales gas is 2.22 MMSCFD. Average fuel consumption at SLS is 0.89 MMSCFD, this fuel is using for power generation system. To reduce fuel consumption, all power supply for SLS will be provide from PLN and EDG as backup. In addition, this option will reduce costs for the operation and maintenance of gas turbines and fuel gas compressors.

Estimate gain from this project will increase of sales gas by 0.6 MMSCFD from SLS field.

At Point A, existing power generator generate by gas turbine generator package PGT-503/504 (GE Frame 3). The power generator consumes 2 MMSCFD of fuel and actual load power required at Point A is 3 MW. In other hand, the power generator in point A is an ageing equipment. To optimize fuel gas consumption, the existing unit will be replaced with gas engine generator (GEG). configuration the GEG is 3 x 1500 kW and led to 0,8 MMSCFD in saving of fuel gas.

Booster compressor KGT-4920 located at Cluster IV, the compressor is used to delivered dry gas to the Point B with discharge pressure 380 psig. The existing compressor is centrifugal multistage compressor driven by gas turbine with fuel consumption 3.7 MMSCFD. To optimize fuel consumption at Cluster IV, the existing compressor will be replaced with reciprocating/screw type compressor with discharge pressure 800 psig. 2.2 MMSCFD fuel gas saving will be obtained from this scenario. The compressed gas from Cluster IV will be not delivered to point B for blending with gas from NSO and then through processing and treating purpose to meet buyer requirement. Gas purification unit will be installed at Cluster IV.

PROCEEDINGS
JOINT CONVENTION BANDUNG (JCB)2021
November 23rd – 25th 2021

As mentioned above, gas purification unit will be installed at cluster IV. Cluster IV is designed to treat raw gas and then deliver to Point B for further process. Currently, portion of PGE fuel at point B is 13 MMSCFD. This project optimization includes installation of CO2 removal unit, TEG Dehydration Unit, H_2S removal. Sales point of gas from PGE is located at Point A (Custody Meter). Potential customer to sales gas directly from APO field is PT PIM or PTGN. This scenario will provide economic benefits for PGE which can increase gas sales by 12 MMSCFD. This option should be seriously considered to prevent economical issue of APO field production and the application of new concept has generated numerous opportunities to extend field life.

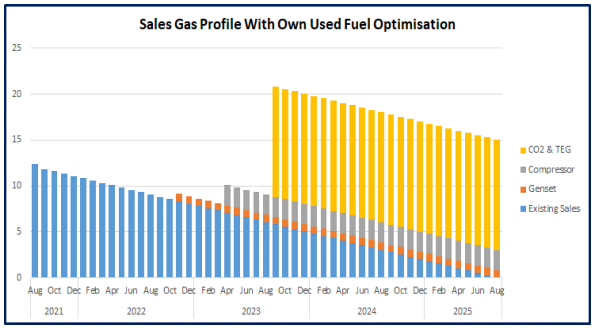

Figure 9. Sales Gas Fuel Optimization APO Field

In addition, with this scenario there will be saving cost $ 6 million annually for utilities services at Point B. It is important to understand the cost reduction at Point B is called cost avoidance. This is one of the right cost reduction strategies to survival and growth for mature gas field. Reduction of fuel gas consumption and cost savings at Point B as a cost reduction strategy enables to PGE to achieve their planned gas production at reduced costs.

Conclusions

1. PGE as a new operator has a lot of challenge to operate Arun mature field. The new operator should be seriously considered innovative method by generating surface facilities to reduce excessive fuel own use and intervention for mature equipment to expand life of production profile.
2. Optimize of existing surface facilities or by intervention of surface equipment including install the new facilities to adapt with current condition is the key to reducing production costs and increase economic value
3. Without facility intervention program to reduce excessive fuel own use, at certain time all the production from this field will be used for fuel gas only.
4. Reduce in fuel consumption and cost reduction for utilities service at Point B is a cost reduction strategy and this is a key to a new operator to dealing with economic issue in mature gas field.
5. Excessive fuel own use and ageing facilities also have more challenging for field operation, either for availability or reliability issue and functional performance.

References

Avida, H., Soedarmo, A. A., and Utama, D. P., 2013, Aceh Operations Mature Field Management: Arun Assets Consolidation and North Sumatera Offshore (NSO) Liquid Handling, SPE-165929.

Luthfi Muhammad, Nugroho, B.A., Setiyadi, Hidajat, I.T., 2019, Rectification of Propane Dehydration System In Aceh Operation Mature Surface Facilities, SPE-196391-MS.

Pathak, P., Fidra, Y., Avida, H., Kahar, Z., Agnew, M., and Hidayat, 2004, The Arun Gas Field in Indonesia: Resource Management of a Mature Field, SPE 87042.

P Horrocks, D Mansfield, K Parker, J Thomson, T Atkinson & J Worlsley, 2010, Managing Ageing Plant A Summary Guide, RR823. www.he.gov.uk.

Suhendro. 2017. Review of 20 Years Hydrocarbon Gas Cycling in the Arun Gas Field. SPE-186280-MS.

Acknowledgements.
The author would like to thank to the management Aceh Upstream Oil and Gas Management Agency (BPMA) their permission to publish this paper. The author would also like to acknowledge for all kind of support from PT PGE team.

PROCEEDINGS
JOINT CONVENTION BANDUNG (JCB)|2021
November 23rd – 25th 2021

Mature Field Rejuvenation by Reactivation of Idle wells in Pertamina's Benakat Area

Guntur Mulyanagara[1], I Gusti Ngurah Aryawan[1], Rakhmadian Abdillah[1]
[1]PT. Pertamina Hulu Rokan

Abstract
In line with Pertamina EP's mission by carrying out the exploitation of the upstream oil and gas sector with an emphasis on commercial aspects and good operations. In May 2019, the Benakat structure was terminated, from KSO Benakat Barat Petroleum to Pertamina EP. Benakat structure has a total of 289 wells, which includes 14 active oil producing wells and 7 water injection wells, with a total oil production of 380 bopd and injection rate of 5000 bwpd. This paper will describe the work that has been done both from the surface or subsurface side to rejuvenate the old Benakat field. The evaluation results from the team show that wells in Benakat they are quite old with high water cut and production facilities that need a lot of repairs. Therefore a program was built, in the form of work stages called 4 pillars. They are optimization of data handover, surface-subsurface potential quadrant optimalization, work plan timeline, and periodic monitoring. Output of program, the gain of increase number of wells from reactivation are 51 wells with a production gain 470 bopd. Meanwhile water injection rate increase up to 15,000 bwpd from 13 water well injection. For the 2019-2021 fiscal year up to May, the production profit from Benakat is around US$ 8.6 million. These results prove that reactivation of suspended wells is an economically attractive undertaking. With low oil prices condition, screening candidates and well services job for reactivating suspended wells is one of the best options, especially in terms of operating cost efficiency.
Keywords: Benakat Structure, Reactivate, Suspended well

Introduction

Benakat area was previously managed by KSO Benakat Barat Petroleum (BBP) since March 16, 2009 and carried out early termination in 2019 (Fig.1). Production of the Benakat field at the time of termination was 380 bopd (14 production wells) with remaining reserves of 1,752 MSTB. Reservoir at Benakat Structure that was produced at that time was in 5 existing layers with the biggest reserve in layer 1st and 2nd. With a large number of reserves and a total of 289 wells, there is a great opportunity to increase production by improving work management at Benakat. From this potential, a work plan is made using the candidate well selection method that has considered the surface and subsurface aspects that are displayed in the surface-subsurface optimal potential quadrant. From this paper, it can be described the stages of work from managing a mature field to its rejuvenation in a relatively short time.

Data and Method

Benakat Structure when handed over to Pertamina had 4 problems. Some problems are:

- Oil production which continued to decline with an operating pattern that was not in accordance with operational excellence.
- Incomplete data collection of wells and facilities.
- Social problems of workers towards former companies.
- The absence of specifics assigned to manage the Benakat field.

From these problems, in priority, the problem of decreasing production becomes the main problem that must be resolved immediately. Then a plan was drawn up to overcome the problem of decreasing production with form of work stages called 4 pillars. They are optimization of data handover, optimal surface-subsurface potential quadrant, work plan timeline, and periodic monitoring.
First pillar of old field management requires integrated data, so the minimum data we have to look for are:

1. Subsurface data (daily and cumulative production data, well profile)
2. Surface data (GS, flowline, well conditions such as wellhead, surface pump, location and road access)
3. Existing contracts and conditions
4. Material stock
5. Social issues

All existing suspended wells are collected to take their value based on the presence of these data parameters. Then an assessment database of well is made for the parameters of the readiness when it will be carried out(Fig.2). Ratings above 80% will directly be a candidate to enter into the 4 quadrants to be grouped based on their potential.

The Pillar number 2 is evaluates its highest potential. Subsurface data will be juxtaposed with a similar method on surface conditions. So that the quadrant wells will be obtained in 4 categories as follows:

1. Subsurface High Potential Quadrant - Ready SF
2. Subsurface High Potential Quadrant - Not Ready SF
3. Quadrant Subsurface Low Potential - Ready SF
4. Quadrant Subsurface Low Potential - Not Ready SF

Then the 4 quadrants(Fig.3) will be translated in the form of wells work plan barchart and surface facilities which will be monitored through weekly meetings to ensure the suitability of the work schedule.

For subsurface analysis, the parameters were evaluated to 9 criterias, such as: last test, reference well production data, scatter zone target layer, injection well, perforation job, downhole pump, well profile, tubing and cementing job. (Fig.4). For surface analysis, the parameters were evaluated to 7 criterias, such as: wellhead, flowline, gasline/electric supply, location, road access, artificial lifting, and gathering station (Fig.5).

PROCEEDINGS
JOINT CONVENTION BANDUNG (JCB)2021
November 23rd – 25th 2021

Output analysis of potential wells compared with the readiness of the surface is put into the form of 3rd pillar, work plan already prepared and planned(Fig. 6).
In line with that, a work plan was also prepared to overcome other problems such as manpower, HSSE, social issues with local residents and budgeting costs arising from efforts to increase the production of the Benakat structure.

The last step or 4th pillar is periodic monitoring every one week to see the progress of the work that has been made a timeline and work options if there are obstacles. Monitoring results are displayed in the S-Curve to see the achievement of work progress against the time and cost targets that have been made based on each stage of work that has been prepared as follows:

1. Collection and analysis of surface/subsurface data on Benakat suspended wells
2. Selection of well candidates with candidate matrix maker based on surface/subsurface data analysis.
3. Making proposals and well programs.
4. Execution of work based on the approved proposal
5. Monitoring of production and well parameters on a regular basis.

From S-Curve data (Fig.7), it can be analyzed that if there is a job late, other options will be sought so that the work can still on track and the target of time can still be achieved.

Result and Discussion

Scatter plot is a well classification based on cut off NP (Oil Cum. Production) and WP (Water cum. Production). Wells in quadrant 1 are wells that have NP and WP, so they are defined as wells with high potential reserves(Fig.8). After we plot the wells, we just have to look at the completeness of the facilities to determine the rig barchart. From the results of mapping the potential quadrant, we get the fastest well candidate that we can execute according to the high subsurface potential and the ready surface. The problem that occurred during execution was that progress was below the target during October 2019 – January 2020 because 1 of 2 rigs in Benakat was transferred to another structure in Pendopo(Fig.9).

This paper reports on the performance of the reactivation wells for the period July 2019 to May 2021, with a period of almost two fiscal years.The number of wells that were reactivated during this period was 65 active oil producing wells and 13 injection wells(Fig.10). The gain of increase number of wells are 51 wells with a production gain of 470 bopd because the current average production is 850 bopd. Meanwhile water injection rate increased up to 15,000 bwpd from 13 water well injection. For the 2019-2021 fiscal year up to May, the production profit from Benakat Barat is around US$ 8.6 million.

Conclusions

Quickly field rejuvenation can be done by following the 4 pillars method as a solution in the Benakat Structure. Work management is an important point to prioritize work according to its potential. These results prove that the reactivation of suspended wells is an economically attractive undertaking. With a low oil prices condition, screening candidates and well services job for reactivating suspended wells is one of the best options, especially in terms of operating cost efficiency.

References

Handayani, N., and Simamora, J.H., 2012, SPE Paper, 149853-MS.
Batohie, G, 2016, SPE Paper, 180792-MS.

Acknowledgements

We thank Pendopo-Adera Subsurface Development Team, Pendopo Field Team and Production Operation Team. This work is fully supported by PT. Pertamina EP Asset 2 in terms of costs and operations.

PROCEEDINGS
JOINT CONVENTION BANDUNG (JCB)2021
November 23rd – 25th 2021

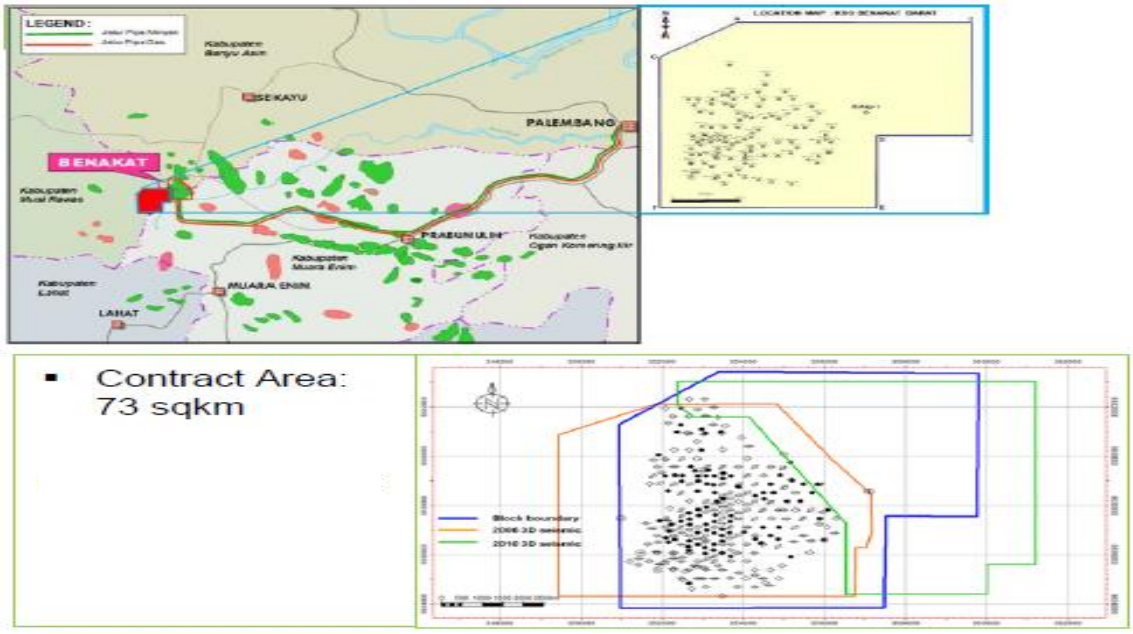

Figure 1: Contract Area Benakat Structure

No.	Well	GS	Last Test before suspend		Flowline (%)	Location (%)	Pump (%)	Artlift	Electrical Line/Gas Line (%)	Electrical Line/Gas Line (%)	Genset (%)	Overall Value	Remarks
			Gross (blpd)	Nett (bopd)									
1	BKB-272		726	67									No well, Far from GS
2	BKB-244	TOS	22	19									No well, Far from GS
3	BKB-190		222	28									No well, Far from GS
4	BKB-113	SPM-69	200	18	100	100	100	PU	100		100	100	
5	BKB-204	SP-204	488	20	100	100	100	PU	100		100	100	
6	BKB-210	SP-06	237	31	100	100	100	PU	100		100	100	
7	BKB-226	SP-03	398	27	100	100	100	PU	100		100	100	
8	BKB-286	SP-03	86	19	0	100	100	PU	100		100	80	
9	BKB-167	SP-03			0	100	100		100		100	80	
10	BKB-098	SP-204	242	12	100	100	100	PU	100		100	100	Social Issues/Road access
11	BKB-238	SP-03	104	11	100	100	100	PU	100		100	100	
12	BKB-025	SP-06			100	100	100		100		100	100	
13	BKB-203	SPM-69	277	8	30	100	100	ESP	100		100	86	
14	BKB-271	SP-04	608	24	100	100	100	ESP	0	Gasline 150m	100	80	2" Stock line gas at workshop
15	BKB-239	SP-04	600	25	100	100	100	ESP	100		100	100	
16	BKB-010	SP-03			0	100	100		100		100	80	
17	BKB-156	TOS	21	13	100	100	100	PU	100		100	100	
18	BKB-069	SPM-69	183	15	85	100	100	PU	100		100	97	
19	BKB-200	SPM-69	260	15	0	100	100	ESP	100		100	80	
20	BKB-174	SP-06	228	7	0	100	100	ESP	100		100	80	
21	BKB-110	TOS	250	15	75	100	100	PU	0	Gasline 100	0	55	2" Stock line gas at workshop

Figure 2: Database Asesment

PROCEEDINGS
JOINT CONVENTION BANDUNG (JCB)2021
November 23rd – 25th 2021

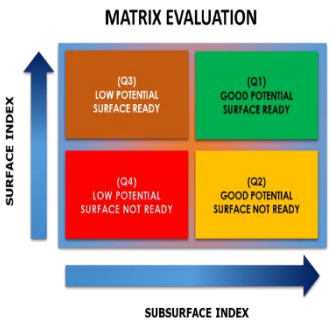

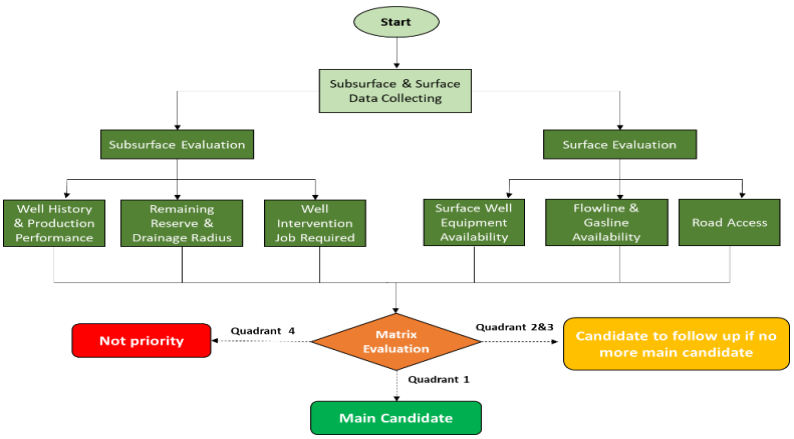

Figure 3: Matrix Evaluation Quadrant

Score	Last Test	Surrounding Well Prod	Scatter Zone Target Layer	Injection Well	Perforation Job	Downhole Pump	Well Profile	Tubing	Cementing Job
1	0	0	4	0	Stimgun	No			Need
2	0<X<=5	0<X<=5	3	RK 2020					
3	5<X<=10	5<X<=10	2	0<X<=500	Yes		No	No	
4	10<X<=15	10<X<=15	1	500<X<=1000					
5	>15	>15	Never produce and Upper OWC	>1000	No	Yes	Yes	Yes	Need

Figure 4: Subsurface Scoring Criteria

Score	Wellhead	Flowline	Gas Line/ Electric Supply	Location	Road Access	Artificial Lifting	Gathering Station
0	No	> 3000 m	> 3000 m	Forbidden Access	Can't Pass at all	No	No Facility
1	Size 1500 psi, ready	2500-3000 m	2500-3000 m	Narrow and need major repair	Need major repair	Artlif ready in other location, no elmot/gasline	Header manifold, Prod tank
2	Size 2000 psi, need stud and bolt	2000-2500 m	2000-2500 m	Narrow and need minor repair	Standard and need repair for rig access	Artlif ready, no elmot/gasline	Header manifold, Prod tank, transfer pump
3	Size 2000 psi, ready	1000-2000 m	1000-2000 m	Standard 50x50 m and need major repair	Standard and good for rig access	Artlif ready, no elmot, gasline ready	Header manifold, Prod tank, transfer pump, test tank
4	Size 3000 psi, ready	500-1000 m	500-1000 m	Standard 50x50 m and need minor repair	Good, wide, social problem	Artlif ready, elmot ready, no gasline	Header manifold, Prod tank and water, transfer pump, test tank, and header pump injeksi
5	Size 5000 psi, ready	0-500 m	0-500 m	Access ready	Good, wide, no social problem	Artlif ready, elmot/gasline and genset ready	Header manifold, FWKO/separator, heater treater, wash tank, prod tank and water, test tank pump transfer dan injection pump

Figure 5: Surface Scoring Criteria

PROCEEDINGS
JOINT CONVENTION BANDUNG (JCB) 2021
November 23rd – 25th 2021

No	Sumur	SP	Start	End	Nett	Loka (%)	Kebutuhan FL	Pump	Jargas	Jarlis	Gensi (%)
11	BKB-117	SP-04	21-Nov-19	26-Nov-19	25	50	1200	ESP			100
12	BKB-27	SP-04	28-Nov-19	3-Dec-19	25	70	700	ESP	200		100
20	BKB-277	SP-03	12-Dec-19	17-Dec-19	25		1100	ESP	100		100
	BKB-173				21		50	ESP			
13	BKB-161		5-Dec-19	10-Dec-19	18	100	900	ESP	300		0
16	BKB-270	SP-06	12-Nov-19	17-Nov-19	17		500	ESP	ok	ok	100
17	BKB-206	SP-03	19-Nov-19	24-Nov-19	17		1500	ESP	ok	ok	100
9	BKB-268	SP-03	7-Nov-19	12-Nov-19	15	100	1000	ESP	200		100
14	BKB-259	SP-04	12-Dec-19	17-Dec-19	15	75	650	PU		200	100
10	BKB-78		14-Nov-19	19-Nov-19		100	1800				0
15	BKB-53		26-Dec-19	31-Dec-19		100	700				0
8	BKB-274	SP-204	31-Oct-19	5-Nov-19	20	100	1500	ESP			100

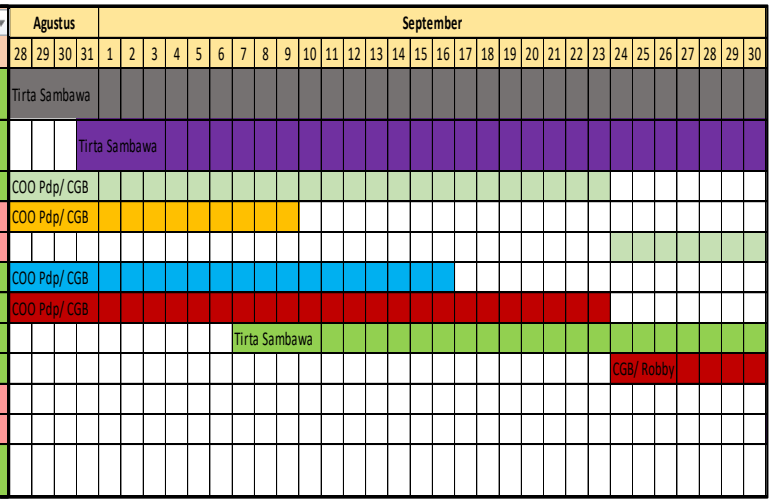

Figure 6: Work Plan Barchart

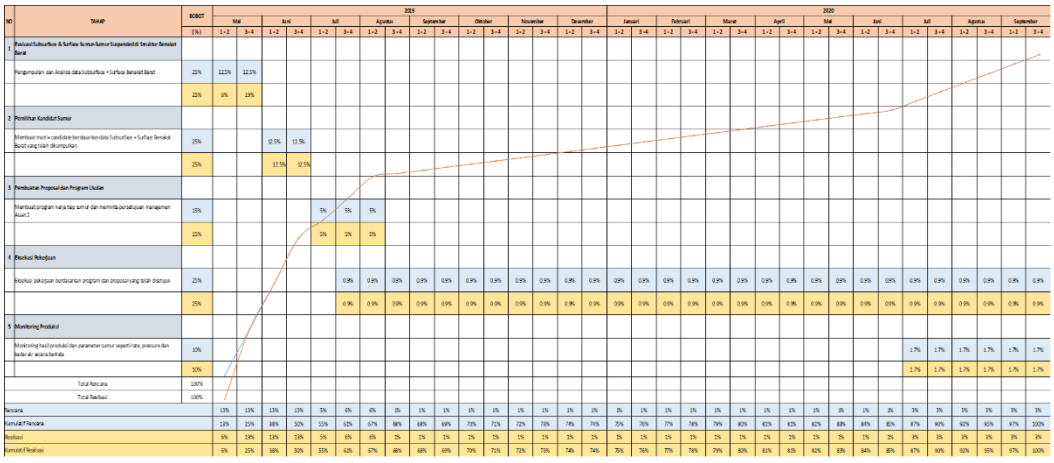

Figure 7: S-Curve

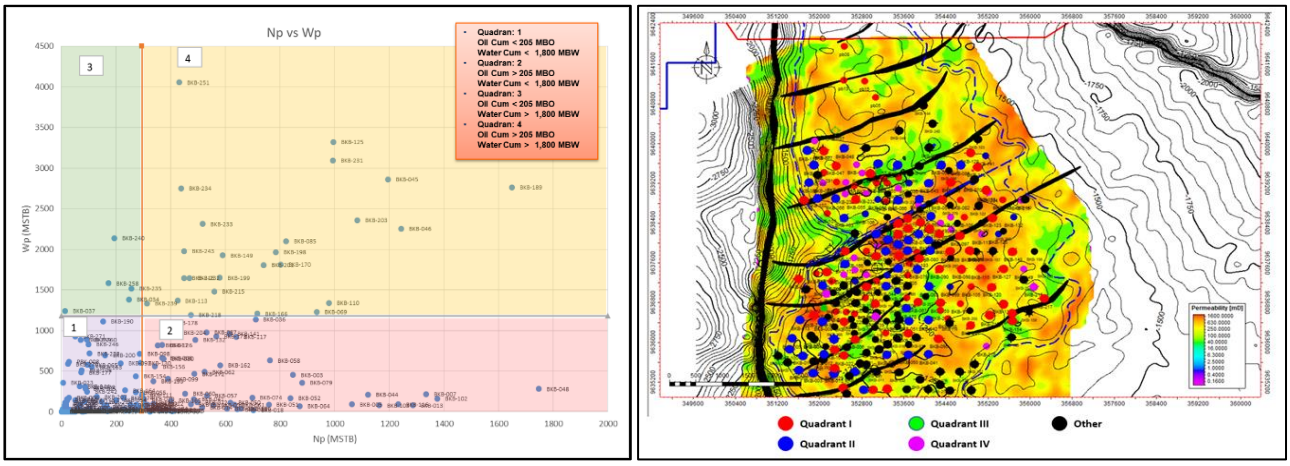

Figure 8: Scatter Plot Quadrant Mapping

PROCEEDINGS
JOINT CONVENTION BANDUNG (JCB) 2021
November 23rd – 25th 2021

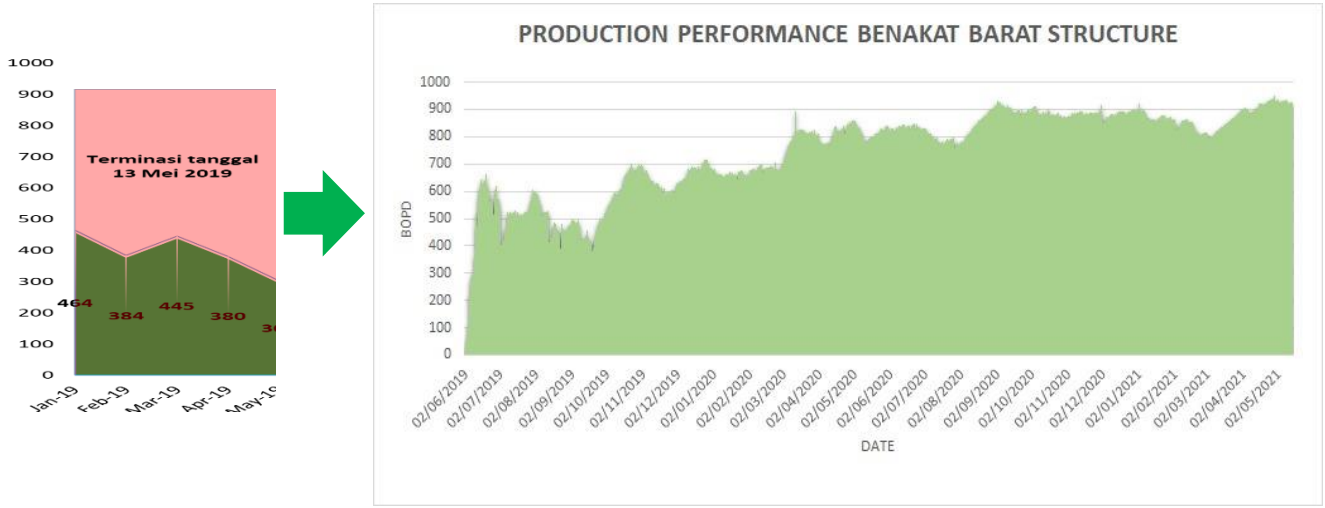

Figure 9: Production Performance Benakat Structure

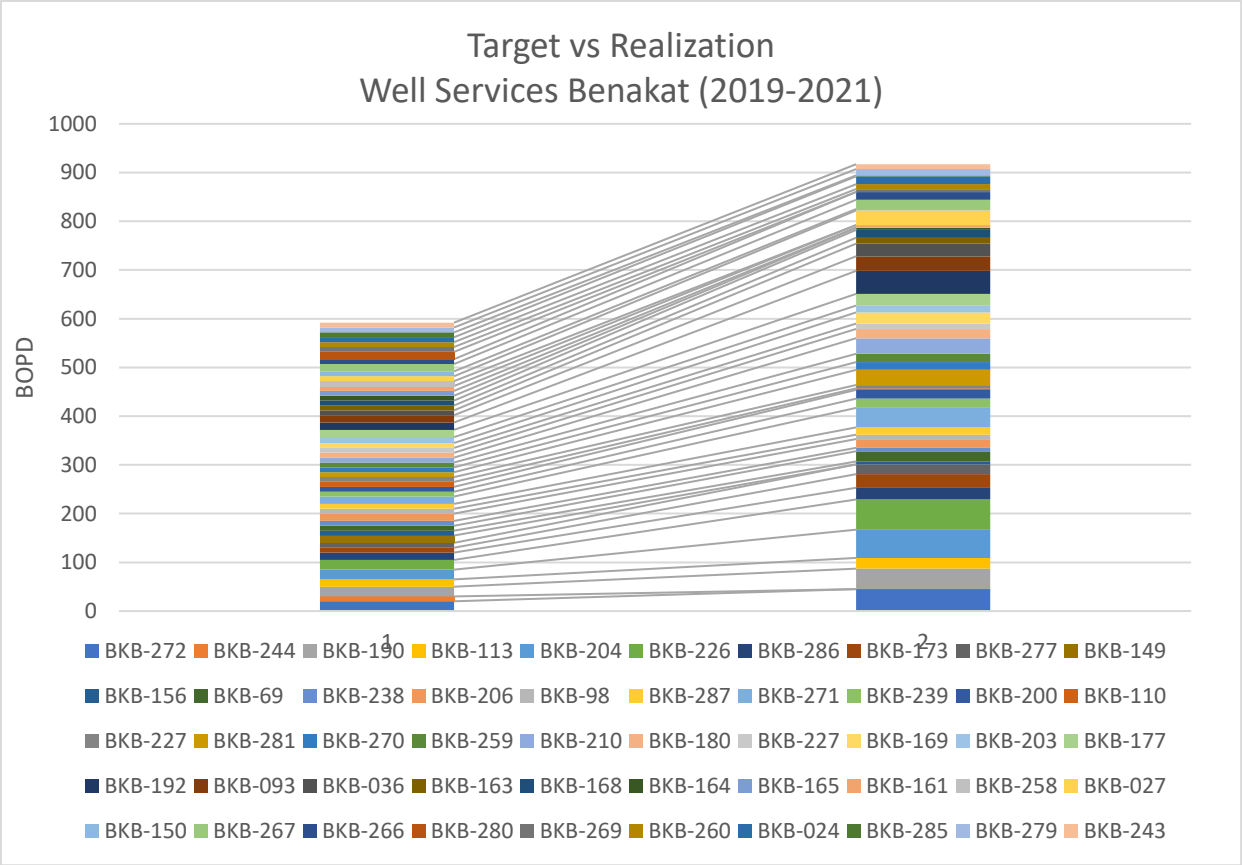

Figure 10: Well Services Realization

PROCEEDINGS
JOINT CONVENTION BANDUNG (JCB)|2021
November 23rd – 25th 2021

Success Story of Mature Field Rejuvenation; a Case Study: New N1 Sand Reservoir in Sungai Gelam-C Area, Jambi

Reza Rahadian[1], Fannopo Rikardo[1], Erwin Dicky Dusyanto[2], Reza Alfajri[1], Oki Musakti[3], Adi Widyantoro[4], Hendra Baskara[1]

[1]Pertamina Hulu Rokan
[2]Pertamina EP Cepu
[3]Pertamina EP
[4]Pertamina Hulu Energi

Abstract

In Sungai Gelam structure, 5 wells have been drilled in last three years. In 2018 was a very dissatisfactory years because 2 wells drilled produced below the production target, which main target is N sand. The main problem occurred was an uncertainty on seismic data. In 2019, 1 well was approved to be executed and performing almost 200% from production target, from new N1 sand. In 2020, 2 out-step wells also produced above production target.

Good understanding of main problem is the key to solve drilling campaign in 2018: seismic data. Velocity anomaly was detected in the northern area of Sungai Gelam because there is discrepancy between seismic and well data. Since then, PSDM reprocessing seismic was going underway parallel to drilling campaign in 2019. The well drilled in 2019 was relocated to be infill drilling to minimize the risk, and creeping out strategy by locating drilling wells in 2020.

Problems and lessons learned in 2018 were taken into consideration in next field development plan. Seismic PSDM reprocessing was also conducted to hopefully resolve the problems. Relocation of key well in 2019 was significantly unlocking potential by new N1 reservoir discovery and later on good understanding of reservoir distribution and properties lead to another 2 wells drilled in 2020. Subsurface model had been updated in every well drilled and showing good accuracy of thickness, properties, and production forecast from actual to prognosed one.

In conclusion, Sungai Gelam C field development has been successfully recovered by the success of last 3 drilled wells and turn into very profitable project. This project is also known and considered to be good practices of internal company's feasibility study.

This paper showing how to deal with database, how to know some pitfalls, and how to overcome the problems. Development strategy shifting of previous mature field is also could be implemented in another field which deal with subsurface uncertainties.

Keywords: Field Rejuvenation, New Layers, Subsurface Uncertainty, Jambi

Introduction

Sungai Gelam C field is an oil and gas field in Jambi, located 10 km to the southeast of Jambi city (**Figure 1**), Indonesia that produces from two main sands, namely an existing N sand productive zone and newly discovery N1 sand, which located below N sand. The N sand has been a main production layer from early 2010, then in 2018, the 2 wells drilled targeting N sand is performing below target. N sand is indicated water out since it found lower than estimated. Those 2 (two) wells is creep-out wells since located outer the existing wells.

Those dissatisfaction drilling campaign story then amend the development strategy of Sungai Gelam C field development. The Pre-Stack Depth Migration (PSDM) seismic reprocessing is also been conducted to solve the uncertainty of the seismic data.

Drilling well in 2019, a SGC-27 well, is particularly got repositioned as categorized to infill well, targeting a N1 sand. By this well, some new insights have been found, then unlocking potential of this reservoir. Another 3 (three) wells have been drilled over 2020-2021, which resulting good production rate.

In this paper, we will share our study and workflow in rejuvenating this old field and gaining highest production rate since this structure was operated.

Data and Method

Project Blue Print

Integrated reservoir characterization work includes geological, geophysical and reservoir studies has been instigated in 2018 for the field development basis of design (Optimasi POFD, 2018).

The Optimasi POFD resulting some drilling commitment: 8 infill wells, 2 injection wells, and 1

step-out well. Most of those planned wells is targeting N sand and part of it is targeting N1 sand. During this project is executed, it is known that N1 sand is having bigger potential than it estimated, which proven by present development is coming from N1 sand.

Infill and Step-out Drillings

Geological model and dynamic simulation show much larger closure prolongs the western area of the field. It suggests potential new closure to be drained by a number of additional wells in the future, including a step-out deep well to prove the existence of Baturaja Formation as a new concept (Rahadian et al., 2019).

The producer wells are mostly focus on layer N and layer N1. However, the major uncertainty is N1 sand distribution as the depositional concept is rather different from N sand, which a strand plain deposit. The N1 sand is not as wide spread as N sand, and having better properties than N sand (Rahadian, 2021).

In SGC-25 and SGC-26 well, which drilled in 2018, the N sand was identified to be shale-out (**Figure 2**), then other sands are evaluated by ratio-gas analysis and approximated there are by-passed zone in M lower zone which containing hydrocarbon but having poor quality property. This proving up oil reservoirs has unlocking potential in another wells.

Pressure Maintenance

The pressure maintenance had been applied in layer N during 2016-2019 by SGC-23 injector well and indicating quite good but slowly respond since permeability of layer N is not good enough (around <10 md). Presently, since the field development scenario has changed, SGC-23 well then converted to be a well producer from layer N1. Due to existing wells located in crestal area, proposed injector well is derived from reservoir simulation sensitivity study that led a well placement in the southern of existing area to maintain N1 sand's formation pressure (**Figure 3**).

The next study will be conducted simultaneously since there are still uncertainties of N1 sand facies, depth structure map, and fluid contact (Rahadian, 2021).

Drilling Results of New Model

S-27 well is repositioned to a triangular position among S-21, S-24, and S-23 wells in order to minimize the structural depth risk. Actual data and result of S-27 well indicating positive results, main target N1 sand is known to be oil contained and having virgin reservoir pressure (1.02 equivalent density), with production naturally flow about 286 BOPD. Subsurface model was then updated especially in dynamic model since the pressure is in initial, since there were many data acquisition taken in S-27 well: PVT, coring program, vertical seismic profiling, and pressure test data.

In 2020, two drilling wells, named S-29 and S-30 are also targeting N1 sand and producing above production target, quite similar from estimated model (actual production: S-29 (240 BOPD) and S-30 (195 BOPD)). Actual reservoir thickness, reservoir pressure, and facies analysis has indicated the good relation to estimated one. This good result increasing confidence level of subsurface model (Rahadian, 2021).

Conclusions

The story of Sungai Gelam C development from 2018-2021 has resulting that we have to honor and check data we use. The failure in early stage of the journey must be identified properly then we could solve in better way, ie: PSDM seismic reprocessing. The successful 3 drilled wells afterwards showed how taking risk in repositioning well with measurable risk is crucial in developing mature field.

Pressure maintenance activity in development phase is recommended to be applied in earlier stage of new sand development.

References

Pertamina EO, 2018, Optimasi POFD Sungai Gelam C, unpublised

Rahadian, R., Dusyanto, E.D., Widyantoro, A., Musakti, O., Baskara, H., 2019, Proceeding of Indonesian Petroleum Association 43rd Annual Convention

Rahadian, R., Widyantoro, A., Musakti, O., Baskara, H., Rikardo, F., 2021, Proceeding of Indonesian Petroleum Association 45th Annual Convention

Acknowledgements

The authors acknowledge Management of Pertamina Hulu Rokan, Direktorat Jenderal Migas, and SKK Migas for permission to present and publish the data and pictures presented in this extended abstract.

PROCEEDINGS
JOINT CONVENTION BANDUNG (JCB)2021
November 23rd – 25th 2021

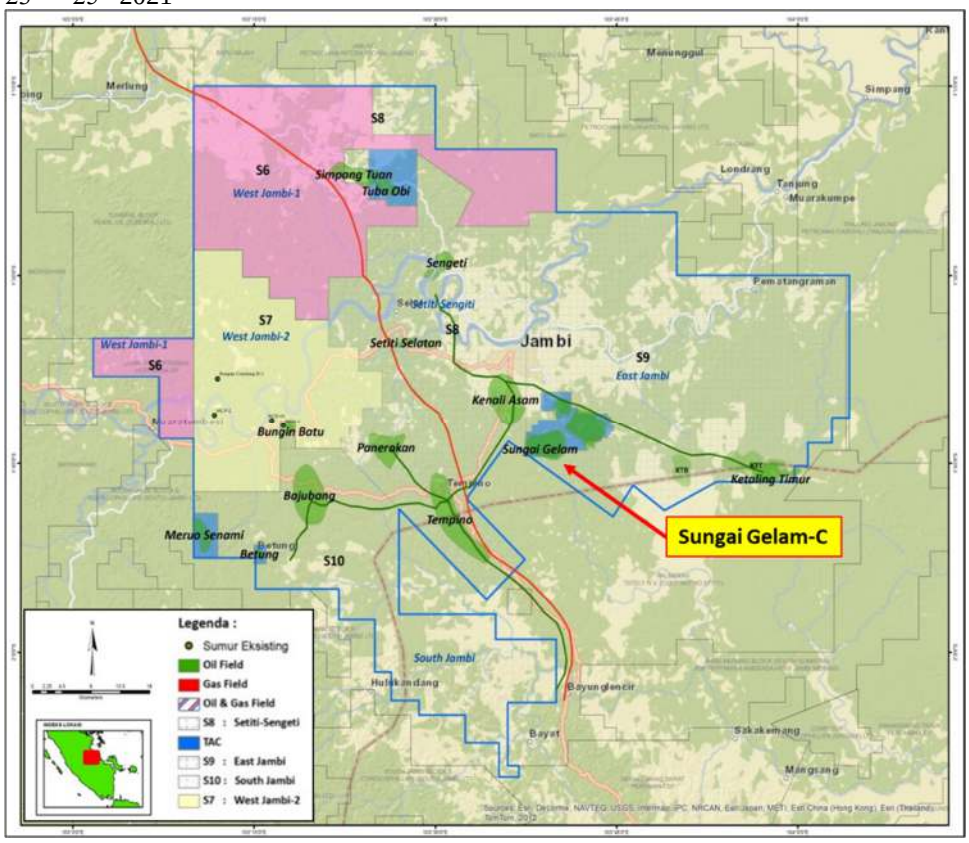

Figure 1 - Sungai Gelam-C field is located about 10 km to the southeast of Jambi city, a capital of Jambi Province.

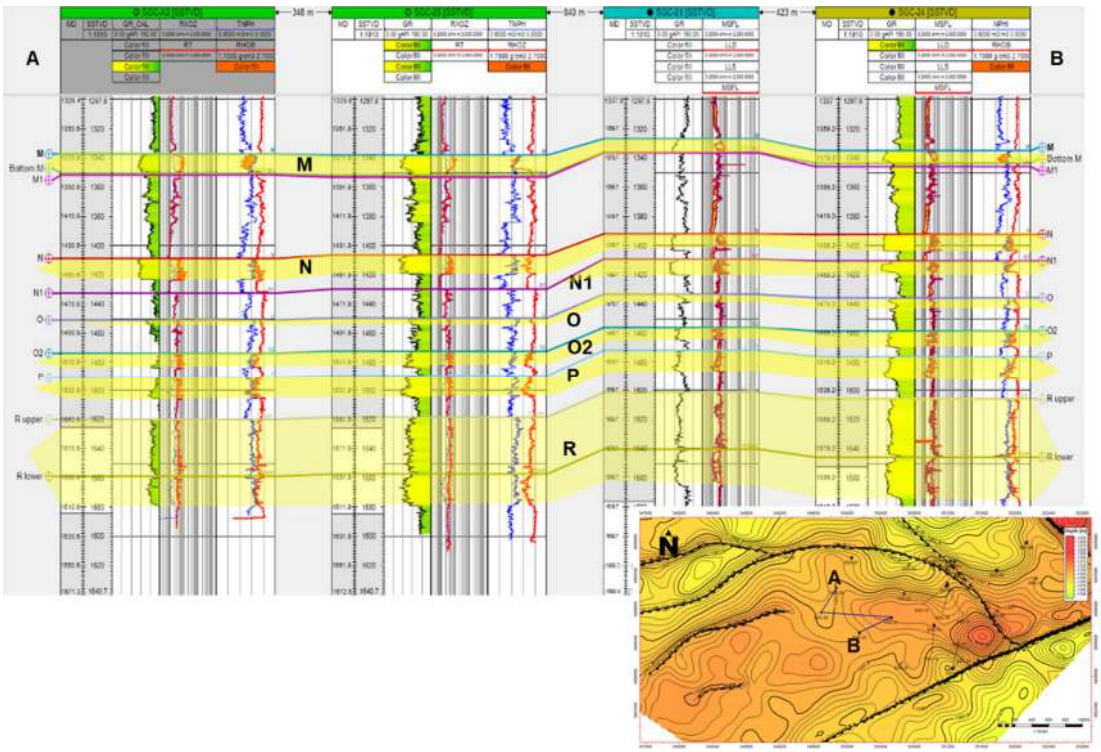

Figure 2 - Well to well correlation of S-25 and S-26 (S-X2) to surrounding wells that indicating N1 layer to be shale-out.

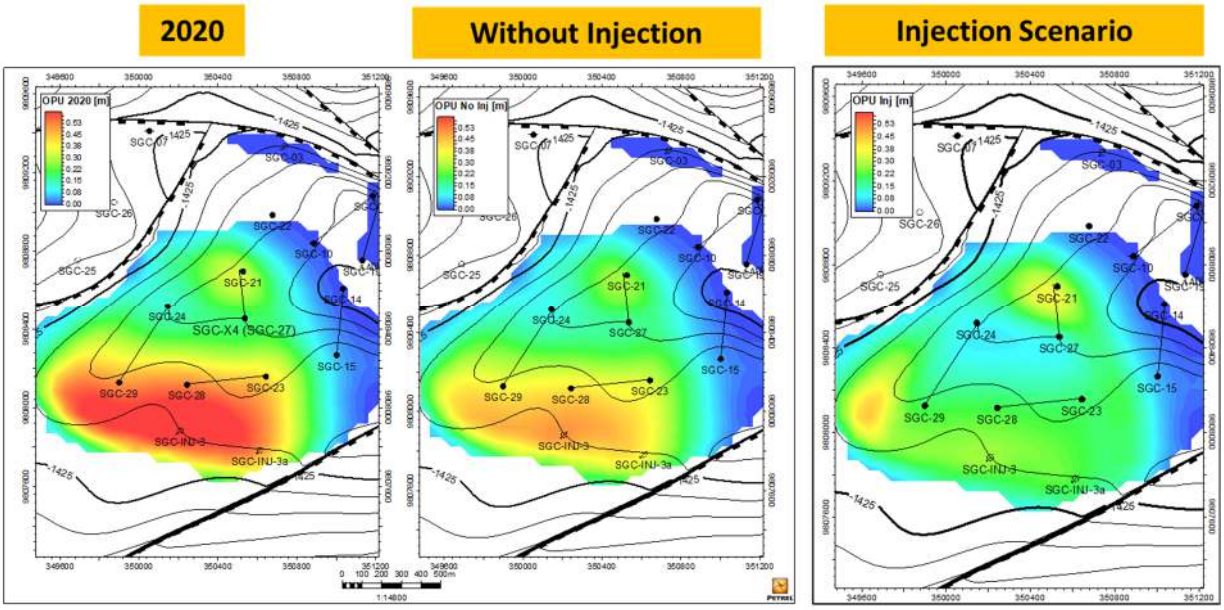

Figure 3 - OPU map showing sensitivity of proposed injector well from reservoir simulation in the southern part existing wells.

PROCEEDINGS
JOINT CONVENTION BANDUNG (JCB)2021
November 23rd – 25th 2021

Peciko Mature Field Rejuvenation Using an Integrated Static-Dynamic Modeling and Unlocking Shallow Targets Potential

Wilsen Supriady Lauwijaya[1], Eros Sidney Erriyantoro[1], Saras Nawangsari[1], Ruth Christiani Basa[1], Yudhistira Adji[1], Yan Muhazir[1]
[1]Pertamina Subholding Upstream Region 3 Zone 8 - Pertamina Hulu Mahakam

Abstract

Peciko is a multilayered offshore gas field located in Mahakam Delta, Indonesia. First discovered in 1983 and has undergone nine (9) field development projects over the years. The current production is supported by baseline production, new well, and well-intervention activities. However, as the remaining hydrocarbon potential exists, a new development project has been launched to drill new wells with 700-meters infill spacing across the field. This paper describes the results of integrated static-dynamic modeling along with seismic reservoir characterization to rejuvenate Peciko mature field. A special geological model has been built by integrating the initial static model, reservoir pressure depletion, and dynamic review analysis to evaluate the remaining gas potential (RGIP). This method yields an RGIP map by layers where the sweet spots for potential infill wells are easily identified. In addition, as resources for future infill wells are limited and no more slots are available in the existing platform, drilling side-track from existing non-productive wells is considered the best option from an economic perspective.

Based on this study, 22 out of 237 infill well candidates have been proposed within three (3) months as a new development project at this field. Several shallow gas reservoirs were also targeted to increase the well resources, making extensive use of vintage 3D seismic data with Amplitude Versus Offset (AVO) and lithoseismic inversion analysis to detect the hydrocarbon potentials. The project has been launched since Q4 2020, and 16 wells have been completed. Despite the pressure depletion model giving a lower reservoir pressure prognosis than the actual condition, the well reserves are still in line with model prediction and have had satisfactory overall results. This methodology has been proven reliable, time-effective and efficient, and has become a game-changer in evaluating and finding the remaining potential at Peciko. Furthermore, it is applicable for mature fields with depletion drive mechanisms, good reservoir connectivity, and clear seismic anomalies.

Keywords: mature field rejuvenation, remaining potential, reservoir pressure depletion, static-dynamic modeling.

Introduction

- *Field Development Context*

Rejuvenating mature assets is crucial in the current low-oil-price scenario, allowing for improved production with limited investments and risks. Nevertheless, in complex integrated reservoir studies, mature field rejuvenation is often very demanding, typically taking several months to complete. Peciko is one of the mature asset gas fields located southeast of the offshore Mahakam Delta, Indonesia. The field has been discovered in 1983 and developed since December 1999 with various development phases, starting from grid wells in the central towards the peripheral area in 2007.

Initial development (Phase 1-5) was designed based on the grid concept to drain the Upper-Main Zone of Peciko field. The latest infill wells (Phase 7 and Phase 9) have been optimized to target narrower infill at Upper-Main Zone and seismic anomalies in Very Shallow Zone and Fresh Water Sand.

- *Geological Context*

Peciko is a multilayered un-faulted field in which the stratigraphy comprises stacked delta front mouth bars in the Upper-Main Zone (2,200 – 3,500 mTVDSS) and fluvial-deltaic channels in the Very Shallow Zone and Fresh Water Sand (600 – 2,200 mTVDSS) (Figure 1).

The Upper-Main Zone (UP-MZ) gas accumulation is 20 kilometers long and 10 kilometers wide, with multiple layering up to 90 layers divided into six (6) stratigraphic units (SU0 to SU5). The main production contributors are 2 to 5 meters' thick mouth bar reservoirs with a lateral extension of 4 to 5 kilometers with intercalations of shaly intervals acting as vertical barriers. At the maximum of progradation of the delta, the stack of mouth bars could reach 15 to 25 meters with good reservoir properties (Duval et al., 1992). The reservoirs at Upper-Main Zone have contributed more than 90% of field production, and all layers have been produced commingle. The production drive mechanisms are divided into two (2) based on the reservoir characterization:

- Peciko Very Shallow Zone and Fresh Water Sand

It is mainly dominated by thick channel facies with water drive mechanism or aquifer support. The reservoir pressure in this interval more likely virgin (0.99-1.00 Deq).

- Peciko Upper-Main Zone

It is mainly dominated by delta front mouth bar facies with depletion drive mechanism. The reservoir pressure range is around 0.15-0.60 Deq, and the depletion rate in this interval depends on the geological area (main lobe, northern lobe, or southern lobe), stratigraphic units, and well density.

PROCEEDINGS
JOINT CONVENTION BANDUNG (JCB)2021
November 23rd – 25th 2021

Peciko current condition is supported by baseline production, new well, and well intervention activities. However, as the remaining hydrocarbon potential exists, a new development project has been launched to drill new wells with 700-meters infill spacing across the field. This paper demonstrates a way of mature field rejuvenation through the integration of static-dynamic modeling along with seismic reservoir characterization to maintain and revitalize the development of the Peciko mature field.

Data and Method

- *Data Availability*

The static geo-model and pressure depletion model (Akbar et al., 2015) was updated in January 2016 with 192 wells, including 23 exploration / delineation wells. Nine (9) seismic horizons have been picked (MF4, MF6, U6, MF7, U7, MF8, MF85, MF9, U9) and used to create the main structural model. This project contains more than 90 sub-layers with 15 to 40 meters' thickness. In addition, 22 wells have been sanctioned in 2020-2021 based on well resources evaluation using the pressure depletion model and 16 wells have been completed in the current field development project (Peciko POD Phase 9).

- *Methodology*

A special geo-model has been built by integrating the initial static model, reservoir pressure depletion, and dynamic review analysis to evaluate the remaining gas potential. The 3D grid of static geo-model was built with 233 x 233 meters' cells size and 60-degree rotation to capture reservoir heterogeneity and accommodate 700 well grid spacing and array, while for the pressure depletion (Deq) model, the size of the cell was reduced to 50 x 50 meters' cells size to obtain more precise results of drainage radius (Rd) during running the sequence of iterative workflow (Internal Study by Erriyantoro and Nawangsari, 2018). This finer grid was needed to capture more detailed heterogeneity in pressure modeling, which hopefully bring the prediction closer to the actual pressure. In addition, the resources of future wells are also calibrated using the latest performance of surrounding wells. Overall, the methodology presented in this paper has been developed to overcome the difficulties in the current context of the Peciko field, i.e. well stakes limitation, slots availability, marginal economic evaluation, and dynamic changes in drilling sequences operation. Having this methodology, the well candidates for future Peciko's development could be identified effectively and efficiently (Figure 2).

(1) Static Modeling - Reservoir Pressure Depletion

Reservoir pressure is the pressure of fluids within the pores of a reservoir, usually hydrostatic pressure, or the pressure exerted by a column of water from the formation's depth to the sea level. Based on the company's rule, the psi is used for the reservoir pressure unit.

For this study, reservoir pressure data acquisition is taken in a psi unit which is then converted into density equivalent (Deq). The conversion of psi to Deq is derived from the pressure gradient with depth (Figure 3). Reservoir pressure (Deq) depletion is the condition where the drop in reservoir pressure resulting from production of reservoir fluids. Deq modeling is a quick approach to forecast field depletion at a given time using the geo-model. As input, the reservoir pressures are normalized to the current condition using pressure depletion rate, depending on the geological area, stratigraphic units, and well density. Laterally, Peciko's reservoirs could be divided into three (3) locations; main lobe area (Platform A, B, C, G, and J), northern lobe area (Platform K), and southern lobe area (Platform E & F) (Figure 4a). The pressure data are amply available for the main lobe; thus, the depletion trend is well-recognized. However, this is not the case for the northern and southern lobe areas where the areas are recently developed, reservoir connectivity is not as wide as the main lobe area, and reservoir depletion is not apparent. Therefore, the decline rate of the main lobe is applied for these areas within the same layer (Figure 4b). With abundant and dense data, the pressures are subsequently propagated by kriging algorithm at the sub-layer level, co-krig by the net-pay map as a trend for geological constraint. Better net-pay means better reservoir quality and larger sand extension, consequently lower pressure values (Figure 5).

(2) *Integrated Static - Dynamic Modeling*

Deq model yields the remaining gas potential (RGIP) map by layers where the sweet spots for potential infill wells are easily identified. The RGIP is the amount of gas that remains in the reservoir after a period of production. It corresponds to the lower RGIP over time (Figure 6a). This condition is only applicable at Upper-Main Zone, where the aquifer is not active, and therefore the Gas-Water Contact (GWC) remains constant. The Remaining Connected Gas in Place (RCGIP) is the amount of gas connected to a well that remains in the reservoir after a period of production. RCGIP from dynamic review (P/Z analysis) per layer has been imposed into static geo-model and the radius is calculated within geo-modeling software through an iterative process to match the volume provided from P/Z analysis continuously until all wells are completed (Akbar et al., 2015). Stacked map of undrained RGIP as the sweet spot area for future infill wells have been produced by excluding the volume drained by the existing wells (booked RCGIP volume) and future wells perforation, assuming a closed tank radius (Figure 6b).

(3) Peciko Well Design and Targeting Concept

Optimization of a field development project through an infill well drilling strategy has been initiated since the early 2000's to manage our mature assets, including Peciko offshore gas field.

As resources for future infill wells are limited and no more slots are available in the existing platform, a side-track well design and combo subsurface targets are considered the best option from an economic perspective. Overall, we could optimize up to 43% for the duration of drilling and 27% for the drilling cost (Table 1).

A new development project of Peciko has been launched since Q4 2020 to produce the remaining potential by drilling new infill wells and unlocking combo targets from Very Shallow Zone (VSZ), Fresh Water Sand (FWS), and Upper-Main Zone (UP-MZ) intervals. Preliminary well candidates were selected based on the ranking of stakes derived from a stacked map of undrained RGIP using the Deq model at UP-MZ (Figure 7). The reservoir targets for each well candidate were reviewed layer by layer thoroughly, considering the most updated fluid content, reservoir pressure depletion, and production data to get more accurate estimate resources.

(4) Peciko Shallow Targets Incorporation

Several shallow gas reservoirs were also targeted to increase the well resources (Figure 8), extensively using vintage 3D seismic data with AVO and lithoseismic inversion analysis by adopting Tunu Shallow methodology to detect the hydrocarbon potentials (Basa et al., 2017).

Tunu Shallow has been used as an analogue for Peciko Shallow as it is composed of the same fluvial deposits with similar reservoir properties. Where the gas-bearing sands for Shallow Zone in Mahakam were mostly categorized as Class III AVO, a detailed seismic interpretation based on angle stacks and gather analysis to separate between the hydrocarbon (HC) and non-HC responses were then executed.

Only the high confidence seismic anomalies were selected for well proposals and must meet the criteria below: (Figure 9).

- The amplitude at Far Stack must be higher than amplitude at Near Stack (brightening effect).
- Check the individual seismic gather at a view trace within the seismic anomalies if the AVO trend is brightening.
- The amplitude extraction at each sub-stack angle must be consistent in shape with one another and in line with geological knowledge.

The well trajectories of selected 700-meters infill candidates would be optimized with Very Shallow Zone (VSZ) targets whenever possible (Figure 10). The selection of parent well to be sidetracked was also a key component for shallow optimization; typically, the wells with the same azimuth towards the shallow anomalies were chosen for better drilling feasibility (after making sure that the parent well candidate has no more remaining potential).

(5) Peciko Well Reserves Estimation

The Deq model at Upper-Main Zone has been updated with the latest wells and production allocation data from December 2015 (Internal Study by Erriyantoro and Nawangsari, 2018). There was no update on the new development project's methodology (Deq model), except for the water saturation (Sw) model. An intensive dynamic review has been undertaken to compensate for any deviation of reservoir pressure derived from the Deq model. Integrated workflow has been performed under a new development project of Peciko field (Figure 11).

The first step is extracting RGIP per-well from Deq model with 700-meters infill spacing and 350-meters drainage radius (Rd) across the field. The first candidates were sorted based on 2020 pressure from Deq model and abandonment pressure assumption 0.10 Deq for Low Low Pressure (LLP) mode and 0.15 Deq for Low Pressure (LP) mode. From 237 infill wells in the first screening, top 33 wells (with 1.1 Bcf cut-off resources) go further to dynamic review to determine the well reserves (Internal Study by Erriyantoro and Nawangsari, 2018). All the data are included in dynamic review and synthesis, including pressure data within the same reservoir pressure units (RPU), recent fluid interpretation, and nearby well behavior. Dynamic pressure for the 2020 year was determined by utilizing trend from the Deq versus time per RPU from production logging tool (PLT) and pressure test (MDT) data. The trend was controlled by the current pressure value estimated from P/Z versus gas production (Gp) plot (gas depletion material balance) and production allocation (Figure 12).

A constant Rd of 350-meters has been applied in the Deq model to obtain the preliminary well resources. The value was then corrected using both statistical data of Rd remaining from the Deq model and Rd deterministic analysis from surrounding wells. Based on the evaluation of 35 wells, the dynamic Rd at Upper-Main Zone layers mostly were larger than the Rd assumption from the Deq model (Rd: 350-meters) (Figure 13).

Result and Discussion

(1) Proposed Well Locations and Associated Reserves

Based on this integrated study, 22 out of 237 infill well candidates with 1.4 Bcf cut-off reserves (after dynamic review and QC) have been proposed within three (3) months as a new development project at Peciko mature field (Figure 14). Most of the well proposals are combo targets, predominantly at VSZ (seismic-driven) and UP-MZ (Deq model).

(2) Well Post-Mortem

Sixteen (16) wells in 2020-2021 have been drilled and completed within less than a year. Netpay prognosis from the static geo-model is considered reliable compared to the actual well results with a good correlation coefficient (R^2:0.80) (Figure 15).

While for the reservoir pressure, the current Deq model gives a lower reservoir pressure prognosis than the actual pressure condition (Figure 16). The declining trend that has been applied on layer level could not accurately capture the variability that occurred on each RPU. It is due to the uncertainty on reservoir connectivity, heterogeneity, and productivity. We still observe a few higher actual pressure at platform MWP-C and SWP-J areas, indicating that the pressure depletion is not as severe as predicted by the Deq model. On the other hand, most of the higher actual pressure (>0.9 Deq) is found at platform SWP-K and SWP-F (peripheral area) on both stratigraphic units (SU) three (3) and four (4). The most underestimated pressure prognosis is due to simplification pressure estimation in the previous Deq model, where it only uses a single pressure depletion in one layer. In reality, within one layer, it may consist of several RPU with different depletion trends. Despite the Deq model giving a lower reservoir pressure prognosis than the actual condition, the actual well reserves are still in line with the model prediction and have had satisfactory overall results (Figure 17).

Conclusions

Integrated static-dynamic modeling along with seismic reservoir characterization has answered the main issues at Peciko mature field. This methodology has been proven reliable, time-effective and efficient, and has become a game-changer in evaluating and finding the remaining gas potential at this field. Twenty-two (22) new wells have been successfully proposed under a new development project within three (3) months with overall satisfactory results. Furthermore, this method is applicable for mature fields with depletion drive mechanisms, good reservoir connectivity, and clear seismic anomalies.

References

Akbar, E., Herwin, H., Schulbaum, L., Roussel, S., Herawati, S., Muhazir, Y., 2015, Integration of Dynamic Synthesis in the Static Model: Enhancing Future Development Plan in the Multi-Layer Deltaic Peciko Mature Field, Proceedings of Indonesian Petroleum Association, 39th Annual Convention.

Basa, R. C., Prabowo, D., Sugiharto, D., Brahmantio, R., 2017, From Hazard to Full Scale Development: Seismic Interpretation Method to Unlock Shallow Gas Potentials in Tunu Field, Mahakam, Proceedings of Indonesian Petroleum Association, 41st Annual Convention.

Duval, B. C., Choppin de Janvry, G., and Loiret, B., 1992, The Mahakam Delta Province: An Ever-Changing Picture and a Bright Futur, Proceedings of the 24th Offshore Technology Conference.

Acknowledgements

We want to thank the management from Subsurface Development and Planning, PT. Pertamina Hulu Mahakam, for allowing us to publish and support this paper. We wish to express our sincere gratitude to the colleagues who have contributed to this project.

PROCEEDINGS
JOINT CONVENTION BANDUNG (JCB) 2021
November 23rd – 25th 2021

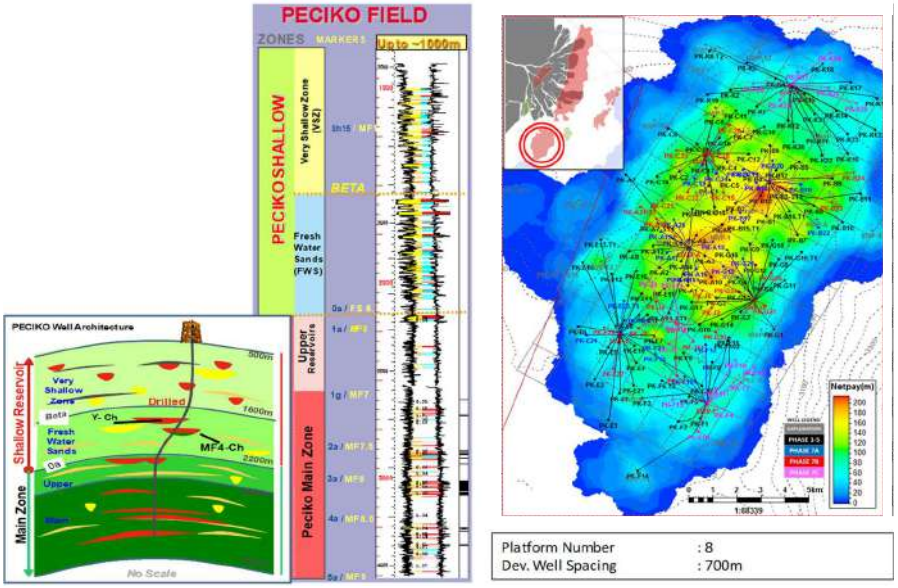

Figure 1: Geological Context of Peciko Field.

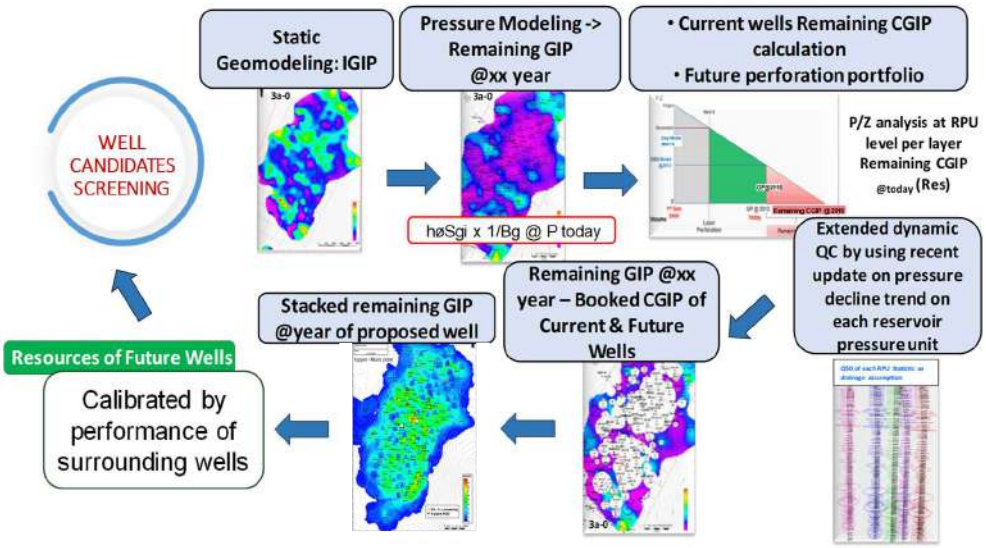

Figure 2: Peciko Depletion (Deq) Method: Static-Dynamic Integrated Workflow.

In PHM, we use psi unit for pressure. But for this model, we convert the psi unit into density equivalent (deq).

○ **dP/dZ = $\rho_f * g$** ⟶ Deq= Pressure (Psi) / mTVDSS*1.422

Typical water (*g*) → 1 g/cc = 0.433 psi/ft = 1.422 psi/m = 0.09806 bar/m

Figure 3: Reservoir Pressure Unit Conversion from Psi (standard unit) to Deq (as a pressure gradient function over the depth).

PROCEEDINGS
JOINT CONVENTION BANDUNG (JCB)2021
November 23rd – 25th 2021

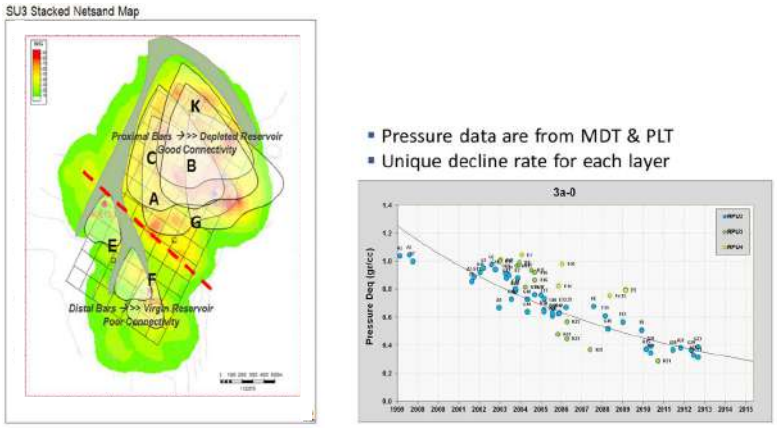

Figure 4: (a) Peciko Main Zone Connectivity. Depletion rate will be depending on geological area (main lobe – MWP-A, B, C, G, & J, northern lobe (SWP-K), and southern lobe (SWP-E & F), stratigraphic units, and well density, (b) Pressure evolution with time in one layer in each area or RPU (Reservoir Pressure Units); main lobe, southern lobe, and northern lobe. Decline rate is used in the pressure modeling to forecast actualized pressure (Akbar et al., 2015).

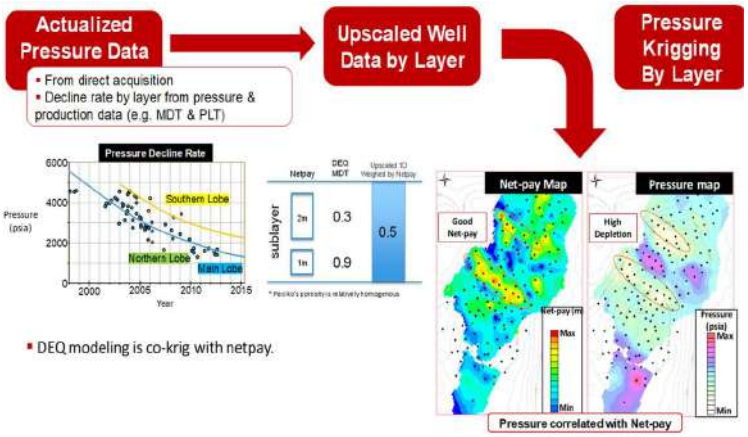

Figure 5: Pressure Depletion Modeling Workflow (Akbar et al., 2015).

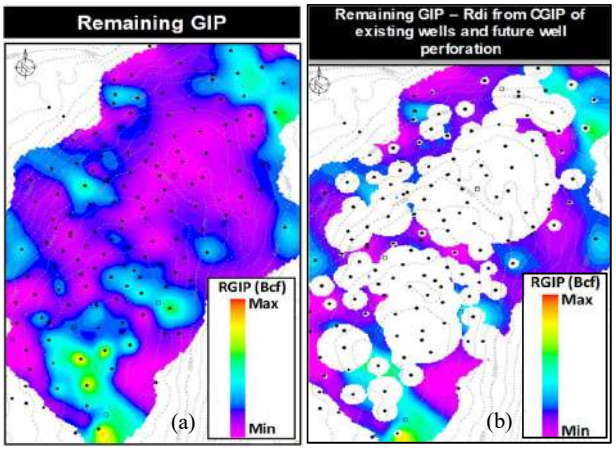

Figure 6: (a) RGIP map which is calculated by the hydrocarbon pore meter (HPM) against the gas formation volume factor (Bg) at a certain time. Where: h = net pay (m), ø = Porosity (%), Sgi = initial gas saturation = 1- Swi, Swi = initial water saturation, and Bg = gas formation volume factor (using Peciko Bg formulas), (b) Undrained RGIP map with the radius match to the remaining CGIP from P/Z analysis and future well perforation (this is an example from one layer) (Akbar et al., 2015).

PROCEEDINGS
JOINT CONVENTION BANDUNG (JCB) 2021
November 23rd – 25th 2021

Table 1: The Comparison of Offshore Drilling Variables for Peciko Side-track and New-Slot Well Architectures.

Variables	Ph9-XXX (Side-track Well)	Ph9-XXX (New-Slot Well)
	P50	P50
Duration (days)	14.07	24.56
Tangible Cost (US$)	201,707	728,436
Intangible Cost (US$)	5,795,412	7,483,551
Drillex Cost (US$)	5,997,119	8,211,987

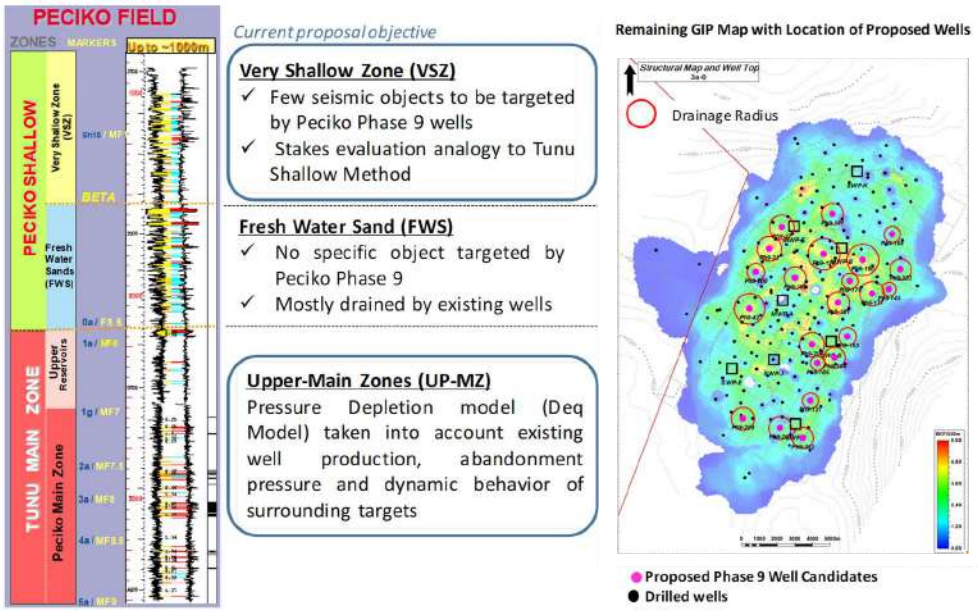

Figure 7. Peciko Well Targeting Concept.

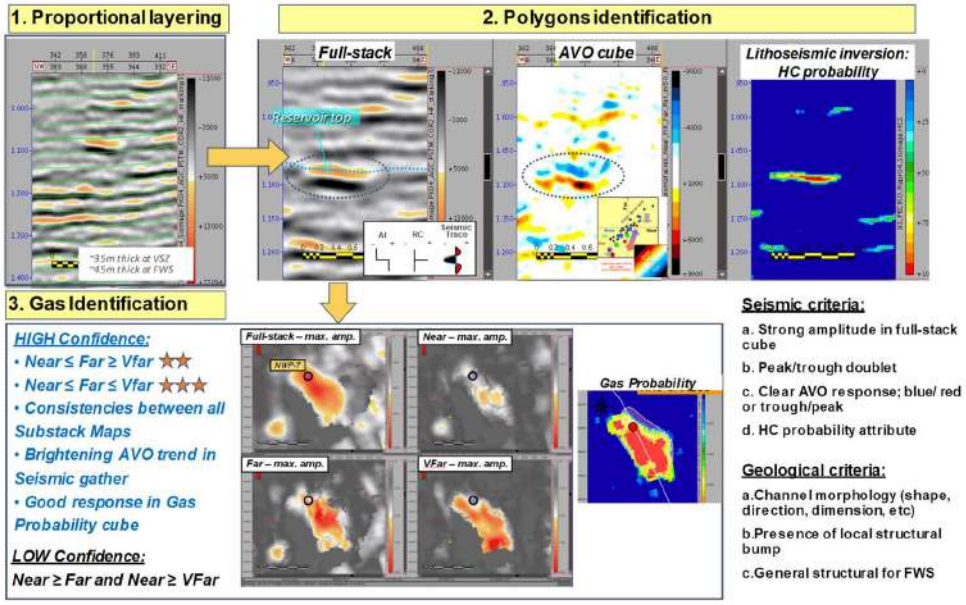

Figure 8: VSZ Seismic Target Determination.

PROCEEDINGS
JOINT CONVENTION BANDUNG (JCB)2021
November 23rd – 25th 2021

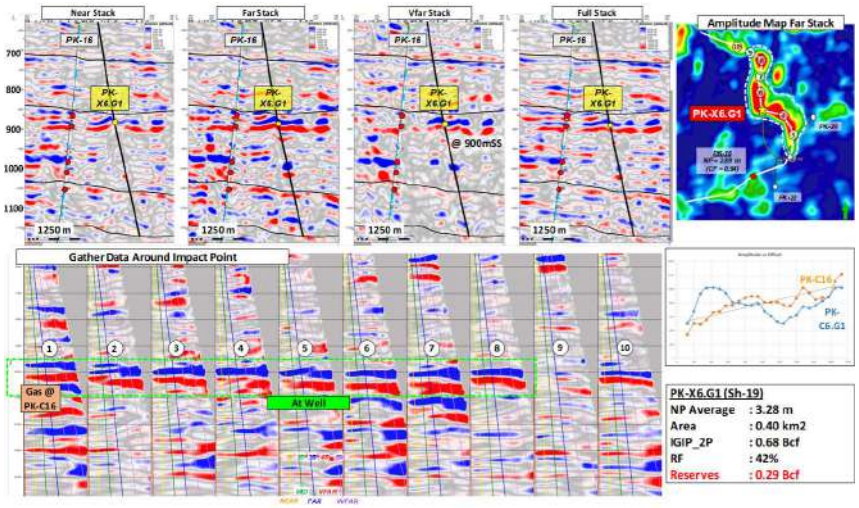

Figure 9: Typical VSZ Seismic Approach Target (Example Case).

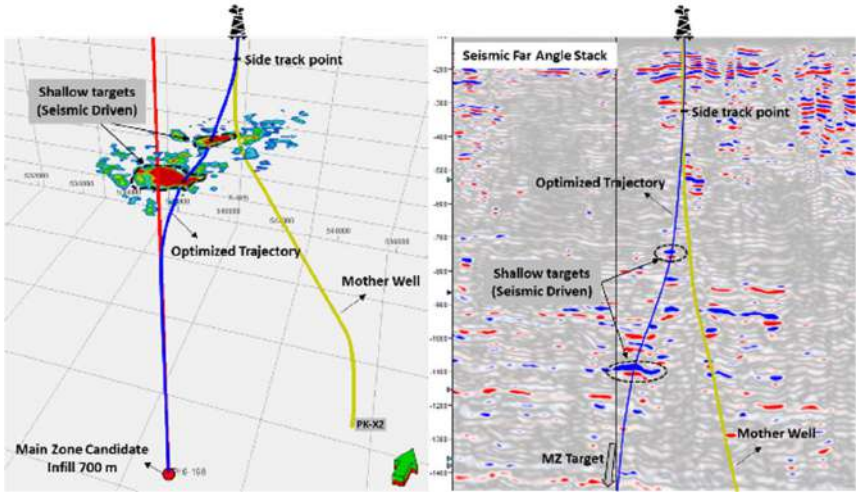

Figure 10: Peciko Well Design and Optimization.

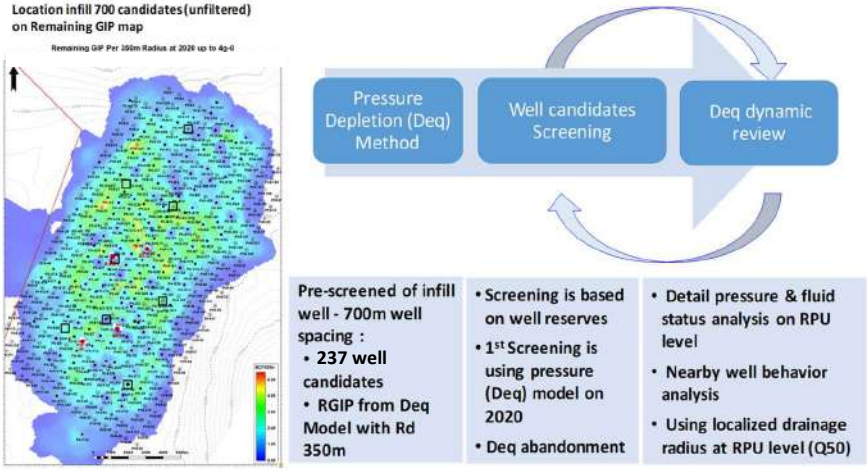

Figure 11: Peciko New Development Project (Peciko Phase 9) Workflow.

PROCEEDINGS
JOINT CONVENTION BANDUNG (JCB)2021
November 23rd – 25th 2021

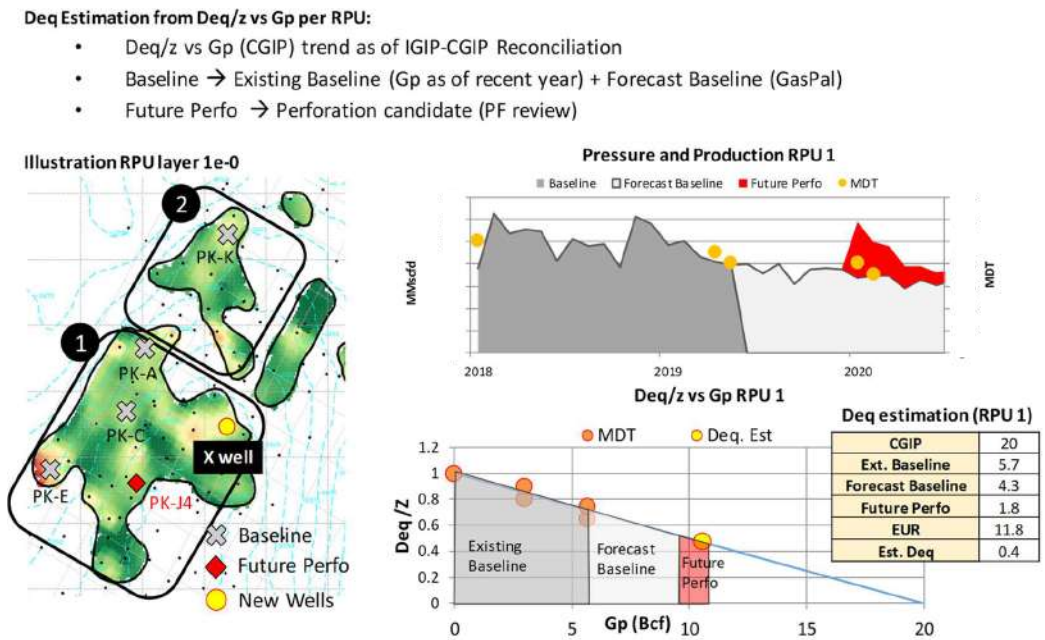

Figure 12: Peciko Dynamic Pressure Review.

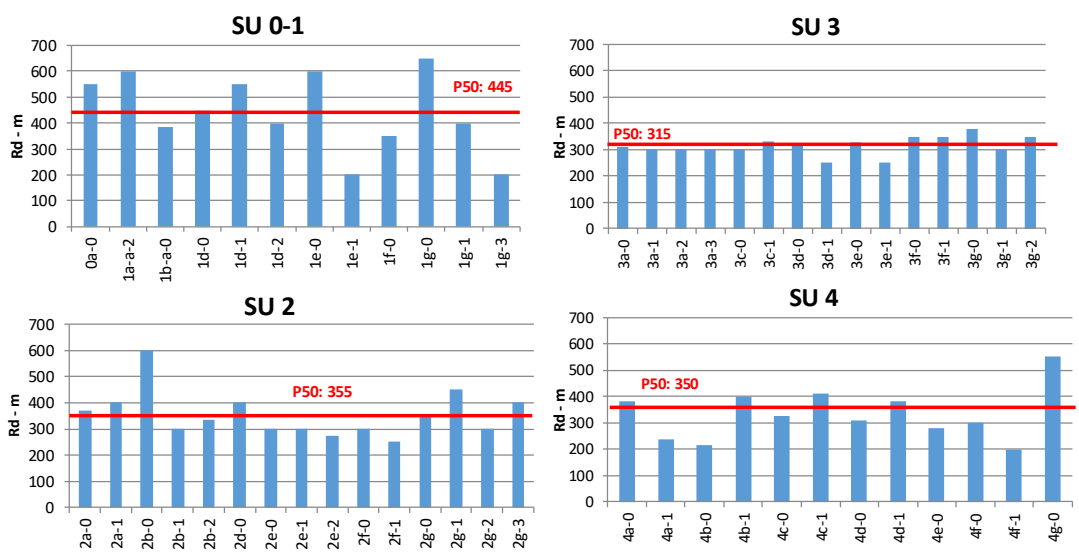

Figure 13: Result of statistic-deterministic approach for Rd per-layer in each stratigraphic unit (SU). Drainage radius (Rd) is coming from remaining gas in place from each well and each layer.

PROCEEDINGS
JOINT CONVENTION BANDUNG (JCB)2021
November 23rd – 25th 2021

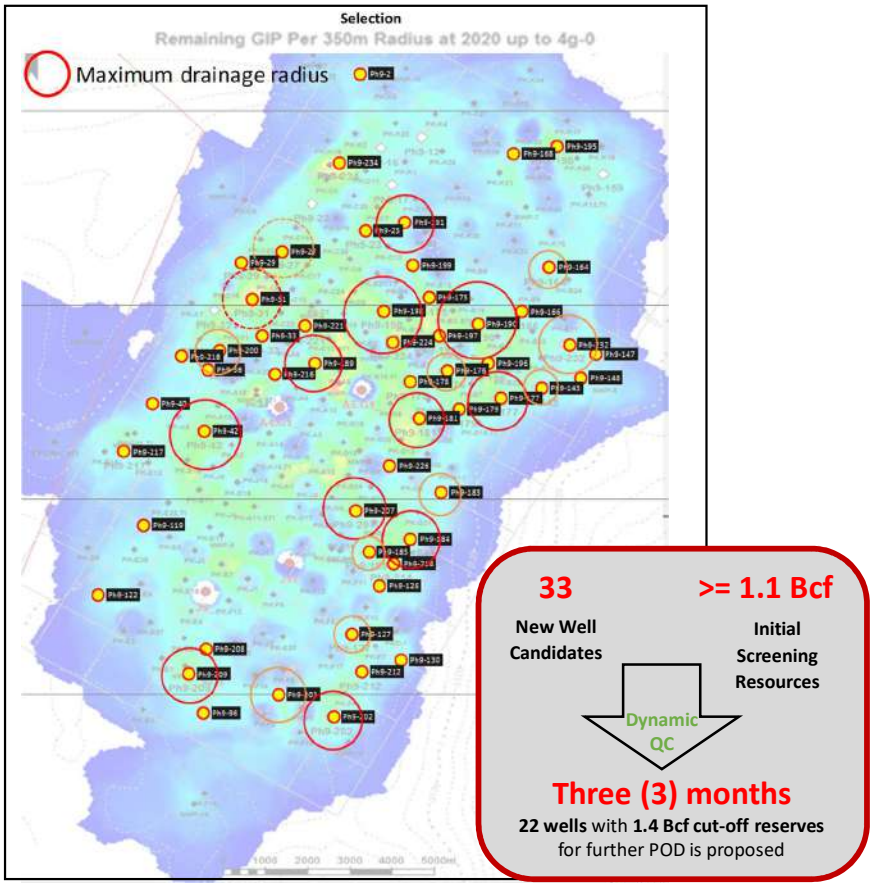

Figure 14: Proposed Well Locations and Associated Reserves.

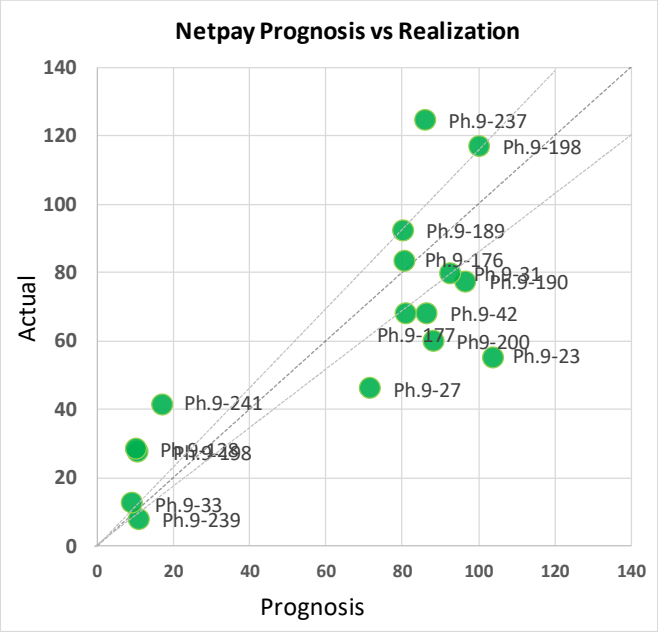

Figure 15: Netpay Comparison (Prognosis vs. Actual).

PROCEEDINGS
JOINT CONVENTION BANDUNG (JCB)2021
November 23rd – 25th 2021

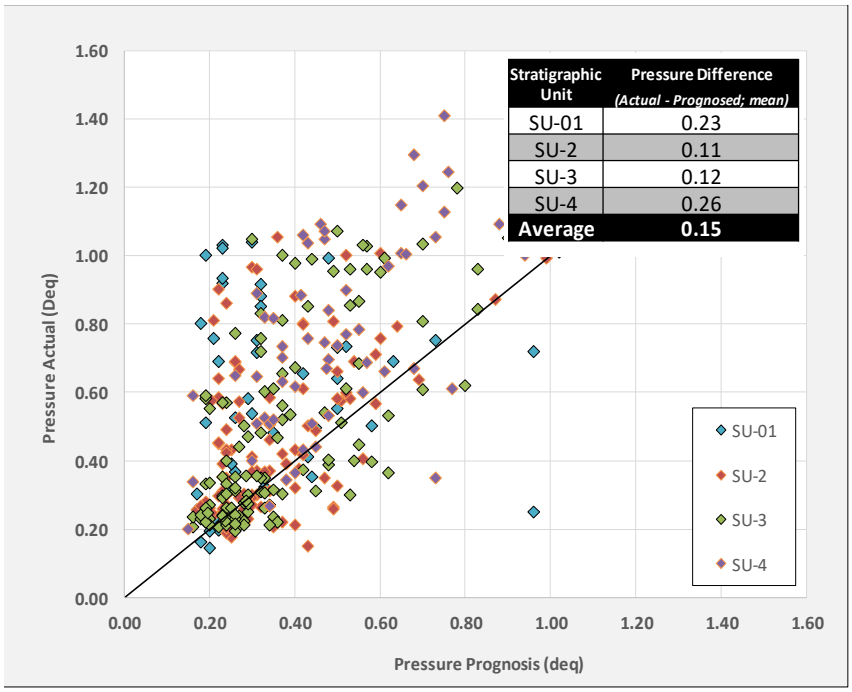

Figure 16: Reservoir Pressure Comparison (Prognosis vs. Actual).

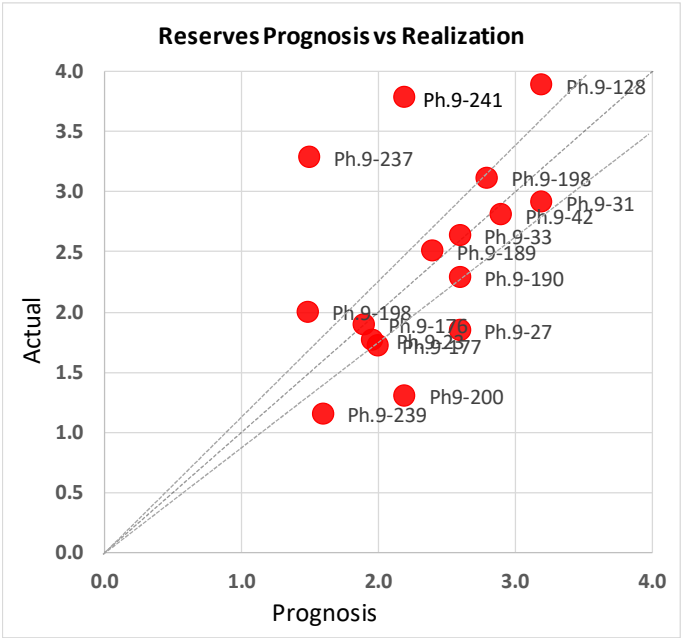

Figure 17: Reserves Comparison (Prognosis vs. Actual).

PROCEEDINGS
JOIN CONVENTION BANDUNG (JCB) 2021
December 1ST – 3rd 2021

Impact of Typhoon Surigae on Oceanographic Parameters in Sangihe-Talaud Waters

N Kusumawardani[1], A A Azani[1], C Iklima[2]*
[1]Bitung Maritime Meteorological Station, Bitung, Indonesia
[2]Toli-toli Aviation Meteorological Station, Toli-toli, Indonesia

**Corresponding Author: niken.kusumawardani@bmkg.go.id.*

Abstract
Tropical cyclones have an influence on the vertical mixing process in the ocean which has a positive impact on water fertility. This research aimed to analyze the impact of Typhoon Surigae on oceanographic parameters around Sangihe-Talaud Waters. The data used are wind direction and speed, sea surface temperature, salinity, sea wave height, and daily composite data of chlorophyll-a concentration from 02 - 30 April 2021 obtained from Aqua-MODIS satellite, NOAA Physical Sciences Laboratory, Copernicus Marine Service, and Ocean Forecast System (OFS) of the Indonesian Agency of Meteorology Climatology and Geophysics. The result shows that Typhoon Surigae only influenced weak upwelling and vertical nutrient mixing which are characterized by the value of sea surface temperature around 26-27 ºC and the value of chlorophyll-a concentration 0.1 - 0.7 mg/m3. Furthermore, Typhoon Surigae led to increased wind speed and significant wave height, creating westwards wind patterns and decreased salinity value. This study also found that Typhoon Surigae caused an increase in chlorophyll-a concentration around the Pacific ocean of Northern Halmahera.

Introduction

The tropical cyclone is one of the meteorological disasters that negatively affect human activities. It usually causes increasing rainfall, strong winds, increasing wave height, and potential for lightning activity (Sofianti and Putranto, 2020). On the other hand, the tropical cyclone gives a positive impact on the vertical mixing process in the ocean. For instance, when Tropical Cyclone Ernie occurred, it caused downwelling shown by the high value of sea surface temperature and low chlorophyll-a concentration. After tropical cyclone Ernie occurs, there is an increase of chlorophyll-a concentration and upwelling occur in the same area (Efendi et al., 2018).

A tropical cyclone is known by several names, such as Typhoon if it formed in the Western Pacific Oceans, Cyclone if it formed around India or Australia, and Hurricane if it formed in the Atlantic Ocean. The Western Pacific Ocean is one of the locations for the formation of tropical cyclones in Northern Indonesia. Tropical cyclones in the northern part of Indonesia usually occur in April, May, June, July, August, September, October, and November (Haryani and Zubaidah, 2012). The Indonesian region is not a good area for the formation process of tropical cyclones. However, the geographical position of Indonesia is adjacent to the formation of cyclone areas (Gaol et al., 2018). For example, Sangihe-Talaud waters are directly adjacent to the Western Pacific Ocean. This causes Sangihe-Talaud waters to get an indirect impact from the occurrence of tropical cyclones around the Western Pacific Ocean.

On April 12th, 2021, the Meteorology, Climatology, and Geophysics Agency of Indonesia (BMKG) gave an early warning of tropical depression 94W in the Pacific Ocean from Northeast Papua. It could increase the probability of heavy rain with strong winds and high sea waves on 13 to 19 April 2021. One of the areas with high potential to be affected is North Sulawesi, especially in Sangihe-Talaud Waters. Tropical depression 94W has become Typhoon Surigae and occurred for 270 hours from 13 to 25 April 2021 (Wicaksono and Nuzula, 2021). However, there is not much research on the impact of tropical cyclones on chlorophyll-a concentration in the northern part of Indonesia. Therefore, this study aimed to analyze the impact of tropical cyclone Surigae on chlorophyll-a concentration in Sangihe-Talaud waters.

Data and Method

Research site

The study area of this research is from Sangihe-Talaud waters to the Pacific Ocean of Eastern Philippines which is located at 123° - 130° E and 2° - 15° N. This research map also shows the Typhoon Surigae trajectory that passes through the research area, as shown in Figure 1.

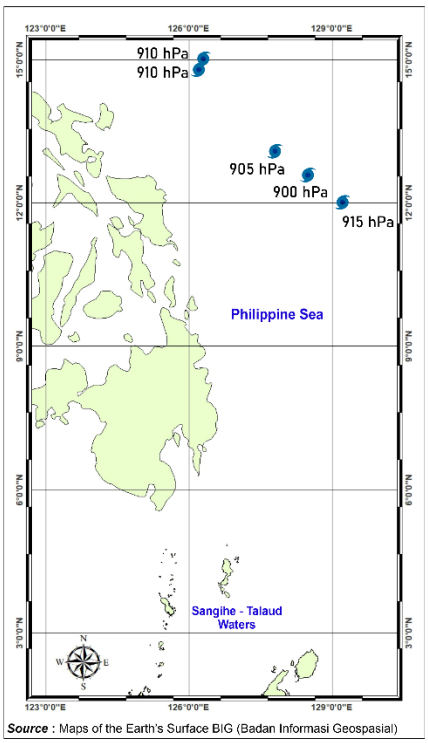

Figure 1. Research Area

Data resources and analysis

The data used in this research consists of typhoon information and oceanographic conditions (sea surface

temperature, sea surface wind, salinity, significant wave height, and chlorophyll-a concentration). The typhoon information is used to identify the movement of the typhoon, especially when the typhoon was near the research area. The typhoon information was obtained from the National Institute of Informatics (NII) Japan's website (http://agora.ex.nii.ac.jp/digital-typhoon/summary/wnp/s/202102.html.en). The typhoon began as a low-pressure area on April 12, 2021. Then, it began to increase its maximum wind speed on April 14, 2021 and was identified as Tropical Storm Surigae. As the storm entered the Philippines Water, its pressure decreased to 915 hPa and its maximum wind speed reached 107 knots so that it could be categorized as a typhoon. The typhoon reached its dissipation phase on April 25, 2021. The Typhoon Surigae information when it influenced the research area is shown in Table 1.

Date	Time (UTC)	Lon	Lat	Max Wind Speed (knot)	Type
17 April 2021	06.00	11.4	130.2	97	Typhoon
17 April 2021	12.00	12.0	129.2	107	Typhoon
17 April 2021	18.00	12.6	128.5	115	Typhoon
18 April 2021	00.00	13.1	127.8	115	Typhoon
19 April 2021	15.00	14.8	12.6	120	Typhoon
19 April 2021	21.00	15.1	126.3	115	Typhoon

Table 1. Typhoon Surigae data when it occurred near research area

The oceanographic conditions are used to analyze the upwelling and vertical mixing process around the waters. To determine the general condition of the water without typhoon disturbances, the monthly average data for the past 2 years (2019-2020) is used. Sea surface temperature data was obtained from NOAA Physical Sciences Laboratory (https://psl.noaa.gov/data/gridded/data.noaa.oisst.v2.highres.html#detail) with a spatial resolution of 0.25 x 0.25. Sea surface wind and salinity data were obtained from Copernicus Marine Service and can be downloaded from https://resources.marine.copernicus.eu/. Sea surface wind data has a spatial resolution of 0.25 x 0.25 and salinity data has a spatial resolution of 0.083 x 0.083.

The monthly significant wave height was obtained from the Ocean Forecast System (OFS) of the Indonesian Agency of Meteorology Climatology and Geophysics. Meanwhile, 3 hours of significant wave height data during Typhoon Surigae was obtained from Copernicus Marine Service (https://resources.marine.copernicus.eu/) with a spatial resolution of 0.083 x 0.083. Chlorophyll-a concentration was obtained from the Moderate Resolution Imaging Spectroradiometer (MODIS) sensor on the Terra satellite (Aqua-MODIS). Moreover, this study also utilizes 8-day composite data to find out the concentration of chlorophyll-a before, during, and after typhoon Surigae happened. This data has approximately 4km x 4km resolution and can be found online on the website https://oceancolor.gsfc.nasa.gov/l3/. All oceanographic data are visualized spatially with Grid Analysis and Display System (GrADS). The flowchart of this research can be shown in Figure 2.

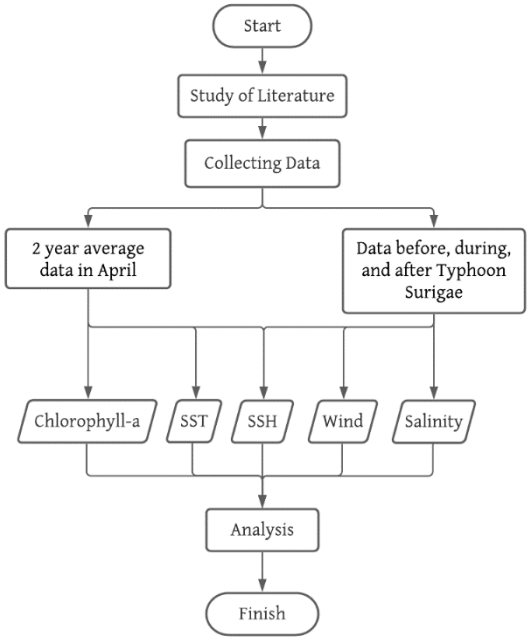

Figure 2. Research Flowchart

Result and Discussion

1. Wind

Sea surface wind is a parameter that has considerable impact due to the activity of Typhoon Surigae. In April, the wind tends to blow from the northeast to the east, indicating the movement of the Asian monsoon. The monthly average value of wind speed in April has a range value of 8 - 15 knots, as shown in Figure 3.

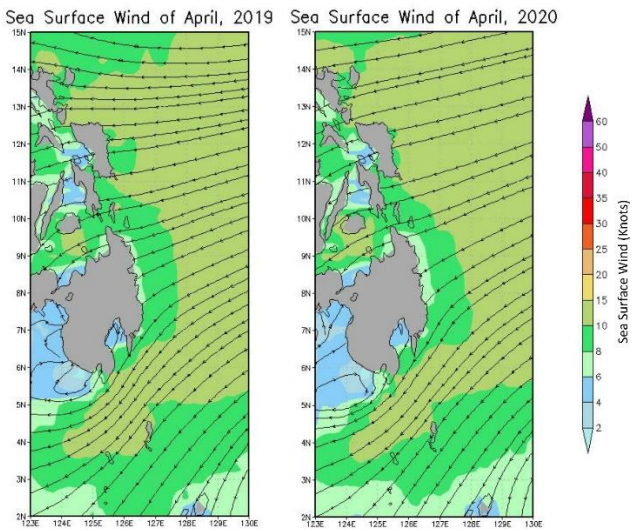

Figure 3. Monthly average sea surface wind condition on April 2019-2020

When a Typhoon Surigae happens, the direction of the wind tends to blow from the west on April 12, 2021. This is also coupled with the formation of a convergence area around the Sangihe-Talaud waters which supports the increase of low-pressure convective activity. When the typhoon began to approach the study area, the daily average wind speed in Sangihe-Talaud waters generally increased up to 10 - 20 knots on April 16. The daily average wind speed still increased on April 18, 2021, until it reached 15 - 25 knots in Sangihe-Talaud waters and up to 30 - 50 knots along the typhoon trajectory as shown in Figure 4. On the same day, maximum wind speed occurred near typhoon Surigae up to 115 knots on 00.00 UTC as shown in Table 1. This difference occurred because the wind speed value shown in Figure 3 is the daily average value, not the maximum value as stated in Table 1. On April 27, the direction of the wind returns blow from the northeast with daily average wind speed decreased to 6 - 10 knots.

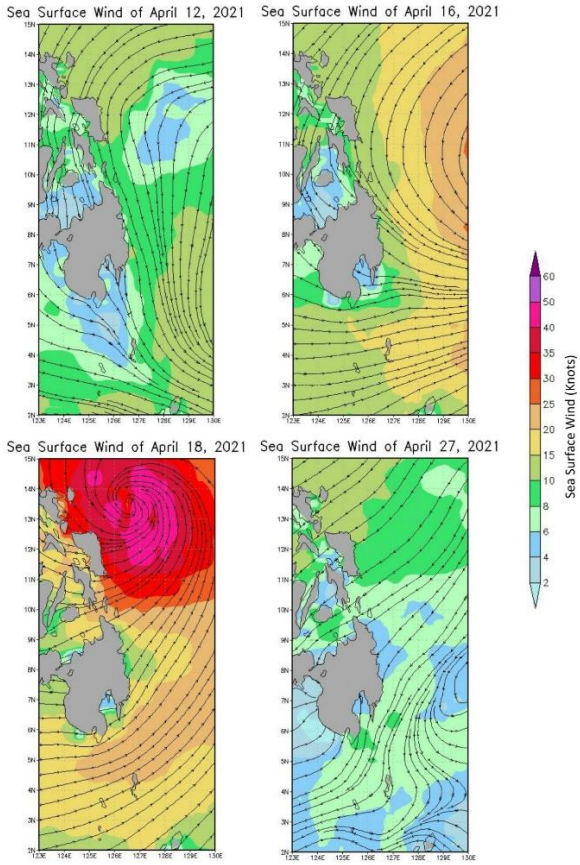

Figure 4. Daily average sea surface wind before (April 12, 2021), during (April 16 and 18, 2021), and after (April 27, 2021) the Typhoon Surigae located near the research area

2. **Sea Surface Temperature (SST)**
   The monthly average sea surface temperature conditions in Sangihe - Talaud waters in April 2020 tended to be warmer than April 2019 where the SST value in April 2020 ranged from 29 – 29.5 °C, as shown in Figure 5.

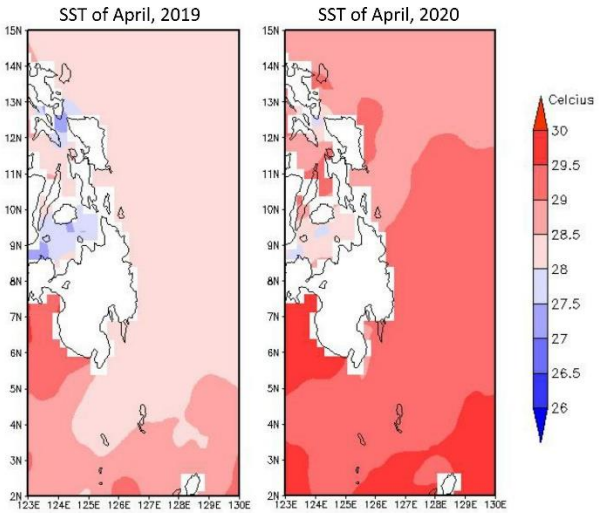

Figure 5. Monthly average sea surface temperature condition on April 2019-2020

Before the occurrence of Typhoon Surigae on April 12, 2021, the SST value in the waters of Sangihe - Talaud was greater than normal, with values ranging from 29.5 – 30 ºC. The high sea surface temperatures trigger the formation of low-pressure areas which cause Typhoon Surigae to form in the waters of Sangihe - Talaud. During Typhoon Surigae on April 18 - 19, 2021, the value of sea surface temperature shows an increase ranging from 29.5 – 30 ºC. On April, 30, the value of sea surface temperature returns to normal, which ranges between 29 – 29.5 ºC.

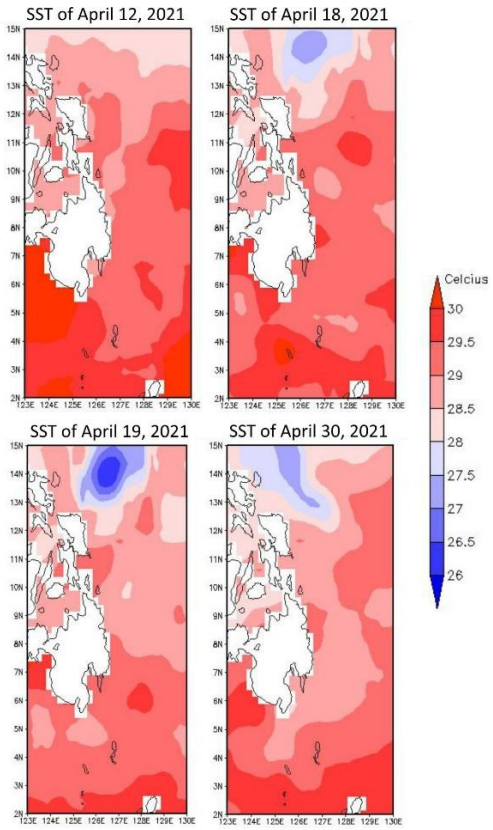

Figure 6. Daily average sea surface temperature before (April 12, 2021), during (April 18 and 19, 2021), and after (April 30, 2021) in Sangihe - Talaud waters

3. **Salinity**

In general, salinity values in Sangihe-Talaud waters tend to be homogeneous. It is also in the range around 33-35 ppt, which is considered as high. This can be seen from the monthly salinity values around these waters during 2019-2020. The lowest salinity distribution was in December 2020, which was in the range of 33-34 ppt. Based on the spatial data distribution, it can be seen that the waters of Sangihe-Talaud tend to be salty with a fairly high salinity value.

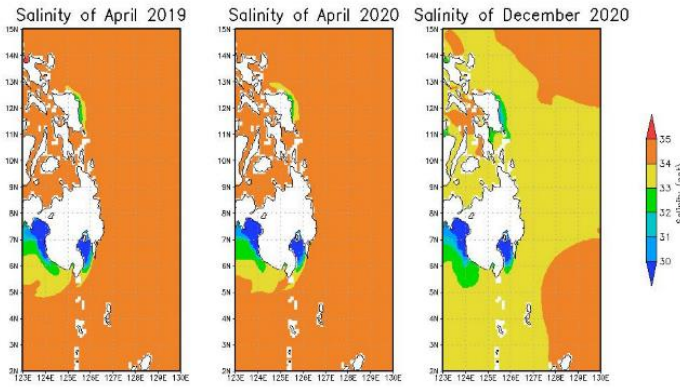

Figure 7. Sample of monthly salinity in the research area.

Meanwhile, during Typhoon Surigae, the salinity value around the Sangihe-Talaud waters was lower than normal, which was around 33-34 ppt. In addition, there was a mixture of salinity values around these waters when Typhoon Surigae was closest to the waters. On April 15 - 20 2021, water with low salinity in the south of the Philippines spread to the Sangihe-Talaud waters by value 30 – 33 ppt. This low salinity value can be caused by high precipitation that occurs in the waters during typhoon events (Suharyo et al., 2020).

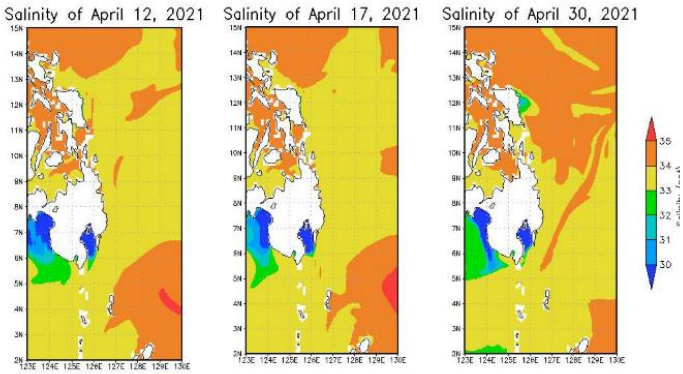

Figure 8. Salinity distribution before (April 12, 2021), during (April 17, 2021), and after (April 30, 2021) Typhoon Surigae located near the research area.

4. **Significant Wave Height**

Significant wave height (SWH) in the Sangihe-Talaud Waters based on monthly wave data for 2019-2020 tends to be in the medium range, which is 1.25 – 2.0 m. The highest waves in these waters occur during the rainy season, which is around December-January-February, with a wave height range of 2.5 – 5.0 m. Meanwhile, the lowest wave height occurred in May 2019, which is in the range of 0.75 – 1.5 m.

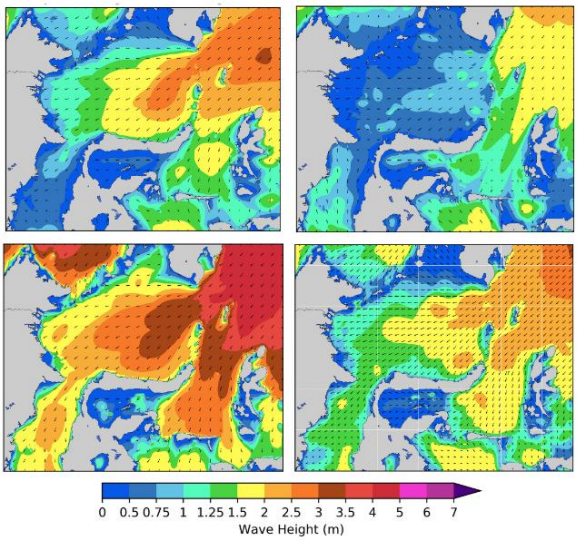

Figure 9. Sample of monthly significant wave height in research area on April 2019 (a), October 2019 (b), February 2020 (c), and April 2020 (d)

The wave height in the Sangihe-Talaud waters at the time of Typhoon Surigae was in the range of the normal height of the waters, which was 1.25 – 2.5 m. However, the presence of the typhoon did have a very significant effect on the wave height in these waters. As of April 17, 2021, at 12.00 UTC, when the wave height value reached 3.0 m. When the typhoon moved away, the wave height was in the low range, which was 0.25 – 1.25 m. The increase in the wave height during Typhoon Surigae was caused by the increase in surface wind speed around Sangihe-Talaud waters which reached 25 knots. Furthermore, the increase of SWH can lead to intensification of vertical mixing, which is essential for a higher increase in biological blooms (Woo et al., 2017).

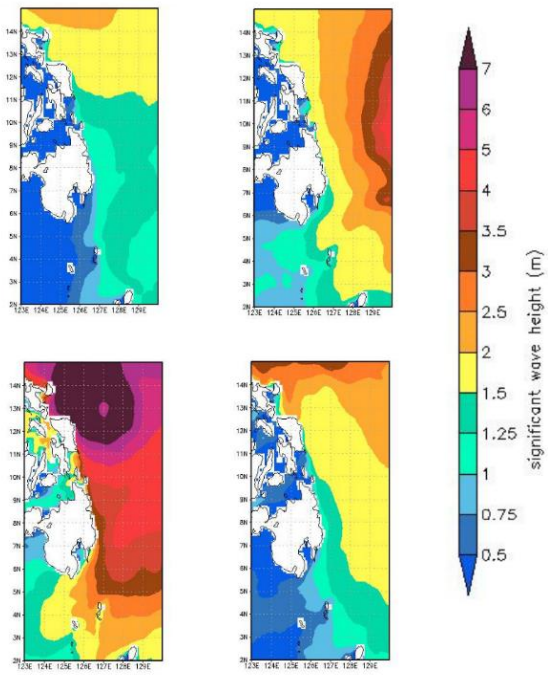

Figure 10. Wave height distribution on April 12, 2021 00.00 UTC (a), April 16, 2021 15.00 UTC (b), April 18, 2021 06.00 UTC, and April 22, 2021 00.00 UTC.

5. **Chlorophyll-a Concentration**

The chlorophyll-a concentration value in Sangihe-Talaud waters for the last 2 years is quite homogeneous. It was only around 0.05 - 0.2 mg/m3. Monthly average values for April 2019 and 2020 also showed the same value. This condition continues to occur up to the border of the Philippine waters. Meanwhile, in the southern part of Sangihe-Talaud waters, specifically in the waters around the Sitaro island until the northern part of the Halmahera coast, the monthly average chlorophyll-a concentration is slightly higher with a range value 0.1 - 0.5 mg/m3.

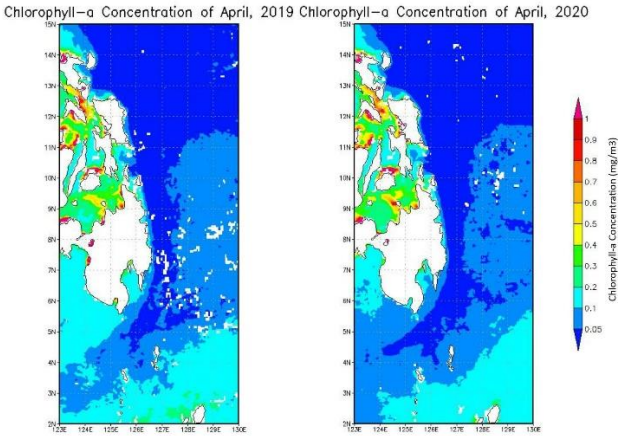

Figure 11. Monthly chlorophyll-a concentration on April 2019-2020

This research used 8-day composite data due to the incomplete data of daily chlorophyll-a concentration. At the beginning period of typhoon Surigae formed (April 1-6, 2021), chlorophyll-a concentration around Sangihe-Talaud waters have a range of values quite similar to the monthly average 2 years ago with a value of 0.1-0.3 mg/m3. When the movement of typhoon Surigae getting closer to the research area (April 7-14, 2021), chlorophyll-a concentration decrease to 0.1-0.2 mg/m3. During the period when typhoons were in the research area (April 15-22, 2021), mostly in the research area there are blank pixels (no value) due to cloud cover brought by Cyclone Surigae (Alianto et.al., 2020). Meanwhile, in the Pacific Ocean of North Halmahera, there was a significant increase in chlorophyll-a with the concentration value of 0.3-0.7 mg/m3. This increase is due to the vertical movement of water masses that contain lots of nutrients to the surface water (Ye, et.al, 2013). After typhoon Surigae moved away from the research area, chlorophyll-a concentration around Sangihe-Talaud waters turned back into 0.05 - 0.2 mg/m3.

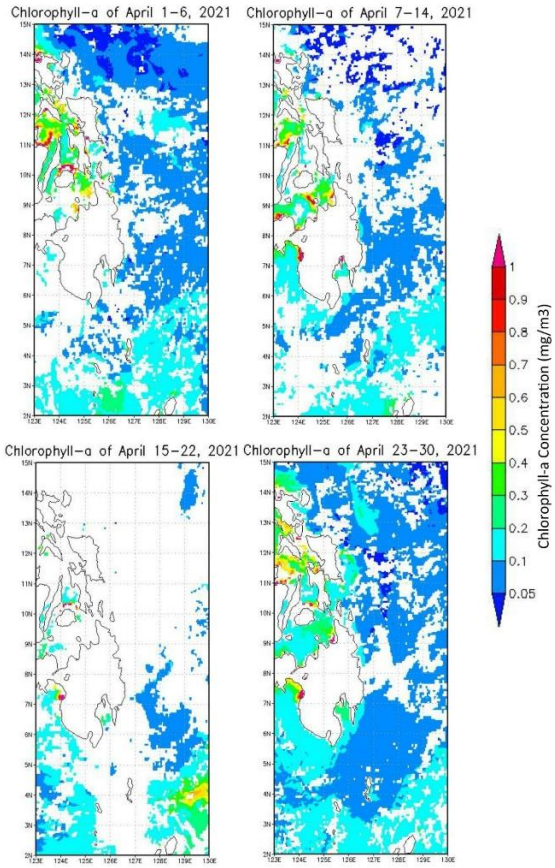

Figure 12. Chlorophyll-a concentration before (a, b), during (c), and after (d) the Typhoon Surigae

6. **Upwelling**

According to Kuttippurath et al. (in Wang, et al., 2021) mostly previous studies have shown that the vertical mixing and upwelling induced by typhoons can uplift the deeper Chl-a to the surface and bring nutrient-rich deeper water up, and increasing ocean productivity in the open ocean. To determine the characteristics of the upwelling area, this study used the analysis based on Table 2.

SST (C)	Chlorophyll-a (mg/m3)	Upwelling Criteria
>27	<1	weak upwelling intensity
26 - 27	1 - 2	moderate upwelling intensity
<26	>2	strong upwelling intensity

Table 2. Upwelling intensity criteria (Gaol, et. al, 2018)

Based on Table 2, it can be assumed that upwelling which occurs during typhoon Surigae around Sangihe-Talaud waters is an upwelling with weak intensity. This also happens around the trajectory area of Typhoon Surigae. During the occurrence of the typhoon, upwelling around Typhoon Surigae trajectory cannot be analyzed due to the incomplete data of chlorophyll-a. After one week, there was still no significant increase in

the amount of chlorophyll around the Typhoon Surigae trajectory.

Conclusions

The oceanographic conditions during Typhoon Surigae in Sangihe-Talaud Waters, such as surface wind, sea surface temperature, salinity, significant wave height, chlorophyll-a concentration, and upwelling, have been examined.

1. The results show that Typhoon Surigae only influenced weak upwelling and vertical nutrient mixing around the research area. It is shown by the result of SST (26 - 29 °C), the result of chlorophyll-a (0.1 - 0.7 mg/m3), and the increase of wind speed and significant wave height when Typhoon Surigae was located near the research area.
2. The increase of rainfall in Sangihe-Talaud Waters decreased the salinity value.
3. Chlorophyll-a concentration did not increase significantly around Sangihe-Talaud waters. However, a significant increase of chlorophyll-a concentration occurred around the Pacific ocean of Northern Halmahera, with a value of 0.3 - 0.7 mg/m3 compared to the monthly average for two years.

References

Alianto., Hamuna, Baigo., 2020, Journal of Applied Geospatial Information, 2, 343-349.

Efendi, U., Fadlan, A., and Hidayat, A.M., 2018, 2nd International Conference on Maritime Sciences and Advanced Technology, 162.

Gaol, S. L., Siadari, E. L., Ryan, M., and Kristianto, A., 2018, Jurnal Meteorologi Klimatologi dan Geofisika, 5.

Haryani, S. N., and Zubaidah, A., 2012, Majalah Ilmiah Widya, 324, 54-58.

Sofiati, I., and Putranto, M.F., 2020, The 9th International Symposium for Sustainable Humanosphere, 572.

Suharyo, G. B., Purba, N. P., Yuliadi, L. P., & Syamsuddin, M. L., 2020, Jurnal Ilmu-Ilmu Perairan, Pesisir, dan Perikanan, 9, 421-427.

Wang, T., and Zhang, S., 2021, Journal of Marine Science and Engineering, 9, 794.

Wicaksono, A., and Nuzula, N. I., 2021, Jurnal Inovasi Sains dan Teknologi Kelautan, 2.

Woo, H. J., and Park, K. A., 2017, Deep Sea Research Part II: Topical Studies in Oceanography, 143, 1–14.

Ye, H. J., Sui, Y., Tang, D. L., Afanasyev, Y. D., 2013, Journal of Marine System, 138-145.

PROCEEDINGS
JOINT CONVENTION BANDUNG (JCB) 2021
November 23rd – 25th 2021

Rare Earth Elements and Economic Mineral Identification Using Micro XRF in Separation Product of Bangka Tins Deposit Processing

Tyto Baskara Adimedha[1], I Gde Sukadana[1], Jana Tjahjana Anggadireja[2], Windi Anarta Draniswari[1]
1 National Innovation and Research Agency, Jl. Lebak Bulus Raya No. 9, Jakarta 12440
2 National Resilience Institute, Jl. Medan Merdeka Selatan No. 10, Jakarta 10110.

Abstract
The mechanical separation of tin processing is conducted in various stages such as density and magnetic separation. The result of those separation process produces several commodities that have certain economic value. Generally, the separation product is classified into 4 groups that are cassiterite, ilmenite, zircon, and monazite concentrate. Analysis of those products had been carried out using grain analysis or geochemical analysis of a bulk sample. However, that kind of analysis is still limited to observation of mineral physical properties and dependent on analyst subjectivity. Quantitative identification can be an aid to minimalize the subjectivity of analysts. The objective of this research is to identify rare earth elements and economic minerals in tin separation products. There are 4 samples as representative of each concentrate analysed using micro XRF M4 Tornado Plus® and completed with mineral identification using AMICS (Advanced Mineral Identification and Characterization Systems). The result shows that tins concentrate consists of cassiterite 96.60% with dominant elements of Sn 85.17%, Ti 3.90%, and Fe 2.11%. Ilmenite concentrate consists of ilmenite 97.83% with dominant elements of Ti 33.67%, Fe 24.97%, and Mn 3.19%. Zircon concentrate consists of Zircon 97.33% with dominant elements of Zr 59.54%, Si 14.88%, Ti2.45%, and Hf 1.52%. Monazite concentrates consist of monazite 91.64%, with dominant element of Ce 32.14%, P 10.52%, La 10.12%, Th 5.49% and Zr 3.47%. Rare earth elements (REE) are found dominantly in monazite concentrate that consists of Ce and La with a radioactive element of Th and Zr as impurities. Quantitative mineral identification can show a better analysis result of element and mineral distribution throughout the concentrate samples and minimalize the bias caused by the analyst subjectivity.

Keywords: Bangka, micro XRF, rare earth elements, tin deposit

Introduction

Bangka Island is one of the islands located in The Southeast Asian Tin Belt that spread from Myanmar, Thailand, Malaysia, and Indonesia[1]. This geological setting causes Bangka Island to become one of the biggest tin deposits in the world. Commodities or mineral that can be extracted from the tin deposits are cassiterite (SnO_2), ilmenite ($FeTiO_2$), rutile (TiO_2), anatase (TiO_2), zircon ($ZrSiO_4$), and monazite ((La, Ce) PO_4)[2].

Before they can be used, tin ore must go through a series of processes both mechanically and chemically. Mechanically, tin ore processing requires some separation process using high tension electrostatic separation to separate conductor and non-conductor factions. Then magnetic separation conductor faction will produce a magnetic fraction of ilmenite 80-90% and the non-magnetic faction of cassiterite 70%. On the other hand, magnetic separation was also applied on non-conductor faction resulting in monazite 40-80% and xenotime 30% as magnetic faction and zircon 20%, and quartz 10% as a non-magnetic faction[3](**Figure 1**). Each of the separation products called concentrate has a certain economic value. Cassiterite is a primary ore of tin and can be used for tin cans, metal coating, alloy, etc. Ilmenite is a source of titanium that important as white pigment colourings. Zircon is mainly applied in the ceramic industry. Monazite and xenotime can be extracted for their rare earth and thorium content that is used as raw materials in the high-tech industry[4].

As a quality assurance, grain mineralogy or geochemical analysis will be conducted for each concentration. This kind of analysis is chosen because it is cheap and fast. However, grain mineralogy analysis is limited to the physical properties of mineral and rely upon analyst subjectivity. Even sometime it is difficult to distinguish K-feldspar and plagioclase in some cases[5]. The geochemical analysis gives us information about the chemical composition but not the mineral contents of a sample. To minimalize the subjectivity of the analyst and to provide better results of mineral contents of rocks and sands, quantitative identification of minerals will become a solution to the problems.

Micro-X-ray fluorescence (Micro XRF) is a method to analyse elemental distribution in a large material up to 15 cm in length and with a level of detail up to 20 µm. Micro XRF analysis has a wide application in material studies including geology[4–6]. In the grain mineral analysis micro XRF has proved that it helps to distinguish K-feldspar, plagioclase, and Ca-bearing plagioclase[5]. Coupled with "Advanced Mineral Identification dan Characterization Systems" (AMICS) software, this analysis will provide mineral composition data and elemental information of each mineral[6]. The objective of this research is to identify rare earth elements and economic minerals in tin separation products using both micro XRF and AMICS analysis so that the disadvantages of grain mineralogy and geochemical analysis can be minimalized.

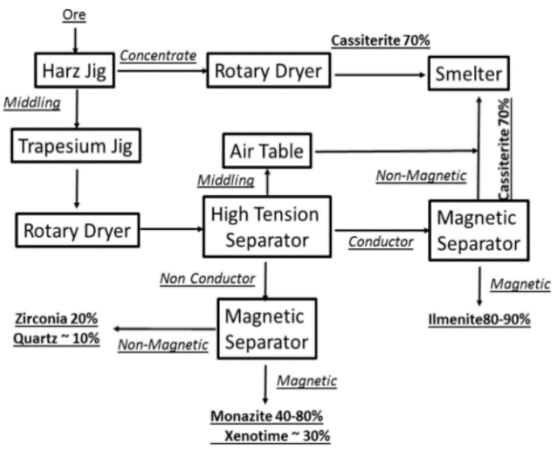

Figure 1 Schematic process of mechanical separation of tin ore processing. The result are mineral concentrates that consist of cassiterite, ilmenite, zircon, and monazite concentrate[3].

PROCEEDINGS
JOINT CONVENTION BANDUNG (JCB) 2021
November 23rd – 25th 2021

Data and Method

There are 4 concentrate samples from tin processing products those are cassiterite, ilmenite, zircon, and monazite concentrates. Each concentrate is in grain form and placed on a glass plate and stuck using tape. This kind of preparation is applied to make only one layer of grains and minimalize stacking grain. Micro XRF analysis is conducted using Bruker M4 Tornado operating at 500 kV, 600 µA. The software is set in area mode then applies a pixel size of 20 µm and acquisition time of 15 ms/pixel. This analysis will give a result of element geochemistry and distribution maps. Furthermore, the element distribution maps are analysed using "Advanced Mineral Identification dan Characterization Systems" (AMICS) software to identify and characterize the mineral composition of the sample. Mineral identification in AMICS is carried out by comparing and classifying the mineral spectrum of the sample and the database spectrum of AMICS. After the classification is completed, we can use any other option in AMICS to get mineral composition data and/or visualize it into the graphic.

Result and Discussion

Micro-XRF analysis was carried out of 4 concentrate samples of tin sand processing that consist of tins, ilmenite, zircon, and monazite concentrates. The result shows the relative elemental mapping of the concentrate samples in which reflected its mineralogical contents. Each concentrate has a minor impurities mineral indicated by the presence of other elements that are not a part of the mineral. The other elements that are found as impurities in a concentrate are varying for each sample (**Table 1**). The tins concentrate has a dominant element of Sn 85.17%, with some impurities of Ti 3.90%, Fe 2.11%, and Si 1.33%. Ilmenite concentrate has dominant elements of Ti 33.64% and Fe 24.97% with some impurities of Mn 3.19% and Si 0.83% (**Figure 2A)**. Zircon concentrate has dominant elements of Zr 59.54% and Si 14.88% with impurities of Ti 2.45% and Hf 1.52%. Monazite concentrate has dominant elements of Ce 32.14%, P 10.52%, La 10.12%, and Th 5.49% with some impurities of Zr 3.47% and Y 1.30%. **Figure 2B** shows that the elemental distribution of dominant element and impurities in monazite concentrate are separated from each other. The data imply that the impurities in the concentrate samples are another mineral that escapes the separation process. The small amount and similar physical properties might not be observed by grain mineralogy analysis.

As comparison the rare earth element composition in monazite sand using Desktop XRF analysis are 9.39 to 12.90% La, 18.27 to 28.20% Ce, and 6.47 to 6,85% Th[8][9][10]. That number are similar to the micro-XRF analysis however, the micro-XRF analysis can add some other information in the sample such as mineralogical mapping throughout the sample.

Table 1. Calculated geochemistry from Micro-XRF analysis of each concentrate.

Element (Wt. %)	Cassiterite Concentrate	Ilmenite Concentrate	Zircon Concentrate	Monazite Concentrate
O	6.07	35.80	19.88	28.62
Al	0.86	0.63	0.73	0.92
Si	1.33	0.83	14.88	3.03
P	-	0.02	-	10.52
S	0.18	-	-	0.12
K	-	-	-	-
Ca	-	-	0.47	-
Ti	3.90	33.67	2.45	2.42
Cr	-	0.16	-	-
Mn	-	3.19	-	-
Fe	2.11	24.97	0.26	1.38
Zn	0.01	0.10	-	-
Sr	-	0.01	-	-
Y	0.01	-	0.26	1.30
Zr	0.09	0.06	59.54	3.47
Nb	0.15	0.32	-	-
Sn	85.17	0.08	-	0.27
La	-	-	-	10.12
Ce	-	-	-	32.14
Hf	-	-	1.52	-
Ta	0.07	-	-	-
W	-	0.05	-	0.07
Pb	0.04	0.11	-	0.12
Th	-	-	-	5.49

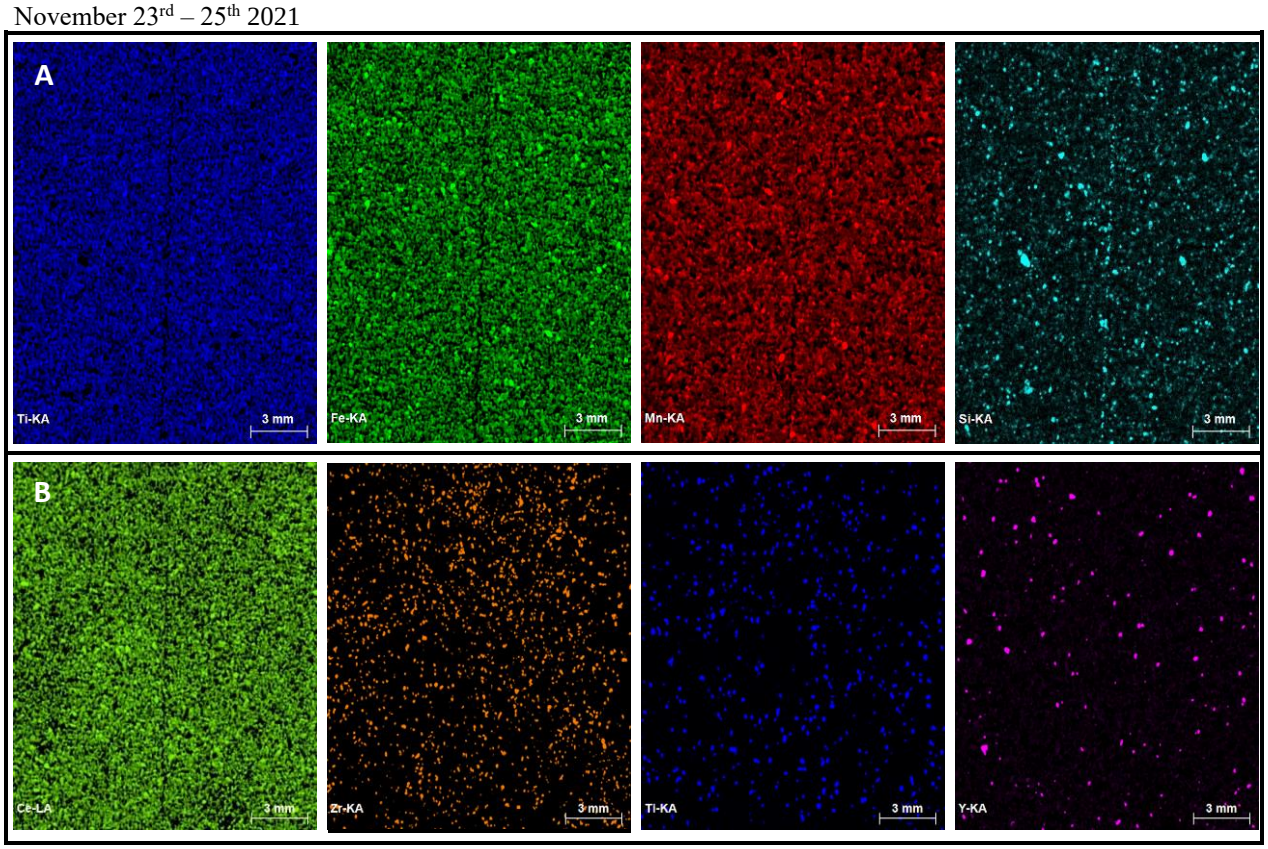

Figure 2. Elemental distribution map as results of micro-XRF analysis. A) Ilmenite concentrate shows dominant element of Fe and TI with impurities of Mn and Si. B) Monazite concentrate showing the dominant element is Ce and the impurities are Zr, Ti, and Y. The dominant and impurities elements are separated each other that implies the different mineralogy.

The mineralogical analysis from AMICS shows that each concentrate has a small number of mineral impurities. The tin concentrate has cassiterite percentages of 96.60% with impurities are rutile and pyrite. Ilmenite concentrate has ilmenite percentages of 97.83% with impurities are rutile and chromite. Zircon concentrate has zircon percentages of 97.33% with impurities are rutile and plagioclase. Monazite concentrate has monazite percentages of 91.64% with impurities are zircon, rutile, ilmenite, and xenotime (**Table 2**). The data indicated that each sample has impurities mineral less than 10%, a very good number for separation products in tin ore processing.

An additional feature that needs to be highlighted is the elemental impurities in a certain mineral. For example, **Figure 3A** shows that in Ilmenite concentrate there are elemental impurities of Mn and Zn that forming Mn-bearing ilmenite and Zn-bearing ilmenite. These detail in elemental information cannot be found in the mineralogical analysis. **Figure 3B** shows that in one grain of xenotime mineral, it is divided into HREE-bearing xenotime in the centre of the grain and non-REE xenotime as a grain coating.

The result explained above indicated that the strength of the micro-XRF analysis is the ability to scan samples relatively quickly to reveal geochemical texture in grain samples that cannot be seen by unaided eye[11]. Coupled with AMICS, micro-XRF maps can also display specific mineralogy such as Mn-bearing ilmenite and Zn-bearing ilmenite in Ilmenite concentrate. Furthermore, the analysis can also present detailed mineralogical texture such as that of HREE-bearing xenotime is coated by non-REE xenotime.

The ability of micro-XRF to analyse large samples up to 15 cm and micro-scale up to 20 µm, fine scale mineralogical composition can be identified and classified in a larger scale across rock sample compared to thin-section or SEM technique[6]. Thus, significantly more chemical, textural, and mineralogical information can be gathered for the purpose to characterize association and alteration of minerals. For consideration, elemental mapping is only feasible for particularly high concentration and contrast. Therefore, for smaller and subtle contrast of elemental concentration, micro-XRF can only provide limited information and cannot yet compete with SEM-EDS or LA-ICP-MS methods[5].

PROCEEDINGS
JOINT CONVENTION BANDUNG (JCB) 2021
November 23rd – 25th 2021

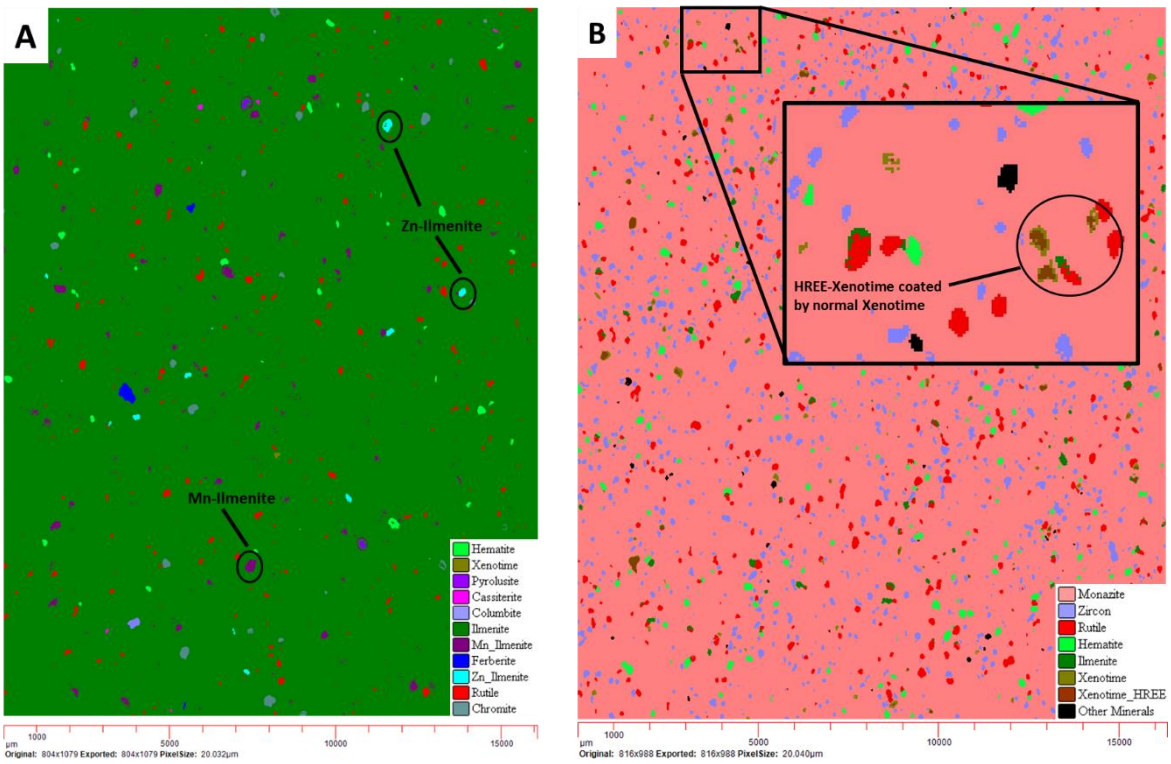

Figure 3. Micro-XRF coupled by AMICS can make such detailed texture of mineralogy analysis A) Ilmenite concentrate show the impurities element in ilmenite minerals forming Mn-bearing ilmenite and Zn-bearing ilmenite. These details cannot be found in grain analysis or geochemical analysis. B). Monazite concentrate show the occurring of heavy REE (HREE) bearing xenotime is coated by normal xenotime.

Table 2. The result of mineralogy identification and characterization was provided by using AMICS.

Mineral	***Cassiterite Concentrate***	***Ilmenite Concentrate***	***Zircon Concentrate***	***Monazite Concentrate***
Cassiterite	96.13	0.02	0.01	-
Ilmenite	0.01	97.85	-	0.52
Mn-Ilmenite		0.63	-	-
Zn-Ilmenite		0.09	-	-
Zircon	0.06	-	97.18	4.53
Monazite	-	-	0.01	90.81
Rutile	1.73	0.80	1.77	2.27
Hematite	0.28	0.22	0.12	1.26
Pyrite	1.33	-	-	-
Chromite	-	0.28	-	-
Quartz	-		0.04	-
Sillimanite	-		0.86	-
Xenotime		0.01	-	0.31
HREE-Xenotime			-	0.19
Other Minerals	0.46	0.10	0.01	0.11

Conclusions

The micro-XRF and AMICS analysis techniques show that there are some impurities element and mineral in concentrate samples of separation product of Bangka tin ore processing. The impurities found in the sample are forming separated individual minerals were detected by AMICS analysis. AMICS analysis shows elemental impurities in certain minerals such as Mn-bearing ilmenite and Zn-bearing ilmenite. Furthermore, AMICS also shows detailed textural information such as coating in a single mineral grain. Paired with AMICS, micro-XRF has proved its ability to identify and characterize the mineralogical composition and textural information of the rock or grain samples. However, micro-XRF still cannot yet compete with SEM-EDS or LA-ICP-MS because of its limitation. Ultimately, improving our ability to identify and characterize minerals within ore deposits is beneficial to improve our understanding of the ore genesis, association of ore and gangue, and proper technique to process the ore minerals.

References

[1] A. Sulastri, "Geochemical Distribution of REE and Grain Size Analysis of Heavy Mineral Associated with Tin Placer-Type Deposit , Bangka," 2020.

[2] R. K. Sianturi, M. N. Heriawan, and Syafrizal, "Analisis Spasi Lubang Bor untuk Mengevaluasi Sumberdaya Timah Aluvial dan Mineral Ikutannya di Pulau Bangka dengan Global

Estimation Variance," *Ris. Geol. dan Pertamb.*, vol. 30, no. 2, pp. 153–170, 2020, doi: 10.14203/risetgeotam2020.v30.1115.

[3] S. Harjanto, "CHARACTERIZATION OF INDONESIA RARE EARTH MINERALS AND THEIR POTENTIAL PROCESSING TECHNIQUES," 2013.

[4] H. Elsner, "Assessment Manual: Heavy Minerals of Economic Importance," Hannover, 2007.

[5] S. Flude, M. Haschke, and M. Storey, "Application of benchtop micro-XRF to geological materials," *Mineral. Mag.*, vol. 81, no. 4, pp. 923–948, 2017, doi: 10.1180/minmag.2016.080.150.

[6] R. D. Barker, S. L. L. Barker, S. A. Wilson, and E. D. Stock, "Quantitative Mineral Mapping of Drill Core Surfaces I: A Method for µXRF Mineral Calculation and Mapping of Hydrothermally Altered, Fine-Grained Sedimentary Rocks from a Carlin-Type Gold Deposit," *Econ. Geol.*, Nov. 2020, doi: 10.5382/econgeo.4803.

[7] L. Germinario, R. Cossio, L. Maritan, A. Borghi, and C. Mazzoli, "Textural and Mineralogical Analysis of Volcanic Rocks by µ-XRF Mapping," *Microsc. Microanal.*, vol. 22, no. 3, pp. 690–697, 2016, doi: 10.1017/S1431927616000714.

[8] I. Rodliyah, S. Rochani, and T. Wahyudi, "EXTRACTION OF RARE EARTH METALS FROM MONAZITE MINERAL USING ACID METHOD," *Indones. Min. J.*, vol. 18, no. 1, pp. 39–45, 2015.

[9] Samin, S. T. Sunanti, and K. Setiawan, "The synthesis and certification of in-house monazite sand certified reference materials (CRM)," *AIP Conf. Proc.*, vol. 2014, no. September, 2018, doi: 10.1063/1.5054552.

[10] S. Virdhian and E. Afrilinda, "Karakterisasi Mineral Tanah Jarang Ikutan Timah Dan Potensi Pengembangan Industri Berbasis Unsur," *Met. Indones. Vol. 36*, vol. 36, no. 2, pp. 61–69, 2014.

[11] C. G. Ryan *et al.*, "Maia Mapper: High definition XRF imaging in the lab," *J. Instrum.*, vol. 13, no. 3, 2018, doi: 10.1088/1748-0221/13/03/C03020.

PROCEEDINGS
JOINT CONVENTION BANDUNG (JCB) 2021
November 23rd – 25th 2021

The Effect of Magnetic Susceptibility value changes against Temperature changes in Geothermal Reservoir based on Time-Lapse Geomagnetic Data

Taufiq[1]
[1]*Research & Technology Innovation, Pertamina (Persero)*

Abstract
Magnetic Susceptibility is a degree to which a material can be magnetized in an external magnetic field. Several factors can be influenced the magnetic susceptibility such as the position of material with respect to magnetic field, frequency of the field, temperature, fluid content, alteration of rock. On geothermal system, magnetic susceptibility is one of the parameter to determine the heat source zone, but in this research, we want to use magnetic susceptibility as a parameter to monitor temperature changes on geothermal reservoir. Based on acquisition in different time (time-lapse magnetic with >10 year) on geothermal field, magnetic susceptibility value changes from -451 to 458 on point RTI065, value changes from -390 to 319 on point RTI072 (geothermal manifestation), value changes from -236 to -751 on point RTI047, value changes from -211 to -346 on point RTI051 (geothermal reservoir), value changes from -261 to -504 on point RTI056, value changes from 169 to 432 on point RTI046 (interest zone). From the reference, temperature decreased from 240^{0}C to 220^{0}C on the production zone. Based on this data, we assumed the magnetic susceptibility can be changed by temperature on the reservoir during production. If this hypothesis solved, time-lapse magnetic can be one of parameter to monitor temperature changes on reservoir and can be parameter to develop the prospect and development geothermal area.

Introduction

Magnetic Susceptibility is a degree to which a material can be magnetized in an external magnetic field. This parameter usually used to guide best practice for geothermal exploration like a combination with gravity data to identify structural geology (IGA, 2014), to identify variation of rock within different magnetic properties at regional scale (Soengkono, 1996), to identify demagnetized rock due to alteration process (IGA, 2014), and to assess the extent of high temperature geothermal reservoirs (Soengkono 1995).

On volcanic area, Magnetic Susceptibilities value can be changed with time. When susceptibilities of volcanic rock will be affected on temperature of rock, susceptibilities value can be changed from the eruption of volcanic mountain until the rock cooling down quickly. But, alteration of rock due to heat factor or material coming up to surface like geothermal manifestation may change the magnetic susceptibility value on the rock.

In this research, we will correlate magnetic susceptibility changes with temperature changes on several years (time-lapse) to determine and to monitor a hydrothermal system on geothermal reservoir (first hypothesis).

Data and Method

2.1 Geological Setting

Research Area is located on active volcanic line quarter-age with elevation 1400-1900 m.a.s.l. The volcanic line spreading from Southwest to Northeast and associated with caldera. This Area is dominated by andesite and basaltic from several old volcanic rocks on Southwest and continue to young volcanic rock on Northeast. Complex erosion processes and structural connections indicate that successive volcanic eruptions ranging from Southwest to Northeast. On this research area, we have several manifestations point with temperature 90°C - 95°C and pH 2.7 – 4 on Northeast and temperature 55°C - 60°C on Southwest.

2.2 Geomagnetic Method

Geomagnetic Method is one of geophysical method that used a potential field (this case a magnetic field) parameters that produced by the earth to determine a magnetic variation of rock on subsurface. Simply processing data from the currently developing precision proton magnetometer is to obtain geomagnetic anomalies ($\Delta \boldsymbol{T}$) from observation data ($|\boldsymbol{T}|$) by correcting/reducing the influence of Earth's main magnetic field ($\boldsymbol{H}$) and its daily variations ($\boldsymbol{T_{vh}}$). If the regional field ($\boldsymbol{F}$) is the approach of Earth's main magnetic field and its daily variations, then the total field anomaly as shown (**Figure 1**) in the textbook (Blakely, 1995) as follows

$$\Delta T = |T| - |F| \quad (1)$$

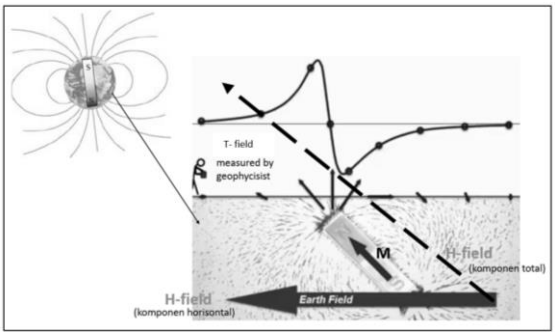

Figure 1: Illustration of Geomagnetic Acquisition on measurement point (Blakely, 1995).

Magnetic surveys can help to:

1. Identify or mapping near-surface volcanic rocks that are often of interest in geothermal exploration
2. Identify near-surface hydrothermal alteration, a magnetic anomaly cannot always be attributed to a single cause since positive magnetic anomalies can be caused by iron sulfides and iron-rich volcanic rock.
3. Ability to detect the depth at which the Curie temperature is reached.
4. Low Magnetic Intensity correlated with the main geothermal activity (Amarson, 2007)

PROCEEDINGS
JOINT CONVENTION BANDUNG (JCB) 2021
November 23rd – 25th 2021

5. The hydrothermal alteration process may alter these to non-magnetic minerals such as hematite, pyrite, leucoxene, or sphere (Browne, 1978), causing the reservoir intervals to become partially or totally demagnetized.

Result and Discussion

In this research, we used geomagnetic data from years "X" totaled 298 points of acquisition. Then, on 2020 (years "2020"), we used 2 (two) unit of magnetometer instrument version GSM 19T with sensor to obtain 130 data on same geomagnetic acquisition point as previous years (years "X"). Both of geomagnetic data then processed (Instrument, Declination/Inclination on each year, IGRF on each year, Varian, and RTP) to get Total Magnetic Anomaly and Susceptibility (Inversion).

2.1 Block-1 (Interest Zone)

Block-1 located on southwest research area, we compare 18 measurement point on years 2020 with years "X", on the chart (see in **Figure 2a**) we can see distribution point on 1-7 increased from previous measurement (years "X") and continue decreased on point 8-18. For example, decreasing magnetic susceptibility value from -381 to -859 on Block-1 point 16 and increasing magnetic susceptibility value from -83 to -1011 on Block-1 point 4, this is interest area because on this area we don't have a well site and manifestation point.

2.2 Block-2, Block-3, Block-4 (Reservoir Zone)

Block-2, Block-3, and Block-4 is located on central research area, on Block-2 we compare 16 measurement point on years 2020 with years "X", on the chart (see in **Figure 2b**) we can see all of distribution point extremely increased from previous measurement (years "X") from left to right area. For Example, increasing magnetic susceptibility value from 307 to 999 on Block-2 point 9, that value increased by effect side of production zone at the top of reservoir.

Block-3 we compare 20 measurement point on years 2020 with years "X", on the chart (see in **Figure 2c**) we can see all of distribution point extremely decreased from previous measurement (years "X") from left to right area. For Example, decreasing magnetic susceptibility value from 263 to -923 on Block-2 point 7, that value decreased by effect of production activity on reservoir zone that caused increasing temperature (based on well data).

Block-4 we compare 20 measurement point on years 2020 with years "X", on the chart (see in **Figure 2d**) we can see distribution point on 1-4 decreased from previous measurement (years "X") and continue increased on point on 5-18. For Example, decreasing magnetic susceptibility value from -221 to 407 on Block-4 point 7, that value increased by effect of production activity on reservoir zone that caused decreasing temperature (based on well data).

2.3 Block-5 and Block-6 (Manifestation Zone)

Block-2, Block-3, and Block-4 is located on central research area, on Block-2 we compare 16 measurement point on years 2020 with years "X", on the chart (see in **Figure 2e**) we can see all of distribution point extremely increased from previous measurement (years "X") from left to right area. For Example, increasing magnetic susceptibility value from 307 to 999 on Block-2 point 9, that value increased by effect side of production zone at the top of reservoir.

Block-6 we compare 35 measurement point on years 2020 with years "X", on the chart (see in **Figure 2f**) we can see all of distribution point increased from previous measurement (years "X"). For Example, increasing magnetic susceptibility value from -256 to -1029 on Block-6 point 24. This condition occurring by effect alteration material coming up to surface then interfere magnetized factor on manifestation area.

Table 1: Magnetic Susceptibility changes on several station interfere by temperature changes on reservoir

Block	Point	Years X	Years 2020	Status
Block-1	16	-381	-859	Decreased
Block-1	4	-83	-1011	Decreased
Block-2	9	307	999	Increased
Block-3	7	263	-923	Decreased
Block-4	7	-221	407	Increased
Block-5	3	-361	-729	Decreased
Block-5	12	-481	567	Increased
Block-6	24	-256	-1029	Decreased

After comparison between time-lapse geomagnetic data on six area or block, we choose several values per point which extremely increased/decreased from years "X" to years 2020 (see **Table 1**). Based on the data, we analyze the magnetic susceptibility controlled by effect of temperature changes, from the data references, temperature decreased from 240^{0}C to 220^{0}C on the production zone from years "X" to years 2020 (see Block-2, Block-3, and Block-4 to compare the

decreasing of magnetic data). First hypothesis we got from this research is magnetic susceptibility can be changed by temperature on the reservoir during production, but we need several years to know the difference of effect temperature against magnetic susceptibility changes (long term period). If this hypothesis solved, time-lapse geomagnetic data can be one of parameter to monitor temperature changes on geothermal reservoir and can be used to develop the prospect on geothermal area

Conclusions

In this research, we conclude:

1. Magnetic Susceptibility changes on reservoir is correlated with increasing of temperature on production activity, its show on central of the research area.
2. On the manifestation zone at Northeast research area, the alteration zone which have shown on the surface show a positive correlation with increasing value of Magnetic Susceptibility measure on surface.
3. In this research, we found the interest zone on Southwest research area which have the decreasing value but not have a production and injection well on there. We assumed that the value changed because controlled by fault or fracture that connected to reservoir on the central area, but this hypothesis must be validated with other method to answer this challenge.

References

Arnason, K., 2007, Short Course II on Surface Exploration for Geothermal Resources, **29**, SC-05.

Blakely, 1995, Cambridge University Press, p.439.

IGA Service GmbH Bochum University of Applied Science, 2014, Best Practice for Geothermal Exploration, 140.

Laily, W., Mawarni, Maryanto, S., Nadhir, A., 2018, Enivrontmental and Earth Science Research Journal, **5 (4)**, 87-93.

Soengkono, S. and Hochstein, M.P., 1995, Proceedings Twentieth Workshop on Geothermal Reservoir Engineering.

Soengkono, S., and Hochstein, M.P., 1996, Proceedings 18th NZ Geothermal Workshop, 243-248.

Utami, P., 2000, Proceedings World Geothermal Congress, 1921-1926.

Wenti, M., Maubana, Sukir, Maryanto, Utami, I.K., Nadir, A., 2019, International Journal of Renewable Energy Research, **9**, 2.

Yunus, D., Syamsu, R., Fikri, F., Faris, M.Y., Reza, M., 2017, E3S Web of Conference, **31**, 02003.

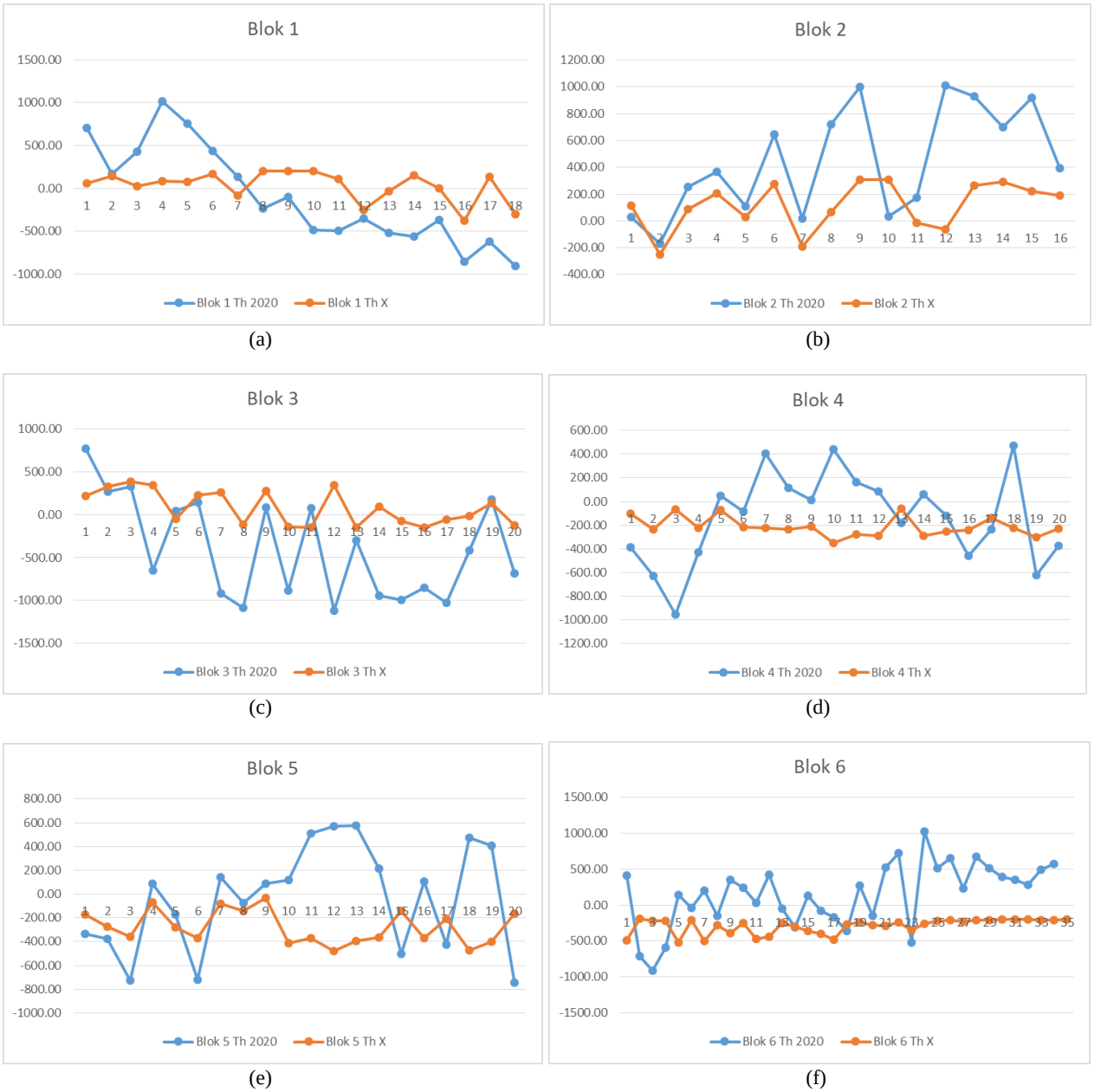

Figure 2: Magnetic Susceptibility Value for different years (effect of geothermal production), Blok 1 (a) located on Southwest, Blok 2 (b),3 (c),4 (d) located on Reservoir Zone, and Block 5 (e),6 (f) located on Manifestation Zone.

PROCEEDINGS
JOINT CONVENTION BANDUNG (JCB) 2021
November 23rd – 25th 2021

INTERPRETATION AND ANALYSIS OF POTENTIAL ALTERATION ZONES HYDROTHERMAL BASE REMOTE SENSING SYSTEM AND GEOGRAPHIC INFORMATION SYSTEM (GIS) IN RANCABALI AND SURROUNDING AREAS, BANDUNG REGENCY, WEST JAVA

Adang Saputra * dan Dadan Wildan *
* Bandung Energy and Mining Polytechnic, KESDM

Abstract

The interpretation and analysis of these hydrothermal alterations using remote sensing or remote sensing has been performed. Remote sensing is a method that is done to collect data or information without touching the object that we will examine. In this study the authors used Landsat 8 OLI/TIRS Satellite Imagery. Remote sensing is widely used for geothermal exploration because it has the advantage that it does not require large costs, it can also access to remote corners. The study aims to map hydrothermal alteration areas regionally in Rancabali Subdistrict and Surrounding Areas, Kab. Bandung, West Java. The study was conducted by processing several image band channels by having a pixel range that can represent hydrothermal alteration minerals in the study area. The methods used in the study were Composite Band and Band Density Slicing. The alteration minerals detected in the study area were yellow to orange using composite images of 4/2, 6/7, 5 and 10. From the results of the study obtained hydrothermal teralterasi rocks reached an area of about 277.24 Km2.

Keywords: Alteration mineral, Landsat, density slicing, hydrothermal, remote sensing

Introduction

The study is located in Rancabali Subdistrict and surrounding areas, Bandung Regency, West Java Province. Geologically, the derah has its own characteristics that make the author interested in studying the region. One of the characteristics of the area is the existence of geothermal minifestation, one of these manifestations found in the Area of Mount Patuha.

The leaves that are Tertiary-aged Volcanoes – Quaternary (M. Koemono kk, 1996). The geothermal potential of the study area is estimated by manifestations with the emergence of hot springs, fumaroles, and teralterasi rocks that occur in several locations.

There are three types of alterations that occur as a reaction between geothermal fluid and the rocks it passes, namely 1) Mineral turnover, 2) Space filling, and 3) Rock dissolution (Browne, 1998; Utami, 2015). With this process can be an important clue in mapping the potential of geothermal, especially those around the manifestation that indicate that there is an active geothermal system (Browne, 1970).

One initial method used in mapping for various needs is by remote sensing methods, especially for mineral exploration, this is done because remote sensing can provide a thorough initial picture of geomorphological conditions, geology, vegetation, and to know other conditions. The use of Imagery is one of the remote sensing methods that are often used, one of which is by utilizing Landsat 8 Operational Land Imager / Thermal Infrared Sensor (OLI / TIRS). Landsat 8 OLI / TIRS image, this image was launched in America, which has 11 kinds of channels (bands) with spatial resolutions ranging from 15 X 15 meters to 100 X 100 meters (United States Geological Survey, 2016).

Landscapeat image analysis is commonly used to determine the conditions on the earth's surface by looking at the reflectance and adsorbtion characteristics of electromagnetic waves from objects on the earth's surface (Sarbins, 1999). In this study, one of its applications used is to find out the existence of hydrothermal alterations that are regional scale.

Data and Methods

The data used in this study is Landsat 8 OLI / TIRS satellite imagery data and secondary data in the form of maps and publications related to geological conditions and mineral alterations in the study area. Software used for processing image data using Er-Mapper, while for complete map creation is used ArcGIS 10.8.

While the method used in this study is the Composite Method of Image and Density Slicing. Composite image is a new image that is from the merger of 3 channels that are able to display the advantages of its constituent channels (Sigit, 2011). This composite image is used given the limitations of the eye in distinguishing color gradations, for it is easier to understand by coloring. Density Slicing method is a method of retrieving a number of pixel values that represent minerals on the surface based on their reflections. Density Slicing is done by correcting the pixel value of the channel to be rationalized, so that the pixel value range becomes 0 - 255. The Threshold Value of each ratio is calculated using values from the pixel value range TH - 255 of each of those ratios (Zhifang et al, 2008).

Threshold Values = Mean + n. Standard Deviation

*n= 1 (confidence level : 92%
2 (confidence level : 95%)
3 (confidence level : 98%)

Results and Discussions

a. Interpretation of Geological Conditions, Geomorphology, and Vegetation

In RGB 432 composite image, where in the red band is filled with band 4 with a length of 0.636-0.636 μm, the green band is filled with a band of 3 wavelengths 0.533 –

0.590 µm, and the Blue band is filled with band 2 with a wavelength of 0.452 – 0.512 µm. By combining the three bands, we can see the condition of vegetation, geomorphology, and geology of the study area regionally. In addition, we can see some geological appearances, such as non-crystalline rocks or sedimentary rocks appear in smoother textures and crystalline rocks appear in rough textures. More details of the RGB 432 composition image map can be seen in Figure 1 below.

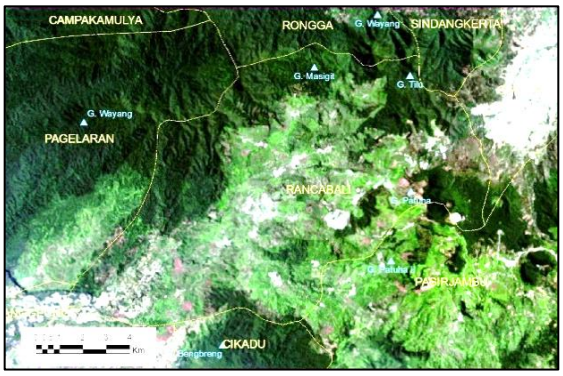

Figure 1. RGB 432 Composite Image that presents vegetation conditions, geomorphology, and geology of the study area

In RGB 567 composite image processing, it looks different from RGB 432 and can show more detailed geology. With the combination of these bands, we can see rocks with coarser and finer textures, where coarser textured rocks are scattered around the body of the volcano, while finer textures are scattered in areas with lower elevations. In addition, it can also observe several main lineages that affect the area with the main directions NW-SE and NE-SW. Vegetation is also seen with differences in plant density which can be seen from the difference in color from light brown to dark brown. In addition, the pattern of river flow, water bodies, residential areas are clearly visible in the image. More details on the image map resulting from the RGB 567 composition can be seen in Figure 2 below.

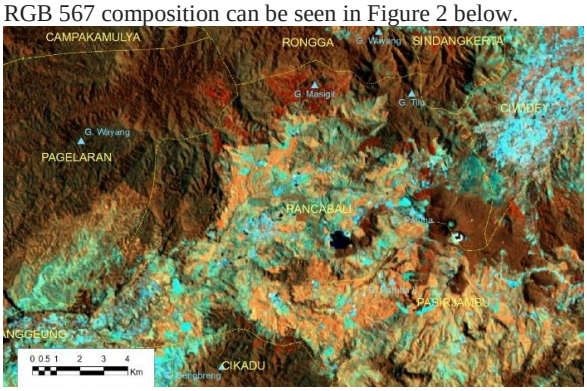

Figure 2. RGB 567 Composite Image showing the geological conditions of the study area

In the RGB image with composite bands 10-11-7, where bands 10 and 11 are infrared bands. Band 10 with a wavelength of 10.60 –11.19 m is placed in the red band, band 11 with a wavelength of 0 11.50 – 12.51 m is placed in the green band, and band 7 with a wavelength of 2.107 – 2.294 m is placed in the blue band. The combination of these bands provides information about rocks or the presence of silica-containing minerals in the study area, this is the effect of the strong reflectance of the wavelength of the image band (Pour and Hashim, 2014). Silica content is shown in the image with a bluish yellow color. The bluish color is more pronounced in the mountain top area, where the silica content is stronger. Concentrations of high silica content are in areas that show high geothermal manifestations, such as in the Patuha Crater, Ciwidey Crater, and Cibuni Crater. More details on the image map of the RGB 10-11-7 composition can be seen in Figure 3 below.

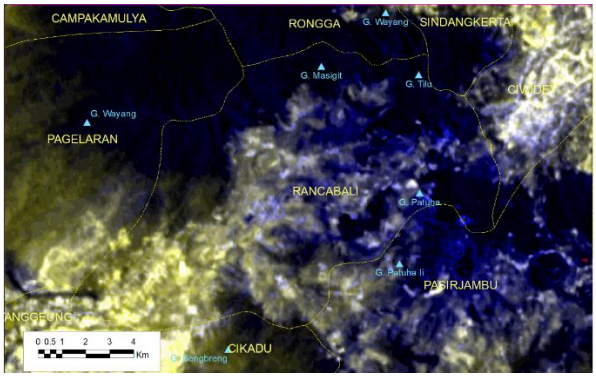

Figure 3. Composite Image RGB 10117 (Blue-yellow color) which shows the condition of Silica rocks or minerals with a bluish-yellow color

b. Appearance of Hydrothermal Alteration Distribution

To see the appearance of hydrothermal alteration, it can be done by combining several bands that have a high reflectance value, namely Band 4 with a wavelength of 0.636 – 0.673 m, band 2 with a wavelength of 0.452 – 0.512 m, band 5 with a wavelength of 0.851 – 0.879 m, band 6 with a wavelength of 1.566. – 1,651 m, band 7 wavelength 2.107 –2,294 m, and band 10 wavelength 10.60 – 11.19 m. These bands can be used to map hydrothermally altered minerals (Pour and Hashim, 2014). The mineral distribution mapping was carried out using the ratio method. In getting the appearance of a certain object, this ratio method is used, namely by dividing the value of the wavelength of a band with other bands. The method is carried out in several bands, namely in band 4 which is ratiod to band 2, band 6 is ratiod to band 7 to produce the value of the reflectance of hydrothermal alteration minerals in the study area.

The ratio of band 4 and band 2 (Figure 4) is recorded in yellow which provides information about the distribution of Ferrugination mineral (limonite) in the study area. Minerals are seen scattered in the area of obedient hydrothermal manifestation in the eastern part of the Rancabali area and its surroundings, the Masigit and Mount Tilu areas in the northern part of Rancabali and its surroundings, and the Gunung Wayang area in the northwest of Rancabali and its surroundings.

The ratio of band 6 and band 7 (Figure 5) is recorded in red which provides information about the distribution of clay and carbonate minerals in the study area. Minerals are seen scattered in the area of obedient hydrothermal manifestation in the eastern part of the Rancabali region and its surroundings, the Masigit and Mount Tilu areas in the northern part of Rancabali and its surroundings, and

PROCEEDINGS
JOINT CONVENTION BANDUNG (JCB) 2021
November 23rd – 25th 2021

the Gunung Wayang area in the northwest of Rancabali and its surroundings, and the southern part of Rancabali and its surroundings.

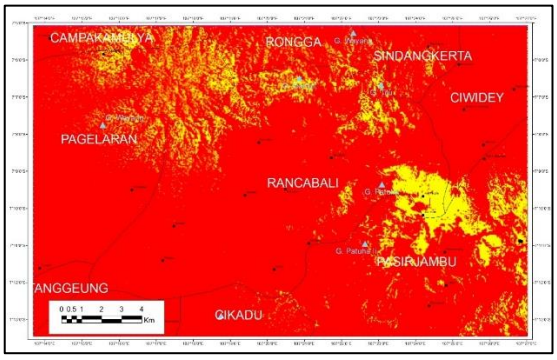

Figure 4. Composite image of 4/2 band ratio (Yellow) showing information on the distribution of Ferrugination (Limonite) in the study area

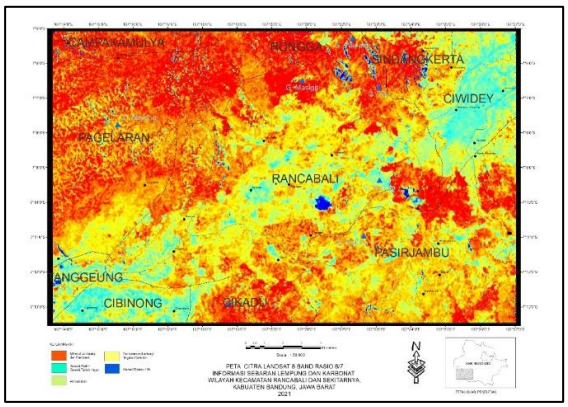

Figure 5. Composite image of 6/7 band ratio (Red Colors) showing information on the distribution of Clay Minerals and Carbonates in the study area

c. Showing Alteration Minerals

1). Displaying Minerals with the Composite Image Method

To see the distribution of hydrothermal alteration minerals in the study area, RGB image composites in bands 4/2, 6/7, 10 are used. The composite results show altered minerals with a cream color appearance (Pour and Hashim, 2014). The distribution of these alteration minerals is found scattered around Mount Patuha and its surroundings, especially the geothermal manifestation area

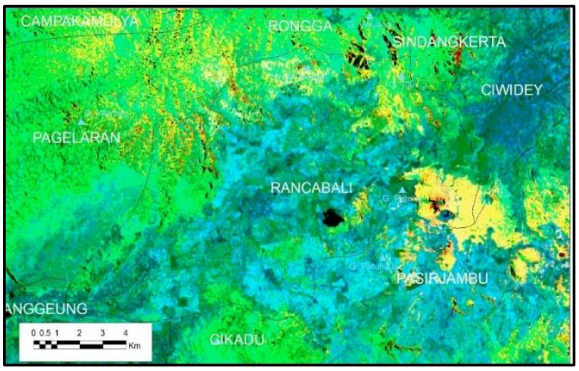

Figure 6. Composite image of RGB band ratio 4/2, 6/7, and 10 which provides main information about hydrothermal alteration minerals with cream color

2). Displaying Minerals with the Density Slicing Method

The Density Slicing method is a method of taking a number of pixel values that represent minerals on the surface based on their reflections. In this study, 4/2, 6/7, and 5/6 ratio images were used which showed the presence of oxide and hydroxide minerals from iron, clay minerals, and carbonate minerals as well as ferromagnetic minerals (Pour and Hashim, 2014). Figure 7 below shows a Ferromagnesian map recorded on a 5/6 band ratio composite image.

- Mineral Ferrugination (Iron Oxides and Hydroxides)

With a combination of 4/2 band ratio in the pixel range of 61.6185 – 255, we can map the distribution of Ferrugination alteration minerals as shown in Figure 4. The distribution of ferrugination group minerals is in mountain areas and geothermal manifestation areas in the Patuha area. In some locations there was a record of identifying this mineral as being caused by the start, where the cloud was also identified as a mineral as well.

- Ferromagnesian Minerals

One of the hydrothermal alteration mineral groups is Ferromagnesian Minerals, minerals can be seen by doing density slicing at a band ratio of 5/6 (Figure 7) with a pixel value range of 64,821 – 255. The distribution of minerals in this group is also concentrated in mountainous areas and craters in the manifestation area. geothermal energy, there is no difference in alteration results between primary and secondary Ferromagnesian minerals.

- Clay Minerals and Carbonates

Density slicing in band ratio 6/7 with pixel range from 62,415–255 (Figure 5), mapped alteration minerals of clay and carbonate groups. The distribution of this mineral is seen spreading in mountainous and hilly areas, as well as in geothermal manifestation areas in the Patuha Mountain Area.

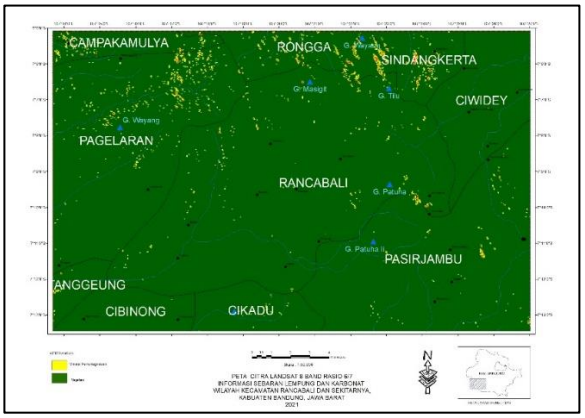

Figure 7. Composite image of 5/6 band ratio (Yellow) showing information on the distribution of Ferromagnesian minerals recorded in yellow in the study area

Conclusion

The interpretation and analysis of Landsar 8 OLI/TIRS imagery is an initial mapping to determine the distribution of hydrothermal alteration minerals. in exploring geothermal potential, minerals, or others.

The process with a combination of several bands that have a pixel range can represent hydrothermal alteration minerals in the study area. The mineral atletion is recorded in different colors. The composite image with a band ratio of 4/2 displays a yellow color which indicates the distribution of Mineral Ferrugination (Iron Oxides and Hydroxides).

The composite image with a band ratio of 5/6 also displays a yellow color which indicates the distribution of ferromagnesian minerals. The composite image with a band ratio of 6/7 displays a pink to dark red color which indicates the distribution of clay minerals and carbonates. Meanwhile, the composite image with the RGB 10117 band displays a bluish yellow color which indicates the distribution of silica minerals.

For future use, the initial mapping using Landsat 8 OLI/TIRS images to determine the distribution of hydrothermal alteration minerals can be used for geothermal potential exploration, mineral exploration, and others. However, it is necessary to consider in choosing an image, which should be avoided for the image of a location with a lot of clouds, vegetation, and the selection of an attractive area for the study location.

Reference

Abubakar, A. J., Hashim, M., Pour, A. B., _, *Using Landsat 8 (OLI) Remote Sensing Data To Map Lithology And Mineralogy For Geothermal Resource Exploration,* Malaysia, Universiti Teknologi Malaysia.

Browne, P. R. L., 1970, *Hydrothermal Minerals as an Aid in Investigating Geothermal Field.Journal of Geothermics*, 2 (1), pp 564 – 570.

Browne, P. R. L., 1998, *Hydrothermal Alteration*, Geothermal Institute, The University of Auckland.

Browne, P. R. L. (1970). Hydrothermal Minerals as an Aid in Investigating Geothermal Field. *Journal of Geothermics*, 2(1), 564-570.

Browne, P. R. L. (1998). *Hydrothermal Alteration.* Geothermal Institute: The University of Auckland.

Cahyati. (2018). Alterasi Hidrothermal Dan Tempreratur Bawah Permukaan Sumur X Lapangan Panasbumi Patuha. *Padjadjaran Geoscience Journal*, 2(6), 514-515.

Fossen, H. (2010). *Structural Geology*. Cambridge University Press.

Gupta, R. P. (2018). *Remote Sensing Geology 3 ed*. Berlin Heidelberg: Springer Varlage.

Hochstein, M. P., & Sudarman, S. (2008). History of geothermal exploration inIndonesia from 1970 to 2000. *Geothermics*, 37(3), 220–266.

Dharmawan, I. P., Firdaus, R. A, Harijokao, **N. A. (2017).** Aplikasi Landsat 8 Oli/Tirs dalam mengidentifikasi Alterasi Hidrotermal Skala Regional : Studi Kasus Daerah Rejang Lebong Dan Sekitarnya, Provinsi Bengkulu, *Proceeding*, Seminar Nasional Kebumian Ke-10.

Iqbal, M., & Juliarka, B. R. (2019). Analisis Kerapatan Kelurusan (Lineament Density) Sebagai Indikator Tingkat Permeabilitas di Lapangan Panasbumi Suoh-Sekincau, Lampung. *Jurnal of Science and Applicative Tecnology*, 3(2), 61-67.

Koesmono, M., Kusnamma, Suwarna, N. (1996). Peta Geologi Lembang Sindang Barang dan Bandarwaru Skala 1 : 250.000, Jawa Barat. Pusat Penelitian dan Pengembangan Geologi.

Nurrochman, Arsy., Febriani, R., Yuliatama, V. P. (2020). Aplikasi Citra *Landsat* 8 OLI/TIRS Dalam Mengidentifikasi Alterasi Hidrotermal Skala Regional; Studi Kasus Kecamatan Suoh dan Bandar Negeri Suoh. J*urnal Geosains dan Remote Sensing (JGRS) Vol 1 No 2 (2020) 89-96.*

Pratama, Y, A., Rifaldy, Mutika, A. (2021). Identifikasi Alterasi Hidrotermal Menggunakan Citra Landsat 8 OLI/TIRS: Studi Kasus Gunung Patuha, Kabupaten Bandung, Jawa Barat. *Bulletin Of Geology, Vol. 5, No. 1*, ITB.

PSDMBP. (2017). *Potensi Panas Bumi Indonesia*. Jakarta: Direktorat Panas Bumi, Direktorat Jenderal Energi Baru, Terbarukan dan Konservasi Energi, Kementerian Energi dan Sumber Daya Mineral.

Putra, I. D., Nasution, R. A. F., & Harijoko, A. (2017). Aplikasi *Landsat* 8 OLI/TIRS dalam Mengidentifikasi Alterasi Hidrotermal Skala Regional: Studi Kasus Daerah Rejang Lebong dan Sekitarnya, Provinsi Bengkulu. *Proceeding Seminar Nasional Kebumian ke- 10, Yogyakarta.*

Rahayu, R., & Candra, D. S. (2014). Koreksi Radiometrik Citra *Landsat*-8 Kanal Multispektral Menggunakan Top of Atmosphere (ToA) Untuk Mendukung Klasifikasi Penutup Lahan. *Prosiding Seminar Nasional Penginderaan Jauh*, LAPAN 762– 768.

Sabins, F. F. (1999). Remote Sensing for Mineral Exploration. *Ore Geology Reviews*. 14, 157-183.

Utami, P. (2011). Hydrothermal Alteration and the Evolution of the Lahendong Geothermal System, North Sulawesi, Indonesia. *Thesis*, The University of Auckland.

PROCEEDINGS
JOINT CONVENTION BANDUNG (JCB) 2021
November 23rd – 25th 2021

Coal macrolithotype identification using Principal Component Analysis (PCA), case study of South Sumatra Basin

Nurdrajat, Syaiful Alam, Budi Muljana, Reza Mohammad Ganjar Gani, Yusi Firmansyah
Affiliation: Laboratory of Stratigraphy, Faculty of Geological Engineering, Padjadjaran University
Corresponding author: nurdrajat@unpad.ac.id

Abstract
The permeability and physical properties of the coal are responsible for the key elements of fracturing and reservoir characterization in coal bed methane (CBM) production. This study examines the reliability of Principle Component Analysis (PCA) in recognizing coal macrolithotypes in the South Sumatera Basin. We used PCA as a method as a function of dimensional reduction and two well logs data. Dimensional reduction of 64%-72% indicates that the original variables are still represented. The swarmplot shows that there are at least two cluster values of PCA that correspond to the coal markers of the basin, which are Suban, Mangus, and/or Petai, according to the result of the analysis.

Keywords: South Sumatra Basin, Coalbed Methane, Principal Component Analysis, Macrolithotypes

Introduction

CBM resources in Indonesia are estimated to be 453 trillion cubic feet (TCF) and are scattered across 11 basins, with the South Sumatera Basin having the highest potential of 183 TCF of CBM resources (Fintaru et al., 2018; Irawan et al., 2017; Sumarno & Bergmann, 2017). The South Sumatera Basin has a coal-bearing structure called Muara Enim Formation. The presence of coal seams had a significant influence on the mapping of oil- and gas-field structures. Based on regional stratigraphy and paleontological data, the age of the Muaraenim Formation is Miocene to Pliocene (Bahtiar & Ningrum, 2012).

The coal as a source of methane gas in the South Sumatera Basin mainly comes from the Muara Enim Formation. As a coal-bearing formation, the Muara Enim Formation has been widely studied in various research topics, including for CBM development in Indonesia (Daulay et al., 2000; Nas & Pujobroto, 2000; Nurdrajat et al., 2018; Susilawati & Ward, 2006). A total of three coal seams, notably Suban, Mangus, and Petai, are deemed economically viable. Among lignite and subbituminous (Ro<0.5%), the coalbed's rank varies. The maceral composition is predominantly huminite, which favors CBM development because of its storage capacity with the assumed its capacity of the coal bed correlated with coal rank (Hermiyanto & Setiawan, 2010; Sosrowidjojo, 2013).

Coal seam permeability as a key parameter for CBM production is largely determined by the macrolithotype of coal which includes bright coal, semi bright coal, semi dull coal, and dull coal. Coal macrolithotype drastically affects the physical characteristics of the main reservoir such as fracture distribution, rock mechanical properties, and gas-carrying properties (Clarkson & Bustin, 1996; Tao et al., 2019; Zhao et al., 2016).

To assess reservoir lithology, geologists in the energy business frequently employ higher-dimensional data from well logs, e.g. gamma-ray, density, resistivity, neutron-porosity, caliper, sonic, spontaneous potential, and coal is no exception. If only one dimension is employed, determining lithology from subsurface data, such as well log, is impossible. To differentiate coal from non-coal lithology in a particular setting, such as a coal-field, mining operators use lower-dimensional data, which includes only a few of them: gamma-ray, density, and resistivity.

As an example, in sequence stratigraphy analysis, which is widely used in oil and gas exploration, it makes use of gamma-ray, resistivity, density, and sonic measurements to define sequence boundaries, among other techniques (Adebayo, 2014; Alam & Setiadi, 2019; Omigie & Alaminiokuma, 2020). Similar to petrophysical analysis, a variety of well log characteristics are utilized to evaluate mineral content, porosity, and lithology, depending on the aim of the investigation. The use of multivariate analysis is essential in these types of analytical situations. The Principal Component Analysis (PCA) is one sort of analysis.

We can examine the inter-relationships of many different parameters or variables all at once using multivariate analysis. Using this approaches is particularly advantageous, as the enable us to change numerous parameters and identify key relationships (Abdi et al., 2013; Jolliffe & Cadima, 2016). Most of the issues in geology include extremely complicated and inseparable forces or parameters which cannot be studied separately. Sometimes, making a meaningful conclusion about which variable is most valuable of a group of possible outcome is impossible. When working upon it, it is often better to try to explore all aspects of the situation and identify the big components.

On the basis of the foregoing explaining of the problem, we apply the PCA technique as an alternative for the determination of the coal macrolithotype in the subsurface, which is carried out using borehole well log data. We validate the Log PCA with coal density to evaluate the robustness of this approach. By selecting input data with parameters sensitive to variations in coal lithology, we hypothesize a number of frequencies in the transformed log that correspond to the coal zone as revealed on the swarmplot with at least two clusters indicated which spread throughout the distribution of PCA values. Thus, this workflow is expected to be able determine coal markers in the South Sumatera Basin.

Data and Method

In order to put the approach to the test, we selected two well log data sets that were dispersed across the South Sumatera Basin, respectively well A and well B. The Muaraenim Formation was penetrated by both wells. Not all dimensions in the well log data are used: rather, only a few dimensions that are sensitive to the presence of coal are taken into consideration. All the processing algorithm was run in Python 3.0 Jupyter Notebook and QGIS.

Well log data has a large number of parameters, which is why its referred as high dimension data in this study, but it is possible to optimize their utilization depending on the

goal. As a result, prior to implementing the PCA approach, it is required to construct assumptions beyond limitation. It has been widely known that density log is the most sensitive metric in coal lithology because lightweight coal varies between 1.1 up to 1.5 gr/cc. Among the other metrics that we assume seem to be sensitive to the presence of coal are gamma-ray (GR), resistivity (LLD), density (RHOB), and sonic (DT), and take data uniformity into account.

Mainly employed in signal processing and machine learning, Principal Component Analysis is a statistical approach. Multivariate statistical approaches like PCA can uncover hidden data properties. A regression model's linearity is assumed in PCA. This approach is also used to extract high-dimensional features from data. Data are subspaced by PCA. It can be used to reduce dimensions of data without compromising its quality.

The eigenvectors of a variance-covariance matrix or a correlation matrix are used in PCA, they can provide important insight into the matrix's structure on their own and are generally evaluated in the same way that factors are (Davis, 2002). Scale affects PCA since the input data is made of GR, LLD, RHOB, and DT units. They must be standardized before applying the PCA method to achieve the best performance. The standardization of each parameter used is needed to remove the unit effect, with the following equation:

$$\bar{Z} = \frac{x-\mu}{\sigma} \text{ .....(1)}$$

This unit effect will affect covariance matrix. Covariance matrix serve as an input to get eigenvectors and eigenvalues. Eigenvalue states how much variation of a variable PC as a new log transformed. Eigenvalue can be obtained with covariance matrix $M$and λ is eigenvalue as a determinant equation:

$$|M - \lambda I| = 0 \text{ .....(2)}$$

And the following equation is to obtain eigenvector v:

$$Mv = \lambda v \text{ .....(3)}$$

The eigenvector is used as a weighting matrix W, which results in data that has smaller dimensions later on in the process. When it comes to data dimensional reduction, PCA's role as a data dimensional reduction function comes into play. The covariance matrix, as well as the eigenvectors and eigenvalues of the two wells, are shown in the following matrix tables:

Table 1. Covariance Matrix of Well A

GR	LLD	RHOB	DT
1.000338	-0.688528	0.657070	-0.181640
-0.688528	1.000338	-0.669308	0.254632
0.657070	-0.669308	1.000338	-0.580286
-0.181640	0.254632	-0.580286	1.000338

Table 2. Covariance Matrix of Well B

GR	LLD	RHOB	DT
1.000449	-0.809686	0.890840	-0.414556
-0.809686	1.000449	-0.745232	0.293003
0.890840	-0.745232	1.000449	-0.529717
-0.414556	0.293003	-0.529717	1.000449

Table 3. Eigenvectors and eigenvalues of Well A

```
Eigenvectors of Well A
[[ 0.51385027 -0.42499681  0.63537009 -0.3894104 ]
 [-0.52852861  0.32212281  0.76130137  0.19316994]
 [ 0.57335861  0.15970925  0.12922852  0.79312852]
 [-0.35759656 -0.83072713 -0.00500614  0.42660529]]

Eigenvalues of Well A
[2.5681044  0.92023658 0.31041559 0.20259387]
```

Table 4. Eigenvectors and eigenvalues of Well B

```
Eigenvectors of Well B
[[ 0.55383445 -0.20489023 -0.73267316 -0.33834515]
 [-0.50810047  0.38984535 -0.14478861 -0.75424848]
 [ 0.55669691 -0.01092335  0.65798589 -0.50697515]
 [-0.35382181 -0.89773118  0.09633729 -0.24414745]]

Eigenvalues of Well B
[2.90356037 0.77215092 0.09492139 0.23116507]
```

The eigenvectors and eigenvalues for each data in well A and B have been calculated in the tables above. To reduce the dimension of the data, eigenvectors were chosen. In the following tables, the contribution of the lambda or eigenvalue shows the percentage of the number of dimension reductions:

Table 5. Persentase or variance of lambda of Well A

```
Variance obtained by each lambda is
 [64.18094195295714, 22.9981500362885, 7.757770666381143, 5.063137344373208]
----------------------------------------
```

Table 6. Persentase or variance of lambda of Well B

```
Variance obtained by each lambda is
 [72.55639970843596, 19.295101042182086, 5.776530644329196, 2.371968605052762]
----------------------------------------
```

To summarize, each Principle Component number indicates the overall variance, with the percentage unit indicating the degree of dimensional reduction. For instance, the PCA logs already reflect 64.18% of the entire original data when using a lambda 1 of 2.568 in Well A. If we utilize lambda 2 of 0.772 in Well B, the PCA log's degree of representation to original data is 19.29%. The linearity combination model's lambda selection is subjective in that sense. The log PCA equation derived is:

$$PCA_A = 0.513 * \bar{Z}_{GR} - 0.424 * \bar{Z}_{LLD} + 0.635 * \bar{Z}_{RHOB} - 0.389 * \bar{Z}_{DT} \text{ .....(4)}$$

$$PCA_B = 0.556 * \bar{Z}_{GR} - 0.010 * \bar{Z}_{LLD} + 0.657 * \bar{Z}_{RHOB} - 0.506 * \bar{Z}_{DT} \text{ .....(5)}$$

Result and Discussion

The following section presents the results of applying the PCA approach to well log data and its provisional confirmation of coal density. The application of the PCA approach to the well log data in this case study leads in the production of two new logs, labeled as Log PCA Well A (Figure 2) and Log PCA Well B (Figure 3).

On the Log PCA Well A curve, the spike deflection is almost identical to that of Log GR and RHOB. When compared to the other logs, Log DT in Well A bears no resemblance to Log PCA in Well A as a whole; yet, the spike deflection in Log PCA is parallel to the spike deflection in Log DT. As a result of the dimension reduction, the Log PCA was able to capture 64.18% (Table 5) of the similarity between the data from the four parameters (GR, LLD, RHOB, and DT). At least, two coal

clusters at depths 4400-4200 m and 3800-3400 m are visible in the Log PCA Well A, as is one spike that also correlates with the existence of coal at depths greater than 4600 m.

The spike deflection on the log curve is more represented in Log PCA Well B than in Log PCA Well A. This can be observed in the percentage expression of the overall summary of parameters employed, which is 72.55% (Table 6), indicating that Log PCA Well B has less dimension reductions than Log PCA Well A. In Log PCA Well B, three clusters of values are more clearly apparent, each likely aligned with the coal markers Suban, Mangus, and Petai. The first coal cluster is located at a depth of 550-650 m, the second at 400-450 m, and the third at 300-350 m.

What makes Log PCA significant is that the presence of a deflection on the curve correlates with a deflection of the curve at low density values, which corresponds to the range of coal density. Future work could validate Log PCA using core data and other coal maceral, taking into account that the PCA technique is also sensitive to the number of input parameters involved. Thus, the Log PCA is projected to be able to more precisely map the coal macrolithotype in order to predict coal in subsurface well log data. This accomplishes the purpose of characterizing the coal reservoir. Fracturing for the CBM field is also influenced by the properties of the coal macrolithotype reservoir, which may be better mapped using PCA and validation of multiple other data sets.

Conclusions

Geologists routinely evaluate the presence of coal using a number of well log data. Frequently, these established approaches are neither representative nor adequate. PCA method creates a new log named Log PCA from the parameters log of GR, RHOB, LLD, and DT. The Log PCA is then used to reduce and transformed the dimensions of data, from a large number of variables to a small number of variables. Dimensional reduction appears to be effective using the PCA, which captures part of the information originally contained in the original variables of well log data. It has been confirmed that the degree of summarization only 64.18% up to 72.55%. Coal ranges are likewise linear in their presence when a deflection curve is included in the Log PCA.

Acknowledgements

We thank to all staff at Laboratory of Stratigraphy, Faculty of Geological Engineering, Padjadjaran University for a great work. The authors do not have any conflict of interest.

References

Abdi, H., Williams, L. J., & Valentin, D. (2013). Multiple factor analysis: principal component analysis for multitable and multiblock data sets. *WIREs Comput. Stat.*

Adebayo, O. F. (2014). Well log sequence stratigraphic and palynological analysis of late Miocene to Pliocene Agbada Formation, Southwestern Niger Delta Basin, Nigeria. *Review of Environment and Earth Science*, *1*(2), 77–98.

Alam, S., & Setiadi, D. J. (2019). Tertiary sequence stratigraphy of Bird Head Area, Eastern Indonesia. *Indonesian Journal on Geoscience2*, *6*(3), 267–278. https://doi.org/DOI: 10.17014/ijog.6.3.267-278

Bahtiar, A., & Ningrum, N. S. (2012). Petrographic Characteristics and Depositional Environment of Coal Seams D (Merapi) and E (Keladi), Muara Enim Formation, South Sumatera Basin. *Indonesian Mining Journal*, *15*(1), 1–13.

Clarkson, C. R., & Bustin, R. M. (1996). Variation in micropore capacity and size distribution with composition in bituminous coal of the Western Canadian Sedimentary Basin. *Fuel*, *75*, 1483–1498.

Daulay, B., Ningrum, N. S., & Cook, A. C. (2000). Coalification of Indonesian coal. *Proceedings of Southeast Coal Geology*, 85–92.

Davis, J. C. (2002). *Statistics and Data Analysis in Geology*. John Wiley & Sons, Inc.

Fintaru, V., Rahmad, B., Setiawan, J., Dewa, A. A., & Ibrahim, M. A. (2018). Macrolithotype and gas content of shallow low-rank coal of Muaraenim Formation at Musi Banyuasin, South Sumatera Basin. *IOP Conference Series: Earth and Environmental Science*.

Hermiyanto, M. H., & Setiawan, R. (2010). Coalbed Methane Potential and Coal Characteristics in Muara Lakitan Area, South Sumatra. *Jurnal Sumber Daya Geologi*, *20*(3), 147–157.

Irawan, C., Nurcahyanto, D., Azmy, I. F., Paju, A., & Ernata, W. M. (2017). Review of Coal Bed Methane Prospect in Indonesia. *Society of Petroleum Engineers*.

Jolliffe, I. T., & Cadima, J. (2016). Principal component analysis:a review and recent developments. *Philosophical Transactions*, 1–16.

Nas, C., & Pujobroto, A. (2000). Vitrinite macerals in Indonesian coal. *Proceedings of Southeast Coal*, 215–226.

Nurdrajat, Sunardi, E., & Arus, E. (2018). Karakteristik Batubara Regresi dan Transgresi Formasi Muara Enim, Cekungan Sumatra Selatan. *Bulletin of Scientific Contribution, Universitas Padjadjaran*, *16*(3), 221–228.

Omigie, J. I., & Alaminiokuma, G. I. (2020). Well log sequence stratigraphic analysis for reservoir delineation and hydrocarbon distribution in the eastern part of the central swamp depobelt, Niger Delta. *Journal of Earth Sciences and Geotechnical Engineering*, *10*(5), 1–14.

Sosrowidjojo, I. B. (2013). Coal Geochemistry of the Unconventional Muaraenim Coalbed Reservoir, South Sumatera Basin: A Case Study from the Rambutan Field. *Indonesian Mining Journal*, *16*(2), 71–81.

Sumarno, T. B., & Bergmann, A. (2017). Coal Bed Methane (CBM) in Indonesia: A comparative analysis of Net Production Sharing Contract (PSC) and Non-Cost Recovery Gross PSC Sliding Scale. *East Meets West SPE Congress*.

Susilawati, R., & Ward, C. R. (2006). Metamorphism of mineral matter in coal from the Bukit Asam deposit, South Sumatera. *International Journal of Coal Geology*, *68*, 171–195.

Tao, S., Pan, Z. J., Chen, S. D., & Tang, S. L. (2019). Coal seam porosity and fracture heterogeneity of macrolithotype in the Fanzhuang Block, southern Qinshui Basin, China. *J. Nat. Gas Sci. Eng.*, *66*, 148–158.

Zhao, J. L., Xu, H., Tang, D. Z., Mathews, J. P., Li, S., & Tao, S. (2016). Coal seam porosity and fracture

heterogeneity of macrolithotype in the Hancheng Block, eastern margin, Ordos Basin, China. *Int. J. Coal Geol.*, *159*, 18–29.

PROCEEDINGS
JOINT CONVENTION BANDUNG (JCB) 2021
November 23rd – 25th 2021

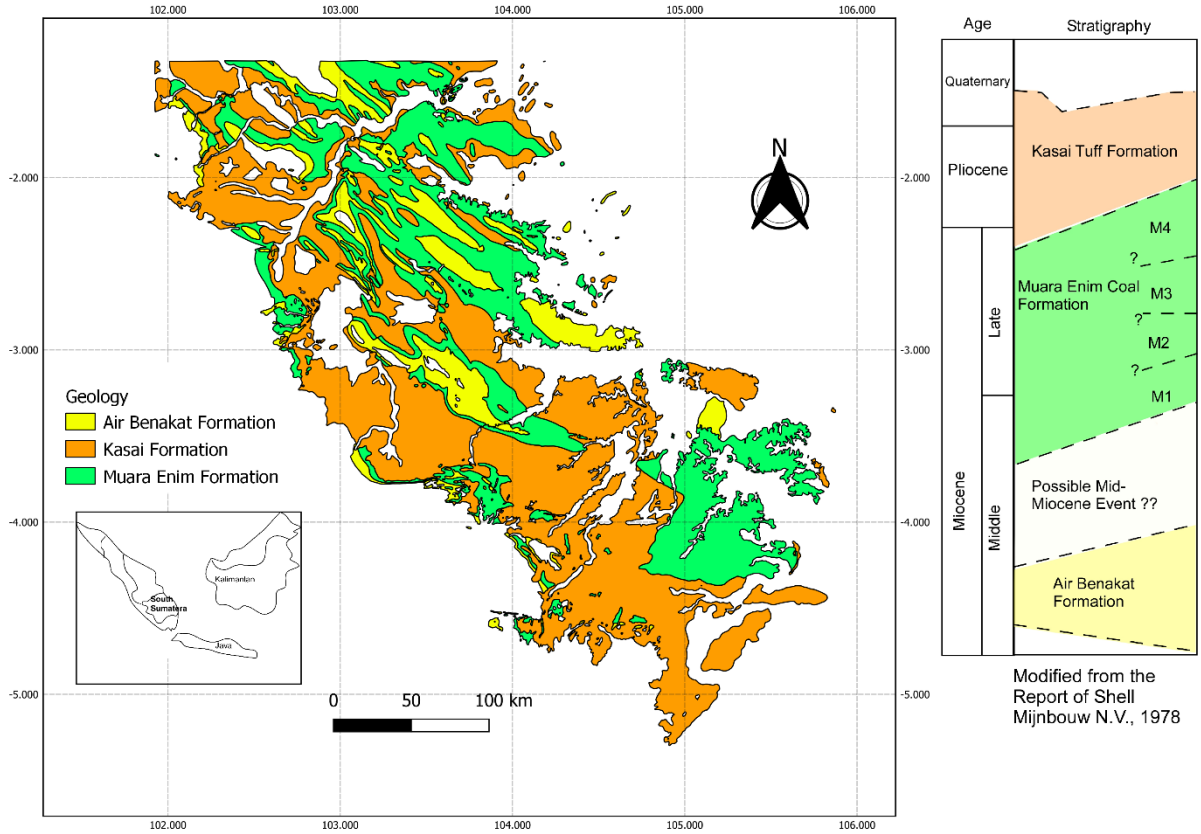

Figure 1. Geology and Stratigraphy of Muaraenim Formation, South Sumatera Basin

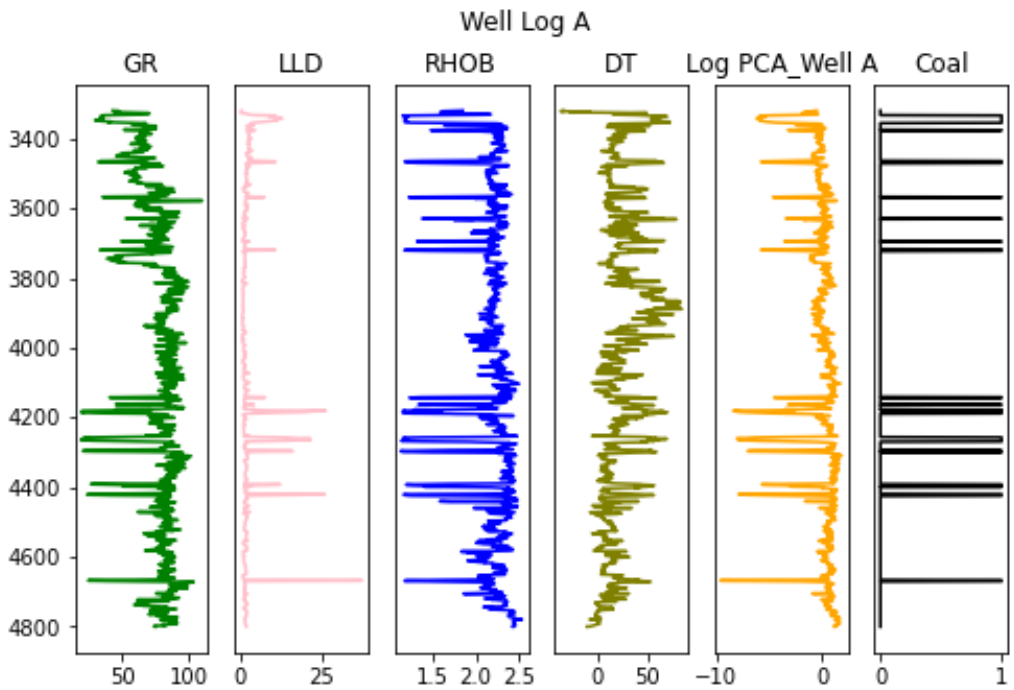

Figure 2. Log PCA of Well A

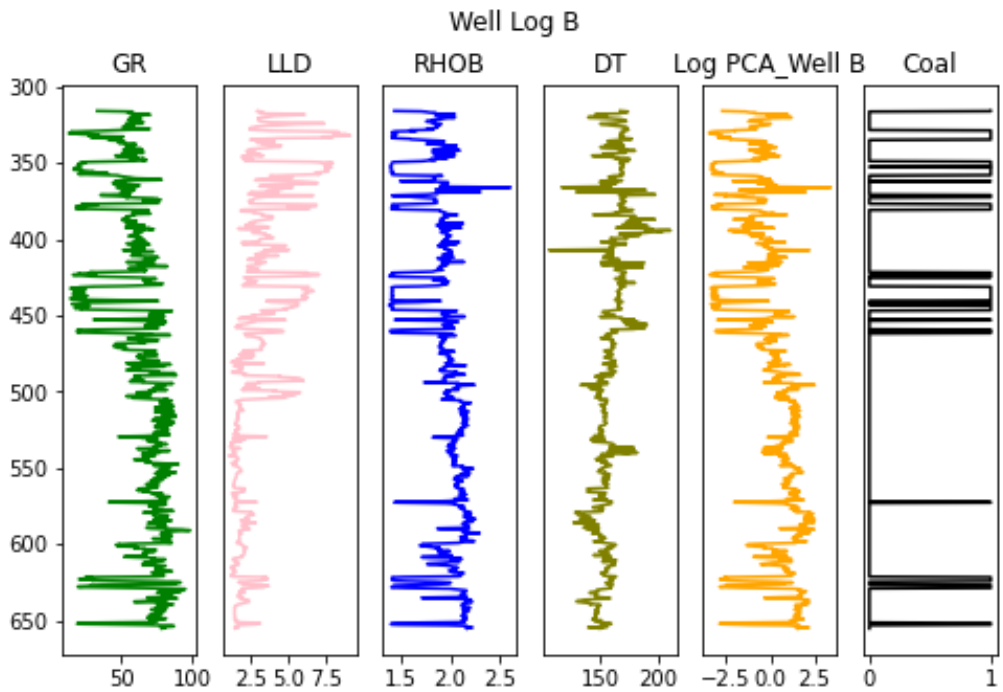

Figure 3. Log PCA of Well B

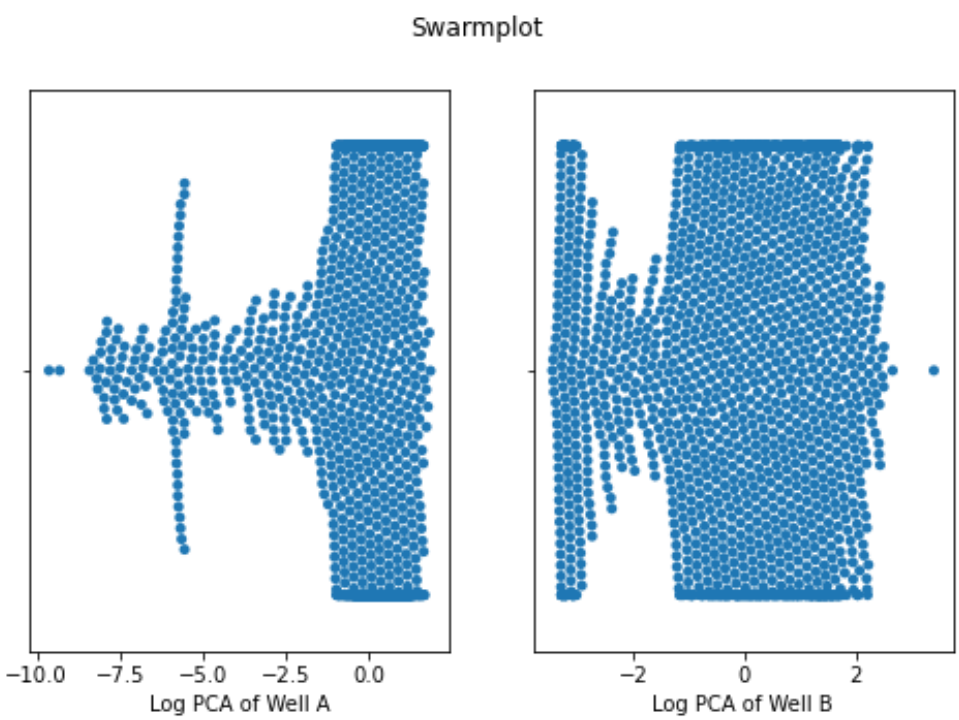

Figure 4. Swarmplot of Log PCA indicating two clusters

PROCEEDINGS
JOINT CONVENTION BANDUNG (JCB) 2021
November 23rd – 25th 2021

Ground Penetrating Radar for Nickel Laterite Exploration: A Case Study in Pakal Island, Indonesia

Muhammad Arief Wicaksono[1], Mordekhai[2], Wahyudi Parnadi[3], Muhammad Chandra R.M.[1]
[1]PT Antam Tbk (Persero), Jl. T.B Simatupang No.1 (12530), Jakarta Selatan, DKI Jakarta
[2] Geovartha Research Group, Jl. Dr Nurdin 1 No.21 (11450), Jakarta Barat, DKI Jakarta
[3]Fakultas Teknik Pertambangan dan Perminyakan, Institut Teknologi Bandung, Jl. Ganesa no. 10, Kota Bandung (40132), Jawa Barat

Abstract
With the increasing demand of batteries for electrical vehicle in world, the interest of nickel laterite exploration and then its exploitation grow significantly. Nickel ore is one of the raw materials for making these batteries, which has high economic values, and is widely found in Indonesia. Therefore, extensive nickel exploration in Indonesia is urgently required to obtain the estimation of its potential resources. Until now, data from boreholes in close proximity to each other are used to calculate Nickel ore resources. To reduce the number of used boreholes and therefore reducing operational costs, Ground-Penetrating Radar (GPR) is suitable method for that purpose due to its cost -and time effectiveness. In this research we analysis two GPR profiles acquired with GSSI SIR-3000 system with unshielded 40 MHz antennas from GPR campaign in Pakal Island. After applying conventional processing steps such as time zero correction, dewow, bandpass filtering f-k filtering, and background removal, radar attributes are assigned. From preliminary results using instantaneous frequency and its comparison with borehole data as validation tool, we obtained interesting results about the boundaries of limonite, saprolite, and bedrocks. The next step will be frequency content clustering in each layer boundary with the aim of clarifying layer boundaries.

Keywords: Nickel laterite; Ground-Penetrating Radar; GSSI SIR-3000; instantaneous frequency; limonite; saprolite

Introduction

Recently, nickel exploration, one of the raw materials for batteries, has been increased in Indonesia as the world demands more batteries for electric vehicles and other electrical instruments. Indonesia is one of the top-rank countries which possess an abundant amount of lateritic nickel resources. Hence, the development of technologies in nickel exploration keeps growing to give efficient exploration costs.

In general lateritic nickel is one of the nickel types that deposited through a long weathering process. The weathering process brings the nickel minerals down and accumulates them into a specific layer called the laterite zone. Several geophysical methods have been utilized throughout the years to scan the subsurface and help to predict the thickness of this potential laterite zone. One of the geophysical methods which can support nickel exploration is the ground-penetrating radar (georadar) method.

The georadar systems deploy transmitting electromagnetic waves and recording its reflected signals to detect electromagnetic property contrast of subsurface.

This research focuses on one of the old georadar data in Pakal Island. Processing steps using several filtering algorithms are applied to clarify the layer boundaries of the laterite zone, including data interpretation on the frequency domain using the Fast-Fourier Transform.

Regional Geology

The research takes place in Pakal Island, East-Northeast Halmahera, North Maluku, Indonesia. Lithologically, East Halmahera consists of ultrabasic rock, which is widely spread all over the island. Pakal is an island that has the morphology of hills with elevation variety until 250 MSL. Stratigraphically the research area is dominated by ultramafic rocks consisting of peridotite and dunite. Dunite rock has a green-yellowish color with fine to very-fine-sized grain, while peridotite has dark grey color. In this rock, gabbro and basaltic fractures occur commonly. The mineralization in the ultrabasic rock produces serpentinite and garnierite.

The general base rocks of the nickel mineral in the area are dunite and harzburgite. They experienced an intense weathering process, indicated by the presence of garnierite and chrysoprase. This presence is due to a high degree of lateritisation.

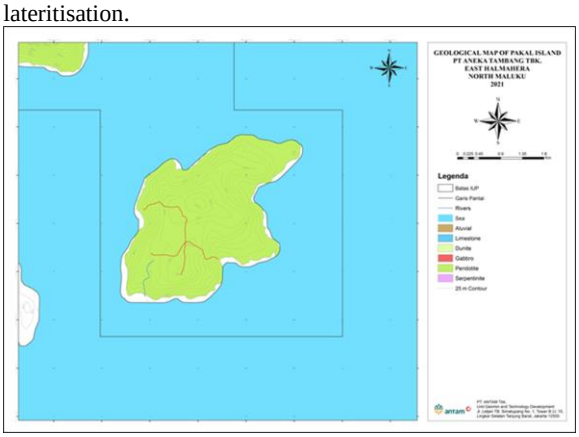

Figure 1: Geological map of Pakal Island

Nickel Laterite of Pakal Island

In general, there are two types of nickel deposits: primary and secondary nickel deposits. The commonly found nickel deposit type in Indonesia is the secondary nickel or nickel laterite. Nickel laterite is a result of a chemical weathering process on an ultramafic rock. The lateritisation process takes millions of years to complete a nickel residue, which is affected by a weathering rate, geological structure, climate, topography, chemical reagents, and surrounding vegetation (Sukaesih, 2015).

The laterite deposit profile of Pakal Island comprises four domains based on the physical appearance and its chemical content, such as

1. Top Soil (TP)
2. Limonite (L) -> High Fe, Low MgO, Low Ni
3. Upper Saprolite (S) -> Low Fe, High Mgo, High Ni
4. Bedrock (BR)

The illustration of chemical content analysis for layer domaining can be seen in Figure 2, while Table 1 shows

PROCEEDINGS
JOINT CONVENTION BANDUNG (JCB) 2021
November 23rd – 25th 2021

the chemical and physical characteristics of the four domains in Pakal Island.

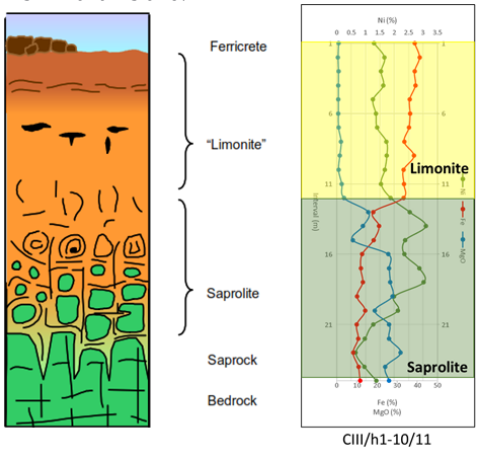

Figure 2. Schematic laterite profile developed on the ultramafic rock after Elias (2002) (left) and the chemical content analysis to determine the four laterite domains in Pakal Island (right)

Table 1. Chemical and physical characteristics of 4 laterite domains in Pakal Island

Characteristic	Top Soil	Limonite	Saprolite	Bedrock
Ni Content	<0.6%	0.8%-1.5%	1.5%-3%	0.3%
Fe Content	>50%	40%-50%	10%-25%	5%
Mg Content	<0.5%	0.5%-5%	15%-35%	35%-45%
Water Content	25%-40%	25%-40%	30%-40%	<5%
Layer Hardness	Soft	Soft	Soft-Medium	Hard
Layer Texture	Unconsolidated, clay grain size	Unconsolidated, clay grain size	Unconsolidated, clay - granule grain size	Massive
Dominant Mineral Composition	Iron Crust	Hematite, Goethite, Manganese Oxide	Garnierite, Silica, Talc	Olivine, Pyroxene

Data and Method

GPR (Ground Penetrating Radar) or georadar method is one of the geophysical methods which utilizes radio waves to investigate the subsurface at a certain depth. Measurement using high frequency will give a better resolution but low penetration. The reflected waves observed in the georadar profile (radargram) are products as responses to layer boundary or other objects in the subsurface which have electromagnetic properties contrasts. The variety of the electromagnetic properties of a layer results from different minerals, textures, wetness, cavity, or fractures.
The georadar equipment works with two antennas, one that acts as the transmitter and the other as the receiver.

The data were acquired using GSSI SIR-3000 with a 40 MHz unshielded antenna. The recording mode used in this data was selective point mode, which is a mode where the transmitter and receiver are moved manually by lifting and dropping the equipment. data were acquired using GSSI SIR-3000 with a 40 MHz unshielded antenna. The recording mode used in this data was selective point mode, which is a mode where the transmitter and receiver are moved manually by lifting and dropping the equipment.

Figure 3. Illustration of measurement with GSSI SIR-3000 40MHz unshielded antenna

In this paper, 2D GPR full-stack sections called radargram were used as the primary input. Figure 4 shows the workflow of this research.

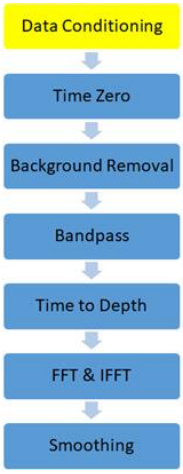

Figure 4. Georadar Research Flow

Time zero correction and background removal Processes are the early processing stages in processing the GPR sections. Time zero correction is applied to correct with time-zero reference. The presence of background noise contained in radargram along the acquisition line was reduced using background removal process. The background noise can result from non-target obstacles such as rocks, cavities, buried rubbish, breakthrough between transmitter and receiver antenna, and multiple reflections between antenna and ground (Khan et al., 2010). The window value of the background removal step used is 100ns. The comparison between raw data and the processed data after background removal is shown in Figure 5.

It is shown in Figure 5 that the continuous horizontal background noise was eliminated to give a clearer georadar section.

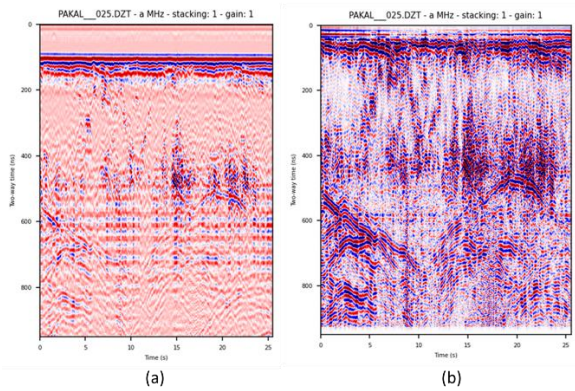

Figure 5. (a) shows the georadar raw data, while (b) depicts the processed data after time-zero and background-removal processing steps.

interpretation with the well data. The time-depth conversion process is done using linear velocity model. The result of time-depth conversion step can be seen in **Error! Reference source not found.**

After the sections have been converted into depth domain, the sections can be overlaid with the well data. From the youngest to the oldest, the well data boundaries plotted consist of 3 parts, such as:

- Top soil – Limonite
- Limonite – Saprolite
- Saprolite – Bedrock

Amplitude domain transformation into the frequency domain was executed to give another view of data interpretation. Previous study shows that this approach has been widely used to assist the subsurface interpretation of the GPR signal. Francke (2000) utilized a GPR data

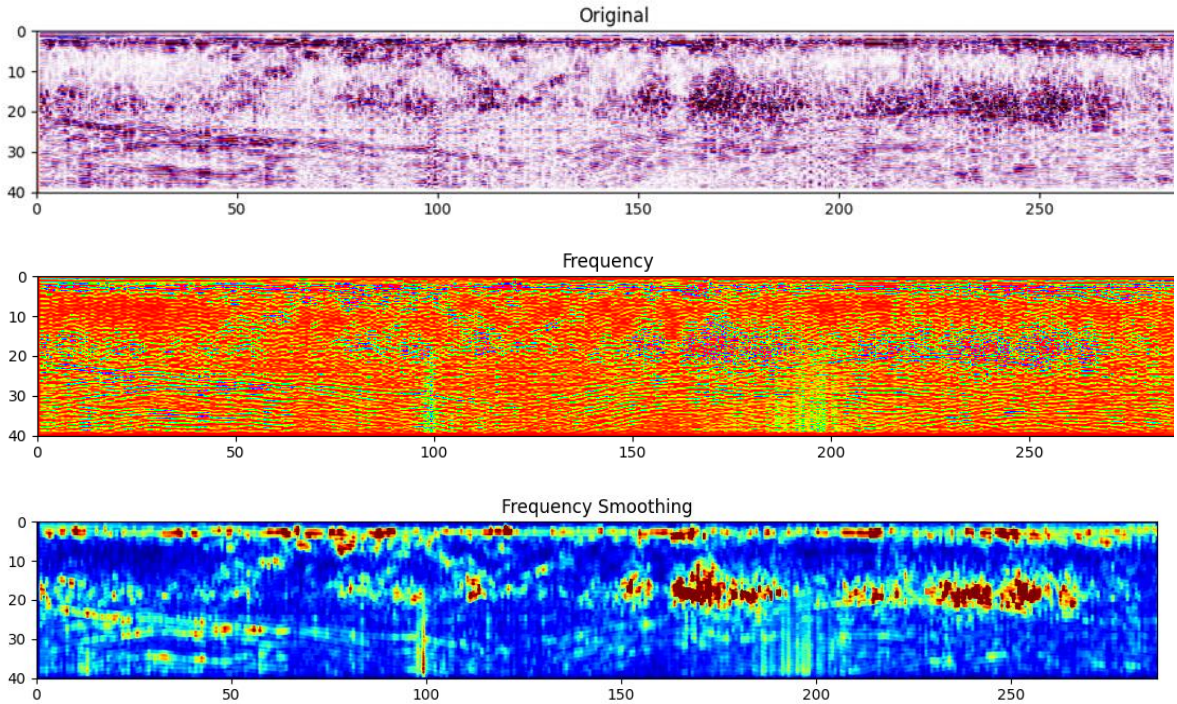

Figure 7. The top section is the georadar section with actual time after time to depth conversion processing step. The middle section shows the frequency-domain radargram after the Fast-Fourier Transform process, while the bottom section shows the frequency-domain radargram after applying the frequency-smoothing step

The time-depth conversion was applied after the bandpass filtering to accommodate the interpretation validated with the wellbore data. Average velocity values are adopted. Figure 7 shows the result of the time-depth conversion step. It can be seen from **Error! Reference source not found.** that the continuous horizontal background noise has been eliminated to give a clearer georadar section.

Furthermore, the bandpass filter method was used to eliminate the coherent noise. The coherent noise contained in the GPR section is the ringing noise. Ringing appears as nearly horizontal and periodic events, which are the most important features enabling us to remove the noise by signal processing (Kim et al, 2007). Based on the trial and error approach, the optimum frequency band which is applied in these sections is between 30 – 200 Hz. The section result after bandpass filter step can be seen in Figure 5.

The time-depth conversion step takes stage after the bandpass filter has been applied, to accommodate the

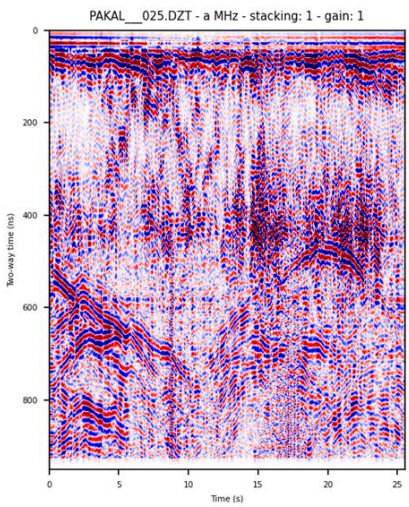

Figure 5. Georadar section after bandpass filter was applied. The frequency band used is 30-200 MHz

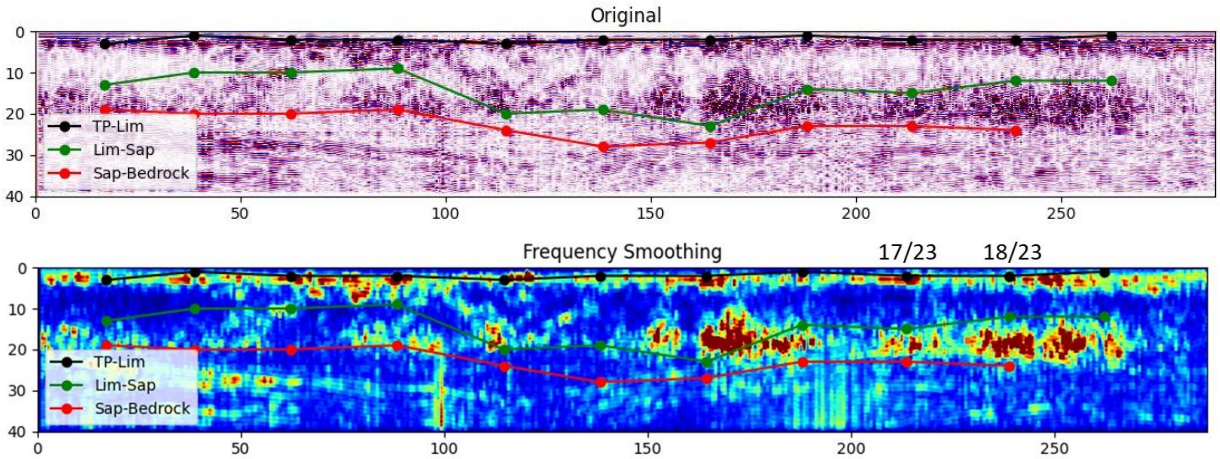

Figure 6. Integration of the boundary of top soil, limonite, saprolite, and bedrock on both time-and-frequency-domain georadar sections. The boundary between top soil and limonite are marked with black line, limonite and saprolite boundary with green line, while saprolite and bedrock boundary is marked with red line. There are spots in the saprolite zone at datum 175-250 meter with a strong frequency amplitude, where in the drillhole data is indicated with saprolite waste (a type of hard saprolite).

processing scheme based on frequency content analysis for laterite investigations, while Panjamani (2014) applied a frequency fast fourier transform to interpret the soil layer interfaces in the absence of borehole data. As seen in **Error! Reference source not found.** the frequency-domain section can delineate more clearly the layer boundaries compared to those in the amplitude domain

Result and Discussion

To give a better understanding of the processed georadar data, 12 drill hole data with 25-meter spacing along the georadar line has been prepared and correlated to both time-domain and frequency domain georadar section. The data integration can be seen in Figure 6.

Based on the drill hole data, the contact between top soil and limonite can be interpreted quite clearly with a layer of high amplitudes along the profile in the time-domain section.
On the bottom part of the section, the contact between saprolite zone and bedrock is quite difficult to determine in the time-domain section. However, this contact can be interpreted more clearly in the frequency-domain section. There is a zone of low frequency range just below the saprolite-bedrock contact. At just above the saprolite-bedrock contact, there are variety of high frequency range. Hence, this frequency difference distinguishes the saprolite and bedrock zone, especially in the saprolite zone at 215-240 meters which shows clusters of high frequency amplitude. In this area, the drillhole 17/23 and 18/23 on Figure 6 shows that the high frequency amplitude in the saprolite zone correlates with layers of saprolite waste. The saprolite waste identifies a saprolite zone which is quite harder than the usual normal saprolite layer in this area, but with lower nickel grade. The drill log of 17/23 and 18/23 can be seen in Table 2.

The most difficult part in the data interpretation is determining the limonite and saprolite zone. The boundary between limonite and saprolite is marked with green line at Figure 6. Based on the georadar section, it is quite difficult to determine the bottom part of the limonite. Neither in the time-domain section nor frequency-domain section shows a clear boundary between limonite and saprolite. The analysis is that in their physical form, limonite zone is often hard to be distinguished from saprolite, because both layers have soft texture (rocky saprolite excluded). The laboratory analysis still gives more accurate result in separating limonite and saprolite zone.

Table 2. Drill log of 17/23 and 18/23

Depth (m)		Drillholes	
From	**To**	**17/23**	**18/23**
0	1	Limonite	Top Soil
1	12	Limonite	Limonite
12	13	Saprolite	Limonite
13	15	Limonite	Saprolite
15	16	Saprolite	Saprolite
16	18	Saprolite	Saprolite Waste
18	24	Saprolite Waste	Saprolite Waste
24	28	Saprolite Waste	Bedrock
28	31.5	Bedrock	

Conclusions

Based on the data result and interpretations, several conclusions have been made:

1. The only laterite zone which can be seen clearly are potentially the rocky saprolite, which is quite different from the earthy saprolite or limonite which has a soft texture.
2. Boundary between limonite and saprolite zone is still hard to be identified, concerning that these two layers can have a very similar physical texture.
3. It is recommended that a georadar measurement using continuous recording is used to give a more detail georadar data section. The selective-point method has low resolution, hence it makes it harder for the geophysicist to interpret the nickel laterite boundaries.

References

Elias, Mick. (2002). Nickel laterite deposits – geological overview, resources and exploitation. CODES Centre of Ore Deposit Research. Special Publication 4. 205-220.

Francke, Jan & Nobes, DC. (2000). Preliminary evaluation of GPR for nickel laterite exploration [4084-02]. PROCEEDINGS-SPIE THE INTERNATIONAL SOCIETY FOR OPTICAL ENGINEERING. 7-13.

Khan, Umar & Al-Nuaimy, Waleed. (2010). Background removal from GPR data using Eigenvalues. Proceedings of the 13th Internarional Conference on Ground Penetrating Radar, GPR 2010. 1 - 5. 10.1109/ICGPR.2010.5550079.

Kim, Jung-Ho & Cho, Seong-Jun & Yi, Myeong-Jong. (2007). Removal of ringing noise in GPR data by signal processing. Geosciences Journal. 11. 75-81. 10.1007/BF02910382.

Panjamani, Anbazhagan & Chandran, Deepu & Burman, Shashank. (2014). Subsurface Imaging and Interpretation using Ground Penetrating Radar (GPR) and Fast Fourier Transformation (FFT). 10.3233/978-1-61499-417-6-254.

Acknowledgements

We would like to express a special gratitude to PT. Antam Tbk. for granting the permission to access the data for this research paper.

PROCEEDINGS
JOINT CONVENTION BANDUNG (JCB) 2021
November 23rd – 25th 2021

Pre-Cenozoic Petroleum System Evaluation from the Aruah Islands Outcrops

Wikan Winderasta, Kirandra Ferari, Hapsari Wahyu Kusumaningsih
PT. Pertamina Hulu Rokan

Abstract

A geological field work in Aruah Islands as part of Joint Study in Rupat Area was conducted in 2020 for an evaluation of Greater Central Sumatra Basin hydrocarbon potential. The island is located about 68 kilometers from port of Bagan Siapiapi, situated at the border of Indonesia's territory and Malaysia in Malacca Strait.

Field observation and rock samples collection were done to provide new data set. The geological field work visited three islands, they are Jemur, Sarang Elang, and Labuhan Bilik Islands. Stratigraphic measured section, structural geology measurement, and sample collection were the main geological field works and conducted at the Jemur Island. The islands lithology is sedimentary assemblage, no granite or crystalline limestone found as originally expected. The sedimentary lithology is dominated by amalgamated quartz sandstone beddings succession with (black) shale interbeds. It is interpreted as dominantly deep-water mass-transport deposits. The outcrop's total measured thickness is approximately 360m thick of stratigraphic record with total of 18 hand specimens were collected. Homoclinal folding structure with general dip above 45o was observed as the result of tilted (compressional) tectonic regime. High degree of fractures density is dominated by pure shear (extensional) tectonic regime. Field interpretation suggested a lithology of Pre-Cenozoic basement, as part of Sibumasu Terrane (fragment of Gondwana Supercontinent, Metcalfe, 2014) that becoming microplate basement of northeastern part of Central Sumatra Basin. Laboratory analyses are included geochemistry, biostratigraphy, petrography, and mineralogy examinations.

Pre-Cenozoic basement lithology implies an opportunity for presence of reservoir and source rock that potentially becomes a possible secondary petroleum system in the Rupat Area (Greater Central Sumatra Basin).

(+) Presence of sandstones as poor to medium quality reservoir.
(+) Presence of black shale as possible source rock type lithology.
(-) Geochemistry analyses so far do not support capability of the black shale as productive source rock. Further data acquisition is required to provide more comprehensive geochemistry analysis.

Outcrop Location in the Context of Regional Geology

Situated in the greater Central Sumatra Basin partially northern area, the Aruah Islands is located on the Malacca Strait. The islands are on the trend of Pre-Cenozoic lithology which is exposed as outcrop in Jemur, Sarang Elang, and Labuhan Bilik Islands. (Figure 1)

The geological field trip guided by University of Padjajaran Team was intended to study the lithology of outcrops and take rock samples for laboratory analysis.

Figure 1: *Aruah Islands is located about 85 kilometers from port of Bagan Siapiapi, situated at the border of Indonesia's territory and Malaysia in Malacca Strait.*

Field observation and interpretation of Aruah Islands lithology was suggesting likely as Pre-Cenozoic basement outcrop. According to Metcalfe (2017) this basement is a part of Sibumasu Terrane (Siam, Burma, Malaysia, Sumatra)[1]. Based on regional study by Metcalfe (2013) of the Sibumasu Terrane, the microplate was a part of Gondwana super continent and have been drifting toward northern position from its original location.[1]

Geoseismic arbitrary cross cection from west to east suggests that Aruah Outcrop could be correlated trough "seismic trend" with either Pre-Cenozoic Basement or as part of Paleogene Syn-Rift Pematang. (Figure 2)

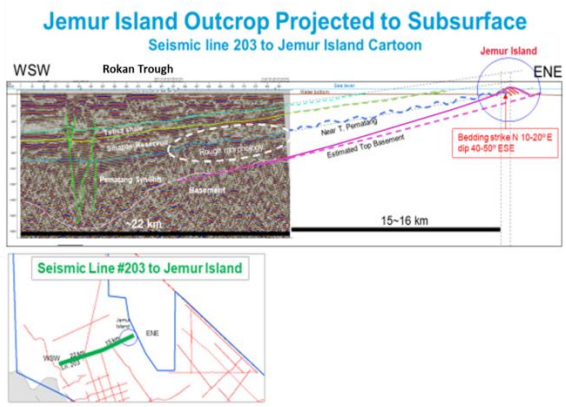

Figure 2: *The 40-50° bedding dip measured in the Jemur Island outcrops might be equivalent to interpreted options, they are:*

- *Near Top Pematang Group (Paleogene section) – interpreted blue horizon, or*
- *Older than Pematang Group or as Pre-Cenozoic Basement section – interpreted purple horizon.*

PROCEEDINGS
JOINT CONVENTION BANDUNG (JCB) 2021
November 23rd – 25th 2021

Geological Field Trip General Findings

The Aruah Island is likely as basement outcrop but based on field observation at all 3 islands, the island is not composed by granite or crystalline limestone as originally expected, but in the fact the outcrops indicate all sedimentary rocks with clear texture and bedding structures.

Geological Structures Observation

Observation and measurement of geological structures (Figure 3) is likely dominated by two tectonic regimes; they are:

- The general bedding strike of the north-south (N10^{O}E - N20^{O}E) trending sedimentary rocks forms a homoclinal fold structure that tilts eastward. The dip is generally above 45° east dipping homoclinal structures indicating the presence of compressional tectonics.
- The east-west and north-south direction joint structures, both are extensional (pure shear tectonic prints) with silicate filling.

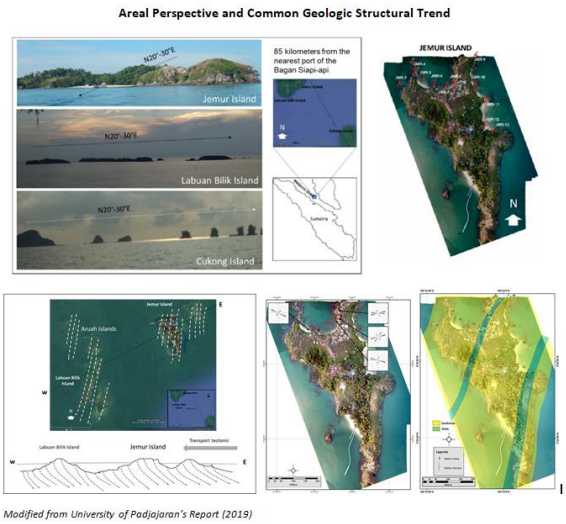

Figure 3: *The main field works were at Jemur Island, with quick spot checks at several islands. General bedding strike NE-SW trend, with common dip of above 45° east dipping indicating the presence of compressional tectonic.*

Lithology and Field Stratigraphy Observation

Stratigraphic measured section was conducted at the outcrops performing description of lithology (Figure 4) as follow:

- The islands lithology is a sedimentary assemblage, no granite or crystalline limestone found. Field observation and interpretation was suggesting deep marine turbidite system deposit.
- Amalgamated quartz sandstone beddings succession with (black) shale interbeds. Outcrop's total measured thickness ~600m (20 hand specimens collected). Geochemical, biostratigraphy and petrographic examinations were completed in the University Padjajaran, Lemigas, and Rumbai laboratories.

Figure 4: *The Aruah Island is likely as basement outcrop, but it is not granite or crystalline limestones. Field observation found all sedimentary rocks: Amalgamated quartz sandstone beddings succession with (black) shale interbeds.*

Sedimentary Structures Description

Very thick clean sandstone succession (Figure 5 & 6) with approximately total 600 m thickness was observed with condition high compacted with fine to coarse size of dominantly quartz grain with pebble fragments as result of offshore to deep water slope sediments and preserving indication of:

- High-density turbidite sedimentary structures (such as intra-formational fold or slump; and fluid-escape structures as dismembered coarse-grained sand injected into the relatively fine-grained sandstone),
- Sandy substrate-offshore deposits sedimentary structures (such as convolution and contorted lamination, current-ripples, and bioturbation), and
- Traction carpet sedimentary structure that be indicated by graded bedding with relict of pebble band.

Figure 5: *Very thick bedded coarse-grained quartz sandstones consist of vertically-stacked sandstone amalgamation indicated by the amalgamation surfaces.*

PROCEEDINGS
JOINT CONVENTION BANDUNG (JCB) 2021
November 23rd – 25th 2021

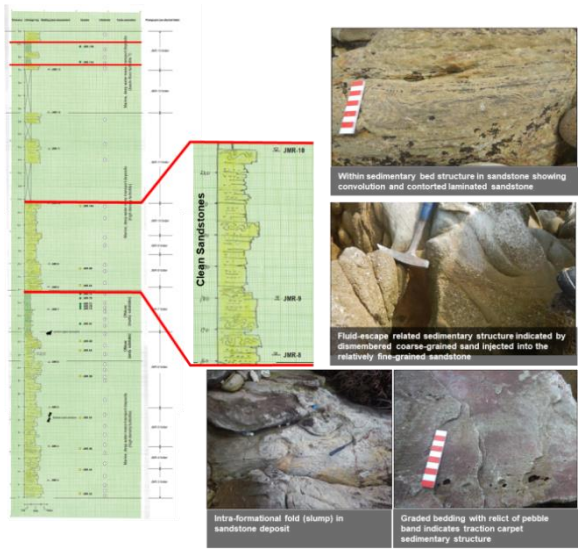

Figure 6: *Thick clean sandstone succession with condition high compacted with fine to coarse size of dominantly quartz grain act as potential reservoir as up to medium quality of porosity.*

Two thick black shale intervals were observed indication of muddy substrate-offshore deposits, characterized by mudstones, black-reddish shale couplets with local bituminous seams (Figure 7).

The first thick black shale interval is located in a bay where seawater pools at high tide. The thickness of the greyish-black substrate-offshore deposits shale interval is about 30 m with alternating fine-grained sandstones with chert intercalations and several number of coal-bituminous seam layers at the lower section, and dominantly massive black shale at the upper section.

Various sedimentary structures were observed in the shale layers such as current-ripple laminated sandstone in association with convolute lamination, and parallel laminated shale and siltstone couplets.

The second interval of shale is located at the bottom of the coastal cliff which is covered by tidal sea water with a thickness of about 20 m. The dominance of greyish black shale with sandstone layering has a parallel laminated shales and siltstone couplets sedimentary structure.

The lithological columns of the two shale intervals can be depicted in Figure 8.

Facies Interpretation

Field interpretation suggested a hypothesis of lithology as Pre-Cenozoic basement as interpreted as part of Sibumasu Terrane, with alternatively, it is possibly part of the Paleogene Pematang Group that was deposited in association with the syn-rift and pre-rift intervals.

Observation and interpretation of Aruah Islands lithology was suggesting a deep marine turbidite system deposit with possibility as diamictites. A measured section was traversed at the north and the northeast part of the island giving approximately 360 m thick stratigraphic record. Ten sandstone samples together with eight shale samples were collected from the outcrops. (Figure 9)

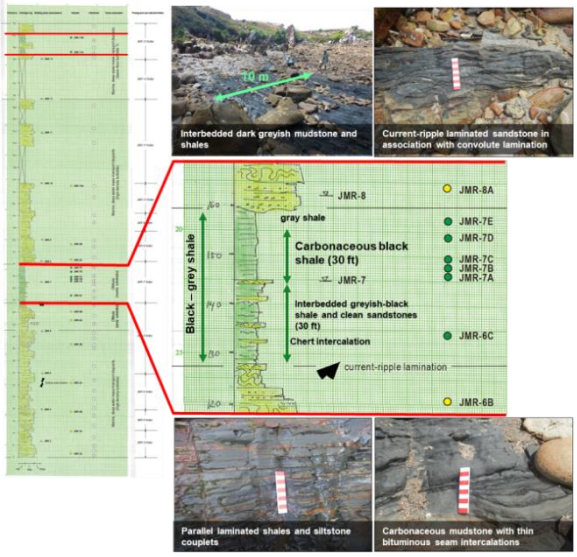

Figure 7: *Two thick black shale intervals act as potential source rock. Bituminous seams indicate organic content in the shale.*

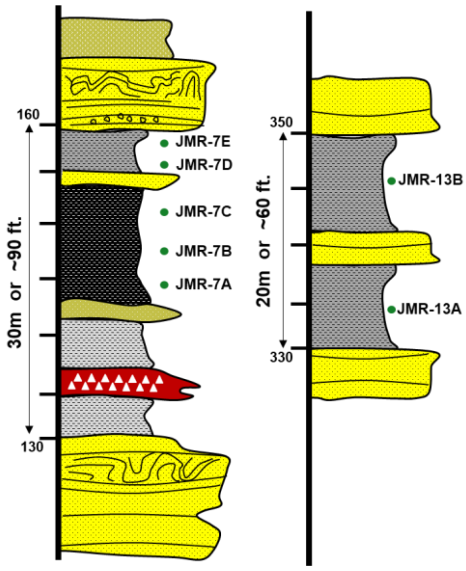

Figure 8: *Two thick black shale intervals act as potential source rock.*

The stratigraphic succession could consequently be divided into three major facies associations (Sunardi et.al, 2019) [3], they are:

- (Facies-1) high-density turbidite, very thick to massive coarse sandstones.
- (Facies-2) sandy substrate-offshore deposits, interbedded convoluted, current-ripple laminated, and bioturbated sandstones.
- (Facies-3) muddy substrate-offshore deposits, interbedded dark-greyish laminated mudstones, black to reddish and greyish shale couplets.

PROCEEDINGS
JOINT CONVENTION BANDUNG (JCB) 2021
November 23rd – 25th 2021

The sedimentary rocks consist of predominant very thick sandstone beds with shale and mudstone interbeds, with proposed six major lithofacies as follow:

- (Lithofacies-1) disturbed sandstones (sandstone showing soft-sediment deformation structures, sand injection, fluid-escape structures, and graded bed sandstones)
- (Lithofacies-2) banded and plane-stratified sandstones
- (Lithofacies-3) cross-stratified sandstones
- (Lithofacies-4) current-ripple laminated sandstones
- (Lithofacies-5) sandstones showing burrows and biogenic structures
- (Lithofacies-6) shale and mudstones (laminated mudstones, reddish mudstones, black shale couplet with thin bituminous seams).

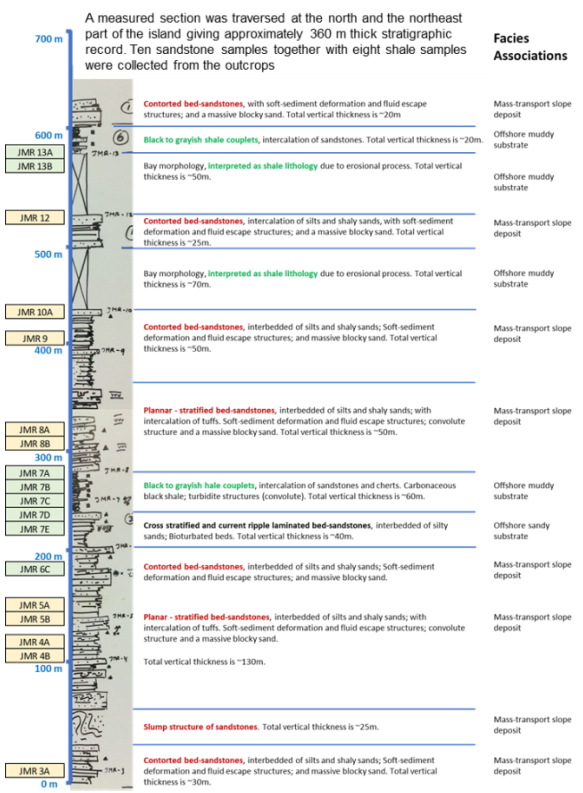

Figure 9: *Stratolith Column shows succession of 3 major facies associations with 6 lithofacies.*

Laboratory Analysis Result

Based on biostratigraphy and petrography analyses, it is concluded that the black shale rocks exposed on surface at the Aruah Islands are considered as age of Mesozoic sandstone and carbonaceous shale lithology. But the geochemistry analyses so far do not fully support the opportunity as possible secondary petroleum system of presence self-source-rock in the Rupat Block.

Biostratigraphy Analysis

Age determination is challenging, due to all samples of carbonaceous shale are barren from micro planktonic/benthic *foraminifera*, and nano plankton (Graha and Lemigas, 2019). Biostratigraphy analysis (Figure 10) suggests the Black Shales exposed on surface are interpreted as Paleogene or older age lithology since no nano fossil found due to probably over maturation or degradation process.

Calcareous nano plankton interpretation indicates mostly barren, but in the 13B samples was found a minor *Sphenolithus cf. moroformis* (NP12-NN9 / Early Eocene – Lower Part of Late Miocene). Lemigas biostratigrapher suggested it is not that species.

But based on University of Padjajaran's report (2019), palynology analysis at the 5 samples found several nano fossil species as determined age of Mesozoic (within Jurassic to Cretaceous Period). The observed non fossils are *Conusphaera Mexicana*, *Rotelapillus sp.*, *Palaeoponthosphaera dorsetensis*, and *Ascidian spicules*. (Figure 11).

Other age dating methods is not recommended due to no igneous/volcanic samples were found, and degraded condition of samples.

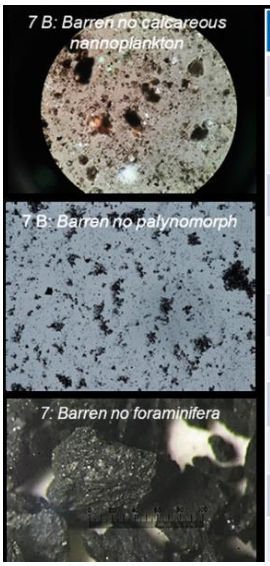

NO	SAMPLES	ANALYSIS	RESULT
1	13A	PALY	barren
2	13B	NANO & PALY	Barren with a minor fossil found
3	7A	FORAM	barren
4	7B	FORAM / NANO & PALY	barren
5	7C	NANO & PALY	barren
6	7D	NANO	barren
7	7E	FORAM	barren
8	7F	FORAM	barren
9	6C	FORAM	barren
10	2	FORAM	barren

Figure 10: *The biostratigraphy analysis observed no nano fossil found due to probably over maturation or degradation process.*

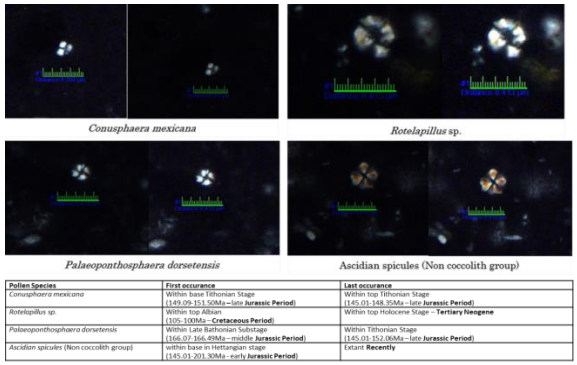

Pollen Species	First occurance	Last occurance
Conusphaera mexicana	Within base Tithonian Stage (149.09-151.50Ma–late **Jurassic Period**)	Within top Tithonian Stage (145.01-148.35Ma – late **Jurassic Period**)
Rotelapillus sp.	Within top Albian (105-100Ma – **Cretaceous Period**)	Within top Holocene Stage – **Tertiary Neogene**
Palaeoponthosphaera dorsetensis	Within Late Bathonian Substage (166.07-166.49Ma – middle **Jurassic Period**)	Within Tithonian Stage (145.01-152.06Ma – late **Jurassic Period**)
Ascidian spicules (Non coccolith group)	within base in Hettangian stage (145.01-201.30Ma - early **Jurassic Period**)	Extant **Recently**

Figure 11: *Palynology analysis found several nano fossils species as determined age of Mesozoic.*

PROCEEDINGS
JOINT CONVENTION BANDUNG (JCB) 2021
November 23rd – 25th 2021

Petrography & SEM (scanned electromagnetic microscope) Analysis

The analysis results show indication of sample degraded condition due to exposure to the surface as indicated by the oxidized process result (ferroan oxide mineral as fracture filling) and insitu secondary diagenesis (abundant kaolinite as dissolution pores filling). Partial carbonaceous materials were replaced by siderite.

The 'Aruah' sandstones are classified into quartz-arenite sandstones that mainly consist of coarse-silt to coarse-grained sands. Compactions are mainly represented by straight to concavo-convex grain contact with only local suture contact. Indication of any incipient metamorphism was not evidently observed.

Sandstone petrography analysis suggests relatively very poor to medium porosity (observed at 5-25%) - Figure 12. Diagenetic events in the sandstone sample can be described as follow:

- Compactions are mainly represented by straight to concavo-convex grain contact with only local suture contact.
- Indication of any incipient metamorphism such as interlocking quartz mosaic with serrated edges and other prominent alteration were not evidently observed.
- The porosity types are classified into: moldic, intergranular, and intragranular, that can be differentiated into: fracture, shrinkage, and dissolution origin.

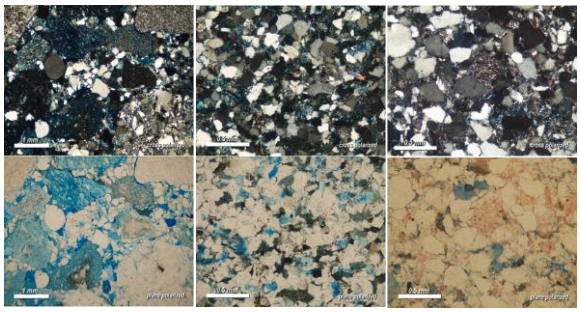

Figure 12: *Sandstone is observed as very poor to medium porosity mainly as intergranular type.*

Shale petrography analysis suggests oxidized process have been occurred and replacement of organic matters with ferrous oxide mineral probably as result of degradation of organic content (Figure 13). Diagenetic events in the shale samples can be described as follow:

- Partial organic and carbonaceous materials were replaced by siderite and pyrite.
- Cementation by ferroan oxide and quartz overgrowth
- Presence of ferroan oxide that filled most of fractures at the carbonaceous shale samples.
- Some mica fragments are found as clay/silt detrital without any lineation/foliation texture appearance as metamorphic indicator.

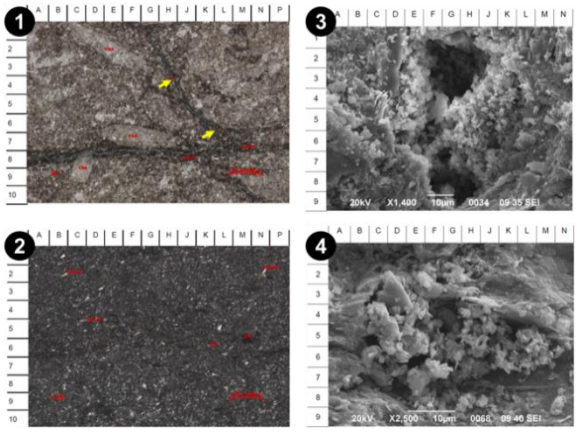

Figure 13: *Shale petrography describe an oxidized argillaceous coal (1) and Claystone (2) – detrital clay mixed with organic matter, with fragments of quartz and rocks. SEM sections show Silty Sandstone (3) composed by quartz and rock fragments, while Shale/argillaceous (4) composed by detrital clay mostly as illite and kaolinite, with fragments of quartz and carbonaceous materials.*

Based on petrography analysis, the lithology in the Aruah outcrops can be defined in the late diagenesis phase, which results in high degree of compaction for performing poor to medium quality of sandstone reservoir. Although the indication of incipient metamorphism is not evidently observed, therefore increasing of porosity may occur due to dissolution and presence of natural fractures.

AP140 Porosity and XRD Analysis

The measurements of AP140 porosity analysis show the samples as tight to poor quality sandstones (5-16 %) with porous shale (12-25%) with relatively low to medium clay mineral content (dominated by illite and kaolinite). (Table 1a).

The XRD (X-ray diffraction) measurements show the samples as tight to poor quality sandstones (5-16%) and relatively porous shales (12-25%) with low to medium clay mineral content (dominated by illite and kaolinite). Both are non carbonates. (Table 1b).

Sample#	Well	Sample No	Sample Description	AP140 method		XRD analysis (RIR Method), value in wt%								
				grain density, gr/cc	Porosity, %	Quartz	plagioclase	K-Feldspar	Clay			carbonate		pyrite
									illite	kaolinite	chlorite	calcite	siderite	
1	Well SB	13B	Shale	2.65	17.5	59.8	3.5	2.2	21.3	7.6	1.6	2.0	2.0	
2		10A	Sandstone	2.66	12.5	90.0	2.3	2.5	3.2	2.0				
3		8B	Sandstone	2.64	8.2	90.0	2.8	3.0	2.3	1.9				
4		7F	Shale	2.63	22.1	83.7	2.0	1.8	3.7	7.2	1.6			
5		7E	Shale	2.68	17.3	73.5	2.9	3.0	14.0	6.1		0.5		
6		7D	Shale	2.68	16.1	77.0	4.1	3.2	9.0	4.7		2.0		
7		7C	Shale	2.62	12.0	80.1	5.7	6.0	6.9	1.3				
8		7B	Spl insufficient for porsity	NA	NA	83.7	3.4	3.6	6.0	3.3				
9		7A	Shale	2.68	24.9	86.3	2.7	2.8	4.4	3.8				
10		6C	Sandstone	2.66	16.3	85.0	2.5	2.0	4.9	5.6				
11		6B	Sandstone	2.64	16.4	86.0	4.3	3.9	3.1	2.7				
12		6A	Sandstone	2.64	16.4	89.0	2.1	2.2	2.2	4.5				
13		5B	Sandstone	2.67	10.1	86.1	2.7	2.2	4.5	3.5	1.0			
14		5A	Sandstone	2.66	6.0	86.1	2.7	2.2	4.5	3.5	1.0			
15		4B	Sandstone	2.71	12.5	88.7	2.0	1.5	5.1	1.8			0.9	
16		4A	Sandstone	2.64	6.8	93.0	2.0	1.7	1.5	1.8				
17		3A	Sandstone	2.64	9.6	89.5	1.9	1.6	3.6	3.4				
18		2	Sandstone	2.66	5.7	93.7	1.7	1.3	2.8	0.5				
19		1	Sandstone	2.67	5.8	92.0	1.7	1.9	1.9	1.0	1.5			

Sample matrix: Core chip sample
Methodic
Cleaning: Soxhlet extraction
Grain volume: Boyle's law grain volume porosimeter
Bulk Volume: Mercury bulk porosimeter
Bulk mineralogy: RIR method

Table 1: *AP140 Porosity Measurement (1a) and XRD Analysis (1b) in sandstone and shale samples.*

PROCEEDINGS
JOINT CONVENTION BANDUNG (JCB) 2021
November 23rd – 25th 2021

Geochemistry Analysis

Geochemistry samples were taken from both shale intervals. TOC (total organic carbon) and RockEvals Pyrolysis measurement performed in the Lemigas Laboratory at the selected outcrop samples to analyze organic richness, maturity, and interpreted environmental of deposition of potential source rock presence.

TOC was measured at 7 sample points and resulted various TOC values (0.2-3.7%) indicates approximately 100ft. thick of rich hydrocarbon source rocks potential (1.4-3.7%) at the middle part of First Black Shale interval. The other shale intervals indicate originally poor or have been degraded or even organic content has been reduced during diagenetic/maturation. (Table 2).

RockEval Pyrolysis at the 4 most higher TOC results a very low volatilized of free hydrocarbon (S1) content (<0.05 mg/gr) and generated hydrocarbon compound (S2) from pyrolysis of kerogen (<0.14 mg/gr). Total potential yield of hydrocarbon (PY=S1+S2) amount is very low (< 0.18 mg/gr). Plot of TOC versus S2 and HI (hydrogen index) of samples considered very poor potential as source rock. The sample based on plot of S2 vs. TOC and HI vs. OI can be defined as Kerogen Type 4 or inertinite/oxidized organic matter. (Figure 14).

Vitrinite reflectance (Ro) data clarify that the thermal maturity are in the late mature to over matured stage (3 samples have 3-4%Ro, but one sample has 1.15%).

Gas Chromatography (GC) done at 3 samples (Table 3) observes degradation level of organic matter. The analysis results show an indication of biodegraded samples due to exposure to surface. Even though the extracted rocks have undergone biodegradation but still leaves pristane and phytane compounds and a small portion of alkanes. (Figure 15).

The extracted rocks are estimated from pristane/phytane ratios to be derived from the source rock, which deposited in anoxic-suboxic of the associated aquatic depositional environment.

No.	Code Sample	Sample Type	General Lithology Description	TOC (%)	S_1	S_2	S_3	PY	S_2/S_3	PI	PC	Tmax (°C)	HI	OI
1	JMR-7A	OC	Shale, med.gray-dark gray, very hard, Non Calcareous	0.34	-	-	-	-	-	-	-	-	-	-
2	JMR-7B	OC	Shale, dark gray, mod.hard, Non Calcareous	1.39	0.04	0.13	0.23	0.17	0.57	0.24	0.01	***	9	17
3	JMR-7C	OC	Shale, black, mod.hard, Non Calcareous	3.71	0.03	0.13	0.71	0.16	0.18	0.19	0.01	***	4	19
4	JMR-7D	OC	Shale, med.gray-dark gray, very hard, Non Calcareous	0.32	-	-	-	-	-	-	-	-	-	-
5	JMR-7E	OC	Shale, med.gray-dark gray, very hard, oxidated, Non Calcareous	0.41	0.03	0.11	0.19	0.14	0.58	0.21	0.01	***	27	47
6	JMR-13A	OC	Shale, med.gray-dark gray, very hard, oxidated, Non Calcareous	0.20	-	-	-	-	-	-	-	-	-	-
7	JMR-13B	OC	Shale, med.gray-dark gray, very hard, oxidated, Non Calcareous	0.44	0.03	0.10	0.31	0.13	0.32	0.23	0.01	***	23	71

Remarks :
TOC : Total Organic Carbon
S_1 : Amount of Free Hydrocarb
S_2 : Amount of Hydrocarbon re
S_3 : Organic Carbon Dioxide
PY : Amount of Total Hydrocarbons = (S_1 + S_2)
PI : Production Index = (S_1/ S_1 + S_2)
PC : Pyrolysable Carbon
Tmax : Maximum Temperature (°C) at the top of S_2 peak
HI : Hydrogen Index = (S_2/TOC) x 100
OI : Oxygen Index = (S_3/TOC) x 100
NDP : No Determination Possible
D/C : Ditch Cuttings
*** : Erroneous reading Tmax due to lack of S_2

Table 2: *Organic richness based on TOC measurement and RockEval Pyrolysis for maturity analysis.*

OIL COMPOSITION AND GAS CHROMATOGRAPHY DATA										
No	Sample ID	Sample Type	EOM(ppm)	SAT	ARO	NSO+Asp	Pr/Ph	Pr/nC17	Ph/nC18	CPI
				WT %						
1	JMR-7B	outcrop	82	15.58	2.60	81.82	1.40	1.16	3.36	-
2	JMR-7C	outcrop	282	2.00	3.00	95.00	2.20	1.86	2.24	-
3	JMR-7E	outcrop	66	5.71	2.86	91.43	1.02	0.83	1.25	-

Remarks
Pr : Pristane
Ph : Phytane
nC17 : normal Alkane C17
nC18 : normal Alkane C17
CPI : Carbon Preference Index (C_{23} +C_{25}+C_{27})= (C_{23} +C_{25}+C_{27})/2* (C_{24} +C_{26}+C_{28})
Sat : Saturate Fraction
Aro : Aromatic Fraction
NSO : Non Polar Fraction

Table 3: *Gas Chromatography (GC) done at 3 samples observes degradation level of organic matter.*

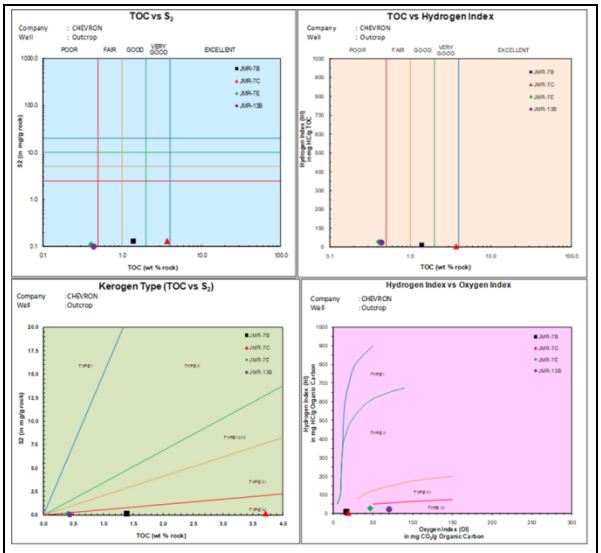

Figure 14: *Organic richness based on TOC measurement and RockEval Pyrolysis for maturity analysis.*

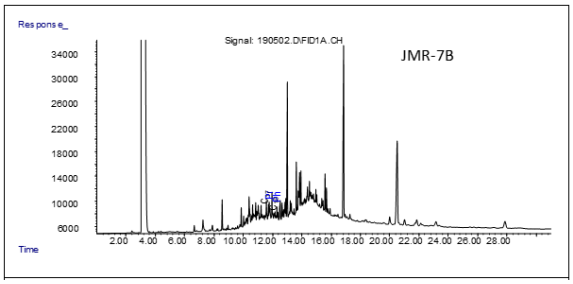

Figure 15: *Gas Chromatography (GC) indicates the samples are biodegraded due to exposure to surface .*

Gas Chromatography Mass Spectrometry (GCMS) results (Figure 16) show an indication of algae and higher plant species biomarkers which is deposited in transition area (estuarine).

- The steranes chromatogram (m/z 217) of JMR-7B, JMR-7C and JMR-7E samples shows clear regular sterane distribution with low indication of higher plant species biomarkers.
- The sterane configuration of C29>C27>C28 which is characteristic of mixed algae and higher plant organic matter.
- Low thermal maturity of hydrocarbons in the extract bitumens is very clearly demonstrated by the presence of the compounds 5a14a17a-sterane 20S which is relatively very low when compared with their 5a14a17a-sterane 20R conter-parts.
- Angiosperm derived biomarkers such as oleananes, C30 oleanoid triterpanes, and other terrestrial indicators, occur in very low concentrations to almost absent in the samples analyzed. This suggests only a minor contribution from terrestrial plants to the source kerogen.

- The dominant of C23 tricyclic terpane (peak no 5) indicate the extracted oil from rocks is produced by algae which deposited in shallow marine environments.
- Ts/(Ts+Tm) ratio (0.46-0.54) and Moretane/Hopane (0.11-0.15) give indicated low of thermal maturity. The possibility of immature sediments is new sediments formed simultaneously with the rework sediments.
- GCMS Biomarker of ion m/z 217 & m/z 191 and steranes show that 7B/7C samples come from same source and deposited in transition depositional environment.

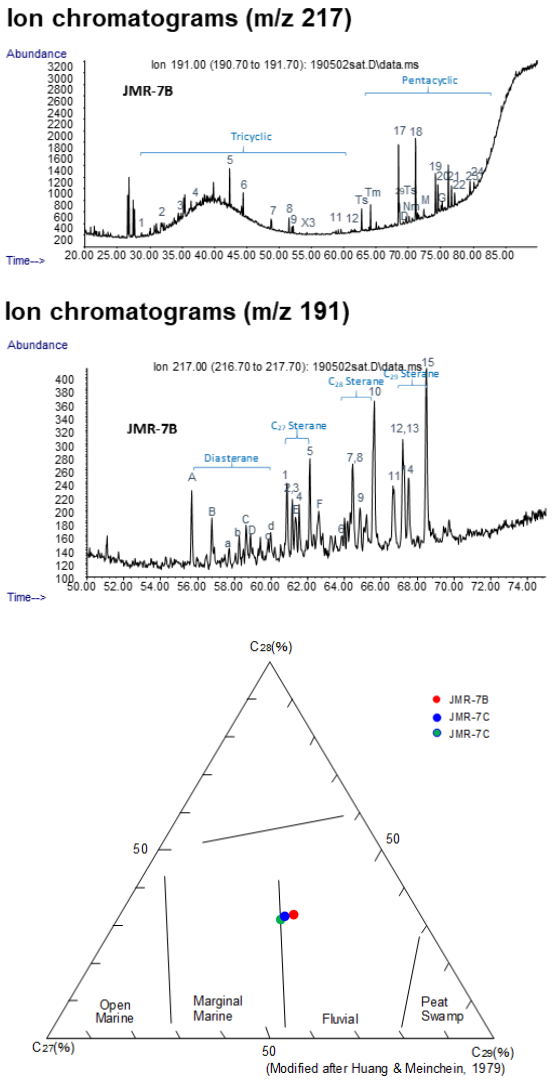

Figure 16: *Gas Chromatography Mass Spectrometry (GCMS) results show an indication of algae and higher plant species biomarkers which is deposited in transition area (estuarine).*

Geochemistry analysis result at the two Black Shale intervals (interpreted as Paleogene or Older lithology) indicates that the Black Shale exposed on surface as inertinite or probably has been over mature. It gives indication of very poor hydrocarbon source rocks potential.

Conclusions

Pre-Cenozoic basement lithology implies an opportunity for presence of reservoir and source rock that potentially becomes a possible secondary petroleum system in the Rupat Area (Greater Central Sumatra Basin).

(+) Presence of sandstones as poor to medium quality reservoir.

(+) Presence of black shale as possible source rock type lithology.

(-) Geochemistry analyses so far do not support capability of the black shale as productive source rock. Further data acquisition is required to provide more comprehensive geochemistry analysis.

Acknowledgment

Author and Co-authors would like to thank you to Ministry of Energi dan Sumbar Daya Mineral, Prof. Edy Sunardi with University of Padjajaran Team, Lemigas Team, Maman Abdul Rahman, Budi Setiawan, Satia Graha, Agus Susianto, Lambok Marpaung, and PT. Pertamina Hulu Rokan.

References

Amlan, M.H., Winderasta, W., Susianto, A., Kurniawan, R. , and Arifin, M.Z.. (2019, August). The Top Seal Capacity of Regional Telisa Shale and Intraformational Seals in Central Sumatra Basin, Association of American Petroleum Geologist Technical Symposium, Volume: The Art of Hydrocarbon Prediction: Managing Uncertainties.[2]

Katz, B.J. and Dawson, W.C. (1997). Pematang-Sihapas Petroleum System of Central Sumatra. Proceedings Petroleum Systems of SE Asia and Australasia Conference, page 685-698.[1]

Metcalfe, I.. (2017). Tectonic evolution of Sundaland. Bulletin of the Geological Society of Malaysia. 63. 27-60. 10.7186/bgsm63201702.[1]

Sunardi, E and Padjajaran University Team (2019). Petroleum Prospectivity of Rupat Area, A Joint Study Final Report (*unpublished*) .[4]

Author:

Wikan Winderasta received his bachelor's degree in Geological Engineering and master's degree in petroleum Geology from Institute Technology of Bandung in 1996 and 2003. He joined Chevron in 1996 with 25 years experiences in the oil and gas industry, including experiences in Exploration & New Venture; Production & Development (Waterflood and Thermal Enhance Oil Recovery); and Unconventional Tight Rock with International experiences in U.S. and Canada. He is currently working in PT Pertamina Hulu Rokan as Senior Earth Scientist for Applied Reservoir Management Team.

PROCEEDINGS
JOINT CONVENTION BANDUNG (JCB) 2021
November 23rd – 25th 2021

Chasing a New Carbonate Fracture Play Type at South Sumatra Basin

Ricky Tampubolon[1], Togi Y Sitinjak[1], Chairatil Asri[1], Rinaldi Imran[1], Bagus Joko Raharjo[1]
[1]Odira Energy Karang Agung

.

Abstract

The newly discovered giant basement fracture gas reservoir in Sakakemang block located in the central part of North Palembang Sub-Basin has been an interesting subject and brings a new perspective in exploration on that basin. However, due to the lack of recent exploration activity, the southern part of this basin, the hydrocarbon potentiality is less known although the remaining potential remains high. This paper will discuss the hydrocarbon potential of the basement fractured in an area located in the southern part of the North Palembang sub-basin, 100 km to the southeast of Sakakemang block.

The geological delineation from Kaliberau discovery trend can be continued, about 100 km to the southeast, called the "X" Structure. The evidence from the well, seismic, and gravity data are integrated to construct the geological model. The previous operator has made a gas discovery from the shallow gas reservoir of Telisa. However, the current operator sees there is a new potential basement fracture at the deeper level.

The "X-1" well drilled 75 m of recrystallized carbonate. While drilling the carbonate, the previous operator experienced a partial loss and the petrophysical analysis reveals the development of secondary porosity. The total gas reading also increased, even higher than the current pay zone at Telisa sand. The seismic facies are showing a widespread carbonate platform, with "X-1" well at the crest of the structure. The thickness of the carbonate can reach >250 m.

The seismic evidence is showing a large (5x10 km), inverted structure from the seismic. This is also supported by the geochemistry and basin modeling evidence. The basin modeling records that there were at least 2 inversion timing, which are Middle Miocene and Plio-Pleistocene. The erosion calculation from basin modeling is showing more than 1000 m sediment has been eroded at the "X" structure. The petrography analysis is showing a feature of type III/IV twinning-calcite, indicating a hot paleotemperature, with intensive microfracture. This inversion history is very important to facilitate the fracture porosity in the basement.

The "X" carbonate reservoir represents a buried carbonate which inverted massively. Without the fracture, there is no chance for this reservoir to develop a matrix porosity. Adjacent to 2 km, the kitchen is able to produce gas. Within the fracture and permeable sand, the gas should be able to reach carbonate. In South Sumatra Basin, there is no current analog that has been discovered in this play type. The discovery of carbonate play type will bring a new play concept into South Sumatra Basin.

Keywords: Basement Fracture, Carbonate, South Sumatra Basin

Introduction

This paper will focus on the topic of basement fracture potential at "X" Structure, at South Sumatra Basin. The "X" Structure is the geological delineation of Kaliberau recent discovery to the southeast.

The "X" Structure represents a large ~50 km^2 structure with a faulted four-way dip type closure. This structure is a result of geological inversion during Middle Miocene and Plio-Pleistocene. Two wells have been drilled on this structure and resulted a discovery in Telisa sand. However, the new operator sees the new play potential from basement.

We did the basin, play, prospect analysis to understand the nature of petroleum system in this area. The "X" Structure is located on the southern edge of the North Palembang Sub-Basin. The sediment is thinning to the northern of the present-day coastal area and Bangka area. The "X" Structure is surrounded by two deeps. These deeps are separated by "X" Structure by a NW-SE reverse fault, dipping to the NE. The

PROCEEDINGS
JOINT CONVENTION BANDUNG (JCB) 2021
November 23rd – 25th 2021

question is whether these deeps are mature to reach hydrocarbon generation window.

Among the reservoirs we identified, Telisa, TAF, and Basement, the thickness and areal extend of reservoir is greatest on the basement layer. However, this basement is never been focused.

This paper aimed to analyze the new carbonate play from seismic, gravity, well, and petrography data.

Data and Method

The data and method used is from seismic, well, gravity, petrography, and XRD data. The interpretation of seismic horizon is carried from biostratigraphy data that used in regional seismic mapping. The geochemistry data is used to build a 1D to 3D basin modeling to understand the nature of the petroleum system.

Result and Discussion

The previous operator targeted TAF as a main objective reservoir. The well resulted in a good reservoir quality of TAF, however the hydrocarbon containment in the TAF layer is insignificant. In contrary, the Telisa sand which above the TAF layer has a significant hydrocarbon containment. The gas in Telisa sand has a 93% of C_1 but also mixture content amount to $C_{11,}$ indicating the gas is not biogenic. Therefore, the source rock identification is very important.

The" X" Structure is an inverted syn-rift structure, as indicating by thickening of Lemat and TAF sand. The geohistory in this area begun from the deposition of carbonate. The carbonate age is unknown, because no fossil recovered from this carbonate. The carbonate is a pre-Tertiary (below the Lemat Fm), and has a widespread distribution, probably in a passive margin in a pre-rift tectonic.

The first Tertiary sediment deposited in this area is Lemat Fm, deposited in a lacustrine environment. This Lemat shale is a very prolific source rock that can generate oil and gas.

The TAF sand has a good reservoir quality because this structure is nearby to the paleohigh as the provenance, probably a metamorphic high. Based on the biostrat data, the TAF is deposited in the shallow marine during a highstand system, so the reservoir has a widespread thick blanket sand as also indicated in the seismic facies.

The Telisa sand is indicating a post inversion deposit during a transgressive succession. The Telisa sand is deposited in a tidal environment. The sand is not widespread as TAF, but more isolated and channelized.

At the top of Telisa sand is Telisa shale, which deposited in a shallow marine during the peak of transgressive sequence, some of these layers are eroded due to a great inversion during Plio-Pleistocene. Based on the 1D modeling and rough calculation from seismic section, there is approximately 1000 m sediment is eroded.

The basin inversion plays a very important role as the tectonic force created a massive fracture from basement to Telisa. There were two episodes of major inversion, which is Middle Miocene and Plio-Pleistocene.

The occurrence of this inversion follows the pre-Tertiary structural suture zone, which is the boundary of plate to plate collision. This collision can be tied to the Sakakemang on the NW area. The suture zone is becoming reactivated in the younger geology time becoming a strike-slip tectonic. This strike slip tectonic is NW-SE oriented and becoming the major hydrocarbon field trend. This is very similar to Sumpal, Dayung, Rayun, Grissik, and Illiran trend which is oriented NW-SE hydrocarbon belt.

This inversion also creates a major deep as the compensation of the uplifted structure. As the result of uplift, the "X" Structure is surrounded by two deeps. To understand the maturity, generation, and expulsion history of the basin we create the petroleum system modeling.

The structural correlation shows that show the context of carbonate basement fracture play can be seen at Figure 1. Interestingly, at "X" Structure, the geochemistry depth plot showing there was a great inversion and erosion at "X" Structure. As we can see at Figure-2, the plot of porosity and vitrinite to depth (y-axis), showing there is a geological event or break consistently from porosity and vitrinite plot at X-1 well.

Normally, increasing to the depth, the porosity will be reduced exponentially with a continuous trend. However, in the X-1 there are two trends of porosity. These 2 trends indicating there is a sedimentation break, which means there is an erosion or uplift. This also applied to vitrinite, normally the vitrinite will be increasing linearly to the depth. However, in X-1 well there is a break of VR trend at top of the TAF (Upper Talang Akar Fm). This section breaks also coincide with the last thickening event. It means this break is indicating the inversion after the deposition of TAF (Figure-2).

PROCEEDINGS
JOINT CONVENTION BANDUNG (JCB) 2021
November 23rd – 25th 2021

To confirm the maturity window at the kitchen, the 3D basin model must be conducted. To conduct the 3D basin model, the surface depth must be created, and the facies map has to be assigned. The basement depth structure is showing that the ”X” Structure is surrounded by two deeps on the west and eastern part, if these deeps reach the maturity window then hydrocarbon can be expelled from the kitchen. From the currently available seismic data, the X- 1 is penetrated the highest elevation of basement surface and the surface geology shows there is an outcrop of older formation, represents the X-1 is the crest of the anticline.

The result of the basin modeling is showing there is a hydrocarbon generation in 20.8 Ma from Lemat as a source rock. The first fluid expelled from Lemat is oil, and later due to increasing thermal and beginning thermal cracking on 19 Ma, gas is expelled from source rock. If there is a reservoir, seal, and trap preserved during the time of migration, the accumulation will occur. To summarize the sequence of basin evolution and timing of generation, migration, and accumulation:

- 20.8 Ma is the start of oil expulsion from Lemat source rock
- 19 Ma is the start of the gas expulsion from Lemat source rock
- 15.5 Ma is the start of the peak of Lemat hydrocarbon generation
- 11.8 Ma is the beginning of accumulation
- Until present day, the Lemat is modelled still in gas maturity window, the hydrocarbon charging is still continuing.

The 2-D basin modeling section at 11.8 Ma when accumulation occurs can be seen at Figure-2.

The cutting study is very important to confirm the presence of basement fracture in X-1 carbonate. The low-density carbonate is obvious from seismic, and the porous carbonate can be seen from AI anomaly, showing a low AI. The low AI is showing a porous carbonate. In order to know how the lithology reflects the geophysical data, we collect petrography analysis from cutting. If it is a porous lithology, we want to know if the porous matrix coming from the matrix, fracture, or combination.

Sample from X-1 cutting was delivered to analyze biostratigraphy, petrography, and XRD. The result of this lab analysis is very important to understand the lithology, type of reservoir, and diagenesis history of carbonate.

The result of petrography is showing a very interesting result. The lithology of the X-1 carbonate is showing a recrystallized limestone or marble. This recrystallized limestone is composed by mostly a deformed twinning calcite (Figure-4). This limestone is heavily fractured, and some fractures are filled by secondary mineral, such as muscovite, indicating an alteration by hot temperature was occurred.

If we compared to the reference from Ferrill et al., (2004), the type of twinning calcite in the X-1 carbonate is categorized as type III. According to the reference, the paleotemperature can reach >200°C, meaning the carbonate was buried deeply and later uplifted.

Normally, this type of rock will give a high density reading in the velocity and gravity. However, the gravity gives a low anomaly density and there is also velocity reversal in the seismic. This is very contrary to the nature of carbonate lithology. However, this will make sense if there is fracture filled with fluid presents in the carbonate.

The XRD is showing an interesting result as the illite mineralogy presents as a dominant portion in clay mineralogy, and smectite is not present at all. The illite mineralogy commonly represents a higher temperature since smectite to illite transformation requires an increasing temperature. This correlate to the burial history of the “X” Structure.

The hydrocarbon indication also shown in the carbonate from CWT and AVO analysis as the class III. This means the chance of success to discovery become higher. This study needs to be tested for the future exploration program.

Conclusions

We have identified a new carbonate fracture play in South Sumatra. Comprehensive study from regional, seismic, gravity, geochemistry, petrography, and XRD show there is anomaly in carbonate basement fracture that may be correlate to the presence of hydrocarbon. This analysis should be tested for the next exploration program.

Acknowledgements

The writers wish to thank Mr Humbang Purba for his guidance and help through this paper.

Reference

Ferrill, David & Morris, Alan & Evans, Mark & Burkhard, Martin & Groshong. Jr, Richard & Onasch, Charles, 2004, Calcite Twin Morphology: A Low-Temperature Deformation Geothermometer. Journal of Structural Geology. 26. 1521-1529. 10.1016/j.jsg.2003.11.028.

PROCEEDINGS
JOINT CONVENTION BANDUNG (JCB) 2021
November 23rd – 25th 2021

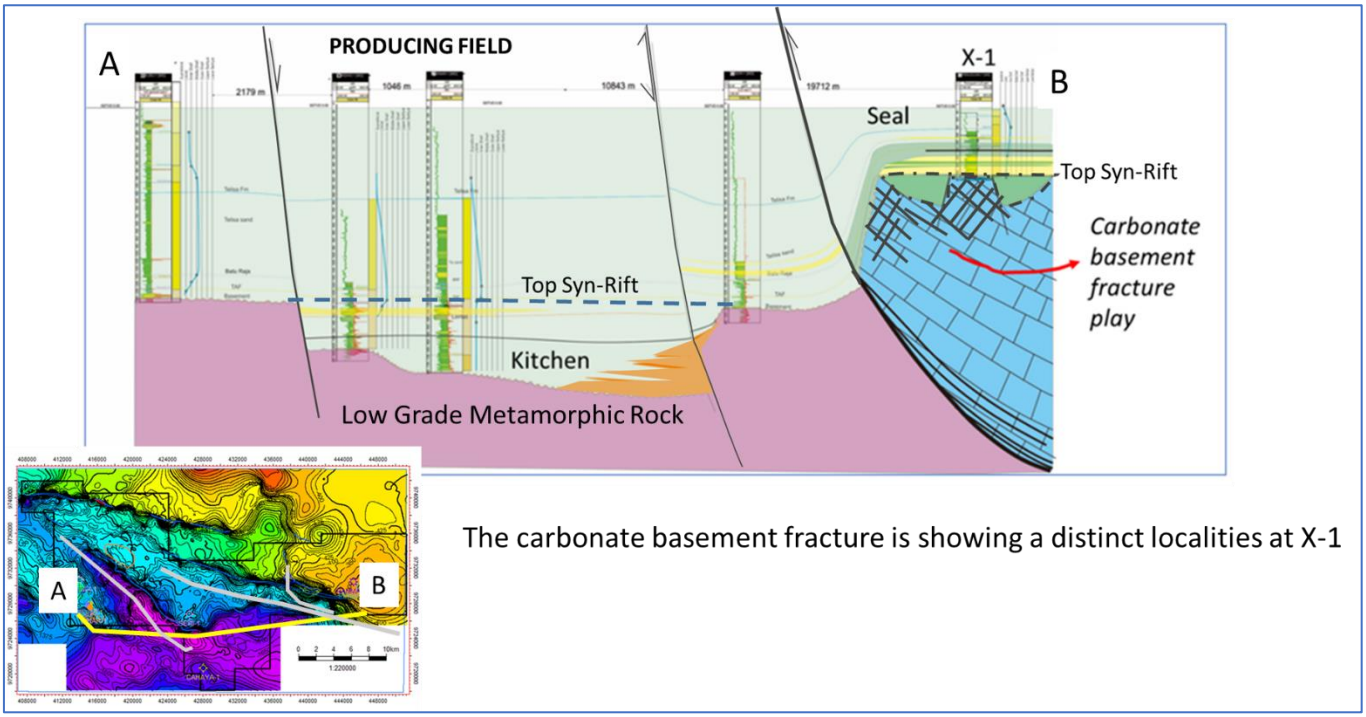

Figure 1: The regional cross section emphasizes the carbonate basement fracture play

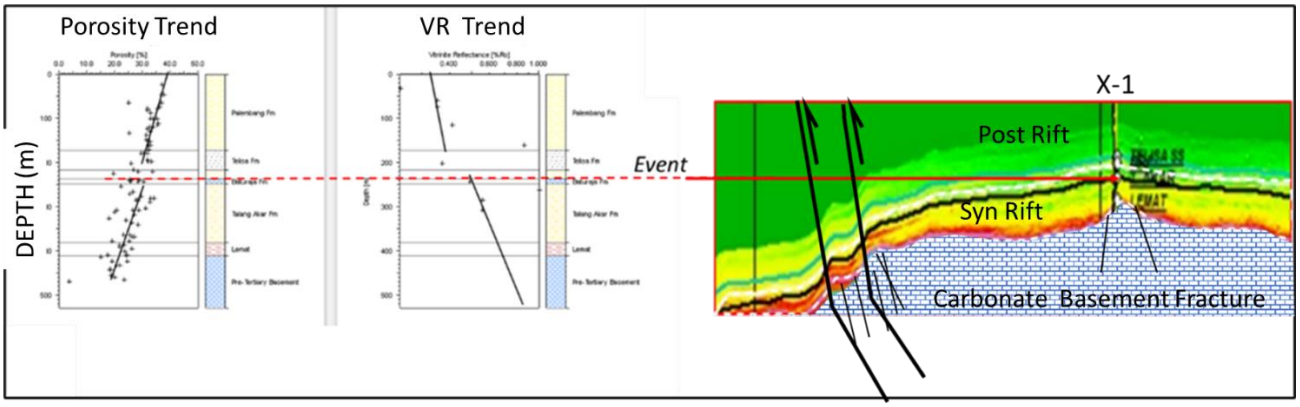

Figure 2: The porosity and vitrinite break that coincides with the last thickening event of syn-rift . This breaks means there is inversion occurs (at Middle Miocene) as we can see as the reactivation of reverse fault from section

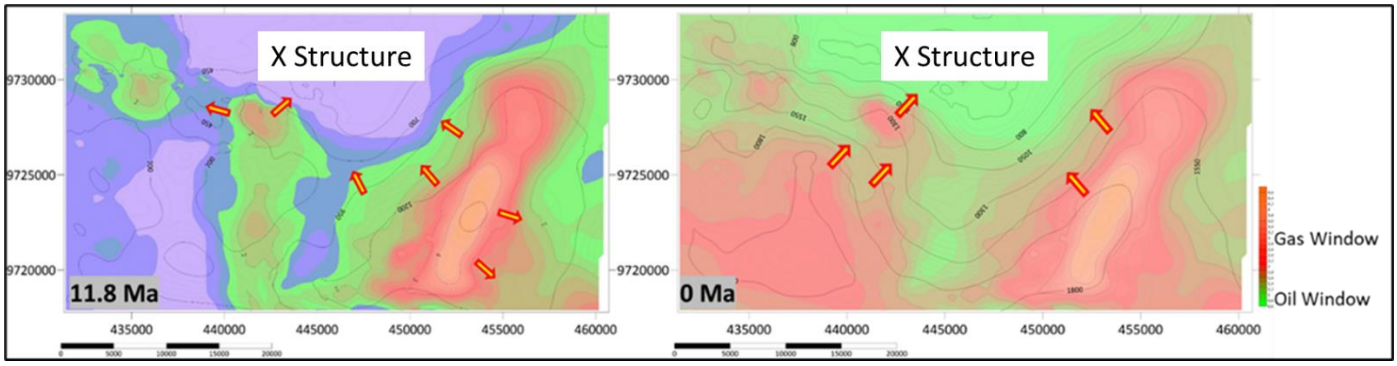

Figure 3: The "X" Structure at 11.8 Ma when the accumulation occurs

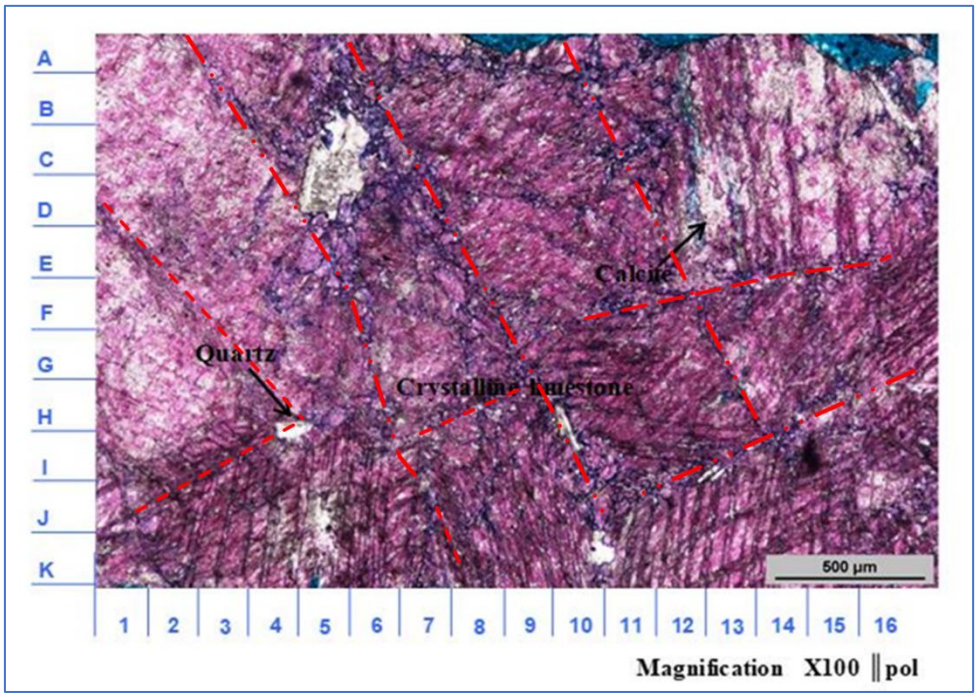

Figure 4: Fractured twinning calcite showing a deformed and highly tectonized carbonate basement

PROCEEDINGS
JOINT CONVENTION BANDUNG (JCB) 2021
November 23rd – 25th 2021

Fractured Reservoir in Baong Formation, North Sumatra Basin, Indonesia

Brianto Adhie Setya Wardhana[1], Hafidl Arsyi[1], Teuku Azransyah[1], Firdiansyah Mawardi[1], Ibnu Hafizh[1] Muhammad Mulyawan[1]

[1] Badan Pengelola Migas Aceh (BPMA)

Abstract

Fracture reservoirs are becoming a major issue throughout the entire world both old and new fields. Many newly discovered oil and gas fields happen to be fractured and their development constitutes a real challenge for E&P industry. North Sumatra Basin (NSB) is one of Indonesia's most profilic sedimentary basins. Baong Formation in NSB is one of the main rocks in the NSB with total content of shale hydrocarbon gas of 4,450 Mmboe and for oil 2,230 Mmbo. Despite of Baong Formation as a source rock in majority of field in NSB, The AR gas reservoir are hosted by fractured Middle Baong Sandstone (MBS) units.

The understanding how naturally fracture can develop in MBS is interested to discuss to expand the exploration in the NSB. This study provides an integrated subsurface data (well log, seismic, drilling report, etc) from several field, outcrop data analogue, and regional literature study. Based on this study fractured MBS can caused inversion tectonic activity, regional uplift in the Middle Miocene was observed by the reactivation of older horst and grabens in NSB and widespread erosion led to regional unconformities. The fracture play in MBS led us to the new exploration view in North Sumatra Basin.

Introduction

North Sumatra Basin is believed to have a good potential of hydrocarbon accumulation and remain challenging for exploration. Although conventional reservoirs dominate the North Sumatra Basin, a new type of sandstone reservoir also exists in the on shore are that has a low matrix porosity (tight) in which natural fractures govern both permeability and porosity.

Although fractures are present at some large scale in all reservoirs, it is only when they have sufficient spacing and length that their effect on fluid flow becomes important. Fractures not only enhance the overall porosity and permeability of many reservoirs, they also create significant permeability anisotropy In order to assess the role of fractures on hydrocarbon production and reservoir permeability an isotropy, characterization of naturally fractured reservoirs has focused primarily on the distribution and orientation of fractures and fluid-flow properties of individual representative fractures in a given reservoir volume.

The occurrence of fractured reservoirs over the world is well acknowledged. A quite significant proportion of world oil reserves is commonly assumed to lie in fractured reservoirs, for instance Firoozabadi (2000) gives an estimation of more than over 20%. Although not or less reported, the proportion is probably equivalent or higher for fractured gas reservoirs if one considers their higher depth in average, often involving a higher occurrence of diagenesis and fracturing phenomena.

The AR gas reservoir are hosted by fractured Middle Baong Sandstone (MBS) units. AR Field is a simple anticlinal structure having about 5 Km long and 1.5 Km wide. Gas was logged to the base of the reservoir at –2,985 meters (-9,653 ft) and the structure may fill to spill point at –2,985 meters (9,790.8 ft). The closure is about 5 kilometers long and 1.5 kilometers wide. AR field penetrated the gas accumulation in the Middle Baong Formation made up of sandstones containing some clay minerals. Two wells were drilled in this field.

Data and Method

Geological analysis from well log and seismic interpretation conducts a comprehensive analysis in this study to compare the characteristic of Baong Formation in another area. The analysis of tectonic regime in NSB combine with proven area of fractured gas reservoir, we get some criteria to analyze another potential area to be reviewed as a potential field that contain fractured sandstone reservoir in Baong Formation.

Some of seismic section was performed as a foundation of a structural style trap that indicate hydrocarbon accumulation. Seismic sections of a proven area in AR field guide us to identify the same situation of another area around the AR field. We also do petrophysical calculation from AR well in order to confirm the presence of the fracture in a proven gas reservoir

Result and Discussion

Regional Geology & Tectonic Review

The North Sumatra Basin, one of the three Sumatra back arc basins, is bounded on the southwest by the Barisan Mountain Front, on the southeast by the Asahan Arch, on the northwest by the Andaman Sea, and on the northeast by the Malacca Platform. The basin exhibits a dominant Northwest/Southeast and Northeast/Southwest structural trend.

Located in tectonically active area within the western margin of Sibumasu continent, NSB underwent several tectonic episodes controlling the basin development. Furthermore, these are also widely recognized from the structural orientation, regional lineaments as well as from the corresponding sedimentary sequences that are observed in outcrop and wells.

Davies (1984) modeled the NSB structural evolution as a product of interactive plate movements during the Tertiary. Major rotational and translational plate movements are responsible for the complex NSB setting and structures.

PROCEEDINGS
JOINT CONVENTION BANDUNG (JCB) 2021
November 23rd – 25th 2021

Daly et al. (1987) and Sosromihardjo (1988) defined that the tectonic model of NSB is principally controlled by the dextral Sumatran coupling fault system forming a major pull-apart basin (Pase sub-basin) bounded by Sigli and Tampur Platforms to the west and east respectively. Both Davies (1984) and Sosromihardjo (1988) agreed that Sumatra underwent rotational movements that modify the structural kinematics during the Tertiary despite their different understanding about the rotational direction of Sumatra.

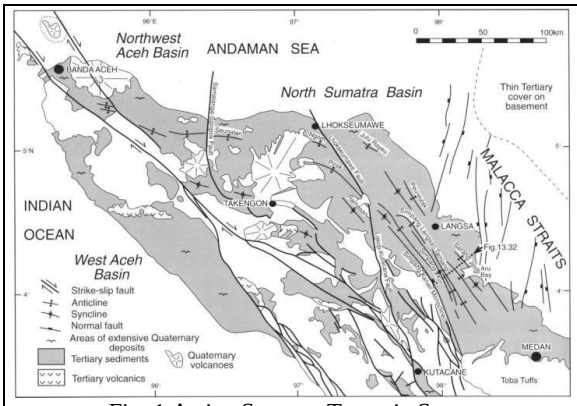

Fig. 1 Active Sumatra Tectonic System

Primary folds and faults of active Sumatra tectonic system are oriented Northwest-Southeast (Figure 1). Compressional or transpressional structures with the deformation intensity are decreasing to eastward across the coastal plain. Convergence subduction of the lithospheric plates between Australian Plate and Asia Plate is oblique resulting in right-lateral offset along Bukit Barisan strike-slip faults.

This Sumatra compressional tectonics overprint an earlier extensional regime, reactivating some pre-existing normal faults as high angle reverse faults and causing structure inversions. Rifting began in the Oligocene, following Eocene and earlier periods of tectonic quiescence. This period of normal faulting controls the distribution of deep gas reservoirs in the Peutu Formation. The intervening Middle Baong gas/condensate sand at AR field was affected by early tensional and later compressional regimes.

Oligocene extension segmented Sumatra into elongated through and horst blocks separated by broad, intervening basins. The upthrown north-south blocks trends are bounded by high angle normal fault systems. Movement on the faults persisted into the Miocene and the uplifts supported reef growth in the Lower Miocene Peutu Formation.

Entering Lower Miocene, the rifting decelerates, and subsequent transgression occurred, submerging the paleohigh and marked the post-rift episodes in NSB (Davies, 1984; Banukarso et al., 2013). Massive deposition of the Peutu limestone and Belumai sandstone equivalent occurred within the highs meanwhile the basinal carbonate and shales were deposited within the lows and submerged platforms (i.e., Matang-Pergidatit area). The transgression endures until Lower Middle Miocene, marked by backstepping carbonate deposition towards the Mallaca Platform (Alexander and Nellia, 1993). The latest tectonic activity occurred starting since Middle Miocene to Present is characterized by predominant compression, uplift, basin shoaling and reversal of sedimentation direction.

Despite the quite established subdivision of NSB tectonic phases from various researchers (rift, post-rift and syn-tectonic/inversion), some discrepancies remain, pertinent on the timing of tectonic events, age of sedimentary sequences and basin definition (Figure 2). Different area of study between researchers and variety of data coverage is accountable to this disagreement. In addition to that, among number of authors, only few of them extended the interpretation towards the Barisan Mountain by taking advantage of surface geology, which made significant differences of regional point of view (e.g., timing of Barisan uplift and southwestward extension of the basin).

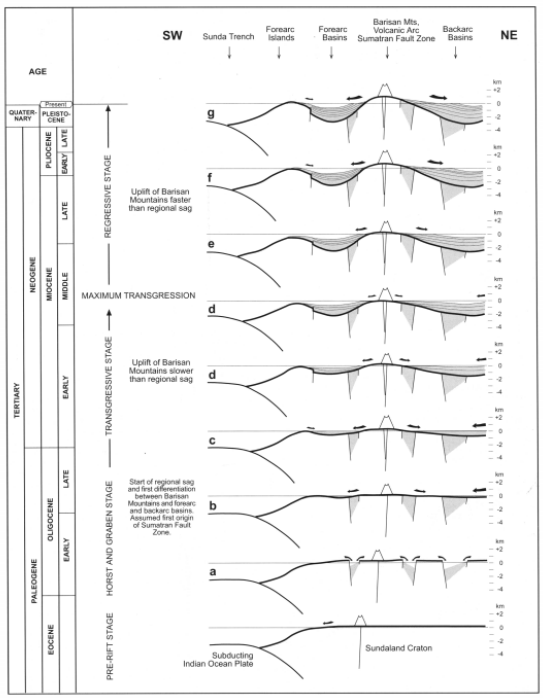

Fig. 2 Palinspastic cross-sections across Sumatra from SW to NE (Barber et al.,2005)

Barber et al. (2005) interpreted that the development of forearc and backarc basins are separating by the Barisan Mountains, which occurred in the latest Oligocene to the earliest Miocene. The starting regional sag resulted in the gradual submergence of the Barisan Mountains and the deepening of the basins in both the forearc and back-arc areas. Marine transgression extended until the Mid-Miocene when the Barisan Mountains still rose above sea level. The Barisan Mountains were uplifted and eroded from the Mid-Miocene onwards, accompanied by marine regression and dextral movements on the Sumatra Fault System, until Sumatra gradually took on its present outline.

In The Middle Miocene, Turbidite sandstone formations started to infiltrate the basins in the back-arc region from the Barisan Mountains until the Pliocene. The fractured turbidite sandstone may occur by the period of the regressive stage when uplift Barisan mountain faster than regional sag.

PROCEEDINGS
JOINT CONVENTION BANDUNG (JCB) 2021
November 23rd – 25th 2021

These movements coincided with the inversion of basin sediments, where the reactivation of faults, the folding of basin sediments, and the development of unconformities in the sequence transpired.

Characteristic of Baong Formation

Sedimentation & Facies

Baong Formation is divided into three sequences, Lower-Middle-Upper Sequence. The lower part of this formation is Baong Shale. A major transgression followed sedimentation of the Peutu Formation. The change from paralic environments in the Peutu limestone to bathyal deposits of the overlying Baong shale reflected a change in tectonic regime as well as a rise in relative sea level. The plate collision along the Sumatra trench became a dominant factor in regional tectonics resulting in reactivating and inversion of pre-existing extensional faults, development of major dextral transcurrent faulting, and compressional folding.

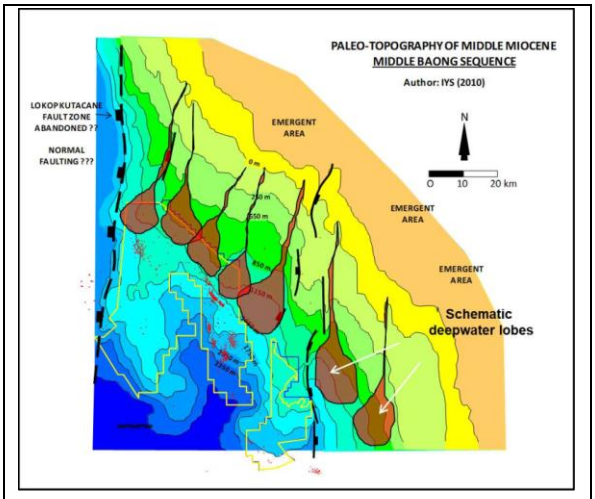

Fig. 3 Provenance of Baong Formation, Northeastward Direction

Regional subsidence accompanied these changes and formed a deep, extensive foreland basin that eventually filled with Baong shale. These basinal shales are onlap pre-existing structural high, including Peutu reefs. This unit consists predominantly of bathyal shale, with local concentrations of planktonic foraminifera forming thin, muddy limestone beds. Foraminifera zones for the Lower Baong vary from zones N-8 to N-11 in the Lower to Middle Miocene.

The middle part of Baong Formation is called Middle Baong sand due to the formation dominantly sandstone. Sands along the eastern basin margin indicate a major low-stand event near zone N-13. The sands derive from the Malacca Platform to the northeast, and they extend southwest. In eastern Block A, the Middle Baong sand is fine-grained and glauconitic. It occurs in three members, but only the second member, the MBS-II sand at AR, has significant hydrocarbon shows.

Middle Baong sedimentation ended with another period of tectonic quiescence. Erosion of pre-existing structural highs resulted in a widespread unconformity within zone N-14. Except for thin local sands above the unconformity, the overlying upper Baong consists of clay-rich mudstone. Paleoenvironment deepened again to bathyal depths, followed by gradual shoaling upward into paralic sands of the overlying Keutapang Formation. These sand prograded northeastward from source terrain in the rising Barisan Mountain (Figure 2).

Middle Baong Sandstone (MBS) in the research area is a member of Baong Formation, in lithostratigraphic dominated by deep sea shale facies. While in the Middle Baong Sandstone contain intercalated with shale. This caused by changing of water depth from bathyal to middle neritic caused by tectonic activity and drop of sea level present at the time of deposition (Situmorang et al, 1994).

Log Analysis & Fracture Indication

The MBS reservoir in AR field includes two sands separated by 11 meters (36.08 ft) of shale break. The upper MBS-IIA Sand is 11 meters (36.5 ft) thick, and the lower MBS-IIB Sand is 218.5 ft thick MBS-IIA has 11.5 % porosity, 1.43 mD and 35.8 % water saturation, while the MBS-IIB has 11.1 % porosity, 0.52 mD and 33.3 % water saturation, respectively. The typical log and the summary of the log analysis are presented in Figure-2.15 and Table-2.4. The porosity of both zones may be slightly underestimated due to formation damage. Sidewall core petrography characterized both MBS-IIA and MBS-IIB as fine to very fine grained argillaceous marine sandstone.

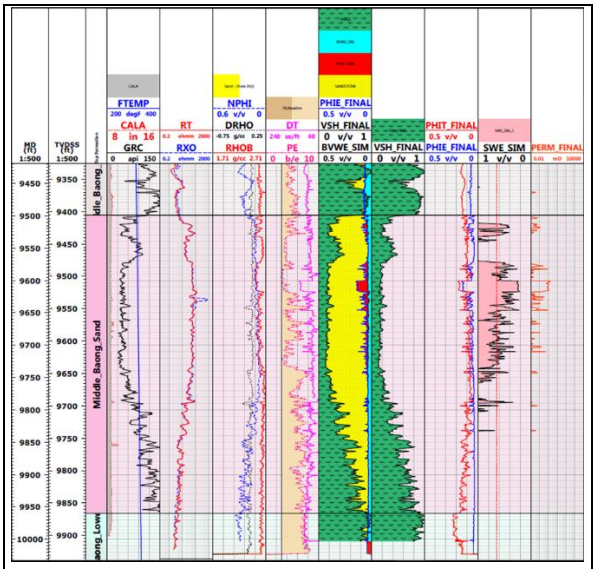

Fig. 4 Petrophysical Calculation Result of AR-1 Well

Based on petrophysical result of Middle Baong Sandstone in AR Field it has to be difficult to perform a good fluid flow with porosity range 8-10% and permeability range 07-1.4 mD. The property shows a low value. In the other hand, we have drilled 2 wells targeted in MBS reservoir and in those intervals dynamic loss occurred several times during 8.5 inch. After logging, we spotted a different pattern of the DT and PEF in MBS interval, although not whole body of

PROCEEDINGS
JOINT CONVENTION BANDUNG (JCB) 2021
November 23rd – 25th 2021

sandstone. The fractured interval was expected from relatively high DT and PEF log value

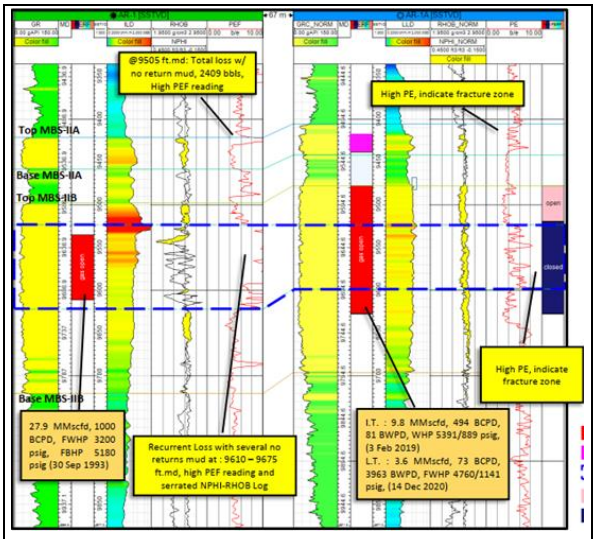

Fig. 5 Well Correlation and Potential Fracture Interval from Log Data

The test of an upthrown, east-west trending fault the closure found 75 meters of gas column in the Middle Baong sand. The sand is over-pressured with an effective mud weight equivalent to approximately 14.1 pounds per gallon. Extensive fracturing resulted in numerous drilling problems with lost circulation followed kick. Multiple cement squeezes and larger volumes of loss circulation material were pumped into the formation to cure lost return.

Seismic Data Review & Interpretation

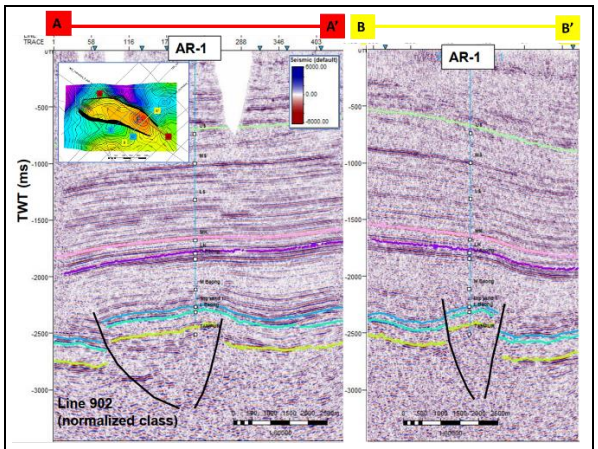

Fig. 6 AR Field Seismic Section

The seismic section from AR field was interpreted to determined structural trap, faults and horizon of a reservoir. The AR field is a simple anticlinal structure, the structure trending west-northwest and east-southeast and it was cut by thrust and normal faults trending northwest-southeast following the structural trend. These are high angle reverse faults and the feature maybe a positive flower structure associated with deeper strike-slip movement. A shallow syncline separates the eastern flank from structurally higher area to the southeast.

From seismic interpretation there is no indication a specific fracture feature from the Formation contain. Tampur until Middle Baong Formation in B-B' section shows some chaotic feature. The intense of chaotic feature are getting more visible in deeper area. It may cause from the tectonic activity in middle Miocene which reactivated the previous rift horst-graben product to build a trap in AR field. These activities are indicated as a period that fracture developed in some Formation with relatively more brittle.

Development Area

Another lead and prospect (figure xx) with same regional tectonic framework in NSB particularly near research area is considered to be the next development. The issue that can be raised related to the tectonic model in the NSB is due to the ranges of existing structural model and evolution. These issues can be broken down into two main categories, the first being related to Paleogene extensional system where different approaches of rifting mechanism have been introduced by various authors (Davies et. al., 1984; Daly et. al., 1987; Sosromihardjo, 1988; Collins et. al., 1996). Secondly, related to subsequent Neogene basin evolution where many researchers pinpoint basin inversion and potential foreland mechanism to explain basin regressive period (Davies, 1984; Daly et al., 1987; Fuse et al., 1996; Banukarso et al., 2013).

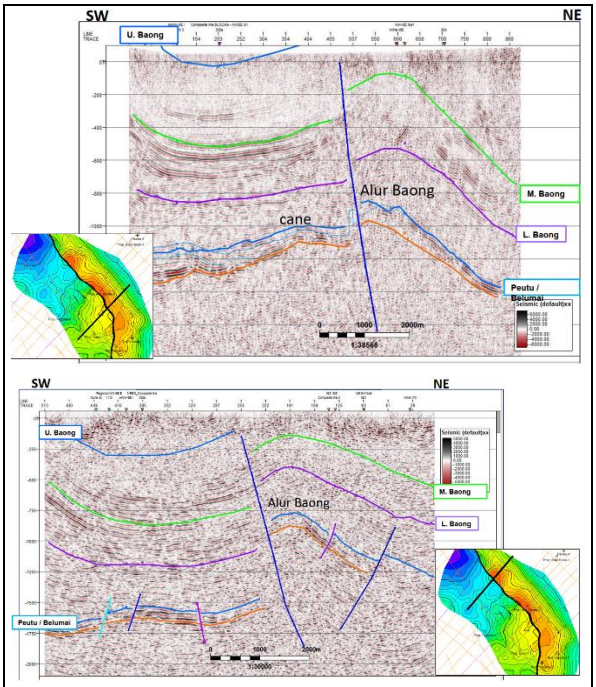

Fig. 7 Seismic Section of Alur Baong Field (Potential Field Area for Baong Formation)

Conclusions

- Fracture is one of the most important geological phenomena that affect the production of hydrocarbon compounds in broken sandstone reservoirs. However,

fracture controlling factors must be combined with well data to achieve accurate fracture modeling.

- The occurrence of fractured reservoirs possibly from latest tectonic activity occurred starting since Middle Miocene to Present which characterized by predominant compression, uplift, basin shoaling and reversal of sedimentation direction.
- In The Middle Miocene, Turbidite sandstone formations started to infiltrate the basins in the backarc region from the Barisan Mountains until the Pliocene. The fractured turbidite sandstone may occur by the period of the regressive stage when uplift Barisan mountain faster than regional sag. These movements coincided with the inversion of basin sediments, where the reactivation of faults, the folding of basin sediments, and the development of unconformities in the sequence transpired.
- The Middle Baong Sandstone have been a proven reservoir in North Sumatra Basin. Based on this study fractured Middle Baong Sandstone have a good reservoir quality for future development
- Middle Baong Sandstone in North Sumatra Basin can be alternated host of fracture reservoir in North Sumatra Basin.
- This study indicates that there is possibility of fractured reservoir developed not only on the research area but also on another research area with high tectonic activity after the Baong Formation deposited.
- The fractured classification in MBS reservoir is very essential to develop the potential of AR field. It's suggested to core some interval in fracture section or run the image log to get a better understanding of fracture behavior.

References

Barber, A. J., Crow, M. J & M. E. M. De Smet, 2005, Tectonic Evolution, 14, 234-259

Davies, P.R., 1984, Tertiary Structural Evolution and Related Hydrocarbon Occurrences, North Sumatra Basin Proc. Indonesia Petroleum Association 13th Ann. Conv., vol. I, p.19-50

Banukarso, M., Meckel, L.D., Citrajaya, N., Raharjo, S., 2013, An Inverted Syn-Rift Play in The Offshore North Sumatra Basin, Proc. Indonesia Association of Geologist, 37th Ann. Conv.

Ariyanto, P., 2018, New Insight into Structural Development of The Block A Area, North Sumatra Basin: Constrain from Subsidence Analysis and Palinspatic Reconstruction. Indonesia Petroleum Association 42 th Ann. Conv.,

Anderson, B.L., J. Bon and H.E. Wahono, 1993, Reassessment of the Miocene Stratigraphy, Paleogeography and Petroleum Geochemistry of the Langsa Block in the Offshore North Sumatra Basin: Proc. Indonesia Petroleum Association 22nd Ann. Conv., vol. I, p.169-190.

Acknowledgements

The authors wish thanks to Head and Deputy Head of Upstream Oil and Gas Management Agency of Aceh (BPMA) for giving permission to publish the data presented in this paper and Medco E&P Malaka Subsurface Team for the contribution to do the research.

PROCEEDINGS
JOINT CONVENTION BANDUNG (JCB) 2021
November 23rd – 25th 2021

A Study of Comparison of the effectiveness between the Process Safety Management Programs Deployed by E&P Companies in Indonesia

Muhammad Riandhy[1,2], Ignatius Gerald Tondi Sinaga[1,3], Handy Suryowicaksono[1,4], Ismail Ghulam Halim[1,5], Iqbal Fauzi[1,6]
1.Enerka Bhumi Pratama, Kawasan Komersial Cilandak Gudang 410, Jakarta Selatan 12560, Indonesia
2.PT. Pertamina Hulu Rokan, Jakarta Selatan 12940, Indonesia
3.Universitas Gadjah Mada, Yogyakarta 55281, Indonesia
4.Institut Teknologi Sepuluh Nopember, Surabaya 60111, Indonesia
5.Universitas Indonesia, Depok 16424, Indonesia
6.Institut Teknologi Bandung, Bandung 40132, Indonesia

Abstract
Oil and gas production has always been a high-risk process, involving highly flammable substances, toxic materials and waste, heavy equipment, and in some areas even hazard by wildlife. Human involvement in this industry is integral, and keeping the workers safe is a challenge that every company has to face. In Indonesia, exploration and production companies are implementing their own Process Safety Management (PSM) program for every aspect of the company to adhere to fit the company's standard of safety. Even a tiny neglect of the PSM may cause material loss of containment, fire, and explosion, some leading to catastrophic events that result in loss of assets. Added to that, fines, sanctions, and stricter regulations may give negative feedback for the respective company. Thus, the importance of proper PSM programs is not to be underestimated. Process safety management program comprises commitment to process safety, understanding hazards involved, managing risks that may occur, and learning from documentations of previous accidents or near misses. It is a comprehensive program that encompasses every essential element involved. Still, some companies' PSM programs held better safety records than the others. The aim of this paper is to compare and give recommendations for the more robust PSM program to be implemented by companies. To be more precise, this paper focuses on PSM programs that are implemented by oil and gas exploration and production companies in Indonesia. The authors focus on more recently updated accident data and latest implementation of the PSM program, as the foregoing program may be outdated and may lead to inaccurate results. The authors aim for this paper to be taken for consideration for further iterations of the PSM program to be implemented by oil and gas companies that operate around the globe, as some of the cases mentioned here might be similar to conditions faced by the company. Furthermore, may this paper sparks the spirit of safety culture to the professionals of the industry and establish the need of safety transparency to the eyes of the public. All of this effort may result in a better safety assurance for the workers involved and industry-wide, erases the connotation of oil and gas as a 'dirty and unsafe' industry. The implementation of a robust PSM program will act as a catalyst for a better oil and gas industry in the future.

Keywords: Process Safety Management, Surface Facilities, Safety Culture

Introduction

Oil and gas production has always been a high-risk process, involving highly flammable substances, toxic materials and waste, heavy equipment, and in some areas even hazard by wildlife. Human involvement in this industry is integral, and keeping the workers safe is a challenge that every company has to face. In Indonesia, exploration and production companies are implementing their own Process Safety Management (PSM) program for every aspect of the company to adhere to fit the company's standard of safety. Even a tiny neglect of the PSM may cause material loss of containment, fire, and explosion, some leading to catastrophic events that result in loss of assets. Added to that, fines, sanctions, and stricter regulations may give negative feedback for the respective company. Thus, the importance of proper PSM programs is not to be underestimated.

Research shows that the incidence rate of failure in the oil and gas industry has increased over the years (Platt & Platt, 1989). From these studies, it can be seen that there are incidents that cannot be predicted so that a preventive technique approach is needed instead of a reactive technique for failures that occur (Nwankwo et al., 2020). One example occurred on the Deepwater Horizon in 2010 which spilled 4 million barrels of crude oil into the Gulf of Mexico. This incident has an impact on the marine environment, abandoned refinery businesses, and led to criminal charges against British Petroleum (BP) of up to 60 billion US Dollars (Norazahar et al., 2014). Other cases also occurred in the Piper Alpha disaster in 1988 which caused the death of 167 people, the Alexander Kielland collapse incident in 1980 which caused the death of 123 people and the BP explosion in Texas in 2005 which resulted in 15 deaths and 180 injuries (Ismail et al., 2014). The root cause of these incidents occurred in process safety failures which consisted of lack of communication, asset problems, poor company management and human factors (Hsu et al., 2015). This can be prevented by implementing Process Safety Management (PSM) in all process facilities (Bridges & Tew, 2010). In this study, a comparative study of the effectiveness of Process Safety Management was conducted based on incidents that had occurred in the oil and gas industry.

20 Elements of PSM based on CCPS

The Center for Process Safety (CCPS) was established by the American Institute of Chemical Engineers (AIChE) in 1985 to research and disseminate technical information for the avoidance of significant chemical catastrophes (Hanida & Azmi, 2017). Risk-based Process Safety (RBPS) was developed by CCPS and named as the framework for the next generation of Process Safety Management (PSM). Figure 1 lists the features of RBPS, which are based on four pillars : commit to process safety, understand hazards and risk, manage risk and learn from experience (*Comparision of Process Safety Management System: CCPS Risk-Based & OSHA PSM*, 2019). Based on the perceived needs, resource requirements, and existing safety culture of the institution, very diverse RBPS actions may arise (NJ, 2007).

a. Process safety culture: Process safety culture has been defined as, "the combination of group values and behaviors that determine the manner in which process safety is managed". Employees at all levels are

dedicated to process safety in this positive environment. This starts at the highest levels of organization and is shared by everyone. Leaders in the field of process safety encourage it.

b. Compliance with standards : A system for identifying, developing, acquiring, evaluating, disseminating, and providing access to process safety-related standards, rules, regulations, and legislation. Internal and external standards, as well as national and international codes and standards, industry association guidelines and practices, and municipal, state, and federal rules and laws, are all addressed by the standards system.

c. Process Safety Competency: To control its process dangers, the firm need the necessary skills and resources in the right areas. Confirmation that the organization as a whole have certain abilities and resources. This knowledge may be put to use in succession planning and change management.

d. Workforce Involvement : Actively committing to established safety standard

e. Stakeholder Outreach: A method for finding, interacting with, and sustaining positive connections with external stakeholder groups. This includes the local community, raw material suppliers, customers, government agencies and regulators, professional societies, contractors, and others.

f. Process Knowledge Management : Documentations and records of any accident

g. Hazard Identification and Risk Analysis: Process safety threats and their possible effects are identified. The dangers associated by various hazard situations are defined. Recommendations for reducing or eliminating risks, reducing possible consequences, and reducing the frequency with which they occur. Depending on the amount of risk, the analysis might be qualitative or quantitative.

h. Operating Procedures: Written instructions for a manufacturing process that explain how the activity should be carried out properly, the consequences of departure from procedures, important safeguards, and exceptional situations and emergencies.

i. Safe Work Practices : Process and operational status monitoring, especially on maintenance and non-routine practices

j. Asset integrity and reliability
Management of operational interfaces. Ensures that critical equipment stays fit for its intended function throughout its service life.

k. Contractor management
Practices to guarantee that contract personnel can execute their tasks safely and that contracted services do not contribute to or exacerbate operational hazards at the site.

l. Training and Performance Assurance
Ensure that workers meet performance standards and to identify where additional training is required

m. Management of Change
Any changes to a process do not inadvertently introduce new hazards

n. Operational Readiness
Before starting or restarting a process, it must be evaluated to verify that it can be started safely. This rule applies to facilities that have been shut down or idled, as well as process modifications and maintenance. This is also true for the start-up of new facilities.

o. Conduct of Operations
Means of carrying out the necessary managerial and operational responsibilities for process safety in a thoughtful, faithful, and systematic manner. Managers ensure that employees complete essential tasks and that performance does not deviate from expectations.

p. Emergency Management
Emergency planning that define actions in an emergency (routes, continuous improvement of strategies) and responses (trainings, how to notify an accident).

q. Incident Investigation
Reporting, tracking, investigating incidents. Provides data for resolution and documentation of recommendations generated by the investigations.

r. Measurements and Metrics
Incidence and near-miss rates, as well as measures that demonstrate how well essential process safety aspects are executed, are leading and lagging indicators of

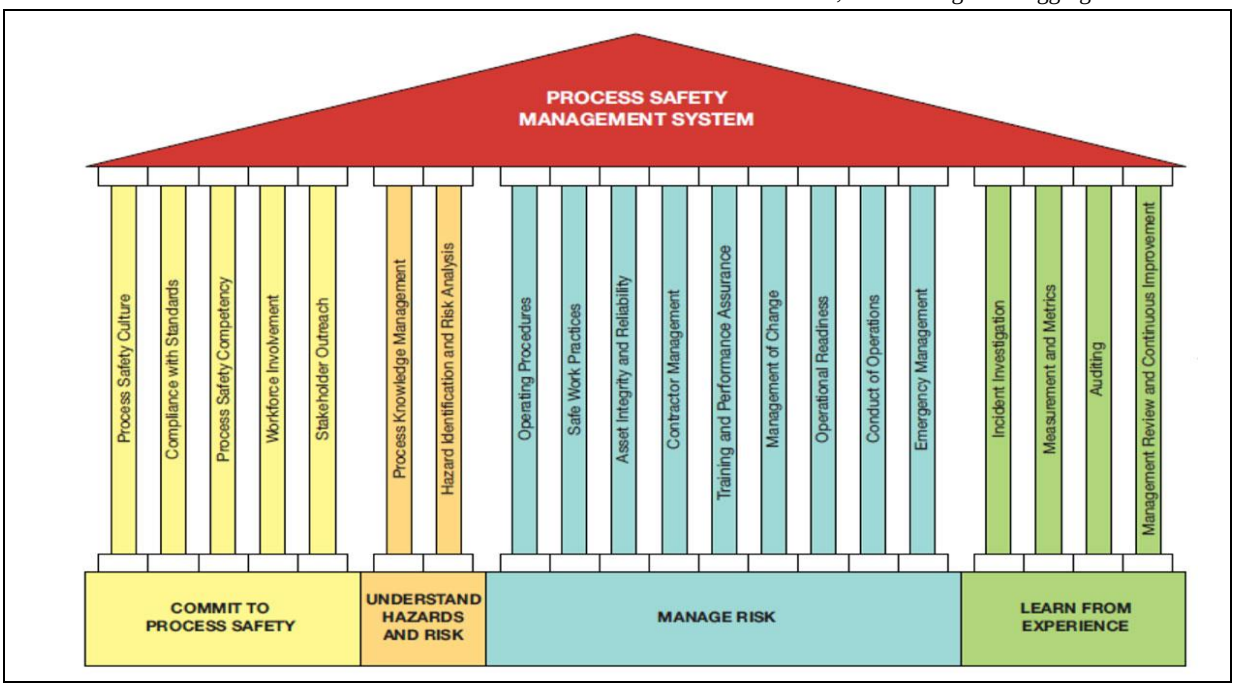

Figure 1: 4 pillars and 20 elements of PSM

PROCEEDINGS
JOINT CONVENTION BANDUNG (JCB) 2021
November 23rd – 25th 2021

process safety performance. This data is utilized to promote process safety improvements.

s. Auditing
Evaluation of safety management system.

t. Management Review and Continuous Improvement
Routine evaluation of whether management systems are performing as intended. Continuously improve current safety system.

Risk & Hazard Potential

Potential hazards are abundant in upstream oil and gas operations. A hazard is defined simply as something that can cause harm, for example gas release, toxic chemical and live electric line. When combined with the likelihood of exposure to the hazard, it becomes a risk. A risk is the probability, high or low, that any hazards will actually cause harm to personnel, environment or assets. Risk can be calculated by multiplying the likelihood of the hazard occurring with the magnitude of the hazard impact. Table 1 shows some of the major hazards and its associated cause normally encountered in upstream operations. These hazards will be the basis for the incident collection used to measure the effectiveness of PSM program in this study.

Overview Surface Facility Operation and Its Associated Hazards

The surface facility operation is very important in the oil and gas industry. It is responsible to process and treat the product from well specification to commercial specification. Simplified diagram of the surface facility process can be seen at Figure – 2.

The first process carried out is the separation of gas from liquid and the separation of water from oil using separator. The separator is a tank a fixed pressure tank that is used to separate the streamflow from the well into gas, oil, and water-based on the density of each substance. There are 3 types of separators used in general at surface facilities, namely High Pressure (HP) Separator, Intermediate Pressure (IP) Separator, and Low Pressure (LP) Separator. The streamflow from the well will first enter the HP Separator and then be separated into gas and liquid phase. The gas which has a low density will flow into the top to flow as the sales product and the liquid which has a heavier density will go down to the bottom of the vessel and enter the next process at the IP Separator. In this equipment, further separation between gas and liquid phase is also carried out. The gaseous phase will come out to the top towards the compressor to increase its pressure to the sales product pressure. The liquid will come out through the bottom of the vessel to the LP Separator. This LP Separator is used to separate 3 phases so this separator is commonly called a 3 phase Separator. The LP Separator is separated into 3, namely oil, water, and gas. The gas will exit through the top and enter the compressor to increase the pressure so that it meets the sales product pressure. Liquid phase consisting of oil and water will be separated in the LP Separator equipment. Because the separation of oil and water may not be perfect then the oil produced from the LP Separator will enter the Oil Treating process. In this process, heating is carried out to reduce the viscosity of the oil so that there is an evaporation of water in the oil. Meanwhile, the water which is separated from the oil will enter the Water Treating process. In this process, the oil still contained in the water is separated. The oil must be separated from the oil at a certain level before it can finally be discharged. From the surface facility description, there are many potential hazards. Referring to API RP 14J, the hazards can be summarized in Hazard Tree shown in Figure 3.

Data and Method

In this study, 2 types of data were used to evaluate the PSM program used by exploration companies, namely incident data as an indicator of the success of the PSM program and data on the PSM program run by each company. Data on incidents that occurred in oil and gas companies in Indonesia were obtained from the media in the form of news from the last 10 years. Data on the PSM program run by each company was obtained from various kinds of literature such as the company's official website and journals.

Result and Discussion

The research was conducted by collecting data in the form of incidents that have occurred based on the potential hazards in the production facilities that have been described previously. The study involved the analysis of each company's method of managing process safety in the facility and clustering to each of the 20 elements and 4 pillars of RBPS process safety management. Some of the companies have multiple items that can be categorized in the same pillar, while at the same time do not have any items to support the other pillars. A total of 5 companies were

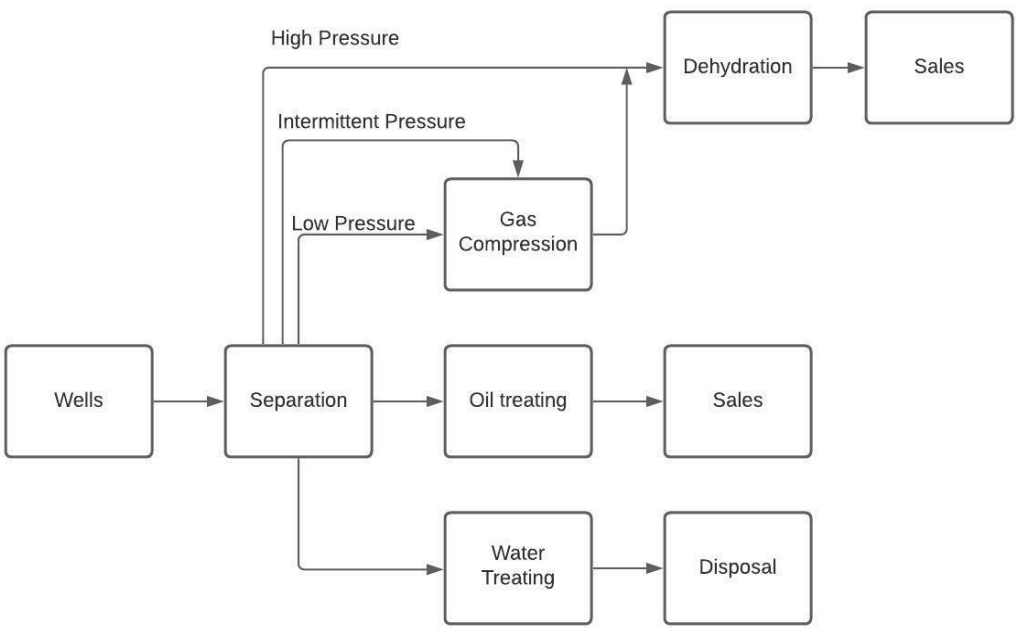

Figure 2: Block Flow Diagram Surface Facility Operation

PROCEEDINGS
JOINT CONVENTION BANDUNG (JCB) 2021
November 23rd – 25th 2021

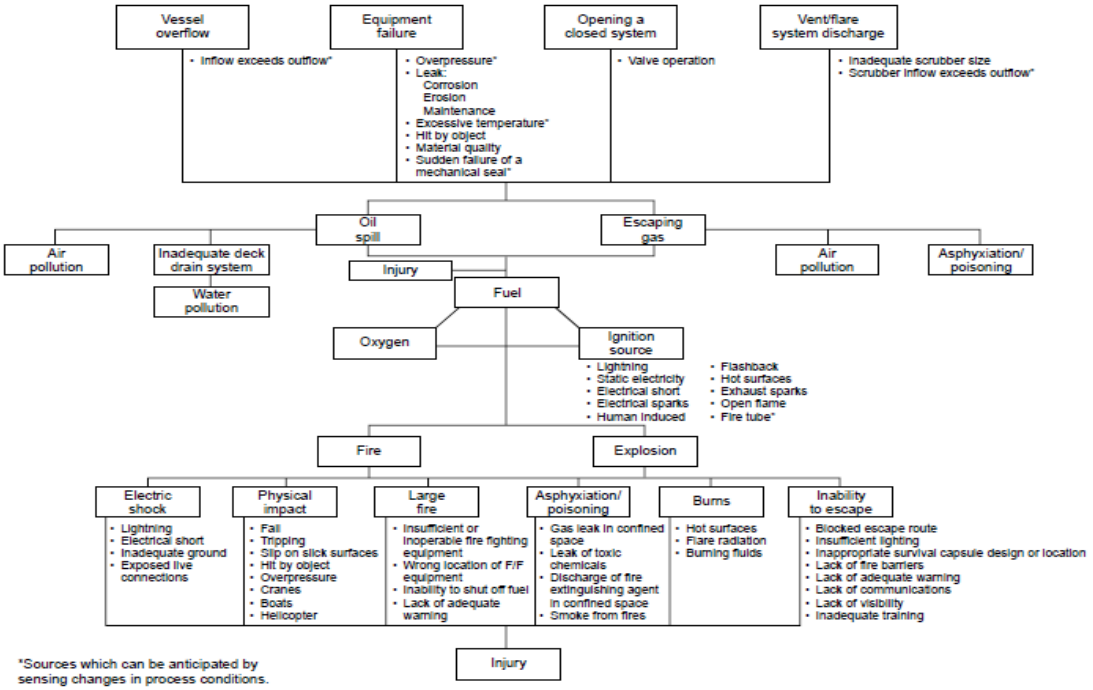

Figure 3: Hazard Tree Surface Facility Operation

selected for this study, and the number of publicly covered accidents in the last 10 years were documented to investigate the relationship -if any- between the number of accidents and the elements supported in the process safety management system.

The comparative framework used within this study uses 20 elements and 4 pillars of RBPS PSM. Under the Commit to Process Safety: Process Safety Culture, Compliance with Standards, Process Safety Competency, Workforce Involvement, and Stakeholder Outreach. Under the Understand Hazards and Risk: Process Knowledge Management and Hazard Identification and Risk Analysis. Under Manage Risk: Operating Procedures, Safe Work Practices, Asset Integrity and Reliability, Training and Performance, Management of Change, Operational Readiness, and Emergency Management. Under Learn from Experience: Incident Investigation, Measurement and Metrics, Auditing, and Management Review and Continuous Improvement.

Accident data used for this study were sourced from public news coverage and excluding close calls or tier 3 events. There is no other information regarding accidents that are not publicized and close call reports from any employees of the selected companies. All of the authors of this study are independent and impartial, which does not give any advantage nor disadvantage to any of the companies assessed. The accident covered in this study is limited to the last 10 years to filter out the possibility of obsolete data as the result of the out-of-date process safety management system employed by the companies prior to the newest.

Table 2 reveals the PSM program E&P companies in Indonesia. Categorized by the four pillars of 20 elements of RBPS process safety management, it appears that all companies have at least one of the elements for each pillars of process safety management. With exception to Pertamina Hulu Energi who does not have its own Engineering Standards.

Based on the count of publicly released incident data visualized in Figure 3, Shell Indonesia leads with 0 public incident. Shell's success is mainly caused by its strong process safety culture reflected by its robust process safety fundamentals and its strong commitment to safety through its Get Zero principles and Safety Culture Awareness program. From fundamental design stand point, Shell Engineering Standards, the DEP provides detail and clear guidance on good engineering practices to design and construct a safe facility. However, this does not means other E&P companies in scope of the study lacks strong process safety culture and commitment. Other companies in scope also have a strong PSM programs. However, the implementation may need to be improved, especially in process safety culture awareness section. This can be done by having a strong, fit for operations process safety fundamentals that is routinely communicated and campaigned topped with strong focus in continuously improving process safety competencies at every level in the organization. Building a strong process safety culture is a long game, therefore the earlier the process starts the better.

PROCEEDINGS
JOINT CONVENTION BANDUNG (JCB) 2021
November 23rd – 25th 2021

Risk and Hazard Potential	Possible Cause
Fire and Explosions	Presence of highly combustible hydrocarbons from loss of containment, oxygen and igniter
Exposure to Harsh Chemicals	Chemicals used in daily operations tend to be hazardous. Long-term exposure to hazardous and volatile chemicals and gases can cause respiratory and mental health issues in employees. In fact, chronic exposure to a common molecule known as hydrogen sulphide has been linked to leukaemia, paralysis, and even death.
Electrical and Other Hazardous Energy	If equipment is not designed, installed, and maintained appropriately, workers may be exposed to uncontrolled electrical, mechanical, hydraulic, or other sources of dangerous energy.
High Pressure Lines and Equipment	Workers may be exposed to compressed gases or high-pressure lines, which pose a risk. Internal line degradation could cause leaks or line bursts, exposing employees to high-pressure threats posed by compressed gases or high-pressure lines. Struck-by risks could be created if connections securing high-pressure lines fail.

Table 1: Risk and Hazard Potential for Production Facility (Insurance, 2021; *Safety and Health Management System in Oil and Gas Industry*, 2021; *Safety Hazards Associated with Oil and Gas Extraction Activities*, 2021; Suda et al., 2015)

Conclusions

A major inference from this study is no one-size-fits-all approach to process safety management. Companies should be thorough when deciding the right system that will be the most suited to the scope of their operations. There is a relation between more pillars covered and lack of accidents, however, every company should thrive to have all pillars in an RBPS process safety management system to maximize the managed area covered by the system.

This study has limitations, namely, the accidents included in the study are public -and by the result, major- accidents. This results in some blind spots for minor reported accidents that do not get coverage by media and close calls which are not reported as accidents but may be beneficial to indicate the weakness in the process safety management in the respective company. Another area to be improved is testimonials from companies studied that can provide insights that are not represented by the number of accidents, namely: the efficiency of the system, the responsiveness of the system, and the process shutdown caused by false-trip that is detected.

PROCEEDINGS
JOINT CONVENTION BANDUNG (JCB) 2021
November 23rd – 25th 2021

PSM Pillar Aspects (CCPS RBPS Based)		PSM Program at E&P Companies in Indonesia			
		Pertamina Hulu Energi	**Conoco Phillips**	**Chevron**	**Shell**
Commit to Process Safety	Process Safety Culture	SUPREME	SPIRIT	Operational Excellence	Safety Culture Awareness
	Compliance with Standards	-	COPSAS	Chevron Engineering Standards (CES)	Shell Design & Engineering Practices (DEP)
	Process Safety Competency	KOMET	COPI Process Safety Fundamental	Process Safety Organizational Capability	Shell Process Safety Fundamental
	Workforce Involvement	Process Safety Campaign	Process Safety Campaign	Process Safety Campaign	Process Safety Campaign
	Stakeholder Outreach	Community Outreach	Community Outreach	Community Awareness & Outreach	Community Outreach
Understand Hazards and Risk	Process Knowledge Management	Process Safety Information	Process Safety Information	Process Safety Information	Process Safety Information
	Hazard Identification and Risk Analysis	Risk Identification (HAZOP/HAZID /QRA)	Risk Assessment	Process Hazard Analysis	Hazard Identification and Risk Analysis
Manage Risk	Operating Procedure	Standard Operating Procedure	Operating Procedures	Operating Procedure and Standard Operating Procedure	Operating Procedures
	Safe Work Practices	Corporate Life Saving Rules	Life Saving Rules	Managing Safe Work	Safe Work Process
	Asset Integrity and Reliability	Process Safety & Asset Integrity Management System	Asset and Operating Integrity	Surface Equipment Reliability & Asset Integrity Practices	Asset Integrity & Process Safety Management
	Training and Performance	Training	Training	Training	Training
	Management of Change	Management of Change	Management of Change	Management of Change	Management of Change
	Operational Readiness	Pre Start-Up Safety Review	Pre Start-Up Safety Review	Pre Start-Up Safety Review	Pre Start-Up Safety Review
	Emergency Management	Emergency Planning and Response	Emergency Preparedness	Emergency Management	Emergency Management
Learn from Experience	Incident Investigation	Accident/Incident Investigation	Incident Reporting and Investigation	Incident Investigation	Incident Investigation
	Measurement and Metrics	Performance Measurement	Process Safety Leading & Lagging Indicators	PSM Visible Scorecards	Performance Monitoring & Reporting
	Auditing	SUPREME Audit	HSEMS Audits	OEMS Audit	SEMS Element Audit
	Management Review and Continuous Improvement	Management Walkthrough	Process Safety Boards	PSM Leadership Engagement	Leadership F2F Engagement

Table 2: Comparison PSM Program

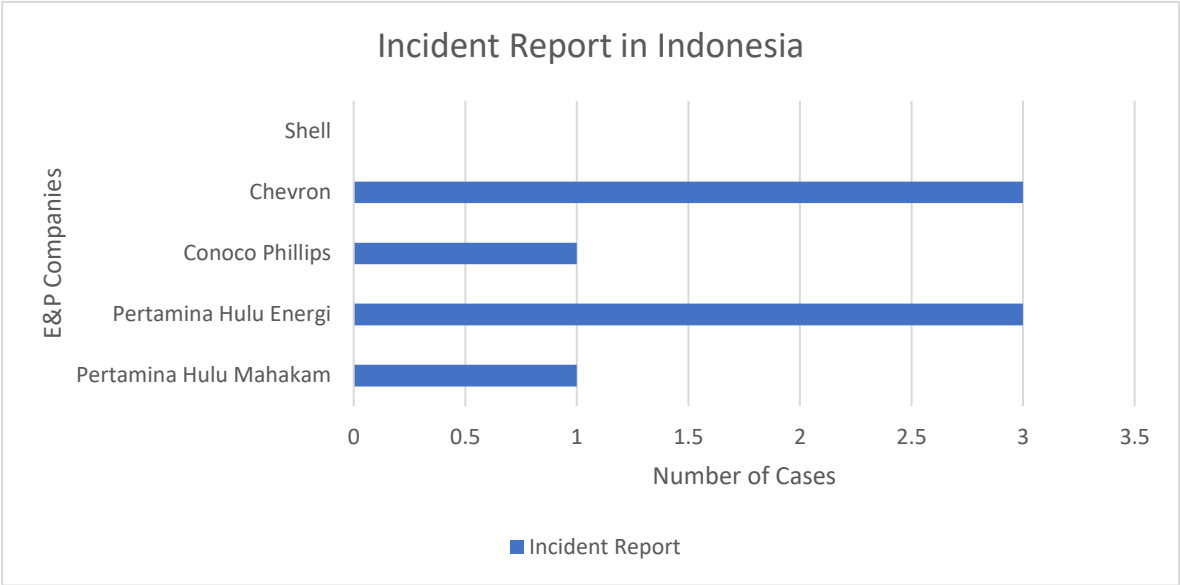

Figure 3: Incident report from several E&P Companies in Indonesia

References

Bridges, W., & Tew, R. (2010). Human factors elements missing from Process Safety Management (PSM). *AIChE Annual Meeting, Conference Proceedings*.

Comparision of Process Safety Management System: CCPS Risk-Based & OSHA PSM. (2019).

Hanida, A., & Azmi, M. (2017). A Journey of Process Safety Management Program for Process Industry. *International Journal of Engineering Technology And Sciences (IJETS)*, *8*(1), 1–9. https://doi.org/10.15282/ijets.8.2017.1.10.1085

Hsu, W. K. K., Huang, S. H. S., & Yeh, R. F. J. (2015). An assessment model of safety factors for product tankers in coastal shipping. *Safety Science*, *76*, 74–81. https://doi.org/10.1016/j.ssci.2015.02.022

Insurance, D. (2021). *Identifying Oil and Gas Industry Hazards*. https://www.danielsinsuranceinc.com/identifying-oil-and-gas-industry-hazards/

Ismail, Z., Kong, K. K., Othman, S. Z., Law, K. H., Khoo, S. Y., Ong, Z. C., & Shirazi, S. M. (2014). Evaluating accidents in the offshore drilling of petroleum: Regional picture and reducing impact. *Measurement: Journal of the International Measurement Confederation*, *51*(1), 18–33. https://doi.org/10.1016/j.measurement.2014.01.027

NJ, H. (2007). *Guidelines for Risk Based Process Safety*. Wiley-AIChE.

Norazahar, N., Khan, F., Veitch, B., & MacKinnon, S. (2014). Human and organizational factors assessment of the evacuation operation of BP Deepwater Horizon accident. *Safety Science*, *70*, 41–49. https://doi.org/10.1016/j.ssci.2014.05.002

Nwankwo, C. D., Theophilus, S. C., & Arewa, A. O. (2020). A comparative analysis of process safety management (PSM) systems in the process industry. *Journal of Loss Prevention in the Process Industries*, *66*(May), 104171. https://doi.org/10.1016/j.jlp.2020.104171

Platt, H. D., & Platt, M. A. (1989). Failure in the Oil Patch: An Examination of the Production and Oil Field Services Industries. *The Energy Journal*, *10*(3), 35–

49. https://doi.org/10.5547/issn0195-6574-ej-vol10-no3-3

Safety and Health Management System in Oil and Gas Industry. (2021). https://www.wipro.com/oil-and-gas/safety-and-health-management-system-in-oil-and-gas-industry/

Safety Hazards Associated with Oil and Gas Extraction Activities. (2021). https://www.osha.gov/oil-and-gas-extraction/hazards#high

Suda, K. A., Shima, N., Rani, A., Rahman, H. A., & Chen, W. (2015). A Review on Risks and Project Risks Management: Oil and Gas Industry. *International Journal of Scientific and Engineering Research*, *6*(8), 938–943.

PROCEEDINGS
JOINT CONVENTION BANDUNG (JCB) 2021
November 23rd – 25th 2021

Extractive Heating Thermal Oxidizers Configuration Design as an Operational Safety Improvement and Energy Conservation in Gas Processing Plant

Nicky Leonard Nasution, PT Pertamina EP Cepu Zona 11.

Abstract

Conservation energy activity in a form of Waste Heat Recovery Unit (WHRU) in Gas Processing Plant (GPP), is a challenge as well as an opportunity for efficiency and cost reduction in Field Operation. This activity is carried out by identifying excess energy, capture the excess energy and transfer the energy to selected equipment that needs the energy, resulting an effective energy usage in production process.

A good example of GPP's equipment that generate excess energy in a form of heat is Thermal Oxidizers (TOx). TOx is an equipment needed to maintain the quality of Gas released to satisfy the regulation of State Minister of Environment, in this equipment acid gas will be purified using thermal oxidation maintained at certain time and high temperature in an oxygen rich situation to ensure the expected oxidation efficiency to prevent harmful gases released into the environment. The excess heat from this activity can be used to heat Hot Oil by using WHRU.

Typical configuration of TOx and WHRU is direct heating or straight through. In this configuration, all of the volume of flue gas generated by TOx will pass through WHRU, since it's located in straight line to outlet stack. Heat will be transferred to Hot Oil by Heat Exchangers tube, until desired Hot Oil temperature achieved, heated Hot Oil then will be circulated to other equipment in needs. By using straight line, the potential risk of failure in equipment involved increased, it is important to find other configuration to minimize this risk.

This paper will address another configuration of TOx and WHRU using Indirect Heating. In this configuration, WHRU is placed outside main line of flue gas. This configuration allowed easy maintenance and reduce the potential of damage to the equipment as well as unplanned shutdown due to upset condition in WHRU.

Introduction

The requirement for environmental regulations of a GPP is growing more stringent nowadays. The awareness of harmful gases released into the environment has increased over time. GPP owners must adapt to the environmental requirement set by the government continuously. To be able to match the emission regulation, TOx are being used in many ways. The majority of GPP used chemical solvents in Acid Gas Removal Unit (AGRU) to absorb acid gas from the gas stream. These solvents then need to be regenerate so it can be recycled back into the AGRU stream and absorb another stream of acid gas. To regenerate the solvents, a high temperature medium is needed to heat the solvent and released the absorbed acid gas. This process can be delivered by a heated Hot Oil into the regenerative system. To achieve this condition, GPP may introduced a heat recovery in the TOx system, the heat recovery system will satisfy the heat requirements to regenerate the solvents as well as reducing overall operating cost by using excess heat from TOx instead of Hot Oil Heater generated by diesel or fuel gas.

Data and Method

Thermal Oxidizers

Thermal Oxidizers (TOx) is an equipment used to destroy harmful gases by thermal oxidation maintained for a fraction of time at high temperature in an oxygen rich environment. This condition is required to ensure the desired oxidation efficiency.

Typical AGRU in a GPP utilized hot oil in the reboilers, the gas released in the vent stream may contain hydrogen sulfide, BTEX (Benzene, Toluene, Ethylbenzene, and Xylene), and hydrocarbons, these gases need to be oxidized before released into the environment.

The utilization of Hot Oil to regenerate solvents is very common in GPP. The majority of GPP with excess fuel gas, may used fired heater to heat the Hot Oil. However, a GPP with fuel gas limitation may equipped a Waste Heat Recovery Unit (WHRU) combined in the TOx to reduce the fuel gas cost.

Thermal Oxidizers Straight Through Design

Thermal Oxidizer Package equipped with WHRU have two main reasons. First, is to oxidize acid gas and harmful hydrocarbon to generate safer flue gas. Secondly, to provide heating medium for hot oil that will be used for process purposes.

The simplest configuration of TOx with WHRU is a Straight Through design, this design used vertical arrangement of Radiant section, convective section, and stack. WHRU is installed at the top of convective section. The configuration also can be arranged at horizontal direction, depends on the availability of space inside GPP.

Acid gas from process area will enter TOx package from the bottom of the stack (burner) along with the fuel gas from other direction. Air is feed from the environment to the burner using Air intake fan. These three gases (acid gas, fuel, and air) will be mixed in the bottom of the TOx. Burner then will burn the mixture of these gases at high temperature, preferably above 1500 degF to ensure all harmful gases (H2S and Hydrocarbon) is burned and perfectly oxidized.

Hot gas from the combustion will rise and the heat energy will be absorbed by WHRU to heat the Hot oil. This hot gas will have a lower temperature due to the heat exchange phenomena and will be discharged to the environment as

PROCEEDINGS
JOINT CONVENTION BANDUNG (JCB) 2021
November 23rd – 25th 2021

flue gas that already fulfilled the environment requirement set by the government.

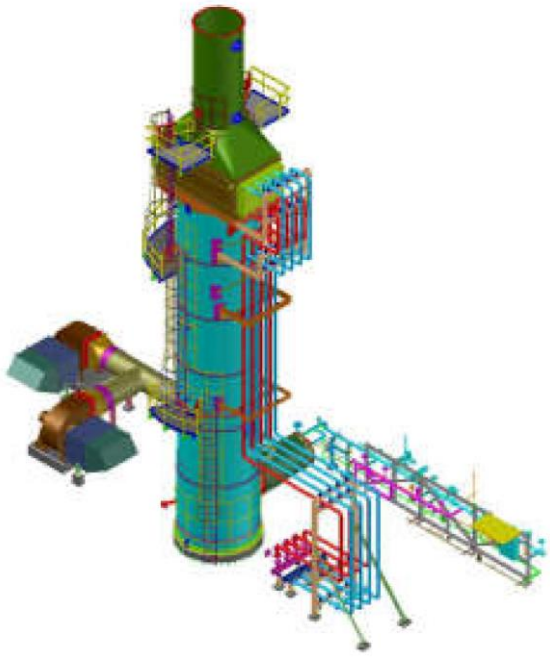

Figure 1: Direct Heating Configuration

Thermal Oxidizers Extractive Design

Thermal Oxidizers with extractive design, used coil outside of the main flue gas path. The flue gas will be pulled by an induced draft fan and will be used to heat the Hot Oil at lower level. This configuration provide easier maintenance as well as safer operability.

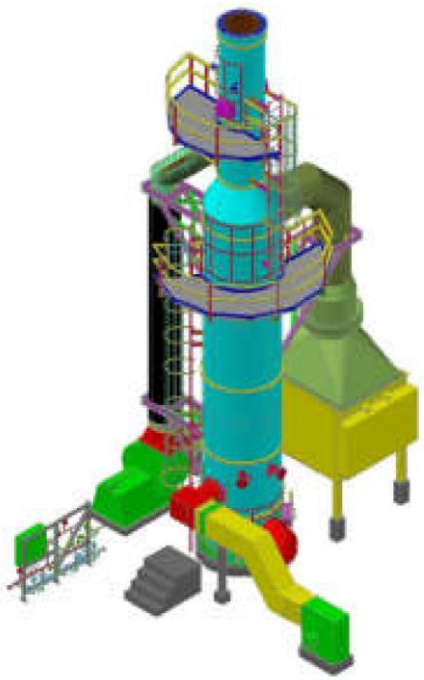

Figure 2: Extractive Heating Configuration

Result and Discussion

Risk of using straight through TOx with WHRU mainly because the WHRU located at main path of the flue gas, if the WHRU tube is broken it will leak the flue gas into the hot gases path, this condition will ignite the Hot Oil and create a combustion resulting a damage into the equipment.

The risk can be minimize by using an extractive design, since the Hot Oil located outside the main path of flue gas. In a case WHRU broken or damaged, the TOx can still be operated while the WHRU is being repaired.

Conclusions

Extractive Heating Configuration provides:

- Operation at various temperatures without changing oil system performance
- Capability to utilize different load configuration
- A well-defined operation envelope
- The ability to continue operation in case there's a failure in the hot oil system

References

Acknowledgements (Optional)
The author would like to express his gratitude toward his colleagues and superior that provide moral encouragement to write these proceedings. The author also would like to send love to his family for their support during the writing process.

PROCEEDINGS
JOINT CONVENTION BANDUNG (JCB) 2021
November 23rd – 25th 2021

The Joint Convention Bandung (JCB) 2021 "Comprehensive Pipeline Maintenance"

1.Aristo Delmayuzar CMRP, SKK Migas, 2. Ali Idham, Pertamina Hulu Rokan, 3.M. Iqbal Ruswandi, Chevron Indonesia Bussines Unit.

Abstract

The Rokan block is one of Indonesia's largest crude oil producers. Rokan block operates and maintains over 530 kilometres of main oil shipping pipelines to transport crude oil from the producing field to the Dumai terminal tank facility. There were pipeline integrity and operational issues in the main shipping lines: aging pipeline networks (more than 45 years old), heavy metal loss due to external corrosion from environment and soil contact, illegal road crossings (RC), Pipeline Hit Incidents (PHI) from public road proximity, and natural factors (land shift, fallen trees, erosion).

CPM Program (comprehensive pipeline repair and maintenance program) in Rokan Block was initiated in 2017 with core goal to continue safe pipeline operation, reduce risk of LOC and reduce the risk of social and environment impact due to pipeline integrity. CPM Program covered all aspects of pipeline maintenance start from inspection programs, life time analysis, priority ranking, planning and executions with main goal to maintain pipeline integrity in acceptable level of services. The focus of activities was to increase rate of proactive repairs (sleeving program), performed road crossing repairs, coating repairs, installed sacrificial anodes, and other interim mitigations until pipelines are either replaced or shut in.

The execution of CPM Program in Main Corridor from 2017 – 2020 has successfully maintain pipeline operation at safe margin (MAWP>MOP), extend pipeline Remaining Life Time (RFT), reduce damage rate from Pipeline Hit Incidents (PHI), reduce Loss Production Opportunity (LPO), and increase Mean Time Between Failure (MTBF).

Keywords: *comprehensive pipeline maintenance, MAWP, pipeline remaining life time, mean time between failure.*

Introduction

The Rokan Block is produce from approximately 75 active oil fields consisting of three major oild fields: Duri, Minas and Bekasap. There are two types of oil production, heavy oil and light oil. The pipeline is used to transport oil production from wells to gathering station for separation between oil, sand and water. Crude oil from the gathering station is transported by pipeline to Dumai storage tank, and then shipped to customers. The following figure shows the simplified process of crude oil transportation system in Rokan Block.

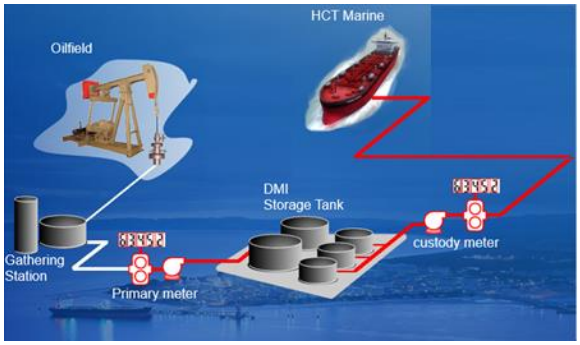

The Rokan Block operates and maintains over 530 kilometres of oil main shipping pipelines ("Main Corridor") to transport crude oil from the producing field to the Dumai terminal tank facility. The existing Main Corridor pipelines were constructed more than 45 years ago located above ground with no community around the area. Current condition reveals that there are many pipeline segments that have been partially/fully buried without proper coating and/or cathodic protection to prevent corrosion.

As part of further pipeline integrity program, In-line Inspection (ILI) and Long-Range Ultrasonic Testing (LRUT) were conducted on the existing aging pipelines to be used as baseline data. The results indicated some pipeline segments were at high risks due to significant metal loss. The Comprehensive Pipeline Maintenance Program ("CPM") was then initiated by PT. Chevron Pacific Indonesia ("CPI") as Rokan Block Operator in 2017 to repair the pipelines and address other threats to support safe operation until lines replaced or shut in. The effort was completed in 2020.

This paper focus on the execution of CPM Program from Y2017 to Y2020 in Main Corridor which was executed by CPI as the Rokan Block Operator until August 2021. The Main Corridors consists of 8 segments as listed and shown in the simplified flow diagram below.

Pipeline Segments	Size (inch)	Length (km)	Built
Balam – Bangko	10"	13	1972
Benar - Bangko	10"	10	1977
Bangko - Dumai	20" / 30"	80	1972
Duri CPS - Dumai	30" / 36"	54	1971
Duri CGS #3 - Dumai	24" / 30"	46	1958
Minas GS#1 - Duri	18" / 30"	76	1958
Libo - Mindal	10"	13	1982
Kotabatak – NBS	12"	33	1995

PROCEEDINGS
JOINT CONVENTION BANDUNG (JCB) 2021
November 23rd – 25th 2021

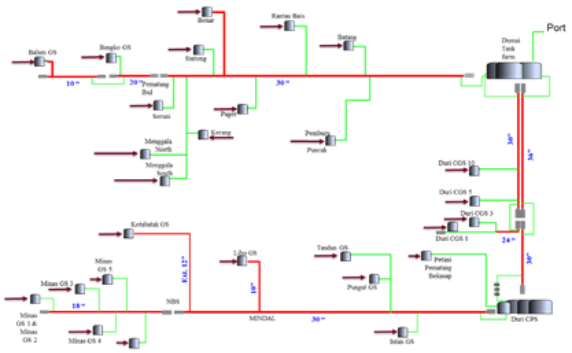

Specifics Problem

The following are main integrity and operational issues for Pipeline in Main Corridors infrastructures:

1. Aging pipeline networks (more than 45 years old)
2. Public encroachment along pipeline Right of Way (RoW)
3. Heavy metal loss due to external corrosion from environment and soil contact
4. Illegal road crossings (RC)
5. Pipeline Hit Incidents (PHI) from public road proximity
6. Natural factors (land shift, fallen trees, erosion)

The pipeline replacement and relocation of existing RoW to new RoW was considered to be the preferred solution to secure and maintain oil shipment through pipelines in Sumatra Operation (SMO). However, due to issue on non-technical issue on Rokan PSC, this solution could not be executed. The Rokan Block Operator was then deploying a so-called Comprehensive Pipeline Maintenance (CPM) Program which covered all aspects of pipeline maintenance, starting from inspection programs, lifetime analysis, priority ranking, planning to executions. The main goal of CPM program was to maintain pipeline integrity in acceptable level of services. The program was focused on activities related to increased rate of proactive repairs (sleeving program), performed road crossing repairs and coating application, installed sacrificial anodes installation, and other interim mitigations until pipelines are either replaced or shut in.

Data and Method

COMPREHENSIVE PIPELINE MAINTENANCE ("CPM") ON MAIN CORRIDORS

CPM Program (comprehensive repair and maintenance program) was initiated to allow safe pipeline operation, reduce risk of LOC and reduce the risk of social and environment impact due to pipeline integrity until the lines replaced or shut-in. As part of CPM Program, The Rokan Block Operator utilized Pipeline Integrity Management System (PIMS) and implemented Risk Based Inspection tools to prioritize the asset integrity program.

1. **Pipeline Integrity Management System ("PIMS")**

The PIMS is pipeline management system in Rokan Block to provide an Integrity Management System for pipelines system that will ensure that all pipelines are designed, installed, operated, maintained, and decommissioned in a manner that protects the safety and health of people, protects the environment, and allows the inherently safe, high quality and cost-effective delivery of the product.

Picture below shows the Pipeline Integrity Flow Process to maintain the pipeline integrity. The main asset integrity pipeline activities including Risk Assessment, Inspection, Monitoring & Testing, Integrity Assessment, and Mitigation & Repair.

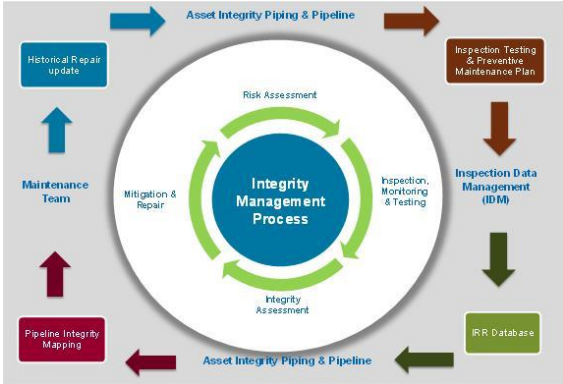

PROCEEDINGS
JOINT CONVENTION BANDUNG (JCB) 2021
November 23rd – 25th 2021

In addition to implementing PIMS, Rokan block operator performed Risk Based Inspection Assessment to prioritize asset integrity program as illustrate on the figure below.

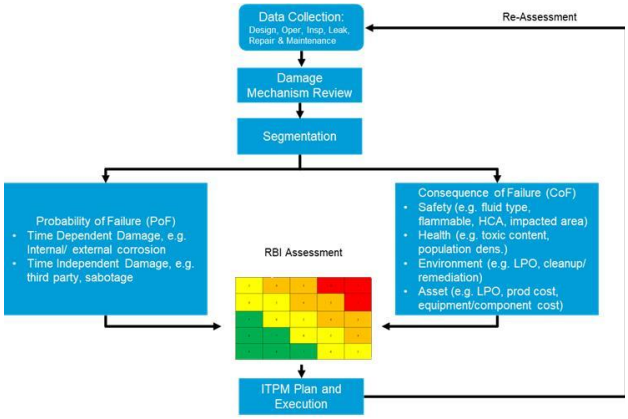

2. CPM - Proactive Repair Program

This section describes the objectives of program repair criteria and key highlighted results related to sleeve installation, road crossing improvement, coating application and guard rail installation.

A. Sleeve Installation

- Objective : Maintain/improve MAWP rating that supports safe operation.
- Repair criteria: Red & orange anomalies based on projection of latest inspection result.

Metal Loss (%)	$MAWP_{current}$
>80%	≤ 1.10 $MAWP_{Limit}$
>60% - 80%	> 1.10 – 1.25 $MAWP_{Limit}$
> 40% - 60%	> 1.25 – 1.50 $MAWP_{Limit}$
<40%	> 1.50 $MAWP_{Limit}$

- Results: Installed sleeve quantity (2018 – 2020) 4,652 pairs (~1.7% total main corridor length).

Visualization of Main Corridors Before and After CPM Program:

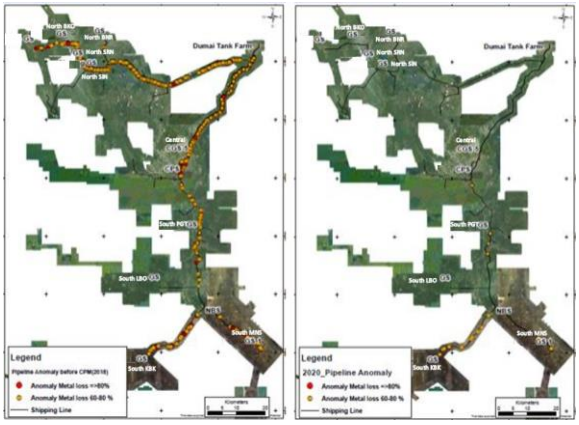

B. Road Crossing Improvement

- Objective : Provide protection against external load/impact on illegal road crossings.
- Criteria : On-site visual inventory for pipe condition (half-buried/buried), road crossing width (vehicle load), and HCA (high consequences area) class.
- Results: Installed sleeve reinforcement and cathodic protection with proper backfill on total 1,580 spots (~3% of total main corridor length).

C. Coating Application

- Objective : Provide protection against external corrosion and mitigate corrosion growth.
- Criteria : Based on projection of latest inspection result on buried/-half-buried pipeline with 50-60% metal loss.
- Results: Applied external coating and installed sacrificial anode cathodic protection along 20.2 km (~6.2% total main corridor length~).

D. Guard Rail Installation

- Objective : Provide protection against pipe hit incident due to vehicle traffic.

PROCEEDINGS
JOINT CONVENTION BANDUNG (JCB) 2021
November 23rd – 25th 2021

- Criteria : Criticality prioritization based on past incidents, road condition, and pipeline position.
- Results: Installed 30.1 km standardized guard rail.

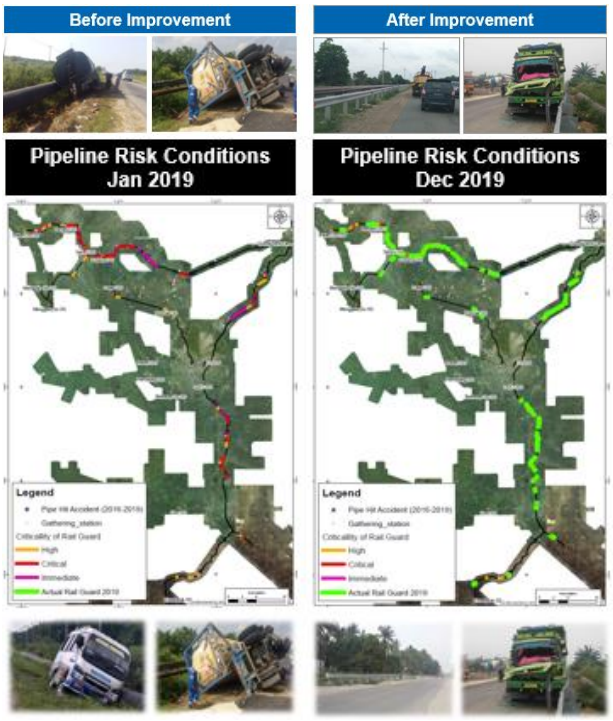

Deliverables or Result of CPM Program (2018 – 2020)

This section summarized the accomplishment of CPM Program from 2018 to 2020 in ensuring safe pipeline operation (MAWP > MOP), extending pipeline Remaining Life Time, reducing damage rate from PHI, reducing loss production opportunity (LPO), and increasing mean time between failure (MTBF).

1. Maintain MAWP above MOP to support safe pipeline operation.
   Avoid degraded MAWP below required operating pressure due to aging pipeline.

Segment	Remaining Life Time - Akhir 2017 Sebelum Perbaikan (Year)	Remaining Life Time - Akhir Tahun 2019 Setelah Perbaikan (Year)	Est MAWP (Block Flow) Akhir Tahun 2017	Est MAWP (Block Flow) Akhir Tahun 2019 (Tanpa Program CPM)	MOP	Cluster	MAWP (Block Flow) Akhir Tahun 2019 (Setelah Program CPM 2018 - 2019)
10" North #1 GS - BD	-3.3	2.5	350	180	240	A	290*
10" North #2 GS - BD	-1.8	3.6	300	150	270	B	350**
20" North Segment #3	-3.8	2.7	300	150	300	B	350**
30" North Segment #4 - Dumai	-3.9	1.1	300	150	300	B	350**
30" Central CPS Segment CGS	-5.7	4.5	200	90	170	C	400
36" Central CGS - Dumai	-0.7	6.8	200	90	170	C	400
24" Central Inter CGS	-2.3	7.5	170	145	1175	D	300
30" Central CGS - Dumai	-6.1	2.1	170	145	170	D	300
18" South GS - South NBS	2	5.6	200	180	200	E	250
30" South NBS - Central	-6.6	2.2	140	120	140	F	400
10" South Infield L	-8.8	4.9	140	120	150	F	400
12" South Infield K	-2.8	5.6	140	120	225	F	400

2. Maintain pipeline services until end of Rokan PSC or until pipeline is replaced.

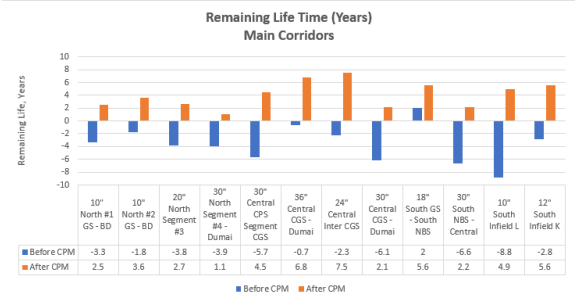

3. Reduce pipeline failure due to integrity issue.
   - Reduced # of leak incidents since 2017 (~20% annually).
   - Improve MTBF and mitigate decline rate in 2019 until 2021
   - Reduced oil spill incidents and mitigate spill volume increase.

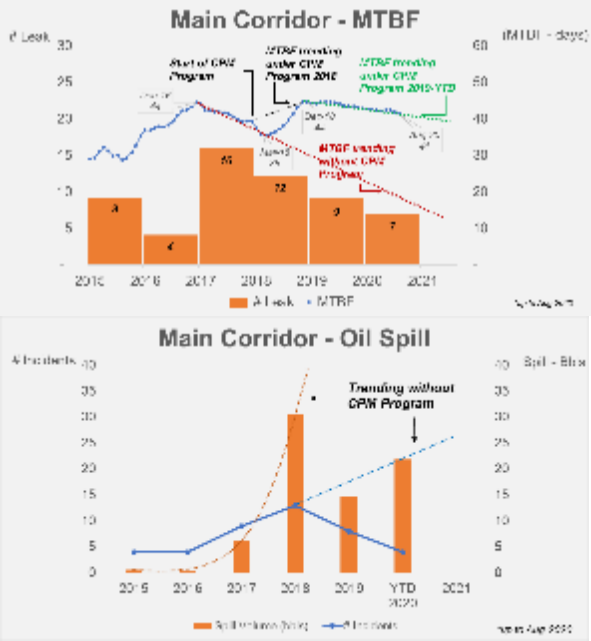

4. More flexibility in mitigating congeal event resulting from sustained MAWP.

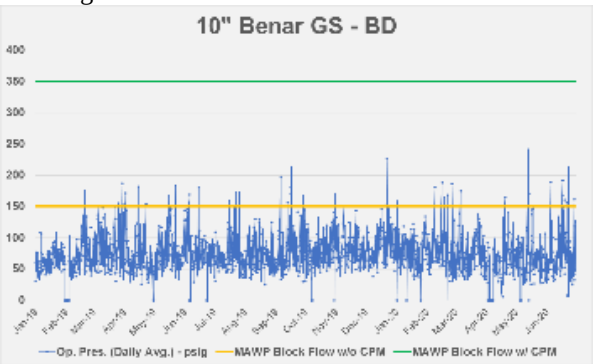

PROCEEDINGS
JOINT CONVENTION BANDUNG (JCB) 2021
November 23rd – 25th 2021

-

5. Reduce LPO due to congeal.

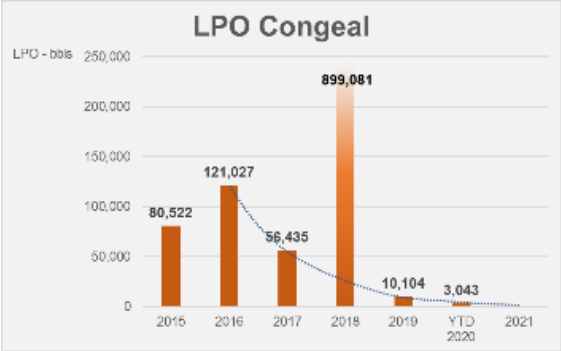

6. Reduce number of damaged inflicted to the pipeline resulting from vehicle strike/accident.

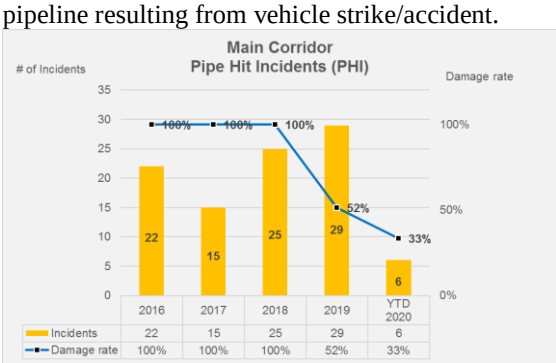

7. Reduce associated repair cost resulting from pipe hit incidents.

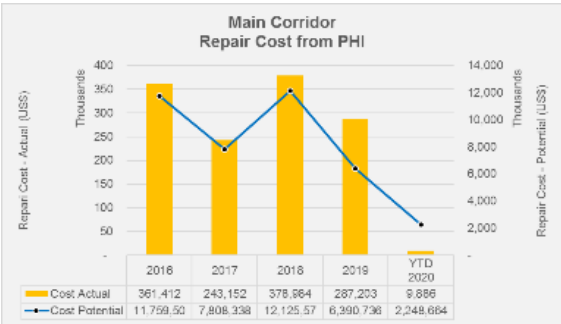

Conclusions

The program to restore pipeline integrity on a campaign basis has proven to be one of the good solutions to contain the massive failure rate. When compared with new replacements, it can be compared in general has several advantages, including:

1. Significant capital cost savings and converted into operational costs.
2. Minimizing social risks, and increase the safety factor.
3. Preventing lost production with an even greater effect.
4. Generating baseline improvements with good learning for future activities.

References

PROCEEDINGS
JOINT CONVENTION BANDUNG (JCB) 2021
November 23rd – 25th 2021

Unlocking Potential of Brownfields through Effective Implementation of Planning & Scheduling

Esi Marlini and Dipta Dwitiya, PT Medco E&P Indonesia.

Abstract

Getting the best out of Brownfields, due to its marginal economics nature, requires accuracy and impactful collaboration in the execution of its activities & projects. Therefore process improvements become highly crucial in the pursuit of operational excellence. This is exactly what is expected from the introduction of Operational Excellence, particularly in the Operating Efficiency Pillar. The focus will be on its sub-pillar which is Planning & Scheduling (P&S). Brownfield operations have long established processes and governance that provide an array of challenges when trying to introduce a new way of working. Therefore this paper tries to share the key learnings during the first year of implementing IP&S in Brownfield operation.

The foundational framework used is the PDCA framework of Plan-Do-Check-Adjust, and then within this framework, there are several elements specified even further with the expectations. The elements in the system basically relate to the establishment of strong Governance, People, Process, or Technology all working together in harmony. This paper will focus on the early stages of developing a solid planning & scheduling system in the organization, where the majority of the groundwork was oriented by the Operational Excellence maturity matrix. The matrix was then converted into actionable items and deliverables within the space of 11 months since the initiative was kicked off.

The foundational phase for the introduction & implementation of P&S was completed within 11 months. Action items and deliverables were produced, and both qualitative and quantitative benefits were gained. There was also a direct connection between P&S and helping the organization achieve its business objectives despite the global challenges that shook the oil & gas industry to its core. Challenges and difficulties were inevitable, but also became the key factor in creating a unified front. Overall, the organization-wide effort played a strong role in the mission of improving operational excellence with P&S as one of its key elements. Everyone was in the same boat, going through the same storm.

In times of unprecedented challenges, Operational Excellence and the Planning & Scheduling sub-pillar became the rock that solidified our organization. It is and shall be a leading practice that helps improve business sustainability, agility, and resilience. Making it a must-have for every organization in any industry wanting to survive and thrive. This paper provides leaders and changemakers with a usable framework in their efforts for the introduction and development of Planning & Scheduling, helping to achieve optimum results while gaining meaningful relationships and experiences along the way.

PROCEEDINGS
JOINT CONVENTION BANDUNG (JCB) 2021
November 23rd – 25th 2021

Background

Getting the best out of Brownfields, due to its marginal economics nature, requires accuracy and impactful collaboration in the execution of its activities & projects. Therefore process improvements become highly crucial. This is exactly what is expected from the introduction of Operational Excellence (OE), particularly in the Operating Efficiency Pillar.

Medco's OE has four main pillars:

1. HSE: Health, Safety, and Environment
2. A&OI: Asset & Operating Integrity
3. CM: Cost Management
4. OEF: Operating Efficiency

Planning & Scheduling (P&S) is a sub-pillar that belongs in the Operating Efficiency pillar. It focuses on making sure all our efforts are constructed thoroughly, and timed accurately, in order to achieve the best possible outcome.

Problem Statement

The main challenge therefore focused on the early stages of implementation. Where it was critical that a strong foundation for further growth had to be established.

Key Factors

There were several key factors that went into the equation. However all of them were covered and governed by this one internal system, called Medco's Operational Excellence Guideline. This became the basic reference to all our efforts. In it, is a maturity matrix filled with expectations that helped us build the system.

Recommendations

As mentioned above, the OE Guideline became the basic reference for our efforts. Within the guideline, is a maturity matrix, complete with elements and expectations in each level of maturity. This paper provides a recommendation for the most critical elements during the early stages of building the foundation for further growth of the OE culture, particularly for the P&S area.

The elements were grouped into the 4 main phases of the continuous improvement cycle more known as the PDCA Framework, short for Plan-Do-Check-Adjust.

The details of how many elements and expectations exist in each can be found in Table 1. While the most important elements during the early stages can be found in Table 2.

Data and Method

This paper shall cover two areas, the first is the 10 most critical elements in the early stages. The second is how the team addressed the most important element of any change initiative, the people. As Kotter (2007) listed in his article, there are 8 important steps in leading change.

Area number 2 was to 'Form a Guiding Coalition', which is built from reliable people having clear roles & responsibilities (Friedman, 2015 and Jones, 2014).

A. 10 Critical Elements of Early-Stage P&S

PLAN

1. Planning & Scheduling Philosophy
A philosophy acts as the basis of all basics. Any vision, mission, objectives, or key results, must be in line with the main philosophy. In this case, the P&S philosophy essentially states that all of the organization's efforts to sustain the business, must be thoroughly planned & scheduled, so as to achieve the best possible outcome.

2. Governance, Roles and Responsibilities
An effective team is one where everyone knows exactly what they are there for, what is demanded of them, and how they are expected to contribute to the team's mission. Therefore, clear responsibilities, with minimum overlaps, and well-quantified outputs from each key person was highly crucial.

3. Planning Components (Planning Tools)
This relates to technology as an enabler. Which essentially means, technology should follow the process. The principle in choosing a tool was something that was readily accessible, highly adjustable, and can serve the purpose. Spreadsheet application, despite all its shortcomings, was chosen.

4. Integrated Planning (Plan Input Standardization)
Consistency is key. Governance in how everyone would input their plans was nothing short of being critical. This aims to establish a minimum standard of quality, where there is a uniform and consistent method for inputting plans and activities. This goes

as detailed as the structure (begins with a verb) of the action sentence.

DO

5. Planning Horizon (Medium Term Plan)
Medium to short term plan is where all the organization's efforts can be made or broken. Therefore, the focus was on the 1 year, down to 7 day planning & scheduling. This was seen as the tactical and operational planning horizon, where things get done and results are created.

6. P&S Communications
A plan is worthless if it is not communicated. Kotter (2007) also listed this as a critical step in leading change (Step #4. Communicate the Vision). The whole organization, especially the key executors must know exactly what is planned, why it is important, the impact it will bring, and how it will be executed.

7. Plan Visualization
Visualization supports the effective understanding of the plan, especially when being communicated. This covers quantification, conditional formattings, and other data visualization techniques aimed to ensure the message is clearly conveyed and understood.

CHECK

8. Plan Performance (Planning Compliance)
Creating a plan is one thing, actually committing and sticking to it, is another. Therefore, periodic reviews are imperative, aimed to ensure plan owners are in full compliance to what is planned at the start of the year. THis does not imply that plans cannot be altered, but changes must also follow a strict process.

9. Key Performance Indicators (KPI)
Reviews need a quantification system, and this is where planning KPIs come into play. This includes Schedule Attainment, Plan Utilization, and Manhour Utilization. All is measured to ensure the schedule is obliged, the plan is used accurately, and that no resource is wasted, therefore enhancing operational efficiency.

ADJUST

10. Planning Program Adjustment
As mentioned in the planning compliance section, adjustments are tolerable. Constraints occur, impacting the execution of a plan and schedule. This however requires a structured approach, therefore minimizing any major disruptions to all the other activities in the approved plan.

B. Building Powerful P&S People

The core P&S team identified an imminent challenge during the early stages. Building a culture, a system, or any effort, requires contribution from the key people involved. The OE initiative was robust and comprehensive, therefore the key players, in this case, the Asset Planners needed to be equipped with the right amount and quality of character, competency, and capability.

The 5Cs was utilized as the foundational framework. The following elaborates each C, and aims to provide practical examples for better understanding. The result was a team of Planners, consisting of 12 personnel that were previously secretaries/admins. This was the main achievement of all the efforts.

1. Care
An essential ingredient to begin with, we have to care enough before we can truly endeavour to improve our operations.
This is shown through the extra efforts taken by the core team in building the system in the beginning, and the constant offering of help.

2. Connection
Aims to build trust with the Planners. This was achieved through having 1-on-1 discussion with them, with the main objective to connect and to understand their strengths, improvement areas, and concerns. This connection was rather harder to be achieved if done through a group setting.
The sessions also involved knowledge sharing, helping them understand the oil & gas operations.

3. Clarity
When we understand what is expected of us, we can contribute better. Effectively managing expectations, provided a sense of clarity for the expected change.
This was achieved through group sessions, aimed to explain the basics of OE and P&S. The desired impact was the Planners' understanding the P&S system before it was implemented to an organization-wide context.
To further assist the process of understanding the technical side of things, explanatory videos on oil and gas operations were also created and distributed.

4. Commitment

Through Connection and Clarity, comes Commitment. This is also shown in the weekly forum conducted with the sole purpose to provide a solid support system for the Planners. Answering any questions, solving any problems, and improving what needs to be improved.
The constant interaction within a nurturing environment significantly contributed in creating commitment. And likewise, through collective commitment, a nurturing environment is created.

5. Continuous Improvement (CI)
The CI mindset is key to any organization's long term success and sustainability (Chandrasekaran, 2019). Business processes that govern how CI is implemented is therefore crucial.
In this case, the PDCA cycle is always referred to. Should there be any problems/opportunities, this triggers a cycle of identifying the root cause, coming up with options, and then trying out which option works best.
Once proven, the existing guideline shall be updated and communicated, to ensure minimum standards are always raised and improved.

Result and Discussion

Key and notable results include the following:

1. 12 Asset Planners, gained from existing personnel, from previously secretaries.
2. 1 P&S Guideline document, developed together with the Planners.
3. MPRP (Monthly Performance Review & Planning), the ultimate ceremony for operational level P&S. This meeting became the core P&S communication event, gathering all key functions and operations, ensuring goals & objectives are well executed and managed.

Overall these 3 results contributed significantly towards the company's success in achieving 2020's business goals, despite the challenges faced globally in the form of COVID-19 pandemic.

Conclusions

The following points became the summary and key findings in this paper.

- It is important to identify which elements are critical in each stage of building a system, especially for building a solid foundation.
- Key personnel must be provided with a strong support system, and effective framework for their professional development. The 5Cs helped with this.
- P&S is a collective effort, therefore a gathering ceremony must exist, in the form of a monthly performance review and planning (MPRP) meeting.

References

Baxter, R. (2015). Operational Excellence Handbook: A Must Have for Those Embarking On a Journey of Transformation and Continuous Improvement. Value Generation Partners: Naples, Florida.

Chandrasekaran, A., Toussaint, J. S. (2019). Creating a Culture of Continuous Improvement. https://hbr.org/2019/05/creating-a-culture-of-continuous-improvement

Friedman, R. (2015). The Best Place to Work: The Art and Science of Creating an Extraordinary Workplace. TarcherPerigee.

Jones, G. (2014). Top Performance Leadership: A dynamic and achievable new approach to delivering first-class, sustainable results. London: How to Books

Kotter, J. P. (2007). Leading Change: Why Transformation Efforts Fail. Harvard Business Review, January 2007, 124-132.

Acknowledgements (Optional)

Thank you and appreciation goes mainly to all the 12 Asset Planners
Additionally, to the core OE team, the Leadership Team, and everyone who has contributed in the development of P&S.

Table 1. Elements and Expectations Within the P&S Sub-Pillar as Grouped in the PDCA Cycle

Cycle	PLAN	DO	CHECK	ADJUST
Elements	5	5	2	1
Expectations	16	15	7	2

PROCEEDINGS
JOINT CONVENTION BANDUNG (JCB) 2021
November 23rd – 25th 2021

PHENOMENA OF SCALING AND CORROSION ON CRUDE OIL PIPELINE WITH VELOCITY PROFILE IN FULLY DEVELOPED CONDITION APPROACH

Sutarno[1,a] , Ekha Panji Syuryana[2] and Mudzakkir H. Basri[3]

[1,2]Program Studi Teknik Metalurgi, Fakultas Teknologi Manufaktur Universitas Jenderal Achmad Yani, Jln, Terusan Gatot Subroto Bandung (samping PINDAD) 40285, Telepon (022) 731274 Bandung-Jawa Barat
[3]PT. Dago Energi Nusantara, Jln. Terusan Bukit Dago Selatan No.29 Kecamatan Coblong, Kota Bandung, Jawa Barat 40135
[a]Email: sutarno@lecture.unjani.ac.id

.

Abstract
Scaling and corrosion phenomena always occur on the internal surface of the crude oil, gas, steam boiler and geothermal pipelines, which have an impact on the flow rate, shutdown frequency, and target maintenance costs and the company's business. In general, this scaling and corrosion phenomenon occurs as a result of crude oil, geothermal, water, gas and steam containing CO_3, OH, HCO_3, Ca^{2+}, Mg^{2+} and Fe^{2+}, CO_3, CO_2, H_2S, O_2, H_2O ions and sulfide compounds respectively.

In this paper, an investigation is carried out by mapping the critical areas for scaling and corrosion in the pipeline based on the crude oil velocity profile approach in steady and fully developed conditions.

Based on the phenomenon of fluid flow, in steady and fully developed conditions, the velocity of crude oil forms a boundary layer where the maximum crude oil velocity is at the center of the pipe or pipe radius = zero, while the interface shear stress of the crude oil-surface internal pipe system is close to zero, which means crude oil is stationary, not moving. In a stationary condition, immobile ion scaling undergoes deposition which has an impact on the reduction in the diameter of the pipeline and the rate of crude oil water.

While at rest, corrosive species ions will react with the pipe surface. Both the formation of scaling and corrosion on the internal surface of the pipeline occur simultaneously and continuously. The mapping of critical areas of scaling and corrosion on the piping surface of the internal system is based on a velocity profile with fully developed conditions and confirmed with maintenance data. Based on the results of the treatment, it is possible to predict the rate of scaling and corrosion, determine the schedule for the maintenance period and the necessary actions to slow down and/or eliminate the process of scaling and corrosion formation, such as adjusting pH and/or adding inhibitors to crude oil. Processing and analyzing the results of the pipeline maintenance period data to predict the trend and rate of scaling and corrosion as well as the manufacture of a maintenance expert system, which is an integral part of excellent operation.

Keywords: Scaling and corrosion phenomena, ion species scaling and crude oil corrosion, pipeline, fully developed profile, excellent operation, expert system maintenance

Introduction

Corrosion of the crude oil pipeline

Crude oil in the form of mud consists of a mixture of organic compounds, hetero atomic compounds (S, N, O), hydrocarbons (C, H), metals and organic compounds (Ni, V, Fe) and inorganic (Na^+, Ca^{2+}, Cl) (https://www.e-education.psu.edu/fsc432/node/5). Hydrocarbon compounds consist of the elements carbon and hydrogen and are the largest organic compounds found in petroleum. Hetero atomic compounds containing sulphur as a source of H2S include mercaptan disulphides, sulphides, thiols, thiophenols, diphenyl sulphide thiophene and dibenzothiophene which are included in the form of organosulfur compounds. While heteroatomic compounds containing oxygen are carboxylic and phenolic, while organometallic compounds such as porphyrins.

Based on its density, crude oil is called light, medium, or heavy which is expressed in specific gravity, which according to the American Petroleum Institute (API), is expressed by the equation

$$°\text{API} = \frac{141.5}{\text{Sp.gr}\frac{60}{60°}} - 131.5 \quad (1)$$

The Specific Gravity of crude oil roughly ranges from 0.82-1 for heavier crudes ranging from 41-10 °API scale. °API gravity higher than 10 means the oil density is less dense than water and will float on it. API gravity lower than 10 means the density of oil is heavier than water and will sink in it. The content of heteroatomic, metallic and inorganic compounds is the species that causes scaling and corrosion on the surface of the internal pipeline.

In general, the problems of scale formation and corrosion and other degradation can be illustrated as shown in Figure 1. Based on Figure 1, the internal system piping interactions are affected by loading in terms of tensile, compression and bending in installations both on land and at sea. From loading and defects during manufacturing are fatigue and fracture mechanics. While the environment such as temperature, pressure, humidity, there are key species scaling and corrosive will have an impact on the occurrence of scaling and corrosion.

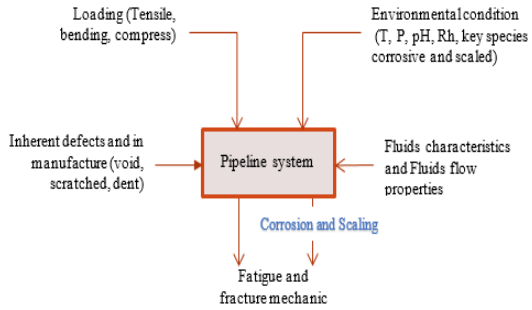

Figure 1. Mapping interaction pipeline and environmental condition

On the internal pipe surface is exacerbated when the pipe surface roughness is getting rougher where species are trapped in the roughness valley. The same is true for the O_2, H_2S, H_2O, Cl- species trapped in the roughness of the pipe, which results in corrosion, such as pitting corrosion, surface corrosion, stress corrosion cracking and others.

As it is known that corrosion and scaling processes are two factors that cause degradation in the pipeline, both for oil and gas as well as in geothermal and boiler pipes due to the interaction of corrosive key species, scaling or a combination thereof. Degradation in the form of thinning of pipe walls, well corrosion are many examples and are commonly found on the surface of internal pipes, while the formation of scale will have an impact on reducing the diameter of the pipeline which inhibits the flow rate of oil and gas or geothermal fluids.

Crude oil is flowed from the oil source reservoir through a pipeline to a refinery center, which is far from the oil source. The interaction of oil with the internal surface of the pipeline has an impact on the simultaneous occurrence of scale formation and corrosion, which is presented in Figure 2. As a result of scale formation and corrosion, the diameter of the pipeline decreases and corrosion such as pitting, stress corrosion cracking, and surface corrosion is unavoidable. Conditions like this can disrupt the oil business, especially related to the transportation of crude oil to refinery centers such as the function and life of the pipeline.

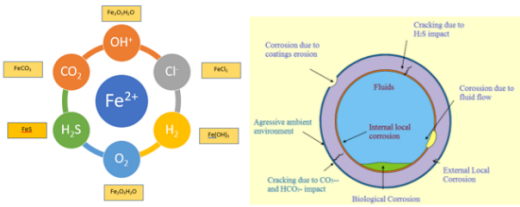

Figure 2. Interaction (a) key species; (b) impact of corrosion and scaling formation

The interaction process between fluids in the form of oil, gas and water vapor with the piping surface of the internal system, for example the simultaneous formation of scale and corrosion, originates from key species such as O_2, CO_2, H_2S, H_2O, Ca^{2+}, Cl- and other elements contained in crude oil. This key species will interact with the internal surface of the pipe to form scale and corrosion simultaneously. The formation of scale due to the presence of CO_2 reacts with the internal surface of the pipe in the form of siderite, $FeCO_3$, calcite, $CaCO_3$, calcium silica $CaOSiO_2$, or ferrosilica, $FeOSiO_2$ and other salts such as $BaCO_3$. Continuous deposition of key species scaling and corrosion processes causes local leakage, thinning of pipe thickness and narrowing of the pipe resulting in the flow rate of crude oil.

Mechanism of scale formation and corrosion

Electrochemically, corrosion is a phenomenon of an oxidation reaction on the surface of the internal pipe (as a substrate) which degrades the anode according to the reaction (Lekan T P at al, 2013;)

$$Fe \rightarrow Fe^{2+} + 2e^- \quad (2)$$

On the surface of the internal steel pipe which contains water with a low concentration of O_2 becomes anodic and oxidized which causes corrosion. Under acidic conditions, if there is O_2 it is reduced according to the reaction

$$O_2 + 4\,H^+ + 4e^- \rightarrow 2H_2O \quad (3)$$

Under neutral or basic conditions, oxygen

$$0.5\,O_2 + H_2O + 2e^- \rightarrow 2OH^- \quad (4)$$

Meanwhile, in an acidic solution,

$$2H^+ + 2e^- \rightarrow H_2 \quad (5)$$

Under conditions of neutral or alkaline water, a reaction occurs

$$2H_2O + 2e^- \rightarrow H_2 + 2OH^- \quad (6)$$

The equation for the reaction of the oxide with H_2S is as follows:

$$Fe_2O_3 + 4H_2S^- \rightarrow 3FeS + 4H_2O + S \quad (7)$$

$$FeS + S \rightarrow FeS_2 \quad (8)$$

$$Fe_3O_4 + 6H_2S \rightarrow 3FeS_2 + 4H_2O + 2H_2 \quad (9)$$

When water combines with CO_2 and H_2S, the surface of the pipeline is represented by Fe2+ reaction

$$Fe^{2+} + H_2CO_3 \rightarrow FeCO_3 + H_2 \quad (10)$$

$$Fe^{2+} + H_2S + H_2O \rightarrow FeS + 2H \quad (11)$$

$FeCO_3$ and FeS or FeS_2 form a thin layer on the internal surface of the pipeline to prevent further corrosion. In the oil and gas production industry, sweet corrosion, acid corrosion, oxygen corrosion, galvanic corrosion, crevice corrosion, erosion corrosion, microbiological corrosion, and stress corrosion cracking are found. Weet corrosion is corrosion that occurs due to CO_2. This CO_2 gas with

water forms H_2CO_3 and will react with Fe to form Fe_3C, $FeCO_3$ or decompose greatly affecting pH.

The presence of CO_2 will have an impact on pitting and mesa corrosion which affects the pipe surface. As an illustration, the reaction process that occurs physically is shown in Figure 3.

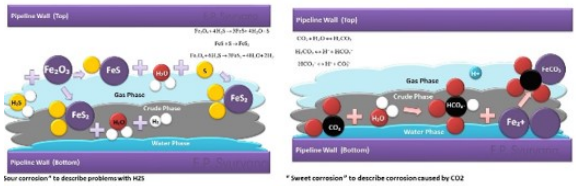

Figure 3. Corrosion (a) pipeline wall upper; (b) pipeline wall bottom

CO_2 gas is a gas dissolved in water and oil. In water, CO_2 dissolves to form carbonic acid:

$$CO_2 + H_2O \leftrightarrow H_2CO_3 \quad (12)$$

$$H_2CO_3 \leftrightarrow H^+ + HCO_3^- \quad (13)$$

$$HCO_3^- \leftrightarrow H^+ + CO_3^- \quad (14)$$

CO_2 gas reacts with water to form H_2CO_3. The presence of CO_2 and HCO_3^- is affected by pH. Corrosion caused by CO_2 gas is pitting, which can be found in turbulent areas. The partial pressure of CO_2 can be used as a benchmark for predicting corrosion. The reaction rate is affected by temperature and pH.

The rate of the reaction can be expressed by the equation:

$$\frac{dS}{dt} = -3{,}000\, x[S_t]^2\, [H^+]^{1.06} x[I] \quad (15)$$

S = total dissolved sulfides in filtrate, ppm; t = time, min; H^+ = hydrogen ion concentration, moles/L; I = Ironite Sponge concentration, lb/bbl (0.351 x kg/m^3).

Transmission of sour gases must be preceded by drying to the dew point, which is below the minimum exposure temperature in the facility. Calculation of CO2 corrosion in a certain regime, according to the equation

$$Log\ (R_{maks}) = 5.8 - \frac{1710}{T} + 0.67\ Log\ (P_{CO2}) \quad (16)$$

where

1. R_{max} is the corrosion rate (mm/year)
2. T is the temperature (°K)
3. P_{CO2} = P x m (CO_2)

CO_2 partial pressure: > 30 psi corrosion will occur, partial pressure (3-30) PSI corrosion can occur, while partial pressure < mild corrosion. In the case of drilling, CO_2 gas is removed by degassers and pH adjustment, with NaOH, to prevent the formation of carbonate scaling. The corrosion rate of steel is expressed by the equation,

$$mpy = (2.831 \text{ x } W)/ (A \text{ x } T) \quad (17)$$

where

W = weight loss (in grams), T = exposure time in days, and A = area of specimen in inch2.

Characteristics and properties of fluids

Two important and critical properties that play a role in corrosion and scaling formation in pipelines are fluid parameters and crude oil fluid flow. The parameters in the fluid are the key corrosive species and scale that cause corrosion on the internal pipe surface, scaling formation and a combination of both.

In a fluid flowing through the pipeline, it is impossible for corrosion and scaling formation to occur. The process of corrosion and scaling formation is only possible when the fluid is at rest so that the key species interact with the internal pipeline surface.

In fluid mechanics, not all fluids move at the same speed in a pipe. The shape of the velocity curve depends on the flow pattern, namely laminar and turbulent. If the flow in the pipe is laminar, the velocity distribution across the cross section will be parabolic with the maximum velocity at the center about twice the average pipe velocity, as shown in Figure 4.

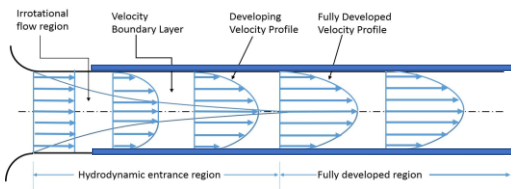

Figure 4. Changes in fluid velocity profile;

Based on Figure 4., there are 2 types of flow, namely viscous flow and convective flow. Convective crude oil flow is perpendicular to the flow direction, while viscous flow is radial. The two streams form a boundary layer. The convective flow velocity profile forms a para-sphere with the largest velocity at the center of the pipe with zero shear stress, while the largest viscous flow is at the crude oil-internal surface of the pipe. Geothermal fluid flow is distinguished by convective momentum in the direction of current and viscous momentum in the direction of radial. The shear force, is proportional to the fluid velocity gradient, expressed as

$$sv_z = \left(\frac{\Delta P}{L} \mp \rho g\right) \frac{R^2 - r^2}{4\eta} \quad (18)$$

The boundary conditions, at r = 0, then the value of x becomes max, and the shear stress, x = 0; while the boundary conditions, at r = R, then the fluid flow velocity, x = 0, and the shear stress, x = max. The flow pattern in the bend pipe shows a turbulent area where friction and cavitation occur which have an impact on erosion-corrosion.

In simple terms crude oil and natural gas fluids characteristics and fluids flow properties as shown in Figure 5. Based on Figure 5, pH, temperature,

PROCEEDINGS
JOINT CONVENTION BANDUNG (JCB) 2021
November 23rd – 25th 2021

moisture content and key species are important factors in the occurrence of corrosion and scaling formation. In addition, the density, viscosity and velocity, flow pattern, radius of the pipeline and the surface roughness of the internal pipeline are important factors in the corrosion process and the formation of scaling.

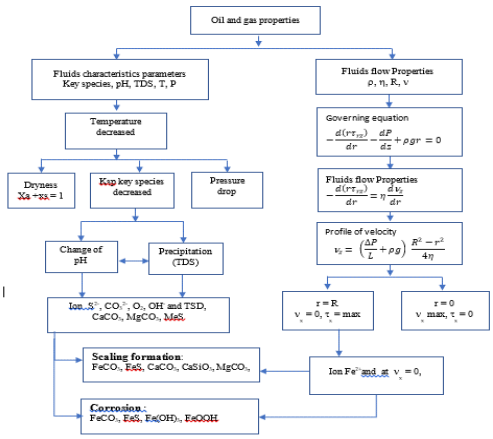

Figure 5. Parameters and fluid flow properties of crude oil

Data and Method

Crude and corrosion key species data

Key species analysis needs to be carried out to control the formation of scale and corrosion on a periodic and scheduled basis so that preventive measures can be taken immediately, as shown in Table 1. the required threshold (NAV).

Table 1. Key species of scale and corrosion

No	Key species	Kadar	Potential to
1	CO_3^{2-}, HCO_3	0.176-0,558	$CaCO_3$
2	Ba^{2+}	0.06-0,294	$BaCO_3$
3	Sr^{2+}	0.23-0.295	$SrCO_3$
4	Ca^{2+}	4.05-5.2251	$CaCO_3$
5	Mg^{2+}	0.367-576	$MgCO_3$
6	Cl^-	55.32-56.8	$FeCl_2$
7	K^{1+}	0.338-1.046	$K2CO_3$
8	Na^{1+}	44.409-96.500	$NaCO_3$
9	SO_4^{2-}	0.551-0.662	$BaSO_4$, Na_2SO_4
10	Fe	0.003-0.007	FeS, Fe_2O3
11	S	0.014-0.301	FeS
12	TSP	0.111-0.140	
13	COD	4.158-5.045	
14	NO^{3-}	0.000-0.004	
15	O_2	-	
16	pH	5.60-6.00	

Pipeline

The type of oil and gas pipe material must meet the dimensional requirements of (1) API 5L Specification (2) API 5LC & 5LD Specification (3) ASME B36.10M Welded and Seamless Forged Steel Pipe and (4) ASME B36.19M Stainless Steel Pipe. The surface roughness of the internal pipe needs to be known to estimate the amount of fluid and total suspended solid buried in the roughness valley.

Flow of fluida

The velocity or flow rate of fluids such as crude oil, viscosity or °API, TDS, key species, pressure, temperature need to be needed for head loss that occurs, especially the fluid-surface interface velocity of the internal pipe.

Parameter proses

Pressure, bases, acids, water and organosulfur compounds and fluid velocity have an important effect on the process of scale formation and corrosion.

Result and Discussion

Key species

The presence of key corrosive and scale species in crude oil will obviously degrade the function and service life of the existing pipeline. The corrosion process in the bag and bottom pipe is shown in Figure 6 and the scaling formation is triggered by corrosive key species such as CO_2, H_2S, O_2, Cl, while the key species for scaling formation are Ca^{2+}, Ba^{2+}, Sr^{2+} ions. Analysis of this method of organic matter must be carried out to ensure the content of key species elements. Besides that, it is also necessary to test COD and TOC and Total suspended solids respectively using the open reflux method per ASTM D 1252, high frequency infrared per GB/T13193 and filtration per GB/T 11901. The standard LOD is 1mg/Liter, 0, 5 mgr/Liter. As for ions such as Cl, basicity, ammonia, Ba, Ca, Fe, Mg, li, K, Na, Sr ions and S. Key species tests must be routine and the results must be processed and presented to interested parties, such as engineering maintenances used to determine periodic maintenance of pipelines

surface roughness

The surface roughness of the pipeline plays an important role in the corrosion process and the formation of scale in the pipeline. The surface roughness of the internal pipeline will be a place for the accumulation of key species of corrosion and scale, especially in the valleys as shown in Figure 6. This accumulation of key species increases along with the roughness and in turn can accelerate the rate of corrosion and scale processes. The surface roughness of the pipeline in fluid mechanics also has an impact on head losses. Large head losses will cause the crude oil flow rate to be slow and require a lot of pumps and large energy.

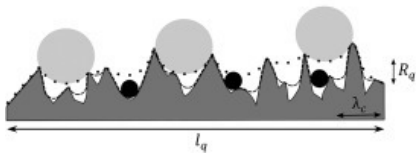

Figure 6. Illustration key species and corrosion and deposit of key species on the internal surface roughness of the pipeline.

Interaction process parameters

The effect of pH on steel corrosion depends on the metal composition, stress, oxygen concentration, and the type of acid that controls the pH. In the high alkaline state, the corrosion reaction is under anodic control and proceeds at high speed. In neutral state and in mild alkaline solution, the corrosion rate is under cathodic control, which provides corrosion protection. The actual corrosion rate depends on the diffusion of oxygen to the metal surface. Corrosion increases with increasing oxygen concentration and abrasion and in the presence of turbulent flow at high velocity. In addition to pH, the process parameters that affect corrosion are temperature, pressure, TDS as shown in Figure 5.

Crude oil flow rate

As it is known that, the flowing fluid has a layered velocity forming a velocity profile like a parabola as shown in Figure 3 where the highest velocity is in the middle, while the lowest velocity is on the surface of the internal pipeline, according to Eq. (18). At r = 0, then the maximum speed, while at r = R, the velocity = 0, which occurs on the surface of the internal pipeline. At zero speed or at rest, the corrosion reaction process and the formation of scaling occur. The surface roughness of the internal pipe causes where key corrosive and scaling species are deposited in the roughness valley.

The flow velocity, density and diameter of the pipeline cause laminar or turbulent flow patterns. If the flow is laminar, then a thin layer that is formed such as siderite and FeS will prevent further corrosion processes. This is also the thin layer formed by the scale that will get thicker over time and reduce the pipe hole to shrink. It is recommended that if the flow pattern is turbulent as shown in Figure 4, then the layers of $CaCO_3$, FeS, and $FeCO_3$ formed will be peeled off and erosion will occur which causes thinning of the pipe thickness, especially this occurs in the Belkan area (Figure 4). As mentioned earlier, that crude oil is in the form of mud because it will be possible to grow and breed bacteria that produce CO_2 and H_2S which are corrosive elements in the presence of H_2O. CO_2 and H_2S react to form $FeCO_3$ and FeS, or with Ca^{2+} to form $CaCO_3$ or with water to form H_2CO_3 which will dissociate into HCO_{3-} and CO_3^{2-} as in pers (1) to pers (12).

Conclusions

The interaction between key species, the surface of the internal pipeline, and parameter conditions such as pH and temperature caused a corrosion process and the formation of scaling that will have an impact on the function and service life of the pipeline. The surface roughness of the internal pipe will become a key species deposit so that the corrosion process and the formation of scaling occur. The process of corrosion and scaling formation is influenced by pH, temperature and water content, H_2S, CO_2 and sulfur.Under fully developed flow conditions, the fluid velocity at the crude oil fluid interface-the internal pipeline surface is zero. In other words, the key species is at rest and the corrosion reaction process and scaling formation occurs. To improve the function and general use of the pipe due to the corrosion process and scaling formation, it is necessary to apply an excellent operation, and an expert system.

References

https://www.e-education.psu.edu/fsc432/node/5, diakses 10 july 2021

George V. Chilingar, Ryan Mourhatch Ghazi D. Al-Qahtani, 2008, The Fundamentals of Corrosion and Scaling for Petroleum and Environmental Engineer, Copyright 0 2008, Gulf Publishing Company 2 Greenway Plaza, Suite 1020 Houston. TX 77046

Lekan Taofeek Popoola, Alhaji Shehu Grema , Ganiyu Kayode Latinwo , Babagana Gutti and Adebori Saheed Balogun, 2013, Corrosion problems during oil and gas production and its mitigation, Popoola et al. International Journal of Industrial Chemistry 2013 2013, Internatonal Journal of industrial chemistry springer open Journal,http://www.industchem.com/content/4/1/35

David R. Gaskell, an introduction to transport phenomena in materials engineering, 2nd, 2013, Momentum press, LLC, New Jersey

Acknowledgements (Optional)

We thank the head of the Department of Metallurgical Engineering and the Dean of the Faculty of Manufacturing Technology for their support so that this paper can be completed.

PROCEEDINGS
JOINT CONVENTION BANDUNG (JCB) 2021
November 23rd – 25th 2021

The awakening of hydrodynamic trapping opportunity to unlock hydrocarbon potential in South Tunu Field, Mahakam Delta

Dhanny Fadlan, Roni Herdiyanto, Adhi Wicaksono, Andrew Ivan Julius Sitorus,Laura Maria Priskila
Pertamina Hulu Mahakam

Abstract

Tunu Field has been a gas producing field for more than 30 years. In Tunu South, which is considered less developed area due to high pressure and relatively deeper burial of deltaic sediment, is suspected to have a different trapping concept. Hydrodynamic trapping that is proven in Peciko, Nilam and Stupa Field is proposed for Tunu South. This paper aims to show the presence of hydrodynamic trapping in Tunu South, to predict and generate hydrodynamic closure map and to find hydrocarbon potential.

Tunu southern wells are used to identify the presence of hydrodynamic trapping. The characteristics of hydrodynamic trapping are observed, such the presence of single gas line accompanied by several water pressure gradients, and the presence of "shoulder effect" or called "pressure belly" in thicker net-sand layer, which is an indication of laterally drained reservoir. Subsequently, evaluation of the hydrodynamic closure can lead to the identification of hydrocarbon potential in the area.

In 2006, a well was drilled in the structural flank to test the hydrodynamic trapping and successfully found the target. However, perforation the reservoir resulted in no flow. The well was suspected to experience reservoir damage due to extremely high mud weight while drilling. In 2012, another well was drilled in the most southern up-dip area and resulted in wet sand. Based on the understanding of well results and 3D seismic interpretation, hydrocarbon closure map is generated, which take into account the high pressure and hydrocarbon potential in the southern area of Tunu is defined.

The knowledge from the study has given essential understanding of hydrodynamic trapping in Tunu South. As a result of that, the area remains interesting for future development strategy to sustain the production life of mature Tunu Field.

Keywords: field development, hydrodynamic trapping, mature field

Introduction

The Tunu Field is one of the largest mature gas field located in Mahakam Delta (Figure 1). This field is being produced more than 30 years. To improve recovery factor and maximize the gas production, intensive drilling campaign has been carried out in this field by gridding well strategy to reach its production peak in 1998. Starting 2002, the infill drilling campaign by reducing spacing has been conducted especially in crestal area to sustain production plateau. Since 2008, this giant field entered into mature field and facing natural decline.

Reservoir in The Tunu Field is dominated by Upper Miocene deltaic system which consists of multi-layer sandstone reservoir (Figure 2). Lateral and vertical connectivity between sand bodies is very limited, particularly in distributary mouthbar facies. Another case for distributary channel, this reservoir has better better reservoir properties with thickness varying between 5 – 20 m. The sedimentation trend in Tunu Field is from West to East which also indicates that in a distal there will be increasing sand deconnection and top overpressure is also getting shallower (Figure 3).

In Tunu South, which is considered less developed area due to high pressure and relatively deeper burial of deltaic sediment, is suspected to have a different trapping concept. Hydrodynamic trapping that is proven in Peciko (Lambert et al, 1999; Ramdhan et al, 2018), Nilam (Jauhari et al, 2012), Stupa (Anshariy et al, 2020) is proposed for Tunu South.

Exploration history in Tunu South was started with the drilling TS-1 well located in the structural flank (Figure 4) to prove hydrocarbon accumulation with hydrodynamic trapping concept. The well has penetrated overpressure zone with extremely high drilling mud weight 2.15 deq. However, maximum reservoir pressure recorded was 1.30 deq and

perforation the reservoir resulted in no flow. The well was suspected to experience reservoir damage.

Another well was drilled in Tunu South (TS-2) in the most southern updip area to prove hydrocarbon extension (Figure 4). The well resulted in thick sand with poor hydrocarbon accumulation. Based on understanding of well results and 3D seismic interpretation, hydrocarbon closure map is generated, which take into account the high pressure and hydrocarbon potential in the Southern Area of Tunu.

Data and Method

Data

The data in this study is using 17 exploration, delineation, and development wells, 3D seismic data, and pressure data. The pressure data need to be filtered into initial condition before production to eliminate depletion. The pressure data is very important to prove hydrodynamic trapping concept.

Method

The hydrodynamic trap could be observed from pressure-depth plot as shown in Figure 5. The tilted hydrocarbon-water contact will be indicated by one hydrocarbon line which indicating one hydrocarbon pool, accompanied by several water lines which indicating a difference in overpressure (Ramdhan et al, 2018). Specifically for lateral reservoir drainage, its presence can be observed from the existence of sand-shale pressure discrepancy and its associated shoulder effect as shown in Figure 6.

The discrepancy shows that the reservoir pressure is less than shale pressure and, permitting the water to flow from shale to sand. Meanwhile, the shoulder effect (O' Connor and Swarbrick, 2008) represents sand-shale pressure continuity since the shale is not entirely impermeable.

The approach to create hydrodynamic closure map is different from the conventional trapping with the flat water contact. Hydrodynamic closure map was utilized in mapping hydrocarbon limit of the tilting contact case. The data required are water head map, depth structure map, and the density of water and hydrocarbon to create pseudo structural map as shown in Figure 7.

The water head data is calculated from the pressure data and distributed into a map with a controlled from understanding of the pressure distribution in Tunu South. The water head map is corrected by the tilting amplification factor (TAF) refer to density of water (1.0 g/cc) and gas (0.2 g/cc). Hydrodynamic closure map is derived from sum dari corrected water head map and value of depth structure map. Therefore, the principle of hydrodynamic map is to correct the structural surface from the tilted water contact condition to a flat water contact which is called a pseudo structural map.

Result and Discussion

This study figures out hydrodynamic trapping occurred in Tunu South from the water head plot which is indicating one gas line accompanied by several water lines and laterally drained reservoir which act as conduit ground water flow communicated to hydrostatic aquifer.

Water Head Plot

The Tunu South is adjacent to The Peciko Fieldm where an intensive study of hydrodynamic trap has been carried out. Gas accumulation in this field is located in the deeper overpressure part and in the flank anticline. Water head-depth plot of gas accumulation in this field shows one gas line accompanied by several water lines which is indicating tilted gas water contact (Ramdhan et al., 2018). Tilting direction is toward the northern direction of the field, which is toward Tunu South.

The same condition was also found in Tunu South, one gas line accompanied by several water lines indicating the occurrence tilting contact. The updip and downdip sections are filled with water while in between are filled with gas (Figure 8). This hydrodynamic trapping indication occurs in the Layer 4d, where the layer consists of a massive spread of distributary channel sand.

Laterally drained reservoir

The presence of high-pressure zone called shoulder effect which overlays hydrostatic reservoir has been recognized. These hydrostatic reservoirs are permeable well-connected sand bodies communicated to the hydrostatic aquifer that can release the overpressure of the enveloping shales (Figure 3). Active lateral reservoir drainage at the present time needs a source of water to maintain the flow. One of possible source of active water flow is dewatering of the shale adjacent to the sand (Grosjean et al, 1994; Lambert, 2003). The shale dissipates their overpressure through the reservoir, this maintaining active lateral drainage. Then, it requires the presence of overpressure in the shales.

The pressure-depth profile shows the shoulder effect as an indication of the presence of lateral reservoir drainage as shown in Figure 9. In Tunu South, lateral

reservoir drainage was identified by pressure-depth profile. The pressure increases with depth in shale and then decreases in sand bodies naturally. This shoulder effect was observed clearly in Tunu South as shown in Figure 9. The well from TS-1 to TS-11 location form West to East shows the shoulder effect occurs at Layer 1, 2, and 3 with high net sand content in these layers. Shoulder effect indication is also decreasing toward distal (East) due to less sand content. Sand bodies indicating active dewatering, thus active fluid flow from Shale. This circumstance makes hydrodynamic trap due to lateral reservoir drainage is plausible to occur in Tunu South.

Hydrodynamic Closure Map (U-Map)

Fluid distribution inside closure in interest area is confirm the coherency of hydrodynamic trapping as shown in Figure 10. Uncertainty remain for closure limit due to lack of data. Some fluid anomalies observed in TS-4 and TS-10 most probably due to facies changes to distributary mouth bar with thin and poor properties sand layer thus causing not filled by hydrocarbon.

Conclusions

The presence of variation of water contact and lateral reservoir drainage are very plausible to proof the hydrodynamic trapping. Single gas line accompanied by several water lines is observed in Layer 4d. Lateral reservoir drainage is shown clearly by pressure-depth profile which indicating shoulder effect as conduit ground water flow.

Hydrocarbon accumulation from hydrodynamic closure map resulting new limit and opening opportunity of hydrodynamic trapping in Tunu South. The knowledge from the study has given essential understanding of hydrodynamic trapping in Tunu South. As a result of that, the area remains interesting for future development strategy to sustain the production life of mature Tunu Field.

References

Jauhari, Usman., Permana, R., Wijanarko, A., and Soenoro, A., 2012, American Association of Petroleum Geologist.

Ramdhan, A.M., Hutasoit, L.M., and Slameto, E., 2018, Indonesian Journal on Geoscience, **5**, 65–80.

Anshariy, A., Hermawan, Endarto, W., Irawan, A., and Utama, F., 2020, Indonesian Petroleum Association.

Grosjean, Y., Choppin de Janvry, G. and Duval, B.C., 1994. Presented at the 14th World Petroleum Congress, May-June 1994, Stavanger, Norway

Lambert, B., Duval, B.C., Grosjean, Y., Umar, I.M. and Zaugg, P., 1999. AAPG, Tulsa, Memoir 78, 297-320.

O'Connor, S.A, Swarbrick, R.E, 2008. Petroleum Geoscience, 14, 115-1

Acknowledgements

The authors thank to Pertamina Hulu Mahakam, SKK Migas, and Migas for their kind support and permission to publish this paper. Thank are also to Agus Ramdhan and Rachman Phasadaon who previously work this study.

PROCEEDINGS
JOINT CONVENTION BANDUNG (JCB) 2021
November 23rd – 25th 2021

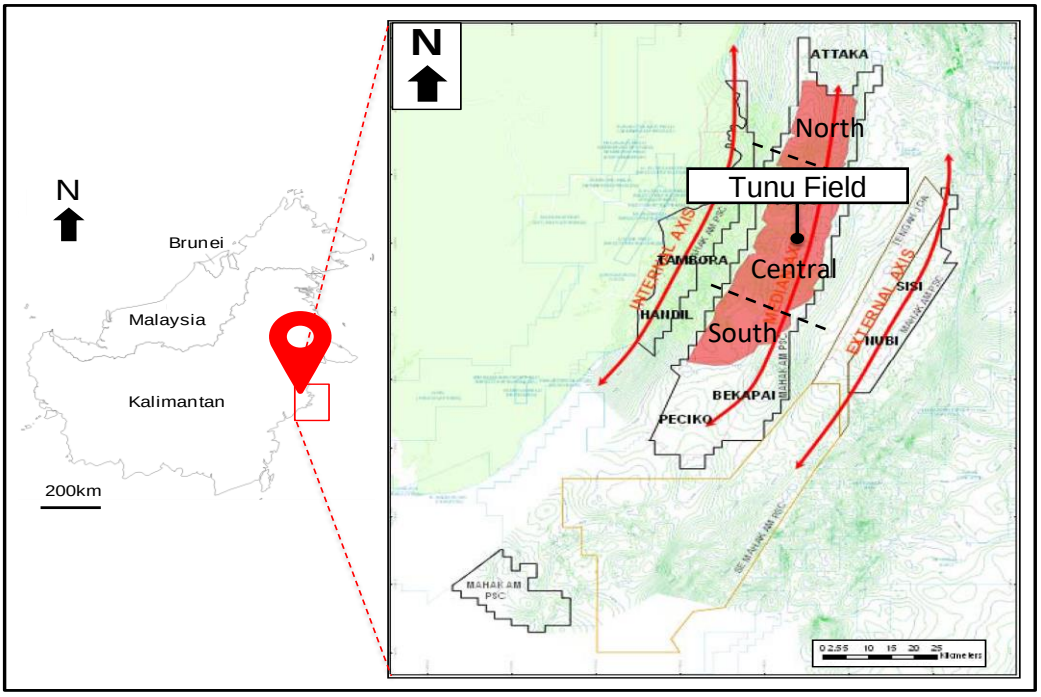

Figure 1: Location map of Tunu Field, Mahakam Delta, which consists of 3 sector, i.e. North, Central, South.

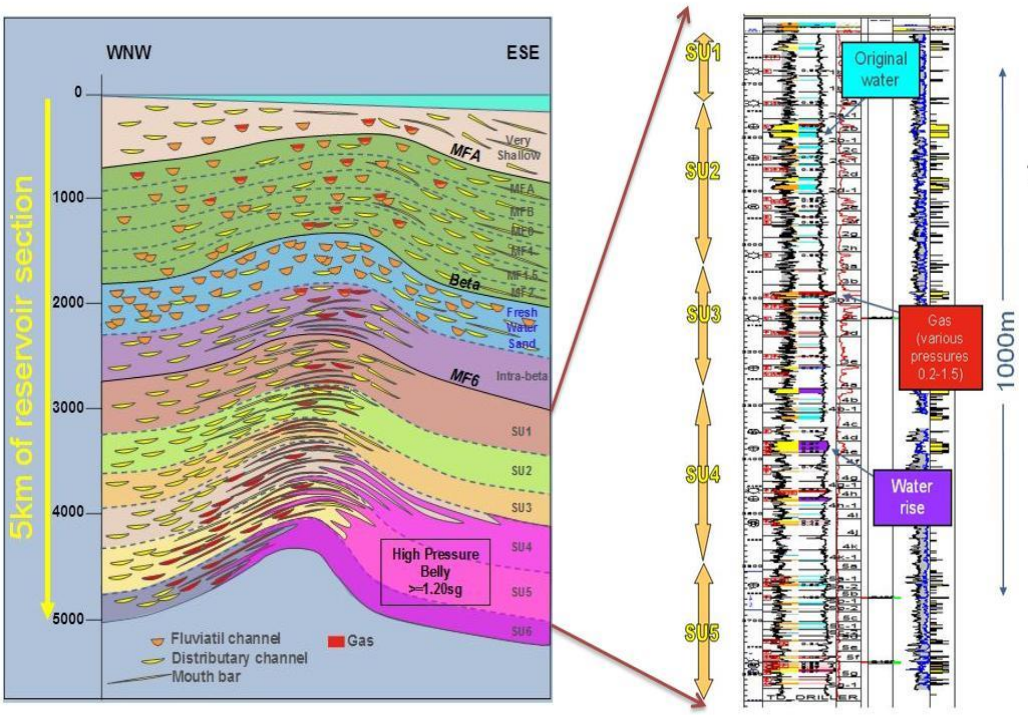

Figure 2: Typical lofs in Tunu Main Zone, showing heterogeneities in reservoir geometry and connectivity

PROCEEDINGS
JOINT CONVENTION BANDUNG (JCB) 2021
November 23rd – 25th 2021

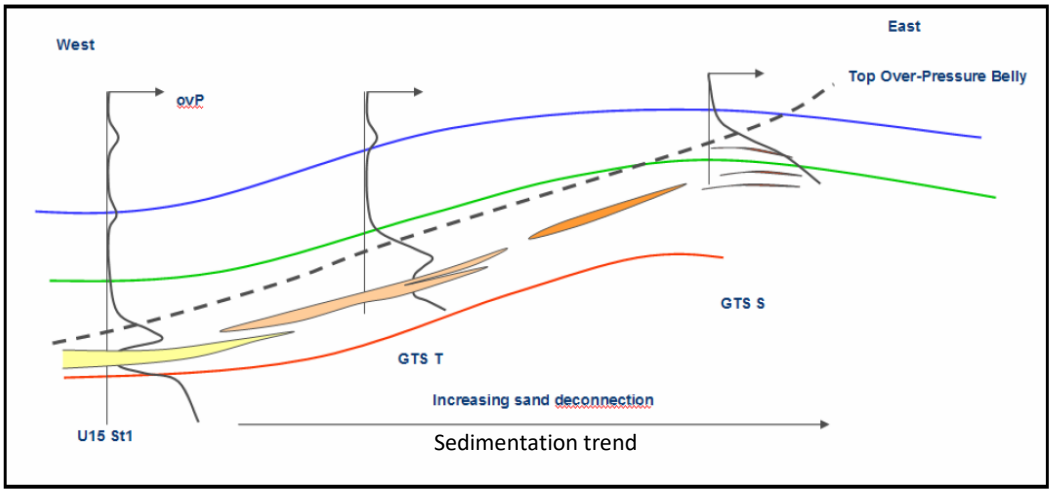

Figure 3: Schematic section from West to East which showing sedimentation trend, increasing sand deconnection, and shallower top overpressure. This schematic also showing "shoulder effect" or "presure belly" in permeable well-connected sand bodies.

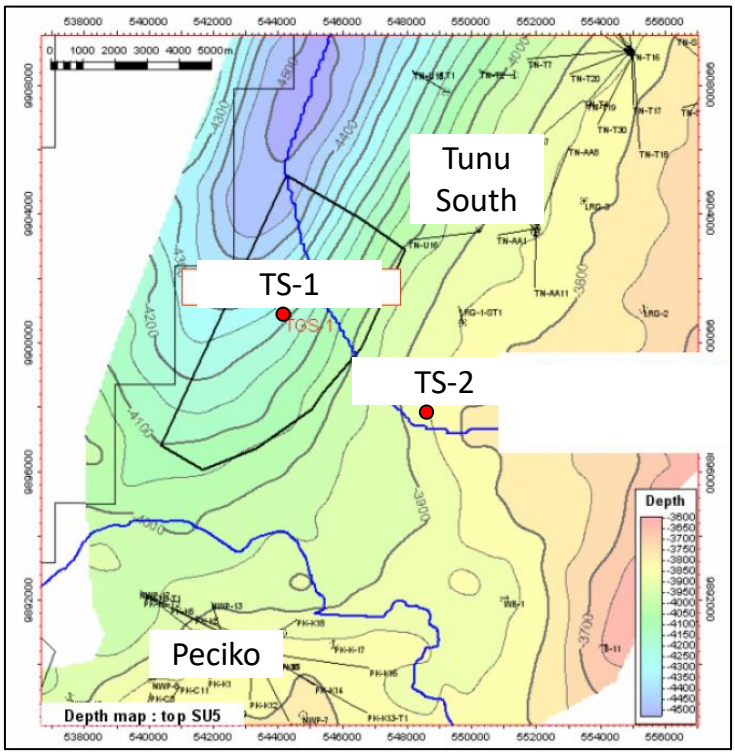

Figure 4: Tunu and Peciko border map. TS-1 well located in the structural flank and TS-2 well located in the most southern updip area.

PROCEEDINGS
JOINT CONVENTION BANDUNG (JCB) 2021
November 23rd – 25th 2021

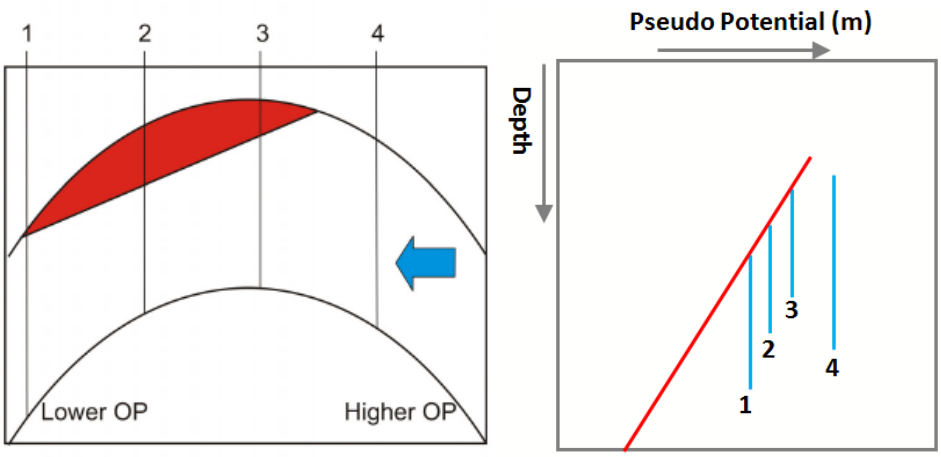

Figure 5: Single hydrocarbon pressure gradient accompanied by several water pressure gradients (Ramdhan et al., 2018).

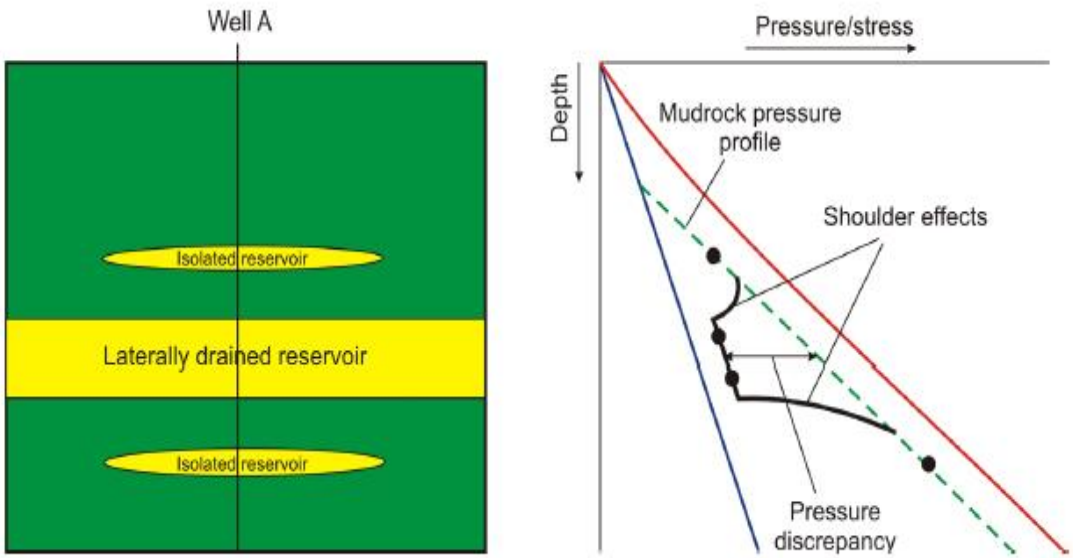

Figure 6: The Schematic of sand-shale pressure discrepancy and shoulder effects as an indication of lateral reservoir drainage (Ramdhan et al., 2018).

PROCEEDINGS
JOINT CONVENTION BANDUNG (JCB) 2021
November 23rd – 25th 2021

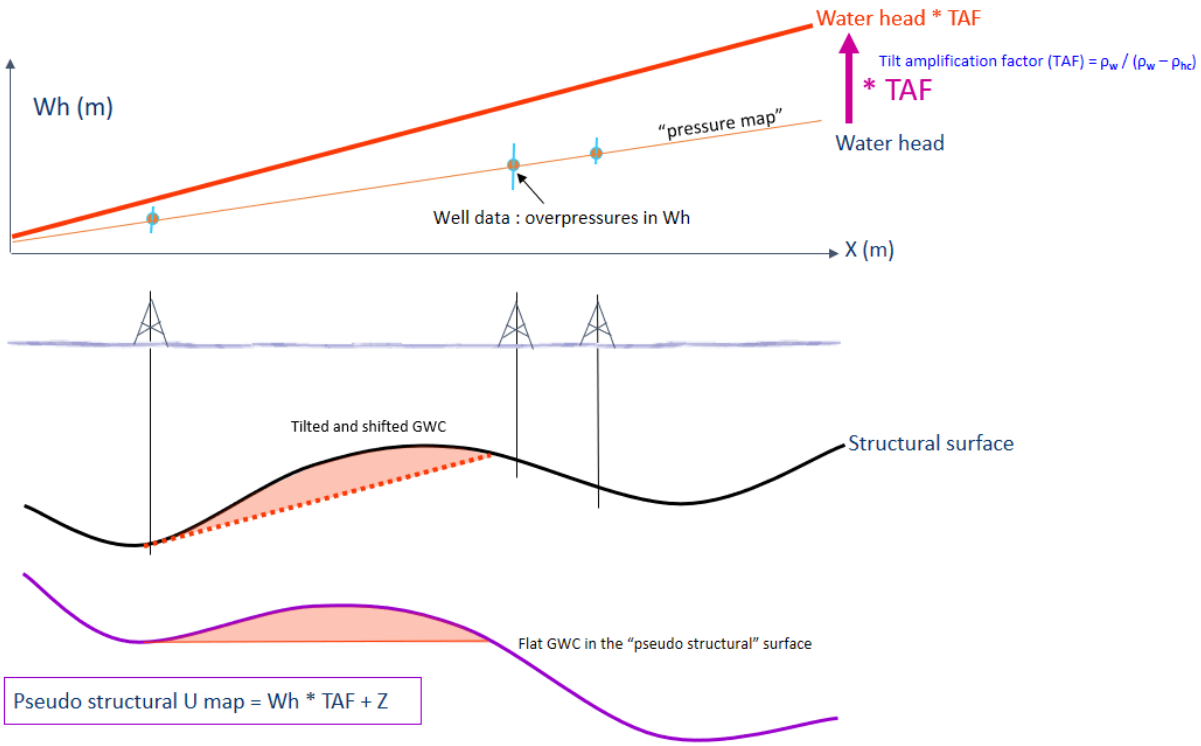

Figure 7: The schematic of generating hydrodynamic closure map by using water head map, depth structure map, and the density of water and hydrocarbon to create pseudo structural surface.

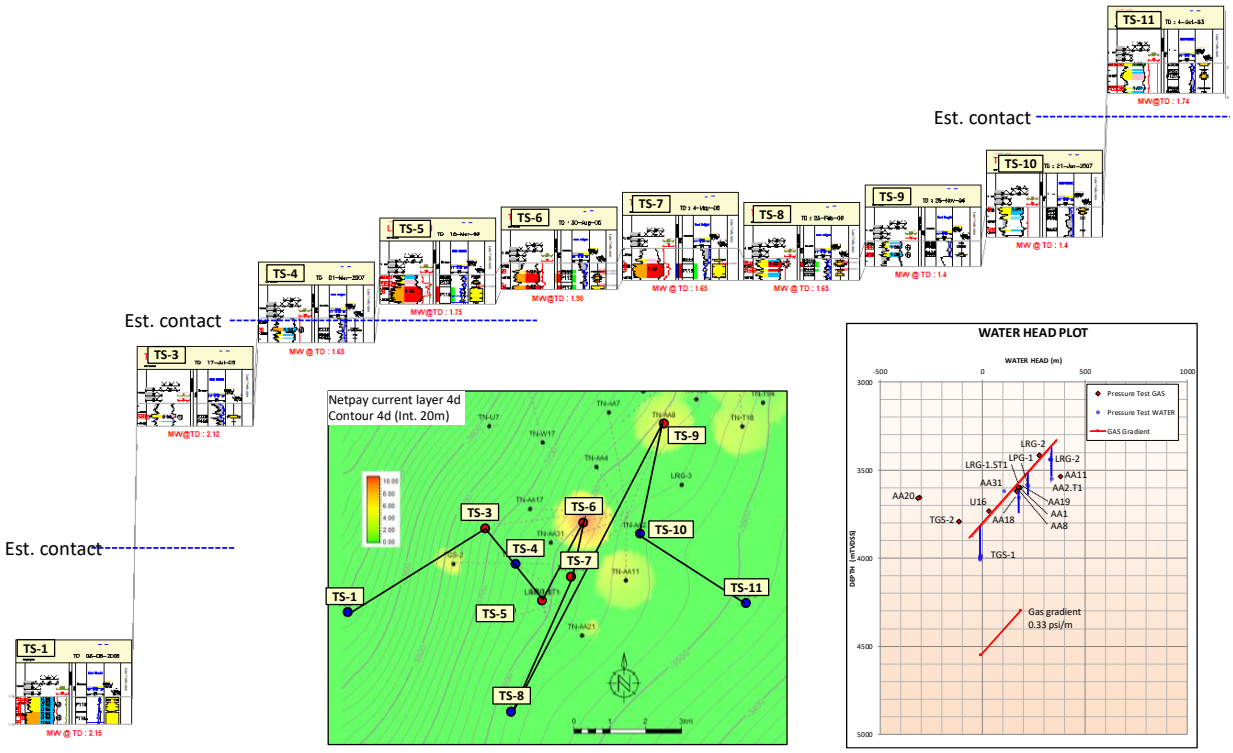

Figure 8: Single gas line accompanied by several water lines and updip and downdip wells were filled by water.

PROCEEDINGS
JOINT CONVENTION BANDUNG (JCB) 2021
November 23rd – 25th 2021

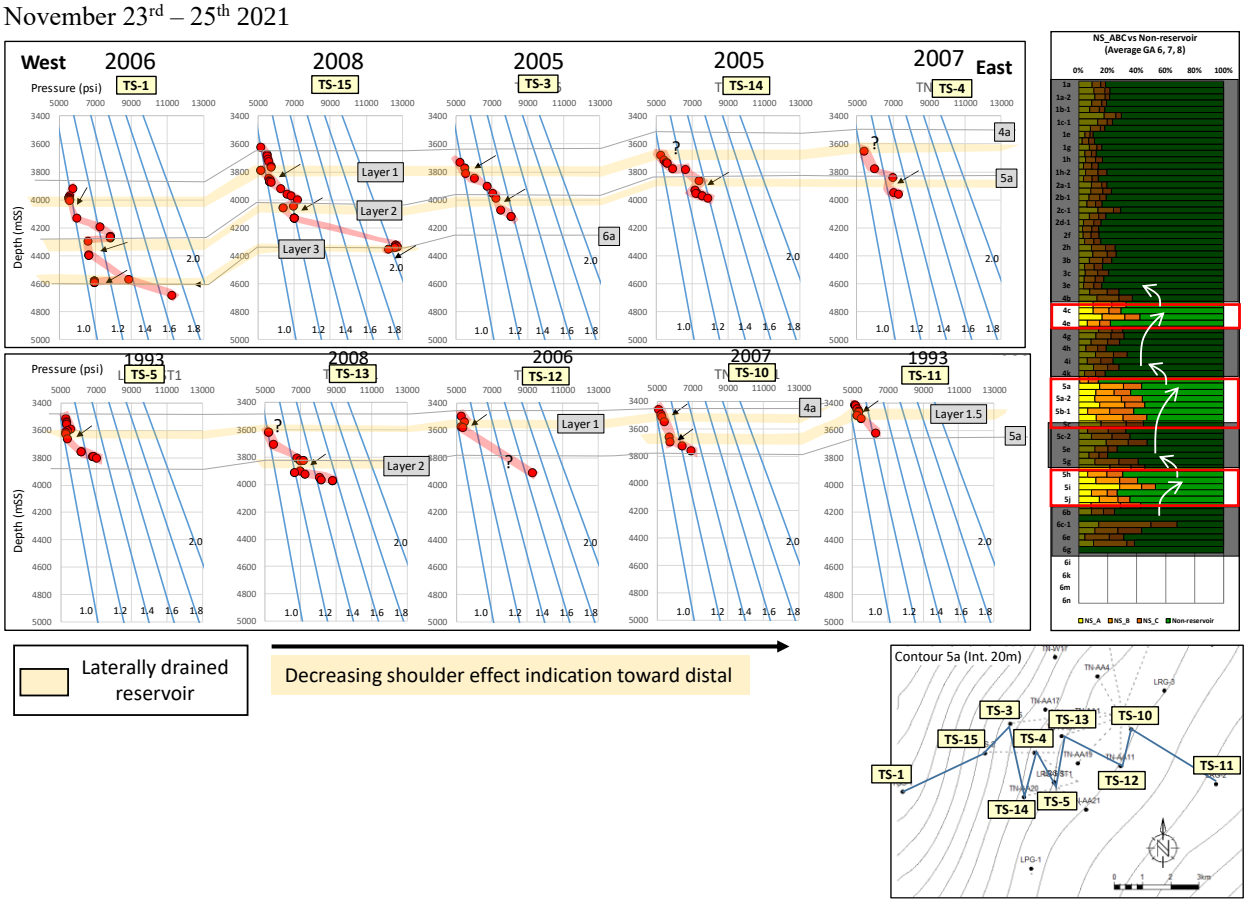

Figure 9: Shoulder effects presence in Layer 1, 2, and 3 which consist of high netsand content. This is indication of presence lateral reservoir drainage.

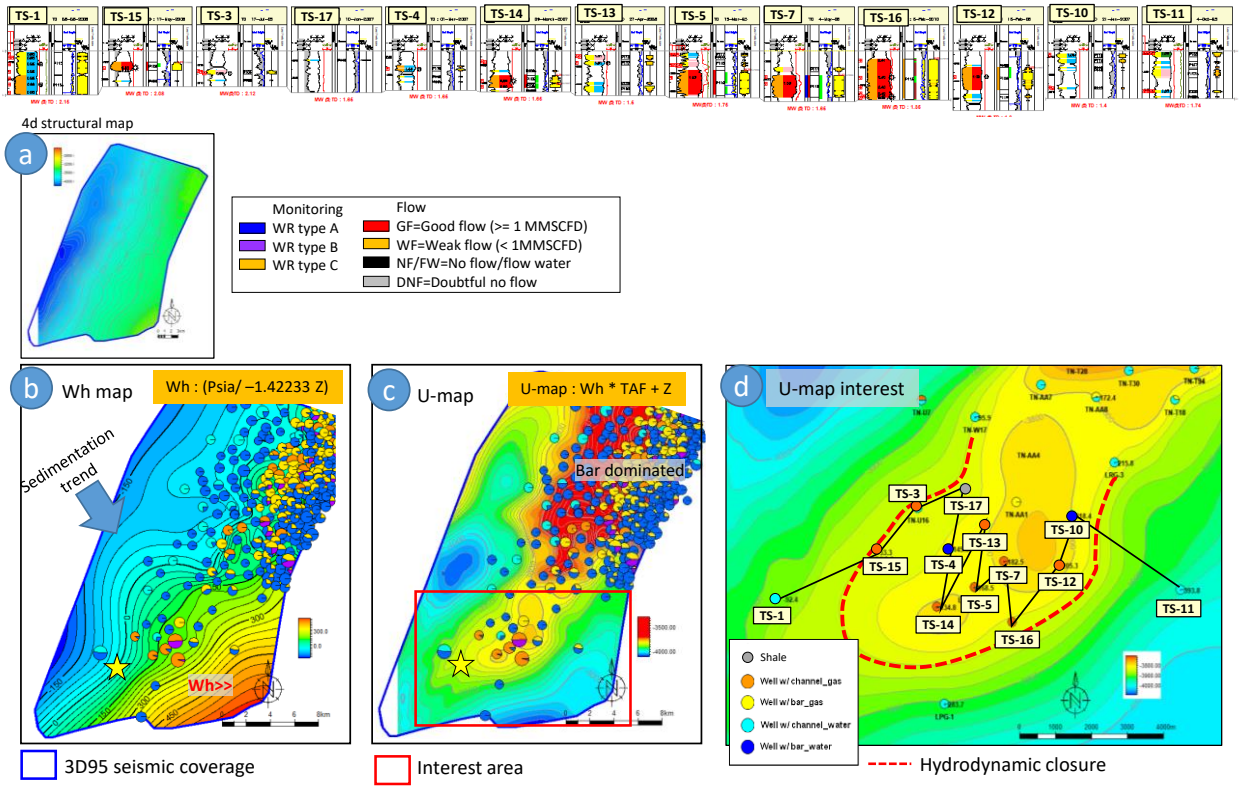

Figure 10: Hydrodynamic closure map (U-Map) workflow and result. a) structural map; b) water head map; c) hydrodynamic closure map in Tunu South; d) hydrodynamic closure map in Tunu South interest area.

PROCEEDINGS
JOINT CONVENTION BANDUNG (JCB) 2021
November 23rd – 25th 2021

Characteristics, Entrapment and Habitat of Hydrocarbon Discovered in the Basement Reservoirs in South Sumatra Basin

Miftah Mazied[1], Rizki Krishna Pratama[1], Poetri Monalia[1], Agung Donurizki[1]
1 PETRONAS Carigali Indonesia

Abstract

This paper presents a basin-scale petroleum system modelling analysis on the basement play in South Sumatra Basin in order to recognize the genesis, entrapment and habitat of the discovered hydrocarbon in this unconventional reservoir. The result of this study will be beneficial for future basement exploration in this basin, especially in improving the prediction of the location and properties of yet-to-find hydrocarbons.

During the study, geochemical data of fluid and rock samples from around 41 wells were evaluated to define the genesis and characteristic of the hydrocarbon. Significant properties were then spatially plotted to recognize the occurrence of any special geochemical trends within specific geological location. 1D and 3D Basin modelling analysis, along with understanding of geology framework, was then used to understand the processes that dictate the geospatial distribution.

The study indicates that the basement is proven to contain both oil and gas. Thermogenic gas concentrated in the basement highs near to the deep kitchens, whereas oil clusters were found in the basement highs near to shallower kitchens. The hydrocarbon entrapment mechanism was mainly by short-distance migration through fault juxtaposition of the fractured basement against the organic-rich source. However, long-distance migrations through carrier beds are also proven to work and should not be ignored. Basin modelling analysis reveals that the type of hydrocarbon phases filling the basement was mostly controlled by type of source rock maturity stage within each kitchen at the time of basement fracturing established.

High concentration of CO_2 is mostly associated with dry gas and mainly controlled by meta-carbonate distribution in the hot and deep grabens. However, to a lesser extent, it was also controlled by magmatic activity locally in few areas of the basin.

Keywords: Basement, Geochemistry, Petroleum System Modelling, South Sumatra Basin.

Introduction

The study area is located in the South Sumatra Basin, one of the most prolific basins in Indonesia which has total discovery of 8.6 BBOE of 2P reserves. The basin covers around 82,000 square kilometers and is situated mostly onshore. Geologically, this basin is a part of a series of tertiary back-arc basins developed over Sumatra and Java Islands as a result of back arc rifting generated by strike slip system in the Paleogene time (Davies, 1984 and Daly et al., 1987).

Almost all stratigraphic levels in the basin are proven as producing reservoir including the Pre-Tertiary Basement with example from Suban, Sumpal, Dayung and Kaliberau Dalam fields. Up to this date, the basement discovery is dominated by hydrocarbon gas with few discoveries of oils. The gas types were found to be wet and dry with high variation in CO_2 content ranging from 5-99%.

Understanding the habitat of hydrocarbon types and properties in this play is still poorly understood as the distribution of the discovered hydrocarbon shows a high variation in its characteristics and it will effect to the high uncertainty in the pre-drill prediction. To overcome this challenge, an integrated of geological, geochemical and basin modelling studies has been conducted and this paper will describe the analysis and findings.

Data and Method

Geochemical evaluation was conducted on both rock and fluid samples. The rock samples was obtained from 17 wells and consist of TOC, rock eval pyrolysis vitrinite reflectance, GC and GC-MS data. The evaluation was done to understand the potential source rock layers, its geochemical properties and the source rock facies.

Oil samples from basement reservoir were obtained from six (6) wells, while gas samples consisted of hydrocarbon and non-hydrocarbon gasses were provided from 18 wells. In this stage, the molecular and isotope properties, as well gas concentration and ratio, were evaluated to understand the character, genesis and the origin of the oil and hydrocarbon gas as well as the non-hydrocarbon gas.

Significant properties were then spatially plotted on maps to recognize the occurrence of any special

geochemical trends within specific geological location. 1D and 3D Basin modelling analysis, along with understanding of geology framework, were then used to understand the processes that dictate the geospatial distribution so that prediction can be made for the location and properties of the yet-to-find hydrocarbon.

Result and Discussion

Hydrocarbon (HC) Size, Types and Characteristics in Basement

Based on the latest IHS data in 2021, in South Sumatra Basin, at least 29 basement discoveries have been made with total of 1.5 BBOE of 2P reserves. The first discovery was made in 1913 where a Pre-Tertiary Carbonate was drilled in Kluang Field by a Dutch company. The most recent discovery was made by Repsol in Kaliberau Dalam field in 2019 where they found a gas accumulation in the Pre-Tertiary Metamorphic Rock. However, so far the significant discoveries were only found from 4 (four) structures which are Suban, Sumpal , Dayung and Kaliberau Dalam.

Gas dominates the discovery which make up 97% of total hydrocarbon resources, while oil is only contributing to 3% of total hydrocarbon resources. There are total of 17 gas discoveries, 6 oil discoveries and 5 oil and gas discoveries.

The analysed oils which collected from South Betara, Hari and Air Serdang Fields are characterized by low sulphur content with API gravity values ranging from 27.2-42° API. The results of this study indicate that these oils were derived from a highly oxidized source rocks that were deposited under fluvio-deltaic environment. This is primarily achieved from their biomarkers which shows high Pr/ph ratio (>3), the predominance of C_{29} over C_{27} and C_{28} steranes and also its low sulphur content. Oil-source rock correlation conducted shows that the oils were originated from the Talang Akar Formation.

Locally in the Musi Platform, a unique oil found from basement was reported by Rashid et al. (1998). The oils are interpreted to be derived from carbonate source rock, possibly from Baturaja or Telisa Carbonate or it can be also from Pre-Tertiary Carbonate. Unfortunately, no geochemistry data available to further re-evaluate this finding.

The gasses found are all thermogenic and consist of wet and dry gasses. The gasses consist mostly of methane with high variation in CO_2 content ranging from 0.1-99%.

HC Habitats and Entrapment

The hydrocarbon type distribution does not seem to be controlled by source rock facies variation as the geochemistry evaluation on rock and fluids indicates that the major contributor of hydrocarbon came from one single source which is fluvio-deltaic Talang Akar. Instead, based on Map of vitrinite reflectance (%Ro) and petroleum system modelling analysis, the variation is more likely to be controlled by type of source rock maturity stage within each kitchen at the time of fracturing or weathering of basement was established.

The vitrinite reflectance map which overlaid by the distribution of HC discovery types (figure 1) shows that the gases are concentrated in the basement highs near to the deep kitchens while majority of oil discoveries were found in the basement highs near to the shallower kitchens indicating a possible control of thermal maturity levels on the variation of hydrocarbon types.

Figure 2 shows an example of charging history through time in one of major kitchen namely Central Palembang Graben. As the fluvio-deltaic Talang Akar source rock is type D/E kerogen, the source rock was capable of generating both oil and gas depending on the maturity window. Oils were expelled first significantly in the early maturity stage at 27 ma and gradually decreases before stop expelling oil before Plio-Pleistocene (5-7 ma). On the other hand, the gases were still generated until present day. Fracturing of the basement occurred mostly due to compressional tectonic event in the Plio-Plistocene, so that only gases would be available from the Central Palembang graben to charge the nearby fractured basement structures.

In the shallower kitchens, where the fluvio-deltaic Talang Akar source rock was still in early to mid-maturity stage in the Plio-Pleistocene time onwards, oils would charge the nearby fractured basement structures.

The majority of discoveries are found on structures facing directly into mature kitchen where the migration are short-distance through fault juxtaposition of the fractured basement against the organic-rich source. However, in few structures such as Air Serdang and SH in the Iliran high, migration of 10 and 20 Km through carrier beds are proven to work.

CO_2 Origin and Habitat

High CO_2 content is one of the main exploration risks for basement exploration in South Sumatra Basin as well as one of significant challenges in the development stage as shown by several discovered structures such as Bungin and Rayun that remains undeveloped due to this issue.

Isotope carbon analysis shows that the origin of high CO_2 was inorganic and it is associated with the dry gas

occurrence (figure 3) indicating both types of gas were generated from hot areas in the basin. A further evaluation on Helium Ratio vs δ13CO_2 (figure 4) on few samples suggests that the inorganic source came from thermal carbonate decomposition, rather than from magmatic degassing.

The interpretation above is supported by the distribution of CO_2 proportion where almost all gas discoveries with high CO_2 content are on trend with the distribution of Pre-Tertiary Carbonate lithology (figure 5), the most likely carbonate section for source of the CO_2 in the area. This trend only applies to pre-tertiary carbonates located in deep areas in the basin near to deep seated faults where the carbonates are exposed to high temperatures and the resulting CO_2 easily migrated upward through the fault zones. On the other hand, the trend does not apply to the pre-tertiary carbonates located in the relatively shallower areas where the temperature was not sufficient enough to decompose the carbonates.

Locally in few areas of the basin, the high CO_2 content is not related at all with the location of Pre-Tertiary carbonates, instead it coincides with the development of Miocene granite intrusion. This leads to a conclusion that the high CO_2 was originated mostly due to thermal decomposition of carbonates with minor contribution from magmatic activity.

Conclusions

This integrated geochemical, geology and petroleum system modelling evaluation suggests that oil found from basement in the South Sumatra Basin are mostly derived from fluvio-deltaic Talang Akar and are characterized by low sulphur content with API gravity values ranging from 27.2-42° API, whereas the gasses are all thermogenic with high variation in CO_2 content ranging from 0.1-99%.

The hydrocarbon type distribution is mostly controlled by the maturity stage in each kitchens. Fractured basement structures near to the hot and deep kitchens have a high probability to contain gas while those located near to the shallower kitchens have a high probability to contain oil.

The entrapment mechanisms could be either by short-distance migration through fault juxtaposition of the fractured basement against the organic-rich source or long-distance migrations through carrier beds.

The high concentration of CO_2 are controlled mainly by the distribution of Pre-Tertiary Carbonate in the hot area in the basin, especially those area located near to the deep seated faults, with minor control from the distribution of Miocene magmatic activity.

References

Daly, M.C., Hooper, B.G.D., Smith, D.G., 1987. Tertiary Plate Tectonic and Basin Evolution in Indoneisa: IPA, 16th, p. 399-426.

Davies, P.R., 1984. Tertiary Structural Evolution and Related Hydrocarbon Occurences, North Sumatra Basin: IPA, 13th, p. 19-50.

Irakli, P., Bilal, S. Arben. B, Alfred, C., Agim, Y., 2017. The Evaluation of The Petroleum Potential in Dumre Region (Albania) Based Upon Dumre-7 Well Result: Muzeul Oltenei Craioa. Oltenia. Studii si comuncari Stiintle Naturii. No. 2/2017, p.13-23.

Rashid, H., Sosrowidjojo, I.B., Widiarto, F.X., 1998, Musi Platform and Palembang High: A New Look At The Petroleum System: IPA, **26th**, p. 225-276.

Huang, Y.R., Zhang, ZH, Liu, J.Y., 2009, Mantle-Derived Gaseous Component in Ore-Forming Fluids of the Xiangshan Uranium Deposit, Jiangxi Province, China: Evidence from He, Ar and C Isotopes. Chemical Geology 266, p. 86-95.

Acknowledgements

The authors thank the Managements of PCINO, SKK Migas and Ditjen Migas for the permission to publish this paper. Special thanks are also directed to colleagues at Exploration Department of PCINO who contributed to the writing of this paper.

PROCEEDINGS
JOINT CONVENTION BANDUNG (JCB) 2021
November 23rd – 25th 2021

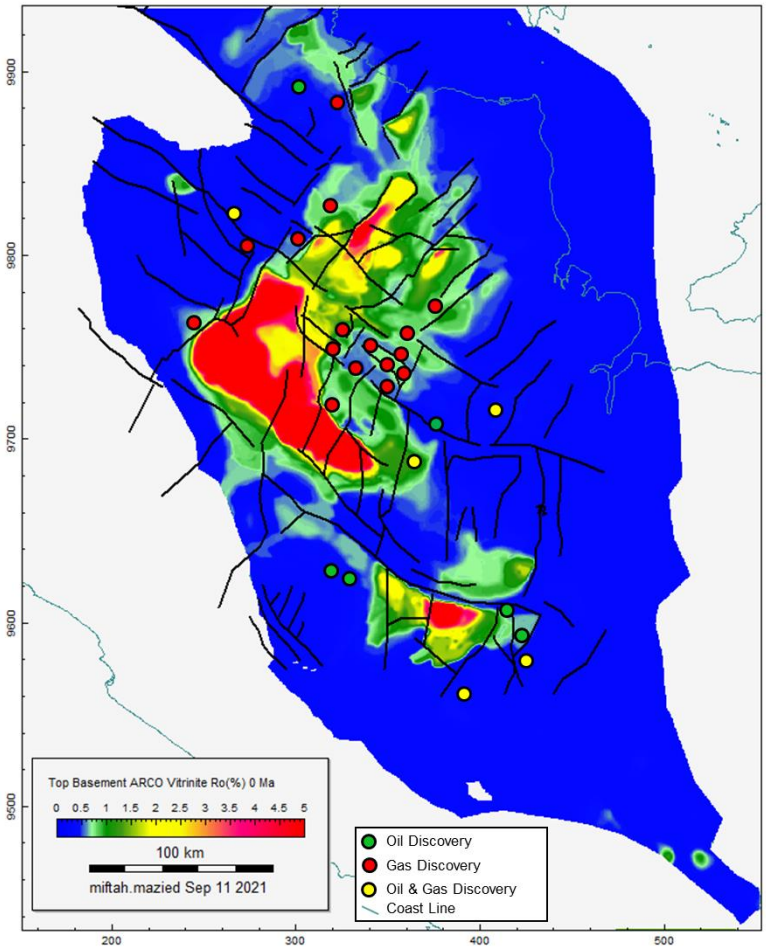

Figure 1: Present day vitrinite reflectance (%Ro) map which is overlain by the distribution of HC discovery types showing gas discoveries located near to deep kitchens while oil discoveries located near to shallower kitchens.

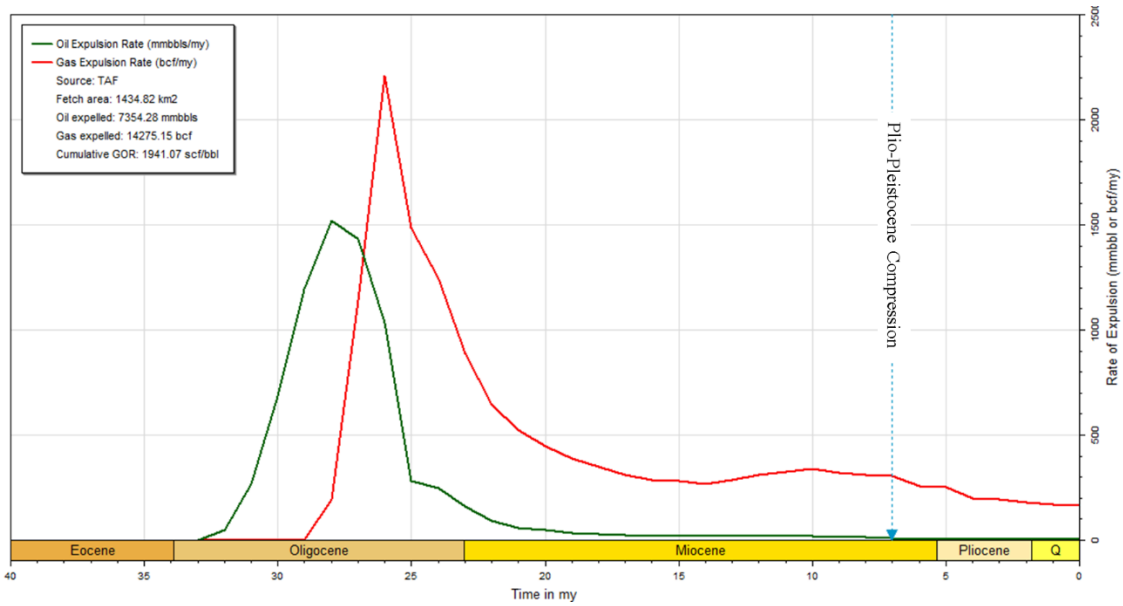

Figure 2: Charging through time from Central Palembang Depression indicating oils stopped expelling before Plio-Pleistocene compression (5-7 ma). On the other hand, the gases were still generated until present day. Fracturing of the basement occurred mostly due to compressional tectonic event in the Plio-Plistocene, so that only gases would be available from the Central Palembang Graben to charge the nearby fractured basement structures.

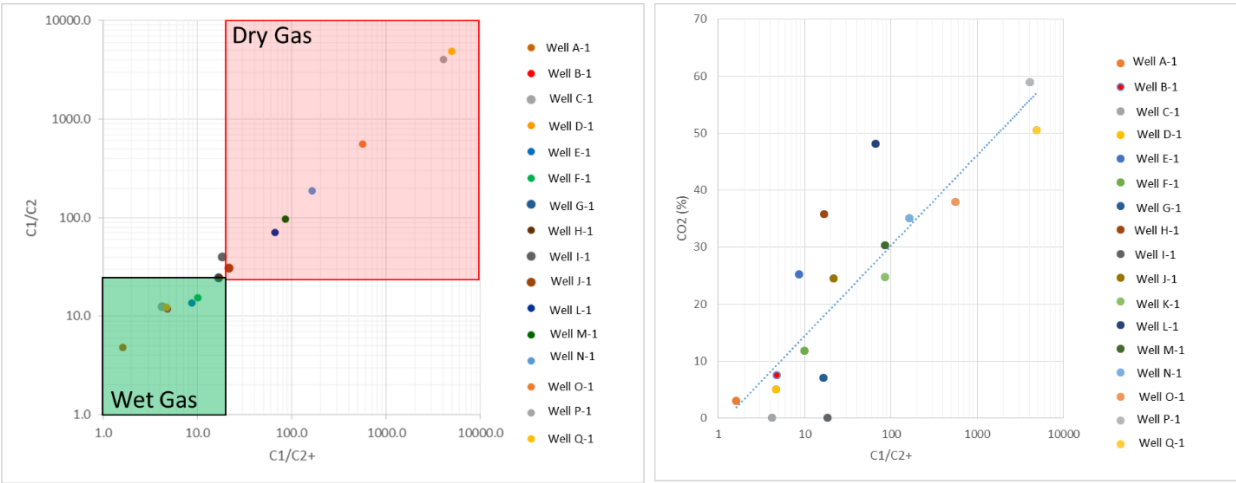

Figure 3: Cross plot of C1/C2+ vs C1/C2 (left side) for wet and dry gas identification (after Irakli et al., 2017) showing that gasses are both wet and dry, and cross plot of C1/C2+ versus CO_2 percentage (right side) showing a correlation between high concentration of CO_2 and the dry gas.

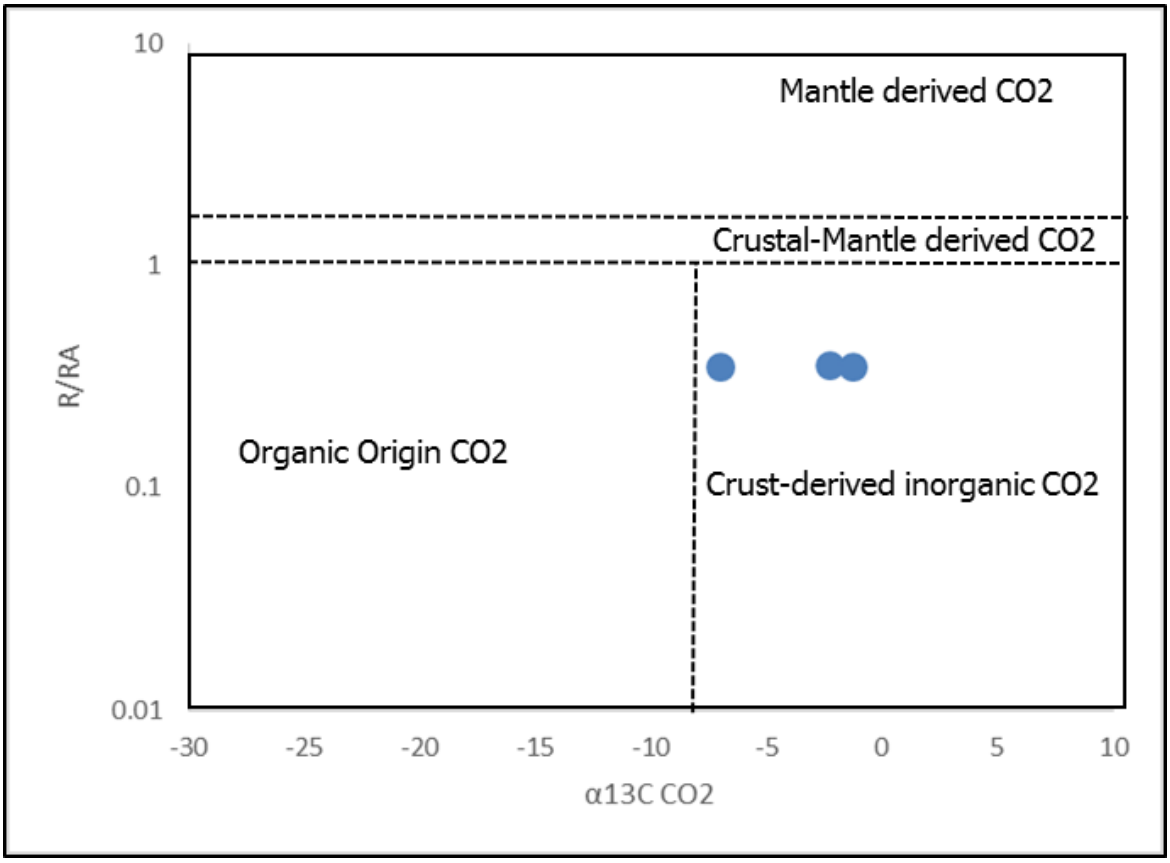

Figure 4: Carbon and helium isotopic identification index of CO_2 from different sources (Hu et al., 2009) showing that the CO2 origin was crust-derived inorganic (thermal carbonate decomposition)

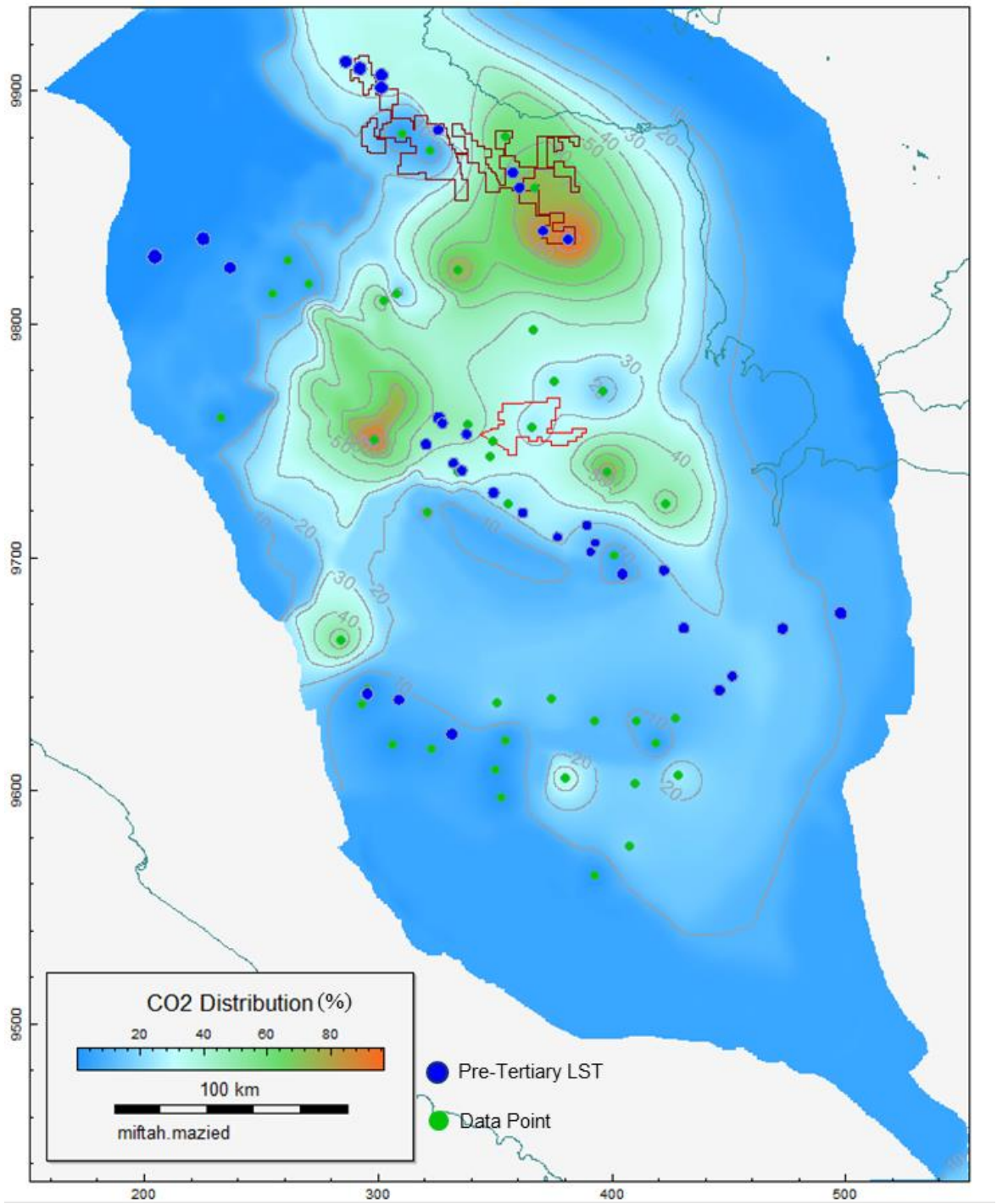

Figure 5: CO_2 percentage distribution map from Basement & TAF in combination with the distribution of Pre-Tertiary Carbonate lithology showing that most location of high CO_2 content are on trend with the location of pre-tertiary carbonate development.

PROCEEDINGS
JOINT CONVENTION BANDUNG (JCB) 2021
November 23rd – 25th 2021

Narrowing Subsurface Depth Uncertainty to Reduce Volumetric Calculation Error and Horizontal Drilling Guidance in Zulu Field, PHE ONWJ

Atmaji Nugroho[1)], Chandra Ageng[1)], Stephanie Cherif [2)], Herman Boro[2)]
[1)]Pertamina Hulu Energi ONWJ, Jakarta 12520, Indonesia
[2)]SGS Subsurface Consultant, Voorburg, Netherland

Abstract

Zulu Field is heavy oil field, located in Offshore North West Java basin, 70 km northwest of Jakarta, Indonesia. It was discovered by ZZZ-1 exploratory well in 1974 and commenced production by installing ZUA platform in 1986. Since then, the development was expanded by seven additional platforms around the structure. Its peak production reached in 1987 with total oil producing was 24,000 bopd, mainly coming from Baturaja carbonate reservoir. Presently the field is producing 2500 bopd, with the intention to gain more oil production by application of waterflood and EOR in the near future.

Zulu Field is partially covered by 3D seismic data, as the consequence of restricted Kepulauan Seribu National Park as well as operational and safety factor due to vicinity to platforms and wells. Eventually, those areas are covered by 2D seismic data. There are also 120 wells included exploratory and development, scattering into the area though concentrated in the northern.

Carbonate reservoir is typically having rough surface and highly undulated morphology. This circumstance creates large gap of depth uncertainty in reservoir depth estimation during drilling, furthermore in horizontal well. Shale out occurrence often experiences in horizontal drilling, causing reduction to the reservoir net to gross. Therefore. it is obliged to quantify depth uncertainty in the whole surface of the reservoir not only for drilling guidance but also for sensitivity in volumetric calculation. The quantification involves seismic attributes, 2D/3D seismic coverage, well distribution variogram and time depth conversion in which might vary on reflector quality, data distribution, horizon picking strategy and rock velocity.

Introduction

Offshore North West Java (ONWJ) basin is considered as one of the great hydrocarbon producers in Indonesia. It has delivered hydrocarbon for almost 50 years with cumulative oil production around 1 BBO. Zulu Field itself is an oil field located in Offshore North West Java (ONWJ) block, approximately 70 km North West of Jakarta, Indonesia (Figure 1). It was discovered by ZZZ-1 exploratory well in 1974 and started production in 1986. The production has reached its peak during mid 90 at 24000 bopd, mainly come from Baturaja Formation. Based on latest study held in 2020, it has enormous Original Oil in Place (OOIP) ranging from 0.85 - 1.4 BBO with only 4% Recovery Factor (RF). Spatially the development takes part into 3 phases; North, Central and South area which is currently is still focused on North development. Whilst Central and South area are going to be developed in the future, integrated with secondary and tertiary recovery implementation such as waterflood and EOR.

Zulu field is consisted of multi stack formation, nevertheless Baturaja Formation is the only reservoir which dominates the oil production. Baturaja Formation is a carbonate reservoir, formed in early Miocene when marine transgression continued and eventually conformably overlain Talang Akar Formation (Ponto et al, 1988). Within its body, it has a wide range heterogeneity, and is composed of mud supported in the lower zone, and grain supported to floatstone – rudstone in the upper zone (Ageng et al, 2018).

As a typical of carbonate lithology, Baturaja Formation has an undulated morphology in the surface. It creates a large depth uncertainty for determining reservoir top whether in structural mapping, casing point and especially horizontal well drilling. ZUA-10 and ZUA-11 horizontal well drilling campaign occurred shale out, which meant the trajectory was out of carbonate body and encountered the upper shale lithology (Figure 2). It absolutely impacted on oil net pay calculation, production rate as well as protuberant operational cost. Though eventually those wells were side-tracked to pursue the good quality reservoir, however drilling cost has exceeded the plan.

An integrated method was approached to minimize the risk of carbonate surface determination. It comprises of seismic attribute, 2D/3D seismic coverage, data distribution, horizon picking strategy, rock velocity and time depth conversion. These parameters are incorporated to quantify the prediction of reservoir top as well as tolerated uncertainty depth in Baturaja Formation.

Data and Method

Regional Tectonic and Stratigraphy

Offshore North West Java (ONWJ) basin is situated in the region that has typical Tertiary backarc settings of tectonic

evolution (Gresko et al, 1995). The tectonic stress and extension are the result from northward movement of the Australian and Indian plates and rotation of Borneo, formed rifts or half-graben complexes along much of the southern margin of the Sunda Shelf plate in Eocene to Oligocene time (Hall, 1997a, b; Longley, 1997; Sudarmono, 1997). The Basement time structure clearly describes the situation during Eocene when the basin started to fill (Figure 3). The basin has 14 sub basins as source pod which primarily supply hydrocarbon to the reservoir (Noble et al, 1997). Sunda and Asri sub basin are the two source pods in the proximity to Zulu Field with distance is only around 20 km. In Figure 4, Baturaja Formation is classified into Lower Cibulakan Group, and developed during Early Miocene, when marine transgression continued and eventually conformably overlain Talang Akar Formation (Ponto et al, 1988). It consists of mud supported in the lower zone, and grain supported to floatstone – rudstone in the upper zone (Ageng et al, 2018). The upper zone has a better properties quality as it was exposed during sea level lowstands where secondary moldic porosity resulted from meteoric water leaching on aragonitic grain (Pertamina, 1996).

Zulu Field is located in the upthrown of the border fault to the Sunda sub basin. The structure is relatively three - way dip closure, bordered with two major faults in the west (Figure 5). Source rock is possibly coming from Banuwati lacustrine facies attains 300 ft thickness in the basin deep (Noble et al, 1997). The major normal fault is suspected to be the conduit to the vertical migration to the reservoir in Zulu Structure. Aside of Baturaja, there are Talang Akar and Massive Formation in which provenly contain hydrocarbon as well, though in only a small scale of portion compared to Baturaja's. The structure is getting more updip to the South, and the fluid contact is still unknown since existing exploration wells hit only full column of oil.

Seismic Data

Zulu Field is partly covered by 3D seismic, which acquired in 2015 by marine streamer with total acreage is approximately 192 km^2. Zulu Field has a crowded surface facility area including platforms, pipline, junction as well as living quarter. The situation generates seismic survey operation limitation and safety issue; hence the 500 m surrounding platform area remains blank. Zulu Field also shares territory with Kepulauan Seribu National Park (Figure 6) in which is prohibited to held all hydrocarbon exploration and exploitation activities. Therefore, blank area and Zulu South are still covered with 80s vintage 2D seismic data, acquired before national park establishment in 2002 (SK Menteri Kehutanan Nomor 6310/Kpts-II/2002, Wikipedia).

Zulu 3D seismic is processed in zero phase and reverse polarity. It has good signal to noise ratio, as no obstacle above target zone; such as carbonate build-up, that interferes wave propagation from source to receiver. The seismic data has parameters; 25 Hz frequency dominant, 6.25 m x 12.5 m bin size, 2 ms sampling rate and 4000 ms record length. Seismic balancing and time shifting were done to adjust 2D seismic amplitude and mis-ties, with 3D seismic set as the benchmarking parameter.

Baturaja reservoir lays down in time 800 – 1000 ms equivalent to -2500 - -2700 ft True Vertical Depth Subsea (TVDSS). As it has a higher Acoustic Impedance compared to the upper shale It is classified as increase impedance reservoir, as. Hence, Baturaja Reservoir top hits the trough reflector, while Baturaja Reservoir base is in peak one.

Well Data

Zulu Field consists of 103 wells, including 80 development and 23 exploration wells. All of those wells have dense distribution, particularly around platform inside northern area. Central and Southern area are predominantly drilled by exploration wells, with distance range from 300 m to 1 km. Gamma ray, resistivity and density logs are used to determine the top and base of the reservoir in each well, though sometimes should be guided by cutting and even core. All reservoir tops are used to create time – depth model using linear regression, which eventually convert structure map from time to depth domain. The wells distribution later on will be used to determine the isotropic spherical model using experimental variogram.

Quantitative Structural Uncertainty

Structural uncertainties are defining a range of values containing with given probability and the possible errors around the estimated value. These uncertainties are strongly related to data availability; the less data, the more uncertainties; and also processing algorithm that is used during interpretation. A thing that should be underlined is; there is no regular workflow in defining structural uncertainties. Interpreters are free to determine the method, algorithm or even creating new technique to measure structural uncertainties.

This method is based on observation of seismic and well data including seismic quality, 2D/3D seismic coverage, well distribution variogram and time depth conversion error. The aim is to quantify the lateral and vertical uncertainties, that possibly happen in the structure. It is standard industry practice to express uncertainties in two sigma (2σ), note that 1σ encompasses 67%, 1.5σ encompasses 80%, and 2σ encompasses 95% of data falling within interval. Figure 7 describes the structural uncertainties workflow.

PROCEEDINGS
JOINT CONVENTION BANDUNG (JCB) 2021
November 23rd – 25th 2021

Seismic Quality Uncertainties

Seismic quality is a result of vertical resolution; might be influenced by processing parameters and geology like layers thickness and fluid content. Empirical vertical seismic resolution has been determined at 76 ft for 3D data and 68 ft for 2D. Figure 8 shows the variation of the wiggle width of the Baturaja Reservoir top in the 3D seismic data. It varies between 10 ms for good data area, yet 20 ms equall to 70 ft for poor data area.

Seismic attributes are utilized to assess lateral variations of picking uncertainty on the characteristics of reflectivity. Those attributes are based on magnitude, sharpness and continuity (Figure 9). Magnitude and sharpness can impact the choice of picking, the higher the magnitude and the sharpness of the reflector, the more certain the picking. Then continuity breaks due to fault, the picking is clearly certain, however when continuity is widely anomalous, the picking might be questioned.

These attributes are then smoothed, normalized and recognized that areas with higher uncertainties set to 1, while the lower uncertainties set to 0. They are all summed up and then normalized one more time to provide qualitative map related to seismic quality and picking uncertainty. This map is weighted with values representing picking misfit. Figure 8 shows that poor quality data wiggle appears flatter compared to the good quality data. This flat wiggle represents higher mispick possibility, with estimated statistical value 35 ft (2σ), while in the other hand, good quality data wiggle represents lower mispick, with estimated statistical value 9 ft (2σ). The inner blank area is simply interpolated from the nearest data, while 26 ft implementation in southern area based on visual investigation from 2D seismic line (Figure 10).

2D Seismic Coverage Uncertainties

3D seismic data is regularly spaced both inline and xline, therefore no uncertainty is considered related to data coverage. Uncertainty increases by the distance between lines, the more line gaps are getting distance, the more uncertainties are getting higher. In the southern area, 2D seismic data is sparsely distributed, ranging from 200 m to 1 km. When two sets of 2D lines are crossing, 5% weighting is applied and when there is only one set of parallel lines a weight of 10% is set. Those weighting factors are coming from the smoothing of the normalized 2D kriging variance map. In the extrapolation zone of the area in the south west, where no seismic data available to constrain the structure, a weighting factor of 45% is estimated (Figure 11).

Time – Depth Conversion Uncertainties

Linear regression method was utilized in Baturaja time to depth conversion. Although it displays several relationships, shown in Figure 12, constant velocity equation with 6022 ft/s was chosen since intercepting with zero axis (0,0) in time - depth crossplot. In that case, the slope is identical to the average of apparent velocities shown in Figure 13, with a very narrow standard deviation around 79 ft. This regression is encompassed by two alternatives, the regular linear regression with constant term (grey dashed line) considering all wells and the regression without three wells (ZU-2, ZV-1 and ZX-1) being isolated from the pool of other wells (blue). When considering only wells in 3D area, the linear regression is equivalent to the grey dashed line meaning that adding wells in 2D areas does not change the regression. When considering only wells in blank areas gives a regression consistent with the use of the constant velocity 6022 ft/s.

The depth conversion uncertainty map results from the kriging process using the same variogram model as for depth residual estimation and the global variance of all wells. The uncertainty map displayed Figure 5 – 36 corresponds to the method using constant velocity for the Baturaja top time to depth conversion and expressed in Sigma (1σ). It is zero at the well location where the map is tied to the geological marker 33 ft far from the well, which is calculated from depth residual linear regression at time - depth conversion. Kriging algorithm is perfectly suited to Zulu data set with its significant number of wells and the confidence resulting from experimental variogram interpretation. An isotropic spherical model with 1250 m as range is used to krige the depth residuals (Figure 14). It was then applied to the whole field uncertainty map shown in Figure 15.

Combination and Final Uncertainties

Uncertainty map that is coming from time – to depth conversion is taking into account the coverage uncertainty linked to the 2D lines spacing in the south to seismic coverage (Fgure 16).

Considering the picking and velocity uncertainties are independent the global uncertainty is calculated as mentioned in Equation below:

$$Unc_{structural} = \sqrt{{Unc_{Picking}}^2 + {Unc_{DepthConv}}^2}$$

Since the picking uncertainty map is not tied to the well, a local adjustment is necessary at the well location to ensure a null value where a geological top is considered for the depth lying (Figure 17).

PROCEEDINGS
JOINT CONVENTION BANDUNG (JCB) 2021
November 23rd – 25th 2021

Result and Discussion

An integrated evaluation of seismic quality, depth conversion and seismic coverage has been effectively disclosing depth prognosis problem whether in well drilling or volumetric calculation. A blind well has been also tested in order to prove the depth uncertainty in real case. NWY-1 exploratory well was drilled and encountered top of Baturaja lower 30 ft than prognosis. It somehow shows the uncertainties estimation is a decent result though precise depth prediction still needs to improve.

Conclusions

This method thoroughly quantifies the depth uncertainties by combining well and seismic parameters. The detailed steps including seismic attributes selection, time depth conversion method, seismic coverage weighting factor and spherical range of well might be different in each case, but the main workflow is supposed to be similar. This evaluation concludes that:

- Seismic quality, time depth conversion and seismic 2D/3D coverage control an important role in determining structural uncertainties
- Depth uncertainties (2σ) are ranging from -35 ft to +35 ft but getting narrower by the close vicinity of wells

References

Noble, R., Pratomo, K., Nugrahanto, K., Ibrahim, A., Prasetya, I., Mujahidin, N., Wu, C. H., and Howes, J., 1997, Petroleum systems of Northwest Java, Indonesia, in Howes, J. V. C., Proceedings of an International Conference on Petroleum Systems of SE Asia & Australasia: Indonesian Petroleum Association, p. 585-600.

Ageng, C., Hafez, M., Kusuma, D., Nugroho, A., Iqbal, M., Nurzaman, Z., A Smart Sector Model Reservoir for Potential Identification of Bypassed Heavy Oil, Baturaja Carbonate, Zulu Field, ONWJ, Proceedings of PIT IAGI 2018

Gresko, M., Suria, C. and Sinclair, **S.,** 1995, Basin evolution of the Ardjuna rift system and its implications for hydrocarbon exploration, offshore Northwest Java, Indonesia, Proceedings *Indonesian Petroleum Association Twenty Fourth Convention*, 24, 147-1 6 1.

Ponto, C. V., Wu, C. H., Pranoto, A., and Stinson, W. H., 1988, Improved interpretation of the Talang Akar depositional environment as an aid to hydrocarbon exploration in the ARII Offshore Northwest Java contract area: Proceedings of the Seventeenth Annual Convention Indonesian Petroleum Association, v. 1, p. 397- 422.

Hall, Robert, 1997a, Cenozoic tectonics of SE Asia and Australasia, *in* Howes, J. V. C., and Noble, R. A., eds., Proceedings of an International Conference on Petroleum Systems of SE Asia & Australasia: Indonesian Petroleum Association, p. 47-62.

Hall, Robert, 1997b, Cenozoic plate tectonic reconstructions of SE Asia, *in* Fraser, A. J., Matthews, S. J., and Murphy, R. W., eds., Petroleum Geology of Southeast Asia: Geological Society Special Publication No. 126, p. 11-23. Hamilton, Warren, 1974, Map of Sedimentary Basins of the Indonesian

Longley, Ian, M., 1997, The tectonostratigraphic evolution of SE Asia, *in* Fraser, A. J., Matthews, S. J., and Murphy, R. W., eds., Petroleum Geology of Southeast Asia: Geological Society Special Publication No. 126, p. 311-339.

Sudarmono, Suherman, T., and Eza, B, 1997, Paleogene basin development in Sundaland and its role to the petroleum systems in western Indonesia, *in* Howes, J. V. C., and Noble, R. A., eds., Proceedings of an International Conference on Petroleum Systems of SE Asia & Australasia: Indonesian Petroleum Association, p. 545- 600.

SK Menteri Kehutanan Nomor 6310/Kpts-II/2002, Wikipedia

Acknowledgements

The authors would like to give a huge gratefulness to General Manager, Sr Manager Subsurface, and Well Operation, Petrophysics and Data Management Manager of PHE ONWJ as well as Legal Council of Pertamina Subholding Upstream Region 2, for the publication approval and permit, advice and remarkable support during this research and paper writing.

PROCEEDINGS
JOINT CONVENTION BANDUNG (JCB) 2021
November 23rd – 25th 2021

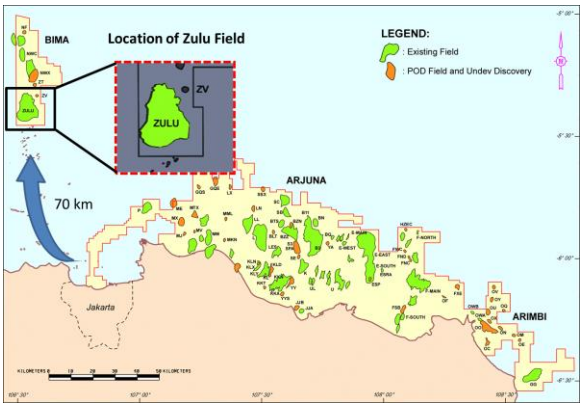

Figure 1. Location of Zulu Field in ONWJ Block

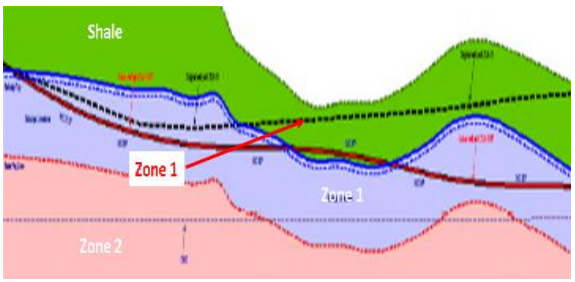

Figure 2. Shale Out Illustration

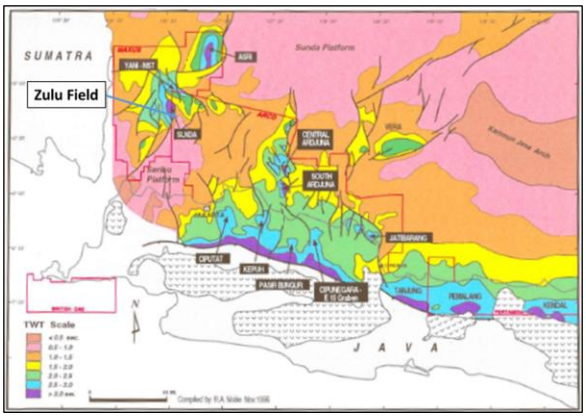

Figure 3. Basement Configuration of ONWJ Basin

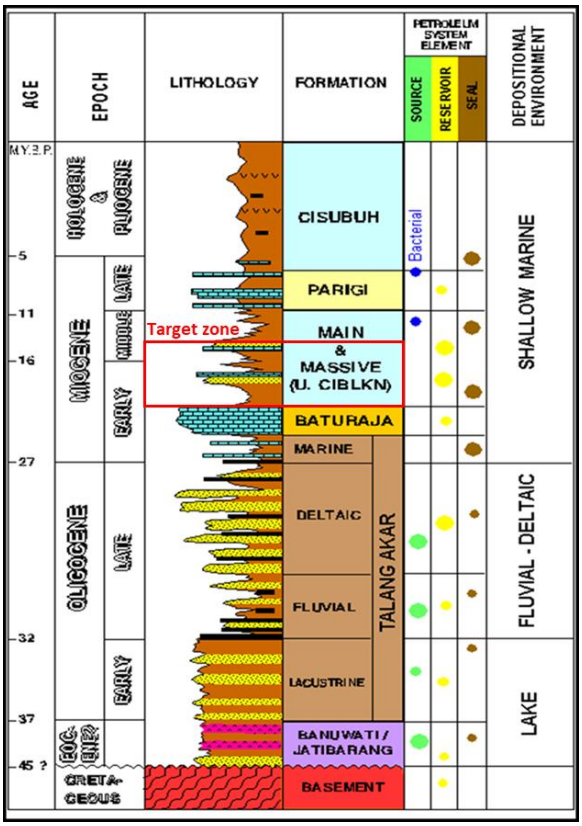

Figure 4. Stratigraphy Column of ONWJ Basin (Noble, 1997)

PROCEEDINGS
JOINT CONVENTION BANDUNG (JCB) 2021
November 23rd – 25th 2021

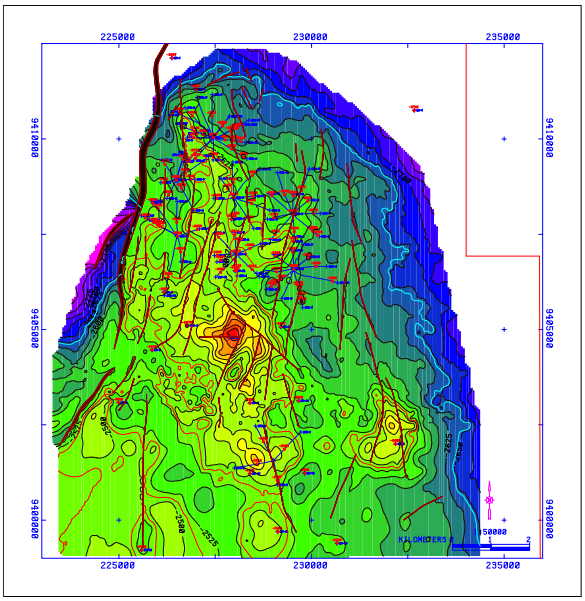

Figure 5. Baturaja Reservoir Depth Structure Map in Zulu

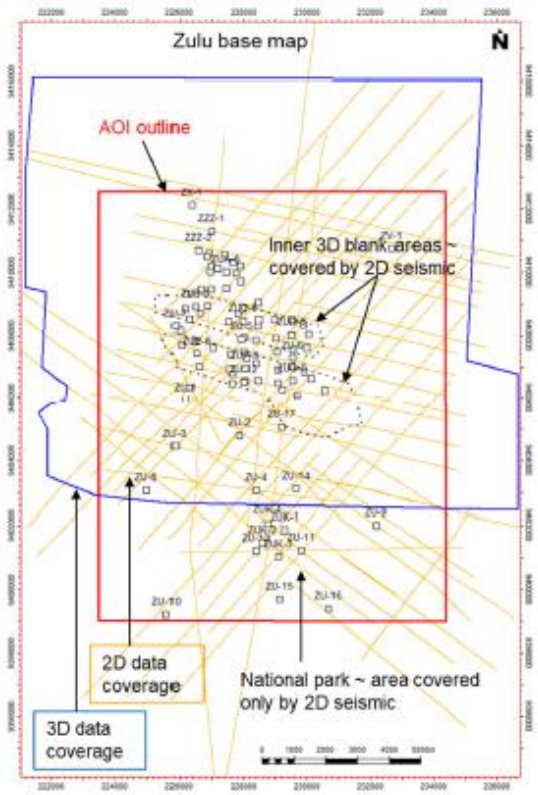

Figure 6. 3D Seismic Data Basemap of KL Field

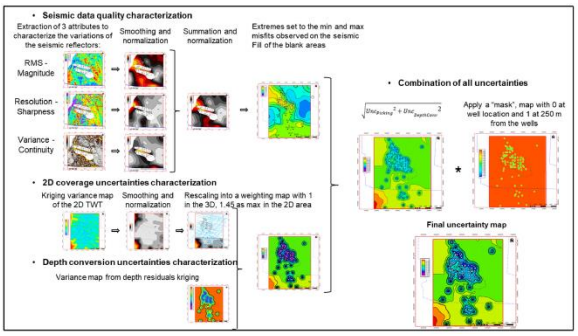

Figure 7. Structural Uncertainties Workflow

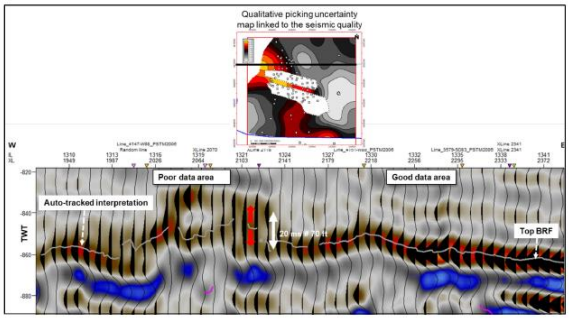

Figure 8. Variation of Seismic Wiggle in Baturaja Top

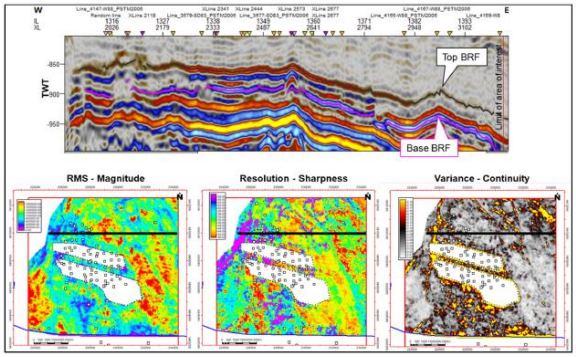

Figure 9. Magnitude, Sharpness and Continuity Attributes to Define Lateral Horizon Picking Uncertainty

PROCEEDINGS
JOINT CONVENTION BANDUNG (JCB) 2021
November 23rd – 25th 2021

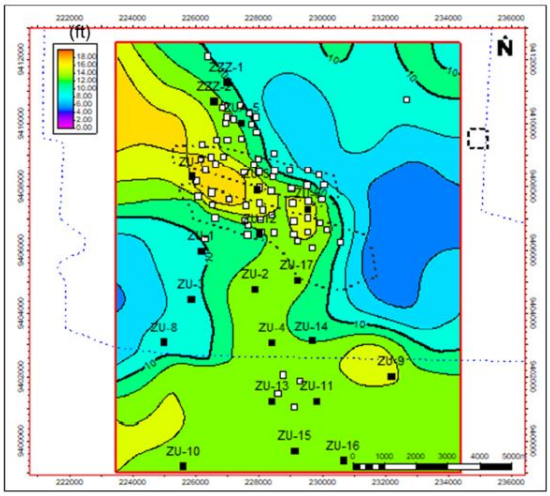

Figure 10. Picking Uncertainty Generated from Seismic Generated from Seismic Attributes Integration

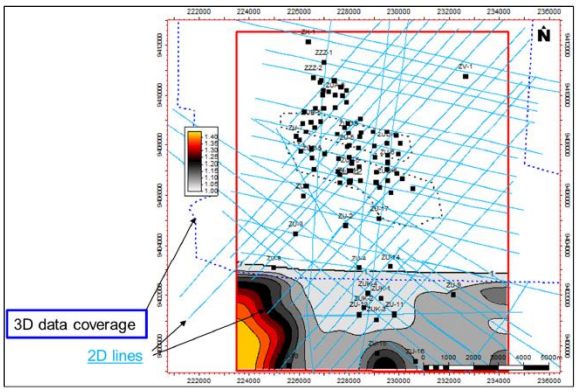

Figure 11. 2D Seismic Coverage Uncertainty in Southern Structure

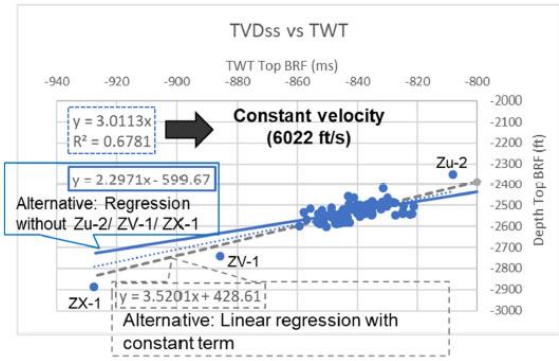

Figure 12. Linear Regression Method of Zulu Time Depth Conversion

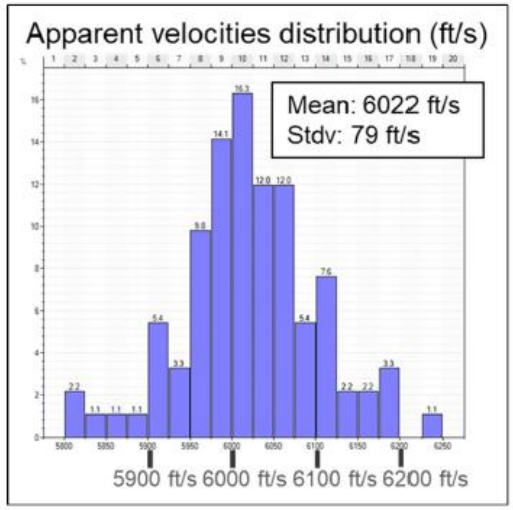

Figure 13. Apparent Velocity Analysis

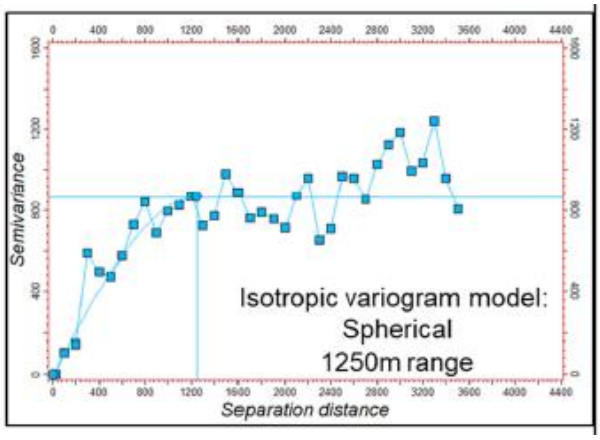

Figure 14. Isotopic Variogram Model with Spherical Range of 1250 m Around Well

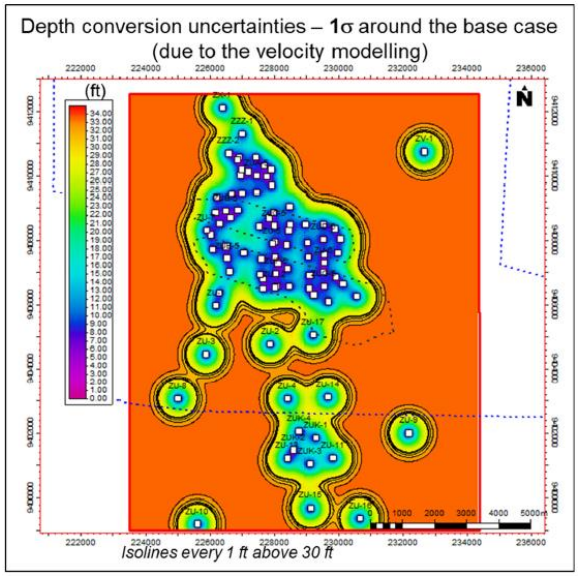

Figure 15. Depth Conversion Uncertainties

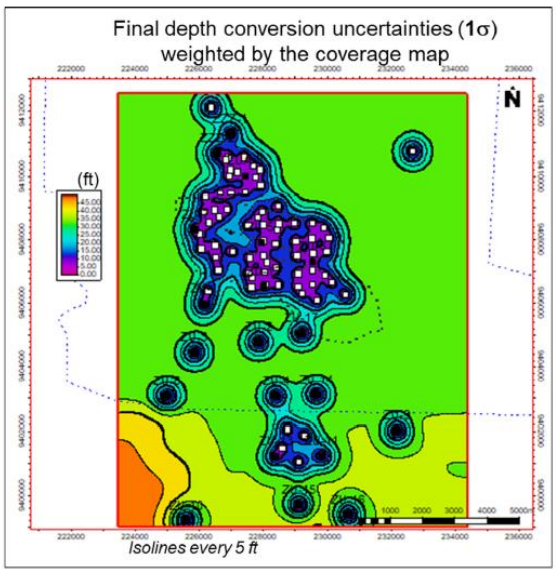

Figure 16. Depth Conversion Uncertainties is Combined with 2D/3D Seismic Coverage

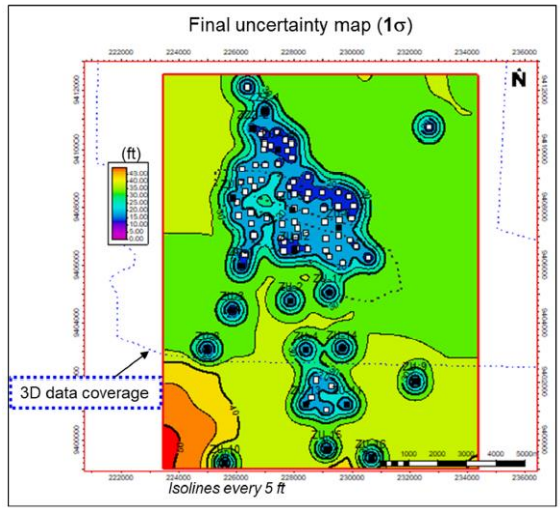

Figure 17. Final Structural Uncertainties (1σ) as Combination of Seismic Quality, Depth Conversion and Seismic Coverage

PROCEEDINGS
JOINT CONVENTION BANDUNG (JCB) 2021
November 23rd – 25th 2021

Duri Steam Flood Fluid Contacts Study: Redefining Oil Water Contacts and Intraformational Top Seals

Wikan Winderasta, Milla Hayati Amlan, Willy Rhauda Paksi
PT. Pertamina Hulu Rokan

Abstract

Duri Field is located in the Rokan Block working area, in Riau Province which is managed by PT. Chevron Pacific Indonesia (PTCPI). The field was discovered in 1941 and started production in 1958. After passing the peak point of production from the primary phase of 65,000 barrels per day in 1965, Duri Field production naturally declined along with the decrease in reservoir pressure. PTCPI started a steam injection pilot project at Duri Field in 1975. Ten years later, this technology was implemented on a large scale and was able to increase production back to 300 thousand barrels per day in 1994. To date, Duri Field has been producing more than 2.6 billion barrels.

The original study of fluid contacts defined that a common original oil water contact (OOWC) depth was at approximately 700 feet true vertical depth subsea which delineated multiple Duri sand reservoirs from the early Miocene Duri and Bekasap Formations. This OOWC depth determined the boundary of Duri Field with covering of all Pertama and Kedua (PK) Sand Reservoir, while the shallower Rindu Reservoir layover above the PK Reservoir with a larger closure area. Further study provided more detail guidance for picking OOWC marker at more than 1,300 wells across Duri Field. A consistent deep resistivity log values at 10, 15, 20 ohms became probabilistic OOWC signatures at the multiple OOWC depth intervals including at Rindu, Pertama, Kedua, and Baji-Jaga-Dalam Reservoirs. About 20 wells were drilled in the Duri Ring area to confirm a more precise boundary of Rindu OOWC and successfully extended the steam flood area on the eastern flank of the Duri Field.

A new study of fluid contacts incorporated historical surveillance logs such as carbon oxygen log in temperature observation wells (TOW) with total 584 active wells that focused on PKBJDM (Pertama, Kedua, Baji-Jaga, Dalam, and Menggala) Sands. This evaluation provided new findings on the most recent lowest known oil (LKO) and the dynamic of current oil water contact (COWC) through steam flood and drainage process. Various levels of fluid contact depth represent different states of heating and production for each area. The intraformational top seals between reservoirs provided new understanding of the presence of multiple fluid contacts in the Duri Field. The new insight of the discovered remaining oil and current oil water contact presents new opportunities for production optimization and further development of steam flood.

1. Introduction

Duri Field is a giant heavy oil field in Riau Province, Sumatra, Indonesia. Duri was discovered in 1941 with active steam flooding beginning in 1985. Petroleum system of Duri Field is described as four elements as follow (Figure 1):

- Migrated oil from Brown Shale source rock to very shallow Duri structure was degraded by microorganism and deposited as heavy oil type with API Gravity 17-23 deg (Katz and Dawson, 1997)[1]
- Medium to excellent sandstone reservoirs (18-30% and up to 4500 mD of permeability) of Sihapas Group.
- Duri trap are capped by Telisa Shale as Regional Seal, with intraformational top seals for deeper reservoirs (Amlan and Winderasta, 2019)[2]. It is a very competent top seal to retain approximately 700 feet hydrocarbon column.
- Giant structural 4-way anticline closure (10x18 km2) as result of inverse fault system.

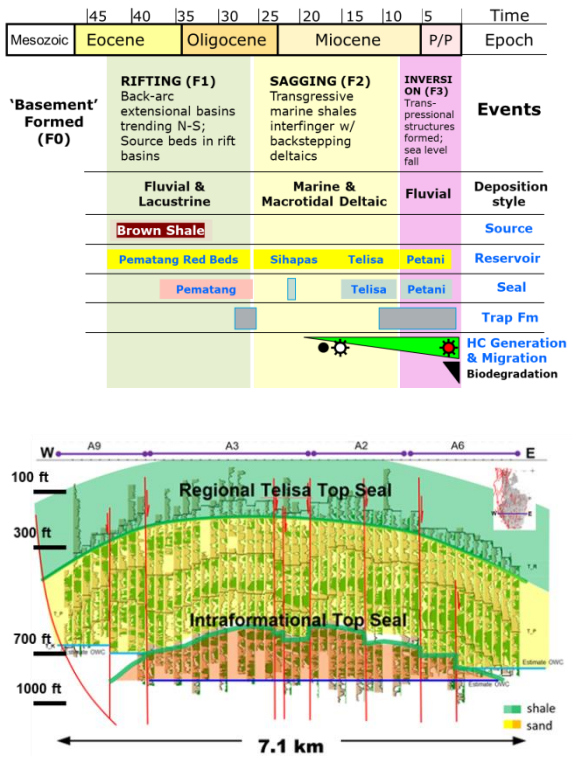

Figure 1: *Petroleum system chart of Central Sumatra Basin and Duri Field show four elements (picture above); and Duri Field Giant Anticline Structure Trap with Regional and Intraformational Top Seals (picture below).*

The structural trap at Duri Field is a complex, asymmetric north-south faulted anticline, with original oil in place about 6 BBO. The producing sands of the Lower Miocene Sihapas Group (Johansen and Semimbar, 2009)[3] lie at a depth range of 300 to 700 ft.

PROCEEDINGS
JOINT CONVENTION BANDUNG (JCB) 2021
November 23rd – 25th 2021

The main reservoir units, from top to bottom, are the 240' Sand, Rindu, Pertama, Kedua, and Baji-Jaga-Dalam sands. These fluvial-deltaic reservoirs are characterized by generally high oil saturation (So 30-80%), thick net pay (30-100 ft./pay sand zone), and very high permeability. (Figure 2).

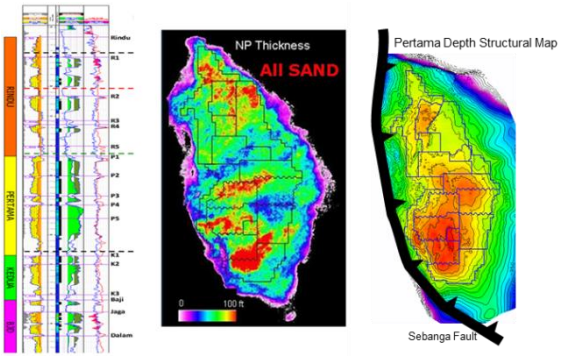

Figure 3: *Type Log, Isochore and Depth Structure Maps of Duri Field.*

Duri Steam Flood has been developed in thirteen areas (about 30,000 acres), in four types of patterns they are inverted 5, 7, 9 spots and irregular patterns (Gael and Putro, 1994)[4].

Relatively low oil gravity performing high oil viscosity when cool (> 100 cP @100 degF). Total more than 10,500 wells have been drilled, consist of around 6,700 producers, 3,000 injectors, and 800 observation wells [6] (Figure 3).

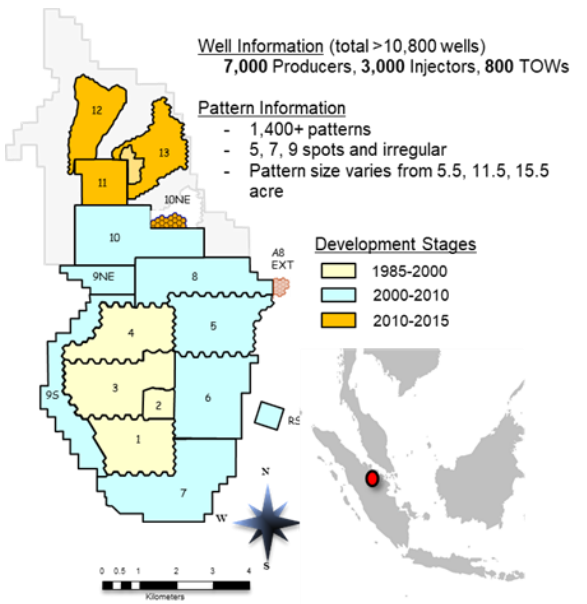

Figure 3: *Duri Steam Flood Pattern Developed Field Map.*

Steam injection improves oil recovery by heating the crude and thereby reducing its viscosity. Steam flooding can also vaporize the oil's light end components, improving fluid mobility. Steam injection also increases reservoir pressure, serving to drive oil toward producing wells.[5] Regular reservoir surveillance is required for steam flood monitoring [6].

Peak producing of steam flood was reached in year 1992 about 290,000 barrels oil per day with over 1 million barrels steam injected per day (Figure 4). Presently, current production is declining to approximately 99,000 barrels oil per day with supported by 290,000 barrels injected steam per day. Total 2.5 billion oils have been produced cumulatively.

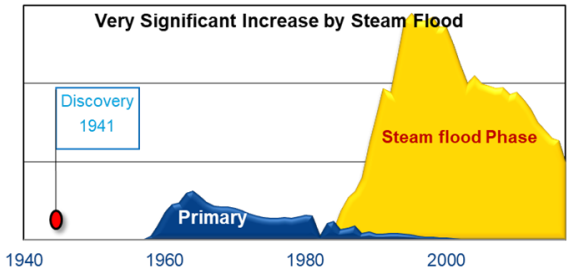

Figure 4: *The graphic shows production profile in primary and EOR steam flood period.*

2. Project Background and Objective

More than 30 years steam injection and production resulted dynamic condition in depth level of fluid contact and oil saturation, as response of injected steam and water displacement to oil zone, water encroachment from natural water aquifer drive and water disposal injection, and oil re-saturation phenomena due to dynamic steam heating.

Historically fluid contacts (OOWC-original oil water contact and COWC-current oil water contact) in Duri Field have been evaluated in several periods of full field studies related development and update of Duri Full Field Model (DFFM) and Duri Temperature Saturation model (DTSM).

OOWC was evaluated based on deep resistivity log in considered pre-steamed wells that represented initial level of fluid contact before steam flood injection and oil production activity. The first COWC was evaluated in 2016 and applied as marker in about 1,100 wells, but the evaluation did not cover all 850 observation wells.

The recent study of COWC (2020-2021) completed evaluation in the total ~700 active observation wells which represent surveillance of current oil saturation that covering all area of Duri Steam Flood Field (A01-13).

The study performed several objectives with in general to obtain clear understanding of fluid contact system dynamically has been working in Duri Steam Flood reservoir. Following are the objectives of study and the its summary in the Table 1:

- Continue study of 2016 COWC effort to understand the dynamic of fluid contact in the mature steam flood field by completing all active observation wells with COWC/LKO marker in PKBJDM based on latest 3 years CO log (2017 to 2020).
- Map the COWC to identify and evaluate areas with significant change of fluid contact level.
- Improve understanding about aquifer water drive and disposal impact to changes of fluid contact level.

PROCEEDINGS
JOINT CONVENTION BANDUNG (JCB) 2021
November 23rd – 25th 2021

- Update and plot COWC/LKO (as official marker under TOPS_CPI set) in observation wells as key well to support steam flood in heating and drainage review.

	OOWC Study	COWC Study	remark
Method	Based on Resistivity log with hard cut off	Based on Current oil saturation log (SOCO log)	
Objective	Pre-Steam wells	Observation wells	
Sand objective	R, PK, BJD, M	P, K, B, J , D, M	No OOWC found in Rindu inside DSF
Marker picked	OOWC (original oil water contact)	COWC (current oil water contact), LKO (lowest known oil)	

Table 1: *Summary table of Project Study - comparison between OOWC (original oil water contact) and COWC (current oil water contact) interpretation method, dataset, sand objectives, and markers picked.*

3. Evaluation Workflow

General workflow for starting step (input data), data interpretation works, and type of delivered evaluation products can be seen in the General Workflow (Figure 5).

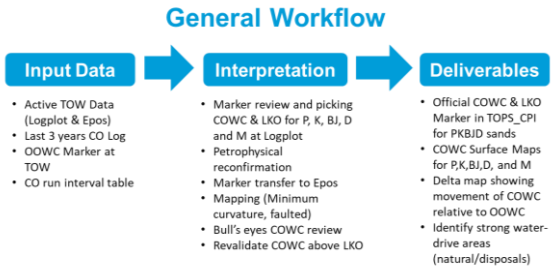

Figure 5: *General workflow (figure above) for starting step (input data), data interpretation works, and type of delivered evaluation products.*

3.1. Input data:

For COWC depth level interpretation (marker picking), the project study team only used active TOW (observation wells) that have at least once survey of CO Log within the last 3 years (2018-2020). The dataset of CO Log represented by SOCO (current oil saturation) with support from other wireline and formation evaluation logs. The wireline logs are such as GRN (gamma ray normalized), DRES (deep resistivity), RHOB (density log), and TEMP (temperature log), while formation evaluation logs are Vshale (volume of shale), SWE (original oil saturation), original net pay flag, and SGPN (steam saturation).

3.2. Interpretation Process:

Those logs were reviewed in LogPlot (a composite well display) that provides historical fluid (oil, steam, and water) changes along the time of steam flood injection, water disposal injection, and oil production for each individual observation well. As necessary, well cross sections were created in EPOS is to understand structural relation for oil water contact level. Several markers of oil water contact were reviewed and interpreted including OOWC, COWC, and LKO for reservoir Pertama (PR), Kedua (KD), Baji (BJ), Jaga (JG), Dalam (DL), and Menggala (MN). The conceptual fluid contacts (OOWC, COWC, and LKO), template of TOW display in LogPlot, and number of total markers picked for each reservoir can be seen in the Figure 6 and Figure 7.

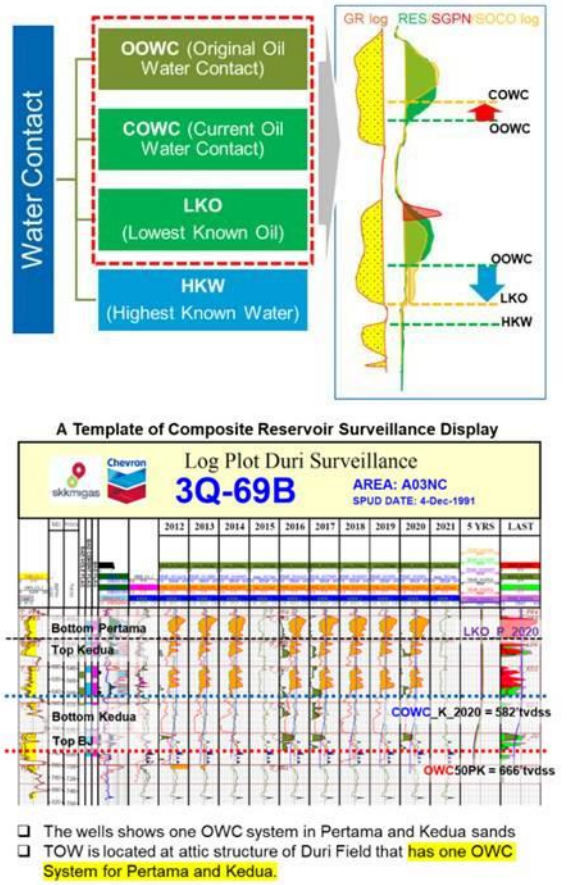

Figure 6: *The conceptual fluid contacts, they are OOWC, COWC, and LKO markers (picture above), and the template of TOW (observation well) display in LogPlot format (picture below). The LogPlot displays static wireline logs are such as GRN (gamma ray normalized) with calculated Vshale (volume of shale), DRES (deep resistivity), RHOB (density log), and calculated SWE (original oil saturation) with original net pay flag. The LogPlot also displays dynamic time lapse wireline surveillance logs of TEMP (temperature log), with formation evaluation logs are including 3-Phase SOCO (current oil saturation from C/O Carbon-Oxygen Log) and SGPN (steam saturation from PNC-Pulsed Neutron Captured Log).*

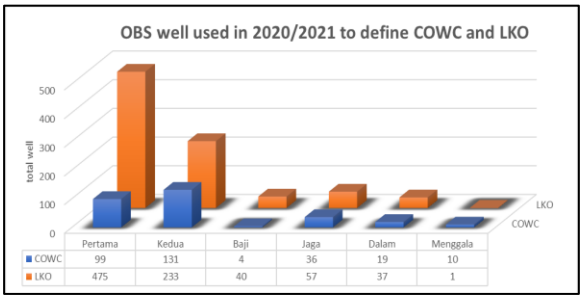

Figure 7: *Number of total COWC (blue bar) and LKO (orange bar) markers picked for each reservoir.*

PROCEEDINGS
JOINT CONVENTION BANDUNG (JCB) 2021
November 23rd – 25th 2021

3.2.1. Data set.

Original oil water contact (OOWC) was reviewed based on DRES log as standard practice since 2006 for building DFFM (Duri Full Field Model).[7] For this study, it is important to benchmark and validate the official OOWC markers depth (marker set OWC50PK, OWC50BJ, OWC50DL, OWC50MN) with SOCO logs that indicate OOWC depth level.

In many cases, we revisit the OOWC picking to the new depth level based on SOCO log reading, especially while the existing OOWC marker was picked based on strong changes in DRES log values from oil to water, but SOCO logs in several years still indicates consistent oil content. Note: The Project Team did not change depth level of OOWC markers in TOPS_CPI.

3.2.2. Top Seal and Oil Water Contacts.

Telisa Formation was deposited regionally as open marine shale dominated unit and in some part was in distributary mouth bar of deltaic system during transgressive cycle in the Early to Middle Miocene Time 22.5-15.5Ma (Yarmanto, 2010)[4]. Telisa Formation contains widespread thick shale and mudstones of condensed section at basinal setting as result of peak transgressive period (16-15.5Ma). Telisa Formation plays the role as regional top seal for the hydrocarbon accumulation in Upper Sihapas Group, the Bekasap and Duri reservoirs directly underneath it.[2]

The role of regional top seal is strongly indicated by the single common oil water contact system within Duri Field's primary hydrocarbon reservoir called Rindu and Pertama-Kedua Reservoirs.

An intraformational top seal was thought to be responsible for hydrocarbon accumulations in deeper reservoirs. The intraformational shale interval in Bekasap and Bangko Formations were thought to contribute as top seal.[2] In Duri Field, this intraformational top seal can hold hydrocarbon accumulations in multiple reservoirs with multiple oil water contacts in Baji-Jaga, Dalam, and Menggala Reservoirs.

3.2.3. Uncertainties and Mitigation.

Current oil water contact (COWC) and Lowest Known Oil (LKO) were reviewed based on SOCO log as new standard interpretation practice in 2020-2021 study. Uncertainties of using SOCO log can be identified based on availability and consistency of SOCO logs trough the time. Several key uncertainties with impacts and mitigation to address its can be seen in the Table 2.

3.2.4. COWC and LKO Markers Interpretation Workflow

The workflow for COWC and LKO markers consists of dataset preparation (data type and well/log selection), data proses (marker interpretation), and result (marker set in official TOPS_CPI and maps). (Figure 8).

Well cross sections of TOW were developed to support COWC and LKO marker picking as well as OOWC depth validation based on consideration of structural position including faulted control for differentiating oil water contact surface blocks.

Uncertainties	Impacts	Mitigation
• Inconsistent SOCO logs trough the time due to different method of SOCO calculation	Misinterpretation of current oil saturation and presence of oil interval	Using only last 3 years SOCO logs (2018-2021 surveys) that already with standard method of calculation by petrophysicist.
• Incomplete coverage of SOCO until TD	Misinterpretation of COWC / fluid level depth level	Ensure bottom of depth of each SOCO log based on database of TOW surveillance logging record.
• Unreliable SOCO calculation in wash out intervals	Misinterpretation of oil saturation and presence of oil → oil re-saturation phenomena	Consulted with petrophysicist during TOW review to ensure the most reasonable interpretation.
• Contradiction between DRES log reading and SOCO log in the possible water zone	Misinterpretation of OOWC depth level and interpreted phenomena of dynamic movement of fluid contact, e.g., COWC move-up or re-saturation (COWC move down and hidden opportunity).	Consulted with petrophysicist during TOW review, especially the result of SWE (effective water saturation) log as initial SW for oil pay flag and OOWC depth level interpretation.
• Depleted SOCO due to steam flood production drainage	Misinterpretation of COWC (be considered of move-up), but evenly created bull-eye on COWC surface map since inconsistent with surrounding COWC depth level.	Defined the phenomena of steam drainage in produced oil interval, and then picked the fluid level as LKO at bottom sand reservoir.

Table 2: *Several key uncertainties with impacts and mitigation. Uncertainties of using SOCO log as product of CO log observation wells can be identified based on availability and consistency of SOCO logs trough the time.*

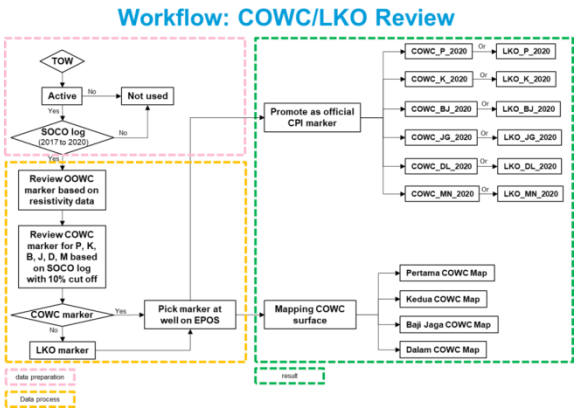

Figure 8: *The workflow for COWC and LKO markers consists of dataset preparation (data type and well/log selection), data proses (marker interpretation), and result (marker set in official TOPS_CPI and maps).*

Interpretation of sub-blocks area that represents multiple COWC surfaces in specific DSF Area was done as pre-computational mapping works. The map gave interpretative understanding of behavior of dynamic oil water contact. The relationship between OOWC depth levels with magnitude of contact movement (COWC) will be summarized as interpretative water drive mechanism, which is classified as degree of qualitative water drive strength.

3.2.5. Conceptual Models of COWC in Duri Steam Flood

Different with OOWC study, in this COWC study, fluid contacts were analyzed for each reservoir: Pertama, Kedua, Baji, Jaga, Dalam, and Menggala. Based on the analysis of the observation wells, there are 4 conceptual models related to the phenomena of water movement in Duri Steam Flood, they are: Steam Flood Depletion, Disposal Impact, Dual System COWC, and Re-saturation Event. (Figure 9).

Those conceptual models require efforts to mitigate any issues and new opportunity.

PROCEEDINGS
JOINT CONVENTION BANDUNG (JCB) 2021
November 23rd – 25th 2021

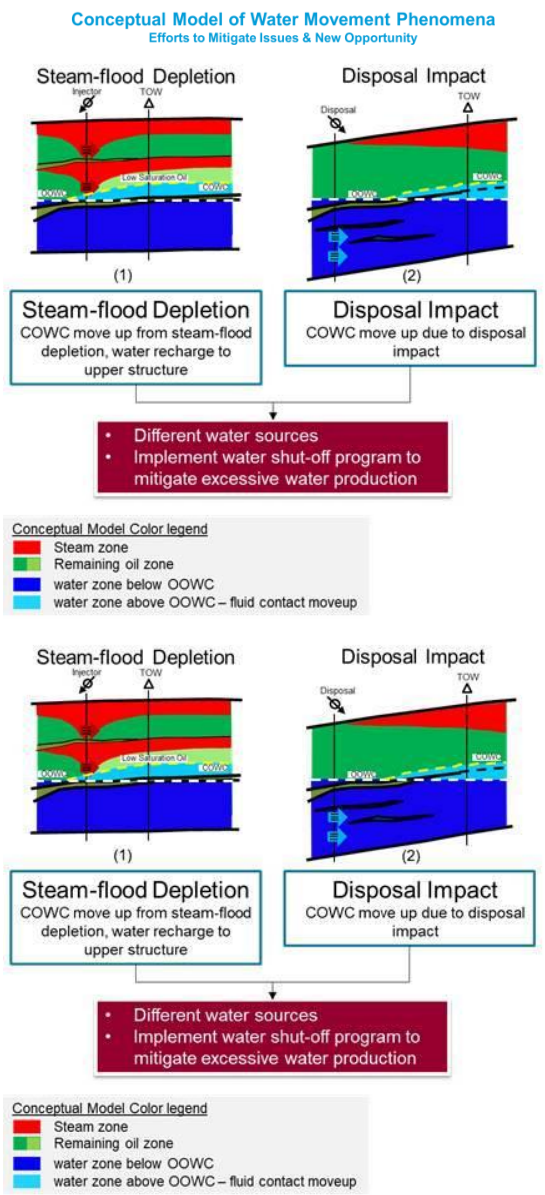

Figure 9: *The Conceptual Models of COWC in Duri Steam Flood - there are 4 conceptual models related to the phenomena of water movement in Duri Steam Flood, they are: Steam Flood Depletion, Disposal Impact, Dual System COWC, and Re-saturation Event. The conceptual models deliver recommendations to support heating and drainage review.*

1. Steam flood depletion. This phenomenon mostly is often found in the upper structure where COWC moves upward because of the oil is depleted and water recharge into the upper structure. The source of water comes from the reservoir.

2. Disposal Impact. This phenomenon is found in the upper structure closed to disposal wells. The move up of COWC depth level is affected by injection of water from disposal wells. Water is injected into the deeper sands (Kedua, Baji, Jaga, and Menggala), and it impacts the upper reservoirs without or only having a thin vertical barrier.

3. Dual System COWC. This phenomenon is found in the Pertama and Kedua (PK) Reservoirs in the flank area which have separate water contact systems. Observation wells on the flank indicate that COWC was found in each reservoir. It is different with attic structure where COWC is found in Kedua only and it has one water contact system. Not only in PK reservoir, but this phenomenon is also found in Baji and Jaga (BJ) reservoirs.

4. Re-saturation Event. The phenomenon of re-saturation was observed in a reservoir with collapse of steam which was affected by the absence of injection or no withdrawal to drain the oil. In some areas, this phenomenon was captured as a hidden opportunity due to the surrounding wells (injector and producer) was drilled too shallow.

The conceptual models deliver recommendations to support heating and drainage review. Several recommendations have been implemented or still ongoing to be evaluated are as follow:

- For the issues of steam flood depletion and disposal impact, it is advisable to implement water shut off program to mitigate excessive water production.
- The lowering pump and revisit zone program are recommended to be implemented in areas with a dual COWC system.
- An interdiction wells program is recommended to mitigate water encroachment in flank areas.
- In addition, for heat management standpoint, it is better to be injected the reservoir by thermal body than by a flow unit.
- The hidden oil opportunities due to re-saturation event can be optimized by deepening the producers or expanding the area if needed.

3.2.6. COWC and LKO markers picking validation.

Prior to finalize the COWC surface map, it is very important to validate the consistency of COWC and LKO markers depth picking. Validation work consists of several review activities in Table 3.

Suspected Incorrect COWC/LKO Markers Picking	Resolution to Validate
Bull's eyes marker appearances: a presence of COWC markers in area with dominantly LKO markers. **Total 91 COWC_P/K markers to be corrected**	Revisit marker picking to ensure areal context such as: - Resolve uncertainty of SOCO curve (current oil saturation from CO Log) by compared to OOWC marker picking (DRES or SWE). - Define a steam flood maturity stage, whether while the fluid contact is related to oil drained by steam and no disposal effect, then assign COWC as LKO marker at the bottom reservoir, instead of considered as a system of broad COWC. - CO Log survey did not penetrate until a complete sand interval. In this case, deleted the COWC marker to avoid inconsistent fluid contact depth level with surrounding. Keep as COWC marker (at 7 wells) as local fluid movement as small compartment closures.
In contrary picking of LKO markers in area with dominantly COWC markers. **Total 53 LKO_P/K markers to be corrected**	1. Mostly due to CO Log survey did not penetrate until a complete sand interval. In this case, deleted the LKO marker to avoid inconsistent fluid contact depth level with surrounding. 2. A re-saturation event. 3. Revisit interpretation as fluid contact change, then changed to COWC marker.

Table 3: *COWC and LKO markers picking validation - Validation work consists of several review activities to ensure the consistency of COWC and LKO markers depth picking.*

PROCEEDINGS
JOINT CONVENTION BANDUNG (JCB) 2021
November 23rd – 25th 2021

3.2.7. Fluid contact compartments.

Based on distribution of the depth of COWC markers, it is interpreted there are at least 10 compartments at Pertama and 6 compartments at Kedua of current fluid contact system (Figure 10).

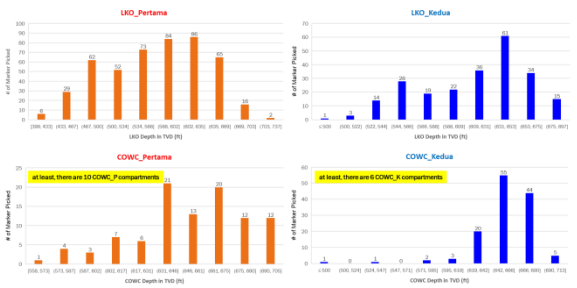

Figure 10: *Based on distribution of the depth of COWC markers, it is interpreted there are at least 10 compartments at Pertama and 6 compartments at Kedua of current fluid contact system.*

3.2.8. COWC Surfaces Maps.

The surfaces were mapped in EPOS Canvas for COWC surfaces of Pertama, Kedua, Baji-Jaga, Dalam, and Menggala.

Pertama COWC Surface Map

In general, for Pertama COWC surface mapping workflow consists of steps to differentiate 2 area of fluid contact system (Figure 11), they are:

1. Area of separated fluid contact system with Kedua that located at the east flank area (A11, A10, A8, A5, A6, and A7) and south-central area of A10. In these areas, its presence COWC_P marker.
2. Area of one fluid contact system with Kedua that located at the attic of Duri at north (A12) and south area (A9, A8, A4, A5, A3, A2, A6, A1, and A7). In these areas, its presence LKO_P marker.

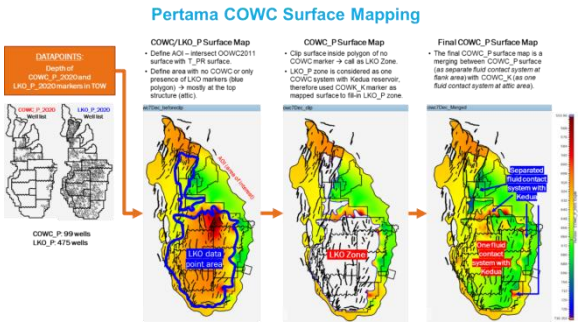

Figure 11: *Pertama COWC surface mapping workflow consists of steps to differentiate 2 area of fluid contact system. The first is area of separated fluid contact system with Kedua. The second is area with presence COWC_P marker that represents one fluid contact system with Kedua.*

Kedua COWC Surface Map

For Kedua COWC surface mapping workflow consists of steps to differentiate 2 area of fluid contact system (Figure 12), they are:

1. Area of fluid contact system of Kedua that located at the flank area (A12, A11, A10, A9, A8, A5, A4, A6, and A7). In these areas, its presence COWC_K marker.
2. Area of fluid contact system in the same depth level with closest COWC_K marker that located at the attic of Duri at north (A12) and south area (A9, A8, A4, A5, A3, A2, A6, A1, and A7). In these areas, its presence LKO_K marker.

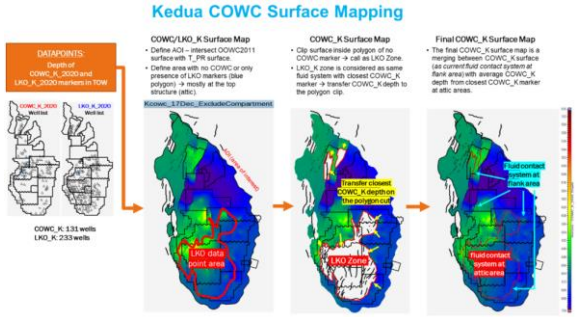

Figure 12: *Kedua COWC surface mapping workflow consists of steps to differentiate 2 area of fluid contact system. The first is area of fluid contact system of Kedua that located at the flank area, which are presence of COWC_K marker. The second is area of fluid contact system in the same depth level with closest COWC_K marker that located at the attic of Duri at north and south area, which are presence LKO_K marker.*

Baji-Jaga, Dalam, and Menggala COWC Surface Maps

For Baji-Jaga, Dalam, and Menggala COWC surfaces mapping workflow was done by differentiating those reservoirs became 3 fluid contacts system (Figure 13), they are:

1. Area of fluid contact system of Baji-Jaga that mainly located at the structurally flank area (A3 and A6) which is presence of COWC_BJ marker. In the attic area (A1 and A2) and west flak (A9) that presence LKO_BJ marker, the fluid contact surface is extended from closest COWC_BJ marker.
2. Area of fluid contact system of Dalam that mainly located at the structurally flank area (A3) which is presence of COWC_DL marker. In the attic area (A1 and A2) and west flak (A9) that presence LKO_DL marker, the fluid contact surface is extended from closest COWC_DL marker.
3. Area of fluid contact system of Menggala that mainly located at all area (A2 and A3) which is presence of COWC_MN marker. Only northwest flak (A3) that presence LKO_MN marker, the fluid contact surface is extended from closest COWC_MN marker

PROCEEDINGS
JOINT CONVENTION BANDUNG (JCB) 2021
November 23rd – 25th 2021

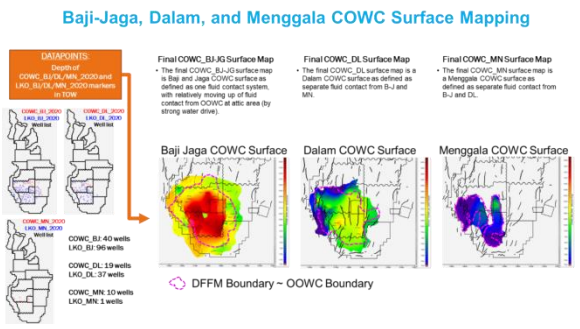

Figure 13: *Baji-Jaga, Dalam, and Menggala COWC surfaces mapping workflow was done by differentiating those reservoirs became 3 fluid contacts system.*

3.3. Thematic Maps and Water Drives Mechanism

3.3.1. Thematic Maps and Conceptual Cross Section

Thematic maps and conceptual cross section were created to display fluid contact changes that show movement of COWC marker relative to OOWC marker. The map is named as Delta Map that been built for Pertama and Kedua reservoirs (Figure 14). Conceptual cross section is a regional section developed base on wells (TOW) from north to south of Duri Field that shows structural position of reservoirs and fluid contacts (Figure 15).

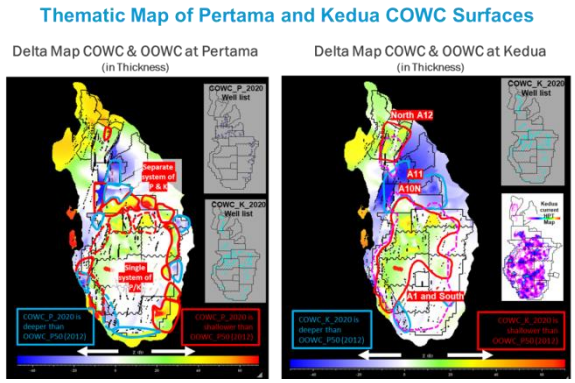

Figure 14: *Delta Maps display fluid contact changes that show movement of COWC marker relative to OOWC marker. The left picture is for Pertama Reservoir, and right picture is for Kedua Reservoir.*

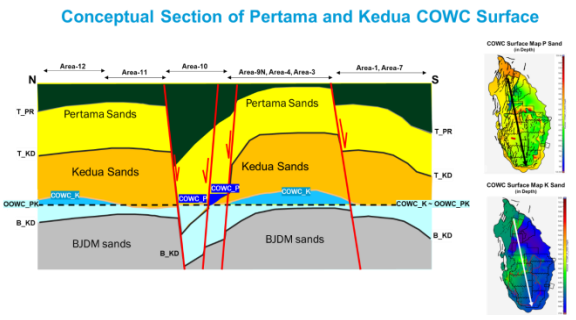

Figure 15: *Conceptual cross section is a regional section developed base on wells (TOW-observation well) from north to south of Duri Field that shows structural position of reservoirs and fluid contacts.*

3.3.2. Identify strong water-drive areas (as natural aquifer, condensed steam, and water disposals)

The water drive strength in the oil reservoir is evaluated based on the intensity of water movement as indicated by changes in the depth level of oil-water contact and the areal distance of water encroachment. Changes in the contact depth level can be in the form of up and down movements shown on the Delta Map of COWC & OOWC for each reservoir.

There are 3 basic water drives in the Duri Steam Flood Field, they are:

1. Natural water drive by aquifer water into oil/steamed reservoir.
2. Artificial water encroachment by injected water
3. Water pushed oil downwards by condensed steam

No-movement of COWC depth level indicates no water drive support in area. Weak to strong water drive by aquifer water below reservoir and water encroachment by injected water from disposal wells expands into oil zone and pushes oil towards producing area and eventually observed in the observation wells. Weak water drive is indicated by small increase or move-down (<10 feet), while moderate strength of water drive move-up or move-down of COWC depth level approximately 10-40 feet from original depth level of OOWC.

The increase or move-down of depth level more than 40 feet and impacted area more than 7-10 patterns indicates strong water drive from aquifer. Very strong water drive, which is extremely increase of COWC level (>80 feet) and sweep the oil in reservoir impacts to 100% water production that so far is not observed in any area of Duri Steam Flood.

Water drive related to the steam flood process, which is a condensed steam due to steam heat collapse pushed oil downward (COWC is deeper than OOWC) in several areas as various strength classification of water drives. As explained in the conceptual model, the collapse of steam is occurred in the relatively higher structure reservoir then pushed oil column downward in the relatively down dip (flank area).

Table 4 shows the generalized classification of water drives strength and mechanisms in the Duri Steam Flood:

Classification of Water Drives and Mechanism in DSF

LEGEND	Water Move	Mechanism	Remarks
No water drive support	No movement (LKO)	Very small expanding water from aquifer do not reach oil zone	At the high structure (attic) or flank area
Weak water drive	COWC 5-10 ft. up/down	Active aquifer	Small expanding water at flank area
		Condense Steam	Water pushed downward oil column and COWC slightly deeper than OOWC
Moderate water drive	COWC 10-40 ft. up/down	Active Aquifer	Significant expanding water at flank area
		Condense Steam	Water pushed downward oil column and COWC slightly deeper than OOWC
Strong water drive	COWC >40 ft. up	Injected Water	Strong expanding water at high structure by disposal wells water injection
		Active Aquifer	Strong expanding water at flank area
Very Strong water drive	COWC > 80 ft. up	Not observed so far	extremely increase of COWC level and swept the oil in reservoir that impacts to 100% water production

Table 4: *It shows the generalized classification of water drives strength and mechanisms in the Duri Steam Flood that described from no water drive support until very strong water drive.*

In Pertama Reservoir, moderate to strong water driver is occurred mostly at the north area (A10) and east flank (A10, A8, A5, A6, and A7) of South Duri high structure, while west (A9) and south flank (A7) area indicate weak water drive.

The higher structure area which Pertama becomes one water contact system with Kedua, weak and no support water drive dominantly presence in the eastern(A5 and A6) and southern area (A1, A2, and A7) with moderate water drives support production withdrawal in the northern (eastern of A9NE) and west area (A4 and A3W).

At the North Duri high structure (A12) relatively weak water drive supports reservoir withdrawal, except a small area in between fault block (A12 north central) that a stronger water drive mechanism is occurred.

Strong water drive in certain parts of area 5/8 and area 7 as active aquifer occurs, while the specific case of injected water in Kedua by disposal wells acts as a water encroachment phenomenon which drives to high increase of COWC level in Pertama and impacts in excessive water production.

A special case of water drive related to the steam flood process, which is a condensed steam that pushed oil downward (COWC is deeper than OOWC) is also observed in several areas (A11, A10N, A8E, and A9S).

In Kedua Reservoir, similar water drives and mechanisms are occurred, except the strong water drive that is not observed presence in Kedua Reservoir so far.

The map of water drive directions and mechanism as well as conceptual section showed structural position of current fluid contacts in Pertama and Kedua Reservoirs can be seen at the Figure 16 and Figure 17.

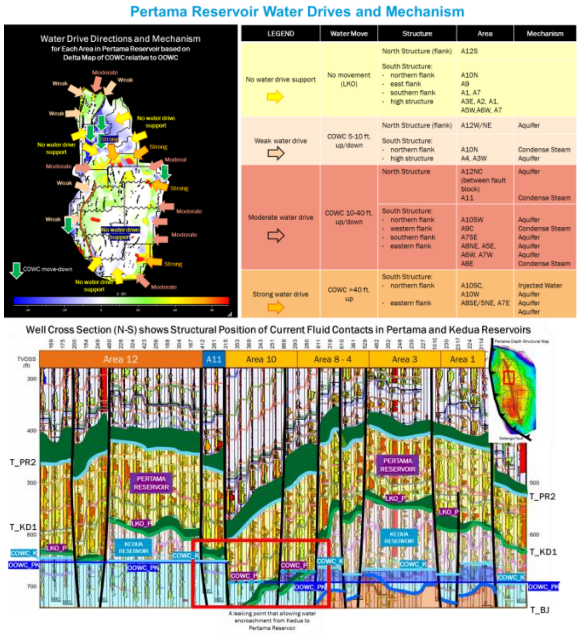

Figure 16: *The maps of water drive directions and mechanism show changes magnitude in the contact depth level of COWC & OOWC represent water drive strength for each reservoir in Pertama (picture above) and tThe conceptual section showed structural position of current fluid contacts in Pertamaand Kedua (picture below).*

3.3. Improved Heat and Drainage Review's Conceptual Models

Two cases of water encroachment from water injection in disposal wells that cross flow to the other oil reservoir are displayed on the following section models in Area 10 (Kedua to Pertama Reservoirs) and Area 2-3 (Baji-Jaga-Dalam-Menggala Reservoirs. (Figure 17).

Recommended heat management and production optimization practices are as follow:

- Interdiction wells to support heat retention in area with Dual system COWC.
- As opportunity to do proactive jobs: water shut-off, lowering pump set, clean out/revisit zone, deepening TD, and area extension.

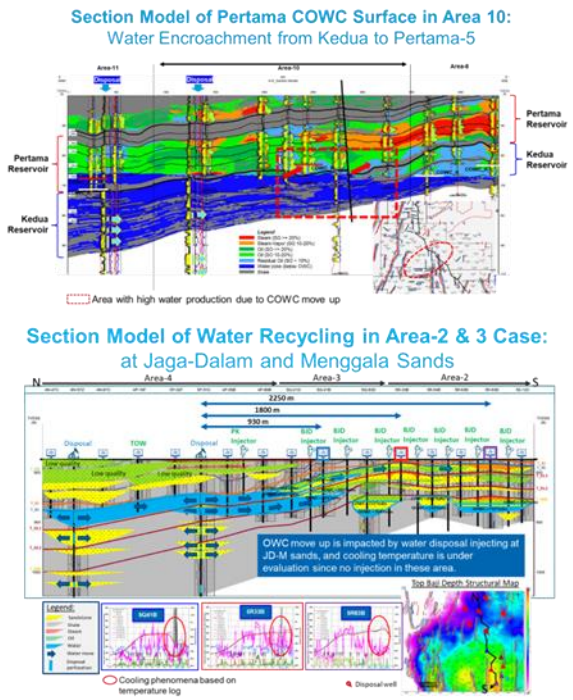

Figure 17: *The case of water encroachment from water injection in disposal wells that cross flow to the other oil reservoir is displayed on the section models in Area 10 (Kedua to Pertama Reservoirs) and Area 2-3 (Baji-Jaga-Dalam-Menggala Reservoirs).*

Conclusions

- Regional Telisa top seal strongly indicates a single common oil water contact system within Duri Field's primary hydrocarbon reservoir (Rindu and Pertama-Kedua). While Bekasap-Bangko intraformational top seals responsible for hydrocarbon accumulations in the deeper reservoirs (Baji-Jaga, Dalam, and Menggala), with multiple oil water contacts system.
- New approach in COWC interpretation in the Duri Steam Flood (DSF) Field: the markers are picked at active observation wells, based on last 3 years C/O log data for P-K-BJ-D-M sands.

- This study resulting 4 (four) types of water movement phenomena in DSF: Steam-flood depletion, Disposal impact, Dual system COWC, and Re-saturation Event.
- The Classification of Water Drives and Mechanism is established to explain the intensity of water movement and its causes.
- Understanding of fluid contact and aquifer water drive in impacted areas were implemented to support pattern heat/drainage review, identify water problem and new oil container (oil re-saturation phenomena).

Acknowledgment

Author and Co-authors would like to thank you to Erry Mastoadji, Erwin Hendardi, and Lenny Puspawati for their insights. We also appreciate PT. Chevron Pacific Indonesia and PT. Pertamina Hulu Rokan.

References

Amlan, M.H., Winderasta, W., Susianto, A., Kurniawan, R. , and Arifin, M.Z.. (2019, August). The Top Seal Capacity of Regional Telisa Shale and Intraformational Seals in Central Sumatra Basin, AAPG Technical Symposium, Volume: The Art of Hydrocarbon Prediction: Managing Uncertainties.[2]

Gael, B. T., Putro, E. S., and Masykur, A. (1994, January). Reservoir Management in the Duri Steamflood. Society of Petroleum Engineers. doi:10.2118/27764-MS.[5]

Johansen, S. and Semimbar, H. (2009). Sand-Rich, Tide-Dominated Systems of the Lower Miocene, Central Sumatra Basin, Indonesia. Proceedings AAPG Hedberg Conference.[3]

Katz, B.J. and Dawson, W.C. (1997). Pematang-Sihapas Petroleum System of Central Sumatra. Proceedings Petroleum Systems of SE Asia and Australasia Conference, page 685-698.[1]

Widyantoro, A., Winderasta, W., Muharam, C., Saptarani, P., and Deemer, A.R., 2001, Reservoir and Heat Management to Optimize Steam Injection in a Mature Multi-Zone Steam Flood in the Duri Field: paper Society of Petroleum Engineers 72136.[4]

Winderasta, W. (2010, May). Application of Dynamic Reservoir Modeling for Horizontal Well Placement in Duri Steam Flood Field's Technology Project. Indonesian Petroleum Association, IPA10-E-091.[7]

Winderasta, W., Lestari, E.S., Budiman, A., and Amlan, M.H. (2018, May). Managing Reservoir Surveillance in Duri Steam Flood Field. 10.29118/IPA18.577.E.[6]

Yarmanto, Noeradi, D., and Hendar (2010). Telisa Deposition Model in Central Sumatra Basin. Proceedings Indonesian Petroleum Association 34th Annual Convention.[4]

Authors:

Wikan Winderasta wikan.winderasta@pertamina.com received his bachelor's degree in Geological Engineering and master's degree in Petroleum Geology from Institute Technology of Bandung in 1996 and 2003. He joined Chevron in 1996 with 25 years experiences in the oil and gas industry, including Exploration & New Venture; Production & Development (Waterflood and Thermal Enhance Oil Recovery); and Unconventional Tight Rock with International experiences in U.S. and Canada. He is currently working in PT Pertamina Hulu Rokan as Senior Earth Scientist for Applied Reservoir Management Team.

Milla Hayati Amlan milla.amlan@pertamina.com received her bachelor's degree in geology from the University of Trisakti Jakarta in 2004 and master's degree in geology from Institute Technology of Bandung in 2012. She joined Chevron in 2005 with 16 years experiences in the oil and gas industry, including Development, Exploration, and Reservoir Management Framework Teams. She is currently working in PT Pertamina Hulu Rokan as Senior Earth Scientist Heat for Heavy oil Asset Optimization Team.

Willy Rhauda Paksi willy.paksi@pertamina.com received her bachelor's degree in geology from Institute Technology of Bandung in 2013. He joined Chevron in 2013 with 8 years experiences in the oil and gas industry, including Development and Optimization for Heavy Oil Teams. He is currently working in PT Pertamina Hulu Rokan as Earth Scientist Drainage for Heavy oil Asset Optimization Team.

PROCEEDINGS
JOINT CONVENTION BANDUNG (JCB) 2021
November 23rd – 25th 2021

Presence of Exsudatinite Macerals in Shelf Area of Kutei Basin: Implication for Geochemical and Basin Modeling Understanding

Hendry Setiawan Lie[1], Yudhistira Shaylendra[2], Sigit Ari Prabowo[1], Asep Heri Patria Kesumajana[3]
[1]: PT Pertamina Hulu Kalimantan Timur ("PHKT")
[2]: LAPI ITB
[3]: Geological Engineering Study Program, Faculty of Earth Sciences and Technology, ITB

Abstract

Kutei Basin is one of prolific basin in Indonesia with Mahakam Delta as significant contributor for all petroleum system in this area including source rock. Primary source rock in the onshore and shelf area of Kutei Basin believed to be coal and carbonaceous shales which containing land-plant organic matter while in the deep-water area, redistributed land plant organic matter which associated with turbidite sands is believed to be the main source rock. While source rock already known, but the level of source rock maturation still under discussion. With this study, we will analysis maturity level and its implication for geochemical analysis and basin modeling in Kutei Basin.

Based on geochemical analysis from 1970 – 2000s exploration wells data that were analyzed in this study, the vitrinite reflectance (Ro) and depth plot shows level maturity of immature until peak mature. As already known, coals and carbonaceous shales contain liptinite macerals. Among the secondary liptinite macerals, exsudatinite become a prominent thing to represent a waxy hydrocarbon generated from coals and carbonaceous facies at low thermal stage. The hydrocarbon zonation told that early generation and storage of oil (including exsudatinite) inside the kerogen started from 0.4% Ro. At 0.55% Ro, source rock could experience early expulsion phase due to massive generation, thermal, and burial sedimentation until it caused intense fracture system and filled with exsudatinite.

Based on these analyses, exsudatinite is believed play important role for geochemical aspects in influencing high HI value and can significantly generate liquid hydrocarbons, therefore the basin modeling analysis can be directly constructed for new insight of Mahakam Delta source rock capability.

Keywords: Exsudatinite, Kutei Basin, Source Rock

Introduction

Source rock studies has been performed in Kutei Basin for many years. Coal and carbonaceous shales are believed as main source rock in Kutei Basin. Generally, Miocene Balikpapan group coal and shale interval is the source rock of the Kutei Basin, had buried more than 2600 m depth (Saller, 2006). From previous study, it is believed top of the oil window is at approximately 3000 m (~10000 ft) and the base of the main gas-generative zone is estimated at 6000 m (~19600 ft) below mud line (Saller et al., 2006).

Based on many studies performed before, there are indication of early maturation of source rock in Kutei Basin that observed from several fields. This early maturation phenomena possibly had significant impact on source rock understanding in Kutei Basin.

The main purposes of this study to revisit current knowledge of source rock behaviour and its implication to basin modeling in North of Mahakam Delta.

Data and Method

This study used previous laboratory analyses on 1062 rock samples from 17 wells. Based on the TOC – HI plot (Fig.1), the richness of organic material in this area can reach more than 1% TOC which classified as fair to very good, even some of sample can reach TOC >10% in coal sample. The coal sample yields good value of TOC and HI, but it also depends on sedimentation or kerogen preservation.

The type of kerogen in this study area is dominated by type II and III, with Early Miocene interval is believed have marine environment source rock origin and Middle – Late Miocene (including Pliocene deep-water) interval is dominated by fluvio deltaic or Terrigenous-Higher Plant source rock origin. Although most of these source rocks are carbonaceous product, HI values can provide more than 300 mg HC/g TOC.

The Ro – Depth plot (Fig.2) show the level of maturity from immature – peak mature of oil window. However, in the Shelf Area of Kutei Basin, early mature seems to be occurred earlier due to the rapid sedimentation as the implication of wide accommodation of Mahakam Delta deposition, plus the presence of the unique macerals of liptinite group (exsudatinite) which later become an interesting discussion for future analysis regarding source rock properties. Source rock properties study will utilize several previous studies from other Kutei Basin and other delta as comparison.

Discussion

Presence of Exsudatinite

The distribution of coastal-plain sediments and organic matter of Mahakam Delta is strongly influenced by tidal and river flow. Domed (ombrogenous) peats fed by rainwater formed on the upper coastal plain and extended to basinward as far as the intertidal zone, where they abut against beach ridges or mangrove swamps (Anderson, 1964). Reworking of coastal plain peats in tidal flat or lagoonal environments resulted in selective separation of soluble and insoluble organic matter and accumulation of liptinite-rich allochthonous drift peats and carbonaceous shales (Allen et al., 1979). These liptinite-rich peats can be further enriched by fresh liptinitic material, such as leaf cuticles and damar resin from resin-producing trees which growing behind the coastal plain. It is believed the forming of exsudatinite was made of those continuously maceral enrichments and provided oil-generative source rocks. Although most Balikpapan Group coals contain abundant vitrinite group macerals, the hydrogen indices of the coals are commonly over 300 mg hydrocarbon/g TOC and the oxygen indices are usually below 15 mg CO2/g TOC (Thompson et al., 1985), and seems no debatable with this current study.

The numbers of exsudatinite presence in other basins have been acknowledged by maceral petrography analysis. The common liptinite constituents like exsudatinite have been found in Merit-Pila coalfield, Sarawak (Abdullah, 1997). Detailed examination of the sample under UV light excitation revealed interesting features which suggest that the generation of liquid hydrocarbons has already taken place at low maturity levels (0.4% Ro). This is demonstrated convincingly by the maceral suberinite and the formation of a secondary maceral, exsudatinite. The presence of laminated coaly sand in deepwater of Kutei cores which interpreted by Saller et al. (2006) have been identified along with cutinite from cuticle/leaf products. It is believed have same precursors with exsudatinite within coal fragments samples.

Hydrocarbon Zonation

Presence of exsudatinite had significant influence on source rock capability understanding. This unique organic material in shelf area extended to deep-water sandstones includes with laminar coaly fragments, pieces of wood, cutinite, and other coaly debris have been identified as prominent TOC value and provided 200 – 300 mg HC/g TOC from HI content. As reported on previous studies regarding coal capability to generate hydrocarbon at very low maturation levels, therefore hydrocarbon zonation will be determined as study result.

Restoration HI and TOC is the first method to be adjusted to determine the primary capacity of source rock deposition. The initial step is to sort out the TOC value and adjusting 1.00% threshold as cut-off for samples that are considered capable of generating hydrocarbons. This is based on the analysis conducted by Lewan (1987) that expulsion events tend to be very low in source rock samples that have TOC value below 1 – 2%, and the source rock is considered to have no capacity to provide expulsion.

The HI_o calculation considers the relationship between the current hydrogen index and the original hydrogen index when immature (HI original). This analysis is specifically data-driven by relying on the distribution of HI data (Justwan and Dahl, 2005). The distribution of Production Index and Bitumen Index from rock samples have also considered to determine projected HI original. After several attempts and considerations, the HI_o value in the Shelf Area of Kutei Basin is estimated at 303 mg HC/g TOC (P95) (Fig.3).

The hydrocarbon zonation in Shelf Area of Kutei Basin is considered from transformed HI analysis (data-driven) and the relationship between organic petrography & vitrinite reflectance (Ro) which conducted by Surdam (1994). Transformed HI is illustrated as decreasing HI curve from HI distribution data and indicated as expelled hydrocarbon from kerogen (HI reactance). Special care was taken in the occurrence of liptinite group (exsudatinite) maceral in the coal samples, due to these macerals can produce waxy oil at the time of hydrocarbon generation at optimal maturity level.

The hydrocarbon zonation shows that the earliest window of oil maturity is at 0.4 – 0.5% Ro, the peak of oil maturity is at 0.5 – 0.6% Ro, and the end of oil maturity along with massive gas expulsion is at 0.6 – 1.0% Ro, while gas expulsion continues at 1.0 – 1.4% Ro. Dry gas occurs at 1.4 – 4% Ro, and so overmature lies at >4% Ro. Detail as shown in fig.4.

The earliest maturity was the first direct cracking from liptinite-rich maceral (exsudatinite), however this process can only occur inside the kerogen composition (early generation). If the source rock was buried and the maturity increases with time, the more liptinite-rich maceral accumulated in the kerogen composition and experienced an early significant expulsion phase at 0.55% Ro. This was proven by the initial opening of secondary porosity in which there were combustion traces of liptinite-rich maceral at a maturity level of 0.55% Ro in shale and coal samples analyzed by Surdam (1994).

Implication for Geochemical and Basin Modeling

The liptinite-rich maceral including exsudatinite is believed play important role for geochemical aspects in influencing high HI value and can significantly generate liquid hydrocarbons. The earliest maturity at 0.4% Ro and based on numerous evidences in coal-bearing source rock basin prove that source rock can

be generated hydrocarbon at low maturity levels. This finding can provide new insights to another hydrocarbon exploration in Shelf Area of Kutei Basin for play concept in deep-water areas, that we still assume in the presence of exsudatinite in Pliocene source rock interval.

The hydrocarbon zonation can be calibrated and validated with 1D basin modeling profile across giant oil field in North of Mahakam Delta. Source rock interval lied at SB-17.5 (Early Miocene) and SB-8.8 (Late Miocene). The early significant oil expulsion at ~0.55% Ro coincides with Transformation Ratio (TR) at 5 – 10%. The Transformation Ratio value suggest a parameter that quantifies the relative progress of hydrocarbon generation (Waples and Tobey, 2015).

Time of expulsion with consideration of hydrocarbon zonation in this paper could make more precise result rather than applying recent conventional maturity level. As of Ro 0.55% stands at early significant oil expulsion, Early Miocene source rock interval occurred early significant oil expulsion at 12.33 Ma and Late Miocene source rock interval occurred at 5.80 Ma. While recent conventional maturity confirmed hydrocarbon expulsion at peak maturity level (0.65% Ro) with ~1.40 million years younger than above, with Early Miocene source rock interval occurred at 10.90 Ma and Late Miocene source rock interval occurred at 4.37 Ma. This difference will make another implication for hydrocarbon generation, preservation, trappings, and overpressure occurrence in Shelf Area of Kutei Basin, especially in North Shelf of Mahakam Delta (Fig.5 and Fig.6).

Conclusions

The presence exsudatinite maceral in source rock of Kutei Basin will give a new insight for future basin modeling work. Based on this study new hydrocarbon maturity zonation can be defined for North of Mahakam Delta which later could have significant role on geochemical and basin modeling study.

References

Abdullah, W. H., 1997, Organic Geochemistry, **27**, 591 – 596.
Allen, G. P., D. Laurier, and J. Thouvenin, 1979, Notes et Mémoires - Compagnie Français des Pétroles, **15**, 1 – 156.
Anderson, J. A. R., 1964, Journal of Tropical Geography, **18**, 7 – 16.
Justwan, H. and B. Dahl, 2005, Petroleum Geology: North-West Europe and Global Perspectives – Proceedings of the 6th Petroleum Geology Conference, 1317 – 1329.
Lewan, M. D., 1987, Migration of Hydrocarbons in Sedimentary Basin, Editions Technip, 30 – 113.
Saller, A., R. Lin, and J. Dunham, 2006, AAPG Bulletin, **90**, 1585 – 1608.
Surdam, R. C., 1994, VICO Reports, Wyoming – USA.
Thompson, S., B. S. Cooper, R. J. Morley, and P. C. Barnard, 1985, Norwegian Petroleum Society, 59 – 73.
Waples, D. and M. H. Tobey, 2015, AAPG Annual Convention & Exhibition, Colorado – USA.

Acknowledgements

The authors would like to acknowledge PT Pertamina Hulu Kalimantan Timur ("PHKT") Subsurface Management in supporting the work and publication of this paper.

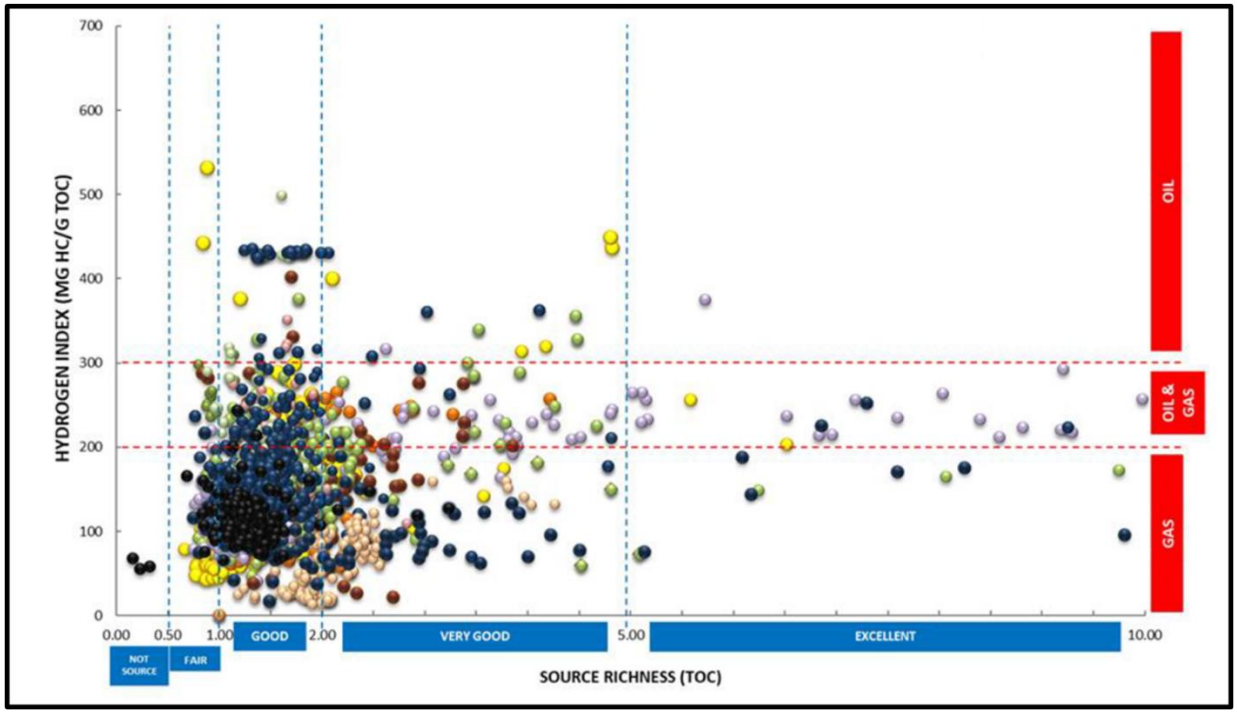

Figure 1: TOC vs HI Plot from wells in Shelf Area of Kutei Basin

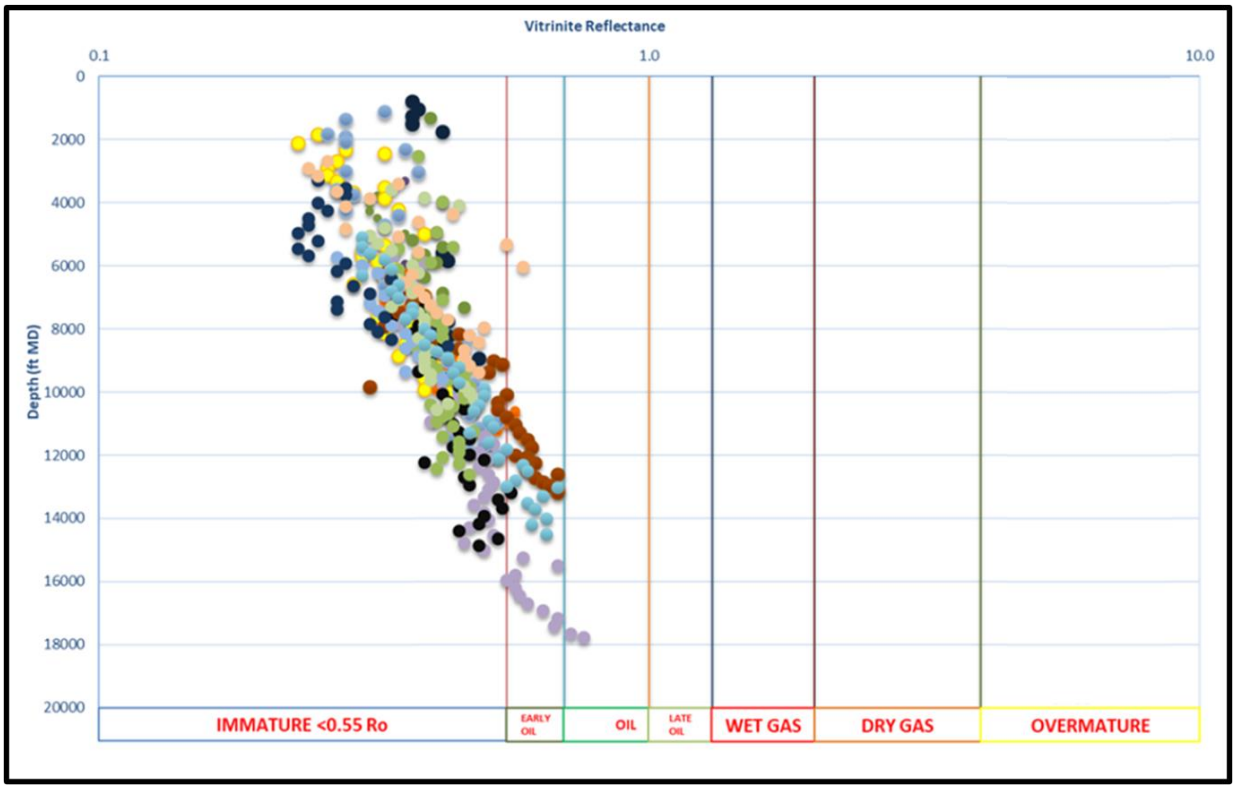

Figure 2: Ro vs Depth Plot from wells in Shelf Area of Kutei Basin

PROCEEDINGS
JOINT CONVENTION BANDUNG (JCB) 2021
November 23rd – 25th 2021

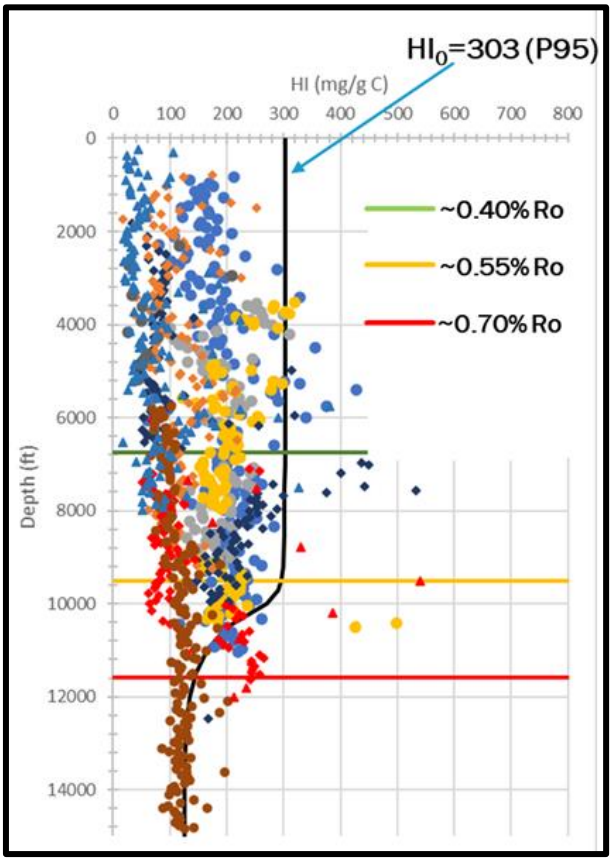

Figure 3: Projected Hydrogen Index original in Shelf Aarea of Kutei Basin

Model	Ro	TR
Immature	0 - 0.4%	0 - 4%
Early Oil Window (Generation & Storage of Liquid HC)	0.4 - 0.5%	0 - 4%
Main Oil Window (Main Generation & Significant Oil Expulsion Phase)	0.5 - 0.6%	4 - >5%
Late Oil Window (Continuous Oil Expulsion & Massive Gas Expulsion)	0.6 - 1.0%	>5 - 50%
Continuous Gas Expulsion	1.0 - 1.4%	>50%
Dry Gas	1.4 - 4%	>50%
Overmature	>4%	>50%

Figure 4: Hydrocarbon zonation in Shelf Area of Kutei Basin

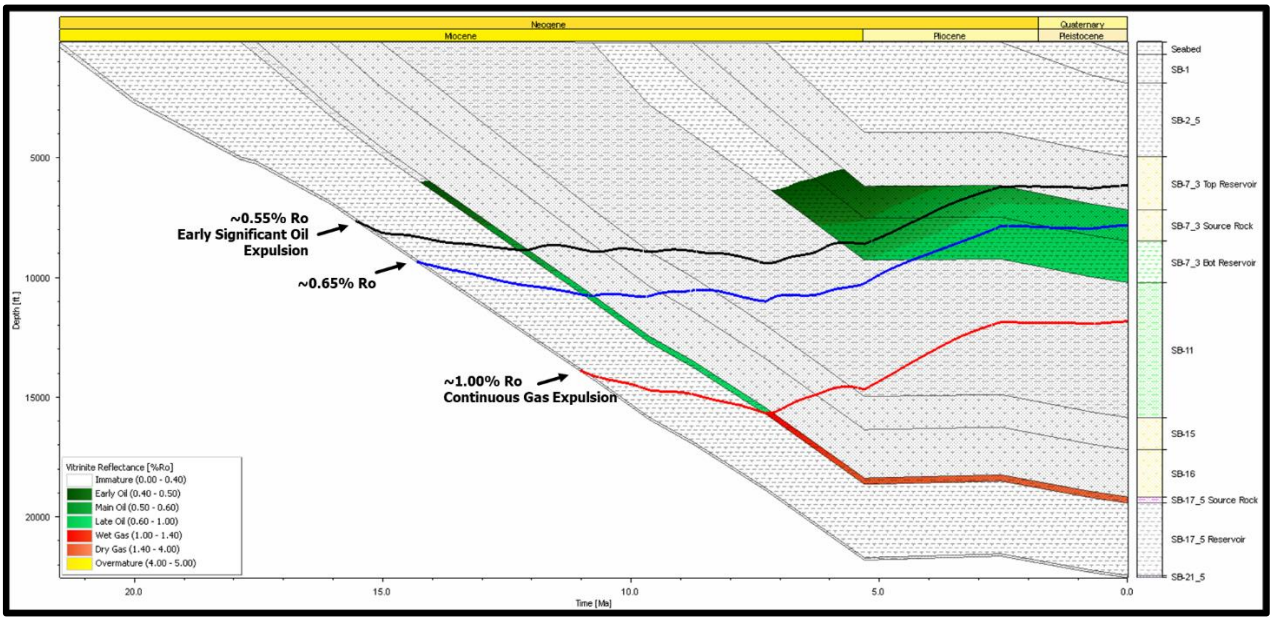

Figure 5: 1D basin modeling with maturity calibration

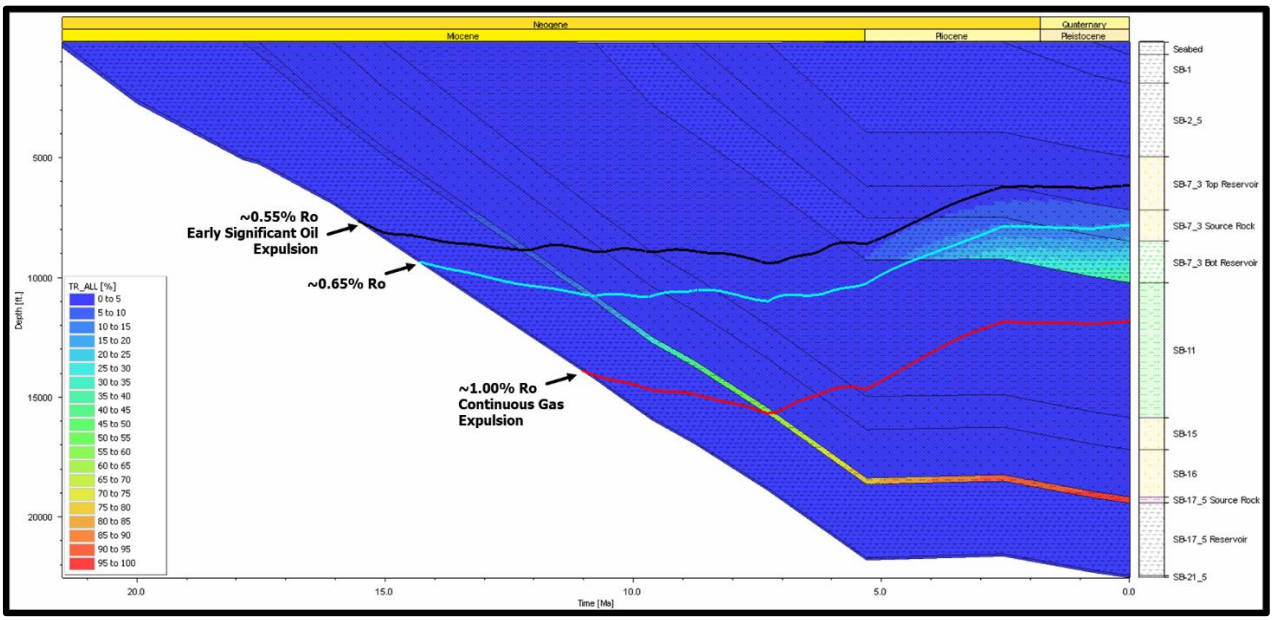

Figure 6: 1D Basin Modeling with transformation ratio calibration

PROCEEDINGS
□O□NT□□ON□□NT□ON□□N□□N□□□□□□2□2□
November 23rd – 25th 2021

Telisa Sand Characterization and Prospects in Langgak Field

Hirzi Farizi[1] Dimas Hadi Prabowo[1] M Yasin Abdulfatah[1] Annisa Palupi[2]

Abstract

The Langgak Field in Mountain Front Kuantan Area, Central Sumatra Basin was discovered in 1975 and has been producing oil since 1979 on Sihapas Sand (Bekasap FM) as the main target. Year by year water cut in Sihapas Sand has been increasing and resulted in a significant decline in production. As an alternative to increase production, the Subsurface team has started to try to open a new zone above Sihapas sand, which is Telisa Sand at Telisa FM and is expected to contribute to more oil production in Langgak Field.

Telisa FM was deposited widely and has been distributed all over Central Sumatra Basin Area from Early to Middle Miocene during a transgressive phase. Telisa FM functions as seal rock for Sihapas Group. The distribution of Telisa FM also has a wide range of thickness (Bangko – Balam = 400-600 feet; Petapahan = 870 feet; Lindai = 500 feet).

The characteristic of Telisa Sand in Langgak has a thin sedimentation of 20 feet, found in a shallow depth, and unconsolidated sand. However, **LGK#31** Mudlog Analysis showed an indication of oil in Telisa Sand, while **LGK#24** CO-Log Analysis Report strongly suggested that Telisa Sand in Langgak has oil with good saturation oil (@813 – 822 ft).

This paper describes the potential of Telisa Sand reservoir in Langgak Field and how the Subsurface team maximized the potential of Tight Telisa Sand in Langgak Field. We used Multicycle Shear Fracturing Technique to increase production, especially in the thin and shallow reservoirs, like Telisa Sand in Langgak Field.

Keyword: **Telisa FM, Central Sumatera Basin, Multicycle Shear Fracturing**

Introduction

The Langgak Field has been producing oil since 1979 in Sihapas Sand as main reservoir. Sihapas zone has been producing oil for several decades, with a significant increase in water cut thus resulting in the decline of production over the years.

Telisa FM has been known as one of the reservoirs in the Central Sumatra Basin area. At the onset, Telisa FM was not the main target of production, because of the thin sedimentation and shaly formation, indicating a tight oil-bearing formation. Moreover, the reservoir characteristic of Telisa Sand in Langgak Field is very shallow, unconsolidated sand, and low resistivity (3 Ω).

The Multicycle Shear Fracturing method would be applied to Telisa Sand in Langgak Field to increase rock permeability, while minimizing unwanted fracturing risks.

PT SPR Langgak[1]
PT NPS Energy Indonesia[2]

Data and Method

Field History

Operated by PT SPR Langgak, The Langgak Field is in the Langgak Block, Mountain Front Kuantan area, Central Sumatra Basin, Riau Province, Sumatra.

The field was discovered in 1975 and commenced production in 1979. The field contains 26 producing wells, 1 swamp well, and 6 P&A wells. The Langgak field is a broad, elongated anticlinal structure and containing 51.94 MMBO of original oil in place with estimated recoverable reserves of 17.56 MMBO (33,8%).

The main productive reservoir is Sihapas A sand with an average of 1,200 feet. Shapes oil is 30.8 degrees API gravity, the viscosity of 14 cp, and pour point 105-110oF. Telisa FM lies above Sihapas A sand, with an average reservoir thickness of 30 feet.

In 2020, PT SPR Langgak has managed to produce oil from Telisa Sand with a total of 71.67 BOPD from 3 wells.

General Geology

The Langgak structure has a 4-way dipped closed anticline with some main fault and a minor splay associated with it. The faulting is post-depositional and is associated with the formation of the Langgak trap. The fault runs along the strike of the north west - south east trending anticline and is downthrown to the northeast.

The Early - Middle Miocene Telisa FM conformably overlies and is partly the lateral time equivalent, of the Sihapas Formation (Figure 1).

The unit comprises a monotonous series of marine clay stones-shales and siltstones with minor limestones and sandstones that were deposited throughout the Central Sumatra Basin at the height of the marine transgression.

Formation Evaluation

Based on CO Log & Sigma analysis result on Telisa Sand, the total porosity of the sandstone reservoir is around 30 – 35 p.u with oil density 0.87 gr/cc. In Telisa Sand interval resulted in a strong oil signal at 813 – 822 feet as an indication of good oil saturation (Figure 2).

Based on mud-log data, there was an obtained trace oil marked (Figure 3). Re-evaluation was carried out in the Telisa formation by lowering the cut-off resistivity from 10 ohm-m to 3 ohm-m manually so that potential wells were obtained.

Telisa reservoir parameters:
· Net sand = 10 - 20 ft
· Net pay = 6 - 14 ft
· Resistivity = 3-5 ohm-m
· Permeabilty = 24.75 mD

Multicyle Shear Fracturing

In the beginning of 2020, SPRL started fracturing projects at Langgak Field. Multicyle Shear Fracturing Method was chosen to reach an objectives :

- Minimize unwanted fracturing risks (Early Screen out, Sand Flowback

PT SPR Langgak[1]
PT NPS Energy Indonesia[2]

After Treatment or Formation Damage).
- Creating Fracture Branch and Network (more possible for the shallow reservoir).
- Enhance the production with less damaging fluid.

Start by dropping cut-off from 10 ohm-m to 3 ohm-m and finding the highest structure of Telisa FM. **LGK#24** was chosen as the pilot well for Telisa FM in Langgak Field, because of its thicker sedimentation compared to other wells, while also showing a good resistivity as an indicator of oil presence.

The objective of fracturing treatment in **LGK#24** is to improve the flow performance of the newly opened Telisa Sand (812-832 feet). The Multicycle Shear Fracturing method is applicable for this type of sedimentation with a thin layer to prevent excessive height growth and breaking the shale barrier (Figure 4).

LGK#27 (820-840 feet) is the 2nd candidate for fracturing stimulation in Telisa zone, Langgak Field. The first Telisa fracturing job has been performed in LGK#24 at the same layer. From the gamma ray log, this Telisa zone has a good barrier at the top and even better at the bottom of the zone, which visually shows a sufficient contrast. This shale barrier is expected to limit the height to grow during fracturing treatment. From resistivity log, it shows an oil indication in cut-off 3 Ω at interest interval.

The 3rd candidate for fracturing stimulation is **LGK#26** (800-820 feet). LGK#26 in overall has cleaner sandstone than other wells, it also has a lower fracture gradient (0.69 psi/ft) compared to others.

Result and Discussion

Based on saturation logging tools and analysis, Telisa is observed to have oil potential (good signal of oil existence) and confirmed by swab test result that this zone has fluid at 90% WC, which is considered as good compared to existing WC in Sihapas Zone (>96%).

Based on the result at LGK#24, LGK#27, and LGK#26, fracturing has increased the production rate/flow performance, based on decline comparison and based on swab test result pre and post Fracturing (Figure 5).

- Based on the single swab test before fracturing treatment, LGK#24 has 120 BFPD and 240 BFPD with 25.79 BOPD initial production after fracturing treatment.
- Result at LGK#27, single swab result before fracturing treatment is dry, because the layer of Telisa sand is too tight. After fracturing treatment based on the single swab test, the gross gluid becomes 345 BFPD with 24.50 BOPD of initial production.
- Gross fluid before frac at LGK#26 is 46 BFPD, and after fracturing treatment the result has increased by 207 BFPD with 21.38 of initial production.
- Multicycle Shear Fracturing method is applicable for the type of sedimentation with a thin layer to prevent excessive height growth and breaking the shale barrier.

Conclusions

- Langgak Field has a Telisa sand layer that is quite widespread (Figure 6).
- After Fracturing Treatment Telisa sand has produced 71.67 BOPD in cumulative from 3 wells.
- Opening another Telisa zone at Langgak Field is recommended to improve oil production.
- Multicycle Shear Fracturing (Figure 7) method is applicable for the type of formation which has a thin layer to prevent excessive height growth and breaking the shale barrier (prevent reaching the water zone).

References

Edward J, et al, 1994, Hydraulic Fracturing of Telisa Formation at Kotabatak Field Central Sumatra, Twenty-Third Annual Convention Proceeding Indonesian Petroleum Association, p 2-3.

Internal SPRL Telisa Fracturing Report, 2020.

Yarmanto, et al, 2010, Telisa Deposition Model in The Central Sumatra Basin, Thirty-Fourth Annual Convention & Exhibition Proceeding Indonesian Petroleum Association, p 6-11.

Acknowledgements

We express our greatest appreciation to the management of PT SPR Langgak's for their support, encouragement, and permission to publish this paper. Notable gratitude to Pak Ikin, Pak Yasin, and all members of the Exploration & Development Department.

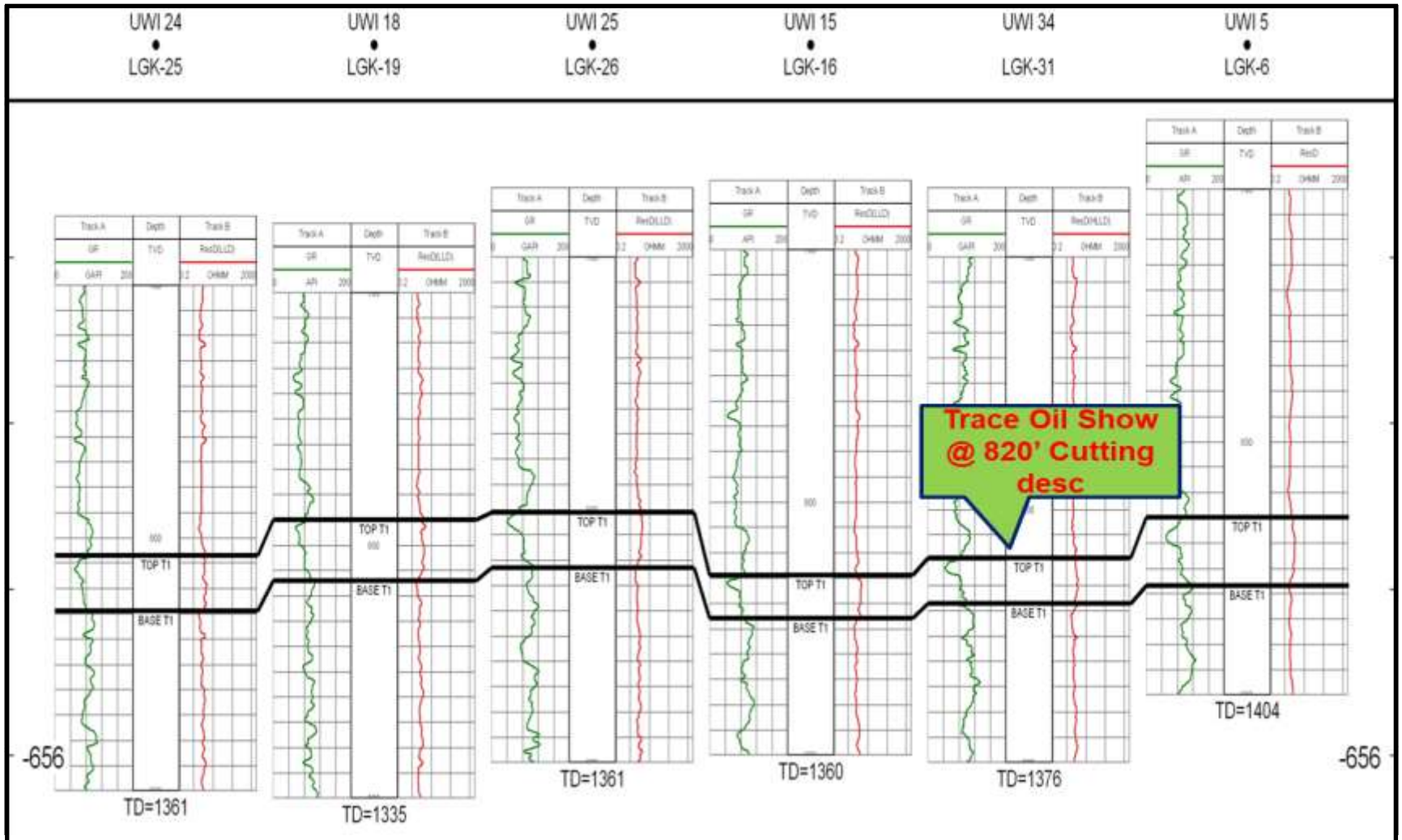

PROCEEDINGS
□O□NT□□ON□□NT□ON□BA N DU N G□(JCB) 2021
November 23rd – 25th□2021

FIGURE 1 - Langgak Field Telisa Structural W-E Cross Section

PT SPR Langgak[1]
PT NPS Energy Indonesia[2]

PROCEEDINGS
□O□NT□□ON□□NT□ON□□□N□□N□□□□□□□2□2□
November 23rd – 25th 2021

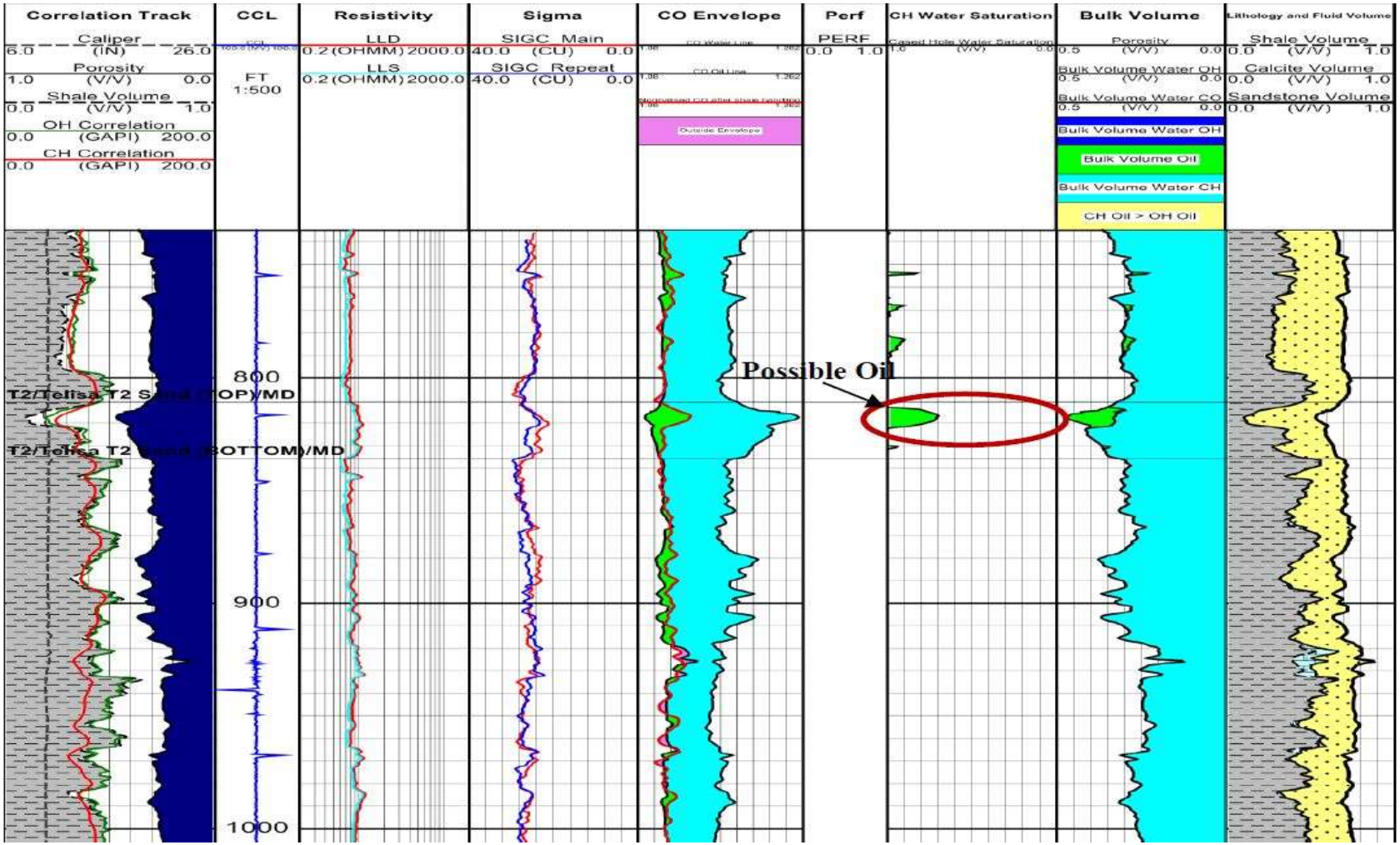

FIGURE 2 - LGK#24 CO Log & Sigma analysis

PT SPR Langgak[1]
PT NPS Energy Indonesia[2]

PROCEEDINGS
□O□NT□□ON□□□NT□ON□□□N□□N□□□□□□2□2□
November 23rd – 25th 2021

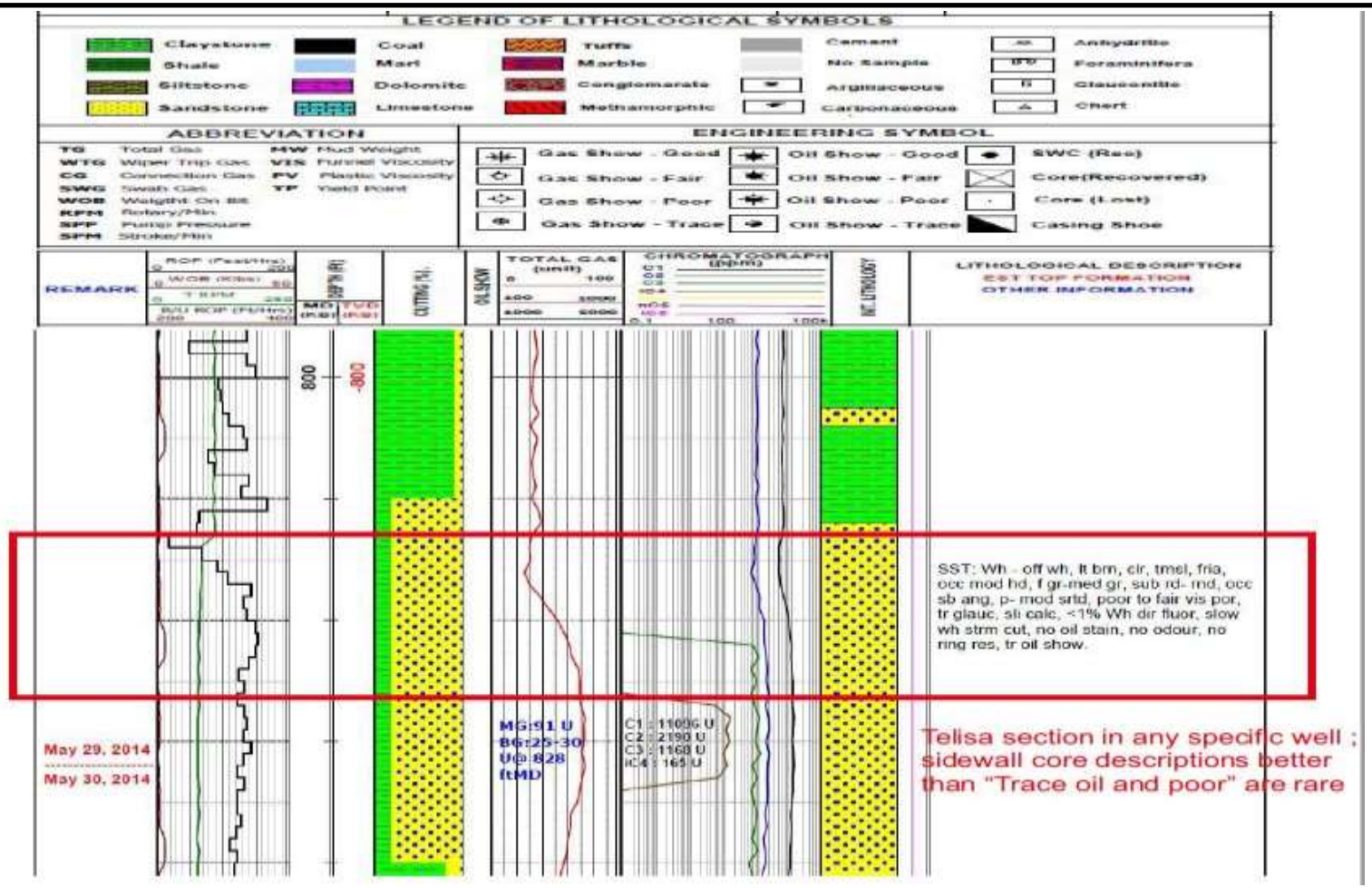

FIGURE 3 - LGK #31 Mud Log Report

PT SPR Langgak[1]
PT NPS Energy Indonesia[2]

PROCEEDINGS
O NT ON NT ON N N 2 2
November 23rd – 25th 2021

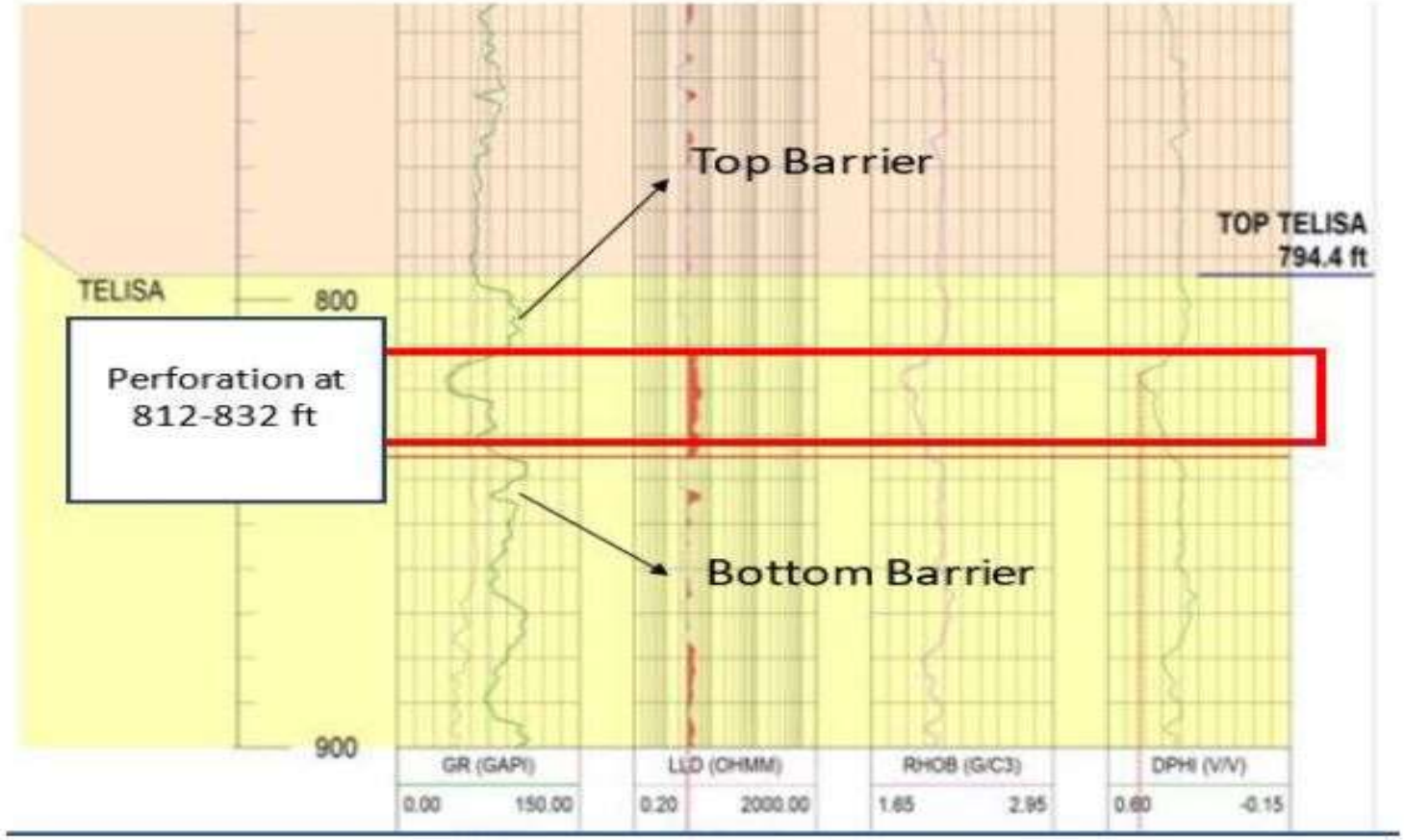

FIGURE 4 – Typical of Telisa Sand in Langgak Field

PT SPR Langgak[1]
PT NPS Energy Indonesia[2]

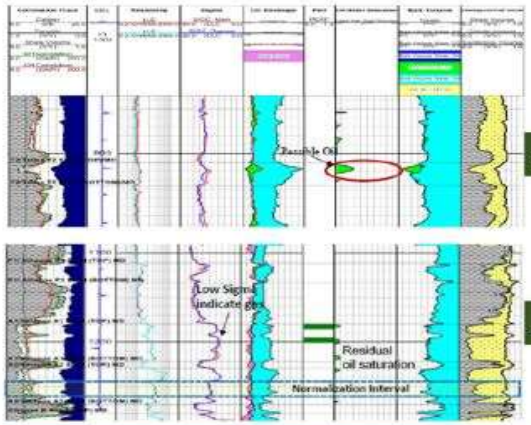

PROCEEDINGS
□O□NT□□ON□□NT□ON□BA N DU N G□(JCB) 2□21
November 23rd – 25th□2021

CO Log LGK #24

Oil Sample LGK #24

Well Number		LGK #24	LGK #27	LGK #26
Date of Execution		16/Feb/20	1/Mar/20	13/Mar/20
Gross Fluid Before Frac	BFPD	120	Dry	46
Gross Fluid After Frac	BFPD	240	345	207
Initial Production	BOPD	25.79	24.50	21.38

FIGURE 5 – Telisa Fracturing Execution Results

PT SPR Langgak[1]
PT NPS Energy Indonesia[2]

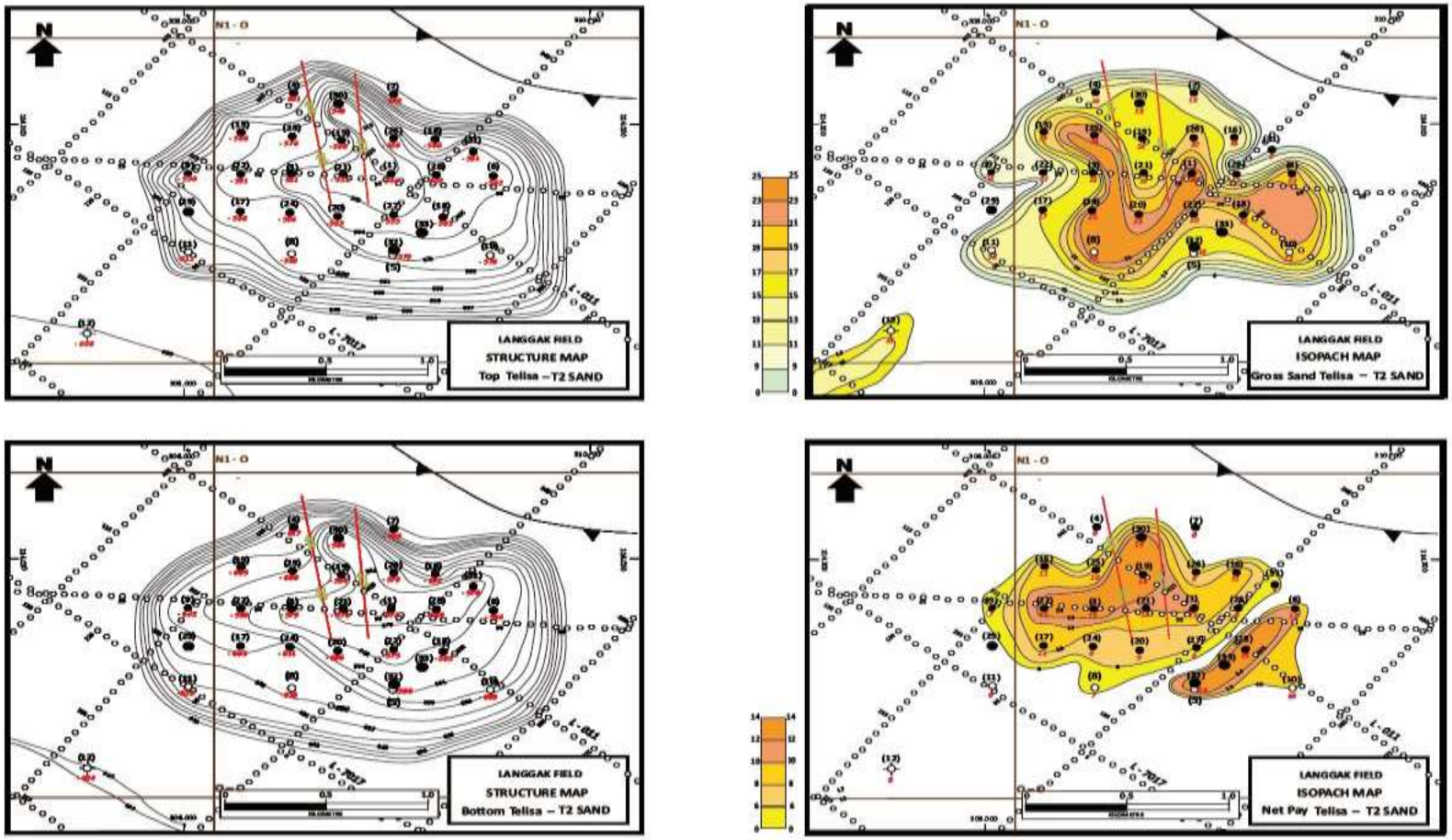

PROCEEDINGS
□O□NT□□ON□□NT□ON□□N□□N□□(JCB □2021
November 23rd – 25th 2021

FIGURE 6 – Langgak Telisa Subsurface Map

PT SPR Langgak[1]
PT NPS Energy Indonesia[2]

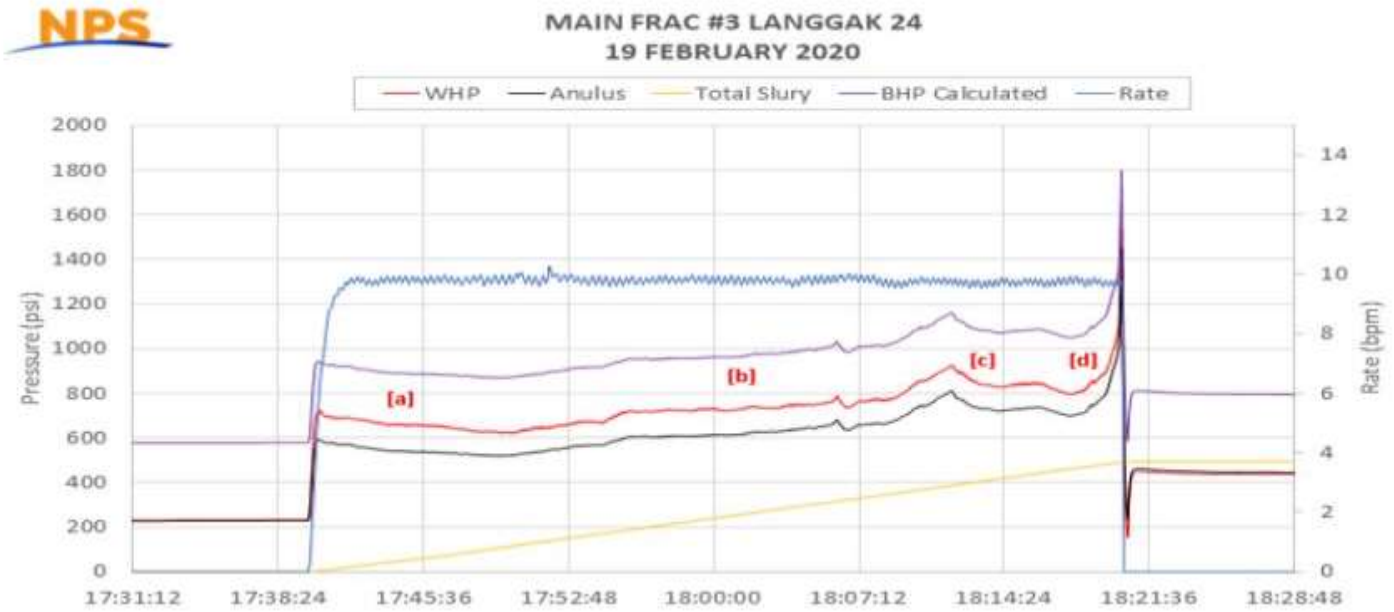

[a] Initial injection, pressure show fracture grows before reaching its barrier

[b] Pressure start to increase indicating growing in length and start packing the formation with proppant

[c] Fracture growth

[d] Rapid pressure increase indicating Near wellbore screenout. Pump Is terminated after Pop-off valve Is activated.

FIGURE 7 – Typical Treatment Summary in 3 Executed Wells

PT SPR Langgak[1]
PT NPS Energy Indonesia[2]

PROCEEDINGS
JOINT CONVENTION BANDUNG (JCB) 2021
November 23rd – 25th 2021

Newly Identified Sub-Basin in Highly Matured Brownfield North-West Java Basin

David Ontosari[1], Miftah[1], Rahmat Budiana[1], Dian Wasugi[1], Adam Dwinanto[1], Yosaphat Ardhita Yudha[1], Rully Firmansyah[1], Erik Wahyu Irawan[1], Ferdy[1], Sidiq Pramada[2], Akmaluddin[3], Salahuddin Husein[3], Jarot Setyowiyoto[3]
1. Pertamina
2. SKK Migas
3. LKFT UGM

Abstract
Since discovered in 1897, North West Java Basin is known for highly prolific hydrocarbon basins sustained from its child sub-basin such as Sunda, Asri, Arjuna, Ciputat, Kepuh, and Jatibarang. These basins filled 296 hydrocarbon fields both onshore and offshore, with cumulative reserves of 5 BBOE.

Data provided from latest satellite gravity - magnetic, newly acquired 1960 Km 2D seismic in 2016 data added existing 1000 km of 2D seismic data in 2013, 31 well post mortems consisted of basin statistic in play assessment, drill chances, field prospectivity evaluation, and palinspastic reconstruction using chronostratigraphic refining markers from nannofossils have resulted newly interpreted two sub-basin in Anggursi area: the South and the North Anggursi sub-Basin. With a range of uncertainty ranging 120-30 Ma of basin formation, this area was previously studied as a simple back-arc basin during Neogene. Based on the new analysis of these newly acquired data, this basin has been analyzed as poly history basin, comprised of syn-rift associated with transtensional during Eocene and Oligocene produced deep-seated old trap with early charged good porosity sands reservoirs, continued with anti-clockwise rotation in Sundaland Orocline during Early- Middle Miocene created clear angular unconformity, and followed by deepening post-rift transgression during Late Miocene and syn-orogenic regression of the sub-basin until the present day.

This new data, analysis, interpretation, and novelty in tectonic reconstruction were strengthened by palinspastic reconstruction of each event, porosity to depth analyzed with attributed seismic for overpressures in the late-synfirt phase due to high sedimentation rate and loading mechanism. From this study, there are some novelties in the basin genetic, basin forming, basin filling, and basin deformation. calculated yet-to-find hydrocarbon from North West Java Basin around 2 BBOE, North Anggursi sub-Basin will be expected to contribute to the discovery of hydrocarbons, especially in the field size of 50-100 MMBO which is a cumulative amount of around 1BBO, a field of 100-250 MMBO and a field of 250-500 MMBO with a cumulative amount of approximately 400 MMBO each.

Introduction

This paper discussed a newly mapped sub-basin in the Northwest Java Basin, named North Anggursi sub-Basin. Regionally, study location situated in the middle of Southwest Sundaland terrane, back-arc Java volcanic Island, offshore Java Sea (Figure 1), located in the north of Cipunegara and Jatibarang sub-basin (Figure 2)

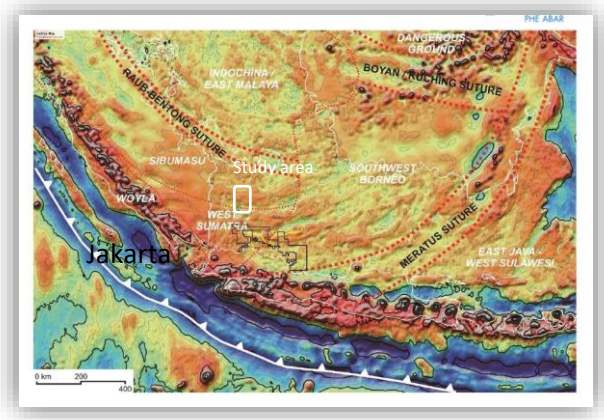

Figure 1. Study location (white box) overlaid with structural geology features and tectonic regime on gravity map. Tectonic blocks in Sundaland (modified from (Breitfeld et al., 2017)) drawn on free-air gravity map (Smith and Sandwell, 1997). Suture zones are bounded by thicker red dashed lines. Block boundaries are indicated by thinner red dashed lines. It appears that basement blocks follow a regional curvature trend (named as Sunda Orocline) formed by Mesozoic tectonic sutures and magmatic belts (Salahuddin, 2018), except the western border of SW-Borneo Block which vaguely and unconvincingly cut those oroclines. Yellow line within Abar – Anggursi area is approximate borderline for granitic basement (to the north) and low- grade metamorphic basement (to the south).

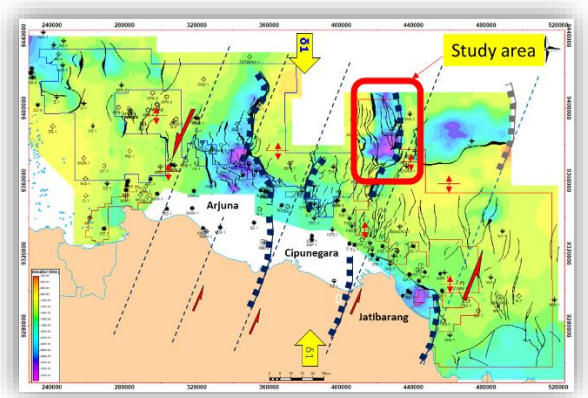

Figure 2. Structural features, sub-basins and tectonic regime surrounding study area

North West Java Basin has been explored and produced mainly in Main and Massive plays. Those two plays are much more exploited than the rest of the plays: Cisubuh, Pre-Tertiary Basement, Pre-Talang Akar Formation (TAF), Parigi, Baturaja, and TAF (Figure 3).

PROCEEDINGS
JOINT CONVENTION BANDUNG (JCB) 2021
November 23rd – 25th 2021

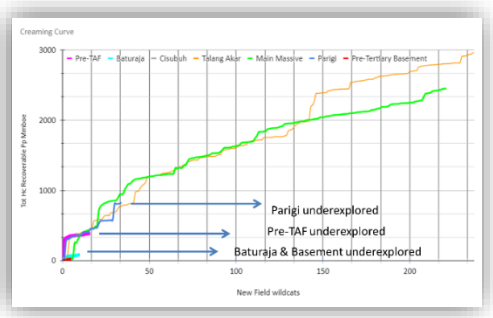

Figure 3. Creaming curve each plays since their first discoveries (data from IHS Markit, 2020)

Even though there are already two plays whose creaming curve level is quite contrasting with the other plays, the overall plays are still below the calculated reserve and there is still a possibility of finding (Figure 4). All plays to date have a reserve of 5 BBOE, consisting of 296 fields and 553 reservoir layers (IHS, 2021). To increase the prospectivity, total reserves and productivity in this area, it is hoped that this new basin mapping can contribute to oil and gas production in the future.

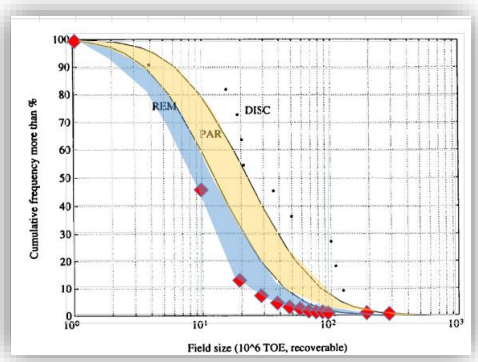

Figure 4. North-west Java field size distribution (red markers) still below remaining reserves / resources (blue area) and still need to push to another discoveries (orange area). Data from IHS Markit (2021), plotted on (Sinding-Larsen and Chen, 1996). It is approximated that North Anggursi sub-Basin will be expected to contribute to the discovery of hydrocarbons, especially in the field size of 50-100 MMBO which is a cumulative amount of around 1BBO, a field of 100-250 MMBO and a field of 250-500 MMBO with a cumulative amount of approximately 400 MMBO each.

Data and Method

Data used in this paper described in the Figure 5. Method used in this paper to identify newly sub-basin is shown in Figure 6.

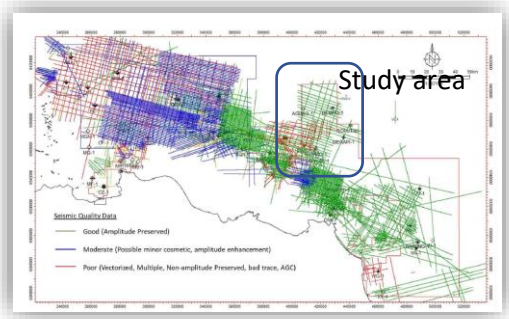

Figure 5. Seismic and well data distribution used in this paper

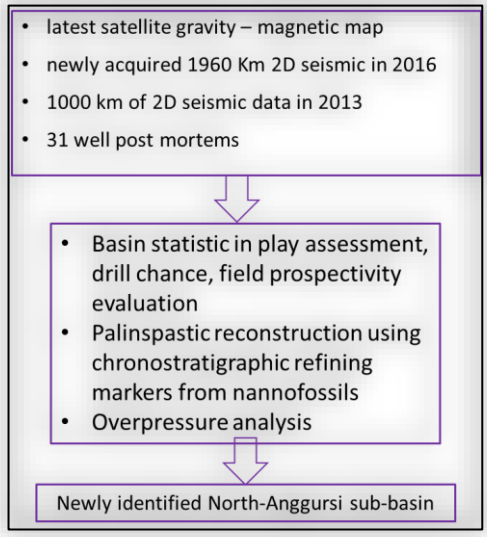

Figure 6. Workflow used in this paper

Result and Discussion

From well-tied seismic, age-sequence marker derrived from biostratigraphic record and data are plotted and interpreted in all seismic lines. For example the representative A-B section crossing perpendicular to the rift axis, show three half-graben geometry in the North-Anggursi sub-Basin. The major bounding fault is situated in the eastern part of the sub-basin (Figure 7).

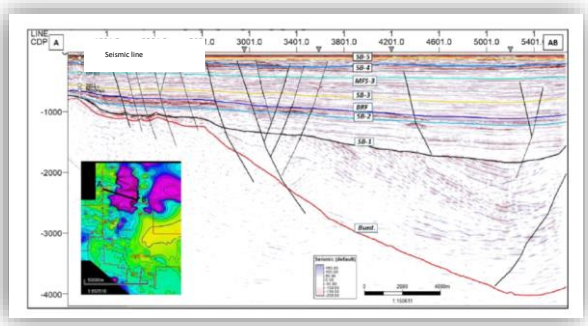

Figure 7. Section A-B crossing perpendicular to rift-axis

Based on the interpretation, Paleogene depositional sequence in the North Anggursi sub-basin is divided into three units, namely Mid Eocene Shale, Late Eocene Sandstone and Early Oligocene Sandstone. The lowest sequence unit Mid Eocene Shale, has a relatively homogeneous lithology seen from its seismic reflection characteristics which generally have a low amplitude. This lithology under the depositional sequence, based on seismic cross-section correlations, was slightly penetrated in the TY-1 well at a depth of 7320 ft MD with quarzt wacke lithology. In addition to the dominant claystone fragments (> 30%), petrographic analysis results indicate the presence of metasediment fragments suspected as provenance of this rock. This depositional sequence division in Figure 8and Figure 9.

PROCEEDINGS
JOINT CONVENTION BANDUNG (JCB) 2021
November 23rd – 25th 2021

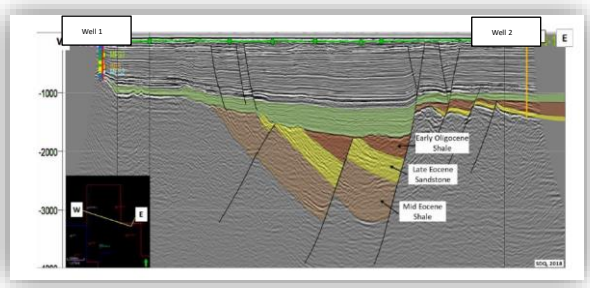

Figure 8. Depositional sequence unit 0 based on seismic section in Anggursi block, the lower part (light brown), middle part (yellow), and upper part (dark brown). Green represent TAF.

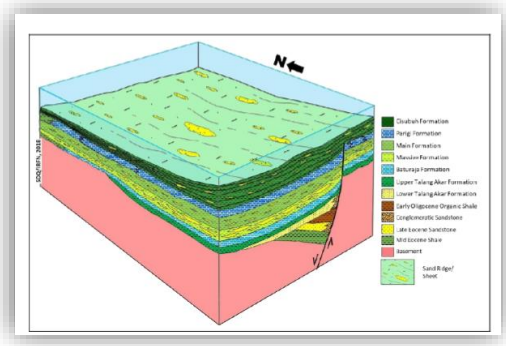

Figure 9. Conceptual deposition model in the center of North Anggursi sub-Basin during Late Pliocene, includes all deposition from Eocene.

This interpretations were tested in Wheeler diagram to create chronostratigraphic chart, shown in Figure 10, palinspatic model was constructed to restore and evaluate deformational processes within North Anggursi sub-basin shown in Figure 11, and tested using the results of estimated pore pressures by the Eaton method from sonic data coinciding with seismic common depth point then modeled in 2D pore pressure sections as shown in Figure 12. To strengthen the prospectivity in the North Anggursi sub-Basin, there are syn-rift and post-rift plays in the parent basin (North West Java Basin) have more chance of success and average field reserves (Figure 13).

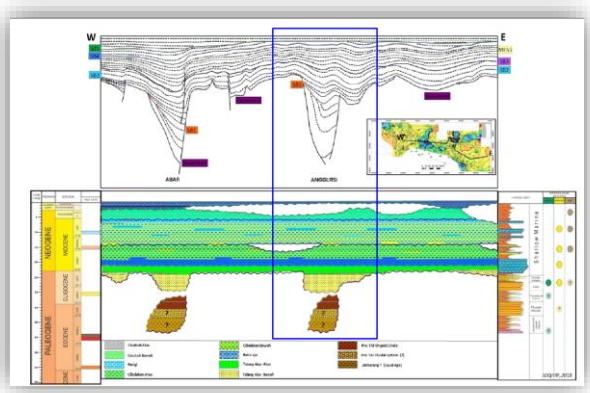

Figure 10. Simplification of seismic section reflection passing through North Anggursi sub-Basin (blue box), trending relatively E-W (upper) and Time stratigraphic Wheeler diagram (lower).

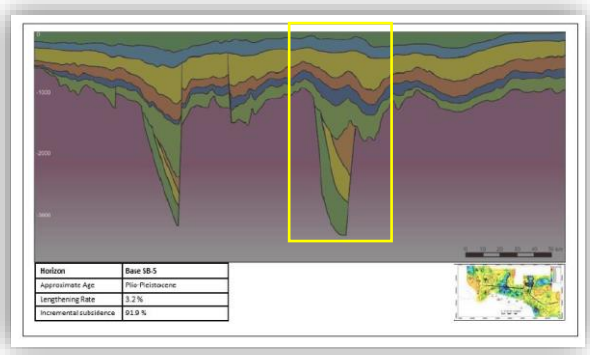

Figure 11. Palinspatic reconstruction on Sequence Boundary 5 (North Anggursi sub-Basin in the yellow box)

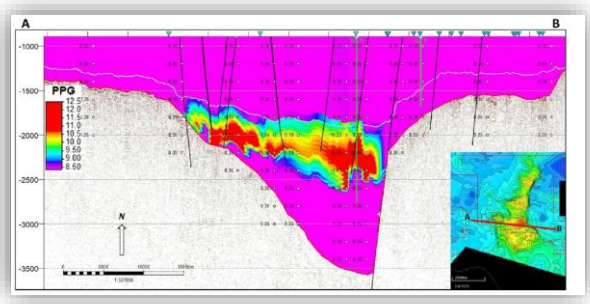

Figure 12. Pore pressure model from seismic velocity data for section A-B in North Anggursi sub-basin

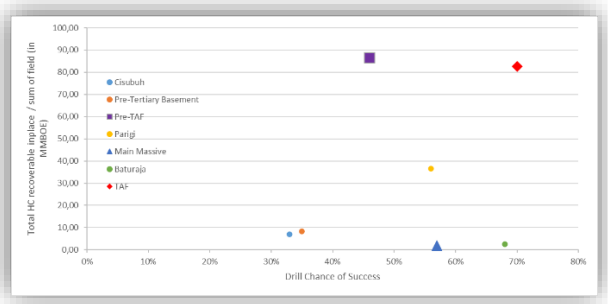

Figure 13. Drill chance of success vs Average each play's field hydrocarbon in-place (IHS Markit 2021)

Conclusions

This new data, analysis, interpretation, and novelty in tectonic reconstruction were strengthened by palinspastic reconstruction of each event, porosity to depth analyzed with attributed seismic for overpressured late-synfirt due to high sedimentation rate and loading mechanism. From this study, there are some novelties in the basin genetic, basin forming, basin filling, and basin deformation. calculated yet-to-find hydrocarbon from North West Java Basin around 2 BBOE, North Anggursi sub-Basin will be expected to contribute to the discovery of hydrocarbons, especially in the field size of 50-100 MMBO which is a cumulative amount of around 1BBO, a field of 100-250 MMBO and a field of 250-500 MMBO with a cumulative amount of approximately 400 MMBO each.

References

IHS Markit, 2020. https://ihsmarkit.com/

IHS Markit, 2021. https://ihsmarkit.com/

Breitfeld, H.T., Hall, R., Galin, T., Forster, M.A., BouDagher-Fadel, M.K., 2017. A Triassic to Cretaceous Sundaland–Pacific subduction margin in West Sarawak, Borneo. Tectonophysics 694, 35–56. https://doi.org/10.1016/j.tecto.2016.11.034

Salahuddin, H., 2018. Oroclinal Wrench Tectonics of Paleogene Back-Arc Rifting in Western Indonesia. Presented at the PROCEEDINGS PEKAN ILMIAH TAHUNAN IAGI 2018, IAGI, Pekanbaru, p. 4.

Sinding-Larsen, R., Chen, Z., 1996. Cross-validation of resource estimates from discovery process modelling and volumetric accumulation modelling: example from the Lower and Middle Jurassic play of the Halten Terrace, offshore Norway, in: Norsk petroleumsforening, Doré, A.G., Sinding-Larsen, R. (Eds.), Quantification and Prediction of Hydrocarbon Resources: Proceedings of the Norwegian Petroleum Society Conference, 6-8 December 1993, Stavanger, Norway, Norwegian Petroleum Society (NPF) Special Publication. Elsevier, Amsterdam ; New York, pp. 105–114.

Smith, W.H.F., Sandwell, D.T., 1997. Global Sea Floor Topography from Satellite Altimetry and Ship Depth Soundings. Science 277, 1956–1962. https://doi.org/10.1126/science.277.5334.1956

Acknowledgements

For this publication, authors expects the study results would be useful and supportive input for the PT. Pertamina Hulu Energi Anggursi management in making decision. We hope that this report is useful as a brief source of information of hydrocarbon potential in Anggursi area, especially for PT. Pertamina Hulu Energi Anggursi, as well as for further development plan by all parties.

PROCEEDINGS
JOINT CONVENTION BANDUNG (JCB) 2021
November 23rd – 25th 2021

Re-Assessment of Oil Family and Its Implication to Unlock New Exploration Opportunity in Pati Trough, North East Java Basin

Danya Zhafira[1], Iwan Bagus Indriyanto[1]; (1) Pertamina Hulu Energi Randugunting

ABSTRACT

Pati Trough is situated in the western part of North East Java Basin. Physiographically, the geometry of Pati Trough is a southwest to northeast trend with Bawean Arch in its north side and West Cepu High in its south side. This basin is categorized as a prolific basin with proven active petroleum system. Hydrocarbon accumulation are proven in some reservoirs and also as oil seepage in the surface.

There are many oil sample data from wells and oil seeps, however the knowledge of oil family in Pati Trough has not been studied comprehensively. Therefore, integrated study was performed using field data (outcrops and seepages) and well data (oil or gas sample). Biomarker approach was used to understand the type of facies, depositional environment, and maturity of source rock. Study revealed that there are at least two types of source facies that had been proven generating hydrocarbon. With those facts, other play is becoming more interesting to re-evaluate i.e. Kujung carbonates play and clastic shallow biogenic play, both of which have not been proven, and it can unlock exploration opportunities in Pati Trough.

Keywords: Biomarker, new target of exploration, Pati Trough, source facies

INTRODUCTION

North East Java basin has been known as one of the basins in Indonesia that has successfully prove its capability of producing oil and gas from almost every formation, mostly in Ngrayong, Tuban, Kujung, and Ngimbang Formation. The Ngimbang Formation itself has not only been known as a reservoir rock, instead it is more often theorized as source rock that is responsible for hydrocarbon expulsion in the area. A number of oil and gas discovery wells are believed to have its reservoir being charged from a source pod in Ngimbang Formation. However, oil family evaluation particularly in Pati Trough area has not been carried out. Thus, geochemistry evaluation is necessary to find out which source rock the hydrocarbon might be generated from and how many oil families there are in this area.

Regional Geological Framework

Java is situated in the south margin of Sunda Plate, in the southeast of Eurasian Plate where Indo-Australia plates subducted in its south during Pre-Tertiary and activated volcanism activity (Ardana, 1993; Sribudiyani et al., 2003; Hall, 2002 in Hall, 2005). Two major structural trends in East Java area are the E-W Sakala trend and NE-SW Meratus trend (Sribudiyani, et al., 2003). East Java basin developed from Late Cretaceous subduction zone to a back-arc basin behind volcanic arc to its south and consists of a series of NE-SW grabens and horsts such as Karimunjawa Arch, Muria Trough, Bawean Arch, Pati Trough, Purwodadi or West Cepu High, and Kening Trough from north to south respectively (Satyana and Djumiati, 2003). Oil and gas generation, migration, and accumulation are related to the present structural framework as the result of intense Paleogene and Neogene tectonic and sedimentologic events (Satyana and Purwaningsih, 2002).

Tectonostratigraphy of the East Java Basin is broadly divided into five tectonic events (Mudjiono and Pireno, 2001), begun with syn-rift depositional system during Paleogene period where terrestrial sandstones were deposited followed by transgressions that changed the facies to shallow marine limestones and then deep marine shales until Early Oligocene which carbonates started deposited. Second, a compression phase during Late Oligocene that occurred as a result of subduction in the south, which caused regression and clastic carbonate sediments were deposited. Third, in Late Oligocene to Early Miocene, there was a sea level rise and limestone was deposited. Fourth, the peak of the transgression occurred in in Early Miocene where reefs and carbonates were deposited. Fifth, in Middle Miocene, a regression began to occur due to compression of the E-W trend and tectonic inversion to the initial deposition of quartz sandstone, followed by sandstone, carbonate, and shale.

Ngimbang Formation as Source Rock

Eocene Ngimbang Formation is believed to have 95% source of oil and gas resources in East Java Basin in its shale, limestone, and coal (Mudjiono and Pireno, 2001 in Fatahillah et al., 2016). In Pati Trough, Ngimbang Formation is also believed to be the main thermogenic source. Located at the north of the West Cepu High, hydrocarbons from Pati Trough kitchen are expected at the right timing to fill traps in the surrounding structures.

PROCEEDINGS
JOINT CONVENTION BANDUNG (JCB) 2021
November 23rd – 25th 2021

Brief Exploration History of Pati Trough

Taking a closer look in Pati Trough area, it is known that there had been successful drilling attempts in discovering the presence of oil during Dutch colonial era in early 1900s. After Indonesia's independence, Pertamina took over the onshore block and drilled a number of wells in which gas and condensate were finally found in 1996 (Fig. 1), along with discoveries in two other wells, as well as gas indication in few other wells in the following years.

DATA AND METHOD

Table 1 is a compilation of geochemistry data taken from onshore wells that are used in this study; 2 crude oil samples from P well, 2 oil samples from condensate of G well, an oil seep sample from T brown field, and 2 oil samples extracted from rock cuttings from S well. All samples had undergone Gas Chromatography (GC) and Gas Chromatography Mass Spectrometry (GCMS) processes and evaluated with fingerprint geochemical approaches to generate biomarker data. Biomarkers are compounds on crude oil that can be used to identify characteristics of source rock, such as lithology, geological age, type of organic matter, and redox conditions, with parameters arranged into several fractions of similar chemical compounds including alkanes and acyclic isoprenoids, sterane and diasterane, terpanes, and aromatic steroids (Peters et al., 2005). From identity of each sample, oil to oil correlation was performed as a method to distinguish oil families in research area and correlation to the rock sample was also carried out to determine the source rock of those oil samples.

Alkanes and Isoprenoids

GC interpretation on alkanes and isoprenoids distribution can provide an indication of the source of organic material (Peters et al., 2005) and height of low carbon value indicates whether crude oil sample has matured. The value of Pristane (Pr) to Phytane (Ph) is a common ratio for indications of depositional environment where a value of more than 3 indicates an environment with oxic conditions, meanwhile value of less than 0.8 indicates an anoxic condition, and values of in between might indicate sub-oxic conditions (Ten Haven et al., 1987 in El Nady, 2014). The crossplot between Pr/n-C17 and Ph/n-C18 can also determine organic materials of the crude oil (Peters et al., 2005).

Steranes

Interpretation of sterane, particularly m/z 217 ion, can be done by observing diasterane in which high level of diasterene indicates shale lithology and low level of diasterane indicates carbonate lithology. Interpretation can also be done by looking at the dominant value between C27 and C29 sterane where C27 dominance indicates marine environment and C29 dominance indicates terrestrial environment (Hunt, 1996 in El Nady et al., 2014). A ternary plot diagram of C27-C28-C29 sterane is also able determine depositional environment (Huang and Meinschein, 1979 in Syaifudin, 2017). A crossplot of C29 $\alpha\beta\beta/(\alpha\alpha\alpha+\alpha\beta\beta)$ with C29 S/(S+R) sterane can be made to reveal maturity level of the organic matter since both sterane ratios increase with increasing thermal maturity (Peters et al., 2005).

Triterpanes

Triterpanes are considered as a powerful tool for correlations due to its resistance to biodegradation (Hunt, 1996 in Nady et al., 2015). Interpretation of triterpanes, particularly m/z 191 ion, can be done by observing whether it has a high trycyclic terpanes as an indicator of marine source rock (Waples, 1991 in Nady et al., 2014), the irregular trend of homohopanes (C31-C35) also indicates carbonate source rock. Ratio of trisnorneohopane (Ts) to trisnorhopane (Tm) indicates more mature oil if Ts is higher than Tm (Hunt, 1996 in Nady et al., 2014). Ratio of C29 norhopane to C30 hopane indicates lithology origin where values of less than 0.5 indicates shale and values of more than 1 indicates carbonate (Waples and Machihara, 1991 in El Nady et al., 2014). Ratio of Oleanane to Oleanane+C30 hopane (Ol/Ol+hopane) with value of more than 0.2 indicates a source of Tertiary age, while value of less than 0.2 indicates a source of Cretaceous age (Peters et al., 1999 in Satyana and Purwaningsih, 2003). C30 moretane/hopane is directly proportional to level of maturity (Waples and Machihara, 1991 in Hakimi et al., 2011). Finding range of thermal maturity can be obtained from Ts/Tm versus moretane/hopane (Mackenzie et al., 1980; Seifert and Moldowan 1986, in Hakimi and Najaf, 2016).

Aromatics

Interpretation of aromatic steroids from GC, the peak height of phenanthere (m/z 178) and methylphenanthrene (m/z 192) in particular, can be used to calculate Methylphenantherene Index (MPI) (Peters et al., 2005), in which a value of vitrinite reflectance called Ro Calculated (Rc) can be obtained from the MPI (Radke et al., 1983 in Hatta, et al., 2013) to be used as maturity indication parameter. MPI-1 versus MPI-2 crossplot is used to determine maturity level (Sonibare et al., 2008 in Fatah, 2014).

RESULT AND DISCUSSION

Lithology

Being characterized roughly by its high diasterane, P and T oil samples are indicated to be originated from a lithology of shale (Fig. 3). The norhopane to hopane ratio shows a very clear distinction, P oil samples have values ranging from 0.52 to 0.65 which supports interpretation of shale as source lithology. In contrast, G oils samples have a ratio of norhopane to hopane on a range of 0.89 to 1.17 which indicates carbonate or marl lithology (Table 1) and a slightly low diasterane (Fig. 3). Regardless, it was observed that there were

no irregular trends on homohopanes which suggests that the lithology is not from carbonate rocks (Fig. 4).

Source Facies and Depositional Environment
Interpretation on the trend of n-alkane and isoprenoid distribution shows an indication of a fluvio-deltaic origin on P oil samples, meanwhile G oil samples show more of a marine origin (Fig. 2). P oil samples have high value of pristane to phytane ratio which is more than 3 and that is indication of source rock that was deposited under oxic condition, whereas G oil samples shows low pristane to phytane with value lower than 3 but more than 0.8 which indicates a source rock that was deposited under sub-oxic condition (Fig. 2; Table 1). Likewise, n-alkane and isoprenoid crossplot showed that P oil samples are dominantly derived from terrestrial organic matter, meanwhile G oil samples have mixed organic source (Fig. 6).

Sterane ternary diagram shows two different cluster of depositional environment (Fig. 7). First cluster is the P and T oil samples with higher concentration of C29 compared to C27 sterane which suggests that oils are related to terrestrial depositional environment (Fig. 3; Table 1), furthermore its sterane distribution have a relatively ascending trend (Fig. 3). Second cluster is the G oil samples that have higher concentration of C27 compared to C29 sterane which indicates that oils are related to estuarine depositional environment (Fig. 3; Table 1) and supported by a relatively descending trend in sterane distribution (Fig. 3).

Maturity and Geological Age
All oil samples indicate that oil are not fully mature, represented by low value of the low carbon on gas chromatograms (Fig. 2). Maturity indicator from sterane crossplot shows that all oil samples are early mature (Fig. 8). Maturity indicator from triterpane crossplot is showing the same result (Fig. 9). Lower Ts compared to Tm is also indicating a less mature oil (Fig. 4; Table 1). Aromatic maturity indicator using MPI revealed that P and T oil samples are more mature than oil samples of G (Fig. 10). Ratio of oleanane to oleanane and hopane shows that all oil samples have a value higher than 20% which indicates Tertiary age (Fig. 4; Table 1).

Extracted Oil from Rock Samples
All rock extract samples from S well plotted on the n-alkane and isoprenoid crossplot are indicating a source deposited under oxic conditions with predominance of terrestrial organic matters input (Fig. 11). Ratio of pristane to phytane showing that both rock samples have values of more than 3 which indicates depositional environment with oxic conditions (Fig. 3, Table 1). The sterane ternary diagram, however, revealed a different outcome where the Kujung rock sample has indication of being deposited in marine-estuarine environment, while Ngimbang rock sample has indication of being deposited in terrestrial-fluviodeltaic environment (Fig. 12). Ratio of norhopane to hopane has a value of 0.64 for Kujung sample and 0.59 for Ngimbang sample which indicates that both samples were originated form a lithology of shale (Table 1).

In a previous study on the Vitrinite Reflectance of Kujung Formation samples from P well, it has already been confirmed that Ro percentage in some of the Kujung interval had not matured and some had just entered the mature stage, with Ro ranging from 0.47 to 0.58. Accordingly, Kujung source rock was classified as early mature (Fig. 13). This data could offer an idea that the oil charging to G condensate samples of Ngrayong Formation were generated from an early mature Kujung calcareous shale or marl. From this data, it can be inferred that in Pati Trough area, source rock is not solely from Ngimbang Formation that were found from most oil in the area, but also from younger formation such as the Kujung Formation.

Biogenic Source Potential
Prior to this study, there had been a study on the sedimentology characters of Ngrayong and Tuban Formation in Pati Trough that had found a content of gypsum, coal, and/or coaly shale present in some outcrops around Pati Trough area e.g. in Ngampel, Mantingan, Soko, Kajar, Pasucen, and Dowan, therefore the Ngrayong Formation can be characterized by any existence of poorly cemented sandstones, tidal shale with lenticular and wavy lamination, coal layer, coaly shale, and gypsum (Purnama et al., 2018). Coal content within those outcrops initiated the idea of biogenic source potential in Pati Trough.

Gas isotope analysis had been conducted from Ngrayong and Tuban Formation gas samples of wells around Pati Trough area using gas dryness and isotope of methane calculation and the outcome is indicating a mixed source of biogenic and thermogenic in which the contribution from biogenic source is 40%. (Purnama et al., 2018). This confirmed that biogenic source had contributed to Ngrayong and upper Tuban reservoir in Pati Trough area.

New Potential Play
In Pati Trough area, Kujung carbonates play had not yet discovered its hydrocarbon presence. The proven Kujung calcareous shale or marl source rock could unlock new potential prospects from Kujung carbonates play e.g. Oligocene to Miocene carbonates in the northernmost part of Pati Trough onshore area and some other Kujung Formation clastics and carbonates in the southern part. Hydrocarbon from Kujung source rock have the tendency to migrate laterally to those reservoirs as it was closer in

comparison to the Eocene Ngimbang source rock (Fig. 14).

Other new potential play is biogenic play for shallow reservoirs such as in Ngrayong Formation or younger that had been seen on seismic in many areas of Pati Trough. Highlighting its narrower age and stratigraphic setting compared to the older source rocks, Ngrayong biogenic-thermogenic mixed source rock is potential to charge hydrocarbon to those shallow reservoirs.

CONCLUSIONS

More than one cluster of oil family can be obtained from all of the examined samples taken from wells in Pati Trough area. All P and T oil samples have negative correlation with G oil samples. Therefore, at least two oil families can be distinguished and those are Tertiary terrestrial-fluviodeltaic shale sourced and Tertiary marine-estuarine calcareous shale or marl sourced.

Overall, Kujung and Ngimbang Formation are the possible thermogenic source rocks in Pati Trough area and have the contribution in generating oil that was found in the Miocene Ngrayong and Tuban Formation reservoir. P and T oil samples are positively correlative to the Ngimbang source rock from S well. G oil samples are positively correlative to Kujung source rock from S well. In addition to the thermogenic source from Ngimbang and Kujung Formation, Ngrayong Formation is also potential to generate hydrocarbon from a contribution of biogenic source.

REFERENCES

El Nady, M. M., Harb, F. M., Mohamed, N. S., 2014, Journal of Egyptian Journal of Petroleum

El Nady, M. M., Mohamed, N. S., Sharaf, L. M., 2015, Journal of Egyptional Journal of Petroleum

Fatah, S. S., 2014, Journal of University of Sulaimani

Fatahillah, Y., Hilyah, A., Utama, W., 2016, Journal of Jurnal Teknik Institut Teknologi Sepuluh Nopember

Hakimi, M. H., Abdullah, W. H., Shalaby, M. R., 2011, GeoArabia, vol. 16

Hakimi, M. H., Najaf, A. A., 2016, Journal of Elsevier Marine and Petroleum Geology 78 (2016) 547-561

Hatta, M. I., Emrizal, M. T., Anita, S., 2013, Proceedings of Semirata FMIPA Universitas Lampung

Mudjiono, R., Pireno, G. E., 2001, Proceedings of Indonesian Petroleum Association 38th Annual Convention and Exhibition

Peters K.E., Walters, C.C., Moldowan, J.N., 2005, Book of Cambridge University Press

Purnama, Y. S., Gunawan, A., Darmawan, W., Rohmana, R. C., Adipradipto, D., Halim, J., Julias, R. H., Rahmanto, B., 2018, Proceedings of Indonesian Petroleum Association 42nd Annual Convention and Exhibition

Satyana, A. H., Purwaningsih, M. E. M., 2002, Proceedings of Indonesian Association of Geologists 31st Annual Conference

Satyana, A. H., and Djumiati, M., 2003, Proceedings of American Association of Petroleum Geologists International Conference

Smyth, H., Hall, R., Hamilton, J., Kinny, P., 2005, Proceedings of Indonesian Petroleum Association 30th Annual Convention and Exhibition

Sribudiyani, Muchsin, N., Ryacudu, R., Kunto, T., Astono, P., Prasetya, I., Sapiie, B., Asikin, S., Harsolumakso, A. H., Yulianto, I., 2003, Proceedings of Indonesian Petroleum Association 29th Annual Convention and Exhibition

Syaifudin, M., 2017, Journal of Journal of Geoscience, Engineering, Environment, and Technology, vol. 1

ACKNOWLEDGEMENTS

Authors wish to thank the management of PHE Randugunting for the data publication permission and support, the geoscientists of PHE Randugunting exploration team for the valuable discussions and insights during analyses, PPPTMGB Lemigas and Badan Afiliasi Teknologi Mineral Universitas Trisakti for conducting the Gas Chromatograms and Mass Spectrometry evaluation in the geochemistry laboratory for tbe studied oil samples in this paper, and IHS Markit for providing reserve cumulative as an overview of past exploration in the area of study in this paper.

PROCEEDINGS
JOINT CONVENTION BANDUNG (JCB) 2021
November 23rd – 25th 2021

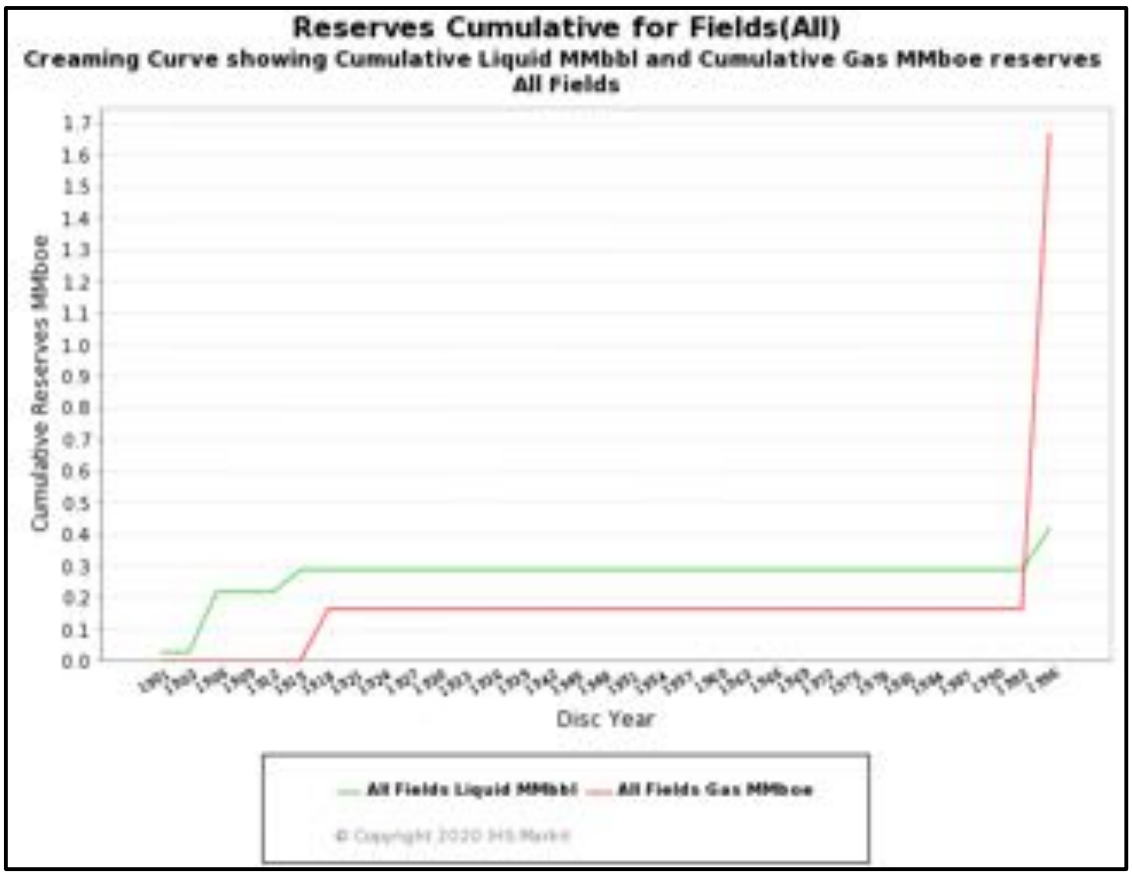

Figure 1 Year 1901-1996 Reserves Cumulative of Fields in Pati Trough Area (IHS Markit, 2020)

Table 1 Geochemical Characteristics of Crude Oils and Source Rock Extracts

No	Well	Sample	Reservoir Age	Bulk Oil Characteristic			Whole Oil Fraction			GC		
				API Gravity at 60°F	Sulphur	Wax	Saturates	Aromatic	NSO	Pr/Ph	Pr/nC17	Ph/nC18
1	P	Crude Oil Sample A	Early Miocene Tuban Carbonate	52.27	0.12	14.08	31.99	2.69	65.32	3.72	1.35	0.38
2	P	Crude Oil Sample B	Early Miocene Tuban Carbonate	46.43	0.12	15.17	41.02	4.63	54.35	3.23	1.62	0.31
3	T	Oil Seep Sample	Early Miocene Tuban Carbonate	21.86	0.13	19.21	54.81	15.58	29.61	3.12	0.83	1.10
4	G	Condensate Sample A	Middle Miocene Ngrayong Sandstone	-	-	-	26.48	3.26	70.26	2.13	1.01	0.59
5	G	Condensate Sample B	Middle Miocene Ngrayong Sandstone	-	-	-	1.0	0.05	99.0	1.35	2.53	1.79
6	S	Extracted Oil from Rock	Early Miocene Kujung Shale	-	-	-	64.00	10.00	26.00	5.42	2.23	0.45
7	S	Extracted Oil from Rock	Early Miocene Ngimbang Shale	-	-	-	40.40	4.10	55.50	4.44	2.97	0.67

No	Well	Sample	Reservoir Age	Sterane					
				Diasterane /Sterane	C27	C28	C29	C29 S/(S+R)	C29 αββ/ (ααα+αββ)
1	P	Crude Oil Sample A	Early Miocene Tuban Carbonate	0.51	14	22	64	0.37	0.31
2	P	Crude Oil Sample B	Early Miocene Tuban Carbonate	0.46	18	21	61	0.32	0.31
3	T	Oil Seep Sample	Early Miocene Tuban Carbonate	0.34	7	24	69	0.39	0.29
4	G	Condensate Sample A	Middle Miocene Ngrayong Sandstone	0.53	43	30	26	0.34	0.32
5	G	Condensate Sample B	Middle Miocene Ngrayong Sandstone	0.43	37	27	36	0.32	0.32
6	S	Extracted Oil from Rock	Early Miocene Kujung Shale	0.25	28	29	43	0.32	0.43
7	S	Extracted Oil from Rock	Early Miocene Ngimbang Shale	0.25	19	27	54	0.42	0.53

No	Well	Sample	Reservoir Age	Triterpane				MPI			Carbon-13 Isotope	
				Tm/Ts	C29/C30	C30 Mor/Hop	Ol/C30 Hop	MPI-1	MPI-2	Rc	Saturates	Aromatic
1	P	Crude Oil Sample A	Early Miocene Tuban Carbonate	1.04	0.65	0.14	0.78	0.71	0.71	0.83	-	-
2	P	Crude Oil Sample B	Early Miocene Tuban Carbonate	1.09	0.64	0.14	0.72	0.75	0.75	0.85	-	-
3	T	Oil Seep Sample	Early Miocene Tuban Carbonate	1.00	0.52	0.15	0.84	0.73	0.75	0.84	-	-
4	G	Condensate Sample A	Middle Miocene Ngrayong Sandstone	1.04	0.89	0.16	0.43	0.33	0.36	0.60	-26.8	-24.1
5	G	Condensate Sample B	Middle Miocene Ngrayong Sandstone	1.19	1.17	0.12	0.27	0.64	0.78	0.78	-26.0	-23.2
6	S	Extracted Oil from Rock	Early Miocene Kujung Shale	1.92	0.64	0.27	0.38	0.50	-	0.70	-26.1	-26.2
7	S	Extracted Oil from Rock	Early Miocene Ngimbang Shale	1.82	0.59	-	0.65	0.49	-	0.69	-27.2	-25.8

PROCEEDINGS
JOINT CONVENTION BANDUNG (JCB) 2021
November 23rd – 25th 2021

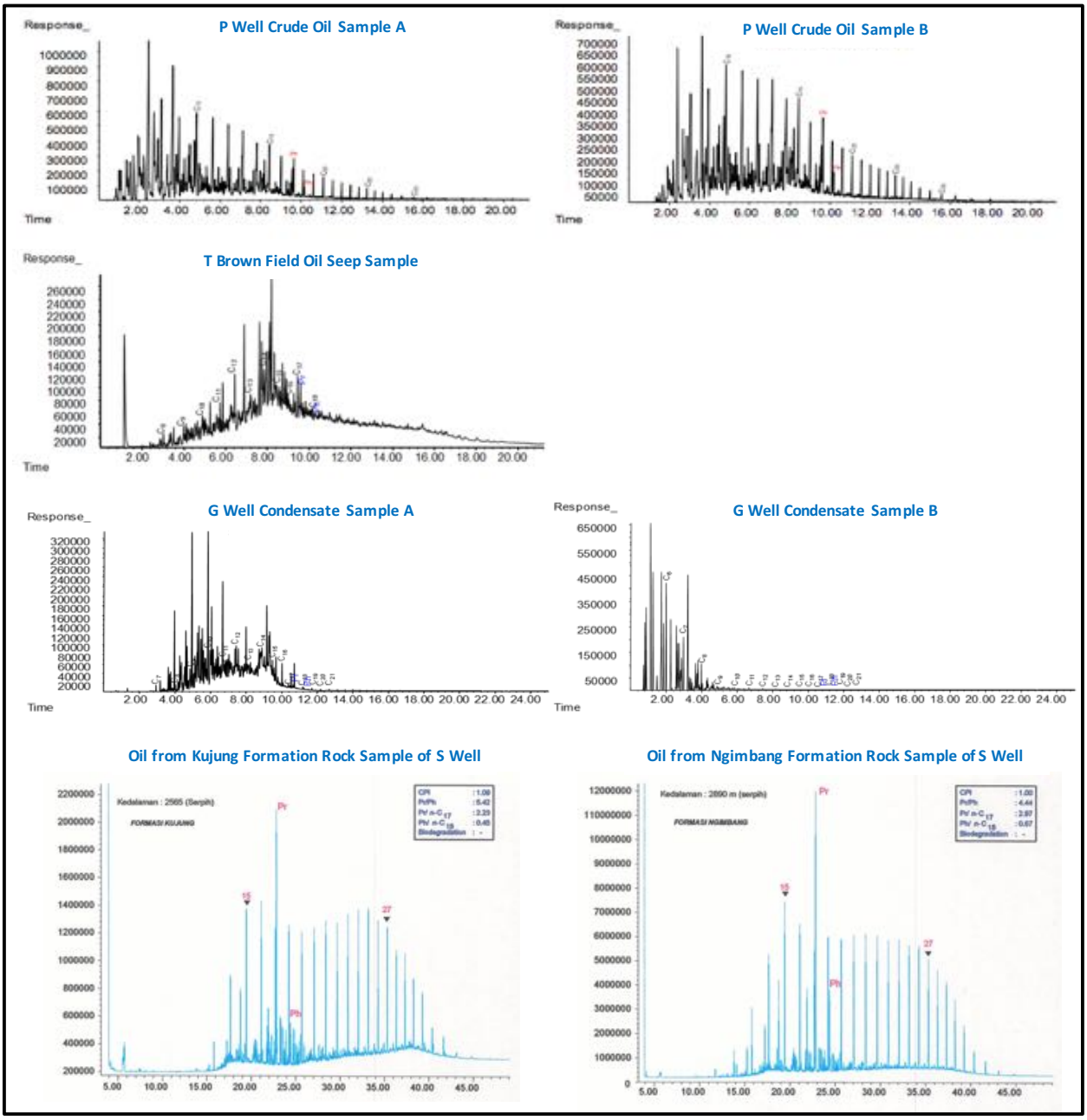

Figure 2 Gas Chromatograms Showing n-Alkane and Isoprenoid Distribution

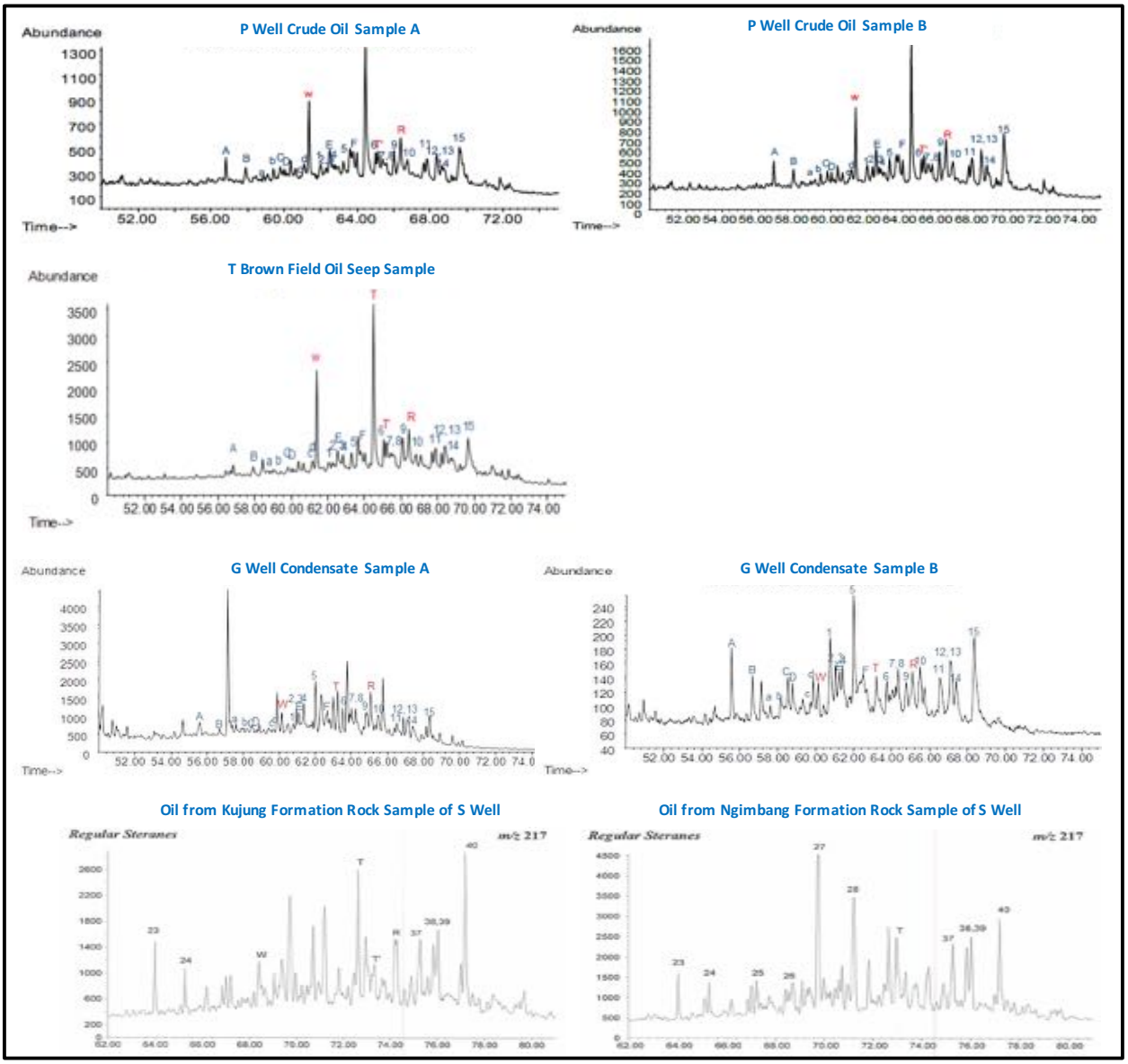

Figure 3 Gas Chromatograms-Mass Spectrometry (m/z 217) Showing Sterane Distribution

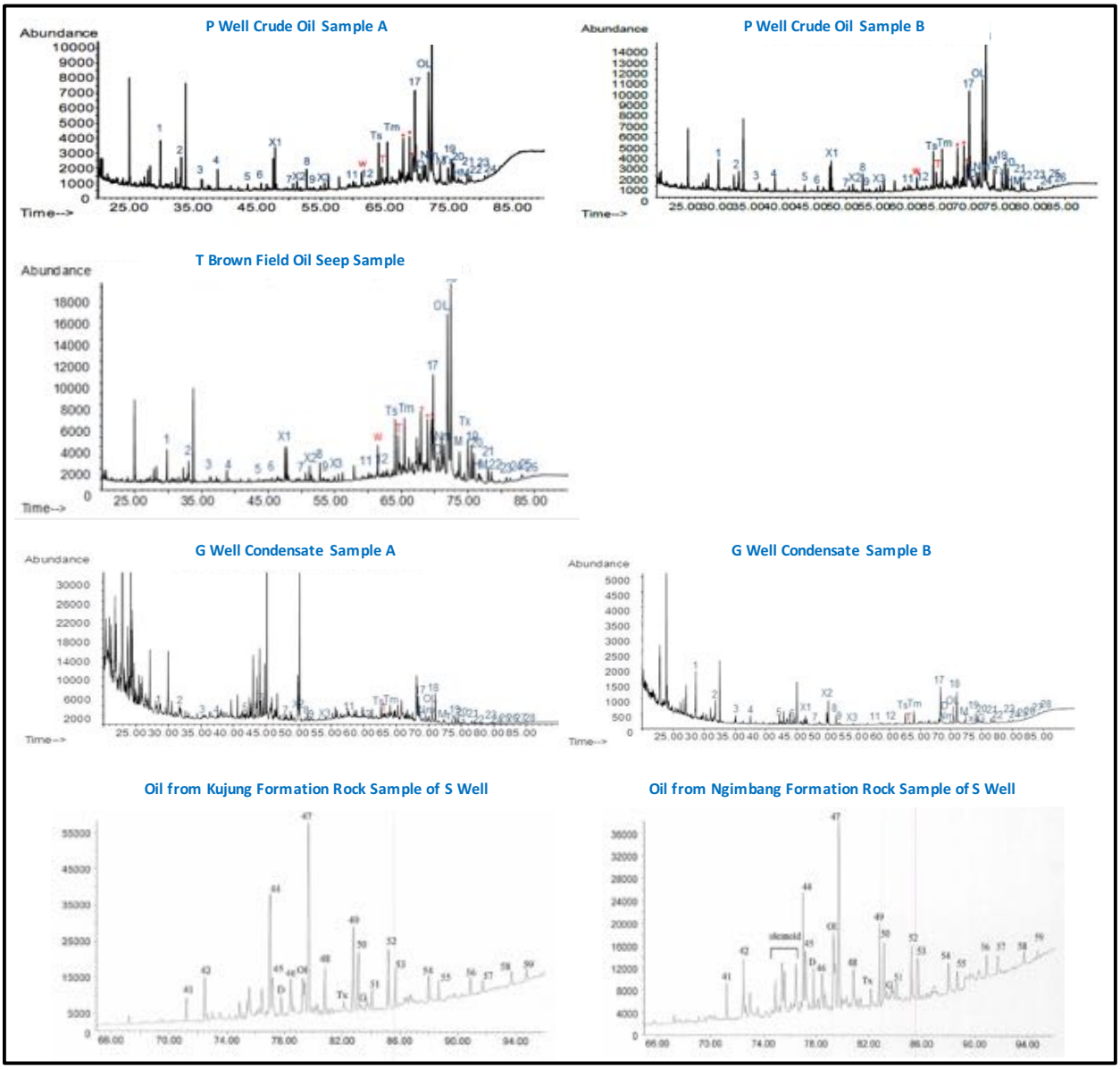

Figure 4 Gas Chromatograms-Mass Spectrometry (m/z 191) Showing Triterpane Distribution

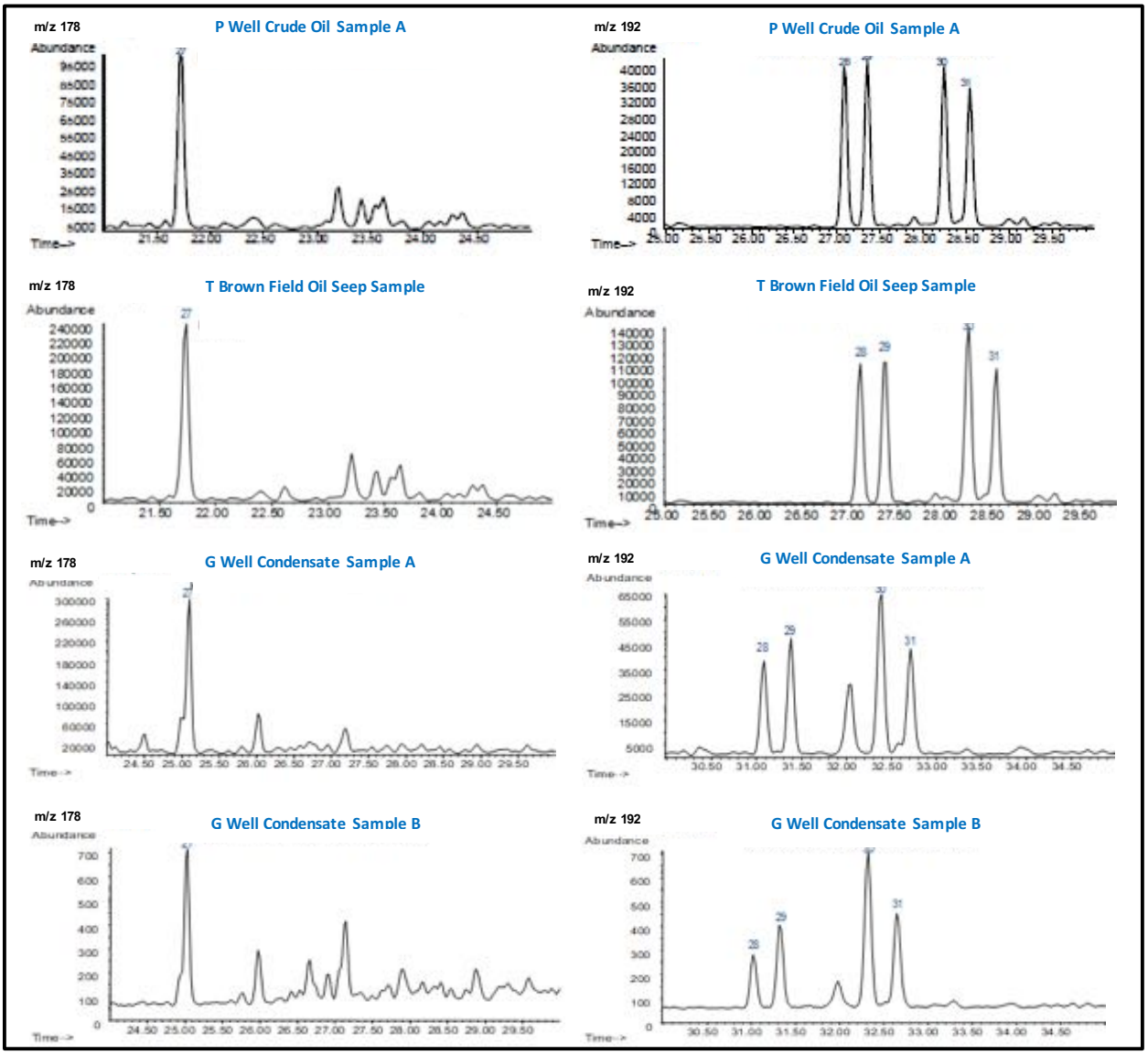

Figure 5 Aromatic Steroid Chromatograms (m/z 178 and m/z 192) Showing Phenanthrene Distribution

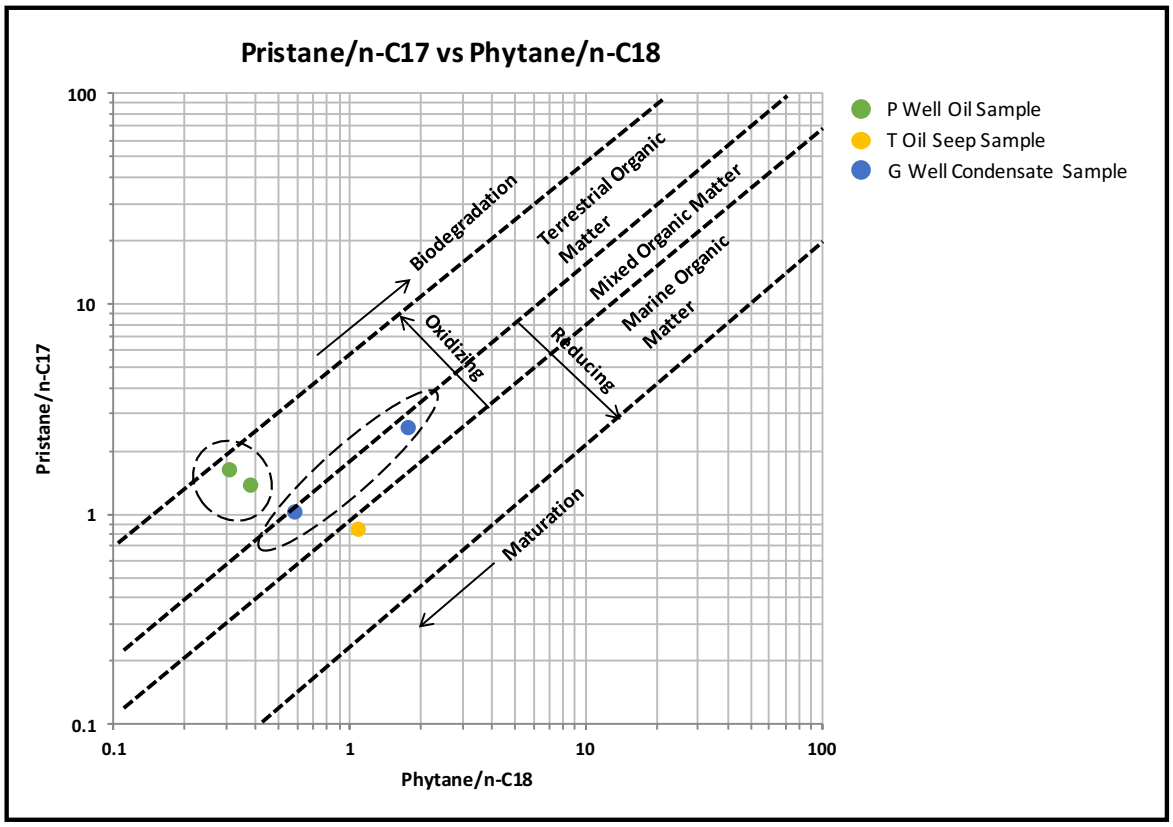

Figure 6 n-Alkane and Isoprenoid Organic Matter Input and Oxidizing/Reducing Environment Crossplot

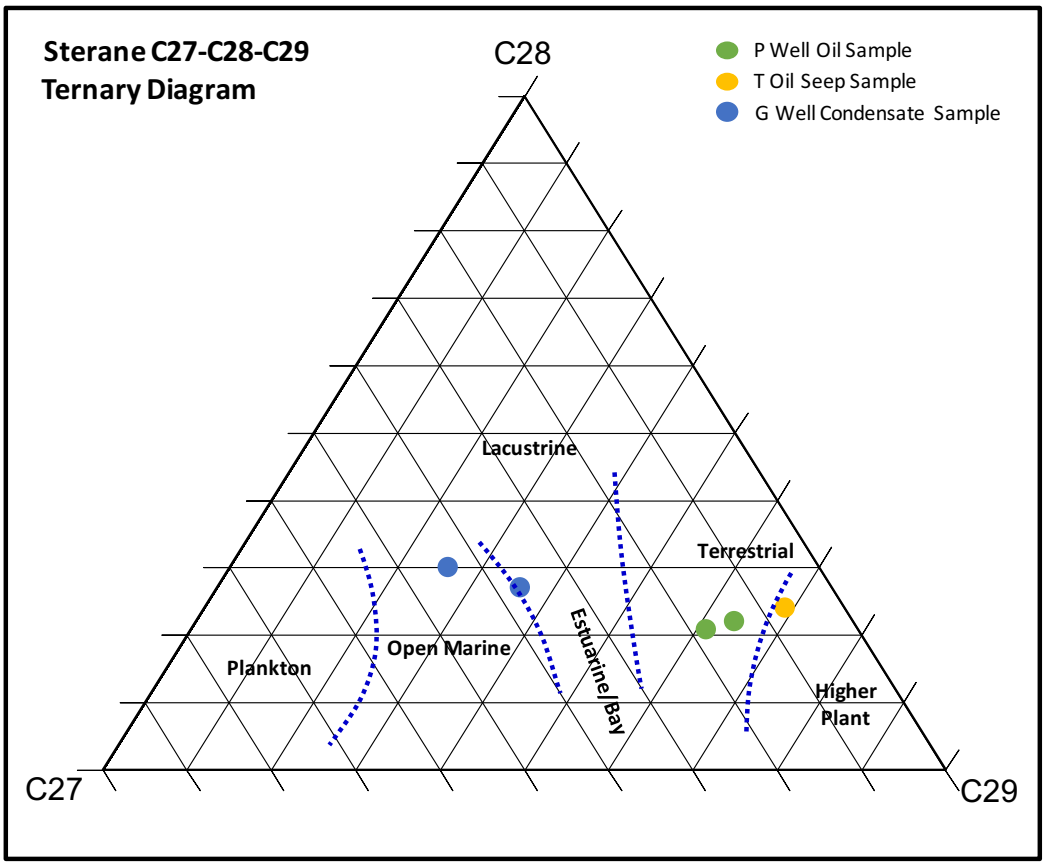

Figure 7 Sterane Depositional Environment Diagram

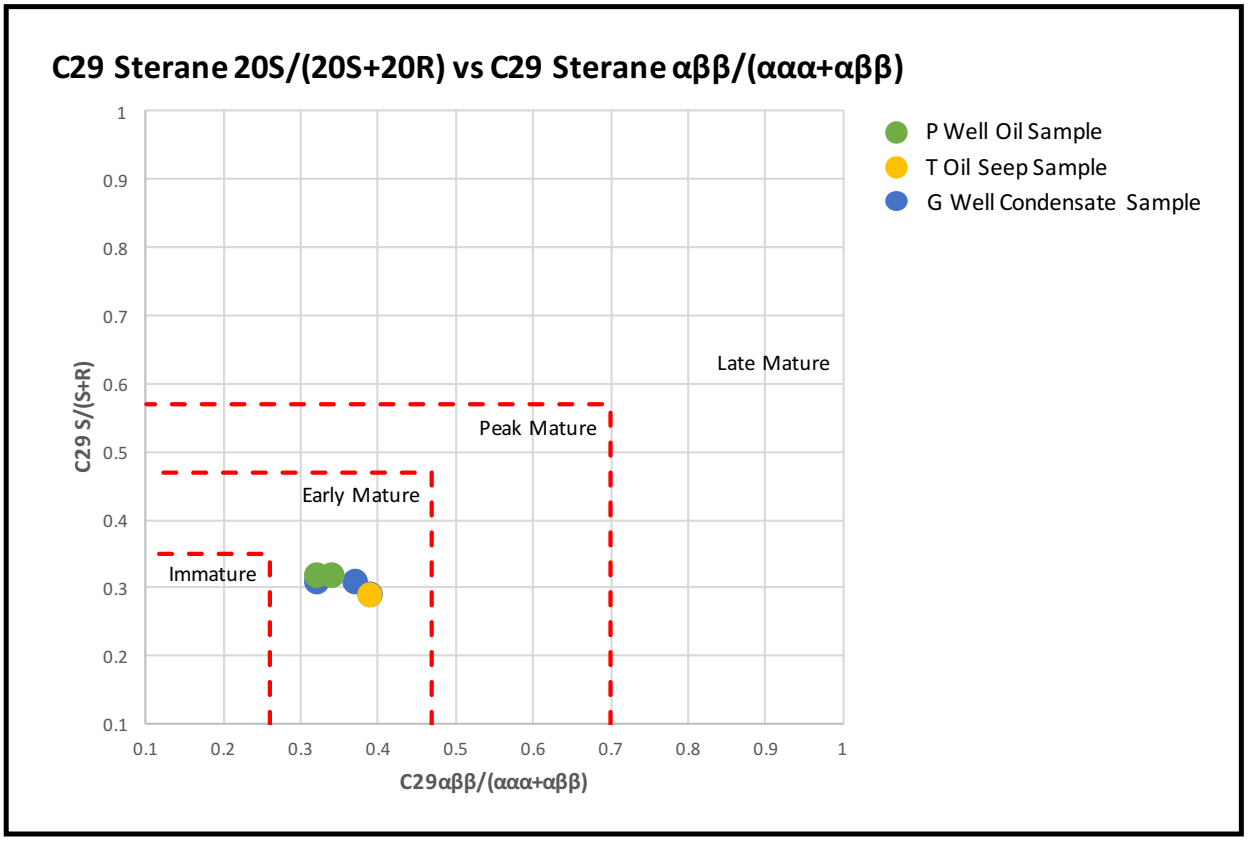

Figure 8 Sterane Maturity Indicator Crossplot

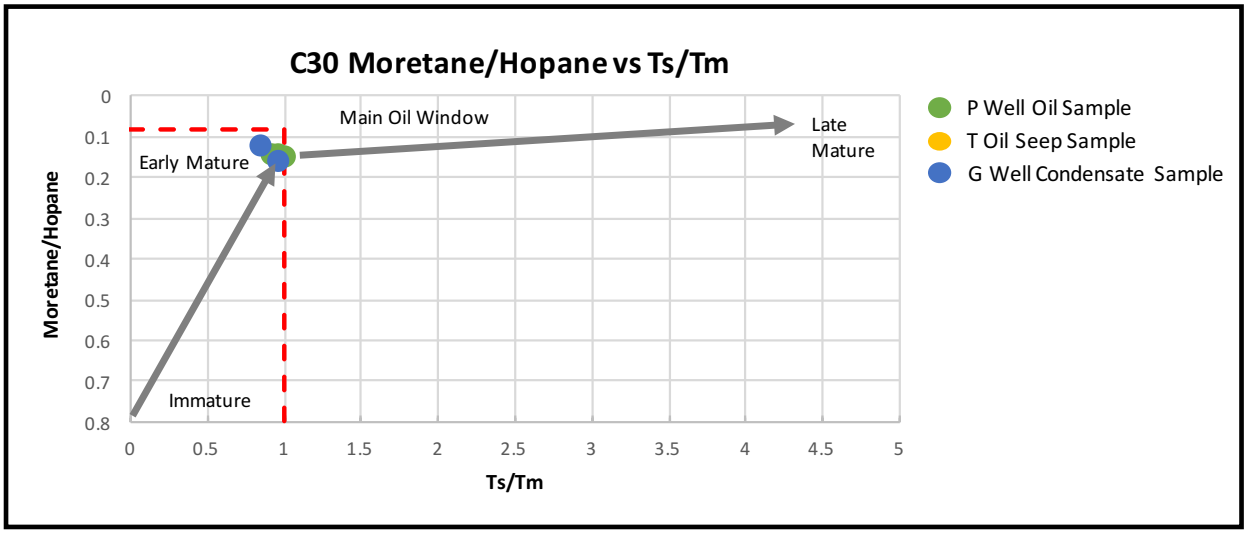

Figure 9 Triterpane Maturity Indicator Plot

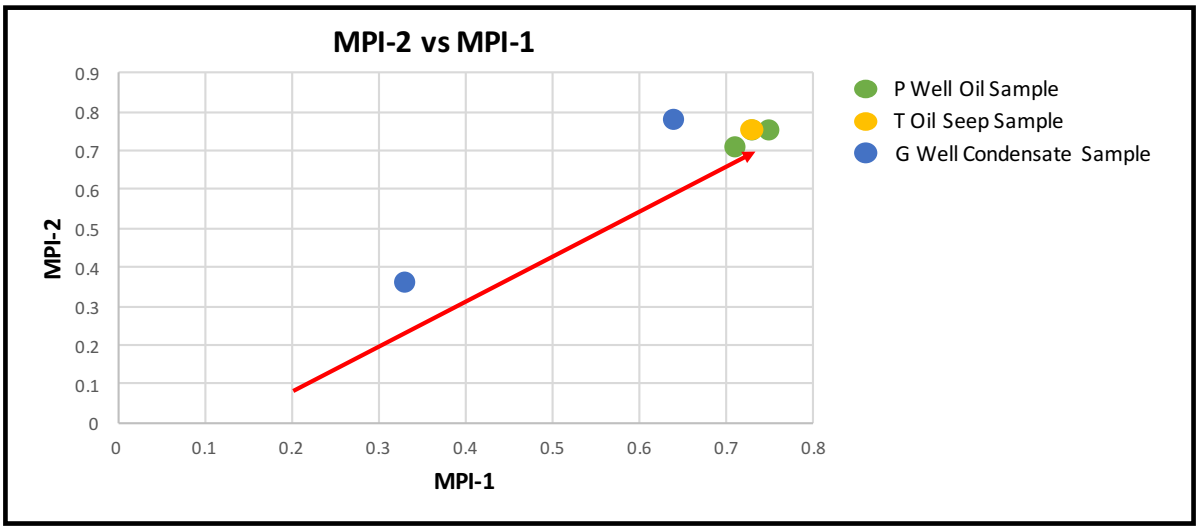

Figure 10 Aromatic Maturity Indicator

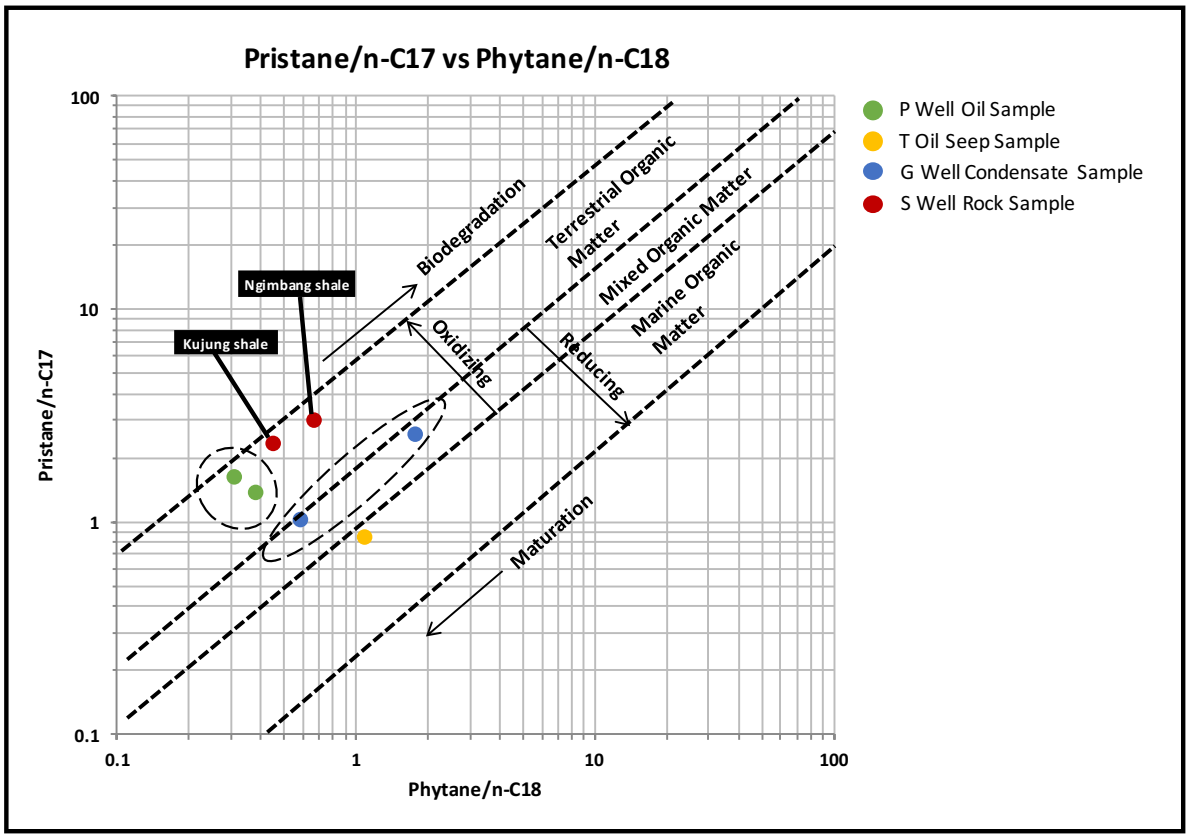

Figure 11 n-Alkane and Isoprenoid Organic Matter Input and Oxidizing/Reducing Environment Crossplot

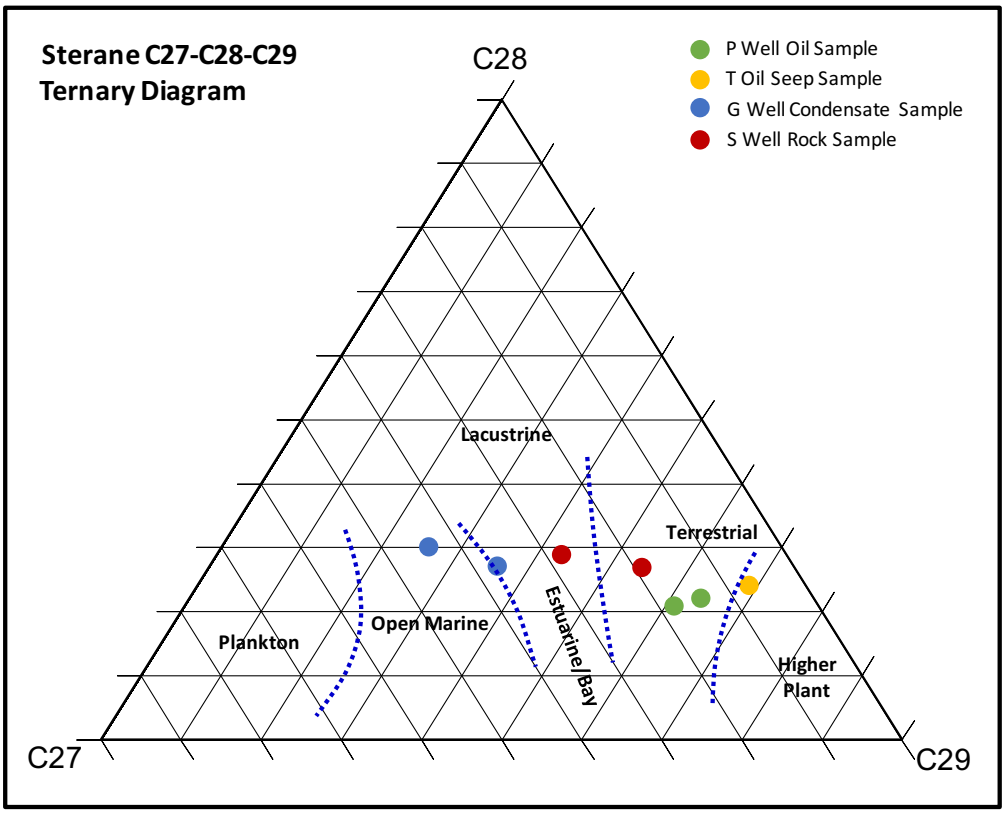

Figure 12 Sterane Depositional Environment Ternary Diagram

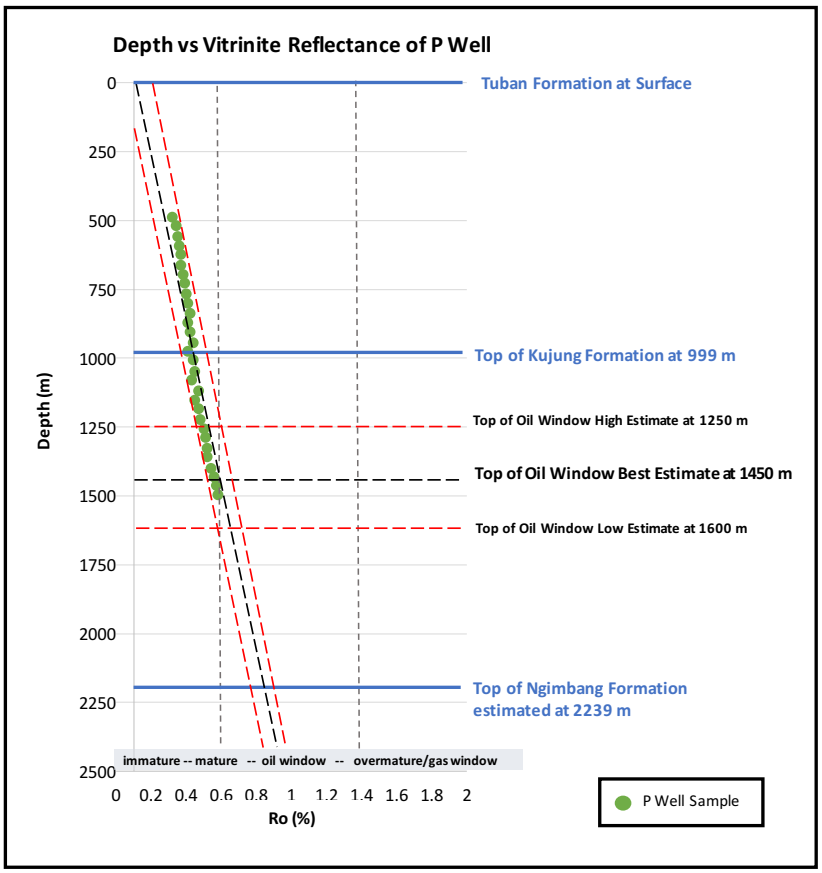

Figure 13 Maturity Profile of P Well Vitrinite Reflectance

PROCEEDINGS
JOINT CONVENTION BANDUNG (JCB) 2021
November 23rd – 25th 2021

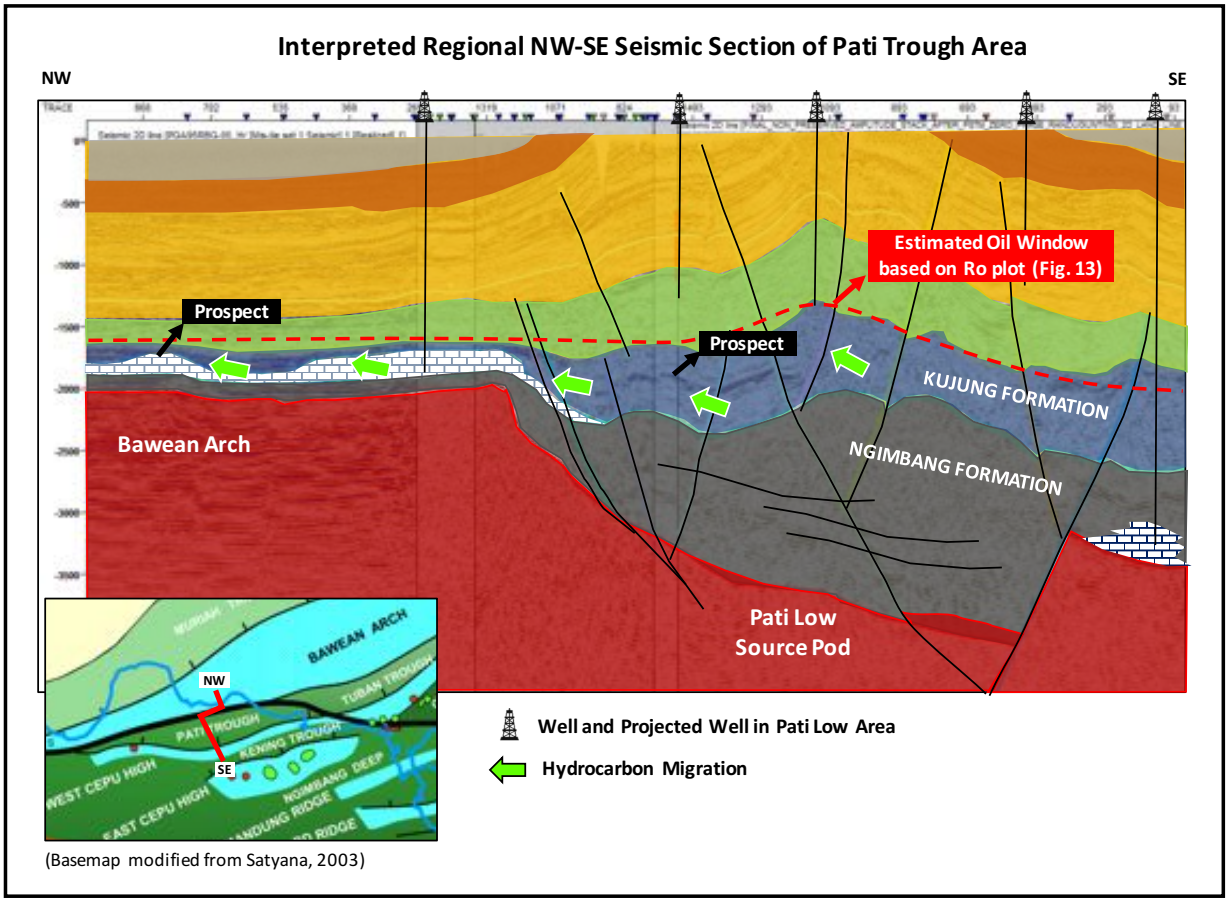

Figure 14 Regional Section Showing Hydrocarbon Migration of Kujung Source Rock to Surrounding Kujung Formation Play

PROCEEDINGS
JOINT CONVENTION BANDUNG (JCB) 2021
November 23rd – 25th 2021

Understanding Source Rock Expulsion at the Edge of Jambi Sub-Basin: Comparison between Ketaling Deep, Gelam Deep and Merang Deep

Belmesty Kamila (1), Yudhistira Shaylendra (2), Asep Heri Patria Kesumajana (3), Arya Nugraha (1), Andri Akbar (1), Mohammad Fery Mustofa (1), Dody Apriadi (1), Ardi Yoga Pradana (1), Haryo Dwi Prabowo (1).

(1) Pertamina Hulu Energi; (2) LAPI ITB; (3) Geological Engineering Study Program, Faculty of Earth Sciences and Technology, ITB

Abstract
Source rock is one of the key components in petroleum system. In South Sumatra back-arc basin, especially near the main depocenter of the basin, source rock maturity and richness are no longer an issue for the hydrocarbon exploration. Various discovered hydrocarbon fields are one of the evidence that the source rock quality and quantity is undeniable. However, on the Eastern edge of the basin, which NW-SE trending strike-slip movement is splitting the basin into multiple smaller rift basin, some might be questioning the maturation of the source rock. On the Eastern edge of Jambi Sub-Basin, South Sumatra Basin, there are several depocenters which have NE-SW direction such as Ketaling Deep, Gelam Deep and Merang Deep. In this area, Talang Akar Formation has proved as a major source rock contributing the hydrocarbon accumulation in vicinity of the basin (Kamila et. al., 2020), therefore understanding of the expulsion mechanism become more critical to adjust and examine it further.

The source rock expulsion occurred due to the increase of the heating condition during syn-rift and the loading of the younger formation as overburden burial. To illustrate the estimation of primary expulsion, one point extraction from each of the deepest depocenter area of Lower Talang Akar Formation are applied, then the extractions are validated using sonic porosity, temperature, and vitrinite reflectance of the nearest well from those extractions. The expulsion in Ketaling Deep, one of the three depocenter, is at 22.38 Ma and become the main source rock for some hydrocarbon accumulation in the northern and southern fields of the region. Applying the Vitrinite Reflectance (Ro) vs Transformation Ratio (TR) vs Expulsion Mass, it is clear that the evidence of the beginning hydrocarbon expulsion in Ketaling Deep is in the earliest of Early Miocene (*Aquitanian*). At that time, the lowest interval of Lower Talang Akar Formation has entered peak mature oil window at 0.70% Ro and only yields Transformation Ratio value as low as 9%. This expulsion mechanism becomes a prominent thing to understand the exact release of hydrocarbon from kerogen, where it is generated, until its movement into the carrier bed or migration conduit.

Keyword: Expulsion, Source Rock, Talang Akar Formation, Ketaling Deep, South Sumatra Basin.

Introduction

South Sumatra Basin is a large pull apart tertiary sediments which also a proven hydrocarbon generating basin. The basin is divided in 3 (three) Sub-Basin, from the North to the South is Jambi Sub-Basin, Central Palembang Sub-Basin, and South Palembang Sub-Basin. Those basins underwent syn-rift sedimentation during Eocene to Early Oligocene and was filled with terrigenous to mixed marine deposits which become the main source rock of the region.

In Jambi Sub-Basin, almost all of the sediment layer is proven as reservoir rock, from the Pre-Tertiary Basement, Gumai, Baturaja until Air Benakat Formation. There are about 20 oil and gas producing fields by various company in this region. Most of the fields are located nearby the main Jambi Depression, encouraged by the proven depocenter as the source of hydrocarbon generation. However, companies worked on the edge of the basin has a small chance for a long migration of the hydrocarbon from the main Jambi Depression to their acreage. Their hope comes from smaller pull apart depocenter near the edge of the basin because without the source of hydrocarbon, all others play component are futile. The intent of this study is to answer some uncertainties of the source rock expulsion.

Expulsion is a method of transferring hydrocarbon from the compacted and impermeable shale source rock to the porous and permeable carrier bed. The abundance and physicochemical characteristics of the generated hydrocarbons available for primary migration are influenced by the burial history of the source rock, the history of the geothermal gradient and the nature and initial amounts of the original organic matter (Verweij, J.M., 1993). In this research, those aspects are quantified using basin modelling software.

Data and Method

The extent of data to elaborate the study are quite massive and comprehensive from well data, final well report, previous research reports, 2D seismic and 3D seismic line. There are 30 wells data in this area, however after checking the detailed report, the available well for study are 11 wells for biostratigraphy analysis, 18 wells for general geochemical analysis, and 25 wells for temperature analysis. The 2D seismic lines are covering almost all research area, however the 3D seismic cube only covered the southern part which are the location of currently producing gas and condensate fields.

The overall workflow for this study is: (1) Build the geological framework, such as the interpretation of horizons and faults, sedimentary facies, and structural framework; (2) Integration of previous research regarding the petroleum system, such as the source rock characteristics, reservoir attribute, trapping mechanism, and prospect and lead inventory; (3) Parameter construction of the basin evolution since the making of the basin until sedimentation of each sediment layers, including calibration of input data such as well data, core dan sidewall core data, seismic data, fault data, and geochemical data; (4) Validation of some representative wells to confirm the conceptual model and also validation with the measured samples; (5) Simulation of those framework, data and parameters into the software and recheck the results.

Building the geological framework was started by surface horizon interpretation and well data calibration. The horizons are picked from Basement, Lower Talang Akar Formation, Upper Talang Akar Formation, Baturaja Formation, Lower Gumai Formation, Gumai Formation, Lower Air Benakat Formation, Middle Air Benakat Formation, Upper Air Benakat Formation, and Lower Muara Enim Formation. Based on the interpretation, the regions are undergoing three phase of deformation which are NE-SW half graben formation accompanied by the deposition of Talang Akar Formation as the syn-rift sediments. After that, the post-rift phase was happened at the time of Baturaja, Gumai, Air Benakat and Muara Enim Formation deposition. Then the syn-orogenic occurred which are dominated by the transpressional fold and resulting several positive flower structures in the area.

Integration of previous research are highly emphasized in the study of oil to oil and oil to source rock correlation. The study shows that the Lower and Upper Talang Akar Formation has a fair to excellent organic content, gas-prone with minor oil kerogen (Type II-III) and immature to late mature sediments (Kamila et al., 2020). The Lower and Upper Talang Akar rock extracts have a correlation with the Air Benakat oils and the Baturaja condensates in this area. Based on the terpane and sterane analysis, The Upper and Lower Talang Akar Foramation are deposited in mixed terrestrial-marine environment. Therefore, in the basin modeling those formation is classified as Type D/E organofacies (Terrigenous, non-marine, wax) with marine clay-rich influenced (Type II-III of kerogen) by Pepper and Corvi (1995).

Parameter constructed in the basin modelling are age vs depth curve, bathymetry vs age curve, lithology model, porosity model, compaction curve, temperature and heat flow model. The age vs depth curve is for the age estimation of each surface in every wells. Combination with the compaction curve is handful for analyzing the erosional effect due to Mio-Pliocene uplift event.

Lithology model per horizon is based on average percentage of lithology per horizon. The lithology model is essential to build burial history and maturation model because those two items depend on the lithology type. Source of the lithology model are mud log, petrography, and side wall core description.

Porosity model is one of the important parameters to reconstruct compaction curve. The compaction process in the sediment rock can be utilized as the erosion determination. The erosion is calculate based on the difference between the exponential compaction curve and porosity distribution with consideration of Normal Compaction Curve (Koesomadinata et al., 1999).

The temperature model is also one of the important factors in burial history, especially for obtaining the maturity model. From the corrected temperature, the gradient geothermal for this area is 5.6°C/100 m. It has differences about 0.5°C/100 m with the uncorrected temperature measurement.

Heat Flow model is the summary of the maturity history based on geological event occurred. The heat flow determination has considered the back-stripping effect, the compaction analysis against the porosity distribution, well temperature and Ro reading. Based on those considerations, the heat flow has peak at the early stage of post-rift, however, at the time of 10 Ma is believed as the critical factor for the heat flow rising due to the emergence of the Barisan Mountain (Figure 1). The basin begun to cool down and followed by the sagging mechanism, until reactivation of magmatism during Plio-Pleistocene occurred (2-0 Ma).

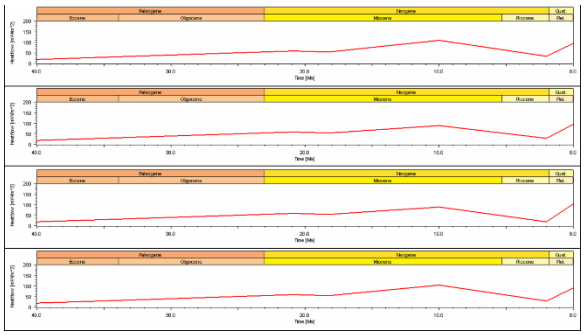

Figure 1 Heat Flow model in four wells inside the study area.

The validation of the basin modeling is conducted using porosity data, bottom hole temperature, Ro data and pressure data. The simulation of those frameworks, all data and parameters are primarily conducted in 1D thermal modeling. After the 1D basin model can represent the thermal maturity, then the 3D modeling was conducted with all input information data which derived from the 1D basin modeling analysis.

Result and Discussion

To understand about the source rock expulsion in this area, 1D basin modeling in Ketaling, Gelam, and Merang Graben are extracted with the overlay of burial history vs Ro model. The exact point locations are selected in the deepest part of each Graben (Graben depocenter). It was assumed that those locations have generated the earliest hydrocarbon generation that was charging onto the shallower intervals.

The source rock maturity from the simulation explained in several colors. White colors indicate that the source rock is immature (Ro <0.55%Ro). The dark green color shows that the source rock has just entered early mature oil window (Ro 0.55 - 0.7%Ro), the green color shows that the source rock entered peak mature (Ro 0.7 - 1.0%Ro), and the light green color shows the source rock entered the late mature (Ro 1.0-1.3%Ro). The red color indicate that the source rock entered gas window (Ro 1.3 - 2.0%Ro). The light red color indicate that the source rock entered dry gas window (Ro 2.0 - 4.0%Ro). And finally, the yellow color shows the area that the source rock is over-mature (Ro >4.0%Ro).

Based on the 1D basin modeling at Ketaling Deep (Figure 2), the basin filling was started in Late Oligocene by the Lower Talang Akar Formation, followed by the sedimentation of the Upper Talang Akar Formation which also the beginning of post rift phase. While the sedimentation kept on going until the Muara Enim Formation, the basin also undergone sagging. Since Pliocene, the graben was slightly uplifted until recently.

The Ketaling Deep started early mature oil window at the end of Oligocene while the Lower Talang Akar was deposited at >3700 m. When the Baturaja Formation was deposited, the deepest area of Ketaling Deep was entering gas window. At recent time, the Gumai Formation is in the

early mature oil window, The Upper Talang Akar is in the late mature oil window to dry gas window, while the Lower Talang Akar have entered the dry gas window to over-mature window.

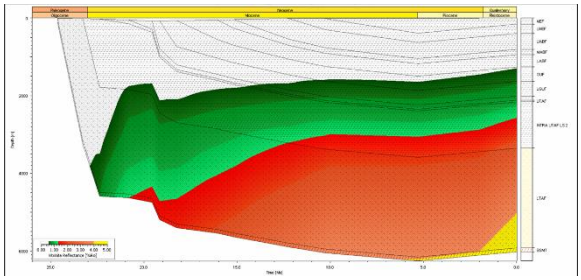

Figure 2 Extraction of 1D Basin Modeling at Ketaling Deep.

Based on the Vitrinite Reflectance (Ro) vs Transformation Ratio (TR) vs Expulsion Mass of Ketaling Deep, the earliest expulsion in Ketaling Deep as the deepest and the largest depocenter in this area occurred at 22.38 Ma. It became the main source rock for some hydrocarbon accumulation in the northern and southern fields of the region. It is clear that the evidence of the beginning hydrocarbon expulsion in Ketaling Deep was in the earliest of Early Miocene (*Aquitanian*). At that time, the lowest interval of Lower Talang Akar Formation had entered peak mature window at 0.70% Ro and yielded TR value as low as 9%.

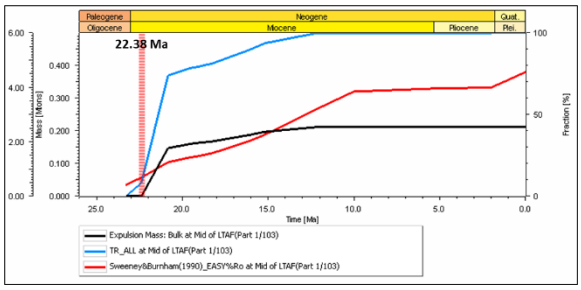

Figure 3 Vitrinite Reflectance vs Transformation Ratio vs Expulsion Mass of Ketaling Deep.

The second largest depocenter in this area is Gelam Deep, which the graben name came from the nearby gas field. The burial history events of the Gelam Deep almost the same with the Ketaling Deep, but the main difference is in the size of the basin. The Ketaling Deep can be as thick as >6000 m, while the Gelam Deep thickness is >4500 m. The Gelam Deep started early mature oil window at Early Miocene when the Upper Talang Akar was deposited (Figure 4). When the Middle Air Benakat was deposited, the deepest part of Merang Deep was entering gas window. At recent time, the Lower Air Benakat is in the early mature oil window, while the Baturaja Formation to Lower Talang Akar Formation is in the gas window.

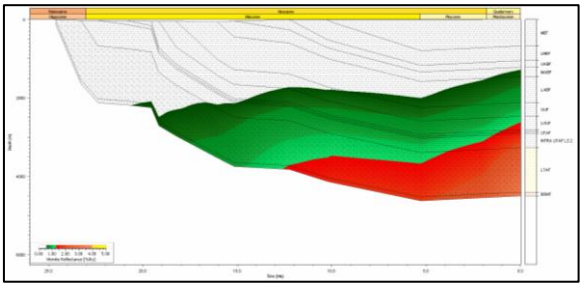

Figure 4 Extraction of 1D Basin Modeling at Gelam Deep.

The expulsion in Gelam Graben occurred at 18.11 Ma (Early Miocene/*Burdigalian*). It became the main source rock for some hydrocarbon accumulations in the Northeastern field of the graben. At that time, the lowest interval of Lower Talang Akar Formation had entered early mature window at 0.66% Ro and yielded Transformation Ratio value as low as 6%.

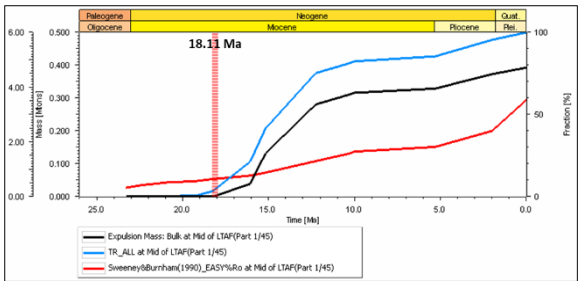

Figure 5 Vitrinite Reflectance vs Transformation Ratio vs Expulsion Mass of Gelam Deep.

The third largest and unproven depocenter in this area is Merang Deep. The thickness of the Merang Deep is about 3750 m (Figure 6). The Merang Deep started early mature oil window at Early Miocene, while the start of gas window only started in Pleistocene. At recent time the Lower Air Benakat is in the early mature oil window, the Baturaja Formation to Lower Talang Akar Formation is in the gas window maturity.

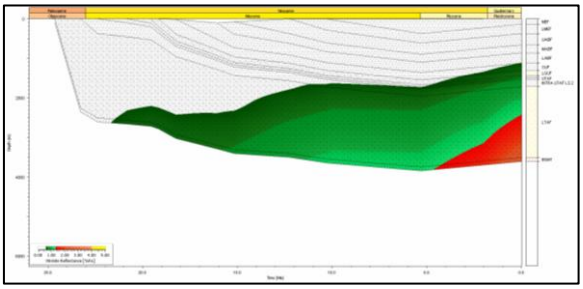

Figure 6 Extraction of 1D Basin Modeling at Merang Deep.

The expulsion in Merang Graben occurred at 15.18 Ma (Middle Miocene/*Langhian*). At that time, the lowest interval of Lower Talang Akar Formation had entered peak mature window at 0.71% Ro and yielded Transformation Ratio value as low as 9.5%.

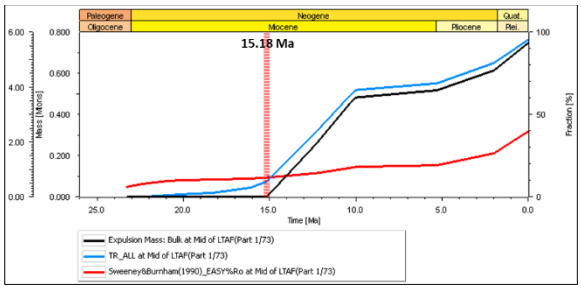

Figure 7 Vitrinite Reflectance vs Transformation Ratio vs Expulsion Mass of Merang Deep.

The summaries of the transformation ratio (blue curves) and the expulsion mass (black-grey curves) of Ketaling Deep, Gelam Deep, and Merang Deep are shown in Figure 8. Although the Ketaling Deep is the largest graben among the three grabens, it is shown that the expulsion mass increased when the rapid sedimentation around 24.65 – 23 Ma of Lower Talang Akar Formation sedimentation. The case was different with comparison of Gelam Deep and Merang Deep which started to expel hydrocarbon at Middle Miocene. It is believed that hydrocarbon products from Gelam and Merang Deep have better preservation than Ketaling Deep since the sedimentation rate of Lower Talang Akar syn-rift is lower than syn-rift deposition in Ketaling Deep.

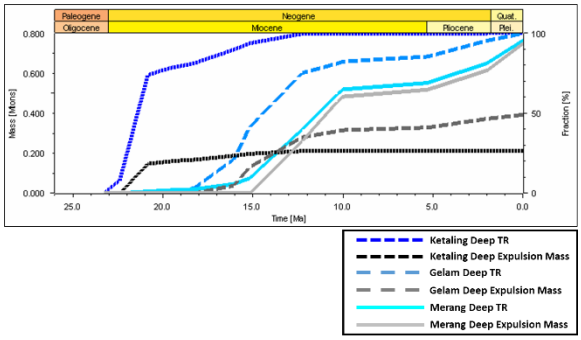

Figure 8 The comparison of Ketaling, Gelam dan Merang Deep.

The A-1 well is located at Northeastern of Gelam Deep and Southwestern of Merang Deep tested as gas with condensate well. This well is a representative well of a gas field in Jambi Sub-Basin and suspected to have gas and condensate accumulation, primarily from Gelam Deep and secondarily from Merang Deep kitchens. The A-1 well is situated on the horst block and showed as ideal petroleum system play. The 1D basin modeling from A-1 well can illustrate the data validation to support all graben extracts clarity (Figure 9).

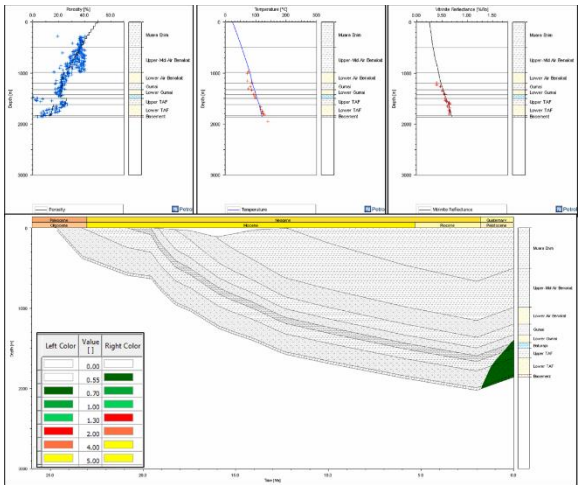

Figure 9 The 1D basin modeling profile of A-1 well.

To expand the understanding of the expulsion in all of the study area, the expulsion mass is illustrated in 3D view. The expulsion mass can also be interpreted as effective source rock expulsion, and can determine the kitchen boundary of the top of Lower Talang Akar Formation.

The top of Lower Talang Akar Formation at Top Gumai Formation Deposition (18.25 Ma) shows that the source rock expulsion only occurred at the center of the Ketaling Deep (Figure 10). When the Lower (Figure 11) and Middle (Figure 12) Air Benakat Formation were deposited, the expulsion was expanding to the greater area of Ketaling Deep, meanwhile the expulsion of Gelam and Merang Deep had not started yet at this time.

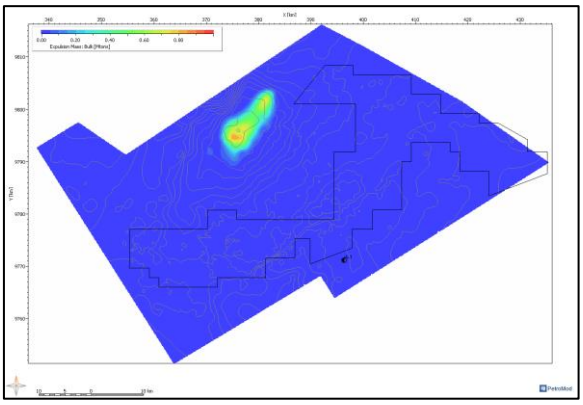

Figure 10 Expulsion mass of Top Lower Talang Akar at Top Gumai Formation Deposition Time Map (18.25 Ma).

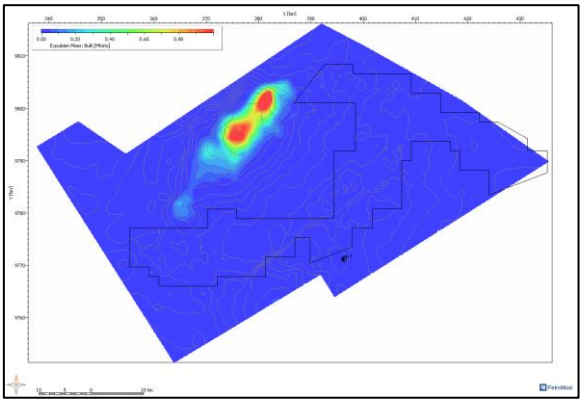

Figure 11 Expulsion Mass of Top Lower Talang Akar Formation at Top Lower Air Benakat Formation Deposition Time Map (16.07 Ma).

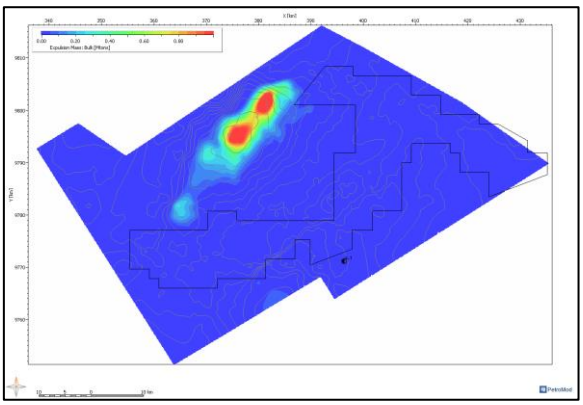

Figure 12 Expulsion Mass of Top Lower Talang Akar Formation at Top Middle Air Benakat Formation Deposition Time Map (15.18 Ma).

At 12.26 Ma while the Upper Air Benakat Formation is being deposited (Figure 13), the expulsion in Gelam dan Merang Deep at Top Lower Talang Akar Formation were start to happen, especially in the inner of depocenter. Continue to the deposition of Lower Muara Enim (Figure 14) until recent time (Figure 15), the expulsion keeps expanding to the edge of Gelam dan Merang Depocenter.

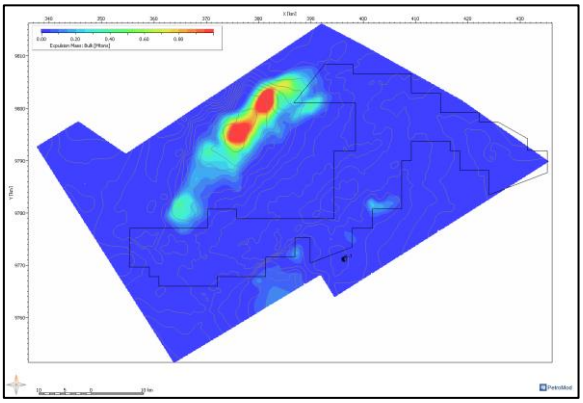

Figure 13 Expulsion Mass of Top Lower Talang Akar Formation at Top Upper Air Benakat Formation Deposition Time Map (12.26 Ma).

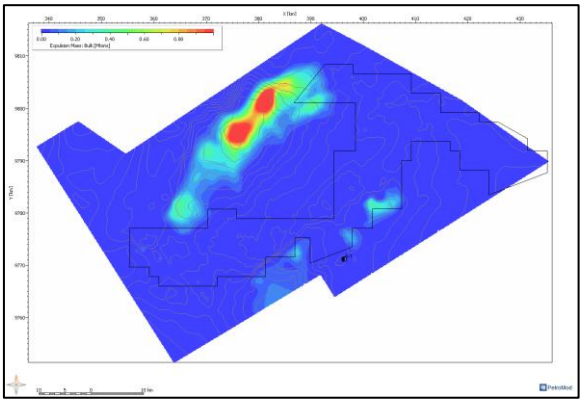

Figure 14 Expulsion Mass of Top Lower Talang Akar Formation at Top Lower Muara Enim Formation Deposition Time Map (10.30 Ma).

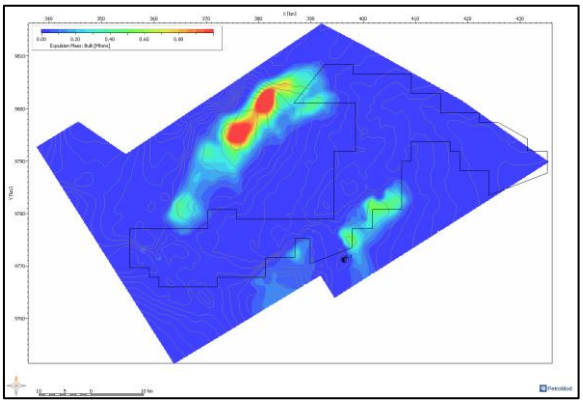

Figure 15 Expulsion Mass of Top Lower Talang Akar Formation Deposition at Recent Time Map (0 Ma).

Conclusions

Improved understanding and prediction of petroleum expulsion from source rocks are achieved and concluded by 3D basin modeling in Ketaling Deep, Merang Deep and Gelam Deep, Jambi Sub-Basin, South Sumatra Basin, Indonesia. Modeling results indicate basin expulsion from the Lower Talang Akar Formation in Ketaling Graben started at the 22.38 Ma (Early Miocene/*Aquitanian*) when petroleum generation exceeded the source rock retention capacity at thermal maturity of >0.70% Ro and transformation ratio by value of >9%. In Gelam Deep, expulsion from the Lower Talang Akar Formation started at the 18.11 Ma (Early Miocene/*Burdigalian*) at thermal maturity of 0.66% Ro and transformation ratio as low as 6%. Meanwhile, in Merang Deep expulsion started at the 15.18 Ma (Middle Miocene/*Langhian*) at thermal maturity of >0.71% Ro and transformation ratio by 9.5%.

While expulsion of Ketaling Deep ceased around the Middle Miocene at about 2.6% Ro, the expulsion of Gelam Deep and Merang Deep kept increase until recently. In the Plio-Pleistocene, tectonic uplift and reactivation of magmatism events did not cease the thermal stress, the pressure and the temperature. And finally, our study indicates that small basin on the edge of the larger basin, has undergone expulsion of the hydrocarbon through thermal maturation by 0.66-0.71%Ro and transformation ratio by ~10%. The A-1

well which described as a representative well with proven gas and condensate field have showed the expulsion capability from Gelam Deep and Merang Deep. It is believed that the major contributing parameters of the expulsion consist of the burial process, local heat flow from Ro information and source rock interval that has been validated by porosity data.

The method and the insights of this study can improve the understanding of source rock expulsion and opening the new play opportunities near the Ketaling Deep, Gelam Deep and Merang Deep. However, this research is not yet perfect, with more data acquired some parameter need to be adjusted and calibrated. Some prediction method also needed to understand about the amount of hydrocarbon expulsion or expulsion efficiency in the study area.

References

Kamila, B., Rachmalia M., Yusriani, A., Mustofa, M. F., Pradana, A. Y., 2020, Source Rock Characterization and Oil to Source Rock Correlation in Jambi Merang Area: New Insights in Jambi Depression – South Sumatra Basin, Proceedings The 49th IAGI Annual Convention and Exhibition, 1-5.

Koesoemadinata, R. P., Qivayanti, S. I. and Kesumajana, A. H. P., 1999, Shale compaction curve from tertiary basins of Western Indonesia, Proceedings IAGI No. 28, IAGI Convention, Jakarta, Indonesia.

Pepper, A. S. and Corvi, P. J., 1995, Simple Kinetic Models of Petroleum Formation. Part I: Oil and Gas Generation from Kerogen, Marine and Petroleum Geology, **12**, 291-319.

Verweij, J. M., 1993, Hydrocarbon Migration Systems Analysis, 83-120.

Acknowledgements

Kind appreciation for those who contributed and supported this study in PHE Jambi Merang and LAPI ITB, as well as everyone else in exploration team.

PROCEEDINGS
JOINT CONVENTION BANDUNG (JCB) 2021
November 23rd – 25th 2021

Tectonic Event in Cenozoic and Its Implication for Hydrocarbon Prospect in Berau Sub Basin, Northeast Borneo, Indonesia

Adi Gunawan[1]
Ahmad Najihal Amal[1]
Alfathony Krisna Budi[1]
Raysita Galuh[1]

PT. Pertamina Hulu Energi [1]

Berau sub basin is the souther onshore of the greater Tarakan Basin Northeat Borneo, The regional tectonic Berau sub basin is re-analyzed to determine new petroleum prospects in such area. This paper present used more than hundred 2D seismic reflection, bouger gravity, wells and geochemical data.

The tectonic system in Berau Sub Basin experienced many poly-deformation histories since Middle Mesozoic until present day. The uplift of Mangkalihat peninsula due to collision between Partenoster and Mangkalihat-Meratus block in Jurassic caused depositional of Pre-Tertiary sediment in proto Berau Sub-Basin. During paleogen, the initiation of Makassar rift resulted extensional phase and formed half graben system in the greater Tarakan Basin.

The half graben and deltaic deposit are considered to be sites of hydrocarbon generation. Working petroleum system in the basin manifested by many oil seeps that can be found in surface Tanjung Redeb city and postmortem wells data shows commercial to sub-commercial and abundant oil and gas show, meanwhile for trap are available especially in roll over anticline, inverted structure and sedimentary wedges. This area dominated by anticline related to oversteeping NW-SE transpressional system between Maratua and North Mangkalihat fault thus forming Oligocene isolated carbonate prospect, and Miocene deltaic prospect , those prospects directly facing with the depocecntre, the hydrocarbon will migrate through border fault and trap in asymmetrical or syncline thrust

Keywords : Berau Sub Basin, Tectonic, Prospect, Hydrocarbon

Introduction

Generally, tectonic evolution can be marked as one of the important factors to determine the presence of hydrocarbon prospect especially in Borneo. The Borneo have many hydrocarbon prospects such as in Kutei Basin, Barito Basin and Serawak Basin (Satyana, 1999) that came from Neogene sediment accumulation (Wijayanti et,al, 2007). In the greater Tarakan Basin, the presence of hydrocarbon prospects remains unclear especially in Paleogene sediment. Early sedimentary fill of the depocentre happened during Middle Eocene to Early Oligocene appeared in the southern part of onshore depocenter of the greater Tarakan Basin is Berau Sub-basin, bounded Mangkalihat, Suikerbrood and Sekatak Highs.

At the present day, the research of hydrocarbon prospectivitity is very limited due to lack of subsurface data and interpretation. Hence, this study, proposed new concept and interpretation to unreveal the new petroleum prospects that highly consider the structural style and timing of tectonic evolution.

Regional Geology

Physiographically, the Berau sub-basin is surrounded Kuching High, Suikerbrood and Sekatak highs. The basin is physiography encompasses a wide variety of faults, structural elements and trends. Tectonics of the basin was initiated by extension and subsidence during the Middle to Late Eocene formed wrench faults and resulted in the formation of major NW-SE oriented arches and has stopped by the end of Early Miocene. Two deep-seated NE-SW sinistral Mangkalihat and Maratua. Were influenced the structural trends in Berau Basin. Recently these faults play an important role arrangement of NWSE, NNW-SSE fold.

Deposition in the Berau sub basin commenced in the Middle Eocene, simultaneously with the rifting of the Makassar Straits which separates Sulawesi from Kalimantan (Lentini and Darman, 1996). The basin subsided and opened to the east. The sea transgressed westwards and shallow marine shales of the Sembakung Formation were deposited, overlying the older Kelay formation basement rocks. The transgression was interrupted by the latest Eocene uplift which resulted in the deposition of coarse clastics of Sujau Formation.

Formation. During Oligocene times a carbonate platform (Seilor Formation) developed and continued into the Early Miocene as the Mangkabua Shales and the reefal Tabalar Limestone. In the middle Miocene, the western basin margins were uplifted and caused open marine conditions to give way to widespread and rapid clastic deltaic deposition, which successively prograded eastwards with time. Periodic and cyclic regression transgression during the middle Miocene to Pleistocene time caused sedimentary switching, leaving marine shales and limestones intercalated with coarse clastic deltaic sediments such as Birang, Latih, Tertiary sedimentary units was tectonically controlled, and each rock unit is separated along their lower and upper contacts by a well-defined conformity on Sajau formation.

Method And Data

The publication attempt to describe and improving exploration play concept in Berau sub basin by integrating newly acquired data from geological mapping, aerogravity map, geochemical, well data, seismic reflection, subsurface mapping to generate structural map and related prospect of petroleum system.

Tectonostratigraphy

The development of tectonostratigraphy in Berau sub basin can be divided into four stage :

Early Jurassic the subduction between Mangkalihat with Partenoster Block resulted NEN-WSW paired metamorphic belt uplift after 195 Ma (Krisnabudi,2020), this emergence had been suspected as provenance for Createaceous Telen Formation and Benggara group with relatively N-S depositional pattern.

Paleocene-Eocene the evolution continued where subduction roll back between Luconia platform with NW Borneo resulted rifting phase and opening Celebes sea, In this period, every graben pocket had been filled by syn-extensional deposits such as Sembakung Fm with shale-siltstone and sandstone facies. The progressive subduction in Southwest Kalimantan in the Early Oligocene led to the uplifting of the Rajang-Embaluh and Suikebrood as a source of sediment towards and Southeast Kalimantan. The source bearing formation overlying by volcanic clastic sujau formation deposits and carbonate Oligocene Sielor and mangakabua formations deposits, after post extensional phase were deposited in the littoral and shallow marine environment.

During Miocene Collision between the Dangerous Ground and Sundaland that impact to sediment prograding system resulted the development of Berau delta to the east, that condition is recorded in latih formation with lithology cross bedded sandstone, carbonaceous shale, coal is generally outcrop in the central of the basin.

In the last stages, transpressional fault system with SE-NW pattern has fully affected since Plio-Plistocene Tectonic uplift. The formation of Latih thrust fault-anticline trigger erosion in the crest of anticline. This process sediment was deposited Sujau Formation with lithology conglomerate, sandstone with thin coal layer

Structural Style

Berau sub-basin have two dominant structural patterns; SE-NW is the main PDZ of Riani Fault Zone (RFZ), North Mangkalihat Fault Zone (NMFZ) and NE-SW that represented echelon fold-thrust system Structural style are controlled by thick-skinned system due to RFZ (Riani Fault Zone) and NMFZ (North Mangkalihat Fault zone) transpressional system. The measurements of strike/dip of shear and fault zone were taken in Tanjung Redeb area, ther oientation of main shear was N 223^0 E – N 242^0 E and normal fault was N 62^0 E – 337^0 E. The main stress (σ1) of fault reconstruction of the structural elements; the relative compression stress of structural geology (fold, fault) also approximately NNW-SSE direction. Therefore, the compressional stress (σ1) of fold, faults and shear have a main structure of direction Berau basin is NW-SE, The existing structure from Paleogene has experienced reactivation and inversion within overstepping sinistral strike slip system Figure 3.

In Neogene, the major regression phase has affected in Miocene due to Kuching high uplift in west area. Based on analysis, the deltaic seq such as Latih Fm in Miocene has possibility as intra-formational source rock and reservoir rocks especially delta plain facies in paleo Berau delta. The last stages, following northwest movement of Australia continental, Borneo experienced anticlock-wise rotation and resulted contractional regime that was triggered by SE-NW overstepping sinistral strike slip fault such as RFZ, NMFZ and MFZ. Based on this event, almost all existing structure experienced reactivation and inversion in Berau sub-basin where structural trap is well developed during this period

Tectonic evolution and structural style in Maratua block, The intensity of this structure had formed asymmetrical anticline and syncline thrust, hence if those prospects directly facing with the depocecntre, the hydrocarbon will migrate through border fault and trap in asymmetrical or syncline thrust.

Hydrocarbon Prospect

The presence of oil seepage in Berau sub-basin has proved that petroleum system has already been working because the source rocks has generated during extensional phase in Paleocene-Middle Eocene eq Sembakung Fm. These units unconformably on the top of Middle Eocene seq and basement high. In Berau sub basin, Oligocene carbonate has considered as reservoir rocks and has possibiity as intra-formational source rocks.

Maturity of the source rock is a related of the subsidence the potential source rock were analysis in the Berau Sub-Basin refers to the Wells which represents the Seilor and Sembakung Formation the paleogen deposits. Based on the TOC VS HI and HI VS Tmax data plots, these data fair to good potential to generate hydrocarbons and interpreted kerogen type III.

Biomarker analyis of the Tanjungredeb oil Seepage sampel based on Sterane (M/Z 217) Plots of the sterane distributions on Huang and Meinschein's paleoenvironment diagram shows that these source rock from the Berau deep situated in the region assigned to oil-derived from source facies deposited within "open marine" to "higher plant" environments. Other data showed on m/z 191 fragmentograms of all the oils display relatively simple distributions of bacterial-derived 17 αβ (H)-hopanes which is dominated by the C30 αβ (H)-hopane (C29 hopane<C30 hopane). This suggests the oils are of clastic origins (Zumberge, 1984; Connan et al., 1986; Price et al., 1987; all in Waples and Machihara, 1991) Figure 4. These oils are classified into two groups of oil based on the contribution of the C30 tricyclic compound with high Oleanana, This suggests that the oils are sourced from source rock facies

with significant contribution from terrestrially-derived organic matter. derived from Seilor formation it is possibly comes from shale deposited in the oligocene marine environment.

The source rock on Berau deep migrates vertically NE-SW locally through complex faults as hydrocarbon pathways to fill on prospects:

(1) Paleogene carbonate prospect is four way dip closure these prospects located in Tanjung Redeb area. In Berau sub basin, carbonate prospect lies within transpression zone. Seilor Limestone prospect that categorized as isolated platform lies in upthrown extensional system which is directly facing with depocentre.

(2) Neogene prospect consists Latih formation Miocene deltaic sediment prospect was mostly influenced by en-echelon fold-thrust due to sinistral strike slip fault movement that formed since 5 Ma. Neogene prospects depends on thick-skineed system where major all prospect lies in roll over anticline it is describe on northwest area. Figure 5.

Conclusion

Through the evolution tectonic research and re-intrepreted seismic section analysis combine with several key well in Berau Sub Basin reveal that area is highly affected by many poly-deformation since Mesozoic. Hence, the structural in Berau Sub Basin have many important roles to determine Hydrocarbon in such area. Extensional phase is one critical factor to create depocentre during Cretaceous to Middle Eocene. During this phase the syn-depositional system deposited and have potential as generated source rock. Meanwhile structural style in Late Neogene have critical factor as trap system. Many Hydrocarbon prospects has delianiated in study area, in south area dominated with asymestrical anticline, southeast area dominated with carbonate that lies in upthrown of normal fault. Based on our study, Berau sub basin should be the superior target for petroleum exploration due to many oil seepage can be trace in onshore area and proven in several discovery wells It is indicated that petroleum system has already working in such area.

References

Hall, R., 2013. Contractional and extension in northern Borneo driven by subduction rollback. Journal of Asian Earth Sciences 76, 399-441.

Hidayati, S., Guritno, E., Argenton, A., Ziza, W., Del Campana, I., 2007, Re-Visited Structural Framework of The Tarakan Sub-Basin Northeast Kalimantan-Indonesia, Proceedings Indonesian Petroleum Association, 31, IPA07-G-109.

Satyana, A.H., Nugroho, D., Surantoko, I., 1999. Tectonic Control on the Hydrocarbon Habitats of the Barito, Kutei, and Tarakan Basins, Eastern Kalimantan, Indonesia: Major Dissimilarities in Adjoining Basins. Journal of Asian Earth Sciences 17, 92-131.

Soesilo, J., Schenk, V., Suparka, E., Abdullah, I.C., 2015, The Mesozoic Tectonic Setting of SE Sundaland Based on Metamorphic Evolution, Proceedings Indonesian Petroleum Association, 39, IPA15-G-205.

Situmorang, R.I. and Burhan, Burhan., 1995, Geological Map of the Tanjung Redeb Quadrangle, Kalimantan.Geological Research and Development Centre, Bandung.

Wijayanti, K.D.H., Surjono, S.S., Soedarmono., 2014, The Paleogeography of Berau Sub-Basin, NE Kalimantan, IAGI Annual Convention and Exhibition 43, Jakarta, Indonesia.

Wilson, M.E.J., Chambers, J.L.C., Evans, M.J., Moss, S.J., Nas, D.S., 1999. Cenozoic Carbonates in Borneo: Case Studies from Northeast Kalimantan. Journal of Asian Earth Sciences 17, 183-201

Sudrajad, Adjat, 2018. Tectonic Control on the Formation of cleat in the coal beds of the Sajau Formation Berau Basin, Northeast Kalimantan. Indonesia Journal on Geoscience, Vol 5, 235 -250

Wijayanti ,Surjono, Soedarmono. The Paleogeography Of Berau Sub Basin, Ne Kalimantan, The 43st IAGI Annual Convention and Exhibition

Balaguru, A., Hall, R., 2009. Tectonic evolution and sedimentation of Sabah, North Borneo, Malaysia. Abstract: AAPG International Conference and Exhibition

A. Krisnabudhi, A. Gunawan, Y. A. Putra, and A. N. Amal, "New insight into Berau Sub-Basin northeast Borneo: basin evolution and tectonostratigraphy and their implication to new exploration play," *Indonesian Petroleum Association Annual Convention and Exhibition, Jakarta, Indonesia*, 2020, pp. 1168-1174

Waples, D. W., 1985, Geochemistry in Petroleum Exploration, 232.

Pertamina-BPPKA, 1996, Vol. V, Tarakan Basin, NE Kalimantan.

PROCEEDINGS
JOINT CONVENTION BANDUNG (JCB) 2021
November 23rd – 25th 2021

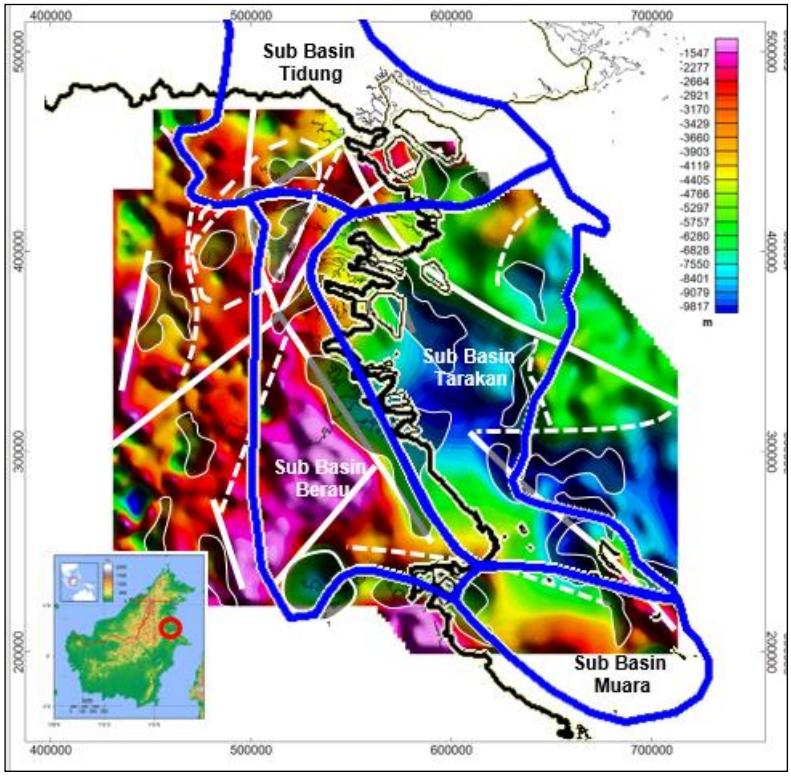

Figure 1. Berau sub basin is located on southern part of greater Tarakan Basin the map is overlaid on aerogravity map and major structure (Pertamina, 2016)

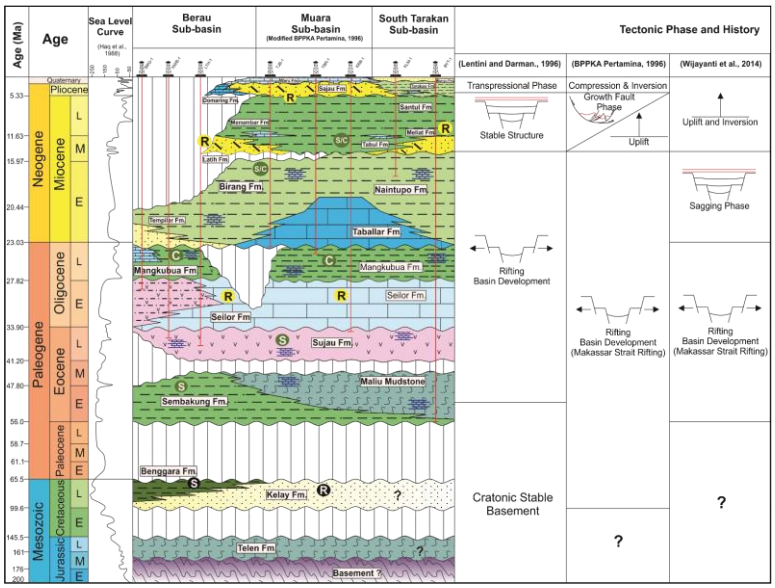

Figure 2. Tectonostratigraphy of Berau sub basin and Petroleum System (modified Krisnabudi, Pertamina-BPPKA, 1996).

PROCEEDINGS
JOINT CONVENTION BANDUNG (JCB) 2021
November 23rd – 25th 2021

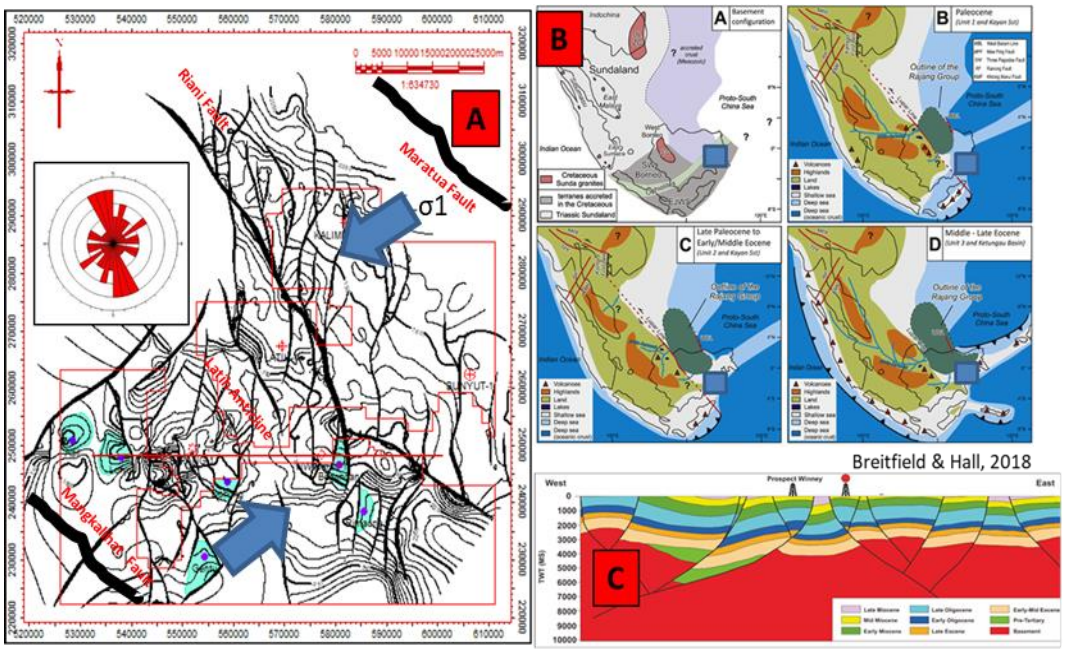

Figure 3. Structure Type of Berau sub basin (A), Tectonic evolution of Kalimantan (Hall, 2018) (B), and . West-east seismic section of Berau Sub-basin .

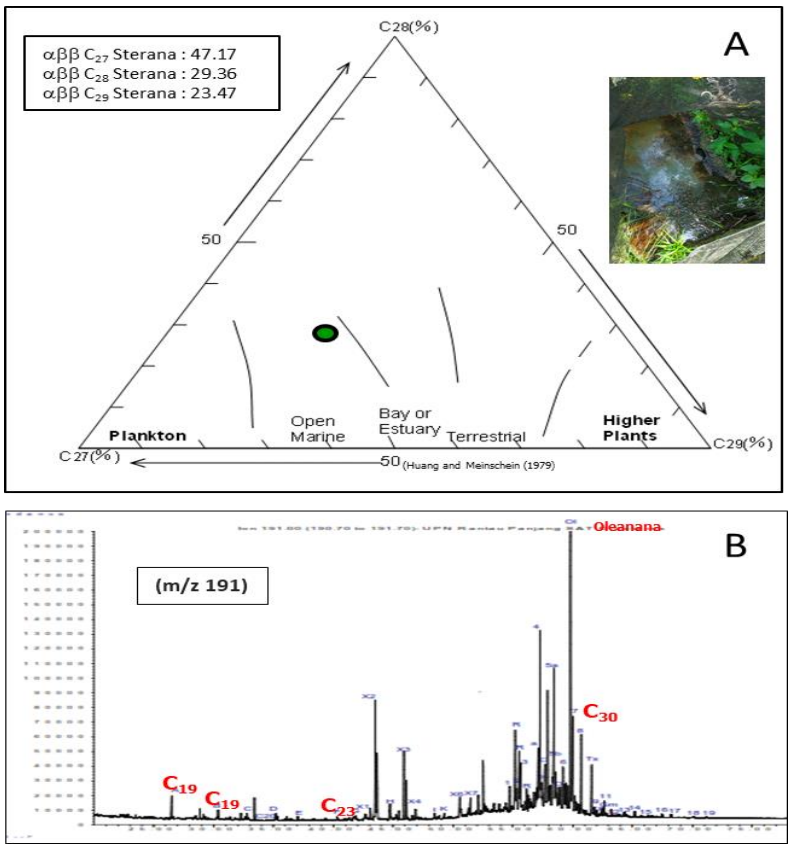

Figure 4. Biomarker analyis of the Tanjungredeb oil Seepage (A) Sterane (M/Z 217) plot (B) M/Z 191 fragmentograms

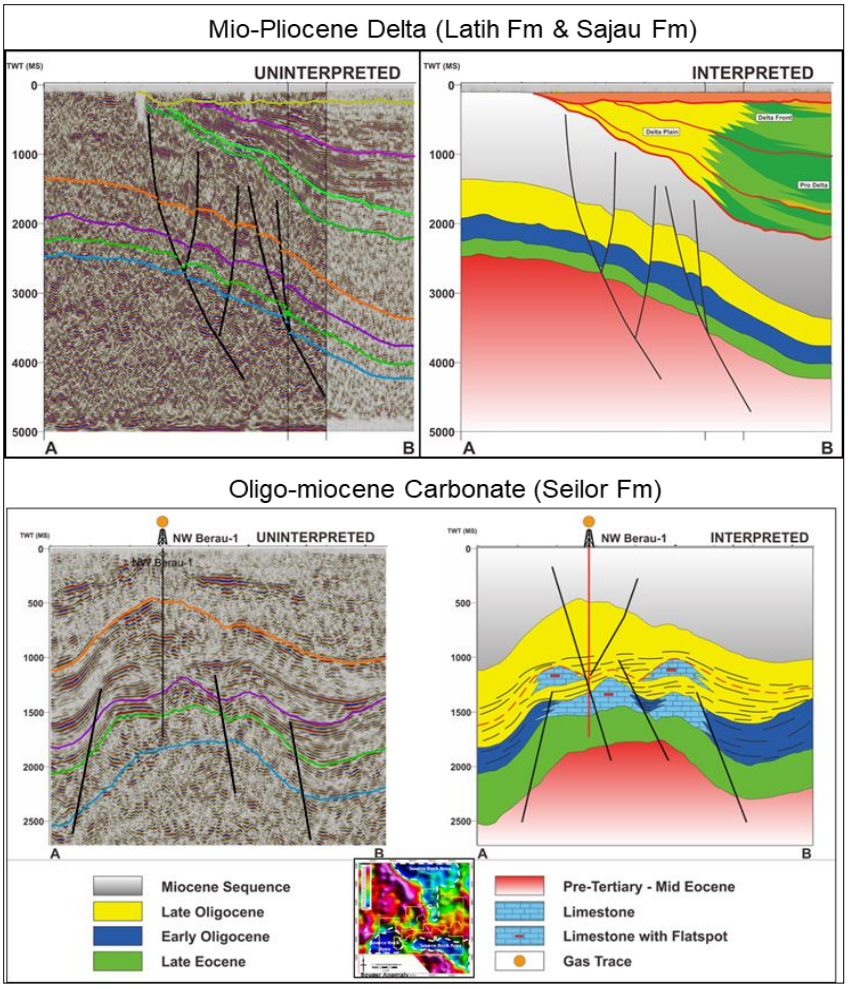

Figure 5. Oligocene Carbonate and Miocene Deltaic Prospects type on Berau Sub basin

PROCEEDINGS
JOINT CONVENTION BANDUNG (JCB) 2021
November 23rd – 25th 2021

"Condition Based Monitoring Data for Maximizing Gas Compressor Output"

Author: Dody Said ST, MBA.

Co-Author: Toni Darmawan MMRE, CPMM

Abstract

There are several condition base monitoring that can be utilized in optimizing the Oil and Gas equipment functions, i.e., Vibration Analysis, Thermography Inspection, Reciprocating Tools Analysis, and Lubricant Analysis.
Compressors are the most widely used equipment in today's gas industries. The reciprocating compressors that can compress a variety of gases, has a wide range of applications with high compression efficiency and stable working pressure.
However, due to its complicated mechanical structure and many vulnerable parts, they need careful maintenance to keep its high performance. There are several of maintenance strategies that can be implemented in maintaining gas compressors and its prime movers. One of them is Predictive Maintenance (PdM) that assesses the equipment's health conditions through diagnostics testing and / or online monitoring. The machine's condition may be inspected and monitored using continuous or intermittent parameter measurements. PdM techniques can detect trend changes in running conditions that could lead to catastrophic failures. They are used to identify early indication of failures, which in turn can provide greater lead-time for taking suitable actions prior to the failure, resulting in reducing unscheduled down time as well as preventing any possible catastrophic failures.
This paper discusses how these multiple technologies could be implemented in maximizing gas compressor and gas engine performances. In 2020 the achieved reliability of the gas compressors in one of the Gas Companies is 93.15 %. It means that most of the maintenance activities are well planned by analyzing detailed collected data from those multiple PdM technologies.

Introduction

Equipment failures are defined as it cannot accomplish its mission or at the extreme end it is stop working.
There are symptoms before the equipment fails to operate such as: disturbing noise, or excessive heats or abnormality in vibration spectrum.
Equipment failure could be detected by implementing condition monitoring utilizing many Predictive Maintenance tools. By doing so we can take appropriate actions in advance so we have a better plan for repairing.
See below figure of PF curve

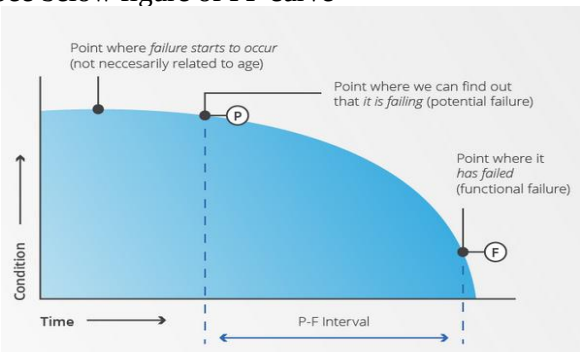

Potential Failure Curve.
The "P" in a P-F curve refers to potential failure (when a piece of equipment could fail based on historical data) or the first point where we can detect that a failure could be occurred.
A P-F curve is a graph that shows the health of equipment over time to identify the interval between Potential failure (P) and Functional failure (F).
Functional failure is the inability of a system to meet a specified performance standard. A complete loss of function is clearly functional failure.

Maintenance and Maintenance strategy.
By definition *Maintenance* is to maintain, to preserve, to protect, to keep in existing condition and to keep from failure or decline. In general term the function of maintenance is to sustain the integrity of physical assets of the company over their planned life by repairing, modifying or replacing them as necessary within the agreed budget for supporting the attainment of the company goals.
In doing so the *life cycle costs* (LCC) and its influencing factors should be the basis for decision making in putting any maintenance strategy in place. Those LCC factors include acquisition costs, running (operation, maintenance and energy) costs, and abandonment costs minus salvage value (if any). Focusing on maintenance costs themselves, it involves cost factors such as: labor, materials, spare part ordering and holding costs, tools and equipment, engineering support costs, contractors and other overhead costs.
Keeping the above factors in perspective, several maintenance strategies can be selected based on the production targets.

PROCEEDINGS
JOINT CONVENTION BANDUNG (JCB) 2021
November 23rd – 25th 2021

Practically a company can either implement the Breakdown, Preventive or Predictive maintenance strategies or a couple, or even all of them.

Predictive Maintenance

Predictive maintenance is generally considered to be the most advanced and intensive type of maintenance. This is because there is a lot of data to be collected and interpreted.

- If there is a measurement that exceeds the limits then we need to analyze the problem to find the root causes. Once we identified the root causes, the work order is generated to make intervention to the equipment before losses its functions. By having those we can better plan the maintenance activities before the failure happen.

Predictive Maintenance Technologies

There are many maintenance strategies that can be implemented depending on the asset criticality and others factors. The first step is to identify criticality of the
Equipment, and then PdM should be directed on to the equipment that have high criticality ranking.
To identify the criticality ranking of the equipment many data should be collected and analyzed such as:

- Safety requirements
- Production loss impacts
- Total work orders
- Maintenance Historical data
- Mean Time between Failures, Mean Time to Repairs, etc.

The risk matrix should be developed as a function of equipment failure frequency and its failure consequences; and the output of this assessment is the equipment criticality ranking. Having these data the maintenance strategy could be identified which of that equipment need reactive maintenance, preventive, predictive even proactive maintenance. Once the predictive maintenance has been decided to be applied to the equipment, then the next step is the suitable PdM Technology selection.

1. Vibration analysis

A vibration monitoring system is a complete system that is capable of acquiring vibration signals according to pre-determined parameters such as sampling frequency, vibration level, recording length, recording intervals and frequency bandwidths. The system should be able to process the recorded vibration and translate the information to intuitive indications for the machine operators, maintenance staff or asset managers.

Used primarily on rotating equipment to find problems such as unbalance, bearing defect, resonance, mechanical looseness, misalignment etc. Measurements can be taken continuously or periodically and subsequently recorded in a data base system. The subject data can then be trended and analyzed to determine the condition of the equipment.

Sample of comressor vibration report analysis.

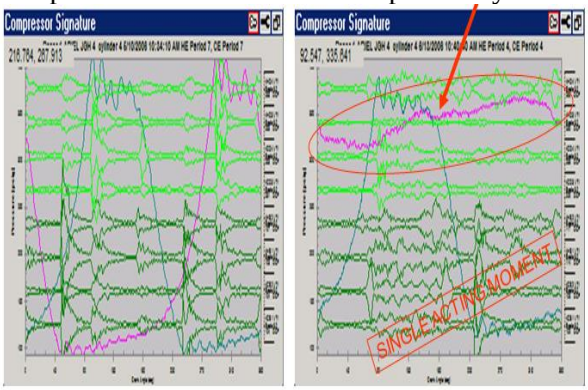

2. Thermography analysis

The principle of infrared thermography is based on the physical phenomenon that any body of a temperature above absolute zero (-273.15 °C) emits electromagnetic radiation. There is clear correlation between the surface of a body and the intensity and spectral composition of its emitted radiation.

This technique is used to detect irregularities by sensing temperatures of objects that are being checked.

Examples of usage include infrared detection of electrical component problems, hot spots, leaks, depositions in storage tanks or vessels, insight to internal processes of equipment, etc.

Sample of Infra-red Thermography report (Turbo Charger of Gas Engine)

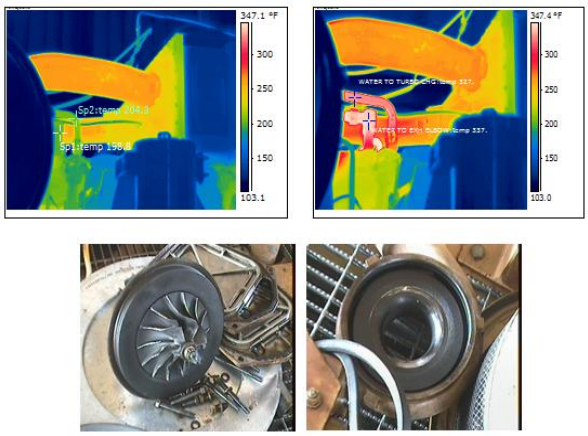

PROCEEDINGS
JOINT CONVENTION BANDUNG (JCB) 2021
November 23rd – 25th 2021

3. Reciprocating Tool analysis

This tool is capable to diagnose the health of any type of reciprocating engine such: low to high speed, spark-ignited or diesel. Some of engine and reciprocating problems that could be detected: Power cylinder condition, ignition system, cylinder and engine performance such as: valve train, carbon in ports, liner wear, piston slap, wrist pin/rod and blow-by / rings. The technique is also be used to find problems associated with discharge or suction compressor valves, compressor valve springs, suction and discharge valve condition, compressor cylinder condition and mechanical looseness.

Sample of reciprocating tool analysis report

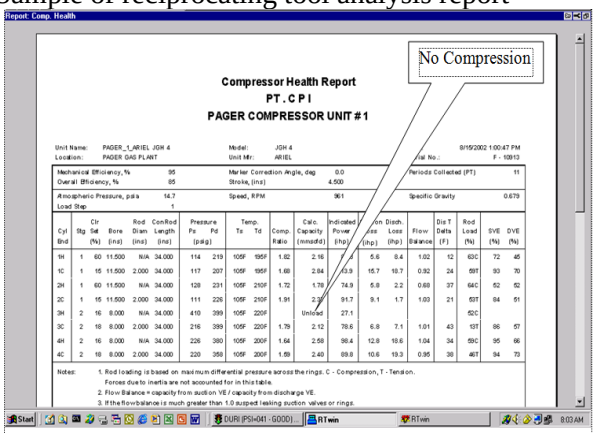

4. Lubricant Analysis

The technique is used to determine the condition of a lubricant and equipment based on the concentration of wear particles found in the lubricant.

The analysis consists of:

1) Fluid properties analysis.

These essential types of oil analysis help to ensure the fundamental quality of the lubricating fluid. The standard to which used oil's properties should be routinely compared to the new oil's properties. Examples of common test include Viscosity, Total Acid Number, and Specific Gravity etc.

2) Fluid contamination analysis

Despite the use of filter and separator, contaminants are the most common destroyer of machine surfaces that lead to failure and down time. It's important to perform basic tests such as particle counting and moisture analysis

3) Fluid wears debris analysis

Unlike fluid properties and contamination analysis, wear debris analysis relates specifically to the health of the machine or unit. The data should be trended and the source of failure should be found.

For example if the Iron count is increased indicates wear originating from cylinder sleeve, rings, gears valve train or the other sources depend of the equipment material. All of data should be compared to the manual.

Sample Oil analysis report:

Ref Oil	Mobil - DTE - 846				
Lab Unit ID	061-CS1001B-P				
Sample Date	24/05/2020	01/04/2020	05/03/2020	03/02/2020	06/01/2020
Sample #	2918187	2918185	3827260	3131263	2893944
Unit Usage - hrs					
Oil Usage - hrs					
Oil Added - l					

Wear	46	61	35	30	35
Visc 40C - cSt	46,650	46,440	45,020	46,260	44,680
Visc 100C - cSt	6,828	6,389	6,535	6,568	6,523
Water K.Fish - ppm	158,000	184,000	136,000	125,000	136,000
Silicon - ppm	2,20	0,00	2,50	2,80	2,60
Iron - ppm	,5	0,0	,4	,7	,9
Copper - ppm	,1000	,3000	0,0000	0,0000	0,0000
Aluminum - ppm	,20	,40	,10	,10	,10
Chromium - ppm	0,00	0,00	0,00	0,00	0,00
Silver - ppm	0,00	0,00	0,00	0,00	0,00
Lead - ppm	1,30	1,10	,10	,40	,10
Sodium - ppm	1,50	0,00	,90	1,20	1,60
DV Visc 40C - cSt					
NAS 1638 - Idx	7	7	7	7	7
RPVOT - min					

Conclusion

In summary, PdM consists of at least three main efforts: surveillance, diagnostic, and remedy. Predictive maintenance strategy with multiple technologies have been implemented in maximizing gas compressor and gas engine performances then achievement is the reliability of the output is 93.15 % in 2020

It means that most of the maintenance activities are well planned by having analyzed detailed information of the gas compressor which was being monitored by those multiple technologies.

PdM has advantages such as:

- Elimination of unnecessary equipment down time and maintenance activities
- Predict when a device is likely to fail
- Reduced lost production attributable to equipment failures
- Reduced spare parts inventory
- Extended operating life of plant & systems
- Increased production capacity
- Reduced overall maintenance costs
- Fewer equipment failures.
- Reduced MTTR
- Increased asset lifetime
- Improved workplace safety.

Predictive Maintenance efforts contribute to the reduction of the down time, maintenance cost as well as the attainment of the company goals.

References

1. Berry, James, "Advance Vibration Diagnostic and Reduction Techniques," Volume 2.

2. Bloch, Heinz P. & Geithner, Fred K, "Machinery Failure Analysis and Trouble Shooting," Volume 2.
3. Central Queensland University, 2004, "Establishing Maintenance Strategy," Maintenance Management
4. Computational System Incorporate, 2003, "Intermediate Vibration Analysis, Training manual."
5. Infrared Training Center, 2005 "An Intermediate course for Thermographers". Level II course manual
6. Marshall Institute, "Preventive/Predictive Maintenance, Training Manual."
7. Noria Corporation, 2005 " Machinery Lubrication I, Training Manual."
8. PT Tiara Vibrasindo Pratama, 2004 "Engine Analysis Training Manual."
9. Stanislavski, M., 1997, "Mechanical Rotating Equipment, "First Edition, Rike Service ,Inc.

The Authors:

Dody Said is Technical Advisor Manager at PT Tiara Vibrasindo Pratama that provides Predictive Maintenance analysis to the customer such as oilcompany, geothermal and other industry in Indonesia. He is the Level I Certified Thermograph, Level I Vibration Analyst and Level I Machinery Lubricant Technician and has more than 15 years experiences in Predictive Maintenance activities. He completed Electrical Engineering and Master of Business Administration from ITB.

Toni Darmawan has more than 30 years of experiences in Design Engineering, Project Management, Primary, Secondary and Tertiary Recoveries Surface Facilities Engineering, Maintenance Management, Operational Assurances. Toni holds a Master of Maintenance Management and Reliability Engineering, Monash University and Certified Professional Maintenance Manager, Association of Facilities Engineering, AFE- USA.

PROCEEDINGS
JOINT CONVENTION BANDUNG (JCB) 2021
November 23rd – 25th 2021

Identification of corrosion products and damage mechanisms from the interior pipeline by using scanning electron microscopy and energy-dispersive X-ray spectroscopy

Muchlis Nurdiyanto
PT. Geoservices Geological & Laboratory Services Division

Abstract
Nowadays, there is a lot of damage caused by corrosion, especially in the industrial sector, especially the geothermal, oil and gas industries. Within the framework of environmental protection, internal corrosion risk assessment is one of the most important activities of modern pipeline corrosion management. In order to assess the risk of internal corrosion of pipelines, it is important to understand corrosion mechanisms and be able to predict whether localized corrosion will be initiated and how it can be prevented. We investigated corrosion products from the interior of the of carbon steel pipeline sample where wall perforation due to corrosion has already occurred. Morphological and compositional studies were conducted by SEM-EDS.

Data Analysis revealing type of corrosion that occurs is pitting corrosion. Pitting corrosion is caused by an inhomogeneous metal composition where in the boundary area corrosion occurs in the form of a well. In addition, under deposit corrosion was also found. This type of corrosion can be prevented by choosing a homogeneous pipe material, applying inhibitors or applying a coating of aggressive substances to the pipe.

Introduction
Pipeline plays an important role in oil and gas industries. Up to now pipeline is perhaps the most economical and efficient means of large scale fluid transportation for crude oil and natural gas compared to rail, truck and tanker transportation in term of the flexibility of routes and large quantities to be moved on. Pipeline is commonly made of carbon steels due to some reasons, i.e. carbon steels have good mechanical properties, low cost and wider availability despite their corrosion resistance is relatively low (Tawancy,et al.2013).

Corrosion is one of the great enemies in the industrial world, some examples corrosion-induced efficacy is a decrease in material strength and repair costs will rise much more than expected. So that a prevention effort is needed against corrosion attacks. Some of the main forms of corrosion are general corrosion, erosion corrosion, stress corrosion cracking, pitting, crevice and galvanic corrosion.

During the last decades a lot of research is being done in order to improve the knowledge of corrosion processes (J. Kittel.,2013). Stainless steel is more resistant to corrosion than carbon steel and most of the important materials of pipe are now constructed from stainless steel.

When studying corrosion it is of great importance to examine the corrosion rate, the kinetics of corrosion, the products that are formed on the surface, the corrosion type and a possible link between degradation products and corrosion. The weight loss technique with metal coupons is one of the most used for the calculation of the corrosion rate. Furthermore, a number of electrochemical methods for corrosion measuring exist and potentiodynamic polarization techniques are among the most popular.

SEM-EDS is one of the main techniques used for examining and analyzing elemental surface component of corrosion-related samples (Little B.J. et al, 2007). The SEM examination provides information about the steel surface, specifically with regard to the morphology and corrosion type, while EDS is used for elemental analysis.

Data and Method
Effects of corrosion on surface morphology and chemical composition of cylinders were examined by combined use of scanning electron microscopy (SEM) and energy dispersive spectrometry (EDS). Both SEM and EDS characterization were carried out by using a Quanta 650 scanning electron microscope. For this purpose small pieces were cut from the cylinders and their surfaces were cleaned with ethanol to remove any deposited corrosion product prior to scanning. An acceleration voltage of 10.0 kV and a working distance of 10.0 µm were used, and samples were placed on stubs and scanned without coating. Aztec Energy software was used to process the EDS data.

Result and Discussion
SEM/EDS is perhaps one of the most popular technique used for examining and analyzing elemental surface component of corrosion-related samples. The SEM examination provides information about the result of the interaction between the corrosive environment and steel pipe, specifically with regard to the morphology of the metal surface, deposits and corrosion products.

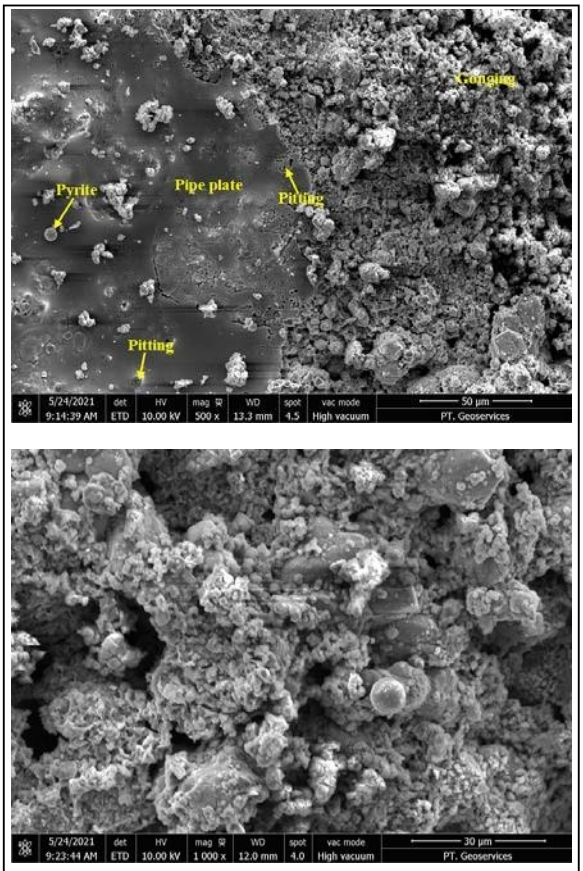

Fig.1. SEM images of stainless steel pipe tube surface

PROCEEDINGS
JOINT CONVENTION BANDUNG (JCB) 2021
November 23rd – 25th 2021

Figures 1 show the sample results of surface scanning by SEM-EDS on the coupons. Each figure shows four scanning electron micrographs taken from the coupons three areas and magnification level at low (500×) and high (1000×) magnification of the areas in the coupons. At high magnifications, the scale consisted of fine crystalline grains that appeared to aggregate (amorphous silica). The shape of the crystals appeared primarily rounded. Data Analysis revealing type of corrosion that occurs is pitting corrosion. Pitting corrosion is caused by an inhomogeneous metal composition where in the boundary area corrosion occurs in the form of a well. In addition, under deposit corrosion was also found.

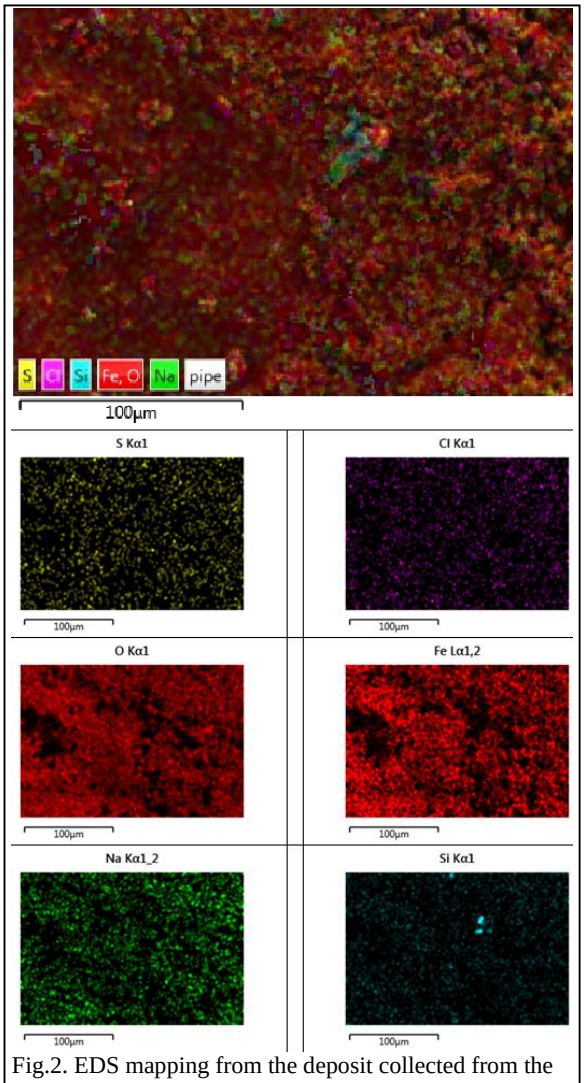

Fig.2. EDS mapping from the deposit collected from the interior of the corroded pipeline.

In corrosion studies EDS is used to provide chemical information about the features being examined by SEM. The result of the EDS analyses scan of the coupons covered with scale deposit was fairly consistent. Often, the relative amounts of elements detected are categorized as major, minor or trace values. Major elements in red and black samples of corrosion products are Fe and O. Minor elements are Na, Cl, S and Si were also found. Debris found contains S and Si. Formation of Silica may explain this abundance of oxygen.

Although EDS indicates only elemental composition, it is possible to postulate the probable nature of the corrosion products and scales. Deposits in pipelines can consist of iron oxide, iron carbonate, iron sulphide, sand, clay and mud (Pickthall, 2005). These scales like this often contain some strontium sulphate. In the present analysis no barium or strontium were detected by EDS. However, the analysis shows probable presence of Fe, Si and Cl scales.

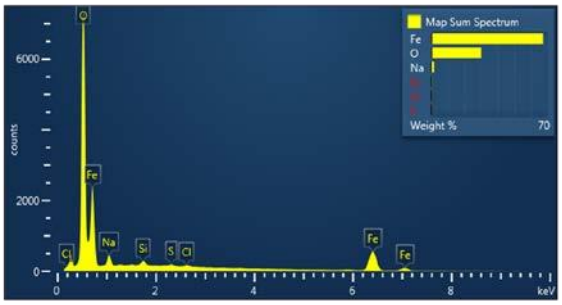

Fig.3. EDS map sum spectrum

Table 1. Elemental composition of coupon surfaces

Element	Apparent Concentration	K Ratio	Wt (%)	Standard Label
O	178.13	0.59943	30.09	SiO2
Na	4.32	0.01825	1.75	Albite
Si	1.17	0.00927	0.49	SiO2
S	0.68	0.00588	0.27	FeS2
Cl	0.87	0.00756	0.36	NaCl
Fe	136.59	1.36594	67.04	Fe
Total			100.00	

SEM itself can be used for surface morphology but does not give any details about the composition of the surface. EDS does not provide data about possible compounds that are formed on the surface but does give elemental composition.

Conclusions

Data Analysis revealing type of corrosion that occurs is pitting corrosion. Pitting corrosion is caused by an inhomogeneous metal composition where in the boundary area corrosion occurs in the form of a well. In addition, under deposit corrosion was also found. Combined effect of pitting corrosion and erosive flow increases corrosion rate along the flow direction. This type of corrosion can be prevented by choosing a homogeneous pipe material, applying inhibitors or applying a coating of aggressive substances to the pipe.

References

Groysman, A. and Erdman, N., 2000,A Study of Corrosion of Mild Steel in Mixtures of Petroleum Distillates and Electrolytes, Corrosion, , 56, 1266-1271.

J. Kittel and S.Gonzalez., 2013, Corrosion in CO2 post combustion capture with alkanolamines-A review. Oil & Gas Science and Technology- Rev. IFP Energies nouvelles, France.

Little B.J., Lee, J.S., 2007, Microbiologically Influenced Corrosion, John Wiley & Sons, Inc., Hoboken, New Jersey, pp. 28-34.

Pickthall, T. and Carlile, A., 2005, Predictive Internal Corrosion Monitoring on a Crude Oil Pipeline: A Case Study, NACE Paper No. 05163

Smart, J. and Pickthall, T., 2004, Internal Corrosion Direct Measurement Enhances Pipeline Integrity, NACE Paper No. 04177

Tawancy HM, Al-Hadhrami LM, Al-Yousef FK., 2013, Analysis of corroded elbow section of carbon steel piping system of oil-gas separator vessel. Case Studies in Engineering Failure Analysis,;1:6–14.

Acknowledgements

In this study the author would like thank to PT.Geoservices for various input and insight to the author and all parties who helped in the research.

PROCEEDINGS
JOINT CONVENTION BANDUNG (JCB) 2021
November 23rd – 25th 2021

Lesson Learned: Fracturing Story Continues in Completely New Telisa Formation in B Structure South Sumatera

Reza Alfajri[1], Areiyando Makmun[1]
Pertamina[1]

Abstract
Telisa is a formation in South Sumatera Basin that was famous for its hydraulic fracturing success. In Pertamina, Telisa is found in TL Structure and was successfully treated with hydraulic fracturing. This year, Pertamina found Telisa as a new formation in B-Structure. It has the lowest net pressure yet highest fluid efficiency among other Telisas. Adding low permeability, low young modulus, and non-ideal reservoir behavior to that list, fracturing this formation becomes quite challenging.

The first Telisa formation in B Structure was found in well B-62. The well can only produce intermittently in a space of two months. However, its water cut was as low as 50%. In order to produce the well continuously and increase its productivity, hydraulic fracturing treatment was planned. Since Telisa is considered soft rock with young modulus around 1 million psi, the treatment was designed to use 20/40 proppant to minimize embedment effect. According to petrophysical analysis this formation has 40 mD permeability, therefore treatment design was designed to be aggressive with fracture width as priority instead of half-length.

After performing breakdown, step rate test, and data frac, treatment was redesigned. It turned out that reservoir permeability is not as high as previously estimated. Transmissibility that was acquired from breakdown test data showed that permeability is less than 10 mD, therefore the treatment was switched from aggressive to conservative with half-length as priority. Step down test, and was later confirmed by data frac, it can be inferred that this well has high entry friction at 1300 psi. Data frac also showed presence of fissures from decline curve with concave up shape. Fluid efficiency and pad ratio calculation was adjusted accordingly to handle this non-ideal reservoir behavior. Final design for fracturing treatment was with total of 65,000 lbs 20/40 proppant to target minimum 1.2 FCD, 0.3 inch fracture width, and 2 lbs/ft2 average proppant concentration. Pre-treatment of hundred mesh sand slug was pumped ahead of proppant slurry to reduce entry friction. During main frac job, sand slug failed to reduce entry friction Job was carried out to 6 ppg proppant concentration before loss prime on one of the frac pumps occurred and eventually screen out at the last proppant stage (7 ppg). Total proppant pumped into formation was 44,701 lbs.

Pumping 70% from designed proppant mass was not too bad, however opportunity for improvements was wide opened. There are three things to be considered for next treatments: perforate formation with highest entry hole size available and increase gel viscosity to handle excessive entry friction, pump more sand slug to deal with fissures, and improve pumping system reliability by installing filter to prevent unwanted solid during pumping and performing horse power test to the frac pumps.

Introduction

B Structure in Pertamina is located in South Sumatera. This structure is well known for its heavy oil properties with viscosity in range of 10 – 350 cp at reservoir condition and 15^0 - 22^0 API. This structure produces from two active formation: Talang Akar and Telisa. Figure 1 shows stratigraphy of South Sumatera Basin. It can be seen that Telisa formation is on top of Baturaja Formation.

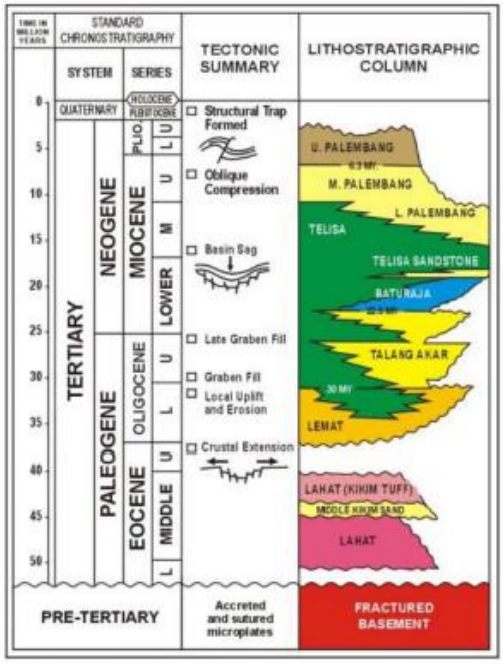

Figure 1 Stratigraphy of South Sumatera Basin (Agarkoesoemah *et al*. 2005)

Telisa formation is closely associated with hydraulic fracturing. In South Balam Field Central Sumatera, this formation has high permeability up to 100 mD. However, hydraulic fracturing is still the completion method chosen for this formation. Poerwanto *et al*. (1995) summarizes that during 1993 to 1994, out of 20 hydraulic fracturing jobs on Telisa Formation in this field, all of the wells generated more than 150 bopd initial production. It means that hydraulic fracturing completion method is suitable for this formation in high permeability Telisa Formation in South Balam Field.

Other Telisa formation with tight properties is in KS Field, Rimau Block, South Sumatera. In this field, Telisa tight sandstone is the primary target of oil production with hydraulic fracturing method as the most suitable completion method (Kamal *et al*. 2018). The results from Telisa wells

in KS Field were also good, considering the wells could not flow without being hydraulically fractured.

New technology of fracturing method called pillar fracturing technique was also performed in Kaji Semoga Field (Azhari *et al*. 2017). This new technique performed in this field resulted better than conventional hydraulic fracturing method by more than ten folds of the wells' peak production.

Telisa formation in B Structure in Pertamina was first discovered in B-062 well. This well was proven in producing oil, however it can't be produced continuously. Figure 2 shows that the well needed 2 – 3 months to be reproduced. Of course operational aspects were also considered to reproduce the well, but the events were evidence that the formation contains oil and the only thing needed was suitable completion method to produce the well continuously. Hence, hydraulic fracturing was then planned and performed.

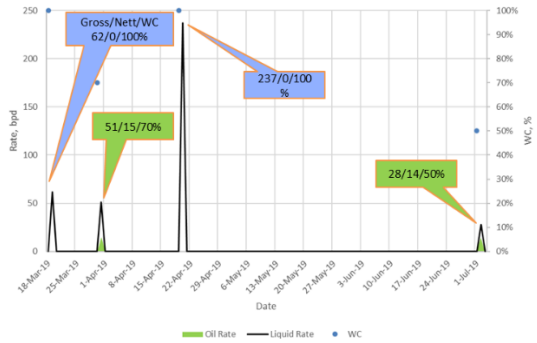

Figure 2 Well B-062 Production Performance

There are three wells that were prepared for hydraulic fracturing pilot in this structure. Two other wells were B-021 and B-020 wells, with more updip position than B-062 wells.

Data and Method

Preparation was made in Well B-062 from cleaning the well by circulation two times well volume, testing and pickling job for fracturing string, to setting and testing packer of fracturing string. Fracturing job sequence that would be performed were breakdown test, step-rate test, data frac (mini frac), and main frac after performing data frac analysis.

Petrophysicist provided permeability data of 40 mD for Telisa formation in this structure, however B-062 cyclic production behavior didn't mirror a 40 mD formation. Performing breakdown test would give transmissibility data that would indicate whether the formation has high or low permeability.

Breakdown test was performed at maximum rate of 17 bpm with maximum tubing pressure of 5200 psi using 4% KCl brine. Total volume injected was 181 bbls. Based on after closure analysis permeability was around 10 mD, tighter than what was predicted from petrophysical analysis. Fracturing design then would need to be switched from aggressive to conservative method with half-length as priority. Figure 3 and 4 show breakdown test pump chart and after closure analysis.

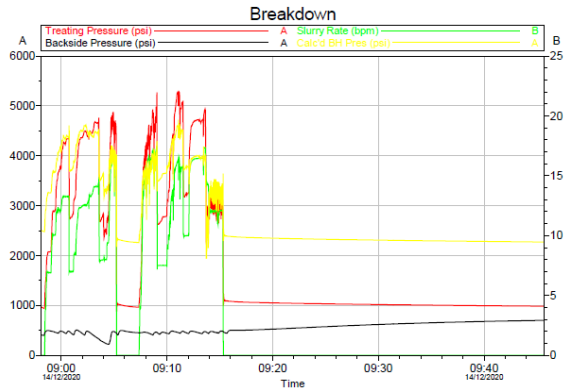

Figure 3 Breakdown Test Well B-062

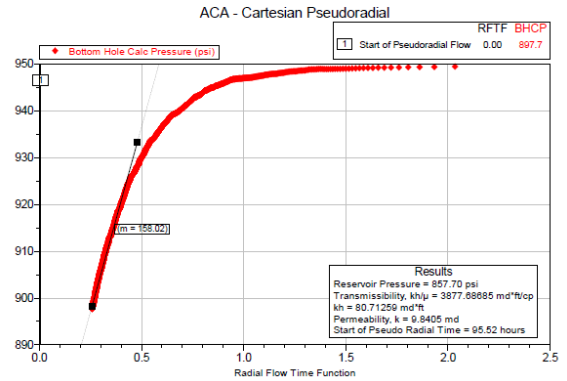

Figure 4 After Closure Analysis (ACA) Well B-062

Step rate test was then executed to know fracture extension rate and pressure and near well bore (NWB) friction. Fracture extension rate and pressure was extracted from step up test and NWB friction was analyzed from step down test. Figure 5 to 8 show step rate test pump chart and the analysis. In Figure 5 step up test started at 1 bpm to 2 bpm for low point analysis and increased per 2 bpm up to 18 bpm. For step down test, 5 points were taken.

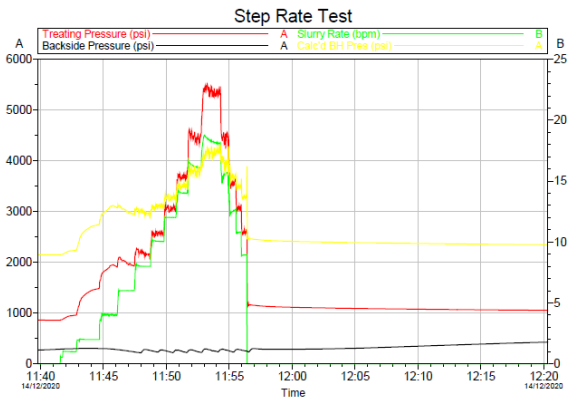

Figure 5 Step Rate Test Pump Chart

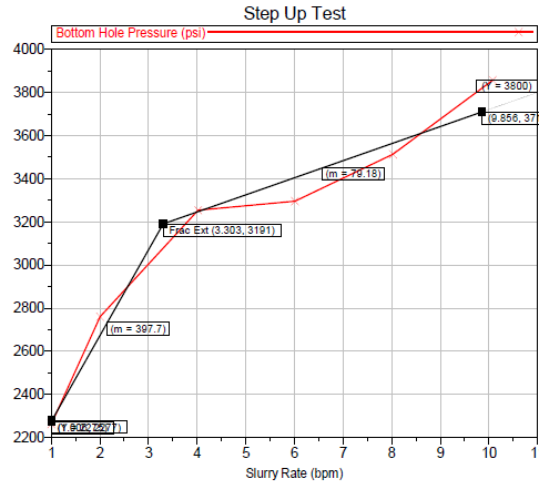

Figure 6 Fracture Extension Rate and Pressure Analysis

Step Down Analysis Input

Surface ISIP, psi:	1165
BH Fluid Density, lb/gal:	7.17
Entry Hole Diameter, in:	0.400
Number of Perfs:	50
Discharge Coefficient:	0.90

Step Down Analysis Results

Effective Perfs:	5.78	Beta Factor:	1.02
Pipe Friction, psi:	2477	Entry Friction, psi:	1731
Perf Friction, psi:	808	NWB Friction, psi:	923
Entry Coeff: 87.74	Perf Coeff: 2.45	NWB Coeff: 216.65	

Step	Rate (bpm)	Pressure (psi)	Pipe Frict (psi)	Entry Frict (psi)	Perf Frict (psi)	NWB Frict (psi)
1	18.15	5392	2477	1731	808	923
2	15.63	4407	1841	1456	599	857
3	12.60	3580	1205	1158	389	769
4	10.83	3056	893	1001	288	713
5	8.93	2608	615	843	196	648

Figure 7 Friction Analysis Results

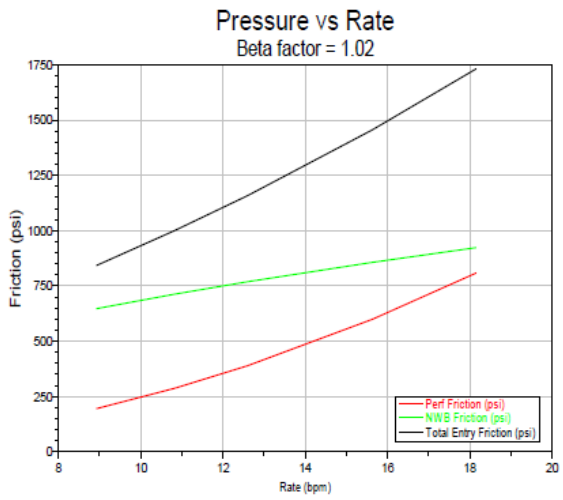

Figure 8 Pressure vs Rate in Friction Analysis

Figure 6 shows that fracture extension pressure was at 3200 psi and fracture extension rate was around 3.5 bpm. So as long as our pressure and rate are more than these numbers, our fracture will keep growing until designed length. Handicap for this well was shown in friction analysis result (Figure 7) that total entry friction for this well was more than 1700 psi. Figure 8 showed that total friction entry was in concave up shape, which means that entry friction was perforation dominated. In order to attempt to ease the NWB friction, hundred mesh (sand slug) would be pumped before pumping designed proppant slurry.

Mini frac was performed to analyze net pressure and fluid efficiency to be later used in final fracturing design. While break down test and step rate test utilized 4% KCL as the pumped fluid, data frac used frac gel. Pumping operated at 16 bpm with total of 231 bbls pumped fluid volume. Figure 9 shows that the gap between pressure before the pump was shut in (around 4200 psi) and the Bottom hole Instantaneous Shut in Pressure (ISIP) (2855) psi was the total NWB friction. It means there are still around 1400 psi NWB friction handicap to handle in this well.

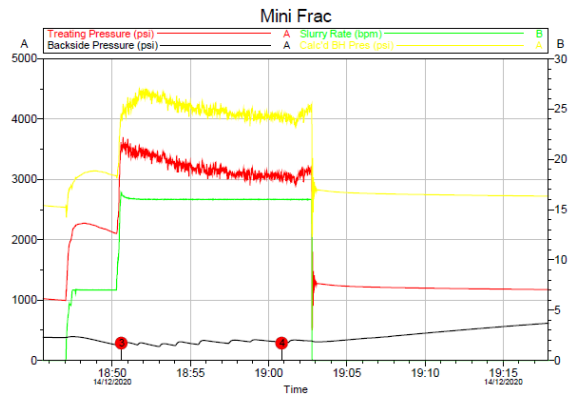

Figure 9 Data Frac Pump Chart

Figure 10 shows mini frac G function analysis. From the chart it can be seen that decline curve shows concave up shape, which indicated presence of fissures in the reservoir. Because of this irregularities, instead of taking G closure from dP/dG or G dP/dG, G time was taken from the interception of the line from bottom hole ISIP to the ¾ point between bottom hole ISIP and closure pressure and the closure pressure line from G dP/dG or dP/dG. This G time was called G^*. From G^* calculation of fluid efficiency was 27%. Fluid efficiency calculation from G closure on G dP/dG curve was 61%. Since this is the first fracturing in Telisa formation B Structure and no previous reference, fluid efficiency for design was the average between G^* calculation and G closure calculation, which was 44%. Pad ratio was then calculated to be 39%. From minifrac data, final design for main frac was laid out as shown in Figure 11 and 12.

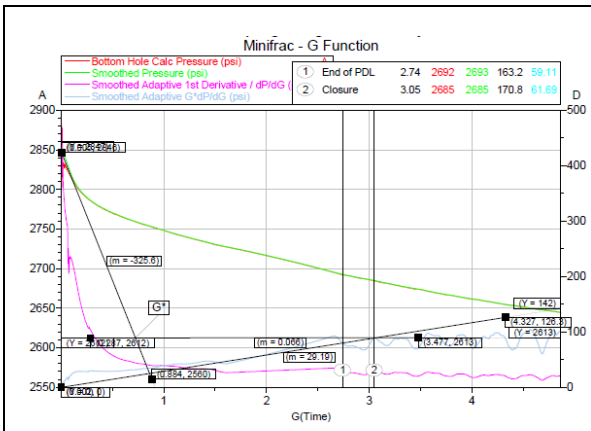

Figure 10 Minifrac G Function Analysis

PROCEEDINGS
JOINT CONVENTION BANDUNG (JCB) 2021
November 23rd – 25th 2021

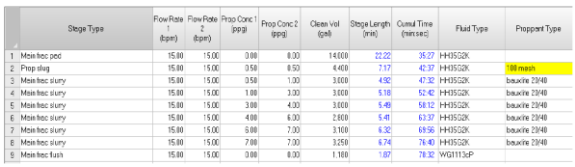

	Stage Type	Flow Rate 1 (bpm)	Flow Rate 2 (bpm)	Prop Conc 1 (ppg)	Prop Conc 2 (ppg)	Clean vol (gal)	Stage Length (min)	Cumul Time (min:sec)	Fluid Type	Proppant Type
1	Main frac pad	15.00	15.00	0.00	0.00	14,000	22.22	35.27	HH35G2K	
2	Prop slug	15.00	15.00	0.50	0.50	4,400	7.17	42.37	HH35G2K	100 mesh
3	Main frac slury	15.00	15.00	0.50	1.00	3,000	4.92	47.32	HH35G2K	bauxite 20/40
4	Main frac slury	15.00	15.00	1.00	3.00	3,000	5.18	52.42	HH35G2K	bauxite 20/40
5	Main frac slury	15.00	15.00	3.00	4.00	3,000	5.49	58.12	HH35G2K	bauxite 20/40
6	Main frac slury	15.00	15.00	4.00	6.00	2,800	5.41	63.37	HH35G2K	bauxite 20/40
7	Main frac slury	15.00	15.00	6.00	7.00	3,100	6.32	69.56	HH35G2K	bauxite 20/40
8	Main frac slury	15.00	15.00	7.00	7.00	3,250	6.74	76.40	HH35G2K	bauxite 20/40
9	Main frac flush	15.00	15.00	0.00	0.00	1,180	1.87	78.32	WG1113cP	

Figure 11 Main Frac Pump Schedule

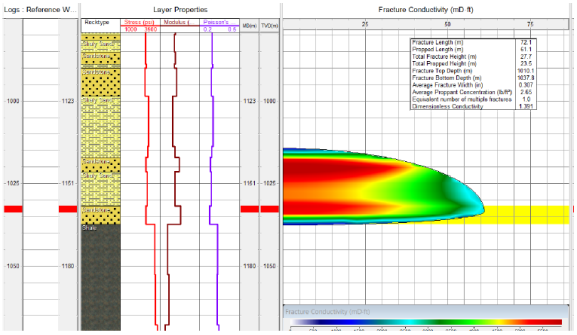

Figure 12 Fracture Geometry Design for B-062

Total proppant that would be pumped was 65 klbs 20/40 proppant preceded by 100 mesh sand slug. From fracture geometry design in Figure 12 showed that dimensionless fracture conductivity (FCD) was more than 1.2, fracture width was more than 0.2 inch, and average proppant concentration was more than 2 lbs/ft^2. These three parameters showed that this design was quite good and ready to be executed.

Result and Discussion

Main frac was then executed with pump chart and event log shown in Figure 13 and 14.

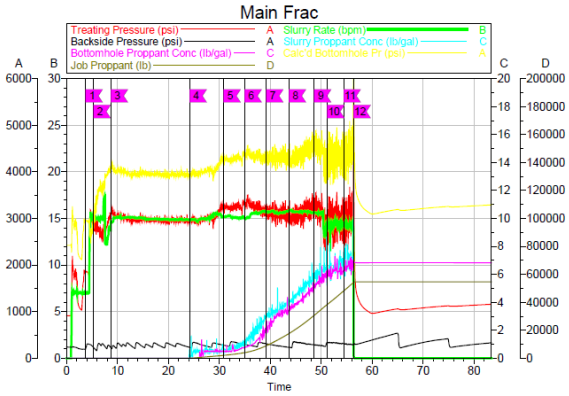

Figure 13 Main Frac Pump Chart

Local Event Log

	Intersection		TP	SR	BP	SPC	BPC	CBP
1	Crosslink Test	3.73	1871	6.993	199.6	0.000	0.000	2967
2	PAD	5.29	3045	15.02	229.9	0.000	0.000	3110
3	Rate adjustment	8.69	3096	14.56	227.4	0.000	0.000	4075
4	0.5 ppg Sand slug	24.17	2937	14.86	233.7	0.309	0.000	3923
5	0.5 - 1 ppg Prioppant	30.82	3296	15.16	280.9	0.610	0.486	4327
6	1 - 3 ppg Proppant	34.96	3361	15.01	297.4	1.097	0.769	4421
7	3 - 4 ppg Proppant	39.20	3146	15.70	306.5	2.946	1.769	4302
8	4 - 6 ppg proppant	43.65	3285	15.84	234.6	4.047	3.455	4509
9	6-7 ppg Proppant	48.61	3353	15.65	291.7	5.802	5.266	4678
10	Rate Decreased	51.19	3133	14.21	330.4	6.134	5.926	4542
11	7 ppg Proppant	54.39	3236	14.32	314.2	6.907	6.301	4643
12	Screen Out	56.34	4976	5.243	307.5	7.864	6.897	6781

Figure 14 Main Frac Event Log

Figure 13 and 14 show that erratic treating pressure started from 3-4 ppg slurry stage that forced a decrease in pumping rate in 6-7 slurry stage, and the pumping ultimately ended because of early screen out at 7 ppg slurry stage on minute 56th. The erratic treating pressure was suspected either due to pump problem or because outside material was accidentally pumped into the fracturing system. Investigation was carried out in order to know the root cause of early screen out as well as erratic treating pressure behavior that preceded the screen out. Figure 15 shows summary of the main treatment.

Main Treatment

Parameter	Value	
Average Rate	15	bpm
Maximum Tubing Pressure	4877	psi
Maximum Annulus Pressure	355	psi
Type of Fluid	**Hybor H3.5411**	
Type of Proppant	**Bauxlite 20/40**	
Fluid Pumped (Clean)	749	bbl
Slurry Pumped	807.00	bbl
Proppant Summary		
Design	65000	lbs
Sand Slug (100 Mesh) pumped	2200	lbs
Proppant pumped	52451	lbs
Proppant in wellbore	7750	lbs
Proppant in formation	44701	lbs

Figure 15 Main Frac Treatment Summary

Figure 15 show that 44,701 lbs proppant was successfully pumped into formation (69% of 65,000 lbs design). After performing investigation, improper suction frac valve condition was found. The root cause for this was solid material that was accidentally pumped during the frac job and stuck inside frac valve (Figure 16). All of the equipment was checked prior to the job and in a good condition. Due to alien material that was found in the investigation, precautions were planned to prevent this to happen in the future by installing screens / filters on the fresh water tank and on suction blender.

Figure 16 Investigation Result Showed Improper Suction Frac Valve Condition due to Unwanted Pumped Solid Material

This early screen out really affected the fracturing result. Well B-062 can only produce half of total fluid pumped during fracturing sequence and then was back to low influx. During unloading, the well's fluid sample indicated fines migration occurred because there was 0.35% basic sediment number (Figure 17).

PROCEEDINGS
JOINT CONVENTION BANDUNG (JCB) 2021
November 23rd – 25th 2021

Figure 17 Fines Migration Occurred After Frac Job

Lesson learned from this first hydraulic fracturing in B Structure Telisa Formation was as follow:

- There was indication of non-ideal reservoir behavior in the presence of fissures.
- High NWB friction (around 1400 psi total NWB friction).
- Fines migration occurred after the job, which means next job clay stabilizer material needs to be evaluated.
- There was so many room of improvement in the operational aspects to make next job better.
    - There was doubt on reliability of frac pumps. Prior to the job, inspection was performed to all the equipment, however for the pumps, hydraulic horse power (HHP) test was not performed. Pump condition was checked by the report of last preventive maintenance. HHP should be performed for the future job.
    - Screens / filters were needed in some locations to prevent outside material to intrude fracturing system.
    - Evaluation on the number of personnels on site for performing fracturing job need to be evaluated to ensure smooth operation for the next job.

Figure 18 shows production performance of Well B-062 after fracturing job. Production under orange shade the well's performance after fracturing job. It can be seen that the well was still in unloading pumped fluid/gel phase. Total fluid recovered was only 564 bbls from total 1408 bbls fluid (980 bbls frac gel) pumped during the job. The well could not be produced anymore due to fines migration combined with the failure in meeting the fracturing design.

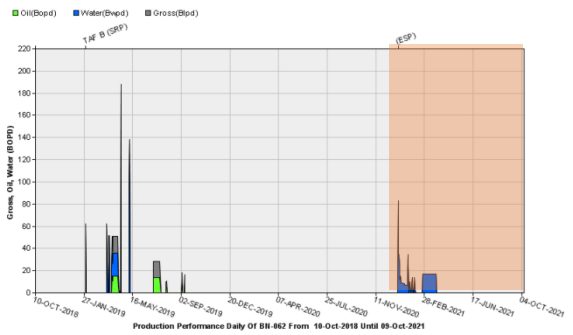

Figure 18 Production performance of Well B-062 after fracturing job

For the next job several mitigations was taken to attempt for a better job execution:

- In order to try to reduce NWB friction, aside from using hundred mesh sand slug during the job, perforation shape charge selection would be taken with more attention. The selection would be more on the hole diameter rather than penetration. The size of 0.4" minimum hole diameter was required, and it can fulfilled because 0.43" diameter was available in B Structure.
- Performing Hydraulic Horse Power (HHP) test for all the frac pump would increase the belief on the reliability of the pump.
- Instead of using 4% KCl brine as clay stabilizer, 7% KCl brine was used to attempt preventing fines migration. The increase of in KCl concentration was decided after the occurrence of fines migration after fracturing job. Laboratory test was needed to confirm the effectiveness of increasing this clay stabilizer.
- Screens / filters were installed when receiving fresh water from vacuum truck and on suction blender to prevent solid material from outside entering fracturing system.
- Additional frac crew would be available for the next job.

With all the lesson learned above, a better job on the operational aspect was expected. This job showed that no matter how good a fracturing design is, proper materials, equipment, personnels, and preparation needs to be paid attention too. If both design and operational aspects of hydraulic fracturing job have already been taken care meticulously, then the result will follow.

Conclusions

Development of Telisa Formation in B Structure is still not conclusive. Further evaluation on subsurface and completion aspect need to be paid more attention. In the completion part for hydraulic fracturing, operational aspects need to be paid attention in the same amount if not more than the design. No matter how good the design is, if operational is a disaster, bad results will follow. However, when unwanted outcome occurred, lesson learned from that experience need to be paid attention to for better jobs in the future.

References

Argakoesoemah, R.M.I et al., 2005, Telisa Shallow Marine Sandstone as an Emerging Exploration Target in Palembang High, South Sumatera Basin. Thirtieth Annual Convention & Exhibition IPA, Jakarta, Indonesia.

Azhari, M., Prakoso, N.F., Ningrum, D., et al., 2017, Unlocking Depleted and Low-Modulus Telisa Sandstone Reservoir with Pillar Fracturing Technique: Well Performance Improvement Comparison with Conventional Fracturing. SPE/IATMI Asia Pacific Oil and Gas Conference & Exhibition, Jakarta, Indonesia.

Kamal, H., Fajar, P.N., Geraldus, Y., et al., 2018, Successful Hydraulic Fracturing Optimisation in Field through Fracture Height Growth Identification and Mitigation, SPE Asia Pacific Oil & Gas Conference & Exhibition, Brisbane, Australia.

Poerwanto, J.H., Sugembong, C.F., Bagzis, J.M, et al., 1995, Application of Hydraulic Fracturing Technologies to the Shallow Telisa Formation, SPE Asia Pacific Oil and Gas Conference & Exhibition, Kuala Lumpur, Malaysia.

Acknowledgements (Optional)
My gratitude to Mr. Areiyando Makmun for his time, insights, and advices during designing and executing this job, and to all of my comrades from Pertamina and service company involved in this project.

PROCEEDINGS
JOINT CONVENTION BANDUNG (JCB) 2021
November 23rd – 25th 2021

Tanjung-Balikpapan Oil Transportation Pipeline Modeling using PertafloSIM – Software developed by Pertamina Upstream Research & Technology Innovation (URTI)

Merry Marteighianti[1], Agus Wibowo Benny[1], Belladonna Maulianda[1], Sudariyanto[1], Welly Setyawan[1], Andre Albert Sahetapy[1], Erma Nur Prastya Ningrum[1], Sumadi Paryoto[1], Hasian P. Septoratno Siregar[2], Darmadi[2]

Abstract

In order to reduce company's dependence on commercial software, PT Pertamina (Persero) represented by the Upstream Research & Technology Innovation department under cooperation with Bandung Institute of Technology has developed in-house software for modeling fluid flow in pipes and wells called PertafloSIM (Steady-State Multiphase Flow Simulator). A study has been conducted to modelling the Tanjung-Balikpapan Oil Transportation Pipeline system using PertafloSIM. The purpose of this study is to test the capability of the PertafloSIM in calculating multiphase flow in pipes including pressure drop calculations based on current flow conditions. The case study used is an oil-water suspension from Tanjung Field which is flowed through a 230 km pipeline to Balikpapan. The regulation of the oil-water suspension ratio also becomes crucial in this transportation system.

The first step is carried out by entering the data reported form the field such as pipe length, outside diameter, inside diameter, elevation, and roughness into PertafloSIM software as well as Oil-Water rate, temperature, API Gravity, Upstream and Downstream Pressure. The PertafloSIM module used in this case study is "Multiphase Black-Oil" which is a module to simulate multiphase flow in pipeline network by using black-oil approach. Furthermore, we run the PertafloSIM software based on the inputted field data and then do a review and analysis.

The results show that changes in inside diameter have the most significant impact compared to other parameters, so we suspect an indication of a narrowing of the pipeline diameter in the field which can be caused by several things such as deposition/scale. We also compare run results between PertafloSIM and PipeSIM Software. Based on the results of study, it shows that PertafloSIM Software is able and reliable to calculate multiphase flow in pipeline.

Introduction

To reduce company's dependence on commercial software, PT Pertamina (Persero) represented by the Upstream Research & Technology Innovation department has developed in-house software for modeling fluid flow in pipes and wells called PertafloSIM (Steady-State Multiphase Flow Simulator under cooperation with Bandung Institute of Technology. PertafloSIM software has proven its capabilities with various types of data compared to commercial software such as PipeSIM. The purpose of this study is to continue testing the capability of PertafloSIM software in calculating multiphase flow in pipes including pressure drop calculations based on current flow conditions.). The case study used is Tanjung-Balikpapan Oil Transportation Pipeline system.

Tanjung field is located in South Kalimatan province of Indonesia, it was discovered in 1937 and located about 230 Km from the nearby Oil Refinery in Balikpapan, East Kalimantan Province (Fig.1). In order to transport Tanjung crude through long hilly pipeline, mixing with water is one of the alternatives that had been chosen, and considered as the most effective way of transport the crude. Mixing ratio of water and Tanjung crude is currently about 65% Tanjung Crude and 35% Water. Mixing of the water and crude is done on a special mixing device, which able to uniformly mix water and crude in the middle of pipe diameter. The regulation of oil-water mixing ratio becomes crucial in this transportation system, it will determine how the flow behavior of the fluid and also the pressure drop of the flow. This condition will be critical for the transport when it flows through uphill and downhill pipeline.

Figure 1: Crude Oil Pipeline Route Tanjung-Balikpapan

Data and Method

Tanjung-Balikpapan Oil Transportation across hilly terrain, which include two main hill about 240 m elevation above sea level. Before refinery, pipeline cross 4.4 Km Balikpapan bay in about 10 m water depth. The pipeline elevation profile is shown in Figure 2. There are 2 Booster Pump between Tanjung to Balikpapan, they are Booster Station I at Batu Butok, and Booster Station II at Longikis. Tanjung-Balikpapan Route Schematic can be seen at Figure 3. The pipeline is 20-inch diameter with total length 237.12 Km.

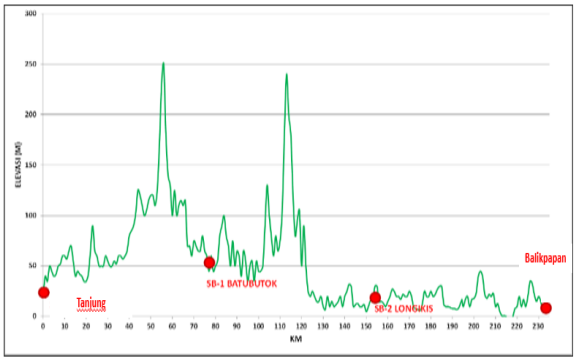

Figure 2: Tanjung-Balikpapan Pipeline Elevation Profile

PROCEEDINGS
JOINT CONVENTION BANDUNG (JCB) 2021
November 23rd – 25th 2021

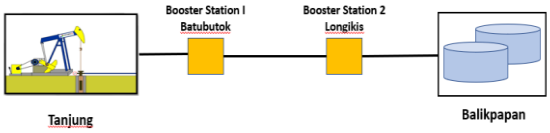

Figure 3: Tanjung-Balikpapan Route Schematic

The first step is carried out by entering data reported from the field such as pipe length, inside diameter, outside diameter, elevation, and roughness, as well as flow rate, temperature, API Gravity and Pressure into PertafloSIM Software. At this stage, the PertafloSIM calculation result will first be validated against the field data, The PertafloSIM module called "Multiphase Black-Oil" will be used in this case study. Furthermore, several scenarios for optimization are carried out such as the sensitivity of the percentage ratio of oil and water as well as pipe diameter. Flow chart of the methodology used can be seen figure 4, while PertafloSIM input data for network model, pipeline segment properties, pipeline elevation profile, and "Source" data can be seen in figure 5 until figure 12.

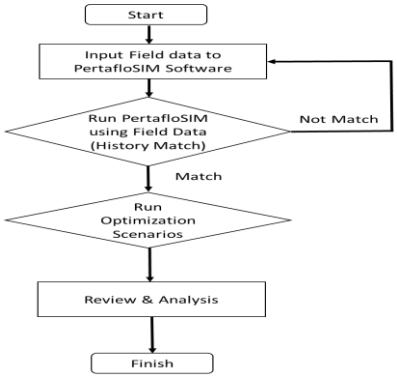

Figure 4: Flow Chart Methodology

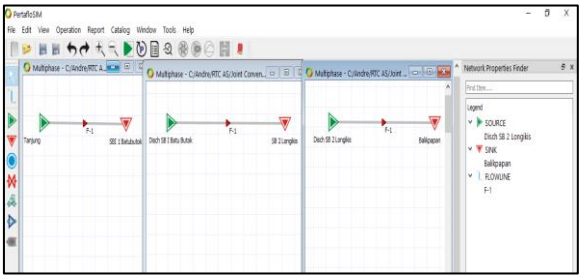

Figure 5: PertafloSIM Network Model

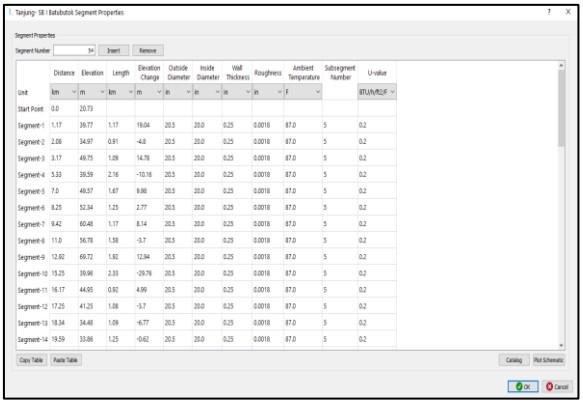

Figure 6: Tanjung – SB I Batubutok Segment Properties

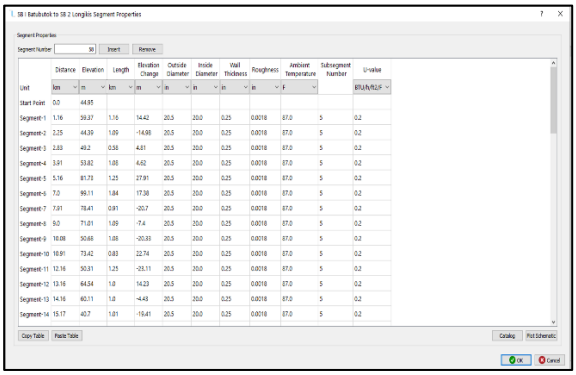

Figure 7: SB I Batubutok – SB II Longikis Segment Properties

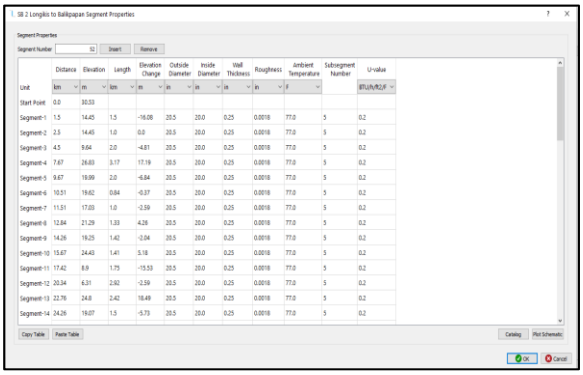

Figure 8: SB II Longikis – Balikpapan Segment Properties.

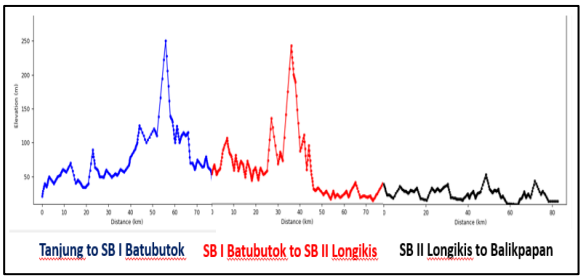

Figure 9: Pipeline Elevation Profile

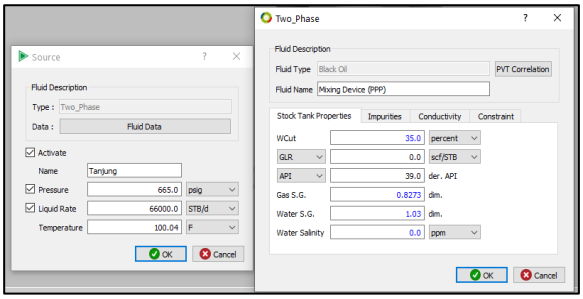

Figure 10: Tanjung "Source" Data

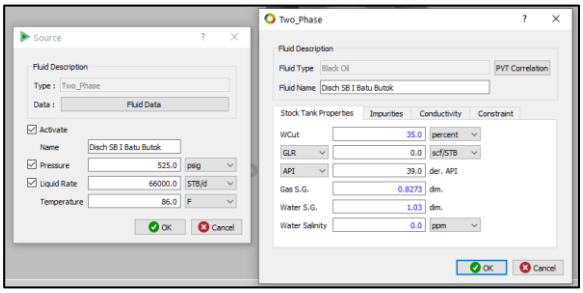

Figure 11: Booster Station I Batubutok Data

PROCEEDINGS
JOINT CONVENTION BANDUNG (JCB) 2021
November 23rd – 25th 2021

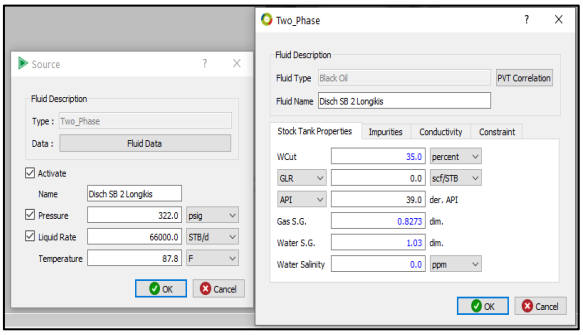

Figure 12: Booster Station 2 Longikis Data

Result and Discussion

The results of the PertafloSIM run using current field data are shown in Table 1, where the outlet pressure/SINK in PertafloSIM has been set as "calculated" so the software will calculate the amount of pressure in the SINK based on input data in SOURCE. The results of the outlet pressure calculation are shown in table 2, where there is a difference between the outlet pressure calculated by PertafloSIM compared to the actual pressure in the field.

PertafloSIM Calculation using current Field Data						
Inlet	Outlet	Inlet Pressure	Outlet Pressure	Pressure Drop	Inlet Temperature	Outlet Temperature
		psig	psig	psig	F	F
Tanjung	SB I Batubutok	665	525.95	139.05	100	91.7
SBI I Batubutok	SB II Longikis	525	441.15	83.85	86	82.8
SB II Longikis	Balikpapan	322	241.91	80.09	87.8	83.8
Actual Field Data						
Inlet	Outlet	Inlet Pressure	Outlet Pressure	Pressure Drop	Inlet Temperature	Outlet Temperature
		psig	psig	psig	F	F
Tanjung	SB I Batubutok	665	420	245	100	86
SBI I Batubutok	SB II Longikis	525	168	357	86	87.8
SB II Longikis	Balikpapan	322	39.2	282.8	87.8	87
Data to be validated						

Table 2: Comparison between PertafloSIM Run Results and Field Data.

Based on this, we tried to take several approaches so that the calculation results of PertafloSIM approach the actual field data, such as changing the oil-water ratio, and pipeline inside diameter. Figure 13 is the result of the sensitivity analysis between the change of Oil-Water ratio from 85%:15%, 75%:25%, 65%:35%, 55%:45%, and 45%:55% to the result of outlet pressure at SB I Batubutok, where it can be seen that the change in the oil-water ratio does not have a significant impact on outlet pressure at SB I Batubutok so that in the end it will not have an impact on pressure drop in Tanjung-SB I Batubutok Pipeline and and also the pipeline as a whole.

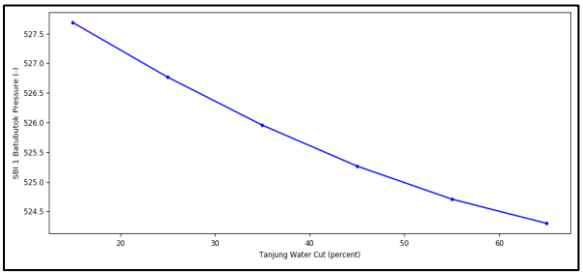

Figure 13: PertafloSIM Sensitivity Analysis Result (Tanjung Water Cut vs Outlet Pressure at SB I Batubutok)

Figure 14 is the result of the sensitivity analysis between the change of inside diameter of Tanjung-SB I Batubutok pipeline to outlet pressure that occur at SB I Batubutok, it can be seen that the inside diameter value which is close to the actual field outlet pressure data is about 17-inch.

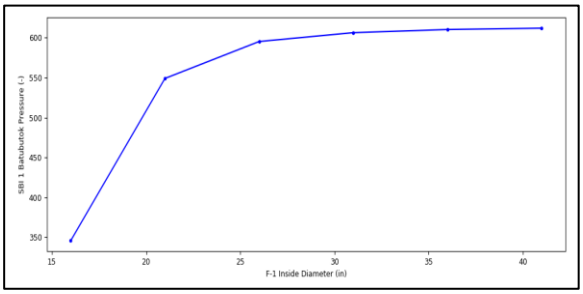

Figure 14: PertafloSIM Sensitivity Analysis Results (Inside Diameter of Tanjung – SB I Batubutok vs Outlet Pressure at SB I Batubutok).

Figure 15 is the result of the sensitivity analysis between the change of inside diameter of SB I Batubutok-SB II Longikis pipeline to outlet pressure that occur at SB II Longikis, the inside diameter value which is close to the actual field outlet pressure data is about 15-inch.

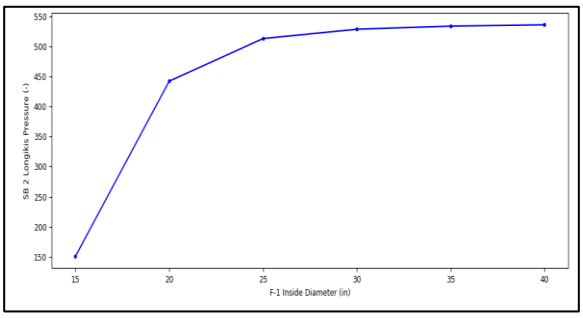

Figure 15: PertafloSIM Sensitivity Analysis Results (Inside Diameter of SB I Batubutok – SB II Longikis vs Outlet Pressure at SB II Longikis).

Figure 16 is the results of outlet pressure at Balikpapan in the form of a node summary, where the inside diameter closest to the actual field data is about 16-inch.

Node Summary

	Name	Type	Pressure	Temperature	Oil Rate	Water Rate	Gas Rate
Unit	-	-	psig	F	STB/d	STB/d	MMscf/d
	Disch SB 2 Longikis	Source	322.0	87.8	42900.0	23100.0	0.0
	Balikpapan	Sink	40.413333	84.47682	42900.0	23100.0	0.0

Figure 16: PertafloSIM Node Summary Results of Outlet Pressure at Balikpapan.

Based on the results of history matching above, changes in inside diameter have the most significant impact compared to other parameters, so we suspect an indication of a narrowing of the pipeline diameter in the field which can be caused by several things such as deposition/scale. The results from Figures 14 to 16 also show that the optimum diameter of the pipeline that produces the lowest pressure drop is around 30-inch.

Table 3 shows PertafloSIM results if not consider two booster pump so that the flow from Tanjung is "direct" to Balikpapan, and then use the above pipeline diameters that match the field data (17-inch, 15-inch, and 16-inch), it can be seen that there was a significant pressure drop from SB I Batubutok to SB II Longikis (about 358.4 psig), while PertafloSIM could not generate the pressure calculation results in Balikpapan, this is presumably because with the existing pipeline diameter and elevation data input, the flow fluid from SB II Longikis cannot reach Balikpapan. Thus,

PROCEEDINGS
JOINT CONVENTION BANDUNG (JCB) 2021
November 23rd – 25th 2021

based on this, it can be a recommendation to operators in the field to operate the SB II Longikis booster pump only.

PertafloSIM Calculation (without booster pump)					
Inlet	Outlet	Inside Diameter	Inlet Pressure	Outlet Pressure	Pressure Drop
		inch	psig	psig	psig
Tanjung	SB I Batubutok	17	665	420	245
SBI I Batubutok	SB II Longikis	15	420	61.6	358.4
SB II Longikis	Balikpapan	16	61.6	NaN	-

Table 3: PertafloSIM Calculation Results using Match Pipeline Diameter and Without Booster Pump.

We also tried to analyze the calculation of the minimum Tanjung pressure to reach Balikpapan without using two booster pumps, Figure 17 shows the sensitivity analysis of changes in Tanjung pressure to changes in Balikpapan pressure, it can be seen that the Tanjung pressure needed to reach Balikpapan without a booster pump is around 900 psig.

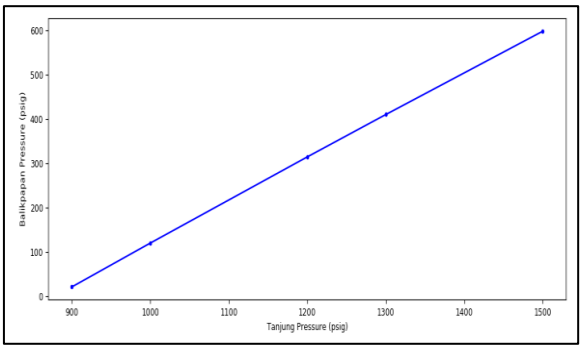

Figure 17: PertafloSIM Sensitivity Analysis Result (Tanjung Pressure vs Balikpapan Pressure) – No booster Pump Consideration.

We also calculated the Tanjung-Balikpapan pressure drop with Commercial Software (PipeSIM) and compared the results with the PertafloSIM calculation (Figure 18), while we used the same inside diameter data as the field data, it can be seen that although there are differences in some pressure points between PertafloSIM and PipeSIM, the pressure drop pattern produced by the two softwares is overall quite similar, so this is a confirmation that if the Tanjung-Balikpapan pipeline data is run with the PipeSIM software, the results will be similar to PertafloSIM..

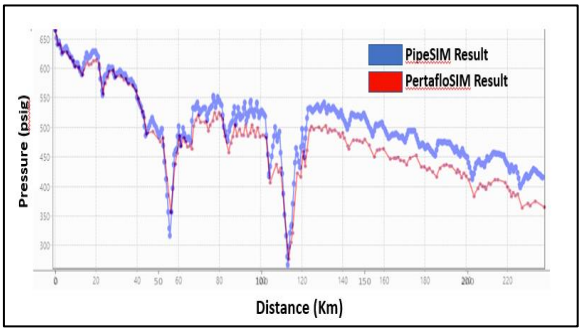

Figure 18: Pressure Drop Comparison between PertafloSIM and PipeSIM

Conclusions

1. A simple pipe modeling and simulation of oil-water flow through a hill was simulated to describe flow behavior such as pressure drop.
2. Regulation of Oil-Water Ratio do not significantly affect the pressure drop performance of the Tanjung-Balikpapan pipeline.
3. Based on the results of history matching to current Field Data, changes in inside diameter have the most significant impact compared to other parameters, so we suspect an indication of a narrowing of the pipeline diameter in the field which can be caused by several things such as deposition/scale.
4. PertafloSIM calculation results show that fluid from Tanjung to Balikpapan can still flow if only activating one booster pump in SB II Longikis and deactivating one booster pump in SB I Batubutok, while without activating two booster pumps, the minimum pressure required at Tanjung is around 900 psig (previously 665 psig).
5. From the results of the comparison of pressure performance between PertafloSIM and PipeSIM both are quite similar, so if the Tanjung-Balikpapan pipeline data is run using the PipeSIM software, the results will be similar to PertafloSIM..
6. More accurate model will be done in future to evaluate other aspects of High Pour Point Transport in pipeline.

References

PERTAMINA Report., 2020, Maintenance and Development PertafloSIM,
PERTAMINA EP Tanjung, 2020, Overview Tanjung Field.
Putra, A. S., and Waspodo, 2004, Society of Petroleum Engineering, SPE 86929

Acknowledgements

The author would like to thank PT PERTAMINA (PERSERO) for permission and support to publish this paper.

PROCEEDINGS
JOINT CONVENTION BANDUNG (JCB)2021
November 23rd – 25th 2021

Temperature Monitoring Operation for Medium Voltage Switchgear by Using Thermal Sensor and Partial Discharge Aler by using Radio Frequency at CPP Gundih Pertamina EP Cepu Field

Febrian Surya Perkasa, Pertamina EP Sukowati Field
Saiful Adib , Pertamina EP

Abstract

CPP Gundih is one of the Central Processing Plant which operated in Pertamina EP Asset 4 – Field Cepu. Electrical power supplied by Gas Turbine Generator (GTG) which distribute by using Medium Voltage Switchgear. During operation, operator or technician cannot measure temperature operation inside switchgear. Temperature inside switchgear should be known for analyze, is there any abnormal for each installation which have potency for failure operation.

If we use Temperature Gun, we cannot measure data of temperature because thickness of panel is thick. By using Temperature Sensor directly on the circuit breaker arms, cable connection bus bar, we can measure temperature operation during Medium Voltage operation with real time condition and directly.

Other side, if there are abnormal condition especially about Partial Discharge condition. Partial Discharge is an electrical discharge or spark that bridges a small portion of the insulation between two conducting electrodes. Partial Discharge can happen at any point in the insulation system, where the electric field strength exceeds the breakdown strength of that portion of the insulating material. Partial Discharge can occur across the surface of insulating material (mainly due to contaminants or irregularities), within gas bubbles in liquid insulation, in voids within solid insulation or around an electrode in gas (corona activity). By using Ultra High Frequency (UHF) antennas, we can measure the wave of Partial Discharge effect and monitor by graphic chart for real time condition. After get the data, we can analyze and can prevent un-planned shut down by Partial Discharge Effect. So, we can do Predictive Maintenance and eliminate failure potency at CPP Gundih.

Introduction

Pertamina EP Asset 4 have three location Central Processing Plant (CPP), two at Donggi – Matindok and one at Gundih, Cepu. CPP Gundih has been operated since 2012 which built by IKPT. Power distribution at CPP Gundih is generated by Gas Turbine Generator (GTG). For distribution, CPP Gundih have Medium Voltage (MV) Switchgear and Low Voltage (LV) Switchgear. During operation, Operation & Maintenance can not measure temperature condition or abnormal condition inside Switchgear Cubicle. The reason why we should measure temperature is to know the condition of bus bar and during operation, the voltage operation is too high which can impact the heating of material inside of Switchgear. That's why, we developed a system which can measure the operation condition of Switchgear by using Thermal Sensor.

Data and Method

This system was created and held during Turn Around CPP Gundih, at September 2019, during all operation was shut down. This activity was started from prepare all the Thermal Sensor and tested for communication operation.

Picture 1.1 Thermal Sensor

And continue for marking each area which the sensor would be installed by Thermal Sensor. Before check or marked the area, make sure the power of switchgear was clear.

Picture 1.2 Object Location

At CPP Gundih, there area five area for Switchgear Cluster. There are SWGR-4100, SWGR-4101, SWGR-4111,SWGR-4112, & SWGR-4113.

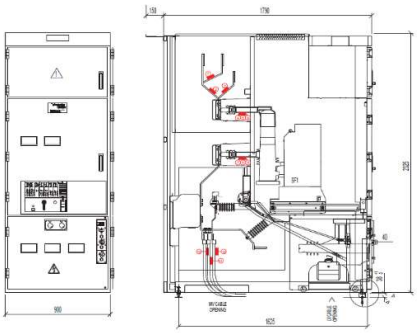

Picture 1.3 Marking Area for MC Set

PROCEEDINGS
JOINT CONVENTION BANDUNG (JCB)2021
November 23rd – 25th 2021

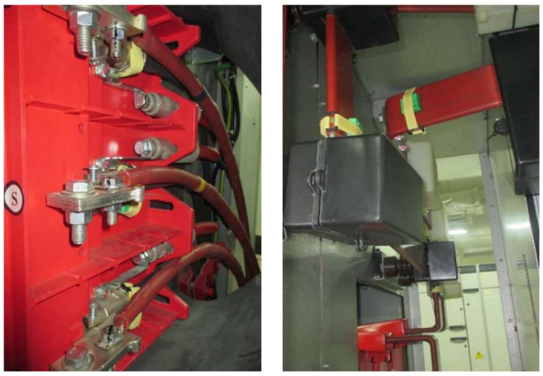

Picture 1.4 Installation on Bus Bar

All the sensor was installed at marking areas, inside the Switchgear.

Picture 1.5 Method of Sensor Installation

After all the sensor was installed, every sensor should be tested to communicate with small router, to check is there any failed communication during send the data.

Picture 1.6 Communication Device

All data was sent to server and displayed at LCD Display which already developed by team and can know each area. Before sending to HMI, all data collect in PLC to generate at HMI display.

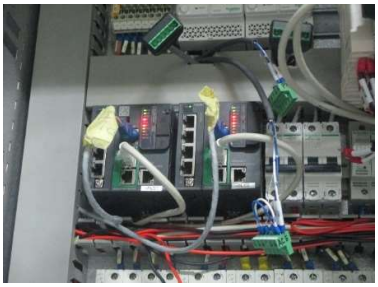

Picture 1.7 PLC Device

Picture 1.8 HMI Device

Result and Discussion

By using this thermal sensor, Temperature Parameter can measured directly with real time condition. With this data, Operation can know if there are some abnormal condition, especially if there are Partial Discharge.

Others, all the data are displayed at LCD and Connected to SCADA Server. Using this device, we can know every data trending if there are some abnormal.

Pengukuran Temperatur pada Koneksi Kabel (°C)		
Sensor 1	Sensor 2	Sensor 3
27	27	28
27	27	28
27	27	29
28	29	27
28	28	28
27	29	29

Pengukuran Temperatur pada Busbar (°C)		
Sensor 4	Sensor 5	Sensor 6
35	35	36
35	35	36
35	34	36
36	35	36
35	36	36
35	36	35

Pengukuran Temperatur pada Contact face (°C)		
Sensor 7	Sensor 8	Sensor 9
37	35	36
36	35	36
36	37	36
37	37	36
36	36	37
35	35	36

PROCEEDINGS
JOINT CONVENTION BANDUNG (JCB) 2021
November 23rd – 25th 2021

Conclusions

With this data, we can do Predictive Maintenance and continue with Preventive Maintenance.
So, failure operation from electrical can minimize and Loss Production Opportunities potency can be eliminated.

References

Schneider Electric

Acknowledgements (Optional)

We would like to thank RAM Pertamina EP Field Cepu, SF-MPE Asset 4 & OM Titis Sampurna for supporting this supervise during installation on site. And authors wish to thank for Schneider Electric Indonesia teams for supporting in this project

PROCEEDINGS
JOINT CONVENTION BANDUNG (JCB)2021
November 23rd – 25th 2021

Eliminated Shutdown Thermal Oxidizer (TOx) by Manipulated Wave Signal of Flame Scanner with UV-IR Wave

Febrian Surya Perkasa, Pertamina EP Sukowati Field
Haritsa Hammami , Pertamina EPCepu Field

Abstract

CPP Gundih is one of the Central Processing Plant which operated in Pertamina EP Asset 4 – Field Cepu. One of the facilities in CPP Gundih is Thermal Oxidizer (TOx) which used for processing / combusting acid gas which generated from sweetening gas process to reduce air polution in many chemical plants that decomposes hazardous gas at a high temperature. For operate TOx, there are some Instrument equipments supported to control, measure and protect during operation.

Previously, TOx in CPP Gundih used Flame Scanner with UV (Ultra Violet) Type to monitor firing operation inside TOx. Output data from Flame Scanner was used to control from PLC. PLC is hardware which have function to control and generate some data by using cause & effect matrix. Unfortunately, during 7 years operation, Flame Scanner which installed at TOx CPP Gundih always override because the signal strength from Flame Scanner was too low (less than 50%) and could not detect actual firing condition inside TOx and this issue was so dangerous because flame scanner triggered cause & effect for shut down system. If the operation didn't do override, TOx will shut down and probably loss production because of this case.

By that case, Maintenance teams tried to solved the problem by manipulating wavelength range of Flame Scanner, concern range of radiation. We replaced existing flame scanner from UV Type became UV – IR (Infa Red), which combination of UV and IR wavelength can cover wider radiation spectrum. All known electromagnetic radiations are customarily arranged monotonically according to their energy in a continuum called the *electromagnetic spectrum*. The electromagnetic spectrum spans many orders of magnitude in energy and, correspondingly, in frequency and wavelength. The optical radiation range is located between microwave radiation and X-rays. The optical radiation range is composed, in order of increasing energy, of infrared, visible, and ultraviolet radiation. Fortunately, after replaced flame scanner by using UV-IR Type, the signal strength was high, above 80% and operation don't do override again.

Introduction

CPP Gundih have some sequence process to generated natural gas become raw gas for selling to buyer. One of important sequence is Thermal Oxidizer (TOx) which which used for processing / combusting acid gas which generated from sweetening gas process to reduce air polution in many chemical plants that decomposes hazardous gas at a high temperature.

TOx equipped which some instrument equipment, especially for measurement and controlling the process. Process control method at TOx used Programmable Logic Controller (PLC) which operated or controlled by using cause & effect diagram , beside used cause & effect , PLC at TOx used Burner Management System (BMS) to control burning sequence inside TOx.

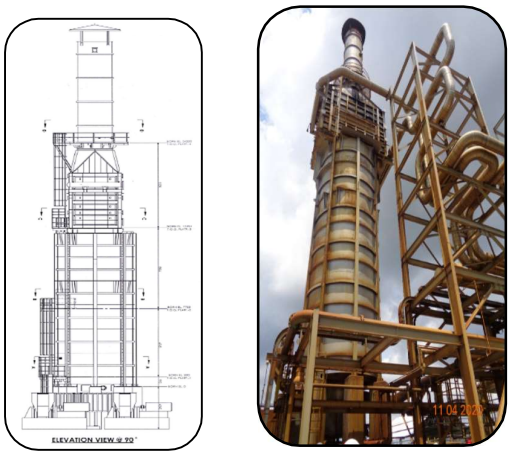

Figure 1. Drawing & Site Condition of Thermal Oxidizer at CPP Gundih

At TOx , there are some sequence process. One of them is burning process, which firing process from acid gas to eliminated Hydrogen Sulfide content and heat transfer for Waste Heat Recovery Unit (WHRU) . During firing process, there are three Flame Scanners used for detection flame condition inside TOx.

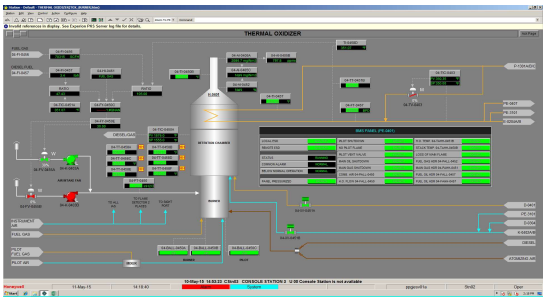

Figure 2. HMI from DCS for Thermal Oxidizer

Unfortunately, previous flame scanner used Ultra Violet (UV) type and cause the logic at PLC should be Override. The cause override was about signal strength from Flame Scanner was to low (less than 20%) and minimum requirement for normal operation should be above 20% to avoid un-planned shutdown. That's why the operation team should override to eliminated un-planned shutdown.

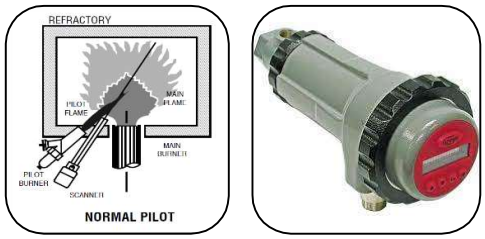

Figure 3 Flame Scanner philosophy and unit type

PROCEEDINGS
JOINT CONVENTION BANDUNG (JCB)2021
November 23rd – 25th 2021

Data and Method

Basic Theory
When acid gas firing inside TOx, gas flame appearance was unpredictable because depend on gas composition. It could be blue flame color or orange color or yellow color. Flame color meaning can be indicative of temperature, type of fuel or the completeness of combustion. For example, a blue flame is the hottest followed by a yellow flame, then orange and red flames. Hydrocarbon gases burn blue whilst wood, coal or candles burn yellow, orange or red. A blue gas flame color is also indicative of complete combustion.

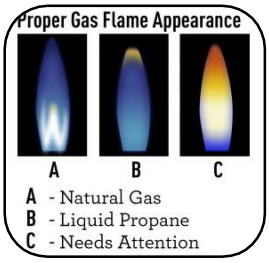

Figure 4 Flame Appearance

Furthermore, type of flame scanner existing used Ultra Violet (UV) Type which have short wave length. The length only from 10 nm – 400 nm . Based on that, the color of firing can not detect by flame scanner and impacted to low signal strength.

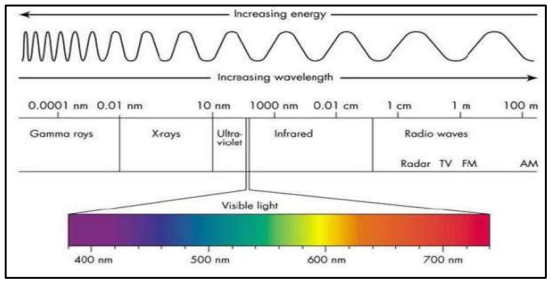

Figure 5 Diagram of Wavelength Flame

Execution
According that condition, Instrument Maintenance team purposed to manipulated flame firing condition by added Infra Red wavelength. We purposed to changed the existing flame scanner, from UV Type become UV-IR Type.

These activities started from collecting existing data from Distributed Control System (DCS) , basic theory about firing inside TOx and gas composition and equipment technical specification. After all fundamental theory already completed, Instrument Team purposed for Management of Change (MOC) to management for final decision about this planning. Continue to purchased material and inspected material before installation.

New Flame Scanner should be tested before install or swab from existing and these activities execute during off line condition to eliminate unstable condition.

Figure 6 Execution Process at TOx

Result and Discussion

After replacement process from UV Sensor to UV-IR Sensor at TOx and did commissioning. The signal strength, can be over 90% because the wavelength from flame scanner can detect flame color.

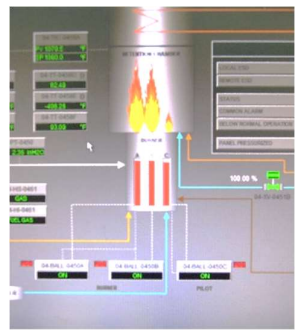

Figure 7 Recent HMI Condition especially about Flame Scanner Strength

By that condition, CPP Gundih can eliminated some high risk potential issue, among others :

a. Eliminated Loss Production Opportunities Gas around 42 MMSCFD
   This potential issue will happen if the Flame Scanner (with UV Type) did not override and will impact TOx will shut down. If TOx shutdown, it means the sales gas will stop to buyer.
   Pertamina EP will loss Rp 4.800.000.000 per day

b. Eliminated Loss Production Opportunities Condensate around 480 BOPD
   This potential issue will happen if the Flame Scanner (with UV Type) did not override and will impact TOx will shut down. If TOx shutdown, it means the processing gas will stop and separated condensate can not process

c. Eliminated Additional Solar Fuel for Turbine Generator Operation
   This potential issue will happen if CPP Gundih shutdown because of TOx and raw gas for Turbine Generator will changed to Solar Fuel

d. Safety issue about Override. Cause override one of the dangerous issue if gas processing still operated

Conclusions

By manipulated wavelength of Flame Scanner at TOx, we can rise up reliability of TOx without override issue and keep the process can run stable and safe.

References

(1) https://en.wikipedia.org/wiki/Ultraviolet
(2) Fireye Flame Scanners, Supersedes February 17, 2015
(3) https://openstax.org/books/college-physics/pages/1-introduction-to-science-and-the-realm-of-physics-physical-quantities-and-units

Acknowledgements (Optional)

We would like to thank RAM Pertamina EP Field Cepu, SF-MPE Asset 4 & OM Titis Sampurna for supporting this supervise during installation on site. And authors wish to thank for Sarana Instrument Indonesia teams for supporting in this project

PROCEEDINGS
JOINT CONVENTION BANDUNG (JCB)2021
November 23rd – 25th 2021

Management of Earthquake Mitigation as Effort to Increase National Oil and Gas Production

Khairil Fikri – PT Pertamina Hulu Energy & Faiz Muttaqy – Institut Teknologi Bandung.

Abstract

Geologically, Indonesia has a complex tectonic setting because it is located between various oceanic plates and continental plates that are actively moving all the time. With the combination of the Indo-Australian plate, the Eurasian plate and the Pacific plate, Indonesia has the potential to experience many earthquakes related to plate movement. Earthquakes that occur due to plate movement in the majority of Indonesia are shallow earthquakes, with a depth of less than 20 km which are very destructive. [1]

Indonesia's earthquake record data from the BMKG records that in 2008 – 2016 there were 5,000 – 6,000 earthquakes in Indonesia. In 2017 the incidence of earthquakes increased to 7,169 times, even in 2018 and 2019 to more than 11,400 times. In 2020 the incidence of earthquakes is still above the annual average of 8.258 times. Even in Jan – Mar 2021 alone there have been 2,108 earthquakes. Exceeds the normal average monthly earthquake event record in the range of 300 – 400 events.[2]

The data shows an increased risk of earthquakes as a warning alert to prioritize proper seismic mitigation management through the readiness of infrastructure and supporting facilities for predictive action (earthquake potential mapping) and corrective action (earthquake handling). In addition to managing seismicity mitigation, synergies from relevant institutions (BMKG, Ministry of Energy and Mineral Resources with Oil and Gas Companies and Oil and Gas Research Institutes) are urgently needed to optimize the potential for earthquakes to become an integrated source of information. As a record & early warning agency, BMKG should refer to an excellent example from the Japan Meteorological Agency (JMA) which monitors earthquakes, volcanoes, and weather in one integrated institution so that it focuses on coordination.

Earthquake is a risk that must be faced and needs to be mitigated properly because it can have a direct impact on upstream oil and gas operations. Studies of rocks excavated from fault zones have revealed crack marks, mineral-filled veins, and other signs that pressure fluctuates freely during and between earthquakes, concluding the theory that hydrocarbon fluid flows play an important role in triggering earthquakes and influencing when earthquakes occur. Including injection of artificial fluids associated with secondary/tertiary recovery operations that can cause earthquakes. Just as seismologists have linked oil and gas waste water wells to the dramatic increase in earthquakes in Oklahoma (USA) in 2009 because of injection of oil and gas wells by operators holding mining rights.[3]

SIG is the Earthquake Intensity Scale. This scale expresses the impact caused by an earthquake. The Earthquake Intensity Scale (SIG-BMKG) was initiated and compiled by accommodating information on the impact of an earthquake based on typical culture or buildings in Indonesia. This scale is structured more simply by having only five levels, namely I-V. GIS-BMKG is expected to be useful in delivering information related to earthquake mitigation and/or rapid response to destructive earthquakes. This scale can make it easier for the public to understand the level of impact caused by an earthquake better & more accurately.

Skala SIG BMKG	Warna	Deskripsi Sederhana	Deskrispsi Rinci	Skala MMI	PGA (gal)
I	Putih	TIDAK DIRASAKAN (Not Felt)	Tidak dirasakan atau dirasakan hanya oleh beberapa orang tetapi terekam oleh alat.	I-II	< 2.9
II	Hijau	DIRASAKAN (Felt)	Dirasakan oleh orang banyak tetapi tidak menimbulkan kerusakan. Benda-benda ringan yang digantung bergoyang dan jendela kaca bergetar.	III-V	2.9-88
III	Kuning	KERUSAKAN RINGAN (Slight Damage)	Bagian non struktur bangunan mengalami kerusakan ringan, seperti retak rambut pada dinding, atap bergeser ke bawah dan sebagian berjatuhan.	VI	89-167
IV	Jingga	KERUSAKAN SEDANG (Moderate Damage)	Banyak Retakan terjadi pada dinding bangunan sederhana, sebagian roboh, kaca pecah. Sebagian plester dinding lepas. Hampir sebagian besar atap bergeser ke bawah atau jatuh. Struktur bangunan mengalami kerusakan ringan sampai sedang.	VII-VIII	168-564
V	Merah	KERUSAKAN BERAT (Heavy Damage)	Sebagian besar dinding bangunan permanen roboh. Struktur bangunan mengalami kerusakan berat. Rel kereta api melengkung.	IX-XII	> 564

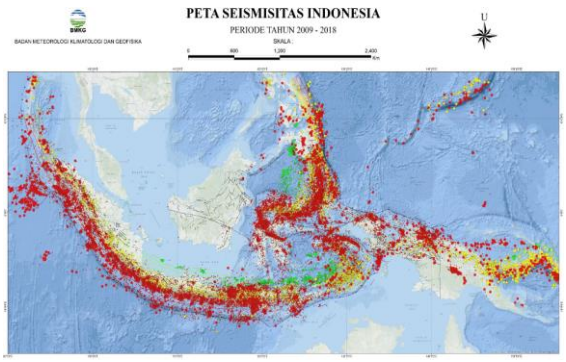

Figure 1: Peta Sebaran Gempa Nasional Data BMKG

Seismic waves generated from earthquakes can also have a positive impact as a stimulus to increase oil and gas production, due to an increase in porosity which allows hydrocarbon fluids to flow more easily. Research has been carried out by firing seismic waves at an oil and gas field through Vibro Seismic Impact Technology (VSIT) & High Resolution Electro Magnetic (HREM), both of which have been carried out massively in many oil and gas fields in the United States & Russia and which have been tested on a limited basis (pilot project) and national oil and gas fields in Indonesia (Sumatra & Kalimantan). [4]

PROCEEDINGS
JOINT CONVENTION BANDUNG (JCB)2021
November 23rd – 25th 2021

Introduction

Indonesia has a complex geological tectonic setting because it is located between various oceanic plates and continental plates that are actively moving all the time. With the combination of the Indo-Australian plate, the Eurasian plate and the Pacific plate, Indonesia has the potential to experience many earthquakes related to plate movement. Earthquakes that occur due to plate movement in the majority of Indonesia are shallow earthquakes, with a depth of less than 20 km which are very destructive.[1]

Earthquakes generally occur without warning and occur rapidly within minutes and seconds. Earthquake events usually consist of 3 phases, namely the initial earthquake (fore shock), the main earthquake (main shock) and the aftershock (after shock). Earthquakes that occur at sea can cause ocean waves. Waves occur due to a change in the form of a fault with an upright (vertical) motion on the seabed due to an earthquake, a large wave is called a tsunami. Earthquakes occur naturally which cannot be avoided and are very difficult to predict or predict, so that when they occur they often cause a lot of loss and loss of life.[5]

Referring to Law Number 31 of 2009 concerning Meteorology, Climatology, and Geophysics and Government Regulation Number 11 of 2016 concerning Meteorology, Climatology and Geophysics Services, which is strengthened by Presidential Regulation Number 93 of 2019 concerning Strengthening and Development of Earthquake Information Systems and Warnings Early Tsunami, the government is obliged to provide meteorological, climatological, and geophysical services consisting of information and services. The information in question consists of public information and special information. One of the public information that must be provided regularly is tectonic earthquake information. Other public information is tsunami early warning.

Earthquake and tsunami early warning information systems are components that are regularly interconnected to form a totality that includes observation of disaster symptoms, analysis of observations, and dissemination of analysis results, in the form of information on tectonic and/or volcanic earthquakes originating from volcanoes in the sea. and tsunami early warning for community decision-making and action. Earthquake and tsunami early warning information systems have a strategic and important role in anticipating and mitigating so that efforts are needed for strengthening and sustainable development to improve the safety of life and property of the Indonesian people from earthquakes and tsunamis.

Indonesia's earthquake record data from the BMKG records that in 2008 – 2016 there were 5,000 – 6,000 earthquakes in Indonesia. In 2017 the incidence of earthquakes increased to 7,169 times, even in 2018 and 2019 to more than 11,400 times. In 2020 the incidence of earthquakes is still above the annual average of 8.258 times. Even in Jan – Mar 2021 alone there have been 2,108 earthquakes. Exceeds the normal average monthly earthquake event record in the range of 300 – 400 events.2

The data shows an increased risk of earthquakes as a warning alert to prioritize proper seismic mitigation management through the readiness of infrastructure and supporting facilities for predictive action (earthquake potential mapping) and corrective action (earthquake handling). In addition to managing seismicity mitigation, synergies from relevant institutions (BMKG, Ministry of Energy and Mineral Resources with Oil and Gas Companies and Oil and Gas Research Institutes) are urgently needed to optimize the potential for earthquakes to become an integrated source of information. As a record & early warning agency, BMKG should refer to an excellent example from the Japan Meteorological Agency (JMA) which monitors earthquakes, volcanoes, and weather in one integrated institution so that it focuses on coordination.

Data and Method

Earthquake is a risk that must be faced and needs to be mitigated properly because it can have a direct impact on upstream oil and gas operations. Studies of rocks excavated from fault zones have revealed crack marks, mineral-filled veins, and other signs that pressure fluctuates freely during and between earthquakes, concluding the theory that hydrocarbon fluid flows play an important role in triggering earthquakes and influencing when earthquakes occur. Including injection of artificial fluids associated with secondary/tertiary recovery operations that can cause earthquakes. Just as seismologists have linked oil and gas waste water wells to the dramatic increase in earthquakes in Oklahoma (USA) in 2009 because of injection of oil and gas wells by operators holding mining rights.[3]

Seismic waves generated from earthquakes can also have a positive impact as a stimulus to increase oil and gas production, due to an increase in porosity which allows hydrocarbon fluids to flow more easily. Research has been carried out by firing seismic waves at an oil and gas field through Vibro Seismic Impact Technology (VSIT) & High Resolution Electro Magnetic (HREM), both of which have been carried out massively in many oil and gas fields in the United States & Russia and which have been tested on a limited basis (pilot project) and national oil and gas fields in Indonesia (Sumatra & Kalimantan). [4]

Currently, oil producing industry facing significant declining production in oil recovery operations by the existing method. Scientifically, natural pressure in the reservoir generated up to 15% recovery of the existing oil contained in the formation and secondary recovery commonly consequences up to 45% recovery factor. The remaining oil is difficult to produce due to its very low mobility. Frequently practical approaches for enhanced oil recovery (EOR) consist of steam, water and gas flooding, surfactants/polymer injection, hydraulic fracturing and layer burning. In the most successful cases, oil recovery can be enhanced by range of 50 – 70% of the total oil in place.

Separately of these EOR techniques has several restrictions, as well as some disagreeable side effects. Intended for illustration, some methods are expensive, requiring shutting down production or may generate damaging environmental consequences. The use of adaptable wave stimulation has been proposed, not as substitute or complimentary tool which, in certain occurrences, may kind conservative methods more effective.

Vibro Seismic Impact Technology (VSIT) applies the principle of vibration (seismic waves) to formations to improve properties of the containing reservoir rock and oil.

The waves are produced by resources of a surface seismic vibrator to stimulate the reservoir. This technology potentially a relative low-cost practice for attractive oil recovery in depleted fields or returning some shut-in wells to production. Comparatively, less supplementary infrastructures are compulsory, and no new wells necessity to be drilled. In Indonesia, VSIT pilot project are still inadequate yet and requires more implementation. Consist of Merbau Trend & Jene field (Sumatera) and Kalimantan.

Vibro Seismic Impact Technology (VSIT) is an alternative EOR technique using seismic waves, which are created by means of a surface seismic vibrator to stimulate the reservoir. The mechanisms responsible for improved recovery remain the subject of further research. However, the following mechanisms have been proposed to explain the change in fluid flow characteristics resulting from the seismic wave stimulation, that is, changes in wettability, coalescence and/or dispersion of oil drops, reduced viscosity and surface tension, and increased permeability.

Result and Discussion

The surface excitation method of reservoir stimulation requires significant further testing. The number of field test or applications conducted is, yet, insufficient. Attempts to use surface sources for oil production stimulation show both positive and negative results, depending on the formations or reservoir characteristics. A correlation between oil rates and earthquakes was observed in the 1970s. It resulted in the first attempts to use the energy of seismic waves to mobilize residual oil spread in the reservoir in the form of drops of different sizes, and to rehabilitate depleted oil fields with high water production.[5]

Vibro Seismic is a technology that can be applied to increase oil recovery and some papers say that this Vibro Seismic research has long been carried out in laboratory studies and applied to the field. Laboratory tests showed that oil displacement can be increased by application of low-frequency vibration. It was also confirmed by field tests of oil production due to Vibro Seismic stimulation impact increased by 30-40%.[8]

However, estimations show that such an increase in oil production does not occur with low-frequency vibration. Most probably some unknown phenomena exist which impact on the mechanism of seismic vibration-induced increases in oil production. The object of this study was the development of an analytical model of Vibro Seismic stimulation to explain the mechanism of residual oil mobilization. Such a model can provide the basis for effective use of vibration stimulation.

The model oil-saturated formation consists of blocks of different sizes. Each large block includes several blocks of smaller sizes. Block sizes depend on the geological processes taking place during their formation, while correlation between their sizes does not depend on properties of constituent materials.

Core measurements taken in the millimeter range and analysis of photographs of layer distribution in open hole taken in the metric range show that correlation between the large and small blocks occurs over a rather small range and varies between 2.91 and 3.43.

Simulation of Vibro Seismic impact on a formation shows that a process of low-frequency energy transfer from larger blocks to smaller ones, producing high-frequency vibration, takes place. These high-frequency vibrations provide conditions under which capillary forces, retaining oil drops in the porous media, are destroyed, improving conditions for oil mobilization. These results agree with experimental data of noise measurements recorded during pilot commercial tests of Vibro Seismic action at different oil fields in Russia. Thus the possibility of residual oil mobilization by applying low-frequency Vibro Seismic stimulation was confirmed both theoretically and in laboratory and field tests. The results received were an essential part of the creation of the technology for Vibro Seismic stimulation of waterflooded, depleted oil reservoirs.[6]

Ariadji (2005) explains the changes that occur in the physical properties of rocks and fluids when Vibro Seismic applied. In the experimental study used a variety of frequency variations to see indicators of change. From the results of the research, the optimum frequency results are 10 Hz and 15 Hz. With this optimum frequency, it can reduce the remaining saturation of oil, increase rock porosity, increase permeability, decrease oil viscosity and change capillary pressure.[7]

Conclusions

Indonesia, which is geographically located in a point prone to earthquakes with high intensity, needs to manage earthquake mitigation so that potential disasters can be avoided early on. In addition, the importance of earthquake mitigation management efforts can also have an impact on the good side of earthquakes on oil and gas activities.

Seismic waves generated from earthquakes can also have a positive impact as a stimulus to increase oil and gas production, due to an increase in porosity which allows hydrocarbon fluids to flow more easily. Research has been carried out by firing seismic waves at an oil and gas field through Vibro Seismic Impact Technology (VSIT) & High Resolution Electro Magnetic (HREM), both of which have been carried out massively in many oil and gas fields in the United States & Russia and which have been tested on a limited basis (pilot project) and national oil and gas fields in Indonesia (Sumatra & Kalimantan). [4]

References

1. Tri Partuti & Ani Umyati, 2019, Jurnal Pengabdian Dinamika, Edisi 6 Volume 1, 1-6.
2. Dwikorita, 2021, Data Gempa Bumi BMKG, 1-3.
3. Tutuka Ariadji, 2018, Simposium IATMI, 1-5.
4. Indra Prasetyo, 2011, Indonesian Petroleum Association – 30th Annual Convention Proceedings (Volume 2), 205
5. Katili, J.A, 1973, Volcanism and Plate Tectonics in Indonesian Island Arc, Tectonophys., v.26
6. G. P. Lopuchov, 1 August 1999, Petroleum Geoscience, 5, 259-263.
7. Stevy Canny Louhenapessy & Tutuka Arijadi, 2020, Petroleum Research 5, 304-314.
8. Tutuka Ariadji, 2005, SPE Asia Pacific Oil Gas Conf. Exhib. – Proc, pp, 161-168.
9. Onnie Ridaliani, Ariadji, Handayani, 2003, IATMI.

PROCEEDINGS
JOINT CONVENTION BANDUNG (JCB)2021
November 23rd – 25th 2021

Thermoelectric Peltier-Based Cooler Generator
As The Option To Optimize Flare Gas Utilization In Mature Fields

Tim Penulis :
Adha Bayu Wijaya (PO)
A.Zainal Abidin (PO)
Rizky Martareza Noor (PO)
Tomi Ardian (PO)
Surpadjrianto (RAM)
Febri Yudha Rahasianto (RAM)
Astika Titistiti (HSSE)

Review, Fasilitator Sr. Spv. Gundih Production	Review, Fasilitator Ast. Man Cepu PO
Hadi Akmalunas	Ardi

Menyetujui,
Manager Cepu Field

Agung Wibowo

PROCEEDINGS
JOINT CONVENTION BANDUNG (JCB)2021
November 23rd – 25th 2021

Thermoelectric Peltier-Based Cooler Generator As The Option To Optimize Flare Gas Utilization In Mature Fields

Ardi, Hadi Akmalunas, Adha Bayu Wijaya, A.Zainal Abidin, Rizky Martareza Noor, Tomi Ardian, Surpadjrianto, Febri Yudha Rahasianto, Astika Titistiti

ABSTRACT

Cepu is a mature field that has been producing since 1877 with a total production of 2,200 BOPD, with the challenge of developing new wells to control the decline in well production coupled with the high water cut in each well. In addition, production facilities in some sub-districts still use conventional equipment with durability and functions that need to be updated and are generally not equipped with the use of gas flares and purification equipment and in actual conditions in which gas is burned directly into the atmosphere. The thermoelectric Peltier is an innovation in the form of a device with a solid-state electric cooling component that functions to pump heat in the air during the cooling process. By being installed on a flowline leading to a flare stack, it is able to maximize the cooling process to enable the collected condensate and sweet gas be reused as a fuel gas engines. On this basis, the use of Thermoelectric Peltier in mature fields has great potential in reducing exhaust emissions of fuel gas/zero flares, heavy hydrocarbons (CH3+) contained in gas flares can be fully condensed and potentially to increase oil recovery from the Cepu field. In addition, the material used is user friendly requires only a power source, easy to be operated as it uses a 9-12 VDC power source, can be applicable in mature fields because it doesn't need spacious place, simply installed on the pipes, low price cost of Rp 5.312 million and is easy to find in the market.

INTRODUCTION

Cepu Field is one of the field clusters located in the PT Pertamina EP area with current production of 2039 BOPD and 59 MMSCFD. The gas field is currently produced from 8 gas wells that producing 56 MMSCFD of crude gas, 41 MMSCFD of gas sales and 387 BCPD of gas. Meanwhile, oil field currently produced from 79 oil wells that produces 3 MMSCFD of gas and 1652 BOPD oil. The majority of these oil fields are mature oil fields with water cuts reaching 98%.

The use of associated gas in the old field is currently used for company needs as generator fuel, while the remaining will be flared if it does not used. According to the Regulation of the Minister of Energy and Mineral Resources No. 31 of 2012 concerning the Implementation of Gas Flaring (Flaring) in Oil and Gas Business Activities, gas flares must go through facilities by means of a liquid trap before it gets burning into the atmosphere which potentially polluting the environment. Some challenges in associated gas use in old fields are caused by using simple existing facilities, namely separators and scrubbers, including:

- Potential for condensate production losses caused by the high liquid content (produced water and condensate) which is still high in the gas flaring.
- Associated gas purification is not optimal to be used as own used generator fuel.
- The high emission of gas flaring is caused by the inadequate dehydration process to liquified the gas flaring.

SELECTED METHODS

This research is a trial and error methods which will be applied in a Gas Flare in the Early Production Facilities (EPF) Field “X”. If this research is successful, it will be developed in other fields in the company under the same field. In general, this research procedure begins with gas testing of three wells in the “X” Field. This test is carried out with a gas chromatograph, resulted from the test; in which the gas composition is obtained. Once the gas composition is obtained, a simulation is carried out to find out the best practice to condense gas to achieve the maximum rate. Simulations were carried out using Aspen Hysys V.8.8 simulator application. A diagram flow of the simulation is shown in Figure-1.

Gas in the Field "X" is obtained by separating liquid and gas in a separator. The output gas from the separator is 0,15 MMSCFD with separator pressure of 17 psi and temperature of 101^0F. Under such conditions, a mass gas of 1.144,82 lb/h was obtained. Gas composition in "X" field has been re-calculated by adding water composition (H_2O). Aspen Hysys V.8.8 is used to obtain the overall gas composition as show in TABLE-1.

Condensate Recovery Solution

When conducting condensate recovery, it is necessary to carry out a process to achieve below the dew point conditions of some hydrocarbon gas components. Because a gas dew point in this field "X" is unknown, the trial and error simulations were performed using Aspen Hysys V.8.8 software in some heat-exchangers.

The use of chiller and fin-fan applications showing that these applications can produce a better result. It also eliminates the use of other separation equipment such as sealer and flare, when producing condensate. The main goal of using chiller and fin-fan is to reduce the temperature of the volatile oil produced, turning its gaseous phase into condensate, which would otherwise waste in a flare. Chiller shows better result of converting gas into condensate, compared to fin-fan. These results were obtained through the simulation process using data obtained from the gathering system. The details of each scenario are as follows:

Fin-fan is a heat exchanger that uses ambient air to cool fluid (air cooler heat exchanger). Heat transfer occurs between the fluids in the tube with the surrounding air without direct contact. The main advantage of fin-fan is no water needed, which means that this cooling equipment does not have to be close to the cold-water supply. In the fin-fan, the heat is transferred from the fluid to the surrounding air without environmental issued, or without enormous costs of water supply and maintenance. The design of the fin-fan is shown in Figure-2.

An air-cooled heat exchanger comprises several parts, namely fans and tubes that arranged in a bank and driver. The fan functions as cooling air to the air cooler, the bank is composed by tubes as a means to process fluids; while the driver functions as a fan drive. The heat transfer that occurs in the fin-fan is just like the ambient of air temperature. Hence, the stability of the ambient air temperature ambiance needs to be noticed.

Fin-fan or water-cooled exchanger is a heat exchanger method in which ambient air is used to cool the process fluid. Therefore, the lowest temperature that can be achieved is about 25^0C. The simulation results using the Aspen Hysys 8.8 software is show in Figure-3.

Based on the simulation in Figure-3, a condensed component comes out the bottom of the scrubber device. The components of condensation is shown in Table-2.

From Table-2, it can be seen that the condensate component is about 46,66 barrels/day consist of high amount of water and less amount of CO_2. At the same time, the hydrocarbon component remains in the gas phase. It shows that the cooling process is still over the dew point of the hydrocarbon which proves that, this method is not suitable to use.

Chiller system is a cooling system that uses the liquid generally water as a cooling medium in the secondary system in which the evaporator in the primary system cooling the liquid (chilled water) in the second cycle and can be used to cool the room through the Air Handling Unit (AHU). The primary system is the central cooling unit using the Steam Compression Cycle (SCC), which consists of main components, like compressor, condenser, expansion valve, and evaporator. Chiller system is a process where expenditure and heat absorption occur. Water entering the Chiller will be cooled and circulated by the pump to the AHU and followed by heat exchange process between air and cold water. Cold air coming out of this unit will be then circulated by the fan to the conditioned room. The design of this fin-fan process is shown in Figure-4.

Chiller can cool down a process fluid to the temperatures below 0 ˚C to conduct condensation on the easily achieved contained condensate. The result of performing sensitivity to the outlet temperature, is displayed in Table-3. By conducting a simulation in which sensitivity is applied to the chiller, it can be seen that the components are condensed from various outlet temperatures, as shown in Table-3.

Based on simulation results in Figure 5, it can be concluded that the lower the temperature, the more condensate obtained. When the chiller reaches the temperature of 0˚C, the highest total liquid was obtained was 53.44 barrels/day, and condensate was 6.58 barrels/day.

After comparing different outlet temperatures, we determined the optimum pipe diameter based on the minimum pressure drop and the maximum result of Condensate production. Table-4 shows the result of pipe sensitivity.

The simulation result in Table-4, it described that fin-fan could not be used because the lowest temperature produced was equal to room temperature. In contrary, the separation process (dehydration) can be obtained with an optimum temperature of 0°C but these conditions can be freezed the liquid. Based on these conditions, the optimum temperature that can be used is at 5°C.

RESULTS

The simulation result, identify that the optimum temperature for the thermoelectric Peltier is at 5°C. Considering of existing condition in early production facilities/EPF and reducing the lower economics issue in a mature field operation, the installation of Peltier Thermoelectric Cooler Generator could be an option for optimizing the associated gas dehydration process. The following details are the advantages by using a Thermoelectric Peltier-based Generator Cooler,

- Relatively safe installation because it does not require hot tapping on existing facilities as the equipment is installed to the facilities that need to be cooled.
- It does not require extra space because the installation is done by attaching it to existing facilities.
- Relatively easy operation is because it uses an energy source in the form of a power source.

Thermoelectric Peltier is a solid-state electric cooling component consisting of two semi-conductor materials (Type-N and Type-P) that a heat pump in the cooling process. When direct current (DC) flows through a device, it carries heat from one side to the other, that makes one side gets cooler while the other gets hotter. Figure-6 and 7 show the component and the work system of the Thermoelectric Peltier.

Based on Figure-8, Thermoelectric Peltier-based Cooler Generator is used as a cold source in existing facilities (separators, scrubbers and other facilities) in order to maximize the separation process (dehydration).

Currently the Peltier Thermoelectric remain limited to its small dimensions which can be seen in Figure-9. However, the main advantages of Peltier coolers if it is compared with the pressure and evaporation technology, is the absence of moving parts or rotating fluids, that makes it long-life span, strong against leakage, has a size that is small, and easily customizable shape. Unfortunately, it is low power efficiency, but now many researchers and companies are trying to develop cheap and efficient Peltier coolers. The most common Peltier Thermoelectric type the market are the TEC-12076 with the following specifications as in Figure-10:

- External dimensions: 40x40x3.75mm
- Internal resistance: 2.1 ~ 2.4Ω (ambient temperature of 23 ± 1 'C, 1kHZ Ac test)
- The maximum temperature difference: Tmax (Qc = 0) above 59 'C.
- Working current: Imax = 4.3-4.6A (rated at 12V)
- Rated voltage: 12V (Vmax: 15V starting current 5.8A)
- Cooling power: Qcmax 55W
- Working environment: temperature range -55 'C ~ 83'C (high ambient temperature drop directly affect the cooling efficiency)

The use of conventional heat exchanger tools, generally related to the limitation of its working environment temperatures and installment inconveniency, that makes them less economical option. Chiller, for example, has maximum output temperature of 39°C and requires more space for its installment.

Therefore, with the implementation of a thermoelectric Peltier-based cooler generator at the scrubber outlet at temperatures of up to 5°C, a more optimal gas dehydration process can be obtained and the gas can be used.

CONCLUSIONS

1. The use of associated gas in the mature field is still quite low. For example, Cepu field using simple separation process (separator & scrubber). Associated gas that is not optimally hydrated will cause potential problems in combustion gas emissions, loss of condensate and cannot be used.
2. Thermoelectric Peltier-based cooler generator is a relatively cheaper equipment, that is more applicable, more portable, and more economical option compared to other heat exchanger technologies such as fin-fans, chillers, and so forth. As an example, Peltier-based cooler generator can still function when surrounding temperature reaches 83°C whereas Chiller is limited to 39°C.
3. The potential uses of Peltier thermoelectric technology for heat exchanger applications in gas flare utilization comprises the monetization of gas flares to increase revenue, the used of gas as generator fuel, and the increase of condensate production by optimizing the separation process in gas flares.
4. Peltier Thermoelectric application has a limitation from its developed size in smaller module. The potential used in a gathering station or production facilities requires further research for installation compatibility.

ACKNOWLEDGEMENTS

The authors are grateful to the Pertamina EP Cepu Region 4 Zone 11 Field Cepu for the data field support to this endeavour.

REFERENCES

AspenTech, 1994-2005, Official Website of AspenTech Company, Aspen Technology. [Online]. Available: www.aspentech.com.

Fares, A. D., 2016, Process Simulation Using Aspen HYSYS V.8.

Fikri, Hafidh Abdurrohman Al, 2016, Efektifitas Modul Peltier Tec-12706 sebagai Generator dengan Memanfaatkan Energi Panas dari Modul Peltier TEC-12706, published by Universitas Muhammadiyah Surakarta.

Hudson Product Corporation, “The Basic of Air-Cooled Heat Exchangers,” 2007.

Kolmetz, Karl, 2015, Kolmetz Handbook of Process Equipment Design: Fin-fan Air Cooler Selection and Sizing, Malaysia: KLM Technology Group.

Smith, P, et al., 2002, Tutorials & Applications HYSYS 3.1, Cambridge: Aspen Technology.

PROCEEDINGS
JOINT CONVENTION BANDUNG (JCB)2021
November 23rd – 25th 2021

TABLE 1
GAS COMPOSITION IN FIELD "X" ALONG WITH WATER CONTENT

Compositions	Value		
	% Mol	% Vol	% Mass
Nitrogen	0,001	0,001	0,001
Carbon Dioxida	0,010	0,016	0,020
Methane	0,112	0,183	0,080
Ethane	0,023	0,060	0,031
Prophane	0,045	0,120	0,089
i-Butane	0,020	0,064	0,052
n-Buthane	0,017	0,051	0,044
i-Penthane	0,010	0,034	0,031
n-Penthane	0,008	0,029	0,026
Hexane	0,008	0,031	0,030
H_2O	0,747	0,412	0,598
Total	1,000	1,000	1,000

TABLE 2
PERCENTAGE OF MOLES OF EACH COMPONENT IN THE FIN-FAN RESULT

MATERIAL STREAM CONDENSATE			
Component	LiqVol Flows	Vapour Phase	Aqueous Phase
Nitrogen	0.0000	0.0000	0.0000
CO2	0.0052	0.0000	0.0052
Methane	0.0000	0.0000	0.0000
Ethane	0.0000	0.0000	0.0000
Prophane	0.0000	0.0000	0.0000
i-Butane	0.0000	0.0000	0.0000
n-Butane	0.0000	0.0000	0.0000
i-Pentane	0.0000	0.0000	0.0000
n-Pentane	0.0000	0.0000	0.0000
N-Hexane	0.0000	0.0000	0.0000
H20	46.6552	0.0000	46.6552

PROCEEDINGS
JOINT CONVENTION BANDUNG (JCB)2021
November 23rd – 25th 2021

TABLE 3
SIMULATION RESULTS USING CHILLER WITH OUTLET TEMPERATURE VARIATIONS

Parameters	Outlet temperature, ^{0}C			
	0	**5**	**10**	**25**
Molar Flow, lb moles/h	38,76	38,42	38,08	37,06
Cumulative Liquid Production, BLPD	53,44	50,94	48,46	46,67
Cumulative Condensate Production, BCPD	6,58	4,10	1,65	0

TABLE 4
POTENTIAL PRODUCTION LIQUID & CONDENSATE

Output Temperature °C	Liquid Production	Condensate Production
	BLPD	**BCPD**
0	53.44	6.58
5	50.94	4.10
10	48.46	1.65

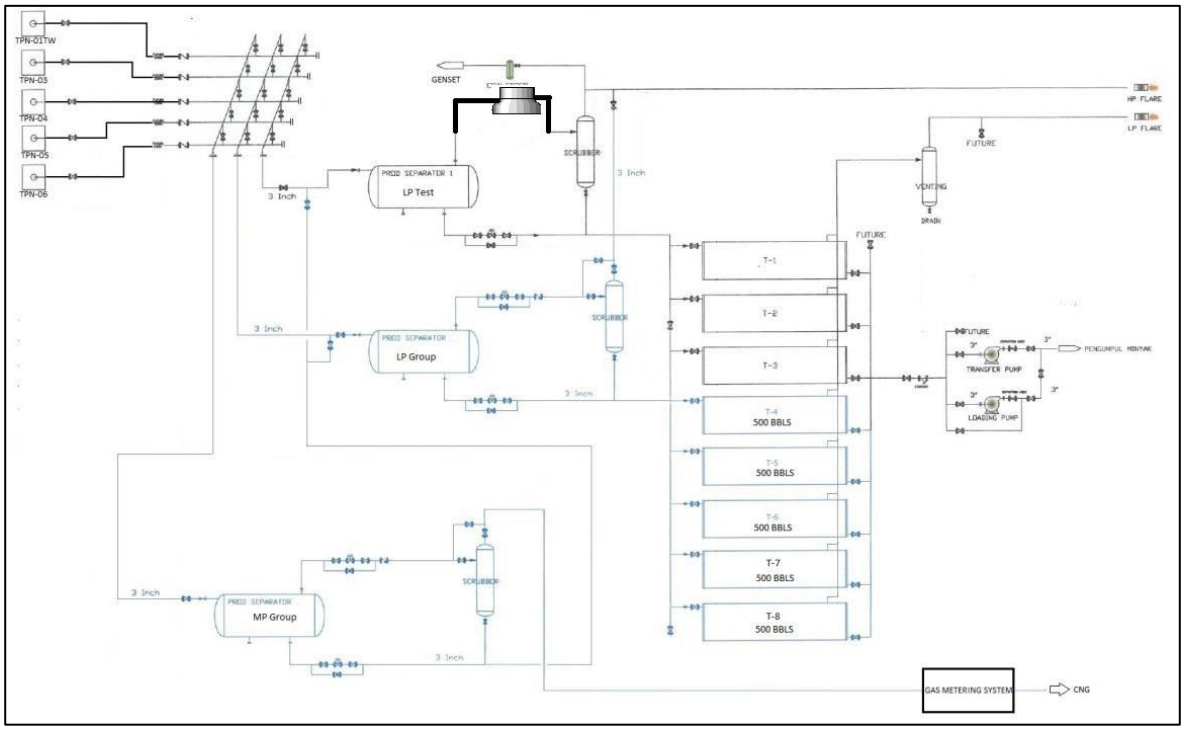

Figure 1 – Flow Diagram

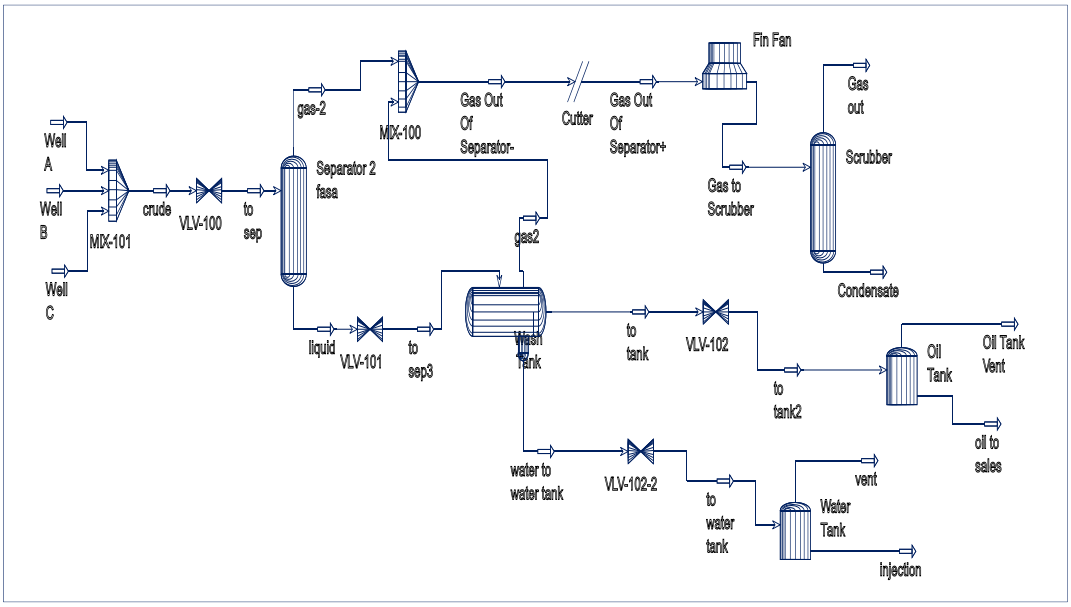

Figure 2 - Design of Fin-fan by Using Aspen Hysys V.8.8

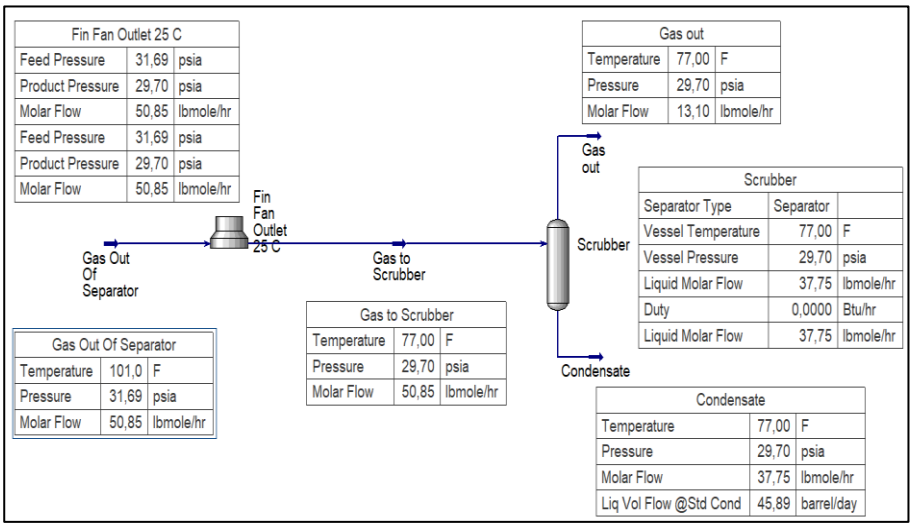

Figure 3 - Simulation Results with Fin-fan

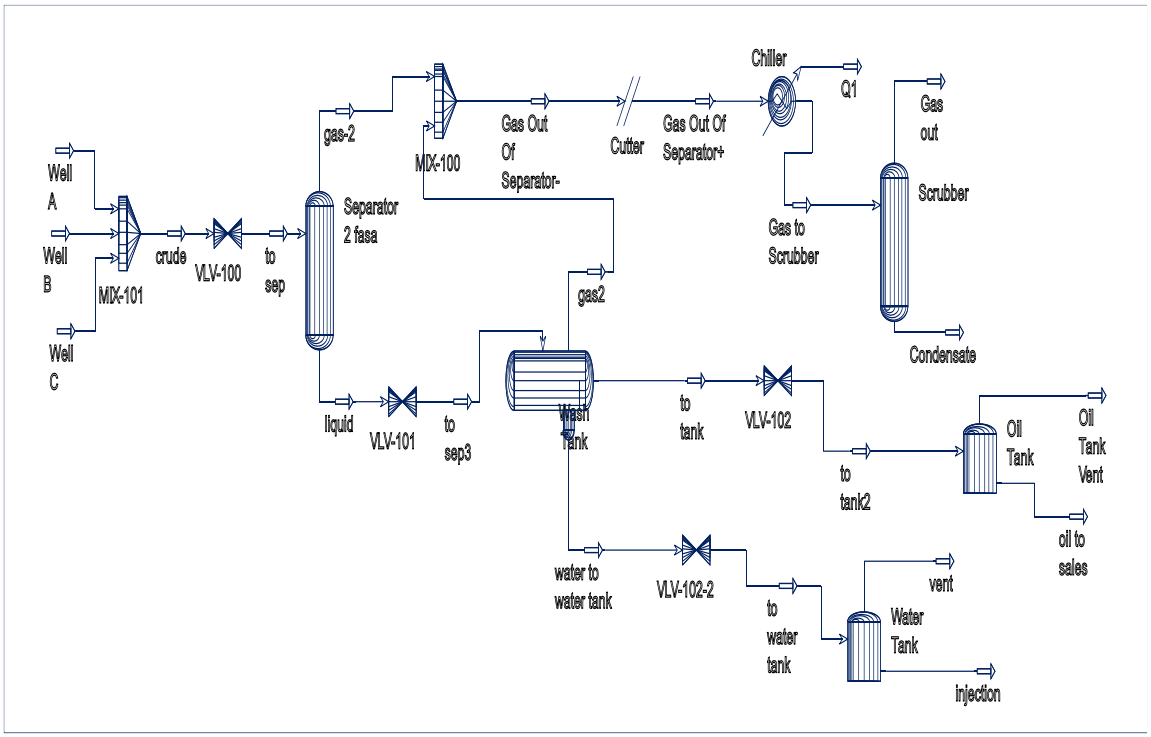

Figure 4 - Chiller Design by Using Aspen Hysys V.8.8.

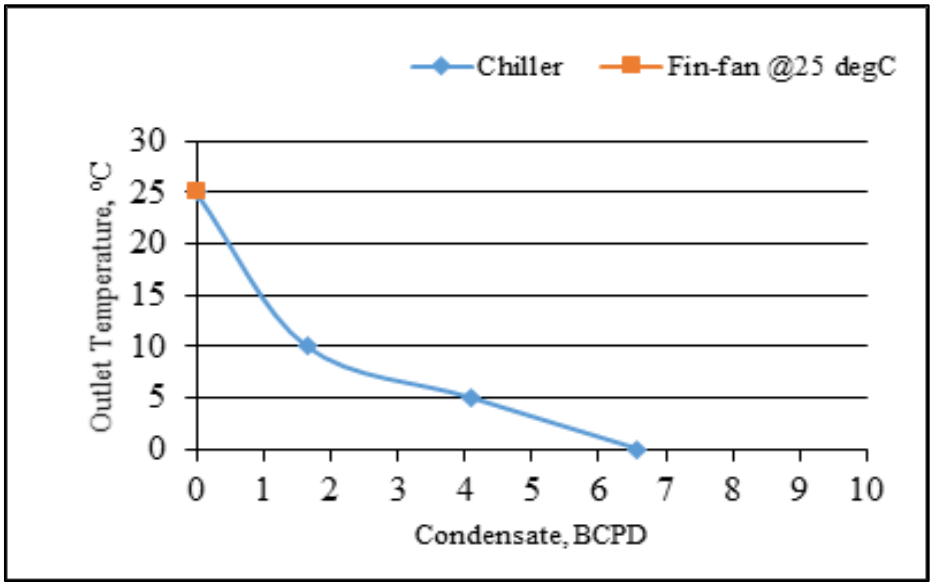

Figure 5 - The sensitivity of Outlet temperature vs. Condensate Results from Simulation

PROCEEDINGS
JOINT CONVENTION BANDUNG (JCB)2021
November 23rd – 25th 2021

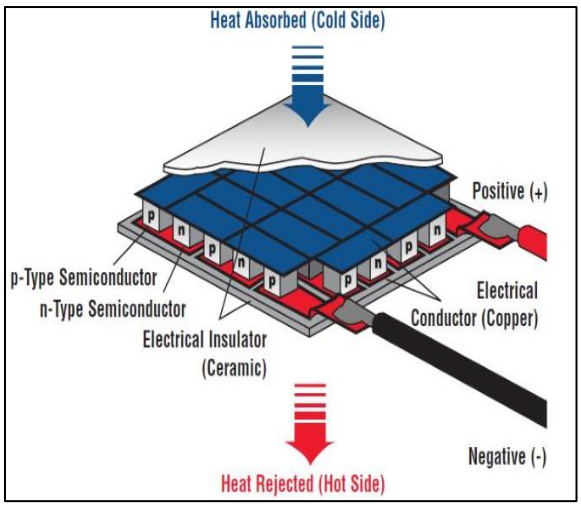

Figure 6 - Component of Thermoelectric Peltier

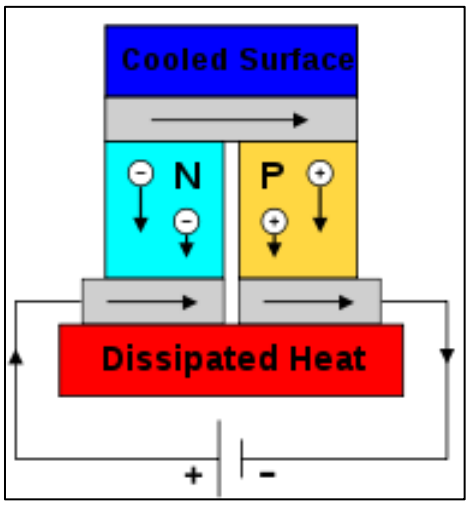

Figure 7 - How to Work the Thermoelectric Peltier

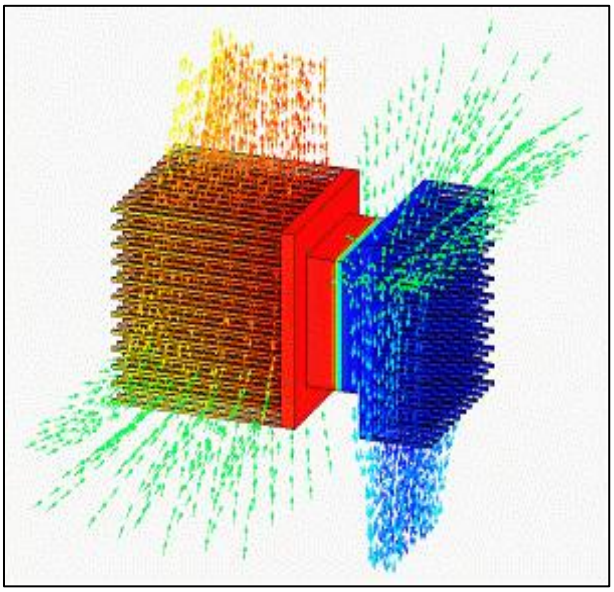

Figure 8 - Cold – Hot Peltier Airflow

PROCEEDINGS
JOINT CONVENTION BANDUNG (JCB)2021
November 23rd – 25th 2021

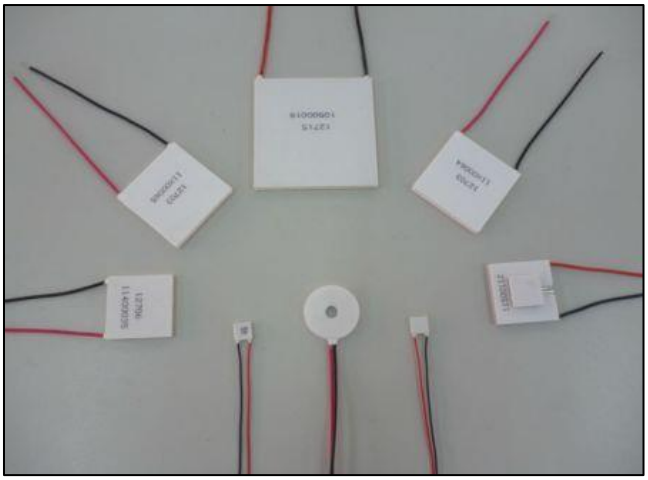

Figure 9 - The Kind of Thermoelectric Peltier

PROCEEDINGS
JOINT CONVENTION BANDUNG (JCB)|2021
November 23rd – 25th 2021

Solvent Stimulation as a Solution for Heavy Oil Production in B Structure Pertamina

Reza Alfajri[1], Arief Hidayat[1]
Pertamina[1]

Abstract
Producing heavy oil requires more efforts than usual. Low degree of API, High viscosity, and high pour point make producing wells with this oil type quite challenging. B Structure oil in Pertamina has 17-23^0 API, 10-222 cp viscosity, and 45^0 C pour point. Producing wells in this structure results in either low production rate or water coning. Altering oil characteristic by pumping suitable chemical would be an ideal solution for this problem. However, the efforts that have been made since 2011 could not meet expectation in terms of production gain and decline of water cut.

Laboratory test was performed to find proper chemical that can alter oil characteristics for this structure. Since oil in B structure contains asphaltene and paraffin, the logical thing to do to achieve this goal is to utilize aromatic solvent. Mixture of xylene and diesel as the main ingredients was chosen. Solubility test with oil from B structure showed that the mixture can dissolve its asphaltene and paraffin content. A dose of surfactant, mutual solvent, and potassium chloride are added into the mixture to condition formation. Compatibility test with brine from B Structure was observed, and neither emulsion nor sediment was formed. The mixture's laboratory tests showed promising result.

Stimulation jobs using solvent mixture mentioned above were performed for three wells in B Structure: well B-104, B-122, and B-121. The problem in well B-122 was the same, i.e. sudden increase in water cut after performing well service. In well B-121 case, it lost its production after water shut off activity. B-104 showed significant oil cut in swab job sample but could not be produced due to its heavy oil characteristics. Stimulation was performed using bullhead method with 6 ft penetration into the formation and minimum 120 minutes of soaking time. The best result out of these three treatments is from well B-121. The well's oil production before treatment was 25 bbls per day and is improved post treatment into 175 bbls/day, with decreasing trend for its water cut. Another improvement also happened in well B-122. Pretreatment oil production for this well was 21 bbls/day and is improved into 76 bbls/day. In B-104 well, which delivered zero production since intervention job, delivered peak oil production of 54 bbls/day. All wells were produced using artificial lift and still have more than 300 m of pump submergence, which means the door for production optimization is wide open.

The success from these stimulation jobs using aromatic solvent provide a solution for heavy oil production in B Structure in Pertamina. Several more wells are already scheduled to receive solvent stimulation treatments. Production monitoring is still on going with production optimization is on the plate. Wells' lifetime is also closely monitored as well as design optimization for stimulation treatment.

Introduction

Even though B Structure oil in Pertamina has been produced since 1959, remaining reserves in B Structure is still quite a lot: 6.43 MMSTB. Currently, wells in the B structure are produced using artificial lifts: ESP and SRP. Based on pump submergence data, these wells can still be optimized by increasing their gross production, which will ultimately result in more oil production. However, this optimization opportunity cannot be carried out because when the well gross production is increased, water coning tends to occur. In addition, there is also the problem of water handling in surface facilities.

Rock properties in B structure tend to be oil wet. Stimulation have been performed by using surfactants to change rock wettability from oil wet to water wet, however the results obtained are far from optimum. Wells' water cut after surfactant stimulation were relatively unchanged. Table 1 shows B Structure overview.

Reservoir Characteristics	
Reservoir formation	Talang Akar Formation (Sandstone)
Reservoir Wettability	Oil Wet
Driving Mechanism	Strong Water Drive
Avg Reservoir Pressure	1500 psi
Avg Reservoir Temperature	200^0 F
Initial Oil in Place	164,137 MMSTB
EUR	37.65 MMSTB
Remaining Reserve	6.43 MMSTB (23% URF)
Fluid Properties	
API	17-23^0 API
Oil Viscosity	10 – 222 cp (@res condition)
Pour Point	46^0 C
Production	
Number of Wells	107 wells (61 on production, 18 suspended wells, 22 water injection wells, 6 plug & abandoned wells)
Average production rate	55,300 bfpd 1800 bopd 7.91 mmscfd 95.69% WC
Average injection rate	53,309 bwipd
Decline rate per year	16.56 %

Table 1 B Structure overview

Oil in B Structure is heavy oil with API values ranging from 17-23^0 API, and viscosity of 10 – 222 cp at reservoir condition. There were cases in wells with small water cuts, when a sample of oil is taken on the surface through a faucet

in the flowline, the sample obtained was only gas. It happened because heavy oil is difficult to flow out of the small diameter of the faucet hole. Therefore, the oil sampling should be done in the separator. Oil from B structure required an assistance to be delivered to refinery unit. In this case, light oil from other structures is utilized as blended oil.

Fig. 1 to 3 show cases of abnormal drops in oil production in three B structure wells, in which water cuts of the three wells rises suddenly. This is thought to be due to the formation of plugging near wellbore due to changes in fluid pressure and temperature from the reservoir to the wellbore. Heavy oil which has a smaller relative permeability makes it difficult to produce. Well stimulation is needed to eliminate damage near wellbore and improve oil relative permeability.

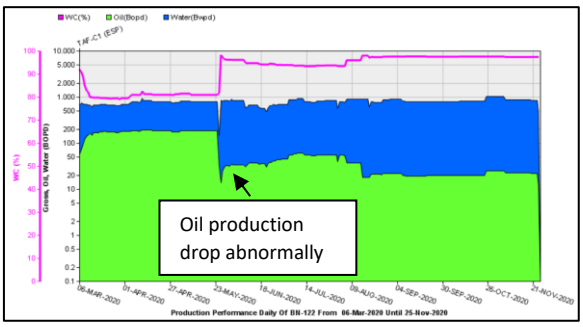

Fig. 1 B-122 Production Profile

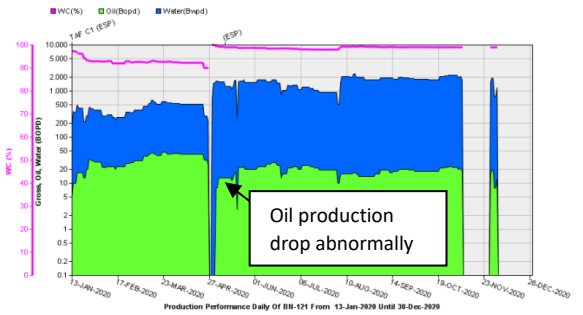

Fig. 2 B-121 Production Profile

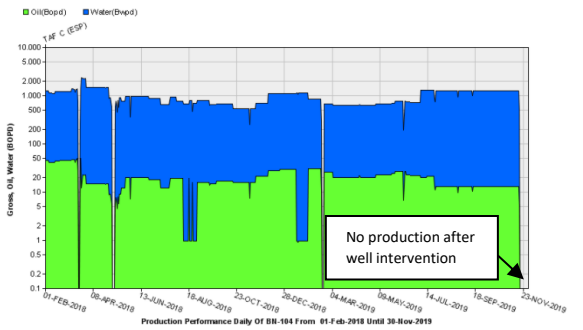

Fig. 3 B-104 Production Profile

Data and Method

Matrix Treatment Selection

Xiong and Holditch 1995 discussed about several fluid options that have been used successfully in matrix treatment (Table 2).

Fluid Type	Specific Fluid	Damage That Fluid Can Remove	Remarks
Acids	HCl	Scale, solid plugging, water block	Used in carbonate sand sandstones with 20% or more calcite, or preflush for HF acid treatment
	Acetic acid	Scale, solid plugging, water block	Same as HCl and in high temperature
	Formic acid	Scale, solid plugging, water block	Same as HCl and in high temperature
	HF	Clays, scales, solid plugging, water block	Sandstones (with HCl or organic acids). Used to cleanup drilling mud damage
	In-situ generated HF acid	Clays, scales, solid plugging, water block	Possibly deep penetration. Sandstones only
Solvents	Mutual solvent	Water block, emulsion, wettability change	Used with other additives such as surfactant to improve hydrocarbon relative permeability
	Aromatic solvent	Asphaltene, paraffin wax, sludge, lubricant plugging	Used with a suspending agent or remove asphalt deposit with dispersant(s) for sludge
	Ethylene diamine tetra acetic acid (EDTA)	Sulfate scale	
Water	Hot water	Paraffin wax	Used with suspending agent(s)

Table 2 Fluid Used in Matrix Treatment Selection (Xiong and Holditch, 1995)

Laboratory test result for crude oil from B structure shows that asphaltene and paraffin content of oil from the B structure is quite high, as shown in Table 3. Matrix treatments suitable for oil containing paraffin wax based on Table 2 are hot water and solvents.

Specific Gravity 60/60 °F	[ ]	0,9170
API Gravity at 60 °F	[ ]	22,8
Kinematic Viscosity at 140 °F	[cSt]	142,4
Kinematic Viscosity at 180 °F	[cSt]	54,45
Kinematic Viscosity at 210 °F	[cSt]	30,70
Pour Point	[°C]	45
Flash Point "ABEL"	[°C]	82
Reid Vapor Pressure at 100 °F	[psi]	solid
Water Content	[%vol]	Nil
Water & Sediment (*)	[%vol]	0,40
Salt Content as NaCl	[%wt]	--
Salt Content as NaCl	[lb/1000 bbl]	> 151
Total Acid Number	[mg KOH/g]	0,053
Strong Acid Number	[mg KOH/g]	Nil
Total Base Number	[mg KOH/g]	0,514
Gross Heat of Combustion	MJ/kg	44,481
Sulfur Content	[%wt]	0,155
Asphaltene Content	[%wt]	0,428
Wax Content	[%wt]	11,51
Congealing Point of Petroleum Wax	[°C]	67
Conradson Carbon Residue	[%wt]	8,360
Ash Content	[%wt]	0,3612
Hydrogen Sulfide	[mg/kg]	0,57
Mercaptane	[mg/kg]	1,97
Total Nitrogen	[%wt]	0,038
Characterization Factor, K_{UOP}	[ ]	12,3
Metal Content: - Vanadium	[mg/kg]	0,47
- Nickel	[mg/kg]	5,25

(*) The result is after free water treatment

The results are summarized as follow:

- API Gravity	[ ]	: 22,8
- Specific Gravity at 60/60°F	[ ]	: 0,9170
- Pour Point	[°C]	: 45
- Sulfur Content	[%wt]	: 0,155
- Asphaltene Content	[%wt]	: 0,428
- Wax Content	[%wt]	: 11,51

Table 3 Laboratory Evaluation of B Structure Crude Analysis

The use of hot water that has been applied in Indonesia to deal with heavy oil problem is by performing steam flood injection. Referring to steam flood study in Pertamina's S Structure, it is necessary to add 15 injector wells to support 26 producer wells at a cost of 1.1 million USD per well. It is equivalent of 16.5 million USD for 15 wells. The well in S Structure has a depth of 300 meters, while the well in B Structure has a depth of 1200 m. The cost of making injection wells in B structure will be higher, it is not

including investment in production facilities such as steam generators. The steam flood in B structure still needs further economic studies, that it cannot be realized in the near future. Besides, prospect zones in B structure have around 200^0 F average reservoir temperature, which means reservoir temperature is still far from its oil pour point, hence no problem temperature wise.

Referring to Table 2, there are three types of solvents: mutual solvent, aromatic solvent, and EDTA. The type of solvent that is suitable for removing asphaltene and paraffin is an aromatic solvent. This fluid is preferred to deal with the heavy oil problem in the B structure.

Fluid Design

Straub et al. 1989 tested the effect of various solvents on paraffin solubility rate (Fig.4). This experiment was carried out at a temperature of 159 F. The results were that xylene was able to dissolve 100% of paraffin to 0% in +/- 4 minutes, followed by condensate +/- 7 minutes, kerosene +/- 8 minutes, light oil +/- 22 minutes, and diesel +/- 30 minutes.

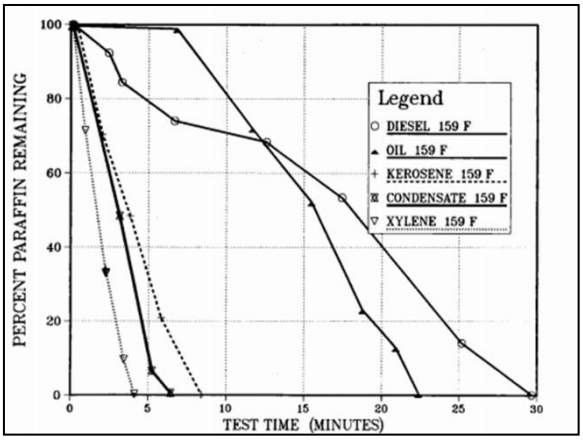

Fig. 4 Effect of Various Solvents on Paraffin Solubility Rate (Straub et al. 1989)

Although xylene is the type of solvent that dissolves paraffin the fastest, the flash point of xylene is low (Table 4).

Solvent Type	Flash Point
Xylene	27 ^{0}C
Condensate	-40 ^{0}C
Kerosene	37.8 ^{0}C
Oil	-20 ^{0}C
Diesel	65 ^{0}C

Table 4 Flash Point of Solvent Types

If the temperature rises to 5.5^0 C above the flash point, the vapor cannot be controlled and has the potential to cause fire. When the job is on site, the ambient temperature can reach 40^0 C. For safety mitigation, xylene is mixed with diesel to increase its flash point. Xylene and diesel are fluids that are compatible with each other. A 50:50 mixture of diesel and xylene makes the flash point 45^0 C (Table 5).

% Diesel	% Xylene	Flash Point ^{0}C
100	0	65
70	30	55
50	50	45
25	75	38
0	100	27

Table 5 Flash Point of Mixture Diesel + Xylene

Solubility test was performed at room temperature, and within two hours a 50:50 mixture of diesel and xylene was able to dissolve B-8 oil samples quite well, 85.42% solubility, as shown in Table 6. In order to maximize solvent stimulation job in B Structure, mutual solvent was added to improve hydrocarbon relative permeability, and a little surfactant was added as demulsifier. Table 7 shows the contents of final fluid mixture that will be used in well stimulation treatment.

Chemical	Temp (^{0}C)	Time (hours)	Solubility (%)
(40% Xylene + 60 % Diesel)	23	2	77.5%
(50% Xylene + 50 % Diesel)	23	2	85.42%
(60% Xylene + 40 % Diesel)	23	2	89.09%
(70% Xylene + 30 % Diesel)	23	2	90%
(80% Xylene + 20 % Diesel)	23	2	92.92%
(90% Xylene + 10 % Diesel)	23	2	93.13%

Table 6 Effect of Mixture Xylene and Diesel on B-008 oil sample

Chemical	Concentration	UoM
Xylene	500	gal/Mgal
Diesel	400	gal/Mgal
Musol	50	gal/Mgal
Surfactant	2	gal/Mgal

Table 7 Contents of Xylene Solvent System

Prior to the stimulation treatment, a solubility test was carried out on the xylene solvent system on samples of oil wells B-008 and B-122 at a formation temperature of 191^0 F. Within 2 hours, Xylene Solvent System was able to properly dissolve paraffin oil samples of 92.03% solubility for samples B-008 and 94.81% solubility for samples B-122. Table 8 shows this solubility test result. *(No sample can be collected from well B-104 & B-121 due to heavy oil damage near wellbore)*

Sample	Chemical	Temp ^{0}F	Time hours	Solubility %
B-008	Xylene Solvent System	191	2	92.03%
B-122	Xylene Solvent System	191	2	94.81%

Table 8 Solubility Test Result of B-008 and B-122 Oil with Xylene Solvent System

PROCEEDINGS
JOINT CONVENTION BANDUNG (JCB)2021
November 23rd – 25th 2021

Result and Discussion

Solvent Stimulation Execution

Here is job procedure for xylene solvent system stimulation:

- Spotted Pumping and Mixing Equipment
- R/U pumping line
- Pressure tested pumping line
- Mix brine with 7% KCl
- Fill up well with 7% KCl water
- Performed pre-injectivity test using brine 7% KCl water.
- Mix Xylene Solvent System
- Pumped Xylene Solvent System
- Pumped displacement 7% KCl
- Soak Xylene Solvent System for 2 hours
- R/D Pumping Line
- R/D Pumping and Mixing Equipment

Xylene solvent system stimulation in B Structure required rig/hoist utilization. Equipments needed for this treatment were as shown in Fig. 5: chemical transport trailer, pump trailer, accessories trailer, acid tank 120 bbl, water tank 120 bbl, and compressor. Examples of injectivity rate test and main treatment job stimulation of solvent are as shown in Fig. 6 and Fig.7. Stimulation was performed using bullhead method with 6 ft penetration into the formation and minimum 120 minutes of soaking time.

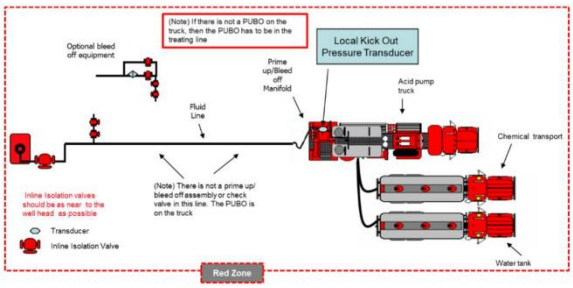

Fig. 5 Equipment Layout for Xylene Solvent System Stimulation Job

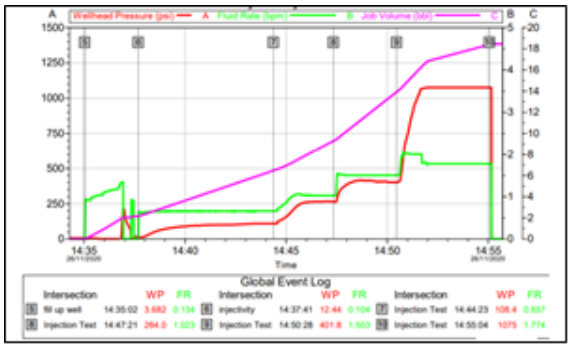

Fig. 6 Injectivity Rate Test Chart of Solvent Treatment B-122

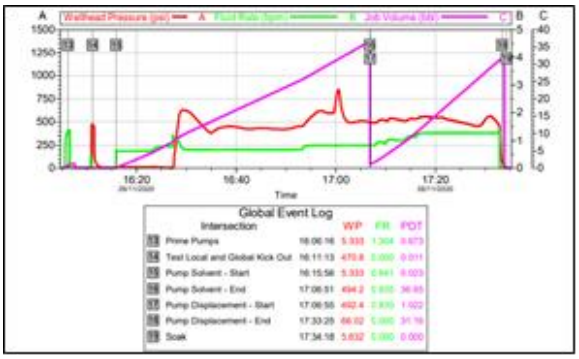

Fig. 7 Main Treatment Chart of Solvent Treatment B-122

Results

The best result out of these treatments was from well B-121. The well's oil production before treatment was 25 bbls per day and was improved post treatment into 175 bbls/day, with decreasing trend for its water cut. Another improvement also happened in well B-122. Pretreatment oil production for this well was 21 bbls/day and was improved into 76 bbls/day with the same pump setting after treatment. In B-104 well, which delivered zero production since well intervention job, delivered peak oil production of 54 bbls/day. All wells were produced using artificial lift and still have more than 300 m of pump submergence, which means the door for production optimization is wide open. Fig. 9 to 11 and Table 9 and 10 show summary of this stimulation project.

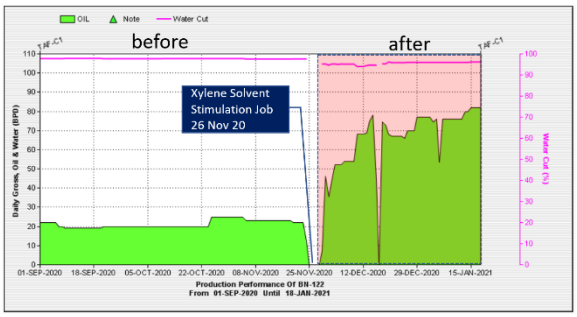

Fig. 9 B-122 Oil Production Comparison after Solvent Stimulation

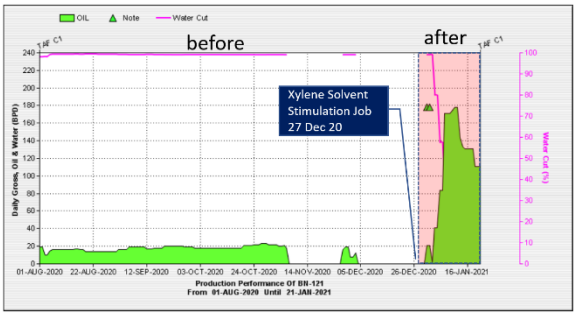

Fig. 10 B-121 Oil Production Comparison after Solvent Stimulation

PROCEEDINGS
JOINT CONVENTION BANDUNG (JCB)2021
November 23rd – 25th 2021

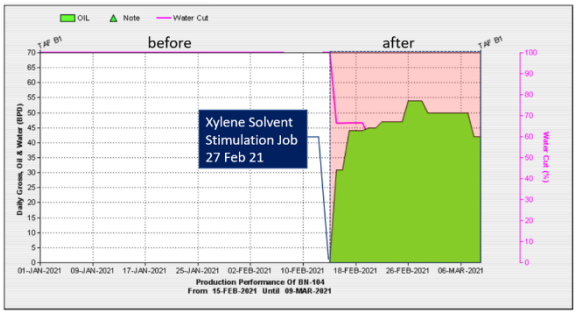

Fig. 11 B-104 Oil Production Comparison after Solvent Stimulation

Well	Average Production (bopd)		Gain (bopd)
	Before	After	
B-122	21	76	+55
B-121	25	175	+150
B-104	0	54	+54

Table 9 Recapitulation of Gain Production

Well	API Gravity	
	Before	After
B-122	17.12	22.19
B-121	19.39	25.01
B-104	19.26	22.15

Table 10 API Gravity Change

Conclusions

The success from these stimulation jobs using aromatic solvent provide a solution for heavy oil production in B Structure in Pertamina. Several more wells are already scheduled to receive solvent stimulation treatments. Production monitoring is still on going with production optimization is on the plate. Wells' lifetime is also closely monitored as well as design optimization for stimulation treatment.

References

Straub, T.J., Autry, S.W., and King, G.E., 1989. An Investigation into Practical Removal of Downhole Paraffin by Thermal Methods and Chemical Solvents. Presentation at the SPE Production Operations Symposium held in Oklahoma City, Oklahoma, March 13-14, 1989. Paper SPE 18889.

Xiong, H and Holditch, S. A., 1995. A Comprehensive Approach to Formation Damage Diagnosis and Corresponding Stimulation Type and Fluid Selection. Presentation at the SPE Production Operations Symposium held in Oklahoma City, Oklahoma, April 2-4, 1995. Paper SPE 29531.

Acknowledgements (Optional)

We would like to express our gratitude to all of our comrades in Pertamina EP Asset 1 for our collaborative efforts in making this project successful.

PROCEEDINGS
JOINT CONVENTION BANDUNG (JCB) 2021
November 23rd – 25th 2021

Innovative Reverse Engineering Approach In Design And Construction Of New Gas Processing Facility In Brown Field Block Through Optimum Utilization Of Excess Materials And Idle Equipment To Improve Capital Stewardship And Inventory Management. Case Study: Field X Associated Gas Recovery Project

.Yudhy, Muhammad Riandhy Anindika. Pertamina Hulu Rokan

Abstract

Successful project management boils down to effectively and efficiently managing resources to meet the project's cost and schedule. The ability to manage project effectively becomes increasingly important to recover capital project expenditures in expiring Production Sharing Contracts (PSC) blocks. The longer the time needed for a project to complete, the higher the project capital and the lower the capital recovery. Referring to look back result of several major capital facility projects, the key challenge in meeting the project cost and schedule is related to procurement of long lead materials and key process equipment. In brown field blocks, there is an opportunity to perform reverse engineering by optimally utilizing the excess materials in the warehouse and idle/unused process equipment to solve the key challenges. As additional benefit, utilization of excess materials and idle process equipment will improve inventory management and capital stewardship, since the cost to relocate and modify the equipment are significantly lower than the cost of buying a new equipment.

Field X Associated Gas Recovery Project (AGRP) provided an excellent case study of successful reverse engineering approach using excess material and idle equipment in design and construction of a new gas processing facility in brown field block. Field X AGRP is designed to recover and process associated gas from X field to be used as fuel gas for the gas turbines at the internal Power Generation Plant. However, based on lesson learned from similar opportunity in the past, the cost of construction and installation of a new gas processing facility using new construction materials and new process equipment is very high, which is uneconomic at the current oil price environment. Therefore, to make the project economic, the project team shall consider the utilization of available excess material in the warehouse and idle/unused equipment into design basis. Project team conducted assessment to several facilities across the concession area to gather equipment specification data of idle process equipment and the size of available excess materials. The gas processing facility design was reverse engineered to optimally utilize the idle process equipment and excess materials.

The utilization of idle equipment and excess material in construction of the gas processing facility has successfully generated cost saving up to 5 times the project cost from avoiding purchase of new equipment and new construction materials. The project successfully recovered associated gas at the rate of 0.5 MMSCFD to be used as fuel to gas turbine and produced 60 BOPD condensate from gas-liquid separation process

Introduction

Field X has been producing associated gas at a rate of up to 1.2 MMSCFD with heating value of around 720 BTU/scf (refer to Table 1 for the detail gas properties). However, before the project was completed, the gas was continuously flared. With the internal power generator being able to process the associated gas with minimum 700 BTU/scf as fuel, there was an opportunity to recover the associated gas and utilize the gas as fuel for the power generator.

Table 1 – Field X Gas Properties

Variable	*Unit*	Field X Associated Gas
Vapor Fraction		0.981542
Temperature	*F*	150
Pressure	*psig*	5
Molar Flow	*MMSCFD*	**1.2**
Mass Flow	*lb/day*	101689
Std Ideal Liq Vol Flow	*barrel/day*	474
Lower Heating Value	*Btu/SCF*	**720.80**

Since Field X did not have a gas processing facility available to recover the associated gas, a new gas processing facility shall be constructed at Field X to take full advantage of the opportunity. However, the opportunity was identified in late 2016 when the oil price was low (~ 50 USD/barrels) and the window to gain return of investment was short, as the concession area will be relinquished to the states in less than 5 years. Therefore, to ensure the decision to invest in constructing a new facility was justified, thorough economic study shall be carried out. The variables to be compared in the economic study was the cost and schedule of constructing the facility using all new materials, the cost and schedule of constructing the facility using available excess materials and existing spare/unused equipment from inactive facilities and the operating cost saving from using the associated gas for power generator fuel. It was found from the study that the cost of constructing the gas processing facility using all new materials will be 5 times higher than using excess materials and will take 700 days longer due to contracting and procurement process for the same operating cost saving. Hence, the alternative to construct the facility using available excess materials and existing spare/unused equipment from inactive facilities was selected as it was the most economic.

PROCEEDINGS
JOINT CONVENTION BANDUNG (JCB) 2021
November 23rd – 25th 2021

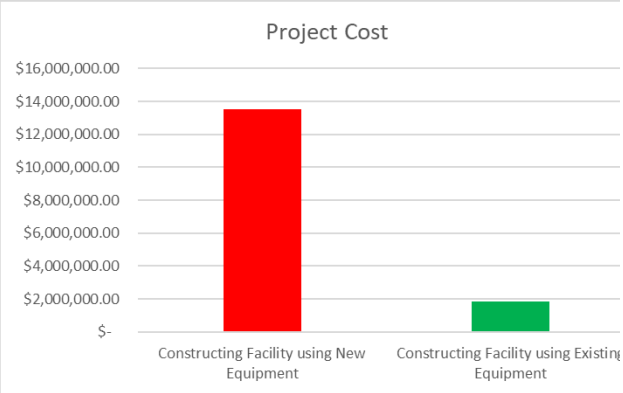

Figure 1 Project Cost Comparison

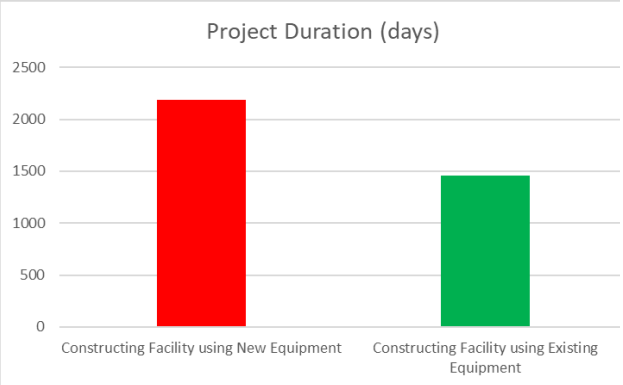

Figure 2 Project Schedule

Using existing materials and equipment to construct a facility posed 3 unique technical challenges that the Project team must be able to solve:

1. The first and most important challenge was the available excess materials or spare equipment size might not match with the required equipment size from engineering calculation.
2. The second challenge was the existing equipment condition that might not be prime to be used for the facility since it was inactive for a long time with minimal maintenance.
3. The last challenge was equipment relocation from the individual equipment location that was scattered all over the concession Area to Field X. The concession area was ~150 km^2 in area which was very wide. The longest distance for equipment relocation travel was more than 100 km.

The creative solutions brought up by the Project team to solve these technical challenges will be discussed further in this paper.

Data and Method

Reverse Engineering

The first step to address the challenge of equipment and material size was to develop a Front-End Engineering Design (FEED) of the facility assuming new equipment was used as baseline. Assuming new equipment will ensure the main objective of the FEED, which was to maximize the dry gas and condensate production from processing the feed associated gas, could be met. In developing the FEED, 3 proprietary simulation software were used:

- A proprietary pipe network simulation software was used to determine the pressure dynamics in the gas pipeline network. The result of the simulation will set the target for the minimum discharge pressure of the gas processing facility to be able to flow to the power generation facility.
- A proprietary process simulation software was used to generate FEED details, such as equipment size and the optimal operating range for the process variables.
- A proprietary gas compressor simulation software was used to design the optimum configuration of the gas compressor.

From the simulation, the optimal design for the baseline was a 3-stage compression process with 2 stages of separation and cooling for the gas prior to entering gas compressor, 2 stages of separation for the liquid phase and throttling for Joule – Thompson cooling at the outlet of the gas compressor to extract the remaining liquid in the gas prior to shipping to the power generation facility. The resulting baseline design for the gas plant facility and the gas compressor are displayed in Figure 3 and Figure 4.

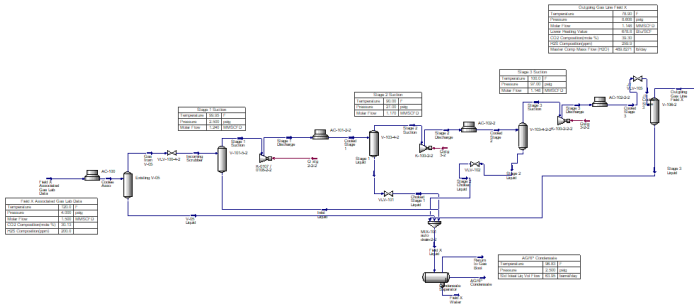

Figure 3 Process Simulation Design for FEED

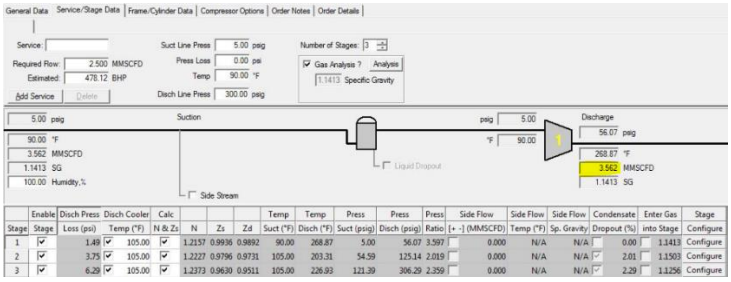

Figure 4 Compressor Simulation Design for FEED

After the baseline was developed, the Project team then re-simulate the process using by changing the size of the major equipment and piping using the available size in stock and compare the simulation result with the baseline result. As an illustration, the available materials and equipment in stock were a 2-stage gas compressor skid with coolers, 2 fin-fan coolers, 2 positive displacement pumps, several 2' diameter vessels and joints of 4", 6" and 8" pipes. Simulations were done using multiple combination scenarios of these materials. Interestingly, the simulation case using available materials resulted in the same production profile as the baseline case, meaning the available materials and equipment were adequate for the construction of the facility. Further assessment were made to verify compliance to applicable engineering standards for gas compressor, piping and pipelines, mechanical and structural construction. Some of the industry engineering standards used to assess the adequacy of the FEED were:

- API 618 Reciprocating Compressors for Petroleum, Chemical, and Gas Industry Services
- API RP 14E Recommended Practice for Design and Installation of Offshore Production Platform Piping Systems
- API RP 686 Machinery Installation and Installation Design
- API Spec 6D Specification for Pipeline and Piping Valves
- API RP 520 Sizing, Selection, and Installation of Pressure-Relieving Devices in Refineries
- API RP 1110 Pressure Testing of Steel Pipelines for the Transportation of Gas, Petroleum Gas, Hazardous Liquids, Highly Volatile Liquids or Carbon Dioxide
- ASME B31.1 Power Piping
- ASME B31.3 Process Piping
- ASME B31.4 Pipeline Transportation Systems for Liquids and Slurries
- ASME B31.8 Gas Transmission and Distribution Piping Systems
- ASME Section VIII, Division 1, Rules for Construction of Pressure Vessels
- NACE MR0175 Petroleum and Natural Gas Industries—Materials for Use in H_2S-Containing Environments in Oil and Gas Production
- AISC 325 Steel Construction Manual
- AISC 326 Detailing for Steel Construction

A more interesting re-engineering case was the gas compressor. The gas compressor available to be used was a 2-stage gas compressor with a cooler mounted on the skid. To yield the most optimum production using the feed associated gas, the gas compressor deployed in the facility must be a 3 – stage gas compressor. The reason was the pressure ratio of the feed associated gas to the target discharge pressure to be able to send the gas to production header exceeded the maximum pressure ratio allowable for the gas compressor. If this was allowed, the discharge temperature will rise above the temperature limit the compressor materials can withstand and cause material failure that would lead to gas compressor major damage. Therefore, to avoid such damage to the gas compressor and be able to recover the optimum gas production, the available gas compressor shall be modified to accommodate additional stage.

The Project team conducted a thorough engineering study to determine the required modification for the gas compressor. From the study, it was found that the cylinder bore of Throw 1 and Throw 3 of the gas compressor shall be modified from 13" to 19.5", while the cylinder bore for Throw 2 shall be modified from 9.25" to 13". The modifications were based on 3-stage compressor design that was simulated using proprietary gas compressor simulation software and has also been validated by the gas compressor manufacturer principal engineer for further technical design assurance. The changes in cylinder were illustrated in Figure 5. The suction and discharge bottle from each stage shall have its dimensions modified to be able to utilize the four throws of a 3-stage compressor. The size of the new bottles were based the simulation result for 3 stage compressor using proprietary gas compressor simulation software. The changes in bottle size dimensions were illustrated in Figure 6. To ensure that the bottles can withstand the pulsation caused by the compressor and verify the simulation results, manual field verification were performed by third party contractor. The summary of result of the verification was illustrated in Figure 7. The bottle size dimension from the calculation was verified to be able to withstand the pulsation from gas compressor operation since the measured vibration was below the API limit. Further manual calculations was performed to verify that the capacity of the existing pressure vessels in the compressor skid were able to accommodate the condensate formed during compression. The result of the calculation was then compared to the expected liquid drop out at each stage from simulation as seen from Table 2. From the calculation, the holding capacity was far greater than the expected liquid drop.

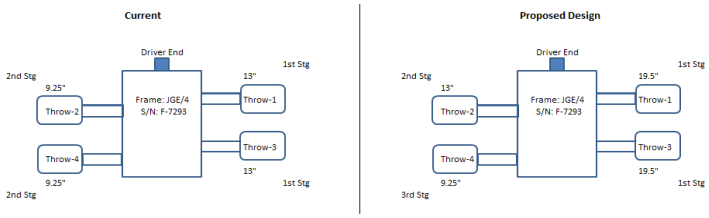

Figure 5 Gas Compressor Cylinder Modification

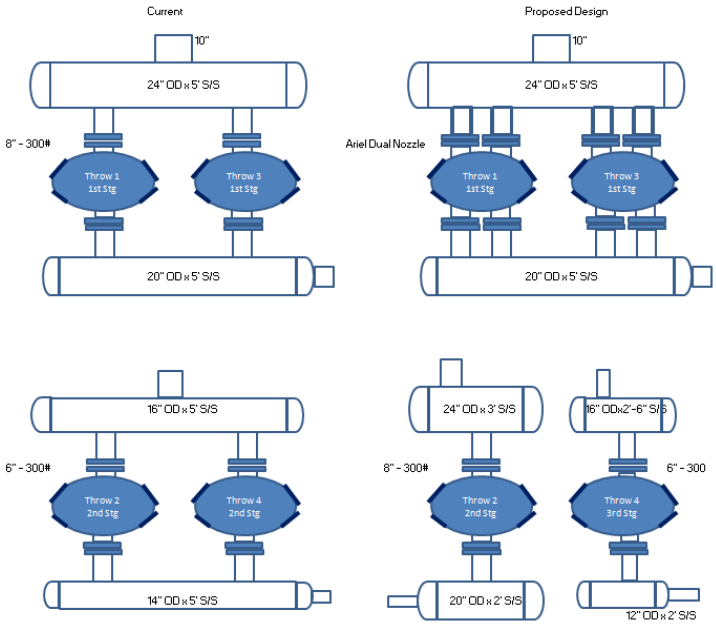

Figure 6 Gas Compressor Bottle Modification

Within the table highest values over the driving speed range will be shown.

Definition:
LC-S/D ... line connection flange suction/discharge side
CC-S/D ... cylinder connection flange suction/discharge side

Location		Basic design	Mod 1 to API limit	Mod 2 empty dampers	Basic design	Mod 1 to API limit	Mod 2 empty dampers
		pk -pk [%]			comparison with API [%]		
1st stage	LC-S	1.6	1.6	-	28	28	-
	CC-S	7.2	7.2	-	100	100	-
	CC-D	7.0	6.2	-	100	89	-
	LC-D	3.0	1.8	-	190	82	-
2nd stage	LC-S	0.34	-	1.5	12	-	64
	CC-S	3.9	-	3.7	59	-	55
	CC-D	4.2	-	3.3	63	-	49
	LC-D	1.5	-	1.6	72	-	73
3rd stage	LC-S	0.79	0.79	1.2	40	40	78
	CC-S	3.3	3.3	2.4	47	47	35
	CC-D	3.5	2.8	2.7	51	39	39
	LC-D	1.7	0.91	0.97	160	79	88

Shaking forces on pulsation damper
Shell – S/D ... forces of entire damper in damper axis suction/discharge side
CP-S/D ... shaking force at cylinder connection flange suction/discharge side

Location		Basic design	Mod1 to API limit	Mod2 empty damper
		kN pp		
1st stage	Shell-S	1.8	1.8	-
	CP-S	0.41	0.41	-
	CP-D	2.0	1.7	-
	Shell-D	8.2	4.5	-
2nd stage	Shell-S	0.49	-	1.0
	CP-S	1.2	-	0.82
	Baffle-S	3.9	-	-
	CP-D	2.4	-	1.6
	Shell-D	3.4	-	0.57
3rd stage	Shell-S	0.94	0.92	1.0
	CP-S	0.81	0.71	0.65
	Baffle-S	3.5	3.1	-
	CP-D	3.8	1.7	1.7
	Shell-D	2.7	2.4	0.70

Figure 7 Pulsation Study

Table – 2 Pressure Vessel Capacity

PROCEEDINGS
JOINT CONVENTION BANDUNG (JCB) 2021
November 23rd – 25th 2021

Vessel	Diameter (in)	Height (ft)	Liquid volume (bbls)	Retention time	Calculated capacity (BOPD)	Simulated Liquid dropout (BOPD)
Inlet Scrubber	28	8.00	2.03	5	584.55	15
1st Stage discharge scrubber	28	7.30	1.85	5	533.41	50
2nd Stage discharge scrubber	28	7.30	1.85	5	533.41	20
3rd Stage discharge scrubber	28	7.00	1.78	5	511.48	15

To ensure the spare equipment will be reliable throughout the facility operational phase, a reliability study was done using Reliability Block Diagram (RBD) modelling using the reliability data of the selected equipment. The reliability data was calculated based on equipment failure history and verified using Maintenance inspection, testing and preventive maintenance (ITPM) records. A baseline of world class reliability of 90% was selected in reference to Society of Maintenance and Reliability Professional (SMRP) Best Practice. Figure 8 displayed the result of the RBD modelling and the calculated system reliability.

Equipment	Inlet Cooler	Inlet separator	Inlet Scrubber	Stage 1 Compressor	Stage 1 Cooler	Stage 1 Discharge Scrubber	Stage 2 Compressor	Stage 2 Cooler	Stage 2 Discharge Scrubber	Stage 3 Compressor	Stage 3Cooler	Stage 3 Discharge Scrubber	JT Valve	Low Temperature Separator	System Reliability
Reliability	0.98	1	1	0.95	0.98	1	1	0.99	1	1	1	1	1	1	0.9032562

Figure 8Equipment Reliability Analysis

The combination of selected spare equipment yield a system reliability of 90.32%, which means they were adequate to sustain a reliable operation.

Equipment Modification and Reconditioning

Based on FEED, several equipment shall be modified to be able to perform its intended function. The major modification was done for the gas compressor, with minor modification on the piping or pipeline to accommodate the usage of excess materials. There were 6 main tasks for the compressor modification, comprised of mechanical modification and control system modification:

1. Cylinder bore modification
2. Pulsation bottles modification
3. Re-staging of gas compressor using new cylinder bore and new pulsation bottles
4. Connection lines for additional cooling for the additional stage
5. Control system upgrade from pneumatic controls to electronic controls
6. Installation, testing and commissioning.

The cylinder bores and pulsation bottles were modified as per engineering study result, then installed back to the gas compressor frame for re-staging of the gas compressor as seen on Figure 9. The additional compression stage needed additional cooling stage to maintain isentropic compression and recover more condensate, therefore additional line was made to connect the discharge line from one of the compressor's outlet to the additional cooling stage assembly (cooler and scrubber), as seen on Figure 10. To better control the gas compressor and for easier integration between gas compressor control systems with the overall plant control system, the pneumatic control system of the gas compressor was upgraded to electronic control system. The new electronic control system has the following capabilities:

- Air-fuel ratio control (AFR) system: to optimize the combustion in the engine and reduce the amount of unburnt fuel the AFR system is required to control the amount of fuel entering the engine. The system operates by sensing the amount of oxygen at the engine exhaust prior to the catalyst. By analyzing the amount of oxygen that exits the combustion chamber, the system can obtain information on the characteristics of the combustion in the cylinder, whether there is too much fuel (too rich) or not enough fuel (too lean). After obtaining the information, the system will adjust the amount of fuel that flows to the carburetor of the engine
- Electronic ignition control system: in contrast to the existing mechanical ignition system, the electronic ignition system will provide better control on how the engine will burn. The ignition control system will be able to be more accurate when setting the ignition timing for the engine. This will be useful in maintaining the NOx emission, as the ignition timing is one of the factors that contribute to the NOx formation. By advancing the timing, combustion occurs earlier in the cycle, which increases the peak pressure. This resulted in higher peak temperatures in the engine cylinders causing higher NOx formation rates. However, by retarding the ignition timing, the peak pressure and temperature will decrease, and it will reduce NOx formation. The ignition control system will be able to better control the ignition timing and consequently the NOx formation.
- Pyrometer and detonation sensors at the engine: primarily, this device will be used to monitor the engine cylinder temperatures and adjust ignition timing when detonation occurs in the cylinder, to avoid damage to power cylinders
- Integration with new PLC system to control sequence and process within engine and compressor as well as process control in the gas plant facility

PROCEEDINGS
JOINT CONVENTION BANDUNG (JCB) 2021
November 23rd – 25th 2021

Figure 9 Gas Compressor Restaging

Figure 10 Additional line to additional cooling stage

Minor modification was made to piping connection to equipment to fully utilize the excess materials for construction. The impact of modification was simulated using proprietary pipe network simulation software to investigate the impact to pressure drop. The simulation result revealed no significant pressure drop from the modification hence it was acceptable to apply. Some examples of these modifications were illustrated in Figure 11. We could see a unique sight of 10" to 8" pipe reduction and a 2" to 6" pipe expansion in the connection between piping to equipment.

Figure 11 Example of Modified Piping Connection

Some of the spare equipment relocated to the AGRP did not need to be modified, however it needed to be reconditioned to restore it to its initial condition. The reconditioning activities included repair, replacement of broken component and repainting. The result of the reconditioning could be seen on the vessels and coolers in Figure 9, Figure 10 and Figure 11 were the vessels and coolers had been restored to its initial condition.

The flowchart for all the activities described above could be found in Figure 12 below.

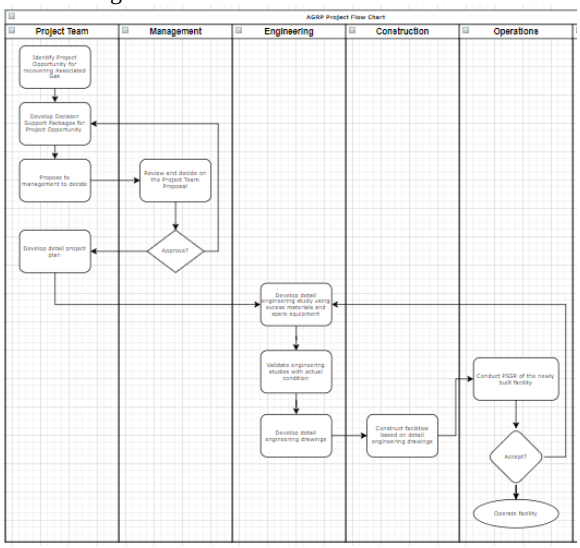

Figure 12 Flow Chart of the Project

Result and Discussion

The primary measure of technical success is the AGRP ability to recover associated gas and condensate and in that respect the project met its objective. The measured gas production and condensate production trends in Figure 13 and 14 respectively has shown that AGRP has been able to recover an average production of 0.5 MMSCFD associated gas and 60 BOPD condensate. While the amount of recovered gas was less than expected in the initial study, it was offset by the 20 BOPD increase in condensate production. With this production rate, the return of investment from reduction in operating cost is expected to break even in 2 years of operation.

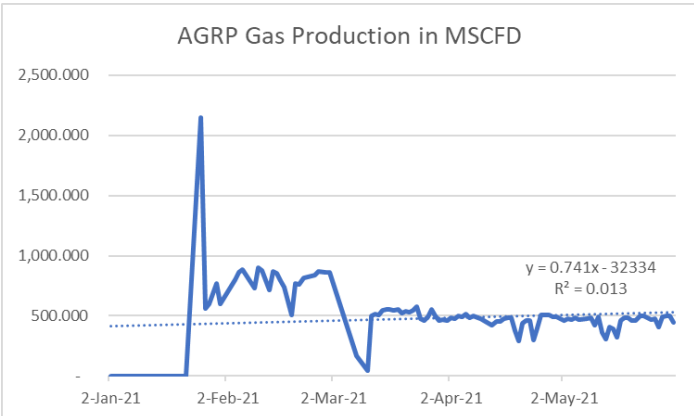

Figure 13 AGR Daily Gas Production

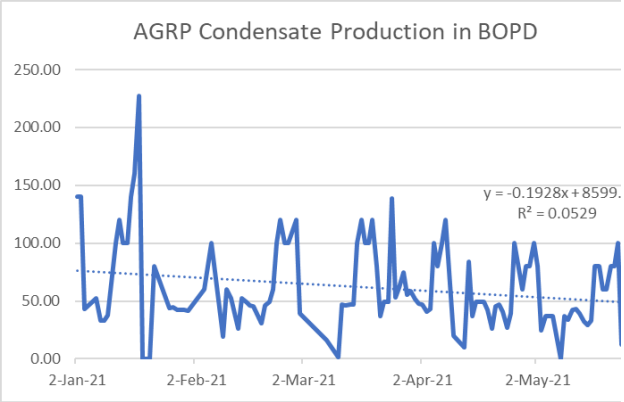

Figure 14 AGRP Condensate Daily Production

Since many of the bulk materials used to construct the facility were from excess materials, the warehouse was able to reduce its inventory level by 8559 items, a pretty significant amount. The total saving from reduced inventory cost and the cost avoidance from buying new bulk materials were more than USD 350,000. Another additional benefit from better inventory management was less sole cost to the Company. The area of operations where the Company operated adopted PSC scheme where the Company will be back-charged if buying something it did not use to increase production.

From project management standpoint, the actual cost and schedule did not differ much from the plan. The project was completed in 3 years 6 months (1278 days) and the total cost was USD 1.9 MM while the plan was to complete the project in 3 years (1095 days) with a total cost of USD 1.8 MM. The additional cost was still within the allowable 10% of the total cost allowed by the Government for cost recovery.

Conclusions

The utilization of idle equipment and excess material in construction of the gas processing facility has successfully generated cost saving up to 5 times the project cost from avoiding purchase of new equipment and new construction materials. As additional benefit, utilization of excess materials and idle process equipment will improve inventory management and capital stewardship, since the cost to relocate and modify the equipment are significantly lower than the cost of buying a new equipment. The facility constructed using the excess materials and spare equipment could perform well too as it successfully recovered associated gas at the rate of 0.5 MMSCFD to be used as fuel to gas turbine and produced 60 BOPD condensate from gas-liquid separation process. All of these were possible due to the creativity of the project team and the strong multi-functional collaboration between support functions

References:

1. Company Project Documents
2. SMRP Best Practices 5th Edition

PROCEEDINGS
JOINT CONVENTION BANDUNG (JCB) 2021
November 23rd – 25th 2021

Analysis Of Salt Content And Calculation Of Compensation Deviation Of Salt Content At SPU To PPP Field X

Diky Pranondo, Instructor In Polytechnic Campus Of Akamigas Palembang

Abstract

Salt content refers to salt contained in crude oil in forms of magnesium, calcium, sodium chloride which are abundant. These salts can be found in two forms; the first is dissolved in water emulsion in oil and the second is in form of crystal and forms solid sediment. The measurement and analysis conducted included fluid level measurement, oil sample taking, and salt content analysis. The tools and materials used in salt content analysis were salt in crude analyzer precision, beaker glass, alcohol mix solvent, xylene and crude oil. This research was based on the data result from observasion in the field. the results of Fluid Level Measurement was 3.580 mm and free water was 420 mm. The samples were taken from two points which are upper and lower. The upper was 7.436 mm and the lower was 9.046 mm. The salt content calculation was 14,7 ptb. The compensation of salt content deviation was US $ 181.33 the same as Rp. 2.564.348,90.

Introduction

Elmusi is a new liquid formed from 2-phase fluids that are not mutually soluble and thus require a method and a long time to sort it out. Emulsion there are usually 2 types, emulsion oil in water and in-water emulsion oil. Emulsions of oil in water (oil in water emulsion) is where the granules oil stuck or trapped in water droplets that affect the quality of water to be purified from the oil. Emulsion oil-in-water (water in oil emulsion) is where the water droplets stuck or trapped in the oil so that it affects the quality of the oil.

Salt content is a parameter that shows the levels of salt content in crude oil. Salt content itself are in the form of magnesium, calcium, and sodium chloride. These salts can be found in 2 forms, namely soluble in water emulsions in crude oil and is shaped crystals can form the suspended solids.

Salt content in crude oil can cause problems during transportation and purification processes, including corrosion, and fouling. To cope with the levels of salt in the oil, then the required water to clean it, the water must then be separated from the oil by adding chemicals to break the emulsion.

Measurement Of Liquid Height

Storage tank used by the Field X is a tank fixed roof where the liquid stored in the tank is a liquid that is volatile. The method used to measure the height of the liquid is the method of innage where the measurement of the referance point to the datum plate.

Sampling Of Oil

Sampling of oil aimed to obtain the oil sample that represents the appropriate purposes. Sampling was done to determine the quality of the oil is full. In sampling oil things that need to be considered as follows :

1. Test Physical And Chemical Properties
2. The Order Of Sampling
3. Hygiene Equipment
4. Transfer Of Sample
5. Composite Sample.

Analysis of The Salt Content

Analysts content of salt is important because it can determine the salt content in the oil is according to the standard or not. How to determine the contents of the salt by the method of electrometris miliampere vs content of salt PTS ASTM D-3230 and the use of tool salt in crude analyzer precision.

The analysis is carried out in the laboratory with the use of tools *in crude analyzer precision* dan *electrometris miliamper* methode vs *salt content in* PTS ASTM D-3230 against the crude oil in the production of whether it is eligible or not.

Compensation Deviation Of The Salt Contents

Compensation of Deviations of Salt Content (PSC) is the fines from the SPU to the PPP on the field X which according to the agreement work. That when the oil in the

PROCEEDINGS
JOINT CONVENTION BANDUNG (JCB) 2021
November 23rd – 25th 2021

transfer from Field X must the following standards :

1. Base sediment and water (BS&W) do not exceed 0,50%.
2. Salt content do not excedd 7,0 Ptb (lbs/1000 bbl).
3. The maximum value of pour point at 80°F.

If it does not meet the standards that have been determined will then be subject to fines, compensation of deviations of salt content (PSC) when the oil in the transfer from the SPU to the PPP has a high content of salt content, which exceed the standard that has been determined.

Penalty Salt Content
Penalty = Salt content actual – Salt content Tolerable

- Compensation deviation of *Salt Content* in US $

$$\text{PSC} = \frac{1{,}15 \text{ x } Penalty \text{ x PPP } Figure \text{ (Barrels)}}{1000}$$

- Compensation deviation of salt content in US $ to IDR

PSC = US $ X Rp. 14.141,75
(the value exchange rate IDR time of observation)

The Methodology Of Observation

Consists of :

- Measurement of height of liquid level
- Gross or Net fluid sent from the Collecting Station (SP) to the collecting station main (SPU).
- Analysis of a sample of fluid.
- Information of salt content in the oil in the tank.
- Shipping information the oil in the amount of the Net from the SPU to the PPP in the field X.

Result and Discussion

The Measurement Of The Salt Content

The measurement of the first stage :

- The value of *Alcohol* 50 ml + *Xylene* 40 ml = 0,414 mA

The measurement of the second stage :

- The value of *Alcohol* 50 ml + *Xylene* 40 ml + *crude oil* 10 ml = 1,17 mA
- The value of (*Alcohol* 50 ml + Xylene 40 ml) + (*Alcohol* 50 ml + *Xylene* 40 ml + *crude oil* 10 ml)

= 1,17 mA – 0,414 mA

= 0,756 mA

The value of 0,756 mA not found in the table of calibration electrometris miliampere vs salt content in PTS ASTM D-3230, then it's made of interpolation as follows :

Figure 1 Interpolation Calibration Values

mA			Ptb	
A	0,710	→	D	14,0
B	0,756	→	E	X
C	0,780	→	F	15,1

$$= \frac{(B-A)/(C-A)}{(E-D)/(F-D)}$$

$$= \frac{(0{,}756 - 0{,}710) \,/\, (0{,}780 - 0{,}710)}{(E - 14{,}0) \,/\, (15{,}1 - 14{,}0)}$$

$$= \frac{(0{,}046) \,/\, (0{,}070)}{(E - 14{,}0) \,/\, (1{,}1)}$$

$$E = 14{,}0 + \left(\frac{0{,}046}{0{,}070}\right) \text{ x } 1{,}1$$

E = **14,7 Ptb**

Figure 2 Compensation deviation of salt content

Tanggal	SALT CONTENT (Ptb)			PPP	PSC US $ 5	PSC Rupiah (Rp.14.141,75) 6
	Actual	Tolerable	Penalty			
	1	2	3=1-2	Daily 4		
1	**8,6**	7	1,6	3.404,524	6.26	88.588,51
2	**8,4**	7	1,4	3.402,271	5.48	77.463,65
3	**8,3**	7	1,3	3.378,484	5.05	71.427,63
4	**9,6**	7	2,6	3.378,960	10.10	142.875,38
5	**9,0**	7	2,0	3.376,410	7.77	109.821,20
6	**8,1**	7	1,1	3.375,623	4.08	57.642,69
7	**8,4**	7	1,4	3.371,631	5.23	74.024,38
8	**8,3**	7	1,3	3.351,912	4.82	68.140,23
9	**8,1**	7	1,1	3.322,617	4.20	59.439,34
10	**7,3**	7	0,3	3.305,396	0.95	13.438,92
11	**7,3**	7	0,3	3.336,229	1.15	16.277,14
12	**9,1**	7	2,1	3.321,757	8.02	113.445,73
13	**9,3**	7	2,3	3.316,772	8.58	121.366,59

Tanggal	Salt Content (Ptb)			PPP	PSC US $	PSC Rupiah (14.141,75)
	Actual	Tolerable	Penalty	Daily		
	1	2	3 = 1-2	4	5	6
14	**8,1**	7	1,1	3.301,760	3.99	56.381,39
15	**8,1**	7	1,1	3.277,285	4.15	58.628,38
16	**9,5**	7	2,5	3.239,816	9.31	131.722,92
17	**10,2**	7	3,2	3.180,168	11.70	165.501,16
18	**8,8**	7	1,8	3.207,410	6.45	91.283,76
19	**7,9**	7	0,9	3.215,401	3.14	44.448,29
20	**9,5**	7	2,5	3.219,225	9.26	133.885,74
21	**8,9**	7	1,9	3.225,183	6.86	97.034,70
22	**7,8**	7	0,8	3.210,050	2.77	39.153,81
23	**7,6**	7	0,6	3.217,008	2.03	28.775,03
24	**7,9**	7	0,9	3.220,284	3.15	44.515,79
25	**8,8**	7	1,8	3.219,795	6.66	94.254,42
26	**8,2**	7	1,2	3.224,738	4.45	62.932,75
27	**9,1**	7	2,1	3.235,949	7.81	110.515,19
28	**9,8**	7	2,8	3.250,115	10.47	147.998,65
29	**8,8**	7	1,8	3.241,826	6.52	92.263,25
30	**8,3**	7	1,3	3.268,096	4.89	69.093,81
31	**8,6**	7	16	3.266,941	6.01	85.008,48
Total				101.863,636	181.33	2.564.348,90

Discussion

Alternative problem solving in lowering the salt content in the oil with the handling of some of the Collecting Station (SP) which is not sending the amount of the net to the Collecting Station Main (SPU) should send in the amount of the net due to minimize the content of salt content in the oil.

When Collecting Station (SP) sends oil in the amount of net automatic oil temperature decreases can result in the oil froze. Therefore, in the process flow of oil in the Collecting Station Main (SPU) to use the heater treater which serves as a heater to maintain a maximum temperature of 60°F and can also maintain the temperature of the oil and can separate oil and water. Then keep the thickness of the oil in the wash tank and the oil should be below the over flow. When the oil flow from the wash tank to the storage tank the oil should be in the settling first and after that do the measurement, sampling and also the quality of the oil.

Content of salt content in the oil Collecting Station Main (SPU) Field X almost entirely exceed the standards imposed compensation deviation salt content (PSC) on the PPP get compensation of US $ 181.33 and in the IDR is 2.564.348,90 On the delivery of oil production by 101.863,636 bbls

References

Long Bob, Gardner Bob. 2004. Guide to Storage Tank and Equipment, Wiley.

Purwaka, Edi. 2012. Surface Production Operation Equipment. Yogyakarta: Powerindo.

Santosa, Eko Budhi. 2012. Pengukuran Minyak. Cepu: BKOPM Pertamina EP Region Sumatera.

Situmorang, Mardame. 2008. Petunjuk Analisis/Uji Fluida Laboratorium Teknik Resevoir SBS. Palembang: PT Pertamina EP Region Sumatera.

Standart Test Method For Salt In Crude Oil (Electrometric Method), ASTM D-3230.

PROCEEDINGS
JOINT CONVENTION BANDUNG (JCB) 2021
November 23rd – 25th 2021

Surviving Triple Shock Hit in Oil and Gas Industry: Maintaining Production under Budget Cuts Condition in Sumatera Asset Pertamina EP

Reza Alfajri[1], M. Taslim[1], Shandy Arfanny Atmanagara[1], Muhammad Linggar Rafsanjani[1]
Pertamina[1]

Abstract
Started on December 2019 the world has been hit by a new global pandemic known as Corona Virus Disease (COVID-19). It impacts every aspect of life, and eventually economy. On March 9th 2020, the oil price saw its biggest fall in 30 years. It triggered severe budget cost-cutting in order for an oil and gas company to survive. Creativity was needed in maintaining production during this financial predicament.

Three approaches were taken to deal with operation cut cost approximately USD 5,000,000. Economic calculation of wells produced by rented lifting was reevaluated. If the well's production fell under economic limit, the lifting for that well would be decommissioned and the fund would be available for other work plans with more production. Shifting preference for production optimization programs such as grossing up a well by converting to or upsizing ESP will cost lower than well intervention programs that requires at least cementing and perforation cost. Lastly, since there is no work travel during this pandemic, sundries fund can be available.

Filtering economic rented lifting well and reallocating sundries fund generated near USD 750,000 and it was converted to six stimulation, six well intervention, three convert to injector, and eight convert to / upsize ESP programs. Since money was tight, number of well intervention program was limited. Therefore well production and optimization were prioritized. A quadrant map that consists of four quadrant based on well's submergence and pump efficiency data was used to determine wells that can be optimized. Wells that still have high pump submergence and either high or low pump efficiency need to be evaluated and ultimately optimized. The simplest form of production optimization were adjusting lifting parameter: increasing frequency for Electrical Submersible Pump (ESP) and Progressive Cavity Pump (PCP), and changing stroke length and / or increasing strokes per minute for Sucker Rod Pump (SRP). The eight convert to / upsize ESP programs were ultimately performed when all maximum lifting parameters for the wells have been met. These overall programs contributed to cumulative 33,437 bbls oil as of December 31st 2020 and will still be increasing. These approaches helps Pertamina EP, especially in Sumatera Asset, to maintain its production under this predicament.

The silver line of COVID-19 global pandemic from business point of view is that creativity in handling budget and its allocation helps to survive this difficult time. The comfort zone of USD 100 / bbl high oil price is long gone. Economic awareness needs to be emphasized, so that it can help when the shock of fallen oil price hit again.

Introduction

In early 2020, the world was hit by a global pandemic that was identified as a new coronavirus (severe acute respiratory syndrome coronavirus 2, or SARS-CoV-2), and later named as Coronavirus Disease-19 or COVID-19 (Qiu et al., 2020). Although it was started in Wuhan China, it was then spread all over the world uncontrollably and very fast. The pandemic stretched all over 2020 and actually were still going on as of this month on September 2021. During 2020 total cumulative cases were more than 80 million and more than 1.8 million total cumulative death. A really huge number that shook the world. Figure 1 shows chart of reported cases and deaths globally from WHO epidemiological update.

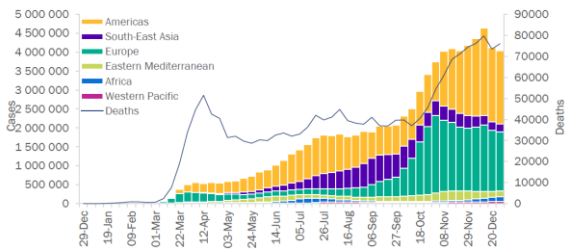

Figure 1 COVID-19 cases reported weekly by WHO Region, and global deaths, as of 3 January 2021 (WHO 2021)

In Indonesia, the coronavirus has infected more than a million people since the first confirmed cases in March 2020 and tens of thousands have died (UNICEF et al. 2021). Total of cases was more than 750,000 and more than 20,000 total deaths during 2020. Figure 2

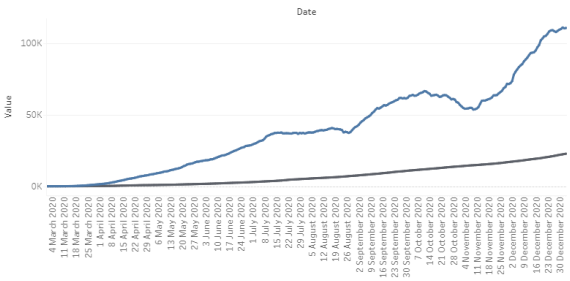

Figure 2 Active Cases and Deaths in Indonesia in 2020 (https://corona.jakarta.go.id/en)

Given the rapid spread of COVID-19, countries across the World have adopted several public health measures intended to prevent its spread, including social distancing (Fong et al. 2020). The effect of this public health measures was gargantuan in every aspects of life: social, work method, and of course economy. The spread of COVID-19 is expected to result in a considerable slowdown of economic activities (Brodeur et al. 2020). The impact on economy hit all kinds of industry including oil and gas.

On April 2020, a historic event happened in oil and gas industry. For the very first time in history US crude oil price plunged below zero (associated press 2020). This negative territory means that oil storage was running out due to global oversupply and other industrial activities that needed fuel were at all time low due to global pandemic. Therefore,

some companies were paying others to take supplies off their hands. Figure 3 shows this historic plunge.

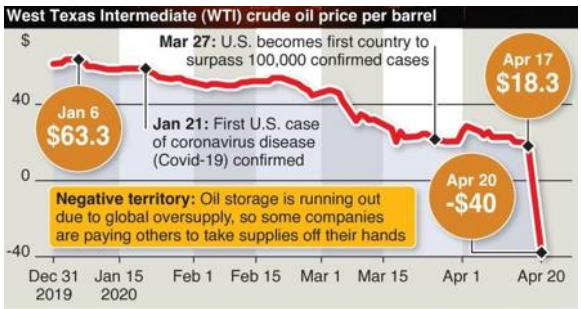

Figure 3 US Crude Oil Historic Plunge below Zero (associated press)

This historic event was also felt around the world, including Indonesia. Revenue from oil and gas (also known as *Penerimaan Negara Bukan Pajak* (PNBP) *minyak* bumi) and Indonesian Crude oil Price (ICP) were on decline trend in the early 2020 (Figure 4). Since global pandemic encouraging a phase of lockdown in order to attempt to minimize the spreading of corona virus, industrial was also laid back. It resulted in decrease of demand for hydrocarbon fuel. So aside from global pandemic that was still spreading and impacting every way of life, oil price was hit to its lowest in the history, oil and gas demand was also decreasing (Figure 5). Oil and gas industry was really hit hard by this shocking triple shock.

Due to this predicament, oil and gas company needed to take extreme measures to survive. Pertamina instructed all of its department and subsidiaries to optimize operational expense without neglecting Health, Safety, Security, and Environment (HSSE) aspect.

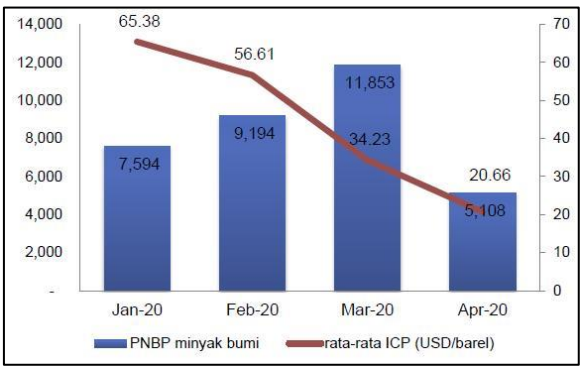

Figure 4 Oil and gas revenue and average ICP Trend in Early 2020

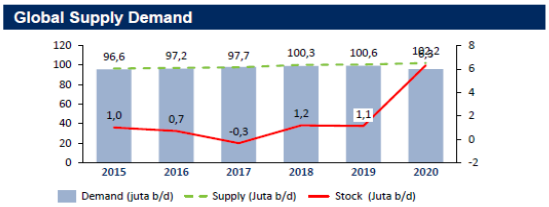

Figure 5 Demand for Oil and Gas was Down and was Up in 2020

With production target in mind and a decrease in operational fund available, creativity was needed in order to survive this pandemic triple shock.

Data and Method

Due to optimizing operational expense up to 28% scenario of well intervention in Asset 1 Pertamina needed to be modified. Figure 6 shows original work plan target for well intervention (WI) and its revised version for Jambi, Lirik, and Ramba Field.

FIELD	TARGET RK WI	TARGET REVISI RK WI
JAMBI	57	36
LIRIK	40	25
RAMBA	81	51

Figure 6 Work Plans (*Rencana Kerja* (RK)) Optimization for Jambi, Lirik, and Ramba Field

In order to pursue production target while also abiding BOD instruction to optimize operational expense, some solutions were discussed and executed. These solutions are:

- Revisit economical evaluation of rented artificial lift in producing well and optimize the utilization.
- Postpone GGR (geology, geophysics, and reservoir) study that would not directly result in production and optimize travel expense fund.
- Optimize well intervention plan in Jambi, Lirik, and Ramba Field.

On April 2020 in Ramba field, the numbers of installed rented ESP (electrical submersible pump) were 34 units and HPU (hydraulic pumping unit) were 23 units. Economic calculation of wells produced by rented lifting was re-evaluated, the summary of this economic evaluation for both types of rented lifting is shown in Table 1. Based on the re-calculation, the minimum economical production of wells produced with rented lifting was 19 BOPD for ESP and 10 BOPD for HPU. Using this calculated economical production cut off, the results of number of population for both type of rented lifting after screening are shown in Figure 7 and 8.

Asset 1			Ramba (Opex 15.57 USD/bbl)			
			ICP 40		ICP 30	
No	Lifting	Biaya Sewa (USD)/unit	Qo (BOPD)	IRR	Qo (BOPD)	IRR
1	ESP	126000	19	15%	33	15%
2	HPU	46000	10	15%	12	15%

Table 1 Summary of Re-evaluation of Economic Calculation of Rented Lifting in Ramba Field

PROCEEDINGS
JOINT CONVENTION BANDUNG (JCB) 2021
November 23rd – 25th 2021

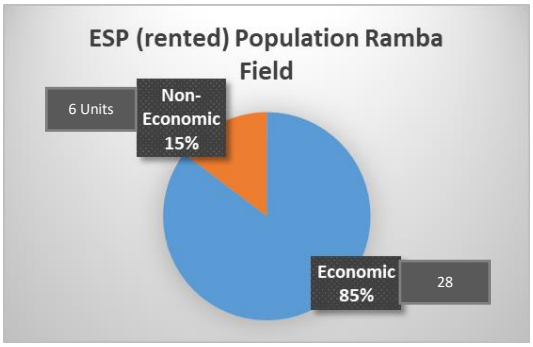

Figure 7 ESP (rented) population in Ramba Field

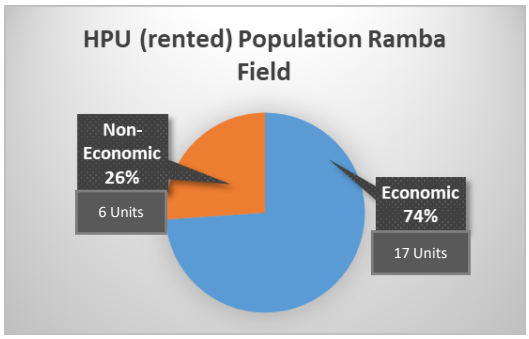

Figure 8 HPU (rented) population in Ramba Field

From the non-economic wells shown in Figure 7 and 8, total of 12 units rented lifting consisting of 6 units of ESP and 6 units of HPU, were either converted to owned lifting method or temporarily suspended for next workover programs. Additional optimization was also made by demobilizing 2 units of rented diesel engine and converting these two power source to company owned power plant. This program started from June to October 2020.

Since global pandemic hit work travel was restricted, only travelling to well sites was allowed to be carried on with strict covid-19 protocols. This policy made some fund available to be relocated to other post such as optimized work plans. Adding rented lifting conversion and postponed GGR study to those freshly made available fund, a total of more than USD 900,000 was saved.

After making the fund available, newly optimized work plans for Jambi, Lirik, and Ramba Field was laid on as shown in Figure 9.

No	Well	Job Description
1	BBT-05	Stimulation and Raparation
2	KAS-284	Reparation
3	KTT-023	Convert to ESP Extreme Well
4	BN-116	Optimation
5	BN-111	Optimation SRP to ESP
6	BN-110	Optimation
7	BN-026	Acidizing
8	BN-099	Reparation
9	TL-01	Reparation
10	NK-31	Optimation SRP to ESP and fishing
11	NK-42	Optimation SRP to ESP
12	BN-122	Solvent Stimulation
13	BN-121	Re-perforated and Stimulation
14	KTB-010	Stimulation
15	KAS-173	Optimation SRP to ESP
16	STT-07	Injection Reparation
17	KTB-011	Injection Stimulation
18	UK-101	Injection Stimulation
Total		

Figure 9 New Optimized Work Plans for Jambi, Lirik, and Ramba Field

Figure 9 shows that there were 18 newly optimized work plans that had been carried out using the freshly made available fund. These work plans could be categorized into three main job types:

- Well optimization

  This job is associated in grossing up the well by converting artificial lift type to a newer or bigger capacity type. There were seven jobs under this type. The job in KTT-023 was converting a conventional ESP to a newer type ESP that is more abrasive resistant. Two jobs in BN-116 and BN-110 were upsizing existing ESP. The remaining jobs in BN-111, NK-31, NK-42, and KAS-173 were converting SRP to ESP.

- Well Stimulation

  This job is performing chemical stimulation to either producer or injector wells. There are five acidizing jobs in BBT-05 and BN-026 (producer wells), and KTB-010, KTB-011, and UK-101 (injector wells). All wells were low on performance due to carbonate scale. Two aromatic solvent jobs were carried out on well BN-122, and BN-121 due to their heavy oil characteristics. There were total seven jobs for this job type.

- Well Reparation

  Well reparation was performed by evaluating and activating other potential layers in an existing wells because their opened interval zone had already been drained enough. There were four well reparation jobs performed on well KAS-284, BN-099, TL-01, and STT-07 (injector well).

Aside from the plans in Figure 9 that would call for rig/hoist for executions, some work plans involving lifting parameter adjustment were also carried out. Increasing operating frequency for ESP and/or increasing stroke per minute (spm) or stroke length (SL) for wells that still have adequate pump submergence were also executed to maintain existing production.

Result and Discussion

Work plans shown in Figure 9 were executed successfully with cumulative production results are shown in Figure 10. Additional note to consider was that injection reparation and stimulation helped a lot in water handling problems in Jambi and Lirik Field in order to also maintain existing production. Figure 11 shows summary from original target to revised target after budget cut, all the way to newly optimized work plans realization.

All of the work plans in Figure 9 contributed oil production gain from producer wells. Jobs executed on injector wells were to maintain existing production by maintaining produced water injection capacity. This work plans were started on August 2020, and since this project was executed under budget cut condition in 2020, the evaluation for contributed production was ended on December 2020. Jobs in 2021 would be carried out utilizing 2021 allocated fund. Figure 12 shows overall cumulative production gain for this surviving from triple shock project, and it can be seen that the production would keep increasing due to the wells are still producing. The effect of this project was even felt on the next year 2021.

PROCEEDINGS
JOINT CONVENTION BANDUNG (JCB) 2021
November 23rd – 25th 2021

No	Well	Job Description	Cum. Gain (BOPD)
1	BBT-05	Stimulation and Raparation	721
2	KAS-284	Reparation	655
3	KTT-023	Convert to ESP Extreme Well	7,091
4	BN-116	Optimation	4,069
5	BN-111	Optimation SRP to ESP	4,757
6	BN-110	Optimation	4,531
7	BN-026	Acidizing	669
8	BN-099	Reparation	1,012
9	TL-01	Reparation	2,461
10	NK-31	Optimation SRP to ESP and fishing	4,263
11	NK-42	Optimation SRP to ESP	417
12	BN-122	Solvent Stimulation	2,228
13	BN-121	Re-perforated and Stimulation	52
14	KTB-010	Stimulation	8
15	KAS-173	Optimation SRP to ESP	805
16	STT-07	Injection Reparation	-
17	KTB-011	Injection Stimulation	-
18	UK-101	Injection Stimulation	-
		Total	33,740

Figure 10 Oil Cumulative Production for the New Optimized Work Plans

FIELD	TARGET RK WI	TARGET REVISI RK WI	OPTIMALISASI RK WI
JAMBI	57	36	43
LIRIK	40	25	26
RAMBA	81	51	61

Figure 11 Summary of Jambi, Lirik, and Ramba Work Plans after the Surviving Triple Shock Project

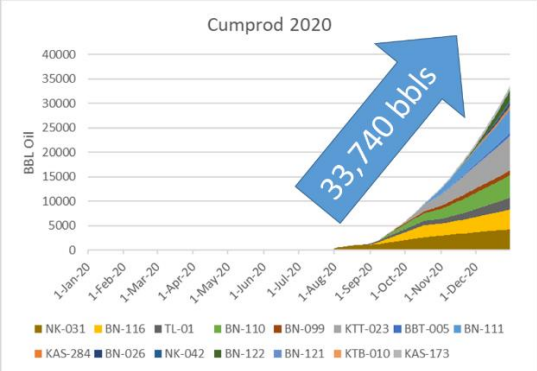

Figure 12 Cumulative production for Surviving Triple Shock Project

Conclusions

1. This triple shock event should trigger survival creativity in optimizing operational fund that involves economic evaluation of every work plan.
2. This survival project was successfully allocating fund more than USD 900,000 to be utilized for work plans to attempt to reach production target.
3. From the newly optimized work plans, 33,740 bbls of cumulative oil production was successfully achieved in 5 months.
4. Based on this invaluable experience from the triple shock hit, a silver line of back to basic method in economic calculation for every project as well as honing business acumen quality could prove to beneficial for the company.

References

Associated Press, 2020, US Crude Oil Historic Plunge Below Zero, Graphic News.

Brodeur, A., Gray, D., et al., 2020, A Literature Review of the Economics of COVID-19, IZA DP, **13411**, 1-61.

Fong, M. W., Gao, H., Wong, J. Y., Xiao, J., Shiu, E. Y. C., Ryu, S., & Cowling, B. J. (2020). Nonpharmaceutical Measures for Pandemic Influenza in Nonhealthcare Settings—Social Distancing Measures. 26(5), 976–984. https://doi.org/10.3201/eid2605.190995

Pemkot DKI, 2020, JAKARTA's COVID-19 RESPONSE TEAM, https://corona.jakarta.go.id/en (accessed on 19 September 2021)

Qiu, Y., Chen, X., et al., 2020, Impacts of Social and Economic Factors on the Transmission of Coronavirus Disease 2019 (COVID-19) in China (Working Paper 494 [pre.]), GLO Discussion Paper, https://www.econstor.eu/handle/10419/215739

UNICEF, UNDP, et al., 2021, Analysis of the Social and Economic Impacts of COVID-19 on Households and Strategic Policy Recommendations for Indonesia, Jakarta.

WHO, 2021, COVID-19 Weekly Epidemiological Update, **21**, 1–17.

Acknowledgements (Optional)

Our gratitude to all of our comrades in Pertamina and all parties involved for the collaboration effort to make this project successful.

PROCEEDINGS
JOINT CONVENTION BANDUNG (JCB) 2021
November 23rd – 25th 2021

Cost Effectiveness of Reliable Power Supply Through DRUPS Implementation

Robi Yasin (Pertamina EP), Jusril Achmad Hidayat (Pertamina EP/ Pertamina (Persero))

Abstract

PT Pertamina EP (PEP) Tanjung Field is a mature oil and gas field in the South Kalimantan area that has problem with high Basic Cost of Electricity Generation. Initially, the electricity demand in Tanjung Field was around 5 MW and then increased to around 8 MW due to the development of the EOR project. The triple shock that has occurred since early March 2020 (down in oil prices, high USD exchange rate, and the COVID-19 pandemic) has pushed the oil and gas field further away from the economic of field. Therefore, an extra strategy is needed so that the field can be operated more economically.

With a surplus of power in the Central Kalimantan PLN area and competitive prices compared to the existing of Basic Cost of Electricity Generation, PLN electricity is an attractive option. However, this is not enough to answer the needs in the oil and gas industry which requires high reliability. The existing PLN electricity services are still not sufficient, because there are still potential blackouts when there is a supply transfer between feeders, including the absence of a power quality control feature that is generated against disturbances that will arise such as voltage sag/dip, undervoltage, voltage fluctuation, harmonic distortion, micro cut, even blackout.

Diesel Rotary Uninterruptible Power Supply (DRUPS) technology was installed to answer the need for better electricity quality. With the DRUPS, the supply transfer process between feeders can be carried out without blackout, even if all feeders from PLN are lost, it can still be handled by the Kinetic Energy Module and Diesel Engine. In addition, the presence of a reactor/active filter combined with a generator at the DRUPS installation can maintain the supply from the above electricity quality disturbances, and can even improve the power factor so as to reduce the kVArh bill charged to customers.

This DRUPS technology can be provided by PLN or through the customer's own investment. The implementation of DRUPS technology at Tanjung Field is the first implementation in the oil and gas industry. The application of DRUPS technology at Pertamina EP Tanjung Field is realized through the Synergy of State-Owned Enterprises (Pertamina – PLN).

Keywords: *Power Quality & Reliability, Cost Effectiveness*.

Introduction

PT Pertamina EP Tanjung Field is a mature field located in South Kalimantan, which has been operating for decades. The Tanjung Field has characteristics such as the characteristics of a mature field in general which is dominated by the use of artificial lifts and additional treatment in the form of pressure maintenance. The large number of artificial lifts in wells which are dominated by artificial lifts with prime mover (using electric motors) as well as the need of pressure maintenance activities using pumps driven by electric motors, makes Tanjung Field require a large enough supply of electricity.

At the beginning of 2019, the Tanjung Field electricity demand was in the range of 5 MW, supplied by 2 Gas Turbine Generators (GTG) – Taurus 60 and 2 Bi-fuel/DGB (Dynamic Gas Blended) Cat 3516B Gensets. As a projection for the coming year, it has been conveyed that there is an additional need for the Enhanced Oil Recovery (EOR) project activity which makes the electricity demand in the Tanjung Field increase to 8 MW.

Initially, the existing generation in Tanjung Field used local gas fuel. However, over time, local gas production from associated gas has decreased, causing the use of fuel to switch to diesel fuel and a small portion of Liquified Natural Gas (LNG) sent from Bontang (distance > 500 km). The change in the use of fuel resulted changes in the cost of electricity generation in Tanjung Field which increased to Rp. 4,711 per kWh. In the end, the cost of electricity generation in Tanjung became one of the largest operational expenses in Tanjung Field, which caused operating costs to increase in Tanjung Field.

The emergence of the triple shock (oil prices fell, the USD exchange rate increased, and the COVID-19 pandemic) made Tanjung Field's high operating costs even more uneconomical. So it is necessary to search for alternative power sources that are more economical/competitive but still pay attention to the reliability aspect to maintain the operational continuity of the Tanjung Field.

The alternative source of electricity available in the Tanjung Field comes from the electricity service provider State Electricity Company / Perusahaan Listrik Negara (PLN) which stated that there is a surplus of electricity supply for the Central South Kalimantan area which is interconnected with the East Kalimantan area (Barito – Mahakam Interconnection). However, the availability of electricity supply is not sufficient to meet the standards of the oil and gas industry, which needs reliability/stability and continuity of electricity supply. This is because the previous PLN electricity has not provided a guarantee of electricity quality (power quality) from disturbances such as overvoltage, voltage dip, voltage

PROCEEDINGS
JOINT CONVENTION BANDUNG (JCB) 2021
November 23rd – 25th 2021

fluctuation, harmonics, micro-cut, even blackout, especially when there is a transfer from a different power source/feeder. So it is necessary to have additional technology (in this case Diesel Rotary Uninterruptible Power Supply (DRUPS)) that can improve the quality of electricity received by the load/customer, especially for oil and gas industry customers.

Data and Method

Diesel Rotary Uninterruptible Power Supply (DRUPS) technology is here to answer the needs related to power quality problems, so that the load will get a continuous supply of quality/reliable electricity (pure sine wave). In the end, this DRUPS technology can answer the electricity needs in the oil and gas industry which demands reliable and continuous electricity quality.
The illustration of regular PLN electricity connection without DRUPS can be seen in Figure 1 as follows:

Figure 1. Illustration of Regular PLN Electricity Connection without DRUPS.

From Figure 1 it can be seen that PLN electricity on Regular service is distributed from the PLN Substation to the Distribution Transformer and from the distribution transformer (owned by PLN for LV customers, owned by customers for MV customers) and then received by the Customer. It can be seen from the illustration that there are no additional components that can guarantee the power quality received by the customer.

By definition, the quality of electricity (Power quality) is described as follows:

a. IEEE 1100-2005: *The concept of powering and grounding sensitive equipment in a manner that is suitable to the operation of that equipment*. [1]
b. IEC 61000-4-30-2008: *Characteristics of the electricity at a given point on an electrical system, evaluated against a set of reference technical parameters*.[2]

In general, the types of disturbances in the quality of electricity (power quality) can consist of:

a. *Overvoltage / surge.*
b. *Voltage dip / Brown-out.*
c. *Voltage fluctuation.*
d. *Harmonic / distortion.*
e. *Microcut / short cut.*
f. *Power Failure / Black-Out.*

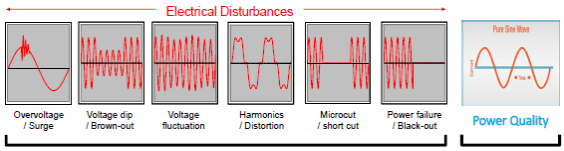

Figure 2. types of electrical disturbances vs. expected power quality. [6]

From the disturbances in the quality of electricity above, DRUPS technology can overcome them and guarantee the load to get good quality electricity (pure sine wave), as shown in Figure 3 as follows:

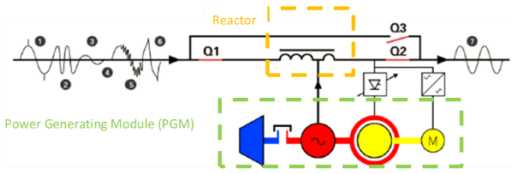

Figure 3. DRUPS Functions. [4]

In general, the main DRUPS system consists of a Power Generating Module (PGM) and a Reactor / Active Filter / Continuous Filter as shown in Figure 3. In more detail, the Power Generating Module (PGM) itself consists of:

1. *Diesel Engine.*
2. *Freewheel Clutch.*
3. *Generator.*
4. *Induction Coupling / Kinetic Energy Module / Energy Transfer Module (ETM) / Flywheel.*
5. *Pony Motor.*
6. *Base.*

The illustration of PGM can be seen in Figures 4A and 4B as follows:

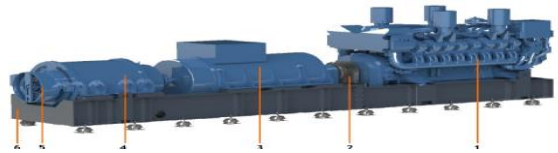

Figure 4A. Typical configuration/topology of Power Generating Module (PGM) on DRUPS unit (1. *Diesel Engine*, 2. *Freewheel clutch*, 3. *Generator*, 4. *Induction Coupling / Kinetic Energy Module (KEM) / Energy Transfer Module (ETM)/ Flywheel*, 5. *Pony Motor*, 6. *Base*). [4]

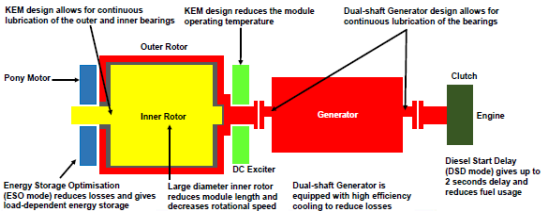

Figure 4B. typical configuration / topology of Power Generating Module (PGM) on the DRUPS unit. [5]

When compared to Static UPS, in terms of space requirements for the same function, DRUPS

PROCEEDINGS
JOINT CONVENTION BANDUNG (JCB) 2021
November 23rd – 25th 2021

technology offers a simpler (compact) installation and space as can be seen in Figure 5 below:

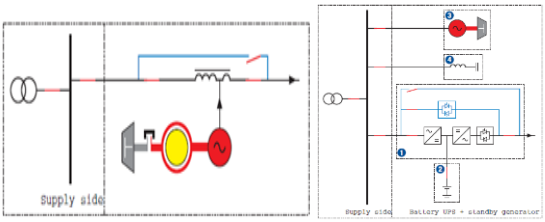

Figure 5. Comparison of DRUPS versus UPS battery system (Static UPS) plus standby generator set. [4]

In general, the principle of DRUPS technology can overcome electrical quality disturbances by applying the following modes (for example):

1. *Utility Mode: Engine Off, Flywheel On RPM 3900/4200 (accelerated by pony motor), Generator (as Synchronous Condenser) On RPM 1500/1800 (coupled with outer rotor KEM).*
2. *Kinetic Energy Module (KEM) flywheel mode + engine start: Engine Start, Flywheel On - Decreasing, Generator On RPM 1500/1800 (coupled with outer rotor KEM).*
3. *Engine Mode / KEM Flywheel Mode: Engine run at RPM 1500/1800, Flywheel On – Increasing to 3900/4200, Generator On RPM 1500/1800 (coupled with outer rotor KEM).*
4. *Preparation (Back to utility mode) / Engine cool down mode: Engine cooling down, Flywheel On – 3900/4200, Generator On RPM 1500/1800 (coupled with outer rotor KEM).*
5. *Utility Mode.*

More specifically, the operating mode naming corresponds to the operating mode naming of the respective DRUPS manufacturer.

The illustration of the stages above can also be explained in Figure 6 as follows:

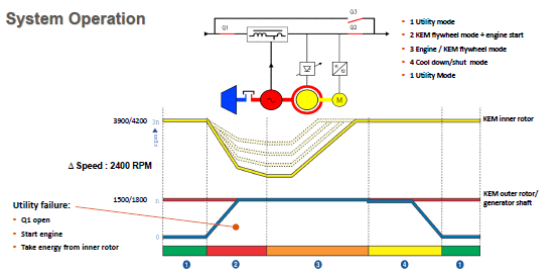

Figure 6. DRUPS system operation (stages of RPM change). [6]

The length of time that can be covered by Kinetic Energy Module/KEM (buffer time before being carried by the Diesel Engine) depends on the amount of load being carried and the size of the Kinetic Energy Module installed. As an illustration for the unit installed at Tanjung Field, the buffer time that can be carried by KEM is of 15 seconds at maximum load (10 MVA). Where the time required to turn on the Diesel Engine itself is 3 seconds, so the available buffer time is more than sufficient.

The existence of a reactor / filter that works with a generator (DRUPS unit) as a synchronous condenser / continuous filter makes the quality of the electricity received by the load to be maintained from interference Overvoltage / surge, Voltage dip / Brown-out, Voltage fluctuation, Harmonic / distortion and also increases the power factor so that it is free from kVArh costs. In addition, the Kinetic Energy Module (KEM) combined with the Diesel Engine makes the system more protected from microcut interference and even black-outs.

Application in the Tanjung Field, DRUPS Technology is provided by PLN with an illustration of the configuration as shown in Figure 7A and Figure 7B below:

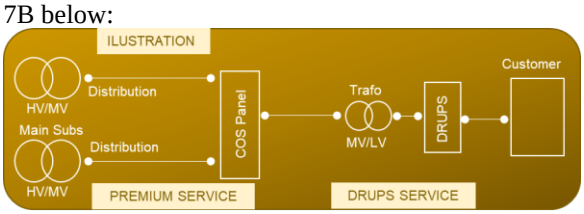

Figure7A. Illustration of PLN Electricity Connection with the DRUPS feature.

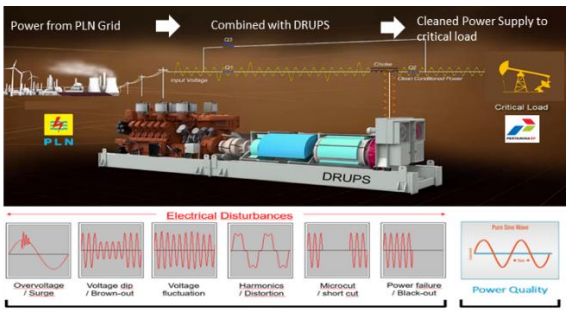

Figure 7B. Configure the interconnection of the PLN – DRUPS network and the PEP network. [6]

The existence of the DRUPS technology provided by PLN has made it easier for PLN customers to access high-quality electricity supplies that are free from electrical disturbances. In addition, the provision of electricity with DRUPS technology involves State-Owned Enterprises (PLN - Pertamina) which makes the synergy of State-Owned Enterprises more optimal.

Result and Discussion

The implementation of PLN electricity connection which is equipped with DRUPS installation in Tanjung Field is packaged under the name Super Ultima II Service. Super Ultima II Services at Tanjung Field consist of Premium Platinum Service 10,380 kVA and DRUPS Service 10,000 kVA (5 x 2 MVA).

In general, the installation of the PLN Main Substation – Substation Connection – Installation of DRUPS (including powerhouses) up to the point of delivery of medium voltage 6.6 kV electricity is the responsibility

of PLN. The customer (PEP Field Tanjung) prepares an incoming panel that will receive PLN's electricity supply and also ensures that the Operational Eligibility Certificate belonging to the customer installation already exists, as well as land that can be used for the construction of the DRUPS powerhouse and its installation.

The process of signing the Super Ultima II Service administration began in August 2019 (Electricity Sale and Purchase Agreement). In implementation, the time required is quite long because it takes time for the DRUPS (import) procurement process, powerhouse construction and new cable network construction which is quite far (about 11 KM) from the nearest main substation. At the end of the construction process, due to the Covid-19 pandemic, the mobilization of personnel and materials become more challenging, so that projects should be completed on time. But in the end, the electricity supply from the PLN Grid combined with the implementation of the DRUPS can be enjoyed by the Tanjung Field in Q2 2020.

The milestones of electricity installation from the PLN Grid combined with DRUPS Technology at the Tanjung PEP Field can be seen in the following picture:

Figure 8. Milestone for Super Ultima II Service Installation at PEP Field Tanjung.

The area of the PLN Grid network – PLN Customer substations – the power house of DRUPS and network interconnection to the PEP Power Plant can be seen in Figure 9 as follows:

Figure 9. PLN network, Powerhouse of DRUPS along with PLN and PEP network interconnection.

The DRUPS unit in Tanjung Field consists of 5 units (5 x 2 MVA) as shown in Figure 10 as follows:

Figure 10. The DRUPS Unit in the Powerhouse Area of the Tanjung Field (PEP) Power Plant.

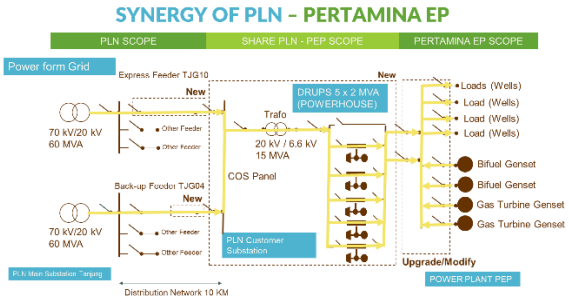

Figure 11. Illustration of the interconnection topology of the PLN – DRUPS – PEP Network.

As shown in Figure 11 above, the electricity supply provided by PLN to PEP is supported by 2 feeder lines from the Tanjung PLN Substation to the PLN Customer Substation located in the PEP Power Plant area. So that with the 2 supplies / feeders, there is an alternative in the supply line from the PLN Substation to the PLN Customer Substation, if one of the lines is interrupted. The switching mechanism between feeders is regulated in the PLN Customer Substation using the Change Over Switch (COS) mechanism automatically. Ideally, COS should work in 300 ms to switch from one feeder to another. At that period, DRUPS will cover the transition, so the electricity still supplied continuosly to the customer (PEP) at the steady voltage 6,6 kV.

From PLN Customer Substation, the receiving voltage which is still 20 kV is lowered into the voltage range used by PEP to a level of 6.6 kV through a step down transformer (20 kV/6.6 kV).

After the step down transformer, the electricity supply is passed into the DRUPS installation (5 x 2 MVA) for conditioning, so that the output voltage from the DRUPS installation is maintained at 6.6 kV. Each DRUPS was controlled by UCP (Unit Control Panel), and to manage all DRUPS (5 Units) the system was controlled by BCP (By-pass Control Panel) so as to manage load sharing between each DRUPS.

In the end, output line from the DRUPS installation then enters the PEP's installation via two incoming lines.

At the beginning of its operation, the mechanism for the entry of PLN electricity into the PEP network was

carried out through a synchronous / parallel mechanism so as to eliminate plant shutdowns when switching power supply sources.

As shown in Figure 8, the on-stream implementation of PLN's electricity supply to the PEP network at the Tanjung Power Plant (due to economic and technical considerations at that time) was carried out by PLN's electricity supply without going through the DRUPS installation (without conditioning). From there, a fairly clear/significant evaluation picture is obtained between PLN electricity supply without DRUPS and DRUPS, especially in terms of power quality and reliability/availability of electricity supply received on the customer load side (PEP). The effectiveness of the DRUPS performance can be shown in the graphs in Figure 12, Figure 13 and Figure 14 as follows:

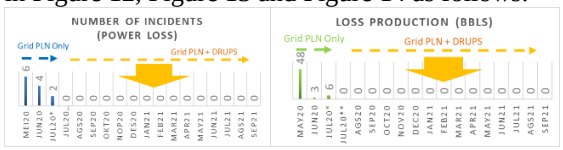

Figure 12. Comparison of Disturbance and Loss Production Opportunity (LPO) between PLN electricity supply without DRUPS and electricity supply with DRUPS.

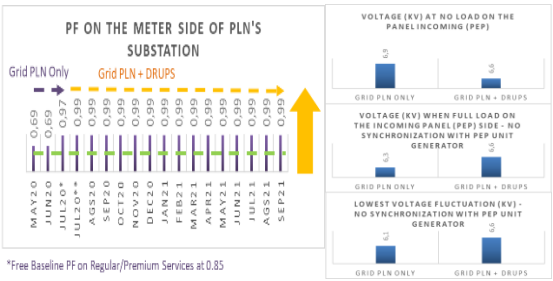

Figure 13. Comparison of PF on the Meter Side of the Substation (PLN Customer Substation) and Voltage on the Customer Load side (PEP) between PLN electricity supply without DRUPS and electricity supply with DRUPS.

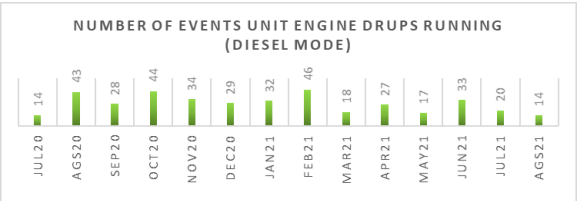

Figure 14. Effectiveness of DRUPS (Diesel Mode Case) performance in reducing disturbances on the upstream side, so that it does not have an impact on the downstream side / customer load (PEP).

The occurrence of Diesel Mode operating in Figure 14, shows a disturbance on the upstream side (DRUPS) caused by voltage fluctuation and frequency fluctuation. However, this disturbance can be suppressed by the DRUPS, so that on the dowstream side, the continuity and quality of electricity that is transmitted to the Tanjung Field PEP network is maintained.

In the evaluation, the connection of PLN electricity combined with the DRUPS equipment resulted in a reduction in the cost of electricity generation to around Rp. 1,800 – 1,900 per kWh (cost efficiency reaches more than Rp 100 M per year) while still getting electricity supply that is free from disturbances in electricity quality (power quality) and continuous (reliability). The evaluation of electricity costs is shown in the following illustration:

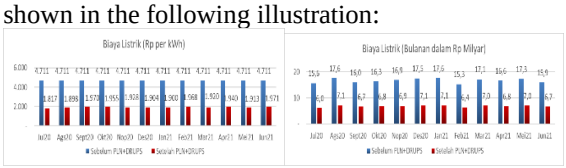

Figure 15. Illustration of Electricity Costs before PLN and after PLN (Super Ultima II) in Tanjung Field (in PEP side).

In Super Ultima II Services Scheme at Tanjung Field, Investment Cost of New Powerline Network (from PLN Grid), PLN Customer Substation, DRUPS Installation (including Powerhouse) are expended by PLN.

Moreover, PEP should expend cost in front such as Connection Cost (*Biaya Penyambungan / BP*, Rp 6,5 billion), Subscription Deposit (*Uang Jaminan Langganan / UJL*, Rp 2,3 billion), operation worthy certificate (*Sertifikat Layak Operasi / SLO*, Rp 300 million), and modification cost (Rp 1,6 billion), which such cost can be paid back from cost efficient for 1,5 months after improvement.

As for the next added value from the installation of DRUPS on PLN electricity connections, there is a Power Factor Correction feature on the side of the PLN Customer Substation meter, so that customers (PEP) are not charged for excess kvarh. Because PLN services in general will charge a kVArh charge if the customer exceeds the set kVArh limit (0.62 x kWh for the current month or PF below the average 0.85). The economic illustration of the DRUPS performance in carrying out power factor correction can be shown in the following illustration:

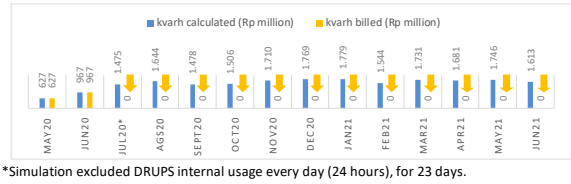

Figure 16. Illustration of Benefit Power factor Correction on the side of the PLN Customer Substation Meter in the Tanjung Field (PEP) Power Plant Area.

The application of DRUPS technology at the Tanjung PEP Field is the first in the Indonesian Oil and Gas Industry, as well as the collaboration for the implementation of the DRUPS from PLN which is the first on stream also in Indonesia. So that it becomes a

pilot / benchmarking for other plants / fields in the oil and gas sector who want to apply similar technology.

Furthermore, the application of DRUPS Technology is not only when it is connected to the PLN Electricity Network, but can also be implemented in multi-source internal power supplies such as between turbines / engines of own power plants with the target of achieving reliability / availability / power quality, especially when switching sources of electricity generation.

Conclusions

1. The implementation of DRUPS combined with power supply from PLN has been successful to resolve the problems described in the introduction, i.e. higher electricity cost due to increase of diesel fuel consumption as the implication of higher electricity demand and lower associated gas produced for gas fuel.
2. The implementation of DRUPS technology in the Tanjung Field is the first in the oil and earth industry. In addition to the application of new technologies related to Power Quality-Reliability & Cost Efficiency, Cost of Electricity Generation was also reduced from Rp. 4,711 per kWh to around Rp. 1,800 – Rp 1,900 per kWh (efficiency more than Rp 100 billion per year). Moreover, this DRUPS technology can be provided by PLN, making the Synergy of State-Owned Enterprises (Pertamina - PLN) much better and of course presenting extraordinary benefits for Indonesia.
3. To obtain power quality that is free from interference with over voltage, voltage dip/sag, harmonics, micro cut, and blackout, DRUPS technology can be used.
4. Users / Customers who need Power Quality & Reliability can request additional DRUPS equipment from PLN or also provide them through their own investment.

References

Institute of Electical and Electonic Engineers, Inc, 2005, Recomended Practice for Powering and Grounding Electronic Equipment, IEEE Standard 1100.

International Electrotechnical Comission, 2008, Electromagnetic compatibility (EMC) – Part 4 – 30: Testing and measurement techniques – Power quality measurement methods, IEC 61000-4-30.

Hitec Power Protection, Diesel UPS/CPS Systems Continuous power. Uninterruptible, continuous and conditioned power supply.

Hitec Power Protection, User Manual UPS System.

Hitec Power Protection, 2016, Presentation PowerPRO2700, Almelo, Netherlands.

Pilar Bahtera Energi, 21st Maret 2019, Presentation Slides: Bussiness Proposal & Solution for Pertamina EP Asset 5.

Dahono, Pekik Argo, 31st July 2019, Presentation Slides: Understanding Voltage Dips: Problem and Soultion, Jakarta.

PROCEEDINGS
JOINT CONVENTION BANDUNG (JCB)|2021
November 23rd – 25th 2021

Optimizing gas production in the existing and new reservoir layer using a combination of compensated neutron log interpretation and selective perforation methods at PSU Field wells, North Sumatra.

Ronald Susanto[1)], Gilang Nuansa Putra[2)], Dian Simatupang[3)], Fadhil Ahmad Fauzan[4)], Hutrido Mas Anyesa[5)], David Christian Karel[6)], Dede Kurniadi[7)]
[1,2,3,4,5,6,7)]PT. Pertamina Hulu Rokan (Regional 1), Zone 1, Jambi

Abstract

PSU Field is one of the areas that are included in PT. Pertamina Hulu Rokan in North Sumatera. It produces gas and has continued to contribute to fulfill the gas demand for the local consumers, especially the industrial market. Based on the information on the decree issued by the Power and Mineral Resources Ministry of Indonesia, the local industries need 81 mmscfd of gas supply until 2024. Out of the total demand, PSU Field of PT Pertamina Hulu Rokan is allowed to supply 7 BBTUD (5,8 mmscfd). Therefore, in order to accomplish the desired gas volume, so PT. Pertamina Hulu Rokan has established some working fields to produce gas: ARB Field and GBG Field.
Producing gas in each of the fields has its own challenges. ARB is challenging because of the increasing gas water contact in the subsurface layer that potentially could have contained hydrocarbons. This condition might have been caused by the incorrect production method which is to produce the well using the commingle layer that could intensify the water production and decrease the oil production. At the same time, GBG field's challenge is the amount of reservoir layers which are thick and have been depleted (maximum recovery factor and decreased pressure). To overcome this challenge, prospecting was needed on the thin reservoir layers. Used methods to minimize the situation is by using a combination method of compensated neutron log interpretation and selective perforation. This method was applied both in ARB-01 and GBG-55 even though each has its different cases.
Case 1 (ARB-01 field) used the combined method of compensated neutron log interpretation and selective perforation and produced low-pressured gas and cumulatively 112.91 mmscf of gas (February 2020-June 2021). In the meantime, Case 2 (GBG-55 field) has produced gas in the new layers cumulatively 51.52 mmscf by using the same method (April-June 2021).
The total revenue from both of the productions is USD 657,720 which is equal to IDR 9,295,556,760. This achievement has also increased the gas well intervention success ratio on the PSU Field workplan by 100% (PPJ-38, PPJ-54, GBG-55, PPJ-60 and ARB-01).
By combining both methods, the problems related to contact fluid change and depleted reservoirs can be prevented in order to optimize the gas production and increase the company's revenue in the midst of the instability of oil price.

Keywords: gas production, gas water contact, commingle layer,depleted reservoir, compensated neutron log, selective perforation, revenue.

Introduction

Location of ARB and GBG fields each has total area and is geographically different.
ARB field is the gas and oil field which is located about 25 km northwest from Pangkalan Brandan. This field is an old field managed by PT. Pertamina from 1975. The wells in this fields counted as many as 113 and has produced gas and oil massively ever since.
As for GBG field is located in the district of Langkat, North Sumatera. The location of the field is ± 95 km northwest of Medan and ± 12 km northeast of Pangkalan Brandan. The total area of this field is about 68.7 km^2. As for the amount of wells inside this field is 60 wells.
Both of these fields were first known as oil producing fields from the deep zones. However, as the time goes by, eventually they were also recognized as oil producing fields from the shallow zones.

Geologically, both of these fields were put to production through Keutapang Formation in which this formation was deposited at the shallow marine depositional environment (foreshore, shoreface, tidal influence). The challenge in searching for the layers that potentially would contain hydrocarbon in Keutapang Formation is the existence of of thin layers that are spread tightly. Therefore a detailed mapping was indispensable. In addition to that, geology structural control of strike slip fault progression has caused the compartment in between reservoirs and directly resulted in varied production performances.

ARB field has reservoir layers that contain oil. The total of OOIP (Original Oil In Place) of ARB fields is 2.2 MMSTB, This amount were calculated from the Keutapang Formation on the sandstone layer at the 480BB, 480OB, 460, 535, 580BB. The drive mechanism of the mentioned sone was the combination of solution gas and water drive mechanism and has produced a recovery factor of 27% and cumulatively has reached 524 MSTB until the year of 2020, leaving a total of 4 MSTB of oil reserve. This achievement has also formed secondary gas cap at the formation. From the obtained oil production and gas solution, the GOR has reached 2265 scf/stb.

Contrarily, GBG field has reservoir layers which contained oil and gas (non-associated), The total of OOIP on the field is 35.7 MMSTB which comes from the summation of OOIP of Keutapang formation at the sandstone zone of 900, 1000A, 00B, 1030A. The total of IGIP (Initial Gas In Place) reached to 198.9 BSCF. This number came from the summation of IGIP from the Keutapang formation on the sandstone zone of 860, 900, 950, 1000B, 1030B, dan 1100.

PROCEEDINGS
JOINT CONVENTION BANDUNG (JCB)2021
November 23rd – 25th 2021

Among the sandstone layers from both of these fields, there were some interesting layers that were found to be used in production: 480BB layer (ARB field) dan 850 layer (GBG field). Through the combination of the methods and technique of compensated neutron log interpretation and selective perforation, there was layer perforation interval that has produced hydrocarbon gas that could evidently increase the company revenue with the transaction process with the local consumer.

Data and Method

The method applied in this study is to map the reservoirs of thin layers so that the pattern of distribution of sandstone reservoirs can be known. Then the interpretation in detail of the results of the CNL running cased hole log is compared to the interpretation of open hole log data. Through data obtained from CNL overlays and open hole logs, the selection of the right perforation interval on the layer to be produced is carried out.

ARB-01 and GBG-55 are two well candidates for the selection of potential gas-containing layers. In the year of 2020 and 2021, well intervention job is carried out on both of these wells. In the previous year, the reservoir layer produced in the ARB-01 well was in the 400OB zone and in the GBG-55 well was in zone 950 of the Keutapang Formation. The characteristics of these two reservoir layers are almost the same: the reservoir fluid is a gas, of which the gas from zone 400OB is the associated gas and the gas from zone 950 is a non-associated gas. In both of these zones, GWC (gas water contact) has reached the top level of its reservoir layer, so that when these two zones are produced, the gas produced is very small and dominated by water production. This is because the draining of hydrocarbons in both zones is large enough to be obtained from the surrounding wells, resulting in GWC levels rising and eventually the reservoir will be dominated by water. In practice, if in the gas reservoir there is already water dominance, then water with greater mobility than gas will make the gas will not be produced properly. In Figure 1 can be seen the current level of GWC which is a reference for the determination of the candidate layer or the next zone to be produced.

From the isopach map zone 850 in Figure 1, it can also be concluded that the thickness in the GBG-55 well tends to be smaller than the thickness of other wells that are on the contour flank, but the advantage is the position of the GBG-55 well is on the top contour of the compartment.

In Figure 2, it can be observed that wells that are more downdip than GBG-55 wells produce water in zone 850, so gbg-55 wells become very interesting to produce because of the good reservoir quality that can be seen from gamma ray values, resistivity, and neutron-density in existing open hole logs. Likewise in the ARB-01 zone 480BB well, structurally this zone was once produced in the PPJ field which is located to the northwest of the ARB field, but in the ARB field this zone includes the virgin zone, and the ARB-01 well is in the second most updip position and has good reservoir quality when viewed from the open hole log in the well itself.

Result and Discussion

Case GBG-55

GBG-55 well has been perforated in the Z-850 layer where the layer is a thin layer (net pay is about 1.5 m). Below the Z-850 (+-5 meter) layer is a thick main gas reservoir (Z-860 series) where the main gas layer is depleted reservoir and has an already high GWC depth. The Z-850 layer is interpreted as a tidal flat deposition environment. The shale break between Z-860 and Z-850 is good in trapping hydrocarbons in the Z-850 layer. Before perforation, compensated neutron log (CNL) was run and interpreted by comparing it with an open hole log. The interpretation confirmed that there was an absence of significant changes of neutron value between the CNL and the neutron open hole log in Z.850 layer, thus, it can be concluded that Z.850 layer is a new potential layer and has cumulatively produced gas of 91.32 mmscf / 92,870 mmbtu (April-August 2021). By producing that amount of gas, PSU Field of PT Pertamina Hulu Rokan has obtained a total revenue of USD 371,481 (USD 4/mmbtu).

Case ARB-01

Some of the wells in ARB Field completed by commingle layer completion method produced formation water. This was possible because the layer containing formation water had a higher productivity index compared to the layer containing the hydrocarbon potential. The last well produced by commingle method and producing formation water was ARB-01. After using a single zone completion method, to confirm the hydrocarbon potential existed in the target layer, the CNL method was applied.
Perforation was applied after the result of the evaluation of CNL in the target layer had been available, then swabbing by a swab tool and static bottom hole pressure measurements were carried out to get useful data for analyzing the productivity index of the well.
By this method, ARB-01 has produced 136.66 mmscf of cumulative gas production and 138,985 mmbtu of energy value. By producing that amount of gas, PSU Field of PT Pertamina Hulu Rokan has obtained a total revenue of USD 555,941 (USD 4/mmbtu).

PROCEEDINGS
JOINT CONVENTION BANDUNG (JCB)2021
November 23rd – 25th 2021

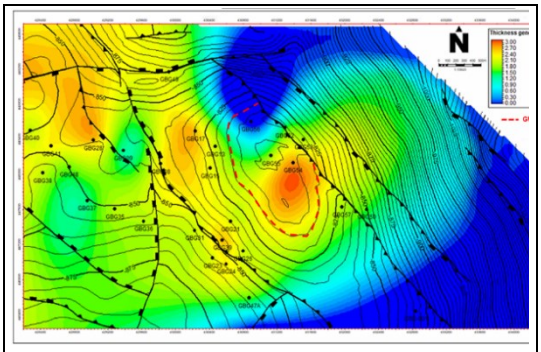

Figure 1: Z.850 GBG field isopach map with current GWC depth

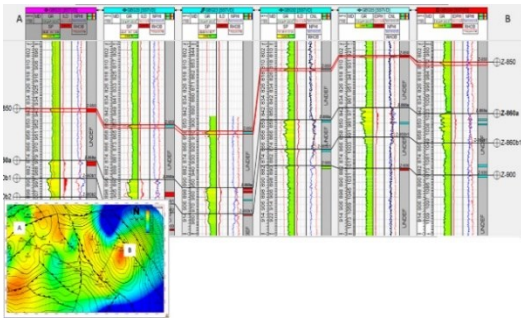

Figure 2: Well log correlation of Z.850 GBG Field

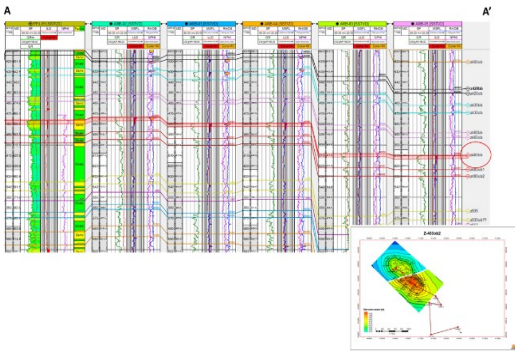

Figure 3: Well log correlation of Z.480BB ARB Field

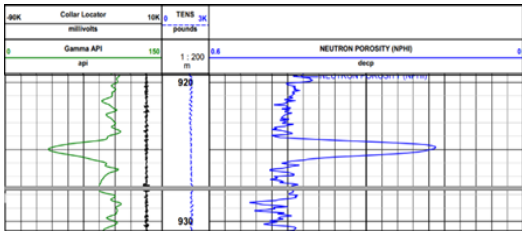

Figure 4: Current CNL (Compensated Neutron Log) of Z.850 sandstone reservoir at GBG-55

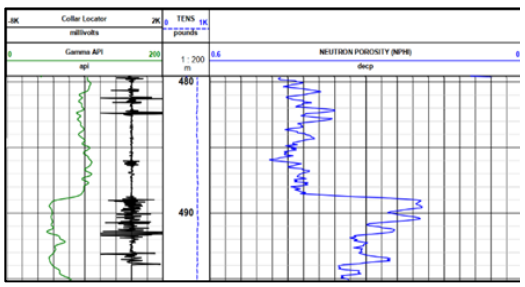

Figure 5: Current CNL (Compensated Neutron Log) of Z.480BB sandstone reservoir at ARB-01

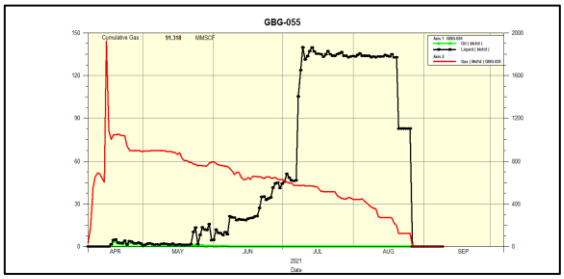

Figure 6: Production Performance of GBG-55

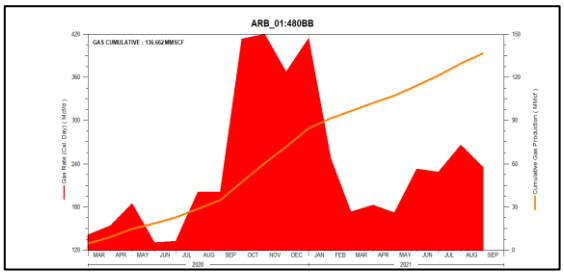

Figure 7: ARB-01 cumulative gas production vs gas rate

Conclusions

The combination of overlay CNL with open hole log and selective perforation method is proven to produce hydrocarbon potential, especially natural gas, in a thin formation layer and make it a new reserve to be developed in other wells and in general can increase the company's revenue through the sale of natural gas to consumers.

References

Dake, L.P., 1978, Fundamentals of Reservoir Engineering, **3**, 86–94.
Hagoort, J.,1988, Fundamentals of Gas Reservoir Engineering, **2**, 17–18.
Kennedy, M., 2015, Practical Petrophysics, **5**, 226-239.

PROCEEDINGS
JOINT CONVENTION BANDUNG (JCB) 2021
November 23rd – 25th 2021

Economic Evaluation for Enhanced Oil Recovery Using Deterministic-Stochastic Particle Swarm Optimization (PSO)

[1]Rahajeng Suryo Rahmadhini, [1]Tutuka Ariadji, and [1]Prasandi Abdul Aziz
[1]Institut Teknologi Bandung

Abstract
The utilization of CO_2 gas from the oil and gas fields or industry for the purposes of Enhanced Oil Recovery has a dual purpose which to increase reserves and also to help deal with the greenhouse effect. The objective is to analyze economic uncertainty in decision making based on stochastic method analysis with the objective function of Net Present Value (NPV).

This research was conducted by two methods, deterministic and stochastic method. In this field development, producers were converted to injector and the economic parameter such as Net Present Value (NPV), Internal Rate of Return (IRR), and Pay Out Time (POT) are feasible to be applied in the field. Then the analysis of the optimal cases is applied to Field X both technically and economically with the stochastic method. This study applied stochastic method Particle Swarm Optimization (PSO) with objective function Net Present Value (NPV) and limit parameters for the number of injection wells and CO_2 injection volume. There are scenarios using different parameter of stochastic method Particle Swarm Optimization (PSO): Inertia Weight and Learning Factor. The changes in the main parameters of Particle Swarm Optimization (PSO) method (Inertia Weight and Learning Factor) indicate that Inertia Weight is the most influential for the simulation.

Keywords: Enhanced Oil Recovery, CO_2, NPV, Particle Swarm Optimization

Introduction

The increase in carbon dioxide is a potential greenhouse gas effect that can generate heat on earth. The increasing concentration of carbon dioxide in the atmosphere can cause global warming which has an impact on an unstable climate that will eventually cause natural disasters in various regions in the world. The utilization of CO_2 gas from the oil and gas fields or industry for the purposes of Enhanced Oil Recovery has a dual purpose which to increase reserves and also to help deal with greenhouse effect.

One of the method to increase oil production is by implementing Enhanced Oil Recovery (EOR) method using CO_2 injection into the reservoir through injection wells so that it can produce oil that can not be produced using the primary or secondary recovery methods. In Indonesia, one of the sources of CO_2 can come from natural gas fields which have high content of CO_2 concentration, such as East Natuna Gas Field, which have more than 72% mole of CO_2 (Muslim et al., 2013).

However, the method that has been used so far is by trial and error all the possibilities, such as a combination of the location of the well, the number of injection wells, and the required injection rate. This takes quite a long time. In this research, a field development optimization study was conducted using stochastic method which can process simulations with various possibilities and the results are more varied. So with this stochastic method, it is expected that the calculation time in optimizing field development can be faster.

Particle Swarm Optimization (PSO) was first introduced by Dr. Eberhart and Dr. Kennedy in 1995 with the purpose of continuously optimizing non-linear functions, the Particle Swarm Optimization (PSO) algorithm is a population-based optimization technique inspired by the social behavior of the movement of birds or fish (bird flocking or fish schooling).

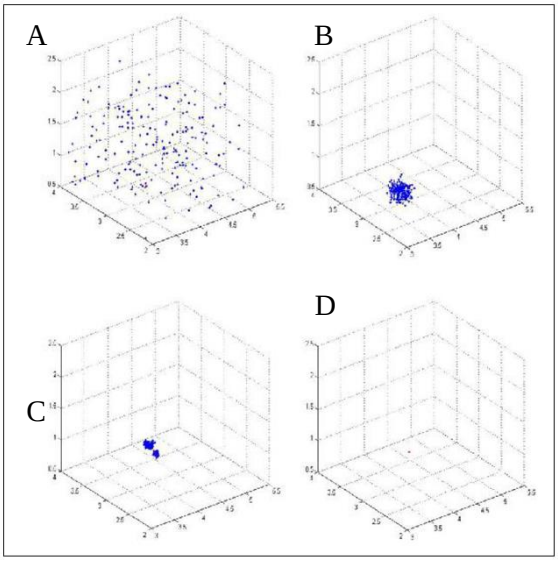

The population movement visualization is shown in Figure 1 starting from Figures A to D where the distribution of particles is seen in finding the best position or value. From the explanation above, it can be said that the PSO algorithm combines local search methods with global search methods (Rosita et al., 2012).

Figure 1: Population Movement Visualization of Particle Swarm Optimization (PSO)

PROCEEDINGS
JOINT CONVENTION BANDUNG (JCB)2021
November 23rd – 25th 2021

Particle Swarm Optimization is a method that memorizes the previous best solution, has the potential to be more effective than other optimization algorithms because it can find the optimal solution faster. However, PSO does not always give better results because it tends to be more exploitative (Sanghyun, 2018).

Data and Method

The deterministic method optimization study is carried out by directly analyzing the results of optimization using software for technically and economically using production sharing contract. Before the Enhanced Oil Recovery method is applied, an in-depth study must be carried out to find out how the optimum CO_2 injection is suitable for use. The data that are used in this study are shown in Table 1.

Table 1. Data Parameter

Parameter	Value
Project life	20 years
Oil price	US$ 60/bbl
Capital cost	13.3 MMUSD/year
Operating cost	0.22 MMUSD/year

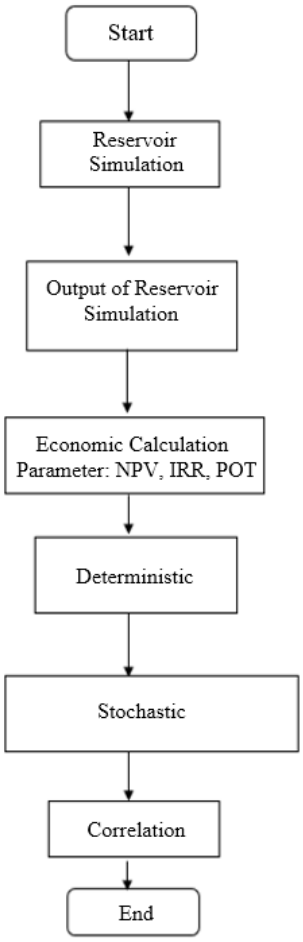

Figure 2: Evaluation Flowchart

This research is carried out data processing flow as shown in Figure 2. In conducting reservoir simulation, limits have been determined for each production and injection well,

such as the number of infill wells, number of injection wells, oil production rate, bottom hole pressure, and CO_2 gas injection rate in each development case.

After reservoir simulation several output parameters are used for the next correlation with stochastic method:

- Oil production cummulative
- Production rate
- Recovery Factor
- CO_2 injection rate
- Recovery Factor

From the output of the reservoir simulation, economic evaluation is conducted to get economic parameter as indicator whether the field development case is feasible or not. The economic parameters are:

- Net Present Value (NPV)
- Internal Rate of Return (IRR)
- Pay Out Time (POT)

The Particle Swarm Optimization of Net Present Value (NPV) objective function method begins with an initialization algorithm consisting of a constant and particle movement. Clerc and Kennedy (2002) suggest the Particle Swarm Optimization (PSO) control parameter value which inertia weight = 0.7298, learning factor C1 and C2 = 1.49618. r1 and r2 are random numbers between 0 and 1.

This study uses Design of Experiment (DoE) to determine the level of influence of several parameters in the simulation. The method used is Plackett-Burman method, which is this method can reduce the number of simulations that must be carried out in finding the level of influence of several parameters to be searched for the level of influence on the calculation time of the objective function.

The inertia weight value that used is in two levels, 0.4 for low and 0.9 for high value. Meanwhile the learning factor parameter uses minimum value of 1 and 1.8 for maximum value.

Table 2 shows the pair of inertia weight and learning factor as input for Design of Experiment to analyze the parameters that affect the search for the objective function NPV.

Table 2. Input Parameter for Design of Experiment

Parameter	Low	High
Inertia Weight	0,4	0,9
Learning Factor	1	1.8

Results and Discussion

After the simulation of objective function (Net Present Value) in stochastic method Particle Swarm Optimization has been done, the results of Net Present Value (NPV) is compared to the number of experiment. And the optimum Net Present Value is 5 MMUSD which the data distribution

PROCEEDINGS
JOINT CONVENTION BANDUNG (JCB)2021
November 23rd – 25th 2021

is more homogeneous than the other part in the graph as shown in Figure 3.

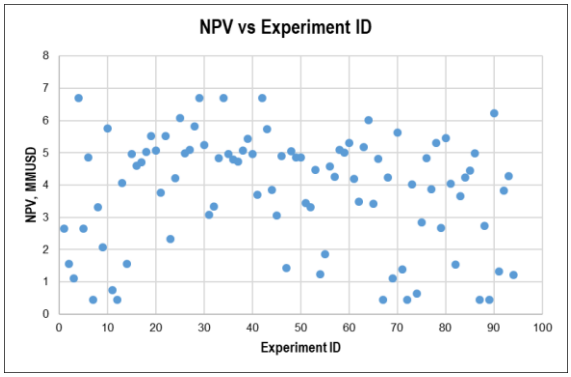

Figure 3: Graphic of Objective Function Net Present Value to the number of experiment stochastic method

Figure 4 shows a Pareto Chart resulting from the simulation based on pairs of the parameter of Particle Swarm Optmization. The chart shows that the inertia weight parameter is the main effect or the parameter that has the most influence on the results compared to the learning factor parameter, because the inertia weight plot is far to the right of the Plackett-Burman coefficient.

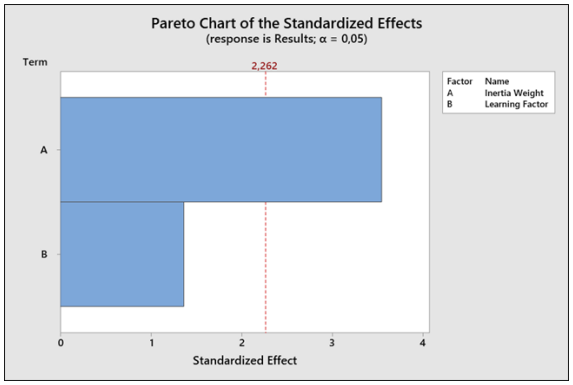

Figure 4: Design of Experiment Analysis Result

Conclusion

Optimization of field development using stochastic method Particle Swarm Optimization (PSO) provides more accurate results in determining the field development plan on economic parameter objective function compared to the method that has been carried out so far, trial error with various possibilities. Based on the results of the analysis in determining the combination of inertia weight and learning factor parameter data using the Plackett-Burman Design of Experiment (DoE) method, inertia weight is the most influential parameter in simulation of objective function value compared to learning factor parameter.

In addition, it will be better to calculate CO_2 produced into the economic calculation so that the results are more accurate and can utilize the CO_2 produced on the other side to save the costs.

References

Clerc, M., and Kennedy, J., 2002, IEEE Transactions on Evolutionary Computation, Vol. 6, No.1.
Muslim, et al., 2013, Opportunities and Challenger of CO_2 Flooding in Indonesia, Society of Petroleum Engineers.
Rosita, A. et al., 2012, ITS Engineering Journal Vol.1.
Sanghyun, L. and Stephen, K.D., 2018, Offshore Technology Conference Asia 2018, Society of Petroleum Engineers.
Telford, J.K., 2007, Design of Experiments, Johns Hopkins Apl Technical Digest, Volume 27.

PROCEEDINGS
JOINT CONVENTION BANDUNG (JCB)2021
November 23rd – 25th 2021

Production Optimization In Peripheral Waterflood Field Using Capacitive Resistance Model (CRM) with Clustering Approach, Pandhawa Field Case Study

Muhammad Hasto Nugroho[1,2], Billal Maydika Aslam [1], Taufan Marhaendrajana[1]
[1]Petroleum Engineering Department, Institut Teknologi Bandung, Indonesia, [2]Medco E&P Indonesia

Abstract
Waterflooding is one of the most effective methods to improve oil recovery in mature fields because of its high success ratio, easy in application and cost efficiency. Development until now has shown that Capacitance Resistance Model (CRM) can be used as alternative from reservoir model and simulation studies. CRM can be used as model to predict reservoir characterization and reservoir performance quickly and accurately with only require historical production and injection data. CRM characterizes the reservoir by calculating the connectivity value and the response delay between the injections well and the production well as unknown parameters. Pandhawa Field is a heterogeneous carbonate reservoir with an average permeability of 65 mD with peripheral waterflood since 20 years ago. By knowing the injection efficiency, the optimization process can be carried out by increasing the water injection rate in injection wells that have high efficiency and vice versa. In this study, the performance of waterflood is analyzed using the Capacitance-Resistance Injection-Production Model (CRM-IP) to determine the connectivity of each injection and production well. This study also discuss CRM-IP implementation on MATLAB programming language and optimization of injection rate allocation for the most optimum cumulative oil production. Result of this study indicate total additional oil 505 MBO will be obtained during 120 months period by conduct redistribution water injection management for each injector. By using CRMIP methodology, waterflood management in this field can be done much faster, therefore decision taken for this field will be more effective. Some proposed solution to reduce dimensionality of field data and improve CRM-IP history match quality is also discussed such as influence radius and clustering producers.

Introduction
One of proven strategy to increase oil recovery in mature field is waterflooding. Water is the most injected fluid to maintain reservoir pressure and push oil from injectors to producers because of it is availability, low cost compared to other techniques and easier to inject.

Reservoir characterization and simulation are the important activities in order to evaluate reservoir performance. Evaluation reservoir performance can be conducted by many methods such as material balance, streamline simulation, numerical simulation, etc. Currently reservoir simulation is one on the methods that is commonly used by petroleum engineers. Reservoir simulation has limitation such as require long time consuming and processing, data uncertainty (geological, petrophysical, reservoir engineering), furthermore to long term response of reservoir management.

Effective reservoir management in waterflooding field needs rapid action regarding injected fluid distribution to improve areal and vertical sweep efficiency during secondary process. Therefore, simpler method that deliver rapid results to counterpart reservoir simulation are important for reservoir management. Capacitance Resistance Model (CRM) is one of verified method to solve the above challenges.

Nowadays CRM arrest various attention because of its ability of rapid evaluation in reservoir performance. Common benefits of CRM application are the low execution time, high level of accuracy adapted to available input data quality, can determine inter-well connectivity, needs no geologic information and fluid flow modelling and can be adapted for an excel spreadsheet (Kansao et al, 2017). Changes in the sweep area will happen along with the injection process. Therefore, it is necessary to re-optimize and even re-modify it to get the optimum oil recovery.

Capacitance Resistance Model Injector-Producer (CRM-IP) was selected because it provides a better insight into the well-to-well connectivity (Yousef et al, 2006) and depending on the heterogeneity of the reservoir, different injectors can impact the production rates of a certain producer with different velocities (Holanda, Gildin, & Jensen, 2015). The CRMs use only production/injection history data to predict performance, which provides simplicity and speed of calculation (Sayarpour et al, 2009). The capacitance–resistance model (CRM) offers the promise of rapid evaluation of waterflood performance.

Noticeably, it will take long time if done manually. In this study, a computer program based on MATLAB was created with only the most recent input of production and injection history data to solve this problem. The program will semi-automatically provide a recommendation output for the optimization of the injection rate at certain wells.

The objective of water injection is to give energy support into reservoir, as well as to increase recovery factor. The water injection is expected to sweep oil that cannot be produced naturally (primary recovery). Furthermore, the water injection can be used to maintain the reservoir pressure.

Capacitance Resistance Model (CRM) is a predictive method that relies upon signal processing, in which water injection rates are treated as input signals and production rates as output signals. The name CRM is derived from its analogy to resistor-capacitor (RC) circuit (Thompson, 2006). Production rates response to a step-change in injection rate is analogous to the voltage change of capacitor in a parallel RC where battery potential is equivalent to the

PROCEEDINGS
JOINT CONVENTION BANDUNG (JCB)2021
November 23rd – 25th 2021

injection rate. CRM may also be viewed as a nonlinear multivariate regression analysis tool, which accounts for compressibility and fluid flow in the reservoir (Yousef et al, 2006). There are unknown parameters in CRM, which are inter-well connectivity as well as time response delay. These parameters reflect connectivity between injector and producer well based on historical injection and production data.

Data and Method

Capacitance resistance model (CRM) characterizes a flooded reservoir by estimating inter well connectivity, time constants and productivity index using production/injection rates for history matching. Figure 1 shows the flow of modeling using Capacitance resistance model (CRM). For this case using the CRMIP model and the figure 2 show the illustration of CRMIP. CRMIP was chosen because it provides a better insight into well to well connectivity (Yousef et al, 2006) and depending on the heterogeneity of the reservoir, different injectors can impact the production rate of a certain producer with different velocities (Holanda et al, 2015).

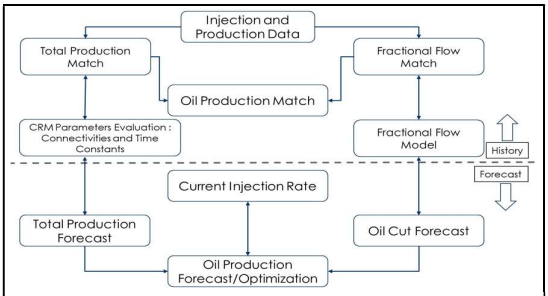

Figure 1. Workflow of CRM

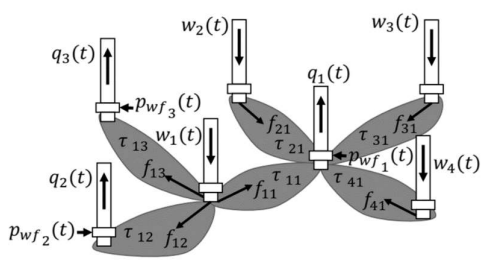

Figure 2. Injector–Producer Pair Based Control Volume, CRMIP (Holanda et. al, 2018)

Modeling using CRM begins with collecting field data such as injection and production rate history, and then predicting total production and oil production using the CRMIP model equation as follows (Sayarpour, 2008)

$$q_{ij}(t_k) = q_{ij}(t_{k-1})e^{\frac{-\Delta t_k}{\tau_{ij}}} + \left(1 - e^{\frac{-\Delta t_k}{\tau_{ij}}}\right)\left[f_{ij}I_i^{(k)} - J_{ij}\tau_{ij}\frac{\Delta p_{wf}^{(k)}}{\Delta t_k}\right] \quad (1)$$

Oil production can be calculated using the empirical oil-cut model. This model is presented by Gentil (2005). This model considering relationship between water oil ratio over time and cumulative injected water. Therefore, the fractional flow of oil can be written as below. Calculation of oil production rate is require evaluation of the value α and β from oil production history each producers.

$$f_o(t_k) = \frac{1}{1+\alpha W_i^{\beta}} \quad (2)$$

Estimation of oil production rate each injector could be calculated using this equation

$$qo_{ij}(t_k) = q_{ij}(t_k)\, f_o(t_k) \quad (3)$$

In CRMIP, for each injector/producer pair, four model parameters exist: $q_{ij(to)}$, τ_{ij}, f_{ij}, and J_{ij}. Make initial estimates for these parameters then this parameter will be optimized to produce the smallest error. The procedure for determining the initial guess of f_{ij} by looking at the distance of the injector to the producer, where the closer distance will have a greater f_{ij} value than those who have farther distance, the number of connectivity (f_{ij}) of one injector to each well must not exceed one or more, can be written as :

$$\sum_{i=1}^{Ni} f_{ij} \leq 1 \quad (4)$$

For this model we use some assumptions such as:

1. Constant Pwf, ΔPwf=0
2. Fluid density are constant and capillary pressure are neglected
3. Immiscible fluid water and oil only

After calculating the total liquid production and oil production, the calibration is carried out between the observed data and the predicted results by minimizing the error by optimizing time constant (τij), connectivity (fij), alpha (α) and beta (β). $fmincon$ function with interior-point algorithm, which already provided in MATLAB optimization toolbox is used to minimize the error. History Match Error can be written as

$$MSE = \frac{\sum_{n=1}^{n_{data}}(q_{act}-q_{est})^2}{n_{data}} \quad (5)$$

A suitable CRM model is obtained after the smallest error is obtained and it is also seen on the chart that the data observe with the estimation results are suitable, then this model will be used to predict oil production for the future. However, it is also important to note that history matching in CRM is an ill-posed problem which can lead to uncertainty of CRM model parameter. The uniqueness of CRM model parameter in history match will depend on the amount of historical rate data available, measurement noise, diffusivity constant, and number of producers per area (Kaviani et. al., 2014).

Result and Discussion

Pandhawa Field is an oilfield located in South Sumatra, Indonesia. Main oil production came from BRF reefal carbonates with minor contribution from TAF and TLS sandstone. Oil gravity produced in Pandhawa Field is considered as light oil with API gravity at 36° API. The reservoir is described as a single continuous zone with minor faults occurrence. The BRF carbonates have good reservoir quality except at several local areas where tight facies occurs and which provides a permeability barrier and stratigraphic entrapment exceeding the simple four-way structural closures. In contrast, the TAF and TLS reservoirs are rather tight.

The Pandhawa Field OOIP is estimated at 230 MMSTB and currently have implemented peripheral waterflood to improve its recovery. There are a total of 238 production wells in Pandhawa field which are divided into 61 clusters. However, for this study we will only consider well that produce from BRF that consist of 58 production wells and 36 injection wells. Production and injection rate history along with voidage replacement ratio (VRR) used in study are given in figure 3(a) and 3(b) respectively. The VRR plot

PROCEEDINGS
JOINT CONVENTION BANDUNG (JCB)2021
November 23rd – 25th 2021

indicates a good balance of injection and production as the values ranging between 1 – 1.2.

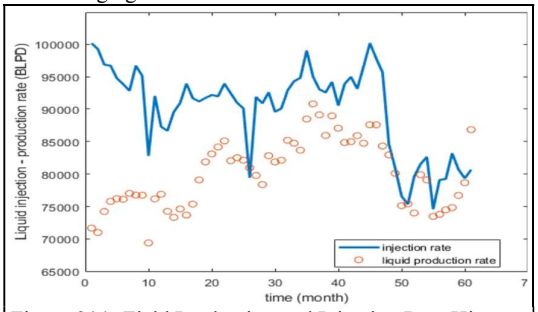

Figure 3(a). Field Production and Injection Rate History

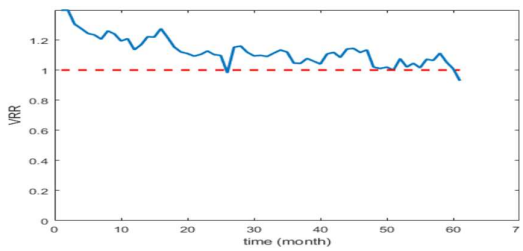

Figure 3(b). Voidage Replacement Ratio

History matching of liquid rates was successfully performed in this analysis. This is conducted to observe whether the liquid produced matches the simulation results. In figure 4 and figure 5, it can be seen that the total liquid rate field and each well generated from calibration of CRM is quite similar trend, however the quality is not yet satisfactory to the actual data. CPU time for history match took only 91.7 seconds on processor 4 core 2.1 GHz.

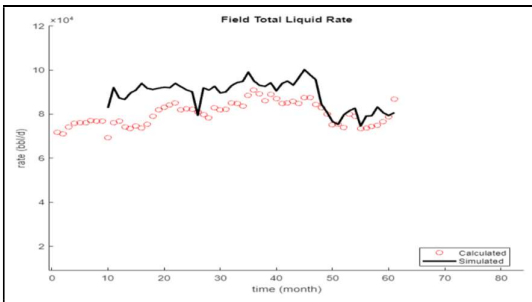

Figure 4. Field Total Liquid Rate History Matching Result

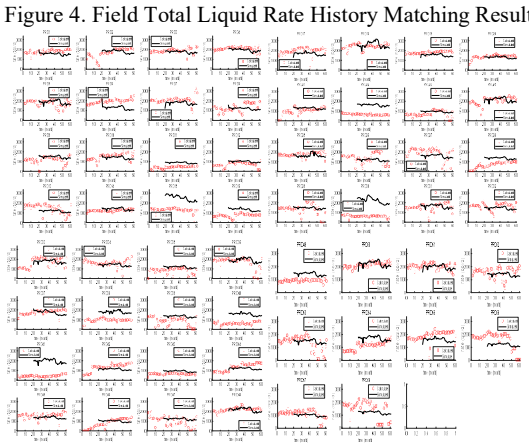

Figure 5. Well Liquid Rate History Matching Result

From the connectivity map in figure 6, it can be seen that due to the scattered distribution of injector the connectivity of injector to producer is quite disordered. However, as injector is intended to be peripheral, general connectivity trend showed that injection is directed to nearest producer. On the other hand, several injection wells show connectivity for producer that are located very far (> 10 km interwell distance) which could make the result unphysical.

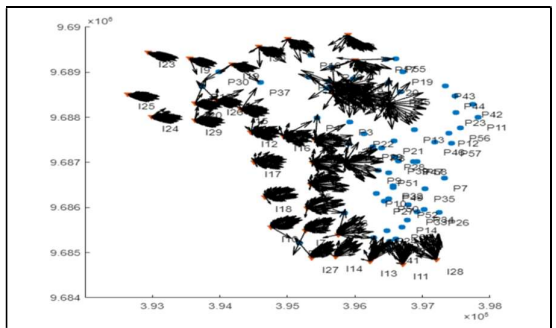

Figure 6. Well Connectivity Map from History Matching

Calculated allocation factor (fij) consistency check can also be done by comparing the values between allocation factor and distance. Generally, further well pairs will have weaker interwell connectivity. Scatter plot of fij versus interwell distance given on figure 7 confirmed this description.

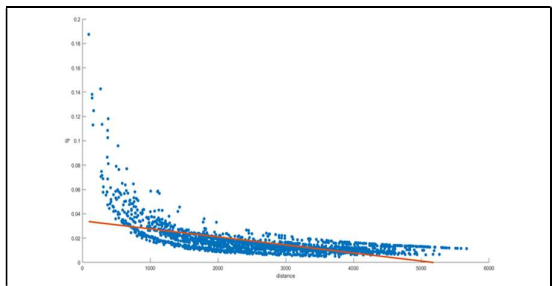

Figure 7. Allocation factor-well pair distance from CRM

In determining the oil rate match, empirical parameter in fractional flow model is calibrated by minimizing the mean square error between predicted oil rates and actual oil rates. Gentil (2005) fractional flow model is used to predict oil rates as it avoid implicit calculation of the fractional flow in each time step. It can be seen in figure 8 and figure 9 that the oil rate data field and each producers is sufficiently matched to the fractional oil flow model used. Calibrated fractional flow model is then used for oil rate forecast and injection allocation optimization.

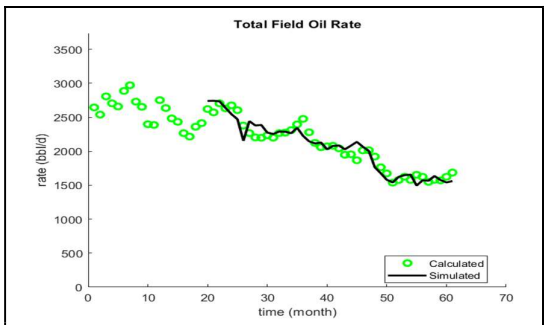

Figure 8. Field Total Oil Rate History Matching Result

PROCEEDINGS
JOINT CONVENTION BANDUNG (JCB)2021
November 23rd – 25th 2021

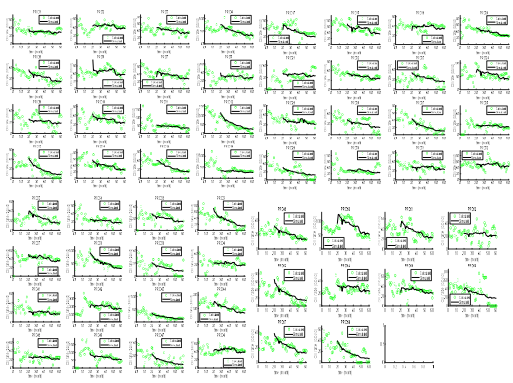

Figure 9. Well Oil Rate History Matching Result

Base case forecast scenario in which no change in allocation rate for injector is carried out to provide base estimate of future reservoir performance. Optimized scenario is then run by the same total injection capacity as in base case, however allocated injection rate will be optimized by interior-point algorithm to obtain maximum cumulative oil produced at the end of forecast period. Maximum injection rate constraint based on history injection rate per well is also imposed to observe achievable value of injection rate and avoid induced fracturing.

Field oil production profile and injection rate allocation for base and optimized scenario are given on figure 10 and figure 11 respectively. By optimizing injection rate allocation, additional 505 Mbbl oil is expected to be recovered, which is equivalent to 0.22% incremental oil recovery factor.

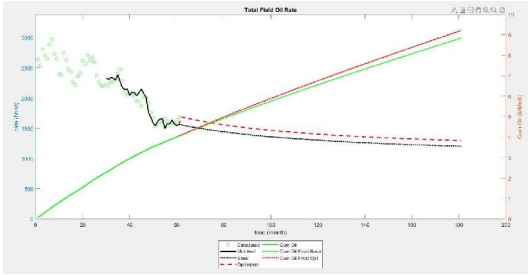

Figure 10. Pandhawa field base and optimized forecast scenario comparison for total oil production rate and oil production cumulative

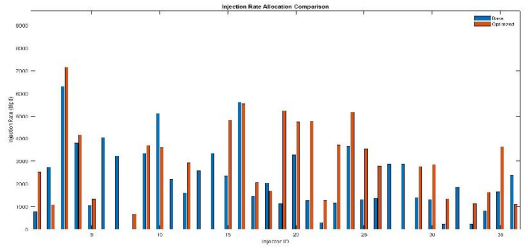

Figure 11. Injection rate allocation comparison between base and optimized case

From interwell connectivity standpoint, optimal allocation rate calculated by CRM can be interpreted as increasing injection support for production wells with the highest oil rate. Producers with the highest oil rate at the start of forecast, hence by CRM logic, the injectors with highest connectivity to these wells will be given priority to increase liquid throughput. Well by well comparison of base and optimized case scenario is provided in figure 12.

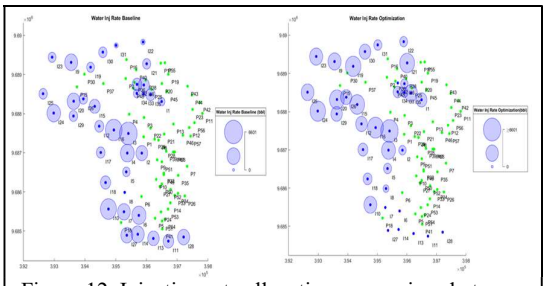

Figure 12. Injection rate allocation comparison between base and optimized case

CRM Improvement

Some workaround has been attempted such as by limiting connectivity only in "influence radius" and clustering well in order to solve CRM issue such as unstable well production data due to shut in period and to make calculation faster than current methodology.

Influence Radius

This method is using limiting connectivity for producers and injector pair that is the maximum distance of possible interwell connectivity. The history match result by implementing influence radius of 2 km is shown on figure 14. Note that influence radius cannot be too small such that a producer is left without injection support as shown in figure 13. The history match result from implementing influence radius did not improve significantly. However, sensitivity analysis of influence radius magnitude can be exercised to infer whether optimal influence radius exists that minimize history match error. Such exercise is planned for future phase.

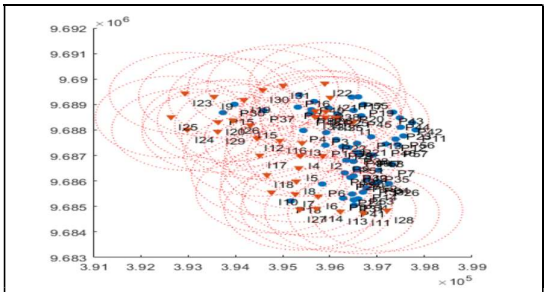

Figure 13. Well influence radius of 2 km

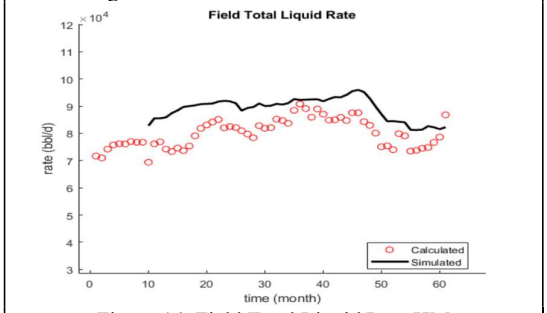

Figure 14. Field Total Liquid Rate HM

PROCEEDINGS
JOINT CONVENTION BANDUNG (JCB)2021
November 23rd – 25th 2021

Clustering Producers

Clustering producers is conducted by merging producers into grouped of wells. It can be seen as compromise between single tank control volume as in CRMT and injector-producers control volume as in CRMIP. Benefit of this approach is that it can reduce unknown parameters significantly therefore give smaller computational cost. The premise is that, due to the waterflood is done in peripheral and producer wells are located non-uniformly, it is possible that once a producer well undergone shut-in, the nearby wells will take the injection support from the closed well. Hence, the production in nearby wells can be represented by single pseudo-well for each cluster. The cluster centers must also represent the major flow path that is happening in the reservoir, which most likely will be directed towards the key wells. Here the key wells are defined as the wells with highest productivity index, or simply can be approached as the well with highest liquid production rate.

This type of clustering scheme can be attempted using several unsupervised clustering algorithm. Weighted K-means is chosen as the most suitable algorithm proposed due to the nature of the clustering scheme. Example of implemented clustering using weighted k-means for six clusters in Pandhawa field is provided in figure 15. The choice of cluster number is an arbitrary input, but several metrics such as silhouette values can be used as guideline for determining the optimal number of cluster.

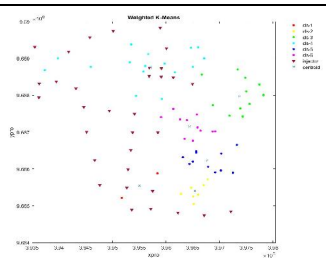

Figure 15. Clustering Producer (weighted k-means)

Result of this method can be seen in figure 16-21 start from liquid history field and well matching, oil history field and well matching, well connectivity map from injectors to clustering wells, baseline production scenario and optimization case. History matching quality of liquid and oil is acceptable and it can be conducted faster 16 time than previous method with similar result. Optimization result using clustering method give smaller number than without clustering, 352 MBO versus 505 MBO.

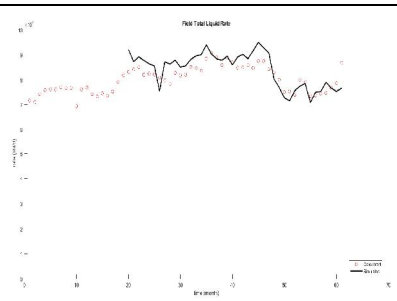

Figure 16. Field Total Liquid Rate HM Result Using Clustering

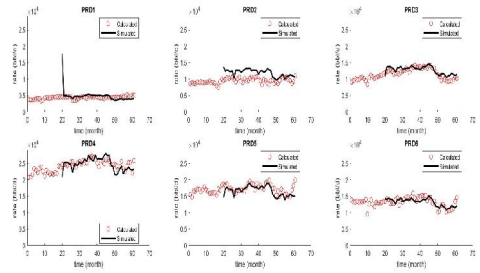

Figure 17. Well Total Liquid Rate HM Result Using Clustering

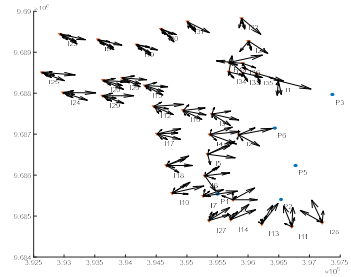

Figure 18. Well Connectivity Map from History Matching

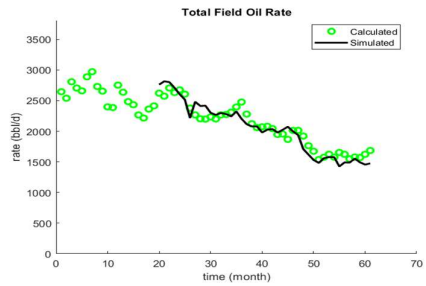

Figure 19. Field Total Oil Rate HM Result Using Clustering

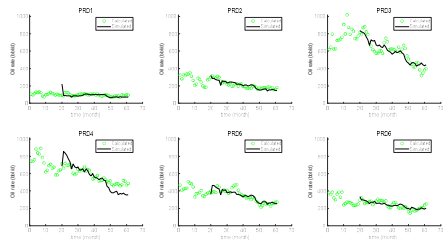

Figure 20. Well Total Oil Rate HM Result Using Clustering

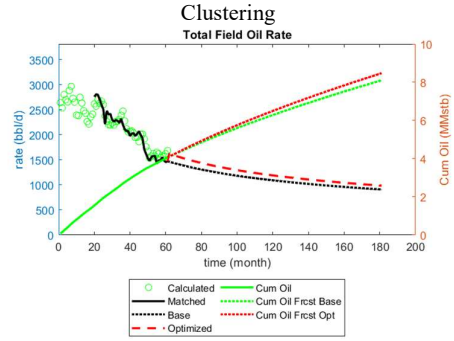

Figure 21. Pandhawa Field Base and Optimized Forecast Scenario Comparison using Clustering

PROCEEDINGS
JOINT CONVENTION BANDUNG (JCB) 2021
November 23rd – 25th 2021

Conclusions

Based on current study, we conclude that

- A computer program for CRM-IP implementation based on MATLAB has been successfully constructed and validated using Pandhawa field data.
- CRM-IP could be used to predict oil reservoir performance with simple and fast, in this study using actual data from Pandhawa field.
- CRM-IP has been shown to analysis injectors and producers performance (effective and ineffective well) in waterflood field by using interwell connectivity estimation.
- Clustering method is success implementing in this study to solve shut in well condition and accelerate time calculation with acceptable result.
- Optimization in Pandhawa field conducted by utilizing interwell connectivity to redistribute injection water with result 352-505 MBO.

Several works are planned to be exercised to further the research progress, such as :

- Optimization algorithm performance comparison for CRM Implementation in Matlab.
- Extension of CRM to include aquifer model such as Carter-Tracy analytical model to aid in uncertainty analysis

References

Daniel Weber, L. W, 2009, SPE Western Regional Meeting.
Gentil, P. H., 2005, Thesis, The University of Texas.
Holanda, R.W., Gildin, E, Jensen, J.L., 2015, SPE Latin American and Carabian Petroleum Engineering Conference.
Kaviani, D., Soroush, M., & Jensen, J, 2014, Journal of Petroleum Science and Engineering.
Rami Kansao, Andres Y, Zamel H, Luigi S, 2017, SPE Europec featured at 79th EAGE.
Sayarpour, M. Zulaga, E Kabir, CS Kabir, L.W. Lake, 2009, Journal of Petroleum Science and Engineering.
Sayarpour, M. Zulaga, E Kabir, L.W. Lake, 2007, SPE Annual Technical Conference and Exhibition.
Thompson, M., 2006, Elsevier E-Book.
Yousef, A. A., Gentil, P.H., Jensen, J.L., Lake, L.W, 2006, SPE Reservoir Evaluation and Engineering.

PROCEEDINGS
JOINT CONVENTION BANDUNG (JCB)2021
November 23rd – 25th 2021

Analysis of the Effect of Tubing Material and External Insulation to Wax Deposition Formation in Vertical Waxy Oil Well

Arsalan Umar [1], Dr. Agus Astra Pramana [1], Dr. Ardian Nengkoda [2]
[1]Department of Petroleum Engineering, Universitas Pertamina, Jakarta, Indonesia
[2]Saudi Aramco

Abstract

Flow Assurance is a nomenclature in the oil and gas industry which can be interpreted as guaranteeing the success of hydrocarbons (oil and gas) flowing from the reservoir to the point of sale and avoiding flow assurance issues, one of them is due to wax deposition (Ansyori, 2013). Waxy oil, also known as HPPO (High Pour Point Oil) is an incompressible type of oil, with high saturate, aromatic, and paraffin content (Joesoef, 1978). In principle, waxy oil will form a wax deposit, either in the pipe or tubing if the temperature of the flowing fluid has touched the Wax Appearance Temperature (WAT), or the highest temperature at which the wax particles begin to precipitate (Ansyori, 2013). This research was conducted using synthetic databases collected from several published journals with the aim of modelling the flow of waxy oil in vertical onshore production wells, identifying problems that may occur during the oil production, simulating the starting point of wax deposition, and comparing several scenarios regarding the factors that affect deposits. The results of this study indicate that one of the most influential parameters in the process of forming wax deposits is when the fluid temperature is below the Wax Appearance Temperature (WAT). The simulation results from the scenarios, it is found that the higher the thermal conductivity of a tubing material, the faster the wax deposition occurs, and produces the highest thickness of wax deposits. Other research results obtained are, with simulations using insulation, show that tubing with an insulating material Fiberglass with a high insulation thickness is proven to be the most effective in preventing the wax deposition process. The presence of wax deposits in the tubing has a negative impact, one of which is a reduction in the inner diameter of the tubing, so that it will reduce the flow rate, and which in the end the wax will create a plug which makes the crude oil unable to be produced again.

Keywords: Flow Assurance, Flow Rate, Temperature Loss, Wax Thickness, Waxy Oil.

Introduction

Flow Assurance includes all sources, processes, facilities and conditions that affect the successful flow of hydrocarbons from the reservoir to the point of processing/sales (PPSDM Migas, 2016). Some of the focuses of flow assurance include gas hydrates, waxy oil, slugging, scale deposits, and heavy oil flow methods. Piping or transportation problems in Indonesia are generally caused by a blockage that interferes with the flow process, the blockage is formed due to the presence of solids or minerals deposited on the pipe wall which causes the inside diameter of the pipe to decrease. Waxy oil is an oil that contains a lot of wax or wax, saturates, and aromatics which at a certain temperature will cause crystallization of the wax. 80% of the global energy needs are oil and gas. Waxy oil production is predicted to increase due to a decrease in conventional oil production, of which around 20% of world oil reserves are waxy oil (Theyab, 2018). The current production of waxy oil has increased from 1960 around 1 million barrels per day up to 24 million barrels per day in 2009 (Chala, 2017).

Waxy oil can cause various complex production problems, because at a certain temperature it can cause wax deposits which will eventually hinder the transportation process. Temperature reduction is the most common cause of wax deposition because wax solubility in hydrocarbon fluids decreases as the temperature is lowered. Wax Appearance Temperature (WAT) is another term for cloud point, which is commonly used for waxy oils. The amount of WAT in waxy oils will be higher than oils that have little or no paraffin. WAT can be interpreted as the highest temperature at which paraffin begins to form crystals for the first time (Emmanuel, et.al, 2016). In accordance with the nature of waxy oil, where when the temperature passes through WAT, it will create wax deposits for the first time which is marked by the start of the rising precipitation curve of the wax deposits (Z.Huang et al., 2015).

There are several factors that cause the formation of wax deposits in pipes or tubing (Prasetyo, A, 2019), namely:

- The composition of wax in crude oil, the more the thickness of the wax deposit increases
- Decrease in temperature, if the temperature drop is high, the wax deposition will increase
- The physical condition of the pipe or tubing, such as roughness; bending; diameter; and inclination
- Flow rates and flow patterns in pipes or tubing

Based on Sousa, A.M et al, 2020, simply the process of forming wax deposits begins with the presence of a

PROCEEDINGS
JOINT CONVENTION BANDUNG (JCB)2021
November 23rd – 25th 2021

thin gel layer around the tubing wall which is formed due to the temperature having passed the WAT, which at a certain time the wax deposit will increase and harden. So, based on this mechanism, the presence of wax deposits in the tubing will cause several problems, including Bern, 1980:

- Decreased production due to reduced tubing diameter
- Tool damage
- The need for experts and materials is increasing
- Increased production cost

Based on the problems that may be caused by the production of waxy oil, this research has a main focus, namely knowing the process of forming wax deposits in tubing. In addition, this research also focuses on efforts to prevent wax deposits from forming in tubing, namely by conducting research on tubing materials used with different heat conductivity, as well as conducting trials on the use of external insulators on tubing with various materials and insulator thicknesses as an effort. prevention or minimizing the rate of decrease in the temperature of the fluid in the tubing to the environment, so that the resulting wax deposits can also be minimized.

The recommendations given are very likely to be carried out, taking into account that the regulation of the flow rate, the selection of tubing materials and the need for insulators related to the prevention of wax deposits will be much easier and is expected to minimize the costs that will later be incurred in remedial action if waxed. has formed in the tubing.

Methodology and Data

- **Methodology**

This research was conducted using synthetic data with some adjustments made. The research begins by collecting data used, such as reservoir fluid data, well schemes, tubing materials and insulating materials used.

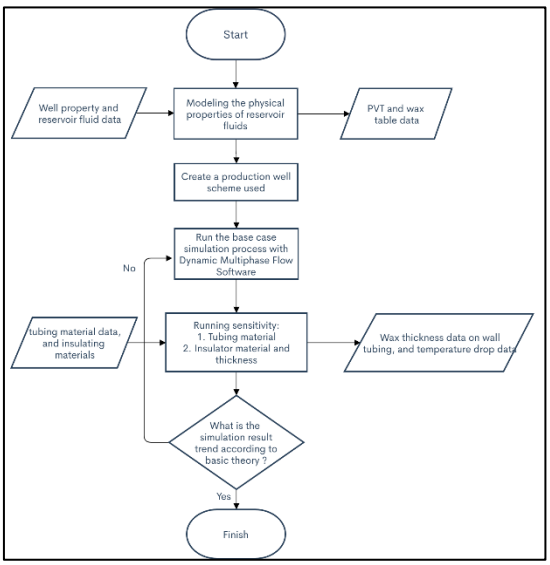

Figure 1. Methodology

- Equation of Fluid Temperature Drop in Tubing

Calculation of temperature distribution can be calculated using Shie & Beggs (2008) correlation, as follows:

$$T = T_d - G_t\left(D - A\left(1 - e^{\frac{D}{A}}\right)\right) \quad (1)$$

where,

$$A = 0.0063 Wt^{0.4882}\, d^{-0.3476} API^{0.2519} \rho_L{}^{2.915} Pwh^{0.2219} \quad (2)$$

Where A = correlation constant; Wt = total mass flow (lb/s); Td = formation temperature (F); Gt = Geothermal gradient; D = depth (ft); and d = tubing diameter (in).

- Equation of Wax Deposit Thickness Rate in Tubing

The rate of formation of wax deposits in tubing is in accordance with Fick's Law of Diffusion, namely:

$$Wm = \rho_w A D_m \frac{dC}{dT}\frac{dT}{dr} \quad (3)$$

Where *Wm* = wax deposition rate (kg/s); ρ_w = *wax density* (kg/m^3); A = tubing area (m^2); *Dm* = diffusion coefficient (m2/s); *dC/dT* = wax concentrate to change of temperature (1/C); and *dT/dr* = temperature radial gradient (C/m).

- Effect of Material on Temperature Loss

Fourier's law examines heat transfer through solid materials whose magnitude is relative to the outer area and wall thickness of the tubing which is also affected by the temperature difference between the inside and outside of the tubing (Serway & Faughn, 2003).

$$q = k\, A\, \frac{dT}{s} \quad (4)$$

Where q = *heat transfer per unit time* (W, Btu/hr); A = *heat transfer area* (m^2, ft^2), k = *thermal conductivity* of tubing material (W/mK or W/mC); dT = temperature difference between fluid and material (C); s = material thickness (m).

- **Data**

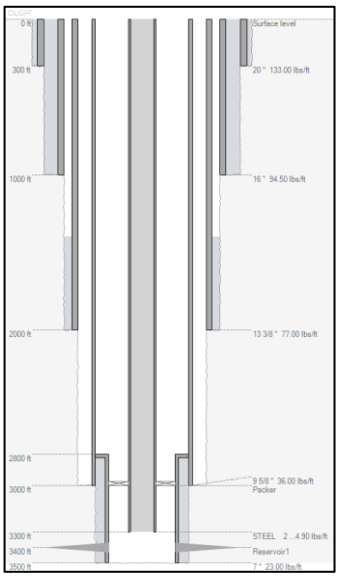

Figure 2. Well Schematic

PROCEEDINGS
JOINT CONVENTION BANDUNG (JCB)2021
November 23rd – 25th 2021

The picture above is a schematic of the well used in the simulation. The well is an onshore vertical well which has 1 reservoir zone.

Reservoir and Production Data	
Reservoir Pressure (psi)	2002
Reservoir Temperature (°C)	62
Surface Temperature (°C)	33
BHP (psi)	1200
Wellhead Pressure (psi)	300
Surface Temperature (°C)	33
Productivity Index (PI) (bbl/d/psi)	1.5
Production Estimation (bbl/d)	1203
Water Cut (fraksi)	0
Fluid Density (kg/m3)	870
Mass Flow (kg/s)	1.9

Table 1. Reservoir and Production Data

The table above is a table of reservoir and production data used in this simulation.

Base Case Data	
Well Type	Vertikal
Mass Flow (kg/m3)	1.9
Water cut (%)	0
Fluid Density (kg/m3)	870
WAT (°C)	50.5
Tubing Interval (ft)	3300
OD Tubing (inch)	2 5/8"
Tubing Thickness (mm)	4.8425
Tubing Material	Carbon Steel
Heat capacity (J/kg-C)	485
Heat Conductivity (W/m-C)	50
Roughness Tubing (ft)	0.000164042
Insulation	No
Duration of Simulation (days)	30

Table 2. Base Case Data

Result and Discussion

- **Reservoir Fluid Simulation**

Reservoir fluid simulation is carried out by entering the composition of oil and natural gas according to known data. Simulations are carried out using PVT-Sim software which aims to determine the distribution of the reservoir fluid properties for each certain temperature and pressure.

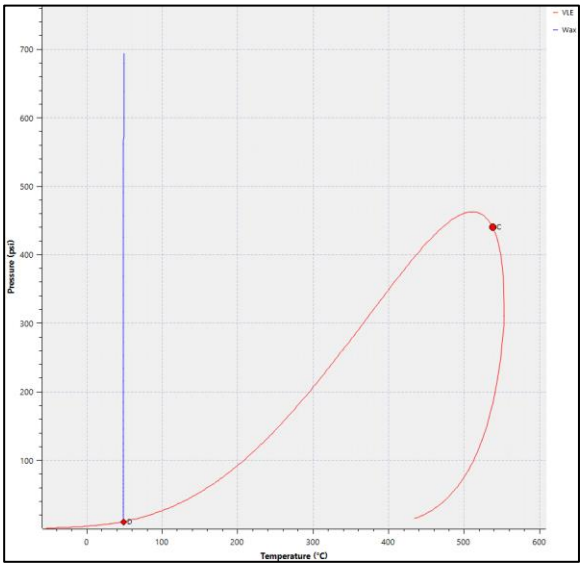

Figure 3. P-T Diagram

The reservoir fluid data used in this simulation is oil with a weight of 31.27°API with a GOR of 150 ft^3/bbl. Figure 4.1 above is a graph of the pressure to temperature curve of the simulated reservoir fluid. Based on the simulation results, the WAT is 48.5 °C and the wax content is 18.2%.

- **Sensitivity of Tubing Material**

The next simulation carried out in this study is the sensitivity of the type of tubing material that has different thermal conductivity values to the decrease in temperature and the resulting wax deposits on the tubing. In the study of tubing material sensitivity, 4 types of materials were used, namely Carbon Steel, Copper, Teflon, and PFA which have different conductivity. However, these four materials have the same diameter, roughness, and thickness, so the resulting output is purely due to the difference in the magnitude of the thermal conductivity.

Material *Tubing*	*Heat Conductivity (W/m-K)*
Carbon Steel	54
Copper	401
Teflon, PTFE	0.4
PFA	0.14

Table 3. Types of Tubing Materials

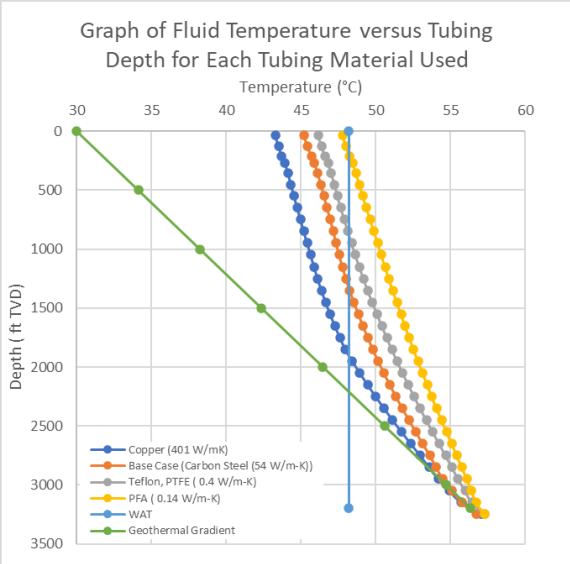

Figure 4. Graph of Fluid Temperature for Each Tubing Material

Figure 4. above is a temperature reduction curve for each type of material used. Based on the graph above, it can be seen that the fastest rate of temperature reduction occurs in tubing with Copper material, then Carbon Steel, then Teflon, and the lowest temperature decrease rate is achieved when tubing uses PFA material. From this figure, it can be seen that for Copper material the temperature drop curve touches the WAT at about 1900 ft TVD depth from the wellhead; for Carbon Steel material at a depth of 1450 ft TVD, for Teflon material at a depth of 900 ft TVD; and for PFA material at a depth of 100 ft TVD from the wellhead.

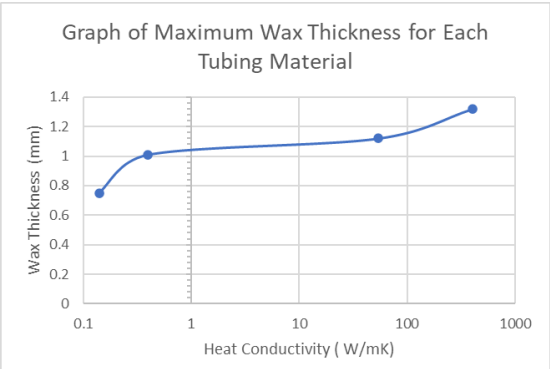

Figure 5. Graph of Heat Conductivity to Wax Deposition Thickness

Figure 5. above is a curve of the thickness of the wax deposits formed in the tubing for each type of material used. Based on Figure 4., it is known that the fastest temperature decrease rate occurs in Copper and Carbon Steel, and the smallest occurs in PFA material. Based on the picture above, it can be seen that the highest wax deposition occurred in Copper material which was 1.31 mm, then for Carbon Steel material was 1.15 mm, then for Teflon material was 0.95 mm, and for PFA material was 0.75 mm at the point where the curve touches the WAT for each material.

This is purely due to the different thermal conductivity of the four types of materials, where the highest thermal conductivity is Copper, which is 401 W/mK, then Carbon Steel, which is 54 W/mK, then Teflon with 0.4 W/mK, and the most small is the PFA with a large 0.14 W/mK. This is in accordance with the theoretical basis used, namely the higher the thermal conductivity of a material used, the material will easily absorb heat from the system and release it to the environment, resulting in the temperature of the system will easily experience a decrease in temperature. Thus, it is easier for the system to experience a decrease in temperature, the faster the fluid will reach WAT, so that wax will form more quickly and with the same simulation time, the wax deposition produced is the thickest compared to materials with low thermal conductivity.

- **Sensitivity of External Insulator Material and Thickness**

After conducting research and simulations regarding the effect of several types of physical properties of the tubing used, the authors conducted further research using Dynamic Multiphase Flow software to model the effect of the use of insulation on the tubing used and the thickness of the insulation on the rate of decrease in the temperature of the fluid in the tubing. and its effect on the process of formation of the resulting wax deposits.

Material and Thickness of Insulator			
Type of Insulator	External Insulator		
Thickness of Insulator	0.1 Inch	0.5 Inch	1 inch
Material Insulator	*Polypropylene Foam (PPF)*		
	Calcium Silicate (CS)		
	Fiberglass ICS)		

Table 4. Insulator Material and Thickness

In this study, three types of materials were used as insulators, namely Polypropylene Foam (PPF), Calcium Silicate (CS), and Fiberglass (FG) using three types of thickness in the simulation, namely 0.1 inch; 0.5 inch; and 1 inch.

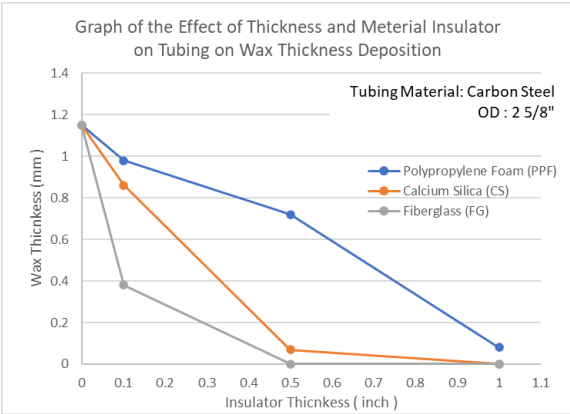

Figure 6. Graph of Insulator Material and Thickness to Wax Deposition Thickness

The three types of insulation provide the same trendline, namely the thicker the insulator, the smaller the wax thickness as the temperature drop in the

system decreases. This is in accordance with Fourier's Law (Equation 4. above), it can be seen that with the type of material, the area of the fluid flowing, as well as the same thermal conductivity, the greater the thickness of a given insulation will produce a smaller or inversely proportional heat transfer, so it seems - if it gives a blanket effect, where the process of heat transfer between the system to the environment will have a smaller rate when compared to a thin insulator thickness. Ignoring the economic factor, it can be seen that when an insulator thickness of 0.1 inch is used, FG material is proven to be effective in preventing wax formation. At a thickness of 0.5 inch, FG and CS materials are proven to be effective in preventing wax formation in tubing, and at a thickness of 1 inch, all three types of materials are proven to be effective in preventing wax formation in tubing.

Conclusions

Based on the research that has been done, it can be concluded that:

- The type of reservoir fluid used has a wax deposition content of 18.3 % , and has been proven to have the potential to form wax deposits in the tubing.
- Based on the sensitivity results of the tubing material used, it was found that the PFA material had the best performance because it produced the smallest wax deposits.
- Based on the sensitivity results of the insulator material, it is concluded that by using the same tubing material, the Fiber Glass insulator material has the best performance because it produces the smallest wax deposits due to low heat conductivity. For the three types of insulator materials, it is also concluded that the thicker the insulator is used, the better it will be in preventing temperature loss to the environment, and preventing wax deposits from forming.

The suggestions given by the author to the research of this final project are:

- Evaluate the simulation results by means of validation to the laboratory and the results of operations in the field.
- Performing simulations by adding more complex parameters or variables, such as the presence of a deviation well or the presence of downhole equipment that can increase restrictions and can be a point where wax is deposited.
- Economic analysis needs to be carried out along with efforts to prevent wax deposition processes in order to obtain the most economical and efficient method.

References

Abdurrahman, M, et al. (2018). *Possibility of wax control techniques in Indonesian oil fields*. AIP Conference Proceedings.

Ajayi, O. E. (2013). *Modelling of controlled wax deposition and loosening in oil and gas production systems.* Norwegian University of Science and Technology.

Azlina, N. (2012). *Simulation of Wax Deposition Model for Various Field.* Universiti Teknologi Petronas (UTP).

Burmantsev, R. et al. (2018). *Managing Wells with Flow Assurance in the Karachaganak Field for Sustainable Production : Transient Simulation Modelling, a Viable Tool.* Society of Petroleum Engineers.

Huang, Z. (2018). *Wax deposition: Experimental Characterizations, Theoretical Modeling, and Field Practices, 1st ed.*

Infochem. (2015). *Multiflash for Windows.* KBC Advanced Technologies Ltd.

Joseph, A., Ajienka, J. A., Essien. E. E .(2018). *Waxy Crude Oil Well Surveillance.* European Journal of Engineering and Technology.

Kasbi, M. (2018). *Thermal Insulationg of Tubing in the Petroleum Industry.* University of Leoben (Austria).

Leontaritis. K. (2003). *Cloud Point and Wax Deposition Measurrement Techniques.* Society of Petroleum Engineers.

Matzain, A., Apte, M.S., & Brill, J.P. (2019). *Investigation of Paraffin Deposition During Multiphase Flow in Pipelines and Wellbores—Part 1: Experiments*. Journal of Energy Resources Technology

Prasetyo, A., Sudono. (2020). "Klasifikasi dan Identifikasi Material terhadap Pengendapan *Wax* pada Sumur Minyak". Cikarang (ID) : Journal of Applied Science.

Semenov, A. (2012). *Wax Deposition Forecast.* Society of Petroleum Engineers.

Seyfaee. A., Lashkarbolooki. M., Mowla. D. (2011). *Investigating of the Effect of Insulation on Wax Deposition in an Iranian Crude Oil Pipeline with OLGA Simulator.* Journal of Dispersion Science and Technology.

Sousa, A.M et al, (2020). *Wax Deposition and Precipitation Forecast*. Society of Petroleum Engineers.

PROCEEDINGS
JOINT CONVENTION BANDUNG (JCB)2021
November 23rd – 25th 2021

Attachment

Komponen	*Mole (%)*	Komponen	*Mole (%)*
C2	0.177	C11	3.733
C3	1.57	C12	4.067
i-C4	1.05	C13	3.53
C4	2.887	C14	2.919
i-C5	2.468	C15	3.2544
C5	3.017	C16	3.63
C6	5.55	C17	3.58
C7	9.8	C18	3.62
C8	11.86	C19	5.01
C9	7.09	C20+	17.23
C10	3.977		

(1)

Komponen	*Mass (%)*
Metana	84.5
Etana	6.5
Propana	4
Butana	2.5
Pentana	1.5
Heksana	0.5
CO2	0.5

(2)

Parameter	*Symbol*	Unit	Nilai
Wax content	-	wt%	19
API Gravity	-	API	31.27
Wax Appearance Temperature	WAT	Celcius	49.62
SG Gas			0.7
SG Minyak			0.86
GOR	-	cuft/bbl	150

(3)

Figure 7. Oil Properties (1); Gas Properties (2); and Reservoir Fluid Properties (3)

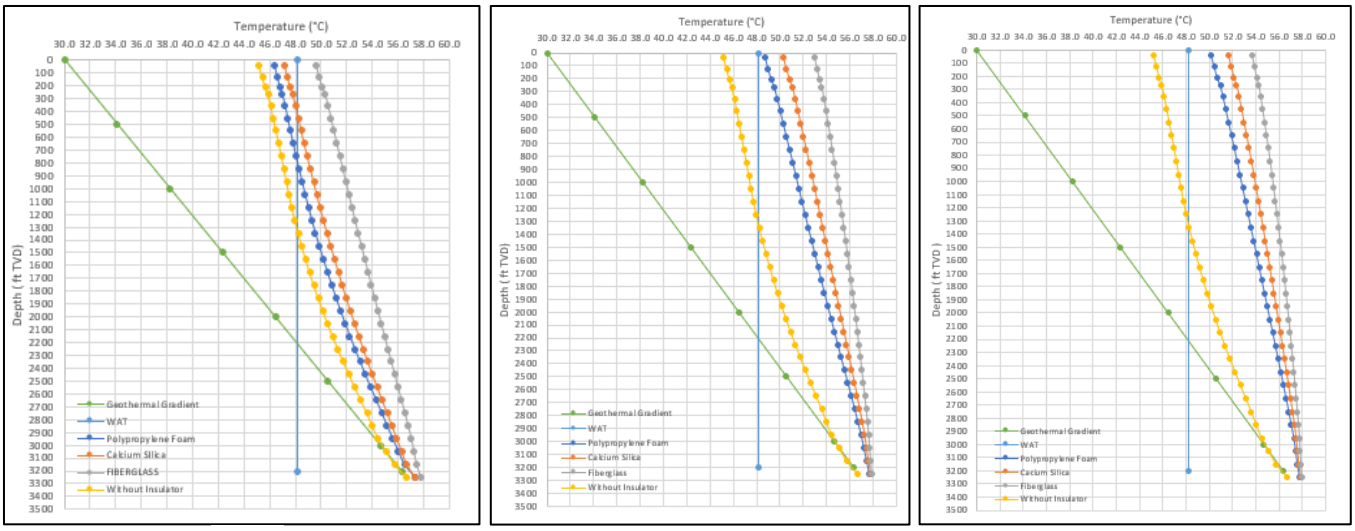

(1) (2) (3)

Figure 8. Fluid Temperature Profile with External Insulator 0.1 inch (1); 0.5 inch (2); and 1 inch (3)

PROCEEDINGS
JOINT CONVENTION BANDUNG (JCB) 2021
November 23rd – 25th 2021

Seismic HC Detection in Fluvio - Deltaic System Using Integrated Quantitative Interpretation by Utilizing Reprocessing Data: Case Study of Intan Field, TAF - Asri Basin, Offshore SE Sumatera

Pranowo Nugroho[1], Hairunnisa[1], Dwandari Ralanarko[1]

[1]*Pertamina Hulu Energi OSES*

Abstract

Along with the development of seismic imaging and increasingly advanced computing technology, the dream of geoscientists to identify reservoir fluids from seismic data will be easier to be accurately and comprehensively conduct. The need for complex seismic data in quality and quantity is a challenge in itself as an initial step for static and dynamic studies to determine how much oil reserves remain. Seismic processing technology and new quantitative seismic methods will further assist in an old oil fairway and mature field such as Fluvio-Deltaic Depositional Environment of Intan Field, Asri Basin, Offshore SE Sumatra. The results of seismic reprocessing show that the quality and quantity of new seismic data have increased sharply compared to old seismic data. This reprocessing data has been using to identify hydrocarbon reservoirs with various quantitative seismic methods. The results of the seismic attribute, AVO, seismic impedance (LambdaRho -VpVs Ratio), lithological impedance (LI), spectral decomposition, RGB blending, and seismic facies results using the Bayesian classification method show that seismic hydrocarbon detection in a Meandering Channel System of sandstone reservoir can be identified accurately through integrated quantitative analysis.

Introduction

Asri Basin has been described as a back-arc, half-graben rift basin (Young and Atkinson, 1993) and a basin with a composite extensional style that begun as an intra-cratonic, "sag style" basin (Aldrich et. al., 1995). Asri Basin is part of a series of Tertiary half-graben developed on the Asian continental margin that has occupied a retro-arc setting since early Neogene times. It covers an area approximately 3500 sq. km and has up to 16,000 feet of sediment ranging from Paleocene to Pleistocene in age. It is bounded to the East by N-S trending fault, downthrown to the West, while the southern margin is marked by a regional NW-SE trending wrench system. There are three major tectonic periods that affected the structural style and depositional systems in the Asri Basin: I) Rift Initiation, II) Syn-Rift, and III) post rift.

Structural control on major axial drainage systems would exert tremendous influence on sand supply to any particular basin at any given time. Basin integration and its control on axial fluvial systems is probably an important part of the story in the stratigraphy of the Asri Basin fill. (Sukanto, et al., 1998) introduce the petroleum system of the Asri Basin, Java Sea, Indonesia. The main reservoir rocks in the Asri Basin are Oligocene to early Miocene fluvial, alluvial, marginal marine, and deltaic sandstones of the Talang Akar Formation (TAF). The TAF of the Asri Basin is divided into Zelda and Gita Member. Typical composite logs of these fields show the vertically stacked sandstone reservoirs. Regional seals are provided by shales at the top of and directly above the TAF by thick mudstones of the succeeding Gumai Fm. The close interplay of the abundant fault and permeability migration pathways, high-quality reservoir, source, and seal facies in a region of high heat flow has thus handled the accumulation of large reserves of oil in the Asri Basin (Figure 01).

The Miocene Gita member of the TAF represent deposits of a post-rift fluvial system that records the northward advance of a late Oligocene to early Miocene marine transgression. Gita reservoirs sandstones is the most prolific hydrocarbon interval and therefore one of the most valuable assets in the Southeast Sumatera Block. If production continues to follow development trends for a mature basin, then the most significant reserve additions will come from exploration and the most productive intervals. One of the candidates is Intan prospect, located at the northwest flank of Asri Basin with a three-way dip structure based on the 2D seismic mapping.

In 1987, a 'final' five-well exploration programmed was undertaken to evaluate the Intan prospect. Intan-01 has prioritized drilled first. It met 76 feet of net oil pay and flow tested a cumulative 5845 BOPD, proving the Asri Basin as a majors oil-bearing area. The development of Intan Field has proposed to recover oil reserves from TAF discovered by Intan-01 well and confirmed in subsequent and appraisal drilling. Since the development of the Intan field began in 1990, near-field exploration has focused primarily on infill prospects using 3D seismic (Wight, et al., 1997).

Seismic Processing

With the success of the discovery of two giant fields in the Asri Basin, namely Intan Field and Widuri Field, the existence of 3D seismic data is an absolute prerequisite for the development program. 3D seismic is an extremely powerful delineation tool that is also cost-effective, particularly when well costs are high. The success is directly attributable to the better structural interpretation made possible by the 3-D survey (Sheriff, 1992). The greatest impact of 3-D surveys has been the ability to match platform size, several wells' slots, and production facilities to the more accurately determined field reserves.

3D seismic data at Intan field was acquired and processed in 1991. The primary lines were recorded using a single boat outfitted with a dual air-gun source and two streamers. The survey was a plan to produce 21-fold coverage on a 6.25 m CMP by 25 m line spacing. After final editing, the 3D volume formed a total of

approximately 15,000 km of 256 channel data. The recording was to 3 seconds at a sample rate of 1ms. The survey was processed using a 2ms sample rate, a record length of 3 seconds, and the nearest 240 channels. The limitations of machine computation when it happened allowed only for the production of seismic post-stack, by using velocity analysis every 500m, 2D Dip Move Out (DMO) in the first process, high-resolution radon de-multiple process has not been applying. Hardware technology and processing parameters were unable to perform processing parameters such as 3D Kirchoff Pre Stack Time Migration (PSTM), high-resolution radon de-multiple, and 5D interpolation.

However, the 1991 3D post stack seismic data with a spacing of inline 25 m, still has excellent geological interpretation results. Seismic amplitude attribute on TAF formation shows that the reservoir zone in the Intan Field can be identified clearly as a braided channel on Zelda Member and meander in Gita Member. The 30 series sand of the Intan field are found within the uppermost part of the Gita Member. The 30-1 sand categorized as meandering fluvial channel sandstones trending northwest southeast.

Processing new seismic data has been complete at the Intan Field for a total area of around 108 km^2 in 2020. The purpose of this reprocessing data is to reveal a new paradigm and provide a better-quality resolution of signal to noise ratio on the seismic data. It is necessary to improve the seismic data quality as input for the static and dynamic model study. This procedure has been designed to convert the original SEG-D raw data from the acquisition (tape format) to hard disk media as an initial step. A comparison of the new seismic flow processing steps with the previous process has shown in Table 01. Based on the processing flow, five steps have a powerful impact on the data compare to the previous one. There are 3D SRME shallow water de-multiple, Tau-Pi deconvolution, high-resolution radon de-multiple, 5D (inline, xline, offset, azimuth, and frequency) interpolation and regularization, and 3D Kirchoff PSTM.

Predictive deconvolution attenuates multiple that involve surface and near surface reflectors. It can remove reverberation or ringing caused by the water layer. The predictive deconvolution predicts a lag (gap) that is equal to the first or second zero crossing. In this study we set 320ms operator length and 16ms gap test for the best Tau-Pi deconvolution parameter. The radon demultiple method is a method for reducing long period multiples mixed with data. The input data has been corrected by NMO, the primary event will be flat (to Zero Offset), while the multiple events is still in a downward and upward curve from the primary data. This happens because the multiple velocities are smaller than the primary velocities at the same depth. Prior to running PSTM, 5D regularization and interpolation should be run to optimize the migration result. 5D interpolation uses a neighborhood of acquired seismic data to predict the missing data. Ideally, data that are missing in one or two of the spatial dimensions can be reconstructed using data that are present and well sampled in the other spatial dimensions. This idea is to put the trace in the correct grid position and then the interpolation will fill up the holes in each offset class.

For quantity of the data, the old seismic parameter has an inline step every two, 25 m each inline, sample interval 2ms with the number of samples per trace is 1500. While the new repro has an inline step 12.5m each inline, sample interval 1ms with the number of samples per trace is 3073, Table 02.

Parameter	OLD	REPRO
Inline step	2	1
Inline interval	25m	12.5m
Sample interval	2ms	1ms
Number of sample per trace	1500	3073

Table 02. New parameter of seismic reprocessing

The final stack result from the reprocessing data qualitatively supplies a better seismic image continuity, makes it easy to interpret the horizon from the 0ms to the basement event, and clear from multiple effects (Figure 02). The spectrum frequencies are more stable, with no low and high frequencies noise at this seismic section. Another QC comes from the time slice result, new repro data showing the good image at closure boundaries in the reservoir zone (Gita) at 1000ms and in the basement zone at 1200ms (Figure 03).

Seismic Amplitude

Seismic amplitude right now is one of the important criteria for recognizing potential hydrocarbon reserves. Recognize and validating an amplitude is the key to bridging between the seismic to lithology and pore-fluid saturation (Hilterman, 2001). Amplitude interpretation must be geologically consistent with the structural analysis. In exploitation perspective, seismic amplitude data is the easiest way to characterize and identify the potential of subsurface reservoirs. An integrated and comprehensive geophysical analysis are needed to support this issue. It started by performing a running seismic amplitude attribute as the first step for an integrated geophysics study. This research will focus on the Gita Member area in the reservoir zone of Gita sand (30-1) TAF.

A seismic attribute is a quantitative measure of a seismic characteristic of interest (Chopra and Marfurt, 2005). Post stack seismic attribute are applied in seismic interpretation data to identify the anomaly, like bright spots effects, frequency anomalies, faults-structural mapping, reveal detail reservoir channels, highlight reservoir trends, and enhance technical presentation. Seismic attribute analysis begins by choosing attributes that are appropriate for the purpose at hand. Certain attributes prove to be most successful for certain objectives. Seismic attributes are cleared when derived from clean seismic data (Barnes, 2016).

To check the quality of seismic amplitude of the new repro data, we try to slice the amplitude attribute map at the Gita horizon. It provides a higher resolution image than the original post stack data. It is due to the new repro data has more inline data every 12.5m compared to the old data that only has 25m inline spacing. The 30-1 meander channel looks better resolution and more continuous compared to the old data. See the black arrows at several places (Figure 03). The yellow color indicates that the

preserve bright amplitude is likely a direct hydrocarbon indicator. The partial angle stack also being used for the QC process, which includes near data (0°-16°), mid data (16°-26°), far data (26°-36°), and ultra-far data (36°-46°). The AVO response (yellow circle) appears increasingly bright from near to ultra-far seismic data (Figure 04), it shown in the slicing attribute amplitude data (Figure 05).

Rock Physics

Seismic data analysis is one of the keys methods for reservoirs characterization and monitoring subsurface pore fluids. While there have been greats advances in 3D seismic data processing, the quantitative interpretation of the seismic data for rock properties still poses many challenges. Quantitative seismic interpretations demonstrate how rock physics can applying to predict reservoir parameters, such as lithologies and pore fluids, from seismically derived attributes (Avseth, et al., 2005).

One of the primary goals of amplitude interpretation is to determine whether a water-saturated rock or a hydrocarbon-saturated rock. (Hilterman, 2001) Thus, a few basics relationships of rock physics are necessary. Before running seismic inversion, it is important to understand the relationship between reservoir properties, seismic amplitudes and also the petrophysical data of the different rock physics.

The first procedure in starting rock physics analysis is to conduct a feasibility study through the cross-plot wells data with various elastic parameters. In this feasibility study, we use tens exploration wells in the Intan area. From those 10 wells, only Laras-01 has an original Vs log. A blind test well was tested on Laras-01 well to figure out how confident the Vs prediction would be for all wells (Figure 06). The procedure for predict Vs log in this study is using Modified Gassmann (sandstone reservoir) while if the calculation was failed, then Greenberg Castagna was applied to the data. The results of the blind test well produce data Vs predictions, which qualitatively look very good compared to the original Vs data log, shown by the cross plot of Vs predicted vs Vs measured and also AI vs Vp/Vs on the Laras-01 well.

This Vs log prediction using those methods then applied to all wells. After that process, a fluid replacement model (FRM) is applied to the cross-plot data. The petro elastic behavior cross plot at 100% Sw showed that the lithology of wet sand, shale, and coal could be well separated. From petro elastic behavior at in situ conditions, we can see that oil saturation can be separated clearly from the wet sand. Low VpVs ratio values and low saturation density indicate the characteristics of hydrocarbon oil. A cross-plot matrix on the INTA-01 well made to figure out which of the best elastic properties parameters to characterize the reservoir.

From the cross-plot results, we obtained several elastic parameters that can characterize the reservoir, such as AI vs VpVs ratio and Lambda-Rho (LR) vs Mu-Rho (MR) with a cut-off VpVs ratio below 2 for oil sand and LR below 15 GPa*g/cc (Figure 07). The AI and SI values in the cross-plot data cannot separate well between sand and shale lithology. It is necessary to try another method like Poisson's Impedance (PI) for solving this issue. (Direzza, et al., 2012) tweaking these methods by varying the C value and dividing it into two categories, namely Lithology Impedance (LI) and Fluid Impedance (FI). We apply using this method at Intan-01 well.

LI is obtained from the correlation coefficient between PI and Vclay, while FI is from the PI and Sw. The maximum values for C on the LI and FI are 1,475 and 1,525 based on the results of the Target Coefficient Correlation Analysis (TCCA) curve as seen from (Figure 08). Then that formula is applying to all the well to see the cut off value of LI and FI. It shows that oil sand, wet sand, and shale can be separated with cut off values for oil sands below 5000 ft/s*g/cc.

AVO Attribute Volume

Since 1970, the bright spot era in seismic data has become a favorite as a powerful tool for direct indicators of the presence of a hydrocarbon. It did not take long to realize that not all hydrocarbon reservoirs were bright. Dim out effects also have the same response as an indicator for hydrocarbons. In 1984, 12 years after the bright spot technology became a commercial tool for hydrocarbon prediction, Ostrander published a breakthrough paper (Ostrander, 1984). He showed that the gas presence in sandstone reservoir capped by a shale would cause an amplitude variation with offset (AVO) in pre-stack seismic data. Then, (Shuey, 1985) confirmed mathematically via approximations of the Zoeppritz equations that Poisson's Ratio was the elastic constant most directly related to the offset-dependent reflectivity for incident angles up to 30°. AVO technology, a commercial tool for the oil industry, was born (Avseth, et al., 2005).

After that, the era of AVO analysis, AVO mapping, and cross-plot data rapidly developed until the end of the '90s. By sequential, (Smith & Gidlow, 1987) with fluid factor analysis, (Rutherford & Williams, 1989) with three AVO classes, (Fatti, et al.,1994) with the fluid factor in term of Vp &Vs, (Castagna & Swan 1997) with intercept and gradient cross plot and then (Goodway, et al., 1997) with the Lambda-Mu-Rho analysis makes AVO is powerful tools for oil hydrocarbon detection. AVO method application in the Intan field was first carried out by (Harmoni, et al., 1996). The purpose of this study is to determine the Intercept (P), Gradient (G), (P * G), and AVO far offset (AVO30 °) to have a better understanding of the AVO response. The impedance value of the sand and carbonaceous shale mapped and separated well. It will make it easier to re-evaluate and review the proposed infill well prospects.

The earlier discussion in (Figure 04) and (Figure 05), shows that the amplitude map in the near, mid, and far data indicating AVO response with an amplitude gets brighter as the offset increases. There is an anomaly bright spot effect that indicated the presence of hydrocarbons. Intercept (P) volume, Gradient (G) volume, Fluid Factor (F), and P*G volume are obtained by deriving them from the angle stack data (Figure 09).

AVO curve analysis at the PSTM gathers data near INTA-01 well shown that there is a strong anomaly amplitude with increasing offset. These can see from the increasing curve magnitude of the analysis on the far offset

data (Figure 10). Whereas in the Susana-01 well, the PSTM gather is flat, with no AVO response, which indicates that there is no hydrocarbon in the well.

Simultaneous Inversion

In line with the AVO growing era, several scientists have succeeded in developing the seismic inversion method. (Connoly, 1999) have succeeded in developing the seismic inversion method with elastic parameters, (Ma, 2001) with the Simultaneous / AVO inversion method and (Whitcombe, et al., 2002) with the Extended Elastic Inversion (EEI) method to complement and develop the acoustic inversion method that has established since (Lindseth, 1979) first introduced it.

Prestack inversion can be used to extract both compression and shear information from P-wave acquisition. It also can be useful in DHI for both carbonate and clastic rocks, and it can be significant to derive elastic rock properties and quick determination for fluid and lithology discrimination of reservoirs (Goodway, et al, 1997; Gray & Andersen, 2000).

Reservoir characterization requires the identification, detection, quantification of thickness, permeability, porosity, and also fluid content. But unfortunately, many of these reservoir parameters are not directly derivable from seismic data. AI and SI estimated using the simultaneous inversion scheme can be used to derive the conventional rock properties such as Vp/Vs or Poisson's ratio (Ma, 2001).

Before performing the pre-stack inversion process on this data, first, we tried to see the relative impedance attribute as an initial screening of the inversion response. Estimated relative AI is calculated by integrating the seismic trace, and then passing the result through a high-pass Butterworth filter. When the extract value amplitude at this relative impedance is compared to the seismic original data, it is clear that the impedance is adequate to describe reservoir 30-1. Low AI values are associated with bright amplitude in the seismic section.

The angle stack data (near, mid, and far) from new seismic reprocessing data are used to build the simultaneous inversion model. The wavelet extracted in each volume. Using common workflow for simultaneous inversion, qualitatively the training data (Vp, Vs, Rho, and Vp/Vs) compared to the input data is quite good. Correlation between synthetic and seismic data at INTA-01 well is 0.96 from window 960ms to end of log (1060ms) while error between synthetic and seismic data is 0.27.

(Figure 11) shows the results of the simultaneous inversion that produces AI, SI, Rho, and Vp/Vs volumes. With these multiple output volumes, another elastic parameter such as Poisson's Ratio (PR), LR-MR, Lambda/Mu (L/M), LI, and FI can be derived mathematically. The analysis of all these attributes shows the consistency of the oil sand presence (indicated by the red polygon area). It is suitable with the rock physics matrix cross-plot, with low AI, low LR, low Vp/Vs ratio, low L/M, low PR, and low LI-FI values. That area is structurally high, especially near to the INTA-01 well.

Seismic Lithology and Fluid Detection

With a good quality of seismic data from seismic reprocessing, it's now easy to quantify and predict lithology and fluid contents. It was imperative to combine deterministic physical models with geostatistical techniques. This method is fundamental for estimate reservoir rock properties derived from seismic data. (Avseth, et al. 2005) explain this procedure by identifying the most likely interpretational, the uncertainty, and then guide the quantitative decision analysis. (Buland & More, 2003) defined a new linearized AVO inversion technique to obtain posterior distributions for Vp, Vs, and density that developed in a Bayesian framework.

In this study, we want to quantify uncertainty in seismic by dividing with the lithology and fluid prediction. By using several elastic parameters from seismic inversion data, this method is based on a supervised Bayesian classification to deliver several probability cubes of predicted rock properties or lithology. The integrated workflow will give us a good understanding of lithology classes. It can also predict a more accurate assessment of fluids and lithology probabilities.

For this project, we just use LR-MR data from simultaneous inversion as an input. As shown in the cross plot (Figure 12), the facies classification has divided into three classes (sand, shale, and coal) and four classes (oil sand, wet sand, shale, and coal). The probability density function cross plot result is applied to the seismic data to obtain the probability volume of each facies. Then it converts to the seismic lithology volume and the seismic fluid volume.

The oil zone (at the red polygon area) in (Figure 13) also shows the same consistency as the other elastic attributes. Indicating that OWC can be justified using this interpretation. The slice results in the 30-1 reservoir zone show that the lithology of sand and shale can be mapped easily, especially with carbonaceous shale-coal in the Yayuk-01 and Susana-01 wells, which cannot distinguish on the AI map and amplitude attribute map. This result is consistent with what (Harmoni, et al., 1996) study done. VpVs ratio map and the Lambda-Mu (LM) map, near the area of that well (Susana-01 and Yayuk-01), also have high VpVs and LM values.

Spectral Decomposition

Spectral decomposition provides a novel means of utilizing seismic data for mapping temporal bed thickness, imaging, and geologic discontinuities over larges 3D seismic surveys. (Partyka, et al., 1999). He introduces spectral decomposition to the industry at large. Oil and gas reservoirs can cause anomalies in the energy and frequency of seismic signals. Strong amplitude anomalies at specifics frequencies have been found easily by using spectral decomposition.

In this study, CWT (Continuous Wavelet Transform) has been applied to the 3D full-stack seismic data to understand the character of a reservoir compared to conventional seismic data. After decomposing the 3D seismic data, several frequencies were gathered from 10-90Hz. 30-1 reservoir images can be identifying starting at 33 Hz frequencies. This CWT seismic data shows good images identifying the hydrocarbon anomalies indicated by

the red circle polygon compared to the legacy seismic data (Figure 14). The bright amplitude anomaly response in the INTA-01 well was not visible in the Yayuk-01 and Susana-01 wells. Both wells have no reservoir and hydrocarbon because its carbonaceous shale (yellow circle) (Figure 14).

Animation through discrete spectral decomposition images helped interpreters understand the stratigraphic setup of this potential reservoir. One of the most common color image techniques is to plot three discrete frequencies against red, green, and blue (RGB) (Chopra & Marfurt, 2005). In this study, three partial stack data at near-mid-far and three spectral components 41 Hz, 56 Hz, and 70 Hz against RGB are plotted (Figure 15). Hydrocarbon anomalies can be seen clearly by applying this RGB blending method from these two data sets. Red color anomalies at near-mid-far, indicating strong amplitude response/AVO anomaly at far offset data. For CWT images, cyan color (high frequency) interpreted to levee complexes. While magenta and yellow indicating the thickest channels and dark colors indicating low reflectivity.

Result and Discussion

Seismic repro data can provide better results than the legacy data, especially in 30-1 reservoir slicing amplitude. The reflector continuity looks acceptable, and the amplitude, frequency, and phase are maintained in preserved condition. There is no issue about multiple and reverberation again since it can be eliminated very well using predictive Tau-Pi deconvolution and radon demultiple. Regularization and interpolation also helpful to fill up the empty trace and set the best full fold coverage.

The AVO analysis on the angle stack data shows that the amplitude value from near to far data is getting bright with the increasing offset. This anomaly also can be seen in the PSTM gather, near the INTA-01 well, which shows the AVO curve, indicates the hydrocarbon presence. While near Yayuk-01 and Susana-01 show flat responses, indicating the absence of hydrocarbon.

Feasibility cross plot results from rock physics analysis show that the sandstone reservoir can be separated very well, especially on Vp/Vs and LR-MR data. Another method tested by using Poisson Impedance since it is difficult to distinguish between AI and SI values in a cross plot. Correlation results between Lithology Impedance (Vclay) and Fluid Impedance (Sw) look favorable.

Lithology and fluid classification using the Bayessian method applied to LR-MR data from the seismic prestack inversion. It gives tremendous results, detecting lithology and hydrocarbon fluid presence. This method successfully identified the ambiguity between lithology sand and carbonaceous shale, also the HC content. The oil sand area has consistent trends compared to other methods.

Apart from the amplitude side, the frequency side of the data was also analyze using spectral decomposition. The oil sand area has an amplitude magnitude that looks brighter. Finally, the RGB blend was tested using three data sets (near-mid-far) and spectral decomposition data sets (41-56-70Hz). The RGB blend looks perspicuously, and when integrated with other methods, it will strengthen the presence of hydrocarbons and lithologies.

Conclusions

With the evolution of the computer technology era and sophisticated seismic processing techniques, hydrocarbon fluids identification and the quantification approach can be easier to execute. 3D seismic reprocessing data is an absolute prerequisite that is currently needed. Qualitatively and quantitatively, these new seismic data look better compared to the previous data. The proposed workflow can simplify the interpretation, better understand the reservoir character, and reduce uncertainty risks by integrating practical techniques.

Several attributes like seismic partial/angle stack, Intercept-Gradient AVO, Fluid Factor, Lambda-Rho Mu-Rho, lithology impedance, litho-fluid detection, seismic facies, and spectral decomposition tested on a 30-1 reservoir. It exhibited tremendous results detecting the presence of hydrocarbons in the Intan field. The OWC of this reservoir can be determined and clearly by integrating the results of this study. It will make a greats impact as an input of the static model in the future step process.

Several types of opportunities were obtained within this seismic QI feasibility study, as follow:

1. Improve communication within the working team, management, or another stakeholder about deliverability and expectations. It could reduce failure chances because of miscommunication and or different expectations between the stakeholders.
2. Provide alternative scenarios or multiple possible solutions to anticipate changes because of the current data, information, technique boundaries to maintain the project completed promptly.
3. Provide credibility because whatever we are doing is systematic, non-random, measurable, and repeatable.

Acknowledgements

We would like to thank Pertamina Hulu Energi OSES and SKK Migas for providing permission and the proprietary data information for this study, Asri Basin working team was instrumental in defining the path of our research, also for Advisors in Pertamina for guidance through each stage of the process. We would also very grateful to acknowledge the Pusat Studi Energi UGM for providing the new reprocessing seismic data and for inspiring our interest in the development of innovative technologies.

References

Aldrich, J.B., Rinehart, G.P., Susandhi, R., Schuepbach, M.A., 1995. Paleogene Basin Architecture of the Sunda and Asri Basins, and Associated Non-Marine Sequence Stratigraphy, Proceedings, International Symposium on Sequence Stratigraphy in SE Asia, p. 261-287.

Avseth, P., Mukerji, T., Mavko, G., 2005. Quantitative Seismic Interpretation: Applying Rock Physics Tools to Reduce Interpretation Risk. Cambridge Univ. Press.

Barnes, A.E., 2016. Handbook of Poststack Seismic Attributes. SEG Library. Geophysical References Volume **21**.

Buland, A., Omre, H., 2003. Bayesian linearized AVO inversion. Geophysics **68**, 185–198.

PROCEEDINGS
JOINT CONVENTION BANDUNG (JCB) 2021
November 23rd – 25th 2021

Castagna, J.P., Swan, H.W., 1997. Principles of AVO crossplotting. Lead. Edge **16**, 337–344.

Chopra, S., Marfurt, K.J., 2005. Seismic attributes-A historical perspective. Geophysics **70**, 3SO-28SO.

Connolly, P., 1999. Elastic impedance. Lead. Edge 18, 438–452.

Direzza, A., Permana, I., 2012. The Application of Poisson Impedance Inversion for Sandstone Reservoir Characterization in the Lower Talang Akar Formation, Case Study Melandong-West Java. AAPG International Comference & Exhibition.

Fatti, J.L., Smith, G.C., Vail, P.J., Strauss, P.J., Levitt, P.R., 1994. Detection of gas in sandstone reservoirs using AVO analysis: a 3-D seismic case history using the Geostack technique. Geophysics **59**, 1362–1376.

Goodway, B., Chen, T., Downton, J., 1997. Improved AVO fluid detection and lithology discrimination using Lamé petrophysical parameters; "λρ", "μρ", & "λ/μ fluid stack", from P and S inversions, in: SEG Technical Program Expanded Abstracts 1997. Society of Exploration Geophysicists, pp. 183–186.

Gray, D., Andersen, E., 2000, Application of AVO and inversion to formation properties: World Oil, **221**, July, 85-90.

Harmony, W. E., Gilmore, H.L., Armon, J.W., Smith, S. W., Danahey, L., Himawan, R., Bowman, T. L., Smith, W., 1996. An example of 3-D AVO for lithology discrimination in Widuri Field, Asri Basin, Indonesia. The Leading Edge. SEG Library.

Hilterman, F.J., 2001. Seismic amplitude interpretation. (Society of Exploration Geophysicists and European Association of Geoscientists and Engineers).

Lindseth, R.O., 1979. Synthetic sonic logs—a process for stratigraphic interpretation. Geophysics **44**, 3–26.

Ma, X.-Q., 2001. Global joint inversion for the estimation of acoustic and shear impedances from AVO derived P- and S-wave reflectivity data. First Break **19**, 557–566.

Ostrander, Wj, 1984. Plane-wave reflection coefficients for gas sands at non-normal angles of incidence. Geophysics 49, 1637–1648.

Partyka, G., Gridley, J. and Lopez, J. (1999) Interpretational Applications of Spectral Decomposition in Reservoir Characterization. The Leading Edge, **18**, 353-360

Rutherford, S.R., Williams, R.H., 1989. Amplitude-versus-offset variations in gas sands. Geophysics **54**, 680–688.

Sheriff, R.E., Geldart, L.P., Telford, W.M., 1992. Applied Geophysics Second Edition. Cambridge university press.

Shuey, R.T., 1985. A Simplification of the Zoeppritz equations. Geophysics **50**, 609–614.

Smith, G.C., Gidlow, P.M., 1987. Weighted stacking for rock property estimation and detection of gas. Geophys. Prospect. **35**, 993–1014.

Sukanto, J., Nunuk, F., Aldrich, J. B., Rinehart, G. P., Mitchell, J., 1998. Petroleum System of The Asri Basin Java Sea Indonesia. Proceeding IPA 26th Annual Convention.

Whitcombe, D.N., Connolly, P.A., Reagan, R.L., Redshaw, T.C., 2002. Extended elastic impedance for fluid and lithology prediction. Geophysics **67**, 63–67.

Wight, A., Friestad H., Anderson, I., Wicaksono, P., Reminton, C.H., 1997. Exploration history of the offshore Southeast Sumatra PSC, Java Sea, Indonesia. Geological Society, London, Special Publications, **126**, 121-142.

Young, R., Atkinson, C.D., 1993. A Review of Talang Akar Formation (Oligo-Miocene) Reservoirs in the Offshore Areas of Southeast Sumatra and Northwest Java, in Clastic Core Workshop, Special Publication of the IPA.,pp. 177-210.

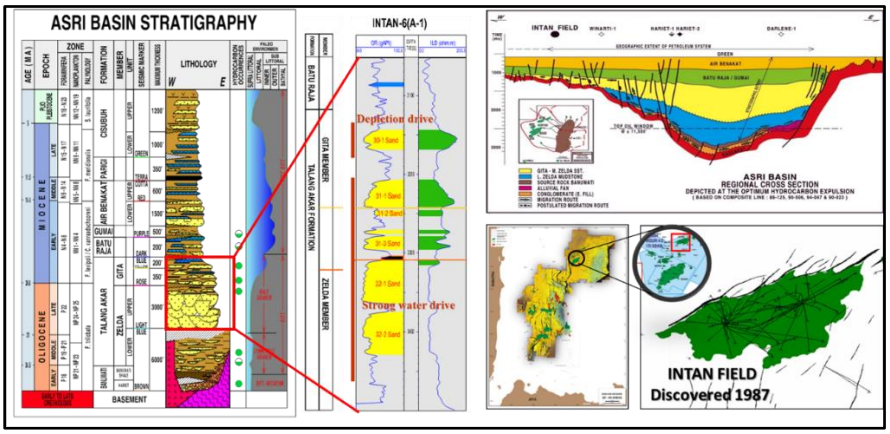

Figure 01. Asri Basin stratigraphy, log type and regional cross section

No	LEGACY DATA (1991)	No	REPROCESSING (2020)
1	Reformat	1	Reformat Field Data to internal format
2	Anti Aliasing Filter	2	3D Geometry & navigation (Bin Size 12.5M x 12.5M)
3	Resample 2ms	3	Designature Minimum Phase
4	Dephasing Filter	4	Gun & Cable Static Correction
5	Spherical Divergence	5	Low cut filter apply
6	Surface Consistent Deconvolution	6	Bad Trace or denoising
7	CMP Gather	7	Swell Noise Removal & Coherence noise removal
8	Veocity Analysis Every 1km	8	Direct Arrival Noise Removal & Linear Noise removal
9	Static Binning 6.25m x 25m	9	Spherical divergence correction
10	Dip Move Out (DMO) Finite Difference	10	Regional velocity analysis every 1km
11	Velocity Analyses Every 0.5km	11	3D SRME or Shallow water demultiple
12	Flexible Binning using 15% bin overlap	12	Shot and cable compensation
13	Normal Move Out (NMO) mute	13	Tau-P Deconvolution
14	Multigate Scaling	14	Denoising
15	Partial Stack	15	1st velocity analysis every 500m X 500m
16	Final Stack	16	High Resolution Radon Demultiple
17	Adjacent Trace Sum in ILINE Direction	17	Residual Noise Attenuation
18	5 Trace Lateral Normalization	18	Regularization & 5D Interpolation
19	Trace Interpolation in XLINE Direction	19	Footprint removal
20	One Pass Migration Based on Finite Diference	20	Residual Shallow water demultiple (if Required)
21	Band Pass Filter	21	3D PSTM for velocity analysis Every 250m X 250m
22	Dynamic Trace Equalization AGC	22	3D Full Kirchhoff PSTM
23	Film Display	23	Final Velocity Picking Every 250m X 250m
		24	High Resolution Radon Demultiple
		25	Output PSTM Gather in SEGY Format
		26	Normal moveout correction (NMO) and Mute
		27	Output Raw PSTM Stack in SEGY Format
		28	Zero Phase Conversion
		29	Random Noise Attenuation
		30	Time variant filter & Time Variant Scaling
		31	Output Filtered & Scaling PSTM Stack in SEGY
		32	SEG-Y Angle Stack (Near, Mid and Far Angle Stack)
		33	Output PSTM Velocity

Table 01. Legacy Data (1991 processing) and New Processing Flow (2020)

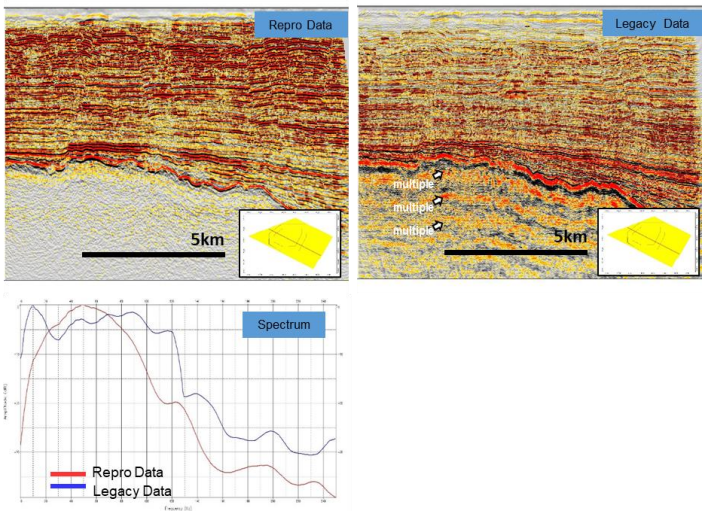

Figure 02. New reprocessing data (left) compared to legacy seismic 1991 data (right). Looks like the S/N ratio improve, less multiple effect, and good continuity reflector at several even. Spectrum from the repro data looks more stable, there is no low and high frequencies noise at this final data stack.

PROCEEDINGS
JOINT CONVENTION BANDUNG (JCB) 2021
November 23rd – 25th 2021

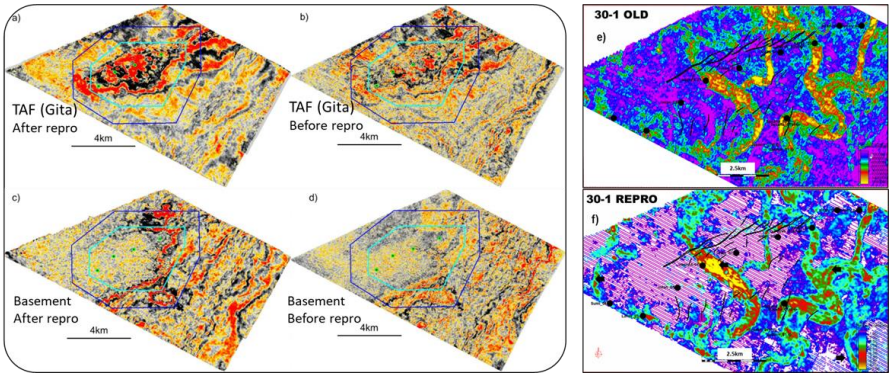

Figure 03. Time slice at 1000ms (near Gita reservoir zone) and at 1200ms (near basement) showing good result and continuity from a) & c) repro data compare to b) & d) legacy seismic data. Horizon slices at 30-1 reservoir showing meandering channel. f) Reprocessing seismic data showing good image result and continuity (black arrows) compared to e) legacy seismic data.

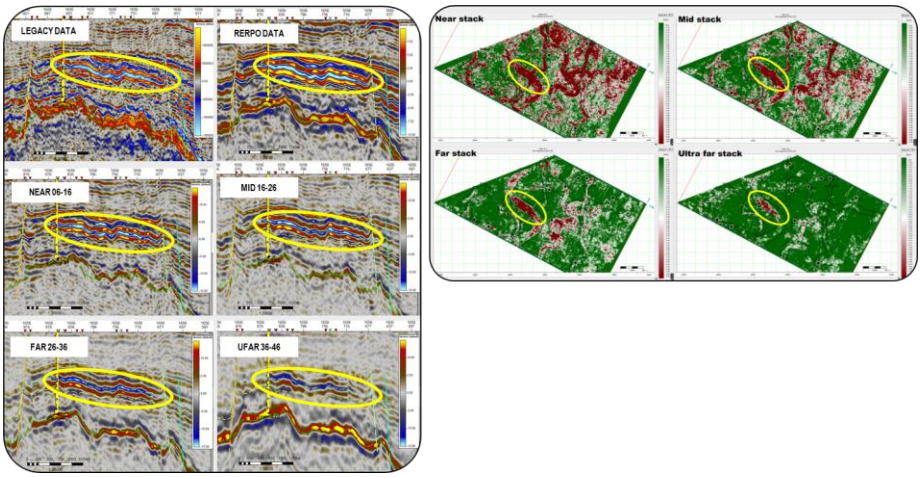

Figure 04. Angle stack data showing the AVO anomaly effect on 30-1 reservoir (yellow circle). The amplitude is getting bright as increasing the angle/offset. Figure 05. Horizon slice on angle stack data showing the AVO anomaly effect on 30-1 reservoir.

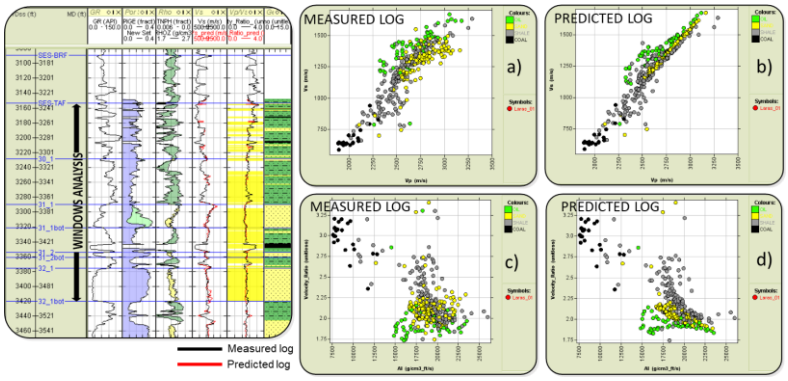

Figure 06. Blind test well on Laras-01 to predict Vs log, predicted log (red curve) qualitatively relative match with the measured log (black curve). Cross plot Vp vs Vs at measured log (a), predicted log (b) and cross plot AI vs VpVs ratio at measured log (c), predicted log (d)

PROCEEDINGS
JOINT CONVENTION BANDUNG (JCB) 2021
November 23rd – 25th 2021

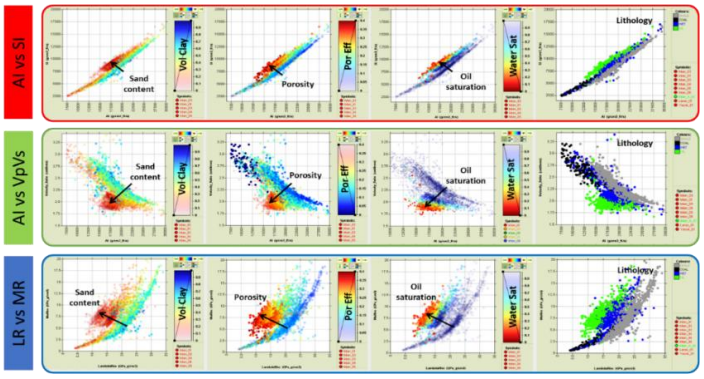

Figure 07. AI vs SI, AI vs VpVs and Lambda-Rho vs Mu-Rho at various color key (Vclay, porosity, lithology, and Sw). From these crossplot analysis, Vp/Vs ratio and LR can distinguish between reservoir and non-reservoir.

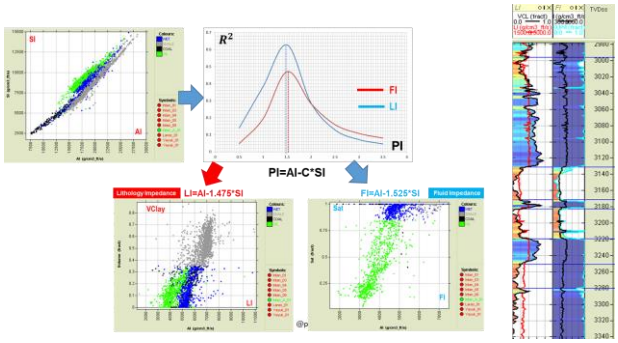

Figure 08. TCCA for Lithology Impedance (corelate with Vclay) and Fluid Impedance (corelate with Sw) at Intan-01 well. The cut off for oil sand is below 5000 ft/s*gr/cc.

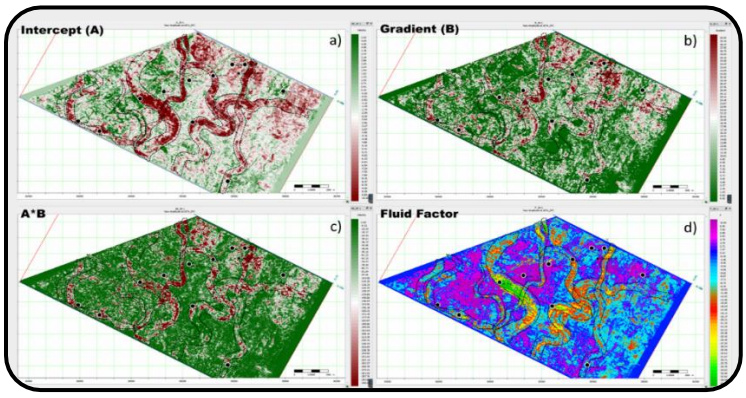

Figure 09. AVO Attribute map a) Intercept (A), b) Gradient (B), c) Product A*B, d) Fluid Factor

PROCEEDINGS
JOINT CONVENTION BANDUNG (JCB) 2021
November 23rd – 25th 2021

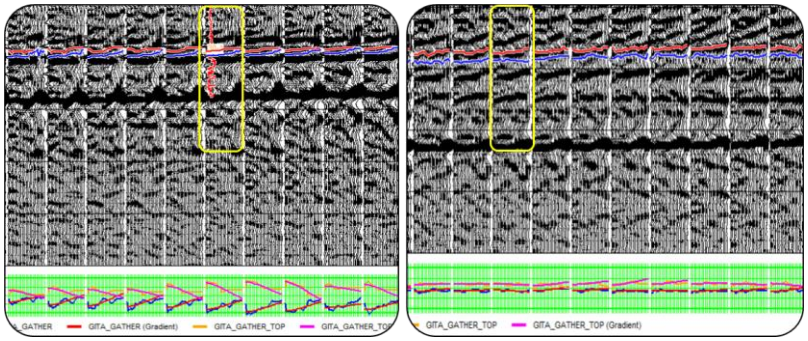

Figure 10. AVO response curve analysis from INTA-01 (left) at 30-1 reservoir showing the anomaly at far offset, while Susana-01 (right) showing flat AVO curve indicating that there is no hydrocarbon at that area.

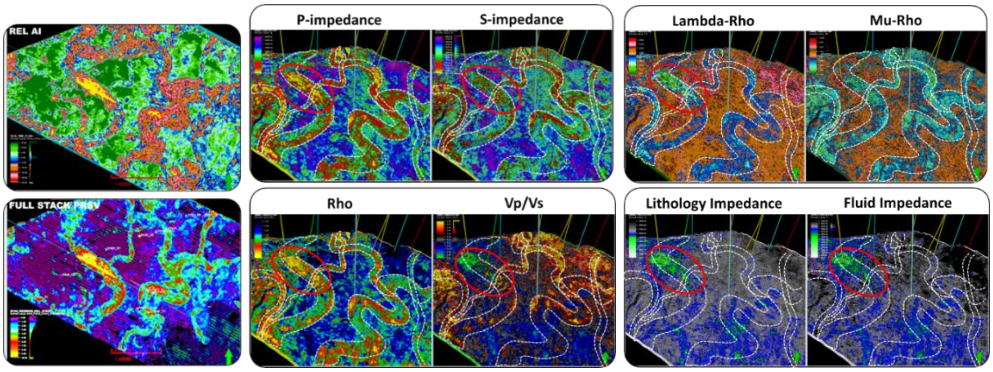

Figure 11. Relative impedance attributes at 30-1 reservoir using low cut frequency 10 Hz compared to original 3D preserve full stack seismic amplitude and Simultaneous Inversion map (AI, SI, Rho, and VpVs Ratio). The hydrocarbon anomaly (red circle) indicated by low value of AI, LR, Vp/Vs, LI, and FI.

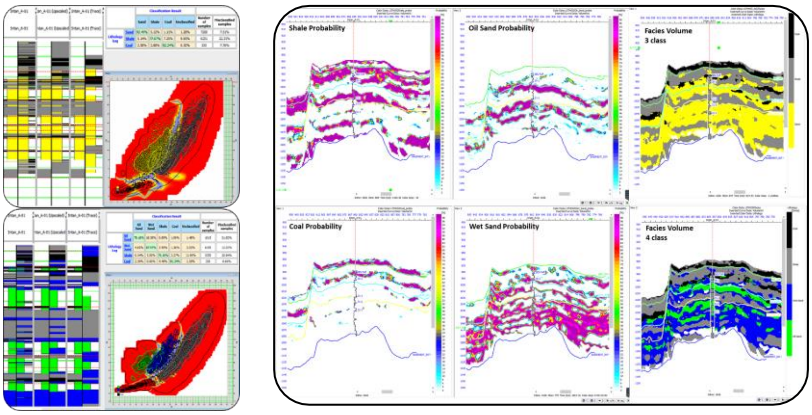

Figure 12. Lithology classification using PDF at 3 classes (Sand, Shale, Coal) and 4 classes (Oil Sand, Wet Sand, Shale, Coal). Probability volume from oil sand, wet sand, coal, and shale based on Bayesian classification.

PROCEEDINGS
JOINT CONVENTION BANDUNG (JCB) 2021
November 23rd – 25th 2021

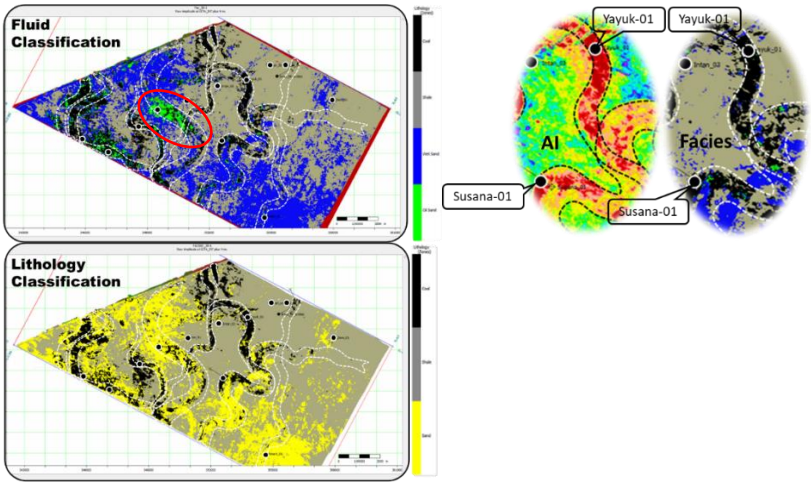

Figure 13. Lithology and Fluid classification map at 30-1 reservoir showing oil sand (green color) accumulated at red ellipse polygon. AI Attribute cannot distinguish between sand and carbonaceous shale, while facies attribute derived from Bayesian classification successfully separate between sand and carbonaceous shale.

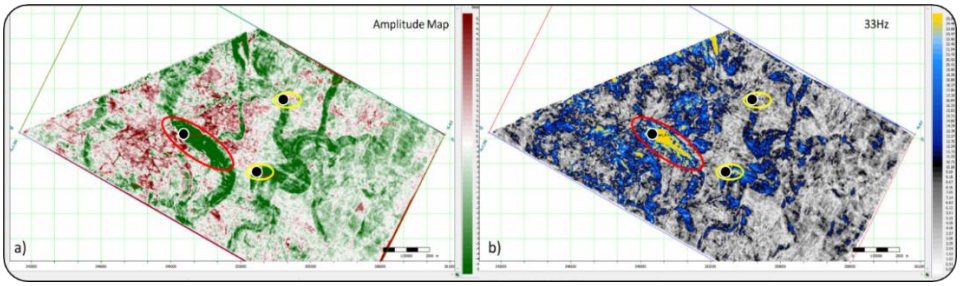

Figure 14. 30-1 CWT attribute map showing high amplitude anomalies (red circle) near INTA-01 well, while the dim amplitude (yellow circle) near the Yayuk-01 and Susana-01 indicating absences of hydrocarbon.

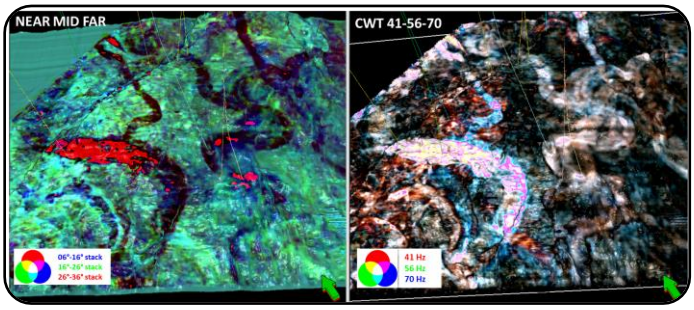

Figure 15. RGB blend at partial stack (left) and CWT map (right) at 30-1 reservoir. Red color anomalies at near-mid-far, indicating strong amplitude response/AVO anomaly at far offset data. For CWT images, cyan color (high frequency) interpreted to levee complexes. While magenta and yellow indicating the thickest channels and dark colors indicating low reflectivity.

PROCEEDINGS
JOINT CONVENTION BANDUNG (JCB) 2021
November 23rd – 25th 2021

Facies and Reservoir Rock Type Analysis of Kujung Unit-I Formation in "Betta" Field, East Java Basin, Indonesia

Asa Fadinda[1], Abdul Haris[2], Agus Guntoro[3]
Department of Reservoir Geophysics, Faculty of Mathematics and Science, Universitas Indonesia[1, 2, 3]

Corresponding Author: Abdul Haris. (Department of Reservoir Geophysics, Faculty of Mathematics and Science, Universitas Indonesia). abdharis@ui.ac.id

Abstract
Kujung Unit-I formation in Betta field is proven to have produced 1.4 – 9.1 MMCFGPD gas which is confirmed to be 100% C1. Where the condition makes kujung Formation Unit I as a secondary target of the reservoir observed. Given the reservoar carbonate rocks are known for their high degree of complexity. So, to understand it requires more detailed attention. Therefore, this study aims to find out the relationship of qualitative analysis (analysis of deposition fasies) and quantitative (reservoir rock type) of carbonate rock reservoirs. Analysis of deposition fasies at research intervals (SB-4 to MFS-4), resulted in fasies associations in the form of interior carbonatreef mound platforms, lagoons/open shelf, barriers (sand shoals – reef shoals), slopes, and deep shelf. The direction of deposition is known to be getting deeper to the Southwest (basinal). Of the three wells, which show the best porosity value of 30-35% are ASA-2 and ASA-3. Then a good permeability value is shown in the ASA-4 well (22 – 32 mD). From the analysis of reservoar rock type (RT) with property value parameters, four groups of rocks produced which are the best (RT-1) showed interconnected pore size (R35) 2.62 – 3.17 µm with flow unit (FZI) 1.7 – 2.7. Then the worst reservoar rock type shows (R35) 0.7 – 0.9 µm (FZI) 0.006 – 0.01. The intervals that produce gas 1.4 – 9.1 MMCFGPD on asa-3 wells are filled by wackstone limestone litofasies – packstones deposited in the open shelf zone, and classified as 4th type rock reservoar (RT-4).

Introduction
Kujung Formation in East Java basin and Ngimbang Formation are oil and gas producing zones that has been proven to produce 9.1 MMCFGPD (limestones in Kujung Unit I), 430 BOPD from Kujung Limestone Unit III, and 16.5 MMCFGPD from the sandstone layers of Ngimbang Formation. Sandstones reservoir at Kujung Formation Unit III is the main target of each drilling of several exploration wells located in field "Betta" while limestone in the Kujung Unit I Formation status is still secondary target. Therefore, it is necessary to conduct further studies related to reservoir characteristics and hydrocarbon potential in the formation. The field "Betta" is located in the East Java Basin, geographically located in the Northern part of Madura Island.
Kujung Formation is the result of stable sea level conditions which support the growth of reefs in the shelf depositional environment, inner to middle neritic. In characterizing reservoirs, carbonate rocks need more detailed attention. Moreover, the lithofacies of carbonate rocks have lots of varieties and are influenced by secondary deformation which will then affect the value of the properties, which are

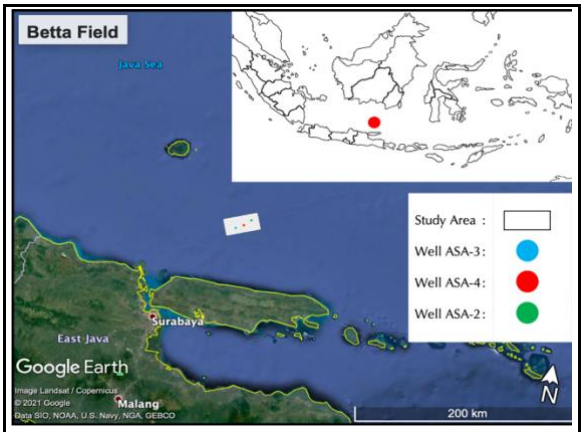

Figure 1. The research location is on the North of Madura Island, part of East Java Basin. This research is supported by three exploration wells (colored points).

porosity and permeability. Based on the value of property measurements on core samples that are often used as a reference, sometimes it still causes errors in the modeling results and actual circumstances. Therefore, it requires a method that can connect between qualitative analysis (depositional facies) and quantitative (property values). This study was conducted by utilizing several data, including three well data along with wireline log, routine core analysis (RCAL), geology final drilling report, biostratigraphy, core, and sidewall core description. All the data are combined to analyze the characterization of reservoir on petrel software.

Data and Method
In characterizing the reservoir, the researchers will combine two methods of analyses, which are qualitative analysis used to interpret the depositional facies of a reservoir and quantitative analysis used for grouping the reservoir property values. The first step that must be done before entering into qualitative and quantitative analysis is to do quality control of the data, as previously mentioned above. After data control stage is completed, it will then be analyzed to create a new project on Petrel software. Furthermore, the determination of marker horizon based on sequence stratigraphy method to divide the zone by the depositional events that has the same age, or usually being named as parasequences. In determining the parasequences, the researchers utilize the rule of electrofacies based on log type. After that, the process is continued by determining the depositional environment of these zones with biostratigraphy data, core and lithology description as the references.
The quantitative analysis divides reservoir groups based on the value of its properties (reservoir rock typing). Reservoir

PROCEEDINGS
JOINT CONVENTION BANDUNG (JCB) 2021
November 23rd – 25th 2021

properties are obtained from RCAL data either sidewall core or conventional core. In this study, the reservoir rock typing that will be applied is by using the R35 Windland method (1972) and also the hydraulic flow unit (HFU) method by Amaefule *et al.* (1993).

It can be explained that Windland (R35) method is to divide the group of reservoir rocks based on the similarity of pore-throat size (in μ) which forms a curve of 35th percentile on mercury intrusion capillary pressure (MICP) on the permeability (*k*) in md vs porosity (φ) in cm^3/cm^3 plot with the following equations:

$$\log(r_{35}) = 0.732 + 0.588\log(k) - 0.864\log(100\phi) \quad (1)$$

Then, Amaefule (1993) describes the equation for reservoir rock typing based on hydraulic flow unit (HFU) method that can expressed by those equations below:

$$\text{RQI} = 0.0314\sqrt{\frac{k}{\phi}} \quad (2)$$

$$\text{PMR} = \phi_z = \frac{\phi}{1-\phi} \quad (3)$$

$$\text{FZI} = RQI/PMR \quad (4)$$

RQI is a reservoir quality index, whereas PMR is matrix pore ratio or commonly referred to normalized porosity index. (*k* in md and φ in cm^3/cm^3). The reservoir rock typing is determined based on the plot on a chart between the RQI vs PMR value, where the plot point that is within one straight slope line are group that have the same hydraulic unit value and rock type. Each hydraulic unit is represented with a unique value of FZI (flow zone unit).

Result and Discussion

Facies and Depositional Environment

The information obtained from the sidewall core report describes ASA-3 wells (Figure 2) where there are variations of lithofacies: packstone, wackstone, mudstone (Dunham classification, 1962), and shale that form a relative pattern fining upwards. As seen in Figure 2 the intervals of 4,350ft - 3,920ft is dominated by shale with thin interbeds of light brown limestones (wackstone, mudstone, and a few packstones at the bottom). After that the interval of 3100 – 3920 ft is dominated by limestones and characterized as blocky pattern where the packstone is at the bottom of the interval and the texture fining increasingly upwards (wackstone and mudstone). The iteration occurred at intervals of 2970 – 3100 ft but with finning upward pattern. After identifying lithofacies based on drilling report data, the information can be led to interpret its deposition environment where it refers to facies associations. Four depositional environment zones were obtained in the study areas which were developed based on description data, fossil analysis of sidewall cores and interpretation processes. Depositional environment in this study area are lagoon and open shelf. Kujung Unit-I formation is deposited in shallow marine deposition environment where the result of sedimentation is very typical due to the influence of eustasy.

Stratigraphy

Stratigraphic correlations connecting between the three wells in the field "Betta" using the principle of sequence stratigraphy method, the markers are determined based on the presence of visible shale and vertical changes in succession of lithofacies in the well data. The area were divided into several 13 parasequence zones based on marker flooding surface boundary (Van Wagoner *et al., 1988)* in this area. In correlation with the three wells (Figure 3), it can be understood that the results of interpretation showed a difference in facies succession at the top of the sequence body. The ASA-3 to ASA-4 well is in the open shelf environment that filled by clastic carbonate, while the closer the NE (ASA-2 well) approaches lagoon zone, which is supported by the presence of thicker shale and depletion of limestones lithofacies.

Rock type identification

In this study, rock typing analysis was conducted using two different methods, Windland method (1972) and hydraulic flow unit method by Amaefule (1993). In determining the classification of rock type using Windland method (R35), done by plotting the value of R35 from 23 data spread from Kujung Unit-I to Kujung Unitt-III Formation based on the order from the smallest to the largest (Figure 4.a). Based on the information, it was then interpreted that in this study area is divided into four rock types, yellow (RT-4), green (RT-3), blue (RT-2), and orange (RT-1). To prove it, the researchers did a plot to classify the four rock types based on MICP curve (Figure 4.b). of the four iso pore-throat curves that have been identified which are 0.5 μm, 0.9 μm, 1.11 μm, 2. 1 μm.

Classification of rock type using HFU method which determines how many rock types to choose, the first step is the same as rock typing with Windland method which is plotting the FZI calculation value (from RQI divided by PMR value) based on the order from the smallest to the largest of its value, as illustrated in (Figure 5. a). The diagram showed the results of interpretation of four rock types. According to Amaefule, (1993) sample rocks plotted on the diagram RQI vs PMR and its position in a slope line is interpreted as a group that has similar flow units. In this study based on rock typing using HFU method obtained sequences based on the bad to the best are: Yellow (HFU-4), green (HFU-3), blue (HFU-2), and red (HFU-1) (Figure 5.b).

Reservoir characterization

The combination of quantitative and qualitative analysis will provide answers on the quality of reservoir where the parameters are large porosity, permeability, pore throat, FZI, and litofacies. In this study the quality of reservoir was divided into four groups (Figure 4C and Figure 5C) into the following:

Excellent reservoir group (Red) based on pore throat 2.14 m μm dominated by wackstone lithofacies and sandstone mouth bars. Where the property has a range of 17-26% porosity and 14.5-1042 mD permeability. Based on flow unit 1.7-2.7 this group is filled by lithofacies similar to large pore throat, namely wackstone and mouth bar sandstone, with a range of 17-22% porosity and 14.5-1042 mD permeability.

Good reservoir group (Blue) based on pore throat 1.3 – 2 μm dominated by lithofacies packstone, wackstone and sandstone. Where the property has a range of 7-31.6% porosity and 0.1 - 13 mD permeability. Based on flow unit 0.07 – 0.3 this group is filled by lithofacies equal to large

pore throat, namely wackstone and sandstone, with a range of 1.3 – 8.4% porosity and 0.1 - 0.4 mD permeability.

Poor reservoir group (Green) based on pore throat 1μm dominated by lithofacies mudstone, wackstone, packstone, and sandstone. Where the property has a range of 1.3 - 31.3 % porosity and 0.04 – 0.5 mD permeability. Based on the flow unit 0.03 – 0.07 this group is filled by lithofacies equal to the size of pore throat, namely wackstone and sandstone, with a range of 1.4 – 31.6% porosity and 0. 01 - 13 mD permeability.

Very poor reservoir group (Yellow) based on pore throat 0.7 – 0.9 μm dominated by lithofacies mudstone and wackstone. Where the property has a range of 1. 4 – 29.7 % porosity and 0.01 – 0. 2 mD permeability. Based on the flow unit 0.006 – 0.01 this group is filled by lithofacies that are equal to the large pore throat, namely wackstone and sandstone, with a range of 22 - 31. 3% porosity and 0.2 – 0.5 mD permeability.

Conclusions

There are several lithofacies in the research area in Kujung Unit-I: mudstone, wackstone, packstone, and shale, where the vertical succession is dominantly finning upwards and blocky at the top with the environment of deposition lagoon to open shelf, where dominated by eustasy influence. Succession in one sequence where equivalent to Kujung Unit-I formation is at the age of Upper Oligocene to Lower Miocene and has 13 parasequences divided by the period of rising sea level. The target zone on the "Betta" field has four groups of reservoir rock type: excellent reservoir group, good reservoir group, poor reservoir group, and very poor reservoir group.

References

Al-Farisi, O., Elhami, M., Al-Felasi, A., Yammahi, F. and Ghedan, S., 2009, October. Revelation of carbonate rock typing—the resolved gap. In *SPE/EAGE Reservoir Characterization & Simulation Conference* (pp. cp-170). European Association of Geoscientists & Engineers.

Amaefule, J. O., Altunbay, M., Tiab, D. et al. 1993. Enhanced Reservoir Description: Using Core and Log Data To Identify Hydraulic (Flow) Units and Predict Permeability in Uncored Intervals/Wells. Presented at the SPE Annual Technical Conference and Exhibition, Houston, 3–6 October. SPE- 26436-MS. https://doi.org/10.2118/26436-MS.

BPPKA, P., 1996. Petroleum Geology of Indonesia'n Basins: Principle, Methods and Application, IV. 1 East Java Basin. *Pertamina BPPKA, Jakarta, 85pp*.

Dunham, R.l. 1962. "Classification of Carbonate Rocks According to Depositional

Ghanbarian, B., Lake, L.W. and Sahimi, M., 2018. Insights into rock typing: A Critical Study. *SPE Journal*, *24*(01), pp.230-242.

Matthews, S.J. and Bransden, P.J., 1995. Late cretaceous and cenozoic tectono-stratigraphic development of the East Java Sea Basin, Indonesia. *Marine and Petroleum Geology*, *12*(5), pp.499-510.

Nichols, G., 2009. *Sedimentology and stratigraphy*. John Wiley & Sons.

Van Wagoner, J.C., Posamentier, H.W., Mitchum, R.M., Vail, P.R., Sarg, J.F., Loutit, T.S., and Hard- enbol, J. (1988) Ann overview of the fundamen- tals of sequence stratigraphy and key definitions, SEPM Spec. Pub., No. 42, pp 39-46.

Windland, H.D. (1972) Oil Accumulation in Re- sponse to Pore Size Changes, Weyburn Field, Saskatchewan: Amoco Production Research Re- port, No. F72-G-2.

Acknowledgements (Optional)

We acknowledge and thank Universitas Indonesia and PUKES MIGAS for granting us the time to put together this technical paper. In addition, we would like to thank several geoscientist mentors that were involved with the petrophysics, geology, and geophysics interpretations including Abdul Haris, Agus Guntoro, and many more colleagues for helping us to supervise this research.

PROCEEDINGS
JOINT CONVENTION BANDUNG (JCB) 2021
November 23rd – 25th 2021

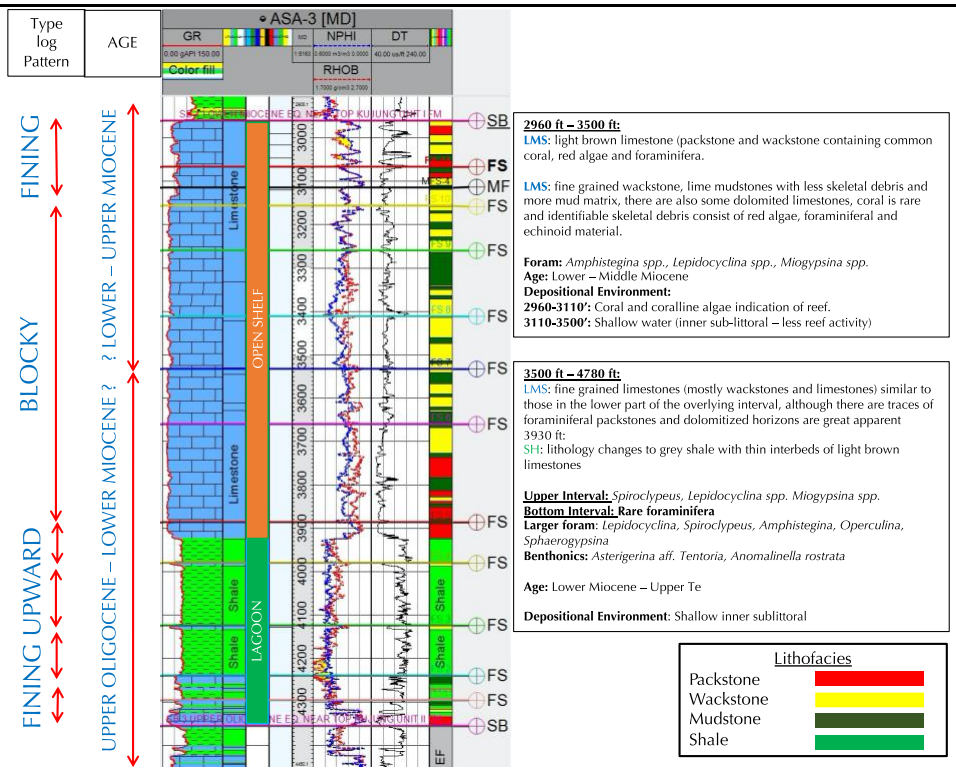

Figure 2. Sedimentary core description of ASA-3 well.

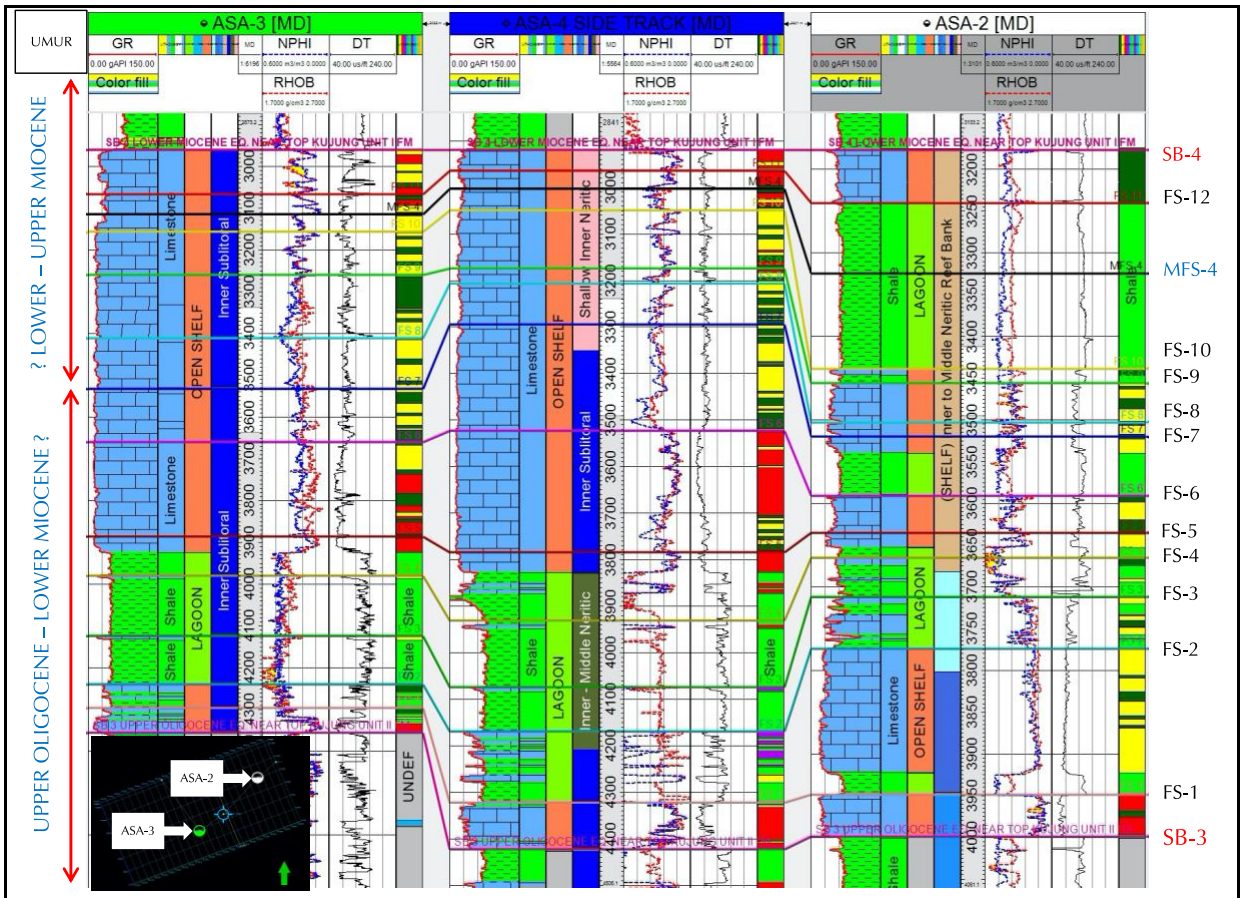

Figure 3. Sequence stratigraphy correlation logs in study area

PROCEEDINGS
JOINT CONVENTION BANDUNG (JCB) 2021
November 23rd – 25th 2021

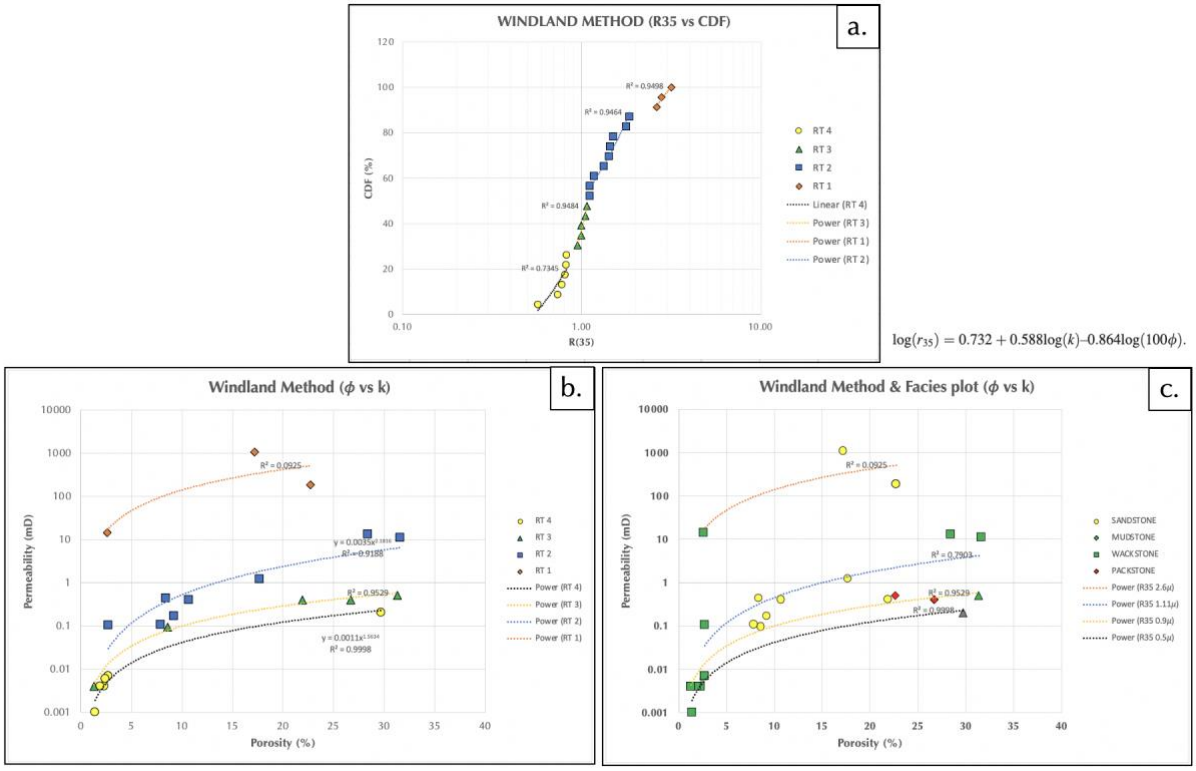

$$\log(r_{35}) = 0.732 + 0.588\log(k) - 0.864\log(100\phi).$$

Figure 4. Rock typing by Windland R-35 method

$$RQI = 0.0314\sqrt{\frac{k}{\emptyset}}$$

$$PMR = \emptyset z = \frac{\emptyset}{(1-\emptyset)}$$

$$FZI = \frac{RQI}{PMR}$$

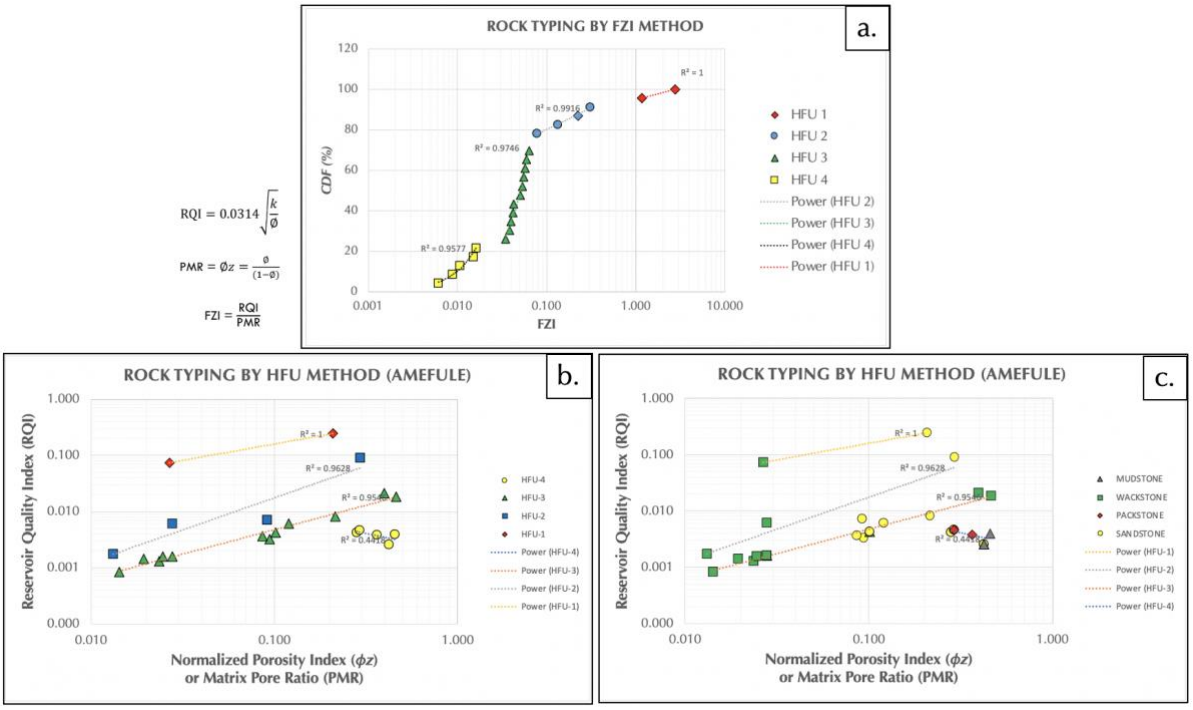

Figure 5. Rock typing by HFU method.

PROCEEDINGS
JOINT CONVENTION BANDUNG (JCB) 2021
November 23rd – 25th 2021

Multi-variate attributes analysis to highlight vsh trend as soft guide into facies modelling

Vania Iqsora Magfirah, Munji Syarif, Hendra Suhendar, Andhy Kurniawan.
Mont D'Or Oil Tungkal Ltd.

Abstract

The following paper presents a simple method in generating volume of shale (VSH) from seismic attributes. Multi-variate statistic methods were used to analyze correlation of seismic attributes and well-log properties to define VSH. VSH is one of rock properties that is considered to have direct link with rock facies. Regression technique was utilized after the establishment function of high correlation between seismic attribute and VSH by using multi-variate analysis was achieved. Intermediate process was introduced by looking up the highest correlation of seismic attributes with other well-log properties (e.g porosity, density, or water saturation) in the case where correlation value of multi-variate matrices is low. This intermediate process should be performed where other rock properties have a high correlation with VSH. Once the intermediate correlation process is established, the seismic attribute – VSH correlation can be properly completed.

In this study case, example of 2 layers-horizon so called direct method (SS-1 & SS-2) and 2 layers- horizon of indirect method (SS-3 & SS-4) is discussed. Result of multivariate analysis from mean envelope relative impedance and RMS relative impedance of the SS-1 and SS-2 zone could correlate directly with VSH, respectively. Whereas, the SS-3 and SS-4 zone indicates direct correlation of RMS relative impedance to NPHI and attribute of mean sweetness corelate to PHIE. Fortunately, these well-log properties of NPHI and PHIE have high correlation with VSH.

In order to established mathematical relationship between rock properties and seismic attributes selected from multivariate analysis, we generate cross plot of each layer and define sensible envelop of the data distribution as an approximation of low – base – high case scenario related to polynomial function which generated later. The proposed method offers fast yet quite robust solution to generate VSH trend as soft-guide into 3D facies modeling whenever data is limited.

Keywords: seismic attributes, multi-variate, volume of shale, seismic facies

Introduction

Seismic attributes are widely used as input to geological model since they could expressing subsurface structure, stratigraphy, and/or rock properties. Analysis of seismic attributes is one of method to find relationship between seismic derived data and rock properties from well log. Since well log can only obtain the rock properties at well location or in vicinity of borehole, the seismic data has become the heart of reservoir characterization both vertically and laterally. However, the wealth of attribute avaibility raises the question what is the meaningful attributes to predict the rock properties? Moreover, in the event of the limited data, the process will be more complicated for the purpose of facies distribution or reservoir delineation.

One of general workflow to find the most related attribute to rock properties is multi-attribute analysis. In this study of the Mengoepeh Field in South Sumatra Basin, our study objectives is to generate volume of shale (VSH) which valuable information for reservoir modeling from seismic data. Since volume of shale has direct representative of the facies distribution or to predict reservoir characteristics, the VSH trend are expected to be helpful guidance in the geological modeling. Using the statistical analysis of multi-variate and cross-plot method, followed by generating polynomial function to predict VSH distribution, we believe that the establishment of seismic attributes to rock properties will be easily achievable.

Mengoepeh Field Overview

The Mengoepeh field is located in the onshore Northern margin of the South Sumatra Basin. The South Sumatra basin was influenced through three major phases, a rifting phase, a sagging phase and lastly a compressional phase. Along with tectonic activities, the South Sumatra basin was also influenced through sea level transgression-regression sequence occurring throughout the tertiary. As a result, the basin contained many different formations; going stratigraphically up, the basement, Lemat, Talang Akar, Batu Raja, Gumai, Muara Enim and Air Benakat Formations (Oldest-Youngest). The main reservoir target within the Mengoepeh field is the Talang Akar formation, which is a fluvial-deltaic deposits during the Late Oligocene-Early Miocene. The formation is composed of interbedded Sandstone, Shale and Coal. The Sandstone is the main reservoir rocks in the formation whereas the shale and coal acts as the source and sealing rocks, respectively (Bishop, 2000). General deposition fairway is coming from Northwest to Southeast of Mengoepeh field. All the stratigraphy and tectonic history in Mengoepeh Field is summarized in **Figure 1**.

PROCEEDINGS
JOINT CONVENTION BANDUNG (JCB) 2021
November 23rd – 25th 2021

In this study, we will discuss four layers or zones in the Talang Akar Formation of the Mengoepeh field. One of the layer is the main oil production reservoir. The other three layers or zones lays above and below this main producing reservoir.

Multi-variate Analysis Method

In the statistical analysis, bivariate analysis is measured by correlation coefficient. This correlation number measures the strength of association between two variables and the direction of the relationship ("Spearman's Rank Correlation Coefficient," 2005). In terms of the strength of relationship, the value of the correlation coefficient (rs) varies between +1 and -1. As the correlation coefficient value goes towards 0, the relationship between the two variables will be weaker. The direction of the relationship is indicated by the sign of the coefficient, namely a+ sign indicates a direct relationship and a- sign indicates an inverse relationship. In the case of more than two variables is measured, the multivariate analysis method is applied.

In this study we used Spearman's correlation to find relation between both seismic attributes and rock properties. Spearman rank correlation is used to measure the degree of association between two variables. The Spearman rank correlation test does not carry any assumptions about the distribution of the data. The following formula is used to calculate the Spearman rank:

$$r_s = 1 - \frac{6\sum D^2}{n(n^2-1)}$$

Correlation:
Rs = Spearman rank correlation
D = the diff. between the ranks of corresponding variables
N = number of observation

Seven set of seismic attributes derived from the 3D post stack seismic data and eight set of petrophysical parameter from well log were analyzed (**Table-1**) using Spearman's correlation to form multivariate matrices. The petrophysical parameters used are derived from 30 wells data with consistent logs. In this case, volume of Shale (VSH) is the main properties to be derived from this analysis. In order to determine which attributes were most related to rock properties. This statistical analysis was applied to 4-zones in the Mengoepeh field. These zones are SS-1, SS-2, SS-3,and SS-4 zone.

Higher correlation number (negative or positive) to VSH in the multivariate matrices means that properties can be pick directly as qualified candidate to cross plot as function of VSH. In this study we were using color bar scale from -1 (white) to +1 (dark blue) to visualize the multivariate correlation matrix.

In the event of the low correlation value to VSH is found or no dominant higher correlation to VSH, the direct establishment of attribute-shale volume relation could not be established. Hence, intermediate process was introduced by looking up the highest correlation coefficient from other rock properties rather than VSH. However, this so-called intermediate property should also have high correlation coefficient number with VSH. Then, the attribute-shale volume correlation can be properly established. We called this indirect approach.

Result and Discussion

In this section we will discuss the multi-variate method using Spearman equation result which reveals that mean envelope relative impedance, relative impedance, and mean sweetness observed to be the most reliable attributes to predict shale volume trend. Based on multivariate matrices result, those set attributes could correlate directly and indirectly to shale volume. Example of direct method is showing from good correlation which found in both the SS-1 and SS-2 zone (**Figure 2a and 3a**). In these zones, the seismic attribute can be directly related to VSH. However, notice from **Figure 3a** there are two candidate that have corelates directly to VSH. In the case having more properties that have relatively high correlation number, we can choose all the properties or we may choose one over the other. In this example we prefer to choose RMS relative impedance to be the nominator as an attribute estimator. In contrast, the low correlation in directly was found in the SS-3 and SS-4 zone that might affected by the tuning thickness (**Figure 4 and 6**). Hence, intermediate process was applied for both zones.

In SS-1 zone, multi-variate method show that mean envelope relative impedance is the most related seismic attributes to VSH (**Figure 2a**).We then cross-plot both properties to established the envelope of relative impedance - VSH distribution. Three set polynomial function is generated to define low-base-high case approximation to predict VSH distribution as shown in **Figure 2b**.

Multi-variate analysis for SS-2 zone observed that RMS relative impedance correlate directly with VSH (**Figure 3a**). We then cross plot both properties to established the envelope of RMS relative impedance to VSH distribution. Three set polynomial function is generated to define low-base-high case approximation to predict VSH distribution as shown in **Figure-3b**.

Another layer, SS-3 zone, shows low correlation between seismic attributes and VSH. In this case, the result suggested that RMS relative impedance is the most related attributes to the NPHI which have high correlation to VSH (**Figure 4**). Therefore, RMS relative impedance was intermediately bridge by NPHI. We then cross plot both properties to

established the distribution envelope from RMS to NPHI and envelope of NPHI to VSH distribution. The distribution envelop from each cross plot is define by three set polynomial function respectively as low-base-high case approximation to predict VSH distribution as shown in **Figure-5**.

Intermediate process was also applied in the SS-4 zone. Multi-variate analysis observed that set of attributes have poor correlation with VSH. The mean sweetness attribute is the most attribute that have a good positive corelation to PHIE directly, which can be bridge to define VSH as intermediate properties (**Figure 6**). Again, we cross plot both properties to established the distribution envelope from mean sweetness attribute to PHIE and the envelope of PHIE to VSH distribution. The distribution envelop from each cross plot is define by three set polynomial function respectively as low-base-high case approximation to predict VSH distribution as shown in **Figure-7**.

The lateral distribution of shale volume are illustrate through the attributes map result which were generated using the established polynomial function from each zone. The shale volume trend map of each zones can be seen in **Figures 8-11**. In our case, the VSH trend is aligned with our depositional model where channel is generally deposited in the NW-SE direction through the area of study, as indicated by VSH trend map. Higher values in VSH map are showing more shaly facies compare to the lower value of VSH which indicates more sandy facies. However, the envelop from those figures indicate that we have wide range of uncertainties in predicting VSH quantitatively. Therefore, the establishment of VSH attributes in this case is to provide soft guidance for facies modeling from seismic data. Even though we can also generate the low and high case VSH distribution using outer band of the define envelope from the cross plot.

In modelling, conditioning facies to seismic can be done within facies modelling algorithms (e.g SIS (Sequential Indicator Simulation), Object-based Method, Multi Point Statistic). However, condition to seismic is very dependent on establishing a robust relationship between a property to be modelled and the seismic parameter. Moreover, the proportion of a facies type within a zone may vary laterally between wells, and/or vertically within a zone as an upward increase or decrease in proportions. Therefore, seismic attributes may represent important guidelines in evaluating such relations. The attribute map generated can be applied into facies modeling process to establish horizontal probability trend of facies proportion.

Conclusions

The applied multivariate method on the multi seismic attributes analysis appears as a simple yet reliable method in delineating shale volume trend. The proposed methods followed by crossplotting and defining distribution envelop zone has been proved in providing VSH trend as desired output. This technique offers a novel and robust solution to generate shale volume trend as soft-guide into 3D facies modeling whenever data is limited.

References

Bishop, M.G., 2000, South Sumatra Basin Province, Indonesia; The Lahat/Talang Akar Cenozoic total petroleum system. Open-File Report 99-50-S.

Spearman's rank correlation coefficient. (2005, December 29). In Wikipedia. https://en.wikipedia.org/wiki/Spearman's_rank_correlation_coefficient

Acknowledgements

The authors thank the Management of Mont D'Or Oil Tungkal Ltd. for granting permission to publish this work. Special thank to subsurface team for their support and critical review of the manuscript.

PROCEEDINGS
JOINT CONVENTION BANDUNG (JCB) 2021
November 23rd – 25th 2021

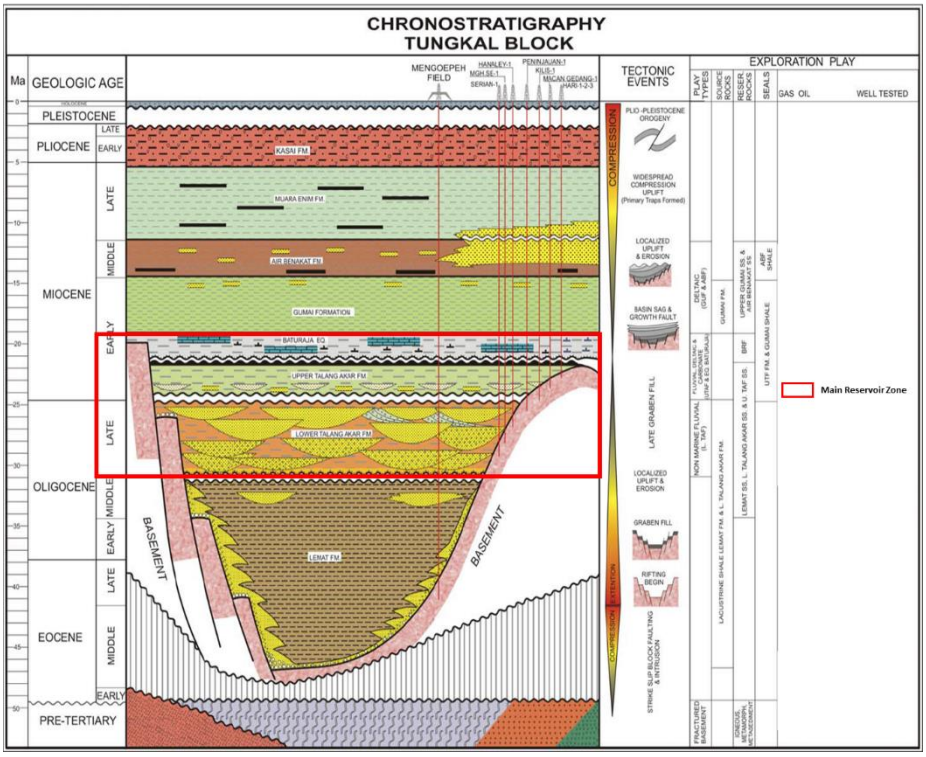

Figure 1 Chronostratigraphy of Mengoepeh Field

Simplify Workflow	Input Data	Expected Result
Quantitative Analysis	**Set of Seismic Attributes** - RMS Relative Impedance - Meane Impedance - RMSE Amplitude - Mean Envelope Average - Mean Sweetness Amplitude - Mean Bandwidth - Mean VpVs **Set of Petrophysical Parameters** - GR - LLS - RHOB - NPHI - VSH - PHIE - LLD - SW	• Understand relationship of set attributes to petrophysical parameters • Established relationship between seismic attribute to facies related petrophysics parameter i.e. VSH • Generate seismic facies maps distribution for each zone

Table 1 List of seismis attributes and petrophysical parameter

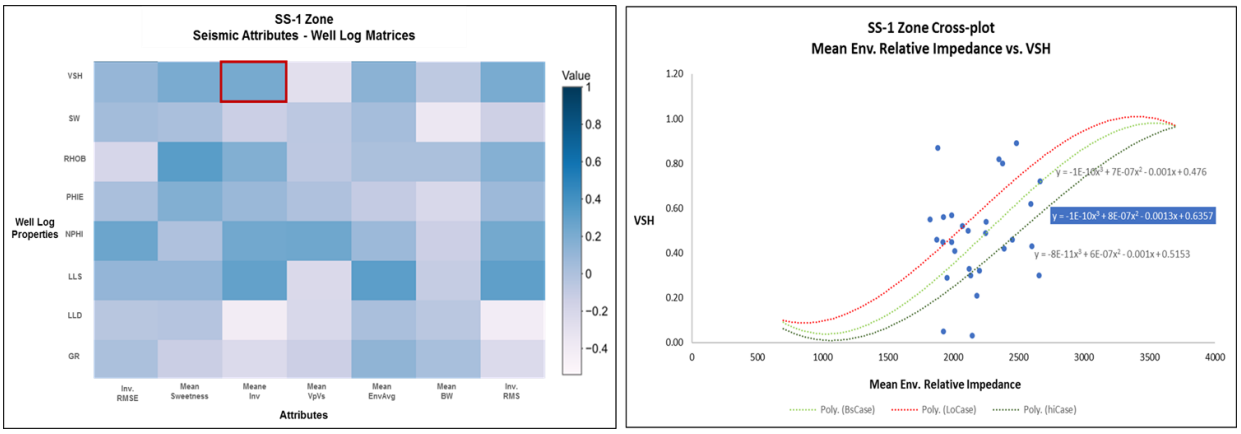

Figure 2 a) Multi-variate analysis result of SS-1 zone; b) Cross-plot of mean envelope relative impedance against VSH

PROCEEDINGS
JOINT CONVENTION BANDUNG (JCB) 2021
November 23rd – 25th 2021

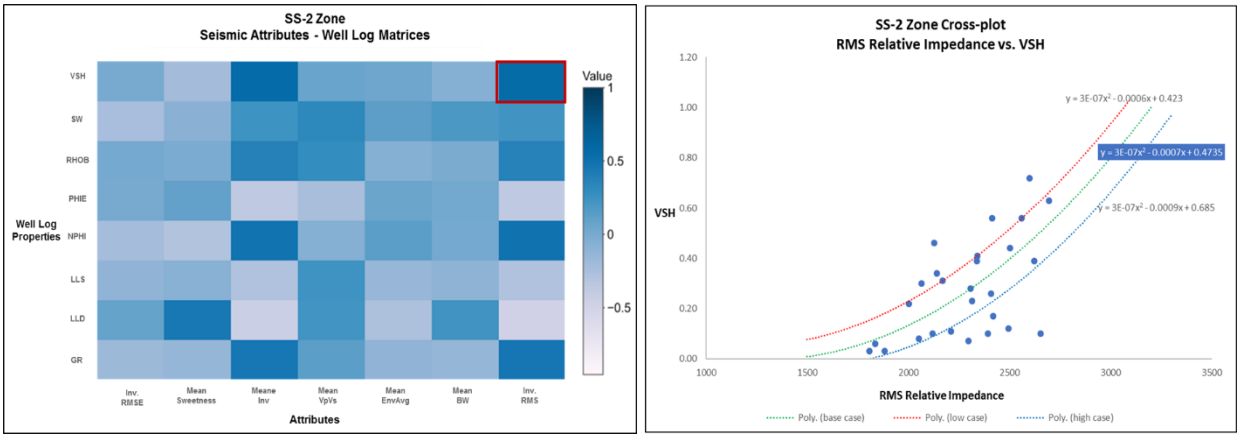

Figure 3 a) Multi-variate analysis result of SS-2 zone; b) Cross-plot of RMS relative impedance against VSH

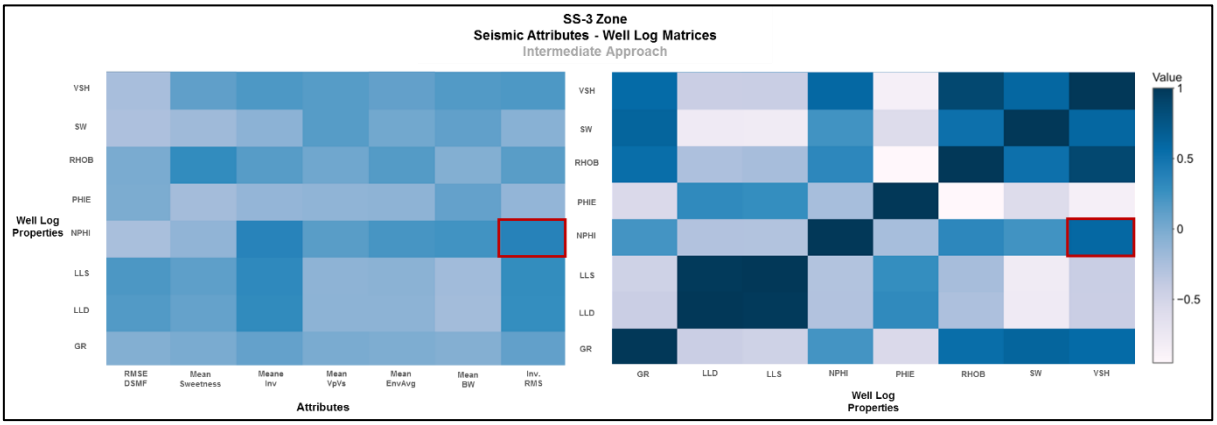

Figure 4 Multi-variate analysis result of SS-3 zone

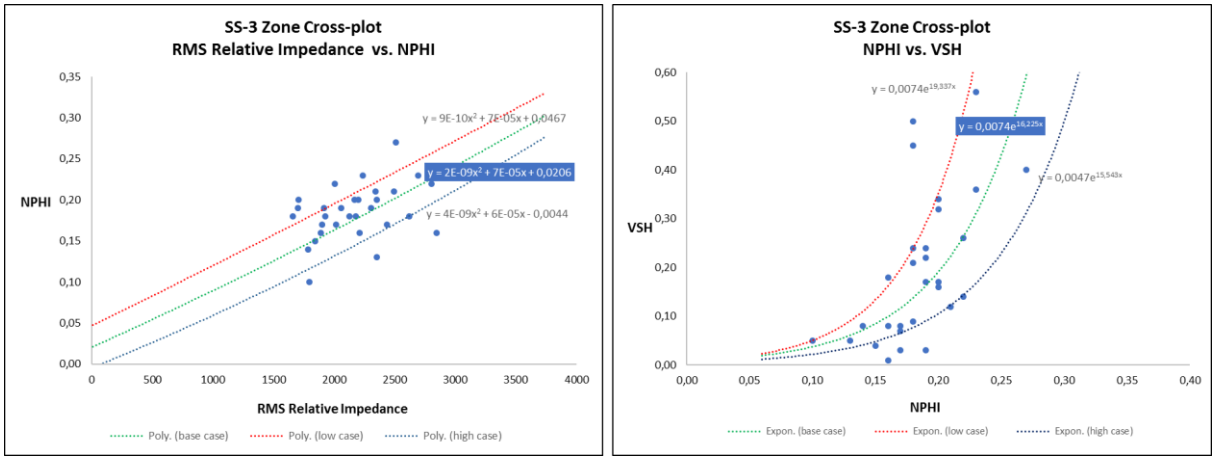

Figure 5 a) Cross-plot of RMS relative impedance to NPHI; b) Cross-plot of NPHI to VSH

PROCEEDINGS
JOINT CONVENTION BANDUNG (JCB) 2021
November 23rd – 25th 2021

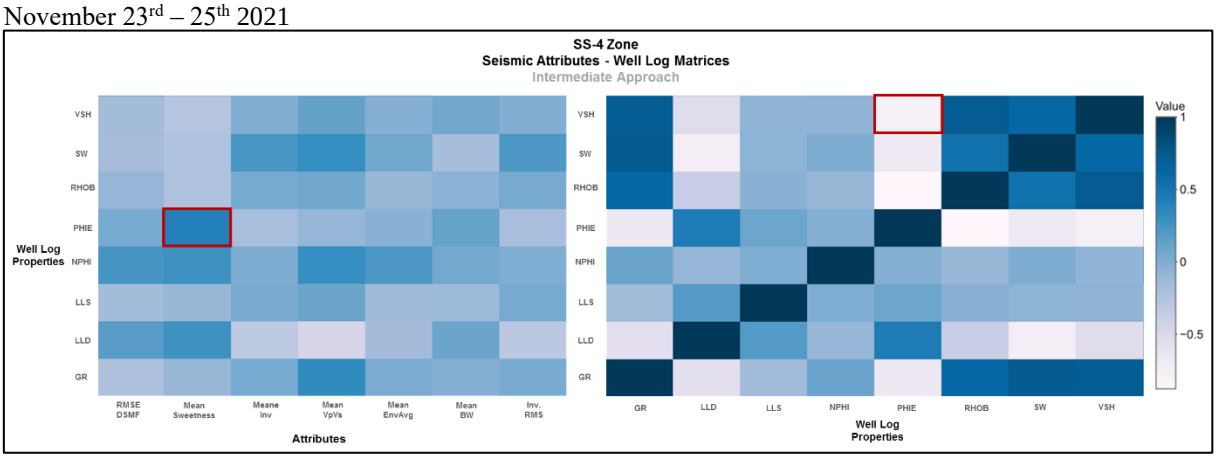

Figure 6 Multi-variate analysis result of SS-4 zone

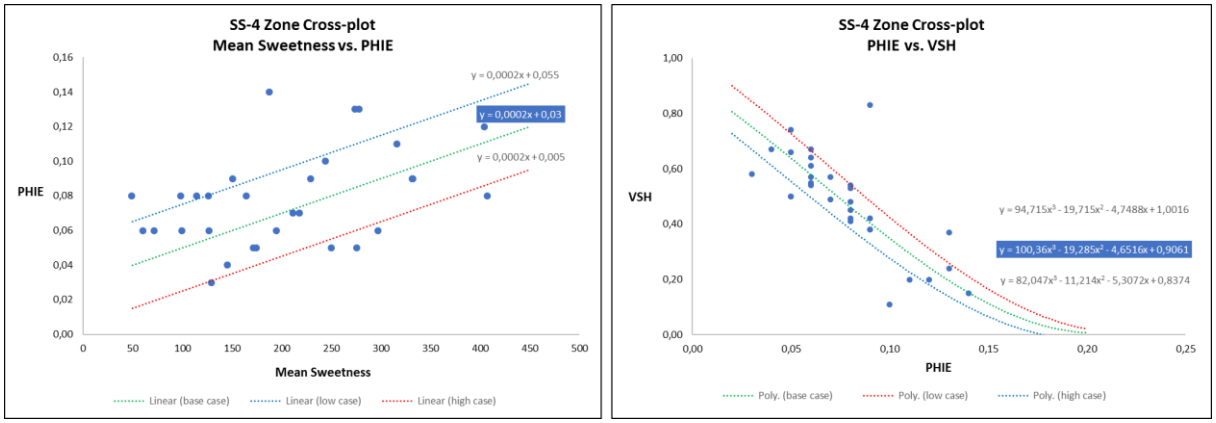

Figure 7 a) Cross-plot of mean sweetness to PHIE; b) Cross-plot of PHIE to VSH

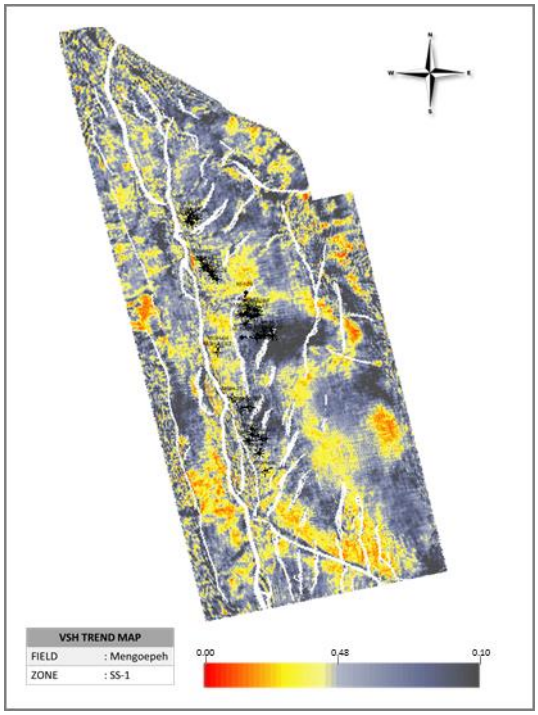

Figure 8 The VSH trend map of SS-1 zone

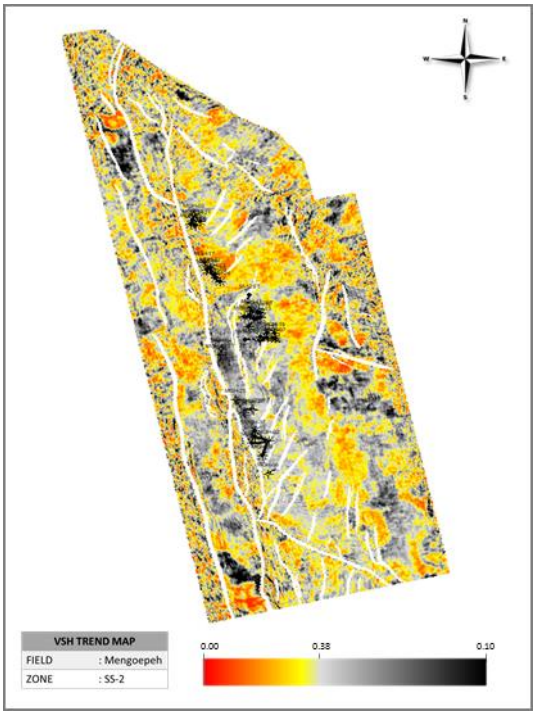

Figure 9 The VSH trend map of SS-2 zone

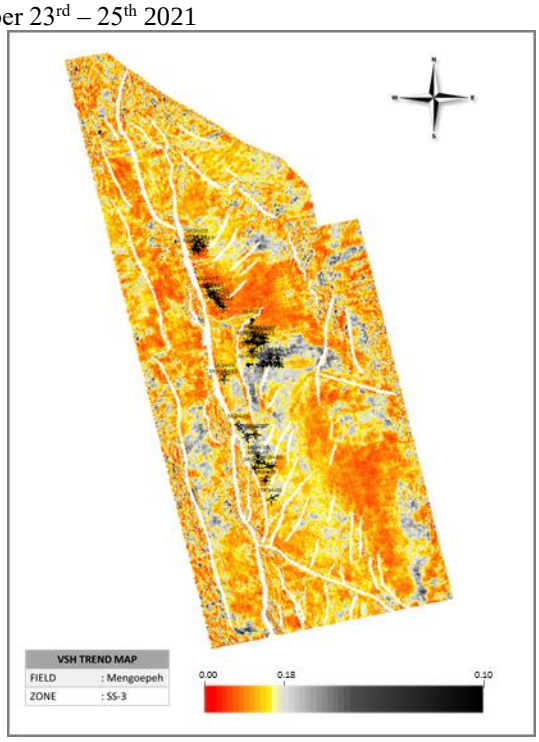

Figure 10 The VSH trend map of SS-3 zone

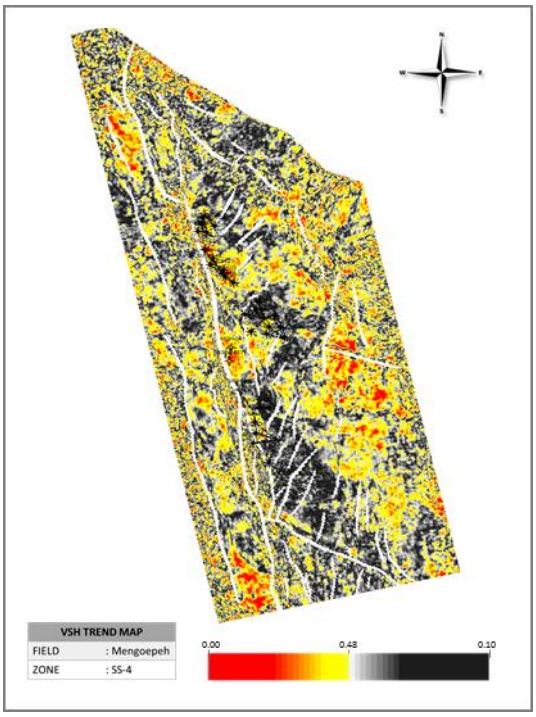

Figure 11 The VSH trend map of SS-4 zone

PROCEEDINGS
JOINT CONVENTION BANDUNG (JCB) 2021
November 23rd – 25th 2021

Analytical and Statistical Interwell Connectivity Analysis in Tight and Complex Reservoir

Richard Arnold, PT Medco E&P Indonesia

Abstract

One of the most important parameters governing waterflood performance is connectivity between producer(s) and injector(s). Several methods have been established to infer interwell connectivity but as all methods have their own limitations, the best practice is always to perform an integrated analysis by applying several methods and comparing their results. This is especially important for tight and complex reservoirs like the TK reservoir highlighted in this study. The methodology implemented in this study was organized into four parts. First, the reservoir of interest was segmented into two and five regions by considering their statics and dynamics characteristics. Next, statistical method with Spearman's correlation was applied to determine the connection between injection and production in each region. Subsequently, streamline simulations were performed to obtain a quick determination of producer/injector connectivity in each region. After inferring the connectivity between producer(s) and injector(s), their actual interactions were validated using production/injection analysis. The input data needed are production/injection data as well as simple geological characteristics. The workflow was performed successfully. Spearman correlation with a time gap quantified the degree of interaction between production and injection both for the entire reservoir as well as for each region. The streamline simulation enabled quick production/injection correlation between several producers and injectors at once. Results from these tools were then compared to results obtained from well-by-well production/injection analysis. Good agreement between the three methods were obtained thereby increasing confidence regarding the reservoir heterogeneity and interwell communication. This methodology provides rapid and easy techniques to obtain a more reliable reservoir heterogeneity characterization and quick identification of interwell connectivity which will be very important input for reservoir management and waterflood optimization. The proposed workflow can be deployed to other complex reservoirs.

Introduction

Interwell connectivity analysis, both qualitatively and quantitatively, is a very important aspect of waterflood evaluation to characterize reservoir heterogeneity and understand how and which injector(s) influence the producer(s), and with that knowledge, formulate the strategy to improve waterflood efficiency. Waterflood optimization strategies here can include water shutoffs, either at producer or injector side, gross production rates adjustments, and/or injection rates optimization.

There are numerous techniques for analyzing interwell connectivity. Conventional methods include interference test, tracer injection, and finite-difference reservoir simulation. Both interference test and tracer test can accurately capture connectivity between producers and injectors. Interference test, however, requires long-term well shut-in which will affect normal field production, whereas tracer injection project is considered expensive and challenging in its execution. The finite-difference reservoir simulation can quantitatively evaluate interwell communication and its dynamic nature, but it is time intensive, tedious, and less reliable for heterogeneous reservoirs.

Due to the disadvantages of these traditional methods, more and more novel techniques are developed to provide quick interpretations of interwell connectivity with only a small amount of data, and for some methods, only production and injection data which is normally available. Refunjol (1996) and Heffer et al. (1997) performed Spearman's rank correlation to quantitatively assess the communication of injector-producer pairs and preferential flow across a reservoir. Soeriawinata and Kelkar (1999) also leveraged Spearman's approach to analyze interwell connectivity, and proposed the constructive and destructive interference of the injected signals using superposition technique. Another statistical method besides Spearman's correlation is Pearson's correlation. Tian and Horne (2016) developed a modified Pearson's correlation coefficient (MPCC) to quantify interwell connection. Albertoni and Lake (2003) performed multivariate analysis to infer interaction between injectors and producers only from the well-rate fluctuations. Yousef et al. (2005, 2006) developed Capacitance-Resistance Model (CRM) which incorporated both flow rate and bottomhole pressure data to provide a more robust evaluation of the correlations between injectors and producers. This method becomes growingly popular and is currently one of the go-to methods for interwell connectivity interpretation. Many researchers modified the CRM to further improve the applicability of this method (Sayarpour, et al., 2009; Nguyen, et al., 2011; Prakasa, et al., 2017; Holanda, et al., 2018). The latest methods developed to interpret interwell communication are machine learning-based (Demiryurek, 2008; Liu, 2019; Ujjwal, 2019).

Despite the advantages to its powerfulness and growing popularity, machine learning is not perfect. Machine learning still has a lot of drawbacks one of which is the need of massive data sets to train on, and these data should be inclusive or unbiased, and of good quality. Machine learning requires enough time to allow the algorithms learn and develop enough to fulfill their objectives with a considerable amount of accuracy and relevancy. This method is also highly susceptible to error, and last but not least, it still has few success stories of applications.

Field Overview

The reservoir of interest in this study is the TK, which is currently operated by PT. Medco E&P Indonesia. This reservoir is located onshore Sumatra, approximately 70 km northwest of Palembang City. TK reservoir can be described as a saturated, low permeability, shaly sandstone reservoir with high heterogeneity. Table 1 summarizes the key properties of this reservoir. Due to the relatively low reservoir permeability, all TLS wells are hydraulically fractured to enable production. After fast production build-

up in the early stage of the production, the reservoir pressure dropped significantly.

Table 1. TK reservoir properties summary

Parameters	Value
Lithology	Sandstone
Depth (ft-TVD)	2,000 – 3,000
Initial Pressure (psia)	1,230
Current Pressure (psia)	500 – 1,230
Initial Temperature (ºF)	175
Porosity (%)	10 – 20
Permeability (mD)	5 – 50
Average Net Pay (ft)	29
Initial Water Saturation (%)	40 – 65
Drive Mechanism	Solution-gas Drive
Production Commencement	Year 2002
Injection Commencement	Year 2009

Considering the weak pressure support from the natural solution-gas drive mechanism, water injection was then established to provide pressure maintenance. However, water injection in TK reservoir is challenging due to the following reasons:

1. low permeability,
2. high reservoir permeability (laterally and vertically),
3. high initial water saturation, and
4. complicated subsurface flow paths due to numerous fractures as the results of hydraulic fracturing in most wells (70+ wells).

Water injection surveillance and performance monitoring is therefore of paramount significance to characterize, manage, and optimize the water injection operation. The surveillance best practice applied in TK reservoir has been reported by Arnold and Asrul (2020). One critical aspect that governs the performance of water injection is interwell connectivity, which is the core subject of this study.

This paper summarizes the interwell connectivity analysis techniques implemented to characterize TK reservoir heterogeneity and determine the connection between injectors and producers. The methodology includes three methods, namely Spearman's rank correlation as the statistical approach, 2D streamline simulation as the semi-analytical approach, and actual production-injection analysis as the observational approach.

Data and Method

Reservoir Segmentation

Prior to evaluating waterflood performance in a heterogeneous reservoir, it is advisable to divide the reservoir into several segments or regions. Reservoir segmentation is important to make the analysis more detailed, accurate, and representative by honoring the reservoir heterogeneity, both laterally and vertically. The segmentation can be done by simple geographic delineation, for example by grouping the regions into: north, south, east, and west. The best practice, however, is to always consider the statics and dynamics characteristics of the reservoir.

Spearman's Rank Correlation

The first interwell connectivity analysis performed in this study is Spearman's correlation. This method is a non-parametric statistical approach that does not require assumptions about the distribution shape of the data (Alabri, 2020). Non-parametric method was applied in this study due to the fluctuative nature of the production and injection rates that make the data to be of unknown distribution. In this method, ordinal data is used, which means the orders or ranks of the data are used rather than the actual values.

Mathematically, Spearman's rank correlation can be expressed as (Hollander, 2013):

$$r_s = 1 - \frac{6\sum_{i=1}^{n} D_i^2}{n(n^2-1)}$$

$$D_i = rank(X_i) - rank(Y_i)$$

where

r_s = Spearman's rank correlation coefficient
Di = difference between the two ranks (*i.e.* X and Y) of each observation
n = number of observations.

The correlation degree between X_i and Y_i can be used according to the standards of r_s shown in Table 2.

Table 2. Spearman's correlation coefficient and degree

Correlation Coefficients	Correlation Degree
$r_s = 0$	no correlation
$0 < \lvert r_s \rvert \leq 0.19$	very weak
$0.20 \leq \lvert r_s \rvert \leq 0.39$	weak
$0.40 \leq \lvert r_s \rvert \leq 0.59$	moderate
$0.60 \leq \lvert r_s \rvert \leq 0.79$	strong
$0.80 \leq \lvert r_s \rvert \leq 1.00$	very strong
1.00	monotonic correlation

The advantages of Spearman's analysis are that it only requires production and injection rates data that are readily available and that, as a statistical tool, it encompasses a massive amount of data and it is not idealistic. It accounts for all the fluctuation of flow rates in one single number which indicates the strength of the well pair connectivity. The weakness of this method, however, is that it does not honor geology and other physical attributes.

2D Streamline Simulation

To validate the results from Spearman's method, we need to compare it with streamline simulation. 2D streamline technique using MBAL software was leveraged in this study. This approach provides a quick and relatively simple method of determining the sweep efficiencies and the interwell connectivity without the need to build complex 3D numerical simulation models.

The simulator models a rectangular reservoir with a combination of no-flow and/or constant pressure boundaries. It assumes that the PVT is constant and the calculated streamlines do not change position with time. The working principles of this method are as follows:

PROCEEDINGS
JOINT CONVENTION BANDUNG (JCB) 2021
November 23rd – 25th 2021

1. the simulator generates image wells to model reservoir boundaries (no flow or constant pressure),
2. calculates the velocity field by time simulation,
3. the resulting streamlines then progress from the injector(s) to the producer(s) over time thereby developing connectivity between the well pairs,
4. once a streamline reaches a producer the water cut will increase, and the more streamlines reaching the producers, the higher the water cuts will become, and
5. track the progression of water along the stream tubes with time.

This method requires the following data:

- well locations,
- reservoir boundaries (no flow or constant pressure),
- well injection and production volumes,
- fluid properties, and
- simple reservoir geological description.

It is worth noting that both Spearman's analysis and streamline simulation are best applied when producers and injectors are kept in constant rate.

Production/Injection Analysis

Production/injection analysis is a traditional approach to infer interwell connectivity. Connectivity between producer(s) and injector(s) is interpreted qualitatively by focusing on the production and injection profiles of the well pairs under investigation. If injection rate increase from a particular injector is followed by liquid production increase from the studied producer(s), then the injector is considered connected to the producer(s) constructively. If changes in injection rates do not change the production rate, even in the slightest, then it will be inferred that the injector is not connected with the producer(s).

Result and Discussion

Reservoir Segmentation

Considering the reservoir heterogeneity, reservoir segmentation strategy is implemented. The reservoir is segmented into two and five regions based on: (1) reservoir characteristics, (2) reservoir pressure, (3) well performance, and (4) well population. In this study, the reservoir is grouped into two regions for Spearman's method and five regions for streamline analysis. Figure 1 and 2 show the areal segmentation of the reservoir for two regions and five regions, respectively.

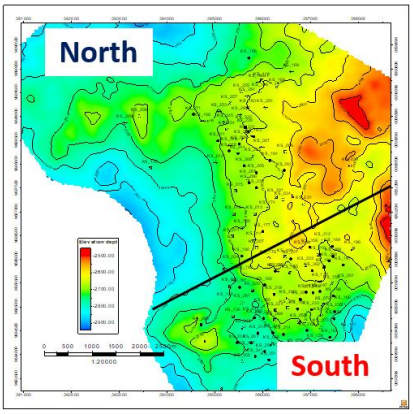

Figure 1: Reservoir north-south segmentation for Spearman's analysis

Spearman's Correlation

Spearman's correlation was performed at both field and regional level. The correlation coefficients were calculated based on the entire injection period of about twelve years. Considering the time required for the injected water to sweep and pressurize the reservoir and ultimately affect the production, time lag was invoked in the calculation process. The results of the field-scale Spearman's analysis is shown in Table 3.

Table 3. Spearman's coefficients for field-scale analysis with time lag invoked

Time Lag (months)	Spearman's Coefficient
0	0.690
1	0.721
2	0.710
3	0.690
4	0.669
6	0.682

From Table 3, two key points can be concluded. Firstly, Spearman's value of approximately 0.70 for all the time lags invoked indicated that the production responded positively and strongly to the injection. It means that, although well-by-well analysis has not been performed, we can safely conclude that there was strong connectivity between the injectors and the producers. The second important observation is that time lag of one month results in the highest Spearman's coefficient which means that it took one month for the injection to finally influence the production strongly.

It is important to note that field-scale analysis results should be refined with regional-scale or pattern-scale analysis. This method therefore was also applied at regional level. The results from the north and south regions are tabulated in Table 4.

PROCEEDINGS
JOINT CONVENTION BANDUNG (JCB) 2021
November 23rd – 25th 2021

Table 4. Spearman's coefficients for regional-level analysis with time lag invoked

Time Lag (month)	Spearman's Value (North)	Spearman's Value (South)
0	0.149	0.676
1	0.145	0.704
2	0.147	0.721
3	0.128	0.730
4	0.117	0.738
5	0.127	0.730
6	0.137	0.755
7	0.148	0.747
8	0.084	0.739
9	0.059	0.717

The results presented in Table 4 show that the performance of northern region differed significantly from that of the southern region. Southern region exhibited a strong, positive relationship between the injection and the production. The time lag required to achieve the highest Spearman's value for the southern region is six months. On the other hand, northern region showed very weak, positive correlation between the injection and the production with no time lag giving the highest Spearman's value. The weak Spearman's correlation at the northern region was predictable due to the following reasons:

- northern region was significantly more depleted than then southern region which necessitated a significantly longer fill-up period for the northern region,
- injection at the northern region was 15 months late from the injection at the southern region,
- injection at the northern region was four times lower than that of the southern region making the sweeping and pressurization less effective, and
- northern region has a large gas cap and area with low permeability which complicated the injection streamline.

Spearman's correlation can also be applied for oil production rate but considering the declining nature of oil flow rate, even at constant injection rate, this analysis was not performed.

Besides quantifying the injection/production connectivity, Spearman's analysis reaffirmed the importance of segmentation in this heterogeneous reservoir. Clearly, field-scale analysis alone was not sufficient to fully describe the reservoir performance and characteristics; regional and pattern-level analysis are required. Also, the northern regions should be further divided into smaller segments to obtain a more robust Spearman's analysis.

2D Streamline Simulation

2D streamline simulation was performed to infer interwell communication after it had been indicated from the Spearman's correlation that the field injection influenced the field production strongly and positively. Streamline analysis was done with 5-regions scheme (A, B, C, D, and E), rather than 2-regions as in Spearman's analysis, to obtain a more accurate evaluation. The streamline results for the whole reservoir and for Region C are depicted in Figure 2 and 3, respectively.

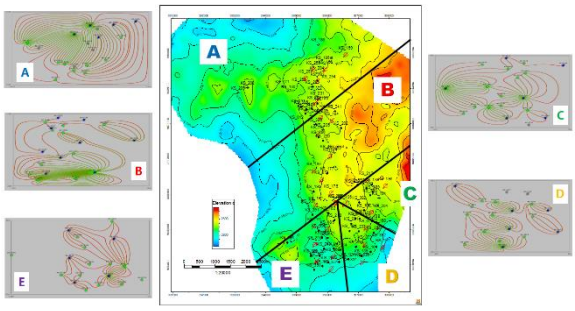

Figure 2: Reservoir segmentation for 2D streamline simulation

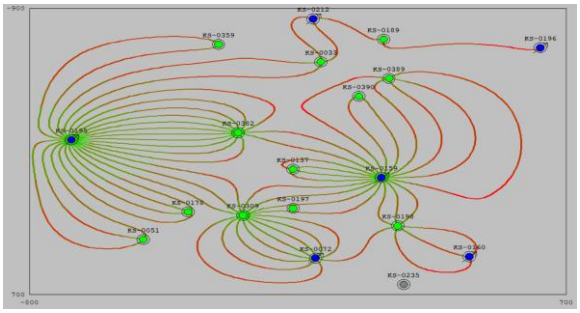

Figure 3: 2D streamline simulation results for Region C

Streamline analysis provides a quick interwell connectivity interpretation but it is important to note that this method takes only a snapshot of the entire production-injection history and uses that for analysis. Due to this limitation, at the time of this writing, this method was applied for semi-qualitative purpose to interpret interwell interaction, rather than deeply quantitative.

Production-Injection Analysis

To validate the results of the Spearman's correlation and the streamline simulation, actual well-to-well production-injection (P/I) analysis was performed. The P/I analysis validated the other methods as illustrated in Figure 4 and 5.

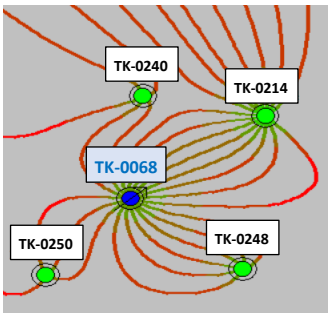

Figure 4: Streamline simulation results showing interwell connectivity between the injector TK-0068 and the four adjacent producers

PROCEEDINGS
JOINT CONVENTION BANDUNG (JCB) 2021
November 23rd – 25th 2021

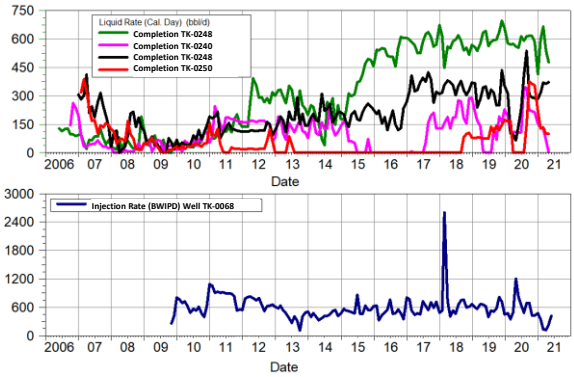

Figure 5: Production-injection profiles indicating strong influence of TK-0068 injection to the production of the adjacent producers

TK-0068 is an injector located at the center of the five-spot pattern with the other four producers, namely TK-0214, TK-0240, TK-0248, and TK-0250. Streamline analysis indicated the communication between the injector with the adjacent producers and this is confirmed by P/I analysis. All the surrounding producers were producing prior to the start of TK-0068 injection. Due to the lack of pressure support, the production of these four producers dropped significantly in 2009. However, after TK-0068 was put to injection, it can be clearly seen that production decline of the four producers were arrested and even reversed. The sweeping effect and pressurization provided by TK-0068 was effectively received by TK-0214 and TK-0248 enabling the two producers to increase production by ESP operation without significant production declines. Unfortunately, TK-0240 and TK-0250 should be produced only intermittently due to high water cut. This high water cut was in part caused by water injection from TK-0068. From this investigation, it can be concluded that water injection can constructively support the production through efficient sweep and pressurization, as in the case of TK-0214 and TK-0248, but it can also destructively impact the production through water breakthrough and/or water channeling, as in the case of TK-0240 and TK-0250. This further emphasizes the importance of interconnectivity analysis as it can be the main input for water injection optimization so that the positive impact of injection can be exploited while avoiding the negative effect of it.

Future Work

Interwell connectivity analysis performed in the TK reservoir is not perfect as it is still on the early stage of maturity. The nearest future works are to conduct the following analyses to enrich and validate the current interpretation of interwell communication:

- reservoir segmentation at a smaller scale,
- 3D streamline simulation,
- 3D reservoir (finite difference simulation),
- capacitance-resistance model (CRM),
- interwell Spearman's correlation, and
- water injection optimization.

Conclusions

In this work, we performed interwell connectivity analysis using production and injection data. The reservoir segmentation is important to make the analysis focused, detailed, and more accurate considering the high heterogeneity of the reservoir under study. Spearman's correlation with a time gap quantified the degree of communication between production and injection rates both for the entire reservoir as well as for each region. This analysis captured a strong correlation between the field-wide injection and production. At regional level, it is shown that the injection influenced the production strongly and positively in the southern region, while injection's effect on production in the northern region was weak. The 2D streamline simulation enabled a quick semi-qualitative assessment of the interwell connectivity between producers and injectors. Results from the two methods were then validated by well-by-well production/injection analysis. Good agreement between the three methods were obtained thereby increasing certainty regarding reservoir heterogeneity and interwell interactions. This methodology provides rapid and easy techniques to obtain a more reliable reservoir heterogeneity characterization and quick identification of interwell connectivity which will be very important inputs for reservoir management and water injection optimization.

References

Refunjol, B. T. (1996). Reservoir characterization of North Buck Draw field based on tracer response and production/injection analysis (Doctoral dissertation).

Heffer, K.J., Fox, R.J., McGill, C.A., and N.C. Koutsabeloulis. "Novel Techniques Show Links between Reservoir Flow Directionality, Earth Stress, Fault Structure and Geomechanical Changes in Mature Waterfloods." SPE J. 2 (1997): 91–98.

Soeriawinata, T., and M. Kelkar. "Reservoir Management Using Production Data." Paper presented at the SPE Mid-Continent Operations Symposium, Oklahoma City, Oklahoma, March 1999.

Tian, Chuan , and Roland N. Horne. "Inferring Interwell Connectivity Using Production Data." Paper presented at the SPE Annual Technical Conference and Exhibition, Dubai, UAE, September 2016.

Albertoni, Alejandro, and Larry W. Lake. "Inferring Interwell Connectivity Only From Well-Rate Fluctuations in Waterfloods." SPE Res Eval & Eng 6 (2003): 6–16.

Yousef, Ali A., Gentil, Pablo H., Jensen, Jerry L., and Larry W. Lake. "A Capacitance Model To Infer Interwell Connectivity From Production and Injection Rate Fluctuations." SPE Res Eval & Eng 9 (2006): 630–646.

Yousef, Ali A., Lake, Larry Wayne, and Jerry L. Jensen. "Analysis and Interpretation of Interwell Connectivity From Production and Injection Rate Fluctuations Using a Capacitance Model." Paper presented at the SPE/DOE Symposium on Improved Oil Recovery, Tulsa, Oklahoma, USA, April 2006.

Arnold, R. and Asrul, F. 2020. Waterflood Surveillance Best Practice in a Tight, Heterogeneous, Water-Sensitive, and Massively Fractured Reservoir. Paper IATMI20-87. Presented at IATMI Simposium 2020, 24 – 25 October 2020

Alabri, S., Ghafram, H., & AlKalbani, M. (2020, November). A Method to Correlate Interactions Between Injectors and Producers. In Abu Dhabi

International Petroleum Exhibition & Conference. OnePetro.

Hollander, M., Wolfe, D. A., & Chicken, E. (2013). Nonparametric statistical methods (Vol. 751). John Wiley & Sons.

Sayarpour, M., Zuluaga, E., Kabir, C. S., Lake, L. W., 2009. The use of capacitance–resistance models for rapid estimation of water flood performance and optimization. Journal of Petroleum Science and Engineering, 69(3-4), 227-238.

Nguyen, Anh P., Kim, Jong S., Lake, Larry W., Edgar, Thomas F., and Byron Haynes. "Integrated Capacitance Resistive Model for Reservoir Characterization in Primary and Secondary Recovery." Paper presented at the SPE Annual Technical Conference and Exhibition, Denver, Colorado, USA, October 2011.

Prakasa, Bona , Shi, Xiang , Muradov, Khafiz , and David Davies. "Novel Application of Capacitance-Resistance Model for Reservoir Characterisation and Zonal, Intelligent Well Control." Paper presented at the SPE/IATMI Asia Pacific Oil & Gas Conference and Exhibition, Jakarta, Indonesia, October 2017.

Holanda, R. W. D., Gildin, E., Jensen, J. L., Lake, L. W., & Kabir, C. S. (2018). A state-of-the-art literature review on capacitance resistance models for reservoir characterization and performance forecasting. Energies, 11(12), 3368.

Demiryurek, Ugur, Banaei-Kashani, Farnoush, Shahabi, Cyrus, and Frank G. Wilkinson. "Neural-Network based Sensitivity Analysis for Injector-Producer Relationship Identification." Paper presented at the Intelligent Energy Conference and Exhibition, Amsterdam, The Netherlands, February 2008.

Ujjwal, Manu , Tummala, Pradeep , Kumar, Viren , Singhal, Manu , and Andrew James. "Rapid Insights into Waterflood Management Using Advanced Analytics and Machine Learning." Paper presented at the SPE/IATMI Asia Pacific Oil & Gas Conference and Exhibition, Bali, Indonesia, October 2019.

Liu, Wei, Liu, Wei David, and Jianwei Gu. "Reservoir Inter-Well Connectivity Analysis Based on a Data Driven Method." Paper presented at the Abu Dhabi International Petroleum Exhibition & Conference, Abu Dhabi, UAE, November 2019.

Acknowledgements

The author expresses sincere thanks to team members of PT Medco E&P Indonesia Resource Development Area-1, Saras N.H., Febrian A., Geraldus Y. S. R. S., Dian U., and Elsa F. S., for their priceless contributions in developing the reservoir presented in this paper. Special thanks to Medco management for allowing the publication of this paper.

PROCEEDINGS
JOINT CONVENTION BANDUNG (JCB) 2021
November 23rd – 25th 2021

Evaluating Oligocene Intra Platform Reef Carbonate Reservoir Potential Using Advance Model of Seismic Facies Analysis and Seismic Inversion – A Case Study Barito Basin Indonesia

Yarris Ibdian Cakra (1,2), Abdul Haris (1), Afriadhi Triwerdhana (2), and Neni Herawati (2)*
(1) University of Indonesia and (2) Pertamina EP

Abstract
Characterizing platform carbonate reservoir is a big challenge and requires more effort due to the lithology complexity. The Oligocene Middle Berai Platform Carbonate in the West of Barito Basin is an under-explored area, which is supported by the 2D seismic of 2015 vintage. The seismic data shows characteristics of mounded reflector configuration and lateral variation of seismic velocity as reef carbonate development indicators. The objective of this study is to evaluate the Intra Platform Reef Carbonate reservoir, where reservoir geometry is determined by facies seismic analysis and validated using Petrographic and Biostratigraphic reports. Thereafter rock properties are extracted using seismic inversion based on an advanced model. The acoustic impedance is expected to describe the development of reefal carbonate reservoirs in more detail, geologically make sense, and further predicting porosity. Validation result provides an overview of the estimated porosity range of reef facies 15-20%, reef debris 7-14%, and muddy facies 3-8%. These methods are effective in understanding the potential of Berai Carbonate Platform with reservoir properties and distribution. The results are successfully and significantly reduced exploration risk.

Introduction

The Berai Carbonate is one of the hydrocarbon reservoir targets deposited in the post-rift phase (Late Eocene – Early Oligocene) of the Barito Basin that has been explored through various studies and exploration drilling since the 1960s. Small amounts of hydrocarbons have been found in the Northern Basin with the structural play concept. In the Southern Basin with the stratigraphic play concept, all six wells were plugged and abandoned as dry holes. Although these attempts failed to find hydrocarbons, they did reveal particularly well-defined reef facies associations which may be useful in further exploration (P.J Pelton, 1974). Berai Carbonate potential reservoir study (Andromeda, 2013), based on Gross Depositional Environment Map shows patch reef and reef debris facies were well developed close to the edge of the basin (Western part of Barito).

In 2015 Pertamina EP acquired 2D regional seismic where covered the under-explored area in West Barito. Prospect evaluation conducted then concluded that Berai Carbonates play in this area was quite promising. Upper Berai Shale as a source rock has a good maturity level and the prospect area was relatively close to the kitchen. Seismic data on the carbonate platform shows some interesting features such as various reflector patterns and lateral interval velocity anomalies. However, the highest risk lies in the reservoir aspect due to the complexity of the carbonate rock and well data limitation for validating. We need a method that can identify and determine the reservoir geometry. Furthermore, the objective of this study is to evaluate the quality and distribution of the Berai Intra Platform Reef Carbonate reservoir.

Data and Method

We used well data consist of gamma ray, sonic, neutron porosity, and spontaneous potential log and 20 lines PSTM 2D seismic data with a density value of 2 km including interval velocity section. In addition, there are petrography and biostratigraphy study reports which relevant to Berai Carbonate. In understanding the reservoir potential, we use qualitative analysis with seismic facies and quantitative analysis with post-stack seismic inversion. The two results of the analysis were validated and then elaborated so that they were able to describe the reservoir in more detail.

2.1 Seismic Facies Analysis

The appearance of carbonate rocks in seismic data contains information about their original depositional environments, lithofacies, diagenesis, source rock, and reservoir potential (Figure 1). The identification of seismic facies is a study in pattern recognition. To characterize seismic facies, we need to describe four aspects or appearances such as the configuration or shape of reflections, the amplitude, the frequency, and the continuity (Macurda, 1997). The aspect that can be used as a reference for the type of facies is reflector configuration such as parallel or subparallel, divergent, progradational, mounded or draped, and onlap or onlap fill. Biostratigraphic information is needed to calibrate the interpretation result.

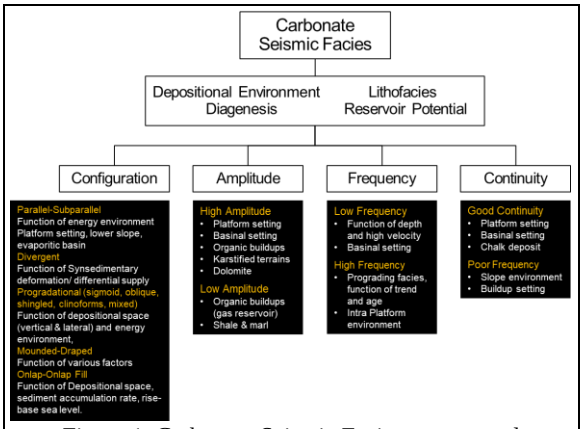

Figure 1. Carbonate Seismic Facies aspects and intepretation

There are eight pairs of well and seismic data that were analyzed for seismic facies and validated using petrographic and biostratigraphic information. The result is used for determining the vertical and lateral reservoir geometry. We use the satellite Bouguer Gravity Anomaly map to elaborate the interpretation of the prospect area to the regional scale.

2.2 Post Stack Inversion with Advance Model

Post stack inversion is a solution for reservoir characterization by integrating wells and seismic data, in the form of acoustic impedance as sensitive rock properties. In this study, we used model-based inversion with Advance Low Frequency Model (ALFM) which calculates well data and seismic interval velocity as external attributes (Figure 2). ALFM has a better geological trend because the lateral information is derived from seismic velocity. In the frontier exploration area where only a few wells are available, the utilization of seismic velocity in the ALFM plays important role in the quality of the results.

PROCEEDINGS
JOINT CONVENTION BANDUNG (JCB) 2021
November 23rd – 25th 2021

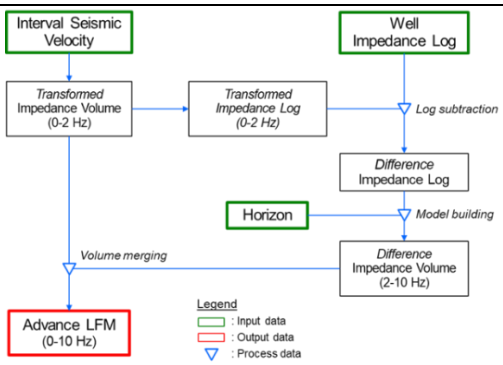

Figure 2. Post stack inversion with advance model workflow

Result and Discussion

Qualitative seismic observations on the Middle Berai Platform carbonate resulted in three types of configurations. There are parallel-subparallel, progradational, and mounded-draped which are all platform interior facies of Middle Berai. Based on the seismic facies' summary in Table 1, we conclude that mounded pattern was interpreted as a patch reef, validated to Barito-01 petrographic and biostratigraphic report. The porosity value range is taken from a study of Berai reservoir prospective which has been calculated from petrophysics analysis and validated by core data (Andromeda, 2013).

Table 1. Carbonate seismic facies summary in North & South Barito consists of depositional environment and porosity range estimation

Reflection Configurations	Depositional Environment	Porosity Range	Reference Well
Parallel Continuous Sub Parallel Discontinuous	• Platform setting • Lagoonal facies (platform interior) • Shale dominated • Mudstone – Wackestone	3-8%	Titan-01, SJ-01, MRD-01, SMD-01, KK-01
Progradational (sigmoid, oblique, shingled)	• Platform setting • Shoal Facies (platform interior) • Related to Reef Debris, Carbonate Shedding • Wackestone – Packestone	10-15%	MRG-01, KTP-01
Mounded - Draped	• Platform setting • Patch Reef (Platform Interior) • Associate with Organic carbonate facies • Packestone - Grainstone	10-20%	BRT-01

Shale Dominated — Carbonate Dominated — Log Index: = Gamma Ray; P-wave; Neutron Porosity; SP

A seismic section on line 007 which is overlaid with seismic velocity intervals in Figure 3 shows a reflection configuration mounded pattern at the middle platform interval which correlates with high-velocity values (4000-5000 m/s). Mounded reflectors can easily be characterized by the appearance of a curve that has the opposite direction of the dipping pattern. Whereas the parallel and shingled patterns have lower velocity values (3200-4000 m/s). Meanwhile, a sub-parallel pattern on line 020 has a relatively high-velocity value (4200-4600 m/s) due to the effect of depth (depth burial). The vertical and lateral geometry of the reefal carbonate reservoir is determined from the reflection mounded pattern and high seismic velocity values.

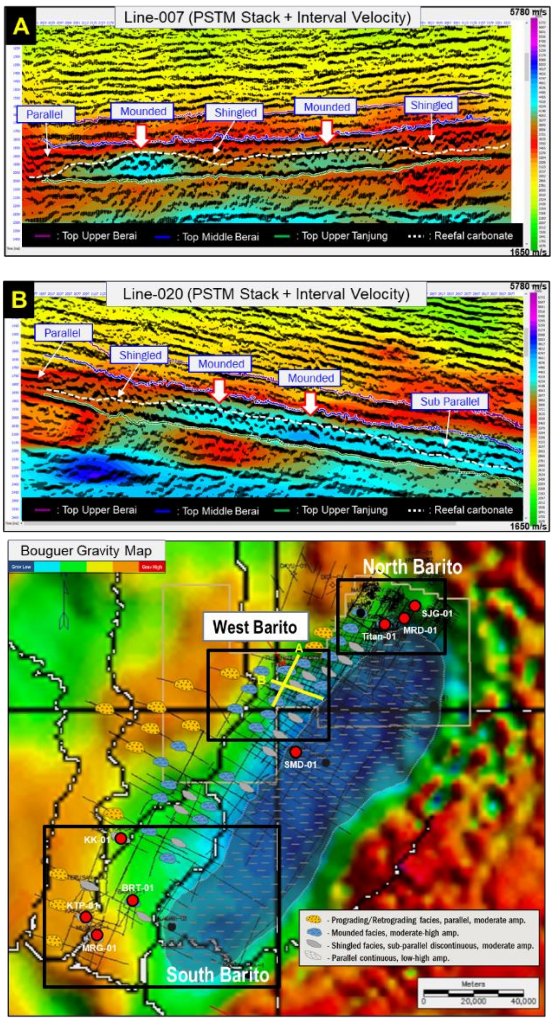

Figure 3. Middle Berai Intra Platform Carbonate interpretation (left) and facies distribution on Barito Basin Bouguer Gravity map (right)

Sensitivity analysis on Titan-01 well in Figure 4 shows that porous carbonate (NPHI 0.1-0.25) has a relatively lower impedance value (6000-9500 m/s.gr/cc) than tight carbonate. P-impedance is a sensitive parameter that can be used to map the distribution of high porosity carbonate reservoirs (10-25%).

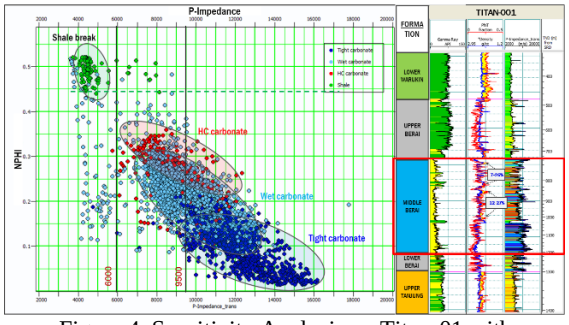

Figure 4. Sensitivity Analysis on Titan-01 with classification of lithofacies on Middle Berai Fm.

PROCEEDINGS
JOINT CONVENTION BANDUNG (JCB) 2021
November 23rd – 25th 2021

ALFM is calculated using seismic velocity interval and Titan-01 as the only reference well that is 40 km from the interest area. Acoustic Impedance section line 007 in Figure 5 shows a clear lateral trend of the P-impedance at 1900-2000 ms (purple-light blue), even though the position of Titan-01 is not in this line. Then we used a model-based inversion algorithm to calculate the PSTM stack preserve, ALFM and Titan-01 well data input with the lowest possible error to obtain optimal results. Porosity estimation is calculated based on the linear relationship between the P-impedance parameter and the NPHI on the sensitivity analysis performed on Titan-01.

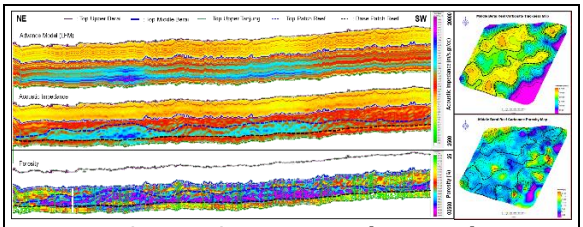

Figure 5. ALFM, Acoustic Impedance, and Porosity section of Line 007 (left). Isochrone Map and Porosity Map of Intra patch reef carbonate Middle Berai (right).

Seismic facies work effectively on good continuity and frequency quality seismic data because thickness and dipping layer are visible to determine patch reef geometry. Another indication of the patch reef is lateral velocity anomaly which has been successfully modeled in ALFM and supported the geological model information. Interpretation of 20 seismic lines resulted in many closures on the isochrone reef carbonate map (Figure 5). Estimated gross reservoir thickness can reach up 480 m with a distribution coverage of 33.000acres. The result of seismic inversion in the form of acoustic impedance is then converted into a porosity value. The value of the distribution of the reef facies porosity is quite valid in the range of 10-20%, reef debris 7-14%, and muddy facies 3-8% which is by following the recent study (Andromeda, 2013).

Conclusions

Based on the results of seismic facies and seismic inversion analysis validated with seismic velocity data and biostratigraphic reports, we have successfully mapped the development pattern of the intra patch reef carbonates reservoir in West Barito. Three closures are in line with the regional trend in the NE-SW trending lagoon zone. Reservoir modeling results indicate that the facies patch reef has the potential to become a good quality reservoir and has a wide coverage distribution. The validation result provides an overview of the estimated porosity range of reef facies 15-20%, reef debris 7-14%, and muddy facies 3-8%. The results of this evaluation are very positive and effective in reducing the risk of exploration in West Barito.

References

Haris, A., Novriyani, M., Suparno, S., Hidayat, R. and Riyanto, A., (2017). *Integrated seismic stochastic inversion and multi-attributes to delineate reservoir distribution: Case study MZ fields, Central Sumatra Basin*. In *AIP Conference Proceedings* (Vol. 1862, No. 1, p. 030180). AIP Publishing LLC.

Anselmetti, F.S., and Eberli, G.P., (1997). *Sonic Velocity in Carbonate Sediments and Rocks*. SEG Geophysical Development Series No 6: Carbonate Seismology Chapter 4, 53-74.

Fitchen, W. M., (1997). *Carbonate Sequence Stratigraphy and its Application to Hydrocarbon Exploration and Reservoir Development*. SEG Geophysical Development Series No 6: Carbonate Seismology Chapter 7, 121-178.

Hampson Russell Software. (2018). *Volume ratio blending: Blending velocity volumes with inversion models in "What is New in HRS10.4"*. CGG GeoSoftware. Calgary. Canada.

Laporan Studi Internal Pertamina EP. (2007). *An Evaluation Study on the Source Rocks, Migration, and Hydrocarbon Potential of the Barito Basin*. Volume II. Jakarta. Indonesia.

Koesoemadinata, R.P., (2008). *Petroleum Basins of Indonesia, The Development of Basins in Indonesia*. Institut Teknologi Bandung - BP MIGAS – IAGI. Bandung.

Macurda, D. Bradford Jr., (1997). *Carbonate Seismic Facies Analysis*. SEG Geophysical Development Series No 6: Carbonate Seismology Chapter 6, 95-120.

Pelton, P. J., (1974). *Exploration of The South Barito Basin Reef Tract, Kalimantan, Indonesia*. Proceeding Indonesian Petroleum Association 3th Annual Convention & Exibition 1974, 153.

Satyana, A.H., (1995). *Paleogene Unconformities in the Barito Basin, Southeast Kalimantan: A Concept for the Solution of the "Barito Dilemma" and a Key to the Search for Paleogene Structures*. Indonesian Petroleum Association, 24th Annual Convention Proceeding.

Society of Petroleum Evaluation Engineers. (1998). *Guidelines for Application of Petroleum Reserves Definitions*. Houston. Texas.

Subekti, Ari et. al., (2015). *New insights into the Kerendan Carbonate Platform: An Oligocene Reservoir from the Upper Kutai Basin, Kalimantan*. Proceeding Indonesian Petroleum Association 39th Annual Convention & Exibition 2013.

Werdaya, A. A. et al, (2013). *Gross Depositional Environment Model of The Berai Carbonate Formation and Its Implication for Reservoir Prospectivity, Barito Basin, South Kalimantan, Indonesia*. Proceeding Indonesian Petroleum Association 37th Annual Convention & Exibition 2013, IPA13-G-001.

Acknowledgements

We would like to thank Afriadhi Triwerdhana for his support and permission to use data belonging to Exploration Pertamina EP. High appreciation for the contributions and ideas of Neni Herawati who assisted in geological evaluation. This research also received many valuable suggestions and input from Abdul Haris, especially in geophysical evaluation and validation of data processing results.

PROCEEDINGS
JOINT CONVENTION BANDUNG (JCB) 2021
November 23rd – 25th 2021

One dimensional stochastic inversion in approach for lateral lithology distribution, case study J-field south sumatra basin

Oddy A. Pranidhana 1, Adi Widyantoro 2, Yona Akbar 3, Rismauly Sitinjak 4
1 RDA Teknologi Indonesia
2 Pertamina EP
3 Pertamina EP
4 Pertamina EP

Abstract

In well - developed hydrocarbon field, understanding reservoir distribution is one of the key factors to ensure successful optimization of a field development plan. The lateral distribution of a certain lithology may be predicted by using the information from the existing well lithofacies log as a reference. ODiSI (One Dimension Stochastic Inversion) is one of the robust methods which able to generate lateral lithofacies distribution. In this study, J-field, a mature hydrocarbon field in South Sumatra Basin, Indonesia, was chosen for ODiSI method application due to its abundant well availability. In the process, four wells were selected as a reference in generating lithofacies log, J-1,J-2, J-3, J-4. while the remaining available wells acted as blind wells to validate the result.

Prior model, consisted of pseudo-wells on each seismic trace location, was initially built as the first step in the vicinity of the reference well. For every single pseudo-well, a lithofacies column was created by using the model of Continuous Time Markov Chain (CTMC), which generated sequences of the layer with different lithofacies and thickness in the time domain. Afterward, sets of parameters composed of the petrophysical, reservoir, and elastic parameters were calculated, where each lithofacies elastic parameter calculation was approached by a different method while remained controlled by rock physics relationship based on data from the reference well. Shale's parameters, for example, were derived by analyzing the linear relationship between three elastic parameters which are Vp – Vs and Density, along with its depth trend. Meanwhile, sand parameters were obtained by utilizing dry rock properties relationships such as bulk and shear moduli and porosity. The parameters prediction on each pseudo – well, play an important role, as it was used in EEI synthetic generation. By examining the lowest misfit between EEI's synthetic and real seismic impedances, pseudo–wells in the prior model were sorted into Best Matched Pseudo Well (BMPW) set. Finally, BMPW set was then become an input for creating probability volume for each lithofacies. The result was validated by the blind wells and produced a decent match for the reservoir intervals.

The proposed ODiSI workflow and method tested in J-field can be the case solution when we do not possess any luxury in conducting any expensive and time-consuming seismic inversion method.

Keywords: Inversion, Lithofacies, Seismic, Stochastic

Introduction

J-field is a mature hydrocarbon field in South Sumatra Basin which has low signal-to-noise quality in its production area, therefore post stack and pre stack analysis are not optimal. Data limitation becomes another challenge in developing this field because J-field has about 200 wells with only one checkshot data, one DSI and eleven sonic data.

As discussed in **(**Connolly and Hughes, 2016**),** ODiSI (One Dimension Stochastic Inversion) is one of the robust methods which able to generate lateral lithofacies distribution. ODiSI method uses not only properties from seismic, but also geology information of the field. In this study, ODiSI method was applied in J-field to ensure optimal lateral lithology distribution.

Pseudo-wells are selected from a prior distribution defined by vertical statistics and rock property trends and relationships. The range of reservoir properties in pseudo-well population, porosity variance, lithofacies type and proportions, vertical stacking patterns, and so on, must encompass the range of possible vertical geologic profiles that may encounter in the reservoir.

Matching large number of pseudo wells to angle stacks can produce high confidence image of reservoir property.

Data and Method

Using four wells we calculated a set of petrophysical, reservoir, and elastic parameters prior to input for ODiSI.

PROCEEDINGS
JOINT CONVENTION BANDUNG (JCB) 2021
November 23rd – 25th 2021

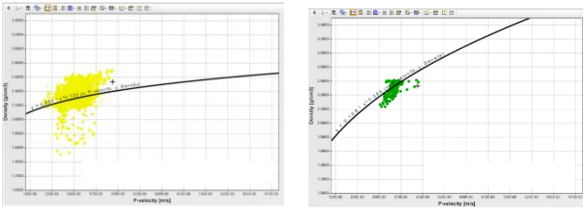

Figure 1. Shale trend and the clean sand trend plotted to ensure the separation and build rock physics model.

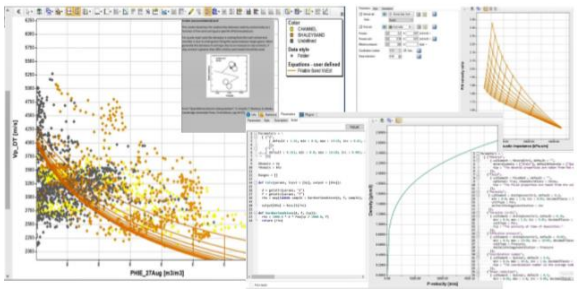

Figure 2. Rock physics model build to separate the non-reservoir and reservoir zone.

Fluid substitutions were done for k-dry control within interval 185 – 225 meters in figure 3.

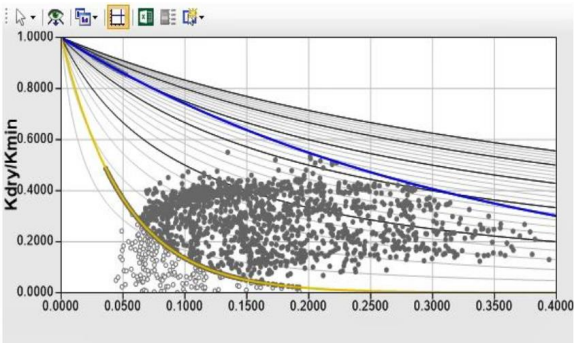

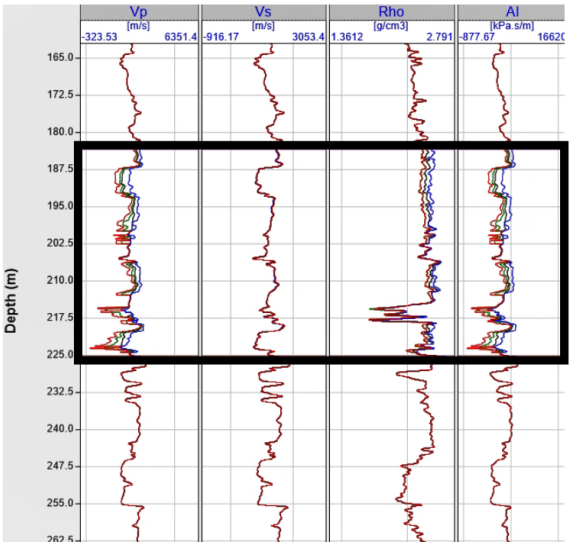

Figure 3. Interval for the reservoir zone use in the pseudo well lithofacies calculation.

A set of lithology definition needed in determining how the inversion will define and calculate throughout the entire field.

In this case we use all four wells and separate by three different lithofacies, Cleans sand, shale (non-reservoir), Bar. Four layers are included in the calculation.

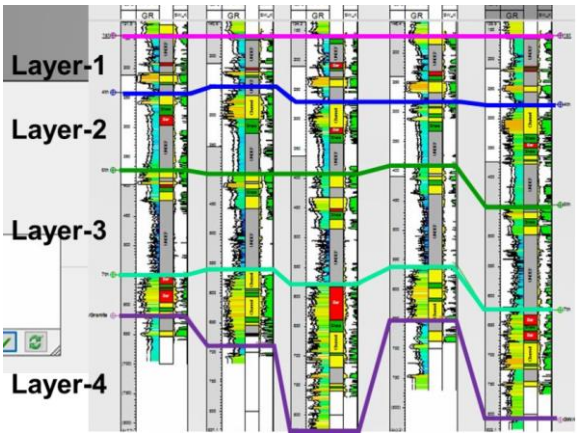

Figure 4. Well correlation for layer define to be included in building the lithofacies model.

Those four layers are further defined as per layer for each of the minimum and maximum thickness in millisecond all together with mean and standard deviation to ensure the accuracy of the inversion and to segregate the slightest difference.

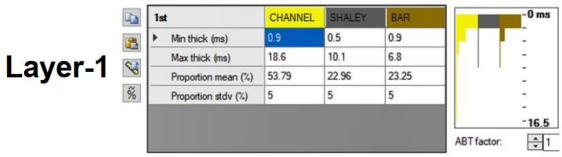

Figure 5. Layer parameterization in defining the thickness of each facies.

This conclude the preparation for the pseudo well, the lithofacies columns are the basis for pseudo wells. From these, a suit of petrophysical and elastic curve are generated by assigning properties to each microlayer using rock physics model calibrated to real data. Each lithofacies modeled separately.

To tie each pseudo wells into seismic we use extended elastic impedance (EEI) concept (Whitcombe et al., 2002) to bridge and act as framework for the trace matching. J-field have a very noisy seismic data and low signal to noise ratio, prior to EEI we done several data conditioning such zero phasing, spectral balancing, and amplitude balancing. To boost the signal to noise ratio.

EEI is a two-term AVO model that assumes that the useful signal component within the data is captured by combination of intercept and gradient. EEI is parameterized by rotation angle in intercept gradient space.

PROCEEDINGS
JOINT CONVENTION BANDUNG (JCB) 2021
November 23rd – 25th 2021

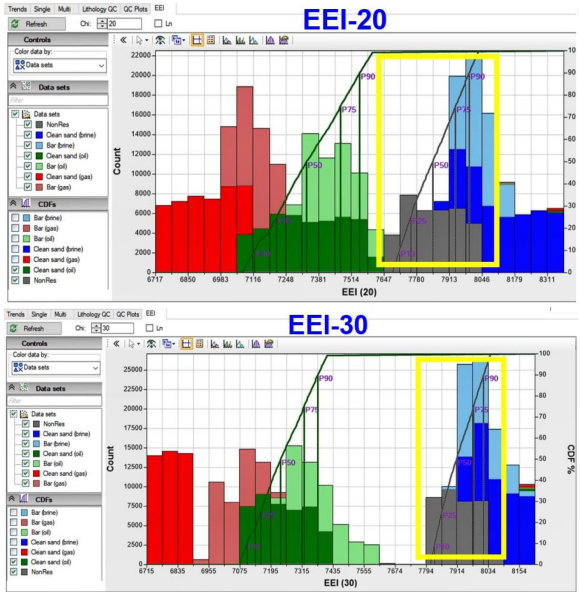

Figure 6. EEI angle are sensitive due to its property drive from intercept and gradient making the angle between them important for any lithology separation.

In this case J-field chi angle for sensitive separation of shale and the reservoir larger than 30 degree.

EEI input are generated based on EEI analysis in obtaining frameworks for the trace matching, we tested 2 different angles for EEI.

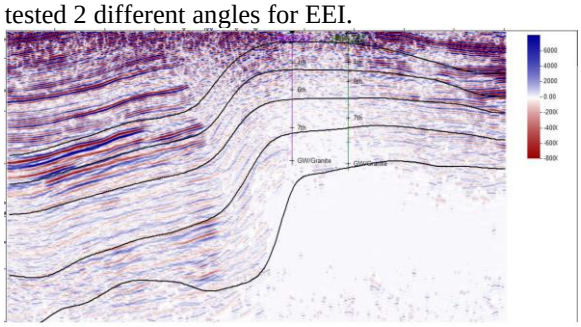

+25 degree

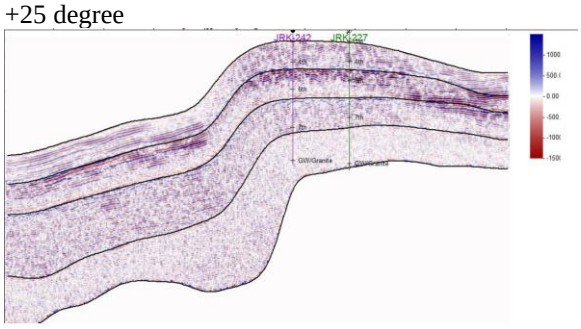

-55 degree

Figure 7. Two different volumes generated to compare the EEI angle and take consideration of following input on ODiSI

+25-degree angle and -50-degree angle created from partial stack seismic.

Thousands of pseudo wells realization has been drawn from each well to create an average from the group of possible outcomes constrained by the rock physics and facies framework define previously. Trace matching process undergone more than 1000 pseudo wells created in each trace. The match quality measured for each macrolayer of each pseudo well. Small static shift is applied to the pseudo wells to optimally align them with the seismic trace and the rms amplitude of the difference (rms error) is calculated. Asset of BMPW is composited from macrolayers with lowest rms error value.

Result and Discussion

The matching proses between pseudo-wells and EEI will result on several output such as probability channel sand distribution and others.

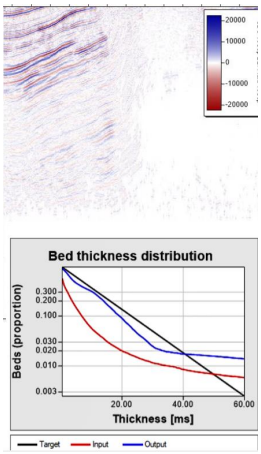

Figure 8. QC tool to make sure the result is close to what target line are.

Post Inversion QC tool adds in lateral continuity to ODiSI inversion results by analyzing facies probabilities of neighboring traces, vertical and lateral continuity is achieved whilst maintaining overall facies proportion and bed thickness

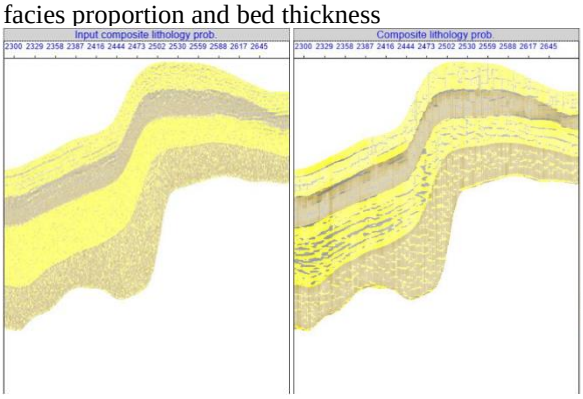

Figure 9. Comparison from input data to composite lithology probability

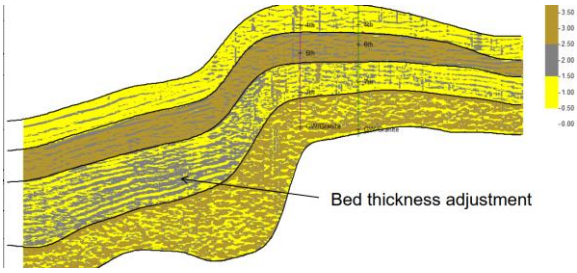

Figure 10. Bed thickness adjustment and final result of probability lithofacies.

Conclusions

Combining pseudo well with litho-sensitive Extended Elastic Impedance (EEI) method, bring new insight to the mature field.

Pseudo wells modeled using CTMC prove that vertical statistic and resolution are maintained throughout the matching process for the field, pseudo well are tied directly to the geologic interpretation.

Proportion between vertical and sand distribution probability are maintained well and displayed clearly, making it more confidence to take on the challenge and use the new insight to the mature field with limited data and poor signal to noise ratio.

References

Grant, S. R., M. J. Hughes, Olatoke, O. J., Philip, Neil, 2019, Stochastic inversion by trace matching for carbonate reservoir property prediction: A Mishrif Reservoir: SEG library, https://library.seg.org

Grant, S. R., M. J. Hughes, Smith, S. R., Gasimov, A., Pickard, M. C., 2017, One-dimensional stochastic inversion for seismic reservoir characterization – A Case Study: SEG library, https://library.seg.org

Connolly, P.A and M. J. Huges, 2016, Stochastic inversion by matching to large numbers of pseudo-wells: Geophysics,81, no. 2, M7-M22

Walker, M., Grant, S. R., Connolly, P.A., Smith, Lindsey, 2016, Stochastic Inversion for facies: A Case Study on The Schiehallion: SEG library, https://library.seg.org

Grimston, O. G., and Connolly, P.A., 2014, Bed Thickness Distributions – The Geology Behind The Geophysics: 76th EAGE Conference & Exhibition, Amsterdam

PROCEEDINGS
JOINT CONVENTION BANDUNG (JCB) 2021
November 23rd – 25th 2021

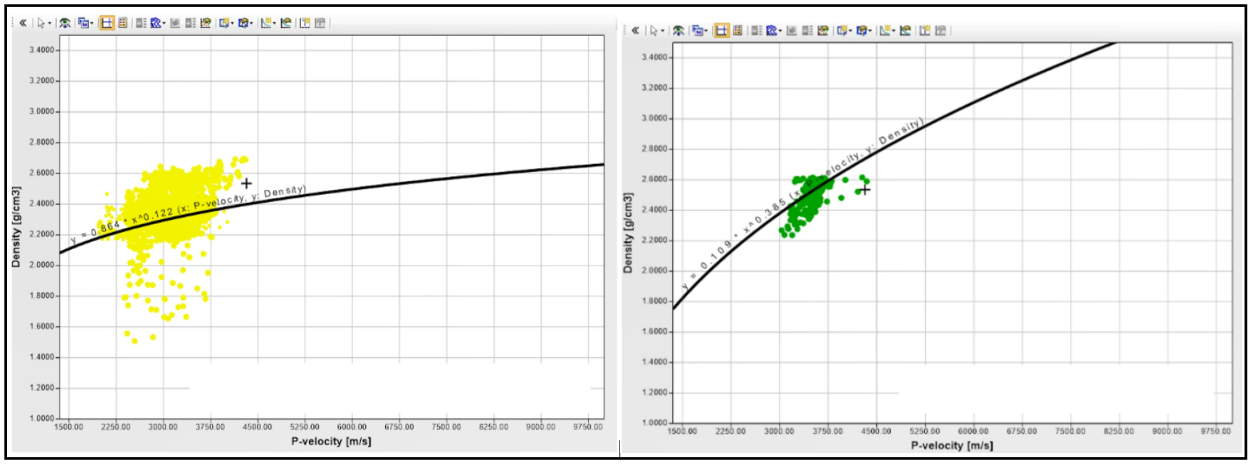

Figure 1. Shale trend and the clean sand trend plotted to ensure the separation and build rock physics model.

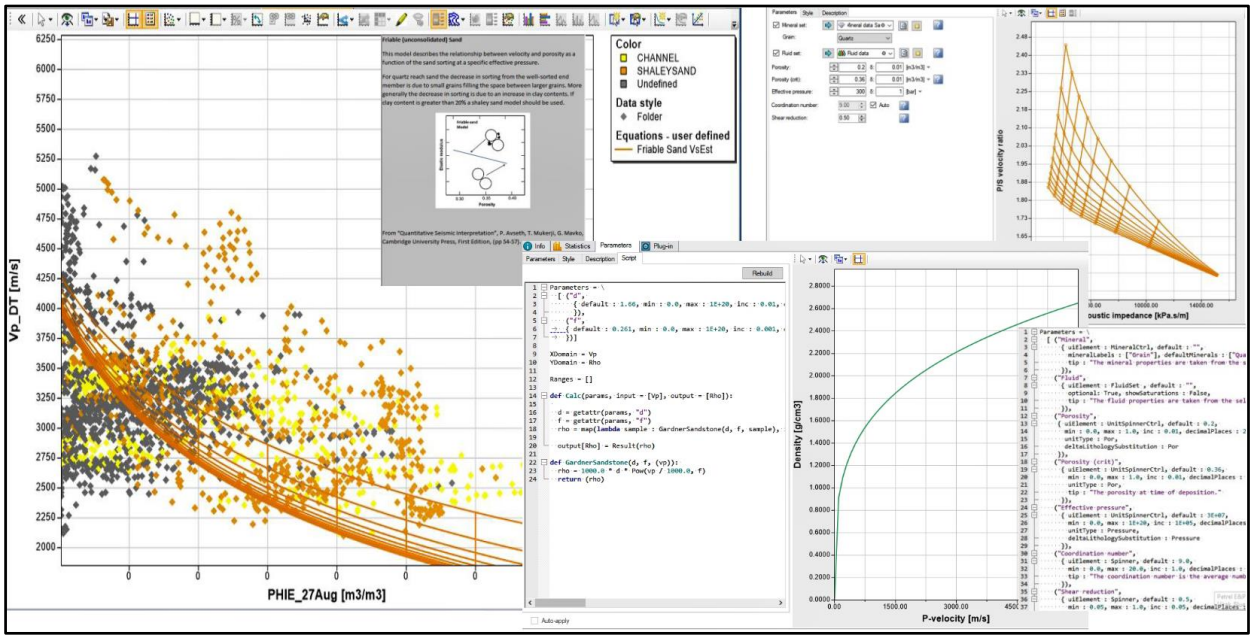

Figure 2. Rock physics model build to separate the non-reservoir and reservoir zone

PROCEEDINGS
JOINT CONVENTION BANDUNG (JCB) 2021
November 23rd – 25th 2021

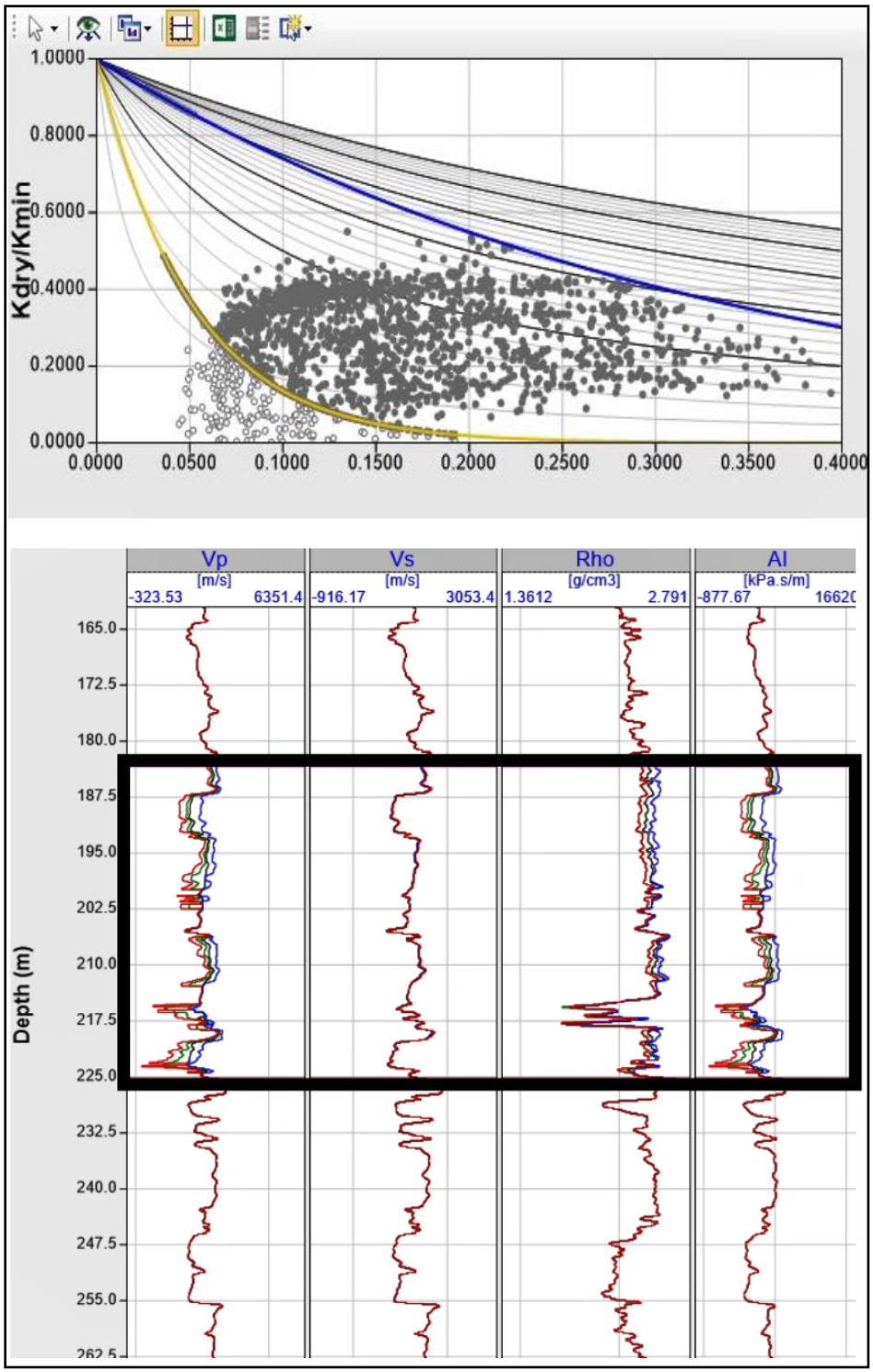

Figure 3. Interval for the reservoir zone use in the pseudo well lithofacies calculation

PROCEEDINGS
JOINT CONVENTION BANDUNG (JCB) 2021
November 23rd – 25th 2021

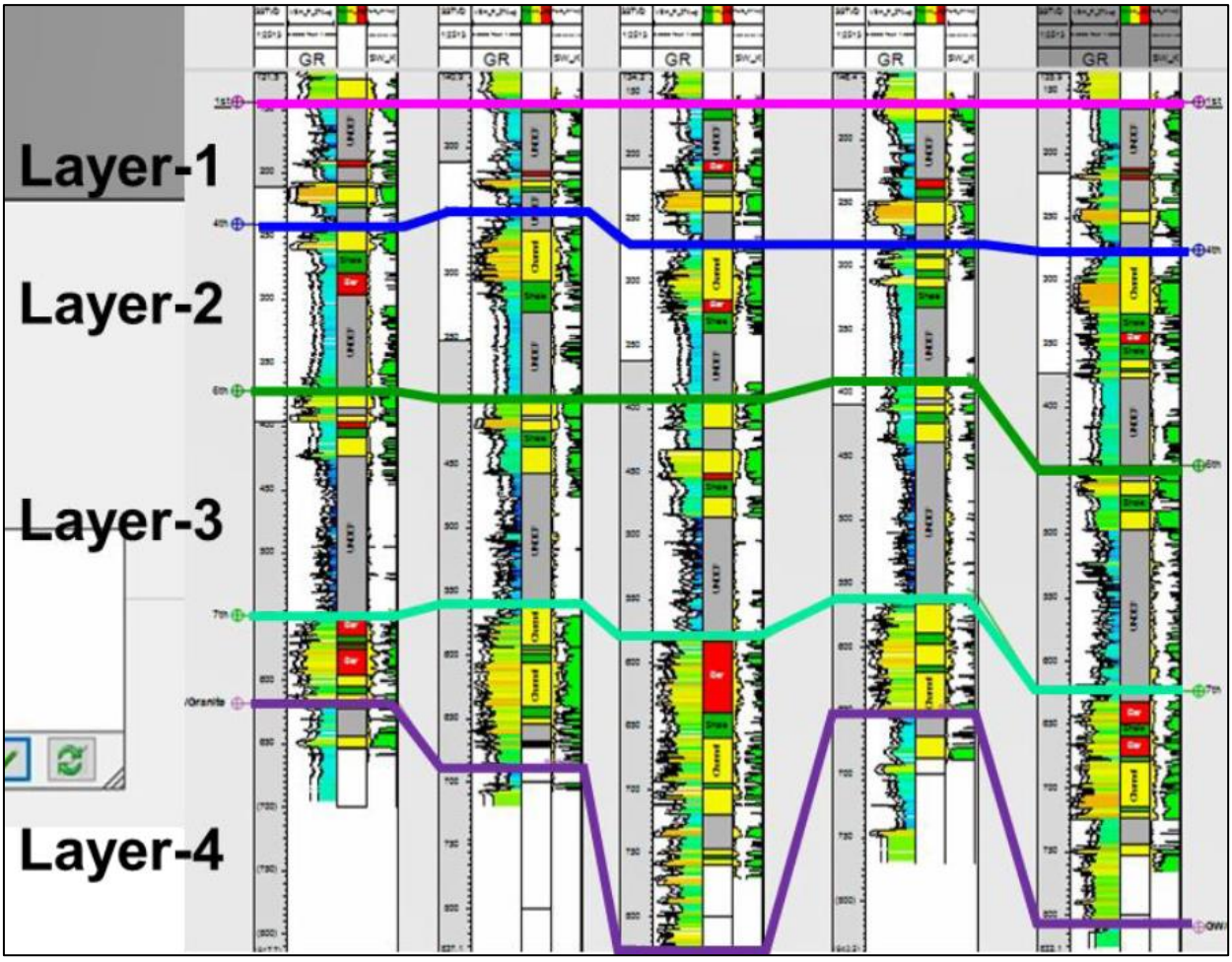

Figure 4. Well correlation for layer define to be included in building the lithofacies model.

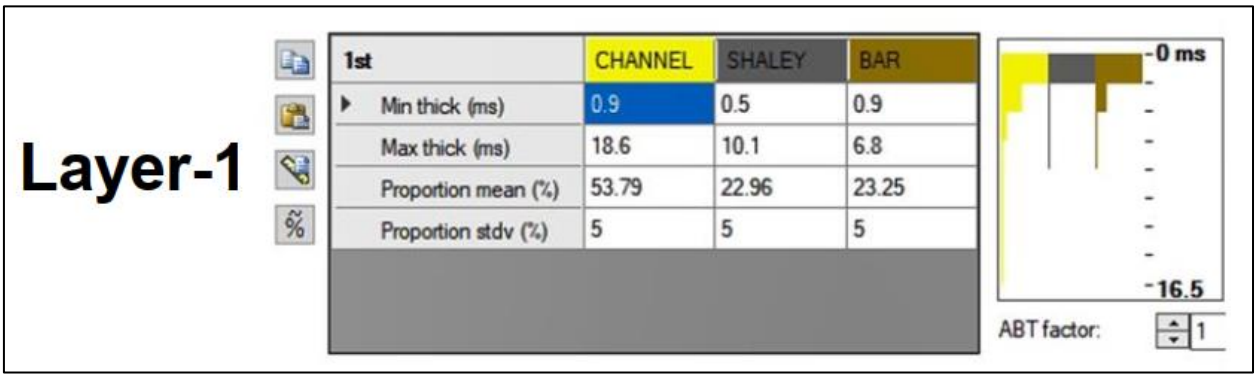

1st	CHANNEL	SHALEY	BAR
Min thick (ms)	0.9	0.5	0.9
Max thick (ms)	18.6	10.1	6.8
Proportion mean (%)	53.79	22.96	23.25
Proportion stdv (%)	5	5	5

Figure 5. Layer parameterization in defining the thickness of each facies

PROCEEDINGS
JOINT CONVENTION BANDUNG (JCB) 2021
November 23rd – 25th 2021

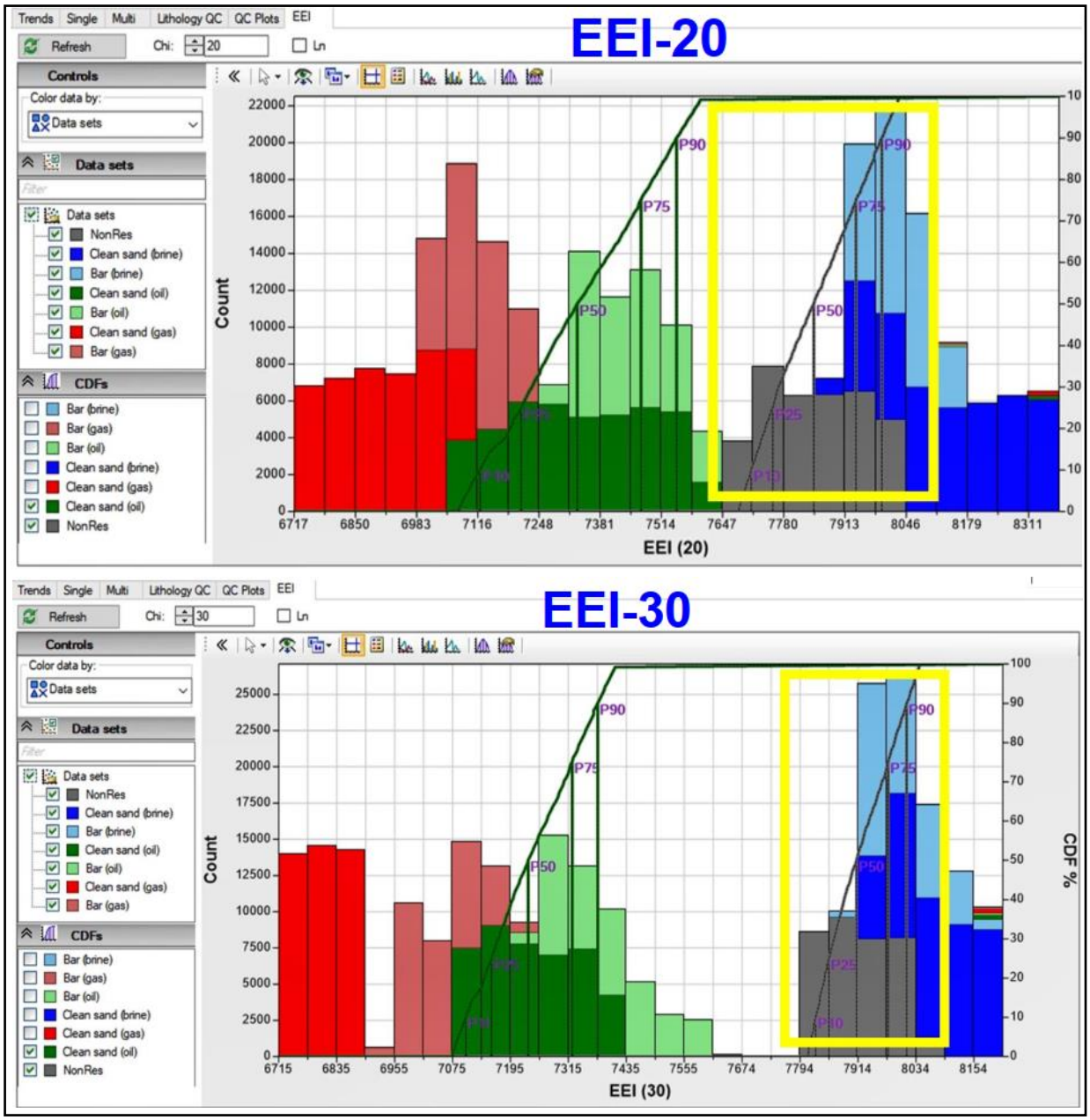

Figure 6. EEI angle are sensitive due to its property drive from intercept and gradient making the angle between them important for any lithology separation.

PROCEEDINGS
JOINT CONVENTION BANDUNG (JCB) 2021
November 23rd – 25th 2021

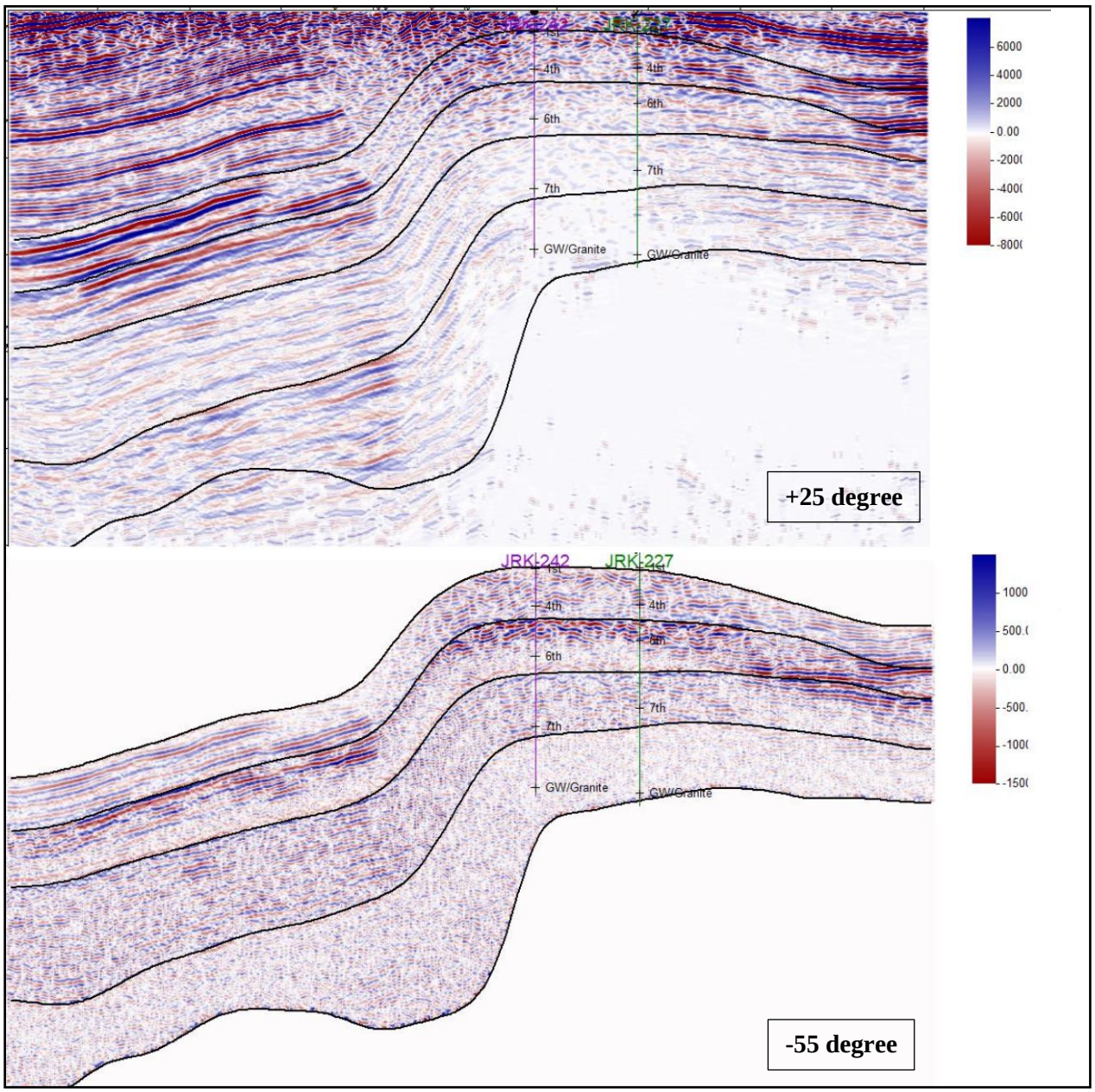

Figure 7. Two different volumes generated to compare the EEI angle and take consideration of following input on ODiSI

PROCEEDINGS
JOINT CONVENTION BANDUNG (JCB) 2021
November 23rd – 25th 2021

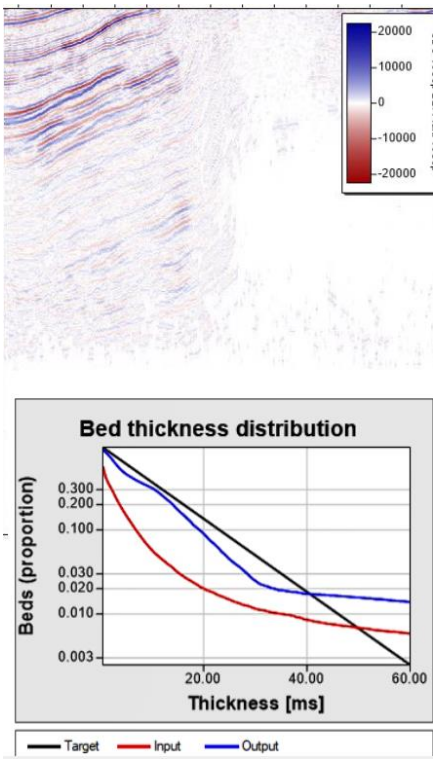

Figure 8. QC tool to make sure the result is close to what target line are.

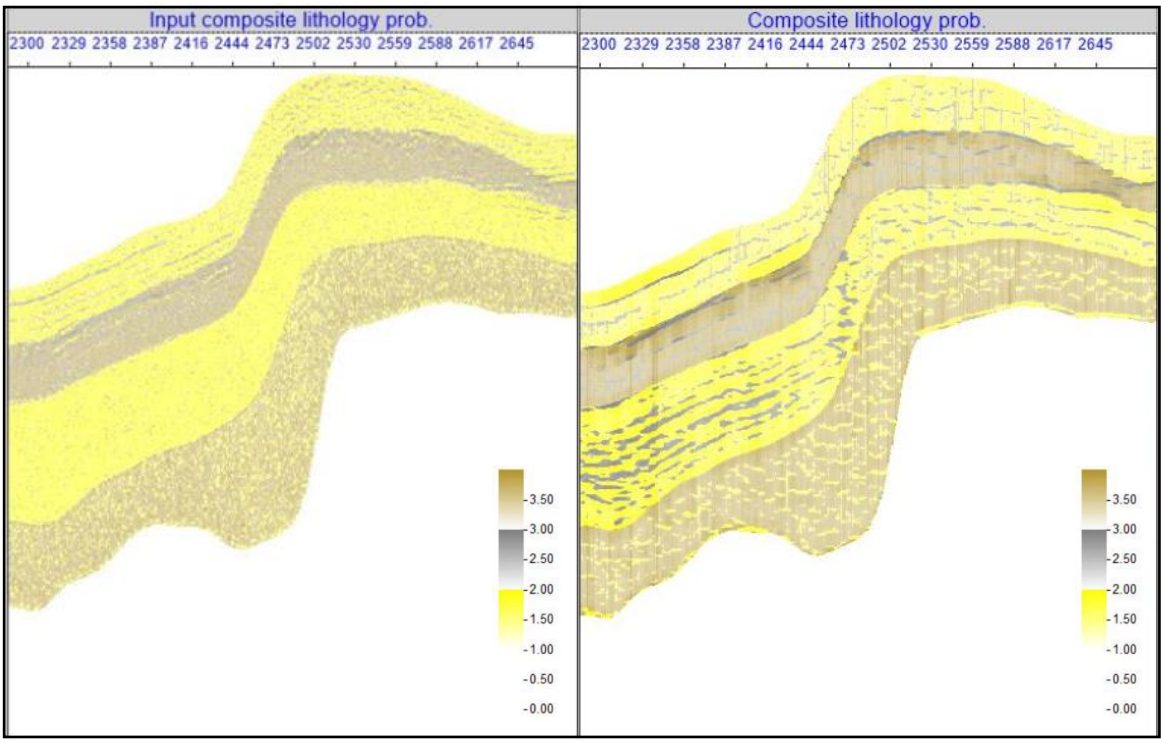

Figure 9. Comparison from input data to composite lithology probability

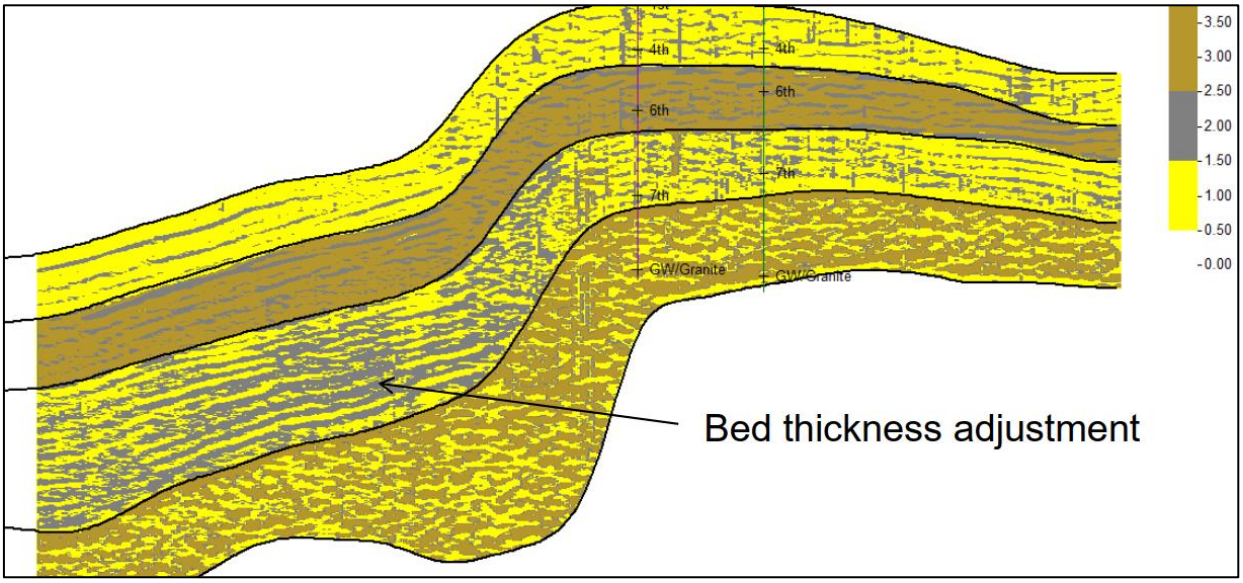

Figure 10. Bed thickness adjustment and final result of probability lithofacies.

PROCEEDINGS
JOINT CONVENTION BANDUNG (JCB) 2021
November 23rd – 25th 2021

Uncertainty Analysis Workflow to Estimate Oil and Gas Reserves as A Guideline for Field Development Planning

Arya Disiyona, SKK Migas

Abstract

It is common practice that estimating resources and reserves for exploration activities is different from the development stage, since has high uncertainty, lack of available data and information, so the method that is often used to estimate resources is probabilistic. However, in development or exploitation period since it is presumed it had more data, the evident of oil & gas discovery, and the presence of commercial hydrocarbons that can be produced, the deterministic method is preferred to be used.

In this paper, the discussion will focus on deterministic applications for field development. Geoscientists assume that the uncertainty at this stage is very low and even tends to be ignored so that the reserve figure used is only a single number. While in this period, uncertainty still exists covering technical aspects, technology application, and commercial valuation with different levels depending on subsurface variables to estimate hydrocarbon reserves. Since 2010, all reserves booked for any field development proposal have always used the deterministic method, however starting in 2018 SKK Migas released the 2nd Revised Pedoman Tata Kerja (PTK) No. 37 on the Plan of Development (POD) and one of its points contains that all subsurface evaluations require to obtain uncertainty analysis & risk management and as well as use multi-scenario methods in calculating hydrocarbons in place. Multi-scenario is a incorporation of probabilistic and deterministic methods for the use of uncertainty analysis of multiple subsurface parameters such as seismic interpretation, petrophysical evaluation, conceptual geology and static modelling. The expected results, for example, are several low case, base case, and high case geological models and are able to provide geological maps for each case.

As a derivative of the PTK-POD implementation, an uncertainty analysis workflow is required to support the use of a multi-scenario method in order to capture all variations of subsurface parameters that have the potential to have an effect on project maturation. The deterministic method is still used as an initial reference in identifying the uncertainty of geological and reservoir parameters through the Tornado Chart. This step is able to reveal which subjects are most sensitive to the Hydrocarbon In-Place value. Once the parameter is selected, the probabilistic calculation will provide a normal distribution curve and show the stability of the parameter distribution in the geostatistical model. In conclusion, the results of the multi-scenario model of low case, base case, and high case in the calculation of reserves are a reflection of the possible risk-outcome that should be considered for decision making in oil and gas projects.

Keywords: Uncertainty Analysis, Field Development, Reserve, Geostatistical Model

Introduction

Exploration and exploitation activities are high-risk businesses. Geological concepts are always uncertain regarding structure, reservoir, seal capacity, facies distribution, etc. Meanwhile, the evaluation of the exploitation and commerciality of hydrocarbons has their respective uncertainties for costs, probability of finding an economical reservoir, technology, and oil/gas prices. The two main different mindsets for the two activities are reflected in the objectives themselves. In exploration is how to find hydrocarbons however in exploitation is how to define the distribution of reservoirs that have economic value.

There are several methods for estimating hydrocarbon resources. In general classification, it can be divided into conventional and geostatistical methods. Conventional methods usually use normal volumetric equations in which each parameter has been determined simply in single number, namely: a). Gross rock volume (GRV) is obtained from a single depth structure map, b) from petrophysical analysis namely average porosity, net to gross ratio, and water saturation numbers, then c) based on the laboratory PVT analysis result that is the average oil/gas formation volume factor. This method has been commonly used in two-dimensional models over the past few decades, but as statistics advances and becomes embedded in the resource calculation process, 2D methods become more precise in estimating hydrocarbon resources.

On the other hand, an explorationist usually uses the conventional method using Monte Carlo Simulation where the process combines probabilistic and deterministic to predict the potential resources in the reservoir. However, this method is only be taken for initial project predictions as a reference for investors

to capture the potential revenue they will receive in the future. Since the objective is to deliver results for high-level decisions, we need to calculate in a simple way and the results are rough numbers. Sometimes, all parameters used to be simulated in a probabilistic process are divided into low values, base values, and high values to create a yield distribution curve.

In geostatistical methods, deterministic and probabilistic processes can be used, especially when combined. The fundamental improvement of this method compared to conventional methods is that we can create three-dimensional models. Recently, three-dimensional modeling is the best method that is popular with all major oil companies and has become an essential part of normal exploration and exploitation activities. Kamali et.al (2013) stated that 3D reservoir models play an important role in geology and petroleum engineering, where each method utilizes geological, mathematical, and statistical information. Modern specialized software programs can model complex and irregular geological volumes in three dimensions. This is done by using geological maps and construction information to create precise models.

Understanding to Uncertainty and Risk

Normally, in the calculation of hydrocarbon resources, the expected number that we will achieve is derived from the average value, although it is possible to get a large variance result. Determining the average number for each parameter is a normal thing for Geologists and Engineers, they sometimes do not take into account the risks that may occur because they do not acknowledge the uncertainty in the distribution of parameters. Savage (2009) says Plans based on the assumption of averages are wrong. An apocryphal example concerns the statistician who drowned while wading through a river whose average depth was only three feet (Figure-1). In Planning for the future, uncertain outcomes are often replaced by a single prediction, called the average. This leads to a class of systematic errors called Flaw of Average, which explains among other things why estimates are always wrong.

In the preparation of development plans, field management decisions are usually made using a deterministic approach. The procedure is to select a single value for each parameter to enter into the appropriate equation and to obtain a single number. Although this approach is very fast, it often leads to one answer and is likely to be a miss leading decision. Since the number of outcomes is only one, the potential risk cannot be measured either. Following provided reserves/resources can be classify to 1P, 2P, and 3P category. Probabilistic procedures are used in some cases for reserve assessment, considering geological uncertainties, or in field evaluations, using Monte Carlo simulations or similar techniques to incorporate economic uncertainties. Probabilistic approach is a rigorous method with comprehensive process, it needs more time consuming since building a robust model. As the uncertainty range parameter input to the software, the outcome will be a distribution model. This approach is quantifying the risk, therefore result numbers of range really informed for decisions.

Figure-2 describes those two main approaches that geologists and petroleum engineers always use to estimate hydrocarbon resources. The two methods have differences in the process and purpose of their application. The Society of Petroleum Engineers (SPE) defines this method as a guideline in the Petroleum Resource Management System (PRMS) document.

People always mix up the terms uncertainty and risk, but they shouldn't. There is nothing uncertain about reality, it is our vision of reality which is about uncertainty. Therefore, uncertainty is not an intrinsic property of the system; it is the result of incomplete knowledge by the observer. Uncertainty is a situation where there is limited knowledge and information that can lead to the target, in this case sometimes there is no key information to understand the possible outcomes to anticipate the worst-case scenario. Risk is a variety of possible conditions as an impact that arises from a situation of uncertainty. Another understanding of risk reflects how uncertain outcomes lead to high potential missed opportunities. Uncertainty cannot also be estimated, it is modeled. Therefore, stochastics takes on its role.

Often there is significant uncertainty in many subsurface input parameters early in the project life cycle. Uncertainty arises since most subsurface parameters are estimated from a small sample of reservoir properties from discovery and appraisal wells. The methodology for measuring the impact of uncertainty is still not well established due to of the amount of variables that have to be considered. Basically, development risk is a function of geological, economic, and technological uncertainty. In this paper we focus on geological uncertainty. In geostatistical models, volume in place and recovery factors are sufficient in risk analysis as a reflection of uncertainty in seismic interpretation, petrophysical evaluation, PVT behavior from laboratory analysis, reservoir pressure data, core analysis, well test results, etc. Recently, the quantification, understanding, and management of subsurface uncertainty has become increasingly important for oil and gas companies as they strive to optimize reserve portfolios, make better field development decisions, and improve day-to-day technical options such as well planning.

PROCEEDINGS
JOINT CONVENTION BANDUNG (JCB) 2021
November 23rd – 25th 2021

As we are very knowledgeable about range of uncertainties in every stage of the oil and gas industry regarding the quality and amount of data at each stage or time. In general, at the exploration stage the range of uncertainty is wide. Analog data usually comes from adjacent fields and the method used is simple Monte Carlo probabilistic which is classified into Low (P90), Best (P50) and High (P10) estimates. Then at the Appraisal and Production stage, additional data were obtained, including over-appraisal wells, additional seismic surveys, and even production data so that the reserve figure becomes more certain and reduces the range of uncertainty. This explanation can be summarized in Figure-3 and the estimation of reserves in the oil and gas field can be more firm when it comes to the abandonment stage.

Multiscenario Concept

The two major approaches in recent reserve prediction are deterministic and probabilistic methods with individual improvements. This method is very common, especially in Indonesia where the deterministic method is included as standard procedure in field development planning before 2018. The advantage of this method is that it is simple, fast, and does not require sophisticated computers. But nowadays, the case of field development is becoming more costly, complex, and unique. Uncertainty is reflected in the challenges and risks and inherent in the complexity of the project, so it seems a must to transform the methodology to a more comprehensive process that is able to capture these difficulties to anticipate any possible impacts in the future.

The probability of uncertainty should be quantified when estimating reserves, and the method that can account for all uncertainties is the Probabilistic method. This method has some inherent problems. They are affected by all input parameters, including the most likely and maximum values for those parameters. However, in one method, it cannot calculate back the input parameter associated with the reserve, only the end result is known but it does not know the exact value of any input parameter. On the other hand, deterministic methods calculate reserves using tangible and explanatory values so that all parameters are exactly known. Susceptibility to deterministic sometimes ignores variability and uncertainty in the input data compared to the probability that it is possible to include more variance in the data. Considering the challenges in such methods, the combination of deterministic and probabilistic methods allows geologists and engineers to solve the problem of reserve estimation. The name of the combination method is the multi-scenario method.

Multiscenario or sometimes called scenario method or multirealization method in PRMS 2011 essentially defines an extension of the deterministic method but range of possible deterministic outcomes or scenarios are described. The scenario method combines elements of a deterministic approach and a fully probabilistic method. It describes a range of possible outcomes for the reservoir, which is consistent with the observed data. The distribution of low case, best case, and high case is made up of several deterministic cases. One result that is physically consistent within this range with in-place volume estimates is called subsurface realization. For the purpose of obtaining recovery factors, we can then define a development scenario for each subsurface realization and subsequently book the recoverable volume in the appropriate category. In the end result, the multi-scenario method makes it possible to select parameters to derive a tornado chart and then utilize the distribution curve that produces statistical calculations, such as minimum and maximum values, mean, most likely value, standard deviation, and percentile (Figure-4). In any scenario, we can extract maps/models for each parameter, such as vshale map, porosity map, sw map, hydrocarbon pore volume, etc.

Uncertainty Analysis Workflow

The availability of data for oil and gas fields is generally insufficient to minimize the uncertainty related to the construction of geological or reservoir models. An understanding of the uncertainties involved in geological modeling is an essential tool to support decisions in field development as they are present in the process. The process is even more critical because most investments are made during the stage when uncertainty is greater (Schiozer et.al., 2004). Deutch (2002) mentions that a geostatistical reservoir model is a “set” of spatially distributed of parameters including (1) structural definition of each stratigraphic layer, (2) facies within each stratigraphic layer, and (3) petrophysical properties such as porosity, permeability, and the residual saturation on a by layer and by facies basis. Each model consists of one realization that is not built for the same facies realization; one porosity realization is associated with each facies realization. The uncertainty created by multiple realizations is realistic when the geological conceptual framework and statistical parameters, such as the variogram and size distribution, are well known. This parameter is not well known early in the reservoir life cycle; therefore, there is more uncertainty than is measured by a set of geostatistical realizations generated with the same of underlying parameters.

A more realistic space of id uncertainty is determined by a combination of scenario-based approaches and conventional geostatistical modeling. As a schematic illustration in Figure-5, the reservoir can fit in any of

different conceptual models (M-I, M-II, or M-III) with probabilities 0.5, 0.3, and 0.2. In scenario-based, there may be different sets of modeling parameters (e.g.: variogram) and some derivations of 3, 2, and 3 sets of possible parameters for a conceptual geological model. After setting specific parameters, geostatistical realizations are generated for each of the eight scenarios.

Meanwhile in the geostatistical uncertainty process, there is a realization of L and equally probable to gives the set of parameters used to create it. Bayes' law, the probability of each realization is calculated by multiplying the probability of each realization (1/L) by the probability of each scenario. A reasonable definition of a scenario and the assignment of conditional probabilities are critical. Scenarios can reflect different aspects of uncertainty, for example, direction of deposition, fault seals, facies quality and fracture density. Scenarios can also reflect uncertainty in critical statistical parameters such as the net-to-gross ratio (low, medium, high) or the range of the variogram. Aspects of large-scale discrete uncertainty are qualified by scenario-based approach, while uncertainty due to incomplete data is quantified by multiple geostatistical realization.

Normally in geostatistical modeling, regardless of whether the method is deterministic, stochastic, or a combination of both, the objective of the process is to have a number of hydrocarbons in place. The integration of work in geostatistical modeling is the result of geophysical interpretation, petrophysical evaluation, and geological interpretation. Through specific processes and certain methodologies, several maps/models will be produced vshale, porosity, water saturation, permeability, hydrocarbon pore volume, etc. In general, geologists or engineers only make one model of each parameter because they think the results are the most correct, but they do not realize that many uncertainties in the model can affect the success of field development. Decisions related to field development and reservoir management are always associated with the risks involved due to the uncertainty present in the process.

The conceptual workflow explained by Deutch (2002) needs sophisticated hardware and applications to capture all these uncertainties. The challenge for calculating uncertainty is that it is time consuming, the more complex the model and the uncertainty, the more time it will take to solve the problem. To manage ambiguity, we need to divide the main parameter groups into two. The first group is large-scale discrete parameters, such as depth structure maps, seismic attributes, seismic inversions, and fracture distributions. Ideally these parameters are used as scenario based however the best possible model is usually been selected. The second group of parameters is part of the uncertainty analysis such as petrophysical parameters (including cut off), statistical variogram, facies shape, fluid contact, formation volume factor, seeds number, and rock typing. This group will be used when the probabilistic process starts.

Figure-6 shows an uncertainty analysis workflow that can be used for geomodelers as a way out of reducing the time required to create geostatistical models while maintaining the quality of the results. This workflow consists of two stages, namely (1) performing a normal deterministic geostatistical modeling to produce hydrocarbons in place then followed by (2) a probabilistic method which include define the uncertainty of the parameters, heavy hitter selection based on the tornado chart, and deciding how many realizations may be required to form the best normal distribution curve.

The most critical to review the uncertainty is when defining incomplete information to some of the parameters used in geostatistical modeling. By heavy hitter selection by using a tornado chart can make it easier for geomodelers to select which parameters may influence the probabilistic process (Figure-7). The objective of heavy hitter selection is to screen out less parameter ranges due to (1) to reduce hardware time consumption to run the application when the number of parameters is few, (2) to avoid ambiguity of the best model number due to the spiky normal distribution curve as a result of statistically very dominant value. Unreal values populated in a certain number can form a "strange" shaped curve due to the narrow range of parameters distribution included in the calculation. The selected 5 to 7 parameters used in the uncertainty analysis yielded a significant impact in reducing almost half the running time of the total 20 parameters.

The required of realization amount depends on the "precision" for uncertainty assessment required. A large amount of realization is required to assess the 1% to 99% percentile of the hydrocarbon in place distribution, but not always. The basic concept, if the running process has reached a solid model, sometimes the number changes are not significant when increasing the realization, and produces a smooth normal distribution curve shape (Figure-8). The best model should have both conditions because they are interrelated. Therefore, there is actually no specific formula that can estimate how much realization is needed.

One of the advantages in the multi-scenario method, based on normal distribution curves, is that the decision to select a certain model is extracted only from the required map, e.g., hydrocarbon pore volume and any petrophysical model at a certain percentile. And another benefit is that iteration from static to simulation can be started earlier because in uncertainty analysis multi-scenario workflows are

able to capture incomplete information of dynamic reservoir modeling.

The output of uncertainty workflow analysis is to select which probability models that able to use for simulation modeling, there are low (P90), best (P50), or high case (P10). However, in normal condition the recommended model is best case as an optimum case which equal to 50% percentile. However, at several conditions when according to the technical evaluation stated reveals (1) the availability data is not sufficient, (2) fewer quality data provided, and (3) remotely location of potential gas buyer can be as one of parameter for choosing of development strategy, the possibly recommended model for simulation is low case model (P90 or 10% percentile) as a part of risk management. In simulation model, engineer will always to assess the uncertainty dynamic data based neither but will not be discussed in this paper.

Discussion and Conclusions

The aim of geostatistical modeling is to utilize a wide variety of data at different scales and accuracy, to build a reservoir model capable of representing geological heterogeneity and also quantifying uncertainty by generating a number of equiprobable models. In the preparation of development plans, management decisions are usually taken using a deterministic approach. The probabilistic approach is often not used because of the amount of time and computational effort required. However, recent hardware and software improvements have made it possible to incorporate more accurate production predictions in the process. Furthermore, uncertainty analysis can also be carried out as one of the workflows of the process itself.

The proposal workflow for uncertainty analysis is important to include a multi-scenario approach to quantifying the impact of uncertainty in the development process. The low, best, and high cases on the results of the multi-scenario method do not always represent the 1P, 2P, and 3P reserve classifications. This condition should also be considered for the type of field, related to its complexity and uncertainty. Usually, cases from multi-scenarios are reflected in the range of reserve numbers from low, best, and high estimates. For green or developing fields, the range may be reflected in the 2P or 3P reserve category, while in mature fields the range may be in the 1P reserves category. This situation describes of uncertainties exist in the field. The green fields due to limited data available possibly need more additional information, such as infill wells, seismic survey, or production data. However in mature fields, probably reservoir pressure itself is depleted, development wells located at optimum position to drain hydrocarbon, and many update dynamic reservoir information are collected, so range of information is narrow reflected proven reserves indicates to entire field.

In addition, recommended model either P90 or P50, from certain selected realization model it can be extracted the map of properties, for example vshale, porosity, permeability, or even HCPV. And the map resulted is typical with deterministic approach.

Meanwhile for deterministic approach, recently since sophisticated hardware easily provided, also can use using geostatistic method, based on stochastic calculation single input properties reservoir in the wells will be distributed through the area but only get single output distribution model either. It takes simple process, fast, single answer but does not quantify the risks. The result model directly able to classified 1P, 2P, or 3P reserves category.

A combination of deterministic and probabilistic approaches with several simplifications in the workflow is allowed based on the required precision, the most common and usual approach is the selection of critical variables through sensitivity analysis. This new proposal approach is already applicable to several fields in Indonesia as a part technical assessment to capture subsurface uncertainties. Accountability of management decisions regarding risk analysis can be accommodated in the uncertainty analysis process. The analysis steps start from selecting scenarios, running multiple realizations, ranking models, then selecting the final model that will be the basis for field development. The methodology described in this paper is applied to geological uncertainty which is the most important parameter of the process; however, research is still needed to address operational and technological uncertainties and also for better reservoir characterization procedures when uncertainty exists.

References

Deutch, C.V., 2002. Geostatistical Reservoir Modeling. Oxford University Press, New York.

Kamali, M.Z., Omdivar, A., Kazemzadeh, E., 2013. 3D Geostatistical Modeling and Uncertainty Analysis in Carbonate Reservoir, SW Iran. Journal of Geological Research, Vol 2013.

Savage, S.L., 2009. The Flaw of Average: Why We Underestimate Risk in the Face of Uncertainty. John Wiley & Sons Inc, Hoboken, New Jersey.

Schiozer, D.J., Ligero, E.L., Santos, J.A.M., 2004. Risk Assessment for Reservoir Development Under Uncertainty. Journal of the Brazilian Society of Mechanical Sciences & Engineering, Vol XXVI.

PROCEEDINGS
JOINT CONVENTION BANDUNG (JCB) 2021
November 23rd – 25th 2021

Acknowledgements

The author would like to thank SKK Migas for approval to publish this paper. Highest appreciation should also be given to the subsurface team who provided useful data and fruitful discussions as well as comprehensive insights on creating uncertainty analysis workflows for field development.

PROCEEDINGS
JOINT CONVENTION BANDUNG (JCB) 2021
November 23rd – 25th 2021

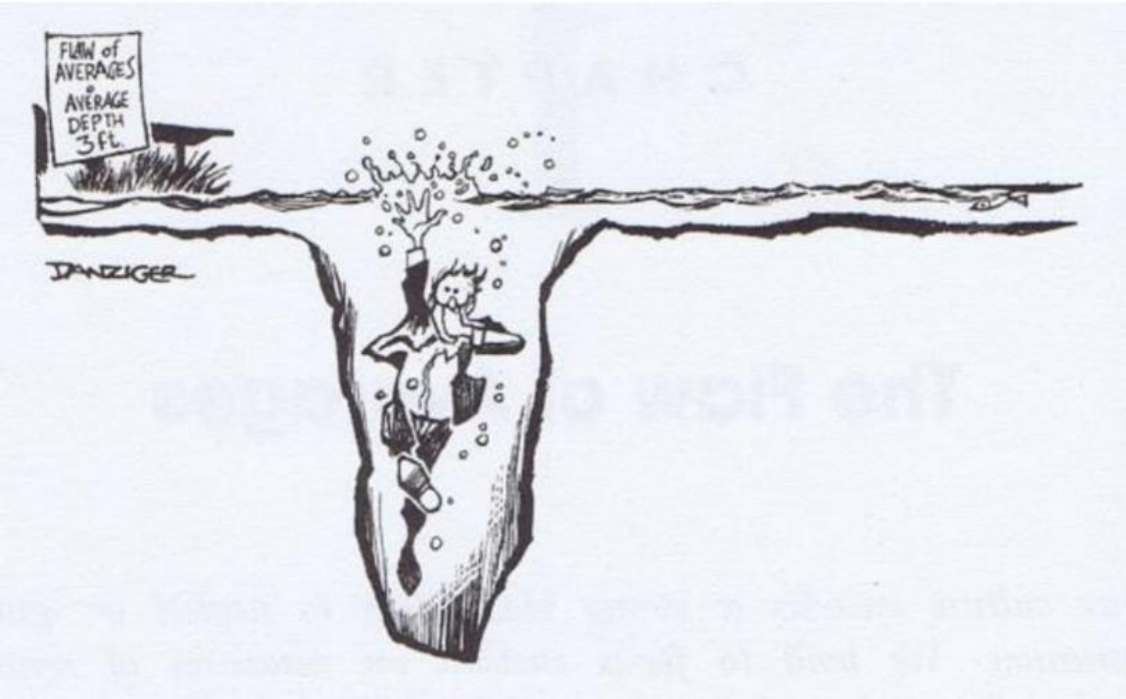

Figure-1: An apocryphal example concerns the statistician who drowned while fording a river that was, on average, only three feet deep, as depicted in the sensitive portrayal by cartoonist Jeff Danziger (Savage, 2009). Miss leading to anticipate for uncertainty in average statement of depth.

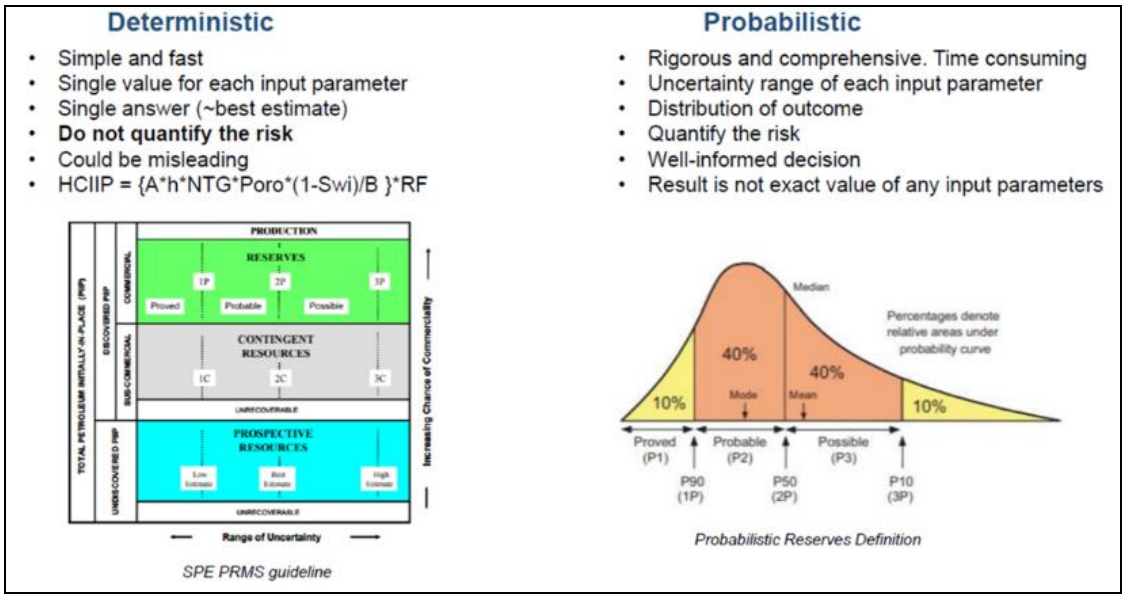

Figure-2: Two general approaches of reserves estimation method with pro and contra. In context of uncertainty analysis will be considered in probabilistic method and more robust process, while deterministic is fast and simple equation.

PROCEEDINGS
JOINT CONVENTION BANDUNG (JCB) 2021
November 23rd – 25th 2021

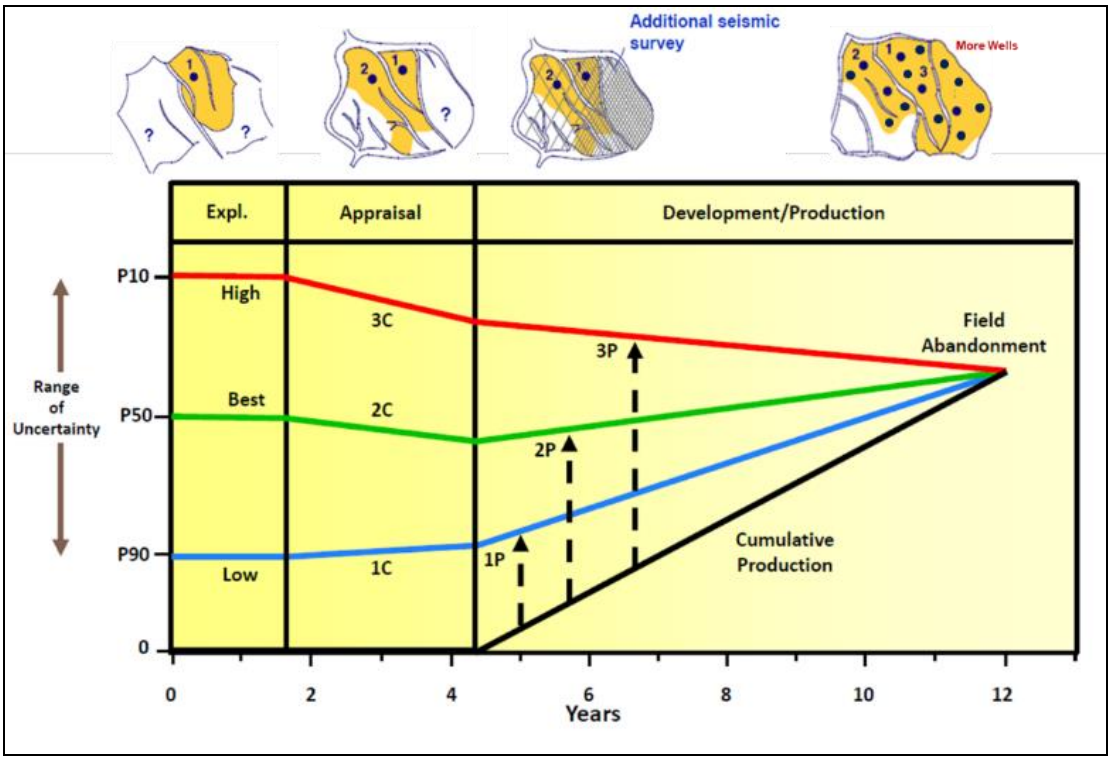

Figure-3: The image gives an understanding of the progression of reserves number during the time. Figures above table describes availability data during each of stage, for example: number of wells, seismic survey, and production data. The uncertainty has the highest range in exploration period with minimum data and will be decreased when the data acquired for appraisal, then the "real" reserves number may be more firmed on abandonment stage.

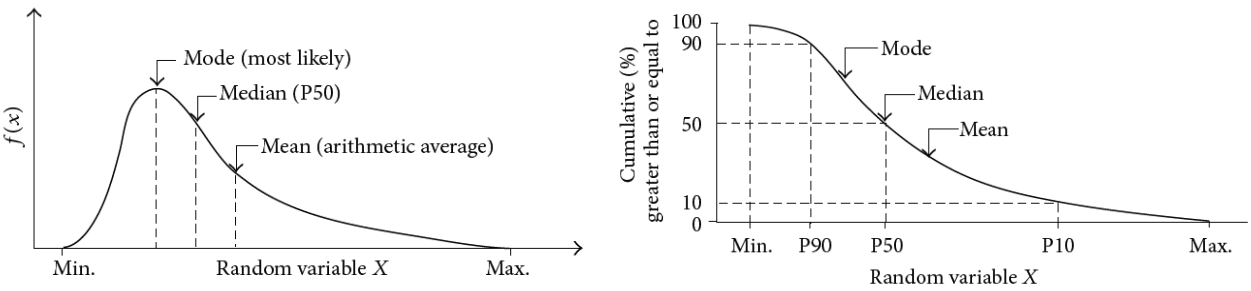

Figure-4: In probabilistic method, we able to see the distribution of number from minimum to maximum with its probability cases as the result of statistical calculation. Left figure is normal distribution curve describes the position of mode, median, and mean variables. Right figure is probability distribution curve describes percentiles variable for any possibility's outcome.

PROCEEDINGS
JOINT CONVENTION BANDUNG (JCB) 2021
November 23rd – 25th 2021

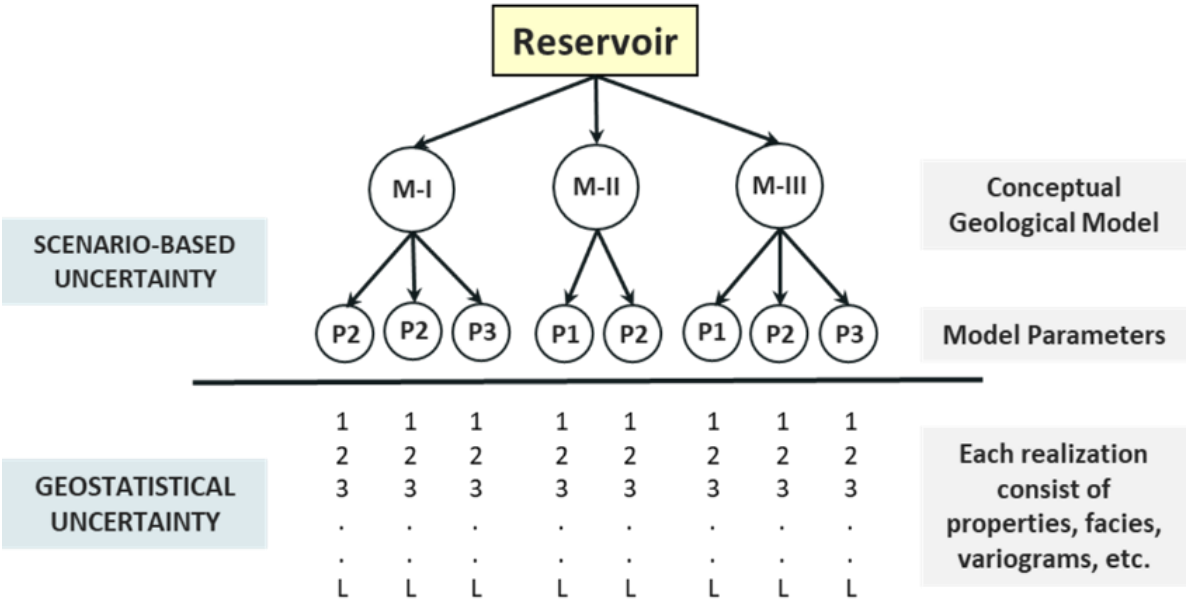

Figure-5: Schematic illustration of combining scenario based and geostatistical based of uncertainty that accommodated in the process of multiscenario method (modify Deutch, 2002).

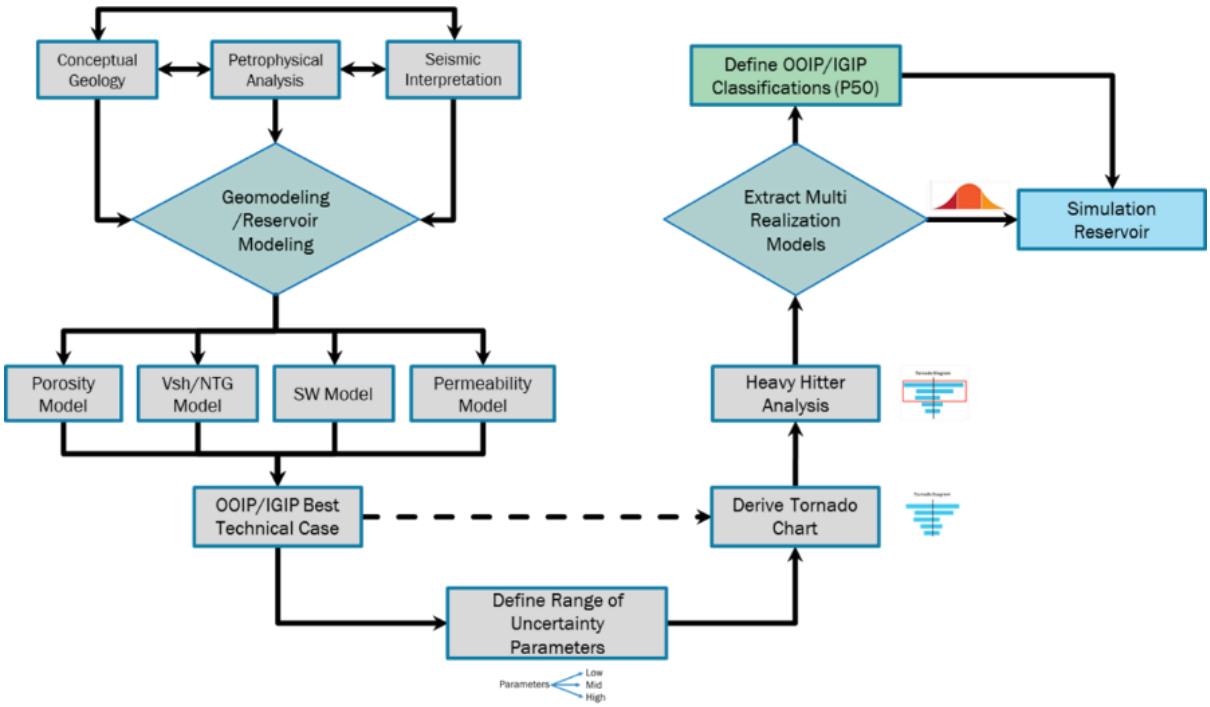

Figure-6: The uncertainty workflow guides to estimate of reserves in geostatistical modelling. Recent hardware able to obtain both deterministic and probabilistic methods. Multiscenario combines these methods to capture scenario base in deterministic and distribute variables to probabilistic process. Common geostatistic modelling with deterministic process resulting a model of porosity, Vsh/Ntg, Sw, permeability, and hydrocarbon in-place. Probabilistic process initiated by defining parameters uncertainty through tornado chart and resulting hydrocarbon distribution numbers in normal distribution curves.

PROCEEDINGS
JOINT CONVENTION BANDUNG (JCB) 2021
November 23rd – 25th 2021

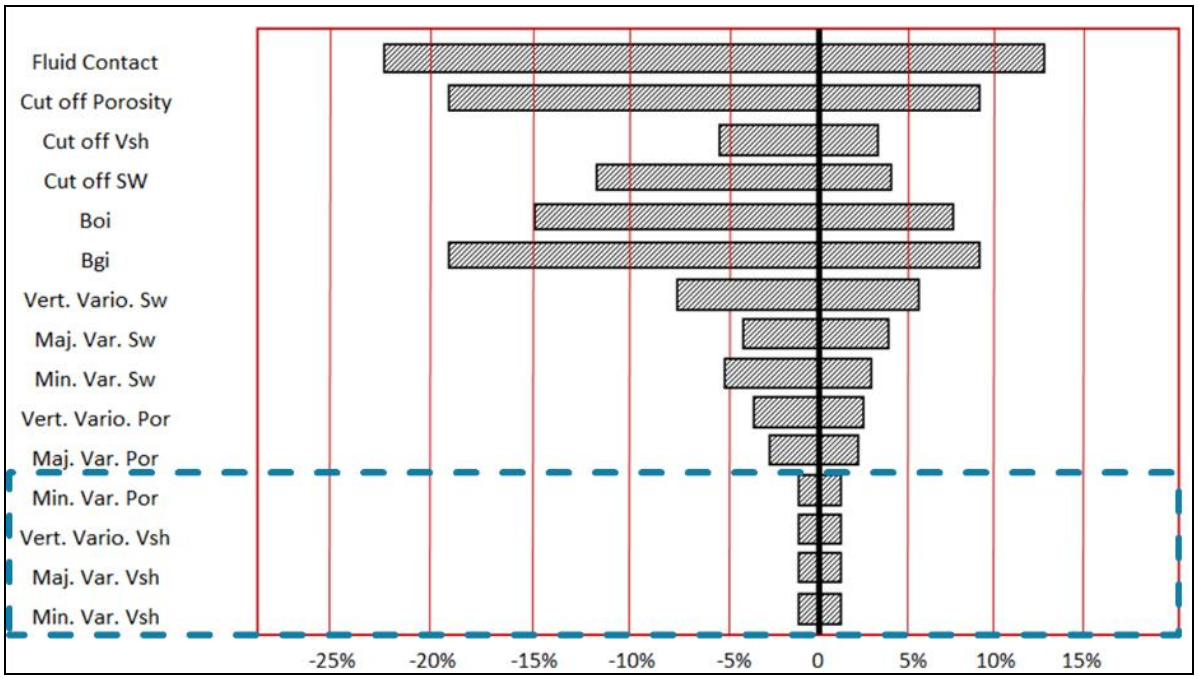

Figure-7: Tornado chart informs the range of variables of geostatistic before to obtain probabilistic Monte Carlo. In order to time effort reduction, unsignificant impact of variables with small range can be screen out and not to be included in running process (dash blue box).

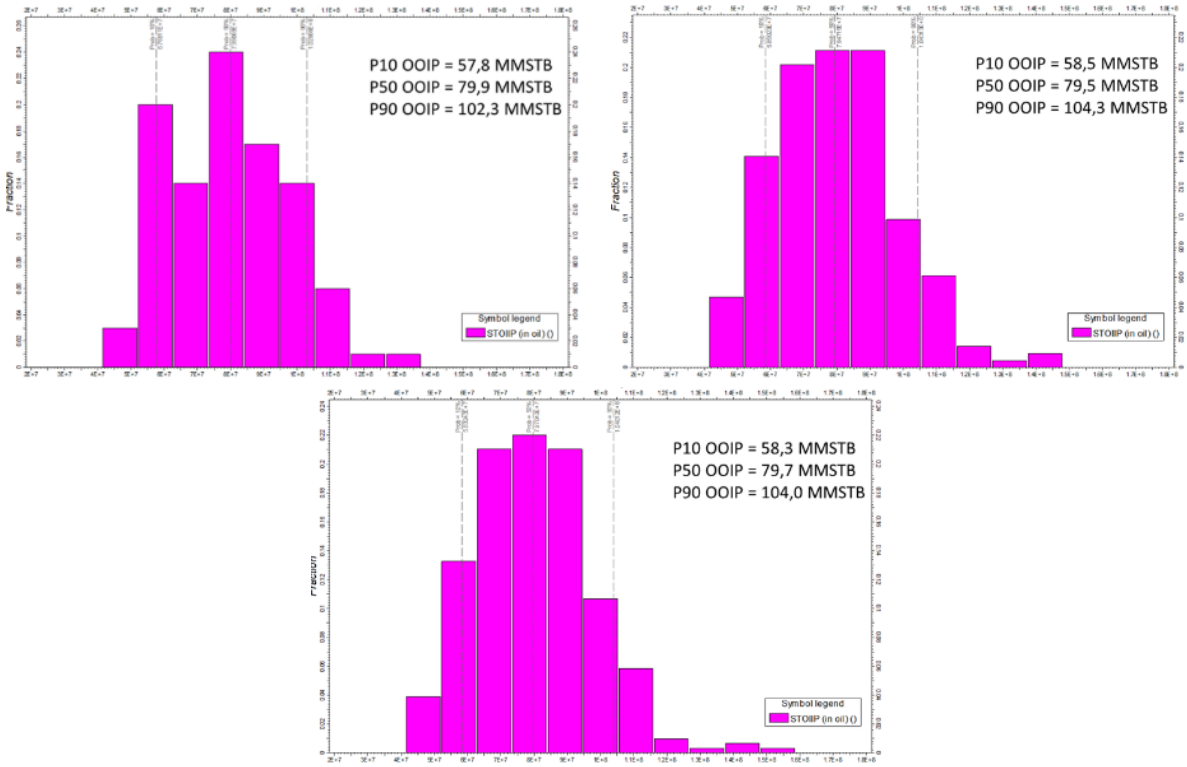

Figure-8: Three figures above describe the amount of realizations or iterations: upper left 100x, upper right 200x, and below 300x. Although each realization gives narrow discrepancy value but better curve indicates better parameter models in geostatistic distribution. 300x iterations are the best curve and model, therefore it can be proceeded to dynamic modelling.

PROCEEDINGS
JOINT CONVENTION BANDUNG (JCB) 2021
November 23rd – 25th 2021

DIGITAL CORE ANALYSIS OF CAPILLARY PRESSURE IN SANDSTONE

Astra Agus Pramana dan *Utami Farahdibah*
Petroleum Engineering, Universitas Pertamina, Jakarta, Indonesia

Abstract
This research aimed to obtain the petrophysical parameters of the capillary pressure in a sandstone from 3D modelling of high-resolution images. By integrating a number of 2D slice results, a plot of capillary pressure vs water saturation was built. When performing digital simulations using 512 x 512 x 512 pixels, the effect on the resulting image was clearly seen using adaptive thresholding. The obtained porosity was 29.5% while the permeability was obtained through iteration was 3942 mD. This quite large value is because the synthetic core was made from coarse sand grains. It was found that at the depth of free water level of 984 ft, the obtained capillary pressure is 167.36 psi with water saturation at 4%.

Introduction
Digital Rock Physics or (DRP) is a method based on digital images because it is an alternative method for finding physical quantities from rocks with more effective and efficient and non-destructive properties. Physical properties of rocks that are usually sought are porosity, specific surface area, permeability, capillary pressure, and saturation. In its development, Digital Rock Physics can show the physical properties of rocks on a micro scale with microstructural parameters such as rock pores, grain size, pore network and surface area. The main goal of rock physics or Rock Physics itself is to find and provide an understanding of model relationships between field data and data transformations obtained from geophysical surveys.

Capillary pressure analysis is one method that is often used in the validation process of a parameter. Rock physical quantities such as porosity, permeability, capillary pressure, and so on are important aspects in petroleum because they are especially useful in determining the quality of a reservoir. The application of DRP applications has been widely used in several sandstone samples from sample data analysis.

Digital images (3D images) on rocks can be obtained by scanning using a CT-Scan tool and combined with simulation software to obtain digital images of the reservoir rock. The projection is then reconstructed into a cross-sectional or incision image. The reconstructed image will then be processed to obtain the desired physical quantity, to obtain this digital image, it is necessary to adjust the physical parameters that can affect the resulting image. Using the help of imaging methods, complex pore geometries can be represented. Therefore, digital rock physics is developing very quickly and has become a potential and valuable resource in determining the relationships between rock properties. This method relies on imaging techniques to obtain high resolution rock representations with 3D samples. The pore spaces and mineral matrices of natural rocks are digitized and then numerically simulated to obtain estimates of various macroscopic rock properties. The volume depiction was obtained using high-resolution micro-scale computer tomography (CT) which was used to capture and visualize the three-dimensional pore geometry structure of the reservoir rock.

Data and Method
The research carried out is pure research or basic research by performing software simulations. The data collection method used is the literature method. The digital simulation used is a DRP software which is used to process data and to iterate over the core samples in order to visualize the core samples in 3D, and also to see how the fluid flows and the direction of the fluid flow. While the data used are digital core data from sandstone originating from synthetic samples or artificial samples made using a mixture of cement and sand.

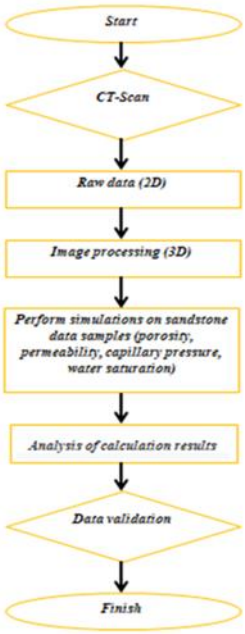

At the beginning of doing this research by doing a micro CT-scan on a sample of sandstone cores. Then from this data will form a digital core data called raw data which is still in 2-dimensional form through an incision on each core slice. Furthermore, the raw data

PROCEEDINGS
JOINT CONVENTION BANDUNG (JCB) 2021
November 23rd – 25th 2021

is processed in A DRP software for image processing so that it can visualize in 3-dimensional form, then from the digital core sample data we initiate and impose limits on the data by segmenting so that the data reads as solids and the data is read as pivot then you can immediately find out the porosity and permeability values obtained, while the capillary pressure and water saturation values are obtained through calculations from the formula discussed in the previous chapter. And the last one is validating the data to find out whether the results that have been studied with the results of digital rock core carbonate data are valid or not.

Result and Discussion

- *Sandstone in Digital Rock Physics*

This type of reservoir has quite high variations in the value of porosity and permeability, so it is very good to be a good quality reservoir. In the sandstone sample in the 3D model it is very important to know to see the microstructure parameters of the rock in the form of pores and rock matrix in detail and to be able to model the pore structure and to be able to know the fluid flow velocity model in the sandstone core sample or sandstone. In this sandstone sample, digital simulation calculations are carried out to calculate the values of porosity, permeability, capillary pressure and water saturation.

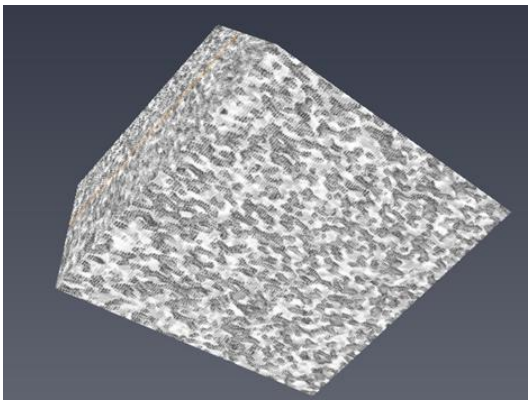

Figure 1. 3D image of a digital core sample

Rock pores are indicated by color (black / white), whereas rock dense matrix is indicated by color (white and gray). This color difference is due to the different density of each mineral.

- DRP Images

To obtain petrophysical data from the micro ct-scan image of core rocks, it is also necessary to verify with laboratory results. For 1 complex core sample it takes 8-12 hours rather than laboratory measurements which take 1-2 days even for relative permeability it may take several months. From this data, it can also be done in parallel for various kinds of petrophysical analysis and also various types of EOR.

By performing simulations using a DRP software from micro ct-scan data, which focuses on visualizing 3-dimensional depictions and to be able to analyze, we must know data properties such as lattice info used, namely 512 x 512 x 512 pixels or in a number of 512 pieces in the form 2 dimensions and voxel size, namely 1 x 1 x 1 to determine the area on the slice so that the results are made into 3 dimensions, then a threshold process is carried out to distinguish between rock pores and the matrix in the sandstone sample. At 512 x 512 x 512 pixels it greatly affects the quality of the resulting digital image because when processing the digital image data it looks clearer than 256 x 256 x 256 pixels.

In a digital image, a set of matrix data is usually called a pixel. Each pixel contains an intensity value with a certain scale so that it can indicate the color in the original image. A digital image that has an increasing number of pixels will produce a good image. From a set of pixel matrices with an intensity value on a gray scale, namely from 0 - 255. Where the value scale of 0 means black this is to show hollow rocks while the 255 value scale means white this is to show its cementation. From the rendering of the information regarding the percentage of the pore content to the total material or the pore with solids / grains to be extracted, then from the digital image it is necessary to convert it with the thresholding stage, which is to determine which rocks have cavities with those without cavities in the rock.

Judging from the porosity and permeability results obtained from the 3D visualization results with the Digital Rock Physics (DRP) method, it can be concluded that the results from rock samples are included in the porous sandstone category and this rock has the ability to pass through fluids to accumulate oil, water, and gases which usually have very good relations between the matrices. With high porosity and permeability values, it can interpret the ideal sandstone layer as reservoir rock.

- *Calculation of Capillary Pressure (Pc) from DRP*

To obtain the value of calculating capillary pressure from free water level 0 - 300 meters by doing trial and error, the capillary pressure formula will be obtained from the following equation (Gibrata, 2019):

$$Pc = Diff\ water\ and\ oil\ Gradient\ x\ HAFWL\ (ft)$$

Where:

Pc = capillary pressure, psi.

Water gradient = 0.495, psi/ft

Oil gradient = 0.320, psi/ft

HAFWL = Height above free water level, ft

PROCEEDINGS
JOINT CONVENTION BANDUNG (JCB) 2021
November 23rd – 25th 2021

Table 1. Capillary pressure calculation results

water gradient=			0.495	psi/ft	
hydrocarbon gradient=			0.33	psi/ft	
wg-hg =			0.165	psi/ft	
HAFWL (m)	HAFWL (ft)	CAPILLARY PRESSURE (Psi)	HAFWL (m)	HAFWL (ft)	CAPILLARY PRESSURE (Psi)
0	0	0	100	328	59.12
0.1	0.328	5.05412	110	360.8	64.532
0.2	0.656	5.10824	120	393.6	69.944
0.3	0.984	5.16236	130	426.4	75.356
0.4	1.312	5.21648	140	459.2	80.768
0.5	1.64	5.2706	150	492	86.18
1	3.28	5.5412	160	524.8	91.592
1.5	4.92	5.8118	170	557.6	97.004
1.7	5.576	5.92004	180	590.4	102.416
2	6.56	6.0824	190	623.2	107.828
4	13.12	7.1648	200	656	113.24
6	19.68	8.2472	210	688.8	118.652
8	26.24	9.3296	220	721.6	124.064
10	32.8	10.412	230	754.4	129.476
20	65.6	15.824	240	787.2	134.888
30	98.4	21.236	250	820	140.3
40	131.2	26.648	260	852.8	145.712
50	164	32.06	270	885.6	151.124
60	196.8	37.472	280	918.4	156.536
70	229.6	42.884	290	951.2	161.948
80	262.4	48.296	300	984	167.36
90	295.2	53.708			

It can be seen from the results of the above calculations that the difference in pressure at HAFWL (Height Above Free Water Level) is within 300 meters or equivalent to 984 ft, the difference in pressure obtained is 167.36 psi. It can be concluded that the height above free water level has an influence on capillary pressure because from the results obtained above, the deeper the free water level is, the greater the pressure difference is obtained, the smaller the HAFWL, the smaller the pressure difference given will be.

- *Calculation of Water Saturation (Sw) from DRP*

One of the very important properties in rocks to know the calculation is the saturation value. After knowing the results of Pc data, then to obtain water saturation (Sw) the formula will be obtained from the following equation (Gibrata, 2019):

$$Sw_{RRT} = \left[\frac{\frac{a}{\frac{Water\ gradient - hydrocarbon\ gradient}{HAFWL\ x\ 3.28}}}{\left(\frac{k}{\emptyset}\right)^{0.5}}\right]^{\left(\frac{1}{b}\right)}$$

Where:

Sw_RRT = *Water saturation of reservoir rock type*, v/v

a = 5 (constant RRT)

b = 2,65 (constant RRT)

HAFWL = *Height above free water level*, ft

k = Permeability, mD

Ø = Porosity, v/v

Table 2. The results of the calculation of water saturation

WHERE:			
a=		5	
b=		2.65	
water gradient=		0.495	psi/ft
hydrocarbon gradient=		0.33	psi/ft
wg-hg =		0.165	psi/ft
Porosity		0.295	
Permeabillity (mD)		3942	
HAFWL (ft)	WATER SATURATION (%)	HAFWL (ft)	WATER SATURATION (%)
0	0	328	0.067794476
0.328	0.918903232	360.8	0.0653995
0.656	0.707413843	393.6	0.063287012
0.984	0.607049384	426.4	0.061404022
1.312	0.544599614	492	0.058176123
1.64	0.500619213	524.8	0.056776406
3.28	0.385399626	557.6	0.055492265
4.92	0.330720988	590.4	0.054308156
5.576	0.315463728	623.2	0.053211349
6.56	0.296698304	656	0.052191296
13.12	0.228411959	688.8	0.051239174
19.68	0.196005974	721.6	0.050347534
26.24	0.175842	754.4	0.049510035
32.8	0.161641472	787.2	0.048721244
65.6	0.124439017	820	0.047976467
98.4	0.106784211	852.8	0.047271631
131.2	0.095798862	885.6	0.046603177
164	0.088062403	918.4	0.045967981
196.8	0.082207382	951.2	0.045363285
229.6	0.0775618	984	0.044786647
262.4	0.073750356		
295.2	0.070544195		

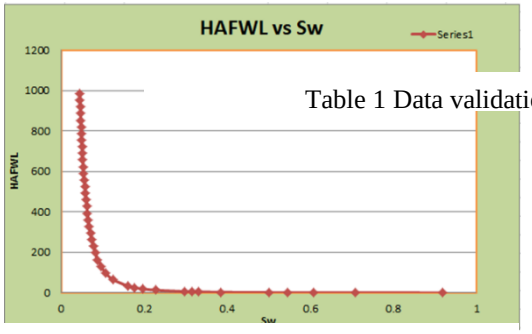

Table 1 Data validation

Figure 2. HAFWL vs Sw

In the graph in Figure 2, we can find out how the vertical distribution of saturation is. And from Figure 1.2 it can also be proven that the minimum water saturation value is 0.04 or about 4% which causes the liquid that sticks to the rock grains so that it can no longer flow due to capillary pressure.

- *Curve of the Pc vs Sw parameters of the DRP*

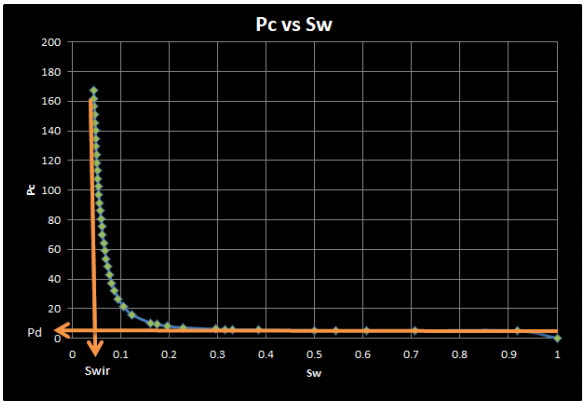

Figure 2. Pc vs Sw

PROCEEDINGS
JOINT CONVENTION BANDUNG (JCB) 2021
November 23rd – 25th 2021

Initially the oil migrates from the source rock to the reservoir. With a Pd of 5 psi to replace the water in the reservoir because initially the water contains 100% Sw and when the oil enters, the Sw will gradually decrease so the oil will increase, when the oil enters there needs to be pressure (Pd) to push the water out from pores. The pressure (Pd) is getting smaller or easier because the values of porosity and permeability are good so that when the water cannot come out again even though the Pc pressure is increased however much, Sw remains at that value. The remaining Sw that cannot come out again is called Swir.

In validating the data in this study using simulation results on carbonate rocks that were examined by researchers using simulation results on sandstone. The core samples used in sandstone are synthetic core samples from a homogeneous mixture of cement and sand, while the core samples used in carbonate rocks are non-homogeneous carbonate rock sample data. Following are the calculation results obtained from the simulation results for carbonate rock and sandstone:

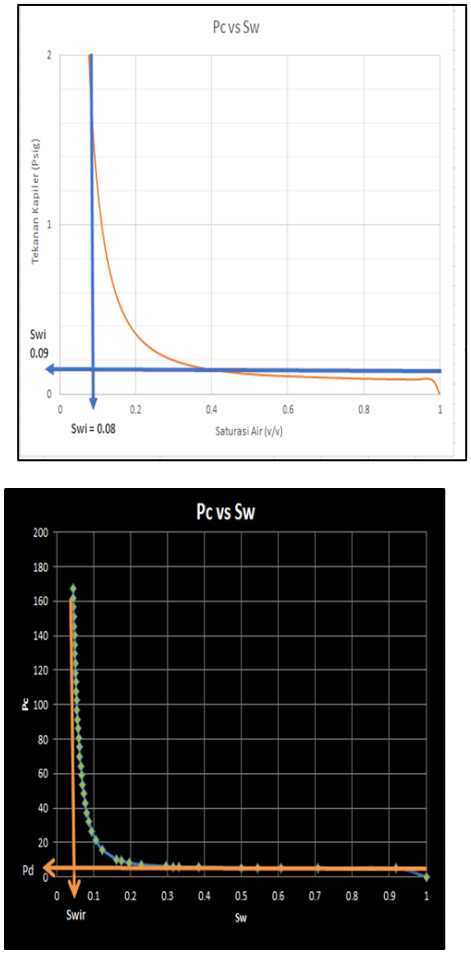

Figure 3. Comparison of carbonate curves and sandstone curves

Perhitungan berdasarkan batuan karbonat				Perhitungan berdasarkan batuan pasir			
Porositas	Permeabilitas (mD)	Pc (Psi)	Sw (%)	Porositas	Permeabilitas (mD)	Pc (Psi)	Sw (%)
0,18	8,10	0	1	0,295	3942	0	1
		0.08646921	0.98			5.05452	0.918903
		0.08831644	0.93603909			5.10824	0.707414
		0.09016386	0.8736958			5.16236	0.607049
		0.09202329	0.8257283			5.21648	0.5446
		0.09383671	0.78145728			5.2706	0.500619
		0.11243096	0.55257328			5.5412	0.3854
		0.13094825	0.45117857			5.8118	0.330721
		0.14947945	0.59072864			5.92004	0.315464
		0.1680157	0.34947832			6.0824	0.296698
		0.18654795	0.3190286			7.1648	0.228412
		0.20508219	0.29536309			8.2472	0.196006
		0.22361644	0.27628687			9.3296	0.175842
		0.24215068	0.26048576			10.412	0.161641
		0.26068495	0.24711849			15.824	0.124439
		0.27921918	0.23561825			21.236	0.106784
		0.29775542	0.22558728			26.648	0.095799
		0.31628767	0.21673725			32.06	0.088062
		0.33482192	0.20885324			37.472	0.082207
		0.35335616	0.2017714			42.884	0.077562
		0.37189041	0.19536432			48.296	0.07375
		0.39042466	0.18955125			53.708	0.070544
		0.4089589	0.18439125			59.12	0.067794
		0.42749515	0.17927859			64.532	0.065399
		0.4460274	0.17473916			69.944	0.063287
		0.46456164	0.17052706			75.356	0.061404
		0.48309589	0.16660725			80.768	0.059711
		0.50163014	0.16294511			86.18	0.058176
		0.52016438	0.1595143			91.592	0.056776
		0.53869863	0.15629146			97.004	0.055492
		0.55723288	0.15325638			102.416	0.054308
		0.57576712	0.15039152			107.828	0.053211
		0.59430137	0.14768154			113.24	0.052191
		0.61283562	0.14511297			118.652	0.051239
		0.63136986	0.14267393			124.064	0.050348
		0.64990411	0.14035387			129.476	0.04951
		0.66843836	0.13814343			134.888	0.048721
		0.6869726	0.13603425			140.3	0.047976
		0.70550685	0.13401882			145.712	0.047272
		0.7240411	0.13209039			151.124	0.046603
		0.74257534	0.13024288			156.536	0.045968
		0.76110959	0.12847078			161.948	0.045363
		0.77964384	0.12676911			167.36	0.044787

From the results of the validation of the carbonate data and the sandstone data that have been studied, this uses the same concept and method of work, but the results of the calculations are slightly different because of differences in digital core data on the rocks being studied respectively. The most visible difference from the results of the comparison above is that the permeability value obtained for the carbonate data itself has a value of 8.10 mD, while for the sandstone data it is obtained a value of 3942 mD, the difference in this value is far enough that it also affects the calculation on Pc and Sw. the shape of the curve is a little different. So it can be concluded that the data under study is valid.

Conclusions

The conclusions in this study are as follows:

1. The 2D image results from the digital core sample data are processed and simulated using DRP software, so a digital core image is formed in 3D using the Digital Rock Physics (DRP) approach.
2. The threshold used is Interactive Thresholding because later the data obtained will be more accurate in processing it so that it can calculate capillary pressure.

3. The calculation results show that the average porosity value of the sandstone sample is 29.5% and the total permeability value is 3942 millidarcy, the permeability value is large because the cores used are synthetic or artificial cores. From the core samples that have been made, the capillary pressure value is 167.36 psi, and the result is a Swir value of 4% and a

Pd value of 5 psi with a free water level range of 0-300 meters.

4. From the results of the analysis and comparing with the carbonate data, the results show that the curves that are compared are almost the same, there is only a slight difference in values between the 2 data samples.

References

Al-Kharusi A.S., M. J. Blunt, 2007, Network Extraction from sandstone and carbonate pore space images, Journal of Petroleum Science and Engineering, 56, 219-231.

Al-marzouqi, H. Digital rock physics using CT scans to compute rock properties. IEEE Signal Process. Mag. 2018, 35, 121-131.

Amabeoku, M.O., Al-Ghandi, T.M., Mu, Y., & Toelke, J. (2013). Evaluation and Application of Digital Rock Physics (DRP) for Special Core Analysis in Carbonate Formations.

Andra, H., Combaret, N., Dvorkin, J., Glatt, E., Han, J., Kabel, M. (2013). Digital rock physics Benchmarks-Part I: Imaging and segmentation Computer & Geosciences, 50, 25-32.

Dvorkin, J. P. 2009. Relevance of Computational Rock Physics. Geophysics Journal. Geophysics Department, Standford University. Standford. USA.

Fourier, D.E.L., 2014. Analysis of Permeability and Tortuosity of Fontainebleau Sandstone and its Models Using Digital Rock Physics Approach. Physics of Earth and Complex System, Faculty of Mathematics and Natural Sciences, Bandung Institute of Technology, Indonesia.

Gibrata, Muhammad. A., 2019. An Integrated Petrophysical Evaluation for Reservoir Characterization and Modelling for Field Development. Dragon Oil, ENOC.

Handoyo, Fatkhan, Fourier, D.E.L.,. 2014. Digital Rock Physics Application: Structure Parameters Characterization, Materials Identification, Fluid Modeling, and Elastic Properties Estimation of Saturated Sandstones. Himpunan Ahli Geologi Indonesia (HAGI) Proceeding. Solo, Bandung Institute of Technology, Indonesia. Department, Stanford University. Stanford. USA.

Xiang-Jun, L., Li-Xi, L., Hong-Lin, Z (2014). Digital Rock Physics of Sandstone Based on Micro-CT Technology. Chinese Journal of Geophysics – Chinese Edition 57(4).

PROCEEDINGS
JOINT CONVENTION BANDUNG (JCB) 2021
November 23rd – 25th 2021

Study of Pore Types Influence for Permeability Value in Carbonate Reservoir Using Differential Effective Medium (DEM) and Adaptive Neuro-Fuzzy Inference System Algorithm

Reza Wardhana[1], Amega Yasutra[1], Dedy Irawan[1], M. Wahdanadi Haidar[2]
[1] *Petroleum Engineering Departement Bandung Institute of Technology*
[2] *PT. Pertamina Hulu Energi*

Abstract
The pore system in a carbonate reservoir is very complex compared to the pore system in clastic rocks. According to measurements of the velocity of propagation of sonic waves in rocks, there are three types classification of carbonate pore classifications: Interparticle, Vugs and Crack. The complexity of these pore types can lead to errors in the calculation or interpretation of the reservoir itself so that characterization of the carbonate reservoir tends to be more difficult.

In this research, elastic modulus modeling will be carried out by taking into account the pore complexity of the carbonate reservoir. Differential Effective Medium (DEM) is an elastic modulus modeling method that takes into account the heterogeneity of pores in the carbonate reservoir. This method adds pore type inclusions gradually into the host material to the desired proportion of the material. In addition, this study will also predict the permeability value of the reservoir using Adaptive Neuro-Fuzzy Inference System algorithm from well logging measurement data as the input and core data from laboratory measurements for training data and validating the predicted results of permeability values in well depths domain. So, the permeability value and pore type variations in well depth domain will be obtained for further interpretation.

Thus we can see which type of pore has a good permeability value in the carbonate reservoir. This kind of thing can also help the engineers to determine a good perforation zone in the well by considering the pores type in the carbonate reservoir and the permeability values that have been predicted before.

Introduction
Carbonate reservoirs consider as one of the main reservoir which produce oil and gas worldwide. Unfortunately, carbonate rocks are more complicated than siliciclastic rocks so that carbonate reservoirs are usually harder to understand compare to sand reservoirs. The difference between the carbonate reservoirs and the sand reservoirs is the distance of deposition. While local deposition happened in carbonate rocks, the grains that comprise siliciclastic rocks may travel hundreds of miles down river systems before deposition and lithification. This local deposition affected significantly carbonate rocks heterogeneity. One of the methods that usually use to characterize carbonate reservoirs is rock physics analysis. This method could determine and calculate pore types of carbonate rocks which are very complex through its elastic moduli. The porosity of carbonate rocks can be divided into three types: Interparticle or reference pores, existing between the carbonate grains and are considered as the dominant pore types in carbonate; stiff pores, represent moldic and vugs pores and are usually formed as a product of dissolved grains and fossils chamber; Cracks, represent micro-fractures and micro-cracks.

To do this research there are several methods to find quantity and distribution of pore type in carbonate reservoir that is Self-Consistent (SC), Kuster-Toksoz (KT), and Differential Effective Medium (DEM) method. In a previous research, *[Candikia et al., 2016]* Has conducted a research entitled comparative study of the Differential Effective Medium (DEM) method with the Kuster-Toksoz (KT) method. In the study it was explained that the Differential Effective Medium (DEM) method was better in determining the carbonate reservoir pore type. Therefore, the authors have a plan to use the Differential Effective Medium (DEM) method to generate pore type logs in the carbonate reservoir.

The next step is the author have to predict permeability value using Adaptive Neuro-Fuzzy Inference System. Fuzzy Logic (FL) that is capable to express the underlying characteristics of a system in human understandable rules is also used. A fuzzy set allows for the degree of membership of an item in a set to be any real number between 0 and 1. This allows human observations, expressions and expertise to be modeled more closely. Once the fuzzy sets have been defined, it is possible to use them in constructing rules for fuzzy expert systems and in performing fuzzy inference. This approach seems to be suitable to well log analysis as it allows the incorporation of intelligent and human knowledge to deal with each individual case. However, the extraction of fuzzy rules from the data can be difficult for analysts with little experience. This could be a major drawback for use in well log analysis. If a fuzzy rule extraction technique is made available, then fuzzy systems can still be used for well log analysis [*Wong et al., 1999 and Kuo et al., 1999*]. With the emergence of intelligent techniques that combine ANN and fuzzy together have been applied successfully in well log analysis [*Huang et al., 2001, Kadkhodaie Ilkhchi et al., 2008, Khaxar et al., 2007,* Johanyák *et al.2007]*. These techniques used in building the well log analysis model normally address the disadvantages encountered in ANN and fuzzy system.

A neural network (NN) is an intelligent tool for solving complex problems. A BPNN is a supervised training technique that sends the input values forward through the network then computes the difference between calculated

PROCEEDINGS
JOINT CONVENTION BANDUNG (JCB) 2021
November 23rd – 25th 2021

output and corresponding desired output from the training dataset. The error is then propagated backward through the net and the weights are adjusted during a number of iterations, named epochs. The training ceases when the calculated output values best approximate the desired values [*Bhatt and Helle, 2002]*.

The basic theory of fuzzy sets was first introduced by *Zadeh, 1965*. In recent years, it has been shown that uncertainty may be due to fuzziness (possibility) rather than probability. FL is considered to be appropriate to deal with the nature of uncertainty in system and human errors, which were not considered in existing reliability theories. Generally, geological data are not clear-cut and habitually are associated with uncertainties. For example, prediction of core parameters from well log responses is difficult and is usually associated with error [*Nikravesh and Aminzadeh, 2003]*. FL derives useful information from this error and applies it as a powerful parameter for increasing the accuracy of the predictions. A fuzzy inference system (FIS) is a method to formulate inputs to an output using FL [*Kadkhodaie Ilkhchi et al., 2006]*.

Data and Method

In this study the author use wireline log data to create pore type models along the reservoir depth that is DTCO, RHOB, PHIE, and Petrophysical parameter such as mineral volume, mineral elastic parameter and fluid saturation in carbonate reservoir. Generally, there is three phase of pore type modelling in carbonate reservoir according [*Xu and Payne 2009]*. Fig 1. Bellow will give us the illustration how we create rock physics pore type log.

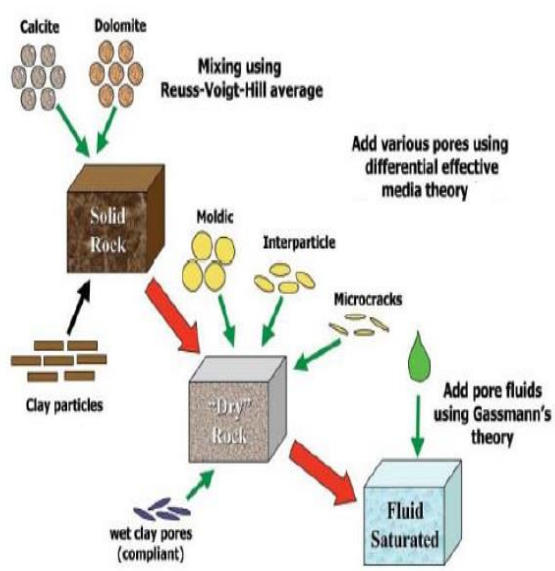

Figure 1: Detailed step of rock physics pore type modelling in carbonate reservoir (Xu and Payne, 2009).

The first step that we have to do to create rock physics pore type model is mixing the mineral and create frame rock model using Voigt-Reuss-Hill method. This is one of method that we use to mix the mineral that contained in carbonate reservoir in order to make background model or usually called solid rock phase. This method is averaging from two methods before that is Voigt method that arrange rock matrix in series and Reuss method that arrange rock matrix in parallel. Solid rock phase is the first step in carbonate reservoir modelling which assumes that the rock not has porosity at all (0% porosity) and all the content in this rock model is 100% mineral such as clay, dolomite and calcite. From this step we could calculate bulk and shear modulus of solid rock phase using Voigt-Reuss-Hill formula bellow *[Mavko et. al., 1998]*:

$$M_V = \sum_{i-n}^{N} f_i . M_i \tag{1}$$

$$\frac{1}{M_R} = \sum_{i-1}^{N} \frac{f_i}{M_i} \tag{2}$$

$$M_{VRH} = \frac{M_V + M_R}{2} \tag{3}$$

Where,

f_i : Mineral fraction

M_i : Elastic modulus of mineral

M_V : Voigt elastic modulus

M_R : Reuss elastic modulus

M_{VRH} : Voigt-Reuss-Hill elastic modulus

The next step method that has been used to input the pore type in the carbonate reservoir is DEM (Differential Effective Medium) method. The theory of DEM method models two-phase composites by incrementally adding a small amount of pores into a matrix. In DEM method, the effective moduli depend on the construction path taken in order to reach the final composite. The DEM method works by put inclusions into the background models. The models are continuously changed as the inclusion added *[Mavko et. al., 1998]*:

$$(1-y)\frac{d}{dy}\left[K^*(y)\right] = (K_2 - K^*)P^{(*2)}(y) \tag{4}$$

$$(1-y)\frac{d}{dy}[\mu^*(y)] = (\mu_2 - \mu^*)Q^{(*2)}(y) \tag{5}$$

PROCEEDINGS
JOINT CONVENTION BANDUNG (JCB) 2021
November 23rd – 25th 2021

Where,

y	: Porosity
dy	: Inclusion of 2nd pore type
$K^*(y)$	: Effective Bulk Modulus of DEM (Phase 3)
K^*	: Bulk Modulus of Solid Rock Model (Phase 1)
K_2	: Bulk Modulus of Dry Rock (Phase 2)
$P^{(*2)}$	: Geometry factor for an inclusion of material
$\mu^*(y)$	: Effective Shear Modulus of DEM (Phase 3)
μ^*	: Shear Modulus of Solid Rock Model (Phase 1)
μ_2	: Shear Modulus of Dry Rock (Phase 2)
$Q^{(*2)}$	: Geometry factor for an inclusion of material

Steps that needed in DEM method are not significantly different than KT method. DEM method also needs a background or matrix, the geometry factor, the elastic moduli of inclusion and fraction of inclusion as inputs. The difference lies on how to use this inputs. The first step is made a matrix or background by using Voight-Reuss-Hill method. Instead of looping aspect ratio, DEM method determined the aspect ratio value as an input to gain the factor geometry.

There are three aspect ratio values that need to be divined such as the aspect ratio of interparticle pores, stiff pores and crack pores. The determination of those three values are based on the Zhao classification who categorized the value of aspect ratio into three groups. The aspect ratio that represents crack pores is range from 0.01-0.02, the interparticle pores range from 0.12-0.15 and stiff pores vary between 0.7-0.8. The third step is to calculate the V_p reference with the assistance of DEM equation where consist the aspect ratio of interparticle pores, fraction of inclusion or porosity, the elastic moduli of matrix and also the elastic moduli of inclusions. This V_p reference is going to be the controller who decides whether the stiff pores are the one to be included into the process or the crack pores. If the V_p reference lower than V_p measurement or V_p from data, then stiff pores must add into the process. But if the V_p reference higher than V_p measurement, then crack pores need to be put into account. After the process has done, the effective elastic moduli are generated and will be compared with the real data to obtain the most representative model.

For the permeability prediction the author use wireline logging data for the input. Before using the log data, we have to normalize using minimum-maximum method so the range of data become 0-1 for every input and target. After we do data normalization, we have to do feature engineering and augmentation to select what kind of log data that have to use as the input. From the 11 feature the author will choose 6 feature which has quite strong correlation like the figure 2 bellow.

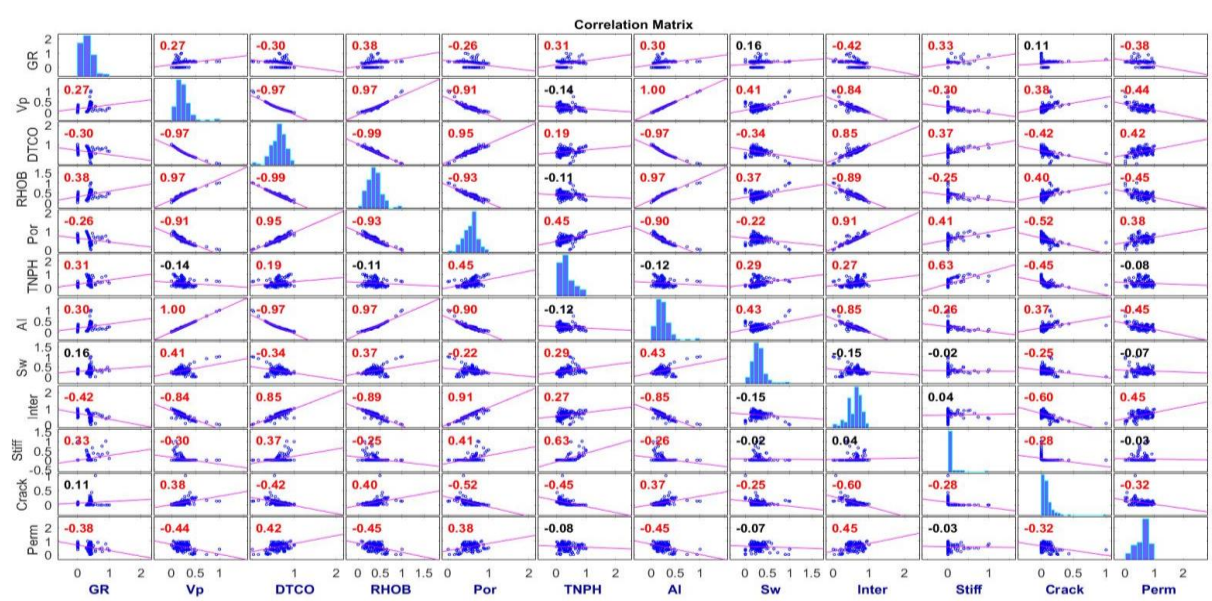

Figure 2: Feature Engineering and Augmentation using matrix Pearson correlation for select the best input for permeability prediction.

PROCEEDINGS
JOINT CONVENTION BANDUNG (JCB) 2021
November 23rd – 25th 2021

From the figure 2 we can see that 6 feature that is (Primary Velocity, DTCO, RHOB, Porosity, Acoustic Impedance and Interparticle Porosity) has a good correlation with the target. After feature selection is finish we have to design Neuro-Fuzzy model in the present research proceeds as following:

1. Removing erroneous and outliers from the raw well log data
2. Organizing data into input data sets including 6 features and 1 output (Permeability)
3. Normalization of input and output data sets (between the ranges 0-1) to renders the data dimensionless and removes the effect of scaling.
4. Dividing the data into: Training and Testing data sets.
5. Clustering the input and output data sets using Fuzzy Subtractive Clustering methods.
6. Fuzzyfication, which involves the conversion of numeric data in real world domain to fuzzy numbers in fuzzy domain, this takes place by building the fuzzy inference system (FIS), which involves setting the membership functions and establishment of fuzzy rules.
7. Defuzzyfication, which is optional, involves the conversion of the derived fuzzy number to the numeric data in real world domain.

Generally, Neuro-Fuzzy Inference System consist of 5 layers that we can see in the figure 3 bellow.

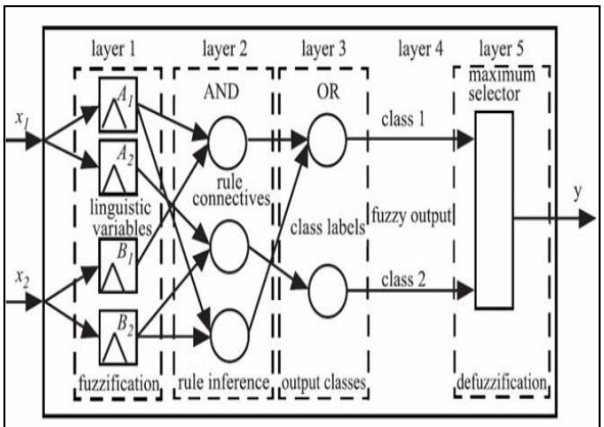

Figure 3: Neuro-Fuzzy Inference System Architecture

Fuzzy modeling technique can be classified into three categories, namely the linguistic (Mamdani-type), the relational equation, and the Takagi, Sugeno and Kang (TSK). Takagi and Sugeno, 1985, is a FIS in which output membership functions are constant or linear and are extracted by a clustering process. Each of these clusters refers to a membership function. Each membership function generates a set of fuzzy if–then rules for formulating inputs to outputs.

Hybrid NF systems combine the advantages of fuzzy systems (which deal with explicit knowledge) with those of NN (which deal with implicit knowledge). On the other hand, Fuzzy Logic (FL) enhances generalization capability of a Neural Network (NN) system by providing more reliable output when extrapolation is needed beyond the limits of the training data.

Fuzzy clustering is necessary to classify the input and output datasets into groups using clustering methods. In this study, a subtractive clustering method, which is a useful and effective way to FL modeling, is used for extraction of clusters and fuzzy if–then rules. The details of subtractive clustering could be found in [*Chiu, 1994*], [*Chen and Wang ,1999*], [*Jarrah and Halawani, 2001*].The important parameter in subtractive clustering which controls number of clusters and fuzzy if–then rules is clustering radius. This parameter could take values between the range of [0, 1]. Specifying a smaller cluster (say 0.1) radius will usually yield more and smaller clusters in the data resulting in more rules. In contrast, a large cluster radius (say 0.9) yields a few large clusters in the data resulting in few rules.

The effectiveness of a fuzzy model is relying on the search for an optimal clustering radius, which is a controlling parameter for determining the number of fuzzy if–then rules. Few rules could not cover the entire domains, and more rules will complicate the system behavior and may lead to low performance of the model. Regarding the permeability model, four centers result from clustering, thus the fuzzy model was established by four fuzzy if-then rules and four membership functions for input and output data. Porosity model, on the other hand, contains five centers (clusters), five rules and five membership functions. Figures 6 and 7 shows the subtractive clusters of permeability and porosity data.

Fuzzy inference is the process of formulating the mapping from a given input to an output using fuzzy logic. The mapping then provides a basis from which decisions can be made, or patterns discerned. The process of fuzzy inference involves setting the membership functions and establishment of fuzzy rules, [*Matlab fuzzy logic user's guide, 2009*].

Setting the Membership Functions (MF). A membership function (MF) is a curve that defines how each point in the input space is mapped to a membership value (or degree of membership) between 0 and 1. The input space is sometimes referred to as the universe of discourse, a fancy name for a simple concept. The only condition a membership function must really satisfy is that it must vary between 0 and 1. The function itself can be an arbitrary curve whose shape we can define as a function that suits us from the point of view of

PROCEEDINGS
JOINT CONVENTION BANDUNG (JCB) 2021
November 23rd – 25th 2021

simplicity, convenience, speed, and efficiency. In this research we have calculate and make the variation of Range of Influence in Fuzzy Subtractive Clustering in MATLAB from 0.01-1 to get the best parameter in ANFIS like we can see on the table below.

R	Training MAPE	Testing MAPE	MF for each Input Data
1	0.09	0.24	2
0.9	0.09	0.24	2
0.8	0.09	0.24	2
0.7	0.09	0.27	3
0.6	0.09	0.26	3
0.5	0.08	0.26	4
0.4	0.09	0.31	4
0.3	0.08	0.31	6
0.2	0.05	0.39	11
0.1	0	0.3	51
0.09	0	0.26	59
0.08	0	0.2	68
0.07	**0**	**0.18**	**70**
0.06	0	0.25	82
0.05	0	0.25	90
0.04	0	0.25	96
0.03	0	0.25	99
0.02	0	0.25	101
0.01	0	0.26	101

Table 1: Variation Range of Influence value in Fuzzy Inference System for getting minimum Mean Absolute Percentage Error.

From the table 1 we can see that range of influence value for 0.07 give the best result for training and testing data and give us 70 membership function for each input in ANFIS algorithm.

For 70 membership function for each input in this research we use Gaussian membership function in the FIS structure, output membership functions are linear equations constructed from inputs. ANFIS is a class of adaptive networks which are functionally equivalent to fuzzy inference systems, where the parameters are chosen so as to tailor the membership functions to the input/output data in order to account for all the variations in the data values. This technique is known as neuro-adaptive learning and is similar to that of neural networks. ANFIS is based on a neuro-adaptive learning technique. Using a given input/output data set, ANFIS constructs a fuzzy inference system whose membership function parameters are tuned (adjusted) using either a backpropagation algorithm alone, or in combination with a least squares type method. This allows fuzzy systems to learn from the data they are modeling.

To describe the ANFIS methodology, the fuzzy inference systems is represented as an adaptive network in the following way. Suppose a fuzzy inference system with two inputs x and y and one output; its rule base contains two fuzzy if-then rules of Takagi and Sugeno's type:

Rule 1: If x is $A1$ and y is $B1$, then $f1 = p1\ x + q1\ y + r1$
Rule 2: If x is $A2$ and y is $B2$, then $f2 = p2\ x + q2\ y + r2$

For the complete ANFIS parameter in this research we can see in the figure 4 for the membership function and figure 5 for ANFIS input-output and structure below.

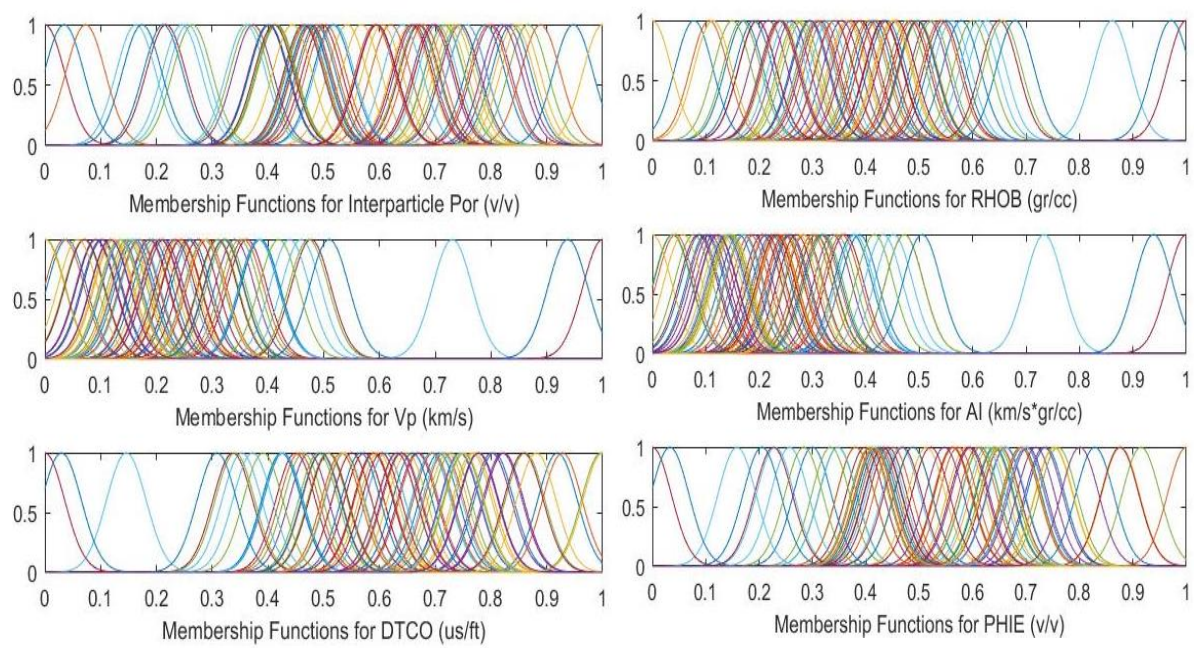

Figure 4: Fuzzy Inference System Membership Function for 6 input in ANFIS Algorithm.

PROCEEDINGS
JOINT CONVENTION BANDUNG (JCB) 2021
November 23rd – 25th 2021

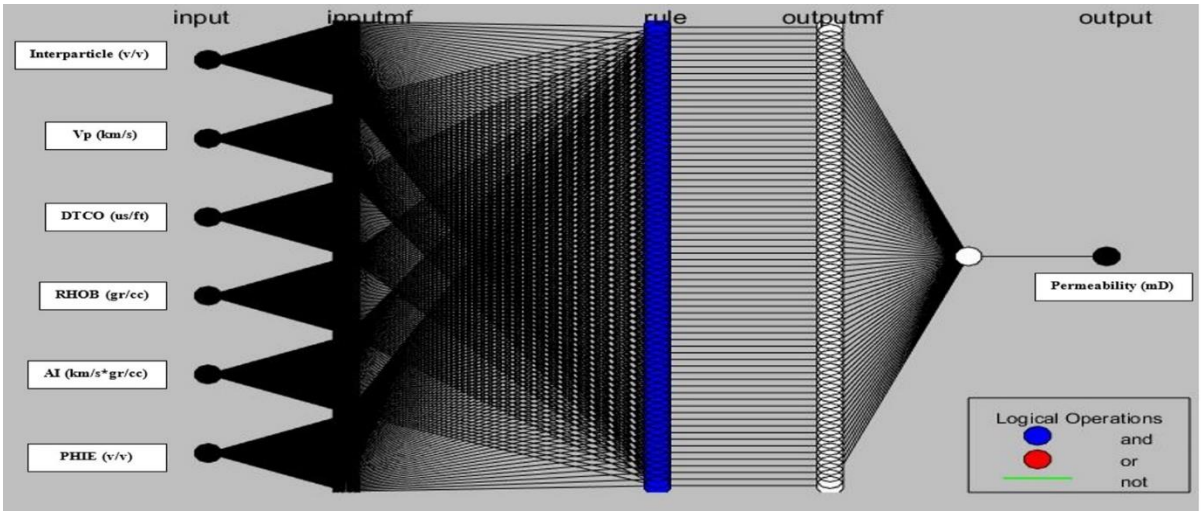

Figure 5: Structure of Neuro-Fuzzy Model for Permeability Prediction.

Result and Discussion

The primary and secondary pore type value using DEM method in this well is calculated. DEM method is used to make models of porous rocks. From this method the type of pores could be calculated. To determine what kind of pore type, the inclusion must be added to the models, and then to compare *V*p reference by *V*p measurement. To calculate *V*p reference we have to make rocks model which has 100% interparticle (dry rock) pores and then the secondary pore type will add step by step with inclusion add each 1% to the dry rock model until *V*p model approach *V*p measurement.

We can calculate *V*p model from DEM equation by extracting effective bulk and shear modulus value to *V*p model equation to ensure that the inclusion we add is appropriate like we can see in the several figure 6 and 7. As we can see in Fig. 6 error value decreases and the trend of cross plot tend to be more linear in DEM method because we have used more accurate input parameters. The more accurate input parameters that we use then RMS error value will decrease and the quantity calculation of secondary pore type will more accurate in each well.

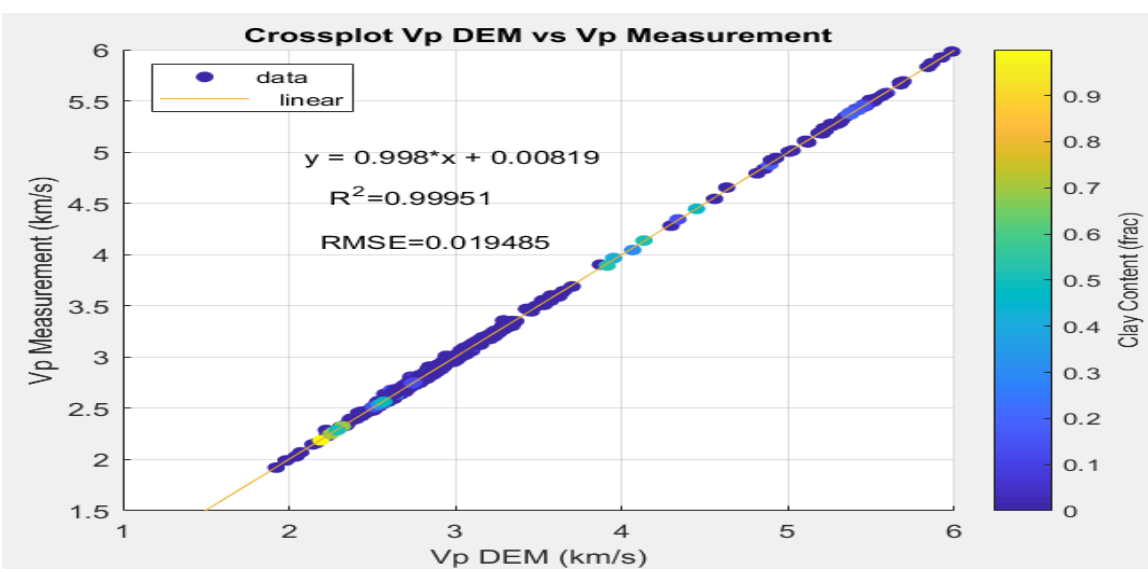

Figure 6: Cross Plot *Vp DEM* vs *Vp Measurement*.

PROCEEDINGS
JOINT CONVENTION BANDUNG (JCB) 2021
November 23rd – 25th 2021

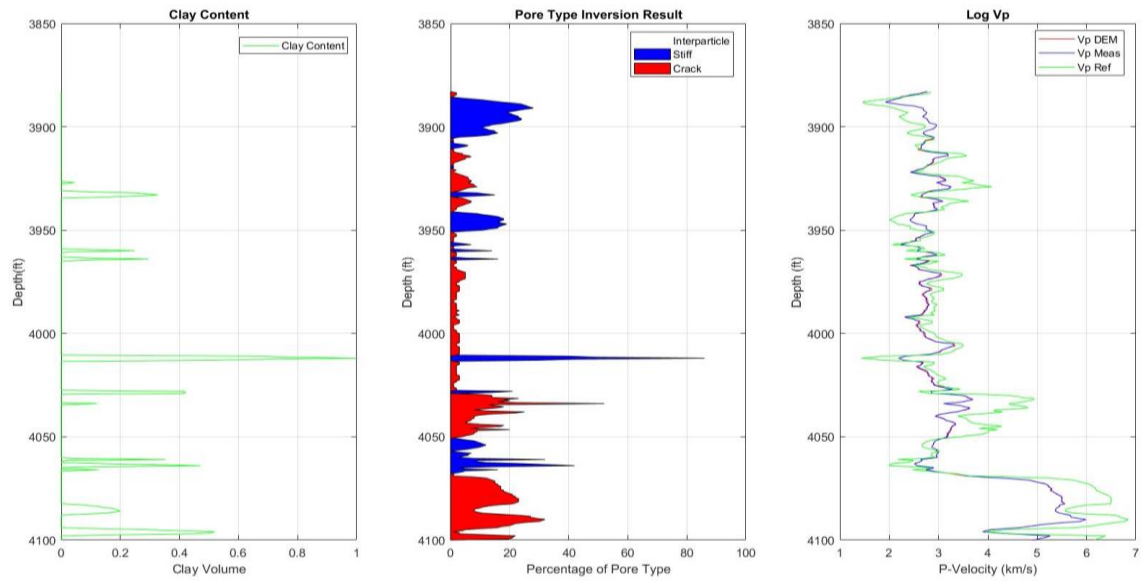

Figure 7: Pore type modelling result for all depth in the well.

From figure 7 in the second coulomb we can see the pore type quantity along the well depth which contain the Primary (Interparticle) and Secondary pore type (Stiff and Crack). We can rely this pore type modelling because we have validated the model quantitatively using P-Velocity which shown in the third coulomb. In the third coulomb we can see the P-Wave from modelling (Vp DEM) and P-Wave from well logging measurement (Vp Measurement) has match enough like we have shown in the figure 6 with the R^2=0.9995 and RMSE=0.01 (1%).

After this pore type modelling is done we have to run ANFIS algorithm to predict permeability in this well using the input that we have got in the feature engineering and augmentation using matrix Pearson correlation. The first step that we have to do is to train the data. In this research we use 100 data training and 36 data for testing from the 136 total data. If the training and testing data show us the minimum error and then we can denormalize the data to the real domain like we can see in the figure 8 and 9 below.

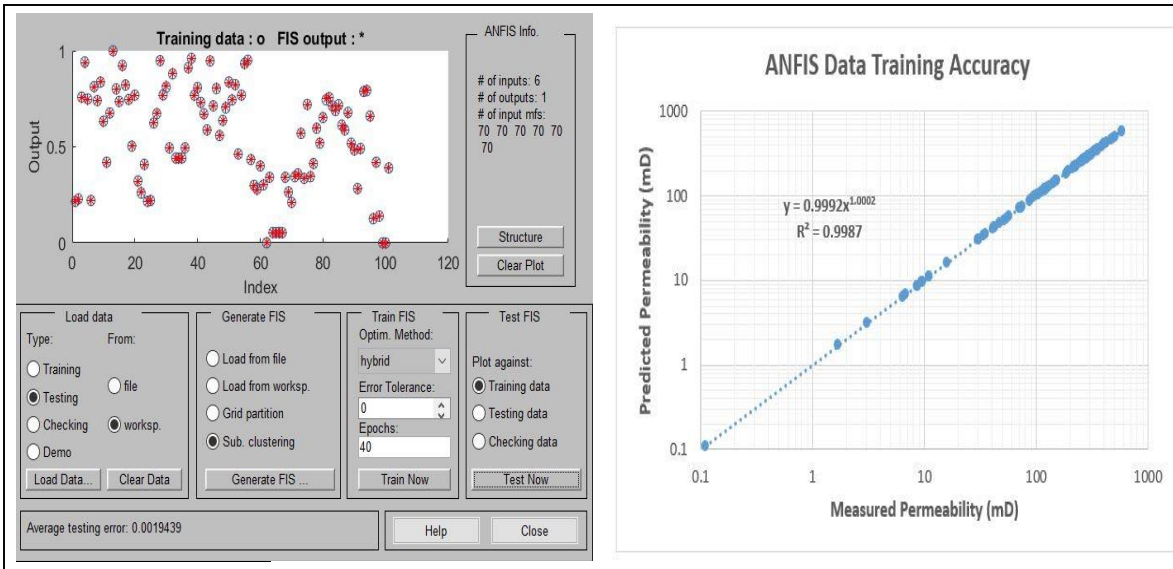

Figure 8: Training data result before denormalization (Left) and
After denormalization (Right)

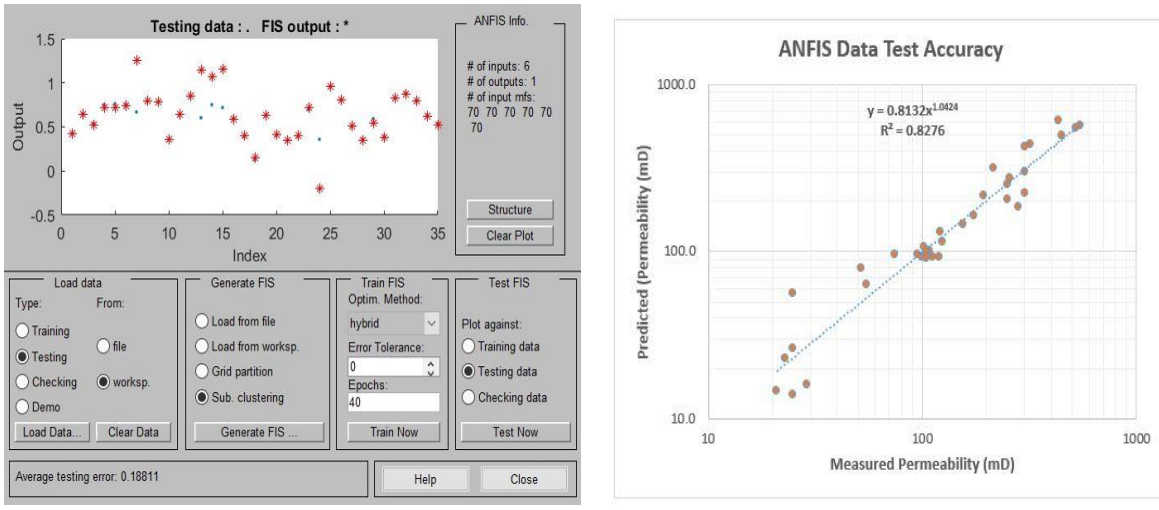

Figure 9: Testing data result before denormalization (Left) and After denormalization (Right)

From the figure 8 the result from training data show us Mean Absolute Percentage Error (MAPE) value 0.0019 with 40 epoch (iteration) that mean the training process has succeeded and the denormalize give us the good value for R^2= 0.9987. After we train the 100 data set we can continue for testing data. In the testing data we use 36 data set for testing. In testing result we got the good enough test result with MAPE value 0.18 and R^2= 0.8276 in figure 9 so we can use this algorithm to predict permeability along the well depth.

After we got the good training and testing score we will calculate the reservoir permeability value for all depth in this well and we will plot it together with pore type result and core data which we got from the laboratory measurement. We can see the final result in the figure 10 which describe the relation of pore type and permeability value in this well. From this final result we can make several decisions for improving our well performance such as where we should decide perforating zone and avoid the wash out zone which relate to the stiff pore.

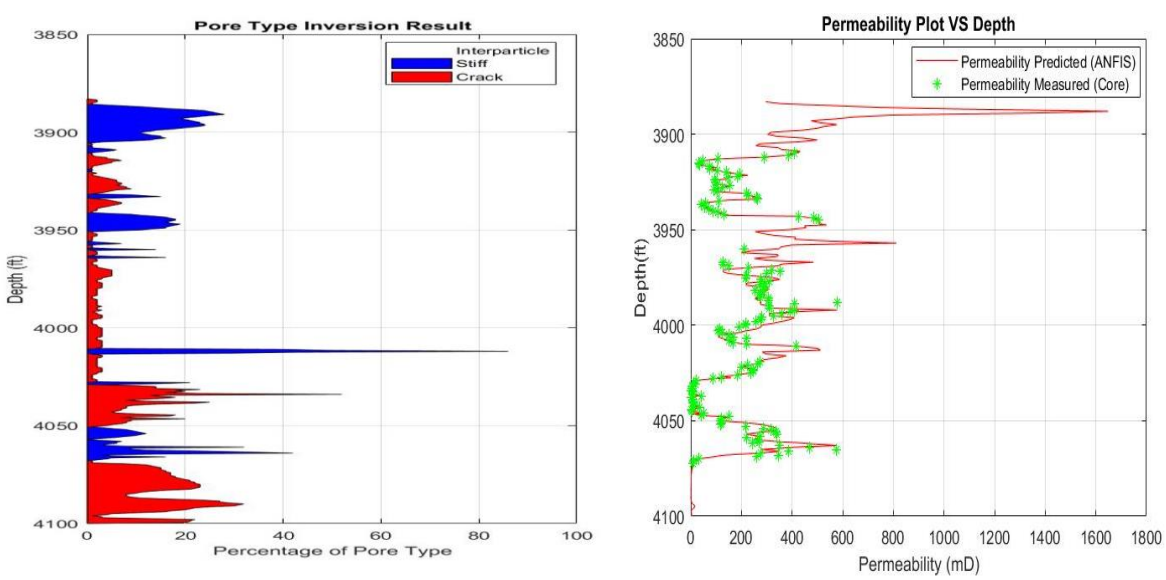

Figure 10: Pore Type Modelling Result (Left) and Permeability Predicted & Measured (Right)

PROCEEDINGS
JOINT CONVENTION BANDUNG (JCB) 2021
November 23rd – 25th 2021

Conclusion

1. Differential Effective Medium (DEM) is a good method for pore type modelling and give us the value of **R^2=0.99951** & **RMSE=0.019485** for X-plot Vp Model against Vp Measured validation.
2. ANFIS algorithm approach in this research has been successfully applied for the prediction of permeability value in carbonate reservoir with value of **R^2=0.9987** for training data and **R^2=0.8276** for testing data.
3. From this research we can see at **figure 10** that Stiff pore (Secondary Porosity) + Interparticle pore (Primary Porosity) has the highest permeability value at **3870 ft - 3900 ft = ± 1600 mD.**
4. Crack pore (Secondary Porosity) + Interparticle pore (Primary Porosity) has the highest permeability value at **4025 ft - 4050ft = ± 20 mD** and at **4075 ft - 4100ft = ± 15 mD.**

References

Bhatt, A., Helle, H.B., 2002.Geophysical Prospecting 50, pp. 645–660.

Candikia, Yuri Nadia, Rosid, M. Syamsu, and Haidar, M. Wahdanadi. 2017. AIP Conference Proceedings 1862, 030185 (2017); doi: 10.1063/1.499128.

Chiu, S., 1994.. Journal of Intelligent and Fuzzy Systems 2, pp. 267–278.

Chen, M.S., Wang, S.W., 1999. Fuzzy Sets and Systems 103, pp. 239–254.

Huang, Y., Gedeon, T.D. and Wong, P.M., 2001. Engineering Applications of Artificial Intelligence, 14(1), pp. 15- 21.

Jarrah, O.A., Halawani, A., 2001. Artificial Intelligence 133, pp. 117–138.

Kadkhodaie Ilkhchi, A., Rezaee, M.R., Moallemi, S.A., 2006.Journal of Geophysics and Engineering 3, pp356–369.

Khaxar, Z. O., Bagheri M., Karkuti, E. A, 2007. International Earthquake symposium, October 22-26, pp. 567-572.

Kuo, H., Gedeon, T.D. and Wong, P.M., 1999. Proceedings of 6th International Conference on Neural Information Processing, vol. 2, pp. 679-684.

Matlab Fuzzy logic toolbox User's Guide, 2009a. Version 4, Fuzzy Logic Toolbox. Math Works,USA, pp 343.

Mavko, G., T. Mukerji, and J. Dvorkin. 1998.. Cambridge University Press.

Nikravesh, M., Aminzadeh, F., 2003. Elsevier, Berkeley, USA, pp 744.

Takagi, T., Sugeno, M., 1985. IEEE Transaction on Systems, Man and Cybernetics 15, pp. 116–132.

Xu, S. and M. A. Payne. 2009. SEG.

Zhao, L., M. Nasser, and D. Han. 2013. European Association of Geoscientists & Engineers, Geophysical Prospecting, 1 – 15.

PROCEEDINGS
JOINT CONVENTION BANDUNG (JCB) 2021
November 23rd – 25th 2021

Probabilistic Lithofacies Class Prediction in Well Data Using Bayesian Framework

Rizky Adityo Prastama[1], Ignatius Sonny Winardhi[1]
[1]Geophysical Engineering, Faculty of Mining and Petroleum Engineering, Institut Teknologi Bandung

Abstract

In hydrocarbon exploration, elastic parameters including P-wave velocity, S-wave velocity, density, and its derivatives are commonly used to classify lithofacies. Since geophysical measurements are often coupled with unwanted noise, the assessment of the uncertainty could be useful in making important decision. Bayesian framework is an ideal solution for uncertainty assessment on probabilistic inversion, especially in a challenging reservoir such as carbonate. In this study, prediction of lithofacies based on elastic parameters is proposed using Bayesian framework. Two wells are processed, each as a training well and target well respectively. Three lithofacies classes from training well is classified based on shear modulus and density cross-plot. Markov-chain approach is performed to get the prior probabilities of each class. Prior probabilities obtained from the stationary condition of transition matrix are 0.088, 0.254, and 0.658 for shale, gas carbonate, and brine carbonate, respectively. Furthermore, Gaussian distribution is constructed to show the likelihood of shear modulus and density values. These information from training well is used to calculate the posterior probability of each lithofacies class in target well. The predicted lithofacies, based on the maximum a posteriori profile, shows similarity to the observed actual lithofacies. The accuracy of lithofacies prediction on the target well, shown by the true positive values of the confusion matrix, demonstrates the performance of the algorithm. For gas carbonate, the true positive value is found to be 73.64%. Result shows that the prediction algorithm works quite well in making inferences of lithofacies class based on the available elastic parameters data in the target well.

Keywords: Bayesian, Carbonate, Lithofacies, Markov-chain, Probabilistic

Introduction

Hydrocarbon exploration have been performed in many types of environments, including carbonate. Around 50% to 60% of world hydrocarbon reserves are located in carbonate reservoir (Burchette, 2012). Other study also revealed that carbonate reservoir is responsible for 50% (Park et al., 1995) of the total identified hydrocarbon basins in Indonesia. However, carbonate reservoir is very challenging due to its physical, chemical, and biological changes over time, resulting in a very heterogeneous rock with poor permeability (Xu & Payne, 2009). Other than that, geophysical measurements are always coupled with noises, especially seismic data. Seismic data is mainly used to get structural and physical properties of the element of petroleum system laterally. Physical properties such as P-wave velocity, S-wave velocity, and density are further analyzed to determine the distribution of hydrocarbon-bearing layer, in this case is carbonate reservoir. With geological challenges mentioned before, combined with noisy data, further exploration in carbonate environment is prone to uncertainty and inaccuracy.

In this study, we review about how to make a prediction of lithofacies class in Bayesian framework on well-to-well basis. There are three lithofacies classes (LFC) in the given area of study: shale, gas carbonate, and brine carbonate. The prediction is performed by calculating posterior probability of each LFC based on the elastic parameter value at given depth. LFC with highest posterior probability is inferred as the most possible LFC to be found in that depth point. The main advantage by using this approach is that we will get a result with its own probability. In other words, we could assess the uncertainty of our exploration for new hydrocarbon resource.

Data and Method

We are going to predict LFC in target well based on information obtained in training well. This work is mainly based on the concept of Bayesian posterior probability. In Bayesian theorem, the posterior probability of an event A to happen can be estimated based on given evidence B by using equation below:

$$p(A|B) = \frac{p(B|A)p(A)}{p(B)} \tag{1}$$

where $p(B|A)$ is likelihood function while $p(A)$ and $p(B)$ are prior probability of event A and evidence B respectively. In our case, we can rewrite the equation as:

$$p(f_i|m_i) = \frac{p(m_i|f_i)p(f_i)}{p(m_i)} \tag{2}$$

PROCEEDINGS
JOINT CONVENTION BANDUNG (JCB) 2021
November 23rd – 25th 2021

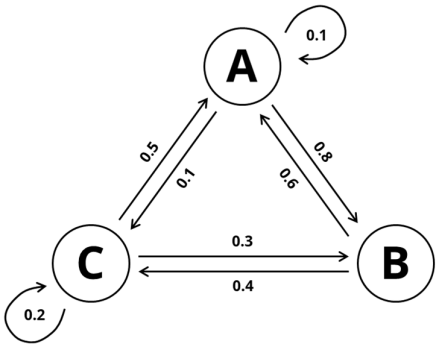

Figure 1: Markov-chain diagram showing how the probability of transition between one state to another.

where f is the LFC class we are going to predict and m is the elastic parameter, both at depth location i. The prior probability of elastic parameter $p(m_i)$ is acting as a normalization factor (Zhao et al., 2014). We can simply write the posterior probability as:

$$p(f_i|m_i) \propto p(m_i|f_i)p(f_i) \tag{3}$$

Since we classify the LFC based on cross-plot, which require at least two elastic parameters m_1 and m_2, we can use conditional independence theorem and modify equation (3) to:

$$p(f_i|m_{1_i}, m_{2_i}) \propto p(m_{1_i}|f_i)p(m_{2_i}|f_i)p(f_i) \tag{4}$$

The two components that we need to estimate on the equation above are the likelihood function and prior probability. The likelihood function $p(m|f)$ represent how likely elastic parameter m is present in the case of LFC f. Naturally, Gaussian or normal distribution can be used in this case. Gaussian distribution is a probability density function that centered on its mean value μ with the width determined by its standard deviation σ. Both μ and σ can be calculated based on cross-plot analysis in training well.

$$p(m_i|f_i) = f(m_i) = \frac{1}{\sigma\sqrt{2\pi}} e^{-\frac{1}{2}\left(\frac{m_i-\mu}{\sigma}\right)^2} \tag{5}$$

The next parameter that should be calculated is the prior probability of each LFC. Markov-chain approach is chosen to estimate the prior probability. Markov-chain itself is a type of series where the probability of upcoming state is only based on the current state. This means that everything that occurred before the current state are neglected. It is natural to see geological sequence as a Markov-chain (Krumbein and Dacey, 1969).

$$p(f_i) = \prod_i p(f_i|f_{i-1}) \tag{6}$$

The Markov-chain concept is capable to illustrate how each LFC is transitioning into another. Figure 1 is a diagram showing the Markov transition between three different classes A, B, and C. The arrow shows the direction of transition and the value is the probability of that transition to be occurred. This diagram could be rewritten into a matrix called transition matrix T. As for the diagram in Figure 1, the transition matrix is:

$$\mathbf{T} = \begin{array}{c|ccc} & A & B & C \\ \hline A & 0.1 & 0.8 & 0.1 \\ B & 0.6 & 0 & 0.4 \\ C & 0.5 & 0.3 & 0.2 \end{array} \tag{7}$$

Furthermore, this transition matrix will be used to calculate the prior probability. Mathematically, the prior probability of each LFC is obtained where:

$$p(f)\mathrm{T} = p(f) \tag{8}$$

The equation above is a stationary condition where $p(f)$ is a matrix containing n-number of prior probabilities, related to each LFC (Larsen et al., 2006).

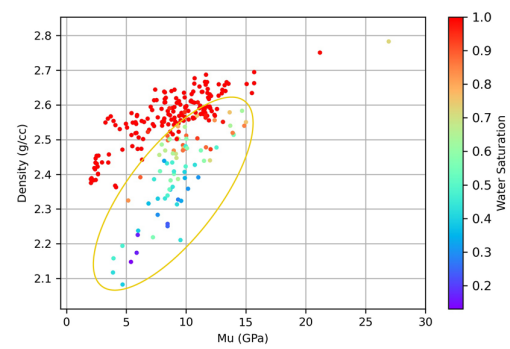

(a)

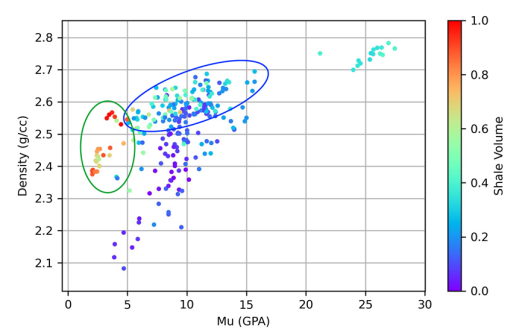

(b)

Figure 2: Cross-plot between shear modulus and density with overlay of (a) water saturation and (b) shale volume. Green, yellow, and blue circle are the class of shale, gas carbonate, and brine carbonate respectively.

PROCEEDINGS
JOINT CONVENTION BANDUNG (JCB) 2021
November 23rd – 25th 2021

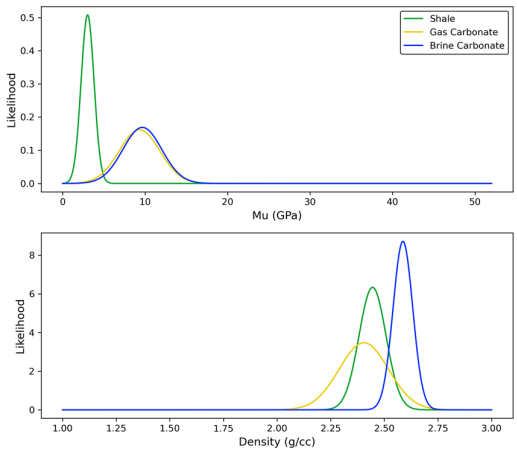

Figure 3: Gaussian distribution of shear density (top) and density (bottom) as a likelihood function to calculate posterior probability.

Result and Discussion

Figure 2a shows the cross-plot between shear modulus and density in training well with overlay color of water saturation. We can clearly see that the data is well separated between hydrocarbon-bearing carbonate (in this case gas carbonate) and the brine carbonate. To further analyze the possibility of other LFC, Figure 2b shows the same elastic parameter but with shale volume overlay. It can be interpreted that there is a little fraction of shale in the area of study that should be taken into account.

The mean and standard deviation of both elastic parameter for each LFC are calculated based on the cross-plot analysis in Figure 2. Figure 3 shows the Gaussian distributions that will be used as likelihood functions. These distributions imply that shear modulus has a crucial role in separating shale from carbonate while density will differentiate the fluid content inside the rock itself.

The prior probability of each LFC is calculated based on quantitative lithofacies interpretation derived from available log data. Figure 4 shows the log data in training well with the sequence of interpreted LFC along the borehole. Based on this sequence, the transition matrix is shown below:

$$\mathbf{T} = \begin{array}{c|ccc} & \text{Sh} & \text{GC} & \text{BC} \\ \hline \text{Sh} & 0.821 & 0 & 0.179 \\ \text{GC} & 0 & 0.800 & 0.200 \\ \text{BC} & 0.238 & 0.254 & 0.658 \end{array} \quad (9)$$

where the first, second, and third row & column belong to shale, gas carbonate, and brine carbonate respectively. For example, there are 82.1% probability of shale transitioning to shale again beneath it and 25.4% probability brine carbonate transitioning to gas carbonate. The stationary condition of the transition matrix above is:

$$p(f) = [0.088 \quad 0.254 \quad 0.658] \quad (10)$$

It can be concluded that the prior probability of shale, gas carbonate, and brine carbonate are 8.8%, 25.4%, and 65.8% respectively. This number is justified by the lack of shale presence in the training well. The brine carbonate is also massively encountered in the training well, giving itself the biggest prior probability among the three LFCs. Now we already have every information that are needed to calculate the posterior probability on target well, based on equation (4).

Posterior probability of each LFC in target well is calculated based on shear modulus and density log. Technically, shear modulus and density value at single depth point are used to generate the likelihood values based on Gaussian distribution. After we get $p(m_{1_i}|f_i)$ and $p(m_{2_i}|f_i)$, we multiply these values with the prior probability $p(f)$ of the corresponding LFC. This process is done iteratively through the whole borehole log data for each LFC. The result is shown in Figure 5. We can see that not only that we get the predicted LFC sequence along the well, but we also calculated its probability. Every predicted LFC along the well are also delivered by its own uncertainty.

Another aspect that should be considered is how well the algorithm predicts the LFC. The assessment of performance could be done by using confusion matrix.

$$\mathbf{C} = \begin{array}{c|ccc} & \text{Sh} & \text{GC} & \text{BC} \\ \hline \text{Sh} & \mathbf{0.474} & 0.079 & 0.447 \\ \text{GC} & 0 & \mathbf{0.736} & 0.264 \\ \text{BC} & 0 & 0.215 & \mathbf{0.785} \end{array} \quad (11)$$

Confusion matrix above shows the ratio or percentage of every match between actual LFC and predicted LFC. For example, there are 47.4% shale is predicted as a shale and 44.7% of shale being predicted as a brine carbonate. Meanwhile, there are no gas carbonate or brine carbonate being predicted as shale, as we seen in the Figure 5. The diagonal of confusion matrix (bold) is called true positive values and these are the value that show the performance of our algorithm. We can see that, in terms of predicting carbonate, the algorithm works quite well with true positive values above 70%. The relatively low (47.4%) true positive value of shale can be caused by limited sample in training well that may not fully represent the elastic properties of the shale itself. On the other hand, in Figure 2, the green circle is extended to higher density value. These several data points, although have high shale volume, might be still related to brine carbonate. This explains why the confusion matrix of shale being predicted as brine carbonate is high (44.7%).

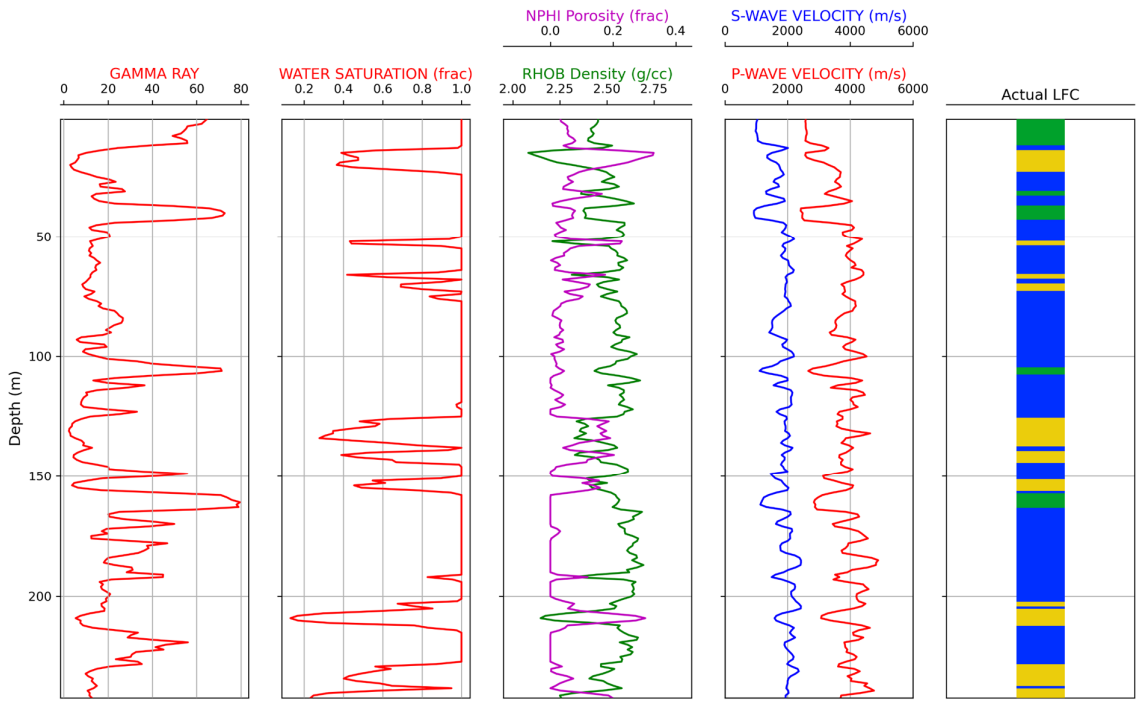

Figure 4: Borehole well log data in training well. The fifth track (right most) shows the interpreted lithofacies class based on the given log information on the other track. Green, yellow, and blue are shale, gas carbonate, and brine carbonate respectively.

Conclusions

We have already seen the advantages in using Bayesian framework for assessing LFC prediction uncertainty in well-to-well basis. Cross-plot analysis plays an important role and has a crucial part in this approach. The chosen elastic parameters should be sensitive enough in separating each LFC that we are interested in. Improvement in prediction may be performed by reanalyzing the cross-plot and changing the elastic parameter that can separate LFCs better.

This work may later be used as a reference for performing lithofacies prediction based on inverted elastic parameters from seismic data.

References

Burchette, T.P., 2012, Geological Society London Special Publications, **370**, 17-37.

Larsen, A. L., Ulvmoen, M., Omre, H., and Buland, A., 2006, Geophysics, **71**, R69-R78.

Krumbein,Y. C., and Dacey, M. F., 1969, Mathematical Geology, **1**, 79-96.

Park, R. K., Matter, A., and Tonkin, P. C., 1995, Proceeding 24th Ann. Conv. Indonesian Petroleum Association (IPA), 163-184.

Xu, S., dan Payne, M. A., 2009, The Leading Edge, **28**, 66-74.

Zhao, L., Geng, J., Cheng, J., Han, D., and Guo, T., 2014, Geophysics, **79**, M25-M34.

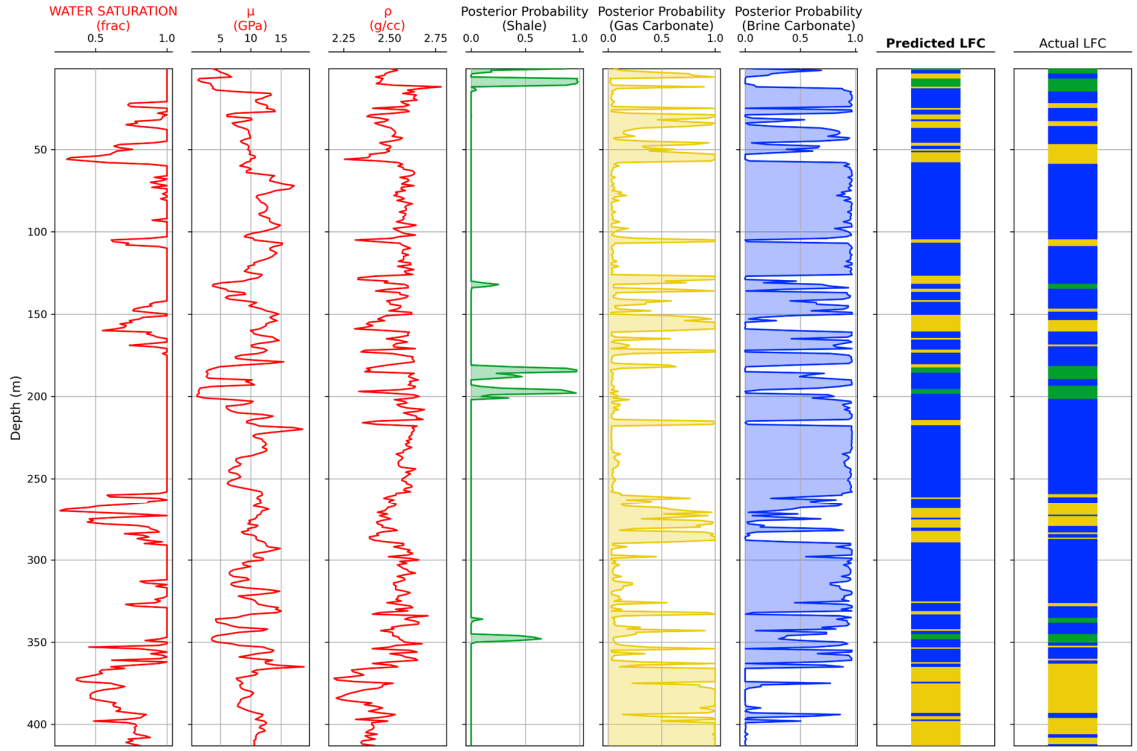

Figure 5: Predicted LFCs (track 7) based on shear modulus (track 2) and density (track 3). The inference of LFC is also called maximum a posteriori (MAP) since it chose the maximum posterior probability between shale, gas carbonate, and brine carbonate. Actual LFC in the last track is obtained from well log interpretation and can be compared with the prediction result to assess the performance of our algorithm.

PROCEEDINGS
JOINT CONVENTION BANDUNG (JCB) 2021
November 23rd – 25th 2021

Implementation of Hybrid Parallel Computation for Complex and Fine Reservoir Model Using Cluster Technology

Budi Darmawan[1] , Ahmad Reizky Azhar[2]
[1]Pertamina Hulu Indonesia. email: budi.darmawan@pertamina.com
[2]Rock Flow Dynamics. email: reizky.azhar@rfdyn.com

Abstract

Pertamina EP plays an important role in maintaining the oil production supply for national energy stability. However, there is big challenge in the field development plan preparation since they are not fully equipped with the advance computing technology to boost the reservoir modeling and simulation phase. To face the challenge, Pertamina EP evaluated the possibility to create a cluster technology that can accommodate high intensity of simulation numbers and high load of simulation process.

This paper described the success story and innovation of a complex simulation and finer scale reservoir model using the hybrid parallel-computing technology with a set of 8 nodes high performing computer. Three models were tested with satisfying results. This paper discusses the parallel scalability of complex computing systems of multi-CPU clusters. Multi-CPU distributed memory computing system is proven to be able to improve and accelerate the reservoir modeling and simulation time when it is used in combination with a new so called "hybrid" approach. In this approach, the common Message Passing Interface (MPI) synchronization between the cluster nodes is being interleaved with a shared memory system thread-based synchronization at the node level.

The model with the longest simulation time has been accelerated by magnitude of 60%. The most exhausted model with highest number of simulation steps has been accelerated by magnitude of 80%. The model with the greatest number of grid (21.7 million active grids) has finally finished its simulation just in 27 minutes where previously was impossible to have it open and run. The successful study case is then followed by the implementation of the cluster computing technology for two pilot POD projects which led to the very good result.

Keywords: POD, Hybrid Parallel Computation, Complex and Fine Reservoir Model, Cluster Technology, multiple reservoir realizations

Introduction

Almost all fields that operated by Pertamina EP has almost 70 years of production history. They are known for its complex multi-reservoirs geology, sophisticated waterflood program of giant proportions, and has more than 150 wells for each reservoir. However, due to extreme complexity, only highly upscaled models have been used as seen in **Figure 1**.

To make plans for infill drilling and various workovers, the most production units were relying on sector models that have necessary spatial resolution but had obvious areal coverage limitations in the areal coverage of the field. Up to now, all the sector models built for planning of infill drilling, workovers, EOR and waterflood optimization were not directly related to the full-field model. In fact, these models can be considered as "single use" tools designed for addressing ongoing challenges of the specific local part of the oil field.

The main reason for such outcome is the fact that the full-field model has much coarser grid. Consequently, its improvements that made for selected sectors cannot be directly integrated.

One of the main goals in advancing the hardware and software technology is to allow the use of comprehensive and detailed geological realm which putting together a self-consistent system for sector and full-field model.

The other important factors influencing large field model development is the calculation time. Upscaling parameters are often chosen based on the available time frame and the computer's performance, not on any physical sense. At the same time, present-day approaches to the hydrodynamic modeling allow us to remove these limitations and perform direct calculations on a geological scale. A combination of several factors, like the availability of more economical parallel computer platforms available on the hardware market and software that efficiently utilizes it to provide optimal parallel performance, helps to reduce the computation time of the reservoir models significantly. For a large reservoir simulation model project implementation, fast calculations should be made possible.

Hierarchic architecture of modern computer clusters

A cluster is a set of computers (referred to as cluster nodes), connected by high-capacity communication channels. Each of the nodes usually contains two (or more rarely four) physical processors and its own Random-Access Memory (RAM), where the operating system is running. Access to the other node's memory is provided via connection lines, and the entire system is entirely integrated from the user point of view. Users communicate with the cluster through the master node that supports system task queues and distributes tasks between the nodes.

These days, the clusters have become economical and easy-to-use machines. It has been demonstrated that the reservoir simulation time can be efficiently scaled on the modern Central Processing Unit (CPU) -based workstations and clusters if the simulation software is implemented properly to support the features of modern hardware architecture. It is fair to conclude that the simulation time is no longer a principal bound for the projects, as it can always be reduced by adding extra computational power. In addition to in-house hardware one can consider simulation resources available on the clouds based on pay-per-use model. This makes the reservoir modeling solutions much more scalable in terms of time, money, human and computational resources. Reservoir engineers from large and small companies can have access to nearly unlimited simulation resources and are able to reduce the simulation time to a minimum whenever needed.

PROCEEDINGS
JOINT CONVENTION BANDUNG (JCB) 2021
November 23rd – 25th 2021

Understanding hybrid
In clusters programming, MPI is de facto the standard interface. The costs of data exchange between the logical processors can be reduced to a minimum if the node just have two processors. Based on this fact, it is found that some of processors can interact more efficiently and caused the MPI programs even more complicated and did not produce significant gain. That changes occurred when the nodes have more than ten logical processors. Loss of performance has reached many-fold numbers and could not be neglected anymore. This led to the development of hybrid applications, where the interaction between the nodes occurs through the MPI, when OpenMP or direct operating system threads are used within the similar nodes to any shared memory platform.

This approach is obviously has the advantages. With the example of a cluster with 20 nodes, 12 cores each. The total number of processors is 240. Traditionally, such a system would use 240 MPI processes which normally leads to limitations due to scalability problems. With the hybrid approach, one needs to use 20 MPI processes (one for each node) and 12 system threads at each node.

Pertamina EP long term Plan of Development (POD) plan for the upcoming 5 years
In order to help maintain national production supply, Pertamina EP has a massive field development plan which consist of waterflood projects from thirty-three structures across Indonesia within 5 years. Some of those structures will also continue to perform tertiary recovery using CO2 and Polymer injection as the Enhanced Oil Recovery effort.

On the other hand, SKKMigas published new Pedoman Tata Kerja (PTK) about POD in 2018 which demand the probabilistic approach which honor and capture the uncertainties, upside and downside potential, subsurface risk and execution mitigation plan. This new approach requires multiple case definitions and evaluations.

The advance technology in hardware development seems promising to help them in current situation. Moreover, there is also massive development in reservoir simulator technology that will enable the process of multiple simulation jobs, allows the running of detailed fine reservoir models, and to integrate geological modeling and dynamic modeling into one complete process, without rebuild the model from the scratch.

Data and Method

Optimal applications for modern high-performance clusters
Internal benchmarking was concluded that 8 nodes with 20 cores per node configuration is the optimum scenario for typical Pertamina EP reservoir model, where the runtime acceleration factor reach the highest improvement as depicted in **Figure 2**. It is better to add more nodes rather than more cores based on the cost point of view. This configuration result is then reported to Pertamina EP IT department as the guidance of the optimum cluster specification requirement that fit their needs.

There are three models tested to get the optimum configuration for the brand-new cluster computer that are going to be built. They are coming from the analog reservoir outside organization which was chosen based on the similarity with the existing fine geological model of Pertamina EP. The resulted cluster setup as can be seen at **table 1** shows that selected configuration is proven to accelerate the simulation time where the first two models with lower number of total active cells can be reduced by the magnitude of 30%, by the addition of the compute nodes where the remaining model is reduced by a factor of 50%. The more complex and higher the active grid numbers, more efficient this parallel computation will be.

This promising benchmark is then become the justification to build the following cluster setup that is now available in Pertamina EP.

The configuration is:

Nodes number	: 8
CPU	: 20 Cores, 2x Intel® Xeon E5-2630v4 2.20 GHz,25M,8.00 GT/s, LGA2011-R3 (85W), DDR4-2133, 10-Cores (Broadwell-EP), 14nm
DRAM	: 64GB DDR4-2133MHz ECC Reg
Interconnection	: FDR Infiniband 56Gb/s
Master node	
CPU	: 20 Cores, 2x Intel® Xeon E5-2630v4 2.20 GHz,25M,8.00 GT/s, LGA2011-R3 (85W), DDR4-2133, 10-Cores (Broadwell-EP), 14nm
DRAM	: 64GB DDR4-2133MHz ECC Reg
Interconnection	: FDR Infiniband 56Gb/s
Capacity	: 60Tb, RAID50

Miscellaneous
Switch Infiniband 56Gb/s 36 port
Switch Ethernet 22 1Gb/s port + 2 10Gb/s port
KVM+IPMI 20 nodes

The main part of the cluster itself are the head node and all the compute nodes which are used for project dispatcher, as well as the engines for the computing and processing purposes. Since the simulator used with this cluster is the one that support hybrid parallel computation, so infiniband was chosen for data interconnection after the ethernet for faster communication between the nodes to access memory. It is because infiniband implement the Remote Direct Memory Access (DMA), which is an operation to access the memory directly from the Network Interface Controller (NIC) without involving CPU and can reach the bandwith up to 100 GB/s.

The network infrastructure was set by assigning a dedicated server for floating license server installation that connect to all system including client's local PC, directory server, head node and compute nodes as shown in **figure 5**. It enables all the users as the client to connect to the cluster anytime and anywhere across the company's network. Cluster that was built by Pertamina EP allows users to run reservoir simulation model start from only using 1 core processor up to 160 cores in total, for each individual user. The cluster nodes can also be allocated up to 8 reservoir engineers who wants to run the reservoir simulation in parallel at the same time.

User Acceptance Test in Pertamina EP organization
As the quality check process, Pertamina EP conducted user acceptance test consists of: physical acceptance test to the

installed hardware components, power redundancy and connection test to from the license server, Application Delivery Platform (ADP), master node and each compute node based on the designated installation topology.
Another evaluation was also conducted for the software implementation in the cluster system. The software selected for this evaluation was the one that can maximize full capability of the installed hardware. This acceptance test was conducted to compare the performance behavior between the existing process using the ADP system, with the proposed new technology using the cluster system.

The evaluation steps consist of:
1) Run full simulation process of selected reservoir model using existing ADP environment.
2) By using the same file, run full simulation process using the new installed High Performing Computer (HPC) cluster system with several power computing configurations using different number of nodes and cores per simulation run.
3) Compare the overall simulation time required by both hardware environment and for each configuration cases.

There were three existing dynamic models selected for the evaluation of the hardware specification setup, as seen in **table 2**. Those models also consider the extreme cases of the complexity and the simulation experiences. The chosen models are Sago structure which has around 500 thousand active grid blocks, Limau Barat – Limau Tengah structure which has around 650 thousand active grid blocks, and one sample model from Rock Flow Dynamics (RFD) that is commonly used for the hardware speed test evaluation which has around 21.7 million active grid blocks. If the performance is acceptable, Pertamina EP will rebuild the dynamic model for each structure using the updated geological static model without upscaling. This was previously impossible because of the limitation of existing hardware and software in Pertamina EP.

Selection of Pilot POD to create standard operating procedures and process guidance
Currently the team is moving forward to a modern approach that is believed to improve the reservoir prediction and expectation using probabilistic and multi-scenario method. This approach is also aligned with the recent SKKMIGAS regulation on POD deliverability in PTK-037/SKKMA000/2018/S0–Rev–02. This method is the attempt to estimate and compensate the uncertainty in reservoir model by combining the deterministic and probabilistic approach so that upside and downside potential can then be discovered and considered for a complete project evaluation.

Pertamina EP EOR department has 33 structures of POD study related to waterflood optimization that need to be completed with the average target of completion of 4 structures per year. An example of reservoir simulation process in Pertamina EP, the model with 500,000 active grid blocks takes approximately 75 minutes to be completed using a full core single workstation. It takes 50 minutes to complete full simulation to run the same model using the server computer of ADP system that is proved provides better computer specs and higher number of cores.

Assuming that if 1 structure need 500 history matching simulation cases in average together with the forecast, then the current ADP system will need 50 days to complete the project. Moreover, the engineering evaluation time to quality check and property adjustment by trial and error can delay the completion of the project which is also depends on the reservoir model complexity and the available computing cores that can be utilized. This means that only 2 structures out of 4 the target structures are feasible to be completed each year.

Therefore, the HPC and robust reservoir simulation that support the latest parallel computing advancement is categorized as urgent. As the result, two of ongoing POD projects are chosen as the pilot implementation of the probabilistic multi scenario simulation to see the improvement that can be achieved in its first year of implementation. Limau Barat and Limau Tengah (LBLT) structure of Pertamina EP Asset 2 and Kenali Asam (KAS) structure of Pertamina EP Asset 1 are chosen for the pilot implementation. The selected reservoir models are chosen based on the complexity, urgency and the most time consuming, where those are the key issues that need to be focused if Pertamina EP wants to improve its business process.

Result and Discussion

Analog Benchmark result from three giga model in terms of simulation time and number of cores effect
The measurements of parallel performance for a different number of CPU nodes and cores were performed for all considered models. From the benchmark test of three different analog reservoir models, the result looks promising where acceleration factor from adding node is around 25 – 50%, as seen in **Table 1**. Slope of simulation runtime from 2 nodes run pack show a relatively more stable variation as shown in **Figure 3**. Two nodes can improve the simulation time from an average of 17 hours with a slope variation of about 8x10-7, to an average of 10 hours with a slope variation of around 3 x 10-7. It was concluded that those typical reservoir model will perform well with the addition of computer cluster.

The first model with 3 million of active grid blocks was chosen to be used for further evaluation. It consists of three phases reservoir model coming from one of Pertamina asset. As shown in **Figure 4**, the simulation was performed in a combination of 4 different nodes configuration ranging from 1 node, then increased by 2 times from 2 nodes, and 4 nodes until 8 nodes. Based on the results described, it is clear that the addition of computing nodes significantly decreases the simulation time. The first attempt using 1 node takes 4 hours and 43 minutes to complete the simulation, while second attempt using 2 nodes takes 3 hours 23 minutes to finish that is approximately takes one hour faster than the first attempt. The third trials using 4 nodes can reduce the simulation time even better with 1 hour 40 minutes needed to complete. Then the fourth attempts can summarize everything with only 1 hour needed to complete the full simulation span. It was concluded that the higher the nodes count will result in better acceleration time. One hour runtime to complete the simulation of 3 million active grid cells that consists of 1360 steps and 25 years of lifespan is surprisingly beyond the initial expectation. Thus, it is a strong justification to strengthen previous evaluation to equip cluster with 8 computing nodes.

Chosen cluster configuration and infrastructure to be implemented in Pertamina EP

Figure 5 shows the configuration that was built in Pertamina EP by stacking 8 nodes into a single system connected to the main master nodes that used as controller and dispatcher. Infiniband was also used to complete and ensure the better communication between the compute nodes. This HPC is connected to the local server network to enable reservoir engineer as the end user to connect to the machine using their local workstations. Information Center and Technology (ICT) team can also monitor the submitted job queue, real time job progress and computing nodes load. Since this HPC will be used to run big data, the simulation results will be stored using a large, dedicated storage

The number of structure completion target was calculated based on the model prepared using the assumptions of grid size, expected runtime and expected number of runs. **Table 3** shows the assumption of required number of storages per study which is 1 TB for a single study with additional of 20% free space and 2 years retention time. Thus, 16.8 TB of the maximum active storage will be needed for this study with consideration that the files that exceeded the retention time will be archived. This table also described that it will takes 5 to 10 months in the first year to complete the projects, and it takes just 5 months the completion of project in the following years, with assumptions that each project may require 300 cases to be run.

User acceptance test result from Pertamina existing fine reservoir model

After the completion of cluster installation in Pertamina EP, user acceptance test was also performed. The objective of this test is for quality check of the selected cluster performance in Pertamina EP using their own existing real field data. This information is written in **Table 2**. Two random reservoir models were selected from the current active POD projects. Since the existing reservoir model is considerably light and less complicated, the huge reservoir model that consist of 21 million active grid blocks which previously used for the benchmark test is also selected to be checked in the user acceptance test.

The first model has around 500 thousand active grid blocks, 107 active wells and 952 timestep. It took very long time to simulate the models in Pertamina EP local ADP system where it resulted to only half of simulation span finished after two and a half hours of running. The test using cluster provided satisfying result with only two hours needed to finish the complete simulation span by using 1 node, and one hour needed for all available nodes.
The second model has around 650 thousand active grid blocks, 129 active wells and around 1000 timestep. The existing ADP system took almost one hour to finish the complete simulation where cluster was proven to improve up to 13 minutes using 1 node. Additional number of nodes was also proven to accelerate even more up to 6 minutes.

The last model has 21 million active grid blocks and 39 wells. The attempts of running the model in ADP system was failed as the model was unable to be run due to its huge size. Cluster shown its main capability in this case where the machine performed very well to open and run this model with runtime significantly accelerated from hours up to become only 27 minutes.

All of these evaluations were successfully concluded the effectiveness of cluster installation in Pertamina EP environment and used as the background of the implementation of the ongoing POD projects.

Pilot POD with cluster implementation results of LBLT and KAS history matching and forecast

The ultimate objective of implementing this cluster technology is to apply full-scale probabilistic approach to determine the uncertainties and true potential of POD projects. Two ongoing projects were selected as the pilot projects based on its urgencies. Both projects were in the static modelling phase when it was decided.

After the implementation, not only geoscientist can work closely with reservoir engineers as they shared the common platform, but it also increases the reliability of the result because they now can model and run a full-field model. Additionally, the application that was used, enables the capability to integrate between the static geological modeling, dynamic modeling and history matching as an extended loop of workflow that can be seen in **Figure 6**. Now the history match will not only be limited to dynamic properties evaluation and adjustments but also to the static modeling part as well.

LBLT field is one of the reservoir models that was selected for pilot implementation. LBLT projects consists of multi tanks model with commingle production was chosen for fully integrated workflow because the model imposed more heterogeneity in both petrophysical modeling and its structural modeling. The workflow, as described in **Figure 7**, will help the static model validation process since all the steps from static modeling until history matching will be performed in connecting loop. This allows more evaluations for all the variables ranges from the selected geological uncertainties.

The total completion time for LBLT field development study was around 6 months. The reservoir model consists of around 700,000 active grid blocks with individual grid dimension of 50 x 50 x 1.4 meters (XYZ). Total 3,150 cases were simulated for the history matching part as shown in **Figure 9**. The number of experimental is quite big because the initial base case model simulation result was very far deviated with the history data. Number of optimization runs are also quite big because there was an issue in the production test and measurement done in the year of 1970-1980s that led to the history misinterpretation.

The process improved by time from the huge deviated liquid profile which gradually improved and finally matched with less than 1% deviation of history to simulation profile. It can also be seen that the workflow used can confirm static uncertainties such as the leaking fault, its transmissibility and fluid contact.

The second model that was selected is KAS. Finally, KAS reservoir also have a full field dynamic model and the simulation is now possible to be performed. KAS model was selected for the implementation of partially integrated workflow since the reservoir does not impose many variations in structural uncertainty. It was later believed that the petrophysical modeling uncertainty will be covered enough by incorporating the percentile 30, 50 and 90 of the deterministic static models, as shown in **Figure 8**. This process is slightly different but still enables user to assess the geological model in limited way.

Total completion time for KAS field development study was around 9 months, slightly longer than LBLT because the model vertical resolution is relatively higher. KAS reservoir model consists of 1,888,359 active grid blocks with individual grid dimension of 50 x 50 x 0.6 meters (XYZ). Total 594 cases were simulated in the history matching part. The number of experimental designs is relatively lower than in LBLT because the quality of the base case is relatively better in representing the history measurement, as can be seen in **Figure 10**. The average simulation time is also three times longer for this field and it requires more time for the evaluation since it has more active wells to be matched. In general, the model history matching progress is gradually improved to very good liquid, oil production profile and region pressure matched as can be seen in the picture.

As result, completion of both fully integrated and partially integrated workflow produced two standard operating procedure workflow options that will be applied for upcoming POD projects in Pertamina EP. The general process of integrated history matching method with help of assisted history matching application started with experimental design and sensitivity analysis to quantify and verify the discovered uncertainties. The experimental design process will normally lead to the more suitable base case model to be used as the first guess for the history matching optimization tool, that will automatically do the majority part of history matching tasks. Eventually, the reservoir engineers can verify the results and do the quality verification to all the completed jobs.

LBLT and KAS projects output along with the generated integrated workflows has been approved and selected as guideline for probabilistic modeling of POD proposal to SKKMIGAS especially for Pertamina EP because it provides user to assess the extended uncertainty evaluation from reservoir static modeling, dynamic modeling until history matching. The output will become the probabilistic solution of matched model that can be used for the field forecast. This approach is proven to provide multiple forecast realizations that is aligned with the background of history matching idea which is non-unique solution. The possible range of outcomes will then be evaluated in terms of decision analysis to decide the maximum production and economically optimum development for the field.

Conclusions

A parallel Hybrid algorithm mixing MPI and system threads at the node level was tested for various full-field models of real oil and gas fields and demonstrated a parallel acceleration record exceeding of 70% in 8 nodes cluster. In the extreme case scenario, an acceleration factor of 80% was reported where a “black oil” model with 21 million active grid blocks was run in a cluster with up to 160 cores. This model also enables the possibility to run the full fine field model that was previously impossible when using existing resource.

Based on the observation, turns out that comparing simulation from the field based on grids with different spatial resolutions, one could conclude that with additional vertical resolution creates noticeable differences in the estimations of internal reservoir energy and, consequently, causes differences in forecast calculations. It appears that the original full-field model with coarser active grid blocks must be upgraded to a model with additional resolution using finer active grid blocks, and this model should become a new base case for all the simulations of fluid and gas migrations, and global history matching at the field level.

It appears that with parallel Hybrid technology, history matching of giant reservoirs gets a significant boost when a higher number of CPU cores/node is used. The most optimum full cluster infrastructure for Pertamina EP is by implementing 8 computing nodes which each node consists of 20-cores Intel Xeon E5-2630 configurations. The proposed technology helps to remove several important performance bottlenecks and solves the “simulation scale problem” related to building, validating up to predicting dynamic models of giant reservoirs.

As a result, nearly “ideal” scalability and record acceleration for clusters have been observed and there is no evidence of the establishment of saturation point in parallel acceleration. The proposed technology allows running history matching of large models into team effort using personal workstations and large corporate cluster systems in the most effective manner.

Most importantly, the requirement to provide probabilistic POD proposal to SKKMIGAS is now become realistic and is easier to be completed. Strengthened by the possibility to couple geological subsurface modeling with dynamic simulation, up to surface production network constraint, allow the complete and realistic binary interaction between all uncertain and certain variables in each asset. It improves the quality of the POD proposal as the final product while also completed the risk evaluation with mitigation plan on downside potential.

Two pilot POD projects as the introduction implementation have been successfully performed which also resulted in the project template and process guideline. Assuming that the duration of this project will be similar with the other upcoming POD projects, then all the thirty-three structures completion target will be able to be done within the expected timeframe.

References

Absalyamov, Bogachev, Glazkova, Kostin, Telishev, Tregub, and Shimonin. 2020. Coupled Static and Dynamic High Resolution Modelling on High Performance Computer Clusters. SPE-201949-MS. https://doi.org/10.2118/187797-MS

Absalyamov, A. V., Bogachev, K. Y., Glazkova, E. A. et al. 2020. Coupled Static and Dynamic High Resolution Modelling on High Performance Computer Clusters. October 26–29, 2020, https://doi.org/10.2118/201949-MS

Telishev, A., Bogachev, K., Shelkov, V. et al. 2017. Hybrid Approach to Reservoir Modeling Based on Modern CPU and GPU Computational Platforms. October 16–18, 2017, https://doi.org/10.2118/187797-MS

K. Bogachev, S. Milyutin, A. Telishev, V. Nazarov, V. Shelkov, D. Eydinov, O. Malinur, S. Hinneh. 2018. High-Performance Reservoir Simulations on Modern CPU-GPU Computational Platforms. Presented at the AAPG international Conference & Exhibition, Cape Town, South Africa, November 4-7, 2018.

Acknowledgements

Management of EOR PT Pertamina EP.

PROCEEDINGS
JOINT CONVENTION BANDUNG (JCB) 2021
November 23rd – 25th 2021

TABLE 1

ANALOG MODEL PROPERTIES FOR BENCHMARK AND RESULT

Field	**A**	**B**	**C**
Area	Indonesia	New Zealand	Siberia
Grid size (cells)	3,000,000	4,700,000	20,000,000
Runtime (hour) with 1 node/ case	11.75	12.9	26
Runtime (hour) with 2 nodes/ case	8.5	7.75	13.12

TABLE 2

USER ACCEPTANCE TEST MODEL PROPERTIES AND EVALUATION RESULT

Nama Project	**Model Complexity**	**Simulation Runtime with ADP (hours)**	**Simulation Runtime with Cluster (hours)**
SAGO	Number of Active Grid: 517,775 Timestep: 952 Wells: 107 Calculated steps: 6,176	02:30:00 (unfinished - terminated at 48% progress due to long simulation time)	- 1 node -> 02:12:03 - 8 nodes -> 00:59:07
LIMAU BARAT - LIMAU TENGAH	Number of Active Grid: 655,556 Timestep: 1,016 Wells: 129 Calculated steps: 1,897	0:52:23	- 1 node -> 00:13:24 - 8 nodes -> 00:06:18 - 5 nodes (2 user A) -> 00:07:14 - 2 nodes (2 user A) -> 00:09:00
SAMPLE PROJECT from Siberia	Number of Active Grid: 21,770,901 Wells: 39 Calculated steps: 762	N/A	- 1 node -> 01:41:06 (unfinished - terminated at 54% progress due to long simulation time) - 8 nodes -> 00:27:07

TABLE 3

NODE REQUIREMENT EXPECTATION TO FULFILL THE 5-YEAR SHORT TERM POD PLAN

Year	**2019**	**2020**	**2021**	**2022**	**2023**
Grid Size	75,496,044	73,896,491	62,009,083	67,786,233	60,517,690
Max grid size	18,795,300	20,962,742	19,462,994	27,118,000	22,417,085
Min grid size	2,553,122	3,539,760	12,622,500	4,222,542	10,721,676
Total struktur	8	6	4	4	4
Node / struktur	1	2	2	2	2
Kebutuhan Node	8	8 *	8	8	8
Max Runtime (hour) / case	24.11	13.28	12.83	15.13	13.72
Min Runtime (hour) / case	11.12	8.05	10.78	8.26	10.21
Max Runtime (hour) / 300 case	7,234.27	3,983.71	3,848.73	4,537.68	4,114.60
Min Runtime (hour) / 300 case	3,336.15	2,415.64	3,233.09	2,477.09	3,062.01
Max Runtime (MONTH) / 300 case	10.05	5.53	5.35	6.30	5.71
Min Runtime (MONTH) / 300 case	4.63	3.36	4.49	3.44	4.25

PROCEEDINGS
JOINT CONVENTION BANDUNG (JCB) 2021
November 23rd – 25th 2021

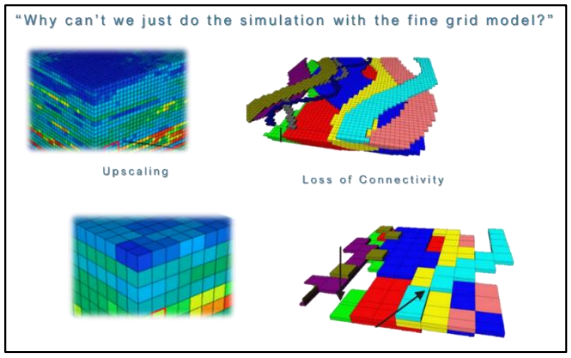

Figure 1 - Fine grid vs upscale grid fundamental.

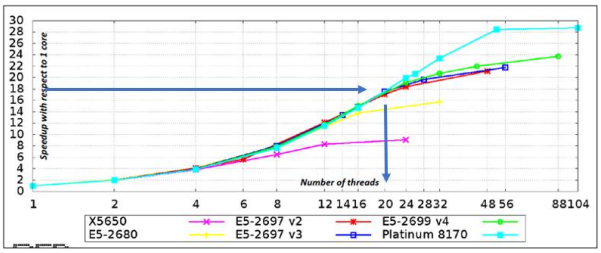

Figure 2 - Parallel computing threads sensitivity in regards with acceleration time.

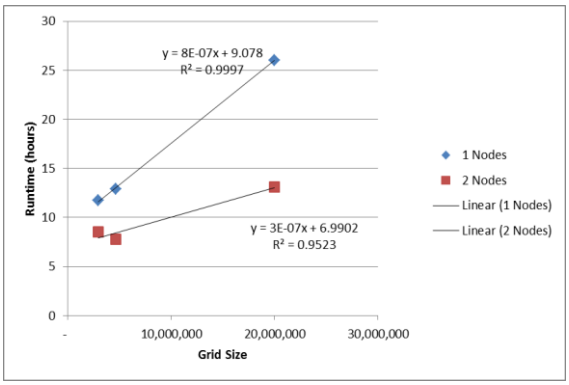

Figure 3 - Benchmark result on cluster configuration selection.

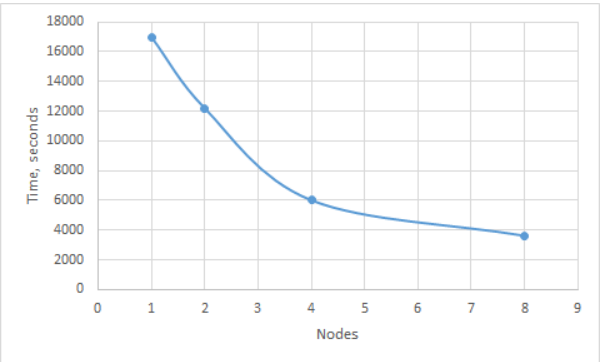

Figure 4 - Further benchmark result of model 1 from Pertamina EP analog reservoir sample.

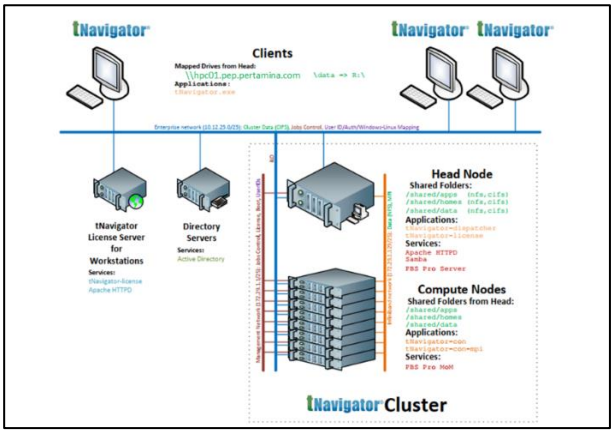

Figure 5 - Cluster infrastructure and flow process in Pertamina EP.

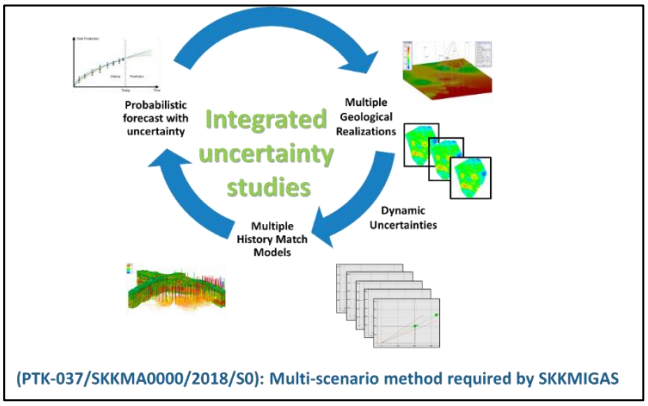

Figure 6 - Probabilistic history matching and forecast standard workflow.

PROCEEDINGS
JOINT CONVENTION BANDUNG (JCB) 2021
November 23rd – 25th 2021

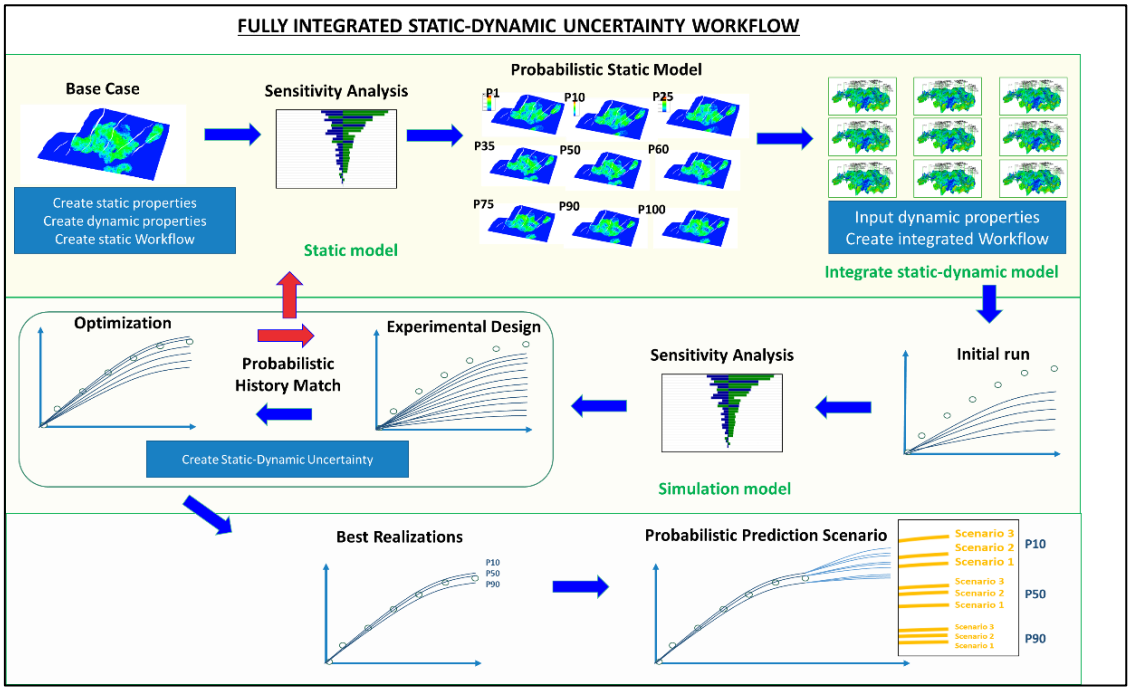

Figure 7 - New guidance and template of probabilistic plan of development process (1. full cycle integration).

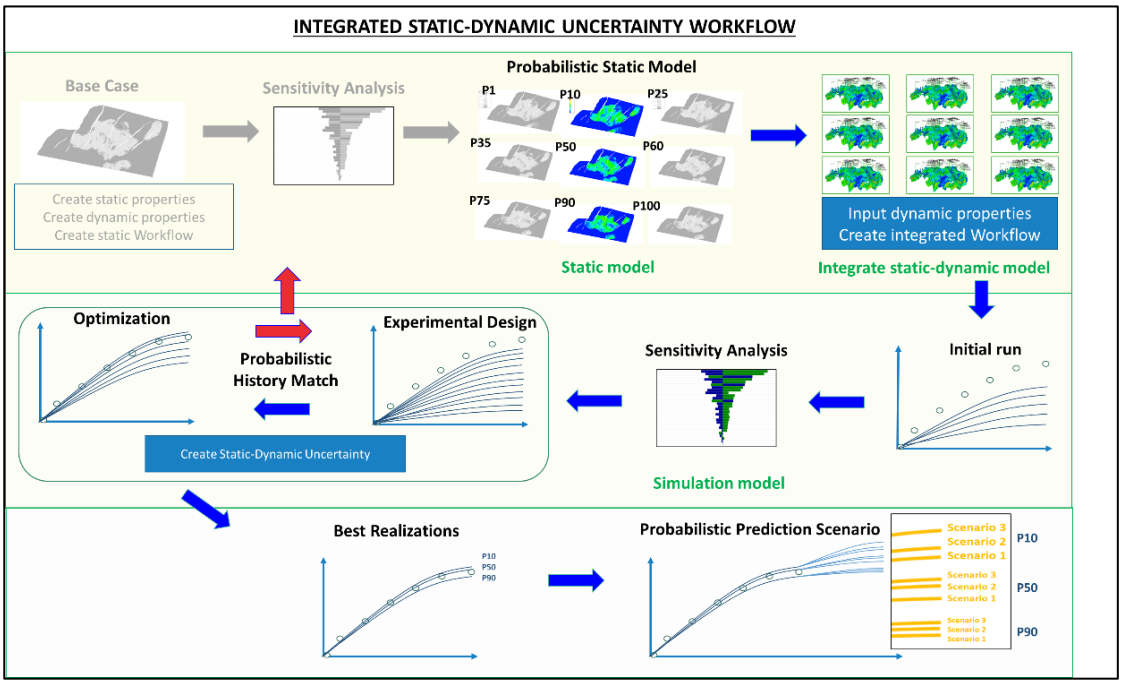

Figure 8 - New guidance and template of probabilistic plan of development process (2. partial integration).

PROCEEDINGS
JOINT CONVENTION BANDUNG (JCB) 2021
November 23rd – 25th 2021

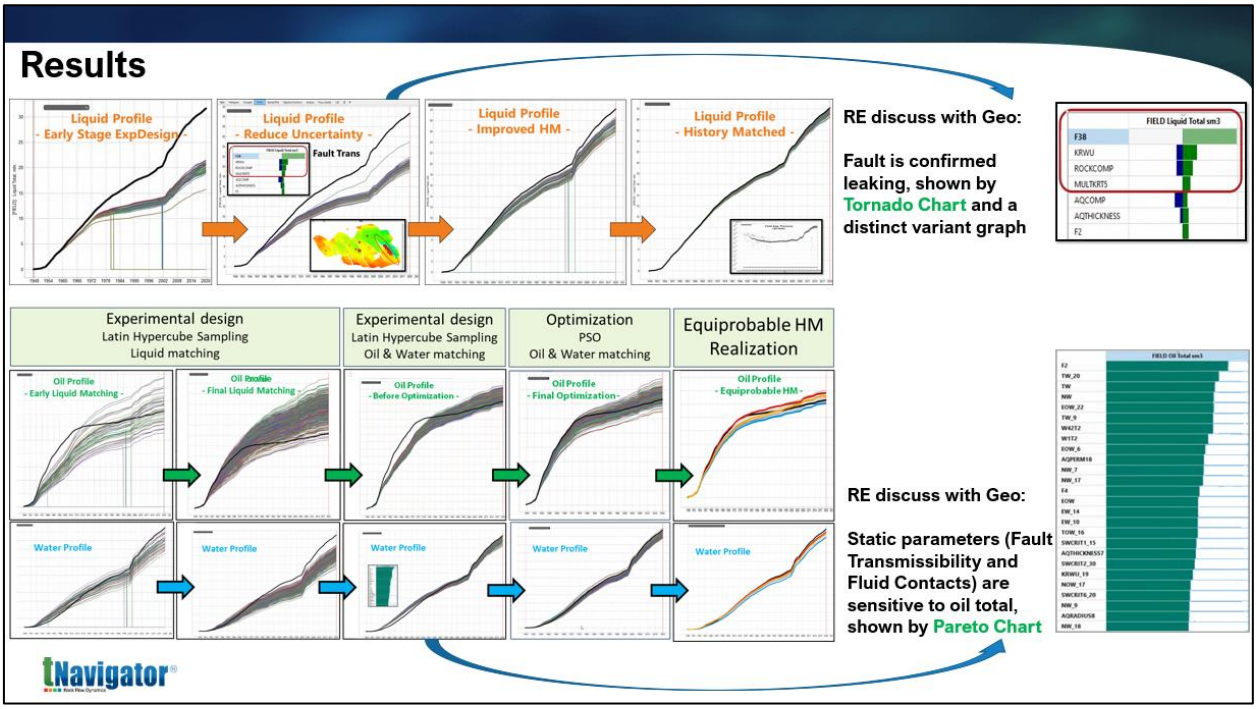

Figure 9 - Pilot projects result (LBLT POD).

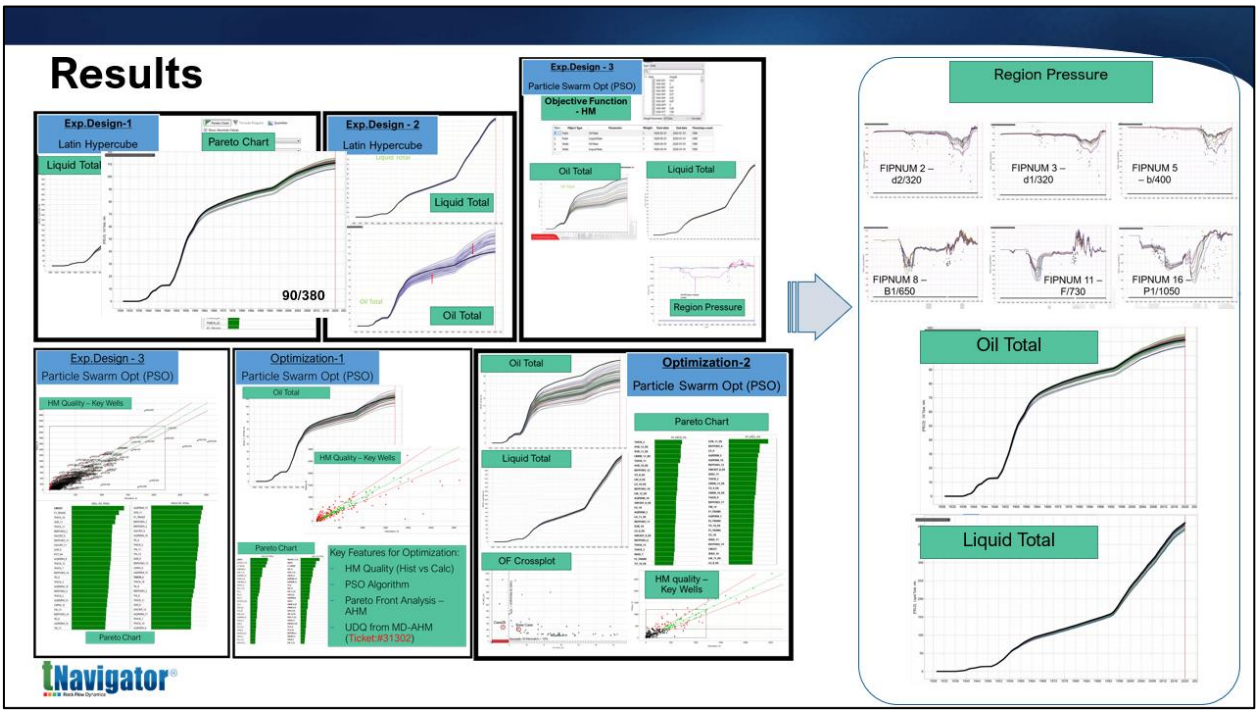

Figure 10 - Pilot projects result (KAS POD).

PROCEEDINGS
JOINT CONVENTION BANDUNG (JCB) 2021
November 23rd – 25th 2021

Understanding the Effect of 3D Layering Methodologies on the Production Profile of Tidal Estuarine Reservoirs

Praja, Ivan T.A. [1)], Indro, Axel P. [1)]
[1)] Rock Flow Dynamics

Abstract

A typical tidal estuarine reservoir comprises inclined interbeds of sandstone and claystone, also known as Inclined Heterolithic Strata (IHS). This sub-seismic feature of naturally inclining beds, combined with considerable heterogeneity, commonly inhibits the horizontal connectivity and ultimately controls the fluid flow behavior within these systems. However, normal datasets from subsurface studies frequently restrict a full IHS characterization and lead to the construction of a conventional, proportionally layered reservoir model. Moreover, once the 3D model is carried forward for simulation purposes, any significant changes to the geomodelling parameters are commonly barred which leads to excessive manual near-well region editing. Therefore, this paper aims to showcase the importance of representing the architectural elements of tidal estuarine deposits in the 3D model and their relation to the 3D layering methodologies and reservoir performance through 3D outcrop studies and multi-scenario reservoir simulation approach.

To demonstrate the effect of 3D layering on the production profile of IHS, 3D scanned outcrops of the Blackhawk Formation, USA, have been studied to produce several realizations of 3D models, including one that matched the morphological features of the outcrops as the truth case. All realizations were then simulated, and history matched to the truth case result as comparative studies.

Using 3 matched realizations to simulate 5-years forecasts, significant divergences prevailed. Cumulatively, there was up to 9% variation in total productions with only 3 producers and 1 injector wells in all realizations. More importantly, evident on both well by well production plots and visually over the time steps, the timing of water breaking-through the producer wells were faster and more uneven on the truth case, contrasting the results from proportionally layered realizations. Naturally, these required varying development strategies and proved that different3D layering methodologies produce quite variations in production forecasting albeit historically matched.

The novelty of this work is to integrate geological concepts, in a form of 3D layering methodology, as one of the most influential variables when modelling tidal estuarine deposits with under-informed conditions. This work can be implemented further in most fields with layering uncertainties to enable an optimum flow estimation, for a better investment decision.

Keywords: Geomodelling; History Matching, Reservoir Simulation; Tidal Estuarine, 3D Outcrop.

Introduction

Estuaries are primarily transgressive features that represent the flooding of incised valleys during the periods of lowstand (McIlroy et al., 2005). These features are known to host economically important deposits in hydrocarbon provinces such as the Athabasca oil-sand in Alberta, Canada (Nardin et al., 2013).

A typical tidal estuarine reservoir shared the similar overall architecture and the inclining nature of the beds to those of prograding point-bars from a fluvial environment. But there is a considerable heterogeneity inherited from the tidal influences which commonly inhibits the lateral connectivity of these reservoirs. Whilst point-bars are sandy and homogenous, the estuarine intertidal deposits are typically heterogenous with rhythmically stacked sandstone and claystone interbeds (figure 1).

The contrasting heterogeneities between the two depositional systems ought to present different 3D grid constructions, particularly the layering. However, this often overlooked, and understandably so, due to the typically insufficient subsurface dataset to fully characterize these geometries.

In a subsurface study, the occurrence of naturally dipping configurations on the other depositional environments, such as the carbonate platforms and delta clinoforms, are likely to be resolved through micro-faunal dating, sequence stratigraphy techniques and seismic imaging (figure 2). In the other hand, IHS are typically sub-seismic and resolved through borehole imaging or dip-meter which are expensive and rarely run while only providing 1D observation. When translated into 3D grid construction, the delta and reefs clinoforms are usually represented in the model as vertical segmentations (zones) whereas the IHS are likely to be represented as dipping-curvilinear layers usually irrespective to the zone boundaries also due to their much smaller scales compared to the previous stratigraphic features. Yet theoretically, the layer configurations will mostly define the production profiles and the reservoir performance of tidal estuarine reservoirs.

PROCEEDINGS
JOINT CONVENTION BANDUNG (JCB) 2021
November 23rd – 25th 2021

This study documents an approach of solving the stated problems with an outcrop-based reservoir analogues study coupled with dynamic simulations from the outcrop-based models. The presented workflow may be replicated in most fields with layering uncertainties to enable an optimum flow estimation, for a better investment decision.

Data and Method

The exposure of rock formations at Blaze Canyon, which located in the southeastern Book Cliffs - Central Utah (USA), is ideal for building reservoir model with 3D outcrop-based data using LiDar and Drones in roughly 1km^2 of area. The location was chosen because it offers a combination of outcrop and well logs observations of the tidal estuarine deposits (figure 3). The Blaze Canyon outcrop itself, represents highly prograding shoreface parasequences and the overlying transgressive incised valley fill deposition of the Campanian Desert Member of the Blackhawk Formation.

The interpreted stratigraphic surfaces on the 3D outcrop model were then brought into 3D modelling suite as polylines, surfaces, and markers. Based on the 3D outcrop data, two versions of 3D grids were created with different 3D layering methodologies, referred as the regular grid model and the dipping grid model in this study. The dipping grid model was matched to the morphological features of the outcrop with curvilinear-inclined 3D layering. The regular grid model was deliberately constructed with conventional horizontal and proportionally layered reservoir model to represent the result of an underinformed subsurface study (figure 4). Both grids are then integrated with sedimentary logs and electrical logs to fill in the grids with facies and petrophysical properties based on controlled geostatistical approach.

Dynamic simulation parameters referred the work of Howell et al (2008) including rock compressibility, equilibrium specifications, pressure and depth settings of the model while the PVT tables were built using correlations (table 1). Two producer wells in the middle and up-dip positions, B-02 and B-01 respectively, one injector well (Inj-01) placed in the down-dip position were then added to each model. After the models were successfully initialized and simulated, the dipping grid simulation result is then set as the truth case or "production history" for other models.

An additional static model based on the dipping grid was also created but with different petrophysical and dynamic properties from the truth case. This enabled direct comparison to determine whether different static parameters or the 3D layering that hold greater significance in dictating the fluid flow behavior in this study.

All in all, three realizations were made in this study, two based on the dipping grid (referred as the truth case and dipping grid model) and one based on the regular grid (referred as regular grid model). Simulated hydrocarbon volume in place for all realizations were kept constant. Figure 5 illustrates the complete workflow of this study.

Result and Discussion

The use of 3D scanned outcrop has allowed thorough observation of the tidal estuarine outcrop at Blaze Canyon, Utah. There are two main depositional environments identified within the studied interval, the wave dominated delta and tidal estuarine environment. Each exhibits different degrees of heterogeneity and architectural complexity. Whilst the stratigraphic framework of the wave dominated delta deposits are usually represented with flat flooding surfaces, the tidal estuarine deposits are encased by sequence boundary at the base and maximum flooding surface at the top but also internally complex with strata termination surfaces which indicate the flooding of the incised valley during a transgressive period (figure 6). Within these strata terminations are the naturally inclining intertidal deposits geometries which commonly hidden from a 1D log-based analysis. All realizations captured similar heterogeneity in terms of facies distributions and properties despite the different 3D layering settings (figure 7).

Simulation results from both regular grid and dipping grid models show similarly good matching quality on field production level (figure 8). However, these results are deceiving as revealed by further investigations on the well-to-well production level. On the regular grid model, well B-02 produced significantly more water compared to B-01 which positioned more up-dip (figure 9). The difference of water production from the producers in regular grid model added up in the field level and made as if the cumulative water production is within the tolerance of a matching criteria. As expected, the dipping grid model showed good matching on the field and well-to-well level despite the different petrophysical properties to the truth case (figure 9).

Sweeping profiles of both dipping grid and regular grid models further explained the phenomenon seen on the well-to-well production profiles (figure 10). By proportionally layering the regular grid, the flow simulation resulted in uniform hydrocarbon sweeping profile. However, in the dipping grid model, there is contrasting 3D layering settings between the tidal estuarine and the surrounding flat layered shoreface facies. Meaning the tidal estuarine reservoirs also rely on vertical permeabilities of the reservoir to laterally flow the hydrocarbon within a zone. This caused severe water-fingering problem and that the water broke-through the well B-01 a lot earlier in the dipping grid model compared to the regular grid model.

To replicate the early breakthrough phenomenon on the dipping grid, several manual editing efforts were conducted to the regular grid model. Relative permeabilities were adjusted and near well permeability multipliers were applied (figure 11). Whilst these history matching measures are common amongst reservoir engineering community, this meant that the geological realism captured in the original model was lost. Also, while having the 3D model redone by the geologists is possible, it usually takes a longer time and therefore often avoided in crunching project deadline. Thus, highlighting integration issue between static and dynamics modelling disciplines.

With the regular grid model historically matched to the truth case, two forecast scenarios were conducted with bottomhole pressure at the end of history matching utilized as the forecast control. The first experiment is a 5-year forecast scenario based on the current well conditions. The second scenario is a 5-year forecast scenario, but one infill wells was added. The infill well was placed where the remaining oil is the highest in both models.

For the first forecast scenario, there was up to 7% of observable difference in cumulative oil production within 5 years with the existing producing wells. The history matched regular grid model shows a rather optimistic result of oil production compared to the dipping grid model. This is due to the water production of B-01 well was still at an optimistic rate at the end of history matching. The result of the first forecast scenario is shown in Figure 12.

The infill case scenario shows an agreement to the first forecast scenario. The history matched regular grid is 9% higher in oil cumulative compared to the dipping grid model. The result of the infill case is shown in Figure 13.

All in all, the results show that different 3D layering schemes produced noticeable differences in the forecast productions and production profiles, probably more than the difference in petrophysical properties. In agreement with Arnold (2008) and Howell et al (2008), different interpretations with very different reservoir parameters may produce equally good history matched models but very different forecast estimates may be produced.

Nowadays, decisions for Field Development Plan are still heavily depending on reservoir simulation results. Multi-scenario approach is now a requirement to better cope the mentioned problems, particularly the lack of data to fully capture the geometrical intricacies and heterogeneities of a reservoir. With a representative range of models presented, a better investment decision is enabled. Whether to go on with acknowledged risks or to gather more data or as this paper demonstrated to do a reservoir analogues study to minimize risks.

Conclusions

An important aspect of the tidal estuarine deposits to be represented well in a model is the complex internal geometries with strata termination surfaces encasing the Inclined Heterolthic Strata (IHS). Ideally, these are then incorporated the reservoir model as 3D layering methodologies which bare as much as importance of the structural framework of the reservoir model. This study highlights the consequence of underrepresenting such features, which held 7% deviation in forecast with 2 producers and 1 injector wells in more or less 1 km2 area. The deviation is punctuated with the addition of an infill well, with up to 9% deviation of forecast from the truth case.

Whilst the importance of applying the complicated dipping grid has been raised, the implementation of such methodology in a real subsurface study is difficult. Moreover, completeness of data is such a luxury that subsurface studies commonly lack. Therefore, two alternatives are suggested based on the result of the study.

First, as this study has demonstrated. Reservoir analogues studies may provide the knowhow on the geometrical intricacies of the reservoirs of interest. In the recent years, the reservoir analogues studies have been benefited from the technological advancements such as LiDar and commercially available drones to scan outcrops which enabled the construction of outcrop-based 3D reservoir models and realistic fluid flow simulations.

Second, by building a rigorous workflow in an integrated static to dynamic modelling suites and iterating the processes in experimental run, some of the 3D model variations may exhibit the similar, or closing towards the expected, fluid flow behavior. The 3D layering uncertainty requires multiple scenarios as proposed solutions. Therefore, multiple grids with different layering scenarios are required to be set as one of the main variables in the experimental design. The second approach requires a capable integrated modelling suite which allows every static model realization to be dynamically initialized upon each iteration and then simulated. The second alternative is reserved for a further work.

Acknowledgement

The authors would like to express their gratitude to Prof. John Howell, University of Aberdeen, CIPR, Virtual Outcrop Group (VOG) and Rock Flow Dynamics. The 3D outcrop model was collected as a part of the SAFARI project by VOG, a collaboration between University of Aberdeen, University of Bergen and a consortium of European oil companies.

References

Arnold D.P., 2008, Ph.D Dissertation, Heriot-Watt University

Baker R.O. et al., 2006, 7th Canadian International Petroleum Conference, PAPER 2006-129

Burgess, P. M., Winefield, P., Minzoni, M., & Elders, C. 2013. Methods for identification of isolated carbonate buildups from seismic reflection data. AAPG Bulletin, 97(7), 1071-1098. https://doi.org/10.1306/12051212011

Howell, J.A., Skorstad, A., Mcdonald, A., Fordham, A., Flint, S.S., Fjellvoll, B. & Manzocchi, T. 2008. Sedimentological parameterization of shallow marine reservoirs. Petroleum Geoscience, 141, 17-34.

McIlroy, D., Flint, S.S., Howell, J.A. & Timms, N. 2005. Sedimentology of the tide-dominated Jurassic Lajas Formation, Neuquén Basin, Argentina. Geological Society, London, Special Publications, 252(1), 83-107.

Nardin, T.R., Feldman, H.R. & Carter, B.J. 2013. Stratigraphic Architecture of a Large-Scale Point Bar Complex in the McMurray Formation: Syncrude's Mildred Lake Mine, Alberta, Canada. In: Hein, F.J., Leckie, D., Larter, S. & Sutter, J.R. (Eds.), Heavy-oil and Oil-sand Petroleum Systems in Alberta and Beyond. American Association of Petroleum Geologists, AAPG Studies in Geology 64, 273-311.

Van Wagoner, J.C. 1995. Sequence Stratigraphy and Marine to Nonmarine Facies Architecture of Foreland Basin Strata, Book Cliffs, Utah, U.S.A. In: Van Wagoner, J.C. & Betram, G.T. (Eds), Sequence stratigraphy of foreland basin deposits, outcrop and subsurface examples from the Cretaceous of North America. American Association of Petroleum Geologists, Memoir 64, 137 - 223.

PROCEEDINGS
JOINT CONVENTION BANDUNG (JCB) 2021
November 23rd – 25th 2021

Parameter	**Value**	**Notes**
Oil PVT		
Correlations	Standing	For Live Oil's Rs, Formation Volume Factor, and Viscosity
Temperature	100	C
Oil SG	0.8	-
GOR	142	Sm3/Sm3
Gas PVT		
Correlations	Lee et al, Standing	For Dry Gas' Viscosity and FVF respectively
Temperature	100	C
Gas SG	1	
Z Factor	0.9	
Water PVT		
Ref. Pressure	1.01	Bars
Ref. FVF	1	
Rock-Fluid		
# of Saturation Regions	1	
Corey Exp	4	Water
	3	Oil-Water
Saturation End Points	0.2	Sorw (Fraction)
	0.2	Swcr (Fraction)
Rel.Perm End Points	1	Kro max
	0.4	Krw max
Equilibrium Specifications		
Datum Pressure	145.6	Bars
Datum Depth	1327.79	Meter
Rock Compressibility	5e-6	1/bar
Rock Ref. Pressure	135.6	Bars
Strategy		
Production History	8	Years
Well Cut Offs	90%	Watercut
# of Wells	1	Injector
	2	Producer

Table 1. Correlation parameters to generate PVT Data and dynamic simulation parameters.

PROCEEDINGS
JOINT CONVENTION BANDUNG (JCB) 2021
November 23rd – 25th 2021

Figure 1. A typical intertidal deposit characterised by rhythmically stacked Inclined Heterolithic Strata (IHS) of sandstone and shale. On the outcrop faces which are not topographically eroded, IHS is observed to have two strata terminations, top-lapping to the capping supratidal coal and down-lapping to a major erosional surface. On most of the sedimentary logs, the succession displays a fining upward pattern and is rooted in several of the logs. The rhythmical appearance suggests alternating energy of tidal influence. The strata were inclined, indicating accreting bodies. These interpretations fit the characteristics of a tidal estuary environment where the high fluvial energy is superimposed by periodical tidal floods.

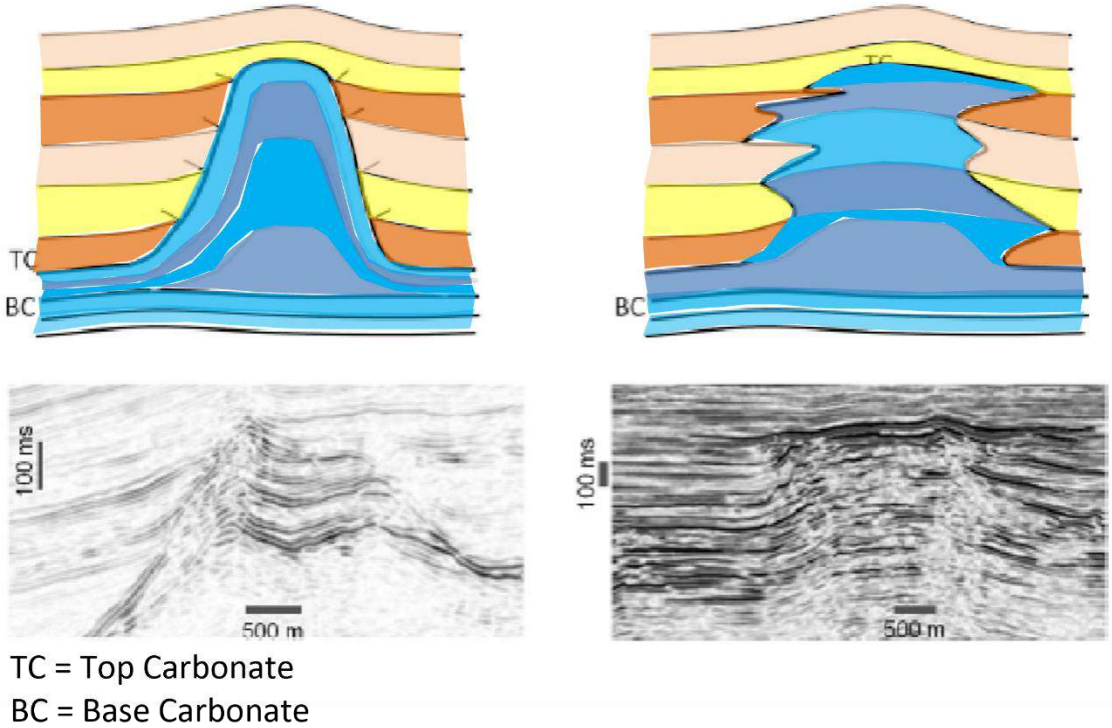

Figure 2. The occurrence of naturally dipping configurations on the carbonate platforms and delta clinoforms, resolved through micro-faunal dating, sequence stratigraphy and seismic imaging (Burgess et al, 2013).

PROCEEDINGS
JOINT CONVENTION BANDUNG (JCB) 2021
November 23rd – 25th 2021

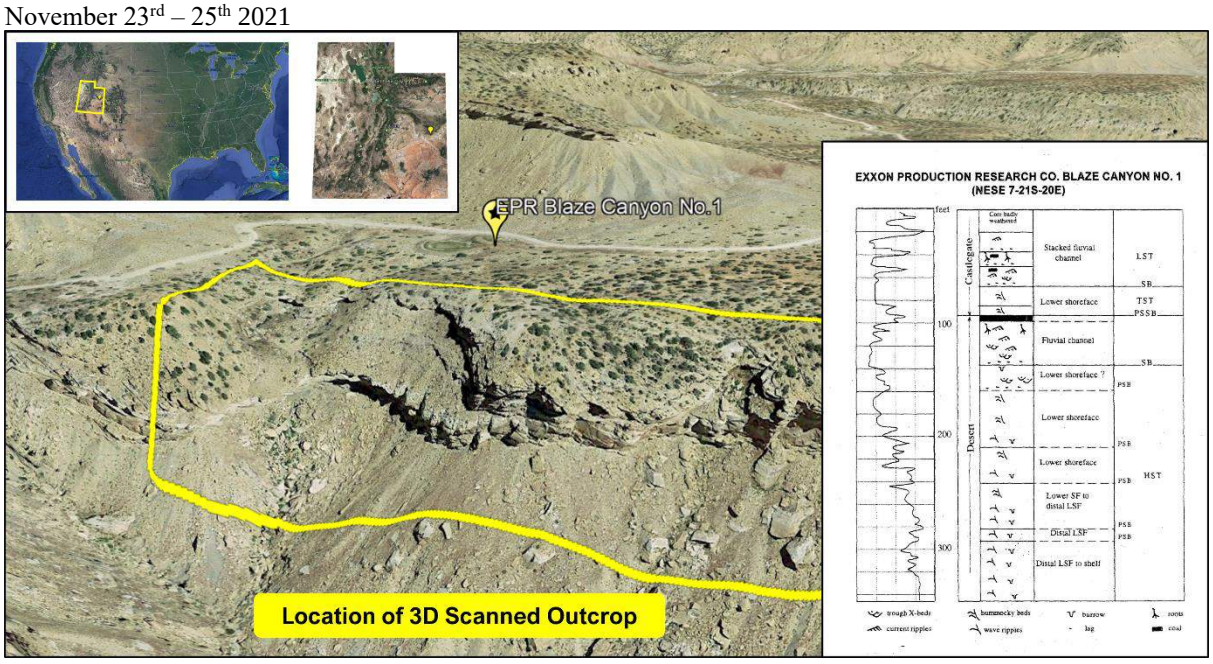

Figure 3. A research well, EPR Blaze Canyon No. 1, was drilled about 350m northwest of the cliff face in the 90s by Exxon Production Research group and published in Van Wagoner (1995) along with numerous sedimentary logs and stratigraphic analysis surrounding the Book Cliffs area. The well was also cored and an array of formation evaluation logs were recorded to allow petrophysical evaluations.

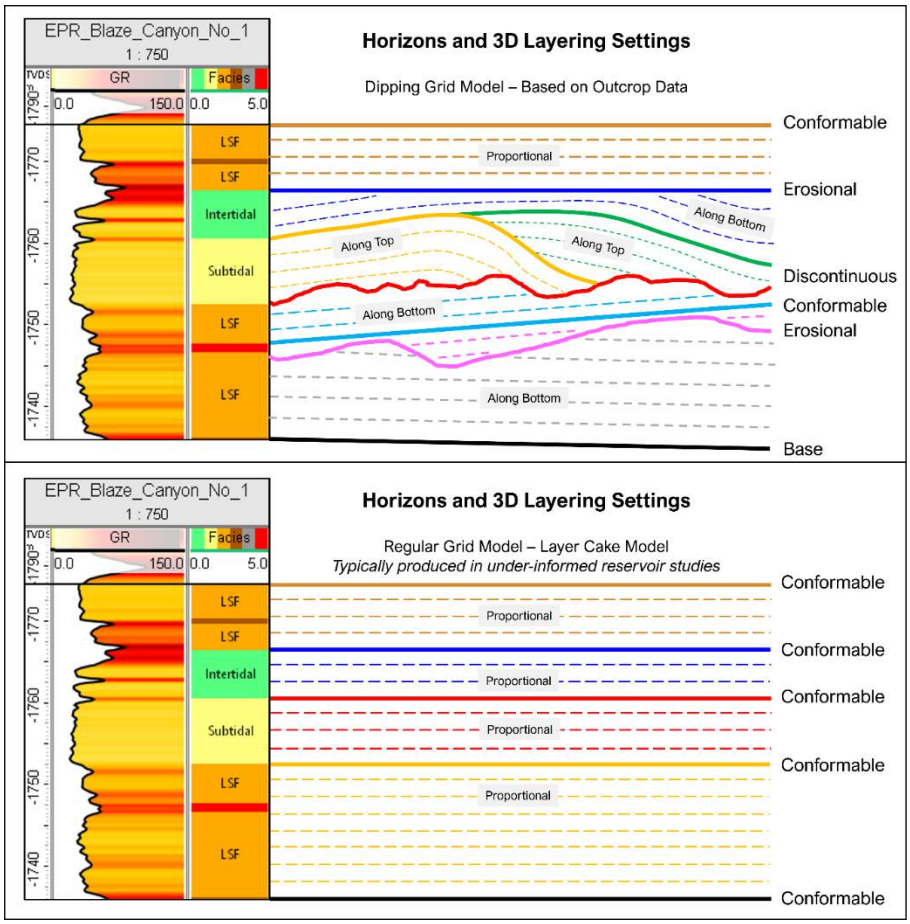

Figure 4. 3D layering settings used as comparative study in this work to create the dipping grid model and the regular grid model.

PROCEEDINGS
JOINT CONVENTION BANDUNG (JCB) 2021
November 23rd – 25th 2021

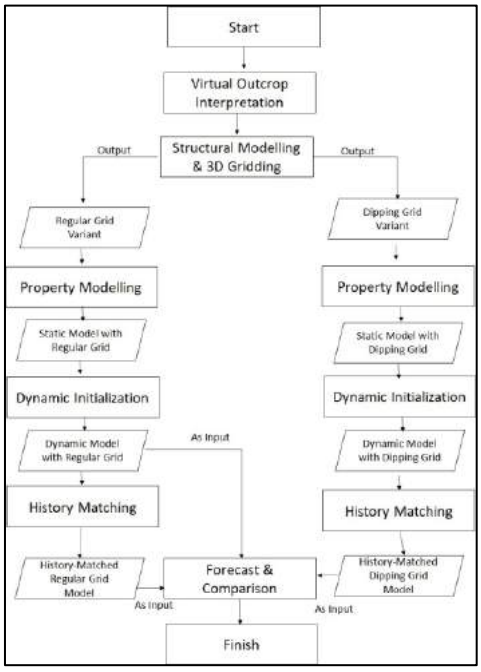

Figure 5. Complete workflow of the study.

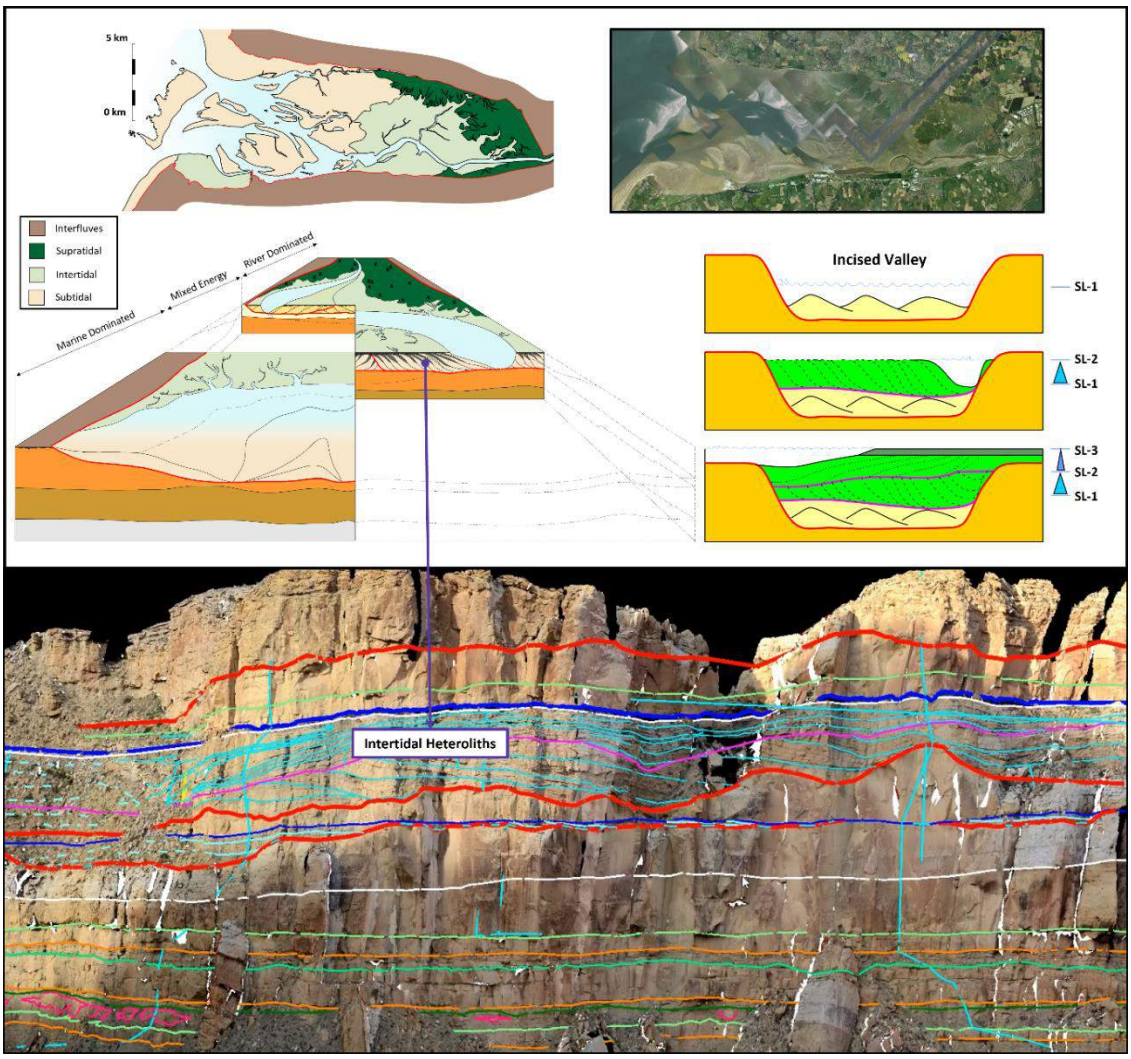

Figure 6. The interpreted 3D outcrop model and conceptual depositional system based on modern analogue of Dee Estuary in Liverpool, UK.

PROCEEDINGS
JOINT CONVENTION BANDUNG (JCB) 2021
November 23rd – 25th 2021

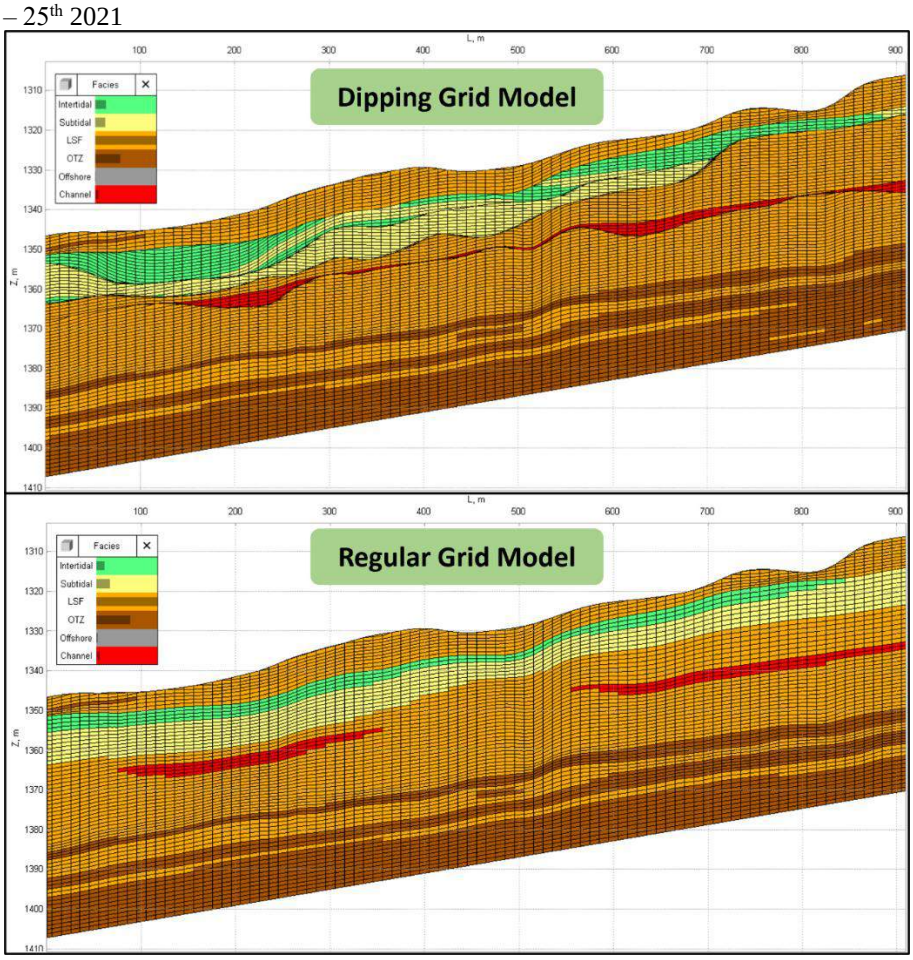

Figure 7. The dipping and the regular grid variants capturing more or less the similar heterogeneity in terms of facies and petrophysical properties.

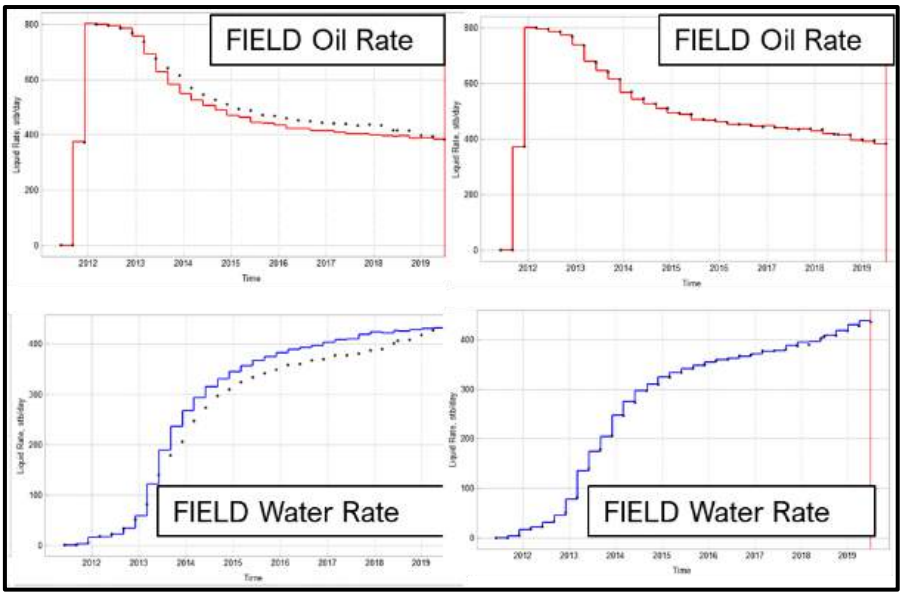

Figure 8. Similar level of matching on field level between regular grid (Left) and dipping grid models (Right).

PROCEEDINGS
JOINT CONVENTION BANDUNG (JCB) 2021
November 23rd – 25th 2021

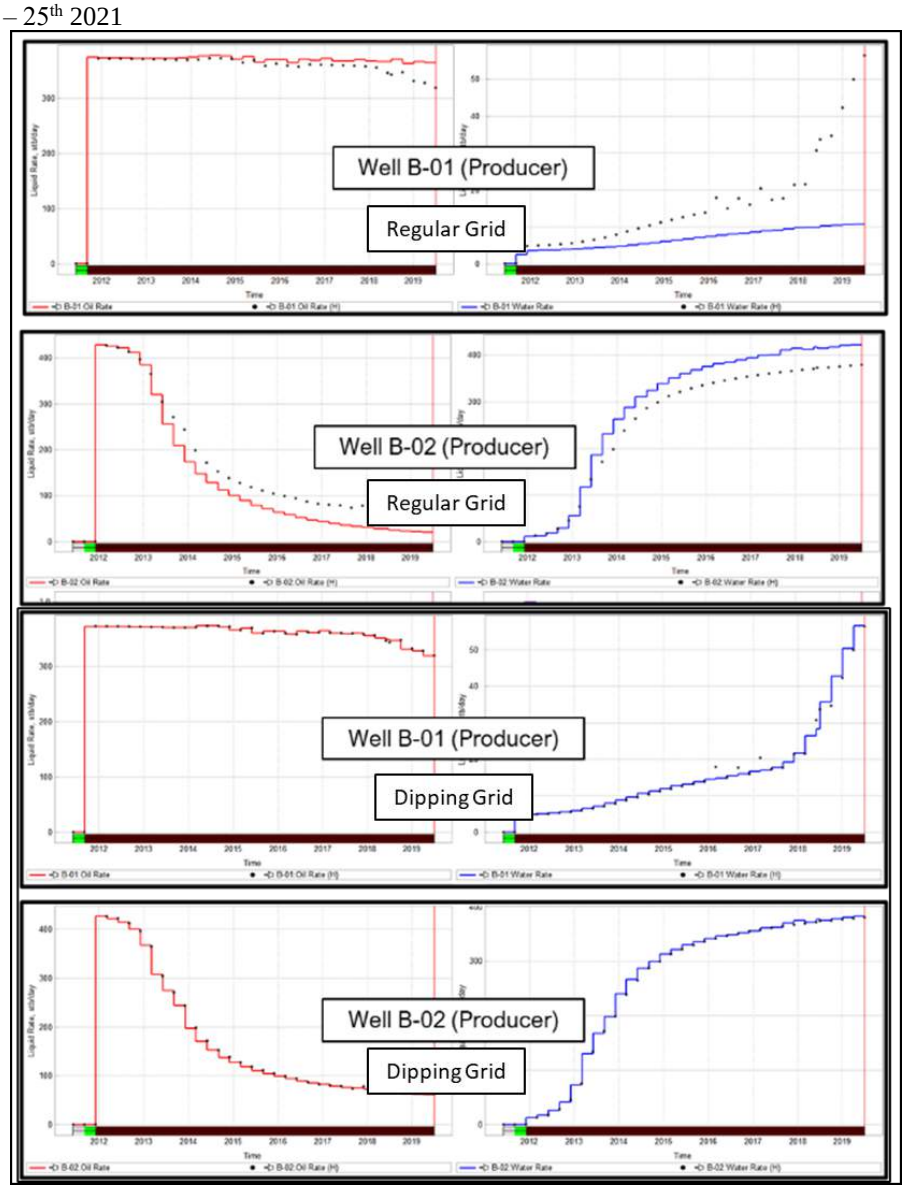

Figure 9. Contrasting level of matching on well-to-well level between regular grid and dipping grid models.

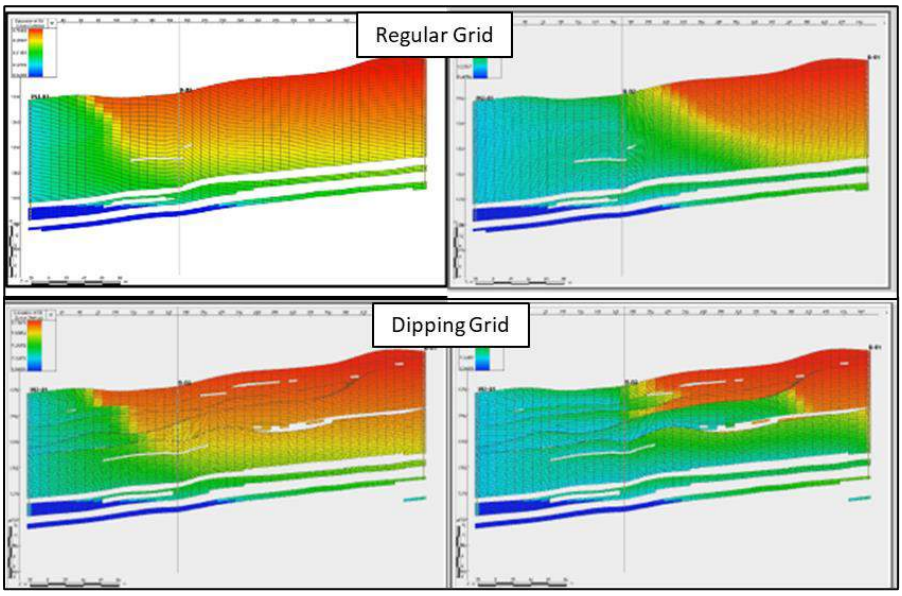

Figure 10. Sweeping profile for both models. Showing different flow uniformity on the well-to-well production profile.

PROCEEDINGS
JOINT CONVENTION BANDUNG (JCB) 2021
November 23rd – 25th 2021

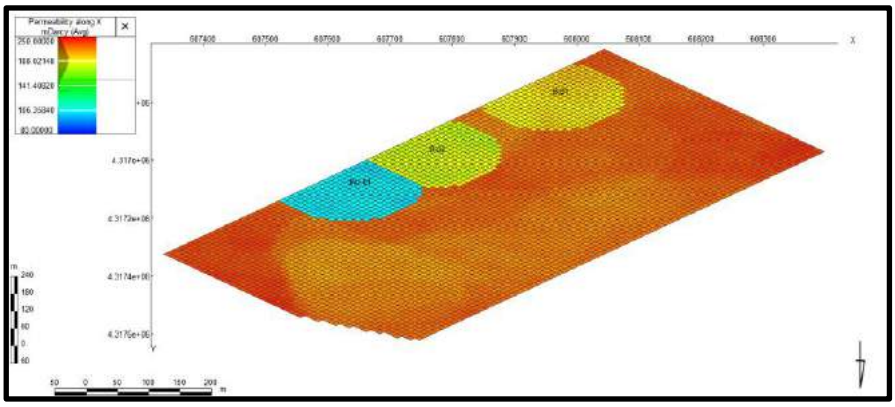

Figure 11. Near well permeability multiplier applied to regular grid model to mimic the water-fingering phenomenon observed on the dipping grid model.

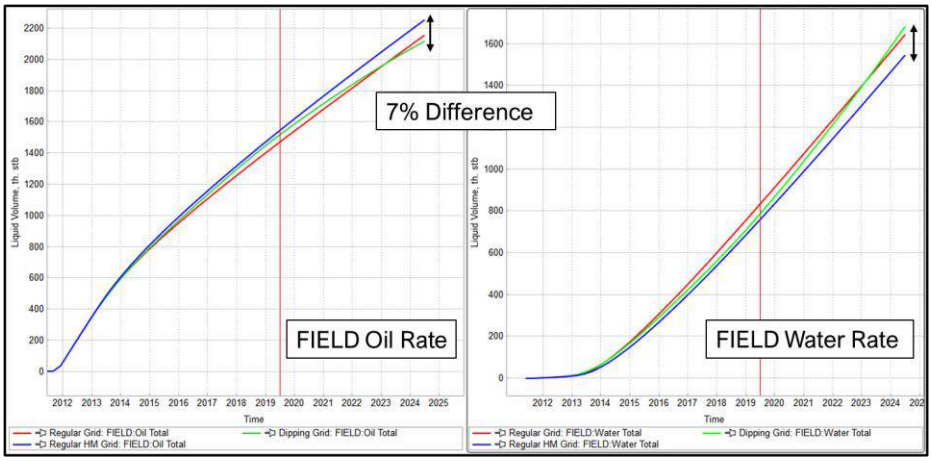

Figure 12. Forecast result comparison for first forecast scenario.

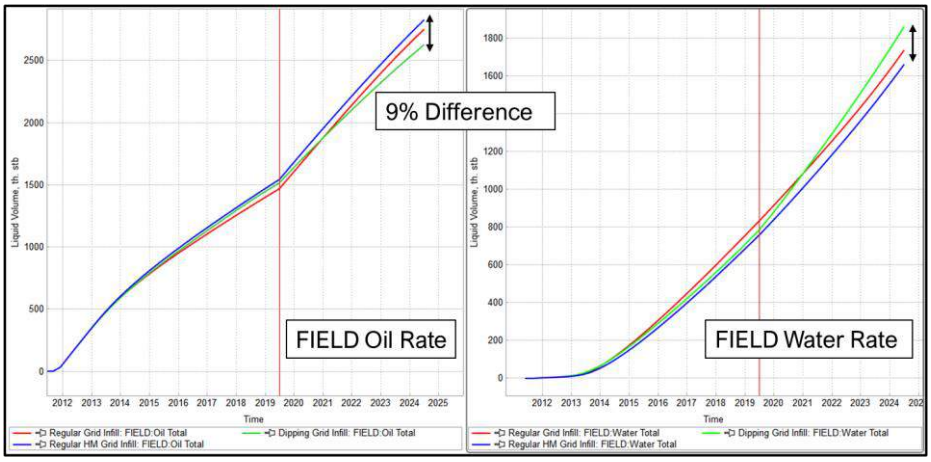

Figure 13. Forecast result comparison for infill case scenario.

PROCEEDINGS
JOINT CONVENTION BANDUNG (JCB) 2021
November 23rd □25th 2021

Immiscible CO2 EOR Injection Coreflooding Optimization using Compositional Simulation Model for Sumatera Light Oil Field

Dimas Rahmadi Giantri Putra [1]

Ruri Muharto[2]

Abstract

Many wells in Sumatra Field have already a decline in production after being produced naturally, but still have oil left in the reservoir. Therefore, there is a technique to produce the remaining oil reserves in the reservoir, it is called EOR (Enhanced Oil Recovery). EOR (Enhanced Oil Recovery) is basically defined as lifting oil with various methods such as Chemical flooding, Thermal Recovery and CO_2 injection.

This paper describes Matching EOS model and Current Pressure CO_2 injection Continous scenario of Coreflooding Simulation based on laboratorium experiment. PVT data of EOS modelling are Differential liberation, Constant Composition Expansion, Separator, Swelling test and MMP using CMG Simulator (Winprop). The PVT data sample used combination from the PVT data initial and PVT data current data property, therefore the fluid model resprents proper current reservoir property to be used in coreflooding simulation scenario.

Matching the scenario experiment data of coreflooding process simulation to get some parameter like injection rate, The value of SORW, Oil Viscosity..Therefore, the simulation model were valid to run sensitivity study over different scenario of injection such as continous CO_2, various slug size, WAG and WAG ratio. Based on the purpose of this paper, this paper can be used for many various sensitivity of coreflooding simulation with one PVT data of laboratorium experiment and one scenario data coreflooding simulation to find the best scenario for the optimum of recovery factor.

From the results of this study, it can be used for field development by upgrading the coreflooding model into a field model and also which scenario is the best for implementing.

Keywords: Enhanced Oil Recovery, Immiscible CO2 Injection, Coreflooding Simulation

Introduction

For further field developments where natural production has been carried out, usually tertiary production will be to do for the next production step. There are several types of tertiary production, there are Chemical Injection, Gas Injection, and Steam Injection.

The tertiary production in this paper is by using CO2 Gas Injection. There are 2 methods for CO2 injection, Miscible CO2 Injection and Immiscible CO2 Injection. To determine whether the injection is Miscbile or Immiscible, it is necessary to know the value of the Minimum Miscibility Pressure (MMP). MMP values can be obtained by slimtube laboratory, and correlation. In this paper, an immiscible CO2 injection will be used because the MMP value is higher than the fracture pressure.

To support tertiary production, a Fullfield simulation model should be done. One of the steps to do a Fullfield simulation model is coreflooding simulation. In this coreflooding simulation, there are several scenarios, there are Continuous CO2 Current Pressure, Continuous CO2 Initial Pressure and WAG Initial Pressure. In this paper,CO2 Coreflooding Simulation uses CMG GEM Simulation

Data and Method

EOS Modelling

To perform a full-field model Simulation CO2 injection simulation, several steps are required, including the following:

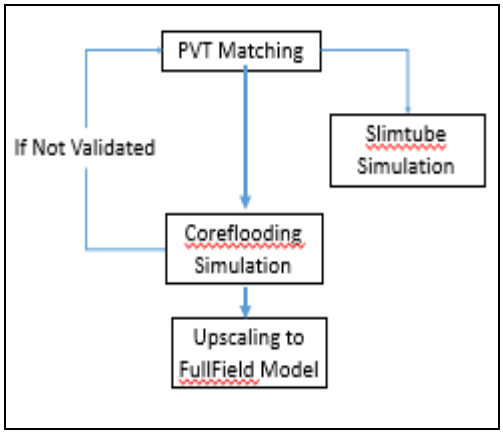

Figure 1: Workflow

PROCEEDINGS
JOINT CONVENTION BANDUNG (JCB) 2021
November 23rd □ □25th 2021

Component	Initial Condition		Current Condition	
	Mol %	Weight %	Mol %	Weight %
CO2	2.38	0.66	1.97	0.43
N2	0.22	0.04	0.24	0.03
C1	23.86	2.43	7.94	0.63
C2	3.32	0.63	1.15	0.17
C3	3.88	1.09	1.98	0.43
i-C4	0.77	0.28	0.72	0.21
n-C4	1.08	0.40	1.38	0.40
i-C5	3.57	1.63	1.13	0.40
n-C5	2.38	1.09	1.22	0.43
C6	4.06	2.21	3.72	1.58
C7+	54.58	89.24	78.55	95.30

Tabel 1 : Initial Composition and Current Condition Composition

The Equation of states Peng Robinson (1978) was used in this paper. By combining PVT data on initial conditions and PVT data on current conditions. PVT matching was performed based of result laboratory data such as Saturation Pressure, Constant Composition Expansion, Differential Liberation, Viscosity, Etc.

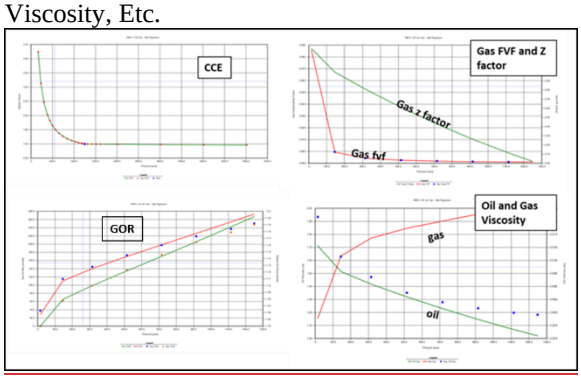

Figure-2 : PVT Matching Initial Composition Data

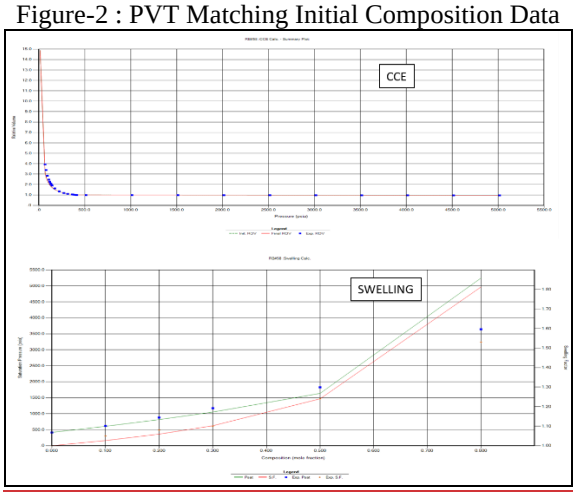

Figure-3 : PVT Matching Current Composition Data

Minimum Miscibility Pressure

Determining the minimum miscibility pressure can be done in two ways, namely the slimtube laboratory experiment and its correlation. The most commonly used method is to graph the oil recovery after 1.2 PV of gas injected at each injection pressure. The three MMP Criteria using the graph are;

1. MMP when the curve starts to bend.
2. MMP at the inflection point with oil recovery greater than 95%.
3. MMP where the oil recovery is greater than 95%.

To determine the MMP by correlation, the correlation used is the correlation of Cronqruist, Yellig and Metcalfe, Holm Jossendal. The MMP for those correlation are 2525 psia, 2300 psia and 2700 psia

In this paper, the MMP value in the laboratory results is 2700 Psia which will then be validated by the results of slimtube simulation

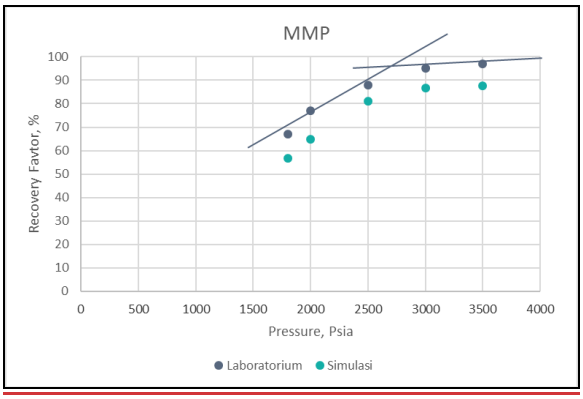

Figure-4: Results of MMP

Coreflooding Simulation Model

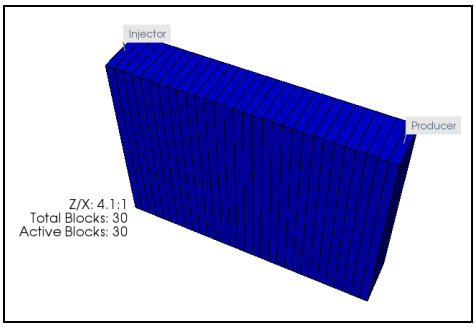

Figure-5: Coreflood Simulation Model with 1 Injector and 1 Producer

Sample Code	Depth	L	K_{He}	Stack Length	Diameter Avg	k avg	ϕ avg
	meter	mm	mD	mm	mm	mD	%
Core 1	811.36	26.86	67.31	195.80	37.7	58.25895	27.8
Core 2	811.65	31.12	68.98				
Core 3	811.70	31.14	64.76				
Core 4	811.86	35.13	52.75				
Core 5	811.94	36.87	52.84				
Core 6	823.55	34.68	52.07				

Tabel-2: Coreflooding Rock Properties

Based on Coreflooding Rock Properties, The model have 68.6 cc with oil saturation 30.1 cc (43.9 %) and water saturation 38.5 cc (56.1 %).

Result and Discussion

In this paper, a WAG scenario will be carried out with an initial pressure of 1250 psia. The steps in this WAG simulation are water injection first until Saturation Oil Residual (SOR) conditions which will then be followed by water injection up to 0.2 PV and gas up to 0.2 PV alternately. And finally flush injection with water until no oil is produced.

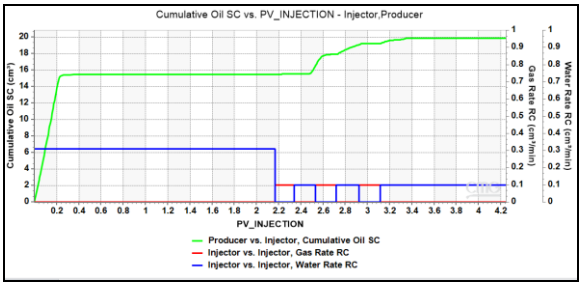

Figure-6: PoreVolume Injection vs Cumulative Oil WAG Scenario Coreflooding

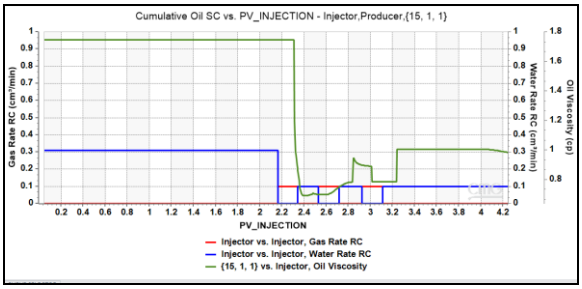

Figure-7 : Oil Viscosity at 15,1,1 Block

From the results of the WAG coreflooding simulation, it is found that the viscosity of the oil is reduced when the gas is injected and the results of the recovery factor are good based on the comparison of the results from the laboratory as follows:

Simulation		Laboratorium	
Recovery Factor Waterflood, %	51.3	Recovery Factor Waterflood, %	51.5
Recovery Factor WAG, %	63.7	Recovery Factor WAG, %	64.4
Incremental, %	12.4	Incremental, %	12.9

Tabel-3: Comparison Matching Between Simulation and Laboratorium

From the results of the WAG simulation which are in accordance with laboratory data, the PVT which used for this model can be used for other scenarios such as WAG injection at current pressure, continous CO_2, various slug size, WAG and WAG ratio to find the optimum scenario

Conclusions

From the results of this paper, this coreflooding simulation can provide output as input for the full-field model such as the PVT , the injection rate that needs to be upscaled, the value of SORW.

References

1. Ahmed, T. (2001): *Reservoir Engineering Hand Book*, 1211.
2. Taber, J.J., Martin, F.D., Seright, R.S. (1997): *EOR Screening Criteria Revisited – Part I : Introduction to Screening Criteria and Enhanced Recovery Field Projects*, New Mexico Petroleum Recovery Researcr Center.
3. Lake, Larry, W. (1989): *Enhanced Oil Recovery*, Prentice Hall Incorporated.
4. Garcia, Marylena. (2005). *OPTIMIZATION OF A CO2 FLOOD DESIGN*. Wasson Field, Texas.
5. Kovarik. (1985): *A Minimum Miscibility Pressure Study Using Impure CO2 and West Texas Oil Systems; Data Base, Correlations and Compositional Simulation*. Arco Exploration and Technology Co.
6. Siregar, Septoratno. (2000): *Teknik Peningkatan Perolehan (Enhanced Oil Recovery)*. Institut Teknologi Bandung.

.

PROCEEDINGS
JOINT CONVENTION BANDUNG (JCB) 2021
November 23rd 25th 2021

PROCEEDINGS
JOINT CONVENTION BANDUNG (JCB) 2021
November 23rd – 25th 2021

RESERVOIR CHARACTER IDENTIFICATION USING EXTENDED ELASTIC IMPEDANCE INVERSION IN "MR" FIELD, NATUNA BASIN

Muhammad Riyo Hanafi[1], Ignatius Sonny Winardhi[1].
[1]Geophysical Engineering, Faculty of Mining and Petroleum, Institut Teknologi Bandung

Abstract

Reservoir character identification is one of the key process in petroleum exploration. One of the petroleum exploration target is one of sedimentary formation in Natuna Basin, Udang Formation. Udang Formation at "MR" Field in Natuna Basin considered as a potential hydrocarbon reservoir. Through regional geology point of view, it consists of interbedded sandstone-shale with braided delta and lacustrine plain as depositional environment, which is a supporting proof of its potential as a reservoir. One of the method to analyze reservoir characteristic is through seismic inversion that modelled subsurface condition. Extended elastic impedance (EEI) inversion is one of inversion type that modify elastic impedance's angle projection, so it could add more possibility of parameter covered in reservoir characterization. Inversion process use sensitive parameters that consist of mu-rho (rigidity) and lambda-rho (incompressibility). These two parameters used to show developed lithology characteristic at "MR Field" linked to hydrocarbon existence. Mu-rho with EEI (84°) and lambda-rho with EEI (336°) shows clear reservoir characteristic along the formation's bed and the formation below and under it. Hence based on the result of EEI inversion, Udang Formation in "MR" Field has a good lateral spreading of high rigidity and low incompressibility that related to the presence of sandstone and possible to be taken as a sign of hydrocarbon presence.

Keywords: Extended Elastic Impedance, Natuna basin, Reservoir Characterization.

Introduction

Petroleum exploration has a close relationship with basin's petroleum system or the field itself to be specific. The petroleum system itself really determined petroleum content whether it is an oil or gas. This act as a basic knowledge needed to consider field's economic value. One of the part on petroleum system is reservoir. Identification of reservoir is an important step in exploration as it related to the petroleum accumulation.

"MR" field is one of the field located in Natuna Basin or West Natuna Basin to be more specific. Natuna Basin already well known with Gabus Formation and Udang Formation as petroleum reservoir (Pangarso, 2010). It related to the lithological content of both the formation itself, which is sedimentary rock consist of interbedded sandstone and shale (Darman & Sidi, 2000). Schon (2015) mentioned that sedimentary rock is an important type of rock in hydrocarbon exploration activity. Hence, as Udang Formation is one of the formation in MR Field, it is intriguing to know the quality and potential. Through this research, reservoir characteristic from MR Field will identified well and there is a possibility for further interpretation through the help of seismic inversion.

Extended elastic impedance (EEI) inversion is an improvement of elastic impedance (EI) inversion. The goal for the inversion is to enhance in fluid separation. EEI developed EI inversion with adding more angle (-90° to 90°). This addition add the inversion's flexibility in contact with seismic parameters. This research aim to show that EEI can be effective to unveiled the reservoir characteristic in "MR" Field especially Udang Formation and furthermore can give an option in processing the seismic inversion. In this research, acoustic impedance – shear impedance (AI-SI) projection used to see the sensitivity of seismic parameter. It is based on Connolly (1999) in Whicombe et al. (2002). This projection applied on AVO analysis will be:

$$EEI(\chi) = AI^{\cos(\chi)} SI^{\sin(\chi)} \quad (1)$$

$$R(\chi) = R_p \cos(\chi) + R_s \sin(\chi) \quad (2)$$

Data and Method

MR-01 well in MR Field is the only well used in this research. The well data consist of density, gamma ray, neutron-porosity, p-wave, s-wave, check shot logs, and tops from each formation. Other than logs, the field also has pre-stack 3D seismic data with angle stack near 6°-16°, mid 17°-27°, and far 27°-36. All of this data used in the processing step.

Before proceeding into seismic inversion process, the process started with sensitivity analysis of seismic attribute cross plot using well log data. The analysis conducted using cross plot of seismic attributes. Attributes used in this research are mu-rho and lambda-rho with the addition of gamma-ray index and density & neutron log as a separating attribute. The result is both of the attributes considered as sensitive parameter showed by its ability in separating between reservoir and non-reservoir (sand and shale lithology).

Other than that, targeted zone condition also considered in the process.

Cross plot showed that lambda-rho (incompressibility) and mu-rho (rigidity) able to differentiate between rocks and higher-lower gamma ray value well. Furthermore, looking from cross plot between lambda-rho and density, targeted zone with the characteristic of low lambda-rho, shows low density and low neutron value. The information relating to sensitivity condition then used as a base for the inversion process to the two parameters.

Tuning thickness, which is a minimum thickness for a layer to be able to be resolved by the seismic, obtained by using equation of wavelength divided by 4. Wavelength calculated using the already known information of average velocity and amplitude. The average of velocity obtained using average of shear wave velocity in the targeted zone. Furthermore, amplitude value obtained by looking at dominant amplitude value from the seismic. Vertical thickness, also called tuning thickness, then calculated using wavelength from average speed of 4956 m/s divide by dominant frequency of 44 Hz. This calculation resulted in more or less tuning thickness 28 m. Compared with sandstone beds thickness on targeted zone (Udang Formation), the thickness is hard to be resolved as it is considered thin layers. However, if all of them grouped as an interbedded sandstone-shale, then it is possible to be resolved as the thickness is more or less 35 m.

Inversion process started with looking at reflectivity from P and S waves. Using calculation with the equation provided by Ursenbach & Stewart (2008) on Thomas (2016), the coefficient value obtained through inversion matrix process from each seismic angle. The result is coefficient showed in the Table 1. Angle data gathered from angle stack are near 11°, mid 22°, and far 31,5°.

Referring to sensitivity processing result, lambda-rho and mu-rho are the focus of inversion step. Correlation angle from each parameter are 336° for lambda-rho and 84° for mu-rho. The value obtained by looping of angle projection range on EEI in order to see which angle suit best to act as correlation angle. Both of the angle then applied into formula (2) to obtained seismic volume from each sensitive parameter.

Well seismic tie on MR-01 well used to get the best suitable connection between the seismic data and well. Seismic volume that correlated with well data are mu-rho and lambda-rho. There are two wavelets used in this process that obtained using well extraction method in full wavelet. After stretching and shifting processes, correlation value obtained are 0,679 for mu-rho and 0,622 for lambda-rho.

Using model based inversion as a method in the inversion, the base model made using lambda-rho and mu-rho seismic volume. Low pass filter used in the process of making the base model. The model then used as a base model after being iterated a few times to obtain the best result. Following base model creation is pre-inversion analysis. It aim to find the best result possible that represented by low error value. Finally, both of the seismic volume (mu-rho and lambda-rho) inversed with EEI in model based method.

Result and Discussion

Based on inversion of each main parameters, mu-rho and lambda-rho, the result of seismic inversion already has a correlation with the well log data (Figure 1). On the target zone, mu-rho value considered as high mu-rho compared to other zone outside of the target. For the parameter that related to fluid, which is lambda-rho, showed relatively low value. Both of this condition can be interpret as hydrocarbon fluid zone. Hydrocarbon show in a sandstone type reservoir shows by higher rigidity is very possible in this type of situation. In order to verify the findings, data slice in the targeted zone used to see in a wider scope.

Data slice conducted in the targeted zone, which is Udang Formation, in each of inversion result. Data used in the slicing process are lambda-rho and mu-rho on the range of target zone (Figure 2). High mu-rho related to sandstone has a lateral expansion throughout southwest – northeast. Lambda-rho shows almost the same pattern with low lambda-rho. This distribution of sandstone and hydrocarbon suspect supported by the time structure map available on the field. Combining the entire information, targeted zone located in the area had a higher elevation and there is a possibility in term of hydrocarbon accumulation through structural trap. This finding shows seismic inversion result that represent reservoir character is correct.

Conclusions

Based on the analysis above, there are several points that can use as a conclusion.

1. From the sensitivity analysis, the most sensitive parameters are mu-rho for lithology and lambda-rho for fluid. This is correlate with well log analysis, where hydrocarbon accumulation found at the targeted zone.
2. From the inversion result, hydrocarbon zone can be found on Udang Formation showed by high mu-rho value (sand) and low lambda-rho (hydrocarbon). From the volume slice showed and confirmed the sandstone beds and hydrocarbon content of target zone mapped around the field. Time structure map shows that the target zone located in a higher elevation compared to the surrounding zone.

3. It is very possible to use the EEI inversion in reservoir characterization especially with more data available that can make the interpretation richer.

References

Burton, D., and Wood, L.J., 2010, AAPG Bulletin, **94(11)**, 1695 – 1712.

Connoly, P., 2010, CSEG Recorder, 7 – 10.

Darman, H. and Sidi, H.F., 2000, Ikatan Ahli Geologi Indonesia.

Doust, H. and Noble, R.A., 2008, Marine and Petroleum Geology, **25**, 103 – 129.

Hendrayana, Y., Pangarso, B., and Asaad, M.A., 2012, IPA 36th Annual Convention & Exhibition Proceedings.

Pangarso, B., Hartadi, E., Sihombing, I., Guttormsen, J., Schmitz, P., Wijayanti, R., and Darmadi, Y., 2010, IPA 34th Annual Convention Proceedings.

Schon, J.H., 2015, Elsevier, 4 – 10.

Thomas, M., Ball, V., Blangy, J. P., and Tenorio, L., 2016, The Leading Edge, **35(5)**, 438 – 444.

Whitcombe, D. N., Connoly, P. A., Reagan, R. L., and Redshaw, T. C., 2002, Geophysics, **67(1)**, 63 – 67.

PROCEEDINGS
JOINT CONVENTION BANDUNG (JCB) 2021
November 23rd – 25th 2021

	Near	Mid	Far
Rp	0,9637	0,3772	-0,3224
Rs	2,6853	0,3915	-2,3908

Table 1: Result of matrix inversion from seismic angles. Value used to calculate reflectivity of p-wave (Rp) and s-wave (Rs).

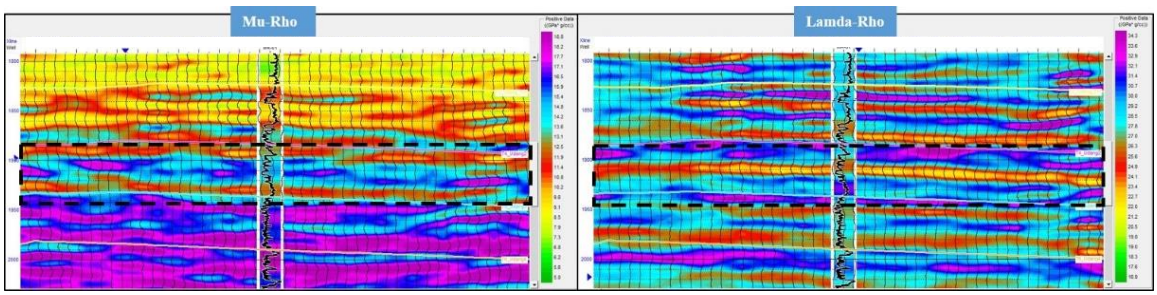

Figure 1: Final inversion result from mu-rho and lambda-rho. Each parameters from the log used in the confirmation of inversion result.

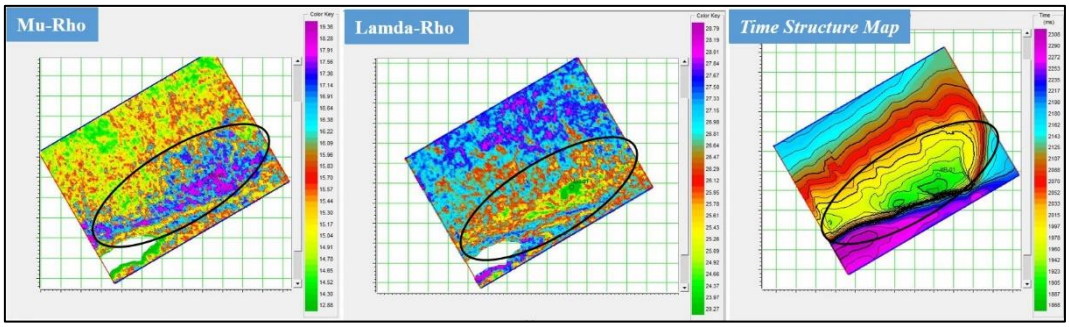

Figure 2: Slices on the targeted zone to verify the anomaly.

PROCEEDINGS
JOINT CONVENTION BANDUNG (JCB) 2021
November 23rd – 25th 2021

Multi-Variant Selection from History Matching to Prediction in Probabilistic Dynamic Model: A Case Study

Ecko Noviyanto[1],Deded Abdul Rohman[1], George Vincent[2], Ivan Praja[2], Kosdar Gideon Haro[2], M. Isa P. Utomo[3], Arif B. Prasetyo[3], Andi Pratama[3]
[1]Pertamina
[2]Rock Flow Dynamics
[3]SKK Migas

Abstract
Multiple history matching approach to quantify remaining oil saturation distribution uncertainty is possible and practical to perform with technological advancement nowadays. This paper presents the selection method to optimize number of forecast variants while preserving the uncertainty. The results are low estimate, best estimate and high estimate of remaining oil saturation distribution for development scenario design and wide-covered representative variants to be used for prediction stage.

Different model variants considered match with historical data are selected based on few criteria such as field total liquid production, field total oil production, region pressure and well total oil production. To be able to measure how similar or different one variant to another, cluster analysis was performed. The clustering was based on significant parameters to objective function which were used to build proxy-equations. In this study, Multi-Dimensional Scaling (MDS) method was used to visualize the result in two-dimensional space. Each variant represented by a point and the distance between points show their degree of similarity. After grouping process finished, different remaining oil saturation distribution were analyzed from P90, P50 and P10 quantile models.

There were 400 variants on final history match stage and then 127 variants were selected based on production and pressure profile similarity. Subsequently, number of forecast variants were optimized to 20 representative variants which cover the range of uncertainty. Three quantiles were selected from cumulative distribution function of these variants to be used for subsurface risk management in designing infill well location or waterflood pattern.

This paper demonstrates the application of extended uncertainty analysis by combining static modelling to dynamic simulation uncertainty variables in Limau Barat Limau Tengah Field which applicable in most development fields. Assisted history matching algorithm used in this study were determined for full field simulation. This paper also introduces the application of probabilistic remaining mobile oil saturation maps in assessing subsurface risk for better decision making in field development.

Introduction

Oil and gas are known as high risk and high gain industry with charateristic of capital-intensive and require advanced technology. It is very difficult and expensive to measure or understand condition in subsurface where hydrocarbon accumulated in magnitude of hundreds or thousands of metres below the surface. Common practice to manage the risk is reservoir modelling which representing the physical features of subsurface condition. Data are gathered and analyzed to be able to mimic historical production and pressure data. Having done this, the reservoir model is used to predict production performance under different scenario. In case of successful development, the reward could bear this high-risk industry while in case of undesirable surprise, expected profit is certainly shrinking. Nowadays, easy-oil become harder to get and more uncertainty in finding and producing hydrocarbon. This unforeseen result actually could be quantified and managed for a better decision.

Popular tool to calculate hydrocarbon volume and predict recoverable reserves are reservoir modeling and simulation. Although static reservoir modelling has been applying probabilistic approach for the last decades, the dynamic reservoir modelling part is still using deterministic approach. As a result, single static reservoir model realization is selected for history matching which provides deterministic remaining oil saturation map to be analyzed for designing development scenario. It's a common practice, that single recovery factor per scenario is used to make business decision out of many possibilities. A significant discrepancy between field development plan and actual reservoir performance occur under this limitation.

Probabilistic approach in reservoir simulation

Capturing the other possibilities of remaining oil saturation distribution map is the main objective of applying probabilistic approach for the reservoir simulation. Having analyzed the potential risk and reward, decision makers could anticipate the worst and best possible outcomes and most importantly eliminate surprises. By assessing the risk, management could reduce the reservoir performance uncertainty by gathering new key data that contribute to uncertainty or consider to proceed with development plan.

Probabilistic approach change the way team work into more blended and synergy among interdisciplinary team. More discussion between geoscientist and reservoir engineer to design uncertainty parameters and their range. Tolerable history matching acceptance criteria prevent unrealistic model modification which has no geological sense. Over fitting in history matching process is unnecessary since historical data which become the reference also have uncertainty. Geoscientist could access the progress of history matching result and evaluate the impact of static uncertainty parameters to quality of mismatch.

Reservoir simulation run time become faster and faster, especially with technology advancement nowadays. This opens the opportunity to analyze fine-scale reservoir model or different realization of reservoir model efficiently (Darmawan, 2021). Combined with methodology and algorithm that effectively perform sensitivity and

optimization, full-field probabilistic study become feasible and practical. Experimental design is a process to perform sensitivity study with few popular algorithms such as; Latin Hypercube, Tornado, Monte Carlo, Placket-Burman and Box-Behnken. Visualization of big data plays an important role to effectively analyze results and get insight from it. For example, tornado diagram visualizes single parameter variation impact while others are kept at base value while Pareto chart visualizes combination parameter variation impact compare to pre-determined objective functions. Further, mismatch between historical produciton and simulations could be minimized by applying Optimization. Example of optimization algorithms are such as; Particle Swarm Optimization, Differential Evolution and Ensemble.

Field application

This study applied probabilistic approach for history matching and prediction of Limau Barat Limau Tengah field and a first-step effort to integtrate static-dynamic uncertainty variables. The field is located onshore in South Sumatra Basin. Depositional environment of the field is fluvio-deltaic with updated geological concept, multi-level reservoirs. Waterflood development will be challenge with the new geological concept, so there are 9 reservoir tanks are prioritized for further development out of 20 reservoir tanks. Production commenced in 1951 and water injection started in 1998. There are 160 wells in total, 80 producing wells, mostly commingled production. Fluid characteristic from the field is 25°API with no gas cap found in the studied tanks. The total original oil in place from 20 tank reservoir is 291.2 MMSTB (P50) with cumulative oil total 45.9 MMSTB per 1st January 2020 and water cut above 94%.

Purpose of this study is to perform probabilistic reservoir simulation for better understanding of the field. Output from this study are different scenario of remaining oil saturation distribution map for risk assessment and optimized number of multi-variant model to be carry out to prediction stage.

Method

A workflow was built to manage probabilistic history matching and prediction for Limau Barat Limau Tengah field as shown in **Figure 1**. Pre-defined static model variations were imported to be integrated with dynamic model uncertainty. Additionally, PVT correlation input data were included as uncertainty to cover laboratory measurement inconsistency. When the reservoir has been characterized in dynamic modeling format, reservoir simulation was performed until match criteria fulfilled. Preparation prior to prediction stage were history match variants selection and development scenario pattern design.

Integrate static-dynamic uncertainty variable and range

Existing probabilistic static model that has been built by geoscientists were imported, excluding its water saturation model. Water saturation model were not imported from the existing static model due to an update applied in this study using J-function approach. The 3D geomodel consists of 7.7 million total cells with dimension 219 x 212 x 156 and block size 50 m x 50 m x 1.4 m. There wasn't upscaling process performed since active cells was only 0.66 million cells. The reservoir properties were rebuilt to be included in uncertainty design for history matching. There were 37 static modelling variables such as variogram parameters for properties distribution and OWC. The reservoir properties are facies (or lithology), porosity and NTG. These variables were then combined with dynamic simulation uncertainty variables such as rock properties, PVT and aquifer properties. Following this, dynamic uncertainty variables and range were determined. The static modelling and the dynamic simulation processes were calculated in a common workflow to automate the multi-realization cases.

Fluid properties and rock properties data obtained from laboratory measurement such as SCAL, RCAL and PVT were analyzed. Flow zone indicator (FZI) technique was applied for rock type classification and later the classification was used to correlate porosity-permeability for each rock type. Relative permeability and capillary pressure data from few samples were normalized and then de-normalized for each rock type. PVT samples were inconsistent each other, possibly due to acquisition time was not at initial condition. It was decided to use correlation with parameter input of oil API and bubble point pressure and gas gravity. The first two parameters were included as uncertainty variable. Existing material balance analysis was used for initial parameter setting of aquifer model and its uncertainty. Subsequently, they were inputted to the integrated modeling software tool including well-related data such as historical well-based production and injection data, field and tank pressure, equilibration data and perforation event.

Manage probabilistic initialization and history matching

Initialization of the integrated probabilistic static model with base case dynamic model has purpose to distribute pressure and saturation for each cell in initial condition. At this stage, calculated OOIP was obtained and then compared with volumetric OOIP from static model. Few methods available for initialization the dynamic model such as; equilibrium, equilibrium+SWATINIT, mix and enumeration method. This probabilistic study was using Equilbrium+SWATINIT method to avoid capillary pressure manual adjustment. After the reservoir was characterized, initialized and equilibrium-validated, probabilistic initial full run without any model modification were ready to perform prior to history matching.

History matching was performed with liquid control, subsequently oil and water profiles were tried to match for both field and well level. Assisted history matching algorithm such as experimental design and optimization were used to manage probabilistic history matching efficiently. Experimental design outputs were sensitivity of single and combination variables. For this study, Tornado experiment was run once and then followed by Latin Hypercube experiment iterations. Tornado diagram and Pareto chart were used to visualize significant parameters compare to objective functions. Prior uncertainty variables and ranges were updated based on this evaluation until historical profile and simulation are overlaid within acceptable range. Further history match was run by Optimization which has pre-determined objective function such as minimizing oil field mismatch and oil well mismatch. In this study, Particle Swarm Optimization (PSO) algorithm was selected to find several local solutions and global solutions. The method is applicable for many uncertain variables and to avoid being trapped at local solution (Kathrada, 2009). Each PSO experiment contained 400 variants which gave result of Pareto chart. The chart was used to screen and rank uncertainty parameter for the following experiment iteration. To determine when experiment has reached optimum result, Pareto front analysis was used.

PROCEEDINGS
JOINT CONVENTION BANDUNG (JCB) 2021
November 23rd – 25th 2021

Manage multi-variant reservoir model for prediction
Pre-defined acceptable match criteria were used for equiprobable history matching variants selection. The criteria were field liquid total and oil total tolerance, qualitative acceptable objective functions and qualitative tank pressure. Afterwards, there are two preparations for transitioning from history matching to prediction stage. First, optimizing number of variant to be carry out to prediction with representative uncertainty range. Another preparation is development scenario design based on few selected remaining hydrocarbon maps. In this study, MDS method was choosen for clusterization analysis which used *k-means* algorithm (Steinhaus 1956, Lloyd 1982). This algorithm minimizes the sum of square error between the points of clusters and their centers. MDS method visualizes how close the model variants are in terms of values of the selected parameters. Validation of this method was tried at smaller model prior to application in Limau Barat Limau Tengah field. Prediction performance of case with and without clusterization were compared as shown in **Figure 2**. Range of oil and water total profiles were similar although variant number have reduced from 89 to 12 models (87%). These selected history matching variants were carried over to prediction stage after the development scenario design was analyzed.

Manage subsurface risk
Cumulative Distribution Function of total oil parameter were established in order to select its P90, P50 and P10 for high, mid and low case determination, respectively. Two-dimensional map of Mobile Oil Per Unit area (NTG*SOIL*PORO*DZ) were established for each representative as subsurface risk assessment in designing development scenario. Risk and reward assessment applied to prioritize development for reservoir tanks. These selected 9 reservoir tanks combined have OOIP and oil cumulative production more than 80% of the whole reservoir tanks. Reservoir tanks with high OOIP and low recovery factor (RF) were suitable for infill primary recovery candidate prior to waterflood secondary recovery. Prediction runs were performed for selected history matching variants from January 2020 to January 2036. Waterflood preparation was estimated ready on January 2026, afterwards full-scale waterflood activity started with pre-defined constraints such as well liquid rate limit, well injection rate limit, botom hole pressure limit for injector, produced water re-injection, group liquid rate limit and economic limit for each well.

Result and Discussion
Static-dynamic model integration
Results of this study are presented from integrating static-dynamic uncertainty to managing multi-variant model run. In collaboration with all subsurface team, initial uncertainty parameters were drafted such as; porosity distribution, contact depth, NTG, facies, permeability multiplier, Kv/Kh multiplier, relative permeability, aquifer properties and fault transmissibiliy. Probabilistic static and dynamic model were recorded within common workflow tool. Afterwards, the probabilistic models were initialized which gave OOIP at 281.7 MMSTB, 289.7 MMSTB and 297.7 MMSTB for P90, P50 and P10 respectively. While volumetric OOIP from static model were 278 MMSTB, 283 MMSTB and 294 MMSTB.

Probabilistic history matching
Initial full run was exercised with liquid control with running time around 75 minutes. Liquid profile from simulation was far from historical data due to over optimistic water profile simulation model as shown in **Figure 3**. Based on this initial performance, dynamic uncertainty variables and range were determined in more detail prior to history matching process. Experimental design was performed with Tornado, Latin Hypercube and Optimization experiment iteratively. There were 400 runs for each iteration to match liquid, pressure, oil and water profile. Pareto chart showed residual oil saturation, aquifer, relative permeability and porosity distribution were the most significant parameters to variable oil field total. Another analysis with Pareto front as shwon in **Figure 4** indicated that further optimization experiment iteration would only give similar result, which means this experiment iteration has reached optimum result of multi-objective functions.

Transitioning from history matching to prediction
Selecting 400 variants to be carried over to prediction required quantitative and qualitative selection techniques as shown in **Figure 5**. The first step was to select probabilistic history matching from the last experiment. These variants were selected based on field liquid total mismatch tolerance 5% and oil total mismatch tolerance 10%. Qualitatively, acceptable objective functions oil wells mismatch < 650 and oil field mismatch < 3 were chosen. Regional or tank level selection was applied only for the tank pressure parameter. Variants with flat tank pressure profile were not selected, which reduced the output to 127 variants for the equiprobable history matching. The following step was variant clusterization to avoid similar variants selection. Assumption was made by taking 20 cluster to represent equiprobable history match variants as shown in **Figure 6**. In this study, the amount has considered sufficient to cover the uncertainty range and also practical to perform within half-day. These unique history matching variants were carried over to prediction stage when development scenario design was finished.

Subsurface risk assessment
OOIP after history matching process were 283.6 MMSTB (P90), 291.2 MMSTB (P50) and 307.4 MMSTB (P10). Compared to before history matching case, OOIP difference were less than 4% and the updated uncertainty range was shifted due to water saturation cut-off elimination. Few wells with perforation at transition zone could only produce sufficient liquid by doing this modification. Recovery factor range with corresponding cumulative oil production were 15.7% to 16.5%. Probabilistic history matching have reduced parameter's uncertainty-range during initial and final history match.

This study considered sufficient and practical to analyze 3 representative maps out of 20 maps for subsurface risk assessment. The P90, P50 and P10 quantile of cumulative oil CDF were determined. The more cumulative oil produced means the less remaining oil in reservoir, therefore low-side MOPU map originated from P10 cumulative oil case. High, medium and low case of MOPU map for 9 prioritized tanks were established and analyzed as shown partially in **Figure 7**. Having examined the risk, the low-side MOPU map was used for waterflood pattern design. Then, adjusted the pattern to actual condition which have considered surface, well and subsurface factors. Prediction of waterflood scenario was applied to 20 selected variants. The range of results represent static and dynamic input data uncertainties and also risk and reward of all variant model possibilities. Different performance behavior among

PROCEEDINGS
JOINT CONVENTION BANDUNG (JCB) 2021
November 23rd – 25th 2021

variants could be analyzed for risk assessment as shown in **Figure 8**. Low case prediction variants in the red circle have key uncertainty parameters such as fluid contact at S Tank 1, aquifer properties and rock properties that drive the reservoir performance. These are focus area of data gathering in the future to reduce reservoir performance uncertainty. Suggestion for future work is focusing on cluster optimization. Optimum number of clusters could be evaluated and then applied to MOPU map for development scenario design.

Conclusions

- Hardware and software advancement nowadays could handle full field probabilistic simulation
- Automatic capillary pressure adjustment enable probabilistic initialization handling in effective and efficient way
- Clustering technique optimizes the number of model variants carried over from history matching to prediction
- Subsurface risk was assessed by evaluating multi-variant MOPU maps for development scenario design
- Probabilistic approach could suggest key reservoir performance uncertainty drivers which are valuable insight for business decision making

References

Darmawan, B., and A. R. Azhar, 2021. Cluster Technology. 45th Indonesian Petroleum Association.

Kathrada, M. 2009. Particle Swarms and Hierarchical Clustering. Doctoral Dissertation. Herriot-Watt University.

Lloyd S. P. 1982. Least Squares Quantization in PCM. IEEE Transactions on Information Theory 28: 129-137.

Steinhaus, H. 1956. Sur la division des corps matériels en parties. Bulletin de l'Académie Polonaise des Sciences Classe III Vol. IV 12: 801-804.

Acknowledgements

This study was the collaboration work of PT. Pertamina EP, Rock Flow Dynamics Indonesia and SKK Migas. Authors acknowledge Asset-2 and Enhanced Oil Recovery Team for valuable input and SKK Migas for constructive meetings to improve the quality of the work. The authors acknowledge Rock Flow Dynamics team for the constant support througout the project.

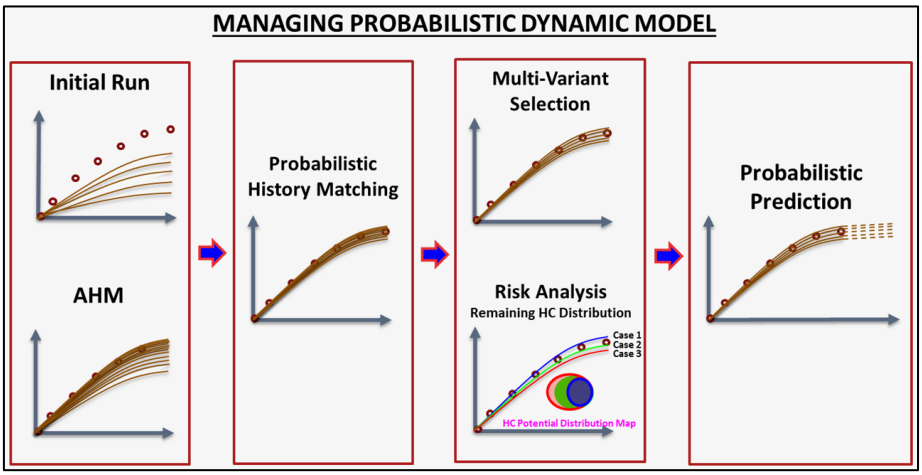

Figure 1. Probabilistic Dynamic Model Workflow

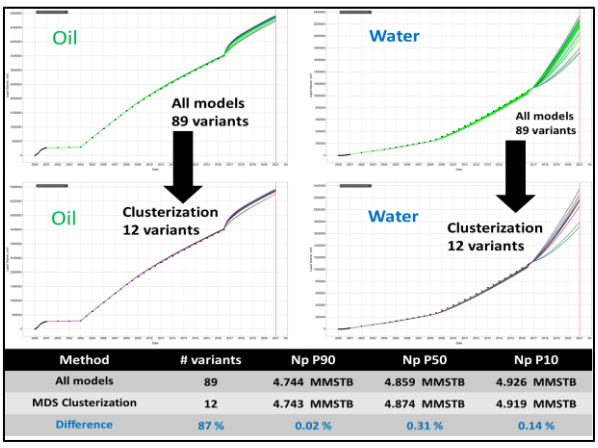

Method	# variants	Np P90	Np P50	Np P10
All models	89	4.744 MMSTB	4.859 MMSTB	4.926 MMSTB
MDS Clusterization	12	4.743 MMSTB	4.874 MMSTB	4.919 MMSTB
Difference	87 %	0.02 %	0.31 %	0.14 %

Figure 2. MDS clusterization validation

PROCEEDINGS
JOINT CONVENTION BANDUNG (JCB) 2021
November 23rd – 25th 2021

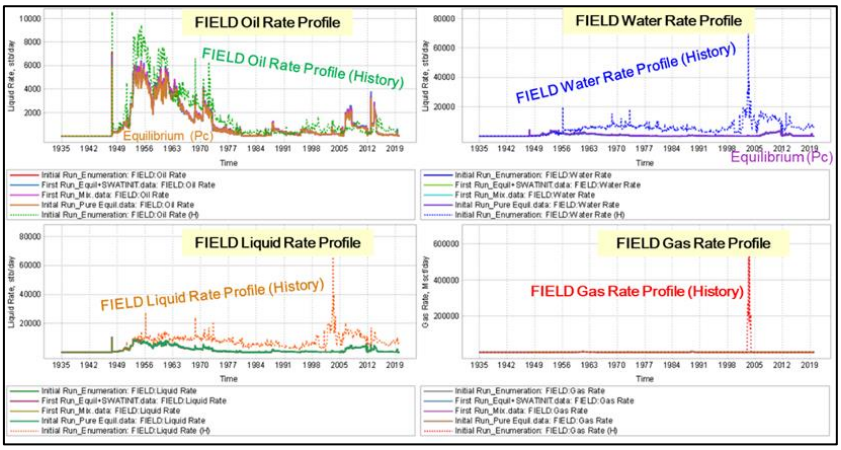

Figure 3. Initial full run

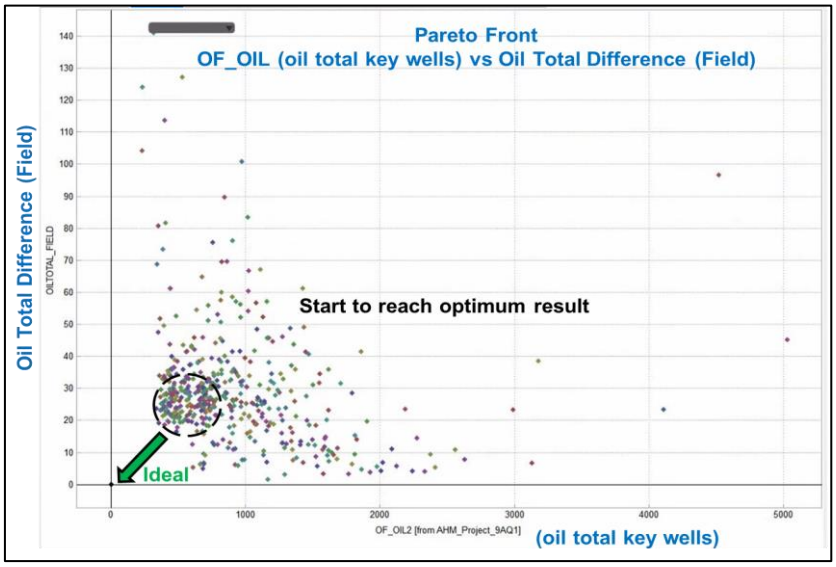

Figure 4. Pareto front analysis

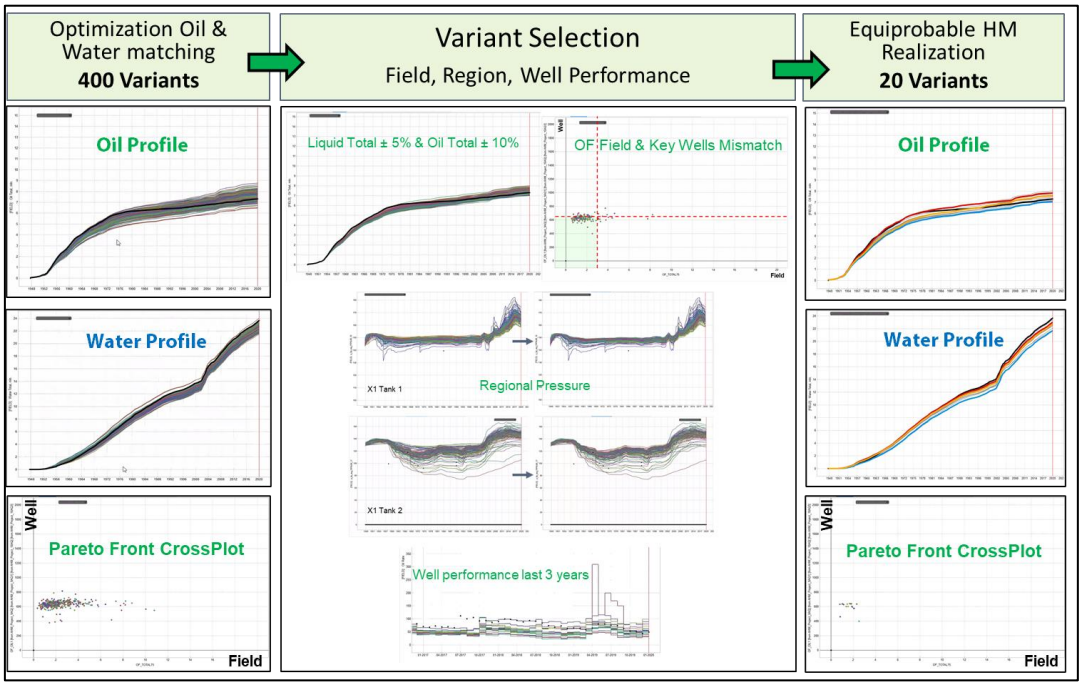

Figure 5. Probabilistic history matching criteria

PROCEEDINGS
JOINT CONVENTION BANDUNG (JCB) 2021
November 23rd – 25th 2021

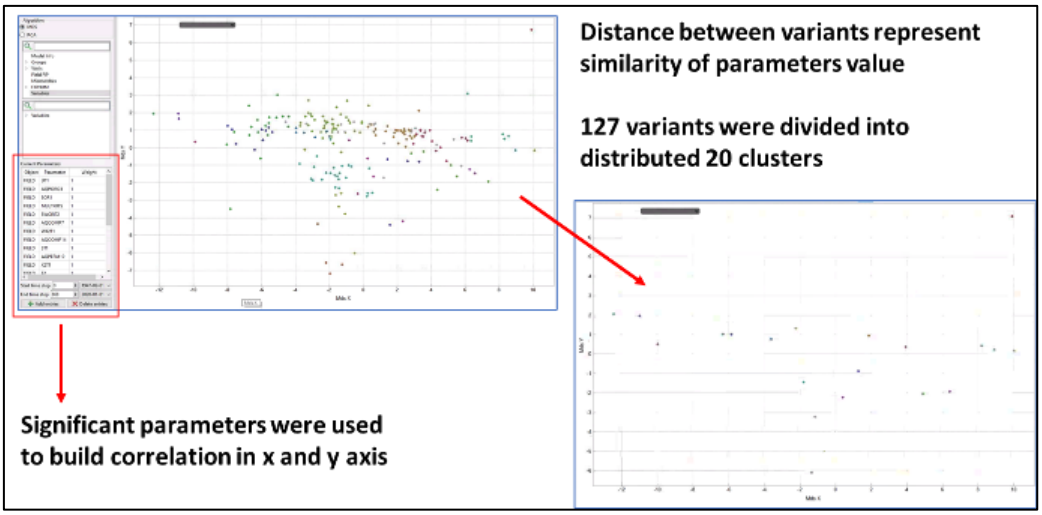

Figure 6. Multi-variant selection

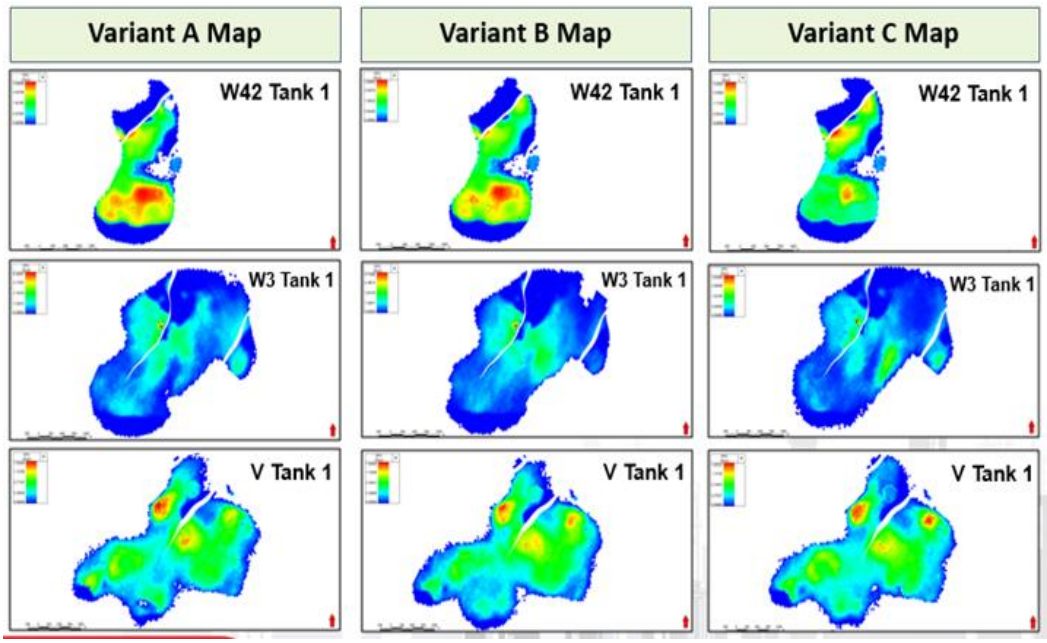

Figure 7. Subsurface risk assessment

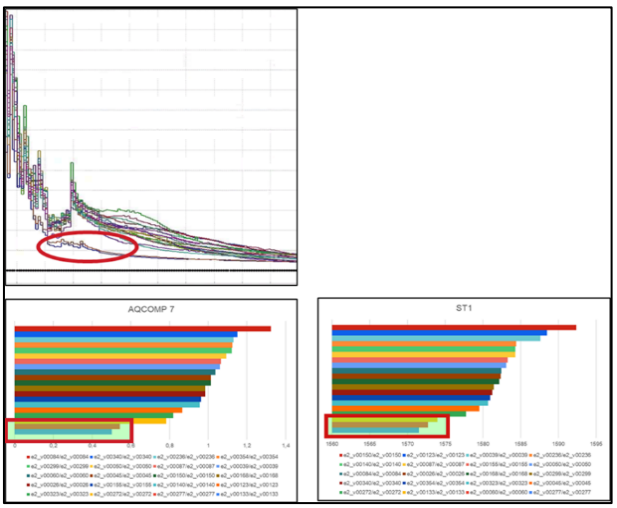

Figure 8. Key uncertainty parameters

PROCEEDINGS
JOINT CONVENTION BANDUNG (JCB) 2021
November 23rd – 25th 2021

An Accurate Simulation Model in a New Virgin Production Layer in Sungai Gelam-C Field: Challenges, Data Analogue, and Further Improvement

Ainun Nu'man Chanif[1], Reza Rahadian[1], Ikhsan Novryan Priatama[1], Kevin Angriawan Pratama[1], Giovanno Leonardo Sihombing[1]

[1]Pertamina Hulu Rokan

Abstract

Defining forecast oil production of new layer N1 sand is challenging. In initial stage of field development, data availability in static to dynamic is limited, especially Special Core Analysis (SCAL). Production test data used to validate model was inadequate in history matching phase. Therefore, new method is needed and conducted to deliver accurate model in proposing new drilling wells.

Regional geological concept and lithology log data indicating that existing N sand and new N1 sand was deposited in same environment so they could be analogized alike. Correlation between static pressure, flowing pressure, and production rate of existing N sand used as an approach to construct the relative permeability curve of new N1 sand. Production rate is predicated on the amount of saturation within the reservoir rock. Increasing water saturation causes in decrease of effective permeability. J-function reconstruction and contact determination are conducted from water saturation versus depth in existing wells' log analysis.

In 2020, two wells were drilled based on latest simulation model, located in outer existing wells with radius around 400-500 meters. In updated static model, there is no major difference to the previous one. The last two wells drilled encountered similar sand facies of marine deposit with thickness of 11.5 meters (15% thicker than estimated), and porosity near 22% (8% bigger than estimated). Like static model, the dynamic model is also had a good accuracy. Static formation pressure, dynamic formation pressure, and multi rate test were being used to validate reservoir simulation by comparing to actual data in the last one year (December 2019-December 2020) which resulting a good relation to the actual production data (oil production cumulative 230.2 MSTB forecast vs 220.7 MSTB actual).

By applying this validation method of data limited-reservoir model will help us to minimize subsurface risk and deliver accurate deliverability of model and production's well performance. This method could be implemented and as a standard of new sand reservoir development.

Keywords: Analogue Method, SCAL, Dynamic Model, Field Development, Minimum Data

Introduction

The Sungai Gelam C field is an oil field in Jambi, Indonesia that produces from two main sands, namely an existing N sand productive zone and newly discovery N1 sand, which located below N sand. In developing the N1 sand, it is necessary to carry out a proper dynamic reservoir simulation, which generally requires complete data in order to obtain accurate forecast results. However, it is common that new sand having limited data such as relative permeability and capillary pressure data. N and N1 sand are belong to Air Benakat Formation, which in deposited in shore environment. Both sands are typically a blocky and thick reservoir.

In this paper, we will describe the process of data validation used in building a dynamic reservoir model, especially for field with the same case. These validation methods generate good result of actual to production forecast. Eventually, it is expected that these methods could be taken into consideration in conducting data analogue in order to reduce the subsurface risk/uncertainty.

Data and Method

Relative Permeability Reconstruction and Fluid Mobility

Relative permeability data is needed in making a representative and accurate reservoir dynamic model. In the absence of these data, relative permeability can be generated using the power-law model. Power-law models have been widely used to represent relative permeability curves because of their simplicity (Lee et al., 1987). The empirical equation as shown below:

$$k_{rw} = a_w \left(\frac{S_w - S_{wc}}{1 - S_{orw} - S_{wc}}\right)^{b_w} \quad \text{.....(1)}$$

$$k_{ro} = a_o \left(\frac{1 - S_{orw} - S_w}{1 - S_{orw} - S_{wc}}\right)^{b_o} \quad \text{.....(2)}$$

From the above equation, From the above equation, several variables are involved in defining the relative permeability. If relative permeability is defined as

normalization of the effective permeability of each phase with absolute oil permeability at unreduced water saturation, then a_o= 1. The connate saturation (S_{wc}), which plays an important role in this procedure, can be established from log evaluations, with the lowest water saturation encountered normally assumed to represent residual oil saturation (S_{orw}) (Larsen, 1990). Lastly for b_w and b_o, this we can do fine adjustments to get a good match with the production data but for reservoirs with few production data, some validations are needed so that unsuitable exponent factors are not entered into the simulation.

For this validation, it is necessary to understand the relationship between exponential factors and fluid mobility which can be seen in the equation below (Larsen, 1990):

$$\lambda_{total} = \frac{k_{rw}}{\mu_w} + \frac{k_{ro}}{\mu_o} \quad (3)$$

$$\lambda_{water} = \frac{k_{rw}}{\mu_w} \quad (3a)$$

$$\lambda_{oil} = \frac{k_{ro}}{\mu_o} \quad (3b)$$

With relative permeability which is a function of saturation, it is possible to plot a graph of mobility vs saturation (see **Table 1** & **Fig. 2**). Based on the relationship from these data, it is possible to perform an exponential factor sensitivity to obtain a suitable relative permeability curve

J-function reconstruction

Capillary pressure is used as the basis for the saturation distribution when running dynamic reservoir simulations, where saturation in the dynamic model is a function of the height above the Water-Oil Contact. The relationship between the two can be seen in (Holmes, 1977):

$$P_c = \frac{h}{144}(\rho_w - \rho_o) \quad (4)$$

From log analysis, saturation gradient above the Water-Oil Contact (WOC) can be derived as the basis for capillary pressure. First, the saturation log data is plotted against the height above the Water-Oil Contact then an equation will be obtained to determine the relationship between h vs S_w (see **Fig. 5**).

By using the saturation gradient trend, it can then be used to find the correlation graph of Pc vs Sw. From these results, a capillary pressure curve is obtained which can be included in the reservoir dynamic model (see **Table 2** & **Fig. 6**).

Result and Discussion

Three different kinds of relative permeability data are entered into the reservoir dynamic simulation for history matching. Because the production data for the N1 sand is still limited, the history match is carried out on the top layer, namely the N sand. In the history match, it is carried out for the liquid rate, oil rate, water rate, and flowing bottom hole pressure. The results of history matching can be seen in **Fig. 3**. Based on the figure, the effect of the difference between b_o and b_w, where the relative permeability data is the most suitable is in Example 3. The table data in Example 3 is used to forecast the N1 sand which incidentally is still virgin but has rock properties like the N sand.

In reservoir dynamic simulation, the use of capillary pressure data also has a very important role, especially for the spread of saturation in the model. If the capillary pressure data is not known, the correlation between the petrophysical log and the height above the Water-Oil Contact can be used as shown in the **Fig. 6**. The result of using this method is a saturation distribution which is then compared with the value of the petrophysical log (see **Fig. 7**).

After all data is entered completely, a forecast is made for the virgin N1 sand by proposing two infill wells and two work over wells. The proposal was successful and then the production realization was monitored for one year, which showed accurate results with cumulative 230.2 MSTB forecast vs 220.7 MSTB actual (see **Fig. 4**).

Conclusions

The results of the exercise show that the use of "b_w" and "b_o" values in the construction of the relative permeability curve have big effect on the wells performance, both in history match and forecast stage. In addition, the saturation distribution in dynamic model of the P_c vs S_w curve could be reconstructed using petrophysical log data. By applying this validation method of limited data-reservoir model will help us to minimize subsurface risk and deliver accurate deliverability of dynamic model. This method could be implemented and as a standard of new sand reservoir development

Nomenclature

k_{rw}	: relative permeability of water, fraction
k_{ro}	: relative permeability of oil, fraction
a_w	: relative permeability of water @ S_{orw}
a_o	: relative permeability of oil @ S_{wc}
b_w	: water exponential or shape factor
b_o	: oil exponential or shape factor
S_w	: water saturation, fraction
S_{wc}	: connate water saturation, fraction
S_{orw}	: residual oil saturation, fraction
λ	: mobility, mD/cp
μ_w	: water viscosity, cp
μ_o	: oil viscosity, cp
ρ_w	: water density, lb/cuft
ρ_o	: oil density, lb/cuft
h	: height above contact, ft
P_c	: capillary pressure, psi

PROCEEDINGS
JOINT CONVENTION BANDUNG (JCB) 2021
November 23rd – 25th 2021

References

Holmes, M., and Tippie, D,. 1977, SPE Annual Fall Technical Conference and Exhibition. 1-12.

Larsen, L., Kviljo, K., and Litlehamar, T., 1990, SPE Formation Evaluation: 360-368.

Lee, T.-Y., and Seinfeld, J.H. 1987, Inverse Prob. Eng.: 711-728.

Acknowledgements

We thank Direktorat Jenderal Migas, SKK Migas and Pertamina Hulu Rokan for permission to publish this paper.

PROCEEDINGS
JOINT CONVENTION BANDUNG (JCB) 2021
November 23rd – 25th 2021

Table 1-Relative Permeability and Mobility Tabulation

1

μ_o	0.273 cp	b_{Oil}	2
μ_w	0.2664 cp	b_{Water}	2
S_{wi}	0.35	a_{Oil}	1
S_{orw}	0.21	a_{Water}	0.4

Example 1

S_{wr} Fraction	$K_{rw,}$ Fraction	K_{ror} Fraction	Mobility Tot. Relative cp^{-1}	Fractional Flow Fraction
0.35	0.00	1.00	3.66	0.00
0.37	0.00	0.90	3.31	0.00
0.39	0.00	0.81	2.98	0.01
0.42	0.01	0.72	2.68	0.01
0.44	0.02	0.64	2.40	0.02
0.46	0.03	0.56	2.15	0.04
0.48	0.04	0.49	1.93	0.07
0.50	0.05	0.42	1.73	0.11
0.53	0.06	0.36	1.56	0.15
0.55	0.08	0.30	1.41	0.22
0.57	0.10	0.25	1.29	0.29
0.59	0.12	0.20	1.20	0.38
0.61	0.14	0.16	1.13	0.48
0.64	0.17	0.12	1.08	0.59
0.66	0.20	0.09	1.07	0.69
0.68	0.23	0.06	1.07	0.79
0.70	0.26	0.04	1.11	0.87
0.72	0.29	0.02	1.17	0.93
0.75	0.32	0.01	1.25	0.97
0.77	0.36	0.00	1.36	0.99
0.79	0.40	0.00	1.50	1.00

2

μ_o	0.273 cp	b_{Oil}	4
μ_w	0.2664 cp	b_{Water}	4
S_{wi}	0.35	a_{Oil}	1
S_{orw}	0.21	a_{Water}	0.4

Example 2

S_{wr} Fraction	$K_{rw,}$ Fraction	K_{ror} Fraction	Mobility Tot. Relative cp^{-1}	Fractional Flow Fraction
0.35	0.00	1.00	3.66	0.00
0.37	0.00	0.81	2.98	0.00
0.39	0.00	0.66	2.40	0.00
0.42	0.00	0.52	1.91	0.00
0.44	0.00	0.41	1.50	0.00
0.46	0.00	0.32	1.16	0.01
0.48	0.00	0.24	0.89	0.01
0.50	0.01	0.18	0.68	0.03
0.53	0.01	0.13	0.51	0.07
0.55	0.02	0.09	0.40	0.16
0.57	0.03	0.06	0.32	0.29
0.59	0.04	0.04	0.29	0.48
0.61	0.05	0.03	0.29	0.67
0.64	0.07	0.02	0.32	0.83
0.66	0.10	0.01	0.39	0.92
0.68	0.13	0.00	0.49	0.97
0.70	0.16	0.00	0.62	0.99
0.72	0.21	0.00	0.79	1.00
0.75	0.26	0.00	0.99	1.00
0.77	0.33	0.00	1.22	1.00
0.79	0.40	0.00	1.50	1.00

3

μ_o	0.273 cp	b_{Oil}	2.6
μ_w	0.2664 cp	b_{Water}	2.2
S_{wi}	0.35	a_{Oil}	1
S_{orw}	0.21	a_{Water}	0.4

Example 3

S_{wr} Fraction	$K_{rw,}$ Fraction	K_{ror} Fraction	Mobility Tot. Relative cp^{-1}	Fractional Flow Fraction
0.35	0.00	1.00	3.66	0.00
0.37	0.00	0.88	3.21	0.00
0.39	0.00	0.76	2.79	0.00
0.42	0.01	0.66	2.42	0.01
0.44	0.01	0.56	2.09	0.02
0.46	0.02	0.47	1.80	0.04
0.48	0.03	0.40	1.56	0.07
0.50	0.04	0.33	1.34	0.11
0.53	0.05	0.26	1.17	0.17
0.55	0.07	0.21	1.03	0.25
0.57	0.09	0.16	0.93	0.35
0.59	0.11	0.13	0.86	0.47
0.61	0.13	0.09	0.83	0.59
0.64	0.16	0.07	0.82	0.71
0.66	0.18	0.04	0.85	0.81
0.68	0.21	0.03	0.90	0.89
0.70	0.24	0.02	0.97	0.94
0.72	0.28	0.01	1.08	0.98
0.75	0.32	0.00	1.20	0.99
0.77	0.36	0.00	1.34	1.00
0.79	0.40	0.00	1.50	1.00

Table 2-Capillary Pressure

ρ_o	42.56 lb/cuft
ρ_w	62.40 lb/cuft
S_{wi}	0.35
S_{orw}	0.21

S_w Fraction	Elevation Fraction	Pc Fraction
0.35	118.41	16.32
0.37	97.56	13.44
0.39	81.28	11.20
0.42	68.40	9.42
0.44	58.07	8.00
0.46	49.69	6.85
0.48	42.84	5.90
0.50	37.18	5.12
0.53	32.46	4.47
0.55	28.50	3.93
0.57	25.15	3.47
0.59	22.30	3.07
0.61	19.86	2.74
0.64	17.75	2.45
0.66	15.94	2.20
0.68	14.36	1.98
0.70	12.97	1.79
0.72	11.76	1.62
0.75	10.70	1.47
0.77	9.75	1.34
0.79	8.92	1.23

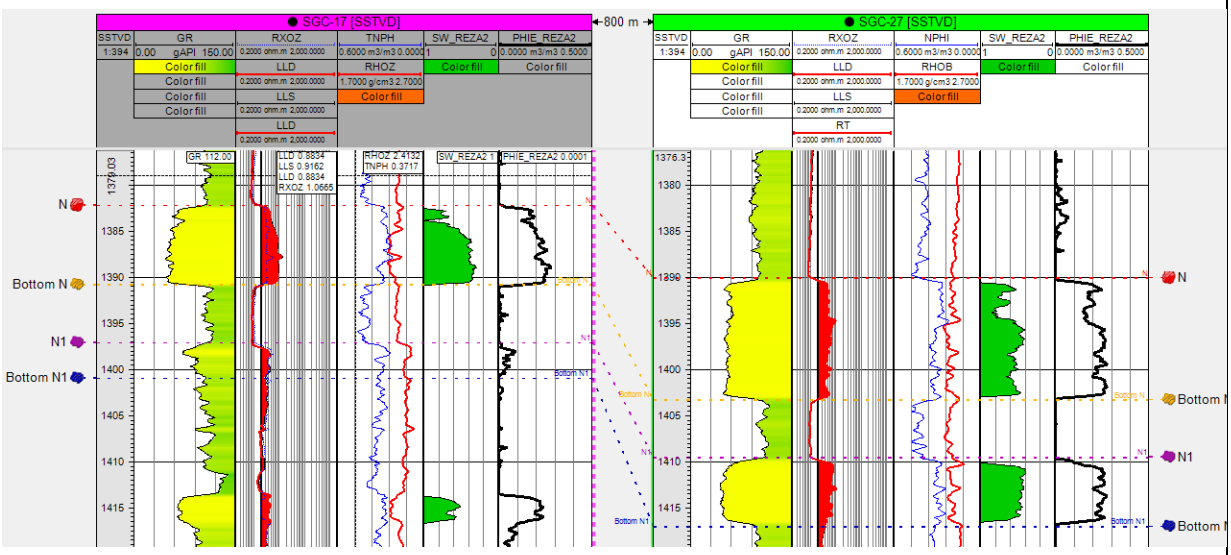

Fig. 1-Well Corelation

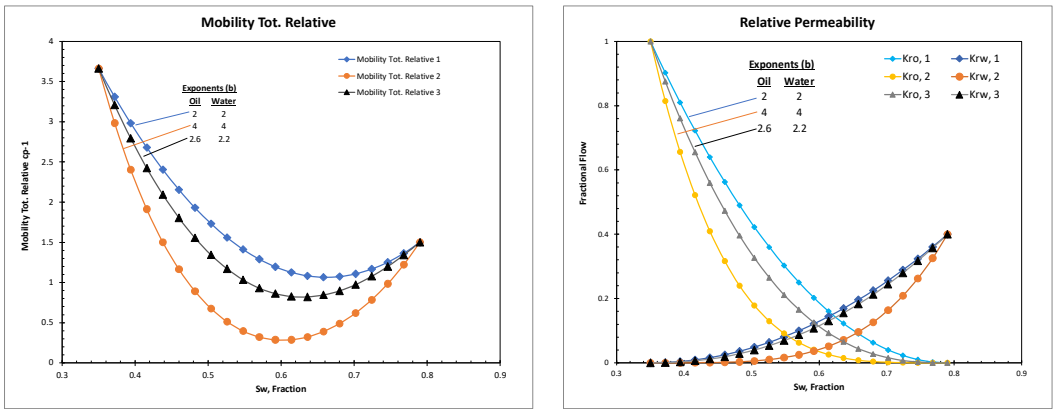

Fig. 2-The Effect of Exponent Factor on Total Mobility

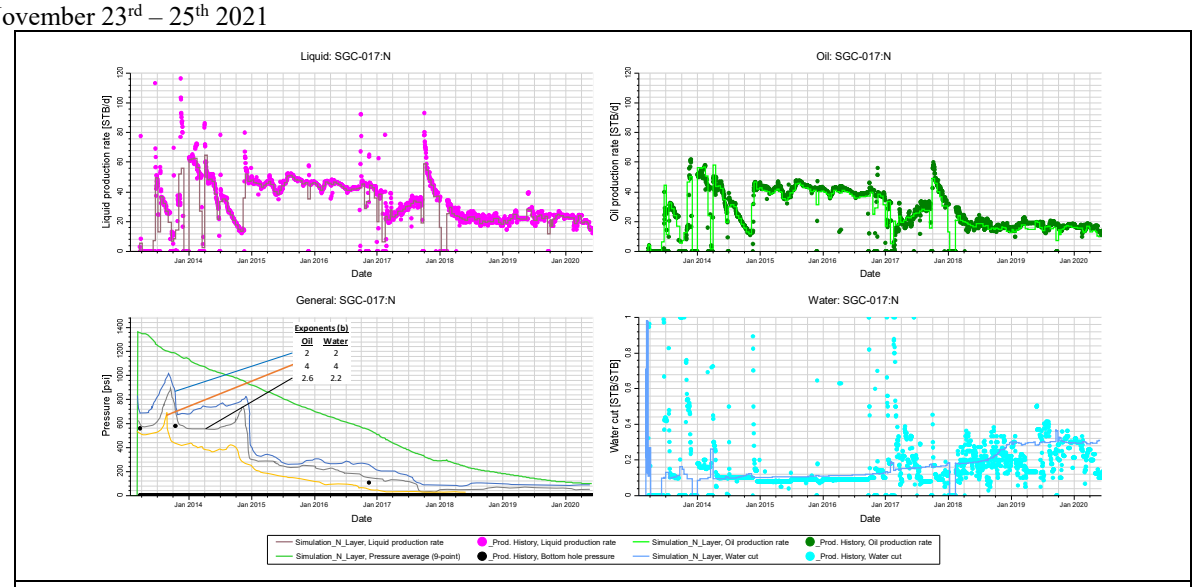

Fig. 3- Relative Permeability Validation using FBHP Data and Production Match of N sand

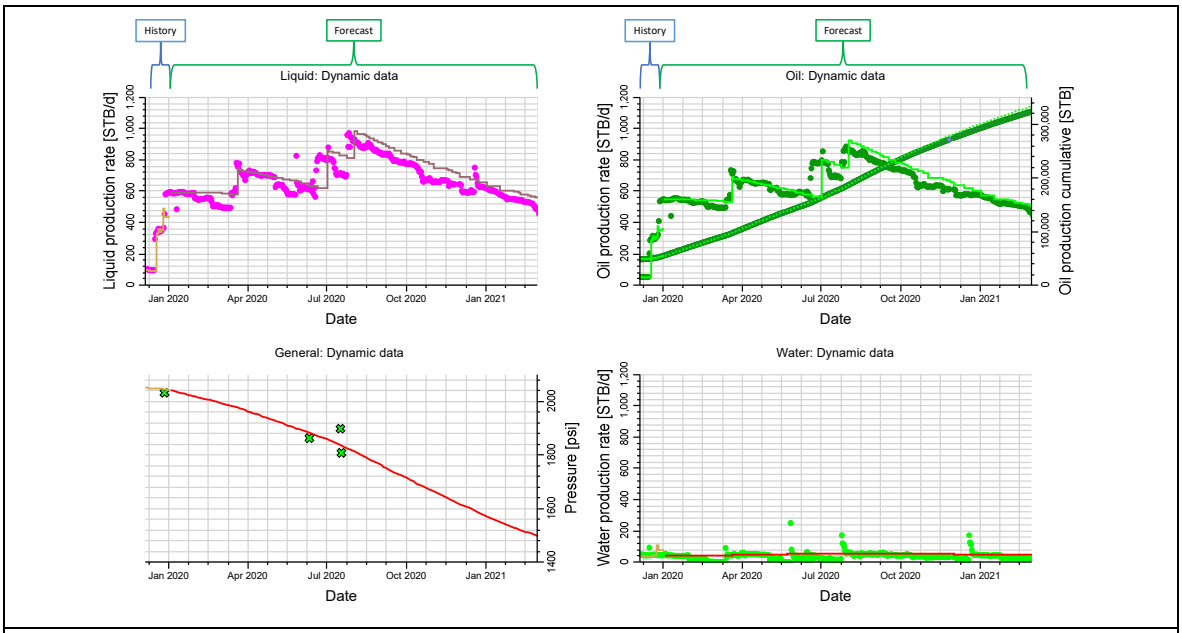

Fig. 4- Sungai Gelam Field Forecast Result in N1 sand

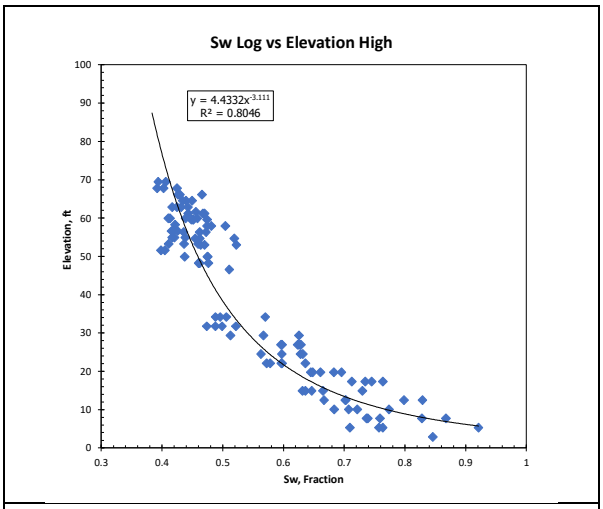

Fig. 5- Sw Loq vs Elevation Height

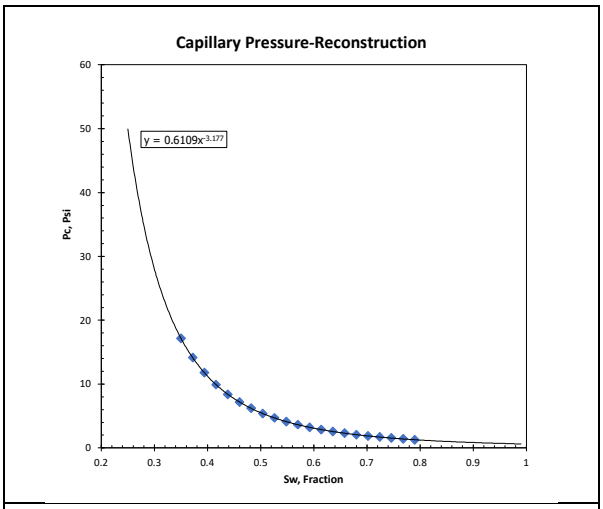

Fig. 6- Capillary Pressure

PROCEEDINGS
JOINT CONVENTION BANDUNG (JCB) 2021
November 23rd – 25th 2021

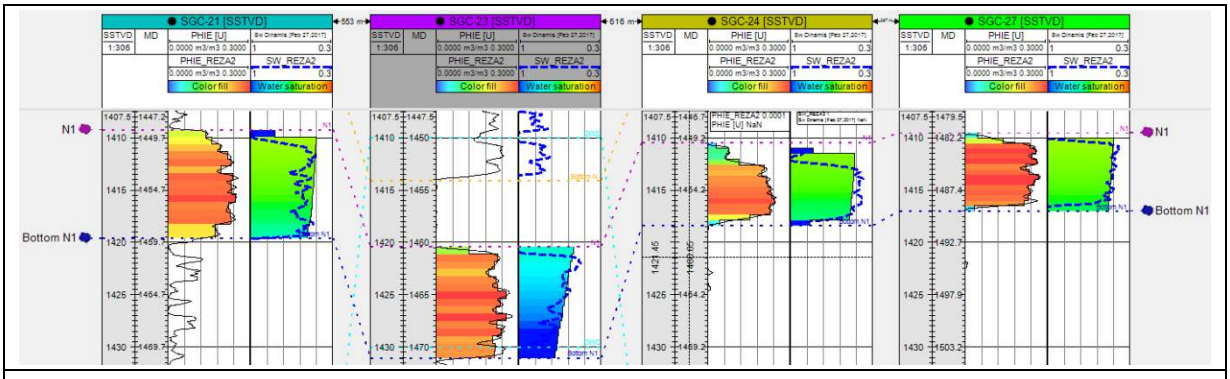

Fig. 7- Sw Model Validation of Capillary Pressure Reconstruction from Petrophysical Log

PROCEEDINGS
JOINT CONVENTION BANDUNG (JCB) 2021
November 23rd – 25th 2021

ANALYZE THE POTENTIAL OF OFFSHORE TIGHT GAS CARBONATE RESERVOIR USING MULTI LAYER RATE TRASIENT ANALYSIS

Muhammad Dwikyriza[1], Hendri Andriyadi[1], Panca Suci W[1], Keiichi Sabase[1], Maulida Aulia F[1], KANGEAN ENERGY INDONESIA. Fabiola Lady K[2], PETROPRO

Abstract

X field is an offshore gas field located in North of Bali. X field is currently developed by 1 subsea deviated well with open hole gravel pack and consist of two reservoir layers. Based on static model, this reservoir has OGIP ratio of around 59% in Layer A and 41% in Layer B and now has recovered 8.6 % of total OGIP. Layer A is known as tight carbonate reservoir with net pay 98–103 ft, and based on core data permeability ranging from 0.2–30 md, meanwhile layer B has better quality of reservoir properties with net pay 53-75 ft, and permeability ranging from 27–1066 md. DST result from exploration well Z-1 indicated that there is small flow from layer A. However, since well Z-1 is commingled, it is difficult to estimate the contribution of each layer properly.

To analyze the gas potential of this tight reservoir layer, Rate Transient Analysis (RTA) is applied in this study. By using this method, production data can be utilized to get estimates of OGIP, production allocation and reservoir properties (skin and permeability) for each layer. Various RTA techniques are used as a default workflow which are Flowing Material Balance, Type-curve analysis, and History matching at multi-well multi-layer model. Result from this study will be used for further development plan of X field.

Keywords: Multilayer Reservoir, Rate Transient Analysis, Tight Gas Reservoir, Flowing Material Balance.

Introduction

X Field was discovered in 1991, approximately 210 miles east of Surabaya and 87 miles north of Bali. It was discovered in 1991 by the drilling of Z exploration well which discovered gas in Paciran Carbonate. A second well, Z-1 was drilled in 2018 as a development well.

Z-1 is deviated subsea commingle well completed with Open Hole Gravel Pack System consist of reservoir layer A and B that produced dry gas. Based on current static model this reservoir has Original Gas in Place (OGIP) ratio of around 59% in Layer A and 41% in Layer B and now has recovered 8.6 % of total OGIP.

Data and Method

Concept of Modern Production Analysis

Modern production analysis method adapted in this study was introduced by Mattar and Anderson (2003) which is known later as Rate Transient Analysis (RTA). Equation behind RTA are combining static material balance with Darcy's flow equation which have same concept of diffusivity equation to perform material balance calculation from production data. This could maximize the utilization of rate and flowing pressure in during reservoir surveillance.

The workflow' employs the method of Flowing Material Balance (FMB), Type curve analysis, and concluded with multilayer model. Through FMB analysis, current connected HC in-place estimation, productivity index, well drainage areas, reservoir pressure trend, and reservoir/well condition can be monitored by flowing production data. Since FMB requires no shut-in pressure data, reservoir performance can also be monitored periodically without shutting the well. To confirm the result from FMB, Type Curve Analysis is conducted to get the dynamic properties of the reservoir such as current permeability, skin, and to identify the flow regime whether it is boundary dominated or still in transient. Both analysis are complimentary and can be used as a basis in multilayer model analysis to obtain production allocation from each layer followed by history matching with commingle historical data.

Fundamental Theory of Multi-Layer Model

Adopted from IHS Markit Harmony Enterprise Manual Book, multilayer material balance and Darcy's flow equation is the main formula behind the RTA for Multi-Layer model. Grid cells are used in the simulation to represent flow in reservoir based on material balance formula.

To define components of mass balance for cell *i* at timestep *n+1*, Mass in place (MIP) for cell *i* at timestep *n+1* can be calculated as:

$$MIP_i^{n+1} = MIP_i\left(p_i^{n+1}\right) = V_{bi}\varphi\left(p_i^{n+1}\right)\rho\left(p_i^{n+1}\right) \quad \text{....(1)}$$

where:

V_{bi} = bulk volume for cell *i*
p_i^{n+1} = pressure for cell *i* at timestep *n+1*
φ = porosity
ρ = density

PROCEEDINGS
JOINT CONVENTION BANDUNG (JCB) 2021
November 23rd – 25th 2021

Then, combined with the Darcy flow formula it become:

$$m_{i,j}^{n+1} = \rho(p)\, q_{i,j}^{n+1} \Delta t = \frac{A_{i,j} k}{L_{i,j}} \frac{\rho(p) k_m(p)}{\mu(p)} \left(p_i^{n+1} - p_j^{n+1}\right) \Delta t \quad .(2)$$

where:

$q_{i,j}^{n+1}$ = flow rate from cell *i* to cell *j* at timestep *n+1*

$A_{i,j}$ = cross-section area between cells *i* and *j*

$L_{i,j}$ = distance between the centers of cells *i* and *j*

μ = viscosity

k = permeability at the initial pressure

$k_m(p)$ = permeability multiplier (permeability at a certain pressure is calculated as $k_{effective} = k \cdot k_m(p)$).

And then, Mass produced at the well during timestep *n+1* (if well penetrates cell *i*) can be calculated as:

$$m_{i,w}^{n+1} = \rho(p)\, q_{i,w}^{n+1} \Delta t = WI \frac{\rho(p) k_m(p)}{\mu(p)} \left(p_i^{n+1} - p_{wb}^{n+1}\right) \Delta t \quad (3)$$

where:

WI = wellbore index (as per Peaceman 1978 or Babu and Oden, 1989)

p_{wb}^{n+1} = pressure at the wellbore at timestep *n+1*

Material balance for cell *i* at timestep *n* can be written as:

$$\underbrace{\sum_j m_{i,j}^{n+1}}_{flow\ to\ other cells} + \underbrace{m_{i,w}^{n+1}}_{flow\ to\ the\ well} = \underbrace{MIP_i\left(p_i^{n+1}\right) - MIP_i\left(p_i^{n}\right)}_{change\ in\ mass\ inplace} \quad .(4)$$

Since the multiple layers assumption are connected through the wellbore, additional modifications are made to model flow in a vertical direction. Refer to equation 2, to account for the fact that the direction of flow may have a vertical component, the equation should be adjusted as:

$$\frac{m_{x\,i,j}}{\Delta t} = \frac{A_{i,j} k_{abs}}{L_{i,j}} \frac{\rho_x(p) k_{rx}(S_x) k_m(p)}{\mu_x(p)} \left(p_i - p_j - \rho_x(p) g h\right) \quad .....(5)$$

Where *h* is a vertical distance between the centers of *cells i and j*. It is also important to note that each phase is in hydrostatic equilibrium.

Remember that wellbore cells are also connected to each other, but this connection is different, because flow in this connection represents flow of the fluid in the pipe, not in the porous media. Phases inside the wellbore are assumed to be mixed and to flow as a single homogeneous fluid. Therefore, pressure drop across the wellbore calculated using this approach:

$$p_i - p_j = \rho_{mix}(p) g h + \frac{q_{mix} \mu_{mix}}{T_m} \approx \rho_{mix} g h \quad .....(6)$$

Where T_m is a high number to represent the high conductivity of the pipe.

Field X Case Study Analysis Workflow

Field X is developed with 1 subsea gas well that produce from layer A and B with commingle completion. Reservoir properties value gap between layer A and B make it difficult to specifically understand the layer proportion. RTA methods is utilized to answer those challenge.

A comprehensive approach in this paper explained details below:

1. Data input: production data (gas rate and calculated sandface pressure from WHP), wellbore diagram, reservoir properties initial (porosity, saturation, thickness, reservoir pressure initial), and welltest result (if any for matching point).
2. Data quality control (QC): Synchronizing sandface pressure calculation and production rate, should follow the relationship between rate and pressure (if the flowrate increase, pressure should be decrease).
3. Perform RTA in an individual well. Trends of FMB and Type curve could estimate connected volume, k, S, well condition, boundary dominated flow identification.
4. History matching in Multilayer Model by changing dynamic properties of reservoir will be confirming k, s, reservoir pressure, and production allocation of each layer.
5. Rate and sand face pressure from each layer will be input back to a new imaginary well for each layer representatively.
6. Conduct Flowing Material Balance analysis using allocated production data for each layer's representative model to validate multilayer result.

Result and Discussion

Due to the nature of Z-1 well (subsea well, commingled, and without downhole gauge) Multi layered material balance could provide the solutions to understand and estimate the reservoir's contribution. According to publication develop by Kuppe, Frank et al [(1)] about "Layered Material Balance" method, there are various advantages which can be summarized as below:

- Good diagnostic tool to determine OGIP in multi-layered reservoirs.
- Accounts for operational effects (i.e. compression, stimulation or re-perforation) on production decline and material balance curves.
- Enables user to QC pressure data.
- Can be used to allocate production between commingled layers (over time).

- Can be used to forecast total or individual layer production

In this paper, Rate Transient Analysis (RTA) is applied as an alternative method to do material balance technique.

Rate Transient Analysis Single Well

Z-1 FMB and type curve result plotted in figure 1. The value of connected pore volume from Layer A and Layer B is determine by FMB result and confirm the boundary in type curve which will be utilized as allocation's reference. FMB plot shows there are two trend data in FMB followed by Productivity Index (PI) plot as well. This condition shows there is PI changing during the production which cannot be fully addressed because the FMB theory is based on Pseudo Steady State condition that have constant PI. Therefore, the stabilized PI trend chosen as matching point, followed by FMB trend, rate and pressure matching. This connected pore volume value is justified by type curve analysis to guarantee that this well has reached the boundary which allowing us to lock the connected gas volume. This means we could only match the data until during the stabilized PI number is achieved in multilayer analysis.

Multilayer Model

Layer A is known as tight carbonate reservoir with net pay 98–103 ft, permeability ranging from 0.2– 30 md meanwhile layer B has better quality of reservoir properties with net pay 53–75 ft, permeability ranging from 27–1066 md refer to core data. Well log of Z-1 and Z well can be seen on figure 2. DST result from exploration well (Z well) indicated that there is small flow from layer A. Multilayer model from RTA method is utilized to obtain the allocation because there is no PLT data in Z-1.

History matching in multilayer model is build using commingled connected volume result and k h range from core data. The result of multilayer history matching showed in figure 3 and figure 4. There are 4 cases that shows the most reasonable matching of layer A and layer B. Based on the outcome of multilayer model, layer A contributes around 0.95% – 9.74% of total production while layer B contributes around 90.26% – 99.05% of total production. The details shown in table 1. This result must be verified using single layer model on the next step.

The result of multilayer model based on several assumption as follows:

- Layers are communicating with each other only through wellbores.
- Gas rate is used as control parameter.
- Not considering the effect of relative permeability because it is single phase (dry gas).
- Initial reservoir pressure of each layer is assumed to be reliable.
- Only consider single value of Productivity Index
- The skin factor from history matching result represents average skin across all layers.

Result Validation

Single layer model of FMB is developed to verify the rate and allocation result. Data input of this model is gathered from production data of each layer, while other properties are based on the average value from all layer. If the connected volume value difference between multilayer model and single layer model is less than 5%, the result stated to be valid. The FMB validation result of each case can be seen on figure 5 for Layer A and figure 6 for Layer B.

Conclusions

- This method can be adopted as an empirical approach to determine production allocation for commingle well.
- Based on best match cases, the range of allocation result are between 0.95 – 9.74% from layer A while layer B contributes around 90 – 99% of total production. Layer A's OGIP is ranging from 11.9% - 13.3% while layer B is ranging from 86.7% - 88.1%
- Simultaneous matches of the material balance and production trend (rate or cumulative production vs. time) are obtained to ensure a representative value of OGIP and k h is generated for each of the two layers.
- Based on the result, Layer A still have potential undrained gas which cannot flow due to tight reservoir properties. This can be used as a reference for production forecasting and planning although it needs PLT data for validation.

References

Kuppe, F, Chugh S, and Connel, P, 2000, SPE 59760, SPE/CERI Gas Technology Symposium, Canada.
IHS Markit, 2021, Harmony Enterprise Manual Book, section Numerical Model Theory.
Anderson, D, Mattar, L, 2003, SPE 84472, SPE ATCE, Denver, USA.
Anderson, D, Mattar, L, 2004, SPE 89939, SPE ATCE, Texas, USA.

Acknowledgements

The author would like to thank Kangean Energy Indonesia to give permission to publish this paper.

PROCEEDINGS
JOINT CONVENTION BANDUNG (JCB) 2021
November 23rd – 25th 2021

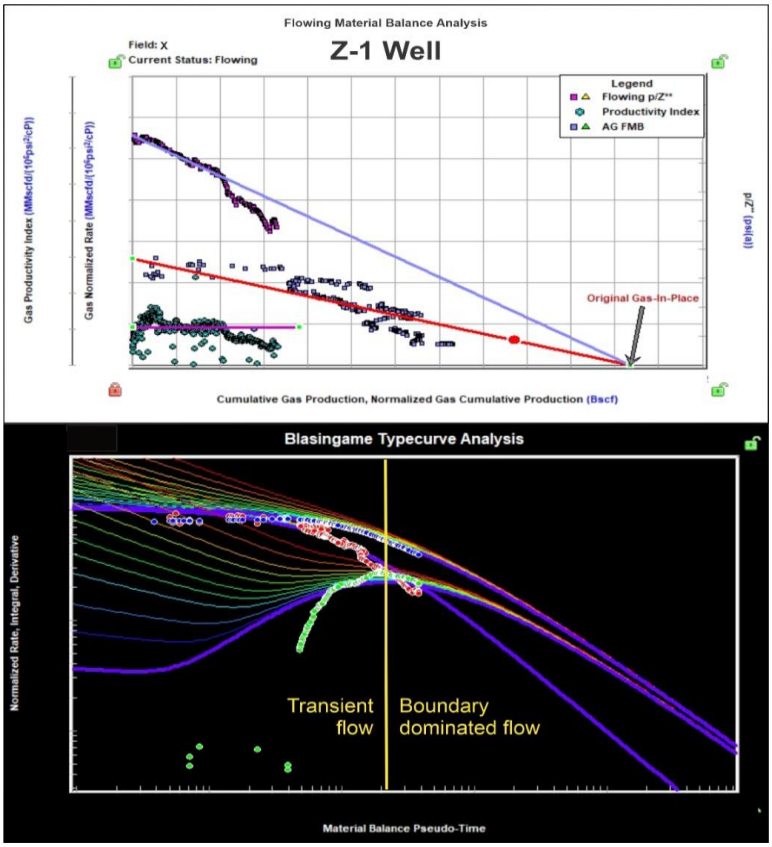

Figure 1: Z-1 Well FMB and Typecurve Result

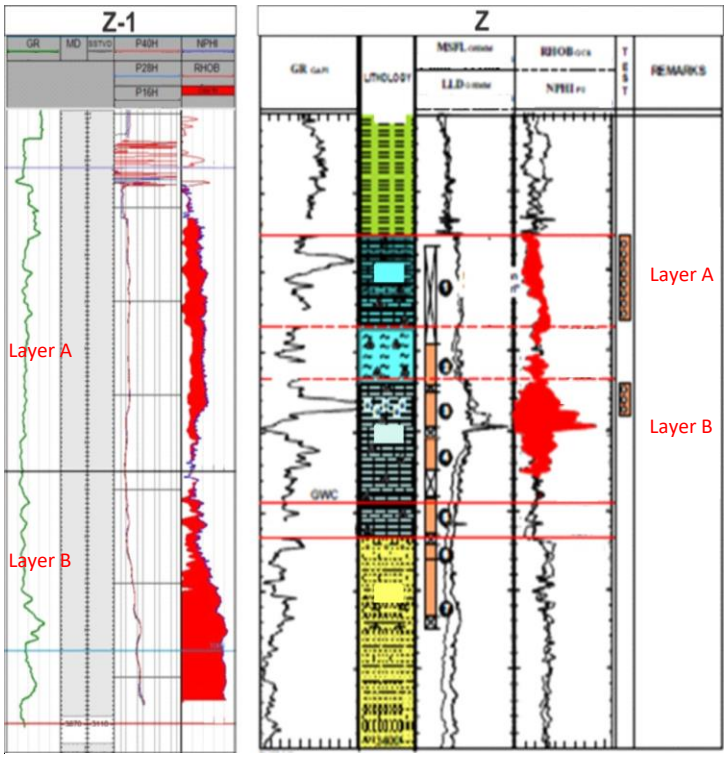

Figure 2: Log Z-1 and Z

PROCEEDINGS
JOINT CONVENTION BANDUNG (JCB) 2021
November 23rd – 25th 2021

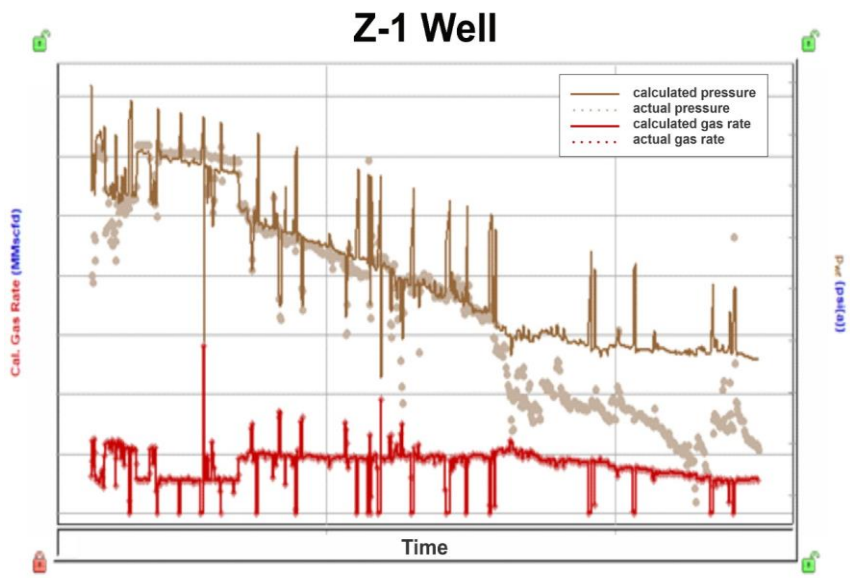

Figure 3: History Matching Z-1 Commingle

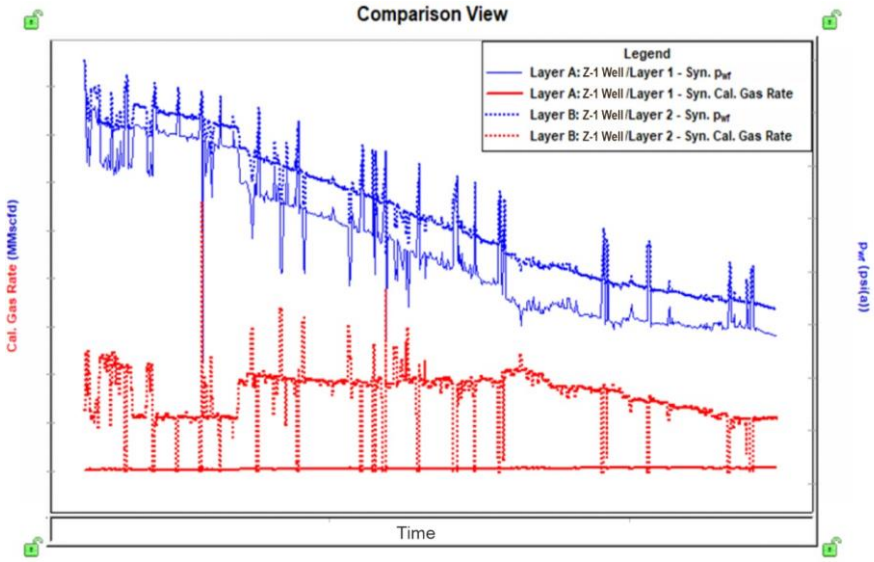

Figure 4: Multilayer Model Result

Layer	Case	Pay zone (ft)	Permeability (md)	Skin factor	OGIP (%)	Flow Contribution (%)
A	1	98	53	15	11,9%	9,74%
	2	103	55	13,5	12,46%	2,55%
	3	103	53	15	12,27%	0,95%
	4	102	57	17	13,33%	5,40%
B	1	64	600	16	88,1%	90,26%
	2	75	530	15	87,54%	97,45%
	3	75	520	15	87,73%	99,05%
	4	59	640	13	86,67%	94,60%

Table 1: Multilayer History Matching Result

PROCEEDINGS
JOINT CONVENTION BANDUNG (JCB) 2021
November 23rd – 25th 2021

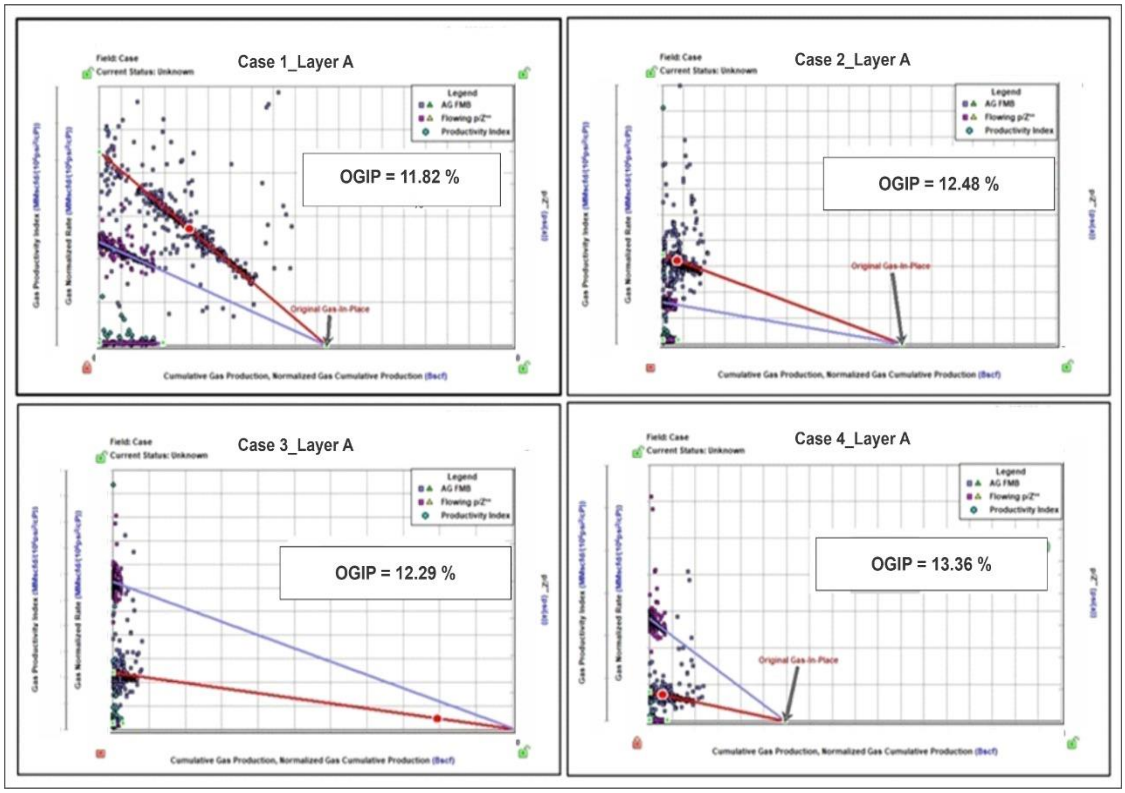

Figure 5: FMB Result Validation Case 1-4 Layer A

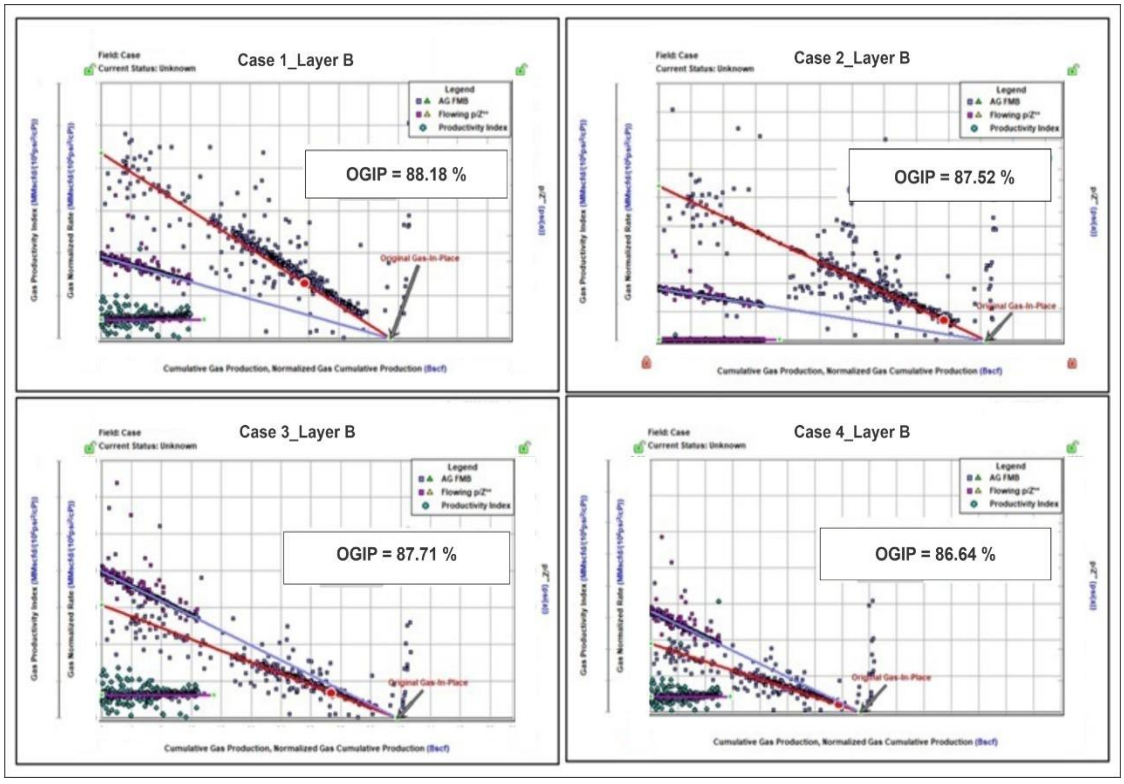

Figure 6: FMB Result Validation Case 1-4 Layer B

ROCEEDINGS
O NT ON NT ON N N 2 2
e ember t 3rd 2 2

r E r E E r I rr d r
S d d Or G r

Barry Majeed Hartono[1], Moh Heri Hermiyanto Zajuli[2], Eddy A. Subroto[1]
[1]Geological Engineering, Faculty of Earth Sciences and Technology, Institut Teknologi Bandung
[2]Pusat Survei Geologi, Badan Geologi

r

The o ene nterv o entr m tr n the e e orm t on h been e no n ro o r e ro th n the b n Mo t o the t d e th the nterv ere o ed on the o r e ro eo hem tr o ever e e orm t on h e o rov de ood eo env ronment re ord d r n the e r r t n n entr m tr n h h the de o t on n o ene dom n ted b the tr ne env ronment Th er re ent det ed ed mento o nd eo hem h r ter t o the tr ne h e o the e e orm t on m e ere t en ever 3 ent meter th tem t r d rom the meter th h e The m e ere n ed or or n etro r h r d r t on nd eo hem n tot or n rbon TO ro d t nd t r te b om r er ob erv t on re t ed to observed the h n e o the o r e o or n m tter OM n t m tr n t nd eo redo ond t on th n the tr ne e The h n e o ed mento o h r ter t re o noted to be t en or the nter ret t on O r t d ho th t ever o r e re ted b om r er r meter re e e t ve to observed the om e de o t on h tor n h h the de o t on er od o e e orm t on o d be rther d v ded t e t nto three er od er od nd h er od h d erent de ree o OM re erv t on n h h the re erv t on be t n er od nd h e the er od e h ve oor OM re erv t on Th eo env ronment t d n erred rom ed mento o nd eo hem ro e o ve n ht nto the b n n me h n m d r n o ene n entr m tr n

rd om r er eo hem tr e e orm t on tr ne eo nv ronment

I r d

Mo t o the h e h dro rbon m t on n e tern ndone re o nd n b r ett n o t nd Nob e 2 t h been e nder tood th t the e b r b n ere ormed on the r Tert r o t nd Nob e 2 r n the b n orm t on e r ed ment t on o rred n the v r o env ronment rom v o tr ne terre tr m r n m r ne nd o en m r ne o t nd Nob e 2 env ronment de end on the eo eo r h ett n o the r t n h env ronment e h b t ood de o t on nd re erv t on o or n m tter OM o th t mo t o the e r n r t de o t m ht t ood o r e ro

entr m tr n rov de ood e m e o etro e m tem th t m n ontro ed b the e r n r t de o t em t n ro th t de o ted n the o O o ene th tr ne ett n e dr nd 3 h e ed ever eo hem t to t d the o r e ro h r ter t h e mo t eo hem t d e o ed on the b t e o the de o t to t o r e ro e t et 5 erm nto et 2 the em t n ro o re ord n orm t on re rd n the de o t on ond t on d r n the e r r t n h n orm t on m ort nt to nder t nd the b n n h tor nd o the re erv t on o OM n the ed ment eo hem nd

ed mento o ro e roved e e t ve to he nder t nd the eo env ronment eter et 2 5 2 M rt et 2 2 o the e r n r t de o t eo env ronment t d e n the em t n ro h ve been ond ted b on e et nd the re e r h e t th t ro n h e orm t on member o em t n ro nto three tho e b ed on no o ed mento o nd eo hem tr n dd t on erm nto nd m 2 h ve o ob erved the evo t on o the eo env ronment o em t n ro vert n eo hem nd or n etro r h d t o ever det ed b om r er ro e te o er too to n erred the evo t on o the tr ne eter et 2 5 h ve not been er ormed There ore th t d m to nter ret the evo t on o the em t n ro tr ne eo env ronment d r n the e r o en n o n det ed b om r er n

D d M d

ere n th t d the eo hem d t re rov ded b t rve eo o nn rve n 2 re h m e ere t en rom meter th h e th tem t m n method ever 3 m re Then eo hem n re er ormed on m e to obt ned b eo hem d t et TO 2 Tm nd b om r er d t b ne ter ne nd ter ne The b eo hem d t re e e ented on erm nto et 2 h e the

ROCEEDINGS
O NT ON NT ON N N 2 2
e ember t 3rd 2 2

or n etro r h d t re v b e on erm nto nd m 2 ever o r e re ted b om r er r meter re m n me red rom r mento r m e n b hed d t rom rtono et 2 2 hemometr n or h er r h ter n n then r n on T 3 22 o t re det ed bo t the o t re v b e on mmer et 2 n o r e re ted b om r er r meter The or thm ed or the n d n or thm h h the m e t or thm nd common ed or ter n n th t me re the d t n e bet een t o o nt n et 2

n dd t on nd or n etro r h n e re o done to ort the de o the eo env ronment evo t on M rt et 2 2 The er ent e o m ner nd rt ve n orm t on re rd n the ond t on d r n the de o t on The m ner re d v ded nto three m n ro h rt rbon te nd m ner The h n e o ed ment r tr t re th n the h e re o noted

G C d

n e the m n o o th t d the e r n r t de o t the eo o ond t on re o ed on the re r t nd e r n r t e en e o n h h e dr nd 3 re erred th ode nd ode ode the te ton e ode th t o rred d r n re Tert r th t om rom e met mor h ro th t ere ormed d e to the m m t on o ever m ro ont nent b o d r n eo o Me o o e dr nd 3 The e ro erved the b ement o nd the ed ment o r e o the e r n r t ed ment t on h e the t re ormed b the m m t on ontro ed the ne t te ton e ode r n the ode o ene O o ene 5 M 2 M n t r t n o rred rom the re t v t on o the rev o tr t re re t n n the orm t on o h r ben th N nd NN or ent t on e dr nd 3 The h r ben rov de ommod t on e or the de o t on o v o tr ne ed ment o em t n ro

em t n ro re re ent the ed ment t on d r n the e r o en n o Th ro on t o three orm t on re e t ve from the o de t o er ed ed ro n h e nd er ed ed on e et e dr nd 3 The o er ed ed re re ent v de o t th t m n om o ed o m d tone t tone nd tone nd on omer te ro n h e re re ent o ener env ronment tr ne env ronment th t re om o ed b or n r h h e Th orm t on o d be d v ded nto three tho e tho e nd on e et th t h ve d t n t h r ter t The te ed ment t on o the em t n ro m r ed b

the de o t on o the er ed ed th tr ne ett n

R d D

Multivariate Analysis

The m t v r te n re t e t th t the de o t on o the tr ne o the e e orm t on o d be d v ded nto three er od re 2 th t re ent m e th m r eo hem nd m ner o h r ter t The re t re te m r to on e et ob erv t on The r t er od h th ne over 5 meter th M 2 to M 2 T b e 2 The e ond er od h th ne over 3 meter M 2 to M 2 There ome eo hem nd m ner o b bre th t re re ented b M 2 M tter ed ment t on de o ted 2 5 meter th h e re re ented b M 2 N to M 2 T b e 2

The Quest for Parameters

Th t d o nd th t the ommon r meter ed b rev o t d e r h e on e et erm nto nd m 2 te ne e t ve to ob erve the evo t on o tr ne de o t on The r h r t o e h b t tt e or no t t on th ht n re n trend to rd the o n er rt re 3 o ever the r n nd h n r t o t h ve moder te en t v t to ho t t on d r n the de o t on o the e e orm t on re 3 n dd t on th t d ho th t de ree o ne O eter et 2 5 nd terr eno t r t o T o rbon erre nd Me er re en t ve to d r m n te e h er od o tr ne de o t on th t ho d t n t ve trend on the h e e en e re 3 omb ned th r n nd h n r t o O nd T re e e t ve to e n the h n e n the o r e o OM nd de o t on env ronment ond t on o the tr ne

The α o e n ne nd 3 meth ter ne th t ere ed b on e et re not v b e n th t d o ever the r t o o tr ter ne TT re e bor ted or n e t h been no n to be e e t ve d r m n te m or mber e eter et 2 5 2 to m nor or no e rtono et 2 2 Th t d e t th t the evo t on o e e orm t on de o t on o d be re e ted b 23 TT 2 2 TT nd 2 25 TT The r t o o 23 TT the mo t en t ve r t o e ted b three d erent trend ob erved re 3

The m er om o t on th t h been b e ted o er ro e to re ord eo env ronment ond t on demon tr ted b on e et erm nto nd m 2 roved not to be e e t ve om red to the b om r er d t n the t d re The re t ve er ent e o n te e n te nd v tr n te o the three er od d no n nt d eren e th n the h e nterv re 3 The

ROCEEDINGS

O NT ON NT ON N N 2 2 e ember t 3rd 2 2

n en t v t o the m er om o t on n the e e orm t on o b re ted to the OM re erv t on e te the d erent o r e o OM the re erv t on o OM o d mod the m er om o t on n ed ment emb r 2

The mo t e e t ve ro e th t rov de eo env ronment re ord or e e orm t on re the m ner o er ent e obt ned rom n th e the m ner o er ent e re re re ented b the r t o o rt m ner t The rt re med to re re ent ood n er od b h h ener ro e h e the m ner re re ent t b e ter ond t on

Lacustrine Deposition: Period I

h e e en e de o ted n er od om o ed b r h e nd r ne m n ted m d tone er tr t re re The bedd n monotono th th ne over to 5 m Th h r ter t m r th tho e h h on t r m n ted m d tone th t re re ent h o tr ne on e et

The ed mento o e m t hed th the de o t on env ronment n erred rom eo hem nd m ner o ro e The h e h re t ve o er 2 2 TT nd 23 TT r t o om red to the

e ond nd th rd h e e en e re 3 The TT nter reted to be der ved rom h her nt eter et 2 5 n dd t on the $_2$ TT ommon enr hed on the n t b e ter o mn h e $_{23}$ TT t b nd nt on m r ne de o t mber e eter et 2 5 There ore the de o t on ond t on o th h e nter reted to be re t ve r rom the h her nt t b e ter o b h o or dee tr ne Th orted b re t ve h h $_2$ TT re 3 h h ommon n the tr e tr ne eter et 2 5 Th env ronment e n the redom n nt n t o t e ero en The m ner o om o t on o e t t b e env ronment th re t ve o er rt m ner rt o re 3 n term o rt nd n t b e env ronment m ner tend to be re t ve enr hed

The h e o m r ed b re t ve o er O 2 nd T 3 nd moder te r n 5 nd h n 2 2 2 th t e t dom n nt terre tr h her nt OM n t onn n nd o eter et 2 5 o ever the terre tr OM n t re t ve o er om red to er od nd The m er om o t on ort the b om r er nter ret t on tr n te th t re re ent terre tr OM o rred n the ed ment 2 b t not the dom n nt m er The dom n nt m er n th r t e en e n te 5 3 3 o o ed b n te 5 23 h h e n the re t ve o O nd T

The dom n nt e n te nd n te on rmed the t b e h o tr ne env ronment

Lacustrine Deposition: Period II

The h e r d h n e nto e ered m d tone The m d tone h d r bro n to r n o or th er tr t re re The bro n o or o d be nd t ve or h o o d n env ronment tho e nd th t re e t tr ne e on e et h re m r h r ter t th the h e de o ted n the er od

o ever b ed on eo hem ro e th nterv h the h he t $_2$ $_2$ TT r t o th t e t n env ronment th n n t b e ter o mn eter et 2 5 o b d e to h her ener o $_2$ $_{25}$ TT r t o re 3 nd te th t the rev o t b e tr e tr ne h h n ed to the re t ve h h ener env ronment th t re ted to v n t or ood n The h h ener o re e ted b m ner o om o t on n h h rt b nd nt th n the nterv re 3

The v bro ht terre tr OM re t n n re t ve h h O 2 T 2 3 nd r n th n the nterv The re t ve h h r t o $_{23}$ TT o orted the ob erv t on n e TT der ved rom terre tr OM mber e etro r h v tr n te nd e n te o rred th not be mo nt re e t ve to nd 2 to 3 Moreover v tr n te b ent n the m dde o th nterv re 3 o b to oor re erv t on o ob erved OM emb r 2 n ontr t n te o rred n tt e mo nt 22 5 2 nd ometme b ent

Lacustrine Deposition: Period III

On the er rt the tho om o ed b d r bro n to r h e th er tr t re nter ered th r ne m n ted m d tone re No br t tho h n e re ob erved Moreover the m er om o t on o d r d h n e nd rem n t b e to the er rt o the h e re 3 o ever eo hem ro e h r n h n T nd O o b re orded ood n event bet een er od nd th t d ed b dden h n e o the e r meter

The t er od o de o t on b to the t b e env ronment t re e ted b the h h r t o $_2$ $_{25}$ TT th t t or tr ne eter et 2 5 The r t o o $_{23}$ TT o be ome o n e t n de re n n terre tr OM n t re 3 erent rom the nterv o er od the h e h re t ve h her $_2$ $_2$ TT r t o e t n n t b e ter o mn M ner o d t o d ve e n t on or h henomenon The r t o o t n th nterv ho no

d eren e to ht h her om red to the r t nterv re 3 There ore th nterv nter reted o tr ne e b re t ve h o er th n the h e rom er od The bro n o or o the h e o b the re t o e o re to the r e d e to the h o ond t on

The nterv o er od dom n ted b e n te nd moder te mo nt o n te 2 2 5 The e om o t on rem n t b e d r the de o t on n er od tr n te on o nd n one m e h h M 2 re 3 The m er om o t on e t th t the env ronment o the h e o b te r rom the nd or e m r n h her nt mo t e e d tr b ted ro nd the tr ne e The r t o o r n h n O nd T n the er rt re o dent th the h e de o ted d r n er od re 3

The Relation between Source Rock Characteristics and Depositional Periods

h e h t o n b t e to re erve the OM de end on the o en er d r n the de o t on O env ronment h ve b d re erv t on o OM be e h ond t on rov de ommod t on or m rob ter to de r de the OM h e no env ronment rov de the be t OM re erv t on emb r 2 Theoret h e e en e de o ted n er od nd h ve ood re erv t on n e the de o t on ond t on re t ve t b e h e de o ted n er od o d h ve oor OM re erv t on d e to the v n t th t br n O_2 to the env ronment

red ted the TO nd 2 v e re re t ve h her n h e e de o ted n er od nd re h e de o ted n er od h the o e t TO nd 2 v e There n tere t n ob erv t on o the m e rom the de o t on bre h h h h TO nd 2 v e to re o b e e n t on or th th t t m re o b e re erv t on o ob erved re 3 the re t o ood n th t br n re t ve o er O_2 not the v n t

C

O r t d ho th t the de o t on o the e e orm t on d r n the o ene not m e n e tr ne de o t on ro e b t om e de o t on h tor n h h the de o t on er od o d be rther d v ded t e t nto three er od The r t er od m r ed b h o tr ne e then h n e nto v en ed tr ne e nd b nto h o tr ne e n the th rd er od h nder t nd n m ort nt n e e h e h ve d erent de ree o OM re erv t on t h been e r ho n th t v n en e e e h ve re t ve oor OM re erv t on re t n n o TO nd 2

Th t d o ho th t O T nd the r t o o 23 TT 2 2 TT nd 2 25 TT omb ned

th d t re e e t ve ro e to nder t nd the evo t on o the tr ne eo env ronment The ne t h en e re to ee more r meter to nder t nd the tr ne de o t on h other b om r er r meter or m ner o e h nder t nd n o d m rove o r no ed e bo t tr ne o r e ro e e the de ree o re erv t on o O M

R r

n M n nd t 2 o rn o M h ne e rn n e e r h 5

o rbonn ere nd Me er nv ronment eo o 22 2

emb r 2 etro e m eo hem tr or e or t on nd rod t on ev er en e m terd m

d M T mone t r e d n nton N t re 2 222

o t nd Nob e 2 M r ne nd etro e m

ROCEEDINGS

O NT ON NT ON N N 2 2

e ember t 3rd 2 2

eo o 3 2

mmer T r er nd n 2

eonto o e tron

rtono M M erm nto broto nd n e t 2 2 ro eed o t Te hn on eren e 2 2

rtono M broto e m n ndr nto M v n h d ono d n r nto 2 2 ro eed o the ntern t on Meet n on Or n eo hem tr

e dr T nd 3 ro eed 22th nn onvent on

erm nto M nd T m 2 O on eren e er e rth nd nv ronment en e 2 2

erm nto M broto nd nto 2 O on eren e er e rth nd nv ronment en e 2

t 5 et n o eo o o et o M 3 3

on e M rr o h M r dden nd ro n ro eed o th nn onvent on 2 2

M rt h onob b m to nd r to 2 2 M r ne nd etro e m eo o 5 5

eter ter nd M Mo do n 2 5 mbr d e n ver t re

eter T oren on nd mber e 2 e r h nd over rt e

mber e eo h m et o mo h m t 25 3

d

The thor o d e to no ed e t rve eo o th t h rov de the d t from the nn rve 2 nd o th re e r h to be re ented on o nt onvent on nd n 2 2

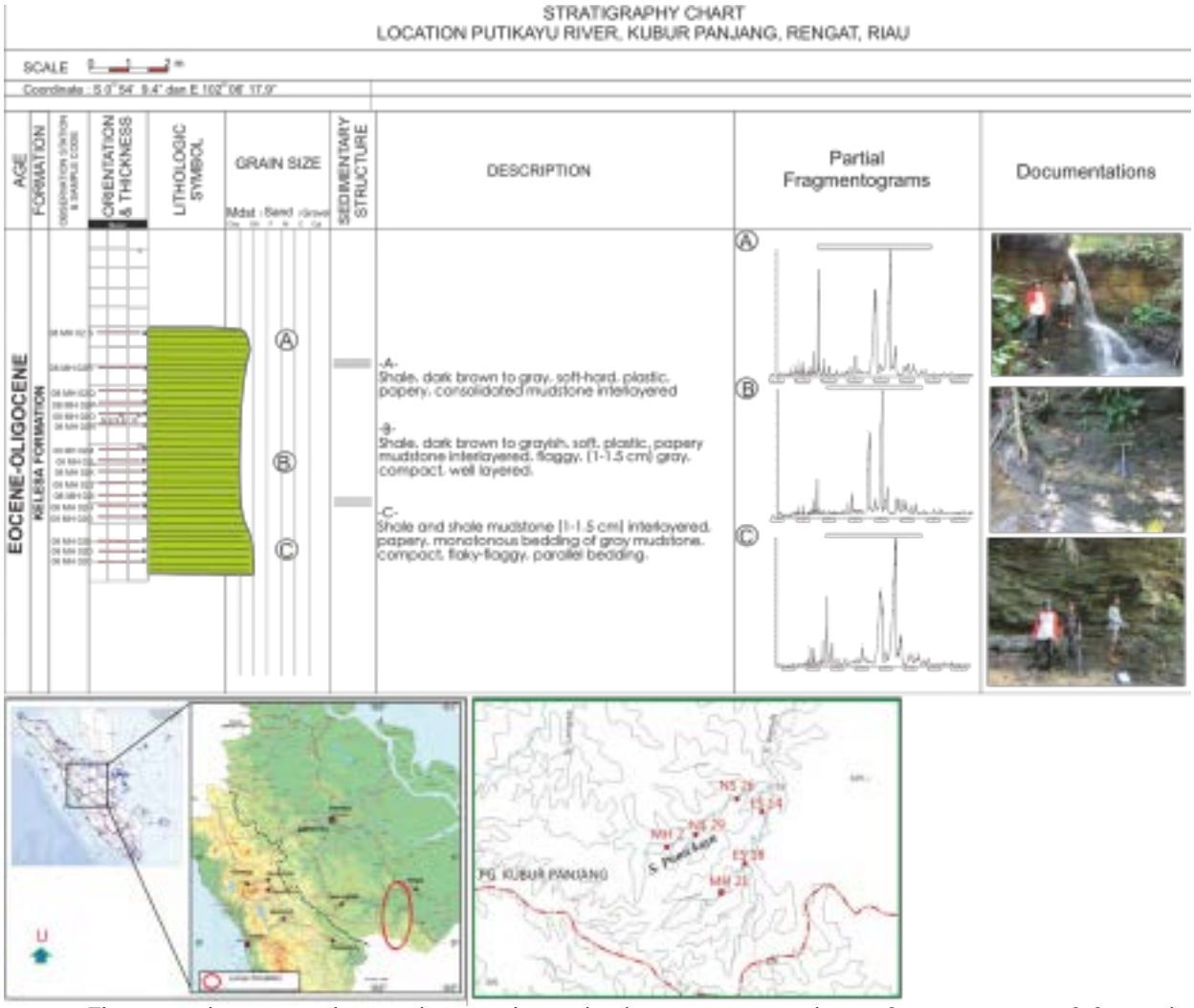

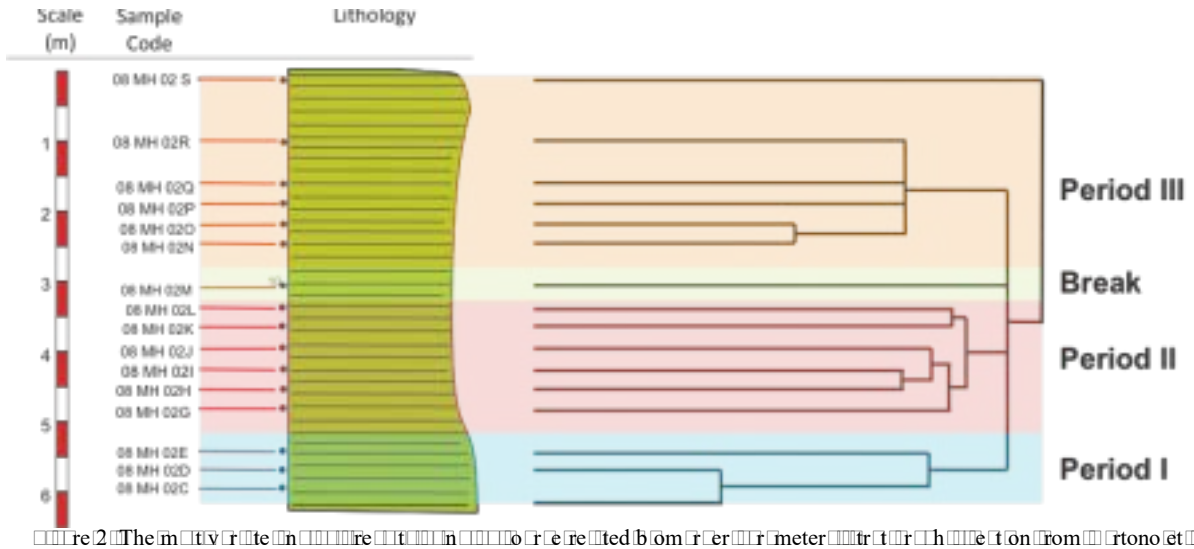

□□□re □□□The □tr□t□r□ h□□□e□ton o□the re□e□r h□re□ (□□ht□□□mod□□ed □rom □erm□□□nto □nd □□m□□□2019 □□ □rtono et al □□2□20 □to □ether □ th□□rt□□□m/ □□91 □r□□mento □r□m□. □n th□□re□e□r h□the h□e□e□en□e th□t □rev□o□□□□nter□reted□□□□□□□□tr□ne□env□ronment□□□□□rther□ d□v□ded□into three□fac□es b□□ed on the□r□□ed□mento□o□□□□□□m□ner□o□□□□□□□nd□□eo□hem□□□□□h□r□□ter□t□□□. □

□□□re 2 □□The □□□t□v□r□□te□□□al□ sis re□□t□us□ng 18□o□r□e□re□□ted b□om□r□er□□□r□meter□□□□tr□t□□r□h□□□e□t□on□rom□□□rtono et□□□□., □ 2□20) □There□re□□t□e□□t three□□er□od□d□r□n□□□e□e□□□orm□t□on□□□□□□tr□ne□de□o□□t□on b□□ed on the□r□□ed□mento□o□□□□□, □m□ner□o□□□□□□□nd□ □eo□hem□□□□□h□r□□ter□t□□□. □

□ROCEEDINGS□□

□O□NT□□ON□ □□NT□ON□□□N□□N□□□□□□□□2□21□□□

□e□ember□1[t□]– 3[rd]2□21□□

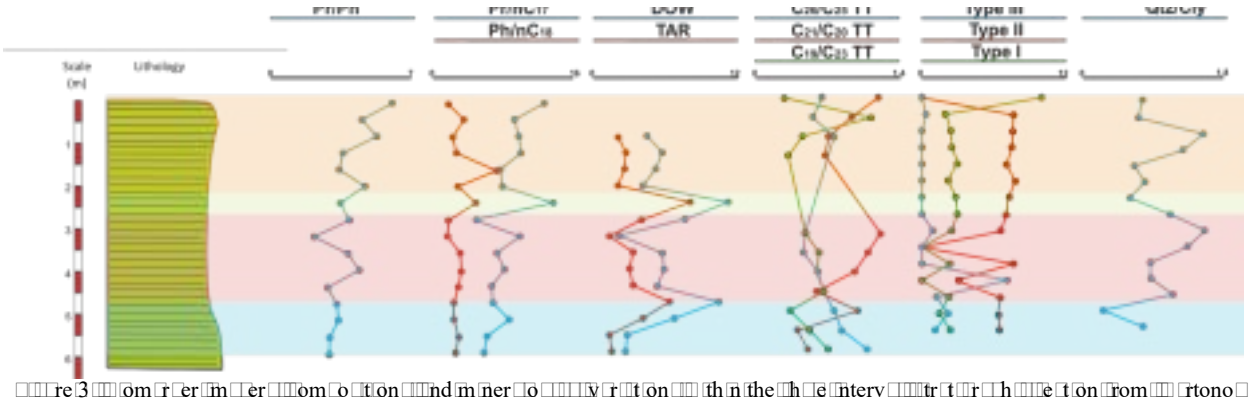

re 3 om r er m er om o t on nd m ner o v r t on th n the h e nterv tr t r h e t on rom rtono et 2 2 h er od h d t n t ttern re ted to de o t on ond t on om r er ho n n the re re en t ve to eo env ronment h n e d r n e e orm t on de o t on

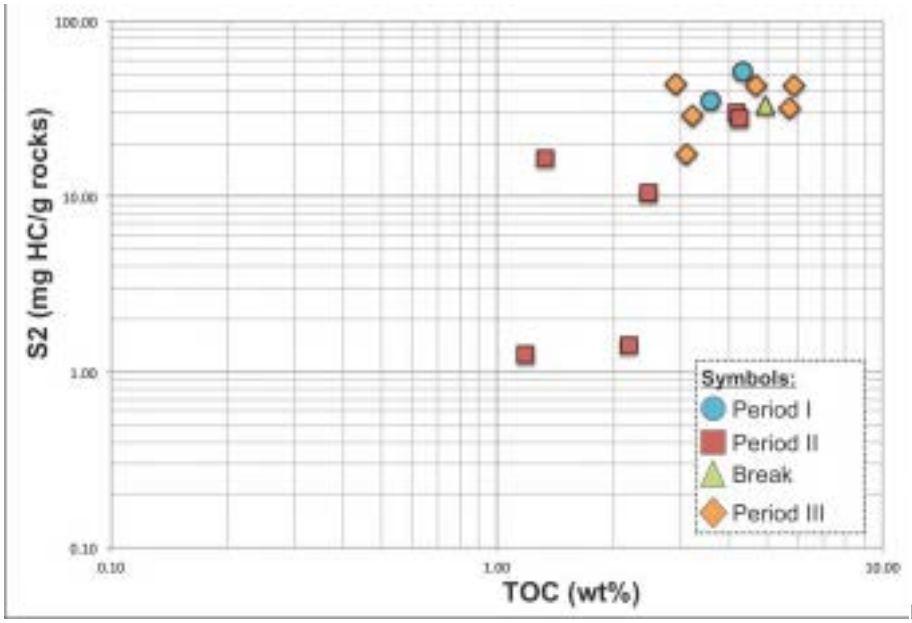

re The ro ot o TO nd 2 v e or h e de o ted n e h er od h e h d erent de ree o OM re erv t on v n en e e e er od h ve re t ve oor OM h e the re t ve t b e h o tr ne e er od nd h ve ood OM re erv t on

PROCEEDINGS
JOINT CONVENTION BANDUNG (JCB) 2021
November 23rd – 25th 2021

Deltaic depositional system in the Kutai Basin: an afterthought

Ery Arifullah[1)]
[1)]*Department of Geology, Universitas Muhammadiyah Kalimantan Timur*

Abstract

The interaction of fluvial, tidal, and wave processes that developed in the Serravallian-Tortonian deposit of the Kutai Basin has been interpreted as a deltaic depositional system. This interpretation is debatable since the interaction of fluvial, tidal, and wave processes is potentially produced not only delta system. Estuary, strand plain, and other non-deltaic systems (e.g., strand plain, shoreface, lagoon, and barrier island) are possibly produced. In addition, those conditions have happened in the Modern Mahakam Delta. Consequently, fluvial, tides, and wave influence discrimination is the main factor in understanding the fluvial-marine transition zone. The challenge is that fluvial discharge coexists with tidal processes, making it challenging to identify the discrimination of importance of the fluvial, tides, and wave processes. It is essential to pay attention to the level of analysis and the scale of observations that will influence the interpretation of the scale of the depositional system in the regional context.

Fluvial proportion

A delta form where sediment-laden rivers enter oceans, enclosed seas, lakes, or lagoons (standing body of water) and supply more sediment than can be distributed by processes that operate within the receiving basin (Elliot, 2005). The result of that process is a shoreline migration and typically advances or prograde into the basin. By that definition, all deltas are, to some degree, fluvial-dominated.

Discrimination of fluvial, tides and wave influence is the main objective at observation. Ichnological and sedimentological study in the modern Mahakam delta (Figure. 1) shows symptoms of fluvial domination's relative importance varies systematically through the river to marine transition (Arifullah, 2005). An increase in the tidal range also causes tidal action to penetrate farther inland, whereas an increase in fluvial discharge causes a decrease the tidal penetration. That situation happened not only in deltaic settings but also in all fluvial-marine transition zones (see Dalrymple et al. 2015; Fig. 1.2; Dalrymple and Choi, 2007, Fig. 9).

The northern distributaries of Modern Mahakam Delta a showed fluvial domination decline in the point when tidal action penetrates farther inland. In this place, the distributary channels are modified to form an estuary and elongate tidal bars in the river's mouth; indeed, some of them have been reworked by a wave. The northern lobe is transgressed lobe. The central part of the delta is purely a tidal channel, tidal bar, and possible tidal ridge. Southern distributaries showed the most active fluvial input activity compared to the central and northern parts. In this place, increase in fluvial discharge and a decrease in tidal penetration. Mid bar and triangular bar are developed in the mouth of the river.

The processes taking place in the modern Mahakam delta are just snapshotted in geological time. The situation in the delta today is very likely to have occurred among the many depositional systems in the Serravallian-Tortonian interval. In that time, fluvial, tides, and wave proportion is always dynamic (see Bachtiar, 2004; Arifullah, 2019). As a result, delta and estuary, strand plains, and other non-deltaic elements potentially developed either alternately vertically and sides by the side in that time (Arifullah, 2019).

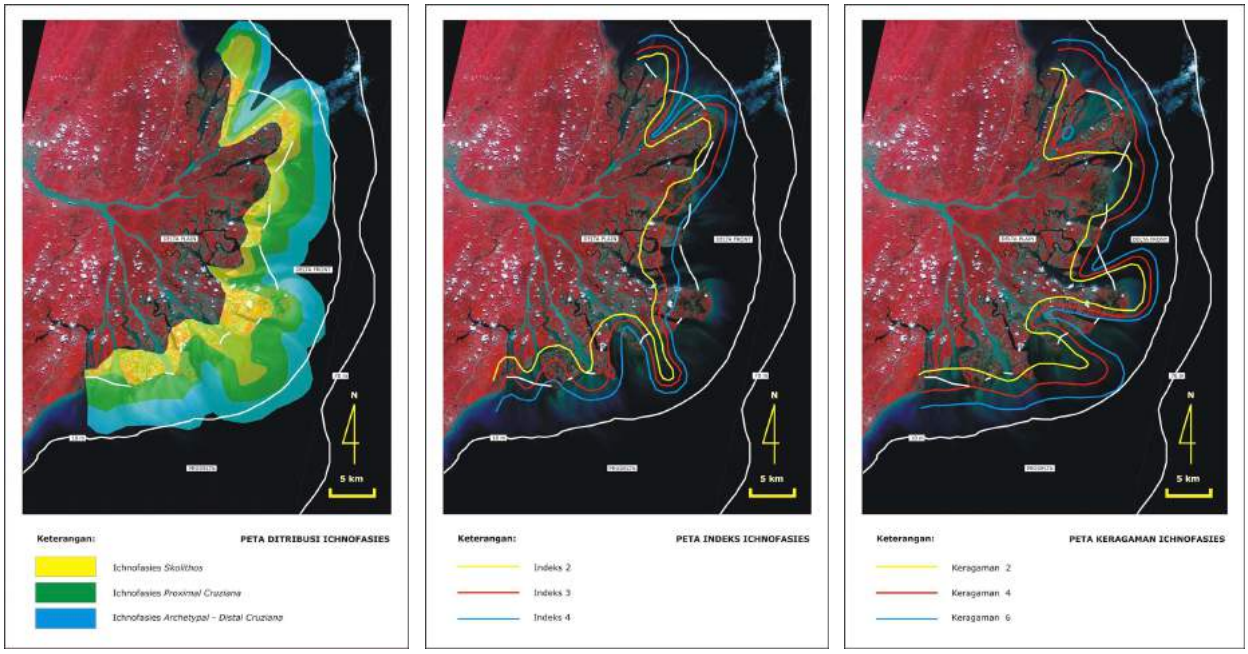

Figure 1 From the left to the right: ichnofacies distribution, bioturbation index and ichnodiversity maps of Modern Mahakam Delta (Arifullah, 2005).

PROCEEDINGS
JOINT CONVENTION BANDUNG (JCB) 2021
November 23rd – 25th 2021

In general, the Miocene deposits in the Kutai Basin are fluvial-marine transition zone systems (see Bachtiar, 2004; Arifullah, 2005; Arifullah, 2019) with variations in the depositional elements and dimensions. Fluvial discharge coexists with tidal processes in the river's lower reaches, making it challenging to identify the discrimination of fluvial and tidal processes. Physical sedimentary structures (e.g., Dalrymple and Choi, 2007; Dalryimple et al., 2015) and biogenic sedimentary structures (i.e., ichnofabric by Arifullah et al., 2019) have been developed in the discrimination of both processes.

There are 17 lithofacies codes of Serravallian-Tortonian deposits in the Kutai Basin (Table 1). However, are these lithofacies the unique characteristic of delta deposits? I think lithofacies could also be a feature for estuaries, strand plains, and non-deltaic deposits. Heterolithic lithofacies include flaser, lenticular, ripple cross-stratification with mud-drape, and symmetrical ripples are some indicators for marine deposit. Despite potential debatable (see Table 2), hummocky cross-stratification is believed to indicate marine deposit. Thus, how to discriminate the fluvial, tides, and wave influence based on those lithofacies?

Scale of analysis

Since the high variability of depositional elements and intricated processes in fluvial-marine transition zone vertically and laterally, then the level of analysis is essential to consider. Terms such as *depositional system, depositional element, depositional environment,* and *facies* are used to mean almost any kind of paleogeomorphic entity. However, using those terms is not essential without an understanding of hierarchy in terms of the scale of the model and their correspondence to the level of analysis.

Interpretation of facies units of ancient sandstone as the deposit of individual channel elements. Also, facies units of interbedding of mudstone and sandstone as the deposit of floodplain element. Both elements are an example of understanding a complex delta plain sequence. This hierarchy has a consequence on the scale of analysis. For example, interpretation of channel elements in terms of bars. Interpretation of bars in terms of bedform migration and aggradation which terms of flow conditions which terms of fluvial regime which in terms of climate and tectonic (Miall, 2006). What is the level of analysis of importance fluvial, tidal, and wave processes by the scale of analysis?

Degree of fluvial, tides and wave domination events include the frequency (mean number of events per period),

Table 1 Lithofacies classification in the Serravallian-Tortonian of Kutai Basin (Arifullah, 2019).

Code	Lithofacies	Sedimentary Structures	Interpretation
C	Coal	Massive, sheets, interbedded with clay	Anoxic condition – swamp
Fr	Silt, clay	Rootlet	Seatearth
Sgc	Gravelly – Coarse Sand	Guttercast	Scourfill
Hm	Silt or clay with sand insert	Bedding, lamination	Suspension dominance interspersed with traction
Hs	Silt or clay insert sand	Bedding, laminate	Traction dominance interspersed with suspension
Mm	Silt or clay	Lamination or massive	Suspension or product of fauna reworking
Se	Sand with scouring	Irregular cross-bedding	Scour fill
Sf	Sand	Synsedimentary fault, microfold	Gravity flow
Sg	Sand	Graded bedding	Gravity flow
Shcs	Sand	Hummocky cross-stratification	Wave and storm
Sl	Sand	Low angle cross-stratification	Antidune
Sp	Sand	Planar cross-bedding	Linguoid, transverse bars, sand waves (low flow regime)
Spm	Sand	Planar cross-bedding with mud drape	Linguoid, transverse bars, sand waves (low flow regime) interspersed with suspension
Sr	Sand	Ripple cross stratification	Ripple migration (traction)
Srm	Sand	Ripple cross-stratification with mud drape	Ripple migration (traction interspersed with suspension)
St	Sand	Trough cross bed	Dunes (upper flow regime).

Table 2 Depositional system where HCS have been reported

Depositional system			References
Continental	Transition	Marine	
Fluvial			Cotter and Graham (1991); Rust and Gibling (1990)
Lacustrine			Eyles and Clark (1986)
	Estuarine-Delta		Arifullah (2005); Arifullah (2019); Bowman and Johnson (2014)
	Intertidal Flat		Yang et al. (2006)
		Shoreface	Dott and Bourgeois (1982); Arifullah (2019)
		Turbidite	Prave and Duke (1990); Monaco (1992); Mulder et al. (2009)
		Pelagic	Seguret et al. (2001)

return interval (mean time between events), spatial distribution, intensity (physical force of the event per area per time), and impact in a given time interval represented in a particular stratigraphic section. It is in the level of interpretation of river regime (see Anderton, 1985) and behavior of the depositional system which controlled by tectonism, climate change, or base-level change (see Miall, 2014, Table 2.1). Thus, it is related to analysis in the depositional system scale.

Suppose the width of the outcrop in Samarinda ranges from 50 - 150 meters and a height of 7 - 10 meters with a thickness interval of 2.52 - 75 meters. In that case, observations on a single outcrop are simply interpretations of local contexts on a broader scale of paleogeomorphic entities. It could be in one outcrop that the fluvial-dominated and another outcrop correlative with it is a more tidal-dominated is in the same paleogeomorphic entity. Consequently, the level of geological analysis (e.g., ichnology, sedimentology) is the more regional scale, not in the local one.

Today ichnofossil is more important for understanding the importance of fluvial, tidal, and wave processes (Dalrymple et al. 2015; Gugliotta et al. 2015; Arifullah, 2019; Arifullah et al. 2021). Not merely lithofacies characterization does but the mapping of ichnofabric, paleocurrent, paleogeographic and statistical analysis are integrated firmly (Arifullah, 2019). The result is a variety of predictable deposition systems such as estuaries, barrier islands, and strand plains.

Conclusion

The probability of what deposition system develops in the fluvial-marine transition zone depends on the degree of dominance of fluvial processes, tides, and waves. Therefore, it is necessary to map discrimination fluvial, tides, and waves processes. The implication is a new interpretation of the depositional system in the Kutai Basin.

References

Anderton, R., 1985, Geological Society, London, Special Publications **18**, 31-47.
Arifullah, E., 2005, M.S, Thesis, Institut Teknologi Bandung.
Arifullah, E., 2019, Ph.D., Dissertation, Institut Teknologi Bandung.
Arifullah, E., Zaim, Y., Aswan., Djuhaeni, 2021, Journal of Mathematical and Fundamental Sciences **53**, 285-304.
Bachtiar, A., 2004, Ph.D., Dissertation, Institut Teknologi Bandung.
Bowman, A.P., Howard, J.D., 2014, Sedimentology **61**, 792–835.
Cotter, E and Graham, J.R., 1991, Sedimentary Geology **72**, 201–224.
Dalrymple, R.W and Choi, K., 2007, Earth Science Review **81**, 135-174.
Dalrymple, R.W., Kurcinka, C.E., Jablonski, B.V.J., Ichaso, A.A., Mackay, D.A., 2015, Development in Sedimentology, Elsevier B.V.
Dott, R.H., Bourgeois, J., 1982, Geological Society of America Bulletin **93**, 663–680.
Elliot, T., 1986, in Reading, H.G., ed., Sedimentary environment and facies, Blackwell Scientific Publication, 113-154.
Eyles, N and Clark, B.M., 1986, Geology **14**, 679–682.
Gugliotta, M., Kurcinka, C.E., Dalrymple, R.W., Flint, S.S., Hodgson, D.M., 2015, Journal of the Geological Society, London, http://dx.doi:10.1144/jgs2015-030.
Monaco, P., 1992, Sedimentary Geology **77**, 123–142.
Mulder, T., Razin, P., Faugeres, J.-C., 2009. Sedimentology **56**, 997–1015.
Miall, A., 2006, Springer-Verlag Berlin Heidelberg, 4th printing.
Miall, A., 2014, Springer International Publishing Switzerland.
Prave, A.R., Duke, W.L., 1990, Sedimentology **37**, 531–539.
Rust, B.R and Gibling, M.R., 1990, Journal of Sedimentary Petrology **60**, 540–548. S
Seguret, M., Moussine-Pouchkine, A., Gabaglia, G.R., Bouchette, F., 2001, Sedimentology **48**, 231–254.
Yang, B., Dalrymple, R.W., Chun, S., 2006, Journal of Sedimentary Research **76**, 2–8.

PROCEEDINGS
JOINT CONVENTION BANDUNG (JCB) 2021
November 23rd – 25th 2021

Jasinga Formation To Proposed New Nomenclature In Stratigraphic Order of the Rangkasbitung Basin

T. Syahrulyati (*), V. Isnaniawardhani (**), M.F. Rosana (**), Winantris (**)

(*) = Universitas Pakuan, (**) = Universitas Padjadjaran.

Contact Details :
tetisyahrulyati@unpak.ac.id
vijaya.isnania@unpad.ac.id
mega.fatima.rosana@unpad.ac.id
winantris@unpad.ac.id

Abstract

The problem of confusion in the nomenclature of the Bojongmanik Formation, where Syahbuddin et al, (1986) divided the Bojongmanik Formation into the Lower Bojongmanik Formation and the Upper Bojongmanik Formation. Meanwhile, Sudjatmiko and Santosa, (1992) divided the Bojongmanik Formation into Sandstone Members of the Bojongmanik Formation; Limestone members of the Bojongmanik Formation and Claystone members of the Bojongmanik Formation, therefore an in-depth study was carried out with an approach to the lithostratigraphic and biostratigraphic characteristics of the Bojongmanik Formation. The research was carried out in the Rangkasbitung Basin, starting from the Leuwiliang area in Bogor Regency to the Bojongmanik area in Lebak Regency, with a research area of ± 595 Km2. The differences in lithostratigraphic characteristics, biostratigraphy, basin geometry and depositional environment can clearly distinguish the Bojongmanik Formation / Upper Bojongmanik Formation from the "Jasinga Formation" / Lower Bojongmanik Formation. with the "Jasinga Formation" (Unit of Claystone with Sandstone and Limestone inserts). The naming of the Lower Bojongmanik Formation and the Upper Bojongmanik Formation has violated the Indonesian Stratigraphic Code rules, paragraph 1 explanation (c), namely: "To avoid duplication, geographic names that have been used for names of official lithostratigraphic units may not be used for names of other official lithostratigraphic units, either the same or different levels even though the position of the geographical names is different from one another". The description of the "Jasinga Formation" is very broad and easy to recognize. So that the requirements to become a new formation have met the Indonesian Stratigraphic Code Rules.

Introduction

There is a confusion of nomenclature in the naming of the Bojongmanik Formation, into the Lower Bojongmanik Formation and Upper Bojongmanik Formation (Syahbuddin et al, 1986), as well as members of the Bojongmanik Formation sandstone; members of the Bojongmanik Formation Limestone and members of the Bojongmanik Formation Claystone, (Sudjatmiko and Santosa, 1992), it is deemed necessary to conduct a more in-depth study, especially an approach to the lithostratigraphic and biostratigraphic characteristics of the Bojongmanik Formation and other rock units that are older, younger, or intertwined.

From this study, the characteristics of the Bojongmanik Formation can be obtained from the beginning of its formation until it was raised to land. The research area covers 9 districts, namely Bojongmanik District, Leuwidamar District, Cisimeut District, Muncang District, Sajira District, Cipanas District, Jasinga District, Cigudeg District and Leuwiliang District, with an area of ± 595 km2 (Figure 1.).

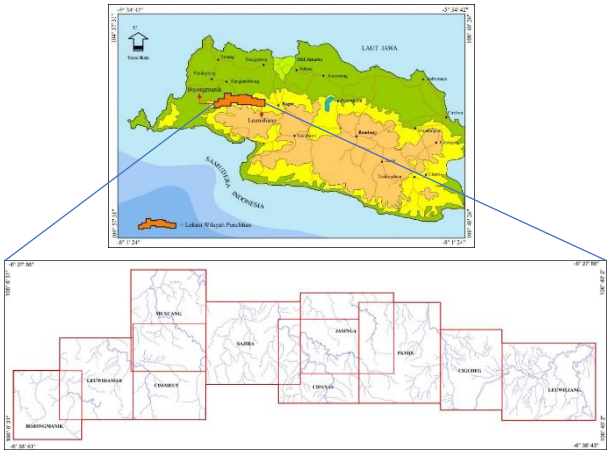

Figure 1. : Location of the research area

In the following discussion, the term Upper Bojongmanik Formation (Syahbuddin et al, 1986) is referred to as BOJONGMANIK FORMATION because, based on its lithological characteristics, it corresponds to the Bojongmanik Formation in the type location. The Lower Bojongmanik Formation (Syahbuddin et al, 1986) is referred to as the "JASINGA FORMATION", because it will be the name of the new formation proposed by Syahrulyati et al (1989).

Data and Method

The principles of geological mapping and the 11-track Stratigraphic Section Measurement (PPS) method were used as the basis for field observations. In the form of petrographic analysis of rock samples that can represent rock units. Analysis of foraminifera fossils using the spot sampling method (Syahrulyati, et.all,2020). Pollen fossil analysis was carried out on rocks with transitional depositional environments – land. The purpose of data collection and analysis is to be able to reveal the differences in the lithostratigraphic and biostratigraphic characteristics of the rocks that make up the Rangkasbitung Basin, especially the Bojongmanik Formation. How are the characteristics of the Bojongmanik Formation different from the "Jasinga Formation" based on the characteristics: lithology, presence of forming fossils, sedimentary structure, age of formation, and depositional environment.

Based on the texture characteristics of the constituent rocks, Jasinga Formation is different from Bojongmanik Formation, with the following characteristics: 1). The "Jasinga Formation" is characterized by the predominance of fine-textured rocks, namely claystone, with insertions of sandstone and limestone. Coal is never found in the form of layers, generally in the form of fibers embedded in claystone or sandstone, as well as mollusk shells are not found throughout the distribution of the "Jasinga Formation". 2).

The Bojongmanik Formation is characterized by the dominance of coarse-textured rocks, namely tuffaceous sandstones, with insertions of claystone and limestone. Coal seams are found with a thickness of between 20 cm to 1.5 meters. In claystone many mollusk shells are found which generally have an incomplete shape.

Sedimentary structure characteristics between the two formations can be distinguished as follows: 1). Sedimentary structures identified and developed in Bojongmanik Formation are parallel lamination, graded bedding and cross lamination. 2). Whereas in "Jasinga Formation" only parallel laminates are found.

From the analysis of planktonic foraminifera microfossils, it (Syahrulyati, et.all,2020) can be seen that the diversity of species and genera of the Bojongmanik Formation is greater than that of the "Jasinga Formation". 1) In Jasinga Formation, 6 (six) genera and 31 species of planktonic foraminifera can be identified, consisting of: Genus *Globorotalia* (10 species), Genus *Globigerioides* (8 species), Genus *Globoquadrina* (5 species), Genus *Globigerina* (4 species), Genus *Orbulina* (3 species) and Genus *Hastigerina* (1 species).

2). In the Bojongmanik Formation, 8 genera and 34 species of planktonic foraminifera (Postuma,J.A.,1971) can be identified, including: Genus *Globorotalia* (8 species), Genus *Globigerinoides* (9 species), Genus *Globoquadrina* (5 species), Genus *Globigerina* (5 species), Genus *Orbulina* (2 species), Genus *Hastigerina* (2 species), Genus *Sphaeroidinella* (1 species), Genus *Sphaeroidinellopsis* (1 species) dan *Cassigerinula chipolensis* (1 species). The characteristics of each formation are shown in Table 1.

Result and Discussion

The results of age analysis based on microfossils show that the age of the "Jasinga Formation" ranges from N9 – N14 (Middle Miocene); while the age range in the Bojongmanik Formation is between N9-N17 (Middle Miocene to Late Miocene). It is interpreted that entering the Late Miocene there is no longer any sedimentation activity that forms the "Jasinga Formation". (Table 1)

Stratigraphic Section Correlation.
From these 11 measurement locations, it is illustrated that the "Jasinga Formation" and the Bojongmanik Formation were formed at the same age, with a congruent relationship to intermingles. In the Leuwiliang block, the Bojongmanik Formation intermingles with the Cibulakan Formation (Syahrulyati,2021). The Cibulakan Formation is a typical sedimentary deposit from the Mandala Continental Shelf. This shows that the Leuwiliang Block is no longer part of the Rangkasbitung Basin as a whole because it has begun to enter the Continental Exposure Mandala system (Martojoyo, 2003).
The lithostratigraphic correlation in the West – East direction was made by connecting the measurement points at PPS locations (Syahrulyati et al,2020) no: TS 3-1, TS 6-1, TS 7-2, TS 8-2, TS 9-1 and TS 10-1. (Figure 1) .
From the cross section of this correlation, it can be seen that there is a lateral discontinuity of rock units, showing that the spread of the "Jasinga Formation" towards the eastern boundary of the study area (Leuwiliang Block) seems to be interrupted by the Bojongmanik Formation. With the result that the Bojongmanik Formation at the edge of the Rangkasbitung Basin runs in two directions. To the west its intertwined with the "Jasinga Formation" while to the East its intermingled with the Cibulakan Formation.
This condition illustrates that the spread of the "Jasinga Formation" has stopped in the Paniis Block due to the high geometry in the Cigudeg Block Area.
Lithotratigraphic Correlation for North – South Direction, correlation was drawn on PPS locations no: TS 6-1, TS 7-2, TS 5-1 and TS 7-2 (Figure 2). From the correlation results, it can be concluded that the Bojongmanik Formation covers the "Jasinga Formation". The contact between the two was intermingled, and was covered in the Genteng Formation disproportionately.
The correlation results show the contact form with a slope towards the North. This gives an illustration that the basic shape of the past bathymetric basin is descending towards the North.
Biostratigraphic correlation is based on the similarity of age based on the microfossil content obtained from each rock unit. However, the presence of a fossil index was not found, so an age range was used. Determination of rock age using planktonic foraminifera fossils, and the depositional environment using bentonic foraminifera fossils.
For the Bojongmanik Formation, in addition to analyzing foraminifera fossils, a palinomorph analysis was also carried out for both age determination and depositional environment. Based on the presence of planktonic fossils, there are 4 (four) biodatums, namely *Hastigerina phraesiphonifera, Globorotalia praemenardi, Globigerina pseudociporaensis* and *Globorotalia mayeri*, (Blow, W.H., 1969).

Conclusions

The "Jasinga Formation" and the Bojongmanik Formation have many differences. The difference concerns: Lithology where the "Jasinga Formation" is more dominated by fine materials in the form of claystone. The Bojongmanik Formation is dominated by coarse material, in the form of sandstone and conglomerate. There is coal with a thickness of between 20 cm to > 1 meter.

Microfossil content, "Jasinga Formation" contains 6 genera and 31 species of planktonic foraminifera, which indicates the age of deposition is in the range of N9 – N14 (Blow, W.H., 1969). The "Jasinga Formation" contains 18 genera and 7 species of benthic foraminifera, indicating the Outer Neritic to Middle Neritic depositional environment (Phelger,1951 classifications).

The Bojongmanik Formation contains 8 genera and 34 species of planktonic foraminifera, which indicates the age of deposition is in the range of N9 – N17. The Bojongmanik Formation contains 19 genera and 5 species of benthic foraminifera, indicating a Middle Neritic - Edge to Transitional Neritic depositional environment (Phelger,1951 classifications).

Depositional Environment "Jasinga Formation", shows the conditions of the Outer Neritic – Middle Neritic. Generally deposited in the "Jasinga Basin". The Depositional Environment of the Bojongmanik Formation, shows the Central Neritic – Transitional condition. Meanwhile, based on the abundance of palinomorphs deposited in the *delta*

plain environment: *mangrove dan back mangrove* (Rahardjo,1994).

Sedimentation mechanism, "Jasinga Formation" Sedimentation, is controlled by fast depositional current velocity on relatively steep slope conditions. The location of deposition is quite far from the source of the material origin. The sedimentation of the Bojongmanik Formation is controlled by a slow current velocity, with relatively gentle slope conditions. The location of deposition is not far from the source of the material origin.

Deployment

The Bojongmanik Formation has two different sources of sedimentation, namely the Cigudeg Block and the Bojongmanik Block.

Stratigraphic contact, fingering contact is only found between the "Jasinga Formation" and the Bojongmanik Formation, and between the Bojongmanik Formation and the Cibulakan Formation.

The "Jasinga Formation" must be separated into separate formations, due to different facies with the Bojongmanik Formation. The "Jasinga Formation" has a wide spread, can be mapped and has lithostratigraphic characteristics that are easily recognizable.

The naming of the Lower Bojongmanik Formation ("Jasinga Formation") and the Upper Bojongmanik Formation (Bojongmanik Formation) has violated the Indonesian Stratigraphic Code rules article 18, paragraph 1 explanation (c).

The name "Jasinga Formation" became a proposal for naming a new formation from the Lower Bojongmanik Formation (Sandstone and Limestone Inserted Claystone Unit).

References

Adams,C.G.,1984. Neogene Larger Foraminifera, evolutionary and geologically events in the context of datum plane, in Ikebe, N., Tsuchi,R.,eds., Pacific Neogene Datum Planes,47 – 67.

Blow, W.H., 1969. Late Middle Eocene to Recent Planktonik Foraminiferal Biostratigraphy. In Bronnimann P. and H.H.Renz (eds.), Proc. Of the 1st Internat. Conf. on Plank. Microfoss. Leiden:E.J.Brill, vol.1,p. 199-422

Martodjojo, S., 2003. Evolusi Cekungan Bogor, Jawa Barat. ITB Press, Bandung, 238 p.

Morley, R. J., 1999. Tertiary Stratigraphic Palynology in Southeast Asia: Current Status and New Directions. Geol. Soc. Malaysia, Bulletin 28, pp. 1-36.

Morley, R. J., 1990. Short Course Introduction to palynology with emphasis on Southeast Asia. Fakultas Biologi UNSOED, Purwokerto, 9-29.

Phleger, Fred & Parker L. Frances., 1969. Foraminifera Species, Part II, Scripps Institution of Oceanography, La Jolla, California.

Phleger, Fred & Parker L. Frances. 1951. Foraminifera Species. Part II, Scripps Institution of Oceanography. La Jolla, California.

Postuma, J.A. 1971. Manual of Planktonic Foraminifera. Elseiver Publishing Company, Amsterdam-London-New York.

Rahardjo, A.T, Polhaupessy, A.A, Wiyono, S, Nugrahaningsih, L, & Lelono, E. B. 1994. Zonasi Polen Tersier Pulau Jawa. Makalah Ikatan Ahli Geologi Indonesia, Pertemuan Ilmiah Tahunan ke, 77-84.

Sudjatmiko dan Santosa 1992. Geologi Regional Lembar Leuwidamar-Jawa (Geology of the Leuwidamar Quadrangle – Jawa). Bandung: Pusat Penelitian dan Pengembangan Geologi, Direktorat Jenderal Geologi dan Sumber Daya Mineral, Departemen Pertambangan dan Energi

Syahrulyati, Asikin, Sudrajat.D, Mudjur Muif., 1989. Perubahan Status Tatanan Stratigrafi Formasi Bojongmanik Suatu Usulan, PIT IAGI XVIII,Desember 1989,Yogyakarta.

Sribudiyani, Asikin dkk, 2003 The Collision Of The East Java Microplate And Its Implication For Hydrocarbon Occurrences In The East Java Basin. Proceedings, Indonesian Petroleum Association Twenty-Ninth Annual Convention & Exhibition

Syahrulyati, Isnaniawardhani, Rosana, Winantris,2020. Bojongmanik Formation Sedimentation Mechanism in the Middle to Late Miocene (N9-N17) in the Rangkasbitung Basin, *Scientific Contribution Oil and Gas* , 43 (3)pp.,115-123

Table 1: Differences in the Characteristics of the Bojongmanik Formation with the "Jasinga Formation"

COMPONENT	JASINGA FORMATION	BOJONGMANIK FORMATION
Lateral Spread	Blocks: Bojongmanik, Leuwidamar, Cisimeut, Muncang, Sajira, Cipanas, Jasinga, Paniis.	Blocks: Bojongmanik, Leuwidamar, Cisimeut, Muncang, Sajira, Cipanas, Jasinga, Paniis, Cigudeg, Leuwiliang
Rock Unit Name	Sandstone and Limestone Inserted Claystone Unit	Satuan Batupasir sisipan batulempung dan Batugamping
Claystone	Dominate the unit	Comes as an insert
Sandstone	Comes as an insert, not conglomerate	Dominate units, conglomerates and tufan
Batugamping	Present as an insert, in the form of alternating bioclastic limestone, crystalline limestone (predominant) and bioturbation limestone	Comes as an insert. in the form of alternating bioturbation limestone (more dominant), bioclastic limestone, and crystalline limestone

COMPONENT	JASINGA FORMATION	BOJONGMANIK FORMATION
Coal	Sometimes coal is found as fibers that enter into claystone or sandstone	Coal can be layered up to about 1.5 meters, often present as fibers that enter the sandstone
Sediment Structure	Generally parallel lamination	Generally graded bedding, cross bedding, and parallel lamination.
Age	N9 to N14 (Middle Miocene)	N9 to N17 (Middle Miocene to Late Miocene)
Depositional Environment	Outer Neritic – Middle Neritic P/B Ratio (44% - 63%) Outer Neritic	Middle Neritic – Edge Neritic – Transition. P/B Ratio (10% - 24.5%) Edge neritic – Middle neritic Based on the abundance of palinomorphs: Lower Intertidal – Lower Intertidal / Mud Flat. Delta front environment
Stratigraphic Relationship and Facies Change	Intermingled with the bottom of the Bojongmanik Formation	The lower part of the Bojongmanik Formation intermingles with the Jasinga Formation. The Bojongmanik Formation is also intertwined with the Cibulakan Formation
Planktonic Foraminifera Fossil Content	Planktonic Foraminifera: Found 31 species, from 6 Genus planktonic foraminifera consisting of: Genus *Globorotalia* (10 species).	Found 34 species from 8 genera of planktonic foraminifera consisting of: Genus *Globorotalia* (8 species) Genus *Globigerinoides* (9 species),

COMPONENT	JASINGA FORMATION	BOJONGMANIK FORMATION
	Genus *Globigerioides*, (8 species) Genus *Globoquadrina*, (5 species) Genus *Globigerina*, (4 species) Genus *Orbulina*, (3 species)Genus *Hastigerina*. (1 species) The absence of *Shpaeroidinellopsis* and *Sphaeroidinella* biostratigraphically characterizes the Jasinga Formation.	Genus *Globoquadrina* (5 species), Genus *Globigerina* (5 species), Genus *Orbulina* (2 species) Genus *Hastigerina* (2 species), Genus *Shpaeroidinellopsis* (1 species) Genus *Shaeroidinella* (1 species). The presence of Shpaeroidinellopsis and Sphaeroidinella biostratigraphically characterizes the Bojongmanik Formation.
Bentonic Foraminifera Fossil Content	Specific Bentonic Foraminifera: There are 18 Genus, 7 species. Benthonic fossils found only in the "Jasinga Formation" *Nonion incicum, Gyroidina soldani, Operculina, Lagena*	There are 19 genera, 5 species. Fossils that are only in the Bojongmanik Formation: C*amerina, Operculina cumingii, Quinquiloculina, Annomalinoides globulosus, Nodosaria*
Pollen Fossil Content	No sampling was carried out, assuming: The Jasinga Formation, which was deposited in the Outer Neritic to Middle Neritic depositional environment, is not a pollen fossil depositional environment, considering that pollen fossils originate from transitional depositional environmental conditions.	Pollen Content: Genus *Rhizopora, Sonneratia,* marker *Florschuetzia meridionalis, Avicennia, Camptostemon, Acrostichum Oncosperma, Spinizonocolpites echinatus.* Backmangrove group *Acrostichum aureum* type, *Acrostichum speciosum* type, *Canthium dicoccum* type, *Oncosperma* type,

PROCEEDINGS
JOINT CONVENTION BANDUNG (JCB) 2021
November 23rd – 25th 2021

COMPONENT	JASINGA FORMATION	BOJONGMANIK FORMATION
		Spinizonocolpites echinatus Mangrove group: *Avicennia* type, *Camptostemon* type, *Florschuetzia levipoli*, *Florschuetzia semilobata*,

COMPONENT	JASINGA FORMATION	BOJONGMANIK FORMATION
		Florschuetzia trilobata, *Zonocostites ramonae*

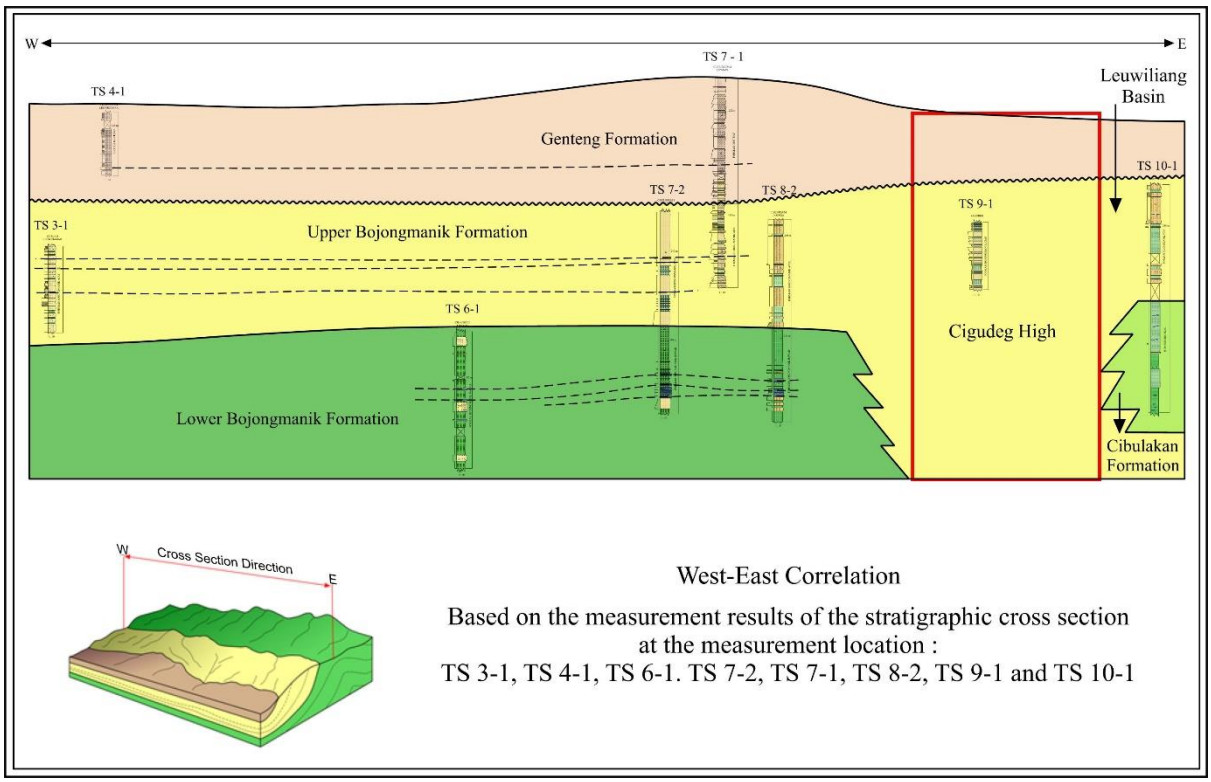

Figure 2 : West – East stratigraphic correlation.

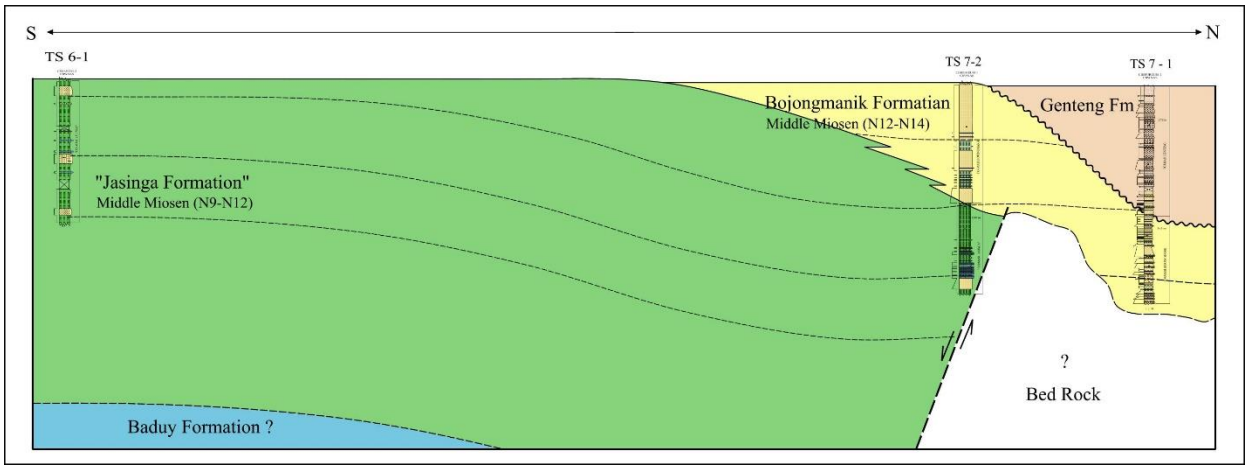

Figure 3 : North – South stratigraphic correlation The measurment stratigraphic section at location TS 6-1, TS 7-2 and TS7-1

PROCEEDINGS
JOINT CONVENTION BANDUNG (JCB) 2021
November 23rd – 25th 2021

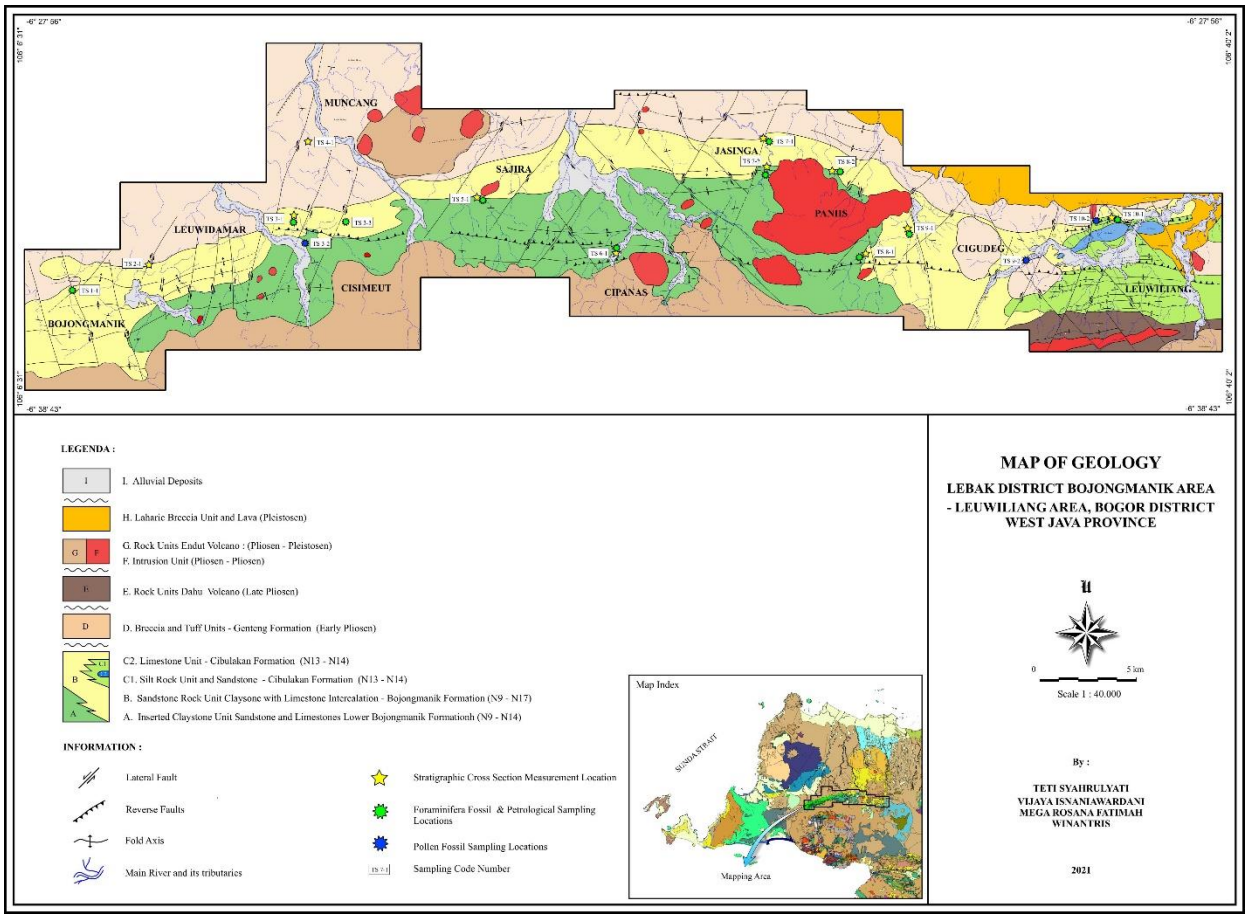

Figure 4 : Geological Map of Research Area

PROCEEDINGS
JOINT CONVENTION BANDUNG (JCB) 2021
November 23rd – 25th 2021

Thrust Fault Evidence to Determine The Structural Geology Correlation Between South Mountains of Eastern Java & Kendeng

[1]Faiz Zain Adli S.T., [1]M. Ghazali Rachman S.T, M.T , [1]Dr. Ir. Carolus Prasetyadi, M.Sc., [1]Gneis Desika Zoenir S.T.
[1]Department of Geological Engineering, Universitas Pembangunan Nasional "Veteran" Yogyakarta, Jl. SWK 104, Condongcatur, Depok, Sleman, Yogyakarta. Author's Email :afaizzain@gmail.com

Abstract

The existence of geological structures with a compression pure regime has been propagated as a model of the new Java Island structure by Robert Hall and his team in several scientific publications. The manifestation was interpreted as a regional thrust fault that affects the morphology and stratigraphic arrangement in Java Island. More specifically, based on Hall's research, et al (2007,2015) the deformation was interpreted as an old volcanic arc overthrust that moved from south to north in Western Java. In this paper, the authors try to analyze the phenomenon of overthrust fault in East Java by integrating data on surface geological structures in the Southern Mountains and Kendeng Zone. The structural data analyzed are the lineaments patter, type of geological structure, and kinematics that work in forming geological structure patterns in the two zones.

The geological structural patterns of the Kendeng Zone clearly show the fold-thrust belt structure as a tectonic manifestation of the compression regime which shows direction of stress is north-south relatively. The morphology of the hills with a relatively western - eastern direction also reinforces the presence of structure phenomena such as folds, fold-thrust fault, and thrust fault. Steep angle fold can be seen well either in the Kendeng Zone, it is supported by characteristic of constituent lithology that is ductile / plastic.

In the Southern Mountains of East Java, the east-west lineament also appears by being shown by the escarpment. Van Bemellen in the book Geology of Indonesia mentions that escarpment is the boundary between Solo Depression that moves down towards the Southern Mountain Zone. However, field data that has been collected around the escarpment shows the presence of the thrust fault (Husein, 2007). The relatively higher morphology of the Southern Mountains could also mean indications of a thrust fault

In Sampung Village, located on the border of West end of Ponorogo and east end of Wonogiri is found a contact between lapilli lithology and clastic limestone underneath. This rare stratigraphic contact is also a strong indication of the existence of an overthrust fault in the Southern Mountains of East Java that was suspected of moving an old volcanic arc northward as expected by Hall and his team in Western Java. But in the Southern Mountains is more dominated by stratigraphy with lithology brittle, so rarely found the presence of folds or hills folded.

Keywords: *Brittle, Ductile, East Java, Overthrust Fault*

Introduction

Compression Tectonic on East Java is believed to play role in architectural formation of lithology and stratigraphy. Subduction of Indo-Australian plate into Eurasian Plate formed the early volcanic arc in Southern part. Following the northward movement, compression tectonic triggered thrust fault in the Middle Miocene until the peak of event in Pliocene-Pleistocene. This event is interpreted happened in several periods Hall et.al (2007) and Clements et.al (2015). Geological Structure as manifestation of compression tectonic regime on East Java is clearly exposed on northern part. The exposed outcrops show clear its evidence in Kendeng Zone. Fold, thrust fault, and fold-thrust fault dominants in shaping the lithology and stratigraphy. In the other hands South Mountain is lack of structure evidences like found in Kendeng Zone.

The lack of structural evidence in southern part becomes question and mystery. Manifestations of compression regime structure must be formed in Southern Mountain either and can be correlated into Kendeng Zone structure though both of them have significant rock mechanic condition. East- west morphology lineaments like valley, hills, and escarpments in Southern Mountain mostly show similar lineaments like in Kendeng Zone has. These condition is inseparable from compression tectonic event that has great impact.

Either the lack outcrop evidence or specific subsurface imaging in Southern Mountain become the obstacle to see thoroughly the structural style of East java from south to north. The sustainability research must be done by collecting tight and integrated data.

This research mostly shows big similarity of compression tectonic evidence between Southern Mountain and Kendeng. The existence of thrust fault is main objective to see thoroughly the structural style on East Java even though there are many differences in field description. In Southern Mountain, the thrust fault is more "hidden" in stratigraphy. The contact between a formation to another make thrust fault evidence clearly unseen and make them seem like conformity or unconformity contact. In Kendeng Zone deformation of lithology is clearly be seen by bedding displacement and/or folded bedding. The most extreme is the rock bedding has steep angle dip.

PROCEEDINGS
JOINT CONVENTION BANDUNG (JCB) 2021
November 23rd – 25th 2021

Data and Method

This research mostly did by geological fieldwork, mapping, sampling and directly measurements. Laboratory analysis is done as supporting such as paleontology for age determination of formation and petrography observation.

Initial study and preparation is done by reviewing previous research and observe the location geomorphology by DEM. Lithology mapping, stratigraphy contact observation, structural geology measurements, and rock sampling are main methods and later the result of each works will be integrated.

Kind of Stratigraphy contact from field observation and geological structure data such as bedding plane inclination, joints, fractures, and faults are key data for interpreting and concluding the possibilities correlation in research area.

Regional Structural Trends & Stratigraphy

This study is taken at two locations; first location is atPohijo Village, Sampung Sub-Districts, Ponorogo District, as representative of Southern Mountain and at Panjeng Village, Gondang Sub-Districs, Bojonegoro District as representative of Kendeng Zone. Both of these locations are on East Java . (Fig.1). Structural trends on Java Island can be divided into four trends; Sumatera trend (northwest – southeast), Meratus trend (northeast – southwest), Java trend (east – west) and Sunda Trend (north – south), Satyana (2004)

Southern Mountain's formation shortly divided into three synthems (Smyth, Hall, Nichols, 2007). The term synthem, defined as an unconformity-bounded stratigraphic package (Rawson et al., 2001 in Smyth, Hall, Nichols, 2007). The three syntems; Synthem One: records the initiation of arc volcanism and the early stages of arc development during the middle Eocene (ca. 45 Ma) to early Oligocene (ca. 34–28 Ma), Synthem Two: records the growth and termination of arc volcanism in the Southern Mountains Arc during the late Oligocene (ca. 28–23 Ma) to the early Miocene (ca. 20 Ma), and Synthem Three: records widespread carbonate growth, accompanied by the erosion and redeposition of rocks from earlier synthems during the middle Miocene (ca. 20 – 10 Ma), with no significant volcanic activity. The explanation about the synthems about can be seen clearly in the stratigraphy succession of Southern Mountain. Yogyakarta and Pacitan can be the good place that record the succession consistently (Smyth, Hall, Nichols, 2007). (Fig.2)

Pelang Formation is the oldest stratigraphic unit found in Kendeng Zone which consist of marl and alternating thin laminae of calcareous sand. In the Middle – Late Miocene there is Kerek Fm consisting of volcanic rich medium to fine-grained sandstone bed alternating with silt and shale that shows a widespread thick deep-sea depositional system. Lie on the Kerek Fm, the Kalibeng Fm is deposited with a dominant marl and shale deposition on the top section with intercalated limestone of Kapung and Klitik Member, Pulunggono & Sukido (1992), Septama, et al (2021). (Fig.2)

Result and Discussion

Sampung Area

Sampung Village located around 25 km to southeast from Mt Lawu. The uniqueness of this location is geomorphological is isolated hills but consist of Tertiary Formations while the plains are filled by Quaternary volcanic rock and sediment. These Tertiary Formations are rock formations that composed Southern Mountain which is located 20 km to south from this location. There is not much previous research explained about this location but Geological Map of Ponorogo Quadrangle by Sampurno & Samodra (1997).

Based on field work this locations consist of volcanic rock such as ignimbrite, pyroclastic flow with gradded bedding structure, and volcanic breccia which they are proximal volcanic facies. They are called Dayakan Fm aged Oligocene-Middle Miocene as the oldest one. Unconformably, lie on this formation are reef limestone, interbedded grainstone, insertion of calcareous sandstone and insertion of calcareous claystone. N14 – N15 (Middle-Late Miocene) is age of this formation and called Sampung Formation. The last is volcanic rocks unit that overlies on Sampung Fm that consists of massive lapilli and intercalation of tuff. It called as Cendono Fm and aged Middle Miocene-Pleistocene. There are two lithodems intruded and it is interpreted as Oligocene-Early Miocene andecite & dacite.

Cendono Fm is unexpected we found overlies on Sampung Fm. There is no equal formation found in Southern Mountain that consists of volcanic rock contact above Miocene limestone formation . Moreover Cendono Fm found on the top of the hill and presumably older than Sampung Fm by Sampurno & Samodra.

.

Kendeng Zone

In this location Kalibeng Fm consists of marl with insertion of calcareous sandstone and calcareous claystone aged N17-N19 (Mid Miocene – Early Pliocene). Volcanic breccia, sandstone, and calcareous tuffacious sandstone found as part of Kalibeng Fm or called as Atas Angin Member. Conformably lies on Kalibeng Fm is Klitik Fm aged N20-N21 (Late Pliocene) which composed by clastic limestone and interbedded calcareous sandstone.

Thrust Fault Evidence

The inconsistency stratigraphy between Sampung Fm and Cendono Fm we suggest as thrust fault contact. This problem cannot be explained by sedimentology concept. Cendono Fm can be equalized by Semilir Fm that exists in Southern Mountain based on lithology characteristics and the time forming. Older rock formation cannot be overlaid on younger rock formation except it is formed by thrust fault

(Fossen,2010). This rock formation contacts shows strike N300E /20 in south part while other bedding plane shows N115E /15 in north part this contact. Two low angle of bedding plane who have same strike direction plus form low angle syncline. A thin layer of breccia that consists of random fragment such as limestone, lithic, and tuff fragment found separates these two formation rocks. This thin layer is strong considered as fault breccia but need microscopic observation. (Fig.3)

In Kendeng Zone thrust fault outcrops easily be seen. The thrust fault also followed by folded rock bedding (fold-thrust fault) from meso to macro scale. Anticline and syncline structure also found in this location. Dip of rock bedding varies, from 32^0 -85^0 . Rock mechanic properties support the forming this kind of structure as compression regime tectonic evidence (Fig.3). Kendeng that consists of very fine to mud grain sedimentary rock is dominant ductile or elastic rock mechanic properties.

Southern Mountain & Kendeng Zone Structural Geology Correlation

Compression regime evidences such as Fold, fold-thrust fault, and thrust fault can be seen well on Kendeng Zone, in other hand this phenomena can be revealed by observing the stratigraphy relations on Southern Mountain. Hypothesis about thrust fault on Southern Mountain interpreted by Hall (2007) and Clements (2015). Furthermore they interpreted the existence of overthrust fault on Southern part that move Oligo-Miocene volcanic arc to north. Husein (2007) also interpreted the creation of the Southern Mountain geomorphology by uplifting.

Inconsistency between Sampung Fm and Cendono Fm we suggest as thrust fault evidence that explained by Hall & Clements before. Sampung village is included in Solo Depression Zone formed isolated hill. The plains around this hill is filled by Quaternary volcanic or sediment deposit. We interpret Sampung isolated hills are part of Southern Mountain. Erosion in million years remained resistance part as hill morphology and depression morphology as gap between Southern Mountain and Sampung Village that filled by quaternary sediment or volcanic sediment. Supported by reversal stratigraphy, this isolated hills are remain of thrust fault body either consider the distance from Sampung Village to the south, this thrust fault called overthrust fault. Probably this is overthrust fault that moved the Oligo-Miocene volcanic arc. Isolated hills at Sampung Village can be called as *klippe* because it is the remain of the overthrus fault from Southern Mountain while the depression morphology between Southern Mountain and Sampung Village is *window* that covered by Quaternarry Sediment.

Uplifting or thrust fault event in Southern Mountain itself interpreted happened in several phases but still unrevealed the exact number Husein (2007), Hall (2007), & Clements (2015).

Consider the overthrust fault existence in southern part and thrust faults in Kendeng Zone, we suggest East Java have structural style that can be correlated thoroughly (Fig.4). Either Surface condition like geomorphology or subsurface is formed by overthrust fault and other compression regime tectonics manifestation. Rock mechanic properties influenced the difference kind of thrust fault in Southern Mountain and Kendeng Zone. Southern Mountain mostly consists of brittle rock formed from volcanic activity or reef building. This brittle rock formation yielded low angle thrust fault that moved rock formation long distance. This kind of rock mechanic properties cannot create fold or fold thrust structure. Contradiction with Southern Mountain, Kendeng Zone mostly consists of ductile rock formations. These rock formations composed by very fine to mud grain sediment material that transported from a high to a basin.

The paleostress after Miocene in Southern Mountain and Kendeng have same trend. North – south trend N of stress in Plio-Pleistocene found in both of them. This data is collected by structure such as fault and fractures that cut Miocene rock in both locations. The thrust fault strike in both location have same direction, east – west trend apparently.

Conclusions

1. Reversal Stratigraphy order between Cendono Fm and Sampung Fm shows thrust fault contact. It's supported by the strike/dip contact and thin layer breccia separated them.
2. The thrust fault in Sampung Village consider as overthrust fault moved from Southern Mountain and eroded which remains isolated hill or *klippe*
3. Thrust fault evidence in Southern Mountain and Kendeng Zone can be united to see East Java geological condition thoroughly on surface or under surface.

We suggest to do advance and continuous research by integration method and collecting detail data.

References

Clements, Hall, Smyth & Cottam,2015,Petroleum Geoscience,**15**, 159-174

Erlangga, et al, 2021.IPA,**55,**-

Fossen, H. 2010, *Structural Geology*, Cambridge University Press, New York, U.S.A., . 152,156, 312, 313, 334, 356, 363

Hall,Clements,Smyth, & Cottam,2007,IPA,**31**, -

Husein & Srijono, 2007, Tinjauan Geomorfologi Pegunungan Selatan DIY/Jawa Tengah: telaah peran faktor endogenik dan eksogenik dalam proses pembentukan ,-,-,-

Pringgoprawiro, H. Dan Sukido, 1992. Geologi Lembar Bojonegoro, Jawa. Pusat Penelitian dan Pengembangan Geologi, Bandung, Indonesia: 1-11.

Sampurno, Samoedra, H.,1997, Peta Geologi Lembar Ponorogo, Jawa, P3G

PROCEEDINGS
JOINT CONVENTION BANDUNG (JCB) 2021
November 23rd – 25th 2021
Satyana, Erwanto, Prasetyadi, 2004 PIT IAGI, **33**, 1-23

Acknowledgements (Optional)

The author thanks to local community of Sampung Village for assisting the field work either local community of Pajeng to be guider in the field.

PROCEEDINGS
JOINT CONVENTION BANDUNG (JCB) 2021
November 23rd – 25th 2021

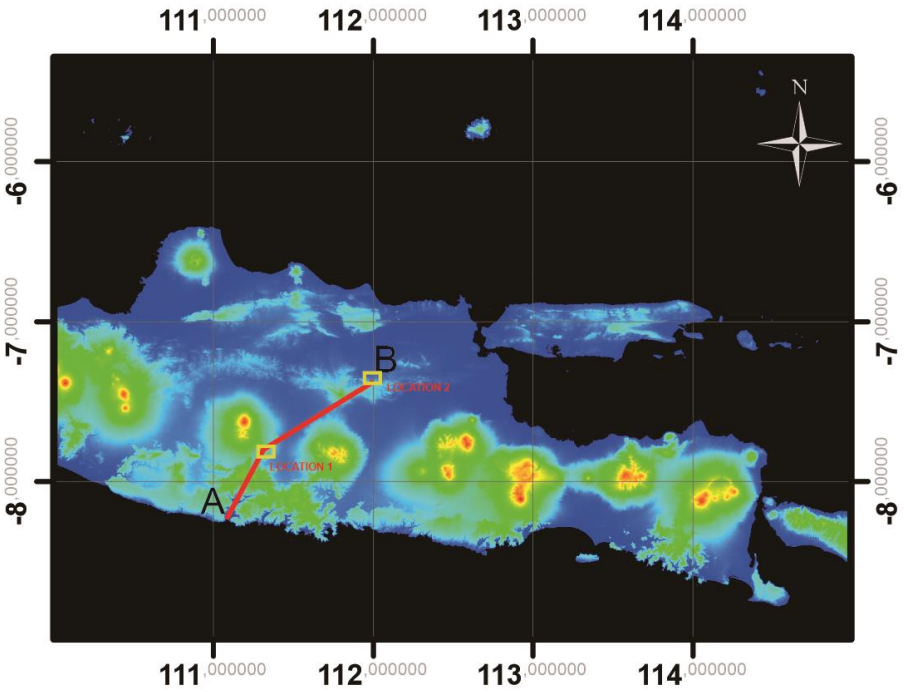

Fig.1. Location and section line of research using SRTM

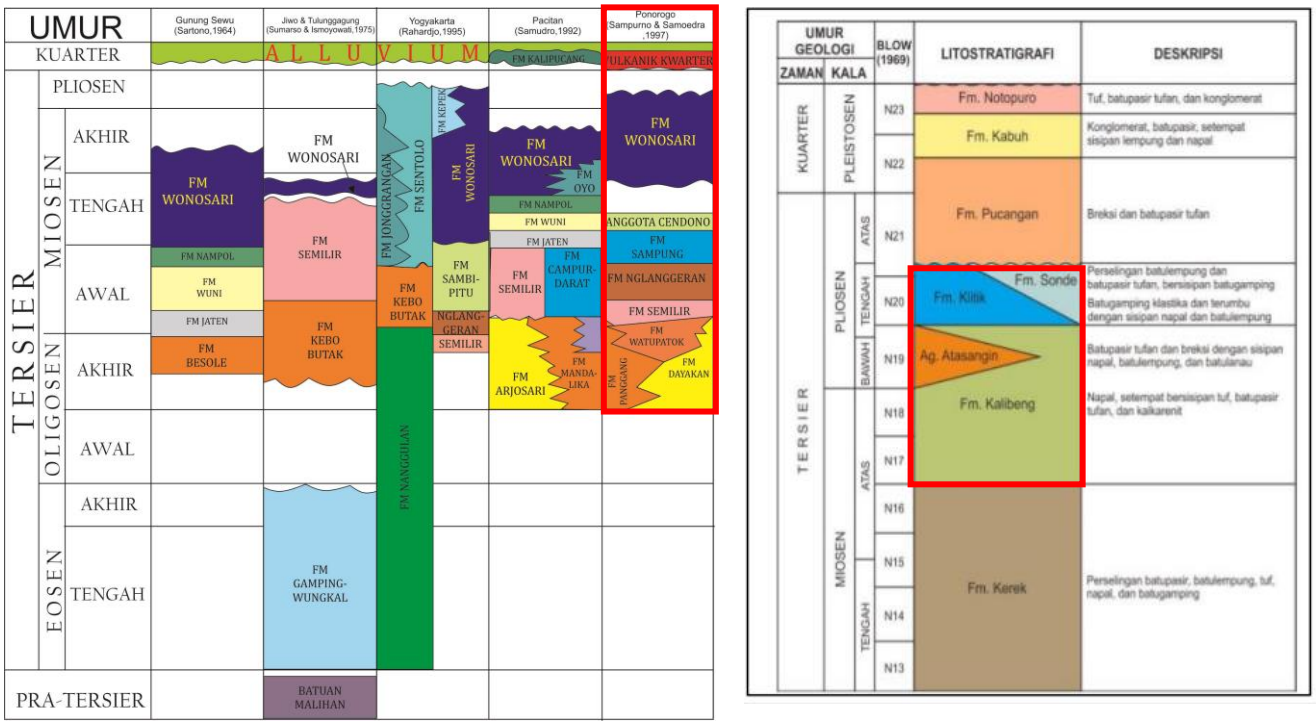

Fig.2. Left : Southern Mountain regional stratigraphy from various sources and redraw by writer. Right : Regional Stratigraphy of Kendeng Zone (red frame is research location regional stratigraphy)

PROCEEDINGS
JOINT CONVENTION BANDUNG (JCB) 2021
November 23rd – 25th 2021

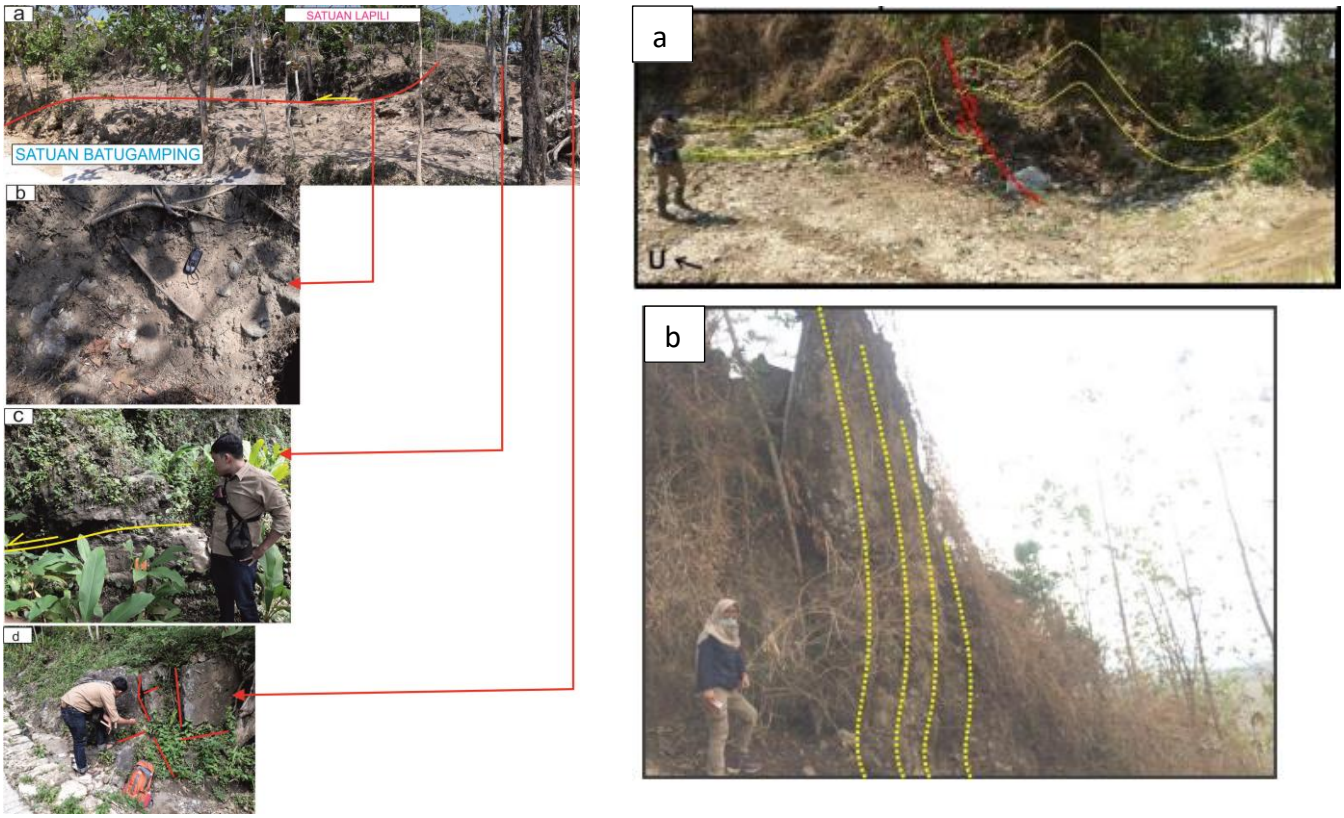

Fig.3. Left : Thrust fault evidence of Sampung Village, represents Southern Mountain thrus fault.that is shown by reversal stratigraphy Right : a) thrust fault evidence of Kendeng Zone, showing fold thrust faults, b) compression tectonics formed steep angle rock bedding.

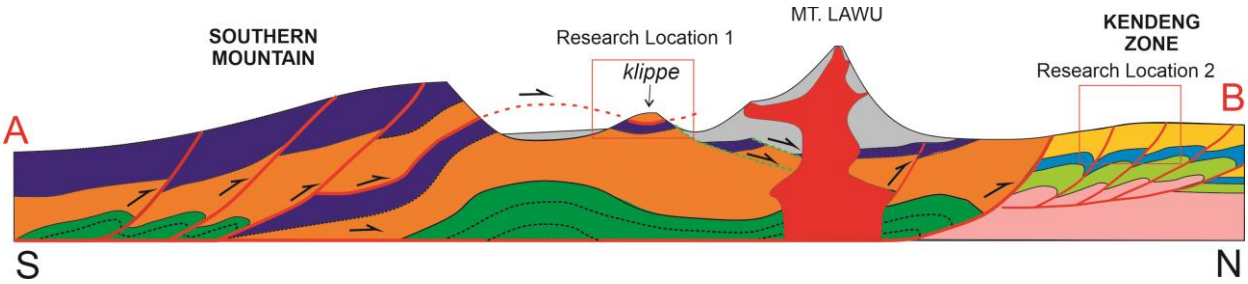

Fig.4. Interpretive model of structural geology correlation between Southern Mountain & Kendeng, East Java

PROCEEDINGS
JOINT CONVENTION BANDUNG (JCB) 2021
November 23rd – 25th 2021

New Concept of Field Development & Enhanced Gas Recovery Using Bioaugmentation Technology in Coalbed Methane Field

Gathuk Widiyanto[1], Byan Muslim Pratama[2], Dahrul Effendi[3], Irawan Sugoro[4]
[1]Pertamina, [2]Lemigas, [3]Tanri Abeng University, [4]BATAN

Abstract
Alternative gas resources to anticipate the national energy crisis is Coalbed Methane. With total reserves throughout Indonesia reaching 453 Tcf, it is a distinct advantage to be able to develop this potential.
Exploration studies that have been conducted since 2003 have not been successful. Technological engineering to increase methane gas production has been carried out, both fracturing and radial jetting methods, but the results are not satisfactory. This is influenced by the characteristics of CBM in Indonesia which is different from the characteristics of CBM in the USA where in terms of maturity, thickness, gas content and brittleness factor and the quality of CBM in Indonesia is still below the USA, it is supported by concessions that still use conventional oil and gas techniques, so that field development using conventional methods will not economical.
Therefore, there is a need for breakthroughs and new concepts to exploit gas from coal. One of the results of research that has been successfully developed is bioaugmentation technology using indigenous methanogenic bacteria. This technology has been tested in the Tanjung CBM field, South Kalimantan by injecting 15000 liters of methanogen or *rumen* fluid into the well in 2 stages, namely 7000 liters and 8000 liters. This effort succeeded in increasing the pressure from an initial 3 psi on 18 December 2017 to 20 psi on the 40th day at the wellhead, indicating that gas was being produced. The results of the post-injection rumen composition test showed that methane gas was still low ranging from 14-15.6%, CO2 content was between 7-7.5% and N2 gas content was still quite high reaching 78%, but it is expected that the N2 content will decrease along with the increase in methane gas content.
The concept of development by injecting liquid methanogen indigenous bacteria using this bioaugmentation technique is proven to increase the recovery of coal methane gas and can be applied for further field development.

Key Word : New Concept Development, Coal Bed Methane, Bioaugmentation, Production Increase

Introduction

Many methods have been applied to produce methane gas in Indonesia, especially in the Tanjung II CBM field. These efforts include hydraulic fracturing and radial jet drilling. The application of radial jet drilling and hydraullic fracturing methods at CBM wells in Indonesia has not been able to increase production. In the WK GMB PHE Metan Tanjung II South Kalimantan, the gas production data from the source of Coal Methane Gas WK (GMB) is still very small, ranging from 0.3 - 0.5 Mscfd per well. Therefore, it is necessary to approach other stimulation methods according to the characteristics of the CBM reservoir. The method is bioaugmentation technology using bacteria

Methane gas can be produced by utilizing indigeneous methanogen microbes such as research in the coal mine area in Indiana - Texas against microorganisms that play a role in the formation of methane gas (Strapoc et al., 2008). Biostimulation is the process of stimulating indigenous microorganism populations of coal by adding nutrients to the reservoir. This method is used to reactivate CBM reservoirs which have decreased production or have not produced. To find out the types of nutrients needed, it is necessary to know the types of indigenous coal microorganisms and reservoir environmental conditions (Jones et al., 2010). Bioaugmentation is the process of inoculating a consortium of microorganisms into a coal reservoir that is already inactive. The application has been carried out in the US and Germany. Addition of microorganisms to formation water to enrich the content of microorganisms in formation water which will later be put back into production wells (Michael, 2008).

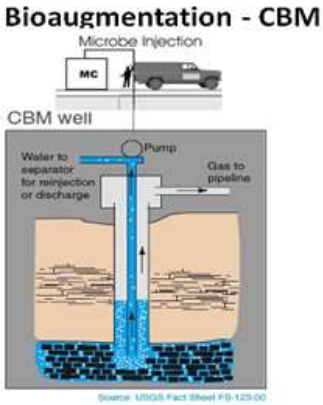

Figure 1. Bioaugmentation Diagram in CBM Well

Data and Method

This study aims to increase methane gas production in CBM wells that are no longer in production (non-productive CBM wells) by utilizing the rumen fluid formula (Bioaugmentation), and gain an understanding of the influence of microbial indigenous (rumen) methane on the formation of methane gas in coal. This pilot project was carried out at TJ-X CBM Y well.

Figure.2. TJ-X CBM-Y Well of CBM Tanjung Field

<u>Production Baseline</u>

Currently, of the 5 GMB wells in Tanjung II Field, only 2 wells are producing, namely TJ-X-CBM-Y wells and TJ-X-CBM-Z wells. The average gas production of TJ-X-CBM-Y wells is 0.23 mscfd and TJ-X-CBM-Z is 0.36 mscfd, while the production of TJ-X-CBM-Y water is 1.25 bwpd at casing pressure 47 psi and TJ-2-CBM-002P amounted to 3.55 bwpd at 10 psi casing pressure.

Table 1. Production of TJ-X-CBM-Y Well and Water Gas

NO	BULAN	KUMULATIF PRODUKSI GAS (MSCFD)	KUMULATIF PRODUKSI AIR (BBL)
1	April-2015	0	316,58
2	Mei-2015	11	73,51
3	Juni-2015	12,84	34,93
4	Juli-2015	7,32	37,25
5	Agustus-2015	6,04	21,37
6	September-2015	4,36	19,49
7	Oktober-2015	6,13	24,88
8	November-2015	6,1	7,80
9	Desember-2015	7,05	38,83
10	Januari-2016	6,48	32,07
11	Februari-2016	4,43	26,91
12	Maret-2016	7,17	44,50
13	April-2016	6,05	40,16
14	Mei-2016	6,06	26,37
15	Juni-2016	4,32	25
16	Juli-2016	5,89	12,5
17	Agustus-2016	2,81	6,25
18	September-2016	0	0
19	Oktober-2016	0	0
20	November-2016	0	0
	Total	104,0	788,40

The activity was carried out by injecting the rumen fluid formula into the test well as much as 14000 liters

In summary, it can be described as follows:

1. . Ensuring microbial population or quality and sufficient volume for injection.
2. Measuring water level in the casing column (annulus) using a sonologist tool to determine the volume of empty space above the fluid level.
3. Perform the injection process by adhering to the Work Procedure or Injection Work Instructions.
4. Injection of rumen fluid must be carried out under formation fracture pressure, to determine the injection pressure (rule of thumb) = 80% of formation fracture pressure (fracture gradient 0.81 ft / psi asi formation fracture pressure 1057 psi at perforation depth. Maximum pumping pressure on the surface is 80% x 1057 psi - 565.5 psi = 280.1 psi).
5. The resistance of rumen bacteria to pressure based on the results of laboratory testing to date is 700 psi, so injection pressure considers this pressure factor.
6. Injection of Nitrogen gas (N2) to push the rumen liquid into the deeper coal seam layer.

Result and Discussion

To analyze the success of this biostimulation pilot and to determine the performance of bacteria, monitoring was carried out during the work by making observations for wellhead pressure, liquid level, BHP, gas composition especially the increase in methane and decrease in CO2 and nitrogen as well as the increase in microbial population which indicated that the bacteria survived and worked.

Well Head Pressure

Based on observations of WHP since post injection of rumen.

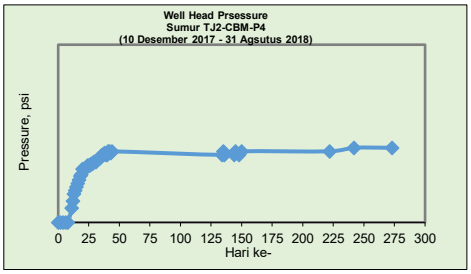

Figure 4. Well head pressure data curve Period-1 TJ-X-CBM-Y well

In the first week the curve still looks zero. On the second week precisely on the 11th day the curve starts to rise slowly at 4 psi. The increase in pressure occurs due to gas production because of microbial activity in the test wells. This condition is like the mini-scale scale laboratory research, where the pressure starts to rise in the second week of the incubation period. The pressure rises slowly until it reaches 19-20 psi in about one month of the incubation period. This position lasts up to 273 days of the incubation period.

Liquid Level

In pre-injection N_2, WHP was 21 psi, surface water, FL 57.63 meters, BHP 573.20 psi. In FL a decline of 57.13 m, where at the beginning of the post rumen injection, the fluid level of 0.5 m changed to 57.63 m. Whereas in BHP there was a pressure increase of 164.02 psi, which was originally at 409.18 psi to 573.20 psi (See Table 3).

This indicates that gas production has occurred, in which the gas produced has accumulated in the tubing / annulus, which in turn the gas will push the fluid level down the well. The data shows that when the gas accumulates it will increase the pressure at the wellhead while at the same time pressing the water level down to the well. When the water level is pushed down the well, it will increase the pressure on the bottom hole of the well.

Table 3. Data on measurement of Sonolog TJ-X-CBM-Y Wells

Analisa	2017	2018				
	Awal pasca injeksi FCR	Monitoring ke-1	Monitoring ke-2	Monitoring Transisi 2 ke 3		Monitoring ke-3
	(10 Desember 2017)	(31 Agustus 2018)	(18 September 2018)	(27 September 2018)	(08 Oktober 2018)	(16 Oktober 2018)
Sonolog:						
- Fluid Level (FL)	0.5 m					
- FL Pra injeksi N2		57,63 m = 189,76 ft	66,01 m			59,59 m (Pra Injeksi N2)
- FL pasca injeksi N2		85,50 m = 280,55 ft				75,89 m (Pasca injeksi N2)
- Bottom Hole Pressure	409,18 psi	573,20 psi	432,10 psi			507,87 psi (Pra injeksi N2)
						490,40 psi (Pasca injeksi N2)
- Well head pressure	0 psig	21 psig	4 psig	4 psig	0 psig	0 psig

The decrease and increase in FL, BHP, and WHP indicates that microbial activity occurs even though it is not optimal, this is made possible by insufficient time for microbes to produce gas as a result of gas release / bleed off in the test wells.

Gas Composition

Based on data obtained from the monitoring activity, there was an increase in the percentage of Methane gas which was very significant, which was originally 15.626% to 90.639%. Whereas the Nitrogen and Ethane occur on the contrary there is a decrease, namely the original 76.841% and 0.002% to 9.355% and 0.005%.

Whereas the CO2 gas which was originally 7.532% became NIL (Table-4).

Table-4. Data of TJ-X-CBM-Y Well gas composition

Analisa	2017	2018				
	Awal pasca injeksi FCR	Monitoring ke-1	Monitoring ke-2	Monitoring Transisi 2 ke 3		Monitoring ke-3
	(10 Desember 2017)	(31 Agustus 2018)	(18 September 2018)	(27 September 2018)	(08 Oktober 2018)	(16 Oktober 2018)
Komposisi gas:	(%)	(%)	(%)	(%)	(%)	(%)
- Methane	15,626	90,639	22,836	24,259	**	23,295
- Ethane	0,002	0,005	0,002	0,001	**	0,001
- Nitrogen	76,841	9,355	76,201	74,061	**	74,315
- CO2	7,532	NIL	0,962	1,679	**	1,629

Keterangan : ** Tidak ada tekanan di kepala sumur

The high percentage of Nitrogen is also likely to be affected by the remaining Nitrogen, which at the time of monitoring is sampling fluid from the test well by injecting nitrogen into the test well. Laboratory data shows that rumen microbes begin with low production of Methane gas and high Nitrogen gas and are followed by CO2. Then with time, gradually the production of Methane gas will increase and conversely the production of Nitrogen will decrease. Nitrogen and CO2 will be reduced by rumen microbes to Methane and as a microbial energy source.

Microbial Population

Observation of microbial activity injected into the test well starts from the beginning after the microbial injection of rumen Phase 2, Monitoring I, and Monitoring III. In monitoring II microbial analysis was not carried out because liquid sampling was not carried out on the test well tubing. Activity of sampling liquid from the tubing of the test well by injecting N2 through annulus. If the N2 injection activity is carried out in close proximity it is feared that it will disrupt microbial activity in producing gas. Overall microbial observations can be seen in Table-5.

Table-5. Analysis data of Total TJ-X-CBM-Y Well Microbial Population

Analisa	2017	2018		
	Awal pasca injeksi FCR	Monitoring ke-1	Monitoring ke-2	Monitoring ke-3
	(10 Desember 2017)	(31 Agustus 2018)	(18 September 2018)	(16 Oktober 2018)
Total Populasi Mikroba :				
- Tangki	$8,40 \times 10^{9}$ cfu/ml	$8,20 \times 10^{8}$ cfu/ml		
- Tubing	$1,07 \times 10^{7}$ cfu/ml	$2,90 \times 10^{7}$ cfu/ml	*	$5,10 \times 10^{6}$ cfu/ml
	$2,62 \times 10^{7}$ cfu/ml	$3,10 \times 10^{7}$ cfu/ml	*	$5,30 \times 10^{6}$ cfu/ml
	$3,02 \times 10^{7}$ cfu/ml	$3,80 \times 10^{7}$ cfu/ml	*	$7,90 \times 10^{6}$ cfu/ml
			*	$2,40 \times 10^{7}$ cfu/ml
Semakin dalam			*	$3,10 \times 10^{7}$ cfu/ml

Keterangan: * tidak dilakukan analisa

The total microbial population in the tank has decreased density, which after the initial rumen injection, the TPM value of 8,40 x 109 cfu / ml dropped to 8,20 x 108 cfu / ml at the time of Monitoring I. It is likely that this happened because non-utilization of produced gas by microbes becomes an energy source. Because the tap on the tank was accidentally opened to avoid the danger of over pressure.

In the initial monitoring after the Phase 2 rumen injection, it showed a decrease in microbial density from initially 8,40 x 109 cfu / ml (in the tank) to 1.07 x 107 cfu / ml up to 3.02 x 107 cfu / ml (in the test well) This indicates there has been dilution in rumen liquid when mixed with formation water in the test well.

Microbial activity shows the same curve pattern in each monitoring. The total microbial population value shows not many significant changes, but still shows changes in density. The deeper the microbial position, the higher the microbial population value (Figure 5).

Each curve in the figure above shows microbial activity while inside the test well. The Monitoring Curve I show a higher value compared to the other 2 curves. This is due to the longer microbial incubation time of the Monitoring curve I compared to the other 2 curves.

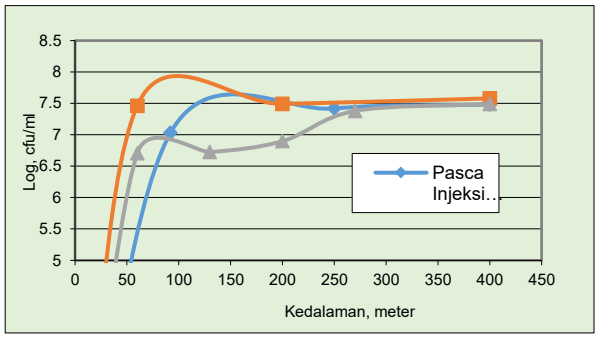

Figure 6. Total TJ-X-CBM-Y Microbial Well Total Curve

Whereas in the Monitoring III curve the TPM value is the lowest compared to the other 2 curves. This is due to the influence of sampling rumen fluids from the test wells at the Monitoring I time and also the relatively short incubation time. Taking the rumen liquid sampling results in the release of gas from the tubing to the well surface, so that microbes cannot utilize the gas needed as an energy source for microbial reproduction. A relatively short time is not enough for microbes to produce and reproduce as expected.

These curves describe microbes taken from the tubing of the test wells. These microbes are in living conditions even though they are far from coal seam sources. The deeper the microbial position, the greater the population level. So that it can be estimated for microbes that are near or in the seam seam of the coal, the greater the chance for life because coal seam can be used as a source of nutrition by microbial rumen fluids.

Conclusions

The pilot project for the utilization of rumen fluid has been successful in producing methane gas in non-productive TJ-X-CBM-Y wells in Tanjung Metan II Field, PHE, South Kalimantan.

Rumen fluid injection is carried out in two stages with a total volume of approximately 14,000 liters.

Dilution occurs in the microbial formula rumen population when mixed with formation water. rumen microbes turned out to be adaptable in reservoir conditions in TJ-X-CBM-Y wells. A coal is utilized by the microbes of rumen fluid as a source of nutrition so that microbes can reproduce and produce gas.

Increased pressure on the well head indicates that microbes are on the move and producing gas. The microbial rumen liquid at the beginning of gas production produces a very dominant Nitrogen composition. Then with the passage of time the composition of Methane becomes dominant compared to other gas compositions.

Gas production in the test wells began on the 11th day of the incubation period after injection of rumen fluid which was indicated by the gradual increase in pressure in the TJ-

X-CBM-Y well to 20 psi on the 44th day of the incubation period. The rumen injection method needs to be retested on CBM wells which are ideal for studies that have been fracturing or radially jetting, and the condition of the well pump is still active.

The bioaugmentation method is proven to be applicable to enhance gas recovery in CBM wells. This method is worthy of consideration as a new concept for developing CBM fields by conducting massive trials in many wells.

.

References

Beckmann *et al*., 2011. Acetogens and acetoclastic methanosarcinales govern methane formation in abandoned coal mines. Appl. Environ. Microbiol. 77:3749–3756

.

Campbell, J. 1983. Biomass Catalysts and Liquid Fuals. Holt Rainheart and Winston ltd, Pensylvania.

De Odarza, M. B. 2000. Rumen Microbiology. *http://www.milkproductioncom/Library/Authors/marybeth_deondarza.html*.13-08-2009. Pukul 15.02.

Fry, L.J., 1973, Methane Digesters for Fuel Gas and Fertilizer, The New Alchemy Institute, Massachusetts, 8th Printing. http:journeytoforever.org/biofuel library/MethaneDigester/MD1.html. 16-05-2009. Pukul 15.17

Hungate, R.E. 1966. The Rumen and Its Microbes. Academic Press : New York.

Jones et al., 2010. Simulation of Methane Generation from Nonproductive Coal by Addition of Nutrients or a Microbial Consortium. Applied and Environmental Microbiology. 76(21): 7013-7022.

Strapoc, et. al., 2008. Methanogenic microbial degradation of organic matter in indiana coal beds. Methane-producing microbial community in a coal bed of the Illinois Basin: Journal of Applied and Environmental Microbiology, v. 74, p. 2424– 2432.

Acknowledgements (Optional)

We would like to thank all those involved in this activity, especially to GM PHE Metan Tanjung II and staff for allowing rumen trials in the CBM Tanjung field, also to the management of UTC Pertamina and Lemigas for supporting on this excellent collaboration.

PROCEEDINGS
JOINT CONVENTION BANDUNG (JCB)|2021
November 23rd – 25th 2021

THERMOGENIC AND BIOGENIC SHALLOW GAS POTENTIAL IN ONSHORE NORTHWEST JAVA BASIN; CASE STUDY AND FUTURE DEVELOPMENT

Mualimin[1] , Ibnu Suhartanto[1], Aji Rahmat Ginanjar[2], Farid Hosni[2], Suryana[2] .
1. Pertamina Hulu Energi 2. Pertamina EP

Abstract

In 2030, Indonesian government targeting one-million-barrel oil per day and twelve billion standard cubic feet (bscf) perday. In order to reach the goal, comprehensive GGR study is needed both to find new hydrocarbon discovery or to maximize existing discovery. One of the future contributions to reach the government target in gas production is shallow gas target in Onshore North West Java Basin (NWJB), that produce from Cisubuh Formation. Cisubuh Formation is widely deposited on both onshore and offshore North West Java Basin. Many references characterized this formation purely as the youngest formation that deposited in North West Java Basin and act as regional seal in petroleum system. Because of that many oil and gas exploration and development plan did not include Cisubuh Formation as a reservoir target, those resulting in poor data in this Formation including log and core data. This study unlocks the hidden potential of Cisubuh Formation as a good reservoir that produce hydrocarbon.

The objective of this study is to understand the depositional setting and facies of Cisubuh Formation and maximizing the seismic data to find the correlation between avo analysis and shallow gas Cisubuh reservoir, and in the end is the upside potential area for hydrocarbon exploration and development of shallow gas Cisubuh Formation. The methods that used in this study are sequence stratigraphy analysis, seismic facies analysis, gas chromatography analysis, and AVO analysis.

The result from sequence stratigraphy and seismic facies analysis show that Cisubuh formation can be divided into three part, the lower part consists of intercalation of sand and shale, middle part consists of massive shale and build up limestone in certain area and the upper part consist of deep marine sandstone and shale and quaternary volcanic facies. From AVO analysis, gas sand in this study area classified as class I, with positive peak amplitude and dimming at mid angle. From gas chromatography analysis, thermogenic gas is found in lower part of Cisubuh Formation, and biogenic gas is found in upper part of Cisubuh Formation. Comprehensive analysis from this study resulting on the distribution map of thermogenic gas in Randegan, Jatibarang and Surrounding area and proposed two upside potential area that have a good potential to produce shallow gas from Cisubuh Formation. While the biogenic gas from seismic anomaly is distributed widely in offshore North West Java Basin in the form of gas pocket.

Massive study of Cisubuh Formation will help for future development of shallow gas exploration in North west Java Basin, currently gas from Cisubuh Formation only produced from thermogenic gas in lower part of Cisubuh Formation, the biogenic gas from upper part Cisubuh Formation also have a great potential to produce shallow gas.

Keywords: AVO analysis, Cisubuh, Onshore North West Java Basin, Shallow Gas

PROCEEDINGS
JOINT CONVENTION BANDUNG (JCB)|2021
November 23rd – 25th 2021

Introduction

Government target of oil and gas production in 2030 must be supported, to reach 1 million bopd and 12 bscf per day we must maintain current production and find new source of oil and gas through conventional and unconventional way. One of the futures of gas production is maximizing from shallow gas target. In Mahakam area ther is Tunu shallow gas zone that produce huge gas from shallow zone, in Sumatera basin there is Air Benakat Formation that have big potential in shallow zone. North west Java basin also have potential in shallow gas production from Cisubuh Formation.

Cisubuh formation is the youngest formation in stratigraphic chart of North West Java Basin, the age is ranged from late Miocene to Pleistocene. Not much research has been done in case of hydrocarbon potential of Cisubuh Formation, because many authors refer this formation purely as regional seal. Although recent study indicate that Cisubuh Formation have a great hydrocarbon potential and not only just as seal, but also good reservoir.

There are many problems in the study of Cisubuh Formation, the main problem is the inheritance idea in every geologist mind that stating Cisubuh formation is a seal formation and not a reservoir.That problem led to another problem such as not many data taken from this formation, many wells did not have wireline logging in this interval, no core data, and no advance wireline logging in this interval.

This study will reveal a hydrocarbon potential from Cisubuh Formation, with hope that in the future the stake holder will know that Cisubuh Formation have a great potential in producing hydrocarbon and led to massive data acquisition in Cisubuh Formation that will help in future comprehensive study in Shallow gas Potential in Onshore North West Java Basin.

Data and Method

The biggest problem to understand Cisubuh potential is lacking drilling data from well log, fmi, core data and others. In order to compensate lacking those data, comprehensive interpretation is needed, those include analysis of:

- Facies and depositional environment from well log data and well report.
- Seismic Facies interpretation from seismic data.
- Seismic interpretation
- Advance seismic analysis with AVO analysis
- Petroleum system analysis.

Well log data and well report data is used to determine sequence stratigraphy analysis of Cisubuh formation, depositional environment, and reservoir characterization in each facies. Seismic data is used to determine seismic facies, building time and depth structure map and attributes map. Individual seismic facies units are produced based on reflection configuration, continuity, amplitude and frequency contents. Seismic facies unit can cross-depositional sequence boundaries. The sequence boundary often reflects sudden shift in the facies distribution. Seismic facies unit also can determine depositional environment with consideration of several factors, such as internal reflection organization, boundary relationships, external geometry and lateral facies relationship.

Integration of well log analysis and avo analysis can increase understanding of facies and fluid analysis. AVO attributes can give better confidence in the result of facies and fluid characterization.

In order for better understanding of shallow gas potential in Cisubuh formation, petroleum system analysis is needed. Its important to determine the elements of petroleum system in Cisubuh formation such as source rock, reservoir rock, seal, trapping mechanism, migration path. Comprehensive analysis of all those method can lead to upside potential area of shallow gas from Cisubuh formation.

Result and Discussion

Based on well log analysis and sequence stratigraphy analysis, Cisubuh formation in deposited in transgressive sequence, it is divided into three main zone, those are (Fig. 1):

1. Lower Cisubuh with characteristic of intercalation of sandstone and shale, massive sand and massive shale.
2. Middle Cisubuh, dominated by massive shale in most of area and carbonate build up facies in several area.
3. Upper Cisubuh, dominated by massive shale, sandstone facies, and turbidite facies in southern area.

Only lower part of Cisubuh Formation is proven to have hydrocarbon. There is undeveloped potential in upper part of Cisubuh Formation within the pocket sand in shallower part that mostly have high amplitude and indicate occurrence of biogenic gas.

Ginanjar et al (2019) divided Seismic facies of Cisubuh Formation into four major facies unit (Fig. 2). Those are:

1. Intercalated sand-shale facies
2. Reefal carbonate Facies
3. Massive shale facies
4. Progradational shelf edge facies.

This classification is based on sedimentary reflection that representing bedding planes, unconformities or discontinuities in the geological record, artefact seismic like diffractions, multiples, etc. and non-sedimentary reflection like fault planes, fluid contacts, etc. Seismic observations need to be calibrated with available geological information in an early phase of the study. Sometimes reflectors are outcropping in the field and a direct tie with some seismic reflections is

available. In this study, seismic stratigraphy analysis is calibrated with well data, including mud log data and wireline log data.

Intercalated sand shale facies are characterized by parallel to sub parallel reflection configuration, reflection amplitude is low to high, indicating of vertical alternation of contrasting lithologies and hydrocarbon anomaly such as gas. Reefal carbonate facies is characterized by parallel to lenticular reflection configuration with mounded/pinnacle external geometry and reflection amplitude is low to high. Massive shale facies are characterized by parallel reflection configuration with homogenous low amplitude. Progradational shelf edge facies are characterized by clinoforms reflection configuraton, it is originated from prograding slope system in standing bodies of water, external geometry is slope front hills, showing successive stages of shelfedge progradation.

Based on integration of facies analysis from well log data and seismic data, Cisubuh formation is divided into several deposition environment, those are :

1. Lower Cisubuh Formation is deposited in shoreface area, ranged from lower shoreface, transition and shelf zone in southern part of study area and upper shoreface in northern part of study area.
2. Middle Cisubuh formation is deposited in shelf zone, characterized by massive shale and carbonate reef build up in several area.
3. Upper Cisubuh formation is deposited in sheld margine to slope area, characterized by massive shale, intercalated limestone and shelf progradation seismic facies.

To improve better understanding in hydrocarbon potential, AVO analysis have been conducted to determine lithology characterization, hydrocarbon detection and fluid parameter analysis. The AVO attribute is commonly applied to illustrate relationship between rock physic properties and seismic. Primary AVO attribute produced the intercept (A) and the reflection-coefficient gradient (B). AVO was classified to be four classes based on different amplitude response of gas-sands enclosed by shale. Class I showed the developments include high acoustic impedance sands and the amplitude decrease with offset. Class I had a positive intercept and a negative gradient. Class II produced sands surrounded by shale with small impedance contrast and the amplitude could either increase or decrease with offset. The intercept of class II value was positive or negative, and on the other hand the gradient was negative. Class III for low acoustic impedance sands that were usually gas sand. The amplitude class III increased along with offset and intercept, while the gradients were negatives. Class IV was added to the AVO class, which was mentioned the standard reflection coefficient as negative and decreases while the offset increases. Meanwhile, the intercept of Class IV was negative and the gradient was positive. The amplitude of the gas sands was expected to increase with offset and give negative value for intercept and gradient.

Before generating AVO attributes, several step have been done for better result, such as gather preconditioning including noise removal, gather flattening and offset scaling. After that intercept (A) and Gradient (B) is generated, then crossplot between intercept and gradient is conducted to determine AVO class (Fig. 3). Based on the crossplot, reservoir from Cisubuh Formation have characteristic of class III AVO that have low acoustic impedance sands and usually is gas sands. The final product is fluid/gas index attributes (Fig. 4) that show the facies and gas potential of Cisubuh Formation. The results then validated with well data (Fig. 5).

Source rock of hydrocarbon in Cisubuh Formation is mainly from Talang Akar Formation that migrated through fault, the trapping mechanism mostly 3 way dip closure, with good potential in main anticline area. Most of the source rock come from Babadan low. Migration is likely in upper Miocene and trap formation is from Pliocene (Fig. 6):.

Based on AVO analysis and petroleum system analysis, there are 5 good potential area that can produce gas from Cisubuh Formation in study area, those are (Fig. 7):

1. Randegan Area
2. Kayu Merah Area
3. Randu Lembayung Area
4. North Bangodua Area
5. Jatibarang Area.

From five area, three area have been proven producing gas from Cisubuh formation, those are, randegan, kayumerah and Jatibarang from several wells. Massive proving up such as perforation in cisubuh interval on those area, drilling step out well in North Bangodua area and Randu lembayung area is needed for better understanding in study of Cisubuh Formation.

The other potential of Cisubuh formation is come from upper part of Cisubuh Formation. There are many small pocket sands that have strong amplitude in seismic. In offshore North west Java Basin, this pocket sand is proven to produce biogenic gas from Cisubuh Formation.

Conclusions

With limitation of well data, an integrated study have been done to understand hydrocarbon potential in Cisubuh Formation. Massive evaluation, massive proving up, and massive collecting data from Cisubuh Formation is needed for better understanding of hydrocarbon potential in Cisubuh Formation.

PROCEEDINGS
JOINT CONVENTION BANDUNG (JCB)|2021
November 23rd – 25th 2021

References

Anggraeni, E. (2010), *Geologi, Studi Fasies, dan Karakterisasi Rekahan Pada Batu Gamping di Daerah Gunung Kromong, Cirebon, Jawa Barat, Institut Teknologi Bandung, unpublished*. Internal

Ginanjar et. al. (2019), Revisitting Cisubuh Formation in Onshore North West Java Basin; New Analysis from Seismic Stratigraphy, Geochemistry, and Subsurface Perspective; Implication for Petroleum System and Shallow Target Hydrocarbon Exploration in Northwest Java Basin;Case Study Randegan Field and Mt. Kromong Area, Proceding of Asia Pacific Oil and Gas Conference, 2019.

Report Pertamina EP (2013), *Eksploasi North West Java Basin* Internal Report POFD Lapangan Randegan (2015), *Plan of Future Development Lapangan Randegan, Pertamina EP Asset 3*.

Praptisih, Kamtono (2014), Karakteristik Batuan Induk hidrokarbon Formasi Cibulakan di daerah Palimana, Cirebon, Jawa Barat. *Bulletin Sumber Daya Geologi* Vol. **9** No.1 2014. Puslit Geoteknologi LIPI Bandung; p.27-40.

Pringgoprawiro, H., Suryo Suwito, P., Roskamil, 1977, The Kromong Carbonate Rocks and Their Relationship with the Cibulakan and Parigi Formation. Paper presented at the 6th Ann. Indonesian Petroleum Association, Jakarta.

Veeken, P.C.H (2014), *Seismic Stratigraphy and Depositional Facies Model*, EAGE Pulications, Netherlands.

Acknowledgements (Optional)

The authors thanks to Pertamina EP for permission to publishing this Paper, and for revisit study team in Pertamina EP region 2, G&G advidors, Mr. Oki, Mr. Anton, Mr. Hendra and Mr. Adi for many sharing knowledges to improve this study.

PROCEEDINGS
JOINT CONVENTION BANDUNG (JCB)2021
November 23rd – 25th 2021

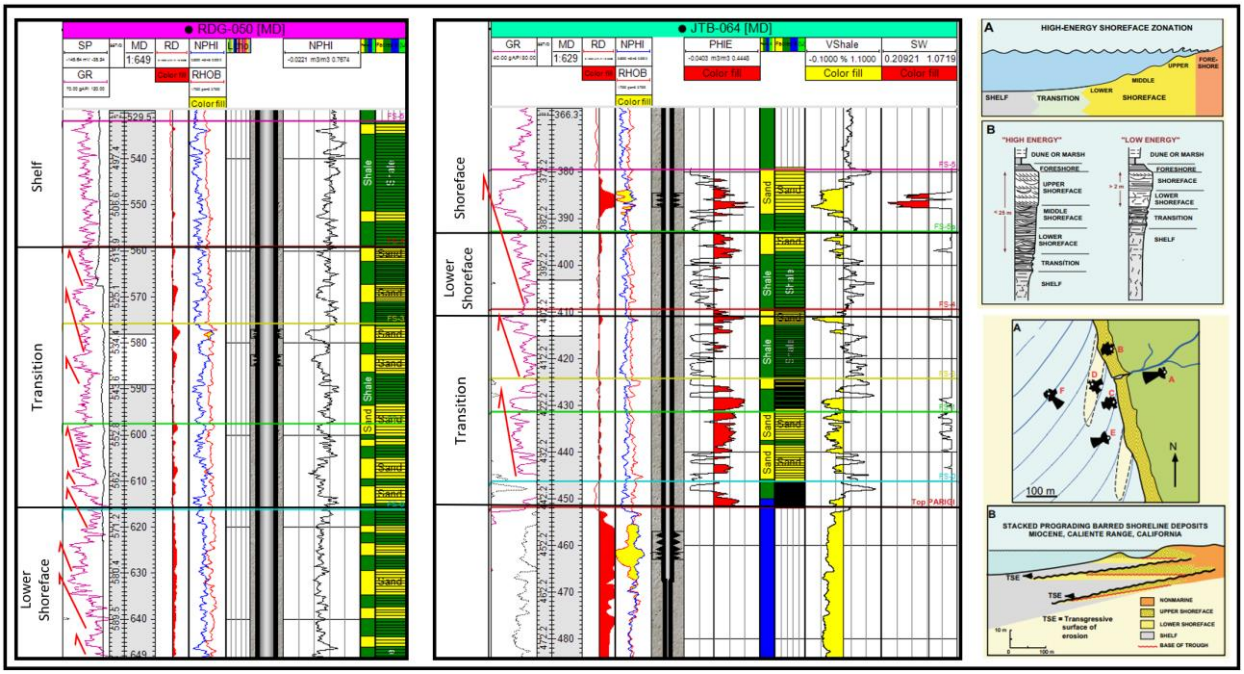

Figure 1: Facies analysis from well log data and depositional environment of lower part Cisubuh Formation

No	Seismic Facies	Seismic Section	Seismic Reflection	Reflection Configuration	Reflection Continuity	Reflection Amplitude	Reflextion Frequency	External Geometry	Interpretation
1	Intercalation Shand-Shale	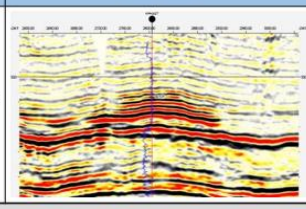	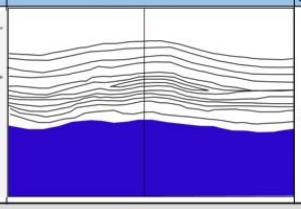	Parallel to Sub Parallel	Continues	High Amplitude	Medium to High Frequency	Sheet	Uniform sedimentation condition in the basin with littele diffrentiation, consist of fine grained deposit, high amplitude and medium to high frequency showing hydrocarbon anomaly.
2	Carbonate build up	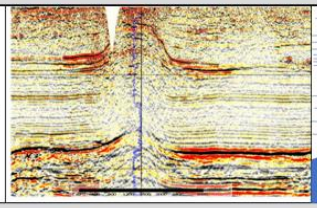	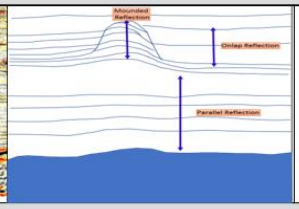	Parallel, Lenticular	Continues, and discontinu es	Low-Medium Amplitude	Medium to High Frequency	Mounded, Pinnacle with high velocity pull up	Represent depositional build up, combined with log data and mudlog data, this unit is confirmed as carbonate build up together with talus
3	Progradational Shelf Edge	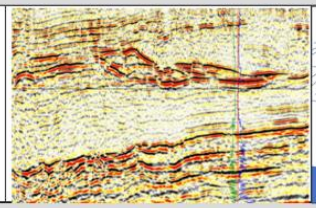	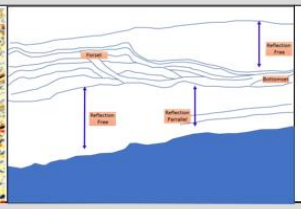	Clinoforms	Discontinu es	Medium-High Amplitude	Medium to High Frequency	Slope Front Fills	This facies show succesive stages of shelfedge progradation, the high amplitude slope front fill is sand, coarser grainedmaterial dumped on the slope area.

Figure 2: Seismic Facies analysis of Cisubuh Formation (Ginanjar et. al., 2019)

PROCEEDINGS
JOINT CONVENTION BANDUNG (JCB) 2021
November 23rd – 25th 2021

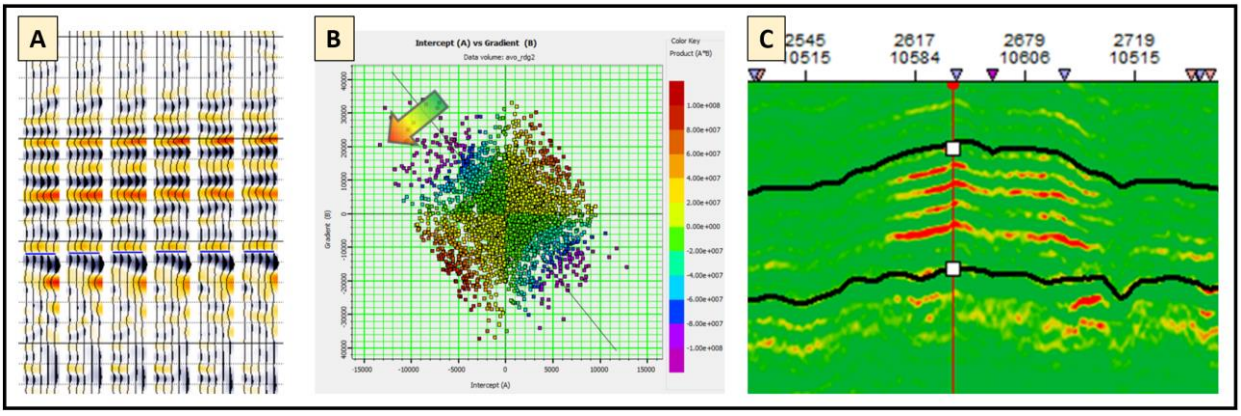

Figure 3: Gather pre-conditioning (A), Crossplot bettween Intercept and Gradient (B), AVO attributes Generation (C)

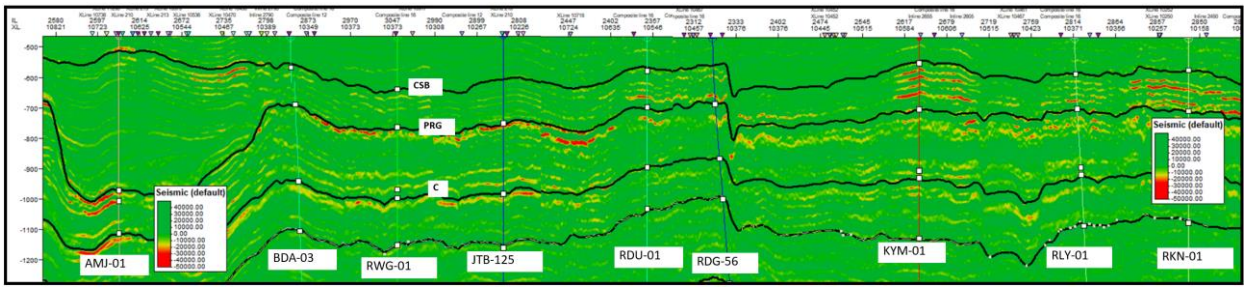

Figure 4: Fluid Index attributes from AVO analysis

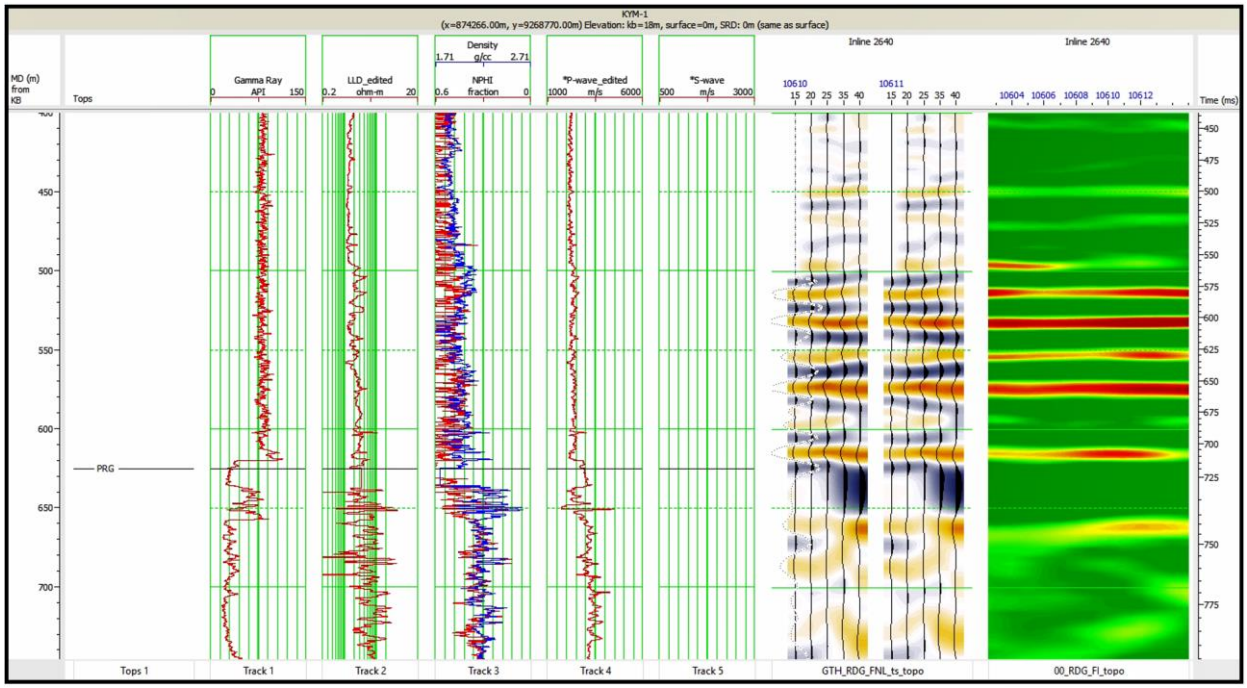

Figure 5: Validation AVO analysis with well data in KYM-01 well.

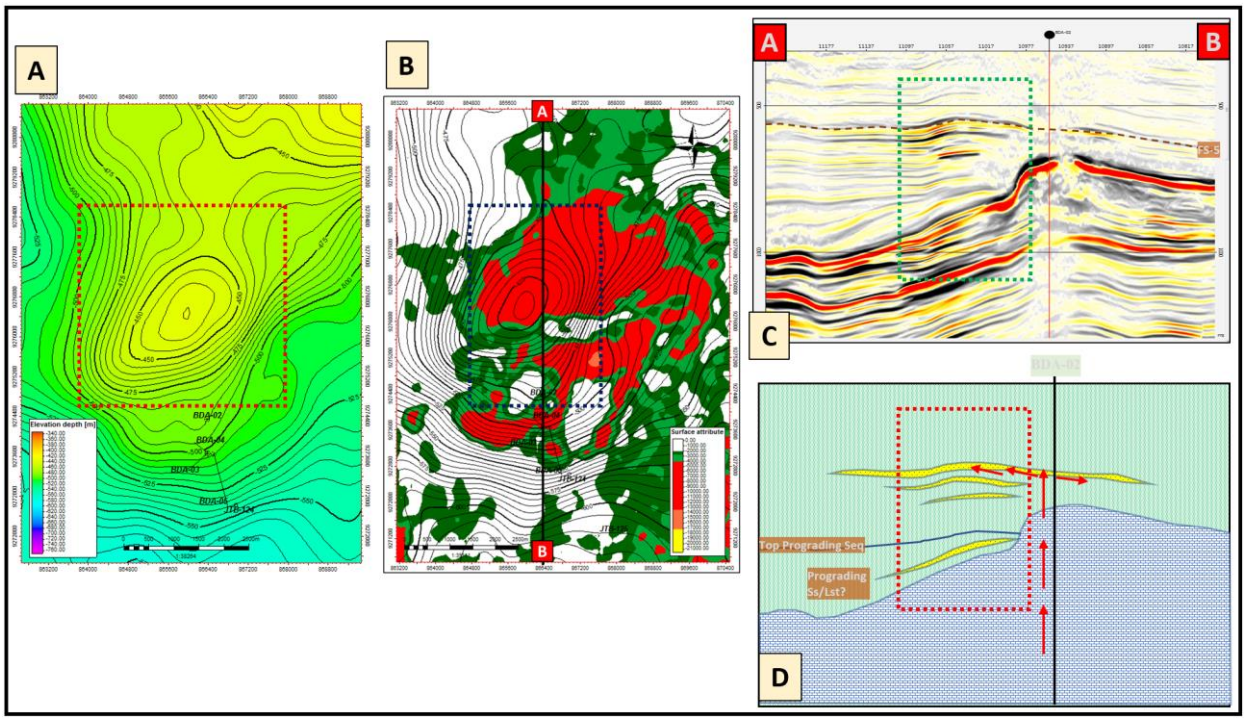

Figure 6: A. Depth Structure map around BDA area, B. Slice fluid index attributes, C. Seismic Section, D. Petroleum system component of seal, reservoir, trap and migration in BDA area.

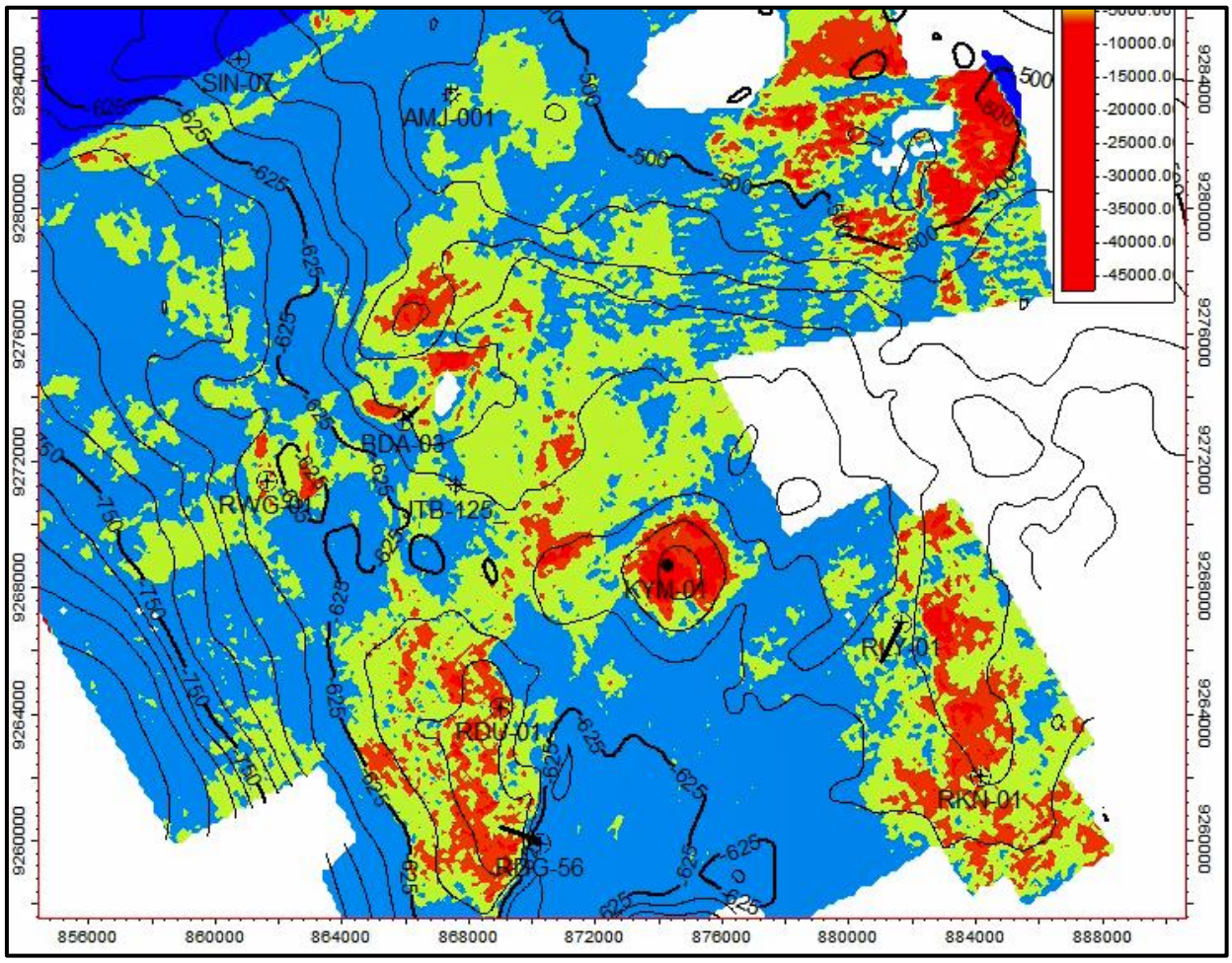

Figure 7: Lateral distribution of Fluid index attributes showing five potential area in generating gas from Cisubuh Formation.

PROCEEDINGS
JOINT CONVENTION BANDUNG (JCB)2021
November 23rd – 25th 2021

Re - Evaluation of Uranium Resources In Batubulan Sector, Melawi, West Kalimantan

Rachman Fauzi, Widodo, Ngadenin, Adhika Junara Karunianto
Center for Nuclear Minerals Research and Technology
Nuclear Energy Research Institution – National Research and Innovation Agency (OR TN – BRIN)
E-mail : rachman.fauzi@batan.go.id

Abstract

Batubulan Sector, Melawi has a relatively high occurrence of uranium. Several exploration activities have been conducted since 1973 in this region. The study is conducted by surface geological mapping, radiometric mapping, borehole logging, and resource estimation in order to determine the subsurface properties, geometry, mineralization direction, and also speculative resources of uranium in Batubulan Sector. Based on these researches show that the geology of Batubulan Sector is composed of metamorphic rocks, metasedimentary rocks, and intrusive rocks which have coarse and fine grain size. Uranium mineralization has been found in a spotted form in the veins with a maximum thickness of 10 cm and also has a high radioactivity concentration which is about 15,000 c/s. The lithologies of the study area consist of metapellite, quarzite, micro biotite, and meta - tuff. Drilling and borehole logging are conducted at four boreholes which have total depth of about 400 m and 75-120 m each. Based on resources estimation shows that the speculative resources of uranium (U_3O_8) in Batubulan Sector are about 540 tonnes. It is necessary to conduct more advanced and more systematic exploration methods in order to estimate the resources of uranium in this area.

Keywords: Batubulan, logging, uranium, radioactive mineral, resource estimation

Introduction

Nuclear energy has become one of the alternative energy sources which is much more effective than other conventional energy sources, such as coal, oil, or natural gas. Radioactive mineral, especially uranium, is one of the critical minerals which can be used as a core element of nuclear fuel. For that reason, uranium resource estimation in all of the potential sectors is necessary to support the sustainable establishment of the development of nuclear power plant in Indonesia.

Batubulan Sector, Melawi has a relatively high occurrence of uranium. Batubulan Sector is located on the banks of Ella River in Ella Ilir District, Melawi Regency, West Kalimantan. The radioactive mineral exploration activities have been conducted in this region from 1973 to 1992 (BATAN – CEA, 1977; PPGN – BATAN, 1985; PPBGN – BATAN, 1992). Those studies concluded that there are significant radiometric anomalies in the veins of magnetite, pyrite, apatite, tourmaline, quartz, and feldspar who intruded metamorphic rocks and magnetite lenses in granite. Those veins have 1.5 – 6 m length and NW – SE direction.

The lithology and uranium mineralization have also been determined on microscopic scale. Generally, The uranium mineralization characteristic is veins – shape which can be found in fractures. Those veins have 1 – 30 cm width, NW – SE strike direction with northwest to vertical dip direction, and also 250 – 15.000 c/s radioactivity. The mineralogy and positive autoradiography analyses determine that the minerals in these veins are uraninite (PPBGN – BATAN, 1992). Therefore, it is necessary to conduct an advance comprehensive study to define and determine the potential for uranium in those areas. The purpose of the study is to determine the subsurface properties, geometry, mineralization direction, and also speculative resources of uranium in Batubulan Sector.

Data and Method

The study is conducted by various methods consisting of literature study, surface geological mapping, radiometric mapping, borehole logging, and resource estimation. The literature study is based on the previous study and exploration report of the study area and surroundings. Surface geological mapping is observing the variety and mineralogy property of the outcrops while emphasizing the occurrences of uranium mineralisation. Radiometric mapping measured the radioactivity of the study area by using RS- 125 spectrophotometry. Core analysis and borehole logging determine the lithology and in - situ radioactivity in four boreholes : BB-01, BB-02, BB-03, BB-04. Furthermore, geological surface interpretation, radiometric measurement, and borehole logging data are used as reference for resource estimation of uranium ore (U_3O_8).

Result and Discussion

Geology of Batubulan Sector

Regionally, the geology setting of Ella Ilir consist of Pinoh Metamorphics (PzRP) and Sepauk Tonalite (Kls) (Figure 1) (Amiruddin and Trail, 1993). Pinoh Metamorphics consist of muscovite – quartz schist, phyllite, slate, hornfels, some metatuff and quartzite. Andalusite, cordierite, and biotite in places; silimanite and garnet rare. Sepauk Tonalite consist of light grey biotite – hornblende tonalite and granodiorite; some diorite, granite, monzodiorite, and quartz diorite. Pinoh Metamorphics are formed in

Paleozoic – Triassic and Sepauk Tonalite are formed in Lower Cretaceous (Tate, 1991; Pieters and Sanyoto, 1993).

The lithology of Batubulan Sector is mainly composed of metamorphic rocks, metasedimentary rocks, and igneous rocks. Metamorphic rocks consist of micro - biotite quartzite, and hornfels. Metasedimentary rocks consist of metapellite, and metatuff. Igneous rocks consist of dolerite. The geological map of the study area is shown in Figure 2.

Metapellite is greyish white, clay – silt grain size, blastopellitic texture, mineralogy consist of quartz, mica, and feldspar, massive structure, parallel dike in place. Metatuff is grey to dark grey color, fine to coarse ash grain size, blastosapmitic texture, mineralogy consist of quartz, feldspar, biotite, rounded blue cordierite in place, poor sorting, quartz feldspar lenses or veins in place with 20 cm length and 0.5 to 1 cm width. Micro – biotite quartz is grey, fine to medium sand grain size, blastopsamitic texture, mineralogy consist of quartz, biotite, feldspar, and muscovite. Hornfels is dark grey, silt to fine sand grain size, massive structure, granoblastic texture, mineralogy consist of quartz and biotite. Hornfels appears as lenses in metatuff. Dolerite is black, fine to very fine crystal size, inequigranular texture, mineralogy consist of olivine.

Geological structures which developed are rock strata, foliation, and faults. The rock layers have NW – SE strike direction and 65 – 83o dipping to SW. Foliations are NW – SE strike direction and 80 – 85o dipping to SW. The faults are indicated by lineaments and mylonitized outcrops.

Radioactive Mineralization

The radioactivity of the outcrops from radiometric mapping in the study area indicated that there are occurrences of radioactive mineralization. Mineralization outcrops which are most likely associated with radioactive minerals in Batubulan Sector are divided into two mineralization types, that are magnetite brecciation and vein type (Figure 3).

Magnetite brecciations in Batubulan Sector are mainly located at the banks of Ella River. There are 3 distinctive magnetite brecciation outcrops identified in study area (B1, B2, and B3). Magnetite brecciation – 01 (B1) is located at the west bank Ella River. This outcrop has > 25 m in height and > 90 m in length. By megascopic observation, B1 is brownish - black, massive structure, uranium mineralization is indicated by high radioactivity (300 – 2,000 c/s), uranium (U) grade is 392.6 ppm and thorium (Th) grade is 0 ppm, found spotted or parallel orientation in place in breccia. Magnetite brecciation – 02 (B2) is located at the west bank of Ella River, 66 meter northward of B1. This outcrop spread continuously to southeastern and northwestern side of the river. The megascopic appearance of B2 is brownish black, massive structure, very resistant, uranium mineralization is indicated by high radioactivity (2,700 c/s), U grade is 380 ppm and Th grade is 0 ppm, formed as mineralization breccia associated with pyrite and tourmaline, 70 cm width, N 125°E /50-70°E orientation. This bedding spread continuously to north west with radioactivity value is 3,000 – 5,000 c/s, U grade is 315 – 699.7 ppm. Borehole BB – 02 is located there. Magnetite brecciation – 03 (B3) is located at the west bank of Ella River, 195 m eastward of B2. B3 is lenses shaped, has 50 m length and more than 5 m width. Uranium mineralization is identified as spotted, parallel with magnetite brecciation orientation. The highest radioactivity measured is 2,000 c/s, U grade is 172 ppm, Th grade is 18.7 ppm.

Other uranium mineralization appeared as boudinage veins found at A6, B14A, B14, B13A, B13, B12, B11, B10, and OC-08. Those veins are collectively grouped into 150 m width mineralization zone (middle zone). Those veins individually have 10 – 50 cm width, NW – SE direction, dipping 75o to vertical to SW. Association minerals between each of the veins are not similar. Vein A6 has N130^{o}E/74°E orientation associated with quartz tourmaline, feldspar, and hematite with 5 – 10 cm width. Radioactivity in this vein is 4,500 c/s and U grade is 662 ppm. Vein B14 has lithology of schistose metapellite, reddish brown color, strong silicification, U mineralization has 0.5 m width, mineralogy consists of feldspatic quartz vein, tourmaline, iron oxide, and pyrite. U mineralization orientation is N130^{o}E /65°E, radioactivity is 12,000 c/s, U grade is 2,965 ppm, and Th grade is 0 ppm. The mineralization beds of middle zone became main target of borehole BB-03 especially at B14 and OC - 08.

Other group of mineralization veins is located in the north of Batubulan Sector, near the estuary of Batubulan River (north zone). Those outcrops are located at C7, C8, C9, and OC9 at the eastern of Ella River. The north zone collectively has 80 m width, consist of centimetric – decimetric sized veins, radioactivity values ranging from 1,000-10,000 c/s, U grade is between 318.7 – 1,026 ppm, Th grade is between 0 - 6.6 ppm. C7 consists of metapellite, mineralization is formed as a vein with 0.1 m width. Mineralogy consists of feldspatic quartz and a little tourmaline, radioactivity is 4,000 c/s, U grade is 519.6 ppm, Th grade is 6.1 ppm, located in place along the vein. C9 appeared as schistose metapellite, light brown color, U mineralization is found in tourmaline vein, molybdenite, pyrite, pyrite vein, and biotite. Its radioactivity is 4,000 – 10,000 c/s, U grade is 609.5 – 1,026 ppm. The north zone became the main target of borehole BB-04. Other outcrops such as OC-07 and OC-06 near Kararu River, also

PROCEEDINGS
JOINT CONVENTION BANDUNG (JCB)|2021
November 23rd – 25th 2021

have relative high radioactivity (750 c/s). Therefore, this location has become a drilling point of BB – 01. The mineralization outcrops and borehole points are shown in Figure 2.

Figure 3: Outcrops of a. B1, b. B2, c. C7, and d. C9

Borehole Logging of BB - 01

Borehole BB – 01 is referred to the orientation of OC – 06 mineralization which has direction of N120^{o}E /80° SW. This borehole has N 45°E azimuth, 65°NE inclination, and 75.11 m depth. The subsurface lithology of BB – 01 is metapellite, fine grained size, grey to light grey color due to silicification, intercalation of quartz and micro muscovite in place, moderately fractured. Mineralization is identified as bedded and pinched vein, associated with feldspatic quartz, pyrite, biotite, and tourmaline. The borehole profile is shown in Figure 4a. Radioactive anomaly measured by RS 125 can be found in several intervals as follows :

- 43,65 m depth : 0.055 m width, radioactivity is 200 c/s associated with pyrite and a little tourmaline.
- 45,20 m depth : 0.02 m width, radioactivity is 300 - 350 c/s associated with pyrite and a little tourmaline.
- 45,60 m depth : 0.02 m width, radioactivity is 200 c/s associated with pyrite and a little tourmaline. U grade is 24.4 ppm and Th grade is 9.9 ppm.
- 45,75 m depth : 0.005 – 0.015 m width, radioactivity is 250 c/s associated with pyrite and a little tourmaline. U grade is 31.3 ppm and Th grade is 9.3 ppm.
- 61,60 m depth : 0.01 – 0.02 m width, radioactivity is 750 c/s associated with pyrite and a little tourmaline. U grade is 31.3 ppm and Th grade is 9.3 ppm.

Based on geophysical well logging, there are radioactive anomalies in several intervals as follows :

- 44,60 - 45,80 m depth : 1.20 m width, radioactivity is < 100 – 647.5 c/s
- 60.95 – 61.20 m depth : 0.25 m width, radioactivity is < 100 – 381.9 c/s
- 68.60 – 69,25 m depth : 0.65 m width, radioactivity is < 100 – 12,071.8 c/s

Borehole Logging of BB - 02

Borehole BB – 02 has N 20°E azimuth, 60°NE inclination, and 85.45 m depth. The subsurface lithology of BB – 01 is metapellite and metatuff, fine grained size, grey to light grey color due to silicification, intercalation of micro quartzite in place, moderately fractured and intensively fractured in particular interval. Mineralization is identified as magnetite brecciation from 1.19 m – 7.50 m interval with radioactivity is 90 c/s. In 7.50 m – 17.48 m interval is identified as sulfide veins (mostly pyrite), centrimetric width, interbedded with feldspatic quartz, but low radioactivity.

U mineralizations are indicated at interval 49.10 – 49.80 m (radioactivity is 750 c/s, spotted, associated with pyrite), also 52,00 m, 67,95 m, 73,80 m, and 80,40 m(radioactivity is 240 c/s, formed as nodules, milimetric to 3 cm sized). The borehole profile is shown in Figure 4b. Based on geophysical well logging, there are radioactive anomalies in several intervals as follows :

- 3,30 - 3,55 m depth : 0,25 m width, radioactivity is < 100 – 175,92 c/s
- 27,90 – 28,10 m depth : 0,20 m width, radioactivity is < 100 – 12.071,8 c/s
- 48,80 – 50,15 m depth : 1,35 m width, radioactivity is < 100 – 1.743,16 c/s

Borehole Logging of BB - 03

Borehole BB – 03 is referred to the orientation of OC – 06 mineralization which has direction of N120^o E/80° SW. This borehole has N 40°E azimuth, 60°NE inclination, and 121.79 m depth. The subsurface lithology of BB – 03 is interbedding of metapellite and hornfels, also dolerite from 103 – 121.79 m depth. This borehole is intensively fractured. Mineralization is identified as magnetite brecciation that has 1.40 m width, mostly consist of magnetite with less sulfide. At interval 28.35 – 32 m there is magnetite breccia zone, feldspatic quartz, and pyrite. Radioactive anomaly barely found, only at interval 70.05 – 70.65 m whose radioactivity of 298.13 c/s maximum. The borehole profile is shown in Figure 5a.

Borehole Logging of BB - 04

Borehole BB – 04 is referred to the orientation of U mineralization that occur intensively at both banks of northern Ella River near Batubulan River estuary. This borehole has N 42°E azimuth, 60°NE inclination, and 121.49 m depth. The subsurface lithology of BB – 04 is biotite quartzite, hornfels, and metapellite (interval 0 – 21.26 m), massive andesite (interval 21.26 – 63.0 m), and Schistose metapellite with feldspatic quartz vein in its fracture (interval 63 – 121.49 m). Schistosities along borehole are very

intensive which some of them are filled by uranium – associated mineralization.

There are mineralization zone at several intervals such as 76.10 – 76.50 m (radioactivity value is 750 c/s), 77.10 – 77.40 m (radioactivity value is 750 c/s), and 109.20 – 110.10 m (radioactivity value is 300 c/s). The mineralization zones in this borehole are mostly associated with pyrite, tourmaline, and quartz. The borehole profile is shown in Figure 5b. Based on geophysical well logging, there are radioactive anomalies in several intervals as follows :

- 75,60 – 76,95 m depth : 1,35 m width, radioactivity is < 100 – 3.012,29 c/s
- 108,70 – 109,65 m depth : 0,95 m width, radioactivity is < 100 – 1361,14 c/s

Resource Estimation

Resource estimation is conducted by using borehole log data, especially collar (borehole coordinate), survey (borehole azimuth and inclination), and quality (geological data at respective depth interval) which be processed by resource modeling software. The resource estimation of uranium ore (U3O8) is shown in Table 1. Based on Table 1 it is shown that the U_3O_8 resource in Batubulan Sector is 540 tonnes.

Conclusions

Uranium mineralization zones in study area are mainly formed as magnetite brecciation or veins which became the reference point for four borehole drilling (BB – 01, BB – 02, BB- 03, and BB – 04). BB – 01, BB – 02, and BB – 04 have convincingly projected the spreading of uranium mineralization zone in the subsurface. Only BB – 03 that did not project potential radioactive mineralization zone due to the geometry of its surrounding mineralization apparently has no lateral spreading to borehole trajectory. Resource estimation of U3O8 from 4 boreholes in Batubulan Sector is 540 tonnes. However, due to the width interval of the ore is very wide (more than 400 m) and lateral spreading of the ore is still based on mineralization orientation, so the resource category is speculative. It is necessary to conduct a more advanced and more systematic exploration methods in order to enhance the resource estimation in Batubulan Sector.

References

Amiruddin and D. S. Trail, 1993, *Peta Geologi Lembar Nanga Pinoh Kalimantan Skala 1 : 250.000*. Bandung: Pusat Penelitian dan Pengembangan Geologi,

BATAN – CEA, 1977, *Prospect to Development Uranium Deposits in Kalimantan : Volume I and II*, Jakarta, unpublished.

Ngadenin, Indrastomo, F.D., Widana, K.S., and Widodo, 2019, Identification of Radioactive Mineral Occurences on Magnetite Veins in Ella Ilir Area, Melawi, West Kalimantan. *Eksplorium Vol. 40 No. 1*, pp 33 – 42, Jakarta : BATAN.

Pieters, P.E. and Sanyoto, P., 1993, *Peta Geologi Lembar Pontianak/Nangataman, Kalimantan Skala 1:250.000*. Bandung: Pusat Penelitian dan Pengembangan Geologi.

PPBGN – BATAN, 1985, Prospeksi Semi Detil dan Sistematik Daerah *Ella Ilir, Kalimantan Barat : Laporan Akhir*, Jakarta, unpublished.

PPBGN – BATAN, 1992, *Laporan Pelaksanaan Kerja Lapangan Untuk Menunjang Kajian Mikroskopis Mineralisasi U di Daerah Batubulan, 1991/1992*, Jakarta, unpublished.

Tate, R.B., 1991, Cross-border Correlation of Geological Formations in Sarawak and Kalimantan. *Bulletin of the Geological Society of Malaysia, vol. 28*, pp. 63–95.

Acknowledgements

This study can be completed with the support and help from other parties. On this occasion, the Authors would like to thank Mr. Ir. Yarianto Sugeng Budi Susilo, M.Si as the Head of the Center for Nuclear Minerals Research and Technology which has provided the Author's opportunity to carry out this research. The Authors also would like to thanks to Mr. Heri Syaeful, MT as the Coordinator of the Exploration Division who has supported and coordinated this research.

PROCEEDINGS
JOINT CONVENTION BANDUNG (JCB)2021
November 23rd – 25th 2021

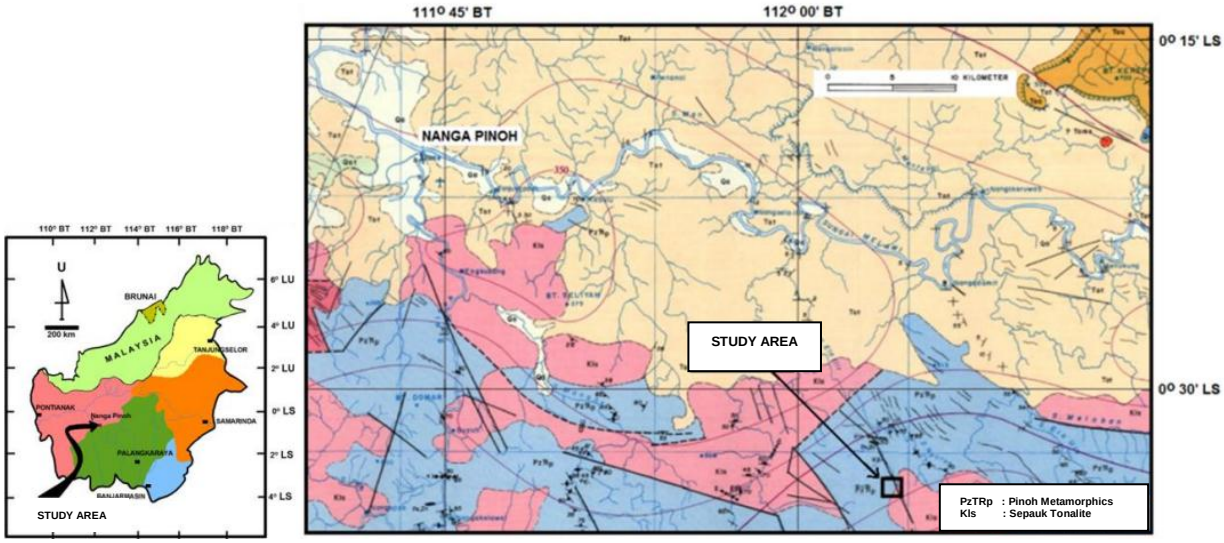

Figure 1: The Regional Geology Map of The Study Area and Its Sorroundings (Modified from Amiruddin and Trail, 1993 in Ngadenin et al., 2019)

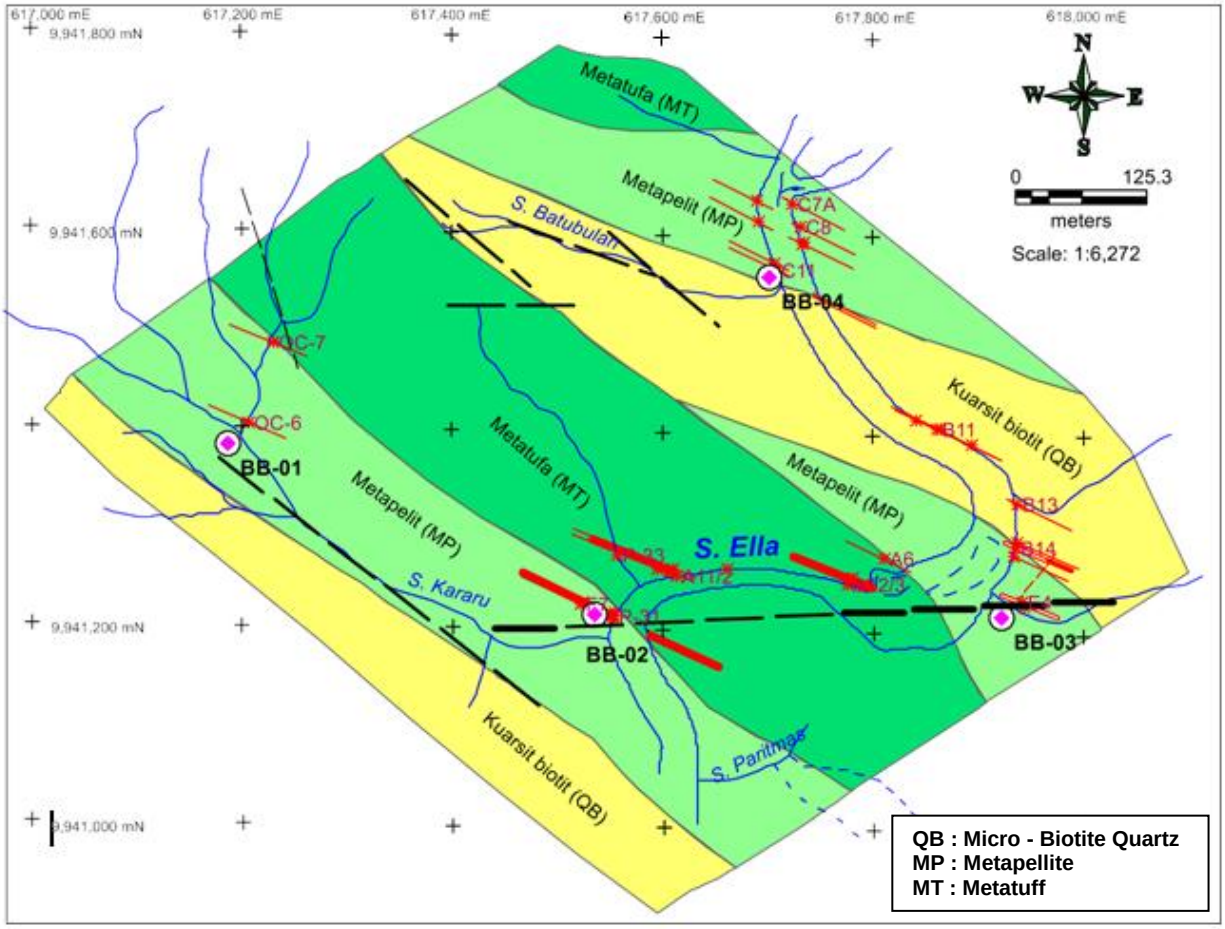

Figure 2: The Geological Map of Batubulan Sector

PROCEEDINGS
JOINT CONVENTION BANDUNG (JCB) 2021
November 23rd – 25th 2021

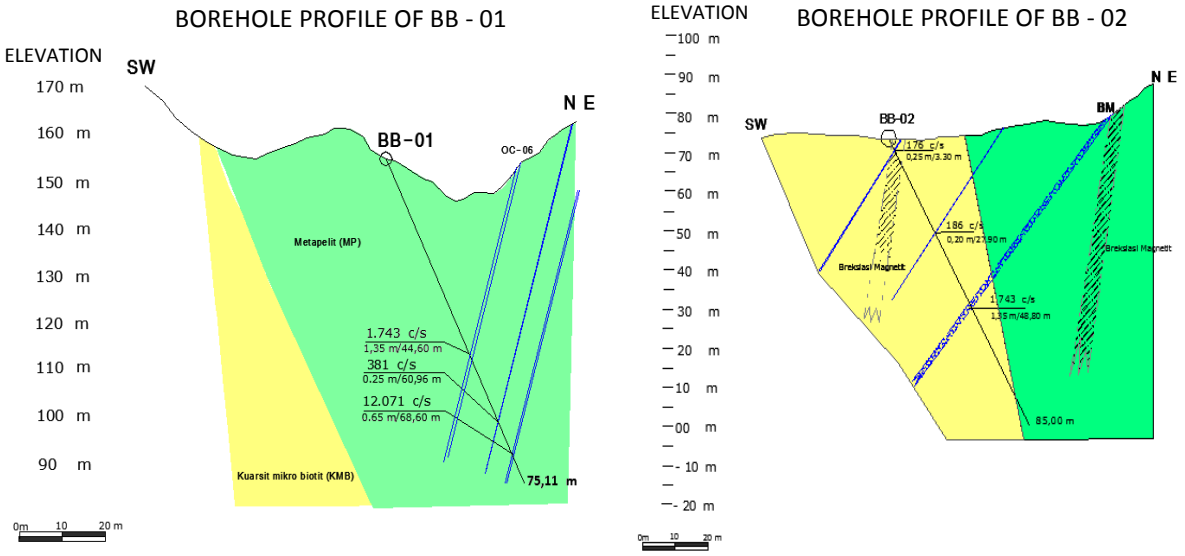

Figure 4: a. Borehole Profile of BB – 01 (left) and b. Borehole Profile of BB – 02 (right)

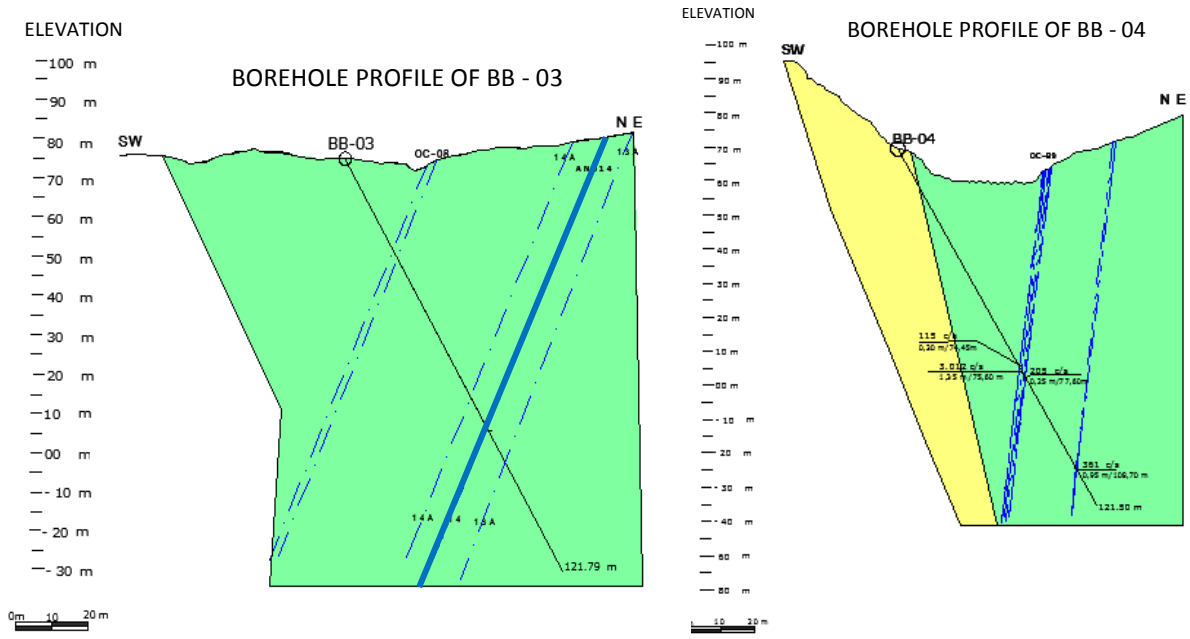

Figure 5: a. Borehole Profile of BB – 03 (left) and b. Borehole Profile of BB – 04 (right)

Table 1: Resource Estimation of Batubulan Sector

Borehole	Ore Name	Volume (m^3)	U_3O_8 Grade (ppm U)	Density (g/cm^3)	Tonnage	Total
BB0-01	ore1	21590	314	3.2	21.6936	**319.3623**
	ore2	4787	278	3.2	4.2585	
	ore3	11942	7678	3.2	293.4102	
BB-02	ore1	10201	105	3.2	3.4275	**107.2755**
	ore2	54345	585	3.2	101.7338	
	ore3	7682	86	3.2	2.1141	
BB-03	ore1	14124	153	3.2	6.9151	**6.9151**
BB-04	ore1	18553	1544	3.2	91.6667	**106.4891**
	ore2	23160	200	3.2	14.8224	
Resources Estimation (tonnes)						**540.04**

PROCEEDINGS
JOINT CONVENTION BANDUNG (JCB)|2021
November 23rd – 25th 2021

A Machine Learning-Based Screening of CO2 Source-Sink Project Performance Parameters for Indonesian Field

Martinus Bhima[1], Leonardo Budhi[1]
[1]Institut Teknologi Bandung

Abstract

CCUS in the form of CO2-EOR can be a win-win solution for Indonesia as a country that still relies its production upon mature oil fields and also as the world's fifth-largest GHGs emitter. The main concern of EOR projects is the time to reach the pilot test for approximately 1.5 years. This paper aims to enhance quick screening and evaluation of technical parameters of CO2-EOR projects in Indonesian fields. The developed CO2 EOR Screening Project by utilizing a supervised learning algorithm assesses the field project candidates by evaluating performance parameters instead of reservoir properties. The parameters were obtained from training data that has been both successful and unsuccessful projects in other fields. These are including OOIP, remaining oil-in-place, recovery factor, and the distance between CO2 source and sink. Each parameter will be normalized and multiplied by its feature importance. The feature importance was determined using random decision forest. Hence, all fields will have a performance grade and be ranked from the highest score to the lowest. Once the field has the final score, it can support the decision of whether the project will be a go/ no-go project. The higher value of most performance parameters result will give a higher final score except for a distance of source-sink. A higher value of source-sink distance will result in a lower final score. This proposed methodology is more likely to be an easier machine learning algorithm than any other method that has been proposed. Besides, the evaluation parameters purely come from economic factors due to the difficulty and limitation to obtain fluid and reservoir parameters, thus there will be more time reduction before the pilot test.

Keywords: CO2 EOR, screening, machine learning, supervised learning,

Introduction

Climate change is an increasingly hot issue in recent times. Natural phenomena that occur such as cyclonic storms, droughts, and the increase in the average temperature of the earth with climate change triggered by increased levels of CO2 gas emissions. CO2 emission levels reached 33.4 Gt at their peak in 2019 [1]. To overcome this emission level, one of the mechanisms developed is Carbon Capture, Utilization, and Storage (CCUS) technology. CCUS is considered as a solution to reduce CO2 emission levels by trapping CO2 in the atmosphere or from fossil power generating sources. The CO2 is processed in such a way that it can become a liquid which is usually stored in mature oil and gas reservoirs. With this mechanism, CO2 stored in the reservoir is also utilized as an EOR medium to increase the level of oil and gas production in a reservoir that is past its prime [2]. To execute this, it is necessary to conduct pilot tests in several potential fields which take a lot of time and money.

For the purpose to reduce time and cost in the pilot tests process that can reach 1.5 years, optimization of performance parameters screening is carried out on the basis of machine learning. Guided learning algorithm that will be used to study data from previous pilot projects and will carry out weighting on existing performance parameters and produce a final value that shows the competence of the reservoir field in carrying out the CCUS project.

Data and Method

This project aims to improve the data pre-processing which consists of training data and test data, and assess each field based on the performance parameters using Random Forest Classification (RFC) tree. Training data is a subset of observations used for the model training process. This dataset is used by the algorithm to learn the parameters of the machine learning model [3]. Meanwhile, the test data is subset of data that is only used to assess the performance of a fully trained model. The prediction accuracy on the test data is an indicator of the model's performance on unseen data encountered in a real-world scenario [3].

In this project, the authors apply random forest method only in processing training data. In random forest algorithm, two highlighted activities were considered. The first is classification and regression which can be determined by observing the y (output) feature whether y is a number/ value or a decision and the second is the importance features where the machine learning algorithms fit a model where the prediction is the weighted sum of the input values.

[RFC scheme]

The methodology of this project consists of two main steps. Firstly, using training data to obtain the

PROCEEDINGS
JOINT CONVENTION BANDUNG (JCB)2021
November 23rd – 25th 2021

importance features value. Secondly, the importance features value will be used to grade the fields.

1. Training data

   The features that the authors consider include original oil in place (OOIP), oil recovery factor (OIL RF), remaining oil (OIL CURREN), and feasible feature. Zero means not feasible and one means feasible fields. Performance parameters are used because the data is relatively easier to be obtained than technical parameters e.g porosity, permeability, viscosity, etc. Using python, training data can be visualized as in the figure below. There is a limitation in training data because these data is a dummy data hence, the value of each parameters is a random value as well. It is because the CCUS activities is very low and currently there is no success story of CCUS in Indonesia yet.

2. Tested data

   The authors evaluate three performance parameters which include OOIP, OIL RF, and OIL CURREN. The tested data is visualized in the Microsoft Excel in the comma separated value (CSV) format as shown in the figure below.

3. Grade calculation

   Based on [4], it used normalization to assess the parameters which have various ranges and differing physical meanings and units, into new dimensionless variables that vary linearly between 0 and 1. These can subsequently be added to produce
   a score used in reservoir ranking. For each relevant property (j) of the reservoir (i) being ranked ($P_{i,j}$), a corresponding normalized parameter ($A_{i,j}$) is calculated according to

$$A_{i,j} = \frac{|P_{i,j} - P_{min,j}|}{|P_{max,j} - P_{min,j}|}$$

Equation 1. Normalization formula for RF

For the recovery factor (RF), and

$$A_{i,j} = \frac{|\log P_{i,j} - \log P_{min,j}|}{|\log P_{max,j} - \log P_{min,j}|}$$

Equation 2. Normalization formula for OOIP and remaining oil

Where, $P_{i,j}$ is the value of the performance parameter j (j = 1 for OOIP and j = 2 for OIL CURREN) for the ith reservoir. After A is calculated, those values will be multiplied by 100 so that the values vary between 1 and 100. Then, the next calculation is determining each field's score using

$$S_i = A_{i,j} \times w_j$$

Equation 3. Score calculation

Where $\sum w_j = 1$ with w_j was obtained from the importance feature values that already generated by training data. Finally, S_i can be summed from each feature and yields a final score of that field.

Result and Discussion

Each feature (OOIP, OIL RF, OIL CURREN) has its own contribution to the decision (feasibility). Importance value can be the indicator of it. Based on the Figure 3, RF has the smallest contribution to the decision but many works of literature said that doesn't mean the smallest value will have the least effect to the decision. Each feature's importance value can be seen in the table below

Feature	Importance
OOIP	0.414
OIL RF	0.177
OIL CURREN	0.409

Table 1. Feature's importance value

These values will be then multiplied to each feature in the test data using [4] calculation. After the calculation of all fields, the authors have ranked the grade of every field as can be seen in the Figure XX. Based on the output, it can take a conclusion that FIELD_Q is the most favorable for CO2 EOR project while FIELD_F is the least favorable for CO2 EOR. It is because FIELD_Q has the biggest OOIP and favorable oil recovery factor and FIELD F has the least of OOIP. Hence, the bigger OOIP, RF, and remaining oil yield a bigger grade of the field.

The advantage of this project are by using random forest classifier its versatility and simplicity make this project suitable for the given problem. This method also provides relative importance it assigns to the input features. By using this supervised learning, a large of data processing can be optimized, hence quicken the CCUS screening. The next advantage is handy and good prediction because RFC uses default hyper-parameters which often produce good prediction.

Meanwhile, some disadvantages were evaluated i.e overfitting. Most of the time this won't happen thanks to the random forest classifier. If there are enough trees in the forest, the classifier won't over-fit the model. A large number of trees can make the algorithm too slow and ineffective for real-time predictions. In general, these algorithms are fast to train but quite slow to create predictions once they are trained hence, limited data and prediction time can be the obstacles for this project.

Conclusions

Based on the field grade using performance parameters, FIELD_Q is the most favorable for CO2 EOR project and FIELD_F is the least favorable for CO2 EOR with the biggest importance value from original oil in place (OOIP) feature. The authors

recommend that technical parameters (rock and fluid properties) should be considered to validate the final score and also image/map/zone classification should be evaluated as well because the data provides zone/ map each field and its coal-fired power plant, we can determine which field is more favorable based on the distance.

References

[1] IEA.
[2] A. Tura, Y. Ning, and Y. H. Nasser, "No Title."
[3] Y. N. Pandey, A. Rastogi, S. Kainkaryam, S. Bhattacharya, and L. Saputelli. 2020.
[4] J. Shaw and S. Bachu, *J. Can. Pet. Technol.*, vol. 41, no. 9, pp. 51–61, 2002, doi: 10.2118/02-09-05.

PROCEEDINGS
JOINT CONVENTION BANDUNG (JCB)2021
November 23rd – 25th 2021

The training data which printed using Python. Zero value in feasible means not feasible and 1 means feasible.

	zone	field_name	OOIP	OIL RF	OIL CURREN	feasible
0	1	#d61f03	3278.5	34	56.004	0
1	1	#27ef31	3942.7	23	2.864	0
2	2	#62ec22	44778.3	18	67.098	1
3	3	#168da9	30659.7	28	42.461	0
4	2	#ab8353	36161.5	34	17.288	0
..	...	...	...	...	...	...
995	3	#f61e70	30736.1	31	46.350	0
996	1	#f0cf48	33423.8	27	56.926	1
997	2	#589028	27539.4	31	20.012	0
998	1	#d00272	24477.4	13	22.655	0
999	3	#a92f65	23210.7	16	16.921	1

Figure 1. Training data for CCUS project

The figure above is the training data to generate the importance feature value and the figure below is the tested data which printed in the CSV format

Zone	FIELD_NAME	Operator	PROD_STAT	GN_HC_TYPE	OOIP	OIL Reserv	OIL RF	OGIP	GAS RESERV	GAS RF	OIL CUM PR	GAS CUM PR	OIL CURREN	GAS CURREN
Zone B	FIELD_A	PT ABC Hulu Energi Ltd	Temporarily shut-in	Oil & Gas Fields	12652	2657	21	19200	4400	23			2.657	4400
Zone B	FIELD_B	PT ABC EP	Producing	Oil & Gas Fields	273	85	31	100500	58000	67	49.92	37083.01	35.08	20916.99
Zone B	FIELD_C	PT ABC EP	Temporarily shut-in	Oil & Gas Fields	44948	8566	19	40500	14300	24	8126	14300	0.44	0
Zone B	FIELD_D	PT ABC EP	Producing	Oil & Gas Fields	659.9	194.4	29	1265000	885000	65	141963	291474696	52.437	593525.304
Zone B	FIELD_E	PT ABC EP	Temporarily shut-in	Oil & Gas Fields	1417	0.425	30	55200	40700	76.43	0.189	8655	0.237	32045
Zone B	FIELD_F	PT ABC EP	Producing	Oil & Gas Fields	46.8	7	15	124080	98560		1148	53000.35	5.852	45559.65
Zone B	FIELD_G	PT ABC EP	Temporarily shut-in	Oil & Gas Fields	30	7.5	25	100000	68000	65	0.081	419.8	7.419	67580.2
Zone B	FIELD_H	PT ABC EP	Producing	Oil & Gas Fields	71.5	14	20	137000	99000		10774	73983.03	3.226	25016.97
Zone B	FIELD_I	PT ABC EP	Temporarily shut-in	Oil & Gas Fields	32.2	8.6	27	123800	101400		1966	26634.12	6.634	74765.88
Zone C	FIELD_J	PT ABC EP	Producing	Oil & Gas Fields	110	22	20		5000		0.233		21.767	5000
Zone C	FIELD_K	PT ABC Hulu Energi Ltd	Temporarily shut-in	Oil & Gas Fields	13061	2351	18	16000	3000	50			2.351	3000
Zone C	FIELD_L	PT ABC EP	Producing	Oil & Gas Fields	181.95	46989	26	637000	477100		9687	92657.48	37.302	384442.52
Zone C	FIELD_M	PT ABC EP	Producing	Oil & Gas Fields	64.4	12.4	19	95700	70500	51	9129	64462.66	3.271	6037.34
Zone C	FIELD_N	PT ABC EP	Producing	Oil & Gas Fields	34657	4086	12	130600	96100		1539	15990	2.547	80110
Zone C	FIELD_O	PT ABC EP	Temporarily shut-in	Oil & Gas Fields	4808	0.962	20	3580	2250	62.5	0.07	410	0.892	1840
Zone C	FIELD_P	PT ABC EP	Producing	Oil & Gas Fields	17302	3612	20.9	43400	34600		1536	11137.1	2.076	23462.9
Zone C	FIELD_Q	PT ABC EP	Producing	Oil & Gas Fields	38985	11306	29	136100	95600		0.891	16152.6	10.415	79447.4

Figure 2. Test data for CCUS project

PROCEEDINGS
JOINT CONVENTION BANDUNG (JCB)2021
November 23rd – 25th 2021

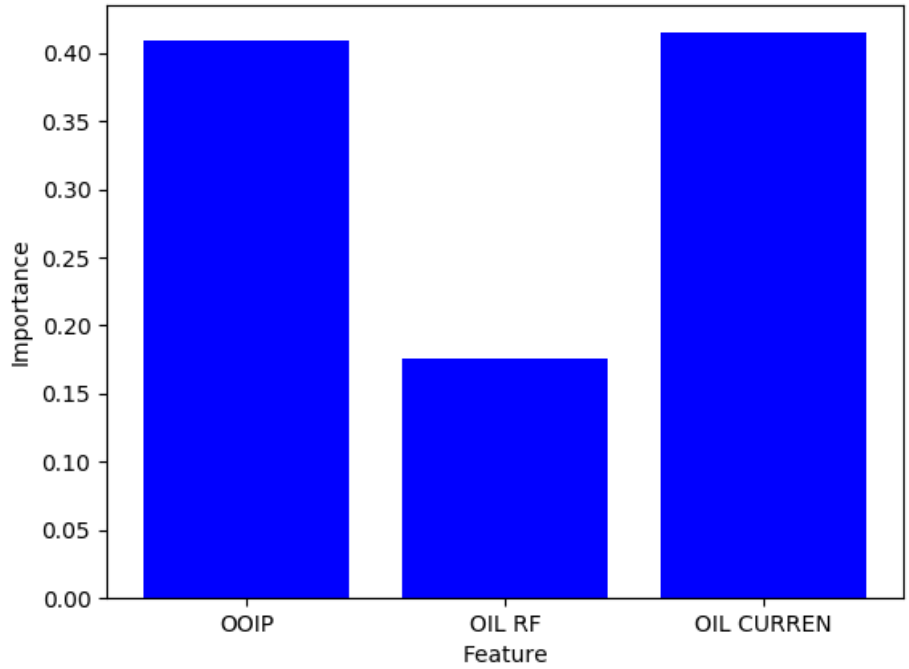

Figure 3. Importance features comparison

	Zone	FIELD_NAME	OOIP	OIL RF	OIL CURREN	Grade
16	Zone C	FIELD_Q	38985.00	29.0	10.415	85.050082
3	Zone B	FIELD_D	659.90	29.0	52.437	74.403123
1	Zone B	FIELD_B	273.00	31.0	35.080	68.294682
11	Zone C	FIELD_L	181.95	26.0	37.302	61.743979
0	Zone B	FIELD_A	12652.00	21.0	2.657	60.792634
15	Zone C	FIELD_P	17302.00	20.9	2.076	60.584459
13	Zone C	FIELD_N	34657.00	12.0	2.547	57.601441
10	Zone C	FIELD_K	13061.00	18.0	2.351	57.200653
2	Zone B	FIELD_C	44948.00	19.0	0.440	52.381360
9	Zone C	FIELD_J	110.00	20.0	21.767	49.148334
14	Zone C	FIELD_O	4808.00	20.0	0.892	46.136572
8	Zone B	FIELD_I	32.20	27.0	6.634	39.874754
4	Zone B	FIELD_E	1417.00	30.0	0.237	38.703518
6	Zone B	FIELD_G	30.00	25.0	7.419	38.430082
7	Zone B	FIELD_H	71.50	20.0	3.226	32.254088
12	Zone C	FIELD_M	64.40	19.0	3.271	30.824258
5	Zone B	FIELD_F	46.80	15.0	5.852	29.651698

Figure 4. Rank of field based on the grade

PROCEEDINGS
JOINT CONVENTION BANDUNG (JCB)2021
November 23rd – 25th 2021

2D Visualization of Subsurface Temperature Flow Condition Using HV2D (Hydrotherm Visualization 2 Dimension) Program Based on Phyton (Case Study: Way Ratai Geothermal Field)

Muhammad Adli[1], Istifani Ferucha[2], Igo Relindo[3], Karyanto[4], Ida Bagus Suananda Yogi[5]
Geophysical Engineering Department, Engineering Faculty, University of Lampung

Abstract

Visualization of the subsurface conditions of the Way Ratai geothermal system was carried out by making the HV2D (Hydrotherm Visualization 2D) program. Hydrotherm Viewer 2D is a program designed to run on all major operating system. HV2D provides simple Graphic User Interface (GUI), which makes easier. The next and back button makes easier for user to find the difference on temperature, saturation, or pressure countour. This program is simulated with a simple and interactive Python programming language that can be used in subsurface resource monitoring activities by displaying 2D cross-sectional results. The data required is in the form of phase and temperature data to identify the characteristics of geothermal reservoirs. The steps taken in making the HV2D program include analyzing the output data of Hydroterm Interactive, making contour data, and making Graphic User Interface (GUI). Based on the secondary data, it can be analyzed that there is a pattern where at the beginning there are X, Y, and Z coordinates, then the data, if detailed, there are time-step and year data filled with temperature data. The visualization showed that the heat flows from middle of the cross-section to the right of the cross-section, and that can be justified by the Margodadi geyser manifestation in the right of the cross-section. A possible interpretation that can be conveyed is the presence of a cover layer or a very thick rock cap that causes the vapor fluid to be unable to penetrate to the surface. A lot of rock data and characteristics are still needed to model the exact heat and fluid flow.

Keywords: Geothermal Reservoir, Temperature Flow, Python, Subsurface Visualization.

Introduction

In general, the geothermal system in Indonesia is formed from a volcanic affiliation system. The appearance of surface manifestations is one of the characteristics of the occurrence of the system (Goff & Janik, 2000). One of the potentials for geothermal energy that is still being developed is the Way Ratai geothermal field located on Mount Ratai, Pesawaran (Donovan, 2018). Based on data from the Directorate of Geothermal in 2017, Way Ratai geothermal resource has potential more than 330 MW with the manifestation of hot springs and hot steam (Direktorat Panas Bumi, 2017). The status of work which is currently still in the exploration stage. This status has not increased due to the unfinished feasibility study for production operations, so this is the background of this research. One of the stages in the feasibility study is the presence of numerical modeling to calculate measured resources into reserves.

The post-processor Hydrotherm Interactive V3.2 software can be used to interpret the simulation results, but the simulation is displayed like a video and is difficult to pause between two years. In addition, on the post-processor it is difficult to zoom in and zoom out, as well as data creation with the dict function which produces a database of temperature data per year.

The difficulty in simulating a numerical model is caused by the large number of field parameters required. The absence of research on numerical models, especially related to hydrothermal fluid flow and heat energy transfer in the Way Ratai geothermal system, is an opportunity for renewal in this research. This study specifically aims to model hydrothermal fluid flow and heat energy transfer in the Way Ratai geothermal system using numerical simulation methods.

In general, the Way Ratai area, Padang Cermin District, Pesawaran Regency, Lampung Province is located in the regional geology of Tanjung Karang. The following will be shown in Figure 1 which is a regional geological map of the Way Ratai geothermal area, Lampung Province. On the geological map the rock research area is dominated by rocks which are the product of young volcanoes (Qhv) consisting of lava rock (andesite-basalt), breccia, and tuff, the Hulusimpang (Tomh) formation consisting of basalt andesite lava, tuff, and tuff. Volcanic breccias were changed with limestones of Oligocene – Early Miocene age, and the inseparable Mount Kasih complex (Pzg) which consists of metamorphic sedimentary and igneous rocks consisting of schist, quartzite, and gneiss. There are two types of schist, quartz mica graphite and amphibole schist.

Fault structure in the Way Ratai geothermal field and its surroundings dominated by fault structures trending northwest-southeast and northeast-southwest is as a normal fault. Beside the two structures normal faults, the study area is also characterized by the main lineaments are northeast-southwest and northwest–

southeast. Straightnesses are present quite a lot, especially in the west, southwest, south and a little in the middle of the area to investigate (Gafoer et. al., 1993).

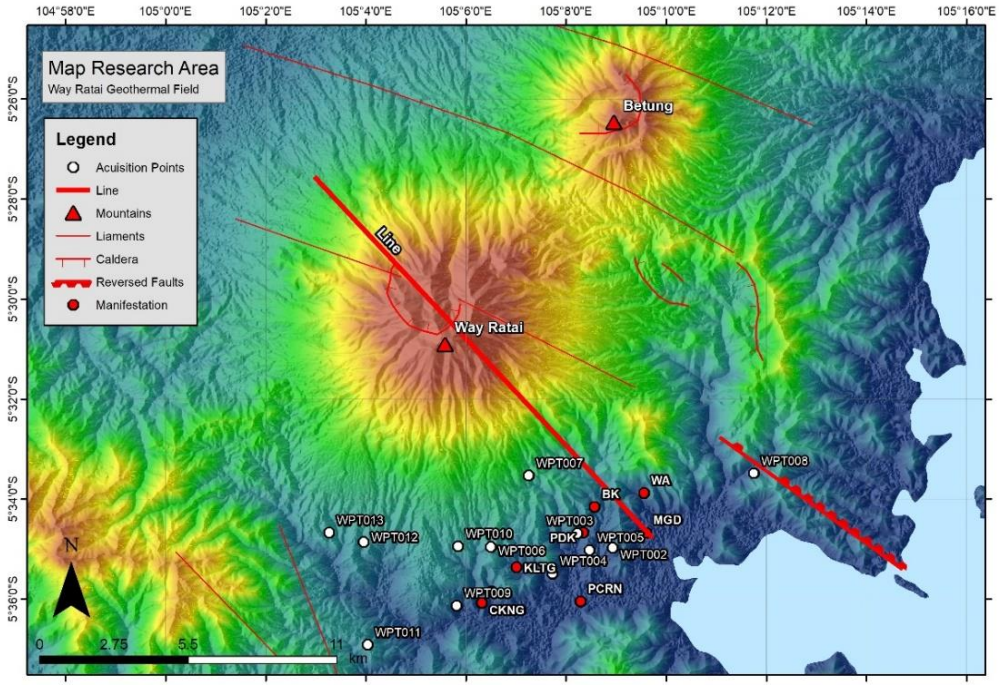

Figure 1: Research Area of Way Ratai Geothermal Field

The heat transfer equation is based on the conservation of enthalpy in the solid and fluid phases of the porous medium in the elemental region. Enthalpy is a derived property containing internal energy and flow energy. Can be defined as:

$$\frac{\partial}{\partial t}[\phi(\rho_w h_w S_w + \rho_s h_s S_s) + (1-\phi)\rho_r h_r] - \nabla \cdot K_a \mathrm{I}\nabla \mathrm{T} + \nabla \cdot \phi(S_w \rho_w h_w V_w + S_s \rho_s h_s V_s) - q_{sh} = 0 \frac{\partial}{\partial t}[\phi(\rho_w h_w S_w + \rho_s h_s S_s) + (1-\phi)\rho_r h_r] - \nabla \cdot K_a \mathrm{I}\nabla \mathrm{T} + \nabla \cdot \phi(S_w \rho_w h_w V_w + S_s \rho_s h_s V_s) - q_{sh} = 0 \quad (1)$$

Where, h is specific enthalpy of the fluid phase (J/kg), h_r is the enthalpy of the solid phase of the porous matrix (J/kg), ρ_r is the density of the solid phase of the porous matrix (kg/m^3), K_a is the effective thermal conductivity of the porous medium. (W/m·^{o}C), I is identity of third order matrix (dimensionless), T is the temperature (^{o}C), and q_{sh} is the flow rate intensity from the enthalpy source (W/m^3). The subscript phases w and s refer to water and steam. Equation (1) relates the rate of change of the fluid and the elbut of the porous medium to a net conductive enthalpy flux, then a net advective flux, and a heat source. The equation is written for unit volumes containing liquid, gas, and solid phases.

$$f(u) = 0 \quad (2)$$

Where f is the residual value vector of the nonlinear finite difference equation (W), u is the unknown 2x1 block vector (pressure, enthalpy) with length Na, and N_a is the number of active points in the mesh. The vectors f and u are of length $2N_a$, which can be divided into two components, since there are two equations with two unknowns for each active point. It can be assumed that all points are active, so $N_a = N_a$ (Kipp, 2008)

Data and Method

This study uses secondary data in the form of a plot type file which will be analyzed for secondary data structures, so that data will be obtained in the form of XYZ coordinates, temperature, as well as year and time-step data. Then the Mesh Grid will be made on the XYZ coordinate data, while the temperature data as well as the year and time-step data will be carried out in the process of classifying the temperature data per year. Based on these two processes will produce the temperature contour of the research location. The next stage is the process of creating a Graphical User Interface (GUI).

This research makes a program with the Python 3.6 programming language because it is easy to do basic research to Machine Learning. Modules are files that contain definitions and statements used for Python. The modules used in this program are the Tkinter module for the Graphical User Interface (GUI) which is used to create button and window displays, the Matplotlib Pyplot Library which is used to create plots based on the MATLAB program, and the Numpy Library which is used for reading data and writing arrays.

PROCEEDINGS
JOINT CONVENTION BANDUNG (JCB)2021
November 23rd – 25th 2021

So that from this stage we will get a GUI to visualize the subsurface temperature flow, which we call Hydroterm Viewer 2D. Where, the flow chart of this research can be seen in Figure 2.

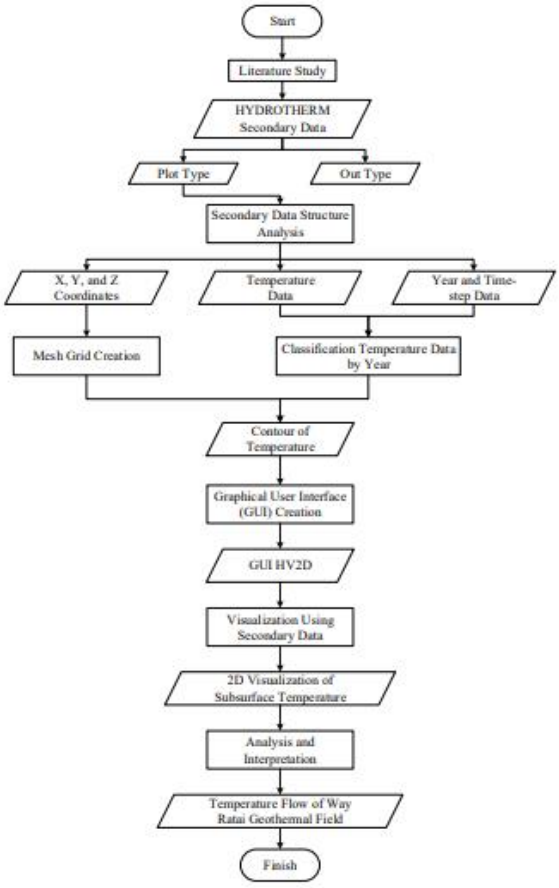

Figure 2: Research Flow Chart

Result and Discussion

- **Hydroterm Viewer 2D Program**

To use Hydroterm Viewer 2D (HV2D) program, first open the "Hydrotherm Viewer 2D.exe" file. Then the main menu window will appear containing a description of the description and options for visualizing the desired data. This program can visualize three types of data processed by the Hydrotherm Interactive v3.2 software, namely temperature, pressure, and water saturation. To start the visualization, select the desired visualization, after that a window will appear that is used to select data.

The data used in this program is the “Out_” file where there are data grid x, grid y, grid z, and the values of temperature formed in the cross-section with tenths of grid x. If you have selected the data, the program will automatically read the data and immediately visualize the data. The data being visualized as well as the “*Selanjutnya*” and “*Sebelumnya*” buttons that are used to move forward and backward years on the data to be visualized. The last process is to create a GUI. Making a GUI using the tkinter module so that HV2D interface looks neat and simple. It can be seen from Figure 3, that the next and back buttons come from the tkinter module which is used to move plot data from the database that was created earlier. Where in the next and back buttons there is a change in the value of the get variable_data_year. Based on those variables, re-plotting is carried out from the data that has changed according to the value at that time.

```
#tombol next dan back
button_next = tk.Button(plttemp,
                        text="Selanjutnya",
                        state = tk.ACTIVE,
                        command = lambda : Btn_Next(data_val_tstep))
button_next.place(x=1000, y=110)
button_next.config(width=10)

button_next = tk.Button(plttemp,
                        text="Sebelumnya",
                        state = tk.ACTIVE,
                        command = lambda : Btn_Back(get_data_year))
button_next.place(x=1000, y=140)
button_next.config(width=10)

def Btn_Next(data_val_tstep):

    global c
    c += 1
    data_val_tstep = get_data_year(0+c)
    fig.clf()
    for b in range(n_tstep):
        ax = fig.add_subplot()
        im = ax.contourf(xx,-zz,data_val_tstep[:,:,b],
                         cmap='jet',vmin = 0, vmax=1000, levels =10)
        fig.colorbar(im , ax=ax)
        ax.set_xlabel("X (Km)")
        ax.set_ylabel("Z (Km)")
        title = "Tahun ke %.0f" % float(tahun_l[c])
        ax.set_title(title)
        ax.axis('equal')
        canvas.draw()

def Btn_Back(data_val_tstep):

    global c
    c -= 1
    data_val_tstep = get_data_year(0+c)
    fig.clf()

    for b in range(n_tstep):
        ax = fig.add_subplot()
        im = ax.contourf(xx,-zz,data_val_tstep[:,:,b],
                         cmap='jet',vmin = 0, vmax=1000, levels =10)
        fig.colorbar(im , ax=ax)
        ax.set_xlabel("X (Km)")
        ax.set_ylabel("Z (Km)")
        title = "Tahun ke %.0f" % float(tahun_l[c])
        ax.set_title(title)
        ax.axis('equal')
        canvas.draw()
```

Figure 3: Next and back button creation.

The results of the HV2D program can be seen in Figure 4. From these images it can be seen that the HV2D program can visualize data properly and correctly, although there are still some shortcomings, namely there are still spaces between the data so that the data does not merge. Then, there is no vector for easy indication of flow movement on the contour. The advantage of HV2D is that it is easy to read the data and interact with buttons to advance or rewind the year on the data used to analyze the movement of the processed heat flow.

Figure 4: Main Menu of HV2D

- **Subsurface Temperature Flow Condition**

Then further research is carried out using secondary data and from numerical results, it can be seen that in

PROCEEDINGS
JOINT CONVENTION BANDUNG (JCB)2021
November 23rd – 25th 2021

the simulation results in Figure 5, showing that heat flows from the middle of the cross-section to the right of the cross-section.

From the HV2D program we can facilitate the analysis of heat flow based on secondary data, where currently the secondary data that obtained is 100,000 years with a fraction of 1,000 years. In HV2D, it can be clearly seen that there is a flow movement in each data fraction by looking at the next year and the previous year using the "*Selanjutnya*" and "*Sebelumnya*" buttons.

Based on the results of the simulation visualization, it can be seen that the heat flow of Way Ratai Mount subsurface moves to the left and right of the cross section which can be seen in the 40,000 to 100,000 years. The heat that moves flows from the middle of Way Ratai Mount towards the right side of the section where there is a point of manifestation of Margodadi (MGD). A possible interpretation that can be conveyed is the presence of a cover layer or a very thick rock cap that causes the vapor fluid to be unable to penetrate to the surface. This research still needs a lot of data to show the real Way Ratai geothermal system model.

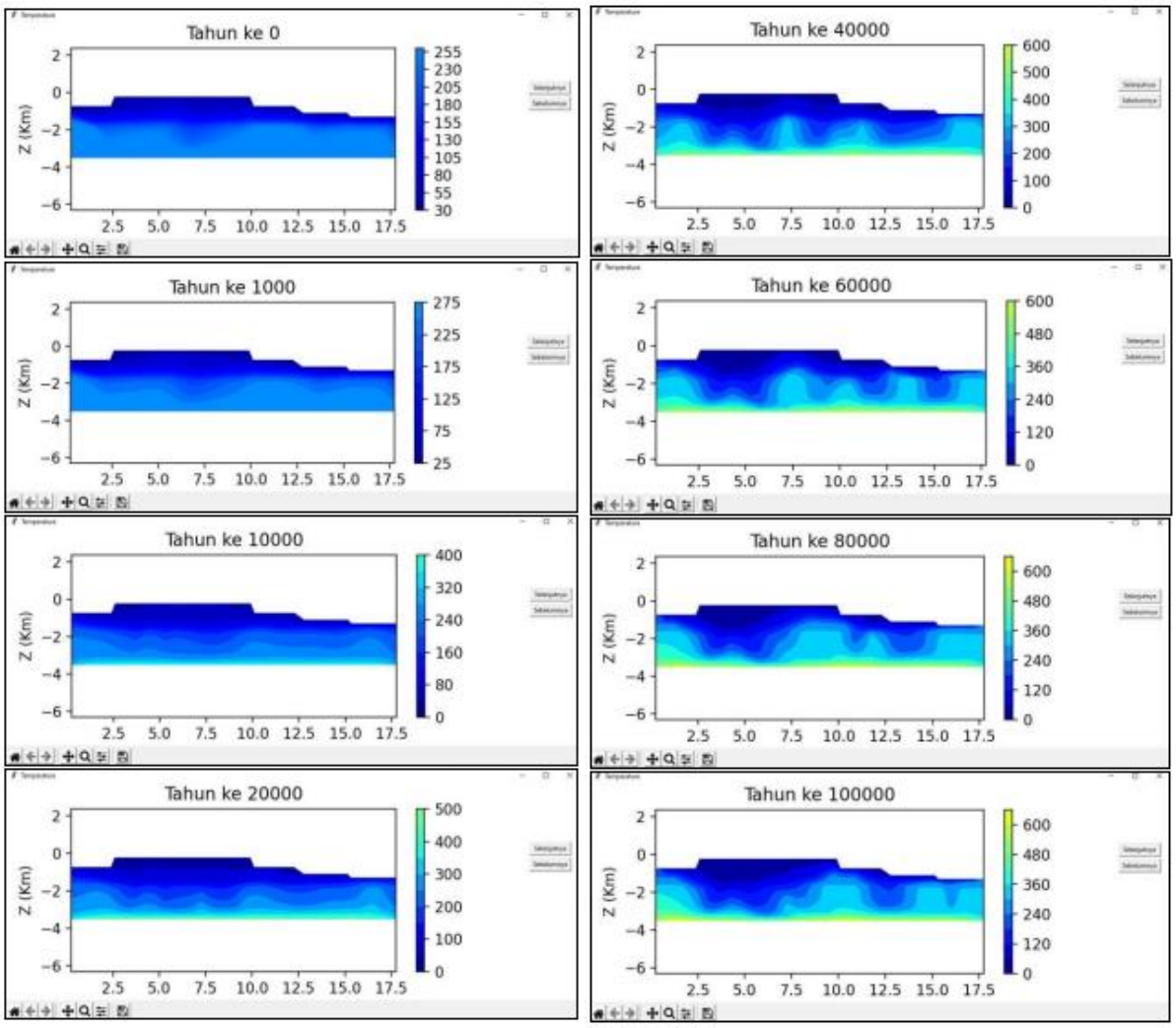

Figure 5: Visualization of temperature flow condition in several sections of time.

Conclusions

- Hydrotherm Viewer 2D is a program designed to run on all major operating system. HV2D provides simple Graphic User Interface (GUI), which makes easier. The next and back button makes easier for user to find the difference on temperature, saturation, or pressure countour.
- The visualization showed that the heat flows from middle of the cross-section to the right of the cross-section, and that can be justified by the Margodadi geyser manifestation in the right of the cross-section.
- A possible interpretation that can be conveyed is the presence of a cover layer or a very thick rock cap that causes the vapor fluid to be unable to penetrate to the surface. A lot of rock data and characteristics are still needed to model the exact heat and fluid flow.

Acknowledgements
The authors would like to thank the Geophysical Engineering University of Lampung and related parties who have provided advice and support in this research.

References

Direktorat Panas Bumi, 2017, *Potensi Panas Bumi Indonesia*. Direktorat Panas Bumi, Direktorat Jenderal Energi Baru, Terbarukan dan Konservasi Energi Kementrian Energi dan Sumber Daya Mineral, Jakarta.

Donovan, R., Karyanto, and Dewanto, O., 2018, Studi Sifat Termal Batuan Daerah Lapangan Panasbumi Way Ratai Berdasarkan Pengukuran Metode Konduktivitas Termal. Jurnal Geofisika Eksplorasi, Vol. 4 No. 3.

Gafoer, S., Amirrudin, A., M., and Sidarto, 1993, Peta Geologi Lembar Tanjungkarang, Sumatera, Skala 1 : 250.000. Bandung: Pusat Penelitian dan Pengembangan Geologi.

Goff, F., and Janik, C. J., 2000, Encyclopedia of Volcano: Geothermal System,Academic Press : A Harcout Science and Technology Company.

Kipp, K. L., Hsieh, P. A., and Charlton, S. R.., 2008, *Guide to Revised Ground-Water Flow and Heat Transport Simulator: HYDROTHERM – Version 3*. Virginia. U.S. Geological Survey.

PROCEEDINGS
JOINT CONVENTION BANDUNG (JCB) 2021
November 23rd – 25th 2021

Early Evaluation of Modified FPSO Utilization in Indonesia Towards Offshore Clusterization

Andi Magfirah[1], A Muhammad Athallah Naufal[1], Daniel Van Vriezer Situmeang[1]
[1]Universitas Pertamina

Abstract

Floating Production Storage and Offloading units (FPSO) has become a dominant application for offshore oil and gas fields when nearby infrastructure does not exist or considered too far away. Exploration and production activities have progressed into unlocking the potential of less attractive reserves in remote areas and challenging environments or known as marginal fields. Many explorations in offshore areas were successfully finding hydrocarbon, but due to certain circumstances, mostly too small reserves combined with lack of nearby infrastructures, these discoveries were considered economically unattractive. In the past, FPSO proven to be attractive option, however for some cases, traditional development using FPSO is still considered not economic. This paper will analyze the new concept of Floating Production Storage and Offloading (FPSO) utilization in unlocking the potential of the marginal field located offshore. By implementing the novel concept of clusterization based on the similarity of field properties, a group of marginal fields will be developed using this field similarity based clusterization concept. Two production development concepts, Conventional Fixed Hub and Novel Moving Hub, will be analyzed. The economic analysis and evaluation for the two concepts in field development concepts are based on the Net Present Value (NPV), Investment Return Rate (IRR), profitability index or Profit to Investment Ratio (PIR), and Pay Out Time (POT). These criteria are used as the economic indicators to screen and rank the concepts to select the most suitable concept for FPSO utilization in offshore areas, specifically for marginal fields. Each model scenario will be tested for its economic sensitivity to understand the critical factors that may affect the selection of clusterization concept using FPSO for marginal field. The result shows that Moving Hub scenario is more flexible and attractive in developing the marginal field across the offshore area that separated in a long-distance. In comparison, the Fixed Hub scenario shows that the pipeline cost will impact significantly as the field distance increase and may deteriorate the project value.

Keywords: Clusterization, Field Development, FPSOs, Marginal Field, Offshore

Introduction

Achieving Indonesia's ambition to produce one million barrels of oil per day (BOPD), the oil and gas industry needs to optimize mature fields or look for other reserves. According to IPA, 2017, Indonesia's hydrocarbon potential accumulates up to 70% of oil and gas reserves located in offshore areas. Therefore, offshore proves that most oil and gas potential is still largely unexplored and not developed optimally.

A marginal field is a field that may not produce enough net income to make it worth developing at a given time; should technical or economic conditions change, such a field may become commercial (Stig Svalheim, 2004). The definition of marginal depends on a combination of technical, commercial, and regulatory issues. In addition, marginal fields have several parameters, such as environmental concerns, political stability, access, remoteness, and the price and price stability of the produced oil, including condensate and/or gas. The marginal field, especially offshore, may have significant reserve that may be economical if located onshore or close to existing producing facilities, however several factors such as lack of nearby infrastructure, technological constraint, metocean challenges, and fiscal levies, may result in prohibitive development cost which turn to be uneconomical.

One of the floating facilities currently widely used is FPSO (Floating, Production, Storage, and Offloading) vessels. In recent days, Floating Production Storage and Offloading (FPSO) vessels have become a trend for offshore field development. It is caused by the convenience the FPSO provides. After being supported by FPSO technology, the industry can move toward efficient production from smaller fields while making production possible in remote areas where pipeline infrastructure did not exist. The flexibility of Floating Production Storage and Offloading, such as relocatable, easy to modify, rapid employment, makes it more be considered to be used offshore. In reality, 70% of FPSOs operating worldwide are converted by utilizing existing tankers through a conversion system.

Currently, there are around 196-200 FPSO facilities worldwide (World Energy Report, 2021). The Floating Production Storage & Offloading (FPSO) market is growing due to increased focus on developing offshore oil & gas production. The global FPSO market is expected to grow at a CAGR of more than 6.1%. The significant factors that drive the market include the increase in offshore drilling activities, flexibility, and installing the offshore assets as an FPSO is less expensive than building or installing permanent structures. Moreover, the FPSO is flexible towards movements. The aggregate

processing and storing facilities are built on a ship, and they can be connected to any pipeline present on an offshore asset.

In Indonesia, FPSO is vital because current exploration is more inclined towards offshore fields. The exploitation of fields that require production facilities over the sea and the optimization of the FPSO are carried out to improve the prospect of its economic value in offshore development in the future. This analysis of FPSO utilization is expected to assist the development of offshore fields for SKK MIGAS decision-making in managing FPSO assets to be used. Referring to the current condition of FPSO utilization in Indonesia, some FPSO is operated in mature fields where the production is already declining and makes the FPSO underutilized. On the other hand, many discoveries in offshore areas were also successfully explored but considered uncommercial or marginal fields. In this case, FPSO has the potential to be utilized. This paper will analyze the utilization of Floating Production Storage and Offloading (FPSO) in the marginal field located offshore.

Data and Method

The research begins by determining the marginal field that will be used as the basis for the use of FPSO. A marginal field is based on the terms and conditions of a production sharing contract that is not yet economical to be developed in a work area with the status of being in production.

After determining the type of marginal field using an economic feasibility test based on the parameters of NPV, IRR, and Payback Period, the FPSO model is developed in marginal areas to increase productivity when produced together. In this case, there are two scenario models that the researcher examines, namely Fixed Hub and Moving Hub. In the development of the Fixed Hub model, the FPSO facility is placed at a central point of the terminal in the middle of the marginal fields area. This development model involves a pipeline network that will be concentrated in the center where the FPSO is located. While the Moving Hub is a novelty model that researchers offer in this study, where the FPSO facility will pick up hydrocarbons in marginal areas in turn, without having to build a pipeline network. Each model scenario will be tested for its economic sensitivity to determine the right model for the development of an integrated FPSO in the future.

Result and Discussion

Field Base Clusterization

Field base clusterization is performed to gather marginal fields that have similar characteristics to be developed together. The clusterization model used is a hypothetical marginal field that is isolated from any other production infrastructure offshore. Using this clusterization method, different fields which are located far apart can be developed together.

Assumption

1. Three hypothetical marginal fields with similarities in their characters are used to build the analysis.
2. Field base case of the marginal field has an IRR less than 7%, profitability index less than 0.2, and still has a positive NPV.
3. Oil and gas production follows the three production phases of production build-up, plateau, and production decline. The forecasting future production trend is assumed based on the exponential decline analysis method.
4. The field is offshore located in remote areas with no near existing facility or pipeline network.
5. Produced gas is used for gas lifting and fuel.
6. Produced water will be injected for pressure maintenance.
7. The base case scenario for the oil price is 50 USD/bbl.
8. The tax and royalty assume to be 50% of taxable income and 10% of gross revenue, respectively.
9. The discount rate for base cases is 10%.

In this paper, the are three marginal fields, namely MG1, MG2, and MG3, owned by three different operators. These marginal fields built for analysis are located in the South China Sea offshore area where no near production or pipeline facility exists (figure 2). The detailed information of each field can be seen in table 1.

The MG1, MG2, and MG3 are an oil fields. The MG1 and MG2 is a light sweet oil with low and high gas content, respectively. The API gravity of MG1 and MG2 are 30 ^{o}API and 32 ^{o}API, respectively. Meanwhile, the MG3 is a sour oil with 0.8% H_2S, 15% CO_2 content, and 28 ^{o}API. The characteristic of the field is vital in designing the FPSO specification.

All the marginal fields have already been discovered with the oil existence that has been proven during the exploration drilling. However, owing to its low hydrocarbon reserve and isolated location, it is not attractive enough to be developed. The economic analysis in the case of conventional development scenario where each operator develops the field independently already been calculated. The result is shown in table 5. It is shown that all of the three fields have very low IRR, which is less than 7% and low PI with less than 0.2. These values indicate that it is not economic to develop the field in a conventional way. In this case, an integrated development scenario will be analyzed to make these marginal field to be possibly develop together.

Field Development

The development of a marginal field needs to consider many technical aspects because it is influenced by various fairly complex parameters. Thus, it is necessary to integrate various key parameters to determine the right scenario model. The main

parameters that affect the feasibility assessment of marginal field development are reservoir characteristics, including reservoir type and size, number of wells, overburden conditions, and others. In addition, metocean data is also very important in identifying scenarios for using FPSOs whose economic parameters are sensitive, including the matter of water depth.

Scenario performance assessment also needs to consider spare capacity on the available surrounding platforms in marginal field areas. This affects the decision to use FPSO in carrying out its functions optimally. If there are facilities with better revenue, the use of FPSO can be canceled. On the other hand, if the use of FPSO is considered more profitable, then equipment replacement is worth reviewing, in order to get as much revenue as possible. In addition, it is also necessary to review how much storage and offloading volume capacity is needed, considering that the scenario will be run on Fixed Hub and Moving Hub models. The drilling constraint factor also needs to be studied in depth. The last complexity consideration that needs to be studied is the level of commercialization, which is of course negotiable on transportation and processing tariffs.

The use of FPSO as the development concept is now well known and a technically feasible option for small field development. In this paper, the development scenario will focus on the production development concept. The production development method uses a development scenario with Floating Production Storage and Offloading (FPSO) with two scenarios, scenario I is to produce all the marginal fields at the same time using Centered Fixed Hub, and scenario II is to produce the field sequentially in an integrated production scheme using a Moving Hub.

Scenario 1: Fixed Hub

Three of the marginal fields will be developed using a centered floating production storage and offloading (FPSO), where each field will transport its production through a pipeline network that is connected to the FPSO (figure 3.a)

Based on the production forecast, each field will be produced for eight years before the NPV become negative. The operators have two options either renting or purchasing the FPSO. In this case, for eight years of production, a rented FPSO is used. The rented cost for the FPSO will be distributed proportionally based on the reserve of each field.

The surface design of the FPSO shall consider the hydrocarbon characteristics from three of the marginal fields. The weather condition that is considered moderate favors an external turret moored system with all the systems that would be required, that is, water injection, gas lift, and storage of the crude oil for export by shuttle tanker. To transport the production, a 20 in. of subsea pipeline should be constructed connected to the FPSO. The FPSO itself is located at the center of the fields. The detailed information of the distance from the field to the production facility is listed in table 3.

Scenario 2: Moving Hub

Three of the marginal fields will be developed using a moving hub of floating production storage and offloading (FPSO) (figure 3.b). Each field will be produced sequentially from one field to another. Three of the operators will join in a unit utilization development scenario to develop the marginal field. All the project will be structured as a joint venture to better manage the capital expenditures and distribute risk between parties.

This area favours an external turret moored system with all the systems that would be required, that is, oil and gas production facility and storage of the crude oil for export by shuttle tanker. The production will start producing from the MG1 field and move to the MG2 and MG3 field, respectively. This sequent adjusted to the field characteristic. Before the move to the MG2 field, owing to the high amount of its gas content, an additional gas compressor will be added for gas injection. While for the MG3 field, H_2S and CO_2 removal systems will be added to process the H_2S and CO_2 from the field. The moving operation is estimated will take seven days.

The flexibility of FPSO to be modified and allocated makes this concept more attractive and can be adjusted to the field conditions. In this case, the authors introduce a dynamic clusterization concept which means that this Moving Hub concept can be implemented in a different cluster. Not necessarily located in the same area, but also can be distributed all over Indonesia offshore area.

Economic Analysis

The economic analysis and evaluation for the two concepts in field development concepts are based on the Net Present Value (NPV), Investment Return Rate (IRR), profitability index, and Pay Out Time (POT). These criteria are used as the economic indicators to screen and rank the concepts in order to select the most suitable concept for FPSO utilization in offshore areas, specifically for marginal fields. The economic analysis is done using the Ms-Excel spreadsheet. The mathematical models are presented in appendix A.

Appendix B. highlight the list of capital and operational expenditure considered in this analysis. It shows the base case of the cost that is used. The oil price and operating expenditure are assumed to be constant the whole year. The 95% uptime and 5% downtime of the production facility are inputted in calculating the revenue.

Scenario 1: Fixed Hub

The total CAPEX that should be invested to implement this scenario is U.S. $205million, U.S. $183million, U.S. $202million for MG1, MG2, and MG3, respectively. The variation is owing to the different size and number of well of each field. It is

found that with 150km distance to the central production facility, the pipeline cost count about 45% - 50% of the total CAPEX (table 3). The NPV obtained from this scenario is U.S $46million, $46million, $45million for MG1, MG2, and MG3, respectively. There is an increase of U.S $5thousand – U.S $13thousand compared if the operators develop each field independently. The result also shows an increase of the IRR, which are 7%, 7%, and 9% for MG1, MG2, and MG3, respectively. The PI and payout time range from 0.23 to 0.25 and 4 – 5 years, respectively. The detailed list of economic parameters shown in table 5.

Scenario 2: Moving Hub

The total CAPEX that should be invested in implementing this scenario is U.S. $296million in total for three fields the whole year. The additional U.S. $49million and U.S $65million of CAPEX is needed when moving to another field. It was consist of the moving cost for FPSO and the drilling cost for the following field. The total NPV obtained from this scenario is U.S $168million, which means that each parties will obtain U.S56million. The IRR for the project using this scenario is 14% and 3 years of payout time. The detailed list of economic parameters shown in table 5.

Sensitivity Analysis

The sensitivity analysis is critical to be taken into account considering the uncertainty of the key input parameters in economic analysis. In this case, variation of 5% within a range of -30% to 30% from the base case is used. The parameter with the steepest slope is the most sensitive (figure 4). It is shown that oil price and and CAPEX is the most sensitive parameters in both scenarios. Comparing these two parameters between two scenarios, the oil price and CAPEX is more sensitive in Fixed Hub scenario. When the analysis focus on the CAPEX itself, it is found that pipeline cost and the parameter of pipe length is the most sensitive variable of CAPEX. As the pipeline cost increase to 45 USD/in-km, the NPV is negative for the Fixed Hub scenario. The length of pipeline that exceed 200km also resulted the negative NPV.

Conclusions

The result shows that in the case of Fixed Hub and Moving Hub, Moving Hub scenario make the highest profit. The sensitive behavior of the pipeline cost itself shown that the Fixed Hub scenario is not suitable for field that located far apart. This condition makes the Moving Hub scenario outstanding. Moving towards the offshore field potential, there are 70% of Indonesia reserves potentially lie in offshore areas. Adopting the concept of Moving Hub will allow the development of any marginal field located over Indonesia offshore area.

Acknowledgement

We would like to thank Ir. Puput Aryanto Risanto, IPM for providing guidance and feedback throughout this project. The meetings and conversations from the perspective of facility engineer were vital in inspiring us to form a comprehensive and objective result. We would also like to thank Mr. Avidianto Setiawan M.Sc., for his support in completing this project.

References

About an FPSO. (n.d.). MODEC. https://www.modec.com/fps/fpso_fso/about/index.html [15 September 2021]

Akinwale, Y. O. & Akinbami J.K. 2016. Economic Evaluation of Nigeria Marginal Oil and Gas Field using Financial Simulation. International Journal of Economics and Policy. ISSN: 2146-4553

Barton, C.M. (2019). FPSO Market Set for Revival. https://www.offshore-mag.com/rigs-vessels/article/14038760/fpso-market-set-for-revival [17 September 2021]

Barton, C.M. et all.2019. 2019 WORLDWIDE SURVEY OF FLOATING PRODUCTION, STORAGE AND OFFLOADING (FPSO) UNITS. Houston. Offshore Magazine

Field Developments and Technical Solutions – Marginal Fields. Society of Petroleum Engineers. (n.d.). Retrieved October 24, 2021, from https://www.spe.org/en/training/courses/field-developments-and-technical-solutions-marginal-fields/.

Hong, C. et all. 2017. Subsea Production Layout: Design and Cost. Norway. ASME 36th International Conference on Ocean, Offshore, and Article Engineering DOI:10.1115/OMAE2017-62488

Kue, Y. N., & Orodu, O.D. 2006. Economic Analysis of Innovative Approaches to Maginal Field Development. China University of Geoscience. Society of Petroleum Engineers DOI:10.2118/106001-MS

IPA. (2017, May 17-19). "Oil and Gas Industry Multiplier Effect." Jakarta, DKI Jakarta: Indonesian Petroleum Association (IPA), May 17-19. Retrieved from http://www.ipa.or.id/assets/images/news/Infographic%202017.pdf.

Journal, G. 2002. FPSO conversion. Marine Engineers Review, JUL., 6.

Khakzad, N., Reiners,G..Safety of Offshore Topside Processing Facilities: The Era of FPSOs and FLNGs. Elsevier Inc.

Newswire, P. R., York, N., & York, N. 2013. Floating Production Storage and Offloading (FPSO) Industry - Global Market Analysis, Competitive Landscape and Planned Projects to 2016. April, 99..

Schmidt, H., Sridhar, R., Rehn, C.F., 2014. Optimal Design of A Concept FPSO. ESD.77/16.888 Multidisciplinary System Design Optimization (MSDO), MIT

The Independent Natural Gas Information Site. (n.d.) Gas Pipeline. Natgas.info http://www.natgas.info/gas-information/what-is-natural-gas/gas-pipelines

Svalheim, S. (2004). *Marginal Field Development - A Norwegian Governmental Perspective*. Retrieved October 24, 2021, from http://www.ccop.or.th/ppm/document/SEM3/10_Marginal%20Field%20_NPD.pdf.

APPENDIX A: **Mathematical Equation for Economic Feasibility Analysis**

- **NPV (Net Present Value)**

$$NPV = \sum_{t=1}^{n} \frac{CF_i}{(1+k)^n}$$

Where:
CF_i = Cash Flow on Year-i
k = Discount Rate
n = Number of Project Life

- **Internal Return Rate**

$$IRR = \sum_{n-1}^{n} \frac{C_t}{(1+k)^n} - C_o$$

Where:
C_t = Net Cash Inflow during Period t
k = Discount Rate
n = Number of Project Life
C_o = Net Cash Inflow on initial

- **Profitability Index (PI)**

$$PI = \frac{Revenue\ @NPV\ Interest\ Rate}{CAPEX}$$

- **Revenue**

$$Revenue = Total\ Oil\ Production * Oil\ Price * Uptime$$

- **POT (Pay Out Time)**

$$POT = t_a + (t_b - t_a)\left(\frac{c_a - 0}{c_a - c_b}\right)$$

Where:
t_a = Cumulative Year @NPV Positive
t_b = Cumulative Year @NPV Negative
c_a = Cumulative Revenue @NPV Positive
c_n = Cumulative Revenue @NPV Negative

APPENDIX B: **Technical Cost Estimates of Development Cost**

OPEX		
Operation and Variable Cost	:	$50,000/Day
Abandonment Cost	:	$1,000,000
CAPEX		
Well Cost	:	$15,000,000/Well
Facility Cost (Renting Cost FPSO)	:	$50,000/Day
Up-Time	:	95%/Year
Down time	:	5%/Year
Moving Cost (7 Days)	:	$200,000/Day
Pipeline Cost	:	$30,000/in-km
FPSO Cost	:	$118,000,000

PROCEEDINGS
JOINT CONVENTION BANDUNG (JCB) 2021
November 23rd – 25th 2021
List of Table

Table 1 Marginal Fields Description

		Marginal Field 1	Marginal Field 1	Marginal Field 1
Field Description	Field Name	MG1	MG2	MG3
	Location	South China Sea	South China Sea	South China Sea
	Province	South China Sea	South China Sea	South China Sea
	Basin	X	X	Y
	Country	Indonesia	Indonesia	Indonesia
	Water Depth (m)	250	300	245
	Operator	OPA	OPB	OPC
	Project	JC-1	JC-2	JC-3
	Life Cycle	Appraisal	Appraisal	Development
	Field Type	Oil Field	Oil Field	Oil Field
	Distance to Shore (m)	351.2	428.6	269.9
	Area (km^2)	36	33	40
	Number of Well	4	3	4
	Expected Facility	FPSO	FPSO	FPSO
	Discovery Year	2015	2017	2013
	Expected Approval Year	2020	2020	2020
	Expected Start-Up Year	2023	2023	2023
Hydrocarbon Characteristic		Sweet Oil	Sweet Oil	Sour Oil
Reserve	Crude Oil (MMbbl)	11.5	10.97	12.2
	Condensate	-	-	-
	Gas (BCF)	2	4	2

Table 3 Flowline Length and Cost Estimation for Fixed Hub Scenario

Fixed Hub				
Flowline length and layout of manifold for FPSO application				
Field	Well	Flowline Length (m)		Total Cost (MUSD)
		Subsea Wellhead to Manifold	Manifold to TDP	
MG1	A1, A2, A3, A4	1400	150000	93,360
MG2	B1, B2, B3	1400	150000	92,520
MG3	C1, C3, C3, C4	1400	150000	93,360

Table 4 Flowline Length and Cost Estimation for Moving Hub Scenario

Moving Hub				
Flowline length and layout of manifold for FPSO application				
Field	Well	Flowline Length (m)		Total Cost (MUSD)
		Subsea Wellhead to Manifold	Manifold to TDP	
MG1	A1, A2, A3, A4	1400	500	3660
MG2	B1, B2, B3	1400	500	2820
MG3	C1, C3, C3, C4	1400	500	3660
			Total Cost	10,140

Table 5 Economic Parameter of Fixed Hub and Moving Hub Scenario

	Independently Developed (Each Field Purchase an FPSO)			FIXED HUB			MOVING HUB
	MG1	MG2	MG3	MG1	MG2	MG3	MG1, MG2, MG3
CAPEX (MUSD)	210,660	195820	207000	205,068	183,145	202,027	295,940
NPV (MUSD)	32,153.5	34,274.5	41,984.7	46,201	46,096	45,813	168,219
IRR (%)	6	5	5.7	7	7	9	14
PI	0.15	0.17	0.19	0.23	0.25	0.23	0.5

PROCEEDINGS
JOINT CONVENTION BANDUNG (JCB) 2021
November 23rd – 25th 2021

List of Figure

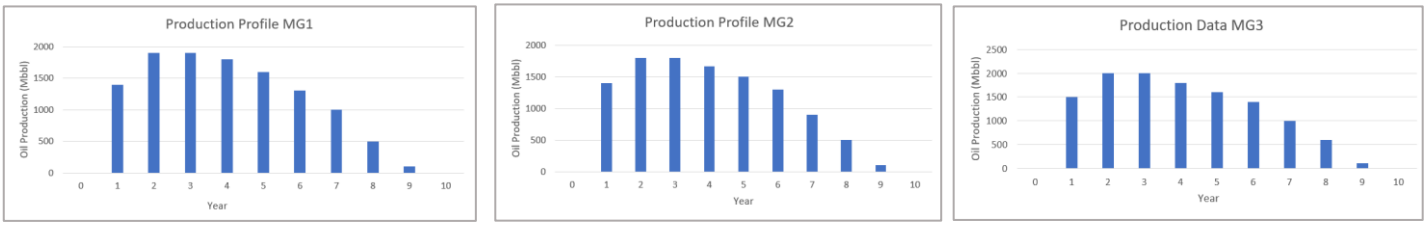

(a) Marginal Field MG1 (b) Marginal Field MG1 (c) Marginal Field MG1

Figure 1Yearly Production of Crude Oil for The Hypothetical Marginal Field

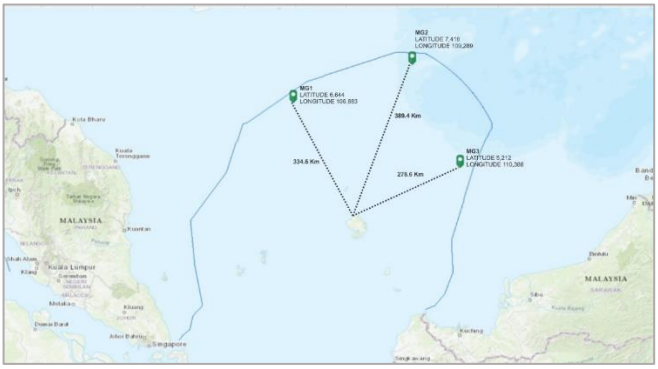

Figure 2 Marginal Field Location

The figure shows the location of the marginal field cluster. The distance to the shore (Riau Island) are 351.2m, 428.6m, 269.9m, for MG1, MG2, and MG4, respectively.

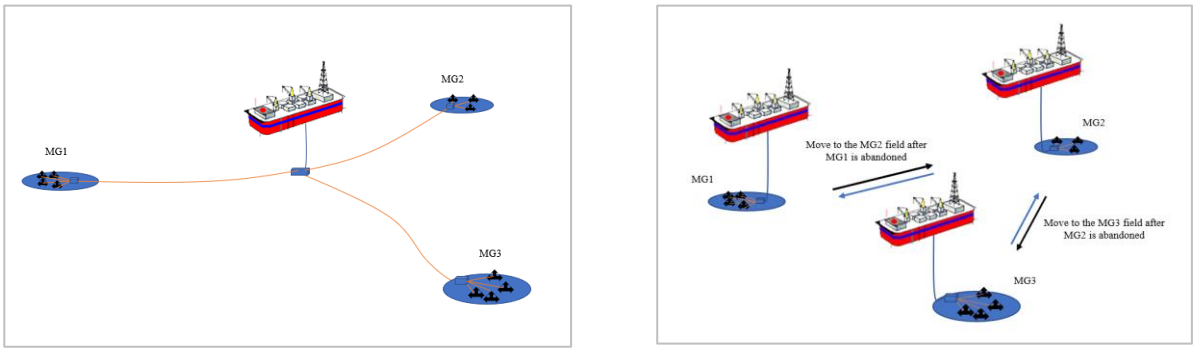

a. Fixed Hub Concept with Central Production Facility b. Moving Hub Concept with Sequential Production Scheme

Figure 3 Production Development Concept.

Figure (a) shows that additional pipeline network need to constructed to implement the concept, while figure (b) shows that the field will produce sequentially, the sequence of the production will be adjusted to gain the most profit.

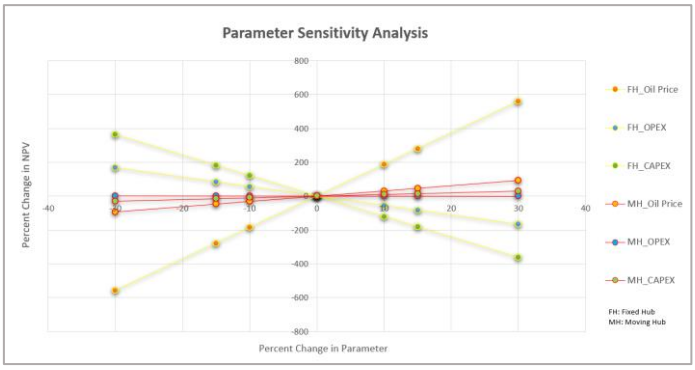

Figure 4 Sensitivity Analysis

The figure shows that the steepest slope is the most sensitive parameter. It shows that the parameter become more sensitive in the Fixed Hub Scenario and more stable in Moving Hub Scenario.

PROCEEDINGS
JOIN CONVENTION BANDUNG (JCB) 2021
December 1ST – 3rd 2021

UNDERSTANDING LAND ACQUISITION AND LOCAL COMMUNITY ISSUES IN INDONESIA GEOTHERMAL EXPLORATION PROJECT

Amrullah Farad Sunaryo[1], Dorman Purba[1] Nabila Azarine Zahraf[1] Erica Prasetyo[1], and Mochamad Risyad Rizkyafdhal[1]

[1]Enerka Bhumi Pratama, Cibis Nine Building 11th Floor, Jakarta Selatan 12560, Indonesia;

ABSTRACT

Indonesia is in the process of increasing geothermal energy utilization in its energy mix. The identified challenges considered by many lies in the exploration phase since most of geothermal prospect in Indonesia has not yet been explored properly. Obviously, in doing exploration activities, any geothermal developers will have to deal with land acquisition and local community issues.

Several potential issues in the land acquisition process are lack of understanding of regulations, failure to determine fair prices, local community resistance, lack of communication skill from both sides, technical incompetence, and environmental impacts. Failure to address these issues will potentially bring failure in getting the required land, which consequently leads to failure in completing the exploration project.

This study aims to discuss in detail several potential problems that might occur in land acquisition activities that are most likely correlated with local community rejection, based on literature review and interview with practitioners who has experiences in land acquisition. This research aims to provide a simple guidance yet useful for geothermal developers to mitigate problems in the land acquisition process. Additionally, this paper also summarizes some aspects related with land requirements, regulations, standards, and case studies, which relevant to geothermal exploration project in Indonesia.

Keywords: *Geothermal, land acquisition, community, exploration, drilling, rejection, livelihood, Indonesi*

1. INTRODUCTION

1.1. Current Development of Geothermal Energy in Indonesia

No	Field	Unit	Total Capacity	Reservoir	Technology
1	Sibayak	Monoblok 2 MW. Unit-2–3, 2 × 5 MW	12 MW	Water dominated	Single-flash
2	Ulubelu	Unit-1–3; 3 × 55 MW	165 MW	Water dominated	Single-flash
3	Salak	Unit-1–3, 3 × 60 MW. Unit 4–6 3 × 65.6 MW	377 MW	Water dominated	Single-flash
4	Wayang Windu	Unit-1: 110 MW Unit 2: 117 MW	227 MW	Water dominated	Single-flash
5	Patuha	Unit 1: 55 MW	55 MW	Water dominated	Single-flash
6	Kamojang	Unit-1: 30 MW Unit 2–3: 2 × 55 MW Unit 4: 60 MW Unit 5: 35 MW	235 MW	Vapor dominated	Dry steam plant
7	Darajat	Unit-1: 55 MW Unit-2: 94 MW Unit 3: 121	270 MW	Vapor dominated	Dry steam plant
8	Dieng	1 × 60 MW	60 MW	Water dominated	Single-flash
9	Lahendong	Unit 1–6: 6 × 20 MW	120 MW	Water dominated	Single-flash
10	Ulumbu	Unit 1–4: 4 × 2.5 MW	10 MW	Water dominated	Single-flash
11	Mataloko	2.5 MW	2.5 MW	Water dominated	Single-flash
Total			1533.5 MW		

Fig. 1. Geothermal Powerplant in Indonesia (N.A. Pambudi, 2017)

Indonesia is a country that has enormous geothermal potential. Indonesia has geothermal energy potential of more than 23.9 Gigawatts (GW) (EBTKE, 2019). This abundance of geothermal resources can help meet the increasing demand and increase the electrification rate. Based on data from the Direktorat Panas Bumi, currently Indonesia has utilized 8.9% or 2,130.6 MW, the utilization of geothermal energy in Indonesia can be considered quite small in terms of the amount of potential it has. Therefore, it is known that the government is targeting an increase in geothermal utilization to 7,241.5 MW or 16.8% in 2025.

If we compared Indonesia's geothermal development with other countries, it is indeed still classified as low. But there are several fields we could find in Indonesia that were successful to install geothermal powerplant as shown in the table below.

There are a lot of issues that make geothermal development is challenging such as government policy, regulation, incentive infrastructure, and predominantly when doing the processes land acquisition. Land plays an important role as a financial asset. The process of land acquisition takes place gradually, which land has the potential to be developed. Even when the process of land acquisition itself goes well, there are still an issue from local community. The purpose of this preliminary study is to discuss in detail several potential problems that might occur in land acquisition activities

1.2. Research Objective and Method

1.2.1 Research Objective

This study aims to discuss in detail several potential problems that might occur in land acquisition activities that are most likely correlated with local community rejection, based on literature review and interview with practitioners who has experiences in land acquisition. This paper also are completed by land requirements, regulations, standards, and it hopefully could be a simple guidance for geothermal developers to mitigate problems in the land acquisition process.

In order to ripen the main questions, this research started by offering question below:

1. What is the land acquisition for?
2. What is the effect on geothermal exploration from regulations that governing land acquisition?
3. How much land is required for infrastructure specifications?
4. How long the land is needed for the geothermal development project?
5. What procedure are needed before buying land?
6. What are the challenges of geothermal land acquisition? How to prevent that?

1.2.2 Research Method

In order to know how several aspects relate to the land acquisition process for a geothermal project in Indonesia and it could be made up as a guidance, the authors conducted a literature review of various sources regarding laws and regulation of geothermal land acquisition, technical aspects that must be concerned, the procedure of land acquisition and challenges that will meet them on geothermal project land acquisition in Indonesia. In addition, we also interviewed practitioners who already had been through the land acquisition process to get the point of view from them based on real experience.

2. RESULTS AND DISCUSSION

2.1 Laws and Regulation

Regulations that greatly affect the process of geothermal land acquisition in Indonesia in terms of exploration are Presidential Regulation Number 71 of 2012 and Government Regulation Number 7 of 2017. Meanwhile, from the investment side, it is influenced by the IFC (International Finance Cooperation) Performance Standard-5.

2.1.1. Presidential Decree No. 71 of 2012

Referring to Presidential Decree No. 71 of 2012, the land acquisition process related to the public interest must be led by a governor where the governor will form a team consisting of the mayor, provincial level task force, agencies requiring land, and other supporting agencies (Dewi et al., 2013).

2.1.2. Republic of Indonesia Law No. 5 of 1990

The prospect of geothermal that is located in conservation areas and protected forests and requires test drilling to make the exploration process limited to land use acquisition. Because there is Law no. 5 of 1990, especially in articles 1, 2, and 3 which emphasize aspects of ecosystem balance.

2.1.3. Government Regulations No. 7 of 2017

In Government Regulation No. 7 of 2017, land acquisition needs to be stated in IPB (Geothermal Exploitation Permit) which consists of commitments and must be approved by the Director General and IPB holders. Exploration commitments that must be fulfilled are in the form of financial guarantees to drill exploration wells.

2.1.4. IFC Performance Standard-5

One of the main investments in the energy sector in Indonesia is funding from the World Bank, where the agency enforces a fairly strict IFC-5 Standard of Work. This standard is the reference for most energy sector loan operators. The essence of this regulation states that displacement of affected people must be strictly avoided. However, if there is something that has a major and significant impact on the wider community, the company can provide compensation in the form of physical compensation including providing cash compensation for affected people including plants and buildings, providing resettlement places and housing, facilitating the relocation process, and livelihood restoration program.

Government Regulation No. 7 of 2017 can be a way out for cases of land use in protected forest areas, because the agency entitled to issue IPB is the Ministry of Energy and Mineral Resources, which must coexist with the Ministry of Environment and Forestry. Therefore, technical design is very important to reduce the impact of changes in forest ecosystems.

2.2 Technical Aspects

Acquisition of land is carried out to do geothermal exploitation activities. For determining whether an area has geothermal prospects, exploration is implemented to determine the presence of hot water or steam in the reservoir. The exploration activity itself is divided into several parts, namely preliminary exploration, further exploration, and exploration drilling (Syahda et al, 2019). The objectives of the preliminary exploration activities are to determine the areas that become geothermal fields that show manifestations on the surface, as well as obtain a geological description of the area. After conducting preliminary exploration, further or detailed exploration, which collects data through field surveys. To sort out the land that will be used for geothermal exploration, data is required using a field survey. The survey consists of geological, geophysical, hydrological, and geochemical surveys (Juanda, 2020). The survey was conducted to identify that an area is likely to contain geothermal sources and has economic value to develop. After that, exploration drilling activities were carried out which proved that there was a presence of geothermal heat below the surface.

Towards conduct drilling, several infrastructures are needed to support geothermal exploration activities.

2.2.1 Access Road

Road access is one of the important things for geothermal exploration. This road access will facilitate the implementation of exploration activities starting from the delivery of tools, equipment, and materials to the area until eventually facilitating mobilization during drilling. Land acquisition at the start of a project is usually based on gaining access from a road built by the government to the desired area where exploration will take place, which is commonly referred to as a drilling site or well pad (Purba D.P.,et.al, 2020).

Geothermal systems are frequently found in volcanic environments, where the terrain is steep and access is difficult. which implies that for usable access roads to be made, massive earth has to be excavated (Miyora, 2015). To open a new road, the construction of this road will destroy forest areas, vegetation, and traffic activities for the general public. The width of land to be used for the construction of this road generally ranges from 8 to 15 meters which will include road and streamline access (Purba D.P.,et.al, 2020).

2.2.2 Well pad

Well pad is a very necessary infrastructure for drilling. This is because the well pad is a well facility which is the main asset in carrying out geothermal development projects. Well

pad contains the basement which is where the hole is drilled. A well pad might have a recirculation pool which is used to fill water from the holes drilled and will be reused for drilling.

According to industry estimates, the average size of a multi-well pad for the drilling and fracturing phase of operations is 0.014 km; 006 km² is the estimated average after the required partial reclamation (SGEIS 2011, chapter 5). The area of the well depends on what type of well will be drilled. Geothermal well types are classified into 3 types based on the size or diameter of the well bore, specifically big hole, standard hole, and slim hole. Slim and standard hole well have a size in width and length each one 40 meters and 50 meters; 70 meters and 120 meters

A well pad is a relatively flat work area within the geothermal field (surface location) that is used for drilling a well or wells and producing from the well once it is completed (TEEIC, 2015). The well location is at least 100 meters from housing, roads, and public construction (BSN,2002). The existence of a gap between the well location and community facilities will mitigate the negative impact of drilling on the community

2.2.3 Base camp, Warehouse, and Site office

Base camp, warehouse, and site office this place was built in the early stages of the project. Base camp it is no less important for geothermal project development. This place is a place to live and rest for workers. All drilling materials, such as casing, liner, wellhead, cementing material, and drilling fluid material, are stored in a warehouse. A site office, on the other hand, is a working space established near the project site (Purba D.P.,et.al, 2020)

This area usually has an area of 42.000. But depending on the number of rigs operating and also the more rigs built, the larger the building area. This place is located not far from the main well drilling area to facilitate project work.

2.2.4 Staging area

Drilling necessitates the use of bulky hardware as well as consumables. This area is used to store various materials used in the construction of well pads and drilling structures. The staging area is usually chosen in the flat area between the well pad and the basecamp, closer to the well pad than to the basecamp. The staging area typically requires much less land than the basecamp and well pad area, which can range from 1.000 to 5.000 (Purba D.P.,et.al,2020).

2.2.5 Period of time the land is used

The development of geothermal projects necessitates a lengthy period of time therefore, the land is used for an extended period of time. According to Permen ESDM No.36 tahun 2017, geothermal exploration activities can take a long time. The time is divided into two parts: preliminary survey and exploration along with pre-feasibility. This activity requires a long duration with a span of approximately 7 years. Then the land is used for exploitation and utilization of geothermal which takes more than 30 years.

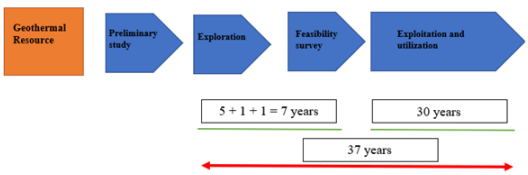

Fig. 2. Indonesia Geothermal Development Period

2.3 Land Acquisition Procedure

It is necessary to know the landowner's status before buying the land for the project. There are two types of land status, they are land state and non-land state. Each of the lands has several procedures that must be done.

2.3.1 State Land

If the land available is state land, there are several processes that should be follow.

2.3.1.1 Valuation Process

After surveying suitable land for the project, it is important to know the land prices in the area. To know the land prices in an area, do a land prices valuation can be a solution. A land prices valuation is conducted to achieve a reference for determining the nominal value. Land prices can be affected by the existing crops and land statuses. It is possible to use consulting services to research prices for the land.

2.3.1.2 Negotiation Process

After getting a land price from the valuation process, The Land Acquisition Team will negotiate with the landowner by giving a benchmark price. The negotiation will be successful if the landowner and the negotiator have a deal on the final price.

2.3.1.3 Ownership Process

To accomplish a successful transaction, the negotiator team need proper legal documentation. There is identification of the legal status of land to acquired that divided into two, forestry area and non-forestry area, and based on (OTP Geothermal, 2013), the documentation needed are:

Forestry Area:

1. Proof of Heritage and Inheritance
2. Surat Pernyataan Penguasaan Fisik Bidang Tanah
3. Signature of adjacent owner
4. Kartu Tanda Penduduk (KTP)

Non-Foresty Area

1. Proof of Heritage and Inheritance
2. Surat Keterangan Tanah signed by the Village Head and subdistrict Head
3. Signature of adjacent owner
4. Kartu Tanda Penduduk (KTP)

2.3.1.4 Purchase and Financial Transaction Process

The process to have legal ownership for forest area and non-forestry would be different but the transaction method will be decided at the discretion of the landowner (OTP Geothermal, 2015). To finalize the transaction process will need a few documents required. The forestry area needs Surat Pelepasan Penguasaan Hak and the non-forestry area needs Berita Acara of Transaction and Surat Pelepasan Hak Ganti Rugi. In the forestry area, the document required the detail of the provision of the peace settlement and should be conducted by a notary. While in a non-forest area will involve a certified notary to legalize the area and payment of compensation will follow en-suite. After this step is done, the payment can be made with several steps: cash-call and transfer by finance, witness allowance (approved documents on rates are available) and photographs of each transaction (OTP Geothermal, 2015).

2.3.2 Non-State Land

If the only suitable land available is non-state lands, there are several steps that should be follow in each agreement.

2.3.2.1 Voluntary Land-Use Agreement
This agreement happens when the local landowner willing to give the land for the project team but in consideration the project team will give the community member the benefit of the project.

2.3.2.1 Land-Purchase through Negotiated Agreement
This agreement happens when the local landowner willing to sell part of their land and the land may be purchased through negotiated agreement following the Land Act.

2.3.2.2 Third-Party Verification
This agreement happens when both voluntary land-use agreements and negotiated purchase agreements will be verified by a third-party Non-Government Organization (NGO) (Asian Development Bank, 2015).

2.4 Challenges in Geothermal Land Acquisition

2.4.1 Based on Literature Review

Based on the literature review, this research categorizes some aspects that can be the main challenges for the land acquisition.

2.4.1.1 Technical

As an engineer, this aspect must be considered before designing land necessity. Land boundaries are often lost/damaged, documentation has not been handled properly, and some lands that do not have official certificate documents are some of the technical challenges that should not be ignored (Pertamina report, 2018). If they had to, they would have caused the potential for reduced land assets, the potential for land misuse, the potential for conflict with the surrounding environment, difficulty to inventory and consolidate company land. Therefore, the developers can use a tool like Pertamina had which is in the form of a GIS (Geographic Information System) based on land acquisition application that records all land data from the procurement process, measurement, payment, and the issuance of land acquisition certificates into a centralized system using the PGE LAND application.

2.4.1.2 Internal (Community) Problem

Internal problem is the most frequent aspect that happens in almost every land acquisition process. Local people generally do not know buying and selling mechanism and lack understanding of the geothermal project (Ginting et al, 2017). These problems can lead to delay the project because the developer must spare extra time and even money to socialize them.

Besides that, land in several regions in Indonesia is not owned by one person but owned communally by one the whole village (Purba et al, 2021). This means that all decisions related to the land must be discussed together and take a long time, especially if one of the community members disagrees. It might take a long time, so the developer has to wait or find another land if it is reasonable.

2.4.1.3 Refusal of Inhabitant

From the previous point, it only happens when people do not know about the geothermal project at all. However, this aspect is one of the resistances that internal residences already know a little bit about a geothermal project but not in detail. They do not meet adequate information from trustworthy sources so they are afraid of being deceived by the company (Purbat et al, 2021). Another example is they are worried that the drilling activity would cause a Lapindo-like even though they have been explained a technical aspect from the developer. These effects might make them unwilling to sell their land, and it causes a delay for the geothermal project (Purbat et al, 2021). Thus, the ultimate task of a facilitator is not to explain the geothermal project in technical terms but to serve as a bridge in any disputes that occur between the people. Moreover, developing direct-use facilities to bring economic impact to local communities while serving as geothermal education media. This campaign is suggested to be conducted in the very early phase of the exploration project to increase local community awareness of the geothermal exploration project before the project itself commenced.

Apart from that, some people do not allow the geothermal project because they think geothermal development can destruct a historical value in the hot spring area (Ginting et al, 2017). Since the developer has to respect everyone's faith, it must pay attention to be careful, maintain and build the value of local community wisdom.

2.4.1.4 Social Environment

Developing geothermal energy does not mean it has not social environment issue. As an engineer, you also have to look forward to this aspect. Before you negotiate a land, you have to think about the condition of land where you want to construct. If you do not notice appropriately, it will cause erosion or even a landslide (Supremenergy, 2017). Hence, mitigation is needed to limit impacts on air, water, agricultural land, and wildlife habitats. In addition, developers have to consider the needs of the local community, such as road improvements, public health, and other facilities like schooling and housing (Supremenergy, 2017).

2.4.2 Based on Practitioners Interview

Referred to the interview section, there are some factors that can be the main challenges for land acquisition. They will be discussed by each practitioner. This section provides info that is not available in the literature review.

2.4.2.1 Dorman Purba

Dorman currently works as an energy consultant in the world bank. He has been active in geothermal projects since 2014, particularly between 2014 and 2017 which he succeeded in two land acquisition projects in North Sumatra and East Nusa Tenggara. Based on his experience, there are some obstacles in the land acquisition process.

1. Technical

There was a case when the landowner whose land in the center of the project. He did not want to sell it, so it could fail the entire project. It could be done after a long time of negotiation until it could meet at a fair price.

2. Price

When we want to acquire the land of the geothermal project, we normally need not only a village, so we have to negotiate

with more than one village. Because every village does not have the same price for a meter of land, the developer has to make a smart plan for the transaction scheme. If it had not been made, the price would have experienced a drastic increase, and it will cause an imbalance in the project balance sheet.

3. Local Community

There were some land owners who lived there, but he had not property rights or place where they live. There were also some landowners when they were in negotiating, and their family members were not there. Moreover, there was customary land where it was not clear who owned it. These aspects will hamper the transaction process. There is no way to solve that unless you want to wait in an unspecified time or you find another location.

4. Government

Land acquisition surely involves the local government coordinating with stakeholders. There was a case when government delivers a different perception as the developer had told about, so it needed extra time to socialize again with the local residences. In the future, the developer has to ensure the understanding of the project is well delivered enough to the government.

5. The Incitement of Other Parties

This is the aspect that the developer does not underestimate because it can happen at every stage of the project. It happens when there are some people in the village whose land which it is not sold while the neighbor's land is sold to the developer, so they become envious. It can be dangerous because they will incite others to do not sell the land, which can hamper another land acquisition process. This problem can be solved through negotiation at a fair price.

There are some tips from Mr. Dorman for geothermal land acquisition in the future, such as training and development of land acquisition for people involved in geothermal projects, land mapping in Indonesia could be improved, and permit access should not be complicated and increase quantity of geothermal practitioner.

2.4.2.2 Vicky Chandra

Vicky is a geologist at PT. Geo Dipa Energy who has been participating in geothermal projects for nine years. He has completely finished a geothermal land acquisition project from 2015 to 2017 in East Nusa Tenggara. Regarding his past experience, he classifies the land acquisition process's resistances into some elements.

1. Technical

As an engineer, you have to be able to design a geothermal land regardless of size. In fact, the land that you finally acquired is not always as you planned before, so you have to be competent in it. Besides that, do not forget to pay attention to other aspects related to technical, such as the environment. In some case, there was a case when drains are blocked by the project, and even worse, causes a landslide. Therefore, you have to master your competencies, not only one field.

2. Price

The land that the developer usually acquired the land where it is plantation land, so lots of plants are growing there. Normally, it has a problem with the pricing. It is very difficult to determine the correct calculation method, so it needs a consultant to help us. However, the landowner sometimes does not agree with the price, and they want a higher price. To solve this problem needs an advanced strategy, and it usually surveys from surroundings.

Besides that, sometimes there is an obstacle in corporate bureaucracy. When the developer has dealt with the landowner, the corporate needs a long time to transfer the money. It should be made easier.

3. The Incitement of Other Parties

As mentioned before, it does not take it easy for the whole project. In this case, what differentiates it from Mr. Dorman is the influence from local NGOs who does not get a project from the developer. It must need dealing a negotiation to overcome this.

There are some tips from Mr. Vicky for geothermal land acquisition in the future such as companies must welcome in society, make an advanced masterplan and great strategy for negotiation, flexibility in internal corporate, enhance a negotiation skill for people who involve in a geothermal project, competent skill for engineering, and can predict the future of the project..

3. CONCLUSION

1. This land acquisition is intended to carry out geothermal development projects. Will be used as the main infrastructure for developing a geothermal exploration project. The land was used for a span of approximately 37 years.
2. Regulations in Indonesia require that an exploration project be financially secure in order to obtain an IPB, where in order to obtain financing, the exploration must comply with the regulation that all affected communities are guaranteed their rights. Throughout the land acquisition, the company will also be supervised by a provincial-level task force.
3. It is important to know the landowner’s status and prepare several documents needed before buying the land. For state land and non-state land have different steps that must be remembered.
4. Regarding both literature review and practitioners interview, several aspects such as technical, refusal of inhabitant, social environment and government are the main obstacles that will hamper the land acquisition process. Hence, the developers should be appropriately flexible in terms of technical aspects and the communication with the local community. Moreover, the government must have the same vision and command in the land acquisition process, simplify the access to permit for the bureaucracy and must develop tools such as the national center of land information system.

4. PATH FORWARD

1. The government, both national and local, must have the same vision and command in the land acquisition process so that there is no misinterpretation during actions in the field. Then, the government simplify the access to permit for the bureaucracy. Then, the government must develop a tool such as the national center of land information system. Actually, Pertamina has made it, and it could be developed further. The system contains spatial (graphical) and non-spatial (physical land information, legal data, financial data, administrative data, environmental visuals), which are managed in digital form. It is built with the purpose of monitoring land availability financially, such as safeguarding the system of

company land assets and non-financially such as eases the status of land acquisition progress, avoids fraud in the land acquisition process, the data consolidation process can be done in real-time. Moreover, the government must increase practitioners in the geothermal sector because the ratio of the number of projects and practitioners involved is very disproportionate.

2. A developer company must make strategic plans as much as possible and must be flexible, and provide spare time. In fact, this land acquisition process takes unpredictable times and many unwanted events occur. The company should also conduct land acquisition training and development for people involved in geothermal projects so that people at least know how to do it.

5. ACKNOWLEDGEMENT

The authors would like to express their deepest gratitude towards PT. Enerka Bhumi Pratama for their support for providing the facilities and the data. Comfortable gratitude for the practitioners that supporting the information of geothermal land acquisition challenges based on their real experience in this research.

REFERENCES

Asian Development Bank. (2015). Building Resilience to Climate Change in PNG: Voluntary Land Use/Negotiated Settlement Framework.

Dewi, A.N.R.P., Chatim, L., Lukito, L., et. al. (2013). What Are the Benefits and Challenges: Land Acquisition Process Based on Presidential Regulation No. 71 Year 2012 Versus IFC Performance Standard 5. *The 37th Indonesian Petroleum Association Proceedings.* Jakarta.

Ginting, Febrianti. "Studi Sosial Potensi Energi Panas Bumi Di Kabupaten Bantul." Publikauma: Jurnal Administrasi Publik Universitas Medan Area 5.1 (2017): 13-17.

Hunt T.M.(2012). Geothermal Resources, Environmental Aspects of. In: Meyers R.A. (eds) Encyclopedia of Sustainability Science and Technology. Springer, New York.

Intenational Council on Mining & Metals. (2015). Land acquisition and resettlement: Lessons learned. Intenational Council on Mining & Metals. London.

International Finance Corporation. (2012). Performance Standard 5: Land Acquisition and Involuntary Resettlement. *In book: IFC Performance Standards on Environmental and Social Sustainability*. World Bank Group. Washington D.C.

Ongau M.T. (2015). Introduction To Geothermal Drilling. Short Course X on Exploration for Geothermal Resources, organized by UNU-GTP, GDC and KenGen, at Lake Bogoria and Lake Naivasha, Kenya.

OTP Geothermal. (2013). Land Acquisition Processes.

Pambudi, Nugroho. (2017). Geothermal power generation in Indonesia, a country within the ring of fire: Current status, future development and policy. http://dx.doi.org/10.1016/j.rser.2017.06.096

Peraturan Pemerintah Republik Indonesia Nomor 7 Tahun 2017 *Panas Bumi untuk Pemanfaatan Tidak Langsung*. 21 Februari 2017. Lembaran Negara Republik Indonesia Tahun 2017 Nomor 30. Jakarta

Peraturan Pemerintah ESDM No. 36 Tahun 2017 tentang Tata Cara Penugasan Survei Pendahuluan Dan Penugasan Survei Pendahuluan Dan Eksplorasi Panas Bumi. 18 Mei 2017. Lembaran Negara Republik Indonesia Tahun 2017 Nomor 36. Jakarta

Peraturan Presiden Nomor 71 Tahun 2012 *Penyelenggaraan Pengadaan Tanah Bagi Pembangunan Untuk Kepentingan Umum*. 8 Agustus 2012. Lembaran Negara Republik Indonesia Tahun 2012 Nomor 156. Jakarta

Pertamina Geothermal Energy.: PGE Land One Map One Solution. Geomatics & ICT, (2021).

Purba, D., Adityatama, D.W., Soedarsa. (2021). A Study on Competency Assessment of the Geothermal Exploration Project Manager in Indonesia. *World Geothermal Congress.* Reykjavik.

Purba D.P.,et.al. (2021). Drilling Infrastructure Construction Challenges in Geothermal Exploration Project in Eastern Indonesia. *World Geothermal Congress.* Reykjavik

Purba D.P.,et.al. (2019). Review on Geothermal Direct Use Application as an Alternative Approach in Community Engagement at Early Exploration Phase in Indonesia. *Workshop on Geothermal Reservoir Engineering Stanford University. Stanford*, California.

Supremeenergy. Rencana Kegiatan Pengusahaan Panas Bumi untuk PLTP Rantau Dedap 250 MW. (2017)

Undang-undang Republik Indonesia Nomor 5 Tahun 1990 *Konservasi Sumber Daya Alam Hayati dan Ekosistemnya*. 10 Agustus 1990. Lembaran Negara Tahun 1990 Nomor 49. Jakarta

Yousefi H., et.al. (2007). Environmental Aspects of Geothermal Energy Development in Iran. Conference: The 5th International Workshop on Earth Sciences and Technology. Fukuoka, Japan.

PROCEEDINGS
JOINT CONVENTION BANDUNG (JCB) 2021
November 23rd – 25th 2021

Soil dynamic response mapping and underground structural modeling in Kertajati-West Java region using Horizontal-to-Vertical Spectral Ratio (HVSR) method

Firda Haifa Fadhilah[1], Tedi Yudistira[2], Yayan Sopyan[3]
Geophysical Engineering Study Program, Bandung Institute of Technology[1]
Global Geophysical Expertise Group, Bandung Institute of Technology[2]
Geological Survei Center[3]

Abstract
The Kertajati area is dominated by soft rocks' geological features, namely Lower Quaternary sedimentary rocks (Qos) and Alluvium Deposits (Qa). The condition of soft rock on top of the dense rock will result in amplification during an earthquake. This earthquake is because the Baribis Fault is in the southwest of the study area, possibly subducts from Purwakarta and Majalengka. Baribis fault is also estimated to have caused the largest earthquake ever recorded on Java which occurred in the 17th century. This study processed microtremor data with the Horizontal to Vertical Spectral Ratio (HVSR) method. HVSR is expected to be a disaster mitigation in the Kertajati region, considering that the West Java International Airport (BIJB) has also been built. HVSR is a seismic method to identify dynamic characteristics of soil. From the data processing results, it is obtained that the dominant frequency values vary in the range of 0.6-18 Hz while the amplification values have a range of 1.2-6.3. The dominant low-value frequencies are in the middle, west, and southeastern study area's, indicating a relatively larger sediment layer thickness. At the same time, the high-value amplification values are dominant in the middle and north side of the area. Then the inversion of the HVSR curve was carried out using the Neighborhood Algorithm method to find out the information on the subsurface V_s value, which was then associated with the characteristics of the subsurface layer. The values of V_s ranged from 53-3027 m/s for a depth range of up to 610 m, with relatively lower values on the study area's middle, southeast, and west sides.

Introduction

This study aims to develop a subsurface V_s model of the Kertajati Region, West Java. Kertajati region is one of the areas that contain soft rock. Those are Lower Quartenary sedimentary rocks (Qos) and Alluvium Deposits (Qa) (Hasibuan & Sudarsono 2009). Geological map as shown in Figure 1 down below.

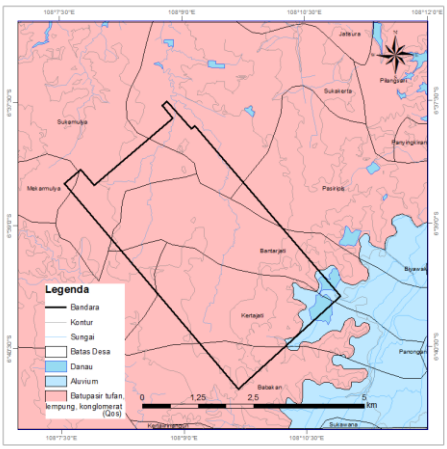

Figure 1. Geological map of Kertajati Region (Modification of Djuri 1995; Hasibuan & Sudarsono 2009)

In terms of geotectonic conditions, Kertajati has a Baribis fault that stretched from Purwakarta and Majalengka (Bemmelen 1949). Processing microtremor data is also expected to be hazard mitigation in Kertajati because the study area has been built an International Airport of West Java. The data that used in this study was microtremor recording data. Microtremor is a short period of vibration that accumulated because of an ocean wave, wind interaction with plants, and the activity of the atmosphere (Toiba et al. 2016). The microtremor data is processed by the HVSR method. HVSR (Horizontal to Vertical Spectral Ratio) is an estimation method for frequency resonance and amplification from ground shaking that is impacted by the surface layer (Nakamura 2019).

Data and Method

HVSR Method

This study processed microtremor data recorded by Pusat Survei Geologi (PSG) on August 16-19th, 2018, at 01.30 – 10.15 a.m. to verify the stability (Cipta et al. 2019). We are using seismometer LE-3D/5s MkIII broadband three components. Every data has a duration of around 30 minutes, with 71 locations spread on study areas.

HVSR method or Nakamura's method is comparing horizontal (A_H) and vertical (A_v) displacement components ([H/V] spectral ratio) from microtremor or earthquake motion (Nakamura 2019). The equation of ellipticity HVSR curve is defined as equation (1) below.

$$HVSR(\omega) = \frac{A_H(\omega)}{A_v(\omega)} \qquad (1)$$

The horizontal components are calculated by quadratic mean square defined as equation (2) below.

$$A_H(\omega) = \frac{\sqrt{A_{NS}^2(\omega) + A_{EW}^2(\omega)}}{2} \qquad (2)$$

A_{NS} is the amplitude spectrum in the north-south direction, and A_{EW} is the amplitude spectrum in the east-west direction. The result of processing HVSR is connecting frequency and amplification (H/V). The peak of the HVSR curve indicates frequency resonance and amplification at the site. Frequency resonance is associated with the thickness of the sediment layer, and the lower the dominant frequency value indicates, the more significant the thickness of sediment will be and vice versa (Nakamura 2008). At the same time, amplification increases the level of ground shaking because of rock contrast impedance and accumulation of wave propagation in basin structure (Semblat et al., 2005). The results of the investigation of the V_s value by the SNI Laboratory 1726 conducted by Badan Standarisasi Nasional resulted in grouping the V_s value to determine soil characteristics, as shown in Table 1.

PROCEEDINGS
JOINT CONVENTION BANDUNG (JCB) 2021
November 23rd – 25th 2021

Table 1. The grouping of the V_s parameters based on the investigation of the V_s value by the SNI 1726 Laboratory (Badan Standarisasi Nasional 2012)

Type	Site Classification	V_s(m/s)
SA	Hard rock	>1500
SB	Rock	750-1500
SC	Very dense soil and soft rock	350-750
SD	Medium soil	175-350
SE	Soft soil	<175

Neighbourhood Algorithm Inversion

Inversion process from HVSR curve using Neighbourhood Algorithm with Dinver software to create V_s subsurface model. The inversion process started with creating 1-D models (initial models) from V_s, depth, and the other parameters. Based on these models, processed forward modelling to produce a calculated HVSR curve. HVSR curves have the minimum misfit associated with the 1-D model V_s-depth is the most representative subsurface feature. Misfit equation defined as (Wathelet 2004).

$$misfit = \sqrt{\sum_{i=0}^{n_f} \frac{(x_{obs\,1} - x_{cal\,i})^2}{\sigma_i^2 n_f}} \qquad (3)$$

More clearly, the inversion with the Neighborhood Algorithm presented by Sambridge (1999a) can be carried out in the following stages.

a) Create an initial model (n_{s0}) in the parameter space.
b) Calculates the misfit function for the newly formed initial model (n_{s0}) and determines the model with the smallest misfit value (n_r) of all the models that have been formed in the previous step.
c) Create a new model with a total (n_s) by doing a uniform random walk on Voronoi cells from each selected n_r or iteration.
d) Back to the second step (step b).

In this inversion process, the following equation can calculate the number of models produced by each data.

$$M = n_{s0} + n_s \qquad (4)$$

This study uses the values of n_{s0} and n_s, i.e. 500 and 75,000. So that the number of models generated each data is 75,500 models. The inversion process is carried out by making many 1-D models of V_s concerning depth and several other parameters, which are then carried out by forwarding modelling to produce the calculated HVSR curve. Then the misfit calculation is carried out for each data. The calculated HVSR curve with the smallest misfit is associated with the most representative 1-D V_s-depth model curve with the associated subsurface feature. For the initial models, parameter ranges of V_s, V_p, depth, Poisson's ratio, and density are shown in Table 2 below.

Table 2. Parameter value initial model for inversion process.

Layer	V_p (m/s)	V_s (m/s)	Depth (m)	Poisson's Ratio	Density (kg/m^3)
1	200-5000	50-750	100	0.2-0.5	2000
2		50-750	100		
3		50-3500	100		
4		50-3500	100		
5		50-3500	200		
6		50-3500	2000		
8		50-3500	*Halfspace*		

Result and Discussion

HVSR Curve Shape

The characteristic of subsurface corresponding HVSR curve peak. In this study, the HVSR curve is classified into four groups: (1) single peak with sharp or broad peak; (2) two peaks, first peak on low frequency (<2 Hz) with broad peak and the other peak on the high frequency (>4 Hz) have sharp or broad peak; (3) three peaks, which indicate stratigraphy complexity of subsurface (Cipta et al. 2018); (4) the absence of any peak (no peak with amplitude > 3) which may reflect the absence of strong impedance contrast (Cipta et al. 2018). The sharp peak on (1) and (2) indicates a strong impedance contrast (Gosar 2010). The broad peak on (1), (2), and (3) suggest a low impedance contrast caused by gradual discontinuity or irregularity of subsurface structure (Uebayashi 2003; Gosar 2010).

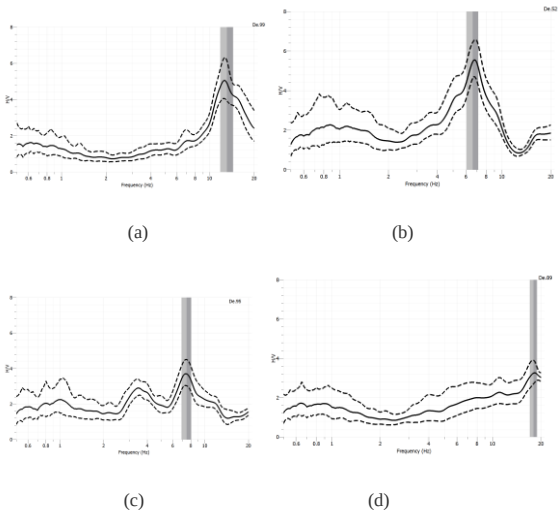

Figure 3. Type of HVSR curve (a) single peak, (b) two peaks, (c) three peaks, (d) flat

The distribution of the type of HVSR curve is shown in Figure 2.

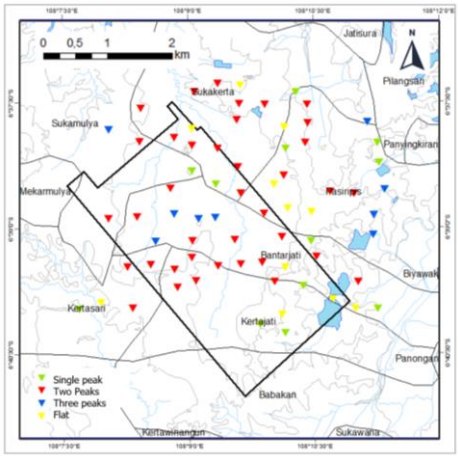

Figure 2. The distribution of the type of HVSR curve

Frequency Resonance

The highest peak on each curve can generate a map of frequency and amplification, as shown in Figures 3 and 4.

PROCEEDINGS
JOINT CONVENTION BANDUNG (JCB) 2021
November 23rd – 25th 2021

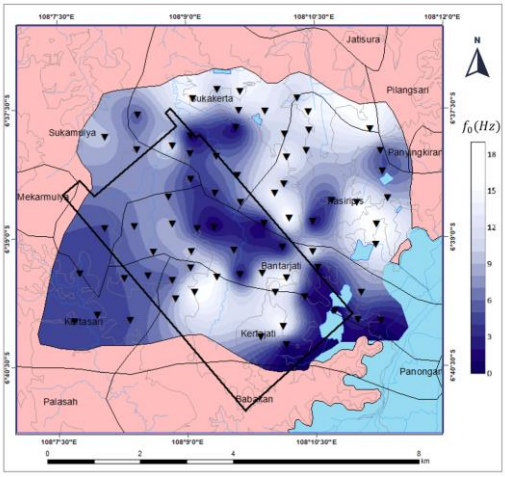

Figure 3. Map of interpolated frequencies

The value of frequencies is dominated by low frequency (<10 Hz) on the middle, western, and southeast sides of the study area. That generally located in the middle and eastern of the Bantarjati region, southern of the Sukakerta region, and eastern of Kertajati. At the same time, the high frequency is distributed over the southern and northeast of the Kertajati region. The low frequency on the middle and eastern of the study area is expected because of Lower Quartenary sedimentary rocks (Qos) in the form of residual soil that consists of three types layer relative thicker than around. Based on the penetrom test from Hasibuan & Sudarsono (2009), The three layers are a layer of clay as the top layer, then underneath a layer of clay sand, and the third layer is a sand layer with a reasonably large thickness. Based on the penetrom test, a vertical cross-section shows a thicker sand layer on the middle side of the Kertajati area (Sudarsono & Hasibuan 2011). At the same time, the low dominant frequency value on the southeast side is associated with Alluvium Deposits (Qa) which consist of layers of silt, sandy silt, and relatively thick sand (Sudarsono & Hasibuan, 2011). This condition was obtained from the penetrom test, which showed alluvium deposits with a relatively greater thickness than the surrounding area.

Amplification

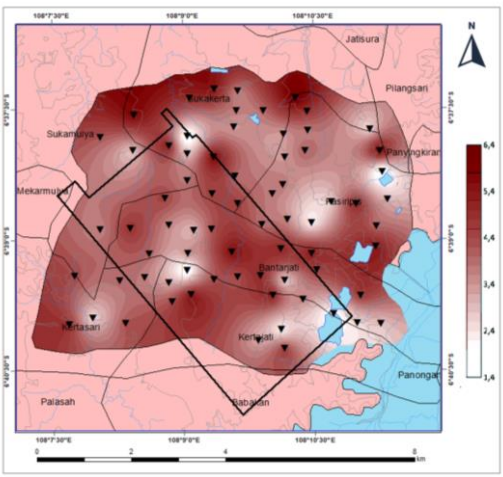

Figure 4. Map of interpolated amplification.

The amplification value in the Kertajati area is relatively low, ranging from 1.4 to 3.4 on the southeast and northeast sides. The medium amplification values in the range of 3.4-4.4 are in the western part. While relatively higher amplification values ranging from 4.4 to 6.4 are located on the middle and north sides of the study area, covering the central part of the Bantarjati region and the south and center of the Sukakerta region. The amplification value of the study area is quite varied. In the same lithology, the amplification value can show different values—the amplification value change when rock deformation occurs (Marjiyono, 2010). The relatively high amplification value in the middle of the study area is thought to be associated with layers resulting from the weathering process of Lower Quaternary Sedimentary (Qos) rocks that form residual soils, which are soft layers. Meanwhile, a high amplification value in the north may be associated with the presence of a sediment layer with a low V_s value in bedrock with a relatively high V_s value.

Model of V_s subsurface

The results of the inversion process using the Neighborhood Algorithm method in the form of a 1-D model of the V_s value and the HVSR curve depicted by the ellipticity value can be seen in Figure 5 below.

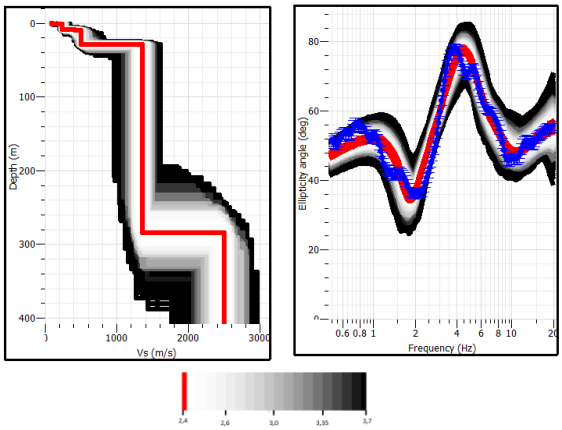

Figure 5. The results of the inversion of the HVSR curve at the MI073 station. (a) 1-D V_s model to depth (b) HVSR curve from observations (blue) and

Based on the model, it is found that the shear wave velocity (V_s) has an enormous value relative to the increasing depth measured in all stations. This condition shows that the greater the depth of the subsurface layer, the more dense the lithological appearance. Sudarsono and Hasibuan (2011) revealed that the Kertajati area has a near-surface appearance in residual soil and soft transported soil and has more dense source rock in more profound depth. Determining the variation of the V_s value with depth, a horizontal cross-sectional mapping of the distribution of the V_s value was carried out at several depths. Horizontal sections at depths of 10, 25, 40, 100, 250, and 1000 m are shown in Figure 6.

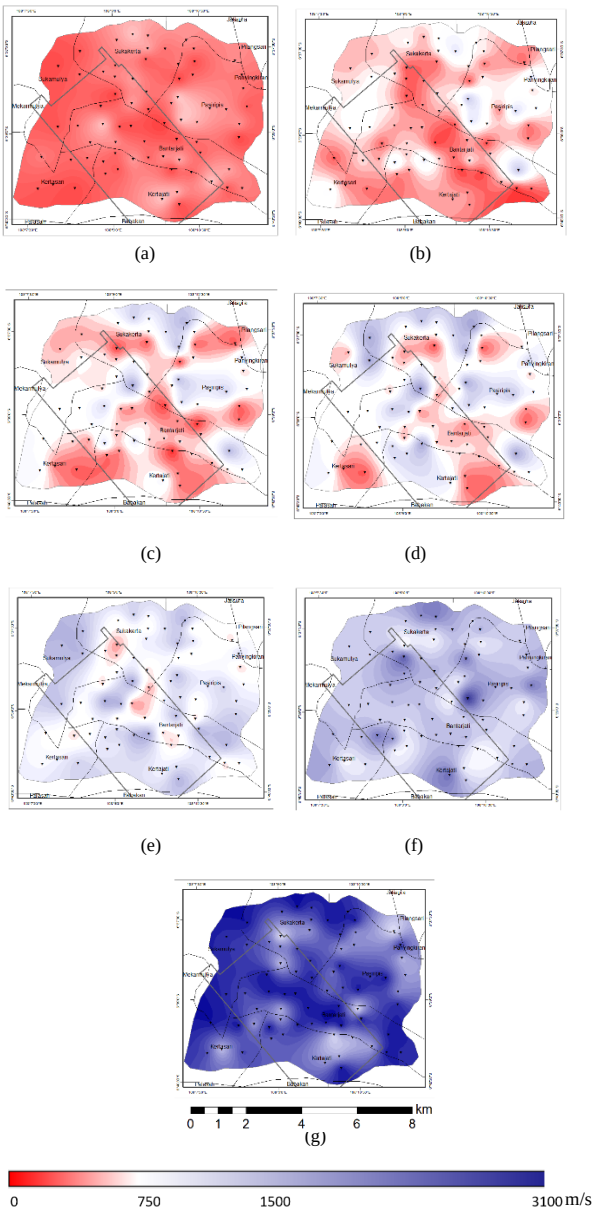

Figure 6. The horizontal cross section of the value of V_s at a depth of a) 10 m, b) 25 m, c) 40 m, d) 80 m, e) 100 m, f) 250 m, g) 1000 m.

Based on the horizontal cross-sectional map of V_s from several depths, it is found that at a depth of 10 m (Figure 6 (a)), the V_s value is relatively low (<750 m/s). It can be concluded that overall the study is a layer of sediment at 10 m depth. This condition is due to geological conditions in the form of residual Lower Quaternary sediments (Qos) with depths ranging from 2.4 m to 14.20 m, with high plasticity properties (Hasibuan & Sudarsono, 2011).

The horizontal cross-section of V_s at 25 m depth (Figure 6 (b)) shows that the study area is still dominated by the appearance of a sedimentary layer, which has a V_s value less than 750 m/s. However, in the east, there are visible layers with V_s values in the range between 750-1500 m/s, which are engineering bedrock.

Figure 6 (c), showing a horizontal cross-section at a depth of 40 m, shows that the layer with a V_s value of less than 750 m/s still dominates. However, the western, eastern, and northern sides have shown layers with V_s in the range of 750-1500 m/s.

The horizontal cross-section with a depth of 80 m in Figure 6 (d) shows that the study area still shows the appearance of sediment in several places, namely, in the middle, southwest, and southeast. This condition indicates that this section has a larger sediment thickness. This cross-sectional map supports the results of relatively low dominant frequency values associated with relatively larger sediment thickness.

The cross-section of the V_s value at 100 m depth (Fig. 6 (e)) shows that the layer's appearance with the V_s value is only on the middle side of the study area, which indicates the possibility of a reasonably large sediment thickness at that point.

The results of the horizontal section at 250 m depth (Figure 6 (f)) are dominated by layers with a V_s range of 750-1500 m/s. At the same time, the horizontal section at 1000 m depth (Figure 6 (g)) is dominated by hard rock features with a V_s value of more than 1500 m/s.

To see the variation of V_s value in more detail in a line, we generate a vertical section of the six lines, as shown in Figure 7 below.

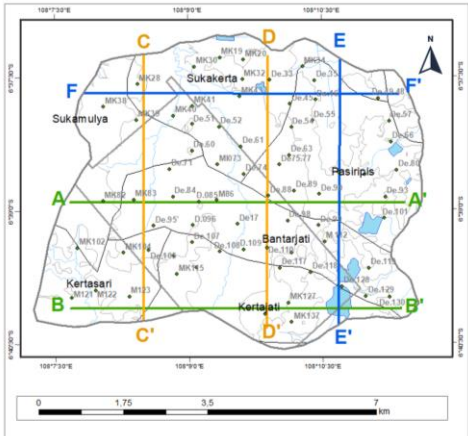

Figure 7. Vertical cross-section trajectory map

The vertical cross-section is varied based on the value classification made by the National Standardization Agency. The red colour shows the value of less than 750 m/s, which in the classification is included in the soft soil (SE), medium soil (SD) and very dense soil / soft rock (SC) or can be referred to as sedimentary layers. A cross-sectional image is shown as follows.

PROCEEDINGS
JOINT CONVENTION BANDUNG (JCB) 2021
November 23rd – 25th 2021

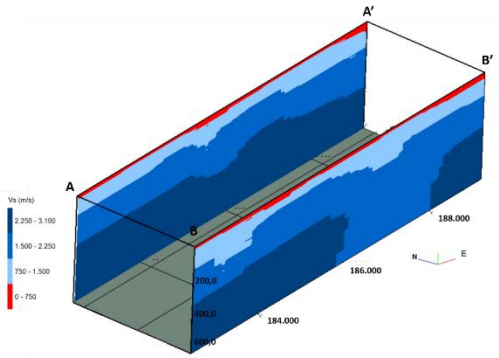

(a)

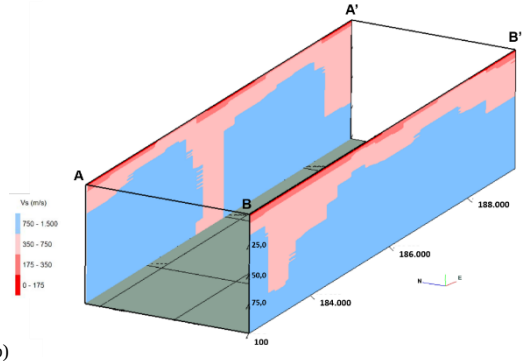

(b)

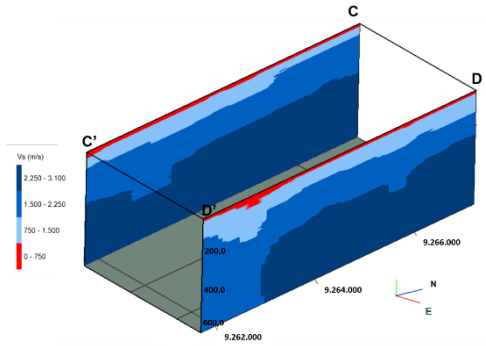

(c)

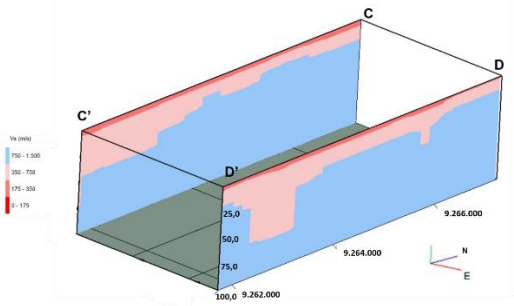

(d)

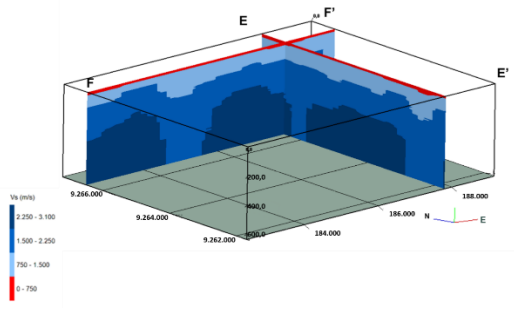

(e)

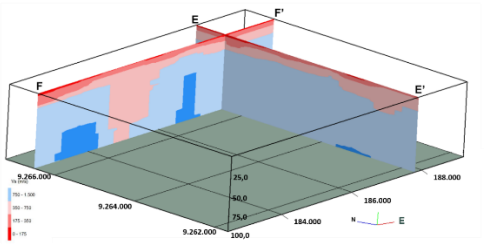

(f)

Figure 8. Cross sectional (a) line AA' and BB' with maximum depth 610 m, (b) line AA' and BB' with maximum depth 100 m, (c) line CC' and DD' with maximum depth 610 m, (d) line CC' and DD' with maximum depth 100 m, (e) line EE' and FF' with maximum depth 610 m, (f) line EE' and FF' with maximum depth 100 m

The vertical section of V_s is sufficient to show the variation of V_s value that changes with depth. The value of V_s gets more significant as the depth increases. The value of shear wave velocity or V_s is associated with the characteristics of subsurface layers that SNI has grouped. This study shows that the subsurface features of the study area that show sedimentary features, namely the value of V_s less than 750 m/s, indicate a relatively low thickness of 20-100 m. It was found that the sediment layer, which has a wave velocity value of V_s less than 750 m/s, is dominated by a sedimentary layer with a V_s value range of 350-750 m/s indicated by a relatively large thickness compared to the layer above it. This condition indicates that the subsurface features of the Kertajati area are dominated by a very dense soil layer or soft rock (SC). Then followed by a layer with a more extensive V_s value range of 750-1500 m/s with a relatively thicker thickness that has a depth in the range of 20-150 m associated with rock layers (SB)—under that layer, followed by a value of V_s higher than 1500 m/s, associated with hard rock to a maximum resolution of 610 m. By making a vertical section, more detailed information is obtained about the precise boundaries of each layer with different characteristics. Thus, it was found that in the research area, the results were quite undulating, especially at the boundary between rocks at a certain depth.

The V_s^{30} value obtained from the average V_s value to a depth of 30 m can classify the soil types of an area. This study carried out classification using the V_s^{30}value grouping based on the National Standardization Agency. The research area is divided into two soil groups: medium soil type (SD) with a value of V_s in the range of 175-350 m/s and very dense soil (SC) or soft rock in the range of 350-750 m/s. The map of the distribution of soil types based on the value of V_s^{30} can be seen in Figure 9 below.

PROCEEDINGS
JOINT CONVENTION BANDUNG (JCB) 2021
November 23rd – 25th 2021

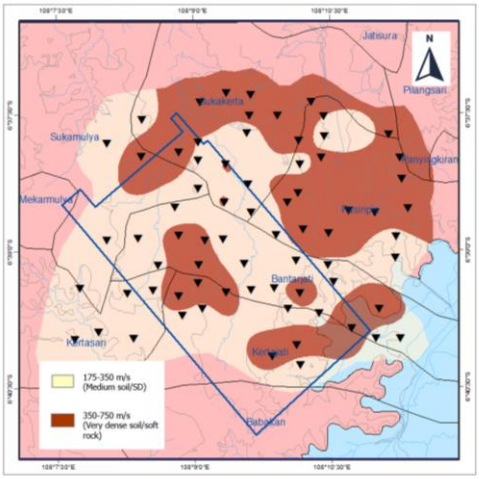

Figure 9. Map of the distribution of soil types based on the value of V_s^{30} in the Kertajati area

The Kertajati area is classified into two types of layers, namely soil with V_s value in the range of 175-350 m/s, which is associated with medium soil (SD) and very dense soil or soft rock (SC) with V_s value in the range of 350-750 m/s. Medium soil types (SD) are relatively scattered on the southwest side of the study area, right at the establishment of West Java International Airport. At the same time, the type of soil in the form of very dense soil or soft rock (SC) is relatively scattered on the northeastern side of the study area. The resulting soil type can be interpreted that the Kertajati area has dominant soil types, namely medium soil (SD) and very dense soil or soft rock (SC) to a depth of 30 m below the surface.

Conclusions

The dominant vibration frequency value (f_0) in the Kertajati region ranges from 0.63 – 18.63 Hz. It has a low dominant frequency values distribution in the southeast, west, and central part of the study area. Meanwhile, the amplification value of (A_0) ranged from 1.26 to 6.33, with relatively moderate to high amplification values spread over the north, west, and central part of the study area. The inversion of the HVSR curve results in the distribution of the subsurface shear wave velocity (V_s) in the Kertajati area ranging from 53 - 3027 m/s with a depth range of up to 610 m, with a relatively low distribution of V_s values on the southeast, southwest and central parts of the study area.

The soil type obtained from the classification is based on the average shear wave velocity (V_s) to a depth of 30 m. The value of V_s^{30} in the study area ranges from 247 – 541 m/s. Thus, it was found that the study area was divided into two rock groups. The value of V_s^{30} with a range of 180-360 m/s is a medium soil group (SD) dominant on the southwest side and a small part on the northeast side. Furthermore, the value of V_s^{30} with a range of 350-750 m/s belongs to the very dense soil or soft rock (SC), which is mainly spread on the northeast side and a small part on the southeast side the study area. In the Kertajati region, the area with a relatively low dominant frequency value (f_0) which is associated with a relatively higher value of sediment thickness, is dominated by the type of sediment in the form of a layer of solid soil or soft rock (SC) which is associated with a V_s value in the range of 350- 750 m/s.

References

Djuri, (1995): Peta Geologi Lembar Arjawinangun, Jawa, sekala 1:100.000. Ed. 2, *Pusat Penelitian dan Pegembangan Geologi*, Bandung.

Hasibuan, G. dan Sudarsono, U., (2009): Geologi Teknik Daerah Kertajati Kabupaten Majalengka, Jawa Barat. *Buletin Geologi Tata Lingkungan (Bulletin of Environtmental Geology*, ***19*(3)**, 125-134.

Bemmelen, R. V. (1949): General geology of Indonesia and adjacent archipelagoes, Government Printing Office, *The Hague Martinus Nijhoff*, **1**.

Toiba, Y., Sili, P. D., dan Maskur, M. (2016): Analisis Mikrotremor Kawasan Palu Barat Berdasarkan Metode Horizontal to Vertical Spectral Ratio (HVSR). *Gravitasi*, ***15*(1)**.

Nakamura, Y. (2019): What is the Nakamura method? *Seismological Research Letters*, ***90*(4)**, 1437-1443.

Cipta, A., Cummins, P., Dettmer, J., Saygin, E., Irsyam, M., Rudyanto, A., dan Murjaya, J. (2018): Seismic velocity structure of the Jakarta Basin, Indonesia, using trans-dimensional Bayesian inversion of horizontal-to-vertical spectral ratios. *Geophysical Journal International*, ***215*(1)**, 431-449.

Nakamura, Y. (2008): On the H/V spectrum, Proceedings of the 14th World Conference on Earthquake Engineering (14WCEE).

Semblat, J. F., Kham, M., Parara, E., Bard, P. Y., Pitilakis, K., Makra, K., dan Raptakis, D. (2005): Seismic wave amplification: basin geometry vs soil

BSN. (2012): Tata cara perencanaan ketahanan gempa untuk struktur bangunan gedung dan nongedung, Badan Standardisasi Nasional, Jakarta, 17-18

Wathelet, M., Jongmans, D., & Ohrnberger, M. (2004): Surface-wave inversion using a direct search algorithm and its application to ambient vibration measurements. *Near surface geophysics*, ***2*(4)**, 211-221.

Gosar, A. (2010): Site effects and soil-structure resonance study in the Kobarid basin (NW Slovenia) using microtremors, *Natural Hazards & Earth System Sciences*, **10(4)**.

Uebayashi, H., (2003): Extrapolation of Irregular Subsurface Structures Using the Horizontal-to-Vertical Spectral Ratio of Long-Period Microtremors. Bull. *Seism. Soc*. **93(2)**, 570–582.

Sudarsono, U., dan Hasibuan, G. (2011): Karakteristik Geologi Teknik Tanah Residu Batuan Sedimen Kuarter Bawah Daerah Kertajati, Majalengka, Jawa Barat Engineering Geological Characteristics of the Residual Soil, Lower Quaternary Sediments in Kertajati Region, Majalengka, West Java. *Jurnal Geologi Indonesia*, ***6*(3)**, 177-189.

Marjiyono, (2012): Estimasi Karakteristik Dinamik Tanah dari Data Mikrotremor. Institut Teknologi Bandung. **39**

Acknowledgements (Optional)

We used Geopsy software to estimated the HVSR curve, and most of the figures were drawn using Surfer, ArcGis, and RockWorks. Inversion processed using Dinver. The core engine is a Neighbourhood Algorithm originally proposed by Sambridge (1999), implemented and improved by Wathelet (2008), and value of horizontal cross-sections of V_s using MATLAB.

PROCEEDINGS
JOIN CONVENTION BANDUNG (JCB) 2021
December 1ST – 3rd 2021

Zonation of Soil Movement Vulnerability Areas Using Remote Sensing: A Case research of Puncak Bogor, West Java

Gilang Diesty Nuarihidayah[1], Eko Sudarsono[2], Jasmine Mustika Sukmawati[3]
[1]Department of Geological Engineering, Faculty of Geological Engineering, Padjadjaran University, Sumedang
[2]Department of Geological Engineering, Faculty of Geological Engineering, Padjadjaran University, Sumedang
[3]Department of Geological Engineering, Faculty of Geological Engineering, Padjadjaran University, Sumedang

Abstract
Indonesia is a country rich in natural resources, but this doesn't prevent Indonesia from various kinds of geological disasters because Indonesia's geographical location is surrounded by a ring of fire. With that, each province has various disasters that occur, one of them is soil movement, the most common disaster in West Java Province. Indonesia's geological characteristics, tropical climate, high rainfall trigger, human intervention with agricultural activities, and uncontrolled infrastructure development the possibility of soil movement. The Puncak Bogor area, the border between Bogor Regency and Cianjur Regency, West Java, is an area that often occurs soil movement disasters that can have an impact on humans. Geological conditions, rainfall, and steep slopes are the main causes of soil movement. Remote sensing technique using Landsat 8 OLI and National DEM (DEMNAS) as input data is the research method used. Analyzing and correlating rainfall data, morphometry, Normalized Difference Vegetation Index (NDVI), Fault and Fracture Density (FFD) to predict zonation of soil movement vulnerability areas. The research area has NDVI values ranging from 0.25 to -0.03 with low to very low vegetation and high-density values, both of which are spread from northwest to southeast. The slopes in the research area are dominated by steep slopes of $16^o – 35^o$ (30% – 70%), and supported by a fairly high intensity of rainfall in October, which is >50 mm/day. It can be concluded that the research area is mostly of a vulnerable zone in the Naringgul District, Bogor Regency, and a very vulnerable zone in Gegerbentang District, Cianjur Regency. Rock types in Regional Geology strengthen the weathering process so that it's easy to soil erosion because it has been mixed with sedimentary rocks. With this, it's hoped that the community will pay attention to infrastructure development and soil movement disaster mitigation activities.
Keyword: Soil Movement, Puncak Bogor, Remote Sensing

Introduction

Indonesia is a country with a high incidence of disasters because its geographical location is surrounded by a ring of fire. With that, each province has various disasters that occur, one of which is in West Java Province, a disaster often occurs is soil movement. Soil movement is the disturbance of soil stability that causes the soil to move down the slope due to the mass of soil or rocks that compose the slope [1]. These disasters often occur in our research area, which is located in Puncak Bogor, on the border between Bogor Regency and Cianjur Regency, West Java, where some of the green lands have been converted into settlements so that it can trigger the potential for soil movements in the area. The soil movement causes damage to building materials and even death to local residents. Therefore, the purpose of this paper is to an analysis of the risk of soil movements around Puncak Bogor to make local residents aware of the dangers of soil movements.

Geological map of the research area in Sheet Bogor, Java and Sheet Cianjur, Java. The lithology that composes this area is dominated by breccia lithology and lava originating from ancient mountains that have been mixed with sedimentary rocks and has a hilly morphology with a sloping to steep slope, fracture structures also affect this area.

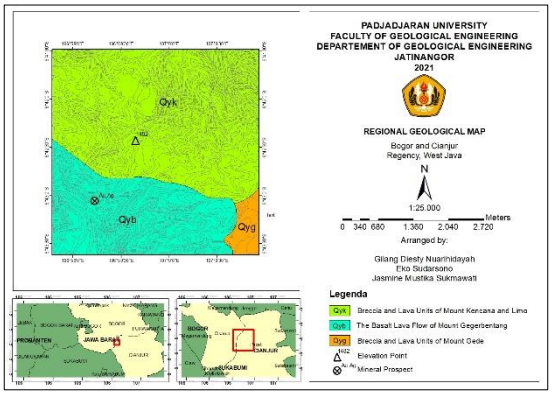

The constituent units in the research area are composed of material from the oldest to the youngest of Mount Gede Volcano:

1. Breccia and Lava units of Mount Kencana and Mount Limo, andesite tuff boulder, andesite breccia, and lava along the Cibeet River and the Cikundul River with lots of pyroxene phenocrysts and basalt lava.
2. The basalt lava flow of Mount Gegerbentang spans with the prospect of Au and Ag minerals.
3. Mount Gede Breccia and Lava Unit, sandstone tuffaceous, shale, breccia, and conglomerate forming the Cianjur plain [2], [3].

Figure 1: Regional Geological Map

PROCEEDINGS
JOIN CONVENTION BANDUNG (JCB) 2021
December 1ST – 3rd 2021

Data and Method

Determination of the soil movement vulnerability zone in the research area is carried out by utilizing techniques of remote sensing using Landsat 8 OLI and the Digital Elevation Map *Nasional* (DEMNAS) as input data. The data will be input in remote sensing software, there are ArcGIS 10.8 and Geomatica 2016 for processing into Normalized Difference Vegetation Index (NDVI) Map, Morphometric Map, and Lineament Density Map. Lineament Density Map generated through digitation and attributing process from lineament data. The output data then performed the next overlay procedure to determine the soil movement vulnerability zone in the research area. In addition to these maps, we also use rainfall data from *Badan Meteorologi, Klimatologi, dan Geofisika* (BMKG) as supporting data.

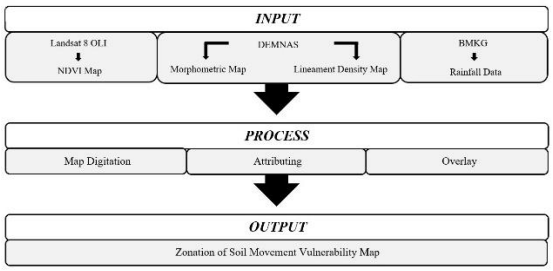

Figure 2: Research Flow Chart

Following are the details of the parameters in determining the soil movement vulnerability zone in the research area:

1. Normalized Difference Vegetation Index (NDVI)

NDVI is an index used to measure the greenness of vegetation and understand the density of vegetation in an area [5]. The working principle of NDVI or vegetation index is based on observations of near infrared light waves (NIR) and red-light waves (Red), which were formulated by Tucker (1979) as follows [6].

$$NDVI = \frac{(NIR - Red)}{(NIR + Red)}$$

Description:
NIR (Near – Infrared Radiation) = Near infrared radiation from pixels
Red = Red light radiation from pixels

The data used to obtain the NDVI value is Landsat 8 OLI that is processed by using ArcGIS 10.8. software. In Landsat 8 OLI, to calculate the NDVI value, you can use the formula:

$$NDVI = \frac{(Band\ 5 - Band\ 4)}{(Band\ 5 + Band\ 4)}$$

The calculation of the NDVI value is done using the Raster Calculator on the ArcToolbox feature in ArcGIS software. The software automatically calculates the two bands to generate the NDVI value.

The NDVI value obtained was then classified using the classification by Wahyunto (2003) to indicate the level of greenery in the research area [7].

NDVI Value	Greenery Level	Color
-1,00 < NDVI < -0,03	Non-Vegetation	
-0,03 < NDVI < 0,15	Very Low Vegetation	
0,15 < NDVI < 0,25	Low Vegetation	
0,25 < NDVI < 0,35	Moderate Vegetation	
0,35 < NDVI < 1,00	High Vegetation	

Table 1: NDVI Classification

Plants in an area can be categorized as high vegetation if the vegetation absorbs most of the Red waves and reflects higher NIR waves, this indicates that the vegetation is actively carrying out photosynthesis. Meanwhile, if the vegetation reflects more the Red wave than the NIR wave, this indicates that the vegetation is not actively carrying out photosynthesis or indicates an area that is categorized as having low vegetation.

2. Fault and Fracture Density (FFD)

FFD method is used in areas formed by interconnecting faults and fractures to assess high structural density by drawing lineament patterns of morphology. In the FFD analysis, the identified structures are the density of lineament rivers or escarpments due to fault activity [8]. The resulting structure develops due to rock deformation during tectonic activity, such as folds and faults. The data used in this research is DEMNAS which has been downloaded through the website (http://tides.big.go.id/DEMNAS/). The software used to extract automatically indrawing lineament are Geomatica 2016 and ArcGIS 10.8. with the output in the form of Lineament Density Map. Making Lineament Density Map begins with extraction of lineament in Geomatica with results of lineament polyline, followed by changing the data into a lineament single line by using the split lineament on the ArcToolbox feature in ArcGIS. The last stage is making a Lineament Density Map using the density map tool on the ArcToolbox too.

The application of this method is in the form of calculating the lineament density pattern to determine the direction of the lineament distribution so that the weak zones of the area are known [9].

With the example of the direction of 0 – 20°, then the formula for calculating the alignment is as follows:

$$0 - 20° = \frac{\Sigma\ Lineament\ length\ in\ direction\ \ 0 - 20°}{\Sigma\ Total\ lineament\ length} \times 100\%$$

3. Morphometry

Morphometry is the quantitative aspect of an area such as slope, slope length, slope shape, altitude, height difference, terrain roughness, abrasion levels and flow patterns [10]. The slope is part of the landform which is one of the factors for the occurrence of soil movements. Assessment is carried out on the slope, so that we know slope size can provide information about processes that affect landforms.

PROCEEDINGS
JOIN CONVENTION BANDUNG (JCB) 2021
December 1ST – 3rd 2021

The data used in morphometric calculations using DEMNAS data with ArcGIS 10.8. software. The data is processed automatically using the feature slope on the ArcToolbox feature in ArcGIS.

The slope value obtained was then classified using the classification by Van Zuidam (1985) [11].

Slope Value	Description	Color
0° – 2° (0% – 2%)	Flat	
2° – 4° (2% – 7%)	Gently Slope	
4° – 8° (7% – 15%)	Sloping	
8° – 16° (15% – 30%)	Moderate Steep	
16° – 35° (30% – 70%)	Steep	
35° – 55° (70% – 140%)	Very Steep	
>55° (>140%)	Extremely Steep	

Table 2: Morphometry Classification

4. Rainfall

Rainfall is one of the major elements of the climate that plays a role against soil movement and erosion [12]. Erosion is one of the factors that cause soil movement. Erosion can be caused by rainwater that falls to the earth and then erodes the surface of the land in its path, resulting in a steeper slope of the land. The rocks and soil that compose the slopes can be weakened through saturation caused by heavy rains.

Rainfall data in the research area were obtained from the *Badan Meteorologi, Klimatologi, dan Geofisika* (BMKG) and the accuweather website (https://www.accuweather.com/en/id/puncak/). The rainfall data can be an indicator of soil movement.

Result and Discussion

1. Normalized Difference Vegetation Index (NDVI)

The results of NDVI data processing produce five levels of greenery with NDVI values generated in the research area ranging from -1.00 to 1.00 which are used to measure the greenness of the vegetation in the research area that will be associated with the possibility of soil movement [7].

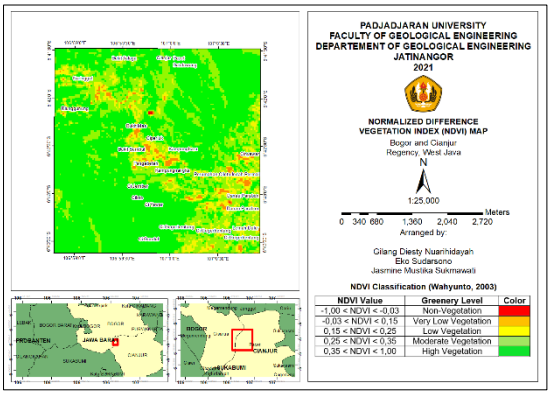

Figure 3: NDVI Map

Research Area with unvegetated land shown in red only occupies a small part of the research area. This land has an NDVI value range of -1.00 to -0.03 which indicates non-vegetated or aquatic objects.

Land with very low vegetation is spread over several areas in the research area. This land is indicated by the orange color and has an NDVI value range of -0,03 to 0,15. Vegetation in this area is very lacking because the area includes residential areas as well as lodging for tourists because considering the location of Puncak Bogor is a tourist destination. Lack of vegetation can trigger soil movement due to lack of strength from plant roots to support the soil if the area has high rainfall conditions and steep slopes.

Land with low vegetation indicated by the yellow color is spread around the residential area. The NDVI value obtained in this area of 0,15 to 0,25 can be in the form of less dense vegetation such as garden areas and courtyards of most houses in the research area. Likewise with the very low vegetation, this area is also still possible for soil movement to occur if there are other contributing factors.

Land with moderate vegetation is spread over several areas in the research area. The land indicated by the light green color has an NDVI value of 0,25 to 0,35 which indicates that this area is quite covered by vegetation. This area can be interpreted in the form of rice fields and farms scattered throughout the research area, which allow soil movement to occur because the vegetation roots from this land are not strong enough and do not penetrate the avalanche plane, so that the strength to bind soil grains is reduced and the soil becomes saturated with water when the weather conditions are wet so that it can allow the occurrence of soil movement.

Land with a high vegetation has an NDVI value of 0,35 to 1,00 which is indicated by a dark green color. This land occupies most of the research area and can be in the form of very dense vegetation such as wilderness. Land conditions like this are very good for resisting soil movement because the roots are strong enough to support the soil so that it is stable when high rainfall on the slopes.

Areas that allow for soil movement are spread from the northwest to the southeast of the research area which have low to very low vegetation with NDVI values ranging from 0,25 to -0,03.

2. Fault and Fracture Density (FFD)

The results of data processing in the software produce a Lineament Density Map which is used in the interpretation of permeability and vulnerability of soil movement in the research area.

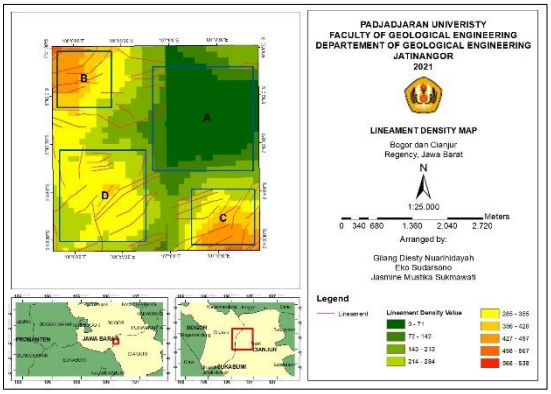

Figure 4: Lineament Density Map

Areas with high density values indicate the area has good permeability so when it rains the area will be vulnerable to soil movement while areas with low density have poor permeability and are not vulnerable to soil movement. In this research, there are three zones, namely areas with high density (Zone B and Zone C), medium density (Zone D), and low density (Zone A). Based on that classification, Zone B in the northwest direction and Zone C in the southeast direction, which is a medium for flowing water in the fractures and is a zone with high geological structure activity because it has a line density as a result of drawing morphological lineament patterns.

3. Morphometry

Results of morphometric data processing produce seven levels of slope with slope values generated in the research area ranging from 0º to >55º (0% to >140%).

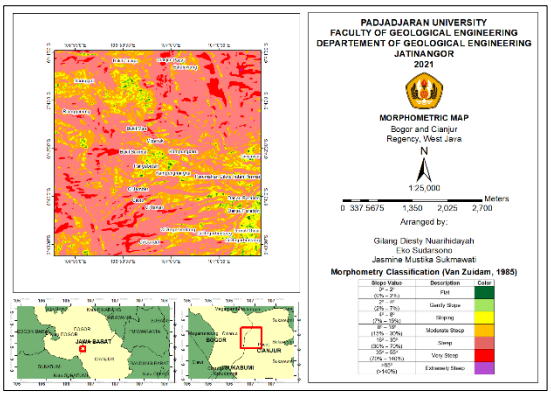

Figure 5: Morphometric Map

Flat land occupies a small part of the research area. This area has slopes ranging from 0° – 2° (0% – 2%) indicated by dark green color. The possibility of soil movement in this area is very small because in general the soil will move if there is a significant slope.

Land with gentle slopes also occupies a small part of the research area. This area has a slope of about 2° – 4° (2% – 7%) indicated by light green color. Similar to flat land, this area is also less likely to occur soil movement.

Sloping land is spread in several areas. This area has a slope of about 4° – 8° (7% – 15%) indicated by yellow color. This area is still possible for soil movement to occur if there are other contributing factors.

Land with a moderate steep is evenly distributed in several areas. This area has a slope of about 8° – 16° (15% – 30%) indicated by the orange color. This area has a higher probability of soil movements than sloping land.

Land with steep slopes occupies most of the research area. This area has a slope of around 16° – 35° (30% – 70%) indicated by the pink color. This area is vulnerable to soil movements because the slopes show a significant slope.

Land with very steep slopes occupies several areas in the research area. This area has a slope of around 35° – 55° (70% – 140%) indicated by red color. This area is very vulnerable to soil movement because the material that composes the slopes will easily move down the slope.

Land with extremely steep slopes has a slope of >55° (>140%) which is indicated by the purple color. In the research area, the slope with an extremely steep slope is only at one point. This area is the most vulnerable to soil movements compared to other slopes because the slopes show almost upright conditions. Material from the top of the slope is very easy to move, therefore it is not allowed to build buildings or roads along this slope.

The slope in the research area is dominated by steep slopes indicated by pink color with slope values ranging from 16° – 35° (30% – 70%). This can allow the research area to be vulnerable to soil movement if it is supported by other factors such as high rainfall, the type of material that composes the slopes is not strong enough, lack of vegetation, and high density.

4. Rainfall

Based on data from the *Badan Meteorologi, Klimatologi, dan Geofisika* (BMKG), the rainfall in the research area is quite heavy which is >50 mm/day. The research area has the highest rainfall forecast in October which is reviewed based on the data listed on the page accuweather. This shows that the research area has a high probability to occur soil movement because in the research area is also supported by other factors such as vegetation, slope, density, and the type of material that composes the slope. High rainfall will cause the slope to lose its strength in supporting the slope structure and the area has good permeability resulting in soil movement.

PROCEEDINGS
JOIN CONVENTION BANDUNG (JCB) 2021
December 1ST – 3rd 2021

5. Zonation of Soil Movement Vulnerability Areas

Zone is obtained based on the greenness of the vegetation, lineament density, and the slope. These three factors are related to each other, when a land is in a condition of less vegetation, then coupled with a significant slope and structure obtained from drawing lineament on rivers or escarpments, can increase the risk of soil movement on the land. These three factors are also supported by high rainfall in the research area so that zonation of soil movement vulnerability map is obtained.

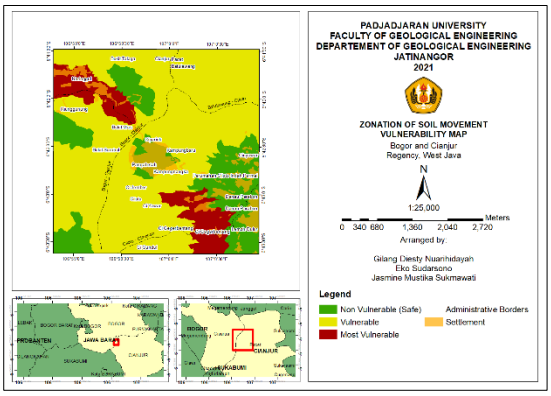

The zone is classified based on three colors, there are green, yellow, and red. Green represents non vulnerable (safe), yellow represents vulnerable, and red represents very vulnerable to soil movement.

Figure 6: Zonation of Soil Movement Vulnerability Map

The green zone or non-vulnerable (safe) zone is land that has high vegetation in the form of wilderness, this greatly reduces the possibility of soil movement because when high rainfall the water will be absorbed by tree roots which also function to bind the soil. In this zone, the land has a rare lineament density and a flat land to sloping. Under these conditions, there is little chance of soil movement.

The yellow zone or vulnerable zone is land that has moderate to high vegetation, the vegetation on this land is in the form of rice fields and farms where rice fields can allow soil movement because the roots of this vegetation are not strong enough so that they cannot withstand water saturation when high rainfall. In this zone there is also a lineament density that is rare to dense and the slope is steep to very steep so that this land allows soil movements to occur.

The red zone or very vulnerable zone is land that has low to very low vegetation in the form of settlements and non-vegetated areas, this is very possible for soil movement to occur because there is absolutely no vegetation that covers this area so that nothing can support the soil when high rainfall. In this zone, the land has a dense lineament density and a steep to very steep slope.

In the research area, there are residential areas spread in vulnerable and very vulnerable zones, so it is necessary to pay attention to infrastructure development and soil movement disaster mitigation activities in very vulnerable zones.

Conclusions

Based on the results of the research, the research area has three zones of vulnerability to soil movements, there are non-vulnerable (safe) zone, vulnerable zone, and very vulnerable zone to soil movement. This is reviewed based on the greenness of the vegetation (NDVI), lineament density (FFD), slope (morphometry), and supported by rainfall. (1) The research area has an NDVI value ranging from 0,25 to -0,03 with a low to very low vegetation spread from the northwest to the southeast of the research area. (2) Judging from the FFD factor, the high-density values are spread in the northwest to southeast direction of the research area which is a medium for flowing water in the fractures in the research area and zones that have high geological structure activity due to the density of the line drawn from the lineament pattern of morphology. (3) Most of the research area is a slope with a steep slope of 16° – 35° (30% – 70%). (4) Based on BMKG data, the rainfall in the research area is quite heavy, which is >50 mm/day with the highest rainfall data estimated in October (page accuweather). These influencing factors are related to each other so that it can be concluded that the research area is mostly a zone vulnerable to soil movement, but what needs more attention is the very vulnerable zone located in the Naringgul District, Bogor Regency and Gegerbentang District, Cianjur Regency, and reinforced by rock types in the Regional Geology of the area in the form of breccia and lava from Volcano Mount Gede which have been mixed with sedimentary rocks which are easily subjected to weathering processes so that they are very vulnerable to soil movement. With this, it is hoped that the community will pay attention to infrastructure development and soil movement disaster mitigation activities.

References

[1] A. W. Skempton and J. Hutchinson, "Stability of Natural Slopes and Embankment Foundations," Soil Mech Fdn Eng Conf Proc, 1969.
[2] A. C. Effendi, Kusnama, and B. Hermanto, "Peta Geologi Lembar Bogor, Jawa," Pus. Penelit. dan Pengemb. Geol. Bandung, 1974.
[3] Sudjatmiko, "Peta Geologi Lembar Cianjur, Jawa," Pus. Penelit. dan Pengemb. Geol. Bandung, 1972.
[4] "Gempabumi Badan Meterologi, Klimatologi, dan Geofisika (BMKG)." https://warning.bmkg.go.id/ (accessed Jul. 10, 2021).
[5] Weier, J. and Herring, D. (2000). Measuring Vegetation (NDVI & EVI). NASA Earth Observatory, Washington DC.
[6] Tucker, C. J. (1979). Red and Photographic Infrared Linear Combination for Monitoring Vegetation. Remote Sensing of Environment, Vol. 43, No. 2, hal. 333-337.
[7] Wahyunto, Sofyan Ritung dan Widagdo. (2003). Teknologi Penginderaan Jauh Untuk Monitoring Sumberdaya Lahan di Daerah Lampung. Laporan Akhir, Bagian Proyek Penelitian Sumberdaya Tanah. Balai Penelitian Tanah. Bogor.
[8] Chemong C.A. and Chenrai P. (2013). Fracture Density Analysis in the Sai Yok Fault, Western Thailand and its Implications for Hydrological Exploration. 142 Research Journal of Applied Sciences, 125-130
[9] Thannoun, R.G. (2013). Automatic Extraction and Geospatial Analysis of Lineaments and their Tectonic Significance in some areas of Northern Iraq using Remote Sensing Techniques and GIS. Mosul University. Iraq
[10] Mangunsukarjo, K. (1984). Inventarisasi Sumberdaya Lahan di Daerah Aliran Sungai Serayu Dengan Tinjauan Secara Geomorfologi.

[11] Van Zuidam, R. A. (1985). Aereal photo-interpretation in terrain analysis and geomorphologic mapping. Netherlands.
[12] Sutedjo, M.M., dan A. G Kartasapoetra. (2002). Pengantar Ilmu Tanah. Jakarta: Bineka Cipta.

PROCEEDINGS
JOIN CONVENTION BANDUNG (JCB) 2021
December 1ST – 3rd 2021

Mitigasi Daerah Rawan Tanah Longsor Menggunakan Teknik Interpretasi Delineasi Unit Morfometri Bentang Lahan (Studi Kasus: Kabupaten Tanah Datar)

*Luthfan Julian Nugroho[*1], Nabila Azarine Zahra[*1], Shabrina Tasha Zahra[*1], Raissa Salsabila Arifin[*1], Julianto[*1].*
*[*1] Geofisika, Fakultas Matematika dan Ilmu Pengetahuan Alam Universitas Indonesia,*

ABSTRACT
West Sumatra is a province in Indonesia that is located above subduction zone of the Indo-Australian Plate and the Eurasian Plate, construct an active tectonic and volcanic area. For example, Tanah Datar Regency on West Sumatra have various geological features such as the Anai Valley and others due to the active tectonism. A region that is close to active tectonic zone is analogous to two sides of the same coin, however, apart from having rich natural resources, the other hand, it also triggers many natural disasters such as landslides. Tanah Datar Regency Frequently encounters several landslide events that result in casualties, losses, and damage to facilities. The method used comprises spatial analysis and descriptive analysis utilizing Geographic Information Systems (GIS) which uses Interpretation and Delineation Techniques for Landscape Morphometric Units, including scores and weights for each parameter and then classified into 3 classes, namely low, medium, and high classes. The higher the weight, the higher the landslide hazard. The findings revealed that Tanah Datar Regency has a landslide hazard class ranging from low to high, therefore provide results in the form of a disaster mitigation map as a recommendation for the government in Tanah Datar Regency.

Keyword: GIS, Landslide, Kabupaten Tanah Datar, Mitigation

ABSTRAK
Sumatera Barat merupakan provinsi di Indonesia yang terletak di atas pertemuan Lempeng Indo-Australia dan Lempeng Eurasia yang mengakibatkannya menjadi daerah yang aktif tektonik dan vulkanik. Seperti pada Kabupaten Tanah Datar, Sumatera Barat memiliki kekayaan geologi yang luar biasa seperti Lembah Anai dan lainnya akibat oleh aktivitas tektonik. Daerah yang dekat dengan zona pertemuan lempeng yang aktif dianalogikan sebagai dua sisi mata koin, yaitu selain memiliki kekayaan sumber daya alam namun di lain sisi juga memicu banyaknya bencana alam seperti tanah longsor. Kabupaten Tanah Datar sering mengalami beberapa kejadian bencana tanah longsor yang mengakibatkan korban jiwa, kerugian, dan kerusakan fasilitas. Metode yang digunakan meliputi analisis spasial dan analisis deskriptif memanfaatkan Sistem Informasi Geografis (SIG) yang menggunakan Teknik Interpretasi dan Delineasi Unit Morfometri Bentang Lahan, meliputi skor dan bobot untuk setiap parameter selanjutnya diklasifikasikan ke dalam 3 kelas, yaitu kelas rendah, sedang, dan tinggi. Bobot yang semakin tinggi akan mempengaruhi tingginya bahaya longsor. Hasil penelitian menunjukan Kabupaten Tanah Datar memiliki kelas bahaya longsor yang variatif dari kelas longsor rendah sampai dengan tinggi, sehingga dapat memberikan hasil berupa peta mitigasi bencana sebagai rekomendasi untuk pemerintah di Kabupaten Tanah Datar.

Kata Kunci: SIG, Tanah Longsor, Kabupaten Tanah Datar, Mitigasi.

PENDAHULUAN

Kabupaten Tanah Datar, Provinsi Sumatera Barat yang beribukota di Batusangkar berada pada posisi 00°17” LS - 00°39” LS dan 100°19” BT - 100°51” BT memiliki luas wilayah 1.336 Km^2 atau 133.600 ha. Secara geografis wilayah Kabupaten Tanah Datar berada di sekitar kaki Gunung Marapi, Gunung Singgalang dan Gunung Sago dan diperkaya pula dengan 25 sungai. Kabupaten Tanah Datar terdiri dari 14 Kecamatan dengan 75 Nagari dan 395 Jorong. Sebelah Utara Kabupaten Tanah Datar berbatasan dengan Kabupaten Tanah Agam dan 50 Kota. Sebelah Selatan berbatasan dengan Kabupaten Solok, Kemudian sebelah Barat berbatasan dengan Kabupaten Padang Pariaman, dan sebelah Timur berbatasan dengan Kota Sawahlunto dan Kabupaten Sijunjung. Jumlah penduduk Kabupaten Tanah Datar berdasarkan hasil Sensus Penduduk Tahun 2020 mencapai 371.704 jiwa.

Sumatera Barat merupakan provinsi di Indonesia yang terletak pada pertemuan Lempeng Indo-Australia dan Lempeng Eurasia yang mengakibatkannya menjadi daerah yang aktif tektonik dan vulkanik yang menyebabkan Kabupaten Tanah Datar, Sumatera Barat memiliki kekayaan geologi yang luar biasa seperti Lembah Sinai, Puncak Aua Sarumpun, Gua Ngalau Pangian dan lainnya. Di samping memiliki kekayaan geologi tersebut, Kabupaten Tanah Datar sering mengalami beberapa kejadian bencana tanah longsor.

Tanah longsor (landslide) adalah bentuk erosi (pemindahan massa tanah) yang pengangkutan atau pemindahan tanahnya terjadi pada suatu saat secara tiba-tiba dalam volume yang besar. Tanah longsor dapat terjadi jika keadaan lereng yang cukup curam, terdapat bidang peluncur yang kedap air dibawah permukaan tanah, dan terdapat cukup air dalam tanah di atas lapisan kedap (bidang luncur) sehingga tanah jenuh air. Tanah longsor dapat mengakibatkan korban jiwa, kerugian, dan kerusakan fasilitas. Oleh karena adanya potensi bencana yang dapat terjadi, perlu adanya upaya pengurangan risiko bencana pada Kabupaten Tanah Datar.

Penelitian ini dilakukan dengan analisis spasial dan analisis deskriptif yang memanfaatkan Sistem Informasi Geografis (SIG) yang menggunakan Teknik Interpretasi dan Delineasi Unit Morfometri Bentang Lahan. Tujuannya agar kita dapat memberikan hasil berupa peta mitigasi bencana yang diharapkan dapat dijadikan acuan untuk pemerintah daerah setempat dalam membuat rencana kontijensi pengurangan bencana.

Penerapan teknologi Sistem Informasi Grafis (SIG) merupakan salah satu upaya mitigasi bencana alam khususnya tanah longsor. Upaya mitigasi bencana tanah longsor adalah meminimalirisir dampak dari bencana dengan cara membuat model penyusunan SIG yaitu analisis data peta yang diperlukan sebagai variabel untuk mendapatkan peta daerah yang memilihi bahaya dan risiko

PROCEEDINGS
JOIN CONVENTION BANDUNG (JCB) 2021
December 1ST – 3rd 2021

tanah longsor. Citra satelit juga dapat dimanfaatkan secara tidak langsung dalam menentukan potensi tanah logsor, menggambarkan permukaan, dan struktur geologi suatu wilayah (Suhendar, 1994).

DATA DAN METODE

Data Digital Elevation Model (DEM) SRTM Sumatera Barat didapatkan dari Badan Informasi Geospasial yang diolah *software* ArcMap 10.8 yang didapatkan lisensinya melalui kerjasama ESRI dan Departemen Geografi, Universitas Indonesia. Data DEM diolah menggunakan *tools* yang disediakan ArcMap sehingga dihasilkan kelas-kelas di setiap parameter yang dianalisis melalui penelitian yang pernah dilakukan Dyah Susanti pada 2019. Data curah hujan didapatkan dari Badan Pusat Statistik yang melampirkan besar curah hujan di setiap stasiun Badan Meteorologi Klimatologi dan Geofisika yang ada di sekitar Sumatera Barat. Data curah hujan yang didapatkan berupa besaran titik yang ditangkap setiap stasiun yang selanjutnya digunakan tools IDW. Metode *Inverse Distance Weighted* (IDW) merupakan metode deterministik yang sederhana dengan mempertimbangkan titik di sekitarnya (NCGIA, 2007). Data geologi didapatkan dari Kementerian Energi dan Sumber Daya Mineral berupa data geologi seluruh indonesia yang dipotong sesuai daerah penelitian di Sumatera Barat. Selanjutnya data yang telah diolah masing-masing akan dilakukan proses *overlay* atau tumpang tindih di ArcMap serta analisis visual melalui Google Earth yang dapat diakses oleh umum sehingga dapat ditarik kesimpulan dari data yang berupa beberapa peta di daerah Sumatera Barat.

Gambar 1. Diagram Alir Pengolahan, (Pengolahan Penulis, 2021)

Pada diagram alir menjelaskan metode penelitian mulai dari mempelajari literatur, pengumpulan data, pengolahan data, rancangan penulisan, dan penarikan kesimpulan.

1. Pengumpulan Data

Pengumpulan data dilakukan dengan diawali studi literatur dengan cara mempelajari buku, jurnal, internet, atau media lain yang berkaitan dengan tema paper yang dibawakan. Diketahui beberapa parameter utama potensi longsor, diantaranya yakni geomorfologi, intensitas hujan, dan jenis batuan. Parameter tersebut dijadikan acuan sebagai komponen utama mengidentifikasi potensi longsor di suatu wilayah. Selanjutnya data acuan dihimpun dari berbagai sumber lembaga nasional penyedia data seperti Badan Informasi Geospasial (BIG), Badan Pusat Statistik (BPS), Badan Meteorologi Klimatologi dan Geofisika (BMKG), dan Kementerian Energi dan Sumber Daya Mineral (KESDM).

2. Pengolahan Data

Pengolahan data yang dilakukan dalam penulisan ini adalah menggunakan metode *Weighted overlay* dan juga interpolasi. Dalam sistem informasi geografis dari parameter yang telah dipelajari. Mengacu pada penelitian sebelumnya yang dikaji oleh Susanti (2019), terdapat beberapa parameter yang sama dengan parameter penelitian ini, di antaranya adalah relief, curah hujan, dan jenis batuan. Ketiga parameter dikaji secara kuantitatif menggunakan skor yang telah ditentukan berdasarkan kelas pada masing-masing parameter (Susanti, 2019). Skor yang di dapat dibuat dalam bentuk peta pada tiap kecamatan di Kabupaten Tanah Datar. Berikut tabel modifikasi terkait parameter penelitian beserta skor menurut Dyah Susanti:

Tabel 1. Tabel Bobot Parameter Data Untuk Potensi Longsor (Pengolahan Penulis Modifikasi dari Dyah Susanti, 2019)

Parameter	Kelas	Skor
Relief	*Flat* *Undulating*	1
	Rolling *Hummocky*	2
	Hillocky *Hilly* *Mountainous*	3
Curah Hujan	120 - 125	1
	125 - 130	2
	121 - 125	3
	126 - 130	4
Batuan	Beku	1
	Metamorf	3
	Sedimen	5

Data keseluruhan disajikan secara konsep dan kuantitas yang diolah ke dalam perangkat lunak berbasis penginderaan jauh ArcGis. Data yang telah dideskripsikan kemudian diproses yang akan menghasilkan benang merah dari masalah di dalam penulisan. Kemudian data akan dibuatkan peta masing-masing guna menghasilkan gagasan baru. Gagasan baru dapat dijadikan referensi sebagai potensi longsor di Kabupaten Tanah Datar Sumatera Barat.

3. Penulisan

Penulisan dilakukan agar penyampaian gagasan dibuat efisien dan efektif. Metode penulisan dijelaskan menggunakan kaidah penulisan ilmiah yang diberikan. Setiap kerangka tulisan dikumpulkan, disusun, dan

ditafsirkan berdasarkan kaidah penulisan ilmiah. Setiap data hasil olah dan proses disajikan menggunakan tabel, gambar, dan diagram agar informasi tersampaikan secara efektif. Hasil olahan kemudian dianalisis dan disintesis yang kemudian dihasilkan sebuah simpulan. Hasil analisis berupa gagasan baru yang ditemukan dalam literatur.

4. Penarikan Kesimpulan

Penarikan kesimpulan dibuat dengan berdasarkan hasil penelitian serta sumber referensi data dan pertimbangan melalui tinjauan pustaka yang tersedia atau bisa disebut penarik kesimpulan metode induktif. Sedangkan, saran atau rekomendasi dibuat berdasarkan kesimpulan.

HASIL DAN PEMBAHASAN

Geomorfologi

Secara umum Kabupaten Tanah Datar dapat dikelompokkan menjadi 4 satuan morfologi yaitu:

1. Dataran yang mempunyai satuan morfologi relatif kecil dan ketinggiannya antara 226-274 meter di atas permukaan laut dengan kemiringan 0-2%.
2. Dataran bergelombang yang terletak pada lembah diantara perbukitan atau pada lereng perbukitan dengan ketinggian antara 365-615 meter di atas permukaan laut dengan kemiringan 2-15%.
3. Perbukitan yang merupakan daerah peralihan antara satuan dataran gelombang dengan satuan perbukitan terjal dan mempunyai ketinggian 612-952 meter di atas permukaan laut dengan kemiringan 15-40%.
4. Perbukitan terjal yaitu daerah puncak-puncak dengan kemiringan >40%.

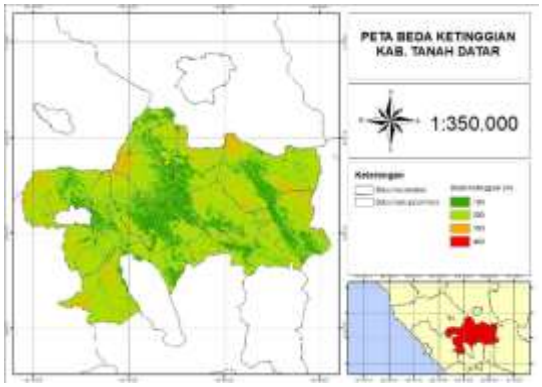

Gambar 2. Peta Beda Ketinggian Kab. Tanah Datar (Modifikasi Data DEM SRTM, 2021)

Pada **Gambar 2** peta beda ketinggian Kabupaten Tanah Datar berdasarkan data dari *Digital Elevation Model* (DEM) Badan Informasi Geospasial terlihat bahwa beda ketinggian daerah tersebut berada pada rentang 200-300 m.

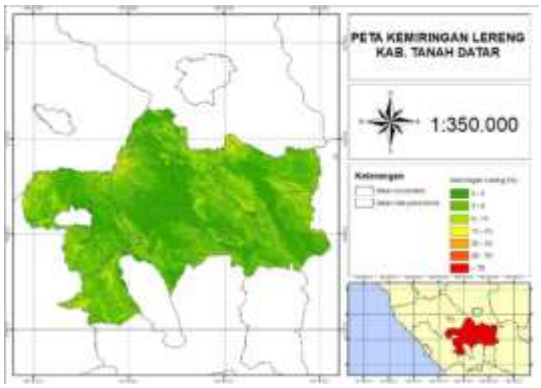

Gambar 3. Peta Kemiringan Lereng Kab. Tanah Datar (Modifikasi Data DEM SRTM, 2021)

Pada **Gambar 3** peta kemiringan lereng oleh data DEM Badan Informasi Geospasial terlihat bahwa kemiringan lereng Kabupaten Tanah Datar yaitu antara 3-15%.

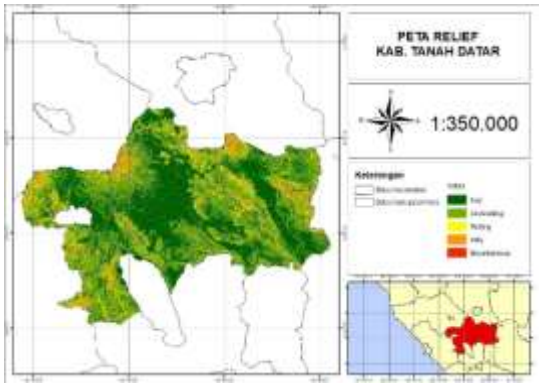

Gambar 4. Peta Relief Kab. Tanah Datar (Modifikasi Data DEM SRTM, 2021)

Pada **Gambar 4** peta relief diatas adalah hasil dari peta beda ketinggian dan peta kemiringan lereng pada Kabupaten Tanah Datar. Dapat dilihat bahwa Kabupaten Tanah Datar didominasi oleh dataran bergelombang dan bergulir, kemudian juga terdapat sedikit perbukitan.

Jenis Batuan

Berdasarkan Peta Jenis Batuan Kabupaten Tanah Datar yang dimodifikasi dari data SHP (sumber data ESDM) didapatkan peta seperti **Gambar 5**. Peta tersebut memberikan informasi bahwa Kabupaten Tanah Datar memiliki litologi batu beku, batu sedimen, dan batu metamorf.

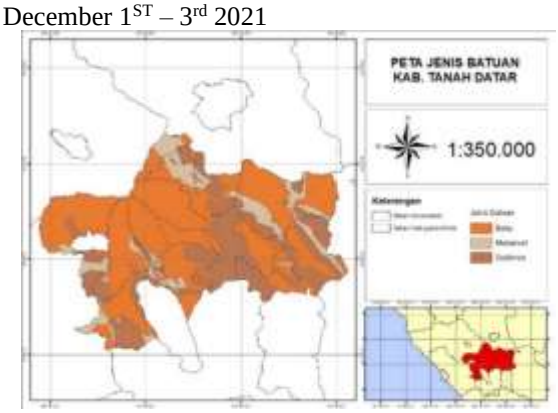

Gambar 5. Peta Jenis Batuan Kab. Tanah Datar
(Modifikasi Data ESDM, 2021)

Kabupaten Tanah Datar, Sumatera Barat secara regional masuk kedalam lembar Solok pada peta geologi Sumatera oleh P.H Silitonga dan Kastowo (1995). Berdasarkan peta geologi, Kabupaten Tanah Datar terdiri dari beberapa jenis batuan, yang terdiri dari:

1. Endapan Aluvial

Strata ini merupakan sedimen yang terendapkan pada zaman kuarter sampai dengan sekarang, yang terdiri dari litologi batu lempung, kerikil, dan bongkah - bongkah batuan yang memiliki umur lebih tua. Endapan ini berada di medan yang rendah pada lingkungan sekitar Danau Singkarak dan sekitar lembah - lembah.

2. Batuan Gunungapi

Batuan Gunungapi pada daerah Kabupaten Tanah Datar berumur kuarter dan Kuarter - Tersier. Strata yang berumur tersier terdiri dari batuan vulkanik tufa, lapili, lava, andesit Gunung Malintang dan andesit Gunung Marapi. Batuan gunungapi berumur kuarter tersebar di sekitar Gunung Marapi di sebelah barat Batusangkar, dan sekitar Gunung Malintang yang berada di utara Batusangkar. Batuan Gunungapi berumur Kuarter - Tersier berupa batuan volkanik aliran lahar dan batuan andesit, basalt. Batuan ini berada di tenggara Danau Singkarak yang membentuk perbukitan kecil.

3. Batuan Metamorf

Batuan Metamorf pada daerah Kabupaten Tanah Datar berumur tersier dan Triassic, batuan metamorf berumur pada daerah Kabupaten Tanah Dasar terdiri pasir kuarsa yang termasuk anggota bawah Formasi Ombilin, batugamping yang merupakan anggota Bawah Formasi Telisa, serpih napalan dari Formasi Sangkarewang dan Konglomerat dari Formasi Brani (Putra et.al., n.d). Batuan Metamorf ini tersebar di daerah selatan dari Batusangkar yang membentang dari barat laut ke tenggara. Batuan Metamorf berumur Triassic pada tanah datar berupa Anggota Batusabak dan serpih dari Formasi Tuhur dan Anggota Batugamping Formasi Tuhur (Putra et.al., n.d). Batuan ini tersebar di daerah sebelah tenggara Danau Singkarak dan di selatan membentuk perbukitan.

Batuan Intrusi ditemukan pada daerah Kabupaten Tanah Datar berumur Triassic, batuan intrusi ini terdiri dari granit, granodiorit, diorit kuarsa dan kuarsa porfiritik (Putra et.al., n.d). Batuan intrusi granit gneiss ditemukan di daerah Danau Singkarak dan batuan intrusi juga dapat ditemukan di sekitar utara Batusangkar dan di selatan kota Padang Panjang yang membentuk bukit yang cukup terjal.

Curah Hujan

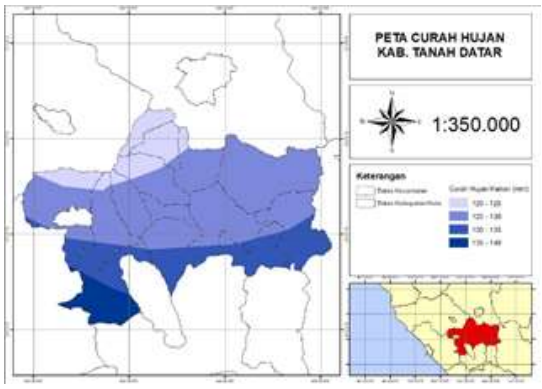

Gambar 6. Peta Curah Hujan Kabupaten Tanah Datar
(Modifikasi Data BMKG dan BPS, 2021)

Curah hujan ialah jumlah air yang jatuh di permukaan tanah selama periode tertentu bila tidak terjadi penghilangan oleh proses evaporasi, pengaliran, dan peresapan. Pada umumnya curah hujan diukur dalam satuan tinggi milimeter (mm) di atas permukaan horizontal. Tinggi air hujan 1 mm berarti air hujan pada bidang seluas 1 m^2 berisi 1 liter. Unsur-unsur hujan yang harus diperhatikan dalam mempelajari curah hujan, yakni jumlah curah hujan dan intensitas atau kekuatan tetesan hujan. Pada peta curah hujan Kabupaten Tanah Datar, kita membagi curah hujan menjadi 4 tingkat. Tingkat pertama dengan satuan tinggi 120 – 125 mm, tingkat kedua dengan satuan tinggi 125 – 130 mm, tingkat ketiga dengan satuan tinggi 130 – 135 mm, dan tingkat empat dengan satuan tinggi 135 – 140 mm. Pada peta tersebut terlihat bahwa persebaran curah hujan didominasi oleh wilayah yang memiliki curah hujan dengan tinggi 125 – 130 mm dan sangat sedikit sekali wilayah yang didominasi dengan curah hujan dengan tinggi 135 – 140 mm. Pada peta tersebut juga ditunjukkan perubahan tinggi curah hujan dari rendah ke tinggi dari arah utara menuju arah selatan.

Analisa Potensi Bencana Longsor

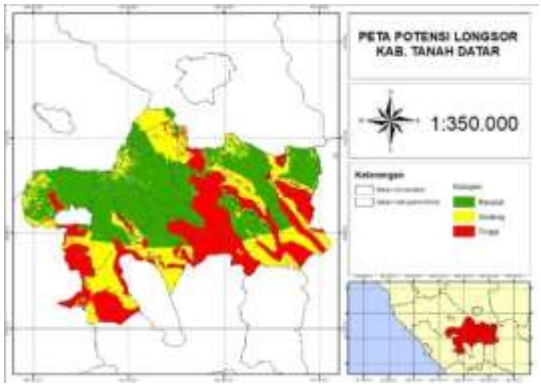

Gambar 7. Peta Potensi Longsor Kab. Tanah Datar
(Modifikasi Penulis, 2021)

PROCEEDINGS
JOIN CONVENTION BANDUNG (JCB) 2021
December 1ST – 3rd 2021

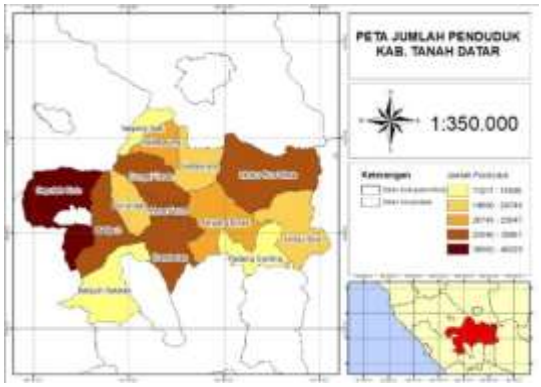

Gambar 8. Peta Jumlah Penduduk Kab. Tanah Datar (Modifikasi Data BPS, 2021)

Berdasarkan pengolahan data yang dilakukan menghasilkan beberapa peta dari beberapa parameter penelitian yang meliputi data geomorfologi, curah hujan, dan jenis batuan di Kabupaten Tanah Datar, Provinsi Sumatera Barat. Masing-masing parameter menghasilkan nilai berskala rendah hingga tinggi sesuai dengan skor dari **Tabel 1.** Kemudian dihasilkan Peta Potensi Longsor di Kabupaten Tanah Datar yang merupakan *overlay* dari ketiga peta parameter di atas (relief, jenis batuan, dan curah hujan). Tingkatan potensi longsor dikategorikan menjadi tiga, yaitu rendah, sedang, dan tinggi. Yang mana pada peta potensi longsor indeks potensi tertinggi hingga terendah dilambangkan dengan warna merah, kuning, dan hijau.

Tabel 2. Tabel Potensi Tanah Longsor (Pengolahan Penulis, 2021)

No.	Kecamatan	Jumlah Penduduk	Potensi Tanah Longsor (Ha)			Luas (Ha)
			Rendah	Sedang	Tinggi	
1	Batipuh	11217	6101,016	2677,587	1561,116	10339,719
2	Batipuh Selatan	14405	25,91627	5426,752	6666,123	12118,79127
3	Lima Kaum	14599	3034,815	30,13696	0	3064,95196
4	Lintau Buo	18671	1590,385	3846,846	6104,233	11541,464
5	Lintau Buo Utara	19771	10750,37	5400,316	2923,931	19074,617
6	Padang Ganting	20744	537,3159	2476,382	4099,401	7113,0989
7	Pariangan	23551	5045,901	508,245	277,4531	5831,5991
8	Rambatan	25047	3258,223	3402,531	3148,052	9808,806
9	Salimpaung	31883	1729,64	3014,817	202,1039	4946,5609
10	Sepuluh Koto	32694	9422,126	3213,907	2760,229	15396,262
11	Sungai Tarab	37180	7561,849	820,1602	0	8382,0092
12	Sungayang	37652	3047,783	1573,256	2551,668	7172,707
13	Tanjung Baru	38061	1601,271	1983,549	31,23062	3616,05062
14	Tanjung Emas	46229	4112,455	942,2372	7661,391	12716,0832
	Total	**371704**	**57819,06617**	**35316,72236**	**37986,93162**	**131122,7202**
		Persentase	44%	27%	29%	100%

Potensi longsor dipetakan berdasarkan 14 kecamatan di Kabupaten Tanah Datar yang dikorelasikan terhadap tingkat kepadatan penduduk di masing-masing kecamatan. Hasil perhitungan menunjukkan bahwa dari 14 kecamatan diindikasikan sebesar 44% kawasan memiliki indeks kerawanan longsor yang rendah, 27% sedang, dan 29% tinggi **Tabel 2.** Selain dihasilkannya peta analisis potensi longsor, dibuat pula peta jumlah kepadatan penduduk yang menunjukkan tingkat kepadatan dari yang tertinggi hingga terendah yaitu coklat tua hingga coklat muda. Pada peta potensi longsor menunjukkan bahwa tingkat potensi longsor tertinggi berada pada Kecamatan Tanjung Emas dengan tingkat potensi tinggi seluas 7661.391 ha. Hal ini dapat ditinjau salah satunya dengan jenis batuan penyusunnya didominasi oleh sedimen, yang didukung dengan curah hujan harian berupa 125 – 135 mm. Curah hujan tergolong sedang – tinggi serta tingginya tingkat kepadatan penduduk berpotensi terhadap penurunan tahanan geser dari tanah. Hal ini didukung oleh pernyataan Paimin dkk. (2006), faktor penurun ketahanan tanah adalah sebagai berikut:

a. Faktor alami, meliputi hujan harian kumulatif 3 hari berurutan, kemiringan lereng lahan, geologi batuan, keberadaan patahan, dan kedalaman tanah sampai lapisan kedap.
b. Faktor manajemen, meliputi penggunaan lahan, infrastruktur, dan kepadatan pemukiman.

Kabupaten Tanah Datar juga merupakan daerah yang memiliki kekayaan alam yang dimanfaatkan sebagai destinasi wisata. Salah satunya adalah Lembah Anai yang merupakan air terjun yang berada di Kecamatan Sepuluh Koto. Lembah Anai yang merupakan akses utama yang menghubungkan Kota Padang dengan Bukittinggi menjadi destinasi wisata yang menarik dikarenakan oleh aksesibilitasnya. Walaupun menjadi destinasi wisata favorit, menurut Zurnida dkk. (2019), kawasan Lembah Anai masih memerlukan akomodasi berupa penginapan serta infrastruktur lainnya yang mendukung kemajuan dari kawasan tersebut.

Lembah Anai yang berada di Kecamatan Sepuluh Koto memiliki relief yang beragam dari *flat* hingga *hilly* serta curah hujan berkisar antara 120 – 135 mm. Berdasarkan peta potensi longsor Kabupaten Tanah Datar, Kecamatan Sepuluh Koto memiliki potensi bervariasi mulai dari rendah hingga tinggi dengan tingkat kepadatan penduduk yang sangat tinggi. Maka dari itu, diperlukannya perhatian terhadap faktor ketahanan tanah agar menekan potensi longsor di daerah tersebut.

KESIMPULAN

Berdasarkan hasil yang didapat dari hasil pengolahan, didapatkan kesimpulan sebagai berikut:

1) Didapatkan hasil potensi tanah longsor di Kabupaten Tanah Datar Sumatera Barat dengan tiga kelompok yaitu potensi tanah longsor berpotensi tinggi dengan luasan total 37.986 ha, potensi tanah longsor berpotensi sedang dengan luasan total 35.316 ha, dan potensi tanah longsor berpotensi rendah dengan luasan total 57.819 ha.
2) Dari total sebaran luasan Kabupaten Tanah Datar Sumatera Barat, didapatkan 29% potensi tanah longsor berpotensi tinggi, 27% potensi tanah longsor berpotensi sedang, dan 44% luasan potensi tanah longsor berpotensi rendah. Dengan potensi tertinggi berada pada Kecamatan Tanjung Emas.
3) Lembah Anai sebagai salah satu destinasi wisata di Kabupaten Tanah Datar memiliki potensi mengalami longsor dilihat dari peta *overlay* dari beberapa parameter (geomorfologi, jenis batuan, dan curah hujan) dan mengkorelasikannya dengan jumlah penduduk di masing-masing kecamatan.
4) Hasil yang berupa peta potensi longsor diharapkan dapat menjadi salah satu pertimbangan kepada pemerintah daerah dalam pembangunan di Kabupaten Tanah Datar

REFERENSI

Arifin, MS, (2010), Modul klimatologi. Jawa Timur: Fakultas Pertanian Universitas Brawijaya.

Badan Pusat Statistik Kabupaten Tanah Datar. (2021). Kabupaten Kabupaten Tanah Datar 2021. Tanah Datar: Badan Pusat Statistik Kabupaten Tanah Datar.

Badan Pusat Statistik Sumatera Selatan. (2021). Provinsi Sumatera Barat 2021. Sumatera Barat: Badan Pusat Statistik Provinsi Sumatera Barat.

Cipta Karya. (2021). Rencana Program Investasi Jangka Mengah Bidang Cipta Karya Kabupaten Tanah Datar. Diakses pada https://sippa.ciptakarya.pu.go.id.

Dyah Susanti, Pranatasari & Miardini, Arina. (2019). Identifikasi Karakteristik dan Faktor Pengaruh pada Berbagai Tipe Longsor. agriTECH.39.97.10.22146.

NCGIA. (2007). Interpolation: Inverse Distance Weighting. http://www.ncgia.ucsb.edu/pubs/spherekit/inverse.html (17 Oktber 20021).

Paimin, dkk. (2009). Teknik Mitigasi Banjir dan Tanah Longsor. Balikpapan: Tropenbos International Indonesia Programme.

Pemerintah Kabupaten Tanah Datar. (2021). Geografis – Profil Pemerintah Kabupaten Tanah Datar. Diakses pada https://tanahdatar.go.id.

Putra, RP, dkk.(n.d). Implikasi Struktur Patahan Singkrak Terhadap Kerusakan Mesjid Nurul Islma dan Fasilitas Umum di Nagari Guguk Malalo, Kecamatan Batipuh Selatan, Kabupaten Tanah Datar, Provinsi Sumatera Barat. Padang: Fakultas Teknik Universitas Negeri Padang

Zurnida, C. S., dkk. (2019). Penerapan Arsitektur Organik pada Resort Hotel di Kawasan Wisata Lembah Anai Kabupaten Tanah Datar Sumatera Barat. Senthong, Vol. 2, No. 1

PROCEEDINGS
JOINT CONVENTION BANDUNG (JCB) 2021
November 23rd – 25th 2021

SEIRA: A Freeware for Joint Tomographic Inversion of Travel Time Based Seismic Refraction and Reflection Data

Putu Pradnya Andika[1,2], Yudha Styawan[1], Ruhul Firdaus[1], Tedi Yudistira[2], Cahli Suhendi[1], Gestin Mey Ekawati[1]
[1]Geophysical Engineering Study Program, Institut Teknologi Sumatera
[2]Geophysical Engineering, Faculty of Mining and Petroleum Engineering, Insitut Teknologi Bandung

Abstract
The massive infrastructure development in the past few decades has challenged us to provide sufficient initial information about subsurface conditions to solve geotechnical engineering problems. To produce the best and accurate solution, active seismic methods are implemented as one of the techniques to estimate subsurface physical parameters with high resolution by estimating the subsurface impedance value based on the variation of seismic wave velocity. In order to support the acquisition technology, we have developed a free and user-friendly software SEIRA to process and model seismic data. This application is written using Python programming language that has some key features, such as determining an initial model that combined the Intercept Time Method (ITM) and plus-minus algorithm, the forward modeling module using pseudo-bending ray tracing, and least-squares inversion methods to solve joint tomography seismic of refraction and reflection arrival time data. The validation of this software is tested using synthetic and field data, and from the obtained results shows that developed and implemented algorithms in SEIRA agree with theory.
Keyword: *seismic tomography, joint inversion, refraction, reflection, geotechnics*

Introduction

Implementation of seismic tomography using travel time data is a well-established inverse modelling technique to determine seismic velocity distribution in the subsurface (Meléndez et al., 2018). In tomographic inversion, the subsurface is divided into cells and each cell is given by starting velocity model and the ray tracing will performed where each ray will pass some number of cells in the velocity model (Lundberg et al., 2015). The final tomographic velocity can be used for various purposes such as site characterization to investigate the physical properties of soil.

Unfortunately, as far as we know, the availability of advanced seismic joint tomography software is limited and not free to use for student or educational purposed. Many free tools are available in code program and without user interface, for some people that have no background in programming will confused to do seismic joint tomography data processing. To solve the problem, we tried to develop a software based on python programming language version 3.7 named SEIRA. Python is chosen because they have so many contributors and the dependencies that help us coding faster.

The preliminary SEIRA have some feature such as visualizing and picking seismic data, interpret depth model from seismic raw data and single or joint tomography from seismic refraction and reflection travel time data.

Then, we also need validate this software to ensure that implementation algorithm in SEIRA confirm with the theories. So, in this part we already validated the result using synthetic and field data measurement.

Method

Joint inversion tomography using seismic refraction and reflection data can improve the resolution of velocity variations for shallow subsurface investigation. We solved the problem using 2D initial velocity model from intercept time method for laterally inhomogeneous media (Pavlenkova, 1973) shown in formula 1. Where Z_1 is depth of first layer, t_i is time intercept from refraction data and V is velocity from first layer and second layer.

$$Z_1 = \frac{t_i}{2} \times \frac{V_1 V_2}{\sqrt{V_2^2 - V_1^2}} \tag{1}$$

Moreover, we can also calculate depth model using the plus-minus method to solve more complex case layer (Hagedoorn, 1958). This method utilizing two approaches for determining the depth layer by plus time analysis and the velocity layer using minus time analysis. To calculate velocity and depth layer, we can use the following formula 2 and 3 respect respectively.

$$\Delta T_D^- = \frac{2(\Delta x)}{V_2} \tag{2}$$

$$Z_{1D} = \frac{T_D^+ V_1}{2\cos(\theta_c)} \tag{3}$$

The initial model velocity parameterization is using regular mesh grid white size $\Delta x \times \Delta z$. T hen, in the forward simulation, first-arrival travel times data in refraction are calculate using ray tracing pseudo-bending method by Um & Thurber (1987) shown in Figure 1. The pseudo-bending algorithms use the Fermat's principle of travel time minimalization that can reduce the computation time while maintaining the accuracy. The concept of ray bending between the specified pair from source and receiver is constructed by starting a three-point guess to the ray path and perturbing it by following equations 4 and 6 respectively:

$$\underline{n'} = \nabla V - \frac{[\nabla V.(X_{K+1} - X_{K-1})](X_{K+1} - X_{K-1})}{|X_{K+1} - X_{K-1}|^2} \tag{4}$$

$$R_c = \frac{-(cV_{mid} + 1)}{4c\underline{n}\,.\nabla V_{mid}} + \left[\frac{(cV_{mid} + 1)^2}{\left(4c\underline{n}\,.\nabla V_{mid}\right)^2} + \frac{L^2}{2cV_{mid}}\right] \tag{5}$$

Where $\underline{n} = \frac{\underline{n'}}{|\underline{n'}|}$, $L = |X_{K+1} - X_{mid}|$ and $c = \left[\frac{1}{V_{k+1}} + \frac{1}{V_{k-1}}\right] / 2$. ∇V is velocity gradient, X_K , X_{K+1}, and X_{K-1} are vectors position point, then n and R are the direction and amount of perturbation. Finally, the new bending position can be solved by equation 6 bellow:

$$X'_k = X_{mid} + \underline{n}.R_C \quad (6)$$

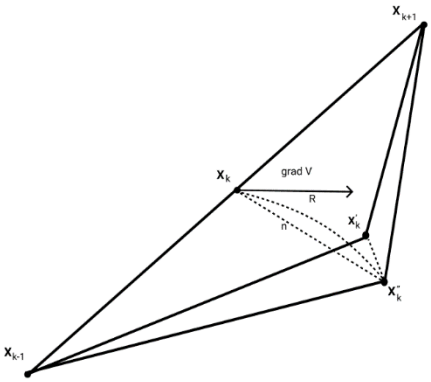

Figure 1. The concept of pseudo-bending ray tracing algorithms modified from Um and Thurber (1987).

Forward simulation in reflection wave has been calculated using the common depth point (CDP) guided by initial model that has been calculated from intercept time or plus-minus method as reference for every depth points.

Then, we applied damped least-squares (DLS) to solve the inversion problem, and the joint tomographic matrix equation can be written in equation 7.

$$\begin{pmatrix} A \\ \alpha I \\ \gamma G \end{pmatrix} \delta m = \begin{pmatrix} \delta t \\ 0 \\ 0 \end{pmatrix} \quad (7)$$

Where A is the matrix length of the ray reflection and refraction in each block, αI is a norm damping which is used to provide solutions for blocks model that aren't passed by seismic rays so that they are biased towards the initial model, γG is gradient damping is used to provide a solution to the block by gives a smooth effects (Nugraha, 2017), δm is the slowness perturbation and δt is the delay time between observation and calculation. At the end, the final velocity written in equation 8 can be reach with maximum iteration or will be stop when RMSE becomes small and convergent.

$$m_{i+1} = m_i + \delta m \quad (8)$$

The main tasks of SEIRA software are to solve 2D modeling and inversion that can be done by single or joint processing. We design the software architecture with different abstraction levels written in Python 3.7 version shown in Figure 2. At the application level, we defined the basic framework that we use to solve complex data handling and processing such as joint inversion. Then, all the abstraction levels can communicate across the interface or independently. In the modelling level presents a data visualization from each task in SEIRA feature. In a question level, we storage many functions of equation that we may needed for scientific data processing. In utilities level, we config data from temporary memory and input or output (I/O) file and how to communicate with the user interface. Also in an external dependencies level, there a list of python module that we need to build the SEIRA software and to avoid program running in single core that make time elapsed getting longer, we improve the performance by implemented multi-thread processing by utilizing the resource from central processing unit (CPU) core in our computer.

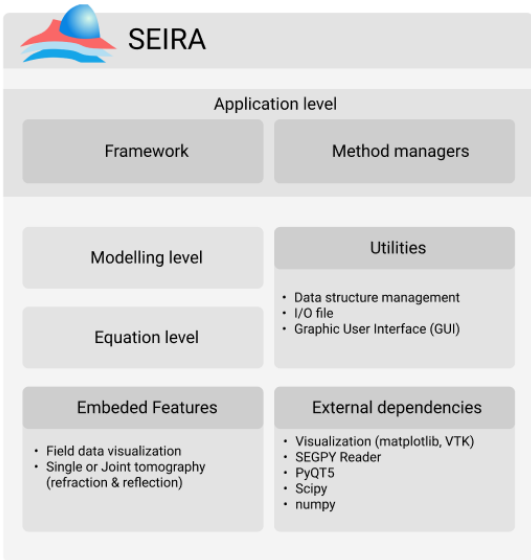

Figure 2. The concept of pseudo-bending ray tracing algorithms modified from Um and Thurber (1973).

The workflow for data processing from raw data to 2D joint tomography can be done by following the flowchart show in figure 3. In the first step, we need to pick of first break from refraction and reflection data from all the trace in each source. For creating the initial velocity model, we can use the depth calculation as a guide.

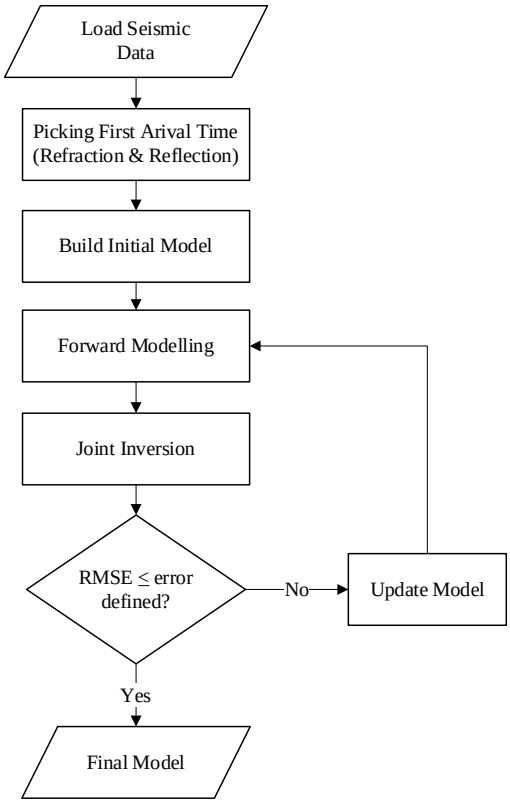

Figure 3. The concept of pseudo-bending ray tracing algorithms modified from Um and Thurber (1973).

PROCEEDINGS
JOINT CONVENTION BANDUNG (JCB) 2021
November 23rd – 25th 2021

Result

In this step, we already have a preliminary result from the SEIRA. This software has several features such as depth model interpretation, single or joint tomography and ray simulations. Then, to validate the result from our product, we do test in synthetic and real dataset as we described below.

To create a synthetic dataset, we made a simple higher positive velocity anomaly in the middle of the model (in Figure 4.a), and we also use starting initial velocity model with lateral velocity change (Figure 4.b), for the details about the model and inversion tomography parameters can be seen table 1. From the result shown in Figure 4, we can interpret the anomaly can clearly detected by the pattern of final model and perturbation velocity in Figure 4.d and Figure 4(e). Furthermore, from the RMS error shown that the curve is convergence.

Table 1. Details parameters for generated travel time data and joint inversion in synthetic model.

Parameters	Value
Synthetic Model	
Source number	25
Source spacing	5 m
Station number	24
Geophone interval	5 m
Joint Inversion	
Number of iterations	5
Number of rays iterations	250
Grid size (x,y)	(3,3)
Block model size (nx, nz)	(43,11)
Norm damping	20
Gradient damping	30

a.

b.

c.

d.

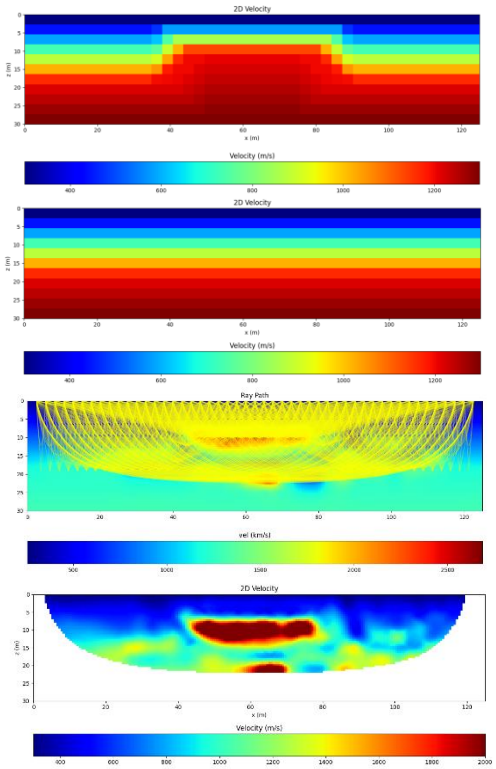

e.

f.

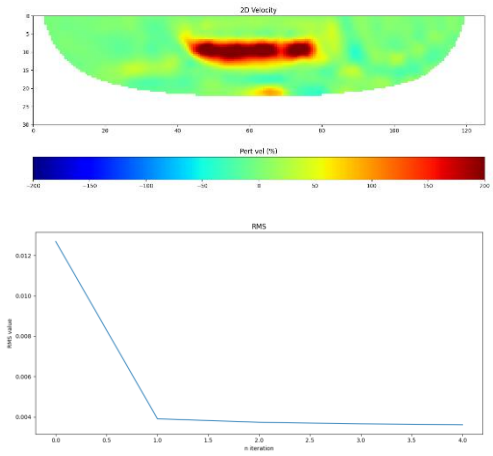

Figure 4. (a) The true model of synthetic data, (b) initial velocity for joint tomography, (c) ray-path data from final velocity model, (d) final velocity model, (e) velocity perturbation change and (f) RMS error for each iteration.

Then, for the field data implementation, we carried out an acquisition data at Institut Teknologi Sumatera campus area with parameters as show in table 2.

Table 2. Details parameters for seismic data acquisition and joint inversion tomography.

Parameters	Value
Acquisition data	
Source number	24
Station number	24
Geophone interval	1
Record length	500 ms
Joint Tomography	
Number of iterations	10
Number of rays iterations	100
Grid size (x,y)	1
Block model size (nx, nz)	(23,5)
Norm damping	20
Gradient damping	30

Figure 5(a) shows the site condition where the depth of the sediment layer is estimated at around 2.5 meters. Then, after calculating the initial model using the ITM, we get the depth model around 3 meters with a velocity approximately 400 m/s as shown in Figure 5(b). After that, we run the joint tomography where the final ray path and final velocity model is shown in figure 5(c) and 5(d). Perturbation velocities is shown in Figure 5(e), we can recognize the pattern around the depth 2 meters indicated as a bedrock from the velocity correction that match the site condition. The RMS error curve also shows that the inverse process is convergence.

a.

PROCEEDINGS
JOINT CONVENTION BANDUNG (JCB) 2021
November 23rd – 25th 2021

b.

c.

d.

e.

f.

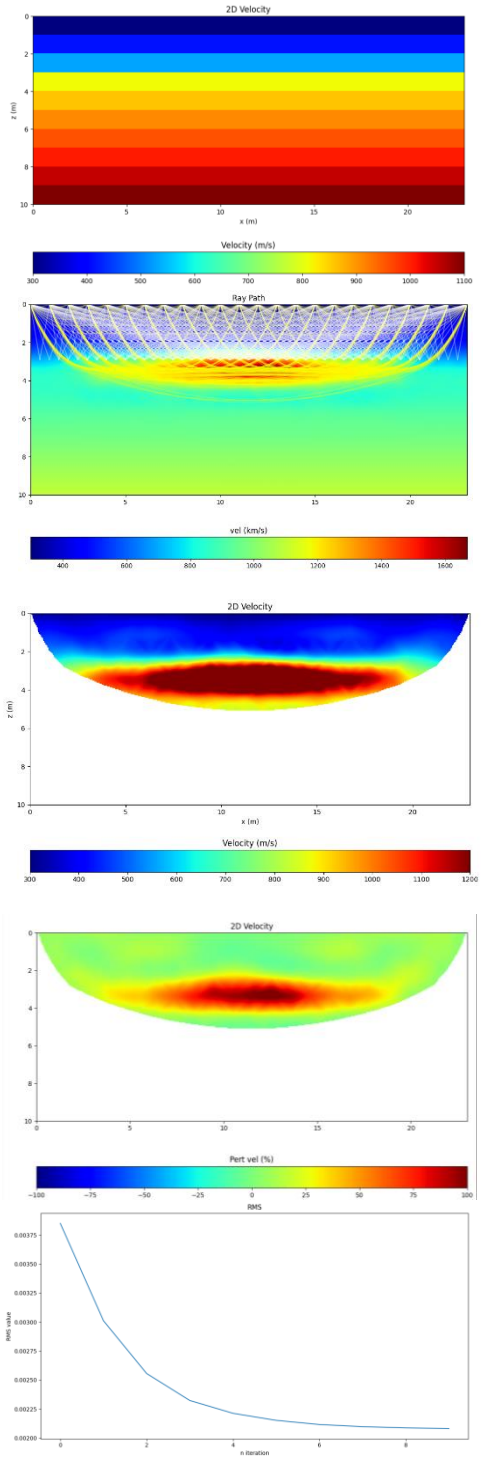

Figure 5. (a) the site condition, (b) initial velocity for joint tomography obtained from intercept method, (c) ray-path of final velocity model, (d) the final velocity model, (e) velocity perturbation change and (f) RMS error for each iteration.

Discussion

From the obtained results, as we explain in the previous section, we validate the developed software by using the synthetic and real dataset and give appropriate results. Nonetheless, the accuracy of seismic tomography has a limitation to image the deeper structure due to limitation of ray-path coverage, especially in seismic refraction. Furthermore, up to now, SIERA also have limitations such as error handling that sometimes makes application force close for sometimes and when parameters not acceptable, the software can't give error details in status bar. This limitation subject to improvement for the next updated version.

Conclusions

We have presented the capability of SEIRA software for various options to do routine joint travel-time tomography based on seismic refraction and reflection data using python programming language. This software consists of three main parts: a tool for visualizing and picking raw seismic data, a tool for interpreting the layering model, and a tool for single or joint tomography inversion. To improve the computing performance to handle huge matrix, we employ the multi-thread schema to utilize the CPU resources. Then, to evaluate that the developed and implemented algorithm in SEIRA agrees with the theory, we validate using synthetic and real datasets and give satisfying results. However, we realize that SIERA still has some limitations as we state above. To make SIERA better, we need optimize the algorithm and software design in the next development.

References

Hagedoorn. J.G, The Plus-Minus Method of Interpreting Seismic Refraction Section. London: Fifteenth meeting of the European Association of Exploration Geophysicists, 1958.

Lundberg, E., Juhlin, C., Zhang, F., & Behrendt, R. (2018). Seismic Reflection, Refraction and Tomography results from 3D seismic data, Forsmark.

Meléndez, A., Korenaga, J., Sallarès, V., Miniussi, A., & Ranero, C. R. (2015). TOMO3D: 3-D Joint Refraction and Reflection Traveltime Tomography Parallel Code for Active-Source Seismic Data Synthetic Test. Geophysical Journal International, 203(1), 158-174.

Nugraha, A. D. (2017). Tomografi Seismik.10. Penerbit ITB Press.

Pavlenkova, N. I. (1973). Interpretation of refracted waves by the reduced travel time curve method. Physics of the Solid Earth, 8, 544-550.

Um, J., & Thurber, C. (1987). A Fast Algorithm for Two-Point Seismic Ray Tracing. Bulletin of the Seismological Society of America, 77(3), 972-986.

Wood, L. C., & Treitel, S. (1975). Seismic signal processing. Proceedings of the IEEE, 63(4), 649-661.

Acknowledgements

We thank to Institut Teknologi Sumatera for providing the research grant (B/338/IT9.C1/PT.01.03/2019) "Hibah Penelitian ITERA SMART 2019" scheme.

PROCEEDINGS
JOINT CONVENTION BANDUNG (JCB) 2021
November 23rd – 25th 2021

Landslide risk-mitigation design: a case study in Lahat-Pagar Alam Highway

Muhammad Fadhli[1], Tommy Julio Lumban Tobing[2], Muhammad Faris Hafiddin[3], Rina Sahara[1]
[1]Geological Engineering Study Program, Sriwijaya University
[2]Balai Besar Pelaksanaan Jalan Nasional V Sumatera Selatan
[3]DMS Program Pamsimas III Kabupaten Lahat

Abstract

Lahat- Pagar Alam highway is a connecting road between districts and provinces in South Sumatra. the area is included in the Talang Akar formation which consists of fine sandstone lithology, claystone, siltstone, and shale stone. When there is fairly high rainfall, the road area is one of the most vulnerable areas to generate landslides in weak planes. of which happened on February 12, 2021. The damage to the catchment zone in the road area is triggered by the presence of slip planes as well as the influence of the anthropogenic process. In this study, slip plane analysis was carried out using the 2 track 2D resistivity method of Wenner Alpha configuration, 2 borehole sampling for subsurface detailed investigation of landslide and field observation for surface investigation. From the results of the 2D resistivity survey, it was found that on paths 1 and 2 there are two-layer zones, namely the Wet Zone with a resistivity value of fewer than 60 Ohms and the Weathered Zone with a resistivity value of 61 ohm-meters to 300 ohm-meters to a depth of 30 meters below the surface. Meanwhile, from the borehole, it is known that there is a gravel and fragmented claystone lithology (1-14) meters, very fine sandstone (14-18) meters, and clay-siltstone (18-30) meters and from calculated of Safety Factor (FK) obtained a value > 1.1 which indicated it is safe from earthquake hazard. With the results of this survey, it can be carried out to prevent and handle landslide disasters in this area, such as the installation of erosion control mats and DPT + Bore Pile and can make for spatial planning, settlement, and infrastructure in the future for Lahat - Pagar Alam highway.

Keywords: Landslide, Lahat-PagarAlam Highway, Electric Resistivity, Mitigation

Introduction

The existence of landslide activity is a problem that is highly considered in efforts to build national infrastructure. Landslide is a disaster activity that occurs influenced by morphological factors, lithology, geological structure, and hydrology (Mulyasari, 2020) to cause the movement of the constituent mass of the slope towards the bottom of the hill by the earth's gravity. The presence of steep slopes and slip fields below the surface is one of the conditions for landslides. Lahat- Pagar Alam Highway is a connecting road between districts and provinces in South Sumatra with relatively high activity as a national road.

Lahat-Pagar Alam highway has a morphological appearance with hilly terrain that is steep to very steep. In the period January-March 2021, there have been at least three landslide activities, with the most significant impact occurring on February 12, 2021 (Figure 1). The existence of landslides that occur is strongly influenced by the inability of the road slopes to accommodate pore water pressure in the fragmented clay layer as a slope constituent material when rain happens.

Based on regional geological conditions, this area is included in the Talang Akar and Alluvium formations, which have a composition of fine sandstone lithology, claystone, siltstone, and shale stone (Figure 2), which has a very weathered physical appearance and has very minimal cover vegetation. If there is high enough rainfall, this road area will be directly affected by landslides; this is also controlled by the presence of slip fields and damage to the catchment zone in the road area.

In this study, we used the Wenner Alpha configuration 2D resistivity method and borehole sampling to determine the derailment field and subsurface structure analysis so that recommendations were obtained in prevention and mitigation efforts Lahat-Pagar Alam highway area.

Data and Method

The research was occurred in the Lahat-Pagaralam highway KM 229+760, precisely in the village of Lubuk Sepang, Lubuk Pinang sub-district, Lahat Regency, South Sumatra, which experienced a landslide on February 12, 2021, with a considerable impact.

This research begins with discussing regional studies and direct field observations conducted to determine the physical condition of the constituent lithology, the slope and direction of the lithological layers, and the current state of the surface of the slopes.

Furthermore, the slip plane analysis was carried out using the 2D resistivity method with the Wenner Alpha configuration and borehole sampling. 2D Resistivity Wenner Alpha configuration uses 2 tracks with a track length of 160 meters with several 32 channels and a distance between electrodes of 5 meters (Figure 3). This method is used in horizontal profiling (mapping), with the final result obtained as a flat profile (Loke, MH 1999). Borehole sampling was carried out with 2 core samples with a depth of 0-30 meters which was carried out to determine the

lithology of the constituents and the depth of the layers of Rock.

Result and Discussion

2D Resistivity Wenner Alpha Configuration

2D resistivity analysis of the Wenner Alpha configuration using 2 tracks with a length of 160 m and 32 channels in the direction of the main road that experienced landslides; The results obtained on track 1 can be interpreted as having two types of zones that form the surface layer of the slope, namely the wet zone and the weathered zone. The wet zones layer has a resistivity value of fewer than 60 ohm-meters, whereas the weathered zone has 61 ohm-meters to 300 ohm-meters. In track 1, it is carried out to a depth of 30 meters (Figure 4).

Furthermore, on track 2, the resistivity results obtained are interpreted as having two surface layer zones, the weathered zone marked with a resistivity value of <50 ohm-meters and the weathered zone marked with resistivity 51 ohm-meters to 98 ohm-meters. In track 2, it is carried out to a depth of 29 meters (Figure 5).

These results align with the natural appearance in the field where the constituent lithology is in the form of fine sandstone and claystone, which is included in the geological Talang Akar formation. In addition, due to anthropogenic processes in the form of logging of vegetation on the slopes, it also dramatically controls the presence of slip fields on the surface of the road slopes.

Borehole Data Analyze

Borehole data conducted using 2 borehole logging with a depth of 30 m showed that the borehole (BH 1) has 3 types of rock lithology that have different characteristics. In BH 1, the results obtained are gravel clay with clay-sand grain sizes (1-4 m), fragmented clay with clay-coarse sand grains (4-9 m), compact claystone with clay-silt grains with (9-14 m), laminated structure sandstone with fine sand-coarse sand (14-18 m), and claystone with clay-silt grains (18-30 m) (Figure 6). While in BH 2 the results obtained are gravel clay (0-3 m), fragmented clay with the grain size of clay-coarse sand (3-5 m), compact claystone with grains of clay – silt (5-8.5 m), sandstone with the grain size of fine sand – coarse sand (8-13 m) and claystone compact with clay-silt grain size (13 – 30 m) (Figure 7). So from the borehole analysis of this data, it can be seen that the slope composition layer on the shoulder of the road has the characteristics of being quickly saturated with water so that the loading factor, very steep slope and high anthropogenic level significantly control the slip field on the road surface slope.

Analysis of Landslide Types and Handling Concepts

From data analysis and field observations, it can be correlation of surface and subsurface in the research area the type of avalanche that occurred was a slide-type characterized by the presence of a shear strain zone so that it was marked by the formation of a slip plane that caused the constituent material to descend the slope. The type of slip plane formed is translational, which has a relatively straight plane. A translational slide in which the moving mass consists of a single unit that is not significantly deformed (Varnes & Cruden (1996).

So in the concept of handling and mitigating landslides in the Lahat-Pagaralam highway area, KM 229+760 can be done with two handling concepts, namely Handling the upper and lower slopes. The handling of the upper slope can be done by:

a) Horizontal Drain Installation

It is the installation of pipes on slopes used to reduce surface water pressure on slopes that can cause landslides. With the installation of a horizontal drain, groundwater will be able to flow out of the surface (Figure 8).

b) Erosion control mat installation

It is an effort made to make a layer of soil to prevent landslides, prevent leakage, and control the direction of surface water flow that seeps through the walls to strengthen the stability of the construction.

The installation of this mattress is combined with geotextiles using plastic sheets or polymers of the type of polyester, polypropylene, or polyethylene. In addition, this mat can maintain its natural shape that can still be planted with vegetation (Figure 9).

Meanwhile, efforts to handle downslope can be made by:

a. Installation of DPT + Bore Pile

It is an Efforts are made to make pile foundations made of concrete using direct drilling on the ground surface to prevent further landslides where bore piles are installed to cut the slip plane. The water pressure that occurs is dissipated through the drainage system behind the retaining wall (Figure 10)

By reducing the upper and lower slopes of the Lahat-Pagaralam highway area KM 229+760, the results of the recapitulation of the FK and Gaya values are obtained with a value of 1.049 -. 1.17, which can be categorized as safe with the provisions of the SF number > 1.1, which is influenced by the PGA result value of 0.3 – 0.4 in earthquake conditions (Table 1).

Conclusions

Based on the results of data analysis using the 2D resistivity method Wenner-Alpha configuration and taking 2 drill hole samples, it can be seen that the road slope surface has two types of zones forming the surface layer of the slope, namely the wet zone with the weathered zone which significantly controls the slip plane. The wet zone has a resistivity value of fewer than 60 Ohms, and the Weathered Zone with a resistivity value of 61 ohm-meters to 300 ohm-meters and the slip plane is between the fragmented clay layer fine sandstone.

From the analysis of landslide types based on data and field observations, it can be seen that the type of landslide that occurred in the Lahat-Pagaralam highway area KM 229+760 is a type of landslide with a type of translational slip plane where the analysis is controlled by the shear strain zone which controls the slip plane. Two methods can be used to handle and mitigate landslide hazards in the Lahat-Pagaralam highway KM 229+760 area, namely upper slope management, which can be done by installing horizontal drains and erosion control mats, while on the lower slopes, it can be done by installing DPT + Bore Pile. The risk mitigation research in the Lahat-Pagaralam highway KM 229+760 area can be used to recommend the design of efforts and mitigation in other areas with a relatively high level of landslide susceptibility.

References

Barber, A.J., Crow, M.J. and Milson, J.S., 2005, Sumatra: Geology, Resources and Tectonic Evolution. London; The Geological Society.

Cruden, DM & Varnes, DJ. 1996. TransportationResearch Board, Washington D.C.

Faloe, P. O, *et. al.* 2019. Environmental Earth Sciences (2019) 78:430. https://doi.org/10.1007/s12665-019-8430-x

Gafoer, S., Cobrie, T. & Purnomo, J., 1986. Center for Geological Research and Development.

Maharani, Intan, *et.al.* 2018 J. Aceh Phys. Soc., Vol.7, No.3 pp.139-143, 2018

Mulyasari, R, *et.al*. 2020. Journal of Exploration Geophysics Vol. 6/No. March 1, 2020: 66-76

Lestari, Endah. 2017. Journal Of Forum mechanics Vol. 2/No.November 2, 2017

Loke, M.H. 1999. Electrical Imaging Surveys for Environmental and Engineering Studies: A practical quide to 2-D and 3-D surveys. Malaysia:Penang.

Varnes, DJ. 1978. Slope movement types and processes. In Special report 176: Landslides: Analysis and Control, Transportation Research Board, Washington, D.C

Widyatmanti, W., Wicaksono, I., Syam, P. D. R., 2016, IOP Conference Series: Earth and Environmental Science, 37(1). https://doi.org/10

Acknowledgements

We are grateful to PT Visi TEKNIKTAMA UNGGUL (KSO) and CV. MERCURI DESIGN CONSULTANT as a data survey contractor in an effort to handle landslides and we would thank you for the Joint Convention Bandung for accepted for our papers.

PROCEEDINGS
JOINT CONVENTION BANDUNG (JCB) 2021
November 23rd – 25th 2021

Table 1. FK Value and Gaya Recapitulation

No	PGA	Percepatan	FK	Mmax	Pmax	Mmax stem	Mmax toe/heel	Vmax stem	Vmax toe/heel
1	0,3	0,108	1,17	400,3	-838,0	-314,4	-186,6	-188,4	736,7
2	0,35	0,126	1,092	441,3	-911,8	-333,3	-383	-199,7	814,7
3	0,4	0,144	1,049	489,7	-991,8	-351	-437,2	-211,3	912,7

Figure 1. The Condisition of Lahat-Pagaralam highway area, KM 229+760 after the landslide on February 12, 2021

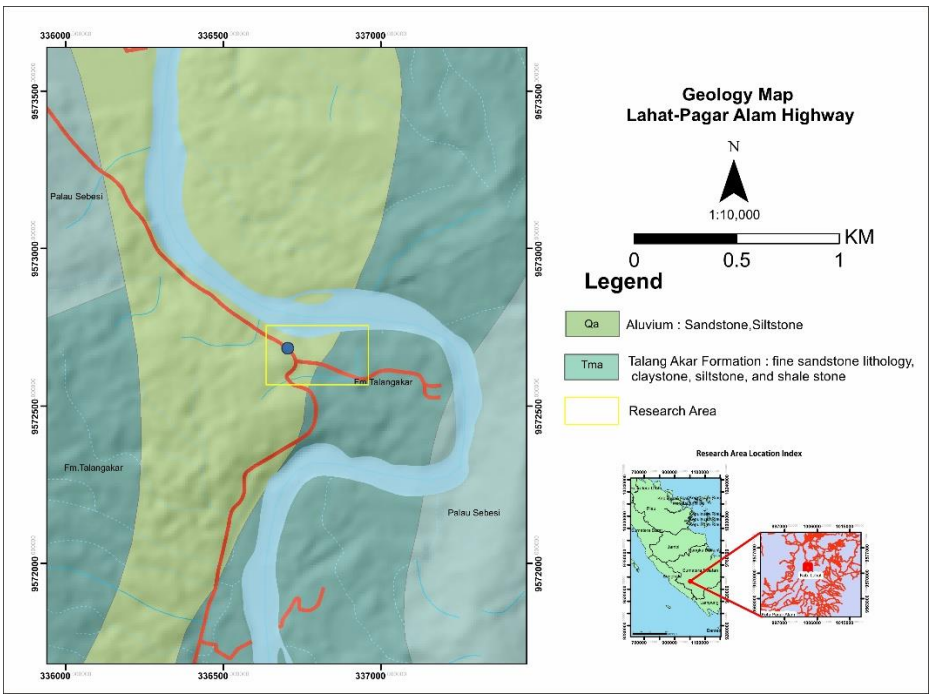

Figure 2. Geology Map of Lahat-Pagaralam highway area, KM 229+760 (Modiefied Frrom Gafoer et al., 1986)

PROCEEDINGS
JOINT CONVENTION BANDUNG (JCB) 2021
November 23rd – 25th 2021

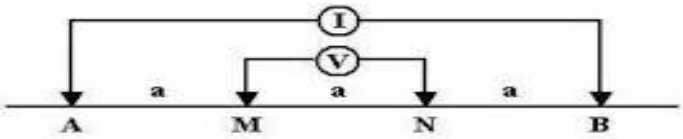

$$\rho_A = 2\pi\, a \frac{V}{I}$$

Figure 3. Illustration of measurement points Configuration Wenner-Alpha (Loke, M.H. 1999).

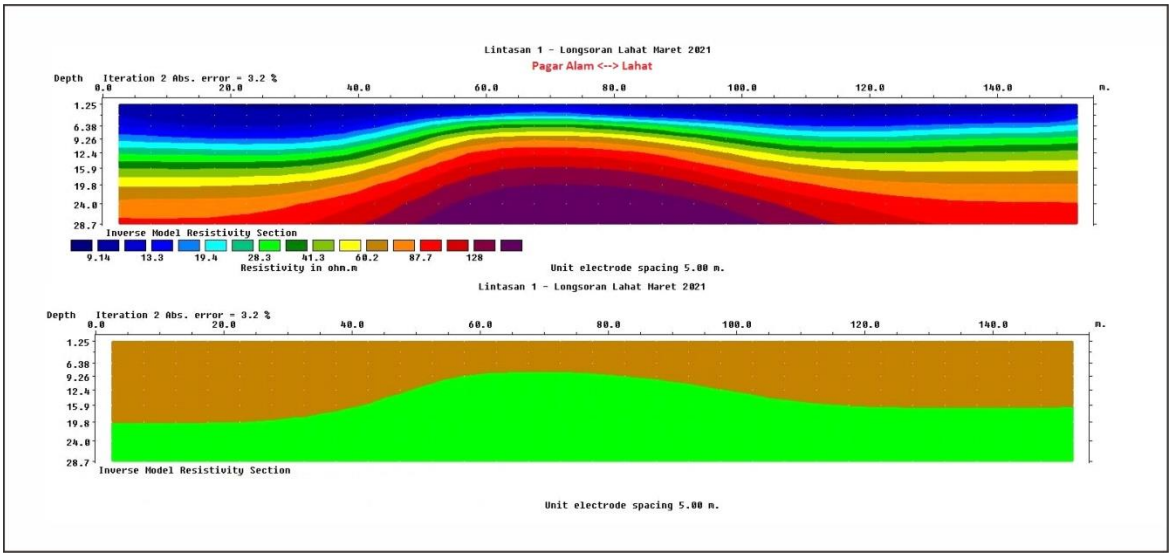

Figure 4. Illustration of Inverse model of resistivity sections along profle lines Track 1

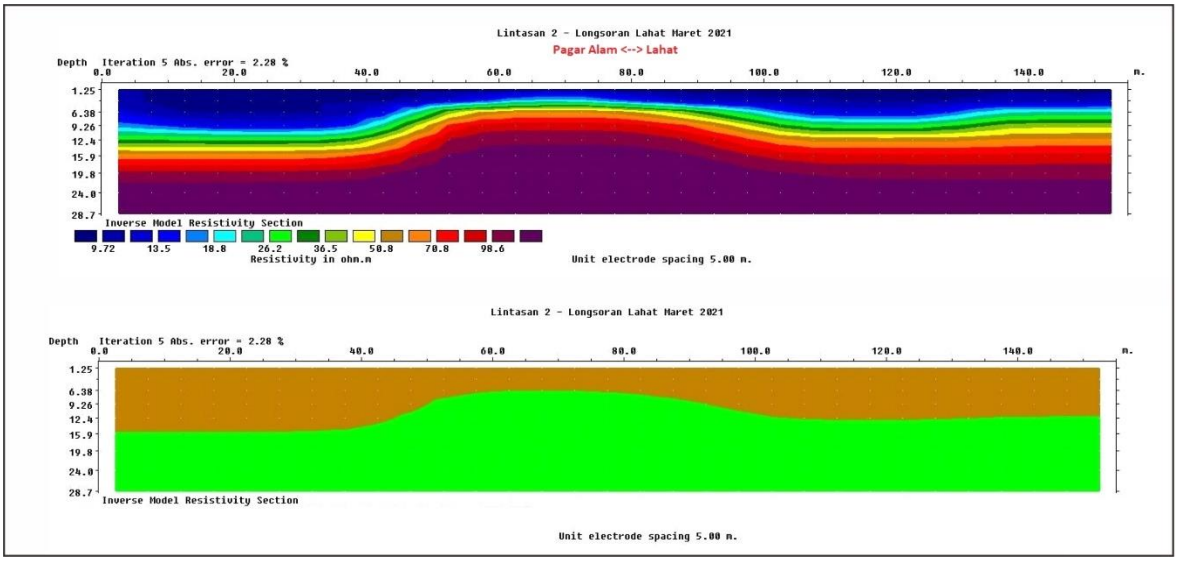

Figure 5. Illustration of Inverse model of resistivity sections along profle lines Track 2

PROCEEDINGS
JOINT CONVENTION BANDUNG (JCB) 2021
November 23rd – 25th 2021

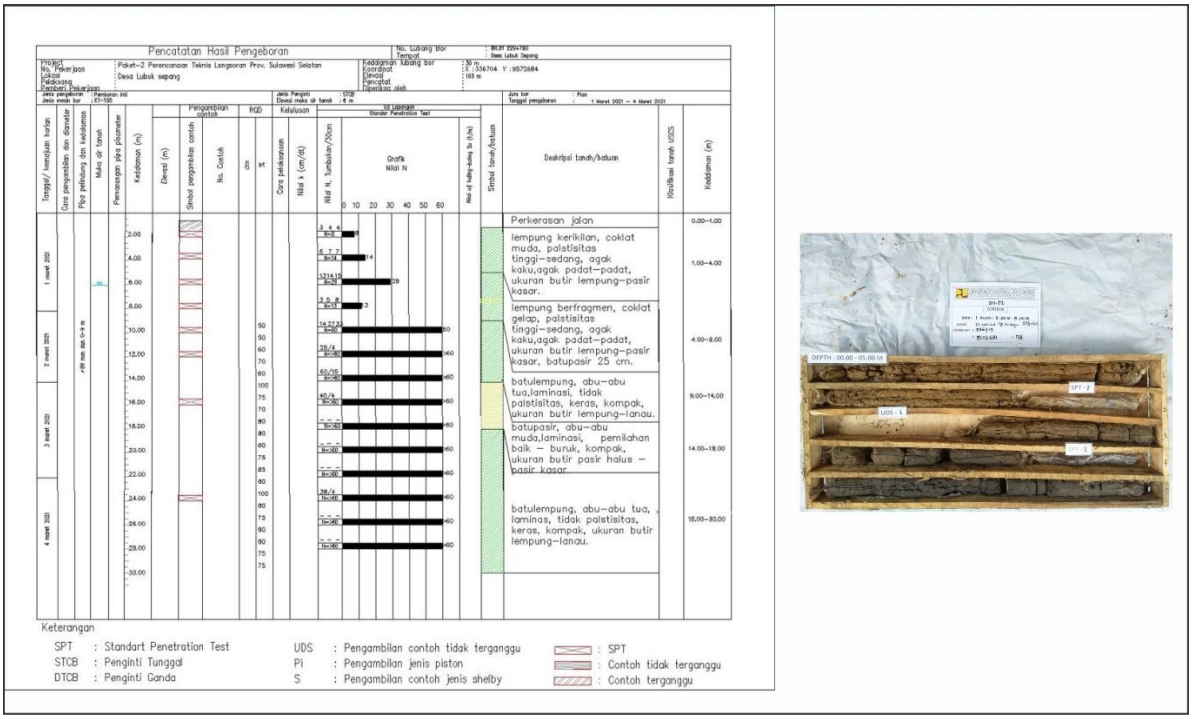

Figure 6. The drill core logs and drilling cores of BH-1

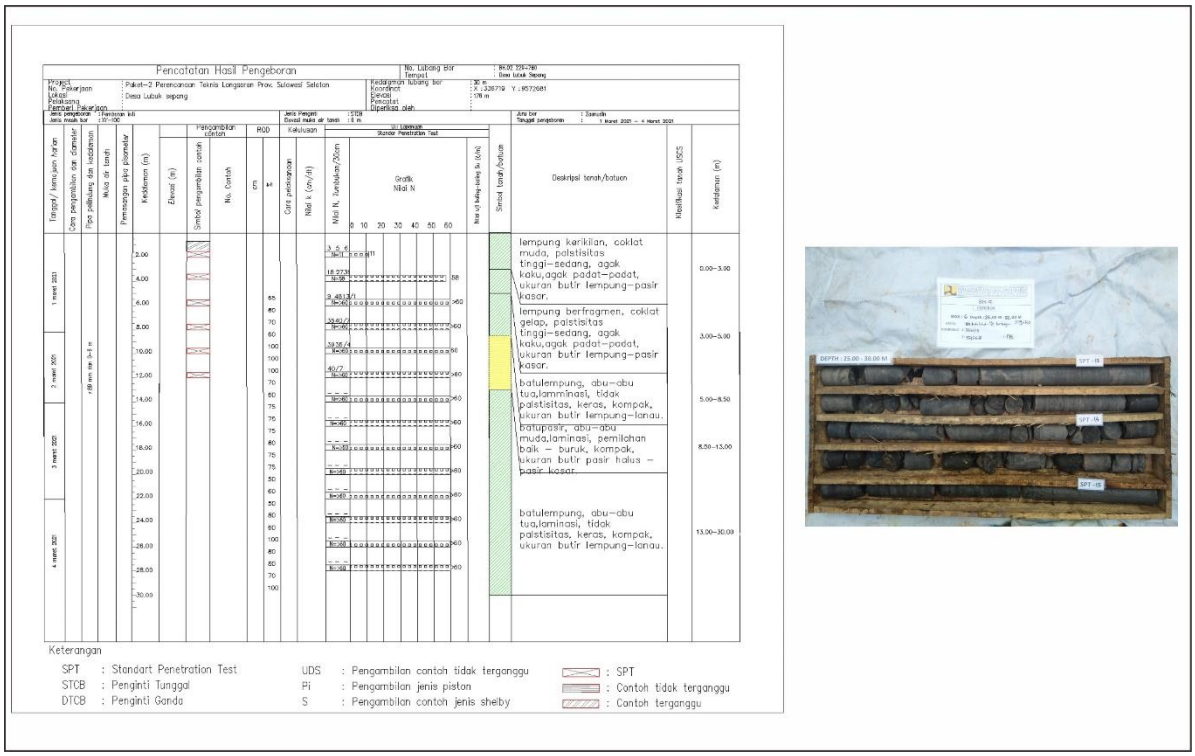

Figure 7. The drill core logs and drilling cores of BH-2

PROCEEDINGS
JOINT CONVENTION BANDUNG (JCB) 2021
November 23rd – 25th 2021

Figure 8. Illustration of Horizontal Drain Installation

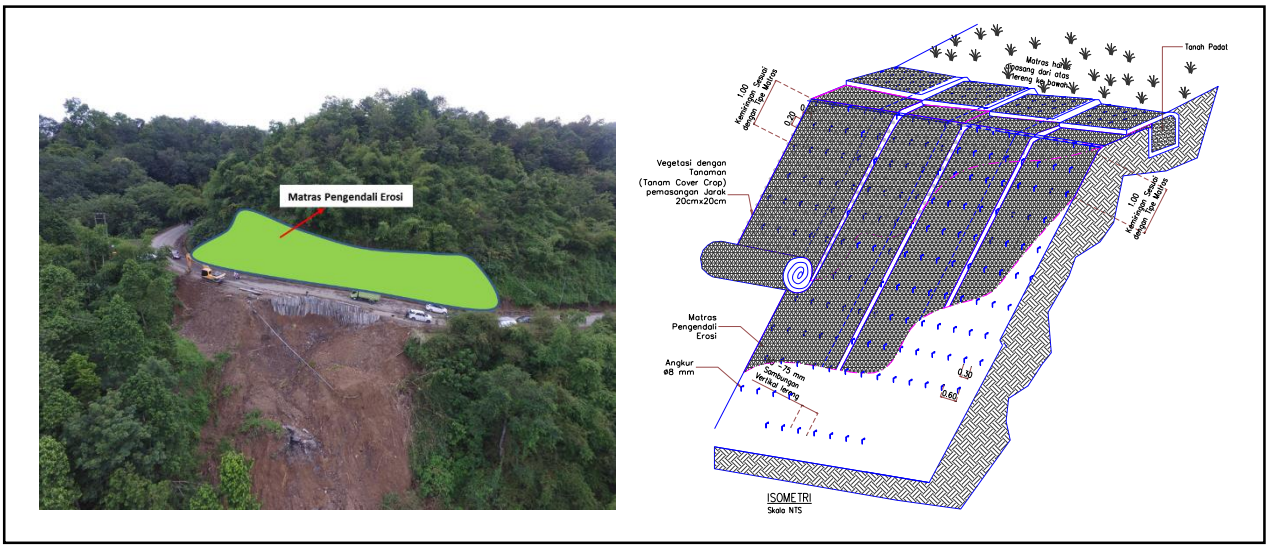

Figure 9. Illustration of Erosion control mat installation

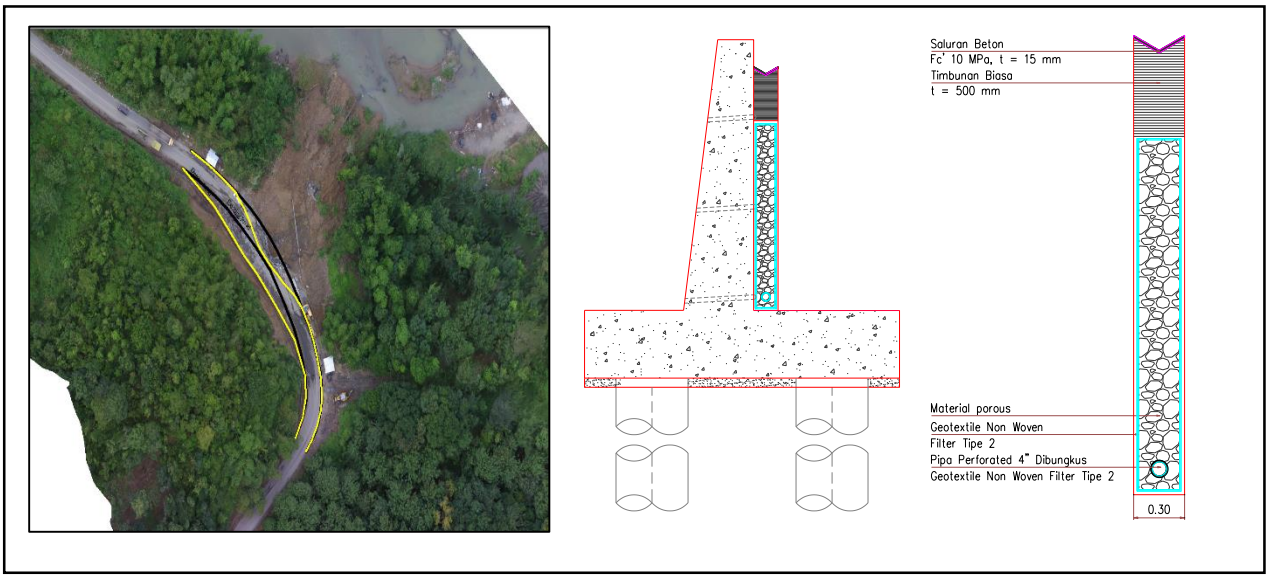

Figure 10. Illustration of Installation of DPT + Bore Pile

PROCEEDINGS
JOINT CONVENTION BANDUNG (JCB)2021
November 23rd – 25th 2021

Disaster Potential Analysis and Earthquake Mitigation related to the Opak Fault at Prambanan Temple, D.I. Yogyakarta

Muhammad Haryo Dwiriandri[1]
Nine Safira[1]
Naila Andriani[1]
[1]*Program Studi Geofisika, Fakultas Matematika dan Ilmu Pengetahuan Alam, Universitas Indonesia, Kampus UI Depok, Indonesia.*

Abstract

The Special Region of Yogyakarta is a province in Central Java that has a lot of potential for natural disasters such as earthquakes and volcanic eruptions. An earthquake is a shaking on the earth's surface caused by a sudden release of energy due to the faulting of the earth's crustal rock along the subduction zone. Tectonic earthquakes have a close relationship with plate tectonic activity. D.I. Yogyakarta region is very prone to earthquake disasters which can be caused by the presence of the Opak Fault that cuts through the D.I. Yogyakarta from the southern coast of the island of Java to the Prambanan temple. The most famous earthquake that hit the Yogyakarta Special Region occurred in 2006 with a magnitude of 5.9 on the Richter scale and lasted for 57 seconds. According to Pinasti & Widjajanti (2019), the area to the west of the dominant fault moves to the northeast and the area to the east is dominantly moves to the southwest at a speed of 2.4 mm/year. For the sake of the effectiveness of earthquake disaster mitigation caused by the Opak fault, this study aims to produce a Map of Earthquake Prone Areas. In making the map, further analysis of earthquake risk is carried out using four main parameters, namely geology, intensity scale, seismicity, and earthquake acceleration. Based on the map, several areas around the Opak Fault are shown which show different levels of potential risk due to earthquake disasters. When viewed from the indicator of the level of disaster vulnerability, the area above the Opak Fault or small fault has the highest level of disaster vulnerability. It is also recognized that the Opak Fault could be a disaster threat to Prambanan Temple.

Keywords : Disaster, Earthquake, Opak Fault, Prambanan.

Introduction

The Special Region of Yogyakarta (D.I.Y.) is one of the provinces in Indonesia that has the potential for earthquakes and volcanic disasters. Disaster mitigation is one of the preventive measures needed to minimize casualties. One form of disaster mitigation can be done by analyzing the potential for disaster and mitigation in the D.I. region. Yogyakarta. due to the presence of the Opak Fault that cuts through the D.I. Yogyakarta from the south of the island of Java to near Prambanan Temple. The existence of this Opak Fault makes the D.I.Y. vulnerable to natural disasters resulting in material losses and loss of life.

Regional Geology

Indonesia is an archipelagic country that is traversed by the confluence of three plates, namely the Eurasian plate, the Pacific plate and the Indo-Australian plate. With the meeting of the three plates, Indonesia's territory is vulnerable to natural disasters. Natural disasters in Indonesia are very diverse. One example of natural disasters that often occur in Indonesia such as earthquakes and volcanic eruptions. An earthquake is a collision activity between the Earth's plates, active faults due to volcanic activity or rock collapse. Earthquakes in Indonesia quite often occur due to plate encounters. In addition, the territory of Indonesia is also traversed by the Ring of Fire which makes the existence of many volcanoes and has the potential to erupt.

Opak Fault

The Opak Fault in D.I. Yogyakarta is dominated by the extension component which is influenced by tectonic and volcanic activity. Meanwhile, the rotational value, dilatation rate, and maximum shear strain rate indicate that the Opak Fault is not entirely a strike slip fault (Pinasti & Widjajanti, 2019).

Tsuji et al (2009) concluded that surface deformation occurred 10 km east of the Opak River. The fault caused the May 2006 earthquake, which is correlated with the position of the epicenter of the aftershock, which is suspected to be a temporary seismic network. Finally, the western part of Yogyakarta experienced subsidence due to this fault (Tsuji et al, 2009).

Methodology

In general, the research method is carried out by conducting a literature study first. Then, a map of earthquake-prone areas is made based on GIS stacking reviews. Then, further analysis is carried out as shown in **Figure 1.**

GIS Stacking Review

The making of an earthquake-prone area map was carried out to obtain further analysis of the risk of an earthquake disaster in D.I. Yogyakarta. There are four main parameters in this map, namely: (1) Geology (rocks, morphology, geological structure), (2) Intensity scale of earthquakes that have occurred, (3) Seismicity, and (4) Earthquake acceleration. Based on each of these parameter weights, contours are made to determine the boundaries of the zone. The earthquake-prone area is divided into five zones as can be seen in **Table 1.**

PROCEEDINGS
JOINT CONVENTION BANDUNG (JCB)2021
November 23rd – 25th 2021

Table 1. Parameters of Weighting Map of Earthquake Prone Areas.

Vulnerability Level	Color
1 – Very Low	Blue
2 – Low	Green
3 – Average	Yellow
4 – High	Orange
5 – Very High	Red

Disaster Risk Analysis of Yogyakarta D.I Earthquake and Surrounding Areas

On the map of the Yogyakarta D.I Earthquake Prone Area (see **Figure 2.**) it can be seen that in the Opak Fault line there are many small faults surrounding the area. According to Pinasti & Widjajanti (2019), the area to the west of the dominant fault moves to the northeast and the area to the east is dominantly moves to the southwest at a speed of 2.4 mm/year.

Judging from the level of vulnerability with the four main parameters previously mentioned, D.I. Yogyakarta has varying levels of vulnerability. The highest vulnerability is indicated by the presence of the Opak Fault. In addition, the location of Prambanan Temple, which is in an orange to red area, indicates that the area is very prone to earthquakes.

The Influence of the Opak Fault on Prambanan Temple

On the analysis map of the existence of the fault and its movement (see Figure 3.) it can be seen that the location of Prambanan Temple is traversed by an opaque fault which cuts from the south of Java Island to approach the location of Prambanan Temple. In this area there are also small faults along the Opak fault line.

To be able to increase resistance to earthquake disasters, adequate research is needed in the aspects of buildings, structural systems, construction materials, and the cultural values contained therein.

Conclusions

- The D.I area of Yogyakarta is passed by the Opak Fault from along the southern coast of Java to the Prambanan Temple complex. Therefore, areas in the fault zone are prone to earthquakes.
- There are four parameters used in making the earthquake-disaster-prone map, namely: (1) Geology (rocks, morphology, geological structure), (2) The intensity scale of earthquakes that have occurred, (3) Seismicity, and (4) Earthquake acceleration .
- The location that is most prone to earthquake risk is in the area around the Opak Fault, while for Prambanan Temple, the area that has the potential to cause damage due to disaster is the Prambanan Temple complex itself.
- The recommendation that can be obtained is that integration of other geophysical data is needed to make it easier to implement.

References

Mujiatun, n.d. MITIGASI BENCANA DI KOTA YOGYAKARTA PROVINSI DAERAH ISTIMEWA YOGYAKARTA. *Geo Educasia - S1*. Available at: http://journal.student.uny.ac.id/ojs/index.php/geo-educasia/article/view/9745/9399 [Accessed April 13, 2021].

Pinasti, A., Widjajanti, N. 2019. PEMODELAN DEFORMASI KAWASAN SESAR OPAK BERDASARKAN DATA GNSS PERIODIK TAHUN 2013 SAMPAI 2018. Available at: http://etd.repository.ugm.ac.id/penelitian/detail/178617 [Retrieved April 13, 2021].

PVMBG, Galeri Pusat Vulkanologi dan Mitigasi Bencana Geologi. (2009) KRB GEMPA D.I.YOGYAKARTA | Galeri Pusat Vulkanologi dan Mitigasi Bencana Geologi. Available at: https://vsi.esdm.go.id/gallery/picture.php?%2F262 [Accessed April 13, 2021].

Tsuji, T., Yamamoto, K., Matsuoka, T., Yamada, Y., Onishi, K., Bahar, A., Meilano, I., Abidin, H.Z. (2009). Earthquake fault of the 26 May 2006 Yogyakarta earthquake observed by SAR interferometry. Earth, Planets and Space volume 61: 29-32. Available at: https://earth-planets-space.springeropen.com/articles/10.1186/BF03353189 [Accessed September 16, 2021].

PROCEEDINGS
JOINT CONVENTION BANDUNG (JCB)2021
November 23rd – 25th 2021

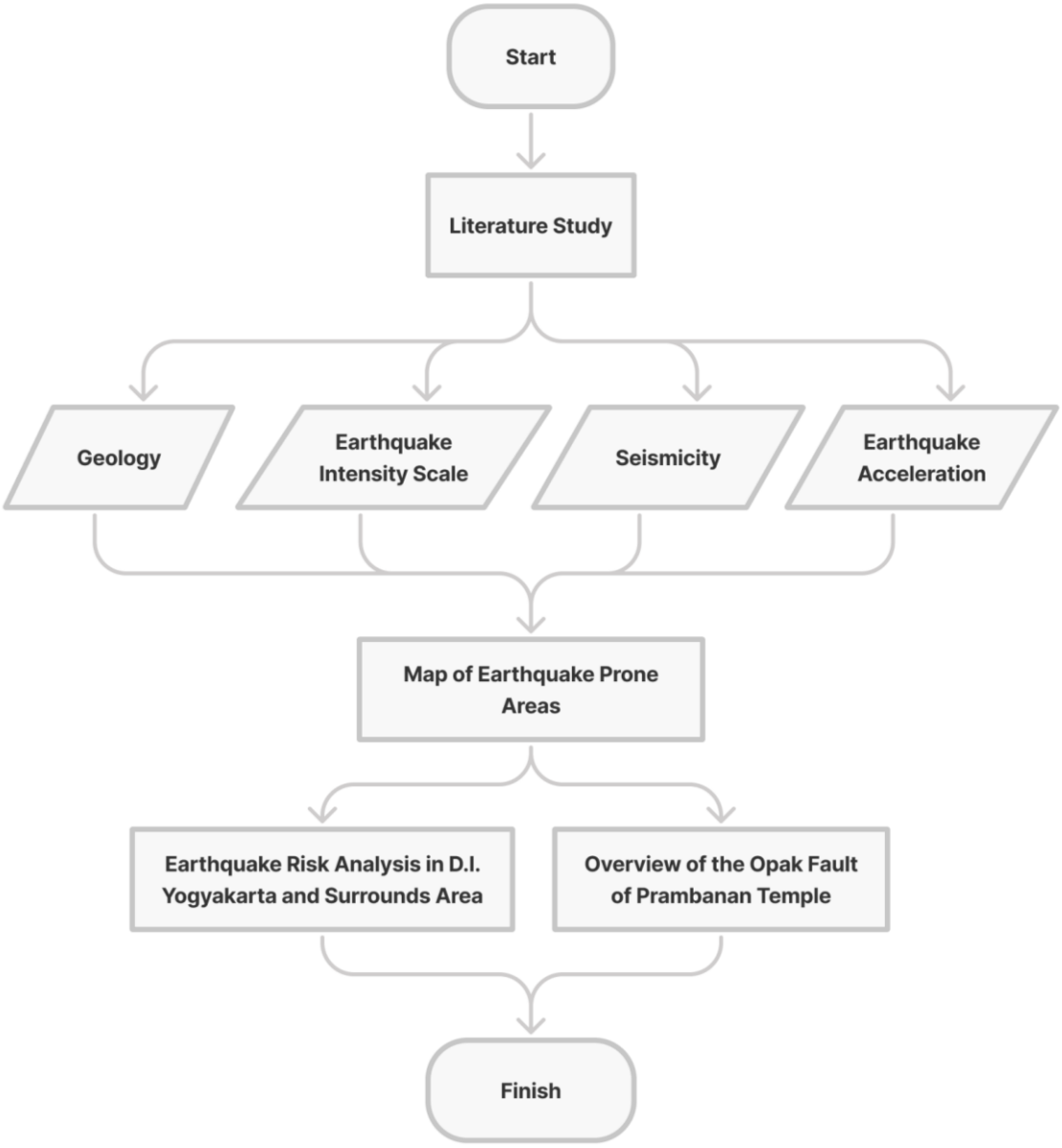

Figure 1. Research Flowchart

PROCEEDINGS
JOINT CONVENTION BANDUNG (JCB)2021
November 23rd – 25th 2021

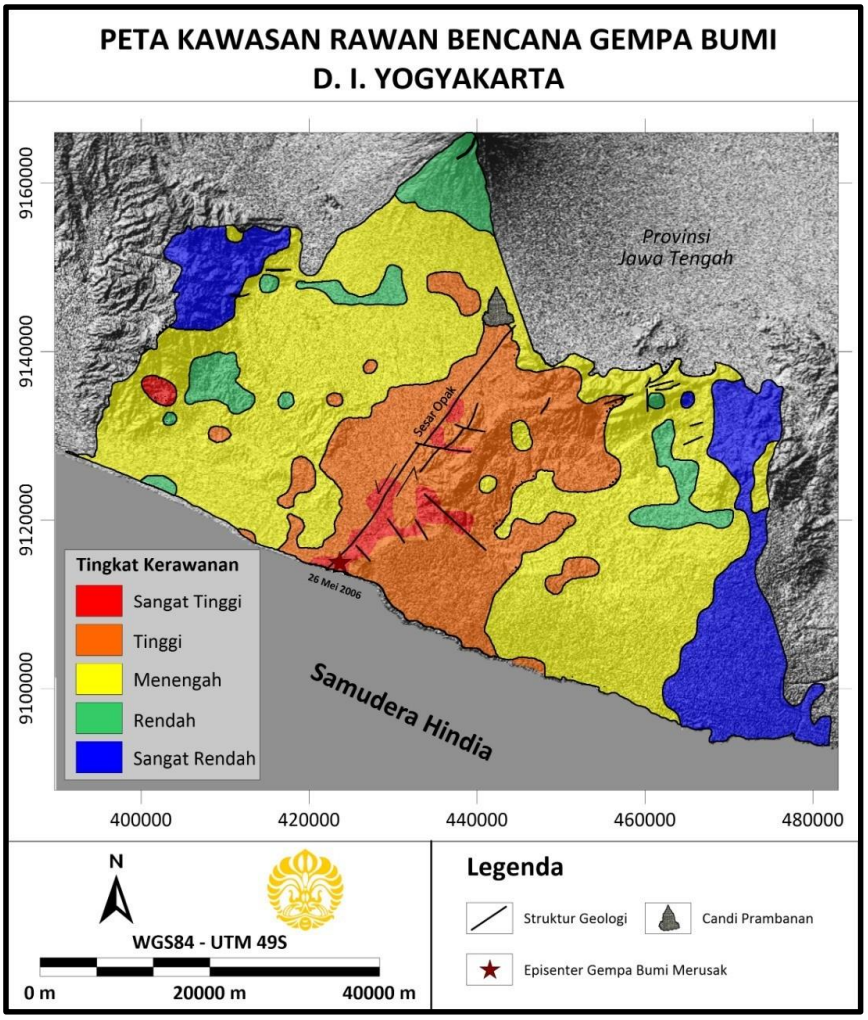

Figure 2. Map of Earthquake-Prone Areas

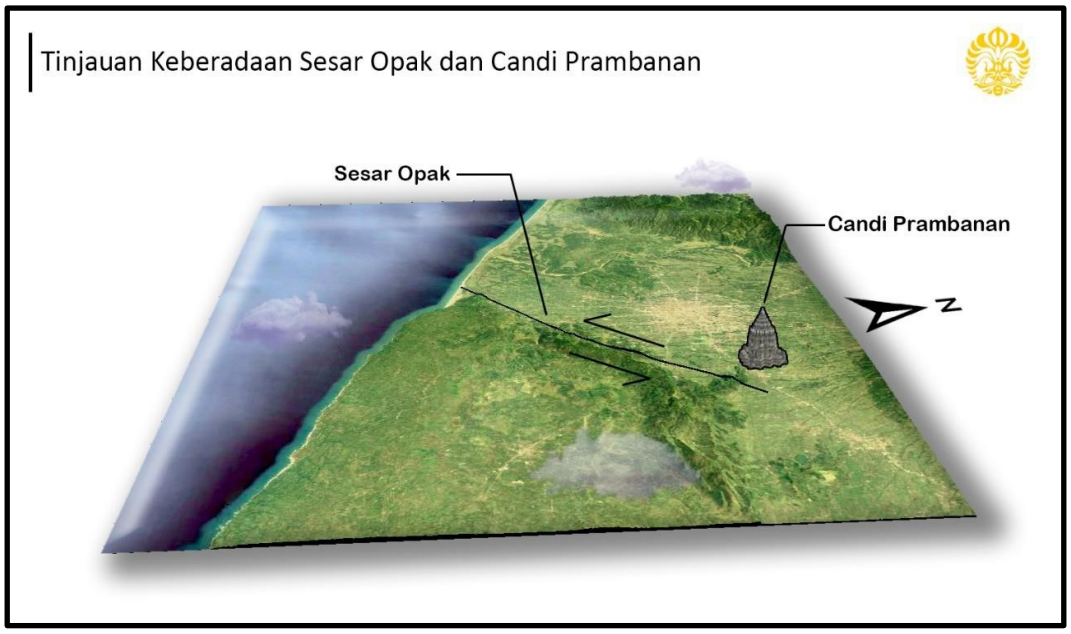

Figure 3. Overview of the Opak Fault and Prambanan Temple

PROCEEDINGS
JOINT CONVENTION BANDUNG (JCB) 2021
November 23rd – 25th 2021

Mapping of Sinkhole Vulnerability Using the Weight of Evidence Method in Semanu District, Gunung Kidul Regency, Yogyakarta

Johanes Timoty Jeremi Terok [1], Bayu Pamungkas[2], Edward Wijaya [3] , Eva Rutia Silaen [4] , Misbahudin,S.T.,M.T. [5]
Geological Engineering, Faculty of Exploration and Production Technology, Pertamina University
E-mail: [1]Jeroktimothy@gmail.com

Abstract

The presence of limestone in the Wonosari Formation, Oyo Formation, and Kepek Formation in Gunung Kidul Regency accommodates the karstification process and triggers the formation of sinkholes. In 2020, 32 sinkhole incidents have been recorded, with some of them spread in Semanu District, which is the largest District. The pattern of sinkhole events is getting more intense with the increasing conversion of land to housing for residents and the decrease in groundwater level due to industrial activities. Semanu District is the center of population, economic, and business activities, so further research is needed to evaluate vulnerability criteria and mapping of sinkhole vulnerability zones to assist in the preparation of regional development strategies as well as non-structural mitigation efforts. In the early stages of the study, delineation of karst distribution was carried out, followed by a determination of the controlling factors for sinkhole events to be used as criteria in the evaluation stage. The criteria used are lithology, geological structure, slope, land use, and hydrological conditions which are evaluated using the Weight of Evidence method. The method is integrated with the principles of Geographic Information Systems to create a sinkhole hazard map which is divided into three classes namely low, medium, and high vulnerability. Industrial estates, housing estates, and agricultural lands that are mapped in the high vulnerability class are recommended to be moved to areas with medium to low vulnerability class with the closest distance. Land use with a high vulnerability class is recommended to be converted into a geotourism area. The results of the vulnerability mapping were validated with the results of previous studies, as well as the distribution location of the sinkhole incident in the study area.

Keywords: Gunung Kidul, Karst, Mitigation, Sinkhole, Weight of Evidence

I.Introduction

1.1 Background

Semanu District is part of Gunung Kidul Regency, Yogyakarta Special Region. This district is located in the southern part of Gunung Kidul Regency with an area of 108.39 km². Administratively, the research area is included in Candirejo Village, Dapadayu Village, Ngeposari Village, Ayahejo Village and Semanu Village. Semanu District is the center of population, economic and business activities in Gunung Kidul Regency. The presence of limestone in the Wonosari Formation, Oyo Formation and Kepek Formation in Gunung Kidul Regency accommodates the karstification process and triggers the formation of sinkholes. Karstification is the process of dissolving, chemical corrosion of rocks by water on limestone, gypsum, rock salt or other soluble rocks which is responsible for the formation of karst phenomena both on the surface and below the earth's surface (Summerfield, 1991). A sinkhole is an area of land that does not have natural external drainage where when it rains all water remains in the hole and flows below the surface (USGS, 2007).

Sinkholes can occur naturally or with the influence of human activities. The natural process that triggers sinkhole is the process of dissolving rocks composed of carbonate minerals below the surface (Allen, 1984). Household activities and industrial activities that utilize groundwater in aquifers with alluvial, fluvial, and estuary sedimentary lithologies for a long time with a lot of intensity (Foley, et al, 2009). Sinkhole formation is controlled by lithology, geological structure, slope, land use, and hydrological conditions. Based on data from the BPBD of Gunung Kidul Regency, in 2020 there have been 32 sinkhole incidents recorded, with some of them scattered in Semanu District. The pattern of sinkhole events is getting more intensive with the increasing conversion of land to housing for residents and the decrease in ground water level due to industrial activities. Therefore, further research is needed, in order to evaluate vulnerability criteria and mapping of sinkhole vulnerability zones to assist in the preparation of regional development strategies as well as non-structural mitigation efforts.

1.2 Aims

Sinkhole vulnerability mapping using the weight of evidence method in Semanu District, Gunung Kidul Regency, Yogyakarta aims to map locations that have the potential for sinkholes. The results of this study are described in the form of a sinkhole hazard map with a scale of 1:1000 m.

1.3 Regional Geology

Based on *figure 1* Gunung Kidul regency is located in the Special Region of Yogyakarta, which is in the southern part of the island of Java. The Gunung Kidul region is part of the Southern Mountains Zone which stretches from the province of the Special Region of Yogyakarta to the southern coast of East Java (Van Bemmelen, 1949). The meeting of the Indo-Australian plate and the Eurasian plate converges on the southern part of the island of Java to form the Southern Mountain Zone. This zone is bounded by Yogyakarta in the west, Surakarta in the north, Wonogiri in the east, and in the south by the Indian Ocean. The period of lithostratigraphic formation of the Southern Mountains is divided into 3 periods, namely the pre-volcanism period, the volcanism period, and the post-volcanism period (Surono, 2009).

The pre-volcanism period occurred in the Paleocene age forming the floor of the Southern Mountains basin, this event was marked by the exposure of the oldest rocks of the Southern Mountain Basin located in the Jiwo Hills. The rock is an assemblage of various metamorphic rocks that are overlain by sedimentary rocks of Eocene age. Then the period of volcanism, occurred at the age of Upper Eocene to Lower Miocene which is characterized by the presence of thick volcanic rocks.

The distribution of these volcanic rocks then formed the Baturagung Mountains. The last post-volcanic period occurred in the Middle Miocene age which marked by the formation of carbonate rocks. The accumulated carbonate rocks then form the karst hills of Gunung Sewu which stretch from the districts of Gunung Kidul, Wonogiri, to Pacitan.

Regionally, the limestone stratigraphy in Gunung Kidul Regency focuses on three formations, namely the Oyo Formation, Wonosari Formation, and Kepek Formation.

a. *The Oyo Formation* is composed of sandy limestone with a layered structure, calcarenite, calcareous sandstone, and marlstone-tuffaceous sandstone aged around the Middle Miocene. Part of the Oyo Formation is aligned with the Wonosari Formation.

b. *The Wonosari Formation* is composed of layered limestone, massive limestone, and reef limestone. This formation is dominated by secondary porosity in the form of cavities resulting from dissolving. This formation sometimes shows a harmonious relationship above the Oyo Formation, while in other places the relationship is not aligned or fingered.

c. *The Kepek Formation* is composed of alternation of clay, sandy marl, and layered limestone deposited in a shallow marine environment and is late Miocene to Pliocene. Kepek Formation and Wonosari Formation have a harmonious relationship in one area, and have finger relationships in many places. The Oyo, Kepek, and Wonosari Formations are considered as a group of formations named Gunungsewu Group.

II. Data and Method

2.1 Data

2.1.1 Lithology

Based on field data observations Widyaningtyas & Putra. 2014 on *figure 2* lithology in Semanu District is divided in two types of rock namely fresh limestone and weathered limestone. The fresh limestone area is in the south and the weathered limestone are in the north. Based on the Geological Map Sheets of Surakarta and Girintoro (Surono and Sudarno, 1992) the Semanu District is located above the Wonosari Formation. This formation consists of limestone lithology, marl-tuffaceous limestone, conglomerate limestone, tuffaceous sandstone, and siltstone. This makes Semanu District became a karst area, so it has the potential for sinkhole phenomena to occur in the area. Limestone lithology is closely related to the sinkhole phenomenon. This is due to the nature of limestone which is easy to dissolve when exposed to water. In addition, in the karst area, there are also river flows below the surface and also hilly hills with a very distinctive shape.

2.1.2 Type of Soil

Based on *figure 3* the type of soil in Semanu District is divided in two characters of soil namely latosol-mediteran red and mediteran red-rendzina. Latosol soil type has a characteristic yellowish red color with a clay texture, usually found in areas that have high rainfall and humidity. Red Mediterranean soil type has a characteristic yellowish red color with low fertility, usually the result of weathering limestone. Rendzina soil type has a characteristic black color, this soil is the result of weathering limestone with high rainfall. The distribution of red mediteran soil types - rendzina is in the northern part, while the distribution of red latosol-mediterranean soil types is in the southern part.

2.1.3 Sinkhole Event Data

Figure 4 is the location of the sinkhole in Semanu District. According to Widyaningtyas & Putra (2014) there have 24 sinkhole incidents in Semanu District. To perform an analysis using Weight of Evidence, the sinkhole data is separated into 2 parts with a share of 60% for analysis and 40% for validating the modeling results.

2.1.4 Lineament

Based on the division of the distance from the straight line by Braathen and Grabielsen (2000) in Widyaningtyas and Putra (2014), a distance of 0-200 m from the lineament is an area that is strongly affected by the structure characterized by the presence of more and more dense cracks towards the structure, at a distance of from 200 m the influence of the structure decreases, indicated by the decrease in the number of cracks and their density as they move away from the structure. Based on *figure 5* there are several lineages in Semanu District, these lineaments have a positive correlation to the sinkhole data in Semanu District. Most of the mapped sinkholes are close to the lineament area with a distance of 0-200 m (near) and 200-400 m (medium).

2.1.5 Slope

Based on the Van Zuidam classification (1985), the Semanu District is mapped mostly to have a moderate slope (8-16°) which is in the southeast, then there is a steep slope (16-35 ^{o}) on several peaks in the southeast. Gently slope (2-4°)-Sloping (4-8°) is mapped in the north and northwest areas (*figure 6)*.

2.1.6 Geomorphology

The geomorphology of the Semanu District area is controlled by the karstification process. Based on *figure 7* here are four types of geomorphological units in this area, namely Karst Plateau, Conical Karst Zone, Polje, and Dry Valley. Karst Plateau is located in the north and spreads to the northwest of Semanu District. This unit makes up 42% of the research area. There is a river on the surface with an annular type. This unit is characterized by a relatively gentle slope, and no perfect conical shape is observed. Conical Karst Zone is located in the southeast. This unit makes up 51% of the research area. In this unit, karst hills are observed with a short distance. Polje is to the west, in the middle of the Karst Plateau. This unit makes up 1% of the research area. This unit is in the form of a sinkhole, Dry Valley is located in the middle of Conical Karst which is in the southeast, namely in the villages of Karangasem, Ponjong, and Dapadayu. This unit makes up 6% of the research area. The appearance of Dry Valley is shaped like a chasm between conical karst (Haripa, et. al. 2020).

2.1.7 Hydrogeology

One of the surface waters that can be found in Semanu District is the Munggi River and also a relatively medium-sized lake that can be found in several villages (*figure 8*). Not infrequently some of the rivers in Semanu the existing water absorbs into the ground, causing a sinker, so that surface water enters through the pores of the soil and passes through permeable karst rock units joins the subsurface water. One of the sources of subsurface water flow comes from surface water seepage, underground rivers also have the same flow system as rivers on the

surface. Semanu District has many karst morphologies, one of which is a cave. The caves in Semanu are indicated as the location of flowing subsurface water, several caves drain subsurface water including Bribin Cave, Buriomah Cave, Grubug Cave, Seropan Cave, Semuluh Cave, Sodong Cave, and others. Of the several caves, Seropan Cave and Semuluh Cave are caves that have a large enough subsurface water discharge so that residents can take advantage of it when the dry season arrives. The karst area aquifer itself is characterized by having secondary porosity which is regulated by the enlargement of the tunnels resulting from the dissolving process.

The potential for underground water is the main commodity for clean water needs in the Semanu subdistrict because this area often experiences drought in the dry season. It was identified that in addition to rivers and lakes there is a lake in Semanu District which often experiences drought during the dry season, besides that the existing water cannot be used because it contains coliform bacteria (fecal coli) which is quite high. The impact of the existence of subsurface rivers is to erode the soil layer on the surface which is carried away by the flow of water so that it has the potential to cause sinkholes in weak zones.

Based on figure 8, there are 2 types of aquifers, namely medium aquifers at a depth of 7-15 m and deep aquifers at a depth of >15 m.

2.1.8 Rainfall

The intensity of hydrological conditions in Semanu District is strongly influenced by the rainfall that falls every year, due to the erratic intensity of rainfall which is one of the triggers for Semanu District to experience frequent droughts. The intensity of the rain in Gunung Kidul Regency in each District has a different intensity every month. Rainfall data were obtained in Gunung Kidul Regency in 2011-2013. Based on the available data, the increase in rainfall occurred in December-March causing quite high humidity conditions, while the lowest rainfall conditions were in September.

Based on the existing map *(figure 9)* the intensity of rain in Semanu District has various levels in several villages, the rainfall ranges from 1500-2000 mm/year. This indicates that the rainfall of 1500-2000 mm/year is not so heavy but fairly even and occurs in almost all villages in Semanu District at a certain time. Meanwhile, in some rural areas, the rainfall intensity ranges from 2500-3000 mm/year and is classified as the heaviest level of rainfall in a certain period. This high and low rainfall will affect the flow of water below and above the surface, this also pushes the average daily temperature in Gunung Kidul Regency which is around 27.7°C, the minimum temperature is 23.2°C and the maximum temperature is 32, 4°.

2.1.9 Land Use

Based on *figure 10* Semanu District has a total land area of 108.39 Km². Based on the land use map, it can be seen that the land in Semanu District consists of 0.017 Km² of offices, 17.44 Km² of settlements, 0.28 Km² of lakes, 2.82 Km² of gardens, 8.15 Km² of non-agricultural shrubs, 0.158 Km² of non-agrialang, 6.81 Km² of rice fields, and 14.97 Km² of fields. There are also 36 places of worship, 2 banks, 4 hospitals, 7 government offices, 1 post office, 11 rivers and roads scattered in several places.

2.2 Method

In the Semanu District, several observations were made on several driving factors that triggered the sinkhole, including observations of rainfall data, hydrogeology, slope, lithology, soil type, lineament, and geomorphology. Each observation data has a different level of influence that can encourage the occurrence of sinkholes in the Semanu District area. Dropout sinkholes occur in cohesive soil, which results from the soil collapse into soil voids formed over bed rock fissures (these may collapse in minutes but the void evolves over months or years by roof stoping mechanisms) (e.g., Sowers, 1996). Another thing that encourages is that the type of rock permeability in every area is good and the permeability is bad will affect the resistance of rock and soil. Better permeability make more water can pass through resulting erosion in the layer at any time in contrast to areas with poor permeability because they are rarely exposed to water, the composition will be stronger.

This WoE method is a quantitative technique based on data, which uses several data combinations to produce a map of the data weighting process, resulting in continuous and categorical formations, based on prior (beginning) and posterior (after) probabilities (Bonham Carter 1994). The WoE method can also combine uncertainty in a type of vulnerability model (type, quality, and calculation of each data).

$$W^{+} = \ln\left[\frac{P\{N_j|S\}}{P\{N_j|\bar{S}\}}\right] = \ln\left(\frac{\frac{P(N_j \cap S)}{P(S)}}{\frac{P(N_j \cap \bar{S})}{P(\bar{S})}}\right) = \ln\left(\frac{\frac{Npix\ landslide\ in\ class}{Npix\ total\ landslide\ area}}{\frac{Npix\ stable\ area\ in\ class}{Npix\ total\ stable\ area}}\right) \quad \ldots(1)$$

$$W^{-} = \ln\left[\frac{P\{\bar{N}_j|S\}}{P\{\bar{N}_j|\bar{S}\}}\right] = \ln\left(\frac{\frac{P(\bar{N}_j \cap S)}{P(S)}}{\frac{P(\bar{N}_j \cap \bar{S})}{P(\bar{S})}}\right) = \ln\left(\frac{\frac{Npix\ landslide\ outside\ class}{Npix\ total\ landslide\ area}}{\frac{Npix\ stable\ area\ outside\ class}{Npix\ total\ stable\ area}}\right) \quad \ldots(2)$$

W+ is a probability weight of ground motion in a certain geofactor class (positive weight). W– is a weight where ground motion should not occur in a geofactor class (negative weight). Nj itself is the number of pixels in the geofactor class J. S is the total number of pixels that contain ground motion data in the entire area, and P is the result of the probability value.

III.Result and Discussion

3.1 Results and Data Processing

The results of data processing that have been carried out produce WoE values as in *table 1*. In the slope parameter, the class with the slope (0–2%) has the highest WoE value with a total of 11 sinkholes that occur in that class. The rainfall parameter have the highest WoE value in the rainfall class (2000 mm/year) where there are 11 sinkhole events in areas with rainfall (2000 mm/year). The distance parameter from straightness has the highest WoE value in the class (> 400 m) with a total of 7 sinkholes that occur in the area. The hydrogeological parameter has the highest WoE value in the deep aquifer class (>15 m) with a total of 12 sinkholes in the deep aquifer class area. Based on lithological parameters, the highest WoE value is found in weathered limestone lithology which has 8 times the number of sinkholes. In the soil type parameter, the highest WoE value was found in the red mediterranean soil and redzina soil types with 10 sinkhole occurrences. In geomorphological parameters, the highest WoE value is found in the karst plateau with 8 sinkhole occurrences in the class area.

Based on Yesilnacar and Typhoon (2005) area under curve (AUC) is a metric used to evaluate the performance of a particular vulnerability model, in this case it is able to predict the probability of sinkhole occurrence or not. Therefore we have to calculate the area under curve (AUC) value of each parameter. The results of the calculation of each parameter are in *table 2*, the slope has an AUC value of 0.5, rainfall has an AUC value of 0.49, the distance from straightness has an AUC value of 0.42, hydrogeology has an AUC value of 0.46, lithology has an AUC value of 0.57, soil types has an AUC of 0.62, and rainfall has an AUC value of 0.45. The greater the AUC value, the parameter has a greater influence than the parameter with a lower AUC value.

The results of the AUC calculation in *table 3* state that the soil type parameter has the greatest influence, while the straightness parameter has the least effect. According to Perrint, et.al (2015) the AUC value of 0.5-1 is in the good category, so the parameters used to model the sinkhole vulnerability area are soil type, slope, lithology and rainfall. Meanwhile the hydrogeological, geomorphological and lineament parameters cannot be used for modeling because they have a value of <5. If these parameters are still included, it will reduce the quality of the sinkhole vulnerability model.

After processing the data based on the parameters of soil type, slope, lithology and rainfall, it produces a Sinkhole Vulnerability Map modeling as in *figure 11* from the results of data processing, there are 3 vulnerability classes, namely low class in green, midium class in yellow, and class in yellow. high in red. The medium-high vulnerability class is located in the middle of the Semanu District area, where most of the residential areas are located in zones with high vulnerability classes. Meanwhile, classes with low vulnerability are found in the North and South areas of Semanu District, where the area is mostly covered by shrubs.

3.2 Map Validation

Validation of this map uses a sinkhole hazard map modeling with sinkhole data that has been separated before doing the modeling. Then it produces the highest WoE value in the high vulnerability class with a WoE value of -1416 and the sinkhole incidence is 7 times in the high vulnerability class (*Table 4*). Then the lowest WoE value is in the low vulnerability class with a WoE value of -86473 which does not have a sinkhole event in that vulnerability class.

After calculating the WoE value, next step is to determine the Area Under Curve (AUC) value (*Table 5)*. The results of the AUC calculation obtained an AUC value of 0.72, based on Perrin, et.al (2015) the AUC value > 5 then the sinkhole vulnerability modeling can be categorized as good. If the AUC value < 5 then the modeling can be categorized as bad, then the model must be remade or add parameters and data for sinkhole events.

3.3 Discussion

Correlation between Geological Condition with Sinkhole Vulnerability Classes

High Vulnerability Cllases tend to be associated with Latosol soil types, steep slopes, rainfall >1500 mm/year, high density of lineament, and Karst Plateau geomorphology.

Low Vulnerability Classes

This class is the area with the lowest probability of sinkhole occurrence. This class is mapped at the southern end and northern end of Semanu District. The geological conditions in this area are limestone, conical karst geomorphological, sloping class (8-16°), and deep aquifer of hydrogeological condition. If validated with sinkhole events, the number of sinkhole occurrences in this area is twice which is very rare compared to other classes. Areas with this class should be utilized for the development of sinkhole disaster impact areas, and especially for land use development centers and regional development strategies. All types of land use development can be maximized in this area. Settlements located in areas of high vulnerability class should be moved to areas with this class of vulnerability.

Medium Vulnerability Classes

This class is an area with a moderate probability of sinkhole occurrence. This class is mapped to the center part of Semanu District. This probability is supported by geological conditions in the form of limestone lithology, Latosol soil type, Conical Karst Zone geomorphological units, and deep aquifers. If validated with sinkhole events, the number of sinkhole events in this area is quite intensive. The use of land in this area can be used for residential areas but it needs strong structural mitigation, such as good irrigation, as well as paying attention to supporting factors for sinkhole events, such as buildings should not be built on Latosol soil.

High Vulnerability Classes

This class is the area with the highest probability of sinkhole occurrence. This class is mapped to the northern part of the research area. This condition is associated with geological conditions such as limestone lithology, Latosol soil type, high density of lineament, shallow aquifers, and high rainfall rates of 2000 mm/year. If validated by sinkhole events, the number of sinkhole events in this area is very intensive. This area is recommended not to be used as a residential area and agricultural activities, but to be used as a geotourism area. The karstification process in this area produces cave products and other beautiful karst features. Even so, the strategy for using geotourism must still pay attention to appropriate structural and non-structural mitigation.

IV. Conclusions

- With a cutoff value of 0.5 in the Under Curve Area, the most influential geological parameters in supporting sinkhole events are soil type, slope, lithology, and rainfall intensity.
- The northern part of Semanu District has the most prone to sinkhole potential. The land use in this area is residential and office areas.
- Areas with a high vulnerability class are recommended to be used as geotourism areas, while residential and office areas are built in low to medium vulnerability classes.
- The value of CR (Consistency Ratio) from the calculation of the weighting of the AHP method has a value of 4% (acceptable).

References

Bonham-Carter, Graeme F., (1994). *Geographic Information Systems for Geoscientists.*

Cahyadi, A., Haryono, E., & Barianto, D. H. (2017). *Hidrogeologi Kawasan Karst Gunungsewu*: Panduan Lapangan Fieldtrip PAAI 2017.

Haripa, R. I., Damayanti, A., & Indra, T. L. (2020). *Property index and hydrophysical conditions of soils at subsidencess in Ponjong, Rongkop and Semanu subdistricts, Gunungkidul district.* International Journal, 19(73), 242-249.

Handayani, A.(2009). *Analisis Potensi Sungai Bawah Tanah di Gua Seropan dan Gua Semuluh untuk Pendataan Sumberdaya Air Kawasan Karst di Kecamatan Semanu Kabupaten Gunung Kidul Propinsi Daerah Istimewa Jogyakarta tahun 2007*.

Perrin,Jerome, Noury Gildas, Charles Cartannaz, & Emily Vanoudheusden. (2015). *A Multicriteria Approach to Karst Subsidence Hazard Mapping Supported by Weight of Evidence Analysis.* Francis : French Geological Survey.

Potro, Sumpeno. (2010). *Rencana Tata Ruang Wilayah Gunung Kidul.* Yogyakarta : BAPPEDA Kabupaten Gunung Kidul.

Sowers, G.F., (1996). *Building on Sinkholes*. ASCE Press, New York.

Surono. (2009). *Litosratigrafi Pegunungan Selatan Bagian Timur Daerah Istimewa Yogyakarta Dan Jawa Tengah*. Pusat Survey Geologi. JSDG Vol.19

Van Zuidam, R. A. (1983). *Guide to Geomorphologic Aerial Photographic Interpretation and Mapping. International Institute for Geo-Information Science and Earth Observation*, Enschede, The Netherlands, 325.

PROCEEDINGS
JOINT CONVENTION BANDUNG (JCB) 2021
November 23rd – 25th 2021

Map and Table Attachments

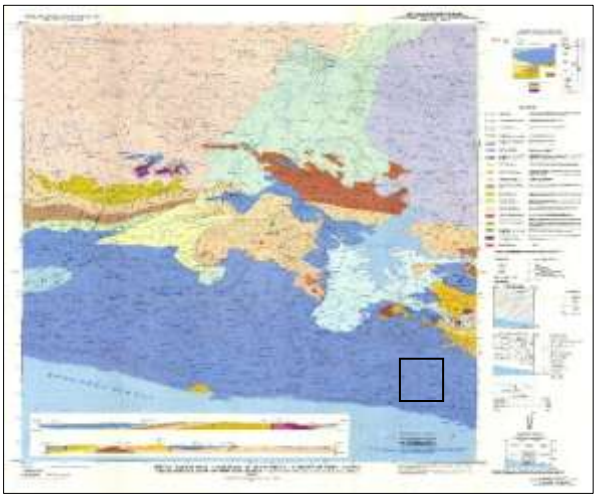

Figure 1: Geological Map Sheet Surakarta-Girintoro, Central Java (Surono dan Sudarno, 1992)

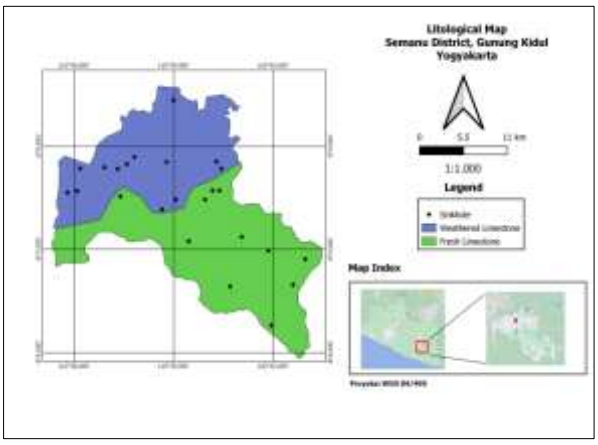

Figure 2: Lithology Map of Semanu District (Modified from Widyaningtyas & Putra, 2014)

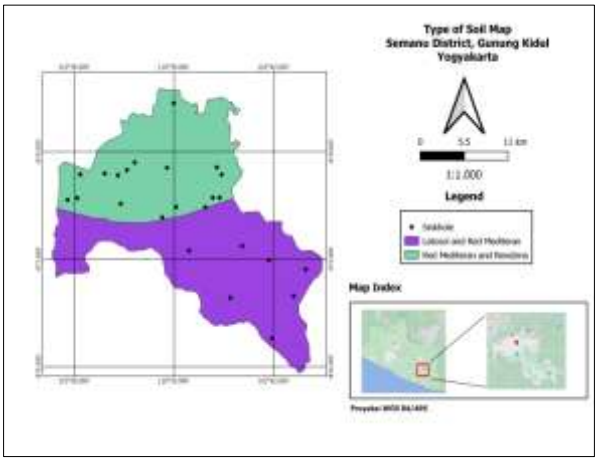

Figure 3: Type of Soil Map of Semanu District (Modified from BAPPEDA Gunung Kidul Regency)

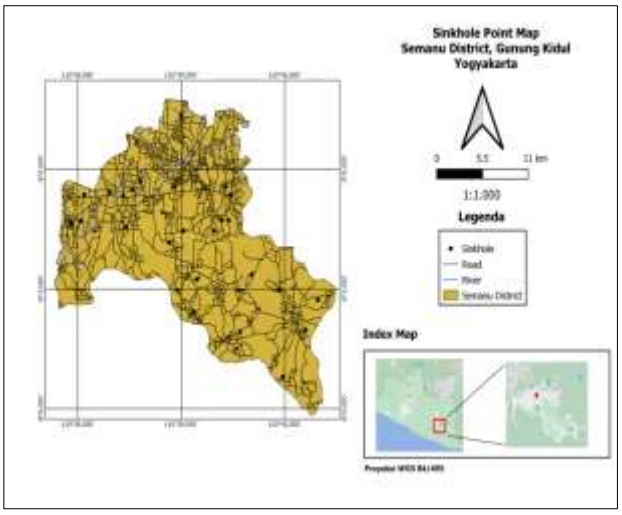

Figure 4: Sinkhole Distribution Map of Semanu District

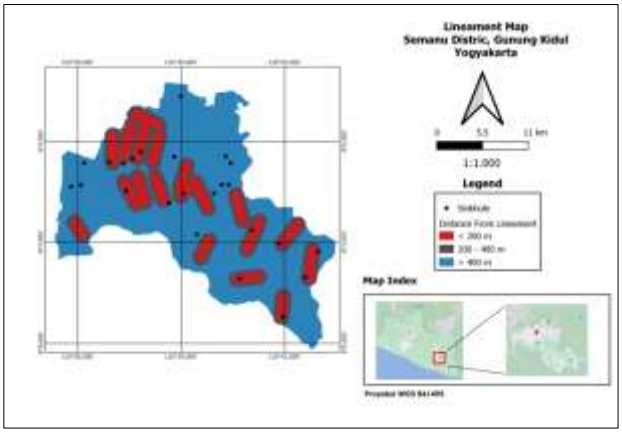

Figure 5: Lineament Map of Semanu District

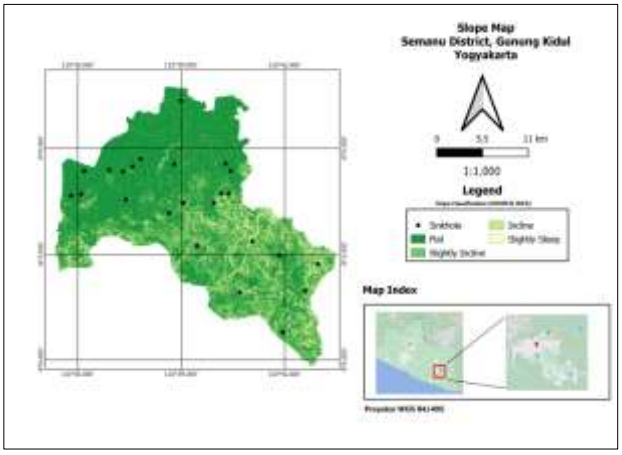

Figure 6: Slope Map of Semanu District

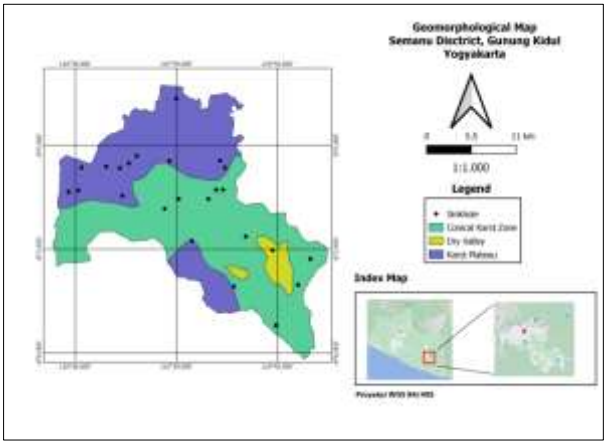

Figure 7: Geomorphology Map of Semanu District (Modified from Haripa,et. Al.2020)

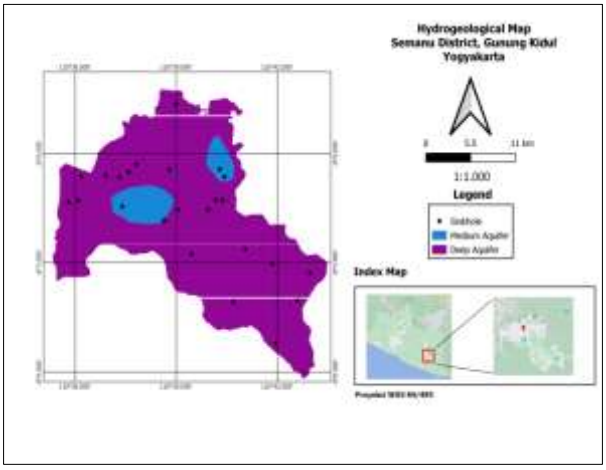

Figure 8: Hidrogeology Map of Semanu District (Modified from BAPPEDA Gunung Kidul Regency)

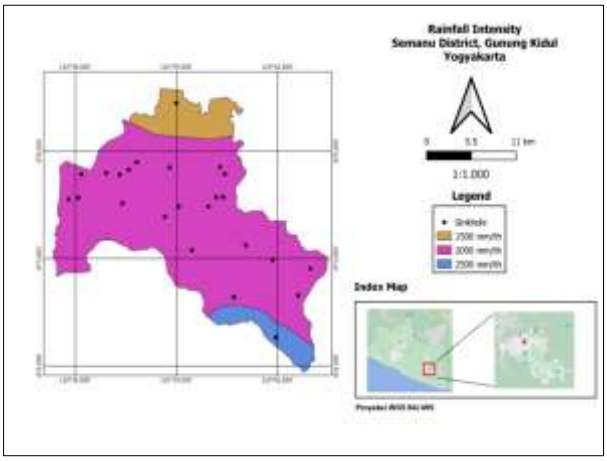

Figure 9: Rainfall Map of Semanu District (Modified from BAPPEDA Gunung Kidul Regency)

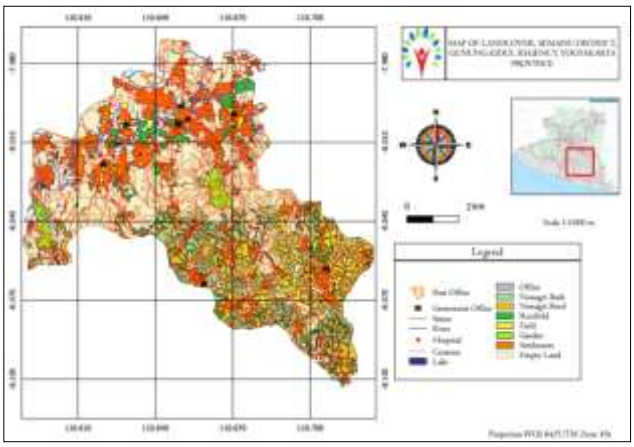

Figure 10: Land Use Map of Semanu District

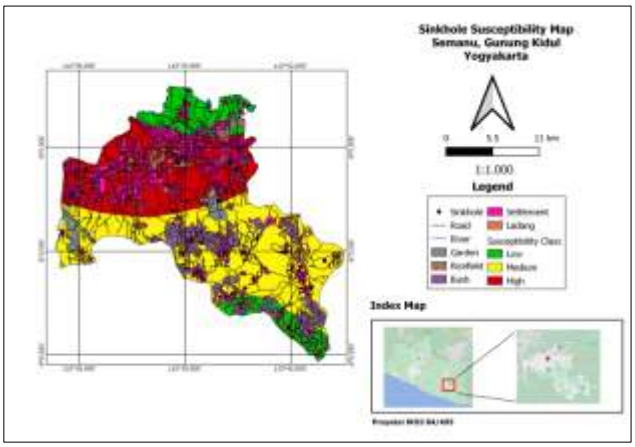

Figure 11: Sinkhole Vulnerability Map of Semanu District

Table 1. WoE Values

Parameter	No.	Kelas	area	factor	sinkhole	tot_sh	class_den	map_den	FR	IVM	W+	W-	C	WeightWOE	x1000
Slope	1	0 - 2 %	938994	0,635011	11	11,63501	1,24E-05	1,01E-05	1,221501	0,200081	-0,40004	-4,09498	3,694934	-0,7444121	-744
	2	2 - 7%	401223	0,271334	3	3,271334	8,15E-06	1,01E-05	0,803765	-0,21845	-5,61245	-0,33762	-5,27482	-9,7141713	-9714
	3	7 - 15%	119780	0,081003	0	0,081003	6,76E-07	1,01E-05	0,066667	-2,70805	-64,4574	-0,00589	-64,4515	-68,890842	-68890
	4	15 - 30%	17842	0,012066	0	0,012066	6,76E-07	1,01E-05	0,066667	-2,70805	-590,533	-0,00081	-590,532	-594,97108	-594971
	5	30 - 70%	842	0,000569	0	0,000569	6,76E-07	1,01E-05	0,066667	-2,70805	-17875,9	-3,8E-05	-17875,9	-17880,338	-1,8E+07
	6	70 - 140%	17	1,15E-05	0	1,15E-05	6,76E-07	1,01E-05	0,066667	-2,70805	-1224835	-7,7E-07	-1224835	-1224839,3	-1,2E+09
	7	> 140%	6	4,06E-06	0	4,06E-06	6,76E-07	1,01E-05	0,066667	-2,70805	-3727030	-2,7E-07	-3727030	-3727034,5	-3,7E+09
	SUM		**1478704**	**1**	**14**	**15**						**-4,43935**			
Rainfall Intensity	1	1500	139174	0,095027	1	1,095027	7,87E-06	9,56E-06	0,823093	-0,19469	-26,8163	-0,09	-26,7263	-38,907779	-38907
	2	2000	1236378	0,844191	11	11,84419	9,58E-06	9,56E-06	1,002159	0,002156	-0,19808	-12,0076	11,80953	-0,3719732	-371
	3	2500	89019	0,060782	1	1,060782	1,19E-05	9,56E-06	1,246596	0,220417	-42,448	-0,08389	-42,3641	-54,545594	-54545
	SUM		**1464571**	**1**	**13**	**14**						**-12,1815**			
Lineamant	1	< 200 m	208050	0,139204	5	5,139204	2,47E-05	1E-05	2,461235	0,900663	-7,69495	-0,48732	-7,20763	-10,214988	-10214
	2	200 - 400 m	252771	0,169126	2	2,169126	8,58E-06	1E-05	0,855032	-0,15662	-11,4336	-0,18799	-11,2456	-14,25297	-14252
	3	> 400 m	1033749	0,69167	7	7,69167	7,44E-06	1E-05	0,741362	-0,29927	-0,96565	-2,33204	1,366395	-1,6409584	-1640
	SUM		**1494570**	**1**	**14**	**15**						**-3,00735**			
Hydrogeology	1	Aquifer Sedang (7-15m)	110020	0,074722	2	2,074722	1,89E-05	1,02E-05	1,851051	0,615754	-26,4746	-0,16089	-26,3137	-52,949118	-52949
	2	Aquifer Dalam (>15m)	1362365	0,925278	12	12,92528	9,49E-06	1,02E-05	0,931272	-0,0712	-0,16089	-26,4746	26,31367	-0,3217741	-321
	SUM		**1472385**	**1**	**14**	**15**						**-26,6354**			
Litology	1	Batugamping lapuk	633746	0,427665	8	8,427665	1,33E-05	1,01E-05	1,31375	0,272885	-1,34809	-1,44178	0,093681	-2,6961887	-2696
	2	Batugamping segar	848130	0,572335	6	6,572335	7,75E-06	1,01E-05	0,765558	-0,26715	-1,44178	-1,34809	-0,09368	-2,8835508	-2883
	SUM		**1481876**	**1**	**14**	**15**						**-2,78987**			
Type of Soil	1	Mediteran Merah dan Redzina	670405	0,455183	10	10,45518	1,56E-05	1,02E-05	1,53128	0,426104	-0,79299	-2,19167	1,398678	-1,5859755	-1585
	2	Latosol dan Mediteran Merah	802421	0,544817	4	4,544817	5,66E-06	1,02E-05	0,556127	-0,58676	-2,19167	-0,79299	-1,39868	-4,3833315	-4383
	SUM		**1472826**	**1**	**14**	**15**						**-2,98465**			
Geomorphology	1	Karst Plateau	508825	0,343887	8	8,343887	1,64E-05	1,01E-05	1,617563	0,480921	-1,70557	-1,23837	-0,4672	-3,4111466	-3411
	2	Connical Karst	970803	0,656113	6	6,656113	6,86E-06	1,01E-05	0,676318	-0,39109	-1,23837	-1,70557	0,467201	-2,4767441	-2476
	SUM		**1479628**	**1**	**14**	**15**						**-2,94395**			

PROCEEDINGS
JOINT CONVENTION BANDUNG (JCB) 2021
November 23rd – 25th 2021

Table 2. Calculation Results Area Under Curve (AUC)

Parameter	woe_value	area	tot_area	tot_area_%	sh	total sh	tot_sh_%	AUC
Slope	-744	938994	938994	0,6350115	11	11	0,7857143	0,249469
	-9714	401223	1340217	0,9063457	3	14	1	0,242263
	-68890	119780	1459997	0,9873491	0	14	1	0,081003
	-594971	17842	1477839	0,999415	0	14	1	0,012066
	-1224839	17	1477856	0,9994265	0	14	1	1,15E-05
	-1788033	842	1478698	0,9999959	0	14	1	0,000569
	-3727034	6	1478704	1	0	14	1	4,06E-06
	SUM	**1478704**			**14**			**0,585386**
Rainfall Intensity	-371	1236378	1236378	0,8441912	11	11	0,8461538	0,357158
	-38907	139174	1375552	0,9392184	1	12	0,9230769	0,084062
	-54545	89019	1464571	1	1	13	1	0,058444
	SUM	**1464571**			**13**			**0,499664**
Lineamant	-1640	1033749	1033749	0,6916698	7	7	0,5	0,172917
	-10214	208050	1241799	0,8308738	5	12	0,8571429	0,09446
	-14252	252771	1494570	1	2	14	1	0,157046
	SUM	1494570			14			0,424423
Hydrogeology	-321	1362365	1362365	0,9252777	12	12	0,8571429	0,396548
	-52949	110020	1472385	1	2	14	1	0,069385
	SUM	**1472385**			**14**			**0,465933**
Litology	-2696	633746	633746	0,4276647	8	8	0,5714286	0,12219
	-2883	848130	1481876	1	6	14	1	0,449692
	SUM	**1481876**			**14**			**0,571882**
Type of Soil	-1585	670405	670405	0,4551828	10	10	0,7142857	0,162565
	-4383	802421	1472826	1	4	14	1	0,466986
	SUM	**1472826**			**14**			**0,629551**
Geomorphology	-2476	970803	970803	0,6561129	8	8	0,5714286	0,187461
	-3411	508825	1479628	1	6	14	1	0,270197
	SUM	**1479628**			**14**			**0,457658**

Table 3. AUC Result

Parameter	Nilai AUC
Type of Soil	0,6295
Slope	0,5853
Litology	0,5718
Rainfall Intensity	0,4965
Hydrogeology	0,4659
Geomorphology	0,4576
Lineamant	0,4244

Table 4. Map Validation Calculation

Class_ID	Kelas	Class	factor	sinkhole	tot_sh	class_den	map_den	FR	IVM	W+	W-	C	WeightWOE	x1000
1	Rendah	88018	0,060864	0	0,060864	6,91E-07	6,91E-06	0,1	-2,30259	-83,8203	-0,0065	-83,8138	-86,4739314	-86473
2	Rendah	133580	0,09237	0	0,09237	6,91E-07	6,91E-06	0,1	-2,30259	-50,7144	-0,01022	-50,7042	-53,3643276	-53364
3	Menengah	700818	0,484615	2	2,484615	3,55E-06	6,91E-06	0,512699	-0,66807	-2,87334	-0,55421	-2,31913	-4,97929986	-4979
4	Tinggi	523719	0,362151	7	7,362151	1,41E-05	6,91E-06	2,032896	0,709462	-0,8456	-2,08923	1,243632	-1,41653988	-1416
SUM		1446135	1	9	10						-2,66017			

Table 5. AUC Calculation

woe_value	area	tot_area	tot_area_%	sh	total sh	tot_sh_%	AUC
-1416	523719	523719	0,362150837	7	7	0,777777778	0,140836436
-4979	700818	1224537	0,846765343	2	9	1	0,430768451
-53364	133580	1358117	0,939135696	0	9	1	0,092370353
-86473	88018	1446135	1	0	9	1	0,060864304
SUM	**1446135**			**9**			**0,724839544**

PROCEEDINGS
JOINT CONVENTION BANDUNG (JCB) 2021
November 23rd – 25th 2021

Coulomb stress transfer and accumulation on the Great Sumatran Fault, over the past 43 years and its implications for seismic hazard

Lasroha Marulitua Panjaitan[1], Cahli Suhendi[1]
[1]Institut Teknologi Sumatera

Abstract

Sumatra is an area with relatively high seismic activity due to the presence of the Great Sumatran Fault (GSF) and its location close to the convergence zone between the Eurasian Plate and the Indo-Australian Plate. The GSF is an active fault with dominant dextral strike-slip faulting, stretching from the Andaman Sea to the Sunda Strait, with a length of ± 1900 km. The purpose of this study is to reveal the heterogeneity of stress and stress changes caused by large earthquakes (Mw≥6) occurred along the fault. The analysis was carried out by modeling static coulomb failure stress (ΔCFS). The earthquakes focal mechanism data used were obtained from the Global Centroid Moment Tensor (GCMT) and the International Seismological Center (ISC) Earthquake Catalog for the 1976-2019 period. The results of the CFS model analysis show that six of the thirteen earthquakes with Mw≥6 occurred in areas in which stress increases resulted from the previous earthquake. This proves that the earthquake triggering hypothesis can be applied to the Sumatra Fault. Information about the heterogeneity of stresses obtained from this study can then be used to mitigate earthquake hazards in Sumatra.

Keywords: Coulomb Failure stress, Hazard Mitigation, Great Sumatran Fault (GSF).

Introduction

Stresses in the earth's crust, tectonic or non-tectonic, can cause earthquakes according to the failure law (Zang & Stephansson, 2010). The main source of tectonic stress is mostly horizontal because it comes from forces due to plate movement (Barber, Crow & Milson, 2005). Information on the state of stress in the earth's crust is important in developing a seismic hazard mitigation strategy. It has been shown in previous studies that the main features of earthquake triggers, barriers, and clustering can be explained by modeling the change in coulomb failure stress (CFS) (King, Stein & Lin, 1994; Lin, Stein, 2004). The released earthquake energy can cause voltage changes by dissipating and redistributing to other areas (Hardebeck & Okada, 2018). Thus, this can trigger slip on other nearby faults and produce widespread aftershocks. In-situ stress information on the earth's crust can be estimated from various sources such as: earthquake focal mechanisms; geological data from fault slips; observation of a series of volcanoes; borehole collapse due to pressure and drilling (Hudson, Cornet & Christiansson, 2003; Fairhurst, 2003; Maury, Cornet & Dorbath, 2013).

In Sumatra, the main source of tectonic stress comes from the subduction of the Sunda megathrust, where the Indo-Australian plate subducts to the northeast of the Sunda shelf with a relative movement of about 60-75 mm/year (Curray, 2005). This convergence is also thought to be the cause of the Great Sumatran Fault (GSF) to have a strike-slip dextral fault (Fitch, 1972). Sieh and Natawidjaja (2000) studied the geomorphology of the GSF in detail and found that along the GSF there are many discontinuities with a width of 4 km to 12 km which divide the GSF into 19 segments. This indicates that the in-situ stress state along the GSF is very heterogeneous. Although there are strong indications of stress heterogeneity along the GSF and its seismicity, very little research has been done on this subject.

In this study, stress heterogeneity along the GFZ was obtained by modeling the change in coulomb failure stress (CFS) using data from the earthquake focus mechanism for the period 1976 to 2019. The results from this modeling can be used for further geomechanical analysis, including stress distribution by large magnitude earthquake which may potentially trigger the next earthquake event and it can be also used for seismic hazard assessment as part of mitigation purposes.

Data and Method

2.1 Focal Mechanisms solution catalog

We used focal mechanisms catalog compiled by Global Centroid Moment Tensor (GCMT) catalog and International Seismological Centre (ISC) bulletin from January 1976 to December 2019. The study area was located at latitudes -6.5° until 6.05° and longitudes 94.73° until 107°. We used earthquake data with Mw≥6. The distribution of the focal mechanisms within the study area is shown in Fig. 1 and Table 1.

2.2. Methodology

Coulomb Failure Stress Change (ΔCFS)

Coulomb stress change is a method used to see the distribution of stress, either released or still accumulating on the fault. When a fault produces an earthquake, it causes a change in stress on the surrounding fault. This indicates that there will be

areas experiencing increased stress which has the potential to trigger slip in local faults elsewhere.

Slip on a fault plane generates surface and internal deformations, which can be estimated from elastic dislocation equation (Okada, 1985; Okada, 1992). The displacement is then converted into strain. Then strain in the medium due to earthquake is converted into stress according to its elastic medium property. The stress is resolved on the surrounding fault planes, perturbing the normal and shear stresses. These perturbations are used with the Coulomb failure function to estimate the stress transfer distribution. In a homogeneous isotropic medium, static Coulomb failure stress change (ΔCFS) calculation is based on the following equation (Harris, 1998).

$$\Delta CFS = \Delta\tau_\beta - \mu'\Delta\sigma_\beta$$

where $\Delta\tau_\beta$ and $\Delta\sigma_\beta$ is the shear and the normal stress change on a plane, respectively. While μ' is the apparent friction coefficient that equals to $\mu' = \mu(1 - B)$, with B similar to the Skempton coefficient B for soils (Harris, 1998). Increase (positive) in stress change corresponds to possible subsequent event location, whereas decrease (negative) in stress change relates to stress shadow.

Result and Discussion

ΔCFS Evolution on GSF

We calculated the stress transfer and accumulative ΔCFS using the parameters described above and shown in Table 1. The ΔCFS evolution since the inception of earthquake series till 2013 earthquake on the GSF is illustrated in Figure 2. A series of snapshots exhibit state of stress field by the initial event, 1977 Mw 6.1, in Figure 2a followed by stress field state (Figure 2a-2l) immediately before each subsequent event. The 1977 earthquake ruptured increased stress to the Southeast-Northwest and Southwest-Northeast, but the next 1979 Mw 6.5 earthquake was not in that positif stress area. It is because this event was located far away from the previous earthquake. Hence, we suggested that the 1979 earthquake is an independent one. Similarly, the 1994 Mw 6.8 earthquake that destroyed most of the Southeast and Northwest is an area of increased stress.

Several earthquake events caused by previous earthquake were the 1995 Mw 6.7 earthquake with an increase in stress of 0.02 bar or 2 kPa. Then the 1996 Mw 6.2 earthquake which was driven by the 1987 Mw 6.4 and 1990 Mw 6.7 earthquakes with an increase in stress of 0.06 bar. The next earthquake event was the 2007 Mw 6.4 earthquake which was driven by the accumulation of stress from the 1977 Mw 6.1 earthquake from the northwest, the 1995 Mw 6.7 earthquake from the southeast, on the same day as Mw 6.3 triggered by a Mw 6.4 earthquake with a stress increase of 0.1 bar. The following events were the 2008 Mw 6.0 earthquake driven by the 1987 Mw 6.4 earthquake and the 1977 Mw 6.1 earthquake with a stress increase of 0.05 bar and the last possible earthquake triggered by the previous earthquake was the 2009 Mw 6.6 earthquake driven by the earthquake. the 1979 Mw 6.5 earthquake and the 1995 Mw 6.7 earthquake where the increased stress was 0.07 bar. the results of modeling the accumulation of coulomb stress changes from thirteen earthquakes are shown in Figure 3 and the results of the cross section on the depth of the earthquake hypocenter can be seen in Figure 4.

Conclusions

The modeling results show a significant interaction between earthquakes, six out of thirteen earthquakes occurred in the positive stress lobe which is an area of increased stress. From the final modeling results, it can be identified areas that have positive stress perturbations that may potentially trigger the next major earthquake to occur again. In addition, from the final calculation of the large earthquake that occurred in January 1976 to December 2019 it was concluded that the area along the SFZ was considered seismically active, which means that in the area there may occur another major earthquake in the future.

References

Okada, Y., 1985, Bulletin of the Seismological Society of America 75, 1135-1154. issn: 0037-1106.

Okada, Y., 1992, Bulletin of the Seismological Society of America 82, 1018-1040. issn: 0037-1106.

Harris, R. A., 1998, Journal of Geophysical Research: Solid Earth 103, 24347-24358. issn: 2156-2202.

Zang, A., & Stephansson, 2010, Springer, Dordrecht. (pp. 37-62).

Barber, A. J., Crow, M. J., & Milsom, J. (Eds.), 2005, Geological Society of London.

King, G. C., Stein, R. S., & Lin, J., 1944, Bulletin of the Seismological Society of America, 84(3), 935-953. (1994).

Lin, J., & Stein, R. S., 2004, Journal of Geophysical Research: Solid Earth, 109(B2).

Hardebeck, J. L., & Okada, T., 2018, Journal of Geophysical Research: Solid Earth, 123(2), 1350-1365.

Hudson, J. A., Cornet, F. H., & Christiansson, R., 2003, International Journal of Rock Mechanics and Mining Sciences, 40(7-8), 991-998.

Fairhurst, C., 2003, International Journal of Rock Mechanics and Mining Sciences, 40(7-8), 957-973.

Maury, J., Cornet, F. H., & Dorbath, L., 2013, Bulletin de la Societe Geologique de France, 184(4-5), 319-334.

Curray, J., 2005, J Asian Earth Sci 25 187–232.

Fitch, T. J., 1972, Journal of Geophysical research, 77(23), 4432-4460.

Sieh, K., & Natawidjaja, D., 2000, Journal of Geophysical Research: Solid Earth, 105(B12), 28295–28326. doi:10.1029/2000jb900120.

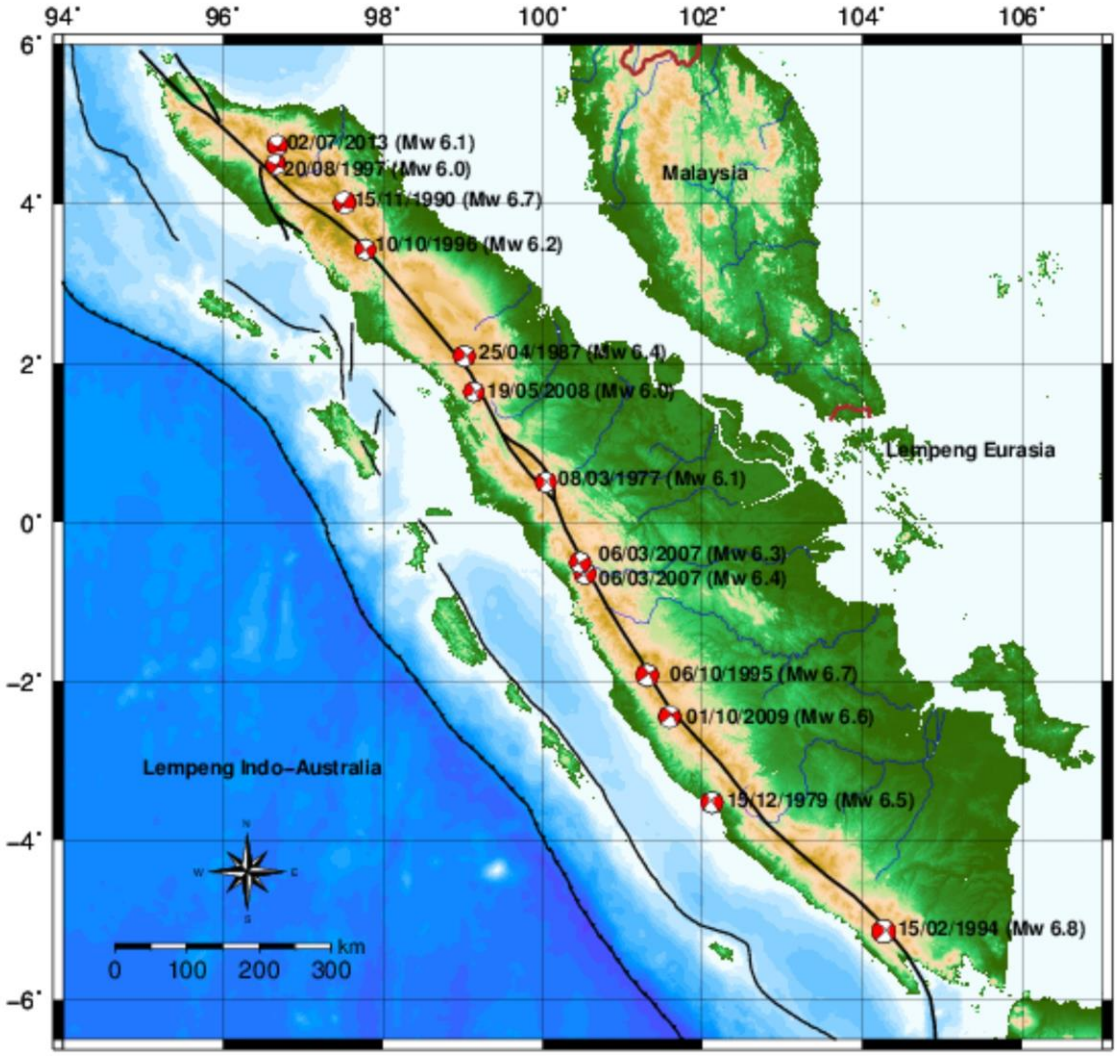

Figure. 1. Thirteen mainshock earthquakes for the period January 1976 to December 2019 along the Great Sumatran Fault (GSF)

Table 1. Mainshock data used in calculating Coulomb stress.

Date	Longitude	Latitude	Depth (km)	Mw	Strike	dip	rake
08/03/1977	100.04	0.5	19.5	6.1	312	80	179
15/12/1979	102.12	-3.53	26	6.5	320	86	-164
25/04/1987	99.02	2.09	21.5	6.4	324	75	172
15/11/1990	97.52	4.02	15	6.7	122	67	178
15/02/1994	104.27	-5.15	16.2	6.8	315	71	176
06/10/1995	101.31	-1.93	16.7	6.7	326	74	-177
10/10/1996	97.78	3.43	22.8	6.2	144	89	-178
20/08/1997	96.66	4.5	15	6	116	87	-165
06/03/2007	100.53	-0.65	20.9	6.4	150	84	-177
06/03/2007	100.47	-0.51	21.9	6.3	149	80	179
19/05/2008	99.14	1.64	16.1	6	331	82	173
01/10/2009	101.59	-2.45	15.1	6.6	323	70	-178
02/07/2013	96.68	4.74	15.9	6.1	129	72	-160

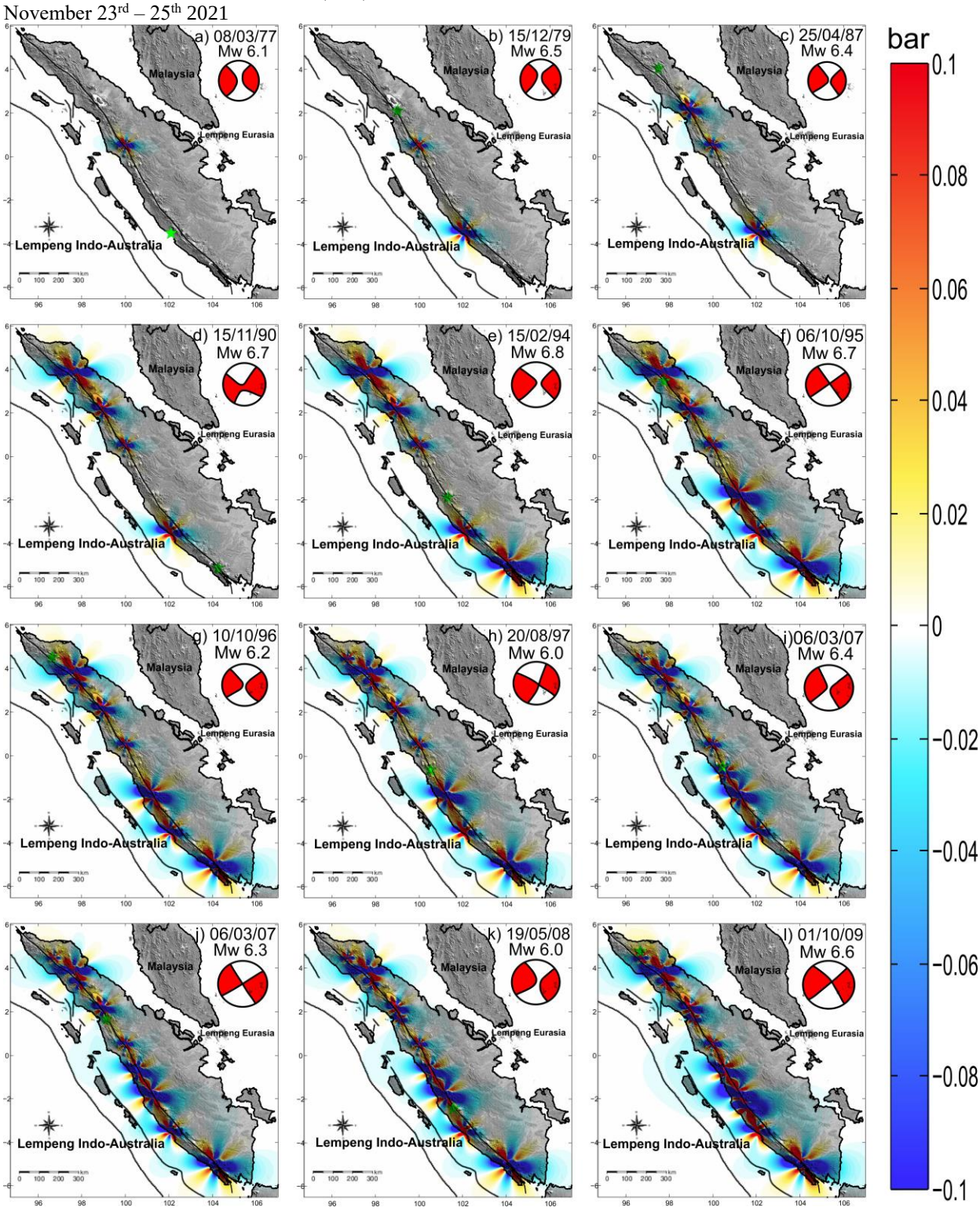

Figure 2. (a-l) ΔCFS evolution since 1976 until 2019. The green star represent of the next earthquake rupture. the label of year in each figure indicates the occurrence time of event.

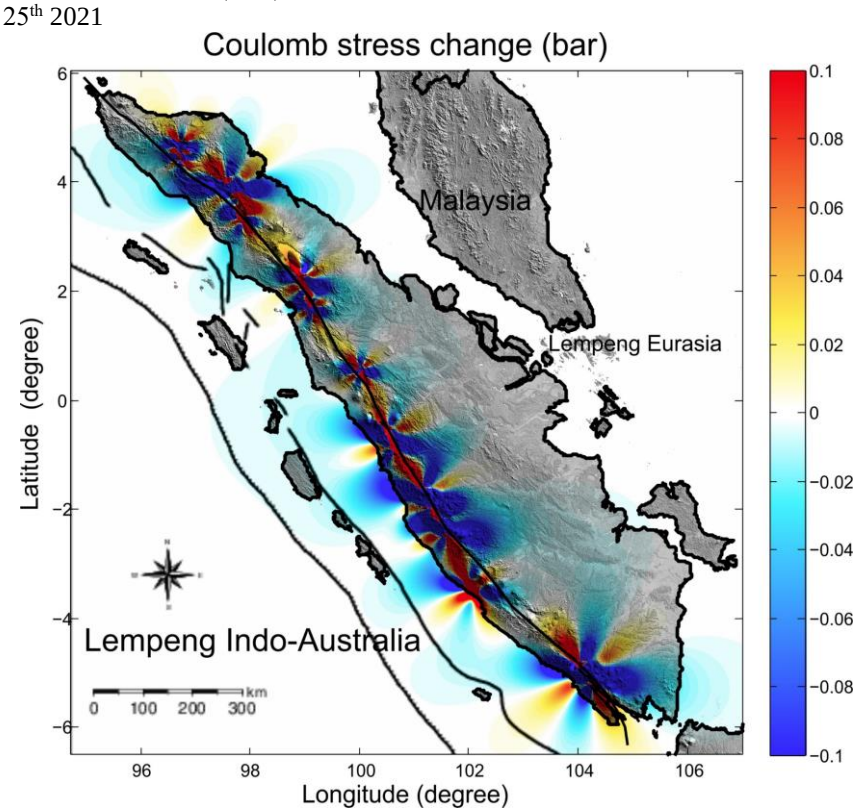

Figure 3. Map views of static Coulomb stress changes along the GSF. They were calculated from slips in four segments with magnitude greater than 6.0 available in the data catalog.

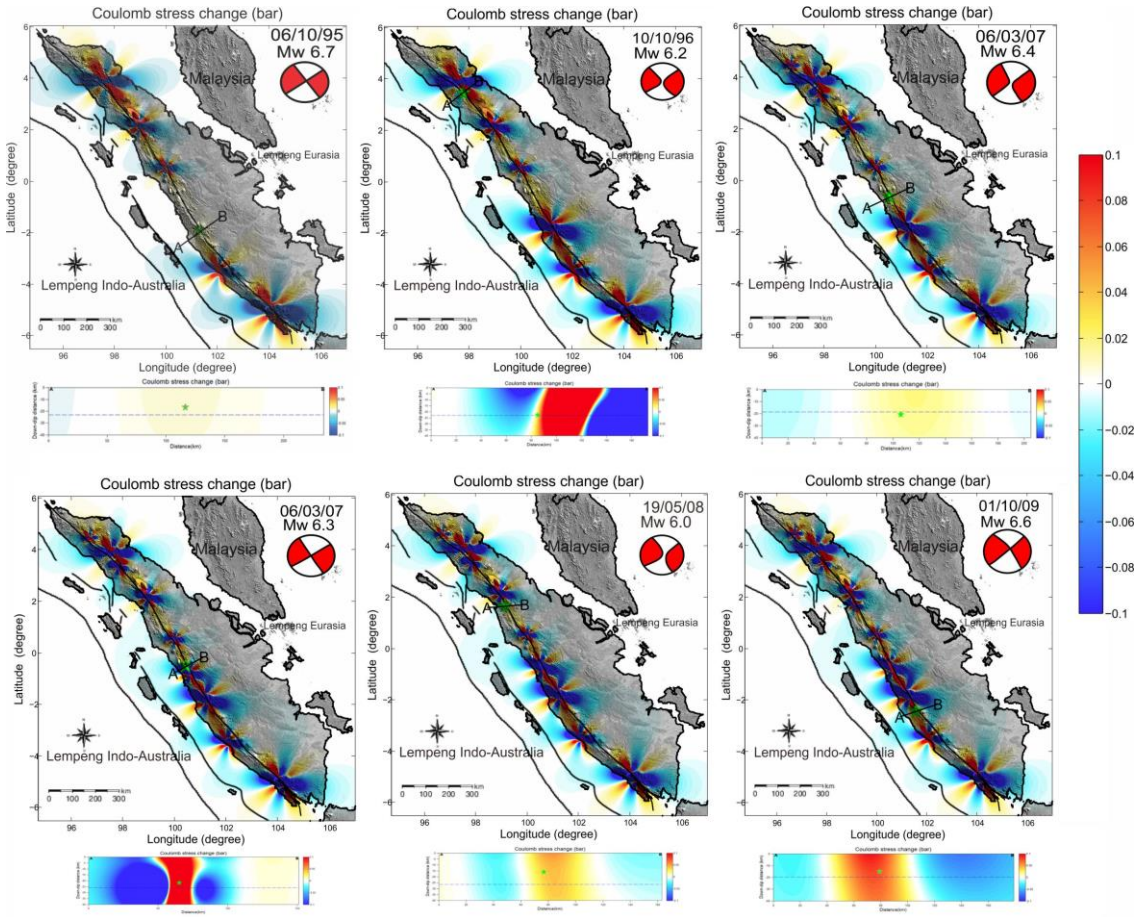

Figure 4. The results of the cross section of the earthquake that occurred because it was triggered by a previous earthquake.

PROCEEDINGS
JOINT CONVENTION BANDUNG (JCB)2021
November 23rd – 25th 2021

Leveraging Artificial Neural Network, Support Vector Regression, and K-Nearest Neighbors for Porosity Prediction in X Well: An Integrated Petrophysics and Machine Learning

Sanggeni Gali Wardhana, Tunggul Mirza Pratama
Faculty of Exploration and Production Technology, Pertamina University

Abstract

One of the most important parts to determine hydrocarbon reserves is the total porosity in the reservoir, which is generated from well data. Total porosity generally calculated using several log data, consisting of density & neutron porosity. The challenge is when the data used to estimate one of the data, either density or neutron, is not obtained clearly. The calculation of the total porosity in the reservoir cannot be done conventionally using an empirical formula. This research aims to create a new total porosity model based on machine learning as an approaching method without using a conventional formula and provide an almost similar result to the conventional formula. In this study, X well data were used at depths of 138 feet to 2812 feet in X well, consisting of Gamma Ray, Resistivity, Sonic, Photoelectric, Neutron, and Density Porosity. Then the calculation is done to determine the total porosity based on the average of neutron and density porosity as the conventional way. The total porosity is up to 0.45, with an average is approximate of 0.15. Then the determined test data is 30%, and training data is 70%. This research conducted using Artificial Neural Network (ANN), Support Vector Regression (SVR), and K-Nearest Neighbors (KNN) as the main method. Root Mean Square Error (RMSE) was determined using the comparison of the model and real porosity data or validation to know the model's error. Based on the result, Artificial Neural Network provides the RMSE up to 0.0254. Based on the Support Vector Regression, the RMSE up to 0.0491, and KNN provides the RMSE up to 0.0179. It can be concluded that KNN provides the best result to predict the total porosity in X well. We hope this research can give advice and example about an applied machine learning in the petrophysics world and help to solve the interpretation problem and minimize the uncertainty with the minimum data.

Keywords**:** Petrophysics, Porosity, ANN, SVR, KNN

Introduction

Porosity is the portion of the total volume of a rock that is porous. By definition, porosity is the ratio between the volume of space contained in the rock in the form of pores to the overall rock volume expressed in units of fractions. Porosity depends on the type of material, material size, pore distribution, cementation, diagenetic history, and composition. Rock porosity decreases with age and depth. But the opposite can happen which is usually caused by the temperature of the rocks. In the two-phase flow of gases and liquids, the fraction is defined as the fraction of the volume of the stream occupied by the gas (Hewitt et al, 1997).

Porosity is divided into primary (precipitation) or secondary (diagenetic or solution) porosity. Primary and secondary porosity can be determined by using neutron, sonic, and density log. These tools do not measure volume directly, but they measure the physical parameters of the formation and relate them to porosity mathematically or empirically. Since sonic instruments only record primary (or matrix) porosity, they can be combined with total porosity tools, such as neutron density or combined density, to determine secondary porosity (Lyons, 1996). Porosity is a measure of the volume in the rock available to hold reservoir fluids. Therefore, the volume of oil, gas and air in a given reservoir depends directly on the porosity value (Oyeneyin, 2015).

Total porosity consists of all the pore space, while effective porosity shows only the interconnected pore space. Porosity could be a hydrocarbon presence indicator. Porosity could be measured by mercury displacement, mercury pump, bulk volume meter, caliper measurement, well loging, etc. (Hyne, 2014). Well logging can measure the physical properties of reservoir directly in the borehole. The porosity measurement can also be done by using magnetic resonance (NMR) (Hyne, 2014., Asquith & Krygowski, 2004) and none of the log measures porosity directly. NMR, Density, and neutron logs are based on nuclear measurement. We can use sonic log for acoustic

PROCEEDINGS
JOINT CONVENTION BANDUNG (JCB)2021
November 23rd – 25th 2021

measurement. Well logging or wireline measurement is one of the most important procedures in hydrocarbon exploration and it is very expensive at most of the time.

Machine learning approach can be done to estimate porosity conditions at a fairly affordable price by using machine learning predictions with several algorithms, there are Artificial Neural Network (ANN), Support Vector Regression (SVR), and K-Nearest Neighbor (KNN). Those methods are very useful, especially to predict the porosity while the data provided is very limited. ANN is one of the largely used method in science and engineering. It is a powerful tool that can perform classification, diagnosis, feature extraction, function approximation, and data optimization.

Nowadays, ANN has been largely used by scientist and engineer to predict data from other provided information. In geophysical world, ANN has been increasingly applied to predict the characteristics of reservoir properties using several well log data. ANN is used to predict rock permeability, normalized oil content, and other reservoir properties (Bhatt, 2002). ANN also be able to predict formation permeability in highly heterogeneous reservoir condition. Another method that can be used to predict reservoir characteristics is SVR and KNN, absolutely those three algorithms have different characters in data predicting data.

The purpose of this study is to apply ANN, SVR, and KNN in predicting the porosity at certain depth. In this case, we use GR, resistivity, sonic, photoelectric, neutron, and density logs as the main data input. The result of this prediction will be compared to the result of conventional formula, which is represent the real data. This study is also aimed to analyze the accuracy model given by the applied method, and we can conclude which method that provides the best result, which is most similar to the real data.

Data and Method

The total porosity prediction process starts from the input predictor data and the predicted or output data. The high level of correlation with the total porosity data is the basis for the predictor data selection. After that, we can normalize the data to adjusting to the appropiate scale to reduce the error in data prediction using the scaling feature (Alasadi & Bhaya, 2017).

Then the datasets are divided or split with 70% train datasets and 30% test datasets. Machine learning algorithm models can be built using train datasets. In this experiment, we use Gridsearch Cross-Validation for Hyperparameter Tuning and Cross-Validation. This step helps select the best hyperparameters from each algorithm based on iterative experiments for a specific range of values. In cross-validation, the data are divided into several folds to find the average value of the accuracy generated from the predictions for each fold to ensure that the model built is consistent.

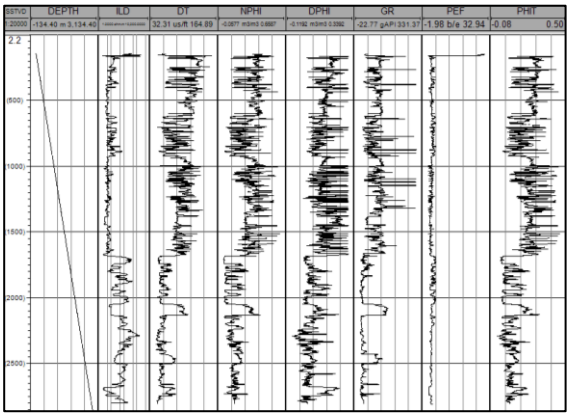

Figure 1. Input data

Then, we can determine the best model based on the results of cross-validation. The best model is used to make predictions using predictors from the test datasets from the splitting well "X" and the overall data well "X" to see the model's performance besides the training datasets. Finally, the total porosity can be predicted.

Table 1. All algorithms performance on training and test dataset

Algorithm	Metric	Training	Test
ANN	RMSE	0.0253	0.0257
	R^2	0.929	0.929
SVR	RMSE	0.0491	0.049
	R^2	0.732	0.739
KNN	RMSE	0.0159	0.022
	R^2	0.971	0.947

PROCEEDINGS
JOINT CONVENTION BANDUNG (JCB)2021
November 23rd – 25th 2021

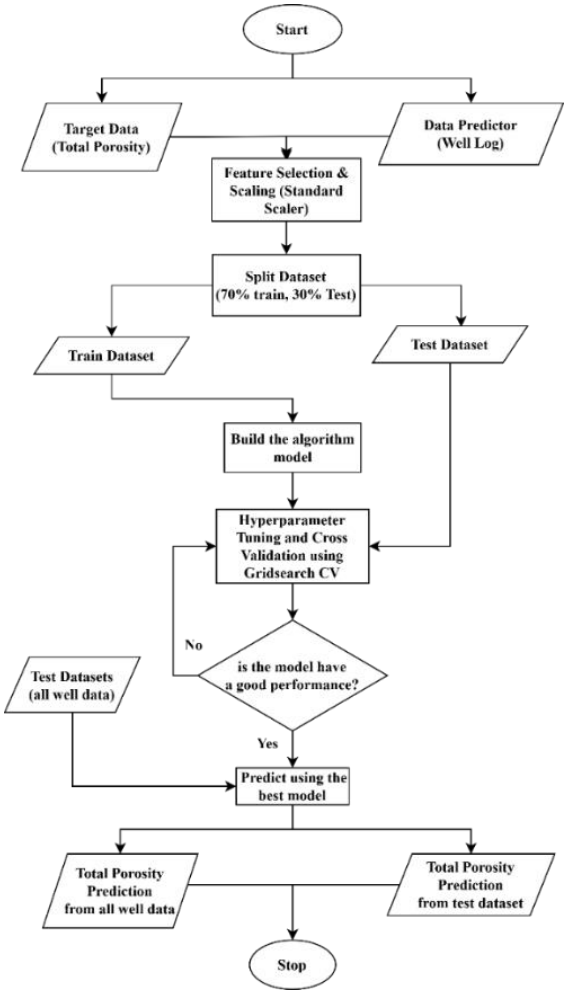

Figure 2 Methodology

Result and Discussion

- Artificial Neural Network (ANN)

ANN algorithm is quite good at predicting the total porosity value, with an RMSE value of 0.0254 and an R2 score of 0.929. In this algorithm, the performance on training and testing datasets shows the same RMSE and R2 scores, which indicates that the ANN performance shows a good fit. For this reason, the prediction results on the overall "X" well data show optimal results with average value of total porosity is 16.1%.

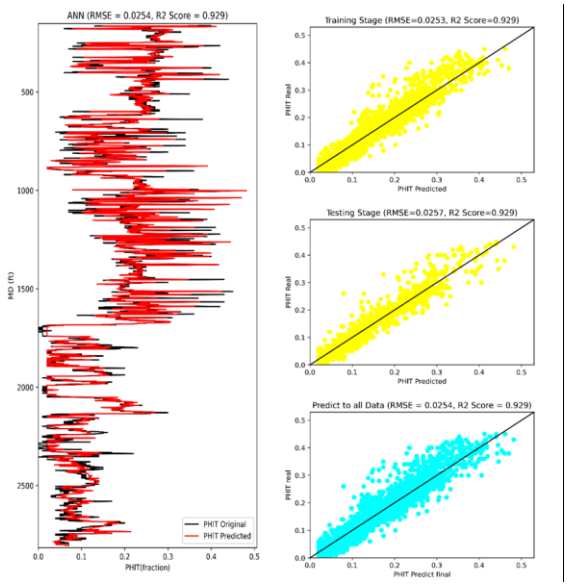

Figure 3 ANN result

- Support Vector Regression (SVR)

The SVR algorithm shows poor predicting in total porosity, with a relatively high RMSE value of 0.0491 and a relatively low R2 score of 0.612. The training stage error is lower than the testing stage error in this algorithm, which indicates the SVR algorithm performance is still slightly overfitting. In addition, this algorithm cannot predict low total porosity values. So that the total porosity prediction results in the all well data "X" shows a relatively high error with the total porosity average of 19.3%.

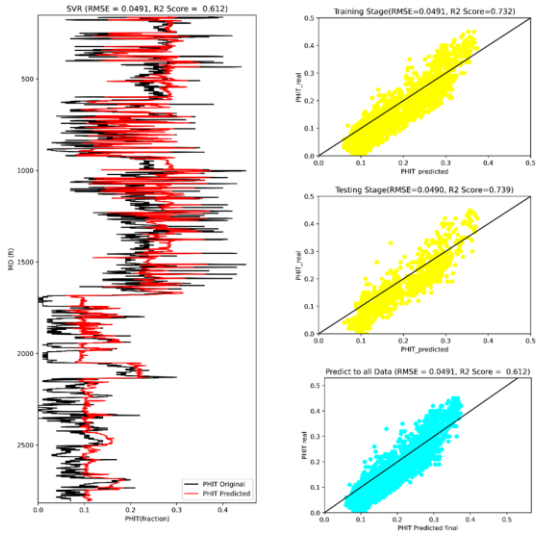

Figure 4 SVR Result

- *K-Nearest Neighbor (KNN)*

In the KNN algorithm, the total porosity value can be predicted well, with an RMSE value of 0.0179 and an R2 score of 0.962. The training

stage error is lower than the testing stage error in this algorithm, which indicates that the algorithm is overfitting. Although the overfitting issues, the results of the KNN algorithm show a perfect prediction of total porosity at all depths of the "X" well data with the average of 16%.

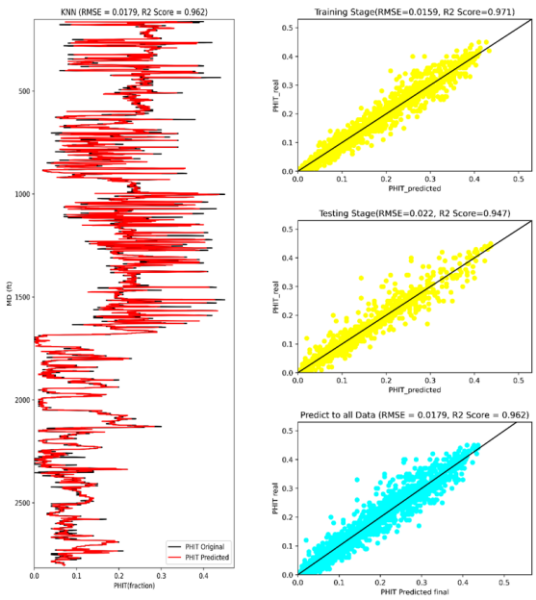

Figure 5. KNN result

Table 2. All algorithm results

Algo	Max	Min	Average	RMSE
ANN	48.2%	2%	16.1%	0.0254
SVR	37.4%	6%	19.3%	0.0491
KNN	43.7%	0%	16%	0.962

Conclusion

- ANN produces total porosity with the RMSE of 0.0254, SVR produces 0.491 RMSE, and KNN produces 0.962 RMSE
- KNN produces the most similar result to real data, so in this case we can conclude that KNN is the best method

References

Alasadi, S. A., & Bhaya, W. S. 2017. Review of data preprocessing techniques in data mining. Journal of Engineering and Applied Sciences.https://doi.org/10.3923/jeasci.2017.4102.4107

Asquith, G., Krygowski, D., 2004. *Basic Well Log Analysis*. The American Associaton of Petroleum Geologists, pp 37-56.

Bhatt, A., 2002. *Reservoir Properties from Well Logs Using Neural Networks*. Norwegian University of Science and Technology.

Cortes, C., & Vapnik, V. 1995. Support-vector networks. Machine learning, 20(3), 273-297.

G.F. Hewitt, G.L. Shires. 1997. *International Encyclopedia of Heat and Mass Transfer*. CRC Press.

Hyne, Norman., 2014. *Dictionary of Petroleum Exploration, Drilling and Production*. Tulsa: Penwell Corporation, pp 394-395.

Lyons, W. C., 1996. *Standard Handbook of Petroleum and Natural Gas Engineering*. Gulf Professional Publishing Vol. 2, Houston.

Mitchell, T. M. 1997. Machine learning. McGraw Hill, 45(37), 870-877.

Oyeneyin. 2015. *Integrated Sand Management for Effective Hydrocarbon Flow Assurance*. 1st Edition Vol. 63. Elsevier

Scholkopf B., and Smola A. 2002. Learning With Kernels. MIT Press.

Shmueli, G., Patel, N. R., Bruce, P. C., & Torgo, L. 2016. Data Mining for Business Intelligence: Concepts. Techniques and Applications Wiley, India.

Wang, L. J., Guo, M., Sawada, K., Lin, J., & Zhang, J. 2016. A comparative study of landslide susceptibility maps using logistic regression, frequency ratio, decision tree, weights of evidence and artificial neural network. Geosciences Journal, 20(1), 117-136.

Wei, B., Sugiura, N., & Maekawa, T. (2001). Use of artificial neural network in the prediction of algal blooms. Water Research, 35(8), 2022-2028.

PROCEEDINGS
JOINT CONVENTION BANDUNG (JCB)2021
November 23rd – 25th 2021

Analyzing Shallow Marine Depositional Environment using Paleotopography Reconstruction and RGB Blending – Case Study: Woolaston and Johnson Formation, Poseidon, Browse Basin.

Iqbal Daffa Pradana[1], Aji Darma Maulana[2], Cecilia Jatu[3], Muhammad Iqbal Ramadhan[4], Firhan Maulana P.[5]
[1]University of Brawijaya, [2]UPN Veteran Yogyakarta, [3]University of Gadjah Mada,
[4]Bandung Institute of Technology, [5]University of Padjadjaran

Abstract

The study of subsurface facies at the geological modeling stage is crucial for the oil and gas industry. Nowadays, the front-lead in geological science is greatly facilitated by technological developments that can graphically support the modeling and visualizing of geological objects. The seismic imaging method is a product of these technological advances. In addition to forming three-dimensional geometry, it is easier to do the offered resolution, and the appearance that is highlighted using this method will be better in the result. In this study, one of the seismic imaging methods: RGB Color Blending, is used to describe circumstances and geological features in terms of depositional fluvio-delta environments. In simple terms, this method mixes (blending) the three primary colors in the electronics world, red (R), green (G), and blue (B), into a new color spectrum. By combining three seismic cubes with identical attributes, a new seismic cube containing information from the three cubes will be created. This study involved two kinds of RGB Color Blending methods, Spectral Decomposition and Energy Based Attribute. Spectral Decomposition is a method that separates three dominant spectrums into three individual cubes. Then will be combined using the RGB Blending method. The two methods will collaborate to assist the visualization and geological modeling of the shallow marine to deltaic environment. The geological features shown using this method will then be delineated, elaborated with a conceptual understanding of the deltaic depositional environment. Several facies have been successfully interpreted, including Distributary Channel, Upper Delta-plain & Coastal plain, Lower delta plain (Marsh, etc), and Pro-delta.

Keywords: Caswell Sub-Basin, Depositional Environment, RGB Blending, Seismic Spectral Decomposition.

INTRODUCTION

The study area is located in Caswell Sub-Basin, Browse Basin precisely situated at an offshore depocenter in the southern Timor Sea region of the North West Shelf, Australia. The Browse Basin and its component structures were formed as extensional half-grabens. The sub-basin forms part of one of a series of northwest-trending extensional basins that made up the Westralian Superbasin during the Carboniferous to Early Permian (Yeates et al., 1987). This basin has undergone six major tectonic phases, which are: Late Carboniferous to early Permian extension, continued by thermal subduction, Late Triassic to Early Jurassic inversion, second time of extension during Early to Middle Jurassic, Late Jurassic to Cenozoic thermal subsidence. From the age of Late Jurassic onwards, the Browse Basin became a passive margin, made it more stable. Some turbidites were deposited within the Caswell Sub-basin, followed also by the deposition of carbonate sediments which were increased, though fluvial-deltaic to nearshore sediments were still deposited on the basin margins. Followed by the last event: the upper inversion.

Petroleum system in the Browse Basin controlled by the Upper Triassic (Inversion 1), and the Lower to Middle Jurassic (Extension 2) structuring events that critical to the development of most hydrocarbon traps, and potential source rocks were deposited during the initial Palaeozoic rift phase and in the Early Triassic, Early to Middle Jurassic, Late Jurassic and Early Cretaceous. The formations of interest to this study are Jamieson and Woolaston formations deposited in Early to Late Cretaceous, consist of massive claystone and sandstone which contained both marine and terrestrially-derived plant material. The more distal sediments have a higher potential for oil.

DATA AND METHOD

This study conducted using 3D Seismic Data of Poseidon Field and 7 wells within the field. After analyzing the 3D Seismic Data and Regional Geology, we found that Woolaston and Johnson Formation has unique geological features that could stand out when applying RGB Blending technique. This leads to the determination of Volume of Interest (VOI) which stretch out from seismic inline of 2077-3898, crossline of 660-3340, and time reference around 2144-3180 ms.

After the volume of interest is determined, the amplitude-spectral of this volume is extracted and investigated to select frequencies (within seismic bandwidth) that will be decomposed for RGB Blending. The method used for extracting the frequencies is Generalized Spectral Decomposition.

Spectral Decomposition is used to describe and consider temporal bed thickness and geological discontinuities in 3-D surveys (Partyka et al., 1999). This technique improves the definition of future seismic tuning resolution and often helps solve information that cannot be resolved in the time domain. Spectral decomposition converts seismic data into the frequency domain using time-frequency transformations that have been in development for decades. Modification (free phase) of the amplitude spectrum is used to delineate layer variations, while the spectrum is used to develop geological discontinuities laterally.

Spectral Decomposition proven to be a perfect approach in estimating the thickness as well as faults. Spectrum decomposition can practically be used to delineate stratigraphic arrangements (such as sandstone channels) and structural arrangements involving complex fault systems in 3-dimensional seismic surveys (Partyka et al., 1999). Spectral decomposition is often used in seismic data processing, including spectral analysis, frequency filtering, wavelet characteristics, etc. Still, in recent years three-dimensional seismic data interpretation has also been applied (Partyka et al., 1999). The frequencies that were selected are shown by the green line in **Figure 3**.

PROCEEDINGS
JOINT CONVENTION BANDUNG (JCB)2021
November 23rd – 25th 2021

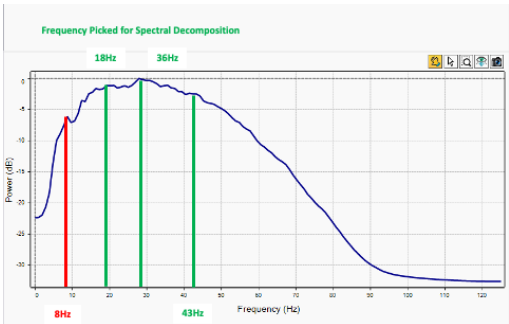

Peak of frequencies within the seismic bandwidth (blue curve) showed by green and red line, whereas the selected frequencies for decomposition is showed by green line.

Figure 1: Spectral-Amplitude of VOI Seismic

A color model is an abstract mathematical model that describes how colors can be represented as tuples of numbers, usually in three/four color components. In its construction, the color model is formed by mixing (blending) various color components. The commonly used models are the RGB model and the CMY model (Silva, 2011).

The RGB model is an additive color model that uses the primary colors red (R), green (G), and blue (B) in various ways to produce a variety of colors tailored to human visual perception. Red, Green, and Blue are the main components of the RGB model. Each component can vary from entirely off (zero saturation) to fully active (full saturation).

To show the stratigraphic features, RGB Blending is introduced by combining these 3 frequency volumes and co-render them by Equation (2.0) below:

$$C_{out}(x,y,z) = C[I_R(x,y,z),\ I_G(x,y,z),\ I_B(x,y,z)]$$

x, y, and z are coordinate position, while I_R, I_G, and I_B are respectively the value of red, green, and blue attribute.

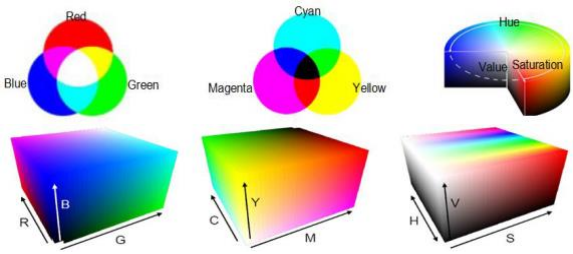

Figure 2: lustration of Color Blending Space RGB (left), CMYK (middle), and HSV (right) taken from (Cao, 2015)

RESULT AND DISCUSSION

In the seismic section shown in Figure 3, the zone of interest (Woolaston and Jonson Fm.) shows a form of marginal depositional environment. Where the NW side are the proximal area (landward), while the SE part goes to distal (basinward). Area around NW of the field is highly controlled by structures that formed after the deposition of interest zone (Woolaston and Jonson Fm.) which can be seen by the faults exist on NW side of the interest zone.

These structures were developed during Upper Jurassic to Tertiary due to thermal subsidence, creating normal faults that displaces this block downward in results (Gradstein et al, 2004). Because of this condition, the seismic need to be restored to the hypothetical initial condition where the NW part of the interest zone must be higher than the SE part.

This could be achieved by flattening surface that locally deposited nearly maximum accommodation space/regionally flat deposition. As Top of Johnson Fm. are deposited relatively flat in this local region, flattening the time structure map of Top Johnson Fm. resulting in a construction of hypothetical paleotopography of formations below it. This shown by **Figure 1-A** where the NW side of the marginal depositional environment has been restored to the hypothetical original position. This means that the analysis of stratigraphic features can be easily delineated in both in seismic sections and time slices.

Seismic Stratigraphic Reconstruction

After the structure control has been restored, each formation below Top of Johnson Fm. were picked, the surfaces were Top of Woolaston Fm (Bottom of Johnson Fm.) and Top of Jamieson Fm. which became the foundation for Woolaston Fm. deposition where the marginal depositional environment is shown by Figure 4-A and 4-B.

Evidence from the well reports (Kronos, Pharos, Proteus, Poseidon-1, Poseidon-2, Boreas, Poseidon North) shows that the Woolaston and Johnson Fm. were deposited in shallow marine depositional environment, where Woolaston Fm. mostly consist of calcareous claystone and minor sandstone, while Johnson Fm. consist of calcilutite grading to argillaceous calcilutite, marl, calcareous claystone and sandstone.

Seismic reconstruction (Base Woolaston Time Structure Map) shows that Woolaston Fm. in the deposition was a marginal environment with channels scouring and eroding Top of Jamieson Fm. (**Figure 4-A, 4-B, 4-C, and 3-D**). The main channel has width of 3km with orientation of NW-SE, deposited sediments (relatively parallel to sub-parallel seismic reflectors) to an open accommodation space in shallow marine environment. Several channel infils can be easily delineated in seicmic section.

The NW and Northern part of Woolaston Fm. indicates a coastal plain, 13-18km wide from the land to the shoreface. Woolaston Fm. believed to be deposited during rising sea level with maximum transgression which validated by the deposition of massive claystone.

In addition, the evidence of seismic data shows that after the deposition of Woolaston Fm. and several formations above, there's a major erosion that eroded the upper section of Woolaston Fm. and the following formations (Fennelon Fm., Puffin Fm., etc). The eroded surface became the base for Johnson Fm. settling (**Base Johnson Time Structure Map on Figure 4-A**), followed by the development of deltaic/estuary with main channel still in NW-SE orientation, while smaller distibutary channel developed on the transitional-shallow marine environment (**Figure 4-D, 4-F, and 4-B**).

There are some differences between the log & well stratigraphic interpretation with the seismic interpretation. This due to most of the well doesn't penetrate the deltaic/estuary area and mostly were around the coastal plain and distal area. While the erosion above Woolaston Fm. need further investigation/evidence from log/stratigraphic analysis.

PROCEEDINGS
JOINT CONVENTION BANDUNG (JCB)|2021
November 23rd – 25th 2021

RGB Blending of Woolaston & Johnson Formation

The RGB blending results from blending 3 spectral decomposed cube which are 18 Hz (Red), 36 Hz (Green), and 43 Hz (Blue) cube. The RGB blending time slice show consistent results as in seismic interpretation. In early deposition of Woolaston Fm. there's no visible distributary channel (**Figure 5-A, Image 1 and 2**). The depositional environment of Woolaston Fm. is interpreted as shallow marine settling, while the upper section shows faint channels (**Figure 5-A, Image 3 and 4**). Meanwhile, a deltaic depositional environment is clearly visible on Johnson Fm., distributary channels (with abandoned channel) can be seen in with major orientation of NW-SE and distribute throughout SW-NE area. Facies association on Johnson Fm. are Main channel with Distributary Channel, upper delta-plain and coastal plain along SW-NE area, Lower delta plain in NE area, and pro-delta to further NE (**Figure 3**).

CONCLUSIONS

From this study we can conclude that the depositional environment in the zone of interest (Woolaston & Johnson Fm.) is shallow marine with a deltaic environment developed in Johnson Fm. The deltaic facies that associated in the formation are Distributary Channel, Upper Delta-plain & Coastal plain, Lower delta plain (Marsh, etc), Pro-delta, where the proximal area are in NW while the distal are further in SE.

REFERENCES

Cao, J., Yue, Y., Zhang, K., Yang, J., dan Zhang, X., (2015), Subsurface Channel Detection Using Color Blending of Seismic Attribute Volumes. International Journal of Signal Processing, Image Processing and Pattern Recognition Vol.8, No.12 (2015), pp.157-170.

Palu, Tehani & Hall, Lisa & Edwards, Dianne & Grosjean, Emmanuelle & Rollet, Nadege & Boreham, Chris & Buckler, Tamara & Higgins, K. & Nguyen, Duy & Khider, Kamal. (2017). Source Rocks and Hydrocarbon Fluids of the Browse Basin.

Silva, S., Santos, B. S., and Madeira J., 2011, Using color in visualization: A survey, Computers & Graphics, vol. 35, no. 3.

Struckmeyer, H.I.M., Blevin, J.E., Sayers, J., Totterdall, J.M., Baxter, K. and Cathro, D.L., 1998, Structural evolution of the Browse Basin: New concepts from deep seismic data. In: Purcell, P.G. and R.R. (Eds), 1998, The Sedimentary Basins of Western Australia 2: Proceedings of the Petroleum Exploration Society of Australia Symposium, Perth, WA, 1998, 345–367.

Partyka, G. A., Gridley, J.M., dan Lopez, J., (1999), Interpretational Application of Spectral Decomposition in Reservoir Characterization, The Leading Edge, vol. 18, No. 3, hal. 353-360.

PROCEEDINGS
JOINT CONVENTION BANDUNG (JCB) 2021
November 23rd – 25th 2021

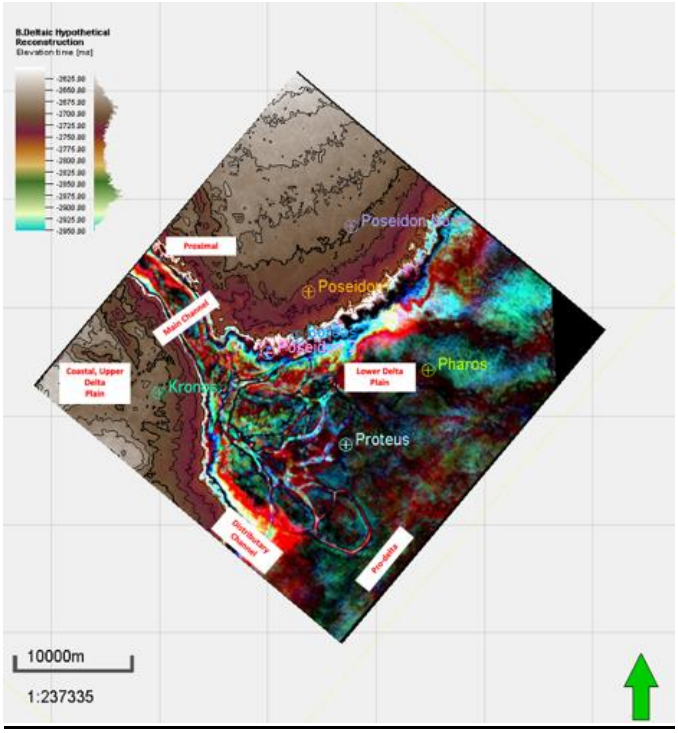

Figure 3: RGB Blending Facies Association Interpretation on -2768ms time slice (Johnson Fm.)

PROCEEDINGS
JOINT CONVENTION BANDUNG (JCB)2021
November 23rd – 25th 2021

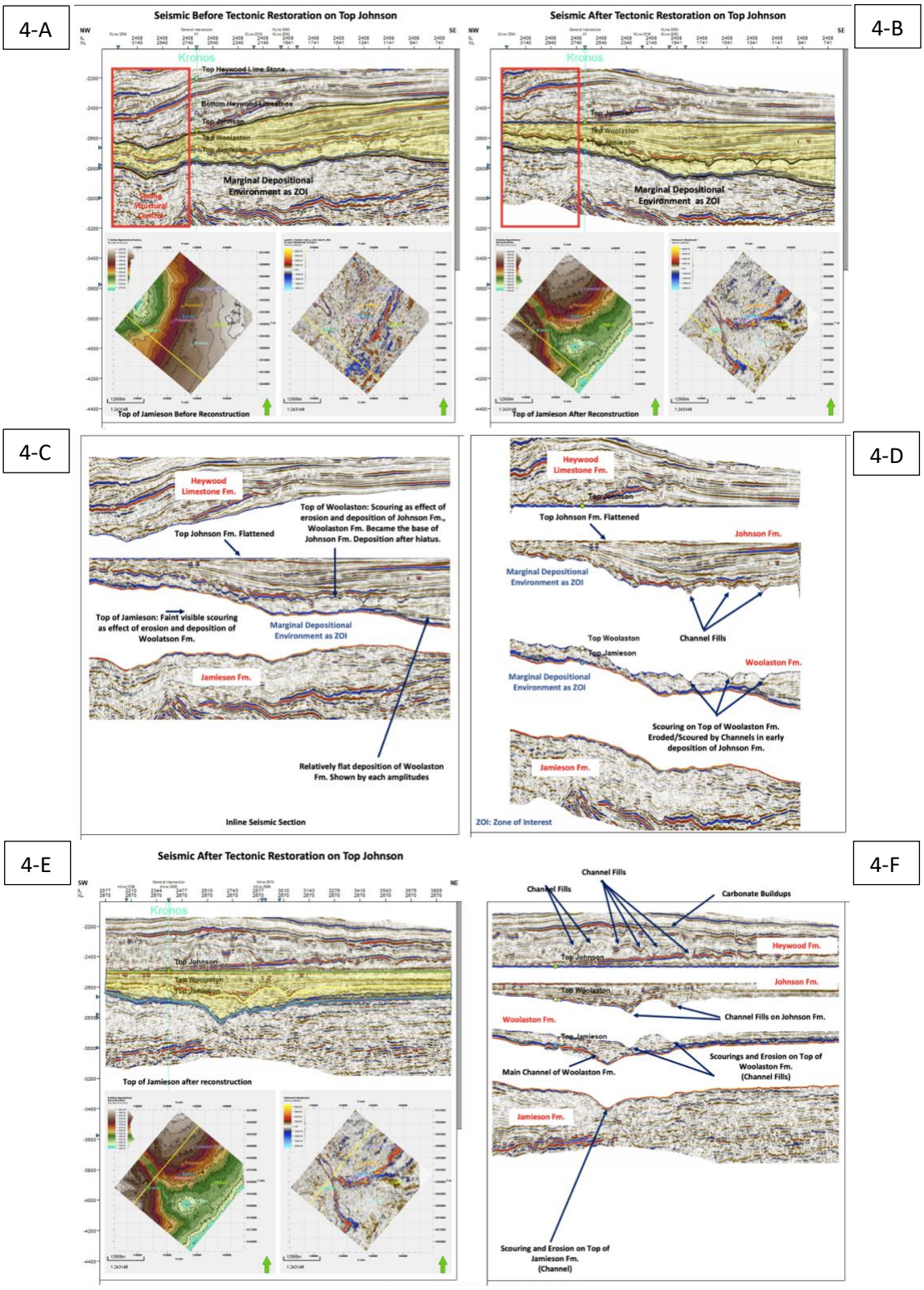

Figure (4-A) seismic inline section along Kronos well, shows a structure controlling the NW side, resulted in the tilting of proximal section of ZOI (Zone of Interest). Figure (4-B, 4-E) shows seismic after restoration of structural control. Figure (4-C, 4-D) shows seismic stratigraphic reconstruction with marginal marine as ZOI.

Figure 3: Seismic Stratigraphic Reconstruction and resulted surfaces of Top Johnson.

PROCEEDINGS
JOINT CONVENTION BANDUNG (JCB)2021
November 23rd – 25th 2021

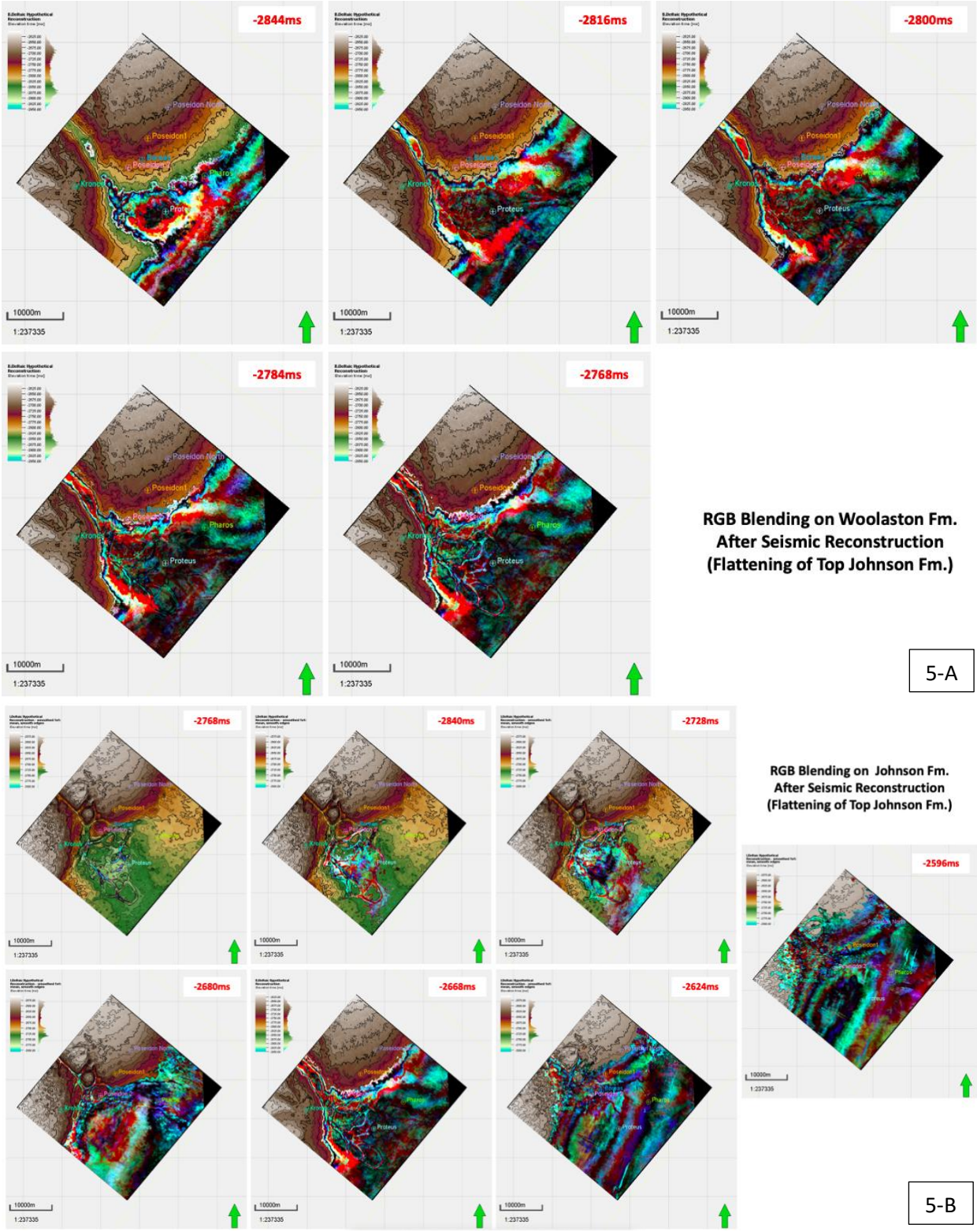

Figure (5-A) shows the RGB blending in Woolaston area, the RGB results on time -2844 to 2800ms shows no visible channel. While around 2784ms some faint channel starts to show. Figure (5-B) shows the deposition of Johnson Fm.

Figure 5: RGB Blending on Woolaston and Johnson Formation.

PROCEEDINGS
JOINT CONVENTION BANDUNG (JCB)|2021
November 23rd – 25th 2021

IDENTIFICATION OF THE SHALLOW HYDROCARBON ZONE USING TILT DERIVATIVE GRAVITY DATA AND THE WENNER-SCHLUMBERGER CONFIGURATION METHOD IN RANTAU PEREULAK AREA, EAST ACEH, ACEH PROVINCE

K. Alfaiz[1], Imaduddin[2], M.K. Jibran[1], Y. Assyifa[1], Z. R. Qauvani[1], S. J. Fahira[2], R. R. Putra[1], N. Khaira[2], S. Futhra[1], A. Zahran[1]
[1]Department of Geophysical Engineering, [2]Department of Geological Engineering, Universitas Syiah Kuala, Banda Aceh 23111 Indonesia

ABSTRACT

The increasing of human needs for oil and natural gas caused the exploration and production are in crucial to be carried out, especially in Aceh. Since the conflict begun between Indonesian Government and GAM, exploration activities have also begun to be rarely carried out. A well of an old oil, which was operated by a Dutch company is being neglected currently. An illegal drilling carried out by the community in Rantau Peureulak area of East Aceh has proved the potential reserves of this old oil well. The gravity method can be applied in the early stages of hydrocarbon exploration to determine the location of hydrocarbon potentials based on variations in the Earth's gravitational field. Through the gravity satellite, it found the anomaly data of free air is obtained with a value range of -31.7 - 80 mGaL. Assuming the rock density in the study area is 2.67 gr / cm3, a Bouguer correction is made to obtain the gravity value by taking it into account the effect of rock mass around the measurement point. The gravity value is later going to be used to calculate the simple Bouguer anomaly value by reducing the free air anomaly value with the Bouguer correction value. The range of values resulting from the simple Bouguer anomaly in the study area ranged from - 92.6 - 51.6 mGa. Based on the results of the SRTM and Tilt Derivative overlay and geological structure showed that the research target location is a zone with a value of 1.5 mGal and there are several minor faults which are assumed to be fault lines where shallow hydrocarbons migrate to the surface. The lateral distribution of shallow hydrocarbon potential shows the presence of 4 (four) rock's layers, namely topsoil, loamy sand, muddy sand, and alluvium sediment with the distribution data of resistivity values obtained from 6 - 100 Ωm. An indication of the presence of shallow hydrocarbon fluid is found in alluvium sediment in the form of sand's layer with a resistivity value of 8 - 40 Ωm at the depth of 60 m. Analysis studies of shallow hydrocarbon potential distribution in the Rantau Pereulak area of East Aceh need to be carried out to understand the residual of potential realities from the field as a guide in determining the best scenario for field's development.

Keywords : Geoelectric, Gravity Satellite, Resistivity, Shallow Hydrocarbon, Tilt Derivative.

INTRODUCTION

Hydrocarbons which consist oil and natural gas are still the main energy sources that support human activities and interests in various aspects. The more needs, the higher the use of hydrocarbon so that hydrocarbon reserves are needed. Therefore, exploration and production activities are very important to fulfill the needs of oil and gas in Indonesia, especially in Aceh. Since the conflict begun between the Indonesian government and GAM (Free Aceh Movement) exploration activities have also begun to be rarely carried out. Many old oil wells have been abandoned after previously being operated by a Dutch company, one of which was in Peurelak, East Aceh. Most of these oil wells still have potential reserves, as evidenced by the illegal drilling of communities around the area to fill the needs of oil and natural gas in Indonesia, especially Aceh.

One of the efforts to increase oil and gas production in the Peureulak area, East Aceh is by mapping shallow hydrocarbon zones by measuring the physical parameters of rocks on the surface and below the surface using both geophysical and geological approaches. Gravity data can be used as the main information in determining the location of 2D geoelectric measurements. Gravity is a leading method in geophysical exploration to determine the presence of hydrocarbon basins based on variations in the value of the acceleration of gravity (Erviantari & Sarkowi, 2008).

The gravity method is used as a preliminary exploration of natural resource targets below the earth's surface by describing a two-dimensional (2D) or three-dimensional (3D) profile through processing gravity field anomaly data, which is known as the Bouguer Anomaly. Based on this model, it can be interpreted as the geological structure of subsurface rock layers that are the target of research (Arif, 2016). To better represent the geological structure, Tilt Derivative Gravity can be used to obtain anomaly boundary data, so that the presence of geological structures in the form of major or minor faults can be identified (Praktik & Pertamina, 2020).

PROCEEDINGS
JOINT CONVENTION BANDUNG (JCB)2021
November 23rd – 25th 2021

Faults can act as a hydrocarbon migration route from source rock to reservoir rock where hydrocarbons accumulate, therefore the straightness of the fault needs to be visualized with DEM SRTM to determine the distribution of shallow hydrocarbon potential in the study area.

Data on the distribution of shallow hydrocarbon potential is used in determining the location of the geoelectric method. In the geoelectric method, electric current is injected into the earth through two current electrodes and the potential difference is measured through two potential electrodes. From the results of current and electric potential differences measurements can be calculated variations in resistivity values in the earth's surface layer below the measuring point (Apparao. A, 1997), so that shallow hydrocarbon characteristics related to thickness, depth, and distribution below the surface can be known in shallow zones (Apparao. A, 1997).

A study on the potential distribution of shallow hydrocarbons in the Rantau Pereulak area, East Aceh needs to be carried out to understand the potential reality that remains from the field. This study is important to be used as a guide in determining the best development scenario in developing the field due to rampant illegal practices in the process of exploration and exploitation of natural resources and also as an effort to overcome problems in the planning sector related to natural resource conservation.

DATA AND METHOD

Regional Geology

The study area in East Aceh Regency when viewed based on the geological map, it is known that East Aceh is included in the North Sumatra Basin (NSB). The North Sumatra Basin (NSB) is a combination of a pull-apart basin and a half-graben basin which is located in the southeastern part of the Eurasian continent's crust. The basin is bounded by the Mergui Ridge to the west and the Malacca Platform to the east. To the south, it is bounded by the Barisan Mountains and to the north, it extends off the coast of Thailand. According to (J.D. Bennet, D.MvC. Bridge, NR Cameron, A. Djunuddin, SA Ghazali, D. H Jeffery, W. Kartawan, W. Keats, NM S, Rocks, 1981), that sediments in the East Peureulak Idi River and Raya are dominated by the Seurula Formation which consists of sandstone, shale, and claystone. This indicates that in this formation the regression phase is still continuing. The depositional environment of this formation is still in the marine environment. Then there is the Julu Rayeu formation which consists of sandstone, claystone, and mudstone containing lignite. Quarter (Alluvial) Formation consisting of sand, gravel, and clay. And also the Baong Formation consists of dark gray shale which is predominantly carbon-rich in forams.

In addition, there is also a marginal oil field in the Rantau Panjang area which is crossed by a long fault from northwest to southeast of Peureulak. The map also shows some of the fault trends and major anticline structures where hydrocarbons may be trapped.

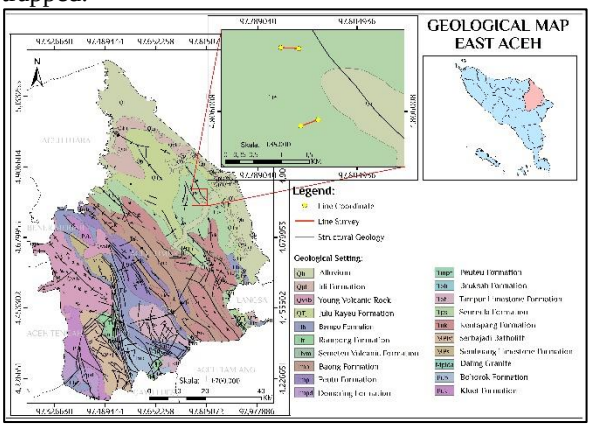

Fig. 1 Geological Map of Study Area - East Aceh Regency (modified by Cameron, 1981)

Tectonic Settings

In general, the North Sumatra Basin was formed in two tectonic phases. The first tectonic activity or rifting phase begins in the Middle Paleogene (Eocene), where the Tampur carbonate Formation is deposited extensively in the marine shelf environment. The North Sumatra Basin experienced crustal extension as a result of a collision between the Indian Continental Plate and the Eurasian Plate. During this period, the horst, graben, and half-graben trending North-South and Northeast-Southwest developed.

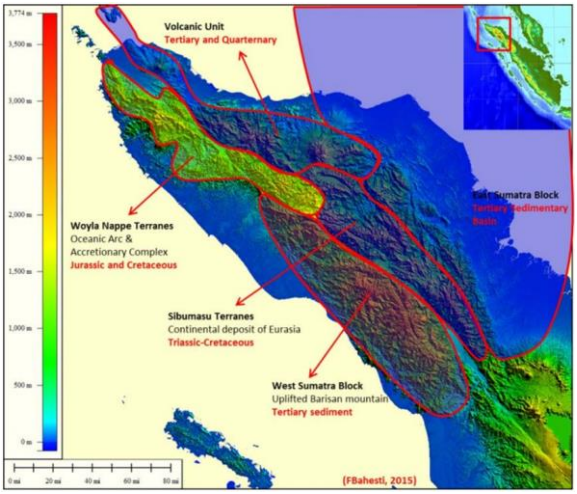

Fig 2. Regional Tectonics North Sumatra Basin

During the Early Oligocene, the collision and subduction of these plates slowed down and changed the extensional regime to a compressional regime resulting in basin inversion, which was shown by regional uplift and misalignment over the Eocene-aged sediments in the North Sumatra Basin. During

PROCEEDINGS
JOINT CONVENTION BANDUNG (JCB)2021
November 23rd – 25th 2021

the Late Oligocene, compressional stress is released resulting in fault blocks along the weak zone formed by faults aged Early Oligocene. This uplifting makes the old sediment (Formation intervened) on structural highs where the depocenter basin or graben make room for the younger clastic sediments, the formation Bruksah/Parapat, Secanggang, and Bampo.

The transitional phase of basin evolution occurred during the Early Miocene and represents a relative tectonic quiescence. This stage is characterized mainly by forced regression and basin filling (down belumai). At the end of the Early Miocene, large ocean transgressions occurred so that the Malacca Platform and Central Horsts sank and became accommodation for the deposition of shallow marine carbonates including reefs (Peutu Formation). Belumai carbonate sedimentation continued during the accumulation of skeletal limestone and reefs around the platform. At the end of the Middle Miocene, transgression reached its maximum level, characterized by very rapid and thick sedimentation in the marine environment of the loam of the Baong Formation. The Bukit Barisan lift was active since the late Middle Miocene, and reached maximum activity in the Plio-Pleistocene. At that time, deltaic to alluvial sedimentation occurred (Keutapang and Seurula Formations).

Regional Stratigraphy

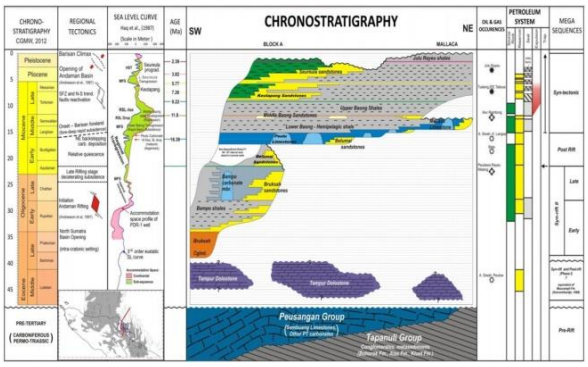

Fig 3. Regional Stratigraphic Map

The stratigraphy of the research area is generally composed of the following formations:

1. Julu Rayeu Formation

The lithology of this formation is in the form of a fine to coarse-grained sandstone and claystone with the presence of mica, wood, and mollusk fragments. The thickness of the formation can reach 550-2200 meters. This formation was deposited in a shallow marine environment.

2. Seurula Formation

The Seurula Formation is the formation that is the target zone in this study. This formation consists of sandstone, shale, and claystone. The sandstone in this formation has a coarser texture than the Keutapang Formation. This indicates that the regression phase is still continuing at that time. The environment of deposition in the marine environment.

3. Keutapang Formation

The Keutapang Formation is composed of alternating shale lithology with claystone to siltstone and the presence of thick limestone and sandstone inserts. The thickness of this formation ranges from 404-1534 meters. The Keutapang Formation is the beginning of a regression cycle from sediments in the North Sumatra Basin that were deposited in a deltaic to the deep-sea environment during Late Miocene.

4. Baong Formation

This formation mostly has shale and sandstone lithology. The shale in this formation is characterized by light gray to dark gray and carbonate. This formation was deposited in the Bathyal environment and has a thickness of 1500-1750 meters.

Method

This study uses data sourced from the Topex Geodetic Satellite (Geosat), where the data obtained is in the form of Free Air Anomaly. Free Air Anomaly is the value of the gravitational anomaly that has been corrected for free air but has not taken into account the effect of rock mass and it is necessary to include the Bouguer correction into the calculation (Astra, 2013). The data used in this study is the Bouguer Anomaly gravity data. The research location is in the Pereulak Rantau Area, East Aceh Regency.

Gravity is one of the geophysical methods used to describe subsurface geological structures based on variations in the earth's gravitational field due to lateral density differences. One application of the gravity method is in the early stages of hydrocarbon exploration where this method is used to estimate the configuration or depth of the basement and the existence of the basin. The theoretical basis for using this gravity method is Newton's law of gravity. The theoretical basis for using the gravity method is Newton's Law, expressed in the following equation:

$$F = G\frac{m_1 m_2}{r^2} \quad \text{.....(1)}$$

Where:
F = Gravitational Attraction (N)
G = Gravitational Constant (6,673 x 10^{-11} Nm^2Kg^2)
m_1 = Mass of object one (kg)
m_2 = Mass of object two (kg)
r = Distance between the two masses (m)

Research using the gravity method can initially be done in three ways; namely land surface, marine, and airborne surveys. However, along with the development of technology, a method for measuring gravity data from satellites has been developed which has several advantages including it does not take much time and finances when compared to field measurements, besides it can easily expand the

research area. Gravity Satellites can detect mineral deposits below the surface by utilizing gravity anomaly data obtained from altimetry satellites such as the Topex/Poseidon, ERS, Envisat, and Jason satellites to measure large-scale topography (Sandwell, 2009).

Bouguer correction is performed on Free Air Anomaly which is the output of gravity satellite data to get a simple Bouguer anomaly value. Through this simple Bouguer anomaly value, it is possible to determine the location of potential hydrocarbons using the Grav2dc. Software.

Non-commercial oil seeps found in the study area indicate the presence of oil and natural gas below the surface, this also means that there is a geological structure in the form of faults or fractures that become the path of migrating hydrocarbons. The structure of the fault can be analyzed using Tilt Derivative data from remote sensing or satellite gravity data. Tilt derivative is a filter to analyze the boundary layer so that it can be seen clearly from the boundary and shape of the target anomaly. In addition, the straightness of the fault can be interpreted with DEM SRTM data visualization so that it can be seen where the distribution of shallow hydrocarbons is in the area so that the geoelectric method measurement location can be determined for further surveys. The software used in data processing in this study is RES2DINV.

The resistivity geoelectric method is a geoelectrical method that studies the electrical resistivity (specific resistance) properties of rock layers within the earth. In this method, electric current is injected into the earth through two current electrodes and the potential difference is measured through two potential electrodes. From the results of current and electric potential differences, measurements can be calculated variations in resistivity values in the earth's surface layer below the measuring point (Apparao. A, 1997). In this method, many electrode configurations are known, including the Wenner configuration, the Schlumberger configuration, the Wenner-Schlumberger configuration, and the dipole-dipole configuration (Hendrajaya, L., & Arif, 1990). Each rock has different characteristics, including electrical properties. One of the rock's properties is resistivity (specific resistance) which indicates the ability of the material to conduct electric current. The greater the resistivity value of a material, the more difficult it is for the material to conduct electric current.

Table 1. The resistivity of rocks and minerals (Telford, W. M., Geldart L. P., Sheriff, 1976)

Material	Resitivity (Ωm)
Limestone	500 – 10.000
Sandstone	200 – 8.000
Shales	20 – 2.000
Sand	1 – 1.000
Clay	1 -100
Marl	10 - 108
Silt	10 – 200
Ground Water	0.5 -300
Dry Gravel	600 – 10.000
Alluvium	10 – 800
Gravel	100 – 600

In geoelectricity, the measured resistivity is apparent resistivity (ρa) (Reynolds, 1997). The apparent resistivity is:

$$(\rho_a) = K\frac{\Delta V}{I} \quad \text{.....(2)}$$

Information :

ρ_a = Apparent Resistivity (Ωm)
K = Geometry Factor (m)
ΔV = Electrode Electric Potential Difference (V)
I = Current Value (A)

The Wenner-Schlumberger configuration is a configuration with a system of constant spacing rules with a note that the "n" factor for this configuration is the ratio of the distance between the C1-P1 or C2-P2 electrodes to the space between P1-P2. If the distance between the potential electrodes (P1 and P2) is a, then the distance between the current electrodes (C1 and C2) is 2na+a. The process of determining the resistivity uses four electrodes placed in a straight line (Priambodo, I. C., Purnomo, H., Rukmana, N., 2011).

Table 2. Geoelectric Method Tools and Materials

No	Tools	Total Unit
1.	Nainura NRD 3000	1 box
2.	Battery DC12 Volt	1 unit
3.	Current Cable	2 rolls
4.	Potential Cable	2 rolls
5.	Meter (200 meters)	2 rolls
6.	Battery Jumper Cable	1 unit
7.	Jumper Cable	2 unit
8.	Hammer	2 unit
9.	GPS (Global Positioning System)	1 unit

Result and Discussion

The satellite gravity data is used to determine locations that have a complex structure or are dominated by many faults, both major and minor faults. So later the processing results of the gravity data can be used as reference data in conducting geoelectric surveys. The reservoir in the research area is located in the Seureula Formation where hydrocarbons accumulate, but due to the presence of a minor fault structure so that the formation of pathways and hydrocarbons in the Seureula Formation will migrate again to the surface to become oil sea pages.

PROCEEDINGS
JOINT CONVENTION BANDUNG (JCB) 2021
November 23rd – 25th 2021

Based on the anomaly data obtained from the altimetry satellite, a free air anomaly map is obtained as shown in Figure 1. It can be seen that the Free Air Anomaly corresponds to the topography, the zone with high topography is indicated by the Free Air Anomaly which has a high value with a range of values ranging from 100 to 231.1 mGal. The low topography also corresponds to the low Free Air

Anomaly, with the anomaly value varying from -31.7 to 80 mGal which is indicated by a dark blue to the light blue zone. The Free Air Anomaly data obtained, has not been able to fully present geological information in the research area, therefore some corrections are needed to see further the presence of the anomaly to be studied, namely the Bouguer correction.

Bouguer correction is used to correct the value of gravity which is affected by the effect of altitude by taking into account the effects of rock mass around the measurement point. Before the Bouguer correction, the rock assumption in the study area was determined, which was 2.67 gr. This assumed rock density value will be used to calculate the Bouguer correction due to the rock density around the study. After obtaining the value of gravity which is influenced by altitude due to differences in mass density in the area around the study, the gravity value is then used to calculate the value of a simple Bouguer anomaly by reducing the value of the Free Air Anomaly with the Bouguer correction value. Based on Figure 2 the range of values generated from the simple Bouguer anomaly in the study area ranges from -92.6 to 51.6 mGal.

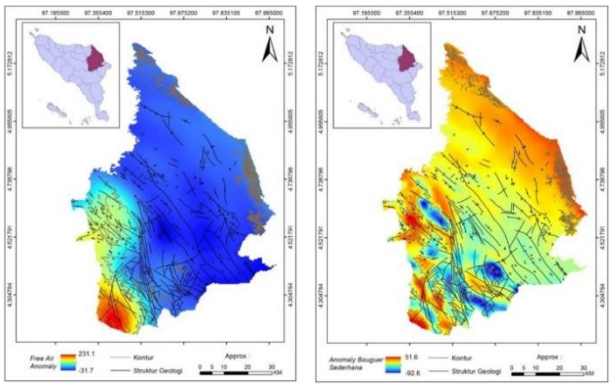

(a) (b)

Fig 4. (a) Free Air Anomaly Map, (b) Simple Bouguer Anomaly overlaid with Geological Structure and Contours

The low simple Bouguer anomaly is characterized by a dark blue to light blue colored zone with a value range of about -92.6 to -30 mGal. Meanwhile, the high simple Bouguer anomaly is indicated by a yellow to the red zone with a value range of about -30 to 51.6 mGal. Zones that have a high simple Bouguer anomaly value may be due to the high density in the area. A simple Bouguer anomaly map can investigate the subsurface density based on the effect of rock mass in the area of the measurement point so as to produce a gravity value that corresponds to the subsurface density. To present the geological structure better, it is necessary to process anomaly data with certain methods in order to obtain the anomalous boundary data that you want to find. Fig. 4 presents Bouguer gravity data after filtering using tilt derivative. Assuming that the fault is the boundary between geological structures, the edges of the structure or fault trace can be represented by a tilt derivative value of 0 rad. Comparison of geological fault structure and tilt derivative will conclude that processing data is well concentrated to many features along with fault structure. Tilt derivative data can clearly show the presence of geological structures, both major and minor faults. The pattern given by the tilt derivative filter indicates the presence of a positive geological structure, ranging from 0 to 1.5 mGal (Fig. 4).

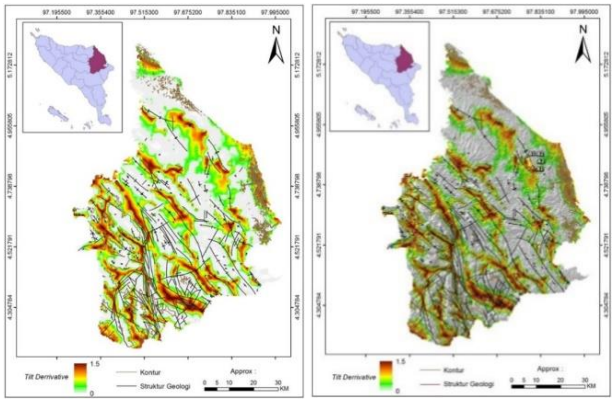

(a) (b)

Fig 5. (a) Tilt Derivative Map, (b) SRTM Overlay and Tilt Derivative and Geological Structure

In the results of the SRTM and Tilt Derivative overlays and geological structures, it can be seen that the pinned location is a zone with a value of 1.5 mGal and several minor faults are assumed to be fault lines where shallow hydrocarbons migrate to the surface. When viewed from a simple Bouguer anomaly map, zones with low-density values are indicated in blue and the average density value is -92.6 mGal -31.7 mGal and when overlaid with a geological structure map, the zone with low-density values is also visible in zones with diverse and quite complex geological structures. To determine whether these geological structures are migration paths from shallow hydrocarbons, they are overlaid again with a Tilt Derivative map so that it is found that the research target location is right on a minor fault with a fairly high Tilt Derivative value and is suspected of being a shallow hydrocarbon migration path.

After obtaining the location of the potential distribution of shallow hydrocarbons as the research target, measurements were carried out using the geoelectric method to determine the characteristics of

shallow hydrocarbons at that location. The length of the geoelectric path in this study is 330 m.

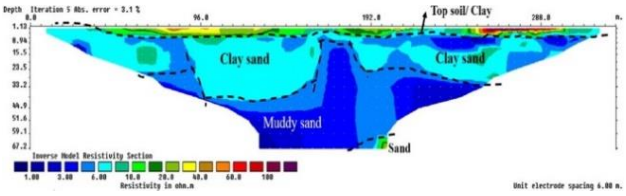

Fig 6. Interpretation of B 2D Geoelectrical Cross Section 1

In section A, it is shown that there are 4 rock layers. The first layer is topsoil mixed with clay with a resistivity value of 10-100 m at a depth of 5 m. The second layer contains clay-sand with a resistivity value of 6-10 m at a depth of 35 m. In the third layer, there is muddy sand with a resistivity value of 6 m in the depth range of 10 to 68 m. In the last layer which has a depth of 60 m, there is a layer with a resistivity value of 8 to 40 m which is indicated as an alluvium deposit. This alluvium deposit is then interpreted as a layer of sand that acts as a hydrocarbon reservoir.

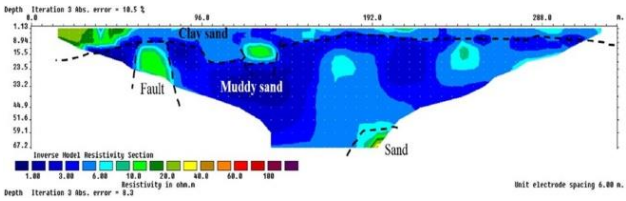

Fig 7. Interpretation of 2D Geoelectrical B-Section 2 Track

In section B, it is shown that there is a fault with a distance of 60 - 78 m at a depth of 10 m. There is also a small fault at a distance of 120 – 138 m. The shallowest depth in section 2 is composed of sand-clay with a depth variation of 20 m from a distance of 0 - 138 m on the line. In addition, at a distance of 138 and 330 m, sand-clay lithology was found at a depth of 9 m. Furthermore, muddy sand was obtained at a depth of 9-68 m with a resistivity value below 6 m. The sand layer which is thought to be a shallow hydrocarbon reservoir is found at a depth of 60 m and deeper. The resistivity values obtained from both paths (A and B) show low resistivity values. It seems clear that resistivity values ranging from 2-10 m may be a barrier to water in the reservoir. indicates the strong presence of reservoir fluid in the shallow hydrocarbons.

CONCLUSIONS

Based on the analysis of the free air anomaly map, we obtained anomalous variations with values ranging from -31.7 to 80 mGal which are marked with dark blue to light blue zones. Sections with low simple Bouguer anomaly values are indicated by dark blue to light blue zones that range in value from -92.6 to -30 mGal. Meanwhile, zones with a high range of values are indicated by yellow to red zones which have a range of values between -30 to 51.6 mGal. In the results of the SRTM and Tilt Derivative overlays and geological structures, it can be seen that the pinned location is a zone with a value of 1.5 mGal and several minor faults are assumed to be fault lines where shallow hydrocarbons migrate to the surface. In the results of the analysis using the geoelectric method, it is shown that there are 4 (four) rock layers, namely topsoil at a depth of 5 m with a resistivity value of 10-100 m, clay sand at a depth of 35 m with a resistivity value of 6-10 m, and muddy sand at a depth of 10-100 m. 68 m with a resistivity value of 6 m, and alluvium deposits at a depth of 60 m with a resistivity value of 8 – 40 m. This alluvial deposit is interpreted as a layer of sand that acts as a shallow hydrocarbon reservoir.

REFERENCES

Apparao. A., 1997, *Developments in Geo-electrical Methods*, National Geophysical Research Institute Hyderabad (ed.).

Blakely, R. J., 1995, *Potential Theory in Gravity and Magnetic Application*, Cambridge University Press.

Dangdangilo, D., Bojonegoro, K., Timur, J., & Wibowo, E., 2019, *Analisa Potensi Shallow*, Jurnal Offshore, *3*(2), 76–85.

Erviantari, D., & Sarkowi, M., 2008, *Jurnal Geofisika Eksplorasi*, *2*(1), 13–20.

Hendrajaya, L., & Arif, I., 1990, *Geolistrik Tahanan Jenis*. Laboratorium Fisika Bumi, Jurusan Fisika FMIPA ITB.

J. D. Bennet, N. R. Cameron, A. et all, Rocks, S. J. T. & R. W., 1981, *Geologic Map 1.250,000 of Aceh Timur Quadrangle, Sumatra*, Pusat Sumberdaya Geologi.

Praktik, L. K., & Pertamina, U., 2020, *Analisis Data Magnetik di Daerah Timor Barat Menggunakan 2D Averaged Power Spectrum , Upward Continuation, dan Tilt Derivative*.

Priambodo, I. C., Purnomo, H., Rukmana, N., & J., 2011, *Aplikasi Metoda Geolistrik Konfigurasi Wenner-Schlumberger pada Survey Gerakan Tanah di Bajawa, NTT. VI* (Bulletin Vulkanologi dan Bencana Geologi), 2.

Sandwell, D. T. and W. H. F. S., 2009, *Journal of Geophysical Research, 114, No. B1, B01411,B01411*.

Sosromihardjo, S. P. C., 1988, *Indonesian Petroleum Association*, Proceedings of the 17th Annual Convention, 187–210.

ACKNOWLEDGEMENTS

With the completion of this research, we would like to thank the East Aceh district for helping us to conduct the research, we also thank Mr. Muzakir, S.Si., M.Si who has guided us in completing this research, and we express our gratitude to all parties who have contributed to this research so that this research can be carried out properly.

PROCEEDINGS
JOIN CONVENTION BANDUNG (JCB) 2021
November 23rd – 25th 2021

Sandstone Reservoir Mapping in the "M" Field of the Northwest Java Basin, Based on Seismic Attributes

Mohammad Syaiful – Pakuan University
Indra Yuliandri – Pertamina Hulu Energi
Ari Samodra – Research Technology Centre of Pertamina

Abstract
Hydrocarbon has been discovered and produced in the "M" Field, located in the Cipunegara Sub-basin, Northwest Java Back Arc Basin, from deeper levels of the Baturaja and Talang Akar Formations since early of 2000s. Oil and gas has also been produced in the shallower level of the Upper Cibulakan Formation in this Northwest Java Basin, but in the other sub-basin, not in the "M" Field in the Cipunegara Sub-basin.

Prior to find hydrocarbon in the Upper Cibulakan Formation of this field, the existing of its reservoir should be evaluated. Based on a limited data of 3 wells and a 3D seismic, several seismic attributes mapping has been used to define the reservoir of sandstone.

RMS amplitude, average amplitude, maximum amplitude, energy half-time, and arc length, have been applied in defining the sandstone reservoir. This sandstone reservoir could be considered further in studying the petroleum system in the area.

Keywords: sandstone reservoir, Upper Cibulakan Formation, seismic attribute.

Introduction

Geologically, research area is located in Cipunegara Sub-basin of Northwest Java Basin, as could be seen in Figure 1. Administratively, the study area is under the authority of West Java Province.

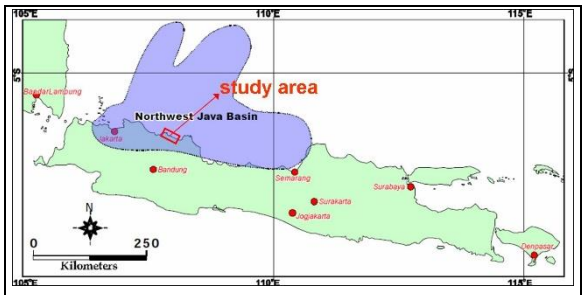

Figure 1: Location map of the research area

Hydrocarbon has been discovered and produced in the "M" Field, located in the northern edge of the Cipunegara Sub-basin, Northwest Java Back Arc Basin, from shallower levels of the Baturaja and Talang Akar Formations, since early of 2000s. These levels had been studied intensively with various attributes (Sukmono et al., 2006).

Oil and gas has also been produced in the shallower level of the Upper Cibulakan Formation in this Northwest Java Basin, but in the other sub-basin, not in the "M" Field in the Cipunegara Sub-basin (see Figure 2).

In the closest area from the studied area, southern edge of the Arjuna Subbasin, Offshore Northwest Java Basin, the Upper Cibulakan Formation is known as Main and Massive Intervals with multiple stacked sandstone reservoirs and hydrocarbon inside them (Purantoro et al., 1994; Butterworth et al., 1995; Posamentier et al., 1998).

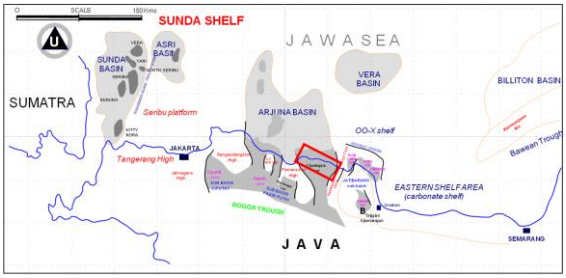

Figure 2: Regional geology of Northwest Java Basin (red square is the research area)

Thus, the objective of this research was to explore the existing of sandstone reservoirs of the Upper Cibulakan Formation in the study area.

Data and Method

Available main data that used in this research are 3 drilled wells and a volume of 3D seismic, as shown in Figure 3.

MSY-1 well was drilled in 2000 and penetrated the Jatibarang Formation or Pre-TAF in its total depth of 2951 mMD. MSY-2 well was drilled in 2003 and penetrated the basement in its total depth of 3107 mMD. MSY-3 is the oldest well that was drilled in 1993 and penetrated the basement in its total depth of 2125 mMD.

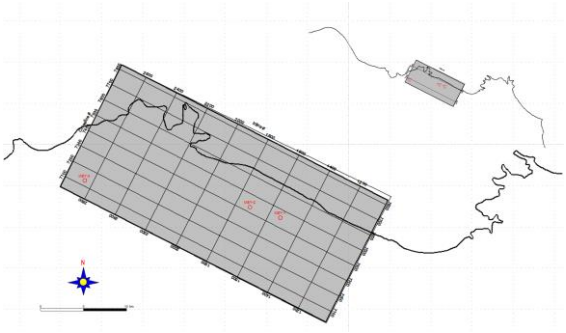

Figure 3: Map of data set

Data of 3D seismic was acquired in 2004-2005 and is down to 2500 ms, consisting of 738 in-lines (in-line 2021 to in-line 2758) and 798 cross-lines (x-line 7032 to x-line 7829).

The methodology of this study is displayed in the flow chart of Figure 4, which is started with the evaluation of both wells and seismic data.

PROCEEDINGS
JOIN CONVENTION BANDUNG (JCB) 2021
November 23rd – 25th 2021

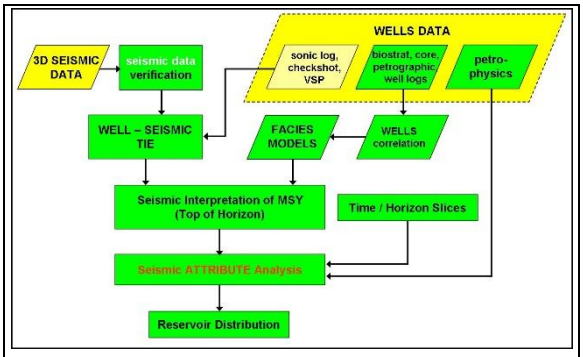

Figure 4: Working flow

All available well data has been analyzed, e.g. biostratigraphy, core data, petrography, and wireline logs. Petrophysical analysis of the MSY sandstone has also been run, while sonic logs and checkshots have been used in integrating wells into 3D seismic volume. In this research, geological evaluation and its result have been used to support and are integrated to the geophysical matter.

Controlled by wells, the seismic interpretation of MSY horizon was done (Figure 5), by picking its horizon top. Due to difficulty in picking top of MSY horizon, easier horizons in the shallower and deeper levels were picked and interpreted earlier, i.e. top of Parigi Formation, top of Upper Cibulakan Formation, and top of Baturaja Formation. MSY horizon is layered between top of Upper Cibulakan dan top of Baturaja Formations.

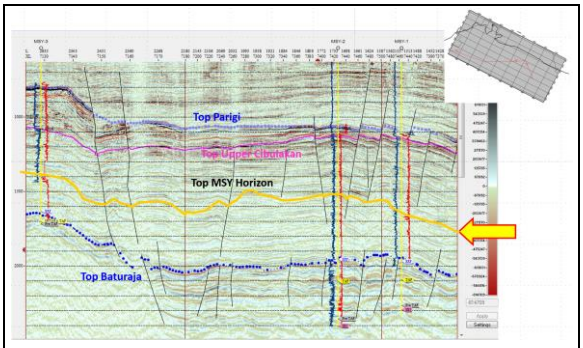

Figure 5: Seismic section

Once the MSY horizon picking was completed, analyses of seismic attributes were applied. The final result is the lateral distribution of the sandstone reservoir. All analyses were performed using 2 main softwares, i.e. GeoGraphix for seismic horizon picking and Petrel for wells correlation and seismic attributes.

Brown (2004) says that seismic amplitude-derived attributes provide stratigraphic and reservoir information, while although frequency-derived attributes are not yet well understood, but there is widespread optimism that they will provide additional useful stratigraphic and reservoir information.

One of the frequency-derived attributes is spectral decomposition. This seismic attribute could be well used in recognizing the lateral distribution of a relatively thin bed reservoir and its fluid. Instead of spectral decomposition, amplitude-derived attributes are used in this study due to the uncertainty of the picked-MSY horizon. Various types of 'window' have been applied in running five amplitude-derived attributes.

RMS (root mean square) amplitude is the square root of sum of the squared amplitudes, divided by the number of live samples as shown in the following formula (Equation 1), where k is the number of live samples.

$$\sqrt{\frac{(\sum_i^n amp^2)}{k}}$$

Equation 1: RMS amplitude

RMS amplitude can map directly to hydrocarbon indications in the data and other geological features which are isolated from background features by amplitude response.

The second amplitude-derived attribute is the average energy, which is the squared RMS amplitude. This attribute is a measure of reflectivity within a time or depth window and can be used to map direct hydrocarbon indicators in a zone.

Average energy is computed using the following formula (Equation 2).

$$(\sum_i^n amp^2)/k$$

Equation 2: Average energy

The third one, maximum amplitude, measures reflectivity within a time or depth window. It returns the maximum positive number in the defined or selected window. It is used to detect positive direct hydrocarbon indicators such as bright spots.

The fourth amplitude-derived attributes is energy half-time, which computes the time or depth required for the energy within a window to reach one-half of the total energy within the entire window. Energy half-time may indicate asymmetric changes in lithology or porosity within a specific zone.

Hybrid attributes are an intriguing combination of amplitude and frequency information (Brown, 2004). One of hybrid attributes which is used in this research is arc length. Arch length is a stratigraphic sequence indicator. It measures reflection heterogeneity, and can be used to quantify lateral changes in reflection patterns. It is calculated using the following formula (Equation 3), where Z is in milliseconds in time domain, or in feet or meters in depth domain.

PROCEEDINGS
JOIN CONVENTION BANDUNG (JCB) 2021
November 23rd – 25th 2021

$$\frac{\sum_{j=i}^{n-1}\sqrt{(amp(j)-amp(j+1))^2+(Z)^2}}{(n-i)\_x\_sample\_rate}$$

Equation 3: Arc length

Interpretation of seismic has been done using 2 different applications, i.e. *GeoGraphic* of Halliburton and *Petrel* of Schlumberger. *GeoGraphix* was used in doing the early steps of subsurface mapping, i.e. horizons picking, including faults defining. Lately, *Petrel* was used to play the various types of amplitude-derived attributes.

Result and Discussion

Based on data of wells, a standard geological evaluation has been done, i.e., sedimentological analysis and biostratigraphical analysis. Only result of these geological analyses is displayed in this paper, not their detail.

Biostratigraphical analysis of 3 wells, MSY-1, MSY-2, and MSY-3, has summarized that the Upper Cibulakan Formation was deposited in the neritic (inner to outer) during Middle Miocene time. Wireline logs interpretation has indicated an intercalation of sandstones and shales, with minor limestones and claystones.

As a result of seismic interpretation, a time structural map of Top MSY horizon has been generated, as shown in Figure 6.

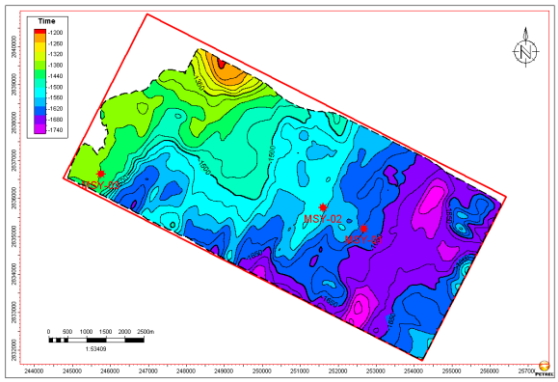

Figure 6: Time structural map of Top MSY horizon

A velocity map is used to convert the time structural map into a depth structural map as shown in Figure 7.

An original velocity map which was taken from the reprocessing seismic volume was used in the beginning; not controlled by wells yet. A "cokriging" facility in the software then was applied in considering depths of wells as the control of the true depths in 3 points. The entire points outside of the wells have been relatively interpolated to the 3 control points.

In the "M" Field, the MSY Horizon is ranging from 1100 m through 1900 m depth. Generally, the horizon is going down from NW to SE. Few closures are recognized in the SE area, e.g. an elongate shape closure in the MSY-2 well, a small closure about 2 km south of the MSY-2 well, and a closure in NE corner of the area.

There are 2 features that possibly could be closures, i.e. the shallower closure in the NW of the area and the deeper one in the SE of the area. Unfortunately, both "closures" have unknown contours that could also be opened to outside of the area.

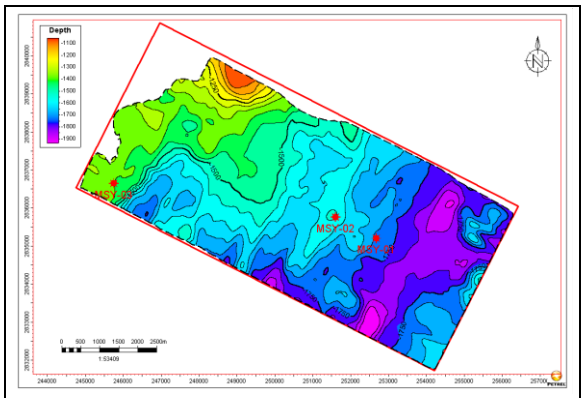

Figure 7: Depth structural map of Top MSY horizon

Five attributes have been selected in trying to define a lateral distribution of sandstone reservoir of the MSY horizon. Four amplitude-derived attributes were run, i.e. RMS amplitude, average energy (window – gross), maximum amplitude (window – selection), and energy half-time (window – distribution). One hybrid attributes (amplitude-frequencyderived) was run, i.e. arc length (window – window).

Several widths of windows of each attribute had been applied to have the most geologically acceptable results. The most acceptable result is the window with 20 ms width (10 ms above and 10 ms below the picked MSY horizon layer), as displayed in the following figures (Figures 8 to 12).

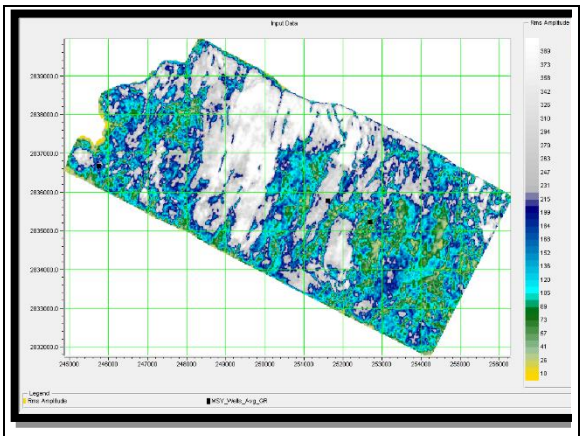

Figure 8: RMS amplitude of MSY horizon

Prior to getting the most acceptable result of window, various widths of windows had been tried in order to have the best one. Some of windows, e.g. 5 ms width (5 ms below the MSY Horizon), 10 ms (5 ms above and 5 ms below the MSY Horizon), 15 ms (5 ms above and 10 ms below the MSY Horizon), 25 ms (10 ms above and 15 ms below the MSY Horizon), and 30 ms (10 ms above and 20 ms below the MSY Horizon).

PROCEEDINGS
JOIN CONVENTION BANDUNG (JCB) 2021
November 23rd – 25th 2021

It is more difficult in, geologically, interpreting the 5 seismic attributes using those widths of windows, than using the most acceptable window of 20 ms width (10 ms above and 10 ms below the MSY Horizon).

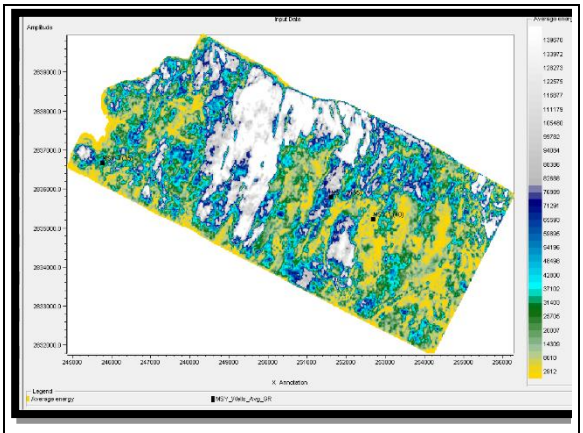

Figure 9: Average energy of MSY horizon

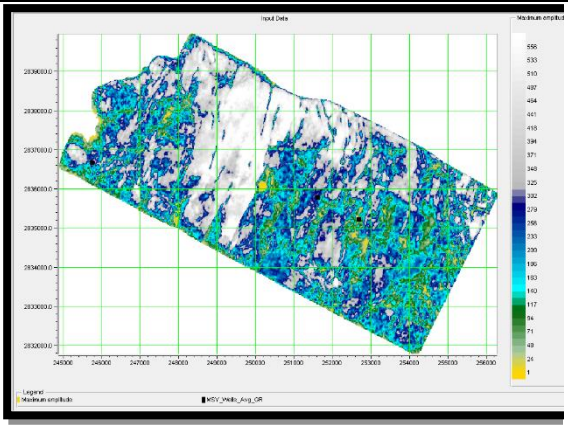

Figure 10: Maximum amplitude of MSY horizon

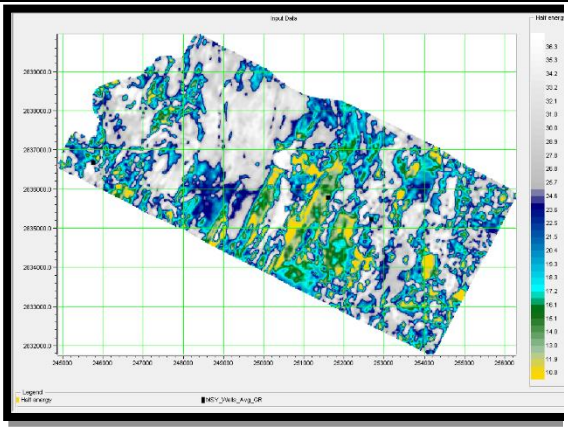

Figure 11: Energy half-time of MSY horizon

By overlaying all 5 seismic attribute maps, a composite map has been generated as shown in Figure 13.

It could be interpreted that sandstone of MSY reservoir is distributed in limited area marked by the yellow arrows in the map of Figure 13 (yellowish or brownish orange in color).

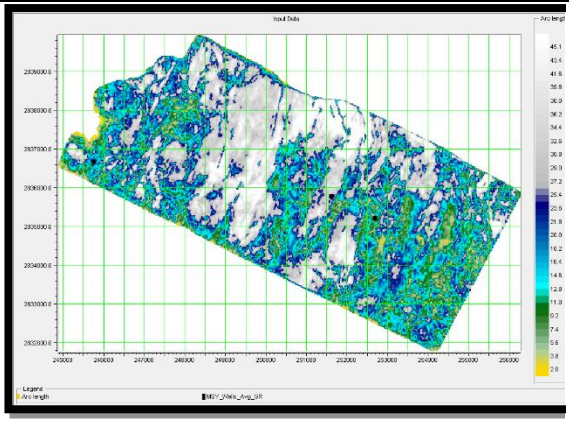

Figure 12: Arc length of MSY horizon

The composite map displays a lateral distribution of MSY sandstone reservoir. It could be interpreted that sedimentation of the MSY sandstone reservoir was directing to the southwest.

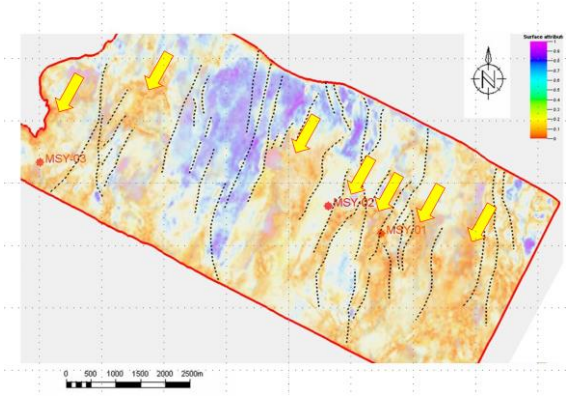

Figure 13: A composite map

Figure 14 shows the composite of attributes map overlaid by the depth structural contours.

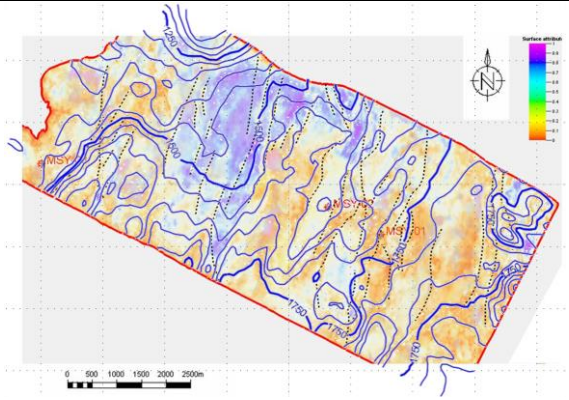

Figure 14: The composite map overlays on its depth structural contours

The accumulation of sandstones is dominantly found in the SE area around the MSY-1 well and between MSY-2 and MSY-1 wells. The MSY Horizon is dipping down from NNW to SSE. Unless stratigraphic trap, no structural trap will be discovered in this area. It means that the area unlikely to be a good prospect for hydrocarbon.

Conclusions

Defining a lateral distribution of MSY sandstone in the area of about 5 km x 10.5 km, based on a limited number of wells and 3D seismic data, has uncertainty. Seismic amplitude-derived attributes could be used in this evaluation, but should be with a note that there is still an uncertainty.

RMS amplitude, average energy, maximum amplitude, energy half-time, and arc length, are possibly not a perfect tool in delineating a sandstone reservoir, but certainly these seismic attributes could decrease the degree of uncertainty.

The MSY Horizon was deposited in the shallow marine or transition zone. All attributes support that this sandstone reservoir was developed from NE (proximal area) to the SW (distal area).

The lateral distribution of MSY Sandstones is spread over the entire area, as supported by the composite map of the 5 seismic amplitude attributes.

The prospective area is in the elongate closure (based on depth structural map) which passes the location of MSY-2 well as a structural play. Second prospect is probably in the smaller closure that located about 2 km south of MSY-2 well.

Finally, the above tools should be integrated with other available data to get a perfect evaluation in exploring hydrocarbon in general.

Acknowledgements

The authors wish to thank Pertamina, BPMIGAS (now SKKMIGAS), and Dirjen Migas of Kementerian ESDM, for permission in using wells and seismic data.

References

Brown, A. R., 2004, AAPG Memoir 42, SEG Investigation in Geophysics No. 9, 541 p.

Butterworth, P. J., R. Purantoro, and J. G. Kaldi, 1995, Proceedings of the International Symposium on Sequence Stratigraphy in SE Asia, p. 311-325

Posamentier, H. W., W. Suyenaga, D. Rufaida, R. Meyrick, and S. G. Pemberton, 1998, Proceedings of 26th IPA Annual Convention, p. 129-153

Purantoro, R., P. J. Butterworth, J. G. Kaldi, and C. D. Atkinson, 1994, Proceedings of 23rd IPA Annual Convention, p. 289-306

Sukmono, S., D. Santoso, A. Samodra, W. Waluyo, and S. Tjiptoharsono, 2006, the Leading Edge, May 2006, Vol. 25, Issue 5, p. 532-538

PROCEEDINGS
JOINT CONVENTION BANDUNG (JCB) 2021
November 23rd – 25th 2021

Carbonate Rock in Paciran Formation, North Rembang Anticlinorium: Geological, Microfacies, and Diagenesis Study based Surficial Data

Dewi Sintia Reka[1], Lorian Aldi Firmansyah[1], Kamila Nuril Izzah[1], Hauzan Naufal Fadli[1], Agus Hendratno[1]
[1]Geological Engineering Department, Engineering Faculty, Universitas Gadjah Mada

Abstract

The limestone of the Paciran formation is known as a gas reservoir in several fields in the northeast java basin. This research aims to determine the geology, study of microfacies, and diagenesis of limestone-based on surficial data in Paciran formation. Research has been conducted in the Kerek area, Tuban Regency, East Java Province, within a study area of 20 km2. Geological mapping has been carried out to determine the distribution of rocks, and 77 limestone samples have been taken for petrographic analysis. Four rock units are obtained based on the geological mapping and measured section; the order from oldest to young is sandy allochem limestone unit, algae grainstone unit, wackestone foraminiferal unit, and sand - gravel deposit unit. The depositional age of the limestone (algae grainstone unit and wackestone foraminiferal unit) is Pliocene, Zanclean (PL1- PL3 planktonic foraminiferal biozones) based on the paleontological analysis. Microfacies in the research area were determined based on Standard Microfacies Types (SMF Types); the result consists of SMF 3, SMF 4, SMF 5, and SMF 12. The depositional environment of the limestone-based SMF is the slope to the toe of the slope. After rock deposition, there have been various diagenetic processes: bioturbation/ichnofossil, cementing, micritization, and dissolving. Limestone in the study area has phytokarst, and lapies, this feature on limestone below the surface can significantly increase the value of rock porosity and permeability, which is suitable for a reservoir.

Keywords: Paciran, limestone, microfacies, carbonate, diagenesis

Introduction

The North Rembang Zone is a physiographical area on Java Island, located in the north of the island of Java, stretching from East Java to Central Java. So, many exploration fields are being developed by companies such as PT. Pertamina EP Asset 4 and ExxonMobil Cepu Ltd. which is currently conducting exploration in the Cepu Area. North Rembang Zone is famous for its abundance of reservoirs in the formations that compose it. In order to discover and maximize the potential for hydrocarbon exploration in this zone, many formations must be investigated. Many potential hydrocarbons were found in the past exploration, which focused on the Kabuh Formation and the Ngrayong Formation. This research aims to find out the potential for the Paciran Formation, which is the youngest part in the physiographic stratigraphic composition of the Rembang Zone. The Paciran Formation is a late miocene-pleistocene rock. The lithological composition of this formation consists of limestone deposits, so that the potential for carbonate hydrocarbons will be investigated in this study using field studies, petrography, and microfacies determination methods. Obtained from field mapping data and supported by paleontological data. The potential for the presence of potential reservoirs in the sandstone formation will be determined mainly by the most critical aspects of the porosity and permeability of the existing rock. The existence of the reservoir aspect will become a new treasure trove of knowledge for oil and gas exploration in Indonesia.

Data and Method

Data collected in the research area consists of stratigraphic measurements, rock samples, petrographic analysis, paleontology analysis, and geological mapping has been carried out to determine the distribution of rocks. Geological outcrops in the research area have been measured, and all samples from each rock unit have been taken. Selected samples have been analyzed via petrographic and paleontological analysis. Description of the data and methodology of this research are as follows:

Geological Mapping

Geological mapping has been carried out to determine the distribution of rocks, and 77 limestone samples have been taken for petrographic analysis. Based on existing data shows the distribution of rocks is shown in Figure 1.

Measured Section

The stratigraphy of the mapping area is divided based on the lithostratigraphy in the form of a unit of rock sequences based on the physical appearance of the rock (texture and structure), the lithological composition of each unit, and petrography. Based on geological mapping and measured section, four rock units are obtained; the order from oldest to young is sandy allochem limestone, algae grainstone, wackestone foraminiferal, and sand - gravel deposit.

Petrographic Analysis

The petrographic analysis is used to determine microfacies, determine the diagenesis, and ascertain the type of rock that composes the research area. Microfacies in the research area were determined based on Standard Microfacies Types (SMF Types) according to Flugel (2009) and facies zone withdrawal according to Wilson (1975).

Paleontology Analysis

Samples from the research location were taken for analysis. This analysis uses the identification of both benthic and planktonic foraminifera. The analysis is helpful to determine the age of the rocks. However, because some units do not contain fossils planktonic foraminifera, then the age of the unit is determined by performing comparability to regional geology and age draw based on analysis of large foraminifera. The comparison is carried out by taking into account lithological characteristics, whether at the bottom, middle, or top of a formation, age differences, or misalignment.

The depositional environment is determined by texture, structure, and pattern. The stratigraphy of each unit is compared with the facies model. This analysis then correlated with the bathymetric observations of each unit deposition using benthic foraminifera fossils.

Result and Discussion

The lithofacies of the research area is the sandy allochem limestone unit, algae grainstone unit, wackestone foraminiferal unit, and the sandy gravel deposit unit.

1. Sandy allochem limestone unit

This unit has a distribution in the Northeastern part of the administrative mapping area in Mliwang village, with a percentage spread of 15% from the area mapping. This unit is exposed to seasonal river valleys and several mines. This unit has an inconsistent relationship with algae grainstone units (Embry & Klovan, 1971) deposited in it. The average unit thickness of 300 – 350 meters is obtained from the reconstruction geological incision A – A' and B – B.'

1. Algae grainstone unit

Algae grainstone units are in the northern part of the mapping area, with the expansion of this unit about 60%, including Mliwang Village and Kedungrejo Village. This unit has a thickness of about 800m - 900m and is obtained from the A-A' and B-B' reconstructions. From the data, the lithological slope obtained by this unit extends relative to the West Sea – Northeast with a relative slope to the Southwest. The sediment structure that developed in this unit is the parallel bedding in grainstone lithofacies and massive structures in some floatstone lithologies. Besides, it is observed that the rest macrofossils are in floatstone lithofacies such as pelecypod fossils. Algae grainstone units were deposited in the Late Miocene, namely at the age of N 18 (Blow, 1969), based on the analysis results of paleontology. The number of fossils is well preserved. Planktonic foraminifera found in this unit are as follows:

- Globigerinoides ruber (d'Orbigny, 1839). It is an identifying fossil at N18.
- Globorotalia Menardii A (Jones & Brady, 1965). It is a fossil marker at N18.
- Globorotalia Plesiotumida (Blow, 1965). It is an index fossil aged N17 to N19.

Then, the content of benthic fossil species found in this unit characterizes the bathymetric environment of the Upper Bathyal. The benthic fossils found as follows:

- Cibicidoides alazanensis (Nuttal, 1932)
- Globobulimina pacifica (Cushman, 1927)
- Laxostomina limbata (Brady, 1881)
- Uvigerina auberiana (d'Orbigny, 1839)

Based on the drawing of microfacies standards in petrographic analysis, the unit algae grainstone in the form of SMF 5: allochthonous bioclastic grainstone (Figure 3) and SMA 12-S sample: limestone with shell concentrations were identified. Based on Wilson's modification of a rimmed carbonate platform model, this unit was deposited in facies zone (FZ) 4, namely slopes.

c. Wackestone foraminiferal

The main constituent of the wackestone foraminiferal unit is the wackestone lithofacies with the presence of several packstone inserts. The distribution of this unit is in the southern part of the mapping area with a spread of about 15%, which includes administratively, namely the Salary Village and Kedungrejo Village. This unit was deposited below, namely the algae grainstone unit; the foraminiferal wackestone unit has a thickness of about 150m - 250m obtained from the A-A' reconstruction. This unit spreads relative to the West-East and the South from the data obtained from the stance and lithological slope. The sedimentary structure that develops in this unit is the parallel bedding of the wackestone and packstone lithofacies.

Based on paleontological analysis results, Wackestone foraminiferal units were deposited in the Pliocene at ages N 19 to N 21 (Blow, 1969). Because most of the rock conditions have crystallized, the number of well-preserved fossils is minimal. It includes fossil species. The following plankton was discovered in this unit:

- Globorotalia miocenica (Palmer, 1945). It is an index fossil aged N19 to N21.
- Sphaeroidinella dehiscens (Parker & Jones, 1965)

The bathymetric environment of the Upper to Middle Batial is then characterized by the content of benthic fossil species found in this unit. The benthic fossils discovered have the following content:

- Bigenerina cylindrical (Cushman, 1922)

- Cibicidoides alazanensis (Nuttal, 1932)
- Laxostomina limbata (Brady, 1881)
- Vaginulinopsis tasmanica (Parr, 1950)

After doing petrographic analysis on this unit and supported by the withdrawal of Standard microfacies (SMF) according to Flugel, 2009. Obtained unit foraminiferal Wackestone in the form of SMF : 3 pelagic wackestone with planktonic microfossil (at the attachment of sample LAF 01) and SMF, namely micro breccia bioclastic packstone (in the appendix of the LAF 31 sample petrography), due to petrographic features have an abundance of mud and microfossils. After obtaining SMF in this unit, based on Wilson's rimmed carbonate platform model, this unit was deposited in the facies zone (FZ) 3, the toe of slope (Figure 3). In the toe of slope area, it is dominated by the size of the finer depositional material, and besides that, the carbonate sediment generated in the form of erosion by sea waves indicated in the facies zone has a lot of fossil content.

d. Sandy gravel deposit

This sandy gravel deposit is a young quarter deposit due to the influence of erosion, sedimentation, and ongoing deposition processes. It lies misaligned above the units described previously—Brownish-gray in color, the very fine to coarse sand and gravel composition.

Based on Standard Microfacies Types (SMF Types), the result consists of SMF 3, SMF 4, SMF 5, and SMF 12. The depositional environment of the limestone-based SMF is the slope to the toe of the slope. After rock deposition, there have been various diagenetic processes: bioturbation/ichnofossil, cementing, micritization, and dissolving (Figure 3). Limestone in the study area has phytokarst, and lapies, this feature on limestone below the surface can significantly increase the value of rock porosity and permeability, which is suitable for a reservoir. The value of porosity and permeability could not be determined because no further analysis was carried out using a porosimeter. In this research, it can only be determined that the porosity and permeability have good rock appearances and petrographic observations (Figure 4).

Conclusions

There are four rock units found in the research area, from oldest to youngest: sandy allochem limestone unit, algae grainstone unit, wackestone foraminiferal unit, and sandy gravel deposit unit. Standard Microfacies Types (SMF Types) shows the result consists of SMF 3, SMF 4, SMF 5, and SMF 12 with the depositional environment of the limestone-based SMF is the slope to the toe of the slope.

References

Bemmelen, R.W. Van. 1949. Vol 1A. Amsterdam: Government Printing Office, The Hague.

Bolli, H.M., et.al. 1985. Cambridge : Cambridge University Press.

Pringgoprawiro, Harsono, 1983, Institut Teknologi Bandung

Wilson, J. L. 1975. Springer-Verlag, Berlin.

Acknowledgments

Thanks to the Geological Engineering Department - Universitas Gadjah Mada for supporting the laboratory analysis.

PROCEEDINGS
JOINT CONVENTION BANDUNG (JCB) 2021
November 23rd – 25th 2021

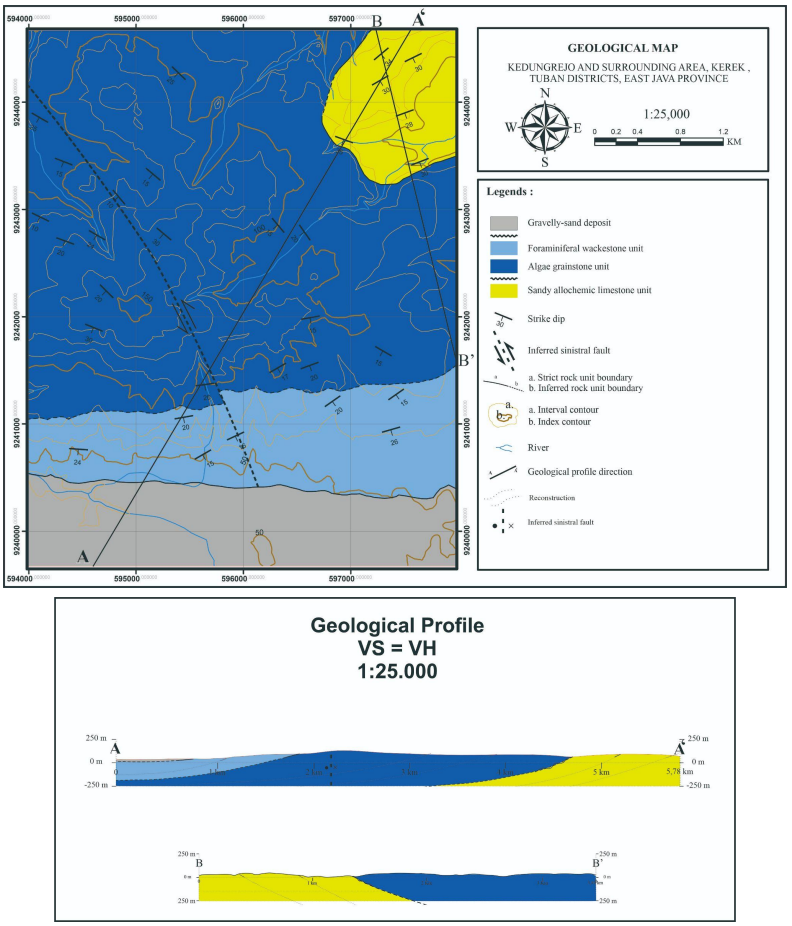

Figure 1: Geological Map of the research area and the geological profile A-A' and B-B'

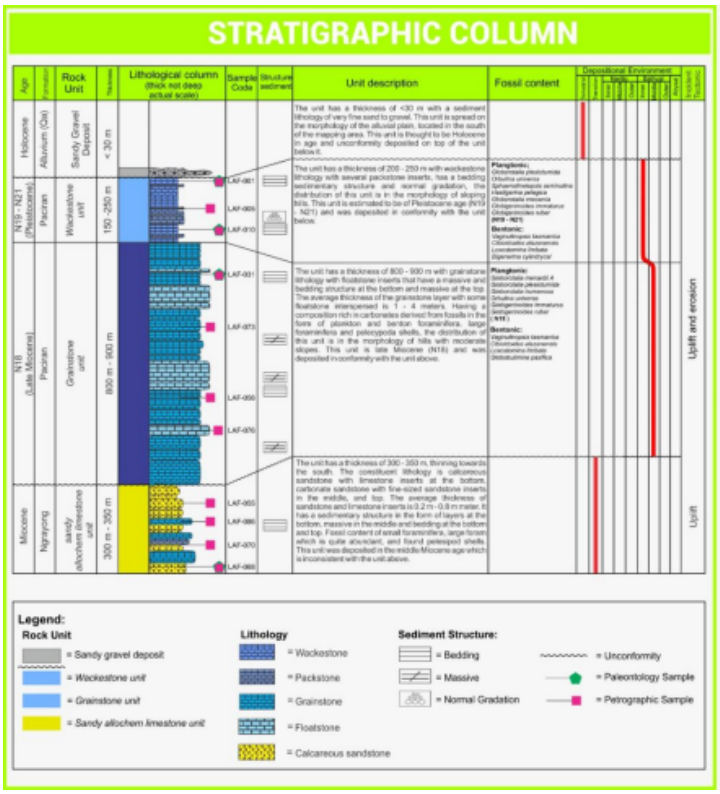

Figure 2: Stratigraphy in the research area

PROCEEDINGS
JOINT CONVENTION BANDUNG (JCB) 2021
November 23rd – 25th 2021

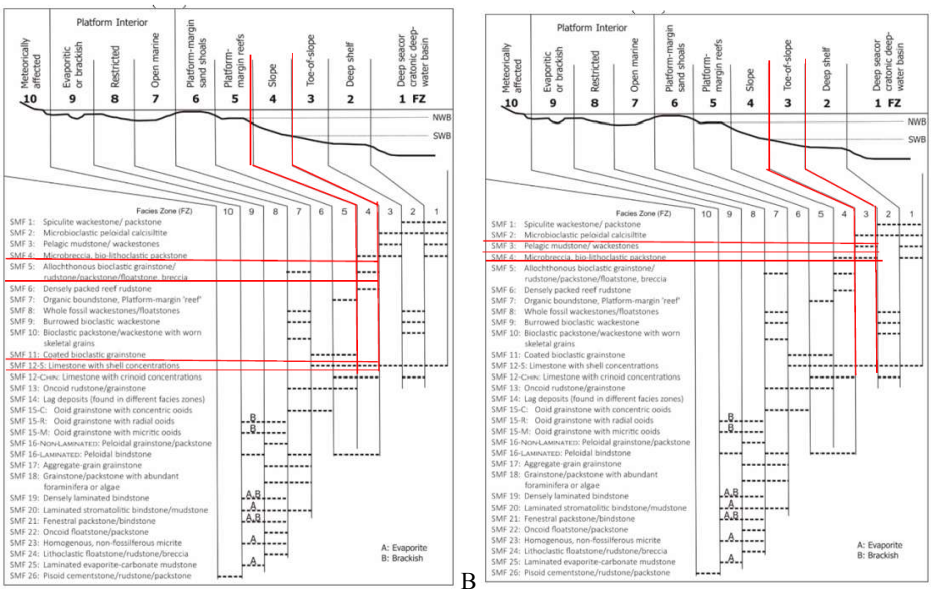

Figure 3: SMF plotting and facies zone with the modified model (Flugel, 2009). (A) Algae grainstone units were deposited in the slope area. (B) Wackestone foraminiferal units deposited in the toe-of-slope area.

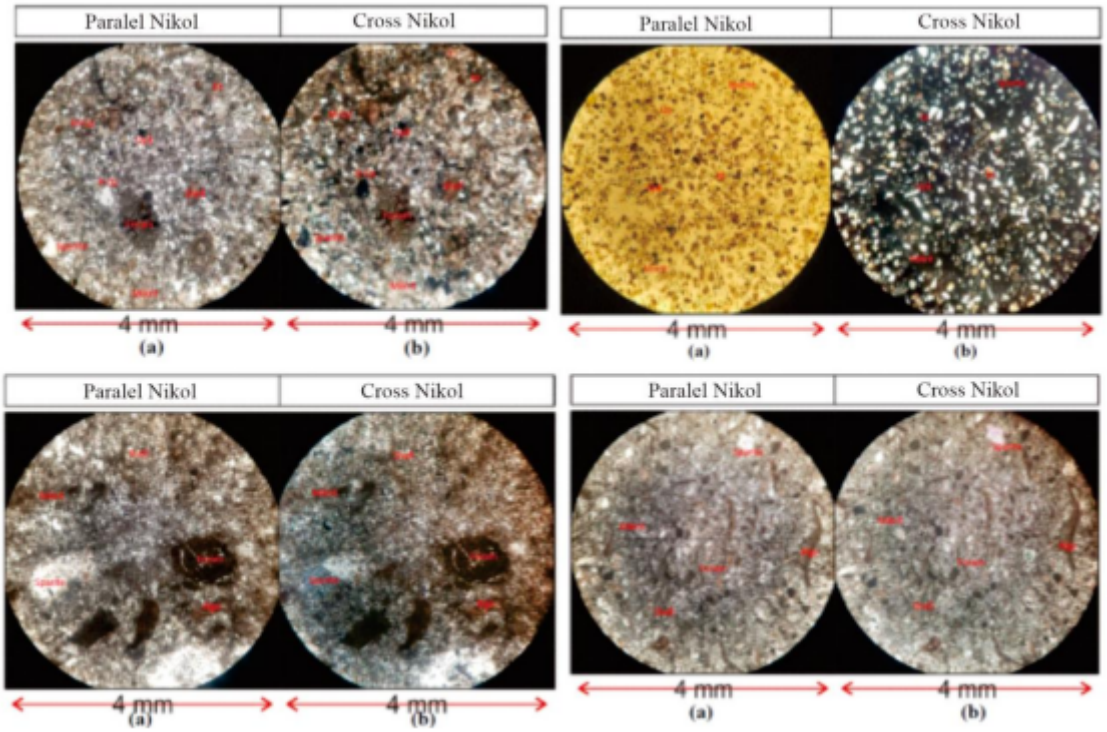

Figure 4: Petrography Analysis

PROCEEDINGS
JOINT CONVENTION BANDUNG (JCB) 2021
November 23rd – 25th 2021

Preliminary Result of Earthquake Hypocenters Relocation with Double Difference Method in Garsela Fault, West Java, based on the Latest Addition of Earthquake Catalog Data by BMKG until 2020

Nararya Pramjana M. 1), Agung Sabtaji 2), Cahyo Aji H. 1), Eny Latifah 1)
1) Physics Undergraduate Program, State University of Malang 2)Balai Besar Meteorologi, Klimatologi dan Geofisika Wilayah 2

Abstract
The Garsela Fault (Southern Part of Garut) which consisted of Rakutai Segment dan Kencana Segmen is already mapped quite well inside the Map of Indonesia's Earthquake Sources and Hazards in 2017, including the length of the fault and and mechanism of the fault respectively. With the latest addition of earthquake catalog data by BBMKG 2nd until the year of 2020, which consisted of 101 earthquake events concentrated within the depth of less than 30 km (very shallow earthquakes), this study has managed to relocate 79 earthquake events using the Double Difference method. Based on the result of the earthquake hypocenter relocation on Garsela Fault, it has shown that the seismicity to be concentrated on top segments of Garsela Fault. Another result of this study is that there is a cluster of earthquakes forming a lineament trending in the north-south direction with an azimuth value of ± 8 degrees, within the area of Mount Malabar into the northern part of District Cisewu, Garut Regency. This lineament is an indication of an unidentified fault existence in Southern Part of Garut Regency.

Introduction

West Java has a complex tectonic structure because it is located above a subduction zone. The subduction zone is formed by the collision of Indo-Australia Plate and Eurasia Plate. This subduction zone causes the emergences of several active faults and volacanoes throughout various locations in West Java, which corelates with West Java's high rate of seismicity. Based on the the statistics for frequency of tectonic earthquake Indonesia from 2009-2019, West Java ranks 8th out of 34 provinces (Sabtaji, 2020). One of the contributors to West Java's high seismicity is Garsela Fault, located in Garut.
Garsela Fault has caused series of earthquakes from time to time in Garut Regency. Hypocenters from these series of earthquakes have been recorded in BBMKG 2nd region's earthquake catalog, using the Seiscomp3 software. Due to 1D velocity model used by the Seiscomp3 software, hypocenter in this catalog data has some degrees of error. These degrees of error came in forms of hypocenter locations distribution that spread around the fault and fixed depth, by the value of 10 km. These two forms of means that in BBMKG 2nd region's earthquake catalog data needs to be improved with hypocenter data which more accurate and more precise.
Garsela Fault was successfully identified back in 2017 (Irsyam dkk, 2017) and the focal mechanism of the fault was identified in 2018 (Supendi dkk, 2018). The identification process of this fault was based on two major earthquakes in Pangelangan in 2016 and Garut Regency 2017. From these two earthquakes, it was found that Garsela Fault consisted of two segments, which are Garsela Kencana and Garsela Rakutai. As new identified fault, a deeper study is needed to obtain the information regarding tectonic condition under Garut Regency.
The existence of Garsela Fault could be a source of danger for a densely populated place like Garut Regency. Indonesia Statistic Agency (Badan Pusat Statistik) recorded, by 2015, Garut Regency is populated by 2.210.017 people (Population of Garut Regency in 2015 by BPS, n.d.). Therefore, an earthquake catalog with data which more accurate and more precise, and also new information regarding tectonic condition under Garut regency are needed to serve as foundation for mitigation plans in Garut Regency. Based on these needs, this study aims to improve in BBMKG 2nd region's earthquake catalog with data which more accurate and more precise and obtain new information regarding tectonic condition under Garut Regency. In order to do that, this study will conduct hypocenter relocation on Garsela Fault with Double Difference Method (DD).

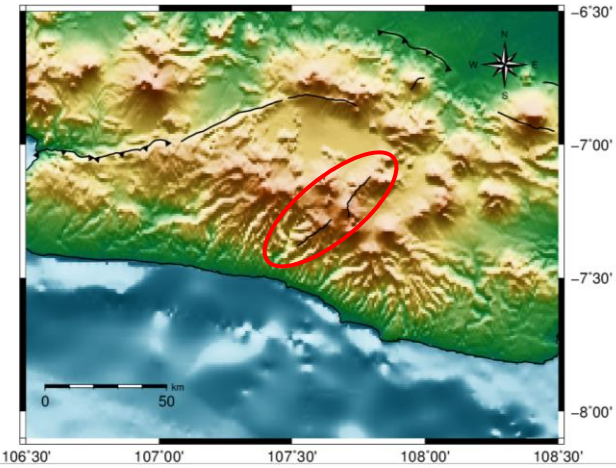

Figure 1. Garsela Fault.

Data and Method

The data used in this study is the earthquake arrival time from the earthquake catalog catalogue in the form of P wave and S wave, determined by the Seiscomp3 software used by BBMKG 2nd region. This catalog recorded series of earthquakes happened around Garut from 2013-2020. Based on the catalog, there are 101 earthquake events that will be relocated by the Double Difference Method.
The Double Difference (DD) method aims to obtain more accurate and more precise hypocenter locations (Waldhauser, 2001). In order to obtained it, DD method used an algorithm to minimize residual time differences (double differences), for a pair of earthquakes at a single location. The algorithm requires that the difference between two events to be small compared to the distance between the hypocenter of the earthquake and a station. In that case, the travel time difference between these two events at a single location independent of un-

modeled velocity heterogeneity along the ray paths between paired events at each station.

The calculation of the residual time from a pair of events can be formulated in the following equation:

$$dr_k^{ij} = (t_k^i - t_k^j)^{obs} - (t_k^i - t_k^j)^{cal} \quad (1)$$

with:

i and j	= two hypocenters in close range
k	= earthquake station
dr_k^{ij}	= residual time between hypocenter I and j on station k.
t^{obs}	= arrival time from observation
t^{cal}	= arrival time from calculation

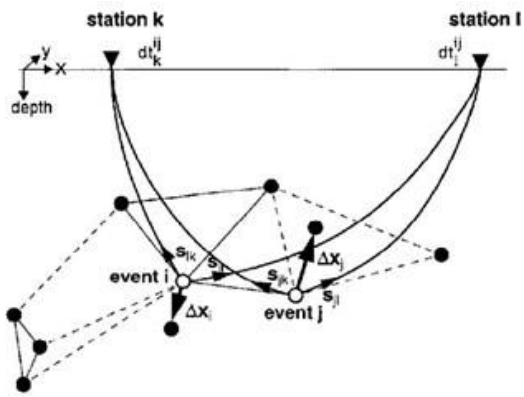

Figure 2 Algorith used in DD

The algorithm used by the DD method is illustrated by Waldhauser and Ellsworth (Figure x). White circles and black circles indicate two events connected by cross-correlation data (solid line) or catalog data (dotted line). It can be seen that event i and j indicated by the white circle are recorded by the same earthquake station (k and l). Since the distances i and j are closer to each other than the earthquake station, it can be assumed that the ray paths of the hypocenters are nearly the same.

Result and Discussion

Hypocenter relocation begun by processing locations of 101 earthquake events from 2013-2020 in Garut Regency. These earthquake events are identified as shallow earthquake, with the value of depth less than 30 km and spread around Garsela Fault. All these earthquake events were recorded by 59 earthquake stations in BMKG's network, located from Lampung Province to the eastern part of West Java.

Relocation process by DD aims to obtain hypocenter location that which are more accurate and more precise. Arrival time data from earthquake catalog was processed by Ph2dt program as one of the steps in HypoDD program. This program identified P Wave and S Wave to be linked as events with the same arrival time.

BMKG's earthquake stations network recorded 101 earthquake events from 2013-2020, from that series of earthquake, 79 earthquake events have been successfully relocated. The remaining 22 earthquake events did not meet the requirement set by Ph2dt program to be linked as events with the same arrival times. HypoDD program used in this study utilized velocity model of AK135. The maps of relocated hypocenter location were generated from Generic Mapping Tool (GMT). The mapping of hypocenter relocation aims to compare hypocenter location distribution before the relocation and after the relocation.

The result of hypocenter relocation needed to undergo a validity test (Jannah and Anggono, 2016). This test was done by comparing histogram of residual time before the relocation and histogram of residual time after the relocation. Histogram of residual time before the relocation showed that the series of arrival time are varried and randomly spread (Figure 3, left). On the other hand, histogram of residual time after the relocation showed that the series of arrival time are close to zero (Figure 3, right). This comparison showed that the residual time between arrival time obtained from observation and arrival time obtain from calculation has decreased, which means hypocenter relocation that has been done obtained hypocenter location distribution which are more accurate and more precise.

The map of hypocenter before the relocation and after the relocation was added with two cross sections to determine the value of depth of the hypocenter. The first cross section is cross section A-A' with length of 111km and the second cross section is cross section B-B' with the length of 82,5 km. The map of hypocenter location before the relocation with cross section A-A' showed hypocenter location distribution which spread and did not follow the lineament of Garsela Fault. It also showed a fixed depth with the value of 10 km (Figure 4, left). On the other hand, the map of hypocenter location after the relocation with cross section A-A' showed hypocenter locations distribution which centered and followed the lineament of Garsela Fault. It also showed a variation of depth with the value of 3-19 km (Figure 4, right). The map of hypocenter location before the relocation with cross section B-B' showed hypocenter location distribution which spread and did not follow the lineament of Garsela Fault. It also showed a fixed depth with the value of 10 km (Figure 5, left). On the other hand, the map of hypocenter location after the relocation with cross section B-B' showed hypocenter locations distribution which centered and followed the lineament of Garsela Fault. It also showed a variation of depth with the value of 3-19 km (Figure 5, right).

Based on the map of hypocenter location after the relocation, it showed there is a cluster of hypocenter that formed a lineament (Figure 6). This lineament is a newfound information, since the discovery of Garsela Fault in 2018. This means that the lineament is formed from shallow earthquakes and micro earthquake which happened since 2018. The lineament is stretched from Mount Malabar to northern part of Cisewu District, Garut Regency, with azimuth value of 8°. This lineament could be an indication of activities from a new fault that needs to be discovered (Sabtaji, 2018). Further study is needed to prove this indication.

Conclusions

Based on the results of the hypocenter relocation from BBMKG 2nd region's earthquake catalog in Garut from 2013-2020 using the Double Difference method, two conclusions can be drawn:

1. The distribution of hypocenter locations after the relocation has improved the earthquake locations. This improvement came in form of more accurate and more precise hypocenter location distribution. The distribution of the hypocenter locations is centered and followed the lineation of the Garsela Fault, and has a more varied depth, from 3 to 19 km, where previously it was dominated by fixed depth.
2. New information regarding tectonic conditions in Garut is in the form of a hypocenter cluster that forms a lineation and stretches from around Mount Malabar to the north end

of Cisewu District, Garut, with azimuth value of 8° The existence of these this lineation indicates activities from a new fault, which is still uncharted.

References

1. Jannah, Iis Nur, dan Titi Anggono. 2016. "APLIKASI METODE DOUBLE DIFFERENCE DALAM RELOKASI HIPOSENTER UNTUK MENGGAMBARKAN ZONA TRANSISI ANTARA BUSUR BANDA DAN BUSUR SUNDA." 5(3): 9.

2. Jumlah Penduduk Kabupaten Garut tahun 2015 versi BPS Kabupaten Garut 2015 NetMonk. (n.d.). Diakses pada 11 Agustus 2021, https://web.archive.org/web/20160903010529/http://www.garutkab.go.id/pub/static_menu/detail/sosbud_demografi_kelompok_usia

3. Irsyam; Widiyantoro; Danny; Irwan; Ariska; Hidayati; Wahyu; Nuraini; Didiek; Lutfi; Sunarjito. (2017). Peta Sumber dan Bahaya Gempa Indonesia Tahun 2017. Bandung: Pusat Penelitian dan Pengembangan Perumahan dan Permukiman, Badan Penelitian dan Pengembangan, Kementerian Pekerjaan Umum dan Perumahan Rakyat.

4. Sabtaji, Agung. 2018. Relokasi Hiposenter Gempa dan Penentuan *Focal Mechanism* di Tenggara Lebak, Banten (Studi Kasus Gempa Tanggal 7-17 Juli 2018). Buletin BBMKG Wilayah 2 tahun 2018.

5. Sabtaji, Agung. 2020. STATISTIK KEJADIAN GEMPA BUMI TEKTONIK TIAP PROVINSI DI WILAYAH INDONESIA SELAMA 11 TAHUN PENGAMATAN (2009-2019). Buletin BBMKG Wilayah 2 tahun 2020.

6. Supendi, Pepen, Andri Dian Nugraha, dan Sri Widiyantoro. 2018b. "Recent destructive earthquakes around Garut area, West Java, Indonesia: An unidentified fault?" Dalam Bandung, Indonesia, 020077. http://aip.scitation.org/doi/abs/10.1063/1.5047362 (Juni 1, 2021).

7. Waldhauser, Felix. 2001. *HypoDD -- A Program to Compute Double-Difference Hypocenter Locations*.

Acknowledgements (Optional)
The completion of this study could not have been possible without the expertise of Agung Sabtaji, S.Si, M.Si, Dr. Cahyo Aji H. M.Si and Dr. Eny Latifah M.Si as respected adviser.
A debt of gratitude is also owed to BBMKG 2nd region that provided the needs of this study and State University of Malang that equipped me with the certain knowledge to complete this study.

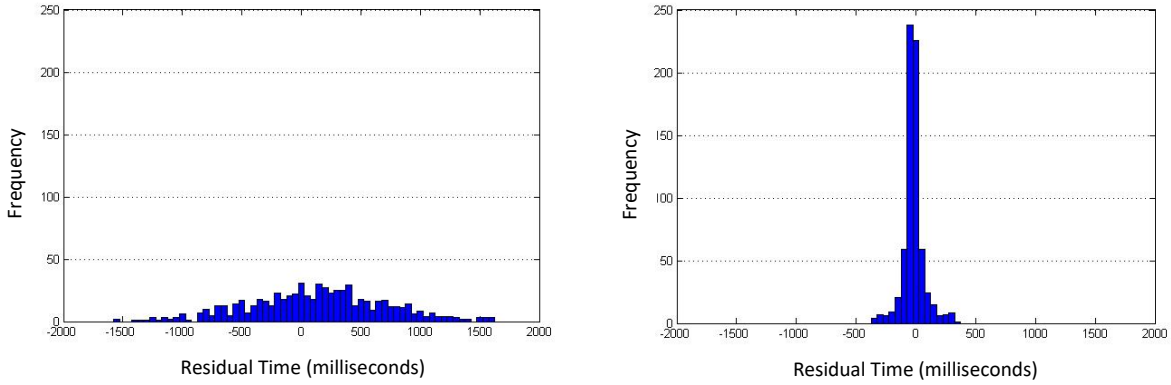

Figure 3 Histogram of residual time before the relocation (left) and histogram of residual time after the relocation (right)

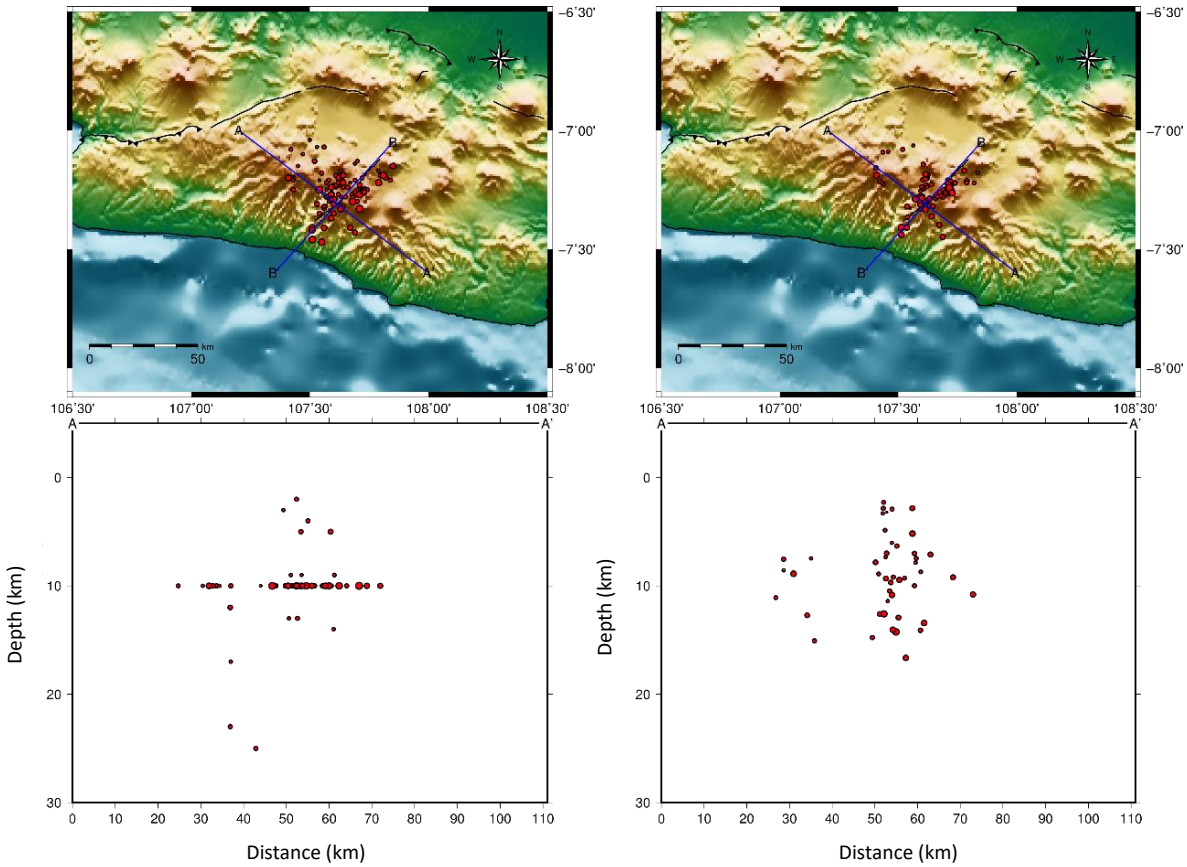

Figure 4 Map of hypocenter location before the relocation (left) and map of hypocenter location after the relocation (right) with cross section A-A'

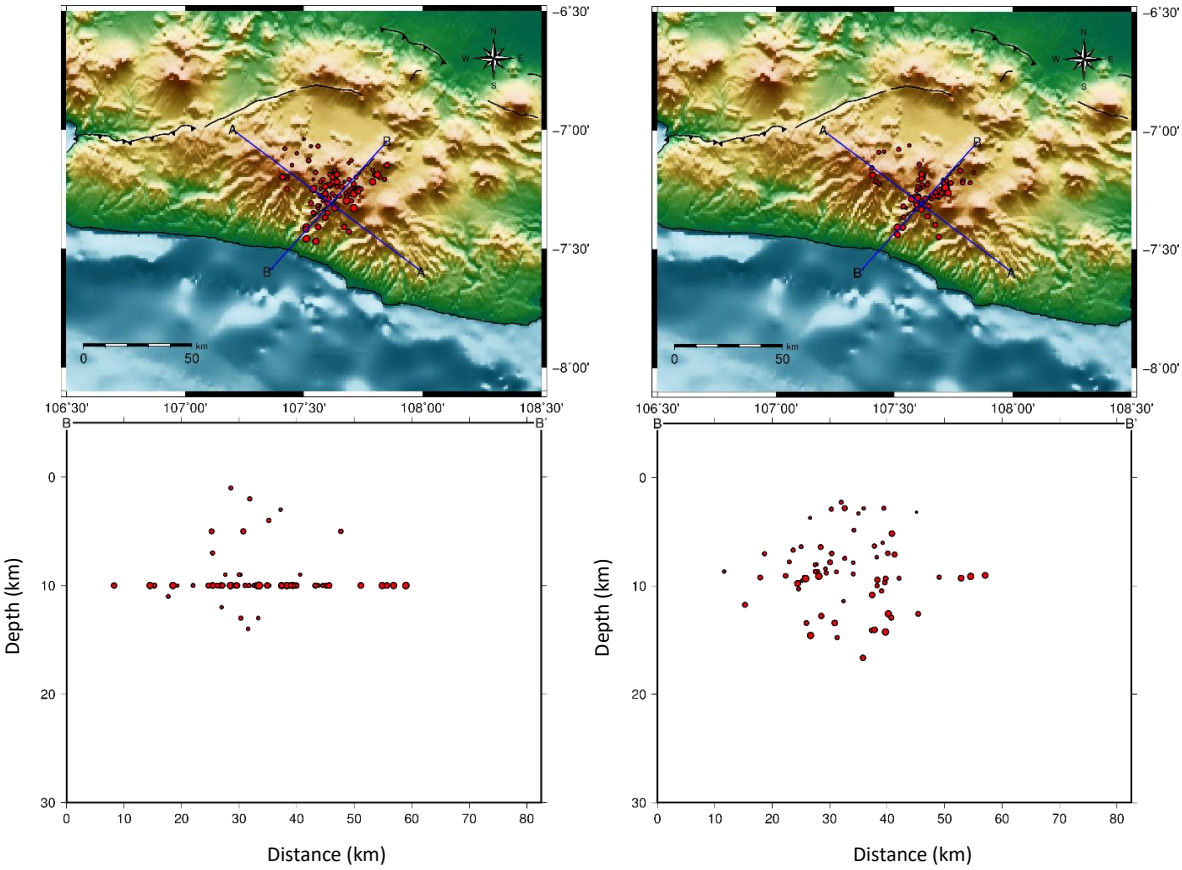

Figure 5 Map of hypocenter location before the relocation (left) and map of hypocenter location after the relocation (right) with cross section B-B'

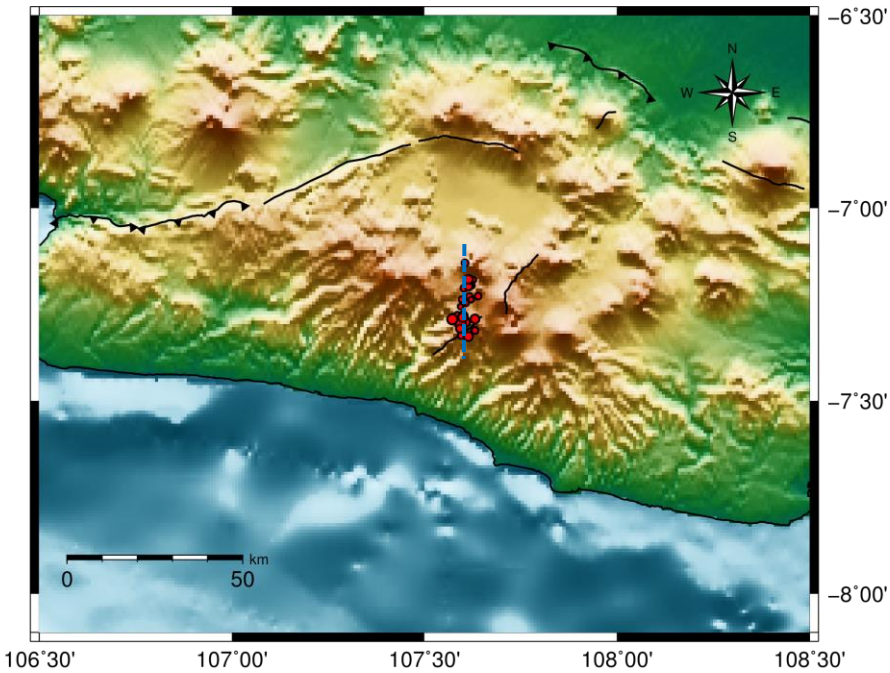

Figure 6 Cluster of hypocenters that formed a lineament

PROCEEDINGS
JOINT CONVENTION BANDUNG (JCB) 2021
November 23rd – 25th 2021

Geochemical Characteristics of Schwaner Mountains Granitoids and their Relationship to Magmatism in the Southwest Borneo Block

Irsyad Auliya' Azhar Ramadhan[1], Mochammad Kivlan Marcellyo Darmaputra[1], Muhammad Bahrun Najah[1], I Gusti Bagus Eddy Sucipta[1]
[1]Geological Engineering, Faculty of Earth Sciences and Technology, Institut Teknologi Bandung, Indonesia

Abstract

The Schwaner Mountains, located in Southwest Borneo, is a complex of igneous and metamorphic rocks. Most of the existing igneous rock products are granitoid rocks. The area was formed by magmatism processes due to various tectonic events. The complexity of tectonic events can be reflected by their geochemical characteristics. Therefore, this study aims to determine the geochemical characteristics of the major, trace, and rare earth elements of granitoid in the Schwaner Mountains and their relationship to magmatism in the Southwest Borneo Block. This study uses granitoid geochemical data in the Schwaner Mountains that have been compiled from several previous studies. The existing data are spatially grouped into three clusters, namely the North Schwaner Zone (NSZ), the South Schwaner Zone (SSZ), and the Northwest Schwaner Zone (NWSZ). The discriminant results of major elements show that the magma series of granitoid rocks in the Schwaner Mountains has a different range in each group. The NSZ has calc-alkaline to high K calc-alkaline series, the SSZ group has high-K calc-alkaline to alkaline series, and the NWSZ group has a range from tholeiitic to alkaline series. Based on the Alumina Saturation Index (ASI), the entire granitoid groups of the Schwaner Mountains has a metaluminous to peraluminous composition. By looking at the relationship of the major, trace, and rare earth elements, we can provide an overview of the tectonic setting in each zone of the Schwaner Mountains. It is found that the granitoid rocks of the SSZ are indicated to have S-type granitoid with ferroan magma and are associated with divergent plate boundaries. Furthermore, the I-type granitoid with magnesian magma has an association with orogenic tectonism. Furthermore, the NSZ and the NWSZ granitoid generally have an I-type character with predominantly metaluminous ASI and magnesian magma. The formation of the A-type granitoid rocks in the SSZ is interpreted to be related to the rifting of the Southwest Borneo Block from Northwest Australia, part of Gondwanaland, during the Jurassic. The separation continued until SW Borneo Block moved further away from the Australian Plate and closer to Sundaland. As a result of this movement, plus subduction from the Paleo-Pacific, the convergent plate boundary interaction during the Cretaceous resulted in the formation of I-type granitoid.

Keywords: geochemical, granitoid rocks, magmatism, Schwaner Mountains, Southwest Borneo Block

Introduction

Borneo (Figure 1) is one of the islands in Indonesia which has a complex geological tectonic history. Schwaner Mountains, located in the southwest part of Borneo, is one of the geological features known as evidence of past tectonic activity in the SW Borneo Block. This area is composed of granitoid and metamorphic rocks resulting from magmatic intrusion from the Cretaceous (Williams et al., 1988; Amiruddin and Trail, 1993; Setiawan et al., 2013), with dimensions of 200 km wide and 200 km long, approximately 500 km (Setiawan et al., 2013), and has a height of 1-2 km (Hennig et al., 2017). As one of the main rocks in SW Borneo, the granitoid of the Schwaner Mountains have geochemical characters that are able to explain the complexity of the history of magmatism in the SW Borneo Block. Granite rocks can be divided into several types, each of which is formed under typical magmatism and tectonic conditions. These characters can be identified from the analysis of geochemical major elements, trace elements, and rare earth elements (REE) which are represented in discriminant diagrams. Through a comprehensive geochemical approach, this paper aims to identify the relationship between granitoid characters in the Schwaner Mountains to magmatism processes in the SW Borneo Block.

Geological Background

The SW Borneo block is a microcontinent block where plate tectonic interactions have occurred since the Late Triassic. On the northern boundary, there is the Crocker-Rajang-Embaluh accretionary complex which is Cretaceous to Early Miocene, while to the south there is the Late Eocene Melawi-Ketungai Basin and the Kutai Basin with a melange-ophiolite zone in Semitau. To the southeast, there is the Meratus-Lok Ulo suture zone (Metcalfe, 2017) which is also the southeastern boundary of the SW Borneo microcontinental block. The Schwaner Mountains, located south of the SW block of Borneo, was formed as a result of various intrusions and volcanic activity that occurred from the Late Triassic to the Cenozoic. The Intermediate to acidic igneous rocks, such as andesite, dacite, rhyolite, tonalite, are associated with

granodiorite and diorite which are formed as dykes, stocks, and sills (Amiruddin and Trail, 1993). The igneous rocks in the Cretaceous intruded the basement of the Paleozoic Pinoh Metamorphic Group. In the northern part of the Schwaner Mountains, there is a Sintang granodiorite complex bounded by the Kuching Suture Zone (Williams et al., 1988; Breitfeld et al., 2020).

Data and Method

This study uses granitoid rocks geochemical data of the major elements, trace elements, and rare earth elements (REE) that are compiled from a survey report of Pusat Sumber Daya Mineral dan Panas Bumi (Muliyana et al., 2018) and previous studies (Williams et al., 1988; Hennig et al., 2017; Beitfeld et al., 2020) in the Schwaner Mountains. Clustering of the Schwaner Mountains samples is also carried out according to their sample location, they are the North Schwaner Zone (NSZ), South Schwaner Zone (SSZ), and the Northwest Schwaner Zone (NWSZ). The analysis was carried out by plotting the data on several discriminant diagrams to determine the characteristics of the granitoid rocks in each zone. Analyses of geochemical rock naming, magma series, and alumina saturation index were used using the main element. Then, trace elements and REE were used to differentiate granitoid type and tectonic environment. The results of the data analyses are then used to interpret the magmatism and tectonics events in the SW Borneo Block.

Result and Discussion

Geochemical Analysis Result

Based on the diagram from Cox et al. (1979), these samples have a chemical composition of diorite to granite. In addition, it is seen that the SSZ granitoid rocks predominantly have alkaline magma affinity, the NSZ has sub-alkaline magma affinity, and the NWSZ granitoid rocks have magma affinities spread from sub-alkaline to alkaline (Figure 2a). Further identification of magma affinity was carried out using the SiO_2 plot against the K_2O diagram from Peccerillo and Taylor (1976). In Figure 2b, it is shown that the SSZ granitoid has a high-K calc-alkaline to alkaline magma affinity, the NSZ granitoid rocks have magma affinity from medium-K calc-alkaline to high-K calc-alkaline, this is confirmed with the AFM diagram which shows a FeO decreasing pattern the Na_2O+K_2O increasing pattern (Figure 2c), and NWSZ granitoid rocks are spread from tholeiitic to alkaline, but are more dominant in high-K calc-alkaline to alkaline affinity. Granitoid rocks in Schwaner Mountains that have alkaline magma affinity, according to the plot of the diagram from Middlemost (1975), generally belong to the medium-K alkaline (Figure 2d).

The classification of granitoid rocks can be an indicator of the petrogenesis process (Whalen et al, 1987; Chappel and White, 2001; Barbarin, 1990). Indications of the presence of A-type granite in the Schwaner Mountains were sought through the diagrams of Whalen et al. (1987). A-type granite is a type of granite that originates from the melting of lower crustal rocks in anorogenic environments such as continental rifts, oceanic ridges, and hotspots (Whalen et al, 1987). Based on the plot (Figure 3a), A-type granite was found in the SSZ sample and a small portion of the NWSZ granitoid sample. Other samples of the Schwaner Mountains granitoid, notably the NSZ and most of the NWSZ, show that they are not part of the A-type granite.

The A/NK versus A/CNK diagram of Shand (1943) was used to identify the alumina saturation index of granitoid rocks. In addition, this diagram is also intended to be used to analyze the 'non-A-type granite' obtained from the plot of Figure 3a. Based on the plot of Figure 3b, the granitoid rocks of the Schwaner Mountains in the NSZ and NWSZ are generally of the metaluminous type, while the SSZ is of the metaluminous to peraluminous type. Metaluminous ASI (A/CNK <1.1) indicates a granite has I-type granite character (Chappel and White, 2001). I-type granite has magma sources from melted infracrustal igneous rocks of mafic to intermediate composition (Barbarin, 1990; Chappel and White, 2001).

A plot of granitoid rocks is made on the $FeO^{tot}/(FeO^{tot}+MgO)$ versus SiO_2 diagram, which is overlaid with areas of A-type granite and Cordilleran granite. The Cordilleran in this diagram is a granite formed by melting magma sources in the subduction (orogenic) zone with an I-type dominant character (Frost et al., 2000). The result in Figure 3c shows that the granitoid rocks in the NWSZ and the NSZ have magnesian Cordilleran granite character, while the SSZ generally falls into two types. The first type is a ferroan A-type granitoid, while the second type is a Cordilleran type with magnesian composition. The results in this diagram confirm that the granitoid rocks in the NWSZ and NSZ have I-type granitoid characters, while in SSZ there is the presence of A-type and I-type granitoid rocks.

Analysis of the tectonic setting made with diagrams from Pearce et al. (1984) to support the relationship of the granitoid character and type of the Schwaner Mountains to the magmatism process. From the plot of Nb versus Y (Figure 4a), it was found that the NWSZ and NSZ granitoid rocks were formed in the arc and syn collision granites volcanic environment, while some SSZ granitoid rocks were formed in the volcanic arc and syn collision granites environment and the other part was formed at the upper boundary

of the ridge segments. Furthermore, in the plot of Rb versus Nb+Y (Figure 4b), it appears that the granitoid rocks in the NWSZ, NSZ, and part of the SSZ are associated with the volcanic character of arc granites, while the SSZ granitoid rocks, which were previously classified in the upper boundary of the ridge segment, are associated with within-plate granite plate (WPG).

Implication to Magmatism in the SW Borneo Block

The magmatism in the NWSZ generally produced the I-type granitoid (Figure 3b-c). The I-type granitoid is related to magmatism associated with convergent plate interactions and is generated magma melting from infracrustal igneous rocks (Chappel and White, 2001). Figure 3c shows that the NWSZ generally belongs to the Cordilleran granite type which is associated with orogenetic processes (Frost et al., 2001) or specifically belongs to the volcanic arc tectonic environment (Figure 4b). The NWSZ is part of the West Borneo block (Sundaland margin) which is subducted with the oceanic plate from the east which is then called Paleo-Pacific subduction in the Triassic until Jurassic (Setiawan et al., 2013). In this study, we also found several samples containing A-type granite in the NWSZ based on their geochemical characters. However, the absence of age data from isotopic dating makes the implications for the history of magmatism still unexplained.

Granitoid rocks in the NSZ are associated with subduction of the Cretaceous paleo-Pacific in SW Borneo with the oceanic plate. SW Borneo Block began to separate from Northwest Australia in the early Jurassic and completely separated in the middle to late Jurassic, then moved relative to the north experiencing paleo-pacific subduction and collision in the north with the West Borneo (Breitfeld et al., 2020). The magma is generated from partial melting of mantle wedge in the subduction zone (Wilson, 1989). As a result, the magma generated formed the I-type granitoid in the NSZ.

the SSZ granitoid rocks have I-type and A-type characters (Figure 3a-c), originating from magmatism associated with subduction and within-plate rifting processes (Figure 4b). The A-type granitoid is associated with rifting events from SW Borneo, which is part of NW Australia and moved relatively northward in the Late Jurassic, before subduction with the Pacific Ocean plate (Paleo-Pacific subduction) in the Early Cretaceous (Hall, 2012; Hennig et al., 2017). Meanwhile, the formation of I-type granitoid in the SSZ is related to the post-collision of SW Borneo with West Borneo (Sundaland margin) Late Cretaceous (Breitfeld et al., 2020). The age is much younger than the A-type granitoid in the same Schwaner zone. The appearance of type I-type granitoid in this zone is not directly related to the Paleo-Pacific subduction, because it is located further west, while the subduction is further east.

Conclusions

Geochemical analyses in this study show that there are 2 major types of granitoid rocks in the Schwaner Mountains. The I-type granitoid rocks with magnesian and metaluminous composition are found in the North Schwaner Zones (NSZ), Northwest Schwaner Zones (NWSZ), and in the South Schwaner Zones (SSZ). Furthermore, the A-type granitoid rocks with ferroan and alkaline composition are found in the SSZ and are indicated in several of the NWSZ samples. Magmatism that produces the I-type granitoid in the NWSZ is associated with Paleo-Pacific subduction in the Triassic-Jurassic. For the same type of granitoid in the NSZ, it is also associated with younger Paleo-Pacific subduction in the Cretaceous when SW Borneo interacted with West Borneo in the north, and with the Paleo-Pacific oceanic plate (paleo-pacific subduction). In contrast to the NWSZ and NSZ, the I-type granitoid in the SSZ is associated with a Late Cretaceous post-collision event in West Borneo (Sundaland margin). Meanwhile, the A-type granitoid rocks in the SSZ are generated by the magmatism when SW Borneo begins to separate from NW Australia through a rifting mechanism so that the granitoid during Jurrasic.

References

Amiruddin and D. S. Trail, 1993, Geology of the Nangapinoh sheet area, Kalimantan Map at 1: 250000 scale, Bandung: Geological Research and Development Centre.

Barbarin, B., 1990, Geological Journal, **25**, 227-238.

Breitfeld H. T., L. Davies, R. Hal, R. Armstrong, M. Forster, G. Lister, M. Thirlwall, N. Grassineau, Juliane Hennig-Breitfeld, M. W. A. van Hattum, 2020, Frontiers in Earth Science, **8**, 1–37.

Chappell, B.W. and A. J. R. White, 2001, Australian Journal of Earth Sciences, **48**, 489-499.

Cox, K.G., J. D. Bell, R. J. Pankhurst, 1979, The interpretation of igneous rocks, Allen & Unwin.

Frost, B. R., C. G. Barnes, W. J. Collins, R. J. Arculus, D. J. Ellis, and C. D. Frost, 2001, Journal Petrol. **42**, 2033–2048.

Hall, R., 2012, Tectonophysics, **570–571**, 1–41.

Hennig, J., H. T. Breitfeld, R. Hall, and A. M. S. Nugraha, 2017, Gondwana Research **48**, 292–310.

Irvine, T. N. and W. R. A. Baragar, 1971, Can. J. Earth Sci. **8**, 523-48.

Middlemost, E. A. K., 1975, Earth Sci. Rev. **11**, 337-64.

Muliyana, T., W. Widodo, R. M. Faisal, and E. Putra, 2018, Evaluasi potensi logam tanah jarang di

Kabupaten Ketapang Provinsi Kalimantan Barat kaitannya dengan endapan timah, Bandung: Geological Research and Development Centre.

Pearce, J. A., N. B. W. Harris, and A. G. Tindle, 1984, Journal Petrol. **25**, 956–983.

Peccerillo, A. and S. R. Taylor, 1976, Contrib. Mineral. Petrol. **58**, 63–81.

Setiawan, N. I., Y. Osanai, N. Nakano, T. Adachi, L. D. Setiadji, and J. Wahyudiono, 2013, Berita Sedimentologi **28**, 4–12.

Shand, S. J., 1943, Eruptive rocks: Their genesis, composition, classification, and their relation to ore-deposits with a chapter on meteorite, John Wiley & Sons.

Whalen, J. B., K. L. Currie, and B. W. Chappell, 1987, Contrib. Mineral. Petrol. **95**, 407–419.

Williams, P. R., C. R. Johnston, R. A. Almond, and W. H. Simamora, 1988, Tectonophysics **148**, 279–297.

Wilson, M., 1989, Igneous petrogenesis a global tectonic approach, Springer.

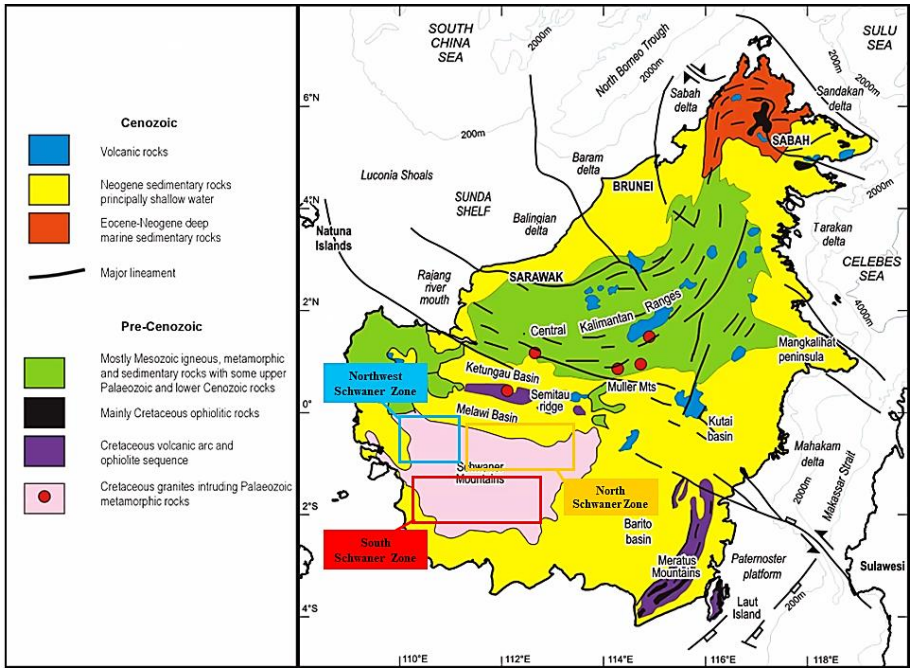

Figure 1: A map showing Borneo (Kalimantan) regional geology (from Amiruddin and Trail, 1993) and each zone of Schwaner Mountains where the samples are collected.

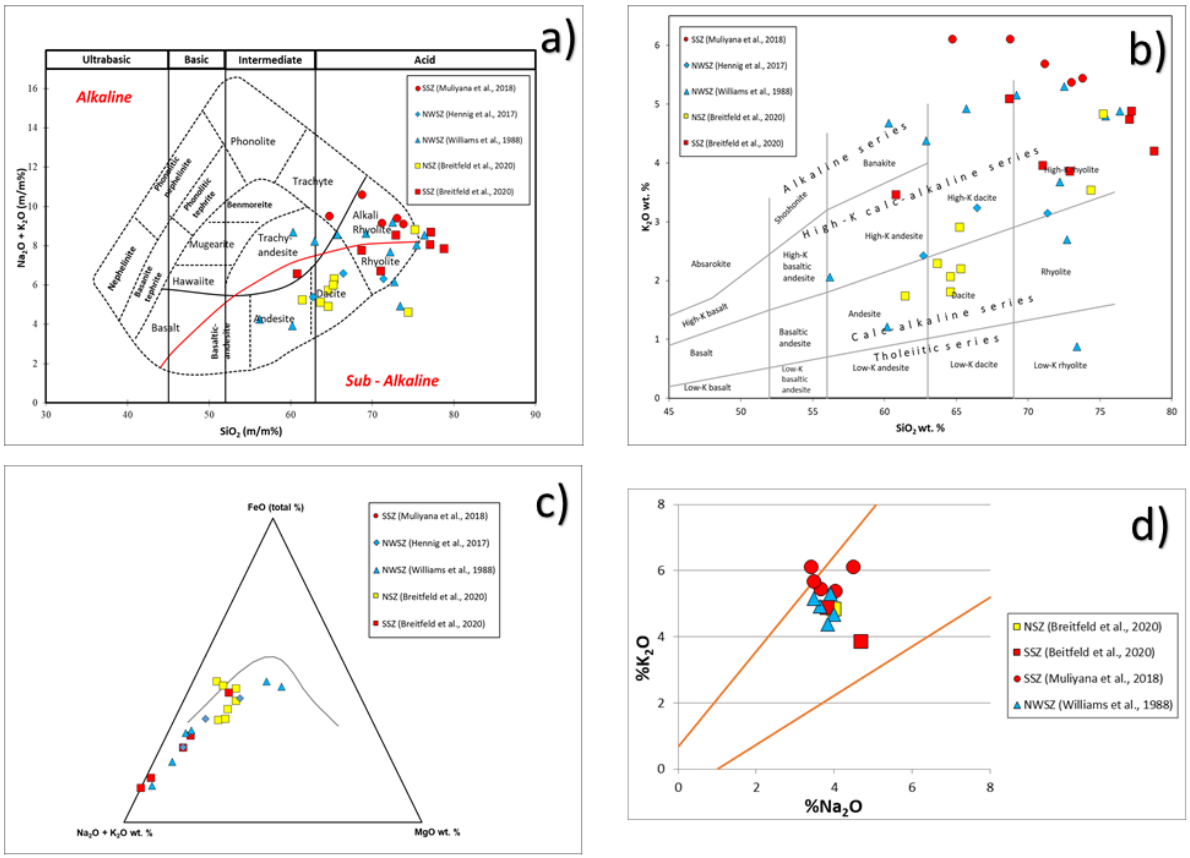

Figure 2: a) Plot Na_2O+K_2O versus SiO_2 (diagram from Cox et al., 1976), b) K_2O versus SiO_2 (diagram from Peccerillo and Taylor, 1986), c) AFM diagram (from Irvine and Baragar, 1971), and d) K_2O versus Na_2O (diagram from Middlemost, 1975) showing magma affinity of granitoid rocks from Schwaner Mountains.

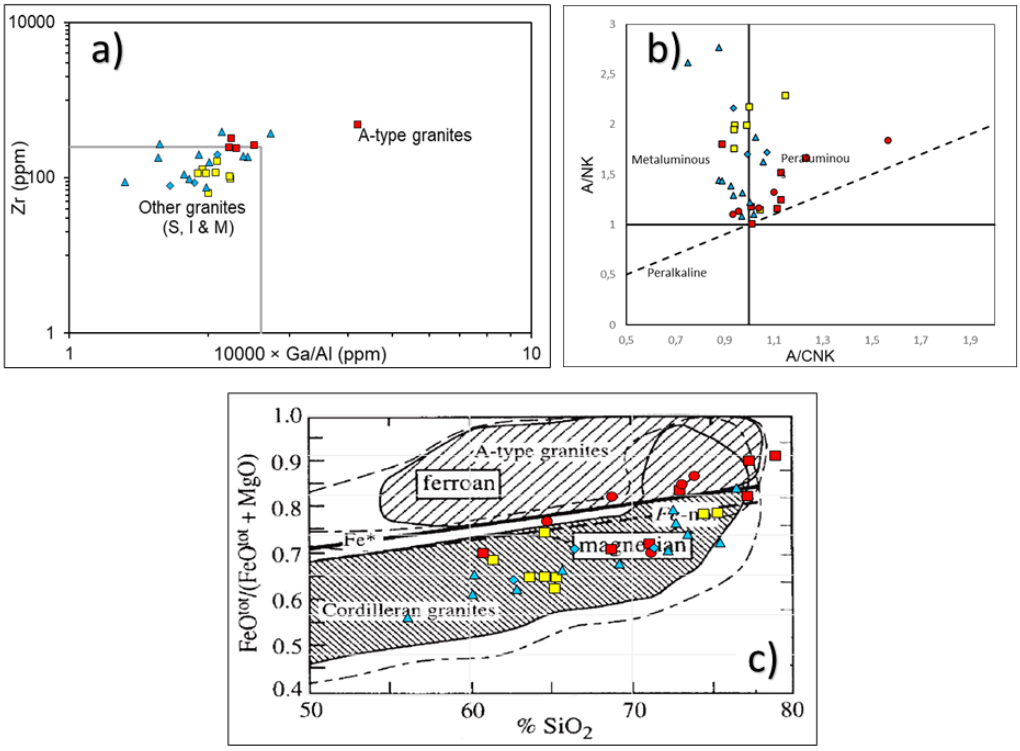

Figure 3: a) Diagrams from Whalen et al. (1987), b) Shand (1943), and c) Frost et al. (2001) to identify the granite type and alumina saturation index of granitoid rocks from Schwaner Mountains. The simbology is the same as in Figure 2.

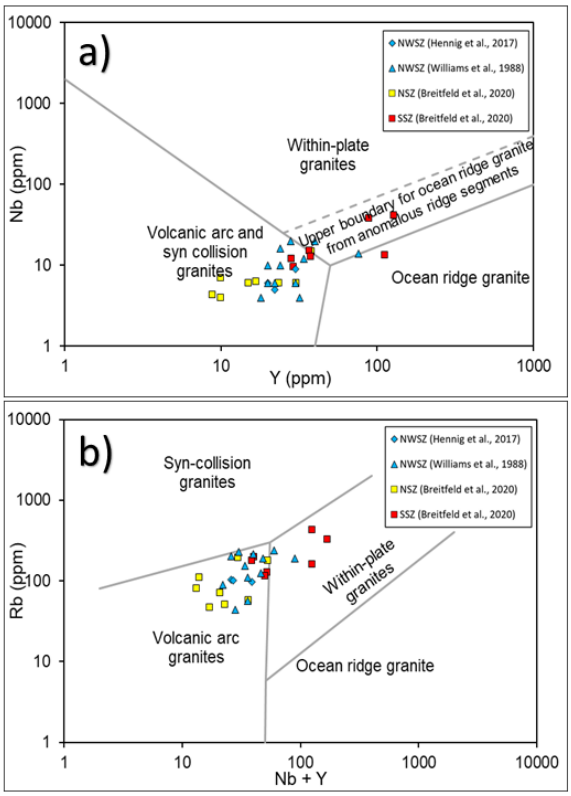

Figure 4: Plot diagrams from Pearce et al. (1984) showing tectonics setting of Schwaner Mountains granitoid rocks.

PROCEEDINGS
JOINT CONVENTION BANDUNG (JCB) 2021
December 1st – 3rd 2021

The evolution of Lamongan Volcanic Complex based on scoria-cone morphometric age analysis and its implication for geological resources and hazard preliminary study.

Eka Febriana Triastiningsih[1],Nisrina Bahiyah Kesuma[1],Mirzam Abdurrachman[1],
[1]Bandung Institute of Technology

Abstract

Lamongan Volcanic Complex consists of 60 scoria-cones spread on the northeast, north, northwest, west, southwest, and south sides surrounding Lamongan Volcano main body. Changes in the characteristics of the scoria cone of the Mount Lamongan Complex have a distribution pattern that relatively follows the fissure vent path, indicated by the type of cone morphology. Therefore, morphometric age group mapping can become one of the methods for disaster approaches and heat source transfer detection for geothermal exploration. Using Digital Elevation Model, SiO2 data from previous researches, as well as the volcanostratigraphy of Lamongan Volcanic Complex, the evolution of Lamongan Volcanic Complex was obtained by analyzing groups of morphometric ages.

Based on morphology characteristics, geochemistry data, and volcanostratigraphy of the research area, three groups of morphometric ages were identified. The first group, which is the youngest, is characterized by gentle slopes for low height-to-width ratio (Hco/Wco) cones, as well as steep slopes for low Hco/Wco cones, with medium-high calc-alkaline affinity, basalt-andesitic volcanic rocks, and was located the furthest from the main body. Meanwhile, the second and third groups are characterized by smaller cones size, steeper slopes, with medium calc-alkaline affinity, more primitive volcanic rocks such as picrobasalt – basalt, and located near to the main body. Based on these morphometric ages, it can be concluded that there was movement in the heat source towards the main body of Lamongan Volcanic Complex. This indicates that the region potential for geothermal exploration will be near the main body of this volcanic complex, though further study should be conducted to fixate the exploration location. The heat source movement towards the main body will also indicates the potential of Lamongan Volcano and Tarub Volcano reactivation, since those volcanoes have been dormant and new possible magmatic supply can triggered them to be active.

Keywords: Lamongan, Morphometry, scoria cones, volcanology, petrology

Introduction

The process of formation of maar lakes and scoria cones in the Mount Lamongan Complex is not yet known with certainty. Padang (1951 in Bronto et al., 1980a) described cones and maars that appeared on the surface associated with magma chambers, namely each referred to as the result of an eccentric eruption, while Kemmerling (1921 in Bronto et al., 1980a) argued that cones and maars were injections. lava that is not directly related to the magma chamber. Structural control plays a very important role in the appearance of eccentric eruptions in the form of cones, springs in the Ranu Segaran area, side eruptions and eruptions that cause parasitic craters (Bronto et al, 1980a). The sudden formation of cones such as Mount Anyar followed by intensive seismic activity causes the need for an understanding of the mechanisms that occur in the Mount Lamongan Complex, which is located in Probolinggo, West Java (Figure 1).

The unknown sequence of formation of each scoria cone makes it difficult to compose vulcanostratigraphy. In addition, scoria cones have a distribution pattern that relatively follows the path of the fissure vent so that several cones can form in the same path. Meanwhile, absolute dating is expensive for a large number of samples, so alternative methods are needed, such as morphometric relative age determination.

Several aspects studied in morphometry are shapes and sizes that can be applied to explain the process of a geomorphological form. Carn (2000) has carried out a cone morphometric measurement method based on the Wood (1980) and Hasenaka and Carmichael (1986 in Kereszturi, 2012) method but has not been further applied, especially regarding the volcanostratigraphic aspect and its relationship to the shape of the cone configuration and the geochemical composition of the rock.

Data and Method

The data used in this study are secondary data and primary data on morphometric measurements. The primary data used were 60 measurement locations. The measurement locations were adjusted to evaluate the results of previous studies in the Mount Lamongan area using the volcanostratigraphy method. From 60 morphometric measurement locations, several samples were selected according to the availability of geochemical data from previous studies. The selection of this sample was based on the representativeness of the Mount Lamongan Complex unit that had been made by previous research (Bronto et al., 1986). Primary data is satellite imagery in the form of DEM

(Digital Elevation Model) as many as 4 pieces taken from the Geospatial Information Agency or DEMNAS.

Wco is the average of the maximum and minimum diameters of the cone. Wco defined by Settle (1979 in Kereszturi and Nemeth., 2012):

Wco = (Wcomax+Wcomin)/2…….…….. (1)

The cone height Hco is defined as the difference between the mean basal height and the maximum crater height or peak height. The Hco/Wco ratio decreases with age because erosion reduces the height of the cone by transporting material around the base of the cone. The width or diameter of the crater Wcr is defined as the average of the maximum and minimum crater diameters. Another indicator of morphological change with time is the mean slope angle (Save). The average slope angle (Save) is derived through morphometric parameters, namely Hco, Wco and Wcr. To find the mean angle (Save) is used (Hasenaka and Carmichael, 1985):

Save = tan−1 (2Hco/(Wco−Wcr))..... (2)

As for the scoria cone which has a crater that is difficult to calculate, such as an open/breaching crater, a complex cone or a cone without a crater, the equation is used:

Save=tan−1 (2Hco/Wco)..... (3)

Result and Discussion

The ratio of Hco/Wco values divided the cones into 3 morphometric age groups based on (Carn, 2000) which was also compared with vulcanostratigraphy including age group 3 (Hco = 0.179 Wco), age group 2 (Hco = 0.124 Wco) and age group 1. The age groups also showed distinctive affinity characteristics, which ranges from the (medium-high K) calc-alkaline to (high-K) calc-alkaline. Based on the Hco/Wco and SiO2 plots, the age distribution is concentrated into two parts, SiO2 < 50 and SiO2 > 50. The effect of SiO2 values is that high SiO2 values have a wide age range of rocks, while at low SiO2 values the age range is narrower. This can be influenced by differences in the level of rock resistance. The plot diagram of Hco/Wco and rock affinity is shown in Figure 2.

The age group 1 cones were formed during the Mount Tarub period along with the formation of maars and Tarub Young Lava deposits. The crust in the Mount Lamongan Complex is still thin so magma rises to the surface and forms a cone with a fast time and high temperature. This causes the cones at age 1 to be dominated by the cinder cone type. The eruptions that occur continuously due to the large supply of magma, cause the size of the cinder cone of age 1 to reach a width of hundreds of meters and reach the final growth phase. A long time lag causes the magma to differentiate to become more acidic, this is indicated by the geochemical content of rocks that are high K calc-alkaline with the dominant process is crystal fractionation. The emergence of the Tarub Fault causes parts of the mountain body to split and create new craters, this is likely to be a source of new magma supply for cone age 2 which has a more alkaline composition. The composition of the cone of age 1 with high SiO2 (> 50 wt.%) has a higher resistance to weathering so that it has a longer/wide life span. So that the erosion process produces river flows and decreases the slope value. The emergence of this age group period is called the Tarub Volcano Period (Figure 3A).

Age group 2 is characterized by a high composition of MgO and high K2O, P2O5, and SiO2 relatively low and has a narrow range. Compared with age group 1, age 2 has a more alkaline composition and indicates that during this period the eruption was no longer active explosive. Some cones show eruption products with different compositions, for example (G. Tangke, G. Cilik, G. Geni, etc.) which indicates a magma mixing/assimilation process that is dominant in age group 2. The emergence of cones in age group 2 was identified as having a long time lag after the formation of cones in age group 1. This is related to the active activity of the Tarub fault which led to the emergence of a new volcanic cone to the west of Mount Tarub, namely Mount Lamongan. In age group 2, the crust of the Mount Lamongan Complex began to thicken and the temperature cooled so that the cone growth was dominated by the assimilation process, followed by crystal fractionation. The types of cones in age group 2 vary widely, including cinder cones and lava-spatter which also have two variations of SiO2 values. The emergence of this age group period is called the Lamongan Volcano Period (Figure 3B).

The activity of Mount Lamongan has begun to decrease so that only a few cones are formed during this period and generally have a picro-basalt composition a distance closer to the slopes of Mount Lamongan. In monogenetic volcanism, the growth of cones with small volumes is more influenced by external factors so that in the age groups 1 and 2 there has been an intensive degradation process and is supported by a gap in the ratio of Hco/Wco with SiO_2 at the transition of ages 2 and 3. External factors such as rock type/ geological substrate, climate and physical characteristics of the cone cause the difference between the ratio of Hco/Wco. Some of the cones of age 1 which had a high SiO2 composition (> 50 wt.%) and final growth eventually had the same Hco/Wco ratio as the cones of age 2.

In contrast to the other groups, the age 3 cone is trending closer to the center of the eruption and has a primitive composition (picrobasalt) and a calc-alkaline medium. Based on the geochemical plots that

have been carried out, it is estimated that group 3 magmas pass through special paths, such as some appearing in the maar or side eruptions. This path has relevance to the vent alignment/magma feeding fracture that encircles the Mount Lamongan Complex (Figure 3C). The location closer to the center of the eruption makes the temperature high and the magma assimilation process becomes less dominant.

After all the analysis, it is indicated there were movements of heat source based on the development of scoria cones in Lamongan Volcano Complex. The younger age of scoria cones grew nearer to the center of the complex, showing that the heat supply in this complex system is moving towards the Lamongan Volcano and Tarub Volcano. This may lead to the reactivation of either Lamongan Volcano, Tarub Volcano, or both of those, which, in either case, demand further research for reactivation probability. In addition to possible future reactivation, the heat source movement is suggested to be monitored and estimated so that if a geothermal plant have to get constructed on this volcanic complex, the mitigation of hazardous events and exploration strategies can be designed in the response to the movement.

Conclusions

The different age groups of Tarub and Lamongan Volcanic Complex can be successfully determined through morphometry and show different rock affinity. These groups show younger age emergence towards the center of the complex near Lamongan and Tarub Volcano, indicating a movement of heat source. This heat source needs to be monitored and get its movement predicted to prevent any hazardous events and an exploration design can be created.

References

Carn, S. ,2000, Journal of Volcanology and Geothermal Research, 95(1- 4), 81-108.

Carn, S.A., D.M.Pyle, 2001, Journal Of Petrology, 42, 9 ,1643–1683.

Kereszturi,G., Németh,K.,2012, Journal of Geomorphology, 45 – 58.

Wood,C.A.,1980a,Morphometric Evolution of Cinder Cones. Journal of Volcanology and Geothermal Research 7, 387– 413.

Wood,C.A., 1980b, Morphometric Analysis of Cinder Cone Degradation. Journal of Volcanology and Geothermal Research, 8, 137–160.

Acknowledgement

We would like to express our gratitude to family, friends, colleagues, and Bandung Institute of Technology for the endless support throughout this research.

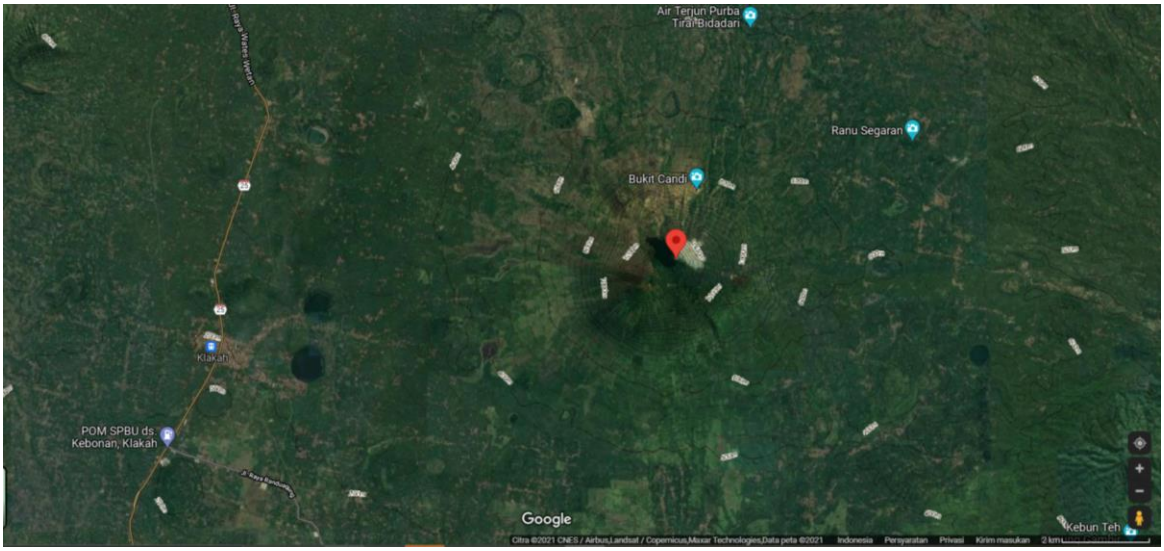

Figure 1. Location of Tarub and Lamongan Volcanic complex (red pinned) in Probolinggo, West Java (source: Google Earth, 2021)

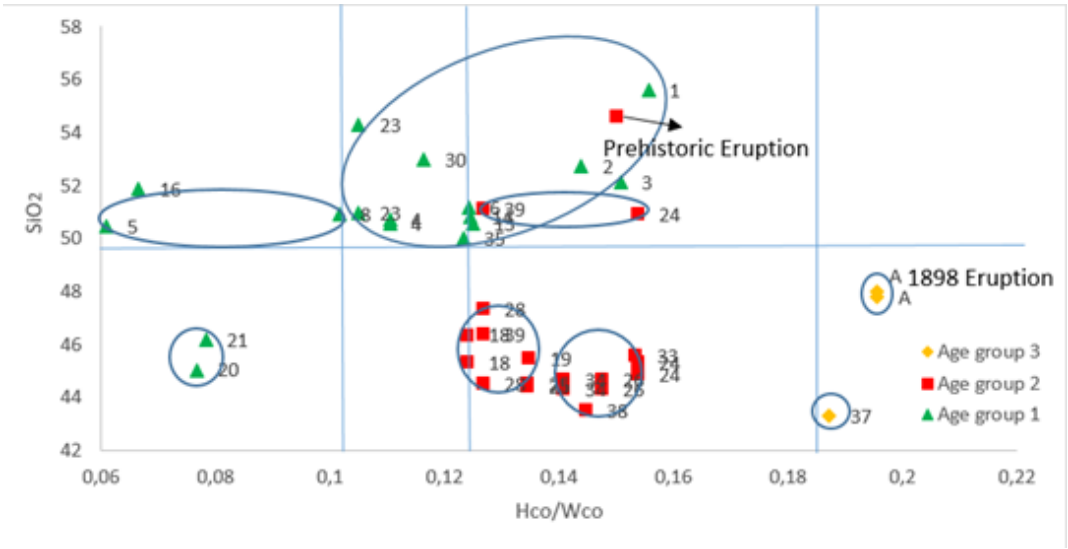

Figure 2. Plot Hco/Wco and SiO2

PROCEEDINGS
JOINT CONVENTION BANDUNG (JCB) 2021
December 1st – 3rd 2021

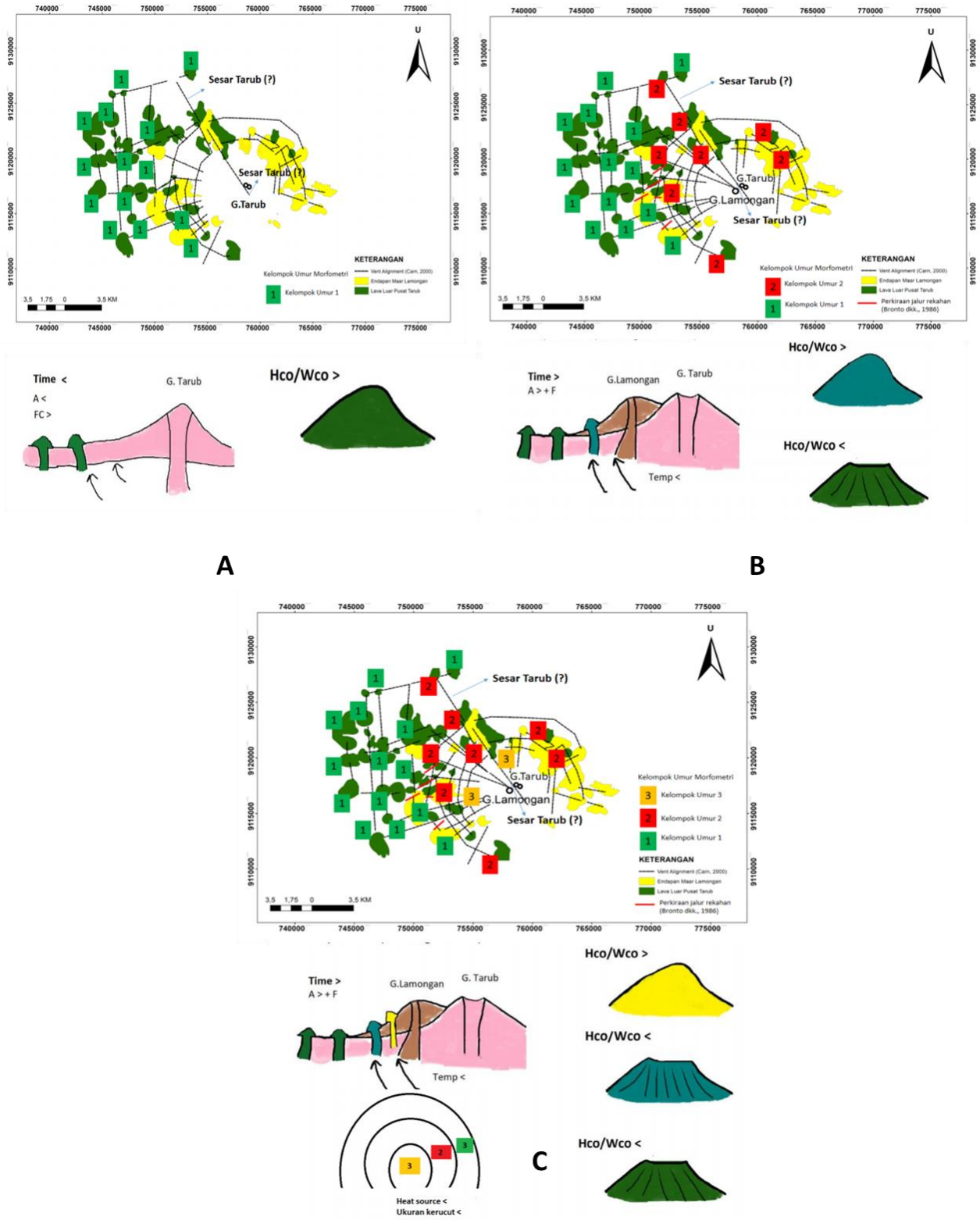

Figure 3. Volcanic activity development based on age group

PROCEEDINGS
JOINT CONVENTION BANDUNG (JCB) 2021
November 23rd – 25th 2021

DETERMINATION OF EARTHQUAKE HYPOCENTER POSITION USING GRID SEARCH METHOD, CASE STUDY: EARTHQUAKE IN MALUKU REGION IN 2021

PENENTUAN POSISI HIPOSENTER GEMPABUMI MENGGUNAKAN METODE GRID SEARCH, STUDI KASUS: GEMPA PADA DAERAH MALUKU PADA TAHUN 2021

Irma Nurliza[1], Adelia Safitri[2], Luscacini Maria[3], Ida Bagus Sunanda Yogi[4]

Abstract
Pada penelitian ini bertujuan untuk menentukan posisi hiposenter gempabumi pada daerah Maluku Tengah yang terjadi pada tahun 2021. Pada penelitian menggunakan satu event dan menggunakan tiga stasiun gempabumi dengan melakukan proses picking waktu tiba gelombang P dan gelombang S, kemudian mencari origin time menggunakan diagram Wadati. Penentuan hiposenter gempa dengan menggunakan Metode Grid Search dengan melakukan pengolahan pada software Matlab dan software Phyton untuk menentukan titik koordinat. Pada penelitian ini dilakukan pencarian hiposenter gempabumi secara regional sehingga dihasilkan nilai RMS Error terkecil yaitu 2.5 s. Dilakukan pengecilan range pengukuran untuk menghasilkan error yang lebih kecil sehingga dihasilkan nilai RMS error yaitu 0.04 s. Kemudian dilakukan konversi guna mendapatkan koordinat lintang dan juga bujur dari hiposenter gempa, sehingga dihasilkan lintang -3.40º LS, bujur 129.36º BT, dan kedalaman 10 km. Sedangkan untuk posisi hiposenter BMKG yaitu lintang -3.39º LS, bujur 129.56º BT, dan 10 km, hasil ini menunjukkan bahwasanya perhitungan sudah dapat mendekati posisi sebenarnya.

Keyword : Gempabumi, Hiposenter, Metode grid search

Abstract
This study aims to determine the position of the earthquake hypocenter in the Central Maluku that occured in 2021. In the study using one event and using three earthquake stations by picking up the P wave and S wave arrival time, then looking for origin time using the Wadati diagram. Determination of earthquake hypocenter using the Grid Search Method by processing the Matlab software and Python software to determine the coordinates. In this research, an earthquake search for regional hypocenter results in the smallest RMS Error, which is 2.5 s. Reducing the measurement range to produce a smaller error resulting in an RMS error value of 0.04 s. Then the conversion is done to get the latitude and longitude coordinates of the earthquake hypocenter, so that the resulting latitude -3.40º latitude, longitude 129.56º east longitude, and depth 10 km. As for the BMKG hypocenter position, namely latitude -3.39º South Latitude, longitude 129.36º East, and 10 km, these results indicate that the calculation can approach the actual position.

Keyword: Earthquake, Hypocenter, Grid search method

Introduction
An earthquake is a violent shaking that spreads to the earth's surface caused by disturbances in the lithosphere (earth's crust). This disturbance occurs because of the accumulation of energy as a result of the shift in the earth's crust itself. The earth's crust has a relatively much lower temperature than the layers below it (the mantle and core of the earth) so that convective flow occurs, i.e. mass with high temperature flows to areas of lower temperature. This high-temperature mass resides in a very viscous, slowly flowing asthenosphere layer. As a result of these movements, the earth's crust is divided into parts in the form of plates that move with each other, which are then called tectonic plates. Earthquakes are generally caused by the release of energy produced by a pressure from moving plates (Meilano, 2011).

Central Maluku, Maluku is located at a position of 2.5º-7.5º South Latitude and 127.25º-132.5º East Longitude. To the north it is bordered by the Seram Sea, to the south by the Banda Sea, to the west by the Buru Sea and to the east by the Papuan Sea, and in the middle by the city of Ambon. The location of the epicenter of the earthquake was at sea, namely in Taluti Bay, the central part of Seram Island which is included in Central Maluku Regency. The area closest to the epicenter of the earthquake is Central Maluku Regency, especially the coastal area of Taluti Bay. The coastal area is mostly composed of Quaternary deposits in the form of coastal and river alluvial. The middle part is mostly composed of the Tehoru Complex Formation in the form of metamorphic rock or green schist facies (Pre-Tertiary age) and the OH Formation in the form of Napal, sandy limestone, sandstone, and tuffaceous marl (Tertiary age). Some of the Pre-Tertiary and Tertiary rocks have undergone weathering. Quaternary deposits and pre-Tertiary and Tertiary rocks that have undergone weathering are generally decomposed, soft, loose, unconsolidated and strengthen the effects of shocks, making them prone to earthquake shocks. Based on the location of the epicenter of the earthquake and its depth, the earthquake event is estimated to be associated with active fault activity in the Taluti Bay area, with a normal fault mechanism at the position of Strike = N 217º E, Dip = 57º, Rake= -85º(Badan Geologi, 2021)

PROCEEDINGS
JOINT CONVENTION BANDUNG (JCB) 2021
November 23rd – 25th 2021

The hypocenter is one of the most important parameters in the seismic field. Based on hypocenter information, it can be estimated that the cause of an earthquake in an area is in the form of magma activity or structural activity such as faults. The hypocenter can be determined by various methods. Several methods for determining the hypocenter are using the inversion method and the Grid Search method (Fauzi, 2010).

Determination of the position of the hypocenter of an earthquake using the Grid Search method is carried out by calculating each sample point that is formed based on the grid (Grandis, 2014). In its calculation, the Grid Search method takes time which depends on the initial parameters in the iteration process. This method is a development of the higherbohood method. For each grid that has been calculated, the error value will be reviewed. If the new error value is smaller than the previous error value, the new value is used as the limit. Thus, the calculation will continue until all grids are successfully calculated and will get the smallest RMS (Root Mean Square) value with the best solution (Nurwidyanto, 2011). Methods for determining the hypocenter have been developed to get results quickly, but in some cases, data processing speed can be found which is often inversely proportional to the accuracy of the results obtained (Arimuko, 2019).

This study aims to determine the position of the earthquake hypocenter in the Central Maluku area, Maluku, Indonesia in 2021 by using the Grid Search method calculation by programming using Matlab and Python software. This study is expected to improve the accuracy of determining the earthquake hypocenter well.

Data and Method

In this study, data on earthquakes that occurred in 2021 in the Maluku area were used, precisely in the central Maluku area. Then in this study used earthquake source data from three stations, which can be accessed on the IRIS page by entering the desired event date range and minimum magnitude. Which includes latitude, longitude, depth, time, region, magnitude, date, month, and also the year of the earthquake.

Gambar 1. Location of Study Area

2.1 Data Processing

In processing data to determine the location of the hypocenter of an earthquake, the process carried out is as follows:

1. Picking P and S wave phases from previously downloaded data using seismograph software.
2. Determine the origin time or earthquake time (t_{obs}) from the available station data using a wadati diagram.
3. Determine the hypocenter of the earthquake using the Grid Search method
4. Verify the results obtained with the hypothetical epicenter
5. Relocating several earthquake events recorded by BMKG.

2.2. *Picking* P and S wave phase

In this study, picking P and S wave phases was done using seismograph software by entering data from several stations that had previously been downloaded and then a graph of earthquake waves recorded at each station would appear where on the graph the X axis is the arrival time of the waves. and the Y axis is the amplitude. Do phase picking of P and S waves where the P wave is the first wave to arrive while the S wave is the wave that comes after the P wave and has a larger amplitude than the P wave.

2.3. Earthquake timing (*origin time*)

Origin time is the initial time of the occurrence of an earthquake in each earthquake event. Then the origin time or earthquake time is determined using the wadati diagram method where this method uses tp and ts-tp data from a number of n stations. Then the two data are plotted so as to produce a point of intersection of the straight line to the data tp and ts-tp, the point of intersection of the straight line is an approximation of the time of the earthquake.

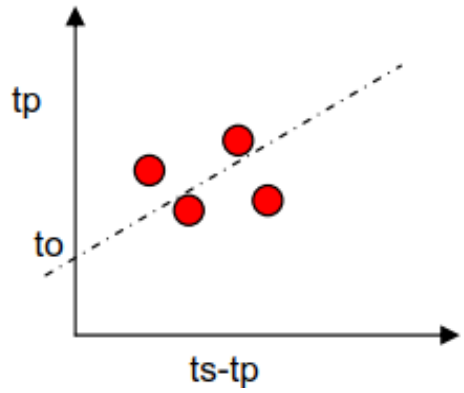

Gambar 2. Tp vs Ts-Tp curve with Wadati method (Lay dan Wallace, 1995).

***2.4. Grid Search* Method**

The method used in determining the hypocenter of the earthquake in Central Maluku is the Grid Search method. the grid search method is the development of a non-linear inversion solution using a global approach. The grid search method is done by making space in an area that is suspected to be the location of the source of the earthquake.

The Grid Search method itself requires time that is related to the initial parameters in the iteration process. In this study, the Grid Search method was carried out on Matlab and Python programming software, with the initial parameter required was the reference time which in this case used the reference time of the P wave, wide range, evaluation step, and also origin time. The wide range used starts from the widest area which will then be narrowed down after knowing the wide range that has the smallest error value from the previous calculation, the calculation will continue until it is known the value of the wide range or area limit which has the smallest RMS (Root Mean Square) value which is the best solution. What needs to be considered when determining a large evaluation step parameter is that the RMS (Root Mean Square) value used is too small. The results obtained from this grid search method will be more accurate if the grid is made more tightly but thus the calculation will take longer.

Result

From the results of data processing carried out using the grid search method with the research area using one target event or earthquake source used. From the data using three stations as shown in table 1.

Tabel 1. Coordinate of station

Station	Latitude	Longitude
KAPI	-5.01	119.75
DAV	7.07	125.58
WRAB	-19.93	134.36

At the stage of calculating the earthquake hypocenter position using the Grid Search method, a regional search for earthquake sources is carried out first or looking for earthquake sources with a large range. The calculation results can be seen in Figure 3. It can be seen that the y-axis is the latitude position in km units and the x-axis is the longitude which uses km units. In this regional calculation, it is not possible to know for sure the position of the hypocenter in the earthquake, but we can see the resulting range in the calculation. In the results of these calculations, it can be seen that the position of the earthquake hypocenter is in the range on the x-axis = 0 km to 7000 km, then for the y-axis it is in the y-axis range = 7000 km to 19000 km with a depth that is between 0 km to 20 km has an RMS value. the smallest error is 2 s. The results obtained from this regional hypocenter calculation cannot be used as a reference because the values obtained in this calculation get results that are not too clear because the range value is still relatively wide and this regional calculation is carried out to obtain the initial approximate location of the earthquake hypocenter position, so that by using the initial estimated position we can determine the position of the earthquake hypocenter.

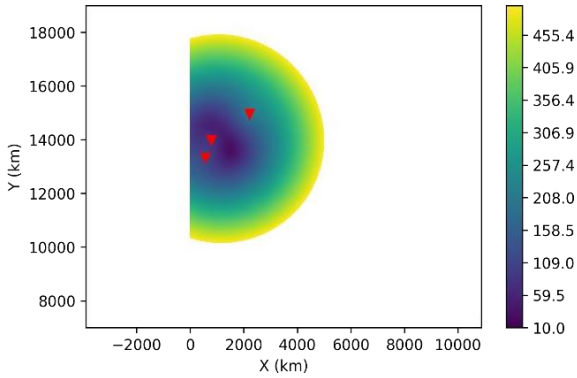

Gambar 3. Earthquake hypocenter position regionally with Grid Search method

To get a more accurate hypocenter position, a range reduction process is carried out from the results of the initial model calculations that have been carried out. From the results of these calculations, the results of the earthquake hypocenter position were on the x axis = 380 km, y axis = 14400 km, and a depth of 10 km. After reducing the measurement range to produce a smaller error, the resulting RMS error value is 0.04 s. Then the conversion is carried out to obtain the latitude and longitude coordinates of the earthquake hypocenter, resulting in a latitude of -3.40º South Latitude, longitude 129.36º East Longitude, and a depth of 10 km. As for the position of the BMKG hypocenter, which is latitude -3.39º South Latitude, longitude 129.56º East Longitude, and 10 km, these results show that the calculation is close to the actual position.

Conclusion

This study uses 3 earthquake observation stations that record the occurrence of earthquake processes, namely KAPI, DAV, and WRAB stations. Then the stages of searching for earthquake sources are carried out regionally or looking for earthquake sources with a large range to get an estimate of the initial earthquake position. 0-20 km has an RMS error value of 0.04 s. Then the conversion is carried out to obtain the latitude and longitude coordinates of the earthquake hypocenter, so that the resulting latitude is -3.40o South Latitude, longitude 129.71o East Longitude, and 19 km. As for the position of the BMKG hypocenter, namely latitude - 3.39o South Latitude, longitude 129.56o East Longitude, and 10 km, these results indicate that the calculation is close to the actual position.

Reference

Arimuko, A.,dkk. 2019. Model Kecepatan 1-D Gelombang P dan Gelombang S dari Data Hasil Relokasi Hiposenter di Wilayah Gunung Sinabung. Jurnal Meteorologi Klimatologi dan Geofisika 5(3).

Badan Geologi Pusat Vulkanologi dan Mitigasi Bencana. 2021. *Analisis Geologi Kejadian Gempa Bumi Di Kabupaten Maluku Tengah, Provinsi Maluku Tanggal 16 Juni 2021*. Diakses pada Minggu, 22 Agusts 2021 *https://vsi.esdm.go.id/index.php/gempabumi-a-tsunami/kejadian-gempabumi-a-tsunami/3645-analisis-geologi-kejadian-gempa- bumi-di-kabupaten-maluku tengah-provinsi-maluku-tanggal-16-juni-2021*

Fauzi. 2010. Analisis Data Seismogram untuk Menentukan Parameter Magnitude Gempabumi. Jakarta: Universitas Islam Negeri Syarif Hidayatullah.

Grandis, H dan Dahrin, D. 2014. Constrain TwoDimensional Inversion of Gravity. ITB Journal 46(1) :113.

Lay, T. and Wallace, T.C., 1995. Modern Global Seismology, Academic Press.

Meilano, I. 2011. Kajian Geodesi terhadap Subduksi di Mentawai. Seminar dan Gladi Posko Bencana.

Nurwidyanto, I, M, dan Setiawan, A, 2011. Inversi linier leastsquare dengan Matlab (Studi Kasus Model Gravitasi Bola Berlapis). Jurnal Berkala Fisika 14(3): 93 -100.

Pratama Putra, Ahmad. 2011. Penataan Ruang Berbasis Mitigasi Bencana Kabupaten Kepulauan Mentawai. Jurnal Penanggulangan Bencana 2(1)

PROCEEDINGS
JOINT CONVENTION BANDUNG (JCB)|2021
November 23rd – 25th 2021

The Influence of Failure Criteria in Geomechanical Wellbore Stability Modelling

Muhammad Archie Antareza[1], Benedictus Dicky Pradnya Agung Pramudhita[1], Sachrul Wahyu Hidayat[2]
[1] Institut Teknologi Sepuluh Nopember, Surabaya, Indonesia
[2]Institut Teknologi Bandung, Bandung, Indonesia

Abstract

Wellbore instability may cause a significant operational and safety issue if not properly managed. Optimization strategy such as trajectory design based on the safe and stable drilling operation can be done through geomechanical approach to make sure the stability of the wellbore can be maintained. This requires detailed knowledge about the geomechanical parameters including the choice of the criteria to determine the onset of the rock failure. The Mohr-Coulomb failure criterion has been widely used and becomes a standard in petroleum geomechanics. Nevertheless, an appropriate selection of failure criteria plays an important factor in wellbore stability modelling. However, the decision as to which failure criterion is adequate for the problem requires a thorough analysis and investigation. This paper aims to compare several failure criteria commonly used in wellbore stability to examine their behaviour for a given problem. Traditionally, a linear-elastic solution is used to compute the near-wellbore stress through which the stability of the wellbore can be assessed upon inserting them into failure criteria. The piece of rocks around the wellbore will be subjected to a high near-wellbore stress concentration in response to the excavation. For a given hypothetical problem, the stress around the wellbore will be first computed and the onset at which the rock will fail will be obtained based on several failure criteria such as Mohr-Coulomb, Mogi-Coulomb, Modified Lade and Drucker-Prager. The chosen failure criteria are found to have produced a considerable range of variability in terms of predicting the onset of wellbore stability. The result also reveals the significant influence of failure criteria on the stability prediction of a wellbore. Triaxial failure criteria such as Mohr-Coulomb tends to give a more conservative value as compared to the true-triaxial failure criteria such as Mogi-Coulomb. This kind of comparison and assessment support the argument on the importance of selecting adequate failure criteria in wellbore stability modelling to predict the onset of rock shear failure.

Keywords: failure criteria, wellbore stability, stress concentration.

Introduction

Wellbore instability is one of the most serious issues affecting drilling and production operations, required when drilling new wells in order to allocate a safe mud window during drilling operations so that it can be produced. Problems caused by wellbore stability are both time-consuming and costly. Drilling-induced fracture at the borehole wall, due to tensile failure, occurs when the least effective principal stress exceeds the tensile strength of the rocks (Gholami et al., 2014). While borehole breakout occurs if the stress concentration at the borehole wall exceeds the shear strength of the rocks. Inability to mitigate wellbore stability issues can result in a significant operational and safety issue such as stuck pipe, drilling fluid loss, well pack-off (Bahrami et al., 2020; Rahimi, 2014). Addressing such challenges necessitates the use of a geomechanical model that incorporates rock elastic and strength properties, in-situ stress and pore pressure and near-wellbore stress. Geomechanical analysis by using failure criteria can provide an insight regarding the mechanical stability of the borehole wall could potentially reduce Non-Productive Time (NPT). McLean and Addis (1990) argued that the choice of failure criteria is important and has a significant impact on the wellbore stability model. In the prediction of wellbore failure, associated with reservoirs and rock formations in general, several failure criteria are typically considered and evaluated. Determining the appropriate failure criteria for maintaining wellbore stability, on the other hand, can be challenging.

Many researchers have investigated the effect of the choice of failure criteria and are primarily concerned with the quantitative comparison to obtain the best fitting parameters for the various rock failure criteria. Al-Ajmi and Zimmerman (2006) conducted wellbore stability analysis using the Mogi-Coulomb failure criterion and compared the result with Mohr-Coulomb failure criterion. Setiawan and Zimmerman (2019) found that the Mogi-Coulomb criterion predicts lower minimum mud weight by incorporating the strengthening effect of the intermediate principal stress. Meanwhile, Rahimi (2014) mentioned that Drucker-Prager failure criterion estimates the upper bounds of the minimum mud weight for the case under investigation, whereas Mogi-Coulomb and Modified Lade predict results that are lower than Drucker-Prager. These studies were carried out with different parameters and wellbore conditions, hence, it is

difficult to justify as to which failure criteria is best representing a general case.

In order to address this, an analysis has been done to investigate the behavior of several failure criteria assuming the same wellbore conditions and in situ geomechanical parameters. This paper investigates four different failure criteria such as Mohr-Coulomb, Mogi-Coulomb, Drucker-Prager, and Modified Lade. These failure criteria are commonly used in wellbore stability modelling. The different radar plots of each failure criteria will be constructed to provide insight regarding the influence of failure criteria on the mechanical wellbore stability.

Near-Wellbore Failure Prediction

In situ stress and near-wellbore stress calculation

To construct a comprehensive wellbore stability model, in-situ and near-field stress of the wellbore needs to be calculated. There are three main steps that need to be done in wellbore stability analysis for an arbitrary oriented wellbore. Firstly, the in-situ stress components need to be transformed from earth coordinate system to wellbore coordinate system. Secondly, near-wellbore stress must be computed depending on the relative wellbore orientation with respect to the in situ stress azimuth. Lastly, the shear failure limit of the rock around the wellbore perimeter is calculated and examined (Setiawan and Zimmerman, 2018).

Traditionally, the Kirsch equation is used to compute the near-wellbore stress. The generalized Kirsch equation proposed by Hiramatsu and Oka (1965) is valid for all wellbore orientations. The equations depends on the in-situ stresses, $\sigma_{x,0}, \sigma_{y,0}, \sigma_{z,0}$; the wellbore geometry in polar coordinate system, r or R_w (radial distance/wellbore radius), angular direction (θ), and the wellbore pressure (p_w). The stress components of the generalized Kirsch can be written as (Fjaer, 2008):

$$
\begin{aligned}
\sigma_\theta &= \frac{\sigma_{x,0}+\sigma_{y,0}}{2}\left(1+\frac{{R_w}^2}{r^2}\right) - \frac{\sigma_{x,0}-\sigma_{y,0}}{2}\left(1+3\frac{{R_w}^4}{r^4}\right)\cos 2\theta - \tau_{xy,0}\left(1+3\frac{{R_w}^4}{r^4}\right)\sin 2\theta - p_w\left(\frac{{R_w}^2}{r^2}\right)\\
\sigma_r &= \frac{\sigma_{x,0}+\sigma_{y,0}}{2}\left(1-\frac{{R_w}^2}{r^2}\right) + \frac{\sigma_{x,0}-\sigma_{y,0}}{2}\left(1+3\frac{{R_w}^4}{r^4}-4\frac{{R_w}^2}{r^2}\right)\cos 2\theta\\
&\quad + \tau_{xy,0}\left(1+3\frac{{R_w}^4}{r^4}-4\frac{{R_w}^2}{r^2}\right)\sin 2\theta + p_w\left(\frac{{R_w}^2}{r^2}\right)\\
\sigma_z &= \sigma_{z,0} - v\left[2(\sigma_{x,0}-\sigma_{y,0})\frac{{R_w}^2}{r^2}cos2\theta + 4\tau_{xy,0}\frac{{R_w}^2}{r^2}sin2\theta\right]\\
\sigma_{r\theta} &= \frac{\sigma_{x,0}-\sigma_{y,0}}{2}\left(1-3\frac{{R_w}^4}{r^4}+2\frac{{R_w}^2}{r^2}\right)\sin 2\theta + \sigma_{xy,0}\left(1-3\frac{{R_w}^4}{r^4}+2\frac{{R_w}^2}{r^2}\right)\cos 2\theta\\
\sigma_{\theta z} &= (-\sigma_{xz,0}\sin\theta + \sigma_{yz,0}\cos\theta)\left(1+\frac{{R_w}^2}{r^2}\right)\\
\sigma_{rz} &= (\sigma_{xz,0}\cos\theta + \sigma_{yz,0}\sin\theta)\left(1-\frac{{R_w}^2}{r^2}\right)
\end{aligned}
\tag{1}
$$

After near-field stress components are obtained, the stability limit of the shear failure can then be calculated using a particular failure criteria. The following section will briefly describe the four different failure criteria, such as Mohr-Coulomb, Mogi-Coulomb, Drucker-Prager, and Modified Lade, considered in this paper.

Mohr-Coulomb Failure Criterion

Mohr-Coulomb is considered to be the most popular and widely used failure criteria for multiple engineering cases, especially in the oil and gas industry. It is one of the conventional triaxial criteria, which only accounts for the minimum and maximum principal stress; the criterion disregards the intermediate principal stress (S_1>S_2=S_3). Specifically, this criterion implies that rock failure occurs toward points where shear stress is greater than the rock's shear strength. The Mohr-Coulomb criterion is represented mathematically as follows (Jaeger, 2007):

$$\sigma_1 = 2S_0\,\frac{\cos\phi}{1-\sin\phi} + \sigma_3\,\frac{1+\sin\phi}{1-\sin\phi} \tag{2}$$

As observed, this failure criteria is popular due to its simple calculation. However, there are situations in which the intermediate principal stress needs to be accounted for to give a more accurate representation of the stress condition. Hence, other options of failure criteria that involves the three principal stress should be considered, i.e. polyaxial stress state (S_1>S_2>S_3).

Mogi-Coulomb Failure Criterion

The importance of the polyaxial stress approach arises from an experiment conducted by Mogi (1971), which confirmed that most fractures occur along the intermediate principal stress direction. It turned out that intermediate principal stress has a strengthening influence on rocks. Mogi implied that $\sigma_{m,2}$, instead of the octahedral normal stress (σ_{oct}), is the mean normal stress that holds against the occurrence of the

fracture plane. The basic form of Mogi failure criterion describes that distortional strain energy is proportional to σ_{oct} and increases monotonically with $\sigma_{m,2}$ until failure occurs (Al Ajmi and Zimmerman, 2005). However, it cannot be coupled with Coulomb's strength parameters (c and ϕ) due to being a power-law function (Al Ajmi and Zimmerman, 2006). To address this issue, Al-Ajmi and Zimmerman (2005) proposed a linear version of the function called the Mogi-Coulomb failure criterion, which is represented by the following formula:

$$\tau_{oct} = a + b\sigma_{m,2} \tag{3}$$

In a triaxial stress condition, the Mogi-Coulomb criterion is equivalent to the Mohr-Coulomb criterion. As a result, this failure criterion can be considered as an extension of Mohr-Coulomb (Rahimi, 2014; Al-Ajmi and Zimmerman, 2005). In addition to Mogi-Coulomb, other researchers have also proposed other polyaxial failure criteria.

Drucker-Prager Failure Criterion

The Drucker-Prager criterion originally stems from a failure criterion developed for soil mechanics called the Von Mises criterion, hence why this criterion is also called the Extended Von Mises criterion (Colmenares and Zoback, 2002; Drucker and Prager 1952). In the beginning, Von Mises criterion was discovered through the unempirical means of rotational symmetry of the deviatoric plane. However, Von Mises criterion does not account for mean normal stress, so it defies experimental observation. In order to make it more relevant to rock mechanics, Drucker and Prager expand the failure criterion by involving mean normal stress into its calculation, which would eventually become the Drucker-Prager criterion known as follows:

$$\sqrt{J_2} = k + \alpha J_1 \tag{4}$$

where α is the material constant for internal friction, k is the material constant for cohesion, J_1 is the mean normal stress, and J_2 is the second invariant of deviatoric stress (Colmenares, 2002). Based on its relationship with the Mohr-Coulomb criterion when observed in the principal stress plane, the criterion can be categorized into two versions, Circumscribed and Inscribed. Aside from its different material constant value, they are distinguished by its position on the deviatoric plane relative to Mohr-Coulomb. The circumscribed Drucker Prager encircles the Mohr-Coulomb hexagon and intersects with its outer apices, while the inscribed Drucker Prager is embedded inside the Mohr-Coulomb hexagon. (Rahimi, 2014; Colmenares and Zoback, 2002)

Modified Lade

The Modified Lade criterion was adjusted by Ewy (1999) from its original counterpart, the Lade strength criterion. Initially developed for cohesionless soil with curved yield surfaces, the original Lade was modified to conform to rock mechanics by considering the material constant m as 0 so that the criterion can calculate linear shear strength increase with increasing mean normal stress invariant (Colmenares and Zoback, 2002). In addition, the cohesion parameter S is also introduced. The modification on Lade criterion is defined as follows (Colmenares and Zoback, 2002; Ewy, 1999):

$$\frac{(I_1'')^3}{I_3''} = 27 + \eta \tag{5}$$

where η is the internal friction parameter and I_1'', I_3'' are the first and third stress tensor invariants respectively, defined by the following equation:

$$\begin{aligned} I_1'' &= (\sigma_1 + S) + (\sigma_2 + S) + (\sigma_3 + S) \\ I_3'' &= (\sigma_1 + S)(\sigma_2 + S)(\sigma_3 + S) \end{aligned} \tag{6}$$

While Modified Lade tends to be inaccurate when tensile stress is considered due to not possessing tension cut off component, this issue does not affect wellbore stability analysis (Rahimi, 2014; Ewy, 1999). This is because tension is not applied to the points of interest which require mud weight.

Result and Discussion

To examine the effects of failure criteria in wellbore stability, radar plots of four different equations have been plotted in Figure 2a. The radar plot represents all possible wellbore orientation from North-East-South-West and from vertical (center of the radar plot) to horizontal wellbore (the outermost ring). The white dot represents the actual wellbore orientation, color-coded contour represents the minimum mud weight to prevent wellbore collapse. An inclined wellbore with 60° deviation towards N 75E with an azimuth of minimum horizontal stress of 45° NE is used in this paper. The rock formation is characterized by a pore pressure of 9 ppg, cohesion of 4.1958 psi, and 31° angle of internal friction. The in situ stress also applies the same values for each failure criteria.

Figures 2b and 2c show the influence of the wellbore inclination and azimuth to the minimum shear failure limit for all failure criteria considered in this paper. The Mohr-Coulomb (MC), Modified Lade (Lade), Drucker-Prager (DP) and Mogi-Coulomb (MgC) are shown as green, blue, red and dark blue, respectively. For all failure criteria, shown in Figure 2b, the trend of minimum shear failure increases as the wellbore becomes more deviated. Nevertheless, they are different in the rate of changes, particularly for Drucker-Prager. Figure 2c shows the profile of the minimum shear failure limit with respect to wellbore azimuth.

When the Mohr-Coulomb criterion is considered, it shows that the color-coded contour produces a unique

symmetric pattern where the minimum value of mud weight is towards the NE-SW direction. This condition requires a mud weight of approximately 10.5 ppg EMW. However, an extra mud weight of higher than 11.0 ppg EMW is necessary when the wellbore has an inclination of more than 70º as indicated by the green curve in Figure 2b. From the inclination and azimuth sensitivity plot, it can be seen that the shear failure limit has an uptrend profile with respect to the change in inclination (Figure 2b) while the azimuthal sensitivity of the shear failure limit shows a horizontal trend with "jagged" profile (Figure 2c).

In Figure 2a, the shear failure limit of Mohr-Coulomb has a similar pattern with that of Drucker-Prager; in which the symmetric pattern is also toward the minimum horizontal stress direction. However, it is obvious that the Drucker-Prager is more sensitive for an inclined wellbore of more than 30º. Moreover, according to the Drucker Prager criterion, the predicted shear failure limit is approximately 13.0 ppg EMW to prevent the hole collapse. In contrast, Mogi-Coulomb and Modified Lade resulted in a much smaller predicted minimum shear failure limit. A 60º inclined wellbore only required 9.0 ppg EMW on Mogi-Coulomb, even the highest shear failure limit is only 10.2 ppg EMW. This may be associated with the fact that Mogi-Coulomb criterion accounts for the strengthening effect of the intermediate principal stress, hence, it predicts a lower minimum shear failure limit of the mud weight as compared to Mohr-Coulomb. The Modified Lade is mainly estimating the lowest minimum required mud weight than other rock failure criteria because of overestimation of rock strength (Rahimi, 2014).

For the case considered in this paper, it is interesting to see that for a wellbore inclination of less than 20º, the influence of the intermediate principal stress considered in the Drucker-Prager is not sensitive, i.e. their profile follows that of Mohr-Coulomb. And also, for wellbore with inclination higher than 20º, from all failure criteria considered in this paper, it is obvious that Drucker-Prager gives the most sensitive minimum shear failure limit compared to the other failure criteria.

Figure 2c shows that the minimum shear failure limit of Mogi-Coulomb and Modified Lade seem to be insensitive with the drilling azimuth, i.e., the azimuth profile is rather flat for both failure criteria. Modified Lade predicts the wellbore only required 9.2 ppg EMW for all possible azimuth. However, for Mohr-Coulomb and Drucker-Prager, the azimuthal sensitivity is more fluctuate.

Conclusions

The result discussed in this paper shows the significant influence of failure criteria on the stability prediction of a wellbore. This assessment supports the argument on the influence of failure criteria in wellbore stability modelling to predict the onset of rock shear failure.

In summary, it can be seen that all of the investigated failure criteria produce different profiles of minimum shear failure limit. Mohr-Coulomb and Drucker-Prager produce a more conservative shear failure limit with the difference of the minimum shear failure limit with that of Modified Lade and Mogi-Coulomb, for the case considered in this paper, is approximately 4.0 ppg EMW. Such a difference would considerably affect drilling design. This may not be true for other cases, therefore, to ascertain the influence of the choice of failure criteria for a given case, the wellbore stability analysis should be performed using as many possible failure criteria, whenever possible. Nevertheless, polyaxial failure criteria considered in this paper, i.e. Mogi-Coulomb, Drucker-Prager, Modified Lade, reflect the actual downhole conditions in which the three principal stresses are likely to influence wellbore instability.

Acknowledgements

The authors would like to thank Enerka for the initiative and Ngurah Beni Setiawan for the fruitful discussion.

References

Al-Ajmi, A. M., and Zimmerman, R. W., 2005, International Journal of Rock Mechanics and Mining Sciences, 42(3), 431–439.

Al-Ajmi, A. M., and Zimmerman, R. W, 2006, Proceedings of the IADC/SPE Asia Pacific Drilling Technology Conference, 1, 537-550.

Bahrami, B., Sadatshojaie, A., and Wood, D. A, 2020, Journal of Energy Resources Technology, 142, 8.

Benz, T., & Schwab, R., Journal of Rock Mechanics and Mining Sciences, 45(7), 1176–1186.

Colmenares, L. B., and Zoback, M. D., 2002, International Journal of Rock Mechanics and Mining Sciences, 39(6), 695–729.

Drucker., and Prager., 1952, Quarterly of Applied Mathematics 10(2), 157-165.

Dusseault, M. B., 2011, KSCE Journal of Civil Engineering, 15(4), 669–678.

Ewy, R. T., 1999, SPE Drilling and Completion, 14(2), 85–91.

Fjaer, E., Holt, R. M., Horsrud, P., Raaen, A. M., Risnes, R., 2008, Elsevier.

Gholami, R., Moradzadeh, A., Rasouli, V., and Hanachi, J., 2014, Journal of Rock Mechanics and Geotechnical Engineering, 6(1), 13–25.

Gholami, R., Moradzadeh, A., Rasouli, V., and Hanachi, J, 2014, Journal of Rock Mechanics and Geotechnical Engineering, 6(1), 13–25.

Jaeger, J. C., Cook, N. G. W., Zimmerman, R. W., 2007, Blackwell Publishing.

Han, Y., Liu, C., Phan, D., AlRuwaili, K., and Abousleiman, Y., 2019, SPE Middle East Oil and Gas Show and Conference, MEOS.

Irawan, S., Bataee, M., and Zare, M. R., 2016, Advanced Materials Research, 1133, 624–628.
McLean, M. R., and Addis, M. A., 1990, SPE/IADC Drilling Conference.
Mehranpour, M. H., and Kulatilake, P. H. S. W., 2016, Geomechanics and Geophysics for Geo-Energy and Geo-Resources, 2(4), 203–229.
Rahimi, R., 2014, Master Thesis, Missouri University of Science and Technology.
Setiawan, N. B., and Zimmerman, R. W., 2018a, International Conference on Oil & Gas Engineering and Technology (ICOGET), 13–14.
Setiawan, N. B., and Zimmerman, R. W., 2018b, International Journal of Rock Mechanics and Mining Sciences, 112, 313–322.
Setiawan, N. B., and Zimmerman, R. W, 2019, 53rd U.S. Rock Mechanics/Geomechanics Symposium.
Setiawan, N. B., 2019, Memoir ISPG.
Setiawan, N. B., 2020, thesis, Imperial College London

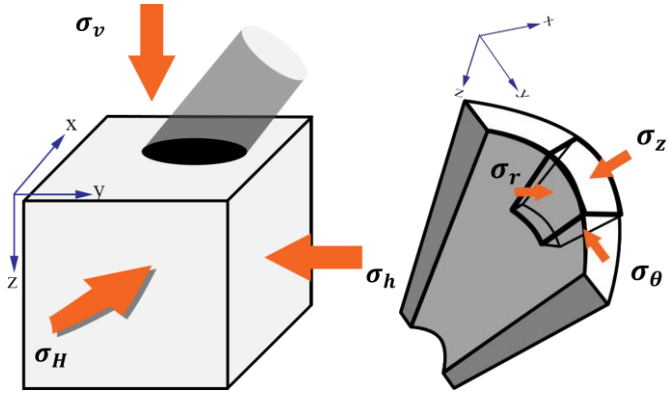

Figure 1: Principal stress and near-wellbore stress ($\sigma_v, \sigma_H, \sigma_h$). The in-situ stress be redistributed around the wellbore to become ($\sigma_\theta, \sigma_r, \sigma_z$) (Modified from Setiawan, 2019).

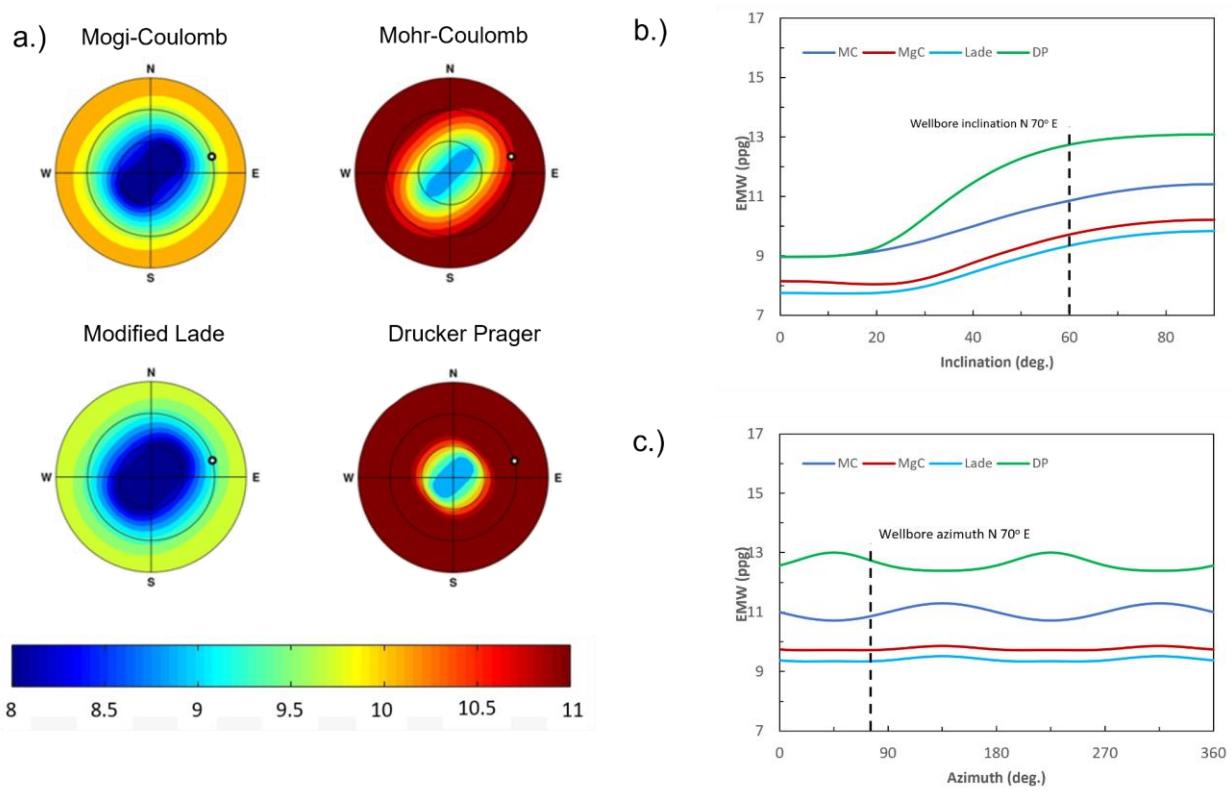

Figure 2: The sensitivity of shear failure limit to avoid wellbore collapse along with the (a) Mohr-Coulomb, Mogi-Coulomb, Modified Lade, and Drucker Prager failure criteria. (b) Inclination and (c) azimuth sensitivity plot.

PROCEEDINGS
JOINT CONVENTION BANDUNG (JCB) 2021
November 23rd – 25th 2021

Geomechanical Evaluation of the Fractures Productivity in Geothermal Resources

Naomi Nadya Angelia S.[1], Muhammad Archie Antareza[2], Marsil Irvan Defri[3], Arif Aulia Fikri[3]
[1] PT. Enerka Bhumi Pratama, Jakarta, Indonesia
[2]Institut Teknologi Sepuluh Nopember, Surabaya, Indonesia
[3]Universitas Pertamina, South Jakarta, Indonesia

Abstract

Geothermal development has seen an increasing trend in the recent years in Indonesia to fulfill the increase in energy demand. Subsurface-related aspects in the development of geothermal resources is an integral part that requires a comprehensive analysis in order to expedite the geothermal development; one of which is their geomechanical aspect. This aspect is mainly associated with the in situ stress in the reservoir that plays an important role for a successful planning, drilling and production of the resources. Although the geomechanical aspect of geothermal may seem to be overlapped with petroleum, there are a subset of problems that is inherently unique to geothermal settings. For instance, the effect of the high temperature on the stability of the wellbore and the examination of the quality of the fractures affecting the productivity of the energy source. One needs to address these unique challenges to ensure the development of the geothermal resources can be optimised. In this paper, one of the cases that will be discussed is regarding the productivity assessment of fractures through geomechanical evaluation. The potential contribution of fractures to the production will be examined by assessing their tendency to open or close under shearing. The stress acting on each fracture will be first computed through which their slip tendency can be determined. Depending on the relative orientation between the fracture and the in situ stress, their slip tendency can be obtained. This integrated yet simple analysis is found to be meaningful in geothermal development. For a given fracture set, the relative magnitude of the in situ stress can potentially lead to a different conclusion if not accurately determined. To ascertain this, a profile showing the maximum shear stress acting for various fracture orientations is then overlapped with the fractures. It is confirmed that fractures will tend to open for the orientation associated with the high shear stress. Hence, detailed knowledge on the in situ stress magnitude and orientation is just as important as the knowledge on the distribution of the fractures.

Keywords: Fracture slip, Geothermal, In situ stress, Shear stress.

Introduction

Geothermal development has seen an increasing trend in recent years in Indonesia to fulfil the increase in energy demand. Based on the Geothermal Director of the Directorate General of EBTKE at the Ministry of Energy and Mineral Resources, geothermal energy had been produced around 8.9 % or 2130.6 MW in 2019. Meanwhile, the government targets an increase in geothermal utilization to 7241 MW or 16.8% in 2025. There are few challenges that come through this target, such as social issues, conservation area, funding, efficiency cost, and risk in the development stage.

Cost efficiency is also related to how much risk is involved at each stage in geothermal development. The exploration and power plant development stage has a higher cost than the other stages. Risk and cost can be diminished by development ini reservoir technology based on geomechanical principles. Reservoir geomechanical have significant processes through years, but mainly focused on the petroleum field. As geothermal energy is widely used and developed, technology for geothermal has started to thrive and geomechanics issues have become an interest. This aspect is mainly associated with the in situ stress in the reservoir that plays an important role for a successful planning, drilling and production of the resources. Challenges must be addressed to optimize the resources.

In this paper, one of the cases that will be discussed is regarding the productivity assessment of fractures through geomechanical evaluation. The potential contribution of fractures to the production will be examined by assessing their tendency to open or close under shearing. The stress acting on each fracture will be first computed through which their slip tendency can be determined. Depending on the relative orientation between the fracture and the in situ stress, their slip tendency can be obtained.

Geomechanics and Geothermal

Geothermal has a unique condition from the traditional oil and gas challenges. A number of geomechanical issues that arise in geothermal development have been identified, especially drilling and production. These issues are associated with the heating-cooling processes, fractures productivity, injection and production in the reservoir.

Drilling and well placement

Similar to oil and gas drilling, the geomechanical aspect has an influence on geothermal drilling,

especially when it comes to managing wellbore stability. The most common problem faced in geothermal drilling is lost circulation due to the presence of fractures. On the other hand, the presence of fractures indicates good reservoir quality in a geothermal system. A geothermal wellbore is considered as high potential when it intersects major fracture systems. Therefore, in geothermal drilling, it is a common practice to directionally orient the wellbore to intersect as many fractures as possible. In other words, the more severe a lost circulation is, the better the wellbore would be. However, this may trigger wellbore instability because of the presence of fractures. According to Carson et al. (1982), fractures is a common feature in geothermal due to the vulnerability of hard rock formations in seismically active regions and abnormal thermal gradients due to convective groundwater flow through fractures. Although lost circulation is a good omen, it is also the most expensive problem and can even lead to increased cost, contributing to Non-Productive Time (NPT), and even well abandonment. On top of that, this problem can cause unbalanced formation pressure and induce borehole wall collapse, which can trigger other follow-up problems, such as casing failure and stuck pipe (Carson et al., 1982; Nugroho et al., 2017; Saleh et al., 2020).

In addition to the drilling challenges related to fractures and lost circulation, the high temperature inherent in a geothermal system can also promote other challenges. Zhou et al. (2018) discussed the thermal shock and tensile stress in rocks due to the cooling effect. The temperature difference between the drilling fluid and the surrounding rocks can induce shear failure or tensile failure around the wellbore (Dusseault, 1993). Wang et al. (1996) proposed a solution to model the effects of temperature and fluid flow on pore pressure and stress. They observed a substantial compressive stress being induced near a borehole when hotter fluid is circulated in the borehole. This may trigger shear failure around the borehole and increase its instability. On the other hand, circulating a cooler mud, such as in geothermal drilling, may improve the stability of the wellbore by reducing the near wellbore tangential stress. However, it is also recognise that the risk of tensile failure increases. Hence it is often observed that the downgoing cooler mud circulated through the drill bit nozzle will promote tensile fracture near the bottom of the hole while the upgoing hotter mud will potential induces breakout near the nearest casing shoe.

Production

One system that plays an important role in geothermal is enhanced or engineered geothermal system (EGS). EGS is very suitable for dry rock, geothermal energy production generally from dry reservoirs with low permeability that can be achieved by circulating water in an engineering fracture network consisting of artificial fractures and pre-existing fractures. Then, one of the important technologies in the development of geothermal resources, especially with the one with low permeability is hydraulic fracturing to improve productivity. The ultimate goal is to enhance the permeability of the reservoir sufficiently high to achieve the economic limit. Li and Lior (2015) developed a simplified model to qualitatively examined the required energy for a typical EGS reservoir. They concluded that the required energy to create a fracture is propotional to the volume of the created fracture represented by a propotionality coefficient that increases with depth due to a larger in situ stress. As an alternative of hydraulic fracturing, which requires the fluid pressure to overcome the minimum principal in situ stress and the tensile strength of the rocks, the hydro-shearing technique will requires a less pressure to induce pre-existing fractures to slip by increasing the pore pressure. Gischig and Preisig (2015) argued as to which mechanisms, i.e. hydrofrac or hydro-shearing, occurs during injection depends on the in situ stress state and the relative orientation of the fractures. The permeability enhacement induces by hydrofrac will tend to be reversible if proppant is not placed to keep the fracture open. Another approach that has gain a lot of attention is identification of an enhance fracture productivity by a so called critically stressed fractures. The concept and modeling of hydroshearing is similar to the evaluation of productivity asessment of a potentially slip fractures due to in situ stress. These are existing fractures that have slipped or has a potential to slip because of the in situ stress acting on them. Hennings et al. (2012) presented a study supporting the argument that fractures that were critically stressed are a good indicator for well productivity. Nygren and Ghassemi (2005) studied the impact of cold water injection on the productivity of critically stressed fractures of a geothermal field. They investigated the impact of injection on the shear initiation of a fractures networks and found that a large temperature difference can induce thermoelastic stress and cause the fracture to slip even below the critical injection rates. Such an approach of identifying the zones with critically stressed fractures can be implemented for predicting zones of enhanced permeability.

Brief methodology to examine fracture productivity by investigating their slip potential is presented in the following section followed by a case example using a hypothetical dataset.

Fractures and in situ stress

The presence of fractures plays an important role in determining the production in geothermal resources. Therefore, the identification of their presence becomes important. One of the best methods to recognize fractures is downhole image log; that allows geoscientists to study and analyze the fractures. The image log can provide a high-resolution image of the near-wellbore fracture from which fracture

PROCEEDINGS
JOINT CONVENTION BANDUNG (JCB)2021
November 23rd – 25th 2021

orientation, i.e. their dip azimuth and dip angle, can be obtained.

To assess fractures productivity, in addition to the fractures orientation, one needs to also understand and quantify the in situ stress. The following equation can be used to estimate the magnitude of in situ stress in isotropic rocks considering the temperature effect (Zhang, 2019):

$$\sigma_h = \frac{\nu}{1-\nu}\left(\sigma_v - \alpha P_p\right) + \alpha P_p + \frac{E}{1-\nu^2}\left(\varepsilon_h + \nu\varepsilon_H\right) + \frac{E\alpha_T}{1-\nu}\Delta\mathrm{T}$$
$$\sigma_H = \frac{\nu}{1-\nu}\left(\sigma_v - \alpha P_p\right) + \alpha P_p + \frac{E}{1-\nu^2}\left(\varepsilon_H + \nu\varepsilon_h\right) + \frac{E\alpha_T}{1-\nu}\Delta\mathrm{T} \quad (1)$$

The equation requires the knowledge of the rock elastic properties such as Young's modulus (E) and Poisson's ratio (ν), the vertical stress (σ_v) as well as the thermal expansion coefficient (α_T). The in situ stress will have to be projected into the fracture plan to obtain the normal and shear stress component acting on the plane. The following relation can be used for the transformation:

$$W = \begin{bmatrix} \cos(90-\beta) & 0 & \sin(90-\beta) \\ 0 & 1 & 0 \\ -\sin(90-\beta) & 0 & \cos(90-\beta) \end{bmatrix} \begin{bmatrix} \cos\alpha & \sin\alpha & 0 \\ -\sin\alpha & \cos\alpha & 0 \\ 0 & 0 & 1 \end{bmatrix} \quad (2)$$

where α and β are the dip azimuth and dip angle of the fracture. The stress acting on the fracture plane σ_f can then be obtained from the in situ stress:

$$\sigma_f = W\sigma_0 W^T \quad (3)$$

in which

$$\sigma_0 = \begin{bmatrix} \sigma_h & 0 & 0 \\ & \sigma_H & 0 \\ & & \sigma_v \end{bmatrix} \quad (4)$$

Result and Discussion

One of the key analyses in geothermal field development is associated with the knowledge of whether or not the fractures set tend to open and, hence, contribute to the production. This kind of analysis requires knowledge of the fracture orientations as well as the in situ stress state. Such a piece of information can be obtained from image log data. The natural fractures appearance from the image log can be identified and their dip angle and azimuth can be inferred.

The underlying concept to evaluate the slip potential of fractures follows that of the Jaeger's plane of weakness. The fractures shear strength limit is characterised by their cohesion and frictional coefficient. In most cases, the cohesion (S_w) of the fractures can be assumed to be zero. Hence, their strength depends only on the frictional coefficient (μ_w). The in situ stress will have to be projected into the individual fracture plane to obtain the normal and shear stress components. If the stress acting on the fracture plane exceeds the shear strength, then the fracture is said to have a tendency to slip.

$$|\tau| = S_w + \mu_w\sigma_n \quad (5)$$

Figure 1 shows an example of a hypothetical fracture set indicating a dominant azimuth orientation of 15-120 degree NE azimuth with varying dip angles. The in situ stress is assumed to be psi. The pore pressure is assumed to be 5000 psi The frictional coefficient is assumed to be . From Figure 1, it is obvious that some of the fractures tend to slip and it is expected the fractures to contribute to production. Most of the fractures that have a dip angle higher than 70 degree tend to be more stable than fractures that have a dip angle less than 70 degree. Moreover, it is also obvious that fractures whose dip is around 70-120 degree NE tend to open compared to the other fractures set. Such an analysis is important for well targeting to ensure the wellbore would primarily intersect those fractures that have a higher tendency to slip.

PROCEEDINGS
JOINT CONVENTION BANDUNG (JCB) 2021
November 23rd – 25th 2021

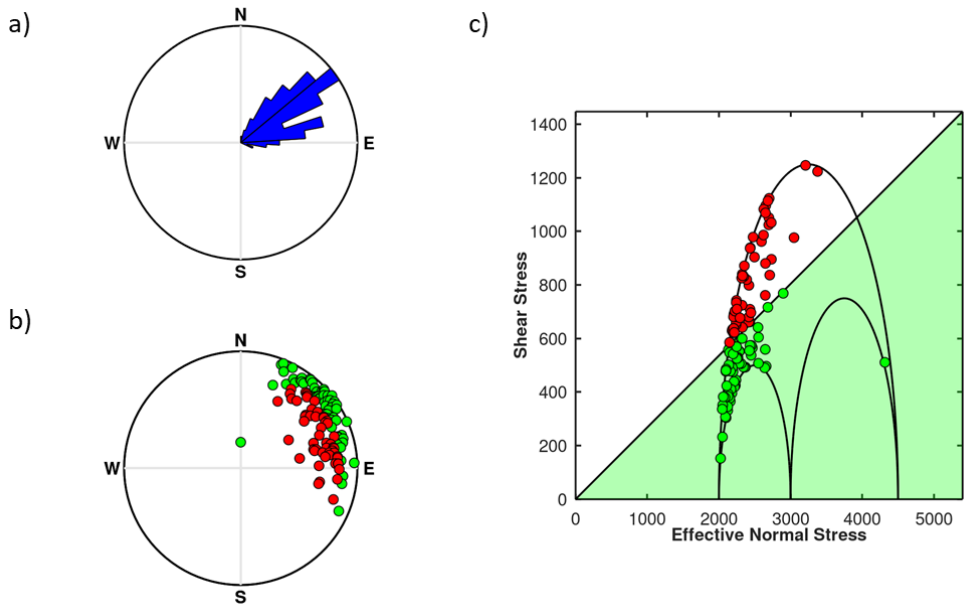

Figure 1. (a) Stereonet indicating the fracture set orientations. (b) Individual fractures orientation is shown as a point reflecting the dip azimuth and dip angle. The red coloured circles are fractures that have a higher tendency to slip and open and the green coloured circles are the stable fracture set. (c) The shear stress vs. effective normal stress plot indicating the unstable fractures (red circle) that lie above the Coulomb failure envelope.

A more detailed examination shown in Figure 2 revealed the distribution of the shear stress acting on the failure plane. The plot suggests that fractures with orientation of SE-NW with a dip angle between 30 to 70 degree will likely to be under stressed and has a higher potential to slip.

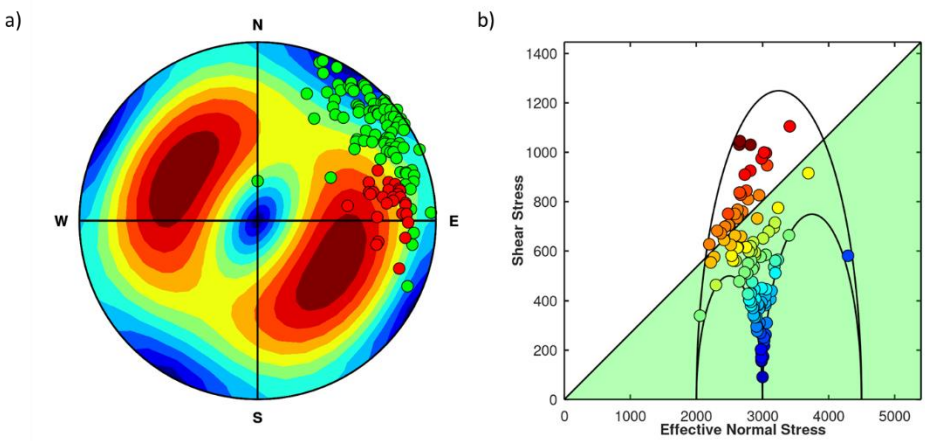

Figure 2. (a) The stereonet plot showing the shear stress overlaid with the potentially open (red circles) and closed (green circles) fractures. (b) The shear stress vs. effective normal stress plot color-coded by the magnitude of the shear stress acting on the fracture plane.

Conclusions

Productivity of a geothermal resources can be assess by studying the quality of the fractures. One approach that can be integrated in fractures evaluation is by examining their slip potential due to the in situ stress. The potential contribution of fractures to the production can be examined by assessing their tendency to open or close under shearing.It is understood that fractures opennes tendency will be associated with the high shear stress. The profile of the shear stress acting on the fracture plane, for all possible fracture azimuth and dip angle, may provide an insight on the preferable orientation of fractures that may contribute to productivity. The concept and

modeling of hydroshearing is similar to the evaluation of productivity asessment of a potentially slip fractures due to in situ stress presented in this paper.

Acknowledgements

The authors would like to thank Enerka for the initiative and Ngurah Beni Setiawan and Marino Baroek for the fruitful discussion.

References

Carson, C. C., 1982, AAPG Bulletin, 66, 188–94.

Dusseault, M. B., 1993, SPE International Thermal Operations Symposium.

Dusseault, M. B., 2011, KSCE Journal of Civil Engineering, 15(4), 669–678.

Ghassemi, A., 2012, Geotechnical and Geological Engineering, 30, 647–664.

Gischig, V. S., Preisig, G., 2015, 13th ISRM International Congress of Rock Mechanics.

Hennings, P., Allwardt, P., Paul, P., Zahm, C., Reid, R., Alley, H., Kirschner, R., Lee, B., Hough, E., 2012, AAPG Bulletin, 96, 753–772.

Li, M., Lior, N., 2015, Journal of Energy Resources Technology, 137(4).

Nugroho, W. A., Hermawan, S., Lazuardi, B. H., Mirza, R., 2017, SPE/IATMI Asia Pacific Oil and Gas Conference and Exhibition.

Nygren, A., and Ghassemi., A., 2005, The 40th U.S. Symposium on Rock Mechanics (USRMS).

Saleh, F. K., Teodoriu C., Ezeakacha, C. P., Salehi, S., 2020, Stanford Workshop on Geothermal Reservoir Engineering.

Wang, Y., Papamichos, E., Dusseault, M. B., 1996, 2nd North American Rock Mechanics Symposium.

PROCEEDINGS
JOINT CONVENTION BANDUNG (JCB) 2021
November 23rd – 25th 2021

Technical MULTI-BASE ROVER Acquisition and BASE MAP DATA-BASED Processing in Overcoming Pitfall of Undercorrected and Overcorrected in Geomagnetic Method

Aji Darma Maulana, Rizki Adilaga, Tedy Wiku Setiaji, Kevin Prastya, Nurwanti Ibtisamah Sagala
Geophysical Engineering, Pembangunan Nasional "Veteran" University Yogyakarta

Abstract

Accuracy in the processing-acquisition method is crucial in geoscience research so that the data obtained represents geological events and increases S/N ratio. Multi-base rover and base map data-based methods are processing-acquisition integrations that offer a product in acquisition and processing stages that correct diurnal anomaly information with precision in detailed zones and identify correction errors (undercorrected or overcorrected). However, this method requires different processing steps compared to single base processing. This method will be tested on three variables with six unique conditions. The conditions are differences in lithology (position function), daily variation trend by weather (position and time functions), and datum values (initial time function) caused by the initial weather conditions. First case has heterogeneous lithology, but similar in daily variation trend and datum values. In this case, the value of lithological variation will be eliminated by shifting the reading graph of each base on the reference datum, so the reading value is no longer affected by lithological differences. Second case has different datum values and daily variation values, but similar in daily variation trends and lithology. The difference in datum value and daily variation value will be eliminated by the shifting method. Processing method in the first and second cases is relatively easy because only one parameter is different and has a stable daily variation, so that the correction can be done by table-based processing method. Third case has differences in daily variation trend, but is similar in lithology and datum values. In third case, it will be effective to do the correction using the base map data-based processing method. Fourth case has differences in lithology and daily variation trend, but is similar in datum values. In this case, the value of lithological variation will be eliminated similar to the first case, then correction of daily variations is carried out using the base map data-based processing method. Fifth case has homogeneous lithology, but differs in datum values and daily variation trends. Therefore, only instantaneous shifting is carried out on the datum value so that the base map data-based processing method can be applied. Sixth case has a condition that is similar to the real world condition which is not possible to carry out the correction steps because the magnetic reading event cannot be separated from the response of daily variations or lithology. This case is assumed to have different lithology, datum values, and daily variation trends. Therefore, an acquisition concept was created as a solution to the sixth case problem, namely by approaching the fourth case, where there is an inability to change geological conditions and daily variation trends so that they are diverted to carry out a countermeasure for differences in datum values. The same datum value can be obtained by taking measurements at a time that is assumed to have stable and relatively same weather conditions which generally occur in the morning.

Keywords: Base Map Data-Based, Multi-Base Rover, Overcorrected, Processing-Acquisition, Undercorrected.

Introduction

The S/N ratio obtained in a series of acquisition steps will greatly affect the processing stages and the resulting output. This study offers a method that can increase the S/N ratio in the geomagnetic method domain. **MULTI-BASE ROVER METHODS** and **BASE MAP DATA-BASED** are processing-acquisition integrations that offer a product of the acquisition and processing stages that can correct diurnal anomaly information with precision in detailed zones, and detect possible errors of correction (undercorrected or overcorrected).

Using three variables, this method will be tested based on six conditions with different parameters. These variables include a **function of position** caused by differences in lithology, where these lithological differences will affect the magnetic intensity (M) of the study area. Second is the **function of position and time**, the function in question is the daily variation, where these parameters will change with changes in position and time function. Changes in magnetic intensity related to position function are caused by local weather differences, while changes related to the time function is caused by changes in the external magnetic field periodically. This external magnetic field can cause the geomagnetic field to vary on a daily basis to produce diurnal variations (Kearey et al, 2002). Third, **the initial time function** which refers to the difference in datum values caused by differences in the initial weather measurements. The six conditions will be explained in the methodology section. This analysis-based research will then be elaborated to produce a conclusion in the form of the most appropriate acquisition method that can compensate for the three different variables.

PROCEEDINGS
JOINT CONVENTION BANDUNG (JCB) 2021
November 23rd – 25th 2021

Data and Method

In the first case study, the correction will be carried out using the data acquisition graph in each base. There are four data graphs with different values but have relatively the same value trend caused by differences in lithology at each base. Correction is carried out by uniforming the datum value or the initial reading value on the graph to a particular constant value which is called the shifting process. This data shifting process aims to eliminate the influence of different lithologies at each base.

In the second case study, there are differences in the datum values on the daily variation graph caused by differences in weather at each base. In this case the correction steps are similar to the first case study, namely by using a data acquisition graph in each base. Correction is done by shifting the data on the datum value, which aims to eliminate the influence of weather differences at each base. Therefore, the shifting results are considered free from the influence of weather differences.

In the third case study, there are different conditions in the daily variation trend parameter, but similar in lithological parameters and datum values. In the third case, the processing stage is carried out using the base map data-based processing method, so that the resulting data is free from the influence of differences in the daily variation trend parameters.

The fourth case study has different conditions on lithological parameters and daily variation trends, but is similar in datum value parameters. In the fourth case, the value of lithological variation will be eliminated by a shifting process using table based processing, then the difference in the daily variation trend will be eliminated using the base map data-based processing method. In figure 1 is shown the conditions at the beginning of the measurement, where there are lithological differences but similar in weather conditions which cause the similarity in datum values. Whereas in figure 2 can be seen that different weather conditions throughout the day at each base cause differences in the daily variation trend.

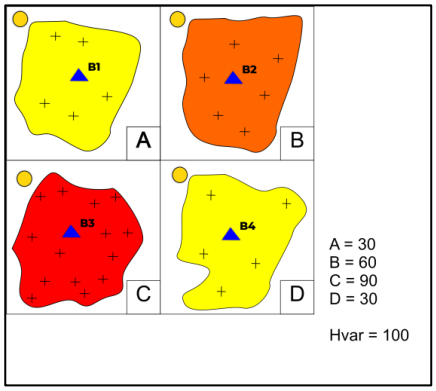

Figure 1. Lithology Condition and Initial Weather Condition in Case 4

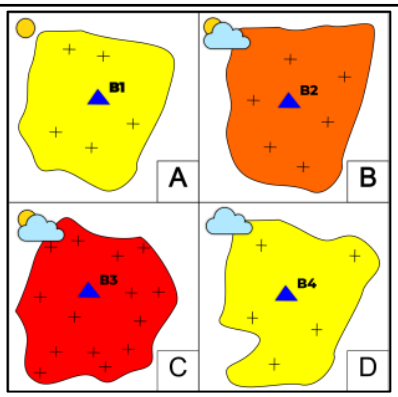

Figure 2. Lithology Condition and Weather Variation Throughout the Day in Case 4

The fifth case study has different parameters of datum values and daily variation trends, with similarities in lithological parameters. In the fifth case study, a table based processing method is applied instantaneously to the data to eliminate the effect of different datum values, then base map data-based processing will be performed to eliminate differences in daily variation trends.

In the sixth case study, there are differences in lithological parameters, datum values, and daily variation trends, where these conditions are close to the actual situation in the field. In this case, it is not possible to separate the event of magnetic readings between lithological responses and daily variations.

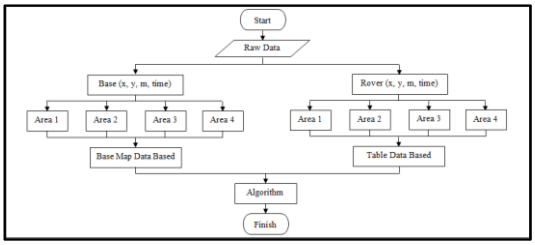

Figure 3. Processing Flowchart

Figure 3 shows the processing flowchart of the steps that will be taken in the processing stage of the magnetic acquisition data. After obtaining the measurement data, then the processing stage is carried out on the base and rover data separately. In the base data that has been corrected for different parameters, a map of the corrected base reading result is obtained in the form of a base map data-based. Meanwhile, the rover data can be processed using table data based methods. After earlier processing stages are done, then the next processing stage is to find the right base data to be used as a correction parameter on the rover data. This processing stage is carried out on the base and rover data simultaneously using the scan and pick method based on the algorithm of the base map data-based method. The algorithm can be mathematically described as follows :

PROCEEDINGS
JOINT CONVENTION BANDUNG (JCB) 2021
November 23rd – 25th 2021

$$\left(\left(\frac{HB_{n+1}rover - HB_{n-1}rover}{TB_{n+1}rover - TB_{n-1}rover}\right) x\ (TR_n rover - TB_{n-1}rover)\right) + (HB_{n-1}rover - HB_1 base)$$

Whereas,

HB_{n+1}rover : magnetic value in base after *n* rover time
HB_{n-1}rover : magnetic value in base before *n* rover time
TB_{n+1}rover : time in base after *n* rover time
TB_{n-1}rover : time in base before *n* rover time
TR_nrover : time at *n* rover
HB_1base : magnetic value at initial base

Result and Discussion

The processing stage of the data acquired in the six existing case studies can be done using two methods. The first method is a table based processing method in which the data processing stage is based on calculations in tables with a value shifting process. The second method is a base map data-based method with a processing stage that refers to the map of the magnetic anomaly readings on each base to determine the correction parameters.

The first case study with the conditions described previously can be corrected by using the table based processing method by shifting process. Figure 4 is the reading graphs for each base with different values due to the difference in lithology. First case has a similar daily variation trend in each base (figure 5).

The second case study with different datum values can be corrected by using the table based processing method similar to the first case. In figure 6 it can be seen that the reading graph of each base has a different value because of the difference in the datum value factor. The difference of daily variation trend in the second case is similar to the first case which can be seen in figure 5.

The third case study obtained a reading graph as in figure 7 with the difference in the values due to differences in daily variation trend. The difference in daily variation trend can be seen in figure 8. Because the difference in the daily variation trend is difficult to correct using table based processing, this third case study will be more effective if the processing stage is carried out. by using a base map data-based.

The fourth case study has a graph as shown in figure 9 with different values caused by differences in lithological parameters and daily variation trend. Also shown is graphs daily variation trend (figure 8). The difference in lithology in this case can be corrected using table based processing, where the data that has been corrected for lithology can be seen in figure 10. Then for differences in daily variation trend will be corrected using base map data-based method.

The fifth case study with different conditions on the datum value and the daily variation trend can be seen in figure 11. The graphic difference in daily variation trend can be seen in figure 12. The processing stage in this case is similar to the fourth case, where the correction is done by shifting the datum value instantaneously (figure 13), so that the base map data-based method can be used to correct the difference in the daily variation trend.

In the sixth case study, a data acquisition graph for each base is shown in figure 14. The conditions in this case differ in the parameters of datum values, lithological conditions, and daily variation trend (figure 12). In this case, there is a condition that makes it impossible to separate the reading events of the three parameters which causes the difference in the magnetic reading value of each base.

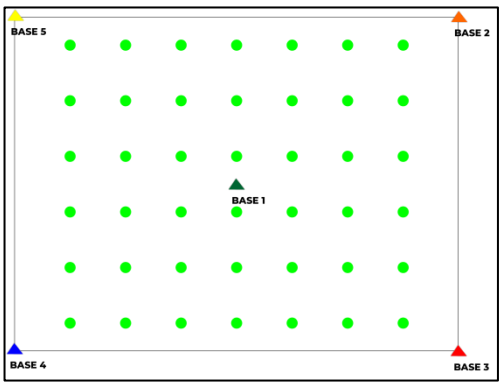

Figure 15. Design Layout for Base Placement in Acquisition Stage

Figure 15 shows the design of placing each base on a large measuring area based on the previously discussed method (multi-base rover). The placement of each base is based on considerations of the accuracy of the data to be obtained, where there are four bases placed at the edges of the measuring area and one base is placed in the middle. Placement of such bases will make the data obtained more accurate because the parameters that affect the reading of magnetic data can be corrected by the processing stage that has been discussed previously, and during the processing of the base map data-based method, the data obtained are interpolated data and not extrapolated.

Conclusions

From this analysis-based research, it can be concluded that the case study closest to the actual situation in the field is the fourth case. The second, third and fifth case studies have the same lithological parameters, where this condition is rare and cannot be controlled. The sixth case study cannot be applied due to complex conditions, where there are differences in lithological parameters, datum values,

and daily variation trends which reading events cannot be separated from one another.

The fourth case study has conditions with different lithological parameters and daily variation trends, where these parameters can not be controlled. This case has a similar parameter in datum value, where this parameter can be controlled by means of quality control at the time of acquisition process. The required quality control can be carried out by making acquisitions at the same time and at relatively the same and stable weather conditions which generally occur in the morning.

In the fourth case study, it will be effective if the processing stage is carried out using the base map data-based method. This processing method uses data on each base that has been processed into a magnetic anomaly map which is then processed using a processing algorithm to eliminate the possibility of undercorrected or overcorrected data. After obtaining the data that has been corrected by these factors, then further data processing on the reading of the rover can be carried out. The processing stage in the rover data is carried out using the scan and pick method based on the algorithm in base map data-based method. This stage aims to find the appropriate data on the base to be used as a correction parameter on the rover data.

References

Kearey, P., et al, 2002, An Introduction to Geophysical Exploration 3rd Edition, London: Blackwell Science Ltd.

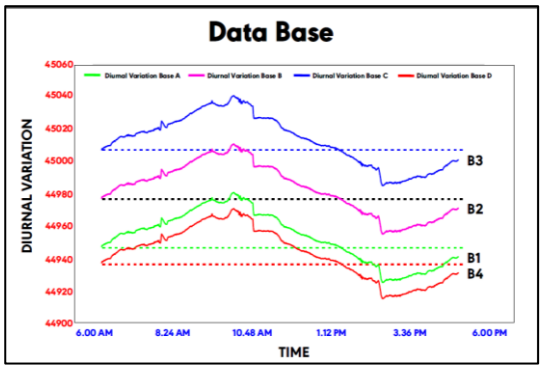

Figure 4. Data Base Case 1

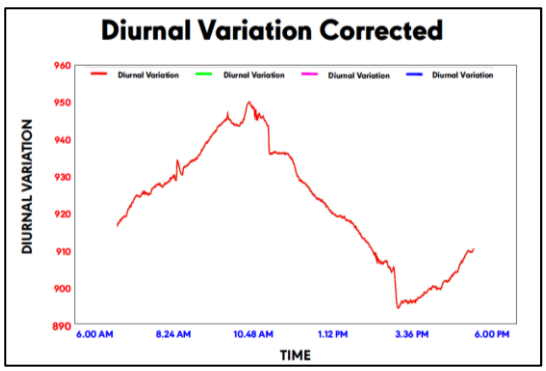

Figure 5. Diurnal Variation Corrected

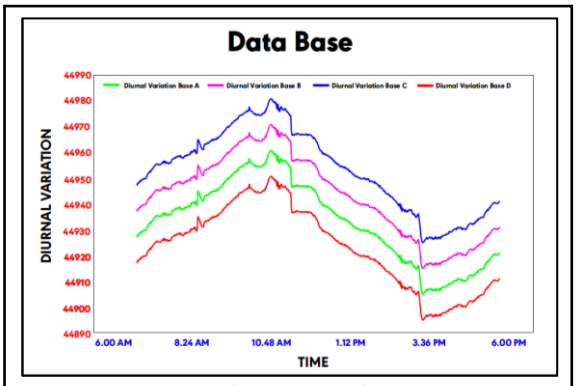

Figure 6. Data Base Case 2

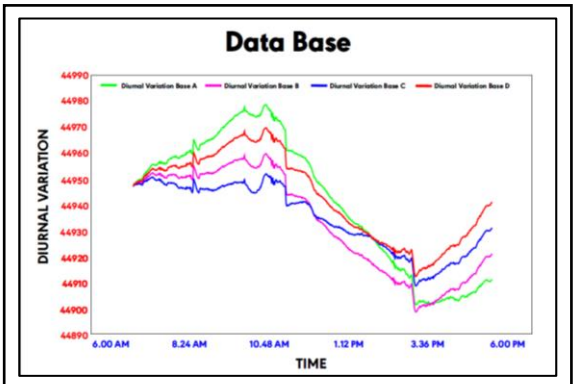

Figure 7. Data Base Case 3

Figure 8. Weather Change Effect 1

Figure 9. Data Base Case 4

Figure 10. Lithology Corrected Data

Figure 11. Data Base Case 5

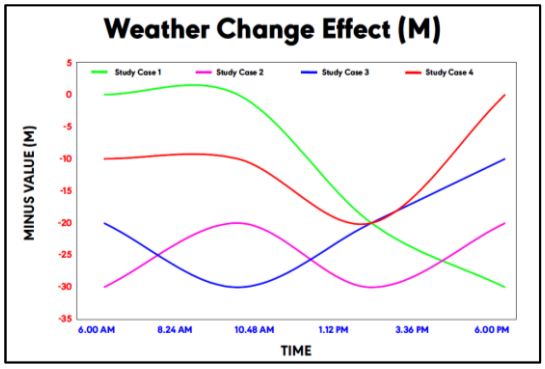

Figure 12. Weather Change Effect 2

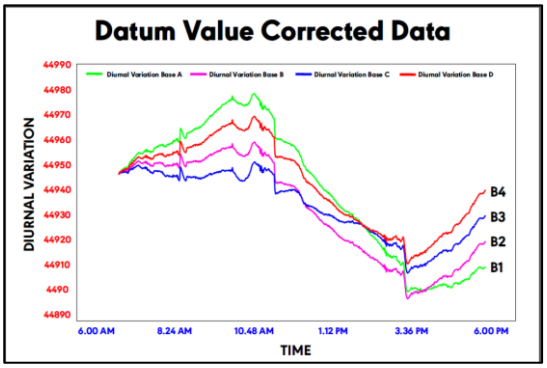

Figure 13. Datum Value Corrected Data

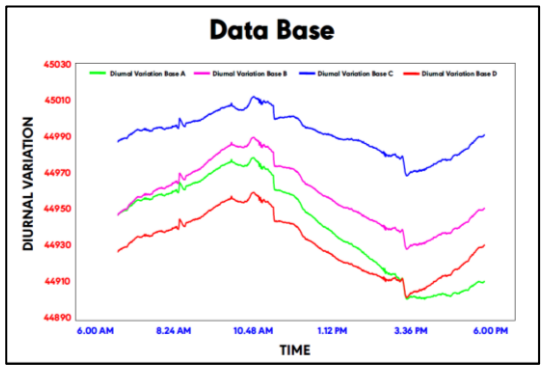

Figure 14. Data Base Case 6

PROCEEDINGS
JOINT CONVENTION BANDUNG (JCB) 2021
November 23rd – 25th 2021

Technical Processing-Acquisition in Geomagnetic Method Study Case : Extends The Measurement Area by The Difference in Base Time

Rizki Adilaga, Aji Darma Maulana, Tedy Wiku Setiaji, Kevin Prastya, Nurwanti Ibtisamah Sagala
Geophysical Engineering, Pembangunan Nasional "Veteran" University Yogyakarta

Abstract

Processing-acquisition is a series of stages that are interconnected with each other in geoscience research activities. The acquisition method that has been applied will affect the data processing method that will be carried out. In this analysis-based research, a case study concept for the acquisition of the geomagnetic method will be presented between two data clusters with adjacent positions but with a very significant measurement time difference (more than one year). The effect of differences in daily variation value that have a measurement time interval of more than one year on the distribution of variations in the lithological value is a problem that arises if the reference datum used in each data cluster is different. Therefore, this study offers a processing-acquisition method that can overcome this problem based on the case study analysis as follows. The first case study uses the assumption that there are two adjacent data clusters (A and B) with homogeneous lithology conditions. However, between cluster A and cluster B, the measurement time difference is one year, which is also assumed to have a daily variation of 50 nT. Therefore, the datum used refers to the daily variation graph of cluster A which has been measured first. It aims to normalize the difference in daily variations for one year. The second case study uses the assumption of the same two data clusters with a daily variation difference of 50 nT. However, they have different lithological states (heterogeneous) with assumed different values of 20 nT. Therefore, the solution used when measuring daily variations in cluster B, which is one year away from cluster A and has lithological difference, is to use two bases (multi-base). Where the first base is placed in the center of cluster A and the second base is placed in the center of cluster B. So it is necessary to correct the lithological difference on the daily variation chart as preconditioning processing before entering the main processing stage. The third case study has exactly the same conditions as the second case study. However, the measurement method used is a single base. Therefore, to correct the difference in daily variation and to maintain magnetic information on the research area, a tie trajectory is needed. Tie trajectory is a path that overlaps with another path (measuring trajectory in cluster A overlaps measuring trajectory in cluster B). It is used to perform shifting correction on the resulting map. The correction uses quality control based on statistical correlation. Based on the accumulation of the three case studies above, case two and three are the case studies that are closest to the real situation in the field. In conclusion, based on the time and cost efficiency-effectiveness, the most appropriate technical processing-acquisition method has been obtained.

Keywords: Geomagnetic, Lithological Difference, Processing-Acquisition, Time Difference.

Introduction

The acquisition stage and processing stage are stages that are interconnected with each other and can not be separated from one another in order to gain a high S/N ratio in the final output of geomagnetic method. In this research, the problem that occurs in the acquisition stage will be discussed using three case studies approaches. In these cases there are two magnetic data clusters with adjacent positions but with a very significant difference in measurement time, over than one year gap. Difference in measurement time can cause changes in the external magnetic field, which then will be causing the geomagnetic field to vary on a daily basis to produce diurnal variations (Kearey et al, 2002). The daily variation that differs in measurement time can cause the reading of magnetic data in the lithological parameter to differ if the reference datum value used in each data cluster is different. In order to resolve this problem, the use of a precise technical processing-acquisition method is necessary.

Data and Method

In this analysis-based research, there are three case studies. These case studies are used to examine the different conditions that might occur during the acquisition stage to extend the measurement area with different time periods.

The first case study has a condition in which there are two adjacent data clusters, namely cluster A and cluster B with similar lithological parameters, but are different in measurement time. The measurement time difference is over one year period. In this one year gap, the difference in daily variation is assumed to have a value of 50 nT (nano Tesla). This value is only an assumption value to make it easier to understand the effects caused by differences in certain parameters

The second case study has two adjacent data clusters that differ in daily variation similar to the first case which is assumed to be 50 nT. This case has

differences in lithological parameters (heterogenous lithology). The different lithological parameter is assumed to have a different value of 20 nT. Two data clusters in this case, namely cluster A that is measured in 2009 and cluster B that is measured in 2010 (1 year measurement time gap). The step used to correct these differences is the multi-base measurement method. This method uses two bases, where each base is placed in the center of each cluster (A and B) as shown in figure 1. Cluster A and Cluster B have different lithological parameters, so it is necessary to eliminate this parameter with preconditioning processing before doing the main processing stages. The preconditioning process can use a table based processing method to do the shifting process of the value differences caused by lithological condition.

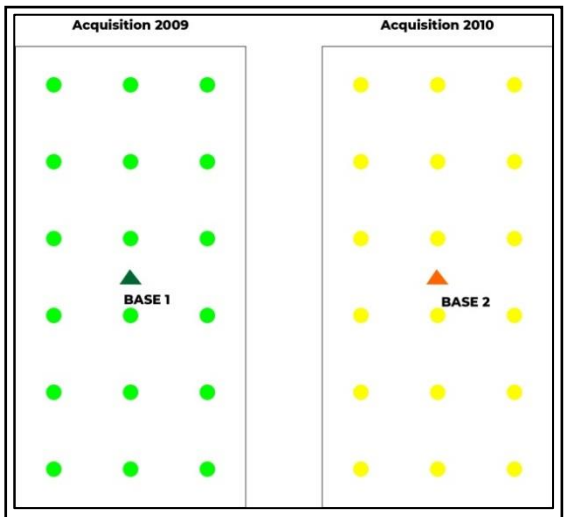

Figure 1. Multi-Base Method

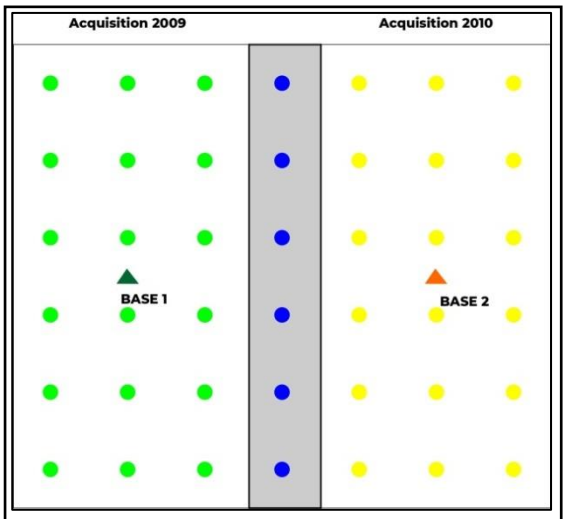

Figure 2. Single Base – Tie Trajectory Method

The third case study with two adjacent data clusters has a condition that is similar to the second case. This case has different parameters in daily variation and lithological condition. The third case has a different method in the elimination process necessary for this problem. The method used in this case is a single base measurement method. However, by using this single base method, it becomes necessary to use a tie trajectory. Tie trajectory is a line or area in the new area of measurement (cluster B) that overlaps with the line or area of the adjacent old area of measurement (cluster A). This tie trajectory can be seen in figure 2 which is drawn by blue dots. This measurement trajectory can be used as a control data to do the shifting correction processing method.

Result and Discussion

The processing-acquisition stage to overcome the problems in those three case studies can be divided into two methods. The first one is multi-base method and the second is single base-tie trajectory method.

The multi-base method in which the acquisition stage is using two bases to acquire the difference in daily variation value. However, the difference in lithological parameters at each base must be eliminated or corrected first. This correction can be done by shifting the initial reading value in each base to the same certain value. This correction process is using a table based processing method. Then, this lithology corrected data can be used as a parameter to do the correction process of the rover data.

The single base-tie trajectory method uses another trajectory or area of measurement that overlaps the adjacent old measurement area. The processing stage is carried out by a method called curve matching, in which the data curve on one trajectory in the old measurement area is matched with the data curve on a tie trajectory in the new measurement area. This curve matching has quality control in the form of an RMS (root mean square) error calculation, where the difference in the data for each path is averaged and then an RMS calculation is carried out so that the resulting data difference is always positive. The graph of the trajectory in the old measurement area (cluster A) can be seen in figure 3, while the graph of the tie trajectory in the new measurement area can be seen in figure 4.

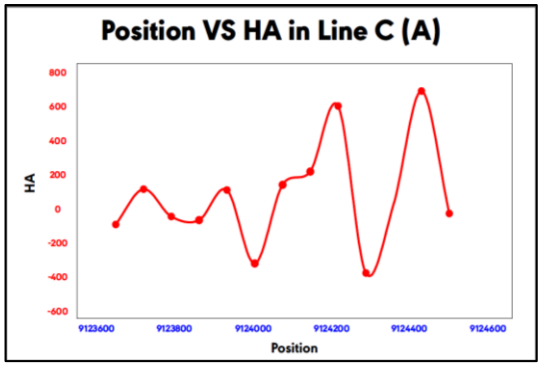

Figure 3. Graph of Position VS HA in Line C (A)

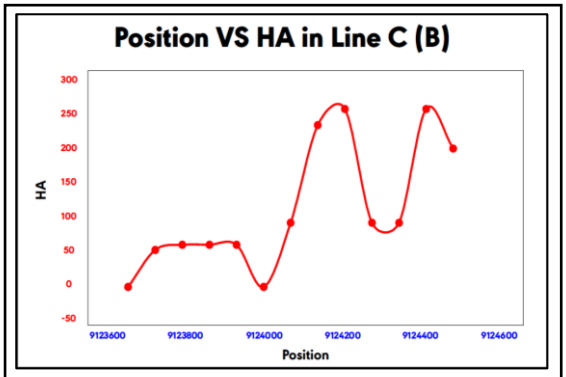

Figure 4. Graph of Position VS HA in Line C (B)

In figure 3 and 4 are shown the method of tie trajectory in the form of a line, whereas the tie trajectory in the form of area can be seen in figure 5 and 6. Figure 5 shows the tie area (area named C) in the old measurement area or cluster A, while figure 6 shows the tie area (area named C) in adjacent new measurement area or cluster B. The choice to use either the tie trajectory or tie area depends on certain conditions, such as time and cost needed to do the acquisition and also depends on how accurate the data is wanted. The tie trajectory method has effectiveness and efficiency in terms of time and cost, but lacks in the accuracy of the data. The tie area method is costly and requires more time, but will produce more accurate data.

Conclusions

The difference in acquisition time of two different magnetic data clusters can cause differences in magnetic values. This difference in magnetic value is caused by periodic changes in the external magnetic field. With this condition, a correction step is needed to eliminate the difference in this parameter.

The offered correction steps consist of two methods, namely the multi-base rover measurement method and the tie trajectory measurement method. The multi-base rover method offers efficiency and effectiveness in terms of energy and time because the rover measurement is carried out only on new measuring areas, but requires more costs because it requires an additional measurement tool in the process. The tie trajectory method is an efficient method in terms of cost because it only requires a single base measurement. However, the tie trajectory method is not efficient in terms of energy and time because it requires an additional measurement line or area that is overlaid with the previous measuring areas.

References

Kearey, P., et al, 2002, An Introduction to Geophysical Exploration 3rd Edition, London: Blackwell Science Ltd.

PROCEEDINGS
JOINT CONVENTION BANDUNG (JCB) 2021
November 23rd – 25th 2021

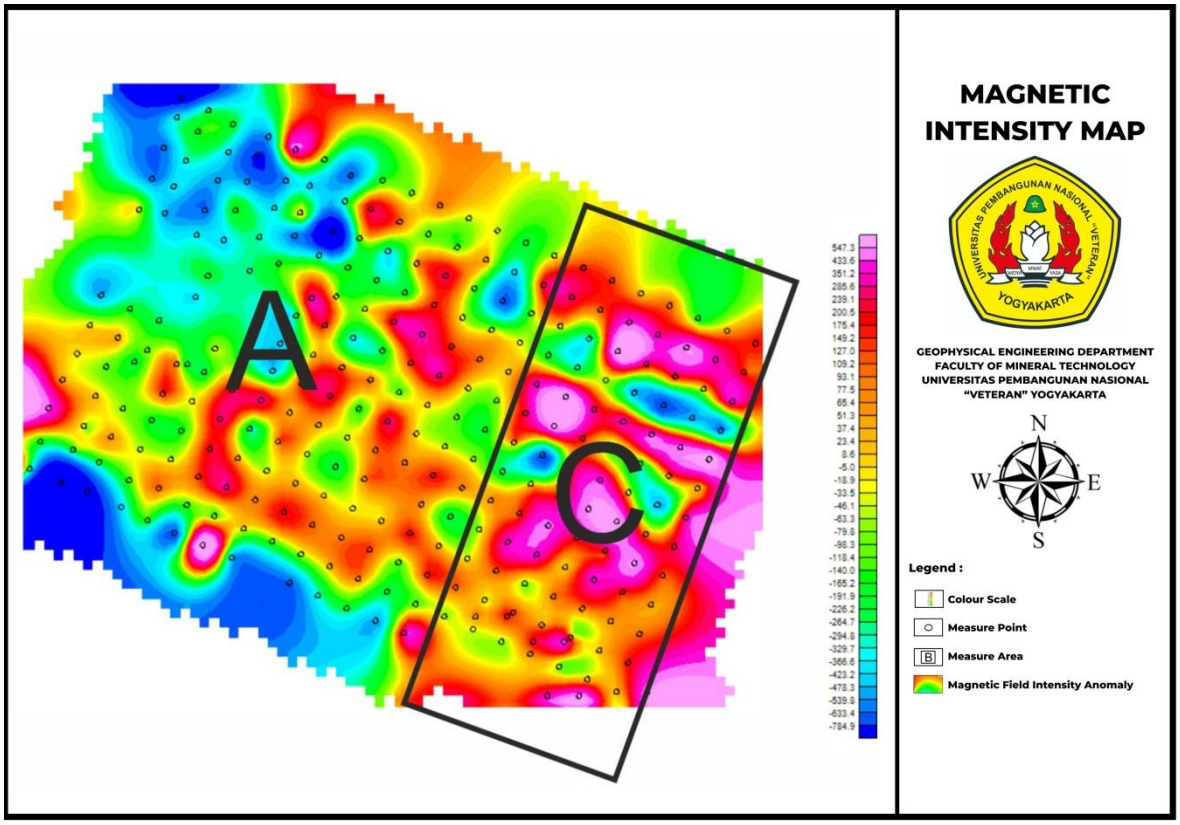

Figure 5. Map of Magnetic Intensity in Cluster A

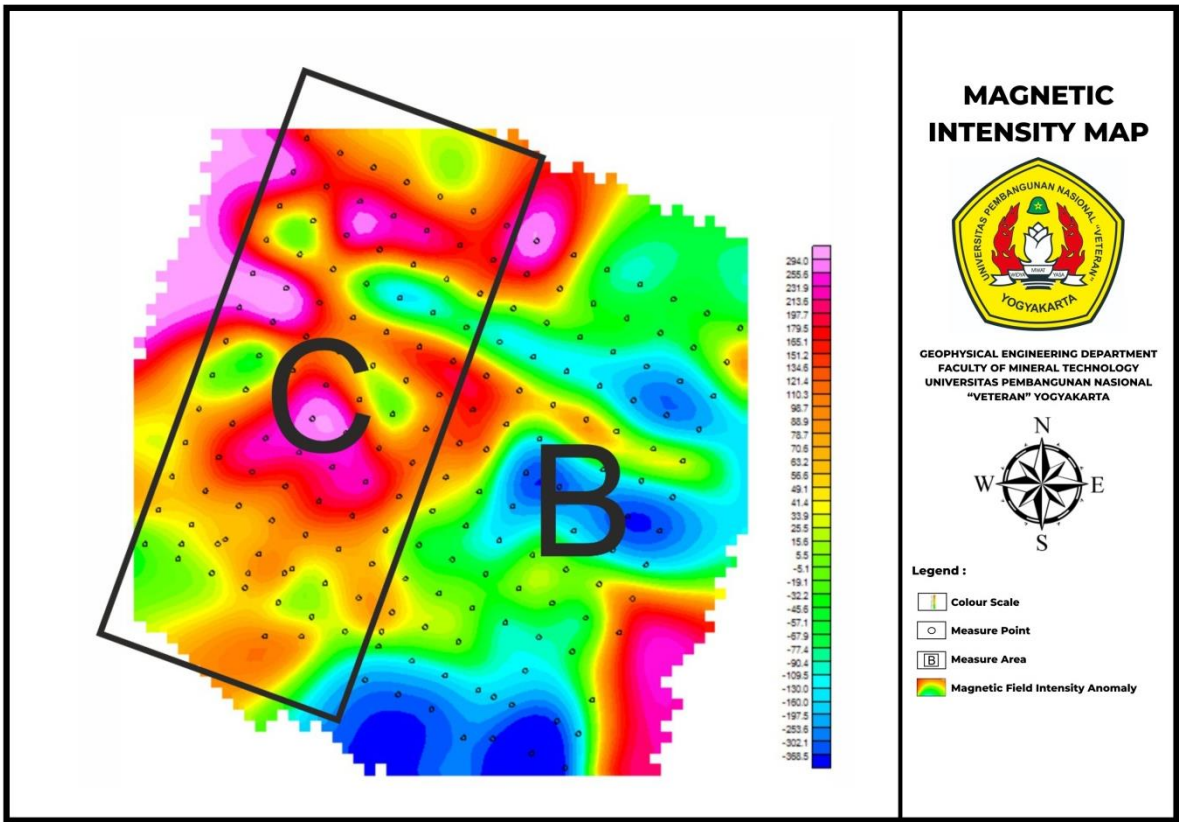

Figure 6. Map of Magnetic Intensity in Cluster B

PROCEEDINGS
JOINT CONVENTION BANDUNG (JCB) 2021
November 23rd – 25th 2021

Basin Identification Using Satellite Data GGMplus (Global Gravity Model plus) V.2013 as a Preliminary Survey of Oil and Gas Field Exploration

Indah Mustika Dewi[1], Dimas Bayu Seto[1], Hangga Bayu Krisna[1], Dewi Sintia Reka[2],
[1]Geophysical Department, FMIPA, Universitas Gadjah Mada
[2]Geological Engineering Department, Engineering Faculty, Universitas Gadjah Mada

Abstract

A gravity survey is an initial survey conducted in oil and gas exploration activity. Gravity anomaly data from GGMplus (Global Gravity Model Plus) is used in this research to determine the presence of sub-basin in the area of interest, which refers to the Karawang Geological Map. The use of GGMplus data refers to its advantages, as it has a high resolution of 200 m. GGMplus Gravity Anomaly data is then processed to calculate the Complete Bouguer Anomaly (CBA) value. Furthermore, spectrum analysis was carried out on CBA data and generated an estimated depth of the regional anomaly source of 14808 m, while the residual anomaly source was at a depth of 290 m. The CBA data is then separated using Upward Continuation Filter to produce Regional Anomaly, while the Residual Anomaly is produced by subtracting CBA with Regional Anomaly. Based on the residual anomaly map, the high anomaly in the southern region indicates the presence of hilly structures from the Bogor zone which are composed of high density rocks, while the low anomaly in the center of the study area is interpreted as sedimentary materials deposited in the sub-basin location which becomes the target of this research. Based on the geological information of the study area, the existence of this sub-basin is influenced by local fault movements in the graben mechanism. Therefore, a derivative analysis is needed that aims to clarify the exact location of the boundaries of the fault structure, which in this study used the first horizontal derivatives and second vertical derivatives methods. 2.5D forward modeling was then carried out to provide a clearer subsurface picture related to the sub-basins in the study area.Thus, it can be concluded that the gravity anomaly map generated from the GGMplus data can be used as supporting data to conduct a preliminary survey of oil and gas exploration.

Keywords: Basin, GGMplus ,Gravity, Kerawang, Satellite

Introduction

The current condition of the oil and gas industry in Indonesia requires the companies to be able to find new sources of basins that can be used as new prospect areas. Before a seismic survey, a preliminary survey is required to locate a hydrocarbon prospect area. The gravity method is one of the geophysical methods that is included in the passive method because the measurements are sourced directly from the gravitational field emitted by the earth. The variations in the earth's gravitational field are caused by differences in the density of rock in each layer of the earth. Because it may illustrate the basin prospect in that location, the gravity method can be utilized as a pre-seismic survey. This research aims to identify basins using Satellite Data GGMplus (Global Gravity Model plus) V.2013. Administratively, the research area is in the Kerawang Regency, West Java Province, Indonesia and the geology of the research area is included in the Karawang geological map which has been mapped by Achdan and Sudana, 1992 (Figure 1). Based on the physiography according to van Bemmelen (1949), Karawang geological map is included in the Lowland Zone of southern Jakarta and the south side of the research location is included in the Bogor physiographic zone. The formations of the research area consist of Jatiluhur Formation (Tms), Sandstone and conglomerate unit (Qav), and alluvium deposits (Qaf). In general, the lithology scattered in the research area is in the form of sandstone, tuff, limestone, claystone, conglomerate, and clay-sandy deposits.

The geological structure found in the research area is in the form of faults and folds in the Jatiluhur Formation, Parigi Formation, and Subang Formation as shown in the figure 1. The faults in the area are normal faults, reverse faults, and transforms. In general, the normal fault in the region is oriented NE - SW, the reverse fault is oriented SE - NW, and the transform is oriented SE - NW and NE - SWt. Meanwhile, the fold structure found in this area is in the form of anticlines and synclines whose fold axes have a SE-NW orientation.

Data and Method

This research is conducted by processing GGMPlus Gravity Data Model which is obtained from the official website of Global Gravity Model plus (GGMplus) Gravity Data Extraction (http://murray-lab.caltech.edu/GGMplus/index.html). GGMPlus data is a gravity model data with a resolution of 200 m provided by the Western Australian Geodesy Group at Curtin University. The type of Gravity field component used in this research is Free Air Anomaly/Gravity Disturbance with longitude latitude as coordinates. We also use Digital Elevation Model

(DEM) which extracting from Arcgis helps calculate terrain correction. There is also a geological map to support data for 2d subsurface modelling.

After that we change the geographic coordinates of the GGMPlus data to UTM coordinates which can then be used as input data for making Local DEM and Regional DEM grids in software Global Mapper. The grid is used to get the terrain correction values. After the terrain correction value is obtained, the process is carried out to obtain the ABL value (Complete Bouguer Anomaly). The ABL data is used as input to perform spectrum analysis.

For advanced processing, we do separation of regional anomalies and residual anomalies, as well as the FHD (first horizontal derivative) and SVD (Second Vertical Derivative) processes. The spectrum analysis process is carried out by making an incision on the ABL map for further calculations to obtain the estimated regional and local depth values. The filter used to separate regional and residual effects is an upward continuation with continuation distance is 1100 m, and kriging gridding method. FHD and SVD processing is carried out on the residual anomaly map with the aim of clarifying the structure contained in the research area. The geological data which has been mentioned before is used to interpret by correlating with the result. And the final result will answer the question about subsurface structure in X field And its relation with existence basin as a preliminary survey of oil and gas exploration.

Elevation value is used to calculate bouguer correction based on the following equation [Eq.1]

$CB=2.\pi.G.\rho.hp$ …….(1)

With ρ is the Bouguer density, G is the universal gravitational constant, and hp is the elevation of point P

Simple Bouguer Anomaly (ABS)

The simple Bouguer anomaly is obtained by subtracting the value of the Free Air anomaly (FA) with the Bouguer correction.

$\Delta gB= \Delta gFA-CB$……. (2)

Terrain Correction

Terrain correction is carried out to limit the Bouguer slab to be more realistic and closer to the actual situation with undulating topographic conditions such as valleys and mountains.

Complete Bouguer Anomaly (CBA)

Complete Bouguer Anomaly (ABL) is the total regional anomaly, residual, and noise, which can be written mathematically as follows.

$\Delta g= gregional+gresidual+noise$ …..(3)

Anomaly separation is used to provide a more specific picture of the desired research target. The three types of data have their own signal characteristics, which has a larger wavelength, indicating a deep anomaly. While has a smaller wavelength, describing the location of the shallow anomaly.

Spectrum Analysis and Anomaly Separation

Spectrum analysis can be used to determine the estimated depth of an anomaly, both regional and residual. Spectrum analysis is done by applying the Fourier transform which can convert a signal into a sum of several sinusoidal signals of various frequencies. In this study, anomaly separation is performed using upward continuation which is a low pass frequency filter.

Second Vertical Derivative

Second Vertical Derivative (SVD) is part of the derivatives analysis that can describe residual anomalies associated with shallow structures such as faults. Therefore, this SVD analysis can be used to identify fault types. The gravitational field satisfies the Laplace equation, therefore the SVD calculation can be derived directly from the Laplace equation for the gravity anomaly on the surface with the equation

$$\nabla_g^2 = \frac{\partial^2 g}{\partial x^2} + \frac{\partial^2 g}{\partial y^2} + \frac{\partial^2 g}{\partial z^2} = 0$$

$$\frac{\partial^2 g}{\partial z^2} = -\left(\frac{\partial^2 g}{\partial x^2} + \frac{\partial^2 g}{\partial y^2}\right) \text{.....(4)}$$

First Horizontal Derivative

The FHD method is carried out by deriving the vertical component of the gravitational potential field (in this case the Bouguer Anomaly) with respect to the horizontal components (x and y). Derivating bouguer anomaly about the x-axis is formulated according to the following mathematical equation.

$$\frac{dg_z(x)}{dx} = \frac{\partial g_z}{\partial x} = \frac{\partial^2 U}{\partial z\, \partial x} \text{ ..... (5)}$$

The equation is then carried out also on the y-axis. The results of each resultant components to get the total FHD anomaly according to the equation following

$$\sqrt{\left(\frac{dg_z(x)}{dx}\right)^2 + \left(\frac{dg_z(y)}{dy}\right)^2} \text{ .....(6)}$$

Result and Discussion

From the complete bouguer anomaly map (Figure 2), the results show that the value of the gravity anomaly ranges from 27 mGal - 57 mGal. The high value of the gravity anomaly is located on the south side of the map, while the low anomaly is distributed to form a circular pattern in the center of the map. Furthermore, an anomaly separation method was carried out on the Complete Bouguer Anomaly Map, which resulted in the Regional Anomaly Map and Residual Anomaly Map. After the comparison, the anomaly trend that refers to the research target can be seen more clearly

on the Residual Anomaly Map. Therefore, in this paper only the residual anomaly map is shown, which can be seen in Figure 3. From the Residual Anomaly Map (Figure 3), it is shown that the gravity anomaly value ranges from -2.2 mGal to 2.6 mGal. In the southern part of the Residual Anomaly Map, there is distribution of a high anomaly with a value range of 1 mGal to 2.6 mGal, which indicates the presence of hilly structures from the Bogor zone which are composed of high density rocks.

as an indication of a folded structure (anticline) in the area. Meanwhile, the low closure anomaly with a value range of -2.2 mGal to - 1 mGal is in the middle area extending to the west as an indication of the existence of a local basin in the area. The contrast of high and low gravity values shown at the bottom of the residual anomaly map indicates the presence of a fault structure in the area. Furthermore, SVD analysis was carried out in the area to determine the type of fault found in the area.

Spectrum analysis was carried out on a complete reduced bouguer anomaly map to get an estimate of the depth value of the regional anomaly source of 14808 m, while the residual anomaly source was at a depth of 290 m. In the southern part of the Residual Anomaly Map, there is a high closure anomaly with a value range of 0.8 mGal to 1 mGal as an indication of a folded structure (Anticline) in the area. Meanwhile, the low closure anomaly with a value range of -0.8 mGal to -0.6 mGal is in the middle area extending to the west as an indication of the existence of a local basin in the area.

The contrast of high and low gravity values shown at the bottom of the residual anomaly map indicates the presence of a fault structure in the area. Furthermore, SVD analysis was carried out in the area to determine the type of fault found in the area. Spectrum analysis was carried out on a complete reduced bouguer anomaly map to get an estimate of the depth value of the source of the anomaly residual.

Further processing in the form of SVD (Second Vertical Derivative) is carried out on the Residual Anomaly Map, which then produces the Residual SVD Anomaly Curve as a quantitative analysis to determine the type of fault structure (fault) in the area.

Conclusions

- Residual anomaly map shows anomalous contrast indicating the occurrence of a basin.

- Analysis of residual SVD derivatives showed that the fault in the study area incision was a normal fault type.

References

Achdan dan Sudana, 1992, Pusat Penelitian dan Pengembangan Geologi, Bandung.

Bemmelen, R.W. Van. 1949. Vol 1A. Amsterdam: Government Printing Office, The Hague.

PROCEEDINGS
JOINT CONVENTION BANDUNG (JCB) 2021
November 23rd – 25th 2021

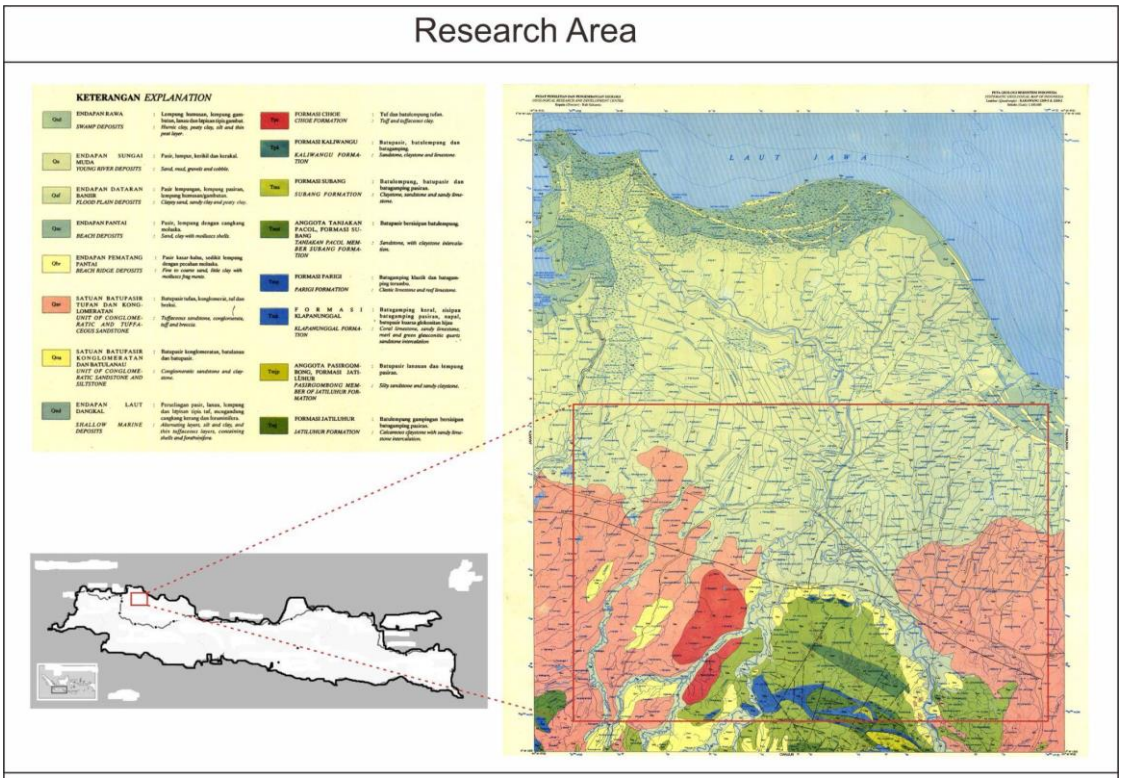

Figure 1: Research area is included in the Karawang geological map which has been mapped by Achdan and Sudana, 1992.

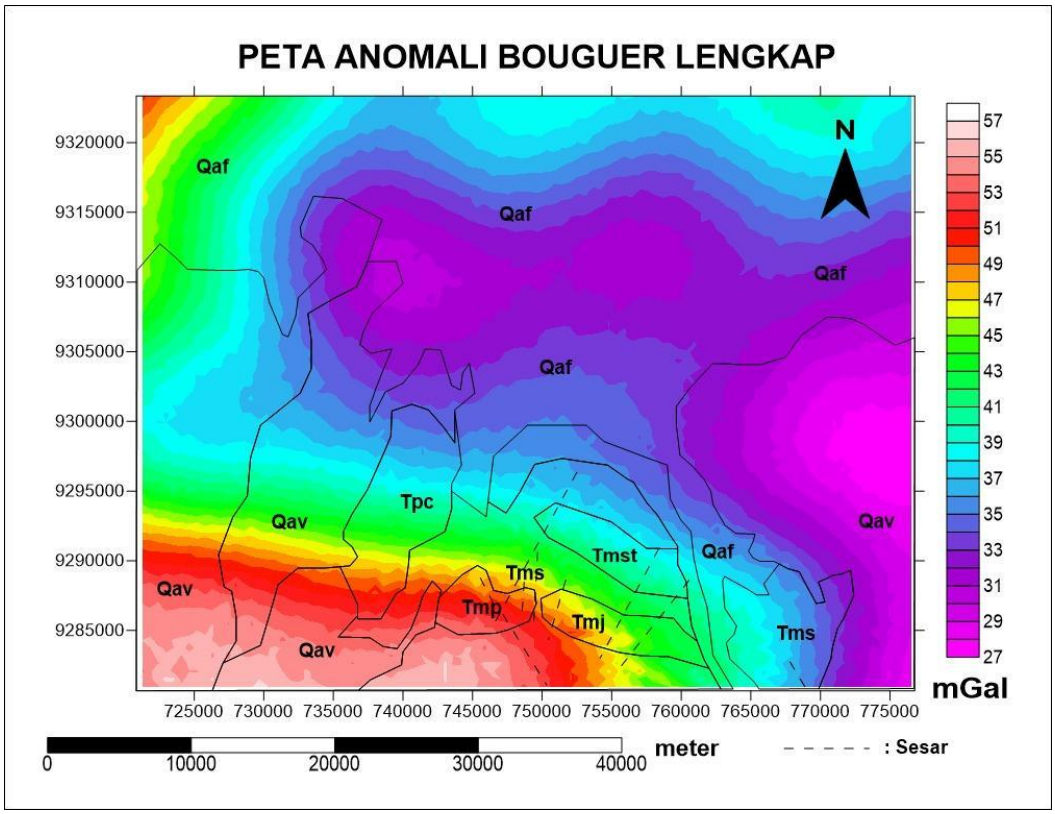

Figure 2: ABL analysis

PROCEEDINGS
JOINT CONVENTION BANDUNG (JCB) 2021
November 23rd – 25th 2021

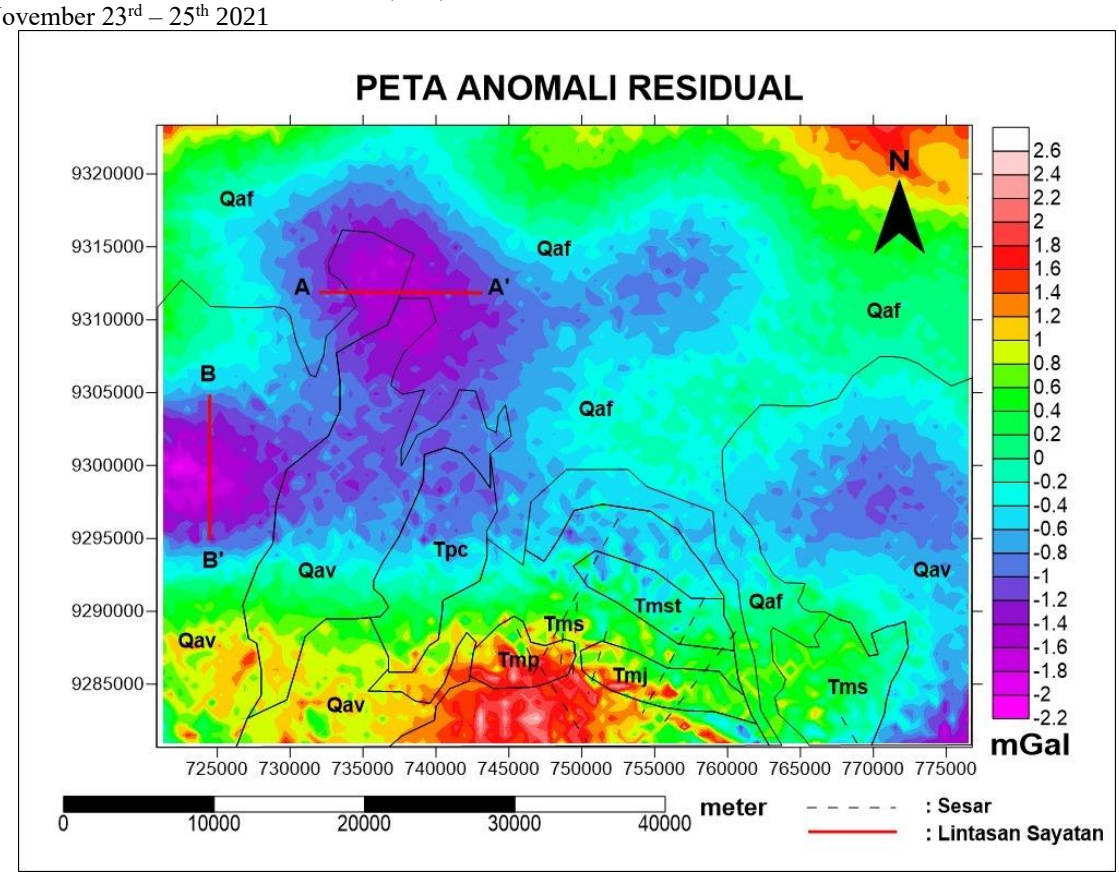

Figure 3: Residual Anomaly Map

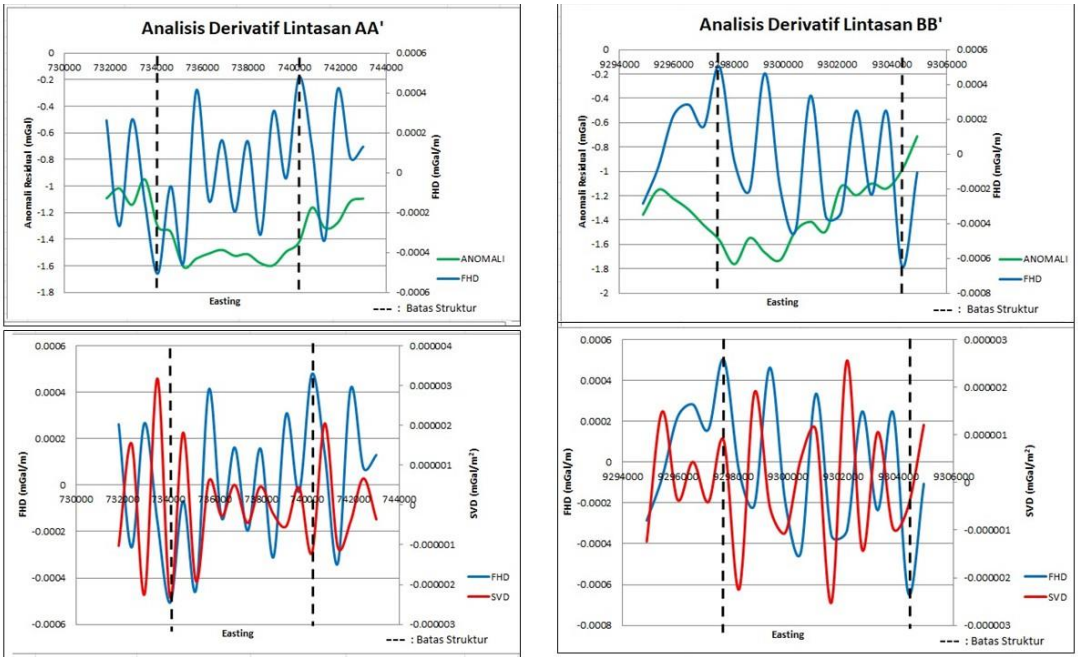

Figure 4: Derivative analysis curve

PROCEEDINGS
JOINT CONVENTION BANDUNG (JCB) 2021
November 23rd – 25th 2021

Study of 2014 – 2019 Water Budget in Ciminyak Sub-Watershed, West Bandung Regency

Diandra Abi Rafdi[1], Mochammad Prahastomi[1], Dyah Nindita Sahdarani[1]
[1]Program Studi Geologi, Fakultas Matematika dan Ilmu Pengetahuan Alam, Universitas Indonesia,
Jl. Margonda Raya Pondok Cina, Depok, 16424, Indonesia

Abstract
The research was conducted in Ciminyak Sub-Watershed, West Bandung Regency, West Java Province, part of the Citarum Watershed. The Ciminyak Sub-Watershed is a critical land area which currently in undergoing recovery. The phenomenon of critical land in the Ciminyak Sub-Watershed can result in underutilization of groundwater. Therefore, an effort is needed to identify the potential of groundwater in the Ciminyak Sub-Watershed so that it can be utilized optimally. This effort can be done by conducting research using the water budget calculation method. Based on the calculation, the largest potential discharge and groundwater reserve occurred in 2016, with the potential discharge of 491,448,694.62 m^3/year and reserve of 465,636,522.42 m^3/year. Based on this study, the phenomenon of critical land that occurs does not significantly affect the potential value of groundwater as the precipitation discharges in the period 2014 – 2016 were higher than the runoff and evapotranspiration discharges. This is supported by the results of the calculation of the water criticality index, which shows the index values in the Ciminyak Sub-Watershed generally classified as "not-critical".

Introduction
The Ciminyak Sub-Watershed is 332 square kilometers and located at 7°3'36.7"S, 107°3'25.6"E and 6°53'27.4"S, 107°33'10.9"E. Regionally, the research area includes in Lembar Cianjur (Sudjatmiko, 1972), Lembar Bandung (Silitonga, 1973), and Lembar Sindangbarang & Bandarwaru (Koesmono, Kusnama, & Suwarna, 1996). The Ciminyak Sub-Watershed is one of the Sub-Watersheds included in the Citarum Watershed recovery program to overcome the critical land problems. The phenomenon of critical land in the Ciminyak Sub-Watershed can result in underutilization of groundwater, because it will affect the runoff water discharge in a water budget system. Underutilization of groundwater will impact on the social and economic life of the surrounding community such as a decrease in production functions, conservation, and other impacts. Therefore, an effort is needed to identify the potential of groundwater in the Citarum Watershed so that the groundwater can be utilized optimally. This effort is carried out by conducting research based on the water budget calculation method. The final result of this study is the potential groundwater discharge (infiltration) and groundwater reserve discharge, which provides information on the availability and demand for groundwater in the Ciminyak Sub-Watershed.

Data and Method
The main object of this research is to determine the potential of groundwater and groundwater reserves in the Ciminyak Sub-Watershed, West Bandung Regency in the 2014 – 2019 period. This study mainly uses secondary data, which obtained from the company or agency providing the data. The list of datasets used in this study can be seen in the flow chart in Figure 1. The method uses water budget calculations based on the precipitation, evapotranspiration, and runoff discharge. These calculations were divided into 7 areas of polygon (rainfall stations) referring to the Thiessen Method. This method forms area of polygonal plane based on the network of rain stations. Each polygonal area represents a value of the calculations (Sudarmadji, Pramono, & Widyastuti, 2019). Precipitation discharge were calculated using the rainfall data from these 7 stations to get the annual average rainfall value (m/year) from January to December. To calculate the evapotranspiration, Thornthwaite Method (1948) was used to calculate monthly evapotranspiration using monthly mean temperature dataset from January to December from a climatological station (Nugroho, 1989). After they were corrected, the monthly evapotranspirations are added up to obtain the annual evapotranspiration value. To calculate the runoff discharge, parameters of the runoff coefficient (C), effective precipitation (I), and the area of each land cover (A) are required. The runoff discharge can be calculated by multiplying the values of C, I, and A by the value of 0.078. Determination of the C value is done by processing secondary data of land cover maps that provide information about land use at each polygonal area.

Infiltration discharge can be calculated by subtracting the precipitation discharge with the evapotranspiration discharge and the runoff discharge. The calculated infiltration discharge value is the groundwater potential contained in the Ciminyak Sub-watershed in a year or period. The calculation of groundwater demands require the population data per sub-district in West Bandung Regency, which obtained from Badan Pusat Statistik. The demands are then calculated by multiplying the number of residents per sub-district, the amount of water needed per day, and 365 (the number of days in a year). The amount of water needed per day refers to the classification of the SK-SNI Air Bersih in 2002 based on the type of city and population. Groundwater reserves are the potential discharge of groundwater remaining after being deducted by the population's water needs in one year.

The water criticality index can be calculated by rationing the amount of groundwater demand and the amount of groundwater availability in percentage (%). The percentage level then grouped based on the classification according to the SK. Menhut No.52/KPTS-II/2001 concerning Guidelines for the Implementation and Management of Watersheds, which divides the levels into four classes : from not critical to very critical.

Result and Discussion
The Ciminyak Sub-Watershed consists of steep mountain reliefs and very steep mountains with flat to steep morphometry (BIG, 2018). Based on studies from Sudjatmiko (1972), Silitonga (1973), Koesmono, Kusnama, and Suwarna (1996), the Ciminyak Sub-Watershed are composed of volcanic, pyroclastic, clastic and carbonate sediments, and alluvial deposits. By the hydrogeological aspect, the research area is dominated by aquifers of small local productivity with low permeability (Badan Geologi, 2018).

Based on the calculation results, the highest precipitation discharge was in 2016. While the lowest discharge occurred in 2015 (Figure 2a). Then, the evapotranspiration discharge increased from 2014 – 2016. While the evapotranspiration discharge decreased from 2016 to 2018. In 2018 – 2019, the evapotranspiration discharge increased significantly (Figure 2b). This is caused by the increasing of temperature significantly where in 2019 the maximum temperature reached 26 degrees Celsius. Based on the calculation, the results shows that the runoff discharge decreased in 2014 – 2015, 2016 – 2017, and 2018 – 2019. While it increased in 2015 – 2016 and 2017 – 2018 (Figure 2c). The discharge of infiltration then can be calculated. Based on the results, the infiltration decreased in 2014 – 2015 and 2016 – 2017. While the increases occured in 2015 – 2016 and 2017 – 2019 (Figure 2d). The fluctuation occurred as the changing of precipitation, evapotranspiration, and runoff discharge in the period 2014 – 2019. Therefore, precipitation, evapotranspiration, and runoff become major influences in infiltration on a water budget system.

Based on calculations, the discharge of groundwater demands were also fluctuated (Figure 3). The decrease occurred in 2014 – 2015 and 2018 – 2019. While the increase occured in 2015 – 2018. This caused by the number of population that keeps changing every year. The increasing population will impact on the increasing demand for groundwater.

Based on the calculation of groundwater reserves, the order of reserves from the largest to the smallest can be determined based on the amount of discharge (Figure 4). The following is the order of groundwater reserves from the largest to the smallest in the period 2014 – 2019 :

- Reserves in 2016, were the largest groundwater reserves with discharge by 465,636,522.42 m^3/year.
- Reserves in 2014, were the second largest groundwater reserves with discharge by 263,644,864.58 m^3/year.
- Reserves in 2019, with discharge by 241,413,990.55 m^3/year.
- Reserves in 2018, with debit of 193,643,119.30 m^3/year.
- Reserves in 2017, with debit of 170,344,666.30 m^3/year.
- Reserves in 2015 were the lowest groundwater reserves with discharge of 15,262,894.04 m^3/year.

Based on the calculation results, in 2014 and 2016 - 2019 the water criticality indexes were classified as not-critical classification. This occurred as the percentage levels of water criticality index were still below 50%. While in 2015 the level reached 62.23%, which classified as the near critical classification with the percentage level range from 50% - 75% (Table 1). Thus, in terms of quantity, the Ciminyak Sub-Watershed still has enough water or has not lacked water, because within the 6 years the infiltration discharges were generally greater than the demands so that there are still remaining reserves that could be used for other necessities.

Conclusions

Based on the results of water budget calculations and graph readings, the largest potential discharge and groundwater reserves occured in 2016, amounted to 491,448,694.62 m^3/year for potential groundwater discharge and reserve discharge of 465,636,522.42 m^3/year. In the 2014 – 2019 period, the quantity of precipitation discharges were still higher than the runoff and evapotranspiration discharges, which indicate that the critical land phenomenon that occurs does not significantly affect the potential value of groundwater. This is supported by the results of the calculation of the water criticality index for 2014 – 2019, where the Ciminyak Sub-watershed generally has a criticality index value which is generally still below 50%. Nevertheless, spatial and land management in the Ciminyak Sub-watershed still needs to be done. Good spatial and land management will be beneficial in maintaining the distribution of land cover so that the runoff value will always be stable and well maintained every year. Furthermore, the aquifer in the Ciminyak Sub-watershed is dominated by tertiary volcanic rocks which have low permeability, making it difficult to pass water. Therefore, it is necessary to conduct further studies to determine the potential zoning of groundwater in the Ciminyak Sub-Watershed.

References

Badan Geologi, 2018, Peta Hidrogeologi Kabupaten Bandung Barat, Provinsi Jawa Barat, Bandung: Pusat Air Tanah dan Geologi Tata Lingkungan, Kementerian ESDM.

Badan Informasi Geospasial (BIG), 2018, Data DEMNAS, http://tides.big.go.id/DEMNAS/DEMNAS.php

Badan Standardisasi Nasional, 2002, Penyusunan Neraca Sumber Daya Bagian 1: Sumber Daya Air Spasial, Standar Nasional Indonesia, SNI 19-6728.1-2002.

Koesmono, M., Kusnama, & Suwarna, N., 1996, Peta Geologi Lembar Sindangbarang dan Bandarwaru, Bandung: Pusat Penelitian dan Pengembangan Geologi.

Nugroho, A., 1989, Beberapa Teori dan Aplikasi Rumus Thornthwaite Untuk Menghitung Jumlah Cadangan Sumberdaya Air, Majalah Geografi Indonesia, 27-38.

Silitonga, P., 1973, Peta Geologi Lembar Bandung, Bandung: Pusat Penelitian dan Pengembangan Geologi.

Sudarmadji, Pramono, H., & Widyastuti, M, 2019, Pengelolaan Sumberdaya Air Terpadu, Gadjah Mada University Press.

Sudjatmiko, 1972, Peta Geologi Lembar Cianjur, Bandung: Pusat Penelitian dan Pengembangan Geologi.

Republik Indonesia, Surat Keputusan Menteri Kehutanan No. 52/KPTS-II/2001 tentang Pedoman Penyelenggaraan Pengelolaan Daerah Aliran Sungai.

Thornthwaite, C., 1948, An approach towards a rational classification of climate, Geograph, Rev., 55-94.

PROCEEDINGS
JOINT CONVENTION BANDUNG (JCB) 2021
November 23rd – 25th 2021

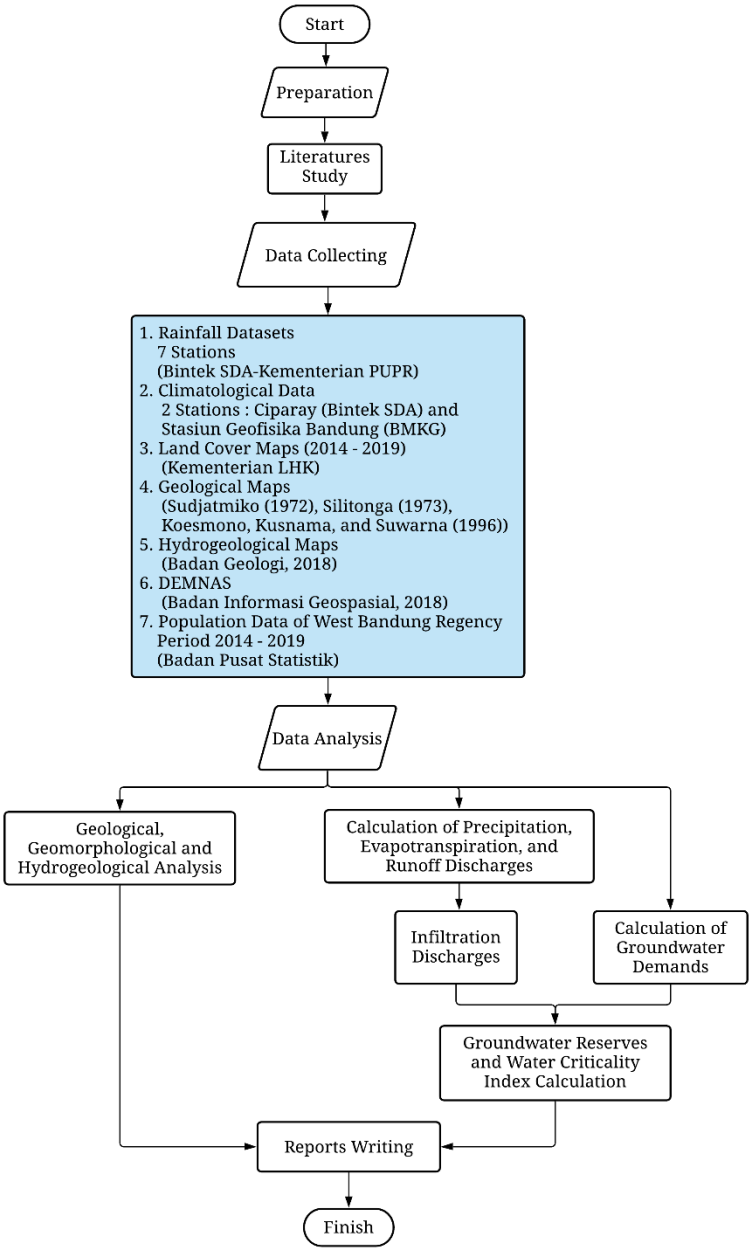

Figure 1. Research Flow Chart

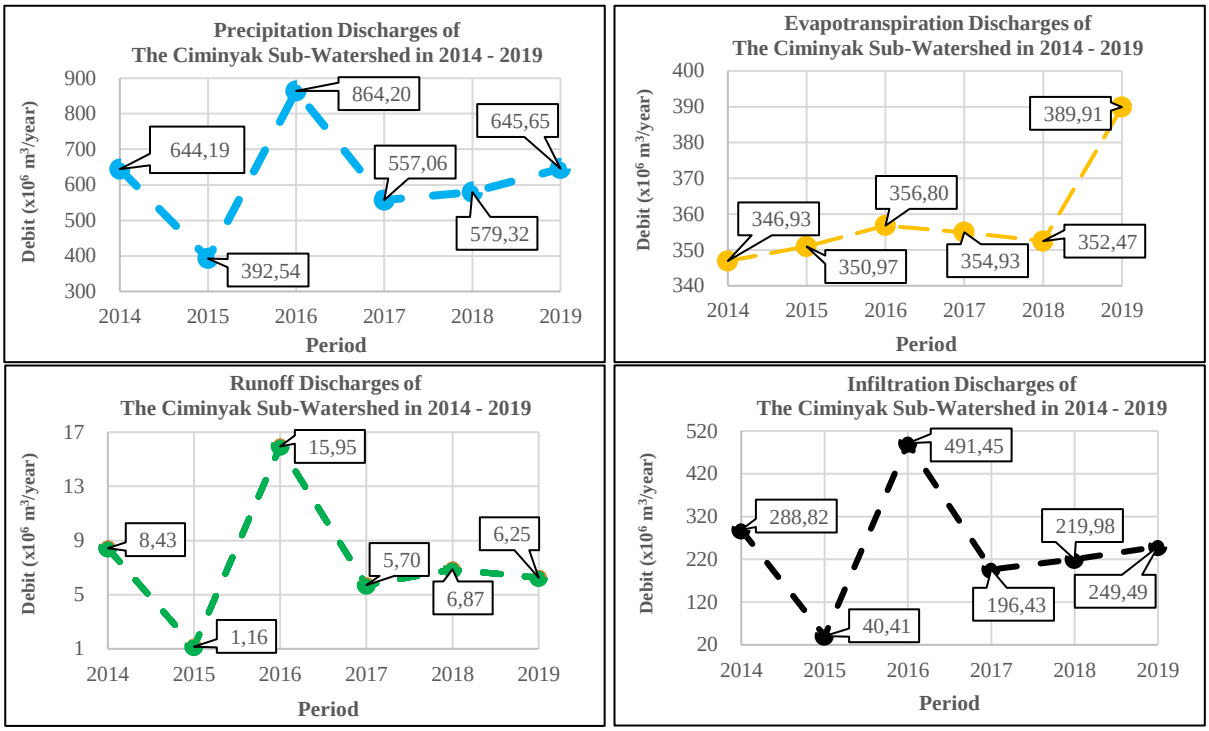

Figure 2. a) Graph of Precipitation (top left). b) Graph of Evapotranspiration (top right). c) Graph of Runoff (bottom left). d) Graph of Infiltration (bottom right) In Ciminyak Sub-Watershed Year of 2014 – 2019

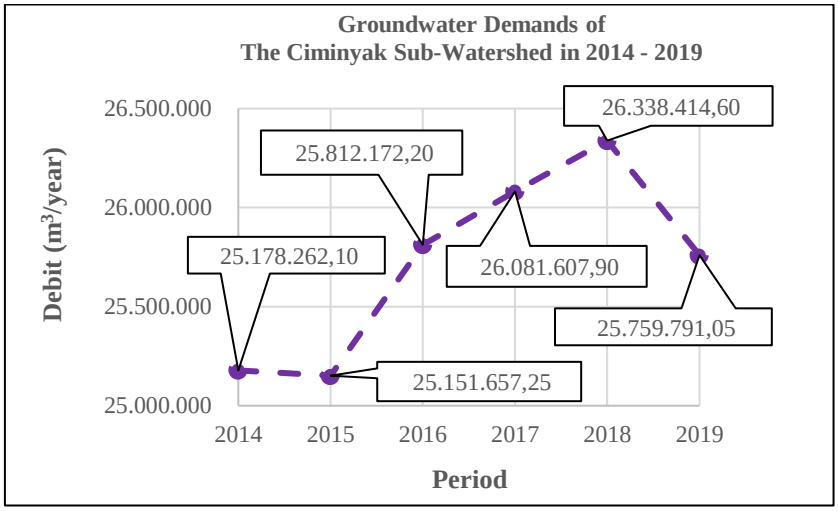

Figure 3. Graph of Groundwater Demands in Ciminyak Sub-Watershed Year of 2014 – 2019

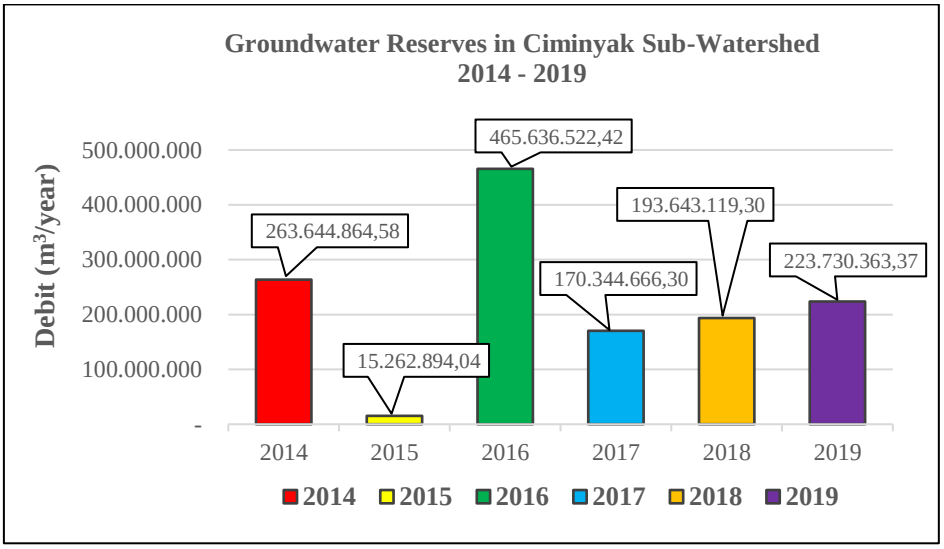

Figure 4. Graph of Groundwater Reserves in Ciminyak Sub-Watershed Year of 2014 – 2019

Table 1. Calculation of Water Criticality Index Year of 2014 – 2019 in Ciminyak Sub-Watershed

Period	Debit (m^3/tahun)		Percentage (%)	Criticality
	Demands	Infiltration		
2014	25.178.262,10	288.823.126,68	8,72	Not Critical
2015	25.151.657,25	40.414.551,29	62,23	Near Critical
2016	25.812.172,20	491.448.694,62	5,25	Not Critical
2017	26.081.607,90	196.426.274,20	13,28	Not Critical
2018	26.338.414,60	219.981.533,90	11,97	Not Critical
2019	25.759.791,05	249.490.154,42	10,32	Not Critical

PROCEEDINGS
JOINT CONVENTION BANDUNG (JCB) 2021
November 23rd – 25th 2021

Utilization of Standard Deviation and Gradient Data on Automatic Processing: Statistical Filtering and Diurnal Correction on Geomagnetic Method Using Python

Aji Darma Maulana[1]
Bayu Setiawan[2,3]
Naila Andriani[3]
[1]*Universitas Pembangunan Nasional "Veteran" Yogyakarta*
[2]*EnerGIS Indonesia*
[3]*Universitas Indonesia*

Abstract

The ability to recognize mathematical and physical processes from reduction and filtering data is crucial to represent the geological condition on the geoscience data. A justification at the interpretation stage could be meaningless if the processing does not satisfy any scientific concept. Conventionally, reduction and filtering processes would take relatively quite a long time and has subjective views. Thus, quantitative algorithm should have been done to higher the research's efficiency and effectivity.

This research offers an automatic processing method based on statistical analysis based on python, which is standard deviation as statistical filtering among the data and noise. The gradient data obtained from diurnal variation graphs are also used as parameter for further statistical filtering. Moreover, this method applied on base-rover magnetic with 17.92% statistical noise which would go through two despiking steps. Both steps characterize the data over individual and standard deviations as noise. Then, the low S/N ratio on diurnal variation is used as the diurnal correction. After all the processing steps, the consumed time for conventional and automatic processing compared to each other. It is also found out that the overcorrected event is getting lower after the despiking applied.

Keywords: Despiking, Magnetic, Standard Deviation, Python.

Introduction

In the geoscience data processing, mathematical and physical phase is very involved in resulting reliable data for further steps. One of geophysical methods that has quite complex processing stage is magnetic method. It is known that magnetic method processing could take times for relatively long, days to weeks. The time needed at this stage could be longer to higher the accuracy. Sometimes, even the processing phase of every processed data is also subjective, based on the geoscientist who processed the data. Due to the subjectivity, the processed data quality may be varied and inconsistent. Therefore, applying new method is needed as the only way to improve every aspect in processing phase.

As the time passes by, the data processing is growing into more modern and efficient way, that is by applying the automation. One of many programming languages, which is also used in this research, is Python. It is easier to understand and use than other programming languages. Moreover, it is a free source software that could be accessed by everyone. By applying automatic processing, the consumed time would be faster than the conventional processing. The accuracy of the processed data would also be higher and more consistent. Hence, the processing phase would be more effective and efficient.

Theory

1.) Magnetic Method

Magnetic method is a passive geophysical method that observe rocks' magnetic behaviour beneath the surface. The object's magnetic behaviour may come as inherent and/or as remanent feature. Inherent feature is a magnetic behaviour as the object has. Meanwhile, remanent feature is a magnetic behaviour due to the nature of ferromagnetic containing object. It also may cause by the magnetic field induction, in this case is the earth's magnetic field (Dentith & Mudge, 2014).

2.) Diurnal Correction

Riddihough (1971) states that the use of diurnal corrections is to separate the temporal variations of the earth's magnetic field from its geographical variations. The diurnal correction aimed to eliminate the daily magnetic field variation, with the formula as follows Eq.

$$H_{\mathrm{D}} = \frac{(tn-t0)}{(t1-t0)}\,(H1 - H0)$$

3.) Standard Deviation

The standard deviation is used to estimate the confidence interval under the given confidence

PROCEEDINGS
JOINT CONVENTION BANDUNG (JCB) 2021
November 23rd – 25th 2021

coefficient, or in the other word is to assess the data reliability (Denisov et al, 2006). It is expressed by Eq.

$$\sigma^{o}{}_{\mathrm{B}} = \frac{B}{2\pi}\frac{\sigma}{So}\sqrt{\sum_{j=0}^{N}\left[\frac{\partial F}{\partial tj}\right]}$$

The standard deviation used in this research is divided into Std+ and Std-, which acts as the upper and lower limit. The Std+ could be obtained by add the standard deviation to the mean while Std- by reduce the mean with standard deviation.

4.) Root Mean Square (RMS)

RMS error values in the geomagnetic field is a measure of how the data spread.

$$RMSE = \sqrt{\sum (fobs - fmodel)^2/N}$$

Data and Method

The data is a quite complete "X" field data between Proton Precession Magnetometer (PPM) Rover and base read of magnetic method. However, there are still some noises in the obtained data. This research aimed to reduce the noises by offering the new QC method, that is despiking technique.

Despiking is a technique to reduce noises, which present as spikes on the time series data graphs. The significant difference of data values are the causes of the spike's appearance. On the magnetic method, these spikes and data could be seen at the base time series data (**Fig.** 1). As seen on **Fig.** 1, Some of the rover data which coincide with the base data that contain spikes. The data is categorized as spikes if it passes the standard deviation value of the base data.

The despiking process consists of two steps, which are the first and the second Despiking (**Fig.** 2). The first Despiking uses standard deviation as noise reduction parameters. If the data passes the standard deviation value, it would be automatically reduced by the interpolation result of the data in between. Furthermore, the second despiking has three options to utilize:

a. Standard deviation with addition of Hvar gradient. Hvar, also known as diurnal variation, obtained from the differences of base and best datum data. So, Hvar gradient is value changes per time unit.

b. Standard deviation obtained from Root Mean Square (RMS) data.

c. Low pass frequency filter. The potential method data, the noise usually associated with high frequency. Therefore, low pass filter could be a despiking method option to reduce noise.

According to early Quality Control (QC), the data uses histograms as the filtered noise indicator. Geostatistically, good quality denoised data would show normal distribution histogram. Additional indicator for QC is by considering the distribution of base data that is not too significant by standard deviation of the Despiked base data.

Result and Discussion

The result obtained from the first Despiking is Diurnal Variation Graph that is free from the highly deviated noise, which is the noise due to the error of the tools when the measurement is being done. This process must be applied to all the denoising processes. The first Despiking result shown by **Fig.** 3, 4, and 5 with the blue line while the raw data could be seen with the red line. The histogram shows the difference from the applied and not applied first Despiking which formed the normal distribution. This situation suits nature characteristics as well.

The next processing stage is the second Despiking. This process has three method options with different approaches. The first option of second Despiking uses the standard deviation from instantaneous Hvar gradient as the filter. This option has the objective to remove the high deflection from Hvar gradient that caused high fluctuation value (highly spike on the graph).

On the other hand, the second option of second Despiking utilizes the standard deviation on the Hvar gradient data obtained from the first Despiking to be the parameter. Whereas the standard deviation obtained based on the RMS. So, the standard deviation would follow the data trend. In this method, the noise is defined as the Hvar that exceeds the standard deviation value based on RMS.

The third option considers the spectrum amplitude as the parameter from the Hvar gradient on the time series data. The noise is associated with high frequency, so this method has the objective to remove it with low pass frequency.

The map construction from the corrected Rover data with diurnal variation subsequently would be obtained automatically with the algorithm (**Fig.** 6). There is significant difference after Despiking applied to the base data which could overcome the pitfall of geomagnetic data interpretation.

Conclusions

The Despiking method aimed to reduce the spikes on the data which represents the noise so the S/N ratio would tend to be higher. The parameters used as the QC factor are the Histogram and the Moving Standard

PROCEEDINGS
JOINT CONVENTION BANDUNG (JCB) 2021
November 23rd – 25th 2021

Deviation. The recorded magnetic data went through the first Despiking using Standard Deviation, then to the second Despiking which was divided into three processes options, which are Hvar Gradient, RMS, and Lowpass filter. The map constructed from all the Despiking processes produces higher resolution with efficient time.

References

Denisov, A.Y., Denisova, O.V., Sapunov, V.A., Khomutov, S.Y. 2006. *Measurement Quality Estimation of Proton-Precession Magnetometers*. Earth Planets Space 58: 707 – 710.

Dentith, M., Mudge, S.T. 2014. Geophysics for the Mineral Exploration Geoscientist. Cambridge University Press, New York.

Jing, L., Lou, L., BiQiang, Z., WeiXing, W., Chen, Y. 2012. *Empirical Modeling of Ionospheric F2 Layer Critical Frequency Over Wakkanai Under Geomagnetic Quiet and Disturbed Conditions*. Science China Technological Sciences 55(5): 1169 – 1177.

Riddihough, R.P. 1971. *Diurnal Corrections to Magnetic Surveys – An Assessment of Errors*. Geophyisical Prospecting 19: 551 – 567.

Acknowledgements

The authors would like to express a lot of gratitude to Allah SWT and Joint Convention Bandung Committees that gave the opportunity to publish this research. Also, the enerGIS party who contributed the algorithm to the automatic processing in this research.

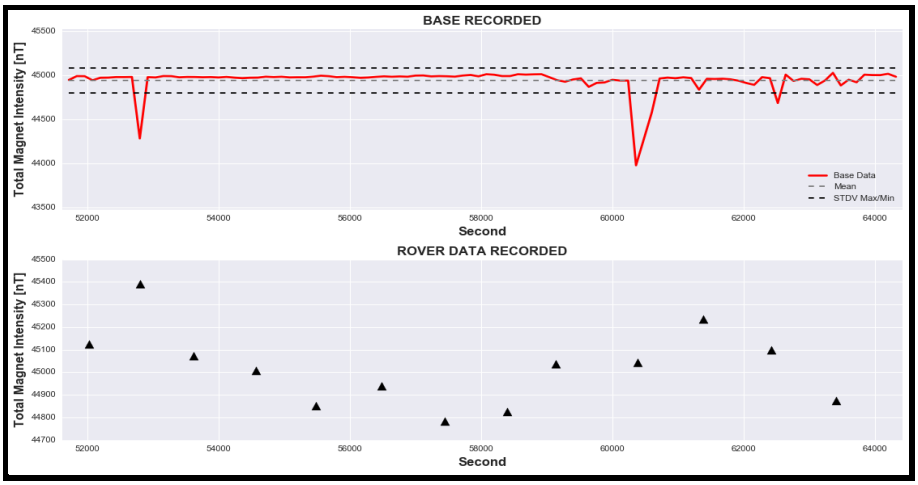

Figure 1. Base data (above) and Rover data (below).
Some of the rover data which coincide with the base data that contain spikes

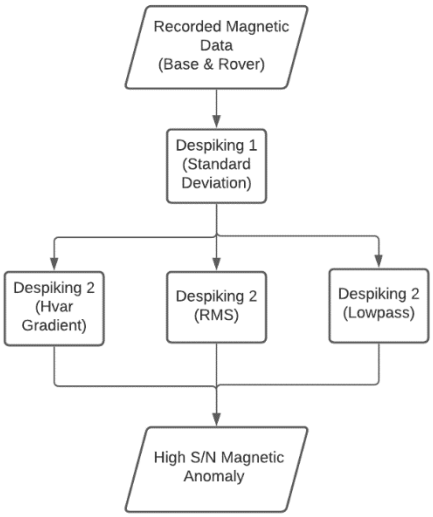

Figure 2. Workflow Diagram

PROCEEDINGS
JOINT CONVENTION BANDUNG (JCB) 2021
November 23rd – 25th 2021

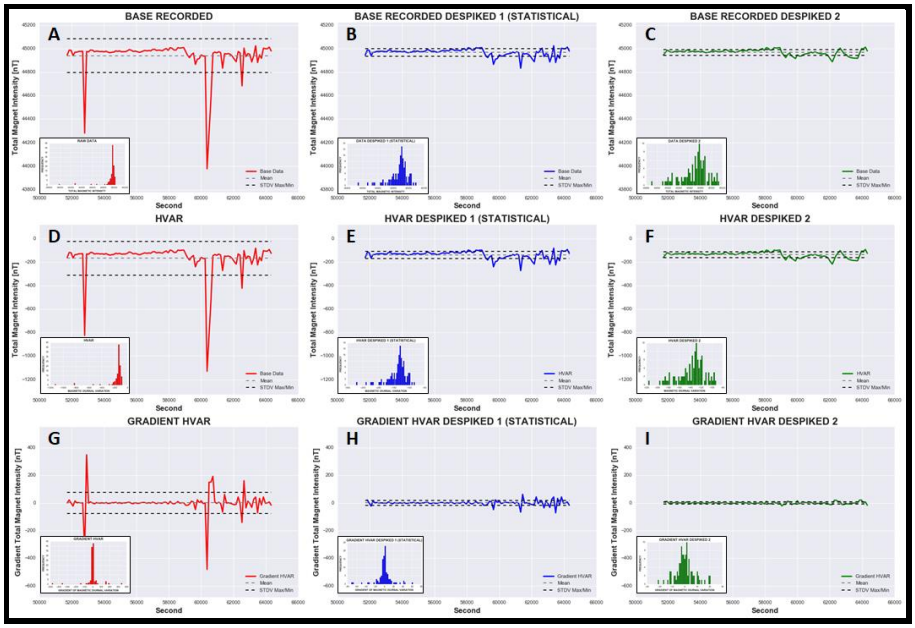

Figure 3. The raw recorded data base, Hvar, Hvar gradient before the first Despiking (A, D, and G) ; after first Despiking (B, E, and H) ; after the second Despiking using standard deviation based. All processes are based on **Hvar gradients** (C, F, and I). For the histogram QC, each graph shows the curves are more likely to formed normal distribution from the red, to blue, and the green with left to right orientation.

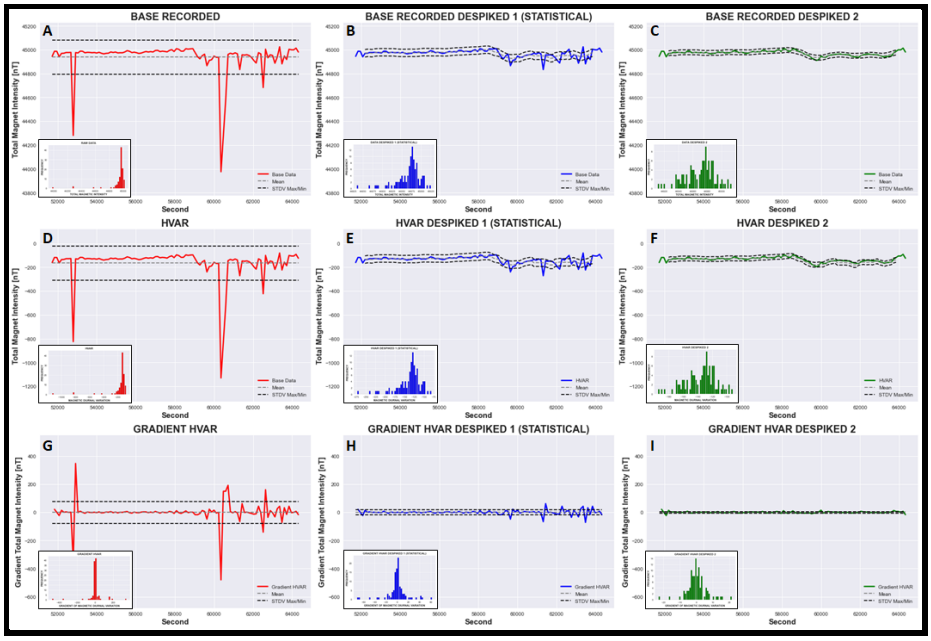

Figure 4. The raw recorded data base, Hvar, Hvar gradient before the first Despiking (A, D, and G) ; after first Despiking (B, E, and H) ; after the second Despiking using standard deviation. All the values are obtained from **RMS** data after first despiking (C, F, and I). For the histogram QC, each graph shows the curves are more likely to form normal distribution from the red, to blue, and the green with left to right orientation.

PROCEEDINGS
JOINT CONVENTION BANDUNG (JCB) 2021
November 23rd – 25th 2021

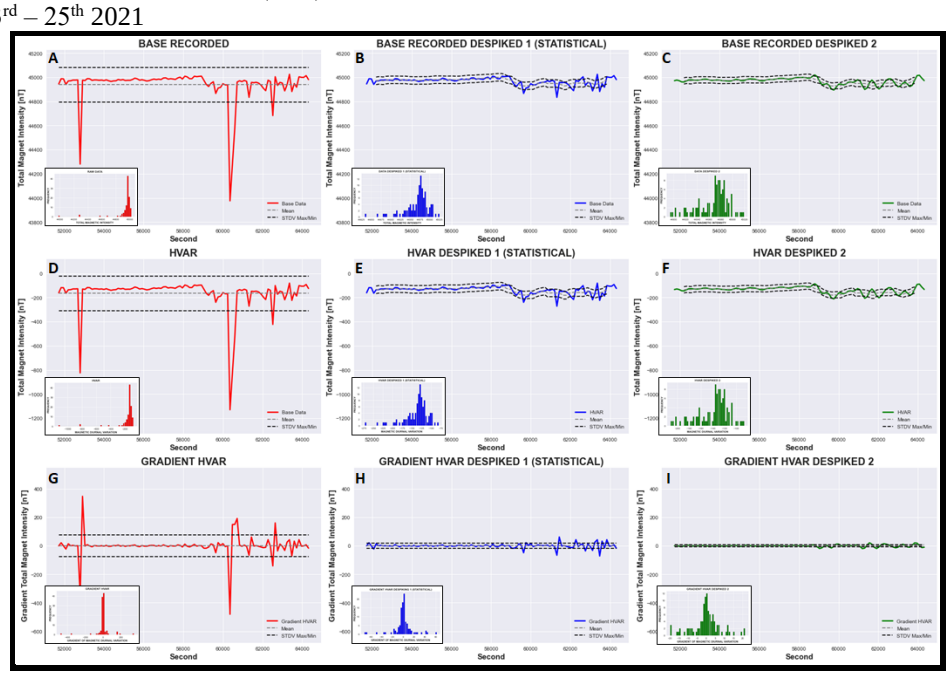

Figure 5. The raw recorded data base, Hvar, Hvar gradient before the first Despiking (A, D, and G) ; after first Despiking (B, E, and H) ; after the second Despiking. These processes are using **low pass filters** (C, F, and I). For the histogram QC, each graph shows the curves are more likely to form normal distribution from the red, to blue, and the green with left to right orientation.

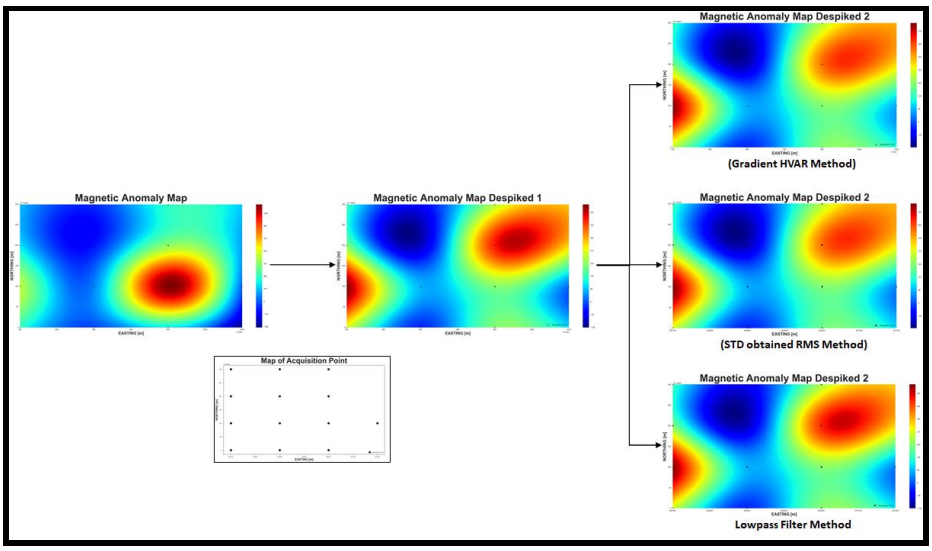

Figure 6. The Magnetic Anomaly map resulted from the magnetic processing. This figure shows the anomaly map before and after the first and second Despiking applied on each method.

PROCEEDINGS
JOINT CONVENTION BANDUNG (JCB) 2021
November 23rd – 25th 2021

Physical and Chemical Characteristics of Groundwater in Ciminyak Sub-watershed, West Bandung Regency

Hans Pintor Sahat Parulian[1], Mochammad Prahastomi[1], Dyah Nindita Sahdarani[1]
[1]Program Studi Geologi, Fakultas Matematika dan Ilmu Pengetahuan Alam, Universitas Indonesia, Jl. Margonda Raya, Pondok Cina, Depok, 16424, Indonesi

Abstract
The research area is located in Ciminyak Sub-watershed, West Bandung Regency, West Java Province. This research was conducted to identify the geological, hydrogeological, and their relationship to the physical and chemical characteristics of groundwater in the Ciminyak sub-watershed. Groundwater samples used are samples taken directly from the research area. The method used in this research is hydrochemical analysis using gibbs, stiff, piper, and durov diagrams. Hydrochemical analysis is carried out in the laboratory to identify the main ions present in groundwater. Other data were also collected, such as electrical conductivity, total dissolved solids, pH, and depth of the ground water table for making water contour maps. In addition, the correlation of field data with the hydrogeological map of the Ciminyak Sub-watershed. The results of the hydrochemical analysis showed that groundwater in the Ciminyak Sub-watershed has a dominant concentration of magnesium cation (Mg) and bicarbonate anion (HCO3). The dominant bicarbonate anion indicates that the water in the study area can be classified as fresh water. Then the other main ions have relatively different concentrations at each location. This is probably caused by the aquifer and geological conditions found in the Ciminyak Sub-watershed.

Introduction
One of the groundwater sources in West Java is the Ciminyak sub-watershed which is the upstream part of the Citarum watershed. The condition of the Citarum watershed is very worrying because high-intensity pollution has occurred from its upstream part (Republika, 2013). One of the locations that is badly polluted is the Saguling Dam, which is part of the Ciminyak Sub-watershed. The pollution that occurs is caused by the Saguling Dam which has a role to filter the dirt transported by the Citarum River. There have been several efforts made by the government, such as revitalizing and normalizing the banks of the Saguling Dam. However, these efforts have not been maximized because the pollution that occurs is still very concerning. Therefore, one of the efforts that can be done is to conduct research on the physical and chemical characteristics of groundwater in the Ciminyak Sub-watershed to determine the water content contained in groundwater in the area. the results of this This research was conducted in the Ciminyak sub-watershed area. Regionally, the Ciminyak sub-watershed is included in the geological map of the Cianjur sheet (Sudjatmiko, 1972), the Bandung sheet (Silitonga, 1973), and the Sindangbarang and Bandarwaru sheet (Koesmono, Kusnama, and Suwarna, 1996). The research area is the upstream part of the Citarum watershed. Based on Republika (2013), the condition of the Citarum watershed has experienced high-intensity pollution starting from the upstream. One of the heavily polluted locations is the Saguling Reservoir, which is part of the Ciminyak sub-watershed. Based on research by Sudarmadji, et al. (2014) in the Citarum River, the reservoir has the ability to restore water quality conditions naturally (natural self-purification capacity). However, this causes pollutants to settle and accumulate which can have a negative impact later on. Various efforts have been made by the government, such as revitalizing and normalizing the banks of the Saguling Dam. However, these efforts have not been maximized because the pollution that occurs is still very alarming.

This study carried out several measurements and analyzes to determine the characteristics of groundwater in the Ciminyak sub-watershed. The physical characteristics to be measured are pH, electrical conductivity, and the amount of dissolved solids. Meanwhile, the chemical characteristics to be analyzed are the main ions present in water, namely K, Ca, Mg, Na, SO4, Cl, HCO3, and CO3. The final result of this research is data on the physical and chemical characteristics of groundwater in the research area. The results of this study are expected to be used to assist in determining the efforts that can be made to overcome the pollution that occurs in the Ciminyak Sub-watershed. study can be used as a preference to determine the next effort that can be done to reduce the pollution that occurs in Ciminyak Sub-watershed.

Data and Method
This study uses primary and secondary data. The primary data used is groundwater samples taken directly from the research area. This sample will be processed in the laboratory to determine the concentration of the main ion contained in it. In addition, data collection on the physical properties of groundwater is also carried out directly in the field, including electrical conductivity, total dissolved solids, pH, and depth of the groundwater table. Then the secondary data used in this research is geological and hydrogeological map data. This data is used as supporting data for the correlation between physical and chemical properties of groundwater with geological and hydrogeological conditions in the study area.

The primary data taken in this study is groundwater. This groundwater sampling follows the standard method of the Indonesian National Standard (SNI) 6989.58:2008 concerning water and wastewater - part 58 : Groundwater sampling method. Groundwater samples that have been taken will then be analyzed in the BALITTANAH Bogor laboratory to identify the main ions contained in it. The results of the main ion in groundwater will then be plotted into several diagrams for further analysis, including: Gibbs diagram, stiff diagram, piper diagram, and Durov diagram. In addition, data taken directly in the field is data on the physical properties of groundwater. Measurement of the physical properties of groundwater is carried out by inserting the TDS-EC meter and pH meter into the

groundwater contained in each well. Then the last data taken directly in the field is the data on the depth of the ground water table. The measurement of the depth of the groundwater table is carried out using a meter and ballast.

The secondary data used in this study are geological and hydrogeological maps. The geological map used is a combination of 3 regional maps, namely the Cianjur geological map (Sudjatmiko, 1972), the Bandung sheet (Silitonga, 1973), and the Sindangbarang and Bandarwaru sheets (Koesmono, Kusnama, and Suwarna, 1996). Some of the maps above were re-digitized to get a map that only shows the research area. Meanwhile, the hydrogeological map used is the hydrogeological map of West Bandung Regency (Kementerian Energi dan Sumber Daya Mineral Republik Indonesia, 2018).

The primary and secondary data that have been obtained will then be correlated with each other. Based on the correlation, it will be known the influence of geological and hydrogeological conditions on the groundwater content in the study area.

Result and Discussion

The geological conditions in the study area are composed of 4 formations, 7 formation members, and 11 rock deposits. The geology of the study area is dominated by breccia lithology with fragments of andesite and tuff, and lithology of limestone deposits. In the study area there are also several geological structures, including 5 normal faults, 3 horizontal faults, and 2 anticlines.

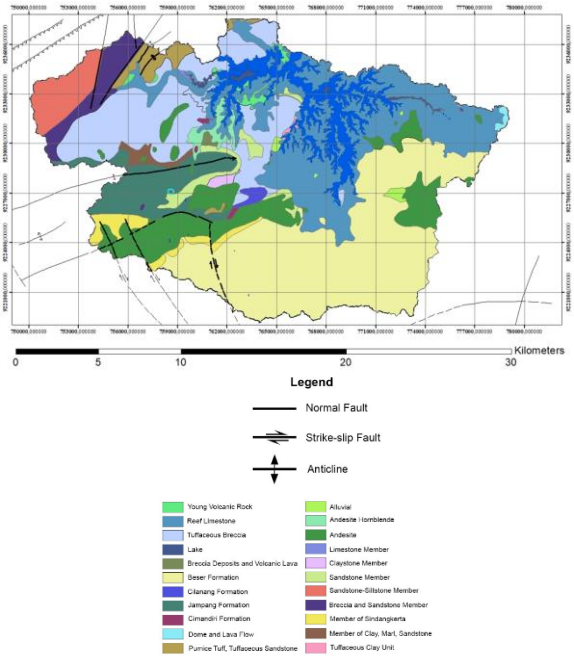

Figure 1. Geological Map of Sub-DAS Ciminyak

The hydrogeology of the research area has several lithological characteristics. The aquifer in the study area is dominated by volcanic rock lithology which covers more than 50% of the total area of the study area. In addition, the aquifers in the study area are also composed of other lithologies such as limestone, igneous and metamorphic rock, solid rock, and loose sediment.

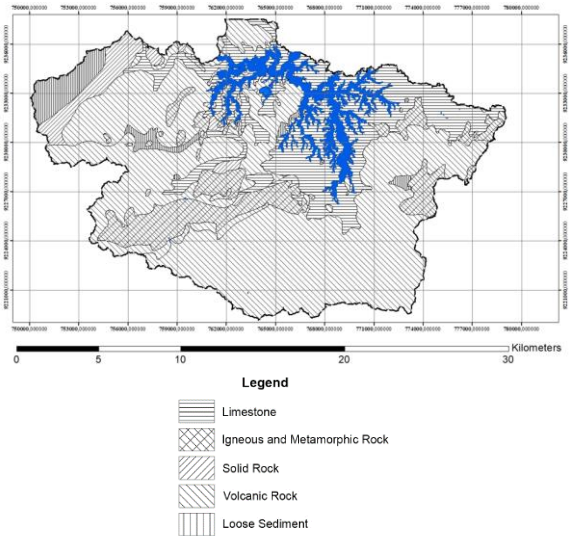

Figure 2. Hydrogeological Map of Sub-DAS Ciminyak

Total Dissolved Solid (TDS) of groundwater in the study area has a value range of 4-536 mg/L. Based on the classification by Freeze and Cherry (1979), all groundwater found in the study area can be classified as fresh water (0,5-1.000 mg/L). Then for Electrical Conductivity (EC) of groundwater in the research area has a value that ranges from 8-1.072 s/cm. Based on the classification by Mandel and Shiftan (1981), groundwater in the study area can be classified into 2 types of water. Water with an EC value between 5-30 s/cm is included in the classification of rainwater where there are 2 groundwater wells in the study area that are included in the classification. Meanwhile, the other 59 wells can be classified as fresh groundwater because they have a range of EC values in the range of 30-2,000 s/cm. Next, the degree of acidity (pH) of groundwater in the study area has a value in the range of 4.9-7.5. Based on the pH value of the groundwater in the study area, there are characteristics where a relatively alkaline pH value (> 7) is found in the central and northern parts of the study area or in the area around the Saguling Dam.

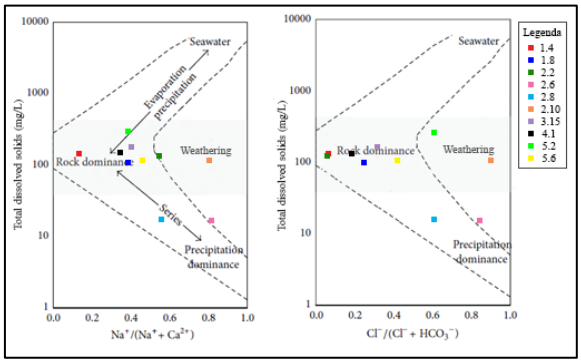

Figure 3. Gibbs diagram plotting result

The results of the Gibbs diagram plot (**Figure 3**) show that the mechanism that controls the chemical content of groundwater in the study area is the interaction between groundwater and rocks. Then there are also 2 samples that are included in the zone of dominance by precipitation or rainwater which indicates that the two samples are heavily influenced by atmospheric water or rainwater (Marandi and Shand, 2018)

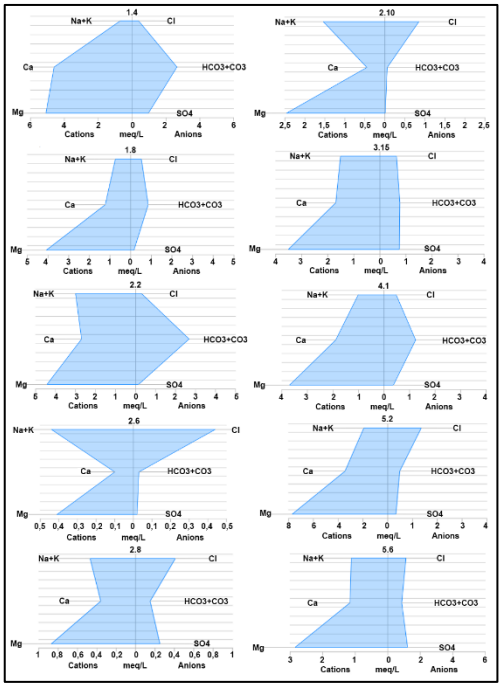

Figure 4. Stiff diagram plotting result

The results of the stiff diagram plot (**Figure 4**) have one characteristic in common, that is high magnesium ion (Mg) concentration. The high Mg ion value is probably caused by the interaction of groundwater with aquifers where the aquifer that dominates the study area consists of igneous and limestone lithology. Mg ion is one of the elements that make up igneous rock and is a generally dissolved ion derived from dolomite minerals which are abundant in limestone. Groundwater characteristics can be divided into 3 based on the location in the study area. Groundwater in the central and southern parts has a fairly high concentration of sodium and chlorine ions. Furthermore, groundwater in the east and west has high concentrations of calcium and carbonate ions. Meanwhile, in the northern part of the study area, the ion concentration is relatively balanced.

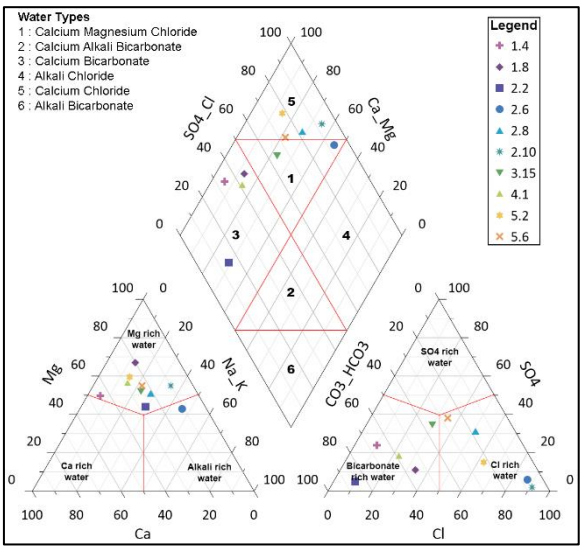

Figure 5. Piper diagram plotting result

The results of the piper diagram plot (**Figure 5**) show that the groundwater in the study area is divided into 3 groundwater facies. The first facies is the mixed facies (Ca-Mg-Cl). This facies includes 2 groundwater samples in wells 2.6 and 3.15. The characteristics of these two samples are different where sample 2.6 is dominated by alkali and chlorine elements while sample 3.15 is dominated by Mg and bicarbonate ions. This is probably due to the different mechanisms that affect groundwater in these two wells, where well 2.6 is heavily influenced by precipitation, while well 3.15 is heavily influenced by interactions with rocks. The next facies is the calcium bicarbonate (Ca-HCO3) facies. This facies includes 4 groundwater samples which have the characteristics of cations dominated by Mg ions and anions dominated by carbonate ions. The chemical content of the sample with the calcium carbonate facies type is much influenced by the interaction between water and rock. The last type of facies is calcium chloride (Ca-Cl). There are 4 samples included in this facies. The cation that dominates the groundwater in this facies is Mg ion and the anion is dominated by Cl ions. Sample 5.6 has a relative anion percentage. Then for samples 2.8 and 5.2 have the characteristics of an intermediate Cl ion percentage. Meanwhile, sample 2.10 has a very high percentage of Cl ions. possibly due to the influence of formation water in the study area which has high Cl ion characteristics.

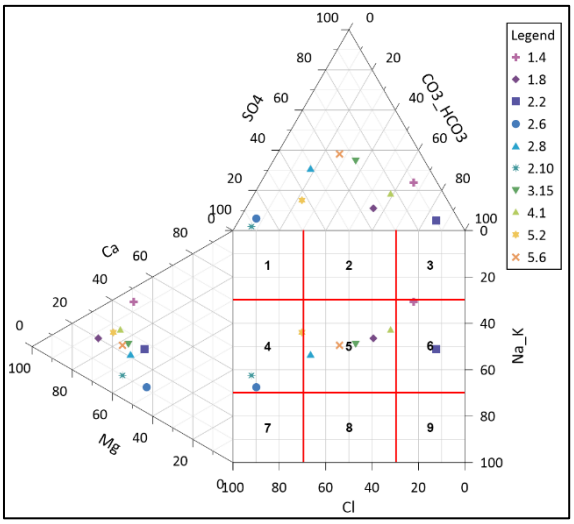

Figure 6. Durov diagram plotting result

The results of the Durov diagram plot (**Figure 6**) using the Lloyd and Heathcote classification (1985) divide the groundwater of the study area into 3 zone groups, namely zones 4, 5, and 6. In zone 4 there are 3 groundwater samples dominated by Na-Cl ions. This indicates a reverse ion exchange process for the Na-Cl ion. Then in zone 5 there are 5 samples of groundwater with a relatively balanced number of ions. This indicates the mixing or dissolution of chemical substances in the water. Then the last is zone 6 which includes 2 groundwater samples. This zone is dominated by Ca-HCO3 ions. Generally indicates a relationship or interaction between water and carbonate rocks (especially dolomite).

The relationship between geology and groundwater characteristics of the research area can be seen based on the Gibbs diagram which shows that the mechanism that most influences the chemical content of groundwater in the study area is the interaction between water and rocks. The high value of magnesium ion concentration is caused by the interaction of groundwater in the study area which is

dominated by igneous and limestone rocks which contain a lot of magnesium ions. Then the high concentration of Cl ions in some samples may be due to the influence of precipitation or mixing by formation water, both of which contain relatively high Cl ions. Meanwhile, the high carbonate ion is probably caused by ion exchange between groundwater and the aquifers in the study area which is composed of limestone.

Conclusions

Based on the results of the analysis of physical characteristics, groundwater in the Ciminyak Sub-watershed can be classified as fresh water. This is because the TDS value in the study area ranges from 4-536 mg/L which is included in the classification of fresh water (Freeze and Cherry, 1979) and is supported by EC values ranging from 8-1072 us/cm which are included as fresh water based on the Mandel and Cherry classifications. Shiftan (1981). Then the groundwater pH in the study area has a slightly acidic value ranging from 4.9 to 7.5. Meanwhile, the chemical characteristics of groundwater in the study area are influenced by the interaction process between groundwater and rocks based on the results of the Gibbs diagram plot (Figure 3). Based on the stiff diagram (Figure 4), groundwater in the study area is dominated by magnesium (Mg) cations. Then based on the results of the piper diagram plot (Figure 5) the groundwater facies of the study area can be classified into 3, namely the mixed water facies of calcium magnesium chloride (Ca-Mg-Cl), the water facies of calcium bicarbonate (Ca-HCO3), and the calcium chloride (Ca-HCO3) facies. Cl). Based on the Durov diagram, groundwater in the study area is divided into 3 zones using the Lloyd and Heathcote classification (1985). Groundwater in the study area is included in zone 4 which is dominated by Na-Cl ions, zone 5 which is not dominated by anions or cations, and zone 6 which is dominated by Ca-HCO3 ions. The chemical characteristics of groundwater are strongly influenced by the lithology of the groundwater aquifers. The high value of Mg ions in groundwater in the study area is due to the contact between water and the lithology that dominates the study area (igneous and sediment rock). In addition, there is also groundwater with high carbonate ion values. Based on the hydrogeological map, the area is composed of aquifers with limestone lithology. However, from the results of the study, further analysis is needed to determine the characteristics of groundwater in more detail.

References

Badan Standardisasi Nasional. 2008. SNI 6989.58:2008. Metoda Pengambilan Contoh Air Tanah. Badan Standardisasi Nasional : Jakarta.

Betageri, V. M. and Patil, R., 2020, Geochemistry of Groundwater.

Caine, J. S., Evans, J. P., Forster, C. B, 1996, Geology, **24**, 1025-1028.

Fetter, C. W. (2014). Applied Hydrogeology (4th ed.). Harlow : Pearson Education Limited.

Freeze dan Cherry. (1979). Groundwater Hydrology. Ann Arbor : Prentice-Hall.

Kementrian ESDM. (2018). Data Shapefile Hidrogeologi Kabupaten Bandung Barat. Skala 1:100.000. Badan Geologi, Pusat Air Tanah dan Geologi Tata Lingkungan.

Koesmono, M., Kusnama, dan N. Suwarna. (1996). Peta Geologi Lembar Sindangbarang dan Bandarwaru, Jawa. Pusat Penelitian dan Pengembangan Geologi.

Lloyd, J. W. dan Heathcote, J. A. (1985). Natural inorganic hydrochemistry in relation to groundwater. Oxford : Oxford Science Pub.

Mandel, S., dan Shiftan, Z. L. (1981). Groundwater Resources: Investigation and development. New York : Academic Press.

Marandi, A. and Shand, P, 2018, Applied Geochemistry, **97**, 209-212.

Maulana, A. N., Miftahussalam, and Purnawati, D. I, 2019, Jurnal Teknomineral, **1**, 63-70.

Pulunggono, A. and Martodjojo, S, 1994, Proceedings Geologi dan Geotektonik Pulau Jawa: 37-50.

Rahadi, F. (2013, June 2). Kondisi Citarum di Hulu dan Hilir. Republika.co.id. https://www.republika.co.id/berita/mnqx3g/kondisi-citarum-di-hulu-dan-hilir

Selley, R. C. dan Sonnenberg, S. A. (2015). Petroleum Geology (3rd ed.). London : Academic Press.

Silitonga, P. H. (1973). Peta Geologi Lembar Bandung, Jawa. Pusat Penelitian dan Pengembangan Geologi.

Sudarmadji, et. al. (2014). Pengelolaan Sumber Daya Air Terpadu.Yogyakarta : Gadjah Mada University Press.

Sudjatmiko. (1972). Peta Geologi Lembar Cianjur, Jawa. Pusat Penelitian dan Pengembangan Geologi.

Todd, D. K dan Mays, L. W. (2005). Groundwater Hydrology (3rd ed.). Berkeley : John Wiley & Sons, Inc.

Water Sampling Steps

Groundwater sampling technique follows the Indonesian National Standard (SNI) 6989.58:2008 concerning water and wastewater – part 58 : Groundwater sampling method. Groundwater sampling technique is as follows:

a. Prepare a sampling tool according to the type of water to be tested

b. Rinse the container with the water sample to be taken 3 (three) times

c. Take a sample of water in accordance with the parameters to be tested

d. Put it in the sample container according to the parameters to be analyzed

e. Immediately carry out tests for physical water parameters such as temperature, turbidity, electrical conductivity, amount of dissolved solids, and degree of acidity.

f. The results of parameter measurements carried out in the field are immediately recorded in the field data notebook

g. Water sampling for laboratory testing is carried out by preservation according to the parameters to be analyzed as contained in attachment C of SNI.

Lampiran C
(normatif)
Tabel cara pengawetan dan penyimpanan contoh air tanah

Tabel C.1 Cara pengawetan dan penyimpanan contoh air tanah

No	Parameter	Wadah penyimpanan	Minimum jumlah contoh yang diperlukan (mL)	Pengawetan	Lama penyimpanan maksimum yang dianjurkan	Lama penyimpanan maksimum menurut EPA
1	Asiditas	P,G (B)	100	Pendinginan	24 jam	14 hari
2	Alkalinitas	P,G	200	Pendinginan	24 jam	14 hari
3	Boron	P	100	Tambahkan HNO_3 sampai pH < 2, didinginkan	28 hari	6 bulan
4	Total Organik Karbon	G	100	Pendinginan dan ditambahkan HCl samapi pH < 2	7 hari	28 hari
5	Karbon dioksida	P,G	100	Langsung dianalisa	-	-
6	COD	P,G	100	Analisa secepatnya atau Tambahkan H_2SO_4 sampai pH < 2, didinginkan	7 hari	28 hari
8	Minyak dan Lemak	G, Bermulut Lebar dan dikalibrasi	1000	Tambahkan H_2SO_4 sampai pH < 2, didinginkan	28 hari	28 hari
9	Bromida	P,G	-	Tanpa diawetkan	28 hari	28 hari
10	Sisa Klor	P,G	500	Segera dianalisa	0,5 jam	0,5 jam
11	Klorofil	P,G	500	Ditempat gelap	30 hari	30 hari
12	Total Sianida	P,G	500	Ditambahkan NaOH sampai pH > 12, dinginkan ditempat gelap	24 jam	14 hari (24 jam jika terdapat sulfida di dalam contoh)
13	Fluorida	P	300	Tanpa diawet	28 hari	28 hari
14	Iodin	P,G	500	Segera dianalisa	0,5 jam	0,5 jam

PROCEEDINGS
JOINT CONVENTION BANDUNG (JCB) 2021
November 23rd – 25th 2021

Groundwater Aquifer Potential Zone Identification by Using Vertical Electrical Sounding Methods in Ngandong Village, Girikerto, Turi, Sleman

Saptono B Samodra[1] , Theo R Siregar[2], Ghiffary R Ramadhan[2], Hatfan A Kharis[2], Rocky T Sembiring[2], Fido F Nurhan[2], Meiliawati Nurbaiti[2]
[1] Lecturer, Department of Geological Engineering, Faculty of Engineering, Universitas Gadjah Mada
[2] Undergraduate Student, Department of Geological Engineering, Faculty of Engineering, Universitas Gadjah Mada

Abstract

Water is an essential part of human need. Most of our activities depends on water. Groundwater represents 97% of freshwater on Earth and makes most of water consumption came from groundwater. But not all locations have a good groundwater resource. Ngandong Village is one of them. Ngandong village is the highest village in Girikerto, Turi, Sleman. Locate above Merapi's spring belt makes Ngandong village facing water shortages and even suffered droughts during dry season. As a community service move, Exploration Geophysics Laboratory of Geological Engineering Department UGM collaborated Kalurahan Girikerto conducting geophysics surveys by measuring and interpretating rock resistivity properties to identify groundwater aquifer potential zone in study area.

Geophysical assessment conducted by using Vertical Electrical Soundings (VES). This configuration used in 3 measurement point VES-01, VES-02, and VES-03 with outer electrode distance with midpoint was 220 meters, 225 meters, and 250 meters respectively.

Based on interpreted resistivity data, lithology in study area consists of interbedding between andesite breccia and andesitic lava with intercalated sand layer. Occurrence of sand layer in study area shown at VES-01 and VES-02 and its interpreted can be an aquifer. This result can be used as a preliminary study to determine location of new well in Ngandong Village. Based on aquifer layer occurrence and accessibility, we recommend drilling a new well in VES-02 at 180-meter depth.

Keywords: Geoelectric, Groundwater, Merapi, Resistivity, VES

Introduction

Groundwater has vital role in human activities. 97% of world's available freshwater resource come from groundwater [1]. Most of water consumption came from groundwater. But finding groundwater in subsurface is quite big problem. Groundwater exploration is much harder than surface water development because we can't see and measure the object below the surface [2]. Therefore, several assessments can be conducted to locate groundwater in subsurface aquifer. One of them is geophysical survey.

In groundwater exploration, geophysical survey carried out to evaluate subsurface condition and predicting aquifer location. Geoelectrical survey is common geophysical assessment for groundwater investigation. Geoelectric survey measures rock resistivity properties by flowing electric current in specific value to determine the rock by its properties [3].

Ngandong Village, Girikerto, Turi, Sleman, Jogjakarta as shown in **Figure 1.a.** is highest village in Kalurahan Girikerto. This village locate on southern side of Merapi Volcano. Based on hydrology settings, Ngandong Village situated above Merapi's spring belt. Besides that, most of water well in this area came from deep aquifer. This situation makes Ngandong Village experienced water scarcity and even drought during dry season. Based on this condition, Ngandong village needs a new water resource to fulfill water needs by doing geoelectrical survey to observe subsurface condition and determine a new borehole.

Geological Settings

The research area is located on the Geological Map of Yogyakarta Region Sheet [4] which can be seen in **Figure 1.b.** This Geological Map is composed of 24 formations, but the formation that composes the research area is only the Young Merapi Volcanic Deposits. This formation is composed of several types of rock, such as agglomerates, tuffs, breccia, and ash [4]. Based on **Figure 1.b.**, no geological structures were found in the research area.

Hydrogeological

Hydrogeology is a study that learns groundwater movement in a particular geological setting. Groundwater is part of the hydrological cycle and can be found under any subsurface condition [5]. It has some benefits, such as: commonly available around settlement, can be used without processing, easy to deliver, and it's not pathogenic in general [6, 7].

The research area, located in Yogyakarta – Sleman Groundwater Basin. This basin is divided into an upper aquifer and a lower aquifer. These aquifers

contain inter-bedded materials, such as middle coarse sands, gravel, silt, clay, and breccia's lenses [8]. These materials originally derived from Young Merapi Volcanic Deposits that formed Yogyakarta Formation and Sleman Formation [9].

The condition of an aquifer is affected by its porosity and permeability [10]. Porosity is a ratio of the volume void contains in the rock, to the bulk rock's volume. It leads to the maximum quantity of how much groundwater can be stored in an aquifer. Permeability is the capability of rock to stream fluids in it, and it affects the flow speed of the groundwater movement through the aquifer.

Data and Method

Geophysical assessment conducted to discover groundwater potential zone. Geoelectrical resistivity method was chosen because this method considered as a promising and most suitable method for groundwater investigation in study area. Vertical Electrical Sounding (VES) was used because it's quite popular for groundwater exploration due to the simplicity of the data acquisition [11]. This method generally works by detecting the surface effects that produce by the flow of electric current inside the earth [11]. Vertical Electrical Resistivity with Schlumberger configuration was used in this study which consist of four electrodes moving sequentially.

In total, three VES point measurements were carried out in the study area, with details in the form of two N – S profiles and one E – W profile. The coordinates of each measurement point shown in Table 1.

Table 1. VES points coordinate

Point	Coordinate	Elevation (m.a.s.l)	Azimuth
VES-01	7° 35' 1,42" LS/ 110° 24' 39.1" BT	954	N 22° E
VES-02	7° 35' 21" LS/ 110° 24' 42" BT	940	N 5° E
VES-03	7° 35' 23,8" LS/ 110° 24' 48,2" BT	939	N 5° E

The study area only consists of one formation and no geological structure found. This makes the determination of measurement points not selected based on geological and geomorphological condition. The availability of land for further construction of drilling well, also non-existence of external factors such as irrigation pipes or other infrastructure (due to the lack of infrastructure being built around this around the mountainside), determined the distribution of measurement points.

Measured vertical electrical soundings (VES) calculated to get true resistivity (ρ). Subsurface overview which includes type, depth and thickness, distribution of aquifers vertically interpreted from true resistivity value. The geoelectric model utilizes data generated from geophysical data acquisition and is combined with geological conditions at the research site. PROGRESS software used to interpret geoelectrical data to calculate resistivity value and layer thickness. Groundwater potential zone can be predicted after we got resistivity and layer thickness results. Based on the resistivity data acquisition, the measurement results from the three VES points are shown in **Figure 2.**

Result and Discussion

Geomorphologically, the study area is located on the lower slope of Mount Merapi. This area characterized by a topography that slopes to the south about 5-10 degrees. About 50-100 meters to east, there was Turgo Hill which is an isolated hill. Turgo hill is a remnant of Old Merapi, located around the sediment of Young Merapi. Bedog tributary from Mount Merapi as border on west a side, is a river that flow through Yogyakarta city. The geological condition of the research area is generally composed of andesite breccia as a result of Young Merapi activity. Based on field observations, the lithology that composes this area is weathered andesite breccia, which leaves soil and andesite fragments that have not been weathered.

Based on the interpretation of geoelectrical data, it can be seen that the rocks in the study area are interbedded between andesite breccia, andesite lava, and sand. From the geoelectrical interpretation, sand layers are found at a depth of about 150 - 170 meters, or at an elevation of 790 m above sea level at VES-01 and VES-02 while no sand layer observed in VES-03. This condition could possible because there is Turgo Hill near VES-03. This isolated hill obstructs sediment material from Mount Merapi. So, there is no sand deposit observed on VES-03. On the other side, thick layer of sand can be found on VES-01 because it's located on northwest side and higher elevation from VES-03. So, possibility of deposition sediment from Merapi in VES-01 is higher than VES-03.

From the geoelectric interpretation above, there is a layer of sand that interpret as an aquifer at the measurement points VES-01 and VES-02. Considering of aquifer depth possibility and the ease of access to drilling tools, it is recommended to drill wells around point VES-02 to a depth of 180 m.

Based on three available profiles, there is a difference between VES-01 & VES-02 profile and VES-03 profile. At VES-01 & VES-02 profile, there is a layer of sand, while in VES-03 it was not found. At VES-02 profile layer of sand between andesite breccia. Deposition time gap between sand layer and andesite breccia caused this condition. Deposition from fluvial environment around the study area is possible as the source of sand layer that presence.

Groundwater recharge based on the geomorphological model and calculations using the Water Table Fluctuation method in this location is characterized by high magnitude supply up to 4270 mm/year with

average rainfall 2801.5 mm/year [12]. It shows that the water supply at the research location is quite good and resistant to changing seasons in Indonesia [12]. From previous data, we can calculate the water supply that can be utilized. Based on Regulation of The Minister of Energy and Mineral Resources the Republic of Indonesia, it was suggested maximum 40% of recharge supply can be extracted [13].

Conclusions

The following conclusions can be drawn based on previous discussion:

1. Ngandong village (administratively in Turi, Sleman, Yogyakarta) is located on the lower slopes of Mount Merapi. It located above the Merapi spring belt based on hydrological system in Yogyakarta
2. Based on acquired VES data, the study area composed by layers of andesite breccias, andesite lava, and sand from Young Merapi volcanic deposit product.
3. approximately at 180 meters there is a layer of sand that can function as an aquifer at 2 measurement points in the research area.
4. The groundwater recharge is quite good and resistant to changing seasons in Indonesia (based on previous researcher), with maximum 40% of recharge supply can be extracted based on Regulation of The Minister of Energy and Mineral Resources the Republic of Indonesia to conserve ground water sustainability.

References

[1] Guppy, L., Uyttendaele, P., Villholth, K.G., Smakhtin, V., 2018, UNU-INWEH Report Series, **4**, p. 1 – 23.
[2] Ramli, M., Sufriadin, Aryanti V.A., Nur, I., Thamrin M., Widodo, S., 2018, JURNAL TEPAT: Teknologi Terapan untuk Pengabdian Masyarakat, **1**, p. 137 – 146.
[3] Wintolo, D., Arifianto, I., Wibowo, J.P., Proceeding Seminar Nasional Kebumian 10.
[4] Rahardjo, W., Sukandarrumidi, Rusidi H.M.D., 1977, Geological Surveys of Indonesia.
[5] Alley, W., 2009, Encyclopedia of Inland Waters, pp 684-690.
[6] Beckie, R., 2013, Reference Module in Earth Systems and Environmental Sciences, p. 1 – 3.
[7] Wagener, E., Lanoix, J., 1959, World Health Organization Monograph, 40, p. 53 – 119.
[8] Putra, D.P.E., Indrawan, I. ASEAN Engineering Journal Part C, **3**, p. 105 – 116.
[9] Putra, D.P.E., Atmaja, R.R.S., Manny, L., 2016, Journal of Applied Geology, **1**, p. 89 – 99.
[10] Todd, D., 1980, John Wiley & Sons, p. 535.
[11] Abdullahi, M., Toriman, M., & Gasim, T., 2015, Journal of Geology & Geosciences, **4**, p. 1 – 3.
[12] Tjahyo, A 2008 Application of Water Table Fluctuation Method to Quantify Spatial Groundwater Recharge Within the Southern Slope of Merapi Volcano, Indonesia *Indonesian Journal of Geography* vol 39, pp 157-171
[13] The Minister of Energy and Mineral Resources the Republic of Indonesia Number 31 of 2018 *Guidelines for Determining Groundwater Conservation Zone*

Acknowledgements

Thanks to the stakeholder of Ngandong Village (Sleman, Yogyakarta), that allowed and helped us to conduct this study.

PROCEEDINGS
JOINT CONVENTION BANDUNG (JCB) 2021
November 23rd – 25th 2021

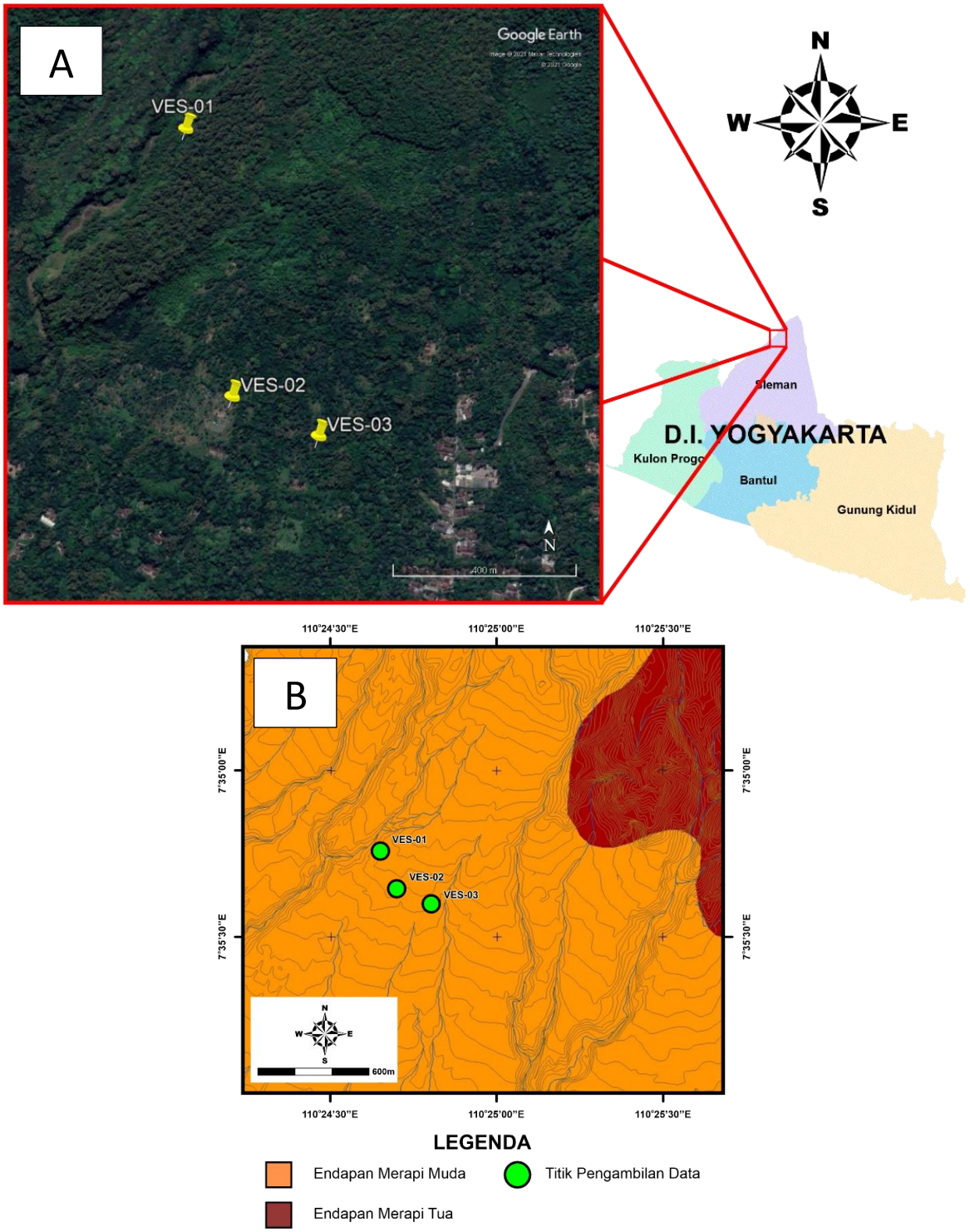

Figure 1. a. Location of the study area with area of interest marked with red square., b. Geological Map of study area, modified from [4]

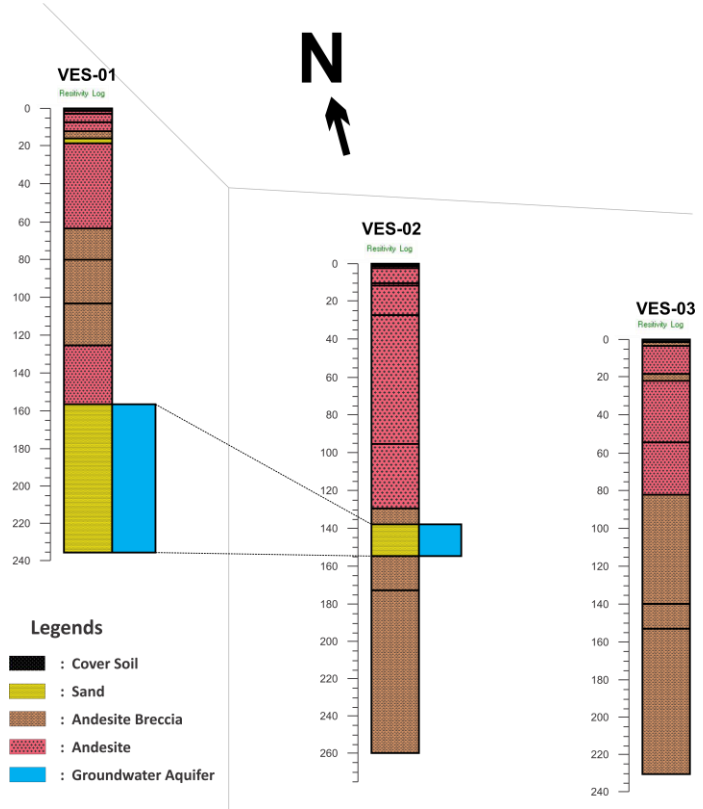

Figure 2. Perspective illustration of VES point correlation VES-01, VES-02, and VES-03

PROCEEDINGS
JOINT CONVENTION BANDUNG (JCB) 2021
November 23rd – 25th 2021

Identification of Badrock Layer Using Resistivity Method with Dipole - Dipole Configuration in Luwuk Area

Rahmad Murdani[1], Muhammad Fajar Rahmani [1], Putra Aliftadira[1], Yunisa Indri Puspita[1], Sandy Kurniawan[1]
Department of Geophysical Engineering University of Pertamina, Jakarta, Indonesia

Abstract

The rapid development of the tourism industry in the Luwuk area has an impact on infrastructure development, especially hotels, resorts, and shopping centers. The foundation plays a critical role in the structure of a building. The foundations are generally located on the bedrock layer. Therefore, research has been carried out that aims to determine the bedrock layer as a building foundation. The Luwuk area consists of several formations including: complex ultramafic where the formation is composed of Harzburgite, Serpentinite, Dunit, Gabron, Basalt, and Diorite; the Bongka Formation composed of conglomerate rock, sandstone, silt, limestone, and marl; Alluvium composed of mud, sand, and kerakal; and the Tolaka Formation composed of rocks of limestone, marl with shale insertion, and sandstone conducted geophysical surveys with the resistivity method using the configuration of the dipole-dipole. The resistivity method is a method of geoelectric that utilizes the properties of the soil layer as a conductor of electricity, which is measured using the injection of an active power supply and the configuration of the dipole-dipole mapping. Data was collected using eight tracks with a track length of 470 meters and a distance between electrodes of 10 meters. Data processing and 2D under the surface modeling were carried out using the Least Square Inversion method with 5 iterations using Res2DInv software. The base layer in this area is composed of limestone and sandstone, based on the initial hypothesis. Based on the modeling results, the area identified as bedrock is located at a depth of 8-16 meters and seen the upper bedrock getting deeper to the northeast with the constituent rocks in the form of sandstone. As a result, a minimum of 8 meters was required to build a sturdy building structure in the area.

Keywords: Bedrock, Development, Foundation, Infrastructure and Resistivity.

Introduction

The development of the tourism industry in Indonesia is growing rapidly. This is because, in addition to the mining sector, tourism plays a significant part in Indonesia's development. With the rapid development of tourism in the Luwuk area, it has an impact on infrastructure development, especially hotels, resorts, and shopping centers. Because the foundation is the lowest structure of a building that is directly attached to the ground and has a role in supporting the load of the building above it, the determination of bedrock is a very important factor in a building.

The research was conducted in the Piondo Toili district of Central Sulawesi's Luwuk Banggai Regency. It is located at 1°27'39.8"S 122°13'35.0"E in terms of geographic coordinates. The research location is shown in Figure 1. Data collection was carried out on 8 tracks with each track length of 470 meters.

Based on this description, research was conducted with the aim to determine the base layer as the building's foundation. Geophysical surveys combined with geotechnical studies can be used to determine the position of the hard soil layer. One of the geophysical survey methods used is the resistivity method using a dipole-dipole configuration and 2D modelling below the surface is carried out using the Least Square Inversion method with 5 iterations using the Res2DInv software. The resistivity method is an effective geophysical method for subsurface imaging. This method is done by injecting current into the subsurface through an intermediary transmitter electrode to determine the potential of the bottom with the recorded data of physical. From the results of research and processing of the Geoelectric method, different resistivity values are obtained in each different rock so that a hard layer distribution model can be obtained that can be used as a building foundation in the Luwuk area.

Data and Method

This research uses the method of resistivity with the principle of injecting current into the subsurface through an intermediary transmitter electrode to determine the potential of the bottom with the recorded data of physical. The pores or minerals in the rock become a medium for the flow to move. Where the current will be easier to move when passing through rocks with conductive properties. The following is the rock resistivity range: Figure 2.

The configuration used in this research is a dipole-dipole configuration with potential electrodes placed 10 meters apart from the current electrode. This measurement is used for mapping the distribution of

bedrock, which focuses the results laterally. The dipole-dipole configuration makes the distance between the C1C2 electrode current and the P1P2 electrode potential equal, as shown in the Figure 3.

To get the value of the apparent resistivity of the configuration of the dipole – dipole then used the equation: $K = \pi a n (n+1) (n+2)$

k = Geometry Factor a = Space n = Number of Electrodes

The data was taken in hilly areas with an altitude of 5–30 meters above sea level. With 8 tracks that have a length of 470 meters each. On the track, there are three south-to-north tracks, three east-west tracks, and two crossing lines running southwest-to-northeast and southeast-to-northwest. With the orientation of paths 4 and 5, which intersect the six paths, it is expected to be able to provide 3D data and target bedrock distribution in the research area Figure 4.

Result and Discussion

The data was collected in hilly areas with a topography of 30-40 meters above sea level, and the research area was located in the Bongka Formation, which is formed of conglomerate rocks, sandstone, silt, marl, and limestone, according to the Surono geological map sheet (1993).

Figure 5. The first three tracks run from south to north, with the first having a resistivity value of 1.55 Ωm to 46.6 Ωm, the second having a resistivity value of 1.86 Ωm to 53.3 m Ωm and the third having a resistivity value of 1.60 Ωm to 50.2 Ωm. Subsurface imaging can be produced up to a depth of 100 - 110 meters using a 470 meter track length. A number > 12.7 Ωm is interpreted as sandstone, which is one of the constituents of the bedrock layer at a depth of 8 – 40 meters above the surface, while a value between 1.56 Ωm and 12.7 Ωm is interpreted as shale stone, which is at a depth of 40 – 100 meters.

Figure 6. The subsurface section of the three tracks above, that stretch from East to West, are in the Bongka Formation and have varying resistivity values. The resistivity range on the fourth track is 1.41 Ωm – 70 Ωm, 1.80 Ωm – 61.6 Ωm on the fifth track, and 1.12 Ωm – 53.0 Ωm on the sixth track. Based on the resistivity value, it is interpreted that the three tracks contain sandstone, silt, and conglomerate rock. Where shale has a resistivity value of resistivities 1.12 Ωm – 13.9 Ωm with a depth of 3 – 80 meters below sea level, and sandstone has a resistivity value of > 13.9 Ωm at a depth of 6 – 30 meters from the surface.

Figure 7. The subsurface section of the seventh trajectory, which runs from Northeast to Southwest, is in the Bongka Formation. The distribution of resistivity values in this path has a resistivity range that varies from 1.87 Ωm – 37.2 Ωm. There are lithologies of sandstone, silt, and conglomerate based on resistivity values in track seven. Where the resistivity value of shale is 1.87 Ωm – 10.3 Ωm at a depth of 22 – 130 meters below the surface, while sandstone is > 10.3 Ωm at a depth of 4 – 22 meters from the surface which is interpreted as bedrock.

Figure 8. The resistivity range for eighth track, which runs from southeast to northwest, is 0.49 Ωm to 31.5 Ωm. Resistivity values > 9.99 Ωm are sandstone, which is interpreted as the hardest layer or bedrock at a depth of 10 – 50 meters below the surface, and 1.61 Ωm – 9.99 Ωm is shale stone at a depth of 50 – 80 meters below the surface.

Conclusions

Based on the initial hypothesis that the rock layers are composed of limestone and sandstone, this study obtained resistivity data on all paths in the Luwuk Banggai which has a resistivity value of 12.7 Ωm – 77.9 Ωm, which is a hard layer with a depth of 8 meters continuously up to 16 meters below the surface. The hard layer lithology in this area ranges from fine to coarse sandstone. As a result, a hard layer suitable for use as a building foundation for infrastructure development has been formed in the area.

References

A. Samouelian, I. Cousin, A. B. Tabbagh, dan G. Richard, "Electrical Resistivity Surveyin Soil Science: a review", Soil and Tillage Research, Elsevier, hal. 173-193, 2005.

Agus,Chandra.2020. "Analisis Data Induced Polarization Dalam Menduga Zona Mineralisasi Logam Daerah Godean, Kabupaten Sleman DIY". reseachgate.net https://www.researchgate.net/figure/Gambar-1-Konfigurasi-Dipole-Dipole-Konfigurasi-dipole-dipole-lebih-banyak-digunakan_fig1_348109650

Baker, D. W., and N. L. Carter, 1972, American Geophysical Union Geophysical Monographs **16**, 157–166.

Castagna, J. P., 1993, The Leading Edge, **12**, 172–179.

College of Education, Zaria,Nigeria", Zaria: Master Thesis, Department of Physics, Faculty of Science, Ahmadu Bello University, 1999.

Grandis Hendra.2017. "*Geolistrik-Resistivitas Batuan"*. Geofisika,net https://geofisika.net/resistivitas-batuan/

Kosloff, D. D., and E. Baysal, 1982, Geophysics, **47**, 1402–1412.

Lodha, G. S., 1974, M.S. thesis, University of Toronto.

Mahartanto,MA. 2021. *Identifikasi Lapisan Keras Menggunakan Metode Geolistrik Konfigurasi Wenner – Schlumberger di Gelanggang Olahraga Institut Teknologi Sumatra*. Research

Repository-ITERA, *http://repo.itera.ac.id/depan/submission/SB2102110010*

Priambodo, I.C., Purnomo, H., Rukmana, N., dan Juanda., .2011. *Aplikasi Metode Geolistrik Konfigurasi Wenner-Schlumberger pada Survey Gerakan Tanah di Bajawa, NTT.* Bulettin Vulkanologi dan Bencana Geologi, Vol 6(2), 2-10.

Surono ,T.O. Simandjuntak, R.L.Situmorang dan Sukido. 1993. "Peta Geologi Lembar Batui Sulawesi Tengah*"*. Pusat Penelitian dan Pengembangan Geologi. Bandung

Suyanto Imam, Utomo Agung Setyo. 2013 . "Analisis Data Resistivitas Dipole-dipole untuk Identifikasi dan Perhitungan Sumber Daya Asbuton*"*. Program Studi Geofisika FMIPA UGM Sekip Utara, Bulaksumur, Yogyakarta

PROCEEDINGS
JOINT CONVENTION BANDUNG (JCB) 2021
November 23rd – 25th 2021

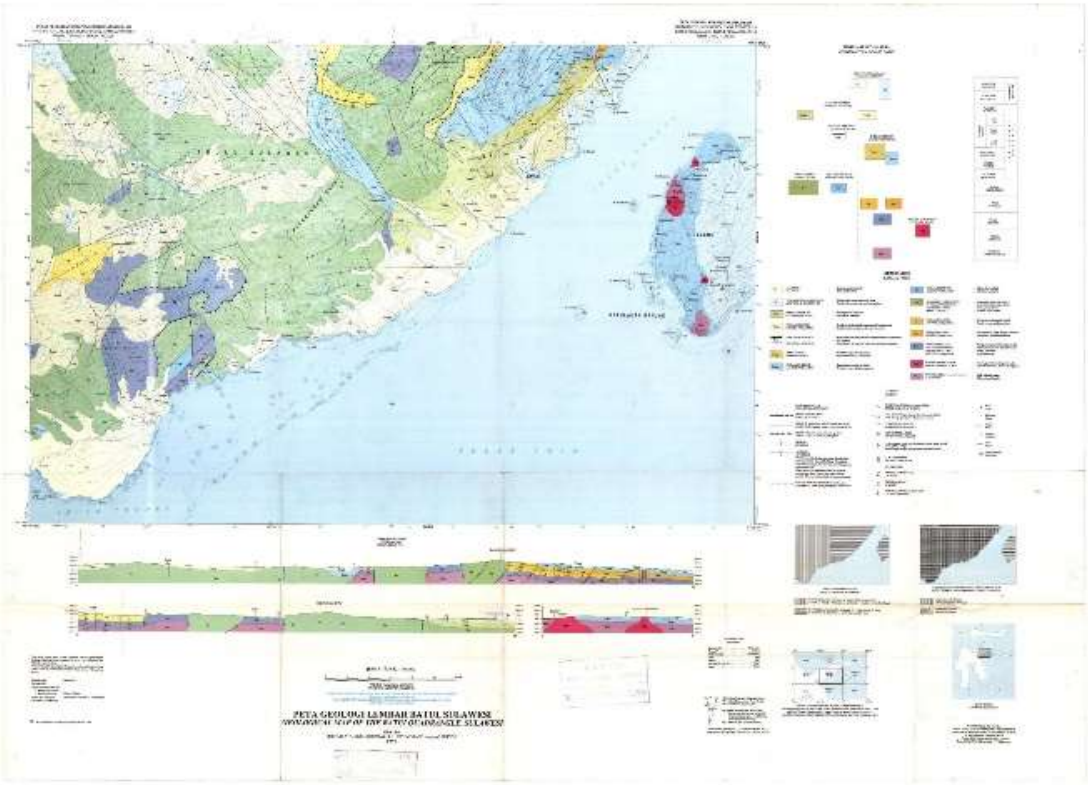

Figure 1: Geological map of the Luwuk (Surono, 1993)

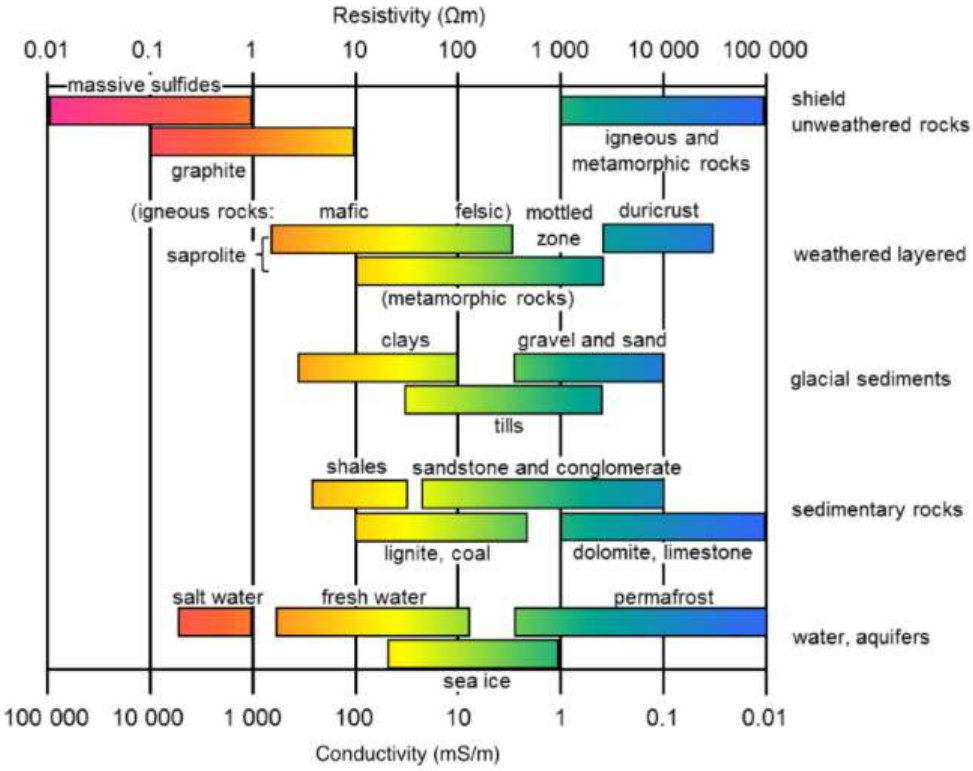

Figure 2: Rock resistivity range (Grandis, 2017)

PROCEEDINGS
JOINT CONVENTION BANDUNG (JCB) 2021
November 23rd – 25th 2021

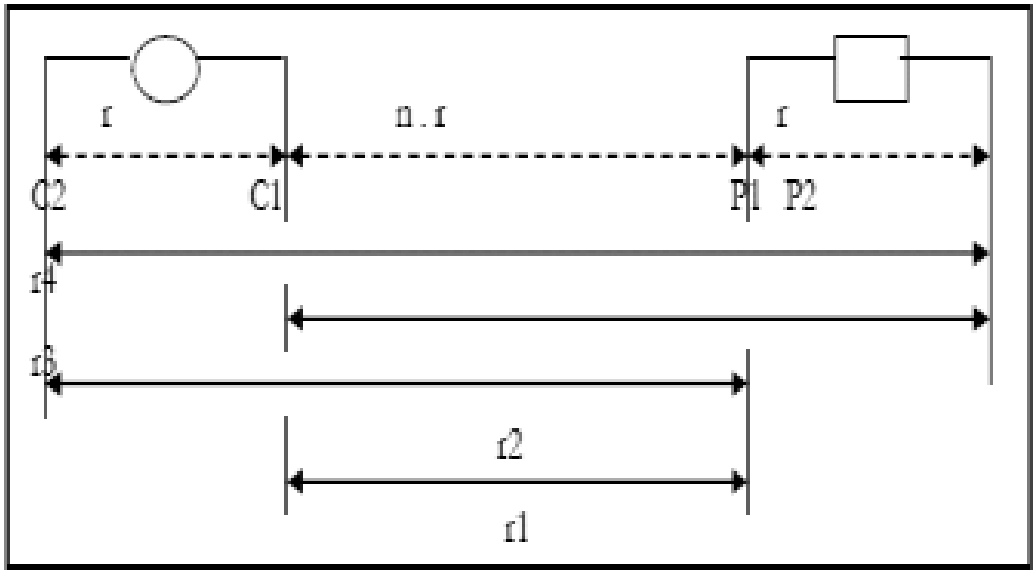

Figure 3: Configuration of the dipole – dipole electrode (Agus Chandra, 2020)

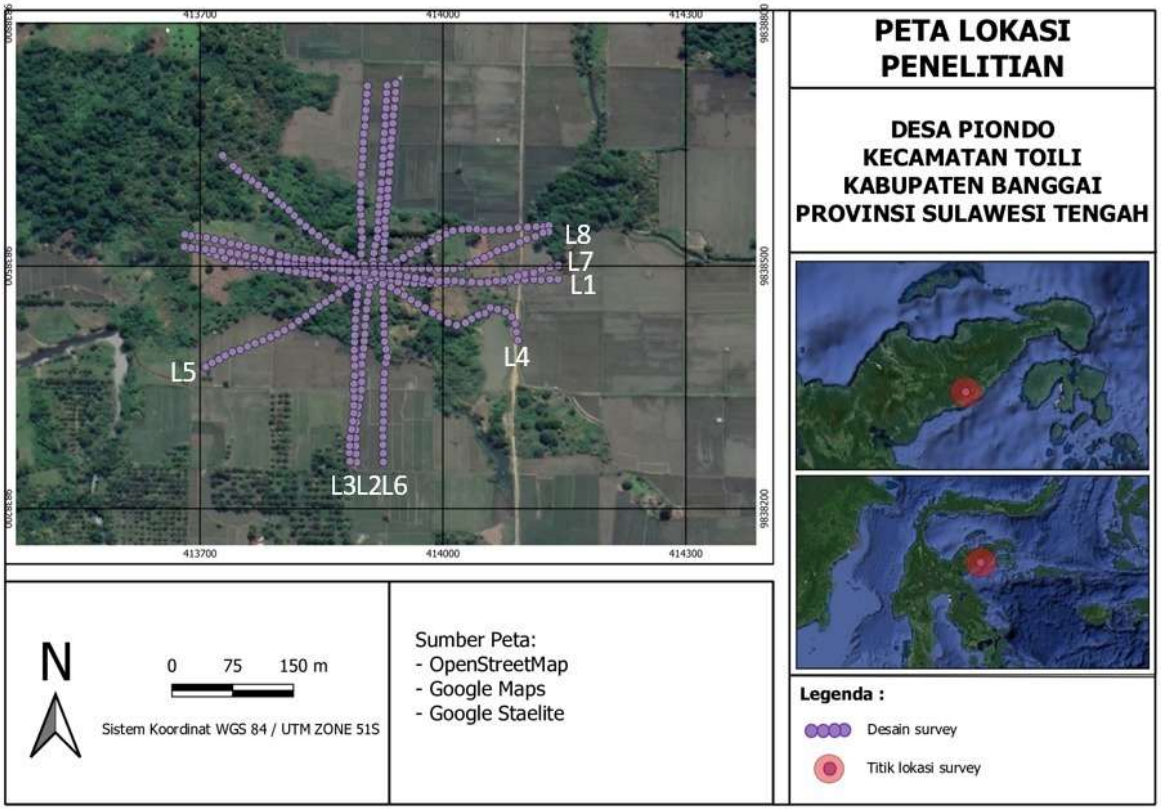

Figure 4: Survey design

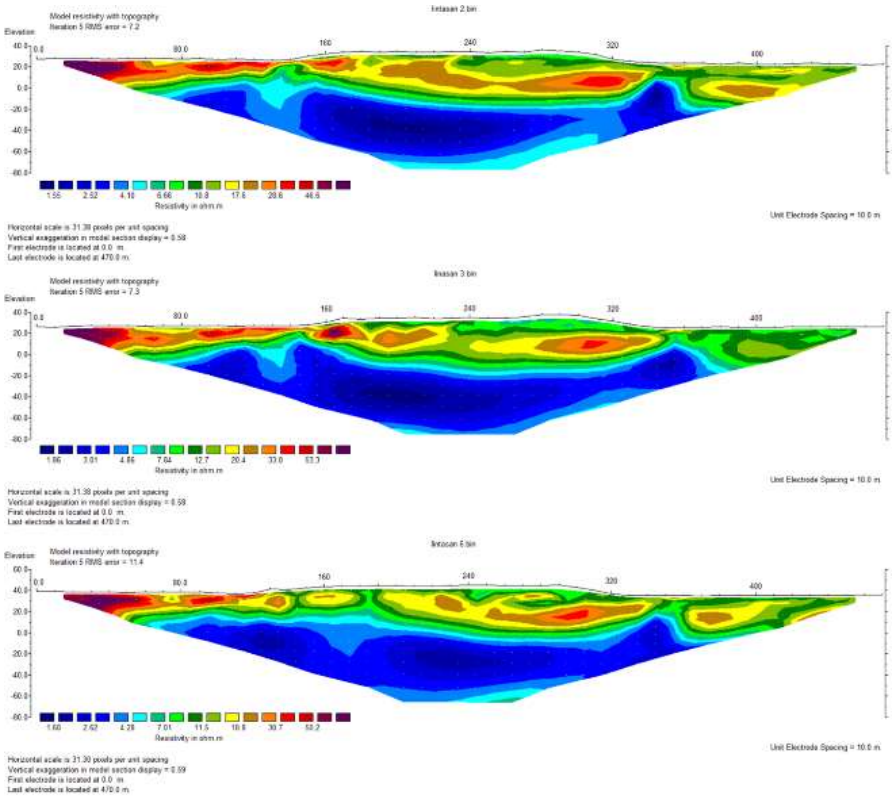

Figure 5: The trajectory of the South to the North

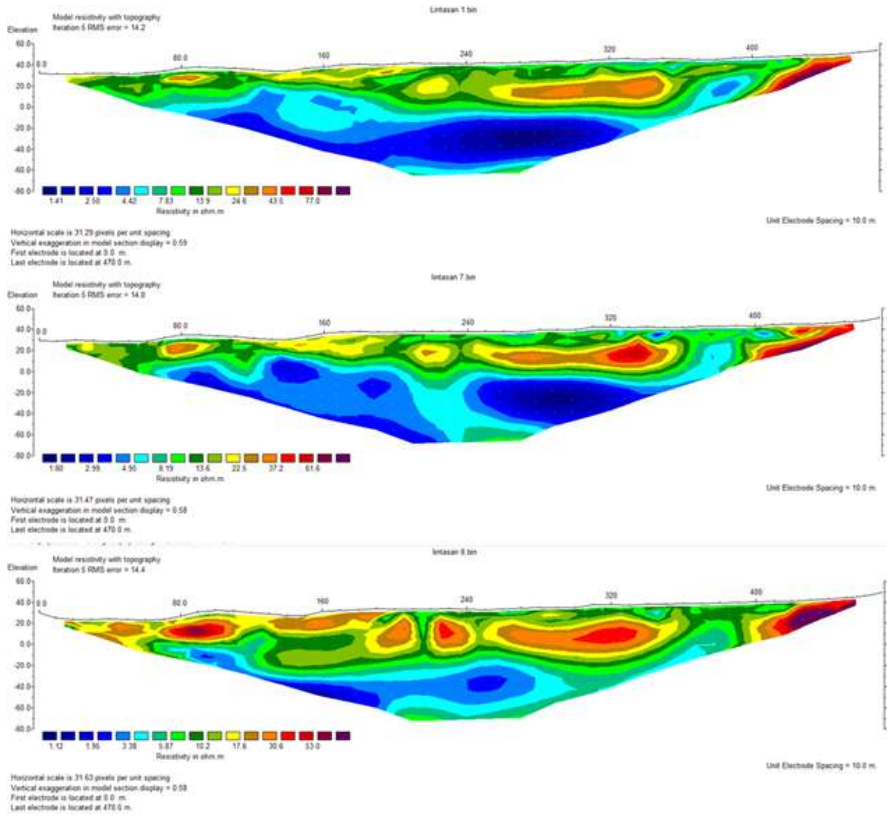

Figure 6: The trajectory of the East to the West.

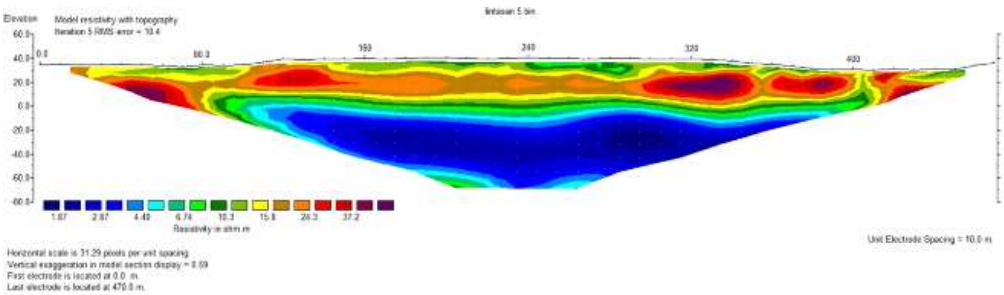

Figure 7: Southwest to Northeast

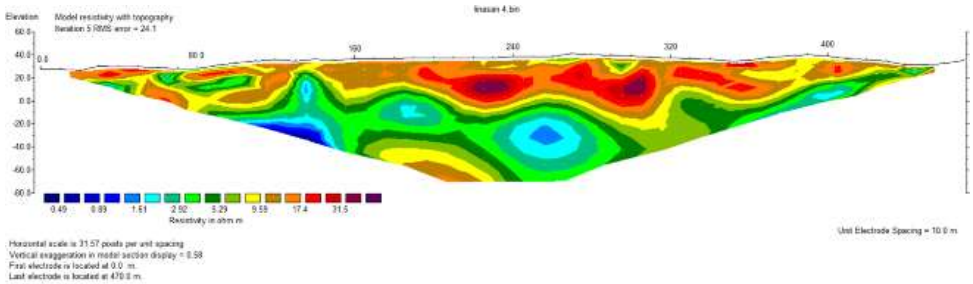

Figure 8: Southeast to Northwest

PROCEEDINGS
JOINT CONVENTION BANDUNG (JCB) 2021
November 23rd – 25th 2021

Analysis of Seismic Hazard Probability against Landslide Vulnerability using Horizontal to Vertical Spectral Ratio (HVSR) in Nogosari, Wukirsari, Imogiri

Dewi Widya Ningsih, Ririn Setyowati, Vira Irnanda, Rizki Nurdianto, Tadeus Ivan Prudish Suba, Refita Khumayroh, Amrupranadi Muhammad[1]
[1]*Geophysical Engineering Department, UPN "Veteran" Yogyakarta*

Abstract
The research area is administratively located in Wukirsari, Bantul, Yogyakarta Special Region. Bantul is generally an area with a flat slope (0-2% slope) which has a height in the eastern part that reaches a steep slope (> 40% slope) and is an area prone to earthquakes and landslides (PVMBG, n.d.). This reasearch aims to analyze the potential for landslides in the research area using the microseismic HVSR (Horizontal to Vertical Spectral Ratio) method. The HVSR method will produce dominant frequency maps (f_0), amplification (A_0), soil vulnerability index (Kg), Peak Ground Acceleration (PGA), and Ground Shear Strain (GSS) which will be used to microzonate landslide prone areas. in the research area of 1x1.2 km2 with a total of 42 points. Based on the processing of the HVSR method, the A0 value range is 1 - 7.4, f0 is 1.5 - 21.8 Hz, kg is 0.07225 - 9.79383 s2 / cm, PGA is 281,658 - 1059.17 gal, and GSS is 0.7x10-4 - 43x10-4. These results are integrated with other parameters for scoring and weighting. Parameters and weight used are slope (3), GSS (3), rainfall (2) and PGA (2). From this analysis, a landslide hazard map is produced where the high level of hazard is located in the middle of the study area, namely at points M29, M32, M34, M35, M38, and M39. This analysis is expected to be able to assist the government in making a directed and precise mitigation design

Introduction

Wukirsari, Imogiri, Bantul areas have morphology in the form of Fault scrap, Hills Slopes and Valleys. The research area consist of 4 main lithology unit, they are Tufaan of Semilir, Breksi Volcanic of Nglanggeran, Carbonatan Sandstone of Sambipitu, Coral Limestone of Wonosari, and there is a structure named Opak fault. Bantul is an area with flat slope (0-2%) that have highs in the eastern part that reaches the steep marbles (>40%) and included in areas prone to earthquake and land disasters landslide (PVMBG, n.d.). This causes the area research is prone to vibrations/shocks

Landslide hazard is a disaster that often happens in Indonesia. It's also supported by the season in Indonesia, which is the wet and dry season. During the rainy season come, the rainwater can fill empty cavities on the ground and resulting in soil is saturated with water so that it can causing landslides.

According to (Priyantari & Suprianto, 2009) in (Julianti, 2018), landslides are usually moving in a particular field, it is called the plane slip zone between the stable zone (bedrock) and the unstable zone (the field that slipping). The field of the slip in, it is common under the earth's surface. The field of slip can be known its existence by analyzing the characteristics of the layer soil.

The method that can be used to find out the potential for landslides, namely by microseismic HVSR measurements. This method is suitable for mitigation hazard. Microseismic HVSR can be used to know the strength of the land based on dominant frequency value and amplification of soil to find out the potential for landslides. This research was conducted with the aim of knowing the zones that are prone to landslides with approaches to geology (lithology and morphology) and geophysics (dominant frequency value (f0), amplification value (A0), soil vulnerability index (Kg), Peak Ground Acceleration (PGA), and Ground Shear Strain (GSS) in Wukirsari, Imogiri, Yogyakarta

- Horizontal to Vertical Spectral Ratio (HVSR)

HVSR method basically has the assumption that the ratio of the horizontal and vertical spectra of the surface vibrations is a function of displacement. It also shows that the characteristics of the surface can be roughly seen at the observed point if the seismic microwave waveform observation is carried out on three components, namely two horizontal components (East-West and North-South) and one vertical component (Depth) (Nakamura Y. , 1989).

Horizontal and vertical amplification factor of the surface sediment based on seismic motion at the surface, which is directly related to the ground motion in the basin area denoted by T_H and T_V (Nakamura Y. , 2000). The magnitude of the horizontal amplification factor is:

$$T_H = \frac{S_{HS}}{S_{HB}} \quad [1]$$

$$T_V = \frac{S_{VS}}{S_{VB}} \quad [2]$$

Because spectrum ratio between the horizontal and vertical components in the bedrock is close to one, the disturbances recorded on the surface sediment layer due to the effects of Rayleigh waves can be eliminated. So there is only the effect caused by the local geological structure or site effect (TSITE). TSITE shows the amplification at the fundamental frequency of the area (Slob, 2007). Based on equations (1), and (2), the amount of TSITE is obtained as:

$$T_{SITE} = \frac{T_H}{T_V} = \frac{S_{HS}}{S_{VS}} \quad [3]$$

so,

$$HVSR = T_{SITE} = \frac{\sqrt{((S_{north}-S_{south})^2+(S_{east}-S_{west})^2)}}{S_{VS}} [4]$$

- Peak Ground Acceleration (PGA)

Peak Ground Acceleration (PGA) is the acceleration value of vibration by the earthquake. Peak Ground Acceleration (PGA) value is calculated based on the magnitude and distance of the earthquake source that has occurred to the calculations point, and the value of soil dominant period in the area. Kanai formulated an empirical formula for ground acceleration at the surface (Edwiza, 2008) as:

PROCEEDINGS
JOINT CONVENTION BANDUNG (JCB) 2021
November 23rd – 25th 2021

$$a = \frac{5}{\sqrt{T_g}} 10^{0.61M - \left(1.66 + \frac{3.6}{R}\right) \log R + 0.167 - \frac{1.83}{R}} \quad [5]$$

- *Ground Shear Strain* (γ)

Ground Shear Strain (GSS) value of soil horizon can describe the ability of the soil material to move during an earthquake. Ground Shear Strain (γ) value can be calculated using the equation:

$$\gamma = \frac{(A_0 d)}{H} \quad [6]$$

where A0 is the amplification factor, H is the soil horizon thickness, and d is the seismic wave that move below the surface. The velocity of seismic wave that move below and around the surface denoted as Vb and Vs. The velocity value of seismic wave that move below the ground surface (V_b) is formulated as:

$$V_b = 4 A_0 H f_0 \quad [7]$$

so the thickness of the layer can be determined by the equation:

$$H = \frac{V_b}{4 A_0 f_0} \text{ atau } H = \frac{V_s}{4 f_0} \quad [8]$$

with

$$V_s = \frac{V_b}{A_0} \quad [9]$$

The following peak ground acceleration (ag) equation:

$$a_g = (2\pi f_0) \quad [10]$$

so seismic displacement from below the surface can be determined using the equation:

$$d = \frac{a_g}{(2\pi f_0)^2} \quad [11]$$

If equations (8), (9), (10), and (11), are entered into equation (6), then obtained:

$$\gamma = \frac{\left(\frac{A_0 a_g}{2\pi f_0}\right)^2}{\left(\frac{V_S}{4 f_0}\right)} \quad [12]$$

or it can be simplified to

$$\gamma = \frac{(A_0 a_g)}{\pi^2 V_s f_0} \quad [13]$$

so the following Ground Shear Strain (γ) equation is:

$$\gamma = (K_g a_g) x 10^{-6} \quad [14]$$

where Kg is the soil vulnerability index:

$$K_g = \frac{\left(\frac{A_0}{f_0}\right)}{(\pi^2 V_s)} \quad [15]$$

- Controlling and Triggering Factors of Landslide

Landslides have two main factors, they are controlling factors and triggering factors. Controlling factors are the factors that affect the condition of material such as geological conditions, slope, lithology, faults, and joints in rocks. The trigger factors are the factors that cause the movement of material such as rainfall, earthquakes, erosion, and human activities (Naryanto, 2013) (Naryanto, 2017).

Data and Method

The methods used by researchers include the acquisition, processing and interpretation is shown in Figure 1.

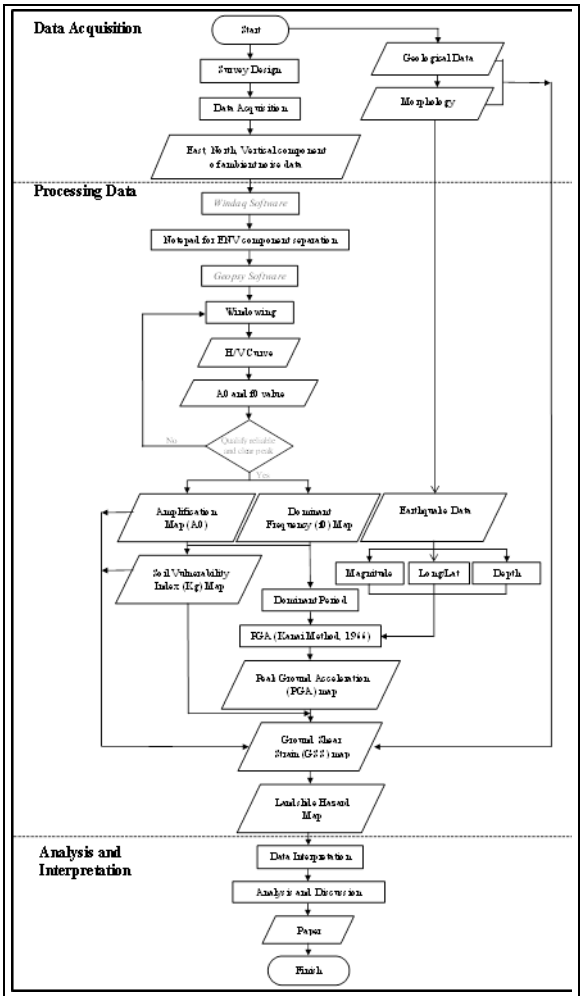

Figure 1: Flow Chart of Research Method

- Acquisition

The research was done in 2 sessions on 8-11 February and 13-15 February 2021. The acquisition area has a plot area of 1x1.2 Km2. Each track consists of 42 measurement points with a space between 200 meters. Adjustment points actualizing by field conditions, which are safe and measurable.

Measurement was done using the LE-3D/20s seismometer with an average measurement time of ±30 – 45 minutes/points. The data acquisition location map is shown in Figure 2.

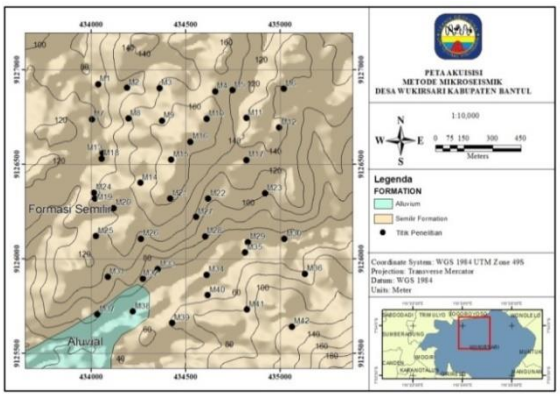

Figure 2: Data Acquisition Location Map

PROCEEDINGS
JOINT CONVENTION BANDUNG (JCB) 2021
November 23rd – 25th 2021

- Processing Data

The measurement data results in Windaq Waveform (.WDQ) format then exported into .CSV format and will be saved in .TXT format. The resulting file consists of 3 components, they are horizontal data (east-west), horizontal data (north-south), and vertical data. The three data are processed using geopsy software for windowing. HVSR was done to get F0 and A0 data.

From f0 and A0 data calculations to get the value of Kg. Based on data from the 2006 Jogja's earthquake (USGS, n.d.), this value was used for the calculation of PGA and GSS. These data are integrated with geological and morphological data to create a landslide hazard in the research area.

Result and Discussion

The results were obtained in the form of an index of vulnerability and disaster vulnerability in the Wukirsasi area, Imogiri, Bantul. This was analyzed based on the H/V curve, amplification (A0), dominant frequency (f0), soil vulnerability (kg), associated with lithology, morphology, population density, and the 2006 Yogyakarta earthquake to determine the Peak Ground Acceleration (PGA) value. Ground Shear Strain (GSS) as the basis for making landslide hazard maps.

- Spectrum Comparison H/V

The result of windowing on the E-W, N-S, and vertical components in the form of an H/V curve containing information on amplification and dominant frequency, then analyzed to determine the value of soil vulnerability. These three values are used to analyze the characteristics of sediments and rocks in the study area. The following is the result of the H/V curve which is considered to represent the research area:

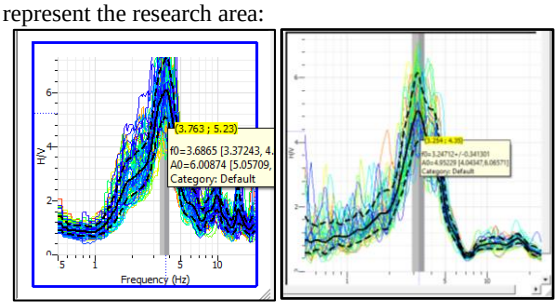

Figure 3: H/V curves of points M29 (left) and M38 (right)

The amplification value affects the character of the rock which is soft or compact. While the dominant frequency affects the thickness of the sediment. The results of both can show the character of the sediment, the thickness of the sediment layer, and the fineness of the sediment grains. These results are used for soil vulnerability analysis. Soil vulnerability will be of high value if it is composed of less compact rock (high A0), relatively large thickness (high H and low f0). This soil vulnerability value can be used for disaster studies such as earthquakes and landslides.

- Amplification Map (A0)

Amplification is the magnification of seismic waves that occurs due to significant differences between layers, in other words, seismic waves will experience magnification, if they propagate from one medium to another, which is softer than the medium that has been passed before (Haerudin, Alami, & Rustadi, 2019).

A high amplification value means experiencing (strengthening) larger waves, which can then be interpreted as soft/less compact rock, and vice versa.
The research area has an amplification value range of 1 – 7.4 which can be seen on the map below:

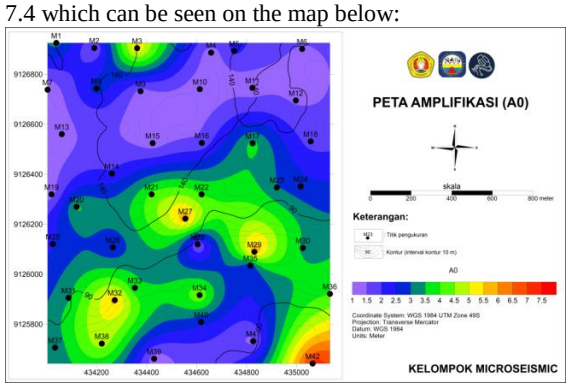

Figure 4: Amplification Map (A0)

From the map above, it is interpreted into 3 zones according to the amplification classification according to (Fitri, 2018) (Table 1). Areas that have low amplification values with a range of 1 – 3, namely the southern and northern parts of the map (purple – blue) have a low risk of damage in the event of vibration or shock. For areas with a value of 3 – 6 have a moderate amplification factor value, then an area with a high amplification value of > 9 has a high risk of damage in case of vibration/shock.

Based on the table below, it can be seen that the research area is dominated by low - medium amplification values, where the level of risk of damage is also low - moderate in the event of vibration or shock. Only the area in the middle of the plot has a moderate to high amplification value.

Table 1. Classification of amplification values based on (Fitri, 2018):

ZONE	CLASSIFICATION	A_0 VALUE	POINT NUMBER
1	Low	A<3	M2 M4 - M16 M18 - M19 M24 - M26 M28 M35 M39 - M41
2	Middle	3≤A≤6	M1 M3 M17 M20 - M23 M27 M30 - M34 M36 - M38
3	High	6≥A≥9	M29 M42
4	Very High	A>9	-

PROCEEDINGS
JOINT CONVENTION BANDUNG (JCB) 2021
November 23rd – 25th 2021

- Dominant Frequency Map (f0)

The dominant frequency (f0) shows the frequency value that occurs most often which is influenced by wave speed and sediment thickness.

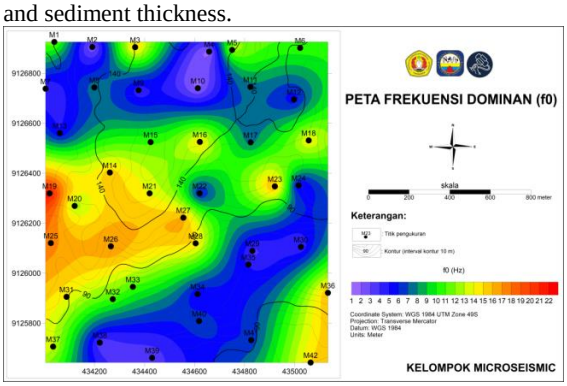

Figure 5: Dominant frequency pattern (f0)

The dominant frequency is inversely proportional to the thickness of the sediment and is directly proportional to the velocity (Mucciarelli & Gallipoli). Areas that have thicker layers of sediment will tend to have a small dominant frequency value. The dominant frequency value in the study area is depicted in Figure 5. The study area has a dominant frequency value of 1.5 – 21.8 Hz, and is classified as shown in the table below:

Table 2. Soil classification based on dominant frequency (Kanai, 1983)

CLASSIFICATION	f_0 (Hz)	POINT NUMBER	DESCRIPTION
IV	6.6 - 20	M1 M3 M5 - M6 M8 M11 M14 - M21 M23 M25 - M28 M31 - M33 M36 - M37 M40 - M42	The thickness of the surface sediment is very thin which is dominated by hard rock
III	4 - 6.6	M9 M12 - M13 M22 M24 M30 M34 - M35	Medium category surface sediment thickness 5 – 10 meters
II	2.5 - 4	M7 M29 M38 - M39	The thickness of the surface sediment is thick category, about 10 – 30 meters
I	<2.5	M2	The thickness of the surface sediment is thick category, about >30 meters

- Soil vulnerability index map (Kg)

Soil vulnerability index (Kg) is obtained from the square of the amplification value (A0) divided by the dominant frequency (f0) which is shown in Figure 6. The value of soil vulnerability index (Kg) in the study area is 0.07225 – 9.79383 s^2/cm. In the research area there are 3 zones, namely a zone with a height of kg 8 – 9.5 s^2/cm which indicates that the zone consists of less compact or impervious rock and has a relatively high potential or disaster risk and can be classified as a hazard zone and very dangerous. then the medium kg zone has a value of 3 – 8 s^2/cm. Furthermore, the low kg zone with a value of 0.07225 – 3 s^2/cm indicates a lower level of risk of damage or disaster-prone because it is composed of more compact/resistant rock.

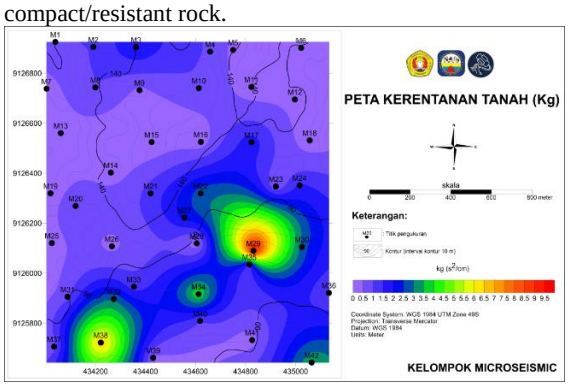

Figure 6: Soil vulnerability index map (Kg)

- Peak Ground Acceleration Map (PGA)

The PGA value in the research area was obtained by calculation using the Kanai's method (Kanai, 1966). To calculate the PGA value, we need an earthquake parameter that has the largest magnitude and also the epicenter distance closest to the microtremor acquisition point. In this study, the earthquake parameters used were the earthquake that occurred on May 26, 2006 in Bantul, DIY with a magnitude of 6.3 on the Richter Scale and an earthquake depth of 12.5 km below sea level. The processing results show PGA values ranging from 281,658 gal to 1059.17 gal as shown in Figure 10.

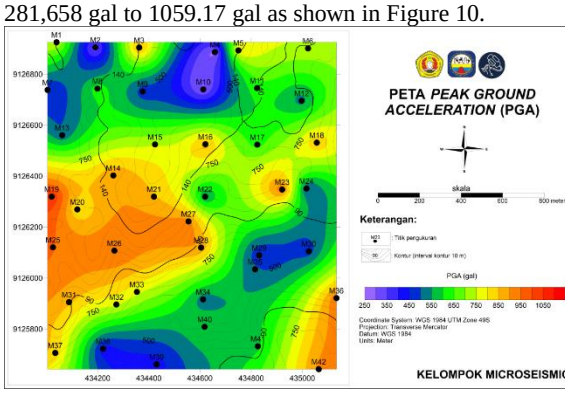

Figure 7. Peak Ground Acceleration Map (PGA)

This PGA value shows the change of velocity over time. Peak Ground Acceleration can also be interpreted as the maximum acceleration felt by a particle/layer when an earthquake occurs. The PGA value can be related to the level of damage in the event of an earthquake. BMKG in Haerudin, Alami & Rustadi (2019) has classified and correlated the MMI scale with PGA values which can be seen in Table 3.

PROCEEDINGS
JOINT CONVENTION BANDUNG (JCB) 2021
November 23rd – 25th 2021

Table 3. BMKG Earthquake Intensity Scale

Skala SIG BMKG	Warna	Deskripsi Sederhana	Deskrispsi Rinci	Skala MMI	PGA (gal)
I	Putih	TIDAK DIRASAKAN (*Not Felt*)	Tidak dirasakan atau dirasakan hanya oleh beberapa orang tetapi terekam oleh alat.	I–II	< 2.9
II	Hijau	DIRASAKAN (*Felt*)	Dirasakan oleh orang banyak tetapi tidak menimbulkan kerusakan. Benda-benda ringan yang digantung bergoyang dan jendela kaca bergetar.	III–V	2.9–88
III	Kuning	KERUSAKAN RINGAN (*Slight Damage*)	Bagian non struktur bangunan mengalami kerusakan ringan, seperti retak rambut pada dinding, genteng bergeser ke bawah dan sebagian berjatuhan.	VI	89–167
IV	Jingga	KERUSAKAN SEDANG (*Moderate Damage*)	Banyak Retakan terjadi pada dinding bangunan sederhana, sebagian roboh, kaca pecah. Sebagian plester dinding lepas. Hampir sebagian besar genteng bergeser ke bawah atau jatuh. Struktur bangunan mengalami kerusakan ringan sampai sedang.	VII–VIII	168–564
V	Merah	KERUSAKAN BERAT (*Heavy Damage*)	Sebagian besar dinding bangunan permanen roboh. Struktur bangunan mengalami kerusakan berat. Rel kereta api melengkung.	IX–XII	> 564

- Ground Shear Strain Map (GSS)

Ground shear strain is a value that indicates the dynamics of the soil or the ability of the soil layer material to shift or move during an earthquake. When an area has a high ground shear strain value, the area has a layer of soil that is easy to move, either stretch or shift; on the other hand, when an area has a low ground shear strain value, the area will be difficult to move and shift. Strain and shift will cause deformations such as soil fractures, landslides, and liquefaction (Syahputri & Sismanto, 2020). Figure 11 shows the distribution of ground shear strain values in the study area, which has a range of $0.7x10^{-4}$ to $43x10^{-4}$.

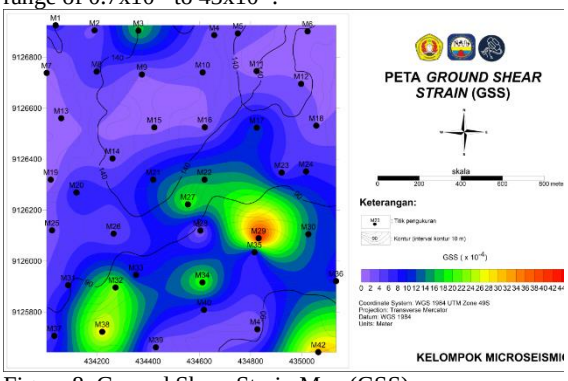

Figure 8. Ground Shear Strain Map (GSS)

Based on the classification table of the relationship between the value of Ground shear strain and soil dynamics according to (Nakamura Y. , 1997) it was identified that the research area has plastic and elastic soil dynamics, so that the research area will have the potential for phenomena such as cracks and soil subsidence. Areas that have high ground shear strain values are at points M29, M42, and M38, which have the potential to have high damage to the study area.

- Landslide Hazard Map

One of the controlling factors for landslides is the slope. Morphological and morphometric analysis was carried out to determine the level of slope in the study area. Figure 9 shows a map of the slope of the study area. The study area has a varied morphology, with a predominance of 25 to >45% slope. With this level of slope, the research area is classified as steep to very steep.

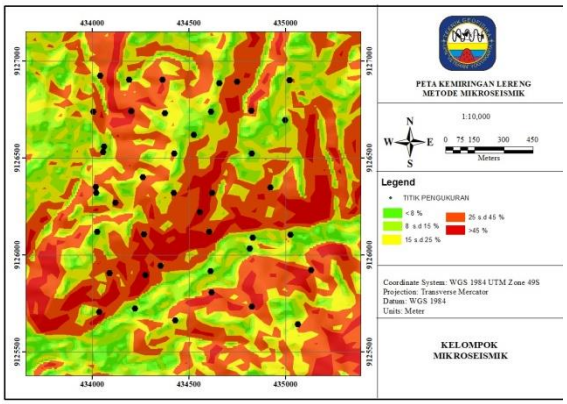

Figure 9. Slope Map

The determination of the level of landslide susceptibility is based on the cumulative score obtained from the overall influence parameters, namely slope, Ground Shear Strain, Peak Ground Acceleration and rainfall, to produce the map shown in Figure 10. In this study, 3 classes of vulnerability were used, namely low, medium and high. The determination of the vulnerability level of the landslide occurrence area in the study area is based on the estimation model of landslide-prone areas by the Directorate of Volcanology and Geological Hazard Mitigation/DVMBG (PVMBG, n.d.) and (Isbakhul Lail, 2019). Based on this analysis, it is known that the parameters that influence the occurrence of landslides, if sorted from the highest, are rainfall, slope, and rock characteristics (GSS and PGA). In this study, the score given is 30% for slope and GSS, then 20% for rainfall and PGA. The rainfall data used is the result of the average rainfall throughout 2019 obtained from the Central Statistics Agency (BPS) data. The scoring of the rainfall parameter is only 1 ranking because the research area is still local so that the rainfall value is considered to be the same. The overall value of this weighting can be seen in Table 4.

Table 4. The value of the weight and score of each parameter

No.	Parameter	Quality	Score	Rank
1	Slope	30%	<8%	1
			8-15%	2
			15-25%	3
			25-45%	4
			>45%	5
2	*Ground Shear Strain* (GSS)	30%	0.000076 - 0.001504	1
			0.001504 - 0.002933	2
			0.002933 - 0.004361	3
3	*Peak Ground Acceleration* (PGA)	20%	280 - 540	1
			540 - 800	2
			>800	3
4	Rainfall	20%	185.5	1

PROCEEDINGS
JOINT CONVENTION BANDUNG (JCB) 2021
November 23rd – 25th 2021

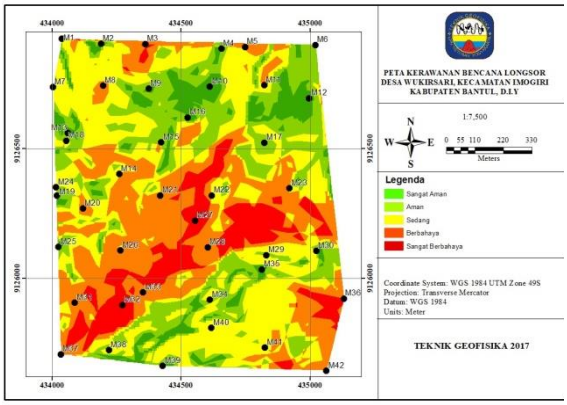

Figure 10. Landslide Hazard Map

Based on the picture above, it can be seen that the area with a high level of vulnerability is located in the middle of the research area, namely at points M29, M32, M34, M35, M38, and M39. The zoning distribution of landslide-prone areas in this study showed similar results to the slope maps, GSS and PGA. Areas with a moderate level of vulnerability are spread from the northwest to the southeast of the study area. Meanwhile, the low-risk area is located in the northeastern part of the study area.

Conclusions

The research area that have high vulnerability index more potential for landslide hazard, they are M29, M32, M34, M35, M38, and M39 points (middle center of the research area).

References

Edwiza. (2008). Analisis terhadap Intensitas dan Percepatan Tanah Maksimum Gempa Sumbar. *Jurnal Geofisika, 1, No.29, Th. XV*, 73-79.

Fitri, D. A. (2018). Pemetaan Zonasi Indeks Kerentanan Seismik pada Daerah Pasca Tambang Di PT.Bukit Asam (Persero) Tbk. Unit Penambangan Ombilin, Sawahlunto. Padang: Universitas Negeri Padang.

Haerudin, N., Alami, F., & Rustadi. (2019). *Mikroseismik, Mikrotremor dan Microearthquake dalam Ilmu Kebumian*. Bandar Lampung: Pustaka Media.

Isbakhul Lail, B. W. (2019). IDENTIFIKASI POTENSI LONGSOR MENGGUNAKAN SISTEM INFORMASI GEOGRAFIS DI KECAMATAN SALEM KABUPATEN BREBES. *Plumula, 7*, 73-85.

Julianti, T. S. (2018). *Analisis Mikroseismik dengan Pendekatan Ground Shear Strain untuk Mikrozonasi Potensi Longsor di Deliksari Sukorejo Kecamatan Gunungpati Kota Semarang*. Semarang: UNNES.

Kanai. (1966). Improved Empirical Formula for Characteristic of Stray [sic] Earthquake Motion. *Proceedings of the Japanese Earthquake Symposium* , (pp. 1-4).

Kanai, K. (1983). *Engineering Seismology*. University of Tokyo.

Mucciarelli, M., & Gallipoli, M. R. (n.d.). The HVSR Technique from Microtremor to Strong Motion: Empirical and Statistical Considerations. *13th World Conferences on Earthquake Engineering.* Vancouver, B.C., Canada.

Nakamura, Y. (1989). A Method for Dynamic Characteristics Estimation of Subsurface using Microtremor on the Ground Surface. *Quarterly Report of Railway Technical Research Institute (RTRI), 30, No.1*.

Nakamura, Y. (1997). *Seismic Vulnerability Indices for Ground and Structures Using Microtremor*. Florence: World Congress on Railway Research.

Nakamura, Y. (2000). *Clear Identification of Fundamental Idea of Nakamura's Technique and Its Application*. Japan: Tokyo University.

Naryanto, H. S. (2013). Analisis dan Evaluasi Kejadian Bencana Tanah Longsor di Cililin, Kabupaten Bandung Barat, Provinsi Jawa Barat Tanggal 25 Maret 2013. *8, No. 1*, 39-49.

Naryanto, H. S. (2017). Analisis Kejadian Bencana Tanah Longsor di Dusun Jemblung, Desa Sampang, Kecamatan Karangkobar, Kabupaten Banjarnegara, Provinsi Jawa Tengah tanggal 12 Desember 2014. *1 No. 1*, 1-10.

Priyantari, N., & Suprianto, A. (2009). *Penentuan Kedalaman Bedrock Menggunakan Metode Seismik Refraksi di Desa Kemuning Lor Kecamatan Arjasa Kabupaten Jember, 10, No.1*, 6– 12.

PVMBG, n. (n.d.). Retrieved Maret 25, 2020, from Peta Zona Kerentanan Gerakan Tanah Kota Yogyakarta dan Bantul: https://vsi.esdm.go.id/gallery/index.php?/category/12

Slob, S. (2007). *Micro Seismic Hazard Analysis*. Netherlands: International Institute for Geo-Information Science and Earth Observation.

Syahputri, A., & Sismanto. (2020, Agustus 17). Identifikasi Potensi Tanah Longsor Menggunakan Metode Mikrotremor Di Dusun Tegalsari Desa Ngargosari Kecamatan Samigaluh Kabupaten Kulon Progo. *Artikel Riset*, 66-71.

USGS. (n.d.). Retrieved Februari 20, 2021, from https://earthquake.usgs.gov/earthquakes/map/?extent=16.80454,-137.19727&extent=55.07837,-52.82227

PROCEEDINGS
JOINT CONVENTION BANDUNG (JCB) 2021
November 23rd – 25th 2021

Identification of Groundwater Potential Zone for Drinking Water Demand in Muara Empayang Village, Lahat Regency, South

Rina Sahara[1], Muhammad Faris Hafiddin[2], Muhammad Fadhli[1], Tommy Julio Lumban Tobing[3]
[1]Geological Engineering Study Program, Sriwijaya University
[2]DMS Program Pamsinas III Kabupaten Lahat
[3]Balai Besar Pelaksanaan Jalan Nasional V Sumatera Selatan

Abstract

Water becomes a daily human need for survival such as drinking water, household needs, agriculture, livestock, and many other things. Along with the increasing number of populations the population compensates for the increasing water needs. Sehingga needs to research to find out the potential of groundwater that is following standardization in clean water that can be drink. The study was conducted in Muara Empayang Village by conducting spatial data analysis using fuzzy logic approaches, geoelectric surveys, and water quality tests according to PERMENKES No.37 of 2017. Fuzzy logic approaches use fuzzy membership and fuzzy overlay operations with slope, geomorphology, elevation, and drainage parameters. Geoelectric surveys use a terameter (resistivity meter) by an electric current into the ground using electrodes and recording their resistance in the response time dimension. From validation results based on fuzzy logic, geoelectric surveys, and water quality tests, the research site has the potential to become an aquifer with flow through space between grains, moderate productive aquifers with widespread spread have moderate to low canes with diverse water levels that can be used as community consumption, but need special treatment to be used as drinking water.

Keywords: Muara Empayang, Groundwater, Drinking water, Fuzzy Logic, Aquifer

Introduction

Groundwater is a very valuable natural resource in everyday life. The increase in the number of people every year has an impact on the increasing need for clean water to support human survival. This raises concerns about the availability of clean water.

Groundwater is part of the hydrological cycle and is in rocks below ground level which includes the discovery, spread, and movement of groundwater with an emphasis on the relationship of regional geological conditions (Danaryanto, et al., 2005). The factor that causes poor groundwater quality is the process of overexploitation.

Identifying groundwater quality includes physical, chemical, and biological parameters. It is strongly influenced by the nature of water, the content of living things, substances, energy, and other components in water. The physical analysis includes smell, taste, amount of solutes, turbidity, temperature, color. While chemistry in the form of Fe, Cd, $CaCo_3$, Mn, NO_2, pH, Zn, CN, SO_4, Pb, and on biological parameters are Total Coliform and Escherichia Coli.

Regionally the location of the study is on the Bengkulu sheet composed of Kasai formation and Plieosen-aged alluvium and quaternary composed of continental sandstone and clay and pyroclastic material (fig. 1). The topography of the research area, in general, is lowlands and low hills with slope slopes from flat to very steep.

This research aims to find out the potential of groundwater as well as the distribution of groundwater spread and quality for drinking water as an effort to meet the needs of the people of Muara Empayang Region, East Kikim Subdistrict, Lahat Regency, South Sumatra.

Data and Method

The research was conducted in Muara Empayang Area, East Kikim Subdistrict, Lahat Regency, South Sumatra (fig.2). The methods used are literature studies and field observations in the form of geological observations, resistivity surveys, physics, chemical, and biological sample tests, and groundwater suitability analysis using fuzzy logic in ArcGIS software (fig. 3). Literature studies discuss the regional geology of the research area which is further carried out field observation in the form of resistivity surveys with 2 trajectories and 2 potential electrodes and distances between spaces of 250 meters using the Schlumberger electrode configuration.

Furthermore, water quality analysis tests were conducted on 2 samples based on physical, chemical, and biological characteristics according to Decree No.32 of 2017 on standard standards of water quality and health. The last fuzzy logic approach with fuzzy membership and fuzzy overlay operating models is available on ArcGIS software. In fuzzy membership and fuzzy overlay, operations used parameters in the form of slope, geomorphology, elevation, and

drainage. Fuzzy membership values are adjusted to the rating. The value of 0 is very bad, 0.5 is medium and 1 is a very good water potential zone (Ratheret al., 2012).

Result and Discussion

Geolistrik Analysis

The geoelectric testing of Schlumberger's configuration was performed to determine the potential of the water. Geolmeasurements are tricks showing electrical resistivity between 5 - 32 Ohm-meters (fig. 4) with clay lithology, sand clay, and clay sand (fig.5). Aquifer system with flow through space between grains, medium productive aquifers with widespread have moderate to low cans with varying water levels (Table 1).

Water Quality Test

Determining the quality water that is worth drinking or not feasible must be analyzed by water quality standards issued by PERMENKES No.37 of 2017, it consists of several parameters, namely Physical, Chemical, and Biological Characteristics.

a) Physical Characteristics

In determining the physical characteristics of water, it includes temperature, turbidity, color, smell, and taste (Todd, 2005). In the research area, water sampling was conducted at two well-point locations with the codes ME-01 and ME-02. The location of ME-01 obtained the results that groundwater in the location of the study does not smell and taste and for color obtained a value of 15 / 50 from the TCU scale. Furthermore, the results of the amount of solid toot (TDS) produced a value of 64 / 1000 units mg/liter and turbidity produced a value of 0.06 / 25 of the NTU scale unit. And from the last parameter that temperature obtained a value of 25℃.

While at the location of ME-02 obtained the results that groundwater in the research location does not smell and taste and has a color content of 13/50 from the TCU scale. Furthermore, in the test results, the amount of toot solid substances (TDS) produced a value of 66 / 1000 from mg/lite units, turbidity with a value equal to the location of ME-01 which is 0.06, and a jar with a value of 25℃ equal to the me-01 sample. In the acquisition of data, using Organoleptic method for odor and taste tests, Direct Reading for TDS tests, SNI 06-6989.25-2005 for turbidity and temperature, and color tests using spectrophotometry methods.

b) Chemical Characteristic

Determining the chemical characteristics of water can be done using the methods ICP-OES, SNI 06-6889, 12-2004, and SNI 6989.11.2019. Quality tests using the ICP-OES method include iron (Fe), cadmium (Cd), manganese (Mn), zinc (Zn), and lead (Pb). The location of ME-01 and ME-02 still qualified according to the health minister's quality standard test. The locations of ME-01 and ME-02 have the same values, namely Iron (Fe) values 0.14, Cadmium < 0.0015, Manganese (Mn) 0.11, Zinc (Zn) < 0.0050 and Timbal (Pb) < 0.0031. Furthermore, SNI 6989.12-2004 elements of $CaCo_3$ obtained results that meet the quality standard where ME-01 has a value of 114 and ME-02 102. And finally based on SNI 6989.11.2019, analysis of NO_2, pH, and SO_4, from the results of NO_2, SO_4 value meets the quality standard that is Me-01 0.01, 31.11, and Me-02 0.01, 42.89, but for pH obtained the results have not met the quality standard with a value of ME-01 6.43 and mE-02 5.58. The standard test parameters of quality and analysis results are in table 2.

c) Biological Characteristic

Determining the biological characteristics of water can be done using a test detection of coliform bacteria content (Todd, 2005. According to Decree No. 37 of 2017, the maximum threshold for total coliform is 50 CFU/100 ml, andE-Coil is 0 CFU/100 ml. In the area of the me-01 and ME-02 research sites, CFU and Escherichia Coli were 200 ml. Therefore, it can be known that groundwater at the peneplain site has been polluted so it is not recommended to be consumed directly. The standard test parameters and analyst results are found in table 3.

Fuzzy Logic Data Analyze

Fuzzy logic is a numerical for spatial modeling problems. A fuzzy system consists of 3 main elements, namely fuzzy set, fuzzy membership, and fuzzy production. The fuzzy theory was introduced by Zadeh, 1965. The membership value of an object ranges between 0 and 1. The value 1 means the full membership of an object and the closer the value of 0 the weaker the membership of the object in the fuzzy set (Kollias et al, 1998).

Fuzzy models use fuzzy membership operations and fuzzy overlays available on spatial analysis of ArcGIS software. In generating a map of groundwater potential by analyzing the interrelationships between spatial data layers and the influence on groundwater systems. The fuzzy membership function curve (Fig. 6) defines a point in a fuzzy membership input interval between 0 and 1. This function helps determine the influence of the lowest to highest parameters.

Fuzzy overlay is a relative relationship and interaction measurement. Fuzzy overlay approach in the form of fuzzy And, fuzzy Or, fuzzy Product, fuzzy Sum and fuzzy Gamma.

1. Fuzzy And: Fuzzy overlay type to find locations that meet a wide variety of criteria.
2. Fuzzy Or: Fuzzy overlay type to find a location that meets one of the criteria.
3. Fuzzy Product: Fuzzy overlay type to find locations with various combined fuzzy membership values.
4. Fuzzy Sum: Fuzzy overlay type for possible locations that correspond to fuzzy membership inputs.
5. Fuzzy Gamma: A very complex fuzzy overlay type with a combination of various spatial sub-data.

In fuzzy membership and fuzzy overlay, operations are used in a suitable combination of slope, geomorphology, elevation, and drainage. Fuzzy membership values are adjusted to the rating. The value of 0 is very bad, 0.5 is medium and 1 is a very good water potential zone. Secondary data processing based on DEMNas data on a scale of 1:40,000. The slope of slopes based on Widyaatmanti classification 2016 to 6 categoy. Geomorphology from elevation consists of 2 landfrom. In addition, DEM data used for elevation classification and high drainage density reflects the basin where fluid flows with a rapid hydrological response to rainfall while low drainage density indicates slow-response basins to rainfall at the research site consisting of flat or almost flat until very steep (fig. 7).

In the fuzzy overlay combine various spatial data, applied fuzzy sum operators, a fuzzy sum approach that shows the location of the study can be used with a value between 0.2 to 1(fig. 8) as well as weighting in table 4.

Conclusions

Based on the results of data analysis using geoelectric surveys, water quality analysis, and fuzzy logic, it can be known that the research site has the potential to meet the needs of the people of Muara Empayang Region, East Kikim Subdistrict, Lahat Regency, South Sumatra. This can be known from the results of fuzzy membership and fuzzy overlay approaches with a value range of 0.2 to 1 that shows low hills topography areas with sloping slopes. Electric surveys show electrical resistivity between 5-32 Ohm-meter with clay lithology, sandy clay, and clay sand can be known the flow of a medium productive aquifer system with widespread has a moderate to low with varying water levels.

Furthermore, in determining water quality, tests of the characteristics of physics, chemistry, and biology are carried out. The physical characteristics of water quality can be used, but in chemical tests, the pH content has not been met because it obtained results less than the quality standard, and biological results do not support water used directly.

From this, the need for further systematics to become water that is worth drinking directly.

References

Danaryanto, Djaendi., et al. 2007. Department of energy and mineral resources geological agency, geological environment center, Bandung.

Gafoer, S., et al. 1992. Geological Research and Development Centre.

Goyal, Sandeep., et al. 2017. Journal of Geomatics, 11, 2.

Kollias, V.J.and D.P., Kollias, 1998. Computers and Electronics in Agriculture, 20, pp. 79–95.

Mallik, Santanu., et al. 2021. Ecological Indicators 121 (2021) 107179.

Rafati, S., and M. Nikeghbal. 2017. The International Archives of the Photogrammetry, Remote Sensing and Spatial Information Sciences, Volume XLII-4/W4, 2017

Rather, J.A., and A.B. Zameer and A. Raouf (2012). Journal of Advances in Remote Sensing and GIS, Vol. 1, No. 2, 2012, 218-233.

Republic of Indonesia. 2017. PERMENKES No.32 of 2017. Jakarta. Government of the Republic of Indonesia.

Todd, D.K., et al. 2005. Groundwater Hydrology, Third Edition. NewYork: John Wiley & Sons

Acknowledgments

We are grateful to Joint Convention Bandung for accepted our paper. We would like to thank all members of JCB Sriwijaya for supported this study.

Table 1. Interpretation result of survey electric resistivity

Titik Duga	Lapisan	Hasil Penafsiran			Perkiraan Litologi	Perkiraan Hidrogeologi
		Kedalaman		Tahan Jenis		
GL.1	1	0,00	5,17	114,39	Tanah Penutup	
	2	5,17	10,21	32,44	Pasir Lempungan	Air Tanah Bebas
	3	10,21	35,85	6,52	Lempung	
	4	35,85	~	19,30	Lempung Pasiran	Akuifer
GL.2	1	0,00	6,49	64,39	Tanah Penutup	
	2	6,49	70,88	5,20	Lempung	
	3	70,88	~	15,82	Lempung Pasiran	Akuifer

Table 2. Fisical and chemistry analysis of water quality

No	Parameter	Satuan	Standar Baku Mutu (Kadar Maksimum)	Hasil	Metode Pemeriksaan
ME 01					
A. Fisika					
1	Bau	#	Tidak Berbau	Tidak Berbau	Organoleptik
2	Rasa	#	Tidak Berasa	Tidak Berasa	Organoleptik
3	Jumlah zat padat terlarut (*TDS*)	mg/liter	1000	64	Direct Reading
4	Kekeruhan	SkalaNTU	25	0,06	SNI 06-6989.25-2005
5	Suhu	°C	Suhu udara ±3	25	SNI 06-6989.25-2005
6	Warna	Skala TCU	50	15	Spektrofometri
B. Kimia					
1	Besi (Fe)	mg/liter	1	0,03	ICP - OES
2	Kadmium (Cd)	mg/liter	0,005	<0,0015	ICP - OES
3	Kesadahan ($CaCo_3$)	mg/liter	500	114	SNI 06-6989.12-2004
4	Mangan (Mn)	mg/liter	0,5	0,06	ICP - OES
5	Nitrit (NO_2)	mg/liter	1	0,01	SNI 6989.11.2019
6	pH (di Laboratorium)	#	6,5 - 8,5	6,43	SNI 6989.11:2019
7	Seng (Zn)	mg/liter	15	<0,0050	ICP - OES
8	Sianida (CN)	mg/liter	0,1	<0,003	Spektrofometri
9	Sulfat (SO_4)	mg/liter	400	31,11	SNI 6989.20:2019
10	Timbal (Pb)	mg/liter	0,05	<0,0031	ICP - OES
ME 02					
A. Fisika					
1	Bau	#	Tidak Berbau	Tidak Berbau	Organoleptik
2	Rasa	#	Tidak Berasa	Tidak Berasa	Organoleptik
3	Jumlah zat padat terlarut (*TDS*)	mg/liter	1000	66	Direct Reading
4	Kekeruhan	SkalaNTU	25	0,06	SNI 06-6989.25-2005
5	Suhu	°C	Suhu udara ±3	25	SNI 06-6989.25-2005
6	Warna	Skala TCU	50	13	Spektrofometri
B. Kimia					
1	Besi (Fe)	mg/liter	1	0,14	ICP - OES
2	Kadmium (Cd)	mg/liter	0,005	<0,0015	ICP - OES
3	Kesadahan ($CaCo_3$)	mg/liter	500	102	SNI 06-6989.12-2004
4	Mangan (Mn)	mg/liter	0,5	0,11	ICP - OES
5	Nitrit (NO_2)	mg/liter	1	0,01	SNI 6989.11.2019
6	pH (di Laboratorium)	#	6,5 - 8,5	5,58	SNI 6989.11:2019
7	Seng (Zn)	mg/liter	15	<0,0050	ICP - OES
8	Sianida (CN)	mg/liter	0,1	<0,003	Spektrofometri
9	Sulfat (SO_4)	mg/liter	400	42,89	SNI 6989.20:2019
10	Timbal (Pb)	mg/liter	0,05	<0,0031	ICP - OES

PROCEEDINGS
JOINT CONVENTION BANDUNG (JCB) 2021
November 23rd – 25th 2021

Table 3. Biology analysis of water quality

Nama Sampel	CFU/100 ml Total Coliform	CFU/100 ml Escheria Coli
ME 01	200	200
ME 02	200	200

Table 4. Thematic parameters of fuzzy membership

Parameter	Class	Fuzzy membership
Geomorphology	Low Hill	0,22
	Low Land	0,24
Slope (%)	0 – 2	1
	3 – 7	1
	8-13	0,85
	14 - 20	0,25
	21 - 55	0,31
	56 - 140	0,16
Elevation (m)	50 - 75	1
	75 - 100	1
	100 - 125	1
Drainage	0 - 14	0,08
	28 - 42	0,04
	42 - 56	0,02

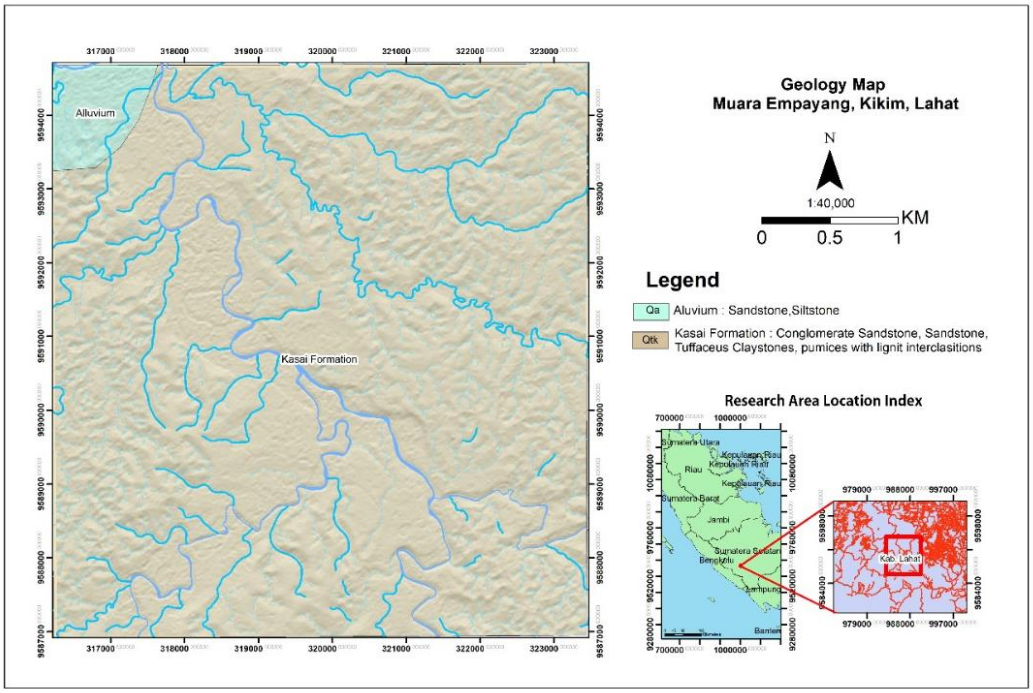

Figure 1. Geology Map Muara Empayang (Modified S. Gafoer, T.C. Amin and R. Pardede, 1992)

PROCEEDINGS
JOINT CONVENTION BANDUNG (JCB) 2021
November 23rd – 25th 2021

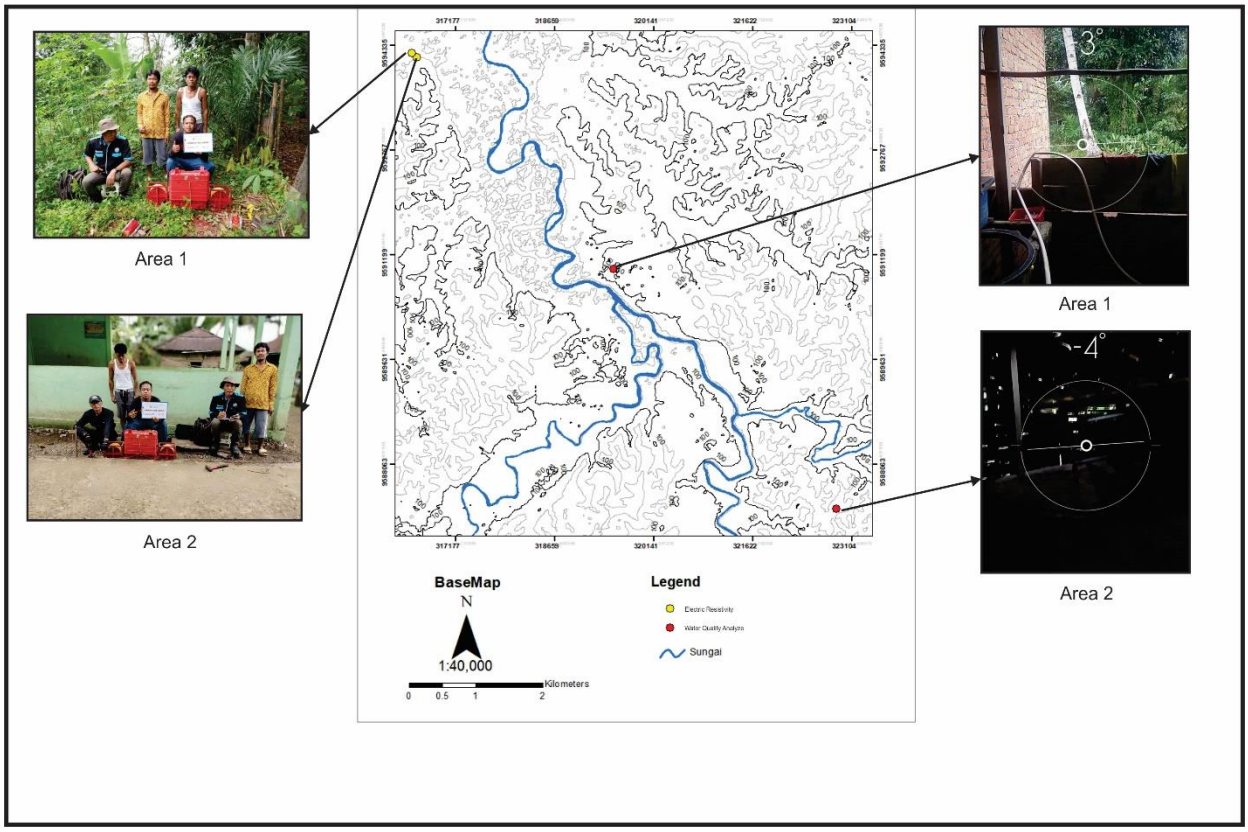

Figure 2. Field observation electric resistivity and water quality analysis at Muara Empayang

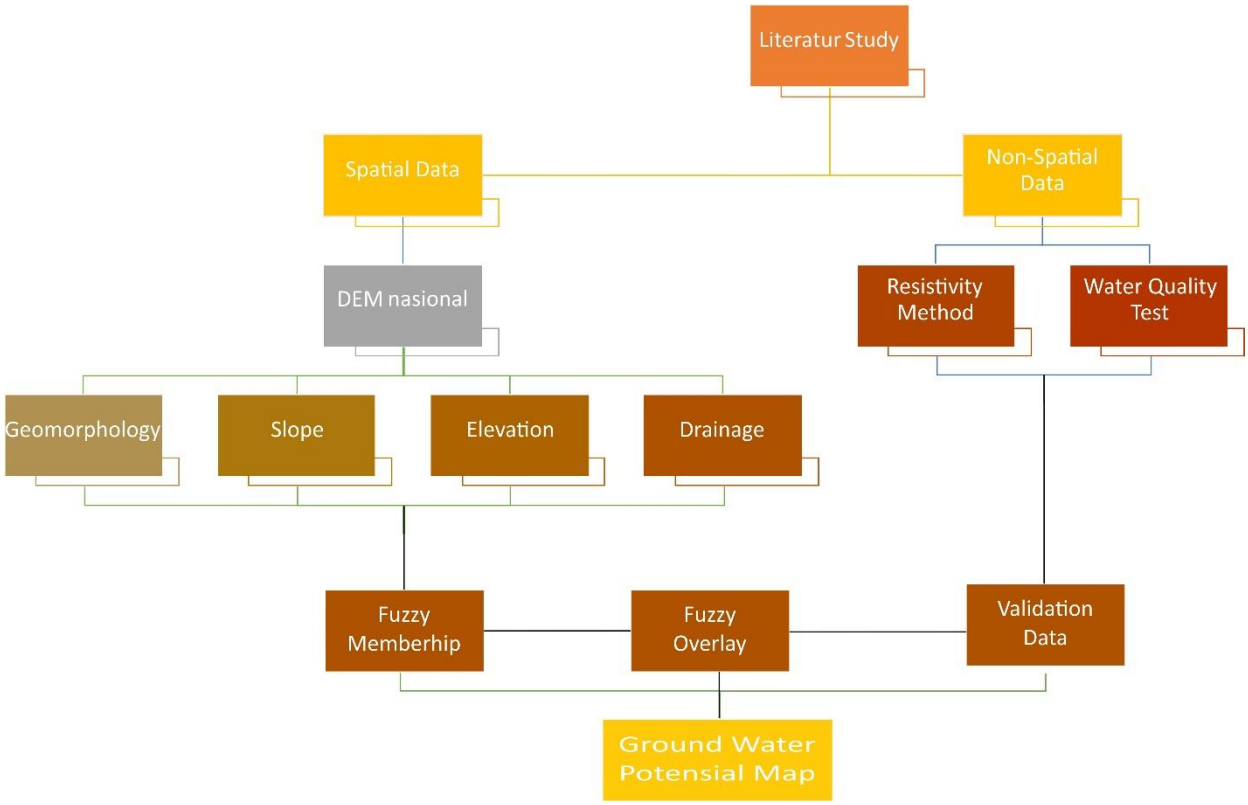

Figure 3. Research Flow

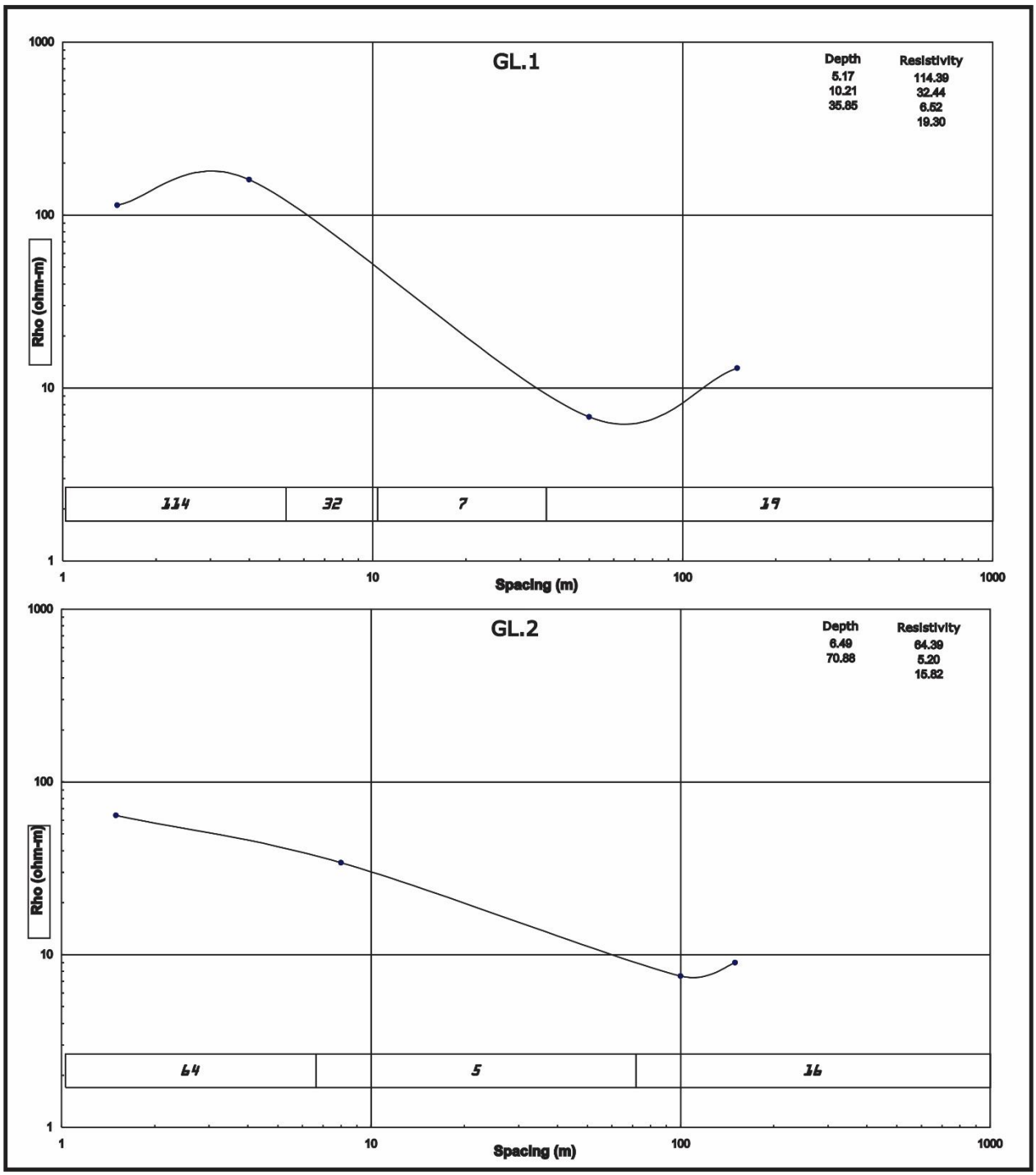

Figure 4. 1D Schlumberger from electric resistivity at Muara Empayang

PROCEEDINGS
JOINT CONVENTION BANDUNG (JCB) 2021
November 23rd – 25th 2021

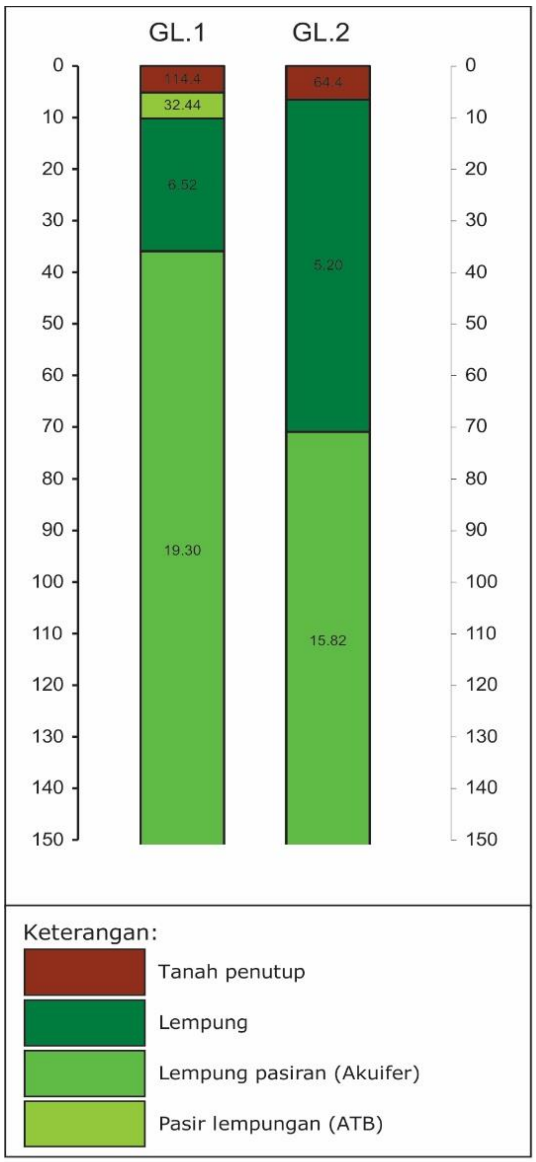

Figure 5. Vertical cross-sectional resistance type point estimate electric resistivity

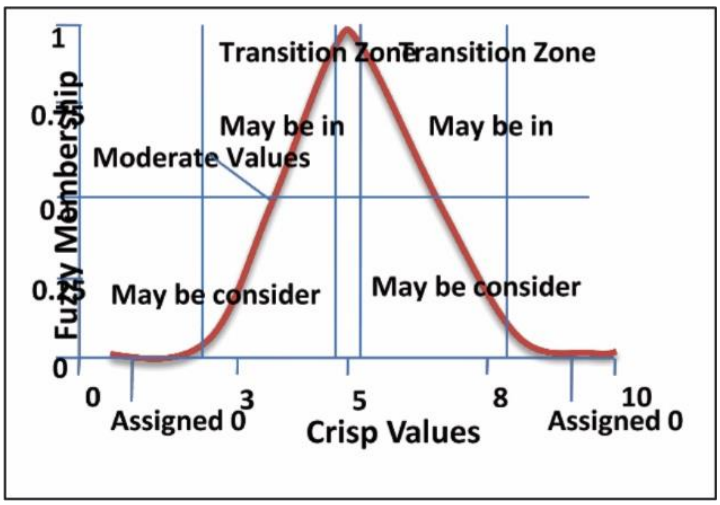

Figure 6. Fuzzy membership function program (Modified Goyal, Sandeep et al, 2017)

PROCEEDINGS
JOINT CONVENTION BANDUNG (JCB) 2021
November 23rd – 25th 2021

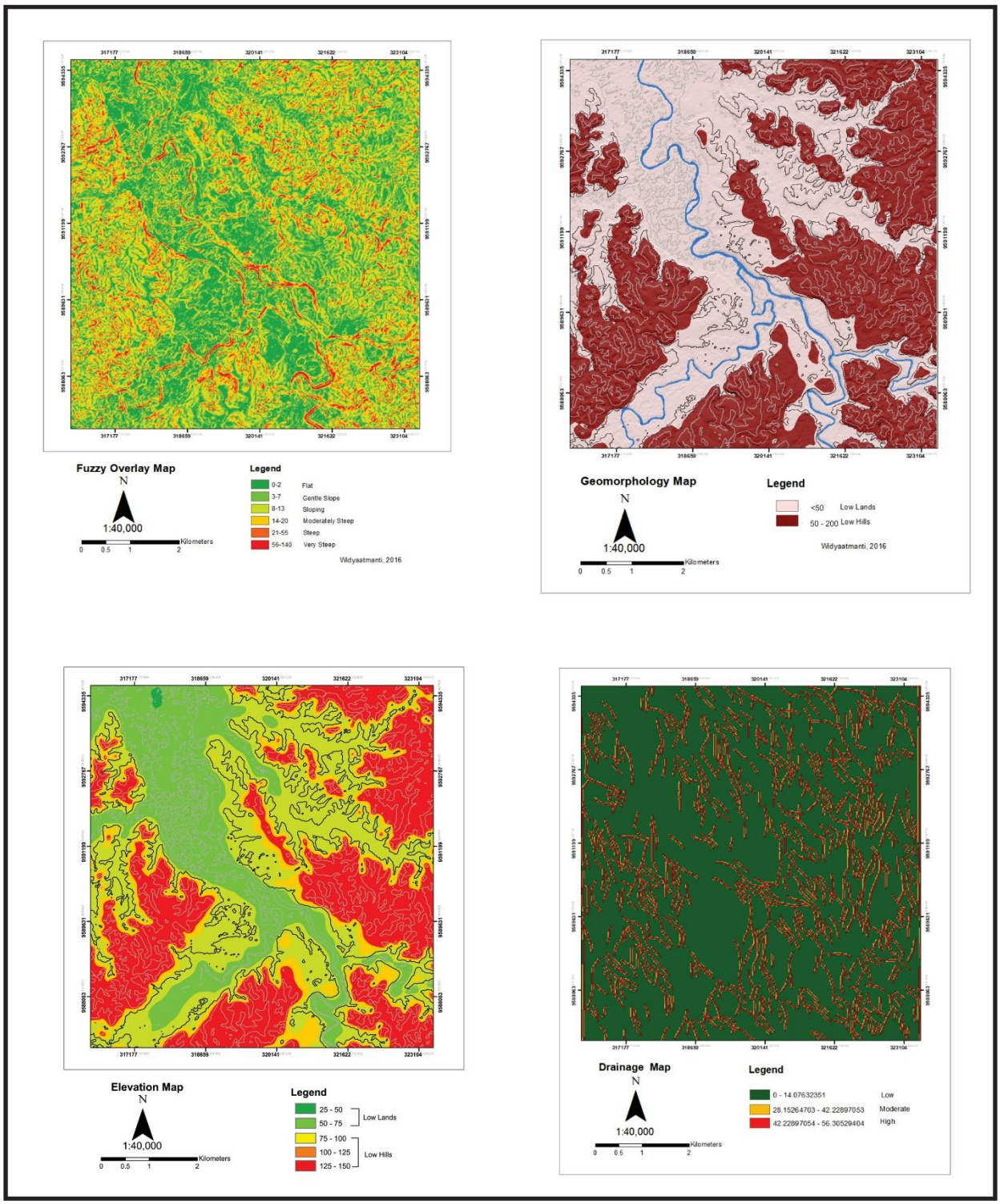

Figure 7. Fuzzy membership parameters

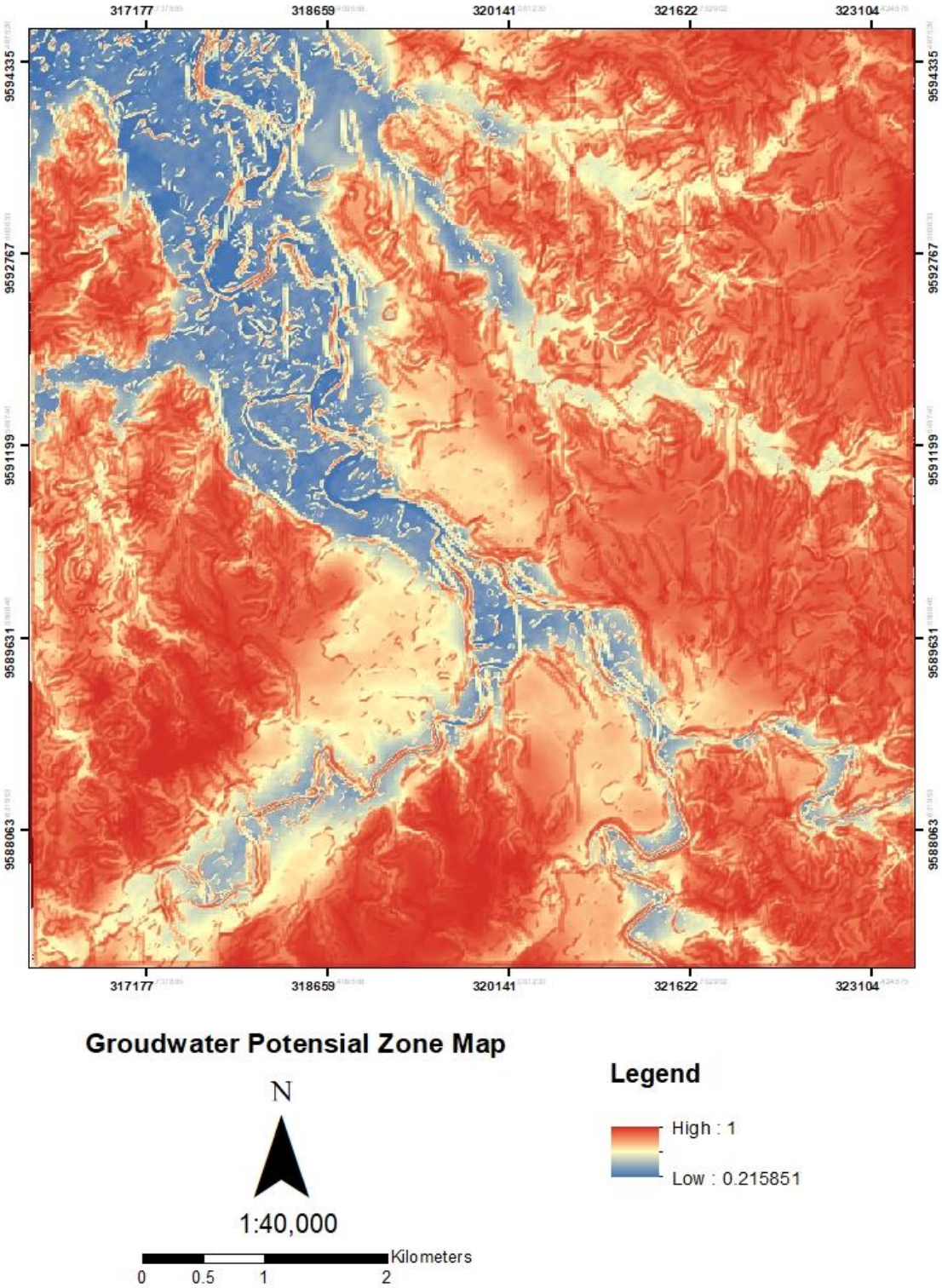

Figure 8. Groundwater potential zone from combination geomorphology, slope, elevation, and drainage.

PROCEEDINGS
JOINT CONVENTION BANDUNG (JCB) 2021
November 23rd – 25th 2021

STUDI KUALITAS AIR TANAH BERDASARKAN SIFAT FISIK DAN KIMIA MENGGUNAKAN ANALISIS HIDROGEOLOGI DAN HIDROKIMIA DI JAKARTA BARAT

Albar Karismawan[1], Dyah Nindita Sahdarani[1], Mochammad Prahastomi M.S[1], Tantowi Eko Prayogi[2]

1. Program Studi Geologi, Fakultas Matematika dan Ilmu Pengetahuan Alam, Universitas Indonesia, Depok, 16424, Indonesia
2. Balai Konservasi Air Tanah (BKAT), Jakarta, Indonesia, Kementrian Energi dan Sumber Daya Mineral (ESDM)

Email: albar.karismawan@ui.ac.id

Abstract : The study of Groundwater in West Jakarta is to determine the quality of groundwater that is commonly used by residents for their daily needs such as drinking, clean up and etc. This study is important because the water consumed by residents does not necessarily meet standard of raw water quality for drinking set by the government through Permenkes No. 492 of 2010, through physical and chemical parameters. The research focuses on examining free aquifers in densely populated housing by using hydrogeological and hydrochemistry analysis. This research aims to condition groundwater by hydrogeology and hydrochemistry method and also mapping water quality. Hydrogeological analysis is used to map ground water level based on groundwater depth measurements measured in community wells with units of meters below ground level (mgmt) and meters below sea level (m.asl).Hydrochemical data uses two data, namely primary and secondary data. Primary data is data taken by the author in the field in 2021 by focusing on free aquifer groundwater wells taken in densely populated housing. Secondary data is data taken by BKAT in 2018-2020 by focusing on groundwater wells for public spaces such as gas stations, parks, and houses of worship. So that the hydro chemical analysis produces two types of maps, the first map is groundwater quality of free aquifers in public spaces through BKAT data, and a map of groundwater quality in densely populated housing in 2021. The results of the hydrogeological research are making a map of the free aquifer zone, and a map of the average change in groundwater level in West Jakarta. While the hydro chemical analysis was carried out to see the conditions of salinity, type of water, the level of seawater intrusion and the total dissolved solids in the study area.Based on measurements made by the author in March 2021, the deepest water depth is in Semanam Village with a depth of 9.3 mgmt., and the shallowest is in Rawa Buaya village with a depth of 0.2 mbmt. Meanwhile, based on the author's measurements, groundwater quality are chagrin. Roa Melaka Village has smelly water, also high in Chloride, Sodium, and Natrium. Duri Kepa and Jelambar Village have high iron pollution, through measurement have 0,4 mg/l and 1,65 mg/l.

Keywords : Free Aquifer, Hydrogeology, Hydro Chemistry, Ground Water Quality

Introduction

Humans depend on clean water in carrying out various activities. These activities include meeting domestic and non-domestic needs. Domestic needs include household needs, bathing, drinking, toileting and so on, as well as non-domestic needs such as markets, industry, agriculture, transportation and so on. To meet the needs of clean water, humans depend on ground water. Groundwater is part of the hydrological cycle that can be found at the bottom of the soil surface (Sen, 2015). Groundwater is stored in soil pores in the pore spaces between grains, cracks, or in the dissolution tunnel (Cahyadi and Hidayat, 2017).

According to the Groundwater Conservation Center of Balai Konservasi Air Tanah (BKAT), the use of ground water in DKI Jakarta in 2015 was 60% of the total clean water needs, and 40% used PAM water. The amount of ground water consumed by residents of DKI Jakarta in that year was 496,356,207m3. Meanwhile, the population of DKI Jakarta in 2015 reached 10,177,924 people (BPS, 2016). This means that every person uses 48.76m3 of groundwater per year. Continuous use of groundwater can cause land subsidence in DKI Jakarta (Djaja, Rais et al. 2004). There was a land subsidence in DKI Jakarta of 0-12 cm per year in the period 1996-2016 (Hutabarat, 2017).

PROCEEDINGS
JOINT CONVENTION BANDUNG (JCB) 2021
November 23rd – 25th 2021

The next problem with groundwater use is the poor quality of water quality standards. Based on the 2015 BKAT, the groundwater conditions in DKI Jakarta in the free aquifer layer were 16 of the 85 monitored wells that met water standards and 69 monitored wells did not meet water quality standards. In 2018, five sub-districts in three different sub-districts in West Jakarta, namely Kalideres, Kebon Jeruk, Taman Sari sub-districts experienced heavy pollution (DKI Jakarta Environmental Service, 2019). According to the DKI Jakarta Environmental Service in 2019, groundwater has a heavy pollution index if the water contains mercury, helium, solids and other chemicals. In addition, there is a sub-district that contains e-coli bacteria in groundwater, namely the Palmerah sub-district (Dayanti, 2017).

The use of ground water needs to be seen from the physical and chemical aspects to determine the quality of water that can be consumed by residents. The standard for using ground water is stated in the Regulation of the Minister of Health number 492 of 2010 concerning the requirements for drinking water quality. Water plays an important role in life, so it is important to study groundwater quality using hydrogeological and hydro chemical analysis

Data and Method

Research on groundwater quality in West Jakarta focuses on free aquifers in densely populated housing. The research was conducted with two types of data, namely primary and secondary data. Primary data are groundwater depth data, laboratory analysis data, and drill core data. Secondary data includes MAT data and groundwater quality in 2019-2020. The authors obtained secondary data through data released by the Center for Groundwater Conservation (BKAT).

In general, the research is divided into four stages, namely the preparation stage, the data collection stage, the data processing stage, and the final stage.

The preparation stage begins with taking care of permits to conduct research, submitting secondary data to the DKI Jakarta Groundwater Conservation Center (BKAT), and preparing sampling equipment such as EC TDS Meters, pH Meters, depth measuring instruments, stationery, and so on related to preparation. The author also prepares software such as ARC GIS 10.6, Ms. Excel which is used to process the data.

Next is the data collection stage. The data collection stage is processing the data obtained by the author such as groundwater depth data, rock drill core data, physical and chemical measurement data in the field, and laboratory analysis data. Next is the data processing stage. The data processing stage aims to find the relationship between the data that has been taken, collect data in the field, make an initial picture of the research, distribute water quality to the data obtained. All data is processed to obtain the actual situation regarding groundwater quality in West Jakarta. Mapping of water quality refers to clean water standards set by the government through Minister of Health Regulation No. 492 of 2010.

The last is the final stage. The final stage of the research is to get the distribution of groundwater quality in West Jakarta using hydrogeological and hydro chemical analysis.

Result and Discussion

1. Hydrogeological Condition

The hydrogeological conditions of the research area based on measurements in the field in March 2021, two conditions were obtained regarding these measurements. The first situation is that the Southeast and Southwest regions have deeper wells than the surrounding areas. This condition is seen in the H3S2 sample which has a depth of 9 mbmt, and H5S4 and H5S5 which has a depth of 4 mbmt. The second condition is that the northern and central parts have shallower wells. This situation is a consideration for determining the area of discharge and recharge.

The affixed areas are found in the sample codes H3S2, H5S4, H5S5, and H8S2. The four samples are located in the Urban-District Semanam, Palmerah, Srengseng, and South Kembangan. In addition, it is identified as a discharge area. Thus, the West Jakarta aquifer zone is divided into two, namely the recharge zone interpreted as brown, and the discharge zone interpreted as green. The recharge areas are located in three sub-districts, namely ± 25% of the Kebon Jeruk area, ± 20% of the Kalideres and Kembangan areas, and ± 10% of Cengkareng and Palmerah. The discharge area is located from the North to the South (Figure 1). The area includes the sub-districts of Taman Sari, Tembora, Grogol Petamburan, Palmerah, Kebon Jeruk, ±90% of the Cengkareng area, ±80% of the Kembangan area, and ±60% of the Kalideres area. So that it can be interpreted to determine the West Jakarta free aquifer

PROCEEDINGS
JOINT CONVENTION BANDUNG (JCB) 2021
November 23rd – 25th 2021

zoning map.

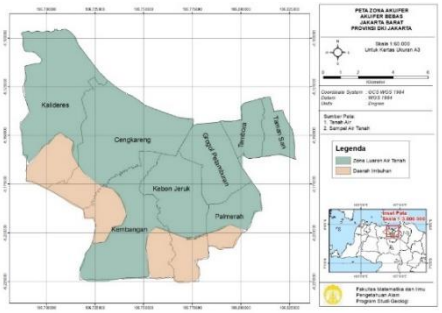

Figure 1. Zone Aquifer Maps in West Jakarta

In the 2021 ground water level measurement, the highest ground water level height in red with the sample code H8S3, and H5S4 is in the sub-districts of Meruya Selatan, and Palmerah. Both samples were measured at an altitude of 17.2 masl and 14.5 masl. The deepest ground water level is dark green with sample codes H2S4 and H2S5, each having a depth of -3.17 masl and -2.02 masl.

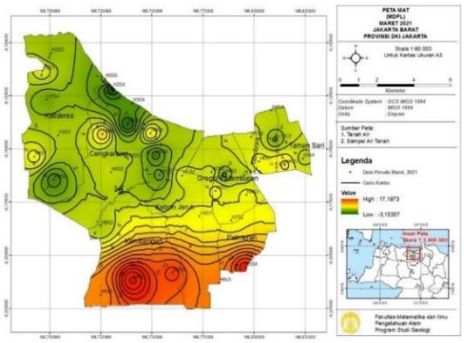

Figure 2. Ground Water Level Map in March 2021

2. Hydrochemistry Analyse

The first analysis in hydrochemistry is salinity. Salinity analysis using laboratory data. The samples used were twelve wells which were taken through groundwater samples from residents in West Jakarta (Figure 3). The reference for salinity classification refers to Todd (1980).

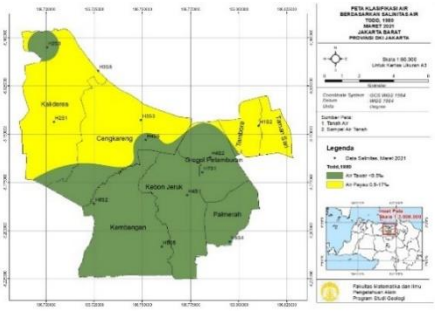

Figure 3 Water Salinity Map

The salinity map shows in green with a percentage of ±60% of the study area classified as fresh water, while the yellow color with a percentage of ± 40% is brackish water (Figure 4.35). Based on the map, the salinity boundaries are located in the sample code H4S2 in Grogol Petamburan, H4S% in Cengkareng, and H8S2 in Kembangan. These boundaries divide into two areas, namely the north and south. The northern region has higher salinity with a 5-17$^{0}/_{00}$. percentile range, while the southern region is below 5$^{0}/_{00}$.

The next analysis is the type of groundwater using total dissolved solids in groundwater or total dissolved solids (TDS). The TDS unit uses S/cm. The data was obtained through direct measurements at the wells of residents of West Jakarta. The TDS parameter used refers to PAHIAA (1986). Based on their distribution, transitional water and brackish water are more commonly found in the northern part of West Jakarta which has a position close to the coast of North Jakarta, compared to the southern part of West Jakarta which has freshwater types (Figure 11). This is caused by several possibilities, the first is that the topography of North West Jakarta is lower than the South so that seawater intrusion may occur, and the H2S5 sample is located at an elevation of -2 meters above sea level. The second possibility is the source rock factor which is geologically regionally coastal embankment deposits (Turkandi, 1992). So that groundwater is affected by the rock of origin.

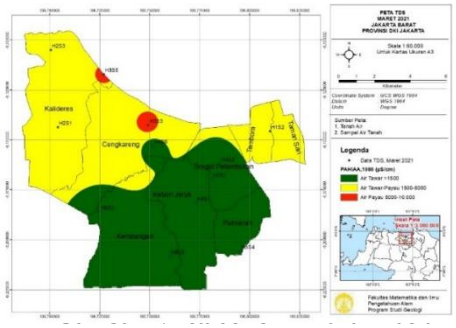

Figure 4. TDS Map

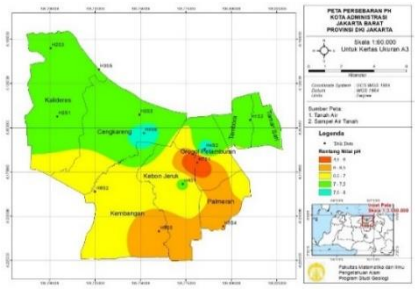

FigurE 5. pH Map in Ground Water Villager Well in West Jakarta

PROCEEDINGS
JOINT CONVENTION BANDUNG (JCB) 2021
November 23rd – 25th 2021

Based on the pH distribution map, the authors divide the pH range into 5 classes, with details of two classes not meeting and three classes meeting the water quality standards for drinking according to the Minister of Health Regulation No.492 of 2010 (Figure 4.38). The first class, which is red, is used for water that has a low pH, which is below 6, which is found in the sample code H7S1 which is located in North Tanjung Duren. The second class orange is used for groundwater with a pH value close to the drinking water standard, namely pH 6-6.5. This class is found in the sample code H5S4 in Palmerah village and H5S5 in Srengseng village. The third class already meets the standards of Permenkes No. 492 in 2010 with a pH close to neutral, namely 6.5-7. This class range is found in the development district with the sample code H8S2.

The fourth class is symbolized in green, and dominates in the North of the research area. This class has a neutral pH of 7-7.5 with sample codes H1S2, H2S1, H2S3, H3S3, H3S5, and H4S1, each located in the villages of Roa Melaka, Pegadungan, Kamal, Kapuk, and Tegal Alur. The last class is the fifth class with the highest pH approaching a weak base, namely 7.5-8 with a blue symbol. In this class, there are sample codes H4S2, and H4S6, which are located in Jelambar and Kedungkaliangke, respectively

Table 1. Charge Balance Eror Equation

Kode Sampel	Kation			Anion			Hasil CBE (%)	Penilaian
	Ca	Mg	Na	SO4	Cl	HCO3		
	(meq/L)	(meq/L)	(meq/L)	(meq/L)	(meq/L)	(meq/L)		
H1S2	8,25	3,675	10,26087	2,3125	22,48571	6,114754	-14,7456	Tidak Diterima
H2S1	5	4,675	12,21739	18,5625	8,657143	9,557377	-24,7108	Tidak Diterima
H2S3	5,4	5,583333	9,73913	4,333333	12,4	14,06557	-18,4262	Tidak Diterima
H3S3	2,9	4,016667	17,95652	6,75	30,22857	8,754098	-28,5955	Tidak Diterima
H3S5	9,85	5,3	16,43478	8,166667	32,22857	6,901639	-18,5696	Tidak Diterima
H4S1	5,3	0,8175	1,478261	0,8125	0,314286	8,229508	-8,30488	Tidak Diterima
H4S2	2,9	0,7075	3	1,208333	2,371429	5,180328	-12,402	Tidak Diterima
H4S6	2,2	0,313333	0,565217	0,75	0,4	2,655738	-7,65985	Tidak Diterima
H5S4	1,15	0,439167	0,73913	0,979167	2,371429	0,918033	-27,2658	Tidak Diterima
H5S5	2,6	0,815	0,695652	0,458333	2,142857	0,983607	7,281284	Tidak Diterima
H7S1	1,7	0,3275	0,521739	2,375	0,428571	0,065574	-3,98014	Diterima
H8S2	2,5	1,391667	0,608696	1,666667	1,6	3,131148	-16,8362	Tidak Diterima

Based on the CBE calculation, the range of values is -3.9% - 7%. Acceptable CBE tolerances have values below 5% and above -5%. Thus, only one data met the criteria, namely the H7S1 sample, and the rest did not have good data quality according to Freeze & Cherry (1979). There are several data factors that affect the quality of the resulting data. These factors include human errors such as improper weighing of solutions by the laboratory so that there can be errors in reading concentrations that are reduced or excessive. The second factor is the contamination of water during sampling, considering that the well is in a toilet for a densely populated house, there could be an impurity factor through cactus washing bathing activities. The third factor is the presence of the main element ion which is not read during the measurement, so it needs to be analyzed further considering that the dominant data is anion so that it indicates the presence of an unreadable cation. The consideration is that the research area is a densely populated residential area that is close to industrial areas such as in the Pegadungan, Durikepa, Kapuk, and Cengkareng villages so that it indicates the presence of heavy metal pollution which is not readable in the chemical research data and further analysis is needed regarding the content of heavy metals such as lead, cobalt, and so on.

Next is the control of soil water content. Control of groundwater content through analysis of groundwater composition using the value of TDS (total dissolved solid) with the ratio value of the main cations of groundwater, namely Na+, K+ and Ca2+ and the main anions, namely Cl- and HCO3 in the Gibs diagram.

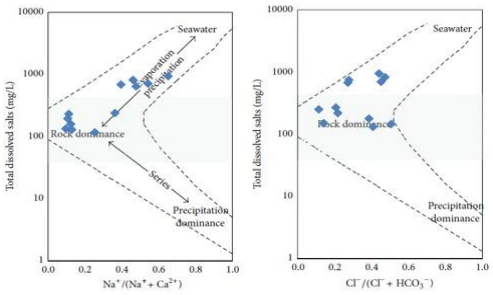

Figure 6. Ground Water Gibbs Diagram at West Jakarta

From the results of the data on the ratio of cations and anions that have been plotted on the Gibbs Diagram of groundwater, it can be interpreted that the study area shows rock dominance (Figure 6) with 7 of 12 samples. The sample is found in the sample number H4S1-H8S2 with a low TDS value of <1000 mg/l

Based on the Gibbs diagram, the research area is affected by weathering of rocks through 7 of the 12 samples studied. Meanwhile, 5 of the 12 samples had TDS values >1000 mg/l and the ratio of cations and anions <1 (Gibbs, 1970). In the Gibbs diagram, it is in the middle between weathering rock and seawater intrusion. However, the position of 5 of the 12 samples is closer to rock weathering.

The next analysis is groundwater facies. The

groundwater facies analysis uses the values of the main cations and anions in groundwater, namely Na+, K+, Ca2+ and Mg2+ and the main anions are Cl-, HCO3- and SO42- and uses a Piper diagram. Each molecule was converted from milligrams per liter (mg/l) to percent milliequivalents per liter (%meq/l) in twelve samples of groundwater from Jakarta residents scattered in West Jakarta.

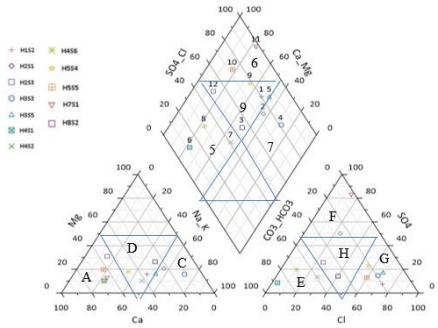

Figure 7. Piper Diagram

The first analysis of the parallelogram Piper Diagram. In the diagram there are two analyzes that can be discussed. First, look at the type of groundwater facies based on cations and anions (Figure 7). Based on the analysis of the Trilinear Piper parallelogram diagram (Figure 2.8), it was found that the dominant classification was 9 with 4 of 12 mixed type groundwater samples with balanced cation and anion content and not exceeding > 50% (Walton, 1970).

The second analysis in the parallelogram diagram is to look at the dominance of cations and anions to see the difference between acids and bases. The graph on the left illustrates that West Jakarta groundwater is classified into classification 1 where alkaline earth elements exceed elements. This condition is referred to as hard water (Philip Kristanto, 2004). The graph on the right depicts the condition of groundwater anions in West Jakarta. In the graph there are 9 out of 12 samples showing a strong acid (SO42- +Cl-) is more dominant than a weak acid (CO32– + HCO3-. The last in the Piper diagram is a triangle diagram to see the dominance of elements in the groundwater facies. In the triangle diagram has cations dominant in group A, namely calcium with 5 of 12 samples, followed by anion with dominant type G. Type G is the type of groundwater anion with chloride dominant.

Next is the relationship between ions using Durov diagram analysis. Based on the Durov Diagram, it can be interpreted that most ions are in Type 5. Type 5 is characterized by no dominant ion between anions and cations, because the water has been mixed well. The second position is Type 2. This type has a dominant ion of Ca, and Mg. The abundance of these elements indicates that groundwater is associated with dolomite and abundant Mg ions.

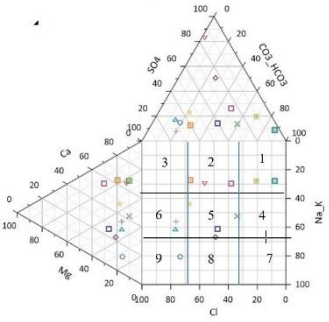

Figure 8. Diagram Durov Hubungan Antar Ion

3. Relation Between Hydrogeology and Hydrochemistry

Through petrography and XRD conducted by Listyani (2016) that rocks have dolomite minerals. According to Bowen (1986) Dolomite is associated with Fe2+, Fe3+, Ca2+, Mg2+, Cl-, and F. This means that groundwater in the study area is affected by underground rock conditions. In addition, the salty conditions in North West Jakarta are influenced by hornblend minerals associated with groundwater.

4. Water Quality Study

a. Kualitas Air Tanah 2019

In 2019, cluster quality of water based on BKAT data using 14 data points. Measurement in 2019 is a yellow zone with 40% area. While the red zone with 8 of the 14 samples measured did not meet the physical and chemical parameters with 45% of the area.

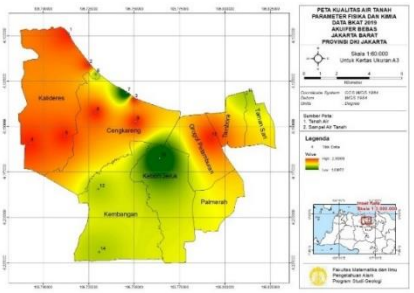

Figure 9. Ground Water Quality in 2019
(**Source:** BKAT, 2021)

b. Kualitas Air Tanah 2020

During the rainy season in March 2020, BKAT measured groundwater quality in West Jakarta. In this period, the authors obtained 12 data points from BKAT. The green zone is seen in measurements in Palmer with code 2, and the Al Ikhlas Mosque in Kapuk with data code number 10 has groundwater quality that meets drinking water standards. There is a difference in the District of Kebon Jeruk into the yellow zone. This change was due to the decrease in pH to 6.4 from the standard stipulation of Permenkes number 492 of 2010 which was 6.5. Joglo area, and Roa Melaka.

Map of groundwater quality for summer season in September 2020, there are three color zones, namely green, yellow and red based on the level of pollution (Figure 10). This map shows that the Kebon Jeruk area experienced a zone change from yellow during the rainy season in March 2020, and turned green during the dry season in August 2020. Changes in the Kebon Jeruk area were observed through an increase in pH from 6.4 to 7.29. It can be seen from this case that the rain in Jakarta tends to be acidic so that it can lower the pH, while during the dry season the influence of the rock layers below the surface is more dominant. Groundwater suitable for consumption is located in Joglo Village, Kembangan District with a code point of 11, and Kebon Jeruk with a code of 14. Next, it is slightly unfit for consumption through the yellow zone because it does not meet the physical parameters in Kembangan with a code point of 10 and Palmmerah with a code point of 12. Water unfit for consumption in the red zone dominates the research area with ±60% with a total of 7 code points, the majority of which are in the northern part of West Jakarta.

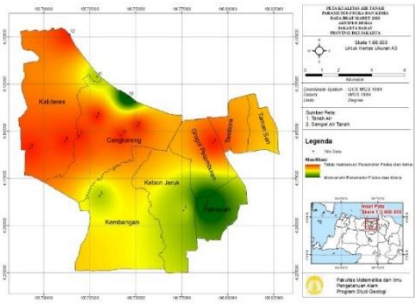

Figure10. Ground Water quality in March 2020 (**Source:** BKAT, 2021)

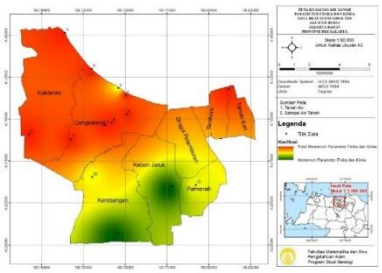

Figure11. Ground Water quality in March 2020 (**Source:** BKAT, 2021)

c. Ground Water Quality in 2021

Groundwater quality in 2021, the authors use data from residents' wells with free aquifer types located in densely populated housing, so they do not take measurements in public areas as BKAT did. However, there are several sample points such as in Urban-District Roa Melaka with code H1S2, Urban-District Tegal Alur with code H3S5, which can be compared with BKAT data (Table 4.18).

The first zone is green and is only located in Kedaungkaliangke Village which meets the quality of raw water for drinking. While the second zone is yellow, as the yellow zone. The yellow category is for samples that do not meet one of the parameters such as the sample code H8S2 which is located in Kembangan Selatan Village with Manganese ion content exceeding the standard, which is 0.46. Then H5S4, and H5S5, which are located in Palmerah Village, and Srengseng Village, respectively, do not meet the standard water pH values of 6.3 and 6.2. The yellow zone dominates the southern part of the research area, covering the sub-districts of Palmerah, Kembangan, 30% Kapuk, and 20% Grogol Petamburan.

The last zone is the red zone, located in the northern part of the research area. The red zone does not meet the physical parameters and the red zone is seen in the sample code H1S2 which is located in the Urban-District Roa Melaka has a TDS of more than 500, namely 1959, the sodium ion value is more than the standard, which is 236 mg/L, and high chloride is 787 mg/L. L. Urban-District Roa Melaka is observed from the BKAT data and the author's data that both do not meet the standard water parameters for drinking. Meanwhile, the Tegal Alur Urban-District has a slightly different development, in 2018-2019 it is a red zone, while in 2020 the rainy season changes to a yellow zone due to the decline in Ammonium and Manganese ions.

The Conditions are not suitable for consumption, with water having iron content that exceeds the standard are found in H4S1 and H4S2 located in the Duri Kepa and Jelambar Urban-Districts. Both sample codes have iron content of 0.4 mg/L and 1.65 mg/L. Some samples have manganese content that exceeds the high limit, namely H2S1, H3S3, and H4S1. The three sample codes are located in the Urban-District of Pegadungan, Kapuk, and Duri Kepa. Each sample contains 0.88 mg/L, 0.74 mg/L, and 2.74 mg/L Manganese.

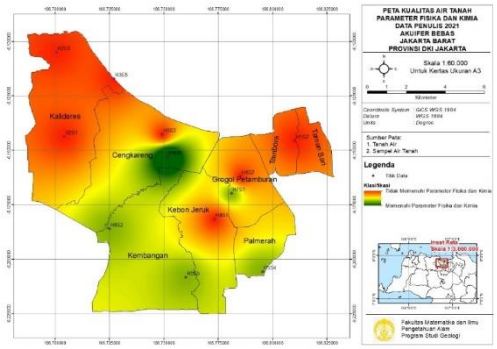

Figure 12 Water Quality Map in 2021

After dissecting the pollution zoning, the next is the facies based on Figure 4.51 the West Jakarta area has a variety of chemical facies. In general, the TDS parameter is divided into two research areas, the North area of West Jakarta has a higher TDS than the South. The northern region, namely the first day to the third day samples had a TDS above 500 ppm, while the fourth to eighth day had a TDS value below 500 ppm.

The next parameter, namely pH as an indicator of acid and alkaline water, divides into three, namely high pH 8, neutral pH 7-8, and acidic below 7. Kedaungkaliang to Cengkareng District. Next is a neutral pH with a range of 7-8, located in North West Jakarta, with sample codes H1S2, H2S1, H2S3, H3S3, H3S5, and H4S1. The last is the Southern region with an acidic pH below 7 with a value of 4.4-6.6. Southern region with sample code H5S4, H5S5, H7S1, and H8S2.

It can be concluded that the ion trend in the North region tends to be more neutral in pH because it has a relatively more balanced ratio of anions and cations. Meanwhile in the Southern region, the pH is relatively more acidic because even though the anion and cation content is not high according to the standards of Minister of Health Regulation No. 492 in 2010, but the ratio of the number of ions is more anions. The middle region with a pH of 8 has a higher number of cations than its anions, namely high hardness and bicarbonate. Especially for the sample code H7S1 which is located in North Tanjung Duren, it has a very low pH value of 4.4. There are several things that affect the low pH including rainwater, decomposition of organic matter (Barus, 2004). In addition, strong acids are more dominant than strong and weak bases

Conclusions

Based on the research and analysis that has been done, the authors obtained several conclusions, there are:

1. Hydrogeological conditions of West Jakarta, namely the recharge area is in the Southwest and Southeast of the study area, and the discharge is North West Jakarta. Based on changes in the average MAT height in masl from 2018-2021, it varies in each Urban-District from decreasing to increasing MAT height. The largest decrease occurred in the Tegal Alur Urban District, which was -0.51 mdpl/year, and the highest increase in groundwater occurred in Kalideres, which was 3.51 mdpl/year.
2. Hydrochemical conditions in the study area based on salinity, there are two types of water, namely fresh water located in the South of West Jakarta and brackish water in North West Jakarta. While the type of water with TDS parameters is that the northern part has brackish water and brackish-fresh water, and the southern part has fresh water. Based on the control of groundwater content through the Gibs diagram, it is known that groundwater is influenced by the type of rock lithology that affects the ionic elements of groundwater. Based on the relationship between ions based on the Durov Diagram, groundwater from the water sample tested for its content has a mixed type with a dominant sample of type 5 with 4 out of 12 samples there is no dominant ion between anions and cations, because the water has been mixed well, followed by type 2 with the same amount. not much different from type 5 with 3 of 12 i.e. the dominant ions are Ca and Mg.
3. The hydrogeological and hydrochemical conditions of the study area are influenced by the lithological conditions of the rock. This condition is observed through a thin section of the rock core data, which contains the mineral hornblende which is associated with Fe2+, Fe3+, Ca2+, Mg2+, Cl-, and F. These conditions affect the saltiness of groundwater in North West Jakarta.
4. Groundwater quality in 2021 in densely populated housing in West Jakarta based on the Permenkes standard number 492 of 2010, there are three quality zones, namely green, yellow, and red. The green zone is groundwater that meets the physical and chemical parameters, the yellow zone does not meet any of these parameters, and the red zone does not meet the physical and chemical parameters. The green zone is located in the Urban-District of Kedaung Kaliangke, Cengkareng District. While the yellow zone

dominates the southern part of the study, such as Kembangan, Palmerah, parts of Kebon Jeruk, and parts of Cengkareng. Meanwhile, the red zone is located in the West Jakarta area, such as Tambora, Kalideres, and parts of Cengkareng.

DAFTAR PUSTAKA

Ashriyanti, Hidanafie. (2011). *Kajian Kerentanan Pada Wilayah Terintrusi Air Laut. (Tesis)*. Program Studi Geografi. Universitas Indonesia

Assegaf, A. 1998. H*idrodinamika Airtanah Alamiah Cekungan Jakarta. (Tesis)*, Program Studi T. Geologi, Program Pasca Sarjana.

Assegaf, A., Hendarmawan, Hutasoit, L.M., Hutabarat, J. (2017). *Salinitas Airtanah Akifer Tidak Tertekan Kedalaman 0 – 20 m Daerah Kalideres – Cengkareng, Jakarta Barat*. Jurnal RISET Geologi dan Pertambangan. Vol.27, No.1, Juni 2017,15 – 25. Pusat Penelitian Geoteknologi Lembaga Ilmu Pengetahuan Indonesia.

Banks, D., Frengstad, B., (2006). *Evolution of groundwater chemical composition by plagioclase hydrolysis in Norwegian anorthosites. Geochem*. Cosmochim. Acta 70, 1337–1355.

Cahyadi, A., dan Hidayat, W. (2017). *Analisis Karakteristik Hidrogeokimia Air Tanah di Pulau Korang Panggang, Kepulauan Seribu, DKI Jakarta*. Jurnal Geografi Vol 9 No.2 (99-108).

Chow, VT, (1988). *Applied Hydrology*. New York: Mc-Graw-Hill Company

Çinar, Ö., & Merdun, H. (2009). *Application of an unsupervised artificial neural network technique to multivariant surface water quality data*. Ecological Research, 24(1), 163–173. doi: 10.1007/s11284-008-0495-z.

Dayanti, M.P. (2017). *Kualitas Air Tanah di Kecamatan Palmerah Jakarta Barat ditinjau dari pola sebaran Escherichia coli*. Jakarta: Universitas Trisakti.

Djaja, R., et al. (2004*). Land subsidence of Jakarta metropolitan area.* Proceedings of the 3rd FIG Regional Conference for Asia and the Pacific.

Fachri, M., Djuhaeni, Hutasoit, L.M., dan Ramdhan, A.M., (2002). *Stratigrafi dan hidrostratigrafi Cekungan Airtanah Jakarta*. Bulletin Geologi, Vol. 34, No. 2, hal 169 – 190

Fatoni, Muhammad, dkk. (2018). *Studi Agihan Salinitas Air Tanah Dangkal di Kecamatan Puring Kabupaten Kebumen Tahun 2016*. Jurnal GeoEco. Vol.4.No.1. Januari 2018. ISSN. 2460-0768

Fetter, C.W. (2014). Applied Hydrogeology, *fourth edition*. USA : Pearson

Firdaus, Bakri, H., dan Raul, J. (2018). *Penentuan Lapisan Akuifer Berdasarkan Hasil Interpretasi Geolistrik (Tahanan Jenis) di Desa Nonong Provinsi Sulawesi Tengah*. Jurnal Geomine, Vol. 6, No. 2: Agustus 2018.

Ge, S., Gorelick, S. M. (2014). *Encyclopedia of Atmospheric Science (Second Edition*). USA: *Academic Pres*

Geriesh, M., (1994). *Hydrogeological and hydrochemical evaluation of groundwater resources in the Suez Canal region*. Egypt. PhD Thesis. Suez Canal University.

Gibbs, J.R., (1970). *Mechanisms controlling world water chemistry. Science* (80-.) 170, 1088–1090.

Hiscock, K.M. and Bense, V.F. (2014). *Hydrogeology: Principles and Practice*, Second Edition. Chichester: John Wiley and Sons Ltd.

Hutabarat, L.E. (2017). *Studi Penurunan Air Tanah (Land Subsidence) Akibat Pengambilan Air Tanah Berlebihan di DKI Jakarta*. Jakarta: UKI Press

Kementrian PUPR. (2017). *Modul Geologi dan Hidrogeologi Pelatihan dan Pencernaan Air Tanah. Pusat Pendidikan dan Pelatihan Sumber Daya Air dan Konstruksi*: Jakarta.

Listiawan, Yudhi, (2015). *Kajian Potensi Intrusi Air Laut Berdasarkan Karakteristik Hidrokimia Airtanah Di Daerah Karangwuni Kecamatan Wates Kabupaten Kulon Progo Provinsi D.I Yogyakarta*. Seminar Nasional ke-II FTG Universitas Padjadjaran.

Listyani, T.R.A, (2016). *Rock's Mineral Control on Groundwater Quality in Jakarta Groundwater Basin. Prosiding Seminar Nasional XI "Rekayasa Teknologi Industri dan Informasi 2016*, Yogyakarta: Sekolah Tinggi Teknologi Nasional

Lubis, R.F., Sakura, Y., and Delinom, R. (2008). *Groundwater Recharge and Discharge Processes in the Jakarta Groundwater Basin, Indonesia*. Springer. Hydrogeology Journal 16: 927–938

Lloyd. J. W., and Heathcote J. A. (1985). *Natural inorganic hydrochemistry in relation to groundwater – An introduction* :Clarrendon Press, England: Oxford, 296p

Martodjojo, S., (1984). *Evolusi Cekungan Bogor, Jawa Barat*, Tesis Doktor, Pasca Sarjana ITB.

Mukhtar, O. dkk. (2015). *Manajemen Air Tanah di Cekungan Air Tanah DKI Jakarta*. Unpad: Bandung. Seminar Nasional Ke – III.

Nettleton, W.D.. Parsons, R.B., Ness, A.O. and Gelderman, F.W., (1982). *Spodosols along the southwest Oregon coast*. Soil Sci. Soc. Am. J., 46: 593-598.

Nurrohim, Ahmad, Tjaturahono, BS. dan Wahyu Setyaningsih. (2012). *Kajian Intrusi Air laut di Kawasan Pesisir Kecamatan dan Kabupaten Rembang.* Jurusan Geografi, Fakultas Ilmu Sosial, Semarang: Universitas Negeri Semarang.

PAHIAA (Panitia Ad Hoc Intrusi Air Asin). (1986). Direkrorat Geologi Tata Lingkungan, Jakarta.

Permenkes No. 492 Tahun 2010 mengenai Standar Mutu Air Tanah

Piper, A. M. (1944). *A graphic procedure in the geochemical interpretation of water analyses. American Geophysical Union Transactions*, V. 25, 914–923.

Samsuhadi. (2009). *Pemanfaatan Air Tanah Jakarta.* JAI Vol 5. No. 1. ejournal.bppt.go.id.

Sen, Z. (2015). *Practical and Applied Hydrogeology. Waltham, UK: Elsevier Stuyfzand*, P. J., (1989). *A New Classification of Water Types, Regional Characterization of Water Quality* (Proceedings of Baltimore Symposium, May – 1989), IAHS – Publication No 182.

Tikhomirov, V. V. (2016). *Hydrogeochemistry Fundamentals and Advances*: Mass Transfer and

Mass Transport.Willey: Canada

Tirtomihardjo, Haryadi. (2012) *Kuantifikasi dan Pemodelan Air Tanah Cekungan Air Tanah Jakarta Provinsi D.K.I Jakarta, Provinsi Jawa Barat, dan Provinsi Banten*. PSD Air Tanah dan Geologi Lingkungan: Bandung

Toth, J. (2016). *A Theoretical Analysis of Groundwater Flow in Small Drainage Basin.* Canada. Journal of Geophysics Research: Vol 68. No.16

Turkandi, T. dkk. (1992). *Peta Geologi Lembar Jakarta dan Kepulauan Seribu*, Jawa skala 1:100.000. Bandung : Dit. P3G, Dit. Geologi dan Sumberdaya Mineral.

Van Bemmelen. R. W, (1949). *Geology of Indonesia*. Vol. 1. General Geology Adjaeent Archipelago. Government office. The Haque

Van Zuidam, et, al (1985). *Guide to Geomorphologic aerial photographic interpretation and mampping*

Yuli Priyana, (2008). *Air Tanah (Groundwater). Diktat Kuliaah, Surakarta*: Universitas Muhammadiyah Surakarta

Walton WC. (1970) *Groundwater resources evaluation*. McGraw Hill Book Co, New York

WHO.(1996).*Total dissolved solids in Drinking-water. Geneva*: World Health Organization.

Zamora, R. Harmadi. dan Wildan. (2015). *Perancangan Alat Ukur TDS (Total Dissolved Solid) Air dengan Konduktivitas Secara Real Time.* Jurnal Sainstek Vol. VII No. 1: 11-15, Juni 2015

PROCEEDINGS
JOINT CONVENTION BANDUNG (JCB)2021
November 23rd – 25th 2021

Geoscience Education in Maros, South Sulawesi: An Overview of Rammang-rammang Geotourism Objects.

Muh. Alifian Al Anshari[1], Nurul Hidayah[2], Andi Vera Febriana[3].
[1]University of Sam Ratulangi, [2,3]Politeknik STIA LAN Makassar

Abstract
Geoscience education is very important for the civil society to learn, geotourism is an effort to introduce Geoscience. Geotourism education serves as service-based geotourism that introduces the basics of science, geological and geoculture potential through the interpretation of geological phenomena existing at a given location. Maros regency is one of geotourism potential in South Sulawesi, where in Maros there are Rammang-rammang geotourism objects. Rammang-rammang, identified as the largest karst in Indonesia, has limestone, sedimentary and crystal rock. Many tourists visit the place, both local and foreign tourists. Apart from the beauty and unique landscape, visitors could learn about the basics of geoscience through the geotourism objects. This paper aims to determine the implication of Rammang-rammang geotourism objects to giving geoscience education to the visitors. This research used mixed descriptive quantitative and qualitative. The data collected by literature review, questionnaire, interview, and observation. The results are the implication of Rammang-rammang for increased geoscience education of the visitors. These results indicate that geotourism could be an alternative geoscience learning media for civil society.

Kata Kunci : Geoscience, Karst, Maros.

Introduction

Indonesia is a very wide country and has a very beautiful landscape, various geological characteristics such as volcanic craters, rivers and waterfalls, the Kaput (Karst) mountains with a network of caves underneath. the gift of a very abundant geological potential. geotourism emerged in the mid-1990s. According to some sources, a geologist from Buckinghamshire Chilterns University in England named Tom Hose was the first to actively introduce the term. He even wrote at the Geological Society in 1996 a paper entitled "Geotourism, or can tourists become casual rock hounds: Geology on your doorstep" (Dirgantara, nd).

Geotourism education itself has a function to provide services to the community, especially local and international residents as a geotourism-based service that generally provides or introduces the basics of science, geological potential and geoculture through the interpretation of geological phenomena that exist in certain locations where one of the objects of the phenomenon The geology is located in the Maros district. Geotourism education is presented in Indonesia as a form of application and also a solution on how to take advantage of wealth and dynamics for tourism, education and economic activities that are environmentally sound. This concept has been popularly promoted as a way of reconciling the conservation of geological and geomorphological phenomena with economic development, especially in developing countries (Camp, 2016).

Matos Regency is one of the areas that has various geotourism potentials. This location is located in South Sulawesi, one of the tourist attractions is Ramang-ramang where Ramang-ramang itself comes from the Makassar language which means a lot of clouds or fog, these rocks are formed due to water activity. in the limestone area, causing plating. Ramang-ramang is also identified as the largest karst in Indonesia, having limestone, sedimentary and crystalline rocks.

This location is visited by many local and foreign tourists, not a few of these locations are used as research sites, in addition to its beauty which is dubbed a rock forest and a landscape that has its uniqueness and characteristics, this location can also support the development of science where visitors can learn about the basics of geoscience through geotourism objects in Ramang-ramang. The thing that becomes the learning material in the Ramang-ramang area is karst rock where Karst is a German term derived from the Slovenian language (kras) which means rocky arid land. This term in the country of origin is actually not related to limestone and the dissolution process, but currently the term kras has been adopted for the term landform resulting from the dissolving process (Haryono, E., & Adji, TN (2017).

This paper aims to provide knowledge from the implementation of the Ramang-Ramang geotourism object that is packaged by providing geoscience education in the form of information from the location made in the results of field observations to visitors. This study uses mixed descriptive, quantitative research methods where this method looks at the results of previous research and also pre-existing theories to become a researcher's reference and connects findings with current observations and also qualitative methods are used as a form of description of researchers who use this method. analysis of the data that has been obtained. The data collection that is applied is done by literature study, questionnaires, interviews, and observations.

The results of this study are where the implications are for the provision of geoscience education for visitors. The results obtained prove that geotourism can be an alternative media for learning geosciences for civil society and students in Indonesia.

Data and Method

The data colledted by literature review and field research in the literature review. This data is based on reviews, summaries, and several library sources in the form of articles, books, journals, and some information from the Internet. As for this field research, it is used to examine the potential for geoscience-based geotourism education that can be found by visitors by technically interviewing visitors, local residents to managers and visiting directly the location of karst rocks. Locations were also analyzed in a secondary manner using geological maps and ecoregions to further describe the characteristics of the location.

PROCEEDINGS
JOINT CONVENTION BANDUNG (JCB)2021
November 23rd – 25th 2021

Result and Discussion

Maros Regency

Maros Regency has an area of 1619.11 KM2 which has 14 sub-districts spread over and oversees 105 villages/kelurahan. One of the districts directly adjacent to the capital city of South Sulawesi. Geographically, Maros Regency is located in the western part of South Sulawesi between 40º45'- 50º07' south latitude and 109º205'-129º12' east longitude (Siduppa, MI). Maros Regency is administratively bordered by:

- North, East Pangkep
- East, Gowa Regency,Bone
- South Regency, Gowa Regency and Makassar City
- West, bordering the Makassar Strait.

The topography of Maros Regency varies from land area to highlands or mountains. Areas that have slopes above 40% or mountainous areas have an area of 49,869 ha or can be said to be 30% and 26.2% are coastal areas. For the classification of rocks in Maros district, they are divided into 4 major groups, namely surface rocks, sedimentary rocks, volcanic rocks and breakthrough rocks (Arif, 2019)

Forest is one form of application of nature tourism. Nature tourism is an area that has the aim to preserve ekosiste and its components and also become one of the functions of an environmental services as a tourist attraction (Rahmawaty,S., & Agriculture, MF (2004). One area that is actively developing the potential of nature tourism is Maros Regency, South Sulawesi Province. And now the Maros district government is developing one of the natural attractions, namely Ramang-Ramang which is located in the middle of Maros district, precisely in the village of Salerang, Lau District, in the form of Krast-based natural tourism objects. This rambling forest was formed about 30 million years ago, but this area has inhabitants estimated to be inhabited by humans at 40 thousand years ago, this is evidenced by the existence of humans in the past which until now can be enjoyed by tourists with handwriting or symbols. on the mountain wall. The state of the ramang-ramang forest in the current era is pure without any changes and touches of human hands, the ramang-ramang forest is pure, the authenticity of krast stone in general and has become a national tourist attraction in Maros district and has supporting facilities for tourists who want to enjoy the beauty of natural tourism such as boats, caffe and photo services for visitors provided by local managers. The following is an illustration of the Ramang-ramang forest.

Rammang-rammang Overview

Figure 1: Access road to Ramang-ramang
Source: Field Documentation

Figure 1 (one) provides a description of the access road to enter the Ramang-ramang cave area which is the only access and is built using tied bamboos.

To enter the Tamang-Ramang forest, it has several accesses at piers 1 and 2, you can use wheeled vehicles and also the provision of boat transportation who wants to use boat transportation. community and managers Rp. 12,000,000.00 to make access to the community and tourists who want to see closely the ramang-ramang forest, for this access requires improvement because the level of security for tourists is very minimal, also seen from the grouping of bamboo which is used for approximately 1 (one) more years the application for government funding has been carried out but has not yet received a definite answer.

Figure 2: Figure 2: the appearance or appearance in the interior of the stone forest.
Source: Field Documentation

From the figure describes the number of rocks that are arranged and solid where the rocks are still original without human touch, so that their uniqueness and beauty are maintained until now according to the picture above.

This Maros forest innew forest indistinct is very famous for its beauty, it is not uncommon for photographers or tourists to take pictures and capture one of these natural resources, become one of the National tourist attractions, and has a variety of plants and animals. live inside so that the ecosystem in the Ramang-ramang area is very good and maintained, exposure to sunlight reflected on the rocks gives a touch of beauty, often this ramang-ramang forest is also a place of research for researchers to see new discoveries in that location. So that in the near future this Ramang-Ramang forest will be closed completely for the construction of supporting facilities in the vicinity.

PROCEEDINGS
JOINT CONVENTION BANDUNG (JCB)2021
November 23rd – 25th 2021

Figure 3: The appearance of a stone that has two different basic colors
Source: Field Documentation

In Figure 3 (three) there is a picture of a large rock that has a different color pattern at the bottom and top indicating a significant difference and uniqueness in the rocks in the ramng-ramang, there are not a few rocks in the ramang-ramang that have two different basic colors as in the picture above.

Inside the Kaur or krast mountains it has many unique features, one of which is a stone that has an irregular color that gives a distinct impression in it, the ramang-ramang itself comes from the Makassar language which means a lot of clouds or fog This rock is formed due to the activity of water in the limestone area, causing plating. The results are as seen in the formation of a very distinctive karst nature, other studies conducted by geologists reveal that these karst rocks have been of Eocene to Miocene age. But formerly this area was receding waters, giving rise to these rocks.

Figure 4: The heart of Ramang-ramang is a valley area and water dam.
Source: Field Documentation

This illustrates the existence of a valley area in the middle of a rocky forest or Ramang-ramang, where there is a lot of floura and fauna that live in this area, this valley is located in the middle rocky area and surrounded by rock crash.

This place is in the middle of a stone forest surrounded by karst rocks, this area becomes a rain valley when entering the rainy season, this water will be filled with water and make karst rocks partly submerged, to find this location takes 10-15 minutes from the entrance, because this is included in the middle of the ramang-ramang forest or can be called the heart of the stone forest.

Figure 5: The striped stone in the middle of the desert
Source: Field Documentation

Figure 5 after entering the heart of the rock forest not far from that point we can get a striped stone which is given the name by the local manager, the same as in Figure 3, these rocks are mutually attached to each other but have different colors.

In the ramang-ramang forest we will find various types of unique rocks, one of which is rocks that stick to each other but have different colors and textures, local managers call them striped stones because they have two different colors. Here, it is very clear that the comparison between the rocks in the ramang-ramang forest and the rocks that stick together and are shaped like melted larvae, one of the typical forms that we can encounter if we want to get out of the ramang-ramang forest.

Figure 6: historical painting or historical archeology on a stone wall
Source: Field Documentation

In Figure 6 (six) depicts the scratches found on the stone wall that provide various symbols of life in ancient times, with this symbol image it becomes a new science that can be learned in history self-explanatory

One form of preservation of prehistoric relics also exists and is proven by several pictures of symbols or paintings from ancient times found on the walls of rambling debt, at a height that is difficult for humans to reach there are images resembling animals carved with orange color that cannot be lost, and also some pictures that we can find near water valleys or rainwater reservoirs, some pictures that resemble symbols of people hunting, eyes and various other symbols

engraved in blue that cannot be lost. for the community to maintain the sustainability of the ramang-ramang forest.

Figure 7: The road to the ramang-ramang location
Source: Field Documentation

Figure 7 (seven) this shows the road access to the rock forest location is very good, and can be passed by all vehicles. Can be seen from a distance this rock looks very clear when it has entered a distance of about 1 Km

The access road to the ramang-ramang forest is monitored very well and can be passed by 2 (two) motorbikes to 8 (eight) wheeled tour buses, from the outside we can already see The beauty of the beautiful stones, the white limestone in this stone forest gives clarity to the carvings, the public and tourists need a distance of approximately 1 kg from the Maros district axis road, but the long journey can be paid off with beautiful views.

Educational Value on Observation
Table 1: The results of field observations of Ramang-ramang

No.	Criteria	Weight (%)	Value
1.	Vulnerability	10	4
2.	Location achievement	10	1
3.	Barriers to site utilization	5	4
4.	Security facilities	10	2
5.	Supporting facilities	5	4
6.	Population density	5	4
7.	Relationship with other values	5	4
8.	Location status	5	4
9.	Distinctiveness	5	4
10.	Conditions for observing geological elements	10	4
11.	Potential for educational/research information	20	2
12.	diversity Geological	10	4

From Observation results show that for vulnerability itself, it is very clear that there is no change in the authenticity of the rocks inside and outside the Ramang-ramang Forest environment, by getting a value of 4, the supporting facilities at the location have a restaurant that can accommodate up to 50 people. visitors and is located above a ramang-ramang forest without destroying rocks but building a restaurant using bamboo with a score of 4, to residents around the ramang-ramang forest Dis around the ramang-ramang (surrounding the location) there are many houses but do not have a population. From the management informant there are 1000 souls getting a value of 4, the relationship with value. Here, we can see the number of pre-historic pictures painted using blue and orange ink that cannot be lost. Culture: *according to the information, the Baruga or the stage studio will be built in the Ramang-raman area as a form of complementing tourist facilities with a value of 4, location status by getting field results because Ramang-Ramang forest is a national tourism which is a natural tourism known in various places. area with a score of 4. Potential for education or research information For the delivery of information for this shady forest and the education provided is not yet available, but access to research inside is given free opportunity to everyone and managers also have a good understanding of the location can value 2.

Interview Results
Tourist
Law of the Republic of Indonesia Number 9 of 1990 in Yoeti (2007), defines tourists as people who carry out tourism activities. Based on the definition of visitors above, the parts included in it are:
1. Tourists, namely temporary visitors who stay at least 24 hours in the country they visit.
2. Travelers (exursionists) are temporary visitors who stay less than 24 hours in the country they visit (including travelers on cruise ships) (Astuti, 2021).

On the joint agenda to conduct an interview with one of the informants, on behalf of Muhammad Fahran (Interview on 17 September 2021), said:

> *It is very large because the geotourism object was formed due to nature and there is no human intervention and it is very interesting to visit there and at the same time provide education for ordinary people at the same time.*

The informant admitted that the rammang-rammang geotourism was very interesting from a natural point of view and also education related to the shape of the rock which is patterned like stripes and there are traces of graffiti on the cave's sky, such as pictures of traces/scribbles left by ancient humans, and the informant suggested that access to the inside of the cave is recommended. the geotourism site has been repaired again because the road access is currently obsolete because it is made of bamboo.

On the joint agenda to conduct an interview with one of the informants, on behalf of Andi Triwijaya kusuma (Interview on 17 September 2021), said:

> *The knowledge I got after visiting Rammang-Rammang in 2016 (1st grade SMA) was to get information about primitive life in the past which was marked by ancient paintings on the stone walls there. The knowledge that was presented by my friend, Duta Wisata Kab. Maros 2018, Andi Naufal explained that there are 280 caves composed of minerals and limestone, and 16 caves that have become prehistoric sites with an area of 43,700 hectares and there are paintings of primitive human palms on the karst walls and have been used as prehistoric and geotourism sites since 2014.*

The informant said that after visiting the geotourism site, the informant received information in the form of education related to primitive life in the past which was marked by the presence of ancient paintings found on the rock walls in the Rammang-Rammang cave.

On the joint agenda to conduct an interview with one of the informants, on behalf of Muhammad Reza Patrio (Interview on 17 September 2021), said:

> *This tour itself certainly provides education because it is one of the evidences of the existence of ancient humans living in Gowa and this is one of the characteristics of this tour that attracts people to look deeper into the history of the rocks or this tour.*

Informants received education related to the existence of ancient humans who had lived and carried out activities in the Rammang-Rammang cave so that both local and foreign people were interested in visiting Rammang-Rammang geoscience.

Local Residents:
Local residents are a group of people who live/live in a certain area and are related by the regulations that apply in that area.

On the joint agenda, conduct an interview with one of the informants, on behalf of Andi Feby Febrianti (Interview on 18 September 2021), said:

> *For information about the type of geoscience about tourist objects, it is still very minimal, where this tourist spot only provides tourist facilities. So, tourists can only see the natural beauty in the area.*

The informants felt that the information provided to both local residents and visitors was still minimal because rammang-rammang geoscience, which is also a prehistoric site and also as a tourist attraction, is more burdensome on the tourist attraction section with the lack of information related to rammang-rammang geoscience education.

On the joint agenda to conduct an interview with one of the informants, on behalf of Ananda Marchfadil Fatah (Interview on 17 September 2021), said:

> *What I know is related to the characteristics of rocks in the Rammang Rammang karst, namely the type of limestone.*

Manager
A manager is a person who manages. On the joint agenda to conduct an interview with one of the informants, on behalf of Imrang (Interview on 16 September 2021), said:

> *The role of geotourism is very large for the surrounding community because we know that to visit the Berua village we need boat access or what we usually call jolloro' and the boat or jolloro' costs ranging from two hundreds to three hundred and fifty thousand.*

The informants realized that the role of rammang-rammang geoscience was very large, both in terms of the existence of relics that could provide information related to education to the community and also the existence of work infrastructure that could improve the local community's economy.

On the joint agenda to conduct an interview with one of the informants, on behalf of Imrang (Interview on 16 September 2021), said:

> *Karst In rammang-rammang is still relatively active. In Rammang-Rammang, he has several sites that can be visited by tourists, the first is the Firefly Cave, Angel Lake, King Kong Cave, Diamond Cave, then there is also a Panrenyaong Karst cave which is ± 500 meters long.*

Informan mendapatkan edukasi dengan adanya geosains rammang-rammang ini dan di ramang-rammang memiliki situs juga yang sering dikunjugi oleh wisatwan sehingga juga memberikan informasi kepada pengunjung.

Conclusions
The karst rock area in Maros district has been proven to provide geoscience education where geotourism education is a form of its application so that it has a function to provide services to the community, especially local and international residents as a geotourism-based service which in general by providing knowledge and introducing basic knowledge about geoscience education can achieve the goal is in the form of education in the field of geoscience.

From the observations we made in the field, it provides an overview and also great potential in providing geoscience education which can be achieved easily in the form of geotourism implications, karst rocks located in Maros district, which is known as the Ramang-ramang area, become a tourist spot as well as a place to visit. the provision of appropriate education with its existence and well-maintained natives are the main factors in supporting the existence of knowledge that can be taken for the surrounding community can also be an economic source with their involvement in managing and completing existing facilities. several indicators of assessment in our field observations of This geotourism implica- tion provides a good assessment and supports its implementation in the future.

Acknowledgments
Thank you to Manager of Rammang-rammang site for permit us to collected the data in site area. And for all the society around the site area.

References
Camp, MCI (2016). Wisata Outbond Ciwangun Indah Camp.

Dirgantara, AR (nd). Peran Interpreter dalam Kegiatan Geowisata: Studi Kasus Gunung Tangkuban Perahu.

Siduppa, Mi Implementasi Program Baznas Microfinance Desa Badan Amil Zakat Nasional Di Kabupaten Maros.

Arief Setia Budi, Arief (2019).Analisis Sektor Basis Di Kabupaten Maros Tahun 2013-2017(Doctoral Dissertation, Universitas Islam Negeri Alauddin Makassar).

Tri Astuti, Fm (2021). Pengelolaan Objek Wisata Danau Ranau Sebagai Aset Desa Banding Agung Kabupaten Ogan Komering Ulu Selatan, Sumatera Selatan, Palembang. Pengelolaan objek wisata danau Ranau Sebagai Aset Desa Banding Agung Kabupaten Ogan Komering Ulu Selatan, Sumatera Selatan, Palembang.

Rahmawaty, S., & Pertanian, MF (2004). Hutan: Fungsi dan peranannya bagi masyarakat.Program Ilmu Kehutanan. Universitas Sumatera Utara

Haryono, E., & Adji, TN (2017). Geomorfologi dan hidrologi karst.

PROCEEDINGS
JOINT CONVENTION BANDUNG (JCB)2021
November 23rd – 25th 2021

THE DEVELOPMENT OF THE DANAU BIRU AREA OF BELITUNG REGENCY AS TOURISM FACILITIES AND EDUCATION ABOUT THE ENVIRONMENT

Rival Akbar Firdaus (1), Nurrahmah Fadlilah (1)
(1) Education of Geography Studi Program, Faculty of Social Science Education, UPI

Abstract

Indonesia is blessed with various geological resources that can be used as a source of income both by the government and the people. This utilization can be in exploration and exploitation to extract various mining goods contained in Indonesian soil. However, in addition to providing benefits, exploitation also causes negative impacts that cannot be avoided through environmental damage. Utilization of various geological resources that are not destructive and many are chosen as an alternative to natural exploitation without destroying it, namely by making geological wealth areas as geotourism objects. Geotourism objects can be formed naturally due to the geological wealth that composes them, even artificially due to human activities such as mining activities. One example of a geotourism object born from mining sites is Danau Kaolin or Danau Biru in Belitung Regency. This lake was formed as a result of kaolin mining activities managed by private parties. The former excavation started a basin which was then filled with rainwater and turned into a lake. The uniqueness lies in the lake's blue water as a result of the interaction between the kaolin in the former excavation and rainwater. This lake can also be used as a means of education for the surrounding community and the broader community regarding the comparison and impact of exploiting mining goods by using them as geotourism objects. The fulfillment of transportation infrastructure to Danau Biru has also been considered good in the sense that it is a geotourism object. This location makes it very easy for tourists to come. The unclear management, ownership by the private sector, and kaolin mining activities that are still active are also the shortcomings of Blue Lake as a geotourism object. The absence of public facilities such as toilets, clean places to eat, gift and souvenir shops, prayer rooms, and adequate trash cans also affect the quality of satisfaction and the number of tourist visits to Danau Biru. The steep morphology due to excavation activities also needs to be addressed to increase tourism carrying capacity for the safety of tourists. In comparison, the potential of Blue Lake as a geotourism object can move the wheels of the economy in the area through MSME activities that meet the basic needs of tourists such as food, beverages, souvenirs, to service needs. Therefore, good management and increasing the value of geotourism objects also benefit various parties to the government. The government and the private sector can work together to manage the area as a geotourism object. In addition to advancing the economy in the area around Danau Biru, this geotourism object can also be a lesson, especially for future generations, on how to take advantage of various natural potentials without destroying them.

Keyword: Kaoline lake, geotourism, sustainable tourism

Introduction

As part of the southeast *Asian Granite Tin Belt*, which divides four granite provinces, Belitung Island is included in two Granite Belt provinces, with East Belitung being the eastern belt and West Belitung being the central belt (Hartono & Najili, 2019). This division forms the basis of the island's rich geological and type c minerals, ranging from tin, kaolin to quartz sand.

Utilization of the geological wealth owned may not be exploited optimally with extractive exploitation such as mining and manufacturing (Hermawan & Ghani, 2018). The impact of this activity has a negative effect in terms of decreasing environmental quality, even ecological damage in the ex-mining area. In the *International Union for the Conversation of Nature* (IUCN) in 1980, a 'World Conversation Strategy' was issued, including three main objectives: maintaining essential ecological processes, maintaining genetic diversity, and ensuring sustainable use of ecosystems/species (Sutiarso, 2018). In this case, the tourism sector can be economically valuable as an alternative solution to the utilization of existing geology. The environment is valuable as a tourism asset in the short term and the long term for future generations. This concerns the relationship between tourism and the environment without destroying resources and harmony.

The change in the trend of community economic activity into the tourism sector does experience ups and downs. Even the unique geological potential will not develop if it is not aligned with the management, marketing, and maintenance so that geotourism can run sustainably. For this reason, it is necessary to have environmental management and good planning so that the geological potential as a tourist attraction on Belitung Island can be optimally utilized with less damage and the possibility of pollution.

Data and Method

The research method used in this research is qualitative analysis. Data collection techniques used include observation, interviews, and literature studies. Observations were made directly in the Blue Lake area and quartz and kaolin sand mining by tracing every point in it. Interviews were conducted with people living near Blue Lake and with people working in the mines.

The discussion includes the general condition of the Blue Lake and its development from the beginning of the mining period to the present. Then enter the discussion of its potential as a geotourism object, including (1) the attractiveness and uniqueness of the Blue Lake; (2) potential as a means of outdoor learning regarding the mining process of quartz and kaolin and their processing; (3) accessibility to the Blue Lake area; (4) facilities to support geotourism activities in the Blue Lake area.

Result and Discussion

Region Setting

The Blue Lake area, which still functions as an active mining site, is located in Perawas Village, Tanjungpandan District, Belitung. Blue Lake is located at coordinates 2°44'16" South Latitude and 107°40'56" East Longitude. The mining location, which is still in the city area makes this location mutually influences the activities of the surrounding community. The distance of Blue Lake to the center of Tanjungpandan City is about 3 km. Affordability, which in addition to moving on the tourism side, also impacts the transportation of minerals such as quartz sand and kaolin as a result of washing and separating tin ore from mining sites. This land is dominated by tailing sand, which has high erosion potential and has low chemical fertility. Landscapes that are not overgrown with large trees are a feature that describes the remains of large mining. The position of the kulong or excavated hole is usually around the valley and follows the tributary's flow. In this regard, there is a distance of about 700 meters from the residential area on Jalan Murai.

In general, the morphology of Belitung Island is dominated by lowlands and hills in the middle. The highest peak on Belitung Island is Mount Sharp, which is 510 meters above sea level, while Blue Lake, which is located in the lowlands, only has an average height of 8 meters above sea level. Geologically, the location of Blue Lake is in the Tanjungpandan Granite formation, with the granite having light gray leaves, having a holocrystalline texture with coarse to very coarse grains. The granite contains many quartz minerals, which both the community and companies usually mine. The granite in the Tanjungpandan Granite Formation is an S-type granite (Pitfield, 1987). The absolute age of the Tanjungpandan Granite Formation is from 208 to 245 million years (Priem et al., 1975).

The mining process in the Blue Lake area is still ongoing until now, where PT carries out this mining. Main Kaolin Assortment. The basic problem is the use of post-mining land. In accordance with Law number 3 of 2021 Article 1, there are two options for post-mining management: conducting reclamation or post-mining activities. Although both are efforts to return the land to its original function, post-mining activities have a broader meaning, restoring environmental functions and social functions. So, if it is developed into a tourist spot, this ex-mining area can continue to be utilized while still prioritizing environmental functions, in addition to sustainable economic value. This is in line with the company's goal to create more benefits in post-mining land. So, by looking at these things, Blue Lake has the potential to be used as one of the geotourism objects in the Belitung Regency.

Attractiveness

The existence of a Danau Biru is the main attraction of this location. The lake was formed due to mining activities to create an ex-excavated hole or commonly called kulong, by the surrounding community. Then, this ex-dug hole is filled with rainwater, which reacts with the kaolin contained in the ex-dug hole and makes the water look blue.

In addition to having the value of beauty, this area can also be used as a means of education for the general public regarding the potential of Indonesia's natural resources and geological wealth. This concept refers to the concept applied at the Ombilin Coal Mine, which is currently used as a tourist attraction. Mining locations that are on the surface make geotourism with the geotrek method suitable to be implemented in this area. Tourists can explore the mining area and ex-excavated lands. In addition, near the mining area, there is also a processing factory that can be used as a mining product processing museum to provide educational value if it is no longer operating.

Access

Access to the Blue Lake area is getting better every year. Initially, road access was only focused on mining areas. This is in accordance with the function of the road that facilitates the distribution and transportation of mining goods. However, the development in 2006-2007 made the residential area around the mining area more integrated. This has continued from 2006 to the present as shown by the hundreds of houses that have been built in this area.

Facilities

Facilities can be divided into three types, namely accommodation, supporting facilities, and supporting facilities. In geological tourism, accommodation is a place to rest and involves the availability of places to eat and cultural events. In this case, lodging is not highly recommended. It is related to the nature of geotourism objects that are still simple and in small units. In addition, Blue Lake is more suitable for being used as a transit geotourism object and various other tourist objects on Belitung Island. However, the existence of places to eat is important enough to meet the needs of tourists.

Furthermore, the supporting facilities need to be built to develop the Blue Lake area as a geotourism object. A tourist attraction requires parking space to store vehicles and transportation that transports tourists when they are at the tourist site. This parking area must provide comfort when tourists park their vehicles, for example, by equipping it with a roof or shade so that parked vehicles are not exposed to the heat of the sun. In geotourism objects, cleaning facilities are also needed to keep the environment clean and not deviate from geotourism destinations. Prayer rooms and toilets are fundamental in a geotourism area to facilitate tourists who want to worship or go to the toilet. Currently, in Blue Lake, there is no prayer room or toilet facilities because its function is still mining. However, there are two supporting facilities that must be built. Besides these two things, information posts and information boards are also needed as an information center if tourists are confused and are not accompanied by a guide. A seat or gazebo is also essential to rest and shade from the hot sun.

Acomodation

Acomodation	Description
Lodging	-
Kantin	-
Cultural Activities	-

From the table above, it can be seen that it has not been fulfilled in terms of

PROCEEDINGS
JOINT CONVENTION BANDUNG (JCB)2021
November 23rd – 25th 2021

accommodation. However, what needs to be noted is that the need for lodging is not too considered a geotourism object.

Facilities

Facilities	Description
Parking area	Yes, but still not well managed
Sarana Kebersihan	-
Musholla/tempat ibadah	-
Toilet	-
Tempat duduk/gazebo	Yes, but it's still a wooden/bamboo seat.
Toko souvenir	-

From the supporting facilities, some of them already exist even though they are still in simple condition. If you want to attract more tourists, of course, the supporting facilities must be more aggressively improved to attract tourists.

Fasilitas Penunjang

Fasilitas Penunjang	Keterangan
Papan penunjuk arah menuju lokasi	Tidak ada
Pusat informasi	Tidak ada
Peralatan pendukung wisata	Tidak ada
Papan informasi	Tidak ada

Conclusions

Post-mining land use is one of the things that is still a problem. The empowerment of post-mining land into a geotourism facility is one way to empower it so that it has economic value and continues to carry out the process of environmental restoration. With this kind of tourism, apart from being a means of entertainment for tourists, it is hoped that it can provide educational value about Indonesia's natural wealth, the processing process, and the process of restoring environmental functions such as their initial function. Blue Lake in Belitung Regency is one of the locations that can maximize its potential for geotourism areas as a follow-up in the future if this area is no longer active as mining.

The challenge of developing the Blue Lake area as a geotourism object is that the construction of facilities that support tourism activities must be carried out properly, as well as the management of geotourism objects that must be carried out in accordance with geotourism objectives, namely as sustainable tourism. In addition, the safety of tourists is the top priority of geotourism according to the principles issued by the National Geographic Society.

References

Hermawan, H., & Ghani, Y. A. 2018. Geowisata: solusi pemanfaatan kekayaan geologi yang berwawasan lingkungan.

Sutiarso, M. A. 2018. Pengembangan Pariwisata Yang Berkelanjutan Melalui Ekowisata.

Priem, et al. 1975. Isotope Geochronology in The Indonesian Tin Belt. Geol. Mijnbouw, 54: 61-7

Pitfield, P. E. J. (1987). South-East Asia Granite Project Report on the geochemistry of the tin islands granites of Indonesia: British Geological Survey Overseas Division Report No. MP/87/9/R, 52 p.

Acknowledgements

The author is grateful to Mrs. Herlina and Mr. Kujor as the original community members of the study area and has acted as resource persons in writing this extended abstract.

PROCEEDINGS
JOINT CONVENTION BANDUNG (JCB)2021
November 23rd – 25th 2021

Development of Colorado Hill Geosite "Ngoro-oro Cliff" and Jurug Gedhe As Potential Geotourism in Ngoro-oro Village, Patuk Subdistrict, Gunung Kidul Regency, Special Region of Yogyakarta

Jabatio Primizakaria [1], Subhan Nur Sya'ban [2], Ongky Suherman Heng [3]*

[1] *Geological Engineering Departement, Fakulty of Engineering, Gadjah Mada University*
[2] *Geological Engineering Departement, Fakulty of Engineering, Gadjah Mada University*
[3] *Geological Engineering Departement, Fakulty of Engineering, Gadjah Mada University*
** email : jabatioprimizakaria@mail.ugm.ac.id*

Abstract

Colorado Hills "Ngoro-oro Cliff" is a huge cliff with measurements 35 meters x 25 meters that shows rock stratigraphy of different colors as a result of chronicled records of complex geological that can be created as geo-tourism. Colorado Hills are uncovered due to street development that cuts through the hills in Ngoro-oro Village. Close to Colorado Hill, there is Jurug Gedhe which is the highest waterfall visit in Gunung Kidul. However, these two locations have not gotten the consideration of different parties properly so that they can be developed optimally. Great potential of Bukit Colorado and Jurug Gedhe encourages the implementation of research on the development of the two locations into geosites using literature study methods and qualitative-quantitative analysis such as weighting geo-tourism potential based on geo-tourism parameters (Kubalikova, 2013) and Geosite Assessment Model (Vujicic et al., 2011). The results of the research with these 3 methods state Colorado Hill and Jurug Gedhe are suitable for geosite with yields of 53% and 74% (Kubalikova, 2013) and Z32 (Vujicic et al, 2011) for both. Therefore, this research aims at these two locations as geosites to support a new geo-tourism area in Ngoro-oro Village, Patuk District, Gunung Kidul Regency, Yogyakarta Special Region.

Keywords: colorado hill, geosite, geo-tourism, jurug gedhe, ngoro-oro cliff

Introduction

The village of Ngoro-oro is an area that has a cliff known as the Colorado Hills. Colorado Hill is an exposed cliff due to the construction of a road that intersects the hill in the village of Ngoro-oro. The cliffs give the appearance of solid and aesthetic rock strata. This makes the Colorado Hills an object of geological study because they are the result of historical records of complex geological processes. The aesthetic appeal of the Colorado Hills also makes it a popular tourist destination for the local community. However, there has been no development or management effort to turn the Colorado Hills into a tourist area at its best, especially as a geotourism. Therefore, this study aims to assess the feasibility of the Colorado Hills and other geosites located in the village of Ngoro-oro so that they can provide recommendations for the direction of development of the area in a tourist area based on geology.

Regional Geology

The regional geology of the research vicinity is generally positioned withinside the Semilir Formation that's in the Southern Mountain Zone. The Southern Mountain Zone consists of lithology withinside the shape of volcanic products and carbonate sediments (Surono, 2008). Surono et al. (2009) divided the stratigraphy of the Southern Mountain Zone into three periods, specifically the pre-volcanism duration, the volcanism duration, and the carbonate duration. Based at the duration, the studies place is withinside the duration of volcanism. The morphology of the Southern Mountain Zone stretches west - east alongside 50 km with a width of forty km orientated north - south (Bronto and Hartono, 2001). In the west and north of the Southern Mountain Zone, it's miles bordered through the Yogyakarta-Surakarta Plain with barriers in the shape of Kali Opak withinside the west and Gawir Baturagung withinside the north. While withinside the south it's miles bounded through the Indian Ocean and the east is bounded through the Gajahmungkur Reservoir.

The Semilir Formation is estimated to be over 460 meters thick (Surono, 2008) with a cover area extending from the western end of the southern mountains, precisely in the Pleret Imogiri area to the upper area of Mount Gajahmungkur at the eastern end. The Semilir Formation has a lithology of tuff, dacitic pumice breccia, tuffaceous sandstone, and shale (Surono, 1992). The Semilir Formation settled in harmony in the Lower Miocene to Middle Miocene over the Kebo Formation and the Butak Formation, interfinger to the Wonolelo Formation with lava, breccia, and conglomerate lithology (Bronto et al., 2008), the Sindet Formation with sandy tuff lithology (Surono, 2009), and the Nglanggeran Formation deposited at the end of the Lower Miocene in an environment dominated by

volcanic breccias, tuffs, agglomerates, basal andesite pillow lavas, autoclastic breccias and hyaloclastite breccias (Surono et al., 1992) supported by different sources (van Bemmelen, 1949; Sumarso and Ismoyowati, 1975).

The depositional environment of the Semilir Formation was initially estimated to be in the deep sea which experienced siltation due to a large supply of sediment accompanied by the uplift of the basin floor to the environment near land or even to land (Surono, 2008).

Detailed stratigraphy shows that the Semilir Formation at the study site consists of seven volcaniclastic facies (Patria, 2018) and andesite breccia facies as additional facies which are only found in the Jurug Gedhe geosite. The seven lithofacies referred to by Patria (2018) are the carbonaceous claystone layered with sandstone, the sandstone layered facies, the tuffaceous sandstone layered facies, the ignimbrite facies, the interspersed tuffaceous siltstone facies with tuffaceous sandstones, the carbonated claystone facies with the tuffaceous sandstones, massive and tuffaceous sandstones. Patria, 2018).

a. The facies of carbonaceous clays stratified with sandstones indicates the environmental conditions of deep-water deposition with an eruptive process with a long pause so that carbonaceous and clay materials can settle between the sandstones which are the products of the eruption.
b. The relatively thin sandstone stratification facies indicates a repeated eruptive process over a short period of time with the deposition environment in the form of shallow seas.
c. The tuffaceous sandstone facies indicates the product of volcanic fallout material in the form of tuff that is transported and re-deposited with sand-sized material in a shallow marine environment.
d. Interspersed with carbonated claystone facies with tuffaceous sandstones indicates the occurrence of repeated eruption events with a long pause in the deep-sea environment so that carbon material is deposited, the eruptive material does not fall directly but undergoes a re-sedimentation process.
e. Massive tuff facies indicates a long-term eruption and produces a lot of volcanic material with a transitional – land-based depositional environment.
f. Interspersed facies of tuffaceous siltstone with tuffaceous sandstones indicates repeated eruptions in shallow marine environments with different depositional energies, tuffaceous sandstones were deposited at greater depositional energy than tuffaceous siltstones. Differences in depositional energy can occur due to the varying amount of sediment supply.
g. The ignimbrite facies indicates that this lithology was formed close to the eruption source because it has old angular rock fragments which were fragmented due to the explosion (Cas and Wright, 1987). In the ignimbrite there is imbrication of carbonaceous material which indicates welding with high pressure and high temperature as a result of the compaction and consolidation process of pyroclastic material. These facies are in a marine depositional environment.
h. The andesite breccia facies at Jurug Gedhe indicates the presence of high depositional energy as a result of erosion of volcanic material through andesite igneous rocks that have already been formed so that the erosion of andesite igneous rocks is transported and deposited through turbidite currents with sand-sized volcanic material. The appearance of the wedged distribution of this facies indicates that the andesite breccia is a product of lower fan deposits (Mutti and Lucchi, 1978) precisely at the edge of the channel.

Stratigraphically, the position of Jurug Gedhe is still located in the Semilir Formation under the geosites BC 1, BC 2 and BC 3. The lithology of Jurug Gedhe consists of tufa breccias and tuffaceous sandstones with andesitic breccias. Each layer is approximately 2 meters to 4 meters thick. While in the Colorado Hills, lithology has been obtained as carbonaceous clay, sandstone, tuffaceous sandstone, and ignimbrite (tuff breccia) (Patria, 2018).

Data and Method

The study was carried out to identify the potential of geotourism areas at geological sites located in Ngoro-oro region, Patuk district, Gunung Kidul regency, Yogyakarta Special Region province. The research method used is a literature study method and a quantitative-qualitative analysis method with an assessment of each geosite based on the parameters of Kubalíková (2013) and the Geosite Assessment Model (Vujičić et al., 2011).

The Kubalíková (2013) analysis method is performed by determining the value of each geosite with predetermined parameters and scores. To find out the eligibility percentage for each geosite, the total score is divided by the maximum of the total value.

$$P(\%) = percentage$$

$$P(\%) = \frac{Total\ value\ of\ assessment\ results}{Total\ value\ of\ all\ parameters} x100\% \quad (1)$$

Geosites that have a percentage of >50% deserve to be prioritized to be developed into geotourism areas. For geosites that have a value of <50%, it has not been recommended to be prioritized as a geotourism area but at any time it can be developed if the weaknesses or shortcomings of the geosite can be overcome by development carried out in the area.

The Geosite Assessment Model Analysis method (Vujičić et al., 2011) is carried out by adding up the main score (MV) scores to get the X-coordinate value and adding up the scoring results from the additional values (AV) to get the Y-coordinate value. Then, the MV and AV values are plotted on the Geosite Assessment Model (GAM) matrix.

$$MV = VSE + VSA + VPr \quad (2)$$

$$AV = VFn + VTr \quad (3)$$

Description:

MV : Main Values
AV : Additional Values
VSE : Scientific/Educational Values
VSA : Scenic/Aesthetic Values
VPr : Protection Values
VFn : Functional Values
VTr : Touristic Values

This method is used to determine the strengths and weaknesses of each geosite so that it can provide recommendations for the direction of developing geotourism areas.

Result and Discussion

The assessment of 4 geosites that have the potential to be developed as geotourism areas in general provides fairly good results based on the parameters method of Kubalíkova (2013) and the geosite assessment model (Vujičić et al., 2011).

Information regarding the 4 geosites studied are as follows:

a. BC 1
BC 1 (Figure 1) is a cliff located in the village of Ngoro-oro with UTM coordinates 49S 448782E 9134109N. This cliff is 15 meters long and 5 meters high with the appearance of a layer of yellowish-brown rock. This cliff faces east with the northern limit in the form of a plain, the southern limit in the form of an elevation, the western limit in the form of a cliff continuity, and the eastern limit in the form of a ravine.

b. BC 2
BC 2 (Figure 2) is a cliff located in the village of Ngoro-oro with UTM coordinates 49S 448852E 9134406N. This cliff is 35 meters long and 25 meters high with the appearance of a layer of reddish yellow-gray brown rock which indicates the presence of various types of different lithologies. This cliff faces east with the northern limit in the form of a plain, the southern limit in the form of an elevation, the western limit in the form of a cliff continuity and the eastern limit in the form of a ravine. Location BC 2 is northeast of location BC 1 with a distance of 220 meters.

c. BC 3
BC 3 (Figure 3) is a cliff located in the village of Ngoro-oro with UTM coordinates 49S 449181E 9135491N. This cliff is 20 meters long and 5 meters high with the appearance of a layer of gray-brown rock. On this cliff, it is seen that there is a layer of rock that is not continuous with grayish white color which is a diagenesis sandstone. This cliff faces east with the northern limit in the form of a plain, the southern limit in the form of a plain, the western limit in the form of a continuous cliff, and the eastern limit in the form of a plateau. Location BC 3 is north of location BC 2 with a distance of 1130 meters.

d. JG
JG (Figure 4) is a waterfall tour that has been managed by the local community and is located in Ngoro-oro Village with the coordinates of UTM 49S 448926E 9135126N. This waterfall flows from the east - west.

Detailed calculations using Kubalíková (2013) parameters for the four geosites were carried out by considering scientific and intrinsic elements, education, economics, conservation, and additional elements can be seen in Figure 5. The final results of calculations using this method are presented in the table below.

Table 1. Geosite value calculation results with parameters from Kubalova (2013)

Geosite Code	Result
BK 1	29%
BK 2	53%
BK 3	35%
JG	74%

Based on the above results, geosites that deserve to be prioritized to be developed into geotourism areas are BC 2 and JG. This is because both geosites meet the criteria of more than 50% based on Kubalíková's (2013) parameters.

The discussion of the results of the assessment using Kubalíková (2013) parameters is as follows:

a. BC 1
The value of scientific and intrinsic elements in the BC 1 geosite is 1.5. This value is the smallest value compared to other geosites. This is because this site does not have a proper uniqueness and has suffered quite intense damage. While on the value of educational and economic elements, this site also does not meet

the criteria significantly where this site does not provide a representative geological process appearance and does not have a good accessibility value. The value for the educational and economic elements on this site is 1. Then for the conservation and additional elements, this site also does not meet the criteria well which has an impact on the value of these two elements being low so that the BC 1 geosite is classified as unfit to be prioritized as a geotourism area.

b. BC 2
The value of scientific and intrinsic elements in the BC 2 geosite is 3.5. This value is the highest value compared to other geosites. This is because this site has a uniqueness that is very rarely found in the form of the appearance of clear rock layers on the cliff and not damaged so it is very good to be used as a geological study location. The representative of the BC 2 site is also very ideal so that it gives a rating of 2.5. Other elements such as economy, conservation, and additional support so that the BC 2 site can be classified as eligible to be prioritized as a geotourism area.

c. BC 3
The value of scientific and intrinsic elements in the BC 3 geosite is 2. This value is at an intermediate level among other geosites. While the elements of education, economics, conservation and addition do not provide significant value so that the impact on the final assessment for this site is of low value. The final value of the BC 3 site is also not much different from the BC 1 site. This causes the BC 3 site to be classified as unfit to be prioritized as a geotourism area.

d. JG
The value of scientific and intrinsic elements in the JG geosite is 2. This value is at an intermediate level among other geosites. However, on other elements such as education, economy, conservation, and additional, this site has the highest value. This is because the JG geosite is a tourist area that has been managed by the community. This area also has good parking, tourism management, and accessibility. However, this tourist area does not emphasize the existing geological value because people still do not know the developing geological potential. The accumulated rating on this site is the highest. Thus, the JG site is classified as feasible to be prioritized as a geotourism area because it meets the criteria.

After an analysis using the parameters of Kubalíková (2013), an analysis was carried out using the method of the geosite evaluation model (Vujičić et al., 2011) on the sites declared suitable for being prioritized according to the parameters of Kubalíková (2013). The elements considered in this method are elements of education, aesthetics, protection, functionality and tourism. The results of calculations with this method are shown in the table below.

Tabel 2. Geosite calculation results with parameters from Vujicic et al (2011)

Geosite Code	*Main value*	*Additional value*	Color Code
BK 1	6,5	6,5	Red
BK 2	8,0	6,75	Green
BK 3	6,75	6,75	Yellow
JG	8,75	8,5	Blue

The calculations then plotted on the Geosite Assessment Model (GAM) matrix which can be seen in Figure 6.

The discussion of the plot results in the Geosite Assessment Model matrix (Vujičić et al., 2011) is as follows:

a. BC 2
The BC 2 site based on the plotting results on GAM is located in the Z32 area with a main value of 8 and an additional value of 6.75 with an accumulated percentage value of 55%. This shows that the BC 2 geosite has great potential as geological tourism but is not ready to be used as a geotourism area that can be accepted by the general public. Thus, the development of the BC 2 site is more emphasized on the existing geological values and by maximizing the aspects of providing tour guide services, making interpretive panels, developing tourism infrastructure, and conducting promotions.

b. JG
The JG site based on the plotting results on GAM is located in the Z32 area with a main value of 8.75 and an additional value of 8.5 with an accumulated percentage value of 64%. This value is the highest value compared to other sites. This value indicates that the JG site is very feasible to be prioritized as a geotourism area with its unique geology and is ready to be opened to serve tourist visitors from various circles.

Conclusions

Based on the results of observations and field data processing carried out on 4 geosites in the village of Ngoro-oro, the conclusions are:

- Assessment using the Kubalikova parameter method (2013) on sites BC 1, BC 2, BC 3, and JG found that sites BC 1 and BC 3 are not eligible to be prioritized as geotourism areas and sites BC 2 and JG are eligible to be prioritized as geotourism areas.
- Assessment using the Geosite Assessment Model method (Vujičić et al., 2011) on the BC 2 and JG sites found that the BC 2 site has a development direction as geological tourism education and the JG site has a development direction as geological tourism education which is ready to serve tourist visitors from various among.
- Based on the two methods used in this study, it was found that the BC 1 and BC 3 sites are still not feasible to be used as geotourism areas. Meanwhile, the BC 2 and JG sites have the potential to be developed as geotourism areas by maximizing the aspects of providing tour guide services, making interpretive panels, developing tourism infrastructure, and conducting promotions.

Therefore, the purpose of the research by the author has been well achieved as evidenced by the acquisition of two geosites that are suitable as geotourism area

References

Bemmelen, R. W. Van, 1949, The Geology of Indonesia, **IA**, 732.

Bronto, S., 2008, Indonesian Journal on Geoscience, **3**, 117–128.

Cas, R. A. F. dan Wright, J. V., 1987, Volcanic Successions, 144.

Hartono, H., 2009, Indonesian Journal on Geoscience, **4**, 157–165.

Kubalíková, L., 2014, Czech Journal of Tourism, **2**, 80–104.

Mutti, E., dan Lucchi, F. R., 1978, International Geology Review, **20(2)**, 125-166.

Patria, A. A., dkk., 2018, Proceedings Pekan Ilmiah Tahunan IAGI 2018.

Patria, A.A., dkk., 2019, Seminar FOSI-IASSEPM Regional Yogyakarta.

Setiawan, B., dkk., 2019, Seminar Nasional AVoER XI 2019, 23-24.

Sumarso dan Ismoyowati, T., 1975, IPA 4th Annual Convention Proceedings, **II**, 19-26.

Surono, 2008, Jurnal Sumber Daya Geologi, **18**, 29-41.

Surono, 2009, Jurnal Sumber Daya Geologi, **19**, 31-43.

Vujičić, M.D., dkk., 2011, Acta Geographica Slovenica, **51**, 361-37.

PROCEEDINGS
JOINT CONVENTION BANDUNG (JCB)2021
November 23rd – 25th 2021

Attachment

Figure 1. BC 1

Figure 2. BC 2

Figure 3. BC 3

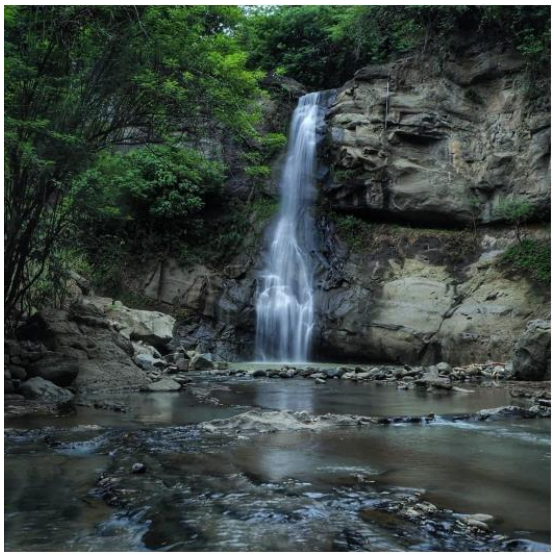

Figure 6. JG

Scientific and intrinsic values	Rules Value	Site 1	Site 2	Site 3	Site 4
Integrity	0 - totally destroyed site, 0.5 - disturbed site, but with visible abiotic features 1 - site without any destruction	0,5	1	0,5	1
Rarity (number of similar sites)	0 - more than 5 sites, 0.5 - 2-5 similar sites, 1 - the only site within the area of interest	0	0,5	0	0
Diversity (number of different partial features and processes within the geosite or geomorphosite)	0 - only one visible feature/processes, 0.5 - 2-4 visible features/processes, 1 - more than 5 visible features/processes	0,5	1	1	0,5
Scientific knowledge	0 - unknown site, 0.5 - scientific papers on national level, 1 - high knowledge of the site, monographic studies about the site	0,5	1	0,5	0,5
Educational values	**Rules Value**	**Site 1**	**Site 2**	**Site 3**	**Site 4**
Representativeness and visibility/clarity of the features/ representativeness and visibility/clarity of the features/ processes	0 - low representativeness/clarity of the form and process, 0.5 - medium representativeness, especially for scientists, 1 - high representativeness of the form and process, also for the laic public	0	1	0,5	1
Exemplarity, pedagogical use	0 - very low exemplarity and pedagogical use of the form and process, 0.5 - existing exemplarity, but with limited pedagogical use, 1 - high exemplarity and high potential for pedagogical use, goedidactics and geotourism	0,5	0,5	0,5	0,5
Existing educational products	0 - no products, 0.5 - leaflets, maps, web pages, 1 - info panel, information at the site	0	0	0	1
Actual use of a site for educational purposes (excursions, guided tours)	0 - no educative use of the site, 0.5 - site as a part of specialized excursions (students), 1 - guided tours for public	0,5	1	0,5	1
Economical values	**Rules Value**	**Site 1**	**Site 2**	**Site 3**	**Site 4**
Accessibility	0 - more than 1000 m from the parking place, 0.5 - less than 1000 m from the parking place, 1 - more than 1000 m from the stop of public transport	0	0,5	0	0,5
Presence of tourist infrastructure	0 - more than 10 km from the site existing tourist facilities, 0.5 - 5 – 10 km tourist facilities, 1 - less than 5 km tourist facilities	0,5	0,5	0,5	1
Local products	0 - no local products related to a site, 0.5 - some products, 1 - emblematic site for some local products	0,5	0,5	0,5	0,5
Conservation values	**Rules Value**	**Site 1**	**Site 2**	**Site 3**	**Site 4**
Actual threats and risks	0 - high both natural and atrophic risks, 0.5 - existing risks that can disturb the site, 1 - low risks and almost no threats	0,5	0,5	0,5	1
Potential threats and risks	0 - high both natural and athrophic risks, 0.5 - existing risks that can disturb the site, 1 - low risks and almost no threats	0,5	0,5	0,5	0,5
Current status of a site	0 - continuing destruction of the site, 0.5 - the site destroyed, but now with management measures for avoid the destruction, 1 - no destruction	0	0	0	1
Legislative protection	0 - no legislative protection, 0.5 - existing proposal for legislative protection, 1 - existing legislative protection (Natural monument, Natural reservation…)	0	0	0	1
Added values	**Rules Value**	**Site 1**	**Site 2**	**Site 3**	**Site 4**
Cultural values: presence of historical/archaeological/ religious aspects related to the site	0 - no cultural features, 0.5 - existing cultural features but without strong relation to abiotic features, 1 - existing cultural features with the strong relations to abiotic features,	0	0	0	0,5
Ecological values	0 - not important, 0.5 - existing influence but not so important, 1 - important influence of the geomorphologic feature on the ecologic feature	0,5	0,5	0,5	1
Total		**29%**	**53%**	**35%**	**74%**

Figure 4 . Geosite value detail calculation with parameters from Kubalova (2013)

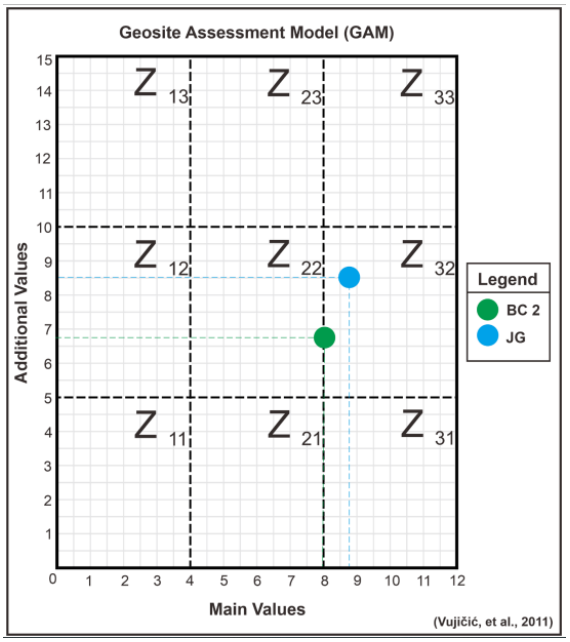

Figure 5. Geosite plotting result on the GAM matrix from Vujičić et al. (2011)

PROCEEDINGS
JOINT CONVENTION BANDUNG (JCB)2021
November 23rd – 25th 2021

Potensi Geowisata Tersembunyi Desa Lubuk Resam, Kabupaten Seluma, Provinsi Bengkulu

Roman Hetu Manggara[1], Budhi Setiawan[1]
Program Studi Teknik Geologi, Fakultas Teknik, Universitas Sriwijaya
romanhetumanggara22@gmail.com

Abstrak

Kabupaten Seluma merupakan salah satu kabupaten di Provinsi Bengkulu yang dilalui oleh jalur lintas barat Sumatera. Kabupaten ini hanya dijadikan tempat persinggahan bagi para pelancong yang melewatinya. Tak heran, karena tidak adanya ikon yang menjadikan kabupaten ini untuk menjadi tempat persinggahan. Padahal jika ditelusuri banyak tempat wisata indah yang dapat menarik para pelancong untuk singgah bahkan bermalam disini. Salah satunya yaitu Desa Lubuk Resam, merupakan desa yang memiliki potensi geowisata yang menakjubkan. Desa ini mempunyai suatu aspek geologi yang menarik yakni adanya sumber mata air panas yang muncul ditengah-tengah pematang sawah, kemudian airnya dialirkan ke sebuah kolam yang dapat dijadikan tempat pemandian. Air yang mengandung belerang dipercaya dapat menyembuhkan berbagai macam penyakit oleh masyarakat setempat. Di lokasi yang sama juga terdapat sebuah Goa Karst yang indah dan memiliki sungai bawah tanah. Masyarakat setempat percaya bahwa Goa tersebut memiliki panjang puluhan kilometer, belum ada ahli yang membuktikan hal ini. Berdasarkan peta geologi lembar Manna dan Enggano (Amin, et al., 1993) Desa Lubuk Resam berada pada formasi Lemau, yang terdiri oleh susunan batugamping. Untuk pengembangan geowisata yang berkelanjutan lokasi ini sangat cocok karna telah mencakup unsur penting dalam konsep geowisata yaitu adanya unsur keragaman geologi, keragaman hayati, dan keragaman budaya. Dalam membantu melihat potensi geowisata Desa Lubuk Resam dapat menggunakan metode kuantitatif (kubalikova, 2013) serta pengambilan data sekunder memakai metode kualitatif observasi lapangan dan penentuan lokasi memakai GPS (*Global Positioning System).* Pengembangan potensi geowisata ini diharapkan mampu menaikan kondisi ekonomi masyarakat setempat serta menjadikan Kabupaten Seluma menjadi salah satu tempat tujuan berwisata untuk wisatawan lokal maupun asing.

Abstrac

Seluma Regency is one of the regencies in Bengkulu Province, traversed by the West Sumatra crossing. This district is only used as a stopover for travelers who pass through it. No wonder because no icon makes this district a stopover place. In fact, if traced, many beautiful tourist attractions can attract travelers to stop and even spend the night here. One of them is Lubuk Resam Village, a village that has amazing tourism potential. This village has an interesting geological aspect, namely the existence of hot springs that appear in the middle of the rice fields, then the water flows into a pond that can be used as a bathing place. Water containing sulfur is believed to cure various diseases by local people. In the same location, there is also a beautiful Karst Cave and has an underground river. Local people believe that the cave has tens of kilometers; there are no experts who prove this. Based on the geological map sheet Manna and Enggano (Amin, et al., 1993), Lubuk Resam village is in the Lemau formation, consisting of limestone composition. For the sustainable development of geotourism, this location is very suitable because it includes important elements in the concept of geotourism, namely the presence of elements of geological diversity, biological diversity, and cultural diversity. In helping to see the geotourism potential of Lubuk Resam Village, quantitative methods can be used (Kubalova, 2013) as well as secondary data collection using qualitative field observations and determining location using GPS (Global Positioning System). The development of tourism potential is expected to improve the economic conditions of the local community and make Seluma Regency a tourist destination for local and foreign tourists.

Kata Kunci: Geowisata, Mata Air Panas, Goa Kecil, Desa Lubuk Resam.

Introduction

Indonesia negara yang kaya akan sumber daya. Posisinya yang strategis mejadikan Indonesia memiliki potensi sumber daya alam yang sangat melimpah, baik sumber daya hayati maupun non-hayati. Kekayaan non hayati berupa bahan galian dan fenomena bentang alam yang luar biasa menakjubkan. Pegunungan menjadi salah satu potensi bentang alam dengan kondisi geologinya yang khas dan unik yang dimiliki Indonesia. Megageodiversity menjadi sebuah sebutan untuk Indonesia, dikarenakan potensi geologinya yang bermacam ragam. Namun, kondisi realita menunjukkan bahwa potensi geologi yang ada belum terkelola secara optimal sampai sekarang ini. Pemanfaatan sumber kekayaan geologi masih berfokus pada eksploitasi bahan galian sebagai penunjang dalam sektor pemenuhan energi, industry dan infrastruktur. Akibatnya dari eksploitasi tersebut berdapak pada menurunya daya dukung lingkungan dan rusaknya situs – situs geologi yang seringkali memiliki daya tarik yang luar bisaa. Pariwisata sebagai hal yang sangat berkembang di Indonesia menjadi strategi dalam Pemanfaatan dan pengembangan potensi geologi, sektor pariwisata diharapkan dapat menjadi alternatif jalan keluar dalam mengoptimalkan aset geologi dengan cara yang berbeda dari yang telah dilakukan sebelumnya. Selama ini aktivitas pariwisata memang tidak bisa lepas dari alam, terutama terkait dengan pengembangan daya tarik wisata. Semua itu berkorelasi terhadap aspek lingkungan alam, tentunya juga tidak lepas dari perspektif geologi dan daya dukung lingkungan. Geowisata muncul sebagai fenomena global baru. Secara luas definisi geowisata mencangkup aspek geografis, social, ekonomi, dan budaya. Sedangkan secara khusus definisi geowisata adalah wisata yang berfokus pada bentang alam dan geologi. Hadirnya geowisata merupakan sebuah solusi

baru dalam memanfaatkan potensi geologi. Tetapi perkembangan geowisata yang masih tergolong baru masih banyak diperlukan upaya dalam pengembangannya.

Keragaman dan keunikan geologi yang dimiliki suatu daerah dapat menjadi potensi penting dalam mendukung program konservasi sumber daya geologi, salah satunya adalah kegiatan pengembangan dan pemanfaatannya sebagai objek wisata berbasis edukasi geologi/geowisata (Agustina, 2020). Geowisata adalah bentuk pariwisata yang menopang karakteristik geografi dari suatu tempat, seperti lingkungan, estetika budaya, warisan dan juga kesejahteraan penghuninya (Kubalikova, 2013). Pengembangan daerah tertentu menjadi suatu kawasan geowisata tentunya akan memberikan dampak yang baik bagi kehidupan masyarakat dalam berbagai aspek kehidupan seperti ekonomi, sosial, dan budaya.

Desa Lubuk Resam adalah desa yang terletak di Kabupaten Seluma, Bengkulu. Desa ini memiliki keragaman wisata yang menarik untuk dijadikan geowisata. Wisata alam merupakan daya tarik utama yang ada di des aini.

Data and Method

Penelitian ini menggunakan metode penelitian dengan memanfaatkan data kuantitatif (kubalikova, 2013) serta dipadukan dengan data sekunder untuk mendukung penelitian. Data sekunder dengan metode kualitatif observasi lapangan dan penentuan lokasi menggunakan GPS (*Global Positioning System).*

Result and Discussion

Lokasi penelitian terletak di Desa Lubuk Resam, Kecamatan Seluma Utara, Kabupaten Seluma, Bengkulu. Untuk mencapai lokasi penelitian dapat melalui Jl. Raya Manna-Bengkulu menggunakan mobil ataupun motor dengan waktu tempuh sekitar 1 jam dari pusat Kota Bengkulu. Kondisi lokasi penelitian secara geografis masih berupa hutan dan lahan perkebunan. Sawit dan kopi merupakan komoditas utama di daerah penelitian dimana bertani dan berkebun merupakan mata pencaharian sebagian besar masyarakat disana. Secara geologi regional, daerah penelitian masuk kedalam peta geologi lembar Bengkulu.

Secara geologi Desa Lubuk Resam mencakup Formasi Lemau dan Formasi Quarter Vulkanik yang didominasi oleh satuan batugamping, batupasir gunungapi epiklastika. Dari hasil observasi lapangan terdapat tiga objek geowisata diantaranya pemandian airpanas, goa kecil, sungai lubukresam. Berikut penilaian mengenai 3 objek tersebut :

Pemandian Air Panas

Lokasi geosite ini terletak pada koordinat 48 240524 E 9562497 S merupakan sebuah kolam pemandian air panas yang terletak di Desa Lubuk Resam yang berjarak 1 jam dari pusat kota Kabupaten Seluma. Pemandian air panas ini termasuk kedalam Formasi Lemau, dengan satuan batuan batugamping. Air panas keluar dari bumi setelah dipanaskan secara geothermal, memiliki suhu diatas titik didih dilihat dari buih-buih yang keluar dari sumber mata air panas.

Gambar 1. Sumber mata air panas

Kelebihan dari mata air panas ini ialah telah dibangun oleh warga desa sebuah kolam untuk pemandian. Kolam pemandian ini sendiri dibangun pada tahun 2020. Air panas langsung disalurkan dari sumber mata air panas menuju kolam pemandian yang berjarak sekitar 100 meter. Air panas mengandung belerang dipercaya memiliki khasiat yang bagus untuk Kesehatan.

Gambar 2. Kolam pemandian air panas

Goa Kecil

PROCEEDINGS
JOINT CONVENTION BANDUNG (JCB)2021
November 23rd – 25th 2021

Gambar 3. Goa Kecil Lubuk Resam

Lokasi site selanjutnya terletak di koordinat 48 241330 E 9562843 S berjarak tidak jauh dari pemandian air panas di Desa Lubuk Resam. Goa Kecil merupakan goa yang tersusun dari batugamping pada Formasi Lemau. Goa Kecil merupakan site yang memiliki kelebihan yang diantaranya adalah suatu objek wisata yang dapat dijadikan edukasi mengenai batugamping, contoh stalaktit dan stalagmite, sungai bawah tanah dan edukasi geologi lainnya. Walau mempunyai nama Goa Kecil namun kenyataannya gao ini memiliki luas yang cukup besar dan panjang.

Sungai Lubuk Resam

Sungai Lubuk Resam merupakan sumber air utama dari Desa Lubuk Resam. Sungai ini terletak ditengah desa yang membagi dua lokasi perumahan warga di Desa Lubuk Resam. Sungai ini cocok dijadikan objek wisata karena memiliki kelebihan yaitu masih sangat terjaga kebersihannya, air yang dingin menyegarkan saat mandi di sungai ini, sungai yang memiliki jeram cocok dijadikan objek wisata arum jeram.

Gambar 4. (a. Sungai Lubuk Resam, b. Jembatan gantung di Sungai Lubuk Resam)

Conclusions

Berdasarkan penelitian yang telah dilakukan dapat diketahui bahwa Desa Lubuk Resam memiliki 3 situs geologi dengan nilai kelayakan masing masing antara lain Pemandian Air Panas (51.6%), Goa Kecil (51.6%), Sungai Lubuk Resam (51.6%) (Tabel 1). Secara keseluruhan hasil penelitian dari keempat area ini memiliki nilai kelayakan (>50%) yang menandakan bahwa area tersebut berpotensi menjadi obyek geowisata.

Namun dari hasil survey yang dilakukan pada 50 masyarakat Bengkulu, 70% dari jawaban mengatakan tidak mengetahui objek wisata yang ada di Desa Lubuk Resam, Kabupaten Seluma, Bengkulu

Gambar 5. Hasil survey mengenai wisata Desa Lubuk Resam

Kesimpulan dan saran yang diperlukan untuk pengembangan – pengembangan Desa Lubuk Resam antara lain :

- Pengembangan infrastruktur seperti jalan, dikarenakan akses yang masih sangat buruk untuk mencapai lokasi

- Pengembangan pengetahuan masyarakat tentang bagaimana mengelola wisata yang baik. Seperti tidak melakukan vandalism dan selalu menjaga kebersihan objek wisata

- Pengembangan promosi tentang Desa Lubuk Resam, sangat amat diperlukan promosi yang ekstra untuk mengenalkan objek wisata ini, terkhususnya dari pemerintah Kabupaten Seluma

Tabel 1. Hasil Penilaian Kelayakan Geowisata

Parameter	Pemandian Air Panas	Goa Kecil	Sungai Lubuk Resam
Nilai Pendekatan Ilmiah Dan Interistik			
A	1	0.5	1
B	1	1	0.5
C	0	0.5	0.5
D	0	0	0
%	50%	50%	50%
Nilai Pendidikan			
A	1	1	1
B	1	1	1
C	0	0	0
D	0	0	0
%	50%	50%	50%
Nilai Ekonomi			
A	0.5	0.5	0.5

B	0.5	0.5	0.5
C	0	0	0
%	33%	33%	33%
Nilai Konservasi			
A	1	1	1
B	1	1	1
C	1	1	1
D	0	0	0
%	75%	75%	75%
Nilai Tambahan			
A	0	0	0
B	1	1	1
C	0.5	0.5	0.5
D	0.5	0.5	0.5
E	0.5	0.5	0.5
%	50%	50%	50%
Total	52%	52%	52%

References

Budi, B. & Bachtiar, T. (2009). Wisata Bumi Cekungan Bandung. Bandung: Truedee Pustaka Sejati.

Gordon, J., (2018). Geoheritage, Geotourism and the Cultural Landscape: Enhancing the Visitor Experience and Promoting Geoconservation. Geosciences, 8(4), p.136.

Hermawan, H., & Brahmanto, E. (2018). GEOWISATA : Perencanaan Pariwisata Berbasis Konservasi. Jawa Tengah: Jawa Tengah: PT Nasya Expanding Management

Kubalikova, L., (2013). Geomorphosite assesment for geotourism purposes, Czech Journal of Tourism. 02/2013 .

PROCEEDINGS
JOINT CONVENTION BANDUNG (JCB)2021
November 23rd – 25th 2021

Geotourism Concept Development based on Environment Sustainability and Social Wisdom in Batu Dinding Amurang, North Sulawesi.

Muh. Alifian Al Anshari[1], Pricilia B. Diamanis[2], Hendra Riogilang[3], Herawaty Riogilang[4], Christo F. Onibala[5]
[1,2,3,4,5]University of Sam Ratulangi.

Abstract
Geotourism is a sustainable natural tourism activity with a main focus on the geological appearance of the earth's surface, in order to encourage understanding of the environment and social wisdom. Indonesia has many geotourism potentials, one of them in North Sulawesi, which is Batu Dinding Amurang. This geological object consists of andesite, volcanic, and sedimentary rock. The rocks are neatly arranged, unfortunately only two attractions are developed, rock climbing and the landscape views on the top. This place has not yet showed the sustainable tourism principles. However, there are many aspects that need to be improved. This paper aims to design the development concept for Batu Dinding Amurang as the new geotourism object in North Sulawesi based on Environmental Sustainability and Social Wisdom. It is designed to represent the development concept of geotourism such as economics, social and esthetics, maintaining cultural integrity, essential ecological process, biological diversity and life support systems. This paper used descriptive qualitative. The data collected by literature review and field research. The results are the development concept of the Batu Dinding Amurang as the new Geotourism object in North Sulawesi.

Keywords: Geotourism, Development, Batu Dinding Amurang.

Introduction

The geographical location of Indonesia is very special, making Indonesia have a very large source of wealth, especially non-biological natural wealth, in the form of a diversity of geological phenomena that stretches from Sabang to Merauke. Geotourism is a type of sustainable and conservation tourism related to the types of natural resources (forms of landscapes, rocks/fossils, geological structures, and earth history) of an area in order to develop insight and understanding of phenomena processes that occur in nature.

Indonesia has a lot of potential from natural resources that can be developed into interesting tourism objects, one of which is Geotourism stone wall Kilo Tiga which is located in the southern Minahasa district of North Sulawesi province. Kilo Tiga Rock Wall or often called Kilo Tiga Cliff, because it is near Kilometer Tiga Village, Amurang District is a natural cliff that towers about 90 meters.
Batu Wall is known as 'Paradise' for rock climbing sports lovers. Batu Wall Kilo Tiga is a natural cliff that is very unique, different from natural cliffs in general. The uniqueness of Batu Wall is like an inverted ladder, besides that the surface structure of the cliff is like a row of blocks that are stacked upside down. As the upper beam overlaps the lower beam, so that the higher you go, the more prominent the surface ofcliff this uniqueis which is a distinctive feature that distinguishes the amurang wall stone from other cliffs.

Figure 1: The Andesit Stone of Batu Dinding
Source: manado.tribunnews.com

Stone Wall has hard rock type andersite. Andesite rocks are formed because lava cools quickly at the surface, generally lava consists of small crystals. So, it can be concluded that andesite is a fine-grained rock that is formed when magma erupts to the surface and crystallizes quickly. Citing the page Minerals Education Coalition, Andesite is a volcanic rock similar to basalt, only lighter in color and contains less iron and magnesium than basalt. Andesite also contains large, striking crystals. This rock type turned out to be the source rock for andesite, a precious gemstone. This rock type is supported by the characteristics of the ecoregion found in the region.

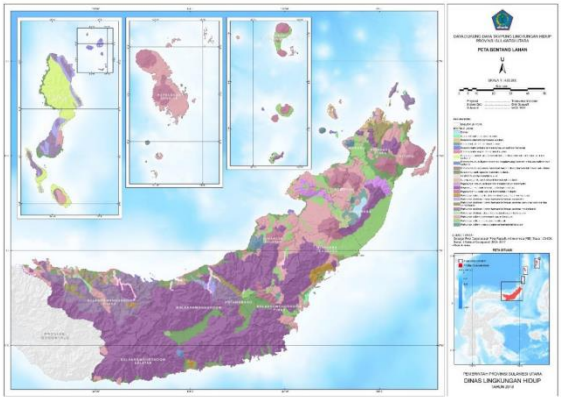

Figure 2: The Ecoregion Map of North Sulawesi
Source: Dinas Lingkungan Hidup Sulawesi Utara

An ecoregion is a large regional ecosystem containing a number of smaller ecosystems. They are geographic zones that represent geographical groups of similar functioning where similar sites (which have the same landform, slope, parent material, and drainage characteristics) can be found in several climatic areas. In one area, these sites will support the same vegetation community, but in another area, the vegetation on the site will be different (Bailey, 1983). As for the Batu Wall Amurang geotourism area in North Sulawesi, it is located in the Structural Hills area of the Manado Complex, with the following general characteristics: Longitudinal

PROCEEDINGS
JOINT CONVENTION BANDUNG (JCB)2021
November 23rd – 25th 2021

Table 1: The Characteristics of Ecoregion
Source: Deputy for Environmental Management, 2013

NO	PARAMETER	DESCRIPTION
1	Location	Western Areas on North Sulawesi
2	Climatology	with Wet Tropical Climate, the average air temperature is 24-28°C. Annual rainfall is 1,500-2,500 mm.
3	Geology	Composed of sedimentary rock and igneous rock. Spread over hilly areas in the outer arc and ring arc tectonic zones.
4	Geomrphlogy	Elevation is predominantly <500 m asl. Reliefs and slopes; hilly, with a relief amplitude of 0-300 m slope of >16%. Formed by tectonic processes so that the layers of the earth's skin undergo changes in shape due to pressure and pull. The form of the layered structure that results between the folded structure of the fault structure, or the magmatic breakthrough that results in the local uplift of the earth's crust that forms a dome structure or other structure.
5	Hydrology	Perennial river flow. River discharge at certain waterfalls can be used as an energy resource.
	Soil and land use	Sour latosol and red-yellow podzolic soil with low to moderate fertility. In some places, Mediterranean soil derived from limestone parent material is found which has good chemical fertility and is productive. Type of closure / land use rather diverse, the forest, scrub, lading and settlement

This paper aims to design the development concept for Batu Dinding Amurang as the new geotourism object in North Sulawesi based on Environmental Sustainability and Social Wisdom. It is designed to represent the development concept of geotourism such as economics, social and esthetics, maintaining cultural integrity, essential ecological process, biological diversity and life support systems.

Data and Method

The data collected through field research and secondary data. The literature review data based on reviews, summaries, and some literature sources (may be articles, books, slides, information from the internet). Field research is carried out to monitor the current situation related to examine the potential design concept for the development of amurang stone wall geotourism by technical interviews with the surrounding community and visiting the location of the stone wall directly.

Result and Discussion

Minahasa Region

South Minahasa Regency is a district in North Sulawesi Province, with the capital city of Amurang. The area is 2,120.8 km2 and is divided into 15 districts. Its territory is bordered by Minahasa Regency in the north, Bolaang Mongondow Regency in the south, the Sulawesi Sea in the west and the Maluku Sea in the east.

Interesting tourism objects in this area, among others; Maruasey River tourist attraction, located in Tangkuney Village, Tumpaan District, about 30 Km from the center of Amurang City. Batu Wall tourist attraction is located in Amurang District, a stone that is ± 70 m high near the Ranoyapo river. The tourist attraction of Bukit Doa Pinaling is located in Pinaling Village, East Amurang District, tourists can feel the combination of natural beauty and a religious touch. Moinit Beach tourist attraction which is located in the south of this district, between Teep and Tawaang villages, Amurang District. This Moinit Beach area keeps a lot of flora and fauna

Figure 3: Bukit Doa (Pray Valley) at Pinaling
Source: Bukit Doa Pinaling

As for the geothermal exploration area by PGE, the Lahendong Area in North Sulawesi is located in the Volcanic Complex Hills area of the Manado, with the following general characteristics:

Cultural Diversity

Kuntung Watuleley

The cultural site of Kuntung Watuleley is a witness to the history of the civilization of the Pinamorongan people when the dotu-dotu began to inhabit this area. Previously, this place was used as a meeting place for the tonaas so that Watuleley itself has always been a place that is very sacred by the community. village people are sometimes very afraid to come to visit carelessly. From a working visit from the North Sulawesi Archeology Center and the Minsel Dispar in 2016, it is known that there is 1 tumotowa stone on the Watuleley hill, 1 stone pedestal and 1 flat stone which is neatly cut on the side of this hill and all of them are still well maintained until now.

Figure 4: Umpak Stone
Source: Berita Manado,com

Traces Culture megalithic
Remains of archaeological indicating human migration and the spread of culture in the North Sulawesi is quite commonly found, generally in the form of websites settlements characterized by megalithic, characterized paleolithic-neolithic, and the site is characterized by neolithic-paleometalik, not least the sites found in the southern Minahasa. Archaeological remains that show past activities in South Minahasa are found in almost all areas that are part of South Minahasa. Existing cultural traces show the same level of time, in the form of a megalithic culture that is quite developed in this region, this is clearly seen from the distribution of megalithic remains which are quite abundant.

The results of data collection on the distribution of megalithic remains in the southern Minahasa region show that South Minahasa is one of the areas with the largest and most varied megalithic distribution. The remaining megalithic remains are stone mortar/stone mortar, menhirs, stone altar, stone tray, and waruga.

Figure 5: Lesung Stone
Source: Sumber: diolah dari dok. Balar Sulut)

Until now, the people who inhabit the southern part of Minahasa (Minsel-ed) which is precisely in the North Talaitad Village, Suluun-Tareran District, South Minahasa Regency, are still doing the home-lifting culture. the Minahasa community which includes the South Minahasa Community, with one leadership command to lift the house or move the house from the old location to the new location. Even women (mothers, ed) often help lift the house.

Figures 6: Mapalus Activities in South Minahasa
Image source : nonapanbaru.sideka.id

Biodiversity
Generally, food crop commodities cultivated by residents are lowland rice, upland rice, corn, peanuts, green beans, soybeans, cassava and sweet potatoes. Horticultural plants (commodities of seasonal vegetables) in South Minahasa Regency have great potential and good quality. South Minahasa Regency also has good potential for annual fruits, biopharmaceuticals (medicinal plants) and ornamental plants. As for plantation crops, both smallholder plantations and large plantations play an important role in the economy of the community in the South Minahasa Regency. Generally, people's plantation crops that are cultivated are coconut, cloves, vanilla, sugar palm, coffee (robusta and arabica), cocoa (chocolate), cassiavera, jatropha and nutmeg although the planting pattern is still simple and is a people's garden that is managed for generations.

The potential for flora and fauna in South Minahasa is quite large which can be seen from the forest area in this area, there are several forests in Minsel and are quite large resources such as examples of production forests. Production forest is a forest that can be used for materials (wood or other products) while still paying attention to its conservation function which is also found in all sub-districts in the southern Minahasa district. In southern Minahasa there are 6 types of forest which have a land area of 51,713.07 ha. Then there is also the potential of mangrove forest areas,especially in Sub Tatapaan has a mangrove forest with an area of approximately 873.6 hectares and 276.7 hectares located in the village of mangrove Sondaken.Hutan is in zone II Bunaken National Park in the village of Sondaken, District Tatapaan As for potential fauna Minsel area, namely the presence of a Yaki population is estimated to exist in the Lolombulan Forest and in the Sinonsayang Forest. Yaki or wolai monkeys or Sulawesi black monkeys (Macaca nigra) are endemic animals to Indonesia that are only found in the northern part of Sulawesi Island and several surrounding islands. South Minahasa Regency is also part of theBunaken National Park, there are 20 dive points with a variety of different marine biota. But most importantly, the coral reefs, flora and fauna are very beautiful. Approximately, there are about 150 species of fish scattered in the dive spots.

Geodiversity
The diversity of geological components in an area, where the presence of distribution, and its condition can reflect the process of Earth's evolution in the area. The South Minahasa Regency has a hilly or mountainous topography in which there are many mineral deposits with important economic values, such as gold. Gold deposits in the South Minahasa Regency are widespread in several sub-districts in addition to other deposits. With the flow of large rivers, it produces sand, gravel and stones which are widely used in physical construction as the main raw materials. The area of South Minahasa Regency has five soil orders, namely Entisols, Inceptisols, Alfisols, Mollisols and Ultisols with very varied geology of the rocks that make up the area of South Minahasa Regency. This is based on the Interim Report of the Preparation of the Drainage Master Plan for the City of Amurang (Anonymous, 2011)

Batu Dinding Amurang
This tourist attraction is located in North Sulawesi which is named Batu Wall Kilo Tiga. This Kilo Tiga Wall Stone Tourism object is located in the Kilometer 3 (Km3) Village area, Amurang District, South Minahasa Regency, North Sulawesi Province. Batu Wall Kilo Tiga is a natural cliff that rises about 90 meters. Kilo Tiga Rock Wall is known as the Heaven for lovers of extreme sport Rock Climbing. The shape is not like natural cliffs in general. Wall Stone has a surface like a row of blocks stacked upside down and like

the upper beam overlapping the lower beam, so that the higher the surface the more prominent the surface. This cliff is its own uniqueness that distinguishes the stone wall of kilo three from other cliffs. Gowisata Batu wall offers rides both beautiful scenery and rock climbing which is so challenging.

Extreme Sport Rock Climbing
The amurang wall will provide a sensation that is enough to trigger adrenaline due to the reversed arrangement of the blocks which is quite stressful for the brain and energy and also the paths are quite difficult. On this exotic Batu Wall cliff, there are several climbing routes with different names. And save an interesting story on each climbing track name. The rock cliffs of Kilo Tiga Amurang are predicted to be the cliffs that have the second highest difficulty level in the world, with an average difficulty level of 10.12.

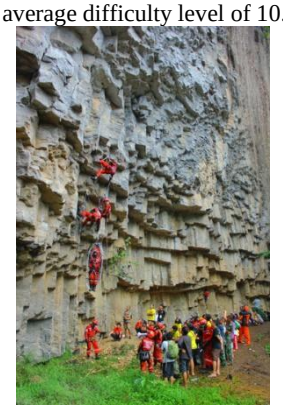

Figure 7: Wall Climbing in Batu Dinding
Source: Kabar sahabat

The beautiful and cool view of the Rocks.
The splendor of the Stone Walls will appear when you see it from a distance. However, you will feel even more awe when you look at the surface up close and see how the blocks in this place come together so perfectly. In addition to the splendor of the Kilo Tiga Rock Wall, the scenery that surrounds this location is very beautiful and cool. Not far from the Batu Wall location, you can find the clarity and freshness of the flow of the Ranoyapo River. This river is also often used forwhite water rafting.

Figure 8: Batu Dinding View
Source: indonesia.tripcanvas.co

Lodging and restaurant facilities are only available in the cities closest toBatu Wall, namely the cities of Amurang and Manado. Some recommended hotels nearBatu Wall Kilo Tigasuch as Minahasa Lagoon Hotel and Manguni Terrace Resort.
The geographical condition of the stone wall kilo three has a height between 0-100 meters above sea level with a topography in the form of mountainous hills, a small part of which is undulating lowlands and has large rivers. Most of the land use around the stone walls is dry land, one of which is plantations.

Geotourism Development Concept

Geotourism activity, is expected to be an appreciation of the significance and uniqueness of the diversity of geological heritage contained in an area to raise awareness of the environment through conservation efforts There are some who were targeted in the development of stone walls Amurang Geotourism is as follows:

1. Facility
Visitor satisfaction is not only based on natural attractions, but also from tourist facilities owned by tourist objects. Facilities that can be developed to support the comfort of the visitors who come to the amurang stone wall tourist location are the Mushola. Food court or culinary center. A large parking area, cleaning and security facilities, equipment and sanitation facilities on site. These facilities will certainly be very helpful for the needs of the visitors who come

2. Rides
In addition to facilities that can support the comfort of visitors, of course, there are also several rides that add to the attraction when visiting the rock walls and existing rides such as park rides with a natural concept, spot for climbing training for beginners, flying fox, enjoying the beauty from the top of the cliff, and cycling where the Batu wall Amurang area has quite a challenging cycling track.

3. Community Empowerment
Community empowerment actually refers to the word empowerment, namely as an effort to actualize the potential that the community already has. In this case, it is like building creative and productive SME sectors so that they can absorb a lot of energy besides empowering the community to be part of the management of Amurang stone wall geotourism.

4. Environmental Processing
In research, spurring the concept ofsanitation attractions for tourism objects, land use for agricultural cultivation plants that are adapted to the characteristics of the land and land use by developing conservation areas to maintain an ecological system so that it is sustainable. support tourism areas such as the development of conservation areas to maintain the ecological system in the area so that it remains sustainable.

5. Challenges and Strategies
In developing the concept of geotourism in the rock walls of Amurang, there are several challenges that become the focus of research on the basecamp location which is occasionally flooded because the soil layer is floodplain soil and the weathering process on the rock structure of the wall is fast so it will be dangerous if the cliff continues continuously used in rock climbing activities, geotourism is not well known among the public, then the human resources for driving geotourism are still few, policies for geotourism management do not yet exist.

After seeing the various challenges that exist, a development strategy is needed that can overcome the existing challenges. Development strategies that can be implemented such as promotion in various mass media, sustainable human resource capacity building construction of gabions to

withstand flooding if the river's water discharge increases, and in collaboration with students and various NGOs/NGOs such as IAGI-MAGI and local communities.

Conclusions

Geotourism is a type of sustainable and conservation tourism related to the types of natural resources (forms of landscapes, rocks/fossils, geological structures, and earth history) of an area in order to develop insight and understanding of phenomena processes that occur in nature. One of them is Kilo Tiga stone wall geotourism which is located in the southern Minahasa district of North Sulawesi province. Kilo Tiga Rock Wall or often called Kilo Tiga Cliff, because it is near Kilometer Tiga Village, Amurang District is a natural cliff that towers about 90 meters.

Batu Wall known as 'Paradise'Stone Wall Kilo Tiga is a natural cliff that is very unique, different from natural cliffs in general. The uniqueness of Batu Wall is like an inverted ladder, besides that the surface structure of the cliff is like a row of blocks that are stacked upside down. As the upper beam overlaps the lower beam, so that the higher you go, the more prominent the surface ofcliff this uniqueis which is a distinctive feature that distinguishes the amurang wall stone from other cliffs.

References

Aryo Sunaryo 2009 Ornamen Nusantara, Kajian Khusus Tentang Ornamen Indonesia. Semarang: Penerbit Effhar Offset Semarang.

Bagyo, dkk 2004 Religi Pada Masyarakat Prasejarah di Indonesia. Jakarta: Puslitbang Arkenas.

Bertling 1931 De Minahassische Waroega en Hockerbestatung. NION: Amasterdam-Denhaag.

Bumipala,2013," Jambore Nasional Panjat Tebing dan Vertical Rescue" https://mapalammtc.wordpress.com/2013/07/19/jambore-nasional-panjat-tebing-dan-vertical-rescue/. Diakses tanggal 18 September 2021 pukul 12.11

Elnusanews/com.2015. "Pameran Seni Budaya Keunggulan Minsel"http://www.elnusanews.com/2015/08/pameran-seni-budaya-tampilkan.html, diakses 10 Agustus 2021 pukul 10.27

Hendratno, A. (2004). Peluang Pemanfaatan Data Geologi dan Sumberdaya Mineral dalam Pembangunan Wilayah. In Seminar Geologi Nuklir dan Sumberdaya Tambang. Jakarta: Pusat Pengembangan Bahan Galian dan Geologi NuklirBATAN. Retrieved from http://www.iaea.org/inis/collection/NCL CollectionStore/_Public/39/123/3912307 6.pdf.

Mas Han, 2020, "Megalitikum di Minahasa Selatan, dari Olah Pangan hingga Ritual Pemujaan" https://www.kompasiana.com/wurihandoko7905/5f40c50f097f3646ef2c8952/megalitik-di-minahasa-selatan-dari-ritual-ke-olah-pangan?page=all&page_images=1. Diakses tanggal 30 Agustus pukul 14.05

Mas Han, 2020, "Mapalus, Budaya Gotong Royong Leluhur yang Tetap Hidup di Masyarakat Minahasa" https://www.kompasiana.com/wurihandoko7905/5f68795cd541df21c35470c3/budaya-mapalus-di-kalangan-masyarakat-minahasa?page=all&page_images=1. Diakses tanggal 8 September 2021 pukul 21.10

Rahma, Filda.2019." Menelusuri Indahnya Minahasa Selatan, dari Bawah Laut Hingga Atas Awan". https://travelingyuk.com/minahasa-selatan/247588/,Diakses pada 22 Agustus 2021 pukul 16.40 Rumah.com.2021." Batu Andesit: Fungsi dan Keunggulannya Sebagai Material Pada Bangunan Rumah". https://www.rumah.com/panduan-properti/batu-andesit-41061, diakses pada 9 september 2021 pukul 22.15.

Ronald Kalalo,2021, "Mengenal Destinasi Wisata Minsel, "KUNTUNG WATULELEY" Jadi Saksi Sejarah Peradaban" https://beritamanado.com/mengenal-destinasi-wisata-minsel-kuntung-watuleley-jadi-saksi-sejarah-peradaban/.Diakses tanggal 9 September 2021 pukul 11.49

Superbook Admin,2018"Keren! Anda Bisa Berlibur Sambil Melakukan Wisata Rohani Ke Tempat-Tempat Berikut" https://www.superbookindonesia.com/article/read/article/Keren%21+Anda+Bisa+Berlibur+Sambil+Melakukan+Wisata+Rohani+ke+Tempat-tempat+Berikut/id/765.html. Diakses tanggal 16 September 2021 pukul 09.1

Urban Places,2021,"Destinasi Wisata Hits yang menarik Banget buat dikunjungi" https://www.superadventure.co.id/news/23565/destinasi-wisata-hits-di-manado-yang-menarik-banget-buat-dikunjungi/. Diakses tanggal 14 Agustus 2021 pukul 20.25

Yudhi Mahesa, 2021," Gagahnya Batu Dinding Kilo Tiga, Surga Bagi Pemanjat Tebing" https://www.kabartravel.id/gagahnya-batu-dinding-kilo-tiga-surga-bagi-pemanjat-tebing/destinasi/. Diakses tanggal 20 Agustus 2021 pukul 13.25

PROCEEDINGS
JOINT CONVENTION BANDUNG (JCB)2021
November 23rd – 25th 2021

Comprehensive Evaluation for Ranah Minang Silokek Geopark to UNESCO Global Geopark (UGG), West Sumatera

Amsal Frans Harapenta Surbakti[1,2], Muhammad Fadhli[1,2] dan Alisha Maulidita[1] Ugi Kurnia Gusti[2,3]
[1] Geological Engineering Program Study, Sriwijaya University
[2] Bumi Sriwijaya Research Group, Palembang
[3] McMaster University, Canada.

Abstract
The implication of determining the Ranah Minang Silokek as a geopark in Sijunjung, West Sumatra, can become a halal tourism destination for tourists and an opportunity to realize an international class conservation area. The utility of establishing a geopark for local communities and governments increases the economic levels, education, and creating an inclusive, safe, and resilient environment through geotourism in supporting the declaration of the Sustainable Development Goals. The research goal is to analyze the potential for extraordinary to boost the enlargement of the Ranah Minang Silokek Geopark sustainably towards the UNESCO Global Geopark from the geology perspective. Spatial analysis, review surveys for quantitative weighing, and feasibility tests using the SWOT method at each site are the study's approaches are performed in this study.

The quantitative review shows the value of scientific, intrinsic, educational, economic, conservation, and supplementary approaches classified as excellent and exciting to develop. The quantitative description is conducted by a feasibility test that displays the strength in exposed granite; therefore, it could be an imperative analog for reservoir basement development in Indonesia. The establishment of a national geopark management agency became a positive opportunity to be an international geopark. Meanwhile, the lack of information is regarding the existence and potential of hidden treasure in the Ranah Minang Silokek geopark and a geosite that had not been well optimized. So, it takes a threat to provide socialization to residents about the importance of conserving the diversity in the geopark to contribute to creating a geopark with UNESCO global geopark standards.

Introduction
Geopark represents the unified local community with a geological heritage of international significance to sustainability and where that heritage is used for its promotion and development (UNESCO, 2011). According to the Ministry of Tourism and Creative Economy (2021), there are six parks with international standards in Indonesia, known as UNESCO Global Geoparks (UGG). Silokek Ranah Minang is one of the candidates for UGG, which currently has a national geopark with a leading and halal tourist destination located in West Sumatra Province, precisely in Sijunjung Regency (Figure 1). Silokek Geopark was designated as a National Geopark on November 30, 2018. The geopark becomes a destination for forty-six natural attractions, twelve cultural attractions, and eight special-interest attractions (LAKIP Disparpora Sijunjung Regency, 2017). Regional tourism development is indicated by an increase in the number of tourists visiting over the years. In 2016, 9,920 tourists entered the Sijunjung area. The following year, there was an increase in the number of tourists to 12,718 tourists. The determination of Silokek to become a national Geopark can open up opportunities to improve the economy and the value of education to the surrounding community and encourage Silokek Geopark to become a UNESCO Global Geopark.

Deciding from the geological aspect, Silokek Ranah Minang Geopark has its charm, indicated by the rocks that compose it. The lithology found in this area has crossed three eras in the geological time scale. The oldest rocks exposed in this area are in the Paleozoic era, precisely in the Carboniferous and Permian periods, consisting of limestone (karst), sedimentary rock, metamorphic rock, and granite intrusion. The morphological condition of the Silokek area will attract tourists who visit with the morphological appearance of towering and elongated karst hills. In the middle of the geopark, it finds a morphological form a depression or basin is formed which forms a river flow at the bottom of the bay. Hardian (2018) stated that Sites of geological diversity (geodiversity) are found in the form of karst caves, waterfalls, karst hills, hot springs, white sand, and others.

Geologically, the study area is composed of Tertiary to Pre-Tertiary rocks. The Kuantan Formation is a basement or bedrock of the Pre-Tertiary age research area, precisely Carbon (Silitonga & Kastowo, 1975). The lithology contained in this formation consists of phyllite rocks (Puku), limestone members (PCkl), and shale members (PCks1). The research of Silitonga and Kastowo (1995) claimed that in the area also found granite, granodiorite lithology, and pre-tertiary rocks (Silitonga and Kastowo, 1995). At the top of this Pre-Tertiary rock, the Sihapas Formation (Tms2) is deposited, a Tertiary rock group consisting of quartz sandstone, carbon shale, siltstone, and conglomerate. The lower members of the Ombilin Formation (Tmol) of Oligocene-Miocene age (Koesoemadinata, 1981) are included in the study area (Figure 2).

This study is conducted to disseminate the potential for the wonderful of geotourism aimed at a broad audience of geosites in Silokek based on geological studies. The approach taken in this research is through spatial analysis and feasibility test using the SWOT method, namely by analyzing various indicators including strengths, weaknesses, opportunities, and threats to tourism objects to be developed.

Method
This research is developed using a state-of-the-art approach, secondary data compilation, and based on three main methods to analyze the tourism potential of the Silokek Ranah Minang Geopark. First, collecting data through field observations aimed at obtaining data on geological conditions in the research area. The geological setting is the main issue that has been discussed about the tectonic regime, sedimentation process, and morphology aspects. Next, spatial analysis is carried out by analyzing Geographic Information System (GIS) data to explore an object from a

bird's perspective from Citra Satellite. The spatial analysis uses the open-source data from Geospatial Information Agency (BIG) with DEMNas data with EGM2008 type. Last, identify potential geological sites (geosite) based on a qualitative assessment through a SWOT approach (Copper et al., 2005). SWOT analysis is utilized to determine the research object's strengths, weaknesses, opportunities, and threats. The visualization of the SWOT analysis leads to a qualitative assessment of each geosite. On the other hand, the presentation of the results of this study is displayed in the distribution map and geosite achievement (geo track) to having a field trip in the Silokek Ranah Minang Geopark.

Result and Discussion

Based on the observations that have been made on seven sites spread over the research location. The survey constructs a SWOT analysis description and geological study related to tectonic, stratigraphic, and processes that influence them. An assessment has been done, investigating the geological setting depicted in the scratches and morphological formations.

SWOT Analysis

SWOT analysis is a qualitative analysis method that coherently describes the strengths and weaknesses of tourism from internal factors and opportunities and threats that may interfere with external factors (Kalantari et al., 2011). SWOT analysis separates internal and external problems and observations in dealing with issues in business development in geotourism. The study of minimizing problems in geotourism, according to Ferrek et al. (1998), is another function of SWOT Analysis. The result of Silokek Ranah Minang towards UGG requires an investigation from this SWOT, which has been carried out with the following achievements and circumstances.

Strength

- Has become a National Geopark Area with 25 types, 12 biodiversity sites, and 17 Cultural Diversity.
- Become one of the Regional Tourism Service Areas (DPP) V tourist destinations/destinations for the Province of West Sumatra, which includes natural, cultural, and artificial tourism.
- There has been participation by the Sijunjung Regional Government by establishing a source center for the Silokek Geopark Information.
- It has also been supported by the existence of a Geopark committee/management and a tourism-aware community (Pokdarwis) in every village with a geosite.
- Geologically 3 times in the era of the geological time scale the oldest rocks in this area were formed in the Paleozoic Era, precisely in the Permian Period (299 – 252 million years ago) and the Carboniferous (359 – 299 million years ago).

Weakness

- There is still a lack of geological research on sites in the Minang Silokek geopark area.
- There is still a lack of research on disaster mitigation in making tracks in the Silokek geopark area.
- The geopark environment is still not well maintained, which is indicated by the polluted flow of the Kuantan River.
- The name of the Silokek Ranah Minang area is still unfamiliar to local and foreign tourists.

Oppurtunity

- There have been government efforts to create geopark areas as learning materials and sources of knowledge, especially earth science.
- Silokek Ranah Minang Geopark has been designated as one of 15 national geoparks.
- There is already a management and inventory unit in the direction of the Silokek Ranah Minang Geopark.

‘**Threat**

- The lack of coordination between each Tourism Community Group (PokDarWis) villages in the vicinity of the Minang area of the Silokek Geopark.
- Each lacks information from the public about the importance of the conservation of assets and geosites in the geopark.
- There is competition for determining national geoparks between various of them in West Sumatra

Deskripsi Geosite

Geosite Catalog is very closely related to geological information and analysis. In the process of determining, it as a national geopark, especially UGG, it certainly requires a detailed description of the geosite in the Silokek Ranah Minang Geopark. This description is undoubtedly an essential point of assessment to support the achievement of geoparks as UGG. This review is shown seven geosites found in the preliminary survey at the study site (Figure 3).

a. Ngalau Basurek

Ngalau Basurek's location of this observation is a cave with limestone lithology and a height of about 30 meters (Figure 4). This location can be reached from the city of Muara Sijunjung about 40 minutes by motorbike. This geosite in terms of infrastructure is quite good because it already has prayer rooms and toilet facilities, but in this case, the geosite in terms of maintenance and cleanliness still lacks because this geosite is quite a lot with indiscriminate scribbles and poor waste management.

b. Air Terjun Kajai

Air Terjun Kajai has a height of 10 meters with a distance of 1 hour from Muara Sijunjung City. This geosite has a pretty exciting beauty and is equipped with parking facilities 200 meters from the geosite (Figure 4). However, this geosite has a reasonably low safety factor value for tourists because the access to the waterfall is a steep slope, and there is no safe access with granite rock lithology.

c. Ngalau Batu Tombuak

Ngalau Batu Tombuak is one of the geosites in the form of a cave within 1.5 hours from Muaro Sijunjung by vehicle, which has limestone lithology (Figure 4). However, this geosite is one of the sites with low maintenance in terms of the other sites. The access reaching this geosite has a high level of vulnerability and is a narrow road. Furthermore, the area is still covered by tall vegetation, which significantly reduces the cave's appearance when visited.

d. Air Terjun Batang Tayeh

Air Terjun Batang Tayeh is one of the sites with excellent management in terms of parking locations for the track to traverse. This site has seven water levels; there is an information board related to each waterfall on the geo-track route at each station (Figure 4). Furthermore, this site at the fifth level of the waterfall already has adequate public facilities such as a bathroom and a prayer room. In front of the sites, tourism management has been informed of the

impact of waste. In creating a healthy tourist area, the area obeys health protocol from the beginning of the entrance to each waterfall level.

e. Granit outcrop

The granite outcrop of this site is one of the most exciting geosites that can be used as a geoeducational (Figure 4) park. The granite rocks exposed in Silokek are the bedrock that becomes the basement of the Ombilin Basin, which is one of the tertiary-aged oil and gas basins in West Sumatra (Koesmawardani, 2020). Natural fractures that appear in granite rocks occur due to the activity of fault movement, which causes the surrounding rock to be under pressure. So, if the granite cannot accept the stress caused by the direction of the fault, it will form fractures prone to landslides. Natural fractures in the granite that appear with reasonably high intensity and density cause granite to have porosity and permeability. So, the existence of this site can also attract students and research on the Basement Reservoir.

f. Pasir Putih

The Pasir Putih geosite is one of the sites in the Silokek Ranah Minang Geopark, which is part of the floodplain of the Batang Kuantan river. This geosite contains a stretch of fine white sandstone, which has an instagramable photo spot. Besides being used as an exciting photo point, this site is also used for local traditional processions (Figure 4).

Conclusions

Based on comprehensive evaluation with SWOT analysis, a direct observation survey accompanied by a description of each geosite in Silokek Ranah Minang Geopark found seven geosites scattered between Sijunjung regency. The SWOT study shows that this geopark has excellent potential to become a UGG with improvements to the deficiencies that have been identified with current opportunities. On the other hand, the role of the local community and local government as actors and stakeholders in regional development is also needed, including those who guard Silokek Ranah Minang as a UNESCO Global Geopark.

References

Amarullah, Deddy, 2007, Pemaparan Hasil Kegiatan Lapangan dan Non Lapangan Pusat Sumber Daya Geologi, 2-3.

Baker, D. W., and N. L. Carter, 1972, American Geophysical Union Geophysical Monographs **16**, 157–166.

Castagna, J. P., 1993, The Leading Edge, **12**, 172–179.

Dinas Pariwisata, Pemuda dan Olahraga Kabupaten Sijunjung, 2017, Laporan Kinerja Instansi Pemerintah.

Ferrell, O., Hartline, M., Lucas, G., Luck, D., 1998, Dryden Press.

Ismail, F.A., Meideliza T., Hardian, D., 2018, Seminar Hasil Kajian Pengembangan Geopark di Kabupaten Sijunjung Sumatera Barat.

Kalantari, Mohsen, F. Bazdar, and S. Ghezelbash, 2011, International Conference on Biology, Environment and Chemistry IPCBEE, **24,** 181-188.

Koesoemodinata R.P. and Matasal Th., 1981, Proceeding IPA Tenth Annual Convention.

Koesmawardani, Wildan, M. Burhannudinnur, G. Maulana, 2020, TRKU Journal, **62**, 645-655.

Kosloff, D. D., and E. Baysal, 1982, Geophysics, **47**, 1402–1412.

Kusuma, Desi Widia., 2019, Jurnal Pembangunan Nagari 18-19.

Silitonga P.H & Kastowo, 1995, Geological Survey of Indonesia, Ministry of Mines.

UNESCO, 2016, UNESCO Global Geoparks, **1.**

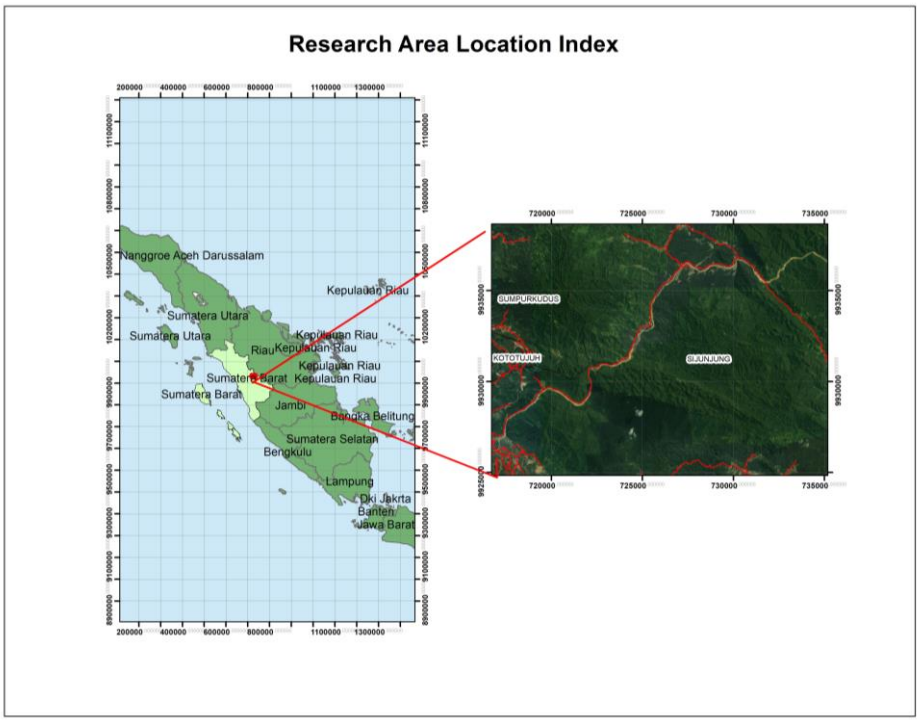

Figure 1: Research area location in Sijunjung Regency, West Sumatera.

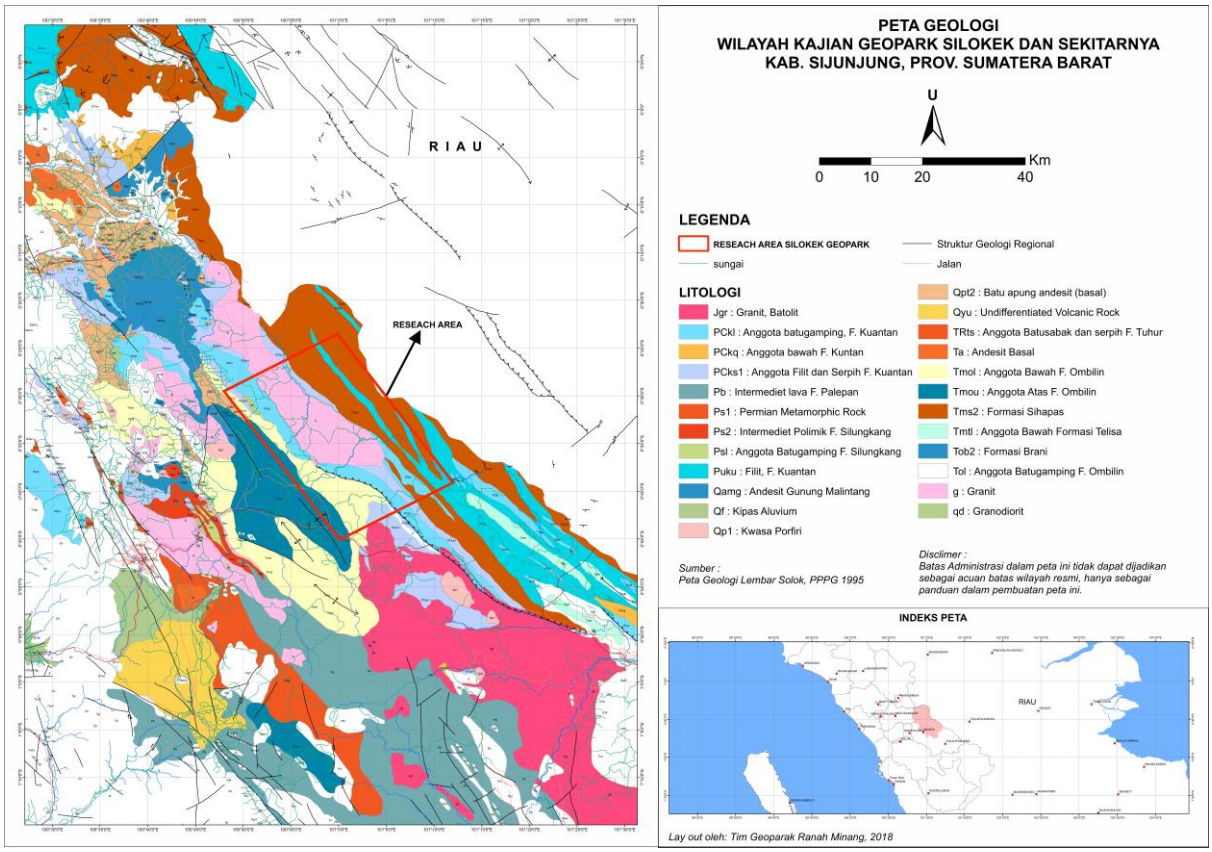

Figure 2: Regional Geology of Silokek Ranah Minang Geopark which was consisted of pre-tertiary – recent sedimentation process (Modified from Kastowo and Silitonga, 1995 in Silokek Geoparak Management, 2019).

PROCEEDINGS
JOINT CONVENTION BANDUNG (JCB)2021
November 23rd – 25th 2021

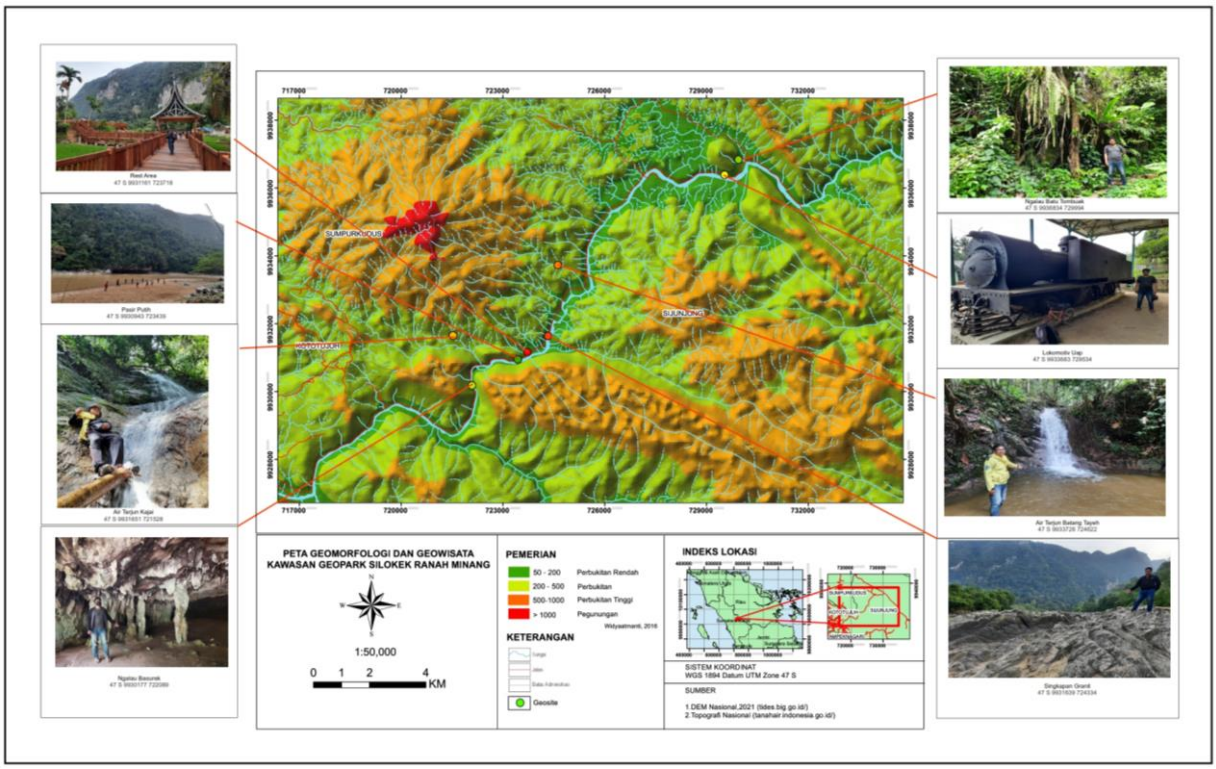

Figure 3: Distribution each geosites in Silokek Ranah Minang Geopark with seven and the dissemination location in a different geotrack.

Figure 4: Geosites point catalog with the description and geological appearance: a) Ngalau Basurek; b) Air Terjun Kajai; c) Ngalau Batu Tombuak; d) Air Terjun Batang Tayeh; e) Granit outcrop; and f) Pasir Putih, which is have a unique and typical of geological process.

PROCEEDINGS
JOINT CONVENTION BANDUNG (JCB) 2021
November 23rd – 25th 2021

Landslide Vulnerability with Remote Sensing Technology at Sekincau Area, West Lampung Regency.

Fani Mulyana Indah Sari.[1] Ghazi Muslim.[1] Ghina Husni Fahira[1] Muhammad Saiful Ruuhulhaq[2] Abdul Wahid Asykarulloh[1]
Padjadjaran University[1] Indonesia University of Education[2]

Abstract

Natural disasters are problems that need to be addressed by the Indonesian population. And an earthquake is a type of disaster that is difficult to know for sure that it will happen. Liwa City is a learning center for natural disasters, especially the monumental earthquake in 1994. The 1994 Liwa earthquake occurred on February 16 at 00:07 local time. It was located in southern Sumatra, Indonesia. The magnitude of the earthquake was put at Mw 6.9, Mw 7.0, or Ms 7.2, according to different sources. The earthquake caused 207 deaths and 2000 injuries. The earthquake took place at the Sumatran Fault Zone. The Sumatran Fault Zone is 1900 km long and highly segmented. It can be divided into about 20 segments.The earthquake occurred in a subparallel strand 2.5 km southwest of the principal trace of the Kumering segment.The focal mechanism is of right-lateral strike-slip faulting. The research here uses the Analytical Hierarchy Process (AHP) method to map Landslide Vulnerability with Remote Sensing Technology at Sekincau Area. This prediction is also reinforced by the presence of soil mechanical data and rainfall data. Liwa itself is the capital of West Lampung Regency. The area of this city covers the entire area of Sekincau. The earthquake that occurred in West Lampung Regency was a shallow earthquake (with a hypocenter 0-90 kilometers) with a magnitude of 5 and 6 on the Richter scale. In residential areas where it is already densely packed with buildings so that the level of water infiltration into the soil is reduced, if it rains with high rainfall, most of the water will become surface runoff which directly enters the water drainage system so that its capacity is exceeded and causes flooding. It will produce an earthquake risk zone for the population with a concrete calculation of the number of houses through satellite monitoring and aerial photography. This research is expected to facilitate and encourage various policy makers to strengthen disaster data and development plans related to the surrounding area.

Keywords: Sekincau Area, Landslide, Remote Sensing, Analytical Hierarchy Process (AHP) and Soil.

Introduction

Landslides are usually defined as ground motions, such as falls, avalanches, and flows. The danger of landslides resulted in many casualties and property. This damage can be avoided if the causal relationship of the event is known. Landslides are a complex natural disaster, involving many factors and need to be studied systematically in order to be evaluated effectively. The landslide susceptibility map depicts areas that are likely to experience landslides in the future by relating some of the main factors that contribute to landslides with the distribution of slope failure that occurred in the past. (Brabb, 1985).

Mapping of landslide susceptibility relies on in-depth knowledge of slope movement and its controlling factors. The validity of a landslide hazard map largely depends on the amount and quality of available data, the scale of work and the selection of appropriate analysis and modeling methodologies. The process of making this map involves several qualitative or quantitative approaches. Efforts to define vulnerability classes by overlaying several spatial data of parameters determining landslide hazard for landslide susceptibility zoning (Kumajas, 2006).

Currently, there are various technologies that can be applied for slope stability analysis, namely geotechnical engineering, photogrammetry, and remote sensing. In case of slope collapse, all the above mentioned technologies can be applied; however it depends on the scale of the project and the reliability of the achievable results. It has recently been discovered that remotely sensed data has become a special tool in the problems mentioned above. There are many published studies and documented reports that utilize remotely sensed data to investigate, predict and monitor slope stability (Ouattara et al., 2004).

1. West Lampung, especially the Sekincau area is an illustration of a dense population which indicates the risk of disasters. Land movement often occurs throughout the year with evidence of landslide-prone points so that it can have a major impact on access between regions.
2. What are the geological conditions and parameter distribution of landslide events in the study area?
3. How to verify landslide susceptibility map with stability calculation in the research area?
4. As a reference for the relevant local government in anticipating and mitigating the occurrence of landslides that have an impact on related areas.
5. Contribute ideas to the community and related local governments as well as for further research.

PROCEEDINGS
JOINT CONVENTION BANDUNG (JCB) 2021
November 23rd – 25th 2021

Data and Method

The landslide vulnerability mapping methodology is based on the assumption that future landslides will occur under the same conditions and circumstances as previous landslides. For this reason, the Analytical Hierarchy Process (AHP) method is used to model the landslide susceptibility map in the research area. The Analytical Hierarchy Process (AHP) is a semi-qualitative method, which involves a matrix-based pairwise comparison of the contributions of different factors (saaty, 1980).

Result and Discussion

The geology of the research area consists of the Ranau Formation (Qtr) and the Sekincau Volcano Formation (Qhv). The Ranau Formation consists of pumice breccia, tuff micaan, pumice tuff, terkersic wood, and Plio-Plistocene uncoated sand deposits, deposited in a terrestrial environment. The Sekincau Volcano Formation (Qhv) is dominated by breccia, lava, and tuff composed of andesite to Holocene basalt, deposited in a terrestrial environment.

The resulting zoning is divided into three, namely low, medium, and high. In this study a process hierarchy analytical model (AHP) was applied to develop a landslide susceptibility map for Sekincau District, West Lampung. In this study, an inventory of the factors causing landslides was carried out using the AHP method, which allows rapid and practical landslide analysis based on data collection and analysis of data that are important for landslide susceptibility. The landslide susceptibility zoning used by the AHP method is used with a weighting of nine parameters. The landslide susceptibility zoning is derived from nine factors that cause landslides to be considered, namely elevation, slope aspect, slope angle, distance from drainage, drainage density, soil type, distance from straightness, NDVI and distance from highway. In terms of elevation, the higher the slope, the higher the probability of landslides. In terms of the distance from drainage, lineaments, and roads, the closer they are, the higher the probability of landslides. In the case of NDVI areas with denser vegetation cover have a higher probability. In terms of slope, steeper slopes have a higher probability of landslides. In terms of the slope aspect, it is known that the research area in the south and southwest has a higher probability. While the lower probability is in the northern region.

Landslide hazard using the AHP method is verified by field data by calculating the safety factor. From the calculation of the safety factor, it is found that slopes in areas with a high level of vulnerability have a safety value of more than three, which means that the slopes in the area are quite stable. Furthermore, the second slope which is in an area with a moderate level of vulnerability has a safety value in the range of one, which means that the slope in the area is not stable enough.

FAKTOR	TANAH	SLOPE	ASPEK	ELEVASI	NDVI	JARAK DARI KELURUSAN	JARAK DARI DRAINASE	JARAK DARI JALAN	DD
TANAH	1	1	8	8	3	5	7	5	6
SLOPE	1	1	8	7	5	3	3	5	6
ASPEK	1/8	1/8	1	1	1/3	5	3	5	1
ELEVASI	1/8	1/7	1	1	1/3	5	3	5	1
NDVI	1/3	1/5	3	3	1	1	3	5	2
KELURUSAN	1/5	1/3	1/5	1/5	1	1	3	5	3
DRAINASE	1/7	1/3	1/3	1/3	1/3	1/3	1	3	1
JALAN	1/5	1/5	1/5	1/5	1/3	1/5	1/3	1	1/2
SUM	3 1/8	3 1/3	21 3/4	20 3/4	11 1/3	20 1/2	23 1/3	34	20 1/2

Weights and ratings are assigned to each attribute layer and its respective class. The summation of these layers is performed and the cumulative scores are regrouped into three classes. The way for this classification is to use an algorithm to separate the landslide susceptibility index into landslide susceptibility classes, namely high, medium, and low.

For landslide susceptibility analysis, using factor weights and ratings from AHP, the landslide susceptibility index (LSI) value is calculated by adding up the ranking of each factor multiplied by the weight of each factor using the following equation:

$$LSI = \sum_{i=1}^{n} (W_i \times R_i)$$

LSI = Landslide susceptibility index

Ri = Class of each category

Wi = Weight of each category

In the slope aspect, the most landslides occur on slopes facing south and southwest. Thus, the slopes facing the Landslide Hazard Map Figure in the south and southwest of the Study Area are highly susceptible to landslides, while the frequency of landslides is lowest on the slopes facing north.

In terms of slope angle, steeper slopes have a greater chance of landslides. Slopes with a slope at a slope of 14°, the ratio is lower. For slopes above 14°, the ratio is higher for landslides. This result means that the probability of landslide increases with the slope angle.

In terms of distance from the drainage and drainage density, a larger distance indicates a high probability of landslides, and for a distance above 1,000 m, indicates a low probability. This result means that the probability of landslide decreases with distance from the drainage.

In the case of soil types, the frequency ratio is highest in andosols and lowest in granitic areas. In terms of distance from straightness, for distances below 5000 m, indicates a high probability of landslide occurrence, and for distances above 500 m indicates a low probability. This result means that the probability of landslide decreases with distance from the straight line.

In terms of distance from the highway, for distances below 500 m, it indicates a high probability of landslide occurrence, and for distances above 500 m indicates a low probability. This result means that the probability of landslide decreases with distance from the highway. In the case of NDVI, slopes covered with vegetation have a lower probability of landslides. In the case of higher elevation areas have a higher probability.

Conclusions

Mapping of landslide susceptibility relies on in-depth knowledge of slope movement and its controlling factors. The validity of a landslide hazard map largely depends on the amount and quality of available data, the scale of work and the selection of appropriate analysis and modeling methodologies. The process of making this map involves several qualitative or quantitative approaches. Efforts to define vulnerability classes by overlaying some spatial data on parameters that determine landslide susceptibility for landslide susceptibility zoning.

Landslides cause great damage and often take many lives. Geologists regard this kind of event as a natural process. However, efforts should still be made to study the origins of this process. On the other hand, the engineers, focused on investigating the causes in terms of soil mechanics principles and developing methods for reliable assessment of slope stability and this method is called slope stability analysis.

References

Brabb, E. E. (1985). Innovative approaches to landslide hazard and risk mapping. http://pubs.er.usgs.gov/publication/70197529

Kumajas, M. (2006). Inventarisasi dan Pemetaan Rawan Longsor Kota Manado–Sulawesi Utara.

Ouattara, T., Couture, R., Bobrowsky, P. T., & Moore, A. (2004). Remote Sensing: Theory and Principles. Geological Survey of Canada, 102.

Saaty, T. L. (1980). The Analytical Hierarchy Process. McGraw Hill, New York.

Acknowledgements (Optional)

The author expresses his deep respect and gratitude to the lecturer who guides in the process of working on the final project, namely Dr. Ir. Dicky Muslim, M.Sc. and Dr. Ir. Emi Sukiyah M.T. and Mr. Prahara Iqbal M. T. as a technical advisor who was very helpful from before to the completion of this research.

PROCEEDINGS
JOINT CONVENTION BANDUNG (JCB) 2021
November 23rd – 25th 2021

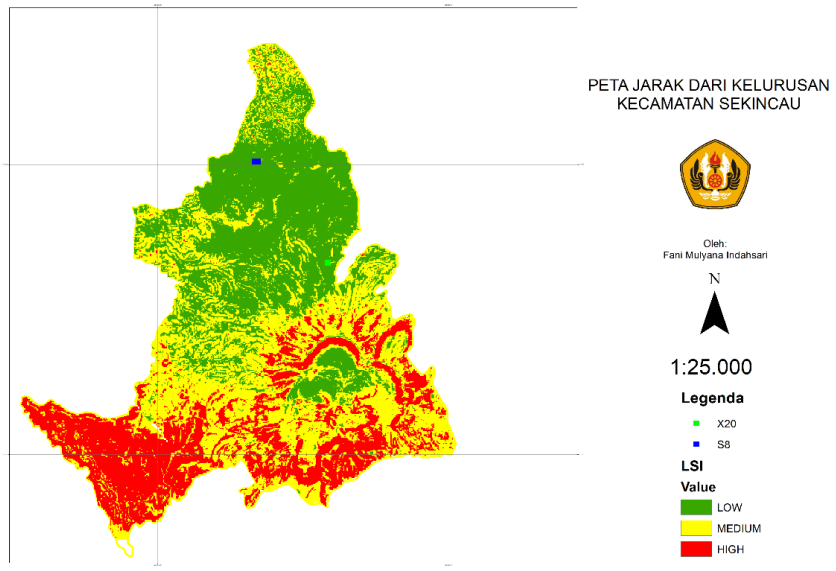

Figure 1: Landslide Hazard Map in Study Area

From the calculation results, it is known that LSI has a minimum value of 0.125 and a maximum value of 2.375. LSI represents the relative vulnerability of landslide events. Therefore, the higher the index, the more vulnerable the area is to landslides. If the LSI value is high, the landslide susceptibility is higher, the lower the landslide susceptibility value is lower. This LSI value is divided into three classes based on the natural fault range representing three different zones in the landslide susceptibility map, namely areas with high vulnerability (HS), medium vulnerability (MS), and low vulnerability (LS).

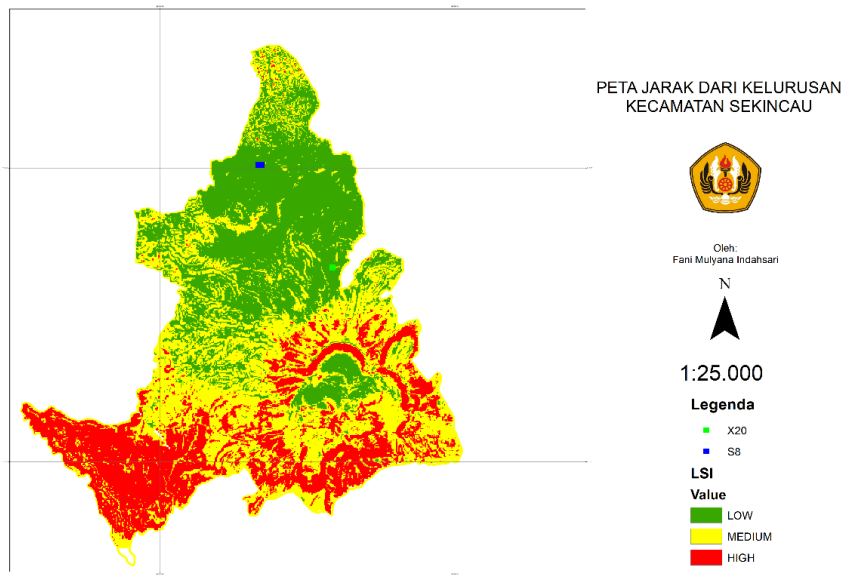

Figure 2: Soil Sampling Location

Landslide susceptibility analysis using GIS and remote sensing methods is then correlated with slope stability calculations from available field data. Slope stability calculations were carried out at two points located in the east and northwest of the study area. The first slope is the X20 slope which is located to the east. Based on the landslide susceptibility zoning, this area is classified as low vulnerability. This is then correlated with the results of the calculation of slope stability which shows values above three which are classified into stable slopes. The second slope is the S8 slope which is located in the west. Based on the landslide susceptibility zoning, this area is categorized as moderate vulnerability. This is then correlated with the results of the slope stability calculation which shows a value in the range of one which is classified into less stable slopes.

PROCEEDINGS
JOINT CONVENTION BANDUNG (JCB) 2021
November 23rd – 25th 2021

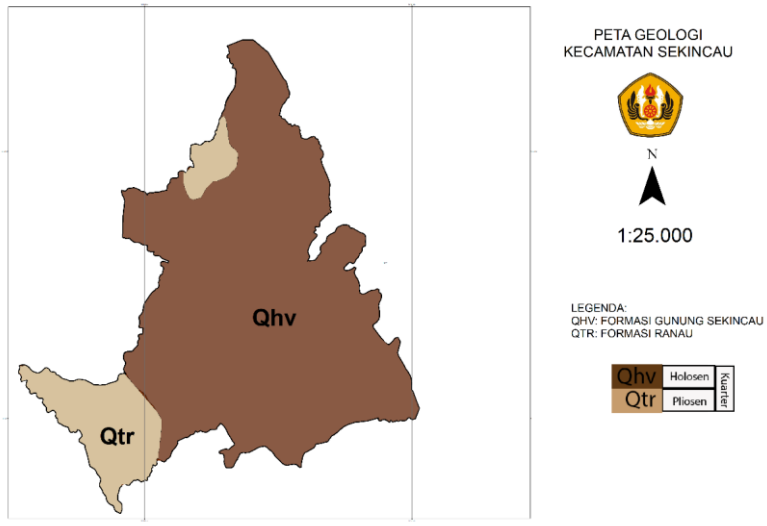

Figure 3: Geological Map of Research Area

Ranau Formation (Qtr): The Ranau Formation includes pumice breccia, micaan tuff, pumice tuff, terkersikan wood, and uncoated sand deposits. The Ranau Formation is Plio-Plistocene in age, deposited in a terrestrial environment, and is located inconsistently above the Hulusimpang Formation.

Sekincau Volcano Formation (Qhv): Dominated by Breccia, lava, and tuff of andesite to basalt composition are the rocks that make up the Sekincau Volcano Formation. This formation is Holocene in age, deposited in a terrestrial environment, and is located unconformably above the Ranau Formation. This formation is composed of weathered soil with large grains of sand-clay, and is brownish red in color.

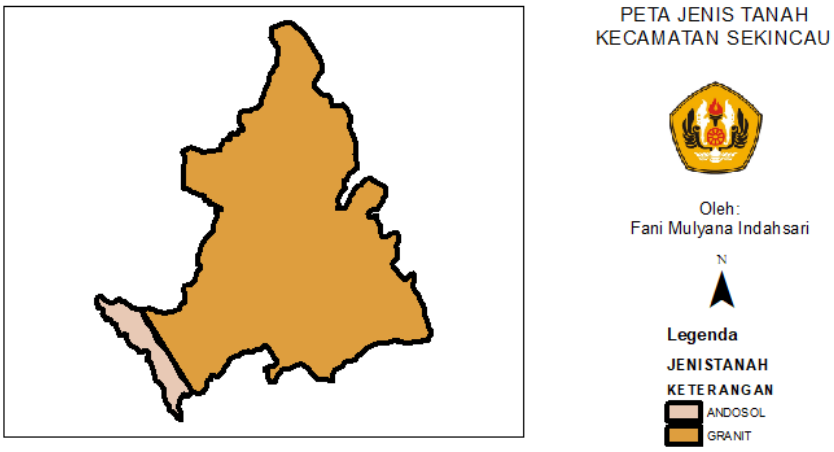

Figure 4: Map of Soil Types in the Study Area

Soil is considered as one of the most relevant parameters in landslide hazard (Marfai, 2021). Different soil types respond differently to erosion agents and carry out mass movements under different natural conditions, and they have varying compositions and structures, which contribute to the strength of the material. The Study Area is divided into two areas shown in the map below.

PROCEEDINGS
JOINT CONVENTION BANDUNG (JCB) 2021
November 23rd – 25th 2021

Identification of Geothermal Manifestation Area at Mount Slamet, Central Java Region by Using Digital Imagery Processing

Anis Sofiyah[1], Sielmy Firdhausyi Al Aziva[1], Ulrike Johanna Hutabarat[1]
[1]Geological Engineering, Pertamina University
Corresponding author: anissofiyah13@gmail.com

Abstract

Indonesia's geographical location in the ring of fire produces a chain of volcanoes that can potentially result in a source of renewable energy, namely geothermal energy. In this study, an early stage of geothermal manifestation identification on a regional scale using digital imagery aims to narrow the exploration target area. The methodologies used in this study are calculation of LST (Land Surface Temperature) to analyze the presence of land surface temperature anomalies, NDVI (Normalized Difference Vegetation Index) that aims to determine vegetation density, and analysis of structural lineament patterns. The results showed that there are several locations identified as possible geothermal manifestations from high-temperature anomalies ranging from 12º-24ºC around the foot of Mount Slamet. The vegetation index value at the same locations range from 0.35 - 1 which are categorized as a low vegetation density level. The lineament trend of the NE-SW direction is identified as a geological structure that accommodates the discharge of geothermal fluids around the foot of Mount Slamet, Central Java.

Keywords: geothermal, renewable energy, digital imagery, LST, NDVI, structural lineament

Introduction

Indonesia is located in the ring of fire, which produces a chain of volcanoes that has potentially become a source of geothermal energy. Geothermal energy is defined as the process of transferring heat source from a place in the earth's crust to the surface as a manifestation of geothermal energy (Hochstein, 2000). The potential of geothermal energy in Indonesia saves 40% of the world's geothermal reserves. The number of geothermal reserves in Indonesia is one of the largest in the world, with potential up to 29,038 MW (KESDM, 2012). This potential can be seen from geothermal manifestations found around volcanic areas, for example, hot springs, water vapor, and altered rocks. One of the volcanoes that has geothermal potential and has been designated as a geothermal working area (WKP) in 2010 is Mount Slamet. The WKP is located in Baturraden District with an estimated reserve of 175 MWe (Direktorat Jenderal EBTKE, 2017)

The research area is located in Mount Slamet with 30 x 30 kilometers square area. Mount Slamet is located among five regencies in Central Java, namely Banyumas, Purbalingga, Pemalang, Tegal and Brebes. The location of Mount Slamet in the tectonic context and structure of central Java can be seen in Figure 2. Mount Slamet is part of a quaternary volcanic arc formed by subduction activities between the Indo-Australian Plate and the Eurasian Plate. The Mount Slamet area has several known geothermal manifestations, for example, hot springs of Pancuran Pitu, Pancuran Telu, Cahaya, Pakujati, and Guci as can be seen in Figure 3.

Identification of manifestations in a geothermal exploration area can be done by remote sensing analysis that utilizes recognition of imagery properties without direct interaction with the objects (Liliesand & Kiefer, 1994; Bates & Jackson, 1987 in Soetoto, 2019: 1). The possibility of detecting geothermal manifestations through remote sensing can be done because of the characteristics of heat emission from geothermal manifestations as mentioned in previous studies (e.g. Cahyono, 2019). Remote sensing analysis can be a preliminary approach prior to conducting a field survey by considering the ratio of costs per unit area that need to be spent. However, field validation is still needed to ensure the accuracy of the remote sensing analysis that has been carried out.

In this study, the identification of geothermal manifestations was carried out by using Landsat 8 OLI/TIRS digital imagery analysis and DEM (Digital Elevation Model). Landsat 8 can be used for the identification of geothermal manifestations because it has Onboard Land Imager (OLI) and Thermal Infrared Sensor (TIRS) sensor. The OLI sensor consists of bands 1-9, while the TIRS sensor consists of band 10 and 11 (USGS, 2019). In this study, band 10 is used to determine the anomaly of the land surface temperature. Meanwhile, band 4 and band 5 are used to determine the level of vegetation density. The DEM data is used to delineate the lineament of the geological structure in the research area which is the discharge of geothermal manifestation fluids.

Data and Method

Data

Landsat 8 Imagery

The Landsat 8 imagery was downloaded from the USGS website (https://www.explorer.usgs.gov) which was acquired on September 25th, 2015, with paths 121 and raw 065. This imagery has a cloud cover of 4.51. The cloud

cover value in this imagery is smaller than other imagery taken from 2015-2021, so the imagery processing results will be better. The Landsat 8 images used are bands 4, 5, 10. Band 4 and band 5 are used for NDVI (Normalized Difference Vegetation Index) analysis, while band on TIRS is used for LST (Land Surface Temperature) analysis.

TIRS (Thermal Infrared Sensor) which consists of band 10 and band 11. The two bands have different characteristic wavelengths that can be captured. Band 10 is able to capture wavelengths 10.60-11.19 µm, while band 11 is able to capture wavelength 11.50-12.51 µm (USGS, 2019). The lower wavelength causes the land surface temperature captured by the Landsat 8 imagery sensor to be more detailed than the higher wavelength. The bandwidth on band 10 is narrower than band 11. This shows the effective wavelength on band 10 will be smaller than band 11. As a result, the land surface temperature captured by TIRS band 10 will produce a more detailed data output than band 11 data output. Therefore, this study uses band 10.

DEM (Digital Elevation Model)

DEM data is used to analyze the morphological lineament which may be caused by geological structures in the study area. The DEM data used are DEMNAS_1308-63, DEMNAS_1308-64, DEMNAS_1308-61 and DEMNAS_1308-62. The data was downloaded from the Geospatial Information Agency website (https://tanahair.indonesia.go.id/demnas/).

Method

Pre-Processing

From the Landsat 8 imagery data that has been obtained, cropping of the images was conducted to reduce area of the processed images. Correction of surface reflectance and TOA radiance is done after the Landsat 8 imagery data was cropped. Surface reflectance correction was carried out on Landsat 8 band 4 and 5 to eliminate atmospheric effects by changing the DN (digital number) value to physical value. Meanwhile, TOA radiance correction was done on Landsat 8 band 10 and band 11 to obtain atmospheric temperature values. Pre-processing of band 4, band 5, and band 10, were done in QGIS software using Semi-Automatic Classification Plugins (Landsat Conversion to surface reflectance and brightness temperature).

Pre-processing of DEMNAS_1308-63, DEMNAS_1308-64, DEMNAS_1308-61, and DEMNAS_1308-62 data was carried out by merging and cropping DEM data according to the research area. After that, the hillshade was made to display the relief of the research area.

Processing

LST (Land Surface Temperature)

According to Sutanto (1984) in Mardiana (2017), the land surface temperature is the external temperature possessed by a particular object. Each object on the earth's surface has electromagnetic wave radiation characteristics depending on the temperature. Land surface temperatures are usually related to the geothermal source below the surface. Therefore, land surface temperature data can be used as an initial analysis to determine geothermal manifestations in the study area. Calculation of land surface temperature is done with the Semi-Automatic Classification Plugins (Landsat Conversion to surface reflectance and brightness temperature) made by Congedo (2013) in QGIS software. The mathematical formulas used in the Semi-Automatic Classification Plugins are as follows:

- Changes the satellite temperature to atmospheric brightness temperature (in celsius) with the following mathematical equation.

  $TB = \frac{K_2}{ln\left(\frac{K_1}{L\lambda}+1\right)}$……..…Equation 1 (USGS, 2019)

  Where:

  TB = TOA (Top of Atmosphere) Brightness Temperature in Celsius

  $L\lambda$ = Spectral Radiance ($\frac{Watt}{m^2 * sr * \mu m}$)

  K1 = Thermal constant in band 10

  K2 = Thermal constant in band 11

- Changes the atmospheric brightness temperature to subsurface temperature.

  $T = \frac{TB}{[1+\left(\lambda * \frac{TB}{\alpha}\right) * ln ln\ (\varepsilon)]}$…..Equation 2 (Weng,2004)

  Where:

  T = Subsurface temperature

  TB = TOA (Top of Atmosphere) Brightness Temperature in Celsius

  λ = Wavelength of emitted radiance

  $\alpha = \frac{h*c}{k}$ =1.4388 x 10^{-2} mK=14388 µm K

  h = Planck's constant

  k = Boltzmann constant

  c = Velocity of light

NDVI (Normal Difference Vegetation Index)

NDVI is an index used to express the density of vegetation in an area. NDVI analysis is necessary because the vegetation is very influential on the temperature on the surface. Areas with high vegetation density values usually have lower surface temperatures than areas with weak vegetation density values. The NDVI value was calculated by using the following mathematical equation:

$NDVI = \frac{\rho_{NIR} - \rho_{red}}{\rho_{NIR} + \rho_{red}}$…….Equation 3 (JARS, 1993)

Where:

ρNIR = reflectance value of near infrared band

ρred = reflectance value of red band

Fault-Fracture Density

DEM data that has been merged and cropped then made a hillshade using the QGIS to show the relief of the earth's surface. Then the hillshade was

PROCEEDINGS
JOINT CONVENTION BANDUNG (JCB) 2021
November 23rd – 25th 2021

processed using the PCI Geomatica application through lineament extraction to obtain the lineament. Lineament extraction was used to create a Fault-Fracture Density (FFD) map using ArcGIS software which shows the lineament density in the area. These lineaments may indicate the existence of geological structures that can play a role as a permeable zone for geothermal fluid circulation, in this case as discharge area.

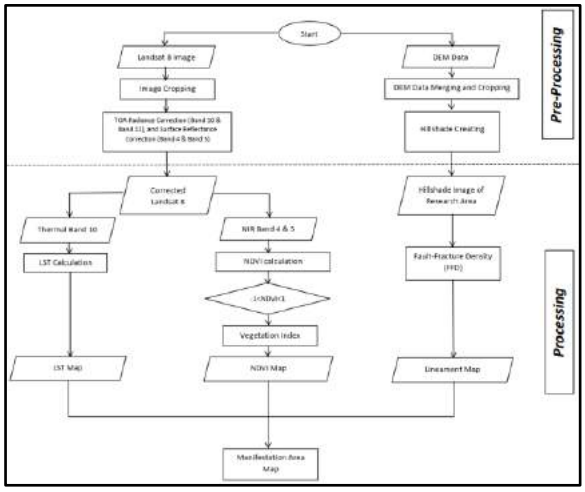

Figure 1: Flowchart Research Method

Result and Discussion

Result

NDVI

In this research, the results of NDVI calculation were classified using the Departemen Kehutanan (2009) reference as follows.

Table 1 Classification of NDVI value ranges on maps (Departemen Kehutanan, 2003)

Value	Category
-1-(-0.03)	Non-vegetated land
-0.03-0.15	Very low density vegetation
0.15-0.25	Low density vegetation
0.25-0.35	Medium density vegetation
0.35-1	High density vegetation

Using the reference from Departemen Kehutanan (2003) as shown in Table 1, the results of the distribution of NDVI zones are shown in Figure 3. The results of NDVI processing in QGIS software are shown in Figure 3, revealing that the Mount Slamet area is dominated by a high level of vegetation density (0.35-1). However, some areas such as the lake and the Mount Slamet crater classified as non-vegetated land with an NDVI value of -1-(-0.03) then in the urban areas, rice fields, and open land are classified as very low vegetation density (-0.03 -0.15) low (0.15-0.25) and medium (0.25-0.35). NDVI values classified as very low to moderate and located on the mountain's slope can indicate geothermal manifestations. However, in the Mount Slamet area, the NDVI value with that classification is in the urban areas, rice fields, and open land, while the slopes of Mount Slamet have a high vegetation density value. Based on these conditions, it can be interpreted that the possibility of geothermal manifestations in the Mount Slamet area there on mountain slopes with dense vegetation. This interpretation is supported by the geothermal manifestation of Pancuran Pitu and Pancuran Telu in the high vegetation area shown in Figure 3. Therefore, other processing is needed to interpret the geothermal manifestation area in the Mount Slamet region.

LST (Land Surface Temperature)

The value of land surface temperature is classified based on statistics which is divided into 4 classes, as follows:

Table 2 Land Surface Temperature Classification

LST Value (°C)	Temperature Level
12-16	Very low temperature
16-24	Low temperature
24-32	High temperature
32-39	Very High temperature

Based on this classification, the LST map of band 10 is obtained as seen on figure 4. LST map of band 10 (Figure 4) shows that the study area has a surface temperature range from 12°-38°C, which is divided into 4 classes (Table 2). LST range values 12-16°C is on mountain slopes, LST range values 16°-24°C is on the lower mountain slopes and the foothill, LST range values 24° - 32°C is on the lowland, LST range values 32°-39 °C is on mountain slope and the crater of Mount Slamet.

In general, locations with high-temperature to very high temperatures can be interpreted as locations for geothermal manifestations. However, after being validated with true-color composite Landsat 8, locations with high to very high LST values are located in urban areas, rice fields, open land, and the crater of Mount Slamet, so the locations do not include the criteria for heat manifestation areas.

Lineament

The lineament map (Figure 5) shows the dominant lineament pattern in the study area with a NE-SW direction. Lineament analysis with fault-fracture density (FFD) resulted in 4 lineament density classes (Table 3). These lineaments indicate the existence of geological structures, one of which can be in the form of fractures. The fracture lineament in the research area works as a way of exiting fluids from below the surface to the earth's surface as a geothermal manifestation. More fractures in a unit area may lead to higher possibility of geothermal manifestation presence. Therefore, areas with high lineament density values can be considered as possible areas for geothermal manifestation.

PROCEEDINGS
JOINT CONVENTION BANDUNG (JCB) 2021
November 23rd – 25th 2021

Table 3 Fracture Fault Density Classification

Lineament Density (km/km^2)	Density Level
≤ *0*	Very low density
0-2	Low density
2-4	High density
>4	Very high density

Discussion

Area with a high vegetation index indicates that a lot of vegetation covers it, so the land surface temperature captured by the TIRS will be covered by vegetation and result in a low LST value. While the area with low vegetation indicates that the area are on open land, urban area, rice fields, and the crater of Mount Slamet, so the surface temperature captured by TIRS causes a high LST value. In general, the initial appearance of geothermal manifestations is done by observing high LST and NDVI value anomalies in the mountain slope area. However, conditions are not always ideal. Geothermal manifestations are found in locations with low LST values due to vegetation, so the surface temperature of the area will be low, such as in Pancuran Pitu and Pancuran Telu, which can be seen in Figure 6. According to the problems, other data is needed, such as geological structure lineaments used to find the existence of lineaments that act as the discharge for geothermal manifestations.

Based on that, it can be interpreted that other areas where geothermal manifestations may be found in the locations covered by vegetation and have low surface temperatures (Figure 6). The interpretation must be completed with the condition that it is on the same lineament as the known manifestation discharge or has a high lineament density.

In this study, validation is not carried out because the COVID-19 pandemic constrained it. However, it is highly recommended to carry out the validation in future studies so that the interpretation of the manifestation area becomes more precise.

Conclusions

Based on the map of the recommendation area, the recommended areas for further examination are areas located to the south and north of the crater of Mount Slamet with characteristic high vegetation density (0.35-1), land surface temperature between 12-21° celsius and high to very high lineament density (4.95-6.61 km/km^2). However, it is still necessary to check the field directly to ensure the identification of the satellite imagery.

References

Bachri, S.,2014, J.G.S.M. Vol. 15 No. 4 November 2014 hal. 215 - 221

Cahyono, B. E., Jannah, N., and Suprianto, A, 2019, NATURAL B, Vol. 5, No. 1, April 2019

Congedo, Luca, 2021, Journal of Open Source Software, 6(64), 3172, https://doi.org/10.21105/joss.03172

Departemen Kehutanan, 2009, Peraturan Menteri Kehutanan Republik Indonesia nomor: P.32/MENHUT-II/2009, Jakarta.

Direktorat Jenderal EBTKE, 2017, Jilid I

Hochstein, M. P., & Browne, P. R., 2000, Encyclopedia of volcanoes, 835-855.

JARS, 1993, Japan Association on Remote Sensing, available at http://www.jars1974.net/pdf/rsnote_e.html.

KESDM, 2012, ESDMMAG, Edisi 07, Hlm. 36.

Mardiana, R., 2017, Undergraduated thesis, Institut Teknologi Sepuluh Nopember.

Soetoto, 2019, Yogyakarta, Penerbit Ombak.

USGS, 2019, LSDS-1574 Version 5.0

Weng, Q., Lu, D., & Schubring, J, 2004, Remote Sensing of Environment, 89(4), 467–483. doi:10.1016/j.rse.2003.11.005

Acknowledgements

The highest appreciation to our supervisor, Mr. Rio Priandri Nugroho, M. MinRes, for the guidance for authors to complete this research. Many thanks to co-authors who have collaborated until the end of the research process. Thank you for our friend, Angelica Maratu, as the proofreader of our paper. Last but not least, thank you to USGS for the free access data.

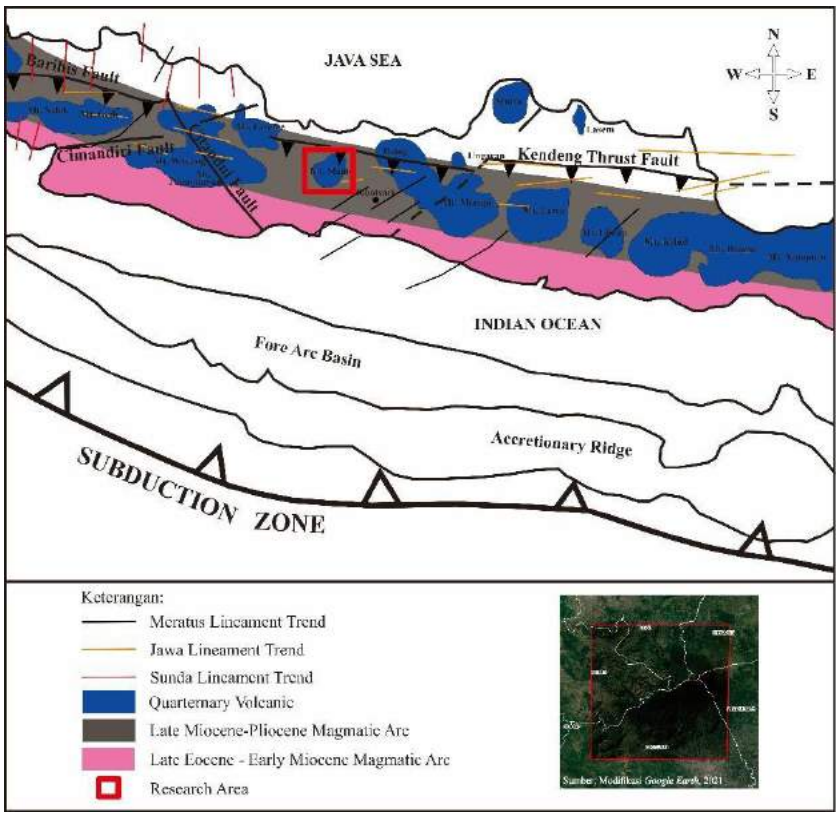

Figure 2: Research Areas on the Structure and Tectonics of Java Island (Modifications from Pulonggono and Martodjojo, 1994; Soeria-atmadja drr., 1994; Simandjuntak and Barber, 1996 in Bachri, 2014)

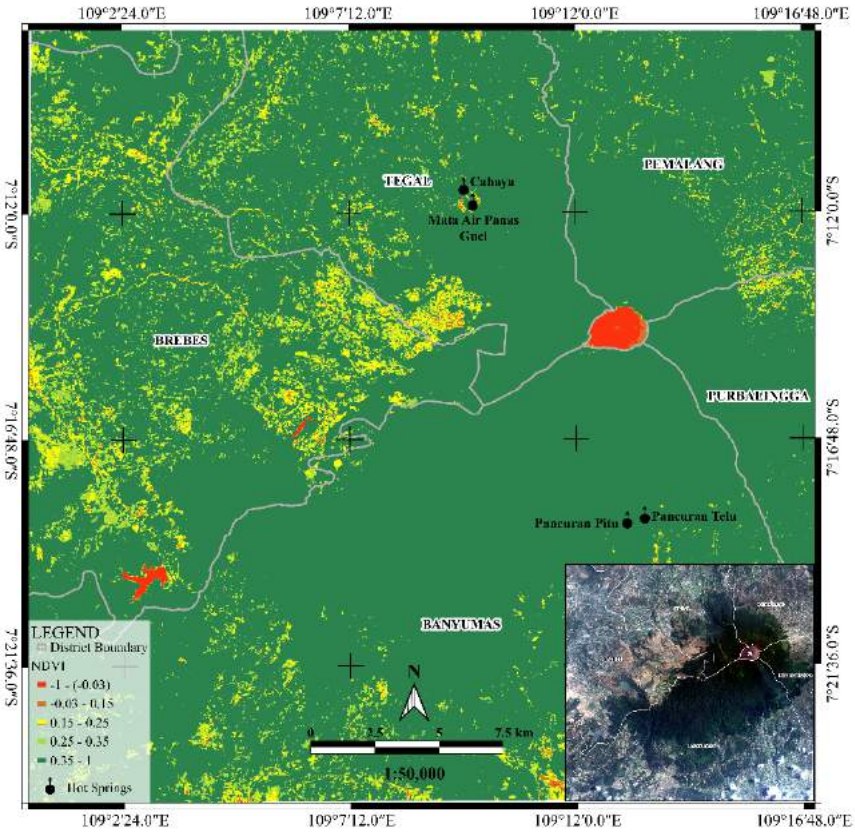

Figure 3: NDVI Map

PROCEEDINGS
JOINT CONVENTION BANDUNG (JCB) 2021
November 23rd – 25th 2021

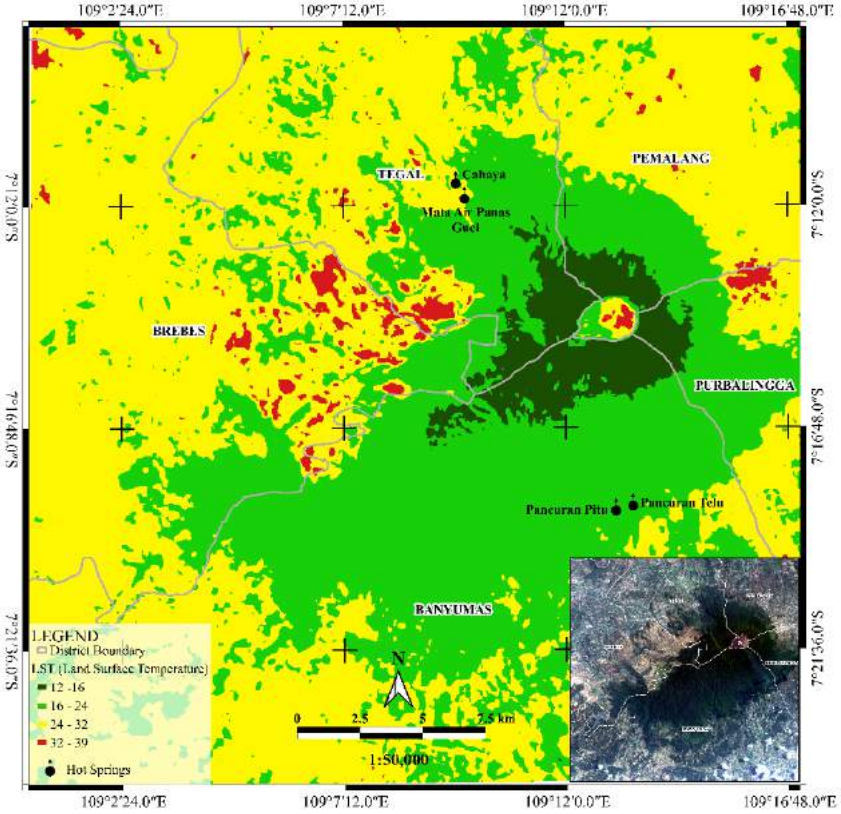

Figure 4: LST Map of Band 10

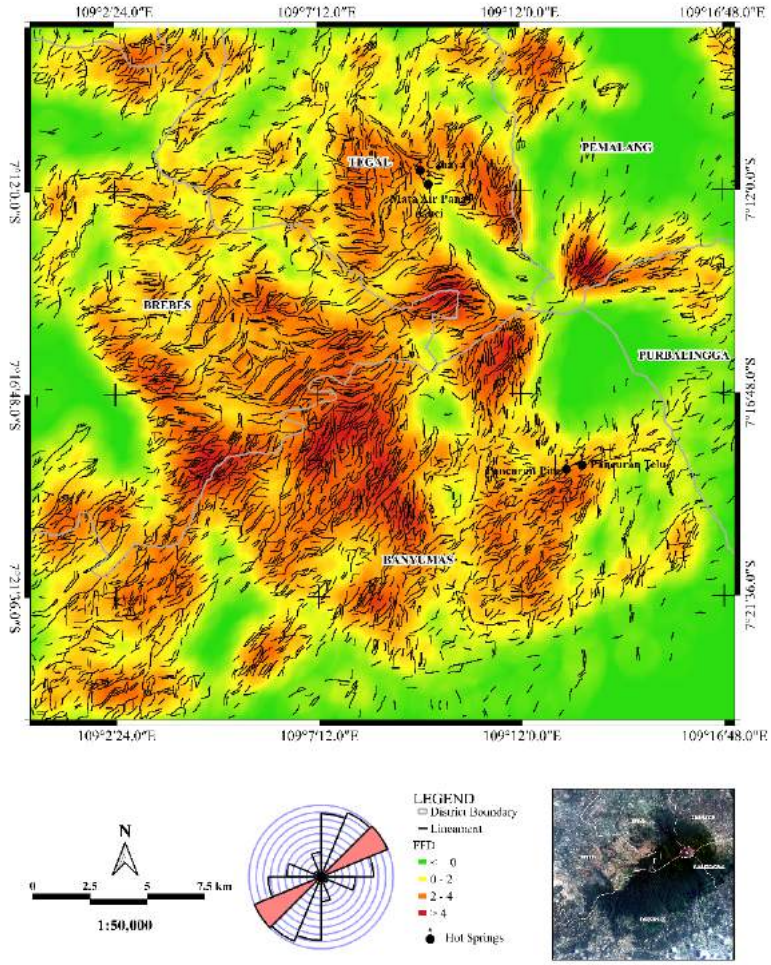

Figure 5: Lineament Map

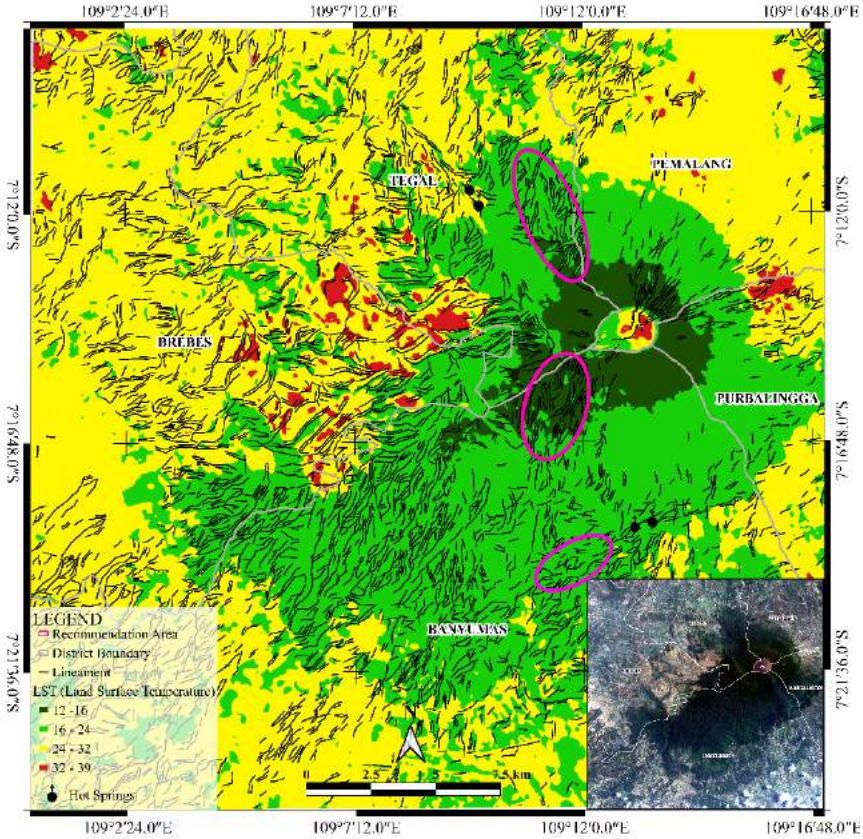

Figure 6: Recommendation Area Map

PROCEEDINGS
JOINT CONVENTION BANDUNG (JCB) 2021
November 23rd – 25th 2021

DIGITAL ELEVATION MODEL DERIVED LANDFORM CLASSIFICATION: STUDY CASE OF CIMANGGUNG DISTRICT, SUMEDANG REGENCY, WEST JAVA PROVINCE

[1]Hilfi Taufiqul Rahman, [1]Gian Haposan, [1]Muhammad Chairil Talib [1]M Reza Ramanda Putra [1]Dinah Rahmaniah

[1]Geological Engineering Department, Faculty of Geological Engineering, Padjadjaran University

Jalan Raya Bandung-Sumedang Km.21, Jatinangor 45363, West Java, Indonesia

ABSTRACT

Application of Geographic Information System (GIS) through Digital Elevation Models (DEMs) for slope and landform analysis was done in Cimanggung, Sumedang, West Java. Data analysis was done through GIS software. This analysis divides the Cimanggung Area into several landform classes based on slope steepness: Flat (0 - 8%), Sloping (8 - 15%), Moderately steep (15 - 25%), Steep (25 - 45%), and Very Steep (> 45%). This classification was based on settlement suitability standards on National Spatial Regulation No. 26/2007. Based on the regulation, land that is suited for public settlement has slope steepness of 0 – 25%. The result shows that about 46,78% of Cimanggung area consisted of Steep to Very Steep Landform and isn't suitable for settlement area according to the National Standard.

INTRODUCTION

Geomorphology can be defined as a science that describes land forms, the processes that act on them and investigates the relationship between landforms and these processes in their spatial order (Zuidam, 1979).

Morphometry is quantitative aspects of an area such as slope steepness, slope shape, elevation, height difference, terrain roughness, valley shape, erosion rate and flow pattern. The shape of the area or slope is an attribute in the formation of a soil map unit.

DEMs or Digital Elevation Models are continuous digital images according to space of the state of the earth's surface relief (Rossiter, 1994). Software tends to be used to analyze DEMs because it is easier and the results are more detailed than using conventional or manual methods.

Utilization of DEMs derived from Landsat imagery in assessing slope shape, slope

length and aspect as input data from slope conditions in the Cimanggung District.

Cimanggung District is located in Sumedang Regency, West Java Province. This location is located at geographical coordinates, namely 6° 57' 20.1096" South Latitude and 107° 49' 3.81" East Longitude. Cimanggung District based on the Geological Map of Sheet Bandung, Java (P.H. Silitonga., P3G, 1973), the disaster area is composed of Young Undegradable Volcanic Products (Qyu) in the form of tuffaceous sand, lapilli, breccia, lava and agglomerates.

The purpose of this study was to classify the regional shape unit class from DEMs by using slope morphometry classification and to assess the quality of the regional shape unit map derived from DEMs as input data from the state of the slopes in the Cimanggung district.

METHODOLOGY

This study involves the slope steepness algorithm in determining the areal morphometry. Slope steepness usually defined by the value change of height from one point to the other such that, slope steepness calculation can be expressed by the formula below.

$$Slope\ degree = \theta \quad \frac{rise}{run} = tan\theta$$

$$Slope\ percents = \frac{rise}{run} \times 100\%$$

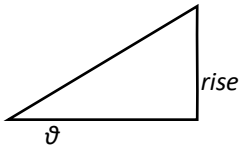

The steepness of the slope can be expressed as degrees and percent. Steepness is produced by dividing the tangent of the height difference by the difference in the distance between the points. While the steepness percentage is produced by dividing the difference in height by the difference in distance between points multiplied by 100 percent.

However, this research uses Digital Elevation Model data derived from satellite imagery, so a slope algorithm method is needed so that the resulting error value can be minimized. DEM data is data in the form of cells that have values of x (longitude), y (latitude) and z (height).

Conceptually, slope steepness algorithm is adjusted to the plane of z value from 3 x3 cell around processing cell or

PROCEEDINGS
JOINT CONVENTION BANDUNG (JCB) 2021
November 23rd – 25th 2021

middle cell. This plane steepness value is calculated using maximum average technique. Plane surface direction is the processing cell aspect.

a	*b*	*c*
d	***e***	*f*
g	*h*	*i*

Surface level change (delta) in horizontal (Δz/Δx) and vertical direction (Δz/ Δy) from middle cell determines the slope steepness. Steepness usually measured in degrees with the algorithm as shown below.

$$Slope\ degrees = ATAN\ (\sqrt{([\Delta z/\Delta x]2 + [\Delta z/\ \Delta y]2)}) \times 57.29578$$

This algorithm can also be expressed as:

$$Slope\_degrees = ATAN\ (riserun) \times 57.29578$$

$$riserun = \sqrt{([\Delta z/\Delta x]2 + [\Delta z/\ \Delta y]2]}$$

Middle cell value (*e*) and eight cell around it determines the horizontal and vertical delta. The cells around the middle cell are identified by letter a to i with e representing the middle cell, the cell that is being calculated or processed.

Steepness algorithm calculation in this study was carried out using the software ArcGIS 10.5 while the total area calculation was done using Microsoft excel.

Slope steepness calculation will then be classified according to settlement suitability standards on National Spatial Regulation No. 26/2007.

Table 1. Slope classification based on National Spatial Regulation No. 26/2007

Steepness (%)	Slope Class	Area (ha)	Area percentage (%)
0 - 8	Flat	443.23	11.04
8 - 15	Gently sloping	679.43	16.92
15 - 25	Moderately Steep	1013.76	25.25
25 - 45	Steep	1313.45	32.71
> 45	Very steep	565.08	14.07
Total		**4014.96**	**100**

RESULT AND DISCUSSION

Location and Total Study Area

Cimanggung District is administratively included in Sumedang Regency with an area of ± 4014.96 ha. In general, the topography of this sub-district are mostly steep slopes with partially plane.

PROCEEDINGS
JOINT CONVENTION BANDUNG (JCB) 2021
November 23rd – 25th 2021

Cimanggung District includes 11 villages in the Sumedang Regency area with the north of this sub-district bordering the Tanjungsari, Pamulihan and South Sumedang Districts. In the east, it is bordered by South Sumedang District and Garut Regency. In the west it is bordered by Jatinangor District and in the south by Bandung Regency and Garut Regency.

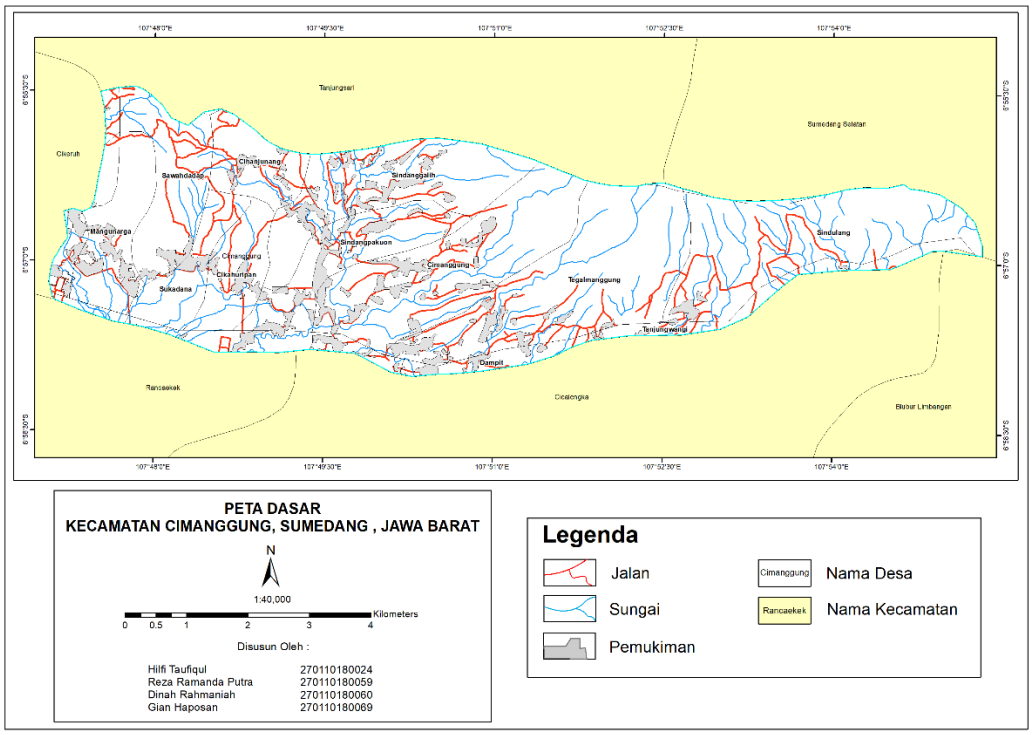

Figure 1. Base Map of Cimanggung District

Slope Characteristics

Slope characteristics and morphographic conditions around Cimanggung District can be seen in Figures 2 and 3, which are the result of

identification of contour maps at a scale of 1: 40,000. From Figure 2 it can be seen that Cimanggung District is located at an altitude of 667.8 – 3000 m above sea level, which according to Van Zuidam (1985) in Cahyadi (2016) is included in the classification of high hills to mountains.

Figure 3 provides the information about the slope characteristic at Cimanggung District. Slope steepness vary from flat, gently sloping, moderately steep, steep, until very steep. Area calculation on slope steepness and pixel amount are shown in table 2.

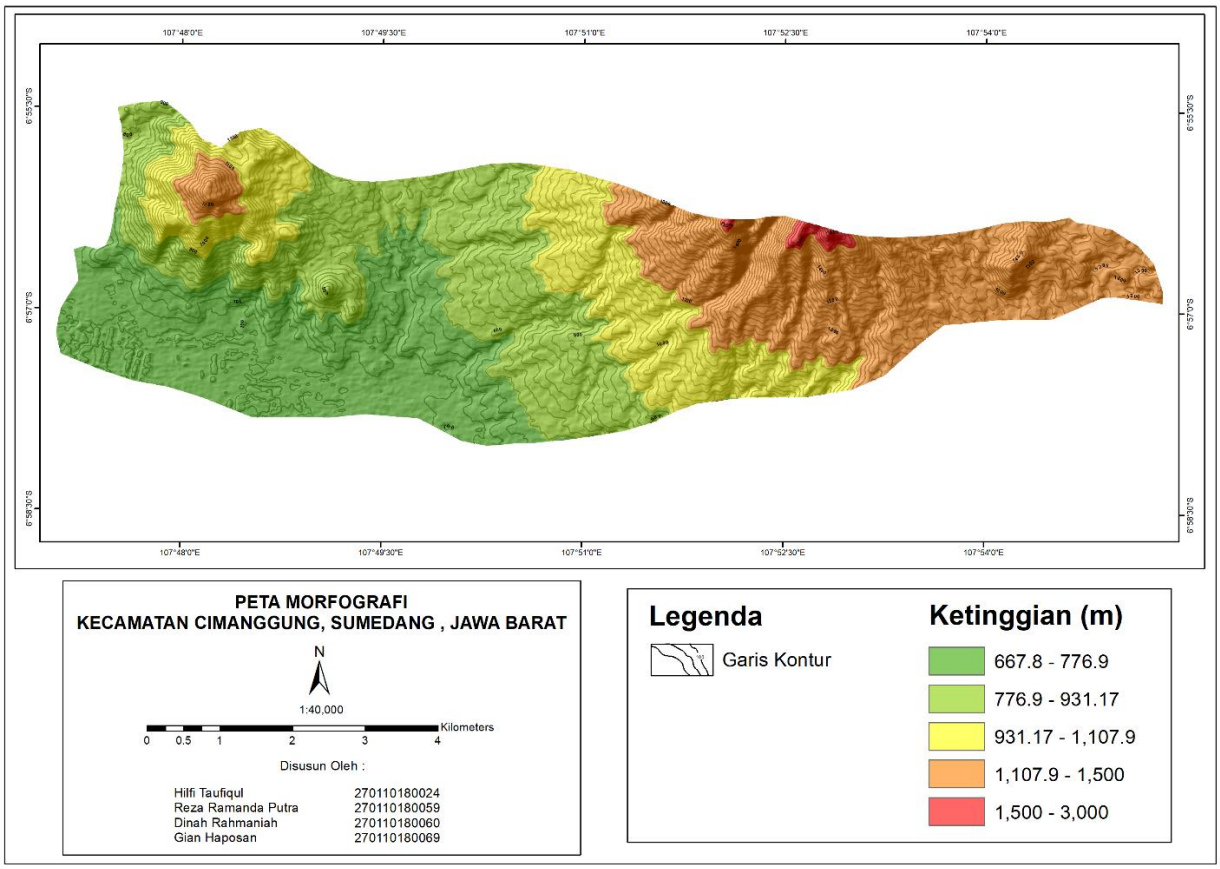

Figure 2. Morphography map of Cimanggung District

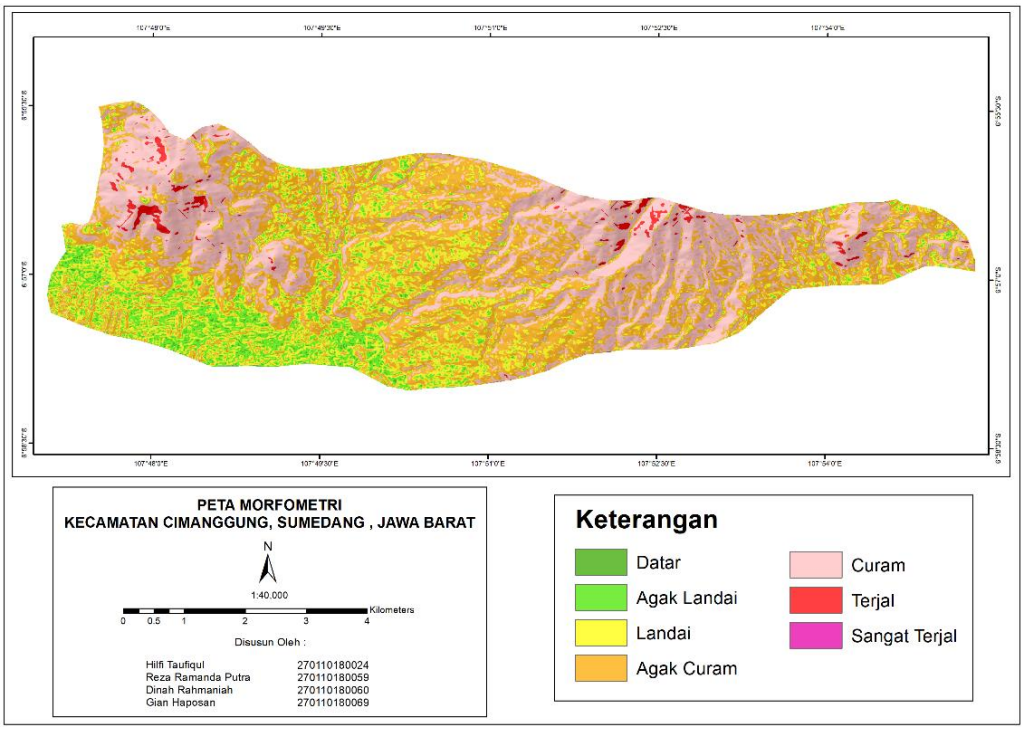

PROCEEDINGS
JOINT CONVENTION BANDUNG (JCB) 2021
November 23rd – 25th 2021

Gambar 3. Morphometry distribution map of Cimanggung District

Table 2. Slope area calculation process

Slope Class	Pixel amount	Spatial Resolution	Area (m²)	Area (ha)
Flat	63580	69,71281434	4432340,736	443,23
Gently Sloping	97461	69,71281434	6794280,598	679,43
Moderately steep	145420	69,71281434	10137637,46	1013,76
Steep	188409	69,71281434	13134521,64	1313,45
Very steep	81058	69,71281434	5650781,304	565,08
Total	**575928**		**40149561.74**	**4014.956174**

Table 2 shown the calculation process on map to the total area attributed to each slope class. To acquire the area in meter square, pixel amount has to be multiplied by spatial resolution which then converted into hectares (ha) and can further multiplied by 100% to acquire the area percentage as shown in table 3.

Table 3. Slope classification on Cimanggung District Area

Steepness (%)	Slope Class	Area (ha)	Area percentage (%)
0 - 8	Flat	443,23	11,04
8 - 15	Gently Sloping	679,43	16,92
15 - 25	Moderately steep	1013,76	25,25
25 - 45	Steep	1313,45	32,71
> 45	Very steep	565,08	14,07
Total		**4014,96**	**100**

Based on our study, around 11,04% of the total Cimanggung area are included in the flat slope class, 16,92% of Cimanggung area are of gently sloping class, around 25,25% are included in the moderately steep slope class, 32,71% of the total Cimanggung area are categorized as steep, and about 14,07% of the total Cimanggung area are included in the very steep category. Based on the regulation, land that is suited for public settlement has slope steepness of 0 – 25%. The result

shows that about 46,78% of Cimanggung area consisted of Steep to Very Steep Landform which aren't suited for settlement purpose.

CONCLUSION

Landform of Cimanggung District can be classified based on the slope steepness into 5 class: Flat (0 – 8%), Gently Sloping (8 – 15%),

Moderately steep (15 – 25%), steep (25 – 45%), and very steep (> 45%) . From 1 : 40.000 base map, it can be seen that Cimanggung area is located on elevation of 667,8 – 3000 m above sea level with varied slope class. This study shows that Cimanggung Area mostly consisted of moderately steep (15 – 25%) – steep (25 – 45%) landform with a total of 46,78% of Cimanggung District.

DAFTAR PUSTAKA

Bermana, Ike. 2006. *Klasifikasi Geomorfologi Untuk Pemetaan Geologi Yang Telah Dibakukan*. Bulletin of Scientific Contribution, Vol 4. No 2.

Burrough, P. A, and McDonell, R. A. 1998. *Principles of Geographical Information Systems* (Oxford University Press, New York), 190 pp.

Cahyadi, H. 2016. *Geomorphology Characteristic of Ciangsana and Surronding Areas, Cikembar Sub-District, Sukabumi Regency, West Java*. Proceeding, Seminar Nasional Kebumian Ke-9.

Rossiter, D.G. 1994. *Geographical Information System. Lecture Notes: Land Evaluation*. Cornell University, College of Agriculture and Life Science. Department of Soil, Crop and Atmospheric science. P 125.

Silitonga, P. H. 1973. *Peta Geologi Lembar Bandung, Jawa, Skala 1 : 100.000*. P3G. Bandung.

Van Zuidam, R. A. 1985. *Aerial Photo-Interpretation in Terrain Analysis and Geomorphological Mapping*. Smith Publisher, The Hague.

Zuidam, R.A. and Zuidam Cancelado, F.I. 1979 and 1985. *Terrain Analysis and Classification Using Areal Photographs, A Geomorphologycal Approach*. Netherland, Enschede: ITC.

PROCEEDINGS
JOINT CONVENTION BANDUNG (JCB) 2021
November 23rd – 25th 2021

Modeling and Analysis of Landslide Susceptibility Using Analytical Hierarchy Process Methods and Geographic Information Systems in Kulon Progo Regency, Special Region of Yogyakarta

Meiliawati Nurbaiti[1] ,Nelly Ariska Septyana[1], Kamila Nuril Izzah[1], Agung Setianto[2]
[1] Undergraduate Student and [2]Lecturer, Department of Geological Engineering, Faculty of Engineering, Universitas Gadjah Mada

Abstract

The number of disasters in Indonesia by the date of August 17, 2021, released by BNPB Indonesia shows that landslides are the third most common disaster after floods and tornadoes, at 20.32%. Landslide is the displacement of slope-forming material which can be in the form of rock, soil debris, or a mixture of both that moves down the slope. Kulon Progo Regency is one of the regencies in Indonesia that often occur landslides due to its high slope and low soil compaction. Thus, it is necessary to model and analyze landslide susceptibility to be able to classify areas in Kulon Progo that are prone to landslides. The purpose of modeling and analyzing this landslide disaster will be useful for the future which can be used as a source of information on disaster mitigation and planning for infrastructure and non-infrastructure development. The method used in this study is the method of overlapping thematic maps using overlay techniques with several spatial and non-spatial data parameters, namely land cover maps from the results of supervised classification of Landsat 8 images in 2020, geological maps, soil type maps, slope maps, rainfall maps along with map attribute data with a scale of 1:50000. These parameters will be weighted using the Analytical Hierarchy Process (AHP) method and then processed using Geographic Information Systems. The results of the AHP weighting and overlaying of all parameter maps are obtained in the form of a Landslide Susceptibility Zone Map in Kulon Progo Regency with very low 11.16%, low 38.41%, medium 32.29%, high 13.84%, to very high 4.30% levels of susceptibility. The analysis results are visualized into a modeling map in 3D to support the information conveyed. Based on the map, the very high landslide susceptibility level is located in areas with slopes of >45°, high rainfall, regosol soil types, and land cover in the form of rice fields and dry fields. The high landslide susceptibility level is located in areas with slopes of 30-45°, high rainfall, andosol soil types, and land cover in the form of bushes. The medium susceptibility level is located in areas with slopes of 15-30°, rainfall medium, mediteran soil type, and land cover in the form of forest and plantations. The low susceptibility level is located in areas with slopes of 8-15°, low rainfall, latosol soil type, and land cover in the form of settlements. While the very low susceptibility level is located in areas with slopes <8°, low rainfall, alluvial soil types, and land cover in the form of reservoirs and waters. The validation stage uses a diffusion matrix by comparing the map of analysis results with the data of observation points in the field. The results showed an accuracy rate of 83.3%, so the map is accurate enough to suspect potential landslide at the research site.

Keywords: Analytical Hierarchy Process, GIS, Kulon Progo, Landslide Susceptibility, Modelling

Introduction

Landslides are natural disasters that often occur in almost all areas of Indonesia, especially in areas with high topography. This disaster took many victims, both lives and property. Landslides occur when land that has a high topography or a slope experiences instability due to certain physical factors such as soil type and slope. The type of soil due to weathering processes that are on impermeable rocks in hills or mountains with moderate to steep slopes has the potential to cause landslides in the rainy season with high quantity of rainfall. If the hills do not have strong and deep rooted perennials, then the area is prone to landslides (Bagus, 2007).

Landslide hazard mapping is very necessary to identify which areas are included in the landslide-prone zone. In practice, this mapping can be done by remote sensing. Mapping in this way utilizes primary and secondary data such as DEM, Landsat images, and spatial data to identify and determine objects on the earth's surface without direct contact. With a relatively high spatial resolution, Landsat images are able to represent the earth's surface and the objects that cover the surface (Cahyono, 2007). The processing of spatial and attribute data utilizes the use of Remote Sensing Integration and Geographic Information Systems as a means of spatial analysis that is useful for analyzing and processing information based on vector and raster data of an area in handling areas that have the potential for landslides.

One of the most widely used methods for assessing landslide susceptibility is the Analytical Hierarchy Process (AHP). By using this method, the parameters determining landslide susceptibility can be systematically processed to determine the level of landslide susceptibility in the study area. By calculating the comparison of paired matrices, the weight of each parameter determining landslide susceptibility can be easily obtained. The results of this AHP calculation will later be processed in a GIS to obtain a Landslide Potential Map.

The purpose of this study was to identify areas with potential for landslides in Kulon Progo Regency by utilizing Landsat 8 imagery and Geographic Information Systems. This research was conducted in Kulon Progo Regency, which annually experiences landslides in various areas. Handling landslides in the Kulon Progo area is still lacking due to limited capabilities and low information education. Efforts

that can be made to anticipate this landslide disaster are making a map of the potential landslide area in Kulon Progo Regency. Making maps based on land cover from remote sensing data from Landsat 8 imagery and supporting data as well as the application of GIS in the calculation of the AHP method. Thus, the preparation for landslide disaster mitigation and future development planning can be based on the Landslide Potential Map of Kulon Progo Regency.

Data and Method

The method used in this study area is the method of overlapping thematic maps by overlaying several spatial and non-spatial data parameters, namely gological maps were analyzed and modified from the Geological Map Sheet Yogyakarta scale 1: 100000 Year 1977 and the Indonesian Topographic Map Bakosurtanal scale 1: 25000. The Slope from Slope Map was analyzed from slope data processed from DEMNAS data and the Indonesian Topographic Map Bakosurtanal scale 1: 25000. The Rainfall Map was analyzed from the 2019 BMKG rainfall data and the Bakosurtanal Indonesia Earth Map at a scale of 1: 25000. The Soil Type Map was analyzed and modified from the Java Island BBSDLP Soil Type Map at a scale of 1: 250.000 and the Bakosurtanal Indonesia Earth Map at a scale of 1: 25000. Furthermore, all maps were weighted AHP (Saaty, 1991) and intersection overlay using ArcGis 10.7 software. Then the division of class intervals into Landslide Hazard Maps with very low, low, medium, high, and high vulnerability levels.

Based on the overlay, the research location are divided into 8 formations. The oldest formations are Naggulan Formation (Middle Eocene – Early Oligocene), Kebobutak Formation (Middle Oligocene – Early Miocene), Andesite (Late Eocene – Early Miocene), Jonggranga Formation (Early Miocene – Middle Miocene), the Sentolo Formation (Middle Miocene – Pliocene), Young Volcanics (Quarter), alluvial and colluvial deposits (Quater) (Rahardjo et al, 1977).

Land cover map processing utilizes Landsat 8 imagery in 2019. The Landsat 8 image was then analyzed using ENVI 5.3 software. Land cover mapping was specially processed using ENVI Classic with a supervised classification method. This method is done by making ROI. In this study, land cover classification is divided into water bodies, settlements, agriculture, gardens, and open land with the chosen ROI tool, namely Maximum Likelihood. The classification checked through RBI maps and Google Earth.

The variables of each parameter determining landslide susceptibility are weighted using the AHP method. According to Saaty (1991), this method is carried out by converting these weights into numbers based on a paired comparison scale. These figures illustrate the magnitude of the influence of one variable on another variable on landslide susceptibility in the study area. These numbers are then presented in a pairwise comparison matrix to calculate the priority weights using the AHP method. Determination of the numbers in the matrix is based on theoretical logic, previous studies related to landslide hazard using the same parameters in the analysis. The weights generated by this method really depend on the accuracy of the author in determining the numbers in the pairwise comparison matrix, therefore, it takes a lot of consideration and benchmarks in determining these numbers. The priority scale table according to Saaty (1991) is presented in Table 1.a.

The results of the weights of each parameter and subparamter are used as a multiplier for each sub---parameter score which has also been calculated AHP. The calculation of the weight parameter of the eigenvalue (λ), the maximum eigenvalue (max) is done by adding up all the multiplication of the number of rows in the initial matrix with the weight or eigenvalue of each flood susceptibility parameter (Saaty, 1990). Test the consistency of the index and ratio. First calculate the consistency index (CI) with the following equation.

$$\text{CI} = \frac{\lambda \text{ maks} - n}{n-1}$$

Next, calculate the consistency ratio (CR) using the following equation.

$$CR = \frac{CI}{RI}$$

The value of Random Consistency Index (RI) (Saaty, 1980) is obtained in the Table 1. b.

The result of this multiplication is a value. These values are then added up and then the class interval classification is carried out with the following formula:

$$\text{Class Interval} = \frac{maximal\ index - minimal\ index}{class\ total}$$

Processing of parameter weights and parameter variables to the division of class intervals is carried out using Arcgis 10.7 software to produce a Landslide Hazard Zone Map, then made into a 3D model using the BlenderGIS application.

The results of the landslide hazard map are validated using the confusion matrix method, which is to compare the results we get from the classification using the system with the actual classification results. For the accuracy of the data at the research location using the calculation of accuration assessment (Kohavi and Provost, 1998) as shown in Equation

$$\text{Accuration} = \frac{\sum Correct\ point\ with\ field\ check}{\sum All\ observation\ points} x\ 100\%$$

Result and Discussion

The AHP model in this research area uses five parameters, namely slope, lithology, rainfall, soil type, and land use (Figure 1.a-e). Matriks of pairwise comparison for each parameter dan subparameter and relationship between these weights can be seen in Table 2 and Table 3. After the parameters were

processed using ArcGis by considering the AHP model, a landslide susceptibility map was created (Figure 1.f). Then using GIS Blender, a 3D model was created by displaying a three-dimensional image of each vulnerability (Figure 2). The results showed that the landslide susceptibility in study ares was divided into five classes, namely very high, high, medium, low, and very low. (Figures 1.f and 2).

Based on the Landslide Susceptibility Map (Figure 2), the areas with very high vulnerability are mostly located in the northern and western areas of the study area. In this area the slope is very high, >45 °, the rainfall is dominated by moderate to high, some composed of alluvial soil types. In the western part, it is common to find high vulnerability, where the slope is high, rainfall is generally moderate, the constituent lithology are carbonate rocks, volcaniclastic sediments rock, and pyroclastics rock which generally contain clay material which is a loose material and in certain types of clay, clay can expand when exposed to water, so that during the rainy season it will be prone to landslides, besides that there is also a transfer of land function into settlements which results in additional loads on the slopes. Most of the research area in the northwest is dominated by moderate vulnerability, where the slope is moderate, land use is in the form of plantations so that when it rains tree roots help in absorbing water, some are composed by Andesite lithology which is compact rock, low porosity and low permeability. From the east to the south, the landslide hazard is at a low-very low level. Although geologically it is composed of lithology in the form of alluvial, colluvial, young deposits of Mount Merapi which are included in loose rock and some of them are carbonate rocks, due to the slope of the slopes ranging from <8°-15° which is classified as a low slope -very low slope and the elevation is low-medium, and the rainfall that occurs is moderate-low, the possibility of landslides is lower. Most of the landslides occur due to very high slopes, loose lithology and clay content, land use diversion, soil type in the form of Regosol, and high rainfall.

The results of research validation using a confusion matrix were carried out by comparing the results of the landslide hazard map using the AHP method with checking field conditions in Kulon Progo Regency (Figure 3) as many as 30 points (Table 4). The results of this validation are followed by an accuration assessment showing an accuracy of 83.3% (fulfil >80%), so the map made can be said to be accurate and in accordance with the actual situation. There is a mismatch of vulnerability between the map and the actual situation due to the possibility that the weighting carried out is not suitable for some areas and the accuracy of the data sources that are not up-to-date may occur later because of activities that affect a landslide susceptibility point at the research area.

Conclusions

Landslide susceptibility in the study area is divided into five namely very high (4.30%), high (13.84), medium (32.29%), low (38.41%), and very low (11.16%), these are displayed in 2D maps and 3D models. The parameters used are slope, lithology, rainfall, soil type, and land cover which AHP analysis is carried out first. The most influential parameter is slope with a weight of 0.39, followed by a lithology weight of 0.27, rainfall 0.19, soil type 0.09, and land use 0.06. The validation showed an accuracy rate of 83.3%, so the map is accurate enough to suspect landslide insecurity at the research area. The accuracy of the results of this AHP depends on the subjectivity of the author in assigning a value to each parameter, the use of AHP in this study is a mathematical method and does not have statistical testing, so it does not have a limit on the truth of the model made. In future research, the use of AHP in determining landslide susceptibility requires updating attribute data in order to get results that are close to the original state. The ways that can be done are using the latest data sources for each parameter used, assigning values to the AHP parameters by experts in their fields, and reviewing important parameters that will be used in determining the landslide susceptibility of the research area. The importance of detailed research to mitigate landslides that are prone to occur on the west side of Kulon Progo Regency.

References

Bakosurtanal, Indonesian Bakosurtanal Earth Map, scale 1: 25000. Jakarta.

BMKG. 2019. BMKG rainfall data for 2019. Jakarta.

Center for Research and Development of Agricultural Land Resources. Soil Type Map of Java Island BBSDLP scale 1: 250000. Bogor.

Geospatial Information Agency, 2008, DEMNAS Kulon Progo Regency accessed in October 2020.

Kohavi, R., F. Provost. 1998 . Editorial for the Special Issue on Applications of Machine Learning and the Knowledge Discovery Process. Glossary of terms.

Rahardjo, Wartono., Sukandarumidi., Rosidi, H. M., 1977. Geological Map Sheet Yogyakarta scale 1: 100000 in 1977. Directorate of Geology, Department of Indonesian Mining.

Saaty T.L., 1990, *An exposition of the AHP in reply to the paper remarks on the Analytic Hierarchy Process*. Management Science 36, p.259-268.

Saaty, T.L., 1980, *Decision making with the Analytical Hierarchy Process*: Int. J. Services Sciences, Vol. 1, No. 1.

USGS. 2019. Landsat 8 image no L1TP 120065 Year 2019 accessed in September 2020.

PROCEEDINGS
JOINT CONVENTION BANDUNG (JCB) 2021
November 23rd – 25th 2021

Table 1: a. The priority scale table (Saaty ,1991) **b.** The value of Random Consistency Index (RI) (Saaty, 1980)

a.

Preference factor	Degree of preference	Explanation
1	Equally	2 factors contribute equally to the objective
3	Moderately	Experience and judgement slightly to moderately favor one factor over another
5	Strongly	Experience and judgement strongly or essentially favor one factor over another
7	Very strongly	A factor is strongly favored over another and its dominance is showed in practice
9	Extremely	The evidence of favoring one factor over another is of the highest degree possible of an affirmation
2,4,6,8	Intermediate	Used to represent compromises between the preferences in weights 1,3,5,7, and 9
Reciprocals	Opposites	Used for inverse comparison

b.

n	1	2	3	4	5	6	7	8
RI	0	0	0,58	0,90	1.12	1.24	1.32	1.41

9	10	11	12	13	14	15
1.45	1.49	1.51	1.53	1.56	1.57	1.59

Figure 1: Map of parameters used to analyze landslide susceptibility in the study area a. Rainfall, b. Geology, c.Slope, d. Soil type, e. Land use. f. Landslide susceptibily map.

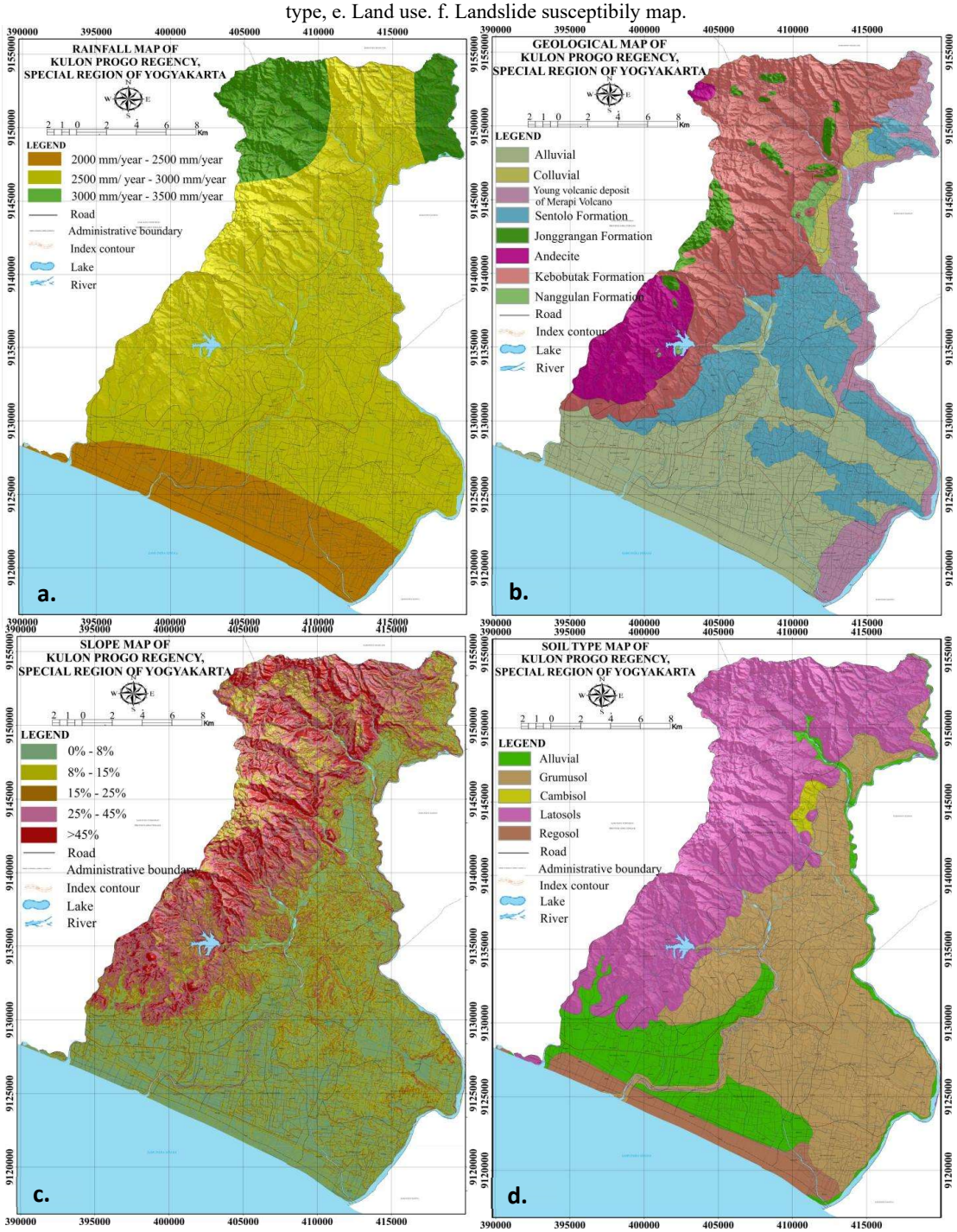

PROCEEDINGS
JOINT CONVENTION BANDUNG (JCB) 2021
November 23rd – 25th 2021

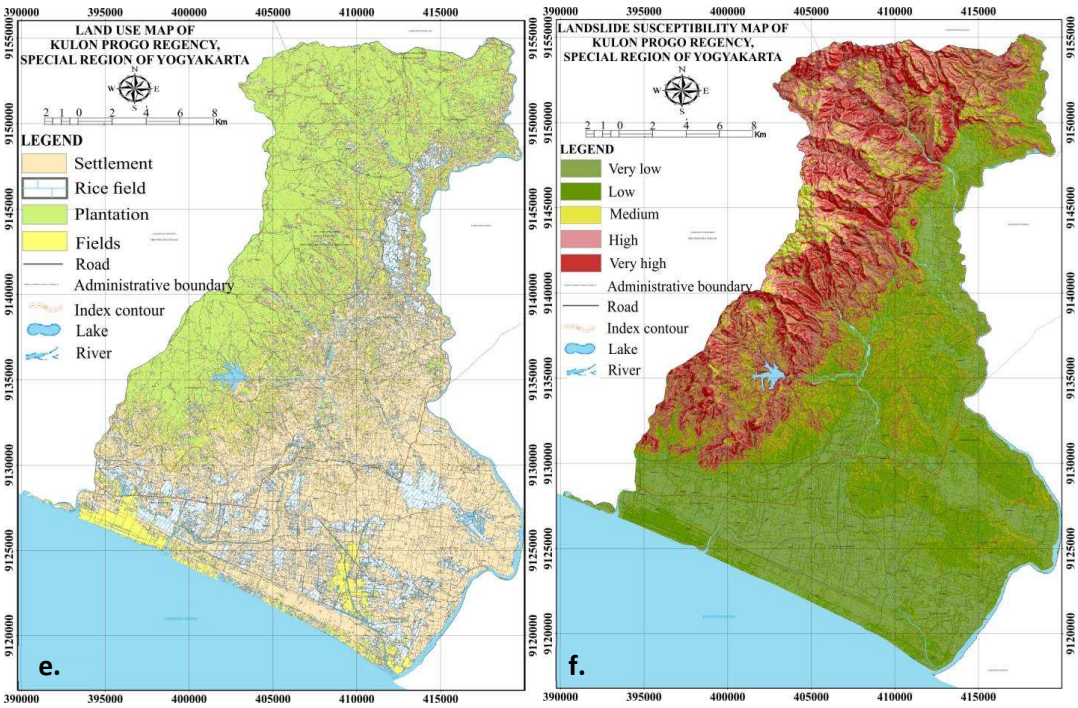

Table 2. Matriks of pairwise comparison and weigh of each parameter.

	Matrix of pair-wise comparison					Weight
	Slope	**Lithology**	**Rainfall**	**Soil type**	**Land use**	
Slope	1					0.39
Lithology	1/2	1				0.27
Rainfall	1/3	1/2	1			0.19
Soil type	1/4	1/3	1/3	1		0.09
Land use	1/4	1/6	1/5	1/2	1	0.06

Table 3. The weight of each sub-parameter uses matrix of ahp pairwise comparison

Parameter	Sub-parameter	Weight	CR
Slope (%)	0-8	0,04	0,0471
	8-15	0,06	
	15-25	0,13	
	25-45	0,29	
	>45	0,48	
Formation	Andecite	0,51	0,0331
	Kebobutak formation, Semilir formation	0,23	
	Sentolo formation , Jonggrangan formation, Nanggulan formation	0,13	
	Young volcanic deposit of Merapi Volcano	0,09	
	Alluvial, colluvial	0,05	

Parameter	Sub-parameter	Weight	CR
Soil type	Alluvial	0,06	0,04691
	Latosols	0,17	
	Cambisols, grumosol	0,33	
	Regosol	0,45	
Land use	Fields	0,37	0,05894
	Rice fields	0,31	
	Settlement	0,17	
	Plantation	0,10	
	Waters	0,05	
Rainfall (mm/year)	1500-2250	0,16	0,0606
	2250-3000	0,25	
	3000-3750	0,59	

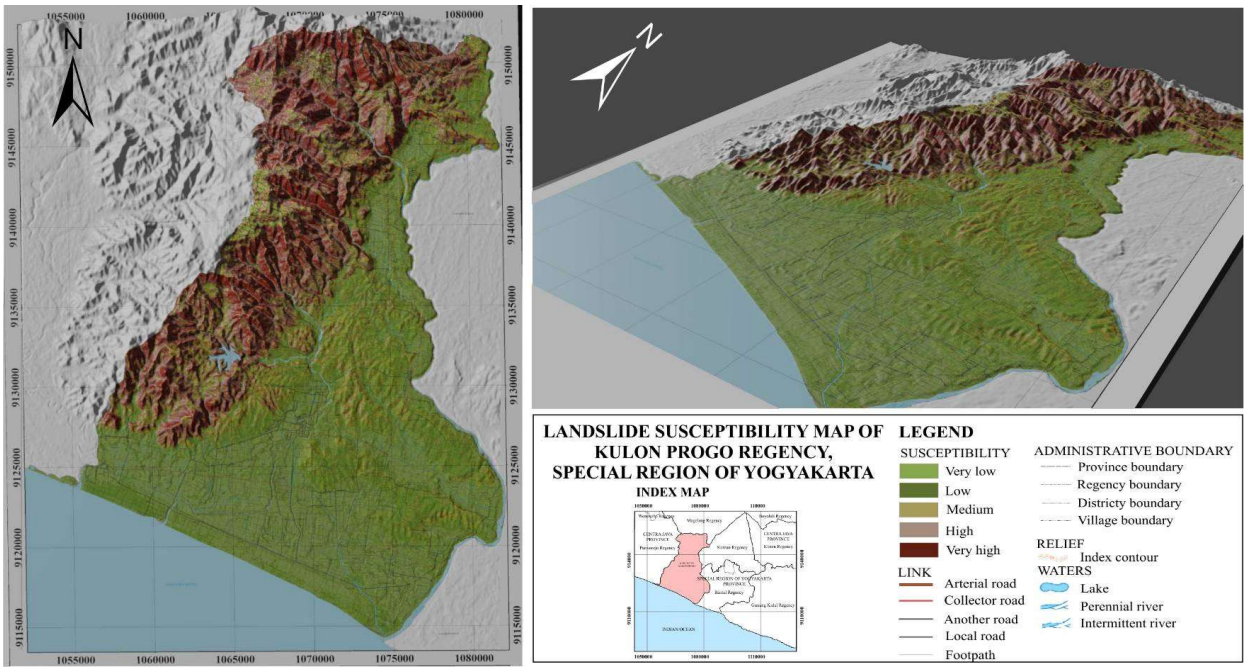

Figure 2. 3D Model of landslide susceptibility in the study area, top view 3D (*left*) and beside view 3D (*right*).

Figure 3. Field documentation (A) Very high vulnerability at Samigaluh District, (B) High vulnerability at Kokap District, (C) Medium vulnerability at Kokap District, (D) Low vulnerability at Wates District, and Very low vulnerability at Sentolo District.

Tabel 4. Result of landslide susceptibility map validation test

	Field data results						Data accuracy	Status
	Class	**Very low**	**Low**	**Medium**	**High**	**Very high**		
Analysis Map Result	**Very low**	4	1				13.3%	
	Low	2	3				10%	
	Medium			6	1		20%	
	High				5		16.7%	
	Very high				1	7	23.3%	
Total							83.3%	Accurate

PROCEEDINGS
JOINT CONVENTION BANDUNG (JCB) 2021
November 23rd – 25th 2021

GIS Analysis to Identify Forest and Land Fire Hazards in North Penajam Paser Regency, East Kalimantan Province

Dewi Mirah Rezki[1], Anggreine Aurelia Porajow[1], Khori Fatimatuz Zahra[1], Zakki Hilal Chalqi[1], Misbahudin[1].*
[1]Geological Engineering Study Program, Faculty of Exploration and Production Technology, Universitas Pertamina

Abstract

The El Nino phenomenon is one of the phenomena that cause forest fires. When El Nino hits, the dry season will be more extended and temperatures will be higher. One area that frequently experiences forest fires is the North Penajam Paser Regency in East Kalimantan. The purpose of this study is to identify areas that have the potential to experience forest fires in North Penajam Paser Regency, especially since this area will become the new capital city of Indonesia, so it is necessary to take appropriate mitigation efforts. The data used are climate data, soil types, and forest and land types. The data is then processed using GIS software such as QGIS. In Geographic Information Systems, several methods for data processing were used, such as overlays and clips. So that the results obtained in the form of points that have the potential to experience forest fires during the dry season in North Penajam Paser Regency, where these points classify into three classes: low, medium, and high categories. The government can use the results of this study to determine mitigation efforts and appropriate evacuation routes. And it can be used to plan where government buildings will be built in to avoid forest fires.

Keywords: El Nino, forest fire, GIS, mitigation

Introduction

Indonesia is a country known as a contributor to the world's lungs. According to the Ministry of Environment and Forestry (2021), forest monitoring results in 2020 show that Indonesia's forest area is 95.6 million ha. One of the islands in Indonesia that has a vast forest is the island of Kalimantan. However, the forest area in Kalimantan is decreasing from year to year. One of the causes is forest fires.

One of the forest fires cases that often occur every year is in North Penajam Paser Regency. In this regency, forest fires have been causing by two factors: intentional factors and natural factors. The deliberate burning of forests causes this conscious factor for land clearing purposes. The natural factor that causes fires in this district is the high temperature during the dry season. In the dry season, the temperature will increase, and the rainfall will decrease. El Nino makes these conditions even worse, making the dry season longer.

According to Sinaga (2021), forest fires affected an area of 1.6 ha in August 2021. Even in September 2019, 60 cases of forest and land fires were reported, with 110 ha of peatland burned that year. According to Pertiwi's (2019) research, there were 16 forest or land fires cases in this area in 2018 from July to September. Forest fires in this area have resulted in numerous losses, including public health conditions disrupted by smog and land damage. Although this district includes the area that will become Indonesia's new capital city, the issue of forest fires in this area appears to be unresolved. The Regional Disaster Management Agency of North Penajam Paser Regency has implemented appropriate mitigation measures, including monitoring, particularly on peatlands. In addition, when forest fires occur, the local government has formed joint officers to extinguish them. However, they discovered several roadblocks during the mitigation process. The lack of high-accuracy data on potential disaster locations makes the mitigation process appear slow, and forest fires continue to occur year after year. In addition, the Head of the Damage Control and Security Section of the East Kalimantan Forestry Service, Shahar Al Haqq, said that one of the obstacles when extinguishing the fire was the difficulty of finding water sources at the fire site. Not only that, when El Nino hits and causes strong winds, the fire tends to spread quickly and overwhelm officials.

After evaluating the disaster mitigation process implemented and witnessing the forest fire disasters that continue to occur year after year, as well as analyzing the magnitude of the disaster's negative impact. As a result, a map of forest and land fire-prone areas are required. There are three parameters to examine the causes of forest fires in this district: forest and land types, climate, and soil types. Using these three parameters was the most influential factor in causing forest fires in the study area. Soil type parameters are also important. This map uses forest and land parameters because shrubs, food crops, and grasslands dominate this area. Then because many forest fires occur during the dry season, it requires rainfall parameters. In addition to these three parameters, it is necessary. This map helps provide information on areas that can experience forest fires and facilitate the mitigation process. Also, this map can use to determine the region’s main priorities in handling forest fires. It can be taken into consideration

by the Government in carrying out sustainable planning and development.

Data and Method

The data processing process in this study refers to the 2016 Indonesian Disaster Risk Book, where the dangers of forest and land fires are made based on the Head of BNPB Regulation Number 2 of 2012. Each parameter used will be scored according to the level of influence of each class using the scoring method. Figure 1 depicts the overall process of creating a Map of Forest and Land Fire Prone Areas.

There are several data used, namely:

1. Soil type data, obtained from the Ministry of Agriculture is shapefile (shp) data with vector data types.
2. Land cover data, obtained from the official ESRI Land Cover 2020 website, and shapefile (shp) data with vector data types.
3. Rainfall data were obtained from the Center for Hydrometeorology and Remote Sensing (CHRS) University of California, Irvine (UCI). This data is shp data with the raster data type. The data used is rainfall data from 2019.
4. Administrative boundary data, this data is obtained from the Indonesia Geospatial Portal website. This data is of type vector data.

Several methods were used in this study, including:

1. Scoring method is a method for assigning a score to each class in a parameter. Analyzing how important these classes are to forest fires must be done to determine each class's score. The class with the most influence receive the highest score. In contrast, the class with the most negligible impact will receive the lowest score. Then the weighting process is carried out, then the overlay process is carried out using GIS processing software. The scoring in this study base on the 2016 Indonesian Disaster Risk Book.
   - Soil type scoring
     Soil type classes were determined using guidelines from the Ministry of Agriculture's Soil Research Center. Organic soils are more flammable than non-organic/mineral soils because they contain carbon gas. When peatlands expose to arid conditions, the water absorption function disruption because its properties are similar to dry wood, making it easy to burn.

Table 1 Soil Type Class Scores

Class	Score
Non-organic/Mineral	0,333
Organic/Peat	1

   - Land type scoring
     The Ministry of Forestry guidelines were used to determine land type classes. A land dominated by shrubs, crops, and dry grasslands will burn more efficiently, whereas trees in forests will be more difficult to burn because large, wet trees require more energy to burn.

Table 2 Land Type Class Scores

Class	Score
Forest, Flooded Vegetation	0,333
Crops	0,666
Grass, Scrub/Shrub	1

   - Rainfall scoring
     Rainfall data used is data in the dry season, from May to October in 2018-2020. During the dry season, there is much dry vegetation. Then, when the rainfall is low, the burning land will be difficult to extinguish, and the strong wind makes the fire quickly spread. As a result, the lowest rainfall receives the highest score.

Table 3 Scores of Rainfall Classes

Class (mm/month)	Score
>250	0,333
125-250	0,666
<125	1

2. Weighting Method, weighting is applied to each parameter that causes forest and land fires. The greater the weight, the greater the influence of the parameter on forest and land fires. The weighting in this study is also base on the 2016 Indonesian Disaster Risk Book.

Table 4 Parameter Weight

Parameter	Weight
Soil type	0,3
Land type	0,4
Rainfall	0,4

3. Overlay Method
   An overlay is a process of combining layers in a GIS processing application in an overlapping manner. This research overlays the three maps; Soil Type Map, Land Type Map, and Rainfall Map. However, before overlaying, it must be ensured that all three maps have the exact resolution. In this study, the three maps have a pixel size of 30 x 30. This size belongs to the

multispectral level, where this level is still quite representative and does not have a too large size. In overlaying, the score and weight values are also involved. The result of the overlay is a Map of Land and Forest Fire Prone Areas in North Penajam Paser Regency. However, this map is not yet equipped with road access and river flow data. So it is necessary to overlay again with shp data of river flow and road access.

Result and Discussion

1. Soil Type Map
   The soil type data were reclassified into two types, namely organic/peat soil and non-organic/mineral soil. Then, a score is given for each type of soil that has been reclassified. Then clip with the map of the administrative boundaries of the Regency so that a new Soil Type Map is obtained. The research area is dominated by non-organic/minerals. Soil type map can be seen in Figure 2.

2. Rainfall Map
   The data used is rainfall data in the dry season, from May to October, from 2018 to 2020. The data was chosen because the rainfall that causes forest fires is rainfall in the dry season. The data is averaged to obtain monthly rainfall data for the dry season using a raster calculator, then clipped with a map of administrative boundaries. Then reclassification is carried out according to the score of each class. So we get a Rainfall Map that has been reclassified. The study area is dominated by rainfall <125 mm/month. The rainfall map can be seen in Figure 3.

3. Land Type Map
   In making this map, each type of land is given a score according to what has been determining. Then reclassification is carried out according to the score and clipping with the administrative boundary map. The type of land in the study area is dominated by forest, but there is also land used for crops. Land Type map can be seen in Figure 4.

4. Forest and Land Fire Vulnerability Class Map
   This map can be seen in Figure 5. Vulnerability Class obtained which divided into three classes:
   - Low Vulnerability Class
     This class covers 88.7% of the study area. The dominance of this area is forest land cover, then rainfall <125 mm/year, and non-organic/mineral soil types., then rainfall <125 mm/year, and non-organic/mineral soil types.
   - Medium Vulnerability Class
     This class covers 6.8% of the research area. This area is dominated by land cover in plantations, then rainfall <125 mm/year, and non-organic/mineral soil types.
   - High Vulnerability Class
     This class covers 4.9% of the research area. This area is dominated by land cover in grass and scrub, then rainfall <125 mm/year, and non-organic/mineral soil types, but there are also organic/peat soil types.

Conclusions

Rainfall and land type are the most influential factors on forest and land fires in this area. Soil type also has an effect but does not have the most significant impact. Low vulnerability classes dominate the research area, but what needs consider is high vulnerability classes. The high vulnerability class dominates by land cover in the form of grass and scrub, then has rainfall <125 mm/month in the dry season and non-organic and organic soil types. High susceptibility classes have the most significant potential for forest fires, so they must be dealt with immediately. This map can be used as initial information for the community, researchers, government, and other interested parties. In addition, this map hopefully can be used in disaster mitigation management planning and regional development planning for national resilience.

References

Amri, M. R et all. (2016). *Risiko bencana indonesia*. Badan Nasional Penaggulangan Bencana.

CHRS. (2018). *Center for Hydrometeorology and Remote Sensing Data Portal*. https://chrsdata.eng.uci.edu/

ESRI. (2020). *ESRI 2020 Land Cover Downloader*. https://www.arcgis.com/apps/instant/media/index.htm?appid=fc92d38533d440078f17678ebc20e8e2.

Indonesia Geospatial Portal. (2021). *Map by region*. https://tanahair.indonesia.go.id/portal-web/download/perwilayah

Ministry of Environment and Forestry. (2021). *Deforestasi Indonesia Turun, Terendah Dalam Sejarah*. https://www.menlhk.go.id/site/single_post/3640/deforestasi-indonesia-turun-terendah-dalam-sejarah.

Pertiwi, D. W. K. (2019). IMPLEMENTASI PERATURAN DAERAH KALIMANTAN TIMUR NOMOR 5 TAHUN 2009 TENTANG PENGENDALIAN KEBAKARAN HUTAN DAN LAHAN DI KABUPATEN PENAJAM PASER UTARA.

Sinaga, D. H. (2021). *Karhutla Seluas 1,6 Ha di Wilayah Penajam Paser Utara Padam*. https://bnpb.go.id/berita/karhutla-seluas-1-6-ha-di-wilayah-penajam-paser-utara-padam.

Acknowledgements

We are very thankful to our supervisor, Mr. Misbahudin, M.T. lecturer in Geological Engineering at Pertamina University, for his generous support, inspiration, and guidance.

PROCEEDINGS
JOINT CONVENTION BANDUNG (JCB) 2021
November 23rd – 25th 2021

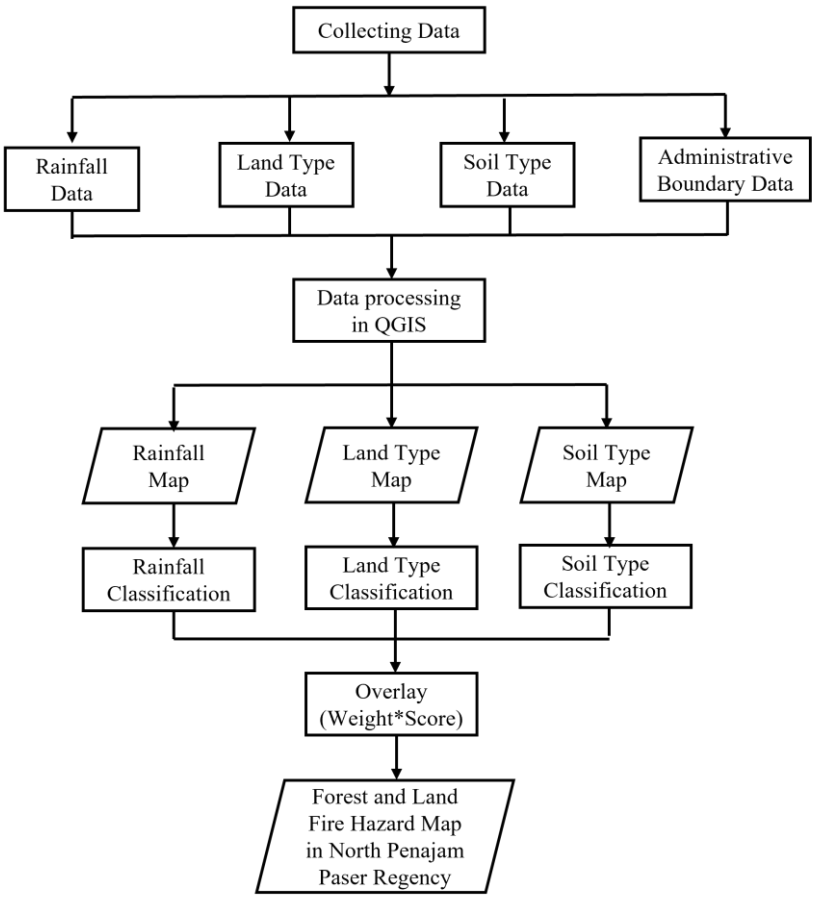

Figure 1 Flow Diagram

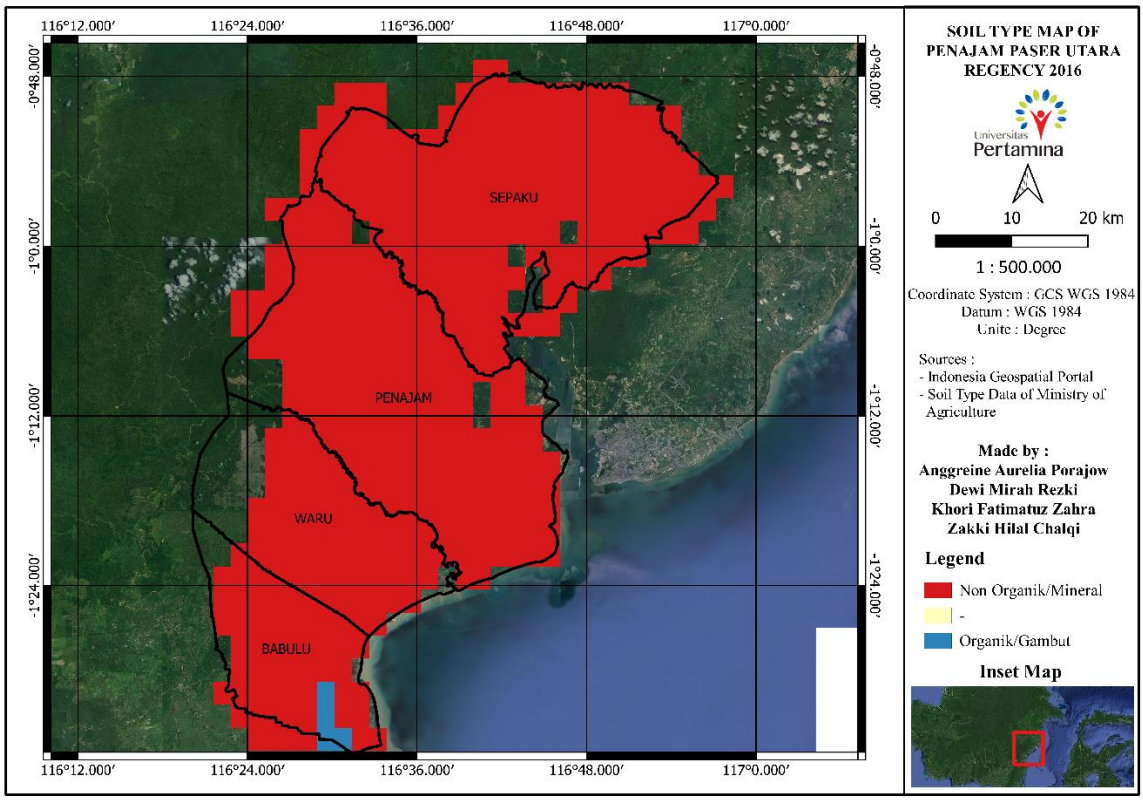

Figure 2 Soil Type Map of North Penajam Paser Regency 2016

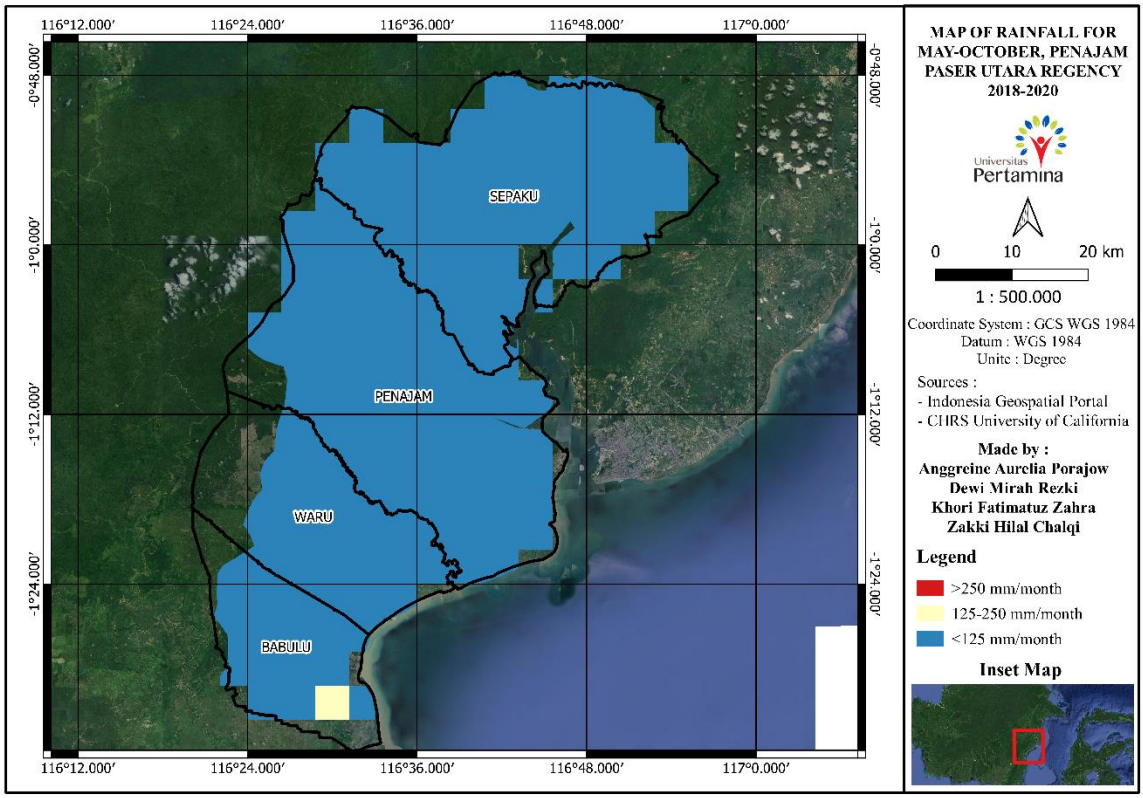

Figure 3 Rainfall Map of North Penajam Paser Regency 2018-2020

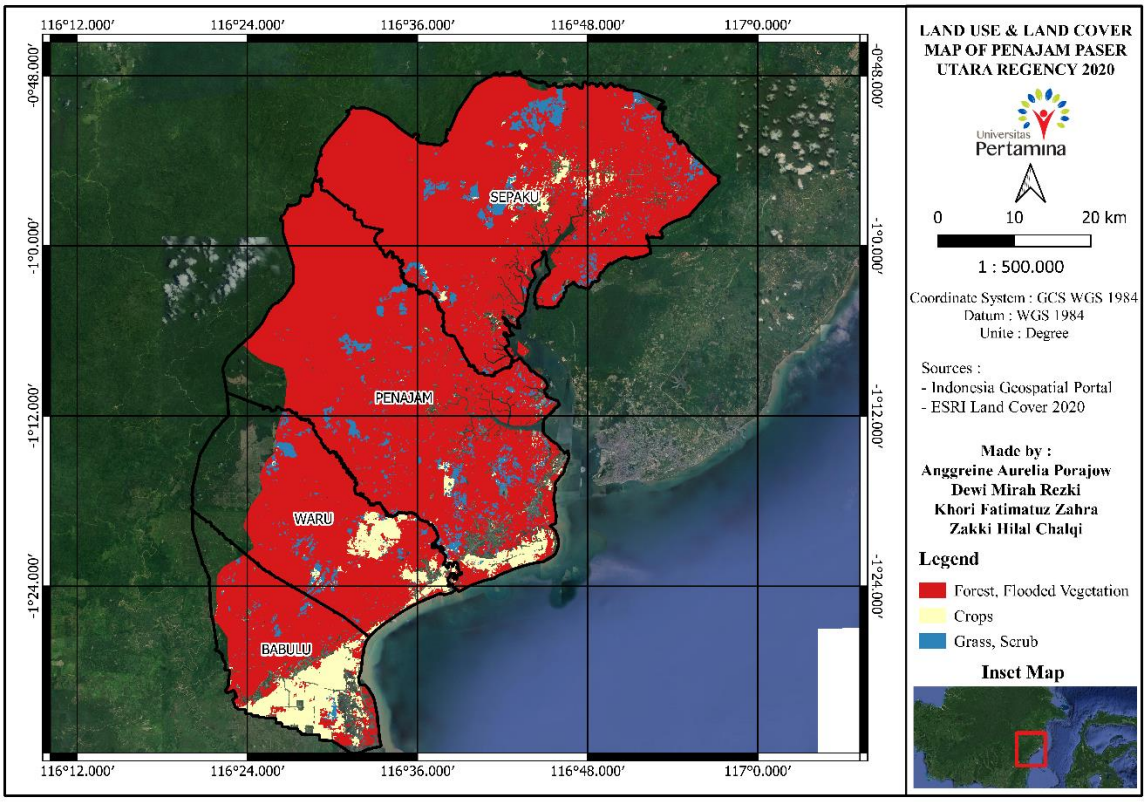

Figure 4 Land Type (Land Use & Land Cover) Map of North Penajam Paser Regency 2020

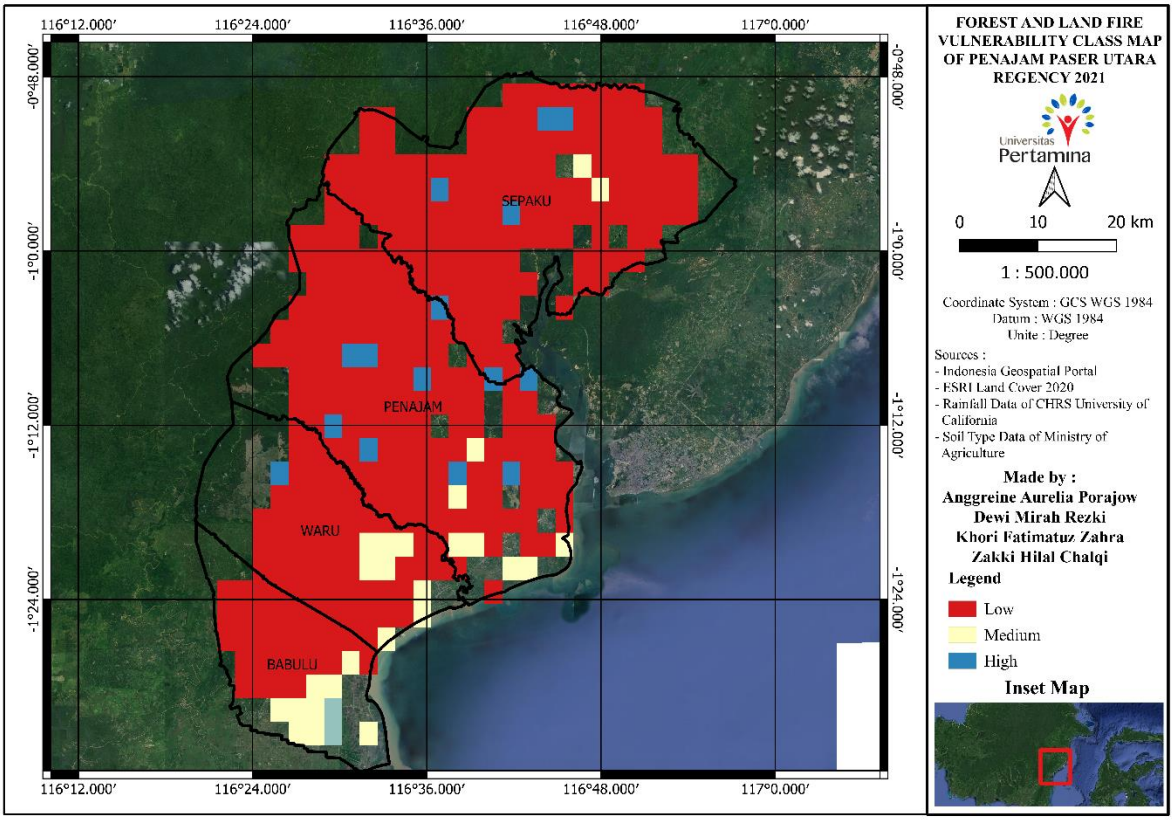

Figure 5 Forest and Land Fire Vulnerability Class Map of North Penajam Paser Regency 2021

PROCEEDINGS
JOINT CONVENTION BANDUNG (JCB) 2021
November 23rd – 25th 2021

Berkaca dari Penurunan Muka Tanah DKI Jakarta sebagai Pertimbangan Pembangunan Ibukota Indonesia di Kalimantan Timur menggunakan Data Sentinel-1

Anzalna Naufal Amaya[1], Athallah Wardhana[1], Siti Marwah[1]
[1]Program Studi Geofisika, Fakultas Matematika dan Ilmu Pengetahuan Alam, Universitas Indonesia.

Abstract
The relocation of the Indonesian capital has been a discussion for quite a long time and has been discussed since President Ir. Sukarno takes office. On August 26, 2019, President Joko Widodo announced that parts of the North Penajam Paser and Kutai Kartanegara Regencies, East Kalimantan would be converted as the new Capital City of Indonesia. The relocation of the capital is based on the level of population density and excessive buildings in DKI Jakarta, causing some areas to experience *Land subsidence*. This study utilizes Sentinel-1 satellite data and other Geographic Information System-based data to identify *Land subsidence* in DKI Jakarta. The processing results are then correlated with regional characteristics as a consideration in the development of the East Kalimantan region, especially North Penajam Paser Regency and Kutai Kartanegara as the new Capital City of Indonesia. The processing is carried out using SNAP (Sentinel Application Platform) and QGIS data processing applications to process Sentinel-1 data which is managed by ESA (European Space Agency). This study utilizes Sentinel-1 data with 4 months period obtained in January 2021 and May 2021. QGIS is used to correlate Sentinel-1 data with lithological data, building density, and land use to identify its effect on *Land subsidence*. Sentinel-1 data shows that *Land subsidence* is more dominant in the North Jakarta area which after being correlated with lithological data is composed of lithology of floodplain deposits and coastal ridge deposits of sediment type. Data obtained from BPS shows that the population density in Jakarta is at a value of 15,906 people/km2 with a total population of 10.56 million people in DKI Jakarta which is included in the high category based on BNPB parameters. About 85% of the area of DKI Jakarta is used as a settlement and is covered by buildings. Data on the population, population density, and area of East Kalimantan have very extreme differences when compared to DKI Jakarta. The total population of East Kalimantan as of 2020 is 3.77 million people who inhabit an area of 127,347 km2, so the population density value of East Kalimantan is around 29 people/km2. With more or less the same lithology, which is composed of sediment, it is recommended that the development for the purposes of the Indonesian capital which will be carried out later in East Kalimantan does not exceed the capacity or capability of the sediment lithology. If the development is carried out excessively, then there is a possibility that *Land subsidence* can also occur in East Kalimantan as its already happened in DKI Jakarta. Moreover, if groundwater exploitation activities are carried out in excess, the rate of *Land subsidence* can be even higher.

Keywords: Land subsidence, DKI Jakarta, East Kalimantan, Capital City, Sentinel-1

Introduction
DKI Jakarta merupakan Ibukota Indonesia yang secara sah telah ditetapkan melalui UU No 10 Tahun 1964, yang mana hal tersebut membuatnya menjadi pusat seluruh kegiatan diantaranya politik, ekonomi dan budaya di Indonesia. DKI Jakarta pada beberapa tahun belakangan hingga 2020 ini merupakan provinsi terpadat di Indonesia mencapai 15.900 jiwa per km2, selain itu, Jakarta juga menyandang predikat sebagai provinsi dengan pendapatan bersih dan pengeluaran per bulan tertinggi di Indonesia serta provinsi dengan Indeks Pembangunan Manusia (IPM) tertinggi di Indonesia dari 2014 - 2019 (Badan Pusat Statistik, 2020). Semua pencapaian tersebut dapat diperoleh meskipun DKI Jakarta merupakan provinsi terkecil di Indonesia dan hanya berperan 0,03% terhadap luas Indonesia. Pencapaian-pencapaian tersebut merupakan bukti bahwa DKI Jakarta benar-benar merupakan pusat kegiatan di Indonesia.

Besarnya kegiatan di DKI Jakarta berdampak terhadap masifnya pembangunan dan meningkatnya kepadatan penduduk Jakarta hingga dinilai pemerintah bahwa DKI Jakarta sudah tidak ideal untuk tetap menjadi ibukota dari Indonesia. Adapun bentuk respon pemerintah Indonesia adalah dengan pengumuman oleh Presiden Joko Widodo pada 26 Agustus 2019 yang menyatakan bahwa sebagian dari wilayah Kabupaten Penajam Paser Utara dan Kutai Kartanegara, Kalimantan Timur akan dialihfungsikan sebagai Ibukota Indonesia yang baru.

Faktor yang mempengaruhi keputusan pemerintah untuk memindahkan Ibukota Indonesia memiliki tanggapan yang berbeda-beda. Terlepas dari faktor yang dinilai pemerintah sangat krusial hingga perlu dilakukannya pemindahan ibukota, seperti segi ekonomi, keamanan ataupun sosial. Salah satu faktor yang perlu dipertimbangkan adalah kebencanaan. Beban yang terlalu berat serta populasi yang berlebihan apabila terus dibiarkan maka dapat mengakibatkan terjadinya penurunan muka tanah atau *Land subsidence* di DKI Jakarta. Bahkan, isu ini telah menjadi permasalahan beberapa tahun belakangan ini. Faktor kebencanaan inilah yang akan dibahas pada penelitian kali ini, terutama berfokus pada penurunan muka tanah atau *Land subsidence*.

Faktor pemicu terjadinya *Land subsidence* di DKI Jakarta dapat dikategorikan menjadi faktor alam dan juga faktor manusia. Faktor alam mengacu pada kondisi geologi regional yang mana DKI Jakarta tersusun atas endapan berumur kuarter diantaranya endapan aluvium, endapan kipas aluvial, endapan pematang pantai, dan endapan tuf Banten (Turkandi dkk, 1992). Endapan yang tergolong muda ini dapat dikatakan memiliki derajat kompaksi yang rendah sehingga akan terus mengalami kompaksi yang memicu terjadinya *Land subsidence*. Selanjutnya faktor manusia yang mengacu pada kondisi masifnya pembangunan akibat peningkatan kepadatan penduduk, dalam kondisi ini beban bangunan yang masif menyebabkan hilangnya air dalam ruang antar pori sehingga tekanan air pori mengalami penurunan dan menghasilkan peningkatan effective stress yang mana akan menekan semua partikel -

partikel penyusun tanah sehingga berdampak pada terjadinya *Land subsidence* (Terzaghi, 1943).

Sejak faktor alam khususnya litologi menjadi faktor pendukung besar atau kecilnya *Land subsidence* yang mungkin akan terjadi di suatu daerah, maka litologi Kalimantan Timur, khususnya Kabupaten Penajam Paser Utara dan Kabupaten Kutai Kartanegara perlu ditinjau juga. Kabupaten Penajam Paser Utara secara geologi termasuk ke dalam Peta Geologi Lembar Balikpapan. Terdapat 5 formasi yang menyusun Penajam Paser Utara, yaitu Alluvium (Qa), Formasi Kampungbaru (Tpkb), Formasi Balikpapan (Tmbp), Formasi Bebulu (Tmbl), dan Formasi Pamaluan (Tomp). Kelima formasi tersebut sudah tersusun dari yang berusia paling muda hingga tua. Kelima formasi tersebut secara garis besar tersusun atas batupasir, batulempung, dan di beberapa formasi yang berusia tua terdapat lapisan batubara (Hidayat & Umar, 1994). Untuk Kabupaten Kutai Kartanegara, kurang lebih terdapat 5 litologi yang menyusun daerah tersebut. Litologi tersebut dari berumur muda hingga tua, adalah sebagai berikut; Alluvium (Qa), Formasi Balikpapan (Tmbp), Formasi Wahau (Tomw), Batuan Terobosan Atas (Toma), Formasi Batu Ayau (Tea). Sama seperti daerah Penajam, Kutai Kartanegara tersusun atas batupasir dan batulempung (Atmawinata, et.al, 1995). Jika dibandingkan dengan litologi penyusun Jakarta, daerah Kalimantan, khususnya Kabupaten Penajam Paser Utara dan Kabupaten Kutai Kartanegara kemungkinan jauh lebih terkompaksi karena berusia lebih tua dari litologi di Jakarta, hal ini mengisyaratkan bahwa litologi Kalimantan sudah mengalami kompaksi lebih lanjut dari litologi Jakarta. Dan kondisi litologi ini menjadi daya dukung pembangunan untuk keperluan ibukota baru.

Data and Method

INSAR Sentinel 1-A

Peta *displacement* muka tanah dibuat dari citra satelit Sentinel 1-A. Citra Sentinel yang digunakan untuk daerah Jakarta terdiri dari 2 data Sentinel. Kedua data tersebut dijadikan sebagai data master dan juga data slave. Data master adalah data yang memiliki tanggal pengambilan data lebih dulu dibandingkan data slave. Penelitian ini menggunakan citra Sentinel tanggal 4 Januari 2021 untuk data masternya dan tanggal 4 Mei 2021 sebagai data slave. Perbedaan tanggal pengambilan data sentinel ini bertujuan untuk melihat perbedaan muka tanah yang terjadi dalam kurun waktu tersebut. Layanan yang digunakan untuk mendapatkan citra satelit Sentinel 1-A pada penelitian ini adalah *Alaska Sentinel Facility* yang dapat diakses melalui ASF Data Search (alaska.edu).

Citra Sentinel 1-A kemudian diolah menggunakan metode INSAR. Metode INSAR pada dasarnya adalah melihat perbedaan fase yang terjadi pada suatu daerah yang sama dalam kondisi waktu yang berbeda. Kepanjangan dari INSAR adalah *Interferometric Synthetic Aperture Radar*. Interferometri itu sendiri secara konsep biasanya diartikan sebagai analisis fase signal radar yang diterima oleh dua antena yang berbeda lokasinya atau waktu perekamannya (Lillesand & Kiefer, 2008). Pengolahan data Sentinel dengan metode INSAR ini diolah menggunakan software SNAP. Informasi yang dihasilkan disebut interferogram, yaitu nilai perbedaan fase pada tiap piksel data. Nilai perbedaan fase tersebut diolah lebih lanjut dan menghasilkan peta *displacement*. Adapun alur pengolahan data pada penelitian ini ditunjukkan pada Gambar 1.

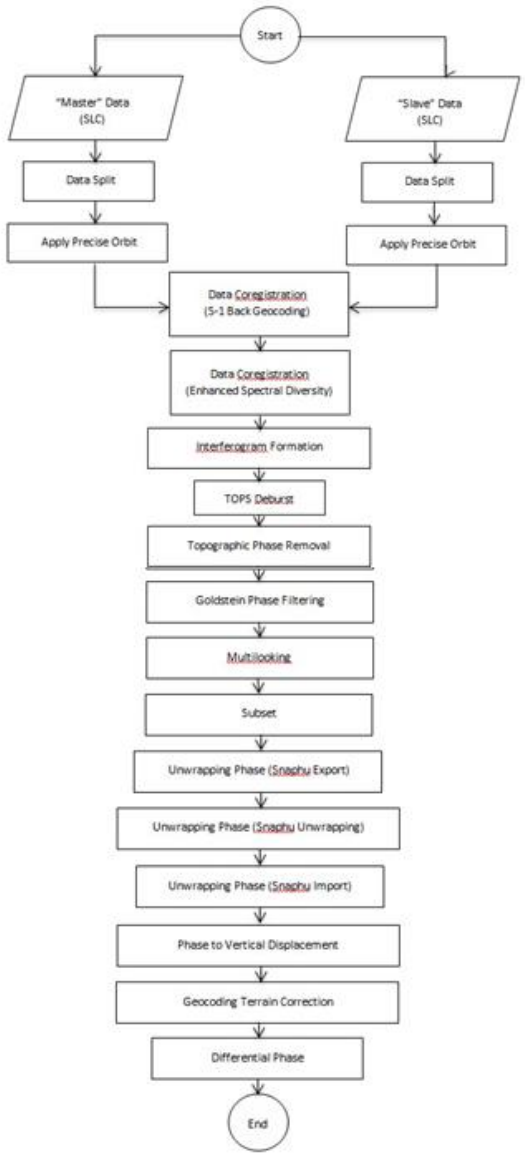

Gambar 1. Alur pengolahan citra satelit Sentinel 1 dengan SNAP.

Pembobotan Kerentanan

Pembobotan kerentanan suatu wilayah dibuat dengan tujuan mengklasifikasi daerah-daerah sesuai tingkat kerentanannya berdasarkan beberapa parameter tertentu. Pembobotan pada penelitian ini mengacu kepada publikasi paper oleh Bhattarai dan Kondoh (2017) yang menggunakan indikator kepadatan penduduk, luas daerah konstruksi, dan PDRB (Produk Domestik Regional Bruto) suatu wilayah seperti yang ditunjukkan pada Tabel 1. Akumulasi ketiga nilai tersebut kemudian dibagi menjadi tiga kategori yaitu rendah (1-1.68) menengah (1.68-2.34), dan tinggi (2.34 – 3.0).

Sistem Informasi Geografis

Data penelitian geosains akan lebih mudah diolah dan disajikan dalam bentuk peta sehingga konsep Sistem Informasi Geografis (SIG) sangat diperlukan. Hal ini dikarenakan data pada konteks geosains umumnya merupakan data spasial. Data pada penelitian ini diolah dan dianalisis menggunakan software QGIS, pengolahan SIG terbuka (*open-source*). Penggunaan software ini bertujuan untuk mempermudah proses identifikasi dan analisis data.

Beberapa hal yang dapat dilakukan antara lain adalah menghitung luas suatu daerah tertentu, memotong data sesuai daerah spasial tertentu, dan mengubah penyajian data menjadi suatu peta yang informatif. Proses ini memanfaatkan data-data spasial yang disediakan oleh Badan Informasi Geospasial (BIG) melalui Indonesia Geospatial Portal.

Tabel 1. Indikator Kerentanan Bencana Penurunan Muka Tanah

Faktor	Indikator	Kelas dan Nilai			
		Bobot	Rendah	Menengah	Tinggi
Kerentanan	Kepadatan Penduduk (per km²)	0,67	0-1000	1000-10000	>10000
	Produk Domestik Regional Bruto	0,24	0-99	100-499	>500
	Luas Daerah Konstruksi (%)	0,09	0-49	50-79	>80

Catatan. Diambil dari "Risk Assessment of Land subsidence in Kathmandu Valley, Nepal, Using Remote Sensing and GIS" oleh Bhattarai, R., Kondoh, A., 2017, Advances in Remote Sensing, 6, 132-146. Hak Cipta 2017 oleh Advances in Remote Sensing.

Result and Discussion

Pengolahan citra Sentinel-1 yang dilakukan menunjukkan hasil penurunan muka tanah yang bervariasi yang ditunjukkan pada Gambar 2. Tabel 2 menunjukkan statistik dari penurunan muka tanah DKI Jakarta. Penurunan muka tanah maksimum teridentifikasi sebesar 0,102 meter atau 10,2 cm dengan rata-rata penurunan muka tanah sebesar 0,021 meter atau 2,1 cm. Mengingat hasil yang diperoleh merupakan hasil dalam interval 4 bulan, dengan laju yang konstan penurunan muka tanah di DKI Jakarta dapat mencapai rata-rata 6,3 cm/tahun. Tren yang dapat dilihat pada peta hasil penelitian adalah terdapat beberapa daerah yang memiliki penurunan muka tanah lebih cepat relatif terhadap daerah lainnya. Kota Jakarta Utara merupakan daerah yang paling mengkhawatirkan disusul oleh Kota Jakarta Barat.

Pemetaan penurunan muka tanah pada periode-periode sebelumnya dengan metode-metode lainnya mendukung hasil penelitian yang telah dilakukan. Menurut Abidin, et al. (2011), penurunan muka tanah di DKI Jakarta secara umum berada pada angka 1-15 cm/tahun bahkan dapat mencapai 20-28 cm/tahun pada daerah dan periode tertentu. Data tersebut diperoleh dengan beberapa metode langsung ataupun tidak langsung, salah satunya adalah pemanfaatan citra satelit. Menurut Tim Penelitian dan Pengembangan *Land Subsidence* PUSFATJA LAPAN (2020), penurunan muka tanah rata-rata DKI Jakarta periode 2015 - 2020 hanya mencapai 0,1 - 8 cm/tahun. Hasil pengukuran rata-rata penurunan muka tanah menggunakan iNSAR pada periode 2017 - 2019 oleh (Ardha, et al., 2021) dapat dilihat pada Tabel 3. Walaupun terdapat variasi nilai dari penelitian-penelitian tersebut akibat beberapa faktor seperti metode dan rentang waktu penelitian, secara umum penurunan muka tanah di DKI Jakarta menunjukkan *trend* atau karakteristik yang sama. Penurunan muka tanah terjadi dengan laju hingga belasan cm per tahun serta Jakarta Utara serta Jakarta Barat merupakan dua daerah dengan tingkat penurunan paling cepat.

Penurunan muka tanah yang bervariasi seperti pada hasil penelitian ini merupakan pengaruh dari beberapa faktor. Faktor yang menyebabkan berpengaruh adalah pengambilan air tanah yang berlebihan dan pembangunan serta pengembangan wilayah yang intens. Selain itu, tanah memiliki tingkat kompresibilitas yang membuatnya secara alami akan memadat. Menurut Hyndman (2011), penurunan muka tanah utamanya disebabkan oleh pengambilan fluida seperti air dan minyak bumi dari lapisan bumi yang akan menyebabkan ruang antar pori batuan terkompaksi secara permanen. Sridharan & Gurtug (2005) menjelaskan bahwa salah satu faktor yang penting dalam aspek geoteknik adalah indeks kompresi atau compressional index (CC) yang kemudian dapat dikorelasikan dengan berbagai parameter seperti liquid limit dan plastic limit. Faktor ini dapat menjadi penghubung antara beban yang ditimbulkan oleh pembangunan dengan terjadinya kompresi tanah. Sebagai contoh, PDAM DKI Jakarta hanya dapat memenuhi 55% kebutuhan air bersih masyarakat. Hal ini menyebabkan masyarakat masih sangat tergantung mengambil air tanah sehingga di beberapa daerah tertentu menyebabkan kerucut depresi air tanah (Badan Pusat Statistik, 2005).

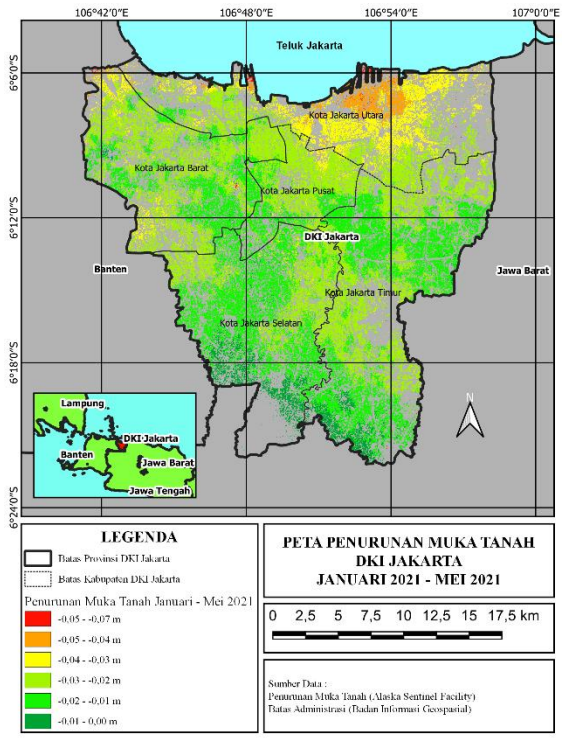

Gambar 2. Peta Penurunan Muka Tanah DKI Jakarta Januari – Mei 2021.

Tabel 2. Rata-Rata Penurunan Muka Tanah DKI Jakarta Januari – Mei 2021

Kabupaten/Kota	Penurunan Muka Tanah (m)		
	Minimum	Maksimum	Rata-Rata
Jakarta Utara	~0	-0,102	-0,032
Jakarta Barat	~0	-0,072	-0,022
Jakarta Selatan	~0	-0,058	-0,017
Jakarta Timur	~0	-0,062	-0,018
Jakarta Pusat	~0	-0,049	-0,22

Ancaman *Land subsidence* yang terjadi di Jakarta berkorelasi erat dengan kondisi kerentanan di Jakarta. Konsep kerentanan merupakan kesadaran bahwa tiap daerah akan merasakan dampak yang berbeda jika terjadi suatu bencana seperti penurunan muka tanah. Banyak penelitian telah menetapkan parameter untuk dapat mengukur tingkat kerentanan ini. Salah satunya adalah Bhattarai dan Kondoh (2017) yang menggunakan PDRB wilayah, persentase lahan terbangun, dan jumlah populasi suatu wilayah sebagai parameter kerentanan terhadap penurunan muka tanah.

Ketiga nilai ini perlu dipertimbangkan dalam rencana pembangunan dan pengembangan suatu wilayah, salah satunya adalah pertimbangan dalam pemindahan Ibukota Indonesia.

Tabel 4 menunjukkan kondisi kerentanan di Kalimantan khususnya Kabupaten Penajam Paser Utara dan Kabupaten Kutai Kartanegara tergolong rendah, berbanding terbalik dengan kerentanan DKI Jakarta yang tergolong tinggi. Kabupaten Penajam Paser Utara memiliki kepadatan populasi 64,07 jiwa/km2, PDRB wilayah sebesar 1.187,77 miliar/km2, dan persentase lahan terbangun sebesar 2%. Untuk di Kutai Kartanegara, kepadatan populasi berada di angka 58,03 jiwa/km2, PDRB wilayah sebesar 13.553,15 miliar/km2, dan persentase lahan terbangun sebesar 0,83%. Sebaliknya, DKI Jakarta memiliki kepadatan populasi di angka 14.371,5 jiwa/km2, nilai PDRB sebesar 487.301,69 miliar/km2, dan persentase lahan terbangun sebesar 90%.

Tabel 3. Rata-Rata Penurunan Muka Tanah DKI Jakarta

City	MAX (m)	MIN (m)	MEAN (m)
West Jakarta	-0.0284142	-0.0041615	-0.0151952
Central Jakarta	-0.0093872	-0.00159568	-0.00389577
South Jakarta	0.00184288	0.016214933	0.0090289
East Jakarta	-0.0138908	-0.0093139	-0.0116630
North Jakarta	-0.0345189	-.006438376	-0.01612811

Catatan. Diambil dari "Utilization of Sentinel-1 satellite imagery data to support Land subsidence analysis in DKI Jakarta, Indonesia" oleh Ardha, M., Suhadha, A. G., Julzarika, A., Yulianto, F., Yudhatama, D., & Darwista, R. Z., 2021, Journal of Degraded and Mining Lands Management, p.2591. Hak Cipta 2021 oleh Journal of Degraded and Mining Lands Management.

Tabel 4. Nilai Kerentanan Wilayah terhadap Penurunan Muka Tanah

Nama Wilayah	Faktor Kepadatan Penduduk			Faktor Lahan Konstruksi			Faktor PDRB			Total Skor
	Kepadatan Penduduk (jiwa/km2)	Kelas	Bobot	Persentase Lahan Konstruksi (%)	Kelas	Bobot	PDRB (miliar/km2)	Kelas	Bobot	
Samboja	63,69	1		2,10	1		519,09	3		1,48
Muara Jawa	55,08	1		2,28	1		374,46	3		1,48
Sanga - Sanga	84,52	1		3,68	1		115,84	3		1,48
Loa Janan	104,74	1		2,32	1		319,72	3		1,48
Loa Kulu	36,74	1		1,13	1		719,99	3		1,48
Muara Muntai	20,89	1		0,22	1		460,87	3		1,48
Muara Wis	8,48	1		0,16	1		549,99	3		1,48
Kota Bangun	32,05	1		0,73	1		567,64	3		1,48
Tenggarong	267,47	1		7,21	1		197,58	3		1,48
Sebulu	47,61	1		2,16	1		426,57	3		1,48
Tenggarong Seberang	155,32	1		6,41	1		216,89	3		1,48
Anggana	18, 58	1		0,58	1		892,75	3		1,48
Muara Badal	49,68	1		2,57	1		466,08	3		1,48
Marangkayu	23,01	1	0,67	0,54	1	0,09	578,55	3	0,24	1,48
Muara Kaman	13,46	1		0,41	1		1692,45	3		1,48
Kenohan	8,9	1		0,07	1		646,29	3		1,48
Kembang Janggut	13,42	1		0,05	1		954,84	3		1,48
Tabang	1,48	1		0,04	1		3853,56	3		1,48
Babulu	101,77	1		3,57	1		142,35	3		1,48
Waru	40,49	1		2,86	1		197,38	3		1,48
Penajam	82,99	1		0,33	1		430,26	3		1,48
Sepaku	31,01	1		0,68	1		417,78	3		1,48
Jakarta Selatan	14430	3		96,71	3		113251,90	3		3
Jakarta Timur	16624	3		88,74	3		134079,33	3		3
Jakarta Pusat	20177	3		98,90	3		38440,48	3		3
Jakarta Barat	19564	3		93,92	3		91323,66	3		3
Jakarta Utara	12708	3		80,32	3		102735,45	3		3

Catatan. Kecamatan di Kutai Kartanegara dan Penajam Paser Utara ditandai dengan warna biru dan merah muda, Kabupaten di DKI Jakarta ditandai dengan abu-abu. Hijau menandakan daerah dengan kerentanan ringan. Merah menandakan daerah dengan kerentanan tinggi.

Risiko bencana *Land subsidence* di DKI Jakarta selain menunjukkan kerentanan yang tinggi juga teramplifikasi oleh bahaya akibat kondisi litologi yang cenderung masih berumur muda dan didominasi oleh batu pasir aluvial atau endapan sungai dan delta. Kondisi litologi ini secara derajat kompaksi masih tergolong rendah jika dibandingkan dengan litologi yang menyusun Kalimantan. Di Kalimantan sendiri, umur litologi cenderung lebih tua dari litologi yang ada di Jakarta, sehingga derajat kompaksi seharusnya sudah jauh lebih tinggi dibandingkan Jakarta. Selain karena umur, litologi yang mendominasi di Kalimantan secara urutan stratigrafi sudah memiliki beberapa lapisan di atasnya sehingga tekanan yang dialami suatu lapisan formasi jauh lebih besar. Dengan kata lain, jika nilai kerentanan Kutai Kartanegara dan Penajam Paser Utara sama dengan nilai kerentanan DKI Jakarta, kemungkinan *Land subsidence* di Kalimantan akan lebih kecil karena litologi yang lebih kompak atau dapat dikatakan lebih kuat untuk menanggung beban yang besar.

Gambar 3 menunjukkan kondisi geologis Kutai Kartanegara dan Penajam Paser Utara. Secara spesifik, daerah di Kabupaten Penajam Paser Utara yang direkomendasikan untuk diadakan pembangunan adalah di atas litologi yang memiliki umur tua karena diasumsikan sudah memiliki derajat kompaksi yang jauh lebih tinggi, seperti Formasi Kampungbaru (Tpkb), Formasi Balikpapan (Tmbp),

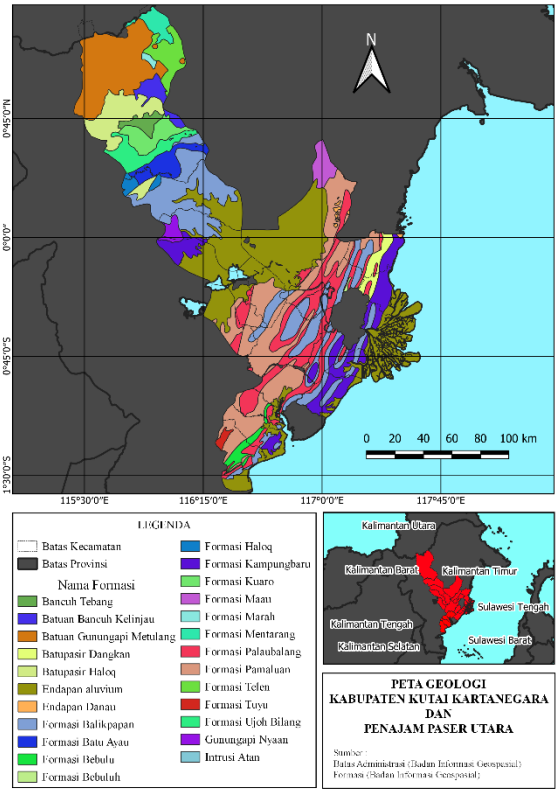

Gambar 3. Peta Geologi Kutai Kartanegara dan Penajam Paser Utara.

Formasi Bebulu (Tmbl), dan Formasi Pamaluan (Tomp). Untuk Alluvium (Qa) tidak disarankan untuk dilakukan pembangunan secara berlebih karena didominasi oleh endapan pasir. Formasi Pamaluan memiliki ketebalan lapisan berkisar antara 1500-2500 meter dan juga memiliki umur tua, yaitu oligosen akhir-miosen tengah. Selain itu, di formasi ini terdapat batulempung yang apabila mendapat tekanan atau kompresi yang tinggi akan terkompaksi dengan sangat baik, sehingga akan menjadikan formasi ini menjadi kandidat kuat untuk dilakukan pembangunan di atasnya karena memiliki karakter yang tahan beban. Untuk daerah di Kabupaten Kutai Kartanegara, hal yang sama harus dilakukan seperti yang telah disarankan di daerah Kabupaten Penajam Paser Utara, yaitu pembangunan dilakukan di atas formasi berumur tua, seperti Formasi

Balikpapan (Tmbp), Formasi Wahau (Tomw), Batuan Terobosan Atas (Toma), Formasi Batu Ayau (Tea). Terlebih lagi di Formasi Balikpapan terdapat batu gamping yang bersifat pejal, hal ini menandakan batu gamping yang ada di daerah ini sudah terkompaksi.

Conclusions

Penurunan muka tanah di Jakarta secara rata-rata terjadi sebesar 6.3 cm/tahun, apabila penurunan muka tanah dalam kurun waktu 4 bulan (batasan penelitian) diasumsikan bernilai konstan. Hal ini diakibatkan oleh pengambilan air tanah yang berlebih, jumlah bangunan, dan tingkat kompresibilitas tanah atau litologi. *Land subsidence* yang terjadi berkorelasi erat dengan kerentanan di Jakarta dan Kalimantan, khususnya daerah Kabupaten Penajam Paser Utara dan Kabupaten Kutai Kartanegara. Nilai kerentanan didapat dari 3 indikator, yaitu kepadatan populasi, PDRB wilayah, dan persentase lahan terbangun. DKI Jakarta memiliki nilai kerentanan yang tinggi yaitu bernilai 3 karena ketiga indikator menunjukkan angka yang tinggi juga. Sedangkan Kutai Kartanegara dan Penajam Paser Utara memiliki nilai kerentanan yang rendah, yaitu sebesar 1.48 karena ketiga indikatornya memiliki nilai rendah. Selain itu, jenis litologi menyumbang peran dalam besar kecilnya *Land subsidence* yang terjadi. Di Jakarta daerah didominasi oleh endapan pasir dan batupasir berumur Kuarter. Sedangkan di Kalimantan didominasi oleh batupasir, batulempung, serta batugamping yang berumur mulai dari Tersier semua kala hingga Kuarter. Untuk daerah yang kemungkinan memiliki ketahanan akan beban yang tinggi adalah Formasi Pamaluan pada Penajam Paser Utara dan Formasi Balikpapan pada Kutai Kartanegara.

References

Abidin, H. Z., Andreas, H., Gumilar, I., Fukuda, Y., Pohan, Y. E., & Deguchi, T, 2011, Nat Hazards, 1753-1771.

Ardha, M., Suhadha, A. G., Julzarika, A., Yulianto, F., Yudhatama, D., & Darwista, R. Z., 2021, Journal of Degraded and Mining Lands Management, 2587-2593.

Atmawinata, S., & Baharuddin, 1995, Peta Geologi Lembar Muara Ancalong, Kalimantan: Skala 1:250.000, Pusat Penelitian dan Pengembangan Geologi.

Badan Pusat Statistik, 2005, Jakarta Dalam Angka 2005, Jakarta: Badan Pusat Statistik.

Badan Pusat Statistik, 2020, Statistik Indonesia 2020, Jakarta: Badan Pusat Statistik.

Badan Pusat Statistik, 2021, Kutai Kartanegara Dalam Angka 2021, Kutai Kartanegara: Badan Pusat Statistik.

Badan Pusat Statistik, 2021, Penajam Paser Utara Dalam Angka 2021, Penajam Paser Utara: Badan Pusat Statistik.

Bhattarai, R., Kondoh, A., 2017, Advances in Remote Sensing, 6, 132-146.

Hidayat, S., & Umar, L, 1994, Peta Geologi Lembar Balikpapan, Kalimantan: Skala 1:250.000, Pusat Penelitian dan Pengembangan Geologi.

Hyndman, D., & Hyndman, D., 2011, Natural Hazards and Disasters, USA: Brooks-Cole.

Lillesand, T. M., Kiefer, R. W., & Chipman, J. W., 2015, Remote Sensing and Image Interpretation: Seventh Edition, John Wiley & Sons, Inc.

Sridharan, A., & Gurtug, Y., 2005, Geotechnical and Geological Engineering, 615-634.

Taniguchi, M., Dkk ., 2008, Science of the Total Environment, 404, 377-392.

Terzaghi, K, 1943, Theoretical Soil Mechanics. New York: John Wiley & Sons, Inc.

Tim Penelitian dan Pengembangan *Land subsidence* Pusat Pemanfaatan Penginderaan Jauh, 2020, Laporan Kemajuan Hasil Pemantauan Penurunan Muka Tanah (*Land subsidence*) di Beberapa Kota Besar di Pulau Jawa Berdasarkan Data Satelit Penginderaan Jauh, Lembaga Penerbangan dan Antariksa Nasional (LAPAN).

Turkandi., Dkk, 1992., Peta Geologi Lembar Jakarta dan Kepulauan Seribu, Jawa, Bandung: Pusat Penelitian dan Pengembangan Geologi.

PROCEEDINGS
JOINT CONVENTION BANDUNG (JCB) 2021
November 23rd – 25th 2021

Indonesia Paleotsunami Database As an Innovation for Tsunami Disasters Mitigation in Indonesia

Ihda Ibtihaj[1], Supriyanto Suparno[2], Muhammad Rizqy Septyandy[1]
[1]Geology Study Program, University of Indonesia, Pondok Cina, Beji, Depok, 16424, Indonesia
[2]Geophysics Study Program, University of Indonesia, Pondok Cina, Beji, Depok, 16424, Indonesia
Corresponding E-mail: supriyanto@sci.ui.ac.id

Abstract
Indonesia's tectonic activity is one of the most active in the world. These conditions make Indonesia prone to earthquakes, tsunamis and volcanic eruptions. Indonesia has been hit by various tsunami events. However, not all characteristic tsunami events are well known and recorded. Knowing the characteristics of a tsunami occurrence is very important to understand the frequency and intensity of tsunamis in the present. This research will create a WebGIS database for paleotsunami in Indonesia. Tsunami events data comes from literature related to tsunami events such as books, journals, reports, final project and others. Making WebGIS in this study will be developed using website programming, namely Hypertext Markup Language, Cascading Style Sheet and JavaScript. The research results obtained 302 tsunami data. The WebGIS created presents a database of tsunami events in Indonesia, a dashboard of Indonesian tsunami statistics and a learn tsunami feature. It is hoped that the results of this database will serve as a means of information for future paleotsunami research needs and as a means of education regarding the potential for tsunamis in Indonesia.

Introduction
Indonesia is one of the world's most active tectonic activities (Latief et al., 2000). Indonesia located at the confluence of four major plates, namely Eurasia, Indo-Australia, the Philippines, and the Pacific (Nugroho et al., 2018). As a result of these conditions, Indonesia is prone to earthquakes, tsunamis, and volcanic eruptions.
Indonesia has experienced a series of tsunami events that have caused thousands of casualties. The danger of a tsunami disaster needs to be studied to undestand the characteristics of its occurrence based on the history of tsunami events. For most of the tsunami events that have hit Indonesia, the tsunami's mechanism and character are not well known (Latief et al., 2000). Knowing the history of tsunami events is essential to understand the frequency and intensity of tsunamis in the present (Dunbar & McCullogh, 2012).
Tsunami deposits are deposits carried by the tsunami, which are left on the coast during the inundation phase or returned to the sea during the backwash phase. These deposits are used to identify past tsunami events (Zaim et al., 2018). Paleotsunami is a tsunami that occurs before historical records or there are no written observations (IOC, 2019). Paleotsunami deposits can be identified using paleotsunami proxies.
Database information related to tsunami events and paleotsunami deposits is very important for further research and tsunami disaster mitigation (Gusiakov, 2001). Tsunami incident data covering Indonesia have been published previously in catalog form including Soloviev and Go (1974), Soloviev et al. (1992), and Iida et al. (1967) (Soloviev & Go, 1974; Soloviev et al., 1992; Iida et al., 1967). The catalog is an international tsunami catalog that records tsunami events in the Pacific Ocean. Information in the catalog is less detailed about tsunami and paleotsunami events that have occurred in Indonesia. Research that contains information on tsunami events in Indonesia has generally been carried out by Meteorogical, Climatological and Geophysical Agency (2019) and Latief et al. (2000) (Meteorogical, Climatological and Geophysical Agency, 2019 and Latief et al. 2000). This research is limited to recording tsunami events in Indonesia and only in general. The older tsunami events are not recorded in the catalog.
Research on tsunamis in Indonesia has not developed an information platform that provides information on all tsunami incidents that have hit Indonesia. Therefore, it is necessary to create a database for the history of tsunami events in Indonesia.This research will be an innovation in tsunami research in Indonesia. The Indonesia Paleotsunami Database will become a tsunami and paleotsunami data integration platform that provides detailed information about the characteristics of tsunamis and paleotsunami deposits in Indonesia.
Indonesia Paleotsunami Database will be made based on WebGIS. WebGIS is a Geographic Information System (GIS) that uses the internet network as the main access to distribute spatial data and information as well as GIS analysis (Abdalla and Esmail, 2019). The use of WebGIS was chosen because this method can be easily accessed by the general public. The results of this database is expected to be a means of information for future paleotsunami research needs as well as a means of education regarding the potential for tsunamis in Indonesia.

Data and Method
Paleotsunami proxy are various criteria used to identify deposits caused by tsunami processes (Chague-Goff et al., 2011) The use of proxies in paleotsunami research has not become a standard thing and is still being developed today. The most common paleotsunami proxy and has been widely used in paleotsunami research is the proxy developed by Goff et al. (2011). Paleotsunami proxy based on Goff et al. (2011) (James-Goff, et al., 2011) are as follows:

1. Grain size ranging from lumps (about 750 m^3 or larger) to fine clay.
2. Sediment with characteristics generally smooth to the top.
3. Sediment units that differ/contrast with other layers.
4. Different lower and upper sub-units that characterize tsunami runup and backwash.

5. Contact with the underlying layer is usually misaligned or erosional.
6. May contain a rip-up clast of reworked material.
7. The loading structure at the bottom of the deposit and can be associated with liquefaction features at the ground surface due to earthquakes.
8. Microscale features may be visible on thin sections but not visible on the stratigraphic scale of the field.
9. Measurement of anisotropy magnetic susceptibility (AMS) combined with grain size analysis.
10. Heavy mineral laminates are close to the bottom of the unit/sub-unit
11. Increased concentration of elements sodium, sulfur, chlorine, calcium, strontium, magnesium, titanium, zirconium in tsunami deposits
12. Possible contamination by heavy metals and metalloids.
13. Geochemical evidence (saltwater content) and microfossil findings extending further inland than the maximum limit should be found on land.
14. Shells of marine organisms and rich layers of shells.
15. Crushed shells, wood, and various other materials are often found "inserted" near or in the upper layers of suspected paleotsunami deposits.
16. It may be associated with vascular plant remains, paleosoil, or buried bone remains.
17. Generally associated with an increase in the appearance of diatoms living in marine environments – brackish water.
18. Found a collection of foraminifera shells (or fossils of other sea creatures) which are increasing in number but in a state of damaged shells.
19. Terrestrial pollen concentrations generally decrease on deposit and/or coastal pollen concentrations increase.
20. The existence of archaeological sites that are overlaid or overlain by layers of sediment.
21. There is a collection of archeological middens, but there are no signs of sudden changes in the conditions of the ancient land and coastal environment.
22. Archaeological sites in the form of buildings that appear to have been damaged by water waves.
23. Archaeological sites that have been re-deposited in inappropriate locations.
24. Replication, layers of coastal archaeological remain and piles of shells that are separated or reworked as a feature of the occurrence of inundation marks.
25. Local folklore about the tsunami.
26. Paleogeomorphological acquisitions.
27. Paleogeomorphology at the time of inundation indicates a small probability of storm pooling.
28. Known and demonstrable or identifiable local or regional tsunamigenic knowledge.
29. Local and regional knowledge of ancient environments can provide ancient storm information.
30. Similar coastal deposits were found regionally indicating regional inundation.

The flow chart of this research is presented in Figure 1. The data used in this study consists of primary and secondary data. Primary data is field data from Bagedur Beach, Lebak, Banten. While, secondary data is literature from research related to tsunamis in Indonesia such as books, journals, reports, final project and others both from the perspective of geoscience, archeology or folklore.

Primary and secondary data that have been collected will be matriculation. Important information about tsunami events that have occurred that will be matriculated. The tsunami event data will be grouped based on the mechanism causing the tsunami and the proxies used in identifying the predicted tsunami deposits.

The data resulting from the matriculation will then be processed into GeoJSON data (Geospatial JavaScript Object Notation). GeoJSON tsunami data will be in the form of a point indicated that at the location of the point the tsunami has occured. In addition, this data will contain attributes about the characteristics of a tsunami event at that location.

The WebGIS Indonesia Paleotsunami Database will be developed using website programming. The programs used are HTML (Hypertext Markup Language), CSS (Cascading Style Sheets), and JavaScript. WebGIS will present attributes related to paleotsunami in Indonesia. The attributes used to present content in WebGIS are as follows:

1. Province / Regional Location
2. Location of the tsunami incident
3. The latitude and longitude of the tsunami / paleotsunami point
4. Location status (there is an unknown deposit or deposit)
5. Physical characteristics (tsunami candidate deposition conditions, or other enabling conditions)
6. Classification of the time of occurrence
   - *Historical* (1800 AD - present)
   - *Prehistorical* (years <1800 AD)
7. Time of occurrence (Date and Year)
8. Validity
   - Fair (1-4 criteria of proxy)
   - Moderate (5-8 criteria of proxy)
   - *Excellent* (> 9 criteria of proxy)
9. Nature of evidence (Primary or Secondary)
10. Description of nature of evidence (sediment deposits, field observations, or community stories)
11. Mechanical Pentarikhan (*Dating Technique*)
12. Type of Pentarikhan (*Dating Method*)
13. Paleotsunami point elevation
14. Inundation zone boundaries
15. The thickness of the sediment/sediment formed
16. The cause of the tsunami
17. Tsunami source location and coordinates
18. Paleotsunami proxy used
19. References

Result and Discussion

Field data results

In the Bagedur Beach area, Lebak, Banten, samples of paleotsunami deposits were taken. There are eight sampling stations. A representative location indicating the presence of paleotsunami deposits is at station BG-06 which is a rice field area around Bagedur Beach with coordinates of -6.80895987° S, 106.01105014° E .

Based on the results of hand drilling, it was found that there is a layer that is a candidate for paleotsunami deposits, namely Sand Layer C (Figure 2). The layer has a thickness of 8 cm. There is a stark contrast between the paleotsunami layers below and above. The paleotsunami layer contains rip-up clasts in the form of shell fragments that are quite a lot compared to the top and bottom. The presence of wood

fragments inserted near the suspected paleotsunami layer was found.

Granulometric analysis was carried out on the sample station BG-06. The sample interval for analysis is 2 cm. The analysis was carried out at a depth of 142-440 cm which is a sedimentary layer. The results of the analysis show that the candidate paleotsunami layer (sand layer C, Figure 2) has a mean value ranging from 2.40 - 2.57 phi (fine sand). Sorting values ranged from 0.87 (medium sorted) - 1.22 (poorly sorted). The skewness value ranges from -1.58 to -1.10 phi (strongly coarse skewed). Kurtosis values range from 1.8 to 2.46 phi (very leptokurtic). The graph of the mean value between the paleotsunami candidate layers (218-226 cm deep) and the layer above it shows a smaller mean value. The smaller the mean value indicates that the grains are getting finer. Thus, in the paleotsunami candidate layer, a smooth upward pattern was found which is the paleotsunami criterion.

X-Ray Fluoresence (XRF) analysis was carried out on samples from station BG-06 at a depth of 221-222 cm, 240-242 cm, 249-251 cm, and 436-437 cm. The results of XRF analysis show that at a depth of 221-222 cm which is part of the C sand layer (paleotsunami candidate) has higher Na, Ca, S, Mg levels than other depths. The high value of these elements indicates that the sediment source comes from the marine environment (James-Goff et al., 2011).

The proxies used in the identification of paleotsunami deposits at Bagedur Beach, Lebak, Banten are proxy numbers 1, 2, 3, 5, 6, 8, 11, 14, 15, 30. Based on the proxies used, the validity of paleotsunami deposits at Bagedur Beach, Lebak, Banten is excellent. The mechanism that caused the tsunami from the paleotsunami deposits found was thought to be an earthquake. The southern region of Java is an active subduction zone so there is a lot of seismic activity. The tsunami events that have occurred in the southern region of Java were predominantly caused by earthquakes (Latief et al., 2000).

Database processing results

The tsunami incident data that was collected and entered into the database amounted to 302 data. Data processing for the database is made matriculated. Data from the literature that is entered into the matriculation is information according to the required attributes.

The distribution of tsunami data in Indonesia, almost all of Indonesia's coasts have been hit by a tsunami. The West Coast of Sumatra Island is the area that has experienced the most tsunamis. The southern regions of Java, North Sulawesi and the Maluku Islands have also experienced many tsunamis. The East Coast of Kalimantan Island is the area least affected by the tsunami. This shows that almost all regions in Indonesia have the potential for a significant tsunami disaster. The results of data grouping show that the causes of tsunamis in Indonesia have several mechanisms, namely earthquakes, volcanism, landslides and combined mechanisms. the recapitulation of the causes of the tsunami in Indonesia is presented in Table 1.

Earthquakes are the mechanism that causes most tsunamis in Indonesia. Based on the database, the occurrence of tsunamis caused by earthquakes mostly occurs in areas associated with the location of active faults. Several active fault zones that are the source of earthquakes that cause tsunamis include the Sunda Megathrust, Banda Megathrust, Flores Rise Fault, North Sulawesi Megathrust, Papua Megathrust, Sangihe Megathrust, and local faults (Harris et al., 2016 and Meteorological, Climatological and Geophysical Agency, 2019).

Volcanism activities that occur in Indonesia have been the cause of the tsunami. The eruption of Mount Krakatau on August 26, 1883, was a volcanic activity that caused tsunami waves that impacted Lampung and Banten (Iida et al., 2017; Mutaqin et al., 2019; Putra, et al., 2016; Putra et al., 2017). The Lampung and Banten regions were also affected by the tsunami on December 22, 2018, due to volcanism from Mount Anak Krakatau. Volcanic activity from Mount Krakatau and Anak Krakatau is one of the pieces of evidences from the past and present that volcanism has the potential to cause tsunamis.

Underwater avalanches are the mechanism that once caused a tsunami in Indonesia. Tsunamis caused by submarine avalanches are rare according to the database. Although rare, tsunamis caused by avalanches are also a risk of disaster.

The Indonesian paleotsunami proxy in this study is a collection of proxies grouped based on the created database. The grouping of proxies is done to find out which proxies are dominant and effectively used in Indonesia. The most widely used proxy is proxy number 28 while the least used is proxy number 23 (Table 2). Based on the grouping of proxy data from the literature used by paleotsunami research in Indonesia, only 28 of the 30 proxies are available. Proxies number 24 and 27 have not been implemented in Indonesia. The validity of the data in this study was determined based on the number of proxies used in identifying tsunami events. The results show that the validity of the tsunami incident data in Indonesia is in three categories, namely Excellent, Moderate and Fair. The number of data validity is Excellent as many as 19, Moderate as many as 53 and Enough as much as 230 validity of this data reflects the quality of tsunami event data based on a large amount of literature and proxies used to identify tsunami events. The more literature and proxies used, the better the validity of the data.

Most of the tsunami events in Indonesia have fair data validity. Tsunamis that occur in historical and prehistorical periods are both classified as fair validity. The validity of this fair data is due to the lack of literature that records in detail the tsunami incident. Improving the validity of tsunami event data in Indonesia can be done by developing paleotsunami research. The development of paleotsunami research can increase the number of proxies used to identify tsunami events in Indonesia so that the validity of the data can be better.

Geological proxies are criteria for the identification of suspected paleotsunami deposits based on geological aspects (James-Goff, et al., 2011). A well-preserved tsunami deposit will be strong evidence that a tsunami has occurred, both for identification now and in the future. The presence of tsunami deposits will make geological proxies workable. The use of geological proxies will make it easier to identify deposits caused by tsunamis because tsunami deposits have distinctive sediment characteristics. The quality of data that uses geological proxies is better than other data that does not apply geological proxies. Based on the database, tsunami events identified by geological proxies have Moderate - Excellent data validity.

The WebGIS created in this research is a web map database of tsunami events in Indonesia. The information presented is data on tsunami events in Indonesia and their characteristics. All information in this WebGIS is open source. The main features of this WebGIS are layer selection, attribute detail information, and data download. WebGIS Indonesia Tsunami Event Database can be accessed via the link https://trc-ui.geosinyal.id/

The initial view of the WebGIS Indonesia Paleotsunami Database will display a Map of Indonesia and data on

tsunami events in Indonesia. The design of this WebGIS display is made informative and attractive so that the general public can easily access and understand the information in WebGIS. In general, the basic appearance of WebGIS consists of a menu bar at the top and widget

The menu bar contains information about WebGIS. In the menu bar you can get information about WebGIS such as about, disclaimer, map legend, download dashboard feature data and tsunami study feature. The data presented in WebGIS is open source, including the overall tsunami incident data, proxies used and reference sources (Figure 3). Widgets in WebGIS are basic features in a Web-based Geographic Information System. These widgets include a layer widget to set the data layer that is cool to display. Then, the widget zooms in and out to zoom in and out on the map. Then, a search widget to search for a specific location, a home widget to return to the home screen, and a my location widget to find out where the user is.

Layer in WebGIS is divided into 2, namely the main layer and additional layers. The main layer is the main data for tsunami events including the "All Data", "Classification", "Validity", "Nature of Evidence", "Deposit Status", and "Tsunami Cause" layers. Meanwhile, the additional layer is a layer that contains supporting data including the "Source Tsunami", "Fault" layer, "Subduction" layer, and " Indonesia's Volcano" layer. The data presented can be selected based on the available layers. The map will only display data according to the layer that is activated. The display of the layer settings that you want to display is presented in Figure 3.

The detailed information feature of tsunami characteristics is a feature of quick access to the attributes of the tsunami database. This feature can be accessed by clicking on the symbol of the desired tsunami event to know in more detail its characteristics. Detailed information will appear after the symbol is clicked. Information will be presented in the form of a pop-up dialog box containing the attributes of the selected tsunami event. The pop-up dialog box display is shown in Figure 4.

The WebGIS comes with a dashboard feature and learn tsunami feature. The dashboard provides statistical infographics and tables of tsunami events in Indonesia. The learn tsunami feature is a tsunami education article on a website view that can be read by the viewer. The existence of this feature as a means of support to facilitate access to WebGIS in order to better understand the data presented.

The Indonesia Paleotsunami Database in this study acts as a data center for tsunami events in Indonesia. In the future, this database is expected to be a tool in tsunami research both for prediction, understanding the characteristics of tsunamis and paleotsunami and the development of other research related to tsunamis in Indonesia. Developments in data quality in the future will be very useful for research in predicting tsunami recurrence. Currently, the data in the database is still limited so that it cannot predict the recurrence of a tsunami in all regions of Indonesia.

Conclusions

Data on tsunami events entered into the database amounted to 302 data. Tsunami events in Indonesia were caused by 255 earthquakes, 26 volcanism, 1 landslide, 10 earthquakes - landslides, 7 earthquakes – volcanism, and 3 volcanism - landslides. There are 28 proxies used to identify tsunami events in Indonesia out of 30 available proxies. Proxy number 28 is the dominant proxy used. The application of geological proxies can improve data quality. The validity of the tsunami data in Indonesia was "Excellent" as many as 19, "Moderate" as 53, and "Fair" as 230. The WebGIS Indonesia Tsunami Event Database can be accessed via the link https://trc-ui.geosinyal.id/. Information that can be accessed in WebGIS is the database of tsunami events and paleotsunami deposits in Indonesia, the Indonesian tsunami statistical data dashboard, and the educational feature for studying tsunamis. The WebGIS Indonesia Paleotsunami Database is an update for tsunami information media in Indonesia to be more comprehensive and informative, which was previously only a note in the catalog. The database in this research will continue to be updated in line with the development of tsunami research in Indonesia

References

Abdalla, R., and Esmail, M., 2019, WebGIS for Disaster Management and Emergency Response, Springer.

Chagué-Goff, C., Schneider, J. L., Goff, J. R., Dominey-Howes, D., and Strotz, L., 2011, Earth-Science Review, **1-2**, 107-122

Dunbar, P. and McCullough, H., 2012, Natural Hazards, **63**, 267–278.

Goff, J., Chagué-Goff, C., Nichol, S., Jaffe, B., and Dominey-Howes, D., 2011, Sedimentary Geology, **243–244**, 70-88.

Gusiakov, V. K., 2001, International Tsunami Symposium, **1**, 263–272.

Harris, R., and Major, J., 2016, Geological Society Special Publication, **441**, 9–46.

Iida, K., Cox, D. C., and Pararas-Carayannis, G., 1967, Preliminary catalog of tsunamis occurring in the Pacific Ocean, Hawaii Institute. of Geophysics.

Intergovernmental Oceanographic Commission (IOC), 2019, Tsunami Glossary, UNESCO.

Latief, H. and Puspito, N.T., 2000, Natural Disaster Science, **22**, 25–43.

Meteorological, Climatological and Geophysical Agency, 2019, Katalog Tsunami Indonesia Per-Wilayah Tahun 416-2018, Earthquake and Tsunami Center Deputy for Geophysics.

Mutaqin, B.W., Lavigne, F., Hadmoko, D.S., and Ngalawani, M.N., 2019, IOP Conference Series Earth and Environmental Science, **256.**

Nugroho, P.C., Pinuji, S.E., Ichwana, A.N., Nugraha, A., Wiguna, S., et al., 2018, Indeks Risiko Bencana Indonesia, National Disaster Management Agency.

Putra, P.S., and Yulianto, E., 2016, Journal of Environment and Geological Disasters, **7**, 19-34

Putra, P.S., and Yulianto, E., 2017, Indonesia Journal of Geology and Mining, **27**, 83-95

Soloviev, S. L., and Go, C. N., 1974, A Catalogue of Tsunamis on the Western Shore of the Pacific Ocean (173-1968), Nauka Publishing House.

Soloviev, S. L., Go, C. N., and Kim, K. S., 1992, Catalog of Tsunamis in The Pacific 1969-1982, Soviet Geophysical Committee.

Zaim Y., Daryono, Sukanta, I.N., Rizal, Y., Aswan, Wahyu, R.O., et al., 2018, Jejak Tsunami Masa Lalu diantara Pangandaran dan Cilacap, Earthquake and Tsunami Center Deputy for Geophysics.

Acknowledgements

The authors would like to thank Geology and Geophysics Study Program University of Indonesia for supporting this research. The authors also would like to thank The Ministry of Research and Technology for providing the Basic Research for Higher Education Grant to fund this research.

PROCEEDINGS
JOINT CONVENTION BANDUNG (JCB) 2021
November 23rd – 25th 2021

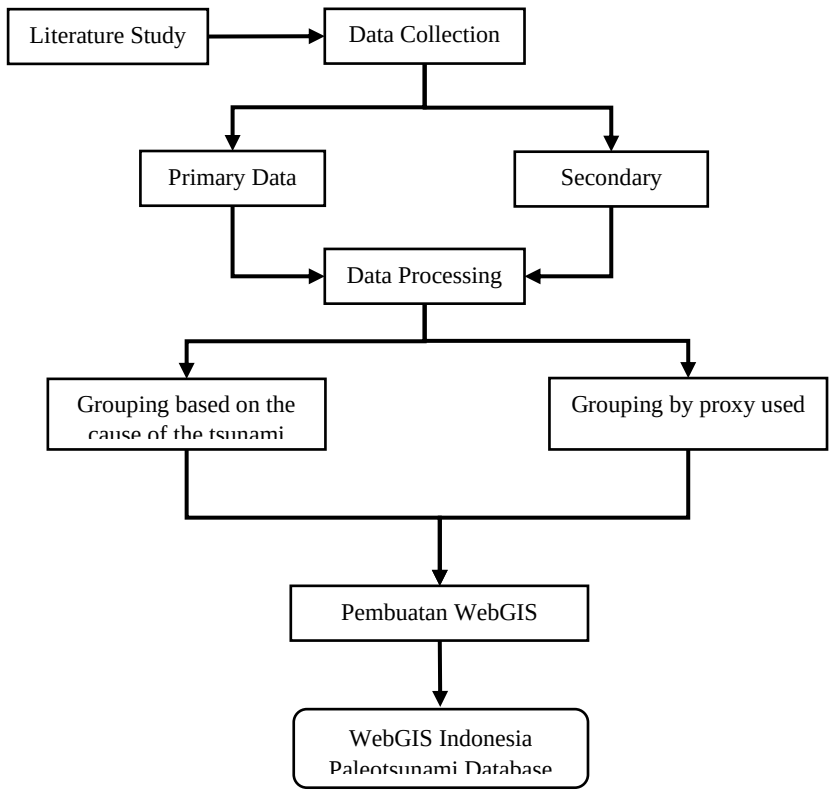

Figure 1: Research flowchart

PROCEEDINGS
JOINT CONVENTION BANDUNG (JCB) 2021
November 23rd – 25th 2021

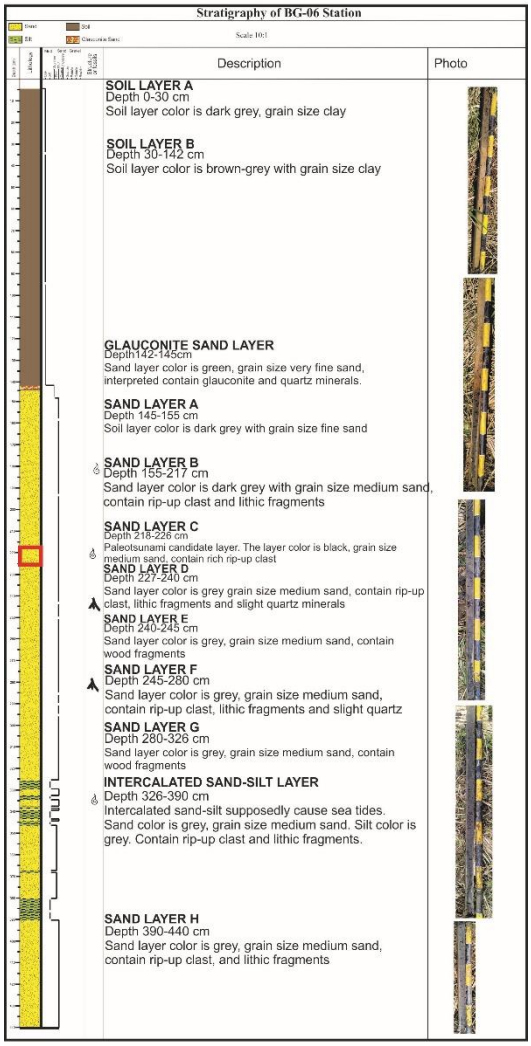

Figure 2: Stratigraphy of paleotsunamai deposit in BG-06 Station

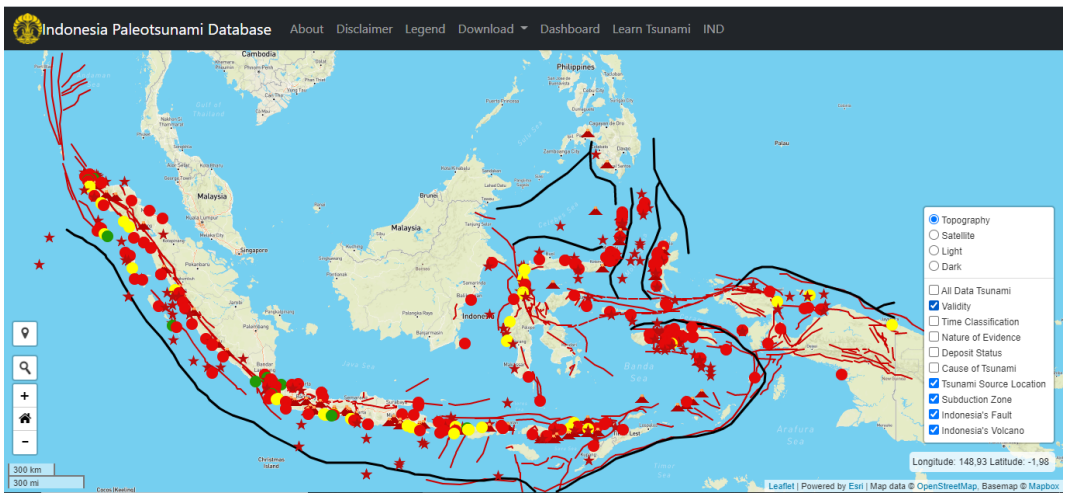

Figure 3: The WebGIS View and layers available in WebGIS

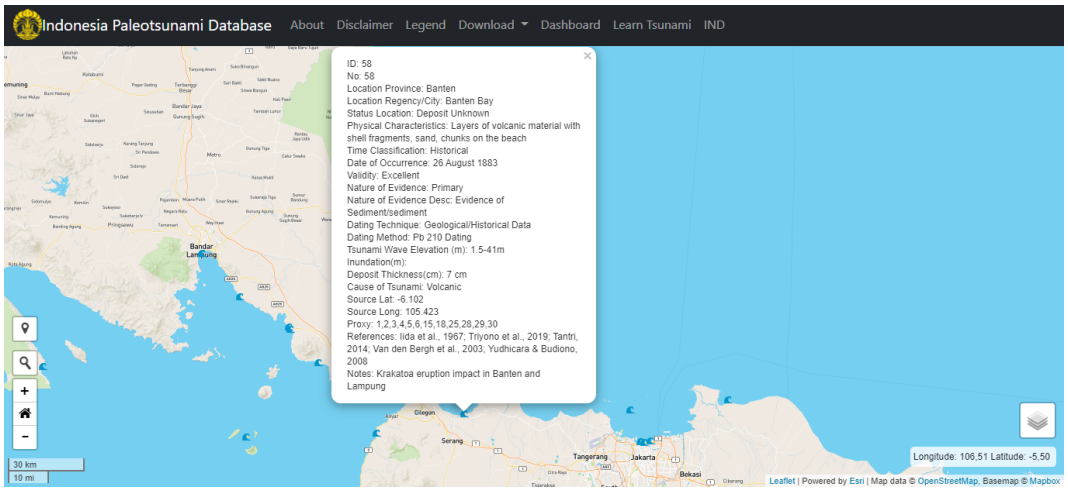

Figure 4: The pop-up box displays the tsunami event attributes

No	The cause of the tsunami	Amount
1	Earthquake	255
2	Volcanism	26
3	Landslides	1
4	Earthquake & Landslides	10
5	Earthquake & Volcanism	7
6	Volcanism & Landslides	3

Table 1: Table of the causes of the tsunami in Indonesia

Proxy No.	Amount	Proxy No.	Amount	Proxy No.	Amount
1	69	11	7	21	1
2	21	12	3	22	24
3	58	13	3	23	1
4	18	14	11	24	0
5	42	15	20	25	48
6	38	16	9	26	2
7	2	17	2	27	0
8	17	18	15	28	74
9	7	19	4	29	44
10	6	20	2	30	63

Table 2: Table of paleotsunami proxy applied in Indonesia

PROCEEDINGS
JOINT CONVENTION BANDUNG (JCB)2021
November 23rd – 25th 2021

A BREAKTHROUGH CONCEPT: ALL-IN-ONE RESERVOIR NANO CONTROLLER TO IMPROVE OIL RECOVERY

Dwi Endah Rachmawati[1], Rahayu Lestari Sugihartini[1], Alltop Amri Ya Habib[1], Mufiid Fatkhurrahman[1], M Raihan Suprajeni[1], Ardian Nengkoda[2], Sutrasno Kartohardjono[1], Andy Noorsaman Sommeng[1]
[1]Department of Chemical Engineering, Faculty of Engineering, University of Indonesia, Depok, Indonesia
[2]Saudi Aramco, Dhahran, Eastern, Saudi Arabia

Abstract

Most fields in Indonesia have reached their mature phase; thus, conventional technologies have challenged further production. The decrease in oil production of the mature field is a natural phenomenon, and many methods have been conducted to solve this issue especially using Enhanced Oil Recovery (EOR). The current popular method for EOR is a thermal method which usually includes flooding the reservoir with steam, gasses, or chemical polymer. This study aims to bring to light a breakthrough concept that contains new nanoparticles application to improve oil recovery. Firstly, as the methodology, a literature study and benchmarking were conducted to identify current EOR technology gaps. Then conceptual technology is designed considering three variables: economic, practicality, and feasibility, mainly because in a mature field, when the oil is trapped in the reservoir, it needs heat to diffuse. The current technologies have proposed various methods that have seen success even in the most challenging field. Unfortunately, such technologies still have a limited range of effects as the problem often happens upon the scale-up of a project. The chemical flooding EOR is reviewed, including the current development and challenges, and finally, nanotechnology is found to be promising to boost reservoir production. A breakthrough new technology in the form of nanoparticle EOR is proposed. The proposed set of nanoparticles can dissipate heat to the reservoir combined with molecular communication to control the reservoir temperature and better mobility (flow) of the oil within the reservoir. The set of nanoparticles consists of nanoparticles A and B (all in one), which are responsible for altering the surface wettability and heating respectively with ultrasonic and electromagnetic sources to activate them.

Keywords: EOR, electromagnetic, graphene oxide, nanoparticles A & B, ultrasonic.

Introduction

In recent years, the oil production in Indonesia has kept on decreasing as more oil fields matured and dried. This matured field cannot be exploited in traditional methods, and the technology to continue the production on this field is commonly called EOR (Enhanced Oil Recovery). There are various methods in doing EOR, but unfortunately, these EOR methods tend to cost significantly higher or have a high degree of difficulty in their field application than the conventional oil production method. This problem is further amplified by the recent pandemic that still hits the nation, making economic leeway for investing in these risky EOR methods more undesirable for Indonesia.

To improve the situation, Indonesia will need EOR technology that is both practical and affordable, and in recent years, the technology that has been growing in popularity is nanoparticle technology. Nanoparticle technology has seen many uses in almost every industry, medical use, automotive, and the petroleum industry. The nanoparticle is a technology for designing tiny materials. In practical use has been seen to have a high surface-to-volume ratio, tiny size for increased penetration, and practically low cost and more ecologically friendly than using common chemicals (Sun, Zhang, Chen, & Gai, 2017). These factors made nanoparticles an exciting field and a potential solution to EOR problems.

In recent years, the application of nanoparticles have been rapidly develop to help EOR processes, such as in chemical flooding, thermal flooding, miscible flooding and microbial flooding tecnologies (Sircar, 2021). One of them is the smart-and nano-hybrid chemical EOR flooding using Fe_3O_4/eggshell nanocomposites that able to improve oil recovery by 8.16% during tertiary recovery. The nanoparticle was synthesized from *Commersomia bartramia* plant through a hybrid chemical solution. It could effectively reduce interfacial tension and change the wettability to water to water when dispersed in CTAB surfactant (Omidi, et al., 2020). However, there are still many challenges in implementation of nano-EOR technique into practice, such as cost-effective, disperse nanoparticles into reservoirs, etc.

In this study, a concept of EOR that will mainly use nanoparticles is given. The concept is given by using nanoparticle combinations that can alter the surface wettability and excitable properties that control the

underground oil flow by heating; thus, the oil can be extracted easily. These excitable properties will be controlled by magnetic influence. Moreover, the combination of ultrasonic and magnetic waves can propagate a longer distance. The concept of this paper will be supported by various related findings from journals and books to prove its possibility for future realization theoretically.

Data and Method

The concept of this study is developed by doing literature studies, which concentrates on classic EOR technologies and the latest development in nanoparticle technologies, and by mentoring professionals and academics in the field. The research is done to create a concept that can improve existing EOR technology. It is conducted theoretically by combining the nanoparticles technologies application with commonly used EOR technology. The advantages and disadvantages of each technology are listed and compared, then applications of nanoparticles technology are applied to improve their advantages or mitigate some of the weaknesses theoretically. The presented result on this paper discussion is based on the strongest candidate where nanoparticles are deemed most crucial and significantly impact current EOR technology. The research is done online with the help of *Remote UI* to obtain the most reliable sources of data. There is no laboratory experiment as the research is done during self–isolation due to the pandemic in Indonesia.

Results and Discussion

Enhanced oil recovery (EOR) is a technique used to increase oil production. One of the techniques to increase the oil production is ultrasonic-based EOR. This technique is used to improve oil extraction and help minimize damage to wellbore formations by supplying mechanical vibrations in an elastic medium. Ultrasonic is energy generated by longitudinal mechanical waves with frequencies above 20 kHz and categorized into low frequencies (20kHz-1MHz)(Shafiai & Gohari, 2020).

Ultrasonic waves are transmitters in an elastic medium. In wave propagation, the amplitude and velocity of the elastic particles change significantly, resulting in stirring, loosening of boundary friction, dispersion, micro-cracking, impact fragmentation, thermal action, and others. The advantages of this mechanical vibration are:

1. Mechanical vibration can damage the cohesion between the embedded particles and the reservoir rock.
2. Mechanical vibration changes the size of the capillary pores, reducing the surface tension of the pores, resulting in capillary expansion and contraction.
3. The impact stress generated by mechanical vibrations causes micro-cracks in the rock formations. When the vibration reaches a certain intensity, the affinity between the crude oil and the rock weakens. Thus, the crude oil is separated from the rock mass.
4. Boundary friction exerts a local heating effect on the fluid. The local heating effect of this boundary friction is the source of the ultrasonic thermal effect. This friction occurs locally and is intense, resulting in enormous localized high temperatures.
5. Reducing the viscosity of crude oil and increasing the seepage rate.

Crude oil is a liquid that contains wax, colloids, asphaltene, and other macromolecular compounds. The action of high-frequency and high-intensity ultrasonic waves causes mechanical vibrations of large molecules, thereby accelerating the formation of relative motion between large molecules. Due to the inertia of the molecule, the molecular chain is broken, and the macromolecule is destroyed, especially in the cavity state, and the depolymerization is more pronounced. For compound polymers in crude oil, depolymerization is sufficiently verified to reduce crude oil viscosity. Of course, this can only happen at a high sound intensity and over a long period. The high temperature generated by the vibration can also reduce the viscosity (Shafiai & Gohari, 2020; Wang et al., 2020).

Based on this explanation, the application of this technology dramatically improves the recovery of oil wells. The construction is simple and does not pollute the oil layer, so it has broad prospects. Ultrasonic-based oil recovery technology has a considerable cost advantage. The cost between the ultrasonic and polymer injection was compared by Meribout, where polymer injection devices can reach 230,000 US$, while ultrasonic devices are much cheaper (90,000 US$) (Meribout, 2018). Thus, applying this technique leads to actual savings in the cost of the oil recovery operation. However, due to the limited range of ultrasonic wave propagation in the reservoir, ultrasonic waves cannot play a role far from the oil well (Shafiai & Gohari, 2020; Wang et al., 2020).

On the other hand, Kundu has researched the use of ultrasonic and electromagnetic waves for medical purposes. The research has proven that, when combined, both ultrasonic and electromagnetic waves could propagate a longer distance (Kundu, 2014). Thus, the idea of this concept is to combine the energy from both ultrasonic and electromagnetic waves in nanoparticle.

The proposed idea is to use electromagnetic waves to activate the nanoparticles. A set of nanoparticles consist of nanoparticle A, and nanoparticle B. Nanoparticle A can alter the surface wettability. In contrast, nanoparticle B has the function of storing energy from electromagnetic waves. The transducer will transmit an electromagnetic induction which will cause electron excitation so that the nanoparticle can release heat to oil and reservoir. After the heat is released, the oil's viscosity will be lowered; thus, the oil flow will increase. Besides, the ultrasonic waves could enlarge the reservoir rock porous, resulting in a higher yield of oil and easier of its transportation.

One of many challenges in oil production is enhanced oil recovery (EOR) from oil-wet carbonate reservoirs. Many oil reserves in the world are found in oil-wet carbonate reservoirs (Jarrahian, Seiedi, Sheykhan, Sefti, & Ayatollahi, 2012). In oil-wet rock, oil tends to stick to the rock due to the hydrophobicity of the walls of porous media. On the other hand, water tends to stick to the rock in a water-wet rock (Hosseini, Sadeghi, & Khazaei, 2017). However, the water-wet reservoir is more efficient because water flooding is far cheaper than organic solvent. Therefore, the chemical injection is conducted to alter the wettability of reservoir rocks.

Nanoparticles can alter the superhydrophobic to super hydrophilicity rock in the reservoir because of their ability to pass through some reservoir rock pores. Hosseini et al. studied an effective method in wettability alteration of carbonate rocks from superhydrophobic to hydrophilic state using TiO_2/SiO_2 nanoparticles with relatively high stability in contact with the salt solution, thermal stability at 150°C, and high durability of the coated surfaces in environmental conditions. Besides, another nanoparticle such as fluorochemical-modified graphene oxide can alter the original liquid-wetting to strong gas-wetting in the gas reservoir (Wang, et al., 2021).

Ultrasonic waves with the fluids in the pores lead to improved oil production rate because they change the permeability of the rock to oil and water. The capillary mechanism is used for this method because peristaltic transport makes mechanical deformation of the pore walls (Salem *et.al.*, 2015). Nanoparticles can deeply penetrate a very long distance through a rock pore. The situation of the reservoir from oil-wet to water-wet will significantly improve oil recovery (Hassan *et.al.*,2020). With the help of nanoparticles, the mobility of oil in the water-wet reservoir is increased with water injection.

The development of magnetic nanoparticles (MNPs) has become one of the main issues, especially in biology, medicine, and engineering. In medical purposes, the use of MNPs can range from MR imaging (Sun, 2008) (Kim, Zeng, Ng, & Brazel, 2009) to localization (Darton, et al., 2008) (Martina, Wilhelm, & Lesieur, 2008), or improving the delivery of drugs to a specific location. This concept can also be used in the EOR method in the oil reservoir. Studies show that MNPs are usually composed of a stabilized metallic core and functionalized by the addition of an outer shell with conjugated functional groups.

In most cases, the metallic core is composed of iron or iron-oxide-based compounds, such as maghemite (γ-Fe2O3) or magnetite (Fe3O4). A magnetic core enables the MNPs to be manipulated using a magnetic field gradient (Williams, 2017). The size of MNPs usually is smaller than 100 nm. MNPs can be synthesized from any material with magnetism (Gupta, Li, & Xiao, 2000). Study found that magnetic field can be used to induce heating around superparamagnetic or ferromagnetic nanoparticles, such as Fe_3O_4 or γ–Fe_2O_3 (Dennis, et al., 2008). In either method, metal (or metal oxide) nanoparticles can be easily combined with several different polymer systems (Glover, et al., 2013).

From the explanation above, we can conclude that graphene oxide-based of super hydrophilic and super paramagnetic nanoparticles can be applied to this concept. Nanoparticle A could be a nano surfactant modified graphene oxide, and nanoparticle B could be an iron oxide/graphene oxide nanocomposite. Both graphene oxide layers could be connected with a crosslinking process (Li, et al., 2018). Thus, we propose an idea of a set of nanoparticles such as illustrated in Figure 1 and the design process as shown in Figure 2.

Conclusions

A set of nanoparticles that consists of nanoparticle A and nanoparticle B with graphene oxide base is predicted to improve the oil recovery. In this concept, the combination of ultrasonic and electromagnetic waves is utilized to activate the nanoparticles.

References

Darton, N., Hallmark, B., Han, X., Palit, S., Slater, N., & Mackley, M. (2008). The in-flow capture of superparamagnetic nanoparticles for targetting therapeutics. Nanomed.: Nanotechnol., Biol. Med., 19-29.

Dennis, C., Jackson, A., Borchers, J., Ivkov, R., Foreman, A., Hoopes, P., . . . Gruettner, C. (2008). The influence of magnetic and physiological behaviour on the effectiveness of iron oxide nanoparticles for hyperthermia. J. Phys. D: Appl. Phys.

Glover, A. L., Bennett, J. B., Pritchett, J. S., Nikles, S. M., Nikles, D. E., Nikles, J. A., & Brazel, C. S. (2013). Magnetic Heating of Iron Oxide Nanoparticles and Magnetic Micelles for Cancer Therapy. IEEE Trans Magn., 231-235.

Gupta, A., Li, X. W., & Xiao, G. (2000). Magnetic and transport properties of epitaxial and polycrystalline chromium dioxide thin films. Journal of Applied Physics, 6073-6078.

Hassan Y M, Guan B H, Zaid H M, Hamza M F, Adil M, Adam A A, Hastuti K. (2020). Crystal, 11, 106.

Hosseini, M. S., Sadeghi, M., & Khazaei, M. (2017). Wettability Alteration from Superhydrophobic to Superhydrophilic via Synthesized Stable Nano-Coating. Surface & Coatings Technology, 79-86.

Jarrahian, K., Seiedi, O., Sheykhan, M., Sefti, M., & Ayatollahi, S. (2012). Wettability Alteration of Carbonate Rocks by Surfactants: A Mechanistic Study. Colloids and Surfaces A: Physicochemical and Engineering Aspects, 1-10.

Kim, D.-H., Zeng, H., Ng, T., & Brazel, C. (2009). T1 and T2 relaxivities of succimer-coated MFe23+O4 (M =Mn2+, Fe2+ and Co2+) inverse spinel ferrites for potential use as phase-contrast agents in medical. MRI, 3899-3904.

Kundu, T. (2014). Ultrasonic and Electromagnetic Waves for Nondestructive Evaluation and Structural Health Monitoring. Procedia Engineering, 395-405.

Li, C., Li, Z., Ye, X., Yang, X., Zhang, G., & Li, Z. (2018). Crosslinking-Induced Spontaneous Growth: A Novel Strategy for Synthesizing Sandwich-Type Graphene@Fe3O4 Dots/Amorphous Carbon with High Lithium Storage Performance. Chemical Engineering Journal, 4-1620.

Martina, M.-S., Wilhelm, C., & Lesieur, S. (2008). The effect of magnetic targeting on the uptake of magnetic-fluid-loaded liposomes by human prostatic adenocarcinoma cells. Biomaterials, 4137-4145.

Meribout, M. (2018). On Using Ultrasonic-assisted Enhanced Oil Recovery (EOR): Recent Practical Achievements and Future Prospects. IEEE Access, 6, 51110–51118. https://doi.org/10.1109/ACCESS.2018.2859774

Omidi, A., Manshad, A., Moradi, S., Ali, J., Sajadi, S., & Keshavarz, A. (2020). Smart- and Nano-Hybrid Chemical EOR Flooding using Fe3O4/Eggshell Nanocomposites. Journal of Molecular Liquids.

Salem A, Abbas A, Salah A, Snosy M F. (2015). Journal of Petroleum and Mining Engineering. 1-19.

Shafiai, S. H., & Gohari, A. (2020). Conventional and electrical EOR review: the development trend of ultrasonic application in EOR. Journal of Petroleum Exploration and Production Technology, 10(7), 2923–2945. https://doi.org/10.1007/s13202-020-00929-x

Sircar, A. (2021). Applications of Nanoparticles in Enhanced Oil Recovery. Petroleum Research.

Sun, C., Lee, J., & Zhang, M. (2008). Magnetic nanoparticles in MR imaging and drug delivery. Adv. Drug Deliv. Rev: Inorganic Nanoparticles Drug Del, 1252-1265.

Sun, X., Zhang, Y., Chen, G., & Gai, Z. (2017). Application of Nanoparticles in Enhanced Oil Recovery: A Critical Review of Recent Progress. Energies.

Wang, Z., Fang, R., & Guo, H. (2020). Advances in ultrasonic production units for enhanced oil recovery in China. Ultrasonics Sonochemistry, 60(March 2019), 104791. https://doi.org/10.1016/j.ultsonch.2019.104791

Wang, Y., Li, Y., Wang, Q., Tang, L., Liang, L., Zeng, Y., . . . Xu, N. (2021). The Influence of Fluorochemical-Modified Graphene Oxide on the Gas-Wetting Alteration of Reservoir Cores. Colloids and Surfaces A: Physicochemical and Engineering Aspects.

Williams, H. M. (2017). The application of magnetic nanoparticles in the treatment and monitoring of cancer and infectious disease. Bioscience Horizons.

PROCEEDINGS
JOINT CONVENTION BANDUNG (JCB)2021
November 23rd – 25th 2021

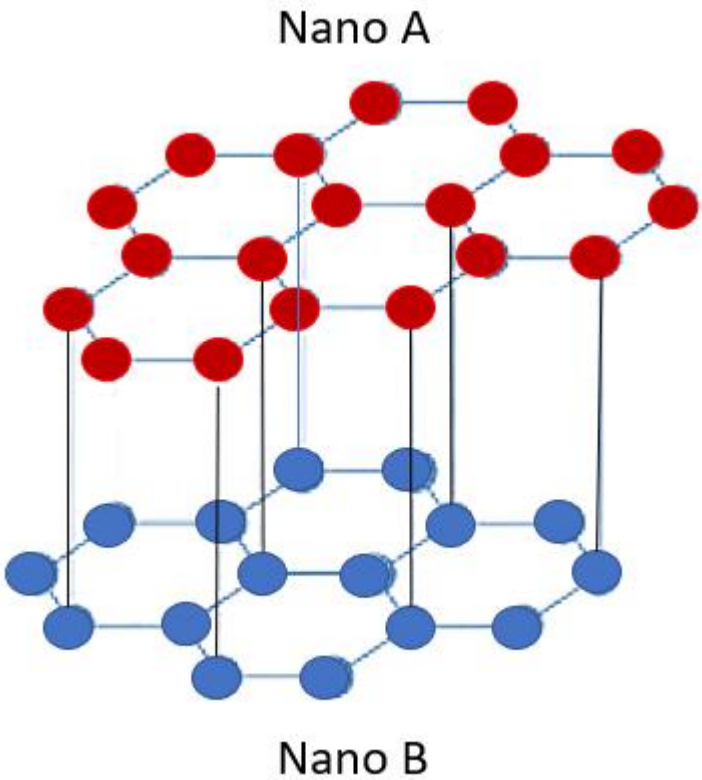

Figure 1: The proposed idea of nanoparticle A and nanoparticle B

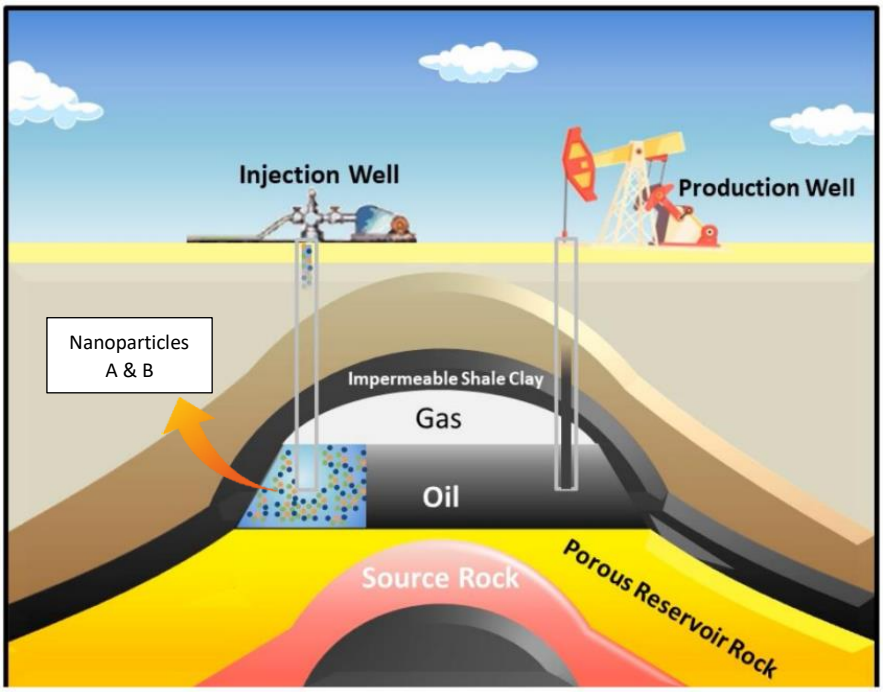

Figure 2: Design Process

PROCEEDINGS
JOINT CONVENTION BANDUNG (JCB)2021
November 23rd – 25th 2021

SIMULATION AND OPTIMIZATION OF STEAM FLOOD USING INJECTION INTERMITTENT

1. *Astra Agus Pramana, Petroleum Engineering, Universitas Pertamina, Jakarta, Indonesia*
2. *Willy Naufalindo Erwin, Petroleum Engineering, Universitas Pertamina, Jakarta, Indonesia*

Abstract
This research is about the simulation and optimization of a steam flood using intermittent injection with the purpose to simulate the steam flood method and design the scenario of steam flood intermittent to make steam flood more optimal in terms of gain lower steam oil ratio and higher oil recovery factor. The method used in this research is reservoir simulation with CMG-STARS software. The simulation results showed the difference in the value of steam oil ratio and the oil recovery factors between steam flood continuously (before optimization) with a steam flood after optimization with intermittent injection. The intermittent steam flood injection resulted in a lower steam oil ratio and a greater oil recovery factor than the continuous steam flood.

Introduction

The need for oil and gas will increase every day, while the level of oil and gas production will continue to decline. Due to the decrease in oil and gas production, this can lead to unmet energy needs of the people in society. Based on this situation, an effort is needed to increase the oil and gas production to meet the community's fuel energy needs. Actions can be made to find potential new oil and gas fields or evaluate the old field to increase production of the area.

Conventional technology in the field of drilling and exploitation of oil in the area is a simple technology. This technology is used by the petroleum industry and can only produce a maximum of 45% of the total petroleum reserves. Meanwhile, about 55% of petroleum left in rock pores cannot be a product made by conventional techniques, so it needs to be applied to the increase in refined petroleum oil or better known as Enhanced Oil Recovery (EOR). (Ko, Chon, Jang, & Jang, 2014)

Enhanced Oil Recovery (EOR) is a production technique applied to old oil and gas fields that have experienced significant production declines. EOR technology has been developed in old oil wells with large and profitable petroleum reserves when advanced oil drains (EOR) are carried out to overcome the decline in oil production. According to the Ministry of Energy and Mineral Resources (2016), about 13 thousand petroleum wells can be done with advanced draining or EOR. Draining the remnants of petroleum in the existing old oil wells is expected to increase national petroleum production and be more practical and economical than drilling new wells.

EOR technology is a method that in the process injects some materials such as gas, steam, or chemicals into underground reservoirs to encourage more oil. EOR technology is very strategically applied in Indonesia. And the EOR method that has long been used in Indonesia is the hot steam injection method.

In its operation, one of the disadvantages of the steam flood is the loss of heat from steam during distribution into the reservoir. It can happen due to the gravity override effect of injected hot steam. Hot steam tends to flow through the porous layer horizontally until eventually, the heat from the steam is trapped into impermeable rocks such as shale. This phenomenon makes the heat from the steam not enough to heat the oil as a whole so that as the steam moves away from the injection well, the heat will decrease, and the superheated steam phase turns into saturated steam and then becomes hot water.

There must be blocking or limiting between the permeable and impermeable layers to anticipate heat loss in the reservoir. The research was conducted by simulation method. The simulation was performed on a reservoir model representing a field with a heavy oil reservoir. Simulations are done with several scenarios. The determination of the scenario is based on the operation of steam injection, namely by distinguishing the interval of injection time or intermittent injection.

The simulation will be conducted on wells in this X-field using CMG-STARS reservoir software expected to be the best scenario for steam flood optimization.

Data and Method

- ***Reservoir Model***

The simulation is run using CMG-STARS simulator software. The reservoir model is designed multi-layered and has homogeneous fluid and rock data using heavy oil field data compiled from research journals as second or third parties. The reservoir model can be seen in Figure 1, which displays an image of the reservoir model with permeability properties. For initial condition data in the reservoir can be seen in Table 1. The area of draining is 5.5

PROCEEDINGS
JOINT CONVENTION BANDUNG (JCB)2021
November 23rd – 25th 2021

acres, and the reservoir thickness is 80 ft. The distance between the producer and the injector is calculated so that it is obtained at 311 ft. And the highest peak of the reservoir or top of the reservoir is at a depth of 700 ft from the ground level.

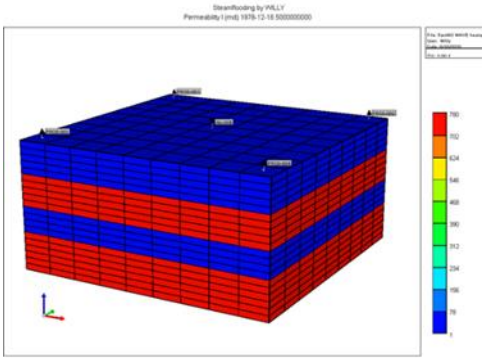

Figure 1. Reservoir model simulation: Permeability, model configuration, and wells location.

Table 1. Initial Reservoir Properties

INITIAL RESERVOIR PROPERTIES		
Properties	**Values**	**Units**
Oil Gravity	**13**	**API**
Top of Formation	**1700**	**ft**
Initial Pressure	**200**	**psi**
Initial Temperature	**140**	**oF**
In-Situ Oil Viscosity at 140 °F	**399**	**cp**
Thickness	**80**	**ft**

This reservoir model assumes no aquifer zone or gas zone either above the oil zone or below the oil zone. The gas phase is not present in the reservoir system because the reservoir pressure is above the bubble point pressure. The thickness of the layer or grid layer on this model is 4 ft and consists of 20 layers. Refer to the 20 layers contained in the reservoir model; there are 11 layers of sand and 9 layers of shale. It is divided into 2 types of zones, namely, pay zone or sand zones and shale zones. Different property values are made to distinguish the shale layer from sand, especially in the components of heat capacity, heat conductivity, porosity, and permeability. Each layer of sand has a uniform porosity of 30%. For sand layer permeability, it has a value that varies between 780-2220 mD, while shale layers have a uniform porosity and permeability value of each layer, which is 3% and 0.05 mD.

For pay zone itself is divided into 2, namely, pay zone 1 and pay zone 2. At the same time, the shale zone is also divided into shale zone 1 and shale zone 2. For more details, the comparison of sand and shale zone components can be seen in Table 2.

Table 2. Rock Properties and Components of Sand and Shale

ROCK & FLUID PROPERTIES		
Property	**SAND**	**SHALE**
Porosity, %	**30**	**5**
Permeability, mD	**780-2220**	**0.5**
Heat Capacity, Btu/(ft3*F)	**35**	**27**
Thermal Conductivity, Btu/(ft*day*F)	**35**	**14**
Oil Saturation	**70%**	**0%**
Layer	**6-10 and 15-20**	**1-5 and 11-14**

- **Grid Model**

The grid-type used in this reservoir modelling is the Cartesian type with a 5-spot inverted injection pattern shown in Figure 2.2. The dimensions of this model's grid are 9 x 9 x 20 consisting of a total of 1620 blocks. Each layer is 4 ft thick. The grid model used is symmetrical square with the reason:

- Compared to IMEX simulators, STARS requires a bigger CPU memory capacity and more storage time process. Thus, due to storage limitations and to save CPU processing time, smaller grid blocks are used.
- The simulation result of 1 square element will be applied to other square elements with the same rock and fluid properties. That way, the steam generator will still work.

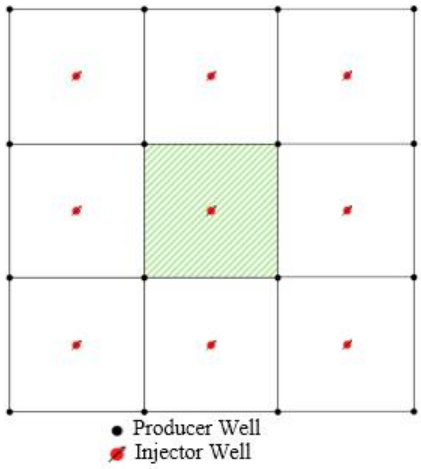

Figure 2. Inverted 5-spot Pattern Scheme

- **Operating Condition**

For the operating condition in this steam flood simulation, the steam temperature is made into 550 oF. It is the highest temperature that can be owned reservoir with reservoir composition in steam or hot water (Hochstein & Sudarman, 1993) and will be a fixed temperature for designed scenarios. At the same

PROCEEDINGS
JOINT CONVENTION BANDUNG (JCB)2021
November 23rd – 25th 2021

time, 70% of steam quality was used in this study. Then for the injected/perforated layer is the same as the bottom layer of the sand zone, namely layer 10 and layer 20.

All 4 production wells have the same pressure constraints and injection rate of 17 psi and MAX 1000 bbl/day. The pressure and injection rate are kept constant at 1500 psi and 300 bbl/day. The economic limit is assumed to be 10 bbl/day per 4 wells or 2.5 bbl/day for the economic limit per well.

Since one of the tasks is to make Steam Flood more optimal in gain lower steam oil ratio and higher oil recovery factor, oil Recovery Factor (Oil RF) and cumulative Steam Oil Ratio (Cum SOR) would be the factors for comparison. In term of getting the best optimization simulation, the various intermittent steam injection from 1 week to 4 weeks was evaluated for different scenarios as proposed in the following:

- Scenario 1 (Intermittent 1 Week). The intermittent scenario was done by injecting steam with periodic time intervals 1 week to reduce excessive use of steam while still producing good sweep effectiveness. Technically, the steam injector was set ON for 1 week, then set off for 1 week, and so on.
- Scenario 2 (Intermittent 2 Weeks).
- Scenario 3 (Intermittent 3 Weeks).
- Scenario 4 (Intermittent 4 Weeks).
- Scenario 5 (Intermittent 4 Weeks).

Result and Discussion

- Base Case

Table 3. Simulation Result of Base Case

BASE CASE SIMULATION RESULTS	
Oil Recovery Factor	69.72%
Cumulative Steam Oil Ratio, bbl/bbl	4.49
Production Age, years	15

As shown in Table 3 above, after the base case simulation was run for 15 years or 5474 days, the oil recovery factor result was quite good at 69.72%. Thus, although it has a high oil recovery factor, the total amount of steam used is still relatively high. It needs to inject the water of 1338.1 Mbbl to obtain the cumulative oil production of 297.25 Mbbl. Therefore, the cumulative steam oil ratio is 4.49 bbl water/bbl oil. So, to produce 1 barrel of oil, it is necessary to inject steam of 4.49 barrels. In this situation, it is required to optimize the steam flood to use a lower cumulative steam oil ratio but still get a high recovery factor.

- ***Optimization Scenario***

The optimization goal is to get a smaller steam oil ratio (SOR) than the base case. Several scenarios are performed to obtain a smaller steam oil ratio by maintaining the operation condition of steam injectors and producers. The scenario is done by injecting steam with intermittent time intervals to reduce excessive use of steam while still producing good sweep effectiveness.

This scenario is applied by assuming that the reservoir still stores enough heat if the steam injection is turned off for some time. What distinguishes one scenario from another is its intermittent time interval.

The interval time is divided into 1 week, 2 weeks, 3 weeks, and 4 weeks. To compare the oil production effectiveness of each scenario with the base case, the production rate limit set on the last day is 10 bbl/day, just like the base case.

This steam flood optimization scenario was applied on the 2800th day of simulation or 7.6th year after the simulation. It was applied at that time because, at that time, instantaneous SOR began to show a very high increase until the SOR ratio touched 30 bbl water/bbl oil.

- ***Comparison Results of Base Case with Optimization Scenario***

From the base case and all optimization scenarios simulation results, the economic limit is set at 10 bbl/day. Therefore, there will be a difference in production age between the base case and optimization scenarios. From the simulation of steam flood optimization, all of them produced a lower cumulative SOR than the base case, with the production length /life being 2.1 - 2.2 years longer than the base case. The comparison result is shown in the following Table 4.

Table 4 Comparison Results of Base Case with Optimization Scenario

Scenario	Oil RF (%)	Cumulative SOR	Production Age	Cumulative Steam Injected (MMbbl)
Base Case	69.72	4.49	15	1.33
1	71.32	3.62	17.8	1.09
2	71.11	3.57	17.8	1.08
3	70.9	3.57	17.5	1.08
4	70.92	3.56	17.6	1.07
5	**71.7**	**3.43**	**17.1**	**1.05**

From 5 optimization scenarios, scenario 5 produces the highest oil recovery factor and the lowest cumulative SOR. Scenario 5 is also the fastest scenario to reach the economic limit when compared to other optimization scenarios. This result means that scenario 5 is the most efficient and effective scenario to apply. The following figure is shown the comparison of heat loss to overburden scenario 5 with base case.

PROCEEDINGS
JOINT CONVENTION BANDUNG (JCB)2021
November 23rd – 25th 2021

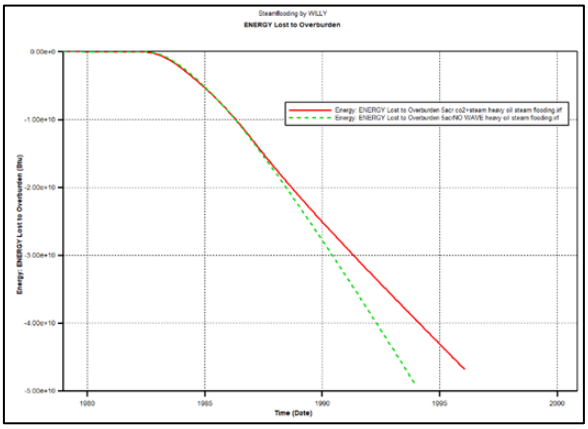

Figure 3 Comparison of Heat Loss to Overburden of Scenario 5 with the Base Case.

Conclusions

After simulating the scenario of steam flooding intermittent steam 1-4 weeks, then obtained several conclusions, including:

1. Intermittent steam flood model simulation is divided into 5 scenarios. That is an intermittent scenario of 1 week, 2 weeks, 3 weeks, 4 weeks.
2. Optimization scenario of intermittent steam flooding can produce a higher oil recovery factor than steam flooding continuously.
3. Scenario 5 with steam flood intermittent is the best optimization scenario. It can produce the lowest cumulative SOR of 3.43 bbl water/bbl oil and produce the highest oil recovery factor of 71.7%.

References

Barillas, J. L., Dutra Jr, T. V., & Mata, W. (2008). Improved Oil Recovery Process For Heavy Oil: A Review Brazillian Journal Of Petroleum And Gas. v. 2, n. 1, 45-54.

Curtis, C., Kopper, R., Decoster, E., Garcia, A. G., Huggins, C., Knauer, L., Waite, M. (2002). Heavy-Oil Reservoirs. In Oilfield Review Autumn (pp. 30-52). Schlumberger.

Fuaadi, I. M., Pierce, J. C., & Gael, B. T. (1991). Evaluation of Steam-Injection Designs for the Duri Steamflood Project. SPE 22995 (pp. 459-477). SPE.

Srochviksit, S., Maneeintr, K. (2016). Simulation on Heavy Oil Production from Steam-Flooding. MATEC Web of Conferences 6. EDP Sciences.

Hochstein, M. P., & Sudarman, S. (1993). Geothermal Resources Of Sumatra. Geothermics, 181-200.

Ko, K. M., Chon, B. H., Jang, S. B., & Jang, H. Y. (2014). Surfactant Flooding Characteristics of Dodecyl Alkyl Sulfate for Enhanced Oil Recovery. Journal of Industrial and Engineering Chemistry, 20, 228-233.

Acknowledgements (Optional)

Follow and obey all the rules by using this template to make your preparation of the extended abstract easier. The committee will not do the ‘editing’ to any part of your submitted extended abstract. We assume that you have submitted as “camera ready”.

PROCEEDINGS
JOINT CONVENTION BANDUNG (JCB)2021
November 23rd – 25th 2021

EOR Development Screening, Strategy and Technology to Optimize Rokan Block Oil Production

(1)Genta Raydiska F., (1)M. Farhan Aflahul M., (1)M. Ilyas Savier A. , (1)Michael Chang K., (1)Reinaldo Raymond, (1)Andy Noorsaman Sommeng, (1)Sutrasno Kartohardjono, (2)Ardian Nengkoda
[1]Departemen Teknik Kimia, Fakultas Teknik, Universitas Indonesia
[2]Saudi Aramco, Dhahran, Eastern, Saudi Arabia

Genta.raydiska@ui.ac.id, muhammad.farhan86@ui.ac.id, muhammad.ilyas82@ui.ac.id, michael.chang@ui.ac.id, reinaldo.raymond@ui.ac.id, petroche@gmail.com

ABSTRACT

Objective:
Rokan Block, with an oil reserve amount of 1.5 billion barrels and an average production capacity of 207,000 BOPD, is one of the backbones of oil production in Indonesia, and it also becomes the future of the country's oil and gas industry. The Rokan Block has nearly 100 other smaller oil fields besides its giant fields known as Duri and Minas Fields. Unfortunately, even with its immense oil production potential, Rokan Block have been experiencing a decline in production. And for that cause, will be the main objective of this paper to overcome the challenges and optimize the Rokan Block oil production, as ongoing development of EOR and EOR technologies is essential for optimizing these mature fields, presenting a critical challenge for Pertamina even if the company retains talent from Chevron's departure.

Methodology:
We have conducted a literature study of various papers and journals that discussing drilling operations using various EOR techniques and the results. After exploring and understanding the various existing EOR techniques, we compare them by looking at several parameters such as lithology, oil properties, effectiveness, and availability. After comparing these parameters and matching them with conditions in Rokan, we can choose the EOR technique that best suits Rokan.

Result & Discussions:
For Duri Field, we recommend In Situ Combustion EOR. Thermal methods such as steam flooding have been primarily used in the Duri Field since 1985 because of their heavy crude oil in shallow reservoirs. However, these methods have specific parameters to be performed with maximum efficiency. The Cyclic Steam Injection is not feasible due to the Duri Field being too shallow for the EOR method to work, while the Steam Assisted Gravity Drainage can be used but sub-optimally as the Duri Field does not fit in the temperature requirement. Hence the In-Situ Combustion EOR method is chosen because its parameter requirements are perfect for Duri Field properties. In this method, the air is injected into the crude oil reservoir. After ignition, the generated heat by combustion keeps the combustion front moving toward the producer well. Combustion front burns all the fuel in its way. Usually, 5 to 10 percent of the crude oil is used as a fuel, and the rest will be produced in the production well. The heat of

the reaction vaporizes initial water and the oil's light components in front of the combustion front. The steam is condensed while distancing from the hot region.

For Minas Field we chose Water Injection EOR. Enhanced Oil Recovery in the Minas Field is severely hampered by its properties, as it renders many processes unsuitable to be used. Carbon dioxide and hydrocarbon flooding has been deemed unusable as it its negatively affected by the field's low reservoir pressure and high reservoir temperature. Chemical flooding methods using surfactant-polymers and polymers are technically feasible, but economically more expensive compared to water or steam injection EOR methods. We chose water injection EOR because the oil's API degree in the field is more suitable to be injected with water EOR.

Novelty:
A new EOR technique to improve efficiency and production of current wells in the Rokan Block.

Keyword: *Enhanced Oil Recovery, Thermal Injection, Chemical Injection, Gas Injection, Lithology.*

PROCEEDINGS
JOINT CONVENTION BANDUNG (JCB)2021
November 23rd – 25th 2021

Laboratory Test of Aqueous Stability and Phase Behavior of Sodium Lignosulphonate (SLS) Surfactant With Intermediate Oil at High Salinity

Tarida Surya Marpaung[1], Rini Setiati[2], Suryono Adisoemarta[3]

[1,2,3]Master Program of Petroleum Engineering, Faculty of Earth Technology and Energy, Universitas Trisakti, Jakarta, Indonesia

Email: taridasuryamarpaung@gmail.com

Abstract

So far, the commonly used surfactant on petroleum industry is petroleum-based surfactant (Petroleum Sulphonate). Although this type of surfactant can perform optimally in reducing Interfacial Tension (IFT), it comes with a high cost, not renewable and not environmentally friendly. That is why plant-based surfactant emerge as alternative on oil recovery effort. One type of alternative plant-based surfactant is Sodium Lignosulphonate (SLS) Surfactant made from lignin. The character of surfactant used on EOR process is important to be identified to make sure it is suitable with the oil condition in reservoir. Surfactant characteristic tests conducted in this laboratory experiment are Aqueous Stability Test and Phase Behavior Test. Based on that, the objective of this research is to identify the characteristic of Bagasse Sodium Lignosulphonate (SLS) Surfactant, by conducting aqueous stability and phase behavior tests, in order to sort the ones that pass the tests to continue to the next stage. There are three variations of brine salinities used in this research namely 90.000 ppm, 100.000 ppm and 100.000 ppm with Bagasse Sodium Lignosulphonate (SLS) Surfactant concentrations of 1%; 1,5%; 2%; 2,5% and 3% with a 1:1 ratio of co-surfactant addition to the SLS surfactant. The results of this research revealed that every surfactant solution involved in Aqueous Stability test has homogenous solubility, which is marked by its transparent color. Based on Phase Behavior Test, surfactant with concentrations of 1,5% and 2,5% with 110.000 ppm salinity were managed to form middle phase with relatively large amount of total emulsion.

Keywords: Aqueous Stability, Bagasse Sodium Lignosulphonate (SLS) Surfactant, High Salinity, Intermediate Oil, Phase Behavior.

Introduction

Surfactant injection is one example of chemical injections used on Enhanced Oil Recovery (EOR) to improve oil production. Surfactant is able to lower water and oil interface tension mechanisms on rock pores and lower capillary force that traps the oil, and finally enables oil to flow out of the rock pores. Surfactant is also able to perform wettability alteration of the rock into water-wet, which cause the rock to be covered by water and release oil droplets from the pores and enable oil production (Rini Setiati, 2017).

Up until now, the commonly used surfactant on petroleum industry is petroleum-based surfactant (Petroleum Sulphonate). Although this type of surfactant can perform optimally in reducing Interfacial Tension (IFT), it comes with a high cost, not renewable and not environmentally friendly. That is why plant-based surfactant emerge as alternative on oil recovery effort (Fitriania, SuryoPurwonoa, & Tawfiequrrahmana, 2017). One type of alternative plant-based surfactant is Sodium Lignosulphonate (SLS) surfactant made from lignin (Setiati, Siregar, Marhaendrajana, & Wahyuningrum, 2018).

The character of surfactant used on EOR process is important to be identified to make sure it is suitable with the oil condition in reservoir. The reason is that surfactant is a highly sensitive chemical compound to temperature, salinity, and other components. Based on that, laboratory test on surfactant characteristic is important and must be conducted before implementing it on a field scale to perform its mechanism. The most common tests of surfactant characteristic on laboratories are Aqueous Stability and Phase Behavior Test.

Aqueous Stability test is conducted to identify the suitability of surfactant and formation water. Test is conducted by mixing surfactant formula with brine, which then observed to witness any changes on the solution and expect it to produce homogenous or clear solution. The reason behind compatibility test is to identify whether a sediment that can plug the rock can be formed (Lemigas, 2008).

Phase Behavior of surfactant/oil/water mixture is the most important factor that the success level of chemical flooding process. The expected ultra-low

IFT on surfactant system is usually measured by testing the microemulsion system phase behavior where area with high solubility is located. Phase behavior is depending on the type and concentration of surfactant, co-surfactant, hydrocarbon and brine (Sandersen, 2012).

Phase behavior is a microemulsion phase nature test formed during oil and water meet with each other. The main objective of this test is to optimize surfactant formulation aimed to be injected on EOR process. Microemulsion can be defined as phase nature that has transparent appearance, thermodynamically stable, a mixture of oil, water/brine, and surfactant (Savero, 2020). Generally the stability formed between hydrocarbon and water is stabilized by surfactant (Chauhan, 2014).

There are three types of microemulsion classification on chemical Enhanced Oil Recovery (cEOR), especially surfactant, namely Winsor Type I (lower phase), Winsor Type II (upper phase) and Winsor Type III (middle phase) (J. Sheng, 2011). As oil-on-water (O/W) microemulsion reach stability with excess oil, it is categorized as Winsor Type I; when water-on-oil (O/W) microemulsion reaches stability with excess water it is categorized as Winsor Type II; if microemulsion reaches oil and water stability it is categorized as Winsor Type III. On optimum salinity condition, stable middle phase microemulsion will be formed and it can lower the remaining oil saturation (Sor). Middle phase microemulsion is also possess ultra-low interfacial tension, wide interface area, thermal stability, and ability to dissolve oil and water (J. J. Sheng, 2015). Generally, Winsor Type III microemulsion is the preferable one on surfactant injection because it can produce the lowest interfacial tension value and improve oil recovery. On the other hand, Winsor Type I and II stabilities are located with either excess of oil or water (J. J. Sheng, 2015).

The conducted laboratory test was formulated based on challenges in research regarding surfactant process flooding by utilizing Sodium Lignosulphonate (SLS) surfactant made from bagasse, that is yet to discover a suitable surfactant characteristic especially on aqueous stability and phase behavior test, with optimum and consistent co-surfactant addition on high salinity intermediate oil. Based on that, the objective of this research is to identify the characteristic of bagasse Sodium Lignosulphonate (SLS) surfactant, by conducting aqueous stability and phase behavior tests, in order to sort the ones that pass the tests to continue to the next stage.

Data and Method

This research consists of a number of testing sequences conducted experimentally by using a mixture of SLS surfactant, brine, and co-surfactant tested on a series of experiments. In this research, similar procedure as mentioned on previous research is conducted to be able to produce a comparison of surfactants with different brine concentration and salinity in order to obtain suitable surfactant solution that would provide valuable insight towards SLS surfactant utilization on EOR, especially on surfactant flooding method.

There are three variations of brine salinity utilized in this research, namely 90.000 ppm, 100.000 ppm and 110.000 ppm Sodium Lignosulphonate (SLS) surfactant made from bagasse with concentrations of 1%; 1,5%; 2%; 2,5%; and 3% which next will be mixed with co-surfactant. The utilized co-surfactant is Ethanol 96% with concentration ratio of 1:1 to SLS surfactant. The utilized oil in this research is intermediate oil obtained from Z field. The temperature used in this test is at 60°C. The tests conducted are initial surfactant screening tests which are Aqueous Stability and Phase Behavior tests. The tools required to conduct this research and to conduct observation are mostly Pipette Tube dan Oven. This research was performed in Universitas Trisakti's Enhanced Oil Recovery (EOR) Laboratory.

Aqueous Stability test is a test to measure compatibility level of surfactant solution and formation water of a reservoir. This test was conducted for 21 days in 60°C heating and ageing inside an oven. Aqueous Stability test was conducted by dissolving surfactants and brines at 90.000 ppm, 100.000 ppm, and 110.000 ppm salinities, each with surfactant and co-surfactant concentrations of 1%; 1,5%; 2%; 2,5%; and 3%. After that, the solutions were inserted inside pipette tubes and observed on the mentioned period of time. The surfactant is categorized as good solubilization surfactant when it is completely dissolved, does not show murkiness, sediments or lumps that would cause clogging during reservoir injection process.

Phase Behavior test is conducted to identify the type of phase and emulsion total volume formed between surfactant solution and oil. Phase behavior test procedures are as follows:

1. Prepare 30 pieces of 5ml Pipette Tube.
2. Prepare SLS surfactant solution previously mixed with brines and co-surfactant, with total samples of 15 with 90.000 ppm, 100.000 ppm, and 110.000 ppm salinities, each of them with surfactant and co-surfactant concentrations of 1%; 1,5%; 2%; 2,5%; and 3%.
3. Prepare ±100 ml of intermediate oil sample (obtained from field Z).
4. Pour the surfactant and oil into the pipette tubes, each of them with a volume of 2 ml.
5. Mix well until they are blended.
6. Set aside and observe the solutions starting from hour 0, up to hour 504 or until both phases reach stable condition and form microemulsion, so that the type of surfactant phase can be determined.

PROCEEDINGS
JOINT CONVENTION BANDUNG (JCB) 2021
November 23rd – 25th 2021

Result and Discussion

All tools used have been calibrated before the research was conducted. Data obtained from Aqueous Stability and Phase Behavior tests, were collected through 504 hours of observation in Universitas Trisakti's Enhanced Oil Recovery (EOR) laboratory.

Aqueous Stability Test (Compatibility Test)

Aqueous Stability test is an experiment conducted visually, where in this research, the clearness of the solution is observed with naked eyes immediately after dissolving surfactant into brine, added with co-surfactant and set aside on a reservoir temperature or 60°C oven.

Surfactant concentration variations utilized in this research are at 1%; 1,5%; 2%; 2,5%; and 3%. The utilized co-surfactant concentration is also at 1%; 1,5%; 2%; 2,5%; and 3% to fulfill 1:1 ratio requirement to surfactant concentration. Brine salinities used in this research are at 90.000 ppm, 100.000 ppm, and 110.000 ppm. Data obtained from Aqueous Stability test can be seen in **Table 1**.

Based on Aqueous Stability test results shown in **Table 1**, we can see that up until 504 hours of observation or 21 days, the ageing surfactant and co-surfactant solutions in 60°C oven, produced clear solution on brines with salinities of 90.000 ppm, 100.000 ppm, and 110.000 ppm, even with increased surfactant concentration from 1% to 3%, the solutions are still transparent. This indicates that the produced surfactant and co-surfactant solutions are compatible with the brine and they can be said as homogenous solutions. If the solution is not dissolved perfectly, it will show a little bit of murkiness or often mentioned as milky solution, because surfactant and brine cannot perfectly dissolved and form a single homogenous solution and create precipitation or sediments on the solution. This finding is supported by a finding mentioned by Eni & Tobing (2013) that the observation conducted on aqueous stability or compatibility tests is to see if there is sediments formed that would possibly cause plugging on rocks.

Phase Behavior Test

Phase Behavior test conducted in this research is aimed to observe emulsion formation, microemulsion volume, and to determine phase type formed between surfactant and co-surfactant with concentrations of 1%; 1,5%; 2%; 2,5%; and 3% (co-surfactant and surfactant SLS ratio is at 1:1), and Intermediate Oil (obtained from Field Z). Brine salinities are at 90.000 ppm, 100.000 ppm, and 110.000 ppm. Tests were conducted for 504 hours or 21 days by observing the formed emulsion and the volume of solution phase formed in Pipette Tubes. The temperature of the oven is at 60°C. Phase behavior test result 90.000 ppm salinity solution can be seen on **Table 2**.

Based on Phase Behavior test result data on 90.000 ppm salinity in **Table 2**, we can see that the middle phase was formed on 2,5% and 3% surfactant and co-surfactant salinities with total emulsion volume respectively at 3,75% and 3,13%. Microemulsion that reaches stability with oil and surfactant is categorized as Winsor Type III. Meanwhile lower phase was identified on surfactant and co-surfactant solutions with concentrations of 1%; 1,5%, and 2% with emulsion total volumes respectively at 2,5%; 2,5%; and 1,25%. In this case, the lower phase or Winsor Type I was formed when surfactant is "dissolved" on oil which increase oil volume (excess oil balance) (J. J. Sheng, 2015). Based on that, surfactant and co-surfactant solutions with concentrations of 1%; 1,5%, and 2% on 90.000 ppm salinities are unsuitable to be used on the next stage of tests because it formed lower phase or Winsor Type I.

Next, similar tests were conducted on 100.000 ppm salinity solution. The surfactant and co-surfactant concentration, oil and solution treatments are similar as the ones performed on 90.000 ppm salinity. Phase behavior test result data on 100.000 ppm salinity can be seen in **Table 3**.

Based on the results of the 100.000 ppm Salinity Research Phase Behavior Test in **Table 3**, it can be seen that there is no Middle Phase but only a Lower Phase in all surfactant + co-surfactant solutions with concentrations of 1%; 1,5%; 2%; 2,5% and 3%. Besides that, the emulsion volumes are relatively low, respectively at 2,50%; 1,25%; 4,38%; 3,75%; and 3,13%. In this case, Lower Phase or Winsor Type I occurred when surfactant "dissolved" on oil and increase oil volume (excess oil balance) (J. J. Sheng, 2015). Based on that, every 100.000 ppm salinity surfactant is unsuitable to be used on the next stage because every one of them formed lower phase or Winsor Type I. This finding shows that surfactant solution is unable to form middle phase because the oil phase is higher than surfactant phase (excess oil balance).

Similar tests were also conducted on 110.000 ppm salinity solutions. The surfactant and co-surfactant concentration, oil and solution treatments are similar as the ones performed on 90.000 and 100.000 ppm salinity, the difference is that in this test, 110.000 ppm salinity solutions were used. Phase behavior test result data on 110.000 ppm salinity can be seen in **Table 4**.

Based on the data from the Phase Behavior Test for Salinity Research of 110.000 ppm in **Table 4**, the type of Middle Phase occurs in a surfactant + co-surfactant solution with a concentration of 1%; 1,5%; and 2,5%, with a total emulsion volume of respectively at 6,25%; 6,88%; and 11,25%.

Microemulsions that reach equilibrium with oil and surfactants are called Winsor Type III. While the Lower Phase type occurs in surfactant and co-surfactant solution with a concentration of 2% and 3% having a total emulsion volume of respectively at 6,25% and 2,50%. In this case, lower phase or Winsor Type I occurred when surfactant "dissolved" on oil and increase oil volume (excess oil balance) (J. J. Sheng, 2015). Therefore, the solution with a concentration of 2% and 3% at a salinity of 110.000 ppm is not feasible to continue in the next test. From a concentration of 1%; 1,5%; and 2,5%, the concentrations used in the next test were only 1,5% and 2,5%. This is because the 1% concentration has the lowest total emulsion volume of the three concentrations. Cost and Time are also act as important consideration to choose the two surfactant and co-surfactant concentrations.

Conclusions

Based on the data obtained from the conducted tests, we can conclude that:

1. The Aqueous Stability test results show that all surfactant + co-surfactant solutions possess transparent solubility up to 504 hours of observation. These solutions have the ability to form homogenous phases.
2. Based on Phase Behavior test, surfactant + co-surfactant solutions with 1,5% and 2,5% concentration at 110.000 ppm salinity are the only solutions that can form middle phase with relatively high total emulsion, respectively at 6.88% and 11,25%.

This is an early-stage of surfactant screening test on the characteristics of SLS surfactants with intermediate oil at high salinity. For the next research, advanced tests such as thermal stability test, surfactant adsorption test, and core flooding test are highly important to obtain more accurate SLS surfactant characteristics.

References

Chauhan, P. D., 2014, Missouri University Of Science And Technology.

Fitriania, SuryoPurwonoa, & Tawfiequrrahmana, A., 2017, Inovasi Teknik Kimia, ***2***, 9–14.

Lemigas, 2008, Prosedur Analisis Surfaktan dan Polimer untuk EOR. Jakarta: Lemigas.

Sandersen, S., 2012, Enhanced Oil Recovery with Surfactant Flooding. Technical University of Denmark (DTU).

Savero, G. N. F., 2020, Universitas Pertamina.

Setiati, R., 2017, Disertasi.

Setiati, R., Siregar, S., Marhaendrajana, T., & Wahyuningrum, D, 2018, Penelitian Dan Karya Ilmiah.

Sheng, J, 2011, Modern Chemical Enhanced Oil Recovery Theory and Practice. Burlington: Gulf Professional Publishing.

Sheng, J. J., 2015, Petroleum.

Acknowledgements

The authors would like to thank Master Program of Petroleum Engineering of Universitas Trisakti, Joint Convention Bandung 2021 (JCB 2021), and the publishers who have published this paper.

PROCEEDINGS
JOINT CONVENTION BANDUNG (JCB)2021
November 23rd – 25th 2021

Table 1: Aqueous Stability Test Results

Brine Salinity (ppm)	Surfactant + Co-Surfactant Concentration (%)	Observation Result of Aqueous Stability Test (Transparent/Milky/Precipitation), Hour						
		0	2	24	48	168	336	504
90.000	1	Transparent	Transparent	Transparent	Transparent	Transparent	Transparent	Transparent
	1,5	Transparent	Transparent	Transparent	Transparent	Transparent	Transparent	Transparent
	2	Transparent	Transparent	Transparent	Transparent	Transparent	Transparent	Transparent
	2,5	Transparent	Transparent	Transparent	Transparent	Transparent	Transparent	Transparent
	3	Transparent	Transparent	Transparent	Transparent	Transparent	Transparent	Transparent
100.000	1	Transparent	Transparent	Transparent	Transparent	Transparent	Transparent	Transparent
	1,5	Transparent	Transparent	Transparent	Transparent	Transparent	Transparent	Transparent
	2	Transparent	Transparent	Transparent	Transparent	Transparent	Transparent	Transparent
	2,5	Transparent	Transparent	Transparent	Transparent	Transparent	Transparent	Transparent
	3	Transparent	Transparent	Transparent	Transparent	Transparent	Transparent	Transparent
110.000	1	Transparent	Transparent	Transparent	Transparent	Transparent	Transparent	Transparent
	1,5	Transparent	Transparent	Transparent	Transparent	Transparent	Transparent	Transparent
	2	Transparent	Transparent	Transparent	Transparent	Transparent	Transparent	Transparent
	2,5	Transparent	Transparent	Transparent	Transparent	Transparent	Transparent	Transparent
	3	Transparent	Transparent	Transparent	Transparent	Transparent	Transparent	Transparent

Table 2: Phase Behavior Test Results at Salinity of 90.000 ppm

Type of Oil	Surfactant Composition	Phase	Volume At Observation Time (Hour)									Total Emulsion (%)	Phase Type
			0	0,5	1	2	24	48	168	336	504		
"Field Z" Oil	1% Surfactant + Co-surfactant	Oil	0	2	2	2	2	2	2	2	2	2,50%	Lower Phase
		Emulsion	4	0,2	0,15	0,125	0,1	0,1	0,1	0,1	0,1		
		Surfactant	0	1,8	1,85	1,875	1,9	1,9	1,9	1,9	1,9		
	1,5% Surfactant + Co-surfactant	Oil	0	2	2	2	2	2	2	2	2	2,50%	Lower Phase
		Emulsion	4	0,15	0,15	0,125	0,125	0,12	0,12	0,1	0,1		
		Surfactant	0	1,85	1,85	1,875	1,875	1,88	1,88	1,9	1,9		
	2% Surfactant + Co-surfactant	Oil	0	2	2	2	2	2	2	2	2	1,25%	Lower Phase
		Emulsion	4	0,1	0,075	0,075	0,05	0,05	0,05	0,05	0,05		
		Surfactant	0	1,9	1,925	1,925	1,95	1,95	1,95	1,95	1,95		
	2,5% Surfactant + Co-surfactant	Oil	0	1,8	1,8	1,85	1,85	1,875	1,9	1,95	1,95	3,75%	Middle Phase
		Emulsion	4	0,3	0,3	0,25	0,25	0,225	0,2	0,15	0,15		
		Surfactant	0	1,9	1,9	1,9	1,9	1,9	1,9	1,9	1,9		
	3% Surfactant + Co-surfactant	Oil	0	1,7	1,7	1,75	1,8	1,8	1,9	1,975	1,975	3,13%	Middle Phase
		Emulsion	4	0,4	0,4	0,35	0,3	0,3	0,2	0,125	0,125		
		Surfactant	0	1,9	1,9	1,9	1,9	1,9	1,9	1,9	1,9		

Table 3: Phase Behavior Test Results at Salinity of 100.000 ppm

Type of Oil	Surfactant Composition	Phase	Volume At Observation Time (Hour)									Total Emulsion (%)	Phase Type
			0	0,5	1	2	24	48	168	336	504		
"Field Z" Oil	1 % Surfactant + Co-surfactant	Oil	0	2	2	2	2	2	2	2	2	2,50%	Lower Phase
		Emulsion	4	0,3	0,3	0,25	0,25	0,1	0,1	0,1	0,1		
		Surfactant	0	1,7	1,7	1,75	1,75	1,9	1,9	1,9	1,9		
	1,5 % Surfactant + Co-surfactant	Oil	0	2	2	2	2	2	2	2	2	1,25%	Lower Phase
		Emulsion	4	0,2	0,13	0,13	0,13	0,08	0,08	0,05	0,05		
		Surfactant	0	1,9	1,88	1,88	1,88	1,93	1,93	1,95	1,95		
	2 % Surfactant + Co-surfactant	Oil	0	2	2	2	2	2	2	2	2	4,38%	Lower Phase
		Emulsion	4	0,2	0,2	0,2	0,2	0,18	0,18	0,18	0,18		
		Surfactant	0	1,8	1,8	1,8	1,8	1,83	1,83	1,83	1,83		
	2,5 % Surfactant + Co-surfactant	Oil	0	2	2	2	2	2	2	2	2	3,75%	Lower Phase
		Emulsion	4	0,2	0,2	0,2	0,2	0,18	0,18	0,15	0,15		
		Surfactant	0	1,8	1,8	1,8	1,8	1,83	1,83	1,85	1,85		
	3 % Surfactant + Co-surfactant	Oil	0	2	2	2	2	2	2	2	2	3,13%	Lower Phase
		Emulsion	4	0,2	0,15	0,15	0,15	0,15	0,13	0,13	0,13		
		Surfactant	0	1,9	1,85	1,85	1,85	1,85	1,88	1,88	1,88		

Table 4: Phase Behavior Test Results at Salinity of 110.000 ppm

Type of Oil	Surfactant Composition	Phase	Volume At Observation Time (Hour)									Total Emulsion (%)	Phase Type
			0	0,5	1	2	24	48	168	336	504		
"Field Z" Oil	1 % Surfactant + Co-surfactant	Oil	0	1,7	1,7	1,8	1,9	1,88	1,9	1,9	1,9	6,25%	Middle Phase
		Emulsion	4	0,5	0,5	0,4	0,4	0,33	0,3	0,25	0,25		
		Surfactant	0	1,8	1,8	1,8	1,8	1,8	1,8	1,85	1,85		
	1,5 % Surfactant + Co-surfactant	Oil	0	1,8	1,8	1,8	1,8	1,8	1,8	1,8	1,8	6,88%	Middle Phase
		Emulsion	4	0,4	0,3	0,3	0,3	0,3	0,3	0,28	0,28		
		Surfactant	0	1,9	1,9	1,9	1,9	1,9	1,9	1,93	1,93		
	2 % Surfactant + Co-surfactant	Oil	0	2	2	2	2	2	2	2	2	6,25%	Lower Phase
		Emulsion	4	0,3	0,3	0,3	0,3	0,25	0,3	0,25	0,25		
		Surfactant	0	1,8	1,8	1,8	1,8	1,75	1,8	1,75	1,75		
	2,5 % Surfactant + Co-surfactant	Oil	0	1,6	1,6	1,7	1,7	1,8	1,8	1,8	1,8	11,25%	Middle Phase
		Emulsion	4	0,7	0,7	0,6	0,6	0,45	0,5	0,45	0,45		
		Surfactant	0	1,8	1,8	1,8	1,8	1,75	1,8	1,75	1,75		
	3 % Surfactant + Co-surfactant	Oil	0	2	2	2	2	2	2	2	2	2,50%	Lower Phase
		Emulsion	4	0,1	0,1	0,1	0,1	0,1	0,1	0,1	0,1		
		Surfactant	0	1,9	1,9	1,9	1,9	1,9	1,9	1,9	1,9		

PROCEEDINGS
JOINT CONVENTION BANDUNG (JCB)2021
November 23rd – 25th 2021

Parameter Analysis of Polymer on Sandstone Reservoir in Indonesia: An Experimental Laboratory Study

Gerry. S[1], Bayu D Prasetiyo[1], Tomi Erfando[1]
[1]R&D Centre for Oil and Gas Technology "LEMIGAS"

Abstract

Polymers are often used to increase oil recovery by improving sweeping efficiency. Screening was carried out as a first step in evaluating the test parameters of several polymers of the Hydrolized Polyacrylaamide (HPAM) type in fluid and sandstone reservoir rocks. The test was carried out using a reservoir fluid classified as light oil (35°API) and at a reservoir temperature (60°C).

There are 5 types of HPAM polymers, namely A1, F1, F2, F3 and P1. The test parameters carried out on these 5 types of polymer include compatibility test for formation water. The rheology polymer test includes concentration vs Tres, shear rate vs viscosity which aims to determine the type of polymer solution being tested is a non-Newtonian or pseudoplastic fluid group. Thermal stability test of polymer for 60 days to determine the stability of the polymer solution whether it is degraded or stable. Filtration testing with criteria FR value < 1.2, screen factor test and adsorption testing using the static method with a standard limit of adsorption value < 400 µg/gr and polymer injectivity test.

From these tests, scoring (range 0-100) was carried out to determine polymer candidates in polymer flooding testing. The F1 polymer candidate for the sandstone reservoir was obtained with a score of 82.25. From the results of the rheology test, the F1 polymer concentration was 2000 ppm. For thermal degradation for 60 days, the polymer F1 2000 ppm experienced a degradation of 15.5%. The results of the F1 2000 ppm polymer static adsorption test were 54.8 µg/gr. For the filtration ratio (FR) value of 1 and the injectivity test results (residual resistance factor / RRF) of 1.With the RRF = 1 value indicating rock permeability after injection of polymer F1 2000 ppm, it tends not to experience plugging due to injection of polymer solution

Keywords: Polymer, sandstone, rheology, injectivity

Introduction

The use of polymer solutions in the application of chemical EOR injection technology have a role in increasing oil recovery effort by improving oil mobility in porous media. The addition of the polymer solution is expected to increase the viscosity value of the displacement fluid so that it can form a "piston like" effect with the aim of increasing volumetric sweep efficiency of the light oil reservoir. (Sheng, 2010; Seright et al, 2008; Shah and Schechter, 1977)

The polymer screening and performance testing must be done before pilot scale implementation in the oil fields. The partially hydrolyzed polyacrylamide (HPAM) polymers were used in this study. There are several tests which have to be passed to make sure the HPAM polymer performance in reservoir condition meet the criteria which will improve the oil recovery of the mature fields. Several test which must be done were screening tests or rheology evaluation such as compatibility tests, viscosity vs. shear rate tests, thermal stability tests, filtration tests, and static adsorption tests. The injectivity tests and coreflooding test were also carried out to know the performance of the polymer injection into the native and/or synthetic core.

The purpose of this study is to investigate the performance of the HPAM polymer injection in increasing oil recovery in light oil reservoir.

Research Methodology

This research study begins to understand the rheological properties of the polymeric material and providing more insight about the adequacy of polymer HPAM from its behavior through porous media (reservoirs). HPAM concentration that were tested were at 500 – 3000 ppm. The material of HPAM was mixed in a injection water (see **Table 1** for injection water composition). The experiment consists of several tests conducted experimentally, started by testing compatibility, shear test, screen factor, filtration, adsorption, thermal degradation, scoring and injectivity (Poettman and Hause, 1978; Lemigas, 2008). All the tests were carried out at 60°C as the reservoir temperature.

- **Compatibility test**
  The solubility of HPAM with various concentrations were visually observed at both

room and 60°C temperature to investigate the phase solution, color changing, and precipitation.

- **Shear test**
  All the rheological experiments were performed on Brookfield DVIII with UL adaptor. For each test (viscosity vs concentration and viscosity vs shear rate), the polymer solutions were prepared with varying concentrations. Concentrations ranged from 500 – 3000 ppm of polymeric material in brine. The viscosity vs concentration of HPAM was measured using shear rate 7 rpm and the viscosity vs shear rate was measured using shear rate from 50 rpm to 250 rpm.
- **Screen Factor**
  Tests were carried out to determine the qualitative size of the polymer and to determine the viscoelastic behavior of the polymer solution (Sorbie, 1991). Viscoelastic is a characteristic that is viscous and elastic when it is deformed (Jouenne, S and Heurteux, 2017).
- **Filtration test**
  A filtration test was conducted to evaluate the polymer solution has free of aggregates which could lead to formation plugging. The measurement of filter test is pumped through 3 µm membrane with a differential pressure of 2 bars.
- **Adsorption test**
  The polymer solutions were prepared to conduct static adsorption test according to Recommended Practice (RP 63) using native core
- **Thermal degradation test**
  Tests were performed during 3 months at 60°C temperature under anaerobic conditions in sealed glass ampoules.
- **Injectivity test**
  HPAM injectivity test was run at concentration 2000 ppm, temperature of 60°C, and slow injection rates of 0.3 cc/min, 0.6 cc/min, and 1 cc/min.

Result and Discussion

Polymer screening on a laboratory scale is carried out to determine the characteristics of polymers in a reservoir. Recent popular material of polymer that assured to accommodate in oil fields is HPAM. HPAM has most often been used to achieve a more favorable mobility ratio and improve macroscopic sweep in chemical EOR by increasing viscosity of the water. When dissolved in fluid, the polymer solutions have a viscosity that depends on many aspects: concentration, molecular weight, temperature, and salinity (Lemigas, 2008). In this study, the investigation of polymer flood has been performed using sandstone reservoir.

The polymer compatibility test for injection water was carried out at room temperature and reservoir temperature of 60°C. The result of that test shown as **Table 2** which shown the good polymer solutions with clearly, no sediment for each of polymer concentrations

The rheological properties of the HPAM polymer solution were evaluated by measuring the apparent viscosity vs concentration and viscosity vs shear rate. This experiment is one of the most prominent screening of an injected chasing fluid during the chemical flooding process. **Figure 1** demonstrates variation shear rate from 7 rpm to 330 rpm was conducted on the viscosity of 1 concentrations each polymer at 60 °C temperature. This result presents HPAM is generally classified as a non-Newtonian fluid, because the viscosity changes when shear rate was applied. Thus, the type of fluid rheology is pseudo-plastic fluid. In this desired condition, pseudo-plastic fluid was known as shear thinning, in which viscosity decreases as shear rate increases.

The experiment result of viscosity vs concentration was demonstrated the viscosity increasing steadily with increasing polymer concentration at 60 °C temperature. This behavior greatly contributes to the shear thickening of the HPAM solution for when the polymer flows at a high shear rate in porous media.

Screen factor test was carried out to determine the quality of the polymer solution. Based on the results of the screen factor test shown in **Figure 2** concluded that higher polymer concentration indicates the polymer solution were long to flow. The equation were used to determine the screen factor (Sorbie, 1991) is:

$$\mathrm{SF} = \frac{\mathrm{t(solution)\ (second)}}{\mathrm{t(solvent)\ (second)}}$$

The filtration test was performed to determine the polymer can flow through the rock pores and evaluating the effect of debris. **Figure 3** informs a volume plot graph against time of the polymer through the filter paper. Each of concentration solution was ensured that polymer hydration had been achieved. The value of the FR for F1 2000 ppm is 1, F2 2000 ppm is 1.2, F3 2500 ppm is 1.1, A1 1500 ppm is 1.02 and P1 2000 ppm is 1.29. This result rapidly indicates F1, F2, F3 and A1 are acceptable as it has no tendency to plug porous media in the reservoir because the requirement of the filtration ratio (FR) value was below 1.2. If the FR value's > 1.2 indicates an indication of polymer causing plugging in rock pores.

Static adsorption test is carried out using native core. Based on each polymer solution, the F1 polymer solution obtained has an adsorption value of 54.8 g/gr and can be seen for the distribution of adsorption on each polymer at **Figure 4**.

The laboratory thermal degradation test was conducted to investigate the remaining viscosity after aging as primary criteria chemicals EOR. F1 presented a good polymer candidate as it performed the remarkable viscosity decay during aging period at 60ºC temperature (see **Figure 5**). The viscosity of F1 2000 ppm maintains a constant value in the last 30 days, and the rest after 3 months of aging period, it increased slowly from 22 cP to 27 cP in the first 20 days. The viscosity of F2 2000 ppm maintains a constant value in the last 30 days, and the rest after 3 months of aging period, it decreases slowly from 20 cP to 14 cP with a viscosity retention percentage of 20%. Thus, more effective preparations should be developed to improve their thermal degradation.

Based on the results of thermal stability test, scoring is carried out on several test parameters and characteristics of the polymer. In Table 3 shows the F1 polymer has a score of 86.5 assuming the F1 polymer price is 3$/kg, the pore volume injected into the reservoir is 0.3.

To understand the performance of the polymer to the rocks, injectivity tests were carried out. The characteristic of the rocks that were used is sandstone native core plugs with permeability range of 1500 to 2500 mD and average porosity of 0.26.

The injectivity tests were carried out using step-up rate of 0.1, 0.3, 0.6 and 1 cc/min. The results of the polymer injectivity can be seen in **Figure 7**. Based on the test results, the polymer has Residual Resistance Factor (RRF) average value 1 (one) which means that the permeability of the core plugs after polymer injection were not changing as much after polymer injection.

Conclusion

The test results for all of the parameters are already meet the criteria for polymer screening as chemical EOR. Based on the polymer screening test and polymer performance test that have been done, polymer concentration (F1) of 2000 ppm is suitable for polymer injection with rule of thumb polymer viscosity should be four times higher than oil viscosity (6.988 cSt) which gives about 22.71 cP. Accordingly, then the conclusion obtained from this study is F1 2000 ppm was selected. F1 with concentration 2000 ppm was resistant in reservoir condition, it shown in thermal stability test (**Figure 5)**. Also the polymer concentration (F1) had the best score of the scoring parameters shown in **Table 3** which gives about 86.5 of 100**.** The results of injectivity test were indicated the rate of injectivity affected the RRF value. Based on these results, this polymer has potential to be implemented on the pilot scale on light oil reservoir.

References

Jouenne, S and Heurteux, G. (2017). Flow of polymer solutions through porous media-prediction of mobility reduction from ex-situ measurements of elasticity. *IOR 2017-19th European Symposium on Improved Oil Recovery*, (April), 1–19.

Lemigas, 2008, Prosedur Analisis Surfaktan dan Polimer untuk EOR, Lemigas, Jakarta.

Poettman, Fred. H., Hause, R., 1978, SPE 7068. 5th Symposium on Improved Methods for Oil Recovery of the Society of Petroleum Engineers of AIME.

Seright, et al., 2008, SPE 115142. SPE Annual Technical Conference & Exhibition.

Shah, D.O., Schechter, R.S., 1977, Improved Oil Recovery by Surfactant and Polymer Flooding.

Sheng, J.J., 2010., Burlington, Massachusetts: Gulf Professional Publishing/ Elsevier.

Sorbie, K. S. (1991). *Polymer-Improved Oil Recovery*. *Springer Science \& Business Media*.

Acknowledgements

Thank you to the Exploitation Department in R&D Center for Oil and Gas Technology “LEMIGAS” for the technical and non-technical supports for this research.

PROCEEDINGS
JOINT CONVENTION BANDUNG (JCB)2021
November 23rd – 25th 2021

Table 1 Brine/water injection composition

Parameter	Result	
ANION		
Klorida	8748	mg/L
Bikarbonat	1970	mg/L
Sulfat	0.16	mg/L
Karbonat	98	mg/L
Hidroksida	0	mg/L
KATION		
Natrium	6150	mg/L
Kalsium	80.2	mg/L
Magnesium	134.2	mg/L
Ferum	0	mg/L
Barium	0	mg/L
Total Dissolve Solid	17550	mg/L

Table 2 Aqueous Stability Polymer

Polymer	Aqueous Stability
F1	Clear, no sediment
F2	Clear, no sediment
F3	Clear, no sediment
A1	Clear, no sediment
P1	Clear, no sediment

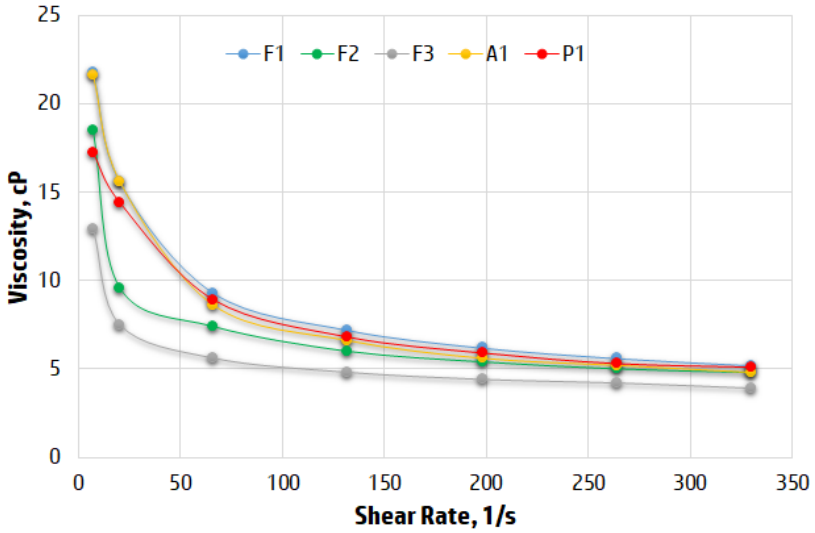

Figure 1 Effect of polymer on shear rate test results

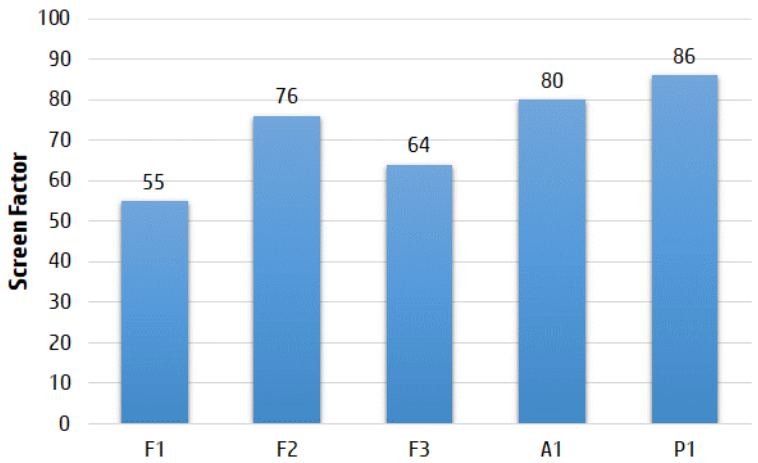

Figure 2 Screen factor test results

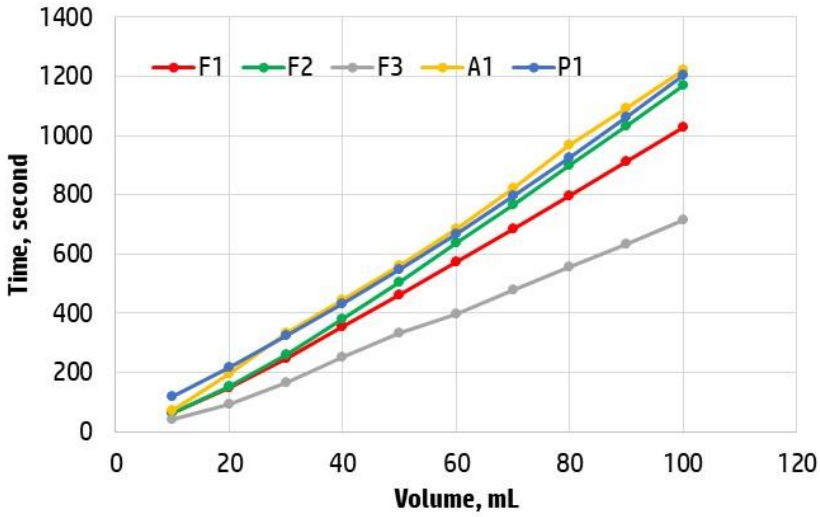

Figure 3 Filter test using 3 µm membrane results

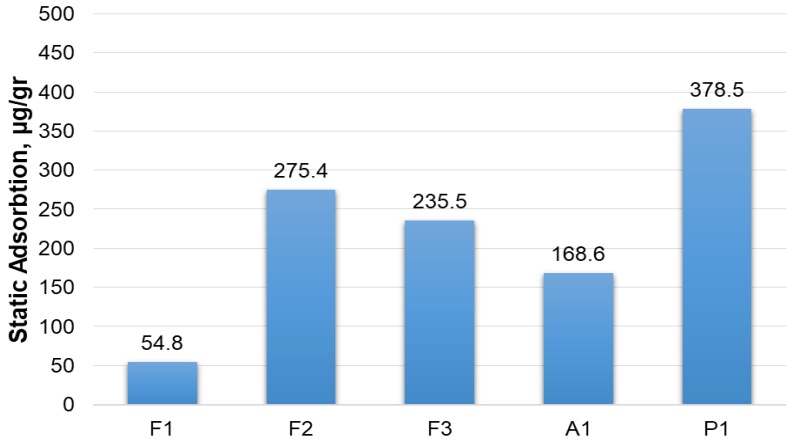

Figure 4 Adsorption static on native core results

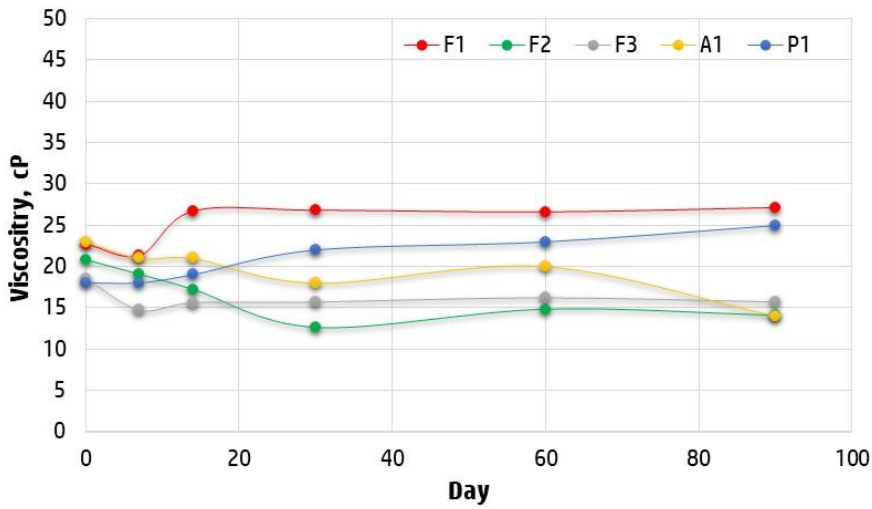

Figure 5 Thermal degradation test results

PROCEEDINGS
JOINT CONVENTION BANDUNG (JCB)2021
November 23rd – 25th 2021

Table 3 Scoring parameter of polymer

PARAMETER	CATEGORY	SCORE	PERCENTAGE	F1		F2		F3		A1		P1	
				Test Result	Score	Test Result	Score	Test Result	Score	Test Result	Score	Test Result	Score
Price (US$/kg)	< 3	20	20	3	15	3	15	3	15	4	10	4	10
	3 - 4		15										
	4 - 5		10										
	> 5		5										
PV Injected, PV	≤0.3	10	10	0.3	10	0.3	10	0.3	10	0.3	10	0.3	10
	0.3 - 0.5		7.5										
	0.5 - 0.8		5										
	> 0.8		2.5										
Concentration, %	≤0.15	15	15	0.2	12	0.25	9	0.2	12	0.15	15	0.2	12
	0.15 - 0.2		12										
	0.2 - 0.3		9										
	0.3 - 0.5		6										
	> 0.5		3										
Screen Factor	≤ 50	10	10	55	7.5	76	2.5	64	5	80	2.5	86	2.5
	50 - 60		7.5										
	60 - 75		5										
	75 - 100		2.5										
FR	<=1	10	10	1	10	1.2	5	1.1	7.5	1.02	10	1.29	5
	1.1 - 1.2		7.5										
	1.2 - 1.3		5										
	> 1.3		2.5										
Static Absorbtion, µg/g	< 100	10	10	54.8	10	275.4	6	235.3	6	167	8	378.5	4
	100 - 200		8										
	200 - 300		6										
	300 - 400		4										
	> 400		0										
Molecule Weight, Million Dalton	<10	10	10	8	10	12	8	20	4	15	6	15	6
	10 - 15		8										
	15 - 20		6										
	20 - 25		4										
	> 25		2										
Thermal Degradation (%)	0 - 10	15	15	15.5	12	14.05	12	16	12	38.6	9	35.6	9
	10 - 20		12										
	20 - 40		9										
	40 - 50		6										
	> 50		3										
		100			86.5		67.5		71.5		70.5		58.5

Table 4. Native core characteristic

Core	D (inch)	L (inch)	W (gr)	Φ	Ka (mD)
1	1.5	6.0	316.0	0.28	764.0

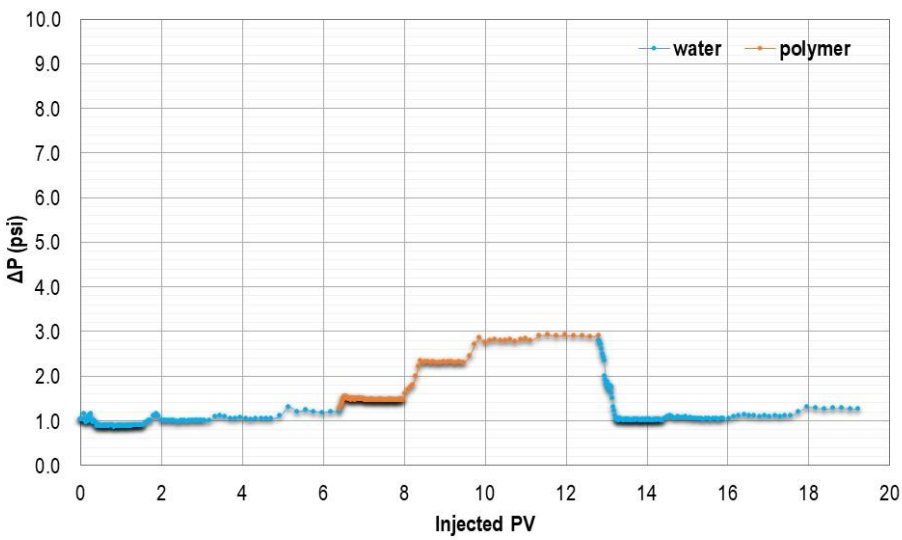

Figure 6. ΔP distribution vs injected pore volume

PROCEEDINGS
JOINT CONVENTION BANDUNG (JCB) 2021
November 23rd – 25th 2021

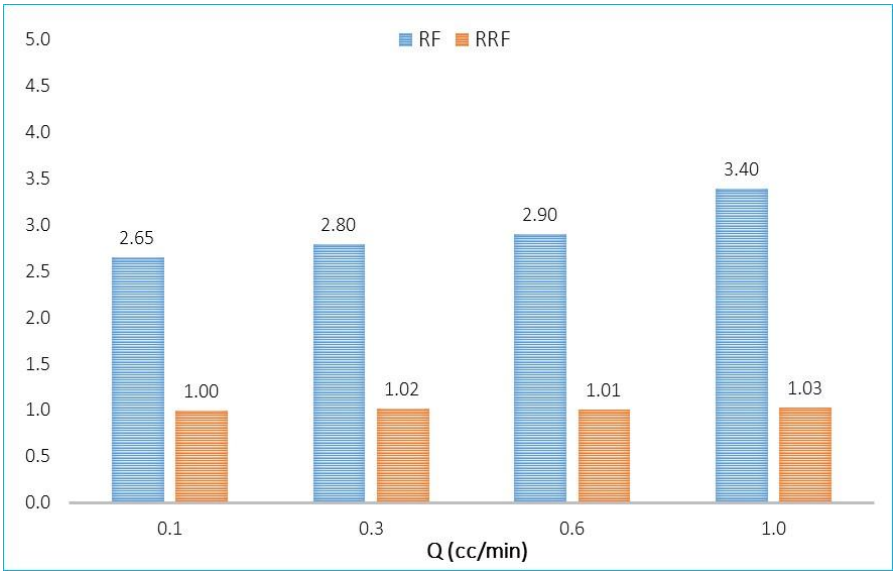

Figure 7. Injectivity test result (RF & RRF)

PROCEEDINGS
JOINT CONVENTION BANDUNG (JCB)2021
November 23rd – 25th 2021

Designing Optimum Salinity and Injection Rates for Low Salinity Water Alternating Hydrocarbon Gas Injection at "B" Structure in "S" Field

Ariel Delano Massie[1], Asep Kurnia Permadi[1], Rochvi Agus Dewantoro[2], Egi Adrian Pratama[3], Muhammad Arif Naufaliansyah[1]
[1]Institut Teknologi Bandung, [2]Bass Oil Sukananti Limited, [3]Curtin University

Abstract
The inability of primary and secondary recovery methods in maximizing oil recovery from existing fields and the lack of new major reserve discoveries have been the two main issues in the oil and gas industry these days. The best solution to solve both problems is by performing enhanced oil recovery (EOR). One of the recent EOR methods that have been developed by many researchers is low salinity water alternating gas (LSWAG) injection. In the LSWAG injection, the type of injection gas that is preferred to be used is hydrocarbon gas. However, there are still limited studies that discuss the implementation of low salinity water alternating hydrocarbon gas injection in prospective fields along with its possible mechanisms.

This study is conducted to design the low salinity water alternating hydrocarbon gas injection at a sandstone reservoir named "B" Structure in "S" Field, Indonesia. Injected water salinity, water injection rate, and gas injection rate are the parameters that become the focus of this study. Sensitivity study through reservoir simulation using a compositional simulator, CMG GEM^{TM}, is performed to study the impact of these parameters on oil recovery by evaluating reservoir dynamic properties and to determine the optimum scenario.

The results of this study conclude that oil recovery increases as the injected water salinity decreases due to wettability alteration towards more water wet. On the other hand, oil recovery increases as the water injection rate and gas injection rate increase due to sweep efficiency improvement. The optimum design of the LSWAG injection, after considering the capacities of field facilities, yields a significant increase of recovery factor from base case. Moreover, this advanced method can reduce cost and gas emission as it utilizes the produced gas.

Keywords: low salinity water alternating hydrocarbon gas injection, salinity, injection rate, recovery factor

Introduction

Enhanced oil recovery (EOR) has been a popular topic in the oil and gas industry these days due to its advantage in extracting more hydrocarbons after primary and secondary recovery. The lack of new major discoveries has forced the oil and gas companies worldwide to maximize the full potential of their existing fields through EOR. One of the EOR methods that have become the center of attention for many researchers is low salinity water injection (LSWI). LSWI is a waterflooding technique in which the salinity of the injected water is made lower than the initial formation water to improve oil recovery. This emerging EOR method could increase the oil recovery of a reservoir up to 20% of original oil-in-place (OOIP) compared to conventional waterflooding (Dang et al., 2015). The benefits of this method in terms of oil recovery have been proved by extensive laboratory experiments and pilot tests. The underlying mechanism of this method is still open for discussion but most of the proposed mechanisms to date indicate that wettability alteration occurs in LSWI and improves the oil recovery.

One of the underlying mechanisms of LSWI that has been widely accepted and used by many researchers is multicomponent ionic exchange (MIE). According to Lager et al. (2008), multivalent cations on the reservoir rock surface bond to polar compounds in the oil phase (resin and asphaltene) forming organo-metallic complexes. At the same time, some organic polar compounds are adsorbed directly to the rock surface displacing the most labile cations. When the low salinity water is injected, MIE takes place, removing the organic polar compounds and organo-metallic complexes from the surface and replacing them with uncomplexed cations (Figure 1). The desorption of the compounds from clay surface leads to a more water-wet surface increasing oil recovery.

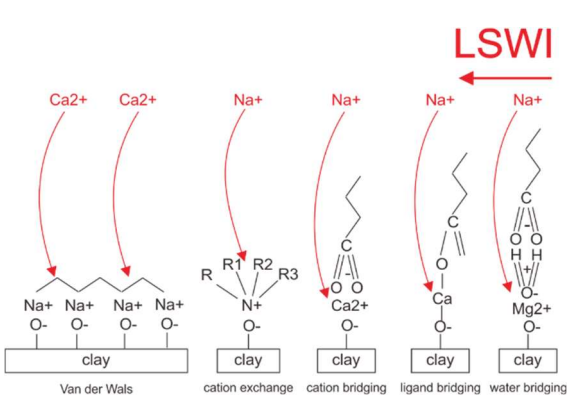

Figure 1: MIE illustration (Lager et al., 2008, modified by Permadi, 2019).

Recent studies on LSWI have discovered another significant benefit from the method when it is combined with another EOR method. One of the promising combinations is LSWI and gas injection, which is called low salinity water alternating gas (LSWAG) injection. LSWAG injection could promote the synergy of the mechanisms underlying LSWI and the mechanisms underlying gas injection (Dang et al., 2014). While LSWI encourages wettability alteration, gas injection enhances sweep efficiency through mobility ratio reduction and un-swept zone sweeping.

Based on its miscibility to the oil phase, gas injection can be classified into miscible and immiscible injection. The following explanation captures the mechanisms for immiscible injection only since the gas flooding process in this study is known to be immiscible. The two main mechanisms are oil swelling and viscosity reduction.

a. Oil swelling
   Oil swelling increases the hydrocarbon saturation in a pore. When the saturation increases, the oil relative permeability and oil mobility in that pore increases as well. It leads

PROCEEDINGS
JOINT CONVENTION BANDUNG (JCB)2021
November 23rd – 25th 2021

to a higher displacement efficiency and eventually higher oil recovery (Holtz, 2016).

b. Viscosity reduction
Viscosity reduction due to immiscible gas injection has been reported in various types of oil reservoirs including undersaturated, saturated, and heavy oils. Ning and McGuire (2004) found that oil viscosity reduction is found to be the dominant mechanism in severely undersaturated reservoirs. They explained that undersaturated oil can dissolve more gas than its initial GOR. When gas is injected into the reservoir, GOR increases, and oil viscosity decreases. Same as oil swelling, viscosity reduction also improves oil mobility.

For one cycle of injection, LSWAG injection consists of two steps, which are injecting low salinity water and injecting gas to the reservoir. The combination of viscosity reduction and oil swelling mechanisms from the gas flooding process has a significant impact on the mobility ratio and thus sweep efficiency of the low salinity waterflooding process (Holtz, 2016). It can be seen from the mobility ratio formula presented below.

$$M = \frac{k_{rw}\mu_o}{\mu_w k_{ro}}$$

Sweep mechanism is more stable when the mobility ratio value is less than 1. As explained before, oil swelling increases k_{ro} and decreases k_{rw}, while the viscosity reduction decreases μ_o. All of which drive the mobility ratio towards a decreased value.

The most common injection gases used in the water alternating gas injection are CO_2 and hydrocarbon gas. Compared with CO_2, hydrocarbon gas is preferable because it is usually directly available from production. In addition, rather than being flared, it is much more environmentally friendly when the produced gas is injected back to the reservoir. On the other hand, CO_2 is an expensive gas and not easily obtained. Moreover, corrosion problems are often reported when using CO_2 (Christensen et al., 2001; Dong et al., 2019). For those reasons, by using hydrocarbon gas as the injectant in its gas flooding process, LSWAG injection can be more attractive to be implemented in the oil fields.

This study is conducted to achieve several objectives that are limited to the application of low salinity water alternating hydrocarbon gas injection at a sandstone reservoir called "B" Structure in "S" Field. The objectives are presented below.

a. To study the impact of injected water salinity, water injection rate, and gas injection rate on oil recovery.
b. To determine the optimum design of injected water salinity, water injection rate, and gas injection rate which gives the highest recovery factor.

Data and Method

"S" Field is an oil field located in South Sumatera Province, Indonesia. The field was found in 1990 with an area of approximately 4,510 acres. The field has two producing structures which are "B" and "T" Structure. This study focuses only on the "B" Structure. This structure consists of three zones (sand layers): "T", "G", and "K" Sand Layers. "T" Sand Layers is the biggest and the main producing layer with 7.364 MMSTB of oil in place. Compared to the "T" Sand Layer, the two other sand layers are relatively small so that they are not included in this simulation study. Therefore, the "B" Structure in this paper only refers to the "T" Sand Layer. 2D Map of the "B" Structure is shown in Figure 2. There are three production wells (B-1, B-3, and B-5) currently producing from the "B" Structure and one suspended well (B-4). The three production wells had been producing 2.254 MMSTB of oil cumulative in total by December 2020.

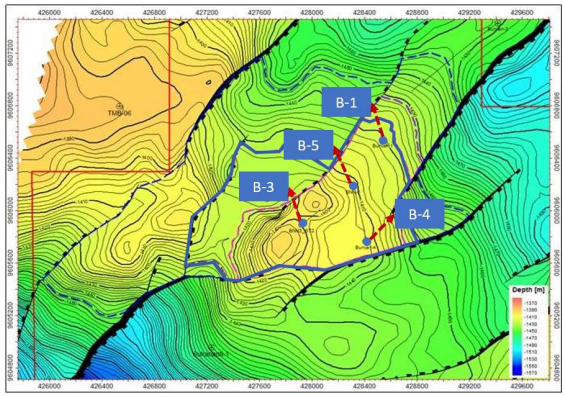

Figure 2: 2D map of "B" Structure.

The reservoir of the "B" Structure is a sandstone reservoir and belongs to Talang Akar Formation. It is reported to initially have 1,700 psig of reservoir pressure and 227 ºF of reservoir temperature. The reservoir has 0.156 of average porosity and 493.7 md of average permeability. It contains light oil with an oil gravity of 33.4 ºAPI and bubble point pressure of 1,205 psi. The drive mechanism of the reservoir is considered to be a strong water drive. The reservoir has formation water with 20,000 ppm salinity and ionic composition as shown in Table 1. The formation water composition indicates that there are divalent ions (Mg^{2+} and Ca^{2+}) in the reservoir that can contribute to ion exchange. The reservoir consists of 5 rock types. Three of them are mix wet and the rest are water wet. The reservoir also contains clay minerals including illite and kaolinite. These characteristics make the reservoir favorable for LSWI and LSWAG injection.

	Components	Concentration (ppm)
Cations	Na^+	7,359.9
	Ca^+	66.8
	Mg^{2+}	13.8
	K^+	74.7
	Ba^{2+}	1.8
	Sr^{2+}	18.7
	Fe^{3+}	3.2
Anions	Cl^-	9,059.4
	HCO_3^-	3,291.7
	SO_4^{2-}	120.9
Total Salinity		**20,010.9**

Table 1: Formation water composition of "B" Structure.

This study was completed by literature review and simulation study. The literature review was conducted to get a comprehensive understanding of the basic theories that are used in this study. The literature review covered the

previous research and publications regarding LSWI, gas injection, water alternating gas (WAG), and LSWAG injection. The simulation study was started by learning the compositional simulator used in this study, namely CMG GEM^{TM}. Afterward, data collection, fluid property modeling, and reservoir modeling were carried out. History matching was then also conducted to validate the reservoir model based on production history data. Finally, production forecasts and sensitivity studies were performed to achieve the objectives of this study.

Due to the unavailability of some experimental data, several assumptions were taken in the LSWAG modeling.

a. Clay mineral content is distributed similarly to all grids.
b. Interpolation range of equivalent fraction for ion exchange ζ(Na-X) is between 0.9378 and 0.6678 based on reservoir model initialization and default value in LSWI wizard menu of CMG GEM^{TM}.

As one of the preliminary steps in reservoir simulation modeling, fluid property or PVT modeling was performed using CMG WINPROP^{TM}. Based on the composition and the properties, the fluid of this reservoir can be categorized as light-medium oil. Fluid model matching to laboratory test results (Constant Composition Expansion and Differential Liberation) was also conducted to validate the model.

Minimum miscibility pressure (MMP) calculation was performed to determine whether the hydrocarbon injection is miscible or immiscible. Due to a lack of experimental data, the MMP was calculated using correlation. Ghorbani's correlation (2013) was chosen to calculate the MMP. Among all the MMP correlations commonly used for hydrocarbon gas, this correlation has criteria that best suit the characteristics of the reservoir fluid and the injection gas in this study. Additionally, unlike many other correlations, this correlation considers the composition of injection gas in its calculation. The calculation result gives 1,951 psi as the MMP value which is higher than the current and even initial reservoir pressure. It suggests that the gas flooding process in this case is immiscible. The MMP in the fluid model was then validated to the calculated MMP.

Reservoir initialization and history matching were performed to ensure that the reservoir model mimics the real condition and could give a valid forecast for this case study. The history matching was conducted by adjusting the aquifer parameters in the reservoir model. Production history data from 1998 until 2020 was used for the history matching process.

After the reservoir model had been validated by history matching, the production forecast for the base case was simulated to see the performance of the reservoir without LSWAG injection. The production forecast was simulated for 15 years, from 1st January 2021 until 1st January 2036, using B-1, B-3, and B-5 well as the production wells. The maximum production liquid rate of each well was limited to the liquid rate value at the end of history matching (546 BLPD for B-1, 2,342 BLPD for B-3, and 120 BLPD for B-5). The minimum bottom hole pressure (BHP) of each well was limited to 100 psi. An economic limit of 15 BOPD was also added to the production constraints of the forecast. The production forecast result is presented in Figure 3. From the oil rate profile of the forecast, compared to the other wells, B-1 produces the lowest oil rate and reaches the economic limit too early in October 2027. Therefore, later in the LSWAG injection cases, B-1 was converted to an injection well in November 2027.

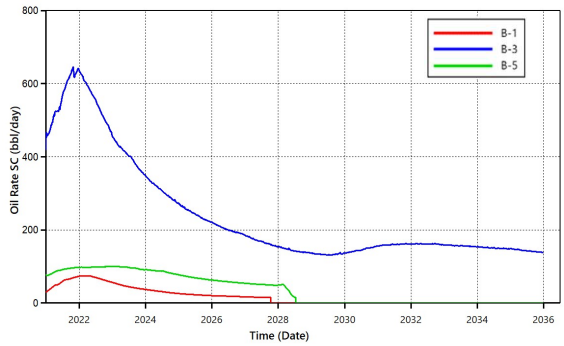

Figure 3: Base case forecast (oil rate profile).

Before proceeding to the other forecasts, LSWAG injection needs to be modeled first in the simulator. The LSWI part of the LSWAG injection was modeled through the LSWI wizard menu in CMG GEM^{TM}. This simulator applies MIE as the main mechanism for LSWI. In the modeling process, formation water composition from ten ion analysis data was inputted into the simulator. A list of geochemical reactions which was obtained from analysis on PHREEQC Software was also entered into the simulator. As listed in Table 2, The geochemical reactions consist of aqueous reactions, mineral reactions, and cation exchange reactions. The cation exchange capacity (CEC) value for this reservoir was calculated using the equation from Seilsepour and Rashidi (2008), and the calculation result gave 237 eq/m^3 of CEC value. Wettability alteration through relative permeability shifting for this reservoir's rock types was modeled as well in the simulator. The interpolant ion used for this study was Na^+. The shifting values can be seen in Table 3 which was obtained from laboratory experiment data that used 1,800 ppm of low salinity water. The initial point of ion exchange equivalent fraction ζ(Na-X) for interpolation was obtained from reservoir model initialization which gave the value of 0.9378. From the initial point and the default value of interpolation range in CMG GEM^{TM}, the end point was assumed to be 0.6678. Figure 4 shows relative permeability shifting modeled in the simulator for one of the reservoir's rock types.

	Reactions
Aqueous Reaction	$H^+ + OH^- \leftrightarrow H_2O$
	$CaHCO_3^+ \leftrightarrow Ca^{2+} + HCO_3^-$
	$NaHCO_3 \leftrightarrow Na^+ + HCO_3^-$
	$MgHCO_3^+ \leftrightarrow Mg^{2+} + HCO_3^-$
	$H^+ + NaCO_3^- \leftrightarrow Na^+ + HCO_3^-$
	$H^+ + MgCO_3 \leftrightarrow Mg^{2+} + HCO_3^-$
Mineral Reaction	$H^+ + \text{Calcite} \leftrightarrow Ca^{2+} + HCO_3^-$
	$H^+ + \text{Dolomite} \leftrightarrow Ca^{2+} + Mg^{2+} + HCO_3^-$
Cation Exchange	$Na^+ + 0.5Ca\text{-}X_2 \leftrightarrow 0.5Ca^{2+} + Na\text{-}X$
	$Na^+ + 0.5Mg\text{-}X_2 \leftrightarrow 0.5Mg^{2+} + Na\text{-}X$

Table 2: Geochemical reactions.

Shifting Parameter	Value
Krw_LSWI/Krw_intial	0.247
Kro_LSWI/Kro_intial	1.098
Sor Reduction	0.039

Table 3: Relative permeability shifting value.

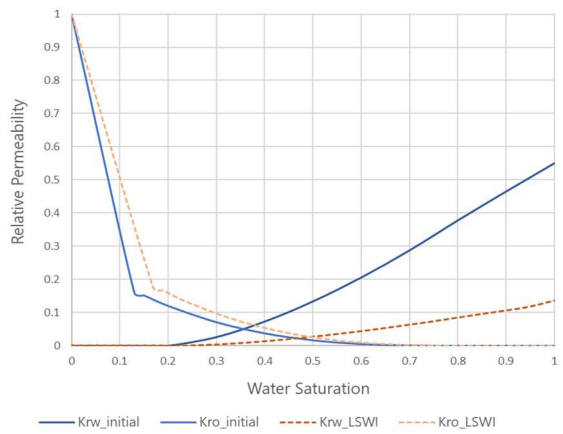

Figure 4: Relative permeability curve of Rock Type 1.

From the LSWI part, the modeling process was continued to the WAG part. The modeling was started by filling the injection gas composition. The injection gas composition was taken from the produced gas composition of the "S" field. The gas composition data are presented in Table 4. WAG ratio of 1:1 and WAG cycle of 1 cycle per year were used for this study. It means that 6 months of gas injection is followed by 6 months of low salinity water injection every year. These values were determined based on the previous study regarding CO_2-LSWAG injection in the "T" Structure of the "S" Field which reported that 1:1 ratio and 1 cycle per year are the optimum values (Syah, 2020). Even though the structure and the injection gas type are different, it is assumed that they are also well applied in this study.

Component	Fraction
CO2	0.1243
N2	0.0086
CH4	0.3735
C2H6	0.0722
C3H8	0.2395
IC4	0.0504
NC4	0.0488
IC5	0.0352
NC5	0.0214
FC6	0.0113
C07+	0.0148

Table 4: Injection gas composition.

A sensitivity study was conducted by forecasting several LSWAG injection cases. These forecasts used the same production constraints (maximum liquid rate, minimum BHP, and economic limit) as those used in the base case forecast. The production wells used in this sensitivity study were also the same as the wells used in the base case (B-1, B-2, and B-3), but this time B-1 was converted to an injection well on 1st November 2027. Besides B-1, the suspended well, B-4, was also used as an injection well which started its LSWAG injection on 1st January 2022. Same as the base case, the LSWAG cases were also forecasted for 15 years. Three parameters were varied in this sensitivity study: injected water salinity, water injection rate, and gas injection rate.

a. Injected water salinity
Injected water salinity is one of the main parameters which affect the performance of low salinity waterflooding. Since LSWAG involves low salinity waterflooding in its process, injected water salinity needs to be included in this sensitivity. There were two salinities used in this sensitivity: 1,800 ppm and 3,600 ppm. Their ionic composition can be seen in Table 5. The ionic strengths of these salinities are still higher than the Critical Total Ionic Strength (CTIS). Therefore, there is no formation damage, and these salinities are safe to use.

b. Water injection rate
Besides salinity, water injection rate also affects the performance of the low salinity waterflooding in LSWAG. The water injection rate in this sensitivity was limited to a maximum of 1,500 BWPD per injection well. This is due to the availability of produced water in "B" structure that can only supply around that quantity. The water injection rate in this sensitivity was then varied to 500 BWPD, 1,000 BWPD, and 1,500 BWPD per well.

c. Gas injection rate
Gas injection rate affects the gas flooding performance in LSWAG. Like the water injection rate, the gas injection rate in this sensitivity was also limited due to the availability of produced gas in the "S" field. The gas injection rate was limited to a maximum of 1 MMSCFD per injection well. Therefore, the gas injection rate in this study was varied to 0.25 MMSCFD, 0.5 MMSCFD, and 1 MMSCFD per well.

	Components	Concentration (ppm)	
		A	B
Cations	Na^+	662.10	1,324.20
	Ca^+	6.01	12.02
	Mg^{2+}	1.24	2.48
	K^+	6.72	13.44
	Ba^{2+}	0.16	0.32
	Sr^{2+}	1.68	3.36
	Fe^{3+}	0.29	0.58
Anions	Cl^-	814.98	1,629.96
	HCO_3^-	296.12	592.25
	SO_4^{2-}	10.88	21.75
Total Salinity		**1,800**	**3,600**

Table 5: Injection water ionic composition.

All permutation cases from the three parameters above were forecasted. In total there were 18 cases forecasted. From those forecasts, the impact of each parameter variation on the recovery factor could be analyzed. The optimum combination which gives the highest recovery factor could also be determined.

Result and Discussion

Simulation result of the LSWAG injection cases is presented in Table 6. From the table, all the 1,800 ppm cases give a higher recovery factor than the 3,600 ppm cases. These results align with the LSWI theory which stated that lower salinity results in more shifting towards water wet and thus more oil recovery. That is because lower salinity promotes

more ion exchanges in the flooding process. Since the simulator used in this study takes MIE as the underlying mechanism of LSWI, the distribution of ion exchange equivalent fraction in the reservoir at the end of forecast can be displayed in a map. Figure 5 presents one pair example of 1,800 ppm and 3,600 ppm cases which have the same values on other parameters (Both used 1,500 BWPD of water injection rate and 0.5 MMSCFD of gas injection rate). Compared to the 3,600 ppm case, the 1,800 ppm case results in a lower ion exchange equivalent fraction ζ(Na-X) which means more ion exchanges have occurred.

Water Inj. Rate (BWPD)	Gas Inj. Rate (MMSCFD)	Recovery Factor (%)	
		1800 ppm	3600 ppm
500	0.25	58.05	58.01
	0.5	58.61	58.59
	1	60.10	60.07
1000	0.25	59.44	59.34
	0.5	60.02	59.92
	1	61.38	61.30
1500	0.25	60.31	60.21
	0.5	61.09	60.84
	1	62.34	62.24

Table 6: Simulation results of LSWAG injection cases.

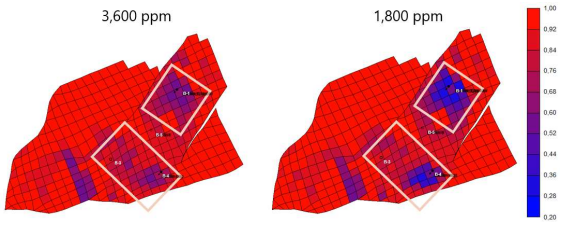

Figure 5: Ion exchange equivalent fraction ζ(Na-X) map of 3,600 and 1,800 ppm case at the end of simulation.

From the sensitivity study result in Table 6, it can be concluded also that recovery factor is directly proportional to water injection rate, meaning the higher the water injection rate, the higher the recovery factor will be. This correlation applies to all gas injection rates and all water salinity. A higher water injection rate means a higher volume of water being injected into the reservoir and more area in the reservoir being swept by the injected water. This improves the macroscopic sweep efficiency of the flooding process. The cation exchange and wettability alteration also take place in a wider area in the reservoir. Figure 6 displays the distribution of ion exchange equivalent fraction at the end of simulation for a pair of simulation cases with the same salinity and gas injection rate but different water injection rate. Compared to the 500 BWPD case, the 1,500 BWPD case shows a wider area impacted by ion exchange and wettability alteration. This result is also confirmed by the oil saturation distribution across the reservoir at the end of simulation. Figure 7 shows the remaining oil saturation across reservoir from B-3 to B-4 at the end of simulation. B-3 is chosen because the incremental of oil recovery mostly comes from B-3. The 1,500 BWPD case gives lower remaining oil saturation than the 500 BWPD case. For water injection rates higher than 1,500 BWPD, it might still give a higher recovery factor. However, as mentioned in the previous section, this sensitivity is limited to a maximum of 1,500 BWPD due to the availability of produced water in the "B" Structure.

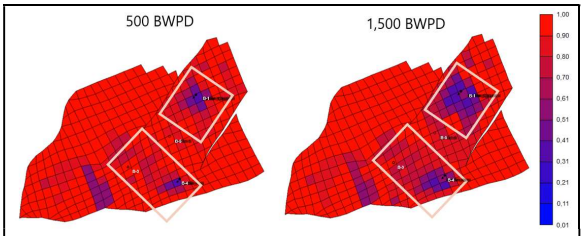

Figure 6: Ion exchange equivalent fraction ζ(Na-X) map of 500 and 1,500 BWPD case at the end of simulation.

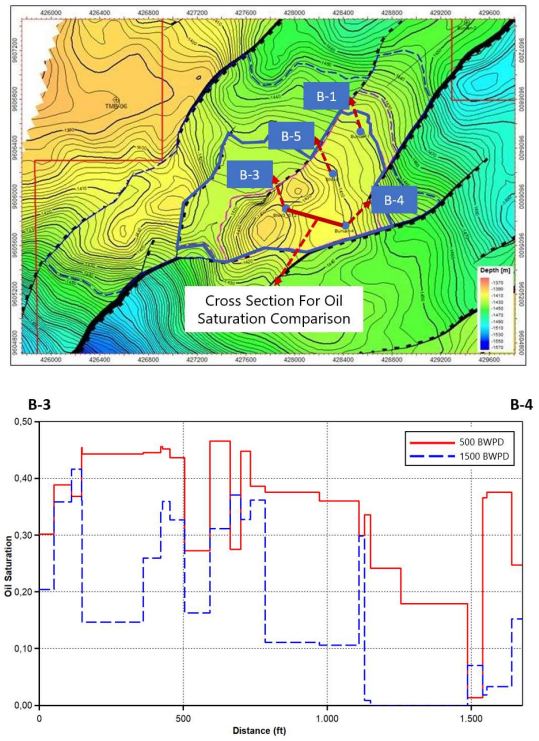

Figure 7: Oil saturation across reservoir of 500 and 1,500 BWPD case at the end of simulation.

Besides water injection rate impact, gas injection rate impact can be inferred as well from the simulation result in Table 6. It shows that recovery factor increases as gas injection rate increases. This linearity applies to all water injection rates and salinity. This is because a higher gas injection rate promotes more viscosity reduction and oil swelling to occur in the reservoir. The mechanisms are viscosity reduction and oil swelling because the reservoir pressure during gas injection has confirmed that the gas flooding process was immiscible. Figure 8 displays viscosity distribution map at the end of simulation for two cases with different gas injection rate but the same injected water salinity and water injection rate (1,800 ppm and 500 BWPD). The figure indicates that higher gas injection rate causes higher viscosity reduction. The viscosity reduction in combination with oil swelling reduces mobility ratio and thus improves sweep efficiency. This result is also proved by the oil saturation distribution across reservoir at the end of simulation. Figure 9 shows that the remaining oil saturation

across reservoir from B-3 to B-4 at the end of simulation in 1 MMSCFD case is lower than that in 0.25 MMSCFD case. Like the water injection rate sensitivity, gas injection rates higher than 1 MMSCFD may give a higher recovery factor, but it is not simulated due to the limitation of produced gas availability in the "S" Field.

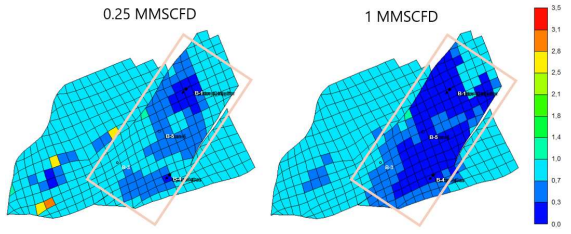

Figure 8: Viscosity (cp) distribution of 0.25 and 1 MMSCFD case at the end of simulation.

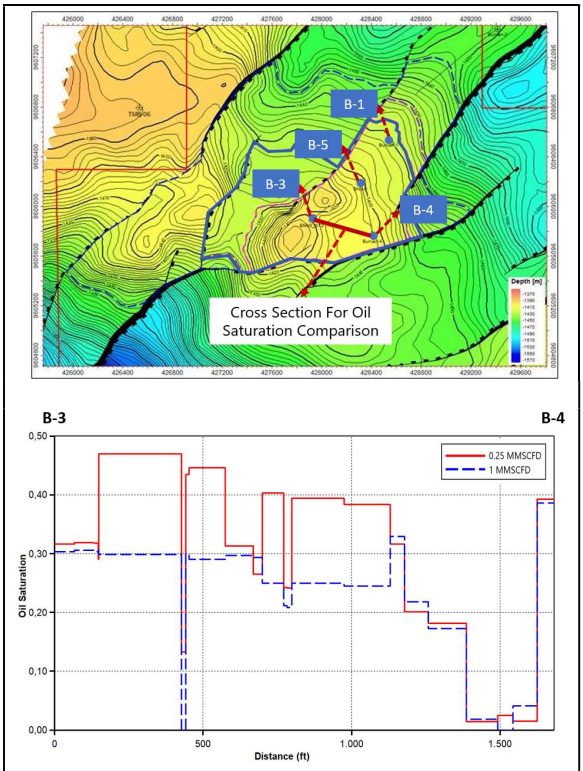

Figure 9: Oil saturation across reservoir of 0.25 and 1 MMSCFD case at the end of simulation.

Finally, based on the simulation result, the optimum design which gives the highest recovery factor is the case that uses 1,800 ppm of injected water salinity, 1,500 BWPD of water injection rate, and 1 MMSCFD of gas injection rate. This optimum design can give 62.34% of recovery factor which means a 7.81% increase from base case. The increase equals 0.56 MMSTB of oil cumulative production. It should be noted that the optimum design is obtained after considering the limitation in the fields such as the availability of produced gas and water. Based on the result, it is known that LSWAG injection is a very promising method to be implemented in terms of oil recovery. Not to mention the utilization of hydrocarbon gas as the injection gas in this method is very good for environment since it reduces flaring activity.

Conclusions

Based on the analysis and discussion above, the following conclusions regarding LSWAG injection implementation at "B" Structure in "S" Field can be taken.

a. Oil recovery is inversely proportional to injected water salinity. It increases as the injected water salinity decreases due to more shifting toward water wet. On the other hand, oil recovery is directly proportional to water injection rate and gas injection rate. The higher the water and gas injection rate, the higher the recovery factor is. It happens because higher injection rates promote mobility ratio reduction and sweep efficiency improvement. This correlation applies until the maximum value of water and gas injection rate which are available in the field.
b. The optimum design for LSWAG implementation at "B" Structure in "S" Field is by using 1,800 ppm of injected water salinity, 1,500 BWPD of water injection rate, and 1 MMSCFD of gas injection rate. This optimum condition considers the availability of water and gas for injection in the field.

To further improve the results of this study, another sensitivity study on operational parameters such as WAG ratio and WAG cycle can be performed. Additionally, production and injection scenario sensitivity such as infill drilling can also be conducted to assess the possibility of better LSWAG performance.

References

Christensen, J. R., Stenby, E. H., & Skauge, A, 2001, SPE Reservoir Evaluation & Engineering, **4**, 97-106.
Dang, T. Q. C., Nghiem, L., Nguyen, N., Chen, Z., and Nguyen, Q. P., 2014, SPE Improved Oil Recovery Symposium, Tulsa, Oklahoma, USA, 12-16 April.
Dang, T. Q. C., Nghiem, L., Nguyen, N., Chen, Z., and Nguyen, Q. P., 2015, SPE Western Regional Meeting, Garden Grove, California, USA, 27-30 April.
Dong, J., Wu, S., Xing, G., Fan, T., Li, H., & Wang, B., 2019, International Petroleum Technology Conference, Beijing, China, 26-28 March.
Ghorbani, M., Momeni, A., & Morady, B., 2013, Petroleum Science and Technology, **31**, 2577-2584.
Holtz, M. H., 2016, SPE Improved Oil Recovery Conference, Tulsa, Oklahoma, USA, 11-13 April.
Lager, A., Webb, K. J., Black, C. J. J., Singleton, M., & Sorbie, K. S., 2008, Petrophysics - The SPWLA Journal of Formation Evaluation and Reservoir Description, **49**, 28-35.
Ning, X. S. & McGuire, P. L., 2004, SPE/DOE Fourteenth Symposium on Improved Oil Recovery, Tulsa, Oklahoma, USA, 17-21 April.
Permadi, A. K., 2019, Scientific Speech, Institut Teknologi Bandung, 23 November.
Seilsepour, M. & Rashidi, M., 2008, World Applied Sciences Journal, **3**, 200-205.
Syah, G. A. A., 2020, B.S.E. thesis, Institut Teknologi Bandung.

Acknowledgments

The authors would like to extend their highest gratitude to Bass Oil Sukananti Limited for providing full support including guidance and field data for this study.

PROCEEDINGS
JOINT CONVENTION BANDUNG (JCB)2021
November 23rd – 25th 2021

Designing Optimum Salinity, Cycle, and Gas-Water Ratio of Low Salinity Water Alternating Hydrocarbon Gas Injection at "B" Structure in "S" Field

Raden Keanu Paranindhia Benedetto[1], Asep Kurnia Permadi[1], Rochvi Agus Dewantoro[2], Egi Adrian Pratama[3], Muhammad Arif Naufaliansyah[1]
[1]Institut Teknologi Bandung, [2]Bass Oil Sukananti Limited, [3]Curtin University

Abstract
In the last decades, injection of brines with modified ionic composition has been developed to improve oil recovery. low salinity water injection (LSWI) is one of the most prominent enhanced oil recovery (EOR) method which can increase oil recovery better than that other conventional chemical EOR methods. As a result of further studies of LSWI, an idea of combining it with other EOR technique was generated. One of the idea is to combine LSWI with gas injection which is known as low salinity water alternating gas (LSWAG) injection. Applying water alternating gas (WAG) in LSWI process means to inject both low salinity water and gas to the reservoir in order to improve the oil recovery. The presence of flue gas produced during production process leads to the idea of utilizing the produced hydrocarbon gas to be used for injection as pure carbon dioxide (CO_2) gas is considered costly.
In this study, the author proposes the idea of modelling low salinity water alternating hydrocarbon gas (Hydrocarbon-LSWAG) injection using compositional model to identify the effects of Hydrocarbon-LSWAG injection operational parameters and to propose the most optimum Hydrocarbon-LSWAG injection scenario to be applied in the sandstone reservoir at "B" Structure in "S" Field, South Sumatera Province, Indonesia. Reservoir simulations and production forecasts were done using CMG GEM™ Simulator during 15 years of production period starting from 1st January 2021 until 1st January 2036 with preliminary work using CMG WINPROP™ for generating the reservoir fluid compositional model. Series of sensitivity analysis were conducted in this study to identify the effects of operational parameters in modelling Hydrocarbon-LSWAG injection and to determine the most optimum Hydrocarbon-LSWAG injection scenario to be applied at "B" Structure in "S" Field to gain promising oil recovery using two injector wells. Water salinity, number of cycle and gas-water injection duration ratio were varied in order to observe the effects of those parameters to oil recovery factor.
The results of this study show that injection using lower water salinity of 1,800 ppm results in higher oil recovery compared to water salinity of 3,600 ppm. The findings of this study also show that the increasing number of Hydrocarbon-LSWAG injection cycle is neither directly or inversely proportional to the improvement of oil recovery. Furthermore, the resulted recovery factor is higher when the LSWI duration is longer than the hydrocarbon gas injection, in this case, with 1:2 ratio of gas-water injection. The most optimum Hydrocarbon-LSWAG scenario to be applied in "B" Structure of "S" Field is by injecting hydrocarbon gas of 0.25 MMSCFD alternating with low salinity water injection of 1000 BPD with injected water salinity of 1,800 ppm by applying one Hydrocarbon-LSWAG injection cycle for each year with gas-water injection duration ratio of 1:2 which results in 60.01% of oil recovery factor. Therefore, Hydrocarbon-LSWAG is suggested to be applied in "B" Structure of "S" Field for further field development.

Introduction
Low salinity water injection (LSWI) is an emerging enhanced oil recovery (EOR) technique that can increase the oil recovery about 5-20% of original oil in place (OOIP) compared to conventional waterflood (Lager et al., 2008). The main recognized effects of LSWI are the decrease of residual oil saturation and the increase of microscopic sweep efficiency (Rotondi et al., 2014). There is an idea to combine LSWI with gas injection which is known as low salinity water alternating gas (LSWAG) injection. LSWAG injection process means to inject both low salinity water and gas to the reservoir in order to improve the oil recovery. The presence of flue gas produced during production process leads to the idea of utilizing the produced hydrocarbon gas to be used for injection as it is easy to obtain. CO_2 gas is not preferable to be used as it is hard to obtain and expensive. Furthermore, CO_2 injection may trigger pipeline corrosion (Dong et al., 2019). However, there are still limited studies that discuss the performance of Hydrocarbon-LSWAG in prospective field as well as its possible mechanisms in recovering additional oil.
Several objectives that will be achieved in the end of this study are to identify the effects of operational parameters of Hydrocarbon-LSWAG injection that contribute to the enhancement of oil recovery, and to propose the most optimum water salinity, number of cycle and gas-water injection ratio scenario of Hydrocarbon-LSWAG injection based on oil recovery performance through simulation studies. Nevertheless, those objectives are limited to the application in sandstone reservoir at "B" Structure in "S" Field.
Some of the underlying mechanisms of LSWI to promote an additional recovery are known as follows:

a. Fines migration
   Tang and Morrow (1999) reported that LSWI may release fines/clay particles from rock surface which leads into increased water-wetness of the rock. Released fine particles from rock surfaces may block the pore throats and subsequently divert the flow of injected water into unswept pores inside reservoir rock.
b. pH increase
   Lager et al. (2006) explained that pH increase during LSWI is caused by carbonate dissolution and cation exchange process. The formation of OH- components in the liquid phase and may result in higher pH and increases oil recovery.
c. Multicomponent ionic exchange (MIE)
   Lager et al. (2006) stated that MIE releases oil component when positively charged multivalent ion which connects to negatively charged clay surface exchanges with a monovalent ion in injected water. Desorption process of polar oil components from clay surface lead into a more water-wet reservoir rock and tends to provide an additional oil recovery.
d. Electrical double layer (EDL) expansion
   Desorption of oil components from clay surface occurs as a result of salinity reduction which causes the EDL

PROCEEDINGS
JOINT CONVENTION BANDUNG (JCB)2021
November 23rd – 25th 2021

expansion between clay surface and oil interfaces (Ligthelm et al., 2009). The clay surface becomes more water-wet and form a more stable water film (Nasralla and Nasr-El-Din, 2012).

e. Salting-in effect
RezaeiDoust et al. (2009) found that salting-in effect describes the increase of organic materials solubility inside the aqueous phase when the water salinity is lowered.

Besides all of the mechanisms mentioned above, geochemical reactions that consist of aqueous reactions, mineral dissolution reactions, and cation exchange reactions also become the main factor in affecting oil recovery improvement through LSWI by supplying cations for the ionic exchange process as a result of mineral dissolutions and support wettability alterations mechanism.

LSWI is an EOR method based on wettability alteration from oil-wet to water-wet conditions and WAG is a proven method for improving gas flooding performance by controlling the gas mobility. Therefore, LSWAG injection promotes the synergy between those underlying mechanisms (multicomponent ionic exchange, wettability alteration, improving displacement efficiency, mobility control, etc.) in enhancing the oil recovery (Dang et al., 2014).

Data and Method

1. Methodology

This study was conducted based on the design framework as shown on **Figure 1**.

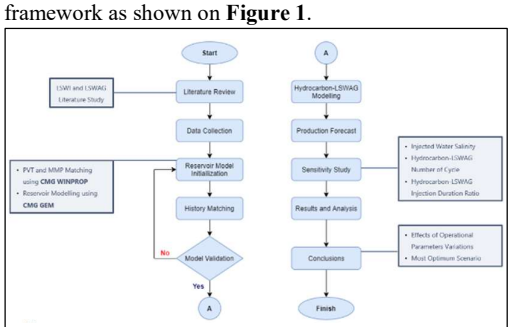

Figure 1: Framework of the Study

In designing the Hydrocarbon-LSWAG injection model, some parameters are assumed to complete the design due to the limitations on experimental data:

a. Clay minerals content is distributed similarly for each grid.
b. Interpolation range of ion exchange $\zeta(Na - X)$ is between 0.9378 and 0.6678 as obtained from the model initialization result.
c. The study is limited to the application in Sandstone Reservoir at "B" Structure in "S" Field.

2. Field Overview

The "S" Field, which is the focus of this study, is located in Kabupaten Ogan Ilir, South Sumatera Province, Indonesia. The field is founded in 1990 with area approximation of 18.25 km^2. Eleven wells are existed in "S" Field with different status that consist of five production wells (B-1, B-3, B-5, T-1, and T-3), an injection well (S-1), two plugged and abandoned wells (T-2 and K-1), and three suspended wells (B-2, B-4, T-4). The 2D map of "S" Field can be seen on **Figure 2**. According to the company, the "S" Field has been producing fluid from four wells and two proven layers since 1992. This field consists of two major structures which are "B" and "T" structures with "B" Structure as the main focus of this study. The cumulative production of "B" Structure is 2.285 MMSTB according to the field status in January 2020. The reservoir of "S" Field is identified as a sandstone reservoir with original reservoir pressure of 1700 psig and a strong water drive reservoir based on material balance analysis. Based on the provided fluid data, the hydrocarbon of this reservoir has an original GOR value of 722 scf/bbl, liquid gravity of 33.4 ºAPI at 60 ºF, and oil viscosity of 0.7342 cP. "B" structure consists of three sand layers including T, G, and K layer. Current productive layers which are used for LSWI implementation in "B" Structure are T and K sand layers. Based on the mineral content analysis data, it shows that the reservoir contains clay minerals especially kaolinite and illite which must be considered for LSWI implementation.

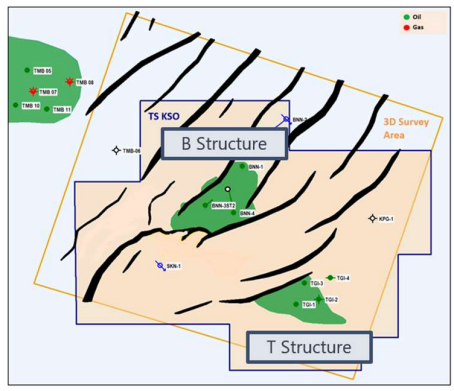

Figure 2: 2D Map of "S" Field

3. PVT Modelling and MMP Determination

In the early process of reservoir modelling, pressure, volume, and temperature (PVT) validation test was conducted by generating a compositional fluid model with C_{7+} as the pseudo-component. In this study, the fluid model was built using CMG WINPROP™ from constant composition expansion (CCE) and differential liberation (DL) tests. The prioritized parameters to be matched in this study are the saturation pressure, gas-oil ratio, relative volume, formation volume factor, and viscosity. Based on the fluid data and phase envelope obtained from this modelling process, the fluid of "B" Structure is identified as light-medium oil.

Minimum miscibility pressure (MMP) is calculated to determine the miscible condition at which the gas is injected to the reservoir. Due to the limited experimental data of "B" Structure in "S" Field, the determination of MMP value is calculated using a correlation proposed by Ghorbani (2013) as the optimum condition for the correlation is fulfilled with the characteristics of "B" Structure. The correlations are shown as follows:

$$\mathrm{MMP} = 44.162 - 4.32\alpha + 0.691\alpha^2 - 0.141$$

$$\alpha = \frac{X_{C2-C6}^{1.68} \times X_{C1}^{0.1}}{(1.8\,T + 32)^{0.5} \times M_{C7+}}$$

$$\beta = Y_{C2+}^{(1.085+0.0056M_{C2+})}$$

This correlation gives MMP value of 1951.27 psi which is identical with the MMP value obtained from cell-to-cell simulation method using CMG WINPROP™ which results in MMP value of 1975 psi with only 1.2% of differences.

4. Reservoir Simulation Modelling

Table 1: Initial Conditions

Parameter	Units	Value
Total Bulk Reservoir	res ft^3	7.954×10^8
Total Pore Volume	res ft^3	1.278×10^8
Total Hydrocarbon Pore Volume	res ft^3	4.951×10^7
Original Oil In Place	std bbl	7.175×10^6
Original Gas In Place	std ft^3	2.365×10^9

Reservoir model initialization was modeled using CMG GEM™ builder format by inputting basic reservoir properties. The initial condition value of the model is obtained with original oil in place (OOIP) of 7.1748 MMSTB. This OOIP value is considered as 2P.

The selected geochemical reactions that are applied in this simulation encompas the aqueous reaction and mineral dissolution or precipitation based on the core flood experiment and PHREEQC Software proposed by Ashraf et al. (2010) in combination with ionic exchange proposed by Dang et al. (2013). The geochemical reactions are as follows:

Table 2: Geochemical Reactions

	Geochemical Reactions
Aqueous Reactions	$H^+ + OH^- \leftrightarrow H_2O$
	$CaHCO_3^+ \leftrightarrow Ca^{2+} + HCO_3^-$
	$NaHCO_3 \leftrightarrow Na^+ + HCO_3^-$
	$MgHCO_3^+ \leftrightarrow Mg^{2+} + HCO_3^-$
	$H^+ + MgCO_3 \leftrightarrow Mg^{2+} + HCO_3^-$
	$H^+ + NaCO_3^- \leftrightarrow Na^+ + HCO_3^-$
Mineral Reactions	$H^+ + \text{Calcite} \leftrightarrow Ca^{2+} + HCO_3^-$
	$H^+ + \text{Dolomite} \leftrightarrow Ca^{2+} + Mg^{2+} + HCO_3^-$
Cation Exchanges	$Na^+ + 0.5Ca - X_2 \leftrightarrow 0.5Ca^{2+} + Na - X$
	$Na^+ + 0.5Mg - X_2 \leftrightarrow 0.5Mg^{2+} + Na - X$

The CEC value was calculated using the equation proposed by Seilsepour and Rashidi (2008) :

$$\text{CEC}\left(\frac{\text{meq}}{\text{kg}}\right) = 628.58 \text{ x fraction clay} + 48.8$$

$$\text{CEC}\left(\frac{\text{meq}}{\text{m}^3}\right) = \text{CEC}\left(\frac{\text{meq}}{\text{kg}}\right) \text{x} \left[\frac{\rho_{\text{rock}}(1-\phi)}{1000}\right]$$

The porosity that being used in the equation is the average porosity of the reservoir by assuming that the porosity value is homogenous for all rock types. The calculated CEC value for LSWI process in this sandstone reservoir is equal to 237 eq/m^3.

After the initialization process of the reservoir model is done, history matching was then conducted using available production history data from three production wells (B-1, B-3, and B-5) from 1992 until 2020 with the reported cumulative oil production of 2.285 MMSTB. The parameters that are used for the history matching of the reservoir model are liquid rate, oil rate, and water rate. Parameters adjustment and refinement during the history matching process were done by modifying the aquifer and water-oil contact (WOC). The history matching process results of cumulative production of the field ("B" Structure) is shown on **Figure 3**.

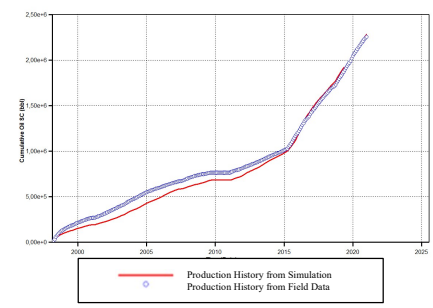

Figure 3: Cumulative Production History Matching

5. Sensitivity Study

The production scenario of this study is forecasted for 15 years of production started from 1st January 2021 to 1st January 2036 to observe the reservoir performance and oil recovery of the field. Production wells that are used are the same as the existing production wells consist of Well B-1, B-3, and B-5. The injection of Hydrocarbon-LSWAG in this study is performed using two injector wells consisting of Well B-4 (suspended well) which begins to inject fluid on 1st January 2022 and by converting Well B-1 into injector well (Convert to Injector or CTI) on 1st November 2027 when the well reaches the economic limit. Several production constraints are applied in this analysis: bottomhole pressure of 100 psi, economic limit of 15 STBD, liquid rate of 546 STBD for Well B-1, liquid rate of 2,342 STBD for Well B-3, and liquid rate of 120 STBD for Well B-5. Those liquid rate constraints are obtained from last production data for each well.

In this study, gas and water injection rates are locked at 1,000 BPD and 0.25 MMSCFD. The water injection rate of 1,000 BPD is obtained from previous study that have been done in this field which concluded that this water injection rate value is the most optimum one. On the other hand, the gas injection rate value of 0.25 MMSCFD is applied based on last gas production data of the field. This decision is made due to the idea that the injected gas used in this study is the hydrocarbon gas produced from the production of the field.

The first analysis to identify the effects of Hydrocarbon-LSWAG injection operational parameters is performed using three comparison studies:

a. Hydrocarbon-LSWAG injection using water salinities of 1,800 and 3,600 ppm are simulated and then being compared with the base case. The number of injection cycle is locked at 1 cycle/year and the gas-water injection duration ratio is locked at 1:1. The composition of the injected water is shown on **Table 3**.
b. Hydrocarbon-LSWAG injection using both injected water salinities of 1,800 and 3,600 ppm are simulated by applying variations in number of injection cycle of 1, 2, and 3 cycles/year. The gas-water injection duration ratio is locked at 1:1.

PROCEEDINGS
JOINT CONVENTION BANDUNG (JCB)2021
November 23rd – 25th 2021

c. Hydrocarbon-LSWAG injection using both injected water salinities of 1,800 and 3,600 ppm are simulated by applying variations in gas-water injection duration ratio of 1:1, 2:1, and 1:2. The number of injection cycle is locked at 1 cycle/year.

Table 3: Injected Water Compositions

	Components	Concentration 1 (ppm)	Concentration 2 (ppm)
Cations	Na^+	662.099	1324.200
	K^+	6.720	13.440
	Ca^{2+}	6.013	12.025
	Mg^{2+}	1.238	2.478
	Fe^{3+}	0.292	0.584
	Sr^{2+}	1.680	3.360
	Ba^{2+}	0.159	0.318
Anions	HCO_3^-	296.124	592.247
	CO^{2-}	0.000	0.000
	OH^-	0.017	0.017
	Cl^-	814.981	1629.961
	SO_4^{2-}	10.876	21.752
Total Salinity		**1800.181**	**3600.363**

The time durations for each number of cycles and gas-water injection duration ratios are shown on **Table 4**.

Table 4: Duration for Each Cycle and Gas-Water Injection Ratio

Number of Cycle/Year	1 Cycle Duration (days)	Ratio 1:1 (days)		Ratio 2:1 (days)		Ratio 1:1 (days)	
		Gas	Water	Gas	Water	Gas	Water
1	365.25	182.625	182.625	243.5	121.75	121.75	243.5
2	182.625	91.3125	91.3125	121.75	60.875	60.875	121.75
3	121.75	60.875	60.875	81.167	40.583	40.583	81.167

Number of Cycle/Year	1 Cycle Duration (months)	Ratio 1:1 (months)		Ratio 2:1 (months)		Ratio 1:2 (months)	
		Gas	Water	Gas	Water	Gas	Water
1	12	6	6	8	4	4	8
2	6	3	3	4	2	2	4
3	4	2	2	2.67	1.33	1.33	2.67

The second analysis is done using permutations of sensitivity study simulations with variations of injected water salinity, number of Hydrocarbon-LSWAG injection cycle, and gas-water injection duration ratio.

Result and Discussion

1. Effects of Operational Parameters

The first study is conducted to identify the effects of Hydrocarbon-LSWAG injection operational parameters that consist of water salinity, number of Hydrocarbon-LSWAG cycle and gas-water injection duration ratio on the improvement of oil recovery. This identification was done by conducting comparison studies as explained in the previous section.

The first comparison was done to identify the effects of the water salinity of the injected low salinity water. The comparison was done to compare the oil recovery resulted from the base case without the application of Hydrocarbon-LSWAG injection, Hydrocarbon-LSWAG injection using 1,800 ppm of water salinity, and Hydrocarbon-LSWAG injection using 3,600 ppm of water salinity. The resulted oil recovery comparison is shown in **Table 5** and **Figure 4**. The comparison results show that the injected water salinity of 1,800 ppm gives better result with 4.27 MMSTB cumulative oil production and 59.577% of oil recovery factor with oil recovery factor improvement of 5.04% from the base case. The results indicate that the increasing value of the injected water salinity is inversely proportional to the improvement of oil recovery. In crude oil-brine-rock systems, the water relative permeability will decrease while the oil relative permeability will increase as the rock surface becomes more water-wet as LSWI influenced the shape and the end points of the relative permeability curves. According to the study done by RezaeiDoust, et al. (2009), lowering the injected water salinity increases the organic materials solubility in the aqueous phase and supports the occurrence of wettability alteration. This phenomenon is known as salting-in effect. Injection using lower water salinity also boosts the occurrence of MIE between the organic material on the surface of the mineral and the invading low salinity water. Polar compound desorption from the clay surface makes the reservoir rocks to be more water wet and cause an increase in oil recovery. **Figure 5** shows the comparison between remaining oil saturation distribution using water salinity of 1,800 ppm and 3,600 ppm. It is shown that Hydrocarbon-LSWAG injection using water salinity of 1,800 ppm promotes better sweep efficiency compared to 3,600 ppm.

Table 5: Oil Recovery Comparison of Water Salinity Variations

Water Salinity (ppm)	Number of Cycle (cycle/year)	Gas-Water Injection Duration Ratio	Np (MMSTB)	RF (%)
	Base Case		3.913	54.534
1,800	1	1 : 1	4.27459	59.577
3,600			4.15695	57.938

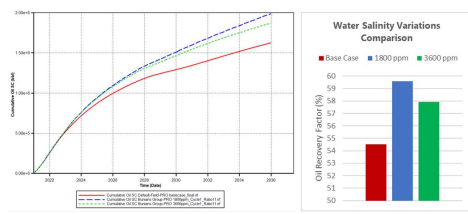

Figure 4: Oil Recovery Comparison of Water Salinity Variations

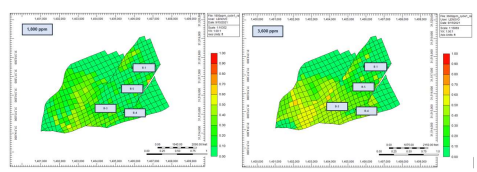

Figure 5: Remaining Oil Saturation Comparison of Water Salinity Variations

The second comparison was done to observe the effect of Hydrocarbon-LSWAG cycle to the oil recovery of the field. The comparison results are shown in **Table 6** and **Figure 6**. For cases with injected water salinity value of 1,800 ppm, the most optimum case is the one with 1 cycle/year (182.625 days of gas injection and 182.625 days of water injection). The case resulted in 4.275 MMSTB of cumulative oil production and 59.577% of oil recovery factor with an improvement of 5.04% from the base case. Nevertheless, the cases with injected

water salinity of 3,600 ppm show that the most optimum case is the one with 2 cycle/year (91.313 days of gas injection and 91.313 days of water injection). The case resulted in 4.158 MMSTB of cumulative oil production and 57.959% of oil recovery factor with oil recovery improvement of 3.43% from the base case. Hence, the comparison results show that increase in number of Hydrocarbon-LSWAG injection cycle is neither directly nor inversely proportional with the improvement oil recovery in this field. The observed results show contradictory pattern with most cases that have been found previously. As in most cases, more WAG cycle results in higher oil recovery. Namani and Kleppe (2011) explained that the longer the duration of the cycle, the supporting pressure that drive the production of the field becomes higher as well. This mechanism may optimize sweep efficiency and support oil production. This contradictory study result may lead to the opinion that the effects of cycle number to oil recovery is uncertain and may result in different behavior at different fields caused by the lateral and areal heterogeneity of the reservoirs.

Table 6: Oil Recovery Comparison of Hydrocarbon-LSWAG Cycle Variations

Water Salinity (ppm)	Number of Cycle (cycle/year)	Gas-Water Injection Duration Ratio	Np (MMSTB)	RF (%)
1,800	1	1 : 1	4.275	59.577
	2		4.274	59.574
	3		4.268	59.480
3,600	1	1 : 1	4.157	57.938
	2		4.158	57.959
	3		4.156	57.927

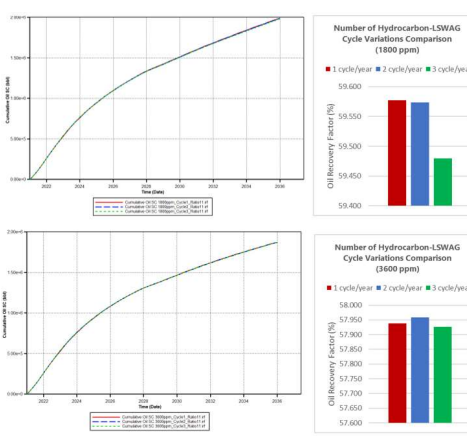

Figure 6: Oil Recovery Comparison of Hydrocarbon-LSWAG Cycle Variations

The third comparison study was done to identify the effects of Hydrocarbon-LSWAG gas-water injection duration ratio to the oil recovery. The results of the third comparison study are shown in **Table 7** and **Figure 7**. The comparison results for both injected water salinity of 1,800 and 3,600 ppm show that the highest oil recovery is obtained from gas-water injection ratio of 1:2 (121.75 days of gas injection and 243.5 days of water injection). The best case for 1,800 ppm water salinity results in 4.306 MMSTB of cumulative oil production and 60.011% of oil recovery factor with 5.48% of oil recovery factor improvement from the base case. Meanwhile, the best case for 3,600 ppm water salinity results in 4.163 MMSTB cumulative oil production and 58.022% of oil recovery factor with 3.489% of improvement from the base case. Therefore, it can be identified that higher oil recovery is obtained in this field when the low salinity water injection duration is twice longer than the duration of hydrocarbon gas injection (gas-water injection duration ratio of 1:2). Longer water injection duration improves the low salinity water performance by increasing the occurrence of mineral dissolutions and ionic exchange reactions. Increase in ionic exchange reactions leads to more oil swept in the reservoir. However, several previous studies found that equal injection duration ratio may also results in better oil recovery as it provides more stable sweep efficiency support. The explanation of different behaviors that were found in different fields regarding injection duration ratio can be related to the fluid composition, injector well locations, and heterogeneity of the reservoir.

Table 7: Oil Recovery Comparison of Gas-Water Injection Duration Ratio Variations

Water Salinity (ppm)	Number of Cycle (cycle/year)	Gas-Water Injection Duration Ratio	Np (MMSTB)	RF (%)
1,800	1	1 : 1	4.275	59.577
		2 : 1	4.221	58.829
		1 : 2	4.306	60.011
3,600	1	1 : 1	4.157	57.938
		2 : 1	4.122	57.453
		1 : 2	4.163	58.022

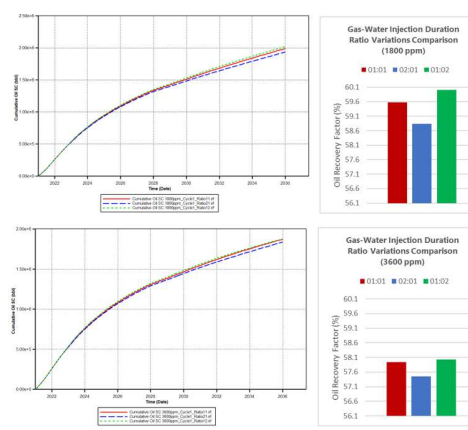

Figure 7: Oil Recovery Comparison of Gas-Water Injection Duration Ratio Variations

2. Optimum Scenario of Hydrocarbon-LSWAG Injection

The determination of the most optimum scenario of Hydrocarbon-LSWAG injection is done by conducting permutation sensitivity study of the injection operational parameters. Those parameters consist of water salinity, number of cycles, and gas-water injection ratio. The oil recovery and recovery factor values resulted from the simulations of the proposed sensitivity permutations can be seen in **Table 8**. From the table, it is observed that the highest oil recovery is obtained from scenario number 9 with injected water salinity of 1,800

PROCEEDINGS
JOINT CONVENTION BANDUNG (JCB)2021
November 23rd – 25th 2021

ppm, 3 cycle/year, and injection ratio of 1:2 (40.58 : 81.17 days). The scenario results in cumulative oil production (Np) and oil recovery factor of 4.31 MMSTB and 60.078% respectively. It means that the scenario has recovery factor value improvement of 5.54% from the base case at which Hydrocarbon-LSWAG is not implemented. Nevertheless, the author suggests to reduce the number of Hydrocarbon-LSWAG injection cycle from 3 cycle/year to 1 cycle/year which indicates that case number 3 is more preferable to be applied. This decision is made by considering that the application of 3 cycles/year may result in higher operational cost and technical difficulties compared to 1 cycle/year. The fact that the oil recovery factors of both scenarios only show 0.067% of difference, which is considered identical, also supports this decision. The comparison between both scenarios is shown in **Figure 8**.

Table 8: Results of Sensitivity Analysis Permutation Scenarios

Scenario	Water Salinity (ppm)	Number of Cycle (cycle/year)	Gas-Water Injection Duration Ratio	Np (MMSTB)	RF (%)
Base Case	-	-	-	3.913	54.534
1	1,800	1	1 : 1	4.275	59.577
2			2 : 1	4.221	58.829
3			1 : 2	4.306	60.011
4		2	1 : 1	4.274	59.574
5			2 : 1	4.227	58.914
6			1 : 2	4.308	60.048
7		3	1 : 1	4.268	59.480
8			2 : 1	4.225	58.887
9			1 : 2	4.311	60.078
10	3,600	1	1 : 1	4.157	57.938
11			2 : 1	4.122	57.453
12			1 : 2	4.163	58.022
13		2	1 : 1	4.158	57.959
14			2 : 1	4.116	57.367
15			1 : 2	4.167	58.080
16		3	1 : 1	4.156	57.927
17			2 : 1	4.122	57.453
18			1 : 2	4.161	57.995

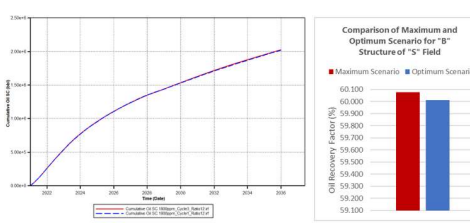

Figure 8: Remaining Oil Saturation Comparison of Water Salinity Variations

As a result, the preferable optimum scenario to be applied in "B" Structure of "S" Field is scenario number 3 with injected water salinity of 1,800 ppm, 1 cycle/year, and injection duration ratio of 1:2 (121.75:243.5 days). The water and gas injection rates are 1000 BPD and 0.25 MMSCFD respectively. This scenario results in cumulative oil recovery (Np) and oil recovery factor of 4.31 MMSTB and 60.01% respectively with oil recovery improvement of 5.47% from the base case.

Conclusions

Based on the results and analysis of this study, several conclusions can be obtained to answer the objectives of this study:

1. According to simulation study results: lowering the injected water salinity improves oil recovery; the number of Hydrocarbon-LSWAG injection cycle in this field is neither directly nor inversely proportional with the improvement of oil recovery; higher oil recovery is obtained from the field when the low salinity water injection duration is twice longer than the duration of hydrocarbon gas injection (gas-water ratio of 1:2).
2. The proposed optimum scenario of Hydrocarbon-LSWAG injection to be applied at "B" Structure in "S" Field is using injected water salinity of 1,800 ppm, applying 1 Hydrocarbon-LSWAG cycle/year, and using gas-water injection duration ratio of 1 : 2 (121.75 : 243.5 days) with water injection rate of 1000 BPD and gas injection rate of 0.25 MMSCFD.

References

Ashraf, A., Hadia, N.J., Torsaeter, O., and Tweheyo, M.T., 2010, SPE Oil and Gas India Conference and Exhibition, January 20–22, 2010.

Dang, C. T., Nghiem, L. X., Chen, Z., and Nguyen, Q. P., 2013, SPE Annual Technical Conference and Exhibition, September 30 – October 2, 2013.

Dong, J., Wu, S., Xing, G., Fan, T., Li, H., and Wang, B., 2019, International Petroleum Technology Conference, March 26–28, 2019.

Lager, A., Webb, K.J., Black, C.J.J., Singleton, M., and Sorbie, K. S., 2006, International Symposium of the Society of Core Analysts, Norway, 12-16 September.

Lager, A., Webb, K. J., Collins, I. R., and Richmond, D. M., 2008, SPE Symposium on Improved Oil Recovery, April 20–23, 2008.

Ligthelm, D. J., Gronsveld, J., Hofman, J., Brussee, N., Marcelis, F., and van der Linde, H., 2009, EAGE Conference and Exhibition, June 8–11

Namani, M., and Kleppe, J., 2011, SPE Enhanced Oil Recovery Conference, July 19–20.

Nasralla, R. A., and Nasr-El-Din, H. A., 2011, SPE Asia Pacific Oil and Gas Conference and Exhibition, September 20–22, 2011.

RezaeiDoust, A., Puntervold, T., and Austad, T., 2010, SPE Annual Technical Conference and Exhibition, September 19–22, 2010

Rotondi, M., Callegaro, C., Masserano, F., and Bartosek, M., 2014, Abu Dhabi International Petroleum Exhibition and Conference, November 10–13.

Tang, G.-Q., and Morrow, N. R., 1999, Journal of Petroleum Science and Engineering, 24(2-4), 99–111.

Acknowledgements

The authors would like to thank the Almighty God for His abundant blessings that are given to the authors during the writing process of this paper. The authors also want to give highest appreciations to:

1. Institut Teknologi Bandung (ITB) for the opportunity that is given to the authors to write and publish this paper.
2. Petroleum engineering study program of ITB for the supports during the research and writing process of this paper.
3. Bass Oil Sukananti Limited for the opportunity and supports especially in conducting Hydrocarbon-LSWAG study so that this paper can be written and published by the authors.

PROCEEDINGS
JOINT CONVENTION BANDUNG (JCB) 2021
November 23rd – 25th 2021

Analysis of Geothermal Existence with Geographic Information Systems in Sangubanyu Village and Surrounding Areas, Batang Regency

Ahmad Syihab Fajarulloh[1], Kartika Luthfia Ariwibowo[1], Yosian Berkat[1], Andrian Nur Habib Musthofa[1], Aldino Maulana Riski[1]
Department of Geological Engineering, Faculty of Engineering, Diponegoro University
syihab.ahmad8@gmail.com

Abstract
Sangubanyu Village is a geothermal potential area in Bawang District, Batang Regency with the main manifestation is hot springs. This manifestation condition is centered on the Sangubanyu hot spring and is located 21 km from the Dieng geothermal area. Geological information on this geothermal potential area is still scant, so a research was conducted with the aim of knowing the geothermal conditions in Sangubanyu by linking geological conditions and analysis of geographic information system. The method used is the analysis of the results of field observations and with secondary data supported by geographic information system processing. The results of this processing show that the lithological conditions in Sangubanyu are dominated by volcanic breccia and with bicarbonate deposits mixed with oxidation products around the hot springs. This condition is supported by its presence in the medium – high land surface temperature zone and based on fault fracture density many fractures or weak zones are found, so it is interpreted that hydrothermal flow in hot springs in Sangubanyu is due to the activation of regional faults which makes many weak zone. Field condition is found many small hot springs with a dominant presence in the south and around the river. The interpretation of Chica-Olma ratio, Kaufman ratio, and Sabin ratio shows that the Sangubanyu area is dominated by iron ions and iron oxide products.

Key Words: Geothermal, Hot spring, Sangubanyu

Introduction

The geothermal sector as a tourism area is experiencing very rapid development. This condition occurs in Sangubanyu Village, Bawang District, Batang Regency (Figure 1), by utilizing geothermal manifestations in the form of hot springs as a bathing tourist area. This has become a trend among the Batang community, with a recorded increase in the level of tourists every year (Dinas Pemuda Olahraga dan Pariwisata Kabupaten Batang, 2018). This condition is also supported by the position of the Sangubanyu hot spring which is located 21 km from the Dieng geothermal area

The existence of hot springs in Sangubanyu Village, needs to be explored in more detail in terms of geology. This is because there is still little information about the occurrence of this geothermal water manifestation from the influence of its geological aspect. Therefore, this research aims to determine the geological conditions (distribution of surface lithology, geological structure and distribution of landforms) from the results of field observations and analysis of satellite imagery or geography infromation system, so as to create a correlation of information on the presence of hot water manifestations in Sangubanyu Village.

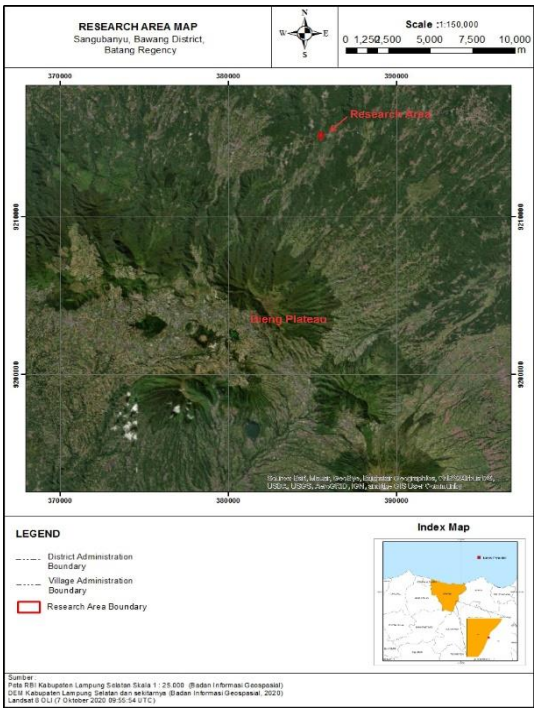

Figure 1. Location of The Research Area

Data and Method

Observations of hot springs in Sangubanyu Village are guided by the regional geology of the Banjarnegara and Pekalongan sheets. According to Condon, et al (1996) explained the regional conditions in the research area consisting of several formations (Figure 2), namely:

a. Kaligetas Formation are composed of volcanic breccia, lava flows, tuff, tuffaceous sandstones, and claystones. Flow breccia with lava inserts and fine to coarse tuff. Locally at the bottom was found claystone containing mollusks and tuffaceous sandstone. Weathered volcanic rock is reddish brown in color and often forms large chunks. About 50-200 m thick.
b. Jembangan Volcanic, composed of andesite lava and volcanic clastic rocks. Mainly hypersthenic-augittic andesites, locally containing hornblend as well as basalt olivine. In the form of lava flows, breccia and pyroclastic flows, lahars and alluvium. Lava and alluvial deposits consist of volcanic debris, lava flows and breccias deposited on gentle slopes some distance from the center of the eruption.
c. Alluvial Fan, is a deposited volcanic debris material.

In addition, the regional structural conditions show a predominance of folds, faults, lineaments and joints

involving Cretaceous to Holocene rocks. The folds in this sheet are in a northwest-southeast direction. The faults found are generally trending northwest-southeast to north-northwest-southeast with some trending northeast-southwest. The types of faults are descending faults, ascending faults and right-hand shear faults that occupy the middle and southern areas of the sheet. The lineage, which is partly suspected to be a fault, has a distribution pattern such as a fault pattern and is generally trending northwest - east southeast and northwest - southeast with some northeast – southwest (Condon, et al 1996).

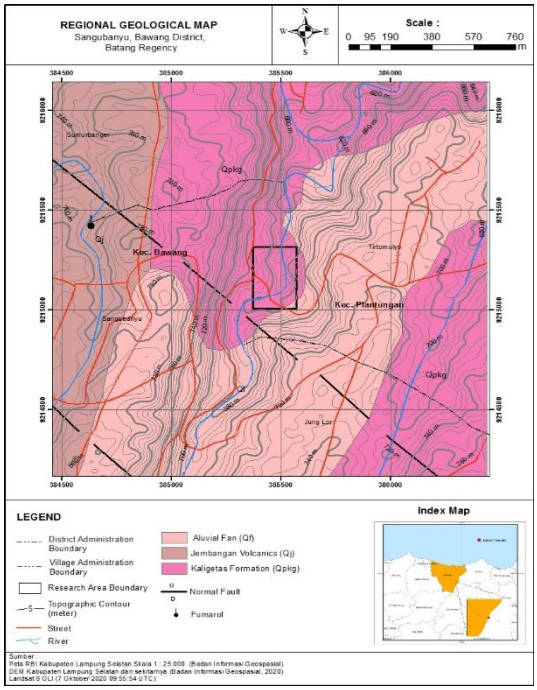

Figure 2. Regional Geology Condition

The method used in this research is the field observation method and geographic information system analysis (satellite image analysis). The explanation of each method is as follows:

a. Field observations, used to determine the distribution of surface lithology, landform conditions, water temperature measurement, and hot spring distribution in Sangubanyu.
b. Geographic information system analysis, by processing image data in the form of Landsat 8-OLI and Digital Elevation Model (DEM), so as to determine the condition of LST (Land Surface Temperature), NDVI, FFD (Fault Fracture Density), and mineral conditions from analysis Chica-Olma ratio, Kaufman ratio, and Sabin ratio

Result and Discussion

Surface Lithology Condition

The type of lithology in the research area is volcanic breccia, which is a rock product of volcanism (Figure 3). Characteristically, it is composed of sand, tuff, and andesite fragments composed of plagioclase, hornblend, biotite, quartz, and aphanite minerals (Thrope and Brown, 1985) (Figure 4). Andesite fragments found have a size of about 1 cm to 1 m. The volcanic breccia is part of the Kaligetas Formation.

The presence of hot springs at the research site causes the volcanic breccia to be altered, this is indicated by the presence of deposits in the form of relatively reddish yellow clay material concentrated around the heat source. It is interpreted that the color change is influenced by oxidation which is controlled by the content of iron minerals and minerals containing iron elements such as hornblend, rocks that undergo oxidation (Figure 5). The precipitate reacts weakly to HCl so that it has low carbonate properties, it is interpreted that this precipitate is an un-lithified travertine deposit. This travertine is an accumulation of calcium carbonate formed by fluids containing HCO3- (bicarbonate), the presence of these travertine deposits indicates that the area is included in the outflow zone.

The presence of this clay material deposit is interpreted quite intensively in the area where the hot springs are found or around the center of the hot springs (Figure 4), which is indicated to come from the feldspar group of minerals in andesite chunks weathered by the presence of hot springs. These springs are often found in the river.

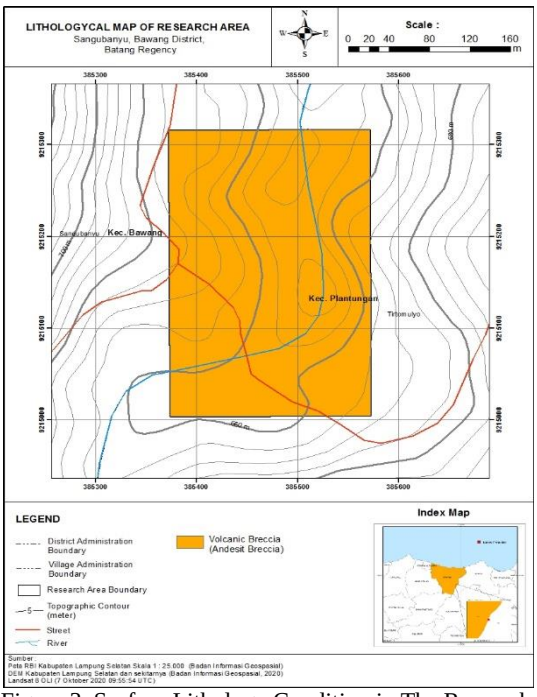

Figure 3. Surface Lithology Condition in The Research Area

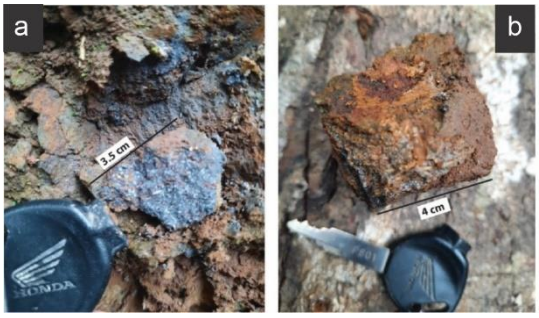

Figure 4. (a) andesite fragments in volcanic breccias with prismatic plagioclase minerals, (b) andesite fragments that are oxidized so that they change color to become longer.

Geologycal Structure Condition

The presence of geological structures in the research area is quite difficult to find on the surface due to weathering factors that are quite intensive, some of the structures that appear in the lithology of volcanic breccia are micro-joints with the type of crushed joints.

PROCEEDINGS
JOINT CONVENTION BANDUNG (JCB) 2021
November 23rd – 25th 2021

The existence of these joints is an indication that there is a geological structure with a larger scale controlling the area. The structural manifestations that can be seen on the surface are on the surface of andesite chunks (Figure 6) and in the presence of a waterfall on the river bank with several joints formed on the river bank (Figure 7). The existence of this structure is indicated as a weak zone area or as a gap for subsurface fluid to reach the surface area.

Figure 5. Accumulation of Iron Oxide deposits in Hot Springs Emerging Areas.

Figure 6. Fracture on The Andesite Rock Surface

Figure 7. Fracture on The Waterfall

Geomorphological Condition

Geomorphological conditions in the research area tend to be volcanic landforms, fluvial landforms, and denudational landforms (Figure 8).

a. Volcanic landforms in the form of hilly morphology resulting from volcanic material deposits or based on the classification of van Zuidam (1985) are included in the sloping wavy topography with a height difference of about 25 m.
b. The fluvial landforms found are morphological, with the Mender river flow. This condition is interpreted as a result of sedimentation activity and the influence of erosion which is quite intensive on the vertical slopes, thus forming the meander of the research area.
c. Denudational landforms (plains morphology) in the research area tend to be due to dominance due to the occurrence of exogenic processes in the form of rock weathering and the influence of human activities.

Figure 8. Morphology Condition

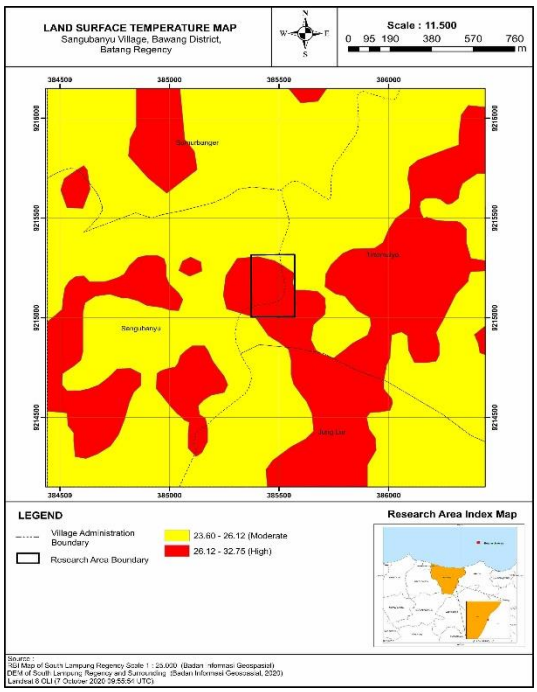

Figure 9. Land Surface Temaperature Condition

Conditions of Land Surface Temperature

Based on measuring water temperature in the field, show that the temperature about 35-37 ^{o}C around hot spring. The data helps to cross check with the result of remote sensing analysis that known as LST (Land Surface Temperature). LST analysis are used to determine the distribution of the estimated surface temperature in the research area (Prayudi, et al 2020). The land surface temperature conditions in the

research area are classified as medium-moderate with a temperature range of about 23.6ºC and included in the high-temperature area with a temperature range of 26.12ºC - 32.57ºC.

This condition is indicated, there is geothermal activity under the surface of the research area and usually the lower the value of the temperature degree, the higher the temperature. The distribution of land surface temperature conditions in the research area is dominated by moderate surface temperatures (Figure 9).

Conditions of Normalized Difference Vegetation Index

NDVI analysis will show the vegetation density index in the research area (Kumar and Silva, 1973). Areas that have geothermal potential will have a low vegetation index in the vicinity, because usually the area of the manifestation will come out of hot springs so that vegetation cannot grow properly. Areas with a low vegetation index will be shown in green gradually turning to yellow, the color still indicates that the vegetation density is sparse. In areas with low vegetation distribution, it is interpreted that there is almost no vegetation in the area and is indicated as a puddle or hot spring outlet, shown in green (Figure 10).

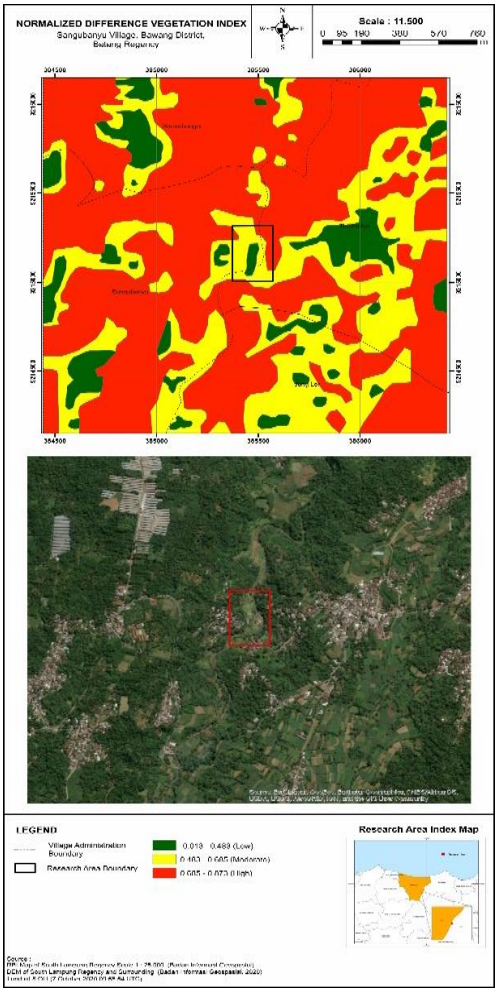

Figure 10. NDVI Condition

Condition of Fault Fracture Density

The results of the FFD (Fault Fracture Density) analysis are in the form of the straightness density distribution in the research area. The straightness can be used as an indication of the presence of geothermal manifestations, because this lineament will play a role in flowing geothermal fluids to the surface. This fluid movement will pass through rock that has a structure in the form of a gap between rocks and will usually change the minerals in the rock it passes through. The FFD results are classified into 3 classes, namely areas with low density values with values ranging from 0-180.44 km/km², medium density values ranging from 180.44-360.89 km/km², and high density values ranging from 360.89-541. ,34 km/km² (Figure 11). Based on the analysis of the straightness level, the conditions in the reseacrh area are interpreted, the geological conditions are quite complex, with the stress direction is NE-SW.

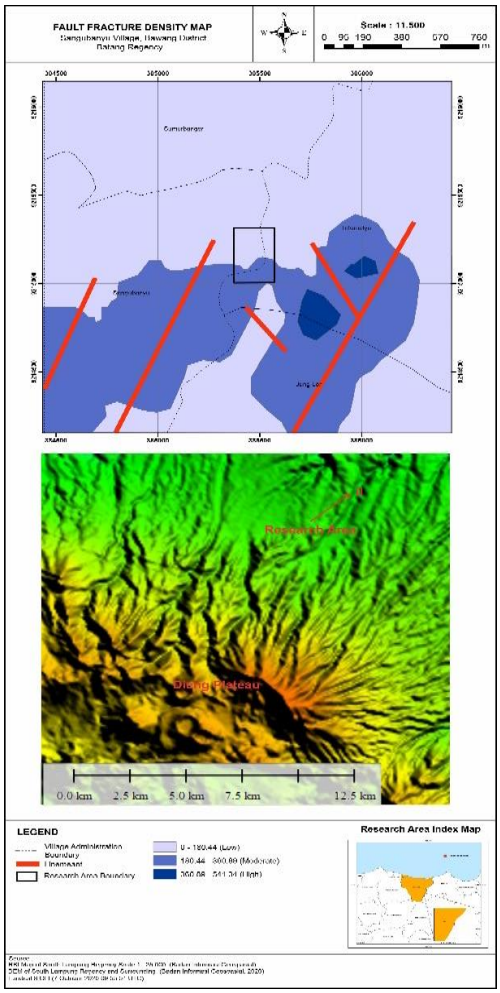

Figure 11. Condition of Fault Fracture Density

Mineral Distribution Analysis

The distribution of these mineral conditions can be determined using band ratio analysis which includes Chica-olma ratio, Abrams ratio, Sabin ratio, and Kaufman ratio (Zhou et all, 2013). The Chica-Olma ratio use 6/7; 6/5; 4/2 band combination, producing a mineral distribution with iron ions (blue), clay minerals (pink), and iron-oxidizing minerals (green). While the Abrams ratio use 6/7; 4/3; 5/4 band combination, by producing a distribution of clay minerals (pink) and iron oxide minerals (green) (Figure 12). Kaufman ratio use 7/5; 5/4; 6/7 band combination, which results in a distribution of hydroxyl minerals (blue) and iron minerals (red). In addition, Sabin ratio use 4/2; 6/7; 6/5 band combination, by producing a distribution of iron oxide (purple), hydroxyl minerals (green), and iron ore minerals (pink).

PROCEEDINGS
JOINT CONVENTION BANDUNG (JCB) 2021
November 23rd – 25th 2021

When viewed from the distribution of minerals based on the band ratio that has been processed, the distribution of alteration is in the middle part which is a river, when adjusted to the map of the location of the research area. This indicates an alteration process caused by the presence of chemical compounds related to hydrothermal carried by river water. The hydrothermal fluid can appear indicated out through the cracks found around the river.

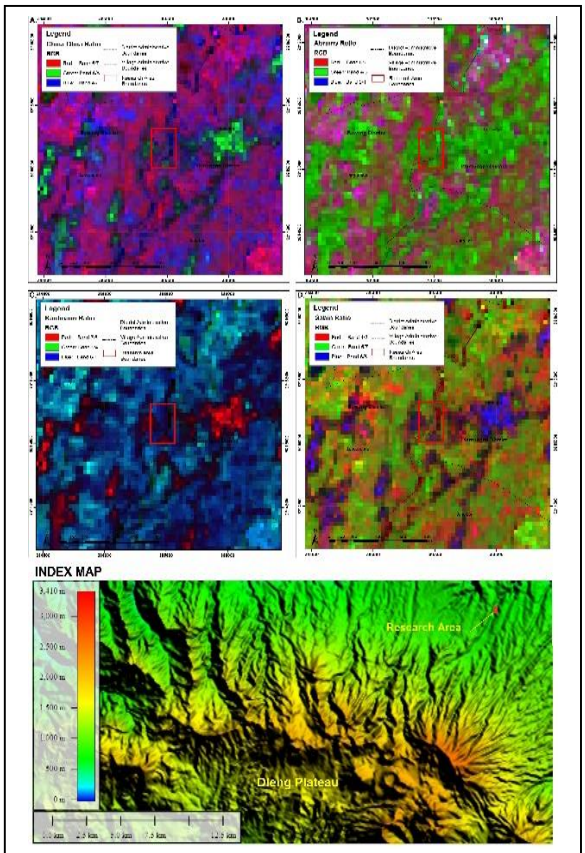

Figure 12. Figure 1. Spectral analysis map result from

Geothermal Potential in the Research Area

Determination of potential is done by combining data that has been analyzed (land surface temperature, nDVI, and FFD) with a raster calculator. The results show the distribution of geothermal potential or areas with the greatest potential will usually have the highest raster calculator values (Figure 13).

Geothermal potential in an area will be controlled by the structure shown on the fault fracture density map because it acts as a pathway for hot springs to emerge to the surface, another factor, namely areas with low vegetation density, will have great potential because plants tend not to be able to live in water conditions. which is concentrated in abundant chemical elements or has a high viscosity under high temperature conditions (Figure 14).

Geothermal potential in the research area is classified into 3 potential classes, namely:

a. The non-potential area (green), characterized by a score of 1-1,5 whose presence tends to be in the northern part of the research area and shows no geothermal manifestations that appear.
b. The area is somewhat potential (yellow), with a score of 1.5-2 and has a distribution in the north and west of the research area. The condition is indicated to be slightly affected by the presence of geothermal manifestations.
c. Potential area (red), is a very dominant area in the research area with a score of 2-3. This fig condition indicates that there is a distribution of manifestations that characterizes geothermal energy.

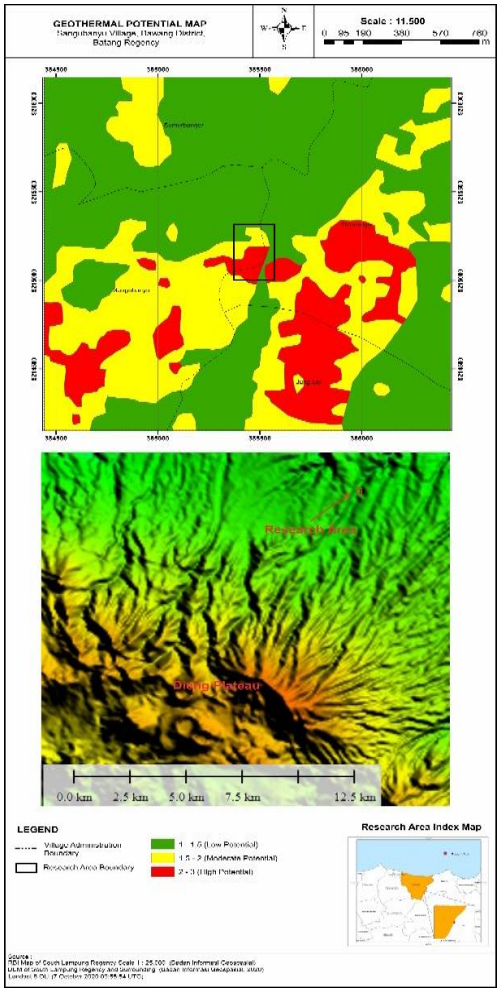

Figure 13. Geothermal Potensial in The Research Area

Figure 14. Hot Springs Manifestation

Conclusions

Lithology of Sangubanyu hot springs area is mainly composed of volcanic breccia (andesite breccia) attribute with interprete NE-SW stress direction providing transport path for hydrothermal fluid to the surface. In addition, from the analysis of satellite images related to the conditions of LST, NDVI, and FFD, it shows that the Sangubanyu bathing area is indeed in the geothermal potential zone, indicated by the distribution of iron oxide minerals from the analysis results that are commonly found.

Suggestion

This research area is generally a bustling tourist area, but some areas and conditions still lack of attention and support to become more developed tourist area. For this reason, it is necessary to review the accommodation area condition. In addition, the research area has also good geothermal conditions, but further research and review about this area is needed to utilize that potential.

References

Condon,W., H., Pardyanto L., Ketner, K.B., Amin, T. C., Gafoer, S., Samodra, H., 1996. *Peta Geologi Lembar Banjarnegara-Pekalongan, skala 1:100.000, Edisi 2*, Pusat Penelitian dan Pengembangan Geologi.

Dinas Pemuda Olah Raga dan Pariwisata. 2018. Daftar Data Koordinat Obyek Pariwisata. Kabupaten Batang.

Kumar, R., and Silva, L. 1973. Light ray tracing through a leaf cross- section. *Appl. Optics 12: 2950-2954*

Prayudi, Diko Sinatrya, Arrofi, Daffa, dan Ali, Rinal Khaidar. 2019. Identifying of Geothermal Manifestation Existence and Characterization Of Sulphidation Type Using Landsat-8 Image Processing Results: Case Study Of Mount Papandayan Area, Garut Regency, West Java Province. *12 PROCEEDINGS, The 7th Indonesia International Geothermal Convention & Exhibition (IIGCE) 2019, Jakarta Convention Center Indonesia, (August 13 -15, 2019)*

Thorpe, R. S., and Brown, G. C. 1985. *The Field Description of Igneous Rocks*. John Willey & Sons, New York

Van Zuidam, R. A. 1985. Aerial Photo-Interpretation in Terrain Analysis and Geomorphological Mapping. *Smith Publisher, The Hague.*

Zhou, J., Liu, L., Jiang, D.,Zhuang, D., Mansaray L.R., Zhang B., (2013), "Targeting Mineral Resources with Remote Sensing and Field Data in the Xiemisitai Area, West Junggar, Xinjiang, China." *Journal Remote Sensing, 5, 7, pp. 3156-3171.*

PROCEEDINGS
JOINT CONVENTION BANDUNG (JCB) 2021
November 23rd – 25th 2021

Distribution and Characteristics of Quarry Mining Type C Based on Geological Mapping and Petrographic Analysis in Jiken District, Blora Regency, Central Java Province

Dewi Sintia Reka[1] , Indah Mustika Dewi[2], Moch Indra Novian[1]
[1]Geological Engineering, Universitas Gadjah Mada
2 Geophysics, Universitas Gadjah Mada

Abstract

Quarry mining type C plays an important strategic role and function in regional economic development efforts. Mining activity is at least one form of income, in addition to being critical to the long-term viability of the industrial manufacturing and construction sectors. One of the prospects for quarry mining type C is in the Wonocolo and Ledok Formation, this formation in research location generally consists of massive limestone and massive sandstone with an area that is capable of being used as a prospect for quarry mining. This study aims to determine the distribution and characteristics of limestone and sandstone in the research location as a quarry mining commodity. Administratively the research location is in Nglebur, Janjang, Bleboh, and Singonegoro Village, Jiken District, Blora Regency, Central Java Province with the area of the mapping is 20 km2, the dimensions of each side 4 km x 5 km. Physiographically, it is included in the Rembang anticlinorium zone. This research was conducted using surface geological mapping methods, lithology determination by describing rocks macroscopically in the field and also based on the petrographic analysis method. According to the geological mapping, the surface is divided into four rock units: glauconitic carbonate sandstone, carbonate sandstone, packstone, and carbonate siltstone. Based on the petrographic analysis, it is found that three rock units have the potential to be quarry mining, it is packstone unit, glauconitic carbonate sandstone unit, and carbonate sandstone unit with a prospect mining area of 17 km2.

Keywords: quarry, mining, type C, jiken, limestone

Introduction

The need for building raw materials is increasing due to the construction of buildings and facilities in all fields. This study aims to determine the distribution and characteristics of limestone and sandstone in the research location as a quarry mining commodity. It is hoped that this research will be able to become a reference in determining the location of the type C minging which estimates the area and product. Geological mapping is required to establish area and thickness of the rock (Murlidhar et all, 2015). Geological reserves based on geological mapping which are important to decide rate of production and to carry out mine planning (Murlidhar et all et all, 2015). Certain test such as petrographic examination of different rocks can identify potential at an earlystage of aggregate quarry (Murlidhar et all et all, 2015). For planning geological exploration, geological mapping is essential to locate bore holes. Geological mapping also provides extent of aggregate deposit from surface mapping (Murlidhar et all, 2015). Administratively the research location is in Nglebur, Janjang, Bleboh, and Singonegoro Village, Jiken District, Blora Regency, Central Java Province with the area of the mapping is 20 km2, the dimensions of each side 4 km x 5 km (Figure 1). Physiographically, it is included in the Rembang anticlinorium zone according to van Bemmelen (1949). In general, according to regional geology, the research location consists of the Wonocolo Formation and the Ledok Formation in the form of carbonate sandstone, carbonate siltstone, and limestone. This type of rock can be used as fill in building buildings or public facilities.

Data and Method

This research was conducted using surface geological mapping methods, lithology determination by describing rocks macroscopically in the field and also based on the petrographic analysis method. At the surface geological mapping stage, rocks were completed at 140 observation points. Petrographic anaysis was determine by polarization microscope Olympus 500x using both plane polarize light (ppl) and cross polarize light (xpl). Rock classification was determine using mixsilisiclastic rock classification by Mount (1985). rock naming in the study area is based on unofficial lithostratigraphy according to the Indonesian Stratigraphy Code (1996). Rock units are divided based on the dominant rock. a Unit boundaries are based on rock contacts found in several places in the research field and the position of the layers. The concept of lithostratigraphy refers to the dominant lithology as a lithological feature. Unit naming is the naming of units in an informal manner in accordance with the Indonesian Stratigraphic Code (1996). In determining rock naming, the author uses rock naming based on field names. Then, to determine the age and bathymetry of rock units by analyzing fossils from field data samples. Rock units are grouped on the basis of observations on various paths traversed in the mapping area.

Result and Discussion

Based on lithological characteristics in the field and analysis of rock thin sections that can be mapped on a 1:25,000 topographic map, the stratigraphy of the mapping area is divided into four rock units which include from young to old according to informal lithostratigraphy: glauconitic carbonate sandstone, carbonate sandstone, packstone, and carbonate siltstone (Figure 2).

Carbonate sandstone unit

This unit is the oldest unit found in this mapping area. This unit consists of carbonate sandstone with an insert of carbonate siltstone. This unit has an erratic orientation of the slope of the layer, there is a relative dip to the north and also a relative dip to the south, this is because in this unit there is control of the special geological structure of the folds.

The naming of this rock unit is based on the dominant lithology in the study area, namely carbonate sandstone. Megascopically, this rock was found in a relatively fresh state. The color of this rock is brownish white to gray with angular to subrounded grain shapes. The cement contains carbonate because it reacts when dropped with 0.1 M HCL solution. The rock composition consists of siliciclastic material, carbonate material, and contains oxide and quartz minerals. Microscopically, the sedimentary rocks of carbonate tuffaceous sandstones are white-brown (PPL) and yellow-brown (XPL), subrounded grain shape, with the dominant texture in the form of grain supported, interparticle porosity type. Based on its composition, the rock consists of a matrix of micrite and sparite and contains oxide minerals, quartz, plagioclase and a small amount of glauconite. There are skeletal grain fragments in the form of small foraminifera. Here the composition of the siliciclastic material is more dominant than the carbonate material. The petrographic name of this rock is Sandy Allochem Limestone Mount Classification (1985). This rock unit occupies 50% of the map with a direction of West to East distribution at the top of the research area which includes Nglebur Village, Singonegoro Village, Bleboh Village, Janjang Village, Jiken District. This unit occupies a steep slope structural hill geomorphological unit. The thickness of this unit is calculated by reconstructing the geological cross section, the measurement results are that this unit is estimated to have a thickness of 400-500 m.

Carbonate glauconite sandstone unit

Megascopically, this rock was found in a relatively fresh state. The color of this rock is brownish white to gray with angular to subrounded grain shapes. The cement contains carbonate because it reacts when dropped with 0.1 M HCL solution. The rock composition consists of siliciclastic material, carbonate material, and contains oxide and quartz minerals. Microscopically, the sedimentary rocks of carbonate tuffaceous sandstones are white-brown (PPL) and yellow-brown (XPL). subrounded grain shape, with the dominant texture in the form of grain supported, interparticle porosity type. Based on its composition, the rock consists of a matrix of micrite and sparite and contains oxide minerals, quartz, plagioclase and a small amount of glauconite. There are skeletal grain fragments in the form of small foraminifera. Here the composition of the siliciclastic material is more dominant than the carbonate material. The petrographic name of this rock is Sandy Allochem Limestone Mount Classification (1985). This rock unit occupies 10% on the map with a direction of West to East distribution at the top of the research area which includes Nglebur Village, Singonegoro Village, Jiken District. This unit occupies a steep slope structural hill geomorphological unit. The thickness of this unit is calculated by reconstructing the geological cross section, the measurement results are that this unit is estimated to have a thickness of 120-160 m.

Packstone unit

Megascopically, this rock was found in a relatively fresh state. The color of this rock is white to yellowish, cement containing carbonate because it reacts when dripped with HCL solution. Good sorting, poor-moderate porosity, mud supported, closed container, massive sedimentary structure. The composition is a carbonate material of very fine sand - medium sand. Microscopically, layered limestone is brownish white (PPL) and gray-brown (XPL), grain size: fragment (2 mm-8mm, matrix < 0.2 mm), mud supported, interparticle porosity type. This incision is composed of fragments in the form of skeletal grains of small foraminifera, as well as a matrix of micrite and sparite. Then non-carbonate materials were also found, namely power minerals and oxide minerals. The composition of carbonate material is more dominant than siliciclastic material. Acting as a micrite is a matrix that is present in the form of carbonate mud, which acts as a sprite is calcite cement with a carbonate crystal shape (Folk, 1965) in the form of equant, morphologies of meteoric cement (James and Choquetta, 1984) in the form of blocky which binds the cavities between fragments and matrix, abundance 36%. Rock name : Limestone packestone (Embry & Klovan, 1971) or Sorted biosparite (Kendall, 2005 (after Folk, 1959). This rock unit occupies 16% on the map with a distribution on the south side of the study area which includes Janjang Village, Bleboh Village and Nglebur Village. This unit is located in the geomorphological unit of structural hills with a rather steep slope. The thickness of this unit is calculated by reconstructing the geological cross section, the measurement results are that this unit is estimated to have a thickness of 150m-180 m.

Carbonate siltstone unit

This unit is in harmony with the packstone unit. The naming of this rock unit is based on the dominant lithology in the study area, namely carbonate siltstone. Megascopically, these rocks are found in a relatively weathered state. The color of this rock is milky white,

cement containing carbonate because it reacts when dripped with HCL solution. Silt grain size, good sorting, closed container with poor porosity, matrix supported, massive sedimentary structure. The composition is a silt-sized carbonate material, and a fine siliciclastic material. The research location has quarry mining prospect potential, the prospect mining area is 17 km2. Microscopically, the layered limestone is brownish white (PPL) and gray-brown (XPL), grain size <0.03 mm – 0.6 mm, subangular-subrounded grain shape, with the dominant texture in the form of matrix supported, interparticle porosity type. Based on its composition, the rock consists of fragments in the form of ooids, quartz, and opaque minerals, as well as a matrix of micrite and sparite as well as the presence of mud and tuff. Rock name: Micritic Mudrock (Mount, 1985). This rock unit occupies 16% on the map with a distribution on the south side of the study area which includes Janjang Village, Bleboh Village and Nglebur Village. This unit is located in the geomorphological unit of structural hills with a rather steep slope. The thickness of this unit is calculated by reconstructing the geological cross section, the measurement results are that this unit is estimated to have a thickness of 150m -180 m.

Based on the petrographic analysis, it is found that three rock units have the potential to be quarry mining, it is packstone unit, glauconitic carbonate sandstone unit, and carbonate sandstone unit (Figure 6). The determination is based on the characteristics and composition of the rock. The estimated thickness of these three units is in the range of 670-840 meters based on the calculation strike dip of the rock and the measured section (Figure 3). From a bird's point of view, we will see an area of about 17 km in the form of rock that has the potential to be a type C quarry mining. The 3-Dimensional map can be seen in Figure 4. These three rocks can be used as backfill and a mixture of building materials or as aggregates for construction purposes. The research location has minimal population and forest so it will be safer if we want to use it as a type C quarry mining location. The research location is also strategic in terms of ease of transportation because it is close to the main Blora-Cepu highway which makes it easier to mobilize.

Conclusions

There are three rock units have the potential to be quarry mining, it is packstone unit, glauconitic carbonate sandstone unit, and carbonate sandstone unit. The estimated thickness of these three units is in the range of 670-840 meters. The area of potential area of Quarry Ming type C is 17km2.

References

Indonesia, K. S. S., 1996, Sandi Stratigrafi Indonesia. Ikatan Ahli Geologi Indonesia, 14.

Murlidhar, D. R., 2015, Jurnal Teknologi, UTM Journal, **78**, 71-79.

Mount, J. (1985). Sedimentology, IAS Journal 32(3), 435-442.

PROCEEDINGS
JOINT CONVENTION BANDUNG (JCB) 2021
November 23rd – 25th 2021

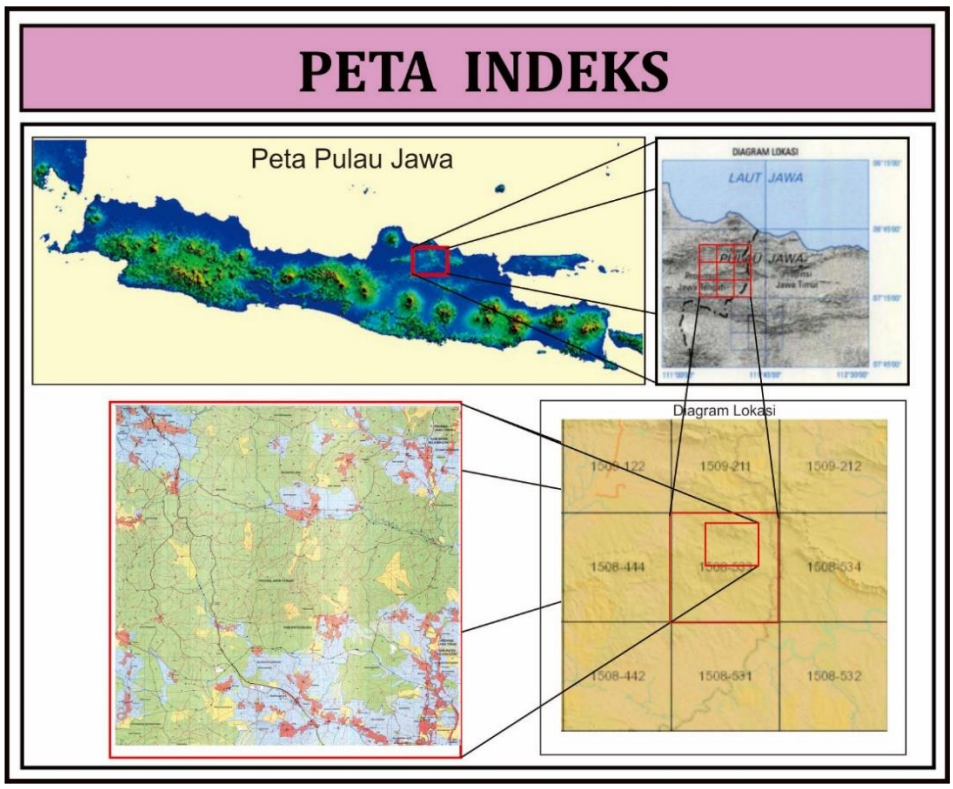

Figure 1: Research location: Jiken, Blora, Central Java

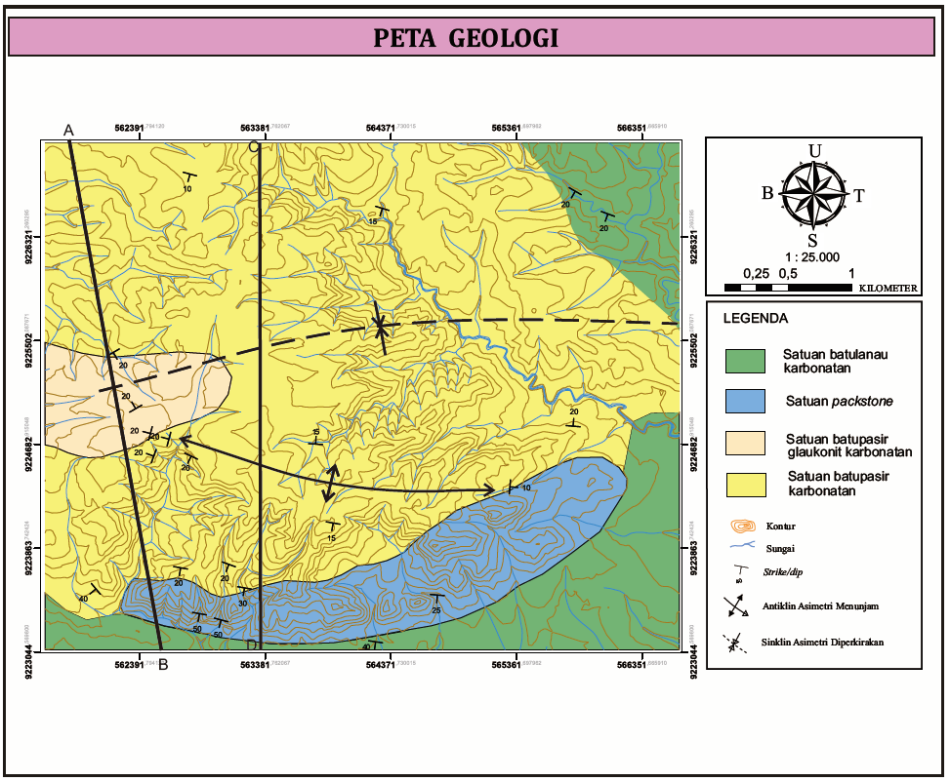

Figure 2: Geological Map of research location

PROCEEDINGS
JOINT CONVENTION BANDUNG (JCB) 2021
November 23rd – 25th 2021

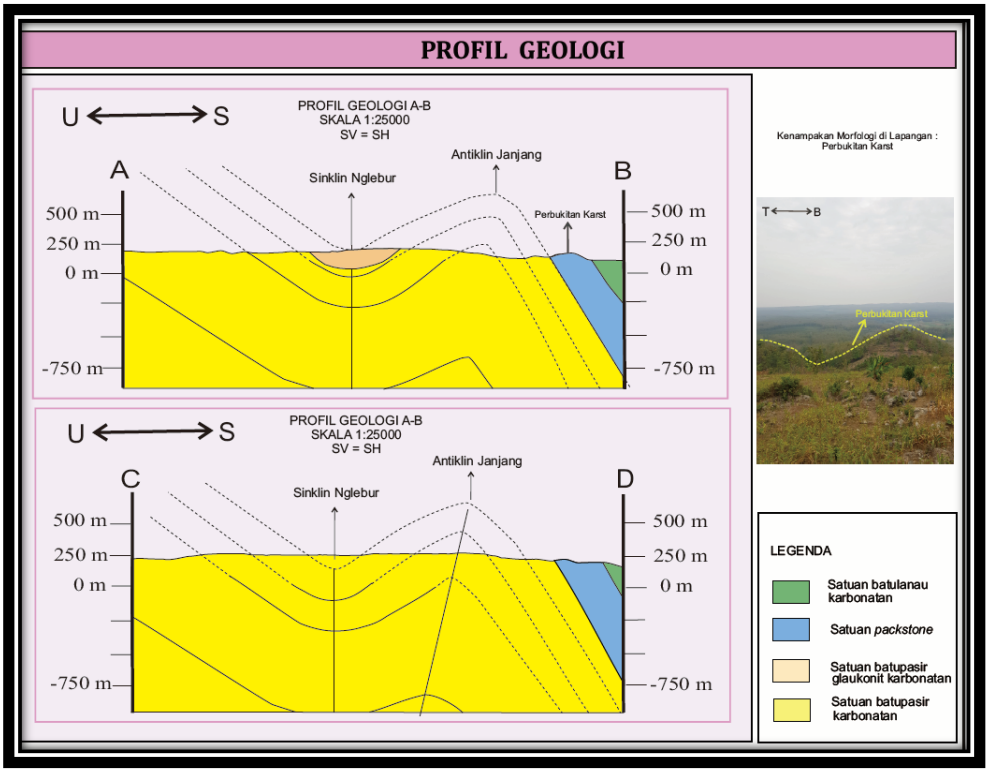

Figure 3: Geological incision of A-B and C-D, it is show the anticline and syncline in research location

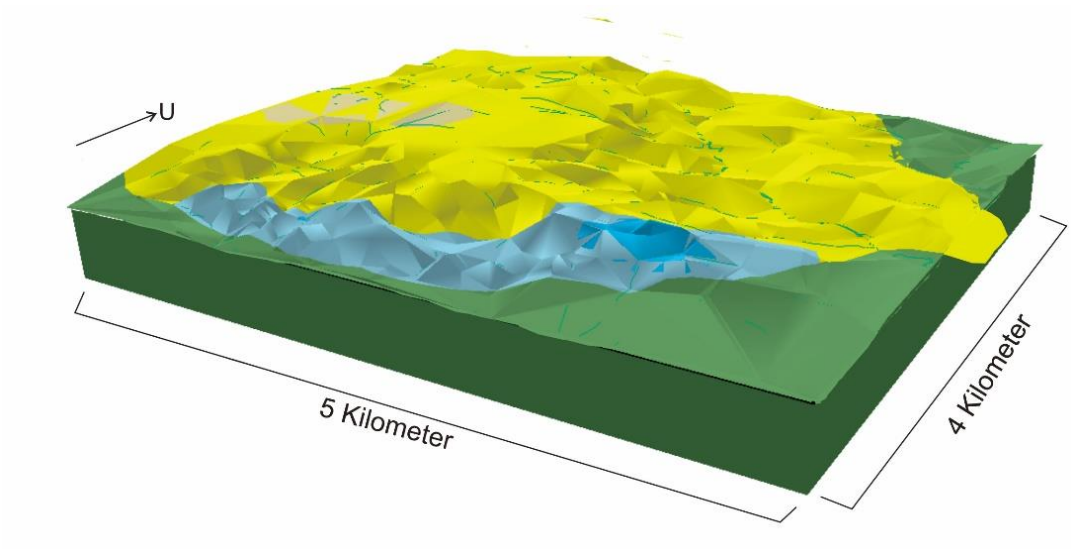

Figure 4: 3-Dimention Geological Map of research location

PROCEEDINGS
JOINT CONVENTION BANDUNG (JCB) 2021
November 23rd – 25th 2021

Figure 5: Limestone outcrop at the south side of research location

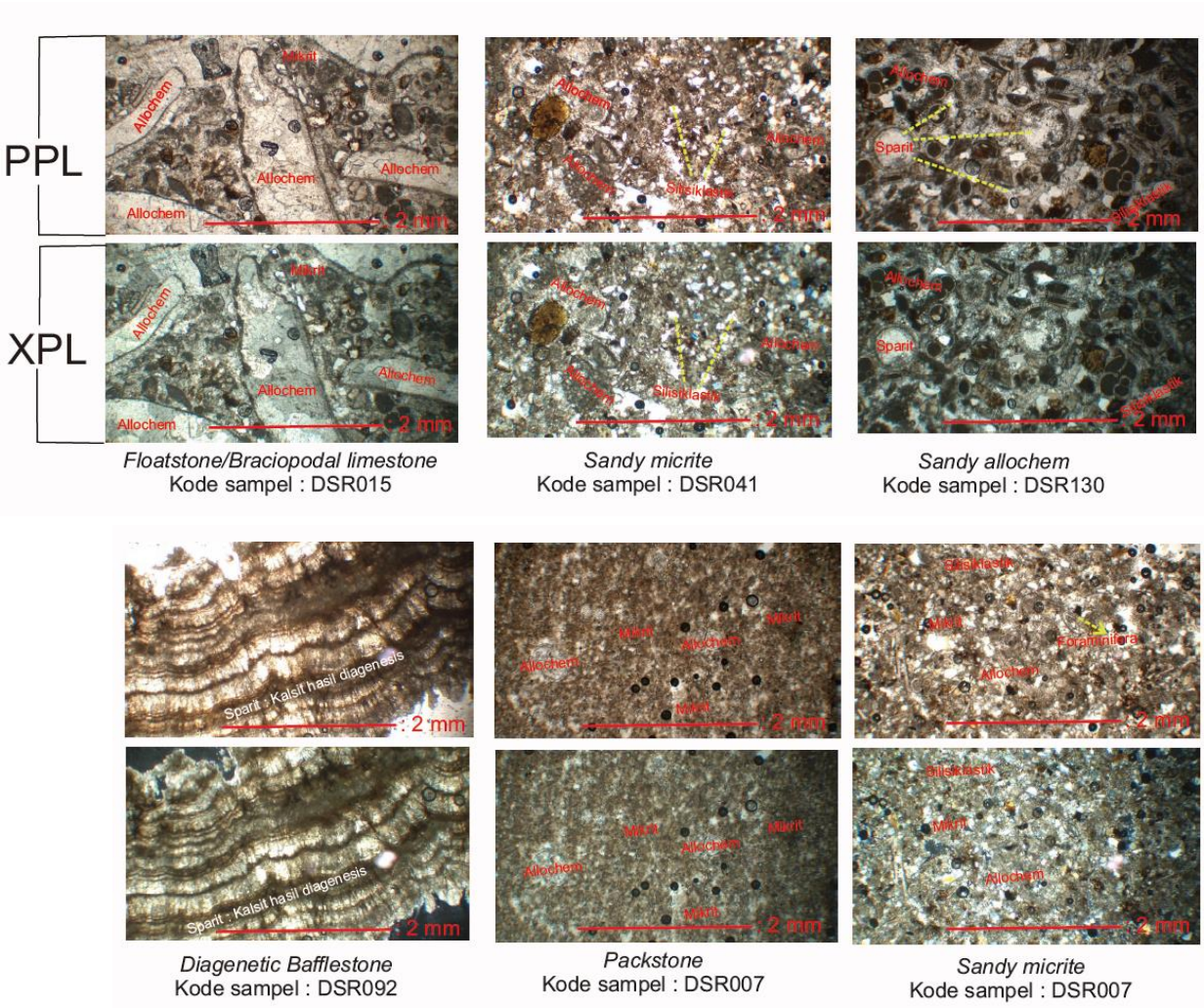

Figure 6: Petrography analysis using polarization microscope Olympus 500x.

PROCEEDINGS
JOINT CONVENTION BANDUNG (JCB) 2021
November 23rd – 25th 2021

EXTENDED REACH DRILLING (ERD) APPLICATION FOR GEOTHERMAL USING MICROHOLE TECHNOLOGY IN INDONESIA

Alfan Khoirul Umam
IATMI SM Universitas Jember, alfanku1811@gmail.com, 085791666049

Abstract

Indonesia is a country traversed by the path of volcanic formation that stretches from Sumatra, Java, Nusa Tenggara, Sulawesi to Maluku. This makes Indonesia a country that has a total geothermal energy potential of around 23,965.5MW or about 40% of the world's geothermal potential. However, until now, Indonesia has only utilized the geothermal potential of 8.9% or 2,130.6MW and there is still much that has not been utilized. This shows that the development of geothermal energy in Indonesia faces many challenges, including the geothermal potential which is spread over 330 location points which are forested areas, both protected forests, production forests, and conservation forests. A technical problem that is often found in geothermal exploration is heat loss. In addition, the high cost of exploration is also an obstacle in geothermal development. From these problems, researchers have an idea, namely the application of extended reach drilling (ERD) using microhole technology. Extended Reach Drilling (ERD) is a directional drilling method in wells that have a Horizontal Displacement to True Vertical Depth (HD/TVD) ratio greater than two, calculated from the depth of the Kick of Point. In this study, the ERD method is applied in geothermal exploration in forest areas. The goal is to drill in areas far from forest areas, without damaging the ecosystem in the area. So that reservoirs at remote points can be reached using this method. In addition, the use of microhole technology can save exploration costs because microhole technology uses small and compatible tools. The data analysis method used in this research is descriptive-quantitative, namely describing the data that has been collected through the study of literature. Furthermore, the results will be made in the form of modeling.

Keywords: *Extended reach drilling, geothermal, microhole, reservoir.*

Introduction

Indonesia is one of the largest archipelagic countries located in Southeast Asia. As a large country, Indonesia faces the challenge of fulfilling energy. This is because the population in Indonesia has reached around 267 million people and is growing by 1.1% every year. In line with the population growth, it can be estimated that Indonesia's national energy needs also increase every year. Pertamina stated that in 2025 it is estimated that the total national energy demand will increase by 2.41 billion BOE (Barrel Oil Equivalent) or an increase of 84 percent of the total national energy demand in 2013 which reached 1.31 billion BOE. Meanwhile, the dominant energy sources used are fossil energy such as oil, natural gas, coal which are included in conventional energy and their availability is limited. Conventional energy, especially fossil energy, over time its availability in nature is increasingly limited. This is because fossil energy cannot be renewed, which if exploited continuously, its availability is running low and can suddenly disappear. So far, the use of fossil energy has caused various problems, including being able to increase greenhouse gas emissions by a large amount if used in a sustainable manner which of course can bring about climate change in the global scope. The Government of Indonesia, through the General National Energy Plan (RUEN) has set a target to realize the optimization of the national energy mix by 2025, where New and Renewable Energy (EBT) accounts for 23% of national energy consumption. The government's target is not impossible to achieve. This is because Indonesia has a variety of renewable energy sources to be developed, one of which is geothermal energy. Geothermal energy in Indonesia can be said to be quite potential if it is developed further. This is because Indonesia is a country traversed by the path of volcanic formation that stretches from Sumatra, Java, Nusa Tenggara, Sulawesi to Maluku. As a result, Indonesia has a total geothermal energy potential of around 23,965.5 MW or about 40% of the world's geothermal energy potential. However, until now, Indonesia has only utilized the geothermal potential of 8.9% or 2,130.6 MW and there is still much that has not been utilized (Directorate General of EBTKE, 2020). This shows that the development of geothermal energy in Indonesia faces many challenges, including based on data taken from the Ministry of Energy and Mineral Resources (KESDM), the geothermal potential is spread over 330 location points which are forested areas, both protected forests, production forests, and forests. conservation. Thus, it creates problems because of policies and permits that can hinder investors from developing geothermal in Indonesia. In addition to these problems, high exploration costs make companies have to think again to continue geothermal development in Indonesia. Therefore, the author has an idea in overcoming these problems, namely by using the application of Extended Reach Drilling (ERD) using microhole technology in geothermal exploration in Indonesia. Extended Reach

PROCEEDINGS
JOINT CONVENTION BANDUNG (JCB) 2021
November 23rd – 25th 2021

Drilling (ERD) is a directional drilling method that is supported by equipment with new methods in the world of drilling. The use of the Extended Reach Drilling (ERD) method in geothermal wells has now been widely applied, but one of them is using slimhole drilling. The use of Slimhole drilling requires a fairly high cost, this has hampered the development of geothermal in the exploration area. For this reason, the author makes Extended Reach Drilling (ERD) modeling using microhole technology. According to research conducted by (Ogbe, 1998) the costs incurred from the use of microhole technology are relatively small. This is evidenced in his research using microhole technology in the development of CBM in remote locations such as Wainwright, Alaska which can result in cost savings of $1.17 million from $1.76 million. microhole orientation can be controlled at the starting point and the effects of gravity, pipe strength and ROP allow some directional drilling capability sufficient to produce a specific layout arrangement. This technique was used successfully in the early development of oil field directed drilling (Foster, 1997). The data analysis method used in this research is descriptive-quantitative method by describing or describing the data that has been collected through the study of literature. Furthermore, the results will be made in the form of modeling. The following flow chart is the implementation stage of this research.

Data and Method

Extended Reach Drilling (ERD)

Extended Reach Drilling (ERD) is a method of directional drilling in wells that have a Horizontal Displacement to True Vertical Depth (HD/TVD) ratio greater than two, calculated from the depth of the Kick of Point. In practice, targets below sea level can be reached from land thanks to the use of this method from an artificial island. In this study, the ERD method is applied in geothermal exploration in forest areas. Where drilling is carried out in areas far from forest areas, without damaging the ecosystem in the area. So that reservoirs at remote points can be reached using this method. In the ERD method in the ERD well design process there are several parameters that must be considered, namely drillstring design, casing design, hydraulics and trajectory of the wellbore.

Drillstring Design

The most optimal drillstring configuration is designed with reference to the trajectory design. The drillstring circuit that will be used is designed based on four parameters, namely thrust, hookload, torque and drag. The four parameters are then compared with the specifications of the rig and pipe used. In general, there are four types of "pipes" that are combined in a drilling series, namely Heavy Weight Drill Pipe (HWDP), drillpipe (DP), and Bottom Hole Assembly (BHA), Drill Collar (DC). In the drillstring design review conducted in this study, the presence of BHA in the drillstring design will be ignored. This is done because the BHA is not too long compared to the overall drillstring length. The length of the BHA does not have a significant effect on drag, torque and pipe weight. In addition to the design process and drilling of ERD wells, the Rotary Steerable System is usually used. Based on these assumptions, the drillstring circuit will consist of DP and HWDP/DC. The placement of DP and HWDP/DC on the drillstring circuit can be done with various variations. To get the optimal circuit, there are four limitations given in the placement of DP and HWDP/DC on the drillstring circuit, these limitations are: 1. Tripping in, tripping out as little as possible. The triping in/out process on the ERD well will take a long time due to the length of the borehole path. The longer the process, the higher the costs. In addition, the possibility for drilling problems to occur is higher. 2. The series of pipes results in minimum rig specification requirements. Rig specifications will decrease if the load on the pipe series that must be borne by the rig decreases. 3. Pipe circuits require as little HWDP/DC as possible. In terms of cost, the use of DP will cost less than the use of HWDP/DC. HWDP/DC has a heavier pounder than DP so the price is more expensive. 4. Pipe circuits require the lowest possible DP quality. The four limitations are technical parameters that must be adjusted to field conditions, such as rig rental time, limited availability of pipes and rigs, and other factors. The four limitations above will be compared with the drillstring design calculations which depend on the drillstring configuration. Drillstring design will focus on placing the HWDP/DC in the lateral session to provide thrust when the drilling process is carried out. HWDP/DC placement in Lateral session will be limited by drag, neutral point, torque and hookload parameters.

Hydraulic

Hydraulics calculations are performed to determine the minimum pump speed required to keep the borehole clean. In this calculation, the pipe rotation speed of 120 RPM is used which is adjusted to the capacity of the TDD and RSS systems owned. The cleanliness of the borehole will be maintained so that the remaining cuttings are around 2% to 5%, according to research conducted by Moore and Larsen which has been modified by Rudi (SPE 57541, 1999).

Wellbore trajectory

The trajectory design of the well refers to the Complex Tangent build curve design with a BUR1 of 30/100 ft, followed by a tangential angle of 68,290 along 8,600 ft. As seen in figure 3, what needs to be noticed is the TVD which reaches 7,704 ft, the lateral side which reaches 12,997 ft and the final angle which reaches 90o. Long lateral sessions with large angles are the hallmark of ERD wells, while the ratio of Trajectory in Field X is 2.54. In this section, more attention should be paid to the problems of drag, torque and hydraulics.

Microhole Technology

Microhole is a wellbore technology that has a hole diameter of less than 4 inches or 10.2 cm in diameter. The concept of using microhole technology, namely reducing the borehole size to the smallest size compatible with good drilling practices and continuous access to instrumentation for subsurface measurements. Microhole technology has limited capabilities in real-time adjustment of azimuth and slope due to small pipe parameters, which cannot accommodate large directional gauges. However, the microhole orientation can be controlled at the starting point and the effects of gravity, pipe strength and ROP allow some sufficient directional drilling capability to produce a specific layout arrangement. Microhole technology provides less torque, less bit weight and lower flow rates for drilling. microholes used as injection or production wells can more flexibly target zones in the reservoir that are (conventionally) stimulated by hydroshearing at stress fracture (as described by microseismicity). In addition, the probability of intersecting the part of the fracture network that is actually connected to the well is greatly increased when using multiple, potentially skewed and directional drilled microholes compared to the probability obtained when using a smaller number of larger diameter conventional wells. High accuracy in directional microhole drilling, however, is not considered an important requirement, as it is an inherent aspect of the proposed concept that the location of the feedzone is essentially unknown and cannot be targeted by the designed well trajectory. Instead, these zones are included in the geothermal exploration process through the generation of extensive hydraulic potential fields, where working fluids find connectivity between injection and production wells. the advantage of smaller bores is that it allows for smaller rigs, pipes and tools, thus requiring less energy and cost.

Result and Discussion

The application of Extended Reach drilling (ERD) using microhole technology can be a new technology in geothermal exploration. This idea is a solution to problems that can hinder geothermal development in Indonesia, such as geothermal potential in forest areas, both protected forests, conservation forests, and production forests. The way it works is by using the ERD-directed drilling method, reservoirs at distant points can be reached. In addition, microhole technology can reduce production costs, which has been one of the problems faced by geothermal companies in Indonesia. Currently, technical problems in geothermal exploration such as heat loss have not found the right solution, for this reason this idea is also designed to deal with heat loss. Heat loss is caused by heat transfer from high temperature to low temperature. the use of insulation is a solution to overcome these problems. In this modeling the researcher uses Rockwool type insulation, this is evidenced by research conducted by (Samsol, et al, 2019), where the smallest heat loss is the type of rockwool material with a thermal conductivity of 0.054 W/mK. A minimum thickness of 50.15 mm is required with a heat loss of 229.92 W/m.

Conclusions

The results of research on the application of Extended Reach Drilling (ERD) using microhole technology in geothermal wells in Indonesia can be concluded as follows:

1. Geothermal potential in Indonesia is spread over 330 location points which are forested areas, both protected forests, production forests, and conservation forests. Thus, the researchers used the Extended Reach Drillling method in geothermal well exploration with the aim that reservoirs at remote points can be reached using this method and do not damage the ecosystems and habitats of animals and plants in the forest.
2. The use of Slimhole drilling requires a fairly high cost, this has hampered the development of geothermal in the exploration area. To overcome this, the researchers used microhole technology because it has a small diameter casing and is compatible.
3. Technical problems such as the occurrence of heat loss are often experienced in geothermal exploration. Heat loss is caused by heat transfer from high temperature to low temperature. the use of insulation is a solution to overcome these problems. In this modeling the researcher uses Rockwool type insulation, this is evidenced by research conducted by (Samsol, et al, 2019).
4. This research is expected to be studied further. In the future, in order to be able to contribute to the development of geothermal energy in Indonesia.

References

Albright, J.N. and D.S. Dreesen, 2000, "Microhole technology lowers reservoir exploration characterization costs," Oil and Gas Journal 98(2):39-41

Cengel, Y. A. (2015). Fundamental of Thermal Fluid Sciences. Biomass Chem Eng, 49(23–6).

Direktorat Jenderal EBTKE. (2020). *Potensi Besar Belum Termanfaatkan, 46 Proyek Panas Bumi Siap*. diakses tanggal 18 Februari 2021, dari URL website: https://ebtke.esdm.go.id/post/2020/03/27/2518/potensi.besar.belum.termanfaatkan.46.proyek.panas.bumi.siap.dijalankan

Foster, M. 1997, "*Rural Alaska natural gas study – A profile of natural gas energy substitution in rural Alaska*," Final Report prepared for the State of Alaska, Department of

Community and Regional Affairs, Division of Energy.

Kreith, F. (2011). Principal of Heat Transfer Seventh Edition (Vol. 2). PROMAT. (n.d.). Calcium Silicate Insulation.

Ogbe, D. O., J.E. Bott, and M. Hawley, 1998, "*Economic analysis of drilling three coalbed methane wells in rural Alaska*." Report to the State of Alaska Department of Natural Resources, Division of Geological and Geophysical Surveys.

R. Rudi R.S, "Equation for Estimating Mud Minimum Rate for Cutting Transport in an Inclined-Until Horizontal Well", SPE – 57541, Middle East Drilling Technology Conference, Abu Dhabi, November 1999.

PROCEEDINGS
JOINT CONVENTION BANDUNG (JCB) 2021
November 23rd – 25th 2021

Remote Sensing for Hydrothermal Alteration Zone Identification Using Landsat 8 OLI/TIRS Satellite Imagery on The Geothermal Prospect Area of Mountain Sirung, East Nusa Tenggara

Rizki Fadhilah Ramadhan[1], Ghina Salsabila[1], Gerald Darshan Mogi[1], Haani Dhiya Ulhaq[1], Rizal Azhari Saputra[1]*
[1]Department of Geological Engineering, Faculty of Exploration and Production Technology, Pertamina University. Jakarta 12220. Indonesia.
[*]email: fadhilahrizki867@gmail.com.

Abstract

Remote sensing techniques are carried out to review the needs of field surveys, thus they can help reduce challenges in exploration activities. Based on the data from the Indonesian Ministry of Energy and Mineral Resources, one of the area that has geothermal potential is Mount Sirung which is located on Pantar Island, Alor District, East Nusa Tenggara. Mount Sirung is an active volcano that has manifestations in the form of hot springs and fumaroles, this indicates the existence of geothermal system with a reservoir dominated by high temperature fluids. The purpose of this study is to identify hydrothermal alteration zone in the Mount Sirung area by applying remote sensing techniques. In this study, the data used is Landsat-8 imagery to analyze the distribution of hydrothermal alteration and altered minerals. Image data processing includes band combination RGB {4-3-2} to visualize geological features. Normalized Difference Vegetation Index (NDVI) method is used to map the distribution of vegetation density with the calculation of (NIR-R)/(NIR+R), band combinations {4/2-6/7-5} {4/2-6/7-10} and {10-11-17} are used to visualize distribution of mineral alteration. Then the density slicing method uses 4/2, 5/6 and 6/7 ratio images to detect the distribution of ferrugination, ferromagnesian, clay and carbonate minerals. The result of this study is a map of mineral alteration distribution in the Mount Sirung area, which is characterized by certain colors. Some of the mineral alteration that can be identified are ferrugination with area about 2,908 km^2, ferromagnesian with area 13.43 km^2, clay and carbonate with area 31.85 km^2 and silica minerals. This is known based on the wavelength value of the identified mineral types using spectral signature analysis by considering the vegetation density of the research area. The conclusion of this study shows that Landsat 8 OLI/TIRS can be used to map hydrothermal alteration for exploration purposes.

Keywords: Hydrothermal Alteration, Landsat 8 OLI/TIRS, Band Combination, Density Slicing, Mount Sirung

Introduction

Subduction is the convergent movement of two tectonic plates and the friction between the plates will melt the surrounding rock into magma (Haldar, 2020). The melt that forms this magma will play a role in being the main component of geothermal energy and the subduction process itself will produce a chain of volcanoes that appear on the surface. The Nusa Tenggara Islands have an active volcano called Mount Sirung which is located on Pantar Island, Alor Regency, East Nusa Tenggara Province and will be the research area in this study. This area is controlled by the subduction of the Indo-Australian Plate under the Sunda-Banda Arc that started 3 million years ago (Bowin et al. 1980; Hamilton 1979; Chamalaun et al. 1976).

Pantar Island is included in the Old Volcanic Hills Geomorphology Unit with an altitude up to 1000 meters above the sea level (high terrain volcano). The geological structure that develops in this area is dominated by a north-south oriented main fault, whose direction is also related to the regional tectonic direction that develops in the Pantar-Alor area. The control of the Puriali and Airmama faults causes the formation of a permeable zone in the Pantar geothermal system. The stratigraphy of this area (**figure 1**) is a product of volcanic eruption deposits and sedimentary rocks. The oldest rocks are volcanic deposits of Late Tertiary age which were deposited on the coast (Nurhadi and Kusnadi, 2015).

According to Rangin and Silver (1990), Pantar Island is included in the tectono-structural unit of the Banda volcanic arc with its geothermal area located in the body of Mount Sirung. This geothermal area is characterized by manifestations in the form of hot springs, hot soil, and fumaroles. The existence of manifestations in the form of hot springs in the study area is an indicator of a geothermal system that has a reservoir dominated by high temperature fluids (> 90°C). Pyroclastic rocks are fundamental indicators of the presence, size, and location of a potential hydrothermal system (Wohletz and Heiken , 1992). So that the geological characteristics of Mount Sirung which is an old volcanic with a main fault can develop the presence of hydrothermally altered rocks. The existence of this hydrothermally altered rocks occurs as a result of the interaction between high-temperature fluids from the hydrothermal system and the surrounding rocks.

The process of alteration that occurs in the Gunung Sirung geothermal area includes mineral replacement and filling spaces (Amir, 2021). Through petrological and petrographic observations, the altered minerals found in drilled wells of the Pantar-Mount Sirung geothermal area consist of Limonite, clay minerals

PROCEEDINGS
JOINT CONVENTION BANDUNG (JCB) 2021
November 23rd – 25th 2021

such as Smectite, Kaolinite, Illite, Sericite, and Chlorite as well as secondary minerals such as Quartz, Calcite, and Anhydrite. Meanwhile, according to research belonging to Nurhadi and Kusnadi (2015) it shows that altered minerals consist of Illite, Halloysite, Na-Alunite, Kaolinite, Montmorillonite, Gypsum, Paragonite, Dickite, Nantronite, and Gybsite are found in the hot soil around Mount Sirung.

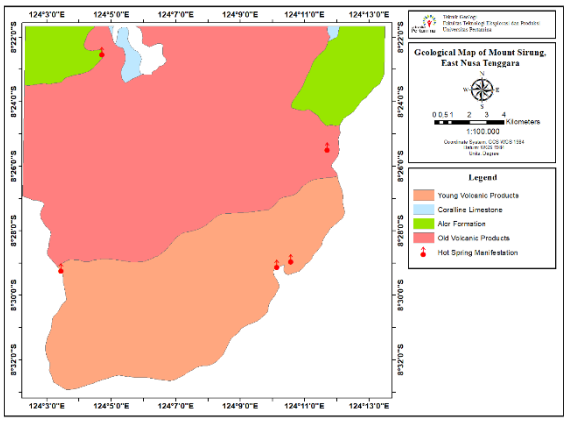

Figure 1. Geological Map of Mount Sirung, East Nusa Tenggara (modified by Koesoemadinata and Noya, 1989).

Data and Methods

1. Data

This research begins with a literature study by analyzing the geological conditions and then carried out by using Landsat 8 to detect the distribution of hydrothermal alteration in the research area. The data used in this study is Landsat 8 OLI/TIRS satellite imagery obtained from the U.S. Geological Survey Earth Resources Observation and Science Center (USGS-EROS). The Landsat 8 image captures the spectral reflectance on path 111 and row 66, the sun's azimuth of 57.89, and the sun's elevation of 56.38 which was recorded on August 29, 2019 with a capture time of 01:53:05.5656790 with cloud cover ranging from 2.98%.

2. Methods

a. Pre-Processing

The Landsat 8 data were subjected to atmospheric and radiometric corrections in the research area. Atmospheric correction in this study uses 2 calibrations, namely using spectral radiance and reflectance. Atmospheric Correction (ToA) or radiometric correction function is to increase the pixel value by considering atmospheric conditions and interference factors, so that information can be read properly (Rajeshwari and Mani, 2014). According to USGS (2019) to obtain these results, the following formula is used:

$$\rho\lambda' = M_\rho \, x \, Q_{cal} + A_\rho \ldots\ldots\ldots(1)$$

This correction is done by calibrating the Digital Number (DN) of the band into spectral reflectance (ToA reflectance).

Then use the formula:

$$L\lambda = M_L \, x \, Q_{cal} + A_L \ldots\ldots\ldots\ldots(2)$$

This correction is done by calibrating the Digital Number (DN) of the band into spectral radiance (ToA radiance) (Ekadinata et al, 2008). This formula is used for {10-11-7} and {4/2-6/7-10} composite RGB maps. Furthermore, Landsat 8 data are corrected for the sun elevation correction. According to USGS (2019) to obtain these results, the following formula is used:

$$\rho\lambda = \frac{\rho\lambda'}{sin\,(\theta)} \ldots\ldots\ldots\ldots\ldots\ldots\ldots(3)$$

In the next stage, the Landsat 8 image is subjected to atmospheric correction using the dark object subtraction method to correct the pixel values in the image that is disturbed by the atmosphere. The atmosphere causes dark objects such as water and shadows to not have a zero pixel value. If the dark object is not zero, then the pixel value is biased. Dark objects such as water have characteristics that absorb the sun's electromagnetic waves very strongly, so that satellite sensors that receive water reflections with low intensity and hue in the image will be dark with a zero pixels value (Ardiansyah, 2015).

b. Processing

At this stage, first step of data processing is carried out using a combination of RGB {4-3-2} bands that have been subjected to atmospheric and radiometric corrections. In the 4-3-2 composite image, band 4 (0.636 – 0.673 m) is positioned in the red channel, band 3 (0.533 – 0.590 m) is positioned in the blue channel and band 2 (0.452 – 0.512 m) is positioned in the blue channel. The combination of these bands can visualize the geological and geomorphological conditions of the research area (Putra et al, 2017).

The next step is calculating of the vegetation index to measure density vegetation obtained from digital signal processing of brightness value data from several satellite image sensor bands (Farras et al, 2017). Normal Difference Vegetation Index (NDVI) is an algorithm for estimating the vegetation index from satellite images (Amliana et al., 2016).

Areas with an NDVI index value close to +1 means that the area has a high level of vegetation density, while -1 means that the area is an unvegetated area or water area. To calculate the value of vegetation density using the NDVI formula. According to USGS

PROCEEDINGS
JOINT CONVENTION BANDUNG (JCB) 2021
November 23rd – 25th 2021

(n.d.) to obtain these results, the following formula is used:

$$NDVI = \frac{(NIR - RED)}{(NIR + RED)}$$

NIR is Near infrared radiation from pixels (band 5) and RED Red light radiation from pixels (band 4).

After processing NDVI, then the band composite method is carried out to detect the distribution of alteration and silicate minerals. This composite method is used to display the appearance of surface features with alteration targets. This research used Hashim Ratio (2015) which is {4/2-6/7-10} to determine alteration mineral in study area. The band used for composite method is RGB {4/2-6/7-5}, {4/2-6/7-10} and {10-11-7}.

This research also used band ratio which was previously used by Sabins (1999) who succeeded in visualizing the distribution of alteration minerals. Thus, the method used in this study is the Sabins Ratio. The ratio used is 4/2, 5/6 and 6/7, which respectively showed the presence of ferrugination, ferromagnetian, clay and carbonate minerals, as well as ferromagnesian minerals (Pour and Hashim, 2015; Jugder and Jalbaa, 2015). This band ratio method is applied for density slicing analysis.

Density Slicing uses computer processing digital data and is obtained from the contrast stretch of each information band (Putra et al. 2017). This classification is carried out using the density slice method at the threshold value of each mineral. After that, the Threshold Value is calculated from the value of each ratio. Thus, density slicing can be carried out using values from the threshold-max pixel value range. The equation for density slicing is as follows:

Threshold Values = Mean + n * Std. Deviation

with: n = 1 (92% confidence level),
2 (95% confidence level).

Composite is used to detect the distribution of alteration minerals in general, then a band ratio and density slicing method is needed to detect the distribution of alteration minerals by type.

Result and Discussion

1. Result

a. Composite Band {4-3-2}

Based on the results of the RGB {4-3-2} composite (**Figure 3**), which can display a visualization of the geological conditions of the research area. The research area is located in a volcanic landscape area and it can be observed that there are volcanic hills/mountains and undulating volcanic hills, namely Mount Sirung.

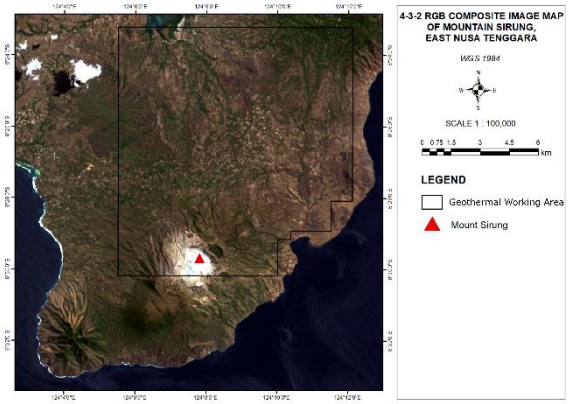

Figure 3. RGB 4-3-2 Composite Image of Mount Sirung.

b. NDVI

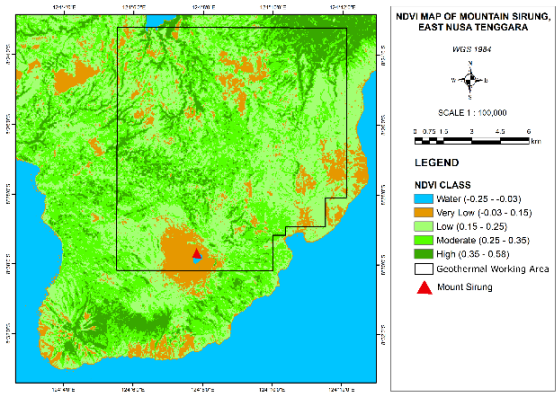

Figure 4. Normalized Difference Vegetation Index Map

Based on the results of the NDVI map, the index value of the vegetation density level in the study area has a value of -0.25 to 0.58. The classification of NDVI index values (Wahyunto, 2006) is divided into 4 classes, namely no vegetation (water), very low vegetation, low vegetation, medium vegetation, and high vegetation. It can be seen in Figure 3 that the condition of the vegetation density level in the study area is dominated by low-medium vegetation density, followed by high, low vegetation density and water bodies.

c. Composite Band {4/2-6/7-5}, {4/2-6/7-10} and {10-11-7}.

The combination of bands 4/2, 6/7, 5 and 10 are used to gather information on rock units, vegetation in drainage, and altered rocks by remote sensing. On the other hand, the combination between 10, 11, 7 is used to get information about the appearance of silica-rich rocks in the study area (Putra and Nasution, 2017). Altered minerals themselves will show different reflectance characters with a result by matching the wavelength of a band or more, there is a clear and different appearance of the alteration minerals from one another, as well as with non-mineral objects (Pour and Hashim, 2015).

PROCEEDINGS
JOINT CONVENTION BANDUNG (JCB) 2021
November 23rd – 25th 2021

The difference between the {4/2-6/7-5}, {4/2-6/7-10} and and {10-11-7}. band combinations lies in the function of band 5 in the form of Near Infrared, which can see the vegetation area clearly, whereas band 10 and 11 which are thermal infrared, has advantages in highlighting its geology features. Meanwhile, the band ratio is done to divide the wavelength value of a band with others, thereby the range is shorter and the appearance of the earth's surface objects is denser, clearer, and better (Pour and Hashim, 2015; Ismail et al., 2020). The ratio of band 4/2, 6/7 is used because the alteration minerals that may exist in the study area are ferrugination minerals and clay minerals as well as carbonates. Band 7 itself can feature rock absorption more clearly because of its function on the Short Wavelength Infrared (Pour and Hashim, 2015).

Based on the RGB Composite Image Map {4/2, 6/7, 5} with a scale of 1:100000 that has been carried out in the Mount Sirung area, it shows the land cover of the drainage system and settlements (barren land) in purple hue, vegetation in turquoise to green, as well as minerals altered in yellow.

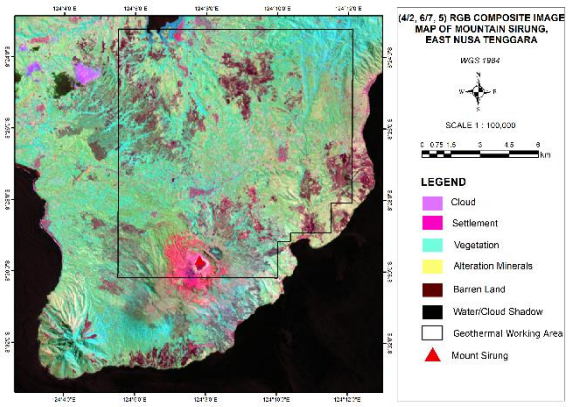

Figure 5. RGB Composite Map {4/2-6/7-5}.

On the other hand, RGB Composite Image Map {4/2-6/7-10} show drainage systems and settlements in purple, vegetation in green and blue, and alteration minerals in yellow and pink. The color range for alteration minerals refers to the silicate content of the mineral, red means high content, pink is medium, and blue is low.

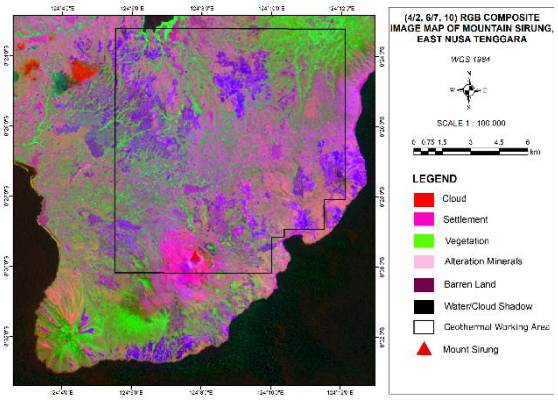

Figure 6. RGB Composite Map {4/2-6/7-10}.

Then, the RGB Composite Image Map {10, 11, 7} shows silica-rich rocks in the form of yellow hue. The stronger the color of yellow, the more silica-rich the study area is, whilst the stronger the blue, the lower the silica content (Pour and Hashim, 2015).

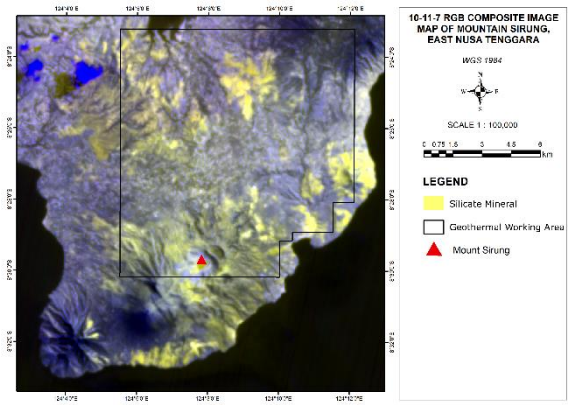

Figure 7. RGB Composite Map {10-11-7}.

The RGB Composite Image Map that has been made shows the vegetation in the study area is a dominant aspect, amidst that the altered minerals are found near Mount Sirung. The distribution pattern of alteration minerals when associated with volcanic facies and stratigraphic units is located in the proximal to distal zone. It is also known that the alteration minerals have moderate silicate content. In general, the presence of silica-rich rocks in the study area aren't that apparent, since the map tends to show the color is bluish yellow.

d. Density Slicing Band Ratio {4/2, 5/6, 6/7}

Density slicing takes a number of pixel values that can indicate the presence of minerals on the earth's surface based on their reflections. In this study, 4/2, 5/6 and 6/7 ratio images or well known as Sabin's ratio (1999) were used, which respectively showed the presence of oxide and hydroxide minerals from iron, clay minerals and carbonate minerals, as well as ferromagnesian minerals (Pour and Hashim, 2015; Jugder and Jalbaa, 2015).

At a band ratio of 4/2 visualize the distribution of ferric-iron bearing minerals, for example limonite. This ratio is useful for oxide and hydroxide minerals mapping because it has absorption in the blue band area and reflectance high in the red band area (Aisabokhae and Tampul, 2019). This distribution is quite interesting if it is associated with rock lithology on geological maps. The distribution of iron oxide and hydroxide minerals (ferrugination) dominates the area with the lithology of young volcanic rocks and the peak of Mount Sirung.

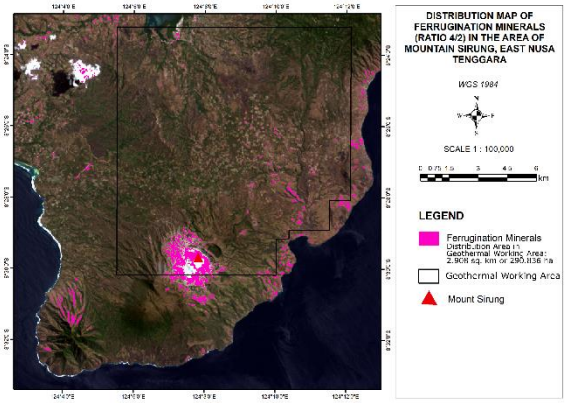

Figure 8. Ferrugination Minerals Distribution Map.

Band ratio 5/6 can be used to identify ferromagnesian mineral groups containing iron and/or magnesium ions. The mineral distribution of the ferromagnesian group is recorded in a wide area, concentrated in the area of the volcanic body around the proximal and distal zones.

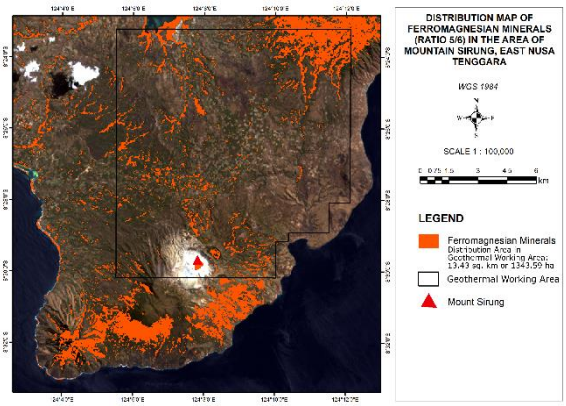

Figure 9. Ferromagnesian Minerals Distribution Map.

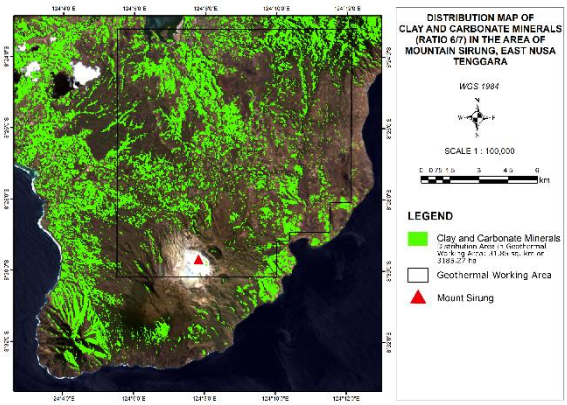

Figure 10. Clay and Carbonate Minerals Distribution Map.

Band ratio 6/7 can be used to identify clay and carbonate minerals such as Kaolinite, Smectite, Illite, Sericite, Chlorite, Halloysite, Nantronite minerals. While carbonate minerals such as calcite.

The results of data processing using the density slicing method, the confidence level in band 4/2 is 95%, band 5/6 is 92% and 6/7 is 92% (**table 1**).

Table 1. Statistic Data of Density Slicing

Band	Min	Max	Mean	SD	TH Value	Confidence Level
Band 4/2	0	1.348692	0.844219	0.106948	1.058115	95%
Band 5/6	0	3.128082	1.112202	0.223747	1.335949	92%
Band 6/7	0	1.642666	1.242311	0.188436	1.430747	92%

By using the density slicing method in band 4/2 which visualizes mineral ferrugination, the pixel value ranges from 1.058115-1.348692, then in band 5/6 which visualizes mineral ferrogination, the pixel value ranges between 1.335949-3.128082, and band 6/7 which visualizes mineral clay and carbonate found the pixel value range between 1.430747-1.642666.

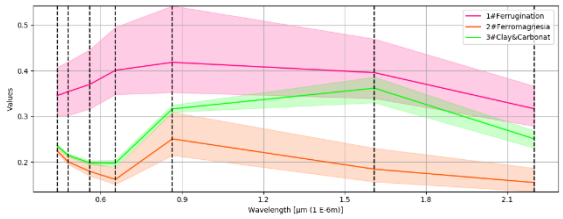

Figure 11. Spectral Signature of Minerals

After that, input training was carried out in areas that have the distribution of these minerals, and it was found that the ferrugination mineral group such as limonite tends to have an absorption feature in the infrared range of 0.4-0.7 µm, then the ferromagnesian mineral group has an absorpion feature in that range. 0.5-0.8 µm, while clay and carbonate minerals have absorption features in the range of 0.7-0.8 µm.

2. Discussion

The distribution of hydrothermal alteration minerals can be visualized through the composite image method using RGB composite map {4/2-6/7-5} and {4/2-6/7-10}. The combination of bands covering {4/2-6/7-5} will visualize hydrothermal alteration minerals in yellow while the combination of the covering band {4/2-6/7-10} will visualize the hydrothermal alteration minerals in pink color. Then the band combination {10-11-7} can visualize the distribution of silicate minerals. The density slicing method will see the wavelengths reflected by minerals that appear on the surface and then converted in the form of pixel values (Putra et al., 2017). The ratios used in this study are 4/2, 6/7, and 5/6, where the three ratios will detect the distribution of alteration minerals that characterize the geothermal field.

The cone of a volcano is divided into 3 facies zones, which include the central zone which means the peak of the volcano, the proximal zone which means along the slopes of the volcano, and the distal zone which means the land around the foot of the volcano (Williams and McBirney, 1979). The alteration minerals detected in this study are scattered in the cones and plains around Mount Sirung with different zone locations.

a) Ferrugination Minerals

Ferrugination alteration minerals consist of iron bearing minerals, so that the oxide and hydroxide mineral groups are included in ferrugination minerals. These minerals are generally scattered in the central zone or the peak of Mount Sirung with an area of about 2,908 km^2.

b) Ferromagnesian Minerals

Ferromagnesian alteration minerals are minerals that have iron and magnesium cations in their essential components. These minerals are generally scattered in the proximal zone or the slopes of Mount Sirung with an area of about 13.43 km^2.

c) Clay and Carbonate Minerals

These minerals are generally distributed in the distal zone or the plains of the foothills of the Mount Sirung with an area of approximately 31.85 km^2.

d) Silicate Minerals

The general distribution of these silicate minerals is in the proximal zone to the distal zone or in the slope area to the foot of the Mount Sirung plain.

Based on the group of altered minerals that are found, the Mount Sirung geothermal field is divided into two zones, namely the oxide zone, which is characterized by the presence of ferrugination and ferromagnesian minerals, and the argillic alteration zone which is characterized by the presence of clay and carbonate minerals.

According to Bateman (1981), a hydrothermal solution is a hot fluid or fluid that comes from the earth's crust and moves up while carrying metal mineral components. The process of transporting hydrothermal solutions that break through to this rock layer will cause chemical reactions, especially when the hot fluid is in direct contact with the surrounding rock. The result of the contact will trigger mineralization and make the surrounding rock undergo hydrothermal alteration. Permeability properties or weak zones in rock layers act as channels to pass hydrothermal fluids and also as spaces for mineralization to occur. The existence of a weak zone is certainly controlled by the geological structure of an area.

Alteration in the Gunung Sirung geothermal field consists of a mineral replacement process and the filling of open spaces. The alteration process begins when the hydrothermal solution which is acidic because it contains sulfuric acid at the geothermal prospect of Mount Sirung moves laterally upwards to break through the rock layers that have been formed (Binsar, M. et al., 2014). The hydrothermal solution will move up to the soil surface and make this solution begin to be affected by low-temperature surface water. The result of the contact between this solution mixing with the surrounding rock will then produce argillic alteration which is characterized by the presence of clay and carbonate alteration minerals. According to Pirajno (1992), alteration of the argillic type is characterized by the presence of high clay mineral content and is formed at low temperatures (<200-250°C). According to Sambari (2017), oxidation is a chemical weathering process caused by the reaction of oxygen to iron minerals in rock, especially if the rock is wet. So that this oxidation zone is interpreted as an area that has ferrugination and ferromagnesian mineral distribution but there is no mineral alteration such as clay and carbonate due to no alteration process occurred but weathering process.

The distribution of altered minerals depends on temperature, fluid composition, and permeability. However, determining the distribution of hydrothermal minerals is not very useful in estimating subsurface temperatures and permeability (Wohletz and Heiken, 1992). Based on the results of the study, mapping the distribution of minerals on the surface of the geothermal field can still estimate the alteration zone as a result of the association of the presence of minerals. This is very useful in geothermal exploration activities (Wohletz and Heiken, 1992). This research based on remote sensing so that the estimation results will be more accurate if it’is balanced with field research and laboratory research. Mount Sirung is an active volcano which has been recorded to have erupted 4 times in the last 20 years so that the results of this eruption can affect the presence of minerals that appear on the surface (Bani et al, 2017).

The minerals detected in this study have similar results with research using drilled well data in Amir's research (2021) and also the results of infrared analysis in Nur Hadi's research (2015). However, several types of minerals were not found in previous research in this study. Another obstacle is the level of vegetation density which can affect the visualization in identifying the distribution of alteration minerals in an area. In tropical areas where high vegetation conditions can affect satellite imagery in detecting and mapping hydrothermal alteration rocks (Siegal and Goetz, 1977). To identify alteration zones from iron oxide and clay zones in areas of high vegetation can affect the identification level of these objects due to the similarity of spectral reflections of minerals (Fraser and Green, 1987). Level of vegetation density greatly affects the analysis of the distribution of minerals because vegetation and minerals have the same characteristics in emitting infrared waves and vegetation covers open areas so that satellites capture wave rays from vegetation.

Conclusions

Based on the result of the study, it was found that the Mount Sirung Geothermal Working Area has mineral alteration, namely the Ferrugination mineral group which is included in the oxide zone that dominates the

volcanic peak area (central zone) with an area of about 2,908 km^2, then Ferromagnesian which is included in the oxide zone that dominates the slope-plain area of the foot of the volcano (proximal-distal zone) with an area of about 13.43 km^2, Clay and Carbonate which is included in the argillic zone that dominates the area of the foot of the volcano with an area of approximately 31.85 km^2, and Silicate which dominates the area of the slopes of the foot of the volcano (proximal-distal zone).This research is based on remote sensing so that there are challenges in the form of dense vegetation in the research area, dense vegetation can affect visualization in identifying alteration minerals in the research area, this is because vegetation and minerals have the same characteristics in emitting infrared waves and vegetation for open areas so that satellites capture wave rays from vegetation. Thus, the estimation results will be more accurate if balanced with field research and laboratory research.

References

Aisabokhae, J., and Tampul, H., 2019, Korean Journal of Remote Sensing, 35(4), 535-544.

Amir, A, 2021, Repository ITB.

Amliana, D. R., Prasetyo, Y., & Sukmono, A. (2016). Jurnal Geodesi Undip, 5(1), 264-274.

Ardiansyah, 2015, PT. Lab SIG Inderaja Islim.

Bani, P., Alfianti, H., Aiuppa, A., Oppenheimer, C., Sitinjak, P., Tsanev, V., and Saing, U.B, 2017, Bulletin of Volcanology, **79.**

Bateman, A.M. dan Jensen, M.L., 1981, John Wiley and Sons, Inc., New York.

Binsar, M. T. A., Aribowo, Y., and Widiarso, D. A., 2014, Geological Engineering E-Journal, 6(2), 338-352.

Bogie, I., and Mackenzie, K.M, 1998, Proceedings, 20th New Zealand Geothermal Workshop. **20**.

Bowin, C., Purdy, G.M., Johnston, C., Shor, G.G., Lawver, L., Hartono, H.M.S., and Jezek, P., 1980, Am Assoc Pet Geol Bull, 64, 868–915.

Chamalaun, F.H., Lockwood, K., and White, A., 1976, Tectonophysics, 30, 241–259.

Dharmawan Putra, Ilham and Firdaus Nasution, Reza Ade and Harijoko, Agung, 2017, Proceeding, Seminar Nasional Kebumian Ke-10 Peran Penelitian Ilmu Kebumian Dalam Pembangunan Infrastruktur di Indonesia 13 – 14 September 2017; Grha Sabha Pramana.

Ekadinata, A., Dewi, S., Hadi, D., Nugroho, D., dan Johana, F, 2008, World Agroforesty Centre. Bogor, Indonesia.

Farras Nabilah, Prasetyo Y, Sukmono, 2017, Jurnal Geodesi Undip 2017. 6,402-412.

Fraser, S. J., and Green, A. A., 1987, International Journal of Remote Sensing, 8(3), 525-532.

Hamilton, W.,1979, U.S. Geol. Surv. Prof. Pap., 1078, 345.

Ismail, N., Wirja, N., Putri, D. R., Nanda, M., and Faisal, F, 2020, Jurnal Rekayasa Elektrika. **16**.

Judger, M., Jalbaa, U., 2015, Mongolian University of Science and Technology.

Koesoemadinata, S., and Noya, N., 1989, Pusat Penelitian dan Pengembangan Geologi, Bandung.

Nurhadi, M., and Kusnadi, D, 2015, PSDG Geologi ESDM.

Pirajno, F. ,1992, Berlin, Springer – Verlag, 709 p.

Pour, A.N., and Hashim, M, 2015, Journal Taibah University of Science, **9**, 155–166.

Pratama, Diyan A. P., Indrawan, I Gde B., and Warmana, I Wayan, 2018, Journal of Applied Geology, vol. 3(2), 2018, pp. 99–108.

Putra, I. D., Nasution, R. A. F., and Harijoko, A, 2017, Proseding Seminar Nasional Kebumian ke-10. **10**, 1812–1826.

Rajeshwari, A dan Mani, N.D, 2014, International Journal of Research in Engineering and Technology. Vol.3 No. 5.

Rangin, C., and Silver, E., 1990, Proceeding of the Ocean Drilling Program, **124**.

S.K. Haldar, 2020, in Introduction to Mineralogy and Petrology (Second Edition), Chapter 9 pages 313-348.

Sabins, F. F. (1999). Ore geology reviews, 14(3-4), 157-183.

Sambari, Villa E. D.G., 2017, Makassar.

Siegal, D.B. and Goetz, A.F.H., 1977, Photogrammetric Engineering and Remote Sensing, 43, pp. 191–196.

USGS, 2019, U.S. Geological Survey, **5**, 54-55

USGS, n.d., U.S. Geological Survey. [Accessed 16 September 2021] available at https://www.usgs.gov.

Wahyunto, W, 2006, Bogor: Informatika Pertanian.Departemen Pertanian.

Williams, H., and McBirney, A. R, 1979, Freeman., 1-391.

Wohletz, K., and Heiken, G., 1992, Berkeley: University of California Press.

Acknowledgements

The writing of this paper can be resolved with the help of various parties. Therefore, the authors would like to thank the supervisor of this research. The greatest appreciation goes to Mr. Rio Priandri Nugroho, M. MinRes. for his advice and knowledge.

PROCEEDINGS
JOINT CONVENTION BANDUNG (JCB) 2021
November 23rd – 25th 2021

Comparison Study of Heat Transfer Flow on Natural Joint Fracture and Hydraulic Fracture

Feninda Amalia Nabilah[1], Adelya Syawjesil Fachyesi[1], Kafa, 'Aisyana N[1], Imam Zulqaishi[1]
[1]Department of Geophysical Engineering, Faculty of Planning and Earth Civil Engineering, Sepuluh Nopember Institute of Technology Surabaya

Abstract
In the Enhanced Geothermal System (EGS) field, to increase thermal conductivity hydraulically, artificial fractures were made to increase the permeability of dry rock constituents of the field. Among the rock types that make up the geothermal field, Zhao & Tso (1993) used granite with natural fracture and Ma et al. (2019) used the granite which formed by artificial fractures due to the impact of Hydraulic Fracturing. This paper aims to understand the different effects of heat productivity on the two rock types with different fracture origins by using the flow rate, confining pressure, and heat transfer coefficient parameters. Heat transfer has a linear relationship with the flow rate and the value of the flow rate can be increased by increasing the confining pressure during hydraulic fractures. The application of hydraulic fracture in the formation of artificial fractures provides advantages because it can modify the temperature, pressure, and injection fluid which can produce finer fractures, to form better permeability to maximize fluid flow rate and heat transfer capability. While natural fractures tend to be rougher and have an irregular direction, they can show a true strike-dip.

Introduction
The current phenomenon of climate change is a very urgent problem to overcome, given the impact caused has reached a global scale. Sustainable infrastructure development, especially in the field of energy is one of the programs that has also been formulated internationally, one of which is through the Paris Agreement agenda. Utilization of sustainable energy based on new-renewable energy (EBT) is one of the points raised in the Paris Agreement. Indonesia has launched utilization of geothermal or geothermal energy in the general national energy plan (RUEN) as one of the one solutions to the problem of climate change 1 Geothermal is a new renewable energy sourced from high heat temperatures below the surface Earth. Generally, heat sources below the earth's surface are associated with volcanic activity and also tectonic. This heat source is also commonly found in hydrothermal complex structures at high temperatures, as well as in hot basement rocks which contain a lot of radioactive elements (Moya, 2018). However, some hot dry rocks also often experience fractures, so it is necessary to build a geothermal system which is further refined or known as EGS: Enhanced Geothermal System (Ma et al., 2019).
In the EGS type geothermal field, artificial fractures that will increase the permeability are produced by hydraulic stimulation, so that the hydraulic thermal conductivity of hot dry rock will be increased. Then, the heat stream flows through the fractured rock mass conductively up until the geothermal system reaches the desired temperature. Due to hydraulic fracturing, the nature of the heat flow in rock masses that have these fractures will be different than in media with standard pores.
From the presence of hydraulic fracture parameters, it will be determined the amount of heat energy that can be extracted from EGS, seen based on the permeability in the fracture. Fractures on hot rock depending on the rock characteristics in the study area. Experimentally, the flow relationship and heat transfer with observed fractures in rocks were modelled by numerical modelling with various types of injection for each different media. In this article, we will discuss the comparison of two rocks that responses to fractures which occur by looking at the comparison of the heat transfer parameters, flow rate, and fracture aperture in natural fracture and hydraulic fracturing.

Hydraulic Fracture
Hydraulic fracturing is a method to allow heat transfer to a reservoir by forming fractures/artificial fractures in hot source rocks. Hydraulic method fracturing becomes interesting to discuss and develop because of the effectiveness of the system related to the fracture characteristics displayed in the rock (fracture geometry). hydraulic method This fracturing is applied to a geothermal reservoir to extract geothermal energy and is assessed as an effective breakthrough (Ma et al., 2019).
Hydraulic fracture is done by pumping or injecting fluid into the wellbore at a rate of high so that the rock formation can receive injection fluids without breaking. Due to the injection, prisoners the flow in the formation also increases and can cause a break-down, so that the fracture is destroyed and another fracture is formed, while the injection fluid flows through it. In general, applications from hydraulic fracturing can be used to increase the flow rate of oil and/or gas from the reservoir which have low permeability as well as those from wells that have been damaged.

Characteristics of Geothermal Field Composing Rocks
Rocks associated with EGS reservoirs are usually hard and compact igneous rocks associated with subsurface heat flows originating from volcanic systems and movements intense plate, so it has low permeability (Cheng, 1979). It makes geothermal energy difficult to extract as a commercial fuel. When applied method 2 Hydraulic Fracturing, it will form fractures in artificial rock that can be a way out of geothermal energy to be extracted (Cho et al., 2013).

Heat Convection Transfer Coefficient The heat transfer mechanism that occurs in the geothermal area applies the heat transfer process automatically convection in the fluid contained in the reservoir. The principle of heat transfer that applies from rock to the fluid is convection by adhering to Newton's law of flow (Newtonian Flow) where the displacement heat occurs continuously and mass and energy transfer is constant (Zhao and Tso, 1993). In mathematical form, this equation is written as follows:

$$q = hA\Delta T, \quad (1)$$

Where q is the heat energy, h is the convective heat transfer coefficient, A is the area of the plane, and T is the change in temperature. Then, in the calculation of heat transfer in

PROCEEDINGS
JOINT CONVENTION BANDUNG (JCB) 2021
November 23rd – 25th 2021

the geothermal case study, another parameter usually is defined in the form of numbers that have no units, namely the Reynolds number (Re), Prandtl number (Pr), and Nusselt number (Nu).

$$Re = UL/v, \quad (2)$$

Where Re is the Reynolds number, U is the velocity, L defines the length, and v defines viscosity. Meanwhile, Pr is the Prandtl number, and alpha is the thermal diffusion. Nu is a Nusselt number, h is the heat convection coefficient, and k is a constant.

$$Pr = v/\alpha, \quad (3)$$

$$Nu = hL/k, \quad (4)$$

Meanwhile, in the paper of Ma et al. (2019), the following heat transfer coefficient equation is used (5), which involves the parameter specific heat capacity (c p) at constant pressure and temperature at the surface sample (Tc). The parameter c p is added because of its relationship with the hydraulic pressure injected to form artificial fractures in coring samples. Meanwhile, for T c is the parameter that previously in Zhao & Tso's (1993) paper it was not taken into account with respect to the temperature scheme equilibrium on rock temperature in the geothermal area.

$$h = \frac{c_{p,w} Q \rho_w (T_{out} - T_{in})}{DL(T_c - (T_{in} + T_{out})/2)}, \quad (5)$$

The discussion in this study is devoted to the topic of conducting a comparative study of heat transfer characteristics in rocks that have natural fractures with rocks with artificial fractures made using the Hydraulic fracturing mechanism. The limitation of the problem in this study is the EGS condition with the assumed granite rock sample as a heat source from an active geothermal potential field, for further analysis of the heat transfer mechanism in geothermal energy sources.

Data and Method

The data used are sourced from data from Zhao & Tso (1993) regarding the mechanism of heat transfer in natural fractures and the data of Ma et al. (2019) which discusses the mechanism of heat transfer in hydraulic fractures. The rock sample used in Zhao & Tso (1993) is a Carnmenellis rock sample granite taken from Cornwall, southwest England with a coarse-medium grain size containing 3 biotite-muscovite minerals. Meanwhile, the sample of Ma et al. (2019) is a sample of granite taken from outcrop of Gonghe, China in a geothermal target area.

Zhao & Tso's (1993) rock coring samples that had natural fractures were then carried out the extension of the fracture extends along the coring, thus forming a fracture as shown in Figure 1.

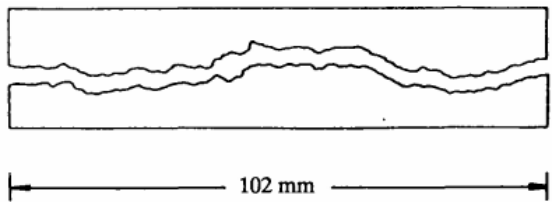

Figure 1. Extension fracture resulting from natural fracture (Zhao and Tso, 1993)

The data generated is in the form of fluid flow rate (flow rate), temperature (temperature), and heat convection coefficients. Meanwhile, for hydraulic fracture testing, the data is in the form of injection values (artificial pressure). The data is then processed and visualized in the form of a graph using Ms. Excel to get the value of the relationship between the parameters associated with the initial formula, namely heat convection coefficient.

Meanwhile, for the coring sample Ma et al. (2019), fractures are formed using the hydraulic fracturing method until the fracture equilibrium phase is obtained. Then, the heat transfer test was carried out by the hydrothermal-mechanics, the schematic of which is shown in figure 2.

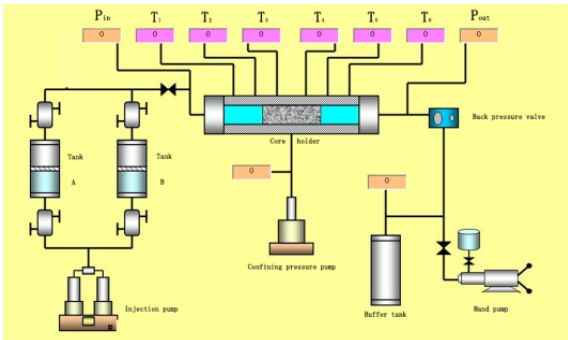

Figure 2. Schematic of a hydro-thermo mechanical device (Ma et al., 2019)

Result and Discussion

The data used from Zhao & Tso's (1993) paper are joint aperture, flow velocity and heat. Data convection coefficient by using two variations of temperature, namely 120℃ and 140℃.

Data on joint aperture, flow velocity and heat convection coefficient derived from research by Zhou & Tso (1993) included in the form of a graph, so that can be seen the relationship between the data. Besides, it is also made a graph of the research data of Ma et al. (2019) which connects the parameters of flow pressure, flow rate, heat transfer coefficient, injection flow rate, and confining pressure. It also includes a graph of the relationship between temperature and fracture toughness from the research data of Chandler et al. (2017).

Graph Analysis Graphic visualization (3-8) represents the results of the comparison of heat transfer parameters in natural joint fractures and hydraulic fractures. There is a trend pattern that shows similarities, namely a positive trend.

On sample natural joint fracture rock which is represented by the visualization of graphs 3 and 4 shows the comparison between value of heat transfer coefficient to the fluid flow rate (water flow rate) in the comparison of the two temperatures of different rocks. It can be seen from the two graphs that at a temperature of 120℃ and 140℃ there is no trend pattern that displays a significant difference.

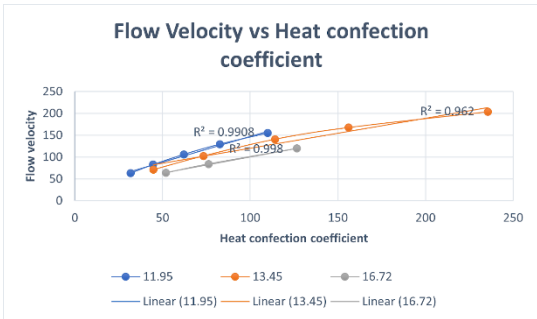

PROCEEDINGS
JOINT CONVENTION BANDUNG (JCB) 2021
November 23rd – 25th 2021

Figure 3. Graph of the relationship between flow velocity and heat convection coefficient for each variation of the natural joint value aperture at 120℃

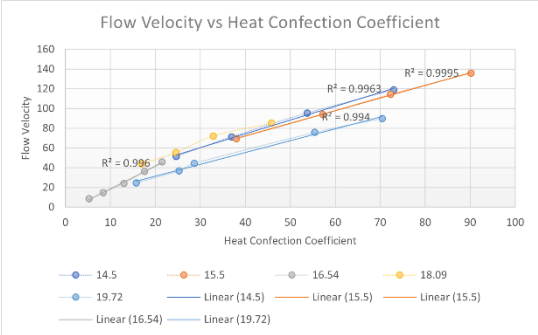

Figure 4. Graph of the relationship between flow velocity and heat convection coefficient for each variation of the natural joint value aperture at 140℃

Meanwhile, the hydraulic fracturing method refers to the data of Ma et al. (2019) visualized on Figure 5 shows a positive relationship between hydraulic flow pressure and flow velocity at fractures in coring rock samples. In graph 5 it is shown that the higher the applied pressure in rock coring samples, resulting in a higher injection flow velocity.

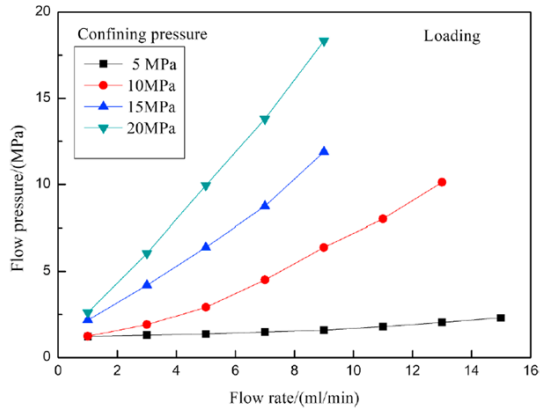

Figure 5. Graph of change in flow pressure with flow rates under different confining pressures (Ma, 2019).

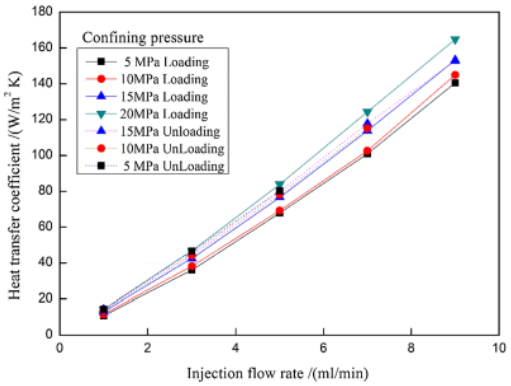

Figure 6. Graph of comparison of heat transfer coefficient with injection rate of water flow using the method Hydraulic fracture (Ma et al, 2019).

Zhao & Tso (1993) stated that a similar trend pattern which shows the difference in rock temperature has no effect on the flow rate water due to the increase in the heat transfer coefficient is proportional to the temperature difference that occurs at rock surface to fluids. This refers to the equilibrium scheme in heat transfer, where heat energy flowing in rock is the same as heat energy flowing through convection currents on the fracture surface equal to the heat energy removed by the fluid.

This matter shows that in order to increase the volume of geothermal fluid that can be extracted, it is necessary to increase the value of hydraulic pressure to create artificial fractures in the reservoir rock. The result was also expressed by previous researchers (Ma et al., 2019 and He et al., 2016). Likewise with the heat transfer coefficient which shows a positive trend with the injection flow rate, as has been discussed in the previous Zhao & Tso (1993) paper. The increase in the fluid flow rate certainly has an effect an increase in the heat transfer element of the fluid, then, when related to the factor loading and unloading as an update in the paper Ma et al (2019) which is a mechanism simulation In-situ stress shows a similar trendline and does not have a significant difference, even though the index R value is higher at pressure loading.

To this end, data from Chandler et al. (2017) which focuses on the discussion on the effect of temperature on fractures formed in anisotropic rocks, where the data used is the granite rock sample data visualized in Figure 8. Based on graph 7 it is known that temperature increase exerts a downward trendline effect on fracture resistance, although it does not show drastic decline. This indicates that an increase in rock temperature results in changes in fracture dimensions in granite, although the difference is in the range of 0.2-0.4 K_{Ic}. Therefore, Chandler et al. (2017) concluded that the sensitivity of the fracture resistance index (fracture toughness) has very little effect on temperature changes.

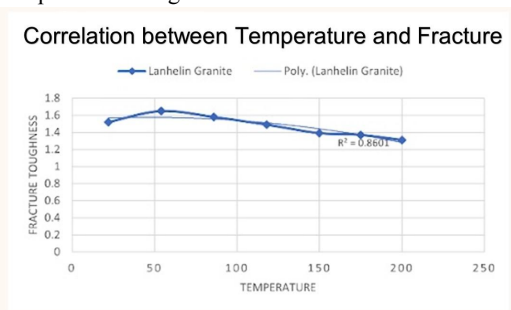

Figure 7. Graph of fracture toughness and temperature relationship in granite (Chandler et al, 2017).

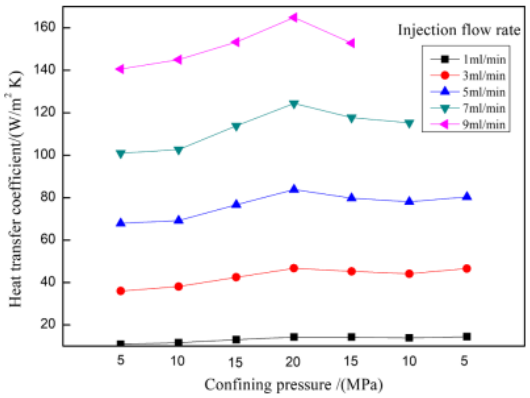

Figure 8. Graph of Heat Transfer with Pressure (Ma et al., 2019).

Then, in Zhao & Tso (1993) the relationship is visualized in a heat transfer comparison graph coefficients with flow velocity are displayed at different joint fracture constant values. Used 4 variations in joint fracture constants, but the graph shows that joint fracture variations do not give significant change in the trendline graph of the relationship between heat transfer and flow rate. Therefore, Zhao & Tso (1993) did not discuss further about the relationship between fracture and heat transfers.

Furthermore, also discussed by Ma et al. (2019) that heat transfer displays inclined graphs constant when related to hydraulic pressure. The slight increase seen in Figure 9 is 9 as a result of the fracture surface smoothing, as the pressure value increases, which makes heat maximum transfer, although not significant. This is related to the permeability of the sample rock, in which when the fracture surface is smoothed, it is possible to increase the permeability of rocks as a passageway for fluids (Neuville et al, 2010).

Natural Joint Fracture with Hydraulic Fracture

The main difference that appears from natural joint fractures with hydraulic fractures is seen in the formula heat transfer used, where the Newtonian Flow formula does not consider the parameters specific heat capacity of water which is an identical parameter of the geothermal injection fluid. This matter influences the morphology of the fractures formed, as well as the direction of these fractures. As mentioned in the chart analysis section, flow injection is important in controlling the fracture dimensions that are optimum use. With high confining pressure will produce fracture characteristics that are finer (smooth), so as to form a higher permeability to maximize fluid flow rate and heat transfer capability.

Meanwhile, in natural fractures (natural joint fractures) usually have fracture characteristics that are high tends to be coarse (rough) and have irregular direction. However, in reality when the simulation area expands into the scope of the geothermal field as described by Liu et al (2020), then the presence of natural joints is actually advantageous because natural joint fractures have directional characteristics fractures that can be viewed from the strike-dip value. Where will the direction of this fracture correspond to the dynamics geology that has occurred in the area (Shi et al, 2019).

In addition to those characters, natural fractures have unmanageable dimensions. So, to maximize it, it is necessary to do an injection which is also concerned with hydraulic fracture and orientation. In this case, it is also influenced by the injection plane factor itself because it will determine the direction and optimization of the fracture, as shown in Figure 11.

In field studies, natural joint fractures will form a separate fracture network group. However, with the incorporation of hydraulic applications fracture at the right point, the natural joint fracture tissue will be able to form a network intact fracture with the ability to drain geothermal resources more optimally This is called a discrete fracture network (DFN). Utilization of DFN will maximize the use of natural fractures (natural fracture) which is the character of geological phenomena in the research area.

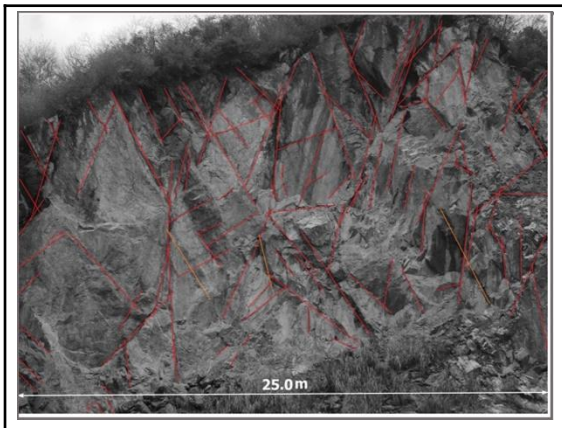

Figure 10. Outcrop at Dapu, Hengyang, China (Feng, et al, 2020)

Furthermore, to exploit the potential of natural fracture by optimizing the induction of hydraulic fracture to form a DFN that can maximize heat transfer flow in the HDR system, it is necessary to pay attention to geomechanical factors, such as in-situ stress, natural fracture density, and orientation of the natural fracture. The research of Shrivastava and Sharma (2018) shows that the higher the natural fracture density value, the greater the possibility of connection between natural fractures when hydraulic fracture is applied. as well as the orientation of the natural fracture which plays a role in regulating the direction of motion of the hydraulic fracture to form a natural fracture network.

In this case, if the strike-dip orientation of the natural fracture is in the same direction as the horizontal in-situ stress, there will be more natural fractures that can be connected to form a DFN.

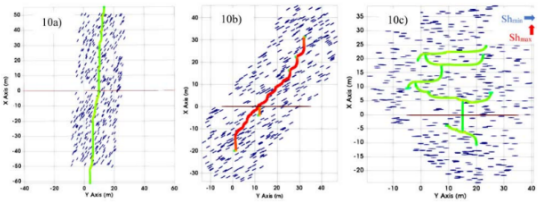

Figure 11. Effect of strike-dip fracture on hydraulic fracture application in forming natural fracture tissue (Shrivastava and Sharma, 2018).

Conclusions

Based on this study, analysis of flow rate, confining pressure, and heat transfer coefficients can be used for researching fracture characteristics in geothermal potential areas with a focus on comparison between natural joint fracture and hydraulic fracture with limited sample of granite indicated by fracture review. From what we observed, we can conclude that:

1. The heat transfer parameter has a strong relationship with the flow rate and the flow rate value can be improved by increasing the confining pressure on the hydraulic fracture simulation.
2. The injection fluid is very affecting to the dimensions of the resulting fracture and the increase in confining pressure will maximize the permeability of rock samples.
3. Because hydraulic fracture can modify the temperature, pressure, and injection fluid used, it provides

advantages for geothermal utilization more than the use of natural joint fractures which tend to have rough morphology and fracture directions irregularly.

4. By combining hydraulic fracture and maximizing discrete fracture network (DFN), it can be capable of generating an increase in exploitable geothermal resources.

References

Chandler, M. R., Meredith, P. G., Brantut, N. & Crawford, B. R., 2017. Geological Society London Special Publications.

Feng, S. et al., 2020. Computers and Geotechnics, 128, 103810.

He, Y., Bai, B., hu, S. & li, X., 2016. Computers and Geotechnic, 80, 312-321.

Liu, H. et al., 2020. Journal of Rock Mechanics and Geotechnical Engineering, 12, 900-916.

Ma, Y. et al., 2018. International Journal of Heat and Mass Transfer, 119, 139-147.

Ma, Y. et al., 2019. Applied Thermal Engineering, 154, 433-441.

Moya, D., Clay Aldás & Prasad Kaparaju. 2018. Renewable and Sustainable Energy Reviews, 94, 889-901

Neuville, A., Toussaint, R. & Jean, S., 2010. Computers Rendus Geoscience, 342, 616-625.

Shi, Y. et al., 2019. Applied Thermal Engineering, 159, 113828.

Shrivastava, K., Sharma, M.M., 2018. SPE Hydraulic Fracturing Technology Conference and Exhibition 2018, HFTC 2018.

Zhao, J. & Tso, C. P., 1993. J. Rock Mech. Min. Sci. & Geomech., 30, 633-641.

PROCEEDINGS
JOINT CONVENTION BANDUNG (JCB) 2021
November 23rd – 25th 2021

Geothermal System Modeling Utah FORGE Site with TOUGH2

D. B. Soebakir[1], M. I. Defri[1], M. D. Paratin[1], D. R. A. Gandini[1], N. Rahmawati[1], A. F. Raharja[1], S. Widyanti[2]

[1]Department of Geophysical Engineering, Pertamina University, Indonesia
[2]Lecturer of Geophysical Engineering Department, Pertamina University, Indonesia

Abstract

The Utah Frontier Observatory for Research in Geothermal Energy (FORGE) Site Geothermal Field is one of the geothermal field that located in Milford, Utah. It is developing with Enhanced Geothermal System (EGS) technology which has an average temperature 200°C. In this study, there are integration data including geological, geophysical, geochemistry, and 58 – 32 well to simulate geothermal system which can determine the characteristic and development this field in the future. Geothermal system simulation using the TOUGH2 simulator, it is expected to reach a natural state condition with temperature and pressure data in 58 – 32 well as an injection well. The results show a natural state condition which are validated by temperature and pressure curves observation and calculation in 58 – 32 well. The reservoir is composed a plutonic rock as granitoid which is characterized low permeability with a value of 1.2 x 10^{-16} m^3, porosity 0.0118%, density 2750 kg/m^3, thermal conductivity 3.05 WmK and specific heat 790 J/KgK. The temperature curve shows a value of thermal gradient 76°C/Km which is fit to the actual condition with a value 73°C/Km and the temperature and pressure curves are in accordance with the observation curve so that it can be reached natural state condition. Natural state condition can be used to assist in developing scenarios in the geothermal field. In addition, it can calculate resources and reserves, and can make well targeting.

Keywords: FORGE Utah Site, conceptual model, natural state, reservoir simulation, TOUGH2

Introduction

The Utah Frontier Observatory for Research in Geothermal Energy (FORGE) Site Geothermal Field is located approximately 322 km south of Salt Lake City and 16 km from northern Milford which was developed by FORGE to utilize Enhanced Geothermal System (EGS) technology. The FORGE program was carried out to extract heat in subsurface where this area has the characteristics of the host rock with low permeability in the form of granitoid. With the host rock having low permeability, it causes hot fluid to propagate in subsurface to that hydraulic fracturing occur in order to extract the heat in subsurface. In addition, there are places for filling deposits in the form of basin at relatively shallow depth. It is proven by previous studies using geophysical survey such as gravity, magnetotelluric (MT) and seismic methods.

Based on Defri (2021) using a gravity method, it shows anomalies with a value of zero in Second Vertical Derivative (SVD) data and the maximum anomaly of SVD is greater than the absolute minimum value which is indicated as a basin (basin fill) in the middle of the Milford Valley. In addition, MT measurements found 5 points in 2012 and 2014 by United States Geological Survey (USGS) to estimate the distribution of resistivity value in subsurface and to characterize the dimensionality structure using 1D modeling and phase tensor. There are 3 classifications of resistivity values where resistivity value of 10 – 20 Ohm.m are interpreted as sedimentary material near surface, 2 – 3 Ohm.m are interpreted as basin fill and 80 – 200 Ohm.m are interpreted as basement. Based on Miller (2018) using seismic data in the central area of the Milford Valley and extending westward, it was identified as a basin.

In 2017, testing was carried out on injection well (58 – 32 Well) to determine the characteristic of subsurface temperature, lithology and permeability with a well depth of 7546 ft. At a depth of 968 m, low permeability rock can be found, namely crystalline rock with a bottom hole temperature of 199°C (Xing et al., 2021)

Integrating several data such as geological, geophysical, geochemistry and well data to develop the conceptual model and numerical model for geothermal system simulation using the TOUGH2 simulator. Geological studies can represent surface condition in the field such as the presence of fault, topography, and lithology. Geophysical studies can determine the characteristic subsurface based on physical properties, namely density and resistivity from the data. Geochemical studies to analyze the manifestation that appear on the surface and with data. Well data can validate subsurface types of lithology and temperatures. Therefore, numerical modeling was carried out with the TOUGH2 simulator in order to reach a natural state condition that matches the temperature and pressure curves between the observation data and calculation data so that it can be

assumed to be in accordance with the actual condition in subsurface.

Data and Method

In this study, data information was obtained in the form of well data and rock physical parameter data from the FORGE Utah Site (https://utahforge.com/laboratory/numerical-modeling/). From several data and other supporting studies, reservoir simulation will be carried out with the TOUGH2 simulator. TOUGH2 is an algorithm simulator for non-isothermal flow in multicomponent, fluid phase and rock parameters (Pruess, 2012). The first stage will create a numerical model in determining the geometry and boundaries of the model, layers in the model, area, parameter distribution and initial rock conditions. Furthermore, the grid system or grid size of the research area will be determined, more grids are made will make better resulting model, the grid used is a block centered grid with the calculated parameters being in the middle of the grid.

The conceptual model that will be made is approached in the form of a numerical model that will be processed using the PetraSim software. In performing a numerical model using TOUGH2-EOS1 it is assumed that this field is in the form of water because there are limited data obtained in the reservoir simulation process. Making a simulation model has a large area 29.7 km^2 from 333500 – 336500 E and 4262000 – 4265000 N with maximum elevation 1800 m until 1500 m with grid size (60 m x 60 m x 66 m) which amounts to 225000 (50 x 50 x 50).

The next step will be input rock physical parameters in the model that has been made. Because the data obtained are limited, therefore the physical input parameters of rock are carried out by trial and error but taking into account the pressure and temperature data will increases if the depth increases. It can be seen in **Table 1** which is the input of rock physical parameters used in the study. After that, input the initial conditions for the geothermal system in the Utah FORGE geothermal field which uses single-phase water using atmospheric pressure and temperature with value 1 atm (1.013 x 10^5 Pa) and 25°C. Of all the parameters that are inputted, the PetraSim software with the TOUGH2 simulator will get the temperature and pressure distribution in a 3D model so that the curve matching will be carried out between the observation and calculation curves. If the results match then it reaches the natural state condition.

Result and Discussion

Based on **Figure 1** is the simulation result between the observation and calculation curves on the pressure and temperature data at the injection well (well 58-32). Well 58-32 functions as an injection well using EGS technology to create fractures because the characteristics of the source rock in the Utah geothermal field are granitoid which have low permeability so that by using the fracture it is easier to drain geothermal fluids. Low permeability will cause the fluid to be trapped in the rock. From the results of curve matching obtained very good results and following the trend, with increasing depth, temperature and pressure will increase. According to (Simmons et al., 2019) states that the temperature gradient in this field is about 73°C/Km which is a very high conductive heat flow around the FORGE Utah Site geothermal field isolated from the Roosevelt Hydrothermal Hot Spring (RHS) by the Opal Mound fault. From the simulation results, the temperature curve shows a thermal gradient of 76°C/Km. Therefore, it can be concluded that from the simulation results of pressure and temperature curves appear to have been fitted and the thermal gradient results are close to the actual so it can be assumed to have reached the natural state condition.

Conclusions

Numerical modeling and conceptual model in the Utah FORGE geothermal field are match to the actual conditions that is validated by the results of the curve between the observation curve and calculation curve at 58 – 32 Well. 58 – 32 Well uses EGS technology by making fracturing because the reservoir composed of low permeability as plutonic rock which makes it difficult for geothermal fluid to flow, thus developing EGS technology in 58 – 32 Well. The result shows the thermal gradient simulation curve in Utah FORGE geothermal field that which are around 76°C/Km and it is close to the actual condition of 73°C/Km.

PROCEEDINGS
JOINT CONVENTION BANDUNG (JCB) 2021
November 23rd – 25th 2021

References

Allis, R., Moore, J., Davatzes, N., Gwynn, M., Hardwick, C., Kirby, S., ... & Simmons, S. F. (2016). *EGS concept testing and development at the Milford, Utah FORGE site*. Proceedings.

Defri, M. 2021. *Analisis Struktur dengan Metode Gayaberat pada Daerah Panasbumi Utah, Amerika Serikat.* Skripsi. Universitas Pertamina.

Faulder, D. D. (1991). *Conceptual geologic model and native state model of the Roosevelt Hot Springs hydrothermal system* (No. SGP-TR-134-18). Idaho National Engineering Laboratory (INEEL), Idaho Falls, ID.

Grant, M.A. dan Bixley, P.F., 2011, *Geothermal Reservoir Engineering Edition 2*, Elsevier, Netherland.

Hardwick, C., dkk. 2018. *Geophysical Surveys of the Milford, Utah, FORGE Site: Gravity and TEM*. GRC Transactions.

Pruess, Karsten. 2012. *Mathematical Modeling of Fluid Flow and Heat Transfer Geothermal Systems – An Introduction in Five Lectures*. Lawrence Berkeley National Laboratory, University of California.

Pruess,K.,Oldenburg,C., and Moridis, G.2012. *TOUGH2 USER'S GUIDE, VERSION 2*. Earth Sciences Division, Lawrence Berkeley National Laboratory University of California, Berkeley, California. page 61-62.

Simmons, S., Kirby, S., Allis, R., & Moore, J. (2020). *Production Chemistry Evidence for an EGS-type Reservoir in Roosevelt Hot Springs and Implications for Utah FORGE*. 45th Workshop on Geothermal Reservoir Engineering (hal. 1-7). Stanford: Stanford Geothermal Program.

Xing, P., dkk. 2021. *Numerical Simulation of Injection Tests at Utah FORGE Site*. Workshop on Geothermal Reservoir Engineering Stanford University, Stanford, California.

Yuono, R., and Daud, Y. 2020. *Reservoir Simulation of Ulumbu Geothermal Field Using TOUGH2 and ITOUGH2 Simulator*. IOP Conference Series: Earth and Environmental Science.

PROCEEDINGS
JOINT CONVENTION BANDUNG (JCB) 2021
November 23rd – 25th 2021

Table 1. Rock Physical Parameter in Utah FORGE Geothermal Field

Rock Type	Density (kg/m3)	Porosity	Permeability (m3)			Thermal Conductivity (W/m.K)	Specific Heat Capacity (J/kg.K)
			X	Y	Z		
Top Boundary	2500	1.0E-07	1.0E-21	1.0E-21	1.0E-21	2.0	1000
Side Boundary	2500	1.0E-07	1.0E-18	1.0E-18	1.0E-18	2.0	1000
Bottom Boundary	2500	1.0E-07	1.0E-20	1.0E-20	1.0E-20	2.0	1000
Granitoid	2750	0.0118	1.2E-16	1.2E-16	1.2E-16	3.05	790
Basin	2500	0.12	1.7E-14	1.7E-14	1.7E-14	2.0	830

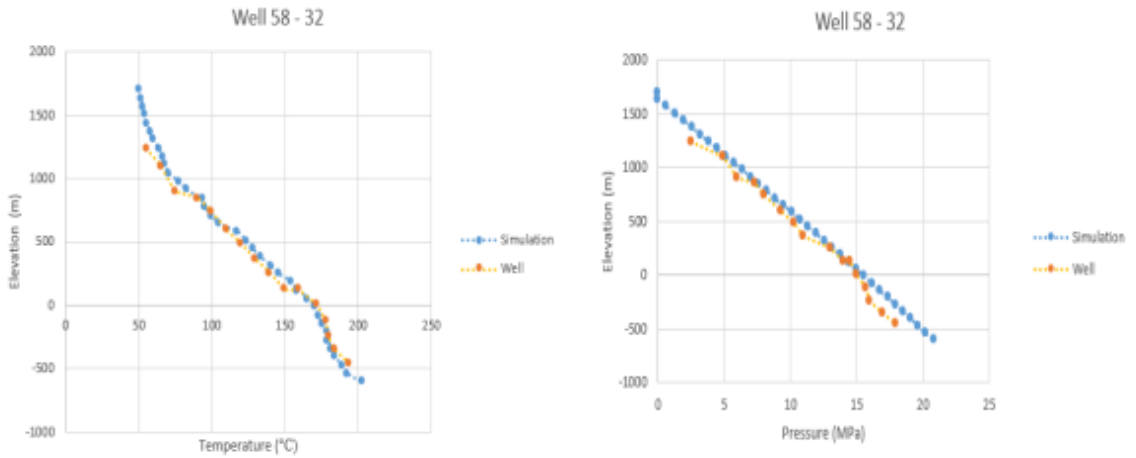

a b

Figure 1. Simulation Result (a) Temperature; (b) Pressure Curves in 58 – 32 Well

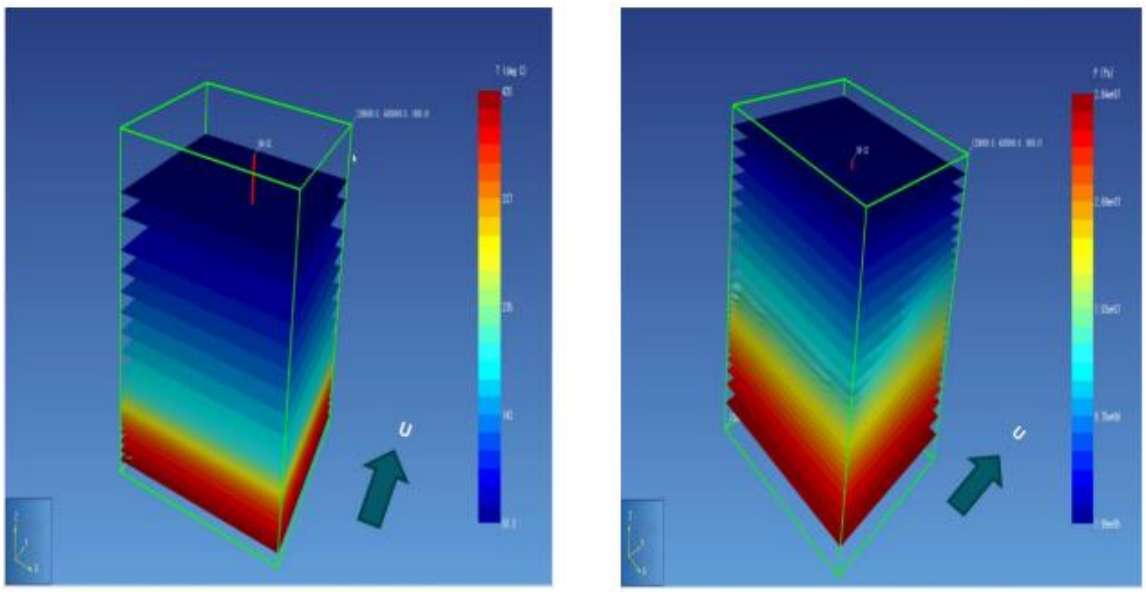

a b

Figure 2. Simulation Result (a) Temperature; (b) Pressure Distribution in 58 – 32 Well

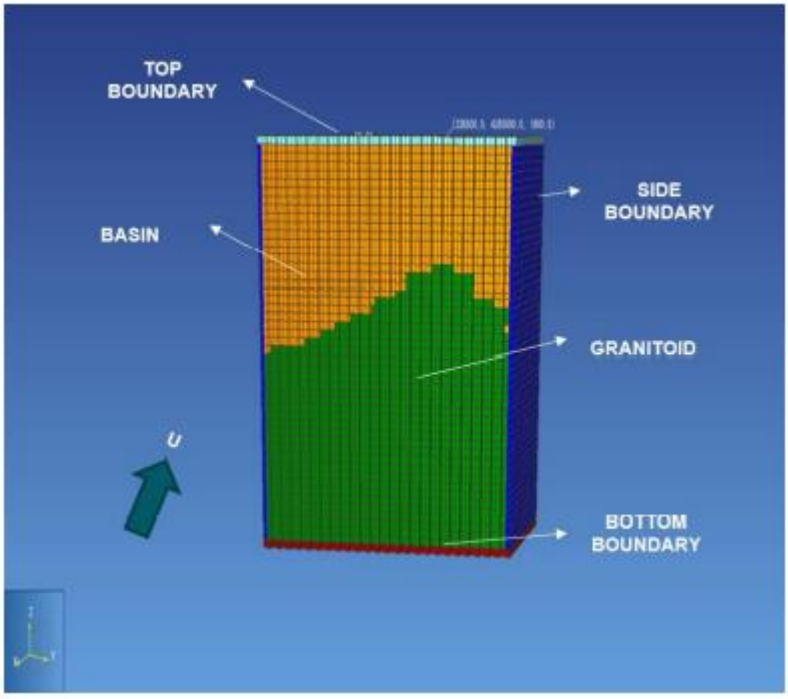

Figure 3. Distribution of Rock Type Vertical Slice View

PROCEEDINGS
JOINT CONVENTION BANDUNG (JCB) 2021
November 23rd – 25th 2021

Metamorphic Basement Reservoir Stimulation Using Hydraulic Fracturing Hybrid Fracs With PAA-CO_2 Combined with Binary Cycle To Develop Non-Volcanic Geothermal System In Sulawesi Area

Muhammad Nur Wahid Fakhrudin[1], Siti Khodijah[1], Syahadun[1]
[1]University of Padjadjaran

Abstract

Geothermal resources are generally related to the mechanism of magma formation, volcanism activities and found in volcanic rock hosts that have high porosity and permeability to flow fluids. Geothermal systems in non-volcanic environments with rocks in the form of metamorphic or plutonic rocks generally have poor permeability and porosity conditions. Based on the lithology association, Sulawesi has 3 geothermal system environments, namely territorial volcanic, plutonic environment and metamorphic environment. The purpose of this paper is to develop non-volcanic geothermal systems in Sulawesi's metamorphic environment. The method is using hydraulic fracturing hybrid fracs with PAA-CO_2 combined with Binary Cycle. The results are non-volcanic geothermal systems can be utilized more efficiently by using hydraulic fracturing hybrid fracs with PAA-CO_2 combined with Binary Cycle. Hydraulic fracturing hybrid fracs with PAA-CO_2 can form secondary porosity and permeability so the heat can be raised to the surface. Binary Cycle to heat or increase the temperature of the working fluid in the geothermal system through a heat exchanger so that the resulting fluid can rotate the turbine.

Keywords: binary cycle, geothermal, hydraulic fracturing, metamorphic, non-volcanic, PAA-CO_2

Introduction

In general, Geothermal system in Indonesia consists of volcanic and non-volcanic geothermal systems. Volcanic geothermal systems are spread along subduction pathways and have high temperatures (>225°C). Non-volcanic geothermal systems are widely distributed on the islands of Kalimantan and Sulawesi, which have low (<125 °C) to moderate (125-225 °C) temperatures. A total of 331 potential geothermal locations have been found, with 166 locations being geothermal areas with medium temperature and 80 geothermal locations at low temperature.

Geothermal systems in non-volcanic environments with rocks in the form of metamorphic or plutonic rocks generally have poor permeability and porosity conditions and the resulting reservoir temperatures reach temperatures of 200°C with varying depths. Geothermal potential in this non-volcanic field generally has a potential of ≤ 50 MW (Kasbani, 2009).

Problem

Currently, the development of geothermal energy to become PLTP in Indonesia is still focused on areas that have high temperatures. The purpose of this paper is looking for a solution to develop non-volcanic geothermal systems in Sulawesi's metamorphic environment.

Geological of Sulawesi

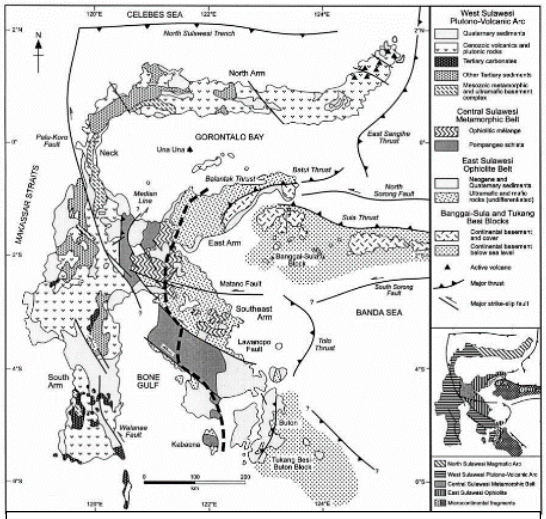

Figure 1: Tectonic Setting of Sulawesi (Hall and Wilson, 2000)

Based on Hall and Wilson (2001), the tectonic of the Sulawesi region can be divided into Western Mandala as the magmatic pathway which is the eastern end of the Sunda Paparan, Central Mandala in the form of poor rock carrying melange rock as part of the Australian block, Eastern mandala is in the form of ophiolite which is a segment of the imitated oceanic crust and sedimentary rocks of Trias-Miocene age and the fourth is the Fragment of the Banggai-Sula-Tukang Besi Continent, eastern and southeastern

PROCEEDINGS
JOINT CONVENTION BANDUNG (JCB) 2021
November 23rd – 25th 2021

islands of Sulawesi which are continental fragments that moved west due to strike-slip faults from New Guinea (Figure 1).

Data and Method

In writing this essay, the authors conducted a study of literature method on books or websites, journals, and papers relating to geothermal energy problems with secondary data. The method is using hydraulic fracturing hybrid fracs with PAA-CO_2 combined with Binary Cycle.

Hydraulic Fracturing Hybrid Fracs with PAA-CO_2

Hydraulic fracturing is often used when dealing with reservoirs (rock nests where fluid is underground) that are hot but have low permeability, so engineers carry out engineering engineering. Fracking is a well stimulation technique in which the rock layers below are cracked with high pressure liquid fluid. Energy mining using fracking is considered to cause minor earthquakes, water pollution, thermal pollution, and also subsidence at a number of points.

As is known, the fracking method requires large amounts of water for the purpose of the injection process along with other materials so that it can cause water scarcity in the area around the mine. In addition, fracking waste fluid consists of various chemical substances so that the waste needs special handling so as not to pollute the environment, especially pollution to surface water and ground water.

Then this problem can be solved by applying PAA-CO_2 Fracturing Fluid, this technology will react with CO_2 in subsurface and will expand by 150% (Jung, et al). The increasing volume will reduce the use of thousands of gallons of water so that the application of this fracs will be more effective.

Binary Cycle

Binary Cycle uses dry steam and flash steam technology. In the Binary Cycle, hot water or steam from production wells never touches the turbine. Geothermal water is used to heat the so-called working fluid in the heat exchanger. The working fluid then becomes hot and produces steam in the form of flash. The steam generated in the heat exchanger is then flowed to rotate the turbine and then drive a generator to produce an electric power source. The hot steam generated in the heat exchanger is referred to as the secondary (binary) fluid. This Binary Cycle is actually a closed system. So, nothing is released into the atmosphere. The advantage of the Binary Cycle is that it can be operated at low temperatures of 90°-1750°C. An example of the application of this type of BCPP technology is at the Mammoth Pacific Binary Geothermal Power Plants in the Casa Diablo geothermal field, USA. It is estimated that BCPP geothermal power plants will be more widely used in the future.

Result and Discussion

Geothermal Condition in Sulawesi

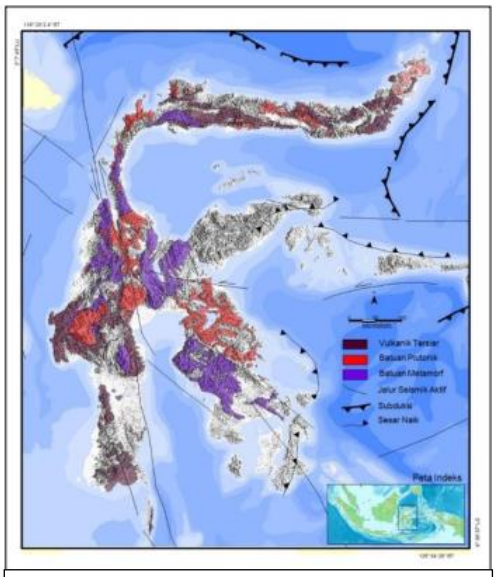

Figure 2: Lithology created geothermal system in Sulawesi (Badan Geologi, 2015)

The rock condition that is influenced by the chemical composition of the geothermal system can affect the manifestation conditions geothermal system. Based on its lithological association, Sulawesi can be divided into 3 geothermal environmental systems namely Tertiary volcanic, plutonic environment and metamorphic environment (Table 1).

Table 2: Calculation of Reservoir Temperature Based on MT Data and Temperature Slope Well (Badan Geologi, 2015)

Lithology	Max Reservoir (m)	Gradient Temperature		T reservoir from well	T reservoir from geothermometer (1)	(2)	(3)	(4)	(5)
					SiO_2	Na-K	Na-K-Ca	Na-Li	K-Mg
Tersier Vulcanic	1000	14°C/100m	65.1°C pada 225 m	173	150	170	160	150	120
		8.8°C/100m	53.3°C pada 100 m	122					
Plutonic	700	29.7°C/100m	53.7°C pada100 m	230	160	210	190	270	120
		28.51°C/100m	84.17°C pada 225 m	220					
Metamorphic	750	32°C/100m	63.18°C pada 100 m	270	140	250	200	250	100
		21.21°C/100m	47.21°C pada 100 m	185					

PROCEEDINGS
JOINT CONVENTION BANDUNG (JCB) 2021
November 23rd – 25th 2021

Note:
(1). Fournier (1981), (2). Fournier (1979), (3). Fournier and Trusdel (1973), (4) Foilac and Michard (1981), (5). Gigenbach (1988).

It can be concluded that among the three lithologies found in Sulawesi, this type of metamorphic lithology has a fairly high temperature condition compared to the others. However, the constraints of utilizing metamorphic rocks as reservoirs are porosity and permeability conditions. However, in controlled areas the structure will form a zone rich in fractures or joins so that it is nest or permeable and able to store hot fluid before it comes out to the surface as a manifestation through fracture pathways. The relatively shallow permeable (reservoir) zone is generally less than 1200 m, and its permeable zone is concentrated only around the structural zone alone in the form of lanes in the orientation of the main geological structure.

Geothermal System in Basement Metamorphic

The Geothermal System available with metamorphic is a hot dry rock geothermal system (Figure 3). In principle, the Hot Dry Rock geothermal system uses heat stored in impermeable rocks, where to extracting heat energy, the system is made to resemble a system convective by making artificial fractures on rock followed by injection of cold water into the impermeable rock layer which contains heat, so the cold water is heated and used for power generation.

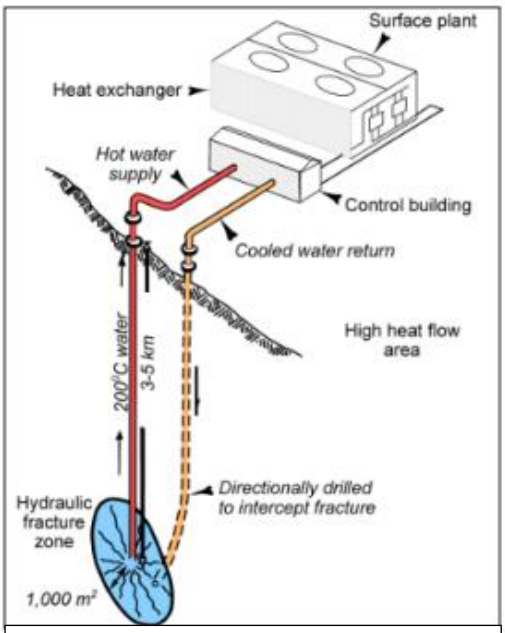

Figure 3: Illustration of the use of the hot dry rock system (Lund, 2007)

Development Design of Non-Volcanic Geothermal System

The following are the designs we offer to overcome the lack of metamorphic rocks which are used as non-volcanic geothermal systems. Where Enhanced Geothermal System with Hydraulic Fracturing will create new porosity and binary cycles to increase fluid temperature (Figure 4).

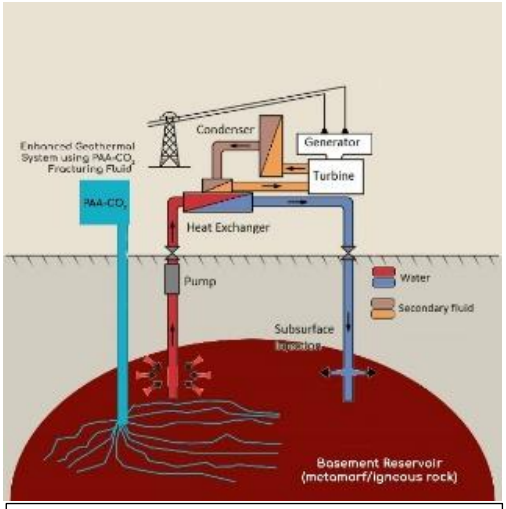

Figure 4: Design of non-volcanic geothermal system

Conclusions

Non-volcanic geothermal systems can be utilized more efficiently by using Binary Cycle technology combined with Hydraulic Fracturing EGS using PAA-CO_2. Binary Cycle to heat or increase the temperature of the working fluid in the geothermal system through a heat exchanger so that the resulting fluid can rotate the turbine. Hydraulic Fracturing combined with PAA-CO_2 in the Enhanced Geothermal System (EGS) technology can form additional permeability and the heat can be raised to the surface.

References

Anonim, 2010. Potensi dan Pengembangan Sumberdaya Panas Bumi Indonesia, Badan Geologi, Kementerian Energi dan Sumber Daya Mineral.

Anonim. 2015. Sistem Panas Bumi Non Vulkanik Sulawesi. Badan Geologi, Kementerian Energi dan Sumber Daya Mineral.

Earle, Steven & Karla Panchuk. 2019. *Physical Geology - 2nd Edition*. BCCampus

Fouilac C. & Michard,G. 1981. *Sodium/lithium ratio in water applied to geothermometry of geothermal reservoirs.* Geothermics, 10, 55-70.

Fournier, R.O., and Truesdell, A.H. 1973. *An Empirical Na-K-Ca Geothermometer for Natural Water*. Geochimica Cosmochimica Acta, vol.37, Pp.1255-1275.

Fournier, R.O., 1981. *Application of Water Geochemistry Geothermal Exploration and Reservoir Engineering, "Geothermal System: Principles and Case Histories".* John Willey & Sons. New York.

Giggenbach, W.F., and Goguel. 1988. *Methods for the collection and analysis of geothermal.*

Hall and Wilson, 2000. *Neogene Sutures in Eastern Indonesia*, Journal of Asian Earth Sciences, 18 (2000) 781 - 808.

Hochstein, M.P., 1990. *Classification and Assessment of Geothermal Resources*, In: Dickson, M.H., and Fanelli, M., 2002: What is Geothermal Energy, Istituto di Geoscienze e Georisorse , Pisa, Italy

Kasbani, 2009. Tipe Sistem Panas Bumi di Indonesia dan Estimasi Potensi Energinya, Badan Geologi, Kementerian Energi dan Sumber Daya Mineral

Lund,J.W., 2007.*Characteristic,Development and Utilization of Geothermal Resources*, GHC-Bulletin.

Montanari D. 2010. *ENGINE Coordination Action. Best Parctice Handbook for the development of Unconventionnal Geothermal Resources with a focus on ENHANCED GEOTHERMAL SYSTEM.*

Acknowledgements (Optional)

The authors would like to thank Akhmad Fauzan, S.T. & Vismaia Isanjarini, S.T. for providing direction and guidance in making this scientific paper.

PROCEEDINGS
JOINT CONVENTION BANDUNG (JCB) 2021
November 23rd – 25th 2021

Potensi Logam Tanah Jarang (LTJ) di Indonesia Berdasarkan Studi Geologi dan Pengembangan Eksplorasinya

Dhea Melvian[1], Refita Khumayroh*[2], Shabrina Tasha Zahra*[3], Fajar Gumelar*[4], Leonardo Budhi Satrio*[5], Ibra Kumara*[6]*
*[1] Teknik Geofisika, FMIPA, Universitas Brawijaya, *[2] Teknik Geofisika, FTM, Universitas Pembangungan Negeri VY *[3] Geofisika, FMIPA, Universitas Indonesia, *[4] Geofisika, FMIPA, Universitas Padjajaran, *[5] Teknik Geofisika, FTTM, Institut Teknologi Bandung*

Abstrak
Rare Earth Element (LTJ) atau Logam Tanah Jarang (LTJ) merupakan salah satu mineral strategis dan termasuk "critical mineral" yang terdiri dari kumpulan 17 jenis unsur di alam. Walaupun disebut "logam tanah jarang" persebarannya luas, namun memang kelimpahannya tidak banyak sehingga eksplorasinya cukup sulit dilakukan. Kebijakan pemerintah Tiongkok untuk membatasi ekspor LTJ sejak tahun 2005 menjadi kendala tersendiri bagi banyak negara konsumen. Sedangkan potensi LTJ di Indonesia saat ini belum banyak dieksplorasi dan dimanfaatkan, padahal permintaan terhadap logam tanah jarang akan meningkat seiring pertumbuhan akan kebutuhan produk industri teknologi tinggi. Metode yang akan digunakan yaitu studi literatur mengenai keberadaan konsentrasi LTJ di Indonesia. Studi ini akan membahas mengenai kelimpahan, geologi dan genesa, eksplorasi, dan potensi LTJ di Indonesia. Saat ini studi terkait LTJ di Indonesia masih terus dilakukan, begitupun dengan eksplorasi guna mencari keberadaan potensinya di Indonesia. Potensi LTJ yang ditemui mulai dari Indonesia bagian barat hingga tengah seperti pada Pulau Sumatra, Jawa, Kalimantan, Sulawesi, hingga Rote. Mineral utama deposit LTJ yang ditemukan di Indonesia adalah *Xenotim*, *Monasit* dan *Zirkon* yang berasosiasi dengan kasiterit yang diperoleh dari penambangan timah aluvial. Mineral logam yang berkaitan dengan LTJ adalah *Timah* (Sn) yang terutama terpusat di wilayah Kepulauan Riau, Bangka Belitung dan sebagian Kalimantan Barat. Sehingga area penambangan *Timah* (Sn) menjadi fokus pengembangan potensi LTJ yang utama terkait tipe plaser serta pada endapan bauksit sebagai hasil lateritisasi pada batuan granitik juga menjadi sasaran. Nantinya hasil penelitian ini dapat dijadikan referensi untuk pengembangan eksplorasi LTJ di Indonesia untuk masa mendatang.

Kata kunci : LTJ, Eksplorasi, Indonesia

Abstract
Rare Earth Element (LTJ) is one of the strategic minerals and includes a "critical mineral" consisting of a collection of 17 types of elements in nature. Although called "rare earth metals" the distribution is widespread, but indeed the abundance is not much so exploration is quite difficult to do. The Chinese government's policy to limit LTJ exports since 2005 has been a constraint for many consumer countries. While the potential of LTJ in Indonesia is currently not widely explored and utilized, even though the demand for rare earth metals will increase as the need for high-tech industrial products grows. The method that will be used is the study of literature on the existence of LTJ concentrations in Indonesia. This study will discuss the abundance, geology and genesa, exploration, and potential of LTJ in Indonesia. Currently, studies related to LTJ in Indonesia are still being conducted, as well as exploration to find its potential in Indonesia. The potential of LTJ encountered ranges from western to central Indonesia as in Sumatra, Java, Kalimantan, Sulawesi, to Rote. The main minerals of LTJ deposits found in Indonesia are *Xenotime*, *Monazite*, and *Zircon* associated with cassiterite obtained from alluvial tin mining. The metal mineral associated with LTJ is *Tin* (Sn) which is mainly concentrated in the Riau Islands, Bangka Belitung, and parts of West Kalimantan. So that the Tin mining area (Sn) becomes the focus of the development of the main LTJ potential related to plaser type and bauxite deposits as a result of lateritisation in granitic rocks are also targeted. Later the results of this research can be used as a reference for the development of LTJ exploration in Indonesia for the future.

Keyword : REE, Exploration, Indonesia

Pendahuluan
Indonesia merupakan salah satu negara yang dilimpahkan unsur tanah jarang. Logam Tanah Jarang (LTJ) merupakan salah satu dari mineral strategis dan termasuk "*critical mineral*" terdiri dari kumpulan dari unsur-unsur *Scandium* (Sc), *Lanthanum* (La), *Cerium* (Ce), *Praseodymium* (Pr), *Neodymium* (Nd), *Promethium* (Pm), *Samarium* (Sm), *Europium* (Eu), *Gadolinium* (Gd), *Terbium* (Tb), *Dysprosium* (Dy), *Holmium* (Ho), *Erbium* (Er), *Thulium* (Tm), *Ytterbium* (Yb), *Lutetium* (Lu), dan *Yttrium* (Y). Di Indonesia, daerah yang memiliki potensi sumberdaya LTJ telah dipetakan oleh Pusat Sumber Daya Mineral Batubara dan Panas Bumi (PSDMBP) yang pada tahun 2019 tercatat ada 29 daerah. Sedangkan mineral-mineral yang terkandung LTJ dapat meliputi *Alanit, Apatit, Bastnaesite, Eudialyte, Fergusonit, Gadolinite, Monasit, Parisit, Xenotime, dan Zircon*. Endapan mineral LTJ terbagi atas dua jenis, yaitu endapan primer dan endapan sekunder. LTJ banyak terdapat di zona *rifting intra-kontinen* dan semakin mendekati batas zona subduksi akan semakin sedikit potensi LTJ-nya (Haxel dkk, 2005).

Adapun mineral pembawa LTJ umumnya berasosiasi dengan batuan granitik. Batuan granit sendiri terbagi atas empat klasifikasi, yaitu tipe-I, tipe-S, tipe-A, dan tipe-M. Granit tipe-A banyak mengandung mineral pembawa LTJ. Logam tanah jarang (LTJ), saat ini menjadi komoditas strategis. Pemanfaatan logam tanah jarang erat kaitannya dengan produk industri teknologi tinggi, seperti industri komputer, telekomunikasi, nuklir, dan ruang angkasa. Penggunaan LTJ akan meluas, terutama unsur tanah jarang tunggal, seperti *Neodymium, Samarium, Europium, Gadolinium*. Saat ini energi bukan lagi sekadar berupa bahan bakar fosil, *Uranium, Plutonium*, angin dan air. LTJ bahkan dikategorikan sebagai cadangan energi. LTJ dianggap sebagai material penting di masa depan. Penggunaan LTJ sangat bervariasi yaitu pada energi nuklir, kimia, katalis, elektronik, paduan logam dan optik. Pemanfaatan LTJ untuk yang sederhana seperti lampu, pelapis gelas, untuk teknologi tinggi seperti *Fosfor*, laser, magnet, baterai, dan teknologi masa depan seperti superkonduktor, pengangkut hidrogen (Haxel dkk, 2005). Penelitian ini akan membahas mengenai kelimpahan dan

eksplorasi mengenai LTJ untuk dijadikan referensi pengembangan eksplorasi LTJ di Indonesia.

Data dan Metode

Studi ini dimulai dengan pengumpulan data yang membahas kelimpahan geologi. Penelitian ini menggunakan teknik pengumpulan data berupa studi literatur. Studi Literatur merupakan penelitian yang dilakukan oleh peneliti dengan mengumpulkan sejumlah buku-buku, majalah yang berkaitan dengan masalah dan tujuan penelitian. Teknik ini dilakukan dengan tujuan untuk mengungkapkan berbagai teori-teori yang relevan dengan permasalahan yang sedang dihadapi/diteliti sebagai bahan rujukan dalam pembahasan hasil penelitian (Danial dan Warsiah, 2009).

Studi dimulai dengan pemumpulan data yang membahas kelimpahan geologi di Indonesia sebagai referensi pengembangan eksplorasi REE untuk masa mendatang.

Hasil dan Pembahasan

1. **Kelimpahan Geologi dan Genesa Indonesia**

   LTJ umumnya berasosiasi dengan batuan atau formasi yang terbentuk dari material Karbonalit yang merupakan batuan karbonat atau alkalin pada sistem ultramafik/ultrabasa. Batuan alkalin itu sendiri umum dijumpai sebagai *dyke* terisolasi. Selain itu, cebakan yang tersusun atas endapan oksida besi-tembaga (Cu) - emas (Au) juga dikenal sebagai salah satu endapan yang mengandung LTJ seperti penemuan cebakan raksasa *Olympic Dam* di Australia. Secara garis besar, endapan LTJ dikaitkan dengan lingkungan batuannya yang terdiri atas jenis batuan beku pegmatit, karbonatit, metamorf, dan plaser (Gunradi, et al, 2019)

   Kondisi LTJ saat ini di Indonesia ada 17 unsur elements diantaranya *Skandium* (Sc), *Yitrium* (Y), *Lanthanum* (La), *Serium* (Ce), *Praseodymium* (Pr), *Neodymium* (Nd), *Promethium* (Pm), *Samarium* (Sm), *Europium* (EU), *Gadolinium* (Gd), *Terbium* (Tb), *Disprosium* (Dy), *Holmium* (Ho), *Erbium* (Er), *Tulium* (Tm), *Iterbium* (Yt), dan *Lutetium* (Lu) (PSDMBP, 2019).

   Indonesia yang terletak pada pertemuan tiga lempeng besar di Bumi, memiliki variasi geologi yang tinggi. Variasi tersebut mengindikasikan potensi keberadaan LTJ pada beberapa cebakan dengan karakteristik tertentu meskipun belum diketahui seberapa besar kandungannya.

   LTJ erat kehadirannya bersama dengan kelimpahan material *Timah* (Sn). Melihat kondisi tersebut, Indonesia memiliki konsentrasi persebaran timah yang cukup besar pada wilayah yang dilalui oleh Sabuk Timah Asia Tenggara antara lain Kepulauan Riau, Bangka Belitung, dan sebagian Kalimantan Barat. Selain itu LTJ juga diperkirakan terdapat pada konsentrasi Bauksit, Nikel, dan Kobalt. Sabuk Timah Asia Tenggara ini merupakan prioritas wilayah studi dan pengembangan untuk eksplorasi LTJ khususnya di Indonesia (Handoko dan Sanjaya, 2018).

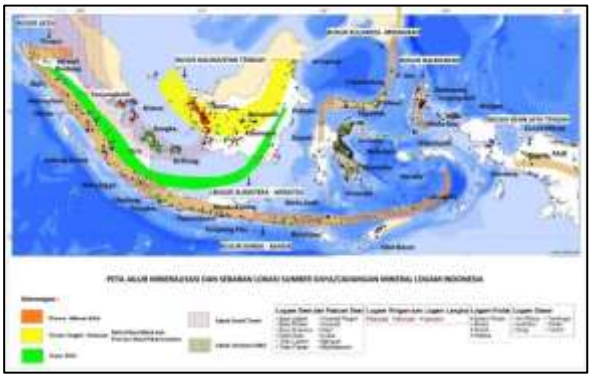

Gambar 1: Peta Jalur Mineralisasi dan Sebaran Lokasi Sumber/Cadangan Mineral Logam di Indonesia (PSDMBP, 2019)

   Genesa LTJ di Indonesia terbagi menjadi cebakan primer yang terkait dengan proses magmatik dan hidrotermal serta endapan sekunder yang terkait dengan proses rombakan dan sedimentasi yang biasanya ditemukan pada residual, plaser, endapan batubara, hasil pelapukan (Syaeful, dkk, 2014).

2. **Pemanfaatan REE saat ini di Indonesia**

   Logam Tanah Jarang (LTJ) merupakan bagian dari pada mineral strategis. LTJ juga merupakan *low critical raw materials* (CRM), ini merupakan material-material yang penting dan keberadaan juga terbatas serta sangat dibutuhkan bagi industri berbasis teknologi tinggi untuk menghasilkan energi yang bersih. penelitian dan usaha pengembangan LTJ di Indonesia sebagai komoditas prioritas tinggi yang bisa diusahakan, baru marak dilakukan dalam lima tahun terakhir.

   Sumber daya hipotetik di Sumatera sekitar 23 juta ton dengan tipe endapan LTJ Laterit, beserta 5 juta ton LTJ dengan tipe tailings. Sedangkan di Kalimantan, sumber daya hipotetik LTJ sekitar 7 juta ton dengan tipe tailings dan di Sulawesi sekitar 1,5 juta ton dengan tipe laterit.

   Memasuki industri modern, unsur tanah jarang merupakan komoditi yang strategis dan signifikan. Pemanfaatan unsur tanah jarang sangat dibutuhkan dalam berbagai macam bidang mulai dari industri elektronik hingga industri transportasi modern. Pada dasarnya manfaat dari LTJ cukup bervariasi namun jika ditarik garis merahnya LTJ didayagunakan pada industri elektronik sebagai katalis kimia untuk pembuatan baterai alat-alat elektronik yang portabel. 20 tahun terakhir terjadi ledakan pembuatan dan penggunaan alat elektronik yang sifatnya portable dan membutuhkan baterai baik itu berupa telepon seluler, laptop, tablet, dll. *Gadget* yang disebutkan yang saat ini sudah menjadi elemen pendukung kehidupan manusia membutuhkan baterai yang salah satu unsur penting pembuatnya adalah LTJ. LTJ juga dimanfaatkan di bidang elektronik untuk pembuatan layar televisi, *chip silicon*, *monitor*, lensa kamera, LED (*light emitting diodes*), CFL (*computer fluorescent lamps*), alat *scanner*, dll (terutama pada lensa LTJ berfungsi sebagai fosfor yang member warna). Pemanfaatan pengembangan LTJ ada di dalam industri elektronik, industri otomotif, dan juga industri pertahanan. Dalam hal industri elektronik, material

LTJ dapat digunakan menjadi magnet permanen untuk pembuatan baterai alat-alat elektronik *portable*, baterai kendaraan listrik, turbin penghasil energi ramah lingkungan, katalis pemecah cairan pada penyulingan minyak mentah, pembuatan layar televisi, *chip silicon*, monitor, lensa kamera, LED (*lighting emitting diode*), CFL *(computer fluorescent lamps*), alat *scanner*, sebagai fosfor yang memberi warna terutama pada lensa, bahan pembuat mesin sinar-X *portable*, tabung sinar-X, MRI (*magnetic resonance imagery*); aplikasi perawatan kanker dan lainnya. Sementara dalam industri otomotif LTJ digunakan dalam pengembangan mobil *hybrid* pada industri kendaraan bermerek nasional yang baru-baru ini direncanakan Pemerintah. Kelompok logam Nd, Pr, Dy, TB merupakan bahan penting dalam pembuatan motor listrik dan generator mobil *hybrid*. Kelompok logam La, Be, Ce merupakan bahan penting dalam pembuatan baterai mobil *hybrid* NIMH. Sementara dalam industri pertahanan LTJ digunakan sebagai motor listrik pada pesawat tempur, tank, dan *control center* (*Global Rare Earth Element Review, Defense National Stockpile Center*). Tabel dibawah akan menjelaskan kegunaan dari masing-masing elemen yang dikelompokkan sebagai LTJ (Cahyo, 2015).

Tabel 2. Pengelompokkan Pemanfaatan LTJ

Z	Elemen	Simbol	Kegunaan
21	Scandium	SC	Instalasi luar angkasa, lampu jalan dengan intensitas tinggi, peralatan dengan performa tinggi.
39	Yttrium	Y	Televisi, aplikasi perawatan kanker, alloy peningkat kekuatan mental.
57	Lanthanum	La	Lensa kamera, elektroda baterai, penyimpanan hidrogen.
58	Cerium	Ce	Alat konventer katalik, kaca berwarna, produksi baja.
59	Praseodymium	Pr	Magnet super kuat, kacamata las, laser.
60	Neodymium	Nd	Magnet ermanen super kuat, mikrofon, motor elektrik dari automobil.
61	Promethium	Pm	Tidak umum dijumpai di alam.
62	Samarium	Sm	Perawatan kanker, tongkat pengontrol reaktor nuklir, laser sinar-X.
63	Europium	Eu	Layar TV berwarna, gelas fluoresen, alat pengetes kaca.
64	Gadolinium	Gd	Alat pelindung reaktor nuklir, alat propulsi nuklit laut, peningkat ketahanan mental aloy.
65	Terbium	Tb	Televisi set, sel matahari, sistem sonar.
66	Dysprosium	Dy	Alat *hard disk* pencahayaan komersil, *transducer*.
67	Holmium	Ho	Laser, pewarna kaca, magnet super kuat.
68	Erbium	Er	Pewarna kaca, penguat sinyal pada kabel fiber optik, penggunaan metalurgi.
69	Thulium	Tm	Laser dengan efisiensi tinggi, mesin sinar-X *portable*, superkonduktor temperatur tinggi.
70	Ytterbium	Yb	Penguat baja *stainless*, alat pengontrol permukaan.
71	Lutetiumm	Lu	*Refining petroleum, LED Light Bulb*, manufaktur sirkuit terintegrasi.

3. Mengenai Eksplorasi LTJ Global dan Indonesia

Tujuan utama dari rangkaian kegiatan eksplorasi adalah menemukan endapan LTJ di suatu daerah. Agar tujuan tersebut tercapai maka diperlukan langkah langkah terencana sehingga dapat ditemukan endapan LTJ secara efektif dengan biaya minimal (efisien). 4 tahapan dalam eksplorasi LTJ, yaitu:

1. Survey Tinjau (*Reconnaissance*) adalah tahap eksplorasi untuk mengidentifikasi daerah-daerah yang berpotensi mengandung endapan LTJ pada skala regional. Peninjauan dimaksudkan untuk mengidentifikasi daerah-daerah anomali atau mineralisasi yang prospektif untuk diselidiki lebih lanjut.
2. Prospeksi (*Prospecting*) adalah tahap eksplorasi dengan mempersempit daerah yang mengandung endapan mineral potensial. Metode yang digunakan adalah pemetaan geologi, studi geokimia, dan geofisika. Tujuannya adalah untuk mengidentifikasi suatu endapan LTJ yang akan menjadi target eksplorasi selanjutnya.
3. Eksplorasi Umum (*General Exploration*) adalah tahap eksplorasi yang merupakan deliniasi awal dari suatu endapan yang teridentifikasi. Tujuannya adalah untuk menentukan gambaran geologi suatu endapan LTJ berdasarkan indikasi sebaran, perkiraan awal mengenai ukuran, bentuk sebaran, kuantitas dan kualitasnya.
4. Eksplorasi Rinci (*Detailed Exploration*) adalah tahap eksplorasi untuk mendeliniasi secara rinci bentuk 3D terhadap endapan LTJ yang telah diketahui dari pemercontohan singkapan, puritan/sumur uji, dan lubang bor.

(PSDMBP, 2019)

Tabel 1. Penggunaan Metode Eksplorasi dalam Setiap Tahapan Eksplorasi

Tahapan	Metode	Keterangan
Survei Tinjau	Inderaja (remote sensing) Geofisika Pemetaan geologi Geokimia endapan sungai aktif Pendulangan	Foto udara, citra satelit, dll Radiometri dan Aeromagnet - 1 conto ± <15 km^2 Mineral yang tahan pelapukan: misalnya *monasit, xenotim* dan *zirkon, kasiterit*, dll
Prospeksi	Pemetaan geologi rinci Geokimia endapan sungai aktif Pendulangan Pemercontoan tanah Geofisika Eksplorasi Pemercontoan batuan	- 1 conto ± < 5 km^2 Mineral yang tahan pelapukan: misalnya *monasit, xenotim* dan *zirkon, kasiterit*, dll "*Ridge and spur*" dan Sistem kisi Ground Radiometri dan Geomagnet Parit/sumur uji, pengeboran
Ekplorasi Umum	Pemetaan geologi rinci Geofisika Pemercontoan tanah Pemercontoan batuan Sistematik untuk analisis geokimia	- - Sistem kisi-kisi Parit/sumur uji, pengeboran -
Eksplorasi Rinci	Pengeboran (lebih rapat sesuai dengan tipe endapan) Geofisika	Logging conto inti bor : litologi, Eksplorasi Rinci ubahan, mineralisasi dan data endapan) geoteknik Logging lubang bor

Salah satu teknologi yang dimanfaatkan untuk melakukan eksplorasi LTJ yang sudah diterapkan di Indonesia yaitu geomarine. Penginderaan atau pemetaan dengan teknologi sonar menggunakan metode eksplorasi geomarine merupakan metode yang

meliputi akuisisi data, pengolahan data, interpretasi dan pengambilan sampel batuan dan sedimen dasar laut, digunakan untuk mengetahui kondisi bawah permukaan dari daerah eksplorasi seismik. Teknologi geomarine dapat mengetahui persebaran REE berdasarkan kondisi geologi daerah penelitian baik dari aspek tektonik, stratigrafi, struktur geologi, dan aktivitas vulkanisme. Seperti halnya yang telah dilakukan oleh Pusat Penelitian dan Pengembangan Geologi Kelautan (PPPGL) di daerah Perairan Sabang Pulau Weh. Bersadarkan penelitian yang telah dilakukan oleh Saputra, Aritonang, dan Mandini (2019) diperoleh bahwa konsentrasi REE ditemukan pada tipe batuan utama, pada proses pembentukan batuan utama berupa mineral minor, dan aktivitas fluida hidrotermal. Eksplorasi keterdapatan REE secara umum dilakukan dengan mengidentifikasi konsentrasinya pada jenis batuan utama (source rock), dan tipe endapan sedimen. Asosiasi persebaran struktur dengan aktivitas vulkanik yang mengandung keterdapatan REE berupa fumarola dapat menjadi metode eksplorasi baru terkhususnya dengan kondisi geologi busur vulkanik.

BATAN Yogya (PSTA) juga telah mampu melakukan uji ekstraksi logam LTJ dari monasit dengan perolehan 80%. Balitbang ESDM (Tekmira) telah mampu mengekstraksi logam Nd dari Nd Karbonat 80%. PSDMBP Badan Geologi rutin melakukan penyelidikan sumber daya LTJ sesuai target RPJM 2015-2019, hasilnya sejumlah indikasi dan sumber daya hipotesis telah dipublikasikan. Belum ada patokan kadar ekonomi endapan LTJ (Lelono, 2021).

Di Indonesia sendiri eksplorasi LTJ masih banyak hambatannya. Ada beberapa faktor yang membuat Indonesia belum bisa maksimal dalam melakukan eksplorasinya. Akurasi cadangan dan sumber daya LTJ mesikpun sudah ada perkiraan jumlahnya perlu dipastikan lagi, perlunya eksplorasi lanjutan yang juga mempertimbangkan aspek bisnis model pengusahaannya, juga harus memastikan tekonologi yang pas untuk mengolah konten yang terdapat unsur radio aktif. Konsorsium nasional LTJ telah dibentuk melibatkan 5 Kementerian atau Lembaga namun kegiatan belum berjalan sebagaimana diharapkan (Mulyana, 2020).

4. Kebijakan Pemerintah Eksplorasi Minerba di Indonesia

Peraturan yang mengatur pengadaan usaha Logam Tanah Jarang di Indonesia adalah PP no 23/2010 mengenai Pelaksanaan Kegiatan Usaha Pertambangan Mineral Dan Batubara. Dalam peraturan tersebut dibahas mengenai bagaimana pengusahaan dari logam tanah jarang, dimana penyelidikan umum eksplorasi bahan galian nuklir dilaksanakan oleh Badan Pelaksana. Badan Usaha ini dapat bekerjasama dengan BUMN, Koperasi, Badan Swasta atau badan lain. Kemudian perijinan lain yang mengatur kegiatan usaha Logam Tanah Jarang di Indonesia adalah rancangan UU Cipta Kerja (Omnibus) Pasal 9A butir 4 yang menyatakan Badan usaha pemegang perizinan terkait pertambangan mineral dan batubara yang menghasilkan mineral ikutan radioaktif, wajib mengolah dan/atau menyimpan sementara mineral ikutan radioaktif sesuai ketentuan peraturan perundang-undangan. Rancangan UU Cipta kerja ini membawa angin segar bagi pengembangan mineral radioaktif di Indonesia salah satunya ialah pengembangan pengusahaan monasit yang sejatinya merupakan penyumbang 90% logam tanah jarang di Indonesia (Tampubolon, 2020).

Namun sayang kebijakan diatas terkunci oleh UU No 3/2020 Minerba Perubahan Pasal 92 yang menyebutkan bahwa Pemegang IUP dan IUPK berhak memiliki mineral, termasuk mineral ikutannya, atau batubara yang telah diproduksi setelah memenuhi iuran produksi, kecuali mineral ikutan radioaktif. Sehingga kegiatan pengusahaan mineral ikutan radioaktif seperti monasit tidak dapat dijalankan. Oleh karena itu perlu adanya harmonisasi UU Cipta Kerja dengan UU Minerba dalam hal Pengajuan Badan Usaha yang dapat mengajukan penugasan kepada Pemerintah untuk melakukan penyelidikan mineral radioaktif atau mengeluarkan Monasit dari daftar mineral Radioaktif (Sukhyar, 2020).

5. Potensi REE di Dunia dan Indonesia

Gambar 2: Lokasi Keterdapatan LTJ Di Dunia (PSDMBP, 2019)

Pada tahun 2009, China melakukan monopoli terhadap produksi LTJ global hingga 97% dalam bentuk mineral karbonat dan oksida besi hidrotermal, monasit dunia sebesar 12 juta ton dan Thorium 500.000 ton. Dengan besarnya jumlah cadangan unsur tanah jarang tersebut, China dapat memanfaatkan unsur tersebut menjadi komoditas utama untuk memasuki era modern, sebagai bahan untuk industri elektronik hingga industri transportasi modern.

Gambar 3: Persebaran Perkiraan Potensi LTJ di Indonesia

Dalam penelitian yang dilakukan oleh Virdhian dan Afrilinda (2014), disebutkan bahwa di Indonesia keberadaan mineral tanah jarang terdapat pada daerah

yang mengandung intrusi granitoid, plaser, dan alluvial. Daerah-daerah yang memiliki ekstensif intrusi granitoid di Indonesia adalah Kepulauan Tujuh, Singkep, Pulau Bangka dan Belitung, Kundur, Karimun Jawa, Sumatera, Pulau Sula Banggai (timur Sulawesi), Kalimantan dan bagian barat Papua (Johari dan Kuntjara, 1991).

Logam tanah jarang di Indonesia diperkirakan mencapai 1,5 miliar ton menurut data Kementerian Energi dan Sumber Daya Mineral pada tahun 2015. Saat ini PT TIMAH, sudah memulai untuk melakukan eksplorasi memisahkan unsur logam tanah jarang dipadukan untuk membuat paduan logam yang pemanfaatannya untuk diaplikasikan dalam beberapa teknologi maju. Namun di Indonesia potensi tersebut belum dapat berkembang secara pesat karena perlu adanya akurasi tingkat cadangan dan sumber daya yang perlu dipastikan lagi jumlah dan kecukupan nya. Lalu perlu dilakukan eksplorasi lanjutan yang juga mempertimbangkan aspek bisnis model pengusahaannya. Dan yang terakhir yang diperlukan yaitu memastikan teknologi yang pas untuk mengolah konten yang terdapat unsur radioaktif. (ESDM, 2015).

Kesimpulan

Dari apa yang telah dilakukan, didapatkan informasi apabila Indonesia mempunyai potensi LTJ yang cukup. Sejauh ini masyarakat sudah mulai banyak menggunakan barang yang menggunakan bahan dasar dari LTJ. Pemerintah sudah melakukan beberapa upaya untuk terus mengembangkan LTJ ini. Namun, sejauh ini masih belum dapat memaksimalkan eksplorasinya dikarenakan beberapa hal. Selain karena teknologi dan sumber kelimpahan yang harus dipastikan jumlahnya, kebijakan pemerintah juga masih membatasi akan ekplorasi LTJ. Diperlukan kajian ulang perihal eksplorasi ini baik dari kebijakan hingga teknologinya.

REFERENSI

Cahyo, Fery. Andika. (2015). *Rare Earth Mineral (REE): Masa Depan Endapan Plaser Dunia*. Geopangea Research Group.

Danial, E, & Warsiah. (2009). *Metode Penulisan Karya Ilmiah*. Bandung: Laboraterium Pendidikan Kewarganegaraan.

Gunradi, R., et al. (2019). *Potensi Logam Tanah Jarang di Indonesia.*1. 17-33. Bandung : Pusat Sumber Daya Mineral, Batubara dan Panas Bumi Badan Geologi Kementerian Energi dan Sumber Daya Mineral.

Handoko, A D dan Sanjaya, E. (2018). *IOP Conf. Ser.: Earth Environ. Sci.* 118**.** 012077.

Johari dan Kuntjara. (1991). *Spectrometry.Encyclopedia of Analytical Chemistry*. pp.9468-9485. The Occurences of Rare Earth Mineral for Electronik.

Kementerian ESDM. (2015). *Rencana Strategis KESDM 2015-2019.*

Lelono, Budi. Eko. (2021). *Potensi dan Pengolahan Logam Tanah Jarang Sebagai Mineral Strategis dan Energi Masa Depan*. Webinar Badan Geologi Kementerian ESDM

Mulyana, Ridwan Nanda. (2020). *Sata Sumber Daya Logam Tanah Jarang di Indonesia*. Badan Geologi.

PSDMBP. (2019). *Potensi Logam Tanah Jarang di Indonesia.* Kementerian ESDM.

PSDMBP. (2019). *Neraca Sumber Daya dan Cadangan Batubara Indonesia 2019*. Kementerian ESDM.

Saputra, I.A.R, Aritonang, S. dan Mandini, M.D. (2019). *Pemetaan Sumber Daya Rare Earth Elements (REE) Untuk Bahan Baku Industri Pertahanan dengan Metode Eksplorasi Geomarine.* Jurnal Teknologi Penginderaan. Volume 1(1).

Sukhyar, Raden. (2020). *Pengusahaan Pertambangan Logam Tanah Jarang*. Pusat Survei Geologi.

Syaeful, H., W. Setiawan K., Sukadana, I. G., dan Adi Gunawan. 2018. Sumatera. *Rare Earth Element Exploration in Indonesia.* Proceedings of Sundaland Resources 2014 MEGI Annual Convention.

Tampubolon,Armin.(2020). *Program Percepatan Penyelidikan Sumber Daya/Cadangan Logam Tanah Jarang*. Pusat Survei Geologi.

Virdhian, Shinta & Eva Afrilinda. (2014). *Karakterisasi Mineral Tanah Jarang Ikutan Timah dan Potensi Pengembangan Industri Berbasis Unsur Tanah Jarang. METAL INDONESIA Vol. 36 No. 2 Desember 2014. ISSN 0126 – 3463.*

PROCEEDINGS
JOINT CONVENTION BANDUNG (JCB) 2021
November 23rd – 25th 2021

Geological Analysis and Hazard Mitigation at Pertamina Geothermal Energy Area Lahendong, North Sulawesi.

Muh. Alifian Al Anshari, Pricilia B. Diamanis[2], Hendra Riogilang[3], Herawaty Riogilang[4].
[1,2,3,4]University of Sam Ratulangi.

Abstract
Pertamina Geothermal Energy Area Lahendong (PGE Lahendong) is an Indonesian geothermal exploration company operating in Lahendong, North Sulawesi. In the exploration process, it must be supported by stable and decent soil conditions, and it is necessary to carry out by geological analysis. The geological analysis aims to know the physical condition and stability of the soil in supporting the feasibility of the geothermal exploration process. Disturbed soil stability can cause geological disasters and damage potential for the equipment. This study aims to conduct a geological analysis in the PGE Lahendong Area in Clusters 5, 13, 24, 4, 27, 26, 32, R1 and R2. The parameters used are subsidence, microseismic, geothermal manifestations and soil movement like landslides and sliding. The data collected through field monitoring and secondary data. The results showed that the PGE Area Lahendong generally has stable soil conditions and is very feasible to continue the operations. Several cluster locations in fields are safe and need to be monitored for the safety of local residents' activities. Meanwhile, cluster locations in hilly areas are relatively safe and it is necessary to carry out routine control on hillsides which have landslide potentials.

Keywords: Geological Analysis, Hazard Mitigation, PGE Lahendong

Introduction

Indonesia is located on the Pacific Ring of Fire which is caused by the interaction between the Eurasian, Pacific, and Indian-Australian plates (Morley, 2012). This condition makes Indonesia one of the countries with abundant geothermal energy potential, which is around 40%. The island of Sulawesi is formed from three large plates, namely the Eurasian, Pacific, and Australian plates since the Mesozoic era (Szentpeteri, 2015). North Sulawesi is one of the arctic arcs of magmatic islands (island arc) due to the subduction of the Sulawesi Sea and the Subduction of the Maluku Sea (Maulana, 2013). This causes North Sulawesi to have several geothermal manifestation points located around the Lahendong area, namely in the Tomohon and Langowan areas.

Geothermal potential can be utilized directly or indirectly. Direct utilization is used in non-electrical sectors such as agriculture, fisheries, health, and others. Meanwhile, indirect utilization is used as a Geothermal Power Plant (Dewi e al. 2019). Pertamina Geothermal Energy Area Lahendong (PGE Lahendong) is an Indonesian geothermal exploration company operating in Lahendong, North Sulawesi. PGE Lahendong Area is located in the Company's Work Area (WKP) Lahendong, North Sulawesi Province, where there are 6 Powerplant units operating commercially since 2001. The current total installed capacity is 120MW, each unit with a capacity of 20MW.

Figure 1: PGE Area Lahendong view.
Source: Pertamina.com

In the exploration process, it must be supported by stable and decent soil conditions, and it is necessary to carry out by geological analysis. The geological analysis aims to know the physical condition and stability of the soil in supporting the feasibility of the geothermal exploration process. Disturbed soil stability can cause geological disasters and damage potential for the equipment. This study aims to conduct a geological analysis in the PGE Lahendong Area.

Data and Method

The data collected through field research and secondary data. Field research is carried out to monitor the current situation related to the implementation of geothermal exploration and the surrounding conditions. Secondary data is used to analyze the characteristics of the area based on the location of the ecoregion, geological mapping, and hydrogeological mapping. The geological parameters used are subsidence, geothermal manifestations and soil movement like erosions and sliding, all geological data except geothermal manifestations are used by secondary data analysis. The data analyze using observation, geological and hydrogeological maps, and the relationship between soil characteristics and its ability. Conclusions are obtained from the analysis of these parameters with the conditions in each cluster, plotted on geological map and analyze the location and character of the soil.

Result and Discussion

Ecorecion Analysis

Ecoregion is a large regional ecosystem containing a number of smaller ecosystems. They are geographic zones that represent geographical groups of similar functioning where similar sites (which have the same landform, slope, parent material, and drainage characteristics) can be found in several climatic areas. In one area, these sites will support the same vegetation community, but in another area, the vegetation on the site will be different (Bailey, 1983). One way to establish reliable production-site relationships is to identify homogeneous geographic strata where similar ecosystems have developed on materials having similar properties (Rowe, 1962). The characteristics of the ecoregion have included geological support factors and hydrogeological factors where all of these factors also play a very important role in facing disaster challenges, especially floods and earthquakes.

PROCEEDINGS
JOINT CONVENTION BANDUNG (JCB) 2021
November 23rd – 25th 2021

In principle, the ecoregion approach also aims to strengthen and ensure horizontal coordination between interdependent regions (upstream-downstream) in hazard mitigation. In addition, the ecoregion approach has the aim of being functionally able to produce a strategic plan for hazard mitigation, including for use in geothermal exploration at Pertamina Geothermal Energy Area Lahendong. Ecoregion maps can describe geological characteristics, flora and fauna, disaster vulnerability, and others.

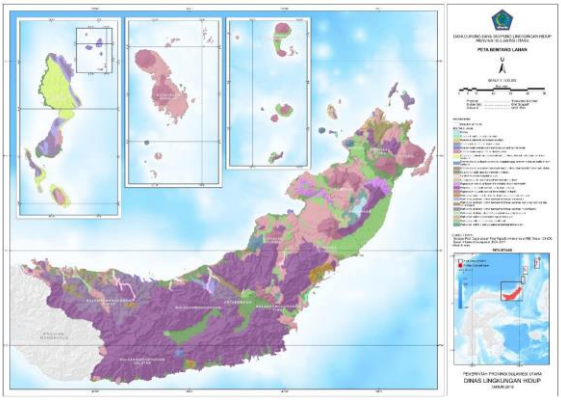

Figure 2: Ecoregion Map of North Sulawesi.
Source: Dinas Lingkungan Hidup Sulawesi Utara

As for the geothermal exploration area by PGE, the Lahendong Area in North Sulawesi is located in the Volcanic Complex Hills area of the Manado, with the following general characteristics:

Table 1: Description of the Ecoregion Map.
Source: Deputy for Environmental Management, 2013.

No.	Parameters	Description
1.	Location	Eastern areas in North Sulawesi
2.	Climatology	Wet tropical climate, average air temperature 14-18C°.annual rainfall 2,000-3,500 mm.
3.	Geology	Composed of outer igneous and pyroclastic rocks. Distributed in mountainous areas in the ring of fire tectonic zone.
4.	Geomorphology	Dominant elevation > 500 masl. Relief and slopes: mountainous, with relief amplitude >300m and slope >16%. Formed by volcanic processes, through volcanic eruptions that produce volcanic cones, lava and pyroclastics.
5.	Hydrology	Abundant water resources with the type of river with a centrifugal radial flow pattern, perennial, potential springs (spring belt), groundwater on the volcanic foot plains (potential)
6.	Soil and Land Use Formed	soil (latosol/alfisol, regosol), generally have moderate to high fertility with low land capability class due to slope resistance. Such characteristics cause this volcanic pefununagn to have various types of land cover/use, such as forests, shrubs, grasslands, fields, and a small number of settlements.
7.	Environmental Hazard	Volcanic eruptions, the dangers of hot cloud bursts, the dangers of toxic gases, the dangers of landslides, and the dangers of soil erosion.

Geological Analysis

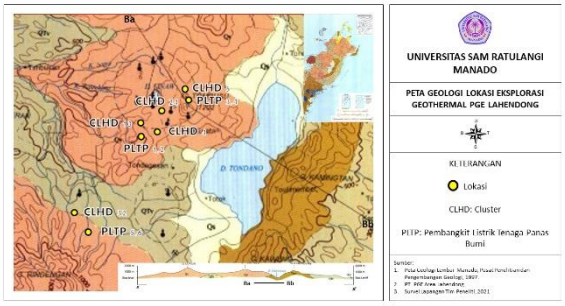

Figure 3: The Geological Map of PGE Area Lahendong.
Source: Geological Map of The Manado Sheet

Generally, the geothermal exploration location of PT Pertamina Geothermal Energy in the Lahendong area is divided into 2 different locations with a fairly close distance, one in the Tomohon area and the other in the Langowan area. Exploration locations in the Tompaso area have 2 lakes, namely Lake Tondano and Lake Linow. Lake Tondano is the largest lake in North Sulawesi Province and one of the lakes with the highest location in Indonesia. Lake Tondano is located in the caldera region of Mount Tondano. Mount Tondano is a mountain located in North Sulawesi, Indonesia, which has a crater with a width of 20 x 30 kilometers which was formed by a large eruption at the end of the Miocene or early Pliocene. Volcanic cones, obsidian flows, and geothermal areas are known to occur in the caldera. Lake Tondano is located on the eastern edge of the caldera. Mount Tondano there are several somma volcanoes that form along the edge of the caldera, namely Soputan, Lokon-Empung, Mahawu, and Sempu. In the Tondano caldera area, there is also the Pangolombian caldera with a size of 5 x 3.5 kilometers which was formed from the eruption of the Somma volcano. Linow Lake is located in Lahendong, Tomohon city. Lake Linow has a characteristic in the form of fairly hot water sourced from geothermal energy around the Tondano caldera. On Lake Linow there is also a fumarole area that is quite large and makes the lake area have a distinctive sulfur smell so that visitors who come are not allowed to bathe in the area. Lake Linow is also famous for its attractive tourism.

Those geothermal exploration areas are located in the Langowan area, Minahasa district. In the area there are many hot springs that are used by local residents both as bathing tourism areas and for other purposes. In Langowan there is also a unique lake called Lake Ranolewo which is known as a 3-color lake because this lake has 3 colors lined up in 3 areas, each side by side and only separated by a few inches of land as a way for visitors.

In terms of geology, the exploration area of the Tomohon area tends to be of the same type, which is located in the area of young volcanic rocks. Generally, young volcanic rocks are characterized by lava, bomb, lapilli, and ash which make up the young stratovolcano ie, Mt. Sopuan, Mt. Mahawu, Mt. Lokon, and Mt. Tangkoko are mainly andesitic composition such as obsidian flows at Taataran and Kiawa village were possibly derived from Mt. Tampusu and Mt. Lengkoan respectively. The areas that enter the area are

PROCEEDINGS
JOINT CONVENTION BANDUNG (JCB) 2021
November 23rd – 25th 2021

Cluster (CLHD) 4, Cluster 5, Cluster 13, Cluster 24, Scrubber, Powerplant unit 1-2, and Powerplant unit 3-4.

As for the exploration area, the Langowan area has different types, the Cluster 32 area is located in the young volcanic rocks area and the Powerplant unit 5-6 area is located in Tondano tuff. Generally, Tondano Tuff has coarse volcanic clastic mainly of andesite composition with angular to subangular components, characterized by abundant pumice fragment, tuff, lapilli tuff, breccia. Very dense ignimbrite with flow structure. This unit occurs around Lake Tondano and Lake Linow in the northern part of the Minahasa region, forming low undulating ridges. Lava flows of trachy-andesitic composition occur in the Mn. Tanuwantik.

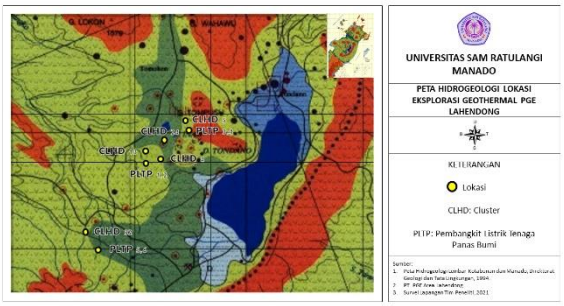

Figure 4: The Hydroeological Map of PGE Area Lahendong.
Source: Geological Map of The Manado Sheet

From a hydrogeological perspective, exploration areas in the Tomohon and Langowan areas tend to have the characteristics of locally productive aquifers and extensive (moderately) productive aquifers. For the locally productive aquifers, it has largely varying transmissivity, generally no exploitable groundwater due to great depth to the groundwater table. Locally, spring yield may reach 100 l/s. for the extensive productive aquifers, it has largely varying transmissivity, water table varies in depth, reaching more than 5 meters below the ground surface. Spring yield may reach more than 500 l/s.

In the area of locally productive aquifers, there are several points of geothermal exploration activities, namely at Cluster (CLHD) 4, Cluster 5, Cluster 13, Powerplant units 1-2, and Powerplant units 3-4. As for the extensive productive aquifers area, there are geothermal exploration activities at Cluster 24 points, Powerplant units 5-6. For cluster 32, it is between the two aquifer boundaries. The characteristics of the aquifer will determine the land's ability to withstand floods and prolonged heavy rains. The more effective the aquifer area, the less potential it is to be affected by flooding. Flood disasters may disrupt the geothermal exploration process, and can also damage or shorten the life of the materials used in exploration. In this geothermal exploration area, it tends to be less prone to flooding even though the land is dominated by rice fields in low-lying areas and is dominated by forests in hilly areas.

Geothermal Manifestations
North Sulawesi Known for their abundant geothermal manifestations, there are many scattered manifestation points. In the vicinity of the research location, there are several manifestation points that have been developed by the surrounding residents. The fumarole in the area around the geothermal development in Langowan is used by residents as a tourism location called Bukit Kasih. Several points in the Langowan area are widely used by residents as hot spring locations. The Tomohon area tends to be found around the Linow Lake area and has predominantly been developed as a tourism place. As for the potential manifestations that can be developed into geothermal areas, there is no such point.

Conclusions
The geothermal exploration area of PT Pertamina Geothermal Energy Area Lahendong is located in the Manado Complex Volcanic Hills ecoregion with geological characteristics located in the area of young volcanic rocks and Tondano Tuff, generally composed of outer igneous and pyroclastic rocks. Distributed in mountainous areas in the ring of fire tectonic zone. Geomorphologically it is formed by volcanic processes, through volcanic eruptions that produce volcanic cones, lava and pyroclastics. As for the landscape, the soil formed (latosol/alfisol, regosol), generally has moderate to high fertility with low land capability class due to slope resistance but has a fairly high productive aquifer capability. Based on geological analysis, it was found that potential disaster vulnerabilities include volcanic eruptions, dangers of hot cloud bursts, dangers of toxic gases, dangers of landslides, and dangers of soil erosion. As for geothermal manifestations around the research area, there is no potential location for the development of geothermal areas.

As a result, it Showed that the PGE area has Lahendong Generally stable soil conditions and is very feasible to continue the operations. Several cluster locations in fields are safe and need to be monitored for the safety of local residents' activities. Meanwhile, cluster locations in hilly areas are relatively safe and it is necessary to carry out routine control on hillsides which have erosion potentials.

Acknowlegments
Thank you to PT Pertamina Geothermal Energy Area Lahendong for permit us to collected the data in site area. the Geological Agency for providing mapping information for us to analyze geological characteristics.

References
Braat, L., de Groot, R., 2012. The ecosystem services agenda: bridging the worlds of natural science and economics, conservation and development, and public and private policy. Ecosystem Services. 1, 4-15.
Ministry of Energy and Mineral Resources, Geological Research and Development Centre. 1997. Geological Map of The Manado Sheet, North Sulawesi.
Ministry of Energy and Mineral Resources, Directorate of Environmental Geology. 1994. Hydrogeological Map of Indonesia in The Manado Sheet, North Sulawesi.
Ministry of Environment and Forestry, Center for Ecoregional Development Control for Sulawesi and Maluku. 2020. Environmental Carrying Capacity of Sulawesi and Maluku Ecoregions.
Ministry of Environment and Forestry, Deputy for Environmental Management. 2013. Description of the Island/Archipelagic Ecoregion Map.
Smithsonian Institution. Tondano: Global Volcanism Program.

PROCEEDINGS
JOINT CONVENTION BANDUNG (JCB) 2021
November 23rd – 25th 2021

Geological and Geochemical Characteristics of Rare Earth Elements Deposits in Ketapang Regency. West Borneo

Mochammad Kivlan Marcellyo Darma Putra[1], Dityas Fergiawan[1], Irsyad Auliya' Azhar Ramadhan[1], Shan Shan Mahendra Syuhada Al-Akbar[1]
[1]Geological Engineering Department of Institut Teknologi Bandung

Abstract
The Southeast Asian Granite Tin Belt is one of the main areas for Rare Earth Elements (REE) exploration in Indonesia extending from Riau islands to West Borneo. Besides containing large tin resources, it is also accompanied by REE-bearing minerals such as monazite, xenotime, zircon, apatite, etc. Many of these minerals are left behind and deposited in the waste material resulting from tin mining. The research area is located in a tin mining area in Tumbangtiti and Sungai Melayu Rayak District, Ketapang Regency, West Borneo. REE geochemical data were obtained from the Center for Mineral, Coal, and Geothermal Resources, Indonesia (PSDMBP). The data was then processed using statistical methods and spider diagrams to determine the correlation between REE concentrations. Based on the data, the largest REE concentration was in the tailing samples but there was no significant difference between the REE amounts in rocks, soils, and tailing samples. The statistical correlation of REE in the tailing samples dominantly showed a strong correlation but there was a weak correlation for Lu. The spider diagram shows an enrichment pattern in most REE concentrations, especially in Tb and Lu, but depleted in Y. In general, there is an enrichment in REE concentrations from rock and soil samples to tailing samples. This is due to the enrichment and resistance of zircon as REE-bearing minerals in tailing deposits. Based on statistical correlations in tailing deposits for Tb and Lu, it is suspected that they have a different mechanism of existence from other REEs, but they both are related.

Introduction
Rare Earth Elements (REE) is a group of elements consisting of the lanthanide group with the addition of Scandium (Sc) and Yttrium (Y) (PSDMBP, 2019). In general, REE can be enriched primarily through partial melting, fractionation, and crystallization of magma and secondarily through weathering and sedimentation processes. REE needs have increased in recent years in line with the rapid development of technology (PSDMBP, 2019). REE is widely used in technological products such as chemical catalysts, superconductors, magnets, and many more. China, as the world's largest REE producer, has reduced REE production (Mancheri, 2015). This has encouraged various countries in the world to explore REE resources, including Indonesia. REE exploration in Indonesia is focused on areas with granite lithology and its weathering results.

Geological Background
The study area is located in Ketapang Regency, West Kalimantan Province, and consisted of six lithological units, namely the Ketapang Complex (JKke), Belaban Granite (Jub), Kerabai Volcanic (Kuk), Sukadana Granite (Kus), Pinoh Metamorphic (PzRp), and Alluvium plus Swamp Sediments (Qa) according to Rustandi & Keyser (1993). The geological process in the study area started with the formation of the Pinoh Metamorphic unit from the Carbon-Triassic. After that, Ketapang Complex from the Middle Jurassic-Early Cretaceous was formed. At the same time in the Late Jurassic, there was an intrusion that formed the Belaban Granite rock unit. Then in the Late Cretaceous, units of Sukadana Granite and Kerabai Volcanic Rocks were formed. The sedimentation process stopped after the Late Cretaceous, resulting in erosion and weathering, until the Holocene Alluvium and Swamp Deposits were deposited unconformably. The research area has a relationship with the Southeast Asian tin belt with the presence of Belaban Granite and Sukadana Granite.

Several previous studies have discussed the potential of REE in granite and its secondary deposits (Murakami, 2008; Kisman, 2014; Hanini, 2017) however, very little research has been done on REE from tailings deposits. Therefore, this study focuses on the presence of REE in tailings deposits in ex-tin mining areas. The presence of REE-bearing minerals such as zircon, which is resistant to erosion and leaching processes, are usually found and deposited in the waste material or tailings from tin mining. From the geochemical studies and correlation analysis conducted, this study is expected to provide a better understanding of REE exploration in the Ketapang Regency. This study can improve the understanding of the geological processes in REE enrichment and strengthen the potencies for exploration of REE in tailings deposits in the future.

Data and Method
This study was conducted using REE geochemical data and mineral grain analysis from Muliyana (2018) in Tumbang Titi and Sungai Melayu District, Ketapang Regency. There are six granite samples. three soil samples, and nine tailing samples but only eight tailing samples that were used in this study. One tailing sample (KTG18M16P) was not used in this study because the data was identified as outlier. The analysis was carried out using a chondrite-normalized spider diagram, mineral grain analysis, and Pearson correlation to determine the pattern of REE enrichment, identified REE-bearing minerals in samples, and the relationship between each REE. The results of the analysis are then used to identify the potential for REE enrichment in the study area.

PROCEEDINGS
JOINT CONVENTION BANDUNG (JCB) 2021
November 23rd – 25th 2021

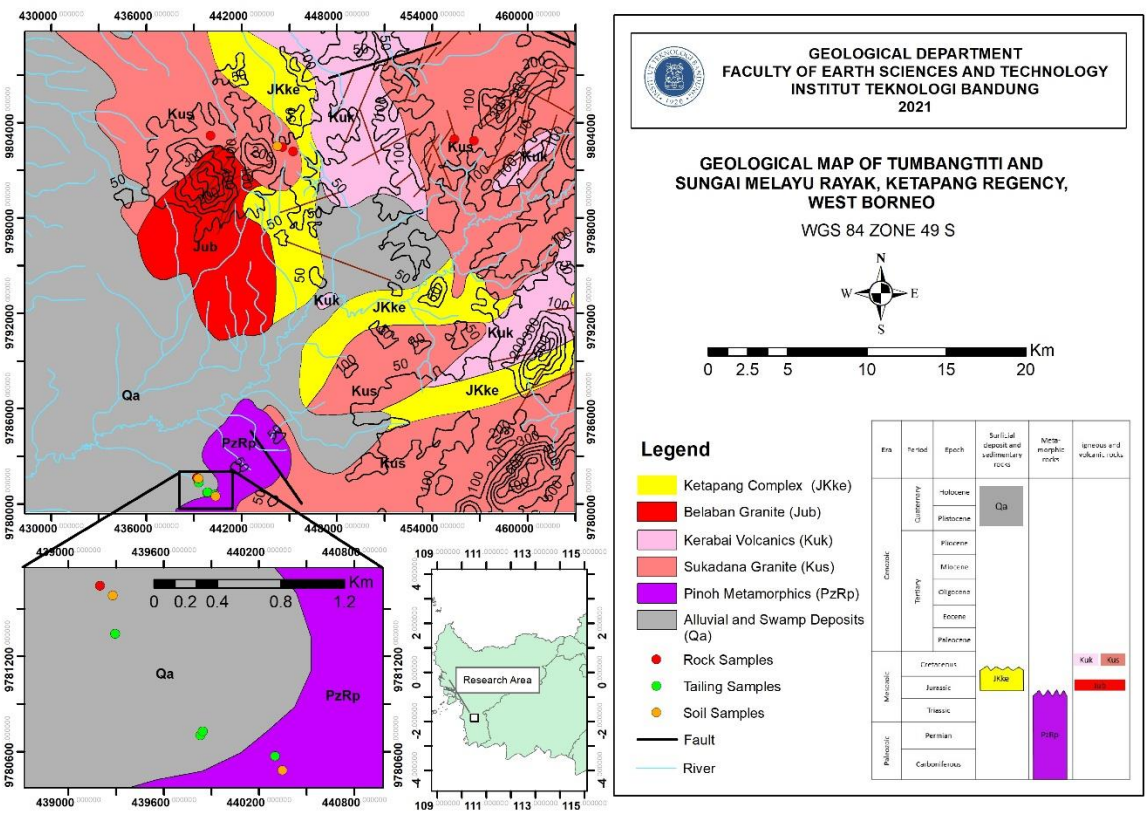

Figure 1. Geological map of the study area (modified from Rustandi & Keyser, 1993)

Tabel 1. Mineral grain analysis from tailing samples (Muliyana, 2018)

No.	Mineral (%)	KTG018M01P	KTG18M02P	KTG18M03P	KTG18M05P	KTG18M06P	KTG18M07P	KTG18M09P	KTG18M11P	KTG18M16P
1	Quartz	56.77	75.71	42.67	71.37	62.94	74.5	56.19	48.8	98.23
2	Cassiterite	1.74	3.19	6.32	2.6	4.87	3.14	6.42	0.27	Trace
3	Zircon	Trace	0.8	5.63	1.23	2.09	0.78	1.93	Trace	Trace
4	Monazite	-	-	-	-	-	-	-	-	0.04
5	Ilmenite	41.46	19.9	45.36	21.56	27.37	20.93	34.75	50.76	1.72
6	Rutile	-	-	Trace	-	-	-	-	-	-
7	Leucoxene	Trace	Trace	Trace	Trace	Trace	Trace	Trace	Trace	Trace
8	Magnetite	0.03	-	-	-	-	-	-	0.17	-
9	Pyroxene	Trace	0.41		3.25	2.74	0.43	0.72	Trace	0.02
10	Pyrite	Trace	-	Trace	-	-	-	-	-	-
11	Iron oxide	Trace	Trace	Trace	Trace	Trace	0.22	Trace	Trace	-
12	Clay	Trace	Trace	-	-	-	-	-	-	-
13	Mica	Trace	-	-	-	-	-	-	-	-
14	Corundum	-	-	Trace	Trace	-	-	-	-	-

Tabel 2. REE data in rock, soil, and tailing samples (Muliyana, 2018)

	La (ppm)	Ce (ppm)	Pr (ppm)	Nd (ppm)	Sm (ppm)	Eu (ppm)	Gd (ppm)	Tb (ppm)	Dy (ppm)	Y (ppm)	Ho (ppm)	Tm (ppm)	Yb (ppm)	Lu (ppm)
KTG18M01R	7.7	14.2	10.9	8.4	3.3	2	11.3	6.5	4.6	5.2	4.9	3.1	4	1.5
KTG18M10R	38.2	71.1	12.9	39.3	9.7	5	11.8	7.4	9.8	30.5	5.3	3	5.6	4.7
KTG18M12R	30.3	57.2	11.6	27.6	5.9	3.1	7.5	5.7	7.6	18.3	5.6	3.4	5	3.9
KTG18M13R	43.6	70.6	14.5	41.1	10.6	2.9	12.4	6.2	11.1	43.1	5.9	3.9	6.5	4.7
KTG18M15R	32.7	64	13.3	34.2	8.6	3	11	6.2	11.3	44.3	5.6	3.6	7.6	5
KTG18M16R	31	58.8	10.4	24.4	6	2.5	7	5.8	7.1	18.8	5.4	3.4	4.8	6.4
KTG18M04S	17	29.8	9.1	12.4	3.3	2.1	6.9	7.4	4.5	6.8	5.3	3.2	3.9	8.4
KTG18M08S	13.3	29.7	13	10.9	3.1	2.4	14.1	8.1	4.8	6.2	5.3	3.1	4.8	4.5
KTG18M14S	11.7	29.5	8.4	12.2	2.5	2.1	5.7	5.8	5.2	6.9	5.6	3	3.7	5.6
KTG18M01P	7	24	0	7.1	0	0	9.7	26.5	0	0.8	0	0	0	53
KTG18M02P	15.3	38.8	0	10.4	0	0	7.4	13.4	0	1.3	0	0	0	29.7
KTG18M03P	26	64	4.2	21.4	0	0	15.3	28.8	0	2.5	0	0	0	59.2
KTG18M05P	44.6	91.5	18.7	40.6	12.4	6.4	16.1	29.4	9.8	15.3	4.4	5.4	8.3	42.9
KTG18M06P	37.1	78.2	16.4	36.5	8.7	3.3	17.4	28.3	6.8	12.8	5.4	3.9	5.8	45.6
KTG18M07P	26.9	55	12.8	28.1	6.6	3.3	12.6	22.8	6.1	9.5	4.3	3.5	5.3	36
KTG18M09P	46.6	98.4	16.8	43.9	9.2	2.8	15.9	29.8	7.4	12.2	4.5	4	5.1	48.9
KTG18M11P	78.5	160.3	23.9	63.7	13.6	3.5	21	30	9.1	18.9	4.2	3.4	6	44.7
KTG18M16P	1015.7	1927	173.5	636.4	128.1	3.4	77.1	15.6	43.5	181.4	8.9	5.5	25.4	8.1

Red = rock samples; brown = soil samples; grey = tailing samples; orange = LREE; green = HREE

PROCEEDINGS
JOINT CONVENTION BANDUNG (JCB) 2021
November 23rd – 25th 2021

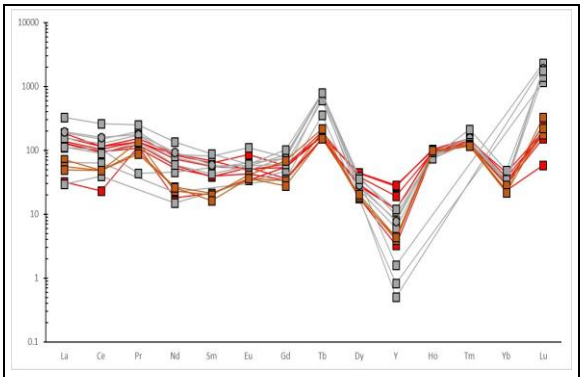

Figure 2. Chondrite-normalized spider diagram for rock, soil, and tailing samples in Ketapang Regency (red = rock samples; brown = soil samples; grey = tailing samples)

Result and Discussion

Mineral Grain Analysis

Mineral grain analysis was carried out on the tailing samples and presented in Table 1. Quartz and ilmenite were the dominant minerals with cassiterite, zircon, magnetite, and pyroxene in small percentages. Rutile, leucoxene, pyrite, iron oxide, clay, mica, and corundum were also found in some samples but mostly as trace minerals. Zircon are REE-bearing minerals and can be found in granitic rocks as accessary minerals (Li, 2017). Zircon has a high degree of resistance to weathering (Ollier, 1984). The presence of iron oxide indicates the weathering product from biotite in granitic rocks.

Distribution and Enrichment Trend of REE

Chondrite-normalized spider diagram are presented in Figure 2. It can be seen that there is an enrichment trend from rock and soil to tailing samples. This occurs as an impact from tin mining activities resulting in the accumulation of zircon as REE-bearing minerals. There is an HREE-enrichment trend due to the presence of zircon.

Rock samples have LREE concentration range from 44.5 to 171.2 ppm and HREE concentration range from 43.1 to 97.6 ppm. Soil samples have LREE concentration range from 64.3 to 71.6 ppm and HREE concentration range from 43.6 to 53.5 ppm. Tailing samples have LREE concentration range from 38.1 to 340 ppm and HREE concentration range from 51.8 to 140.8 ppm. LREE/HREE comparison is used to know the trend of REE enrichment based on chemical properties. If LREE/HREE is below 1 then there is a trend of HREE. If LREE/HREE is more than 1 then there is a trend of LREE. Based on the data, the average of LREE/HREE in rock, soil, and tailing samples is 1.81, 1.42, and 1.37. It shows that there is decreasing LREE/HREE from rock to tailing samples. This is interpreted as enrichment of zircon in soil and tailing deposits that containing HREE.

Statistical Correlation of REE

Pearson correlations are presented in Table 3 and 4. Pearson correlation was used to determine each REE correlation in rock and tailing samples. Soil sample data are not used in this study due to an insufficient amount of data. Pearson correlation coefficient values range from -1 as a negative correlation to 1 as a positive correlation. A positive correlation means that the REE will occur together meanwhile negative correlation means that the REE are opposite each other and will not occur together. A positive correlation can be stronger if the coefficient value is closer to 1. A negative correlation can be stronger if the coefficient value is closer to -1. According to Sidibe et al., (2019), coefficient value $r > 0.6$ or $r < -0.6$ is considered as strong correlation, whereas $0.4<r<0.6$ or $-0.6<r<-0.4$ is considered as moderate correlation, and $r<0.4$ or $r>-0.4$ is considered as weak correlation

In rock samples, all LREE have a strong positive correlation with all the REE except Tb. Gd only shows a strong positive correlation with Pr while against other LREE shows a weak dominant positive correlation. Tm shows moderate correlation to all LREE and varies from strong positive to strong negative correlation in HREE. Tb shows the dominance of weak positive correlation except for Eu and Gd (strongly positive), Tm (moderately positive), and Ho and Lu (weak negative). Eu shows correlation range from strong to moderate positive correlation except for Sm (weak positive). Lu shows the dominance of strong positive correlation in LREE except in Pr (weak positive) and Sm (moderately positive). But Lu shows the concentration range from moderately positive to weak negative correlation in HREE.

In tailing samples, all REE except Lu, Eu, and Tb shows the dominance of a strong positive correlation. Eu shows a moderate positive correlation with Ce and Tb. Tb shows a moderate positive correlation with La, Ce, Sm, and all HREE except Gd and Lu. Lu shows a weak positive to weak negative correlation to all REE except Tb that has a strong positive correlation. It is happening because of the leaching and weathering processes in tailing that makes much REE ions got leached and washed away by rivers or groundwater. For Lu, it is indicated that most of the Lu concentrations are present and concentrated in zircon as zircon are associated with HREE-enriched REE patterns and can be enriched in the granitoid weathered crust (Murakami, 2008). Lu also has relatively more compatible properties than other REEs so when magma fractionation and crystallization it tends to combine to form REE-bearing minerals Due to zircon resistance, Lu doesn't get leached and washed away along with other REE.

PROCEEDINGS
JOINT CONVENTION BANDUNG (JCB) 2021
November 23rd – 25th 2021

Tabel 3. Pearson correlation for REE concentration in rock samples

	La	Ce	Pr	Nd	Sm	Eu	Gd	Tb	Dy	Y	Ho	Tm	Yb	Lu
La														
Ce	0.978													
Pr	0.694	0.610												
Nd	0.967	0.952	0.812											
Sm	0.917	0.876	0.884	0.973										
Eu	0.582	0.637	0.409	0.682	0.636									
Gd	0.118	0.018	0.719	0.309	0.492	0.273								
Tb	0.060	0.059	0.298	0.233	0.340	0.702	0.691							
Dy	0.862	0.855	0.882	0.934	0.943	0.509	0.419	0.168						
Y	0.813	0.795	0.886	0.882	0.914	0.388	0.452	0.116	0.988					
Ho	0.842	0.791	0.682	0.784	0.722	0.141	0.005	-0.385	0.783	0.781				
Tm	0.532	0.441	0.575	0.462	0.475	-0.327	0.076	-0.566	0.584	0.657	0.861			
Yb	0.659	0.676	0.806	0.754	0.777	0.281	0.401	0.038	0.936	0.960	0.700	0.626		
Lu	0.749	0.810	0.161	0.624	0.545	0.293	-0.353	-0.209	0.557	0.538	0.581	0.382	0.457	

Blue = strong correlation; yellow = moderate correlation; white = weak correlation; orange = LREE; green = HREE

Tabel 4. Pearson correlation for REE concentration in tailing samples

	La	Ce	Pr	Nd	Sm	Eu	Gd	Tb	Dy	Y	Ho	Tm	Yb	Lu
La														
Ce	0.997													
Pr	0.911	0.882												
Nd	0.984	0.973	0.965											
Sm	0.877	0.843	0.982	0.928										
Eu	0.627	0.578	0.849	0.710	0.903									
Gd	0.892	0.895	0.875	0.913	0.798	0.600								
Tb	0.558	0.570	0.611	0.613	0.554	0.455	0.805							
Dy	0.809	0.768	0.968	0.883	0.988	0.940	0.747	0.532						
Y	0.910	0.880	0.994	0.956	0.993	0.867	0.848	0.568	0.973					
Ho	0.669	0.620	0.905	0.781	0.894	0.853	0.684	0.472	0.933	0.893				
Tm	0.654	0.604	0.895	0.759	0.923	0.961	0.640	0.492	0.968	0.895	0.950			
Yb	0.705	0.656	0.922	0.795	0.951	0.978	0.680	0.490	0.983	0.929	0.939	0.989		
Lu	0.025	0.074	-0.045	0.031	-0.132	-0.212	0.356	0.744	-0.165	-0.103	-0.183	-0.184	-0.203	

Blue = strong correlation; yellow = moderate correlation; white = weak correlation; orange = LREE; green = HREE

Conclusions

From analysis and data processing, it can be concluded that the REE in the study area is accommodated in zircon according to mineral grain analysis and spider diagram that shows there are HREE-enrichment patterns. The presence of iron oxide indicates the weathering product from biotite in granitic rocks. This is reinforced by evidence of decreasing LREE/HREE from rock to tailing samples and dominance of strong positive correlation in tailing samples. Our study shows that tailing samples has a potential concentration of REE as tin mining by-product in Ketapang Regency, West Borneo, and need more study and exploration activities to know the economic level of REE deposits in tailing.

Acknowledgements

The authors want to acknowledge Pusat Sumber Daya Mineral Batubara dan Panas Bumi for allowing and providing the REE geochemical data in Ketapang Regency, West Borneo.

References

Hanini, F. I. 2017. Tugas Akhir Institut Teknologi Bandung.
Kisman, Widi, B. N. Pusat Sumber Daya Mineral Batubara dan Panas Bumi, Bandung.
Li, Y. H. M., Zhao, W. W., Zhou, M. 2017. Journal of Asian Earth Sciences, 148, 65-95.
Mancheri, N. A., 2015. Resource Policy, 46, 262-271.
Muliyana, T., 2018, Pusat Sumber Daya Mineral Batubara dan Panas Bumi, Bandung.
Murakami, H., and Ishihara, S., 2008, Resource Geology, 58(4), 373-401.
Ollier, C. 1984. Longman Group
PSDMBP. 2019, Pusat Sumber Daya Mineral Batubara dan Panas Bumi, Bandung.
Rustandi, E., and F. De Keyser., 1993, Peta geologi lembar Ketapang, Kalimantan, Scale 1:250,000. Pusat Penelitian dan Pengembangan Geologi, Bandung.
Sidibe, M., and Yalcin, M. G., 2019, Journal of African Earth Sciences, 149, 348-366.

PROCEEDINGS
JOINT CONVENTION BANDUNG (JCB) 2021
November 23rd – 25th 2021

Control of Protolith Geochemistry on Critical Elements Enrichment in Ni-Laterite Deposits: A Novel Approach for Critical Elements Exploration in Indonesia

Rahmat Agung Purnama[1], Ifan Dandi Nurshafara[1], Irsyad Auliya' Azhar Ramadhan[1], Barry Majeed Hartono[1], Devito Pradipta[1]

[1]Geological Engineering, Faculty of Earth Sciences and Technology, Institut Teknologi Bandung

Abstract

Critical elements are a group of elements that have a strategic role in the economic development of a country. Nickel (Ni) and scandium (Sc) are the elements that are considered as critical elements that are usually found in Ni-laterite deposits and become the main focus of exploration in Indonesia. The enrichment of critical elements in Ni-laterite is controlled by several factors, and one of the factors is protolith geochemistry. Therefore, this study compiles and analyze geochemical data from the protoliths, specifically ultramafic rocks, from several publications in Indonesia to observed the genesis of ultramafic rocks (e.g. magma source, affinities, and differentiation) and its relation with the presence of critical element-bearing mineral in the protolith that will undergo laterization. Normative minerals are also calculated from geochemical data. This study shows that several trace elements, the pattern of light rare earth elements (LREE) on spider diagrams, and correlations between elements (e.g. negative correlations of Sc and Ni) could be indicators to ultramafic protoliths that tend to be enriched in critical elements in Ni-laterite. Further detailed petrographic analysis, isotope geochemistry, and even laterite geochemistry study are needed to validate the proposed method. Despite the limited data and analysis, this study improved the understanding of the geochemistry and genesis of protoliths and their relations with critical elements enrichment, so these approaches are applicable in the early stages of critical element exploration in Ni-laterite deposits.

Keywords: critical elements, geochemistry, nickel laterite, protolith, trace elements and rare earth elements, ultramafic rocks

Introduction

Critical elements are commodities that have strategic roles in economic development in a country. Nickel (Ni) and scandium (Sc) are some commodities that are classified as critical elements in Indonesia (Ditjen Minerba, 2021, https://youtu.be/uAKur08M6P8). These commodities commercially occurred in two types of deposits, primary deposits in the form of sulfide deposits and secondary deposits in the form of Ni-laterite deposits (Subagja et al., 2016). In Indonesia, Ni- and Sc-enrichment occurs mainly in form of laterite deposits which are the product of lateritization of ultramafic rocks. Many factors affect the enrichment of these elements in laterite deposits, such as climate, geological structure, and groundwater level (Robb, 2005; Golightly, 2010). However, other factors such as initial concentrations of Ni and Sc in ultramafic rock protoliths are rarely studied. Such study is important since the initial concentration of these elements in protolith possibly controls the enrichment of these elements in laterite deposits (Ahmad, 2006), while the initial concentration of Ni and Sc are possibly controlled by the petrogenesis of ultramafic rocks. Therefore, in this study, the geochemical characteristics and petrogenesis of ultramafic rocks in Indonesia (occurred as ophiolite and melange) are studied and compared to relate the enrichment of Ni and Sc in the laterite with its protolith geochemistry. With a comprehensive petrogenesis study and geochemical characterization, this study seek several new elements as indicators of ultramafic rocks that will become host rocks for Ni and Sc enriched laterite deposit.

Geological Background

Ni-enrichment in laterite deposits is controlled by its protolith which is the ultramafic rock. However, these rocks need to cropped out so that the host rocks undergo lateritization (Robb, 2005; Golightly, 2010). The tectonic events in the area play an important role in the uplifting of the ultramafic rocks so the tectonic events of each study area are considered (Figure 1).

Sulawesi Island is a tectonically active island due to its position at the conjunctions of three tectonic plates, namely the Eurasian Plate, the Indo-Australian Plate, and the Pacific Plate. Ultramafic rocks are distributed in the eastern part of the Sulawesi mandala as part of the ophiolite complex which was exposed due to the thrust belt displacement as formed by the collision of the Banggai-Sula Microcontinent in the Late Miocene (Hamilton, 1979; Kadarusman et al., 2004). The Cyclops Mountains are ophiolitic mountains in the north coast of the mainland Papua. The subduction in

Eocene resulted in the spreading of the fore-arc and back-arc basins of the Cyclops Mountains and formed ultramafic and basaltic rocks from the Oligocene to the Miocene. The compression phase with a north-south direction continues until obduction occurs which makes the ultramafic rock uplifted. Then in the Pliocene, back thrusting occurred which caused the uplift of basaltic rock in the back-arc basin. This ultramafic rock was then exposed to form the Cyclops Mountains and undergoes laterization later (Monnier et al., 1999). Timor Island is a non-volcanic area of the outermost Banda Arc series which is part of the Indo-Australian Plate. The island is formed by the subduction of the Late Miocene by the Indo-Australian Plate to the north beneath the Eurasian Plate in the Banda Arc and formed ultramafic rocks in the "supra-subduction" zone (Falloon et al., 2006). The collision during the Pliocene formed a melange complex that is distributed in the northern part of Timor (Falloon et al., 2006; Audley-Charles, 2011).

Data and Method

This study compiles geochemical data that encompass major elements, trace elements, and rare earth elements (REE) from several previous publications in South Sulawesi (Maulana et al., 2015), Southeast Sulawesi (Irzon and Baharudin, 2016), Timor (Falloon et al., 2006), and Irian Jaya (Monnier et al., 1999). Then, data are corrected by its LOI (lost of ignition) values to remove weathering effect (Wilson, 1989). In this study, the research area which is called "productive" is defined to have economical Ni-laterite deposits with relatively high Ni content (Ni content > 1.3%; based on Berger et. al., 2011) and also shown by mining activities (e.g. Sulawesi). The geochemical characteristics of ultramafic rocks, in the areas referred as "productive" and "non-productive", are compared to determine the factors controlling the genesis of the protolith. Petrogenesis study that includes magma affinity, magma conditions, and tectonic setting, were carried out using bivariate geochemical plots and spider diagrams (chondrite normalization numbers by Sun and McDonough, 1989). Normative mineral analysis was also carried out as part of the petrogenesis study with formula from Hollocher (2004). With a strong understanding of the geochemical character and petrogenesis, several new elements to distinguish ultramafic rocks that are associated with critical element enrichment in Ni-laterite deposits are proposed with a relatively high confidence level.

Results and Discussion

Magma Affinity

Based on the plot of SiO_2 vs total alkali (Figure 2a), all ultramafic rocks have a subalkali affinity. Specifically, harzburgite and dunite from the Cyclops Mountains and lherzolite from Southeast Sulawesi were classified as picrobasalt. In South Sulawesi, dunite and harzburgite are classified as basalt. The harzburgite and lherzolite in Timor are classified as picrobasalt and basalt (Figure 2a). Further determination of magma affinity was carried out by cross-plot of SiO_2 and K_2O (Figure 2b). This plot shows that all rock samples, whether in "productive" areas or not, have no differences in terms of magma affinity because all samples have tholeiitic affinity. Thus, magma affinity does not affect the enrichment of Ni and Sc elements in Ni-laterite deposits.

Magma Condition

Other factor, such as the redox condition is considered by using spider diagrams (Figure 3a-d). Negative Eu anomalies are absent in all ultramafic samples from the Cyclops Mountains, Timor, and South Sulawesi with only one lherzolite sample from Southeast Sulawesi exhibit the negative anomaly (Figure 3b). The absence of negative Eu anomaly in most samples indicates that the ultramafic rocks may have originated from oxidative magma (under reductive condition, Eu present in the form of Eu^{2+} resulting on negative anomaly; Henderson, 1984; Gill, 2010), indirectly related with high content of H_2O. The presence of H_2O affects magma fractionation by suppressing crystallization in orthopyroxene and made Sc concentrated in clinopyroxene. The presence of H_2O in magma contributes to both Ni- and Sc-enrichment as it forms Ni-substitution minerals such as olivine, serpentine, and clinopyroxene in which Sc is mostly concentrated (Ahmad, 2008; Wang et al., 2021). This is because the H_2O is closely related to Mg presence contained in the mineral which will increase the substitution of Ni for Mg through the supergene enrichment process when exposed to the surface (Robb, 2005; Golightly, 2010).

In addition, magma fractionation process should also be considered that is represented by the ratio of LREE (light REE), which is represented by La, to HREE (heavy REE), which is represented by Lu in this study. Magma fractionation tends to enrich LREE relative to the HREE (Wilson, 1989; Gill, 2010). Based on the ratio value of La/Lu < 1 (Figure 3), harzburgites from the Cyclops Mountains, South Sulawesi, and Timor indicate relatively less intesive magma fractionation. Magma that crystallized into dunite in Cyclops Mountains relatively more fractionated compared to the South Sulawesi reflected by the high La/Lu ratio. The La/Lu ratio in the lherzolite from Southeast Sulawesi are higher than in Timor, indicating more intensive fractionation of lherzolite magma in Southeast Sulawesi. Different magma fractionation between regions possibly affects the enrichment of Ni and Sc in ultramafic protoliths. Thus, the LREE/HREE ratio could be an early indicator in

determining the enrichment of Ni and Sc elements in laterite deposits from specific protolith.

Tectonic Settings

Regional petrogenesis aspects such as the tectonic setting of each magmatic ultramafic rock are also considered. The magma affinities of all ultramafic rocks are tholeiitic magmas that are possibly related with mantle origin (Wilson, 1989; Gill, 2010). Cross plot of Nb/Y vs Zr/Y (Figure 4) is used to interpret the tectonic setting, especially magma sources (Condie, 2005). The ultramafic rocks from Southeast Sulawesi and South Sulawesi have plume origin, while those from Cyclops Mountains and Timor falls on the transition zone between plume and non-plume. The transition character is possibly influenced by another petrogenesis aspects that enriched high field strength elements (HFSE), especially Zr and Nb (Wilson, 1989). According to Monnier et al., (1999), High Zr could be the result of addition of H_2O from dissolved amphibole which then moves into the magma.

Proposed Elements: Rare Earth Element

In the previous discussion, all samples shares relatively similar petrogenetic aspects. However, differences on magma fractionation are observed between the "productive' and "non-productive" protolith. Such fractionation are reflected by the character of ratio LREE/HREE. In the REE, plots of La/Lu against La/Gd in harzburgite and lherzolite displays different trends for each region (Figure 5). The harzburgite and lherzolite retrieved from Sulawesi, assummed to be enriched in Ni shown by active mining (Kementerian ESDM, 2020), display identical trends to that of Timor (Figure 5a & 5b). This could be indicator that could prove the productivity of the Sulawesi and Timor, observed from its protolith.

Proposed Elements: Transitional Group

Separationsare observed in the cross plot of the transition element group, Ni/V vs Cr/V (Figure 6). Samples from Timor display similarities to Sulawesi with a relatively high V composition in the harzburgite and lherzolite (Figure 6a-b). Prominent amount of V in both areas suggest that the area are potentially more enriched with critical elements than those from Cyclops Mountains. Dunite also displays similar phenomenon, with samples from Sulawesi are high on V compared to Cyclops Mountains (more adequate data are needed). Vanadium itself is a compatible element that is usually associated with ilmenite (Wilson, 1989; Gill, 2010) that tends to form under conditions of oxidative magma (Rene, 2008), in which high oxygen content in magma is related with H_2O. The high H_2O content catalyzed the formation of H_2O-rich minerals during fractionation so that the rock will be more susceptible to weathering and serpentinization. With the increasing potential for weathering and serpentinization in ultramafic rocks, the potential for Ni-enrichment in the laterite will also be higher. The oxidative condition is also supported by the absence of negative Eu anomalies in most ultramafic rocks (Figure 3). Thus, the relatively high V content indicator, Sulawesi and Timor samples could be more economical by its potential of Ni-enrichment than the Cyclops Mountains.

Mineralogical Control on Ni- and Sc-Enrichment in Ultramafic Rocks

The cross-plot of normative minerals with critical elements Ni and Sc (Figure 7) suggest that olivine is negatively correlated to Sc (Figure 7a) and positively correlated to Ni (Figure 7b). The relatively higher ratio of La/Lu does not affect the amount of olivine in the ultramafic rock though the higher La/Lu ratio indicates the more intensive magma fractionation (Figure 7c). In addition, ultrmafic rocks with high diopside tend to be enriched with Sc (Figure 7d). This critical elements enrichment relationship can be correlated with the normative mineral properties that carry the element. For example, olivine that is typically high in Mg have higher potential to be substituted by Ni, while diopside provides accommodation for Sc to be enriched in a rock (Robb, 2005; Sanematsu et al., 2014). Particular fractionation processes will result in higher H_2O content as it suppresses the formation of orthopyroxene and plagioclase, but becomes a supporting factor for the formation of clinopyroxene (e.g. diopside). Therefore, it can be indirectly said that the relatively high H_2O conditions will affect the Sc-enrichment in ultramafic rocks as reflected by the presence of diopside.

Relation between Ni and Sc in Ultramafic Rocks

Ni-enrichment is one consequence of magma originating from peridotite mantle sources as the Mg content in olivine will be subtituted by Ni (Wilson, 1989). For the Sc composition, high Sc is generally found in rocks that have abundant clinopyroxene minerals because Sc can replace Fe in pyroxene (Sanematsu et al., 2014). The relationship between Ni and Sc in each ultramafic rock are observed (Figure 8a-b). In this study, Sc and Ni has shown negative correlation in harzburgite and lherzolite that was interpreted as the control of mineralogy. Although the amount of clinopyroxene affects the higher value of Sc, however, this mineral has less degree of substitution than olivine as it will be substituted by Ni for lesser amount.(Ahmad, 2008). The plot of Fe_2O_3 against Sc in harzburgite rocks (Figure 8c) shows various trend for each area. This trend is probably due to the Fe content in ultramafic rocks not only associated with clinopyroxene, but also with other Fe-

bearing minerals unrelated to Sc such as olivine, ilmenite, and magnetite.

Conclusions

Our study shows that the ultramafic rocks that tend to be associated with critical enrichment in the laterite could be distinguished from the "nonproductive" one by the proposed elements. It is clearly shown by the separation of ultramafic rock samples from Southeast Sulawesi, South Sulawesi, and Timor from the Cyclops Mountains based on two element groups, which are REE group (La, Lu, and Gd) and the transition element group (Ni, Cr, and V). Such approaches are valid since the comparisons made on ultramafic rock samples are based on the similarity of petrogenic aspects.

These separations are possibly related to the different petrogenic processes in each rock. The "productive" areas (Sulawesi and Timor) tend to have the same petrogenesis process so that the protolith will rich be in H_2O that promotes higher Mg content to be substituted by Ni. Protolites that are already rich in Ni will potentially produce higher Ni in laterite. While the "non-productive" group (Cyclops Mountains) tends to have relatively low H_2O inhibiting the Ni substitution. The negative correlation between Ni and Sc is also observed as the consequence of different mineralogical compositions. The mineralogy becomes an important control in the search for productivity of Ni and Sc content in Ni-laterite deposits in an area.

This research is a part of preliminary study phase in the regional exploration for Ni-laterite based on protolith geochemistry. Laterite geochemical data, as well as more detailed analyzes such as petrographic and isotopic analysis of ultramafic rocks need to be carried out to support the indicators this proposed to distinguish between "productive" and "non-productive" groups. In addition, the proposed geochemical indicators could be new reference in the initial study of Ni and Sc regional exploration in Indonesia as an effort to fullfil the demands of critical elements for economical development.

References

Ahmad, W., 2008, Nickel laterites: Fundamental of chemistry, mineralogy, weathering processes, formation, and exploration, Vale Inco – VITSL.

Ahmad, W., 2008, Fundamentals of chemistry, mineralogy, weathering processes and laterite formation, Vale Inco.

Audley-Charles, M. G., 2011, Geological Society of London, Special Publications, **355**, 241-266.

Berger, V. I., D. A. Singer, J. D. Bliss, and B. C. Moring, 2011, Ni-Co laterite deposits of the world-database and grade and tonnage models, US Geological Survey.

Condie, K. C., 2005, Earth as an evolving planetary system, Elsevier.

Ditjen Minerba, 2021, Webinar: peluang mineral kritis Indonesia, 25th January 2021, https://youtu.be/uAKur08M6P8.

Falloon, T. J., R. F. Berry, and P. Robinson, 2006, Australian Journal of Earth Sciences, **53**(4), 637-649.

Gill, R., 2010, Igneous rocks and processes: A practical guide, Wiley-Blackwell.

Golightly, J. P., 2010, Society of Economic Geologists Special Publications, **15**, 451-485.

Hamilton, W. B., 1979, Tectonics of the Indonesian Region, US Geological Survey Professional Paper 1078.

Henderson, P., 1984, Rare earth element geochemistry (developments in geochemistry), Elsevier.

Hollocher, K., 2004, CIPW Norm Calculation Program, Geology Department, Union College.

Irzon, R. and Baharuddin, 2016, Jurnal Eksplorium, **37**(2), 101-114.

Kadarusman, A., S. Miyashita, S. Maruyama, C. D. Parkinson, and A. Ishikawa, 2004, Tectonophysics, **392**, 55-83.

Kementerian Pekerjaan Umum, 2010, Peta hazard gempa Indonesia 2010 sebagai acuan dasar perencanaan dan perancangan infrastruktur tahan gempa, Kementerian Pekerjaan Umum.

Kementerian Energi dan Sumber Daya Mineral Republik Indonesia, 2020, Peluang investasi nikel Indonesia.

Le Bas, M. J., R. W. Le Maitre, A. Streickeisen,, and B. Zanettin, 1986, Journal of Petrology, **27**(8), 745-750.

Maulana, A., A. G. Christy, and D. J. Ellis, 2015, Journal Chemie der Erde Geochemistry, **75**(1), 73-87.

Monnier, C., J. Girardeau, M. Pubellier, M. Polve, H. Permana, and H. Bellon, 1999, Journal Mineralogy and Petrography, **65**(1), 1-28.

Peccerillo, A. and S. R. Taylor, 1976, Contribution to. Mineralogy and Petrology, **58**, 63-81.

Rene, M., 2008, Acta Geodynamica et Geomaterialia, **5**(3), 239-247.

Robb, L., 2005. Introduction to ore-forming processes, Blackwell Publishing.

Sanematsu, K., C. Arcilla, A. Maulana, and K. Zhaw, 2014, Abstract of Asian Oceania Geology Symposium.

Sun, S. S. and W. F. McDonough, 1989, Geological Society, London, Special Publications, **42**(1), 313-345.

Subagja, R., A. B. Prasetyo, and W. M. Sari, 2016, Metalurgi, **2**, 103-115.

Wang, Z., M. Y. Li, Z. Liu, and M. Zhou, 2021, Ore Geology Reviews, **128**, 1-16.

Wilson, M., 1989, Igneous petrogenesis, Springer.

PROCEEDINGS
JOINT CONVENTION BANDUNG (JCB) 2021
November 23rd – 25th 2021

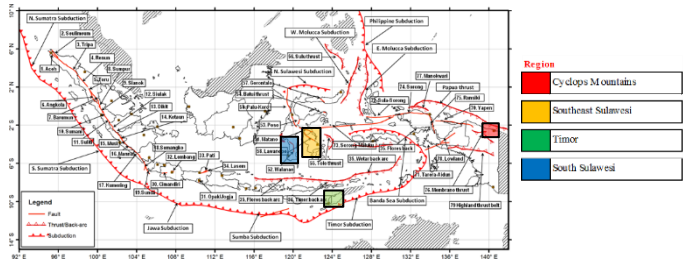

Figure 1: Map shows research areas and its tectonic settings in Indonesia (Kementerian Pekerjaan Umum, 2010).

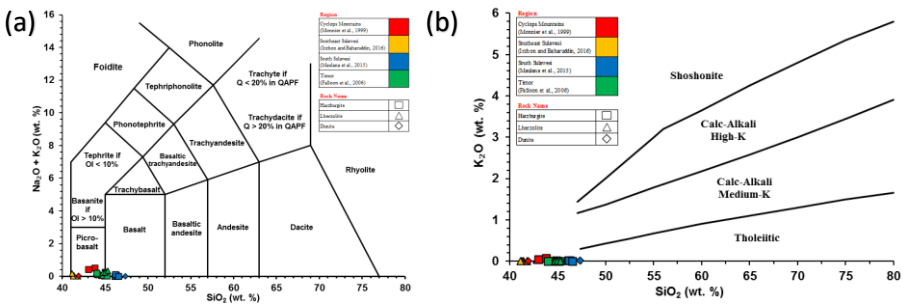

Figure 2: a) Plot of SiO_2 vs total alkali (adaptation from Le Bas et al., 1986) and b) plot of SiO_2 vs K_2O (adaptation from Peccerillo and Taylor, 1976).

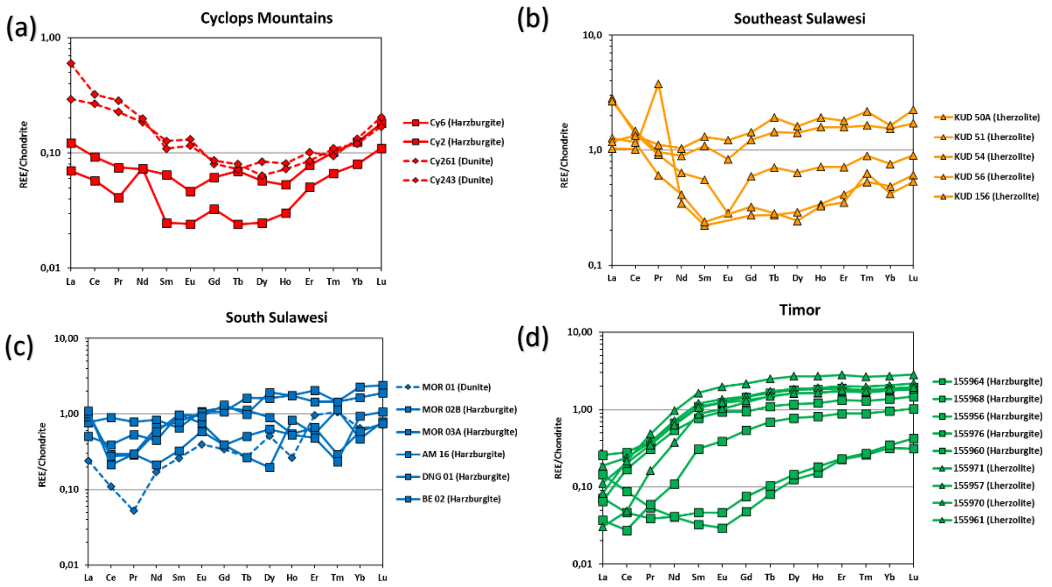

Figure 3: REE chondrite normalized (Sun and McDonough, 1989) spider diagrams for sample from a) Cyclops Mountains, b) Southeast Sulawesi, c) South Sulawesi, dan d) Timor.

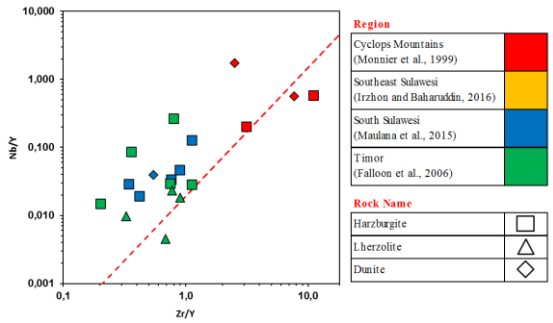

Figure 4: Plot of Nb/Y vs Zr/Y to determine source of magma from plume or non-plume (adaptation from Condie, 2005).

PROCEEDINGS
JOINT CONVENTION BANDUNG (JCB) 2021
November 23rd – 25th 2021

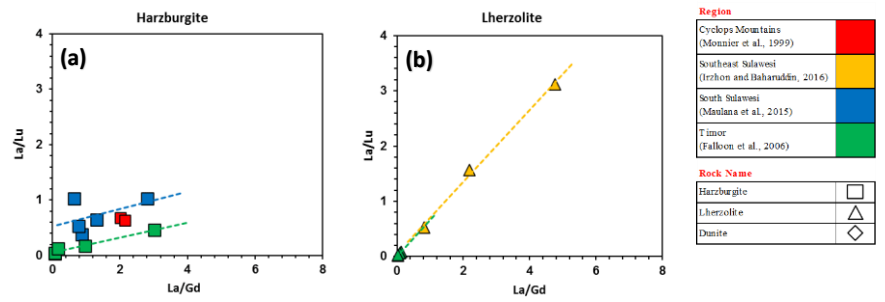

Figure 5: Plot of La/Gd vs La/Lu in: a) harzburgite, and b) lherzolite. These plots show similar trends between Sulawesi and Timor.

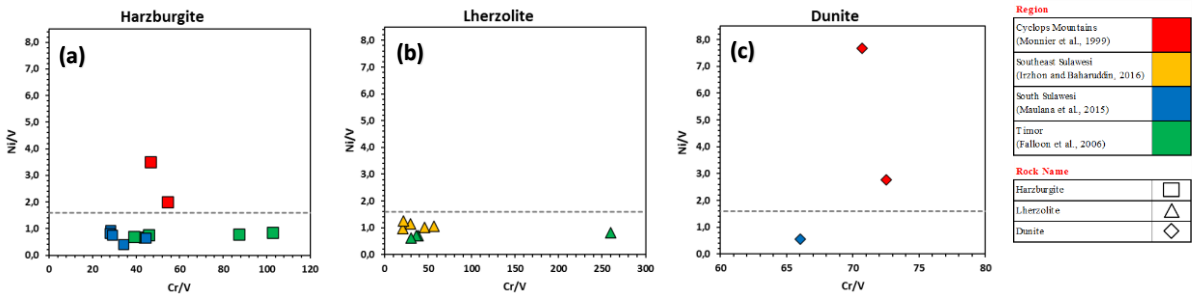

Figure 6: Plot of Cr/V vs Ni/V in: a) harzburgite, b) lherzolite, and c) dunite. These plots show the existence of separation lines between 'productive area' with 'non-productive area'.

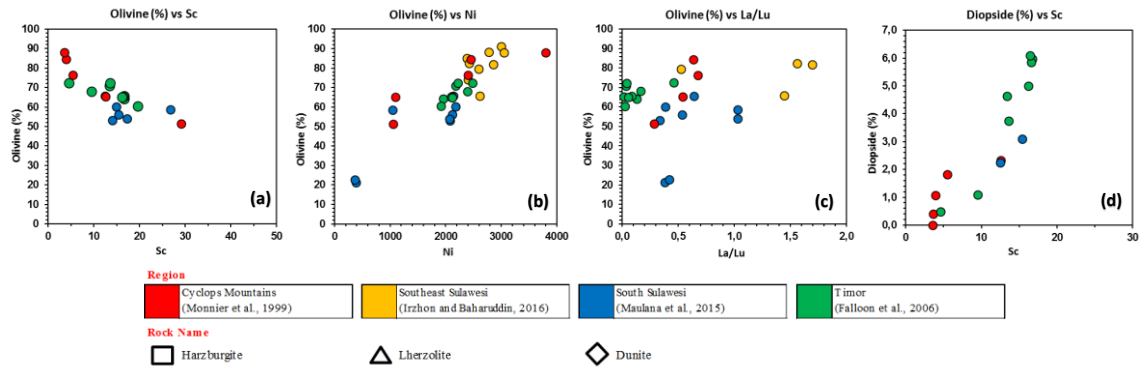

Figure 7: Plot of normative mineral with critical elements and REE: a) olivine (%) vs Sc, b) olivine (%) vs Ni, c) olivine (%) vs La/Lu, dan d) diopside (%) vs Sc to identify the tendency of Sc and Ni enrichment influenced by the presence of normative minerals in ultramafic rocks.

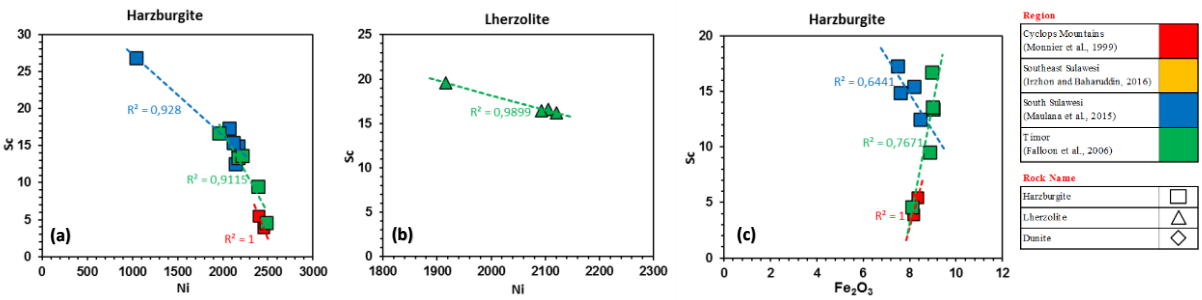

Figure 8: Plot of a) Sc vs Ni in harzburgite, b) Sc vs Ni in lherzolite, and c) Sc vs Fe_2O_3 plot in harzburgite, to identify the tendency and its relation to Ni and Sc enrichment.

PROCEEDINGS
JOINT CONVENTION BANDUNG (JCB) 2021
November 23rd – 25th 2021

Structural Control on Primary Tin Deposit at Paku Area, Payung Subddistrict, South Bangka District, Bangka Belitung Province

Fajar Hari Cahyana[1)], Favian Avila Restiko[1)], Teguh Nur Hidayat[2)]
[1)]Department of Geological Engineering UPN "Veteran" Yogyakarta. [2)]PT. Timah Tbk

Abstract
Bangka Island is one of the largest tin producers in the world. Tectonically, Bangka is part of the Bentong-Raub suture zone, so that there is a lot of primary tin mineralization. Primary tin deposits on Bangka Island are formed from acidic magma fluids resulting from the collision process. One of the primary tin deposits on Bangka Island is located in Paku, Payung District, South Bangka Regency. This study aims to determine the effect of geological structure on primary tin mineralization in the village of nails. The method used is surface mapping. In addition, analyst of the surface data was carried out using XRF (X-Ray Fluorescence), XRD (X-Ray Diffraction), Petrography, and Mineragraphy. The Paku area is composed of rock units from old to young, namely Litodem Filite Pemali Complex, Tanjunggenting Sandstone, and Alluvial Deposits. Based on the results of XRD analyst, the set zones are Quartz ± sericite; Quartz + Sericite + Illite ± Dickite ± Halloysite ± Tourmaline; Quartz + Kaolinite + Dickite ± Illite-Smrctite; and Kaolinite + Montmorillonite + Illite-Smectite. Based on the results of XRF analyst, it was found that the tin content varied greatly, but the highest levels were found in hydrothermal breccias. The geological structure that develops has several directions, namely NE- SW, NW-SE, and E-W. Tin mineralization that is present is commonly found in the ENE-WSW and N-E veinlets, in addition to developing in veinlets, tin mineralization is present in anti-dilational breccia which is the product of compression of the N-E trending stress. Based on field data and laboratory analyst results, primary nail tin deposits include exogreisen deposits.

Keywords: **primary tin deposit, anti dilational jogs, exogreisen**

Introduction

Currently, Tin is still one of the important metal commodities in the industrial world. Industrial demand encourages increased exploration activities in prospective areas to find new large tin resources. The South Asia Tin Belt is one of the most profitable tin prospecting areas ever discovered with the highest production record in world history since 1800 (Schwartz, 1995). The presence of tin deposits in the Southeast Asian Tin Belt is spread along with the Sibumasu Block (Sino, Burma, Malaya, Sumatra), East Malaya, and several other terraces. Indonesia has the same area as primary tin reserves that have been discovered, especially on Bangka Island. The existence of these prospects is influenced by the setting and tectonic events triggered by the collision between the Sibumasu Block and East Malaya-Indochina. The collision produced a suture called the Bentong-Raub Suture Zone (BRSZ), which is spread along the amalgamation zone from the Bangka Belitung Islands in the southeast to Burma - Thailand in the Northwest. (Metcalfe, 2011). Primary Tin or Greisen deposits are produced from late magmatic to post magmatic metasomatism processes that are formed in the granitic freezing phase (Pollar, 1983 in Pirajno, 2009). According to Scherba (1970) Greisen deposits are formed through three phases, namely the alkaline phase, the Greisen phase, and the urate phase. According to Corbett and Leach (1997) mineralization is closely related to the formation of geological structures, mineralization of syn mineralization structures. The tectonic activity that forms the structural pattern on Bangka Island is divided into three orientations, namely, northwest-southeast (Late Paleozoic), north-south (Triassic - Jurassic), and north-south (Cretonic) (Katili, 1967).

Administratively, the research location is in the IUP PT. Tin in the Paku Region, Payung District, South Bangka Regency, Bangka Belitung Province. The research location is in the southeast of the island of Bangka with a distance of 80 Km from the head office of PT. Timah Tbk Pangkal Pinang or about 1 hour 49 minutes using a motorized vehicle.

Figure 1. Research Area (Source: Google Maps)

Data and Methods

Regional studies are carried out comprehensively by researchers. Especially in terms of the characteristics of Bangka primary tin deposits, and their control factors. Tentative interpretations of lithology and fault lines were also developed by the researcher using google earth to determine regional deformation and lithological variance. Surface geological mapping aims to collect factual data in the form of rock units, geological structures, alteration, and mineralization. Then, the petrographic analyst determines the specific lithology type and identifies the alteration minerals present in the sample. The rock samples were then analyzed by XRD to find out the alteration minerals that occurred in more detail. Quantitative XRF analyst was needed to determine the variance and the number of elements that formed the sample out. Analyst is used to see ore minerals.

Regional Stratigraphy

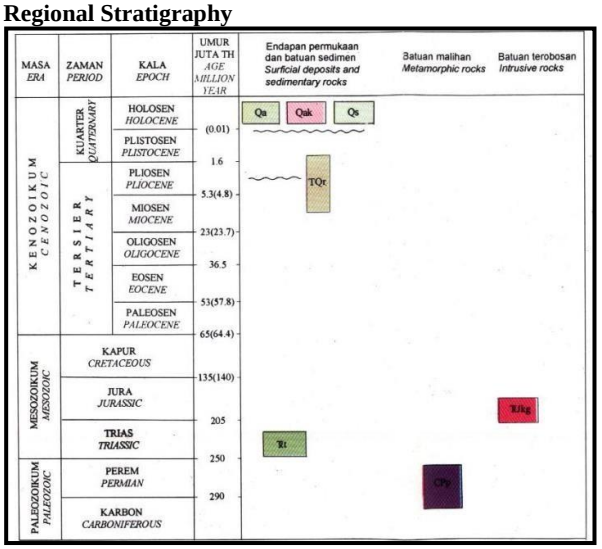

Figure 2. Stratigraphic of South Bangka (Margono,1955)

On Bangka Island there are two geological maps, namely the Geological Map of North Bangka Sheet according to (Mango & Djamal, 1994) and the Geological Map of South Bangka Sheet according to (Margono, 1995). According to (Margono, 1995) the regional stratigraphy of South Bangka

PROCEEDINGS
JOINT CONVENTION BANDUNG (JCB) 2021
November 23rd – 25th 2021

Island is composed of several rock formations or units in sequence from young to old as follows:

1. (QA) Alluvium

Alluvium consisting of mud, clay, sand, gravel, and gravel found as sediment in rivers, swamps, and beaches

2. (Qs) Swamp Sediments

Swamp deposits consisting of mud, silt, and sand

3. (TQr) Ranggam Formation

The Ranggam Formation consists of alternating sandstone, claystone, and conglomerate. Sedimentary structures in sandstones are criss-crossed, parallel waters and layered layers, locally found 0.5 m thick coal lenses and containing secondary tin sand mixed with quartz sandstone. Claystone contains plant debris and peat lenses. Conglomerate has components of granite, quartz, and metamorphic rock. This unit is of Late Miocene-Early Pleistocene age and was deposited in a fluvial environment that overlaps unconformably above the older formations.

4. Klabat Granite

Kelabat granite consists of biotite, granodiorite, and genesisan granite. Biotite granite has a pophyritic texture with medium-coarse crystalline grains, feldspar denocris up to 4cm in length and shows a foliated structure. The name of this unit comes from its type location in Teluk Klabat. This unit is of Late Triassic-Early Jurassic age and breaks through the Tanjung Genting Formation and the Malihan Pemali Complex.

5. Tanjunggenting Formation

The Tanjunggenting Formation consists of alternating sandstone and claystone. Sandstone has a fine-medium grain size, well separated with a thickness of 2-60cm with a cross-sedimentary structure and wavy lamination, locally found fine sandstone lenses. This unit is Early Triassic and deposited in a shallow marine environment? The overlap is not in harmony with the metamorphic rock.

6. Malihan Pemali Complex

The Malihan Pemali complex consists of phyllite, schist, and quartzite. Filite has a leafy structure and is veined with quartz. The schist has a leafy structure, fractured, where the fracture is filled with quartz or iron oxide, interspersed with quartzite. Quartzite is composed of quartz and feldspar. This unit is thought to be of Perem age because it is inconsistently superimposed on the Tanjung Genting Formation.

Regional Tectonic

Bangka Island is part of the Indochina-Malaya block east of Bangka Island as part of the Indochina-Eastmalaya block which is included in the Sunda Continental Block. The eastern Indochina-Malaya block is part of the Gondwana that broke away in the Late Silurian Period. In the Late Silurian Period, there was a rifting event on the edge of Gondwana which consisted of the South China, Tarim, Indochina, and North China blocks which caused the Paleo-Tethys Ocean to form in the Devonian Period.

Bangka Island is closely related to the phenomenon of amalgamation of the Sundaland building blocks, including the Indochina-Malaya Timur block and Sibumasu. Bangka Island is close to the Raub-Bentong suture resulting from the confluence of the East Indochina-Malaya microcontinent.

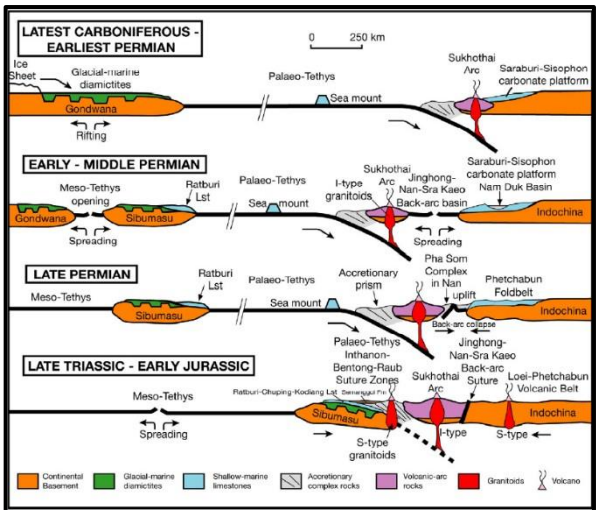

Figure 3. Tectonic Of Sundaland,(Metcalfe,2011)

Result and Discussion

Stratigraphic of Research Area

The research area is composed of three rock units, namely Litodem Filite Pemali Complex, Tanjunggenting Sandstone Unit, and Alluvial Sediment Unit. Pemali Complex Phyllite Litodem with Late Carbon – Early Permian age composed by lithology in the form of sandstone, slate, and phyllite. The Tanjunggenting Sandstone Unit has an Early Triassic – Late Triassic age composed of alternating sandstones and claystones. The Quaternary Alluvial Sediment Unit is composed of alluvial deposits resulting from fluviatile processes and tailings deposits.

Geological Structure of Research Area

The geological structure is closely related to the formation of mineralization in an area. According to Corbett and Leach (1997), the structures that influence the mineralization process are divided into three, namely, pre-mineralized structures, syn-mineralized structures, and post-mineralized structures.

The geological structure that developed at the research site was formed due to tectonic processes that occurred on Bangka Island. Based on the analyst of tectonic joints, two stresses are obtained, namely, the first stress has a northeast-southwest orientation, the second stress is formed with a north-northwest-south-southeast orientation. The geological structures found in the field are in the form of layers, joints, veins, and faults. The geological structure in the study area which is influenced by north-north-north-south-south-south-east trending controls alteration and mineralization in the study area. The geological structure that controls alteration and mineralization is formed as a result of the transpression process produced by fault segmentation with a northwest-southeast trend that forms a structural zone in the form of anti-dilatational jogs. In addition to these zones, mineralization in the study area is found in the structural zone in the form of tension fractures, jogs, massive veins, and lodes.

Alteration

Hydrothermal alteration is a mineral change process that occurs due to the reaction between hydrothermal fluids and side rocks so that they reach a new equilibrium. Hydrothermal alteration can be formed when the fluid ratio is greater than the rock ratio, meaning that the concentration of hydrothermal fluid greatly affects the alteration that will be formed. In addition to the fluid concentration factor, the hydrothermal alteration can be formed due to a combination of several controlling factors such as permeability,

PROCEEDINGS
JOINT CONVENTION BANDUNG (JCB) 2021
November 23rd – 25th 2021

temperature, pressure, side rock types, and others. As a result of some of these factors will form hydrothermal alteration which forms alteration zoning with different patterns and characteristics from one another.

Based on the results of petrographic and XRD analyst, the research area can be divided into four alteration zones based on the mineral assemblage. The alteration pattern that develops follows the existing structural pattern in the research area which functions as a channel way. Alteration zones from the middle to the edge are sequential as follows: alteration zone of quartz ± sericite, zone of alteration of quartz + sericite + illite ± dickite ± halloysite ± tourmaline, zone of quartz + kaolin + dickite ± illite-smectite, and alteration zone of kaolin + montmorillonite ± illite -smectite.

Quartz ± Sericite Zone (Silisik Alteration)

Quartz ± sericite mineral assemblage zone is characterized by the presence of quartz minerals, sericite which can be observed in the field and the results of XRD and petrographic analyst. This alteration zone develops in fault breccia lithology, slate, phyllite, and metasandstone of the Pemali Complex Phyllite Litodem. The altered metasandstone is characterized by a brownish color and is characterized by an abundance of secondary quartz minerals. Based on the results of XRF analyst in this alteration zone, it shows high levels of Sn > 5600 ppm. High Sn content mainly develops in silica oxide veins and hydrothermal breccias.

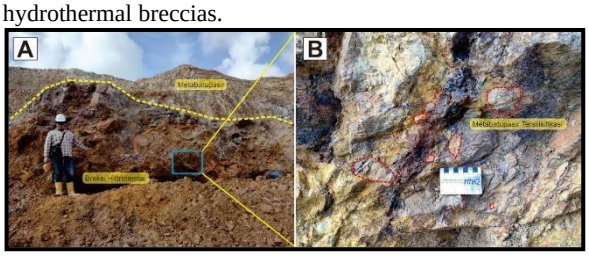

Figure 4. Figure Outcrop Alteration Quartz ± Sericite(A) Figure Lithology Alteration Quartz ± Sericite (B)

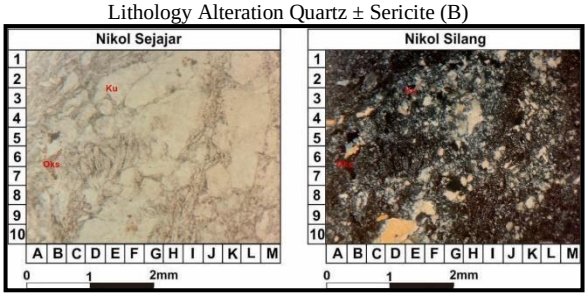

Figure 5. Figure Thin Section Alteration Quartz ± Sericite

Based on a thin section of the metasandstone, the sandstone changed to beige in color with a crystal size of <0.1 mm – 0.5 mm. Composed of silica (quartz) minerals and oxide minerals. Quartz minerals have a percentage of 88% and oxide minerals have a percentage (12%) based on the mineral set, so they are included in the Quartz ± Sericite (Silicification) alteration type.

Quartz + Sericite + Illite ± Dickite ± Halocyte ± Tourmaline Zone (Greisen Alteration)

The assemblage zone of quartz + sericite + illite ± dickite ± halloysite ± tourmaline is characterized by the presence of quartz, illite, and tourmaline veins which can be observed in the field. Based on XRD analyst there are also other minerals such as halloysite and Dickite. This alteration zone develops in metasandstone, slate, and phyllite lithologies. The rocks that have undergone this alteration are greenish- white in color and abundant in secondary quartz and illite minerals, however, at several observation sites, tourmaline veins with a geometry of sheet veins were found. Based on XRF analyst, this zone contains levels of Sn as silica oxide veins with levels of 1200 – 2200 ppm.

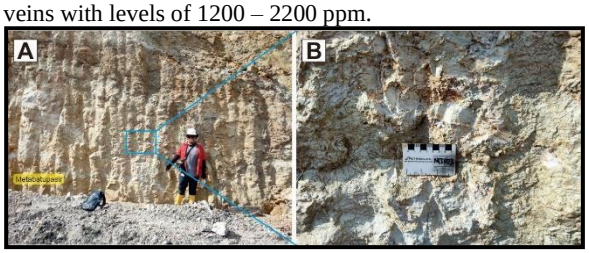

Figure 6. Figure Outcrop Alteration quartz + sericite + illite ± dickite ± halloysite ± tourmaline (A) Figure Lithologi Alteration quartz + sericite + illite ± dickite ± halloysite ± tourmaline(B).

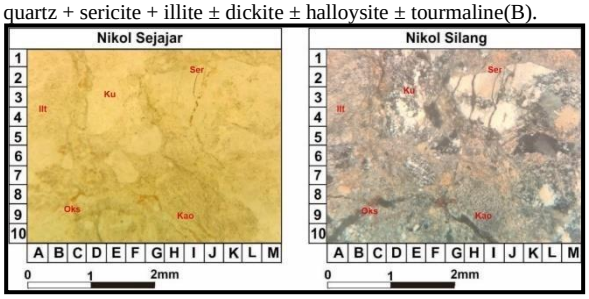

Figure 7. Figure Thin Section Alteration quartz + sericite + illite ± dickite ± halloysite ± tourmaline.

Based on the analyst of thin slices of altered rock on LP 191 it shows a cream color with crystal size <0.1 mm – 1.5 mm. Based on this rock incision, it shows a strong alteration intensity. This rock is composed of quartz minerals (15%), sericite minerals (20%), oxide minerals (5%), and clay minerals/kaolin and illite? (55%). Based on the mineral assemblage, this rock belongs to the alteration type of quartz + sericite + illite ± dickite ± halloysite ± tourmaline (Greisen).

Quartz + Kaolin + Dickite ± Ilite-Smectite Zone (Argilic Alteration 1)

The assemblage zone of quartz + kaolin + dickite ± illite-smectite is characterized by the presence of quartz minerals and an abundance of clay minerals. This assemblage zone develops in phyllite lithology and sandy metatubules with brownish-white lithology color with an abundance of quartz, illite, kaolin, and Dickite minerals. In this zone, many quartz veins are found that fill the joint. The results of XRF analyst showed that in this zone the levels of Sn ranged from <200-400 ppm.

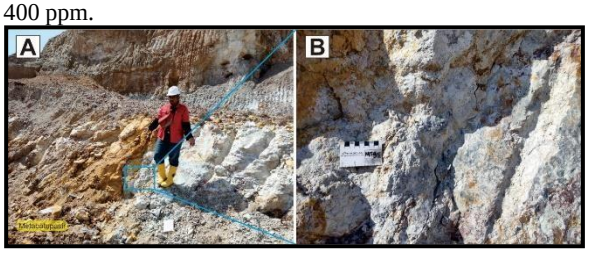

Figure 8. Figure Outcrop Alteration quartz + kaolin + Dickite ± illite-smectite.

PROCEEDINGS
JOINT CONVENTION BANDUNG (JCB) 2021
November 23rd – 25th 2021

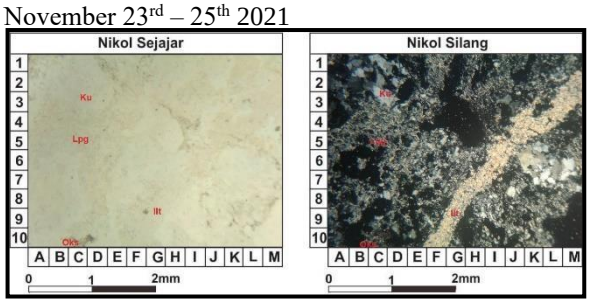

Figure 9. Figure Thin Section Alteration quartz + kaolin + Dickite ± illite-smectite.

Based on the analyst of the thin slices of the altered rock on LP 183 it showed a cream color with a crystal size of <0.1 – 0.5 mm. Based on a thin incision, it shows that the rock has changed strongly. This rock is composed of quartz minerals (25%), oxide minerals (5%), clay minerals/kaolin? (30%), clay minerals/illite (25%), and illite veins? (15%). Based on the zoning of this lithological alteration, it is included in the Quartz + Kaolin + Dikite ± Illite-Smectite mineral set.

Kaolin + Montmorillonite ± Ilite-Smectite Zone (Argilic Alteration 2)

The mineral assemblage zone of kaolin + montmorillonite ± illite-smectite was formed in the last phase of the hydrothermal process by spreading a wide alteration zone. The mineral assemblage zone of kaolin + montmorillonite ± illite-smectite in the field can be observed with the abundant presence of clay minerals such as kaolin illite, and montmorillonite which when held have a soft characteristic. This alteration zone is found in the Tanjunggenting Sandstone Unit with a white-yellowish color. Based on the XRF analyst of this zone, it shows that the Sn content is very small, namely < 200 ppm.

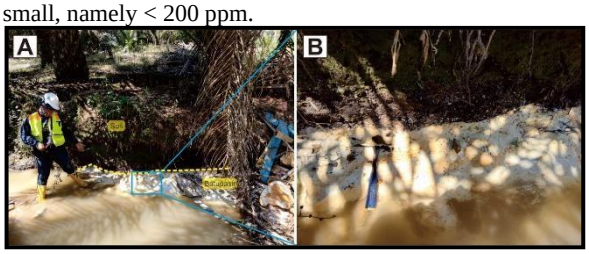

Figure 10. Figure Outcrop Alteration kaolin + montmorillonite ± illite-smectite(A) Figure Lithologi Alteration kaolin + montmorillonite ± illite-smectite(B).

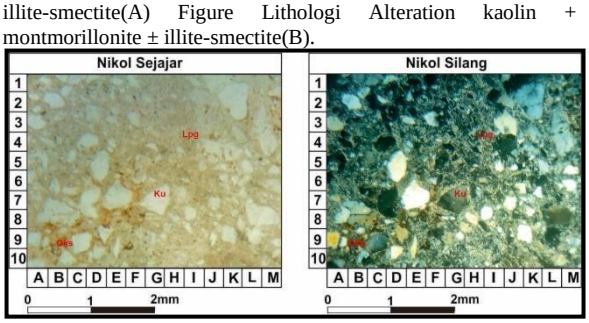

Figure 11. Figure Thin Section Alteration kaolin + montmorillonite ± illite-smectite.

Based on petrographic analyst of siliciclastic sedimentary rocks at LP 32, it shows the absorption color of white – brown with clastic texture with grain size <0.1 – 0.7 mm supported by a matrix with a rounded stern shape. The degree of sorting between poorly processed grains shows the contact between floating contact grains, the point contact which is composed of quartz minerals (60%), oxide minerals (10%), and clay minerals (30%) (Illite ?). Clay minerals and oxide minerals are present as a result of hydrothermal alteration processes. Based on the petrographic analyst, rock names include graywacke (Pettijohn 1975). Based on the mineral assemblage zone, this rock belongs to the kaolin + montmorillonite ± illite-smectite mineral zone.

Mineralization

Elemental Sn mineralization at the study site is present in two structural systems, tensional structure, and compression structure **(See Figure 16)**. The compressional structures in the study area are anti-dilatational jogs and massive veins. Meanwhile, the tensional structure of the carrier of Sn mineralization is in the form of veins with jogs and lode geometries with Sn levels ranging from 1000 to 8000 ppm. The mineralization present in the anti-dilatational jogs and massive veins forms a fault breccia lithology that undergoes a hydrothermal process with Sn levels ranging from 1200 to 21000 ppm **(See Figure 18)**. Based on it can be seen that the present mineralization is controlled by two structures. The Sn element formed in the compressional structure has an Sn content greater than that formed in the tensional structure **(See Figure 16)**.

Based on mineragraphic observations at four locations of ore mineral observations found in the research area in the form of cassiterite, arsenopyrite, pyrite, galena, chalcopyrite, goethite, and hematite. The ore minerals in the form of cassiterite and galena are disseminated in arsenopyrite minerals. The ore minerals are then replaced by Fe-carrying ore minerals in the form of goethite and hematite which are formed as a result of the oxidation process. At several observation locations, chalcopyrite minerals were found scattered **(See Figure 13&14)**.

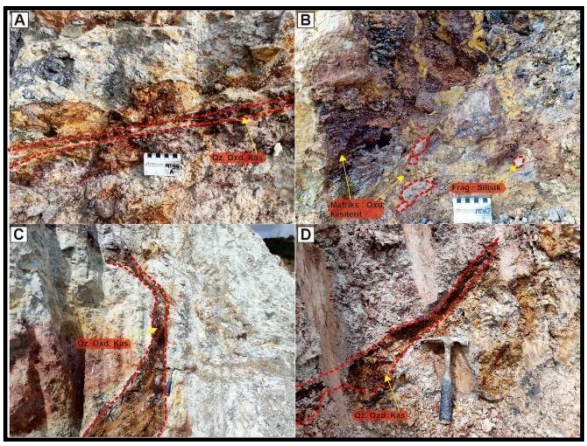

Figure 12. Figure Single Vein Quartz-oxide(A) Figure Fragmen Breccia Hydrotermal(B) Figure Geometry Lode Vein Jog Quartz-Oxide(C)Figure Single Vein Quartz-oxide(D).

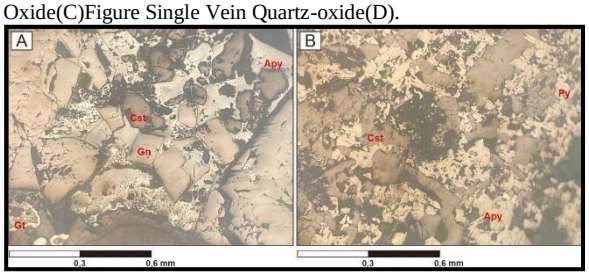

Figure 13. Figure Mineragrafi Cassiterite,Galena,Arsenopyrite,and Ghoetite(A) Mineragrafi Cassiterite,Pyrite,and Arsenopyrite(B).

PROCEEDINGS
JOINT CONVENTION BANDUNG (JCB) 2021
November 23rd – 25th 2021

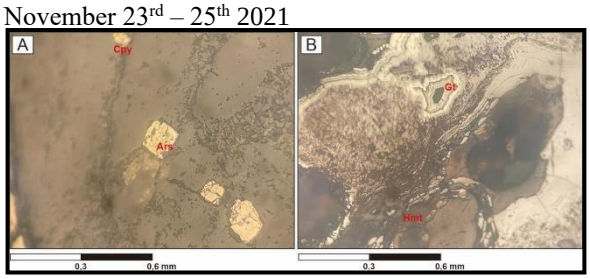

Figure 14. Figure Mineragrafi Arsenopyrite and Chalcopyrite(A) Figure Mineragrafi Ghoetite and Hematite(B).

Elemental Ore Geochemistry

Geochemical analyst was carried out by making a graph of the relationship between the elements of Sn and the elements of Pb, Zn, As. This analyst was carried out as supporting data in interpreting the characteristics of primary tin deposits in the study area.

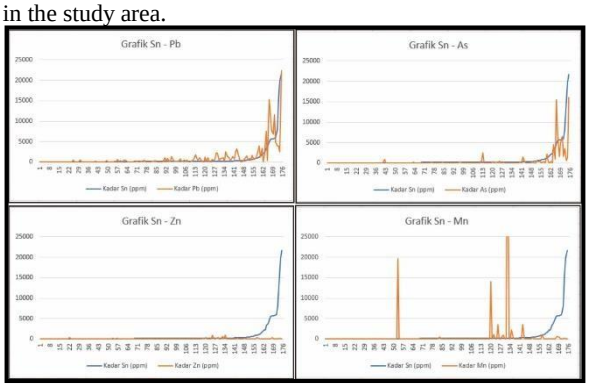

Figure 15. Figure Relationship Between The Elements Of Sn and the elements of Pb, Zn, As.

Based on the picture above, it shows that Sn shows the alignment of increasing levels, when Sn levels are high, Pb and As elements are also high. This shows that the presence of Sn in the field is associated with Pb and As elements. While the comparison graph of Sn with Zn and Mn does not show the alignment of the increase in levels. It can be interpreted that the presence of Sn elements in the field is not associated with both Zn and Mn elements **(See Figure 15)**.

Discussion

The mineralization present in the study area is present in two types of geological structures, namely compressional structures and tensional structures. The compressional structures found in the research area are anti-dilation exercises, tarpaulin veins, and massive veins with an east-northeast-southwest orientation. The tensional structure in the research area is in the form of veins with jogs and lode geometries with northnortheast – southwestsouthwest orientations **(See Figure 16&18)**.

Mineralization in the study area has an Sn content that varies with each geometry formed. Mineralization in the quartz-tourmaline veins that form sheeted veins has Sn elements in the range of 112 - 145 ppm, in the quartz veins - oxide minerals - cassiterite with jogs and lode geometries have Sn levels in the range of 1000 - 8000 ppm. While the anti-dilatational jogs geometry contains Sn with levels of 1200 – 22000 ppm **(See Figure 18)**.

The mineralization that forms the jogs and lode geometries is a product of the tension fracture of the Riedel system. The mineralization formed from the tension fracture has a northeast-southwest orientation. The mineralization geometry is interpreted as a tensional zone of the Bukit Panjang Right Strike Slip Fault which is referred to as a tension fracture. While the mineralization formed in the geometry of anti-dilatational jogs and massive veins is a product of compression from the Bukit Panjang Right Strike Slip Fault, in the horizontal fault system according to Riedel, it is the main fault that undergoes segmentation so as to form anti-dilatational jogs with rocks experiencing brecciation to form hydrothermal breccias**(See Figure 16)**.

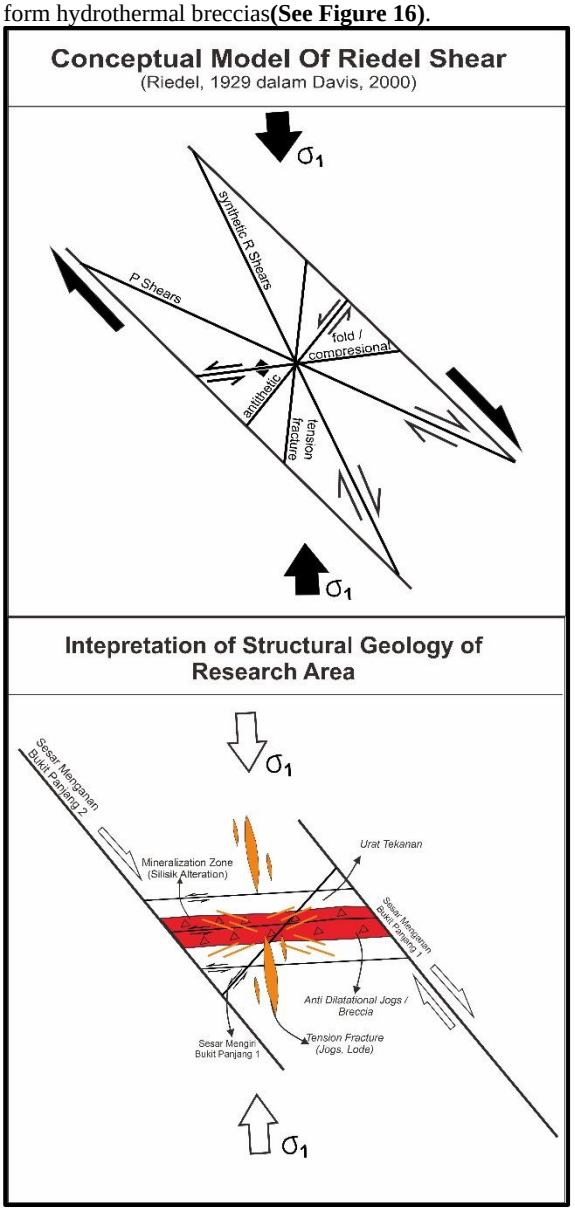

Figure 16. Geological Stucture Model Controlling Primary Tin Deposit In The Research Area.

Based on the analyst of Sn content using XRF, there are differences in levels between the mineralization formed in the tensional structure and the compressional structure. Mineralization present in anti-dilatational jogs geometry and massive vein with eastnortheast – westnorthwest orientation has higher Sn content than mineralization present in veins with jogs and lode geometry**(See Figure 16)**. The difference in Sn levels in the two structures is caused because the fluid will be more concentrated in the compressional structure, because the fluid formed in the compressional structure has a high temperature and temperature so that the Sn element will be more concentrated, but has a relatively small geometry. Meanwhile, the tensional structure has a relatively large geometry for the size of the tensional fracture product but has a relatively lower Sn content.

Based on the results of data obtained in the field and analyst of XRD, XRF, petrography, and mineragraphy, it can be concluded that the sediment in the study area refers to Scherba (1970) in Pirajno (2009) is an Exogreisen Deposit Type. Mineralization zoning refers to Mel'nicov (1965) in Taylor (1979) based on elemental associations including the

PROCEEDINGS
JOINT CONVENTION BANDUNG (JCB) 2021
November 23rd – 25th 2021

Zone of Active Deposition which is formed at a depth of 500-700 meters with hard deformation conditions or in brittle rocks**(See Figure 17)**.

Table 1. Characteristic Primary Tin Deposit in Research Area.

Source Rock	Granite ?
Host Rock	Phyllite, Metasandstone, Slate, Sandstone, Claystone
Altered Mineral	Tourmaline, Quartz, Sericite, Illite, Kaolinite, Dickite, ,Halloysite, Montmorillonit, Illite-Smectite
Major Commodity	Sn
Other Commodity	Pb, As, Zn,Mn, Cu, Mo, Fe
Vein geometri	Sheeted vein, Stockwork,Lode, Massive vein, Jogs, Anti Dilatation Jogs
Control Alteration and Mineralization	Fault, Joint

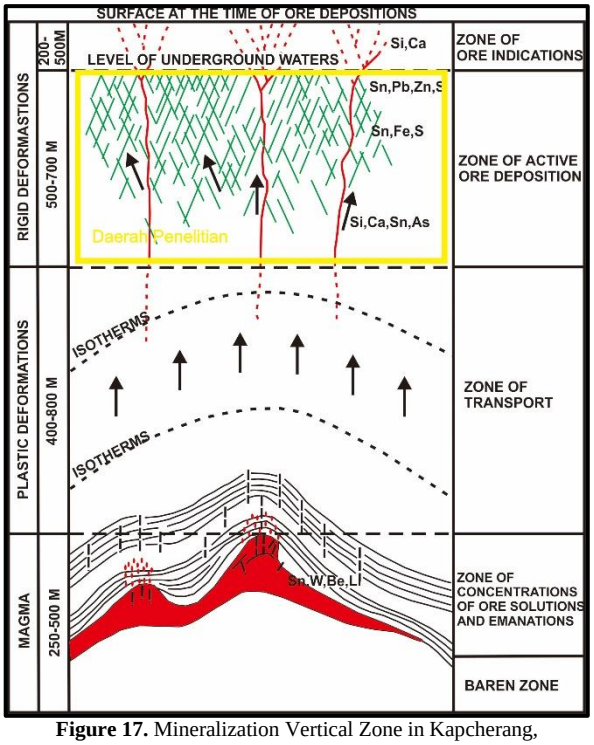

Figure 17. Mineralization Vertical Zone in Kapcherang, Transbaikalia, U.S.S.R (Mel'nicov, 1965 in Taylor, 1979).

Conclusions

Based on the results obtained, mineralization in primary tin deposits is controlled by faults formed by the transpression process which forms anti dilatational jogs with NNE - WSW orientation. In addition, mineralization in the study area is also found in joints with geometry of tension fracture, jogs, lode, and massive vein. The highest grade of mineralization is found in the anti-dilational jogs structure.

References

Corbett & T. Leach. 1997. Southwest Pacific Rim Gold-Copper Systems: Structure, Alteration, and Mineralization. *Short Course Manual Draft as at 2 May 1997.*

Davis, dkk. 2000. Conjugate Riedel Deformation Band Shear Zones. *Journal of Structural Geology. 22 Arizona. Hal 169 -191.*

Katili, et al. 1967. Structure and Age Of The Indonesian Tin Belt With Special Reference To Bangka. *Elsevier Publishing Company.*Hal 1-16.

Mangga, A.S. dan Djamal, B. 1994.*Peta Geologi Lembar Bangka Utara dan Bangka Selatan, Sumatra*. Bandung: Pusat Penelitian dan Pengembangan Geologi.

Margono, dkk.1995.Peta Geologi Lembar Bangka Selatan, Sumatra. Bandung: Pusat Penelitian dan Pengembangan Geologi.

Metcalfe, I. 2011. Tectonic Framework and Phanerozoic Evolution of Sundaland. *Gondwana Research, Vol. 19*

Pirajno., 2009, *Hydrothermal Processes and Mineral Systems*: Springer Science + Bussines Media B.V.

Schwartz, 1995. The Southeast Asian Tin Belt. Germany: *Elsevier Scientific Publishing Company*

Scherba. 1970. Greisens. *International Geology Reviews 12: 2 page 114 – 150.*

Taylor, R.G. 1979. *Geology of Tin Deposits.* New York: Elsevier Scientific Publishing Company

Acknowledgements

The authors would like to thank the Institute for Research and Community Service (LPPM) Universitas Pembangunan Nasional Veteran Yogyakarta, Indonesia, for providing funds for this research. We also thank Riza, Sefrian, Angga and Hafizh, final-year geology students of Teknik Geologi UPN "Veteran" Yogyakarta, for their help during internship at PT. Timah Tbk

PROCEEDINGS
JOINT CONVENTION BANDUNG (JCB) 2021
November 23rd – 25th 2021

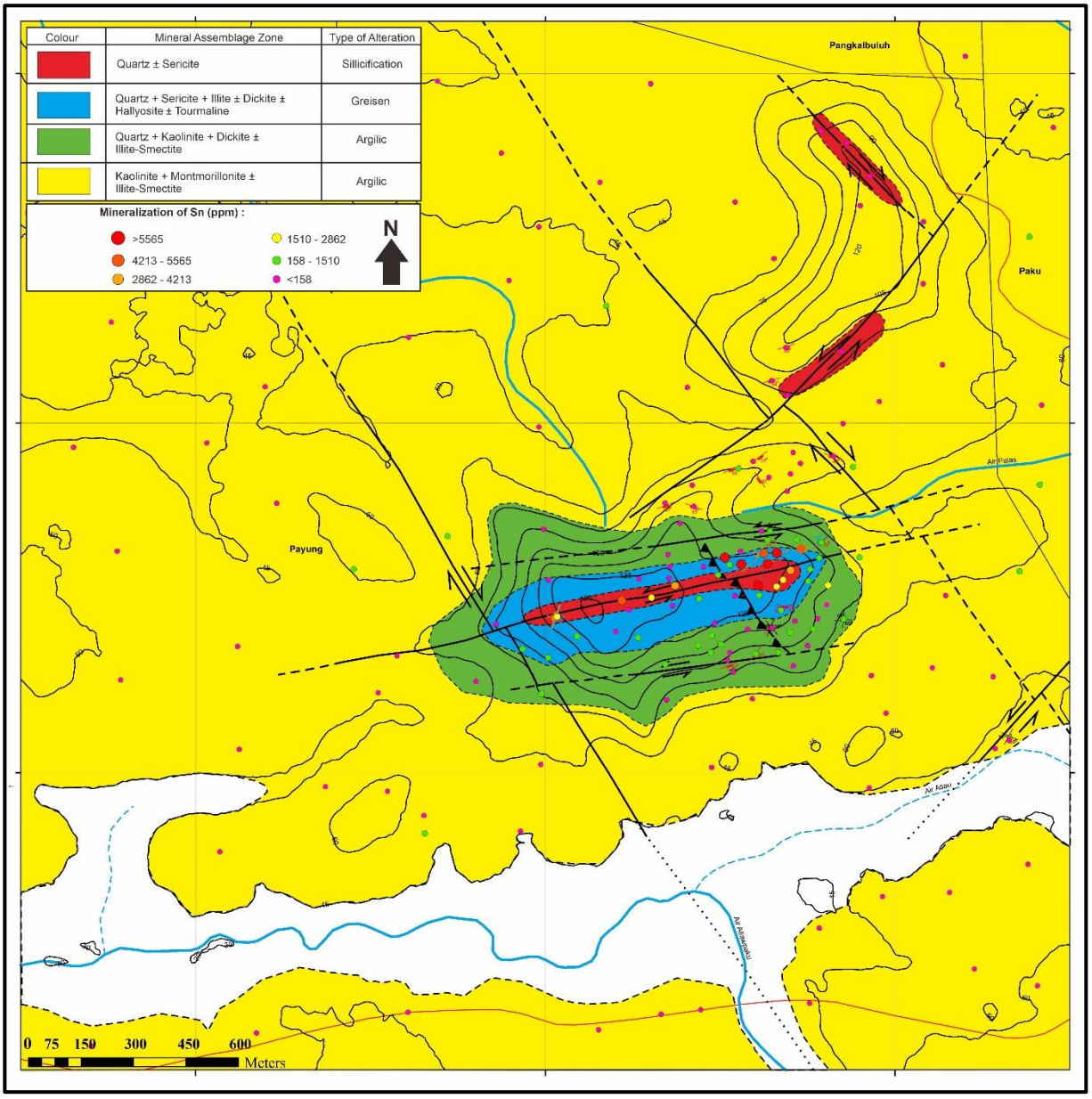

Figure 18. Alteration and Spread Elements Sn In Research Area

PROCEEDINGS
JOINT CONVENTION BANDUNG (JCB) 2021
November 23rd – 25th 2021

Best Time Depth Conversion Output Determination using Single Function vs. 2D and 3D Multi-Function Velocity Modeling: Comparative Studies on Posseidon Seismic Data

Aji Darma Maulana[1], Ghozi Farhanda Putra[2], Nine Safira[3], Jefri[3], Tris Arfiadinarti[3]
[1]UPN Veteran Yogyakarta, [2]University of Brawijaya, [3]University of Indonesia

Abstract

Geological modeling performers in oil and gas exploration, in this case, geoscientists, often undervalue the time-to-depth conversion stage. This stage is one of the main parameters in modeling the distribution of reservoir physical properties before continued with volumetric calculations of oil and gas resources/reserves. Using the Multi-Function Velocity Model, it is expected that the results of the time-to-depth conversion have better spatial precision compared to the Single-Function Velocity Model. This method was implemented in the Browse Basin, Australia. The data used in this study includes two types of data, namely drilling well data and post-stack time migration (PSTM) 3D seismic data. To perform the time-depth conversion stage, Average Velocity data is needed. Average Velocity modeling is done in 1 dimension, 2 dimensions, and 3 dimensions. This is done to produce a function that can change the time domain to the depth domain. Quality Control of velocity modeling results is done by calculating the error value before and after adjustments are made to the well top of each horizon. Furthermore, the results of Quality Control will be ranked as well as making conclusions from each of the advantages and disadvantages of the velocity model. Velocity modeling in 3 dimensions has the combined advantages of 1D and 2D velocity modeling methods. By using the 3-dimensional velocity modeling method, we can apply the time-depth conversion to the lateral and vertical variations accurately and precisely with a minimum error value of zero.

Keywords: Time-to-depth conversion, Single-Function, 2D-3D Multi-Function, Velocity Model, 3D Seismic

Introduction

In general, geological modeling performers in oil and gas exploration, in this case, geoscientists, often undervalue the time-to-depth conversion stage. This stage is one of the main parameters in modeling the distribution of reservoir physical properties, then continued with volumetric calculations of oil and gas resources/reserves. On the other hand, comprehensive analysis is required to obtain accuracy and precision in the time-to-depth conversion and velocity modeling steps. Using the Multi-Function Velocity Model, it is expected that the results of the time-to-depth conversion have better spatial precision compared to the Single-Function Velocity Model. Moreover, to increase the capability and volumetric accuracy of the time-to-depth conversion results, the 3D Multi-Function Velocity Model is applied. Consequently, we examine a comparative study between Single Function and 2D & 3D Multi-Function Velocity Modeling.

Single-Function is a time-to-depth conversion method that solely applies one equation to the entire research area. The method has two types, namely linear equations and polynomial equations. Using the root mean square error (RMS Error), the quality control of the single-function method can be performed. This method is very suitable when executed on well log data that has good quality of checkshot data. However, if more than one well data is used in the research area with low-quality checkshot data, an accumulation of errors will later happen. Thus, the method will always have an accumulated error value if implemented in a research area with a lot of well data. Hence, the multi-function method can be a solution to the shortcomings of the single-function method.

In contrast, the multi-function utilizes multiple equations in the application in the research area. This method can provide a detailed description of the time-to-depth relation (TDR) in each area of influence of the well data. In its application, the method is divided into two types, namely 2D and 3D Multi-Function. 2D Multi-Function is represented in the form of a velocity surface. On the other hand, 3D Multi-Function is described in the form of a velocity cube. With the third dimension, the time-to-depth conversion process can be carried out volumetrically at one time with better accuracy.

This method was implemented in the Browse Basin, Australia. In general, the Browse Basin is intracratonic basin as a result of rifting that occurred during the Late Carboniferous of the Westralian Superbasin consisting of the Caswell, Barcoo and Seringapatam, Scott Plateau, and Yampi and Leveque shelf sub-basins (Yeates et al., 1987; Longley et al. , 2002; Geoscience Australia 2021). Struckmeyer et al (1998) explained that this basin was formed through 6 tectonic phases, namely: Extensional phase 1 in the Middle-Early Permian Carbon; Thermal subsidence phase 1 in the Late-Triassic Silurian; Inversion Phase 1 in Late Triassic-Early Jurassic; Extensional phase 2 in the Early-Middle Jurassic; Thermal subsidence phase 2 in the Late Jurassic-Cenozoic; Inversion phase 2 in the Middle Miocene-Holocene. The Browse basin stratigraphy can be seen in Figure 1.

The research area is located at Latitude 13◦34'24.825”S - 13◦44'16.88”S and Longitude 122◦11'30.24”E - 122◦23'56.48”E which is located in blocks WA-315-P and WA-398 -P. This research focuses on 7 wells namely Kronos, Boreas, Poseidon 1, Poseidon 2, Poseidon North, Pharos, and Proteus wells.

PROCEEDINGS
JOINT CONVENTION BANDUNG (JCB) 2021
November 23rd – 25th 2021

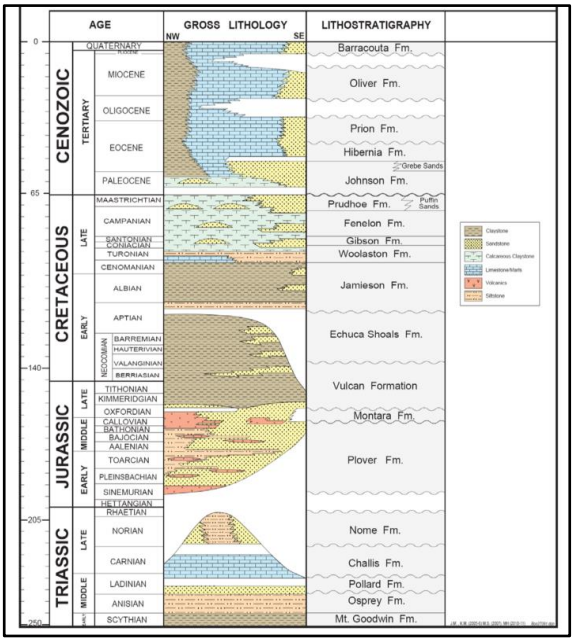

Figure 1. Browse basin stratigraphic column (Warrington, 2011)

Research Data

The data used in this study includes two types of data, namely drilling well data and post-stack time migration (PSTM) 3D seismic data. Seismic data has a range of Inline 2077-3898 and Xline 660-3340. The distribution and completeness of the well data used can be seen in **Table 1.**

Table 1. Inventory of Posseidon Region Well Data.

Well Log / Well Name		Kronos	Posseidon 2	Boreas	Posseidon 1	Posseidon North	Pharos	Proteus
Gamma Ray [API]		✓	✓	✓	✓	✓	✓	✓
Neutron Porosity [%]		✓	✓	✓	✓	✓	✓	✓
Density [g/cc]		✓	✓	✓	✓	✓	✓	✓
Resistivity [ohm.m]	Deep	✓	✓	✓	✓	✓	✓	✓
	Shallow	✓	✓	✓	✓	✓	✓	✓
DT Sonic [us/ft]		✓	✓	✓	✓	✓	✓	✓

Methodology

Time Depth Relation Correction is needed to extrapolate two-way-time data (TWT) and its relation to depth using a polynomial method. The polynomial method is a velocity function that depicts the time-depth relationship of a field irrespective of the number of layers present in the subsurface but does not take account of the local variation of velocities at the shallower layers (Ogbamikhumi & Aderibigbe, 2019). This study will focus on the accuracy for each average velocity modeling that consists of 1D, 2D, and 3D, then continued with comparing for strengths and weaknesses each other to find out which method is more suitable for use in volumetric calculations.

The picking horizon is the stage of developing the horizon continuity model. We carried out this stage to produce 10 top formation horizons which include: (1) Water bottom, (2) Top Oliver, (3) Top Reed Limestone, (4) Top Dampier Limestone, (5) Top Heywood Limestone, (6) Top Johnson, (7) Top Woolaston, (8) Top Jamieson, (9) Horizon 8, and (10) Horizon 9 in 10-20 increments. Quality control picking is given several conditions, namely: (1) Consistency of picking at certain phases, (2) Accuracy in determining picking on top markers, and (3) Adjustments can be made provided that they do not exceed certain phases.

To perform the time-depth conversion stage, Average Velocity data is needed. Average Velocity modeling is done in 1 dimension, 2 dimensions, and 3 dimensions. This is done to produce a function that can change the time domain to the depth domain. The formula for calculating the average velocity value can be seen in **Equation 1.** 1-dimensional modeling will produce a single function in the time-depth conversion process. This single function is created by combining seven time-depth relations (TDR) corrections in one graph which is then performed by polynomial regression to obtain the best average function equation that describes the 7 time-depth relations (TDR). Using the coefficient of determination helps justify the determination of the regression order of the polynomial. Then the best results will be applied to the Time Depth Conversion process.

By applying 2D Average Velocity modeling, it will produce a map of the distribution of the average velocity variation on each horizon. So that the process of making 2D Velocity modeling will be adjusted to the number of existing horizons. The gridding method used in the 2D Velocity Model is a convergent interpolation. This method is used to prevent the bullseye effect on the average velocity variation map. Furthermore, the 2D velocity model is applied to each of the relevant horizons.

3D Modeling Average Velocity Modeling will produce a 3D model of the average velocity variation that covers the entire surface area and the entire depth of the target to be carried out by TDC. Because the velocity distribution method uses the follow-layer method, this is heavily controlled by the shape and undulation of each horizon that has been considered. The gridding method used is convergent interpolation according to the 2D velocity modeling method.

$$V_{avg} = Z*2000/TWT \qquad \textbf{(Eq. 1)}$$

with:

V_{avg} = Average velocity [ms]
Z = Depth [m]
TWT = Two-way-time [ms]

Depth conversion is the conversion of seismic reflection data from the recorded two-way travel time (TWT) domain to the actual depth domain (Chautru, 2018). By converting the time domain to depth, geological structural ambiguity can be reduced by validating the presence of structural traps, spill points, and volumetric calculations for resource reserve estimation (Etris et al., 2001). In general, the calculation formula used to convert the time domain to depth can be seen in Equation 2.

PROCEEDINGS
JOINT CONVENTION BANDUNG (JCB) 2021
November 23rd – 25th 2021

$$Z = V_{avg} \cdot TWT/2 \qquad \textbf{(Eq. 2)}$$

with:
V_{avg} = Average velocity [m/s]
Z = Depth [m]
TWT = Two-way-time [ms]

We utilized this stage as validation and determination of the quality of the velocity model which will produce the best results with the highest fit and the lowest error. Quality Control of velocity modeling results is done by calculating the error value before and after adjustments are made to the well top of each horizon. So that it produces a residual map or a Time Depth Conversion error map (**Table 2**). Furthermore, the results of Quality Control will be ranked as well as making conclusions from each of the advantages and disadvantages of the velocity model.

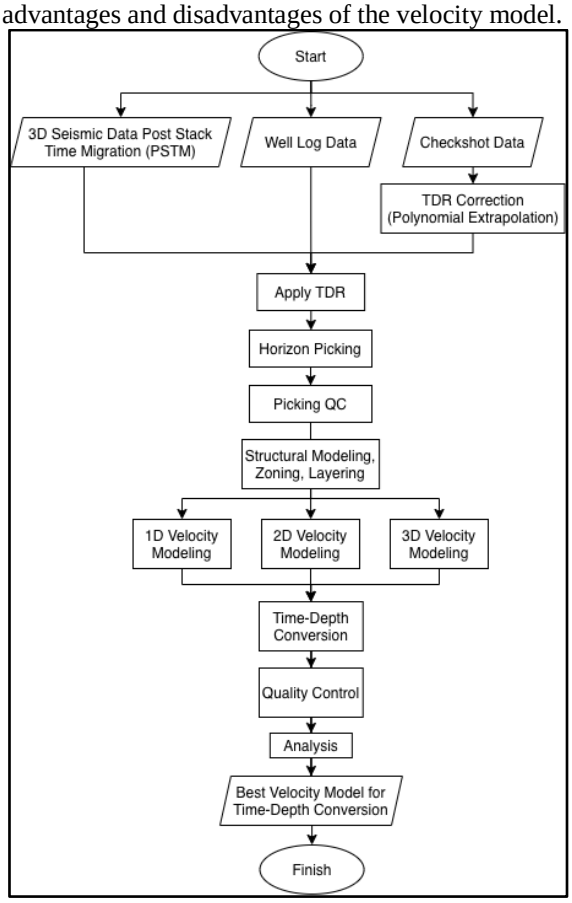

Figure 2. Research Flowchart

Result and Discussion

The results obtained from 1D, 2D, and 3D velocity modeling will be compared and sorted. The order refers to the advantages and disadvantages of each model. One-dimensional modeling has the advantage that the modeling process is relatively fast and light. In addition, the modeling can be applied to perform conversions in time and depth domain variations, such as fault surfaces. However, 1-dimensional modeling does not have lateral variations. This happens because the 1-dimensional model is classified as a single function which is the best average model that represents the entire research area. Consequently, the error and accuracy values will be spread evenly. However, 1-dimensional modeling with more than one time-depth relation (TDR) data will be difficult to get an error value equal to zero.

In 2D velocity modeling **(Figure 4)**, more accurate time-depth conversion results are obtained for each surface. In addition, lateral variations can be well controlled by referring to the gridding method and geological concept used. This modeling method will generally shorten the time but depends on the number of surfaces to be processed. One of the drawbacks is that there are no vertical variations other than the variations that already exist on the reference surface. This is because the modeled velocity is a plane attached to the target surface. Consequently, the 2D velocity modeling method cannot apply the time-depth conversion to faults. The level of accuracy can be maximized with the error value reached. In addition, the critical success factors for modeling include accuracy in the stages of picking horizons for each well top target.

Velocity modeling in 3 dimensions (**Figure 5**) has the combined advantages of 1D and 2D velocity modeling methods. By using the 3-dimensional velocity modeling method, we can apply the time-depth conversion to the lateral and vertical variations accurately and precisely with a minimum error value of zero. This is because the velocity variations in this model are located on the x, y, and z axes. Of course, the accuracy of the Time Depth Conversion process also depends on the quality of the picking horizon and the TDR correction that has been made. However, there are shortcomings in the 3D modeling process, which requires computer specifications that are strong enough to spread velocity in 3D and require a longer time than 1 dimension and 2 dimensions.

Conclusions

- Single function 1D only gets vertical variation. This method can be applied in modeling the fault surface. Because the error values are spread evenly, it will be difficult to get a zero error value.
- 2D is a multi-function velocity model but only has lateral variations. The maximum accuracy of this model depends on the results of QC picking. Lateral variations can be controlled using gridding methods and geological concepts. This model is not capable of performing a time-depth conversion fault and is relatively long if the horizon is increasing.
- 3D is a multi-functional model that is rich in vertical variations. This model tends to be more accurate in all areas and depths. However, the lack of this model is only a matter of time-consuming and requires powerful hardware.

- A good modeling sequence based on advantages and disadvantages is 3D, 2D, and 1D modeling.

References

Blevin, J.E., Boreham, G.J., Summons, R.E., Struckmeyer, H.I.M., Loutit, T.S., 1998. An effective lower Cretaceous petroleum system on the north west shelf: evidence from the Browse basin. In: PURCELL, P.G., PURCELL, R.R. (Eds.), The Sedimentary Basins of Western Australia: Proceedings of the Petroleum Exploration Society of Australia 2. Perth, 1998, pp. 397-420.

Geoscience Australia. (2021). *Regional Geology of the Browse Basin | Geoscience Australia*. Available at: <https://www.ga.gov.au/scientific-topics/energy/province-sedimentary-basin-geology/petroleum/acreagerelease/browse> [Accessed 26 June 2021].

Jablonski, D., Saitta, A.J., 2004. Permian to Lower Cretaceous plate tectonics and its impact on the tectono-stratigraphic development of the Western Australian margin. APPEA J., 287-328.

Ogbamikhumi, A., & Aderibigbe, O. (2019). Velocity modelling and depth conversion uncertainty analysis of onshore reservoirs in the Niger Delta basin. Journal Of The Cameroon Academy Of Sciences, 14(3), 239. doi: 10.4314/jcas.v14i3.7

Rollet, N., Abbott, S., Lech, M.E., Romeyn, R., Grosjean, E., Edwards, D., Totterdell, J., Nicholson, C., Khider, K., Nguyen, D., Bernardel, G., Tenthorey, E., Orlov, C. And Wang, L. (2016). A regional assessment of CO2 storage potential in the Browse Basin: Results of a study undertaken as part of the National CO2 Infrastructure Plan. Record 2016/17. Geoscience Australia, Canberra.

Struckmeyer, H.I.M., Blevin, J.E., Sayers, J., Totterdell, J.M., Baxter, K. And Cathro, D.L. (1998). Structural evolution of the Browse Basin, North West Shelf: new concepts from deep-seismic data. The Sedimentary Basins of Western Australia II: Petroleum Exploration Society of Australia.

Tovaglieri, Federico., Gorge, Annette D. 2014. Stratigraphic architecture of an Early-Middle Jurassic tidally influenced deltaic system (Plover Formation), Browse Basin, Australian North West Shelf. Marine and Petroleum Geology 49 (2014) 59-83.

Yeates, A.N., Bradshaw, M.T., Dickins, J.M., Brakel, A.T., Exon, N.F., Langford, R.P., Mulholland, S.M., Totterdell, J.M. & Yeung, M., 1987. The Westralian Superbasin: an Australian link with Tethys. In: McKenzie, K.G. (ed.) International Symposium on Shallow Tethys 2. Rotterdam, Netherlands. 199-213.

PROCEEDINGS
JOINT CONVENTION BANDUNG (JCB) 2021
November 23rd – 25th 2021

Table 2. Residual Time Depth Conversion.

Kronos		Posseidon 2		Boreas		Posseidon 1		Posseidon North		Pharos		Proteus	
Well Top	Residual (Meter)	Well Top	Residual (Meter)	Well Top	Residual (Meter)	Well Top	Residual (Meter)	Well Top	Residual (Meter)	Well Top	Residual (Meter)	Well Top	Residual (Meter)
Water Bottom	3,17	Water Bottom	2,84	Water Bottom	24,12	Water Bottom	44,16	Water Bottom	3,14	Water Bottom	46,69	Water Bottom	36,74
Oliver	13,43	Oliver	5,8	Oliver	2,18	Oliver	4,61	Oliver	4,5	Oliver	26,63	Oliver	13
Reed Limestone	8,75	Reed Limestone	51,2	Reed Limestone	12,26	Reed Limestone	21,5	Reed Limestone	34,1	Reed Limestone	124,33	Reed Limestone	44,83
Dampier	26,5	Dampier	0,47	Dampier	10,26	Dampier	19,17	Dampier	27,77	Dampier	4,25	Dampier	38,66
Heywood	3,48	Heywood	4,26	Heywood	1,52	Heywood	2,26	Heywood	3,15	Heywood	11,65	Heywood	17,22
Johnson	45,26	Johnson	5,6	Johnson	2,8	Johnson	3,6	Johnson	4,85	Johnson	13,18	Johnson	4,27
Woolaston	10,66	Woolaston	17,8	Woolaston	2,36	Woolaston	4,32	Woolaston	1,17	Woolaston	18,39	Woolaston	61,54
Jamieson	0,06	Jamieson	22,74	Jamieson	24,05	Jamieson	10,05	Jamieson	8,72	Jamieson	45,36	Jamieson	83,55
Horizon 8	24,88	Horizon 8	6,9	Horizon 8	1,36	Horizon 8	5,78	Horizon 8	17,97	Horizon 8	11,36	Horizon 8	38,03
Horizon 9	16,88	Horizon 9	5,25	Horizon 9	7,89	Horizon 9	19,07	Horizon 9	3,28	Horizon 9	10,02	Horizon 9	2,01

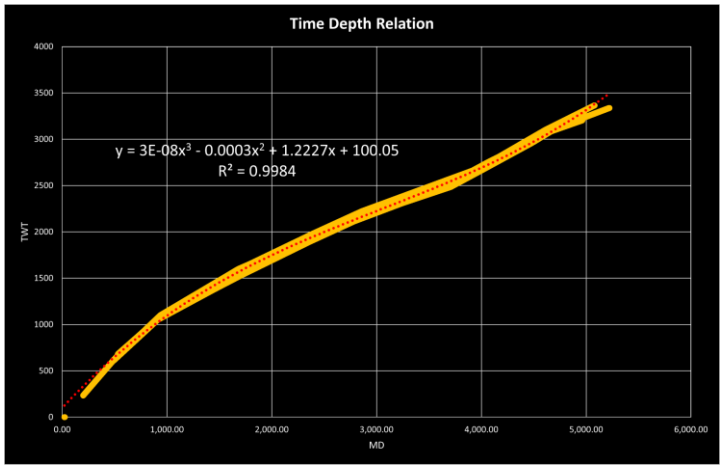

Figure 3. Graph of TDR Correction for all Wells in the Research Area.

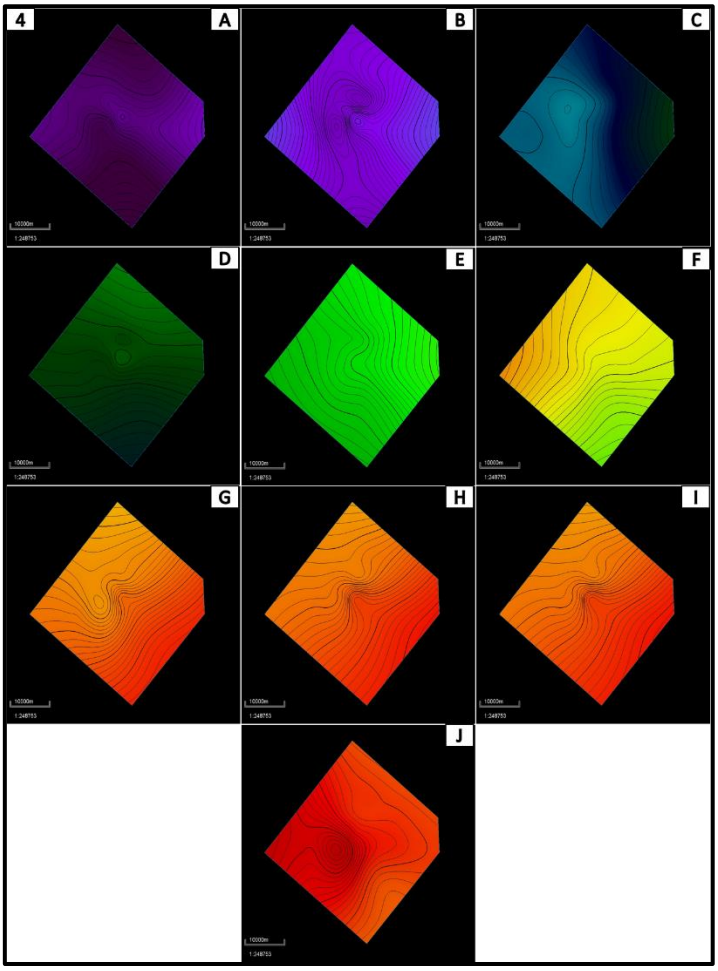

Figure 4. 2D Velocity Modelling.

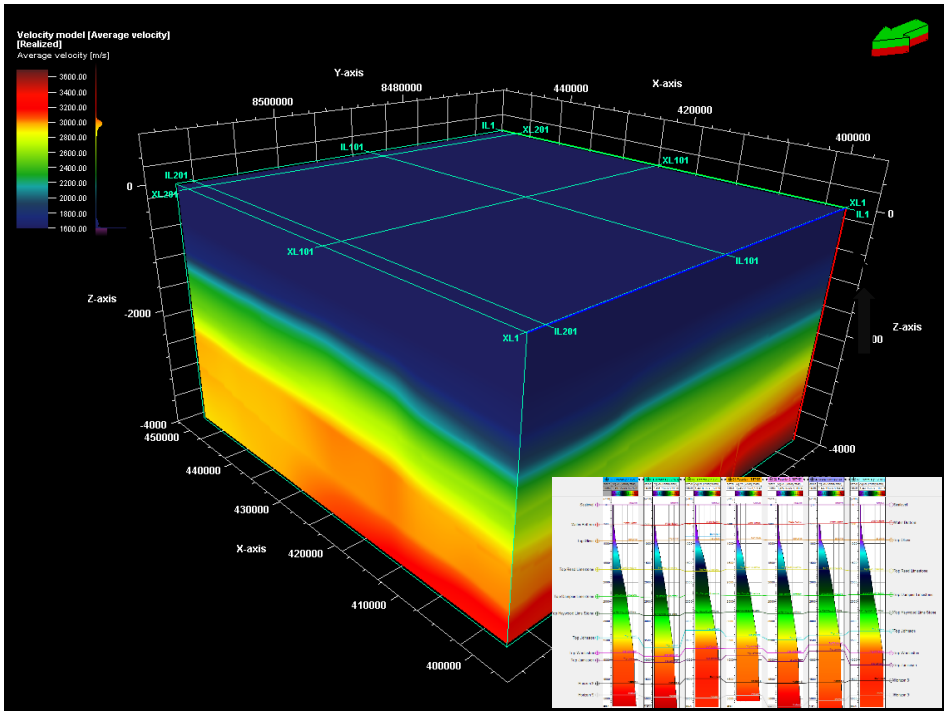

Figure 5. Cross-section of 3D Velocity Model in the Research Area and Velocity Modeling Results on the Cross-section of the Well in the Research Area.

PROCEEDINGS
JOINT CONVENTION BANDUNG (JCB) 2021
November 23rd – 25th 2021

Source Rock Potential of Nampol Formation in Sumbermanjing Area, Malang, East Java, Indonesia

Carolus Prasetyadi[1)], Achmad Subandrio[1)], M. Gazali Rachman[1)], Antu Ridha Falkhan Barizi[1)], Muhamad Muslim[1)]
[1)]Department of Geological Engineering UPN "Veteran" Yogyakarta.

Abstract
Nampol Formation of the Southern Mountains of eastern Java (Indonesia) has a distribution from its type location in Pacitan to the South Malang area. In the research area, this formation consists of clastic limestone with black shale inserts, claystone, siltstone, carbonate sandstone and claystone which are interpreted to be deposited in a restricted platform interior environment with closed water circulation. A total of three samples were analyzed to evaluate the organic matter content, kerogen type, thermal maturity, and hydrocarbon generating potential. Samples were taken from clastic carbonate deposits of the Nampol Formation. Based on the results of geochemical analysis, the three samples from the Nampol Formation have a TOC content of 3.48 – 26.18 wt% and possess good to excellent hydrocarbon generating potential. Hydrogen Index (HI) values for the studied samples ranged from 43 to 86 mg HC/g TOC and S1+S2 results ranged from 1.52 to 19.55 mg HC/g rock, indicating that the sample has the potential to produce gas. All three samples were dominated by Type III kerogen and were thus considered gas prone based on the HI vs. Tmax diagrams. The three samples were categorized as thermally immature based on Tmax pyrolysis analysis and Vitrinite Reflectance (VR) values in the range of 0.44 to 0.46 %Ro. Based on the results obtained, the black shale and coal in the Nampol Formation has the capability to generate hydrocarbon but are considered as an immature source rock that can be predicted to produce gas at its peak maturity.

Keywords : Malang, Nampol Formation, source rock, TOC

Introduction
Nampol Formation of the Southern Mountains of eastern Java (Indonesia) has a distribution from its type location in Pacitan to the South Malang area. According to Samodra & Wiryosujono, (1989), Nampol Formation is 100 m thick which is composed of coarse to fine-sized clastic sedimentary rocks with alternating volcaniclastic rocks and lignite. Recent research has discovered that in the regional stratigraphic setting of the Southern Mountains of East Java there is the Nampol Formation which is considered to possess the capability to become a potential source rock with the discovery of organic material in the lithology of black shale, siltstone, claystone and coal inserts. The presence of black shale and black claystone in the Nampol Formation is demands further investigation through geological mapping and geochemical analysis to determine to total quantity organic matter, type of kerogen, and source rock thermal maturity.

The research area is located in the eastern part of Southern Mountain, more precisely in Sumbermanjing District, Malang Regency, East Java Province. It is located approximately 50 km from the Malang City which can be reached within 1 hour 30 minutes (Figure 1). The focus of this research is on the Nampol Formation possibilty to become a potential source rock due to their organic matter content.

The main objectives of this research is to investigate the possibility of potential source rock.

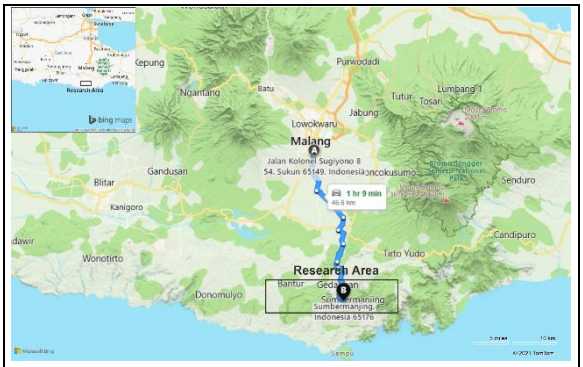

Figure 1. Research Location

Data and Methods
Data collection in this study used 3 methods consisting of surface geological mapping, measuring section (MS), and rock sampling. The selected samples are then analyzed in the laboratory to determine total quantity organic matter, type of kerogen, and source rock thermal maturity. Analysis was carried out on 3 samples of source rock. Samples that taken were calcareous claystone, black shale, and shale coal with the size of a fist. The outcrop is initially dredged with a scrapper to a depth of ±20-30 cm to get samples that have not been contaminated. After being taken, the fresh sample was immediately wrapped in aluminum foil and put in a tight plastic bag to maintain sample quality (Figure 2).

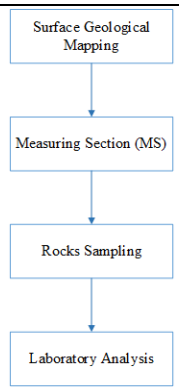

Figure 2. Research Flow Chart

Regional Stratigraphy
The Southern Mountains of East Java are generally composed of rocks with Neogene to Quaternary age. This area is mostly dominated by volcanic rock and limestone. Rock sequences are arranged based on detailed stratigraphy through selected paths and presented in a stratigraphic column (Figure 3).
The stratigraphic order from oldest to youngest is as follows:
1. Arjosari Formation (Tma)

The Arjosari Formation consists of turbidite deposits or sediments that are influ-enced by shearing symptoms that alternate with volcanic rocks, of Late Oligocene Early Miocene age. At the bottom of the formation consists of

breccia of various materials, sandstone, tuffaceous sandstone, claystone, sandy marl, and calcareous claystone, with pumice and limestone breccias inserted. The upper part is interspersed with volcanic breccia, lava, and tuff. Based on its fossil content, the Arjosari Formation is thought to be in the late Oligocene – Late Early Miocene. The Arjosari Formation has a fingering relationship with the Mandalika Formation.

2. Mandalika Formation (Tomm)

The Mandalika Formation is composed of volcanic rock with clastic (volcanic) inserts in a shallow marine environment. At the bottom of this formation is composed of repeating volcanic breccias, lava, tuff with inserts of tuffan sandstone, claystone and polymic breccias. In the center of the formation, it is composed of repeating volcanic breccias, lava and diminishing clastic sediments. At the top of the formation is composed of pillow lava with basalt breccia inserts and tuffan claystone.

3. Intrusive Rocks (Tomi)

According to Samodra et al., (1992), breakthrough rocks intrusive the above formation with lithology in the form of: dacite, andesite, basalt, and diorite. This intrusive rock is in the form of stock, fractured, and localized appearance of a volcanic neck so that it affects the intruded rocks with the age of the Late Oligocene to the end of the Early Miocene, namely the Arjosari and Mandalika Formation. This intrusive rock affects the formation of hydrothermal altered rock and low grade met-amorphic in the rock that is breached. This intrusive rock is estimated to be of Late Oligocene to early Middle Miocene age because the younger formations (Jaten, Wuni, Nampol, Oyo, and Wonosari Formation) are not affected.

4. Jaten Formation (Tmj)

This formation is composed of terrestrial clastic sediments to shallow (restricted) seas containing debris from land and lignite inserts. The bottom of the unit is composed of conglomerate sandstone, quartz sandstone, tuffaceous sandstone, con-glomerate, mudstone; interspersed with claystone and bituminous shale. The upper part is fine clastic sediment in the form of siltstone, claystone and sandy marl with tuff insertion. Fossil content in interspersed with carbonated claystones:, Planorbulina sp., Cancris, sp., Elphidium, sp., Quiqueloculina, sp., Dentalina, sp., ostracods, pelecypods and gastropods.

5. Wuni Formation (Tmw)

The Wuni Formation is composed of volcanic rock from Middle Miocene volcanic activity, with the insertion of clastic sediments of volcanic origin, deposited in a shallow marine environment around the Early Miocene highlands. This unit is composed of volcanic breccia and tuff; inserts tuffaceous sandstone, tuffaceous silt-stone, claystone, limestone, and lignite. Fossils in this unit are very rare. Based on its stratigraphic position which is younger than the Jaten Formation, this unit is thought to be in the middle of the Middle Miocene.

6. Nampol Formation (Tmn)

This unit is a collection of coarse to fine clastic rocks, interspersed with volcanic rocks and lignite. The bottom of this unit is composed of repeating tuffaceous sandstone, siltstone, and claystone, with volcanic breccia, conglomerate sandstone, and lignite inserted. The upper part is more calcareous, consisting of repeating sand-stone, siltstone, claystone; inserts tuff and lignite. The Nampol Formation is formed in a shallow marine environment adjacent to the loop area with a formation thick-ness of about 100 m.

7. Oyo Formation (Tmo)

The Oyo Formation is a collection of clastic limestones whose formation is influenced by volcanic activity. Consists of tuffaceous sandstone, calcareous sandstone, calcareous siltstone, sandy limestone, conglomerate limestone; inserting sandy tuff, marl and conglomerate limestone; inserts sandy tuff, marl and reef limestone. The lower part of the unit is generally tuffaceous, the higher the tuff element decreases and turns into limestone. Based on the fossil content of small planktonic foraminifera, the Oyo formation has a Middle Miocene age. This formation is formed in a marine environment with a depth of 20-100 m.

8. Wonosari Formation (Tmwl)

This unit is a limestone deposit that is late Middle Miocene and formed in a shallow marine environment. The lower part of the unit is more clastic in nature; consists of sandy limestone (calcarenite) with calcareous sandstones. The upper part is com-posed of reef limestone, interspersed with calcarenite, marl, and conglomerate lime-stone. This formation is very rich in small planktonic foraminifera which based on the assemblage they contain have an age of N13-N16 or Middle Miocene to early Late Miocene.

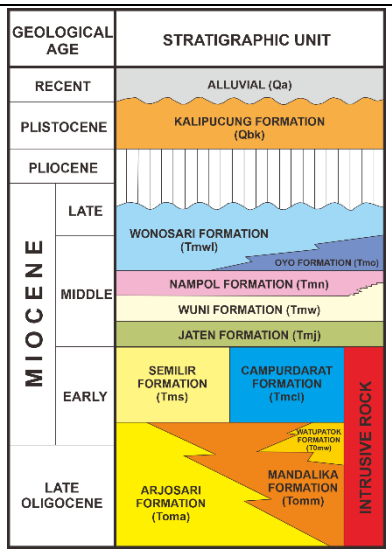

Figure 3. Southern Mountain East Java stratigraphic column (Samodra & Wiryosujono, 1989).

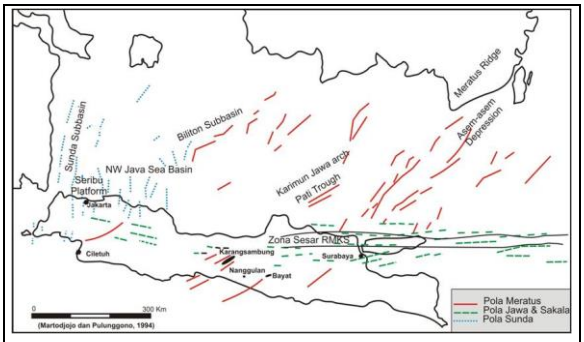

Figure 4. The main structural pattern of Java Island (Pulunggono & Martodjojo, 1994)

PROCEEDINGS
JOINT CONVENTION BANDUNG (JCB) 2021
November 23rd – 25th 2021

Regional Strutural Geology

There are three major structural patterns in Java (Pulunggono & Martodjojo, 1994). First, the northeast-southwest direction (Meratus direction) which was formed in the Late Cretaceous - Early Eocene age. Second, north-south direction (Sunda direction) which was formed in the Early Eocene - Early Oligicene age. Third, the west-east direction (Javanese direction) which was formed at the Late Oligocene age by compression forces from the subduction in the southern part of Java Island (Figure 4).

Result and Discussion

Lithological Characteristics

The rock sampling locations were at the observation sites FB-01 and MM-05 on the stratigraphic measuring section track of Bambang River and Sumbernanas River. Meanwhile, for the rock sample, DA-62 is on the selected observation location in Sekarbanyu District, Sumbermanjing, Malang (Figure 5).

The outcrop of the Nampol Formation in Sekarbanyu at location DA-62 is composed of calcarous claystone, siltstone, clastic limestone, and black shale. Calcareous claystone, grey fresh color, containing shell fragments. Siltstone, grey colored. Clastic limestone, milky white colored, containing mollusk shell fragments. Black shale with parallel lamination structure, containing organic material and shell fragments (Figure 6).

The outcrop of the Nampol Formation on the Bambang River traverse at location FB-01 is composed of intercalation of clastic limestones and calcareous claystones. Clastic limestone is yellowish white with a large grain size of fine sand (1/8-1/4 mm), with a layer thickness of ± 1 m. Calcareous claystone, grey fresh color, contains lignite inserts and shell fragments (Figure 7).

The outcrop of the Nampol Formation on the Sumbernanas River traverse at location MM-05 is composed of clastic limestone and calcareous claystone. Clastic limestone is yellowish white with a large grain size of fine sand (1/8-1/4 mm), with a layer thickness of ± 1 m. Calcaroeus claystone, grey colored, contains lignite inserts and shell fragments (Figure 8).

Potential Source Rock

The results of TOC analysis (Table 1) on the source rock samples in the study area showed TOC values of 3.48 – 26.18 wt.% were categorized as good to very good in gener-ating hydrocarbons according to Peters (1986) and Waples (1985). The cross-plot of TOC values was carried out on the values of S1+S2 to determine the total generating potential of hydrocarbons that could be produced by each sample. The plotting results show that the total hydrocarbon potential that can be produced for the sample 'LP01' is not good; 'LP62' is fair; and 'LP05' is good (Figure 9).

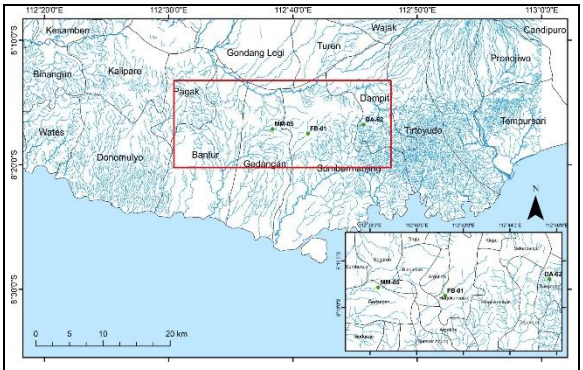

Figure 5. Map Samples are marked with a green dot.

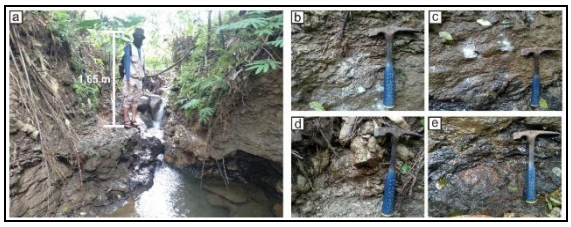

Figure 6. Location of source rock sampling. (a) Location : DA-62 (Sekarbanyu). (b, c, d) Calcareous claystone, siltstone, and clastic limestone. (e) Black shale sampled for geochemical analysis.

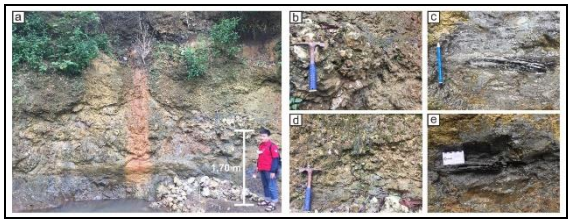

Figure 7. Location of source rock sampling. (a) Location : FB-01 (Bambang River, Argotirto). (b,c,d) Intercalation of clastic limestone and carbonated claystone. (e) Sampled lignite inserts for geochemical analysis.

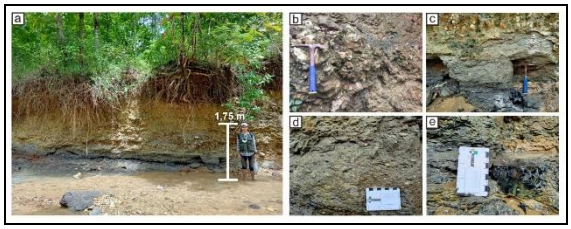

Figure 8. Location of source rock sampling. (a) Location : MM-05 (Sumbernanas River, Ringinsar) (b,c,d) Clastic limestone and calcareous claystone. (e) Sampled lignite inserts for geochemical analysis.

PROCEEDINGS
JOINT CONVENTION BANDUNG (JCB) 2021
November 23rd – 25th 2021

Table 1. Results of TOC and Rock-Eval Pyrolysis analysis on rock samples in the Nampol Fm.

	Sample ID	Lithology	TOC (wt.%)	mg/gm rock			Tmax (°C)	Oil Production Index (OPI)	Potential Yield (S_1+S_2)	Hydrogen Index	Oxygen Index	%Ro
				S_1	S_2	S_3						
1	LP 1	Calc. claystone	3,48	0,04	1,48	0,38	430	0,03	1,52	43	11	0,44
2	LP 62	Shale	4,01	0,22	3,44	2,19	417	0,06	3,66	86	55	0,46
3	LP 05	Shaly Coal	26,18	0,27	19,28	11,82	408	0,01	19,55	74	45	0,45

S_1 = Free Hydrocarbons
S_2 = Pyrolysable Hydrocarbons
S_3 = Organic CO_2
Oil Production Index = Transformation Ratio = $S_1/(S_1+S_2)$
Tmax = Temperature of Maximum S_2
Oxygen Index = (S_3/TOC) x 100
* Pyrolysis by Rock Eval II; TOC content by Leco Analyzer
Hydrogen Index = (S_2/TOC) x 100
*** = Not Detected

The diagram of the content of Total Organic Carbon (TOC) versus Potential Yield (PY) (Figure 6) shows the potential for hydrocarbons in the study area which is indicated by the level of richness of organic material content. This diagram shows that two samples from the Nampol Formation showed good organic material quality with TOC values of 3.48 wt% and 4.01 wt% and PY of 1.52 and 3.66 mgHC/g, respectively. Another sample showed very good organic material quality with a TOC value of 26.18% and a PY value of 19.55 mgHC/g. The three samples tend to form gas (gas prone) with one of the samples, code LP 05, possess the possibility to become a potential or effective source rock.

Based on the hydrogen index (HI) and of S2/S3 values, it can be infered that the type of organic material in the three samples is Type III kerogen (Figure 7). This kerogen contains humic organic matter derived from woody plants containing cellulose from land plants (equivalent to vitrinite in coal (Waples & Curiale, 1999).

The thermal maturity of rock samples was determined using vitrinite reflectance (VR) and Rock-Eval Pyrolysis analyses. From the results of the analysis of vitrinite reflectance in rock samples, values of <0.5%Ro are obtained. The rock samples are thermally immature to become hydrocarbon source rocks, according to Peters and Cassa (1994) classification of source rock maturity based on vitrinite reflectance value. Meanwhile, Rock-Eval pyrolysis data revealed that the maximum kerogen-breaking temperature for the three samples' was ranged from 408 to 430°C. The rock samples are classified as Immature source rock according to Tissot & Welte (1978)'s Tmax classification and its relationship with the source rock's thermal maturity (Table 2).

Table 2. Guidelines for quantity, quality and maturity of source rock determination for immature source rocks.

Quantity		TOC	S1	S2
Poor		<0,5	<0,5	<2,5
Fair		0,5 – 1	0,5 – 1	2,5 – 5,0
Good		1 – 2	1 – 2	5 – 10
Very Good		2 – 4	2 – 4	10 – 20
Excellent		>4	>4	>20
Quality		HI	S2/S3	Kerogen Type
-		<50	<1	IV
Gas		20 – 200	1 – 5	III
Oil and Gas		200 – 300	5 – 10	II/III
Oil		300 – 600	10 – 15	II
Oil		>600	>15	I
Thermal Maturity		VR (%)	Tmax (°C)	TAI
Immature		0,2 – 0,6	<435	1,5 – 2,6
Mature	Early	0,6 – 0,65	435 – 445	2,6 – 2,7
	Peak	0,65 – 0,9	445 – 450	2,7 – 2,9
	Late	0,9 – 1,35	450 – 470	2,9 – 3,3
Over mature		>1,35	>470	>3,3

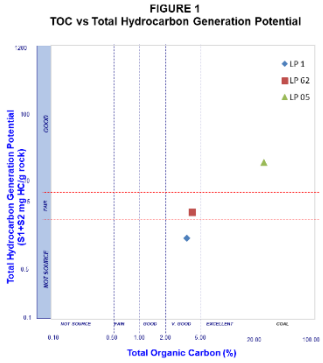

Figure 9. Cross-plot between Total Organic Carbon (TOC) and Potential Yield (PY) content.

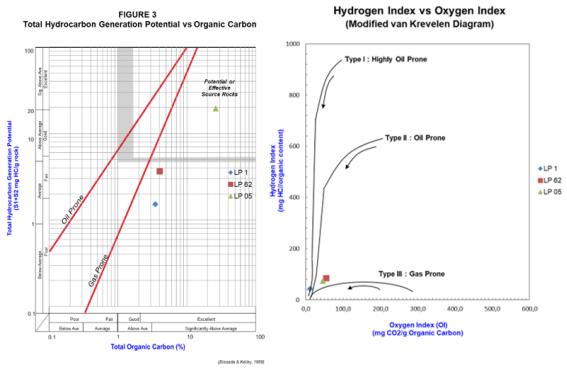

Figure 10. Diagram of Total Organic Carbon (TOC) versus Potential Yield (PY) content (**left**). Cross plot between Oxygen Index (OI) and Hydrogen Index (HI) values (**right**). All three samples is gas prone.

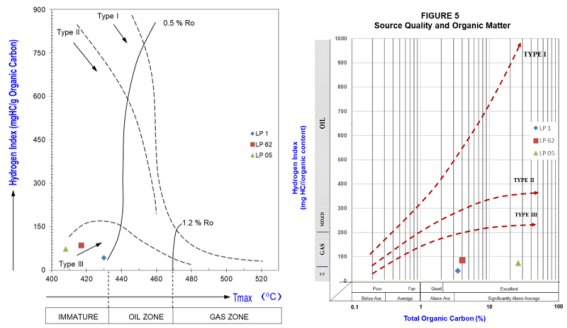

Figure 11. Cross plot between Tmax and Hydrogen Index (HI) values (left). Cross plot between TOC and Hydrogen Index (HI) values (right). The organic material from three samples were all classified as type III kerogen.

Conclusions

Based on the results obtained, it can be concluded that black shale and coal in the Nampol Formation are immature source rocks but have the capability to generate hydrocarbons where at the peak of their maturity, can be predicted its tendency to produce gas. For further research, it is envisaged to discover the possibility of oil seeps presence in the Southern Mountains, allowing for the correlation between oil and source rock.

References

Peters, K. E., & Cassa, M. R. (1994). Applied source rock geochemistry. In *The Petroleum System: From Source to Trap* (Vol. 60, Issue January 1994, pp. 93–120). American Association of Petroleum Geologists.

Peters, Kenneth E. (1986). Guidelines for evaluating petroleum source rock using programmed pyrolysis. *AAPG Bulletin*, *70*(3), 318–329.

Pulunggono, A., & Martodjojo, S. (1994). Perubahan tektonik Paleogen-Neogen merupakan peristiwa tektonik terpenting di Jawa. *Proc. Geologi Dan Geoteknik Pulau Jawa, Yogyakarta*, 37–49.

Samodra, H., & Wiryosujono, S. (1989). *Tinjauan tatanan stratigrafi dan tektonik Pegunungan Selatan Jawa Timur antara Pacitan–Ponorogo*. P3G, Bandung.

Tissot, B. P., & Welte, D. H. (1978). *Petroleum formation and occurrence—A new approach to oil and gas exploration* (1st ed., Vol. 2). Springer-Verlag Berlin Heidelberg. https://doi.org/10.1016/0146-6380(80)90028-5

Waples, D. W. (1985). *Geochemistry in petroleum exploration*. IHRDC Press, Boston, MA. https://www.osti.gov/biblio/5563367

Waples, D. W., & Curiale, J. A. (1999). Oil-Oil and Oil-Source Rock Correlations. In E. A. Beaumont & N. H. Foster (Eds.), *Treatise of Petroleum Geology/Handbook of Petroleum Geology: Exploring for Oil and Gas Traps.* (pp. 8-4-8–71). AAPG Special Volumes.

Acknowledgements

The authors would like to thank the Institute for Research and Community Service (LPPM) Universitas Pembangunan Nasional Veteran Yogyakarta, Indonesia, for providing funds for this research. We also thank Falkhan, Muslim, Defa, and Guntor, final-year geology students of Teknik Geologi UPN “Veteran” Yogyakarta, for their help during our fieldwork.

PROCEEDINGS
JOINT CONVENTION BANDUNG (JCB)2021
November 23rd – 25th 2021

The GEOSTAT Application version 2.0 Development for Determination of Aftershocks Earthquake Decay Based on MATLAB

Takhul Bakhtiar and Iman Suardi
Program Studi Geofisika, Sekolah Tinggi Meteorologi Klimatologi dan Geofisika, Indonesia

Abstract

The emergence of large magnitude earthquakes will certainly be followed by a series of aftershocks. Therefore, we need an application that is easy and simple to find out when the event ends. The GEOSTAT Application version 2.0 is the result of the development of The GEOSTAT Application which was redeveloped using MATLAB to solve problems with determining the end time of aftershocks. Applications that have a Graphical User Interface (GUI) display contain several methods such as Omori, Mogi I, Mogi II and Utsu method to determine the decay of aftershocks. The GEOSTAT Application version 2.0 can be operated properly on the user's device and helps the user in knowing the end of aftershocks simply and easily which is usually calculated manually.

Keywords*:* MATLAB, Omori, Mogi I, Mogi II, Utsu, Earthquake Decay Application

Introduction

The complex tectonic structure in Indonesia cause seismic activity in Indonesia to be classified as very high (Pusgen, 2017). This can be seen based on three major tectonic plates encounters in the world, namely The Eurasian Plate, The Indo-Australian Plate and The Pacific Plate (Ibrahim et al., 2010). So, this can result in a large magnitude earthquake followed by a collection of aftershocks (Riga and Balocchi, 2017). The emergence of a large earthquake followed by aftershocks will certainly cause panic in the community when the aftershocks end. Academics, researchers and related agencies will certainly conduct studies and research to determine the end time of aftershocks. In order to support and assist academics, researchers and related agencies to solve these problems, a simple and easy application is needed.

The GEOSTAT Application version 2.0 is here as a solution to answer these problems. This application is a development of The GEOSTAT Application which serves to determine the level of earthquake risk in an area. The GEOSTAT Application version 2.0 contained several facilities such as models to determine the end time of aftershocks such as the Omori model (1894), Mogi I (1962), Mogi II (1962) and Utsu (1957).

Data and Method

Application development is carried out to improve the existing facilities in The GEOSTAT Application version 2.0. One form of application development is to add functionality in this application. The upgraded facility in this application is the aftershocks decay. The application development process requires much software such as MATLAB as the main component in making source code and Graphical User Interface, Canva as a tool for designing application Microsoft Excel as a container for storing earthquake data. There are several stages carried out on developing the GEOSTAT application:

1. Literature study.
2. Create source code m-file, creating a fig-file for Graphical User Interface (GUI) independently or pure script and designing the latest application features.
3. System test and application validation.

Authors use data after Ambon earthquake on September 25 2019, at 23:46:44 Universal Time Coordinate (UTC) with a magnitude 6.5 Mw. This data used for system test and application validation. The data was obtained from the BMKG earthquake catalog data repository from 26 September 2019 to 25 October 2019, coordinate 2.21 until 5.35°LS and 125.28 until 132.12°BT. The test data is useful to find out if the system in the application can run smoothly, well and correctly.

Table 1. List of aftershocks earthquake after 30 minutes mainshock

Date	Time (UTC)	Depth (Km)	Magnitude
26/09/2019	00:00:08.7	10	3.9
26/09/2019	00:03:55.8	10	4.3
26/09/2019	00:04:45.0	10	4
26/09/2019	00:11:33.7	10	4
26/09/2019	00:12:40.3	10	4
26/09/2019	00:15:11.9	10	4.7
26/09/2019	00:23:29.2	10	4,.2
26/09/2019	00:27:43.8	10	3.9
26/09/2019	00:28.46.3	10	4

The latest features in The GEOSTAT Application version 2.0 require validation tests to re-check the

PROCEEDINGS
JOINT CONVENTION BANDUNG (JCB)2021
November 23rd – 25th 2021

operation of the existing system in the application. In knowing this, some research results that have been done previously are needed to be re-tested using the application. The following research is used to test The GEOSTAT Application version 2.0:

1. Penentuan Waktu Berakhirnya Gempa Bumi Susulan untuk Gempa Bumi Biak 16 Juni 2010 (Awaludin, 2011).
2. Waktu Berakhirnya Gempa Bumi Susulan untuk Gempa Bumi Sulawesi 28 September 2018 (Pahlevi, 2020).

Foreshocks are some earthquake event that precedes the main earthquake in a series of earthquakes with magnitude smaller than the Mainshock. Mainshock. Mainshock is an earthquake event with the most energetic magnitude or the strongest due to the release of previously accumulated energy. Aftershocks are series of earthquake events that follow the mainshock with a smaller magnitude than the mainshock. Aftershocks can occur over a period of days, months or even years. The greater magnitude of the mainshock, the more the series of small earthquakes that follow it and the longer the aftershock event ends (Riga and Balocchi, 2017).

The relationship between time and frequency to determine the level of aftershocks activity can be presented in the formula (Omori, 1894)

$$n(t) = \frac{a}{t+b} \qquad (1)$$

The time span for aftershocks to end if they occur ≥100 days can be determined using this formula Mogi I (Mogi, 1962)

$$n(t) = a.t^{-b} \qquad (2)$$

While the time span of the end of aftershocks that occurred within a period of < 100 days can be determined by the following formula Mogi II (Mogi, 1962)

$$n(t) = a.e^{-bt} \qquad (3)$$

In addition, the formula can be used to determine the end time of aftershocks (Utsu, 1957)

$$n(t) = \frac{a}{t+c^b} \qquad (4)$$

Where *n(t)* is the accumulation of aftershocks *n* calculated in the time span *t.* Then, *t* is the time span for aftershocks, while *a* and *b* are constants, while *c* is 0.01. Several formulas used to determine the end time of aftershocks provide a correlation between the frequency of aftershocks and the time of aftershocks. Both are expressed as the dependent variable (*y*) and the independent variable (*x*). Supranto (2008) explains that the dependent variables and the independent variables can be formulated into a linear relationship which is solved by the least squares method.

$$\bar{Y} = a + b\bar{X}_i$$

Supranto (2008) explains that to find out the constants *a* and *b*, it can be solved with the formula

$$a = \bar{Y} - b\bar{X}_i$$

and

$$b = \frac{n\Sigma X_i Y_i - \Sigma X_i \Sigma Y_i}{n\,\Sigma X_i^2 - (\Sigma X_i^2)}$$

Supranto (2008) also explains that to find out the correlation between constants *a* and *b*, it can be known by using the formula

$$r = \frac{n\Sigma X_i Y_i - \Sigma X_i \Sigma Y_i}{\sqrt{n\,\Sigma X_i^2 - (\Sigma X_i^2)}\sqrt{n\Sigma Y_i^2 - (\Sigma Y_i)^2}}$$

The interpretation of the correlation value between constants *a* and *b* can be seen through the following table (Sugiyono, 2007)

Table 2. The correlation value of the dependent variable and the independent variable (Sugiyono, 2007)

Value	Definition
0.00 - 0.19 or 0.00 - (-0.19)	Very Low
0.20 - 0.39 or (-0.20) - (-0.39)	Low
0.40 - 0.59 or (-0.40) - (-0.59)	Medium
0.60 - 0.79 or (-0.60) - (-0.79)	Strong
0.80 - 1.00 or (-0.80) - (-1.00)	Very Strong

Result and Discussion

When the system test process and application upgrade have been completed, the user can operate the GEOSTAT application in several stages:

1. Search for aftershocks earthquake
2. Save in excel that has been provided by the author.
3. Classify the magnitude frequency with the time of aftershocks and open this application, it will appear as shown in Figure 3 and Figure 4.

PROCEEDINGS
JOINT CONVENTION BANDUNG (JCB)2021
November 23rd – 25th 2021

4. Select the method to use.
5. Enter parameters such as magnitude, classification of earthquake grouping time intervals, date and time of mainshock occurrence.
6. Calculate and the calculation results will appear as shown in Figure 6.

In the development process this application has advantages where the level of accuracy application calculation is more detailed by presenting specific end time of aftershocks in the area (Figure 4). This specific time can help people to find out more detailed information so that the people become more prepared and alert.

System validation test is needed to determine system performance in processing calculations. The following are the results of the application system validation test.

Table 3. The first comparison results of calculating end time aftershocks

Method	Awaludin (2011)	GEOSTAT
Omori	37 Days	387 Days
Mogi I	1056 Days	1057 Days
Mogi II	19 Days	19 Days
Utsu	1029 Days	1030 Days

Table 4. The first comparison results of correlation calculation

Method	Awaludin (2011)	GEOSTAT
Omori	5.26524	0.932
Mogi I	-0.8702	-0.87021
Mogi II	-0.94687	-0.93094
Utsu	-0.8707	-0.97072

Table 5. The second comparison results of calculating end time aftershocks

Method	Pahlevi (2020)	GEOSTAT
Omori	183 Days	184 Days
Mogi I	340 Days	340 Days
Mogi II	17 Days	17 Days
Utsu	334 Days	334 Days

Table 6. The second comparison of correlation calculation results

Method	Pahlevi (2020)	GEOSTAT
Omori	0.96	0.96369
Mogi I	-0.97	-0.97202
Mogi II	-0.95	-0.95586
Utsu	-0.97	-0.97206

From some the tables above, it can be seen that the system giving good results and accuracy. However, there was an error in Awaludin (2011) research. An error occurred on Awaludin (2011) research for the calculation of Omori with correlation results that exceeded the range of values between -1 to 1.

So, this affected the calculation with the expiration time of aftershocks for 37 days. Meanwhile, based on the calculation of The GEOSTAT Application version 2.0, it shows good accuracy results with a correlation value close to 1, which is 0.932. So the time for aftershocks to expire is 387 days.

The thing that needs to be considered in determining the independent and independent variables are the time interval for collecting earthquake frequency data and magnitude earthquake. The greater the magnitude of the mainshock, the longer the duration of the aftershock. This is because the duration of the aftershock loading is inversely related to the earthquake frequency.

Conclusions

The GEOSTAT Application version 2.0 can runs well and assist users in calculating the end time of aftershocks which are calculated manually. In addition this application can calculate and knowing the end time of aftershocks simply and easily.

References

Abdelnaby, A. E., 2012, Dissertation, University of Illinois at Urbana-Champaign
Awaludin, A., 2011, Skripsi, Fakultas Sains dan Teknologi UIN Syarif Hidayatullah.
Ibrahim, G., P. Sendjaja and Subarjo, 2010, BMKG.
Mogi, K., 1962, Bulletin Earthquake Research Institute, **40**, 107-124.
Omori, F., 1894, Journal of Colloid Science, **7**, 111-200.
Pahlevi, M. I., 2020, Skripsi, Fakultas Sains dan Teknologi UIN Syarif Hidayatullah.
Pusgen, 2017, Pusat Litbang Perumahan dan Pemukiman.
Riga, G. and P. Balocchi, 2017, Open Journal of Earthquake Research, **6**, 135-157.
Sugiyono, 2007, ALFABETA.
Supranto, J., 2008, Erlangga.
Utsu, T., 1957, Journal of The Seismological Society of Japan, **10,** 35-45.

PROCEEDINGS
JOINT CONVENTION BANDUNG (JCB)2021
November 23rd – 25th 2021

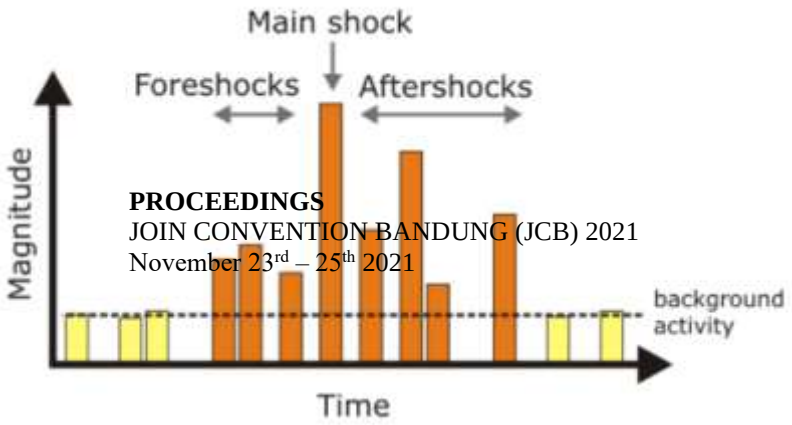

PROCEEDINGS
JOIN CONVENTION BANDUNG (JCB) 2021
November 23rd – 25th 2021

Figure 1: Sequence of foreshocks, mainshock and aftershocks earthquake events (Abdelnaby, 2012)

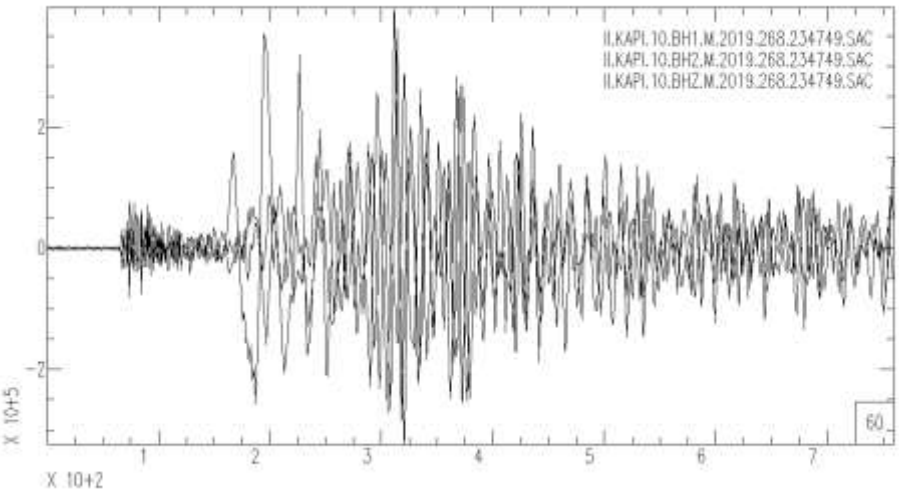

(a)

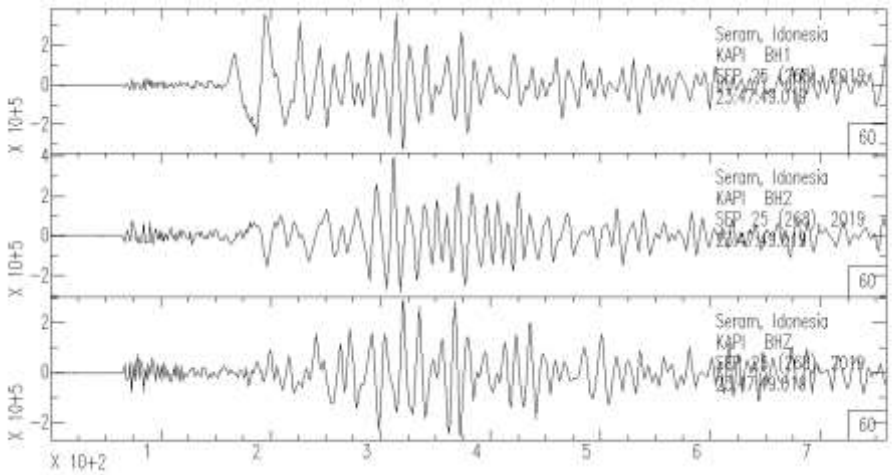

(b)

Figure 2. (a) Mainshock earthquake seismogram magnitude 6.5 Mw and (b) Mainshock earthquake recording on 3 components seismogram.

PROCEEDINGS
JOINT CONVENTION BANDUNG (JCB) 2021
November 23rd – 25th 2021

Figure 3: The splash screen of the GEOSAT Application version 2.0

Figure 4: Main menu display

PROCEEDINGS
JOINT CONVENTION BANDUNG (JCB)2021
November 23rd – 25th 2021

Figure 5: Earthquake decay menu display

Figure 6: Calculation result display

PROCEEDINGS
JOINT CONVENTION BANDUNG (JCB) 2021
November 23rd – 25th 2021

The Feasibility Study of Reservoir Geomechanics from Brittleness Evaluation

Benyamin Elilaski Nababan [1], Harnanti Yogaputri Hutami [2], Fatkhan [3], Sonny Winardhi [4].
[1,2] Geophysics for Natural Resource Research Group, Geophysical Engineering Program, Institut Teknologi Sumatera.
[3,4] Geophysical Engineering Departement, Faculty of Mining and Petroleum Engineering, Institut Teknologi Bandung.

Abstract
A detailed understanding regarding the rock Brittleness Index is useful in oil and gas exploration as upfront information to determine the rock fracture gradient. Researchers have proposed several methods to estimate the rock Brittleness Index. However, different methods may yield different results and, hence, lead to varying interpretations regarding the Brittleness Index classification. This paper estimates the Brittleness Index of an Indonesian gas well using three approaches based on the log data and Rock Physics Modeling and to assess the consistency of the methods. In this study, the rock's brittleness is estimated based on the elastic parameters obtained from the log data as well as the rock physics method and mineralogical data. In the case that the acoustic data is unavailable, the acoustic log data was first estimated using Rock Physics Modeling using Voigt-Reuss-Hill, Kuster-Toksöz, and Biot-Gassman methods. These elastic property-based methods were then compared with the Brittleness Index obtained from the mineralogical method. The results obtained in this study suggest that the elastic property-based and the mineralogical-based methods produced a consistent Brittleness Index. However, they are different in terms of their vertical resolution. It is observed that the Brittleness Index estimated using the actual log data produced a higher resolution index as compared to the one estimated based on the mineralogical data. The Brittleness Index estimation based on the elastic parameters from the log data suggests that the rocks can be classified as less ductile to less brittle, while the Rock Physics Modeling suggests a generally less ductile type of rocks. To optimize the hydraulic fracturing design and planning, it is advised that the TOC data be combined with the Brittleness Index to identify the most suitable depth for an effective and optimum hydraulic fracturing. For further investigation in the future, it is necessary to log geomechanical and direct sample tests in the laboratory from the sample/core to obtain the best geomechanical model of the hydrocarbon shale formation in the study area.

Introduction

A detailed understanding regarding the rock Brittleness Index is significant in oil and gas exploration as upfront information to determine the rock fracture gradient. Brittleness of the shale formation plays an important role in evaluating the interval potential area for hydraulic fracturing. Brittleness, a measure of rock's ability to fracture, is a complex function of lithology, mineral composition, TOC, effective stress, reservoir temperature, diagenesis, thermal maturity, porosity, and type of fluid (Wang and Gale 2009). Therefore, brittleness is one of the key mechanical properties of rocks, and is included in most of petrophysical reports of unconventional shale reservoirs (Hucka and Das 1974). However, the absence of a universally accepted definition and measurement of brittleness has led to various methods or models for its quantification (Göktan 1991).

One of the key parameters in shale gas exploration are brittle and fracture. The shale should have contained more quartz than clay minerals to keep the fractures open during the production process. We estimated the Brittleness indicator of gas-saturated shale interval which are Poisson's Ratio and Young's Modulus. Both of them are affected by the kerogen content (high TOC), the maturity of kerogen, and also the fluid type saturated within the pore space.

In this case, we observed that our TOC were about 2-3% and within immature and early mature level of maturity according to the vitrinite reflectance plot analysis. Thus, the brittleness indicators in this work are estimated from mineral composites of shale intervals and assumed to be fully gas-saturated. This work aimed to be the feasible study for evaluating the sweet spot the gas shale layers using the integrated analysis of petrophysical and also estimated elastic properties from rock physics model of shale intervals by utilizing limited data source.

Data and Method

We classify the Rock Brittleness Index into four categories according to their interval values of rock mechanical properties, mineral composition, TOC and others (Perez Altamar and Marfurt 2014), this classification is similar to review wells included in shale formations as below:

- Ductile = < 0.16
- Less ductile = 0.16 - 0.32
- Less brittle = 0.32 - 0.48
- Brittle = > 0.48

Minerals acted as the most significant factor in controlling brittle rock behavior (Ye, Tang and Xi 2020). The most brittle area has abundant quartz and the least brittle has abundant clay mineral (Jarvie, et al. 2007). According to that, we estimated the brittleness of our area using the following equation [1] by incorporating the information of mineral composition and TOC.

$$BI_{modification} = \frac{F_{Quartz}}{F_{Quartz}+F_{Clay}+F_{TOC}+F_{Composite}} \quad [1]$$

Next, we evaluate the average value brittleness using the combination of Poisson's Ratio and Young's Modulus as the controlling mechanical properties (Grieser and Bray 2007) using the following equation [2]-[4].

PROCEEDINGS
JOINT CONVENTION BANDUNG (JCB) 2021
November 23rd – 25th 2021

$$E_{brittleness} = \frac{E - E_{min}}{E_{max} - E_{min}} \quad [2]$$

$$v_{brittleness} = \frac{v - v_{max}}{v_{min} - v_{max}} \quad [3]$$

$$BI_{average} = \frac{E_{brittleness} - v_{brittleness}}{2} \quad [4]$$

Finally, we incorporated the complex information of porosity, mineral composition, TOC, and type of fluid to get the best estimation of brittleness index using the rock physics model. The modified of our rock physics schemes (Fig. 1) aims to discriminate the ductile and brittle interval layers using the information of elastic wave parameters which are transformed into mechanical properties of Poisson's Ratio and Young's Modulus.

Due to limited data in modelling our gas-saturated shale rock, we had carefully done several steps to get the best model in delineating the sweet spot according to brittleness index from the targeted well. Firstly, estimating the bulk modulus of matrix mineral (Km) which mostly composed of quartz, clay, and several minor minerals from SX-ray Diffraction (XRD) Dataset. The value of Km plays significant role in calculating saturated bulk modulus later. Therefore, this part should be handled properly depicting the real condition of our rocks. Then, putting the matrix minerals bulk modulus together with the aspect ratio of rocks into the bulk modulus of dry rock (Kdry) calculation using Kuster-Toksöz approach. Finally, we obtained Vp and Vs of gas-saturated rock from Gassmann equation and calculated two mechanical properties of rock, which are Poisson's ratio and Young's Modulus. Both of properties obtained were assumed to be the best fit parameters in the model which represents the condition of minerals composing rock, fully gas-saturated rock, and pore space of rock.

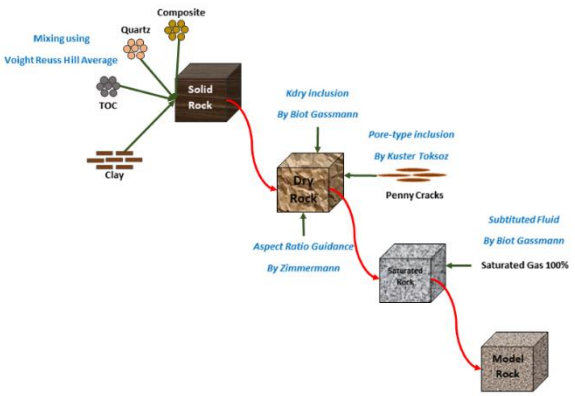

Figure 1 Rock physics Modeling scheme in research

Result and Discussion

Herein this paper, we discussed the rock Brittleness Index from three approaches in order to get the best technique of which should be used as the quick look when delineating the brittleness index of rocks from such limited resources.

<u>Brittleness Index Based on Elastic Property Data Log.</u>

Based on the modulus of elasticity information from the log data, the corrected Brittleness Index value is in the range of 0.001 - 0.795 where the brittleness of the rock in the research well has a ductile to brittle type. Where rock brittleness is dominated by rocks that are less ductile to less brittle with an average Britleness Index value of 0.294 (Fig. 2). The potential location of the maximum fracture zone is localized at 7 depth points with different thicknesses with the level of rock brittleness from less brittle to brittle with an average Brittleness Index of 0.425. The maximum brittleness of rocks tends to have high seismic wave velocities, high Young's modulus, and low Poisson Ratio (Fig. 3). This indicates that the potential zone as the maximum fracture point tends to have high seismic wave velocities associated with its excellent ability to penetrate rock layers with high brittleness.

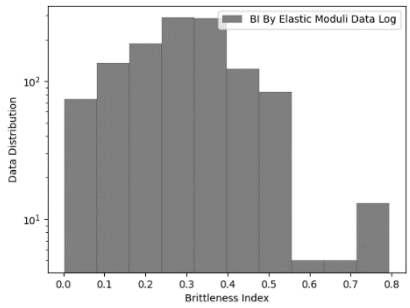

Figure 2 Histogram of Brittleness Index Data log

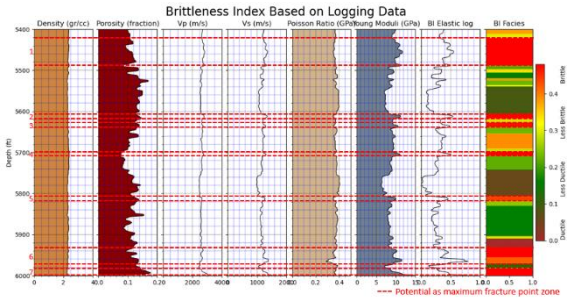

Figure 3 Brittleness Index Interpretation Based on Elstic Properties of Data Log with Maximum Fracturing Point Location

<u>Brittleness Index Based on Elastic Property Rock Pyhsics Modeling.</u>

In this paper, Rock Physics Modeling is proposed to reconstruct seismic wave velocity based on modeling rock physical parameters and mineralogy distribution information (XRD Mineral) at some depth points which is used as a seismic velocity validator from well log data. Applying the Voigt-Reuss-Hill and Kuster-Toksoz Boundary Method, we propose that the rock matrix has a soft pore type (Fig. 4a), This is related to the mineral composition which is dominated by low density mineral composition (composite mineral), with a flat pore geometry seen from the ratio of the longest pore axis to the shortest pore axis of rock porosity with a penny crack inclusion shape represented by the Zimmerman aspect ratio distribution (Fig. 4b) so that it is very representative of the condition of the research well is dominated by shale lithology, and the fill pore fluid which is composed of gas fluid.

From the justification of these parameters, we proceed to the Biot-Gassmann Modeling stage and get the view that the gas fluid substitution carried out in the research well does not provide a very significant change between the primary wave velocity of the modeling data and the log data. Meanwhile, a very significant change was confirmed in the relationship

PROCEEDINGS
JOINT CONVENTION BANDUNG (JCB) 2021
November 23rd – 25th 2021

between the secondary velocity of the modeling data and the log data due to the limitation of the static saturation properties of the modeling fluid on the dynamic properties of the secondary wave velocity of the log data (Fig. 5). Bulk modulus and shear modulus of saturated rock conditions to the seismic velocity of the results of the saturation conditions in the wells of this study have a directly proportional relationship. Overall, we found a positive relationship between the modeling seismic wave velocity (V_P and V_S) and the log data, with the view that the seismic wave velocity of the saturated rock will be greater than the seismic wave velocity of the log data.

Based on the velocity model, we return to the relationship between the elastic properties of the rock brittleness distribution. Based on the modulus of elasticity information from the modeling results, the corrected Brittleness Index value is in the range of 0.241 – 0.502 where the brittleness of the rock in the research well has a ductile to brittle type. Where the rock brittleness is dominated by less ductile rocks with an average Brittleness Index value of 0.294 (Fig. 6). The potential location of the maximum fracture zone is localized at 4 depth points with different thicknesses with the level of rock brittleness from less brittle to brittle with an average Brittleness Index of 0.384. The maximum brittleness of rocks tends to have high seismic wave velocities, high Young's modulus, and low Poisson Ratio (Fig. 7). This shows that the potential zone as the maximum fracture point tends to have high seismic wave velocities associated with its excellent ability to penetrate rock layers with maximum brittleness.

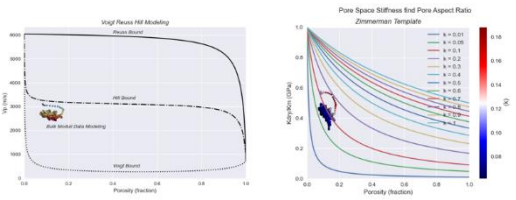

Figure 4 (a) Voigt Reuss Hill Modeling (Mavko, Mukerji and Dvorkin 2020), (b) Pore aspectratio distribution using Zimmerman's constant pore space stiffness (Russell and Smith 2007)

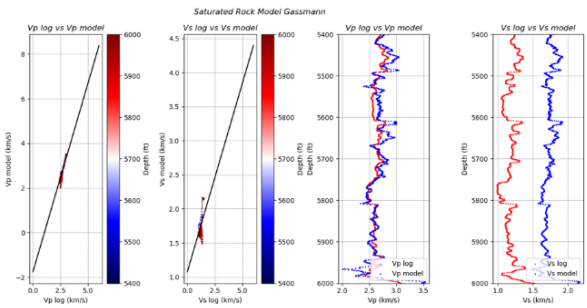

Figure 5 Seismic velocity Modeling Results with Biot Gasmann Modeling

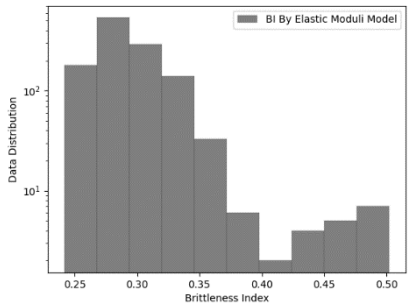

Figure 6 Histogram of Brittleness Index Rock Physics Modeling

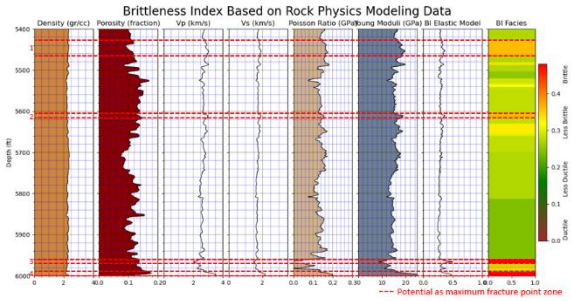

Figure 7 Brittleness Index Interpretation Based on Elstic Properties of Rock Physics Modeling with Maximum Fracturing Point Location

<u>Brittleness Index Based on Mineralogical Rock Pyhsics Modeling.</u>

Based on mineralogy information from Rock Physics Modeling, the corrected Brittleness Index value is in the range 0.140 - 0.354 where the rock brittleness in the research well has a ductile type to less brittle. Where rock brittleness is dominated by less ductile rocks with an average Britleness Index value of 0.191 (Fig. 8). The potential location of the maximum fracture zone is localized at 3 depth points with different thicknesses and the level of brittleness of the rock is less brittle 0.230 (Fig. 9). The maximum brittleness of rocks tends to have a relatively high distribution of non-clay minerals (Quartz + Composite) (23.3 - 23.6 %), relatively low clay minerals (73.0 - 74.6 %), and relatively high Total Organic Carbon content (2.2 - 3.4%) as a determining factor for the optimum and economical fracturing potential zone (Fig. 10).

The results of applying the Brittleness index using the elastic properties of rocks with log data provide more complex and dynamic results, when compared to the results of the Brittleness Index modeling which is limited to several data on the constituent minerals and related physical properties (11b). This affects the vertical resolution of the brittleness of the rock facies in the study area, where the vertical resolution of the Brittleness Index using the elastic properties of log data is better than the vertical resolution of the Brittleness Index using the elastic properties and mineralogy of Rock Physics Modeling (Fig. 11a).

PROCEEDINGS
JOINT CONVENTION BANDUNG (JCB) 2021
November 23rd – 25th 2021

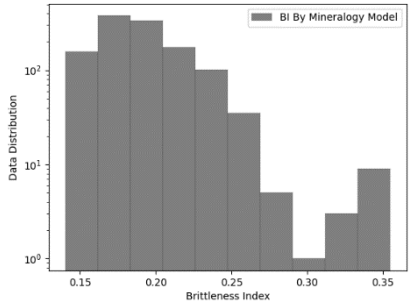

Figure 8 Histogram of Brittleness Index Mineralogy

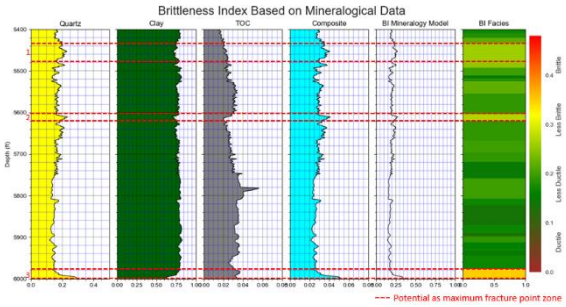

Figure 9 Brittleness Index Interpretation Based on Mineralogical Properties of Rock Physics Modeling with Maximum Fracturing Point Location

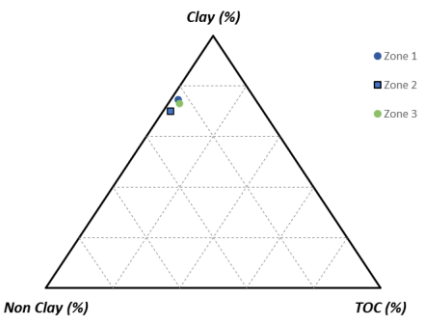

Figure 10 Mineral Composition at Maximum Fracture Point based on Mineralogical Modeling

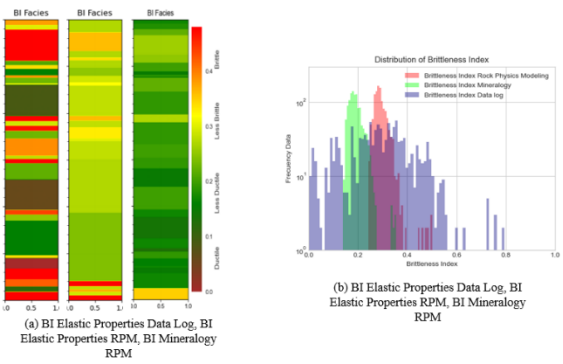

(a) BI Elastic Properties Data Log, BI Elastic Properties RPM, BI Mineralogy RPM

(b) BI Elastic Properties Data Log, BI Elastic Properties RPM, BI Mineralogy RPM

Figure 11 Brittleness Index Interpretation

Conclusions

In this paper, the application of the 3 methods we propose provides maximum consistency to the resulting vertical resolution based on the distribution of rock brittleness index in the review wells. This estimate can be applied and becomes a quick look in seeing the potential for rock to fracture if core data is not available. To optimize the hydraulic fracturing design and planning, it is advised that the complete TOC data be combined with the Brittleness Index to identify the most suitable depth for an effective and optimum hydraulic fracturing. For further investigation in the future, it is necessary to log geomechanical and direct sample test in the laboratory from the sample/core to obtain the best geomechanical model of the hydrocarbon shale formation in the study area.

References

Göktan, R. 1991. Mining Sci. & Technol 13 (3): 237–241.
Grieser, B.,, and J. Bray. 2007. SPE Production and Operations Symposium.
Hucka, V., and B. Das. 1974. International J. Rock Mechanics and Mining Sciences 11 (10): 389–392.
Jarvie, D., M.R.J. Hill, T.E. Ruble, and R.M. and Pollastro. 2007. American Association of Petroleum Geologists Bulletin 91, 475–499.
Mavko, G., T. Mukerji, and J. Dvorkin. 2020. Cambridge university press.
Perez Altamar, R., and K. Marfurt. 2014. Application to the Barnett Shale Interpretation 2(4), T1-T17.
Russell, B. H., and T. Smith. 2007. CREWES Research Report Vol. 19.
Wang, F.P., and J.F.W. Gale. 2009. Gulf Coast Association of Geological Societies Transactions 59, 779–793.
Ye, Y., S. Tang, and Z. Xi. 2020. Energies 13, 388.

Acknowledgements

Thank you to bli Ngurah Beni Setiawan Ph.D. from Imperial College, London for the insights of both knowledge and life lessons to the author.

PROCEEDINGS
JOINT CONVENTION BANDUNG (JCB) 2021
November 23rd – 25th 2021

Evaluating Potential Reservoirs in the Gumai Formation at West Air Komering Area with Multi-Inversions Method

Lutfi Fauzan Erwin[1], Sondang Samosir[2], Ivan Teguh Andhika Praja[3], Waskito Pranowo[1], Kosdar Gideon Haro[3]
[1]Department of Geophysical Engineering, Pertamina University, Jakarta 12220, Indonesia
[2]Tiarabumi Petroleum, Jakarta 10150, Indonesia
[3]Rock Flow Dynamics, Jakarta 12920, Indonesia

Abstract
The Gumai Formation is often regarded as a regional seal to the prolific Baturaja and Talang Akar Formations. However, new discoveries were found in the Gumai Formation that makes it an interesting intra-field exploration target. Therefore, this paper aims to compare the result of seismic inversion methods, their effects on the distribution of lithology and porosity within the Gumai Formation in West Air Komering Area and see how they impact the prospectivity evaluation in the later stage.

The principle of seismic inversion is to transform seismic reflection amplitudes into impedance values that can be used as a guidance to distribute porosity, lithology, and fluid saturation. However, different inversion methods may induce non-unique AI results, especially when dealing with low-contrasts lithologies within the Gumai Formation. Therefore, a comparative study between several inversion methods is necessary to cross correlate between the results. Several deterministic inversion methods were chosen comprises Model-Based Inversion (MBI), Fast Track "Colored" Inversion (CI), and Linier Programming Sparse-Spike (LPSS) Inversion. The inversion results were then calibrated with the well data and subsequently used as input to the 3D static model to evaluate possible in-place volumes estimates after.

Results from LPSS and MBI shows many similarities whilst CI produced different result particularly in the southwestern part of the studied area. Despite many similarities, LPSS shows a blockier impedance compared to MBI. Overall, a high impedance anomaly in all inversion results indicates shaly sandstones. In general, the accumulation of shaly sandstones and relatively high porosity are observed in northeastern part of this area. There is a quite large range between the calculated volumetrics when each inversion result was used as input for the 3D property modelling.

This paper demonstrates a multi-scenario geophysical approach in evaluating intra-field potential which applicable to similar fields. By using multi-scenario method, risks and interpretation uncertainties are well captured. This will enable a better investment decision that also comply with the latest regulations from Indonesian Government.

Introduction
West Air Komering area is located in the southern part of the South Sumatera basin as one of Indonesia's most prolific hydrocarbon-bearing basins. The main hydrocarbon discoveries in the South Sumatera basin are concentrated in Talangakar and Baturaja formations. However, with the recent exploration activities, new discoveries in both stratigraphical and structural traps in the Gumai formation were found, making it an interesting intra-field exploration target.

Gumai formation consists predominantly of shales with intercalated sandstones. A multi-sequence stratigraphy was identified within the Gumai formation from the seismic and well logs data. Three seismic inversion methods were applied, which are Model-Based Inversion (MBI), Fast-track "Colored" Inversion, and Linear Programming Sparse-Spike Inversion. In the later stage, reservoir modelling was performed by incorporating well log analyses and seismic interpretation results into petrophysical and facies models. This paper demonstrates how seismic inversion methods affecting potential evaluation in shaly sand reservoir, which is applicable to similar fields.

Data and Method
This study was using the data from 3 wells and a 3D seismic cube covering an area of 52.8 km^2. Petrophysical analyses were conducted to produce porosity and lithology logs that are crucial for evaluating potential reservoirs. Furthermore, integrated geological and geophysical investigations were performed by assessing well log data, well correlations, and seismic characteristics to provide a structural and stratigraphic framework.

After having a better understanding of the study area and the correlation between acoustic impedance with other physical properties, several deterministic seismic inversions were carried out. Seismic inversion has been widely used in the petroleum industry for subsurface geological inferences (e.g., lithology, porosity) based on seismic analysis tied to well logs (Das, 2016). The most basic and commonly used one-dimensional model for the seismic trace is referred to as the convolutional model, which states that the seismic trace S(t) is simply the convolution of the earth's reflectivity RC(t) with a seismic source function W(t) with the addition of a noise component N(t) (Russel, 1988) as shown below:

$$S(t) = RC(t) * W(t) + N(t)$$

The acoustic impedance (AI) at the nth layer can be expressed as:

$$AI_{(n+1)} = AI_{(n)} \frac{1 + RC_{(n)}}{1 - RC_{(n)}}$$

One of the most commonly used deterministic inversion methods is model-based inversion. This is an interesting method since it updates the model rather than the seismic data itself in the inversion process. First, the acoustic

impedance model is built using well data with the seismic horizons guide and then compared with seismic data. Subsequently, the comparison results are used to iteratively updates the model to better match the seismic data. Once the process is finished, the model should become a cube containing absolute impedance values. This process was done by generalized linear inversion (GLI), which will derive a model that fits well with seismic in the least-squares sense.

Another method, Linear Programming Sparse-Spike inversion, points out that if high-resolution deconvolution is applied to seismic data, the reflectivity estimation will only be accurate in band-limited seismic frequency (missing high & low-frequency content). Recovering the missing frequency is considered a problem of non-uniqueness because of the infinite pairs of velocity and depth that will give in the same time value. Therefore, the layered geological model / blocky impedance model is added as a constraint in the form of a sparse-spike reflectivity function. This can be achieved by using the L1 norm algorithm as the sum of the seismic trace's absolute values that are minimized (frequency domain constraint) to generate a reliable frequency band and sparse reflectivity.

Finally, there is the fast-track "coloured" inversion method based on empirical studies that unconstrained sparse-spike inversion can be approximately modelled as a convolutional process, with an operator whose amplitude spectrum maps the mean seismic spectrum to the mean earth AI spectrum and has a phase of -90º (Lancaster & Whitcombe, 2000). To perform this inversion method, design the linear trend operator in the frequency domain as a "desired output" shown on a log/log scale using AI log from well(s). Apply inverse fast-Fourier transform to have the operator in the time domain, then convolve it to the seismic cube. Just like sparse-spike inversion, the result of fast-track "coloured" inversion is relative impedance. If needed, add the low-frequency AI model to relative impedance to have the absolute impedance.

Each inversion method has its own unique nature based on its processes and algorithm. By comparing them, we can have a comprehensive and quantitative analysis of our area of interest and see the major trend resulted from all inversion methods. All of the results from the inversion method explained above will be used as inputs to build reservoir models.

Result and Discussion

In most cases, a hydrocarbon reservoir is associated with a low acoustic impedance anomaly since it often has the same lithology as the surrounding area. In this case, the sandstone reservoir is surrounded by shale stone. Sandstone has more compact characteristics than shale stone, making it have a greater acoustic impedance value than shale stone. This phenomenon was confirmed by the cross-plot analysis between AI and GR logs.

Model-based inversion method result shows a relatively high impedance anomaly in the north-eastern area. This method gives a good resolution result, but sometimes, it can be too dependent on the initial guess / low-frequency acoustic impedance model. Linear programming sparse-spike creates a broad-band, high-frequency result but without very thin layers often created by model-based inversion method. Therefore, it is shown as a blockier impedance model compared to model-based inversion. The method also shows a relatively high impedance anomaly in the north-eastern area. Meanwhile, fast-track "coloured" inversion produced different results, especially in the southwestern area. This method is directly linked to seismic data, simple, fast, and robust. Consequently, it is considered imprecise compared to other methods.

The differences happened because of the nature of each method. Model-based inversion, as the name suggests, is highly dependent on the low-frequency model. Linear programming sparse-spike only considered large spike (Poisson-Gaussian series), whilst the background spike (Gaussian series) is ignored. Fast-tack "coloured" inversion is the only method presented in this paper that did not use wavelet anywhere in the processes.

From all of the inversion results, the shaly sandstone reservoir and relatively high porosity associated with high impedance anomaly are located in the north-eastern part of this area. Based on paleontological study, the early Miocene Gumai formation is deposited in the marine environment at inner to middle neritic (Yuliansyah et al., 2014). It has the possibility of sandstone presence in the transgression period. Looking at the geometry of the reservoir guided with a gross depositional environment map, it is interpreted as having formed in a delta-front environment.

All inversion results are used as inputs for reservoir models resulted in a wide range of stock tank oil initially in-place (STOIIP) values. For comparison, considered fast-track "coloured" inversion result as a baseline, the differences in STOIIP calculation values are 11% and 51% for linear programming sparse-spike and model-based inversion, respectively.

Conclusions

- Each deterministic inversion method has its own distinct characteristics. Therefore, differences in the results between each method are expected to some extent.
- Based on seismic inversions analyses using Model-based, Linear Programing Sparse-spike, and Fast-track "Colored" inversion methods show us the distribution of relatively high impedance anomaly and interpreted as a sand reservoir having formed in a delta-front environment.
- A wide range of stock tank initially in-place values are identified by incorporating seismic inversion result in reservoir model creation.

References

Das, B., and R. Chatterjee, 2016, Georesursy = Georesources, **18**, 306-313.

Lancaster, S and Whitcombe, D., 2000, 70th SEG Annual Meeting, 1572-1575.

Russell, B.H., 1988, Society of Exploration Geophysicist: Course Notes Series, 2.

Yuliansyah, Z., Bagus, S.M., and Yuda, F.Y., 2014, Jurnal Geofisika Ekplorasi, 2, 41-50.

PROCEEDINGS
JOINT CONVENTION BANDUNG (JCB) 2021
November 23rd – 25th 2021

Acknowledgements
The authors would like to thank Geophysical Engineering Department of Universitas Pertamina for supporting this research, Tiarabumi Petroleum for permission to publish this research, and Rock Flow Dynamics for facilitating the tNavigator software.

PROCEEDINGS
JOINT CONVENTION BANDUNG (JCB) 2021
November 23rd – 25th 2021

Appendix

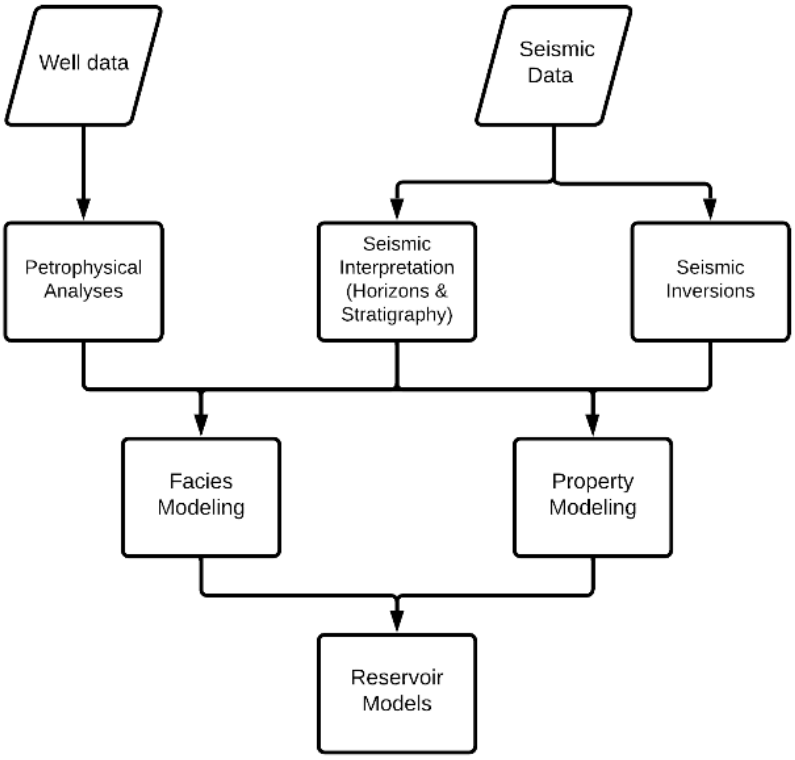

Figure 1: Workflow of the study

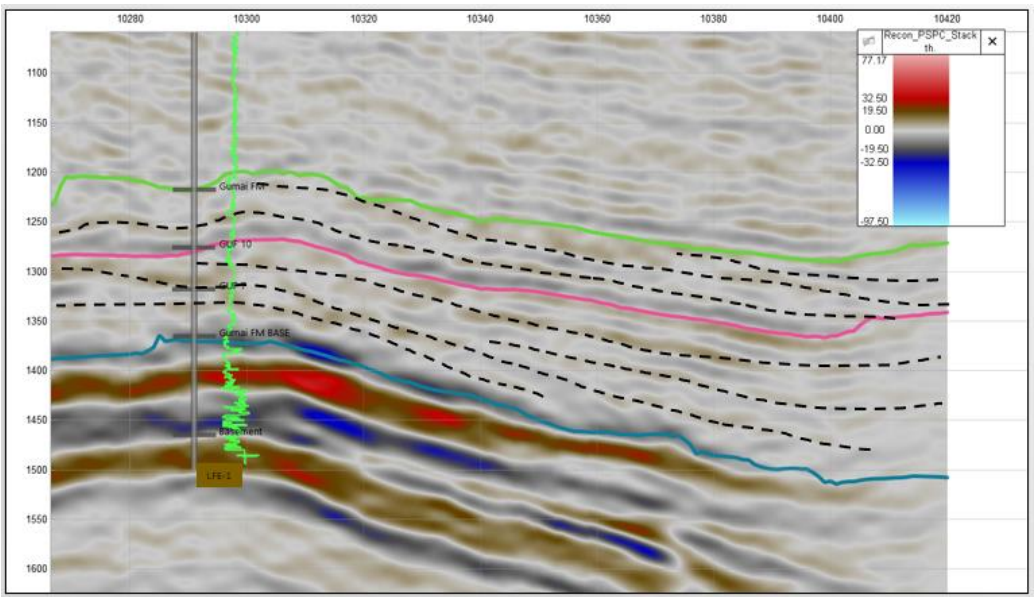

Figure 2: Seismic stratigraphy of Gumai formation showing two different sequences within the formation

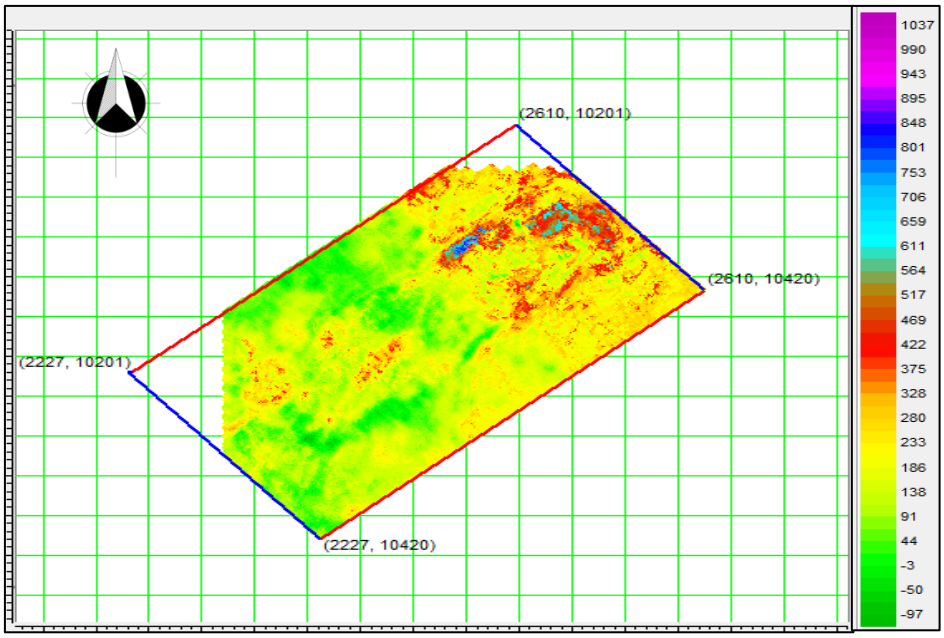

Figure 3: Horizon slice showing average amplitude of relative impedance value from Model-based Inversion

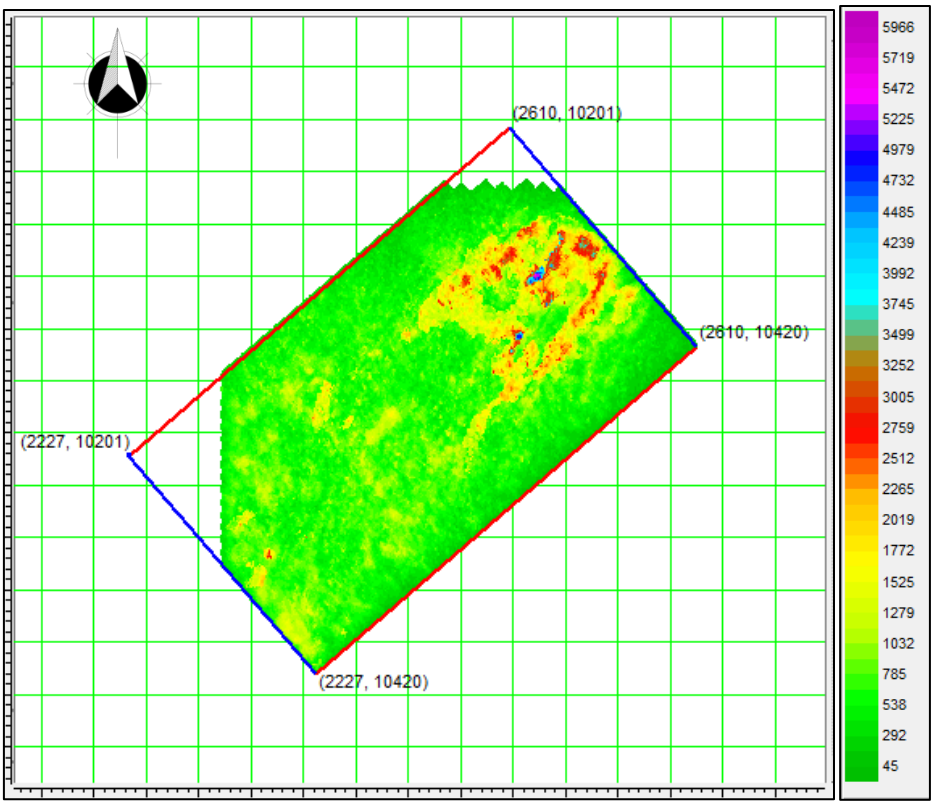

Figure 4: Horizon slice showing average amplitude of relative impedance value from Linear Programming Sparse-spike Inversion

PROCEEDINGS
JOINT CONVENTION BANDUNG (JCB) 2021
November 23rd – 25th 2021

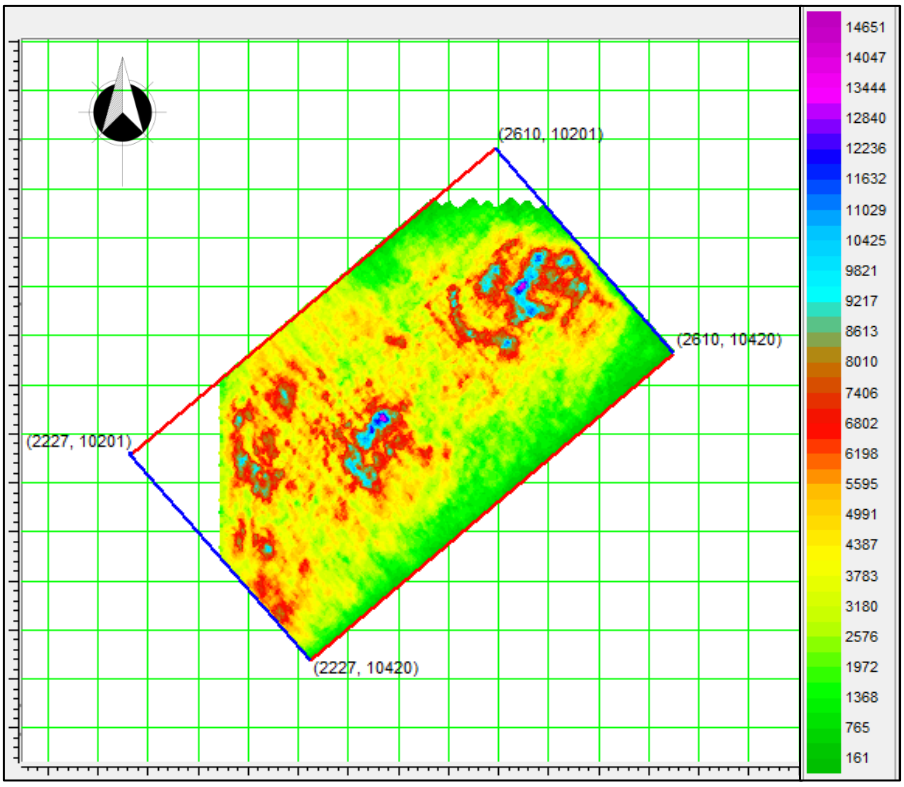

Figure 5: Horizon slice showing average amplitude of relative impedance value from Fast-track "Coloured" Inversion

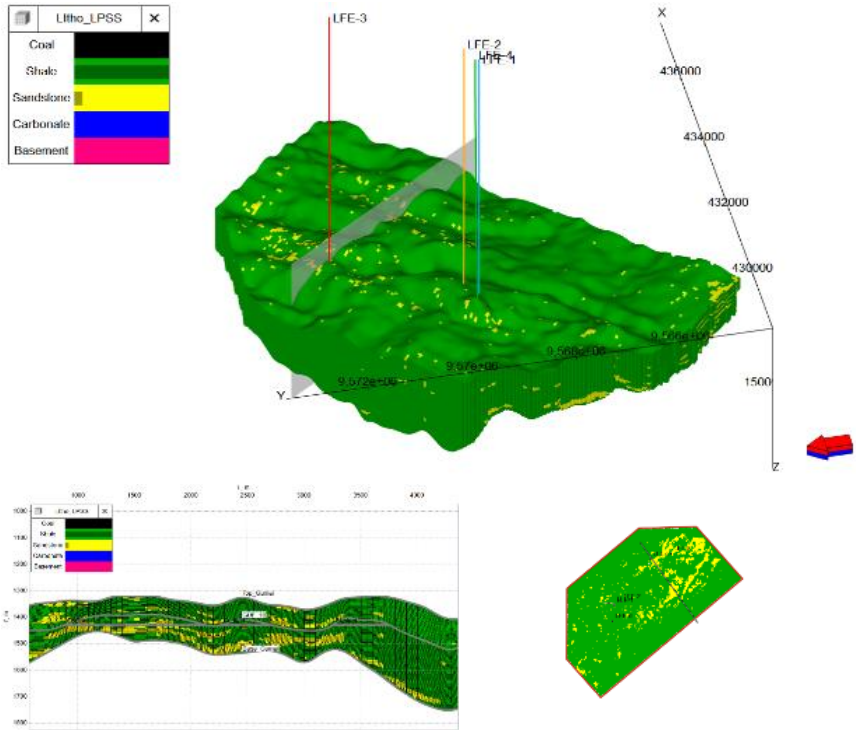

Figure 6: An example of facies model using seismic inversion result.

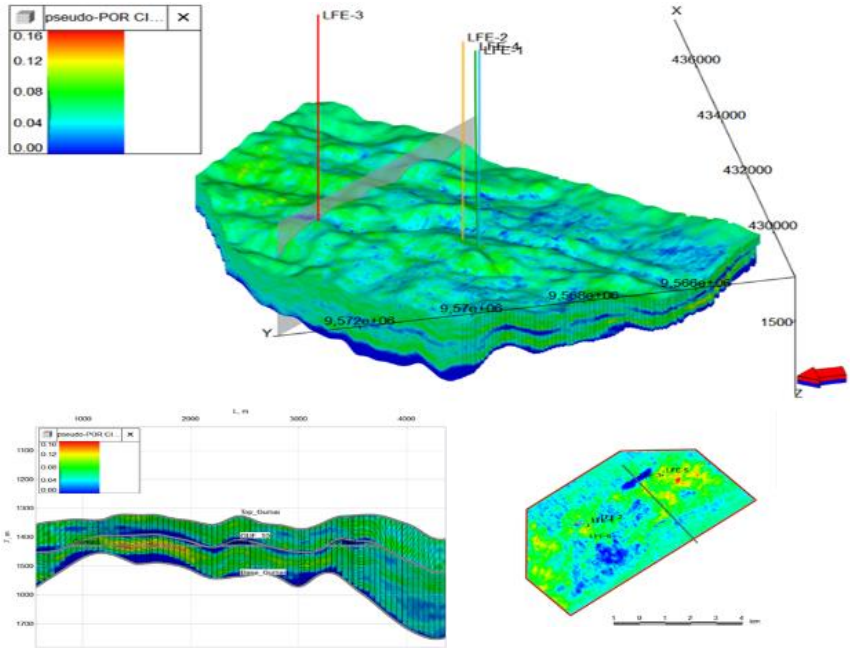

Figure 7: An example of porosity model using seismic inversion result.

PROCEEDINGS
JOINT CONVENTION BANDUNG (JCB) 2021
November 23rd – 25th 2021

Detection of Gas Reservoir at Banyuasin Field by using Amplitude versus Offset (AVO) Analysis

Andiani Latania[1], Eleonora Agustine[1], Humbang Purba[2], Ricky A Tampubolon[3]
[1]Department of Geophysics, Universitas Padjadaran
[2]PPPTMG Lemigas
[3]Odira Energy Karang Agung

andianilatania55@gmail.com

Abstract

Banyuasin Field is indicated to have gaseous hydrocarbons based on well data. The purpose of this study is to examine the distribution of gas hydrocarbons in the Telisa and Talang Akar Formation, which are reservoir rocks that are dominated by sandstone lithology. Amplitude versus Offset (AVO) analysis is used as a method in this study, based on the response to changes in amplitude at the offset/angle. To determine AVO responses towards seismic data, gradient analysis and AVO product were performed using the intercept and gradient attributes. Gradient analysis is made by making intercept-gradient graphs in determining the type of fluid based on the AVO class. The AVO product is a result of multiplication between the intercept and gradient so that the distribution of gas hydrocarbons on a seismic cross-section can be seen. Based on the results of the analysis on the Telisa Top Formation in Zone 1, AVO response of class III was obtained, which indicated the presence of gas hydrocarbon and Zone 2 AVO response of class II P and I was obtained which indicated the presence of wet sand. The top of the Talang Akar Formation in both target zones is identified as an AVO class IV response, indicating the presence of coal. The difference in response is caused by the impedance contrast of the sandstone in the target zone. For gas hydrocarbons, the impedance response of sandstone is small because the layer of porous sandstone is filled with gas. This causes magnitude of Vp to become smaller than Vs which causes the amplitude to increase as the offset/angle increases and AVO product has positive value on the seismic section.

Keywords: AVO, gas, intercept, gradient

Introduction

The Banyuasin field is located in the South Sumatra Basin which is a field with gas hydrocarbon potential (Figure 1). The existence well production wells have proven the presence of hydrocarbon (Figure 2 and Figure 3). However, it is still necessary to conduct field development studies to find new potentials and optimize the distribution of gaseous hydrocarbons laterally through a reservoir characterization approach. In the study area, the reservoirs targeted for gas production are the sandstones of the Telisa formation and the sandstones of the Talang Akar formation. Laterally, the gas-saturated reservoir can be identified quantitatively.

Amplitude versus Offset (AVO) is one of the seismic interpretation methods that can characterize gas hydrocarbon reservoirs by amplitude response to the offset. The Reservoir saturated gaseous hydrocarbons cause Vp response to get decreased and the Vs tends to have a constant velocity. This gives the effect of increasing the amplitude (bright spot) and the response provides information that the reservoir is saturated with gaseous hydrocarbons (Castanga and Swan, 1997).

Data and Method

1. Data

In this study, the data used include: 2D Pre-stack gather seismic data with preserve amplitude, well recordings (gamma ray, sonic, density) and petrophysics data (water saturation) as validators for the presence of gaseous hydrocarbons.

2. Geological Regional

Banyuasin Field is located in the South Sumatera Basin with formed the early Tertiary from the Eocene to Oligocene. Where Telisa Formation as a cap rock and reservoir rock. The Talang Akar Formation is the main reservoir to produce hydrocarbons. Both formations are dominated by sandstone lithology.

3. Method

3.1. Gradient Analysis

The conditioned seismic data were used in classifying the AVO class as has been done by Rutherford and William (1989) are divided into three classes later developed by Ross and Kinmann (1995) and Castagna, et al (1997). Picking data is carried out in the target zone adjacent to the well. So that it will be plotted in the intercept and gradient graph that is adjusted to the AVO class classification. In the graph, the point distribution will be obtained as an amplitude response for each angle change and the graph formed is a response model based on velocity data. Detection of the presence of gas can be shown from the amplitude response which is getting stronger for each angle shown in the class 3 AVO response.

PROCEEDINGS
JOINT CONVENTION BANDUNG (JCB) 2021
November 23rd – 25th 2021

3.2 Product AVO

Aki-Richard made an equation that became the basis of AVO by separating Vp, Vs, and density and was able to explain the relationship with the amplitude of the physical characteristics of rocks such as the following equation.

$$R(\theta) = A + B\ sin^2\theta$$

Product AVO is an attribute that is the result of multiplication between intercept and gradient (A*B) which can be used to determine the distribution of Direct Hydrocarbon Indicator (DHI), especially bright spots (Wibowo, 2020).

Result and Discussion

Gradient Analysis

Gradient analysis by using angle gather data has aim of seeing the amplitude response at every angle change that occurs. These responses can be categorized according to AVO classification which can knowing the type of fluid contained in the target zone.

The results of gradient analysis at APOLLO-1 well have amplitude response of Telisa Formation shows an increase in the amplitude value (Figure 4). This indicates the reservoir is saturated with gaseous hydrocarbons and can be categorized as a class III AVO anomaly response. Due to the influence of Vp, which decreases drastically as it passes through the porous sandstone filled with gas. Vs response from the beginning has seen constant changes that tend to have a faster velocity than the Vp impedance response with low value, known as the bright spot.

The results of the gradient analysis in the APOLLO-4 well have amplitude response in the Telisa Formation shows that there is a polarity reversal (Figure 5). This can be caused by the difference in impedance of the upper layer which is higher than the reservoir layer, which is the response of wet sand with gas fluid which is tight. This response is categorized as an AVO class II P anomaly with a change in polarity at the mid stack angle.

Top Talang Akar Formation for APOLLO-1 and APOLLO 2 have AVO response is decrease in amplitude at each change of angle because of their dimming effect. This indicates the presence of a coal seam that has a low density and velocity so that the ratio of Vp and Vs is not very significant. Such a response can be categorized as class IV response AVO anomalies.

The results of the overall gradient analysis of the wells in the study area are as shown in table 1.

Product AVO

AVO product is used to detect the distribution of gaseous hydrocarbons in the target reservoir. In zone 1 of the Telisa Formation, it indicates the presence of gaseous hydrocarbons with a positive anomaly response of 0.7-1 (Figure 6). In Zone 2, the Talang Akar Formation gives a positive anomaly response of 0.6-0.9 (Figure 7). Based on the AVO analysis that has been carried out, it can be seen that the two target reservoirs have a stronger amplitude anomaly response (brightspot) as the angle increases.

AVO product can show the distribution of gas on a seismic cross section with a positive AVO product value. Zone 1 has a range value of 0.6 – 1 and Zone 2 has a value of 0.6 – 0.9. This is influenced by the depth of the reservoir. Because the deeper the level of rock compaction, the greater the value of the acoustic impedance will increase. This is evident in Zone 1 which has a depth of about 220-240 m providing a greater AVO product response value compared to Zone 2 which has a depth of 1100-1360 m.

Conclusions

The gaseous hydrocarbon saturated reservoir is known from the increase in the amplitude value for each angle can be classified as AVO class III response. The response was obtained in the Top Telisa Formation in Zone 1 and in the Talang Talang Akar Formation in Zone 2 of the study area. Distribution of gaseous hydrocarbon saturated reservoirs is laterally in the Top Telisa Formation in Zone 1 and Talang Akar Formation in Zone 2 with a positive AVO product response shown.

References

Castagna, J. P., & Swan, H. W. (1997). Principles of AVO crossplotting. *The leading edge*, *16*(4), 337-344.

Rutherford, S. R., and Williams, R. H. 1989. Amplitude-Versus-Offset Variations in Gas Sand. Jurnal Geofisika SEG. Vol. 54: 680 – 688

Sukmono, S. (2007). Application of multi-attribute analysis in mapping lithology and porosity in the Pematang-Sihapas groups of Central Sumatra Basin, Indonesia. *The Leading Edge*, *26*(2), 126-131.

Wibowo, R. C., Ferucha, I., Sarkowi, M., & Dewanto, O. (2020). Prediksi Fluida Hidrokarbon Menggunakan Amplitude Versus Offset (AVO) di Lapangan "CHA", Cekungan Sumatera Selatan. *Jurnal Geologi dan Sumberdaya Mineral*, *21*(4), 217-225.

Acknowledgements

The author would like to thank PPPTMGB Lemigas, Geophysics Department, Universitas Padjadjaran, and related parties who have provided advice and support in this research.

PROCEEDINGS
JOINT CONVENTION BANDUNG (JCB) 2021
November 23rd – 25th 2021

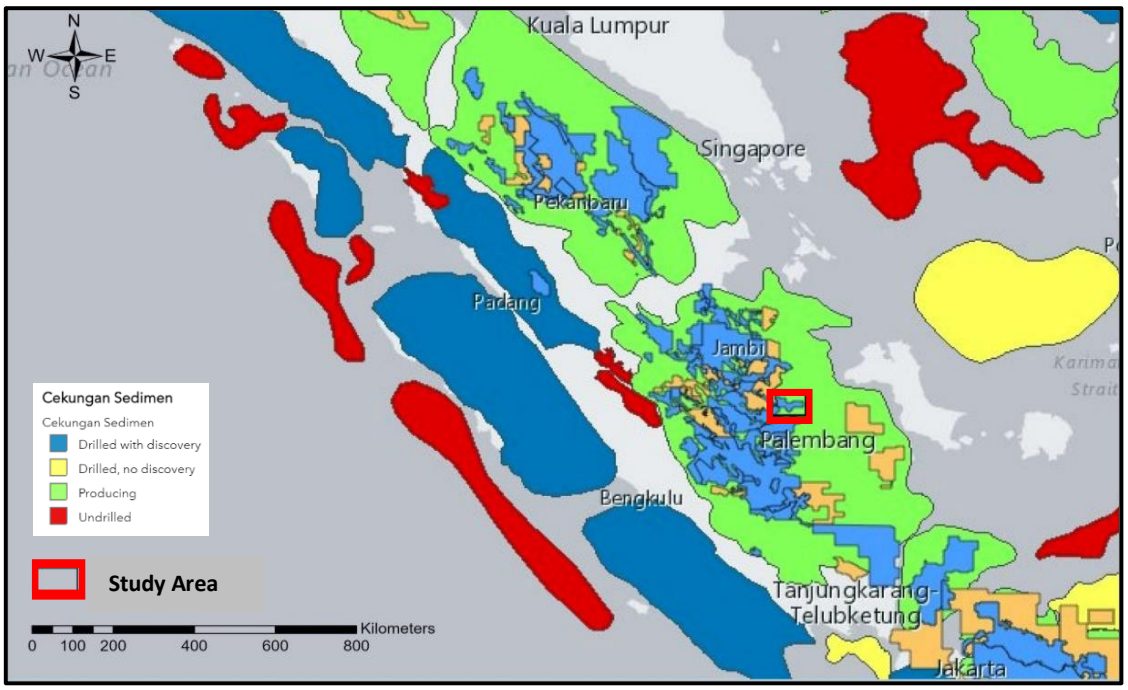

Figure 1: Location of Banyuasin Field Research Area, South Sumatra Basin (Basemap ESDM One Map, 2020)

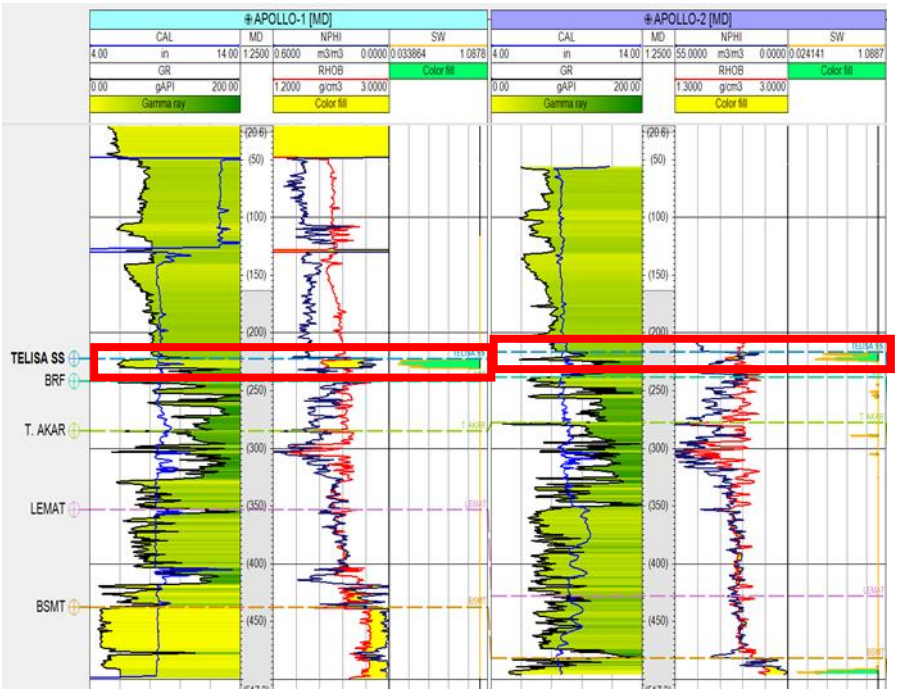

Figure 2: Well Information in Zone 1, Banyuasin Field

PROCEEDINGS
JOINT CONVENTION BANDUNG (JCB) 2021
November 23rd – 25th 2021

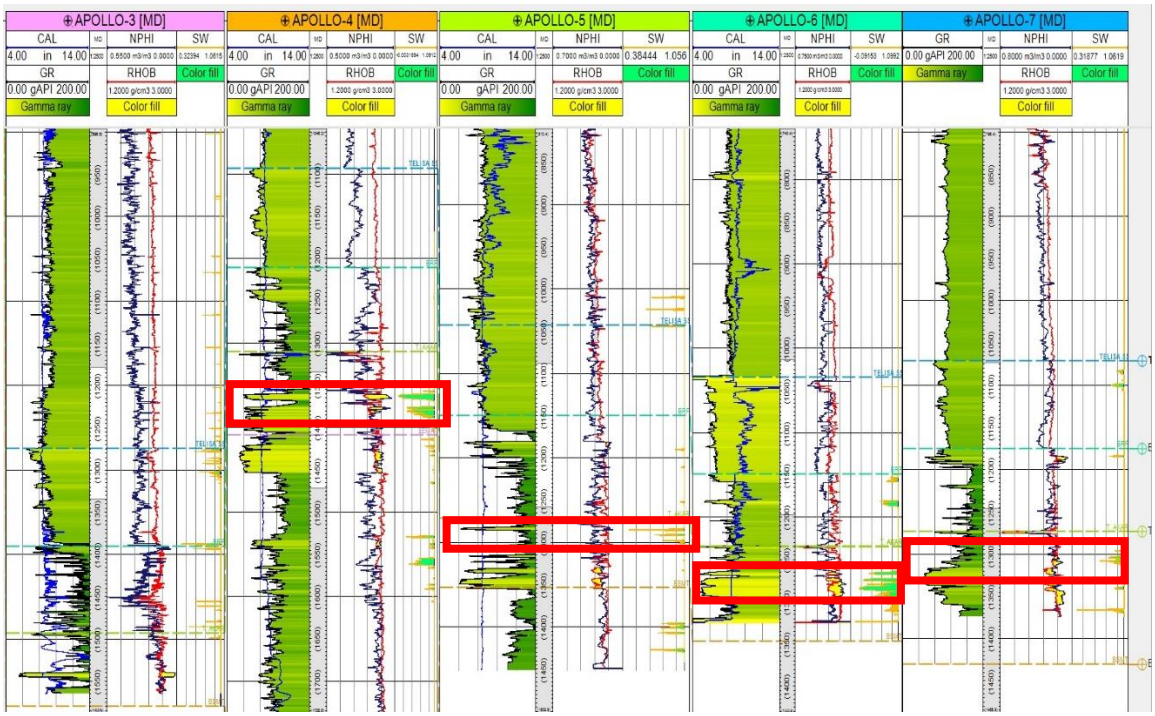

Figure 3: Well Information in Zone 2, Banyuasin Field

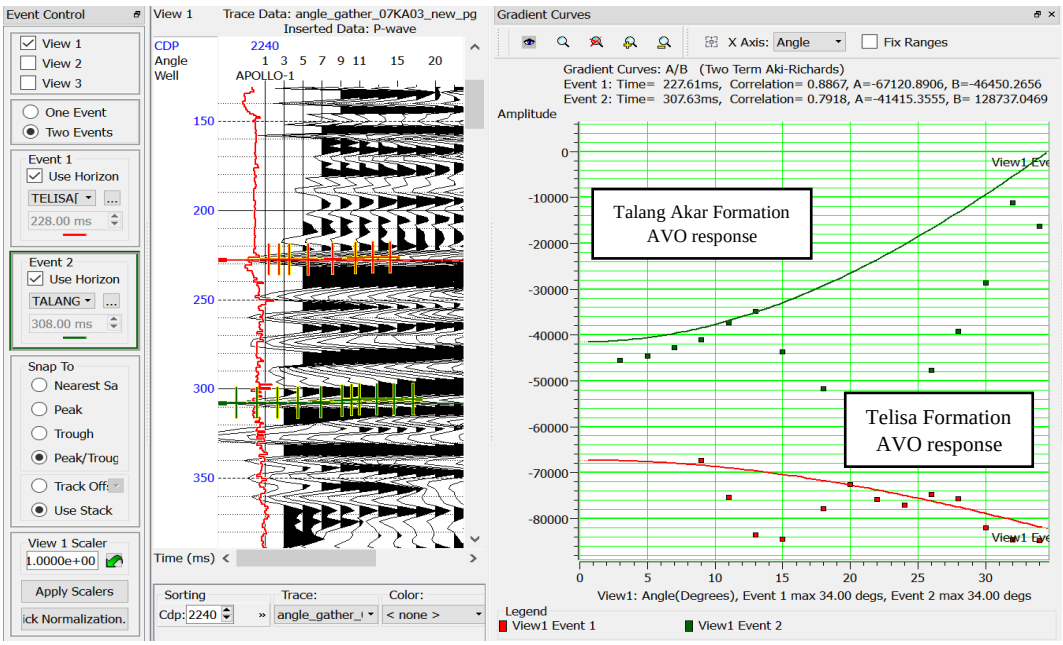

Figure 4: Gradient Analysis in APOLLO-1, Zone 1

PROCEEDINGS
JOINT CONVENTION BANDUNG (JCB) 2021
November 23rd – 25th 2021

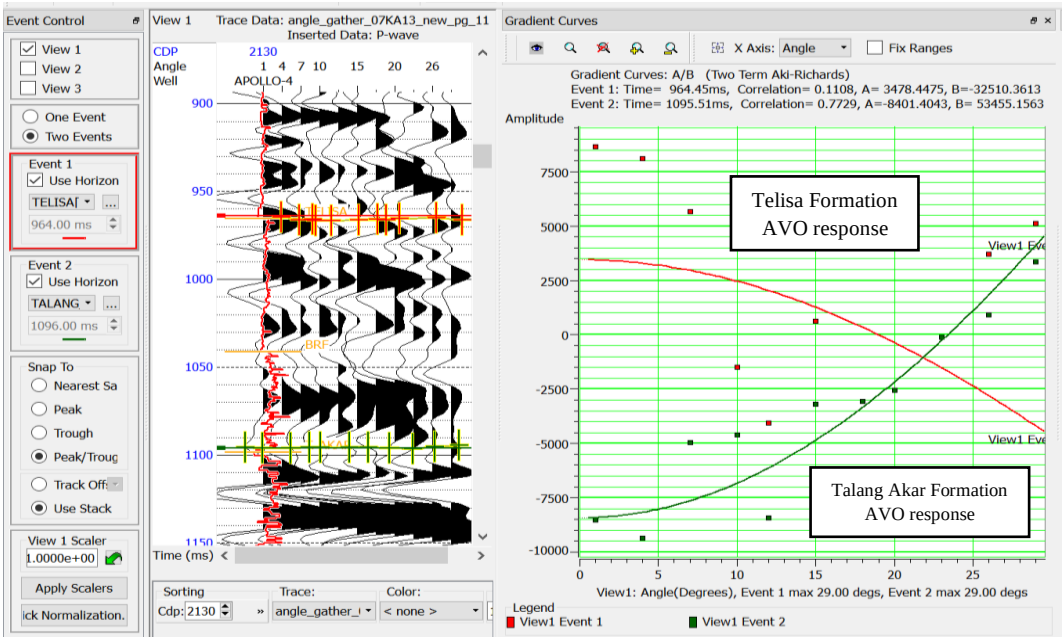

Figure 5: Gradient Analysis in APOLLO-4, Zone 2

Seismic Trace	Well	AVO Class	
		Telisa	Talang Akar
07KA03	APOLLO-1	III	IV
07KA04	APOLLO-2	III	IV
07KA07	APOLLO-3	II P	IV
07KA13	APOLLO-4	II P	IV
07KA14	APOLLO-5	II P	IV
07KA15	APOLLO-6	II P	IV
07KA18	APOLLO-7	I	IV

Table 1: AVO class classification results based on gradient analysis of wells in the study area

PROCEEDINGS
JOINT CONVENTION BANDUNG (JCB) 2021
November 23rd – 25th 2021

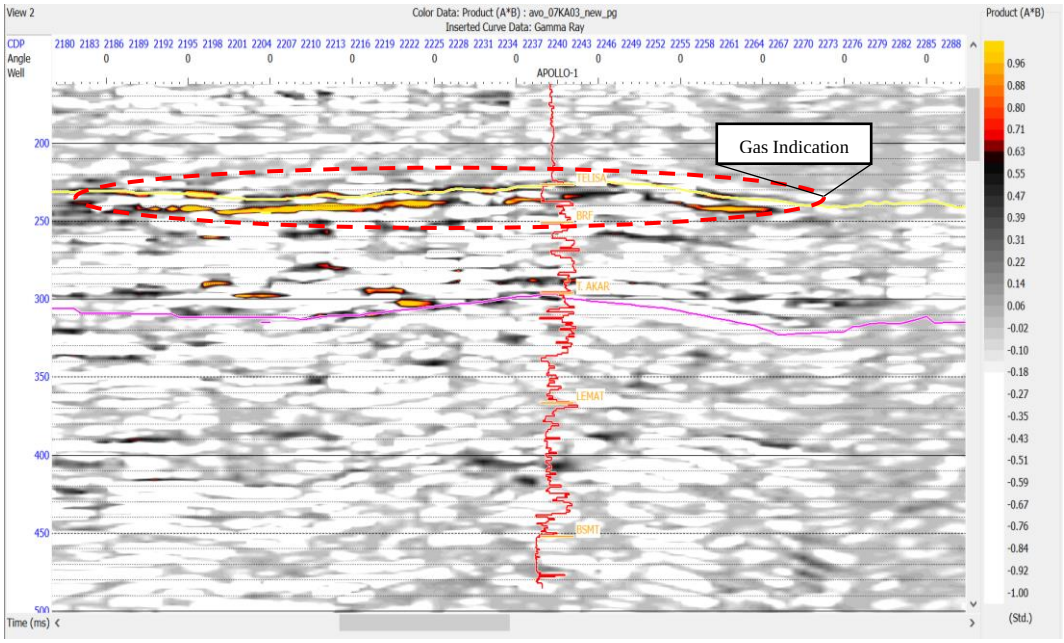

Figure 6: Product AVO in APOLLO-1, Zone 1

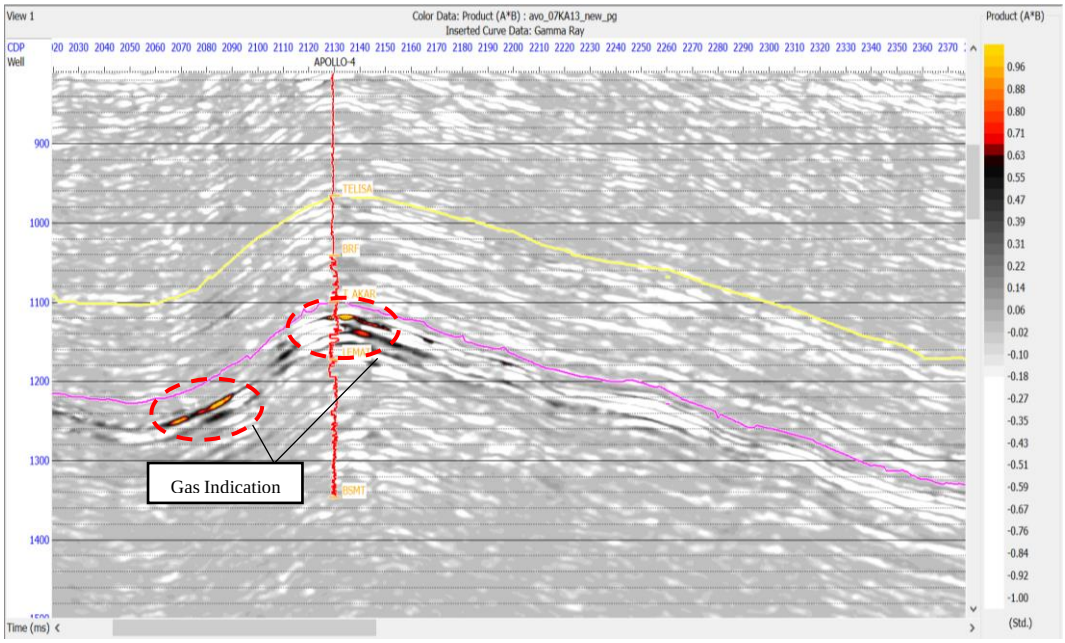

Figure 7: Product AVO in APOLLO-4, Zone 2

PROCEEDINGS
JOINT CONVENTION BANDUNG (JCB) 2021
November 23rd – 25th 2021

Porosity Prediction of a Carbonate Reservoir in KF Prospect, North East Java Basin Based on The Integration of Seismic Attribute and Acoustic Impedance Inversion

Khusnul Fitroh[1], Ahmad Khairul Azmi[1], Fitriyanda Herawan[2]
1 Universitas Islam Negeri WalisongoSemarang
2 Pertamina Hulu Energi Tuban East Java

Abstract
Porosity prediction is still an obstacle and a challenge for geologists and geophysics in the carbonate reservoir of KF prospect, although the surrounding field has high hydrocarbon production. Well data, seismic data, there are still not many that can be used as a reference for reservoir characterization due to the lack of exploration wells around the RF prospect. As a consequence, the prediction of porosity is difficult to map, and this results makes it difficult to interpret hydrocarbon traps and determine prospects for new wells.
In order to have a better porosity prediction, data integration of geological data, well log data, the latest seismic data, seismic attribute extraction and utilization of acoustic impedance inversion are used to optimize the geological interpretation. Regional geology data provide the understanding that the structural trap is coming from E-W direction. The structures that develop in the East Java Basin are mostly in the form of anticlines and faults and stratigraphy are found when carbonate unit onlap and cover high sections of bedrock. In addition, the well log data shows the determination of the formation boundary location in the prospect and greatly contributes as an input to the acoustic impedance inversion process. Besides that, extraction of seismic attribute, in this case, it uses the instantaneous phase attribute which shows the continuity of the seismic layer laterally and the continuity of the seismic trace which contributes to the clearer carbonate build-up on the seismic reflector which is then reinforced by regional stratigraphy which shows that there is a carbonate build-up in high areas.
By doing the well seismic tie, it is obtained seismic data at true depth and the role of the instantaneous phase attribute is also very useful in the picking process, because the discontinuity of the seismic traces is seen more clearly so it makes the picking process easier. And to predict porosity, an inversion model is built to produce a map of the distribution of the porous zone in the target area from the interpolated well logs and target horizon.
Based on this analysis, the distribution of high porosity or porous zones is found in the northern and southern areas of the fault. The construction of acoustic impedance inversion models and structural map are interpreted as important factors in determining porous zones, and can be interpreted using integrated geological and geophysical data.

Introduction

KF prospect is located in the North East Java Basin which is one of the oil and gas prospect areas that can be targeted by new exploration wells, with carbonate lithology as a reservoir that located in the Tuban Formation (Figure 1). The Tuban Formation of North East Java Basin has been managed by PT. Pertamina Hulu Energi Tuban East Java.

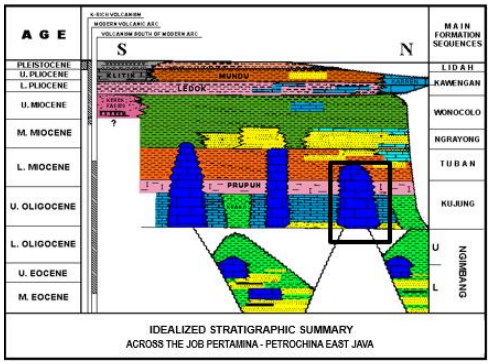

Figure 1: Stratigraphy regional of North East Java Basin (Pertamina – Petro China East Java, 2009)

In developing information regarding the distribution of reservoirs in the stage of determining the location of optimal wells can use seismic attributes and seismic inversions. Both methods are considered suitable for mapping and knowing the subsurface state so that the area of hydrocarbon prospects can be known.

Regional Geology

The North East Java Basin tectonics are in the back arc basin (Figure 2).

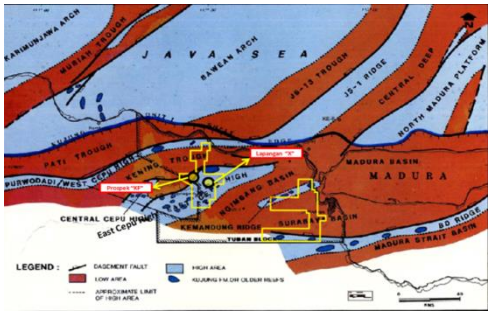

Figure 2: North East Java Basin Tectonics (JOB Pertamina -PetroChina East Java, 2009)

PROCEEDINGS
JOINT CONVENTION BANDUNG (JCB) 2021
November 23rd – 25th 2021

The basin formed in East Java is divided into three mandala structures each from north to south are Paparan Utara, Tinggian Tengah, and South Basin. Paparan Utara is composed by Bawean Arc back arc basin, Sunda Arc System, Northern Platform Central High, Southern Basin Bawean Arc, and Paparan Utara to Madura / North Kangean. Tinggian Tengah consist of Kujung, Madura, Kangean and Lombok Heights, while in the South divided into several Zones namely: Rembang Zone, Randublatung Zone and Kendeng Zone.

Data and Method

The study used methods of seismic attributes and acoustic impedance inversions where the data used are:

- Well data as many as 5 data that have data log neutron porosity, gamma ray, resistivity, density and some have checkshot and top markers.
- 3D post-stack time migration seismic data with depths up to more than 8000ft.

The process of data processing begins with cross plot analysis of log data to find out the character of the reservoir and the location of the reservoir depth. Horizon interpretation is performed on top tuban formations and carbonate formations with markers and log data as references. Below is a flow chart of the study:

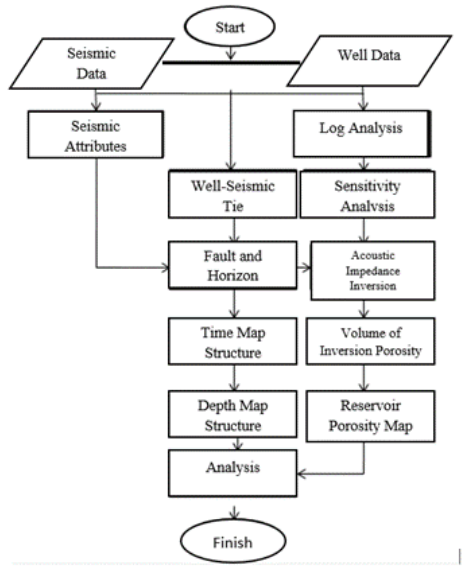

Figure 3: Flow Chart of the Study

Seismic attributes and acoustic impedance inversions are used to analyze physical lithology and the presence of reservoir hydrocarbon fluids.

Result and Discussion

- Well Log Analysis Cross plot Analysis

The results of the log response can be clearly seen the presence of KF prospect areas in carbonate tuban formations that are stratigraphically carbonate rocks precisely from the range of 2152 ms - 2450 ms. Figure 4 shows the result of P-wave log analysis and density logs in KF wells.

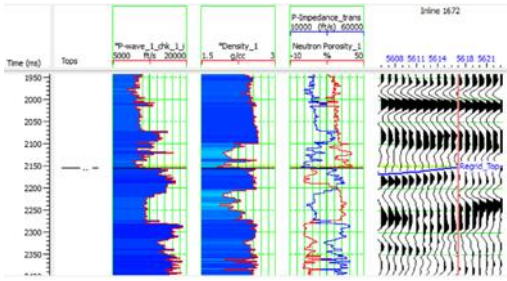

Figure 4: The Result of P-wave Log Analysis and Density Logs in KF Wells

- Cross plot Analysis

Cross plot analysis was conducted to present all acoustic impedance values on top carbonate to base carbonate precisely at a time of 2152 ms to 2450 ms with acoustic impedance values ranging from 24.000 ((ft/s)*(g/cc)) – 56.000 ((ft/s)*(g/cc)). Figure 5 is the result of cross plot analysis of neutron porosity log and P-impedance log.

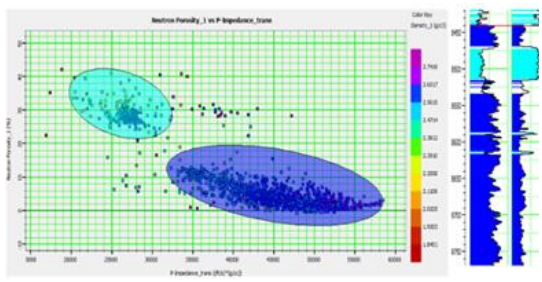

Figure 5: The Result of Cross plot Analysis of Neutron Porosity Log and P-impedance Log

The circled zone in light blue is a target zone with an Acoustic Impedance value of around 24,000((ft/s)*(g/cc)) - 32,000((ft/s)*(g/cc)) that has a high neutron porosity of 22% – 44%. While the dark blue circled zone is a bad reservoir zone in the range of acoustic impedance values >33,000 ((ft/s*(g/cc)) which has a range of neutron porosity values <15%.

- Well-Seismic Tie

Well Seismic Tie is a process of binding seismic data with well data that aims to equalize seismic domains in the form of time into the depth domain of well data. The ultimate aim of this binding process is to find out the position or reservoir horizon of Tuban carbonate on seismic data so that when picking the seismic horizon can be done precisely.

PROCEEDINGS
JOINT CONVENTION BANDUNG (JCB) 2021
November 23rd – 25th 2021

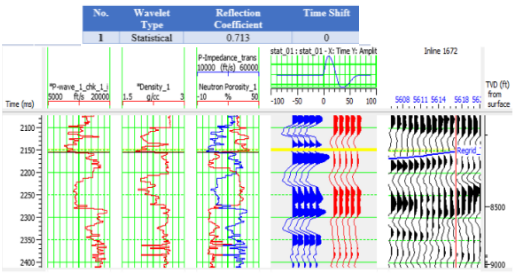

Figure 6: Well Seismic Tie Result

- Instantaneous Phase Attributes

The result of the extraction of this instantaneous attribute is a cross-section of seismic that aims to show the continuity of the layer laterally and the irregularity of the seismic trace (Figure 7).

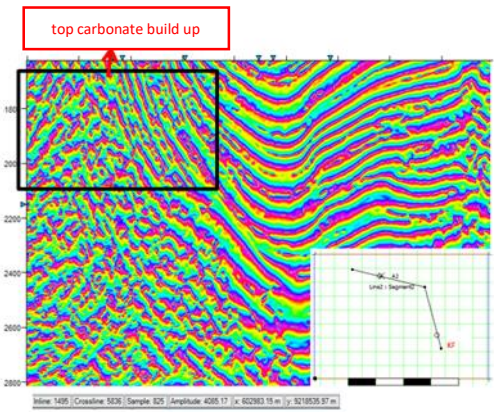

Figure 7: Cross section results trace instantaneous phase attribute

The area in the black box is the result of extraction of the attributes of the targeted research area so that it will make it easier to find the top build up carbonate. The inversion process is carried out on the top tuban of the carbonate reservoir.

- Acoustic Impedance Inversion

The inversion process is carried out on the top tuban of the carbonate reservoir. Control well data in performing inversion is well data that penetrates the entire Tuban carbonate formation, namely KF wells. The main purpose of the inversion is to see the lateral distribution of the acoustic impedance value derived from the KF well to the KF prospect area. The inversion method used is the Inversion Based Model (Figure 8).

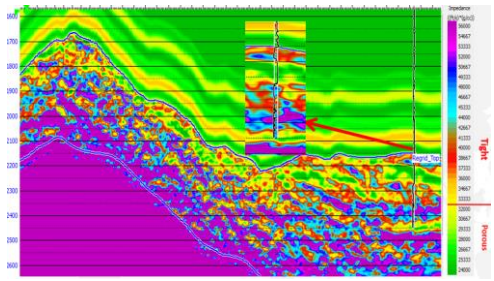

Figure 8: Acoustic Impedance Inversion Cross-Section Result

The distribution of low acoustic impedance values and high acoustic impedance values at each depth, where low acoustic impedance values are green - yellow and high acoustic impedance values are blue-purple. The effect of changes in acoustic impedance (AI) values can be analogous to rock hardness and inversely proportional to porosity. The inversion results are separated by a range of low and high acoustic impedance values. Where the target acoustic impedance value is a low value ranging from 24,000 - 32,000 ((ft/s)*(g/cc)) which is green - yellow, it has a higher porosity. While the range of high acoustic impedance values between >33,000 ((ft/s) (g/cc)), it has a smaller porosity. This is because the existing structure in the prospect area has differences that cause differences in the acoustic impedance value of the inversion process.

- Porosity Volume

The volume of porosity is done to find out the actual porosity value that exists in the target area. The distribution of carbonate porosity values in seismic volumes is derived from the conversion of acoustic impedance values to porosity values through the equation on the cross plot between the P-Impedance trans log and the neutron porosity log. The equation produces a mathematical equation: y = mx + c (-0.00100642 x AI + 51.0727). The mathematical equation is then used to convert the volume of acoustic impedance into the volume of porosity (Figure 9).

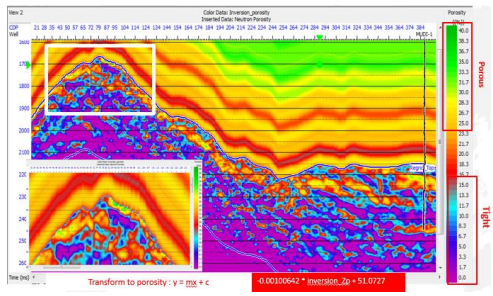

Figure 9: Cross Section of Porosity Volume Distribution

PROCEEDINGS
JOINT CONVENTION BANDUNG (JCB) 2021
November 23rd – 25th 2021

The range of small porosity values is purple – light blue which has a value of <15% indicated as shale rock, while high porosity is red – green which has a range of values ranging from 25% - 40% indicated as rock carbonate.

- Proposed New Well

This carbonate reservoir dispersal pattern is further used to plan the location of the most optimal new well. The conclusion of the location of the most optimal well exploration is done by looking at the distribution pattern of the spread of high dominant porosity values of 25%-- 40% scattered on the top carbonate (green color) which is interpreted as the best reservoir accumulation area where the area is geologically indicated as carbonate build up, so that the most optimal and detailed well prospect zone can be obtained.

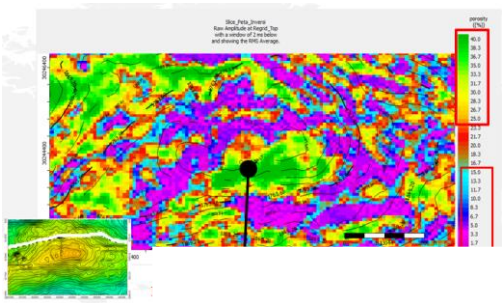

Figure 10: Map Of the distribution of porosity distribution and the location point of the proposed new well (black)

The location of the new proposed well point is depicted with a small black circle symbol on the map. If viewed from the point of the location, it is around the seismic cross-section on inline 1495 and xline 5830.

Conclusions

Based on the results of processing and interpretation of data on research that has been done on KF Prospects it can be concluded that low Acoustic Impedance values ranging from 22,000 - 32,000 ((ft/s)*(g/cc)) have porosity ranging from 25 - 40%. While the high Impedance value of >33,000 ((ft/s)*(g/cc)) has a smaller porosity <15%. The best well position on the KF prospect is right on the Top carbonate at inline 1495 xline 5830 depth of 6000 ft

References

Brown, A.R. 2000. AAPG Memoir 42 SEG Investigations in Geophysics, No. 9, Oklahoma

Ellis, Darwin V., and Singer Julian M. 2008. *Well Logging for Earth Scientist. Netherlands.*

Pertamina BPPKA, 1996. *Petroleum Geology Of Indonesians Basin : Principles, Methods, And Application, Vol IV : East java basin*. Pertamina BPPKA

Rider, Malcolm. 1996. *The Geological Interpretation Of Well Logs Second Edition*. Scotland : Interprint Ltd

Russell, B.H. 1988. *Introduction to Seismic Inversion Methods*. Calgary. Canada

Russell, B.H. 1991. *Introduction to Seismic Inversion Methods*, third edition, Volume 2, S.N. Domenico, Editor Course Notes Series

Sukmono S. 2007. FIKTM, Institut Teknologi Bandung

Veeken, P.C. H., 2007. *Seismic Stratigraphy, Basin Analysis and Reservoir Characterisation*. Amsterdam: Elsevier

Van Bammelen. 1948 *The Geology Of Indonesia* Vol. IA. Government Printing Office The Hague

Acknowledgements (Optional)

The author thanked PT. Pertamina Hulu Energi which has given permission to publish it as well as the UIN Walisongo Semarang Physics Study Program which provides full support

PROCEEDINGS
JOINT CONVENTION BANDUNG (JCB) 2021
November 23rd – 25th 2021

Geothermal System Modeling of Roosevelt Hot Springs (RHS), Utah Using TOUGH2 Simulator

D.R.A. Gandini[1], N. Rahmawati[1], A.F. Raharja[1], D.B. Soebakir[1], M.I. Defri[1], M.D. Paratin[1], S. Widyanti[1]

[1]Department of Geophysical Engineering, Faculty of Exploration and Production Technology, Pertamina University

Abstract

Roosevelt Hot Springs (RHS) is a two-phase geothermal system located in the western side of Mineral Mountains, Utah. Previous study stated that the composition of the fluid has not changed since it was first produced in 1984, except for the effects of steam loss and injection fluid through well 14-2. To know the current condition of the geothermal system below the surface, conceptual model and reservoir simulation are made. The conceptual model is based on the results of geological, geophysical, and geochemical surveys that have been carried out in this area in previous studies. Furthermore, reservoir simulation using TOUGH2 is carried out by combining information of rock physical properties, initial conditions, boundary conditions, as well as sinks and sources to reach the natural state which is characterized by the similarity of the temperature to depth curve from the simulation results carried out with data from one exploration well and two monitoring wells. From the simulation results, it is known that the fractured granitoid reservoir is located at a shallow depth and is limited by the Opal Mound fault in the west which has low permeability. The heat source located in the eastern side of the RHS system, which is just below the Mineral Mountains, makes the fluid in the reservoir the hottest and has a temperature between 175-230°C.

Keywords: Reservoir simulation, geothermal system, TOUGH2, natural state, Roosevelt Hot Springs

Introduction

The Roosevelt Hot Springs (RHS) is a two-phase geothermal system located in Utah, United States of America. This geothermal system is located between the Mineral Mountains in the east and the central part of the Milford Valley in the west (Simmons, et al., 2018). The reservoir covering an area of about 32 km^2 is formed in fractured Precambrian gneiss and Tertiary granite by a fault intersection of the Opal Mound Fault and the Negro Mag Fault (Christensen et al., 1983; Ward et al., 1978; Moore and Nielson, 1994). The geothermal system is believed to be driven by heat from a young intrusion related to rhyolite domes emplaced beneath the Mineral Mountains, which is a 250 km^2 pluton, the largest and youngest in Utah (Lynne et al., 2005).

In 1984, fluids discharged from three production wells are used at tbe Blundell 1 flash plant which generates approximately 26 MW of electrical power (Blackett and Ross, 1992). Additional generation was installed in 2006 by commissioning of Blundell 2 binary plant which generates more 10 MW. Analysis obtained from reservoir fluid prior to production shows that fluid obtained from well 14-2 has the highest temperature and represents hydrothermal fluid in the geothermal system. However, during the production period, well 14-2 was used as an injection well. The reservoir fluid composition has likely not changed since 1984, except for the effects of steam-loss and mixing with the injection fluid (Simmons et al., 2018). This effect is the result of the pressure drop in the reservoir due to the fluid production process and the close distance between the injection well 14-2 and the reservoir. If sorted, the production wells that are most affected are wells 54-3, then wells 45-3 and 28-3. Meanwhile, production wells 13-10 are not affected even though they have been operating for years.

After the geothermal system has been producing for almost 40 years, it is very important to maintain the condition of the geothermal reservoir so that it can continue to produce. Because we cannot see its conditions below the surface with naked eyes, a reservoir modeling simulation was carried out in this study to determine the recent of the geothermal system, which was lastly carried out by Faulder (1991) and Yearsley (1994). Reservoir modeling will be carried out based on geological, geophysical, geochemical, and well data available using a software simulator named TOUGH2. This simulator will test the reservoir model based on previous conceptual model and predict the response of the geothermal system for various production scenarios.

Reservoir Modeling and Natural State Simulation

Reservoir modeling and simulation combine the information of rock physical properties, initial conditions, boundary conditions, as well as sinks and sources to reach the natural state. Initial condition is a state before the geothermal system is formed. While boundary condition is a special condition created around the simulation model of the geothermal system, especially around the reservoir, to keep fluid or heat accumulating in the geothermal system. For this reason, this boundary condition is set by using a constant pressure and temperature. To prevent the fluid or heat escaping the reservoir model, it is also assumed that the area around the reservoir is low permeability rock. Sinks and sources are other information needed in the simulation. Sink is a fluid that enters the geothermal system, such as natural recharge or reinjection wells. While the source is the fluid or heat that comes out of the geothermal system, such as manifestations or production wells. Natural state is a natural condition in a geothermal reservoir where no production or injection has been carried out which disrupts the reservoir state. In reservoir simulation, to know whether this condition is reached, it is necessary to do a curve matching

by looking at the similarity of the temperature and pressure data with depth based on the reservoir simulation result and well data.

Data and Method

Based on the conceptual model of Simmons, et al. (2018), the subsurface conditions in the study area consist of three main rock types, namely Precambrian gneiss, Tertiary pluton, and basins containing sedimentary deposits. The temperature rise at the shallow depth of the well data indicates the upper part of the reservoir. The main meteoric recharge comes from rainfall on the summit and west side of the Mineral Mountains. The extensive fracture coupled with the complex east-west graben associated with the Negro Mag fault allows meteoric water to circulate to depths controlled by the presence of an open fracture. The intersection of the Opal Mound and Negro Mag faults produces a naturally fractured and intensive geothermal reservoir for thermal fluids. The outflow of the hot springs occurs over the Opal Mound horst and is centered at the confluence of the Opal Mound and Negro Mag faults. The hot fluid then mixes and dilutes with cold water in the shallow aquifer as it flows down a hydrological gradient into the Milford Valley (Faulder, 1991).

The simulation carried out using TOUGH2 requires an initial model based on a conceptual model which is then divided into several blocks/grids. Each grid has rock physical parameter information from geological data. The coordinate limits used are adjusted to the area of the geothermal system as contained in the conceptual model and reservoir simulation that has been carried out by previous studies. The simulation model used has a size of 10 x 10 x 6 km^3 in total, consisting of 1000 blocks with a size of 1 x 1 x 0.6 km^3.

The initial model used in this study was made based on geological, geophysical, and well data from previous studies. This model consists of 10 layers with the same thickness and a total depth of 6000 m. The first layer is assumed to be the top boundary with initial conditions such as a pressure of 1.26 Pa and a temperature of 100°C. The surroundings of the model are assumed to be the side boundaries which have the same initial conditions as the top boundary. The pressure and temperature values will increase with depth so that the lowest layer which is assumed to be the bottom layer has the highest value of initial condition.

In addition, rock parameters for simulation models such as porosity, density, permeability, thermal conductivity, and specific heat capacity are also required. Then, the latest well data in the research area from previous studies also needs to be used. Production wells 54-3, 28-3, 13-10, and 45-3 are known to produce fluids with a total of 240-290 kg/s. Meanwhile, injection wells 14-2, 12-35, and 82-33 injected a total of 244 kg/s and an enthalpy of 400 kJ/kg of which 25-40% was injected by well 14-2.

Result and Discussion

Reservoir simulation performed on the initial model were carried out for 35,000 years. This number is determined based on the estimated time the first time this geothermal system was formed. The simulation results obtained are the distribution of the current pressure and temperature values. The distribution of temperature values from the simulation results shows a quite good and logical condition for this geothermal system in Figure 2. It is also known that the temperature near the surface is quite high, indicating a convective heat transfer or reservoir zone. The simulated temperature gradient is 73°C/km with a reservoir temperature around 175-230°C.

After the simulation is run, curve matching is performed to see whether the temperature and pressure curves to depth from the simulation results are in accordance with the available well data or not. Due to the absence of temperature and pressure data from production or injection wells, curve matching is only performed with data from exploration and monitoring wells in the geothermal system area. Well 52-21 is an exploration well located in the southern side of the RHS geothermal system. The OH-1 well is a monitoring well located in the western side of the RHS geothermal system and the Opal Mound fault. The OH-7 well is a monitoring well located in the northeast side of the RHS geothermal system. If the distance between the three wells and the reservoir of the RHS geothermal system is compared, well OH-1 is the closest while well 52-21 is the farthest.

In the curve matching, the blue dots represent the simulated temperature values while the orange dots represent the values from the well data. All of the temperature curve matching from the simulation show an increase in the temperature value with depth which is quite compatible with the well data. Although curve matching cannot be done with pressure data because it is not available, the fit of this temperature curve is enough to prove that the simulation model has reached the natural state.

Conclusions

The RHS geothermal system has a reservoir formed by the fault intersection of the Opal Mound and Negro Mag faults. The Opal Mound fault also acts as a hot fluid flow path to the surface. The heat source zone is in the eastern side of the RHS geothermal system, at the bottom of the Mineral Mountains. In the RHS geothermal system, there are high temperatures at shallow depths which can be interpreted as convection heat transfer zone. The simulation results of reservoir modeling and curve matching show a good curve match even though it is only using the temperature data. This is enough to tell that the reservoir simulation model for the RHS geothermal system have reached the natural state condition. To continue, history matching can be done for the next study.

References

Blackett, R. E., and Ross, H. P., 1992, Utah Geological Association Publication, **21**, 261-280.

Christensen, O. D., Capuano, R. M., and Moore, J. N., 1983, Journal of Volcanology and Geothermal Research, **16**, 99-129.

Energy and Geoscience Institute at the University of Utah, 2018, Utah FORGE: Rock Properties [data set]. Retrieved from https://dx.doi.org/10.15121/1452765.

Energy and Geoscience Institute at the University of Utah, 2019, Utah FORGE: Earth Model Native State Simulation Results [data set]. Retrieved from https://dx.doi.org/10.15121/1557419.

Faulder, D. D., 1991, PROCEEDINGS 16th Workshop on Geothermal Reservoir Engineering, **SGP-TR-134**, 131-142.

PROCEEDINGS
JOINT CONVENTION BANDUNG (JCB) 2021
November 23rd – 25th 2021

Idaho National Laboratory, 2020, Utah FORGE: Data for 3-D Model Development - Lithology, Temperature, Pressure, and Stress [data set]. Retrieved from https://dx.doi.org/10.15121/1605155.

Lynne, B. Y., Campbell, K. A., Moore, J. N., and Browne, P. R. L., 2005, Sedimentary Geology, **179**, 249-278.

Moore, J. M., and Nielson, D. L., 1994, Utah Geological Association Publication, **23**, 25-36.

Simmons, S. F., Kirby, S., Allis, R., Moore, J., and Fischer, T., 2018, PROCEEDINGS 43th Workshop on Geothermal Reservoir Engineering, **SGP-TR-213**, 1-7.

Ward, S. H., Parry, W. T., Nash, W. P., Sill, W. R., Cook, K. L., Smith, R. B., Chapman, D. S., Brown, F. H., Whelan, J. A., and Bowman, J. R., 1978, Geophysics, **43**, 1515–1542.

Yearsley, E., 1994, Geothermal Resource Council TRANSACTIONS, **18**, 617-622.

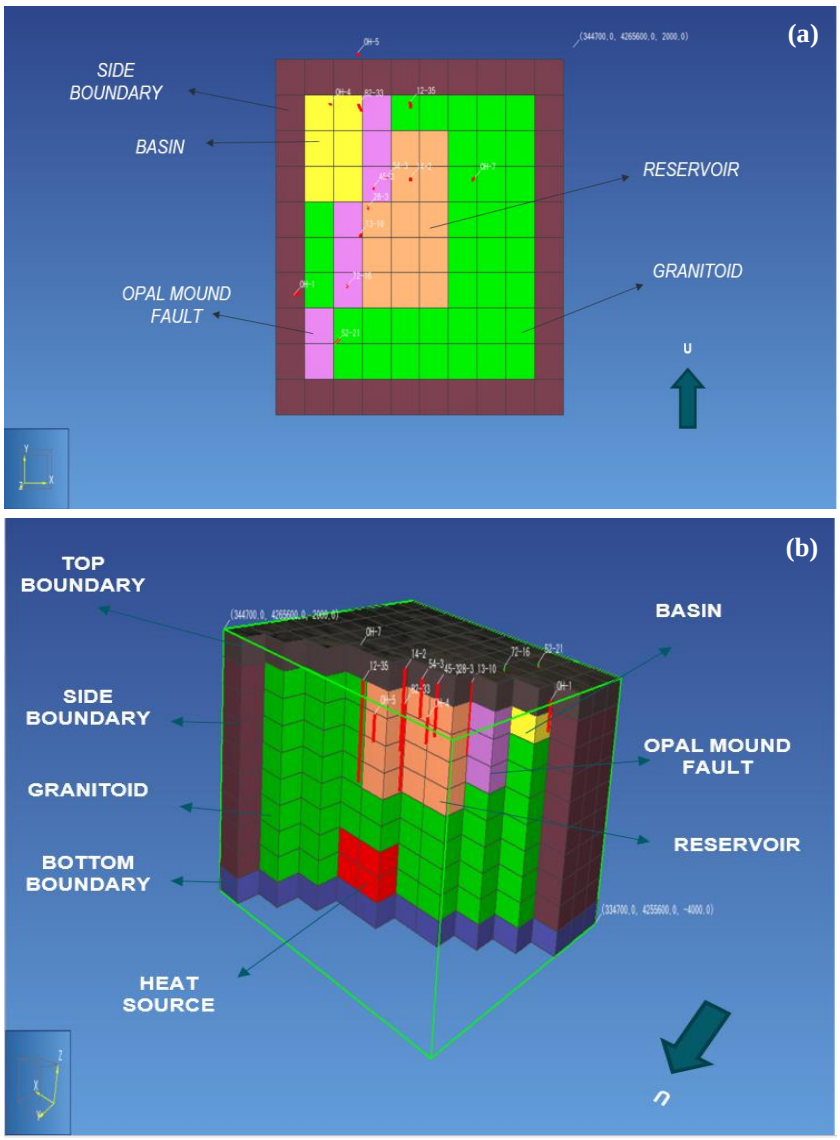

Figure 1: Map view (a) and cross section (b) of the RHS geothermal system simulation model. The model is made based on Simmons et al. (2018) conceptual model with production, injection, exploration, and monitoring wells located in the study area.

PROCEEDINGS
JOINT CONVENTION BANDUNG (JCB) 2021
November 23rd – 25th 2021

Tabel 1: Physical rock parameters used in the reservoir modeling

Rock Type	Density (Kg/m^3)	Porosity	Permeability (m^3)			Thermal Conductivity (W/m.K)	Specific Heat Capacity (J/Kg.K)
			X	Y	Z		
Top Boundary	2500	$1.0e^{-7}$	$1.0e^{-21}$	$1.0e^{-21}$	$1.0e^{-21}$	2.0	1000
Side Boundary	2500	$1.0e^{-7}$	$1.0e^{-18}$	$1.0e^{-18}$	$1.0e^{-18}$	2.0	1000
Bottom Boundary	2500	$1.0e^{-7}$	$1.0e^{-20}$	$1.0e^{-20}$	$1.0e^{-20}$	2.0	1000
Granitoid	2750	0.0118	$1.2e^{-16}$	$1.2e^{-16}$	$1.2e^{-16}$	3.05	790
Basin	2500	0.12	$1.7e^{-14}$	$1.7e^{-14}$	$1.7e^{-14}$	2.0	830
Reservoir	2750	0.13	$1.2e^{-13}$	$1.2e^{-13}$	$1.2e^{-13}$	3.05	790
Opal Mound Fault	2750	0.12	$1.2e^{-14}$	$1.2e^{-14}$	$1.2e^{-14}$	2.0	790
Heat Source	2750	$3.0e^{-1}$	$1.2e^{-14}$	$1.2e^{-14}$	$1.2e^{-14}$	3.05	1000

Source: Utah FORGE data set, 2018, 2019, 2020

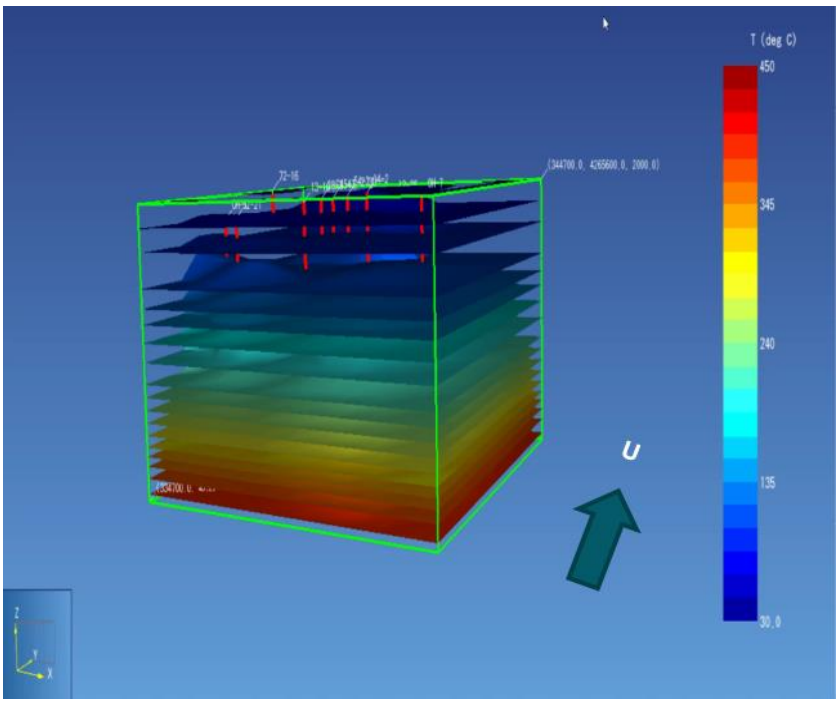

Figure 2: Temperature distribution of the simulation result shows the condition of RHS geothermal system

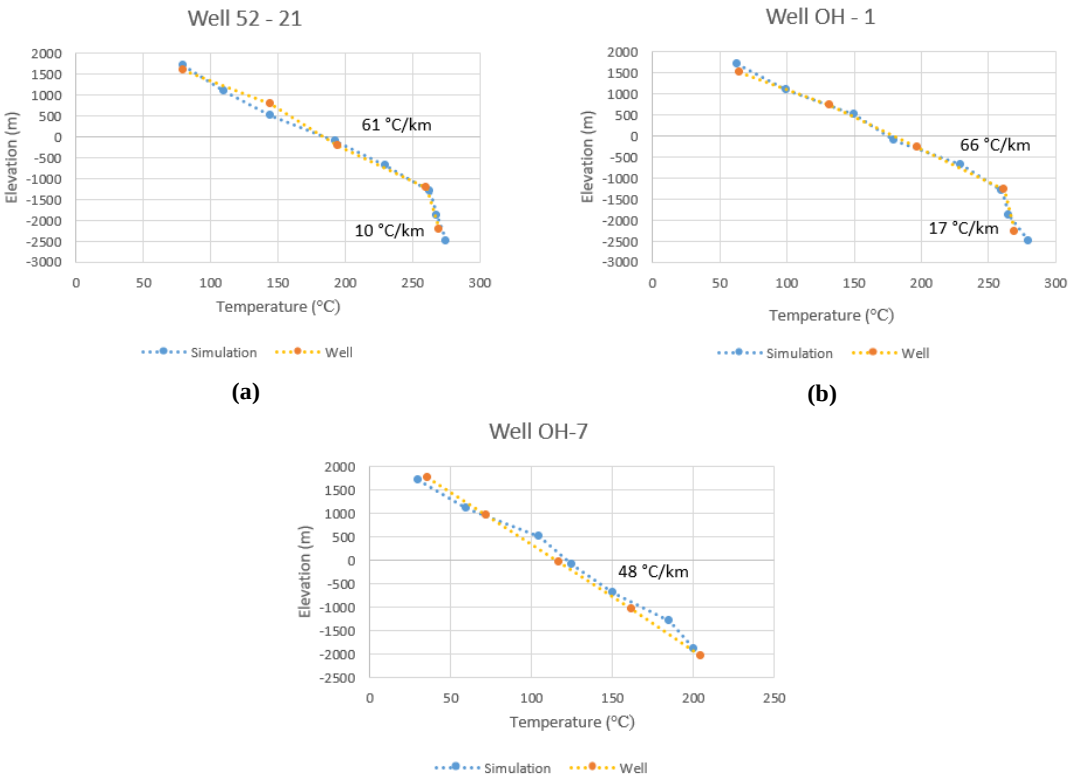

(a) **(b)** **(c)**

Figure 3: Curve matching for well 52-21 (a), OH-1 (b), and OH-7 (c). Blue dots represent the simulated temperature values while orange dots represent the values from well data. The temperature gradiens for each curve are shown near the curve.

PROCEEDINGS
JOINT CONVENTION BANDUNG (JCB) 2021
November 23rd – 25th 2021

Implementation of Mechanical Earth Model in Predicting the Maximum Water Injection Flow Rate in Mature Field

Muhammad Mursalin[1], Febry Romario[1], Aldo Setiawan[1], Dhany Firmansyah[1], Bagas Juniar Kusuma Negara[1]
Politeknik Akamigas Palembang[1]

ABSTRACT

Fracture can occur at shale zone, when fluid injection pressure to reservoir sand target exceeds fracture pressure. Consequence, fluid injected to reservoir target will not be optimum. Therefore, we must determine the fracture pressure that will apply. This study was performed in order to build fit purpose 1D mechanical earth model which will be used to determine or predict injection pressure and maximum injection flow rate, in order to prevent fracture growth from targeted reservoir sand to the enclosing shale interval. Required data to build 1D mechanical earth model in this study namely gamma ray log, density, sonic compression, sonic shear and repeat formation test (RFT). Then, mohr stress diagram applied to determine the safety factor and reservoir simulation done to predict flow rate maximum of water injection at inverted five spot pattern and inverted seven spot patterns with three scenarios. Based on calculation, then obtained vertical stress (S_v) > Maximum Horizontal Stress (SH_{max}) > Minimum Horizontal Stress (Sh_{min}), with average value of S_v, SH_{max}, Sh_{min} is 0.827 psi/ft, 0.731 psi/ft, 0.696 psi/ft, which mean normal stress regime. Fracture pressure that obtained at intact reservoir (cap rock) is 1521.19 psi, and safety factor obtained is 12% or maximum injection pressure is 1460.7 psi. The result of reservoir simulation performed with three scenarios at inverted five spot pattern and inverted seven spot patterns show that second scenario provide the best result with apply flow rate water injection is 53000 STB/D pressure reached is 1453 psi and at inverted seven spot patterns with apply flow rate water injection is 56000 STB/D pressure reached is 1458 psi.

Keywords: *Mechanical Earth Model, Fracture Pressure, Water Injection*

INTRODUCTION

Mario Field is one of the largest waterflood fields in South East Asia, which is located in the Riau Province of Indonesia. This field has been in production for more than 59 years since its discovery in 1944 (Hao et al., 2011). It is planned that water injection will be carried out in this field at injection well X, zone Mr 2 (2276–2390 ft). Before carrying out water injection, an important step that must be prepared in advance is to build a 1D mechanical earth model to determine the maximum injection pressure from the waterflood to prevent fracture of the shale interval in the target reservoir (PT. CPI, 2011).

Most water injection wells in water flooded reservoirs have fractured over time. These fractures have a significant effect on reservoir performance (oil production rate, oil-water ratio, and ultimate recovery). If the injection pressure increases beyond the minimum horizontal (fracture pressure) or vertical stress in the formation around the borehole, fractures will form (Gadde, & Sharma, 2001). Oil recovery and reservoir sweep are affected by a fracture because the injected fluid enters the fractured layer, then water breakthrough will occur quickly which causes little oil recovery to be achieved (Kyunghaeng, Chun, & Sharma, 2011).

To build a 1D mechanical earth model, data logging and field test data are needed such as gamma-ray, density, sonic compression, sonic shear, and repeat formation tests. The mechanical earth model that has been generated, including fracture pressure, will be used as a constraint to perform injection simulation on Petrel 2009 software which will be used to predict the maximum flow rate of water injection in the inverted five spots and inverted seven-spot patterns.

DATA AND METHOD

Water injection planned to be done at injection well X, zone Mr 2 (2276–2390 ft). before doing water injection, important step that must be done is to determine the pressure gradient fracture by building 1D mechanical earth model (MEM). Value of fracture pressure previously obtained at depth critical (Mr 1) shale zone will be used as a limitation in the application of water injection, then a simulation is carried out by building an appropriate reservoir model on the Mario Field depth structure map, then three field scenarios are made to predict the maximum flow rate when water injection is done on pattern inverted five spots and inverted seven spots with limitations fracture pressure. If the injection pressure increases beyond the minimum horizontal (fracture pressure) or vertical stress in the formation around the borehole, the fracture will occur (Gadde, & Sharma, 2001). Oil recovery and reservoir sweep are affected by a fracture because the fluid injected enters the fractured layer, then water breakthrough will occur quickly which causes little oil recovery to be achieved. (Kyunghaeng, Chun, & Sharma, 2011). The flow chart of this research can be seen in Figure 1.

1D Mechanical Earth Model Construction

Analysis of 1D Mechanical Earth Model Construction begins by calculating the vertical stress by integrating bulk density (RHOB) at all depths and

regressing to ground level. Then, combined with the log data. It was found that the vertical stress was 2402.56 psi or the gradient overburden stress was 0.877 psi/ft. And then, determine the normal compaction trend using log sonic data in the shale interval with a Vshale value of 0.6. Then, the normal compaction trend is used as input into the pore pressure calculation. The pore pressure value obtained is calibrated against field tests such as the repeat formation test (Setiawan, & Vera, 2016).

The tensile strength of the formation is used to evaluate the tensile failure of boreholes due to stress concentration. Tensile strength usually ranges from 1/12 to 1/8 of the UCS (Rafieepour, & Jalalifar, 2014). In this study, the tensile strength applied is 1/10 of UCS to determine the rock strength properties of the injection well X. In determining the minimum horizontal stress (Sh_{min}) there are two methods used, namely the eaton method (in sand and shale lithology using a combination of pore profiles pressure), and matthew & kelly method (only on shale lithology), assuming hydrostatic (shale pore pressure). The Matthew & Kelly curves were adjusted to the Eaton curves for the shale fracture, by adjusting the value of the coefficients of the stress matrix. In determining the maximum horizontal stress (Sh_{max}) in the Mario Field, it is assumed that it is based on analog data from the nearest field.

A previous study from Kotabatak Field stating that the calibration borehole enlargements by comparing the difference between collapse mud weight and mud weight used during drilling indicate that the difference between the minimum and maximum horizontal stress, using a comparison σ_H/σ_h with a value of 1.05 resulted in a calibration consistent (Yi, Goodman, Williams, & Hilarides, 2008).

The ratio of these values will be used in this field. Based on the results of calculations and analysis of vertical stress, pore pressure, minimum horizontal stress, and maximum horizontal stress. Based on Anderson's (1951) classification, this Mario field is in the normal fault stress regime where $S_v > SH_{max} > Sh_{min}$. Figure 2 shows the geomechanics model of the injection well X.

Maximum Injection Pressure

Determination of the maximum injection pressure aims to prevent the occurrence of debris in the reservoir to the caprock. As long as there is sufficient stress contrast between the reservoir and the caprock, the applied pressure will always seek the least resistance into the reservoir section. (Setiawan, & Vera, 2016). Determination of maximum injection pressure is divided into two parts, in the intact reservoir and in the fault area. Based on the results of the calculations that have been carried out, the maximum injection pressure in the intact reservoir at a critical depth is 1661.38 psi. Then by applying the Mohr stress diagram, we get a safety factor of 12% or a maximum injection pressure of 1460.7 psi. Then, from the results of calculations that have been carried out, it is found that the maximum injection pressure in the fault area is 1521.19 psi. Then by applying the Mohr stress diagram, we get a safety factor of 20% or a maximum injection pressure of 1220.7 psi.

Prediction of Maximum Flow Rate of Water Injection

After knowing the fracture pressure and establishing reservoir modelling, the next step is to predict the maximum flow rate of water injection in the inverted five-spot and inverted seven-spot pattern by simulating the reservoir for three years, and making several field scenarios by adjusting the injection flow rate to see if the injection flow rate whether the fracture pressure reaches the fracture pressure or not because if the fracture pressure is reached, the fluid injected into the target zone that has been determined will spread to other zones and of course something like this is not desirable to happen.

Inverted Five Spot Pattern Field Development Scenario

Figure 3.a is inverted five-spot patterns in the Mario field using one existing well, namely an injection well and 4 additional production wells. And the following picture below is an illustration of the inverted five-spot patterns on the Mario field.

Inverted Five Spot Pattern Scenario 1

In this scenario (Figure 3.b), the strategy for field development is to set the water injection rate of 40000 STB/D. The pressure is reached at 1263 psi, which indicates that there is no fracture, so it is still at a safe level in the application of the injection rate. The cumulative oil production in this scenario is 23.4 MMSTB, the cumulative water produced is 23 MMSTB and the water cut reaches 80% after producing for 3 years.

Inverted Five Spot Pattern Scenario 2

In this scenario (Figure 3.c), the strategy for field development is to set the water injection rate to 53000 STB/D. The pressure is reached at 1453 psi, which indicates that there is no fracture, so it is still at a safe level in the application of the injection rate. The cumulative oil production in this scenario is 24.6 MMSTB, the cumulative water produced is 33.6 MMSTB and the water cut reaches 84.1% after producing for 3 years.

Inverted Five Spot Pattern Scenario 3

PROCEEDINGS
JOINT CONVENTION BANDUNG (JCB) 2021
November 23rd – 25th 2021

In this scenario (Figure 3.d), the strategy for field development is to set the water injection rate of 60000 STB/D. The pressure is reached at 1560 psi, which indicates that a fracture has occurred because it has exceeded the maximum injection pressure so that the rate is not feasible to apply. The cumulative oil production in this scenario is 25.6 MMSTB, the cumulative water produced is 39 MMSTB and the water cut reaches 86% after producing for 3 years.

From the development scenario that has been carried out, it can be concluded that the best scenario is scenario 2, because with the application of a flow rate of 53000 STB/D the pressure achieved is still below the fracture pressure (1460,7 psi) which is 1453 psi and is still at a safe level to apply.

Inverted Seven Spot Pattern Field Development Scenario

Figure 4.a is the inverted seven-spot patterns in the Mario field using one existing well, namely an injection well and 6 additional production wells. And the following picture below is an illustration of the seven-spot pattern on the Mario field.

Inverted Seven Spot Pattern Scenario 1

In this scenario (Figure 4.b), the strategy for field development is to set the water injection rate to 45,000 STB/D. The pressure is reached at 1295 psi, which indicates that there is still no fracture, so it is still at a safe level in the application of the injection rate. The cumulative oil production in this scenario is 25 MMSTB, the cumulative water produced is 27.4 MMSTB and the water cut reaches 84% after producing for 3 years.

Inverted Seven Spot Pattern Scenario 2

In this scenario (Figure 4.c), the strategy for field development is to set the water injection rate to 56,000 STB/D. The pressure is reached at 1458 psi, which indicates that there is still no fracture, so it is still at a safe level in the application of the injection rate. The cumulative oil production in this scenario is 26 MMSTB, the cumulative water produced is 37 MMSTB and the water cut reaches 86.4% after producing for 3 years.

Inverted Seven Spot Pattern Scenario 3

In this scenario (Figure 4.d), the strategy for field development is to set the water injection rate to 60,000 STB/D. The pressure is reached at 1520 psi, which indicates that there is still no fracture, so it is still at a safe level in the application of the injection rate. The cumulative oil production in this scenario is 26.35 MMSTB, the cumulative water produced is 40.8 MMSTB and the water cut reaches 87% after producing for 3 years.

From the development scenario that has been carried out, it can be concluded that the best scenario is scenario 2, because with the application of a flow rate of 56,000 STB/D the pressure achieved is still below the fracture pressure (1460,7 psi) which is 1458 psi and is still at a safe level to apply.

RESULT AND DISCUSSION

From the three field scenarios that have been carried out in predicting the maximum flow rate. In the five-spot pattern, the second scenario is the best by applying an injection flow rate of 53,000 STB/D and the pressure achieved is 1453 psi. in the seven spot pattern, the second scenario is the best by applying an injection flow rate of 56,000 STB/D and the pressure achieved is 1458 psi, where the pressure is close to fracture pressure by applying a safety factor of 12% which is 1460,7 psi.

CONCLUSIONS

The conclusions obtained from this study are as follows:

1. Based on the calculation and analysis of the 1D mechanical earth model, the Mario Field is currently in the normal fault stress regime where $S_v > SH_{max} > Sh_{min}$.
2. Using log data to identify pore pressure trends that can be used to estimate pore pressure. Where the pore pressure is part of geomechanic properties.
3. Fracture pressure prediction is calculated using 2 methods, namely the Eaton method (on sand and shale lithology), using a combination (profile pore pressure), and the Matthew & Kelly method (only on shale lithology), assuming hydrostatic (shale pore pressure).
4. The maximum injection pressure in the intact reservoir is 1661.38 psi and at the fault area is 1521.19 psi.
5. The safety factor obtained from the Mohr stress diagram at the intact reservoir is 12% or 1460,7 psi and at the fault area is 26% or 1220.7 psi.
6. In the five spot pattern, the second scenario is the best by applying an injection flow rate of 53,000 STB/D and the pressure achieved is 1453 psi.
7. In the seven spot pattern, the second scenario is the best by applying an injection flow rate of 56,000 STB/D and the pressure achieved is 1458 psi.

There are several things that are suggested for further research, namely as follows:

1. Determine wellbore stability, in directional or horizontal wells.
2. Determine the stable mud weight window.
3. Comparing the economics of the five spot pattern and seven spot pattern cases in a water injection project.

PROCEEDINGS
JOINT CONVENTION BANDUNG (JCB) 2021
November 23rd – 25th 2021

REFERENCES

Gadde, P.B., & Sharma, M.M. (2001). Growing Injection Well Fractures and Their Impact on Waterflood Performance. SPE, 71614.

Hao, C., Shook, G.M., Taimur, M., Dwarakanath, V., Smith, B.R., Muhammad, S., Masduki, A., Mario, C.C., & Putra, K.A.D. (2011). Interwell Tracer Test to Optimize Operating Conditions for a Surfactant Field Trial: Design, Evaluation and Implications. SPE, 144899.

Kyunghaeng, L., Chun, H., & Sharma, M.M. (2011). Impact of Fracture Growth on Well Injectivity and Reservoir Sweep During Waterflood and Chemical.

Rafieepour, S., & Jalalifar, H. (2014). Drilling Optimization Based on a Geomechanical Analysis Using Probabilistic Risk Assessment, a Case Study from Offshore Iran. Rock Engineering and Rock Mechanics: Structure in and on Rock Masses, PP. 1415-1452.

Setiawan, P., & Vera, R. (2016). 1D Mechanical Earth Model Petapahan Field. Chevron Pacific Indonesia, Unpublished.

Yi, X., Goodman, H.E., Williams, R.S., Hilarides, W.K., & Chevron. (2008). Building a Geomechanical Model for Kotabatak Field With Applications to Sanding Onset and Wellbore Stability Predictions. IADC/SPE, 114697.

ACKNOWLEDGEMENTS

We would like to express our deepest gratitude to Mr. Roni Alida, S.T as a Head of Petroleum Engineering Department at Politeknik Akamigas Palembang and all of Petroleum Engineering Lecturers who have supported and guided the author in order to completing this paper.

PROCEEDINGS
JOINT CONVENTION BANDUNG (JCB) 2021
November 23rd – 25th 2021

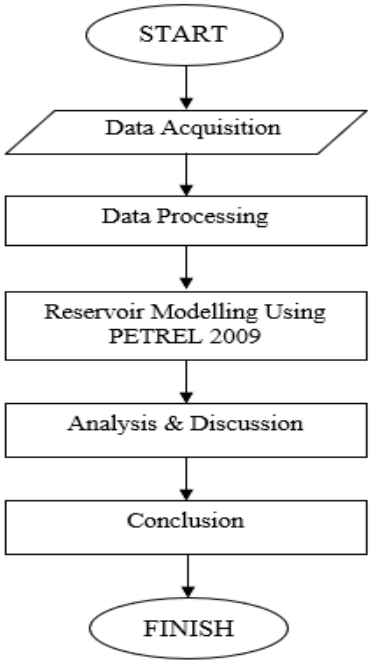

Figure 1: Research Flowchart

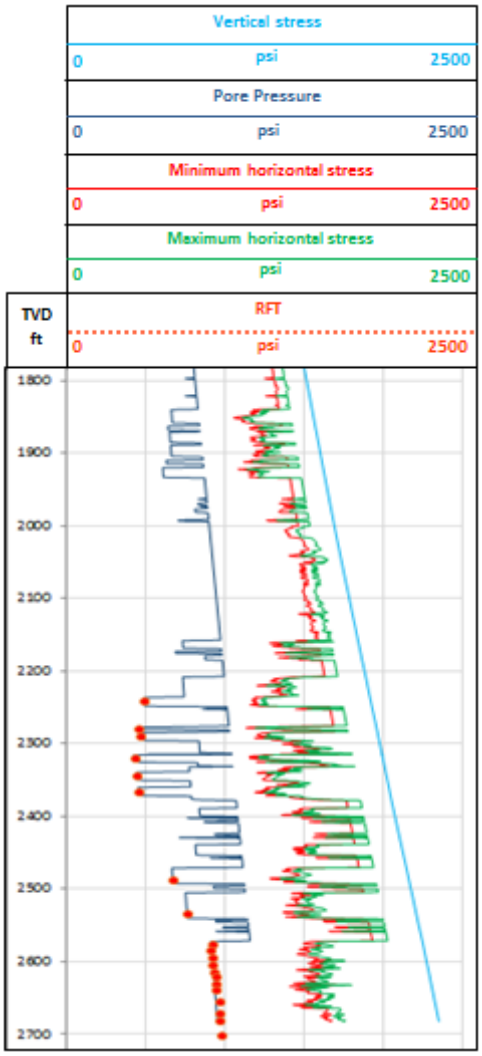

Figure 2: Geomechanic Model

PROCEEDINGS
JOINT CONVENTION BANDUNG (JCB) 2021
November 23rd – 25th 2021

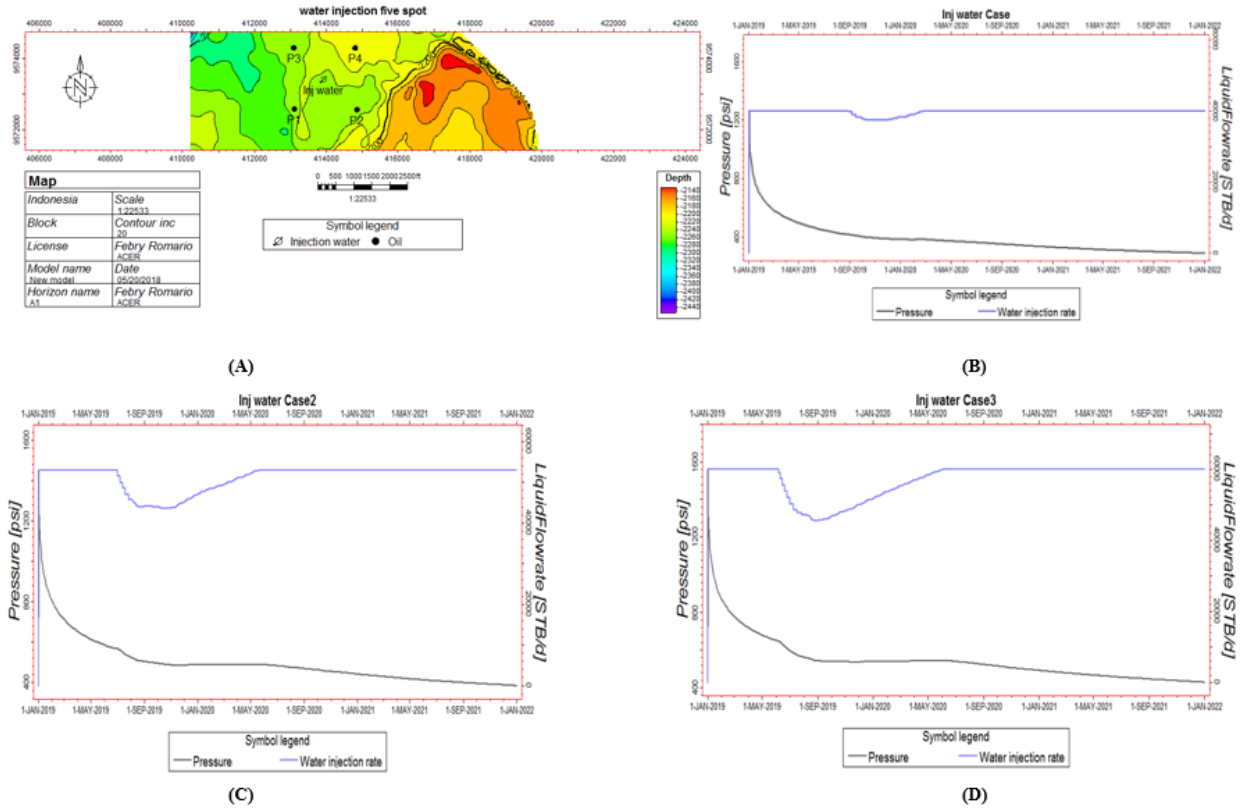

Figure 3: (a) Well Point on the Mario Field with Inverted Five-Spot Pattern; (b) Pressure Profile and Water Injection Rate Scenario 1 in Inverted Five-Spot Pattern; (c) Pressure Profile and Water Injection Rate Scenario 2 In Inverted Five-Spot Pattern; (d) Pressure Profile and Water Injection Rate Scenario 3 In Inverted Five-Spot Pattern.

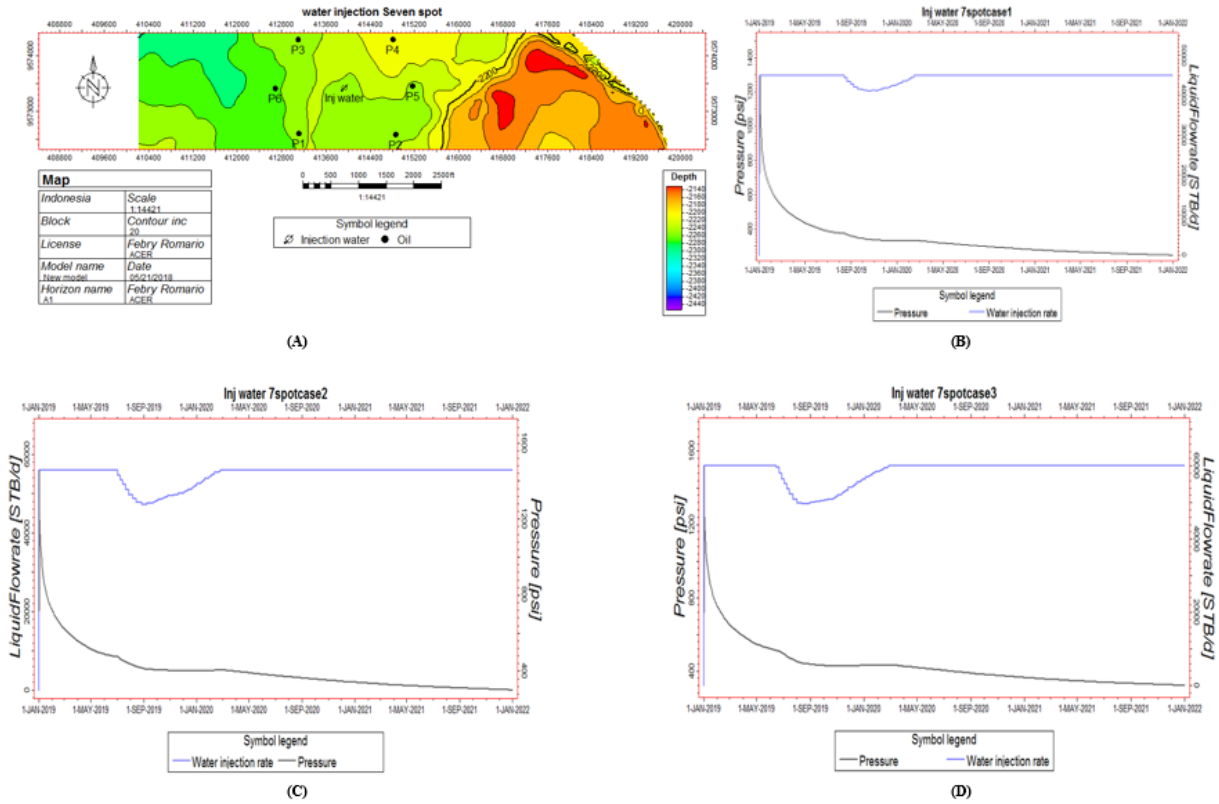

Figure 4: (a) Well Point on the Mario Field with Inverted Seven-Spot Pattern; (b) Pressure Profile and Water Injection Rate Scenario 1 in Inverted Seven-Spot Pattern; (c) Pressure Profile and Water Injection Rate Scenario 2 In Inverted Seven-Spot Pattern; (d) Pressure Profile and Water Injection Rate Scenario 3 In Inverted Seven-Spot Pattern.

PROCEEDINGS
JOINT CONVENTION BANDUNG (JCB)2021
November 23rd – 25th 2021

Sequence Stratigraphy and Paleogeography of Carbonate Rocks on Field "X", North Madura Platform, North East Java Basin

Achmad Yusqi Maulana[1], Ildrem Syafri[1], Reza Mohammad Ganjar Gani[1], Riszky Baisal Risyad[2]
[1] Geological Engineering Faculty, Padjadjaran University , Sumedang
[2] Pertamina Hulu Energi West Madura Offshore

Abstract
"X" area is the working area of Pertamina Hulu Energi located in the North Madura Platform physiography on the North East Java Basin. This research is focused on the Ngimbang Formation, the Kujung Formation, and also the Rancak Formation. The concept of sequence stratigraphy with the correlation method is applied in this study, and the objectives to be achieved are (1) determination of sequence boundary markers, (2) seismic facies mapping, and (3) sequence stratigraphic and paleogeographic models to describe general depositional environments. Based on the analysis, 5 sequence boundaries (SB), 4 maximum flooding surface (MFS), dan 2 Transgressive surface (TS) are determined based on the analysis of paleobathymetri and well log data to create a cross-correlation. Based on the analysis of electrofacies and seismic facies, 3 depositional environment could be identified namely, Backreef Lagoon, Shelf Margin, and Slope on the Rimmed Carbonate Platform. Sediment supply direction is derived from the Northern part of the research area which shown by the progradation pattern to the South from the Line 8 seismic profile North – South trending. Through predetermined sequence markers, the deposition model for the "X" area is divided into 4 deposition model in each sequence interval. The domination of shelf margin progradation towards basinward event at most successive younger sequence, indicates that the movement of the sea level curve is relatively Transgressive in the early Oligocene - Middle Miocene range.
Keywords : North Madura Platform, Sequence Stratigraphy, Seismic Stratigraphy, Rimmed Carbonate Platform

Introduction

The location of the research area is in the "X" area which is part of the North East Java Basin on the North Madura Shelf. This research is focused on carbonate rock formations of tertiary age (Early Oligocene to Middle Miocene) namely the Ngimbang Formation, Kujung Formation, and also the Rancak Formation which have been proven as hydrocarbon reservoir layers in several oil and gas fields in the North East Java Basin.

This study uses the concept of sequence stratigraphys as the main research method. Sequence stratigraphy analysis was carried out to identify the lateral and vertical distribution of facies and provide a more comprehensive understanding of the geological evolution of the North East Java Basin.

The North East Java Basin is bounded to the west by the Karimunjawa Arc, the North West Java Basin, to the south by a volcanic arc, to the east by the Lombok Basin and to the north by the Paternoster Heights. Based on its position, the North East Java Basin can be classified as a back-arc basin and is located on the southeastern boundary of the Eurasian Plate (Mudjiono and Pireno, 2002). The structural trends and depositional history of Tertiary sedimentation in the "X" field are largely controlled by the bedrock configuration formed by tectonic events in the Late Cretaceous to Early Tertiary. The lithology of the study area is dominated by a succession of Tertiary and younger sedimentary deposits (Figure 1). In general, the stratigraphy of North East Java Basin are :

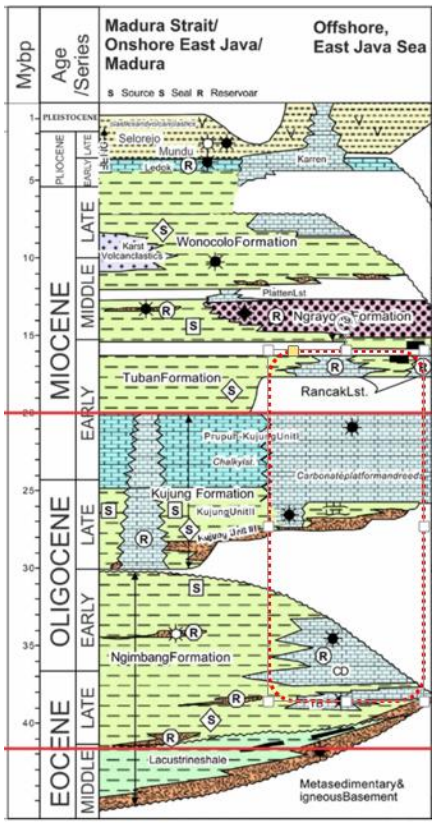

The red box showing the Carbonate Formation Interval which was the main focus of this research

Figure 1: Regional Stratigraphic Chart of North East Java Basin

Basement
The basement bedrock consists of a wide variety of intrusive and extrusive igneous rocks, including gabbro, andesitic basalt, and metamorphic tuff and some untreated Pre-Tertiary sediments. The lithology of the bedrock is estimated to be of Cretaceous age.

Ngimbang Formation
This formation consists of clastic deposits with the materials are shale, claystone, minor platform carbonate and rare low relief carbonate build-up. The depositional environment of this formation is interpreted from shallow sea to fluvial deltaic. The process of sedimentation in this formation took place during the Eocene period.

PROCEEDINGS
JOINT CONVENTION BANDUNG (JCB) 2021
November 23rd – 25th 2021

Kujung Formation

The Kujung Formation was deposited in harmony above the Ngimbang formation with a lithology dominated by limestone consisting of coral fragments, molluscs, foraminifera fossils, and bioclastic in the reef area. This formation was deposited in the late Oligocene to early Miocene.

Rancak Formation

The Rancak Formation is equivalent to the Tuban Formation which has broad spreading characteristics along the East Java Basin. The main constituent lithologies include sandstone, limestone, and shale. The Rancak Formation is interpreted as a mixture of exposed siliciclastic carbonates with delta progression associated with exposure and build-up carbonates. This formation is early Miocene in age.

Data and Method

The concept of sequence stratigraphys with the correlation method is intended to be able to determine (1) the determination of sequence boundary markers, (2) seismic facies mapping, and (3) stratigraphic and paleogeographic sequence models to describe the general depositional environment in the "X" area. This research was conducted based on lithofacies analysis, facies association, paleobatymetry, seismic facies, subsurface mapping, and depositional modeling based on predetermined sequence markers.

This research was carried out qualitatively in the form of descriptive research methods followed by analytical methods. Descriptive method is a method of interpretation of data based on a valid and relevant theoretical basis. After the descriptive interpretation is carried out, it is continued with the analysis stage which will provide a better understanding of the relationship between a descriptive analysis and other descriptive analysis, so that a comprehensive qualitative analysis can be carried out on the research data. The research flow includes data input, interpretation, and analysis in the research described in the research diagram (Figure 2).

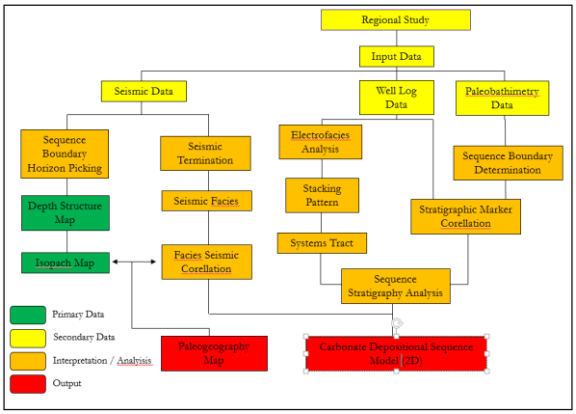

Three main data input are all secondary data provided by PHE WMO for the quantitative analysis

Figure 2: Research Workflow

Result and Discussion

Well Log Analysis

Interpretation results at the interval of the research area from wireline log data of 7 wells consisting of Gamma Ray logs, resistivity, bulk density, and neutron porosity obtained 3 main lithologies, namely sandstone, claystone, and

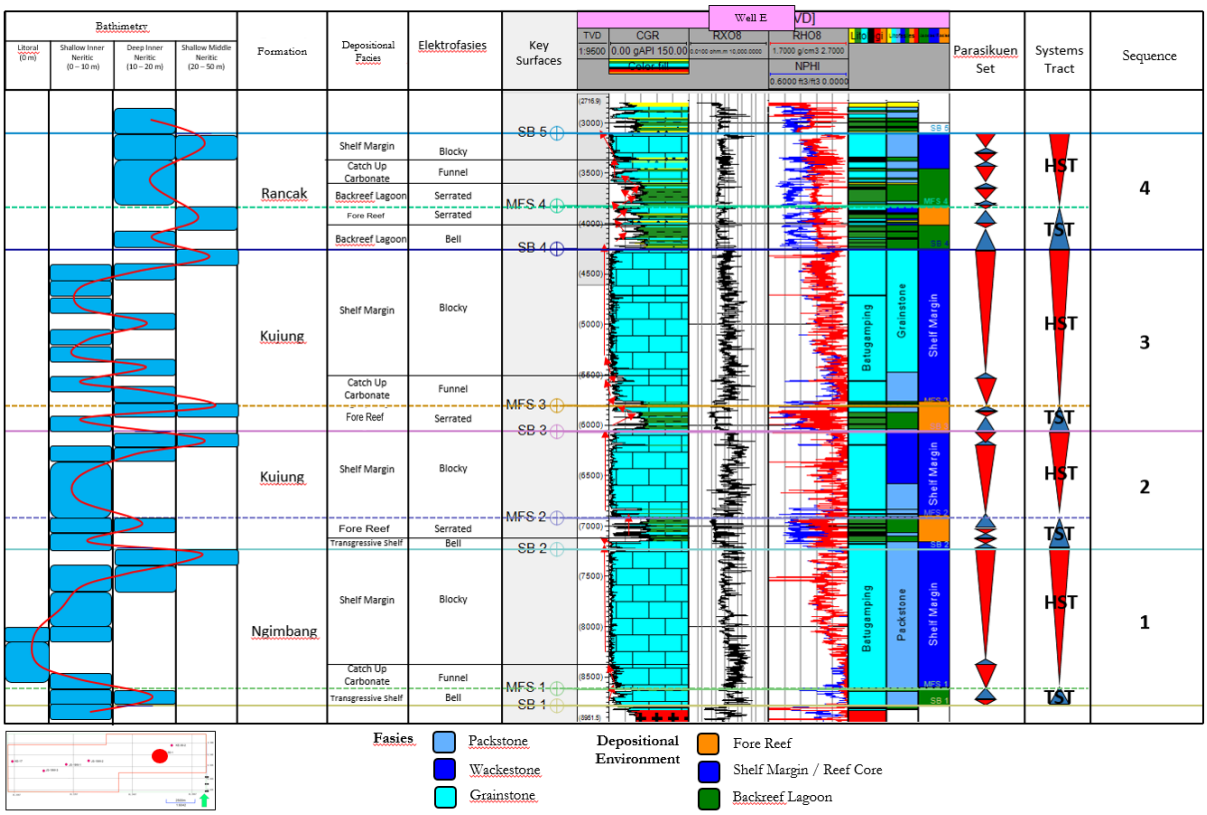

The sequence marker interpretation based on the paleobathimetry data. The depositional facies determined based on the paleobathymetri data and also the electrofacies interpretation.

Figure 3: Well E Electrofacies and Sequence Marker Interpretation

PROCEEDINGS
JOINT CONVENTION BANDUNG (JCB) 2021
November 23rd – 25th 2021

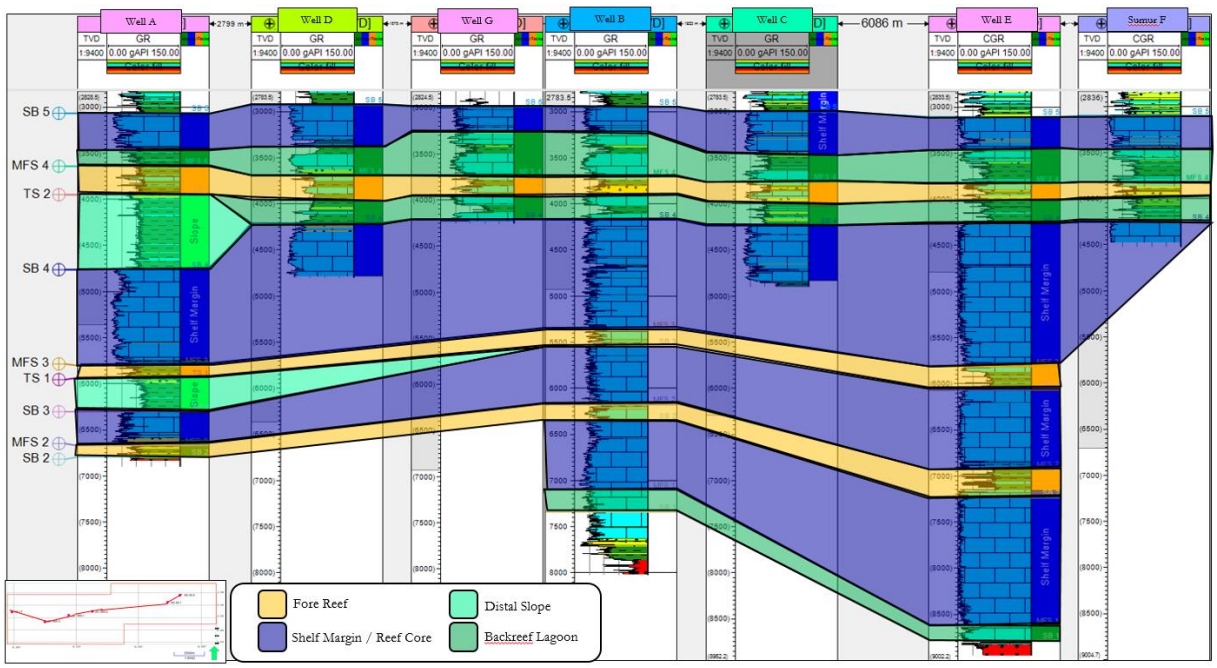

The depositional environment correlation mainly based on the electrofacies and sequence marker interpretation. Distal slope environment only showed on the Well A, indicating that the position of Well A located on the basinward part of Madura Paltform

Figure 4: Depositional Environment Corellation

limestone. After interpreting the lithology, the vertical facies determination was carried out based on the electrofacies method (Kendall, 2003). There are 4 electrofacies patterns found in the gamma ray log, namely bell pattern, funnel pattern, serrated pattern, and blocky/cylindrical pattern (Figure 3).

Well Log Corellation

Well log correlation was carried out to correlate stratigraphic markers and sedimentation facies correlations for each sequence. Well correlations are mainly based on stratigraphic markers. Stratigraphic markers were determined based on the cyclicity pattern and the lithological log pattern (Figure 4). There are 11 stratigraphic markers in the succession of the Ngimbang Formation to the Rancak Formation in the seven wells of the study area, each of which separates one system tract from another. Each system tract has distinctive log characteristics and can also indicate specific depositional environments and processes.

The sequence stratigraphy framework of the well log data is based on the correlation cross-section of the wells in the West – East direction. This cross section shows a significant change in depositional facies in the western area of the study. Distal slope depositional facies are only found in Well A which is located in the eastern area of the study (Figure 4). Distal slope depositional facies on the rimmed carbonate platform are only found in the distal region of a carbonate platform which is characterized by hemipelagic deposits which are interpreted as a 700 feet thick serrated electrofacies pattern in well A (Figure 4). This deposit facies indicates a deposit from the Lowstand Systems tract which can only be formed in a slope environment (Handford, 1993).

Seismic Analysis

Based on the results of seismic analysis of the research area, in general there are 4 seismic facies found in the study area, namely Parallel and Subparallel, Sigmoid Progradation, Mounded, and Chaotic (Table 1). These four seismic facies describe different depositional characteristics, including the depositional environment in the area. Based on the stratigraphic markers in the well log analysis and integrated with the termination seismic analysis and the seismic facies on the seismic data, a 2D carbonate sequence deposit model was made on a seismic cross-section that passed through the seven research wells in a relatively West-East direction (Figure 7). The purpose of this modeling is to determine the framework for the formation of reef bodies or carbonate bodies and to identify lateral stacking patterns formed on seismic lines.

Seismic Facies Description	Example From the Data	Refection Geometry / amplitude characteristics	Interpretation	Predicted Depositional Environment
A Sigmoidal		Clinoforms Continuous - Semicontinous Medium amplitude		Shelf Margin
B Parallel		Bedded Continous High - Medium Amplitude		Shelf Deposit
C Mounded		Mound – shaped Semi continous to Discontinous High – Medium Amplitude		Carbonate Build Up
E Chaotic		Chaotic Low Amplitude		Reef Core (Bioherm)

There are four seismic facies identified on the research area. This seismic facies determined by the seismic wavelet characteristics and also the geometry.

Table 1: Seismic Facies on Research Area

PROCEEDINGS
JOINT CONVENTION BANDUNG (JCB)2021
November 23rd – 25th 2021

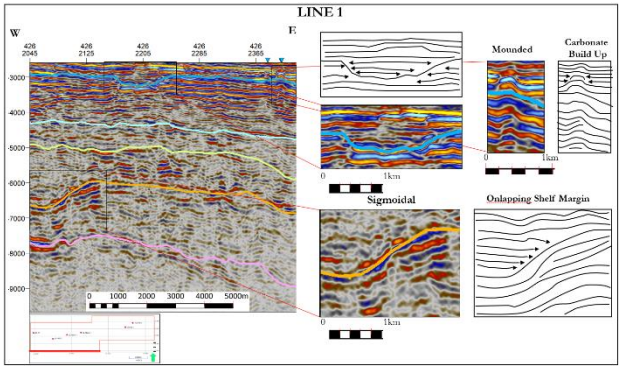

The mounded facies interpreted as a carbonate build up, and the sigmoidal interpreted as a shelf margin. The onlapping termination on the sigmoidal facies representing the distal slope deposit onlapping to a sequence boundary.

Figure 5: Seismic Facies Interpretation on Line 1

In the carbonate sequence deposit model, the Stacking Pattern showed the systems tract that develops in the deposit. Aggradation patterns and progradation patterns in carbonate rock bodies / reefs are strongly associated with the Highstand Systems tract. Retrogradation patterns in carbonate rock bodies / reefs are strongly associated with the Transgressive Systems tract. In addition to the Stacking Pattern, termination patterns such as Onlap, and Toplap, can be identified on the seismic trajectory. The Onlap termination pattern is associated with the Lowstand Systems tract phase where the deposits distal to the basin generally have Onlap characteristics to the exposure slope. The Toplap Termination pattern indicates the presence of a layer that has eroded the top and is overwritten by a younger layer. The eroded layer indicates the presence of a hiatus in depositional time which may indicate the presence of sequence boundaries. Therefore, the Toplap termination pattern is associated with the presence of a sequence boundary.

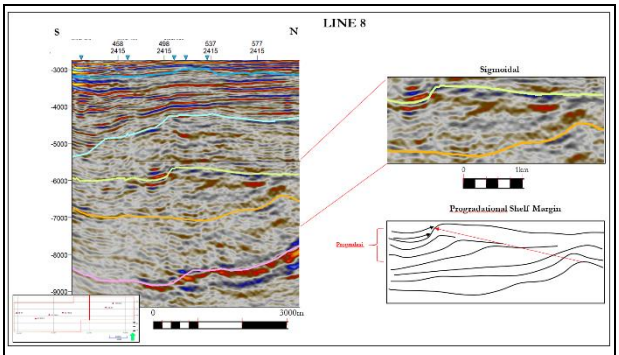

The sigmoidal facies interpreted as a progradational shelf margin characterized by a thick sedimen deposit and a basinward movement of the shelf margin

Figure 6: Seismic Facies Interpretaion on Line 8

Seismic Facies Corellation

Seismic facies correlation was conducted to find out the map view distribution of the facies distribution in the study area. Seismic reflection configurations can indicate bedding patterns that develop as a result of depositional energy processes. Seismic facies analysis was carried out in 9 lines representing the study area, which were spread out and covered the entire study area. There are 4 seismic cross-sectional lines with a north-south direction, and 5 seismic cross-section lines with a west-east direction. In each of these seismic sections, seismic facies zoning is carried out for each sequence on the basemap of the research area so that later seismic facies can be correlated with the same internal configuration.

In the seismic facies correlation of each sequence, it is known that there are 3 main correlations, namely Sigmoidal, Mounded - Chaotic, and Parallel - Subparallel seismic facies. Some Chaotic facies are correlated with Mounded facies because they both describe the formation of growing reef bodies.

Palegeography Map

The Depth Structure Map that has been made per sequence boundaries is used as the basis for making an isopach map per sequences obtained from the depth value of the upper limit of the sequence minus the depth value at the lower limit of the sequence, so that a thickness value is obtained. The purpose of making this map is to determine the direction of sediment influx, lateral facies distribution and determine changes in the basin in the study area from time to time. The isopach map will be integrated with the interpretation of the seismic facies correlation and will be the basis for making a depositional model of the research area and from the depositional model a facies interpretation and analysis of facies changes will be carried out over time which is depicted on the paleogeographic map.

1. Sequence 1

In sequence 1, based on the isopach map, it shows that the Fore reef environment has a relatively thicker thickness compared to other environments which is characterized by sigmoidal seismic facies. The sigmoidal facies which is interpreted as a progradation deposit has a fairly thick thickness. The carbonate growth zone has a higher elevation on the Depth Structure Map so that this carbonate growth zone has a relatively thinner thickness compared to other environments that receive sediment influx. As for the Lagoon environment, the thickness is thinner than the Fore reef area but thicker than the carbonate growth area in some areas (Figure 8).

2. Sequence 2

In sequence 2, the progradation stacking pattern showed very clearly which is characterized by a thick deposit of basinward movement of the shelf margin of sequences 2 that illustrated in the seismic section of Line 8 (Figure 6). This is clearly illustrated on the isopach map which indicates a thickening in the center of the study area. Massive sediment supply in the slope area is caused by regressive sea level events so that clastic sediment influx can increase and be deposited in the slope area and make a progradational stacking pattern (Figure 8).

3. Sequence 3

In sequence 3, some areas of carbonate growth, especially in the center of the research area, were not recovered from growth in the previous sequence and the average area of carbonate growth was reduced. The carbonate growth zone has a higher elevation on the Depth Structure Map so that

PROCEEDINGS
JOINT CONVENTION BANDUNG (JCB)2021
November 23rd – 25th 2021

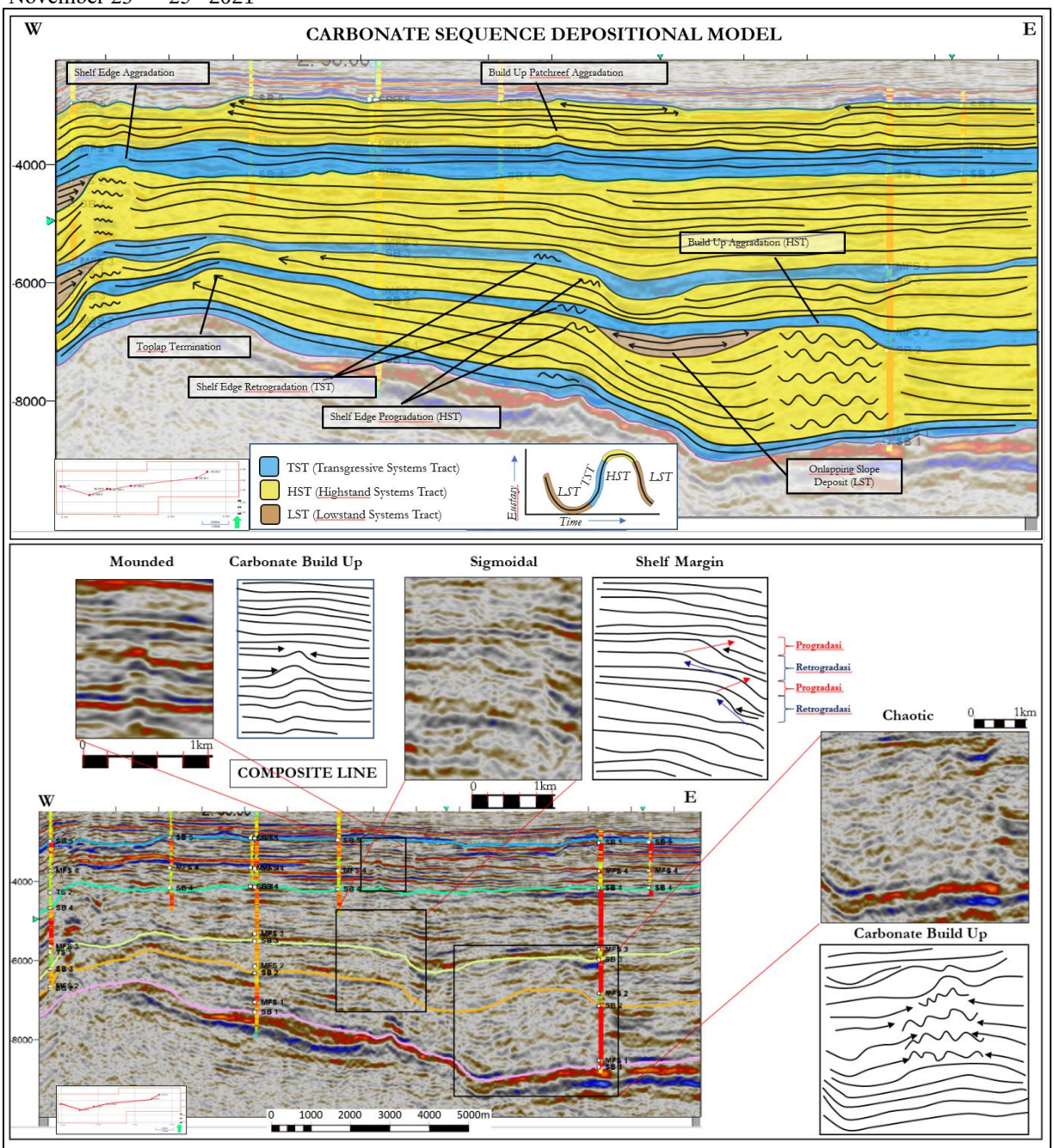

The High Stand Systems Tract (HST) associated with the carbonate build up and the progradational shelf margin, the Low Stand Systems Tract (LST) associated with the onlapping distal slope deposit to the shelf margin, and the Transgressive Stand Systems Tract (TST) associated with the retrogradational pattern of the shelf margin

Figure 7: Sequence Depositional Model and The Corellation with Seismic Facies

this carbonate growth zone has a relatively thinner thickness compared to other environments that receive sediment influx. The carbonate growth zone which is mostly located at the shelf margin is characterized by a fairly thin thickness along the shelf margin. As for the Lagoon environment, the thickness is thinner than the Fore reef area but thicker than the carbonate growth area in some areas (Figure 8).

4. Sequence 4

In sequence 4, the direction of movement of the shelf margin is towards the basin. In this sequence, new carbonate growth was found which was interpreted as Patchreefs complex. It is estimated that in this sequence a regressive event occurs in the study area which is characterized by the presence of incised valley areas in the continental shelf area which is characterized by onlapping termination at the boundary of sequence 5 on the seismic line 1 (Figure 5) and a thinner thickness compared to the surrounding area as shown in the isopach sequence 4 map (Figure 8).

PROCEEDINGS
JOINT CONVENTION BANDUNG (JCB)2021
November 23rd – 25th 2021

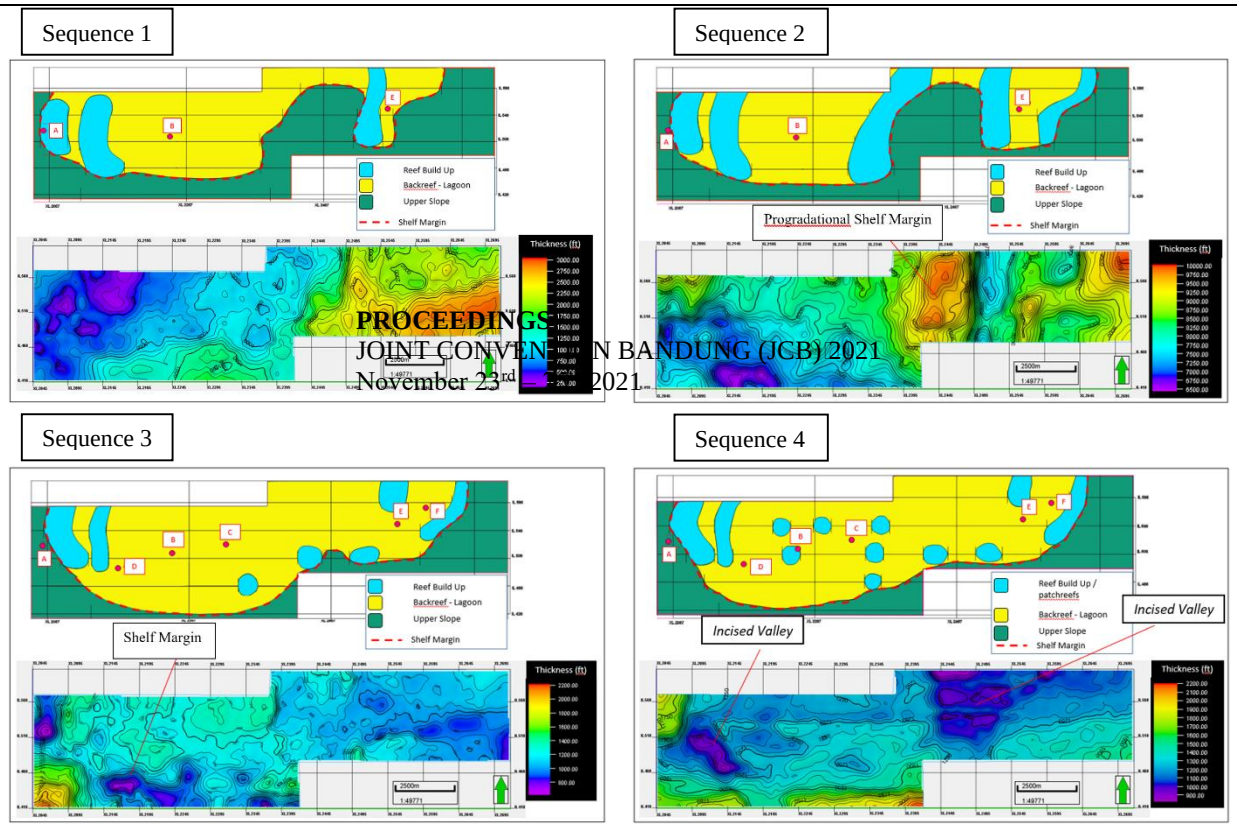

The Paleogeography evolution trough all 4 sequence boundaries could be identified by focusing on the shelf margin, and carbonate reef position.

Figure 8: Paleogeography Map on all 4 Sequence Boundary

PROCEEDINGS
JOINT CONVENTION BANDUNG (JCB)2021
November 23rd – 25th 2021

Conclusions

There are 5 sequence boundaries, 4 maximum flooding surface (mfs), and 2 transgressive surface (ts) determined based on changes in the depositional environment from Shallow Middle Neritic to Deep Inner Neritic or Shallow Inner Neritic in wells E and F. The depositional environ ment of the study area is a margin reef platform on a rimmed carbonate platform with environmental presence in the form of Backreef Lagoonal, Shelf Margin, and Slope. The history of depositional sequences is observed from changes in the depositional environment periodically, namely changes in the shelf margin and the similarity of the carbonate growth location and its relationship with the relative movement of sea level. It can be concluded that regressive event occurred in sequence 1, 2, and 4, and a transgressive event occurred in sequence 3.

References

Handford, C. R., & Loucks, R. G. (1993). AAPG Memoir Vol 57, (1993): 3-41.

Kendall C (2003). USC Sequence Stratigraphy Web. University of South Carolina.

Mitchum Jr, R. M., and P. R. Vail. AAPG Memoir Vol 26. (1977): 135-143.

Mudjiono., R., dan Pireno., G. E. 2002. 28th Annual Convention Proceeding. Indonesian Petroleum Association

Schlager, W. (1992). AAPG Memoir Vol 34.

Van Wagoner, J. C., Mitchum, R. M., Campion, K. M., & Rahmanian, V. D. (1990). AAPG Memoir Vol 7. (1990): III-55.

PROCEEDINGS
JOINT CONVENTION BANDUNG (JCB) 2021
November 23rd – 25th 2021

Turbidite Deposit Characteristics of Semilir Formation on Ngoro-Oro Area, Patuk, Gunungkidul, Special Region of Yogyakarta

Joseph Emmanuel Ardine 1, Muhammad Iqbal Maulana 2, Ardhya Narendra Kusuma Nugroho 3, Angela Hotmaida Rosalline 4, James Christopher Chang 5, Muchamad Ocky Bayu Nugroho 6
1,2,3,4,5,6 Department of Geological Engineering, Faculty of Mineral Technology, National Development University 'Veteran' Yogyakarta

Abstract

The research area is located in Ngoro-Oro Village, Patuk, Gunungkidul, Special Region of Yogyakarta. The research area belongs to the Southern Mountain Zone which is dominated by clastic sedimentary rocks and carbonates mixed with tertiary volcanic rocks (Bemmelen, 1949). The Tertiary volcanic rocks are the part of the Early Miocene Semilir Formation that composed by tuffaceous sandstone units deposited in the marine environment by Turbidite and Debris Flow mechanisms. The methods of this study are field observation and detailed measured stratigraphic column. In this research area is developed high density turbidite and low density turbidite. There are found some turbidite facies such as Classical Turbidite (CT), Massive Sandstone (MS), Pebbly Sandstone (PS), and Conglomerate (CGL) so it is quite strongly interpreted as Channeled Portion of Suprafan Lobes-Lower Fan (Walker, 1978) depositional environment with coarse-grained/sand rich turbidite characteristic. The presence of turbidite deposits of this area is possibly controlled by tectonic activity. That was showed with discontinuous NW-SE oriented fault, and it was cut by debris deposits. geological process during deposition will be summarized in a 2-Dimensional model of the depositional environment, detailed measured stratigraphic column, and sedimentation patterns of the research area.

Introduction

Research area is located at Ngoro-oro Village, Patuk District, Gunung Kidul Regency, Daerah Istimewa Yogyakarta Province. Ngoro-Oro is well-known for its geological outcrops which show good example of sedimentary structures. sedimentary structure that exists in the research area are graded bedding, parallel lamination, wavy lamination, convolute, stratification, and load structure. Those structure indicates turbidite deposits. Turbidite is fine-grained sediment (or sedimentary rock) that gradually changes from coarse- to fine-grained and that was deposited by turbidity currents (DiPietro, 2013). The fact that this is correlated to the volcanism period in Southern Mountain Stratigraphy, especially on Semilir Formation (Surono, 2009).

The aim of this study is to describe the characteristic of the turbidite deposits that existed on research area. The method of this study is by fieldwork continue with studio. Fieldwork is collecting data covered measuring stratigraphic section, rock description, and geological structure analysis. Whereas, studio work is stratigraphic log drawing and conceptual model building. All outcrops' data will be presented in detailed lithological profiles. Those profiles will be analyzed to obtain the characteristic of turbidite deposits. The characteristic of turbidite deposits is depicted by 2-dimensional model and local stratigraphic column.

Regional Geology of Gunungkidul

Physiography

Haryono and Day (2004), stated that Gunungkidul, physiographically, is situated in southern plain of Java Island that stretched across 85 km east-west with gentle slope to the south, and cliff 25-100 m high on the southern part of the island. Gunung kidul located in Southern Mountain Zone that generally consisted of clastic sedimentary and carbonates rocks mixed with rocks from Tertiary volcanism activities (Surono, 2009). Southern Mountain is southern physiographic unit of Java that stretched from Ciletuh Gulf in West Java to Blambangan Peninsula in the most eastern part of East Java. This zone divided into 3 subzone, Baturagung Subzone, Wonosari Subzone, and Gunung Sewu Subzone.

Stratigraphy

Southern Mountain stratigraphy (Figure 1) can be divided into three periods from old to young, the pre-volcanism period that consisted of metamorphic rock unit (basement) and Wungkal-Gamping Formation, the volcanism period that consisted of Kebo-Butak Formation, Semilir Formation, and Nglanggeran Formation, and post-volcanism period or carbonate period that composed of Sambipitu Formation, Oyo Formation, Wonosari, and Kepek Formation (Yuwono and Akmaludin, 2015).

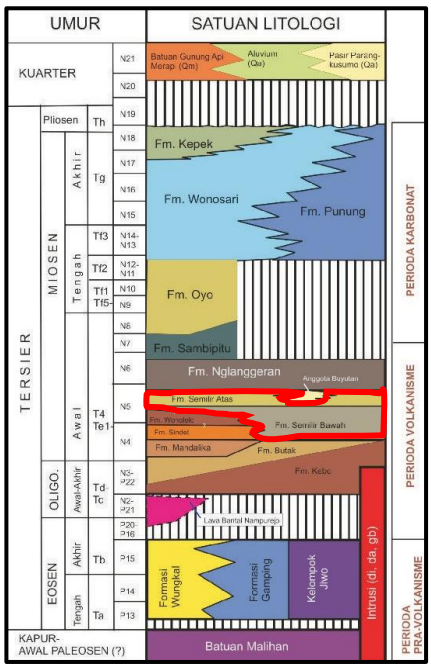

Figure 1. Southern Mountain Stratigraphy (Surono, 2009)

Based on Surono (2009) and Mulyaningsih (2011), at the beginning, the Semilir Formation is part of deep marine sedimentary rock that composed of sandstone,

PROCEEDINGS
JOINT CONVENTION BANDUNG (JCB) 2021
November 23rd – 25th 2021

tuff, tuffaceous sandstone, tuff breccia, lapilli tuff, agglomerate, andesite breccia, claystone, siltstone, and shale dating Oligocene-Early Miocene (Figure, 1). Fragment that formed breccia and sandstone typically acidic pumice. Stratification (bedding) and structure that indicates turbidite were found at the research area. The presence of fossils is pretty rare in this formation, and this indicates that the deposition happened relatively in a short period or at the very deep environment (on or under the CCD Zone) that resulted in carbonate fossils already dissolved before deposited. Semilir Formation conformably deposited over Kebo-butak Formation and well exposed a lot in Baturagung escarpment area, under the peak of Semilir.

Geological Structure

Regionally, geology structures formed in Gunungkidul Regency are strike-slip faults that formed during Miosen or Neogen Compressional Wrenching Period, especially in the sandstone unit Semilir Formation at Pathuk District (Dally et al. 1991 in Albi, 2011). Neogen Compressional Wrenching Period controlled the forming of submarine slope morphology. This morphology is the key factor of the occurrence turbidity system. The formation of the strike-slip fault also resulting in the formation of minor structures as subsidiary faults from major faults. According to the studies that has been done in the past by Kaeliana (2020), geological structure that formed in Gembyong, Ngoro-Oro Village, Pathuk District, Gunungkidul Regency, Special Region of Yogyakarta is a normal right strike-slip fault with southwest-northeast orientation. Structures in this region also affecting the formation of minor faults around it.

Data and Method

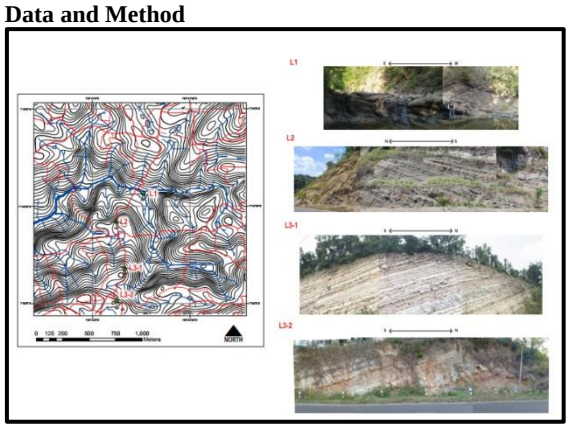

Figure 2. Research Area Path Map

Methods used in this research are field observation and detailed measured stratigraphic column. Field observation includes outcrop observation and taking data such as lithology name, photos, sedimentary structures, sedimentary thickness, and bedding measurement. Lithologies are named from megascopic observation. The bed measurements show an east-west strike with a dip direction pointing to the south. This measurement makes data collecting is taken from the oldest to the youngest of the outcrop. Furthermore, the research area is divided into 4 stations of observation (Figure 2). Each line of observation is used to make a detailed measured stratigraphic column or a profile. This profile will be used in the future for sedimentary pattern analysis, determining turbidite character, and interpret the depositional environment of the area. Bouma Sequence (1962) is referred for the Turbidite deposits, Lowe (1982) is used for the low-density turbidite, and Walker (1973) for high-density turbidite. The Walker (1988) depositional model is used to interpret the depositional model of the area.

Result and Discussion
Result

Station 1

Station 1 (Attachment 1) is divided into four outcrops, each outcrop is treated to be an observation site. Outcrop A (49S. 449080E, 9135183N) has a dimension of height 2 meters and wide of 5.5 meters. Outcrop A extends from east to west with lithology of sandstone, carbonaceous breccia, and siltstone. The bedding on the outcrop shows a strike/dip value of N 109˚ E/19˚ and can be found sedimentary structure of loading structures, graded bedding, and wavy lamination. Outcrop B (49S. 449021E, 9135145N) has a dimension of height 2 meters, and wide of 10 meters. This outcrop extends from north to south with the lithologies of sandstone and breccia. Sedimentary structures that can be found in this outcrop are clastic lens, graded bedding, parallel lamination, slump, and debris-cut reverse fault Outcrop C (49S. 449050E, 9135102N) has a dimension of height 3 meters, wide of 25 meters. The outcrop extends from northwest to southeast and consisted of pebbly sandstones, conglomerates, and sandstone. Those lithologies have sedimentary structures of inverse graded bedding, and loading structures. Outcrop D (49S. 449080E, 9135029N) has a dimension of height 15 meters and wide of 4 meters, extends from west to east. The lithologies of this outcrop consist of claystone, tuffaceous sandstones, and lapilush sandstones. The sedimentary structure of this area are parallel lamination and stratified structures. In Station 1 can be recognized low density turbidite by four Bouma's Turbidite Sequences with Ta-Tb Intervals (Bouma, 1962). Ta's Intervals can be characterized by massive sandstone and Tb's Intervals can be recognized by sandstone with parallel lamination structure. In this station also developed high density turbidite from R2, R3, S1, and S2 facies (Lowe, 1982). R2 facies characterized by inversely graded gravel layer, R3 by normally graded gravel layer, S1 by traction structures with plane lamination, and S2 by horizontal bedding with inverse grading.

Station 2

Station 2 (Attachment 2) (49S, 448782E, 9134874N) has one outcrop with the dimension of height 7 meters and wide of 45 meters showing a fairly good outcrop condition. The outcrop is dominated by very fine sandstone and siltstone with primary structure, stratified. Interbedded sandstone-siltstone that fining upwards were found several times in this station and blanks twice with a thickness of 300 and 60 cm. Unique sedimentary structures such as lenses are present in one layer of claystone, also calcite veins were present in one layer of siltstone, as well as several layers containing carbonaceous material in the matrix. In Station 2 can be recognized one Bouma's Turbidite Sequences with Ta-Tb Intervals, and six Ta Intervals (Bouma, 1962). Ta's Intervals can be characterized by massive sandstone and Tb's Intervals can be recognized by sandstone with parallel lamination structure.

PROCEEDINGS
JOINT CONVENTION BANDUNG (JCB) 2021
November 23rd – 25th 2021

Station 3-1

Station 3-1 (Attachment 3) (49S. 448856E, 9134433N) with the dimensions of height 7 meters and wide of 75 meters shows a very good appearance of various lithologies dan sedimentary structures. The lithologies on this site are siltstone, lapilush sandstone, interbedded siltstone-medium sandstone, carbonate sandstone, interbedded fine-medium sandstone, calcareous sandstone, siderite layer, and tuff. Not only the lithologies, there are many sedimentary structures such as wavy and parallel lamination on tuffaceous sandstone, tuff, and sandstone, graded bedding on sandstone and tuff also reverse graded bedding on 411 cm thick volcanic breccia, convolute, stratified, and massive structure. The bed boundaries are clear, erosional, and gradational in some parts. . In this station can be found three Ta-Tb Intervals, and 12 Ta Intervals with overall repeating Ta, Tb, Tc Intervals and Tc, Td Intervals (Bouma, 1962). Ta's Interval (Bouma, 1962) can be recognized from massive sandstone, and Tb Intervals (Bouma, 1962) can be recognized by sandstone with parallel lamination structure. In this station also developed high density turbidite from R2, (Lowe, 1982). R2 facies characterized by inversely graded gravel layer.

Station 3-2

Station 3-2 (Attachment 4) (49S. 448787E, 9134130N) is located not far from 3-1 has a height of 6 meters and a wide of 35 meters. This station is dominated by tuffaceous material. Claystone, tuffaceous sandstone, and sandstones. Sedimentary structures found in this station are massive, stratified, and parallel lamination also can be found graded bedding and convolute in someplace. Station 3-2 Profile shows 14 Ta's Intervals and with some Tb's Intervals of Bouma's Turbidite Sequences (Bouma, 1962) with epiclastic materials dominating the profile as Tuff. Ta's Interval in this sequence characterized by tuff with massive structure, and some massive sandstone. No high density turbidite is found in this station.

Discussion

Turbidite Characteristic

There are two kinds of turbidite deposits in the research area, it is high-density turbidite and low-density turbidite. High-density turbidite deposits are the facies of the R2, R3, S1, and S2 (Lowe, 1982). The High-density turbidite is well developed on the older lithologies on station 1 (Station 1 3rd Lithology on Attachment 1). Further from Station 1 is dominated by low-density turbidite with facies interval of Ta-Tb (Bouma, 1962). On station 2 the deposit that showed in this area is Low-density turbidite which is characterized by interbedded siltstone-sandstones and also claystone with Ta-Tb Facies Interval (Bouma, 1962). The appearance of claystone can be determined by the turbidite sedimentary gap. Station 3-1 is dominated by Low-density turbidite with a little appearance of High-density turbidite (Station 3-1 36th Lithology on Attachment 3). At the station, 3-1 can be recognized R2 Lowe's Turbidite facies (Lowe, 1982), and the repetition of Ta, Tb, Tc, and Ta, Tb (Bouma, 1962). The High-density turbidite facies appearances can be interpreted as starting point to the volcanic phase on the area. This can be explained in Station 3-2 where it is dominated by low-density turbidite with Ta-Tb (Bouma, 1962) Facies. As a whole the characteristic of turbidite deposit on the research area is at the start is dominated by high-density turbidite with gradually changed to low-density turbidite. Incompleteness Bouma Sequences Facies in the research area indicate rapid sedimentation with a high sediment supply.

The discussion about depositional environment interpretation is based on facies model and depositional environment model of Walker (1984). Referring to Walker (1984) model, Station one showed Peebly Sandstone facies (PS) and conglomerates (CGL), station 2 showed mostly Classical Turbidite Facies (CT). Station 3-1 showed Massive Sandstone facies (MS), and Classical Turbidite Facies (CT).and Station 3-2 showed Classical Turbidite Facies (CT). The Depositional Environment Interpretation of the research area based on the Walker (1984) facies interpreted as Channeled Portion of Suprafan Lobes up to Lower Fan (Walker, 1984).

Turbidite deposits of the research area are composed by siliciclastic material and volcaniclastic material. Where the domination shift from siliciclastic material to volcaniclastic happens gradually over time. The interpretation of the boundary that separates between these material can be found on Station 3-1 36th Lithology (Attachment 3), which is a Volcanic Breccia with pumices as fragments and characterized as high-density flow turbidite. Later after 36th Lithology on Station 3-1, the dominance of tuffaceous and tuffaceous sandstone are more dominant and easier to recognize the volcanic material (Attachment 3). The sedimentation pattern that develops in this area is rapid sedimentation with a high sediment supply, and related to volcanic activity on Miocene, and also fining-upward stacking pattern.

Figure 3. Left picture is discontinous reverse fault in Station 1 ($N105^0$ $E/85^0$). Right picture is slickenside (rake 85^0).

Turbidite deposits that have been observed show coarse-grained/sand-rich type (Bouma, 2004). There is can be found some evidence that can be to support the statement. The first evidence is about the high ratio between the sandstone with shale also the appearance of the shale that thin and doesn't dominate the research area (Bouma, 2004) (Attachments1,2,3,4). The ratio between the sandstone with shale is declining as long as the outcrop gets younger (Bouma, 2004). In the Early Miocene periods the research area was an active margins area. It can be marked due to the high of volcanic activities (Surono, 2009). On the other side, tectonics activities are becoming one of the control factors of turbidite development. This showed by the appearance of NW-SW faults that cut by high-density turbidite at station 1 (Figure 3). Refers to Bouma (2004), the characteristic and

PROCEEDINGS
JOINT CONVENTION BANDUNG (JCB)2021
November 23rd – 25th 2021

controlling factor system of the turbidite in the research area is an ancient submarine fan has medium to small in size, also has a narrow shelf, and small transportation distances (can be seen by the abudance of angular grain), located at the active margin, have a progradation pattern, and is also not influenced by the seawater level. The fining upward domination pattern shows strong evidence if the area is coarse-grained/sand-rich type (Bouma, 2004).

2D Depositional Model

Based on field data that have been taken and processed, the next step is making a depositional environment model concept and local stratigraphic column. This model (Figure 4) represents the order of the turbidite depositional development in the research area. In the beginning, it has been deposited the first turbidite deposit on station 1. Then duet o the effect of the tectonic at the moment and making a reverse fault that triggers the shelf to make the other turbidite deposit as long as the shelf is unstable. This can be seen from the discontinuity of the reverse fault on station 1 that cut by newer material.tectonic interference is implicated on the increase of volcanic activities. These activities have a huge part in interference the sediment supply. On the Local stratigraphic column (Figure 5), we can see the transition between siliciclastic and volcaniclastic

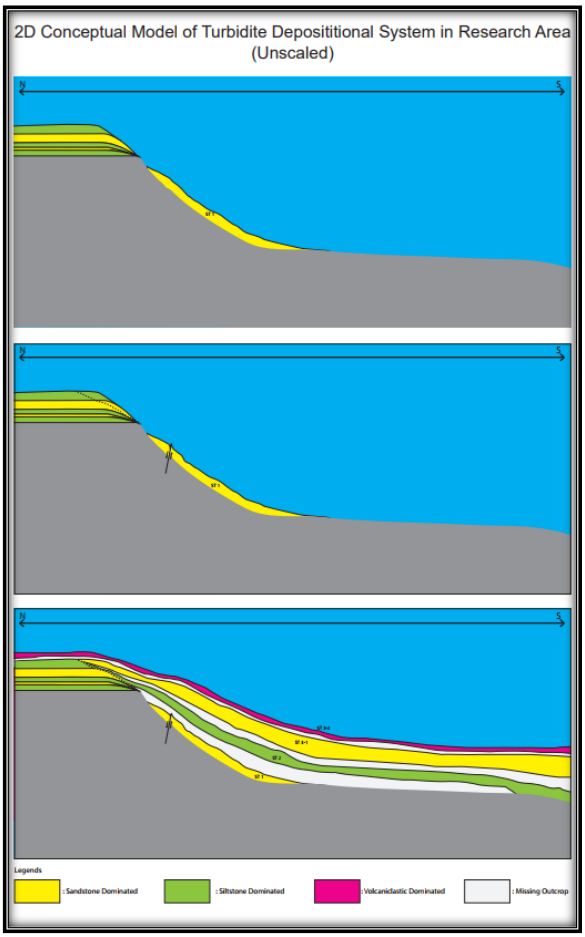

Figure 4. 2D Concept Model of Depositional System in Research Area (Unscaled)

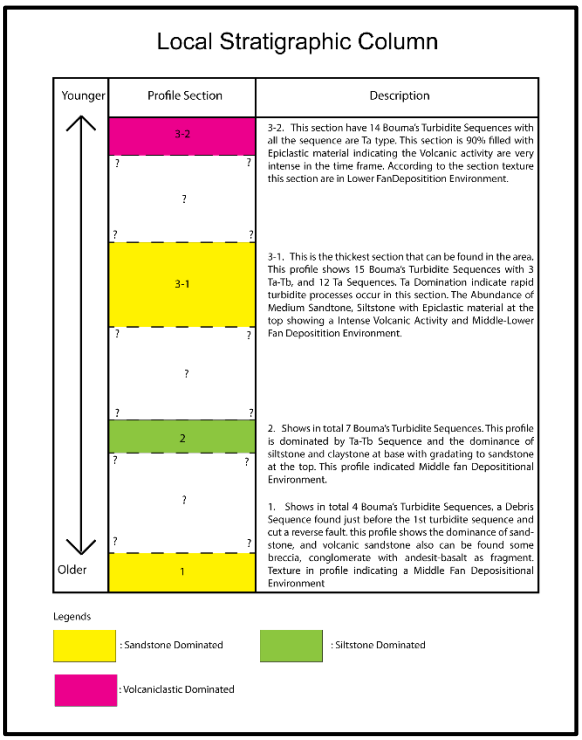

Figure 5. Local Stratigraphy Column

Conclusion

Turbidite deposits in the research area characterized by the early part of the turbidite deposition are dominated by high-density turbidite, as long as come to the late part of the turbidite deposition is changed to low-density turbidite. Turbidite facies that can be recognized from the outcrop are R2, R3, S1 and S2 (Lowe 1982), Ta-Td (Bouma, 1962), and Pebbly Sandstones (PS), Conglomerates (CGL), Classical Turbidite (CT), and Massive Sandstone (Walker, 1984).). The Depositional Environment Interpretation of the research area based on the Walker (1984) facies interpreted as Channeled Portion of Suprafan Lobes up to Lower Fan (Walker, 1984). Turbidite deposits in the research area belong to coarse-grained/sand-rich type (Bouma, 2004). There is a transition from the grade of domination between siliciclastic (Older) material and volcaniclastic material (Younger) indicates volcanic activity that intensifies during the late deposition. The increasing volcanic activities affect the sedimentation to be rapid sedimentation with a high sediment supply. Most of the stacking pattern in this area is a fining-upward pattern. Besides of volcanic activities, the interference of tectonic can be interpreted as the trigger of the turbidity current. It can be seen on the deposition-cut reverse fault because of the turbidite deposition.

References

Albi, D., 2011, Geologi Dan Studi Lingkungan Pengendapan Satuan Batupasir Formasi Semilir Daerah Patuk, Kecamatan Patuk, Kabupaten Gunung Kidul, Provinsi D.I.Yogyakarta, Thesis, UPN "Veteran" Yogyakarta.

Bouma, A.H., 1962, Sedimentology of Some Flysch Deposits: A Graphic Approach to Facies Interpretation, Amsterdam: Elsevier.

Bouma, A.H., 2004, Geology Society, **222**, 9-22.
Dipietro, J.A., 2013, Geology and Landscape Evolution: General Principles Applied to the United States, Second Edition, Amsterdam: Elsevier.
Ghibaudo, G., 1992, Sedimentology, **39**, 423-454.
Haryono, E and M. Day, 2004, Journal of Cave and Karst Studies, **66**, 62-69.
Kaeliana, F. A., 2020, Geologi Dan Studi Kualitas Airtanah Berdasarkan Parameter Fisika Dan Kimia Daerah Ngoro-Oro Dan Sekitarnya, Kecamatan Patuk, Kabupaten Gunungkidul, D.I. Yogyakarta, Thesis, UPN "Veteran" Yogyakarta.
Lowe, D.R., 1982, Journal of Sedimentary Petrology, **52**, 279-297.

Mulyaningsih, S., et al, 2011, Jurnal Teknologi Technoscientia, **4**, 64-78.
Setiadji, L.D. et al, 2006, Resource Geology, **56**, 267-292.
Shanmugam, G., 1996, Journal of Sedimentary Research, **66**, 2-10.
Shanmugam, G., 2000, Marine and Petroleum Geology, **17**, 285-342.
Shanmugam, G., 2002, Earth-Science Reviews, **58**, 311-341.
Surono, 2009, Jurnal Sumber Daya Geologi, **19**, 209-211.
Van Bemmelen, R.W., 1949, The Geology of Indonesia, Hague: Government Printing.
Walker, R. G., 1984, Geoscience Canada, **1**, 1-9.
Yuwono, F. S. and Akmaludin, 2015, Proceeding Seminar Nasional Kebumian 8, 391-399.

Acknowledgments
Thanks to Talitha, Satya, Safira, Nabila, and Cahyo for helping when collecting data. UPN "Veteran" Sedimentology Labrotary for providing places for analysis data. And all the people that support us during the paper development.

ATTA M'BENGUE

DEPARTMENT OF GEOLOGICAL ENGINEERING
FACULTY OF MINING TECHNOLOGY
UNIVERSITY OF NATIONAL DEVELOPMENT "VETERAN YOGYAKARTA"
2011

MEASURED STRATIGRAPHIC SECTION

LOCATION : Nguren Area, Sidorejo Village, Kalirejo Sub-district, Kulon Progo Regency, Special Region of Yogyakarta
COORDINATE : Begin: 7.6.2.0 S, 110.1.1.0 E
End: 7.6.2.0 S, 110.1.1.0 E
SCALE : 1 : 50

DATE : 4 September 2010
MEASURED AND DESPICTED BY : Andhyoka Tama

SEDIMENTARY STRUCTURE:
- Tractional sedimentation
- Suspension sedimentation
- Parallel lamination
- Cross lamination
- Convolute
- Wavy lamination
- Lenticular bedding
- Flaser bedding
- Reverse graded bedding
- Graded bedding
- Crude bedding
- Cross bedding

LITHOLOGY
- Mudstone
- Claystone
- Coal
- Sandstone
- Coal Sandstone
- Conglomerate
- Breccia
- Limestone
- Volcanic Breccia
- Volcanic Tuff
- Andesite Porphyry

BED BOUNDARY
- Conformable
- Unconformable

LEGEND
- 1 : Coal
- 2 : Mudstone
- 3 : Claystone
- 4 : Sandstone
- 5 : Coal sandstone
- 6 : Conglomerate
- 7 : Volcanic breccia
- 8 : Volcanic breccia coarse
- 9 : Volcanic breccia

SAMPLE NUMBER	LITHOLOGY	SEDIMENTARY STRUCTURE (GRAIN SIZE: Mud, Sand, Gravel, Boulder)	DESCRIPTION	PHOTO	FORMATION / MEMBER
24.1 - 27			**24 Tuffaceous sandstone.** Light yellowish brown, very fine-grained, tuffaceous, well sorted, massive, hard.		Sewoh Of Kaliurang Lower Hill Fan
24.0 - 24.1			**23 Tuffaceous sandstone.** Light grey, very fine-grained, tuffaceous, well sorted, massive, hard, contains coal fragments, 0.1 cm thick.		
23.9 - 24.0			**22 Coal.** Black, 0.1 cm thick.		
23.8 - 23.9			**21 Tuffaceous sandstone.** Light grey, very fine-grained, tuffaceous, well sorted, massive, hard, contains coal fragments, 0.1 cm thick.		
23.7 - 23.8			**20 Coal.** Black, 0.1 cm thick.		
23.6 - 23.7			**19 Coal.** Black, 0.1 cm thick.		
23.5 - 23.6			**18 Coal.** Black, 0.1 cm thick.		
23.4 - 23.5			**17 Tuffaceous sandstone.** Light grey, very fine-grained, tuffaceous, well sorted, massive, hard, contains coal fragments, 0.1 cm thick.		
23.3 - 23.4			**16 Coal.** Black, 0.1 cm thick.		
23.2 - 23.3			**15 Coal.** Black, 0.1 cm thick.		
23.1 - 23.2			**14 Coal.** Black, 0.1 cm thick.		
23.0 - 23.1			**13 Coal.** Black, 0.1 cm thick.		
22.9 - 23.0			**12 Coal.** Black, 0.1 cm thick.		
22.8 - 22.9			**11 Coal.** Black, 0.1 cm thick.		
22.7 - 22.8			**10 Coal.** Black, 0.1 cm thick.		
22.6 - 22.7			**9 Coal.** Black, 0.1 cm thick.		
22.5 - 22.6			**8 Coal.** Black, 0.1 cm thick.		
22.4 - 22.5			**7 Coal.** Black, 0.1 cm thick.		
22.3 - 22.4			**6 Coal.** Black, 0.1 cm thick.		
22.2 - 22.3			**5 Coal.** Black, 0.1 cm thick.		
22.1 - 22.2			**4 Coal.** Black, 0.1 cm thick.		
22.0 - 22.1			**3 Coal.** Black, 0.1 cm thick.		
21.9 - 22.0			**2 Coal.** Black, 0.1 cm thick.		
21.8 - 21.9			**1 Coal.** Black, 0.1 cm thick.		
21.7 - 21.8			**23 Conglomerate.** Medium grey-reddish, very coarse-grained, very poorly sorted, massive, very hard, contains coal fragments, 0.1 cm thick, contains granitic boulders.		Conglomeratic (CG) / Chocoladé Portion Of Sparkling Lake Hill Fan
21.6 - 21.7			**22 Sandstone.** Dark reddish-brown, medium-grained, very poorly sorted, massive, very hard, contains coal fragments, 0.1 cm thick, contains granitic boulders.		
21.5 - 21.6			**21 Sandstone.** Dark reddish-brown, medium-grained, very poorly sorted, massive, very hard, contains coal fragments, 0.1 cm thick, contains granitic boulders.		
21.4 - 21.5			**20 Sandstone.** Dark reddish-brown, medium-grained, very poorly sorted, massive, very hard, contains coal fragments, 0.1 cm thick, contains granitic boulders.		
21.3 - 21.4			**19 Sandstone.** Dark reddish-brown, medium-grained, very poorly sorted, massive, very hard, contains coal fragments, 0.1 cm thick, contains granitic boulders.		
21.2 - 21.3			**18 Sandstone.** Dark reddish-brown, medium-grained, very poorly sorted, massive, very hard, contains coal fragments, 0.1 cm thick, contains granitic boulders.		
21.1 - 21.2			**17 Sandstone.** Dark reddish-brown, medium-grained, very poorly sorted, massive, very hard, contains coal fragments, 0.1 cm thick, contains granitic boulders.		
21.0 - 21.1			**16 Sandstone.** Dark reddish-brown, medium-grained, very poorly sorted, massive, very hard, contains coal fragments, 0.1 cm thick, contains granitic boulders.		
20.9 - 21.0			**15 Sandstone.** Dark reddish-brown, medium-grained, very poorly sorted, massive, very hard, contains coal fragments, 0.1 cm thick, contains granitic boulders.		
20.8 - 20.9			**14 Sandstone.** Dark reddish-brown, medium-grained, very poorly sorted, massive, very hard, contains coal fragments, 0.1 cm thick, contains granitic boulders.		
20.7 - 20.8			**13 Sandstone.** Light brown, very fine-grained, well sorted, massive, very hard, contains coal fragments, 0.1 cm thick.		Pelaby Sandstone (PS) / Chocoladé Portion Of Sparkling Lake Hill Fan
20.6 - 20.7			**12 Sandstone.** Light brown, very fine-grained, well sorted, massive, very hard, contains coal fragments, 0.1 cm thick.		
20.5 - 20.6			**11 Sandstone.** Light brown, very fine-grained, well sorted, massive, very hard, contains coal fragments, 0.1 cm thick.		
20.4 - 20.5			**10 Sandstone.** Light brown, very fine-grained, well sorted, massive, very hard, contains coal fragments, 0.1 cm thick.		
20.3 - 20.4			**9 Sandstone.** Light brown, very fine-grained, well sorted, massive, very hard, contains coal fragments, 0.1 cm thick.		
20.2 - 20.3			**8 Sandstone.** Light brown, very fine-grained, well sorted, massive, very hard, contains coal fragments, 0.1 cm thick.		
20.1 - 20.2			**7 Sandstone.** Light brown, very fine-grained, well sorted, massive, very hard, contains coal fragments, 0.1 cm thick.		
20.0 - 20.1			**6 Sandstone.** Light brown, very fine-grained, well sorted, massive, very hard, contains coal fragments, 0.1 cm thick.		
19.9 - 20.0			**5 Sandstone.** Light brown, very fine-grained, well sorted, massive, very hard, contains coal fragments, 0.1 cm thick.		
19.8 - 19.9			**4 Sandstone.** Light brown, very fine-grained, well sorted, massive, very hard, contains coal fragments, 0.1 cm thick.		
19.7 - 19.8			**3 Sandstone.** Light brown, very fine-grained, well sorted, massive, very hard, contains coal fragments, 0.1 cm thick.		
19.6 - 19.7			**2 Sandstone.** Light brown, very fine-grained, well sorted, massive, very hard, contains coal fragments, 0.1 cm thick.		
19.5 - 19.6			**1 Sandstone.** Light brown, very fine-grained, well sorted, massive, very hard, contains coal fragments, 0.1 cm thick.		
19.4 - 19.5			**23 Sandstone.** Light brown, very fine-grained, well sorted, massive, very hard, contains coal fragments, 0.1 cm thick.		
19.3 - 19.4			**22 Sandstone.** Light brown, very fine-grained, well sorted, massive, very hard, contains coal fragments, 0.1 cm thick.		
19.2 - 19.3			**21 Sandstone.** Light brown, very fine-grained, well sorted, massive, very hard, contains coal fragments, 0.1 cm thick.		
19.1 - 19.2			**20 Sandstone.** Light brown, very fine-grained, well sorted, massive, very hard, contains coal fragments, 0.1 cm thick.		
19.0 - 19.1			**19 Sandstone.** Light brown, very fine-grained, well sorted, massive, very hard, contains coal fragments, 0.1 cm thick.		
18.9 - 19.0			**18 Sandstone.** Light brown, very fine-grained, well sorted, massive, very hard, contains coal fragments, 0.1 cm thick.		
18.8 - 18.9			**17 Sandstone.** Light brown, very fine-grained, well sorted, massive, very hard, contains coal fragments, 0.1 cm thick.		
18.7 - 18.8			**16 Sandstone.** Light brown, very fine-grained, well sorted, massive, very hard, contains coal fragments, 0.1 cm thick.		
18.6 - 18.7			**15 Sandstone.** Light brown, very fine-grained, well sorted, massive, very hard, contains coal fragments, 0.1 cm thick.		
18.5 - 18.6			**14 Sandstone.** Light brown, very fine-grained, well sorted, massive, very hard, contains coal fragments, 0.1 cm thick.		
18.4 - 18.5			**13 Sandstone.** Light brown, very fine-grained, well sorted, massive, very hard, contains coal fragments, 0.1 cm thick.		
18.3 - 18.4			**12 Sandstone.** Light brown, very fine-grained, well sorted, massive, very hard, contains coal fragments, 0.1 cm thick.		
18.2 - 18.3			**11 Sandstone.** Light brown, very fine-grained, well sorted, massive, very hard, contains coal fragments, 0.1 cm thick.		
18.1 - 18.2			**10 Sandstone.** Light brown, very fine-grained, well sorted, massive, very hard, contains coal fragments, 0.1 cm thick.		
18.0 - 18.1			**9 Sandstone.** Light brown, very fine-grained, well sorted, massive, very hard, contains coal fragments, 0.1 cm thick.		
17.9 - 18.0			**8 Sandstone.** Light brown, very fine-grained, well sorted, massive, very hard, contains coal fragments, 0.1 cm thick.		
17.8 - 17.9			**7 Sandstone.** Light brown, very fine-grained, well sorted, massive, very hard, contains coal fragments, 0.1 cm thick.		
17.7 - 17.8			**6 Sandstone.** Light brown, very fine-grained, well sorted, massive, very hard, contains coal fragments, 0.1 cm thick.		
17.6 - 17.7			**5 Sandstone.** Light brown, very fine-grained, well sorted, massive, very hard, contains coal fragments, 0.1 cm thick.		
17.5 - 17.6			**4 Sandstone.** Light brown, very fine-grained, well sorted, massive, very hard, contains coal fragments, 0.1 cm thick.		
17.4 - 17.5			**3 Sandstone.** Light brown, very fine-grained, well sorted, massive, very hard, contains coal fragments, 0.1 cm thick.		
17.3 - 17.4			**2 Sandstone.** Light brown, very fine-grained, well sorted, massive, very hard, contains coal fragments, 0.1 cm thick.		
17.2 - 17.3			**1 Sandstone.** Light brown, very fine-grained, well sorted, massive, very hard, contains coal fragments, 0.1 cm thick.		

Attachment 1 Teams 1 Profile

DEPARTMENT OF GEOLOGICAL ENGINEERING
FACULTY OF MINING TECHNOLOGY
UNIVERSITY OF NATIONAL DEVELOPMENT "VETERAN YOGYAKARTA"
2011

MEASURED STRATIGRAPHIC SECTION

LOCATION : Nguren Area, Sidorejo Village, Kalirejo Sub-district, Kulon Progo Regency, Special Region of Yogyakarta, Indonesia
COORDINATE : Begin: 7.6.2.0 S, 110.1.1.0 E
End: 7.6.2.0 S, 110.1.1.0 E
SCALE : 1 : 50

DATE : 4 September 2010
MEASURED AND DESPICTED BY : Andhyoka Tama

SEDIMENTARY STRUCTURE:
- Tractional sedimentation
- Suspension sedimentation

LITHOLOGY
- Mudstone
- Claystone
- Coal
- Sandstone

BED BOUNDARY
- Conformable
- Unconformable

LEGEND
- 1 : Coal
- 2 : Mudstone
- 3 : Claystone
- 4 : Sandstone
- 5 : Coal sandstone
- 6 : Conglomerate
- 7 : Volcanic breccia
- 8 : Volcanic breccia coarse
- 9 : Volcanic breccia

SAMPLE NUMBER	LITHOLOGY	SEDIMENTARY STRUCTURE (GRAIN SIZE: Mud, Sand, Gravel, Boulder)	DESCRIPTION	PHOTO	FORMATION / MEMBER
16 - 17			**152 Sandstone.** Tuffaceous, very fine-grained, massive.		Sewoh Of Kaliurang Lower Hill Fan
15.9 - 16			**151 Sandstone.** Tuffaceous, very fine-grained, massive, hard.		
15.8 - 15.9			**150 Sandstone.** Tuffaceous, very fine-grained, massive, hard.		
15.7 - 15.8			**149 Sandstone.** Tuffaceous, very fine-grained, massive, hard.		
15.6 - 15.7			**148 Sandstone.** Tuffaceous, very fine-grained, massive, hard.		
15.5 - 15.6			**147 Sandstone.** Tuffaceous, very fine-grained, massive, hard.		
15.4 - 15.5			**146 Sandstone.** Tuffaceous, very fine-grained, massive, hard.		
15.3 - 15.4			**145 Sandstone.** Tuffaceous, very fine-grained, massive, hard.		
15.2 - 15.3			**144 Sandstone.** Tuffaceous, very fine-grained, massive, hard.		
15.1 - 15.2			**143 Sandstone.** Tuffaceous, very fine-grained, massive, hard.		
15.0 - 15.1			**142 Sandstone.** Tuffaceous, very fine-grained, massive, hard.		
14.9 - 15.0			**141 Sandstone.** Tuffaceous, very fine-grained, massive, hard.		
14.8 - 14.9			**140 Sandstone.** Tuffaceous, very fine-grained, massive, hard.		
14.7 - 14.8			**139 Sandstone.** Tuffaceous, very fine-grained, massive, hard.		
14.6 - 14.7			**138 Sandstone.** Tuffaceous, very fine-grained, massive, hard.		
14.5 - 14.6			**137 Sandstone.** Tuffaceous, very fine-grained, massive, hard.		
14.4 - 14.5			**136 Sandstone.** Tuffaceous, very fine-grained, massive, hard.		
14.3 - 14.4			**135 Sandstone.** Tuffaceous, very fine-grained, massive, hard.		
14.2 - 14.3			**134 Sandstone.** Tuffaceous, very fine-grained, massive, hard.		
14.1 - 14.2			**133 Sandstone.** Tuffaceous, very fine-grained, massive, hard.		
14.0 - 14.1			**132 Sandstone.** Tuffaceous, very fine-grained, massive, hard.		
13.9 - 14.0			**131 Sandstone.** Tuffaceous, very fine-grained, massive, hard.		
13.8 - 13.9			**130 Sandstone.** Tuffaceous, very fine-grained, massive, hard.		
13.7 - 13.8			**129 Sandstone.** Tuffaceous, very fine-grained, massive, hard.		
13.6 - 13.7			**128 Sandstone.** Tuffaceous, very fine-grained, massive, hard.		
13.5 - 13.6			**127 Sandstone.** Tuffaceous, very fine-grained, massive, hard.		
13.4 - 13.5			**126 Sandstone.** Tuffaceous, very fine-grained, massive, hard.		
13.3 - 13.4			**125 Sandstone.** Tuffaceous, very fine-grained, massive, hard.		
13.2 - 13.3			**124 Sandstone.** Tuffaceous, very fine-grained, massive, hard.		
13.1 - 13.2			**123 Sandstone.** Tuffaceous, very fine-grained, massive, hard.		
13.0 - 13.1			**122 Sandstone.** Tuffaceous, very fine-grained, massive, hard.		
12.9 - 13.0			**121 Sandstone.** Tuffaceous, very fine-grained, massive, hard.		
12.8 - 12.9			**120 Sandstone.** Tuffaceous, very fine-grained, massive, hard.		
12.7 - 12.8			**119 Sandstone.** Tuffaceous, very fine-grained, massive, hard.		
12.6 - 12.7			**118 Sandstone.** Tuffaceous, very fine-grained, massive, hard.		
12.5 - 12.6			**117 Sandstone.** Tuffaceous, very fine-grained, massive, hard.		
12.4 - 12.5			**116 Sandstone.** Tuffaceous, very fine-grained, massive, hard.		
12.3 - 12.4			**115 Sandstone.** Tuffaceous, very fine-grained, massive, hard.		
12.2 - 12.3			**114 Sandstone.** Tuffaceous, very fine-grained, massive, hard.		
12.1 - 12.2			**113 Sandstone.** Tuffaceous, very fine-grained, massive, hard.		
12.0 - 12.1			**112 Sandstone.** Tuffaceous, very fine-grained, massive, hard.		
11.9 - 12.0			**111 Sandstone.** Tuffaceous, very fine-grained, massive, hard.		
11.8 - 11.9			**110 Sandstone.** Tuffaceous, very fine-grained, massive, hard.		
11.7 - 11.8			**109 Sandstone.** Tuffaceous, very fine-grained, massive, hard.		
11.6 - 11.7			**108 Sandstone.** Tuffaceous, very fine-grained, massive, hard.		
11.5 - 11.6			**107 Sandstone.** Tuffaceous, very fine-grained, massive, hard.		
11.4 - 11.5			**106 Sandstone.** Tuffaceous, very fine-grained, massive, hard.		
11.3 - 11.4			**105 Sandstone.** Tuffaceous, very fine-grained, massive, hard.		
11.2 - 11.3			**104 Sandstone.** Tuffaceous, very fine-grained, massive, hard.		
11.1 - 11.2			**103 Sandstone.** Tuffaceous, very fine-grained, massive, hard.		
11.0 - 11.1			**102 Sandstone.** Tuffaceous, very fine-grained, massive, hard.		
10.9 - 11.0			**101 Sandstone.** Tuffaceous, very fine-grained, massive, hard.		
10.8 - 10.9			**100 Sandstone.** Tuffaceous, very fine-grained, massive, hard.		
10.7 - 10.8			**99 Sandstone.** Tuffaceous, very fine-grained, massive, hard.		
10.6 - 10.7			**98 Sandstone.** Tuffaceous, very fine-grained, massive, hard.		
10.5 - 10.6			**97 Sandstone.** Tuffaceous, very fine-grained, massive, hard.		
10.4 - 10.5			**96 Sandstone.** Tuffaceous, very fine-grained, massive, hard.		
10.3 - 10.4			**95 Sandstone.** Tuffaceous, very fine-grained, massive, hard.		
10.2 - 10.3			**94 Sandstone.** Tuffaceous, very fine-grained, massive, hard.		
10.1 - 10.2			**93 Sandstone.** Tuffaceous, very fine-grained, massive, hard.		
10.0 - 10.1			**92 Sandstone.** Tuffaceous, very fine-grained, massive, hard.		
9.9 - 10.0			**91 Sandstone.** Tuffaceous, very fine-grained, massive, hard.		
9.8 - 9.9			**90 Sandstone.** Tuffaceous, very fine-grained, massive, hard.		
9.7 - 9.8			**89 Sandstone.** Tuffaceous, very fine-grained, massive, hard.		
9.6 - 9.7			**88 Sandstone.** Tuffaceous, very fine-grained, massive, hard.		
9.5 - 9.6			**87 Sandstone.** Tuffaceous, very fine-grained, massive, hard.		
9.4 - 9.5			**86 Sandstone.** Tuffaceous, very fine-grained, massive, hard.		
9.3 - 9.4			**85 Sandstone.** Tuffaceous, very fine-grained, massive, hard.		
9.2 - 9.3			**84 Sandstone.** Tuffaceous, very fine-grained, massive, hard.		
9.1 - 9.2			**83 Sandstone.** Tuffaceous, very fine-grained, massive, hard.		
9.0 - 9.1			**82 Sandstone.** Tuffaceous, very fine-grained, massive, hard.		
8.9 - 9.0			**81 Sandstone.** Tuffaceous, very fine-grained, massive, hard.		
8.8 - 8.9			**80 Sandstone.** Tuffaceous, very fine-grained, massive, hard.		
8.7 - 8.8			**79 Sandstone.** Tuffaceous, very fine-grained, massive, hard.		
8.6 - 8.7			**78 Sandstone.** Tuffaceous, very fine-grained, massive, hard.		
8.5 - 8.6			**77 Sandstone.** Tuffaceous, very fine-grained, massive, hard.		
8.4 - 8.5			**76 Sandstone.** Tuffaceous, very fine-grained, massive, hard.		
8.3 - 8.4			**75 Sandstone.** Tuffaceous, very fine-grained, massive, hard.		
8.2 - 8.3			**74 Sandstone.** Tuffaceous, very fine-grained, massive, hard.		
8.1 - 8.2			**73 Sandstone.** Tuffaceous, very fine-grained, massive, hard.		
8.0 - 8.1			**72 Sandstone.** Tuffaceous, very fine-grained, massive, hard.		
7.9 - 8.0			**71 Sandstone.** Tuffaceous, very fine-grained, massive, hard.		
7.8 - 7.9			**70 Sandstone.** Tuffaceous, very fine-grained, massive, hard.		
7.7 - 7.8			**69 Sandstone.** Tuffaceous, very fine-grained, massive, hard.		
7.6 - 7.7			**68 Sandstone.** Tuffaceous, very fine-grained, massive, hard.		
7.5 - 7.6			**67 Sandstone.** Tuffaceous, very fine-grained, massive, hard.		
7.4 - 7.5			**66 Sandstone.** Tuffaceous, very fine-grained, massive, hard.		
7.3 - 7.4			**65 Sandstone.** Tuffaceous, very fine-grained, massive, hard.		
7.2 - 7.3			**64 Sandstone.** Tuffaceous, very fine-grained, massive, hard.		
7.1 - 7.2			**63 Sandstone.** Tuffaceous, very fine-grained, massive, hard.		
7.0 - 7.1			**62 Sandstone.** Tuffaceous, very fine-grained, massive, hard.		
6.9 - 7.0			**61 Sandstone.** Tuffaceous, very fine-grained, massive, hard.		
6.8 - 6.9			**60 Sandstone.** Tuffaceous, very fine-grained, massive, hard.		
6.7 - 6.8			**59 Sandstone.** Tuffaceous, very fine-grained, massive, hard.		
6.6 - 6.7			**58 Sandstone.** Tuffaceous, very fine-grained, massive, hard.		
6.5 - 6.6			**57 Sandstone.** Tuffaceous, very fine-grained, massive, hard.		
6.4 - 6.5			**56 Sandstone.** Tuffaceous, very fine-grained, massive, hard.		
6.3 - 6.4			**55 Sandstone.** Tuffaceous, very fine-grained, massive, hard.		
6.2 - 6.3			**54 Sandstone.** Tuffaceous, very fine-grained, massive, hard.		
6.1 - 6.2			**53 Sandstone.** Tuffaceous, very fine-grained, massive, hard.		
6.0 - 6.1			**52 Sandstone.** Tuffaceous, very fine-grained, massive, hard.		
5.9 - 6.0			**51 Sandstone.** Tuffaceous, very fine-grained, massive, hard.		
5.8 - 5.9			**50 Sandstone.** Tuffaceous, very fine-grained, massive, hard.		
5.7 - 5.8			**49 Sandstone.** Tuffaceous, very fine-grained, massive, hard.		
5.6 - 5.7			**48 Sandstone.** Tuffaceous, very fine-grained, massive, hard.		
5.5 - 5.6			**47 Sandstone.** Tuffaceous, very fine-grained, massive, hard.		
5.4 - 5.5			**46 Sandstone.** Tuffaceous, very fine-grained, massive, hard.		
5.3 - 5.4			**45 Sandstone.** Tuffaceous, very fine-grained, massive, hard.		
5.2 - 5.3			**44 Sandstone.** Tuffaceous, very fine-grained, massive, hard.		
5.1 - 5.2			**43 Sandstone.** Tuffaceous, very fine-grained, massive, hard.		
5.0 - 5.1			**42 Sandstone.** Tuffaceous, very fine-grained, massive, hard.		
4.9 - 5.0			**41 Sandstone.** Tuffaceous, very fine-grained, massive, hard.		
4.8 - 4.9			**40 Sandstone.** Tuffaceous, very fine-grained, massive, hard.		
4.7 - 4.8			**39 Sandstone.** Tuffaceous, very fine-grained, massive, hard.		
4.6 - 4.7			**38 Sandstone.** Tuffaceous, very fine-grained, massive, hard.		
4.5 - 4.6			**37 Sandstone.** Tuffaceous, very fine-grained, massive, hard.		
4.4 - 4.5			**36 Sandstone.** Tuffaceous, very fine-grained, massive, hard.		
4.3 - 4.4			**35 Sandstone.** Tuffaceous, very fine-grained, massive, hard.		
4.2 - 4.3			**34 Sandstone.** Tuffaceous, very fine-grained, massive, hard.		
4.1 - 4.2			**33 Sandstone.** Tuffaceous, very fine-grained, massive, hard.		
4.0 - 4.1			**32 Sandstone.** Tuffaceous, very fine-grained, massive, hard.		
3.9 - 4.0			**31 Sandstone.** Tuffaceous, very fine-grained, massive, hard.		
3.8 - 3.9			**30 Sandstone.** Tuffaceous, very fine-grained, massive, hard.		
3.7 - 3.8			**29 Sandstone.** Tuffaceous, very fine-grained, massive, hard.		
3.6 - 3.7			**28 Sandstone.** Tuffaceous, very fine-grained, massive, hard.		
3.5 - 3.6			**27 Sandstone.** Tuffaceous, very fine-grained, massive, hard.		
3.4 - 3.5			**26 Sandstone.** Tuffaceous, very fine-grained, massive, hard.		
3.3 - 3.4			**25 Sandstone.** Tuffaceous, very fine-grained, massive, hard.		
3.2 - 3.3			**24 Sandstone.** Tuffaceous, very fine-grained, massive, hard.		
3.1 - 3.2			**23 Sandstone.** Tuffaceous, very fine-grained, massive, hard.		
3.0 - 3.1			**22 Sandstone.** Tuffaceous, very fine-grained, massive, hard.		
2.9 - 3.0			**21 Sandstone.** Tuffaceous, very fine-grained, massive, hard.		
2.8 - 2.9			**20 Sandstone.** Tuffaceous, very fine-grained, massive, hard.		
2.7 - 2.8			**19 Sandstone.** Tuffaceous, very fine-grained, massive, hard.		
2.6 - 2.7			**18 Sandstone.** Tuffaceous, very fine-grained, massive, hard.		
2.5 - 2.6			**17 Sandstone.** Tuffaceous, very fine-grained, massive, hard.		
2.4 - 2.5			**16 Sandstone.** Tuffaceous, very fine-grained, massive, hard.		
2.3 - 2.4			**15 Sandstone.** Tuffaceous, very fine-grained, massive, hard.		
2.2 - 2.3			**14 Sandstone.** Tuffaceous, very fine-grained, massive, hard.		
2.1 - 2.2			**13 Sandstone.** Tuffaceous, very fine-grained, massive, hard.		
2.0 - 2.1			**12 Sandstone.** Tuffaceous, very fine-grained, massive, hard.		
1.9 - 2.0			**11 Sandstone.** Tuffaceous, very fine-grained, massive, hard.		
1.8 - 1.9			**10 Sandstone.** Tuffaceous, very fine-grained, massive, hard.		
1.7 - 1.8			**9 Sandstone.** Tuffaceous, very fine-grained, massive, hard.		
1.6 - 1.7			**8 Sandstone.** Tuffaceous, very fine-grained, massive, hard.		
1.5 - 1.6			**7 Sandstone.** Tuffaceous, very fine-grained, massive, hard.		
1.4 - 1.5			**6 Sandstone.** Tuffaceous, very fine-grained, massive, hard.		
1.3 - 1.4			**5 Sandstone.** Tuffaceous, very fine-grained, massive, hard.		
1.2 - 1.3			**4 Sandstone.** Tuffaceous, very fine-grained, massive, hard.		
1.1 - 1.2			**3 Sandstone.** Tuffaceous, very fine-grained, massive, hard.		
1.0 - 1.1			**2 Sandstone.** Tuffaceous, very fine-grained, massive, hard.		
0.9 - 1.0			**1 Sandstone.** Tuffaceous, very fine-grained, massive, hard.		

Attachment 1 Teams 1 Profile

DEPARTMENT OF GEOLOGICAL ENGINEERING
FACULTY OF MINERAL TECHNOLOGY
UNIVERSITY OF NATIONAL DEVELOPMENT "VETERAN' YOGYAKARTA
2021

MEASURED STRATIGRAPHIC SECTION

LOCATION : Ngoro-oro Area, District Pathuk, Gunungkidul Regency, Indonesia
LINE : Station 3 Location 1
FORMATION : Semilir Formation
SCALE : 1 : 20

DATE	MEASURED AND DESPICTED BY
10 September 2021	Ameliorate Team

SEDIMENTARY STRUCTURE: Massive/Stratified; Paralel Lamination; Convolute; Wavy Lamination; Graded bedding; Reverse graded bedding; Coal chips

LITHOLOGY: Sandstone; Tuff-Volcanic Clast; Siltstone; Volcanic breccia; Claystone; Carbonate Rocks

BED BOUNDARY: Contrast; Gradational

LEGENDS
f :fresh
w :weathered
F :fragmen
M :matrix
C :cement
S :sialis mineral
Fr :feromagnesian mineral
Ta :other mineral

FORMATION: SEMILIR FORMATION

THICKNESS (m)	BED	DESCRIPTION
>250	168	**168. Sandstone,** f:yellowis, medium sand, angular, poorly sorted, grain supported, F:lapili, quartz, Massive
55	167	**167. Interbedded Sandstone-Tuff** **Sandstone,** f:grey, fine-medium sand, angular, poorly sorted, grain supported, F:lapilush, quartz, stratified **Tuff,** f:grey, silt, C:silica, stratified
18	166	**166. Sandstone,** f:grey, fine sand, F:quartz, stratified
162	165	**165. Sandstone,** f:grey, medium sanf, angular, poorly sorted, grain supported, F:lapili, quartz, lithic, hornblende, M:clay sized material, C:silica, Lamination
28	164	**164. Tuff,** f:white, silt, Stratified
23	163	**163. Tuff,** f:grey, silt, F:quartz, Stratified
25	162	**162. Siltstone,** f:grey, silt, C: Silica ,Stratified
44	161	**161. Sandstone,** f:grey, medium sand, angular, poorly sorted, grain supported, F:quartz, lithic, M:clay sized material, C:silica, Stratified
36	160	**160. Sandstone,** f:grey, medium sand, angular, poorly sorted, grain supported, F:quartz, lithic, M:clay sized material, C:silica, Stratified
30	159	**159. Siltstone,** f:grey, silt, stratified
18	158	**158. Sandstone,** f:grey, fine sand, C:silica, Stratified
10	157	**157. Siltstone,** f:grey, silt, stratified
134	156	**156. Sandstone,** f:grey, medium sand, angular, poorly sorted, grain supported, F:quartz, lithic, M:clay sized material, C:silica, Convolute
5	155	**155. Interbeded of Tuffaceous Sandstone and Tuff** **Tuff,** f:grey, w:brown, clay-silt, C:silica **Tuffaceous sandstone,** F:grey, w:brown, very fine-fine sand, C:silica wavy lamination
4,5	154	**154.Tuffaceous sandstone,** F:grey, w:brown, very fine-fine sand, C:silica wavy lamination, erotional
22	153	**153.Tuff,** f:grey, w:brown, clay-silt, C:silica
5	152	**152.Tuffaceous sandstone,** F:grey, w:brown, very fine-fine sand, C:silica wavy lamination
36	151	**151.Tuff,** f:grey, w:brown, clay-silt
56	150	**150.Tuff,** f:white, w:brown, silt-clay
17	149	**149.Tuffaceous sandstone,** f:grey w:yellowish, fine sand-medium sand, subangular-angular, poorly sorted, matrix supported, F:lithic, quartz, hornblende, coal, M:clay sized material, C:silica gradational contact
33	148	**148.Siltstone,** f:white, w:yellowlish, silt
26	147	**147.Tuffaceous sandstone,** f:grey, w:yellow, fine-medium sand, subrounded-angular, well sorted, grain supported, F:lithic, quartz, honrblende, M:clay sized material, C:silica
19	146	**146.Calcareous sandstone** f:grey, w:yellow, fine-medium sand subrounded-angular, poorly sorted, matrix supported, F:lithic, hornblenda, coal, M:clay sized material, C:carbonate
24	145	**145.Clay stone,** f:grey, w:yellow, C:silica
142	144	**144.Tuffaceous sandstone,** f:grey, w:yellow, fine-medium sand, subrounded-angular, well sorted, grain supported, F:lithic, quartz, honrblende, M:clay sized material, C:silica, wavy lamination
41,5	143	**143.Claystone,** f:dark grey, w:grey, clay-silt, C:silica
25	142	**142.Tuffaceous sandstone,** f:grey, w:dark grey, silt-fine sand, C:silica parallel lamination, gradational
11	141	**141.Tuff,** f:grey, w: dark grey, clay-silt, C:silica
25	140	**140.Tuffaceous sandstone,** f:grey, w:brown, fine sand-medium sand, subangular -angular, poorly sorted, matrix supported, F:pumice, lithic, coal, hornblende, M:clay sized material, C:silica wavy lamination, gradational contact
36	139	**139.Tuffaceous siltstone,** f:white, w:brown, clay-silt, C:silica
52	138	**138.Tuffaceous sandstone,** f:grey, w:brown, silt-very fine sand, F:lithic, M:Clay sized material, C:silica stratified
65	137	**137.Tuffaceous sandstone,** f:grey, w:brown, very fine sand-fine sand, subrounded-angular, well sorted, grain supported, F:lithic, quartz, M:clay sized material, C:silica, parallel lamination
43	136	**136.Tuffaceous sandstone,** f:grey, w:brown, clay-very coarse sand, subangular-angular, poorly sorted, matrix supported, F:lithic, silt, M:clay size material, C:silica, wavy lamination
28	135	**135.Tuffaceous sandstone,** f:grey, w:brown, very fine-fine sand, C:silica, parallel lamination
9,4	134	**134.Tuffaceous sandstone,** f:grey, w:brown, very fine sand, C:silica, stratified
6	133	**133.Sandstone,** f:grey, w:brown, very fine sand- fine sand, C:Silicastratified
25,1	132	**132.Siltstone,** f:grey, w:brown, C:silica, stratified
28	131	**131.Tuffaceous sandstone,** f:grey, w:brown, fine sand-medium sand, subangular -angular, well sorted, grain supported, F:quartz, lithic, hornblende, M:clay sized material, C:silica, wavy lamination
27,3	130	**130.Tuffaceous sandstone,** f:grey, w:brown, silt-fine sand, C:silica,stratified
129,5	129	**129.Tuffaceous sandstone,** f:grey, w: browny yellow, fine sand-medium sand, subagnular-angular, well sorted, grain supported, F:quartz, lithic, hornblenda, M:clay sized material, C:silica, wavy lamination
	128	**128.Sandstone,** f:grey, fine sand, F:pyroxene
65	127	**127.Tuff,** f:light grey, silt, MS:quartz
23	126	**126.Siltstone,** f:grey, silt, F:quartz, massive
55	125	**125.Sandstone,** f:grey, medium sand, angular, poorly sorted, grain sorted, F:quartz, M:clay sized material, C:silica convolute
12	124	**124.Interbeded of Sandstone and Siltsone** **Sandstone,** f:grey, fine sand, F: pyroxene **Siltstone,** f:grey, silt, stratified
33	123	**123.Lapili sandstone,** f:grey, medium sand, angular, poorly sorted, grain supported, F:, M:clay sized material, C:silica parallel lamination
13	122	**122.Sandstone,** f:grey, medium sand, angular, poorly sorted, grain supported, F:, coal, M:clay sized material, C:silica erosional contact
20	121	**121.Sandstone,** f:grey, fine sand, F:palgioclase, pyroxene
137	120	**120.Lapili sandstone,** f:grey, angular, poorly sorted, grain supported, F:,hornblende, M:clay sized material, C:silica
13	119	**119.Siltstone,** f:grey, silt, stratified
10	118	**118.Lapili sandstone** , f:grey, medium sand, angular, poorly sorted, grain supported, F:, M:clay sized material, C:silica parallel lamination
31	117	**117.Tuff,** f:grey, silt, S:quartz,
16	116	**116.Sandstone,** f:grey, fine sand, angular, poorly, sorted, grain sorted, C:silica
16	115	**115.Sandstone,** f:grey, medium sand, angular, poorly sorted, grain sorted, F:quartz, M:clay sized material, C:silica
5	114	**114.Sandstone,** f:grey, fine sand, angular, poorly sorted, grain sorted, C:silica
16	113	**113.Sandstone,** f:brown, medium sand, angular, poorly sorted, grain supported, F:quartz, M:clay sized material, C:silica parallel lamination
12	112	**112.Sandstone,** f:grey, fine sand, angular, poorly sorted, grain sorted, C:silica
	111	**111.Sandstone,** f:grey, medium sand, angular, poorly sorted, grain sorted, F:quartz, M:clay sized material, C:silica
	110	**110.Tuff,** f:light grey, silt, massive
22	111	
56	110	
9,5	109	**109.Sandstone** , f:light grey, w:brown, very fine-fine sand, subrounded, poorly sorted, matriks supported, F:coal, quartz, M:clay sized material, C=silica, stratified
7,4	108	**108.Sandstone,** f:grey, w:brown, very fine sand, C:silica, stratified
5,1	107	**107.Tuffaceous sandstone,** f:light grey, W:dark grey, fine sand-coarse sand, poorly sorted, matrix supported, F:silt, coal, lithic, quartz, plagioclase, hornblende, M:clay sized material, C:silica, stratified
	106	**106.Tuff,** f: grey, w: brown, fine sand, rounded, well sorted, grain supported, S:plagioclase, quartz, Fr:hornblende, stratified
	105	**105.Siltstone,** F:black, W:brown massive
	104	**104.Tuff,** f:light grey, w: brown, fine sand, rounded, well sorted, grain supported, S:plagioclase, quartz, Fr:hornblende, stratified
12,5	103	**103.Tuff,** f:grey, w: dark brown, fine sand, round, well sorted, grain supported, S:plagioclase, quartz, Fr:hornblende, stratified, coal chip
1,2	102	**102. Clay stone,** f:brown, w:yellow, C:silica
4,9	101	**101.Tuff,** f:grey, w: brown, fine sand, rounded, well sorted, grain supported, S:plagioclase, quartz, Fr:hornblende, stratified
29,3	100	**100.Tuff,** f:white, w: brown, fine sand, rounded, well sorted, grain supported, S:plagioclase, quartz, Fr:hornblende, stratified, coal scratch
10,7	99	**99.Tuf,** f: white, w: brown, silt, stratified
7,2	98	**98.Tuffaceous sandstone,** F:grey, w:brown, fine sand-coarse sand, rounded, poorly sorted, matriks supported, F:quartz, hornblende, M:clay sized material, C: silica paralel lamination, coal scratch, coal chip
10,4	97	**97.Tuff,** f:white,, w:dark grey, fine sand, rounded, well sorted, grain supported, S:plagioclase, quartz, Fr:hornblende
39,7	96	**96.Tuffaceous sandstone** f: dark grey, w:brown, medium sand-coarse sand, rounded, poorly sorted, matrix supported, F:quartz, plagioclase, hornblende, M:clay sized material, C:silica,parallel lamination
6,5	95	**95.Tuff,** f:grey, w:brown, fine sand, rounded, well sorted, grain supported, S:plagioclase, quartz, Fr:hornblende, stratified
102,8	94	**94.Tuff,** f:white, w:brown, silt, stratified
52,5	93	**93.Tuff,** f:light grey, w:brown, fine sand, rounded, well sorted, grain supported, S:plagioclase, hornblende, Fr:hornblende parallel lamination
19,2	92	**92.Tuff,** f:light grey, w:brown, fine sand, rounded, well sorted, grain supported, S:plagioclase, Fr:hornblende stratified
9,8	91	**91.Tuff,** f:white, w: brown, fine sand, subrounded, well sorted, grain supported, S:plagioclase, quartz, Fr:hornblende, T: lithic, parallel lamination
9,1	90	**90.Tuff,** f:dark grey, W:brown, fine sand, rounded, well sorted, grain supported, S:plagioclase,quartz, F:hornblende, stratified
40,5	89	**89.Tuff,** f:light grey, w:brown, silt, stratified
3,7	88	**88.Tuff,** f:white, w:brown, fine sand, rounded, well sorted, grain supported, S:plagioclase, Fr:hornblende, wavy lamination
35,4	87	**87.Tuff,** f:dark grey, w:brown, fine sand, subrounded, well sorted, grain supported, S:plagioclase, quartz, Fr:hoenblende, stratified
48,7	86	**86.Tuff,** f:light grey, w:brown, silt, convolute
7	85	**85.Tuff,** f:light brown, w: brown, fine sand, subrounded, well sorted, grain supported, S:quartz,plagioclase, Fr:hornblende, T:lithic stratified
5	84	**84.Tuff,** f:white,w:brown, silt, stratified
41,2	83	**83.Tuff,** f:white,w:brown, silt, stratified
34,5	82	**82.Tuff,** f:grey, w:brown, fine sand, rounded, well sorted, grain supported, S:plagioclase, quartz, Fr:hornblende, parallel lamination
5	81	**81.Tuff,** f:white, w:brown, fine sand, rounded, well sorted, grain supported, S:plagioclase, Fr:hornblende, stratified
2	80	**80.Tuff,** f:white, w:yellow browny, silt, parallel lamination
4,1	79	**79.Siltstone,** f:grey, w:brown, silt, stratified
32,6	78	**78.Tuff,** f:white, w:dark yellow, silt, parallel lamination
17,5	77	**77.Tuff,** f:grey, w: dark grey, fine sand, rounded, well sorted, grain supported, S:quartz, plagioclase, Fr:hornblende stratified
13,4	76	**76.Tuff,** f:grey, w:dark grey, fine sand, rounded, well sorted, grain supported, S:quartz, plagioclase, F:hornblende, stratified
68,6	75	**75. Tuffaceous sandstone,** f: grey, w:brown, medium-coarse sand, rounded, well sorted, grain supported, F:quartz, lithic, M:clay sized material, C:silica
10,9	74	**74.Tuff,** f:grey, w:brown, fine sand, rounded, well sorted, grain supported, S:quartaz, Fr: hornblenda stratified
13,6	73	**73.Tuff,** f:grey, w:brown,silt stratified
9,3	72	**72.Tuff,** f:grey, w:brown,silt stratified
7,8	71	**71.Tuff,** f:grey, w:dark grey,silt stratified
5,3	70	**70.Tuff,** f:light grey, w:brown, coarse sand, rounded, well sorted, grain supported, S:quartz,plagioclase, Fr:hornblende, Ta:lithic parallel lamination
15,1	69	**69.Tuff,** f:grey, w:brown, fine sand, subrounded, good supported, grain suported, S:plagioclase, Fr: hornblende stratified
11,2	68	**68.Tuff,** f:grey, w:brown, fine sand, rounded, well sorted, grain suported, S:plagioclase, Fr:hornblende, T:lithic, paralel lamination, sisipan pasir
26,3	67	**67.Tuff,** f:white, w:brown, silt, stratified
8,4	66	**66.Tuff,** f:light grey, w:brown, fine sand, rounded, well sorted, grain supported, S:plagiocase, Fr:hornblenda, T:lithic, stratified
5,5	65	**65.Tuff,** f:grey, w:brown, fine sand, subrounded, well sorted, grain supported, S:plagioclase, Fr:hornblende stratified
6,4	64	**64.Tuff,** f:brown grey, w:brown, fine sand, subrounded, well sorted, grain supported, S:plagioclase, Fr: hornblende. stratified
7,5	63	**63.Tuff,** f:grey, w:grey, fine sand, subrounded, well sorted, grain supported, S:plagioclase, Fr:hornblende, T:lithic. stratified
16,3	62	**62.Tuff,** f:grey, w:brown, silt, parallel lamination
2,8	61	**61.Tuff,** f:white, w: yellow brown, fine sand, subrounded, well sorted, grain supported, S:quartz,plagioclase, F:hornblende, T:lithic stratified
7,6	60	**60.Tuff,** f:grey, w:brown, fine sand, rounded, well sorted, grain supported, S:plagioclase, quartz, Fr:hornblene, stratified
20,4	59	**59.Tuff,** f:grey, w: dark brown, silt. parallel lamination
10,8	58	**58.Tuff,** f:grey, w:brown, fine sand, rounded, well sorted, grain supported, S:plagioclase, quartz, Stratified
11,6	57	**57.Tuff,** f:grey, w:brown, fine sand-lapilus, subrounded, poorly sorted, matrix supported, S:plagioklas, quartz, Fr=hornblende Stratified
330,3	56	**56.Sandstone,** f: grey, w:brown, subangular-angular, poorly sorted, matrix supported, fine-coarse sand, F=lithic, quartz, hornblende, M=clay sized material, C=silica, paralel lamination, gradded bedding, convolute
11	55	**55.Siltstone,** f:grey, w:brown, silt, C=silica, stratified, gradational contact
7	54	**54.Tuffaceous sandstone,** f:grey, w:brown, very fine-fine sand, C=silica,coal chip, lamination, gradational contact
66	53	**53.Siltstone,** f:grey, w:brown, silt, C=silica, stratified
32	52	**52.Tuffaceous sandstone,** f:grey, w:brown, very fine-fine sand, C=silica, paralel lamination
13	51	**51.Siltstone,** f:grey, w:brown, silt, C=silica, stratified
11	50	**50.Tuffaceous sandstone,** f:grey, w:yellow, fine sand-very fine sand, C=silica, stratified
16,2	49	**49.Tuff,** f:grey, w:brown, clay-silt, C=silica, gradational contact
23,1	48	**48.Sandstone,** f:grey, w:yellow, very fine-fine sand, C=silica lamination, gradational contact
109,2	47	**47.Tuff,** f:grey, w:black, clay-silt, C=silica, convolute, erosional contact
108,3	46	**46.Tuffaceous sandstone,** f:grey, w:yellow, fine-medium sand, subrounded-rounded, well sorted, grain supported, F=lithic, quartz, hornblend, M=clay sized material, C=silica, paralel lamination
57,1	45	**45.Siltstone,** f:grey, w:brown, silt, C=silica, gradational contact
81,6	44	**44.Sandstone,** f:grey, w:browny yellow, very fine sand-fine sand, subangular-subrounded, well sorted, grain supported, F=lithic, quartz, hornblende, plagioclase, M=clay sized material, C=silica coal chip, graded bedding, wavy lamination, gradational contact
136,5	43	**43.Tuff,** f:grey, w:yellow, clay-silt, C=silica, wavy lamination, convolute bedding, gradational contact
209,6	42	**42.Sandstone,** f:grey, w:browny yellow, very fine sand-fine sand, subangular-subrounded, wlell sorted, grain suported, F=lithic, quartz, hornblende, plagioclase, M=clay sized material, C=silica, gradational contact
84,17	41	**41.Sandstone,** fine-medium sand, f:white, w:yellow, subrounde-sub angular, F=lithic, quartz, plagioclase, hornblende, M=clay sized material, C=silica wavy lamination
51	40	**40.Clacareous sandstone,** f:putih, w:yellow. Fie sand-coarse sand, well sorted, grain supported, F=litic, hornblende, quartz, skeletal grain, M=very fine sand size material, C=carbonat ,stratified, erosional contact
503,7	39	**39.Sandstone,** f:white, w:dark grey, medium sand-very coarse sand, subangular-angular, poorly sorted, matrix supported, F=lithic, quartz, pumice, plaiokclas, M= fine sand, C=silica, paralel lamination
18,9	38	**38.Siderite**
179,46	37	**37.Gravely sandstone** , f:white, w:dark brown, medium sand-granule, poorly sorted, subangular-angular, matriks supported, F:lithic, quartz, plagioklas, M=fine sand sized material, C=silica, paaralel lamination
411,3	36	**36.Volcanic breccia** , f:white, w:yellow, coarse sand-cobble, poorly, angular, matrix supported, F=lithic, pumice, M=fine sand sized material, C=silica, reverse graded bedding
	35	**35. Interbedded Fine Sandstone - Medium Sandstone** **Sandstone,** f:grey, medium sand, angular, poorly, closed, F=quartz, C=silica, stratified **Sandstone,** f:grey, fine sand, angular, poorly, closed, F=quartz, C=silica, stratified
25	34	**34. Sandstone,** f:grey, medium sand, angular, poorly, closed, F=quartz, C=silica, Stratified
77	33	**33. Tuff,** f:grey, silt, MS=quartz, stratified
17	32	**32. Lapilush sandstone,** f:grey, silt-medium sand, angular, poorly, closed F=lapili,Quartz,C=silica, stratified
	31	**31. Lapilush sandstone,** f:grey, silt-medium sand, angular, poorly, closed F=lapili,Quartz,C=silica, stratified
	30	**30. Interbedded Fine Sandstone - Medium Sandstone** **Sandstone,** f:grey, fine sand, angular, poorly, closed, F=hornblende,lapili,Quartz, C=silica, Stratified **Sandstone,** f:grey, medium sand, angular, poorly, closed, F=quartz,Hornblende, C=silica, Stratified
	29	**29. Interbedded Fine Sandstone - Medium Sandstone** **Sandstone,** f:light brown, fine sand, angular, poorly, closed, F=quartz, C=silica, Stratified **Sandstone,** f:brown, medium sand, angular, poorly, closed, Stratified
	28	**28. Sandstone,** f:brown, medium sand, angular, poorly, closed, F=hornblende, Stratified
	27	**27. Sandstone,** f:lightbrown, fine sand, angular,poorly, closed, C=silica, Stratified
	26	**26. Sandstone,** f:grey, medium sand, angular, poorly, close, F=coal, Stratified.
	25	**25.Interbedded Sandstone-Siltstone, Sandstone,** f:grey, fine sand, angular, poorly, closed, F=quartz, C=silica, Stratified. Siltstone, **Siltstone,** f:grey, silt, C=silica, Stratified
29	24	**24. Lapilush sandstone,** f:light brown, very fine-medium sand, angular, poorly, close, F=lapili,coal; C=silica, Stratified
24	23	**23. Sandstone,** f:brown, medium sand, angular,poorly, closed, F=coal, stratified
16	22	**22. Sandstone,** f: grey, fine sand, angular, poorly, close, F=coal, stratified
8	21	**21. Tuffaceous Sandstone,** f:grey, medium sand, angular, poorly close, M=silt, M=clay sized, C=silica, Stratified
69	20	**20. Tuff,** silt,Ms=quartz, Lamination, Graded Bedding
133	19	**19. Lapilush sandstone,** f:grey, very fine-medium sand, angular, poorly, close, F=lithic, lapili,Quartz; C=silica, Stratified
16	18	**18. Sandstone,**f: brown, fine-medium sand,angular, poor, close, F=quartz, C=silica, Stratified
7	17	**17. Claystone,** f:black, clay, C=silica
132	16	**16. Lapilush sandstone,** f:grey, silt-fine sand, angular, poorly, grain, F=lapili,pyroxene,; M:clay sized; C=silica, Massive
	15	**15.Interbedded Siltstone-Lapilush Sandstone** **Siltstone,** f:grey, silt, F=hornblende,Quartz; C=silica, Stratified **Lapilush sandstone,** f:brown, silt-fine sand, angular, poorly, grain, F=lapili,Quartz,Plagioclase M:clay sized; C=silica, Stratified
38	14	**14. Calcareous sandstone,** f:grey, medium sand, angular, poorly, close, F=lapili,coal; M=clay sized; C=catbonate, Stratified
	13	**13.Interbedded Sandstone-Siltstone, Sandstone,** f:grey, fine-coarse sand, angular, poor, grain, F=lapili, coal,Pyroxene,Plagioclase; M=clay sized; C=silicate, Stratified. **Siltstone,** f:grey, silt, - F=hornblende,Quartz; C=silica, Stratified
95	12	**12. Sandstone,** f:grey, fine-coarse sand, angular, poor, grain, F=lapili, coal,Pyroxene,Plagioclase; M=clay sized; C=silica, Stratified
5	11	**11. Lapilush sandstone,** f:brown, silt-fine sand, angular, poorly, grain, F=lapili,Quartz,Plagioclase,; M=clay sized; C=silica, Stratified
42	10	**10. Siltstone,** f:grey, silt, F=lapili, Hornblende,Quartz; M=clay sized; C=silica, Stratified
11	9	**9. Lapilush sandstone,** f:grey, silt-fine sand, angular, grain, F=lapili,Quartz,coal; M=clay sized. C=silica, Stratified
21	7	**8. Lapilush sandstone,** f:grey, silt-fine sand, angular, grain, F=lapili,Quartz,coal; M=clay sized. C=silica, Stratified
	7	**7. Lapilush sandstone,** f:light brown, silt-fine sand, angular, grain, F=lapili,Quartz, M=clay sized. C=silica, Stratified
15	6	**6. Interbedded Siltstone-Sandstone** **Siltstone,** f:dark grey, silt, F=hornblende,Quartz, C= silica, Stratified **Sandstone,** f:yellow, medium sand, angular, grain, poorly, F=quartz, Plagioclase; M=clay sized;S=silica, Stratified
66	5	**5. Lapilush sandstone,** f:white, fine sand-silt, angular, grain, F=quartz ,lapili;M=clay sized; C=silica, Stratified
16	4	**4. Sandstone,** f:brown, fine sand, angular, poorly, grain, F=quartz,M=clay sized, C=silica, Stratified
	3	**3. Interbedded Siltstone-Sandstone** **Siltstone,** f:grey, silt, F=hornblende,Quartz; C=silica, Stratified **Sandstone,** f:grey, fine-medium, angular, poorly, grain, F=quartz,Hornblende; M=clay sized, C=silica, Stratified
14	2	**2. Lapilush Sandstone** f:white, fine sand-silt, angular, grain, F=quartz ,lapili;M=clay sized; C=silica, Stratified
38	1	**1. Siltstone,** f:grey, silt, F=hornblende,Quartz; C=silica, Stratified

FACIES (Walker, 1984) / DEPOSITIONAL ENVIRONMENT (Walker, 1984):
- Classical Turbidite (CT) — Smooth Portion of Suprafan Lobes-Mid Fan
- Massive Sandstone (MS) — Smooth Suprafan Lobes-Mid Fan
- Classical Turbidite (CT) — Smooth to Chaneneled Suprafan Lobes-Mid Fan

Attachment 3. Station 3-1 Profile

DEPARTMENT OF GEOLOGICAL ENGINEERING
FACULTY OF MINERAL TECHNOLOGY
UNIVERSITY OF NATIONAL DEVELOPMENT "VETERAN' YOGYAKARTA
2021

MEASURED STRATIGRAPHIC SECTION

LOCATION : Ngoro-oro Area, District Pathuk, Gunungkidul Regency, Indonesia
LINE : Station 3, Location 2
FORMATION : Semilir Formation
SCALE : 1 : 20

DATE	MEASURED AND DESPICTED BY
10 September 2021	Ameliorate Team

SEDIMENTARY STRUCTURE: Massive/Stratified; Paralel Lamination; Convolute; Coal scratch; Graded bedding

LITHOLOGY: Sandstone; Tuff-Volcanic Clast; Claystone

BED BOUNDARY: Contrast

LEGENDS
f :fresh
w :weathered
F :fragmen
M :matrix
C :cement
S :sialis mineral
Fr :feromagnesian mineral
Ta :other mineral

FORMATION: SEMILIR FORMATION

THICKNESS (cm)	BED	DESCRIPTION
	35	**35. Tuff,** f:grey, w:dark brown, medium sand, angular, well sorted, grain supported, S:Quartz, F:Hornblende, A:ash, Massive.
56	35	**34. Tuffaceous Sandtone,** f:grey, w:brown, fine sand, rounded, well sorted, grain supported, F:Quartz, tuff, M:clay sized, C:Silica, Massive.
3	34	**33. Tuff,** f:grey, w:dark brown, medium sand, angular, well sorted, matrix supported, S:Quartz, F:Hornblende, A:ash, Massive, coal chip.
41	33	**32. Coaly Sandtone,** f:grey, w:dark brown, fine sand, rounded, well sorted, grain supported, F:Quartz, tuff, M:clay sized, C:Silica, Massive, coal chip.
17.3	32	**31. Tuff,** f:grey, w:dark brown, medium sand, angular, well sorted, matrix supported, S:Quartz, F:Hornblende, A:ash, Massive.
11.6	31	**30. Tuff,** f:grey, w:dark brown, silt, rounded, well sorted, matrix supported, S:Quartz, F:Hornblende, Stratified.
14.9	30	**29. Tuff,** f:grey, w:dark brown, medium sand, angular, well sorted, grain supported, S:Quartz, F:Hornblende, A:silt, Massive.
8.6	29	**28. Tuff,** f:grey, w:dark brown, silt, rounded, well sorted, matrix supported, S:Quartz, F:Hornblende, Stratified.
27.9	28	**27. Tuff,** f:grey, w:dark brown, silt, medium sand, rounded, poorly sorted, matrix supported, S:Quartz, F:Hornblende, A:Lithic, Graded bedding,coal chip, coal scratch
261.12	27	**26. Tuff,** f:grey, w:dark brown, silt, rounded, well sorted, matrix supported, S:Quartz, F:Hornblende, Massive.
		25. Claystone, f:black, w:dark brown, clay, F:clay sized material, Stratified.
		24. Tuff, f:grey, w:dark brown, silt, rounded, well sorted, matrix supported, S:Quartz, F:Hornblende, Massive.
		23. Tuffaceous Sandtone, f:grey, w:dark brown, very fine-fine sand, rounded, well sorted, grain supported, F:Quartz, tuff, M:clay sized, C:Silica, Lamination, coal chip, coal scratch.
		22. Tuff, f:grey, w:dark brown, silt, rounded, well sorted, matrix supported, S:Quartz, F:Hornblende, Massive, coal chip.
		21. Tuff, f:grey, w:dark brown, silt, rounded, well sorted, matrix supported, S:Quartz, F:Hornblende, Convolute, coal chip.
19.6	26	**20. Tuffaceous sandstone,** f:grey, w:brown, fine-medium, poorly sorted, matrix supported, sub rounded, F=ash,quartz,M=clay sized material,C=silica lamination, coal chip
5.2	25	
38.3	24	**19. Sandy Tuff,** f:grey, w:dark brown, medium sand, angular, poorly sorted, grain supported, S:Quartz, F:Hornblende, A:Lithic, Convolute stratified.
16.6	23	**18. Tuff,** f:grey, w:dark brown, silt, rounded, well sorted, matrix supported, S:Quartz, F:Hornblende, Convolute stratified.
17.8	22	**17. Claystone,** f:black, w:dark brown, clay, F:clay sized material, Massive.
22.5	21	**16. Tuff,** f:grey, w:dark brown, silt, rounded, well sorted, matrix supported, S:Quartz, F:Hornblende, Massive.
31.6	20	**15. Claystone,** f:black, w:dark brown, clay, F:clay sized material, Massive.
16.4	19	**14. Tuff,** f:grey, w:dark brown, silt, rounded, well sorted, matrix supported, S:Quartz,F:Hornblende, Convolute lamination.
31.2	18	**13. Sandy Tuff,** f:grey, w:dark brown, medium sand, angular, poorly sorted, grain supported, S:Quartz, F:Hornblende, A:Lithic, Convolute lamination.
3.5	17	
9.4	16	
2.7	15	**12. Tuff,** f:grey, w:dark brown, silt, rounded, well sorted, matrix supported, S:Quartz, F:Hornblende, Stratified.
74.3	14	**11. Tuff,** f:grey, w:dark brown, medium sand, angular, well sorted, matrix supported, S:Quartz, F:Hornblende, A:ash, Stratified.
		10. Claystone, f:black, w:dark brown, clay, F:clay sized material, Massive.
		9. Tuff, f:grey, w:dark brown, silt, rounded, well sorted, matrix supported, S:Quartz, F:Hornblende, Stratified.
32.3	13	**8. Tuff,** f:grey, w:dark brown, medium sand, angular, poorly sorted, matrix supported, S:Quartz, F:Hornblende, A:ash, Stratified, coal chip, coal scratch.
54.5	12	**7. Sandy Tuff,** f:grey, w:dark brown, medium sand, angular, poorly sorted, grain supported, S:Quartz, F:Hornblende, A:Lithic, Massive.
		6. Tuff, f:grey, w:dark brown, silt, rounded, well sorted, matrix supported, S:Quartz, F:Hornblende, Massive.
25.8	11	**5. Tuffaceous Sandtone,** f:grey, w:dark brown, very fine-fine sand, rounded, well sorted, grain supported, F:Quartz, tuff, M:clay sized, C:Silica, Lamination, coal chip.
9.5	10	
9.8	9	
18.2	8	**4. Claystone,** f:black, w:dark brown, clay, F:clay sized material, Stratified.
4.2	7	**3. Tuff,** f:grey, w:dark brown, medium sand, angular, poorly sorted, matrix supported, S:Quartz, F:Hornblende, A:ash, Stratified.
26	6	
2.1	5	
1.8	4	**2. Tuff,** f:grey, w:dark brown, silt, rounded, well sorted, matrix supported, S : Quartz, F:Hornblende, Stratified.
13.7	3	
11.3	2	
16.8	1	**1. Tuff,** f:grey, w:brown, medium sand, grain supported, well sorted, M:Quartz, F:Hornblende, ash, stratified, coal chip

FACIES (Walker, 1984): Classical Turbidite (CT)
DEPOSITIONAL ENVIRONMENT (Walker, 1984): Lower Fan

Attachment 4. Station 3-2 Profile

PROCEEDINGS
JOINT CONVENTION BANDUNG (JCB) 2021
November 23rd – 25th 2021

Study of the History of Mount Patiayam, Central Java, Based on the Stratigraphy of Volcanic Rocks

Widyawan N. Muhammad[1], Almira R. R. Ayu[1], Kamila N. Izzah[1], Dewi S. Reka[1], Agus Hendratno[1]
[1]Geological Engineering Department, Engineering Faculty, Universitas Gadjah Mada

Abstract

The Muria Peninsula is an area with an interesting geological history. This area was once separated from Java Island by the Muria Strait to form Muria Island until it was finally connected to Java Island due to the sedimentation process forming the Muria Peninsula. The research area is located on Mount Patiayam on the Muria Peninsula together with the Mount Muria complex, Mount Genuk, and several maars around Mount Muria such as Maar Bambang, Maar Gunungrowo, and Maar Gembong. The Mount Muria complex has a fairly complex geological history, so the area around Mount Muria is an important and interesting part to explore. The study was conducted in the central and eastern parts of Mount Patiayam with an area of 40 km^2. The method used is the surface geological mapping method. This includes observing based on the topographic appearance of the mapping area, there are three geomorphological units, namely a volcanic cone unit, a pyroclastic flow fan unit, and a volcanic foot plain unit. The distribution of lithology at the study site shows that the stratigraphic sequence of the mapping locations from old to young is marl units that are not older than the Middle Miocene, Patiayam tuffaceous sandstones of Pliocene-Pleistocene age, Patiayam pyroclastic breccia units, Patiayam tuff units, Patiayam tuff lapilli units, lava units Patiayam, then in the northeastern part of the Muria tuffaceous sandstone unit, and finally, Muria pyroclastic deposits, which stratigraphically cover the volcanic rocks of Patiayam and Muria tuffaceous sandstones. The results of paleontological analysis of marlstones show that the deposition began in a shallow marine environment that progressed to a lagoon-restricted marine environment, until it turned into a terrestrial environment at the Pleistocene age, reinforced by the discovery of Stegodon fossils in the Patiayam tuffaceous sandstone unit. This study will strengthen the study of the Muria strait that separated Mount Muria and the island of Java in the past.

Keywords: Muria Strait, Pati, Patiayam, stratigraphy, volcanic rock

Introduction

The Muria Peninsula is an area with an interesting complex geological history. Muria Peninsula located in the north of Java Island located in Kudus and Pati Regency, Central Java. A lot of research is published about this location, it shows that the research of the Java Island is still an interesting topic among researchers. The existence of a mountain on Java Island, as well as the content and characteristics of its magma, will provide information about the formation of Java Island. The Mount Muria complex and its surroundings are a one-of-a-kind feature that is still worth exploring. Mount Muria is a mountain that was once separated from Java Island; however, due to continuous sedimentation, Mount Muria and Java Island merged to form the single entity we see today. Mount Patiayam, which is part of the Mount Muria complex and thus is located on the south flanks of Mount Muria, is a mountain that has not been the focus of much research. In general, research only focuses on the portion of Mount Muria that has been explored for its characteristics as a large complex. Many things need to be explored in the stratigraphy of rocks found on Mount Patiayam in order to add to the repertoire of knowledge about stories and evidence regarding the existence of Mount Muria, which was previously separated from Java.

Soekmono (1967) stated that Muria Peninsula, where Mount Patiayam is located, was an island separated from Java. Intense sedimentation has closed this strait, forming an alluvial plain stretched from Pati in the east to Demak in the west. Zaim and Delaune (1990) stated that Mount Patiayam was a stand-alone volcanic system, not a parasitic cone of Mount Muria. Mulyaningsih et al. (2009) confirmed what Zaim and Delaune (1990) have said by comparing the composition of volcanic rocks of Mount Patiayam with Mount Muria and Lasem. The result is that rocks from Mount Patiayam are more similar to volcanic rocks from Mount Lasem than Muria, but because Mount Muria and Lasem are 60 km apart, volcanic rocks found on Mount Patiayam are its own volcanic product.

Telling about the mechanism of the formation of a present-day landscape that we can observe can increase knowledge and strengthen previous opinions. This tracing and verification action will be beneficial for the mitigation of possible disasters that occur because the present is the key to the past.

Data and Method

Data and methods used in this research are:

a. Field mapping

This method aims to identify the outcrops, take the rock samples, and measure the stratigraphy observed on the field. The data acquired in this method are used for making a geological map.

b. Laboratory analysis

Petrographic and paleontological analysis is conducted to determine the mineral of rocks found on Mount Patiayam, and to determine the deposition

environment and relative age of the rocks found on Mount Patiayam. Petrographic and micropaleontologic analyses of the samples were carried out at the Geological Engineering Department of Universitas Gadjah Mada. Petrographic analysis was conducted on 11 thin section samples that represent all of the rock units found in the study area, and the paleontologic analysis was conducted on the rocks found in the marl unit.

Result and Discussion

Based on the data observed from the field, there are seven rock units observed in the field, as follows, from oldest to youngest: marl unit, Patiayam tuffaceous sandstone unit laying unconformably over the marl unit, pyroclastic breccia unit, Patiayam tuff unit, Patiayam tuff lapilli unit, Patiayam lava unit, then in the northeastern part of the Patiayam Mountain deposited Muria tuffaceous sandstone unit overlaying Patiayam units, and finally Muria pyroclastic deposits. The geological map of the Patiayam area is shown in Figure 1.

The oldest rock unit found in the study area is the marl unit composed of black claystone and marl. This unit is only observed along the Gondoharum river valley. The composition of this lithology is clay-sized siliciclastic material and apparently organic material that causes the lithology color to be black, indicating that the rock was deposited in a reductive environment. This could be an indication that the environment of the Patiayam area before volcanism is a transitional environment, probably a reductive marshy environment.

Overlying the black claystone, marl has been deposited too. Paleontological analysis performed on the marl sample revealed a fossil species of foraminifera dominated by benthic foraminifera, which provides early clues that the rock was deposited in a shallow marine environment. The benthic foraminifera species encountered were *Quinqueloculina* sp., *Cibicides praecinctus*, and *Elphidium* sp. which indicates that the rock was deposited in a restricted marine – lagoon shallow marine environment. This reinforces the hypothesis that the Patiayam area was a shallow marine – transitional environment that could constitute a narrow strait, akin to Muria Strait in the 8th -15th century (Rajiyowiryono and Sutawidjaja, 2010). This could mean that before the last appearance of Muria Strait, there have been at least an older Muria Strait, indicated by lithology found on the proximity of Patiayam Mount. Also found is benthic foraminifera *Bathysiphon* sp. which characterizes a deep-sea environment, but it is interpreted that this species is the result of a reworking or upwelling process so that it is mixed with other fossils. Meanwhile, the only planktonic foraminifera species found was *Globigerinoides immaturus*, which characterizes the N8-N23 age range (Bolli and Saunders, 1985), that is early Miocene – present age. Because the age range is too wide to determine the relative age, it is determined that the age of this rock formation is no older than N8 zone. Some microfossils found on this rock unit are shown on Figure 3.

Above the marl unit, there is a tuffaceous sandstone unit, which unconformably overlain the marl unit. The contact between the two of them is shown in Figure 2, in which we could see the erosional contact denoted by a red dashed line. This unit has a parallel bedding, cross-bedding, and normal graded structure which indicates that the depositional process is traction, with a flow regime that can form parallel and cross-beds. It is possibly deposited by streamflow, indicated by good sorting and imbrication structures that were visible at coarser grain sizes. Another texture such as scouring is visible too. The composition of this lithology is andesite, tuff, pumice, and feldspar fragments, as well as plagioclase, hornblende, pyroxene, and opaque mineral fragments which shows that the origin of the grains is a volcanism process. Pyroclastic rocks such as tuff and pumice fragments were deposited as primary volcanic deposits, then it was transported and deposited, probably deposited on the early Muria Strait on distal Patiayam volcanic facies. Other than tuffaceous sandstone, this unit is intercalated by tuff, which gradually thickens upward. Stegodon trigonocephalus has been found on this unit, indicating that the relative age of this rock unit is Pleistocene epoch.

In some places, overlaying the tuffaceous sandstone unit is a massive breccia unit which is denoted by the dominant presence of volcanic andesite breccia, with massive, normal-graded, scouring, and parallel bedding structures, probably deposited on a flow regime, such as lahar flow. On some fragments, many leucite phenocrysts can be observed.

Tuff unit is found overlaying breccia and tuffaceous sandstone units. This rock unit has a parallel bedding structure, sometimes massive. The rock was formed by pyroclastic fall, characterized by uniform grain size, and the presence of layering indicates several eruption episodes that produce ash that lithified into tuff. In some places, there are massive tuff outcrops that are about 2 meters thick, indicating a large-scale eruption, but some outcrops only show a layer of tuff as thick as 15 cm, which indicates a more weak eruption. The composition of this lithology is lithic fragments of igneous rock, hornblende, plagioclase, and clinopyroxene. On the center of the Patiayam Mountain, the lithology is dominated by the lapilli tuff unit, which has a massive to parallel bedding structure. This unit is stratigraphically younger than the tuff unit. Tuff and lapilli tuff are the main primary volcanic rocks of Patiayam, besides andesitic lava, probably closing the early Muria Strait even further by its primary volcanic products.

The youngest unit of Patiayam volcanic units is the andesite lava unit. The composition of this lithology is plagioclase which is dominated by andesine and labradorite, giving us a clue that the rock composition is richer in Ca elements and tends to be intermediate-

mafic Other than plagioclase, there are hornblende, pyroxene, chlorite as a pseudomorph, and opaque minerals. In some places, autoclastic breccia structures are sometimes found which have been sufficiently weathered, thus making identification difficult in the field. The vesicular structure of scoria is commonly found, which indicates that magma tends to contain a lot of volatile material which causes the formation of vesicles.

The Muria tuffaceous sandstone is pretty similar to Patiayam tuffaceous sandstone, except there are no vertebrate fossils found. Muria pyroclastic sediments consisted of largely unconsolidated ash to bomb sized grains. A resume of petrographic composition analyzed is shown on Table 1.

The inferred geological history of Mount Patiayam is started with a swamp/restricted marine environment thriving in the vicinity of the pre-volcanism Patiayam area, indicated by marl and black claystone. Patiayam volcanism did begin later, on the distal facies of the volcano deposited tuffaceous sandstone and laharic breccia, probably deposited on the early Muria Strait by fluvial processes, making the strait narrower. Patiayam volcanism intensifies over time, producing pyroclastic rocks like tuff, lapilli tuff, and andesite lava. Then Muria volcanism started, either concurrent with or after Patiayam volcanism deposited its volcanic products as Muria tuffaceous sandstone and pyroclastic deposits. Then, the mountains are eroded, exposing underlying rocks. There is also deposition of silty-clayey alluvial deposits as a product of sedimentation that closed the late Muria Strait. The visualization of the geological history is shown on Figure 4.

Conclusions

There are 7 rock units found on Mount Patiayam, from oldest to youngest: marl, Patiayam tuffaceous sandstone, Patiayam volcanic breccia, Patiayam tuff, Patiayam lapilli tuff, Patiayam lava, Muria tuffaceous sandstone, and Muria pyroclastic deposits. Based on the micropalaeontological analysis, the oldest rock is no older than N8, equal to the early Miocene. The discovery of black claystone and marl indicates that the vicinity of pre-volcanism Mount Patiayam was a reductive marshy environment - shallow sea that could constitute a narrow strait akin to Muria Strait in the 8th-15th century CE.

References

Bolli, H., Saunders, J. B., 1985, Plankton Stratigraphy, Cambridge, 155-262.

Mulyaningsih, S., Bronto, S., Kusnaedi, A., Simon, I., Prasetyanto, I. W., 2014, Indonesian Journal on Geoscience, **3**, 75–88,.

Rajiyowiryono, H. and Sutawidjaja, I. S., 2010, Majalah Geologi Indonesia **25**, 73-81.

Soekmono, R., 1967, Indonesia, **4**, 2-7

Zaim, Y., Delaune, M., 1990. Géodynamique, **5**, 135-150

PROCEEDINGS
JOINT CONVENTION BANDUNG (JCB) 2021
November 23rd – 25th 2021

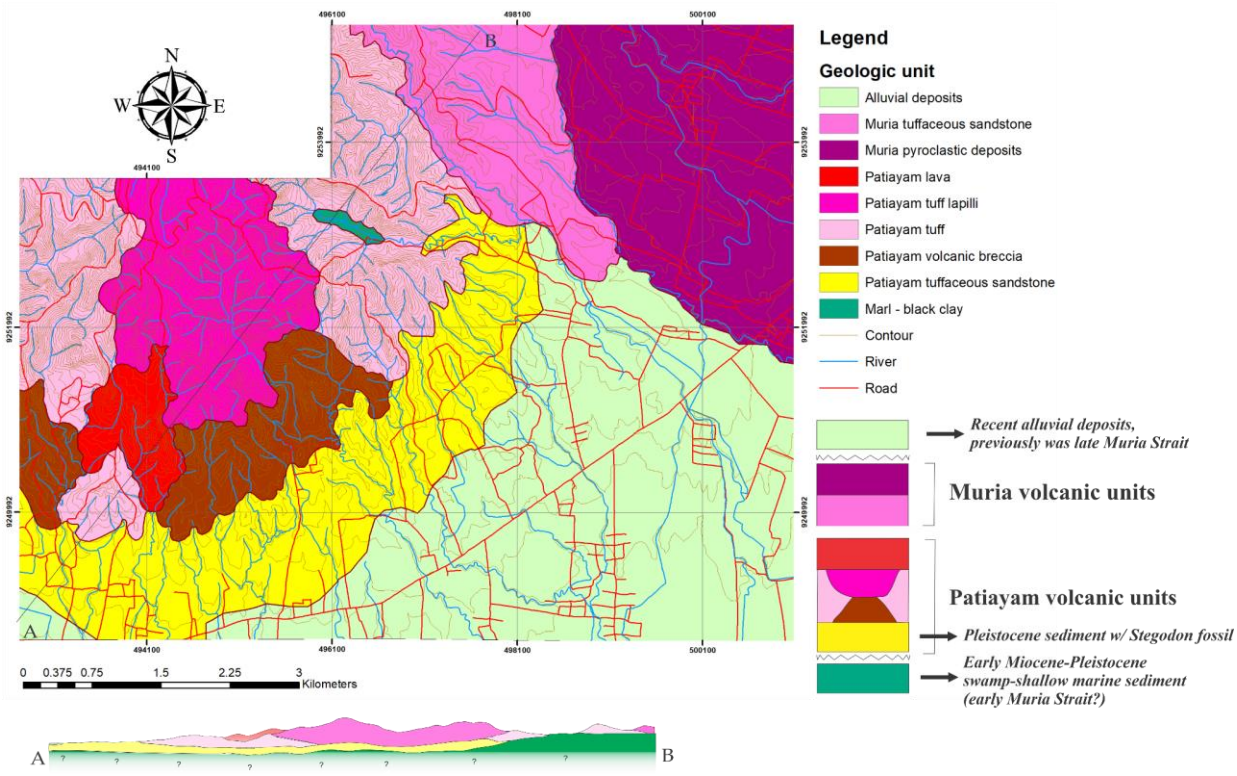

Figure 1. Geological map of the study area

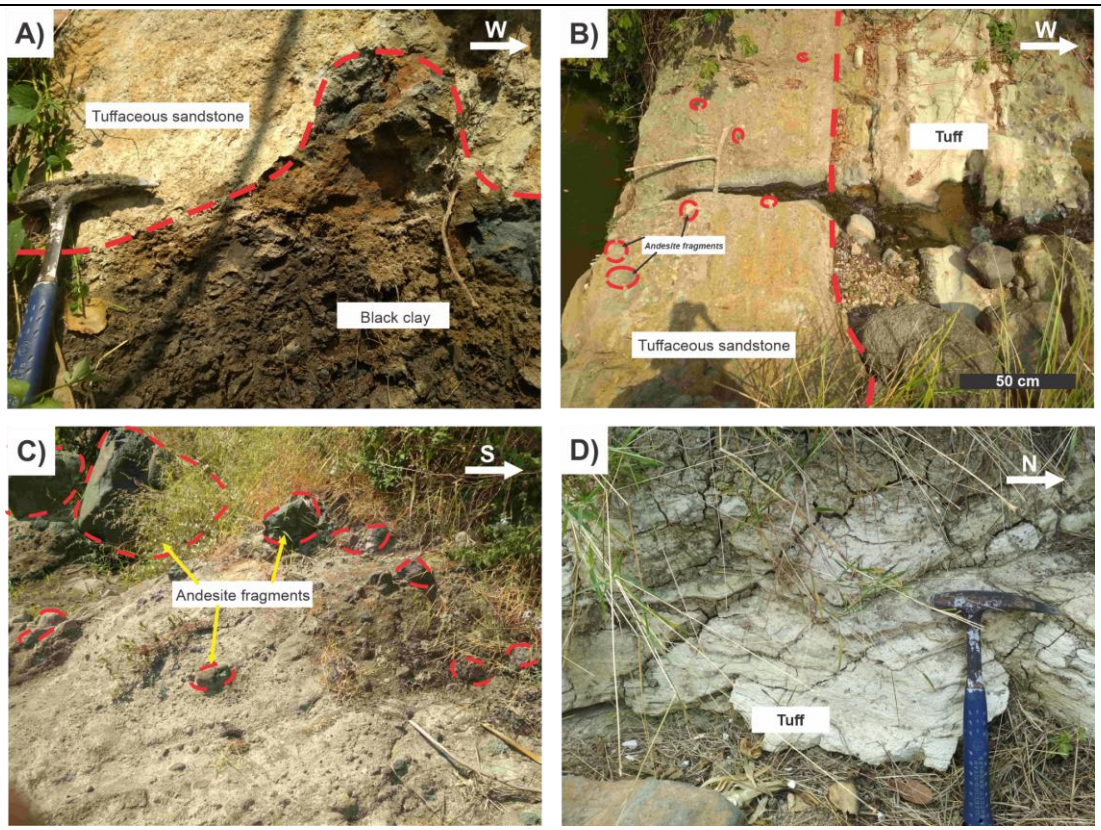

Figure 2. A.) Contact between black claystone (below) and tuffaceous sandstone (above) B.) Outcrop showing contact between tuffaceous sandstone and tuff that exhibits planar bedding C.) Outcrop showing andesite breccia with andesite fragments denoted by dashed red lines D.) Patiayam tuff outcrop.

PROCEEDINGS
JOINT CONVENTION BANDUNG (JCB) 2021
November 23rd – 25th 2021

STA	Lithology	Sample code	Mineral assemblage										
			Pl	Px	Hb	Opq	Hem	Chl	Qz	Leu	Clay	Fossils	Glass frag.
1	Patiayam breccia	WNM-07	○	□	□	△	△	△	-	□	△	-	-
2	Patiayam breccia	WNM 52	○	□	-	△	△	△	-	-	△	-	-
3	Patiayam lava	WNM-103A	○	△	□	△	□	□	-	-	-	-	-
4	Patiayam lava	WNM-103B	○	□	△	△	△	△	-	-	-	-	-
5	Patiayam lava	WNM-109A	○	□	-	△	△	△	-	-	-	-	-
6	Patiayam lava	WNM-109B	○	□	□	△	△	△	-	-	-	-	-
7	Patiayam tuff	WNM-179	○	△	-	△	△	□	-	-	□	-	□
9	Patiayam tuffaceous sandstone	WNM-86B	○	□	-	△	△	△	-	-	△	-	△
10	Tuff	WNM-86A	○	□	-	△	△	△	-	-	△	-	□
11	Marl	WNM-132	□	□	-	□	-	-	□	-	-	△	-
12	Breccia	WNM-93	○	□	□	-	△	△	-	-	-	-	-
13	Muria tuffaceous sandstone	ARRA-06	□	□	△	△	△	-	△	-	○	-	△
14	Muria tuffaceous sandstone	ARRA-39	○	□	□	△	-	△	-	-	-	-	△

- Not present
△ Few (1-10%)
□ Moderate (10-30%)
○ Many (30-50%)
⦿ Abundant (>50%)

Pl = Plagioclase; Px = Pyroxene; Hb = Hornblende; Opq = Opaque; Hem = Hematite; Chl = Chlorite; Qz = Quartz; Leu = Leucite

Table 1. A resume of petrographic analysis of samples studied.

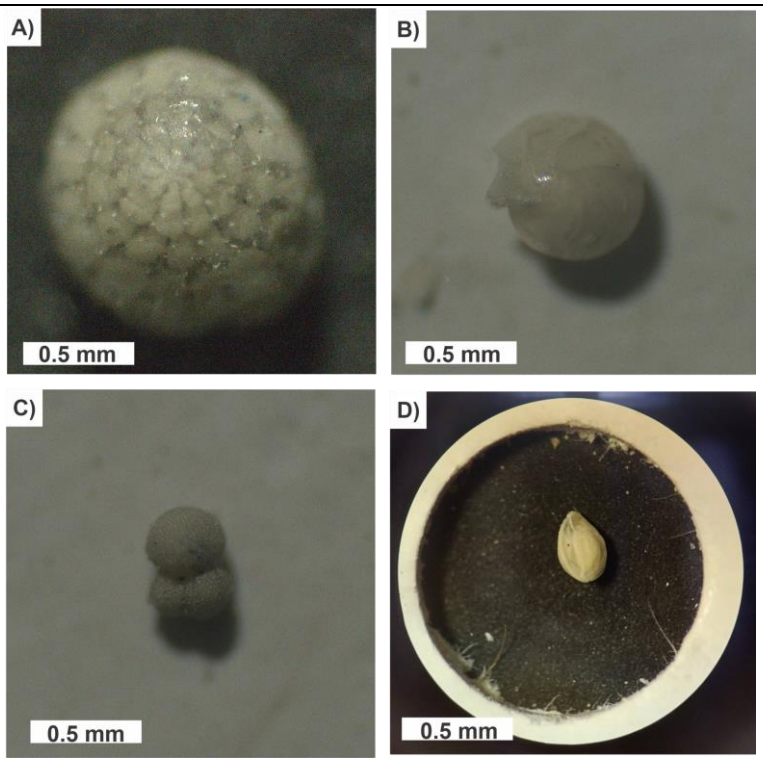

Figure 3. Microfossils found on marl sample. A.) *Rotalinoides compressiusculus* B.) *Cibicides* sp. C.) *Globigerinoides immaturus* D.) *Quinqueloculina seminula*.

PROCEEDINGS
JOINT CONVENTION BANDUNG (JCB) 2021
November 23rd – 25th 2021

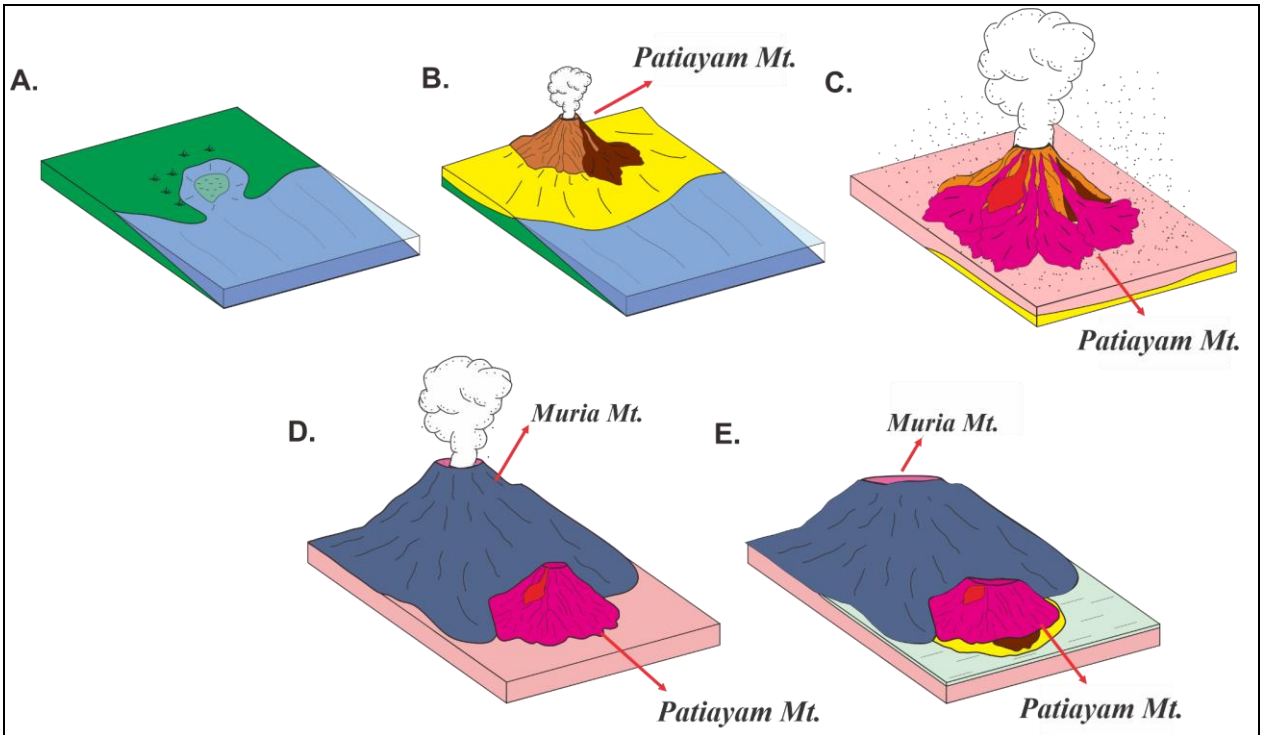

Figure 4. A.) A lagoon/restricted marine environment is thriving in the vicinity of the pre-volcanism Patiayam area indicated by marl and black claystone. B.) Patiayam volcanism has started, on the distal facies of the volcano has deposited tuffaceous sandstone and laharic breccia. C.) Patiayam volcanism intensifies, producing pyroclastics e.g. tuff and lapilli tuff, and andesite lava. D.) Muria volcanism started, deposited its volcanic products e.g. Muria tuffaceous sandstone and tuff. E.) The mountains are eroded, exposing underlying rocks. There is also deposition of silty-clayey alluvial deposits.

PROCEEDINGS
JOINT CONVENTION BANDUNG (JCB) 2021
November 23rd – 25th 2021

Integrated Study of Hydrocarbon Reservoir Potential in Halang Formation, South Serayu Basin

Amsal Frans Harapenta Surbakti[1,2], Selvia Maharani Kusuma[1,2], Zuhaida Jasmine Zahari[2]
[1] *Geological Engineering, Sriwiijaya University, Palembang*
[2] *Bumi Sriwijaya Research Group, Palembang.*

Abstract
Tectonic complexity and its implications for the potential of hydrocarbons in Southern Java are still challenging in exploration activities, specifically in oil and gas carrier formation. The Halang Formation in Purworejo, Central Java, part of the South Serayu Basin, is recently the oil and gas exploration target. The study is conducted to identify the potential for a hydrocarbon reservoir at the Halang Formation to supply the community's energy needs. The research develops with literature study, measuring section (MS), turbidite facies analysis formed biostratigraphy, rock porosity observation on thin sections, and calculate the porosity values.
The Halang Formation is a marine deposit in the Outer Neritic to Lower Bathyal zone with characteristic turbidite sequence series from Late Miocene to Early Pliocene. The association of turbidite facies expresses various detailed depositional processes for interpreting the submarine fan environment; thus, it is a good approximation for analyzing potential hydrocarbon reservoirs. Based on outcrop investigations, the facies in the study area classify into the Upper fan to the Lower fan. The facies are part of the submarine fan system with a proximal channel depositional environment on the inner fan to the distal inner fan channel fan levee. The characteristics of the facies are coarse fraction deposits such as breccia, conglomerate, sandstone, and sandy silt. Constructed on petrographic observations, the lithology of sandstone (sublitharenite and feldspathic arenite) and claystone. The porosity obtained is intergranular porosity with an average calculation of 15.6% - 21.5% with a good to outstanding classification. Hopefully, the study can become a new alternative to become a reservoir in oil and gas exploration in South Serayu Basin.

Introduction
Middle Java is constructed by two main basins: North Serayu Basin and South Serayu Basin. Oil and gas exploration in the Northern Middle Java in the North Serayu Basin, known as terra-incognita, is indicated by oil seepage on the surface (Satyana, 2007). In contrast to the North Serayu basin, the South Serayu Basin has minimal exploration tendencies. The South Serayu basin is composed of sedimentary material that spreads relatively east-west which develops from the upstream of the Bigowoto River to the eastern part of the Citaduy River with morphological variations (Husein et al., 2013). Physiographically, from the northeast to west, this basin is bounded by the Kulon Progo Mountains and the valley formed by the Cawung river (Figure 1). The South Serayu Basin is split into two areas separated by the Jatilawang Plain and geometrically forms a left-stepping en echelon which indicates a sinistral strike-slip fault with an east-west orientation (Van Bemmelen, 1949; Husein et al., 2013).

According to Hall (2012), based on the geological condition, the South Serayu basin has Paleogene Totogan formation after the Sundaland and East Java micro-continent collision and formed by submarine gravitational process become the polymict fragment with clay matrix as well as exposed pre-tertiary rocks in Karangsambung. In the Late Oligocene, volcanic material was deposited to discover a volcanic arc and a rifting process in the North Serayu Basin (Hall, 2012). Middle Miocene, there was a decrease in volcanic activity due to counter-clockwise rotation in Sundaland. In Late Miocene, there was the reactivation of volcanic activity in the South and North Serayu basins. Generally, reactivation resulted in the deposition of Halang Formation sandstones that spanned the study concern.

The Halang Formation consists of alternating rock units of sandstone and calcareous sandstone accompanied by alternating claystone, marl, tuff, and breccias deposited in the Middle Miocene to Late Miocene to Late Miocene to (Asikin, 1992; Van Bemmelen and Lunt, 1999) (Figure 2). Astuti (2013) discusses that the Halang Formation forms an upward stacking pattern that describes its deposition's progradation process. Halang Formation in Husein et al. (2013) referred to as reservoir rock in the petroleum system in the North Serayu Basin with hydrocarbon traps in the form of anticline and rhyme faults. Satyana (2007) states that the petroleum system phenomenon follows the toe-thrusting concept associated with Neogene lifting. Various facts, existing research, and evidence in the field survey interest in discussing oil and gas exploration in the South Serayu Basin in Purworejo, Central Java.

Data and Method
Analysis is conducted with state of the art, field survey, petrography analysis, facies interpretation, and stratigraphy modeling based on the outcrop and lithology. The study's approach is concerned with mapping the surface and acquiring the sedimentary structure, measuring section, composite profile, and depositional environment. Determining the composite profile has been done in three measurements in Halang Formation (Figure 3). The thin section sample is observed for understanding the porosity by using ImageJ Software. The porosity percentage should be considered in constructing the stratigraphy sequence (Nostratia et al., 2019). Stratigraphy sequence is interpreting with the measuring section and the outcrop profile. Data synthesis is done by interpreting facies, depositional environment, and period of the Halang Formation turbidite deposits. The turbidite depositional facies are based on the Bouma sequence (1962), while the turbidite deposit facies, according to Walker (1973) and Mutti (1992), results in a depositional environment model based on Walker (1988). The correlation model and rock porosity visualized the results, which is a potential area in hydrocarbon exploration.

Result and Discussion
The results of this study are shown in several studies, including outcrop analysis with three lines, petrographic

analysis, and calculation of the potential for hydrocarbons obtained at the research site.

Outcrop Investigation

First Track
The facies on first track are dominated by thick layers of sandstone and interluding claystone with the appearance of andesite breccia in several places, the total thickness of rock layers on this track is 20 meters in Purbayan River (Figure 3, 4). The interlayering of sandstone and claystone is arranged in thin layers with a thickness of sandstone ranging from 10-200 cm at medium to fine grain sizes (0-0.5 mm), and a claystone thickness ranging from 5-100 cm. At the third meter, massive andesite breccia deposits were deposited with a medium to fine-grained containing tuff sand matrix. Sandstone has the characteristics of the grayish-white, matrix-supported fabric, well-sorted, well rounded, and compact while claystone is cream to brown in color, matrix-supported fabric, well-sorted, well rounded, and compact. There are three turbidite facies on this track, namely massive sandstone, breccia, and classic turbidite facies.

Looking at the characteristic description deposited by the surface outcrop on first track, it can be interpreted that the segmented facies on this track, which is assessed from the broad or detailed appearance, shows a mega turbidite and high-density turbidite lithofacies package with successive processes starting from inertia flow (laminar state), which gravitates coarse sand - gravelly deposits, then the next process is the result of suspension flow and traction to form normally graded sand deposits and continued with debris flow which precipitates coarse materials first until the flow gradually becomes turbidity current (Shanmugam and Moiola, 1997). These lithofacies are the result of accumulated interpretations of Postma et al. (1988) and the facies have associations with the lower to upper parts of the submarine fan.

Second Track
The next trajectory is the Pamriyan River track (Figure 3). The oldest deposits are composed of carbonate siltstone deposits with good continuous bedding with a total thickness of up to 12 meters (Figure 4). Siltstone has a brownish-beige physical appearance on the fresh side and grays on the weathered part, matrix-supported fabric, well-sorted, well rounded, and compact. The older layer that was deposited on top was sandstone with fine to medium grain size. The interpretation of the sedimentation process that deposited these facies is a suspension current to traction with a low density and low energy depositional current strength. Seeing the characteristic features deposited on this trajectory, it is interpreted that there are two facies on the Purbayan river trajectory, namely massive sandstone facies (Interval Ta) and pelagic deposits (Interval Te) as the last interval in the Bouma sequence. In the stratigraphic column it can be seen that the physical characteristics of the sediment from the turbidite deposits in this path are dominated by silt or siltstone and thick sandstone.

However, on this line no sediment structure was found, this could be an indication that the deposition process lasted quite a long time with constant energy and sediment supply, as well as dense flow material so that the sediment formed became massive and thick with similar characteristics. This trajectory shows the character of the depositional environment of the channel portion of supra fan lobes on the mid fan to the distal inner fan channel levee (Walker, 1984). The coarsening upward depositional pattern shows a progradation and shallowing up process.

Third Track
In Kaligede River finds total thickness of the rock layer with almost 15 meters with the thickness of the sandstone layer ranging from 10-200 cm, and the thickness of the claystone ranging from 5-50 cm (Figure 4). On third track shows a depositional pattern that tends to fining upwards, so it still shows indications of sea-level rise which forms vertical deepening up deposits. The Track is dominated by the deposition of coarse grain facies, where this facies is formed with a depositional pattern that experiences changes in current strength (not stagnant) that is not balanced with the accommodation space, where the sediment supply is sometimes greater than the accommodation space. According to the classification of turbidite deposits by previous researchers, the characteristics of the track indicate the track study area has characteristics of massive sandstone and classic turbidite (Walker, 1978). While referring to the lithofacies classification according to Shanmugam and Moiola (1997), third track includes several massive sand lithofacies and normally graded sand facies as in first track.

The association of lithological characteristics based on the three lines (Figure 3), tracks have almost the same characteristics, namely explaining the characteristics of turbidite facies, including the lithological characteristics of alternating sandstone and silt with parallel lamination structure, wavy lamination, graded bedding and convolute. There is a breccia lithology with andesite fragment, limestone, basalt and volcanic coarse sandstone matrix (Figure 4). The characteristics of the pelagic siltstone lithology are gray to cream with high carbonates properties. Sediment processes in these three tracks are deposited with suspension currents to traction currents which are from low to high density product. Volcanic material indicates a product of volcanic activity, while carbonate properties are the influence of the marine environment.

Petrography Analysis

First Track Petrography
The results of the microscopic petrographic analysis of thin sections, in general, are the lithology of the rocks in this path in the form of felspathic arenite (Pettijohn, 1972). The lithology of this rock incision is fine sand – medium sand (0.125 - 0.5 mm). Overall, the texture of this lithology is massive; the degree of roundness is angular to rounded (Powers, 1953). The uniformity of grains in this rock is well sorted (After Folk, 1965), and the relationship between grains is point contact and prolonged contact. Fragments (70%) present in this rock are k-feldspar, quartz, rock fragments, opac, and planktonic and benthic foraminifera, rounded angular shape, matrix (10-20%), cement (10-15%), and porosity (21%). 5% in intergranular and intragranular forms.

Second Track Petrography
The petrographic analysis has displayed the lithology of the rocks in this path in the form of felspathic arenite (Pettijohn, 1972) with fine incision sand – medium sand (0.125 - 0.5

mm). The texture of this lithology is massive; the degree of roundness is angular to rounded (Powers, 1953); well-sorted (After Folk, 1965); and the relationship between grains is point contact and prolonged contact. The rock fragment is k-feldspar, quartz, rock fragments, opac minerals, and planktonic and benthonic foraminifera, rounded angular shape, matrix (10-20%), cement (15-20%), and porosity (15.5%) in intergranular and intragranular forms.

Third Track Petrography

The thin section obtained the lithology of the rocks in this path in the form of sublitharenite (Pettijohn, 1972) with massive structure and fine-medium sand (0.125 - 0.5 mm). The degree of roundness is angular to rounded (Powers, 1953). The uniformity is well sorted (After Folk, 1965), and the relationship between grains is point contact and prolonged contact. K-feldspar, quartz, rock fragments, opac minerals, and planktonic and benthonic foraminifera, rounded angular shape, matrix (10-20%), cement (10-15%), and porosity (15.6%) in intergranular and intragranular forms are found as the fragment.

Rock Characteristic and Correlation

The results of facies analysis carried out on three tracks in the study area, it can be interpreted that the facies model of the depositional environment describes the rock units in general in the form of a middle to upper submarine fan system deposit package which in detail includes classical turbidite and massive sandstone facies and channel and levee depositional environments. The characteristics of these rocks are quite ideal geometries to become hydrocarbon reservoirs.

In making the biostratigraphy correlation model, it uses a key bed in the form of fossil bio-data that has been obtained from the results of the biostratigraphy analysis as described before. The use of a key bed in the form of a fossil datum is used because there is no lithostratigraphic key bed that can be the key to bio-zoning. The distance of each segment of the stratigraphic column, which is quite far, causes inaccuracies if only using lithostratigraphic correlations. The research data are stratigraphic units located in different areas; the correlation function is carried out to determine the equivalence of each of these stratigraphic units. Each stratigraphic column position in the correlation model has been adjusted to the bathymetric position from the results of the paleontological analysis. The fossil contained in the sample becomes the reference for the withdrawal of biozonation on each track to be correlated. The correlation clarifies the depositional characteristics of the facies, also shows vertical and horizontal depositional patterns based on the biozonation sequence of deposits from biostratigraphy analysis, which is not discussed in detail in this paper.

Hydrocarbon Potential

The evaluation of potential hydrocarbons in the study area refers to previous researchers (Astuti, 2013) who argue that the Halang Formation sandstone has the potential as a reservoir. Also proven based on field data and laboratory analysis which shows the porosity category is 15-21%. From the results of facies analysis carried out on 3 tracks in the study area, it can be interpreted that the facies model of the depositional environment describes the rock units in general in the form of a middle to upper submarine fan system deposit package which in detail includes classical turbidite and massive sandstone facies and channel and levee depositional environments.

In deep water sediment deposition, channel and levee deposit complexes have proven to be a depositional environment with enormous potential to become a reservoir for hydrocarbon accumulation, supported by a petrographic analysis that supports the Halang formation sandstone as a good reservoir. According to Husein, 2013 in his research, the classical turbidite facies where claystone with high organic content in the Walker model (1973) facies can be interpreted as potential source rock, while the sandstone facies that fills the channel of the Halang Formation acts as a reservoir. So that the results of the facies analysis in the research area have the potential as a playing target for hydrocarbons in the South Serayu Basin. Looking at the results of the stratigraphic correlation analysis, as well as rock characteristics and petrographic analysis of the three tracks in the research area state that the best track that has the highest probability of becoming a reservoir is, the middle to upper Miocene massive sandstone facies deposits on track 1 and the younger part of track 3, the western to the southern part of the study area. However, further research is needed to understand and ensure more deeply the reservoir potential of the research area. The next suggestion is to conduct further studies to understand the evolution of the structure in the research area as well as to understand the sealing capability of the younger formations and continue with updating the Geological Chance Factor (GCF) and Probability of Success.

Conclusions

The research concludes that:

1) The rock units in the study area are divided into three units: interlayering siltstone, sandstone, massive sandstone, and andesite breccia. Late Miocene to Early Pliocene deposits was deposited in several submarine fan facies systems, precisely at the Upper fan to Lower fan in the depositional environment of the proximal channel on an inner fan to distal inner fan channel fan levee.
2) The analysis results show that the porosity obtained from the four sandstone samples has a good to excellent rating, so that it is considered a potential hydrocarbon reservoir.
3) The deposits found in the study area, namely the proximal channel and levee, can become hydrocarbon play targets in the South Serayu Basin.
4) Based on lithological characteristics, petrographic analysis, field observation and stratigraphic analysis, the best reservoir among the three tracks is the second and some part of the first trac.

References

Asikin, S., Handoyo A., Pratistho B., dan Gafoer, 1992, Direktorat Geologi, Bandung.

Astuti, B.S, 2013, Thesis, Universitas Gadjah Mada, Yogyakarta.

Blow, W.H., 1969, Proceeding First Int. Conf. Planktonic Micro Fossilles, E.J. Brill-Leiden, **1**, 199-422.

Bouma, A, 1962, Elsevier Publication **168.**

Darul, N, 2017, Thesis, Universitas Pakuan, Jawa Tengah.

Folk, R.L., and W.C. Ward., 1957, Journal of Sedimentary Petrology, **27**, 3-26.

Husein S., Jyalita J., Azis M., 2013, Proceedings of Seminar Nasional 6th Jurusan Teknik Geologi Fakultas Teknik UGM, Yogyakarta.

Hall, R, 2012, Ocean.Tectonophysics, **570–571**, 1–41.

Lunt, P., G. Burgon, A. Baky, 2009, Journal of Asian Earth Sciences, **34**,100-113.
Mutti, E., 2011, Proceeding International Conference and Exhibition, Milan, Italy, October 23-26.
Nosratia, A., A. Kadkhodaieb, A. Aminia, A. Chehrazic V. Mehdipourd T. Moslemnezhada, 2019, Journal of Natural Gas Science and Engineering, **65,** 1-15.
Pettijohn, F.J., 1975, Harper and Row, 3rd, New York.
Postma, H., and J. J. Zulstra, 1988, Elsevier Sci. Publication, **27**, Amsterdam.
Powers, M.C., 1953, A. Jurnal of Sedimentary Petrology, **23**,117-119.
Satyana, A.H, 2007, Central Java, Proceeding Indonesian Petroleum Association 31st Annual Convention and Exhibition, Jakarta.
Shanmugam, G., 2012a, Handbook of Petroleum Exploration and Production, Elsevier, **9**. 524.
Shanmugam, G., and R.J. Moiola, 1997, AAPG Bulletin, **81**, 476-491.
Van Bemmelen, R. W, 1949, **IA**, Martinus Nijhoff.Belanda.
Walker dan Mutti, E., 1973., S.E.P.M. lecture notes series, **4**,119 -137.
Walker, R. G., 1978. Bulletin American Assoc. Petrol Geology, **62,** 932-966.
Walker, R.G. and James, N.P, 1978, Geology Association of Canada, 239-263.
Walker, R.A., 1981, Facies Models, Ainsworth Press Limited, Kitchener, Ontario, Canada, p.211.
Walker, R. A., 1984, Geological Association of Canada Publication, Bussiness and Economic Service, Canada.

Acknowledgements
The writers are eternally grateful for the lecturers of Geological Engineering in Sriwijaya University either Bumi Sriwijaya Research Group's member or Ugi Kurnia Gusti, M. Sc in discussing this final manuscript.

PROCEEDINGS
JOINT CONVENTION BANDUNG (JCB) 2021
November 23rd – 25th 2021

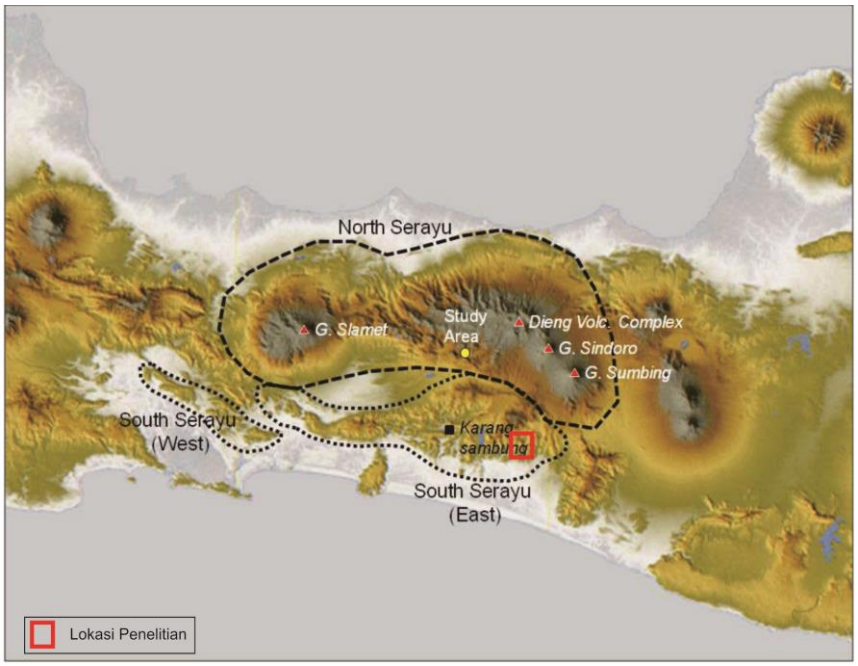

Figure 1: The research area is located in the South Serayu Basin in the Purworejo region, Central Java (modification of Husein et al., 2013).

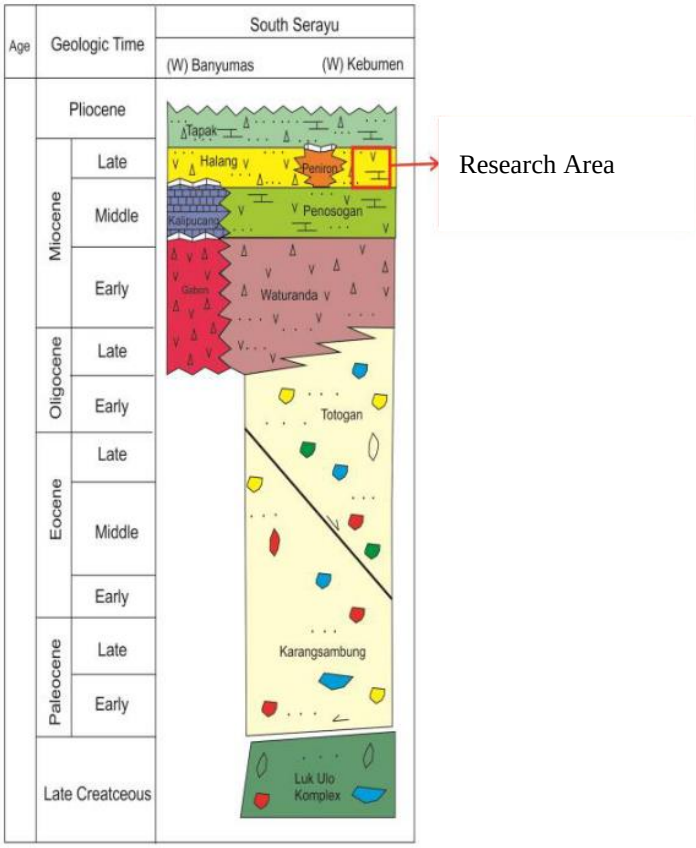

Figure 2: Cenozoic tectonostratigraphic of the Serayu Zone (Modified from Asikin et al., 1992a; Asikin et al., 1992b; Condon et al., 1996; Djuri et al., 1996; Lunt et al., 2009; Hall, 2012 in Husein, 2013). Halang Formation is a formation consisting of turbidite deposits.

PROCEEDINGS
JOINT CONVENTION BANDUNG (JCB) 2021
November 23rd – 25th 2021

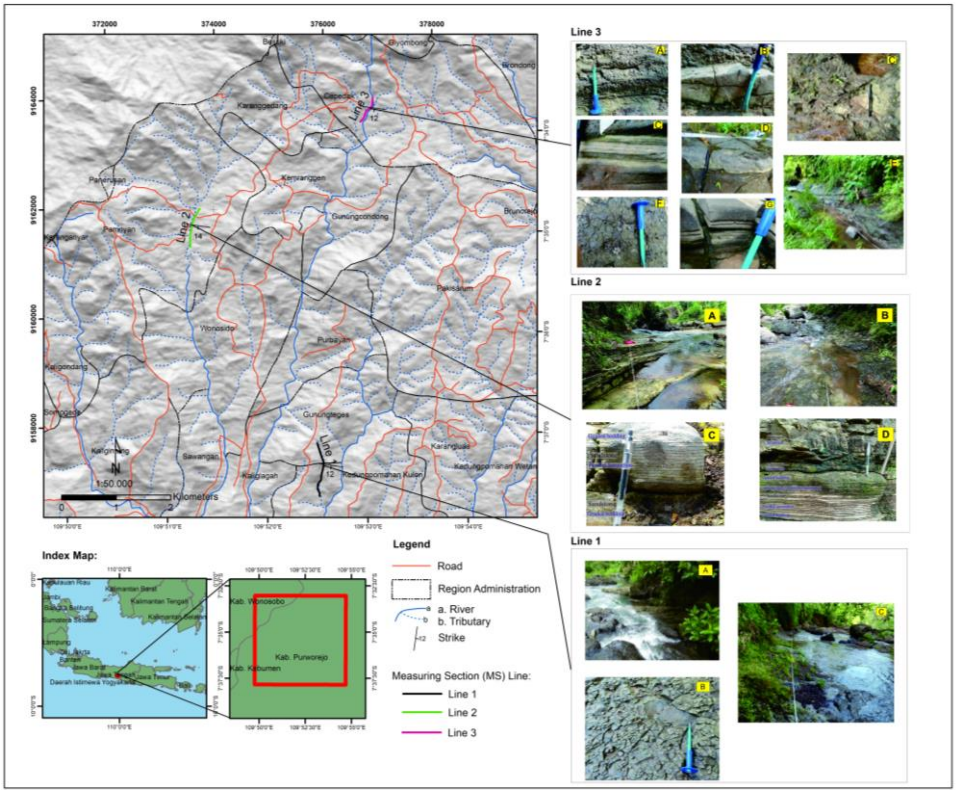

Figure 3. The Measuring Section track with the first line in Purbayan River finds interlayering thick sandstone with clay and andesite breccia with N101°E/12. The second measurement takes in Pamriyan River with no sediment structure, composed of carbonate siltstone with thick sandstone, and having Ta – Te of Bouma sequence (1962). The last point tracking in Kaligede River discovers fining upwards of sediment and the thickness of massive sandstone.

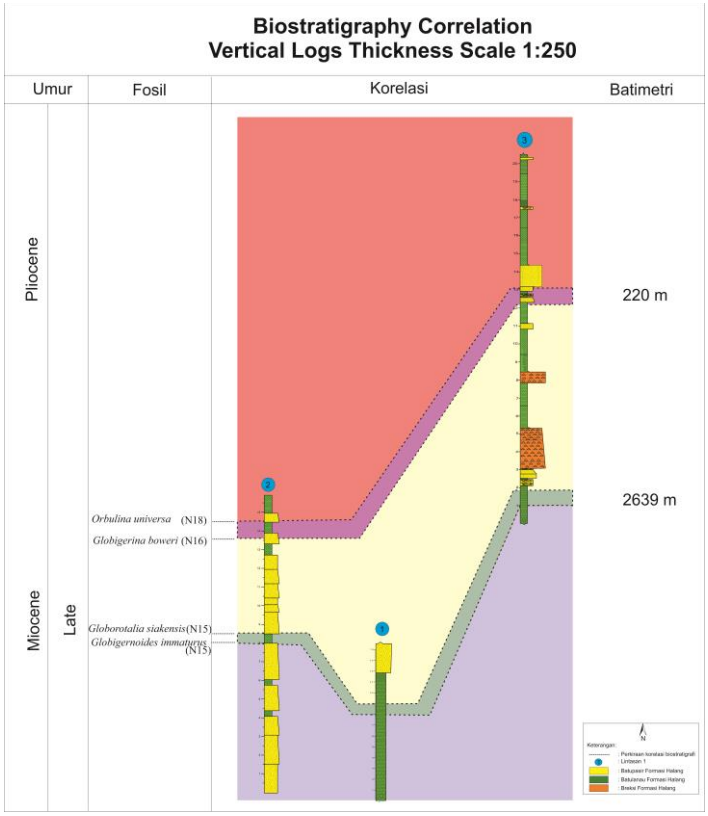

Figure 4: Biostratigraphy correlation based on outcrop profile data on three lines in the Halang Formation which describes the potential attachment as a reservoir. The correlation is based on the presence of benthonic fossils in studio analysis found with the bathymetry environment at 220 m and 2639 m.

PROCEEDINGS
JOINT CONVENTION BANDUNG (JCB) 2021
November 23rd – 25th 2021

Chemostratigraphy of Paleozoic Carbonate in Natar, South Lampung, Indonesia

Darwin Jansen Parningotan Sihombing[1,a], Danni Gathot Harbowo[2,4], Bambang Priadi[2], Luki Ardhianto[3]

[1] *Department of Geological Engineering, Institut Teknologi Sumatera, Wayhui, Lampung, Indonesia.*
[2] *Department of Geological Engineering, Institut Teknologi Bandung, Bandung, Indonesia.*
[3] *PT Aneka Sumberbumi Jaya, Lampung, Indonesia.*
[4] *Sedimentology, Stratigraphy, and Geodynamic Research Group, Institut Teknologi Sumatera, Wayhui, Lampung, Indonesia*
[a] *Corresponding author:*

Abstract
Located in Natar, South Lampung, there is paleozoic carbonate included in the Gunungkasih Formation members. It is supposed to explain the geological history's uniqueness to the paleoenvironment during the Paleozoic age in western Indonesia. We concern with identifying the lithofacies by chemostratigraphy. We used several representative core data in this area. We determined the correlation of chemostratigraphy by CaO, MgO, SiO_2, Fe_2O_3, and Mn concentration. It is to interpret the paleozoic paleoenvironment. The chemical range in stratigraphy is CaO 47.4-55.3 %; MgO 0.51-8.12 %; SiO_2 0.21-1.20 %; up to 0.12% of Fe_2O_3; and up to 162 ppm of Mn. We concluded that the paleoenvironment of this unit was dominated by massive paleozoic coral reef facies that formed in the margin of warm-shallow marine.

Keywords: Paleozoic carbonate, chemostratigraphy, paleoenvironment, South Lampung.

Introduction

The research was conducted in Natar, South Lampung, with the object of research being paleozoic carbonate rocks in the form of marble which are members of the Gunungkasih Formation. The local geological setting consists of the Paleozoic Gunungkasih Fm., surrounded by quarternary pyroclastic rocks (Figure 1). One of them is marble rock, also known as paleozoic carbonate rock. It is presumed that the marble rocks in the study area can explain the unique geology related to the paleoenvironment during the Paleozoic age in western Indonesia (Mangga et al., 1993; Natalia et al., 2020; Zulkarnain, 2011)

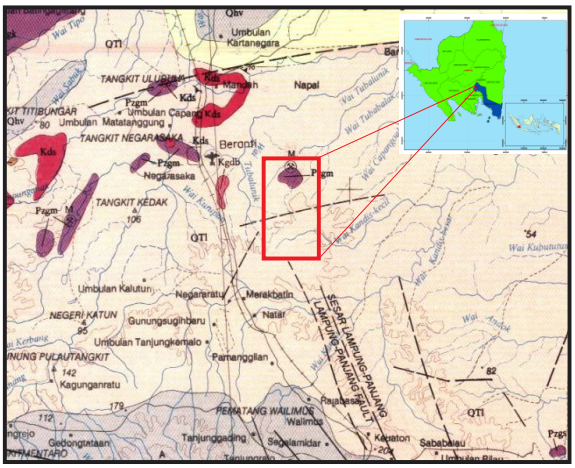

Figure 1. Geological Map of the Tanjung Karang Sheet (Mangga, et al., 1993), red box shown the area of interest.

Chemostratigraphy is an application for stratigraphy with geochemical data on core rocks. Rock identification can be used with geochemical data and core data in the form of chemostratigraphy. Comparison of the abundance of calcium oxide is one of the results that need to be obtained to determine the characteristics of marble rocks with impurity rocks.

Data and Methods

The study used primary data in the form of core descriptions and secondary data in geochemical data. The method used is chemostratigraphy from the correlation of core and geochemical data (refer to Melezhik et al., 2015; Rowe et al., 2012).

Geochemical data is secondary data from a marble (limestone) mining company in the Natar area. Geochemical data are contained in two data 1st wells DH1 (Table 1) and 2nd wells DH4 (Table 2). This data is analyzed from X-ray fluorescence (XRF) analysis of marble cores.

Geochemical data analysis uses geochemical test data on core samples by testing marble rocks with excellent physical characteristics without any iron oxide impurities or the slightest intrusion of andesite. So the samples taken and tested have different thicknesses. The geochemical data obtained in this research are geochemical data that are measured only for CaO, MgO, SiO_2, Fe_2O_3, and Mn concentrations. At the same time, other elements are not reconsidered because the percentages are minimal.

Table 1. Geochemical data of marble rock 1st well (DH1).

WELL GEOCHEMICAL DATA DH1							
WELL	Depth From (m)	Depth To (m)	CaO (wt %)	MgO (wt %)	SiO2 (wt %)	Fe2O3 (wt %)	Mn (ppm)
SDH01_01	5.65	6.20	53.2	2.08	0.21	0.02	23
SDH01_02	6.20	6.70	47.6	6.22	0.54	0.05	162
SDH01_03	6.70	7.30	55.3	0.65	0.22	0.00	17
SDH01_04	7.30	8.20	55.2	0.71	0.25	0.00	7
SDH01_05	8.20	11.20	55.3	0.52	0.24	0.00	10
SDH01_06	11.20	12.90	54.0	1.33	0.26	0.01	10
SDH01_07	12.90	14.20	54.9	0.58	0.27	0.00	7
SDH01_08	14.20	15.60	54.8	0.84	0.35	0.03	19
SDH01_09	16.10	18.40	54.0	0.69	0.67	0.05	20
SDH01_10	19.10	20.30	53.9	0.51	0.55	0.05	32
SDH01_11	23.00	24.95	52.4	2.26	0.36	0.03	40
SDH01_12	26.30	27.70	51.6	2.91	0.58	0.10	27
SDH01_13	27.70	30.70	50.2	4.24	0.52	0.12	35
SDH01_14	30.70	32.30	50.8	3.78	0.38	0.07	45
SDH01_15	32.90	35.00	52.1	2.88	0.36	0.05	37
SDH01_16	36.00	38.00	51.5	3.15	0.34	0.04	22
SDH01_17	43.60	45.90	47.4	8.12	0.29	0.02	22
SDH01_18	45.90	48.50	51.3	3.30	0.51	0.06	18
SDH01_19	48.50	50.40	51.0	3.98	0.35	0.02	13
SDH01_20	53.20	55.50	49.8	2.41	1.20	0.06	62
SDH01_21	55.50	58.55	51.6	1.92	0.69	0.11	41

Chemostratigraphy was carried out by correlation and analyzing core descriptions with geochemical concentrations of marble cores from two different wells. The

PROCEEDINGS
JOINT CONVENTION BANDUNG (JCB) 2021
November 23rd – 25th 2021

results of chemostratigraphy analysis are described by the characteristics of marble rocks with impurity rocks and the abundance of calcium oxide with other geochemical concentrations (Melezhik et al., 2014).

Table 2. Geochemical data of marble rock 2nd well (DH4).

WELL GEOCHEMICAL DATA DH4							
WELL	Depth From (m)	Depth To (m)	CaO (wt %)	MgO (wt %)	SiO2 (wt %)	Fe2O3 (wt %)	Mn (ppm)
SDH04_01	0.30	1.50	51.9	2.64	0.47	0.04	39
SDH04_02	3.00	5.00	54.3	0.57	0.37	0.01	14
SDH04_03	5.00	7.00	54.7	0.56	0.6	0.01	19
SDH04_04	7.00	9.00	54.4	0.82	0.36	0.01	11
SDH04_05	9.80	11.10	54.5	0.68	0.26	0.01	17
SDH04_06	11.40	13.20	54.1	1.08	0.33	0.01	13
SDH04_07	13.20	15.10	55.0	0.77	0.24	0.01	17
SDH04_08	16.40	18.40	54.4	0.68	0.39	0.02	26
SDH04_09	18.40	19.90	54.7	0.98	0.28	0.00	9
SDH04_10	20.60	22.80	54.8	0.78	0.25	0.01	10
SDH04_11	22.90	25.10	54.1	1.13	0.30	0.01	10
SDH04_12	25.10	27.40	52.3	2.68	0.24	0.01	10
SDH04_13	27.40	29.90	54.8	0.97	0.31	0.00	14
SDH04_14	30.20	32.60	55.0	0.73	0.29	0.00	6
SDH04_15	32.60	34.90	52.2	1.80	0.52	0.02	22
SDH04_16	34.90	37.20	52.4	0.90	0.82	0.05	37
SDH04_17	37.30	39.20	54.1	0.51	0.54	0.08	41
SDH04_18	43.10	46.00	54.7	0.79	0.29	0.01	11
SDH04_19	46.00	47.50	54.9	0.60	0.38	0.01	10
SDH04_20	52.20	54.60	49.5	4.36	0.54	0.09	39
SDH04_21	54.60	56.00	48.4	4.57	0.73	0.07	53
SDH04_22	56.20	57.00	49.0	5.51	0.42	0.22	38
SDH04_23	57.50	59.30	51.5	2.71	0.56	0.19	48
SDH04_24	60.00	63.50	50.8	3.57	0.64	0.10	36
SDH04_25	63.50	65.00	47.1	8.04	0.58	0.04	21
SDH04_26	65.00	67.50	49.3	5.13	0.43	0.03	18

Result and Discussion

The two data cores DH1 and DH4, the distance between the two wells is ± 116 meters. The coordinates of the well DH1 are at point 5º 14' 1.0" S, 105º 12' 47.6" E elevation ± 75 masl, and depth 59 meters. Coordinates of the well DH4 are at point 5º 14' 44.2" S, 105º 12' 50.5" E elevation ± 75 masl, and depth 69 meters (Figure 2).

The results of the description and analysis of cores in both wells show the characteristics of three rocks, namely marble, intrusion of andesite, and tuff. The characteristics of marble rocks are light gray to bluish-white color, non-foliated structure, crystalline, granoblastic texture, reacting with HCl in the presence of calcite minerals and some impurities such as iron oxide. Some parts are brittle and break easily. The characteristics of andesite intrusion are dark gray to greenish aphanitic, and there are calcite veins due to breaking through marble rocks. The characteristics of tuff are brown, and the grain size is ash-lapilli (1/16 – 64 mm), altered condition with the presence of pyrite mineral, open packed with marble rock fragments are calcareous.

The marble rock formed by contact metamorphism is shown by granoblastic and crystalloblastic texture (refer to Thomann and Hoffer, 1991). We suggest the protolith of the marble rock is originated from limestone indicated by the presence of a texture (relict) in the form of algae remains; the paleo-environment of this unit is controlled by massive paleozoic coral reef facies formed on the edge of warm shallow seas. (Winter. J. D., 2001; Titisari, A. D. & Kurniawati, S., 2018).

Geochemical core data in the DH1 well show geochemical concentrations with 21 data and different depths. The measured data starts from a depth of 5.65 meters to 58.55 meters. The lowest abundance of CaO is at a depth of 43.60-45.90 meters with a concentration of 47.4%, MgO concentration (8.12%), SiO2 concentration (0.29%), Fe2O3 concentration (0.02%) and Mn (22 ppm) and the largest at a depth of 8.20 – 11.20 meters with a concentration of 55.3%, MgO concentration (0.52%), SiO2 concentration (0.24%), Fe2O3 concentration (0.0%) and Mn (10 ppm).

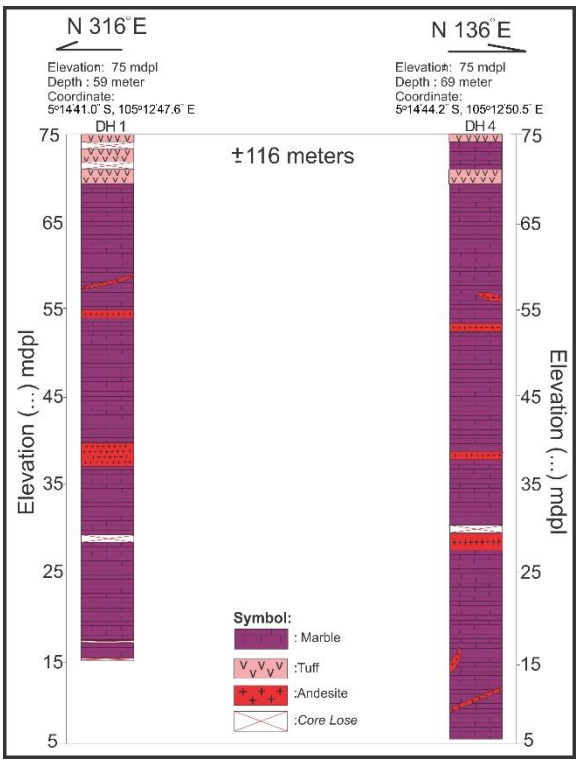

Figure 2. Illustration of a well from the data core.

Core geochemical data in the DH4 well show geochemical concentrations with 26 data and different depths. The measured data starts from a depth of 0.03 meters to 67.50 meters. The lowest abundance of CaO is at a depth of 63.5-65 meters with a concentration of 47.1%, MgO concentration (8.04%), SiO2 concentration (0.58%), Fe2O3 concentration (0.04%) and Mn (21 ppm) and the largest at a depth of 13.20 – 15.1 meters with a concentration of 55.0%, MgO concentration (0.77%), SiO2 concentration (0.24%), Fe2O3 concentration (0.01c%) and Mn (17 ppm). Based on the available geochemical data, diagrams can be made to determine the relationship between the abundance of calcium oxide (CaO) and impurity minerals (MgO, SiO2, Fe2O3, and Mn) originating from intrusion of andesite rocks. So it can be proven that these impurity minerals cause the decrease in the abundance of calcium oxide in marble.

In the analysis of the relationship of geochemical data in the DH1 and DH4 wells, it was shown that the abundance of calcium oxide (CaO) was inversely proportional to the abundance of MgO, SiO_2, Fe_2O_3, and Mn. Its means that

PROCEEDINGS
JOINT CONVENTION BANDUNG (JCB) 2021
November 23rd – 25th 2021

when the abundance of CaO is higher, the abundance of MgO, SiO_2, Fe_2O_3, and Mn is lower, and vice versa when its abundance higher, the abundance of CaO is lower; this is evidenced in the geochemical data relationship diagram (see Figure 3).

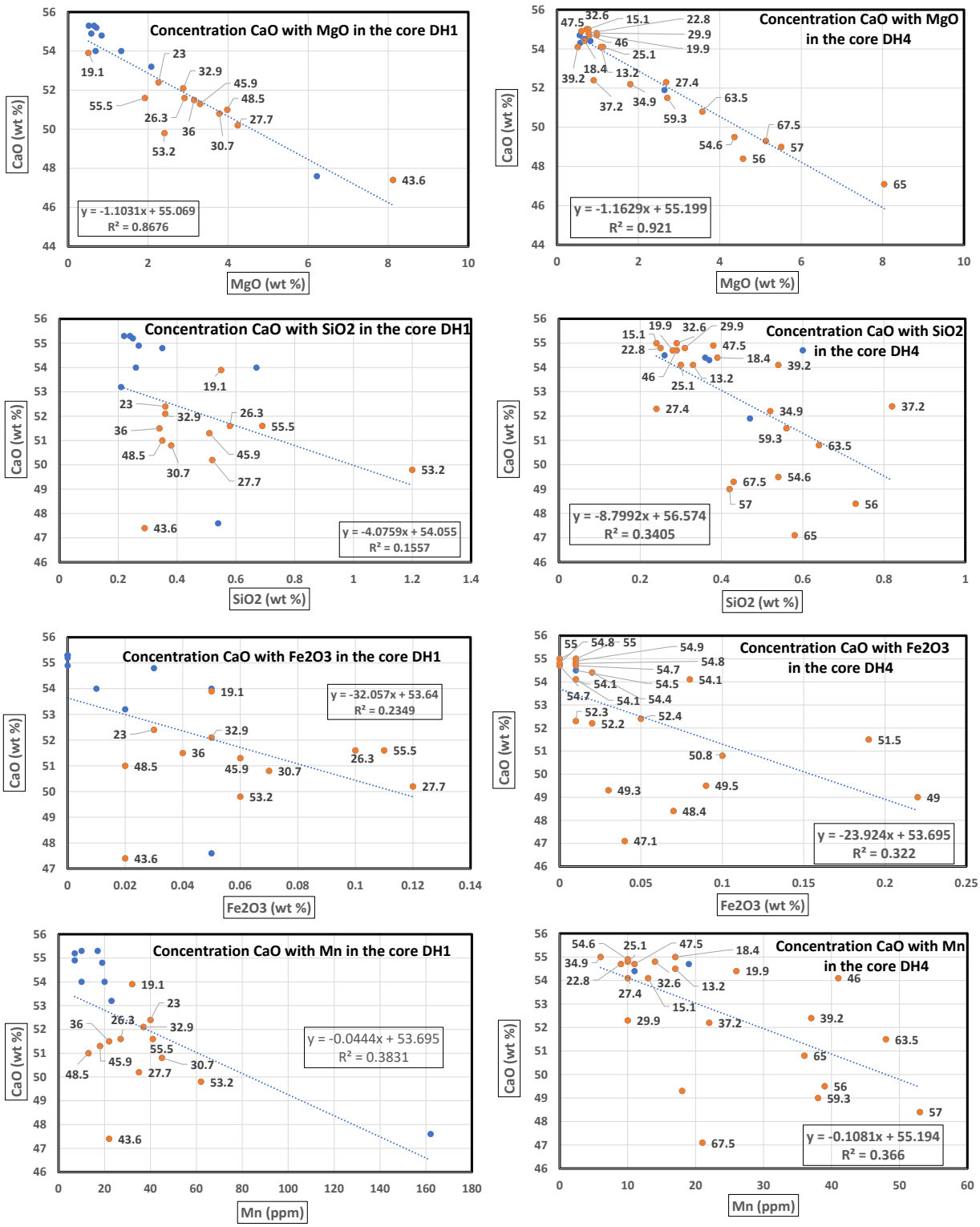

Figure 3. Corelation of CaO concentration with MgO, SiO_2, Fe_2O_3, and Mn of Well DH1 and DH4.

In the diagram, there is a dot symbol with two colors, and the blue dot describes the abundance of CaO before intense with andesite intrusion based on the core description. The blue orange dot describes the abundance of CaO after intense with intrusion of andesite. This figure describes the depth of the well.

Conclusions

PROCEEDINGS
JOINT CONVENTION BANDUNG (JCB) 2021
November 23rd – 25th 2021

As the results, we determined the correlation of chemostratigraphy by CaO, MgO, SiO_2, Fe_2O_3, and Mn concentration to interpreted the paleozoic paleoenvironment. The chemical range in stratigraphy is with 47.4-55.3 % of CaO; 0.51-8.12 % of MgO; 0,21-1.20 % of SiO2; up to 0.12% of Fe2O3; and up to 162 ppm of Mn. We concluded that the paleoenvironment of this unit was dominated by massive paleozoic coral reef facies that formed in the margin of warm-shallow marine.

References

Baker, M. B., 2017. The Application of Marble and Granite as Building Materials in Jordan. Jordan Journal of Civil Engineering, 11(2), pp. 234-238.

Mangga, S.A., Amirudin, Suwarti, T., Gafoer, S., dan Sidarto. 1993. Geology of The Tanjungkarang Quadangle, Sumatera, Scale 1:250.000, Pusat Penelitian dan Pengembangan Geologi, Bandung.

Natalia, H.C., Harbowo, D.G. and Ikhram, R., 2021. Potensi Geodiversity di Sekitar Kawasan Anak Krakatau-Way Kambas, Provinsi Lampung, Sebagai Kandidat Geopark Indonesia. Journal of Science and Applicative Technology, 5(1), pp.47-57.

Haylay Tsegab and Chow Weng Sum., 2019, Chemostratigraphy of Paleozoic Carbonates in the Western Belt (Peninsular Malaysia): A Case Study on the Kinta Limestone, Universiti Teknologi PETRONAS.

Melezhik, V.A., Roberts, D., Fallick, A.E., Gorokhov, I.M. and Kusnetzov, A.B., 2005. Geochemical preservation potential of high-grade calcite marble versus dolomite marble: implication for isotope chemostratigraphy. Chemical Geology, 216(3-4), pp.203-224.

Melezhik, V.A., Kuznetsov, A.B., Pokrovsky, B.G., Solli, A., Gorokhov, I.M., Fallick, A.E., Lindahl, I., Konstantinova, G.V. and Melnikov, N.N., 2014. Chemostratigraphic insight into deposition of the Melkedalen Marble, Narvik Nappe Complex, North-Central Norwegian Caledonides. Norwegian Journal of Geology/Norsk Geologisk Forening, 94(1).

Rowe, H., Hughes, N. and Robinson, K., 2012. The quantification and application of handheld energy-dispersive x-ray fluorescence (ED-XRF) in mudrock chemostratigraphy and geochemistry. Chemical Geology, 324, pp.122-131.

Thomann, W.F. and Hoffer, R.L., 1991. Progressive contact metamorphism of the middle Proterozoic Castner Marble, Franklin Mountains, West Texas. Rocky Mountain Geology, 29(1), pp.71-80.

Titisari, A. D. & Kurniawati, S., 2018. Genesa Marmer Daerah Besole, Kecamatan Besuki, Kabupaten Tulungagung, Provinsi Jawa Timur Berdasarkan Karakteristiknya. Proceeding Seminar Nasional Kebumian Ke-11, Yogyakarta: 5-6 September 2018, Hal. 745-751.

Winter, J. D., 2001. An Introduction to Igneous and Metamorphic Petrology. New Jersey: Prentice-Hall Inc, p.p 411,433-440.

Zulkarnain, I., 2011. Geochemical Evidence of Island-Arc Origin for Sumatra Island; A New Perspective based on Volcanic Rocks in Lampung Province, Indonesia. Indonesian Journal on Geoscience, 6(4), pp.213-225.

Acknowledgements

Authors are grateful to all the colleagues that have had pleasure and honor to work with in limestone mining PT Aneka Sumberbumi Jaya. Without their participation and feedback, this study would not have been possible.

PROCEEDINGS
JOINT CONVENTION BANDUNG (JCB) 2021
November 23rd – 25th 2021

Coastline Shift Identification with Remote Sensing and GPR in Bagedur Beach, Lebak District, Banten

Muhammad Arif Rahman[1], Gamma Abdul Jabbar[1], Maryadi[1]
[1]Program Studi Geologi dan Geofisika, Fakultas Matematika dan Ilmu Pengetahuan Alam, Universitas Indonesia, Jl. Margonda Raya Pondok Cina, Depok, 16424, Indonesia

Abstract
Bagedur Beach is one of many beaches in southern Java that potentially affected by tsunami. In paleotsunami study, morphological features of beach can inform the probability deposition of tsunami sediment also the coastline location included in the calculation of some tsunami parameters. Location of coastline can be identified with remote sensing and understanding of subsurface with GPR. Remote sensing is used to understand recent beach morphological features that can be compared to paleo-beach. Paleo-beach can be interpreted by comparing beach features in subsurface imaging with the morphological features of recent (surface) beach. GPR profiles that record subsurface condition with high resolution can be grouped into several radar facies. Certain radar reflection and geometry can characterize beach features that can be seen in recent beach. Interpretation of processed GPR profile show that there are iteration of beach features such as beach, ridge, swale, and coastal plain either in paleo- or recent beach. The movement of those features landward or seaward can conclude of coastline shift. Coastline shift can be associated with earthquake that causes tsunami.

Introduction
As a country where several plate tectonics converge, Indonesia is one of the most active in terms of geological activity, resulting both positive and negative impact. One of the negative side is geological disaster that commonly happen all around the country (BNPB, 2016). Indonesia as an archipelago country that vulnerable to tsunami, one of the area is Southern Java. Java is the most populated island in Indonesia. Understanding disaster that could and had happen could help preventing huge impact to general population.

Tsunami study in Indonesia start to rise since tsunami events in Aceh 2004 and Pangandaran 2006 that devastases coastal area (Aswan et al, 2017). Recent paleotsunami study in Southern Java bring new information about sediment that deposited in coastal area from tsunami transportation (Putra et al, 2015; Zulkarnain et al, 2017) and tsunami inundation modelling (Deng, 2018). To give better understanding about tsunami that happened before or could happen in the future, information about tsunami parameters need to be studied (Ishimura and Yamada, 2019), one of them is inundation distance. Inundation is a factor that measured the horizontal extend of tsunami transportation landward starting from coastline. Location of coastline play a huge role in measuring inundation distance of tsunami, if the tsunami happen recently, the inundation distance could easily be measured from recent coastline landward, but in paleotsunami, the tsunami maybe happen in paleo-coast environment. Paleomorphological features can be identified from subsurface condition, one of the method to obtain subsurface condition is with Ground Penetrating Radar (GPR) (Gouramanis et al, 2015). The restriction of poor exposure because extensive vegetation can be overcome by GPR (Bristow et al, 2000) and high resolution imagery with shallow depth is suitable with the object of study. The aim of this study are locating paleocoastline using GPR (subsurface condition) and remote sensing (surface condition).

Data and Method
The study area located in Bagedur Beach, located in west side of Java, specifically in Malingping Districts, Banten District. Starting from Binuangen estuary to Pasir Putih Beach. In terms of identifying subsurface morphology, field activity of GPR data acquisition conducted, divided into four lines oriented perpendicular from the beach (Figure 1), in hope to identify various subsurface beach feature. GPR used in this study has frequency of 100 Hz. Each profile have various length and depth, ranging from 83-133 meters and 1 to -13 mdpl respectively. Three of the profiles located in swale and the rest lie north in coastal plain. GPR data processing done using Prism 2.0 with background removal, ormsby bandpass, and gain function. Other than subsurface condition, surface recent morphological feature also identified using remote sensing (Google Earth). River feature mainly identified such as river path, river branches, and flow direction. Shifting of coastline obtained by comparing the subsurface morphology with surface morphology and other evidences.

Figure 1: GPR survey design consist of four line oriented perpendicular from coastline.

Result and Discussion
Surface morphology features that can be seen clearly from remote sensing in area of study is the shape of a river (Figure 2). An active river path can be seen flowing water from northeast eventually move south into the sea (Figure 2d). Few hundred meters to north, there is a dried up river branch which have been covered with vegetation and shift into ricefield (Figure 2c). The river branch shift eastward with a difference lie on the active river path continuing flow south and the dried up river flowed west. Dried river branch have similarity with recent river branch (Figure 2d), both have two branches, one flowing west (paralel to the beach) and the other flowing south (meeting of river and sea). Branch that flow west in dried river, can be traced continuously until connected into a isolated swamp (swale) (Figure 2b). It show that the swamp once had been supplied by the same river coming from northeast. The active river path shows the same pattern as the dried up river by split up paralel and perpendicular to the beach, with the paralel branch forming

PROCEEDINGS
JOINT CONVENTION BANDUNG (JCB) 2021
November 23rd – 25th 2021

a lake that interpreted as a swale and the perpendicular acting as a location where the river meet the sea . With the assumption that present morphology acting as a guide to interpret the past, it can be concluded that there was a coastline shift where the coast move towards the sea.

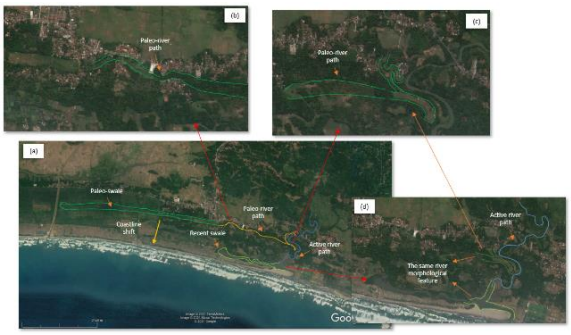

Figure 2: Satelite imagery of research area showing a paleo-swale (green) and recent swale (light green) (a). A dried up river path that lead to active river path (b). River path that connect active river path to paleo-swale (c). Similarity of shape between two river branches (d).

Subsurface information obtained by interpreting processed GPR profiles. From four profiles, six radar facies (RF) can be identified by defining the reflection of radar based on reflection properties and geometry of the reflection (Figure 3).

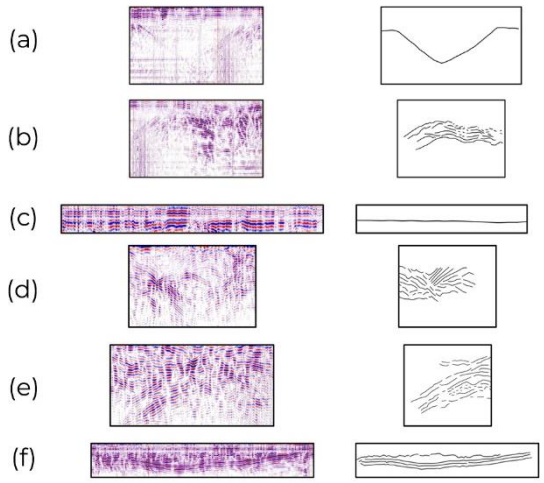

Figure 3: Six radar facies identified from four GPR profiles.

Radar facies 1 (Figure 3a) have continuous and low amplitude properties with bowl-like shaped. Low amplitude indicate low reflection coefficient, that affected by existence of seawater in the sediment acting as conductor. Based on those properties, RF 1 interpreted as a swale with depth of 1.25-5 meters and 61-84 meters wide.

Radar facies 2 (Figure 3b) have discontinuous and high amplitude properties with ripply structure. This facies interpreted as dunes. RF 2 can be found near RF 1 (swale) and acting as barier between beach and coastal plain.

Radar facies 3 (Figure 3c) have continuous reflection and very low amplitude, interpreted as water table. Low amplitude meaning the water acting as conductor, interpreted as seawater. This facies extend horizontally continuously across profile 2 and 3.

Radar facies 4 (Figure 3d) have discontinuous, low amplitude, subhorizontal properties with bowl-like shape filled with v-shaped sediment. This facies interpreted as trough cut and fill that is a part of paleo-river (dried up river path). RF 4 feature have 1.5-2 meters in depth and 25-30 meters in wide dimensions.

Radar facies 5 (Figure 3e) have continuous and high amplitude properties with gently slope landward. RF 5 contains clinoform with few undulation. It is interpreted as backshore part of paleo-beach.

Radar facies 6 (Figure 3f) have continuous and very high amplitude properties with very gentle slope forming a plate-like shaped. This feature interpreted as shallow swale or coastal plain.

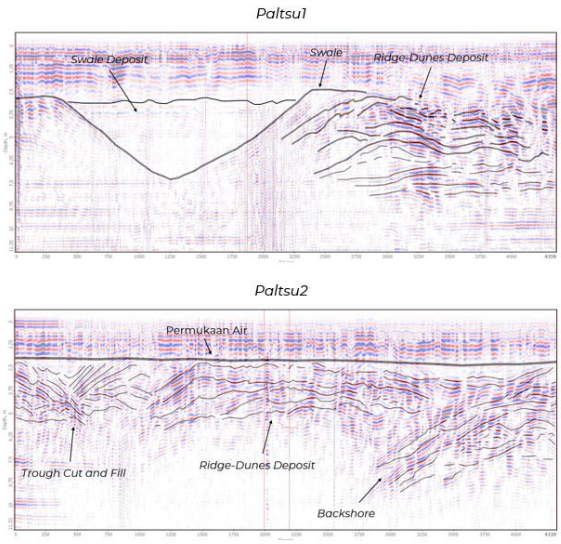

Figure 4: GPR Paltsu1 (Line 1) and Paltsu2 (Line 2) line drawing interpretation.

Paltsu1 (Figure 4) GPR profile located far east taken in a river path that had been covered by a ricefield leading to an isolated swamp. RF 1 and RF 2 can be identified in the profile showing a ridge-swale contact. Deposit inside the swale showing a blurry reflection that affected by saline water. The swale has a depth starting from 2.5 meters to the deepest part in 7.5 meters.

Paltsu2 (Figure 4) located in the middle and more towards the south compared to Paltsu1 and Paltsu3. Paltsu2 consist of RF 2, RF 3, RF 4, and RF 5. Trough cut and fill in Paltsu2 interpreted as the same as swale deposit in Paltsu1 because both was a river path that had been dried up. Furthermore, both RF 2 in Paltsu1 and Paltsu2 is also the same dunes feature extending west-east, meaning features in both profile is the same except backshore that had been found in Paltsu2. This dunes-backshore contact is one of the key in locating paleo-coastline location.

Paltsu3 (Figure 5) located north than other profiles, specifically in ricefield near public settlement. The aim of

acquisition in this area is to confirm that deposit in the north is dominated by mud. Water table at Paltsu3 is shallower at around 1 meter compared to Paltsu2 at 2 meters. There are almost no reflection below 3.75 meters, it is interpreted as a result of mud containing saline water in those area that absorb most of the wave. A shallow swale or coastal plain lie above the mud at shallow depth, about 1.25-2.5 meters.

Paltsu4 (Figure 5) located far west in study area with no features can be identified except two slope, one gently sloping seaward and the other moderately steep slope landward. Both of the slope could be connected forming a deep swale, or the gentle slope is a part of shallow swale and the moderately steep is a part of the same backshore as in Paltsu2. If the pattern of features is the same between Paltsu1, Paltsu2, and Paltsu 3, the latter interpretation is possible. However, it should be confirm with other methods.

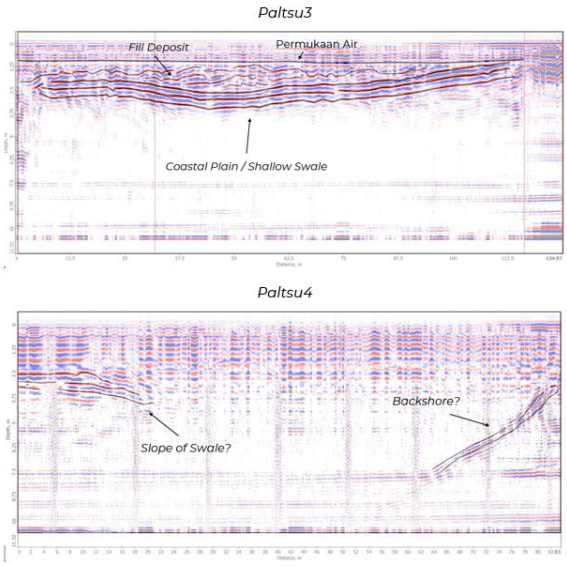

Figure 5: GPR Paltsu3 (Line 3) and Paltsu4 (Line 4) line drawing interpretation.

Figure 6: Beach dunes that separating the beach with coastal plain.

In locating the paleo-coastline in area of study, the presence of dunes-backshore is important because it can be compared to the same feature in the surface. Figure 6 shows a dunes that separating beach in the south and coastal plain in the north, showing a similarity with dunes deposit in Paltsu2. That dunes is extending west-east and can be found from main river (west) to Danau Talanca (east). The distance from dunes-backshore contact (Figure 6) to coastline is measured around 205 meters. With the same assumption that is used in remote sensing, where the present is a guide to interpret the past, the paleo-coastline would be located around 205 meters southward from backshore in Paltsu2.

Conclusions

Based on remote sensing and GPR analysis, it can be concluded that there are a shift of coastline seaward. Remote sensing analysis showing some similarity between dried up (in the north) and active (continuing to the south) river path/branches. Those similarity show a iteration of feature in the same area, such as river that branches into two, one flowing west forming a lake/swamp, and the other meets the sea. Those evidence indicate a flow of river changes more towards the sea. Subsurface analysis with GPR found a dunes-backshore contact at Paltsu2 profile that have similarity with the dunes-backshore contact that is found at the surface. Measured distance from surface dunes-backshore contact to surface coastline is around 205 meters. Therefore, using that information, the location of paleo-coastline is interpreted around 205 meters southward from the dunes-backshore contact that is found in GPR Paltsu2 profile.

References

Aswan, Zaim, Y., Rizal, Y., Sukanta, I. N., Anugrah, S. D., Hascaryo, A. T., Gunawan, I., Yatimantoro, T., Weniza, Hidayanti, Hawati, P., Santoso, W. D., & Nurochim. (2017). Age determination of paleotsunami sediments around Lombok Island, Indonesia, and identification of their possible tsunamigenic earthquakes. Earthquake Science.

Bristow, Charlie S., Chroston, P. Neil, Bailey, Simon D., 2000, The structure and development of foredunes on a locally prograding coast: insights from ground-penetrating radar surveys, Norfolk, UK. International Association of Sedimentologists.

Deng, Han. (2018). Assessing Tsunami Risk in Southwest Java, Indonesia: Paleo-Tsunami Deposits and Inundation Modeling. BYU Scholars Archive.

Gouramanis, C., Switzer, A. D., Polivka, P. M., Bristow, C. S., Jankaew, K., Dat, P. T., Pile, J., Rubin, C. M., Yingsin, L., Ildefonso, S. R., & Jol, H. M. (2015). Ground penetrating radar examination of thin tsunami beds - A case study from Phra Thong Island, Thailand. Sedimentary Geology.

Ishimura, D., & Yamada, K. (2019). Palaeo-tsunami inundation distances deduced from roundness of gravel particles in tsunami deposits. Scientific Reports.

Putra, P. S., Yulianto, E., Praptisih, Supriatna, N., Trisuksmono, D., Amar, Nurhidayati, A. U., Ridwan, J., & Griffin, J. (2015). Paleotsunami Study in the South Coast of Jawa. Prosiding Pemaparan Hasil Penelitian.

Zulkarnain, D. A., Amijaya, H., & Yulianto, E. (2017). Karakteristik endapan paleotsunami di pesisir binuangeun, daerah wanasalam, banten. Proceeding, Seminar Nasional Kebumian Ke-10.

PROCEEDINGS
JOINT CONVENTION BANDUNG (JCB) 2021
November 23rd – 25th 2021

A New Concept of Sedimentation Process and Ancient Volcanic Activity of Semilir Formation in Ngoro-Oro and Nglanggeran, Gunung Kidul, Yogyakarta

Andika Nugraha[1], C. Prasetyadi[2], Hirundini Rustica Absari[2], Jessica Astrid Kartika[2]
[1]PT. Sebuku Iron Lateritic Ores, [2]Universitas Pembangunan Nasional "Veteran" Yogyakarta

Abstract
Intensive volcanism activity from Semilir Formation is well recorded and widespread. Therefore, studying to enhance understanding of past geological processes in the Southern Mountains is an exciting thing. The studied area is situated in the Ngoro-oro area, Nglanggeran, using the Stratigraphic Cross Sections method. The results were analyzed using a volcano stratigraphic approach and presented in a structured stratigraphic section. The lithology in this area is composed of thick and firmly welded lapillistone, coarse tuff, fine tuff, calcareous tuff, volcanic sandstone rich in charcoal, calcareous volcanic sandstone, and claystone with several erosional contacts.
Furthermore, various sediment structures include massif, parallel stratification, parallel lamination, cross lamination, diffuse lamination, convolute, ripple, flaser, and reverse graded bedding. The lithology is a primary pyroclastic product and a post-eruption sedimentation product. The lithofacies is divided into pyroclastic flow (p-f), pyroclastic surge (p-s), pyroclastic fall (p-f), resedimented mass flow (rs-mf), and resedimented traction (rs-t). The lithology was deposited by mass flow, traction, and suspension mechanisms and showed the valley-pond filling geometry. The lithological arrangement was deposited in the transitional at the estuarine area with the eruption source originating from the north and located in terrestrial. The eruption product is from a plinian type eruption with a caldera in a destructive phase and occurred repeatedly. The product of volcanic activity caused local scale regression in the past.

Introduction
The Southern Mountains Region in Java island was chosen for studied area by geological researchers and students to study geology because of variation of well-preserved exposed lithologies, from metamorphic rock of Basement, volcanic deposits and intrusion rocks of Kebo Butak, Semilir, Nglanggeran, and Sambipitu Formation, to carbonate rocks of Oyo, Wonosari, and Kepek Formation (Surono, 1989). These formations are in age from Late Cretaceous to Pliocene. So it can tell the condition of Java Island in the past and evolution until today.

The Semilir Formation is attracting considerable due to deposits are the result of huge Early Miocene eruption (Smyth et al., 2011) and widely spreading from the western part of the Baturagung Range (Parangtritis, Yogyakarta) to the Pacitan Regency (Surono, 2008). It is dominated by pyroclastic rocks, which are grouped into four lithological units. They are sandstone, lapilli tuff, pumice breccia, and andesitic pumice breccia. The research is located at good outcrops in Ngoro-oro, Nglanggeran, Gunung Kidul Regency, Yogyakarta, Indonesia. The study was conducted in an area located in Easting 48871 and Northing 34437. (Figure 1). Based on these studies, We hope that our research will help enhance the understanding of past geological processes in the Southern Mountains.

Data and Method
This research used outcrop observation, rock sampling, and laboratory analysis to collect data. Measurement of the measured stratigraphic cross-section was carried out to determine the sedimentation process and the interpretation of the depositional period. The measurement of the stratigraphic cross-section at the exposed location is carried out by making continuous lithological records, where rock samples are observed in megascopic and petrographic analysis to determine differences in their characteristics.

Result and Discussion
Lithology in the Ngoro-oro area by volcaniclastic rocks can be grouped into pyroclastic deposits, sedimentation deposits, and volcanogenic deposits. Pyroclastic deposits are formed directly in a hot state by primary eruption processes such as flow gusts and falls. Re-sedimentation deposits formed by the rapid deposition of post-eruption autoclastic or pyroclastic materials that do not show significant textural changes and show a composition that tends to be uniform. Volcanogenic deposits formed from the erosion of existing volcanic deposits with a long pause in primary eruptions. Studies of volcaniclastic deposits need to pay attention to the process of clastic formation, the process of transportation and deposition of clastic as well as textural evidence that shows deposition during hot conditions.

The lithological arrangement presented in the measured stratigraphic cross-section is 42.42 m and the lithological arrangement can be grouped into four columns (Figure 2 and 3). The column division is based on physical characteristics (texture and sedimentary structure) and the average thickness of a lithology. The explanation of the column is carried out by paying attention to the direction of the layer's slope and starting from the fourth column with the oldest lithological arrangement to the first column with the youngest lithological arrangement.

The fourth column has 7.15 meters of thickness composed by alternating thin fine tuff with parallel layered structures with coarse-fine-sized carbonate volcanic sandstones rich in charcoal and pumice with parallel layered structures, ripple, flaser, and diffuse lamination, also local claystone inserts. The third column has 6.69 meters of thickness composed by alternating fine tuff and coarse tuff with parallel layered structures, cross lamination, convolute, and

parallel lamination with volcanic sandstone rich in charcoal and pumice with parallel lamination and cross lamination structures and local insertions of lapilli with parallel lamination and cross structures lamination. The second column has 19.6 meters of thickness composed of thick and well-welded lapilli with normal graded bedding on the bottom which is rich in lithic and reversed graded bedding on the top which is rich in pumice with crystal tuff

lenses. The first column has 8.98 meters of thickness composed by alternating lapilli with parallel lamination structure, cross lamination and diffuse lamination, fine and coarse tuff with a parallel layered structure, cross lamination, convolute and parallel lamination with charcoal-rich volcanic sandstone, and pumice with parallel lamination, cross lamination structure, and diffuse lamination and local claystone inserts. Lithological features can be seen in Figure 4.

Petrographic analysis was carried out on pumice breccia, pumice sandstone, carbonaceous sandstone, carbonate pumice breccia, and tuff (Table 1). Based on the classification of After Schmid (1981), these samples belong to the Tuffites group (mixed pyroclastic epiclastic). The rock names for mixtures of pyroclastic and epiclastic fragments in the research area are Tuffaceous Sandstone and Tuffaceous Siltstone. The presence of carbonate cement in the carbonate pumice breccia belongs to the epiclastic group.

Studies of volcaniclastic deposits need to consider the process of clastic formation, the process of transportation, and deposition of clastic as well as textural evidence that shows deposition during hot conditions. Volcanic sandstones were both non-carbonated and present as sedimentation and volcanogenic deposits. Re-sedimentation deposits are characterized by their relatively homogeneous composition, rich in pumice and charcoal as a product of an eruption, and the cross-lamination and parallel lamination sedimentary structures reflecting high energy. Fine tuff is present as falling pyroclastic deposits. In addition, this lithology together with coarse tuff is also present as pyroclastic surge and fall deposits. Lapilli is present as pyroclastic flow deposits resulting from explosive eruptions characterized by their very thick appearance, crystal tuff lenses, and welding from welding under hot conditions. These deposits can be compared to ignimbrite/pumice and ash deposits. Pyroclastic flow deposits are characterized by their relatively thick appearance and welding as a result of welding under hot conditions while pyroclastic surge deposits are characterized by their appearance associated with pyroclastic flow deposits, well layered, relatively thin, and high energy sedimentary structures such as cross lamination, convolute, and parallel lamination. Based on the appearance of the field, pyroclastic surge deposits can be divided into two, namely base surge deposits which precede pyroclastic flow deposits, and ash cloud surge deposits which superimpose flow pyroclastic deposits. Genetically, flow and surge deposits are deposits that form together in one eruption.

The sedimentation mechanism is a reflection of the transportation process and rock sedimentation by various agents, such as air, air, wind, and volcanic gases. There are three mechanisms of sedimentation, namely mass flow, traction, and suspension. In mass flow, particles and fluids are mixed, move, and interact together. This mechanism is characterized by a thick appearance, poorly sorted, and supported matrices. In traction, the particles are free to move in a flowing stream and are characterized by sedimentary structures such as cross lamination and ripple, which are well layered and relatively well sorted. In suspension, particles are suspended in a fluid and generally occur in very fine-sized rocks. All of these mechanisms were observed in all volcaniclastic rocks in the Ngoro-oro area.

The environmental approach with the model from McPhie; 1993 (Figure 5) shows that the depositional conditions of Ngoro-oro is in the shoreline environment. This is also shown from the lithofacies in the form of carbonate composition, relatively fine-sized volcanogenic material, also ripple and flasher sediment structures that reflect the estuarine-transitional environment. The transitional environment shows a systematic succession of mass flow of re-sedimentation, mass-flow pyroclastic, and traction of re-sedimentation lithology with the contacts of each depositional sequence bounded by erosional contacts. In this environment, traction and suspension sedimentations are dominant and deposition may occur in deltas or other offshore environments. This environment is an important environment for volcanoes that are near the coast or volcanic islands.

In general, the lithological arrangement from the fourth column to the first column shows a gradation of volcanism processes that were initially not very active in the old part to become very active and destructive in the young. In the first column, the well-developed volcanogenic deposits and the lack of pyroclastic deposits show that the volcanism activity is relatively calm. In the second column, volcanism activity is increasing. This resulted in the number of volcanogenic deposits starting to decrease and the number of pyroclastic deposits starting to increase. In the third column, evidence of intensive and more explosive volcanism compared to the previous eruption is recorded. This eruption was also sudden due to the striking difference in succession when compared to the previous succession shown in the first and second columns. The source of the eruption comes from land and is shown by the presence of charcoal as a remnant of roasted vegetation and carried away by the eruption process. The source of the eruption is a caldera and has experienced a Plinian eruption and is destructive. This is shown by the abundance of sour pumice. The filling of the channel as a material transportation route is shown from the aspect geometry valley-confined filling of the lapilli which shows a flat top contact and a thinning layer in the north. The transitional environment on this coastline is a distal environment that is far from the source. This is also shown from the minimal concentration of heavy lytic material deposited. Even if they exist, they are relatively subtle and are found locally. In the fourth column, volcanism activity after the eruption of the third column continues. Pyroclastic flow deposits that are thick and higher than the past sea level are thought to have caused the sea level to be covered so that the height of the plains increases and the sea level decreases. This is shown from the succession in the fourth column to the second column. The volcanism activity is getting higher and lower. This is thought to be due to the effect of the eruption on the third column having exhausted the magma stored in the volcano. The close genetic relationship between sedimentation deposits in the marine/transition environment and flow pyroclastic

deposits from the terrestrial environment is good evidence showing that pyroclastic flow deposits fill valleys and will follow drainage channels to reach the sea, have a transport range of several kilometers, formed around volcanic islands and has a history of eruptions capable of reaching the coast.

PROCEEDINGS
JOINT CONVENTION BANDUNG (JCB) 2021
November 23rd – 25th 2021

Conclusions

Ngoro-oro area is part of the Semilir Formation, composed of pyroclastics and post-eruption re-sedimentation deposits. Pyroclastic deposits show the results of pyroclastic processes of flow, surge, and fall. The mechanisms of transportation and sedimentation of sediment by mass flow, traction, and suspension. Based on the sediment structure in the field, the depositional environment at the study area is the transitional environment, precisely on the shoreline. From measurable stratigraphic measurements, it can be concluded that the source of the eruption is a caldera that has a Plinian eruption type and is destructive. The lithological arrangement from the fourth column to the first column shows a gradation of volcanism processes which were initially not very active in the old part to become very active and destructive in the young one.

References

Atmadja, R.S., R.C. Maury, H. Pringgoprawiro, M. Polve, and B. Priadi, 1994, Journal of Southeast Asian Earth Science, **9**, 13-27.

Nugrahini, A., V. Isnaniawardhani, A. Sudradjat, and N. Sulaksana, 2019, , International Journal of GEOMATE, **16**, 154-162.

Song, Sheng-Rong, and Huann-Jih Lo, 2002, Journal of Asian Earth Science **21**, 23-38.

Smyth, H.R., Q. G. Crowley, R. Hall, P. D. Kinny, P. J. Hamilton, and D. N. Schmidt, 2011, Lithos **126**, 198-211.

Smyth, H.R., R. Hall, and G.J. Nichols, 2008, Journal of Sedimentary Research, **78**, 335-356.

Figure and Table

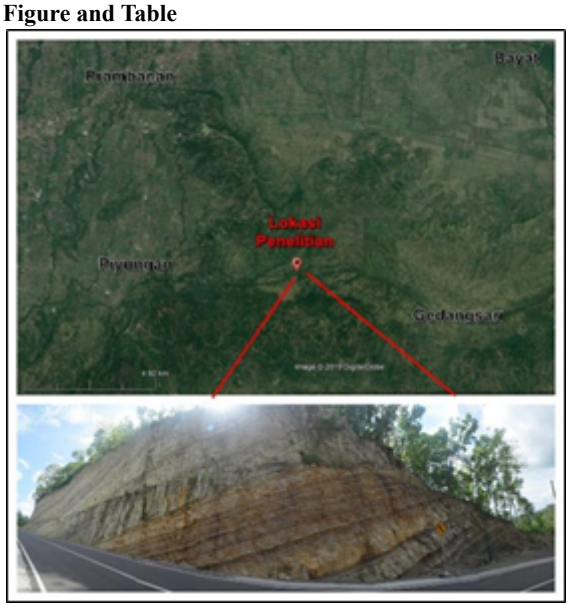

Figure 1. Location of the Ngoro-oro area the appearance of the stratigraphic cross-section measurement location.

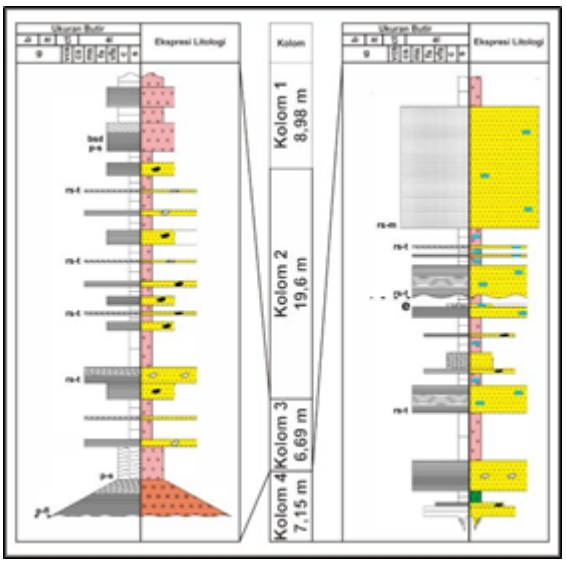

Figure 2.The lithological arrangements of the third column and the fourth column which are lithological arrangements are older and are located under the first and the second columns.

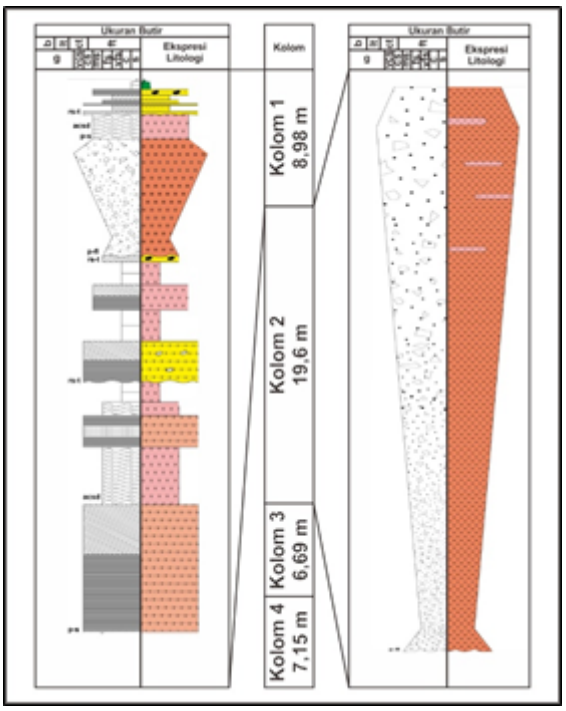

Figure 3. The lithological arrangement of first and second columns which is a younger lithological arrangement and is located above the third and the fourth column.

PROCEEDINGS
JOINT CONVENTION BANDUNG (JCB) 2021
November 23rd – 25th 2021

Figure 4. a. Lithological arrangement at the bottom of the stratigraphic cross-sectional measurement. b. Flaser sedimentary structures in carbonate volcanic sandstones. c. Pumice welded firmly to lapilli. d. Cross lamination sedimentary structure in volcanic sandstone with oxidized charcoal fragments.

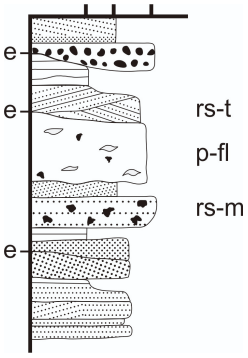

Figure 5. Succession of volcaniclastic deposits in shoreline environments based on the McPhie model (1993), rs - resedimented syn-eruptive deposit; t - traction; m - mass flow; p - pyroclastic deposit; fl - flow.

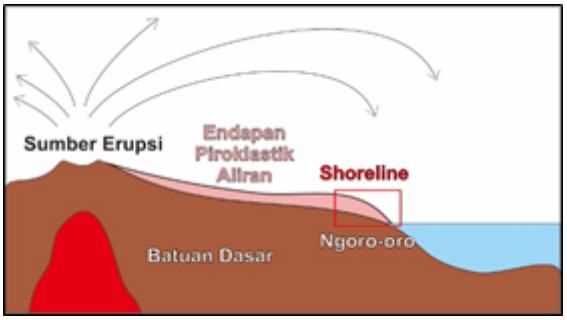

Figure 6. Ngoro-oro Area Depositional Environment Scheme.

PROCEEDINGS
JOINT CONVENTION BANDUNG (JCB) 2021
November 23rd – 25th 2021

Table 1. Petrography Analysis Description of selected rock samples

NO.	DESCRIPTION	IMAGES	
		OBJECTIVE LENS 4X	OBJECTIVE LENS 10X
1	**PUMICE BRECCIA** **Grain size:** 0,1-2,5 mm (Sand) **Composition:** Fiamme Tuff (1%), Plagioclase (20%), Pyroxene (1%), Vitric Tuff (43%), Crystal Tuff (20%), Quartz (5%), Lithic Tuff (10%) **Petrography name:** *Tuffaceous sandstone (After Schmid, 1981)*	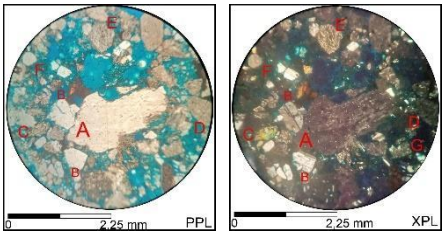	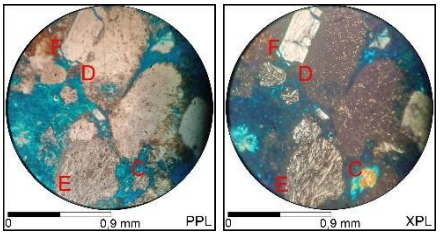
2	**PUMICE SANDSTONE** **Grain size:** 0,1-0,5 mm (Sand) **Composition:** Plagioclase (1%), Pyroxene (2%), Vitric Tuff (10%), Quartz (35%), Lithic Tuff (45%), Glass (3%), Fossil (1%), Charcoal (3%) **Petrography name:** *Tuffaceous sandstone (After Schmid, 1981)*	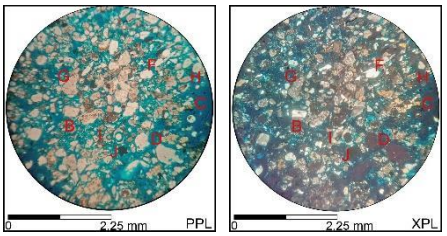	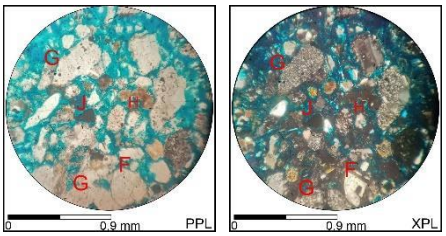
3	**CARBONACEOUS SANDSTONE** **Grain size:** 0,1-0,5 mm (Sand) **Composition:** Plagioclase (10%), Pyroxene (5%), Vitric Tuff (5%), Quartz (30%), Lithic Tuff (20%), Charcoal (5%), Crystal Tuff (25%) **Petrography name:** *Tuffaceous sandstone (After Schmid, 1981)*	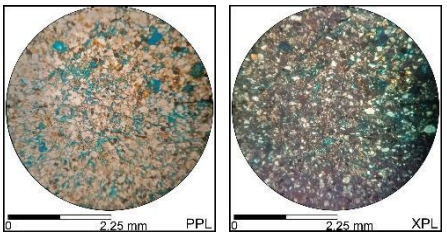	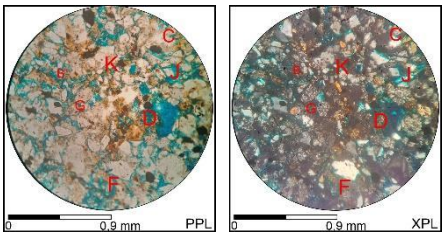
4	**PUMICE BRECCIA RICH IN CHARCOAL** **Grain size:** 0,1-1 mm (Sand) **Composition:** Plagioclase (10%), Crystal Tuff (10%), Quartz (30%), Carbonate (40%), Charcoal (5%), Hornblende (5%) **Petrography name:** *Sandstone (After Schmid, 1981)*	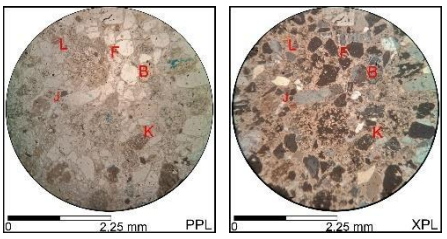	
5	**TUFF** **Grain size:** >0,2 mm (Sand-Clay) **Composition:** Plagioclase (10%), Pyroxene (5%), Charcoal (20%), Fossil (2%), Dust grain sized material (43%), Quartz (20%) **Petrography name:** *Tuffaceous siltstone (After Schmid, 1981)*	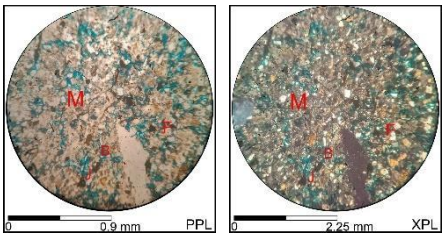	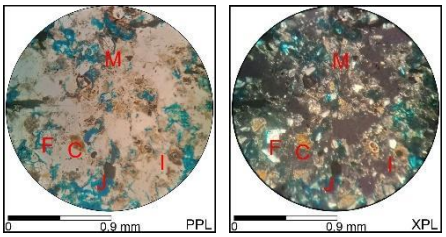

Notes: Fiamme Tuff (A), Plagioclase (B), Pyroxene (C), Vitric Tuff (D), Crystal Tuff (E), Quartz (F), Lithic Tuff (G), Charcoal (H), Fossil (I), Charcoal (J), Crystal Tuff (K), Hornblende (L), Dust grain sized material (M)

PROCEEDINGS
JOINT CONVENTION BANDUNG (JCB) 2021
November 23rd – 25th 2021

Morphotectonic Segmentation Analysis Using GIS Approach in Muaro Kalaban Region, West Sumatra

Muhammad Rizky Tanjung [1], Kevin Nabil Hibatullah[2], Ugi Kurnia Gusti[3]
Geological Engineering, Sriwijaya University, Palembang[1,2]
Mc Master University, Hamilton, Canada[3]

Abstract

Morphotectonic analysis using a GIS approach is an effective method for inferring patterns and spatial variations of tectonic activity. Muaro Kalaban has a complex morphology with various tectonic processes that influence it. This study was intended to determine the relationship between morphology and tectonic activity in the Muaro Kalaban area. The flow of this research is carried out through a series of interpretations divided into 3 segments, making maps of morphological distribution, the direction of lineament patterns, interpretation of lineament in satellite imagery, and field mapping. Muaro Kalaban is heavily influenced by tectonic activity. Tectonic processes that produce strike-slip fault structures, normal faults, and rising faults form a variety of valleys and hills lineaments with various orientations. The general lineament pattern of the study area shows the similarity in the NE-SW (Northeast-Southwest) direction with the main force in the NW-SE (Northwest-Southeast) direction with different lineament intensities. Field identification relates the morphology resulting from the process of formation of the left horizontal fault of Muaro Kalaban with the restraining bands phenomenon that results in the formation of the geometry of the folds. Muaro Kalaban is influenced by various active tectonisms that affect the process of morphological formation, whether in the form of hills or valleys.

Keywords: Morphology, Tectonics, Muaro Kalaban, Lineament, Fault.

Introduction

Muaro Kalaban is geographically located in Sawahlunto City, West Sumatra Province. Geologically, Muaro Kalaban is in the Ombilin Basin which is located in the Barisan Mountains. The Ombilin Basin is formed from two types of microplates, namely the Mergui continental microplate which formed Sundaland in the Late Triassic with Malacca and East Malaya. Then continued with the Woyla oceanic microplate accretion during the Late Mesozoic (Pulunggono and Cameron, 1984). The location of Muaro Kalaban can be seen in Figure 1.

Muaro Kalaban geologically belongs to the Ombilin Basin. Koesoemadinata and Matasak (1981) explained that the Ombilin Formation consists of gray carbonate and carbonate clay rocks with alternating thin layers of carbonate sandstone. The Ombilin Basin is stratigraphically based on Pre-Tertiary rocks consisting of the Silungkang Formation and the Tuhur Formation. Then proceed with Tertiary deposition consisting of the Brani Formation, Sangkarewang Formation, Sawahlunto Formation, Sawahtambang Formation, and Ombilin Formation (Koesoemadinata and Matasak, 1981; Situmorang, et al. 1991; Yarmanto and Fletcher, 1993).

The Silungkang Formation consists of lithology in the form of limestone and andesitic volcanic rocks. The andesite rock in this formation is part of the Mergui microplate. Silitonga and Kastowo (1975) stated that the andesite rocks in this formation were interpreted to be of the Permian-Carbon age. Meanwhile, according to Barber and Crow (2005), Silungkang andesite is interpreted to be associated with rocks found in the Palepat Formation, South Sumatra.
The Tuhur Formation is also a member of the Mergui microplate. The Tuhur Formation is of the Triassic age which is characterized by its characteristic lithology in the form of slate. According to Koesoemadinata and Matasak (1981), the quartzite and slate of the Tuhur Formation intermingle with the volcanic Silungkang Formation.
The Sawahtambang Formation is stratigraphically the youngest deposited, located above the Sawahlunto Formation and the Brani Formation with the presence of erosional fields (Koning, 1985; Situmorang, et al., 1991). This formation consists of Tertiary rocks that were deposited during the Oligocene (Koesoemadinata and Matasak, 1981; Koning, 1985; Situmorang, et al. 1991; Yarmanto and Fletcher, 1993).

The Ombilin Basin is part of the Central Sumatra Basin, which is precisely located in the Barisan Mountains, Sumatra Island. The Ombilin Basin forms a geological structure in the form of a graben as a result of tectonic activity at the beginning of the Tertiary (Widayat, et al., 2015).
Mulyana (2005), states that there are four phases in the development of the Ombilin basin as follows:

1. Early Eocene-Early Oligocene
At this time the formation of the Ombilin basin began with the occurrence of a transtensional motion due to the regional duplex fault, namely the graben in the northwest part of the Ombilin basin. The fault pattern plays a role in controlling the formation of the first basin so that the formation of faults trending northwest-southeast, north-south, northeast-southwest, and west-east.

2. Late-Early Miocene Oligocene
In this phase, the rotation of the island of Sumatra starts counterclockwise. The first rotation occurred at 20º-25º centered on In addition, at this time it was also marked by the occurrence of an initial transgression accompanied by an increase in the part of the Ombilin basin and in another part a decrease as a place for deposition of the constituent rock materials of the Ombilin Formation. Early Miocene-Middle Miocene, volcanic activity in the India block increased, followed by an uplifting process. Thus, the normal -

PROCEEDINGS
JOINT CONVENTION BANDUNG (JCB) 2021
November 23rd – 25th 2021

subduction pattern in Sumatra changes to an oblique subduction pattern.

3. Late Middle Miocene-Resen
The second stage of rotation was followed by the break-up and accretion of oceanic crust from the Andaman Sea. At the time of the Late Middle Miocene, the movement of the Indo-Australian plate that led to the west coast of Sumatra was constant. Then, rotate again with the trend N135ºE. This also has an impact on increasing the angle of subduction from N40º to 60º which has an impact on the occurrence of uplifting on the Bukit Barisan and continued volcanic activity to Resen.

Data and Method
The method used in this research is through a series of morphological and tectonic analysis work. The morphological analysis includes the interpretation of the morphological distribution of the Muaro Kalaban area and the creation of a morphological cross-section of each volcanic body. The interpretation of the morphological distribution of Muaro Kalaban is carried out by compilation of the IFSAR satellites (5m resolution), TERRASAR-X (5m resolution), and ALOS PALSAR (11.25m resolution), by adding mass point data resulting from stereo-plotting so that the spatial resolution is 0.27-arcsecond (8 meters).) plus the 2008 EGM vertical datum.

The tectonic analysis includes lineament interpretation from satellite imagery using parameter classification algorithms (Thannoun R.G. 2013), depiction of rosette diagrams, and geological identification of the research area that results in the distribution of geological structures. Previous research by several researchers was used to support the analysis of this study.

Result and Discussion
There are three main segments in the study area (Fig. 2). Segments are divided horizontally based on observations of the density of the lineament pattern. The segment division aims to divide the research area into three main focuses so that the interpretation carried out is more detailed by covering several results (lineament and structural geology) and can describe the tectonic developments that occur.

1. Segment 1
Based on the lineament analysis carried out in segment 1, this area has a Lineament Density (LD) which tends to be less dense with the orientation of the main pattern in the NE-SW direction (Figure 3b). The direction of this structure is caused by the compression phase acting in the SE-NW direction. It is interpreted that the Northwest tends to be dominated by the normal Saranggangang fault with a positive morphology with a maximum height above 500 meters (Figures 4b and 4c), which are classified as high hills (Widyatmanti, 2016). On the Southwest and Northeast sides, it is interpreted that there are normal faults of Bukit Airdingin and Bukit Kaampat, with morphology in the form of evidence (Widyatmanti, 2016) which tends to be lower with a range of 250 meters (Figure 4d).

2. Segment 2
This region has a main lineament orientation with an NNE-SSW direction (Figure 5b). By observing the geological map, the SSE section in segment 2 has a lineament that tends to be denser and towards SSW the lineament density is decreasing. The direction of this structure is caused by the compression phase in the fourth phase when the Late Miocene worked in the SSE-NNW direction. It is interpreted that in the southern part of this segment is dominated by the Bukit Batutarpus fault and folds with hilly morphology (Widyatmanti, 2016). The elevation in this area ranges from 380-450 meters (Figures 6b and 6c). On the west side, it is interpreted that there are normal faults in Guguk Gapo and Muaro Kalaban. With a morphology in the form of hills that tend to be lower in the range of 250-450 meters (Figure 6d). Meanwhile, in the middle of this segment, folds were found from the restraining bands which were characterized by positive and negative morphology. Both types of morphology are influenced by uplifting on the Bukit Barisan during the Middle Miocene to Resen.

3. Segment 3
This area has the same orientation of the main lineament as segment 2, which is in the NNE-SSW direction (Figure 7b). Based on the geological map, the southwestern parts of segment 3 tend to have a lineament density that tends to be denser than the areas in the western part. This straightness is caused as a result of the compression force acting in the SSE-NNW direction. In the eastern part of this segment, it is interpreted that there is a normal fault in the Tampunik Hill which is characterized by very striking morphological changes (Figure 8d). The compression that occurred during the Middle Miocene to Resen in Sumatra caused uplifting which led to the formation of the Uplift Fault around Parhatianbaras Hill, Padanglawas Hill, and Iban Hill. Thus, it produces a positive morphology with elevations ranging from 250-520 meters (figures 8b and 8c). Thus, based on the classification of Widyatmanti (2016) segment 3 is an area of hills to high hills.

Muaro Kalaban Fault is interpreted based on several supporting elements, namely the existence of lineaments and differences in morphological expressions as well as the presence of an accompanying structure (Figure 9) in the form of a 2nd order drag fold (Moody and Hill, 1956).

Based on the measurement results from the data of structural elements carried out in the field, the wing positions are N22ºE/21º and N259ºE/27º (Figure 10). From these data, a stereographic kinematics analysis of the structure was carried out. The results of the analysis show that this 2nd order drag fold has a hinge line with a trend (trend) of N55ºE and a plunge of 12º and a hinge surface of N55ºE/87º. Based on the naming of the fold according to the classification of Lisle and Leyshon (2004), it was found that this type of fold can be categorized as an Upright Gentle Plunging Fold.

The formation mechanism of the Muaro Kalaban Horizontal Fault occurs as a result of a compression tectonic activity that causes a lateral shift which in one part experiences a mechanism in the form of a collision and forms a fold or is generally known as a pop-up structure according to Legg, M. R., et al (2007). Meanwhile, according to Cunningham (2007), such strike-slip tectonic products are called restraining bands. The morphology that expresses the formation process of the Muaro Kalaban Drag Fault and its relationship to the presence of restraining bands in the form of the Muaro Kalaban Fold can be seen in (Figure 11).

Conclusions
1. The general orientation of the lineament of the study area formed in 3 main segments shows the similarity in the direction of NE-SW (Northeast-Southwest) with the main force of NW-SE (Northwest-Southeast).

2. The structural pattern of segment 1 is caused by the compression phase acting in the SE-NW direction. It is interpreted that the Northwest tends to be dominated by

ascending faults with positive morphology with a maximum height of above 500 meters.
3. The direction of the segment 2 structure is caused by the compression phase in the fourth phase when the Late Miocene worked in the SSE-NNW direction. It is interpreted that the southern part of this segment is dominated by rising faults and folds with hilly morphology.
4. Compression that occurred during the Middle Miocene to Resen in Sumatra caused uplifting resulting in a positive morphology with elevations ranging from 250-520 meters in segment 3.
5. The presence of the Muaro Kalaban Fault is evidenced by the accompanying structure on the N22ºE/21º and N259ºE/27 flank position data. So the results of the analysis show that this 2nd order drag fold has a hinge line with a direction (trend) of N55ºE and a plunge of 12º and a hinge surface of N55ºE/87º. This type of fold can be categorized as an Upright Gentle Plunging Fold. (Lisle and Leyshon, 2004)

References

Barber, A.J., Crow, M.J., and Milsom J.S., 2005, Geological Society.
Katili, J., 1975, Tectonophysics.
Koesoemadinata., R.P., Matasak., 1981, Procc. Indon, Petrol Assoc.
Koning. T., 1985, Proc. Indon. Petrol. Assoc., 14th Annual Con.
Legg, M.R. et al., 2007, Geological Society, London, Special Publications, 290, 143.
Lisle, R. J. and Leyshon, P. R, 2004, Stereographic Projection Techniques for Geologists and Civil Engineers, 2nd ed. viii+112 pp.
Moody, J. D., dan Hill, M. J., 1956, Bulletin of the Geological Society of America 67, 1207 – 1246.
Mulyana, Budi., 2005, thesis, Padjajaran University.
Pulunggono, A., and Cameron, N.R., 1984, Proc. . Petrol. Assoc. Conv., 13th Annual Con.
Lisle, R. J. and Leyshon, P. R, 2004, Stereographic Projection Techniques for Geologists and Civil Engineers, 2nd ed. viii+112 pp.
Moody, J. D., dan Hill, M. J., 1956, Bulletin of the Geological Society of America 67, 1207 – 1246.
Mulyana, Budi., 2005, thesis, Padjajaran University.
Pulunggono, A., and Cameron, N.R., 1984, Proc. . Petrol. Assoc. Conv., 13th Annual Con.
Situmorang. B., Yulihanto. B., Guntur. A., Himawan. R., dan Gamal Jakob., 1991, Proc. Indon. Petrol. Assoc. Twentieth Annual Con.
Thannoun, R. G. 2013, International journal of enhanced research in science technology & engineering, 2.
Widyatmanti, Wirastuti et al., 2016, IOP Conf. Ser.: Earth Environ. Sci. 4.
Yarmanto dan Fletcher, G., 1993, proceedings IPA

PROCEEDINGS
JOINT CONVENTION BANDUNG (JCB) 2021
November 23rd – 25th 2021

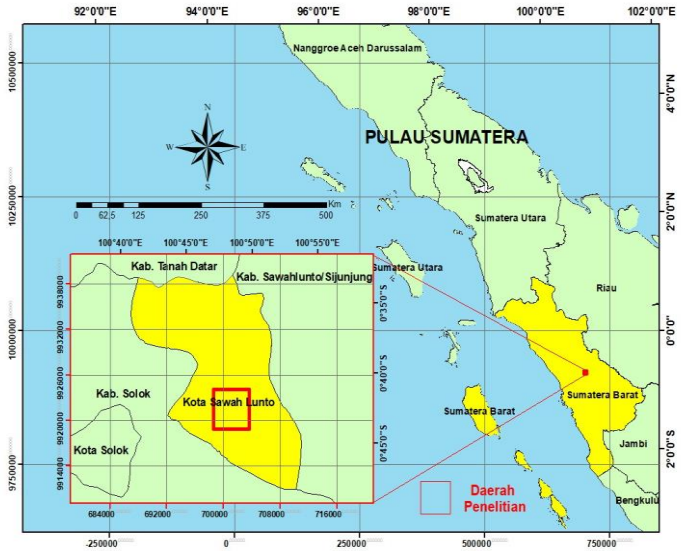

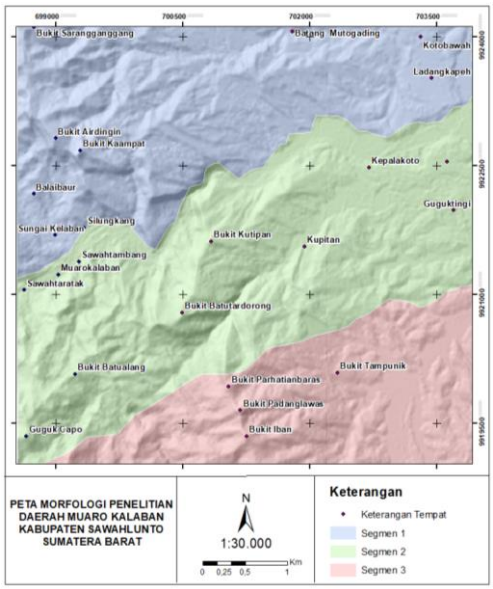

Figure. 1 (left). Location of Muaro Kalaban; **Figure. 2** (right) Research Morphology Map

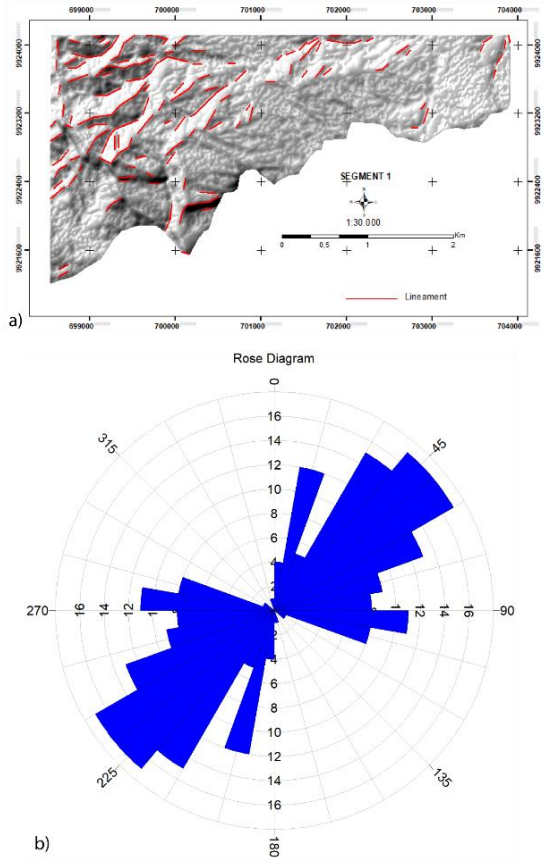

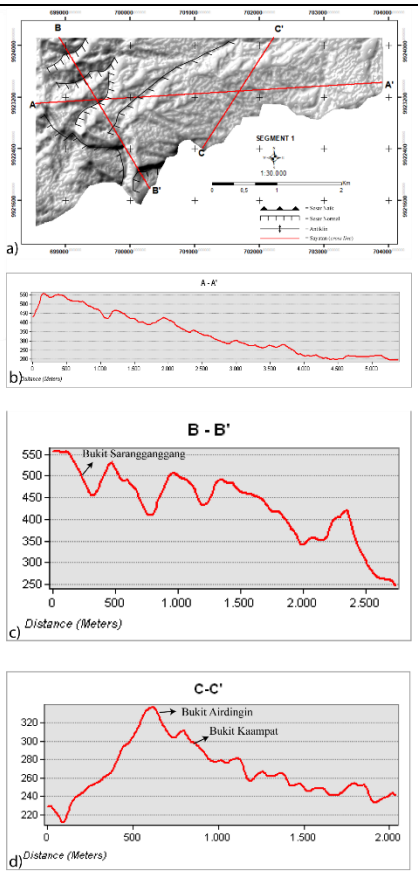

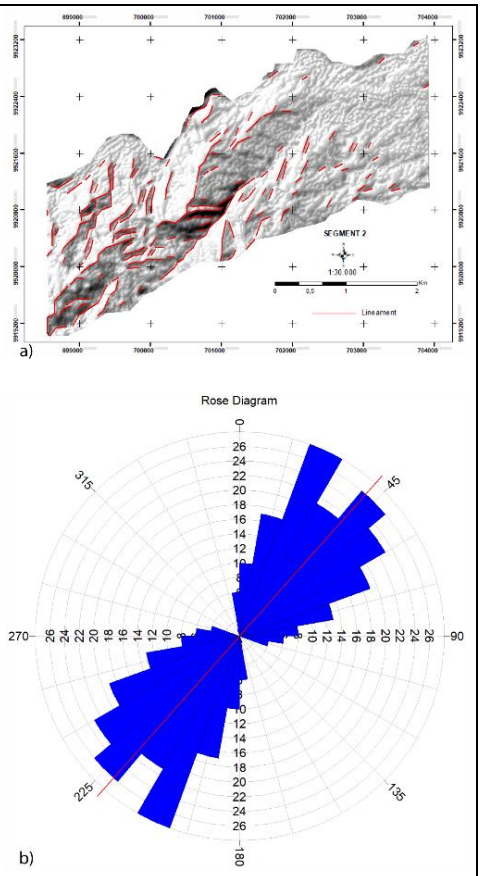

Figure 3 (left): a) Lineament pattern of segment 1; b) The general pattern of the lineament of segment 1; **Figure 4** (center): a) Cross section in segment 1; b) A-A' cross section; c) B-B' cross section; d) C-C' cross section; **Figure 5** (right): a) Lineament pattern of segment 2; b) The general pattern of the lineament of segment 2.

PROCEEDINGS
JOINT CONVENTION BANDUNG (JCB) 2021
November 23rd – 25th 2021

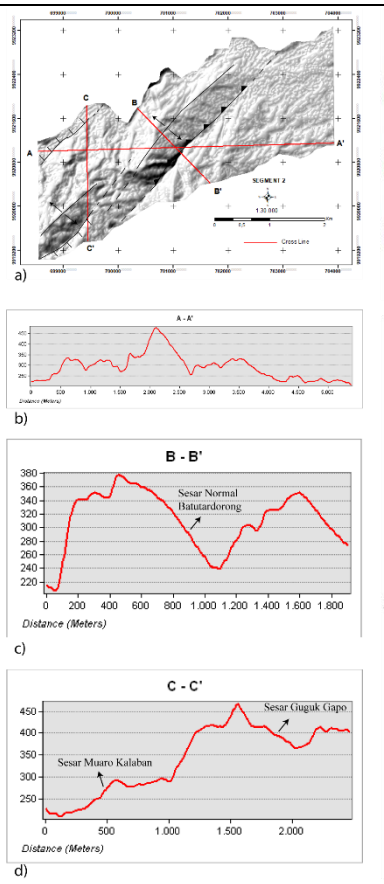

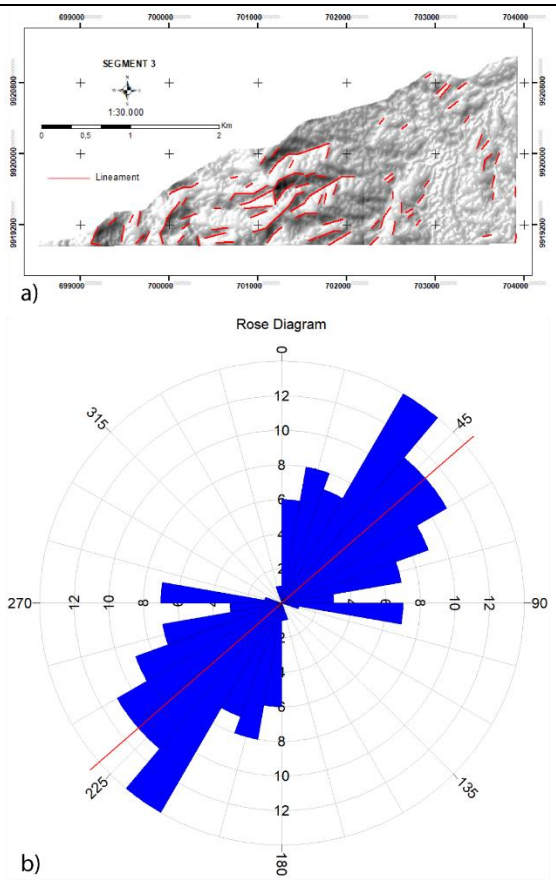

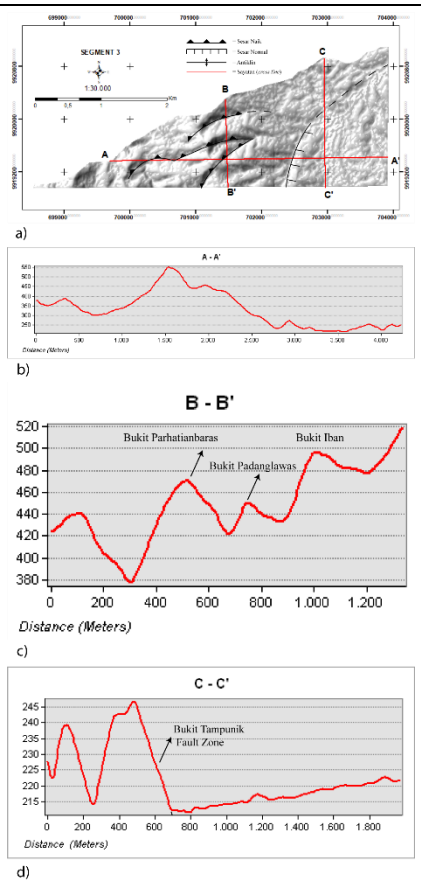

Figure 6 (left): a) Lineament pattern of segment 2; b) The general pattern of the lineament of segment 2; **Figure 7** (center) : a) Lineament pattern of segment 3; b) The general pattern of the lineament of segment 3; **Figure 8** (right): a) Lineament pattern of segment 3; b) The general pattern of the lineament of segment 3.

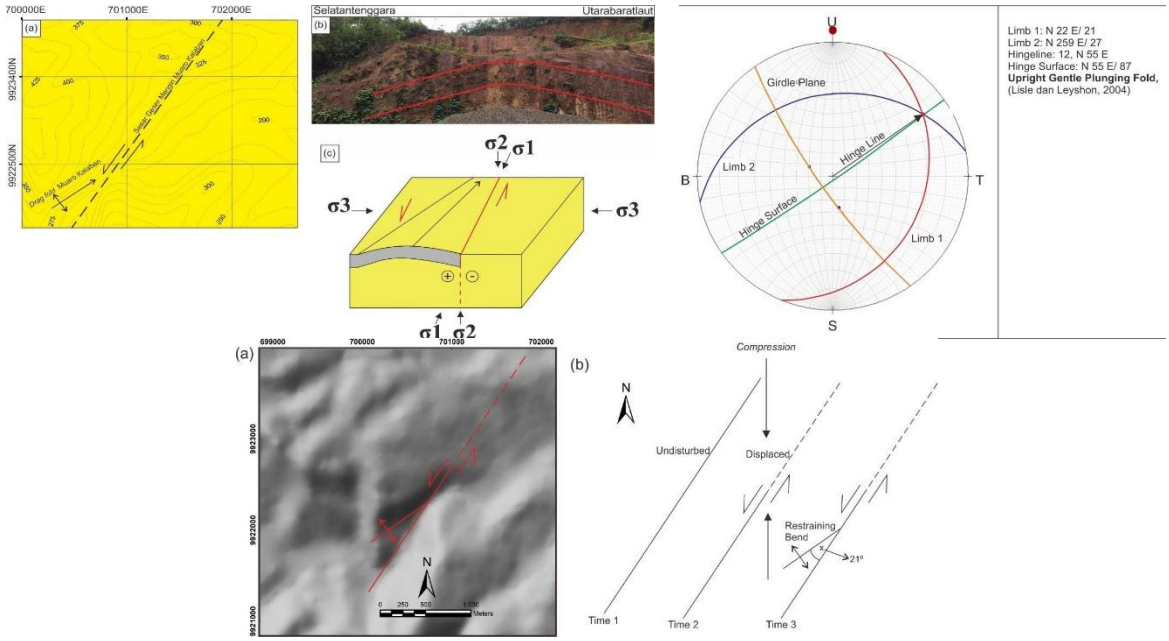

Figure 9 (left): a) Structure restraining bands on the geological map; b) Antiklin fold interpretation based on field mapping; c) The schematic model of the left horizontal fault with a 2nd order drag fold (modification from Cunningham, 2007); **Figure 10**: Stereographic kinematics analysis results from the Muaro Kalaban drag fold which shows the axis in the Northeast-Southwest direction and has a plunging value of 12º; **Figure 11**: a) Digital Elevation Model (DEMNAS) map of the location of the Muaro Kalaban Fault; b) the structural evolution model of the Left Horizontal Fault formation controlled by the transpression regime forming 2nd order drag folds (modification from Cunningham, 2007).

PROCEEDINGS
JOINT CONVENTION BANDUNG (JCB) 2021
November 23rd – 25th 2021

Thrust Fault Deformation Phases, Insight from Analogue Sandbox Modelling

Terry Alfa Furqan (Institut Teknologi Bandung)
Benyamin Sapiie (Institut Teknologi Bandung)

Abstract

Blind fault is one of the threats that lurks beneath the surface. Predicting when blind faults intersect with topography (rupturing) is a monumental achievement in disaster mitigation related to crustal deformation. The main problem is that the concealment of the blind fault below the surface makes it difficult to observe its development. One effort that can be done to study it is through analog sandbox modeling.

Analog sandbox modeling can be done to investigate how the rock behavior in the upper crust by using loose sand as an analog material. This study was carried out by integrating several derivative analysis results from Particle Image Velocimetry (PIV) analysis to see how the evolution of the material displacement vector during the deformation process and its repetition/cycle pattern. As is done in paleoseismology but in a more detailed order of observation.

This study aims to determine where the concentration of observations should be made to estimate when the blind fault will rupture. By using this event as a reference, all events that occurred before the rupture can be valuable information to predict its occurrence. Furthermore, in this study, we will identify what happens during the cycle of thrust faults within fold and thrust belt.

Keywords: Analogue Sandbox Modelling, Thrust Fault, Deformation, Blind Fault

Introduction

Earth deformation occurs in multiscale, from less than 1 second earthquake rupture to millions years of plate movement. Natural field observation can only provide a mere snapshot of such long history. Not to mention, that our knowledge regarding the physics of earthquake and earth deformation is still incomplete. In order to overcome such limitation, simulation using sandbox analogue modelling is one of the solution.

Within fold-thrust belt (FTB) which develops in sequence (the fault in the hinterland is the oldest fault and the fault in the foreland develops the youngest - Baum, 1983; Boyer, 1986; Boyer and Elliott, 1982), blind faults are generally found in the foreland. Blind faults are active faults whose propagation has not yet reached the surface and are generally expressed through the presence of folding without fault separation (Boyer and Elliott, 1982; Yeats et al., 1997). This fault was phenomenal when in 2007 the Kashiwazaki–Kariwa Nuclear Power Plant (7,965 MW) in Japan, which is one of the largest nuclear power plants in the world, was forced to stop operating due to the development of new active fault in the vicinity from a blind fault. (IAEA, 2007; Okumura, 2008 in McCalpin, 2009). From this we can learn that the potential losses that can be caused by blind faults are unanticipated surface deformations. If the geometric development of the blind thrust is recognized, so that it can be anticipated, it will certainly be very helpful in efforts to mitigate the potential for disasters related to its development.

In the past decade, a digital image analysis method called Particle Image Velocimetry (PIV) has been used to observe the deformation process in analog sandbox modeling in detail (Adam et al., 2013; Dotare et al., 2016; Marshak et al., 2019; Sapiie et al., 2018; Yamada et al., 2011). PIV is a digital image processing technique to extract object displacement vectors from two consecutive images by using a cross-correlation technique from several pixels as a reference. This approach makes it possible to observe displacement vectors in the order of sub-millimeters with a resolution of up to 0.01 mm (Adrian and Westerweel, 2011). In this study, PIVlab™ software was used (Thielicke and Stamhuis, 2014) to perform PIV analysis.

This study was conducted to identify the character of the early stages of blind thrust development. This can be a reference in observing the blind thrust activity of the earth's surface. In the future, further studies can be carried out in the form of the relationship between this modeling and observations of deformation on the surface. In this study, a series of analog sandbox modeling experiments will be conducted to identify how the behavior of material movement is related to the development of factoring fault deformation. An analog sandbox modeling experiment with a simple arrangement was carried out which was analyzed using the PIV method, then processed using the

ParaView™ visualization software (Ahrens et al., 2019) and Matlab™.

Data and Method

Analog sandbox modeling experiment was conducted in a 2 m x 0.5 m box, with glass on both long sides and at the base. A metal plate is used as indenter at the back of the box which is driven by an electric motor and moves at a speed of 5 cm per hour. Using the terminology of Kopp and Kukowski, (2003), this type of analog sandbox modeling tool is of the "dynamic backstop" type. The modeling material used in this experiment is dry, loose, quartz sand with grain sizes ranging from 150–250 um originating from the Ngrayong Formation. The sand was given an organic dye to help the process of observing the resulting model. Modeling material is placed by leveling it using a leveling tool to reduce the influence of hand pressure when leveling the material. The initial thickness of the modeling material before deformation is at a value of 4 cm with a variation of less than 2 mm (<5%). The initial length of the model before deformation is 20 cm. To avoid out-of-sequence thrust development (OOST Baum, 1983; Morley, 1988) and as an indicator that the factoring fault development has reached the extreme limit of the modeling tool, a rigid 3.7 cm high ramp is used at the end of the models. The deformation was recorded using a D-SLR camera with an interval of 30 seconds.

In this study, seven (7) iterations of analog sandbox modeling experiments were conducted to test the consistency of the resulting model. From each experimental result, PIV digital image processing was performed (Figure 1).

After the first fault is formed, the displacement data extraction is carried out on the footwall of the first fault. This footwall will develop into hangingwall from the 2nd fault, when the fault is active. However, not all parts of the footwall (of n-th fault) will develop into HW (n+1-th fault). As for the intersection of these two criteria, it can only be known after the n+1 fault plane is observed. To extract the displacement values during the deformation process, the "Plot Selection Over Time" module in ParaView™ is used. To determine where this extraction should be carried out, it is necessary to first identify the presence of two faults qualitatively. The zone between the two targets becomes the hanging wall of the most recent active fault and it is in this zone that measurements are taken. The value of the displacement at each point in a hangingwall is not entirely the same. Therefore, data collection is carried out in one zone and then the values obtained are averaged. If the location of data collection is correct, it will obtain narrow upper and lower quartile data that is close to the average value.
The results of this extraction are plotted into a time-displacement graph. Time on the x-axis can represent a given cumulative strain. This is done by replacing the total time into the percentage of maximum cumulative strain that occurs. This step is repeated for each footwall of the fault that develops in the model. A displacement curve is obtained which is used to determine the deformation phase. Because this study is focused on each fault, the movement of each hangingwall of the fault must be isolated. To do this, the frame of reference of observation must be changed from the ramp at the end of the model to the footwall of the fault. Mathematically this is done by reducing the hangingwall displacement curve from the nth fault with the hangingwall displacement from the n+1 fault.

Other information that can be extracted from the results of the PIV analysis is the shear strain distribution map. To obtain it, it can be done by calculating the displacement data using the "vorticity" module. Vorticity shows the rotation that occurs in the flow field (Means et al., 1980). When there are two zones with different movements, a vortex will develop between them. This vortex can rotate clockwise or counterclockwise. This can represent a concentration of shear strain (Dotare et al., 2016; Marshak et al., 2019). By using vorticity, it can be known exactly when the fault plane reaches the surface (rupturing) which is analogous to the condition of stable strength.

One of the problems in analog modeling is reproducibility, because analog sandbox modeling is very sensitive to the effects of edge effects and the effects of material laying techniques. To overcome this, a strong evaluation method is needed. For this reason, a total deformation profile (TDP) analysis was carried out. TDP is obtained by combining the displacement profiles of each image frame. These displacement profiles were obtained using the "Plot over line" module in ParaView™ and each profile was combined in a stack according to the order of the picture frame numbers using Matlab™. With the TDP, we can find out whether the cycle of development of the factoring fault occurs in a self-similar manner and there is no out-of-sequence development (Figure 1).

Result and Discussion

The initial stage of the thrust fault development begins with a distributed lateral movement and gradually dissipates towards the foreland which is reflected in the displacement field in both the cross-sectional view and the map view (Figure 2). During its development, there are not many changes that occur on the surface, but folds are formed with a very gentle slope. If we look at the TDP plots (Figure 1), it shows that this lateral movement is very strong, due to its wide range, and its intermittent or intermittent occurrence - hereinafter referred to as intermittent

lateral movement (ILM). The vector of this lateral movement is in the direction of the slope of the detachment. When this ILM occurs, particularly during the second and subsequent faults, the detachment progresses beyond the active fault (Figure 2). This shows that the footwall is not always at rest when the factoring fault is active.

Geometrically, a fault can be defined as a plane of discontinuity between two objects resulting from movement whose vectors are different from each other, both in magnitude and direction. Thus, in the side view displacement field of the model, the fault will be a clear boundary having a contrasting color between the two blocks (Figure 3A and B). Reinforced by vorticity observations, there is a concentration of shear stress or fractures that are interconnected from the bottom to the surface. This condition is defined as the occurrence of fracture of the factoring fault.

The surface rupture development of the thrust fault was marked by a very significant increase in the value of the hangingwall displacement and a drastic decrease in the value of the hangingwall displacement from the previous fault which was ended by the achievement of stable hangingwall displacement conditions. During its development, there is a tendency of the fractures that make up this fault plane to change in terms of shape and position in order to achieve the most efficient conditions in moving the hangingwall. This event occurs during the process towards a stable hangingwall displacement condition.

When the hangingwall movement is stable, the entire shortening budget is used to move the hangingwall to a higher elevation. During its development, there is a tendency to increase the intensity of the occurrence of ILM as occurred at the beginning of the development of the first fault. From the pattern of movement, the intermittent behavior of ILM reflects the stick-slip movement which is the result of the interaction between the sand grains and the glass sheet on the bottom.

The end of the thrust fault development is marked by a gradual decrease in the hangingwall displacement velocity after reaching the maximum displacement value and stable conditions. This was triggered by a shortening distribution to initiate ILM for the next fault. When the next fault reaches its maximum displacement value, the previously active fault will stop. From this we can see that there is a cycle in the development of the thrust fault.

Conclusions

By using surface rupture development as a reference, the development of the thrust fault can be mapped into at least 3 phases and its development occurs cyclically with slices in phase 1 and phase 3.

(1) The beginning of the fault development begins with lateral compaction which is reflected by the development of detachment to reach an area of at least twice the thickness of the layer accompanied by ILM. The occurrence of this ILM reflects the stick-slip movement at regular intervals and does not deform the material significantly, but forms folds with a very gentle slope. This stage is terminated by the cessation of the ILM event and all movement is concentrated on the (prospective) hangingwall of the fault that is about to develop.

(2) Immediately after the concentration of movement on the hangingwall, a fracture forms along the discontinuity boundary of this movement. Not only in the middle, but also growing near the surface and detachment. These fractures are not necessarily arranged in a straight line, but may develop in a stepwise fashion. Thus, a reorganization of the position and size of the fracture can occur in order to obtain a fault plane that requires the most optimal shortening budget in moving the hangingwall. This event occurred in a very short time and was marked by a very significant spike in the value of the displacement in a short time. The end of this reorganization was marked by the achievement of the highest hangingwall displacement value.

(3) In the presence of a fault plane to move the hangingwall with an optimal shortening budget, then the entire existing shortening budget is used to move the hangingwall. At this stage the hangingwall displacement value has the same value as the backstop and tends to be in a stable number. As the internal stability of the developing compressive wedge is achieved, the hangingwall displacement decreases. This decrease in value is due to the strength limit of the detachment being reached in response to ILM on the footwall. The end of this decline is marked by an increase in the value of the hangingwall displacement of the next fault which initiates the development of the next fault.

With regard to the use of analog sandbox modeling as an approach to study the development of blind faults, it can be done by concentrating observations in Phase 1 or Phase 3.

References

Adam, J., Klinkmüller, M., Schreurs, G., and Wieneke, B. (2013): Quantitative 3D strain analysis in analogue experiments simulating tectonic deformation: Integration of X-ray computed tomography and digital volume correlation techniques, *Journal of Structural*

Geology, **55**, 127–149.

Adrian, R. J., and Westerweel, J. (2011): *Particle Image Velocimetry*, Cambridge University Press, New York, 586 pp.

Ahrens, J., Bauer, A., Boeckel, B., Choudhary, A., Demarle, D., Geveci, B., Lipsa, D., Loring, B., Maxwell, T., Moreland, K., Nouanesengsy, B., Philip, S., Patchett, J., Pouderoux, J., Quammen, C., Shetty, N., Sherman, B., Waldon, S., Westphal, M., Whiting, E., Zagaris, G., Avila, L., Osterdahl, K., Mckenzie, S., and Jordan, S. (2019): The ParaView Guide Community Edition Utkarsh Ayachit With contributions from, retrieved from internet: http://paraview.orghttp//kitware.com.

Baum, B. (1983): Out of sequence, *Nature*, **305**(5930), 90.

Boyer, S. E. (1986): Styles of folding within thrust sheets: examples from the Appalachian and Rocky Mountains of the U.S.A. and Canada, *Journal of Structural Geology*, **8**(3–4), 325–339.

Boyer, S. E., and Elliott, D. (1982): Thrust systems., *American Association of Petroleum Geologists Bulletin*, **66**(9), 1196–1230.

Dotare, T., Yamada, Y., Adam, J., Hori, T., and Sakaguchi, H. (2016): Initiation of a thrust fault revealed by analog experiments, *Tectonophysics*, **684**, 148–156.

Kopp, H., and Kukowski, N. (2003): Backstop geometry and accretionary mechanics of the Sunda margin, *Tectonics*, **22**(6), 11–16.

Marshak, S., Haq, S. S. B., and Sen, P. (2019): Ramp initiation in fold-thrust belts: Insight from PIV analysis of sandbox models, *Journal of Structural Geology*, **118**(June 2018), 308–323.

McCalpin, J. P. (2009): *Paleoseismology*, Academic Press, London, **95**.

Sapiie, B., Hadiana, M., and Alfa-Furqan, T. (2018): Understanding Mechanics of Fold-Thrust-Belt Trough Sandbox Modelling, *PROCEEDINGS PEKAN ILMIAH TAHUNAN IAGI 2018*, Pekanbaru.

Thielicke, W., and Stamhuis, E. J. (2014): PIVlab – Towards User-friendly, Affordable and Accurate Digital Particle Image Velocimetry in MATLAB, *Journal of Open Research Software*, **2**.

Yamada, Y., McNeill, L., Moore, J. C., and Nakamura, Y. (2011): Structural styles across the Nankai accretionary prism revealed from LWD borehole images and their correlation with seismic profile and core data: Results from NanTroSEIZE Stage 1 expeditions, *Geochemistry, Geophysics, Geosystems*, **12**(7).

Yeats, R. S., Sieh, K. E., and Allen, C. A. (1997): *The Geology of Earthquakes*, Oxford University Press, New York.

PROCEEDINGS
JOINT CONVENTION BANDUNG (JCB) 2021
November 23rd – 25th 2021

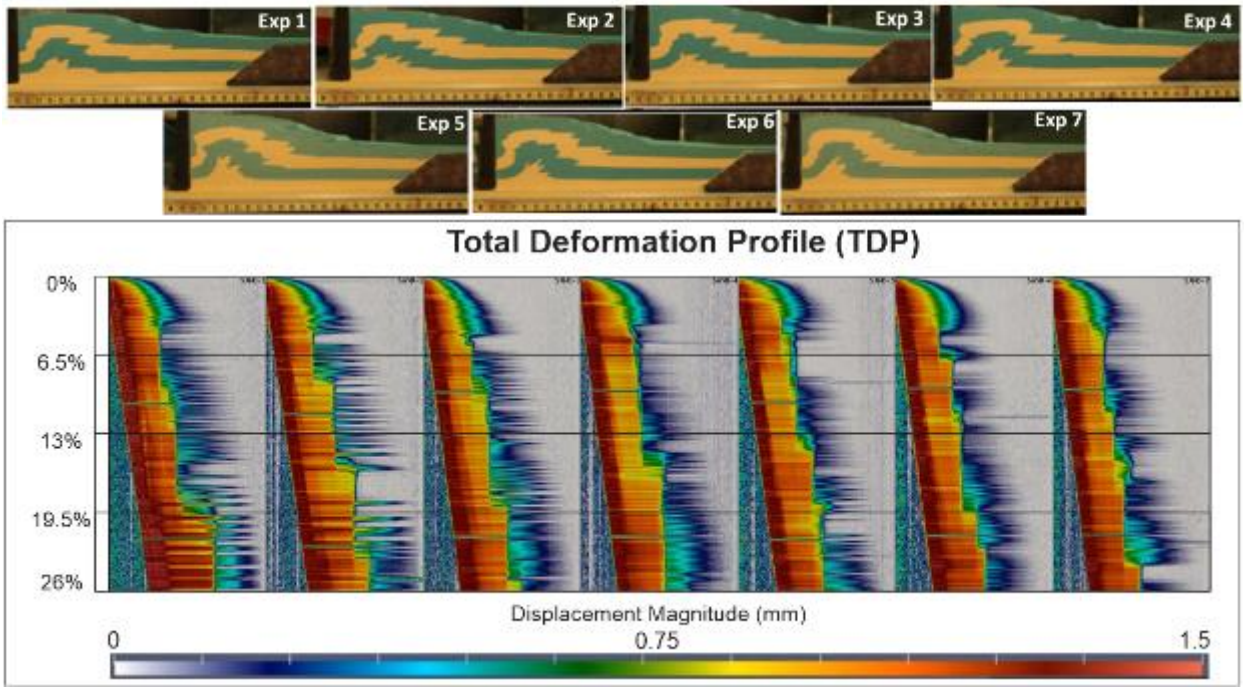

Figure 1: End Result of sandbox experiments along with the total deformation profile

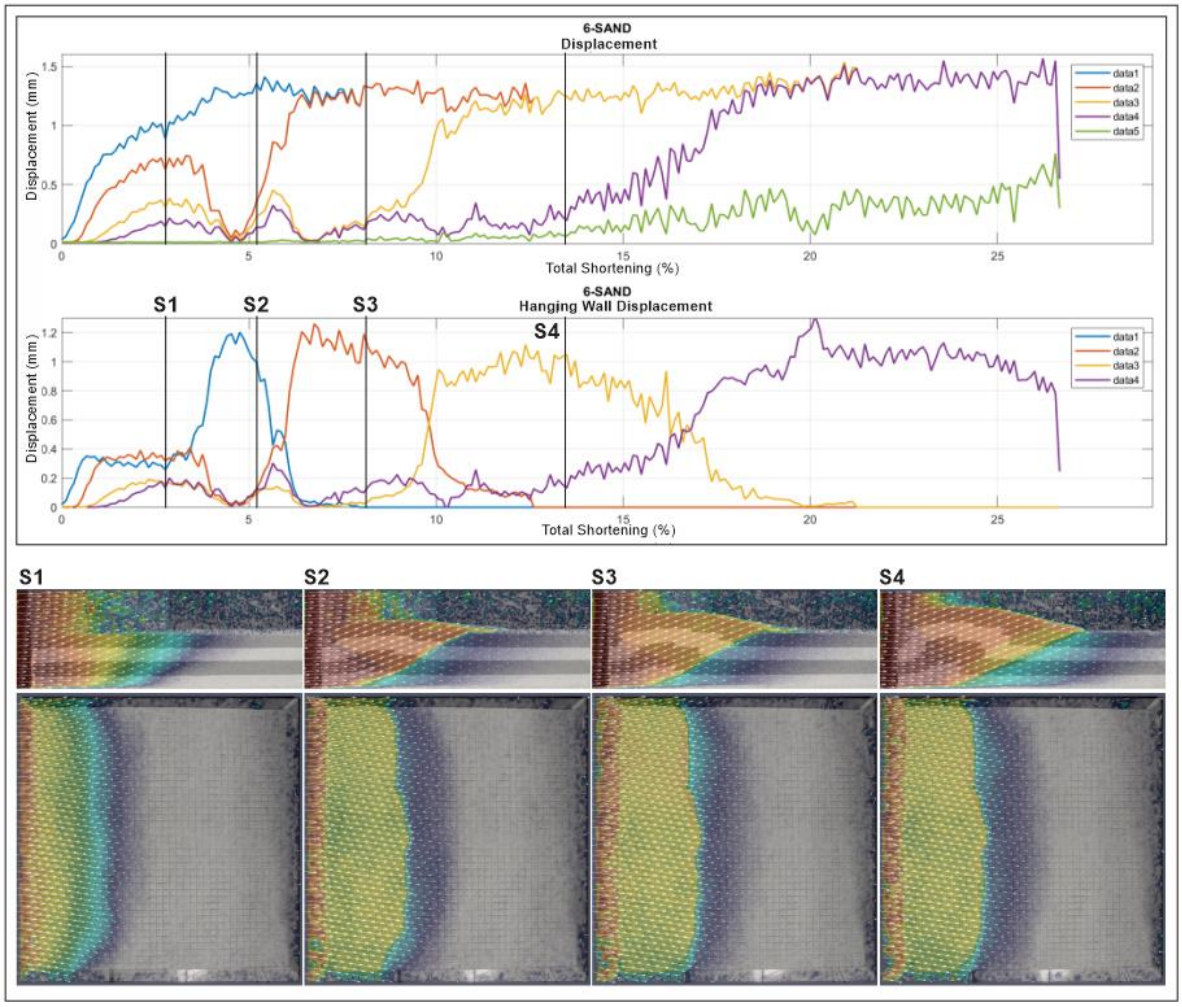

Figure 2: Ilustration of Phase 1 Occurence

PROCEEDINGS
JOINT CONVENTION BANDUNG (JCB) 2021
November 23rd – 25th 2021

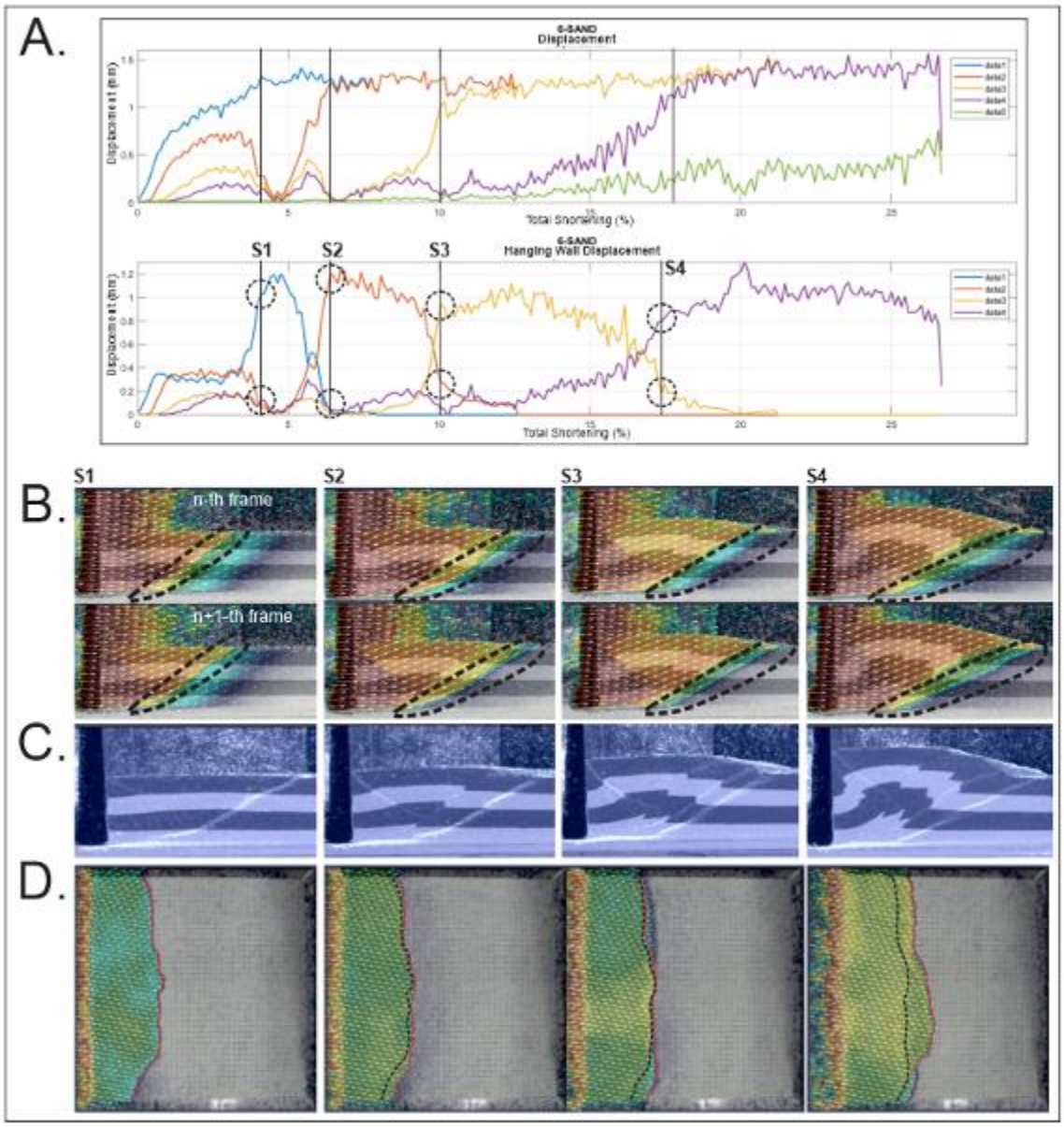

Figure 3: Ilustration of Phase 2 and 3

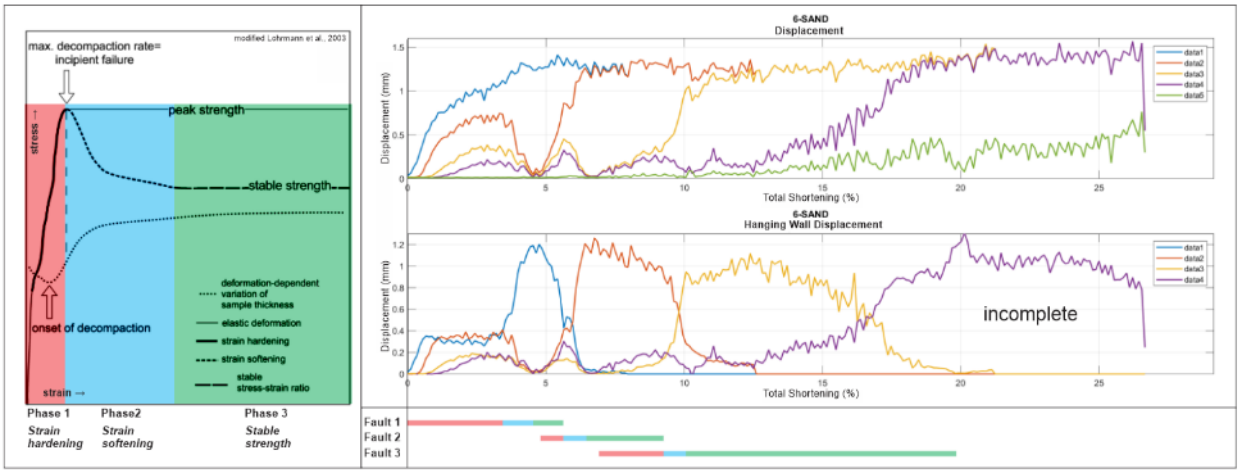

Figure 4: Correlation between phases and material characteristic

PROCEEDINGS
JOINT CONVENTION BANDUNG (JCB) 2021
November 23rd – 25th 2021

IDENTIFICATION OF SIULAK FAULT MOVEMENT AS PART OF THE SUMATERA FAULT SEGMENT THAT AFFECTING THE MORPHOLOGY IN KERINCI DISTRICT

Naufal Abdullah, Hari Wiki Utama, Tobi Prayoga, Ardo Parajo, dan Vidra Chartyne Nolwa
Teknik Geologi, Fakultas Sains dan Teknologi, Universitas Jambi
Jalan Raya Jambi - Ma. Bulian, KM.15, Mendalo Indah, Jambi, 36361

Abstract

Kerinci regency is located in the western part of West Sumatera. This island was formed from subduction process activity of the Indo-Australian plate and the Eurasian plate. The impact of this process divided Sumatra Island into several zones: 1) Front Arc Basin, 2) Magmatic Arc Zone, and 3) Back Arc Zone, which resulted in a complex distribution of rocks and tectonics. Kerinci Regency is located in the magmatic arc zone which is passed by the Sumatran fault along the Bukit Barisan, stretching from the northwest-southeast of Sumatera Island. According to Natawidjaja (2018), The Sumatran fault is composed of 55 segments. One of the segments is the Siulak Fault which is selected as the object of research. The method used in this study is the interpretation of DEM Aster Data in the analysis of geological structure lineaments, which are overlaid with a regional geological map of the Sungai Penuh sheet to determine the position of faults and lithology at the research location. Field data retrieval is carried out directly using a geological compass of several fault line points and stereographic analysis of faults. From the data obtained, The impact of the Siulak fault movement on the morphology of the Kerinci Regency can be seen.

Introduction

Indonesia is a country with an area that has a complicated geological order, because Indonesia is located on three large plates (mega plates), named: Hindi-Australia at south, the Pacific at the east, and Eurasia at the north. The three plates have shifted in the mid-oceanic ridge or MOR (Mid Oceanic Ridges), with speed directions that vary from one to another from the Mesozoic to the present. As the result of complex plate movements, Indonesia has an area characterized by continuous changes in plate composition, collision paths, faults, and shifting arcs. From this reflection, this geological condition causes the level of seismicity, volcanoes, and tectonic movements that are still on going.

The location of the island of Sumatra is on the Eurasian continental plate. This island is integrated with the ocean that moves north-northeast. From this meeting, the subduction zone is still active at the northwest of the Andamans to the southern end of the Semangko Bay, which is known as the Benioff line under the island of Sumatra. The Sumatran fault divided the segmented island of Sumatra. These segments have a length of 1900 kilometers by following the oblique pressure of the Eurasian and Indo-Australian (Simandjuntak and Barber, 1996).

Kerinci is the result of a complex tectonic subduction of the Indo-Australian plate with the Eurasian plate that forms the front arc zone, magmatic arc, and back arc zone. As the result of this process, the Sumatran fault is formed with one of its segments, the Siulak fault, which is interesting to be studied throroughly.

Based on the physiography, the island of Sumatra (Figure.1) is divided into several physiography, including the Bukit Barisan Zone, the Semangko Fault Zone (Sumatra), the plain and hill zone, the Thirty Hill zone, the outer arc zone, and the Sunda exposure zone. The Bukit Barisan Zone is a hilly zone with a southeast-northwest orientation and has an elongated pattern of about 1,650 km with a width of 100 km. This zone is generally associated with the active volcanoes, such as Mount Kerinci, Mount Singgalang, Mount Tandikat, Mount Marapi, Mount Kapanasan, Mount Bongsu, Mount Sibungan, which are scattered in the hills and surrounding areas, which are spread out following an elongated hill pattern line. Bukit Tigapuluh zone is a zone associated with morphological forms experiencing low to the east, dome-shaped morphology or the height of the descending fault section. The Sumatran fault zone is a zone with an elongated pattern from this zone following the pattern of the Bukit Barisan zone. The outer arc island zone is a tectonic activity from the subduction zone causing the emergence of an island arc named magmatic arc (Van Bemmelen, 1949).

The research area includes the Sumatran fault zone with an elongated pattern with a northwest-southeast direction. There are 19 segments that extend from the northern tip of Aceh to the southern tip of Lampung, one of the Sumatran fault segments is included in the research area, named the Siulak fault segment with a northwest-southeast direction.

PROCEEDINGS
JOINT CONVENTION BANDUNG (JCB) 2021
November 23rd – 25th 2021

Figure 1. Physiography of Sumatra Island (Van Bemmelen, 1949).

Data and Method

This study used the DEM aster data interpretation method in analyzing the lineament of the geological structure overlaid with a regional geological map of the Sungai Penuh sheet to determine the position of faults and lithology at the study site. The data were taken directly at several points in Kerinci Regency where fault data was collected using a geological compass, with the lineament interpretation of DEM aster data overlaid with regional geological maps of Sungai Penuh and Painan so that we know the fault lines measured and analyzed stereographically.

Result and Discussion

The data collected by direct observation and measurement at five observation points in the Kerinci area. Based on the results of the field research, it is derived that at the observation of location one there is a fault plane position of N 234 ^{0}E/54^0 and Bearing N 51^{0}E and rake 16^0. In the second observation location, there is a minor fault that cuts the main fault with a fault plane position of N 111^{0}E/59^0 and Bearing N 154^{0}E and rake 55^0. In the third observation location the fault plane position is N 355^{0}E/67^0 and Bearing N 173^{0}E and rake 18^0. In the fourth observation location the fault plane position is N 300^{0}E/43^0 and Bearing N 122^{0}E and rake 15^0. Finally, in The last observation location the fault plane position of N 332^{0}E/36^0 and Bearing N 141^{0}E and rake 21^0 was found. Therefore, it can be assumed as a horizontal dominant fault because the rake value obtained is <45^0.

Based on the geological map of the observation area (Fig. 2) the rocks that make up the fault area are volcanic breccia and conglomerates in bandan formations, which are the product of mapped moss, granite, and pyroclastic volcanoes. The existence of the Siulak Fault is one of the causes of the tectonic activity of the island of Sumatra.

From the stereographic analysis, it was found that the Siulak fault is a left-down fault oriented towards northwest-southeast with a compression force direction of northeast-southwest. This fault movement resulted in the formation of the Kerinci valley. After the Siulak fault was formed, it is followed by a minor fault that cuts perpendicular to the main fault. This condition shaped the morphological form of Kerinci Lake and terraced waterfalls in the area.

Conclusions

Based on the results of research in Kerinci Regency on the Siulak Fault, it is found that the Siulak Fault has a northwest-southeast orientation with a left-down movement resulting in an extensional force that causes the formation of the Kerinci Valley and other morphologies

References

Bemmelen, R.W. Van, 1949, *the Geology of Indonesia*, Vol. 1 A, Government Printing Office, The Hague, Amsterdam.

Natawidjaja, D.H. 2018. Updating Active Fault Maps and Sliprates Along The Sumatran Fault Zone Indonesia, *IOP Conf. Series : Earth and Environmental Science*, 118012001.

Shancharlo, E, T, H. 2018. Kontrol Keberadaan Manifestasi Air Panas Di Utara Barat Laut Danau Kerinci, Jambi: Hasil Studi Pendahuluan. Jurnal Teknik Kebumian. Universitas Jambi.

Simanjuntak, T.O. and Barber, A.J., 1996. Contrasting tetonic styles in the Neogene orogenic belts of Indonesia. In: Hall, R. and Blundell, D.J. (Eds), *Tectonic evolution of Southeast Asia*, Geological Society Special Publication. London, p. 185-201.

PROCEEDINGS
JOINT CONVENTION BANDUNG (JCB) 2021
November 23rd – 25th 2021

Appendix

Figure 2. The appearance of the fault structure in the field

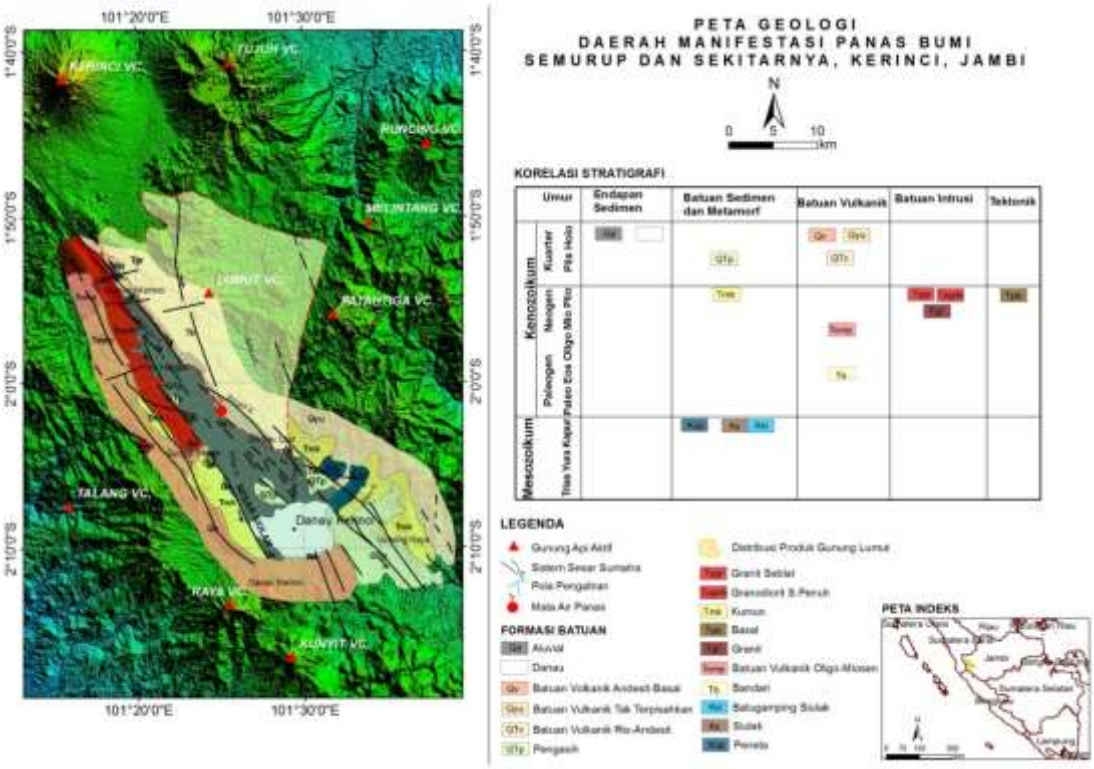

Figure 3. Geological map of the Siulak fault area, Kerinci, Jambi (Shancharlo et al, 2016).

PROCEEDINGS
JOINT CONVENTION BANDUNG (JCB) 2021
November 23rd – 25th 2021

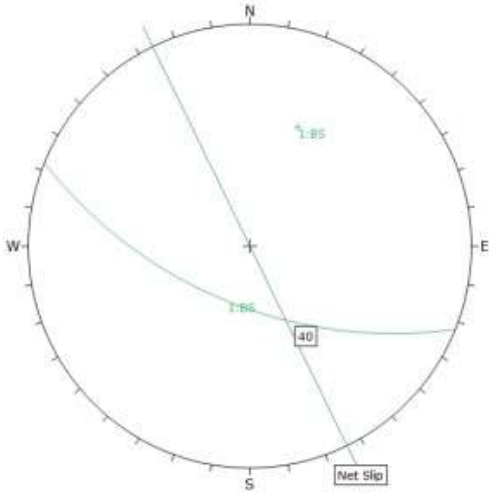

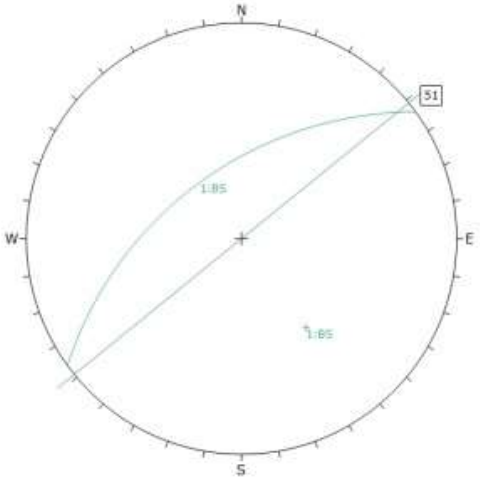

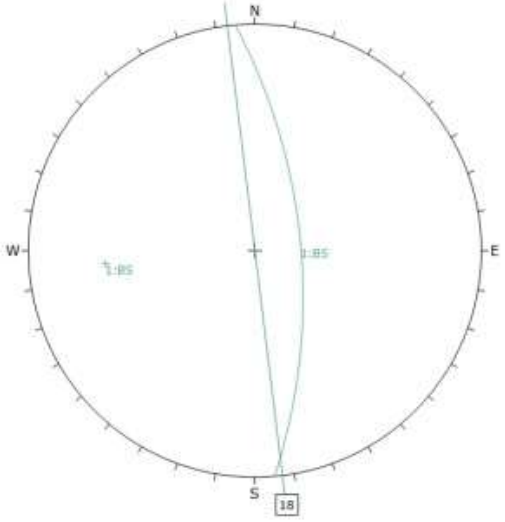

PROCEEDINGS
JOINT CONVENTION BANDUNG (JCB) 2021
November 23rd – 25th 2021

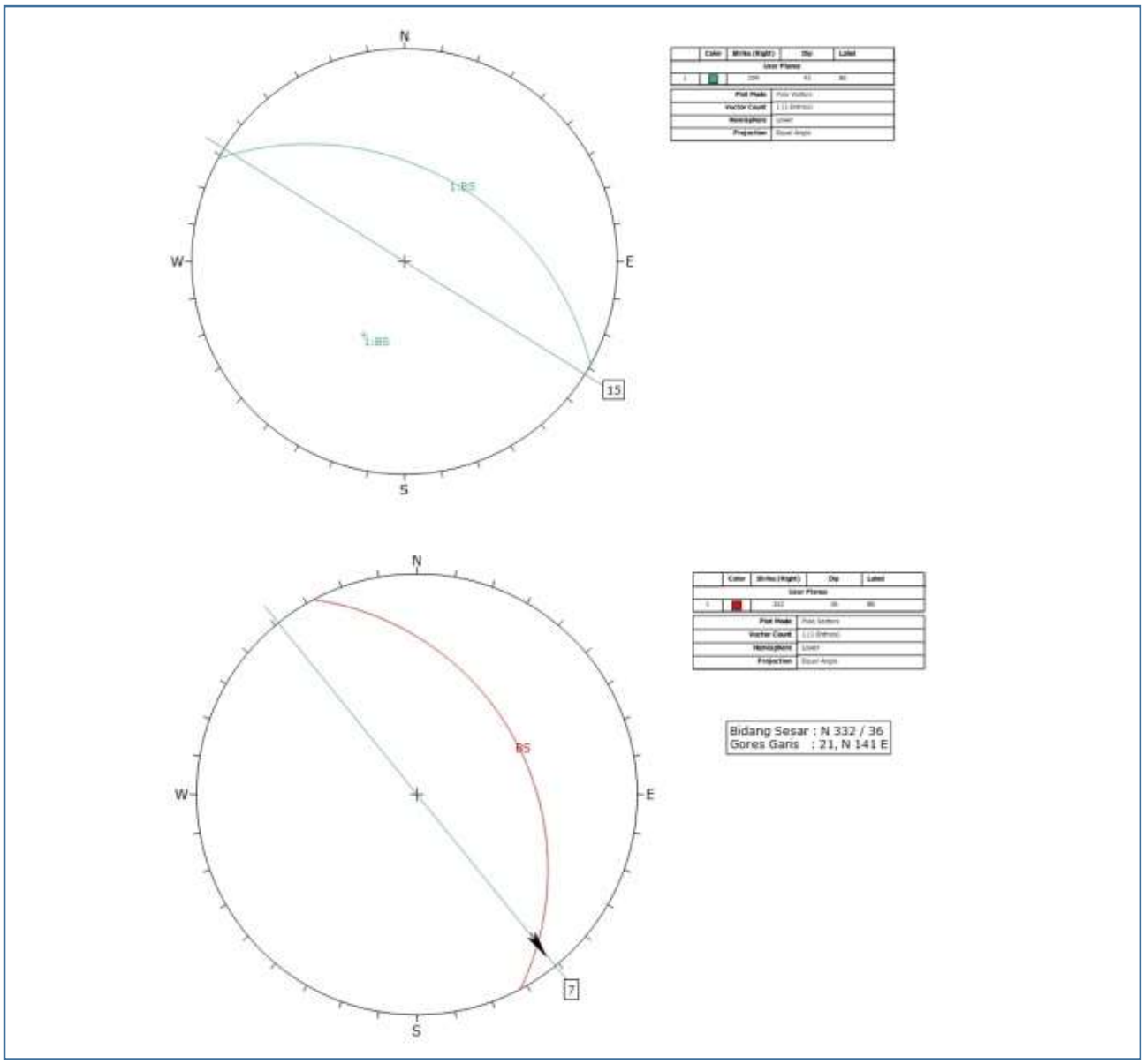

Figure 3. Stereographic analysis of the Siulak fault

PROCEEDINGS
JOINT CONVENTION BANDUNG (JCB) 2021
November 23rd – 25th 2021

IDENTIFICATION OF DIRECTION OF DISTRIBUTION QUARTZ VEINS BASED ON THE GEOLOGICAL STRUCTURE ANALYSIS IN PLAMPANG AREA AND SURROUNDING, KOKAP SUB-DISTRICT, KULONPROGO REGENCY, SPECIAL REGION OF YOGYAKARTA

Fandy Sealtiel Reka[1], Richard Markus Isliko[1], I Gusti Ngurah Adi Prasetia[2], Ohkita[3].
[1] Institut Sains & Teknologi AKPRIND Yogyakarta.
[2] Himpunan Mahasiswa Teknik Geologi "GAIA" Institut Sains & Teknologi AKPRIND Yogyakarta.
[3] MGEI-SC IST AKPRIND Yogyakarta.

Abstract

Generally consisting of the Kulonprogo Mountains, sedimentary and volcanic rocks, the formation of the Kulonprogo Mountains is related to the interaction between the Indo-Australian plate in the South which subducts under the Eurasian plate in the North, with on tectonic processes that work, it directly affects the formation of volcanic pathways and tectonic structures, both faults and fractures due to tectonic activity. This volcanic activity produces volcanic rocks in Kulonprogo which generally contain a lot of economical ore deposits.

The method used in this research is a geological mapping of the surface to determine the distribution of rocks, the direction of veins, and intensity of alteration as well as a polished incision analysis in the Plampang area and surrounding, Kokap sub-district, Kulonprogo Regency, Yogyakarta special region.

Based on the analysis of the result, the research area has lithology in the form of igneous andesite aphanitic and porphyry aphanitic andesite, including the Old Andesite Formation. The geomorphic unit that works is of denudational origin with hills and denudational slopes sub-units (D2), isolated hills (D4). It has two alteration patterns, namely the chlorite-clay mineral-calcite zone and the mineral clay zone. The geological structure in the form of faults is the Plampang 1 Left Slip Fault, the Plampang 2 Left Slip Fault, the Plampang 3 Left Slip Fault which is relatively NorthEast-SouthWest, Normal Right Slip Fault Descending Plampang 4 in Southeast-Northwest direction, and the Normal Right Slip Fault Descending Plampang 5 in the NorthEast-SouthWest direction. The direction of distribution of quartz is west-east (metallic minerals such as pyrite, galena), SouthWest-NorthEast, and NorthWest-SouthEast (presence of metallic mineral pyrite) controlled by the Plampang 2 Fault. while the direction of the Quartz vein is SouthWest-NorthEast (presence of metallic mineral pyrite, galena), NorthWest-SouthEast (presence of metallic mineral pyrite) is controlled by the Plampang 4 Normal Right Slip Fault and is in propilitik alteration and fills fractures in aphanitic andesite rocks. Observation of vein-type showed that there were two types of quartz vein texture formed, namely Banded-Crustiform Veins and Massive Veins. The gangue minerals that developed descriptively that could be observed were chlorite, quartz, and clay minerals.

Keywords: Structure, Quartz and Alteration

Introduction

In general, the rocks that make up the Kulon Progo Mountains consist of sedimentary and volcanic rocks, the formation of the Kulon Progo Mountains is related to the interaction between the Indo-Australian plate in the South which subducts under the Eurasian plate in the North, with ongoing tectonic processes at work, it directly affects the formation of volcanic and volcanic pathways. tectonic structures, both faults, and fractures due to tectonic activity. This volcanic activity resulted in volcanic rocks in Kulonprogo that developed in the Sunda – Banda magmatic arc path during the Oligocene – Miocene (Soeria Atmaja et al., 1994 in Widagdo et al, 2017). Van Bemmelen (1949), referred to all the volcanic rocks in Kulonprogo as the Old Andesite Formation (OAF/Old Andesite Formation). The study of geological structures in the Kulonprogo Mountains was carried out to determine the types of geological structures that exist and their influence on the formation of mineralization. By taking into account the paleo-volcanism factors and the intensity of the geological structures that develop regionally in this area, hydrothermal solutions can form at the end of the magma freezing cycle and generally accumulate in lithologies with high permeability or in weak zones/fractures (Bateman, 1981). Fredy et al, 2017), will form a hydrothermal deposit system controlled by a fracture system. The interaction between the hydrothermal solution and the rock through which the wall rocks pass will cause the primary minerals to change into secondary alteration minerals. The existence of this alteration and mineralization zone will assist in planning the development of mineral exploration for ores containing sulfide mineral ores. One of the indicators that influence the presence of precious ore mineral carrier veins is the fracture structure (joints, faults). The growing joint network is an avenue for late-magmatic to fill and deposit ore minerals. Quartz veins are one of the most common types of veins,

quartz veins are dominated by quartz minerals and several other minerals. The study of the direction of distribution quartz veins is very important for economic mineral exploration. Identification of the direction of distribution of quartz veins controlled by geological structures in area Kulonprogo Mountains, D.I. Y province. Yogyakarta, which emphasizes more on proving that there are rocks that undergo alteration and mineralization processes in the area with the intensity of the geological structure that develops regionally in this area, it is possible for hydrothermal solutions to form at the end of the magma freezing cycle and will form a deposit system. Hydrothermal control controlled by the fracture system or accumulated in lithology that has high permeability, in the Kulonprogo area in Kalirejo Village has undergone an alteration and mineralization process which indicates the presence of economical metal minerals, for that it is necessary to identify the direction of distribution of veins containing economic minerals.

Data and Method

Data collection techniques are in the form of combination primary data or data from direct observations in the field and added with secondary data from literature or related references in the research area summarized in a research flow chart. Primary data taken include field data in the form of geological data such as lithology, geomorphology, geological structure data (measurement of mineral-filled joints), alteration data, mineral observations on quartz veins megascopic and quartz vein texture, secondary data, the compiler summarizes from some related literature, such as books, research journals, scientific papers, e-books, and from the internet, as well as teaching materials.

Result and Discussion

Geology and Geomorphology

The research location is in the Plampang area and its surroundings, Kokap District, Kulonprogo Regency, Special Region of Yogyakarta Province. The morphology of the research area is in the form of denuded hills, weak wavy to hilly. The joints that form quartz veins trending Southeast-Northwest, West-East, Northeast-Southwest. Data collection in the research area includes geological data (lithology, geological structure, alteration) especially those related to the title of the study, namely data on joints filled with quartz veins. In the study area, most of the intermediate igneous rocks were found in the form of andesite. Based on the results of geological observations carried out in the study area, there were 30 observation locations (Figure 1) and found two lithological units, namely aphanitic andesite which were then intruded by younger igneous rocks, namely porphyriaphanitic andesite with plagioclase minerals that became phenocrysts (Figure 2). The type of lithology found in the research area which is a product of igneous rock resulting from andesite intrusion and andesite lava, it can be concluded that the lithology of the research area is included in the Old Andesite Formation (late Oligocene-early Miocene). According to Suyono (2004), the rocks included in the Old Andesite Formation are shallow intrusive rocks of andesite and dacite, andesite breccia, tuff, and lava with compositions ranging from basaltic andesite to andesitic. So it is very possible in the research area to find andesite igneous rocks. In general, the morphology in the study area is a denudational geomorphic unit (based on the classification of Van Zuidam 1983) which is divided into hills and denudational slope geomorphic units (D2), isolated hills (D4) (Figure 3). Therefore, it can be interpreted that morphological expression is the influence of lithological factors that are resistant to denudational processes. The lithological factor in question is andesite igneous rock. So that the hilly protrusions found at the research site can reflect igneous rock intrusion. The intrusion of igneous rocks produces andesite igneous rocks which are physically resistant to weathering processes. This causes the formation of a moderately wavy hillside morphology and several isolated hills in the study area.

Geological Structure

Geological structures, in this case, faults and joints in the study of vein genesis, can be analyzed and interpreted as a pathway to the rise of hydrothermal solutions and cavity filling processes in fault gaps. The geological structure that developed in the research area found and the results of the fault analysis are Plampang 1 Left Slip Fault, the Plampang 2 Left Slip Fault, the Plampang 3 Left Slip Fault, the Plampang 4 Normal Right Slip Fault, and the Plampang 5 Normal Right Slip Fault. Regionally, the geological structure is developing in a northeast-southwest and southeast-northwest direction. The presence of the main faults formed in this study area can explain by the Reidel shear concept (Mc Clay, 2007 in Widagdo et al, 2017), Reidel shear faults consist of a synthetic fault system (R) and an antithetic fault (P). The results of the research in the study area show that the formation is included in the secondary fault system (synthetic fault). The Plampang 4 Normal Right Slip Fault is formed with a north-south trending main that controls the quartz veins trending Northeast-Southwest and Northwest-Southeast, the Plampang 2 Left Slip Fault is formed with north-south main stress that controls the quartz veins that have a southwest-northeast direction, West-East, Southwest-Southeast. The faults that are formed produce tension/ gash fracture and shear joints, these joints serve as a pathway for hydrothermal solutions to rise to the surface and fill the cracks and form quartz veins. In the study area,

quartz veins fill in tension joints or open joints with a dimension of ± 25 cm of vein width and some fill in a shear joint with a dimension of ± 5 cm of veins. The Plampang 4 Normal Right Slip Fault produces a gash fracture with a northwest-southeast trend, the second shear fracture with a northwest-southeast trend is filled with quartz veins, while the Plampang 2 left horizontal fault produces a gash fracture with a west-east west-southeast trend and a shear fracture with a west-southeast trend. The two northeast-southwest joints are filled with quartz veins, these faults are factors controlling the direction of the distribution of quartz veins in the study area. Meanwhile, if using the Riedel Shear Model system (in Corbett and Leach, 1997), the dominant joints develop in the study area. Including tension fractures filled with quartz veins (Figure 4).

Alteration and Quartz Vein Direction

Alteration observations carried out at the research site aim to map and determine the boundaries of the alteration area and at the same time observe the alteration mineral associations found in each of the alteration patterns encountered. The research area consists of two alteration patterns, namely the chlorite-clay mineral zone - calcite (chlorite is green and has a glossy soil), and the mineral clay zone. The physical appearance of alteration in rock (Figure 5), while the distribution of alteration types in the study area can be seen in (Figure 6).

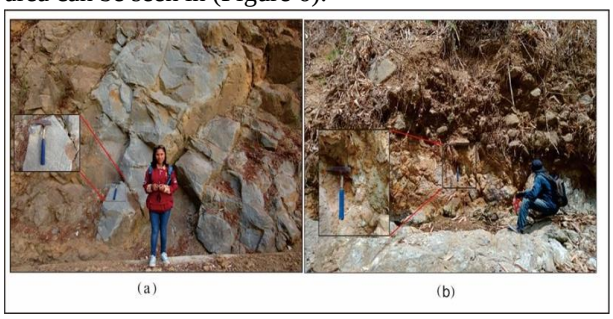

Figure 5. The appearance of the chlorite –clay mineral-calcite zone (a), the appearance of the mineral clay zone (b).

Alteration distribution mapping shows that there are two types of alteration that developed in the research area, namely the chlorite-clay mineral-carbonate zone and the mineral clay zone. By genesis, chlorite is an altered mineral originating from the alteration process due to a hydrothermal solution that changes the mafic minerals that exist in the rock it passes through. While clay minerals are a change from plagioclase minerals and carbonate content shows the effect of the reaction of Ca elements and volatile elements from the remaining magma in the form of CO2 gas and the presence of meteoric water factors in hydrothermal fluids that alter side rocks. Meanwhile, the clay minerals zone, which is by genesis, are altered minerals derived from feldspar minerals such as plagioclase minerals. In the study area, several types of quartz vein textures were found which will later be associated with several classifications as parameters for determining the temperature of the hydrothermal solution in the residual magma that develops into a hydrothermal solution (Table 1). Subsequent hydrothermal solutions with a certain temperature will have a certain alteration effect, the most important of which is knowing the temperature of the hydrothermal solution then we can determine the type/form of mineralized deposits (Figure 7). Quartz vein position data retrieval conducted at the study site aims to determine the direction of the quartz vein and the slope of the quartz vein, and megascopic observations of metallic minerals in the veins using a loupe, data on the position of quartz and metal mineral content found in the study area (Table 2). The distribution of the direction of the Quartz vein in the study area is controlled by the Plampang 2 Left Horizontal Fault and the Plampang 4 Right Horizontal Fault. At the Plampang 2 Left Horizontal Fault produces joints filled with quartz veins with a West-East direction with metal mineral content in the form of pyrite, galena, direction Southwest - Northeast, and Northwest-Southeast contain metallic minerals in the form of pyrite. Meanwhile, the Right Horizontal Fault Down 4 produces joints filled with quartz veins with a southwest-northeast trend with the metal mineral content of pyrite, galena, and northwest-southeast has pyrite metal mineral content . on the quartz veins associated with barite minerals (quartz veins 10) trending northeast-southwest with pyrite mineral content, galena mineragraphic analysis on barite veins showed the presence of pyrite, sparite, chalcopyrite and the presence of gold in the incision. The graphite mineral is embedded in the quartz and pyrite bed mass and is present in barite veins by 50%, characterized by a light cream color, 0.2-5 mm coarse-grained, subhedral-anhedral shape, evenly distributed in the rock and chalcopyrite with a percentage of 20% color. yellow, irregular shape, anhedral, bidirectional cleavage, coarse-grained 1-3 mm. From the results of the mineragraphic incision analysis, it can be observed that pyrite is present to replace chalcopyrite (Figure 8). According to Sangadji (2017) in the research area of quartz veins associated with pyrite trending Northwest-Southeast (quartz vein 8) a mineragraphic analysis showed that pyrite was present with characteristics of a gray, white, angular shape, 0.6-1 mm, cut by veinlets, metallic minerals present in the form of pyrite with 5% presence, anhedral form, light beige color, isotropy, fine-grained size 0.05-0.25 mm, anhedral shape.

PROCEEDINGS
JOINT CONVENTION BANDUNG (JCB) 2021
November 23rd – 25th 2021

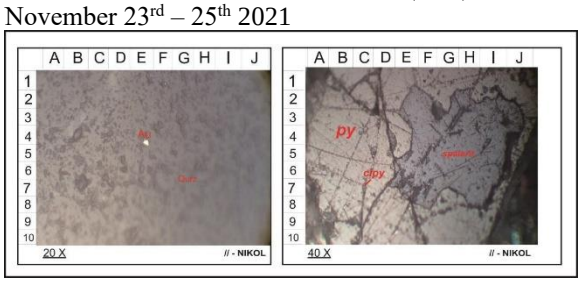

Figure 8. Mineragraphic polishing incision. Au: Gold Cpy: chalcopyrite and Py: Pyrite

Conclusions

The research area has lithology in the form of igneous andesite aphanitic and porphyry aphanitic andesite, which are comparatively included in the Old Andesite Formation. The research area has geomorphological units of denudational origin with sub-units of hilly geomorphic hills and denudational slopes (D2), isolated hills (D4). The study area has a structural orientation in the form of faults, namely Plampang 1 Left Horizontal Fault, Plampang 2 Left Horizontal Fault, Plampang 3 Left Horizontal Fault which is relatively northeast-southwest, Plampang 4 Right Downward Fault, Southeast-Northwest Trending, and Right Downward Fault Plampang 5 is trending northeast-east, southwest-west. The direction of the distribution of quartz veins which is west-east (metal minerals such as pyrite, galena), southwest-northeast and northwest-southeast (pyrite metal minerals) is controlled by the Plampang 2 Fault Left Horizontal Fault, while the direction of the quartz veins is Southwest-Northeast (metal mineral pyrite, galena), Northwest-Southeast (pyrite metal mineral) controlled by the Plampang 4 Normal Right Slip Fault. The type of quartz vein texture found in the study area consists of Banded-Crustiform Vein and Massive Vein based on the classification of hydrothermal mineral deposits according to Lindgren (1933) which is summarized in Sutarto (2004). The research area has undergone alteration with a chlorite-clay mineral-calcite zone and a mineral clay alteration zone.

References

Bateman, A.M., 1956, *Economic Mineral Deposits, 2rd Edi*, John Wiley & Son, Inc. New York, hal 916.

Bemmelen, R. W. van. (1949). *The Geology of Indonesia, Vol. IA. General Geology*. Martinus Nijnhoff, The Hague. Netherlands.

Corbertt, G.J., Leach, T.M. 1997. Southwest Pasific Rim Gold-Copper Systems : Structure, Alteration, and Mineralization. Short Course Manual.

Fredy, Prasetyadi, Gazali, Reyzananda., 2017, Kontrol Struktur Terhadap Model Urat Kuarsa Pembawa Mineral Sulfida Di Kali Mojo, Pacitan, Jawa Timur , Seminar Nasional Kebumian XI-FTM UPN "Veteran" , Yogyakarta.

Sutarto., 2004., "Endapan Mineral"., Laboratorium Petrologi dan Bahan Galian Teknik Geologi, Fakultas Teknologi Mineral, Universitas Pembangunan Nasional "Veteran"., Yogyakarta

Suyono, Slamet., 2004., Geologi Dan Mineralisasi Logam Pada Intrusi Andesit Oligosen Akhir Daerah Sangon, Kulonprogo Daerah Istimewa Yogyakarta., Teknik Geologi, Jurusan Ilmu-ilmu Teknik, Univertas Gajah Mada., Yogyakarta.

Sangadji, I, 2017, Studi Karakteristik Urat Kuarsa Sebagai Parameter Penentuan Suhu Larutan Hidrotermal Di Dusun Plampang, Desa Kalirejo, Kecamatan Kokap, Kabupaten Kulon Progo, Daerah Istimewa Yogyakarta, Seminar, Fakultas Teknologi Mineral, Institut Sains & Teknologi AKPRIND.

Van Zuidam, et, al 1983. Guide to Geomorphologic aerial photographic interpretation and mampping.

Widagdo, A., Pramumijoyo, S., Harijoko, A., Setiawan, A., 2017, Kajian Pendahuluan Kontrol Struktur Geologi Terhadap Sebaran Batuan-Batuan Di Daerah Pegunungan Kulonprogo-Yogyakarta, Proseiding Seminar Nasional KebumianKe-6, T. Geologi UGM, Yogyakarta.

Acknowledgements

Thank you to the departemen of Geological Engineering FTM IST AKPRIND Yogyakarta for the permission and research support, HMTG GAIA and SC MGEI IST AKPRIND and all parties involved who cannot be mentioned one by one.

PROCEEDINGS
JOINT CONVENTION BANDUNG (JCB) 2021
November 23rd – 25th 2021

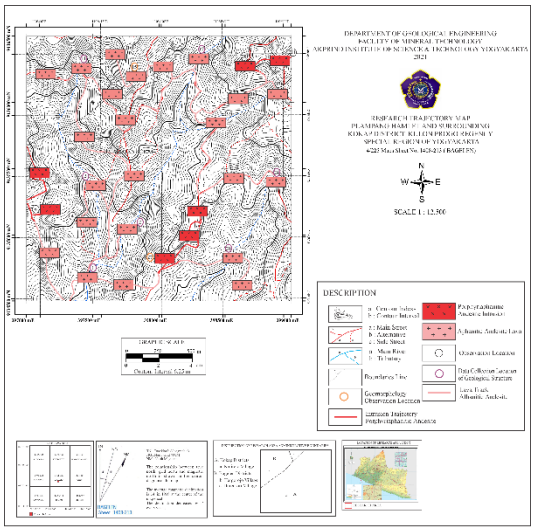

Figure 1. Research trajectory map

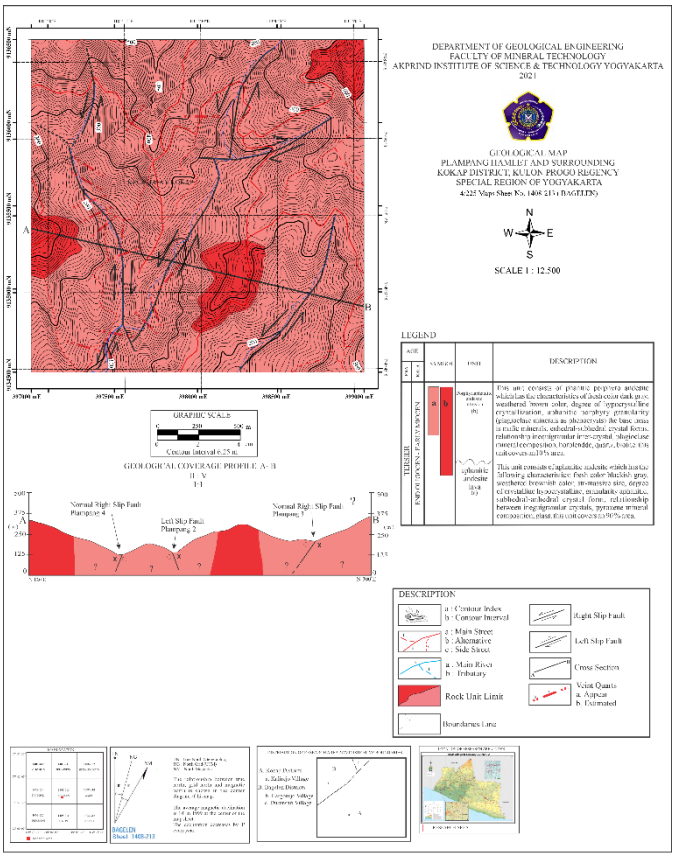

Figure 2. Geological map of the research area

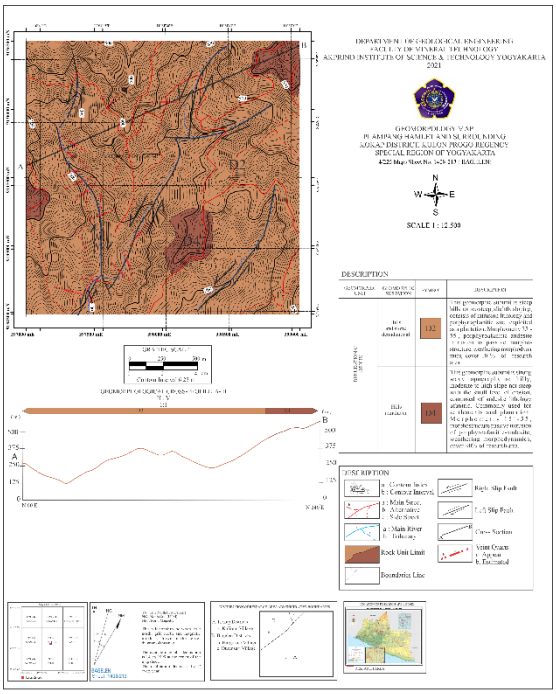

Figure 3. Geomorphological map of the research area

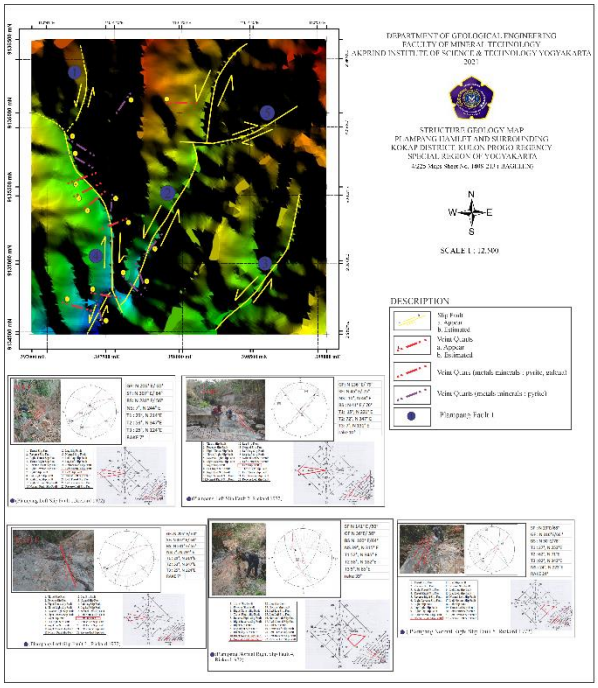

Figure 4. Geological Map Structure of the research area

PROCEEDINGS
JOINT CONVENTION BANDUNG (JCB) 2021
November 23rd – 25th 2021

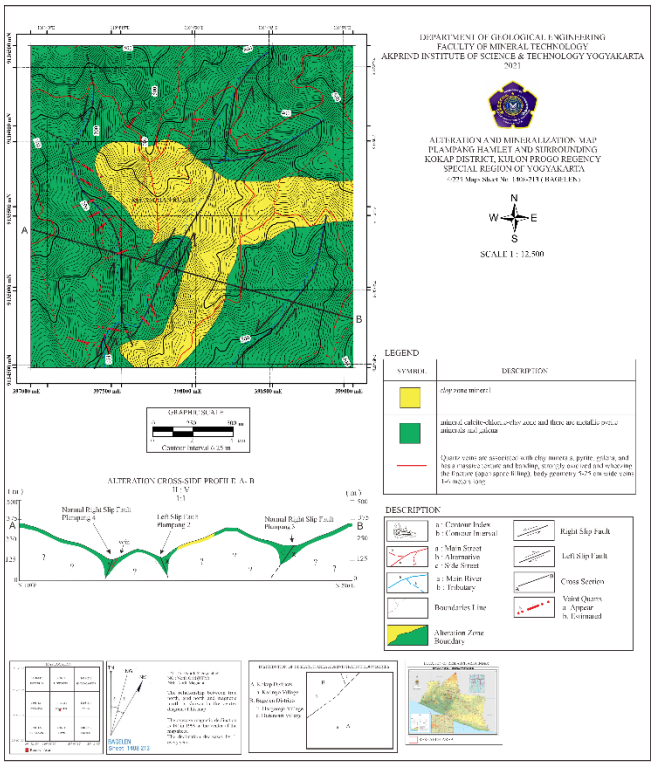

Figure 6. Research area alteration map

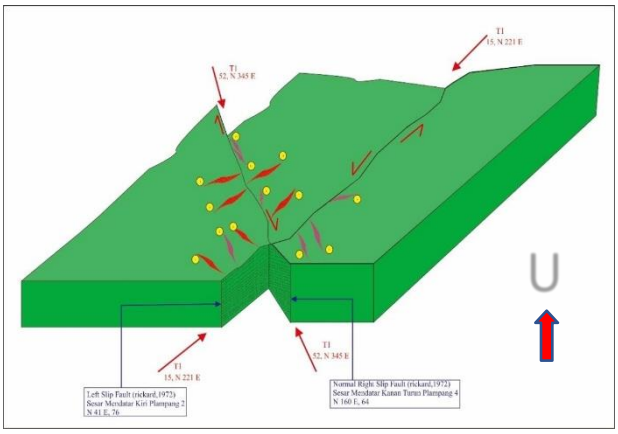

Figure 7. Interpretation of geological structure patterns and direction of distribution of quartz veins

Type of quartz vein	Discriptions	Picture			
Vein Banded-Crustiform (quartz vein 8)	✓ Color; blackish brown with a slight reddish gradation. ✓ Alteration of the body veins; silicification- weak prophylactic. ✓ Textures; Vein Banded-Crustification (Lindgren, 1933, in Sutarto, 2004), with a layer thickness of approximately 2.5 cm. ✓ Structural geometry: Tension Fracture with a width of 5 cm. length of exposed veins about 3 m. It has the appearance of following the previously formed joint geometry in a north-south direction ✓ Secondary minerals; chlorite, quartz. Clay minerals. ✓ Metallic mineral: pyrite with very fine size can be observed using a loupe.	 The direction of veins N 58°E	*Vein massive* (quartz vein 3)	✓ Blackish brown color and there is a slight reddish gradation, ✓ Alteration in the vein body: silicification- weak propylytic. ✓ Texture: massive, 25 cm thick ✓ Structural geometry: Tension Fracture with a width of 25 cm, length of exposed veins about 1 m. Has the appearance of following the previously formed joint geometry in a west-east direction. ✓ Secondary minerals: chlorite, clay minerals, quartz. ✓ Metallic minerals: pyrite with very fine size, can be observed using a loupe, and galena ✓ Genesis: formed as an open space inviting deposit due to the geological structure in the form of solid.	 The direction of veins N 70° E
	✓ Genesis: formed as an open space infilling deposit due to the presence of geological structure in the form of joints.				

Tabel 2 Several types of quartz vein textures found in the study area

Number of veins	Strike	Dip	Metallic logam
1	N 104°E	60°	Pyrite, galena
2	N 355°E	66°	Pyrite
3	N 280°E	70°	Pyrite,galena
4	N 315°E	71°	Pyrite
5	N 330°E	66°	Pyrite
6	N 50°E	74°	Pyrite
7	N 248°E	60°	Pyrite,galena
8	N 190°E	75°	Pyrite
9	N 58°E	70°	Pyrite,galena
10	N 60°E	65°	Pyrite,galena
11	N 70°E	50°	Pyrite,galena
12	N 120°E	70°	Pyrite
13	N 123°E	64°	Pyrite
14	N 45°E	65°	Pyrite

Tabel 2 Data on the position of quartz veins and metal mineral content

PROCEEDINGS
JOINT CONVENTION BANDUNG (JCB)2021
November 23rd – 25th 2021

Integrated Strategy in Increasing Energy Sector Investment (Coal Bed Methane) in Indonesia

Salsabilla Aurelia Azzahra[1], Angela Benedicta Horta[2], Ferdinandus Klea Latuan[2], Suci Nur Hidayah[2], Usholia[1], Lailatul Pitriyah[3]
[1]Accounting Department, UPN "Veteran" Yogyakarta, Indonesia
[2]Petroleum Engineering Department, UPN "Veteran" Yogyakarta, Indonesia
[3]Management Department, UPN "Veteran" Yogyakarta, Indonesia
Corresponding email address: salsabillaaurelia99@gmail.com

Abstract

According to Indonesia Energy Outlook, Indonesia experienced a decline in oil production since 2000, while gas production showed fluctuation but was dominated by the decline. One of the reasons for the decline in oil and gas production is that production wells in Indonesia are generally old, while production of new wells is relatively limited. Seeing the sluggish condition of Indonesia's oil and gas production, it is necessary to develop other alternative energy sources, one of which is Coal Bed Methane (CBM). CBM development certainly requires high costs. Therefore, funding assistance from investors is needed. Investment in the CBM sector is urgent when it is no longer aims to make CBM into a commodity but also as a component of country development. This paper presents a comprehensive methodology to attract investors, particularly for developing in the CBM field. Regulation Enhancement through Government Regulation Number 79/2014 and Ministry of Energy and Mineral Resources (MoEMR) Regulation Number 4/2017, a reliable Reserve Analysis to support the potential of abundant CBM resources with a total of 453 trillion cubic feet, an attractive First Tranche Petroleum (FTP), Tax Income, Depreciation Method, Contractor Share, and Investment Credit, as well as a proportional Risk-Sharing between the government and investors, is an integrated step needed to attract investors. The presence of an investment in the CBM sector has made CBM development not only contributing to meeting domestic energy needs but also contributing to the development of the environment and human resources around the development area. In addition, when investment can be a component of driving development in certain regions, the strategies offered in this paper can assist the government (central and regional in particular) in dealing with crises, especially crises during a pandemic like nowadays.

Keyword: Coal bed methane, Driving development, Economy, Investment.

Introduction

According to Indonesia Energy Outlook that published by the Kementerian ESDM (2010), Indonesia has experienced a decline in oil production since 2000, while gas production shows a fluctuation but is more dominated by a decline. One of the reasons for the decline in the oil production wells in Indonesia, in general, is mature, while the production of new wells is relatively limited (Indonesia Energy Outlook Kementerian ESDM, 2019). The decline in production of oil and gas causing the position of Indonesia is no longer a net exporter of oil, causing the separation of Indonesia from the Organization of the Petroleum Exporting Countries (OPEC) in 2009. Seeing the condition of Indonesian oil and gas production, it is necessary to develop other alternative energy. One of the alternative energy sources is Coal Bed Methane (CBM).

Coal Bed Methane (CBM) is defined as a gas that is formed during the coalification process to change the organic material into coal. This gas is produced by microbiological or thermal processes as a result of increased heat at deeper depths during coal formation (S. K. Haldar, 2018). In the Schlumberger Oilfield Glossary, CBM is defined as natural gas which is dominated by methane (CH_4) and originates from coal formations, which will be absorbed into the surface of the matrix pores between coal and fractures due to pressure rise.

Several reasons drive the need for CBM development in Indonesia. The main reason is that the high potential of CBM in Indonesia is not matched by appropriate utilization. It is recorded that of a total of 51 exploration areas, only 17% have committed to being developed (C. Irawan, et al., 2017). Reporting from the website of the Ministry of Energy and Mineral Resources (2010) the government targets production for CBM in 2015 to reach 500 million (MMSCFD), but ESDM (2015) reports CBM production only reaches around 0.5-0.6 MMSCFD. The realization of CBM development is still very small when compared to the potential of CBM in Indonesia. The second reason is viewed from a regulatory perspective, based on Government Regulation No. 79 of 2014 concerning National Energy Policy and Regulation of the Minister of Energy and Mineral Resources No. 4 of 2017 concerning National Vital Object in the Field of Energy and Mineral Resources, the government supports the development of New and Renewable Energy. Apart from that, air pollution due to the use of

fossil energy which continues to increase from year to year requires the government to look for alternative energy sources immediately therefore, this is the third and the last reason for the need for CBM development in Indonesia. This paper discusses several strategies that can be made to attract investors so that the potential of CBM can be utilized appropriately.

.

Data and Method

The method used to write this paper is the literature review. The five fiscal policies suggested in this paper initially come from various literature and data that have already been collected. The combination of the five fiscal policies that is giving 35% tax income to the state, investment credit, 78% contractor share, appropriate depreciation method, FTP 5%, and proportional risk-sharing combined into one integrated strategy, will be a stimulus to attract investors to invest in the CBM sector. The increasing number of investors who are willing to invest in the CBM industry will play a major role in the development of CBM in Indonesia. On the other hand, investment becomes urgent since CBM development does not only benefit one party. The potential that is developed to the maximum and massive CBM development will have an impact on meeting energy needs, driving development in Indonesia, as well as a solution to facing the energy crisis caused by Covid-19 in Indonesia (Figure 1).

Result and Discussion

Regulation Enhancement

Government Regulation No. 79 of 2014 concerning the National Energy Policy is a form of government support for the development of new energy in Indonesia. Article 1 paragraph 9 emphasizes the creation of energy independence by maximizing the use of energy potential in Indonesia. In addition, the government also supports companies engaged in oil and gas and coal as stipulated in article 24 paragraph 2, point g.

The development of energy sources based on oil and gas, electricity, mineral coal, and new and renewable energy is regulated as vital energy in the Regulation of the Minister of Energy and Human Resources No. 4 of 2017. National Vital Object in the Sector of Energy and Mineral Resources, hereinafter referred to as Obvitnas in the field of ESDM, are areas/locations, buildings/installations, and/or businesses relating to the livelihoods of many people, state interests, and/or sources of state revenue is positioned in the field of energy and mineral resources (ESDM No. 4 of 2017, Article 1, paragraph 1). Based on this understanding, CBM development is certainly something that must be done as a form of realization of the above regulations. The emphasis on the importance of developing CBM is then emphasized again in article 2, point C MoEMR Regulation No. 4 of 2017 that coal minerals are included in vital object.

Reserve Analysis

Indonesia has abundant potential CBM resources with a total amount of 453 TCF. This total number makes Indonesia the second largest country in Asia with CBM potential after China (Table 1). (T. B. Sumarno, 2017). The prospect of potential CBM areas in Indonesia is divided into two areas, namely the Sumatra and Kalimantan areas. Of the 51 CBM exploration contract areas, C. Irawan (2017) wrote that only 17% were able to fulfil commitments, and the rest encountered obstacles or challenges in fulfilling commitments. To maximize CBM management, it is necessary to accurately measure CBM reserves. One of the methods is volumetric calculation of gas reserves based on the nature of stored gas adsorbed in coal can be calculated based on the formula:

$$GIP = 1359{,}7 \times (A \times h) \times Gc \times \rho b \qquad (1)$$

Y. K. Dalimunthe (2019) wrote that GIP (MMSCF) stands for In-place gas or gas reserves adsorbed in coal, A (acre) represents the area of drainage, Gc (SCF/ton) stands for average Gas Content, and ρb (g/cc) indicates density average coal.

First Tranche Petroleum (FTP)

The definition of FTP itself is part of the oil produced which is shared between the government and contractors before being reduced by Cost Recovery (P. V. Wimar 2016). Determining the amount of FTP value is regulated in a Decree of the Minister of Energy and Mineral Resources based on blocks. Currently there are two ESDM Ministerial Decrees that use 10% and 5 % of FTP. Systematically, the FTP calculation is written as follows (P. V. Wimar, 2016).

$$FTP = 20\% \times Gross\ Revenue \qquad (2)$$
$$FTP\ Go\ vernment = (1 - Share) \times FTP \qquad (3)$$
$$FTP\ Contractor = Share \times FTP \qquad (4)$$

Based on the number of FTP that used by the MoEMR, FTP 5% was the number that proposed in this paper.

Tax Income

Income tax or what is known as taxable income is a tax imposed on individuals or individuals and entities concerning income received or earned during a tax year. The amount of income tax for CBM is different for each block, which is stipulated in a Decree of the Minister of Energy and Mineral Resources. Currently, there are 2 Ministerial Decrees, namely the Decree of the Minister of Energy and Mineral Resources Number 1834K/13/HEM/2008 for the “Indragiri CBM” block with the amount received by the government after tax of 60% and the contractor at 40% and the block “CBM Bentian Besar” the amount received by the government after tax is 55% and contractors 45%, and the Decree of the Minister of Energy and Mineral Resources No. 1736K/13/HEM/2008 for the “GMB Sekayu” block with the amount received by the government after tax

is 55% and the contractor is 45%. Tax income 35% was choosen as solution to encourage the investor.

Depreciation Method
Depreciation written by Faneisya Pesak (2018) is a periodic and systematic allocation of the acquisition cost of the asset during different periods that will benefit from the use of the asset concerned. Under SAK 2017, depreciation is recognized even if the fair value of the asset exceeds its carrying amount as long as the asset's residual value does not exceed its carrying amount. The most commonly used depreciation method is:

Straight-Line
The depreciation rate is constant over the time the depreciation occurs.

Depreciation = Investation/ (Depreciation Period) (5)

Depreciation uses the consideration that the longer the fixed assets are used, the lower the quality of the assets will be (Dhafinda Diakinan, 2019). Elijah Acquah - Andoh (2019) writes the most ideal depreciation method for the CBM industry namely the straight-line method with a period of 5 years.

Contractor Share
D. D. Diara (2019) describes that the Contractor's Share or part of the contractor is the right of the contractor's share, which comes from gross income after deducting pre-tax costs multiplied by Equity to be Split. This contractor's share right after being deducted by the sharing tax before Cost Recovery is called the Net Contractor Share, and when added with all the parts issued, it is called the Total Contractor Share. At the end of 2015, the Ministry of Energy and Mineral Resources issued a new policy to accelerate the CBM industry, MoEMR Regulation No. 38 of 2015. The regulation regulates the choice of fiscal system for CBM as a result of negotiations between the government and CBM contractors. In a net PSC that is similar to the PSC for conventional hydrocarbons, the share of the yield on the net PSC CBM has been modified. The contractor share becomes 55 for the government and 45 for CBM contractors to attract CBM investors (T. B. Sumarno, 2017). Elijah Acquah-Andoh (2019) added that with a share contractor of 78%, it was able to attract investors with a ratio greater than the existing net PSC CBM. This amount is also used in this paper as one of the fiscal policies that offers by the writer.

Investment Credit
Investment credit itself is an additional return on capital costs in a certain amount, which is directly related to production facilities, which is given as an incentive for the development of certain oil and/or natural gas fields. The determination of the amount of investment credit itself is the same as for other upstream incentives as stipulated in the Decree of the Minister of Energy and Mineral Resources. Currently, there are 2 Ministerial Decrees relating to Coal Bed Methane, namely, the Minister of Energy and Mineral Resources Decree No. 1834K/13/HEM/2008 for the "CBM Indragiri" block and the "CBM Bentian Besar" block, and the Minister of Energy and Resources Decree. Mineral Number 1736K /13/HEM/2008 for the block “GMB Sekayu” with an investment credit of 0% (Figure 2).

Risk Sharing
In “An Introduction to Risk Management” (Crane et al., 2013) it is explained that risk can be defined as an opportunity for loss or an unfavourable outcome related to an action taken. According to Wanqin Wang, et al (2019), based on the risk characteristics in the life-cycle of a CBM project, a risk assessment index system can be obtained. There are six main risks in the form of policy and legal risk, resource characteristic risk, technical technology risk, economic operational risk, management and organizational risk, and security risk and emergency protection.

The six risks are the first level index that can be derived into the second level index through on-site investigations, literature review, and related laws and policies. The system index will then be reviewed in consultation with an expert. As a result, a CBM project risk assessment index system is obtained, consisting of 6 first-level indexes and 45 derivative indices (Figure 3). SEWM (Structure Entropy Weight Method) was introduced in this study because the SEWM assignment method combines objective and subjective, as well as quantitative and qualitative analysis. This method can reduce the computation workload and be able to obtain higher accuracy, especially for the number of indexes contained in the CBM project risk assessment system.

Integrated Strategy in Increasing Investment in the Energy Sector (Coal Bed Methane) in Indonesia
There are several reasons why CBM in Indonesia should be prioritized and utilized to its maximum potential. With the presence of Government Regulation No. 79 of 2014 concerning the National Energy Policy related to the development of new energy in Indonesia, the administrative processes related to new energy, especially CBM, should no longer encounter significant difficulties. The gas emission from CBM also shows a smaller number since CBM energy produced from coal seams in the form of gas, which makes CBM not produce gas emissions as high as the result of burning coal and petroleum from gas emission of oil and gas energy sector.

Ministerial Regulation No. 79 of 2014 concerning National Energy Policy and Regulation of the Minister of Energy and Human Resources No. 4 of 2017, clearly shows the government's support for CBM

development. The development of coal bed methane in Indonesia must be supported by investment in the CBM sector. This investment is important because the capital that must be spent for the CBM development process is not small. In addition, the CBM industry in Indonesia is classified as an industry with little development, thus making CBM a capital-intensive industry.

The selection of five fiscal policies and proportional risk sharing is determined based on several literature reviews. Determination of the first tranche petroleum (FTP) at 5%, provision of 35% *tax* income to the state, 78 % contractor share, and the 5-year straight-line depreciation method proved not to provide a significant reduction in government revenue and proved more attractive to investors in the coal bed methane industry, based on the paper Coalbed Methane Development in Indonesia: Design and Economic Analysis of Upstream Petroleum Fiscal Policy. Providing FTP, tax income, contractor share, and the 5-year straight-line depreciation method will be more effective when combined with providing incentives to contractors and a balanced risk-sharing. The provision of incentives can be given in the form of investment credit, which has been regulated in Government Regulation No. 27 of 2017. The provision of investment credit will encourage the development of a work area. The existence of risk-sharing with the SEWM (Structure Entropy Weight Method*)* method between the government and contractors will also further reduce the risk of failure in the coal bed methane industry.

Conclusions

The existence of MoEMR Regulation No. 4 of 2017 and Government Regulation No. 79 of 2017 emphasized that the position of CBM is no longer only a commodity but also vital energy. The determination of CBM as vital energy must be supported by the high investor, and to gain the investor could be achieved through the strategy of 5 fiscal policies combined with balanced risk-sharing, which will have an impact on Indonesia. The provision of 5% FTP, investment credit, 35% tax income to the state, 78% contractor share, depreciation method, and balanced risk-sharing are expected to attract investors in the coal bed methane (CBM) industry. The high interest of investors in investing in the CBM industry will encourage meeting energy needs, driving development in Indonesia, and becoming a solution to the energy crisis caused by Covid-19 in Indonesia.

References

Andoh, E. A., H. A. Putra, A. O. Ifelebuegu, and A. Owusu, 2019, Energy Policy **131**, 156–162.

Crane, L., G. Gantz, S. Isaacs, D. Jose, and R. Sharp, 2013, Introduction to Risk Management **2,** 1**–2.**

Dalimunthe, Y. K., D. Marshal, and R. Sitaresmi, 2019 Jurnal Petro 2019, **08 No. 3**, 132– 133.

Diara, D. D., 2019, Laporan Kerja Praktik, Universitas Pertamina.

Haldar, S. K., 2018, Mineral Exploration: Principles and Application, **2**, Elsevier.

Irawan, C., D. Nurcahyanto, F. Azmy, A. Paju, and W. M. Ernata, 2017, OnePetro, **SPE-186343-MS**, 2-3.

Kementerian ESDM, 2010, Pusat Data dan Informasi ESDM KESDM, **2**, 28–29

Kementerian ESDM, 2019, Pusat Data dan Informasi ESDM KESDM, **11,** 2.

Pesak, F., H. Sabijono, and N. Gerungain, 2018, Jurnal Riset Akuntansi Going Concern **13(3),** 458–459.

Sumarno, T. B., 2017, **316655803**, Researchgate, 1–13.

Wang, W., S. Lyu, Y. Zhang, and S. Ma, 2019, Energies 2019, **12,3931**, 5–6.

Wimar, P. V., 2016, Undergraduate Thesis, Universitas Trisakti.

PROCEEDINGS
JOINT CONVENTION BANDUNG (JCB)2021
November 23rd – 25th 2021

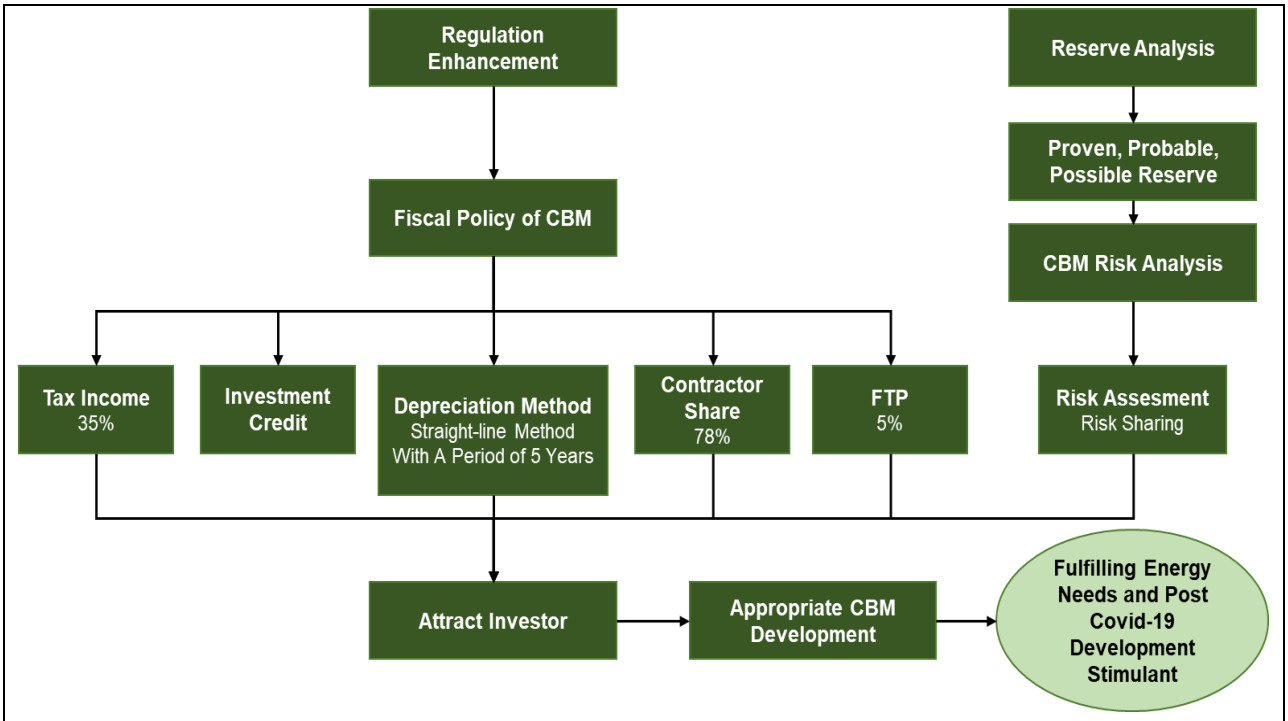

Figure 1: Integrated Strategy in Increasing Investment in the Energy Sector (Coal Bed Methane) in Indonesia

Table 1: Summary of Potential CBM Reserves in Indonesia (Sumarno, T.B. and Bergmann, A., 2017)

No	Basin	Province	Target Formation	Completeable Coal Thickness (m)	Coal Rank (Ro%)	Average Depth (m)	High Graded Area (km^2)	CBM Resources	
								Completeable (Tcf)	Concentration (Bcf/m^2)
1	S.Sumatra	S.Sumatra	M.Enim	37	0.47	762	7350	183	25
2	Barito	Barito	Warukin	28	0.45	915	6330	102	16
3	Kutei	Kutei	Prangat	21	0.50	915	6100	80	13
4	C. Sumatra	C. Sumatra	Petani	15	0.40	762	5150	53	10
5	N. Tarakan	N. Tarakan	Tabul	15	0.45	701	2734	18	6
6	Berau	Berau	Latih	24	0.45	671	780	8.4	11
7	Ombilin	Ombilin	Sawaht	24	0.80	762	47	0.5	11
8	Pasir/Asem	Pasir/Asem	Warukin	15	0.45	701	385	3	8
9	NW Java	NW Java	T. Akar	6	0.70	1524	100	0.8	8
10	Sulawesi	Sulawesi	Toraja	6	0.55	610	500	2	4
11	Bengkulu	Bengkulu	Lemau	12	0.40	610	772	3.6	5
Total							**30248**	**453**	**15**

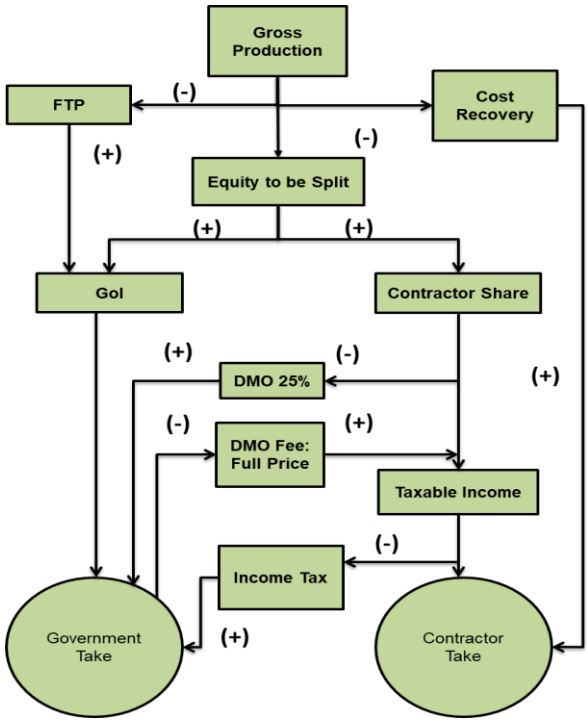

Figure 2: CBM Production Sharing Contract Scheme in Indonesia (Sumarno, T.B. and Bergmann, A., 2017)

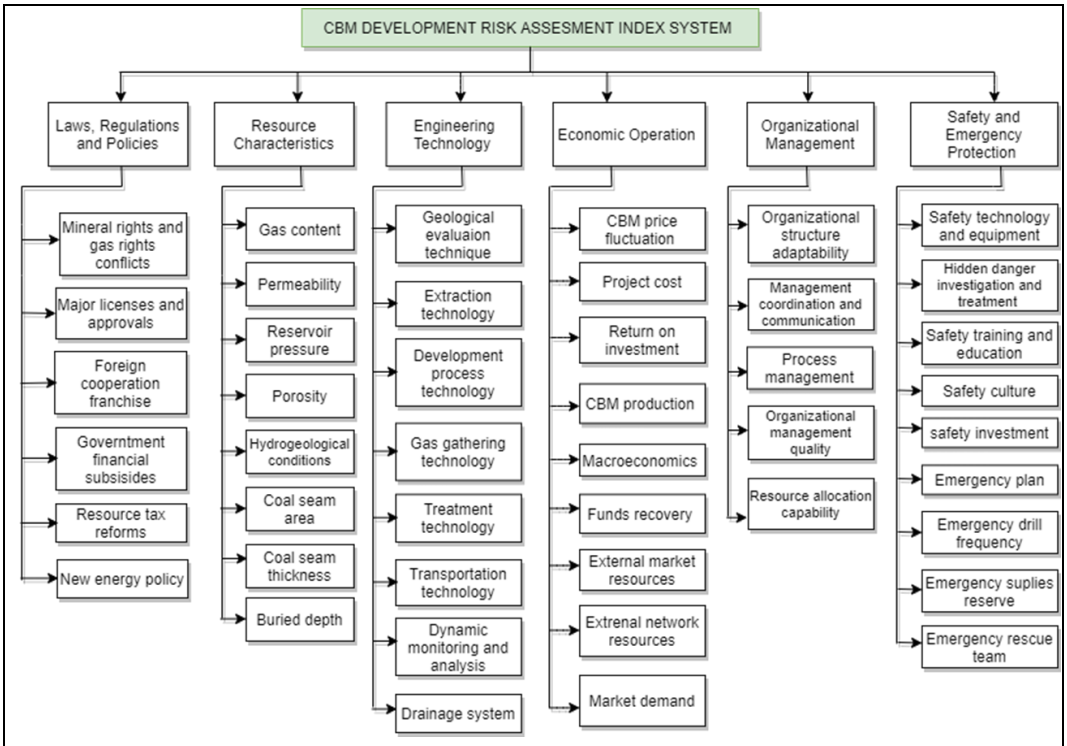

Figure 3: CBM Project Risk Analysis Index System (Wang, W. et al., 2019)

PROCEEDINGS
JOINT CONVENTION BANDUNG (JCB) 2021
November 23rd – 25th 2021

Distribusion of Manifestasion GeothermalEnergy in Solok Selatan

Muhammad Fadhli[1], Rina Sahara[1], Ugi Kurnia Gusti[2]
[1]Geological Engineering Study Program, Sriwijaya University
[2] School of Earth, Environment, and Society, McMaster University.

Abstract
The distribution of geothermal energy in Indonesia reaches 40% of all Indonesia's geothermal reserves. Sapan Maluluang, South Solok is one of the areas that has a promising geothermal manifestation. This area has structural hills that surround the depression area which characterizes areas that have several geothermal surface manifestations. A combination of morphotectonic analysis and field observation of surface manifestation were used to understand the distribution of potential geothermal distribution in the study area. morphometric was carried out to analyze how the morphotectonic control in the research area used dem data input. Smf and Vf were used to understand the landscape evolution and tectonic control to the present morphological condition. In addition, field observation is carried out on how the condition of the source of manifestation found at the research site and observations of the lithology and geological structures control. In the dem data analysis, morphotectonic analysis elements were calculated, such as valley height-weight ratio (Vf) which resulted in 0.02 – 2.38 values of mountain front sinuosity (Smf) which had a value of 1.1-1.3. The research area is heavily controlled by active tectonics. Based on the results of field observation, it is known that there are 5 geothermal manifest sources in the form of hot springs which have a temperature of 175˚C -185℃ and are controlled by the lithologies of the volcanic rocks of Mount Kerinci. In addition, from the lineament analysis at the research site, it was found that the NW-SE lineament was in the same direction as the Sumatran fault zone.
Keywords: Geothermal Solok, Morphotectonic, Lineaments, Geothermal Manifestation

Introduction

Indonesia is one of the countries that have the greatest geothermal potential with a distribution of 25,875 MW or 40% of Indonesia's entire geothermal reserves. Sapan Maluluang, South Solok is one of the areas that have geothermal manifestations. Regionally the research site is on the Bukit Barisan column which is characterized by the existence of a fault zone associated with a row of active volcanoes northwest-southeast. The Sumatra Fault Zone is composed of Pre-tertiary rocks to late-quarter volcanic rocks in the form of metamorphic rock complexes and volcanic rock units (Figure 1)

The collision zone of the Indo-Australian Plate and the Eurasian plate forms a cluster of rows of hills that extends from the north to the south of Sumatra island (Barber et al. 2005). The active tectonics of the Indo-Australian plate move sharply against the Eurasian plate moving southward at a rate of movement of 7 cm/year. The research area experienced several times the lifting, folding, and switching events in the Mesozoic era, resulting in the deposition of shallow seas to the deep in the eastern part and the Cretaceous in the west. Cretaceous tectonic events were accompanied by regional uplift, alignment, and switching. The alignment that occurs controls the formation and development of basins between volcanoes. During Tertiary, volcanism activity produces eruptions and leads at the bottom are sea parts and at the top become sea stacking.

Regional structural patterns consist of the fault and folding structures in the general northwest-southeast direction. While the direction of the anticlinal axis and sinking of Tertiary rocks is almost the same as the direction of the crease of pre-tertiary rocks that flow. Depression in the magmatic arc of Sumatra, occupying the eastern part of the Barisan Mountains and Bukit Barisan Anticlinlin. This depression has straightness with the Ombilin Basin, Sinamar Basin, sub-Kiliran Basin along Bukit Barisan (Rosidi et al, 1996).

The main fault of part of the Sumatra fault is the shear fault and some normal faults are northwest-southeast. The research site is in the Suliti Segment with tectonic basins located in the North Labuh Estuary. The Suliti segment has a length of 95 Km.

In addition, the characteristics of the landscape can identify geological processes that occur at the research site. A collection of plains, plateaus, hills, mountains, slopes, rivers represent the founding of research sites. Topography of the research site consisting of hills to mountains from the southern end of Muaralabuh to the north of Muaralabuh. The area of active tectonics and quaternary volcanism is related to the shape of the manifestation of hot water and the appearance of ancient caldera seen from structural basins influenced by down warping tectonic regions which control the distribution of geothermal distribution in the study area.

Data and Method

The research is developed using, a combination of morphotectonic analysis and field observation of surface manifestation were used to understand the distribution of potential geothermal distribution in the study area (Figure 2). Morphometric was carried out to analyze how the morphotectonic control in the research area used DEM data input. Vf and Smf were used to understand the landscape evolution and tectonic control to the present morphological condition berdasarkan watershed function (Van Noordwijk et al., 2004). In addition, field observation is carried out on how the condition of the source of manifestation found at the research site and observations of the lithology and geological structures control, was carried out by observing the morphology formed by the geological structures that formed an area, that is what is called "Morphotectonic" (Hancock (1994)).

- Vf (Valley Floor Widht to Height Ratio)

The calculation of the ratio of the width of the valley floor and between the two heights, which this method was first introduced by Bull and McFadden (1977) as a geomorphic index used to discriminate between the V-shaped valley floor and the U-shaped valley floor (Rebai, 2013). With the calculation of the Vf index, it can be seen that there is a lifting process in an area. in the study area.

$$Vf = \frac{2Vfw}{Eld+Erd-2Esc} \quad (1)$$

PROCEEDINGS
JOINT CONVENTION BANDUNG (JCB) 2021
November 23rd – 25th 2021

- Smf (Mouintain Front Sinousity)

Calculation of the face of the mountain and the ridge so that it can be seen the level of erosion formed so that it can be used as a parameter whether the area is controlled by high tectonics or not. The SMF concept was first introduced by Bull and McFadden (1977).

$$Smf = \frac{Lmf}{Ls} \quad (2)$$

- Ld (Lineameant Density)

Lineament density is used to determine the relationship between structure density areas formed by the interconnections of fractures or lineament and faults. The permeability rate of the rocks formed is known, which can identify active tectonically.

$$Ld = F/A \quad (3)$$

Result and Discussion

Geomorphology Unit

The landscape is a collection of plains, plateaus, hills, mountains, slope slopes, rivers, and others. Tectonic forces influence the formation of landscapes at work on earth. Therefore, the landscape approach can identify geological processes that occur at the research site. The study results showed that the study's location was influenced by complex tectonic forces, the formation of the topography of the hills to the mountains from the south of the Muaralabuh. Regions of active tectonics and quaternary volcanism are closely related to the manifestations of hot water. This is seen from structural basins that are affected by the tectonic area of down warping so that the emergence of manifestations of Sapan Maluluang hot water is 850 m high (Figure 3).

Vf (Valley Floor Widht to Height Ratio)

The calculation of the morphotectonic index is based on the analysis of the ratio of the valley floor and the height of a flanking morphology. In the measure, the valley morphology formed can be V and U-shaped. This method was introduced by Bull and McFadden (1977). The analysis of the VF index is used to determine whether or not there is a level of lifting activity in a watershed. If the value of Vf < 0.5, then it is included in the high uplift level (High), the medium uplift level (Medium) has a value > 0.5 to < 1, and the value > 1 is included in the low tectonic level (Low) (Keller and Pinter, 2002; Hamdouni, 2008; Sukiyah, 2015).

The calculation result of Vf Batang Ampalu Watershed on the location numbers 3, 5, 6, 7, 10, and 14 shows high uplift rates with Vf values ranging from 0.18 to 0.47. While the locations numbers of 1,4,8,9,11 and 12 have moderate uplift rates with the value of Vf in a range from 0.63 to 0.94 and have lower uplift rates in locations number 2 and 13 with the value of Vf in the field from 1.04 to 1.35. Next, a result of Vf Aia Manyuruak Watershed on location numbers 15 shows high uplift rates with Vf values in a range from 0.29. While the location numbers of 17,18,19 and 20 have moderate uplift rates with the value of Vf in the field from 0.52 to 0.59 and have lower uplift rates in location number 16 with the result, Vf values 1.04

Furthermore, the calculation result of Vf Batang Bangko Jernih and Batang Bangko Keruh Sub Watershed the locations number 22,23,24,25,35,36,37,38 and 39 have the Vf values of 0.10 to 0.41 that tend to show high uplift rates. While the location of Batang Bangko Jernih and Batang Bangko Keruh Sub Watershed number 26, 27, and 40, a moderate uplift rate have occurred, shown by the Vf value in the range from 0.73 to 0.78. They are obtained on the downstream part of Way Batang Suliti watershed, in the Nothern part of the researched area. The have calculation result Vf values 0.22 show high uplift rates in location number 56. While location numbers 54, 55, and 58 have moderate uplift rates with Vf values ranging from 0.53 to 0.56 and have lower uplift rates in locations number 57,59, and 60 with the value of Vf in a range from 1.25 to 2.38.

Moreover, locations Batang Kapur Watershed, locations number 42,43,44, and 45, have a high uplift rate with the value ranging from 0.12 to 0.37, and location number 41 has a lower uplift rate with a value of value 1.05. At the same time, the result of Vf Batang Liki Watershed shows high uplift rates in locations number 29,30,31,32,33, and 34 with the value ranging from 0.02 to 0.40 and have lower uplift rate number in location number 28. At the end of Batang Bangko Watershed, locations number 45,46, 47, 51, and 52 45 have a high uplift rate with values ranging from 0.10 to 0.40. While the number of the location of 48,49,50 and 53 have moderate uplift rates. While location numbers 50 and 53 have reasonable uplift rates with Vf values ranging from 0.59 to 0.62 and lower uplift rates with the value of Vf range from 1.20 to 1.76 in location numbers 48 and 49. The result expressed low to high uplift in the area as shown in Table 1 and Figure 4.

Smf (Mouintain Front Sinousity)

The calculation of the morphotectonic index is in front of the mountain, and the back of the hill, which is seen from the tendency to erosion, so it can develop to find out how an area is controlled by high or low tectonic activity. This method was first introduced by Bull and McFadden (1977). Based on the calculation, the results can be categorized that an area has an active tectonic level if it has an Smf value < 1.5, while if it has a value > 3.0, it is classified as an area with a tectonic level that is no longer active (Hamdouni et al., 2008).

The Calculation of Mountain Front Sinusity was done by determined the Smf through observing the topography and position of the mountain front of Batang Ampalu, Aia Manyurak, Batang Sulit, Batang Bangko keruh dan Batang Liki Watershed (Figure 5) to know the level of tectonic activity on the research area. The Smf calculation indicates that all segment watershed in the researched area is dominated by active fault. The Overall Smf calculation result of six segments produces Smf values ranging from 1.1 to 1.3. Most of them are situated in an active tectonic activity level, and This can be described from Smf values of active tectonic such as Segment A (1.2), B (1.1), C (1.04), D (1.1), E (1.3) and F (1.1). According to SMF Index (Hamdouni et al., 2008), this area is controlled by active tectonics (Table 2).

Ld (Lineameant Density)

Lineament density is performed to sharpen the determination of zone high dominant lineament intensity describing the permeability rate of the rocks formed. The Calculation result of the Lineameant density will produce contour maps based on the absolute value of lineament with Extraction in Software PCI Geomatica.

The interconnections, fractures or lineament, and faults can be used as evidence that active tectonic activity passes the area. The result calculation shows that the highest lineament density values range from 0.25 Km - 5.92 Km with the primary orientation that is northwest-southeast and north-south was in the same direction as the Sumatran fault zone and then be related in the are found geothermal manifestations in the research area. (figure 6).

Geothermal Surface Manisfestasion

In the research are geothermal surface manifestations as hot spring, mud poll, altered rock, steaming ground, steam-heated water, solfatara, and fumaroles. In the research area, five geothermal manifest sources are found in the form of hot springs, which have a temperature of 175˚C -185℃ and are controlled by the lithologies of the volcanic rocks of Mount Kerinci (figure 7).

Conclusions

The calculate of Uplift Values in the area (Vf) Obtained the level of removal at the research site has a value with a range of 0.02-2.38, so it can be known that the research area was experiencing a relatively high level of removal. While in the analysis of mountain face sinusitis (Smf), the level of tectonic activity that controls the research area has a value with a range of 1.1-1.3 so that it can be categorized as areas with high tectonics.

Furthermore, the analysis of lineament density can be supporting data in knowing the permeability rate of the rocks formed with values ranging from 0.25 Km - 5.92 Km with the primary orientation that is northwest-southeast and north-south the same direction the Sumatran fault zone.

Moreover, The formation of a down warping zone controls the depression, and then field observation results found manifestations with a temperature of 175 C˚ – 185 C. According to the calculated Morphotectonic Indexes (Vf and SMF) and Surface manifestation, those areas become the path for the appearance of Distribution Potential Geothermal Resources.

References

Barber, A. C. 2005, Geological Society Memoir, 282 pp.

Bull, B.W., and McFadden, L., 1977, Proceedings of the 8th Annual Geomorphology Symposium, 23-24, p.115-138.

El Hamdouni R,Irigaray C, Fernandez T, Chacon J, Keller E A (2008), Geomorphology, 96 (1-2):150-173.

Gentana, Dwi et.al.,2019. Jouurnal on Geoscience Vol 6 No 3 December 2019:291-309.

Keller, E.A. and Pinter, N., 1996.Active Tectonics; earthquakes, uplift and landscape (2nd edition), Prentice-Hall, Inc., New Jersey

Rimando, Jeremy M. & Lindsay, M.Schoenbohm. 2019. Geomorphology 350 (2020) 106908.

Rimando, J.M., Schoenbohm, L.M., Costa, C.H., Owen, L.A., Cesta, J.M., Richard, A.D., Gardini, C.E., 2019. Tectonics 38 (3), 916–940.

Rosidi, H.M.D.Tjokrosaputra and Pandowo, B. 1996. GSI

Silva, P. G. 1988. M.S Thesis Comlutense University, Madrid.

Silva, P. G.,1994. Dissertaitin, Complutense University Madrid.

Sukiyah, E., Syafri, I., Sjafrudin, A., Nurfadli, E., Khaerani, P., and Simanjuntak, P.A.D., 2015. Proceeding of the 36th Asian Confenrence on Remote Sensing, Philippine, October, 19-23, p.1-10.

Yuliandini, A., and Putra, A, 2013. Journal of Physics Unand Vol. 2, No. 4, October 2013

Acknowledgements

We are grateful to Joint Convention Bandung accepted for our papers. We would like to thank all members of the Bumi Sriwijaya Research Group for supported this study.

Tabel 1. Vf (Valley Floor Widht to Height Ratio) calculation shows low-moderate-high uplifit rates. Determination of Uplifit Rates follow (Keller and Pinter, 2002; Hamdouni, 2008; Sukiyah, 2015) clasification

No	Vfw	2Vfw	Eld	Erd	Esc	2Esc	Vf	Watershed	Uplift Rate
1	132	264	620	1066	600	1200	0.54	Sungai Ampalu	M
2	37	74	731	704	690	1380	1.35	Sungai Ampalu	L
3	13	26	1006	1050	970	1940	0.22	Sungai Ampalu	H
4	26	52	756	784	735	1470	0.74	Sungai Ampalu	M
5	7	14	999	976	969	1938	0.38	Sungai Ampalu	H
6	19	38	919	1024	906	1812	0.29	Sungai Ampalu	H
7	11	22	621	624	599	1198	0.47	Sungai Ampalu	H
8	8	16	868	873	862	1724	0.94	Sungai Ampalu	M
9	7	14	758	766	751	1502	0.64	Sungai Ampalu	M
10	10	20	956	991	917	1834	0.18	Sungai Ampalu	H
11	17	34	1241	1224	1208	2416	0.69	Sungai Ampalu	M
12	10	20	665	667	650	1300	0.63	Sungai Ampalu	M
13	25	50	835	833	810	1620	1.04	Sungai Ampalu	L
14	26	52	938	954	865	1730	0.32	Sungai Ampalu	H
15	3	6	1081	1078	1069	2138	0.29	Aia Manyuruak	H
16	49	98	711	761	705	1410	1.58	Aia Manyuruak	L
17	25	50	810	785	751	1502	0.54	Aia Manyuruak	M
18	13	26	755	753	729	1458	0.52	Aia Manyuruak	M
19	21	42	1182	1154	1130	2260	0.55	Aia Manyuruak	M
20	34	68	781	785	725	1450	0.59	Aia Manyuruak	M
21	60	120	954	754	743	1486	0.54	Batang Bangko jernih	M
22	15	30	871	920	856	1712	0.38	Batang Bangko jernih	H
23	27	54	964	981	904	1808	0.39	Batang Bangko jernih	H
24	25	50	1980	2073	1934	3868	0.27	Batang Bangko jernih	H
25	33	66	1660	1639	1551	3102	0.34	Batang Bangko jernih	H
26	39	78	832	843	784	1568	0.73	Batang Bangko jernih	M
27	27	54	641	625	598	1196	0.77	Batang Bangko jernih	M
28	64	128	1000	1040	962	1924	1.10	Batang liki	L
29	18	36	1221	1227	165	330	0.02	Batang liki	H
30	12	24	1804	1698	1673	3346	0.15	Batang liki	H
31	19	38	1303	1415	1269	2538	0.21	Batang liki	H
32	28	56	1095	1175	1065	2130	0.40	Batang liki	H
33	14	28	850	885	831	1662	0.38	Batang liki	H
34	23	46	1073	1088	995	1990	0.27	Batang liki	H
35	15	30	1660	1663	1625	3250	0.41	Batang Bangko Keruh	H
36	11	22	1885	1936	1805	3610	0.10	Batang Bangko Keruh	H
37	12	24	1822	1880	1795	3590	0.21	Batang Bangko Keruh	H
38	11	22	1656	1659	1614	3228	0.25	Batang Bangko keruh	H
39	9	18	1391	1388	1343	2686	0.19	Batang Bangko keruh	H
40	54	108	1123	1116	1050	2100	0.78	Batang Bangko keruh	M
41	31	62	945	942	914	1828	1.05	Sungai Kapur	L
42	22	44	1394	1421	1323	2646	0.26	Sungai Kapur	H
43	12	24	1503	1600	1454	2908	0.12	Sungai Kapur	H
44	13	26	852	838	810	1620	0.37	Sungai Kapur	H
45	19	38	1020	997	935	1870	0.26	Sungai Kapur	H
46	13	26	959	1023	864	1728	0.10	Batang Bangko	H
47	21	42	879	852	813	1626	0.40	Batang Bangko	H
48	60	120	736	752	710	1420	1.76	Batang Bangko	M
49	39	78	650	625	605	1210	1.20	Batang Bangko	M
50	13	26	895	915	883	1766	0.59	Batang Bangko	M
51	13	26	908	942	891	1782	0.38	Batang Bangko	H
52	18	36	1350	1379	1311	2622	0.34	Batang Bangko	H
53	26	52	812	770	749	1498	0.62	Batang Bangko	M
54	38	76	738	768	685	1370	0.56	Batang Suliti	M
55	18	36	705	733	683	1366	0.50	Batang Suliti	M
56	11	22	760	788	723	1446	0.22	Batang Suliti	H
57	19	38	618	633	611	1222	1.31	Batang Suliti	L
58	17	34	779	791	753	1506	0.53	Batang Suliti	M
59	15	30	571	577	562	1124	1.25	Batang Suliti	L
60	19	38	633	643	630	1260	2.38	Batang Suliti	L

PROCEEDINGS
JOINT CONVENTION BANDUNG (JCB) 2021
November 23rd – 25th 2021

Tabel 2. Smf (Mountain Front Sinousity) calculation shows Tectonic Activity Level

Segment of Mountaint Front	Lmf	Ls	Smf	Tectonic Active Level
A	8310	6896	1.205046	Active
B	4280	3662	1.16876	Active
C	7476	7169	1.042823	Active
D	3635	3109	1.169186	Active
E	4705	3470	1.355908	Active
F	4755	4086	1.16373	Active

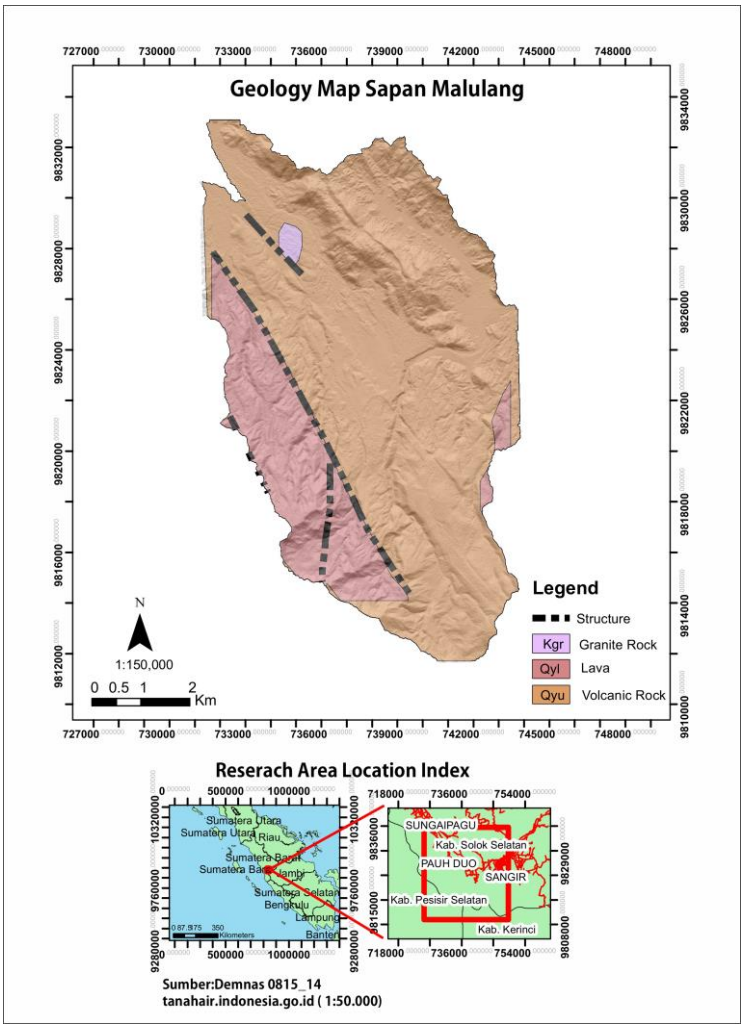

Figure 1. Geology Map of Sapan Malulang Solok Selatan (Modiefied From Rosidi et al., 1996)

PROCEEDINGS
JOINT CONVENTION BANDUNG (JCB) 2021
November 23rd – 25th 2021

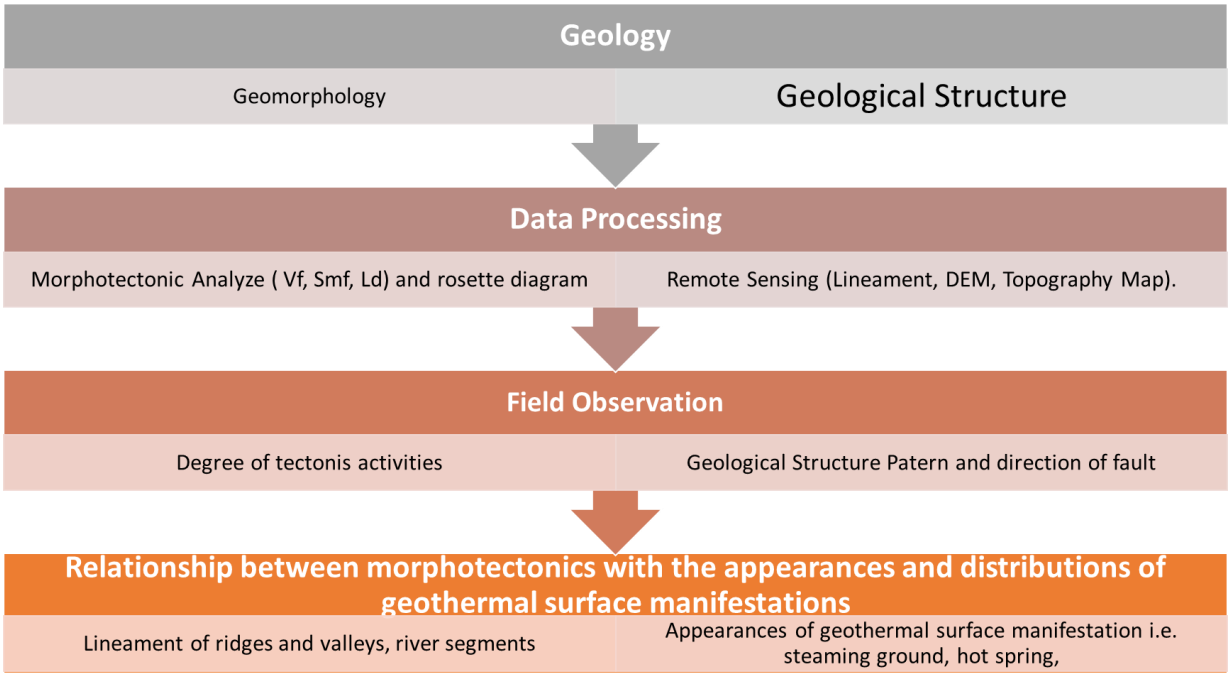

Figure 2. Flow Chart of Research Stage

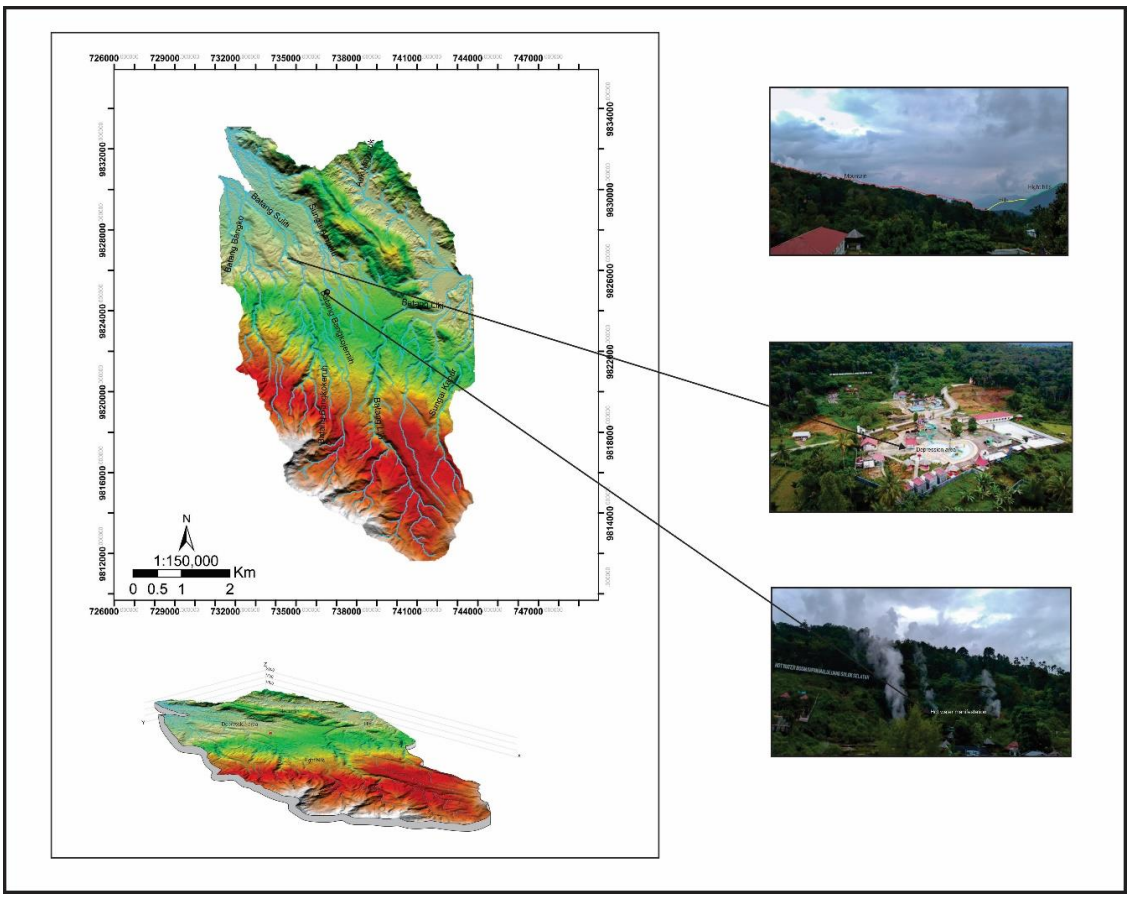

Figure 3. Ilustrasion of Morphology of steep hill and valley, triangular facet, and depression area (Based on field Observation)

PROCEEDINGS
JOINT CONVENTION BANDUNG (JCB) 2021
November 23rd – 25th 2021

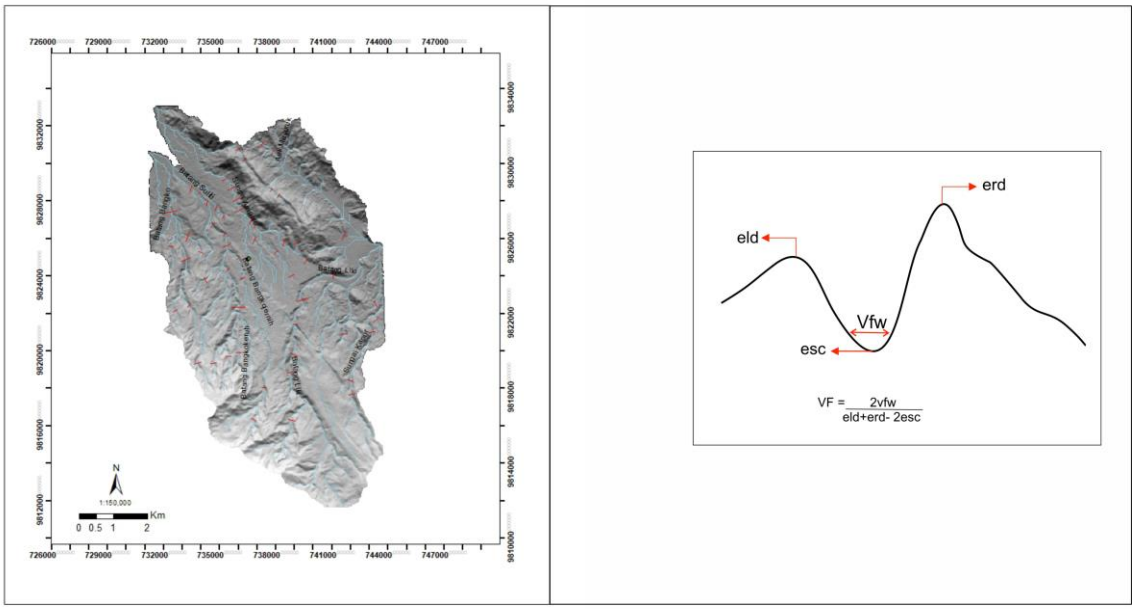

Figure 4. Ilustrasion of Valley floor width to valley height ratio calculation (Vf) calculation method

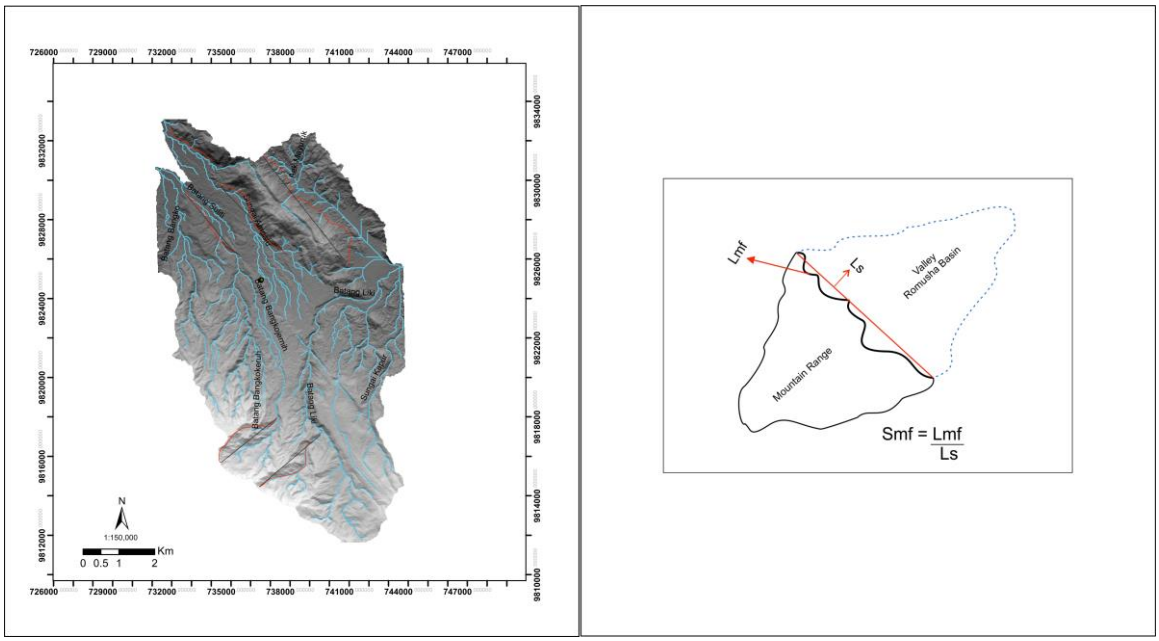

Figure 5. Ilustrasion of Mountain Front Sinousity (Smf) calculation method

PROCEEDINGS
JOINT CONVENTION BANDUNG (JCB) 2021
November 23rd – 25th 2021

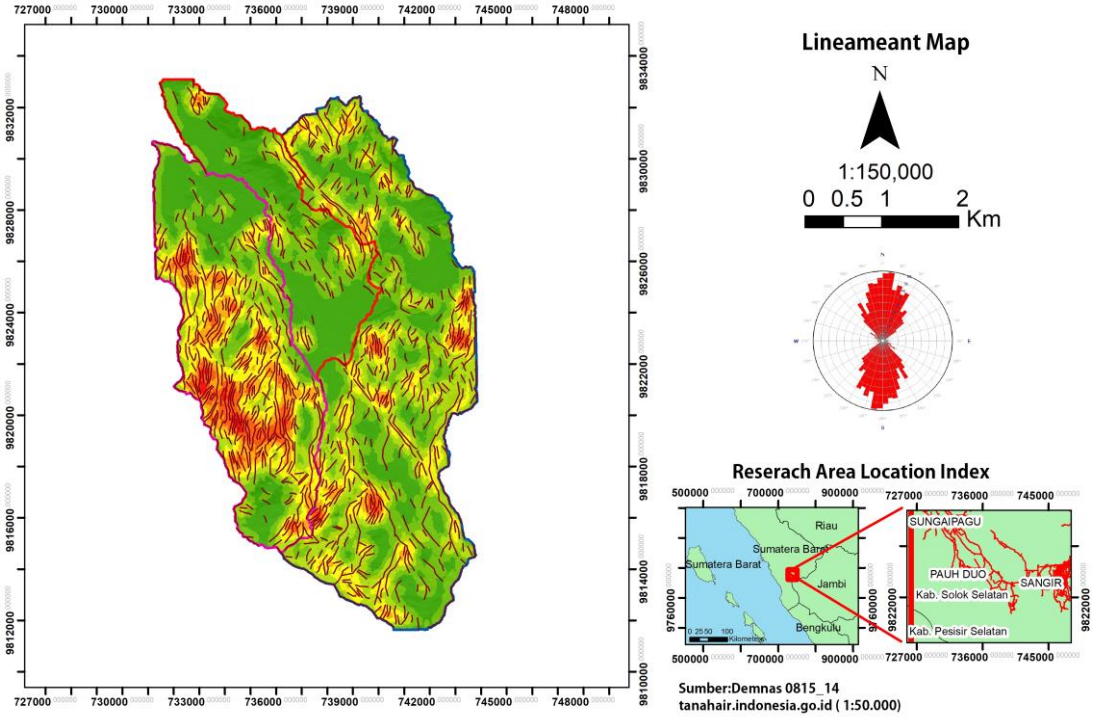

Figure 6. Map of lineament density (Ld) shows areas that have low to high density

Figure 7. Ilustrasion of geothermal surface manifestations at the observation area

Gedung Penunjang Lantai 2 PPPTMGB "LEMIGAS,
Jl. Ciledug Raya No.Kav. 109, RT.7/RW.5, Cipulir,
Kec. Kebayoran Lama, Kota Jakarta Selatan,
Daerah Khusus Ibukota Jakarta 12230

Welcome to the HAGI-IAGI-IAFMI-IATMI 2021 JCB!

This has been a tough year for the Oil Industry. It started previous year with a pandemic, business is slowing down in general, unemployment and high inflation rate becomes a nightmare for almost every country who has been struggling to overcome the economic crisis. The good news is Crude Oil price hopefully will average around $60+ per barrel in 2021. This represents a rebound from the 2020 yearly average of $41 per barrel, but it is still lower than pre-Covid levels.

This year, the 4th Joint Convex 2021 is held with the theme of "Strategic Alliance Acceleration in Natural Resources Utilisation and Hazard Mitigation for National Resilience". The theme couldn't be more accurate in delivering all the issues and opportunities we need to address. As Indonesia's population and economy continue to grow, the demand for energy -in which oil and gas play a significant role- will also continue to grow.

In the current global oil and gas environment, both countries and investors are in strong competition. Countries must compete globally to win foreign investment as the current global opportunities exceed the total available capital, specifically in the energy sector. And the investors still see strong competition to secure the best of these resources. Both must make a choice as it is a long-term commitment that is made and the success of a project is a joint responsibility that depends on know-how, technology and experience from the operating company and stable environment, efficient regulations, and equitable fiscal terms from country.

In this Joint Convex meeting we will have panel discussions on how Strategic Alliance can accelerate the process of increasing Resources-to-Production ratios, special talks related to latest issues in the global market, and technical presentations on the future landscape of the oil and gas industry in Indonesia.

We invite you to joint this great event as sponsor, 400+ papers/posters will be presented covering multi-disciplinary topic geology, geophysics, petroleum engineering, and production facility, 1000+ professionals will attend the seminar and exhibitions, including the top management from all KKKS who has working area throughout Indonesia. And not to forget the prestigious 5-star venue in the beautiful city of Bandung will ensure your company brand exposure in the industry.

Look forward to seeing you in the 2021 Joint Convex!

Ir. Ari Iskandar, S.T. – JCB 2021 Chairman

ISBN 978-979-8126-46-8
9 789798 126468